

NASA Technical Memorandum 105595

1N-82

136185

P.401

Bibliography of Lewis Research Center Technical Publications Announced in 1991

(NASA-IM-105595) BIBLIOGRAPHY OF
LEWIS RESEARCH CENTER TECHNICAL
PUBLICATIONS ANNOUNCED IN 1991
(NASA) 401 p

N73-14773

Unclass

63/82 013.145

October 1992

NASA

Bibliography of Lewis Research Center Technical Publications Announced in 1991

October 1992



National Aeronautics and
Space Administration

Lewis Research Center
Cleveland, Ohio 44135

PREFACE

This year, NASA Lewis Research Center celebrated its 50th year of aerospace and aeronautical research. Special activities included a ground-breaking ceremony, a time-capsule-closing ceremony, and a public open house to showcase the accomplishments of Lewis researchers. In recognition of these accomplishments and of Lewis' contributions to the city of Cleveland, Cleveland City Council and Mayor Michael White officially proclaimed October 25, 1991, as NASA Lewis Research Center Day in Cleveland.

Making the results of our research available to others has always been part of Lewis' 50-year history. In 1991, Lewis Research Center's 1893 research authors (1424 civil servants and 469 on-site contractor and university staff) published 788 technical publications that were announced to and reached the worldwide scientific community. This was our highest number of technical publications since 1963 and 129 more than last year's production of 659. Included in this total were more symposium/seminar presentations (367), more papers for Lewis-hosted conferences (176), and more theses (11) than at any other time, as well as the most high-numbered technical memorandums since 1973 (133). In addition to this total, 10 technical videos and 198 contractor-authored research reports were produced at NASA Lewis.

In 1991, Lewis authors published approximately 57 percent of their research contributions in outside publications and the remainder as NASA research reports. Seventy-six percent of Lewis-authored society presentations and journal articles were addressed to members of the following 10 societies—AIAA, ASME, SAE, American Society of Engineering Education (ASEE), IEEE, NASA, AIChE, American Nuclear Society (ANS), American Chemical Society (ACS), and Ohio Aerospace Institute (OAI).

Sometimes Lewis scientists and engineers write books or manuals that are of lasting reference value. In 1991 Lewis published two of these reference publications:

- NASA RP-1248, Monograph on Propagation of Sound Waves in Curved Ducts by Wojciech Rostafinski
- NASA RP-1255, Fundamentals of Fluid Film Lubrication by Bernard J. Hamrock

Lewis hosted 18 research conferences and workshops in 1991. Ten of these resulted in NASA Conference Publications:

- NASA CP-10078, Computational Fluid Dynamics, March 12-14
- NASA CP-10063, Aeropropulsion '91, March 20-21
- NASA CP-10070, Seals Flow Code Development, March 26
- NASA CP-3125, Space Electrochemical Research and Technology, April 9-10
- NASA CP-3121, Space Photovoltaic Research and Technology—1991, May 7-9
- NASA CP-10084, Magnetoplasmadynamic Thruster Workshop, May 16
- NASA CP-10088, Workshop on Engineering Turbulence Modeling, August 21-22
- NASA CP-10082, HITEMP Review—1991: Advanced High Temperature Engine Materials Technology Program, October 29-30
- NASA CP-3132, Space Communications Technology Conference—Onboard Processing and Switching, November 12-14
- NASA CP-10089, Workshop on Grid Generation and Related Areas, November 14-15

Three of these publications were published at Lewis and made available to the attendees when they registered at the conferences: Aeropropulsion '91, HITEMP Review, and Space Communications Technology. Other conferences and workshops hosted or sponsored by Lewis in 1991 included

- Microgravity Vibrations Isolation Workshop, April 23-24
- 1991 Space Cryogenics Workshop, June 18-20
- The Fourth Annual International Conference on Laser Anemometry Advances and Applications, August 5-9
- Thermal & Fluids Analysis Workshop, August 19-23

- Advanced Space Exploration Initiative (SEI) Technologies, September 3–6
- NASA/Federal Aviation Administration (FAA) Tailplane Icing Workshop, November 4–5
- Lewis CADAM Users' Conference, December

Many of Lewis' researchers patent their inventions. In 1991, 25 patents were applied for and 20 patents were issued. Some of the patents issued in 1991 were given for a thin solar cell lightweight array; substituted 1,1,1/triaryl 2,2,2/trifluoroethanes and processes for their synthesis; arc-textured high-emittance radiator surfaces; furnace for tensile/fatigue testing; quick action clamp; method of making carbide/fluoride/silver composites; brominated graphitized carbon fibers; extended temperature range rocket injectors; probe apparatus with inflatable seal; high temperature, flexible, pressure-activated, rush seal; method of intercalating large quantities of fibrous structures; method of producing a plug type heat flux gauge; selective emitters; and method of preparing a thermal barrier coating.

In 1991, Lewis Research Center received three R&D 100 Awards. Since they were established by Research and Development magazine in 1962, Lewis has won 62 of these prestigious awards. This year's awards were given to Kenneth Bowles and Carl Lowell for the "Inert Gas Post Cured (IGPC) Crosslinked Polymer," to D.R. Englund, Jih-Fen Lei, and C.O. Hulse for the "PdCr Strain Gauge," and to Richard Patterson, the Lewis contact for this project, for the "Optical Fiber Current Sensor" developed jointly by the National Institute of Standards and Technology, NASA Lewis Research Center, the Navy's David Taylor Research Center, and the 3M Company.

Lewis researchers also received some awards for their publications. The 1991 Lewis Distinguished Publication Award was presented to Richard Seasholtz, Steven Schneider, and Frank Zupanc for their paper entitled "Spectrally Resolved Rayleigh Scattering Diagnostic for Hydrogen-Oxygen Rocket Plume Studies." In addition, Joseph Stephens, Donald Petrusek, and Robert Titran received the Charles Hatchett Award. Out of over 5000 entries, their paper, "Refractory Metal Alloys and Composites for Space Power Systems," was chosen by an international panel to be the most significant scientific and engineering paper on the metal niobium published in 1989 or 1990.

A few of the other awards received by Lewis engineers in 1991 follow. Six researchers received Silver Snoopy awards this year for their contributions to astronaut safety in the manned flight program. Those distinguished were Christos Chamis, Robert Hendricks, James Gauntner, Gary Halford, John Koudelka, and Isam Yunis. Margaret Proctor was named Young Engineer of the Year during the National Engineer's Week. Charles Trefny and Richard Dewitt were recognized by the National Aero-Space Plane Joint Program Office for their contributions to technology development for the NASP Program. John Adamczyk, Richard Mulac, Karen Pischel, Anthony Hackenberg, and Richard Sensiba received CRAY Research's Gigaflop Award and were named finalists in the Computerworld Smithsonian Awards for their research and development of a numerical simulation model for the core compressor of a jet propulsion engine.

All of the publications in this collection were announced in the 1991 issues of STAR (Scientific and Technical Aerospace Reports) and IAA (International Aerospace Abstracts). Some 1991 publications will be announced in the 1992 issues of STAR and IAA and will thus appear in the 1992 Lewis Bibliography. However, a few Lewis-authored publications are not included in this compilation because of FEDD (For Early Domestic Dissemination) and ITAR (International Traffic in Arms Regulations) considerations which limit their announcement and distribution.

The arrangement of the material is by NASA subject category, as noted in the Contents. In addition, the various indexes will help locate specific publications by subject, author, contractor organization contract number, and report number.

Richard E. Texler
Chief, Technical Information Services Division

TABLE OF CONTENTS

AERONAUTICS For related information see also *Astronautics*.

01 AERONAUTICS (GENERAL)	1
02 AERODYNAMICS	1
Includes aerodynamics of bodies, combinations, wings, rotors, and control surfaces; and internal flow in ducts and turbomachinery. For related information see also <i>34 Fluid Mechanics and Heat Transfer</i> .	
03 AIR TRANSPORTATION AND SAFETY	18
Includes passenger and cargo air transport operations; and aircraft accidents. For related information see also <i>16 Space Transportation</i> and <i>85 Urban Technology and Transportation</i> .	
04 AIRCRAFT COMMUNICATIONS AND NAVIGATION	20
Includes digital and voice communication with aircraft; air navigation systems (satellite and ground based); and air traffic control. For related information see also <i>17 Space Communications, Spacecraft Communications, Command and Tracking</i> and <i>32 Communications and Radar</i> .	
05 AIRCRAFT DESIGN, TESTING AND PERFORMANCE	20
Includes aircraft simulation technology. For related information see also <i>18 Spacecraft Design, Testing and Performance</i> and <i>39 Structural Mechanics</i> . For land transportation vehicles see <i>85 Urban Technology and Transportation</i> .	
06 AIRCRAFT INSTRUMENTATION	21
Includes cockpit and cabin display devices; and flight instruments. For related information see also <i>19 Spacecraft Instrumentation</i> and <i>35 Instrumentation and Photography</i> .	
07 AIRCRAFT PROPULSION AND POWER	21
Includes prime propulsion systems and systems components, e.g., gas turbine engines and compressors; and onboard auxiliary power plants for aircraft. For related information see also <i>20 Spacecraft Propulsion and Power, 28 Propellants and Fuels</i> , and <i>44 Energy Production and Conversion</i> .	
08 AIRCRAFT STABILITY AND CONTROL	36
Includes aircraft handling qualities; piloting; flight controls; and autopilots. For related information see also <i>05 Aircraft Design, Testing and Performance</i> .	
09 RESEARCH AND SUPPORT FACILITIES (AIR)	37
Includes airports, hangars and runways; aircraft repair and overhaul facilities; wind tunnels; shock tubes; and aircraft engine test stands. For related information see also <i>14 Ground Support Systems and Facilities (Space)</i> .	

ASTRONAUTICS For related information see also *Aeronautics*.

12 ASTRONAUTICS (GENERAL)	39
For extraterrestrial exploration see <i>91 Lunar and Planetary Exploration</i> .	
13 ASTRODYNAMICS	40
Includes powered and free-flight trajectories; and orbital and launching dynamics.	
14 GROUND SUPPORT SYSTEMS AND FACILITIES (SPACE)	40
Includes launch complexes, research and production facilities; ground support equipment, e.g., mobile transporters; and simulators. For related information see also <i>09 Research and Support Facilities (Air)</i> .	
15 LAUNCH VEHICLES AND SPACE VEHICLES	43
Includes boosters; operating problems of launch/space vehicle systems; and reusable vehicles. For related information see also <i>20 Spacecraft Propulsion and Power</i> .	
16 SPACE TRANSPORTATION	44
Includes passenger and cargo space transportation, e.g., shuttle operations; and space rescue techniques. For related information see also <i>03 Air Transportation and Safety</i> and <i>18 Spacecraft Design, Testing and Performance</i> . For space suits see <i>54 Man/System Technology and Life Support</i> .	
17 SPACE COMMUNICATIONS, SPACECRAFT COMMUNICATIONS, COMMAND AND TRACKING ...	44
Includes telemetry; space communications networks; astronavigation and guidance; and radio blackout. For related information see also <i>04 Aircraft Communications and Navigation</i> and <i>32 Communications and Radar</i> .	

N.A.—no abstracts were assigned to this category for this issue.

18 SPACECRAFT DESIGN, TESTING AND PERFORMANCE	46
Includes satellites; space platforms; space stations; spacecraft systems and components such as thermal and environmental controls; and attitude controls. For life support systems see <i>54 Man/System Technology and Life Support</i> . For related information see also <i>05 Aircraft Design, Testing and Performance</i> , <i>39 Structural Mechanics</i> , and <i>16 Space Transportation</i> .	
19 SPACECRAFT INSTRUMENTATION	49
For related information see also <i>06 Aircraft Instrumentation</i> and <i>35 Instrumentation and Photography</i> .	
20 SPACECRAFT PROPULSION AND POWER	50
Includes main propulsion systems and components, e.g., rocket engines; and spacecraft auxiliary power sources. For related information see also <i>07 Aircraft Propulsion and Power</i> , <i>28 Propellants and Fuels</i> , <i>44 Energy Production and Conversion</i> , and <i>15 Launch Vehicles and Space Vehicles</i> .	

CHEMISTRY AND MATERIALS

23 CHEMISTRY AND MATERIALS (GENERAL)	87
24 COMPOSITE MATERIALS	90
Includes physical, chemical, and mechanical properties of laminates and other composite materials. For ceramic materials see <i>27 Nonmetallic Materials</i> .	
25 INORGANIC AND PHYSICAL CHEMISTRY	104
Includes chemical analysis, e.g., chromatography; combustion theory; electrochemistry; and photochemistry. For related information see also <i>77 Thermodynamics and Statistical Physics</i> .	
26 METALLIC MATERIALS	107
Includes physical, chemical, and mechanical properties of metals, e.g., corrosion; and metallurgy.	
27 NONMETALLIC MATERIALS	113
Includes physical, chemical, and mechanical properties of plastics, elastomers, lubricants, polymers, textiles, adhesives, and ceramic materials. For composite materials see <i>24 Composite Materials</i> .	
28 PROPELLANTS AND FUELS	124
Includes rocket propellants, igniters and oxidizers; their storage and handling procedures; and aircraft fuels. For related information see also <i>07 Aircraft Propulsion and Power</i> , <i>20 Spacecraft Propulsion and Power</i> , and <i>44 Energy Production and Conversion</i> .	
29 MATERIALS PROCESSING	127
Includes space-based development of products and processes for commercial applications. For biological materials see <i>55 Space Biology</i> .	

ENGINEERING For related information see also *Physics*.

31 ENGINEERING (GENERAL)	129
Includes vacuum technology; control engineering; display engineering; cryogenics; and fire prevention.	
32 COMMUNICATIONS AND RADAR	131
Includes radar; land and global communications; communications theory; and optical communications. For related information see also <i>04 Aircraft Communications and Navigation</i> and <i>17 Space Communications, Spacecraft Communications, Command and Tracking</i> . For search and rescue see <i>03 Air Transportation and Safety</i> , and <i>16 Space Transportation</i> .	
33 ELECTRONICS AND ELECTRICAL ENGINEERING	136
Includes test equipment and maintainability; components, e.g., tunnel diodes and transistors; microminiaturization; and integrated circuitry. For related information see also <i>60 Computer Operations and Hardware</i> and <i>76 Solid-State Physics</i> .	
34 FLUID MECHANICS AND HEAT TRANSFER	147
Includes boundary layers; hydrodynamics; fluidics; mass transfer; and ablation cooling. For related information see also <i>02 Aerodynamics</i> and <i>77 Thermodynamics and Statistical Physics</i> .	
35 INSTRUMENTATION AND PHOTOGRAPHY	170
Includes remote sensors; measuring instruments and gauges; detectors; cameras and photographic supplies; and holography. For aerial photography see <i>43 Earth Resources and Remote Sensing</i> . For related information see also <i>06 Aircraft Instrumentation</i> and <i>19 Spacecraft Instrumentation</i> .	
36 LASERS AND MASERS	179
Includes parametric amplifiers. For related information see also <i>76 Solid-State Physics</i> .	

37 MECHANICAL ENGINEERING	179
Includes auxiliary systems (nonpower); machine elements and processes; and mechanical equipment.	
38 QUALITY ASSURANCE AND RELIABILITY	191
Includes product sampling procedures and techniques; and quality control.	
39 STRUCTURAL MECHANICS	195
Includes structural element design and weight analysis; fatigue; and thermal stress. For applications see <i>05 Aircraft Design, Testing and Performance</i> and <i>18 Spacecraft Design, Testing and Performance</i> .	
GEOSCIENCES For related information see also <i>Space Sciences</i> .	
42 GEOSCIENCES (GENERAL)	N.A.
43 EARTH RESOURCES AND REMOTE SENSING	N.A.
Includes remote sensing of earth resources by aircraft and spacecraft; photogrammetry; and aerial photography. For instrumentation see <i>35 Instrumentation and Photography</i> .	
44 ENERGY PRODUCTION AND CONVERSION	206
Includes specific energy conversion systems, e.g., fuel cells; global sources of energy; geophysical conversion; and windpower. For related information see also <i>07 Aircraft Propulsion and Power</i> , <i>20 Spacecraft Propulsion and Power</i> , and <i>28 Propellants and Fuels</i> .	
45 ENVIRONMENT POLLUTION	N.A.
Includes atmospheric, noise, thermal, and water pollution.	
46 GEOPHYSICS	N.A.
Includes aeronomy; upper and lower atmosphere studies; ionospheric and magnetospheric physics; and geomagnetism. For space radiation see <i>93 Space Radiation</i> .	
47 METEOROLOGY AND CLIMATOLOGY	N.A.
Includes weather forecasting and modification.	
48 OCEANOGRAPHY	N.A.
Includes biological, dynamic, and physical oceanography; and marine resources. For related information see also <i>43 Earth Resources and Remote Sensing</i> .	
LIFE SCIENCES	
51 LIFE SCIENCES (GENERAL)	N.A.
52 AEROSPACE MEDICINE	215
Includes physiological factors; biological effects of radiation; and effects of weightlessness on man and animals.	
53 BEHAVIORAL SCIENCES	N.A.
Includes psychological factors; individual and group behavior; crew training and evaluation; and psychiatric research.	
54 MAN/SYSTEM TECHNOLOGY AND LIFE SUPPORT	215
Includes human engineering; biotechnology; and space suits and protective clothing. For related information see also <i>16 Space Transportation</i> .	
55 SPACE BIOLOGY	N.A.
Includes exobiology; planetary biology; and extraterrestrial life.	
MATHEMATICAL AND COMPUTER SCIENCES	
59 MATHEMATICAL AND COMPUTER SCIENCES (GENERAL)	215
60 COMPUTER OPERATIONS AND HARDWARE	215
Includes hardware for computer graphics, firmware, and data processing. For components see <i>33 Electronics and Electrical Engineering</i> .	
61 COMPUTER PROGRAMMING AND SOFTWARE	216
Includes computer programs, routines, and algorithms, and specific applications, e.g., CAD/CAM.	
62 COMPUTER SYSTEMS	217
Includes computer networks and special application computer systems.	

63 CYBERNETICS	218
Includes feedback and control theory, artificial intelligence, robotics and expert systems. For related information see also <i>54 Man/System Technology and Life Support</i> .	
64 NUMERICAL ANALYSIS	221
Includes iteration, difference equations, and numerical approximation.	
65 STATISTICS AND PROBABILITY	N.A.
Includes data sampling and smoothing; Monte Carlo method; and stochastic processes.	
66 SYSTEMS ANALYSIS	223
Includes mathematical modeling; network analysis; and operations research.	
67 THEORETICAL MATHEMATICS	N.A.
Includes topology and number theory.	
PHYSICS For related information see also <i>Engineering</i> .	
70 PHYSICS (GENERAL)	224
For precision time and time interval (PTTI) see <i>35 Instrumentation and Photography</i> ; for geophysics, astrophysics or solar physics see <i>46 Geophysics</i> , <i>90 Astrophysics</i> , or <i>92 Solar Physics</i> .	
71 ACOUSTICS	224
Includes sound generation, transmission, and attenuation. For noise pollution see <i>45 Environment Pollution</i> .	
72 ATOMIC AND MOLECULAR PHYSICS	228
Includes atomic structure, electron properties, and molecular spectra.	
73 NUCLEAR AND HIGH-ENERGY PHYSICS	229
Includes elementary and nuclear particles; and reactor theory. For space radiation see <i>93 Space Radiation</i> .	
74 OPTICS	229
Includes light phenomena and optical devices. For lasers see <i>36 Lasers and Masers</i> .	
75 PLASMA PHYSICS	231
Includes magnetohydrodynamics and plasma fusion. For ionospheric plasmas see <i>46 Geophysics</i> . For space plasmas see <i>90 Astrophysics</i> .	
76 SOLID-STATE PHYSICS	231
Includes superconductivity. For related information see also <i>33 Electronics and Electrical Engineering</i> and <i>36 Lasers and Masers</i> .	
77 THERMODYNAMICS AND STATISTICAL PHYSICS	237
Includes quantum mechanics; theoretical physics; and Bose and Fermi statistics. For related information see also <i>25 Inorganic and Physical Chemistry</i> and <i>34 Fluid Mechanics and Heat Transfer</i> .	
SOCIAL SCIENCES	
80 SOCIAL SCIENCES (GENERAL)	N.A.
Includes educational matters.	
81 ADMINISTRATION AND MANAGEMENT	237
Includes management planning and research.	
82 DOCUMENTATION AND INFORMATION SCIENCE	238
Includes information management; information storage and retrieval technology; technical writing; graphic arts; and micrography. For computer documentation see <i>61 Computer Programming and Software</i> .	
83 ECONOMICS AND COST ANALYSIS	238
Includes cost effectiveness studies.	
84 LAW, POLITICAL SCIENCE AND SPACE POLICY	N.A.
Includes NASA appropriation hearings; aviation law; space law and policy; international law; international cooperation; and patent policy.	
85 URBAN TECHNOLOGY AND TRANSPORTATION	238
Includes applications of space technology to urban problems; technology transfer; technology assessment; and surface and mass transportation. For related information see <i>03 Air Transportation and Safety</i> , <i>16 Space Transportation</i> , and <i>44 Energy Production and Conversion</i> .	

SPACE SCIENCES For related information see also *Geosciences*.

88 SPACE SCIENCES (GENERAL)	N.A.
89 ASTRONOMY	N.A.
Includes radio, gamma-ray, and infrared astronomy; and astrometry.	
90 ASTROPHYSICS	238
Includes cosmology; celestial mechanics; space plasmas; and interstellar and interplanetary gases and dust. For related information see also <i>75 Plasma Physics</i> .	
91 LUNAR AND PLANETARY EXPLORATION	241
Includes planetology; and manned and unmanned flights. For spacecraft design or space stations see <i>18 Spacecraft Design, Testing and Performance</i> .	
92 SOLAR PHYSICS	242
Includes solar activity, solar flares, solar radiation and sunspots. For related information see <i>93 Space Radiation</i> .	
93 SPACE RADIATION	N.A.
Includes cosmic radiation; and inner and outer Earth's radiation belts. For biological effects of radiation see <i>52 Aerospace Medicine</i> . For theory see <i>73 Nuclear and High-Energy Physics</i> .	

GENERAL

Includes aeronautical, astronautical, and space science related histories, biographies, and pertinent reports too broad for categorization; histories or broad overviews of NASA programs.

99 GENERAL	242
SUBJECT INDEX	A-1
PERSONAL AUTHOR INDEX	B-1
CORPORATE SOURCE INDEX	C-1
CONTRACT NUMBER INDEX	D-1
REPORT/ACCESSION NUMBER INDEX	E-1

Bibliography of Lewis Research Center Technical Publications Announced in 1991

01

AERONAUTICS (GENERAL)

A91-48605 National Aeronautics and Space Administration. Lewis Research Center, Cleveland, OH.

NASA'S HIGH SPEED RESEARCH PROGRAM - AN INTRODUCTION AND STATUS REPORT

HOWARD L. WESOKY (NASA, Lewis Research Center, Cleveland, OH), MICHAEL J. PRATHER (NASA, Goddard Institute for Space Studies, New York), and GERALD G. KAYTEN (NASA, Washington, DC) SAE, Aerospace Technology Conference and Exposition, Long Beach, CA, Oct. 1-4, 1990. 26 p. refs (SAE PAPER 901923) Copyright

NASA's High Speed Research Program (HSRP) gives attention to the potential environmental effects of a next-generation SST in three areas of concern: atmospheric pollution, airport community noise, and sonic boom. Research has accordingly been undertaken in such fields as the validation of ozone depletion predictions, the feasibility a 90-percent NO(x) emissions reduction to minimize ozone-layer impacts, economically viable compliance with FAR 36 Stage 3 airport community noise levels, and the comparative advantages of efficient subsonic flight over land masses or low-sonic-boom-optimized configurations. Interim HSRP milestones for 1991 and 1992 are noted. O.C.

02

AERODYNAMICS

Includes aerodynamics of bodies, combinations, wings, rotors, and control surfaces; and internal flow in ducts and turbomachinery.

A91-10339*# National Aeronautics and Space Administration. Lewis Research Center, Cleveland, OH.

OSCILLATING CASCADE AERODYNAMICS BY AN EXPERIMENTAL INFLUENCE COEFFICIENT TECHNIQUE

DANIEL H. BUFFUM (NASA, Lewis Research Center, Cleveland, OH) and SANFORD FLEETER (Purdue University, West Lafayette, IN) Journal of Propulsion and Power (ISSN 0748-4658), vol. 6, Sept.-Oct. 1990, p. 612-620. Previously cited in issue 03, p. 262. Accession no. A89-14976. refs Copyright

A91-12521*# National Aeronautics and Space Administration. Lewis Research Center, Cleveland, OH.

EFFECT OF ACOUSTIC EXCITATION ON STALLED FLOWS OVER AN AIRFOIL

K. B. M. Q. ZAMAN (NASA, Lewis Research Center, Cleveland, OH) AIAA, Aeroacoustics Conference, 13th, Tallahassee, FL, Oct. 22-24, 1990. 12 p. refs (AIAA PAPER 90-4009) Copyright

The effect of acoustic excitation on poststalled flows over an

airfoil, i.e., flows that are fully separated from near the leading edge, is investigated. The excitation results in a tendency toward reattachment, which is accompanied by an increased lift and reduced drag, although the flow may still remain fully separated. It is found that with increasing excitation amplitude, the effect becomes more pronounced but shifts to a Strouhal number which is much lower than that expected from linear, inviscid instability of the separated shear layer. Author

A91-13047*# National Aeronautics and Space Administration. Lewis Research Center, Cleveland, OH.

THE AERODYNAMICS OF AN OSCILLATING CASCADE IN A COMPRESSIBLE FLOW FIELD

D. H. BUFFUM (NASA, Lewis Research Center, Cleveland, OH) and S. FLEETER (Purdue University, West Lafayette, IN) ASME, Transactions, Journal of Turbomachinery (ISSN 0889-504X), vol. 112, Oct. 1990, p. 759-767. refs (ASME PAPER 89-GT-271) Copyright

Fundamental experiments are performed in the NASA Lewis Research Center Transonic Oscillating Cascade Facility to investigate and quantify the aerodynamics of a cascade of bioconvex airfoils executing torsion mode oscillations at realistic reduced frequency values. Both steady and unsteady airfoil surface pressures are measured at two inlet Mach numbers, 0.65 and 0.80, and two incidence angles, 0 and 7 deg, with the harmonic torsional airfoil cascade oscillations at realistic high reduced frequency and unsteady data obtained at several interblade phase angle values. The time-variant pressures are analyzed by means of discrete Fourier transform techniques, with these unique data compared with predictions from a linearized unsteady cascade model. The experimental results indicate that the interblade phase angle has a major effect on the chordwise distributions of the airfoil surface unsteady pressure, with the effect of reduced frequency, incidence angle, and Mach numbers somewhat less significant. Author

A91-14429*# National Aeronautics and Space Administration. Lewis Research Center, Cleveland, OH.

3D COMPUTATION OF HYPERSONIC NOZZLE

H. T. LAI (NASA, Lewis Research Center; Sverdrup Technology, Inc., Cleveland, OH) AIAA, International Aerospace Planes Conference, 2nd, Orlando, FL, Oct. 29-31, 1990. 23 p. refs (Contract NAS3-24105; NAS3-25266) (AIAA PAPER 90-5203)

Numerical results of a NASP-like nozzle configuration are presented. The nozzle has characteristically a very large area ratio designed to operate in the hypersonic regime. The overall flowfield consists of the internal expansion from a stagnation reservoir and the external exhaust plume in a quiescent environment. The solutions were obtained for two experimental conditions at an underexpanded pressure ratio of 44000 and an overexpanded pressure ratio of 2495. These conditions produce flows expanding to high Mach numbers in the hypersonic range. At the nozzle entrance, the flow has a supersonic Mach number of 4.3 in the inviscid region. In the external expansion and exhaust regions, the flow expands to a maximum Mach number of 12.3 for the case of high pressure ratio, whereas a shock wave exists for the low pressure ratio case. The solutions from these three-dimensional calculations were compared to the experimental data for pressure distributions. Author

02 AERODYNAMICS

A91-21065*# National Aeronautics and Space Administration. Lewis Research Center, Cleveland, OH.

NAVIER-STOKES SIMULATION OF TRANSONIC BLADE-VORTEX INTERACTIONS

N.-S. LIU (NASA, Lewis Research Center, Cleveland, OH; Scientific Research Associates, Glastonbury, CT), F. DAVOUDZADEH, W. R. BRILEY, and S. J. SHAMROTH (Scientific Research Associates, Inc., Glastonbury, CT) ASME, Transactions, Journal of Fluids Engineering (ISSN 0098-2202), vol. 112, Dec. 1990, p. 501-509. refs

(Contract NAS2-12635)

Copyright

Transonic strong blade-vortex interaction is numerically analyzed by solving the unsteady two-dimensional Navier-Stokes equations using an iterative implicit second order scheme. The dominant processes during the interaction are the development of large transverse pressure gradients in the upper leading edge region and the development of disturbances at the root of the lower surface shock wave. As a result of this interaction, high pressure pulses are emitted from the leading edge, and acoustic waves are radiated from the lower surface in a region originally occupied by a supersonic pocket. In addition, severe load variations occur when the vortex is within one chord length of the blade.

Author

A91-21242* National Aeronautics and Space Administration. Lewis Research Center, Cleveland, OH.

FLOW STUDIES IN CLOSE-COUPLED VENTRAL NOZZLES FOR STOVL AIRCRAFT

JACK G. MCARDLE (NASA, Lewis Research Center, Cleveland, OH) and C. FREDERIC SMITH (NASA, Lewis Research Center; Sverdrup Technology, Inc., Cleveland, OH) SAE, Aerospace Atlantic Meeting, Dayton, OH, Apr. 23-26, 1990. 22 p. (SAE PAPER 901033) Copyright

Flow in a generic ventral nozzle system was studied experimentally and analytically with the PARC3D computational fluid dynamics program (a full Navier-Stokes equations solver) in order to evaluate the program's ability to predict system performance and internal flow patterns. A generic model of a tailpipe with a rectangular ventral nozzle, about one-third of full size, was tested with unheated air at steady-state pressure ratios up to 4.0. Measurements showed about 5.5 percent flow-turning loss and reasonable nozzle performance coefficients. The flow turned more than the designed 90 deg, causing an aftward axial component in the total thrust. Flow behavior into and through the ventral duct is discussed and illustrated with paint streak flow visualization photographs. PARC3D graphic images are shown for comparison with the experiment photographs. The program successfully predicted internal flow patterns; it also computed thrust and discharge coefficients within 1 percent of measured values.

Author

A91-21393*# National Aeronautics and Space Administration. Lewis Research Center, Cleveland, OH.

AN ALGEBRAIC RNG-BASED TURBULENCE MODEL FOR THREE-DIMENSIONAL TURBOMACHINERY FLOWS

K. R. KIRTLEY (NASA, Lewis Research Center; Sverdrup Technology, Inc., Brook Park, OH) AIAA, Aerospace Sciences Meeting, 29th, Reno, NV, Jan. 7-10, 1991. 13 p. refs

(Contract NAS3-25266)

(AIAA PAPER 91-0172)

An algebraic eddy viscosity turbulence model based on Renormalization Group (RNG) theory for complex three-dimensional turbomachinery flows is presented. Modifications are made to the baseline RNG model for wakes and separated flows. The model has several advantages over popular algebraic models most notably its lack of empirically determined coefficients. The model is used to compute the mean flow in a low speed axial compressor rotor. The agreement with blade boundary layer and radial flow experimental data is very good and shows improvement over the Baldwin-Lomax model. The development of the tip leakage vortex is also well predicted. The computed wake decay also compares favorably with recent experimental data.

Author

A91-21493*# Wichita State Univ., KS.

EXPERIMENTAL WATER DROPLET IMPINGEMENT DATA ON MODERN AIRCRAFT SURFACES

MICHAEL PAPADAKIS (Wichita State University, KS), MARLIN D. BREER, NEIL C. CRAIG (Boeing Co., Wichita, KS), and COLIN S. BIDWELL (NASA, Lewis Research Center, Cleveland, OH) AIAA, Aerospace Sciences Meeting, 29th, Reno, NV, Jan. 7-10, 1991. 13 p. Research supported by FAA. refs

(Contract NAG3-566)

(AIAA PAPER 91-0445) Copyright

An experimental method has been developed to determine the water droplet impingement characteristics on two- and three-dimensional aircraft surfaces. The experimental water droplet impingement data are used to validate particle trajectory analysis codes that are used in aircraft icing analyses and engine inlet particle separator analyses. The aircraft surface is covered with thin strips of blotter paper in areas of interest. The surface is then exposed to an airstream that contains a dyed-water spray cloud. The water droplet impingement data are extracted from the dyed blotter paper strips by measuring the optical reflectance of each strip with an automated reflectometer. Preliminary experimental and analytical impingement efficiency data are presented for a NLF(1)-0414F airfoil, a swept MS(1)-0317 airfoil, a swept NACA 0012 wingtip and for a Boeing 737-300 engine inlet model.

Author

A91-22499*# National Aeronautics and Space Administration. Lewis Research Center, Cleveland, OH.

A STEADYING EFFECT OF ACOUSTIC EXCITATION ON TRANSITORY STALL

K. B. M. Q. ZAMAN (NASA, Lewis Research Center, Cleveland, OH) AIAA, Aerospace Sciences Meeting, 29th, Reno, NV, Jan. 7-10, 1991. 16 p. Previously announced in STAR as N91-13420. refs

(AIAA PAPER 91-0043) Copyright

The effect of acoustic excitation on a class of separated flows with a transitional boundary layer at the point of separation is considered. Experimental results on the flow over airfoils, a two-dimensional backward-facing step, and through large angle conical diffusers are presented. In all cases, the separated flow undergoes large amplitude fluctuations, much of the energy being concentrated at unusually low frequencies. In each case, an appropriate high frequency acoustic excitation is found to be effective in reducing the fluctuations substantially. The effective excitation frequency scales on the initial boundary layer thickness and the effect is apparently achieved through acoustic tripping of the separating boundary layer.

Author

A91-24360*# National Aeronautics and Space Administration. Lewis Research Center, Cleveland, OH.

CONTROL OF FLOW SEPARATION AND MIXING BY AERODYNAMIC EXCITATION

EDWARD J. RICE and JOHN M. ABBOTT (NASA, Lewis Research Center, Cleveland, OH) IN: ICAS, Congress, 17th, Stockholm, Sweden, Sept. 9-14, 1990, Proceedings. Vol. 1. Washington, DC, American Institute of Aeronautics and Astronautics, Inc., 1990, p. 543-553. refs

Copyright

The recent research progress in the control of shear flows using unsteady aerodynamic excitation conducted at the NASA Lewis Research Center is reviewed. The program is of fundamental nature concentrating on the physics of the unsteady aerodynamic processes. This field of research is a fairly new development with great promise in the areas of enhanced mixing and flow separation control. Enhanced mixing research reported in this paper include influence of core turbulence, forced pairing of coherent structures, and saturation of mixing enhancement. Separation flow control studies included are for a two-dimensional diffuser, conical diffusers, and single airfoils. Ultimate applications of this research include aircraft engine inlet flow control at high angle of attack, wide angle diffusers, highly loaded airfoils as in turbomachinery, and ejector/suppressor nozzles for the supersonic transport. An argument involving the Coanda Effect is made here that all of the

above mentioned application areas really only involve forms of shear layer mixing enhancement. The program also includes the development of practical excitation devices which might be used in aircraft applications. Author

A91-24519* # Kansas Univ., Lawrence.

MODERN DEVELOPMENTS IN SHEAR FLOW CONTROL WITH SWIRL

S. FAROKHI (Kansas, University, Lawrence), R. TAGHAVI (Sverdrup Technology, Inc., Cleveland, OH), and E. J. RICE (NASA, Lewis Research Center, Cleveland, OH) IN: ICAS, Congress, 17th, Stockholm, Sweden, Sept. 9-14, 1990, Proceedings. Vol. 2. Washington, DC, American Institute of Aeronautics and Astronautics, Inc., 1990, p. 2111-2122. Previously announced in STAR as N90-22000. refs (Contract NCC3-56; NAG3-1098) Copyright

Passive and active control of swirling turbulent jets is experimentally investigated. Initial swirl distribution is shown to dominate the free jet evolution in the passive mode. Vortex breakdown, a manifestation of high intensity swirl, was achieved at below critical swirl number ($S = 0.48$) by reducing the vortex core diameter. The response of a swirling turbulent jet to single frequency, plane wave acoustic excitation was shown to depend strongly on the swirl number, excitation Strouhal number, amplitude of the excitation wave, and core turbulence in a low speed cold jet. A 10 percent reduction of the mean centerline velocity at $x/D = 9.0$ (and a corresponding increase in the shear layer momentum thickness) was achieved by large amplitude internal plane wave acoustic excitation. Helical instability waves of negative azimuthal wave numbers exhibit larger amplification rates than the plane waves in swirling free jets, according to hydrodynamic stability theory. Consequently, an active swirling shear layer control is proposed to include the generation of helical instability waves of arbitrary helicity and the promotion of modal interaction, through multifrequency forcing. Author

A91-26192* # National Aeronautics and Space Administration. Lewis Research Center, Cleveland, OH.

THE AERODYNAMIC CHARACTERISTICS OF VORTEX INGESTION FOR THE F/A-18 INLET DUCT

BERNHARD H. ANDERSON (NASA, Lewis Research Center, Cleveland, OH) AIAA, Aerospace Sciences Meeting, 29th, Reno, NV, Jan. 7-10, 1991. 39 p. Previously announced in STAR as N91-15303. refs (AIAA PAPER 91-0130) Copyright

A Reduced Navier-Stokes (RNS) solution technique was successfully combined with the concept of partitioned geometry and mesh generation to form a very efficient 3-D RNS code aimed at the analysis-design engineering environment. Partitioned geometry and mesh generation is a pre-processor to augment existing geometry and grid generation programs which allows the solver to (1) recluster an existing gridlife mesh lattice, and (2) perturb an existing gridfile definition to alter the cross-sectional shape and inlet duct centerline distribution without returning to the external geometry and grid generator. The present results provide a quantitative validation of the initial value space marching 3-D RNS procedure and demonstrates accurate predictions of the engine face flow field, with a separation present in the inlet duct as well as when vortex generators are installed to suppress flow separation. The present results also demonstrate the ability of the 3-D RNS procedure to analyze the flow physics associated with vortex ingestion in general geometry ducts such as the F/A-18 inlet. At the conditions investigated, these interactions are basically inviscid like, i.e., the dominant aerodynamic characteristics have their origin in inviscid flow theory. Author

A91-26327* # National Aeronautics and Space Administration. Lewis Research Center, Cleveland, OH.

ICING CHARACTERISTICS OF A NATURAL-LAMINAR-FLOW, A MEDIUM-SPEED, AND A SWEPT, MEDIUM-SPEED AIRFOIL
COLIN S. BIDWELL (NASA, Lewis Research Center, Cleveland,

OH) AIAA, Aerospace Sciences Meeting, 29th, Reno, NV, Jan. 7-10, 1991. 32 p. refs (AIAA PAPER 91-0447) Copyright

Tests were conducted in the Icing Research Tunnel at the NASA Lewis Research Center to determine the icing characteristics of three modern airfoils: a natural-laminar-flow, a medium-speed, and a swept medium-speed airfoil. The tests measured the impingement characteristics and drag degradation for angles-of-attack typifying cruise and climb for cloud conditions typifying the range that might be encountered in flight. The maximum degradation occurred at the cruise angle-of-attack for the long, glaze ice condition for all three airfoils with increases over baseline drag being 486 percent, 510 percent, and 465 percent for the natural-laminar-flow, the medium-speed, and the swept, medium-speed airfoils, respectively. For the climb angle-of-attack, the maximum drag degradation (and total extent of impingement) observed were also for the long, glaze ice condition and were 261 percent, 181 percent, and 331 percent, respectively. The minimum drag degradation (and extent of impingement) occurred for the cruise condition and for the short, rime spray with increases over baseline drag values being 47 percent, 28 percent, 46 percent, respectively. Author

A91-26330* # National Aeronautics and Space Administration. Lewis Research Center, Cleveland, OH.

PREDICTION OF ICE SHAPES AND THEIR EFFECT ON AIRFOIL PERFORMANCE

JAIWON SHIN (NASA, Lewis Research Center, Cleveland, OH), BRIAN BERKOWITZ (NASA, Lewis Research Center, Cleveland; Sverdrup Technology, Inc., Brook Park, OH), HSUN H. CHEN, and TUNCER CEBECI (California State University, Long Beach) AIAA, Aerospace Sciences Meeting, 29th, Reno, NV, Jan. 7-10, 1991. 22 p. refs (AIAA PAPER 91-0264) Copyright

Calculations of ice shapes and the resulting drag increases are presented for experimental data on an NACA 0012 airfoil. They were made with a combination of LEWICE and interactive boundary-layer codes for a wide range of conditions which include airspeed and temperature, the droplet size and liquid water content of the cloud, and the angle of attack of the airfoil. In all cases the calculated results account for the drag increase due to ice accretion and, in general, show good agreement with data. Author

A91-26331* # National Aeronautics and Space Administration. Lewis Research Center, Cleveland, OH.

IMPROVED VISUALIZATION OF FLOW FIELD MEASUREMENTS

JEFFREY HILTON MILES (NASA, Lewis Research Center, Cleveland, OH) AIAA, Aerospace Sciences Meeting, 29th, Reno, NV, Jan. 7-10, 1991. 36 p. refs (AIAA PAPER 91-0273) Copyright

A capability is proposed that makes it feasible to apply to measured flow field data the visualization tools developed to display numerical solutions for computational fluid dynamic problems. The measurement monitor surface (MMS) methodology was used for the analysis of flow field measurements within a low-aspect-ratio transonic axial-flow fan rotor acquired with two-dimensional laser anemometry. It is shown that the MMS method may be utilized to generate input for the multidimensional processing and analytical tools developed for numerical flow field simulation data. Thus an experimenter utilizing an interactive graphics program could illustrate scalar quantities such as Mach number by profiles, contour lines, carpet plots, and surfaces employing various color intensities. Also, flow directionality can be shown by the display of vector fields and particle traces. R.E.P.

A91-27801* # National Aeronautics and Space Administration. Lewis Research Center, Cleveland, OH.

EXPERIMENTAL INVESTIGATION OF OSCILLATING CASCADE AERODYNAMICS

DANIEL H. BUFFUM (NASA, Lewis Research Center, Cleveland,

02 AERODYNAMICS

OH) and SANFORD FLEETER (Purdue University, West Lafayette, IN) *Journal of Aerospace Power* (ISSN 1000-8055), vol. 5, July 1990, p. 275-282. refs

A series of experiments are performed in the NASA Lewis Transonic Oscillating Cascade Facility to provide fundamental data quantifying the high subsonic and transonic steady and oscillating aerodynamics of a biconvex airfoil cascade at realistic reduced frequency values for all interblade phase angles. This is accomplished by developing and utilizing an unsteady aerodynamic influence-coefficient technique in which only one cascaded airfoil is oscillated at a time. The vector summation of the resulting airfoil-surface unsteady pressures (measured on a dynamically instrumented airfoil) makes it possible to determine the unsteady aerodynamics of an equivalent cascade with all airfoils oscillating at any specified interblade phase angle. Author

A91-28590* National Aeronautics and Space Administration. Lewis Research Center, Cleveland, OH.

NUMERICAL SIMULATIONS OF SUPERSONIC FLOW THROUGH OSCILLATING CASCADE SECTIONS

DENNIS L. HUFF (NASA, Lewis Research Center, Cleveland, OH) and T. S. R. REDDY (Toledo, University, OH) IN: *Developments in theoretical and applied mechanics. Vol. 15 - Proceedings of the 15th Southeastern Conference on Theoretical and Applied Mechanics*, Atlanta, GA, Mar. 22, 23, 1990. Atlanta, GA, Georgia Institute of Technology, 1990, p. 187-194. refs

Copyright

A finite difference code has been developed for modeling inviscid, unsteady supersonic flow by solution of the compressible Euler equations. The code uses a deforming grid technique to capture the motion of the airfoils and can model oscillating cascades with any arbitrary interblade phase angle. A flat plate cascade is analyzed, and results are compared with results from a small-perturbation theory. The results show very good agreement for both the unsteady pressure distributions and the integrated force predictions. The reason for using the numerical Euler code over a small-perturbation theory is the ability to model 'real' airfoils that have thickness and camber. Sample predictions are presented for a cascade of loaded airfoils and show appreciable differences in the unsteady surface pressure distributions when compared with the flat plate results. Author

A91-30014*# National Aeronautics and Space Administration. Lewis Research Center, Cleveland, OH.

THREE-DIMENSIONAL VISCOUS FLOW COMPUTATIONS OF HIGH AREA RATIO NOZZLES FOR HYPERSONIC PROPULSION

D. R. REDDY and G. J. HARLOFF (NASA, Lewis Research Center; Sverdrup Technology, Inc., Brook Park, OH) *Journal of Propulsion and Power* (ISSN 0748-4658), vol. 7, Jan.-Feb. 1991, p. 84-89. refs

(Contract NAS3-24105; NAS3-25266)

Copyright

The PARC3D code was selected by the authors to analyze a variety of complex and high-speed flow configurations. Geometries considered for code validation include ramps and corner flows, which are characteristic of inlets and nozzles. Flows with Mach numbers of 3-14 were studied. Both two- and three-dimensional experimental data for shock-boundary-layer interaction were considered to validate the code. A detailed comparison of various flow parameters with available experimental data is presented; agreement between the solutions and the experimental data in terms of pitot pressure profiles, yaw-angle distributions, static pressures, and skin friction is found to be very good. In addition, two- and three-dimensional flow calculations were performed for a hypersonic nozzle. Comparison of the wall pressure results with the published solutions is made for the two-dimensional case. Author

A91-34135*# National Aeronautics and Space Administration. Lewis Research Center, Cleveland, OH.

ROLE OF ARTIFICIAL VISCOSITY IN EULER AND NAVIER-STOKES SOLVERS

APARAJIT J. MAHAJAN (NASA, Lewis Research Center, Cleveland, OH; Duke University, Durham, NC), EARL H. DOWELL, and DONALD B. BLISS (Duke University, Durham, NC) *AIAA Journal* (ISSN 0001-1452), vol. 29, April 1991, p. 555-559. refs

(Contract NAG3-724)

Copyright

A method is proposed to determine directly the amount of artificial viscosity needed for stability using an eigenvalue analysis for a finite difference representation of the Navier-Stokes equations. The stability and growth of small perturbations about a steady flow over airfoils are analyzed for various amounts of artificial viscosity. The eigenvalues were determined for a small time-dependent perturbation about a steady inviscid flow over an NACA 0012 airfoil at a Mach number of 0.8 and angle of attack of 0 deg. The method has been applied to inviscid flows here, but as discussed is also applicable to viscous flows. The movement of the eigenvalue constellation with respect to the amount of artificial viscosity is studied. The stability boundaries as a function of the amount of artificial viscosity from both the eigenvalue analysis and the time-marching scheme are also presented. The eigenvalue procedure not only allows for determining the effect of varying amounts of artificial viscosity, but also for the effects of different forms of artificial viscosity. Author

A91-37421*# National Aeronautics and Space Administration. Lewis Research Center, Cleveland, OH.

COMPUTATIONAL ANALYSIS OF UNDEREXPANDED JETS IN THE HYPERSONIC REGIME

ANDREW T. HSU (NASA, Lewis Research Center; Sverdrup Technology, Inc., Cleveland, OH) and MENG-SING LIOU (NASA, Lewis Research Center, Cleveland, OH) *Journal of Propulsion and Power* (ISSN 0748-4658), vol. 7, Mar.-Apr. 1991, p. 297-299. Previously cited in issue 21, p. 3483, Accession no. A88-50604. refs

Copyright

A91-40561*# National Aeronautics and Space Administration. Lewis Research Center, Cleveland, OH.

HOT GAS INGESTION TEST RESULTS OF A TWO-POSTER VECTORED THRUST CONCEPT WITH FLOW VISUALIZATION IN THE NASA LEWIS 9- BY 15-FOOT LOW SPEED WIND TUNNEL

ALBERT L. JOHNS, GEORGE NEINER, TIMOTHY J. BENCIC (NASA, Lewis Research Center, Cleveland, OH), JOSEPH D. FLOOD, KURT C. AMUEDO (McDonnell Aircraft Co., Saint Louis, MO) et al. *AIAA, SAE, ASME, and ASEE, Joint Propulsion Conference*, 26th, Orlando, FL, July 16-18, 1990. 27 p. Previously announced in STAR as N91-21116. (AIAA PAPER 90-2268) Copyright

A 9.2 percent scale STOVL hot gas ingestion model was tested in the NASA Lewis 9 x 15-foot Low-Speed Wind Tunnel. Flow visualization from the Phase 1 test program, which evaluated the hot ingestion phenomena and control techniques, is covered. The Phase 2 test program evaluated the hot gas ingestion phenomena at higher temperatures and used a laser sheet to investigate the flow field. Hot gas ingestion levels were measured for the several forward nozzle splay configurations and with flow control/life improvement devices (LIDs) which reduced the hot gas ingestion. The test was conducted at full scale nozzle pressure ratios and inlet Mach numbers. Results are presented over a range of nozzle pressure ratios at a 10 kn headwind velocity. The Phase 2 program was conducted at exhaust nozzle temperatures up to 1460 R and utilized a sheet laser system for flow visualization of the model flow field in and out of ground effects. The results reported are for nozzle exhaust temperatures up to 1160 R and contain the compressor face pressure and temperature distortions, the total pressure recovery, the inlet temperature rise, and the environmental effects of the hot gas. The environmental effects include the ground plane contours, the model airframe heating, and the location of the ground flow separation. Author

A91-40721* # National Aeronautics and Space Administration. Lewis Research Center, Cleveland, OH.

A NEW LAGRANGIAN RANDOM CHOICE METHOD FOR STEADY TWO-DIMENSIONAL SUPERSONIC/HYPERSONIC FLOW

C. Y. LOH (NASA, Lewis Research Center, Cleveland, OH) and W. H. HUI (Waterloo, University, Canada) IN: AIAA Computational Fluid Dynamics Conference, 10th, Honolulu, HI, June 24-27, 1991, Technical Papers. Washington, DC, American Institute of Aeronautics and Astronautics, 1991, p. 209-216. Research supported by NASA and NSERC. refs (AIAA PAPER 91-1546) Copyright

Glimm's (1965) random choice method has been successfully applied to compute steady two-dimensional supersonic/hypersonic flow using a new Lagrangian formulation. The method is easy to program, fast to execute, yet it is very accurate and robust. It requires no grid generation, resolves slipline and shock discontinuities crisply, can handle boundary conditions most easily, and is applicable to hypersonic as well as supersonic flow. It represents an accurate and fast alternative to the existing Eulerian methods. Many computed examples are given. Author

A91-40730* # Virginia Polytechnic Inst. and State Univ., Blacksburg.

GENERALIZED CONJUGATE-GRADIENT METHODS FOR THE NAVIER-STOKES EQUATIONS

KUMUD AJMANI, WING-FAI NG (Virginia Polytechnic Institute and State University, Blacksburg), and MENG-SING LIOU (NASA, Lewis Research Center, Cleveland, OH) IN: AIAA Computational Fluid Dynamics Conference, 10th, Honolulu, HI, June 24-27, 1991, Technical Papers. Washington, DC, American Institute of Aeronautics and Astronautics, 1991, p. 319-327. refs (AIAA PAPER 91-1556) Copyright

A generalized conjugate-gradient method is used to solve the two-dimensional, compressible Navier-Stokes equations of fluid flow. The equations are discretized with an implicit, upwind finite-volume formulation. Preconditioning techniques are incorporated into the new solver to accelerate convergence of the overall iterative method. The superiority of the new solver is demonstrated by comparisons with a conventional line Gauss-Siedel Relaxation solver. Computational test results for transonic flow (trailing edge flow in a transonic turbine cascade) and hypersonic flow ($M = 6.0$ shock-on-shock phenomena on a cylindrical leading edge) are presented. When applied to the transonic cascade case, the new solver is 4.4 times faster in terms of number of iterations and 3.1 times faster in terms of CPU time than the Relaxation solver. For the hypersonic shock case, the new solver is 3.0 times faster in terms of number of iterations and 2.2 times faster in terms of CPU time than the Relaxation solver. Author

A91-40740* # National Aeronautics and Space Administration. Lewis Research Center, Cleveland, OH.

NUMERICAL FLUX FORMULAS FOR THE EULER AND NAVIER-STOKES EQUATIONS. II - PROGRESS IN FLUX-VECTOR SPLITTING

WILLIAM J. COIRIER (NASA, Lewis Research Center, Cleveland, OH) and BRAM VAN LEER (Michigan, University, Ann Arbor) IN: AIAA Computational Fluid Dynamics Conference, 10th, Honolulu, HI, June 24-27, 1991, Technical Papers. Washington, DC, American Institute of Aeronautics and Astronautics, 1991, p. 422-438. Previously announced in STAR as N91-22084. refs (AIAA PAPER 91-1566) Copyright

The accuracy of various numerical flux functions for the inviscid fluxes when used for Navier-Stokes computations is studied. The flux functions are benchmarked for solutions of the viscous, hypersonic flow past a 10 degree cone at zero angle of attack using first order, upwind spatial differencing. The Harten-Lax/Roe flux is found to give a good boundary layer representation, although its robustness is an issue. Some hybrid flux formulas, where the concepts of flux-vector and flux-difference splitting are combined, are shown to give unsatisfactory pressure distributions; there is still room for improvement. Investigations of low diffusion, pure

flux-vector splittings indicate that a pure flux-vector splitting can be developed that eliminates spurious diffusion across the boundary layer. The resulting first-order scheme is marginally stable and not monotone. Author

A91-41738* # Ohio State Univ., Columbus.

SUPERSONIC JET MIXING ENHANCEMENT BY VORTEX GENERATORS

M. SAMIMY, M. F. REEDER (Ohio State University, Columbus), and K. B. M. Q. ZAMAN (NASA, Lewis Research Center, Cleveland, OH) AIAA, SAE, ASME, and ASCE, Joint Propulsion Conference, 27th, Sacramento, CA, June 24-26, 1991. 13 p. refs (AIAA PAPER 91-2263) Copyright

Experiments were conducted to explore the effects of vortex generators, in the form of tabs projecting normally into the jet, on the mixing and the far-field noise characteristics of a jet. A converging-diverging nozzle with a design Mach number of 1.36 was used in the experiments. The flow regimes from subsonic to highly underexpanded supersonic conditions were studied. One, two, and four tabs were used and some of the findings of previous investigators were examined and confirmed. The tabs eliminated screech noise from moderately overexpanded cases to highly underexpanded cases. Detailed flow visualizations and measurements showed that two tabs bifurcated the jet at all Mach numbers. While the effect of two tabs was persistent and the jet remained bifurcated, the distortions produced by one and four tabs disappeared by a streamwise distance of approximately 16 jet diameters. Two and four tabs significantly increased the entrainment of ambient air into the jet. Author

A91-42814* # National Aeronautics and Space Administration. Lewis Research Center, Cleveland, OH.

INFLUENCE OF THICKNESS AND CAMBER ON THE AEROELASTIC STABILITY OF SUPERSONIC THROUGHFLOW FANS

JOHN K. RAMSEY (NASA, Lewis Research Center, Cleveland, OH) Journal of Propulsion and Power (ISSN 0748-4658), vol. 7, May-June 1991, p. 404-411. Previously announced in STAR as N89-25957. refs Copyright

An engineering approach was used to include the nonlinear effects of thickness and camber in an analytical aeroelastic analysis of cascade in supersonic axial flow (supersonic leading-edge locus). A hybrid code using Lighthill's nonlinear piston theory and Lane's linear potential theory was developed to include these nonlinear effects. Lighthill's theory was used to calculate the unsteady pressures on the noninterference surface regions of the airfoils in cascade. Lane's theory was used to calculate the unsteady pressures on the remaining interference surface regions. Two airfoil profiles were investigated (a supersonic throughflow fan design and a NACA 66-206 airfoil with a sharp leading edge). Results show that compared with predictions of Lane's potential theory for flat plates, the inclusion of thickness (with or without camber) may increase or decrease the aeroelastic stability, depending on the airfoil geometry and operating conditions. When thickness effects are included in the aeroelastic analysis, inclusion of camber will influence the predicted stability in proportion to the magnitude of the added camber. The critical interblade phase angle, depending on the airfoil profile and operating conditions, may also be influenced by thickness and camber. Compared with predictions of Lane's linear potential theory, the inclusion of thickness and camber decreased the aerodynamic stiffness and increased the aerodynamic damping at Mach 2 and 2.95 for a cascade of supersonic throughflow fan airfoils oscillating 180 degrees out of phase at a reduced frequency of 0.1. Author

A91-42820* # Sverdrup Technology, Inc., Brook Park, OH.

LARGE-SCALE ADVANCED PROPELLER BLADE PRESSURE DISTRIBUTIONS - PREDICTION AND DATA

N. NALLASAMY, O. YAMAMOTO, S. WARSI (Sverdrup Technology, Inc., Brook Park, OH), and L. J. BOBER (NASA, Lewis Research Center, Cleveland, OH) Journal of Propulsion and Power (ISSN

02 AERODYNAMICS

0748-4658), vol. 7, May-June 1991, p. 452-461. Previously cited in issue 20, p. 3084, Accession no. A89-47026. refs
Copyright

A91-43631*# National Aeronautics and Space Administration. Lewis Research Center, Cleveland, OH.

3-D NAVIER-STOKES ANALYSIS OF CROSSING, GLANCING SHOCKS/TURBULENT BOUNDARY LAYER INTERACTIONS

D. R. REDDY (NASA, Lewis Research Center, Cleveland, OH) AIAA, Fluid Dynamics, Plasma Dynamics and Lasers Conference, 22nd, Honolulu, HI, June 24-26, 1991. 13 p. Previously announced in STAR as N91-24130. refs
(Contract NAS3-25366)
(AIAA PAPER 91-1758) Copyright

Three dimensional viscous flow analysis is performed for a configuration where two crossing and glancing shocks interact with a turbulent boundary layer. A time marching 3-D full Navier-Stokes code, called PARC3D, is used to compute the flow field, and the solution is compared to the experimental data obtained at the NASA Lewis Research Center's 1 x 1 ft supersonic wind tunnel facility. The study is carried out as part of the continuing code assessment program in support of the generic hypersonic research at NASA Lewis. Detailed comparisons of static pressure fields and oil flow patterns are made with the corresponding solution on the wall containing the shock/boundary layer interaction in an effort to validate the code for hypersonic inlet applications.

Author

A91-44259*# National Aeronautics and Space Administration. Lewis Research Center, Cleveland, OH.

A DESIGN STRATEGY FOR THE USE OF VORTEX GENERATORS TO MANAGE INLET-ENGINE DISTORTION USING COMPUTATIONAL FLUID DYNAMICS

BERNHARD H. ANDERSON (NASA, Lewis Research Center, Cleveland, OH) and RALPH LEVY (Scientific Research Associates, Inc., Glastonbury, CT) AIAA, SAE, ASME, and ASEE, Joint Propulsion Conference, 27th, Sacramento, CA, June 24-26, 1991. 35 p. Previously announced in STAR as N91-24131. refs
(AIAA PAPER 91-2474) Copyright

A reduced Navier-Stokes solution technique was successfully used to design vortex generator installations for the purpose of minimizing engine face distortion by restructuring the development of secondary flow that is induced in typical 3-D curved inlet ducts. The results indicate that there exists an optimum axial location for this installation of corotating vortex generators, and within this configuration, there exists a maximum spacing between generator blades above which the engine face distortion increases rapidly. Installed vortex generator performance, as measured by engine face circumferential distortion descriptors, is sensitive to Reynolds number and thereby the generator scale, i.e., the ratio of generator blade height to local boundary layer thickness. Installations of corotating vortex generators work well in terms of minimizing engine face distortion within a limited range of generator scales. Hence, the design of vortex generator installations is a point design, and all other conditions are off design. In general, the loss levels associated with a properly designed vortex generator installation are very small; thus, they represent a very good method to manage engine face distortion. This study also showed that the vortex strength, generator scale, and secondary flow field structure have a complicated and interrelated influence over engine face distortion, over and above the influence of the initial arrangement of generators.

Author

A91-44545*# National Aeronautics and Space Administration. Lewis Research Center, Cleveland, OH.

AN ANALYSIS OF THE VISCOUS FLOW THROUGH A COMPACT RADIAL TURBINE BY THE AVERAGE PASSAGE APPROACH

JAMES D. HEIDMANN (NASA, Lewis Research Center, Cleveland, OH) and TIMOTHY A. BEACH (NASA, Lewis Research Center; Sverdrup Technology, Inc., Cleveland, OH) ASME, International Gas Turbine and Aeroengine Congress and Exposition, 35th,

Brussels, Belgium, June 11-14, 1990. 11 p. Previously announced in STAR as N90-14206. refs
(ASME PAPER 90-GT-64)

A steady, three-dimensional viscous average passage computer code is used to analyze the flow through a compact radial turbine rotor. The code models the flow as spatially periodic from blade passage to blade passage. Results from the code using varying computational models are compared with each other and with experimental data. These results include blade surface velocities and pressures, exit vorticity and entropy contour plots, shroud pressures, and spanwise exit total temperature, total pressure, and swirl distributions. The three computational models used are inviscid, viscous with no blade clearance, and viscous with blade clearance. It is found that modeling viscous effects improves correlation with experimental data, while modeling hub and tip clearances further improves some comparisons. Experimental results such as a local maximum of exit swirl, reduced exit total pressures at the walls, and exit total temperature magnitudes are explained by interpretation of the flow physics and computed secondary flows. Trends in the computed blade loading diagrams are similarly explained.

Author

A91-45548*# Toledo Univ., OH.

FLUTTER ANALYSIS OF CASCADES USING A TWO DIMENSIONAL EULER SOLVER

T. S. R. REDDY, MILIND A. BAKHLE (Toledo, University, OH), DENNIS L. HUFF (NASA, Lewis Research Center, Cleveland, OH), and TIMOTHY W. SWAFFORD (Mississippi State University, Mississippi State) AIAA, Fluid Dynamics, Plasma Dynamics and Lasers Conference, 22nd, Honolulu, HI, June 24-26, 1991. 21 p. refs

(Contract NAG3-3139; NAG3-1137; NAG3-983)
(AIAA PAPER 91-1681) Copyright

Flutter analysis of a cascade of blades in compressible flow is presented, with each blade of the cascade modeled as a typical section having pitching and plunging degrees of freedom. The aerodynamic forces are obtained from an unsteady, 2-D cascade solver based on the Euler equations. To reduce the computational time, an influence coefficient technique and a pulse response technique are also used to obtain the unsteady force coefficients for any frequency and phase angle. The predicted steady and unsteady aerodynamic forces for selected cascade geometries and flow conditions correlate well with the available experimental and analytical data.

R.E.P.

A91-45792*# National Aeronautics and Space Administration. Lewis Research Center, Cleveland, OH.

THE EFFECT OF VARYING MACH NUMBER ON CROSSING, GLANCING SHOCKS/TURBULENT BOUNDARY-LAYER INTERACTIONS

W. R. HINGST (NASA, Lewis Research Center, Cleveland, OH) and K. E. WILLIAMS AIAA, SAE, ASME, and ASEE, Joint Propulsion Conference, 27th, Sacramento, CA, June 24-26, 1991. 12 p. refs

(AIAA PAPER 91-2157) Copyright

Two crossing side-wall shocks interacting with a supersonic tunnel wall boundary layer have been investigated over a Mach number range of 2.5 to 4.0. The investigation included a range of equal shock strengths produced by shock generators at angles from 4.0 to 12.0 degrees. Results of flow visualization show that the interaction is unseparated at the low shock generator angles. With increasing shock strength, the flow begins to form a separated region that grows in size and moves forward and eventually the model unstarts. The wall static pressures show a symmetrical compression that merges on the centerline upstream of the inviscid shock locations and becomes more 1D downstream. The region of the 1D pressure gradient moves upstream with increasing shock strengths until it coincides with the leading edge of the shock generators at the limit before model unstart. At the limiting conditions the wall pressure gradients are primarily in the axial direction throughout.

O.G.

A91-45813* National Aeronautics and Space Administration. Lewis Research Center, Cleveland, OH.

MIXING OF MULTIPLE JETS WITH A CONFINED SUBSONIC CROSSFLOW - SUMMARY OF NASA-SUPPORTED EXPERIMENTS AND MODELING

JAMES D. HOLDEMAN (NASA, Lewis Research Center, Cleveland OH) AIAA, SAE, ASME, and ASEE, Joint Propulsion Conference, 27th, Sacramento, CA, June 24-26, 1991. 49 p. Previously announced in STAR as N91-24202. refs (AIAA PAPER 91-2458) Copyright

Experimental and computational results on the mixing of single, double, and opposed rows of jets with an isothermal or variable temperature mainstream in a confined subsonic crossflow are summarized. The studies were performed to investigate flow and geometric variations typical of the complex 3D flowfield in the dilution zone of combustion chambers in gas turbine engines. The principal observations from the experiments were that the momentum-flux ratio was the most significant flow variable, and that temperature distributions were similar (independent of orifice diameter) when the orifice spacing and the square-root of the momentum-flux ratio were inversely proportional. The experiments and empirical model for the mixing of a single row of jets from round holes were extended to include several variations typical of gas turbine combustors. Author

A91-45818* National Aeronautics and Space Administration. Lewis Research Center, Cleveland, OH.

RESULTS FROM COMPUTATIONAL ANALYSIS OF A MIXED COMPRESSION SUPERSONIC INLET

J. D. SAUNDERS (NASA, Lewis Research Center, Cleveland, OH) and T. G. KEITH, JR. (Ohio Aerospace Institute, Brook Park) AIAA, SAE, ASME, and ASEE, Joint Propulsion Conference, 27th, Sacramento, CA, June 24-26, 1991. 17 p. refs (AIAA PAPER 91-2581) Copyright

A numerical study was performed to simulate the critical flow through a supersonic inlet. This flowfield has many phenomena such as shock waves, strong viscous effects, turbulent boundary layer development, boundary layer separations and mass flow suction through the walls (bleed). The computational tools used in this study were two full Navier-Stokes (FNS) codes. The supersonic inlet that was analyzed in this study is the Variable Diameter Centerbody (VDC), inlet. This inlet is a candidate concept for the next generation supersonic transport. Application of the code to the inlet geometry involved effort in generating an efficient grid geometry and specifying boundary conditions, particularly in the bleed region and at the outflow boundary. Results for a critical inlet operation compare favorably to Method of Characteristics predictions and experimental data. Author

A91-45819* National Aeronautics and Space Administration. Lewis Research Center, Cleveland, OH.

EVALUATION OF PANEL CODE PREDICTIONS WITH EXPERIMENTAL RESULTS OF INLET PERFORMANCE FOR A 17-INCH DUCTED PROP/FAN SIMULATOR OPERATING AT MACH 0.2

D. R. BOLDMAN, C. IEK, D. P. HWANG, R. J. JERACKI (NASA, Lewis Research Center, Cleveland, OH), M. LARKIN (Pratt and Whitney Group, East Hartford, CT) et al. AIAA, SAE, ASME, and ASEE, Joint Propulsion Conference, 27th, Sacramento, CA, June 24-26, 1991. 18 p. Previously announced in STAR as N91-25106. refs (AIAA PAPER 91-3354) Copyright

An axisymmetric panel code was used to evaluate a series of ducted propeller inlets. The inlets were tested in the Lewis 9 by 15 Foot Low Speed Wind Tunnel. Three basic inlets having ratios of shroud length to propeller diameter of 0.2, 0.4, and 0.5 were tested with the Pratt and Whitney ducted prop/fan simulator. A fourth hybrid inlet consisting of the shroud from the shortest basic inlet coupled with the spinner from the largest basic inlet was also tested. This later configuration represented the shortest overall inlet. The simulator duct diameter at the propeller face was 17.25 inches. The short and long spinners provided hub-to-tip ratios of 0.44 at the propeller face. The four inlets were tested at a nominal

free stream Mach number of 0.2 and at angles of attack from 0 degrees to 35 degrees. The panel code method incorporated a simple two-part separation model which yielded conservative estimates of inlet separation. Author

A91-46181* National Aeronautics and Space Administration. Lewis Research Center, Cleveland, OH.

PRIMITIVE VARIABLE, STRONGLY IMPLICIT CALCULATION PROCEDURE FOR VISCOUS FLOWS AT ALL SPEEDS

K.-H. CHEN (NASA, Lewis Research Center, Cleveland; Toledo, University, OH) and R. H. PLETCHER (Iowa State University of Science and Technology, Ames) AIAA Journal (ISSN 0001-1452), vol. 29, Aug. 1991, p. 1241-1249. Previously cited in issue 16, p. 2482, Accession no. A90-38666. refs (Contract AF-AFOSR-89-0403) Copyright

A91-48816* Toledo Univ., OH.

SEMIANALYTICAL TECHNIQUE FOR SENSITIVITY ANALYSIS OF UNSTEADY AERODYNAMIC COMPUTATIONS

DURBHA V. MURTHY (Toledo, University, OH) and KRISHNA R. V. KAZA (NASA, Lewis Research Center, Cleveland, OH) (Structures, Structural Dynamics, and Materials Conference, 29th, Williamsburg, VA, Apr. 18-20, 1988, Technical Papers. Part 3, p. 1307-1316) Journal of Aircraft (ISSN 0021-8669), vol. 28, Aug. 1991, p. 481-488. Previously cited in issue 12, p. 1820, Accession no. A88-32314. refs Copyright

A91-52315* National Aeronautics and Space Administration. Lewis Research Center, Cleveland, OH.

APPLICATION OF AN EFFICIENT HYBRID SCHEME FOR AEROELASTIC ANALYSIS OF ADVANCED PROPELLERS

R. SRIVASTAVA, D. L. HUFF (NASA, Lewis Research Center, Cleveland, OH), LAKSHMI N. SANKAR (Georgia Institute of Technology, Atlanta), and T. S. R. REDDY (NASA, Lewis Research Center, Cleveland; Toledo, University, OH) Journal of Propulsion and Power (ISSN 0748-4658), vol. 7, Sept.-Oct. 1991, p. 767-775. Previously cited in issue 08, p. 1099, Accession no. A90-22153. refs (Contract NAG3-730) Copyright

A91-53754* Florence Univ. (Italy).

MULTIGRID CALCULATION OF THREE-DIMENSIONAL VISCOUS CASCADE FLOWS

A. ARNONE (Firenze, Università, Florence, Italy), M.-S. LIOU, and L. A. POVINELLI (NASA, Lewis Research Center, Cleveland, OH) IN: AIAA Applied Aerodynamics Conference, 9th, Baltimore, MD, Sept. 23-25, 1991, Technical Papers. Vol. 1. Washington, DC, American Institute of Aeronautics and Astronautics, 1991, p. 297-311. refs (AIAA PAPER 91-3238)

A three-dimensional code for viscous cascade flow prediction has been developed. The space discretization uses a cell-centered scheme with eigenvalue scaling to weigh the artificial dissipation terms. Computational efficiency of a four-stage Runge-Kutta scheme is enhanced by using variable coefficients, implicit residual smoothing, and a full-multigrid method. The Baldwin-Lomax eddy-viscosity model is used for turbulence closure. A zonal, nonperiodic grid is used to minimize mesh distortion in and downstream of the throat region. Applications are presented for an annular vane with and without end wall contouring, and for a large-scale linear cascade. The calculation is validated by comparing with experiments and by studying grid dependency. Author

A91-54027* Lockheed Engineering and Sciences Co., Hampton, VA.

A COMPARISON OF ARROW, TRAPEZOIDAL AND M WING CONCEPTS USING A MACH 2 SUPERSONIC CRUISE TRANSPORT MISSION

GLENN L. MARTIN, DAVID C. TICE (Lockheed Engineering and

02 AERODYNAMICS

Sciences Co., Hampton, VA), DON C. MARCUM, JR. (NASA, Langley Research Center, Hampton, VA), and JONATHAN A. SEIDEL (NASA, Lewis Research Center, Cleveland, OH) AIAA, AHS, and ASEE, Aircraft Design Systems and Operations Meeting, Baltimore, MD, Sept. 23-25, 1991. 11 p. refs (AIAA PAPER 91-3102) Copyright

The present analytic study of the potential performance of SST configurations radically differing from arrow-winged designs in lifting surface planform geometry gives attention to trapezoidal-wing and M-wing configurations; the trapezoidal wing is used as the baseline in the performance comparisons. The design mission was all-supersonic (Mach 2), carrying 248 passengers over a 5500 nautical-mile range. Design constraints encompassed approach speed, TO&L field length, and engine-out second-segment climb and missed-approach performance. Techniques for improving these configurations are discussed. O.C.

A91-54061*# McDonnell-Douglas Research Labs., Saint Louis, MO.

VSTOL GROUND EFFECTS TESTING WITH FLOW VISUALIZATION AND IMAGE ENHANCEMENT

JEROME T. KEGELMAN (McDonnell Douglas Research Laboratories, Saint Louis, MO) and ALBERT L. JOHNS (NASA, Lewis Research Center, Cleveland, OH) AIAA, AHS, and ASEE, Aircraft Design Systems and Operations Meeting, Baltimore, MD, Sept. 23-25, 1991. 12 p. refs (Contract NAS3-25629)

(AIAA PAPER 91-3145) Copyright

A remotely controlled high-energy fiber-optic light delivery technique is employed to examine the implementation of a laser-light-sheet flow-visualization system. During testing, video data are enhanced in real time using digital image processing techniques. A summary of test results for an advanced VSTOL configuration in ground effect, and techniques for the generation of 3D reconstructions for the flowfield are outlined. The system performed well during all phases of the test and proved to be an extremely useful asset to the overall test program. The most useful application of the flow visualization system was the interactive real-time flow field analysis made during the actual testing. P.D.

A91-56115* National Aeronautics and Space Administration, Lewis Research Center, Cleveland, OH.

A NAVIER-STOKES STUDY OF SHOCK-BOUNDARY LAYER INTERACTION AND FLOW SEPARATION INSIDE A TRANSONIC COMPRESSOR

CHUNILL HAH (NASA, Lewis Research Center, Cleveland, OH) and STEVEN L. PUTERBAUGH (USAF, Aero Propulsion Laboratory, Wright-Patterson AFB, OH) IN: International Symposium on Air Breathing Engines, 10th, Nottingham, England, Sept. 1-6, 1991, Proceedings. Vol. 1. Washington, DC, American Institute of Aeronautics and Astronautics, 1991, p. 152-162. refs Copyright

A numerical study to evaluate a three-dimensional Navier-Stokes method as a tool to predict the detailed flowfield inside a low-aspect-ratio compressor at off-design rotor speed has been conducted. The flow field inside a state-of-the-art transonic compressor is used for the purpose of the evaluation. The experimental study shows that the rotor has higher peak efficiency at 90 percent rotor speed than at 100 percent rotor speed. The details of the flow structure inside the low-aspect-ratio compressor (three-dimensional shock structure, shock-boundary layer interaction, tip leakage vortex, etc.) and the overall aerodynamic performance at various operating conditions are numerically analyzed, and the results are compared with the available experimental data. The numerical results also indicate that the rotor has higher peak efficiency at 90 percent rotor speed than at 100 percent rotor speed. This is due to the reduced shock strength and the reduced interactions among passage shock, tip-clearance vortex and blade boundary layer. Author

A91-56152* National Aeronautics and Space Administration, Lewis Research Center, Cleveland, OH.

THREE-DIMENSIONAL FLOWS IN A TRANSONIC COMPRESSOR ROTOR

LONNIE REID (NASA, Lewis Research Center, Cleveland, OH), MARK L. CELESTINA (Sverdrup Technology, Inc., Cleveland, OH), KENNETH DEWITT, and THEO KEITH (Toledo, University, OH) IN: International Symposium on Air Breathing Engines, 10th, Nottingham, England, Sept. 1-6, 1991, Proceedings. Vol. 1. Washington, DC, American Institute of Aeronautics and Astronautics, 1991, p. 514-527. refs Copyright

This study involves an experimental and numerical investigation of the three-dimensional flows in a transonic compressor rotor. A variety of data which could be used, in a complementary fashion, to validate/calibrate the computational fluid dynamics turbomachinery code and improve understanding of the flow physics, were acquired. Detailed radial survey data which consisted of total pressure, total temperature, static pressure and flow angle were obtained at stations upstream and downstream of the rotor blade. Detailed velocity and turbulence profiles were obtained upstream of the rotor and used as the upstream boundary conditions for the numerical analysis. Calibrated flush-mounted hot film probes were used to measure wall shear stress on the hub and casing walls upstream of the rotor. The blade-to-blade shear-stress angle distributions were obtained at two axial locations on the rotor casing, using flush-mounted hot film probes. A numerical analysis conducted using a three-dimensional Navier-Stokes code was compared with the experimental results. Author

N91-10842*# National Aeronautics and Space Administration, Lewis Research Center, Cleveland, OH.

COMPUTATIONAL FLUID DYNAMICS AT THE LEWIS RESEARCH CENTER: AN OVERVIEW

ROBERT M. STUBBS IN NASA, Ames Research Center, NASA Computational Fluid Dynamics Conference. Volume 1: Sessions 1-6 p 49-61 Sep. 1989

Avail: NTIS HC/MF A20; 25 functional color pages CSDL 01A

Lewis is a multidisciplinary Center with strong research and development programs in aeronautical and space propulsion, power, space communications, space experiments and materials. Computational fluid dynamics (CFD) is playing an important and growing role in most of these areas. Described here is how CFD is integrated into these programs and highlights elements of the CFD activities. Examples are presented of codes developed to predict flow fields in advanced propulsion systems and several of the code validation experiments are described. The CFD effort at Lewis ranges from basic research on new and improved algorithms through code development to the application of these codes to specific engineering problems. Because of the substantial improvement in CFD's predictive capability, its use at Lewis is on a steep growth path, spreading rapidly into new areas which had not traditionally taken advantage of the techniques of numerical simulation. Multidisciplinary codes and the future direction of CFD at Lewis are discussed. Author

N91-10849*# National Aeronautics and Space Administration, Lewis Research Center, Cleveland, OH.

NUMERICAL SIMULATION OF NONLINEAR DEVELOPMENT OF INSTABILITY WAVES

REDA R. MANKBADI (Cairo Univ., Egypt) IN NASA, Ames Research Center, NASA Computational Fluid Dynamics Conference. Volume 1: Sessions 1-6 p 183-191 Sep. 1989 (E-4658) Avail: NTIS HC/MF A20; 25 functional color pages CSDL 01A

The nonlinear interactions of high amplitude instability waves in turbulent jets are described. In plane shear layers Riley and Metcalf (1980) and Monkewitz (1987) have shown that these interactions are dependent, among other parameters, on the phase-difference between the two instability waves. Therefore, here researchers consider the nonlinear development of both the amplitudes and the phase of the instability waves. The development

of these waves are also coupled with the development of the mean flow and the background turbulence. In formulating this model it is assumed that each of the flow components can be characterized by conservation equations supplemented by closure models. Results for the interactions between the two instability waves under high-amplitude forcing at fundamental and subharmonic frequencies are presented here. Qualitative agreements are found between the present predictions and available experimental data. Author

N91-10854*# National Aeronautics and Space Administration. Lewis Research Center, Cleveland, OH.

TIME DEPENDENT VISCOUS INCOMPRESSIBLE NAVIER-STOKES EQUATIONS

JOHN W. GOODRICH In NASA, Ames Research Center, NASA Computational Fluid Dynamics Conference. Volume 1: Sessions 1-6 p 255-270 Sep. 1989

Avail: NTIS HC/MF A20; 25 functional color pages CSCL 01A
Information on time dependent incompressible Navier-Stokes equations is given in viewgraph form. Information is given on streamfunction equations for unsteady incompressible flow, the streamfunction algorithm for unsteady incompressible flow, and a multigrid solver for the laminar implicit equations. Author

N91-10866*# National Aeronautics and Space Administration. Lewis Research Center, Cleveland, OH.

PROGRESS TOWARD THE DEVELOPMENT OF AN AIRFOIL ICING ANALYSIS CAPABILITY

MARK G. POTAPCZUK, COLIN S. BIDWELL, and BRIAN M. BERKOWITZ (Sverdrup Technology, Inc., Mayfield, OH.) In NASA, Ames Research Center, NASA Computational Fluid Dynamics Conference. Volume 1: Sessions 1-6 p 473-487 Sep. 1989

Avail: NTIS HC/MF A20; 25 functional color pages CSCL 01A
The NASA-Lewis aircraft icing analysis program is composed of three major sub-programs. These sub-programs are ice accretion simulation, performance degradation evaluation, and ice protection system evaluation. These topics cover all areas of concern related to the simulation of aircraft icing and its consequences. The motivation for these activities is twofold, reduction of time and effort required in experimental programs and the ability to provide reliable information for aircraft certification in icing, over the complete range of environmental conditions. In addition to the analytical activities associated with development of these codes, several experimental programs are underway to provide verification information for existing codes. These experimental programs are also used to investigate the physical processes associated with ice accretion and removal for improvement of present analytical models. The NASA-Lewis icing analysis program is thus striving to provide a full range of analytical tools necessary for evaluation of the consequences of icing and of ice protection systems. Author

N91-10867*# National Aeronautics and Space Administration. Lewis Research Center, Cleveland, OH.

THE BREAKUP OF TRAILING-LINE VORTICES

DAVID JACQMIN In NASA, Ames Research Center, NASA Computational Fluid Dynamics Conference. Volume 1: Sessions 1-6 p 489-494 Sep. 1989

Avail: NTIS HC/MF A20; 25 functional color pages CSCL 01A
It is now known that Batchelor's trailing-line vortex is extremely unstable to small amplitude disturbances for swirl numbers in the neighborhood of 0.83. The results of numerical calculations are presented that show the response of the vortex in this range of swirl numbers to finite amplitude, temporal, helical disturbances. Phenomena observed include: (1) ejection of axial vorticity and momentum from the core resulting in the creation of secondary, separate vortices; (2) a great intensification of core axial vorticity and a weakening of core momentum; and (3) the production of azimuthal vorticity in the form of a tightly wrapped spiral wave. The second phenomenon eventually stabilizes the vortex, which then smooths and gradually returns to an axisymmetric state. The calculations are mixed spectral-finite-difference, fourth-order

accurate, and have been carried out at Reynolds numbers of 1000 to 2000. Some linearized results are also discussed in an attempt to explain the process of vortex intensification. Author

N91-10880*# National Aeronautics and Space Administration. Lewis Research Center, Cleveland, OH.

SIMULATION OF TURBOMACHINERY FLOWS

JOHN J. ADAMCZYK In NASA, Ames Research Center, NASA Computational Fluid Dynamics Conference. Volume 2: Sessions 7-12 p 195-204 Sep. 1989

Avail: NTIS HC/MF A22; 30 functional color pages CSCL 01A
Significant advancements have been made in the last five years in the ability to model turbomachinery flows of engineering interest. This advancement can be directly attributed to the second generation of supercomputers like the Cray XMP and Cray 2 and advanced instrumentation techniques. Early on, the National Aeronautics and Space Administration Lewis Research Center recognized the potential gains in turbomachinery performance and life that could be achieved by taking advantage of this technology and instituted a comprehensive research program in turbomachinery flow modeling. This activity combined the areas of fluid flow analysis, computational fluid dynamics, and experimental fluid mechanics. As a result of this activity, Lewis has become an internationally recognized leader in turbomachinery flow modeling. Many of the research activities conducted under this program are utilized by industry. The presentation gives an overview of this program and provides sample illustration of simulation performed to date. Author

N91-10883*# National Aeronautics and Space Administration. Lewis Research Center, Cleveland, OH.

AUTOMATED DESIGN OF CONTROLLED DIFFUSION BLADES

JOSE M. SANZ In NASA, Ames Research Center, NASA Computational Fluid Dynamics Conference. Volume 2: Sessions 7-12 p 231-244 Sep. 1989 Previously announced in IAA as A89-15967

Avail: NTIS HC/MF A22; 30 functional color pages CSCL 01A
A numerical automation procedure was developed to be used in conjunction with an inverse hodograph method for the design of controlled diffusion blades. With this procedure a cascade of airfoils with a prescribed solidity, inlet Mach No., inlet air flow angle and air flow turning can be produced automatically. The trailing edge thickness of the airfoil, an important quantity in inverse methods, is also prescribed. The automation procedure consists of a multi-dimensional Newton iteration in which the objective design conditions are achieved by acting on the hodograph input parameters of the underlying inverse code. The method, although more general in scope, is applied to the design of axial flow turbomachinery blade sections, both compressors and turbines. A collaborative effort with U.S. Engine Companies to identify designs of interest to the industry will be described. Author

N91-10884*# National Aeronautics and Space Administration. Lewis Research Center, Cleveland, OH.

NUMERICAL ANALYSIS OF FLOW THROUGH OSCILLATING CASCADE SECTIONS

DENNIS L. HUFF In NASA, Ames Research Center, NASA Computational Fluid Dynamics Conference. Volume 2: Sessions 7-12 p 245-257 Sep. 1989 Previously announced in IAA as A89-28413

Avail: NTIS HC/MF A22; 30 functional color pages CSCL 01A
The design of turbomachinery blades requires the prevention of flutter for all operating conditions. However, flow field predictions used for aeroelastic analysis are not well understood for all flow regimes. The present research focuses on numerical solutions of the Euler and Navier-Stokes equations using an ADI procedure to model two-dimensional, transonic flow through oscillating cascades. The model prescribes harmonic pitching motions for the blade sections for both zero and non-zero inter-blade phase angles. The code introduces the use of a deforming grid technique for convenient specification of the periodic boundary conditions. Approximate nonreflecting boundary conditions have been coded for the inlet and exit boundary conditions. Sample unsteady

02 AERODYNAMICS

solutions have been performed for an oscillating cascade and compared to experimental data. Also, test cases were run for a flat plate cascade to compare with an unsteady, small-perturbation, subsonic analysis. The predictions for oscillating cascades with non-zero inter-blade phase angles are in good agreement with experimental data and small-perturbation theory. The zero degree inter-blade phase angle cases, which were near a resonant condition, differ from the experiment and theory. Studies on reflecting versus non-reflecting inlet and exit boundary conditions show that the treatment of the boundary can have a significant effect on the first harmonic, unsteady pressure distributions for certain flow conditions. This code is expected to be used as a tool for reviewing simpler models that do not include the full nonlinear aerodynamics or as a final check for designs against flutter in turbomachinery. Author

N91-10885* National Aeronautics and Space Administration. Lewis Research Center, Cleveland, OH.

ANALYSIS OF THREE-DIMENSIONAL VISCOUS FLOW IN A SUPERSONIC THROUGHFLOW FAN

RODRICK V. CHIMA / In NASA, Ames Research Center, NASA Computational Fluid Dynamics Conference. Volume 2: Sessions 7-12 p 259-272 Sep. 1989

Avail: NTIS HC/MF A22; 30 functional color pages CSDL 01A

A 3-D Navier-Stokes code was developed for analysis of turbomachinery blade rows and other internal flows. The Navier-Stokes equations are written in a Cartesian coordinate system rotating about the x-axis, and then mapped to a general body-fitted coordinate system. Streamwise viscous terms are neglected using the thin layer assumption, and turbulence effects are modeled using the Baldwin-Lomax turbulence model. The equations are discretized using finite differences on stacked C-type grids and are solved using a multistage Runge-Kutta algorithm with a spatially varying time step and implicit residual smoothing. Calculations were made of the flow around a supersonic throughflow fan blade. The fan was designed as a key component in a supersonic cruise engine. The 3-D calculations were done on a 129x29x33 grid and took 50 minutes of cpu time. Comparisons with the quasi-3-D results show minor differences in loading due to 3-D effects. Particle traces show nearly 2-D flows near the pressure surface, but large secondary flows within the suction surface boundary layer. The horseshoe vortex ahead of the leading edge is clearly seen. Author

N91-10887* National Aeronautics and Space Administration. Lewis Research Center, Cleveland, OH.

A NUMERICAL STUDY OF THE HOT GAS ENVIRONMENT AROUND A STOVL AIRCRAFT IN GROUND PROXIMITY

THOMAS J. VANOVERBEKE and JAMES D. HOLDEMAN / In NASA, Ames Research Center, NASA Computational Fluid Dynamics Conference. Volume 2: Sessions 7-12 p 291-310 Sep. 1989 Previously announced in IAA as A88-48752 Original contains color illustrations

Avail: NTIS HC/MF A22; 30 functional color pages CSDL 01A

The development of Short Takeoff Vertical Landing (STOVL) aircraft has historically been an empirical- and experience-based technology. A 3-D turbulent flow CFD code was used to calculate the hot gas environment around an STOVL aircraft operating in ground proximity. Preliminary calculations are reported for a typical STOVL aircraft configuration to identify key features of the flow field, and to demonstrate and assess the capability of current 3-D CFD codes to calculate the temperature of the gases ingested at the engine inlet as a function of flow and geometric conditions. Author

N91-10888* National Aeronautics and Space Administration. Lewis Research Center, Cleveland, OH.

CFD ANALYSIS FOR HIGH SPEED INLETS

TOM BENSON / In NASA, Ames Research Center, NASA Computational Fluid Dynamics Conference. Volume 2: Sessions 7-12 p 311-319 Sep. 1989

Avail: NTIS HC/MF A22; 30 functional color pages CSDL 01A

The increased national interest in high speed flight has

increased research for high speed propulsion components. The highly 3-D flows present in supersonic/hypersonic inlets are currently being studied at NASA-Lewis both experimentally and computationally using a family of steady Parabolized Navier-Stokes (PNS) and Navier-Stokes (NS) solvers and unsteady NS solvers. Some of the results of these efforts are presented with an emphasis on the comparison of the computational and experimental results. The flow in high speed inlets typically involves the interaction of compression shock waves and boundary layers on the internal surfaces. The fundamentals of these interactions have been studied experimentally for many years, while more recently, computations have been used to study these complex 3-D flow fields. Attempts to control the flow through boundary layer bleed are being investigated computationally prior to wind tunnel experiments. The ultimate goal is the higher performing inlets required for high speed flight. Author

N91-10894* National Aeronautics and Space Administration. Lewis Research Center, Cleveland, OH.

FLUX SPLITTING ALGORITHMS FOR TWO-DIMENSIONAL VISCOUS FLOWS WITH FINITE-RATE CHEMISTRY

JIAN-SHUN SHUEN (Sverdrup Technology, Inc., Cleveland, OH.) and MENG-SING LIOU / In NASA, Ames Research Center, NASA Computational Fluid Dynamics Conference. Volume 2: Sessions 7-12 p 437-450 Sep. 1989 Previously announced in IAA as A89-28409

Avail: NTIS HC/MF A22; 30 functional color pages CSDL 01A

The Roe flux difference splitting method was extended to treat 2-D viscous flows with nonequilibrium chemistry. The derivations have avoided unnecessary assumptions or approximations. For spatial discretization, the second-order Roe upwind differencing is used for the convective terms and central differencing for the viscous terms. An upwind-based TVD scheme is applied to eliminate oscillations and obtain a sharp representation of discontinuities. A two-state Runge-Kutta method is used to time integrate the discretized Navier-Stokes and species transport equations for the asymptotic steady solutions. The present method is then applied to two types of flows: the shock wave/boundary layer interaction problems and the jet in cross flows. Author

N91-11675* National Aeronautics and Space Administration. Lewis Research Center, Cleveland, OH.

EFFECT OF ACOUSTIC EXCITATION ON STALLED FLOWS OVER AN AIRFOIL

K. B. M. Q. ZAMAN Oct. 1990 14 p Presented at the 13th Aeroacoustics Conference, Tallahassee, FL, 22-24 Oct. 1990; sponsored in part by AIAA (NASA-TM-103183; E-5563; NAS 1.15:103183; AIAA PAPER 90-4010) Avail: NTIS HC/MF A03 CSDL 01A

The effect of acoustic excitation on post-stalled flows over an airfoil, i.e., flows that are fully separated from near the leading edge, is investigated. The excitation results in a tendency towards reattachment, which is accompanied by an increased lift and reduced drag, although the flow may still remain fully separated. It is found that with increasing excitation amplitude, the effect becomes more pronounced but shifts to a Strouhal number which is much lower than that expected from linear, inviscid instability of the separated shear layer. Author

N91-11676* National Aeronautics and Space Administration. Lewis Research Center, Cleveland, OH.

NUMERICAL STUDY OF UNSTEADY SHOCKWAVE REFLECTIONS USING AN UPWIND TVD SCHEME

ANDREW T. HSU (Sverdrup Technology, Inc., Brook Park, OH.) and MENG-SING LIOU Aug. 1990 16 p (NASA-TM-103251; E-5680; NAS 1.15:103251) Avail: NTIS HC/MF A03 CSDL 01A

An unsteady TVD Navier-Stokes solver was developed and applied to the problem of shock reflection on a circular cylinder. The obtained numerical results were compared with the Schlieren photos from an experimental study. These results show that the present computer code has the ability of capturing moving shocks. Author

N91-13420*# National Aeronautics and Space Administration. Lewis Research Center, Cleveland, OH.

A STEADYING EFFECT OF ACOUSTIC EXCITATION ON TRANSITORIAL STALL

K. B. M. Q. ZAMAN 1991 17 p. Proposed for presentation at the 29th Aerospace Sciences Meeting, Reno, NV, 7-10 Jan. 1991; sponsored by AIAA (NASA-TM-103689; E-5908; NAS 1.15:103689; AIAA PAPER 91-0043) Avail: NTIS HC/MF A03 CSCL 01/1

The effect of acoustic excitation on a class of separated flows with a transitional boundary layer at the point of separation is considered. Experimental results on the flow over airfoils, a two-dimensional backward-facing step, and through large angle conical diffusers are presented. In all cases, the separated flow undergoes large amplitude fluctuations, much of the energy being concentrated at unusually low frequencies. In each case, an appropriate high frequency acoustic excitation is found to be effective in reducing the fluctuations substantially. The effective excitation frequency scales on the initial boundary layer thickness and the effect is apparently achieved through acoustic tripping of the separating boundary layer. Author

N91-13421*# National Aeronautics and Space Administration. Lewis Research Center, Cleveland, OH.

A REVIEW OF ICE ACCRETION DATA FROM A MODEL ROTOR ICING TEST AND COMPARISON WITH THEORY

RANDALL K. BRITTON (Sverdrup Technology, Inc., Brook Park, OH.) and THOMAS H. BOND 1991 35 p. Presented at the 29th Aerospace Sciences Meeting, Reno, NV, 7-10 Jan. 1991; sponsored by AIAA

(Contract NAS3-25266; RTOP 505-68-11) (NASA-TM-103712; E-5930; NAS 1.15:103712; AIAA PAPER 91-0661) Avail: NTIS HC/MF A03 CSCL 01/1

An experiment was conducted by the Helicopter Icing Consortium (HIC) in the NASA Lewis Icing Research Tunnel (IRT) in which a 1/6 scale fuselage model of a UH-60A Black Hawk helicopter with a generic rotor was subjected to a wide range of icing conditions. The HIC consists of members from NASA, Bell Helicopter, Boeing Helicopter, McDonnell Douglas Helicopters, Sikorsky Aircraft, and Texas A&M University. Data was taken in the form of rotor torque, internal force balance measurements, blade strain gage loading, and two dimensional ice shape tracings. A review of the ice shape data is performed with special attention given to repeatability and correctness of trends in terms of radial variation, rotational speed, icing time, temperature, liquid water content, and volumetric median droplet size. Moreover, an indepth comparison between the experimental data and the analysis of NASA's ice accretion code LEWICE is given. Finally, conclusions are drawn as to the quality of the ice accretion data and the predictability of the data base as a whole. Recommendations are also given for improving data taking technique as well as potential future work. Author

N91-14309*# National Aeronautics and Space Administration. Lewis Research Center, Cleveland, OH.

RESULTS OF A SUB-SCALE MODEL ROTOR ICING TEST

ROBERT J. FLEMMING, THOMAS H. BOND, and RANDALL K. BRITTON (Sverdrup Technology, Inc., Brook Park, OH.) 1991 31 p. Presented at the 29th Aerospace Sciences Meeting, Reno, NV, 7-10 Jan. 1991; sponsored by AIAA

(Contract RTOP 505-68-11) (NASA-TM-103709; E-5935; NAS 1.15:103709; AIAA PAPER 91-0660) Avail: NTIS HC/MF A03 CSCL 01/1

A heavily instrumented sub-scale model of a helicopter main rotor was tested in the NASA Lewis Research Center Icing Research Tunnel (IRT) in September and November 1989. The four-bladed main rotor had a diameter of 1.83 m (6.00 ft) and the 0.124 m (4.9 in) chord rotor blades were specially fabricated for this experiment. The instrumented rotor was mounted on a Sikorsky Aircraft Powered Force Model, which enclosed a rotor balance and other measurement systems. The model rotor was exposed to a range of icing conditions that included variations in temperature, liquid water content, and median droplet diameter,

and was operated over ranges of advance ratio, shaft angle, tip Mach number (rotor speed) and weight coefficient to determine the effect of these parameters on ice accretion. In addition to strain gage and balance data, the test was documented with still, video, and high speed photography, ice profile tracings, and ice molds. The sensitivity of the model rotor to the test parameters, is given, and the result to theoretical predictions are compared. Test data quality was excellent, and ice accretion prediction methods and rotor performance prediction methods (using published icing lift and drag relationships) reproduced the performance trends observed in the test. Adjustments to the correlation coefficients to improve the level of correlation are suggested. Author

N91-14310*# National Aeronautics and Space Administration. Lewis Research Center, Cleveland, OH.

NUMERICAL SIMULATION OF ICE GROWTH ON A MS-317 SWEEP WING GEOMETRY

M. G. POTAPCZUK and C. S. BIDWELL Jan. 1991 24 p. Presented at the 29th Aerospace Sciences Meeting, Reno, NV, 7-10 Jan. 1991; sponsored in part by AIAA

(Contract RTOP 505-68-10) (NASA-TM-103705; E-5928; NAS 1.15:103705; AIAA PAPER 91-0263) Avail: NTIS HC/MF A03 CSCL 01/1

An effort to develop a 3-D ice accretion modeling method was initiated. This first step towards creation of a complete aircraft icing simulation code builds on previously developed methods for calculating 3-D flow fields and particle trajectories combined with a 2-D ice accretion calculation along coordinate locations corresponding to streamlines. The types of calculations necessary to predict 3-D ice accretion is demonstrated. Results of calculations using 3-D method for a MS-317 swept wing geometry are projected onto a 2-D plane parallel to the free stream direction and compared to experimental results for the same geometry. It is anticipated that many modifications will be made to this approach, however this effort will lay the groundwork for future modeling efforts. Results indicate that rime ice shapes indicate a difficulty in accurately calculating the ice shape in the runback region. Author

N91-15134*# National Aeronautics and Space Administration. Lewis Research Center, Cleveland, OH.

AERODYNAMICS AND HEAT TRANSFER INVESTIGATIONS ON A HIGH REYNOLDS NUMBER TURBINE CASCADE

TAHER SCHOBELI (Texas A&M Univ., College Station.), ERIC MCFARLAND, and FREDERICK YEH 1991 13 p. Proposed for presentation at the 36th International Gas Turbine and Aeroengine Congress and Exposition, Orlando, FL, 3-6 Jun. 1991; sponsored by ASME

(NASA-TM-103260; E-5937; NAS 1.15:103260) Avail: NTIS HC/MF A03 CSCL 01/1

The results of aerodynamic and heat transfer experimental investigations performed in a high Reynolds number turbine cascade test facility are analyzed. The experimental facility simulates the high Reynolds number flow conditions similar to those encountered in the Space Shuttle Main Engine. In order to determine the influence of Reynolds number on aerodynamic and thermal behavior of the blades, heat transfer coefficients were measured at various Reynolds numbers using liquid crystal temperature measurement technique. Potential flow calculation methods were used to predict the cascade pressure distributions. Boundary layer and heat transfer calculation methods were used with these pressure distributions to verify the experimental results. Author

N91-17000*# National Aeronautics and Space Administration. Lewis Research Center, Cleveland, OH.

NATURALLY OCCURRING AND FORCED AZIMUTHAL MODES IN A TURBULENT JET

GANESH RAMAN, EDWARD J. RICE, and ELI RESHOTKO (Case Western Reserve Univ., Cleveland, OH.) 1991 18 p. Proposed for presentation at the 1991 Joint ASME-JSME Fluids Engineering Conference, Portland, OR, 24-26 Jun. 1991; cosponsored by ASME and Japanese Society of Mechanical Engineers

02 AERODYNAMICS

(Contract NAS3-25266; RTOP 505-62-52)
(NASA-TM-103692; E-5911; NAS 1.15:103692) Avail: NTIS
HC/MF A03 CSCL 01/1

Naturally occurring instability modes in an axisymmetric jet were studied using the modal frequency technique. The evolution of the modal spectrum was obtained for a jet with a Reynolds number based on a diameter of 400,000 for both laminar and turbulent nozzle boundary layers. In the early evolution of the jet the axisymmetric mode was predominant, with the azimuthal modes growing rapidly but dominating only the end of the potential core. The growth of the azimuthal was observed closer to the nozzle exit for the jet in the laminar boundary layer case than for the turbulent. Target modes for efficient excitation of the jet were determined and two cases of excitation were studied. First, a jet was excited simultaneously by two helical modes, m equals plus 1 and m equals minus 1 at a Strouhal number based on jet diameter of 0.15 and the axisymmetric mode, m equals 0 at a jet diameter of 0.6. Second, m equals plus one and m equals minus 1 at jet diameter equals 0.3 and m equals 0 at jet diameter equals 0.6 were excited simultaneously. The downstream evolution of the hydrodynamic modes and the spreading rate of the jet were documented for each case. Higher jet spreading rates, accompanied by distorted jet cross sections were observed for the cases where combinations of axisymmetric and helical forcings were applied.

Author

N91-17002*# National Aeronautics and Space Administration.
Lewis Research Center, Cleveland, OH.

OPTICAL MEASUREMENT OF PROPELLER BLADE DEFLECTIONS IN A SPIN FACILITY

JOHN K. RAMSEY, ERWIN H. MEYN, ORAL MEHMED, and
ANATOLE P. KURKOV Oct. 1990 11 p
(Contract RTOP 505-63-1B)

(NASA-TM-103115; E-5439; NAS 1.15:103115) Avail: NTIS
HC/MF A03 CSCL 01/1

A nonintrusive optical system for measuring propeller blade deflections has been used in the NASA Lewis dynamic spin facility. Deflection of points at the leading and trailing edges of a blade section can be obtained with a narrow light beam from a low power helium-neon laser. A system used to measure these deflections at three spanwise locations is described. Modifications required to operate the lasers in a near-vacuum environment are also discussed.

Author

N91-19044*# National Aeronautics and Space Administration.
Lewis Research Center, Cleveland, OH.

IMPROVED VISUALIZATION OF FLOW FIELD MEASUREMENTS

JEFFREY HILTON MILES 1991 36 p Presented at the 29th
Aerospace Sciences Meeting, Reno, NV, 7-10 Jan. 1991;
sponsored by AIAA Original contains color illustrations
(NASA-TM-103679; E-5896; NAS 1.15:103679; AIAA PAPER
91-0273) Avail: NTIS HC/MF A03; 3 functional color pages
CSCL 01/1

A capability was developed that makes it possible to apply to measured flow field data the visualization tools developed to display numerical solutions for computational fluid dynamic problems. The measurement monitor surface (MMS) procedure was applied to the analysis of flow field measurements within a low aspect ratio transonic axial flow fan rotor obtained with 2-D laser anemometry. The procedure generates input for the visualization tools developed to display numerical solutions for computational fluid dynamics problems. The relative Mach number contour plots obtained by this method resemble the conventional contour plots obtained by more traditional methods. The results show that the MMS procedure can be used to generate input for the multidimensional processing and analysis tools developed for data from numerical flow field simulations. They show that an experimenter can apply the MMS procedure to his data and then use an interactive graphics program to display scalar quantities like the Mach number by profiles, carpet plots, contour lines, and surfaces using various colors. Also, flow directionality can be shown by display of vector fields and particle traces.

Author

N91-19045*# National Aeronautics and Space Administration.
Lewis Research Center, Cleveland, OH.

INFLIGHT SOURCE NOISE OF AN ADVANCED FULL-SCALE SINGLE-ROTATION PROPELLER

RICHARD P. WOODWARD and IRVIN J. LOEFFLER 1991
20 p Presented at the 29th Aerospace Sciences Meeting, Reno,
NV, 7-10 Jan. 1991; sponsored by AIAA

(Contract RTOP 535-03-01)
(NASA-TM-103687; E-5906; NAS 1.15:103687; AIAA PAPER
91-0594) Avail: NTIS HC/MF A03 CSCL 01/1

Flight tests to define the far field tone source at cruise conditions were completed on the full scale SR-7L advanced turboprop which was installed on the left wing of a Gulfstream II aircraft. This program, designated Propfan Test Assessment (PTA), involved aeroacoustic testing of the propeller over a range of test conditions. These measurements defined source levels for input into long distance propagation models to predict en route noise. Inflight data were taken for 7 test cases. The sideline directivities measured by the Learjet showed expected maximum levels near 105 degrees from the propeller upstream axis. However, azimuthal directivities based on the maximum observed sideline tone levels showed highest levels below the aircraft. An investigation of the effect of propeller tip speed showed that the tone level of reduction associated with reductions in propeller tip speed is more significant in the horizontal plane than below the aircraft.

Author

N91-19046*# National Aeronautics and Space Administration.
Lewis Research Center, Cleveland, OH.

ICING CHARACTERISTICS OF A NATURAL-LAMINAR-FLOW, A MEDIUM-SPEED, AND A SWEEP, MEDIUM-SPEED AIRFOIL

COLIN S. BIDWELL 1991 32 p Presented at the 29th
Aerospace Sciences Meeting, Reno, NV, 7-10 Jan. 1991;
sponsored by AIAA

(Contract RTOP 505-68-10)
(NASA-TM-103693; E-5912; NAS 1.15:103693; AIAA PAPER
91-0447) Avail: NTIS HC/MF A03 CSCL 01/1

Tests were conducted at the Icing Research Tunnel at the NASA Lewis Research Center to determine the icing characteristics of three modern airfoils, a natural laminar flow, a medium speed and a swept medium speed airfoil. Tests measured the impingement characteristics and drag degradation for angles of attack typifying cruise and climb for cloud conditions typifying the range that might be encountered in flight. The maximum degradation occurred for the cruise angle of attack for the long glaze ice condition for all three airfoils with increases over baseline drag being 486 percent, 510 percent, and 465 percent for the natural laminar flow, the medium speed and the swept medium speed airfoil respectively. For the climb angle of attack, the maximum drag degradation (and extent of impingement) observed were also for the long glaze ice condition, and were 261 percent, 181 percent and 331 percent respectively. The minimum drag degradation (and extent of impingement) occurred for the cruise condition and for the short, rime spray which increases over baseline drag values of 47 percent, 28 percent and 46 percent respectively.

Author

N91-19047*# National Aeronautics and Space Administration.
Lewis Research Center, Cleveland, OH.

PREDICTION OF ICE SHAPES AND THEIR EFFECT ON AIRFOIL PERFORMANCE

JAIWON SHIN, BRIAN BERKOWITZ, HSUN CHEN, and TUNCER
CEBECI (California State Univ., Long Beach.) 1991 23 p
Presented at the 29th Aerospace Sciences Meeting, Reno, NV,
7-10 Jan. 1991; sponsored by AIAA

(Contract RTOP 505-68-10)
(NASA-TM-103701; E-5924; NAS 1.15:103701; AIAA PAPER
91-0264) Avail: NTIS HC/MF A03 CSCL 01/1

Calculations of ice shapes and the resulting drag increases are presented for experimental data on a NACA 0012 airfoil. They were made with a combination of LEWICE and interactive boundary-layer codes for a wide range of conditions which include air speed and temperature, the droplet size and liquid water content of the cloud, and the angle of attack of the airfoil. In all cases,

the calculated results account for the drag increase due to ice accretion and, in general, show good agreement. Author

N91-19053*# National Aeronautics and Space Administration. Lewis Research Center, Cleveland, OH.

ACOUSTIC RADIATION FROM LIFTING AIRFOILS IN COMPRESSIBLE SUBSONIC FLOW

HAFIZ M. ATASSI, SHANKAR SUBRAMANIAM (Notre Dame Univ., IN.), and JAMES R. SCOTT 1990 22 p Presented at the 13th Aeroacoustics Conference, Tallahassee, FL, 22-24 Oct. 1990; sponsored by AIAA Previously announced in IAA as A91-12427 (Contract RTOP 505-62-52) (NASA-TM-103650; E-5830; NAS 1.15:103650; AIAA PAPER 90-3911) Avail: NTIS HC/MF A03 CSCL 01/1

The far field acoustic radiation from a lifting airfoil in a three-dimensional gust is studied. The acoustic pressure is calculated using the Kirchhoff method, instead of using the classical acoustic analogy approach due to Lighthill. The pressure on the Kirchhoff surface is calculated using an existing numerical solution of the unsteady flow field. The far field acoustic pressure is calculated in terms of these values using Kirchhoff's formula. The method is validated against existing semi-analytical results for a flat plate. The method is then used to study the problem of an airfoil in a harmonic three-dimensional gust, for a wide range of Mach numbers. The effect of variation of the airfoil thickness and angle of attack on the acoustic far field is studied. The changes in the mechanism of sound generation and propagation due to the presence of steady loading and nonuniform mean flow are also studied. Author

N91-19054*# National Aeronautics and Space Administration. Lewis Research Center, Cleveland, OH.

IMPLEMENTATION OF CONTROL POINT FORM OF ALGEBRAIC GRID-GENERATION TECHNIQUE

YUNG K. CHOO, DAVID P. MILLER, and CHARLES J. RENO (Cleveland State Univ., OH.) 1991 13 p Presented at the 3rd International Conference on Numerical Grid Generation in Computational Fluid Dynamics and Related Fields, Barcelona, Spain, 3-7 Jun. 1991; sponsored by the UPC, Catalonia Univ., and ESA (Contract NCC3-153) (NASA-TM-103748; E-5997; NAS 1.15:103748) Avail: NTIS HC/MF A03 CSCL 01/1

The control point form (CPF) provides explicit control of physical grid shape and grid spacing through the movement of the control points. The control point array, called a control net, is a space grid type arrangement of locations in physical space with an index for each direction. As an algebraic method CPF is efficient and works well with interactive computer graphics. A family of menu-driven, interactive grid-generation computer codes (TURBO) is being developed by using CPF. Key features of Turbo (a TURBO member) are discussed and typical results are presented. Author runs on any IRIS 4D series workstation.

N91-19057*# National Aeronautics and Space Administration. Lewis Research Center, Cleveland, OH.

THREE-COMPONENT LASER ANEMOMETER MEASUREMENT SYSTEMS

LOUIS J. GOLDMAN Washington Jan. 1991 20 p (NASA-TP-3080; E-5526; NAS 1.60:3080) Avail: NTIS HC/MF A03 CSCL 01/1

A brief overview of the different laser anemometer (LA) optical designs available is presented. Then, the LA techniques that can be used to design a three-component measurement system for annular geometries are described. Some of the facility design considerations unique to these LA systems are also addressed. Following this, the facilities and the LA systems that were used to successfully measure the three components of velocity in the blading of annular-flow machines are reviewed. Finally, possible LA system enhancements and future research directions are presented. Author

N91-19063*# National Aeronautics and Space Administration. Lewis Research Center, Cleveland, OH.

DEVELOPMENT OF A LASER-INDUCED HEAT FLUX TECHNIQUE FOR MEASUREMENT OF CONVECTIVE HEAT TRANSFER COEFFICIENTS IN A SUPersonic FLOWFIELD

A. ROBERT PORRO, THEO G. KEITH, JR. (Toledo Univ., OH.), WARREN R. HINGST, RANDALL M. CRISS, and KIRK D. SEABLOM Mar. 1991 60 p (Contract RTOP 505-62-52) (NASA-TM-103778; E-6049; NAS 1.15:103778) Avail: NTIS HC/MF A04 CSCL 01/1

A technique is developed to measure the local convective heat transfer coefficient on a model surface in a supersonic flow field. The technique uses a laser to apply a discrete local heat flux at the model test surface, and an infrared camera system determines the local temperature distribution due to heating. From this temperature distribution and an analysis of the heating process, a local convective heat transfer coefficient is determined. The technique was used to measure the load surface convective heat transfer coefficient distribution on a flat plate at nominal Mach numbers of 2.5, 3.0, 3.5, and 4.0. The flat plate boundary layer initially was laminar and became transitional in the measurement region. The experimental results agreed reasonably well with theoretical predictions of convective heat transfer of flat plate laminar boundary layers. The results indicate that this non-intrusive optical measurement technique has the potential to obtain high quality surface convective heat transfer measurements in high speed flowfields. Author

N91-20044*# National Aeronautics and Space Administration. Lewis Research Center, Cleveland, OH.

NASA LOW-SPEED CENTRIFUGAL COMPRESSOR FOR 3-D VISCOUS CODE ASSESSMENT AND FUNDAMENTAL FLOW PHYSICS RESEARCH

M. D. HATHAWAY, J. R. WOOD, and C. A. WASSERBAUER (Sverdrup Technology, Inc., Brook Park, OH.) 1991 15 p Presented at the 36th International Gas Turbine and Aeroengine Congress and Exposition, Orlando, FL, 3-6 Jun. 1991; sponsored by the American Society of Mechanical Engineers (Contract DA PROJ. 1L1-61102-AH-45) (NASA-TM-103710; E-5938; NAS 1.15:103710; AVSCOM-TR-91-C-003; AD-A242473) Avail: NTIS HC/MF A03 CSCL 01/1

A low speed centrifugal compressor facility recently built by the NASA Lewis Research Center is described. The purpose of this facility is to obtain detailed flow field measurements for computational fluid dynamic code assessment and flow physics modeling in support of Army and NASA efforts to advance small gas turbine engine technology. The facility is heavily instrumented with pressure and temperature probes, both in the stationary and rotating frames of reference, and has provisions for flow visualization and laser velocimetry. The facility will accommodate rotational speeds to 2400 rpm and is rated at pressures to 1.25 atm. The initial compressor stage being tested is geometrically and dynamically representative of modern high-performance centrifugal compressor stages with the exception of Mach number levels. Preliminary experimental investigations of inlet and exit flow uniformly and measurement repeatability are presented. These results demonstrate the high quality of the data which may be expected from this facility. The significance of synergism between computational fluid dynamic analysis and experimentation throughout the development of the low speed centrifugal compressor facility is demonstrated. Author

N91-20045*# National Aeronautics and Space Administration. Lewis Research Center, Cleveland, OH.

TRANSONIC AERODYNAMICS OF DENSE GASES M.S. Thesis - Virginia Polytechnic Inst. and State Univ., Apr. 1990

SYBIL HUANG MORREN Jan. 1991 84 p (Contract RTOP 591-41-21) (NASA-TM-103722; E-5953; NAS 1.15:103722) Avail: NTIS HC/MF A05 CSCL 01/1

Transonic flow of dense gases for two-dimensional,

02 AERODYNAMICS

steady-state, flow over a NACA 0012 airfoil was predicted analytically. The computer code used to model the dense gas behavior was a modified version of Jameson's FL052 airfoil code. The modifications to the code enabled modeling the dense gas behavior near the saturated vapor curve and critical pressure region where the fundamental derivative, Γ , is negative. This negative Γ region is of interest because the nonclassical gas behavior such as formation and propagation of expansion shocks, and the disintegration of inadmissible compression shocks may exist. The results indicated that dense gases with undisturbed thermodynamic states in the negative Γ region show a significant reduction in the extent of the transonic regime as compared to that predicted by the perfect gas theory. The results support existing theories and predictions of the nonclassical, dense gas behavior from previous investigations. Author

N91-21060*# National Aeronautics and Space Administration. Lewis Research Center, Cleveland, OH.
COMPRESSIBLE FLOWS WITH PERIODIC VORTICAL DISTURBANCES AROUND LIFTING AIRFOILS Ph.D. Thesis - Notre Dame Univ.

JAMES R. SCOTT Jan. 1991 214 p
(Contract RTOP 505-62-52)
(NASA-TM-103742; E-5984; NAS 1.15:103742) Avail: NTIS HC/MF A10 CSCL 01/1

A numerical method is developed for solving periodic, three-dimensional, vortical flows around lifting airfoils in subsonic flow. The first-order method that is presented fully accounts for the distortion effects of the nonuniform mean flow on the convected upstream vortical disturbances. The unsteady velocity is split into a vortical component which is a known function of the upstream flow conditions and the Lagrangian coordinates of the mean flow, and an irrotational field whose potential satisfies a nonconstant-coefficient, inhomogeneous, convective wave equation. Using an elliptic coordinate transformation, the unsteady boundary value problem is solved in the frequency domain on grids which are determined as a function of the Mach number and reduced frequency. The numerical scheme is validated through extensive comparisons with known solutions to unsteady vortical flow problems. In general, it is seen that the agreement between the numerical and analytical results is very good for reduced frequencies ranging from 0 to 4, and for Mach numbers ranging from .1 to .8. Numerical results are also presented for a wide variety of flow configurations for the purpose of determining the effects of airfoil thickness, angle of attack, camber, and Mach number on the unsteady lift and moment of airfoils subjected to periodic vortical gusts. It is seen that each of these parameters can have a significant effect on the unsteady airfoil response to the incident disturbances, and that the effect depends strongly upon the reduced frequency and the dimensionality of the gust. For a one-dimensional (transverse) or two-dimensional (transverse and longitudinal) gust, the results indicate that airfoil thickness increases the unsteady lift and moment at the low reduced frequencies but decreases it at the high reduced frequencies. The results show that an increase in airfoil Mach number leads to a significant increase in the unsteady lift and moment for the low reduced frequencies, but a significant decrease for the high reduced frequencies. Author

N91-21061*# National Aeronautics and Space Administration. Lewis Research Center, Cleveland, OH.
EXPERIMENTAL STUDY OF BOUNDARY LAYER TRANSITION ON A HEATED FLAT PLATE

K. H. SOHN, E. RESHOTKO (Case Western Reserve Univ., Cleveland, OH.), and K. B. M. Q. ZAMAN 1991 17 p Prepared for presentation at the 1991 Joint ASME-JSME Fluids Engineering Conference, Portland, OR, 24-26 Jun. 1991
(Contract NAG3-230; RTOP 505-62-52)
(NASA-TM-103779; E-6050; NAS 1.15:103779) Avail: NTIS HC/MF A03 CSCL 01/1

A detailed investigation to the document momentum and thermal development of boundary layers undergoing natural transition on a heated flat plate was performed. Experimental results of both

overall and conditionally sampled characteristics of laminar, transitional, and low Reynolds number turbulent boundary layers are presented. Measurements were done in a low-speed, closed-loop wind tunnel with a freestream velocity of 100 ft/s and zero pressure gradient over a range of freestream turbulence intensities from 0.4 to 6 percent. The distributions of skin friction, heat transfer rate, and Reynolds shear stress were all consistent with previously published data. Reynolds analogy factors for momentum thickness Reynolds number, $Re(\theta)$ less than 2300 were found to be well predicted by laminar and turbulent correlations which accounted for an unheated starting length and uniform heat flux. A small dependence of turbulence results on the freestream turbulence intensity was observed. Author

N91-21062*# National Aeronautics and Space Administration. Lewis Research Center, Cleveland, OH.

COMPUTATIONAL FLUID DYNAMICS SYMPOSIUM ON AEROPROPULSION

Washington Jan. 1991 687 p Symposium held in Cleveland, OH, 24-26 Apr. 1990 Supersedes NASA-CP-10045 Original contains color illustrations
(NASA-CP-3078; E-5296; NASA-CP-10045; NAS 1.55:3078)

Avail: NTIS HC/MF A99; 10 functional color pages CSCL 01/1

Recognizing the considerable advances that have been made in computational fluid dynamics, the Internal Fluid Mechanics Division of NASA Lewis Research Center sponsored this symposium with the objective of providing a forum for exchanging information regarding recent developments in numerical methods, physical and chemical modeling, and applications. This conference publication is a compilation of 4 invited and 34 contributed papers presented in six sessions: algorithms one and two, turbomachinery, turbulence, components application, and combustors. Topics include numerical methods, grid generation, chemically reacting flows, turbulence modeling, inlets, nozzles, and unsteady flows.

N91-21115*# National Aeronautics and Space Administration. Lewis Research Center, Cleveland, OH.

AN EXPERIMENTAL COMPARISON OF NONSWIRLING AND SWIRLING FLOW IN A CIRCULAR-TO-RECTANGULAR TRANSITION DUCT

B. A. REICHERT, W. R. HINGST, and T. H. OKIISHI (Iowa State Univ. of Science and Technology, Ames.) Jan. 1991 15 p Presented at the 29th Aerospace Sciences Meeting, Reno, NV, 7-10 Jan. 1991; sponsored in part by AIAA Previously announced in IAA as A91-21466

(Contract RTOP 505-62-91)
(NASA-TM-104359; E-6149; NAS 1.15:104359; AIAA PAPER 91-0342) Avail: NTIS HC/MF A03 CSCL 01/1

Circular-to-rectangular transition ducts are used as exhaust system components of aircraft with rectangular exhaust nozzles. Often, the incoming flow of these transition ducts includes a swirling velocity component remaining from the gas turbine engine. Previous transition duct studies have either not included inlet swirl or when inlet swirl was considered, only overall performance parameters were evaluated. Circular-to-rectangular transition duct flows with and without inlet swirl were explored in order to understand the effect of inlet swirl on the transition duct flow field and to provide detailed duct flow data for comparison with numerical code predictions. A method was devised to create a swirling, solid body rotational flow with minimal associated disturbances. Coefficients based on velocities and total and static pressures measured in cross stream planes at four axial locations within the transition duct, along with surface static pressure measurements and surface oil film visualization, are presented for both nonswirling and swirling incoming flow. In both cases the inlet centerline Mach number was 0.35. The Reynolds number based on the inlet centerline velocity and duct inlet diameter was 1,547,000 for nonswirling and 1,366,000 for swirling flow. The maximum swirl angle was 15.6 deg. Two pair of counter-rotating side wall vortices appeared in the duct flow without inlet swirl. These vortices were absent in the swirling incoming flow cases. Author

N91-21116*# National Aeronautics and Space Administration. Lewis Research Center, Cleveland, OH.

HOT GAS INGESTION TEST RESULTS OF A TWO-POSTER VECTORED THRUST CONCEPT WITH FLOW VISUALIZATION IN THE NASA LEWIS 9- X 15-FOOT LOW SPEED WIND TUNNEL

ALBERT L. JOHNS, GEORGE NEINER, TIMOTHY J. BENCIC, JOSEPH D. FLOOD, KURT C. AMUEDO, and THOMAS W. STROCK (McDonnell-Douglas Corp., Saint Louis, MO.) Jul. 1990 27 p Presented at the 26th Joint Propulsion Conference, Orlando, FL, 16-18 Jul. 1990; sponsored in part by AIAA, SAE, ASME, and ASEE Original contains color illustrations (Contract RTOP 505-62-71) (NASA-TM-103258; E-5690; NAS 1.15:103258; AIAA PAPER 90-2268) Avail: NTIS HC/MF A03; 1 functional color page CSCL 01/1

A 9.2 percent scale Short Takeoff and Vertical Landing (STOVL) hot gas ingestion model was designed and built by McDonnell Douglas Corporation (MCAIR) and tested in the Lewis Research Center 9 x 15 foot Low Speed Wind Tunnel (LSWT). Hot gas ingestion, the entrainment of heated engine exhaust into the inlet flow field, is a key development issue for advanced short takeoff and vertical landing aircraft. Flow visualization from the Phase 1 test program, which evaluated the hot ingestion phenomena and control techniques, is covered. The Phase 2 test program evaluated the hot gas ingestion phenomena at higher temperatures and used a laser sheet to investigate the flow field. Hot gas ingestion levels were measured for the several forward nozzle splay configurations and with flow control/life improvement devices (LIDs) which reduced the hot gas ingestion. The model support system had four degrees of freedom - pitch, roll, yaw, and vertical height variation. The model support system also provided heated high-pressure air for nozzle flow and a suction system exhaust for inlet flow. The test was conducted at full scale nozzle pressure ratios and inlet Mach numbers. Test and data analysis results from Phase 2 and flow visualization from both Phase 1 and 2 are documented. A description of the model and facility modifications is also provided. Headwind velocity was varied from 10 to 23 kn. Results are presented over a range of nozzle pressure ratios at a 10 kn headwind velocity. The Phase 2 program was conducted at exhaust nozzle temperatures up to 1460 R and utilized a sheet laser system for flow visualization of the model flow field in and out of ground effects. The results reported are for nozzle exhaust temperatures up to 1160 R. These results will contain the compressor face pressure and temperature distortions, the total pressure recovery, the inlet temperature rise, and the environmental effects of the hot gas. The environmental effects include the ground plane contours, the model airframe heating, and the location of the ground flow separation. Author

N91-22084*# National Aeronautics and Space Administration. Lewis Research Center, Cleveland, OH.

NUMERICAL FLUX FORMULAS FOR THE EULER AND NAVIER-STOKES EQUATIONS. 2: PROGRESS IN FLUX-VECTOR SPLITTING

WILLIAM J. COIRIER and BRAM VANLEER (Michigan Univ., Ann Arbor.) 1991 19 p Presented at the 10th Computational Fluid Dynamics Conference, Honolulu, HI, 24-27 Jun. 1991; sponsored by AIAA (Contract RTOP 505-62-52) (NASA-TM-104353; E-6138; NAS 1.15:104353; AIAA PAPER 91-1566) Avail: NTIS HC/MF A03 CSCL 01/1

The accuracy of various numerical flux functions for the inviscid fluxes when used for Navier-Stokes computations is studied. The flux functions are benchmarked for solutions of the viscous, hypersonic flow past a 10 degree cone at zero angle of attack using first order, upwind spatial differencing. The Harten-Lax/Roe flux is found to give a good boundary layer representation, although its robustness is an issue. Some hybrid flux formulas, where the concepts of flux-vector and flux-difference splitting are combined, are shown to give unsatisfactory pressure distributions; there is still room for improvement. Investigations of low diffusion, pure flux-vector splittings indicate that a pure flux-vector splitting can

be developed that eliminates spurious diffusion across the boundary layer. The resulting first-order scheme is marginally stable and not monotone. Author

N91-23083*# National Aeronautics and Space Administration. Lewis Research Center, Cleveland, OH.

NASA AEROPROPULSION RESEARCH IN SUPPORT OF PROPULSION SYSTEMS OF THE 21ST CENTURY

JOSEPH A. ZIEMIANSKI and EDWARD A. WILLIS (Sverdrup Technology, Inc., Brook Park, OH.) 1991 26 p Presented at the 36th International Gas Turbine and Aeroengine Congress and Exposition, Orlando, FL, 3-6 Jun. 1991; sponsored by ASME (Contract RTOP 505-62-12) (NASA-TM-104403; E-6226; NAS 1.15:104403) Avail: NTIS HC/MF A03 CSCL 01/1

A review is given of the NASA's ongoing and planned research and technology programs leading to advanced air breathing propulsion systems of the next century. The primary focus is on efforts being performed or sponsored by NASA-Lewis, with emphasis on civil, subsonic, and supersonic transportation systems which should begin to enter service within 10 to 20 years. Subsonic transport propulsion program elements, including ducted UltraHigh Bypass (UHB) engines and high efficiency cores are discussed in terms of goals, technical issues and problems, approaches and plans. Similarly, The Supersonic Cruise Propulsion Program is reviewed via discussion of near term and far term goals; barrier issues such as NOx and noise reduction and the consequent Phase 1 (near term) research plans are described; and finally, emerging technologies such as the supersonic through-flow fan are considered for their potential long term impact. Author

N91-23086*# National Aeronautics and Space Administration. Lewis Research Center, Cleveland, OH.

SIMULATION OF ICED WING AERODYNAMICS

M. G. POTAPCZUK, M. B. BRAGG, O. J. KWON, and L. N. SANKAR (Georgia Inst. of Tech., Atlanta.) 1991 17 p Presented at the 68th Fluid Dynamics Panel Specialists Meeting, Toulouse, France, 29 Apr. - 1 May 1991; sponsored by AGARD (Contract RTOP 505-68-10) (NASA-TM-104362; E-6158; NAS 1.15:104362) Avail: NTIS HC/MF A03 CSCL 01/1

The sectional and total aerodynamic load characteristics of moderate aspect ratio wings with and without simulated glaze leading edge ice were studied both computationally, using a three dimensional, compressible Navier-Stokes solver, and experimentally. The wing has an untwisted, untapered planform shape with NACA 0012 airfoil section. The wing has an unswept and swept configuration with aspect ratios of 4.06 and 5.0. Comparisons of computed surface pressures and sectional loads with experimental data for identical configurations are given. The abrupt decrease in stall angle of attack for the wing, as a result of the leading edge ice formation, was demonstrated numerically and experimentally. Author

N91-23087*# National Aeronautics and Space Administration. Lewis Research Center, Cleveland, OH.

ICING SIMULATION: A SURVEY OF COMPUTER MODELS AND EXPERIMENTAL FACILITIES

M. G. POTAPCZUK and J. J. REINMANN 1991 29 p Presented at the 68th Fluid Dynamics Panel Specialists Meeting, Toulouse, France, 29 Apr. - 1 May 1991; sponsored by AGARD (Contract RTOP 505-68-10) (NASA-TM-104366; E-6164; NAS 1.15:104366) Avail: NTIS HC/MF A03 CSCL 01/1

A survey of the current methods for simulation of the response of an aircraft or aircraft subsystem to an icing encounter is presented. The topics discussed include a computer code modeling of aircraft icing and performance degradation, an evaluation of experimental facility simulation capabilities, and ice protection system evaluation tests in simulated icing conditions. Current research focussed on upgrading simulation fidelity of both experimental and computational methods is discussed. The need

02 AERODYNAMICS

for increased understanding of the physical processes governing ice accretion, ice shedding, and iced airfoil aerodynamics is examined.

Author

N91-23089*# National Aeronautics and Space Administration. Lewis Research Center, Cleveland, OH.

A STUDY OF THREE DIMENSIONAL TURBULENT BOUNDARY LAYER SEPARATION AND VORTEX FLOW CONTROL USING THE REDUCED NAVIER STOKES EQUATIONS

BERNHARD H. ANDERSON and SAEED FAROKHI (Kansas Univ., Lawrence.) 1991 8 p Presented at the Turbulent Shear Flow Symposium, Munich, Fed. Republic of Germany, 9-11 Sep. 1991 (Contract RTOP 505-62-52) (NASA-TM-104407; E-6233; NAS 1.15:104407) Avail: NTIS HC/MF A02 CSCL 01/1

A reduced Navier Stokes (RNS) initial value space marching solution technique was applied to vortex generator and separated flow problems and demonstrated good predictions of the engine face flow field. This RNS solution technique using FLARE approximations can adequately describe the topological and topographical structure flow separation associated with vortex liftoff, and this conclusion led to the concept of a subclass of separations which can be called vorticity separations: separations dominated by the transport of vorticity. Adequate near wall resolution of vorticity separations appears necessary for good predictions of these flows.

Author

N91-23162*# National Aeronautics and Space Administration. Lewis Research Center, Cleveland, OH.

COMPUTATIONAL MODELING AND VALIDATION FOR HYPERSONIC INLETS

LOUIS A. POVINELLI in AGARD, Hypersonic Combined Cycle Propulsion 10 p Dec. 1990 Previously announced as N90-22011

Copyright Avail: NTIS HC/MF A20; Non-NATO Nationals requests available only from AGARD/Scientific Publications Executive CSCL 01/1

Hypersonic inlet research activity at NASA is reviewed. The basis is the experimental tests performed with three inlets: the NASA-Lewis Mach 5, the McDonnell Douglas Mach 12, and the NASA-Langley Mach 18. Both 3-D parabolized Navier-Stokes and Navier-Stokes codes were used to compute the flow within the three inlets. Modeling assumptions in the codes involve the turbulence model, the nature of the boundary layer, shock wave boundary layer interaction, and the flow spilled to the outside of the inlet. Use of the codes in conjunction with the experimental data are helping to develop a clearer knowledge of the inlet flow physics and to focus on the modeling improvements required in order to arrive at validated codes.

Author

N91-24107*# National Aeronautics and Space Administration. Lewis Research Center, Cleveland, OH.

EULER FLOW PREDICTIONS FOR AN OSCILLATING CASCADE USING A HIGH RESOLUTION WAVE-SPLIT SCHEME

DENNIS L. HUFF, TIMOTHY W. SWAFFORD, and T. S. R. REDDY (Toledo Univ., OH.) 1991 19 p Presented at the 36th International Gas Turbine and Aeroengine Congress and Exposition, Orlando, FL, 3-6 Jun. 1991; sponsored by ASME (Contract RTOP 535-03-01)

(NASA-TM-104377; E-5933; NAS 1.15:104377) Avail: NTIS HC/MF A03 CSCL 01/1

A compressible flow code that can predict the nonlinear unsteady aerodynamics associated with transonic flows over oscillating cascades is developed and validated. The code solves the two dimensional, unsteady Euler equations using a time-marching, flux-difference splitting scheme. The unsteady pressures and forces can be determined for arbitrary input motions, although only harmonic pitching and plunging motions are addressed. The code solves the flow equations on a H-grid which is allowed to deform with the airfoil motion. Predictions are presented for both flat plate cascades and loaded airfoil cascades. Results are compared to flat plate theory and experimental data.

Predictions are also presented for several oscillating cascades with strong normal shocks where the pitching amplitudes, cascade geometry and interblade phase angles are varied to investigate nonlinear behavior.

Author

N91-24124*# National Aeronautics and Space Administration. Lewis Research Center, Cleveland, OH.

THREE-DIMENSIONAL EULER TIME ACCURATE SIMULATIONS OF FAN ROTOR-STATOR INTERACTIONS

A. A. BORETTI (Fiat Research Center, Orbassano, Turin, Italy) Dec. 1990 30 p

(Contract NASA ORDER C-99066-G)

(NASA-TM-102528; ICOMP-90-08; E-5338; NAS 1.15:102528)

Avail: NTIS HC/MF A03 CSCL 01/1

A numerical method useful to describe unsteady 3-D flow fields within turbomachinery stages is presented. The method solves the compressible, time dependent, Euler conservation equations with a finite volume, flux splitting, total variation diminishing, approximately factored, implicit scheme. Multiblock composite gridding is used to partition the flow field into a specified arrangement of blocks with static and dynamic interfaces. The code is optimized to take full advantage of the processing power and speed of the Cray Y/MP supercomputer. The method is applied to the computation of the flow field within a single stage, axial flow fan, thus reproducing the unsteady 3-D rotor-stator interaction.

Author

N91-24130*# National Aeronautics and Space Administration. Lewis Research Center, Cleveland, OH.

THE 3-D NAVIER-STOKES ANALYSIS OF CROSSING, GLANCING SHOCKS/TURBULENT BOUNDARY LAYER INTERACTIONS

D. R. REDDY 1991 14 p Presented at the 22nd Fluid Dynamics, Plasma Dynamics and Lasers Conference, Honolulu, HI, 24-26 Jun. 1991; sponsored by AIAA

(Contract RTOP 505-62-52)

(NASA-TM-104469; E-6318; NAS 1.15:104469; AIAA PAPER 91-1758) Avail: NTIS HC/MF A03 CSCL 01/1

Three dimensional viscous flow analysis is performed for a configuration where two crossing and glancing shocks interact with a turbulent boundary layer. A time marching 3-D full Navier-Stokes code, called PARC3D, is used to compute the flow field, and the solution is compared to the experimental data obtained at the NASA Lewis Research Center's 1 x 1 ft supersonic wind tunnel facility. The study is carried out as part of the continuing code assessment program in support of the generic hypersonic research at NASA Lewis. Detailed comparisons of static pressure fields and oil flow patterns are made with the corresponding solution on the wall containing the shock/boundary layer interaction in an effort to validate the code for hypersonic inlet applications.

Author

N91-24131*# National Aeronautics and Space Administration. Lewis Research Center, Cleveland, OH.

A DESIGN STRATEGY FOR THE USE OF VORTEX GENERATORS TO MANAGE INLET-ENGINE DISTORTION USING COMPUTATIONAL FLUID DYNAMICS

BERNHARD H. ANDERSON and RALPH LEVY (Scientific Research Associates, Inc., Glastonbury, CT.) 1991 36 p Presented at the 27th Joint Propulsion Conference, Sacramento, CA, 24-27 Jun. 1991; sponsored by AIAA, SAE, ASME, and the American Society for Electrical Engineers

(Contract RTOP 505-62-52)

(NASA-TM-104436; E-6275; NAS 1.15:104436; AIAA PAPER 91-2474) Avail: NTIS HC/MF A03 CSCL 01/1

A reduced Navier-Stokes solution technique was successfully used to design vortex generator installations for the purpose of minimizing engine face distortion by restructuring the development of secondary flow that is induced in typical 3-D curved inlet ducts. The results indicate that there exists an optimum axial location for this installation of corotating vortex generators, and within this configuration, there exists a maximum spacing between generator blades above which the engine face distortion increases rapidly.

Installed vortex generator performance, as measured by engine face circumferential distortion descriptors, is sensitive to Reynolds number and thereby the generator scale, i.e., the ratio of generator blade height to local boundary layer thickness. Installations of corotating vortex generators work well in terms of minimizing engine face distortion within a limited range of generator scales. Hence, the design of vortex generator installations is a point design, and all other conditions are off design. In general, the loss levels associated with a properly designed vortex generator installation are very small; thus, they represent a very good method to manage engine face distortion. This study also showed that the vortex strength, generator scale, and secondary flow field structure have a complicated and interrelated influence over engine face distortion, over and above the influence of the initial arrangement of generators. Author

N91-25106*# National Aeronautics and Space Administration. Lewis Research Center, Cleveland, OH.

EVALUATION OF PANEL CODE PREDICTIONS WITH EXPERIMENTAL RESULTS OF INLET PERFORMANCE FOR A 17-INCH DUCTED PROP/FAB SIMULATOR OPERATING AT MACH 0.2

D. R. BOLDMAN, C. IEK, D. P. HWANG, R. J. JERACKI, M. LARKIN, and G. SORIN (Pratt and Whitney Aircraft, East Hartford, CT.) 1991 18 p Presented at the 27th Joint Propulsion Conference, Sacramento, CA, 24-27 Jun. 1991; sponsored by AIAA, SAE, ASME, and the American Society for Electrical Engineers (Contract RTOP 535-03-10) (NASA-TM-104428; E-6261; NAS 1.15:104428; AIAA PAPER 91-3354) Avail: NTIS HC/MF A03 CSCL 01/1

An axisymmetric panel code was used to evaluate a series of ducted propeller inlets. The inlets were tested in the Lewis 9 by 15 Foot Low Speed Wind Tunnel. Three basic inlets having ratios of shroud length to propeller diameter of 0.2, 0.4, and 0.5 were tested with the Pratt and Whitney ducted prop/fan simulator. A fourth hybrid inlet consisting of the shroud from the shortest basic inlet coupled with the spinner from the largest basic inlet was also tested. This later configuration represented the shortest overall inlet. The simulator duct diameter at the propeller face was 17.25 inches. The short and long spinners provided hub-to-tip ratios of 0.44 at the propeller face. The four inlets were tested at a nominal free stream Mach number of 0.2 and at angles of attack from 0 degrees to 35 degrees. The panel code method incorporated a simple two-part separation model which yielded conservative estimates of inlet separation. Author

N91-26121*# National Aeronautics and Space Administration. Lewis Research Center, Cleveland, OH.

CONTROL OF AN AXISYMMETRIC TURBULENT JET BY MULTI-MODAL EXCITATION

GANESH RAMAN, EDWARD J. RICE, and ELI RESHOTKO (Case Western Reserve Univ., Cleveland, OH.) 1991 8 p Presented at the Eighth Symposium on Turbulent Shear Flows, Munich, Fed. Republic of Germany, 9-11 Sep. 1991; sponsored by the Turbulent Shear Flow Committee (Contract RTOP 505-62-52) (NASA-TM-104483; E-6243; NAS 1.15:104483) Avail: NTIS HC/MF A02 CSCL 01/1

Experimental measurements of naturally occurring instability modes in the axisymmetric shear layer of high Reynolds number turbulent jet are presented. The region up to the end of the potential core was dominated by the axisymmetric mode. The azimuthal modes dominated only downstream of the potential core region. The energy content of the higher order modes (m is greater than 1) was significantly lower than that of the axisymmetric and $m = +$ or -1 modes. Under optimum conditions, two-frequency excitation (both at $m = 0$) was more effective than single frequency excitation (at $m = 0$) for jet spreading enhancement. An extended region of the jet was controlled by forcing combinations of both axisymmetric ($m = 0$) and helical modes ($m = +$ or -1). Higher spreading rates were obtained when multi-modal forcing was applied. Author

N91-26122*# National Aeronautics and Space Administration. Lewis Research Center, Cleveland, OH.

A STUDY OF HIGH SPEED FLOWS IN AN AIRCRAFT TRANSITION DUCT Ph.D. Thesis - Iowa State Univ.

BRUCE A. REICHERT Jun. 1991 270 p (Contract RTOP 505-62-91) (NASA-TM-104449; E-6290; NAS 1.15:104449) Avail: NTIS HC/MF A12 CSCL 01/1

The study of circular-to-rectangular transition duct flows with and without inlet swirl is presented. A method was devised to create a swirling, solid body rotational flow with minimal associated disturbances. Details of the swirl generator design and construction are discussed. Coefficients based on velocities and total and static pressures measured in cross stream planes at four axial locations within the transition duct along with surface static pressures and surface oil film visualization are presented for both nonswirling and swirling incoming flows. A method was developed to acquire trace gas measurements within the transition duct at high flow velocities. Statistical methods are used to help interpret the trace gas results. Author

N91-27129*# National Aeronautics and Space Administration. Lewis Research Center, Cleveland, OH.

AN EXPERIMENTAL TRACE GAS INVESTIGATION OF FLUID TRANSPORT AND MIXING IN A CIRCULAR-TO-RECTANGULAR TRANSITION DUCT

B. A. REICHERT, W. R. HINGST, and T. H. OKIISHI (Iowa State Univ. of Science and Technology, Ames.) 1991 14 p Presented at the 27th Joint Propulsion Conference, Sacramento, CA, 24-27 Jun. 1991; sponsored by AIAA, SAE, ASME, and ASEE (Contract RTOP 505-62-91) (NASA-TM-104499; E-6356; NAS 1.15:104499; AIAA PAPER 91-2370) Copyright Avail: NTIS HC/MF A03 CSCL 01/1

An ethylene trace gas technique was used to map out fluid transport and mixing within a circular to rectangular transition duct. Ethylene gas was injected at several points in a cross stream plane upstream of the transition duct. Ethylene concentration contours were determined at several cross stream measurement planes spaced axially within the duct. The flow involved a uniform inlet flow at a Mach number level of 0.5. Statistical analyses were used to quantitatively interpret the trace gas results. Also, trace gas data were considered along with aerodynamic and surface flow visualization results to ascertain transition duct flow phenomena. Convection of wall boundary layer fluid by vortices produced regions of high total pressure loss in the duct. The physical extent of these high loss regions is governed by turbulent diffusion. Author

N91-28136*# National Aeronautics and Space Administration. Lewis Research Center, Cleveland, OH.

EVALUATION OF A TECHNIQUE TO GENERATE ARTIFICIALLY THICKENED BOUNDARY LAYERS IN SUPERSONIC AND HYPERSONIC FLOWS

A. R. PORRO, W. R. HINGST, D. O. DAVIS, and A. B. BLAIR, JR. (National Aeronautics and Space Administration. Langley Research Center, Hampton, VA.) Washington Aug. 1991 28 p (Contract RTOP 505-80-21) (NASA-TP-3142; E-5660; NAS 1.60:3142) Avail: NTIS HC/MF A03 CSCL 01/1

The feasibility of using a contoured honeycomb model to generate a thick boundary layer in high-speed, compressible flow was investigated. The contour of the honeycomb was tailored to selectively remove momentum in a minimum of streamwise distance to create an artificially thickened turbulent boundary layer. Three wind tunnel experiments were conducted to verify the concept. Results indicate that this technique is a viable concept, especially for high-speed inlet testing applications. In addition, the compactness of the honeycomb boundary layer simulator allows relatively easy integration into existing wind tunnel model hardware. Author

02 AERODYNAMICS

N91-29150* # National Aeronautics and Space Administration. Lewis Research Center, Cleveland, OH.

PROGRESS TOWARD SYNERGISTIC HYPERMIXING NOZZLES
D. O. DAVIS and W. R. HINGST 1991 11 p Presented at the 27th Joint Propulsion Conference, Sacramento, CA, 24-27 Jun. 1991; sponsored by AIAA, SAE, ASME, and ASEE Previously announced as A91-45800
(Contract RTOP 505-62-40)

(NASA-TM-105169; E-6461; NAS 1.15:105169; AIAA PAPER 91-2264) Copyright Avail: NTIS HC/MF A03 CSCL 01/1

Mean flow measurements were obtained for air-to-air mixing downstream of swept and unswept ramp wall mounted hypermixing nozzle configurations. Aside from the sweep of the ramps, the two nozzle configurations studied are identical. The nozzles inject three parallel supersonic jets at a 15 deg angle (relative to the wind tunnel wall) into a supersonic freestream. Mach number and volume fraction distributions in a transverse plane 11.1 nozzle heights downstream from the nozzle exit plane were measured. Data are presented for a freestream Mach number of three at a matched static pressure condition and also at underexpanded static pressure condition (pressure ratio = 5). Surface oil flow visualization was used to study the near wall flow behavior. The results indicate that the swept ramp injectors produce stronger and larger vortex pairs than the unswept ramp injectors. The increased interaction between the swept ramp model's larger vortex pairs yields better mixing characteristics for this model. Author

N91-31106* # National Aeronautics and Space Administration. Lewis Research Center, Cleveland, OH.

EXPERIMENTAL INVESTIGATION OF TURBULENT FLOW THROUGH A CIRCULAR-TO-RECTANGULAR TRANSITION DUCT Ph.D. Thesis - Washington Univ.

DAVID O. DAVIS Sep. 1991 217 p

(Contract NAG3-376; RTOP 505-62-52)

(NASA-TM-105210; E-6522; NAS 1.15:105210) Avail: NTIS HC/MF A10 CSCL 01/1

Steady, incompressible, turbulent, swirl-free flow through a circular-to-rectangular transition duct was studied experimentally. The cross-sectional area remains the same at the exit as at the inlet, but varies through the transition section to a maximum value approximately 15 percent above the inlet value. The cross-sectional geometry everywhere along the duct is defined by the equation of a superellipse. Mean and turbulence data were accumulated utilizing pressure and hot-wire instrumentation at five stations along the test section. Data are presented for operating bulk Reynolds numbers of 88,000 and 390,000. Measured quantities include total and static pressure, the three components of the mean velocity vector, and the six components of the Reynolds stress tensor. In addition to the transition duct measurements, a hot-wire technique which relies on the sequential use of single rotatable normal and slant-wire probes was proposed. The technique is applicable for measurement of the total mean velocity vector and the complete Reynolds stress tensor when the primary flow is arbitrarily skewed relative to a plane which lies normal to the probe axis of rotation. Author

N91-32074* # National Aeronautics and Space Administration. Lewis Research Center, Cleveland, OH.

AN EXPERIMENTAL STUDY OF NATURAL AND FORCED MODES IN AN AXISYMMETRIC JET Ph.D. Thesis - Case Western Reserve Univ.

GANESH RAMAN, EDWARD J. RICE, and ELI RESHOTKO (Case Western Reserve Univ., Cleveland, OH.) Sep. 1991 196 p
(Contract RTOP 505-62-52)

(NASA-TM-105225; E-6091; NAS 1.15:105225) Avail: NTIS HC/MF A09 CSCL 01/1

The experiment consisted of two parts. The first part was an effort to study naturally occurring instability modes in the axisymmetric shear layer of a high Reynolds number turbulent jet. Untripped (transitional) and tripped (turbulent) nozzle exit conditions, both with 0.1 percent core turbulence, were studied. For the turbulent nozzle exit boundary layer case, the core turbulence, was varied systematically from 0.1 to 5 percent of the

jet exit velocity. The region up to the end of the potential core was dominated by the axisymmetric mode. The azimuthal modes grew rapidly but dominated only downstream of the potential core region. For the jet excited by natural disturbances, the energy content of the higher order modes (m is less than 1) was significantly lower than that of the axisymmetric and $m = +/-1$ modes. The initial boundary layer had a profound effect on the natural jet evolution and its excitability. The shorter potential core allowed the jet in the transitional case to support helical disturbances closer the nozzle exit than the turbulent case. The natural jet evolution was found to remain unaffected for varying initial core turbulence over the range of 0.15 to 5 percent of the jet velocity. Target modes for efficient excitation of the jet were determined from the results of the naturally occurring jet instability mode experiments. The second part of this work describes an effort to control the axisymmetric shear layer by artificially exciting target modes. Under optimum conditions, two-frequency excitation is indeed more effective than single frequency plane wave excitation as far as jet mixing is concerned. At high amplitudes of fundamental and subharmonic forcing, the subharmonic augmentation and the axial location of the peak were independent of the initial phase difference. Two-frequency excitation also has its limitations, since axisymmetric waves are damped beyond the potential core. Higher spreading rates are obtained when multi-modal forcing is applied. Author

N91-32075* # National Aeronautics and Space Administration. Lewis Research Center, Cleveland, OH.

UNSTEADY FLOWFIELD OF A PROPFAN AT TAKEOFF CONDITIONS

M. NALLASAMY (Sverdrup Technology, Inc., Brook Park, OH.) and J. F. GROENEWEG 1991 14 p Presented at the 6th International Symposium on Unsteady Aerodynamics, Aeroacoustics and Aeroelasticity of Turbomachines and Propellers, Notre Dame, IN, 15-19 Sep. 1991; sponsored by the International Union of Theoretical and Applied Mechanics
(Contract NAS3-25266; RTOP 535-03-10)

(NASA-TM-105223; E-6540; NAS 1.15:105223) Avail: NTIS HC/MF A03 CSCL 01/1

The unsteady flowfield of a propfan operation at takeoff conditions with angular inflow is examined by solving the three-dimensional Euler equations. The operating conditions considered are: Mach no. = 0.31, advance ratio = 1.6, and inflow angle to the propfan = 8.3 deg. The predicted results clearly show the cyclic variations of the blade power and thrust coefficients due to angular inflow. The flow changes from blade passage to passage are illustrated in terms of static pressure contours. The predicted blade surface pressure waveforms were compared with flight measurements. The predictions at the inboard radial station, $r/R = 0.68$, show reasonable agreement with flight data. At the outboard radial station, $r/R = 0.95$, where the interactions of the tip vortex, the tip-region flow and the blade wake appear to result in a complex nonlinear measured response. The prediction shows poor agreement. Author

03

AIR TRANSPORTATION AND SAFETY

Includes passenger and cargo air transport operations; and aircraft accidents.

A91-17218* National Aeronautics and Space Administration. Lewis Research Center, Cleveland, OH.

ICING TESTS OF A MODEL MAIN ROTOR

THOMAS H. BOND (NASA, Lewis Research Center, Cleveland, OH), ROBERT J. FLEMMING (Sikorsky Aircraft, Stratford, CT), and RANDALL K. BRITTON (NASA, Lewis Research Center; Sverdrup Technology, Inc., Cleveland, OH) IN: AHS, Annual Forum, 46th, Washington, DC, May 21-23, 1990, Proceedings.

Volume 1. Alexandria, VA, American Helicopter Society, 1990, p. 267-281. refs
Copyright

A NASA-sponsored consortium conducted an experimental program to investigate the characteristics of a model rotor under icing conditions. This project resulted in the first U.S. test of a heavily instrumented model rotor conducted in the controlled environment of a refrigerated wind tunnel, the NASA Lewis Icing Research Tunnel. The tunnel entry used a powered force model with a 1.83-m-diameter main rotor, with 0.124-m-chord main rotor blades fabricated specially for this experiment. Test conditions included a range of liquid water content and median volume droplet diameters that fell within the FAA and DOD icing envelopes. The test data show the effects of icing on rotor lift, rotor torque, blade loads, and vibration. Ice shapes and ice dimensions were taken, and molds were made of three ice shapes. High-speed movies were taken to document ice shedding. The results have been compared with analytical accretion predictions. Author

A91-22500* National Aeronautics and Space Administration. Lewis Research Center, Cleveland, OH.

A REVIEW OF ICE ACCRETION DATA FROM A MODEL ROTOR ICING TEST AND COMPARISON WITH THEORY

RANDALL K. BRITTON (NASA, Lewis Research Center; Sverdrup Technology, Inc., Brook Park, OH) and THOMAS H. BOND (NASA, Lewis Research Center, Cleveland, OH) AIAA, Aerospace Sciences Meeting, 29th, Reno, NV, Jan. 7-10, 1991. 34 p. Previously announced in STAR as N91-13421. refs
(AIAA PAPER 91-0661) Copyright

An experiment was conducted by the Helicopter Icing Consortium (HIC) in the NASA Lewis Icing Research Tunnel (IRT) in which a 1/6 scale fuselage model of a UH-60A Black Hawk helicopter with a generic rotor was subjected to a wide range of icing conditions. The HIC consists of members from NASA, Bell Helicopter, Boeing Helicopter, McDonnell Douglas Helicopters, Sikorsky Aircraft, and Texas A&M University. Data was taken in the form of rotor torque, internal force balance measurements, blade strain gage loading, and two dimensional ice shape tracings. A review of the ice shape data is performed with special attention given to repeatability and correctness of trends in terms of radial variation, rotational speed, icing time, temperature, liquid water content, and volumetric median droplet size. Moreover, an in-depth comparison between the experimental data and the analysis of NASA's ice accretion code LEWICE is given. Finally, conclusions are shown as to the quality of the ice accretion data and the predictability of the data base as a whole. Recommendations are also given for improving data taking technique as well as potential future work. Author

A91-26190* Sikorsky Aircraft, Stratford, CT.

RESULTS OF A SUB-SCALE MODEL ROTOR ICING TEST

ROBERT J. FLEMMING (Sikorsky Aircraft, Stratford, CT), THOMAS H. BOND (NASA, Lewis Research Center, Cleveland, OH), and RANDALL K. BRITTON (NASA, Lewis Research Center; Sverdrup Technology, Inc., Cleveland, OH) AIAA, Aerospace Sciences Meeting, 29th, Reno, NV, Jan. 7-10, 1991. 31 p. Previously announced in STAR as N91-14309. refs
(AIAA PAPER 91-0660) Copyright

A heavily instrumented sub-scale model of a helicopter main rotor was tested in the NASA Lewis Research Center Icing Research Tunnel (IRT) in September and November 1989. The four-bladed main rotor had a diameter of 1.83 m (6.00 ft) and the 0.124 m (4.9 in) chord rotor blades were specially fabricated for this experiment. The instrumented rotor was mounted on a Sikorsky Aircraft Powered Force Model, which enclosed a rotor balance and other measurement systems. The model rotor was exposed to a range of icing conditions that included variations in temperature, liquid water content, and median droplet diameter, and was operated over ranges of advance ratio, shaft angle, tip Mach number (rotor speed) and weight coefficient to determine the effect of these parameters on ice accretion. In addition to strain gage and balance data, the test was documented with still, video, and high speed photography, ice profile tracings, and ice

molds. The sensitivity of the model rotor to the test parameters is given, and the result to theoretical predictions are compared. Test data quality was excellent, and ice accretion prediction methods and rotor performance prediction methods (using published icing lift and drag relationships) reproduced the performance trends observed in the test. Adjustments to the correlation coefficients to improve the level of correlation are suggested. Author

A91-26193* National Aeronautics and Space Administration. Lewis Research Center, Cleveland, OH.

NUMERICAL SIMULATION OF ICE GROWTH ON A MS-317 SWEPT WING GEOMETRY

M. G. POTAPCZUK and C. S. BIDWELL (NASA, Lewis Research Center, Cleveland, OH) AIAA, Aerospace Sciences Meeting, 29th, Reno, NV, Jan. 7-10, 1991. 23 p. Previously announced in STAR as N91-14310. refs
(AIAA PAPER 91-0263) Copyright

An effort to develop a 3-D ice accretion modeling method was initiated. This first step towards creation of a complete aircraft icing simulation code builds on previously developed methods for calculating 3-D flow fields and particle trajectories combined with a 2-D ice accretion calculation along coordinate locations corresponding to streamlines. The types of calculations necessary to predict three-dimensional ice accretion is demonstrated. Results of calculations using 3-D method for a MS-317 swept wing geometry are projected onto a 2-D plane parallel to the free stream direction and compared to experimental results for the same geometry. It is anticipated that many modifications will be made to this approach, however, this effort will lay the groundwork for future modeling efforts. Results indicate that rime ice shapes indicate a difficulty in accurately calculating the ice shape in the runback region. Author

A91-35107* Massachusetts Inst. of Tech., Cambridge.

MODELING OF SURFACE ROUGHNESS EFFECTS ON GLAZE ICE ACCRETION

R. JOHN HANSMAN, JR., KEIKO YAMAGUCHI (MIT, Cambridge, MA), BRIAN BERKOWITZ (Sverdrup Technology, Inc., Middleburg Heights, OH), and MARK POTAPCZUK (NASA, Lewis Research Center, Cleveland, OH) Journal of Thermophysics and Heat Transfer (ISSN 0887-8722), vol. 5, Jan. 1991, p. 54-60. NSF-supported research. Previously cited in issue 10, p. 1433. Accession no. A89-28451. refs
(Contract NAG3-666; NGL-22-009-640) Copyright

N91-20120* National Aeronautics and Space Administration. Lewis Research Center, Cleveland, OH.

NASA'S AIRCRAFT ICING TECHNOLOGY PROGRAM

JOHN J. REINMANN In its Aeropropulsion 1991 24 p Mar. 1991

Avail: NTIS HC/MF A24 CSCL 01/3

NASA's Aircraft Icing Technology Program is aimed at developing innovative technologies for safe and efficient flight into forecasted icing. The program addresses the needs of all aircraft classes and supports both commercial and military applications. The program is guided by three key objectives: (1) to numerically simulate an aircraft's response to an in-flight icing encounter; (2) to provide improved capabilities and techniques for ground and flight icing testing; and (3) offer innovative approaches to ice protection. The fundamental research focuses on topics that directly support stated industry needs, and work is performed closely with industry to assure a rapid and smooth transfer of technology. The progress toward the three stated strategic objectives is reviewed. Author

N91-23098* National Aeronautics and Space Administration. Lewis Research Center, Cleveland, OH.

ENGINE TECHNOLOGY CHALLENGES FOR A 21ST CENTURY HIGH SPEED CIVIL TRANSPORT

ROBERT J. SHAW 1991 13 p Proposed for presentation at the 10th International Symposium on Air Breathing Engines, Nottingham, England, 1-6 Sep. 1991; sponsored by AIAA

04 AIRCRAFT COMMUNICATIONS AND NAVIGATION

(Contract RTOP 537-02-00)
(NASA-TM-104363; E-6159; NAS 1.15:104363) Avail: NTIS
HC/MF A03 CSCL 01/3

Recent NASA funded studies by Boeing and Douglas suggest an opportunity exists for a 21st Century High Speed Civil Transport (HSCT) to become part of the international air transportation system. However, before this opportunity for high speed travel can be realized, certain environmental and economic barrier issues must be overcome. These challenges are outlined. Research activities which NASA has planned to address these barrier issues and to provide a technology base to allow U.S. manufacturers to make an informed go/no go decision on developing the HSCT are discussed.

Author

04

AIRCRAFT COMMUNICATIONS AND NAVIGATION

Includes digital and voice communication with aircraft; air navigation systems (satellite and ground based); and air traffic control.

N91-23102*# National Aeronautics and Space Administration. Lewis Research Center, Cleveland, OH.

CHARACTERISTICS OF A FUTURE AERONAUTICAL SATELLITE COMMUNICATIONS SYSTEM

PHILIP Y. SOHN, ALAN STERN, and FRED SCHMIDT (Ball Corp., Bloomfield, CO.) 1991 30 p Presented at the Advanced Network and Technology Concepts for Mobile, Micro, and Personal Communications, Pasadena, CA, 30-31 May 1991; sponsored by JPL

(Contract RTOP 679-40-00)
(NASA-TM-104389; E-6200; NAS 1.15:104389) Avail: NTIS
HC/MF A03 CSCL 17/7

A possible operational system scenario for providing satellite communications services to the future aviation community was analyzed. The system concept relies on a Ka-band (20/30 GHz) satellite that utilizes multibeam antenna (MBA) technology. The aircraft terminal uses an extremely small aperture antenna as a result of using this higher spectrum at Ka-band. The satellite functions as a relay between the aircraft and the ground stations. The ground stations function as interfaces to the existing terrestrial networks such as the Public Service Telephone Network (PSTN). Various system tradeoffs are first examined to ensure optimized system parameters. High level performance specifications and design approaches are generated for the space, ground, and aeronautical elements in the system. Both technical and economical issues affecting the feasibility of the studied concept are addressed with the 1995 timeframe in mind.

Author

05

AIRCRAFT DESIGN, TESTING AND PERFORMANCE

Includes aircraft simulation technology.

A91-35427*# National Aeronautics and Space Administration. Lewis Research Center, Cleveland, OH.

ELEVATOR DEFLECTIONS ON THE ICING PROCESS

RANDALL K. BRITTON (NASA, Lewis Research Center, Cleveland, OH) AIAA Student Journal (ISSN 0001-1460), vol. 27, Winter 1989-1990, p. 8-18. refs

Copyright

The effect of elevator deflection of the horizontal stabilizer for certain icing parameters is investigated. Elevator deflection can severely change the lower and upper leading-edge impingement limits, and ice can accrete on the elevator itself. Also, elevator

deflection had practically no effect on the maximum local collection efficiency. It is shown that for severe icing conditions (large water droplets), elevator deflections that increase the projected height of the airfoil can significantly increase the total collection efficiency of the airfoil.

R.E.P.

A91-52835* National Aeronautics and Space Administration. Lewis Research Center, Cleveland, OH.

V/STOL GETS A LIFT

TOM BIESIADNY (NASA, Lewis Research Center, Cleveland, OH) Aerospace America (ISSN 0740-722X), vol. 29, Sept. 1991, p. 52-55.

Copyright

The concept of a supersonic STOVL that could offer enhanced mission capability, survivability, operational flexibility, and utility over conventional aircraft is presented. Emphasis is currently on design studies, CFD work, small- and large-scale wind tunnel tests, simulation activities, flight experiments, and ground environment experiments. Propulsion system technology centers about the adaptation of existing or off-the-shelf engines. Concepts under study include separate flow in hover, gas-driven lift fan, and shaft-driven lift fan. NASA is examining generic valve and ducting configurations with airflow at ambient temperature and at temperatures up to 1000 F to gather pressure loss and heat transfer data. Advanced civil rotorcraft technologies examined include high-efficiency/dual-mode components such as torque converters; lightweight, quiet transmissions; and variable geometry power turbines; along with dual-function or convertible engines.

R.E.P.

A91-53871*# National Aeronautics and Space Administration. Lewis Research Center, Cleveland, OH.

OVERVIEW OF THE NASA-SPONSORED HSCT PROPULSION SYSTEM STUDIES

WILLIAM C. STRACK (NASA, Lewis Research Center, Cleveland, OH) AIAA, Applied Aerodynamics Conference, 9th, Baltimore, MD, Sept. 23-25, 1991, 14 p. refs
(AIAA PAPER 91-3329) Copyright

A brief overview of the NASA-sponsored HSCT propulsion system studies is presented that includes objectives, approach, schedules, and a summary of interim results highlighting the NASA in-house studies. Seven propulsion system concepts have been considered to date and comparatively evaluated on a first-order basis using takeoff gross weight (TOGW) as the main discriminator. Only two concepts have been screened out thus far and it is apparent that TOGW is not a strong discriminator. However, the first-order screening process did not account for differences in propulsion installation effects or climb-noise suppression penalties-both of which may strongly influence the screening process.

Author

N91-15146*# National Aeronautics and Space Administration. Lewis Research Center, Cleveland, OH.

REVIEW OF THE TRANSMISSIONS OF THE SOVIET HELICOPTERS

LEV I. CHAIKO Dec. 1990 14 p Prepared in cooperation with Army Aviation Systems Command, Cleveland, OH
(Contract DA PROJ. 1L1-61102-AH-45; RTOP 505-62-OK)
(NASA-TM-103634; E-5803; NAS 1.15:103634; AVSCOM-TM-90-C-015) Avail: NTIS HC/MF A03 CSCL 01/3

A review of the following aspects of Soviet helicopter transmissions is presented: transmitted power, weight, reduction ratio, RPM, design configuration, comparison of different type of manufacturing methods, and a description of the materials and technologies applied to critical transmission components. Included are mechanical diagrams of the gearboxes of the Soviet helicopters and test stands for testing gearbox and main shaft. The quality of Soviet helicopter transmissions and their Western counterparts are assessed and compared.

Author

AIRCRAFT INSTRUMENTATION

Includes cockpit and cabin display devices; and flight instruments.

A91-19580* John Carroll Univ., Cleveland, OH.

DIGITAL ANGULAR POSITION SENSOR USING WAVELENGTH DIVISION MULTIPLEXING

KLAUS FRITSCH (John Carroll University, Cleveland, OH), GLENN BEHEIM, and JORGE SOTOMAYOR (NASA, Lewis Research Center, Cleveland, OH) IN: Fiber optic and laser sensors VII; Proceedings of the Meeting, Boston, MA, Sept. 5-7, 1989. Bellingham, WA, Society of Photo-Optical Instrumentation Engineers, 1990, p. 453-460. refs (Contract NAG3-571)

Copyright

Future aircraft will use fly-by-light control systems with fiber-linked optical sensors for such measurands as temperature, pressure, and linear and angular position. A digital optical sensor is described which was developed to transmit the angular position of such slowly rotating parts as a throttle of fuel flow control valve on an aircraft. The sensor employs a reflective code plate with ten channels providing a resolution of 0.35 degrees. Two light-emitting diodes with overlapping spectra are used as light sources. A single microoptic multiplexer-demultiplexer composed of a GRIN rod lens and a miniature grating is used to disperse the spectrum and recombine the spectral components from each channel after reflection by the code plate. The results of preliminary environmental tests of this unit are discussed. The sensor has been operated for brief periods of time between -60 C and +125 without adverse effects. Preliminary vibration tests indicate that the unit will work properly at the maximum vibration levels expected in a jet-engine environment. Author

N91-27157* National Aeronautics and Space Administration. Lewis Research Center, Cleveland, OH.

THE NASA LEWIS INTEGRATED PROPULSION AND FLIGHT CONTROL SIMULATOR

MICHELLE M. BRIGHT and DONALD L. SIMON 1991 13 p Presented at the Flight Simulation Technologies Conference, New Orleans, LA, 12-14 Aug. 1991; sponsored by AIAA (Contract RTOP 505-62-50) (NASA-TM-105147; E-6423; NAS 1.15:105147; AVSCOM-TR-91-C-037; AD-A240071) Avail: NTIS HC/MF A03 CSCL 14/2

A new flight simulation facility was developed at NASA-Lewis. The purpose of this flight simulator is to allow integrated propulsion control and flight control algorithm development and evaluation in real time. As a preliminary check of the simulator facility capabilities and correct integration of its components, the control design and physics models for a short take-off and vertical landing fighter aircraft model were shown, with their associated system integration and architecture, pilot vehicle interfaces, and display symbology. The initial testing and evaluation results show that this fixed based flight simulator can provide real time feedback and display of both airframe and propulsion variables for validation of integrated flight and propulsion control systems. Additionally, through the use of this flight simulator, various control design methodologies and cockpit mechanizations can be tested and evaluated in a real time environment. Author

AIRCRAFT PROPULSION AND POWER

Includes prime propulsion systems and systems components, e.g., gas turbine engines and compressors; and onboard auxiliary power plants for aircraft.

A91-14430* National Aeronautics and Space Administration. Lewis Research Center, Cleveland, OH.

NUMERICAL STUDY OF SUPERSONIC COMBUSTORS BY MULTI-BLOCK GRIDS WITH MISMATCHED INTERFACES

YOUNG J. MOON (NASA, Lewis Research Center; Sverdrup Technology, Inc., Cleveland, OH) AIAA, International Aerospace Planes Conference, 2nd, Orlando, FL, Oct. 29-31, 1990. 13 p. refs

(Contract NAS3-25266)

(AIAA PAPER 90-5204) Copyright

A three-dimensional, finite-rate chemistry, Navier-Stokes code has been extended to a multi-block with mismatched interface code for practical calculations of supersonic combustors. To ensure global conservation, a conservative algorithm was used for the treatment of mismatched interfaces. The extended code was checked against one test case, i.e., a generic supersonic combustor with transverse fuel injection, examining solution accuracy, convergence, and local mass flux error. After testing, the code was used to simulate the chemically reacting flow fields in a scramjet combustor with parallel fuel injectors (unswept and swept ramps). Computational results were compared with experimental shadowgraph and pressure measurements. Fuel-air mixing characteristics of the unswept and swept ramps were compared and investigated. Author

A91-14466* National Aeronautics and Space Administration. Lewis Research Center, Cleveland, OH.

EXPERIMENTAL INVESTIGATION OF A SINGLE FLUSH-MOUNTED HYPERMIXING NOZZLE

D. O. DAVIS, W. R. HINGST, and A. R. PORRO (NASA, Lewis Research Center, Cleveland, OH) AIAA, International Aerospace Planes Conference, 2nd, Orlando, FL, Oct. 29-31, 1990. 11 p. refs

(AIAA PAPER 90-5240) Copyright

Reported herein are the results of an experimental wind tunnel investigation of a circular supersonic jet ($M_j = 3.47$) injected at a 10 degree angle into a supersonic freestream. Measurements were made for nominal freestream Mach numbers of 1.6, 2.0, 2.5 and 3.0. Three jet total pressures were run at each freestream Mach number, resulting in twelve separate operating conditions. The measurements indicate the presence of two pairs of contra-rotating vortices. One pair follows the jet trajectory and tends to split the jet into two streams. A smaller pair, rotating in an opposite sense, develops in the near wall region. Reported results include Mach number and volume fraction distributions in the cross plane, as well as jet penetration and mixing efficiency. Author

A91-19448* Toledo Univ., OH.

CASCADE FLUTTER ANALYSIS WITH TRANSIENT RESPONSE AERODYNAMICS

MILIND A. BAKHLE, APARAJIT J. MAHAJAN, THEO G. KEITH, JR. (Toledo, University, OH), and GEORGE L. STEFKO (NASA, Lewis Research Center, Cleveland, OH) AIAA, Aerospace Sciences Meeting, 29th, Reno, NV, Jan. 7-10, 1991. 16 p. refs (Contract NSG-3139)

(AIAA PAPER 91-0747) Copyright

Two methods for calculating linear frequency domain aerodynamic coefficients from a time-marching Full-Potential cascade solver are developed and verified. In the first method, the Influence Coefficient method, solutions to elemental problems are superposed to obtain the solutions for a cascade in which all blades are vibrating with a constant interblade phase angle. The elemental problem consists of a single blade in the cascade

07 AIRCRAFT PROPULSION AND POWER

oscillating while the other blades remain stationary. In the second method, the Pulse Response method, the response to the transient motion of a blade is used to calculate influence coefficients. This is done by calculating the Fourier transforms of the blade motion and the response. Both methods are validated by comparison with the Harmonic Oscillation method and give accurate results. The aerodynamic coefficients obtained from these methods are used for frequency domain flutter calculations involving a typical section blade structural model. An eigenvalue problem is solved for each interblade phase angle mode and the eigenvalues are used to determine aeroelastic stability. Flutter calculations are performed for two examples over a range of subsonic Mach numbers using both flat plates and actual airfoils. Author

A91-23642* McDonnell Aircraft Co., Saint Louis, MO.

STOVL HOT GAS INGESTION CONTROL TECHNOLOGY

K. C. AMUEDO, B. R. WILLIAMS, J. D. FLOOD (McDonnell Aircraft Co., Saint Louis, MO), and A. L. JOHNS (NASA, Lewis Research Center, Cleveland, OH) ASME, Transactions, Journal of Engineering for Gas Turbines and Power (ISSN 0022-0825), vol. 113, Jan. 1991, p. 68-74.

(ASME PAPER 89-GT-323) Copyright

A comprehensive wind tunnel test program was conducted to evaluate control of Hot Gas Ingestion (HGI) on a 9.2 percent scale model of the McDonnell Aircraft Company model 279-3C advanced Short Takeoff and Vertical Landing (STOVL) configuration. The test was conducted in the NASA-Lewis Research Center 9 ft by 15 ft Low Speed Wind Tunnel during the summer of 1987. Initial tests defined baseline HGI levels as determined by engine face temperature rise and temperature distortion. Subsequent testing was conducted to evaluate HGI control parametrically using Lift Improvement Devices (LIDs), forward nozzle spray angle, a combination of LIDs and forward nozzle spray angle, and main inlet blocking. The results from this test program demonstrate that HGI can be effectively controlled and that HGI is not a barrier to STOVL aircraft development. Author

A91-28265* National Aeronautics and Space Administration. Lewis Research Center, Cleveland, OH.

CRUISE NOISE OF AN ADVANCED SINGLE-ROTATION PROPELLER MEASURED FROM AN ADJACENT AIRCRAFT

RICHARD P. WOODWARD, IRVIN J. LOEFFLER, and RICHARD J. RANAUDO (NASA, Lewis Research Center, Cleveland, OH) IN: Inter-noise 89 - Engineering for environmental noise control; Proceedings of the International Conference on Noise Control Engineering, Newport Beach, CA, Dec. 4-6, 1989. Vol. 1. Poughkeepsie, NY, Noise Control Foundation, 1989, p. 243-248. refs

Copyright

Results are reported from flight measurements of the noise from a full-scale SR-71 advanced single-rotation turbofan model mounted on the wing of the NASA Lewis Propfan Test Assessment (PTA) aircraft (a modified Gulfstream II). Data obtained on the PTA with an outboard microphone boom and by the NASA Lewis acoustically instrumented Learjet flying along several sidelines relative to the PTA are presented in tables and graphs and briefly discussed. It is found that the PTA-boom and Learjet sound levels are in good agreement at Mach 0.69 and altitude 20,000 ft, but the Learjet values are significantly lower than the boom levels at Mach 0.79 and altitude 36,000 ft. T.K.

A91-29452* National Aeronautics and Space Administration. Lewis Research Center, Cleveland, OH.

AN UPDATE OF ENGINE SYSTEM RESEARCH AT THE ARMY PROPULSION DIRECTORATE

GEORGE A. BOBULA (NASA, Lewis Research Center; U.S. Army, Propulsion Directorate, Cleveland, OH) IN: Rotary Wing Propulsion Specialists' Meeting, Williamsburg, VA, Nov. 13-15, 1990, Proceedings. Alexandria, VA, American Helicopter Society, 1990, 15 p. Previously announced in STAR as N91-11752. refs

Copyright

The Small Turbohaft Engine Research (STER) program provides a vehicle for evaluating the application of emerging

technologies to Army turboshaft engine systems and to investigate related phenomena. Capitalizing on the resources at hand, in the form of both the NASA facilities and the Army personnel, the program goal of developing a physical understanding of engine system dynamics and/or system interactions is being realized. STER entries investigate concepts and components developed both in-house and out-of-house. Emphasis is placed upon evaluations which evolved from on-going basic research and advanced development programs. Army aviation program managers are also encouraged to make use of STER resources, both people and facilities. The STER personnel have established their reputations as experts in the fields of engine system experimental evaluations and engine system related phenomena. The STER facility has STER program provides the Army aviation community the opportunity to perform system level investigations, and then to offer the findings to the entire engine community for their consideration in next generation propulsion systems. In this way results of the fundamental research being conducted to meet small turboshaft engine technology challenges expeditiously find their way into that next generation of propulsion systems. Author

A91-29775* National Aeronautics and Space Administration. Lewis Research Center, Cleveland, OH.

TURBOFAN ENGINE DEMONSTRATION OF SENSOR FAILURE DETECTION

WALTER C. MERRILL, JOHN C. DELAAT, and MAHMOOD ABDELWAHAB (NASA, Lewis Research Center, Cleveland, OH) Journal of Guidance, Control, and Dynamics (ISSN 0731-5090), vol. 14, Mar.-Apr. 1991, p. 337-349. refs

Copyright

In the paper, the results of a full-scale engine demonstration of a sensor failure detection algorithm are presented. The algorithm detects, isolates, and accommodates sensor failures using analytical redundancy. The experimental hardware, including the F100 engine, is described. Demonstration results were obtained over a large portion of a typical flight envelope for the F100 engine. They include both subsonic and supersonic conditions at both medium and full, nonafter burning, power. Estimated accuracy, minimum detectable levels of sensor failures, and failure accommodation performance for an F100 turbofan engine control system are discussed. Author

A91-30015* National Aeronautics and Space Administration. Lewis Research Center, Cleveland, OH.

EXPERIMENTAL INVESTIGATION OF PROPPAN AEROELASTIC RESPONSE IN OFF-AXIS FLOW WITH MISTUNING

ORAL MEHMED (NASA, Lewis Research Center, Cleveland, OH) and DURBHA V. MURTHY (Toledo, University, OH) Journal of Propulsion and Power (ISSN 0748-4658), vol. 7, Jan.-Feb. 1991, p. 90-98. Previously cited in issue 05, p. 628, Accession no. A89-17941. refs

Copyright

A91-37593* National Aeronautics and Space Administration. Lewis Research Center, Cleveland, OH.

SENSOR FAILURE DETECTION FOR JET ENGINES

WALTER C. MERRILL (NASA, Lewis Research Center, Cleveland, OH) IN: Control and dynamic systems. Vol. 33 - Advances in aerospace systems dynamics and control systems. Pt. 3. San Diego, CA, Academic Press, Inc., 1990, p. 1-34. Previously announced in STAR as N89-13432. refs

Copyright

The use of analytical redundancy to improve gas turbine engine control system reliability through sensor failure detection, isolation, and accommodation is surveyed. Both the theoretical and application papers that form the technology base of turbine engine analytical redundancy research are discussed. Also, several important application efforts are reviewed. An assessment of the state-of-the-art in analytical redundancy technology is given.

Author

A91-41653* National Aeronautics and Space Administration. Lewis Research Center, Cleveland, OH.

CFD ANALYSIS OF A HYDROGEN FUELED RAMJET ENGINE AT MACH 3.44

BEVERLY DUNCAN (NASA, Lewis Research Center; Sverdrup Technology, Inc., Brook Park, OH) AIAA, SAE, ASME, and ASEE, Joint Propulsion Conference, 27th, Sacramento, CA, June 24-26, 1991. 12 p. refs

(AIAA PAPER 91-1919)

The full Navier-Stokes solver, RPLUS, has been used to compute the flow field of a ramjet engine in the low supersonic operating regime. Computations have been made for the case where hydrogen is transversely injected and ignited using nine species and eighteen reactions to model the combustion process. The flow fields for two methods of hydrogen injection have been computed and compared to the available experimental data. The purpose of these computations was to assess the mixing effectiveness of the injected hydrogen with the primary supersonic stream. Results indicate significant ignition delay resulting from the poor mixing dynamics in the combustor section. Author

A91-41671* Case Western Reserve Univ., Cleveland, OH.

FEEDBACK LINEARIZATION FOR CONTROL OF AIR BREATHING ENGINES

STEPHEN PHILLIPS (Case Western Reserve University, Cleveland, OH) and DUANE MATTERN (NASA, Lewis Research Center, Cleveland; Sverdrup Technology, Inc., Brook Park, OH) AIAA, SAE, ASME, and ASEE, Joint Propulsion Conference, 27th, Sacramento, CA, June 24-26, 1991. 12 p. refs

(Contract NAG3-1232)

(AIAA PAPER 91-2000) Copyright

The method of feedback linearization for control of the nonlinear nozzle and compressor components of an air breathing engine is presented. This method overcomes the need for a large number of scheduling variables and operating points to accurately model highly nonlinear plants. Feedback linearization also results in linear closed loop system performance simplifying subsequent control design. Feedback linearization is used for the nonlinear partial engine model and performance is verified through simulation. Author

A91-41788* CFD Research Corp., Huntsville, AL.

A CFD STUDY OF JET MIXING IN REDUCED FLOW AREAS FOR LOWER COMBUSTOR EMISSIONS

C. E. SMITH, M. V. TALPALLIKAR (CFD Research Corp., Huntsville, AL), and J. D. HOLDEMAN (NASA, Lewis Research Center, Cleveland, OH) AIAA, SAE, ASME, and ASEE, Joint Propulsion Conference, 27th, Sacramento, CA, June 24-26, 1991. 15 p. Previously announced in STAR as N91-23185. refs

(Contract NAS3-25967)

(AIAA PAPER 91-2460) Copyright

The Rich-burn/Quick-mix/Lean-burn (RQL) combustor has the potential of significantly reducing NO(x) emissions in combustion chambers of High Speed Civil Transport aircraft. Previous work on RQL combustors for industrial applications suggested the benefit of necking down the mixing section. A 3-D numerical investigation was performed to study the effects of neckdown on NO(x) emissions and to develop a correlation for optimum mixing designs in terms of neckdown area ratio. The results of the study showed that jet mixing in reduced flow areas does not enhance mixing, but does decrease residence time at high flame temperatures, thus reducing NO(x) formation. By necking down the mixing flow area by 4, a potential NO(x) reduction of 16:1 is possible for annual combustors. However, there is a penalty that accompanies the mixing neckdown: reduced pressure drop across the combustor swirler. At conventional combustor loading parameters, the pressure drop penalty does not appear to be excessive. Author

A91-41799* National Aeronautics and Space Administration. Lewis Research Center, Cleveland, OH.

THERMAL AND STRUCTURAL ASSESSMENTS OF A CERAMIC WAFER SEAL IN HYPERSONIC ENGINE

MIKE TONG (NASA, Lewis Research Center, Cleveland; Sverdrup

Technology, Inc., Brook Park, OH) and BRUCE STEINETZ (NASA, Lewis Research Center, Cleveland, OH) AIAA, SAE, ASME, and ASEE, Joint Propulsion Conference, 27th, Sacramento, CA, June 24-26, 1991. 10 p. Previously announced in STAR as N91-13456. refs

(AIAA PAPER 91-2494) Copyright

The thermal and structural performances of a ceramic wafer seal in a simulated hypersonic engine environment are numerically assessed. The effects of aerodynamic heating, surface contact conductance between the seal and its adjacent surfaces, flow of purge coolant gases, and leakage of hot engine flow path gases on the seal temperature were investigated from the engine inlet back to the entrance region of the combustion chamber. Finite element structural analyses, coupled with Weibull failure analyses, were performed to determine the structural reliability of the wafer seal. Author

A91-41815* National Aeronautics and Space Administration. Lewis Research Center, Cleveland, OH.

A THREE-DIMENSIONAL NAVIER-STOKES STAGE ANALYSIS OF THE FLOW THROUGH A COMPACT RADIAL TURBINE

JAMES D. HEIDMANN (NASA, Lewis Research Center, Cleveland, OH) AIAA, SAE, ASME, and ASEE, Joint Propulsion Conference, 27th, Sacramento, CA, June 24-26, 1991. 12 p. Previously announced in STAR as N91-23186. refs

(AIAA PAPER 91-2564) Copyright

A steady, three-dimensional Navier-Stokes average passage computer code is used to analyze the flow through a compact radial turbine stage. The code is based upon the average passage set of equations for turbomachinery, whereby the flow fields for all passages in a given blade row are assumed to be identical while retaining their three-dimensionality. A stage solution is achieved by alternating between stator and rotor calculations, while coupling the two solutions by means of a set of axisymmetric body forces which model the absent blade row. Results from the stage calculation are compared with experimental data and with results from an isolated rotor solution having axisymmetric inlet flow quantities upstream of the vacated stator space. Although the mass-averaged loss through the rotor is comparable for both solutions, the details of the loss distribution differ due to stator effects. The stage calculation predicts smaller spanwise variations in efficiency, in closer agreement with the data. The results of the study indicate that stage analyses hold promise for improved prediction of loss mechanisms in multi-blade row turbomachinery, which could lead to improved designs through the reduction of these losses. Author

A91-42556* McDonnell-Douglas Research Labs., Saint Louis, MO.

FLOW VISUALIZATION STUDIES OF THE INTERNAL FLOW CHARACTERISTICS IN A SIMULATED MIXED FLOW

VECTORED THRUST ASTOVL ENGINE CONFIGURATION
K. R. SARIPALLI (McDonnell Douglas Research Laboratories, Saint Louis, MO), P. J. FERRARO, J. D. FLOOD (McDonnell Aircraft Co., Saint Louis, MO), R. E. GREY (NASA, Lewis Research Center, Cleveland, OH), and J. A. WAZYNIK (Pratt and Whitney Group, East Hartford, CT) AIAA, Fluid Dynamics, Plasma Dynamics and Lasers Conference, 22nd, Honolulu, HI, June 24-26, 1991. 13 p. (AIAA PAPER 91-1689) Copyright

The characteristics of internal flowfields in a Mixed Flow Vektored Thrust (MFVT) propulsion system for Short Take Off and Vertical Landing (STOVL) fighter aircraft were investigated using flow visualization techniques. A highly parametric 14 percent scale transparent model was used to simulate the MFVT propulsion system. The working medium was water. The mixing between the fan and core flow was studied using flow visualization for a variety of geometrical and flow parameters including three bypass ratio variations. The flow visualization technique involves the use of laser light sheet for illumination and fluorescent dye or air bubbles as tracers. Results indicate the existence of a strong vortex flowfield in the hover mode of operation that is responsible for good mixing between the fan and core flows. Author

07 AIRCRAFT PROPULSION AND POWER

A91-44050* # National Aeronautics and Space Administration. Lewis Research Center, Cleveland, OH.

STATIC PERFORMANCE TESTS OF A FLIGHT-TYPE STOVL EJECTOR

WENDY S. BARANKIEWICZ (NASA, Lewis Research Center, Cleveland, OH) AIAA, SAE, ASME, and ASEE, Joint Propulsion Conference, 27th, Sacramento, CA, June 24-26, 1991. 11 p. Previously announced in STAR as N91-24201. refs (AIAA PAPER 91-1902) Copyright

The design and development of thrust augmenting STOVL ejectors has typically been based on experimental iteration (i.e., trial and error). Static performance tests of a full scale vertical lift ejector were performed at primary flow temperatures up to 1560 R (1100 F). Flow visualization (smoke generators and yarn tufts) were used to view the inlet air flow, especially around the primary nozzle and end plates. Performance calculations are presented for ambient temperatures close to 480 R (20 F) and 535 R (75 F) which simulate seasonal aircraft operating conditions. Resulting thrust augmentation ratios are presented as functions of nozzle pressure ratio and temperature.

Author

A91-44153* # Florida Univ., Gainesville.

EFFECTS OF NOZZLE LIP GEOMETRY ON SPRAY ATOMIZATION AND EMISSIONS ADVANCED GAS TURBINE COMBUSTORS

GERALD J. MICKLOW, SUBIR ROYCHOUDHURY (Florida, University, Gainesville), and H. L. NGUYEN (NASA, Lewis Research Center, Cleveland, OH) AIAA, SAE, ASME, and ASEE, Joint Propulsion Conference, 27th, Sacramento, CA, June 24-26, 1991. 12 p. refs

(AIAA PAPER 91-2201) Copyright

A parametric study is conducted to investigate the effect of nozzle lip geometry on nozzle fuel distribution, emissions and temperature distribution for a rich burn section of a rich burn/quick quench/lean burn combustor. It is seen that the nozzle lip geometry greatly affects the fuel distribution, emissions and temperature distribution. It is determined that at an equivalence ratio of 1.6 the NO concentration could be lowered by a factor greater than three by changing the nozzle lip geometry.

R.E.P.

A91-44250* # National Aeronautics and Space Administration. Lewis Research Center, Cleveland, OH.

FUEL-RICH, CATALYTIC REACTION EXPERIMENTAL RESULTS

JIM ROLLBUHLER (NASA, Lewis Research Center, Cleveland, OH) AIAA, SAE, ASME, and ASEE, Joint Propulsion Conference, 27th, Sacramento, CA, June 24-26, 1991. 22 p. Previously announced in STAR as N91-24203. refs (AIAA PAPER 91-2463) Copyright

Future aeropropulsion gas turbine combustion requirements call for operating at very high inlet temperatures, pressures, and large temperature rises. At the same time, the combustion process is to have minimum pollution effects on the environment. Aircraft gas turbine engines utilize liquid hydrocarbon fuels which are difficult to uniformly atomize and mix with combustion air. An approach for minimizing fuel related problems is to transform the liquid fuel into gaseous form prior to the completion of the combustion process. Experimentally obtained results are presented for vaporizing and partially oxidizing a liquid hydrocarbon fuel into burnable gaseous components. The presented experimental data show that 1200 to 1300 K reaction product gas, rich in hydrogen, carbon monoxide, and light-end hydrocarbons, is formed when flowing 0.3 to 0.6 fuel to air mixes through a catalyst reactor. The reaction temperatures are kept low enough that nitrogen oxides and carbon particles (soot) do not form. Results are reported for tests using different catalyst types and configurations, mass flowrates, input temperatures, and fuel to air ratios.

Author

A91-45326* # National Aeronautics and Space Administration. Lewis Research Center, Cleveland, OH.

TRANSIENT FLOW THRUST PREDICTION FOR AN EJECTOR PROPULSION CONCEPT

COLIN K. DRUMMOND (NASA, Lewis Research Center, Cleveland,

OH) Journal of Propulsion and Power (ISSN 0748-4658), vol. 7, July-Aug. 1991, p. 465, 466. Abridged. Previously cited in issue 21, p. 3272, Accession no. A89-49688. refs Copyright

A91-45780* # National Aeronautics and Space Administration. Lewis Research Center, Cleveland, OH.

A LINEAR CONTROL DESIGN STRUCTURE TO MAINTAIN LOOP PROPERTIES DURING LIMIT OPERATION IN A MULTI-NOZZLE TURBOFAN ENGINE

DUANE MATTERN (NASA, Lewis Research Center, Cleveland; Sverdrup Technology, Inc., Brook Park, OH) and PETER OUZTS (NASA, Lewis Research Center, Cleveland, OH) AIAA, SAE, ASME, and ASEE, Joint Propulsion Conference, 27th, Sacramento, CA, June 24-26, 1991. 10 p. refs (AIAA PAPER 91-1997) Copyright

The implementation of multi-variable control systems on turbofan engines requires the use of limit protection to maintain safe engine operation. Since a turbofan engine typically encounters limits during transient operation, the use of a limit protection scheme that modifies the feedback loop may void the desired 'guarantees' associated with linear multi-variable control design methods, necessitating considerable simulation to validate the control with limit protection. An alternative control design structure is proposed that maintains the desired linear feedback properties when certain safety limits are encountered by moving the limit protection scheme outside of the feedback loop. This proposed structure is compared to a structure with a limit protection scheme that modifies the feedback loop properties. The two design structures are compared using both linear and nonlinear simulations. The evaluation emphasizes responses where the fan surge margin limit is encountered.

Author

A91-45782* # Maine Univ., Orono.

THREE-DIMENSIONAL CALCULATION OF THE MIXING OF RADIAL JETS FROM SLANTED SLOTS WITH A REACTIVE CYLINDRICAL CROSSFLOW

N. S. WINOWICH (Maine, University, Orono), H. L. NGUYEN (NASA, Lewis Research Center, Cleveland, OH), and S. A. MOEYKENS AIAA, SAE, ASME, and ASEE, Joint Propulsion Conference, 27th, Sacramento, CA, June 24-26, 1991. 12 p. refs (Contract NAG3-1115)

(AIAA PAPER 91-2081) Copyright

A numerical model that calculates the 3D chemically reacting flowfield in an experimental low emission combustor is described. The ICED-ALE finite volume computational methodology is employed in this study. Radial jets issuing from slanted slots interact with a cylindrical axially flowing mainstream to produce a bulk swirl velocity downstream of the slot region. The swirl pattern at a given axial station is composed of a clockwise rotating region near the wall and a counterclockwise rotating region extending from the combustor centerline. The jet radial penetration and downstream swirl velocity axial development are shown to depend principally on the jet-to-mainstream momentum flux ratio.

R.E.P.

A91-45788* # Pratt and Whitney Aircraft Group, West Palm Beach, FL.

DESIGN AND EXPERIMENTAL EVALUATION OF COMPACT RADIAL-INFLOW TURBINES

A. J. FREDMONSKI, F. W. HUBER (Pratt and Whitney Group, West Palm Beach, FL), R. J. ROELKE (NASA, Lewis Research Center, Cleveland, OH), and S. SIMONYI (Sverdrup Technology, Inc., Brook Park, OH) AIAA, SAE, ASME, and ASEE, Joint Propulsion Conference, 27th, Sacramento, CA, June 24-26, 1991. 12 p. refs

(AIAA PAPER 91-2127) Copyright

The application of a multistage 3D Euler solver to the aerodynamic design of two compact radial-inflow turbines is presented, along with experimental results evaluating and validating the designs. The objectives of the program were to design, fabricate, and rig test compact radial-inflow turbines with equal or better efficiency relative to conventional designs, while having 40 percent less rotor length than current traditionally-sized radial

turbines. The approach to achieving these objectives was to apply a calibrated 3D multistage Euler code to accurately predict and control the high rotor flow passage velocities and high aerodynamic loadings resulting from the reduction in rotor length. A comparison of the advanced compact designs to current state-of-the-art configurations is presented. Author

A91-45789* # National Aeronautics and Space Administration. Lewis Research Center, Cleveland, OH.

COMPARISON OF A QUASI-3D ANALYSIS AND EXPERIMENTAL PERFORMANCE FOR THREE COMPACT RADIAL TURBINES

P. S. SIMONYI (NASA, Lewis Research Center, Cleveland; Sverdrup Technology, Inc., Brook Park, OH) and R. J. BOYLE (NASA, Lewis Research Center, Cleveland, OH) AIAA, SAE, ASME, and ASEE, Joint Propulsion Conference, 27th, Sacramento, CA, June 24-26, 1991. 14 p. refs (Contract NAS3-25266) (AIAA PAPER 91-2128)

An experimental aerodynamic evaluation of three compact radial turbine builds was performed. Two rotors which were 40-50 percent shorter in axial length than conventional state-of-the-art radial rotors were tested. A single nozzle design was used. One rotor was tested with the nozzle at two stagger angle settings. A second rotor was tested with the nozzle in only the closed down setting. Experimental results were compared to predicted results from a quasi-3D inviscid and boundary layer analysis, called MTSB (Merid/Tsonic/Blayer). This analysis was used to predict turbine performance. It has previously been calibrated only for axial, not radial, turbomachinery. The predicted and measured efficiencies were compared at the design point for the three turbines. At the design points the analysis overpredicted the efficiency by less than 1.7 points. Comparisons were also made at off-design operating points. The results of these comparisons showed the importance of an accurate clearance model for efficiency predictions and also that there are deficiencies in the incidence loss model used. Author

A91-45791* # National Aeronautics and Space Administration. Lewis Research Center, Cleveland, OH.

EXPERIMENTAL AND ANALYTICAL STUDIES OF FLOW THROUGH A VENTRAL AND AXIAL EXHAUST NOZZLE SYSTEM FOR STOVL AIRCRAFT

BARBARA S. ESKER (NASA, Lewis Research Center, Cleveland, OH) and JAMES R. DEBONIS (NASA, Lewis Research Center, Cleveland; Sverdrup Technology, Inc., Brook Park, OH) AIAA, SAE, ASME, and ASEE, Joint Propulsion Conference, 27th, Sacramento, CA, June 24-26, 1991. 20 p. Previously announced in STAR as N91-25175. refs (AIAA PAPER 91-2135) Copyright

Flow through a combined ventral and axial exhaust nozzle system was studied experimentally and analytically. The work is part of an ongoing propulsion technology effort at NASA Lewis Research Center for short takeoff, vertical landing (STOVL) aircraft. The experimental investigation was done on the NASA Lewis Powered Lift Facility. The experiment consisted of performance testing over a range of tailpipe pressure ratios from 1 to 3.2 and flow visualization. The analytical investigation consisted of modeling the same configuration and solving for the flow using the PARC3D computational fluid dynamics program. The comparison of experimental and analytical results was very good. The ventral nozzle performance coefficients obtained from both the experimental and analytical studies agreed within 1.2 percent. The net horizontal thrust of the nozzle system contained a significant reverse thrust component created by the flow overturning in the ventral duct. This component resulted in a low net horizontal thrust coefficient. The experimental and analytical studies showed very good agreement in the internal flow patterns. Author

A91-45799* # National Aeronautics and Space Administration. Lewis Research Center, Cleveland, OH.

ANALYTICAL COMBUSTION/EMISSIONS RESEARCH RELATED TO THE NASA HIGH-SPEED RESEARCH PROGRAM

H. L. NGUYEN (NASA, Lewis Research Center, Cleveland, OH) AIAA, SAE, ASME, and ASEE, Joint Propulsion Conference, 27th, Sacramento, CA, June 24-26, 1991. 18 p. refs (AIAA PAPER 91-2252) Copyright

A combustion analysis program aimed at upgrading and applying advanced computer programs for gas turbine applications is discussed. 2D and 3D codes, KIVA-II and LeRC-3D, have been used to provide insight into the combustion process and combustor design. The computations performed through these codes show their capability to produce reasonable results, despite such deficiencies in the current models as accurate chemical kinetics modeling of hydrocarbon combustion and turbulence and turbulence combustion interaction modeling. O.G.

A91-45800* # National Aeronautics and Space Administration. Lewis Research Center, Cleveland, OH.

PROGRESS TOWARD SYNERGISTIC HYPERMIXING NOZZLES

D. O. DAVIS and W. R. HINGST (NASA, Lewis Research Center, Cleveland, OH) AIAA, SAE, ASME, and ASEE, Joint Propulsion Conference, 27th, Sacramento, CA, June 24-26, 1991. 10 p. refs (AIAA PAPER 91-2264) Copyright

Mean flow measurements have been obtained for air-to-air mixing downstream of swept and unswept ramp wall-mounted hypermixing nozzle configurations. Aside from the sweep of the ramps, the two nozzle configurations investigated are identical. The nozzles inject three parallel supersonic jets at a 15-deg angle (relative to the wind tunnel wall) into a supersonic freestream. Mach number and volume fraction distributions in a transverse plane 11.1 nozzle heights downstream from the nozzle exit plane were measured. Data are presented for a freestream Mach number of three at a matched static pressure condition and also at an underexpanded static pressure condition (pressure ratio equal to 5). Surface oil flow visualization was used to investigate the near-wall flow behavior. The results indicate that the swept ramp injectors produce stronger and larger vortex pairs than the unswept ramp injectors. The increased interaction between the swept ramp model's larger vortex pairs yields better mixing characteristics for this model. Author

A91-54051* # National Aeronautics and Space Administration. Lewis Research Center, Cleveland, OH.

COMPARISON OF TURBINE BYPASS AND MIXED FLOW TURBOFAN ENGINES FOR A HIGH-SPEED CIVIL TRANSPORT JONATHAN A. SEIDEL, WILLIAM J. HALLER, and JEFFREY J. BERTON (NASA, Lewis Research Center, Cleveland, OH) AIAA, AHS, and ASEE, Aircraft Design Systems and Operations Meeting, Baltimore, MD, Sept. 23-25, 1991. 17 p. refs (AIAA PAPER 91-3132) Copyright

A comparison of the turbine bypass engine and the mixed flow turbofan for a Mach 2.4 cruise application is presented. A parametric assessment is conducted for each cycle. Parameters that are investigated for the turbine bypass engine include design bypass, combustor exit temperature, and overall pressure ratio. Parameters that are investigated for the mixed flow turbofan include fan pressure ratio, mixer design pressure ratio, and combustor exit temperature. The engines are analyzed for a 5000-nautical-mile, all supersonic cruise mission to determine the aircraft takeoff gross weights. The effects of takeoff noise, cruise emissions, the addition of subsonic cruise legs, and constrained supersonic cruise altitudes are also evaluated. P.D.

A91-56109* National Aeronautics and Space Administration. Lewis Research Center, Cleveland, OH.

PROPULSION CHALLENGES FOR A 21ST CENTURY ECONOMICALLY VIABLE, ENVIRONMENTALLY COMPATIBLE HIGH-SPEED CIVIL TRANSPORT

ROBERT J. SHAW (NASA, Lewis Research Center, Cleveland, OH) IN: International Symposium on Air Breathing Engines, 10th, Nottingham, England, Sept. 1-6, 1991, Proceedings. Vol. 1. Washington, DC, American Institute of Aeronautics and Astronautics, 1991, p. 93-103. Previously announced in STAR as

07 AIRCRAFT PROPULSION AND POWER

N91-23098. refs

Copyright

Recent NASA funded studies suggest an opportunity exists for a 21st Century High Speed Civil Transport (HSCT) to become part of the international air transportation system. However, before this opportunity for high speed travel can be realized, certain environmental and economic barrier issues must be overcome. These challenges are outlined. Research activities which NASA has planned to address these barrier issues and provide a technology base to allow the U.S. manufacturers to make an informed go/no go decision on developing an HSCT are discussed.

Author

N91-11752*# National Aeronautics and Space Administration. Lewis Research Center, Cleveland, OH.

AN UPDATE OF ENGINE SYSTEM RESEARCH AT THE ARMY PROPULSION DIRECTORATE

GEORGE A. BOBULA Nov. 1990 18 p Presented at the Rotary Wing Propulsion Specialists' Meeting, Williamsburg, VA, 13-15 Nov. 1990; sponsored in part by the American Helicopter Society, Inc. Prepared in cooperation with Army Aviation Systems Command, Cleveland, OH

(Contract DA PROJ. 1L1-62211-A-47-A; RTOP 505-62-OK)

(NASA-TM-103278; E-5726; NAS 1.15:103278;

AVSCOM-TR-90-C-021; AD-A229668) Avail: NTIS HC/MF A03 CSCL 21/5

The Small Turboshaft Engine Research (STER) program provides a vehicle for evaluating the application of emerging technologies to Army turboshaft engine systems and to investigate related phenomena. Capitalizing on the resources at hand, in the form of both the NASA facilities and the Army personnel, the program goal of developing a physical understanding of engine system dynamics and/or system interactions is being realized. STER entries investigate concepts and components developed both in-house and out-of-house. Emphasis is placed upon evaluations which have evolved from on-going basic research and advanced development programs. Army aviation program managers are also encouraged to make use of STER resources, both people and facilities. The STER personnel have established their reputations as experts in the fields of engine system experimental evaluations and engine system related phenomena. The STER facility has demonstrated its utility in both research and development programs. The STER program provides the Army aviation community the opportunity to perform system level investigations, and then to offer the findings to the entire engine community for their consideration in next generation propulsion systems. In this way results of the fundamental research being conducted to meet small turboshaft engine technology challenges expeditiously find their way into that next generation of propulsion systems.

Author

N91-13455*# National Aeronautics and Space Administration. Lewis Research Center, Cleveland, OH.

MEASUREMENTS AND PREDICTIONS OF A LIQUID SPRAY FROM AN AIR-ASSIST NOZZLE

DANIEL L. BULZAN, YESHAYAHOU LEVY, SURESH K. AGGARWAL, and SUSHEEL CHITRE (Chicago Univ., IL.) 1991 12 p Presented at the 29th Aerospace Sciences Meeting, Reno, NV, 7-10 Jan. 1991; sponsored by ASAA

(Contract RTOP 505-62-41)

(NASA-TM-103640; E-5821; NAS 1.15:103640; AIAA PAPER

91-0692) Avail: NTIS HC/MF A03 CSCL 21/5

Droplet size and gas velocity were measured in a water spray using a two-component Phase/Doppler Particle Analyzer. A complete set of measurements was obtained at axial locations from 5 to 50 cm downstream of the nozzle. The nozzle used was a simple axisymmetric air-assist nozzle. The sprays produced, using the atomizer, were extremely fine. Sauter mean diameters were less than 20 microns at all locations. Measurements were obtained for droplets ranging from 1 to 50 microns. The gas phase was seeded with micron sized droplets, and droplets having diameters of 1.4 microns and less were used to represent gas-phase properties. Measurements were compared with predictions from a

multi-phase computer model. Initial conditions for the model were taken from measurements at 5 cm downstream. Predictions for both the gas phase and the droplets showed relatively good agreement with the measurements.

Author

N91-13456*# National Aeronautics and Space Administration. Lewis Research Center, Cleveland, OH.

THERMAL AND STRUCTURAL ASSESSMENTS OF A CERAMIC WAFER SEAL IN HYPERSONIC ENGINES

MIKE T. TONG (Sverdrup Technology, Inc., Brook Park, OH.) and BRUCE M. STEINETZ 1991 11 p Proposed for presentation at the 27th Joint Propulsion Conference, Sacramento, CA, 24-27 Jun. 1991; cosponsored by AIAA, ASME, SAE, and ASEE

(Contract RTOP 505-63-113)

(NASA-TM-103651; E-5840; NAS 1.15:103651) Avail: NTIS HC/MF A03 CSCL 21/5

The thermal and structural performances of a ceramic wafer seal in a simulated hypersonic engine environment are numerically assessed. The effects of aerodynamic heating, surface contact conductance between the seal and its adjacent surfaces, flow of purge coolant gases, and leakage of hot engine flow path gases on the seal temperature were investigated from the engine inlet back to the entrance region of the combustion chamber. Finite element structural analyses, coupled with Weibull failure analyses, were performed to determine the structural reliability of the wafer seal.

Author

N91-13457*# National Aeronautics and Space Administration. Lewis Research Center, Cleveland, OH.

AN AD100 IMPLEMENTATION OF A REAL-TIME STOVL AIRCRAFT PROPULSION SYSTEM

PETER J. OUZTS and COLIN K. DRUMMOND 1990 20 p Presented at the 4th Annual Conference of the Applied Dynamics International Users' Society of the Central/Northeastern Regions, Warren, MI, 1-2 Oct. 1990

(Contract RTOP 505-62-71)

(NASA-TM-103683; E-5901; NAS 1.15:103683) Avail: NTIS HC/MF A03 CSCL 21/5

A real-time dynamic model of the propulsion system for a Short Take-Off and Vertical Landing (STOVL) aircraft was developed for the AD100 simulation environment. The dynamic model was adapted from a FORTRAN based simulation using the dynamic programming capabilities of the AD100 ADSIM simulation language. The dynamic model includes an aerothermal representation of a turbofan jet engine, actuator and sensor models, and a multivariable control system. The AD100 model was tested for agreement with the FORTRAN model and real-time execution performance. The propulsion system model was also linked to an airframe dynamic model to provide an overall STOVL aircraft simulation for the purposes of integrated flight and propulsion control studies. An evaluation of the AD100 system for use as an aircraft simulation environment is included.

Author

N91-14349*# National Aeronautics and Space Administration. Lewis Research Center, Cleveland, OH.

COMBUSTOR TECHNOLOGY FOR FUTURE AIRCRAFT

ROBERT R. TACINA 1990 17 p Presented at the 26th Joint Propulsion Conference, Orlando, FL, 16-18 Jul. 1990; cosponsored by AIAA, SAE, ASME, and ASEE Previously announced in IAA as A90-47219

(Contract RTOP 535-05-01)

(NASA-TM-103268; E-5707; NAS 1.15:103268; AIAA PAPER 90-2400) Avail: NTIS HC/MF A03 CSCL 21/5

The continuing improvement of aircraft gas turbine engine operating efficiencies involves increases in overall engine pressure ratio increases that will result in combustor inlet pressure and temperature increases, greater combustion temperature rises, and higher combustor exit temperatures. These conditions entail the development of fuel injectors generating uniform circumferential and radial temperature patterns, as well as combustor liner configurations and materials capable of withstanding increased thermal radiation even as the amount of cooling air is reduced. Low NO(x)-emitting combustor concepts are required which will

employ staged combustion. The development status of component technologies answering these requirements are presently evaluated. Author

N91-15174*# National Aeronautics and Space Administration. Lewis Research Center, Cleveland, OH.

OPTICAL MEASUREMENT OF UNDUCTED FAN FLUTTER

ANATOLE P. KURKOV and ORAL MEHMED 1990 11 p
Prepared for presentation at the 36th International Gas Turbine and Aeroengine Congress and Exposition, Orlando, FL, 3-6 Jun. 1991; sponsored in part by the American Society of Mechanical Engineers
(Contract RTOP 505-63-1B)
(NASA-TM-103285; E-5741; NAS 1.15:103285) Avail: NTIS HC/MF A03 CSCL 21/5

A nonintrusive optical method is described for flutter vibrations in unducted fan or propeller rotors and provides detailed spectral results for two flutter modes of a scaled unducted fan. The measurements were obtained in a high-speed wind tunnel. A single-rotor and a dual-rotor counterrotating configuration of the model were tested; however, only the forward rotor of the counterrotating configuration fluttered. Conventional strain gages were used to obtain flutter frequency; optical data provided complete phase results and an indication of the flutter mode shape through the ratio of the leading- to trailing-edge flutter amplitudes near the blade tip. In the transonic regime exhibited some features that are usually associated with nonlinear vibrations. Experimental mode shape and frequencies were compared with calculated values that included centrifugal effects. Author

N91-19097*# National Aeronautics and Space Administration. Lewis Research Center, Cleveland, OH.

THE SELECTION OF CONVERTIBLE ENGINES WITH CURRENT GAS GENERATOR TECHNOLOGY FOR HIGH SPEED ROTORCRAFT

JOSEPH D. EISENBERG 1990 27 p Presented at the Vertical Lift Aircraft Design Conference, San Francisco, CA, 17-19 Jan. 1990; cosponsored by American Helicopter Society Previously announced in IAA as A90-46933
(Contract RTOP 505-69-51)
(NASA-TM-103774; E-6041; NAS 1.15:103774) Avail: NTIS HC/MF A03 CSCL 21/5

NASA-Lewis sponsored two studies to determine the most promising convertible engine concepts for high speed rotorcraft. These studies projected year 2000 convertible technology limited to present gas generator technology. Propulsion systems for utilization on aircraft needing thrust only during cruise and those aircraft needing both power and thrust at cruise were investigated. Mission calculations for the two contractors involved were based upon the fold tilt rotor concept. Analysis and comparison of the General Electric concepts (geared UDF, clutched fan, and Variable Inlet Guide Vane (VIGV) fan), and the Allison Gas Turbine concepts (clutched fan, VIGV fan, variable pitch fan, single rotation tractor propfan, and counter rotation tractor propfan) are presented. Author

N91-19098*# National Aeronautics and Space Administration. Lewis Research Center, Cleveland, OH.

WIND TUNNEL WALL EFFECTS IN A LINEAR OSCILLATING CASCADE

DANIEL H. BUFFUM and SANFORD FLEETER (Purdue Univ., West Lafayette, IN.) 1991 14 p Proposed for presentation at the 36th International Gas Turbine and Aeroengine Congress and Exposition, Orlando, FL, 3-6 Jun. 1991; sponsored by ASME
(Contract RTOP 535-05-01)
(NASA-TM-103690; E-5909; NAS 1.15:103690) Avail: NTIS HC/MF A03 CSCL 21/5

Experiments in a linear oscillating cascade reveal that the wind tunnel walls enclosing the airfoils have, in some cases, a detrimental effect on the oscillating cascade aerodynamics. In a subsonic flow field, biconvex airfoils are driven simultaneously in harmonic, torsion-mode oscillations for a range of interblade phase angle values. It is found that the cascade dynamic periodicity -

the airfoil to airfoil variation in unsteady surface pressure - is good for some values of interblade phase angle but poor for others. Correlation of the unsteady pressure data with oscillating flat plate cascade predictions is generally good for conditions where the periodicity is good and poor where the periodicity is poor. Calculations based upon linearized unsteady aerodynamic theory indicate that pressure waves reflected from the wind tunnel walls are responsible for the cases where there is poor periodicity and poor correlation with the predictions. Author

N91-20084*# National Aeronautics and Space Administration. Lewis Research Center, Cleveland, OH.

AN IMAGING SYSTEM FOR PLIF/MIE MEASUREMENTS FOR A COMBUSTING FLOW

C. C. WEY, B. GHORASHI, C. J. MAREK, and C. WEY (Sverdrup Technology, Inc., Brook Park, OH.) 1990 13 p Presented at the 6th International Symposium on Heat and Mass Transfer, Miami, FL, 10-12 Dec. 1990; sponsored by Miami Univ.
(Contract NAS3-25266; RTOP 505-61-52)
(NASA-TM-103714; E-5887; NAS 1.15:103714) Avail: NTIS HC/MF A03 CSCL 21/5

The equipment required to establish an imaging system can be divided into four parts: (1) the light source and beam shaping optics; (2) camera and recording; (3) image acquisition and processing; and (4) computer and output systems. A pulsed, Nd:YAG-pumped, frequency-doubled dye laser which can freeze motion in the flowfield is used for an illumination source. A set of lenses is used to form the laser beam into a sheet. The induced fluorescence is collected by an UV-enhanced lens and passes through an UV-enhanced microchannel plate intensifier which is optically coupled to a gated solid state CCD camera. The output of the camera is simultaneously displayed on a monitor and recorded on either a laser videodisc set of a Super VHS VCR. This videodisc set is controlled by a minicomputer via a connection to the RS-232C interface terminals. The imaging system is connected to the host computer by a bus repeater and can be multiplexed between four video input sources. Sample images from a planar shear layer experiment are presented to show the processing capability of the imaging system with the host computer. Author

N91-20086*# National Aeronautics and Space Administration. Lewis Research Center, Cleveland, OH.

AEROPROPULSION 1991

Mar. 1991 574 p Conference held in Cleveland, OH, 20-21 Mar. 1991
(Contract RTOP 505-62-00)
(NASA-CP-10063; E-5954; NAS 1.55:10063) Avail: NTIS HC/MF A24 CSCL 21/5

For the 50th anniversary, a review was provided of recent accomplishments of the ongoing programs at Lewis Research Center. The Lewis Aeropropulsion Program has the charter to develop advanced airbreathing propulsion technology for applications of national interest. To implement this program, Lewis concentrates its basic research in the critical disciplines of internal fluid mechanics, instrumentation and control, and structures and materials. The efforts are focused on developing new science, often implemented through advanced computer codes. Carefully designed experiments provide the data required to validate the advanced codes. Recent results and planned accomplishments in these areas are reviewed. From this firm foundation technology is investigated for a number of applications including propulsion, high performance and hypersonic aircraft, rotorcraft, and general aviation.

N91-20088*# National Aeronautics and Space Administration. Lewis Research Center, Cleveland, OH.

OVERVIEW OF SUPERSONIC CRUISE PROPULSION RESEARCH

R. J. SHAW In its Aeropropulsion 1991 30 p Mar. 1991
Avail: NTIS HC/MF A24 CSCL 21/5

Significant advances in propulsion performance are required if supersonic transport vehicles are to become an important part of

07 AIRCRAFT PROPULSION AND POWER

the 21st century international air transportation system. The objective of the NASA Lewis Supersonic Cruise propulsion research is to provide the critical propulsion technologies to the industry in a timely fashion to contribute to the design of economically viable and environmentally acceptable high-speed civil transport (HSCT).

Author

N91-20089*# National Aeronautics and Space Administration. Lewis Research Center, Cleveland, OH.

OVERVIEW OF HIGH PERFORMANCE AIRCRAFT PROPULSION

PETER G. BATTERTON and THOMAS J. BIESIADNY *In its* Aeropropulsion 1991 18 p Mar. 1991

Avail: NTIS HC/MF A24 CSCL 21/5

The basic overall scope of the Lewis High Performance Aircraft Propulsion Research and Technology effort is presented. High performance fighter aircraft of interest include supersonic fighters with such capabilities as short take off and vertical landing (STOVL) and/or high maneuverability. The effort is primarily focused on component-level experimental and analytical research. This research is designed to provide databases for verification of design technology and for calibration of the CFD tools available for design use. Examples from each of the research areas are discussed, and a brief look at future directions for high performance aircraft research and technology is presented.

Author

N91-20090*# National Aeronautics and Space Administration. Lewis Research Center, Cleveland, OH.

FLOW VISUALIZATION AND HOT GAS INGESTION CHARACTERISTICS OF A VECTORED THRUST STOVL CONCEPT

ALBERT L. JOHNS, GEORGE H. NEINER, TIMOTHY J. BENCIC, DAVID M. FRICKER, and JEROME T. KEGELMAN (McDonnell-Douglas Research Labs., Saint Louis, MO.) *In its* Aeropropulsion 1991 17 p Mar. 1991

Avail: NTIS HC/MF A24 CSCL 21/5

Hot gas ingestion, the entrainment of heated engine exhaust into the inlet flow field, is the key development issue for advanced short takeoff and vertical landing aircraft. A 9.2 percent scale short takeoff and vertical landing (STOVL) hot gas ingestion model was designed and built by McDonnell Douglas Corporation (MCAIR) and tested in the NASA Lewis Research Center 9 by 15 foot Low Speed Wind Tunnel (LSWT). The test was conducted over a range of headwind velocities from 10 to 23 kn and nozzle exhaust temperatures from 500 to 1000 F. The model was also tested over a range of model heights above the ground plane (0.20 to 12 in.) and a range of nozzle pressure ratios from 1.3 to 4.00. A copper vapor laser was used to create an illuminated flow field for flow visualization with the model in and out of ground effects. Results are presented showing the flow field visualization which occurs when the model was in and out of ground effects. The effect of hot gas ingestion on the compressor face temperature rise and several other parameters are also presented. The environmental effects of the hot gas on the ground and its effect on the acoustic loads as a function of the model height above the ground are also presented.

Author

N91-20091*# National Aeronautics and Space Administration. Lewis Research Center, Cleveland, OH.

HIGH ALPHA INLETS

RICHARD R. BURLEY, BERNHARD H. ANDERSON, C. FREDERIC SMITH, and GARY J. HARLOFF (Sverdrup Technology, Inc., Cleveland, OH.) *In its* Aeropropulsion 1991 14 p Mar. 1991

Avail: NTIS HC/MF A24 CSCL 21/5

The high alpha inlet research effort at Lewis is part of the High Alpha Technology Program (HATP) within NASA. A key goal of HATP is to develop concepts that provide a high level of control and maneuverability for high performance aircraft at low subsonic speeds and angles-of-attack above 60 degrees. The approach, which consists of both experimental and computational efforts, utilizes the F-18 High Alpha Research Vehicle (HARV) as well as subscale models to obtain the experimental data base needed for validation of the computational codes. As the propulsion center

within NASA, the overall objectives of the Lewis effort is to develop and enhance inlet technology that will ensure high performance and stability of the propulsion system during the aircraft maneuvers at low speeds and high angles-of-attack. An overview is presented of the existing Lewis technology for achieving high inlet performance at low subsonic speed/high angle-of-attack conditions and the plans to extend this technology to advanced, highly maneuverable aircraft. The discussion is divided into six parts: the scope of the HATP effort; the inlet challenge for highly maneuverable aircraft, the Lewis data base, the Lewis computational effort, future plans, and concluding remarks.

Author

N91-20092*# National Aeronautics and Space Administration. Lewis Research Center, Cleveland, OH.

OVERVIEW OF HYPERSONIC/TRANSATMOSPHERIC VEHICLE PROPULSION TECHNOLOGY

JOHN E. ROHDE *In its* Aeropropulsion 1991 11 p Mar. 1991

Avail: NTIS HC/MF A24 CSCL 21/5

Significant progress is being made in attaining many of the enabling technologies critical to the development of future hypersonic vehicles such as the single-stage-to-orbit National Aerospace Plane (NASP) X-30 vehicle and others. In the NASP program, slush hydrogen was safely produced and transferred in modestly large quantities. Inlet testing has demonstrated that a high-performance configuration can be developed, and configurations were developed that reduce cross-talk between engine modules and improve unstart margins. Tests of a hydrogen-fueled ramjet engine model were conducted to investigate engine operability and dynamics, and future tests are planned to demonstrate a closed-loop engine control system. Nozzle tests have identified large transonic-drag losses in the nozzle, which were then reduced significantly through the use of external burning. In other research areas, such as engine seals, advanced materials, and para-to-ortho hydrogen conversion, promising concepts were identified and continuing efforts are adding to these technologies. In the General Hypersonics program an improved understanding is being gained of the physics of inlets, combustors, and nozzles and are developing advanced materials and computational codes that predict the characteristics of both reacting flows and metal matrix composites structures. The High-Mach Turbine-Engine (HiMaTE) component technology program has identified the turboramjet and the air-turboramjet as the most promising combined-cycle engines for more detailed assessment. Efforts are continuing to define critical components for development and testing to demonstrate technology readiness and to establish cycle feasibility. Studies are being conducted to assess the potential benefit of using these combined-cycle engines to power the first stage of two-stage-to-orbit (TSTO) vehicles and other hypersonic vehicles.

Author

N91-20093*# National Aeronautics and Space Administration. Lewis Research Center, Cleveland, OH.

OVERVIEW OF NASP NOZZLE RESEARCH

CHARLES J. TREFNY, RICKEY J. SHYNE, and JEANNE D. CARBONI *In its* Aeropropulsion 1991 16 p Mar. 1991

Avail: NTIS HC/MF A24 CSCL 21/5

Problems facing the National Aerospace Plane (NASP) nozzle at transonic and low supersonic conditions are discussed. An overview of NASP nozzle research at Lewis Research Center is given. Experimental facilities and computational techniques currently in use are reviewed. External burning as a means to reduce transonic drag and initial results of external burning experiments are discussed.

Author

N91-20094*# National Aeronautics and Space Administration. Lewis Research Center, Cleveland, OH.

A COMPARISON OF CFD PREDICTIONS AND EXPERIMENTAL RESULTS FOR A MACH 5 INLET

LOIS J. WEIR and D. R. REDDY *In its* Aeropropulsion 1991 16 p Mar. 1991

Avail: NTIS HC/MF A24 CSCL 21/5

Flow through a high-speed, nominally two-dimensional inlet is

characterized by highly complex, three-dimensional flow phenomena including strong secondary flows and shock/boundary layer interactions. Experimental and analytical data are presented for a Mach 5 mixed compression inlet that exhibits such three-dimensional flow characteristics. The two-dimensional inlet model, designed to provide performance information in the Mach 3 to 5 speed range for an over-under turbojet plus ramjet propulsion system, was also instrumented to provide computational fluid dynamic (CFD) code calibration and validation data, and, in particular, to provide some detailed data in regions where three-dimensional phenomena dominate the local flow field. Calculations of the inlet flow field presented include three-dimensional parabolized and full Navier-Stokes code analyses, with and without bleed. The CFD analyses predicted flow migration up the inlet sidewalls due to glancing shock/boundary layer interactions, which, in turn, developed patterns of vortical flow in the inlet. This vortical flow was at least partially captured by the cowl, which set up large regions of low-energy flow in the corners underneath the cowl. As the vortical flow stream passed through the strong cowl shock, its vorticity appeared to be somewhat dissipated and the low-energy flow was compressed against the cowl. Comparisons between analytical predictions and experimental results are presented for rakes located in regions of vortical flow, separation, or both in the corners between the cowl and the sidewalls. Both experimental and analytical results indicated that porous bleed upstream on the inlet sidewalls and in the corners of the cowl had little effect on the vortical flow entering the inlet; however, bleed removed farther downstream near the shoulder (after the rotational flow had passed through the cowl shock) appeared to remove the low-energy flow on the cowl and sidewalls rather effectively. Author

N91-20103*# National Aeronautics and Space Administration. Lewis Research Center, Cleveland, OH.

ADVANCED AEROPROPULSION CONTROLS TECHNOLOGY
CARL F. LORENZO *In its* Aeropropulsion 1991 25 p Mar. 1991

Avail: NTIS HC/MF A24 CSCL 21/5

The NASA Lewis research activities in the area of propulsion control as driven by the trends and needs of advanced aircraft are discussed. Special emphasis is placed on research to develop design methodologies for integrated flight and propulsion control. Research thrusts in hypersonic propulsion control and dynamics in support of the National Aerospace Plane are also covered, and a new concept for system critical component life-extending control is discussed. Author

N91-20105*# National Aeronautics and Space Administration. Lewis Research Center, Cleveland, OH.

PROPULSION AEROELASTICITY, VIBRATION CONTROL, AND DYNAMIC SYSTEM MODELING
BRUCE M. STEINETZ *In its* Aeropropulsion 1991 11 p Mar. 1991

Avail: NTIS HC/MF A24 CSCL 21/5

Aeropropulsion research in the Structural Dynamics Branch of Lewis Research Center is aimed at addressing two key objectives: (1) conceiving and implementing innovative structural concepts to enhance the performance of advanced aeropropulsion systems; and (2) developing and validating analytical techniques to define the limits of dynamic performance of advanced aeroengines, prior to costly full-scale testing. Aeroelasticity, vibration control, and dynamic systems are the three research areas that make up the Structural Dynamics Branch. In the aeroelasticity technical area, researchers use both analytical and experimental means to extend and define the structural performance limits of advanced propulsion systems, including future ultra-high-bypass ducted turbofans, advanced turboprops, and high power-density turbopumps. Vibration control researchers are developing and evaluating active control systems and the required high-speed robust electronic controls to minimize unwanted shaft vibration of both turbine-engines and rocket engine turbopumps. Researchers in the dynamic systems technical area are developing a new class of high-temperature dynamic engine seals required for advanced

hypersonic (e.g., National Aerospace Plane) engines, as well as developing advanced space mechanism technology to enable future space missions. Central to each of the branch's technical areas is the development of advanced computational methods which, with the aid of modern computer science, will fundamentally improve solution speed and accuracy of large scale structural dynamics problems. Author

N91-20106*# National Aeronautics and Space Administration. Lewis Research Center, Cleveland, OH.

COMPUTATIONAL SIMULATION OF PROPULSION STRUCTURES PERFORMANCE AND RELIABILITY

DALE A. HOPKINS *In its* Aeropropulsion 1991 10 p Mar. 1991

Avail: NTIS HC/MF A24 CSCL 21/5

The chronicle of aeropropulsion development reveals a deliberate evolution during which new engine designs have been derived by incremental improvements of successful previous systems. Aerospace vehicles envisioned near the turn of the century and beyond demand advances in propulsion systems of more revolutionary than evolutionary significance. The systems of tomorrow require unprecedented levels of performance, durability, reliability, and operational economy. Achieving these requirements presents a significant challenge to develop enabling computational structures technology. The aim of computational structures technology is to transform the engine development process by empowering computational simulation to have the principle role. The arena of computation structures technology for aeropropulsion has produced some noteworthy recent gains, and even more extraordinary advances are still to be realized. The essential elements in this endeavor are the following: (1) fundamental theoretical models that more completely represent the complex physics governing engine structural performance; (2) computational techniques that provide accurate and efficient solutions of the governing models and which exploit the potential of emerging computer technology; and (3) integrated strategies for simulation that allow engine structural models of varying fidelity to be evaluated as a continuous and adaptive process. Author

N91-20112*# National Aeronautics and Space Administration. Lewis Research Center, Cleveland, OH.

OVERVIEW OF ROTORCRAFT AND GENERAL AVIATION PROPULSION TECHNOLOGY

JOHN J. COY and JOSEPH D. EISENBERG *In its* Aeropropulsion 1991 14 p Mar. 1991

Avail: NTIS HC/MF A24 CSCL 21/5

An overview of NASA's propulsion research that is aimed at applications for rotary winged flight and general aviation is presented. The strategic goal of this research effort is to provide innovative technologies that will strengthen the nation's competitive stance in the world market for the civil sector, and also provide superior rotorcraft for U.S. military use. The NASA Lewis tactical plan for achieving this strategic goal is the following: (1) to reduce fuel consumption of small engines by 30 percent through use of advanced cycles (including higher pressure and temperature operation) and with improved turbomachinery components technology and ceramic materials; (2) to contribute to fuel savings through weight savings and to reliability by developing advanced technology for transmissions; (3) to contribute to aircraft safety by providing advanced anti-icing and deicing technology; and (4) to achieve high-speed capability through advanced propulsion systems. Author

N91-20113*# National Aeronautics and Space Administration. Lewis Research Center, Cleveland, OH.

TURBOMACHINERY AND COMBUSTOR TECHNOLOGY FOR SMALL ENGINES

LAWRENCE J. BOBER and RICHARD W. NIEDZWIECKI *In its* Aeropropulsion 1991 25 p Mar. 1991

Avail: NTIS HC/MF A24 CSCL 21/5

The goal of the Small Turbine Engine Technology Program is to significantly increase thermal efficiency, reliability, and durability of future small gas turbine engines. Significant fuel savings can

07 AIRCRAFT PROPULSION AND POWER

be achieved through component and cycle improvements as well as through the use of regeneration and uncooled ceramic materials. Recent efforts to identify new regeneration concepts have not been successful, and as a result, no active regenerator research is in progress. Development of uncooled ceramic technology is taking place at the NASA Lewis Research Center under the Department of Energy funded Advanced Turbine Technology Applications Project (ATTAP). Component research is emphasized and includes work on the compressor, combustor, and turbine.

Author

N91-20114*# National Aeronautics and Space Administration. Lewis Research Center, Cleveland, OH.

ROTARY ENGINE TECHNOLOGY

EDWARD A. WILLIS and JOHN J. MCFADDEN *In its* Aeropropulsion 1991 11 p Mar. 1991
Avail: NTIS HC/MF A24 CSCL 21/5

The original goal in this program was to combine some of the better features of reciprocating and gas-turbine engines; thus, obtaining a superior powerplant for light aircraft and a host of related uses. Based on a series of engine and aircraft/mission studies conducted in the early 1980's, the rotary (Wankel) engine was perceived to have many of the desired features and was judged to be capable of considerable further development. At the time, existing automotive rotary engines had demonstrably high power outputs in a compact, smooth-running, and reliable package but were less fuel efficient than comparable reciprocating engines. Accordingly, the basic thrust of the NASA Rotary Engine Technology Enablement Program was (and is) to bring the rotary's efficiency up to the level of a comparably sized diesel, without sacrificing its other desirable features.

Author

N91-20116*# National Aeronautics and Space Administration. Lewis Research Center, Cleveland, OH.

OVERVIEW OF SUBSONIC TRANSPORT PROPULSION TECHNOLOGY

JOHN F. GROENEWEG *In its* Aeropropulsion 1991 13 p Mar. 1991

Avail: NTIS HC/MF A24 CSCL 21/5

The major elements of the NASA Lewis Research Center's Subsonic Transport Propulsion Research Program are summarized. Ultra-high-bypass ratio cycles and high-efficiency cores are being investigated for propulsive and thermal efficiency improvements, respectively. Overall efficiency gains are sought subject to the constraints of noise and emissions goals. Elements of the research program including key technical issues are discussed along with the planned sequence of the activities.

Author

N91-20117*# National Aeronautics and Space Administration. Lewis Research Center, Cleveland, OH.

ULTRA-HIGH BYPASS RESEARCH

CHRISTOPHER J. MILLER, JAMES H. DITTMAR, and ROBERT J. JERACKI *In its* Aeropropulsion 1991 14 p Mar. 1991

Avail: NTIS HC/MF A24 CSCL 21/5

An overview of the ultra-high bypass research at the NASA Lewis Research Center is presented. Over the past decade, the program was focused on unducted rotors and precipitated several development efforts in industry. In this area, forward swept unducted rotors are the concluding effort. Forward sweep can reduce the tip vortex strength and has a potential for reducing the noise of counter-rotating unducted rotors. The aerodynamic performance can also be improved slightly over an aft-swept blade. The future direction of the program is toward ultra-high bypass ratio ducted machines, and short cowls as a particular item. Short cowls can have less aerodynamic drag and less weight, but many allow more noise to be radiated. In general, the aerodynamic research effort will be to provide higher efficiencies, sufficient flow conditioning, and attached flow at high angles of attack. Acoustically, the research is directed towards developing an understanding of fan acoustics in short ducts. The reduced duct length means that there might be insufficient duct length for acoustic cutoff. With less length and less cowl thickness, the space

for acoustic treatment is limited, requiring integrated aeroacoustic designs.

Author

N91-20118*# National Aeronautics and Space Administration. Lewis Research Center, Cleveland, OH.

HIGH-EFFICIENCY CORE TECHNOLOGY

ROBERT M. PLENCNER and GERALD KNIP, JR. *In its* Aeropropulsion 1991 12 p Mar. 1991

Avail: NTIS HC/MF A24 CSCL 21/5

Studies were undertaken to determine the potential benefits from implementing aircraft turbine engine core technology well beyond that being developed for the next generation of long-haul subsonic transport engines (i.e., entry into service date of 1993). These core improvements, projected for year 2010 technology, include the use of very high-pressure-ratio cycles, advanced lightweight materials with minimal cooling requirements, and improved component efficiencies. The studies indicate that a large improvement is possible with engines using these advanced cores as compared to the current turbine engine designs. The results of the studies are presented, and the key challenges to achieving the predicted improvements in performance are identified.

Author

N91-20119*# National Aeronautics and Space Administration. Lewis Research Center, Cleveland, OH.

MULTIDISCIPLINARY RESEARCH OVERVIEW (IHPTET/NPSS)

LESTER D. NICHOLS and SUSAN M. JOHNSON *In its* Aeropropulsion 1991 20 p Mar. 1991

Avail: NTIS HC/MF A24 CSCL 21/5

The Integrated High Performance Turbine Engine Technology (IHPTET) Program and the Numerical Propulsion System Simulation (NPSS) Program are two aeropropulsion multidisciplinary efforts at NASA Lewis that complement each other. The IHPTET initiative is an experimental program to advance engine development and double propulsion system capability by the turn of the century. NASA Lewis is contributing, with the Department of Defense and seven major aerospace contractors, to the development of these advanced, military, high-performance engines in the areas of compressors, combustors, turbines, nozzles, controls, mechanical systems, instrumentation, materials, structures, and computational fluid dynamics. The NPSS effort is a computational, long-range program with the goal of reducing the cost and time of development for advanced-technology propulsion systems. This goal will be achieved through a cooperative effort of NASA, industry, universities, and other government agencies to develop the necessary technologies for integrating disciplines, components, and high-performance computing into a user-friendly simulation environment. This simulation allows for comprehensive evaluation of new concepts early in the design phase, before a commitment to hardware is made. It also allows for rapid assessment of field-related problems, particularly where operational problems are encountered during conditions that are difficult to simulate experimentally. Data generated from the IHPTET engines will be used to help validate NPSS computations.

Author

N91-20122*# National Aeronautics and Space Administration. Lewis Research Center, Cleveland, OH.

IMPAC: AN INTEGRATED METHODOLOGY FOR PROPULSION AND AIRFRAME CONTROL

SANJAY GARG, PETER J. OUZTS, CARL F. LORENZO, and DUANE L. MATTERN (Sverdrup Technology, Inc., Brook Park, OH.) 1991 28 p Prepared for presentation at the American Control Conference, Boston, MA, 26-28 Jun. 1991; sponsored in part by American Automatic Control Council

(Contract RTOP 505-62-50)

(NASA-TM-103805; E-6035; NAS 1.15:103805) Avail: NTIS HC/MF A03 CSCL 21/5

The National Aeronautics and Space Administration is actively involved in the development of enabling technologies that will lead towards aircraft with new/enhanced maneuver capabilities such as Short Take-Off Vertical Landing (STOVL) and high angle of attack performance. Because of the high degree of dynamic coupling between the airframe and propulsion systems of these

types of aircraft, one key technology is the integration of the flight and propulsion control. The NASA Lewis Research Center approach to developing Integrated Flight Propulsion Control (IFPC) technologies is an in-house research program referred to as IMPAC (Integrated Methodology for Propulsion and Airframe Control). The goals of IMPAC are to develop a viable alternative to the existing integrated control design methodologies that will allow for improved system performance and simplicity of control law synthesis and implementation, and to demonstrate the applicability of the methodology to a supersonic STOVL fighter aircraft. Based on some preliminary control design studies that included evaluation of the existing methodologies, the IFPC design methodology that is emerging at the Lewis Research Center consists of considering the airframe and propulsion system as one integrated system for an initial centralized controller design and then partitioning the centralized controller into separate airframe and propulsion system subcontrollers to ease implementation and to set meaningful design requirements for detailed subsystem control design and evaluation. An overview of IMPAC is provided and detailed discussion of the various important design and evaluation steps in the methodology are included. Author

N91-20126*# National Aeronautics and Space Administration. Lewis Research Center, Cleveland, OH.

PERFORMANCE OF A HIGH-WORK, LOW-ASPECT-RATIO TURBINE STATOR TESTED WITH A REALISTIC INLET RADIAL TEMPERATURE GRADIENT

ROY G. STABE and JOHN R. SCHWAB Mar. 1991 31 p
(Contract RTOP 505-62-3B)
(NASA-TM-103738; E-5975; NAS 1.15:103738) Avail: NTIS HC/MF A03 CSCL 21/5

A 0.767-scale model of a turbine stator designed for the core of a high-bypass-ratio aircraft engine was tested with uniform inlet conditions and with an inlet radial temperature profile simulating engine conditions. The principal measurements were radial and circumferential surveys of stator-exit total temperature, total pressure, and flow angle. The stator-exit flow field was also computed by using a three-dimensional Navier-Stokes solver. Other than temperature, there were no apparent differences in performance due to the inlet conditions. The computed results compared quite well with the experimental results. Author

N91-21137*# National Aeronautics and Space Administration. Lewis Research Center, Cleveland, OH.

INTEGRATED FLIGHT/PROPULSION CONTROL SYSTEM DESIGN BASED ON A DECENTRALIZED, HIERARCHICAL APPROACH

DUANE MATTERN, SANJAY GARG (Sverdrup Technology, Inc., Brook Park, OH.), and RANDY BULLARD 1989 41 p Presented at the Guidance, Navigation and Control Conference, Boston, MA, 14-16 Aug. 1989; sponsored by AIAA Previously announced in IAA as A89-53301
(Contract RTOP 505-62-50)
(NASA-TM-103678; E-5895; NAS 1.15:103678; AIAA PAPER 89-3519) Avail: NTIS HC/MF A03 CSCL 21/5

A sample integrated flight/propulsion control system design is presented for the piloted longitudinal landing task with a modern, statistically unstable fighter aircraft. The design procedure is summarized. The vehicle model used in the sample study is described, and the procedure for partitioning the integrated system is presented along with a description of the subsystems. The high-level airframe performance specifications and control design are presented and the control performance is evaluated. The generation of the low-level (engine) subsystem specifications from the airframe requirements are discussed, and the engine performance specifications are presented along with the subsystem control design. A compensator to accommodate the influence of airframe outputs on the engine subsystem is also considered. Finally, the entire closed loop system performance and stability characteristics are examined. Author

N91-21140*# National Aeronautics and Space Administration. Lewis Research Center, Cleveland, OH.

INTEGRATED FLIGHT/PROPULSION CONTROL DESIGN FOR A STOVL AIRCRAFT USING H-INFINITY CONTROL DESIGN TECHNIQUES

SANJAY GARG and PETER J. OUZTS 1991 33 p Presented at the American Control Conference, Boston, MA, 26-28 Jun. 1991; sponsored in part by the American Automatic Control Council (Contract RTOP 505-62-50)
(NASA-TM-104340; E-6113; NAS 1.15:104340) Avail: NTIS HC/MF A03 CSCL 21/5

Results are presented from an application of H-infinity control design methodology to a centralized integrated flight propulsion control (IFPC) system design for a supersonic Short Takeoff and Vertical Landing (STOVL) fighter aircraft in transition flight. The emphasis is on formulating the H-infinity control design problem such that the resulting controller provides robustness to modeling uncertainties and model parameter variations with flight condition. Experience gained from a preliminary H-infinity based IFPC design study performed earlier is used as the basis to formulate the robust H-infinity control design problem and improve upon the previous design. Detailed evaluation results are presented for a reduced order controller obtained from the improved H-infinity control design showing that the control design meets the specified nominal performance objectives as well as provides stability robustness for variations in plant system dynamics with changes in aircraft trim speed within the transition flight envelope. A controller scheduling technique which accounts for changes in plant control effectiveness with variation in trim conditions is developed and off design model performance results are presented. Author

N91-22126*# National Aeronautics and Space Administration. Lewis Research Center, Cleveland, OH.

APPLICATION OF MIXING-CONTROLLED COMBUSTION MODELS TO GAS TURBINE COMBUSTORS

HUNG LEE NGUYEN 1990 13 p Presented at the Joint Symposium on General Aviation Systems, Ocean City, NJ, 11-12 Apr. 1990; sponsored by AIAA and FAA Original contains color illustrations
(Contract RTOP 537-02-11)
(NASA-TM-103236; E-5649; NAS 1.15:103236) Avail: NTIS HC/MF A03; 5 functional color pages CSCL 21/5

Gas emissions were studied from a staged Rich Burn/Quick-Quench Mix/Lean Burn combustor were studied under test conditions encountered in High Speed Research engines. The combustor was modeled at conditions corresponding to different engine power settings, and the effect of primary dilution airflow split on emissions, flow field, flame size and shape, and combustion intensity, as well as mixing, was investigated. A mathematical model was developed from a two-equation model of turbulence, a quasi-global kinetics mechanism for the oxidation of propane, and the Zeldovich mechanism for nitric oxide formation. A mixing-controlled combustion model was used to account for turbulent mixing effects on the chemical reaction rate. This model assumes that the chemical reaction rate is much faster than the turbulent mixing rate. Author

N91-23179*# National Aeronautics and Space Administration. Lewis Research Center, Cleveland, OH.

EFFECTS OF INLET DISTORTION ON THE DEVELOPMENT OF SECONDARY FLOWS IN A SUBSONIC AXIAL INLET COMPRESSOR ROTOR Ph.D. Thesis - Toledo Univ., OH

ALBERT K. OWEN Apr. 1991 340 p Prepared in cooperation with Army Aviation Systems Command, Cleveland, OH Original contains color illustrations
(Contract DA PROJ. 1L1-61102-AH-45; RTOP 505-62-52)
(NASA-TM-104356; E-5583; NAS 1.15:104356; AVSCOM-TR-90-C-012; AD-A240930) Avail: NTIS HC/MF A15; 16 functional color pages CSCL 21/5

Detailed flow measurements were taken inside an isolated axial compressor rotor operating subsonically near peak efficiency. Laser anemometer measurements were made with two inlet velocity

07 AIRCRAFT PROPULSION AND POWER

profiles. One profile consisted of an unmodified baseline flow, and the second profile was distorted by placing axisymmetric screens on the hub and shroud well upstream of the rotor. A primary flow is defined in the rotor and deviations from this primary flow for each inlet flow condition identified. A comparison between the two flow deviations is made to assess the development of a passage vortex due to the distortion of the inlet flow. A comparison of experimental results with computational predictions from a Navier-Stokes solver showed good agreement between predicted and measured flow. Measured results indicate that a distorted inlet profile has minimal effect on the development of the flow in the rotor passage and the resulting passage vortex. Author

N91-23180*# National Aeronautics and Space Administration. Lewis Research Center, Cleveland, OH.

MULTI-HEAT ADDITION TURBINE ENGINE Patent Application
LEO C. FRANCISCUS, inventor (to NASA) and THEODORE A. BRABBS, inventor (to NASA) (Sverdrup Technology, Inc., Brook Park, OH.) 30 Jan. 1991 12 p
(NASA-CASE-LEW-15094-1; NAS 1.71:LEW-15094-1;
US-PATENT-APPL-SN-647902) Avail: NTIS HC/MF A03 CSCL 21/5

A multi-heat addition turbine engine (MHATE) incorporates a plurality of heat addition devices to transfer energy to air and a plurality of turbines to extract energy from the air while converting it to work. The MHATE provides dry power and lower fuel consumption or lower combustor exit temperatures. NASA

N91-23183*# National Aeronautics and Space Administration. Lewis Research Center, Cleveland, OH.

ADVANCED ICE PROTECTION SYSTEMS TEST IN THE NASA LEWIS ICING RESEARCH TUNNEL
THOMAS H. BOND, JAIWON SHIN, and GEERT A. MESANDER (Oklahoma City Air Logistics Center, Tinker AFB, OK.) 1991 12 p Presented at the 47th Annual Forum and Technology Display, Phoenix, AZ, 6-8 May 1991; sponsored by American Helicopter Society
(Contract RTOP 505-68-11)
(NASA-TM-103757; E-6013; NAS 1.15:103757) Avail: NTIS HC/MF A03 CSCL 21/5

Tests of eight different deicing systems based on variations of three different technologies were conducted in the NASA Lewis Research Center Icing Research Tunnel (IRT) in June and July 1990. The systems used pneumatic, eddy current repulsive, and electro-expulsive means to shed ice. The tests were conducted on a 1.83 m span, 0.53 m chord NACA 0012 airfoil operated at a 4 degree angle of attack. The models were tested at two temperatures: a glaze condition at minus 3.9 C and a rime condition at minus 17.2 C. The systems were tested through a range of icing spray times and cycling rates. Characterization of the deicers was accomplished by monitoring power consumption, ice shed particle size, and residual ice. High speed video motion analysis was performed to quantify ice particle size. Author

N91-23184*# National Aeronautics and Space Administration. Lewis Research Center, Cleveland, OH.

MODEL ROTOR ICING TESTS IN THE NASA LEWIS ICING RESEARCH TUNNEL

ROBERT J. FLEMMING, RANDALL K. BRITTON (Sverdrup Technology, Inc., Brook Park, OH.), and THOMAS H. BOND 1991 27 p Presented at the 68th Meeting of the Fluid Dynamic Panel Specialists Meeting on the Effects of Adverse Weather on Aerodynamics, Toulouse, France, 29 Apr. - 1 May 1991; sponsored by AGARD
(Contract RTOP 505-68-11)

(NASA-TM-104351; E-6136; NAS 1.15:104351) Avail: NTIS HC/MF A03 CSCL 21/5

Tests of a lightly instrumented two-bladed teetering rotor and a heavily instrumented sub-scale articulated main rotor were conducted in the NASA Lewis Research Center Icing Research Tunnel (IRT) in August 1988 and September and November 1989. The first was an OH-58 tail rotor which had a diameter of 1.575 m and a blade chord of 0.133 m, and was mounted on a NASA

designed test rig. The second, a four bladed articulated rotor, had a diameter of 1.83 m with 0.124 m chord blades specially fabricated for the experiment. This rotor was mounted on a Sikorsky Aircraft Powered Force Model, which enclosed a rotor balance and other measurement systems. The models were exposed to variations in temperature, liquid water content, and medium droplet diameter, and were operated over ranges of advance ratio, shaft angle, tip Mach number (rotor speed), and weight coefficient to determine the effect of these parameters on ice accretion. In addition to strain gage and balance data, the test was documented with still, video, and high speed photography, ice profile tracing, and ice molds. Presented here are the sensitivity of the model rotors to the test parameters and a comparison of the results to theoretical predictions. Author

N91-23185*# National Aeronautics and Space Administration. Lewis Research Center, Cleveland, OH.

A CFD STUDY OF JET MIXING IN REDUCED FLOW AREAS FOR LOWER COMBUSTOR EMISSIONS

C. E. SMITH, M. V. TALPALLIKAR (CFD Research Corp., Huntsville, AL.), and J. D. HOLDEMAN 1991 17 p Presented at the 27th Joint Propulsion Conference, Sacramento, CA, 24-27 Jun. 1991; sponsored by AIAA, SAE, ASME, and ASEE Original contains color illustrations
(Contract NAS3-25967; RTOP 537-02-21)

(NASA-TM-104411; E-6238; NAS 1.15:104411; AIAA PAPER 91-2460) Avail: NTIS HC/MF A03; 2 functional color pages CSCL 21/5

The Rich-burn/Quick-mix/Lean-burn (RQL) combustor has the potential of significantly reducing NO(x) emissions in combustion chambers of High Speed Civil Transport aircraft. Previous work on RQL combustors for industrial applications suggested the benefit of necking down the mixing section. A 3-D numerical investigation was performed to study the effects of neckdown on NO(x) emissions and to develop a correlation for optimum mixing designs in terms of neckdown area ratio. The results of the study showed that jet mixing in reduced flow areas does not enhance mixing, but does decrease residence time at high flame temperatures, thus reducing NO(x) formation. By necking down the mixing flow area by 4, a potential NO(x) reduction of 16:1 is possible for annual combustors. However, there is a penalty that accompanies the mixing neckdown: reduced pressure drop across the combustor swirler. At conventional combustor loading parameters, the pressure drop penalty does not appear to be excessive. Author

N91-23186*# National Aeronautics and Space Administration. Lewis Research Center, Cleveland, OH.

A THREE-DIMENSIONAL NAVIER-STOKES STAGE ANALYSIS OF THE FLOW THROUGH A COMPACT RADIAL TURBINE

JAMES D. HEIDMANN 1991 13 p Presented at the 27th Joint Propulsion Conference, Sacramento, CA, 24-27 Jun. 1991; sponsored by AIAA, SAE, ASME, and American Society for Electrical Engineers

(Contract RTOP 505-05-10)

(NASA-TM-104420; E-6254; NAS 1.15:104420) Avail: NTIS HC/MF A03 CSCL 21/5

A steady, three dimensional Navier-Stokes average passage computer code is used to analyze the flow through a compact radial turbine stage. The code is based upon the average passage set of equations for turbomachinery, whereby the flow fields for all passages in a given blade row are assumed to be identical while retaining their three-dimensionality. A stage solution is achieved by alternating between stator and rotor calculations, while coupling the two solutions by means of a set of axisymmetric body forces which model the absent blade row. Results from the stage calculation are compared with experimental data and with results from an isolated rotor solution having axisymmetric inlet flow quantities upstream of the vacated stator space. Although the mass-averaged loss through the rotor is comparable for both solutions, the details of the loss distribution differ due to stator effects. The stage calculation predicts smaller spanwise variations in efficiency, in closer agreement with the data. The results of the study indicate that stage analyses hold promise for improved

prediction of loss mechanisms in multi-blade row turbomachinery, which could lead to improved designs through the reduction of these losses. Author

N91-24201*# National Aeronautics and Space Administration. Lewis Research Center, Cleveland, OH.

STATIC PERFORMANCE TESTS OF A FLIGHT-TYPE STOVL EJECTOR

WENDY S. BARANKIEWICZ 1991 12 p Presented at the 27th Joint Propulsion Conference, Sacramento, CA, 24-27 Jun. 1991; cosponsored by AIAA, SAE, ASME, and the American Society for Electrical Engineers (Contract RTOP 505-62-71) (NASA-TM-104437; E-6131; NAS 1.15:104437; AIAA PAPER 91-1902) Avail: NTIS HC/MF A03 CSCL 21/5

The design and development of thrust augmenting STOVL ejectors has typically been based on experimental iteration (i.e., trial and error). Static performance tests of a full scale vertical lift ejector were performed at primary flow temperatures up to 1560 R (1100 F). Flow visualization (smoke generators and yarn tufts) were used to view the inlet air flow, especially around the primary nozzle and end plates. Performance calculations are presented for ambient temperatures close to 480 R (20 F) and 535 R (75 F) which simulate seasonal aircraft operating conditions. Resulting thrust augmentation ratios are presented as functions of nozzle pressure ratio and temperature. Author

N91-24202*# National Aeronautics and Space Administration. Lewis Research Center, Cleveland, OH.

MIXING OF MULTIPLE JETS WITH A CONFINED SUBSONIC CROSSFLOW. SUMMARY OF NASA-SUPPORTED EXPERIMENTS AND MODELING

JAMES D. HOLDEMAN 1991 49 p Presented at the 27th Joint Propulsion Conference, Sacramento, CA, 24-27 Jun. 1991; sponsored by AIAA, SAE, ASME and the American Society for Electrical Engineers (Contract RTOP 537-02-21) (NASA-TM-104412; E-6239; NAS 1.15:104412; AIAA PAPER 91-2458) Avail: NTIS HC/MF A03 CSCL 21/5

Experimental and computational results on the mixing of single, double, and opposed rows of jets with an isothermal or variable temperature mainstream in a confined subsonic crossflow are summarized. The studies were performed to investigate flow and geometric variations typical of the complex 3-D flowfield in the dilution zone of combustion chambers in gas turbine engines. The principal observations from the experiments were that the momentum-flux ratio was the most significant flow variable, and that temperature distributions were similar (independent of orifice diameter) when the orifice spacing and the square-root of the momentum-flux ratio were inversely proportional. The experiments and empirical model for the mixing of a single row of jets from round holes were extended to include several variations typical of gas turbine combustors. Combinations of flow and geometry that gave optimum mixing were identified from the experimental results. Based on results of calculations made with a 3-D numerical model, the empirical model was further extended to model the effects of curvature and convergence. The principle conclusions from this study were that the orifice spacing and momentum-flux relationships were the same as observed previously in a straight duct, but the jet structure was significantly different for jets injected from the inner wall of a turn than for those injected from the outer wall. Also, curvature in the axial direction caused a drift of the jet trajectories toward the inner wall, but the mixing in a turning and converging channel did not seem to be inhibited by the convergence, independent of whether the convergence was radial or circumferential. The calculated jet penetration and mixing in an annulus were similar to those in a rectangular duct when the orifice spacing was specified at the radius dividing the annulus into equal areas. Author

N91-24203*# National Aeronautics and Space Administration. Lewis Research Center, Cleveland, OH.

FUEL-RICH, CATALYTIC REACTION EXPERIMENTAL RESULTS

R. JAMES ROLLBUHLER 1991 23 p Presented at the 27th Joint Propulsion Conference, Sacramento, CA, 24-27 Jun. 1991; sponsored by AIAA, SAE, ASME, and the American Society for Electrical Engineers (Contract RTOP 537-01-11) (NASA-TM-104423; E-6256; NAS 1.15:104423; AIAA PAPER 91-2463) Avail: NTIS HC/MF A03 CSCL 21/5

Future aeropropulsion gas turbine combustion requirements call for operating at very high inlet temperatures, pressures, and large temperature rises. At the same time, the combustion process is to have minimum pollution effects on the environment. Aircraft gas turbine engines utilize liquid hydrocarbon fuels which are difficult to uniformly atomize and mix with combustion air. An approach for minimizing fuel related problems is to transform the liquid fuel into gaseous form prior to the completion of the combustion process. Experimentally obtained results are presented for vaporizing and partially oxidizing a liquid hydrocarbon fuel into burnable gaseous components. The presented experimental data show that 1200 to 1300 K reaction product gas, rich in hydrogen, carbon monoxide, and light-end hydrocarbons, is formed when flowing 0.3 to 0.6 fuel to air mixes through a catalyst reactor. The reaction temperatures are kept low enough that nitrogen oxides and carbon particles (soot) do not form. Results are reported for tests using different catalyst types and configurations, mass flowrates, input temperatures, and fuel to air ratios. Author

N91-25148*# National Aeronautics and Space Administration. Lewis Research Center, Cleveland, OH.

THE DESIGN/ANALYSIS OF FLOWS THROUGH TURBOMACHINERY: A VISCOUS/INVISCID APPROACH

D. P. MILLER and D. R. REDDY (Sverdrup Technology, Inc., Brook Park, OH.) 1991 12 p Presented at the 27th Joint Propulsion Conference, Sacramento, CA, 24-27 Jun. 1991; sponsored by AIAA, SAE, ASME, and the American Society for Electrical Engineers (Contract RTOP 505-62-10) (NASA-TM-104447; E-6288; NAS 1.15:104447; AIAA PAPER 91-2010) Avail: NTIS HC/MF A03 CSCL 21/5

The development of a design/analysis flow solver at NASA Lewis Research Center is discussed. The solver is axisymmetric and can be run inviscidly with assumed or calculated blockages, or with the viscous terms computed. The blade forces for each blade row are computed from blade-to-blade solutions, correlated data or force model, or from a full three dimensional solution. Codes currently under development can be separated into three distinct elements: the turbomachinery interactive grid generator energy distribution restart code (TIGGERC), the interactive blade element geometry generator (IBEGG), and the viscous/invicid multi-blade-row average passage flow solver (VIADAC). Several experimental test cases were run to validate the VIADAC code. The tests, representative of typical axial turbomachinery duct axisymmetric wind tunnel body problems, were conducted on an SR7 Spinner axisymmetric body, a NASA Rotor 67 Fan test bed, and a transonic boattail body. The results show the computations to be in good agreement with test data. L.K.S.

N91-26146*# National Aeronautics and Space Administration. Lewis Research Center, Cleveland, OH.

CFD ANALYSIS OF JET MIXING IN LOW NOX FLAMETUBE COMBUSTORS

M. V. TALPALLIKAR, C. E. SMITH, M. C. LAI (Wayne State Univ., Detroit, MI.), and J. D. HOLDEMAN 1991 11 p Presented at the 36th International Gas Turbine and Aeroengine Congress and Exposition, Orlando, FL, 3-6 Jun. 1991; sponsored by ASME Original contains color illustrations (Contract NAS3-25834; RTOP 537-02-21) (NASA-TM-104466; E-6313; NAS 1.15:104466; ASME-91-GT-217) Avail: NTIS HC/MF A03; 1 functional color page CSCL 21/5

The Rich-burn/Quick-mix/Lean-burn (RQL) combustor was identified as a potential gas turbine combustor concept to reduce

07 AIRCRAFT PROPULSION AND POWER

NO(x) emissions in High Speed Civil Transport (HSCT) aircraft. To demonstrate reduced NO(x) levels, cylindrical flamel tube versions of RQL combustors are being tested at NASA Lewis Research Center. A critical technology needed for the RQL combustor is a method of quickly mixing by-pass combustion air with rich-burn gases. Jet mixing in a cylindrical quick-mix section was numerically analyzed. The quick-mix configuration was five inches in diameter and employed twelve radial-inflow slots. The numerical analyses were performed with an advanced, validated 3-D Computational Fluid Dynamics (CFD) code named REFLEQS. Parametric variation of jet-to-mainstream momentum flux ratio (J) and slot aspect ratio was investigated. Both non-reacting and reacting analyses were performed. Results showed mixing and NO(x) emissions to be highly sensitive to J and slot aspect ratio. Lowest NO(x) emissions occurred when the dilution jet penetrated to approximately mid-radius. The viability of using 3-D CFD analyses for optimizing jet mixing was demonstrated. Author

N91-27159*# National Aeronautics and Space Administration. Lewis Research Center, Cleveland, OH.

EFFECT OF TABS ON THE EVOLUTION OF AN AXISYMMETRIC JET

K. B. M. Q. ZAMAN, M. SAMIMY, and M. F. REEDER (Ohio State Univ., Columbus.) 1991 14 p Presented at the Eighth Symposium on Turbulent Shear Flows, Munich, Fed. Republic of Germany, 9-11 Sep. 1991; sponsored by the Technical Univ. of Munich

(Contract RTOP 505-62-52)

(NASA-TM-104472; E-6125; NAS 1.15:104472) Avail: NTIS HC/MF A03 CSCL 21/5

The effect of vortex generators, in the form of small tabs at the nozzle exit, on the evolution of an axisymmetric jet was investigated experimentally over a jet Mach number range of 0.34 to 1.81. The effects of one, two, and four tabs were studied in comparison with the corresponding case without a tab. Each tab introduced an indentation in the shear layer, apparently through the action of streamwise vortices which appeared to be of the trailing vortex type originating from the tips of the tab rather than of the necklace vortex type originating from the base of the tab. The resultant effect of two tabs, placed at diametrically opposite locations, was to essentially bifurcate the jet. The influence of the tabs was essentially the same at subsonic and supersonic conditions indicating that compressibility has little to do with the effect. Author

N91-27164*# National Aeronautics and Space Administration. Lewis Research Center, Cleveland, OH.

MODERN CFD APPLICATIONS FOR THE DESIGN OF A REACTING SHEAR LAYER FACILITY

S. T. YU (Sverdrup Technology, Inc., Brook Park, OH.), C. T. CHANG, and C. J. MAREK 1991 13 p Presented at the 29th Aerospace Sciences Meeting, Reno, NV, 7-10 Jan. 1991; sponsored by AIAA Previously announced in IAA as A91-21540 (Contract NAS3-25266)

(NASA-TM-104523; E-6396; NAS 1.15:104523; AIAA PAPER 91-0577) Avail: NTIS HC/MF A03 CSCL 21/5

The RPLUS2D code, capable of calculating high speed reacting flows, was adopted to design a compressible shear layer facility. In order to create reacting shear layers at high convective Mach numbers, hot air streams at supersonic speeds, rendered by converging-diverging nozzles, must be provided. A finite rate chemistry model is used to simulate the nozzle flows. Results are compared with one-dimensional solutions at chemical equilibrium. Additionally, a two equation turbulence model with compressibility effects was successfully incorporated with the RPLUS code. The model was applied to simulate a supersonic shear layer. Preliminary results show favorable comparisons with the experimental data. Author

N91-27165*# National Aeronautics and Space Administration. Lewis Research Center, Cleveland, OH.

ANALYTICAL COMBUSTION/EMISSIONS RESEARCH RELATED TO THE NASA HIGH-SPEED RESEARCH PROGRAM

H. LEE NGUYEN 1991 12 p Presented at the 27th Joint Propulsion Conference, Sacramento, CA, 24-27 Jun. 1991; sponsored by AIAA, SAE, ASME, and ASEE (Contract RTOP 537-02-20)

(NASA-TM-104521; E-6392; NAS 1.15:104521; AIAA PAPER 91-2252) Avail: NTIS HC/MF A03 CSCL 21/5

Increasing the pressure and temperature of the engines of new generation supersonic airliners increases the emissions of nitrogen oxides to a level that would have an adverse impact on the Earth's protective ozone layer. In the process of implementing low emissions combustor technologies, NASA Lewis Research Center has pursued a combustion analysis program to guide combustor design processes, to identify potential concepts of greatest promise, and to optimize them at low cost, with short turn-around time. The approach is to upgrade and apply advanced computer programs for gas turbine applications. Efforts have been made to improve the code capabilities of modeling the physics. Test cases and experiments are used for code validation. To provide insight into the combustion process and combustor design, two-dimensional and three-dimensional codes such as KIVA-II and LeRC 3D have been used. These codes are operational and calculations have been performed to guide low emissions combustion experiments. Author

N91-29181*# National Aeronautics and Space Administration. Lewis Research Center, Cleveland, OH.

DIVERGENCE THRUST LOSS CALCULATIONS FOR CONVERGENT-DIVERGENT NOZZLES: EXTENSIONS TO THE CLASSICAL CASE

JEFFREY J. BERTON Aug. 1991 19 p

(Contract RTOP 537-01-22)

(NASA-TM-105176; E-6472; NAS 1.15:105176) Avail: NTIS HC/MF A03 CSCL 21/5

The analytical derivations of the non-axial thrust divergence losses for convergent-divergent nozzles are described as well as how these calculations are embodied in the Navy/NASA engine computer program. The convergent-divergent geometries considered are simple classic axisymmetric nozzles, two dimensional rectangular nozzles, and axisymmetric and two dimensional plug nozzles. A simple, traditional, inviscid mathematical approach is used to deduce the influence of the ineffectual non-axial thrust as a function of the nozzle exit divergence angle. Author

N91-29187*# National Aeronautics and Space Administration. Lewis Research Center, Cleveland, OH.

EXPERIMENTAL STUDY OF CROSS-STREAM MIXING IN A CYLINDRICAL DUCT

A. VRANOS, D. S. LISCINSKY, B. TRUE (United Technologies Research Center, East Hartford, CT.), and J. D. HOLDEMAN 1991 15 p Presented at the 27th Joint Propulsion Conference, Sacramento, CA, 24-27 Jun. 1991; sponsored by AIAA, SAE, ASME, and ASEE Previously announced as A91-45815 (Contract NAS3-25967; RTOP 537-02-21)

(NASA-TM-105180; E-6478; NAS 1.15:105180; AIAA PAPER 91-2459) Avail: NTIS HC/MF A03 CSCL 21/5

An experimental investigation of cross stream injection and mixing was conducted with application to a low NO sub x combustor for the High Speed Civil Transport (HSCT). Mixing in a cylindrical chamber was studied for transverse injection from slanted slot and round orifice injectors. Momentum ratio, density ratio, and number were studied. Quantitative measurement of injectant concentration distributions were obtained by planar digital imaging of the Mie scattered light from an aerosol seed uniformly mixed with the injectant. The unmixedness, defined as the ratio of the r.m.s. concentration fluctuation to mean concentration in a plane perpendicular to the main flow direction, was found to be primarily a function of momentum ratio and injector spacing. An optimum spacing is indicated. Unmixedness is also a function of orifice size, or mass flow ratio, but the mass flow dependence can be accounted for by normalizing the unmixedness with its maximum theoretical value. The data indicate that a density ratio greater

than unity retards mixing. It was found that above a certain momentum flux ratio, mixing with slanted slot injectors was better than with round hole injectors. Author

N91-29188*# National Aeronautics and Space Administration. Lewis Research Center, Cleveland, OH.

A LINEAR CONTROL DESIGN STRUCTURE TO MAINTAIN LOOP PROPERTIES DURING LIMIT OPERATION IN A MULTI-NOZZLE TURBOFAN ENGINE

DUANE MATTERN (Sverdrup Technology, Inc., Brook Park, OH.) and PETER OUZTS 1991 28 p Presented at the 27th Joint Propulsion Conference, Sacramento, CA, 24-27 Jun. 1991; sponsored by AIAA, SAE, ASME, and ASEE Previously announced as A91-45780

(Contract NAS3-25266; RTOP 505-62-50)
(NASA-TM-105163; E-6452; NAS 1.15:105163; AIAA PAPER 91-1997) Avail: NTIS HC/MF A03 CSCL 21/5

The implementation of multi-variable control systems on turbofan engines requires the use of limit protection to maintain safe engine operation. Since a turbofan engine typically encounters limits during transient operation, the use of a limit protection scheme that modifies the feedback loop may void the desired 'guarantees' associated with linear multi-variable control design methods, necessitating considerable simulation to validate the control with limited protection. An alternative control design structure is proposed that maintains the desired linear feedback properties when certain safety limits are encountered by moving the limit protection scheme outside the feedback loop. This proposed structure is compared to a structure with a limit protection scheme that modifies the feedback loop properties. The two design structures are compared using both linear and nonlinear simulations. The evaluation emphasizes responses where the fan surge margin limit is encountered. Author

N91-30141*# National Aeronautics and Space Administration. Lewis Research Center, Cleveland, OH.

THE NAVY/NASA ENGINE PROGRAM (NNEP89): A USER'S MANUAL

ROBERT M. PLENCNER and CHRISTOPHER A. SNYDER Aug. 1991 118 p

(Contract RTOP 505-69-50)
(NASA-TM-105186; E-6484; NAS 1.15:105186) Avail: NTIS HC/MF A06 CSCL 21/5

An engine simulation computer code called NNEP89 was written to perform 1-D steady state thermodynamic analysis of turbine engine cycles. By using a very flexible method of input, a set of standard components are connected at execution time to simulate almost any turbine engine configuration that the user could imagine. The code was used to simulate a wide range of engine cycles from turboshafts and turboprops to air turbojets and supersonic cruise variable cycle engines. Off design performance is calculated through the use of component performance maps. A chemical equilibrium model is incorporated to adequately predict chemical dissociation as well as model virtually any fuel. NNEP89 is written in standard FORTRAN77 with clear structured programming and extensive internal documentation. The standard FORTRAN77 programming allows it to be installed onto most mainframe computers and workstations without modification. The NNEP89 code was derived from the Navy/NASA Engine program (NNEP). NNEP89 provides many improvements and enhancements to the original NNEP code and incorporates features which make it easier to use for the novice user. This is a comprehensive user's guide for the NNEP89 code. Author

N91-30142*# National Aeronautics and Space Administration. Lewis Research Center, Cleveland, OH.

COMPARISON OF A QUASI-3D ANALYSIS AND EXPERIMENTAL PERFORMANCE FOR THREE COMPACT RADIAL TURBINES

R. S. SIMONYI (Sverdrup Technology, Inc., Brook Park, OH.) and P. J. BOYLE 1991 15 p Presented at the 27th Joint Propulsion Conference, Sacramento, CA, 24-27 Jun. 1991; sponsored by AIAA, SAE, ASME, and ASEE Previously announced as A91-45789

(Contract NAS3-25266; RTOP 535-05-10)
(NASA-TM-105155; E-6441; NAS 1.15:105155; AIAA PAPER 91-2128) Avail: NTIS HC/MF A03 CSCL 21/5

An experimental aerodynamic evaluation of three compact radial turbine builds was performed. Two rotors which were 40 to 50 percent shorter in axial length than conventional state of the art radial rotors were tested. A single nozzle design was used. One rotor was tested with the nozzle at two stagger angle settings. A second rotor was tested with the nozzle in only the closed down setting. Experimental results were compared to predict results from a quasi-3D inviscid and boundary layer analysis, called Merid/Tsonic/Blayer (MTSB). This analysis was used to predict turbine performance. It has previously been calibrated only for axial, not radial, turbomachinery. The predicted and measured efficiencies were compared at the design point for the three turbines. At the design points the analysis overpredicted the efficiency by less than 1.7 points. Comparisons were also made at off-design operating points. The results of these comparisons showed the importance of an accurate clearance model for efficiency predictions and also that there are deficiencies in the incidence loss model used. Author

N91-31178*# National Aeronautics and Space Administration. Lewis Research Center, Cleveland, OH.

A HIGH-FREQUENCY SERVOSYSTEM FOR FUEL CONTROL IN HYPERSONIC ENGINES

DONALD L. SIMON Aug. 1991 11 p

(Contract DA PROJ. 1L1-61102-AH-45; RTOP 505-62-OK)
(NASA-TM-104333; E-6098; NAS 1.15:104333; AVSCOM-TR-91-C-016; AD-A241468) Avail: NTIS HC/MF A03 CSCL 21/5

A hydrogen fuel-flow valve with an electrohydraulic servosystem is described. An analysis of the servosystem is presented along with a discussion of the limitations imposed on system performance by nonlinearities. The response of the valve to swept-frequency inputs is experimentally determined and compared with analytical results obtained from a computer model. The valve is found to perform favorably for frequencies up to 200 Hz. Author

N91-31181*# National Aeronautics and Space Administration. Lewis Research Center, Cleveland, OH.

JET-A REACTION MECHANISM STUDY FOR COMBUSTION APPLICATION

CHI-MING LEE, KRISHNA KUNDU, and WALDO ACOSTA (Army Aviation Systems Command, Cleveland, OH.) 1991 13 p Presented at the 27th Joint Propulsion Conference, Sacramento, CA, 24-27 Jun. 1991; cosponsored by AIAA, SAE, ASME, and ASEE Previously announced in IAA as A91-45810

(Contract DA PROJ. 1L1-62211-A-47A; RTOP 537-01-11)
(NASA-TM-104441; E-6279; NAS 1.15:104441; AVSCOM-TR-91-C-029; AIAA PAPER 91-2355) Avail: NTIS HC/MF A03 CSCL 21/5

Simplified chemical kinetic reaction mechanisms for the combustion of Jet A fuel was studied. Initially, 40 reacting species and 118 elementary chemical reactions were chosen based on a literature review. Through a sensitivity analysis with the use of LSENS General Kinetics and Sensitivity Analysis Code, 16 species and 21 elementary chemical reactions were determined from this study. This mechanism is first justified by comparison of calculated ignition delay time with the available shock tube data, then it is validated by comparison of calculated emissions from the plug flow reactor code with in-house flame tube data. Author

AIRCRAFT STABILITY AND CONTROL

Includes aircraft handling qualities; piloting; flight controls; and autopilots.

A91-22950* National Aeronautics and Space Administration. Lewis Research Center, Cleveland, OH.

INTEGRATED FLIGHT/PROPULSION CONTROL SYSTEM DESIGN BASED ON A CENTRALIZED APPROACH

SANJAY GARG, DUANE L. MATTERN (Sverdrup Technology, Inc., Cleveland, OH), and RANDY E. BULLARD (NASA, Lewis Research Center, Cleveland, OH) Journal of Guidance, Control, and Dynamics (ISSN 0731-5090), vol. 14, Jan.-Feb. 1991, p. 107-116. Previously cited in issue 23, p. 3620, Accession no. A89-52611. refs

Copyright

A91-29466* National Aeronautics and Space Administration. Lewis Research Center, Cleveland, OH.

AN EXPERT SYSTEM TO PERFORM ON-LINE CONTROLLER RESTRUCTURING FOR ABRUPT MODEL CHANGES

JONATHAN LITT (NASA, Lewis Research Center; U.S. Army, Propulsion Directorate, Cleveland, OH) IN: Rotary Wing Propulsion Specialists' Meeting, Williamsburg, VA, Nov. 13-15, 1990, Proceedings. Alexandria, VA, American Helicopter Society, 1990, 10 p. refs

Copyright

This paper presents the work in progress on an expert system utilized to tune and reconfigure airframe/engine control systems on-line in real time in response to structural or battle damage failures. The closed loop system is monitored constantly for changes in performance and structure, which detection prompts the expert system to select and apply a particular control restructuring algorithm based on the severity and type of damage. Control restructuring algorithms that have been implemented handle most failure cases involving actuator damage (control mixer) and many instances where the system dynamics are altered as well (modified control mixer). R.E.P.

A91-31030* National Aeronautics and Space Administration. Lewis Research Center, Cleveland, OH.

CIVIL AIR TRANSPORT - A FRESH LOOK AT POWER-BY-WIRE AND FLY-BY-LIGHT

GALE R. SUNDBERG (NASA, Lewis Research Center, Cleveland, OH) IN: NAECON 90: Proceedings of the IEEE National Aerospace and Electronics Conference, Dayton, OH, May 21-25, 1990. Vol. 3. New York, Institute of Electrical and Electronics Engineers, Inc., 1990, p. 1365-1368. Previously announced in STAR as N90-21283.

Power-by-wire (PBW) is a key element under subsonic transport flight systems technology, with potential savings of over 10 percent in gross take off weight and in fuel consumption compared to today's transport aircraft. The PBW technology substitutes electrical actuation in place of centralized hydraulics, uses internal engine bleed air to supply cabin comfort. The application of advanced fiber optics to the electrical power system controls, to built-in-test (BITE) equipment, and to fly-by-light (FBL) flight controls provides additional benefits in lightning and high-energy radio frequency (HERF) immunity over existing mechanical or even fly-by-wire controls. The program plan is reviewed and a snapshot is given of the key technologies and their benefits to future aircraft, both civil and military. Author

A91-38547* National Aeronautics and Space Administration. Lewis Research Center, Cleveland, OH.

EFFECTS OF HORIZONTAL TAIL ICE ON LONGITUDINAL AERODYNAMIC DERIVATIVES

R. J. RANAUDO, A. L. REEHORST, T. H. BOND (NASA, Lewis Research Center, Cleveland, OH), J. G. BATTERSON (NASA,

Langley Research Center, Hampton, VA), and T. M. O'MARA (George Washington University, Washington, DC) Journal of Aircraft (ISSN 0021-8669), vol. 28, March 1991, p. 193-199. Previously cited in issue 10, p. 1441, Accession no. A89-28454. refs

Copyright

A91-49676* National Aeronautics and Space Administration. Lewis Research Center, Cleveland, OH.

NEURAL NETWORK APPLICATION TO AIRCRAFT CONTROL SYSTEM DESIGN

TERRY TROUDET, SANJAY GARG, and WALTER C. MERRILL (NASA, Lewis Research Center, Cleveland, OH) IN: AIAA Guidance, Navigation and Control Conference, New Orleans, LA, Aug. 12-14, 1991, Technical Papers. Vol. 2. Washington, DC, American Institute of Aeronautics and Astronautics, 1991, p. 993-1009. Previously announced in STAR as N91-27167. refs (AIAA PAPER 91-2715) Copyright

The feasibility of using artificial neural network as control systems for modern, complex aerospace vehicles is investigated via an example aircraft control design study. The problem considered is that of designing a controller for an integrated airframe/propulsion longitudinal dynamics model of a modern fighter aircraft to provide independent control of pitch rate and airspeed responses to pilot command inputs. An explicit model following controller using H infinity control design techniques is first designed to gain insight into the control problem as well as to provide a baseline for evaluation of the neurocontroller. Using the model of the desired dynamics as a command generator, a multilayer feedforward neural network is trained to control the vehicle model within the physical limitations of the actuator dynamics. This is achieved by minimizing an objective function which is a weighted sum of tracking errors and control input commands and rates. To gain insight in the neurocontrol, linearized representations of the nonlinear neurocontroller are analyzed along a commanded trajectory. Linear robustness analysis tools are then applied to the linearized neurocontroller models and to the baseline H infinity based controller. Future areas of research identified to enhance the practical applicability of neural networks to flight control design. Author

A91-49793* National Aeronautics and Space Administration. Lewis Research Center, Cleveland, OH.

APPLICATION OF AN INTEGRATED FLIGHT/PROPULSION CONTROL DESIGN METHODOLOGY TO A STOVL AIRCRAFT

SANJAY GARG and DUANE L. MATTERN (NASA, Lewis Research Center, Cleveland, OH) AIAA, Guidance, Navigation and Control Conference, New Orleans, LA, Aug. 12-14, 1991. 11 p. refs (AIAA PAPER 91-2792) Copyright

The application of an emerging Integrated Flight/Propulsion Control design methodology to a STOVL aircraft in transition flight is reported. The methodology steps consist of: (1) design of a centralized feedback controller to provide command tracking and stability and performance robustness considering the fully integrated airframe/propulsion model as one high-order system; (2) partition of the centralized controller into a decentralized, hierarchical form compatible with implementation requirements; and (3) design of command shaping prefilters from pilot control effectors to commanded variables to provide the overall desired response to pilot inputs. Intermediate design results using this methodology are presented, the complete point control design with the propulsion system operating schedule and limit protection logic included is evaluated for sample pilot control inputs, and the response is compared with that of an 'ideal response model' derived from Level I handling qualities requirements. C.D.

N91-20133* National Aeronautics and Space Administration. Lewis Research Center, Cleveland, OH.

A METHOD FOR PARTITIONING CENTRALIZED CONTROLLERS

PHILLIP SCHMIDT, SANJAY GARG (Sverdrup Technology, Inc., Brook Park, OH), and CARL F. LORENZO Apr. 1991 9 p

(Contract RTOP 505-62-01)
(NASA-TM-4276; E-5800; NAS 1.15:4276) Avail: NTIS HC/MF
A02 CSCL 01/3

The notion of controller partitioning is described. Conditions are developed under which the input/output behavior of a multi-input multi-output centralized controller can be exactly matched by two separate subsystem controllers interconnected through output crossfeed. A systematic method is developed for determining a controller partitioning which best approximates the input/output behavior of the centralized controller for the general case when the exact matching conditions are not satisfied. The controller partitioning procedure is demonstrated for a centralized integrated flight/propulsion controller designed in a previous study. Author

N91-22135*# National Aeronautics and Space Administration. Lewis Research Center, Cleveland, OH.

LIFE EXTENDING CONTROL: A CONCEPT PAPER

CARL F. LORENZO and WALTER C. MERRILL 1991 17 p
Presented at the American Control Conference, Boston, MA, 26-28 Jun. 1991; sponsored by the American Automatic Control Council (Contract RTOP 505-62-50)
(NASA-TM-104391; E-6206; NAS 1.15:104391) Avail: NTIS
HC/MF A03 CSCL 01/3

The concept of Life Extending Control is defined. Life is defined in terms of mechanical fatigue life. A brief description is given of the current approach to life prediction using a local, cyclic, stress-strain approach for a critical system component. An alternative approach to life prediction based on a continuous functional relationship to component performance is proposed. Based on cyclic life prediction an approach to Life Extending Control, called the Life Management Approach is proposed. A second approach, also based on cyclic life prediction, called the Implicit Approach, is presented. Assuming the existence of the alternative functional life prediction approach, two additional concepts for Life Extending Control are presented. Author

N91-23053*# National Aeronautics and Space Administration. Lewis Research Center, Cleveland, OH.

CIVIL AIR TRANSPORT: A FRESH LOOK AT POWER-BY-WIRE AND FLY-BY-LIGHT

GALE R. SUNDBERG In National Aeronautics and Space Administration, Technology 2000, Volume 1 p 263-267 Mar. 1991 Previously announced as N90-21283
Avail: NTIS HC/MF A18 CSCL 01/3

Power-by-wire (PBW) is a key element under subsonic transport flight systems technology with potential savings of over 10 percent in operating empty weight and in fuel consumption compared to today's transport aircraft. The PBW technology substitutes electrical actuation in place of centralized hydraulics, uses internal starter-motor/generators and eliminates the need for variable engine bleed air to supply cabin comfort. The application of advanced fiber optics to the electrical power system controls, to built-in-test (BIT) equipment, and to fly-by-light (FBL) flight controls provides additional benefits in lightning and high energy radio frequency (HERF) immunity over existing mechanical or even fly-by-wire controls. The program plan is reviewed and a snapshot is given of the key technologies and their benefits to all future aircraft, both civil and military. Author

N91-27167*# National Aeronautics and Space Administration. Lewis Research Center, Cleveland, OH.

NEURAL NETWORK APPLICATION TO AIRCRAFT CONTROL SYSTEM DESIGN

TERRY TROUDET (Sverdrup Technology, Inc., Brook Park, OH.), SANJAY GARG, and WALTER C. MERRILL 1991 20 p
Presented at the Guidance, Navigation and Control Conference, New Orleans, LA, 12-14 Aug. 1991; sponsored by AIAA (Contract RTOP 505-62-50)
(NASA-TM-105151; E-6435; NAS 1.15:105151) Avail: NTIS
HC/MF A03 CSCL 01/3

The feasibility of using artificial neural networks as control systems for modern, complex aerospace vehicles is investigated

via an example aircraft control design study. The problem considered is that of designing a controller for an integrated airframe/propulsion longitudinal dynamics model of a modern fighter aircraft to provide independent control of pitch rate and airspeed responses to pilot command inputs. An explicit model following controller using H infinity control design techniques is first designed to gain insight into the control problem as well as to provide a baseline for evaluation of the neurocontroller. Using the model of the desired dynamics as a command generator, a multilayer feedforward neural network is trained to control the vehicle model within the physical limitations of the actuator dynamics. This is achieved by minimizing an objective function which is a weighted sum of tracking errors and control input commands and rates. To gain insight in the neurocontrol, linearized representations of the nonlinear neurocontroller are analyzed along a commanded trajectory. Linear robustness analysis tools are then applied to the linearized neurocontroller models and to the baseline H infinity based controller. Future areas of research are identified to enhance the practical applicability of neural networks to flight control design. Author

N91-32143*# National Aeronautics and Space Administration. Lewis Research Center, Cleveland, OH.

APPLICATION OF AN INTEGRATED FLIGHT/PROPULSION CONTROL DESIGN METHODOLOGY TO A STOVL AIRCRAFT

SANJAY GARG and DUANE L. MATTERN (Sverdrup Technology, Inc., Brook Park, OH.) 1991 12 p Presented at the Guidance, Navigation and Control Conference, New Orleans, LA, 12-14 Aug. 1991; sponsored by AIAA Previously announced in IAA as A91-49793
(Contract RTOP 505-62-50)

(NASA-TM-105254; E-6583; NAS 1.15:105254; AIAA PAPER 91-2792) Avail: NTIS HC/MF A03 CSCL 01/3

Results are presented from the application of an emerging Integrated Flight/Propulsion Control (IFPC) design methodology to a Short Take Off and Vertical Landing (STOVL) aircraft in transition flight. The steps in the methodology consist of designing command shaping prefilters to provide the overall desired response to pilot command inputs. A previously designed centralized controller is first validated for the integrated airframe/engine plant used. This integrated plant is derived from a different model of the engine subsystem than the one used for the centralized controller design. The centralized controller is then partitioned in a decentralized, hierarchical structure comprising of airframe lateral and longitudinal subcontrollers and an engine subcontroller. Command shaping prefilters from the pilot control effector inputs are then designed and time histories of the closed loop IFPC system response to simulated pilot commands are compared to desired responses based on handling qualities requirements. Finally, the propulsion system safety and nonlinear limited protection logic is wrapped around the engine subcontroller and the response of the closed loop integrated system is evaluated for transients that encounter the propulsion surge margin limit. Author

09

RESEARCH AND SUPPORT FACILITIES (AIR)

Includes airports, hangars and runways; aircraft repair and overhaul facilities; wind tunnels; shock tubes; and aircraft engine test stands.

A91-14454*# National Aeronautics and Space Administration. Lewis Research Center, Cleveland, OH.

A UNIQUE HIGH HEAT FLUX FACILITY FOR TESTING HYPERSONIC ENGINE COMPONENTS

MATTHEW E. MELIS and HERBERT J. GLADDEN (NASA, Lewis Research Center, Cleveland, OH) AIAA, International Aerospace

09 RESEARCH AND SUPPORT FACILITIES (AIR)

Planes Conference, 2nd, Orlando, FL, Oct. 29-31, 1990. 8 p. refs

(AIAA PAPER 90-5228) Copyright

This paper describes the Hot Gas Facility, a unique, reliable, and cost-effective high-heat-flux facility for testing hypersonic engine components developed at the NASA Lewis Research Center. The Hot Gas Facility is capable of providing heat fluxes ranging from 200 Btu/sq ft per sec on flat surfaces up to 8000 Btu/sq ft per sec at a leading edge stagnation point. The usefulness of the Hot Gas Facility for the NASP community was demonstrated by testing hydrogen-cooled structures over a range of temperatures and pressures. Ranges of the Reynolds numbers, Prandtl numbers, enthalpy, and heat fluxes similar to those expected during hypersonic flights were achieved. I.S.

A91-26112* National Aeronautics and Space Administration. Lewis Research Center, Cleveland, OH.

TRANSONIC WIND-TUNNEL WALL INTERFERENCE PREDICTION CODE

PAMELA S. PHILLIPS and EDGAR G. WAGGONER (NASA, Langley Research Center, Hampton, VA) Journal of Aircraft (ISSN 0021-8669), vol. 27, Nov. 1990, p. 915, 916. Previously cited in issue 16, p. 2603, Accession no. A88-40722. refs Copyright

A91-37417* Sverdrup Technology, Inc., Cleveland, OH. **TEST-CELL PRESSURE EFFECTS ON THE PERFORMANCE OF RESISTOJETS**

D. H. MANZELLA (Sverdrup Technology, Inc., Cleveland, OH), P. F. PENKO (NASA, Lewis Research Center, Cleveland, OH), K. J. DE WITT, and T. G. KEITH, JR. (Toledo, University, OH) Journal of Propulsion and Power (ISSN 0748-4658), vol. 7, Mar.-Apr. 1991, p. 269-274. Previously cited in issue 18, p. 3008, Accession no. A88-44820. refs (Contract NAG3-577) Copyright

A91-47847* National Aeronautics and Space Administration. Lewis Research Center, Cleveland, OH.

THE NASA LEWIS INTEGRATED PROPULSION AND FLIGHT CONTROL SIMULATOR

MICHELLE M. BRIGHT (NASA, Lewis Research Center, Cleveland, OH) and DONALD L. SIMON (NASA, Lewis Research Center; U.S. Army, Propulsion Directorate, Cleveland, OH) IN: AIAA Flight Simulation Technologies Conference, New Orleans, LA, Aug. 12-14, 1991, Technical Papers. Washington, DC, American Institute of Aeronautics and Astronautics, 1991, p. 448-458. refs (AIAA PAPER 91-2969) Copyright

A new flight simulation facility has been developed at NASA Lewis to allow integrated propulsion-control and flight-control algorithm development and evaluation in real time. As a preliminary check of the simulator facility and the correct integration of its components, the control design and physics models for an STOVL fighter aircraft model have been demonstrated, with their associated system integration and architecture, pilot vehicle interfaces, and display symbology. The results show that this fixed-based flight simulator can provide real-time feedback and display of both airframe and propulsion variables for validation of integrated systems and testing of control design methodologies and cockpit mechanizations. Author

A91-51858* National Aeronautics and Space Administration. Lewis Research Center, Cleveland, OH.

AN ELECTRONIC PRESSURE PROFILE DISPLAY SYSTEM FOR AERONAUTIC TEST FACILITIES

MARK R. WOIKE (NASA, Lewis Research Center, Cleveland, OH) IN: International Instrumentation Symposium, 36th, Denver, CO, May 6-10, 1990, Proceedings. Research Triangle Park, NC, Instrument Society of America, 1990, p. 117-124. Previously announced in STAR as N90-15964. refs Copyright

The NASA Lewis Research Center has installed an Electronic Pressure Profile Display system. This system provides for the

real-time display of pressure readings on high resolution graphics monitors. The Electronic Pressure Profile Display system will replace manometer banks currently used in aeronautic test facilities. The Electronic Pressure Profile Display system consists of an industrial type Digital Pressure Transmitter (DPI) unit which interfaces with a host computer. The host computer collects the pressure data from the DPI unit, converts it into engineering units, and displays the readings on a high resolution graphics monitor in bar graph format. Software was developed to accomplish the above tasks and also draw facility diagrams as background information on the displays. Data transfer between host computer and DPI unit is done with serial communications. Up to 64 channels are displayed with one second update time. This paper describes the system configuration, its features, and its advantages over existing systems. Author

N91-11770* National Aeronautics and Space Administration. Lewis Research Center, Cleveland, OH.

A UNIQUE HIGH HEAT FLUX FACILITY FOR TESTING HYPERSONIC ENGINE COMPONENTS

MATTHEW E. MELIS and HERBERT J. GLADDEN 1990 10 p Presented at the 2nd International Aerospace Planes Conference, Orlando, FL, 29-31 Oct. 1990; cosponsored by AIAA, and NASP (Contract RTOP 763-01-41) (NASA-TM-103238; E-5657; NAS 1.15:103238) Avail: NTIS HC/MF A02 CSCL 14/2

A major concern in advancing the state-of-the-art technologies for hypersonic vehicles is the development of an aeropropulsion system capable of withstanding high thermal loads expected during hypersonic flights. Consequently, there is a need for experimental facilities capable of providing a high heat flux environment for testing compound concepts and verifying analyses. A hydrogen/oxygen rocket engine was developed to provide a high enthalpy/high heat flux environment for component evaluation. This Hot Gas Facility is capable of providing heat fluxes ranging from 200 (on flat surfaces) up to 8000 Btu per sq ft per sec (at a leading edge stagnation point). Gas temperatures up to 5500 R can be attained as well as Reynolds numbers up to 360,000 per ft. Test articles such as cowl leading edges, transpiration-cooled seals, fuel injectors, and cooled panel concepts can be evaluated with gaseous hydrogen as coolant. This facility and its configuration and test capabilities are discussed. Results from flow characterization experiments are also shown and their implications considered. Author

N91-20099* National Aeronautics and Space Administration. Lewis Research Center, Cleveland, OH.

INSTRUMENTATION AND CONTROLS OVERVIEW

NORMAN C. WENGER In its Aeropropulsion 1991 8 p Mar. 1991

Avail: NTIS HC/MF A24 CSCL 14/2

The Lewis Research Center has had a long history of research directed toward advancing the Nation's capability in the areas of propulsion research instrumentation and propulsion controls. Some of the major advances from this research are highlighted as well as some of the planned research that will strongly impact the future capabilities. Efforts on research instrumentation and controls, as well as, efforts in high-temperature electronics are covered. The goals, scope, and major thrusts in each of the research areas are stressed. Author

N91-20121* National Aeronautics and Space Administration. Lewis Research Center, Cleveland, OH.

RECENT ADVANCES IN LEWIS AEROPROPULSION FACILITIES

FRANK J. KUTINA, JR. In its Aeropropulsion 1991 12 p Mar. 1991

Avail: NTIS HC/MF A24 CSCL 14/2

Guided by the aeropropulsion strategic plan, Lewis Research Center was systematically refurbishing and upgrading its aeropropulsion facilities through a combination of research and development and construction of facilities funding. Currently, much of the work is accomplished as a part of the NASA Aeronautical

Facility Revitalization Program. The total effort is addressing issues of improved flight simulation, improved productivity, capability to support advanced aeropropulsion systems, increased computational capability, and recertification. An overview of the changes brought about by this effort is presented. Author

N91-29199*# National Aeronautics and Space Administration. Lewis Research Center, Cleveland, OH.

CALCULATED PERFORMANCE OF THE NASA LEWIS ICING RESEARCH TUNNEL

LARRY A. VITERNA Aug. 1991 23 p

(Contract RTOP 474-12-10)

(NASA-TM-105173; E-6469; NAS 1.15:105173) Avail: NTIS

HC/MF A03 CSCL 14/2

The Icing Research Tunnel is used extensively to test many classes of aircraft under atmospheric icing conditions. Because of the need to test models at higher Reynolds numbers, a new fan rotor was designed to increase test section wind speed. A preliminary study was made of the present fan rotor to suggest possible methods to increase tunnel wind speed. The results of that study are presented. Author

N91-30163*# National Aeronautics and Space Administration. Lewis Research Center, Cleveland, OH.

THE NASA LEWIS RESEARCH CENTER INTERNAL FLUID MECHANICS FACILITY

A. R. PORRO, W. R. HINGST, C. A. WASSERBAUER, and T. B. ANDREWS Sep. 1991 23 p

(Contract RTOP 505-62-52)

(NASA-TM-105187; E-6487; NAS 1.15:105187) Avail: NTIS

HC/MF A03 CSCL 14/2

An experimental facility specifically designed to investigate internal fluid duct flows is described. It is built in a modular fashion so that a variety of internal flow test hardware can be installed in the facility with minimal facility reconfiguration. The facility and test hardware interfaces are discussed along with design constraints of future test hardware. The plenum flow conditioning approach is also detailed. Available instrumentation and data acquisition capabilities are discussed. The incoming flow quality was documented over the current facility operating range. The incoming flow produces well behaved turbulent boundary layers with a uniform core. For the calibration duct used, the boundary layers approached 10 percent of the duct radius. Freestream turbulence levels at the various operating conditions varied from 0.64 to 0.69 percent of the average freestream velocity. Author

12

ASTRONAUTICS (GENERAL)

A91-13991*# National Aeronautics and Space Administration, Washington, DC.

VIBRATION ENVIRONMENT - ACCELERATION MAPPING STRATEGY AND MICROGRAVITY REQUIREMENTS FOR SPACELAB AND SPACE STATION

GARY L. MARTIN (NASA, Microgravity Science and Applications Div., Washington, DC), CHARLES R. BAUGHER (NASA, Marshall Space Flight Center, Huntsville, AL), and RICHARD DELOMBARD (NASA, Lewis Research Center, Cleveland, OH) IAF, International Astronautical Congress, 41st, Dresden, Federal Republic of Germany, Oct. 6-12, 1990. 9 p.

(IAF PAPER 90-350) Copyright

In order to define the acceleration requirements for future Shuttle and Space Station Freedom payloads, methods and hardware characterizing accelerations on microgravity experiment carriers are discussed. The different aspects of the acceleration environment and the acceptable disturbance levels are identified. The space acceleration measurement system features an

adjustable bandwidth, wide dynamic range, data storage, and ability to be easily reconfigured and is expected to fly on the Spacelab Life Sciences-1. The acceleration characterization and analysis project describes the Shuttle acceleration environment and disturbance mechanisms, and facilitates the implementation of the microgravity research program. B.P.

A91-41980*# National Aeronautics and Space Administration. Lewis Research Center, Cleveland, OH.

PRELIMINARY RESULTS FROM THE ADVANCED PHOTOVOLTAIC EXPERIMENT FLIGHT TEST

DAVID J. BRINKER, RUSSELL E. HART, JR. (NASA, Lewis Research Center, Cleveland, OH), and JOHN R. HICKEY (Eppler Laboratory, Inc., Newport, RI) IN: IEEE Photovoltaic Specialists Conference, 21st, Kissimmee, FL, May 21-25, 1990, Conference Record, Vol. 2. New York, Institute of Electrical and Electronics Engineers, Inc., 1990, p. 1213-1218.

Copyright

The Advanced Photovoltaic Experiment is a space flight test designed to provide reference cell standards for photovoltaic measurements and to investigate the solar spectrum and the effect of the space environment on solar cells. After a flight of 69 months in low earth orbit as part of the Long Duration Exposure Facility set of experiments, it was retrieved in January 1990. The electronic data acquisition system functioned as designed, measuring and recording cell performance data over the first 358 days of flight, limited by battery lifetime. Significant physical changes are also readily apparent, including erosion of front surface paint, micrometeoroid and debris cratering, and contamination. I.E.

A91-45781*# National Aeronautics and Space Administration. Lewis Research Center, Cleveland, OH.

THE RATIONALE/BENEFITS OF NUCLEAR THERMAL ROCKET PROPULSION FOR NASA'S LUNAR SPACE TRANSPORTATION SYSTEM

STANLEY K. BOROWSKI (NASA, Lewis Research Center, Cleveland, OH) AIAA, SAE, ASME, and ASEE, Joint Propulsion Conference, 27th, Sacramento, CA, June 24-26, 1991. 20 p. refs

(AIAA PAPER 91-2052)

Two nuclear thermal rocket (NTR) technology options are examined - one derived from the graphite-moderated reactor concept developed by NASA and the AEC under the Rover/NERVA (Nuclear Engine for Rocket Vehicle Application) programs, and a second concept, the Particle Bed Reactor. The paper also summarizes NASA's lunar outpost scenario, compares relative performance provided by different lunar space transportation system concepts, and discusses important operational issues (e.g., reusability, engine 'end-of-life' disposal, etc.) associated with using this important propulsion technology. Author

A91-45807*# National Aeronautics and Space Administration. Lewis Research Center, Cleveland, OH.

SYNERGISTIC USE OF HIGH AND LOW THRUST PROPULSION SYSTEMS FOR PILOTED MISSIONS TO MARS

JAMES H. GILLAND (NASA, Lewis Research Center, Cleveland; Sverdrup Technology, Inc., Brook Park, OH) AIAA, SAE, ASME, and ASEE, Joint Propulsion Conference, 27th, Sacramento, CA, June 24-26, 1991. 12 p. refs

(AIAA PAPER 91-2346)

The use of high-thrust, relatively-low-specific-impulse systems, such as chemical or nuclear thermal propulsion, in conjunction with low thrust, high-specific-impulse nuclear electric propulsion (NEP), has been considered for a representative piloted Mars mission. It is concluded that the single-burn option in an all-propulsive mission scenario does not yield a significant performance advantage in reduced trip time for reasonable masses. The multiple burn option allows significant reductions in trip time relative to the NEP system, and may provide a performance advantage over nuclear thermal propulsion depending upon the system assumptions. The combined systems serve to reduce NEP power requirements for fast trip times, and to reduce high thrust systems' sensitivity to mission opportunity. It is considered that 5

12 ASTRONAUTICS (GENERAL)

kg/kWe systems can provide significant improvements in mass and trip time over the single systems at power levels of 5 to 10 MWe. O.G.

N91-19112*# National Aeronautics and Space Administration. Lewis Research Center, Cleveland, OH.

SPACE REACTOR/STIRLING CYCLE SYSTEMS FOR HIGH POWER LUNAR APPLICATION

PAUL C. SCHMITZ (Sverdrup Technology, Inc., Brook Park, OH.) and LEE S. MASON 1991 11 p Presented at the 8th Symposium on Space Nuclear Power Systems, Albuquerque, NM, 6-10 Jan. 1991; cosponsored by New Mexico Univ, Strategic Defense Initiative Organization, DOE, and AF (Contract RTOP 590-13-11) (NASA-TM-103698; E-5920; NAS 1.15:103698) Avail: NTIS HC/MF A03 CSCL 10/2

An analysis is performed to mathematically model a 550 kWe lunar base power supply which uses a SP-100 reactor coupled with Stirling converters. The reactor is placed in an excavation to keep activated coolant in the hole and to allow maintenance of the components outside the hole. Two technology levels are considered. They are 1050 and 1300 K heater head Stirling converts. It is found that for a 1050 K converter the total mass which provided 1000 volts DC at 250 m is 14,366 kg while the 1300 K system mass is 12,104 kg. The radiation area of the 1050 and 1300 K systems are 641 and 356 sq m respectively. Comparisons are made with Brayton and thermionic systems with both near term and advanced technology considered. Author

N91-22139*# National Aeronautics and Space Administration. Lewis Research Center, Cleveland, OH.

VISION-21: SPACE TRAVEL FOR THE NEXT MILLENNIUM

GEOFFREY A. LANDIS, ed. (Sverdrup Technology, Inc., Brook Park, OH.) Apr. 1990 600 p Symposium held in Cleveland, OH, 3-4 Apr. 1990 (NASA-CP-10059; E-5838; NAS 1.55:10059) Avail: NTIS HC/MF A25 CSCL 22/1

The papers from this symposium, that was held at the NASA Lewis Research Center on April 3-4, 1990, are presented. The theme selected for the symposium was space travel for the next millennium. It was hoped that the participants would allow their focus to consider possible advances in technologies for space travel not just for currently envisioned projects, but for possibilities beyond the next generation and the next thousand years. About half of the contributed papers focussed on propulsion and the other half on other issues related to space travel.

13

ASTRODYNAMICS

Includes powered and free-flight trajectories; and orbital and launching dynamics.

A91-22966*# National Aeronautics and Space Administration. Lewis Research Center, Cleveland, OH.

SATELLITE RELOCATION BY TETHER DEPLOYMENT

GEOFFREY A. LANDIS and FRANK J. HRACH (NASA, Lewis Research Center, Cleveland, OH) Journal of Guidance, Control, and Dynamics (ISSN 0731-5090), vol. 14, Jan.-Feb. 1991, p. 214-216. Previously announced in STAR as N89-26877. refs Copyright

Several new uses of satellite tethers are discussed, including: (1) using tether extension to reposition a satellite in orbit without fuel expenditure by extending a mass on the end of a tether; (2) using a tether for energy storage to power the satellite during eclipse; and (3) using a tether for eccentricity pumping to correct perturbations in the orbit and as a means of adding energy to the orbit for boosting and orbital transfer. Author

A91-49764*# National Aeronautics and Space Administration. Lewis Research Center, Cleveland, OH.

THE DYNAMIC EFFECTS OF INTERNAL ROBOTS ON SPACE STATION FREEDOM

JEFFREY H. MILLER (NASA, Lewis Research Center, Cleveland; Sverdrup Technology, Inc. Brook Park, OH), CHARLES LAWRENCE, and DOUGLAS A. ROHN (NASA, Lewis Research Center, Cleveland, OH) IN: AIAA Guidance, Navigation and Control Conference, New Orleans, LA, Aug. 12-14, 1991, Technical Papers. Vol. 3. Washington, DC, American Institute of Aeronautics and Astronautics, 1991, p. 1865-1878. Previously announced in STAR as N91-22604. refs

(AIAA PAPER 91-2822) Copyright

Many of the planned experiments of the Space Station Freedom (SSF) will require acceleration levels to be no greater than microgravity (10 exp -6 g) levels for long periods of time. Studies have demonstrated that without adequate control, routine operations may cause disturbances which are large enough to affect on-board experiments. One way to both minimize disturbances and make the SSF more autonomous is to utilize robots instead of astronauts for some operations. The present study addresses the feasibility of using robots for microgravity manipulation. Two methods for minimizing the dynamic disturbances resulting from the robot motions are evaluated. The first method is to use a robot with kinematic redundancy (redundant links). The second method involves the use of a vibration isolation device between the robot and the SSF laboratory module. The results from these methods are presented along with simulations of robots without disturbance control. Author

N91-19115*# National Aeronautics and Space Administration. Lewis Research Center, Cleveland, OH.

AUTOMATIC CONTROL STUDY OF THE ICING RESEARCH TUNNEL REFRIGERATION SYSTEM

ARTHUR W. KIEFFER and RONALD H. SOEDER Washington Feb. 1991 27 p (Contract RTOP 505-62-3B)

(NASA-TM-4257; E-5588; NAS 1.15:4257) Avail: NTIS HC/MF A03 CSCL 13/2

The Icing Research Tunnel (IRT) at the NASA Lewis Research Center is a subsonic, closed-return atmospheric tunnel. The tunnel includes a heat exchanger and a refrigeration plant to achieve the desired air temperature and a spray system to generate the type of icing conditions that would be encountered by aircraft. At the present time, the tunnel air temperature is controlled by manual adjustment of freon refrigerant flow control valves. An upgrade of this facility calls for these control valves to be adjusted by an automatic controller. The digital computer simulation of the IRT refrigeration plant and the automatic controller that was used in the simulation are discussed. Author

14

GROUND SUPPORT SYSTEMS AND FACILITIES (SPACE)

Includes launch complexes, research and production facilities; ground support equipment, e.g., mobile transporters; and simulators.

A91-10176*# National Aeronautics and Space Administration. Lewis Research Center, Cleveland, OH.

SYSTEMS ANALYSIS OF MARS SOLAR ELECTRIC PROPULSION VEHICLES

J. M. HICKMAN, H. B. CURTIS, B. H. KENNY, and R. J. SEFCIK (NASA, Lewis Research Center, Cleveland, OH) AIAA, Space Programs and Technologies Conference, Huntsville, AL, Sept. 25-27, 1990. 22 p. refs (AIAA PAPER 90-3824)

Mission performance, mass, initial power, and cost are

14 GROUND SUPPORT SYSTEMS AND FACILITIES (SPACE)

determined for solar electric propulsion vehicles across a range of payload masses, reference powers, and mission trajectories. Thick radiation shielding is added to arrays using indium phosphide or III-V multijunction solar cells to reduce the damage incurred through the radiation belts. Special assessments of power management and distribution systems, atmospheric drag, and energy storage are made. It is determined that atmospheric drag is of no great concern and that the energy storage used in countering drag is unnecessary. A scheme to package the arrays, masts, and ion thrusters into a single fairing is presented.

Author

A91-11471* National Aeronautics and Space Administration. Lewis Research Center, Cleveland, OH.

NATIONAL SPACE TEST CENTERS - LEWIS RESEARCH CENTER FACILITIES

RONALD R. ROSKILLY (NASA, Lewis Research Center, Cleveland, OH) AIAA, Space Programs and Technologies Conference, Huntsville, AL, Sept. 25-27, 1990. 6 p. Previously announced in STAR as N90-26030.

(AIAA PAPER 90-3593) Copyright

The Lewis Research Center, NASA, presently has a number of test facilities that constitute a significant national space test resource. It is expected this capability will continue to find wide application in work involving this country's future in space. Testing from basic research to applied technology, to systems development, to ground support will be performed, supporting such activities as Space Station Freedom, the Space Exploration Initiative, Mission to Planet Earth, and many others. The major space test facilities at both Cleveland and Lewis' Plum Brook Station are described. Primary emphasis is on space propulsion facilities; other facilities of importance in space power and microgravity are also included.

Author

A91-27356* National Aeronautics and Space Administration. Lewis Research Center, Cleveland, OH.

PROPOSAL FOR A SUN-FOLLOWING MOONBASE

G. A. LANDIS (NASA, Lewis Research Center, Cleveland, OH) British Interplanetary Society, Journal (ISSN 0007-084X), vol. 44, March 1991, p. 125, 126. refs

Copyright

A new concept for a manned lunar facility is proposed, where the moon base moves across the moon to follow the sun. Such a facility has advantages of continuous solar power, no reduced activity period during the lunar night, and constantly new territory to sample.

Author

A91-27702* New Mexico Univ., Albuquerque.

PRELIMINARY ASSESSMENT OF THE POWER REQUIREMENTS OF A MANNED ROVER FOR MARS MISSIONS

MOHAMED S. EL-GENK, NICHOLAS J. MORLEY (New Mexico, University, Albuquerque), ROBERT CATALDO, and HARVEY BLOOMFIELD (NASA, Lewis Research Center, Cleveland, OH) IN: Engineering, construction, and operations in space II; Proceedings of Space 90, the Second International Conference, Albuquerque, NM, Apr. 22-26, 1990. Vol. 2. New York, American Society of Civil Engineers, 1990, p. 1278-1287. refs

(Contract NAG3-992)

Copyright

A preliminary study to determine the total mass and power requirements of a manned Mars rover is presented. Estimates of the power requirements for the nuclear reactor power system are determined as functions of the number of crew members, the emergency return trip scenario in case of a total malfunction of the reactor system, the cruising speed and range of the vehicle, and the specific mass of the power system. It is shown that the cruising speed of the vehicle and the soil traction factor significantly affect the traversing power requirement and therefore the mass of the nuclear power system. The cruising speed of the vehicle must be limited to 14.5 and 24 km/hr for power system specific masses of 150 kg/kWe and 50 kg/kWe, respectively, for the

nuclear power system mass not to exceed 50 percent of the total mass of the rover. R.E.P.

A91-36239* National Aeronautics and Space Administration. Lewis Research Center, Cleveland, OH.

THRUST STAND FOR HIGH-POWER ELECTRIC PROPULSION DEVICES

T. W. HAAG (NASA, Lewis Research Center, Cleveland, OH) Review of Scientific Instruments (ISSN 0034-6748), vol. 62, May 1991, p. 1186-1191. refs

Copyright

This paper describes a new high-power thrust stand developed for use with high-power (up to 250 kW) magnetoplasmadynamic (MPD) thrusters, which is installed in a high-vacuum MPD facility at Lewis Research Center. The design of the stand is based on inverted pendulum configuration, with the result of large displacements and high resolution. Calibration results showed that thrust measurements were linear and repeatable to within a fraction of 1 percent. The thrust stand was used for testing water-cooled MPD thrusters at power levels up to 125 kW. The thruster, however, is quite well suited for testing other types of electric propulsion devices. I.S.

A91-41987* National Aeronautics and Space Administration. Lewis Research Center, Cleveland, OH.

DESIGN CONSIDERATIONS FOR LUNAR BASE PHOTOVOLTAIC POWER SYSTEMS

J. M. HICKMAN, HENRY B. CURTIS, and GEOFFREY A. LANDIS (NASA, Lewis Research Center, Cleveland, OH) IN: IEEE Photovoltaic Specialists Conference, 21st, Kissimmee, FL, May 21-25, 1990, Conference Record. Vol. 2. New York, Institute of Electrical and Electronics Engineers, Inc., 1990, p. 1256-1262. Previously announced in STAR as N91-14259. refs

A survey was made of factors that may affect the design of photovoltaic arrays for a lunar base. These factors, which include the lunar environment and system design criteria, are examined. A photovoltaic power system design with a triangular array geometry is discussed and compared to a nuclear reactor power system and a power system utilizing both nuclear and solar power sources.

Author

A91-41988* National Aeronautics and Space Administration. Lewis Research Center, Cleveland, OH.

DESIGN CONSIDERATIONS FOR MARS PHOTOVOLTAIC POWER SYSTEMS

GEOFFREY A. LANDIS and JOSEPH APPELBAUM (NASA, Lewis Research Center, Cleveland, OH) IN: IEEE Photovoltaic Specialists Conference, 21st, Kissimmee, FL, May 21-25, 1990, Conference Record. Vol. 2. New York, Institute of Electrical and Electronics Engineers, Inc., 1990, p. 1263-1270. refs

Copyright

Considerations for operation of a photovoltaic power system on Mars are discussed with reference to Viking Lander data. The average solar insolation at Mars is 590 W/sq m, which is reduced yet further by atmospheric dust. Of major concern are dust storms, which have been observed to occur on local as well as on global scales, and their effect on solar array output. While atmospheric opacity may rise to values ranging from 3 to 9, depending on storm severity, there is still an appreciable large diffuse illumination, even at high opacities, so that photovoltaic operation is still possible. If the power system is to continue to generate power even on high-optical-opacity (i.e., dusty atmosphere) days, it is important that the photovoltaic system be designed to collect diffuse irradiance as well as direct. Energy storage will be required for operation during the night. Temperature and wind provide additional considerations for array design. I.E.

A91-52343* National Aeronautics and Space Administration. Lewis Research Center, Cleveland, OH.

EVALUATION OF COMPONENTS, SUBSYSTEMS, AND NETWORKS FOR HIGH RATE, HIGH FREQUENCY SPACE COMMUNICATIONS

ROBERT J. KERCZEWSKI, WILLIAM D. IVANCIC, and JOHN E.

14 GROUND SUPPORT SYSTEMS AND FACILITIES (SPACE)

ZUZEK (NASA, Lewis Research Center, Cleveland, OH) AIAA, NASA, and OAI, Conference on Advanced SEI Technologies, Cleveland, OH, Sept. 4-6, 1991. 12 p. refs
(AIAA PAPER 91-3423) Copyright

The development of new space communications technologies by NASA has included both commercial applications and space science requirements. At NASA's Lewis Research Center, methods and facilities have been developed for evaluating these new technologies in the laboratory. NASA's Systems Integration, Test and Evaluation (SITE) Space Communication System Simulator is a hardware-based laboratory simulator for evaluating space communications technologies at the component, subsystem, system, and network level, geared toward high frequency, high data rate systems. The SITE facility is well-suited for evaluation of the new technologies required for the Space Exploration Initiative (SEI) and advanced commercial systems. This paper describes the technology developments and evaluation requirements for current and planned commercial and space science programs. Also examined are the capabilities of SITE, the past, present, and planned future configurations of the SITE facility, and applications of SITE to evaluation of SEI technology. Author

A91-52350* # Pratt and Whitney Aircraft Group, West Palm Beach, FL.

DESIGN OF AN ADVANCED EXPANDER TEST BED

ARTHUR I. MASTERS (Pratt and Whitney Group, West Palm Beach, FL) and WILLIAM K. TABATA (NASA, Lewis Research Center, Cleveland, OH) AIAA, NASA, and OAI, Conference on Advanced SEI Technologies, Cleveland, OH, Sept. 4-6, 1991. 9 p.
(Contract NAS3-25960)

(AIAA PAPER 91-3437) Copyright

The Advanced Expander Test Bed (AETB) is the key element for development of technology for future space engines. The AETB will be used to validate the high pressure expander cycle concept, investigate system interactions and conduct investigations of advanced mission focused components and new health monitoring techniques. The AETB will use oxygen/hydrogen propellants and a split expander cycle with nominal operation at a combustion chamber pressure of 1200 psia, a mixture ratio of 6.0, and an equivalent vacuum thrust of 20,000 lbf. It will function over a wide range of conditions including throttling to 5 percent thrust, operation at a mixture ratio of 12.0, and operation in tank head idle and pumped idle modes. Author

A91-52396* # National Aeronautics and Space Administration, Lewis Research Center, Cleveland, OH.

TEST FACILITIES FOR HIGH POWER ELECTRIC PROPULSION

JAMES S. SOVEY, ROBERT H. VETRONE, STANLEY P. GRISNIK (NASA, Lewis Research Center, Cleveland, OH), ROGER M. MYERS, and JAMES E. PARKES (NASA, Lewis Research Center; Sverdrup Technology, Inc., Cleveland, OH) AIAA, NASA, and OAI, Conference on Advanced SEI Technologies, Cleveland, OH, Sept. 4-6, 1991. 22 p. refs

(AIAA PAPER 91-3499) Copyright

Electric propulsion has applications for orbit raising, maneuvering of large space systems, and interplanetary missions. These missions involve propulsion power levels from tenths to tens of megawatts, depending upon the application. General facility requirements for testing high power electric propulsion at the component and thrust systems level are defined. The characteristics and pumping capabilities of many large vacuum chambers in the United States are reviewed and compared with the requirements for high-power electric-propulsion testing. Author

N91-22171* # National Aeronautics and Space Administration, Lewis Research Center, Cleveland, OH.

DESIGN STRATEGIES FOR THE INTERNATIONAL SPACE UNIVERSITY'S VARIABLE GRAVITY RESEARCH FACILITY

SHEILA G. BAILEY, FRANCIS P. CHIARAMONTE, and KENNETH J. DAVIDIAN *In its Vision-21: Space Travel for the Next Millennium*

p 416-427 Apr. 1990

Avail: NTIS HC/MF A25 CSCL 14/2

A variable gravity research facility named 'Newton' was designed by 58 students from 13 countries at the International Space University's 1989 summer session at the Universite Louis Pasteur, Strasbourg, France. The project was comprehensive in scope, including a political and legal foundation for international cooperation, development and financing; technical, science and engineering issues; architectural design; plausible schedules; and operations, crew issues and maintenance. Since long-term exposure to zero gravity is known to be harmful to the human body, the main goal was to design a unique variable gravity research facility which would find a practical solution to this problem, permitting a manned mission to Mars. The facility would not duplicate other space-based facilities and would provide the flexibility for examining a number of gravity levels, including lunar and Martian gravities. Major design alternatives included a truss versus a tether based system which also involved the question of docking while spinning or despinning to dock. These design issues are described. The relative advantages or disadvantages are discussed, including comments on the necessary research and technology development required for each. Author

N91-27175* National Aeronautics and Space Administration, Lewis Research Center, Cleveland, OH.

FURNACE FOR TENSILE/FATIGUE TESTING Patent

PAMELA K. BRINDLEY, inventor (to NASA) 14 May 1991 11 p. Filed 19 Mar. 1990

(NASA-CASE-LEW-14848-1; US-PATENT-5,015,825; US-PATENT-APPL-SN-382885; US-PATENT-CLASS-219-390; US-PATENT-CLASS-73-826; US-PATENT-CLASS-374-49; US-PATENT-CLASS-374-50; INT-PATENT-CLASS-F27B-5/14; INT-PATENT-CLASS-F27D-11/10; INT-PATENT-CLASS-G01N-3/08) Avail: US Patent and Trademark Office CSCL 14/2

Mechanical properties of short test specimens are tested in tension and fatigue using an improved electrical resistance heating furnace having a short length that mounts between the grips of a typical testing machine. The furnace includes a ceramic inner liner having an oval cross section to reduce heat loss at the ends. The furnace is divided into a plurality of individually controlled heating zones. Provision is made to supply an inert gas to the volume around the specimen in the center of the furnace.

Official Gazette of the U.S. Patent and Trademark Office

N91-30186* # National Aeronautics and Space Administration, Lewis Research Center, Cleveland, OH.

POWER SYSTEMS TESTING

Aug. 1991 17 p. Original contains color illustrations

(Contract RTOP 474-74-10)

(NASA-TM-104513; E-6383; NAS 1.15:104513) Avail: NTIS HC/MF A03; 11 functional color pages CSCL 14/2

The Space Station Freedom (SSF) will give the U.S. a permanent manned presence in space in 1999. The SSF underwent its final design concept in 1991. Launches of hardware will begin in late 1995, and the SSF will become operational in the manned configuration in 1997. Additional Space Shuttle flights between 1997 and 1999 will complete the SSF. Along with international partners, a crew of four astronauts will conduct long-term experimentation in the microgravity environment of the orbiting spacecraft. Lewis Research Center, along with its prime contractor, will provide the electrical power system (EPS) for SSF. Two major testing facilities at the Lewis Research Center will support the Lewis EPS. The Power Systems Facility provides test beds for life testing the station batteries and the power management distribution system testbed. This testbed simulates two channels of the EPS. The Space Power Facility at the Lewis Plum Brook Station is the largest vacuum chamber in the world. Within this chamber, a simulated space environment, testing of full-size EPS components will occur. Author

LAUNCH VEHICLES AND SPACE VEHICLES

Includes boosters; operating problems of launch/space vehicle systems; and reusable vehicles.

A91-45793* # National Aeronautics and Space Administration. Lewis Research Center, Cleveland, OH.

A REVIEW OF CANDIDATE MULTILAYER INSULATION SYSTEMS FOR POTENTIAL USE ON WET-LAUNCHED LH2 TANKAGE FOR THE SPACE EXPLORATION INITIATIVE LUNAR MISSIONS

RICHARD H. KNOLL, ROBERT J. STOCHL, and RAFAEL SANABRIA (NASA, Lewis Research Center, Cleveland, OH) AIAA, SAE, ASME, and ASEE, Joint Propulsion Conference, 27th, Sacramento, CA, June 24-26, 1991. 20 p. refs (AIAA PAPER 91-2176) Copyright

The storage of cryogenic propellants such as liquid hydrogen (LH2) and liquid oxygen (LO2) for the future Space Exploration Initiative (SEI) will require lightweight, high performance thermal protection systems (TPSs). For the near-term lunar missions, the major weight element for most of the TPSs will be multilayer insulation (MLI) and/or the special structures/systems required to accommodate the MLI. Methods of applying MLI to LH2 tankage to avoid condensation or freezing of condensable gases such as nitrogen or oxygen while in the atmosphere are discussed. Because relatively thick layers of MLI will be required for storage times of a month or more, the transient performance from ground-hold to space-hold of the systems will become important in optimizing the TPSs for many of the missions. The ground-hold performance of several candidate systems are given as well as a qualitative assessment of the transient performance effects. Author

A91-45812* # National Aeronautics and Space Administration. Lewis Research Center, Cleveland, OH.

THERMAL PERFORMANCE OF A LIQUID HYDROGEN TANK MULTILAYER INSULATION SYSTEM AT WARM BOUNDARY TEMPERATURES OF 630, 530, AND 152 R

ROBERT J. STOCHL and RICHARD H. KNOLL (NASA, Lewis Research Center, Cleveland, OH) AIAA, SAE, ASME, and ASEE, Joint Propulsion Conference, 27th, Sacramento, CA, June 24-26, 1991. 21 p. Previously announced in STAR as N91-25159. refs (AIAA PAPER 91-2400) Copyright

The results are presented of a study conducted to obtain experimental heat transfer data on a liquid hydrogen tank insulated with 34 layers of MLI (multilayer insulation) for warm side boundary temperatures of 630, 530, and 150 R. The MLI system consisted of two blankets, each blanket made up of alternate layers of double silk net (16 layers) and double aluminized Mylar radiation shields (15 layers) contained between two cover sheets of Dacron scrim reinforced Mylar. The insulation system was designed for and installed on an 87.6 in. diameter liquid hydrogen tank. Nominal layer density of the insulation blankets is 45 layers/in. The insulation system contained penetrations for structural support, plumbing, and electrical wiring that would be representative of a cryogenic spacecraft. The total steady state heat transfer rates into the test tank for shroud temperatures of 630, 530, 152 R were 164.4, 95.8, and 15.9 BTU/hr, respectively. The noninsulation heat leaks into the tank (12 fiberglass support struts, tank plumbing, and instrumentation lines) represent between 13 to 17 pct. of the total heat input. The heat input values would translate to liquid H2 losses of 2.3, 1.3, and 0.2 pct/day, with the tank held at atmospheric pressure. Author

A91-54054* # National Aeronautics and Space Administration. Lewis Research Center, Cleveland, OH.

THE DESIGN AND PERFORMANCE ESTIMATES FOR THE PROPULSION MODULE FOR THE BOOSTER OF A TSTO VEHICLE

CHRISTOPHER A. SNYDER and JAIME J. MALDONADO (NASA,

Lewis Research Center, Cleveland, OH) AIAA, AHS, and ASEE, Aircraft Design Systems and Operations Meeting, Baltimore, MD, Sept. 23-25, 1991. 13 p. refs (AIAA PAPER 91-3136) Copyright

A NASA study of propulsion systems for possible low-risk replacements for the Space Shuttle is presented. Results of preliminary studies to define the USAF two-stage-to-orbit (TSTO) concept to deliver 10,000 pounds to low polar orbit are described. The booster engine module consists of an over/under turbine bypass engines/ramjet engine design for acceleration from takeoff to the staging point of Mach 6.5 and approximately 100,000 feet altitude. Propulsion system performance and weight are presented with preliminary mission study results of vehicle size. R.E.P.

A91-54088* # National Aeronautics and Space Administration. Lewis Research Center, Cleveland, OH.

OVERVIEW OF THE BETA II TWO-STAGE-TO-ORBIT VEHICLE DESIGN

ROBERT M. PLENCNER (NASA, Lewis Research Center, Cleveland, OH) AIAA, AHS, and ASEE, Aircraft Design Systems and Operations Meeting, Baltimore, MD, Sept. 23-25, 1991. 11 p. refs (AIAA PAPER 91-3175) Copyright

A design concept for fully reusable two-stage-to-orbit (TSTO) vehicle is reviewed in terms of adapting the Beta vehicle to revised mission requirements. The Beta II vehicle is discussed in terms of study-mission requirements such as horizontal takeoff and landing, a 10,000-lb payload, and a 120-nm polar orbit. The fully reusable TSTO concept specified in the study is found to be feasible with a moderate gross lift-off weight particularly if air-breathing propulsion is incorporated. C.C.S.

A91-54099* # National Aeronautics and Space Administration. Lewis Research Center, Cleveland, OH.

MACH 6.5 AIR INDUCTION SYSTEM DESIGN FOR THE BETA II TWO-STAGE-TO-ORBIT BOOSTER VEHICLE

ANTHONY C. MIDEA (NASA, Lewis Research Center; Sverdrup Technology, Inc., Cleveland, OH) AIAA, AHS, and ASEE, Aircraft Design Systems and Operations Meeting, Baltimore, MD, Sept. 23-25, 1991. 12 p. refs (Contract NAS3-25266) (AIAA PAPER 91-3196)

A preliminary, two-dimensional, mixed compression air induction system is designed for the Beta II Two-Stage-to-Orbit booster vehicle to minimize installation losses and efficiently deliver the required airflow. Design concepts, such as an external isentropic compression ramp and a bypass system, are developed and evaluated for performance benefits. The design is optimized by maximizing installed propulsion/vehicle system performance, and the resulting system design operating characteristics and performance are presented. The air induction system design has significantly lower transonic drag than similar designs, and only requires approximately 1/3 of the bleed extraction. In addition, the design efficiently provides the integrated system required airflow, while maintaining adequate levels of total pressure recovery. The excellent performance of this highly integrated air induction system is essential for the successful completion of the Beta II booster vehicle mission. Author

N91-25159* # National Aeronautics and Space Administration. Lewis Research Center, Cleveland, OH.

THERMAL PERFORMANCE OF A LIQUID HYDROGEN TANK MULTILAYER INSULATION SYSTEM AT WARM BOUNDARY TEMPERATURES OF 630, 530, AND 152 R

ROBERT J. STOCHL and RICHARD H. KNOLL 1991 21 p Presented at the 27th Joint Propulsion Conference, Sacramento, CA, 24-27 Jun. 1991; sponsored by AIAA, SAE, ASME, and the American Society for Electrical Engineers (Contract RTOP 593-21-00) (NASA-TM-104476; E-6323; NAS 1.15:104476; AIAA PAPER 91-2400) Avail: NTIS HC/MF A03 CSCL 22/2

The results are presented of a study conducted to obtain experimental heat transfer data on a liquid hydrogen tank insulated

15 LAUNCH VEHICLES AND SPACE VEHICLES

with 34 layers of MLI (multilayer insulation) for warm side boundary temperatures of 630, 530, and 150 R. The MLI system consisted of two blankets, each blanket made up of alternate layers of double silk net (16 layers) and double aluminized Mylar radiation shields (15 layers) contained between two cover sheets of Dacron scrim reinforced Mylar. The insulation system was designed for and installed on a 87.6 in diameter liquid hydrogen tank. Nominal layer density of the insulation blankets is 45 layers/in. The insulation system contained penetrations for structural support, plumbing, and electrical wiring that would be representative of a cryogenic spacecraft. The total steady state heat transfer rates into the test tank for shroud temperatures of 630, 530, 152 R were 164.4, 95.8, and 15.9 BTU/hr respectively. The noninsulation heat leaks into the tank (12 fiberglass support struts, tank plumbing, and instrumentation lines) represent between 13 to 17 pct. of the total heat input. The heat input values would translate to liquid H₂ losses of 2.3, 1.3, and 0.2 pct/day, with the tank held at atmospheric pressure.

Author

N91-31196* National Aeronautics and Space Administration. Lewis Research Center, Cleveland, OH.

THE INTERNATIONAL SPACE UNIVERSITY'S VARIABLE GRAVITY RESEARCH FACILITY DESIGN

SHEILA G. BAILEY, FRANCIS P. CHIARAMONTE, and KENNETH J. DAVIDIAN Sep. 1991 36 p
(Contract RTOP 506-41-11)

(NASA-TM-105224; E-6541; NAS 1.15:105224) Avail: NTIS HC/MF A01 CSCL 22/2

A manned mission to Mars will require long travel times between Earth and Mars. However, exposure to long-duration zero gravity is known to be harmful to the human body. Some of the harmful effects are loss of heart and lung capacity, inability to stand upright, muscular weakness and loss of bone calcium. A variable gravity research facility (VGRF) that would be placed in low Earth orbit (LEO) was designed by students of the International Space University 1989 Summer Session held in Strasbourg, France, to provide a testbed for conducting experiments in the life and physical sciences in preparation for a mission to Mars. This design exercise was unique because it addressed all aspects concerning a large space project. The VGRF design was described which was developed by international participants specializing in the following areas: the politics of international cooperation, engineering, architecture, in-space physiology, material and life science experimentation, data communications, business, and management.

Author

16

SPACE TRANSPORTATION

Includes passenger and cargo space transportation, e.g., shuttle operations; and space rescue techniques.

A91-52470* National Aeronautics and Space Administration. Lewis Research Center, Cleveland, OH.

SPACE ENGINE SAFETY SYSTEM

WILLIAM A. MAUL and CLAUDIA M. MEYER (NASA, Lewis Research Center, Cleveland; Sverdrup Technology, Inc., Brook Park, OH) AIAA, NASA, and OAI, Conference on Advanced SEI Technologies, Cleveland, OH, Sept. 4-6, 1991. 10 p. refs (AIAA PAPER 91-3604) Copyright

A rocket engine safety system is designed to initiate control procedures which will minimize damage to the engine and vehicle or test stand in the event of an engine failure. This report describes the features and the implementation issues associated with rocket engine safety systems. Specific concerns of safety systems applied to a space-based engine and long duration space missions are discussed. Examples of safety system features and architectures are given from recent safety monitoring investigations conducted

for the Space Shuttle Main Engine and for future liquid rocket engines. Also, a general design and implementation process for rocket engine safety systems is presented.

Author

N91-21182* National Aeronautics and Space Administration. Lewis Research Center, Cleveland, OH.

FIRE SUPPRESSION IN HUMAN-CREW SPACECRAFT

ROBERT FRIEDMAN and DANIEL L. DIETRICH (Sverdrup Technology, Inc., Brook Park, OH.) May 1991 14 p Presented at the Halon Alternatives Technical Working Conference, Albuquerque, NM, 30 Apr. - 1 May 1991; sponsored in part by New Mexico Univ.; and by The Center for Global Environmental Technologies

(Contract NAS3-25266; RTOP 323-53-62)

(NASA-TM-104334; E-6100; NAS 1.15:104334) Avail: NTIS HC/MF A03 CSCL 06/11

Fire extinguishment agents range from water and foam in early-design spacecraft (Halon 1301 in the present Shuttle) to carbon dioxide proposed for the Space Station Freedom. The major challenge to spacecraft fire extinguishment design and operations is from the micro-gravity environment, which minimizes natural convection and profoundly influences combustion and extinguishing agent effectiveness, dispersal, and post-fire cleanup. Discussed here are extinguishment in microgravity, fire-suppression problems anticipated in future spacecraft, and research needs and opportunities.

Author

17

SPACE COMMUNICATIONS, SPACECRAFT COMMUNICATIONS, COMMAND AND TRACKING

Includes telemetry; space communications networks; astronavigation and guidance; and radio blackout.

A91-11472* National Aeronautics and Space Administration. Lewis Research Center, Cleveland, OH.

A TECHNOLOGY ASSESSMENT OF ALTERNATIVE COMMUNICATIONS SYSTEMS FOR THE SPACE EXPLORATION INITIATIVE

DENISE S. PONCHAK, JOHN E. ZUZAK, WAYNE A. WHYTE, JR., RODNEY L. SPENCE, and PHILIP Y. SOHN (NASA, Lewis Research Center, Cleveland, OH) AIAA, Space Programs and Technologies Conference, Huntsville, AL, Sept. 25-27, 1990. 24 p. Previously announced in STAR as N90-27736. refs (AIAA PAPER 90-3681) Copyright

Telecommunications, Navigation, and Information Management (TNIM) services are vital to accomplish the ambitious goals of the Space Exploration Initiative (SEI). A technology assessment is provided for four alternative lunar and Mars operational TNIM systems based on detailed communications link analyses. The four alternative systems range from a minimum to a fully enhanced capability and use frequencies from S-band, through ka-band, and up to optical wavelengths. Included are technology development schedules as they relate to present SEI mission architecture time frames.

Author

A91-14056* National Aeronautics and Space Administration. Lewis Research Center, Cleveland, OH.

ADVANCED COMMUNICATIONS TECHNOLOGY SATELLITE (ACTS)

RICHARD T. GEDNEY, DAVID L. WRIGHT, JOSEPH R. BALOMBIN, PHILIP Y. SOHN (NASA, Lewis Research Center, Cleveland, OH), WILLIAM F. CASHMAN (General Electric Co., Astro-Space Div., Princeton, NJ) et al. IAF, International Astronautical Congress, 41st, Dresden, Federal Republic of Germany, Oct. 6-12, 1990. 17 p. refs (IAF PAPER 90-481)

The ACTS, to be launched by NASA in 1992, is described with a focus on its multibeam antenna, baseband processor,

17 SPACE COMMUNICATIONS, SPACECRAFT COMMUNICATIONS, COMMAND AND TRACKING

microwave matrix switch, rain fade compensation, and Ka-band components. Four system applications of the satellite technology are discussed, including a baseband processor for Very Small Aperture Terminal (VSAT) services, aeronautical mobile system, high data-rate communications, and a thin-route system for personal communications. Circuit capacity per unit spacecraft weight are compared for ACTS-type operational systems and conventional satellite systems. It is pointed out that for some of the services, the ACTS technologies may have more immediate application internationally rather than in the U.S. V.T.

A91-52344*# National Aeronautics and Space Administration. Lewis Research Center, Cleveland, OH.

OVERVIEW OF KA-BAND COMMUNICATIONS TECHNOLOGY REQUIREMENTS FOR THE SPACE EXPLORATION INITIATIVE
EDWARD F. MILLER (NASA, Lewis Research Center, Cleveland, OH) AIAA, NASA, and OAI, Conference on Advanced SEI Technologies, Cleveland, OH, Sept. 4-6, 1991. 10 p. refs (AIAA PAPER 91-3424) Copyright

Four exploration architectures are reviewed, and Ka-band technology requirements are identified to meet the data traffic needs and schedule. These requirements include high-frequency transmitters at 0.5 to 200 W; antennas with 5 m and 9 m diameter, with multiple beams and/or scanning beams; and spacecraft receivers with a noise figure of 2 dB. O.G.

A91-52377*# National Aeronautics and Space Administration. Lewis Research Center, Cleveland, OH.

A COMPARISON OF OPTICAL TECHNOLOGIES FOR A HIGH DATA RATE MARS LINK
RODNEY L. SPENCE (NASA, Lewis Research Center, Cleveland, OH) AIAA, NASA, and OAI, Conference on Advanced SEI Technologies, Cleveland, OH, Sept. 4-6, 1991. 14 p. refs (AIAA PAPER 91-3469) Copyright

Several optical systems, based on Nd:YAG, GaAs, and CO₂ laser sources and employing both direct and heterodyne detection, are analyzed in order to assess their feasibility in providing high data rate (10-1000 Mbps) Mars-to-earth communications. The rms pointing/tracking accuracy is shown to be a critical parameter in defining the Mars-earth optical link. Data obtained reveal that unless, extremely small rms pointing and tracking errors can be achieved (sigma less than .2 microrad), the most promising optical implementation appears to be the Nd:YAG laser using direct detection and high order PPM modulation. O.G.

A91-52424*# National Aeronautics and Space Administration. Lewis Research Center, Cleveland, OH.

DATA COMPRESSION FOR FULL MOTION VIDEO TRANSMISSION
WAYNE A. WHYTE, JR. (NASA, Lewis Research Center, Cleveland, OH) and KHALID SAYOOD (Nebraska, University, Lincoln) AIAA, NASA, and OAI, Conference on Advanced SEI Technologies, Cleveland, OH, Sept. 4-6, 1991. 11 p. refs (AIAA PAPER 91-3533) Copyright

Clearly transmission of visual information will be a major, if not dominant, factor in determining the requirements for, and assessing the performance of, the SEI communications systems. Projected image/video requirements which are currently anticipated for SEI mission scenarios are presented. Based on this information and projected link performance figures, the image/video data compression requirements which would allow link closure are identified. Finally several approaches which could satisfy some of the compression requirements are presented and possible future approaches which show promise for more substantial compression performance improvement are discussed. Author

A91-52425*# Loral AeroSys, Seabrook, MD.
TECHNOLOGIES FOR UNATTENDED NETWORK OPERATIONS

ALLAN JAWORSKI, JIDE ODUBIYI, MARK HOLDRIDGE (Loral AeroSys, Seabrook, MD), and JOHN ZUZKEK (NASA, Lewis Research Center, Cleveland, OH) AIAA, NASA, and OAI,

Conference on Advanced SEI Technologies, Cleveland, OH, Sept. 4-6, 1991. 9 p. refs (AIAA PAPER 91-3534) Copyright

The necessary network management functions for a telecommunications, navigation and information management (TNIM) system in the framework of an extension of the ISO model for communications network management are described. Various technologies that could substantially reduce the need for TNIM network management, automate manpower intensive functions, and deal with synchronization and control at interplanetary distances are presented. Specific technologies addressed include the use of the ISO Common Management Interface Protocol, distributed artificial intelligence for network synchronization and fault management, and fault-tolerant systems engineering. R.E.P.

A91-52427*# Hughes Aircraft Co., El Segundo, CA.
DEVELOPMENT OF TECHNOLOGY NEEDS FOR THE SEI TNIM NETWORK

M. R. WACHS (Hughes Aircraft Co., El Segundo, CA) and J. E. ZUZKEK (NASA, Lewis Research Center, Cleveland, OH) AIAA, NASA, and OAI, Conference on Advanced SEI Technologies, Cleveland, OH, Sept. 4-6, 1991. 10 p. (AIAA PAPER 91-3536) Copyright

A comparison of the salient features of the SEI with previous space exploration programs shows the need for a telecommunications, navigation and information management (TNIM) system level reoptimization. An approach is developed that takes the various candidate mission plans and decomposes them into architectural building blocks, many of which are common to several of the plans. Once identified, each of these blocks can then be parametrically examined with respect to performance benefit, cost, technology, and schedule risk tradeoffs. As the Space Exploration Initiative plan is established, these TNIM building blocks may be fused into an optimized system architecture. R.E.P.

A91-52458*# National Aeronautics and Space Administration. Lewis Research Center, Cleveland, OH.

MILLIMETER WAVELENGTH COMMUNICATIONS APPLICATIONS FOR THE SEI
DENISE S. PONCHAK, JOHN E. ZUZKEK, RODNEY L. SPENCE, and WAYNE A. WHYTE, JR. (NASA, Lewis Research Center, Cleveland, OH) AIAA, NASA, and OAI, Conference on Advanced SEI Technologies, Cleveland, OH, Sept. 4-6, 1991. 25 p. refs (AIAA PAPER 91-3589) Copyright

The potentially complex missions of the Space Exploration Initiative (SEI) require advanced lunar and Mars Telecommunications, Navigation, and Information Management (TNIM) systems to provide data, voice, and image transmissions. The objectives of the study are to determine which SEI telecommunications applications will benefit from millimeter wave technology, assess the state-of-the-art in millimeter wave technology and describe the technology development shortfalls with respect to potential mission time frames. The assumptions for the analysis as well as other issues, not related to performance, are also presented. Author

A91-53188*# National Aeronautics and Space Administration. Lewis Research Center, Cleveland, OH.

ATDRS PAYLOAD TECHNOLOGY R & D
G. ANZIC, D. J. CONNOLLY, G. FUJIKAWA, M. ANDRO, R. R. KUNATH, and G. R. SHARP (NASA, Lewis Research Center, Cleveland, OH) IN: GLOBECOM '90 - IEEE Global Telecommunications Conference and Exhibition, San Diego, CA, Dec. 2-5, 1990, Conference Record. Vol. 2. New York, Institute of Electrical and Electronics Engineers, Inc., 1990, p. 1149-1155. Previously announced in STAR as N90-28596. Copyright

Four technology development tasks were chosen to reduce (or at least better understand) the technology risks associated with proposed approaches to Advanced Tracking and Data Relay Satellite (ATDRS). The four tasks relate to a Tri-Band Antenna feed system, a Digital Beamforming System for the S Band

17 SPACE COMMUNICATIONS, SPACECRAFT COMMUNICATIONS, COMMAND AND TRACKING

Multiple-Access System (SMA), an SMA Phased Array Antenna, and a Configuration Thermal/Mechanical Analysis task. The objective, approach, and status of each are discussed. I.E.

N91-21184*# National Aeronautics and Space Administration. Lewis Research Center, Cleveland, OH.

GAS MONOLITHIC RF MODULES FOR SRSAT DISTRESS BEACONS

MICHAEL A. CAULEY Apr. 1991 8 p Presented at the International Symposium on Optical Engineering and Photonics in Aerospace Sensing, Orlando, FL, 1-5 Apr. 1991; sponsored in part by the Society of Photo-Optical Instrumentation Engineers (Contract RTOP 342-02-00)

(NASA-TM-104338; E-6107; NAS 1.15:104338) Avail: NTIS HC/MF A02 CSCL 17/2

Monolithic GaAs UHF components for use in SRSAT Emergency Distress beacons are under development by Microwave Monolithics, Inc., Simi Valley, CA. The components include a bi-phase modulator, driver amplifier, and a 5 watt power amplifier.

Author

18

SPACECRAFT DESIGN, TESTING AND PERFORMANCE

Includes satellites; space platforms; space stations; spacecraft systems and components such as thermal and environmental controls; and attitude controls.

A91-23077* Maxwell Labs., Inc., San Diego, CA. HIGH VOLTAGE INTERACTIONS OF A SOUNDING ROCKET WITH THE AMBIENT AND SYSTEM-GENERATED ENVIRONMENTS

ROBERT A. KUHARSKI, GARY A. JONGEWARD, KATHERINE G. WILCOX, THOMAS V. RANKIN (Maxwell Laboratories, Inc., San Diego, CA), and JAMES C. ROCHE (NASA, Lewis Research Center, Cleveland, OH) (IEEE, DNA, JPL, et al., Annual Conference on Nuclear and Space Radiation Effects, 27th, Reno, NV, July 16-20, 1990) IEEE Transactions on Nuclear Science (ISSN 0018-9499), vol. 37, pt. 1, Dec. 1990, p. 2128-2133. refs Copyright

EPSAT (environment power system analysis tool) is used to examine the design of SPEAR III, which is scheduled to fly in early 1991. It will test high-voltage designs in both ambient and system-generated environments. Two of the key questions that the experiment hopes to address are whether or not the earth's magnetic field can cause the current that a high-voltage object draws from the plasma to be far less than the current that would be drawn in the absence of the magnetic field and under what neutral environmental conditions a discharge from the high-voltage object to the plasma will occur. The EPSAT program makes it possible to perform a variety of analyses on a preliminary or conceptual-level description of a system in a short period of time. The calculations presented on SPEAR III are all done for a conceptual-level description. The calculations indicate that the experiment will produce the conditions necessary to address these questions. I.E.

A91-29799*# General Dynamics Corp., San Diego, CA. THE COLD-SAT EXPERIMENT FOR CRYOGENIC FLUID MANAGEMENT TECHNOLOGY

J. R. SCHUSTER (General Dynamics Corp., Space Systems Div., San Diego, CA), J. P. WACHTER (Ford Aerospace Corp., Space Systems Div., Palo Alto, CA), and D. M. VENTO (NASA, Lewis Research Center, Cleveland, OH) JANNAF Propulsion Meeting, Anaheim, CA, Oct. 2-4, 1990, Paper. 16 p. (Contract NAS3-25062)

The COLD-SAT spacecraft design experiments are described. COLD-SAT will be placed into an initial 1300 km circular orbit by

an Atlas commercial launch vehicle. Electric power, experiment control and data management, attitude control, and propulsive accelerations for the experiments will be provided by the three-axis-controlled spacecraft bus. To provide data on the effects that low gravity levels might have on the heat and mass transfer processes involved, low levels of acceleration will be created. The COLD-SAT experiment will be configured into a module. The spacecraft experiment module will include three liquid hydrogen tanks; fluid transfer, pressurization and venting equipment; and instrumentation. Since the largest tank has helium-purged MLI to prevent ingress and freezing of air on the launchpad, it will contain all the liquid hydrogen at the point of launching. The hydrogen tanking system used for the Centaur upper stage of the Atlas will load and top off this tank. Atlas, with its liquid hydrogen upper stage, large payload fairing, and large launch margin, simplifies COLD-SAT design and integration. O.G.

A91-30019*# National Aeronautics and Space Administration. Lewis Research Center, Cleveland, OH.

SOLAR ARRAY ORIENTATIONS FOR A SPACE STATION IN LOW EARTH ORBIT

GEOFFREY A. LANDIS and CHENG-YI LU (NASA, Lewis Research Center, Cleveland, OH) Journal of Propulsion and Power (ISSN 0748-4658), vol. 7, Jan.-Feb. 1991, p. 123-125. refs Copyright

A large portion of the drag of a space station in LEO is generated by its solar array; for a baseline 25-kW solar array in 334-km orbit, 1800 kg of reboost propellant/year is needed to counteract solar array drag. A study is conducted of the drag reduction potential of three possible solar array orientations: sun-pointing, sun-pointing during illumination/edge-on during eclipse, and edge-on during entire orbit. An 18.5-percent drag-makeup propellant reduction is found to be obtainable with the sun-pointing/edge-on eclipse orientation technique. O.C.

A91-42522*# National Aeronautics and Space Administration. Lewis Research Center, Cleveland, OH.

A CHARGING STUDY OF THE ACTS SATELLITE USING NASCAP

JOEL L. HERR (NASA, Lewis Research Center, Cleveland; Sverdrup Technology, Inc., Brook Park, OH) AIAA, Fluid Dynamics, Plasma Dynamics and Lasers Conference, 22nd, Honolulu, HI, June 24-26, 1991. 12 p. refs (Contract NAS3-25266)

(AIAA PAPER 91-1471) Copyright

The results of a charging study conducted with the NASA Charging Analyzer Program (NASCAP) using a model of the Advanced Communications Technology Satellite (ACTS) are presented. The electrostatic discharge mechanisms are described including the field and potential threshold values that were monitored during the NASCAP simulation. Particular attention is given to the charging behavior of the ACTS inclined antennas. The data obtained indicate that the possibility of a discharge occurring in the immediate vicinity of the antennas is minimal when the semiconducting paint layer on the antenna's front surface has sufficient surface conductivity. It is shown that the metallized multilayer insulating blanket ACTS design provides good electrostatic discharge control. O.G.

A91-45550*# National Aeronautics and Space Administration. Lewis Research Center, Cleveland, OH.

PRELIMINARY THERMAL DESIGN OF THE COLD-SAT SPACECRAFT

HUGH ARIF (NASA, Lewis Research Center, Cleveland, OH) AIAA, Thermophysics Conference, 26th, Honolulu, HI, June 24-26, 1991. 38 p. Previously announced in STAR as N91-25161. (AIAA PAPER 91-1305) Copyright

The COLD-SAT free-flying spacecraft was to perform experiments with LH2 in the cryogenic fluid management technologies of storage, supply and transfer in reduced gravity. The Phase A preliminary design of the Thermal Control Subsystem (TCS) for the spacecraft exterior and interior surfaces and components of the bus subsystems is described. The TCS was

composed of passive elements which were augmented with heaters. Trade studies to minimize the parasitic heat leakage into the cryogen storage tanks are described. Selection procedure for the thermally optimum on-orbit spacecraft attitude was defined. TRASYS-2 and SINDA'85 verification analysis was performed on the design and the results are presented. Author

A91-45808* National Aeronautics and Space Administration. Lewis Research Center, Cleveland, OH.

MASS COMPARISONS OF ELECTRIC PROPULSION SYSTEMS FOR NSSK OF GEOSYNCHRONOUS SPACECRAFT

V. K. RAWLIN (NASA, Lewis Research Center, Cleveland, OH) and G. A. MAJCHER (Cleveland State University, OH) AIAA, SAE, ASME, and ASEE, Joint Propulsion Conference, 27th, Sacramento, CA, June 24-26, 1991. 46 p. refs (AIAA PAPER 91-2347) Copyright

A model was developed and exercised to allow wet mass comparisons of three-axis stabilized communications satellites delivered to geosynchronous transfer orbit. The mass benefits of using advanced chemical propulsion for apogee injection and north-south stationkeeping (NSSK) functions or electric propulsion (hydrazine arcjets and xenon ion thrusters) for NSSK functions are documented. A large derated ion thruster is proposed which minimizes thruster lifetime concerns and qualification test times when compared to those of smaller ion thrusters planned for NSSK applications. The mass benefits, which depend on the spacecraft mass and mission duration, increase dramatically with arcjet specific impulse in the 500-600 s range, but are nearly constant for the derated ion thruster operated in the 2300-3000 s range. For a given mission, the mass benefits with an ion system are typically double those of the arcjet system; however, the total thrusting time with arcjets is less than one-third that with ion thrusters for the same thruster power. Author

A91-49810* National Aeronautics and Space Administration. Lewis Research Center, Cleveland, OH.

THE EFFECT OF THE NEAR EARTH MICROMETEOROID ENVIRONMENT ON A MIRROR SURFACE AFTER 20 YEARS IN SPACE

MICHAEL J. MIRTICH (NASA, Lewis Research Center, Cleveland, OH) and WILLIAM R. KERSLAKE (Sverdrup Technology, Inc., Brook Park, OH) IN: Materials degradation in low earth orbit (LEO); Proceedings of the Symposium, 119th Annual Meeting of the Minerals, Metals, and Materials Society, Anaheim, CA, Feb. 17-22, 1990. Warrendale, PA, Minerals, Metals, and Materials Society, 1990, p. 107-122. refs Copyright

The effect of micrometeoroid impact on the optical properties of polished metals and thin film coatings has been simulated by accelerating micron-sized particles to hypervelocities in a shock tube. The degradation of these properties after exposure to simulated meteoroids was determined as a function of impacting kinetic energy/area of the particles. A calibrated sensor, 2000-A Al/stainless steel, was developed to detect the micrometeoroid environment and to evaluate the degradation of the optical properties of thin aluminum films in space. No changes in the optical properties of the highly reflective surface sensor on SERT II, launched in 1970, were measured during 19 years in space. These results are found to be in agreement with the 1969 Micrometeoroid Flux Model. It is concluded that a highly reflective surface should lose less than 1 percent of its specular reflectance in near-earth orbit during 19 years. O.G.

A91-53403* National Aeronautics and Space Administration. Lewis Research Center, Cleveland, OH.

DEVELOPMENT OF A VIBRATION ISOLATION PROTOTYPE SYSTEM FOR MICROGRAVITY SPACE EXPERIMENTS

K. A. LOGSDON, C. M. GRODSINSKY, and G. V. BROWN (NASA, Lewis Research Center, Cleveland, OH) (Microgravity research: Material and fluid sciences; Proceedings of Symposium 11 of the COSPAR 28th Plenary Meeting, The Hague, Netherlands, June 25-July 6, 1990. A91-53401 23-29) Advances in Space Research

(ISSN 0273-1177), vol. 11, no. 7, 1991, p. 9-16. Previously announced in STAR as N91-19324. refs

Copyright

The presence of small levels of low-frequency accelerations on the Space Shuttle orbiters has degraded the microgravity environment for the science community. Growing concern about this microgravity environment has generated interest in systems that can isolate microgravity science experiments from vibrations. This interest has resulted primarily in studies of isolation systems with active methods of compensation. The development of a magnetically suspended, six-degree-of-freedom active vibration isolation prototype system capable of providing the needed compensation to the orbital environment is presented. A design for the magnetic actuators is described, and the control law for the prototype system that gives a nonintrusive inertial isolation response to the system is also described. Relative and inertial sensors are used to provide an inertial reference for isolating the payload. Author

N91-19156* National Aeronautics and Space Administration. Lewis Research Center, Cleveland, OH.

AEOLIAN REMOVAL OF DUST TYPES FROM PHOTOVOLTAIC SURFACES ON MARS

JAMES R. GAIER and MARLA E. PEREZ-DAVIS In NASA, Goddard Space Flight Center, 16th Space Simulation Conference Confirming Spaceworthiness Into the Next Millennium p 379-396 Nov. 1990

Avail: NTIS HC/MF A20 CSCL 22/2

Dust elevated in local or global dust storms on the Martian surface could settle on photovoltaic (PV) surfaces and seriously hamper their performance. Using a recently developed technique to apply a uniform dust layer, PV surface materials were subjected to simulated Martian winds in an attempt to determine whether natural aeolian processes on Mars would sweep off the settled dust. Three different types of dust were used. The effects of wind velocity, angle of attack, height above the Martian surface, and surface coating material were investigated. It was found that arrays mounted on an angle of attack approaching 45 deg show the most efficient clearing. Although the angular dependence is not sharp, horizontally mounted arrays required much higher wind velocities to clear off the dust. From this test it appears that the arrays may be erected quite near the ground, but previous studies have suggested that saltation effects can be expected to cause such arrays to be covered by soil if they are set up less than about a meter from the ground. Particle size effect appear to dominate over surface chemistry in these experiments, but additional tests are required to confirm this. Author

N91-19160* National Aeronautics and Space Administration. Lewis Research Center, Cleveland, OH.

SIMULATION OF MARTIAN DUST ACCUMULATION ON SURFACES

MARLA E. PEREZ-DAVIS, JAMES R. GAIER, ROBERT KRESS, and JUSTUS GRIMALDA (Massachusetts Inst. of Tech., Boston.) In NASA, Goddard Space Flight Center, 16th Space Simulation Conference Confirming Spaceworthiness Into the Next Millennium p 447-456 Nov. 1990

Avail: NTIS HC/MF A20 CSCL 22/2

Future NASA space missions include the possibility of manned landings and exploration of Mars. Environmental and operational constraints unique to Mars must be considered when selecting and designing the power system to be used on the Mars surface. A technique is described which was developed to simulate the deposition of dust on surfaces. Three kinds of dust materials were studied: aluminum oxide, basalt, and iron oxide. The apparatus was designed using the Stokes and Stokes-Cunningham law for particle fallout, with additional consideration given to particle size and shape. Characterization of the resulting dust films on silicon dioxide, polytetrafluoroethylene, indium tin oxide, diamondlike carbon, and other surfaces are discussed based on optical transmittance measurements. The results of these experiments will guide future studies which will consider processes to remove

18 SPACECRAFT DESIGN, TESTING AND PERFORMANCE

the dust from surfaces under Martian environmental conditions.

Author

N91-19165*# National Aeronautics and Space Administration. Lewis Research Center, Cleveland, OH.

THE EFFECT OF THE LOW EARTH ORBIT ENVIRONMENT ON SPACE SOLAR CELLS

DAVID J. BRINKER, JOHN R. HICKEY (Eppley Lab., Inc., Newport, RI.), and DONALD K. BRASTED Nov. 1990 8 p Presented at the 5th International Photovoltaic Science and Engineering Conference, Kyoto, Japan, 26-30 Nov. 1990; sponsored in part by Japan Society of Applied Physics, Inst. of Electrical Engineers of Japan and Foundation for Adv. of Intern. Science, Kyoto, Japan (Contract RTOP 506-41-11)

(NASA-TM-103735; E-5973; NAS 1.15:103735) Avail: NTIS HC/MF A02 CSCL 22/2

The results of a space flight experiment designed to provide reference cell standards for photovoltaic measurements as well as to investigate the solar spectrum and the effect of long-term exposure of solar cells to the space environment are presented. This experiment, the Advanced Photovoltaic Experiment (APEX), was launched into low Earth orbit as part of the Long Duration Exposure Facility in 1984 and retrieved 69 months later. APEX contained over 150 solar cells of a wide variety of materials, designs and coverglasses. Data on cell performance was recorded for the first year-on-orbit.

Author

N91-20184*# National Aeronautics and Space Administration. Lewis Research Center, Cleveland, OH.

DESIGNS FOR THE ATRSS TRI-BAND REFLECTOR ANTENNA

SHUNG-WU LEE, MARTIN L. ZIMMERMAN (Illinois Univ., Urbana.), GENE FUJIKAWA, and G. RICHARD SHARP 1991 7 p Proposed for presentation at the 1991 IEEE AP-S International Symposium and URSI Radio Science Meeting, London, Ontario, 24-28 Jun. 1991

(Contract RTOP 316-60-13)

(NASA-TM-103754; E-6008; NAS 1.15:103754) Avail: NTIS HC/MF A02 CSCL 20/14

Two approaches to design a tri-band reflector antenna for the Advanced TDRSS are examined. Two reflector antenna configurations utilizing frequency selective surfaces for operation in three frequency bands, S, Ku, and Ka, are proposed. Far-field patterns and the antenna feed losses were computed for each configuration. An offset-fed single reflector antenna configuration was adapted for conceptual spacecraft design. CADAM drawings were completed and a 1/13th scale model of the spacecraft was constructed.

Author

N91-20727*# National Aeronautics and Space Administration. Lewis Research Center, Cleveland, OH.

THE ENVIRONMENT WORKBENCH: A DESIGN TOOL FOR SPACE STATION FREEDOM

GARY A. JONGEWARD, ROBERT A. KUHARSKI, THOMAS V. RANKIN, KATHERINE G. WILCOX (Systems Science and Software, La Jolla, CA.), and JAMES C. ROCHE In NASA, Lyndon B. Johnson Space Center, Fourth Annual Workshop on Space Operations Applications and Research (SOAR 90) p 684-687 Jan. 1991

(Contract NAS3-25347)

Avail: NTIS HC/MF A14 CSCL 22/2

The environment workbench (EWB) is being developed for NASA by S-CUBED to provide a standard tool that can be used by the Space Station Freedom (SSF) design and user community for requirements verification. The desktop tool will predict and analyze the interactions of SSF with its natural and self-generated environments. A brief review of the EWB design and capabilities is presented. Calculations using a prototype EWB of the on-orbit floating potentials and contaminant environment of SSF are also presented. Both the positive and negative grounding configurations for the solar arrays are examined to demonstrate the capability of the EWB to provide quick estimates of environments, interactions, and system effects.

Author

N91-20728*# National Aeronautics and Space Administration. Lewis Research Center, Cleveland, OH.

FINDINGS OF THE JOINT WORKSHOP ON EVALUATION OF IMPACTS OF SPACE STATION FREEDOM GROUND CONFIGURATIONS

DALE C. FERGUSON, DAVID B. SNYDER, and RALPH CARRUTH (National Aeronautics and Space Administration. Marshall Space Flight Center, Huntsville, AL.) In NASA, Lyndon B. Johnson Space Center, Fourth Annual Workshop on Space Operations Applications and Research (SOAR 90) p 689-694 Jan. 1991

Avail: NTIS HC/MF A14 CSCL 22/2

At the workshop, experts from the plasma interactions community evaluated the impacts of environmental interactions on the Space Station Freedom (SSF) under each of the proposed grounding schemes. The grounding scheme chosen for the SSF power system was found to have serious implications for SSF design. Interactions of the SSF power system and structure with the low Earth orbit (LEO) plasma differ significantly between different proposed grounding schemes. Environmental constraints will require modification of current SSF designs under any grounding scheme. Maintaining the present negative-grounding scheme compromises SSF safety, structural integrity, and electromagnetic compatibility. It also will increase contamination rates over alternative grounding schemes. One alternative, positive grounding of the array, requires redesign of the primary power system in work package four. Floating the array reduces the number of circuit changes to work package four but adds new hardware. Maintaining the current design will affect all work packages; however, no impacts were identified on work packages one, two, or three by positively grounding or floating the array, with the possible exception of extra corona protection in multi-wire connectors.

Author

N91-21185*# National Aeronautics and Space Administration. Lewis Research Center, Cleveland, OH.

A NEW FABRICATION METHOD FOR PRECISION ANTENNA REFLECTORS FOR SPACE FLIGHT AND GROUND TEST

G. RICHARD SHARP, JOYCE S. WANHAINE, and DEAN A. KETELSEN Washington Mar. 1991 19 p Presented at the 13th International Communications Satellite Systems Conference, Los Angeles, CA, 11-15 Mar. 1990; sponsored by AIAA Previously announced in IAA as A90-25627 Original contains color illustrations

(Contract RTOP 650-60-20)

(NASA-TP-3078; E-5176; NAS 1.60:3078) Avail: NTIS HC/MF A03; 2 functional color pages CSCL 22/2

Communications satellites are using increasingly higher frequencies that require increasingly precise antenna reflectors for use in space. Traditional industry fabrication methods for space antenna reflectors employ successive modeling techniques using high- and low-temperature molds for reflector face sheets and then a final fit-up of the completed honeycomb sandwich panel antenna reflector to a master pattern. However, as new missions are planned at much higher frequencies, greater accuracies will be necessary than are achievable using these present methods. A new approach for the fabrication of ground-test solid-surface antenna reflectors is to build a rigid support structure with an easy-to-machine surface. This surface is subsequently machined to the desired reflector contour and coated with a radio-frequency-reflective surface. This method was used to fabricate a 2.7-m-diameter ground-test antenna reflector to an accuracy of better than 0.013 mm (0.0005 in.) rms. A similar reflector for use on spacecraft would be constructed in a similar manner but with space-qualified materials. The design, analysis, and fabrication of the 2.7-m-diameter precision antenna reflector for antenna ground tests and the extension of this technology to precision, space-based antenna reflectors are described.

Author

N91-21194*# National Aeronautics and Space Administration. Lewis Research Center, Cleveland, OH.

MAGNETIC BEARINGS WITH ZERO BIAS

GERALD V. BROWN and CARLOS M. GRODSINSKY In NASA, Langley Research Center, Aerospace Applications of Magnetic

Suspension Technology, Part 1 p 165-182 Mar. 1991
 Avail: NTIS HC/MF A17 CSCL 22/2

A magnetic bearing operating without a bias field has supported a shaft rotating at speeds up to 12,000 rpm with the usual four power supplies and with only two. A magnetic bearing is commonly operated with a bias current equal to half of the maximum current allowable in its coils. This linearizes the relation between net force and control current and improves the force slewing rate and hence the band width. The steady bias current dissipates power, even when no force is required from the bearing. The power wasted is equal to two-thirds of the power at maximum force output. Examined here is the zero bias idea. The advantages and disadvantages are noted. Author

N91-21206* National Aeronautics and Space Administration. Lewis Research Center, Cleveland, OH.

MICROGRAVITY VIBRATION ISOLATION: AN OPTIMAL CONTROL LAW FOR THE ONE-DIMENSIONAL CASE

RICHARD D. HAMPTON, CARLOS M. GRODSINSKY, PAUL E. ALLAIRE, DAVID W. LEWIS, and CARL R. KNOSPE (Virginia Univ., Charlottesville.) In NASA, Langley Research Center, Aerospace Applications of Magnetic Suspension Technology, Part 2 p 413-476 Mar. 1991

Avail: NTIS HC/MF A17 CSCL 22/2

Certain experiments contemplated for space platforms must be isolated from the accelerations of the platform. An optimal active control is developed for microgravity vibration isolation, using constant state feedback gains (identical to those obtained from the Linear Quadratic Regulator (LQR) approach) along with constant feedforward gains. The quadratic cost function for this control algorithm effectively weights external accelerations of the platform disturbances by a factor proportional to $(1/\omega)^2 \exp 4$. Low frequency accelerations are attenuated by greater than two orders of magnitude. The control relies on the absolute position and velocity feedback of the experiment and the absolute position and velocity feedforward of the platform, and generally derives the stability robustness characteristics guaranteed by the LQR approach to optimality. The method as derived is extendable to the case in which only the relative positions and velocities and the absolute accelerations of the experiment and space platform are available. Author

N91-24225* National Aeronautics and Space Administration. Lewis Research Center, Cleveland, OH.

ENVIRONMENTAL INTERACTIONS OF THE SPACE STATION FREEDOM ELECTRIC POWER SYSTEM

HENRY K. NAHRA and CHENG-YI LU (Rockwell International Corp., Canoga Park, CA.) 1991 8 p Presented at the European Space Power Conference, Florence, Italy, 2-6 Sep. 1991; sponsored by ESA, the Politecnico di Milano, the Italian Space Agency, and the European Power Electronics

(Contract RTOP 474-12-10)

(NASA-TM-104373; E-6177; NAS 1.15:104373) Avail: NTIS HC/MF A02 CSCL 10/2

The Space Station Freedom operates in a low earth orbit (LEO) environment. Such operation results in different potential interactions with the Space Station systems including the Electric Power System (EPS). These potential interactions result in environmental effects which include neutral species effects such as atomic oxygen erosion, effects of micrometeoroid and orbital debris impacts, plasma effects, ionizing radiation, and induced contamination degradation effects. The EPS design and its interactions with the LEO environment are briefly described and the results of analyses and testing programs planned and performed thus far to resolve environmental concerns related to the EPS and its function in LEO environment. Author

N91-25161* National Aeronautics and Space Administration. Lewis Research Center, Cleveland, OH.

PRELIMINARY THERMAL DESIGN OF THE COLD-SAT SPACECRAFT

HUGH ARIF 1991 39 p Presented at the 26th Thermophysics Conference, Honolulu, HI, 24-26 Jun. 1991; sponsored by AIAA

(Contract RTOP 506-48-00)

(NASA-TM-104440; E-6247; NAS 1.15:104440; AIAA PAPER 91-1305) Copyright Avail: NTIS HC/MF A03 CSCL 22/2

The COLD-SAT free-flying spacecraft was to perform experiments with LH2 in the cryogenic fluid management technologies of storage, supply and transfer in reduced gravity. The Phase A preliminary design of the Thermal Control Subsystem (TCS) for the spacecraft exterior and interior surfaces and components of the bus subsystems is described. The TCS was composed of passive elements which were augmented with heaters. Trade studies to minimize the parasitic heat leakage into the cryogen storage tanks are described. Selection procedure for the thermally optimum on-orbit spacecraft attitude was defined. TRASYS-2 and SINDA'85 verification analysis was performed on the design and the results are presented. Author

19

SPACECRAFT INSTRUMENTATION

A91-45816* Aerojet-General Corp., Sacramento, CA.

SPACE SHUTTLE MAIN ENGINE NOZZLE MOUNTED OPTIC FOR THROAT PLANE SPECTROSCOPY

R. L. BICKFORD (Aerojet, Propulsion Div., Sacramento, CA), D. B. DUNCAN (Duncan Technologies, Auburn, CA), and G. MADZSAR (NASA, Lewis Research Center, Cleveland, OH) AIAA, SAE, ASME, and ASEE, Joint Propulsion Conference, 27th, Sacramento, CA, June 24-26, 1991. 11 p. refs (AIAA PAPER 91-2524) Copyright

A program intended to develop a flight-capable nozzle mounted optic for monitoring emissions from metals entrained in the Space Shuttle Main Engine (SSME) flowfield is described. The optic will collect light emitted from metal atoms within the high-temperature, high-pressure SSME chamber and transfer the optical signal to a high-resolution spectrometer via a fiber-optic cable. The nozzle mounted optic makes it possible to conduct earth-to-orbit monitoring of flowfield emissions without requiring modifications to the SSME. O.G.

A91-52467* National Aeronautics and Space Administration. Lewis Research Center, Cleveland, OH.

TECHNOLOGY READINESS ASSESSMENT OF ADVANCED SPACE ENGINE INTEGRATED CONTROLS AND HEALTH MONITORING

MARC G. MILLIS (NASA, Lewis Research Center, Cleveland, OH) AIAA, NASA, and OAI, Conference on Advanced SEI Technologies, Cleveland, OH, Sept. 4-6, 1991. 16 p. refs (AIAA PAPER 91-3601) Copyright

An evaluation is given for an integrated control and health-monitoring (ICHM) system that is designed to be used with hydrogen-oxygen rocket engines. The minimum required ICHM functions, system elements, technology readiness, and system cost are assessed for a system which permits the operation of H-O engines that are space-based, reusable, and descent-throttleable. Only the advanced sensors and some engine-dependent software are not found to be ready for applications to laboratory demonstration. Other systems related to the minimum functions are more developed, bringing the total system readiness to the conceptual design stage. Based on the evaluation of the H-O ICHM, it is estimated that the minimum system requirements for demonstration on an engine system testbed will require an investment of 30-45 million dollars over 6 years. C.C.S.

A91-52468* National Aeronautics and Space Administration. Lewis Research Center, Cleveland, OH.

FIBER-OPTIC APPLICATIONS FOR SPACE-BASED ROCKET ENGINES

AMY L. SOVIE, DOUGLAS P. BEWLEY, and MARC G. MILLIS

19 SPACECRAFT INSTRUMENTATION

(NASA, Lewis Research Center, Cleveland, OH) AIAA, NASA, and OAI, Conference on Advanced SEI Technologies, Cleveland, OH, Sept. 4-6, 1991. 8 p. refs
(AIAA PAPER 91-3602) Copyright

The use of fiber-optic technology is discussed with respect to the instrumentation systems for space-based rocket engines. Optical fiber technologies are reviewed with specific attention given to the reliability, light weight, small fiber diameter, and operating life of the components in the space environment. An optical system can facilitate the incorporation of an optical health-monitoring system, increase the space available for necessary redundancy, and safe high-bandwidth communications that are immune to the effects of electromagnetic radiation. C.C.S.

N91-12417*# National Aeronautics and Space Administration. Lewis Research Center, Cleveland, OH.

PRESENTATION ON A SPACE ACCELERATION MEASUREMENT SYSTEM (SAMS)

THEODORE L. CHASE In NASA, Marshall Space Flight Center, Measurement and Characterization of the Acceleration Environment on Board the Space Station 20 p Aug. 1990
Avail: NTIS HC/MF A99 CSCL 14/2

The primary objective of the Space Acceleration Measurement Systems (SAMS) project is to provide an acceleration measurement system capable of serving a wide variety of space experiments. The design of the system being developed under this project takes into consideration requirements for experiments located in the middeck, in the orbiter bay, and in Spacelab. In addition to measuring, conditioning, and recording accelerations, the system will be capable of performing complex calculations and interactive control. The main components consist of a remote triaxial optical storage device. In operation, the triaxial sensor head produces output signals in response to acceleration inputs. These signals are preamplified, filtered and converted into digital data which is then transferred to optical memory. The system design is modular, facilitating both software and hardware upgrading as technology advances. Two complete acceleration measurement flight systems will be build and tested under this project. Author

20

SPACECRAFT PROPULSION AND POWER

Includes main propulsion systems and components, e.g., rocket engines; and spacecraft auxiliary power sources.

A91-10107*# Pratt and Whitney Aircraft Group, West Palm Beach, FL.

THE ADVANCED EXPANDER TEST BED

ARTHUR I. MASTERS (Pratt and Whitney Group, West Palm Beach, FL) and WILLIAM K. TABATA (NASA, Lewis Research Center, Cleveland, OH) AIAA, Space Programs and Technologies Conference, Huntsville, AL, Sept. 25-27, 1990. 9 p.
(AIAA PAPER 90-3708) Copyright

The principal goals and design concepts of the Advanced Expander Test Bed (AETB) program are briefly reviewed. The AETB is planned as the focal point for the development and demonstration of high-performance oxygen/hydrogen engine technology and advanced component technology for the next space engine. The engine will operate at pressures up to 1200 psia over a wide range of conditions, easily accommodating mission-focused components. The discussion covers design requirements, design approach, conceptual design, the AETB cycle, and the AETB control system. V.L.

A91-10174*# National Aeronautics and Space Administration. Lewis Research Center, Cleveland, OH.

EVOLUTIONARY USE OF NUCLEAR ELECTRIC PROPULSION

K. J. HACK, J. A. GEORGE, J. P. RIEHL (NASA, Lewis Research Center, Cleveland, OH), and J. H. GILLAND (Sverdrup Technology,

Inc., Cleveland, OH) AIAA, Space Programs and Technologies Conference, Huntsville, AL, Sept. 25-27, 1990. 21 p. refs
(AIAA PAPER 90-3821)

Evolving new propulsion technologies through a rational and conscious effort to minimize development costs and program risks while maximizing the performance benefits is intuitively practical. A phased approach to the evolution of nuclear electric propulsion from use on planetary probes, to lunar cargo vehicles, and finally to manned Mars missions with a concomitant growth in technology is considered. Technology levels and system component makeup are discussed for nuclear power systems and both ion and magnetoplasmadynamic thrusters. Mission scenarios are described, which include analysis of a probe to Pluto, a lunar cargo mission, Martian split, all-up, and quick-trip mission options. Evolutionary progression of the use of NEP in such missions is discussed. Author

A91-10338*# National Aeronautics and Space Administration. Lewis Research Center, Cleveland, OH.

TURBINE BLADING DESIGNED FOR HIGH HEAT LOAD SPACE PROPULSION APPLICATIONS

K. C. CIVINSKAS, R. J. BOYLE (NASA, Lewis Research Center, Cleveland, OH), and H. V. MCCONNAUGHEY (NASA, Marshall Space Flight Center, Huntsville, AL) Journal of Propulsion and Power (ISSN 0748-4658), vol. 6, Sept.-Oct. 1990, p. 598-611. Previously cited in issue 04, p. 491, Accession no. A89-16486. refs
Copyright

A91-13447*# National Aeronautics and Space Administration. Lewis Research Center, Cleveland, OH.

HIGH TEMPERATURE SUPERCONDUCTIVITY TECHNOLOGY FOR ADVANCED SPACE POWER SYSTEMS

KARL A. FAYMON, IRA T. MYERS, and DENIS J. CONNOLLY (NASA, Lewis Research Center, Cleveland, OH) Space Power - Resources, Manufacturing and Development (ISSN 0883-6272), vol. 9, no. 2-3, 1990, p. 185-194. refs
Copyright

In 1987, the Lewis Research center of the NASA and the Argonne National Laboratory of the Department of Energy joined in a cooperative program to identify and assess high payoff space and aeronautical applications of high temperature superconductivity (HTSC). The initial emphasis of this effort was limited, and those space power related applications which were considered included microwave power transmission and magnetic energy storage. The results of these initial studies were encouraging and indicated the need of further studies. A continuing collaborative program with Argonne National Laboratory has been formulated and the Lewis Research Center is presently structuring a program to further evaluate HTSC, identify applications and define the requisite technology development programs for space power systems. This paper discusses some preliminary results of the previous evaluations in the area of space power applications of HTSC which were carried out under the joint NASA-DOE program, the future NASA-Lewis proposed program, its thrusts, and its intended outputs and give general insights on the anticipated impact of HTSC for space power applications of the future. Author

A91-13766*# National Aeronautics and Space Administration. Lewis Research Center, Cleveland, OH.

SATELLITE ECLIPSE POWER BY LASER ILLUMINATION

GEOFFREY A. LANDIS (NASA, Lewis Research Center; Sverdrup Technology, Inc., Cleveland, OH) IAF, International Astronautical Congress, 41st, Dresden, Federal Republic of Germany, Oct. 6-12, 1990. 6 p. refs
(IAF PAPER 90-053) Copyright

A method is proposed to eliminate the energy storage system required to power a satellite in geosynchronous orbit during eclipse. An array of high-power CW lasers is situated at one or more ground locations in line of sight of the satellite, preferably on mountaintops. The lasers are provided with a tracking system, and lenses or mirrors of sufficient size to reduce the beam spread

due to diffraction. As the satellite enters eclipse, the laser arrays illuminate the solar arrays on the satellite to a level sufficient to provide operating power. Author

A91-13868* National Aeronautics and Space Administration. Lewis Research Center, Cleveland, OH.

NUCLEAR POWER SYSTEMS FOR LUNAR AND MARS EXPLORATION

R. J. SOVIE and J. M. BOZEK (NASA, Lewis Research Center, Cleveland, OH) IAF, International Astronautical Congress, 41st, Dresden, Federal Republic of Germany, Oct. 6-12, 1990. 11 p. Previously announced in STAR as N90-26873. (IAF PAPER 90-200) Copyright

Initial studies of a variety of mission scenarios for the new Space Exploration Initiative, and the technologies necessary to enable or significantly enhance them, have identified the development of advanced space power systems whether solar, chemical or nuclear to be of prime importance. Lightweight, compact, reliable power systems for planetary rovers and a variety of surface vehicles, utility surface power, and power for advanced propulsion systems have been identified as critical needs for these missions. These mission scenarios, the concomitant power system requirements, and the power system options considered are discussed. The significant potential benefits of nuclear power are identified for meeting the power needs of the above applications. Author

A91-13908* National Aeronautics and Space Administration. Lewis Research Center, Cleveland, OH.

REACTIONLESS ORBITAL PROPULSION USING TETHER DEPLOYMENT

GEOFFREY A. LANDIS (NASA, Lewis Research Center; Sverdrup Technology, Inc., Cleveland, OH) IAF, International Astronautical Congress, 41st, Dresden, Federal Republic of Germany, Oct. 6-12, 1990. 10 p. refs (IAF PAPER 90-254) Copyright

Examples of tether propulsion in orbit without the use of reaction mass are discussed. These include (1) using tether extension to reposition a satellite in orbit without fuel expenditure by extending a mass on the end of the tether; (2) using a tether for eccentricity pumping to add energy to the orbit for boosting and orbital transfer; and (3) length modulation of a spinning tether to transfer angular momentum between the orbit and tether spin, thus allowing changes in orbital angular momentum. Author

A91-19218* National Aeronautics and Space Administration. Lewis Research Center, Cleveland, OH.

DROPSIZE CORRELATION FOR CRYOGENIC LIQUID-JET ATOMIZATION

ROBERT D. INGEBO (NASA, Lewis Research Center, Cleveland, OH) AIAA, Aerospace Sciences Meeting, 29th, Reno, NV, Jan. 7-10, 1991. 6 p. Previously announced in STAR as N91-12064. refs (AIAA PAPER 91-0284) Copyright

Momentum transfer from high velocity nitrogen gas flow to liquid-nitrogen jets was investigated. A correlation of aerodynamic and liquid-surface forces with characteristic drop diameter was obtained for cryogenic liquid-jet breakup in Mach 1 gas flow. Nitrogen gas mass-flux was varied by using three differently sized two-fluid fuel atomizers with different nozzle diameters. Author

A91-21498* National Aeronautics and Space Administration. Lewis Research Center, Cleveland, OH.

SPECTRALLY RESOLVED RAYLEIGH SCATTERING DIAGNOSTIC FOR HYDROGEN-OXYGEN ROCKET PLUME STUDIES

R. G. SEASHOLTZ, F. J. ZUPANC, and S. J. SCHNEIDER (NASA, Lewis Research Center, Cleveland, OH) AIAA, Aerospace Sciences Meeting, 29th, Reno, NV, Jan. 7-10, 1991. 10 p. refs (AIAA PAPER 91-0462) Copyright

A Rayleigh scattering diagnostic has been developed to measure gas density, temperature, and velocity in the exhaust plume of 100 N thrust class hydrogen-oxygen rockets. The

spectrum of argon-ion laser light scattered by the gas molecules in the plume (predominantly water vapor) is measured with a scanning Fabry-Perot interferometer. The gas density is determined from the total scattered power, the gas temperature from the spectral width, and the velocity from the shift in the peak of the spectrum from the frequency of the incident laser light. The diagnostic has been demonstrated in a rocket test cell and a discussion of results is given. Author

A91-26063* National Aeronautics and Space Administration. Lewis Research Center, Cleveland, OH.

AN EVOLUTIONARY PATH TO SATELLITE SOLAR POWER SYSTEMS

GEOFFREY A. LANDIS (NASA, Lewis Research Center; Sverdrup Technology, Inc., Cleveland, OH) Space Power - Resources, Manufacturing and Development (ISSN 0883-6272), vol. 9, no. 4, 1990, p. 365-371. refs Copyright

A difficulty with proposals for satellite solar power systems is the absence of a plausible evolutionary pathway to development of systems on the scale required. One possible pathway is discussed, where the required technologies are developed and refined on an incremental scale. The initial stages of the process are development of ground-based photovoltaic power and of beamed power systems for space use. Author

A91-30010* National Aeronautics and Space Administration. Lewis Research Center, Cleveland, OH.

EXPERIMENTAL EVALUATION OF RESISTOJET THRUSTER PLUME SHIELDS

LYNNETTE M. CARNEY (NASA, Lewis Research Center, Cleveland, OH) and ALLAN B. BAILEY (Calspan Corp., Arnold AFB, TN) (International Electric Propulsion Conference, 20th, Garmisch-Partenkirchen, Federal Republic of Germany, Oct. 3-6, 1988, Proceedings, p. 513-526) Journal of Propulsion and Power (ISSN 0748-4658), vol. 7, Jan.-Feb. 1991, p. 49-55. Previously cited in issue 21, p. 3295, Accession no. A89-47487. refs (Contract NASA ORDER C-30004-J) Copyright

A91-30013* National Aeronautics and Space Administration. Lewis Research Center, Cleveland, OH.

PERFORMANCE AND LIFETIME ASSESSMENT OF MAGNETOPLASMA DYNAMIC ARC THRUSTER TECHNOLOGY

JAMES S. SOVEY and MARIS A. MANTENIEKS (NASA, Lewis Research Center, Cleveland, OH) Journal of Propulsion and Power (ISSN 0748-4658), vol. 7, Jan.-Feb. 1991, p. 71-83. Previously cited in issue 04, p. 491, Accession no. A89-16485. refs Copyright

A91-31025* National Aeronautics and Space Administration. Lewis Research Center, Cleveland, OH.

ADVANCED LAUNCH SYSTEM (ALS) - ELECTRICAL ACTUATION AND POWER SYSTEMS IMPROVE OPERABILITY AND COST PICTURE

GALE R. SUNDBERG (NASA, Lewis Research Center, Cleveland, OH) IN: NAECON 90; Proceedings of the IEEE National Aerospace and Electronics Conference, Dayton, OH, May 21-25, 1990. Vol. 3. New York, Institute of Electrical and Electronics Engineers, Inc., 1990, p. 1346-1350. Previously announced in STAR as N90-21271.

To obtain the Advanced Launch System (ALS) primary goals of reduced costs and improved operability, there must be significant reductions in the launch operations and servicing requirements relative to current vehicle designs and practices. One of the primary methods for achieving these goals is by using vehicle electrical power system and controls for all aviation and avionics requirements. A brief status review of the ALS and its associated Advanced Development Program is presented to demonstrate maturation of those technologies that will help meet the overall operability and cost goals. The electric power and actuation systems are highlighted as a specific technology ready not only

20 SPACECRAFT PROPULSION AND POWER

to meet the stringent ALS goals (cryogenic field valves and thrust vector controls with peak power demands to 75 hp), but also those of other launch vehicles, military and civilian aircraft, lunar/Martian vehicles, and a multitude of commercial applications. I.E.

A91-31026* National Aeronautics and Space Administration. Lewis Research Center, Cleveland, OH.

ELECTROMECHANICAL ACTUATION FOR THRUST VECTOR CONTROL APPLICATIONS

MARY ELLEN ROTH (NASA, Lewis Research Center, Cleveland, OH) IN: NAECON 90; Proceedings of the IEEE National Aerospace and Electronics Conference, Dayton, OH, May 21-25, 1990. Vol. 3. New York, Institute of Electrical and Electronics Engineers, Inc., 1990, p. 1351-1353.

(Contract NAS3-25799)

The advanced launch system (ALS), is a launch vehicle that is designed to be cost-effective, highly reliable, and operationally efficient with a goal of reducing the cost per pound to orbit. An electromechanical actuation (EMA) system is being developed as an attractive alternative to the hydraulic systems. The controller will integrate 20 kHz resonant link power management and distribution (PMAD) technology and pulse population modulation (PPM) techniques to implement field-oriented vector control (FOVC) of a new advanced induction motor. The driver and the FOVC will be microprocessor controlled. For increased system reliability, a built-in test (BITE) capability will be included. This involves introducing testability into the design of a system such that testing is calibrated and exercised during the design, manufacturing, maintenance, and prelaunch activities. An actuator will be integrated with the motor controller for performance testing of the EMA thrust vector control (TVC) system. The EMA system and work proposed for the future are discussed. I.E.

A91-36832* National Aeronautics and Space Administration. Lewis Research Center, Cleveland, OH.

POWER ELECTRONIC APPLICATIONS FOR SPACE STATION FREEDOM

ROY L. PICKRELL (NASA, Lewis Research Center, Cleveland, OH) and IGOR LAZBIN (Analex Corp., Fairview Park, OH) IN: PESC '90 - Annual IEEE Power Electronics Specialists Conference, 21st, San Antonio, TX, June 11-14, 1990, Record. Vol. 2. New York, Institute of Electrical and Electronics Engineers, Inc., 1990, p. 628-635.

Copyright

NASA plans to orbit a permanently manned space station in the late 1990s, which requires development and assembly of a photovoltaic (PV) power source system to supply up to 75 kW of electrical power average during the orbital period. The electrical power requirements are to be met by a combination of PV source, storage, and control elements for the sun and eclipse periods. The authors discuss the application of power electronics and controls to manage the generation, storage, and distribution of power to meet the station loads, as well as the computer models used for analysis and simulation of the PV power system. The requirements for power source integrated controls to adjust storage charge power during the insolation period current limiting, breaker interrupt current values, and the electrical fault protection approach are defined. Based on these requirements, operating concepts have been defined which then become drivers for specific system and element design. I.E.

A91-37424* National Aeronautics and Space Administration. Lewis Research Center, Cleveland, OH.

COMMENT ON 'NEGATIVE MATTER PROPULSION'

GEOFFREY A. LANDIS (NASA, Lewis Research Center; Sverdrup Technology, Inc., Cleveland, OH) Journal of Propulsion and Power (ISSN 0748-4658), vol. 7, Mar.-Apr. 1991, p. 304. refs
Copyright

A91-37929 National Aeronautics and Space Administration, Washington, DC.

NASA'S FUTURE SPACE POWER NEEDS AND REQUIREMENTS

A. D. SCHNYER (NASA, Washington, DC) and RONALD J. SOVIE (NASA, Lewis Research Center, Cleveland, OH) IN: IECEC-90; Proceedings of the 25th Intersociety Energy Conversion Engineering Conference, Reno, NV, Aug. 12-17, 1990. Vol. 1. New York, American Institute of Chemical Engineers, 1990, p. 13-17. Copyright

The National Space Policy of 1988 established the U.S.'s long-range civil space goals, and has served to guide NASA's recent planning for future space mission operations. One of the major goals was to extend the human presence beyond earth's boundaries and to advance the scientific knowledge of the solar system. A broad spectrum of potential civil space mission opportunities and interests are currently being investigated by NASA to meet the espoused goals. Participation in many of these missions requires power systems with capabilities far beyond what exists today. In other mission examples, advanced power systems technology could enhance mission performance significantly. Power system requirements and issues that need resolution to ensure eventual mission accomplishment are addressed, in conjunction with the ongoing NASA technology development efforts and the need for even greater innovative efforts to match the ambitious solar exploration mission goals. Particular attention is given to potential lunar surface operations and technology goals, based on investigations to date. It is suggested that the nuclear reactor power systems can best meet long-life requirements as well as dramatically reduce the earth-surface-to-lunar-surface transportation costs due to the lunar day/night cycle impact on the solar system's energy storage mass requirements. The state of the art of candidate power systems and elements for the lunar application and the respective exploration technology goals for mission life requirements from 10 to 25 years are examined. I.E.

A91-37930 National Aeronautics and Space Administration. Lyndon B. Johnson Space Center, Houston, TX.

POWER SYSTEM REQUIREMENTS AND DEFINITION FOR LUNAR AND MARS OUTPOSTS

D. A. PETRI (NASA, Johnson Space Center, Houston, TX), R. L. CATALDO, and J. M. BOZEK (NASA, Lewis Research Center, Cleveland, OH) IN: IECEC-90; Proceedings of the 25th Intersociety Energy Conversion Engineering Conference, Reno, NV, Aug. 12-17, 1990. Vol. 1. New York, American Institute of Chemical Engineers, 1990, p. 18-27.

Copyright

Candidate power systems being considered for outpost facilities (stationary power systems) and vehicles (mobile systems) are discussed, including solar, chemical, isotopic, and reactor. The current power strategy was an initial outpost power system composed of photovoltaic arrays for daytime energy needs and regenerative fuel cells for power during the long lunar night. As day and night power demands grow, the outpost transitions to nuclear-based power generation, using thermoelectric conversion initially and evolving to a dynamic conversion system. With this concept as a guideline, a set of requirements has been established, and a reference definition of candidate power systems meeting these requirements has been identified. I.E.

A91-37931* National Aeronautics and Space Administration. Lewis Research Center, Cleveland, OH.

MICROWAVE BEAM POWERED MARS AIRPLANE

KARL A. FAYMON (NASA, Lewis Research Center, Cleveland, OH) IN: IECEC-90; Proceedings of the 25th Intersociety Energy Conversion Engineering Conference, Reno, NV, Aug. 12-17, 1990. Vol. 1. New York, American Institute of Chemical Engineers, 1990, p. 28-33. refs

Copyright

The feasibility of an unmanned Mars airplane that receives its primary power from an RF (microwave) beam located on the Martian surface has been analyzed. An onboard rechargeable electrochemical storage system is to be used for special

maneuvers, and possible range extension when the airplane is out of the line-of-sight of the microwave source antenna is included as a back-up to the microwave system. The weight of the onboard microwave beam receiving system, relative to other power systems, and the ability to recharge the onboard energy storage system in flight result in a payload capability independent of range and significant mission flexibility. Such an airplane, its onboard power system, its methods of utilization, and the transmitting station requirements to support various Martian exploration operations are presented. The status of microwave beam technology is given, in addition to the technology advances required for the microwave-beam-powered Mars airplane. The concept is thought to be feasible, but advances in microwave technology are required. It is concluded that the payload capability gives the Mars airplane significant operational flexibility and utilization. I.E.

A91-37932* New Mexico Univ., Albuquerque.

A COMPARISON OF ENERGY CONVERSION SYSTEMS FOR MEETING THE POWER REQUIREMENTS OF MANNED ROVER FOR MARS MISSIONS

MOHAMED S. EL-GENK, NICHOLAS MORLEY (New Mexico, University, Albuquerque), ROBERT CATALDO, and HARVEY BLOOMFIELD (NASA, Lewis Research Center, Cleveland, OH) IN: IECEC-90; Proceedings of the 25th Intersociety Energy Conversion Engineering Conference, Reno, NV, Aug. 12-17, 1990. Vol. 1. New York, American Institute of Chemical Engineers, 1990, p. 34-39. refs
(Contract NAG3-992)
Copyright

Several types of conversion systems of interest for a nuclear Mars manned application are examined, including: free-piston Stirling engines (FPSE), He/Xe closed Brayton cycle (CBC), CO₂ open Brayton, and SiGe/GaP thermoelectric systems. Optimization studies were conducted to determine the impact of the conversion system on the overall mass of the nuclear power system and the mobility power requirement of the rover vehicle. The results of an analysis of a manned Mars rover equipped with a nuclear reactor power system show that the free-piston Stirling engine and the He/Xe closed Brayton cycle are the best available options for minimizing the overall mass and electric power requirements of the rover vehicle. While the current development of Brayton technology is further advanced than that of FPSE, the FPSE could provide approximately 13.5 percent lower mass than the He/Xe closed Brayton system. Results show that a specific mass of 160 is achievable with FPSE, for which the mass of the radiation shield (2.8 tons) is about half that for He/Xe CBC (5 tons). I.E.

A91-37933* National Aeronautics and Space Administration. Lewis Research Center, Cleveland, OH.

PROGRAMMATIC STATUS OF NASA'S CSTI HIGH CAPACITY POWER STIRLING SPACE POWER CONVERTER PROGRAM

JAMES E. DUDENHOEFER (NASA, Lewis Research Center, Cleveland, OH) IN: IECEC-90; Proceedings of the 25th Intersociety Energy Conversion Engineering Conference, Reno, NV, Aug. 12-17, 1990. Vol. 1. New York, American Institute of Chemical Engineers, 1990, p. 40-46. Previously announced in STAR as N90-22606. refs
Copyright

An overview is presented of the NASA Lewis Research Center Free-Piston Stirling Space Power Converter Technology Department Program. This work is being conducted under NASA's Civil Space Technology Initiative (CSTI). The goal of the CSTI High Capacity Power element is to develop the technology base needed to meet the long duration, high capacity power requirements for future NASA space initiatives. Efforts are focused upon increasing system thermal and electric energy conversion efficiency at least fivefold over current SP-100 technology, and on achieving systems that are compatible with space nuclear reactors. The status of test activities with the Space Power Research Engine (SPRE) is discussed. Design deficiencies are gradually being corrected and the power converter is now outputting 11.5 kWe at a temperature ratio of 2 (design output is 12.5 kWe). Detail designs were completed for the 1050 K Component Test Power Converter

(CTPC). The success of these and future designs is dependent upon supporting research and technology efforts including heat pipes, gas bearings, superalloy joining technologies and high efficiency alternators. An update of progress in these technologies is provided. Author

A91-37939* National Aeronautics and Space Administration. Lewis Research Center, Cleveland, OH.

NUCLEAR TECHNOLOGY AND THE SPACE EXPLORATION MISSIONS

HENRY W. BRANDHORST and RONALD J. SOVIE (NASA, Lewis Research Center, Cleveland, OH) IN: IECEC-90; Proceedings of the 25th Intersociety Energy Conversion Engineering Conference, Reno, NV, Aug. 12-17, 1990. Vol. 1. New York, American Institute of Chemical Engineers, 1990, p. 84-89. Previously announced in STAR as N90-22847.

Copyright

The strategy for a major exploration initiative leading to permanent human presence beyond earth orbit is still being developed; however enough is known to begin defining the role of nuclear technologies. Three broad areas are discussed: low power (less than 10 kWe) rover/vehicle power systems; integrated, evolutionary base power systems (25 to 100 kW) and nuclear energy for electric propulsion (2 to 100 MWe); and direct thermal propulsion (1000s MW). A phased, evolutionary approach is described for both the moon and Mars, and the benefits of nuclear technologies relative to solar and their integration are described. Author

A91-37940* National Aeronautics and Space Administration. Lewis Research Center, Cleveland, OH.

NUCLEAR POWER TECHNOLOGY REQUIREMENTS FOR NASA EXPLORATION MISSIONS

HARVEY S. BLOOMFIELD (NASA, Lewis Research Center, Cleveland, OH) IN: IECEC-90; Proceedings of the 25th Intersociety Energy Conversion Engineering Conference, Reno, NV, Aug. 12-17, 1990. Vol. 1. New York, American Institute of Chemical Engineers, 1990, p. 90-93.

Copyright

It is pointed out that future exploration of the moon and Mars will mandate developments in many areas of technology. In particular, major advances will be required in planet surface power systems. Critical nuclear technology challenges that can enable strategic self-sufficiency, acceptable operational costs, and cost-effective space transportation goals for NASA exploration missions have been identified. Critical technologies for surface power systems include stationary and mobile nuclear reactor and radioisotope heat sources coupled to static and dynamic power conversion devices. These technologies can provide dramatic reductions in mass, leading to operational and transportation cost savings. Critical technologies for space transportation systems include nuclear thermal rocket and nuclear electric propulsion options, which present compelling concepts for significantly reducing mass, cost, or travel time required for Earth-Mars transport. I.E.

A91-37970* National Aeronautics and Space Administration. Lewis Research Center, Cleveland, OH.

AUTOMATED ELECTRIC POWER MANAGEMENT AND CONTROL FOR SPACE STATION FREEDOM

JAMES L. DOLCE, PAMELA A. MELLOR, and JAMES A. KISH (NASA, Lewis Research Center, Cleveland, OH) IN: IECEC-90; Proceedings of the 25th Intersociety Energy Conversion Engineering Conference, Reno, NV, Aug. 12-17, 1990. Vol. 1. New York, American Institute of Chemical Engineers, 1990, p. 269-274. Previously announced in STAR as N90-23125. refs

Copyright

A comprehensive automation design is being developed for Space Station Freedom's electric power system. It strives to increase station productivity by applying expert systems and conventional algorithms to automate power system operation. An integrated approach to the power system command and control problem is defined and used to direct technology development in:

20 SPACECRAFT PROPULSION AND POWER

diagnosis, security monitoring and analysis, battery management, and cooperative problem-solving for resource allocation. The prototype automated power system is developed using simulations and test-beds.

Author

A91-37972* National Aeronautics and Space Administration. Lewis Research Center, Cleveland, OH.

AUTONOMOUS POWER EXPERT SYSTEM

MARK J. RINGER and TODD M. QUINN (NASA, Lewis Research Center; Sverdrup Technology, Inc., Cleveland, OH) IN: IECEC-90; Proceedings of the 25th Intersociety Energy Conversion Engineering Conference, Reno, NV, Aug. 12-17, 1990. Vol. 1. New York, American Institute of Chemical Engineers, 1990, p. 278-283. Previously announced in STAR as N90-25187. refs

(Contract NAS3-25266)

Copyright

The goal of the Autonomous Power System (APS) program is to develop and apply intelligent problem solving and control technologies to the Space Station Freedom Electrical Power Systems (SSF/EPS). The objectives of the program are to establish artificial intelligence/expert system technology paths, to create knowledge based tools with advanced human-operator interfaces, and to integrate and interface knowledge-based and conventional control schemes. This program is being developed at the NASA-Lewis. The APS Brassboard represents a subset of a 20 KHz Space Station Power Management And Distribution (PMAD) testbed. A distributed control scheme is used to manage multiple levels of computers and switchgear. The brassboard is comprised of a set of intelligent switchgear used to effectively switch power from the sources to the loads. The Autonomous Power Expert System (APEX) portion of the APS program integrates a knowledge based fault diagnostic system, a power resource scheduler, and an interface to the APS Brassboard. The system includes knowledge bases for system diagnostics, fault detection and isolation, and recommended actions. The scheduler autonomously assigns start times to the attached loads based on temporal and power constraints. The scheduler is able to work in a near real time environment for both scheduling and dynamic replanning.

Author

A91-38003* National Aeronautics and Space Administration. Lewis Research Center, Cleveland, OH.

AN ANALYSIS OF SPACE POWER SYSTEM MASSES

BARBARA H. KENNY (NASA, Lewis Research Center; Sverdrup Technology, Inc., Cleveland, OH), RONALD C. CULL, and M. D. KANKAM (NASA, Lewis Research Center, Cleveland, OH) IN: IECEC-90; Proceedings of the 25th Intersociety Energy Conversion Engineering Conference, Reno, NV, Aug. 12-17, 1990. Vol. 1. New York, American Institute of Chemical Engineers, 1990, p. 484-489. Previously announced in STAR as N90-25184. refs

(Contract NAS3-25266)

Copyright

Various space electrical power system masses are analyzed with particular emphasis on the power management and distribution (PMAD) portion. The electrical power system (EPS) is divided into functional blocks: source, interconnection, storage, transmission, distribution, system control and load. The PMAD subsystem is defined as all the blocks between the source, storage and load, plus the power conditioning equipment required for the source, storage and load. The EPS mass of a wide range of spacecraft is then classified as source, storage or PMAD and tabulated in a database. The intent of the database is to serve as a reference source for PMAD masses of existing and in-design spacecraft. The PMAD masses in the database range from 40 kg/kW to 183 kg/kW across the spacecraft systems studied. Factors influencing the power system mass are identified. These include the total spacecraft power requirements, total amount of load capacity and physical size of the spacecraft. It is found that a new utility class of power systems, represented by Space Station Freedom, is evolving.

Author

A91-38019* Sverdrup Technology, Inc., Brook Park, OH. **RAPID THERMAL CYCLING OF NEW TECHNOLOGY SOLAR ARRAY BLANKET COUPONS**

DAVID A. SCHEIMAN (Sverdrup Technology, Inc., Brook Park, OH), BRYAN K. SMITH (NASA, Lewis Research Center, Cleveland, OH), RICHARD M. KURLAND, and HANS G. MESCH (TRW Space and Technology Group, Redondo Beach, CA) IN: IECEC-90; Proceedings of the 25th Intersociety Energy Conversion Engineering Conference, Reno, NV, Aug. 12-17, 1990. Vol. 1. New York, American Institute of Chemical Engineers, 1990, p. 575-580. refs

(Contract NAS3-25226)

Copyright

NASA Lewis Research Center is conducting thermal cycle testing of a new solar array blanket technologies. These technologies include test coupons for Space Station Freedom (SSF) and the advanced photovoltaic solar array (APSA). The objective of this testing is to demonstrate the durability or operational lifetime of the solar array interconnect design and blanket technology within a low earth orbit (LEO) or geosynchronous earth orbit (GEO) thermal cycling environment. Both the SSF and the APSA array survived all rapid thermal cycling with little or no degradation in peak performance. This testing includes an equivalent of 15 years in LEO for SSF test coupons and 30 years of GEO plus ten years of LEO for the APSA test coupon. It is concluded that both the parallel gap welding of the SSF interconnects and the soldering of the APSA interconnects are adequately designed to handle the thermal stresses of space environment temperature extremes.

I.E.

A91-38020* National Aeronautics and Space Administration. Lewis Research Center, Cleveland, OH.

MONOLITHIC AND MECHANICAL MULTIJUNCTION SPACE SOLAR CELLS

RAJ K. JAIN and DENNIS J. FLOOD (NASA, Lewis Research Center, Cleveland, OH) IN: IECEC-90; Proceedings of the 25th Intersociety Energy Conversion Engineering Conference, Reno, NV, Aug. 12-17, 1990. Vol. 1. New York, American Institute of Chemical Engineers, 1990, p. 581-586. refs

Copyright

Monolithic and mechanically stacked tandem solar cells have been fabricated with encouraging AM0 efficiencies summarized as: monolithic GaAs/Ge: 19.1 percent (28 C, 4 sq cm); monolithic InP/Ga0.47In0.53As: 22.2 percent (25 C, 0.296 sq cm); monolithic AlGaAs/GaAs/InGaAs: 27.6 percent (80 C, 0.2 sq cm, 100 X); mechanically stacked GaAs/GaSb: 30.8 percent (25 C, 0.049 sq cm, 100 X); and mechanically stacked GaAs/CuInSe2: 23.1 percent (25 C, 4 sq cm). Significant improvement in tandem cell efficiencies nearing to theoretical predictions has been projected with the improvement in cell material quality and processing. Thin-film cells offer improved specific power. It is pointed out that both the monolithic and mechanically stacked cells have their own problems as to size, processing, current-voltage matching, weight, etc. More information is needed on the effect of temperature and radiation on the cell performance. Proper reference cells and full spectrum range simulators are required to measure efficiencies correctly.

I.E.

A91-38023* National Aeronautics and Space Administration. Lewis Research Center, Cleveland, OH.

COMPONENT AND PROTOTYPE PANEL TESTING OF THE MINI-DOME FRESNEL LENS PHOTOVOLTAIC CONCENTRATOR ARRAY

MICHAEL F. PISZCZOR, CLIFFORD K. SWARTZ (NASA, Lewis Research Center, Cleveland, OH), and MARK J. O'NEILL (ENTECH, Inc., Dallas, TX) IN: IECEC-90; Proceedings of the 25th Intersociety Energy Conversion Engineering Conference, Reno, NV, Aug. 12-17, 1990. Vol. 1. New York, American Institute of Chemical Engineers, 1990, p. 598-603. refs

Copyright

The mini-dome Fresnel lens concentrator array, a high-efficiency, lightweight space photovoltaic array concept, is described. The three critical elements of the array concept are

the Fresnel lens concentrator, the prismatic cell power cover, and the photovoltaic cell. Prototype concentrator lenses have been fabricated and tested, with optical efficiencies reaching 90 percent. Work is progressing on the design and fabrication of the panel structure. The impact of recent advances in 30 percent-efficient multijunction photovoltaic cells on array performance is also discussed. Near-term performance goals of 300 w/sq m and 100 w/kg are now feasible. I.E.

A91-38040* Virginia Polytechnic Inst. and State Univ., Blacksburg.

MODELING OF SPACE STATION ELECTRIC POWER SYSTEM WITH EMTP

KWA-SUR TAM, LIFENG YANG (Virginia Polytechnic Institute and State University, Blacksburg), and NARAYAN V. DRAVID (NASA, Lewis Research Center, Cleveland, OH) IN: IECEC-90; Proceedings of the 25th Intersociety Energy Conversion Engineering Conference, Reno, NV, Aug. 12-17, 1990. Vol. 2. New York, American Institute of Chemical Engineers, 1990, p. 104-109. refs

(Contract NAG3-1120)

Copyright

The authors provide an introduction to using the electromagnetic transients (EMTP) program to model aerospace power system components. A brief general overview of EMTP is presented. The modeling of the dc/dc converter unit in the space station electric power system is described as an illustration. I.E.

A91-38041* Analytical Engineering Corp., North Olmsted, OH. **AN EXPERT SYSTEM FOR SIMULATING ELECTRIC LOADS ABOARD SPACE STATION FREEDOM**

GEORGE KUKICH (Analytical Engineering Corp., North Olmsted, OH) and JAMES L. DOLCE (NASA, Lewis Research Center, Cleveland, OH) IN: IECEC-90; Proceedings of the 25th Intersociety Energy Conversion Engineering Conference, Reno, NV, Aug. 12-17, 1990. Vol. 2. New York, American Institute of Chemical Engineers, 1990, p. 110-114. Previously announced in STAR as N90-22325. refs

Copyright

Space Station Freedom will provide an infrastructure for space experimentation. This environment will feature regulated access to any resources required by an experiment. Automated systems are being developed to manage the electric power so that researchers can have the flexibility to modify their experiment plan for contingencies or for new opportunities. To define these flexible power management characteristics for Space Station Freedom, a simulation is required that captures the dynamic nature of space experimentation; namely, an investigator is allowed to restructure his experiment and to modify its execution. This changes the energy demands for the investigator's range of options. An expert system competent in the domain of cryogenic fluid management experimentation, was developed. It will be used to help design and test automated power scheduling software for Freedom's electric power system. The expert system allows experiment planning and experiment simulation. The former evaluates experimental alternatives and offers advice on the details of the experiment's design. The latter provides a real-time simulation of the experiment replete with appropriate resource consumption. Author

A91-38076* National Aeronautics and Space Administration, Lewis Research Center, Cleveland, OH.

EFFECT OF KOH CONCENTRATION ON LEO CYCLE LIFE OF IPV NICKEL-HYDROGEN FLIGHT BATTERY CELLS

JOHN J. SMITHRICK (NASA, Lewis Research Center, Cleveland, OH) and STEPHEN W. HALL (U.S. Navy, Naval Weapons Support Center, Crane, IN) IN: IECEC-90; Proceedings of the 25th Intersociety Energy Conversion Engineering Conference, Reno, NV, Aug. 12-17, 1990. Vol. 3. New York, American Institute of Chemical Engineers, 1990, p. 16-21. Previously announced in STAR as N90-21116. refs

Copyright

A breakthrough in the low-earth-orbit (LEO) cycle life of

individual pressure vessel (IPV) nickel hydrogen battery cells is reported. The cycle life of boiler plate cells containing 26 percent potassium hydroxide (KOH) electrolyte was about 40,000 LEO cycles compared to 3500 cycles for cells containing 31 percent KOH. The effect of KOH concentration on cycle life was studied. The cycle regime was a stressful accelerated LEO, which consisted of a 27.5 min charge followed by a 17.5 min charge (2 x normal rate). The depth of discharge (DOD) was 80 percent. The cell temperature was maintained at 23 C. The next step is to validate these results using flight hardware and real time LEO test. NASA Lewis has a contract with the Naval Weapons Support Center (NWSC), Crane, Indiana to validate the boiler plate test results. Six 48 A-hr Hughes recirculation design IPV nickel-hydrogen flight battery cells are being evaluated. Three of the cells contain 26 percent KOH (test cells) and three contain 31 percent KOH (control cells). They are undergoing real time LEO cycle life testing. The cycle regime is a 90-min LEO orbit consisting of a 54-min charge followed by a 36-min discharge. The depth-of-discharge is 80 percent. The cell temperature is maintained at 10 C. The cells were cycled for over 8000 cycles in the continuing test. There were no failures for the cells containing 26 percent KOH. There were two failures, however, for the cells containing 31 percent KOH. Author

A91-38077* National Aeronautics and Space Administration, Lewis Research Center, Cleveland, OH.

EFFECT OF LEO CYCLING ON 125 AH ADVANCED DESIGN IPV NICKEL-HYDROGEN BATTERY CELLS

JOHN J. SMITHRICK (NASA, Lewis Research Center, Cleveland, OH) and STEPHEN W. HALL (U.S. Navy, Naval Weapons Support Center, Crane, IN) IN: IECEC-90; Proceedings of the 25th Intersociety Energy Conversion Engineering Conference, Reno, NV, Aug. 12-17, 1990. Vol. 3. New York, American Institute of Chemical Engineers, 1990, p. 22-27. Previously announced in STAR as N90-21808. refs

Copyright

An advanced 125 Ah individual pressure vessel (IPV) nickel-hydrogen cell was designed. The primary function of the advanced cell is to store and deliver energy for long-term, low earth-orbit (LEO) spacecraft missions. The new features of this design are: (1) use of 26 percent rather than 31 percent potassium hydroxide (KOH) electrolyte, (2) use of a patented catalyzed wall wick, (3) use of serrated-edge separators to facilitate gaseous oxygen and hydrogen flow within the cell, while still maintaining physical contact with the wall wick for electrolyte management, and (4) use of a floating rather than a fixed stack (state-of-the-art) to accommodate nickel electrode expansion. Six 125-Ah flight cells based on this design were fabricated by Eagle-Picher. Three of the cells contain all of the advanced features (test cells) and three are the same as the test cells except they don't have catalyst on the wall wick (control cells). All six cells are in the process of being evaluated in a LEO cycle life test. The cells have accumulated about 4700 LEO cycles (60 percent DOD 10 C). There have been no cell failures; the catalyzed wall wick cells, however, are performing better. Author

A91-38082* National Aeronautics and Space Administration, Lewis Research Center, Cleveland, OH.

IMPEDANCES OF NI ELECTRODES AND NI/H₂ CELLS FROM DIFFERENT MANUFACTURERS

MARGARET A. REID (NASA, Lewis Research Center, Cleveland, OH) IN: IECEC-90; Proceedings of the 25th Intersociety Energy Conversion Engineering Conference, Reno, NV, Aug. 12-17, 1990. Vol. 3. New York, American Institute of Chemical Engineers, 1990, p. 48-53. refs

Copyright

The consistency of impedance measurements within each group of flightweight Ni/H₂ cells being tested for Space Station Freedom confirms that impedance measurements are reproducible provided that the same conditions of cycling and storage are maintained. However, electrodes and cells from different manufacturers vary widely, even with the same cycling and storage conditions. Measurements on cells from two manufacturers that have been

20 SPACECRAFT PROPULSION AND POWER

cycled for 500-800 cycles show that there are not only major changes upon cycling, but there are substantial differences in the behavior of cells from different manufacturers with cycling. I.E.

A91-38088* National Aeronautics and Space Administration. Lewis Research Center, Cleveland, OH.

NASA AEROSPACE FLIGHT BATTERY SYSTEMS PROGRAM
MICHELLE A. MANZO and PATRICIA M. O'DONNELL (NASA, Lewis Research Center, Cleveland, OH) IN: IECEC-90; Proceedings of the 25th Intersociety Energy Conversion Engineering Conference, Reno, NV, Aug. 12-17, 1990. Vol. 3. New York, American Institute of Chemical Engineers, 1990, p. 85-89. Previously announced in STAR as N90-26397. refs
Copyright

The major objective of the NASA Aerospace Flight Battery Systems Program is to provide NASA with the policy and posture to increase and ensure the safety, performance and reliability of batteries for space power systems. The program plan has been modified in the past year to reflect changes in the agency's approach to battery related problems that are affecting flight programs. Primary attention in the Battery Program is being devoted to the development of an advanced nickel-cadmium cell design and the qualification of vendors to produce cells for flight programs. As part of a unified Battery Program, the development of a nickel-hydrogen standard and primary cell issues are also being pursued to provide high-performance NASA Standards and space qualified state-of-the-art primary cells. The resolution of issues is being addressed with the full participation of the aerospace battery community.

Author

A91-38140* National Aeronautics and Space Administration. Lewis Research Center, Cleveland, OH.

UPDATE ON RESULTS OF SPRE TESTING AT NASA

JAMES E. CAIRELLI, DIANE M. SWEC (NASA, Lewis Research Center, Cleveland, OH), ROBERT C. SKUPINSKI, and JEFFREY S. RAUCH (NASA, Lewis Research Center; Sverdrup Technology, Inc., Brook Park, OH) IN: IECEC-90; Proceedings of the 25th Intersociety Energy Conversion Engineering Conference, Reno, NV, Aug. 12-17, 1990. Vol. 5. New York, American Institute of Chemical Engineers, 1990, p. 237-244. refs
Copyright

The space power research engine (SPRE I), a free-piston Stirling engine with a linear alternator, was tested as a candidate for high-capacity space power. A portion of the test data from the SPRE I, essentially in its baseline configuration while operating with helium at heat exchanger metal temperature ratios ranging from 1.6 to 2.4 and mean cycle pressures of 7.5 and 15.0 MPa, are presented. HFAST computer code predictions are presented for comparison. The measured results at 7.5 and 15 MPa, from the first day, from the first day of testing, at temperature ratios from 1.6 to 2.0 agreed fairly well with the HFAST code predictions; within -8.8 percent to +11.9 percent for PV power and -2.7 to +1.07 percentage points for PV efficiency. Measured compression-space pressure amplitude was 5.1 to 11.1 percent below predictions; although these results were within the error bands, there was poorer agreement than observed for previous tests, and the transducer calibration is suspect. All of the dynamic pressure transducer calibrations will be verified before testing is resumed. Measured pressure phase angles were within -1.95 percent to +5.37 percent of the predictions, which is much closer than previously observed. The poor agreement of the measured heat flow to the heater with the code appears to be due to thermocouple degradation. I.E.

A91-38158* National Aeronautics and Space Administration. Lewis Research Center, Cleveland, OH.

LUNAR ORBITING MICROWAVE BEAM POWER SYSTEM

EDGAR H. FAY (NASA, Lewis Research Center; Sverdrup Technology, Inc., Brook Park, OH) and RONALD C. CULL (NASA, Lewis Research Center, Cleveland, OH) IN: IECEC-90; Proceedings of the 25th Intersociety Energy Conversion Engineering Conference, Reno, NV, Aug. 12-17, 1990. Vol. 6. New

York, American Institute of Chemical Engineers, 1990, p. 4-10. refs

Copyright

A microwave-beam power system using lunar orbiting solar-powered satellite(s) and surface rectenna(s) is investigated as a possible energy source for the moon's surface. The concept has the potential of achieving reduced system mass by placing the power source in orbit. This can greatly reduce and/or eliminate the 14-d energy storage requirement of a lunar surface solar system. Also, propellants required to de-orbit to the surface are greatly reduced. To determine the practicality of the concept and the most important factors, a zeroth-order feasibility analysis is performed. Three different operation scenarios employing state of the art technology and forecasts for two different sets of advanced technologies are investigated. To reduce the complexity of the problem, satellite(s) are assumed to be in circular equatorial orbits around the moon, supplying continuous power to a single equatorial base through a fixed horizontal rectenna on the surface. State of the art technology yields specific masses greater than 2500 kg/kW, well above projections for surface systems. The specific masses are on the order of 100 kg/kW using advanced technologies, which is within the range of projections for surface nuclear (20 kg/kW) and solar systems (500 kg/kW). Further studies examining optimization of the scenarios, other technologies, such as laser transmitters and nuclear sources, and operational issues, such as logistics, maintenance, and support, are being carried out to support the Space Exploration Initiative (SEI) to the moon and Mars. I.E.

A91-38163* National Aeronautics and Space Administration. Lewis Research Center, Cleveland, OH.

PRELIMINARY FLIGHT TEST RESULTS FROM THE ADVANCED PHOTOVOLTAIC EXPERIMENT

DAVID J. BRINKER (NASA, Lewis Research Center, Cleveland, OH) and JOHN R. HICKEY (Eppley Laboratory, Inc., Newport, RI) IN: IECEC-90; Proceedings of the 25th Intersociety Energy Conversion Engineering Conference, Reno, NV, Aug. 12-17, 1990. Vol. 6. New York, American Institute of Chemical Engineers, 1990, p. 36-41. Previously announced in STAR as N91-11058. Copyright

The Advanced Photovoltaic Experiment is a space flight test designed to provide reference cell standards for photovoltaic measurement as well as to investigate the solar spectrum and the effect of the space environment on solar cells. After a flight of 69 months in low earth orbit as part of the Long Duration Exposure Facility set of experiments, it was retrieved in January, 1990. The electronic data acquisition system functioned as designed, measuring and recording cell performance data over the first 358 days of flight, limited by battery lifetime. Significant physical changes are also readily apparent, including erosion of front surface paint, micrometeoroid and debris catering and contamination.

Author

A91-38184* Cleveland State Univ., OH.

FURTHER TWO-DIMENSIONAL CODE DEVELOPMENT FOR STIRLING SPACE ENGINE COMPONENTS

MOUNIR IBRAHIM (Cleveland State University, OH), ROY C. TEW, and JAMES E. DUDENHOEFER (NASA, Lewis Research Center, Cleveland, OH) IN: IECEC-90; Proceedings of the 25th Intersociety Energy Conversion Engineering Conference, Reno, NV, Aug. 12-17, 1990. Vol. 6. New York, American Institute of Chemical Engineers, 1990, p. 329-335. refs
Copyright

The development of multidimensional models of Stirling engine components is described. Two-dimensional parallel plate models of an engine regenerator and a cooler were used to study heat transfer under conditions of laminar, incompressible oscillating flow. Substantial differences in the nature of the temperature variations in time over the cycle were observed for the cooler as contrasted with the regenerator. When the two-dimensional cooler model was used to calculate a heat transfer coefficient, it yields a very different result from that calculated using steady-flow correlations. Simulation results for the regenerator and the cooler are presented. I.E.

A91-38933* # National Aeronautics and Space Administration. Lewis Research Center, Cleveland, OH.

SP-100 NUCLEAR SPACE POWER SYSTEMS WITH APPLICATION TO SPACE COMMERCIALIZATION

J. M. SMITH (NASA, Lewis Research Center, Cleveland, OH) IN: Space commercialization: Launch vehicles and programs; Symposium on Space Commercialization: Roles of Developing Countries, Nashville, TN, Mar. 5-10, 1989, Technical Papers. Washington, DC, American Institute of Aeronautics and Astronautics, Inc., 1990, p. 106-120. refs
Copyright

The technology of the SP-100 space nuclear power system program is compared to that of more familiar solar-power systems. The SP-100 program develops, validates, and demonstrates the technology for space nuclear power systems in the range of 10 to 1000 kilowatts electric for use in future military and civilian space missions. Mission applications, including earth orbiting platforms and lunar/Mars surface power, are enhanced or made possible by SP-100 technology. Attention is given to the SP-100 reference flight system design, the SP-100 nuclear reactor and nuclear-reactor shield, the platform-mounted, tethered, and free-flying reactors, and installation, operation, and disposal options, as well as lunar-Mars surface applications. The SP-100 is presented as one of the nuclear energy sources needed for long-life, compact, lightweight, continuous high power independent of solar orientation, specific orbits, or missions. P.D.

A91-41670* # National Aeronautics and Space Administration. Lewis Research Center, Cleveland, OH.

LINEAR QUADRATIC SERVO CONTROL OF A REUSABLE ROCKET ENGINE

JEFFREY L. MUSGRAVE (NASA, Lewis Research Center, Cleveland, OH) AIAA, SAE, ASME, and ASEE, Joint Propulsion Conference, 27th, Sacramento, CA, June 24-26, 1991. 11 p. refs
(AIAA PAPER 91-1999) Copyright

The paper deals with the development of a design method for a servo component in the frequency domain using singular values and its application to a reusable rocket engine. A general methodology used to design a class of linear multivariable controllers for intelligent control systems is presented. Focus is placed on performance and robustness characteristics, and an estimator design performed in the framework of the Kalman-filter formalism with emphasis on using a sensor set different from the commanded values is discussed. It is noted that loop transfer recovery modifies the nominal plant noise intensities in order to obtain the desired degree of robustness to uncertainty reflected at the plant input. Simulation results demonstrating the performance of the linear design on a nonlinear engine model over all power levels during mainstage operation are discussed. V.T.

A91-41780* # National Aeronautics and Space Administration. Lewis Research Center, Cleveland, OH.

NUMERICAL STUDY OF HIGH-AREA-RATIO H₂/O₂ ROCKET NOZZLES

S. C. KIM (NASA, Lewis Research Center; Sverdrup Technology, Inc., Cleveland, OH) AIAA, SAE, ASME, and ASEE, Joint Propulsion Conference, 27th, Sacramento, CA, June 24-26, 1991. 12 p. refs
(Contract NAS3-25266)
(AIAA PAPER 91-2434) Copyright

Calculations were made for high-area-ratio H₂/O₂ rocket nozzles by using the RPLUS code which employs an implicit finite volume, lower-upper symmetric successive over-relaxation scheme to solve the Navier-Stokes equations and the species equations in a coupled manner. The combustion processes of hydrogen and oxygen are modeled by an 8-species and 18-step reaction mechanism, and the turbulence is simulated by the Baldwin-Lomax turbulence model with a pressure gradient correction on the van Driest's damping constant in the inner-layer model. The calculated results for two different rocket nozzles are presented as contours, profiles, and performance values. The predicted specific impulse

and thrust agree well with the experimental data and those from the industry standard code. It is demonstrated that the RPLUS code can be used for analysis of rocket nozzles. Author

A91-41878* # National Aeronautics and Space Administration. Lewis Research Center, Cleveland, OH.

PHOTOVOLTAIC POWER FOR SPACE STATION FREEDOM

COSMO R. BARAONA (NASA, Lewis Research Center, Cleveland, OH) IN: IEEE Photovoltaic Specialists Conference, 21st, Kissimmee, FL, May 21-25, 1990, Conference Record. Vol. 1. New York, Institute of Electrical and Electronics Engineers, Inc., 1990, p. 30-35. Previously announced in STAR as N90-21812. refs

Space Station Freedom is described with special attention to its electric power system. The photovoltaic arrays, the battery energy storage system, and the power management and distribution system are also discussed. The current design of Freedom's power system and the system requirements, trade studies, and competing factors which lead to system selections are referenced. This will be the largest power system ever flown in space. This system represents the culmination of many developments that have improved system performance, reduced cost, and improved reliability. Key developments and their evolution into the current space station solar array design are briefly described. The features of the solar cell and the array including the development, design, test, and flight hardware production status are given. Author

A91-41989* National Aeronautics and Space Administration. Lewis Research Center, Cleveland, OH.

THE MINI-DOME FRESNEL LENS PHOTOVOLTAIC CONCENTRATOR ARRAY - CURRENT STATUS OF COMPONENT AND PROTOTYPE PANEL TESTING

M. F. PISZCZOR, C. K. SWARTZ (NASA, Lewis Research Center, Cleveland, OH), M. J. O'NEILL, A. J. MCDANAL (Entech, Inc., Dallas, TX), and L. M. FRAAS (Boeing High Technology Center, Seattle, WA) IN: IEEE Photovoltaic Specialists Conference, 21st, Kissimmee, FL, May 21-25, 1990, Conference Record. Vol. 2. New York, Institute of Electrical and Electronics Engineers, Inc., 1990, p. 1271-1276. refs
Copyright

NASA Lewis and ENTECH have been developing a high-efficiency, lightweight space photovoltaic concentrator array. The emphasis of the program has shifted to fabrication and testing of the minidome Fresnel lens and other array components. Prototype lenses have been tested for optical efficiency, with results around 90 percent, and tracking error performance. The results of these tests have been very consistent with the predicted analytical performance. Work has also progressed in the fabrication of the array support structure. Recent advances in 30 percent efficient stacked cell technology will have a significant effect on the array performance. It is concluded that near-term array performance goals of 300 W/sq m and 100 W/kg are feasible. I.E.

A91-41990* Boeing Co., Seattle, WA.

LIGHTWEIGHT CONCENTRATOR MODULE WITH 30 PERCENT AMO EFFICIENT GAAS/GASB TANDEM CELLS

J. E. AVERY, L. M. FRAAS, V. S. SUNDARAM, N. MANSOORI, J. W. YERKES (Boeing High Technology Center, Seattle, WA), D. J. BRINKER, H. B. CURTIS (NASA, Lewis Research Center, Cleveland, OH), and M. J. O'NEILL (Entech, Inc., Dallas, TX) IN: IEEE Photovoltaic Specialists Conference, 21st, Kissimmee, FL, May 21-25, 1990, Conference Record. Vol. 2. New York, Institute of Electrical and Electronics Engineers, Inc., 1990, p. 1277-1281. refs
Copyright

A concept is presented for an aerospace concentrator module with lightweight domed lenses and 30 percent AMO efficient GaAs/GaSb tandem solar cell circuits. The performance of transparent GaAs cells is reviewed. NASA's high-altitude jet flight calibration data for recent GaSb cells assembled with bulk GaAs filters are reported, along with subsequent Boeing and NASA measurements of GaSb I-V performance at various light levels and temperatures. The expected performance of a basic

20 SPACECRAFT PROPULSION AND POWER

two-terminal tandem concentrator circuit with three-to-one voltage matching is discussed. All of the necessary components being developed to assemble complete flight test coupons are shown. Straightforward interconnect and assembly techniques yield voltage matched circuits with near-optimum performance over a wide temperature range. I.E.

A91-42002* Kopin Corp., Taunton, MA.

23.5 PERCENT THIN-FILM SPACE CONCENTRATOR CELLS
B. D. DINGLE, R. P. GALE, R. W. MCCLELLAND, M. B. SPITZER (Kopin Corp., Taunton, MA), H. B. CURTIS, and D. J. BRINKER (NASA, Lewis Research Center, Cleveland, OH) IN: IEEE Photovoltaic Specialists Conference, 21st, Kissimmee, FL, May 21-25, 1990, Conference Record. Vol. 2. New York, Institute of Electrical and Electronics Engineers, Inc., 1990, p. 1346-1349. Copyright

Thin-film AlGaAs-GaAs double-heterostructure concentrator cells were fabricated which exhibit total-area conversion efficiencies as high as 23.5 percent AM0 at 100 suns, 25 C. This is one of the best space concentrators measured to date at NASA and is designed for a thin-film cell without a prismatic coverglass. This solar cell structure consists of a GaAs/AlGaAs film less than 5 micron thick mounted to a glass cover/superstrate, with coplanar back-side contacts. The coverglass is not prismatic. The CLEFT process, a method for mechanically separating epitaxial layers from their substrate, is used to process these cells into thin films. The advantages of single-crystal GaAs are thereby retained, while reducing weight and cutting cost by allowing for substrate reuse. Thin-film cells also have better thermal management capabilities and can be stacked for use in tandem structures. Cell fabrication and performance are described, and directions for further improvements are identified. I.E.

A91-42004*# National Aeronautics and Space Administration. Lewis Research Center, Cleveland, OH.

PHOTOVOLTAIC SUPERIORITY FOR SPACE STATION FREEDOM POWER IN THE 21ST CENTURY

SHEILA G. BAILEY (NASA, Lewis Research Center, Cleveland, OH), GEOFFREY A. LANDIS (Sverdrup Technology, Inc., Brook Park, OH), and MARIA A. PERINO (Aeritalia S.p.A., Turin, Italy) IN: IEEE Photovoltaic Specialists Conference, 21st, Kissimmee, FL, May 21-25, 1990, Conference Record. Vol. 2. New York, Institute of Electrical and Electronics Engineers, Inc., 1990, p. 1356-1361. refs

Complete power systems capable of delivering 75 kW of continuous power in low earth orbit have been compared. Performance, liabilities, and advantages are discussed for a shielded nuclear system, a solar dynamic system, and photovoltaic systems, both current Freedom Si design and near-term GaAs/Ge with NaS storage. System components include power generation, storage (if required), heat rejection, power conversion and distribution, structural support, and shielding (if required). Performance parameters indicate the substantial advantage of the GaAs/Ge photovoltaic system, which does not require altering the support structure of the current Freedom design. I.E.

A91-42725* National Aeronautics and Space Administration. Lewis Research Center, Cleveland, OH.

PROBABILISTIC MODELING FOR SIMULATION OF AERODYNAMIC UNCERTAINTIES IN PROPULSION SYSTEMS

A. HAMED (NASA, Lewis Research Center, Cleveland; Cincinnati, University, OH) and C. C. CHAMIS (NASA, Lewis Research Center, Cleveland, OH) (Computational technology for flight vehicles; Proceedings of the Symposium on Computational Technology on Flight Vehicles, Washington, DC, Nov. 5-7, 1990. A91-42703 18-59) Computing Systems in Engineering (ISSN 0956-0521), vol. 1, no. 2-4, 1990, p. 373-390. Previously announced in STAR as N90-21036. refs

(Contract NASA ORDER C-99066-G)
Copyright

The numerical simulation of the probabilistic aerothermodynamic response of propulsion system components to randomness in their environment was explored. The reusable rocket engine turbopumps

were selected as an example because of the severe cryogenic environment in which they operate. The thermal and combustion instabilities, coupled with the engine thrust requirements from start up to shut down, lead to randomness in the flow variables and uncertainties in the aerodynamic loading. The probabilistic modeling of the turbopumps' aerodynamic response was accomplished using the panel method coupled with fast probability integration methods. The aerodynamic response in the form of probabilistic rotor blades and splitter loading were predicted and the results presented for specified flow coefficient and rotor preswirl variance. Possible future applications of the aerothermodynamic probabilistic modeling in engine transient simulation, condition monitoring, and engine life prediction are briefly discussed. Author

A91-43397# National Aeronautics and Space Administration. Lewis Research Center, Cleveland, OH.

EVALUATION OF THERMAL CONTROL COATINGS FOR USE ON SOLAR DYNAMIC RADIATORS IN LOW EARTH ORBIT

JOYCE A. DEVER (NASA, Lewis Research Center, Cleveland, OH), ELVIN RODRIGUEZ (Cleveland State University, OH), WAYNE S. SLEMP (NASA, Langley Research Center, Hampton, VA), and JOSEPH E. STOYACK (LTV Missiles and Electronics Group, Grand Prairie, TX) AIAA, Thermophysics Conference, 26th, Honolulu, HI, June 24-26, 1991. 12 p. Previously announced in STAR as N91-22367. refs

(AIAA PAPER 91-1327) Copyright

Thermal control coatings with high thermal emittance and low solar absorptance are needed for Space Station Freedom (SSF) solar dynamic power module radiator (SDR) surfaces for efficient heat rejection. Additionally, these coatings must be durable to low earth orbital (LEO) environmental effects of atomic oxygen, ultraviolet radiation and deep thermal cycles which occur as a result of start-up and shut-down of the solar dynamic power system. Eleven candidate coatings were characterized for their solar absorptance and emittance before and after exposure to ultraviolet (UV) radiation (200 to 400 nm), vacuum UV (VUV) radiation (100 to 200 nm) and atomic oxygen. Results indicated that the most durable and best performing coatings were white paint thermal control coatings Z-93, zinc oxide pigment in potassium silicate binder, and YB-71, zinc orthotitanate pigment in potassium silicate binder. Optical micrographs of these materials exposed to the individual environmental effects of atomic oxygen and vacuum thermal cycling showed that no surface cracking occurred. Author

A91-44106# National Aeronautics and Space Administration. Lewis Research Center, Cleveland, OH.

LAUNCH VEHICLE PERFORMANCE USING METALLIZED PROPELLANTS

BRYAN PALASZEWSKI (NASA, Lewis Research Center, Cleveland, OH) and RICHARD POWELL (NASA, Langley Research Center, Hampton, VA) AIAA, SAE, ASME, and ASEE, Joint Propulsion Conference, 27th, Sacramento, CA, June 24-26, 1991. 15 p. Previously announced in STAR as N91-24304. refs

(AIAA PAPER 91-2050) Copyright
Metallized propellant propulsion systems are considered as replacements for the solid rocket boosters and liquid sustainer stages on the current launch vehicles: both the Space Transportation System (STS) and the Titan 4. Liquid rocket boosters for the STS were analyzed as replacements for current solid rocket boosters. These boosters can provide a liquid propulsion system within the volume constraints of a solid rocket booster. A replacement for the Space Shuttle Main Engines using metallized 02/H2/A1 was studied. The liquid stages of the Titan 4 were also investigated; the Aerozine-50 (A-50) fuel was replaced with metallized storable A-50/A1. A metallized propellant is similar to a traditional liquid propellant. However, it has metal particles, such as aluminum, that are suspended in a gelled fuel, such as hydrogen, RP-1, A-50 or monomethyl hydrazine (MMH). The fuels then undergo combustion with liquid oxygen or nitrogen tetroxide (NTO). These propellants provide options for increasing the performance of existing launch vehicle chemical propulsion systems by increasing fuel density or specific impulse or both. These increases

in density and specific impulse can significantly reduce the propulsion system liftoff weight and allow a liquid rocket booster to fit into the same volume as an existing solid rocket booster. Also, because gelled fuels are akin to liquid propellants, metallized systems can provide enhanced controllability over solid propulsion systems. Gelling of the propellant also reduces the sensitivity to impacts and consequently reduces the propellant explosion hazard. Author

A91-44151*# National Aeronautics and Space Administration. Lewis Research Center, Cleveland, OH.

FLOW VISUALIZATION OF A ROCKET INJECTOR SPRAY USING GELLED PROPELLANT SIMULANTS

JAMES M. GREEN, DOUGLAS C. RAPP, and JAMES RONCACE (NASA, Lewis Research Center, Cleveland; Sverdrup Technology, Inc., Brook Park, OH) AIAA, SAE, ASME, and ASEE, Joint Propulsion Conference, 27th, Sacramento, CA, June 24-26, 1991. 17 p. Previously announced in STAR as N91-24306. refs (Contract NAS3-25266) (AIAA PAPER 91-2198) Copyright

A study was conducted at NASA-Lewis to compare the atomization characteristics of gelled and nongelled propellant simulants. A gelled propellant simulant composed of water, sodium hydroxide, and an acrylic acid polymer resin (as the gelling agent) was used to simulate the viscosity of an aluminum/PP-1 metallized fuel gel. Water was used as a comparison fluid to isolate the rheological effects of the water-gel and to simulate nongelled RP-1. The water-gel was injected through the central orifice of a triplet injector element and the central post of a coaxial injector element. Nitrogen gas flowed through the outer orifices of the triplet injector element and through the annulus of the coaxial injector element and atomized the gelled and nongelled liquids. Photographs of the water-gel spray patterns at different operating conditions were compared with images obtained using water and nitrogen. A laser light was used for illumination of the sprays. The results of the testing showed that the water sprays produced a finer and more uniform atomization than the water-gel sprays. Rheological analysis of the water-gel showed poor atomization caused by high viscosity of water-gel delaying the transition to turbulence. Author

A91-44156*# National Aeronautics and Space Administration. Lewis Research Center, Cleveland, OH.

A DUAL-COOLED HYDROGEN-OXYGEN ROCKET ENGINE HEAT TRANSFER ANALYSIS

KENNETH J. KACYSKI, JOHN M. KAZAROFF, and ROBERT S. JANKOVSKY (NASA, Lewis Research Center, Cleveland, OH) AIAA, SAE, ASME, and ASEE, Joint Propulsion Conference, 27th, Sacramento, CA, June 24-26, 1991. 16 p. Previously announced in STAR as N91-24302. refs (AIAA PAPER 91-2211) Copyright

The potential benefits of simultaneously using hydrogen and oxygen as rocket engine coolants are described. A plug-and-spool rocket engine was examined at heat fluxes ranging from 9290 to 163,500 kW/sq m, using a combined 3D conduction/advection analysis. Both counterflow and parallel flow cooling arrangements were analyzed. The results indicate that a significant amount of heat transfer to the oxygen occurs, reducing both the hot-side wall temperature of the rocket engine and also reducing the exit temperature of the hydrogen coolant. The total heat transferred to the oxygen was found to be largely independent of the oxygen coolant flow direction. The reduction in combustion chamber wall temperatures at throttled conditions is especially desirable since the analysis indicates that double temperature maxima, one at the throat and another in the combustion chamber, occur with a traditional hydrogen-only cooled engine. A dual-cooled engine eliminates any concern for overheating in the combustion chamber. Author

A91-44198*# National Aeronautics and Space Administration. Lewis Research Center, Cleveland, OH.

GROUND TESTING OF THE NONVENTED FILL METHOD OF ORBITAL PROPELLANT TRANSFER - RESULTS OF INITIAL TEST SERIES

DAVID J. CHATO (NASA, Lewis Research Center, Cleveland, OH) AIAA, SAE, ASME, and ASEE, Joint Propulsion Conference, 27th, Sacramento, CA, June 24-26, 1991. 32 p. Previously announced in STAR as N91-24547. refs (AIAA PAPER 91-2326) Copyright

The results are presented of a series of no-vent fill experiments conducted on a 175 cu ft flightweight hydrogen tank. The experiments consisted of the nonvented fill of the tankage with liquid hydrogen using two different inlet systems (top spray, and bottom spray) at different tank initial conditions and inflow rates. Nine tests were completed of which six filled in excess of 94 percent. The experiments demonstrated a consistent and repeatable ability to fill the tank in excess of 94 percent using the nonvented fill technique. Ninety-four percent was established as the high level cutoff due to requirements for some tank ullage to prevent rapid tank pressure rise which occurs in a tank filled entirely with liquid. The best fill was terminated at 94 percent full with a tank internal pressure less than 26 psia. Although the baseline initial tank wall temperature criteria was that all portions of the tank wall be less than 40 R, fills were achieved with initial wall temperatures as high as 227R. Author

A91-44204*# National Aeronautics and Space Administration. Lewis Research Center, Cleveland, OH.

ANODE POWER DEPOSITION IN AN APPLIED-FIELD SEGMENTED ANODE MPD THRUSTER

R. M. MYERS (NASA, Lewis Research Center, Cleveland; Sverdrup Technology, Inc., Brook Park, OH), A. J. KELLY, R. G. JAHN (Princeton University, NJ), and A. D. GALLIMORE (AIAA, SAE, ASME, and ASEE, Joint Propulsion Conference, 27th, Sacramento, CA, June 24-26, 1991. 13 p. NASA-supported research. refs (AIAA PAPER 91-2343) Copyright

Anode heat flux measurements of a water cooled segmented anode applied-field MPD thruster were made to investigate anode heat transfer phenomena. Pure argon and argon-hydrogen mixtures were used as propellants for a variety of thruster currents, propellant mass flow rates, and axial applied magnetic field strengths. The thruster was operated in two modes; with all four segments active, and with two of the segments floating. In addition, thrust and specific impulse were determined for each operating condition. The results show that the heat flux to the anode increases monotonically with axial magnetic field strength and thruster current. Between 50 and 75 percent of the anode heat flux is transported by the current carrying electrons. Convective and radiative heat transfer account for the remaining portion of the power deposited in the anode. The addition of hydrogen to the argon propellant results in the reduction of the fraction of anode power deposited by the anode fall to a level equivalent to that deposited by convection and radiation. Author

A91-44228*# Analex Corp., Fairview Park, OH.

A PRESSURE CONTROL ANALYSIS OF CRYOGENIC STORAGE SYSTEMS

C.-S. LIN (Analex Corp., Fairview Park, OH), N. T. VAN DRESAR, and M. M. HASAN (NASA, Lewis Research Center, Cleveland, OH) AIAA, SAE, ASME, and ASEE, Joint Propulsion Conference, 27th, Sacramento, CA, June 24-26, 1991. 9 p. Previously announced in STAR as N91-24460. refs (AIAA PAPER 91-2405) Copyright

Self-pressurization of cryogenic storage tanks due to heat leak through the thermal protection system is examined along with the performance of various pressure control technologies for application in microgravity environments. Methods of pressure control such as fluid mixing, passive thermodynamic venting, and active thermodynamic venting are analyzed using the homogeneous thermodynamic model. Simplified equations suggested may be used to characterize the performance of various pressure control systems and to design space experiments. Author

20 SPACECRAFT PROPULSION AND POWER

A91-44246*# National Aeronautics and Space Administration. Lewis Research Center, Cleveland, OH.

CARBON MONOXIDE AND OXYGEN COMBUSTION EXPERIMENTS - A DEMONSTRATION OF MARS IN SITU PROPELLANTS

DIANE L. LINNE (NASA, Lewis Research Center, Cleveland, OH) AIAA, SAE, ASME, and ASEE, Joint Propulsion Conference, 27th, Sacramento, CA, June 24-26, 1991. 18 p. Previously announced in STAR as N91-24303. refs (AIAA PAPER 91-2443) Copyright

The feasibility of using carbon monoxide and oxygen as rocket propellants was examined both experimentally and theoretically. The steady-state combustion of carbon monoxide and oxygen was demonstrated for the first time in a subscale rocket engine. Measurements of experimental characteristic velocity, vacuum specific impulse, and thrust coefficient efficiency were obtained over a mixture ratio range of 0.30 to 2.0 and a chamber pressures of 1070 and 530 kPa. The theoretical performance of the propellant combination was studied parametrically over the same mixture ratio range. In addition to one dimensional ideal performance predictions, various performance reduction mechanisms were also modeled, including finite-rate kinetic reactions, two-dimensional divergence effects and viscous boundary layer effects. Author

A91-44247*# National Aeronautics and Space Administration. Lewis Research Center, Cleveland, OH.

IN-SITU PROPELLANT ROCKET ENGINES FOR MARS MISSIONS ASCENT VEHICLE

ELIZABETH A. RONCACE (NASA, Lewis Research Center, Cleveland, OH) AIAA, SAE, ASME, and ASEE, Joint Propulsion Conference, 27th, Sacramento, CA, June 24-26, 1991. 8 p. Previously announced in STAR as N91-24305. refs (AIAA PAPER 91-2445) Copyright

When contemplating the human exploration of Mars, many scenarios using various propulsion systems have been considered. One propulsion option among them is a vehicle stage with multiple, pump fed rocket engines capable of operating on propellants available on Mars. This reduces the earth launch mass requirements, resulting in economic and payload benefits. No plentiful sources of hydrogen on Mars have been identified on the surface of Mars, so most commonly used high performance liquid fuels, such as hydrogen and hydrocarbons, can be eliminated as possible in situ propellants. But 95 pct of the Martian atmosphere consists of carbon dioxide, which can be converted into carbon monoxide and oxygen. The carbon monoxide oxygen propellant combination is a candidate for a Martian in situ propellant rocket engine. The feasibility is analyzed of a pump fed engine cycle using the propellant combination of carbon monoxide and oxygen. Author

A91-44281*# National Aeronautics and Space Administration. Lewis Research Center, Cleveland, OH.

THE DEVELOPMENT OF A POST-TEST DIAGNOSTIC SYSTEM FOR ROCKET ENGINES

JUNE F. ZAKRAJSEK (NASA, Lewis Research Center, Cleveland, OH) AIAA, SAE, ASME, and ASEE, Joint Propulsion Conference, 27th, Sacramento, CA, June 24-26, 1991. 12 p. Previously announced in STAR as N91-24787. refs (AIAA PAPER 91-2528) Copyright

An effort was undertaken by NASA to develop an automated post-test, post-flight diagnostic system for rocket engines. The automated system is designed to be generic and to automate the rocket engine data review process. A modular, distributed architecture with a generic software core was chosen to meet the design requirements. The diagnostic system is initially being applied to the Space Shuttle Main Engine data review process. The system modules currently under development are the session/message manager, and portions of the applications section, the component analysis section, and the intelligent knowledge server. An overview is presented of a rocket engine data review process, the design requirements and guidelines, the architecture and modules, and the projected benefits of the automated diagnostic system. Author

A91-44283*# National Aeronautics and Space Administration. Lewis Research Center, Cleveland, OH.

THE APPLICATION OF NEURAL NETWORKS TO THE SSME STARTUP TRANSIENT

CLAUDIA M. MEYER and WILLIAM A. MAUL (NASA, Lewis Research Center; Sverdrup Technology, Inc., Brook Park, OH) AIAA, SAE, ASME, and ASEE, Joint Propulsion Conference, 27th, Sacramento, CA, June 24-26, 1991. 15 p. Previously announced in STAR as N91-23205. refs (Contract NAS3-25266) (AIAA PAPER 91-2530) Copyright

Feedforward neural networks were used to model three parameters during the Space Shuttle Main Engine startup transient. The three parameters were the main combustion chamber pressure, a controlled parameter, the high pressure oxidizer turbine discharge temperature, a redlined parameter, and the high pressure fuel pump discharge pressure, a failure-indicating performance parameter. Network inputs consisted of time windows of data from engine measurements that correlated highly to the modeled parameter. A standard backpropagation algorithm was used to train the feedforward networks on two nominal firings. Each trained network was validated with four additional nominal firings. For all three parameters, the neural networks were able to accurately predict the data in the validation sets as well as the training set. Author

A91-45776*# National Aeronautics and Space Administration. Lewis Research Center, Cleveland, OH.

REVIEW AND TEST OF CHILLDOWN METHODS FOR SPACE-BASED CRYOGENIC TANKS

DAVID J. CHATO and RAFAEL SANABRIA (NASA, Lewis Research Center, Cleveland, OH) AIAA, SAE, ASME, and ASEE, Joint Propulsion Conference, 27th, Sacramento, CA, June 24-26, 1991. 26 p. Previously announced in STAR as N91-25351. refs (AIAA PAPER 91-1843) Copyright

The literature for tank chilldown methods applicable to cryogenic tankage in the zero gravity environment of earth orbit is reviewed. One method is selected for demonstration in a ground based test. The method selected for investigation was the charge-hold-vent method which uses repeated injection of liquid slugs, followed by a hold to allow complete vaporization of the liquid and a vent of the tank to space vacuum to cool tankage to the desired temperature. The test was conducted on a 175 cubic foot, 2219 aluminum walled tank weighing 329 pounds, which was previously outfitted with spray systems to test nonvented fill technologies. To minimize hardware changes, a simple control-by-pressure scheme was implemented to control injected liquid quantities. The tank cooled from 440 R sufficiently in six charge-hold-vent cycles to allow a complete nonvented fill of the test tank. Liquid hydrogen consumed in the process is estimated at 32 pounds. Author

A91-45779*# National Aeronautics and Space Administration. Lewis Research Center, Cleveland, OH.

POWER ELECTRONICS FOR LOW POWER ARCJETS

JOHN A. HAMLEY and GERALD M. HILL (NASA, Lewis Research Center, Cleveland, OH) AIAA, SAE, ASME, and ASEE, Joint Propulsion Conference, 27th, Sacramento, CA, June 24-26, 1991. 16 p. Previously announced in STAR as N91-25172. refs (AIAA PAPER 91-1991) Copyright

In anticipation of the needs of future light-weight low-power spacecraft, arcjet power electronics in the 100- to 400-W operating range were developed. Power topologies similar to those in the higher 2-kW and 5- to 30-kW power range were implemented, including a four-transistor bridge-switching circuit, current-mode pulse-width modulated control, and an output current averaging inductor with an integral pulse generation winding. Reduction of switching transients was accomplished using a low inductance power distribution network, and no passive snubber circuits were necessary for power switch protection. Phase shift control of the power bridge was accomplished using an improved pulse width modulation to phase shift converter circuit. These features, along with conservative magnetics designs, allowed power conversion

efficiencies of greater than 92.5 percent to be achieved into resistive loads over the entire operating range of the converter.

Author

A91-45783# National Aeronautics and Space Administration. Lewis Research Center, Cleveland, OH.

PRESSURE MEASUREMENTS IN A LOW-DENSITY NOZZLE PLUME FOR CODE VERIFICATION

PAUL F. PENKO (NASA, Lewis Research Center, Cleveland, OH), IAIN D. BOYD (NASA, Ames Research Center; Eloret Institute, Moffett Field, CA), KENNETH J. DEWITT (Toledo, University, OH), and DANA L. MEISSNER AIAA, SAE, ASME, and ASEE, Joint Propulsion Conference, 27th, Sacramento, CA, June 24-26, 1991. 17 p. refs

(AIAA PAPER 91-2110) Copyright

Measurements of Pitot pressure were made in the exit plane and plume of a low-density, nitrogen nozzle flow. Two numerical computer codes were used to analyze the flow, including one based on continuum theory using the explicit McCormack method, and the other on kinetic theory using the method of direct-simulation Monte Carlo (DSMC). The continuum analysis was carried to the nozzle exit plane and the results were compared to the measurements. The DSMC analysis was extended into the plume of the nozzle flow and the results were compared with measurements at the exit plane and axial stations 12, 24 and 36 mm into the near-field plume. Two experimental apparatus were used that differed in design and gave slightly different profiles of pressure measurements. The DSMC method compared well with the measurements from each apparatus at all axial stations and provided a more accurate prediction of the flow than the continuum method, verifying the validity of DSMC for such calculations.

Author

A91-45784*# National Aeronautics and Space Administration. Lewis Research Center, Cleveland, OH.

NONEQUILIBRIUM IN A LOW POWER ARCJET NOZZLE

ROGER M. MYERS (NASA, Lewis Research Center, Cleveland; Sverdrup Technology, Inc., Brook Park, OH) and DIETER M. ZUBE AIAA, SAE, ASME, and ASEE, Joint Propulsion Conference, 27th, Sacramento, CA, June 24-26, 1991. 23 p. refs (AIAA PAPER 91-2113) Copyright

Emission spectroscopy measurements were made of the plasma flow inside the nozzle of a 1-kW-class arcjet thruster. The thruster propellant was a hydrogen-nitrogen mixture used to simulate fully decomposed hydrazine. Atomic electron-excitation, vibrational, and rotational temperatures were determined for the expanding plasma using relative line intensity techniques. The atomic excitation temperature decreased from 18,000 K at a location 3 mm downstream of the constrictor to 9000 K at a location 9 mm from the constrictor, while the molecular vibrational and rotational temperatures decreased from 6500 K to 2500 K and from 8000 K to 3000 K, respectively, between the same locations. The electron density, measured using hydrogen H-beta line Stark broadening, decreased from about 10 to the 15th cu cm to about 2 x 10 to the 14th cu cm during the expansion. The results show that the plasma is highly nonequilibrium throughout the nozzle, with most relaxation times equal or exceeding the particle residence time.

Author

A91-45785*# National Aeronautics and Space Administration. Lewis Research Center, Cleveland, OH.

ION BEAM SPUTTERING IN ELECTRIC PROPULSION FACILITIES

JAMES S. SOVEY and MICHAEL J. PATTERSON (NASA, Lewis Research Center, Cleveland, OH) AIAA, SAE, ASME, and ASEE, Joint Propulsion Conference, 27th, Sacramento, CA, June 24-26, 1991. 28 p. refs (AIAA PAPER 91-2117) Copyright

Experiments were undertaken to determine sputter yields of potential ion beam target materials, to assess the impact of charge exchange on beam diagnostics in large facilities, and to examine material erosion and deposition after a 957-hour test of a 5 kW-class ion thruster. The xenon ion sputter yield of flexible

graphite was lower than other graphite forms especially at high angles of incidence. Ion beam charge exchange effects were found to hamper beam probe current collection diagnostics even at pressures from 0.7 to 1.7 mPa. Estimates of the xenon ion beam envelope were made and predictions of the thickness of sputter deposited coatings in the facility were compared with measurements.

Author

A91-45787*# National Aeronautics and Space Administration. Lewis Research Center, Cleveland, OH.

MICROANALYSES OF EXTENDED-TEST XENON HOLLOW CATHODES

TIMOTHY R. VERHEY (NASA, Lewis Research Center, Cleveland; Sverdrup Technology, Inc., Brook Park, OH) and MICHAEL J. PATTERSON (NASA, Lewis Research Center, Cleveland, OH) AIAA, SAE, ASME, and ASEE, Joint Propulsion Conference, 27th, Sacramento, CA, June 24-26, 1991. 47 p. refs (AIAA PAPER 91-2123) Copyright

Four hollow cathodes have been examined using boroscopy, scanning electron microscopy, energy dispersive X-ray analysis, and X-ray diffraction analysis to characterize the life-limiting phenomena that resulted from their extended operation. The first pair of cathodes was operated for approximately 500 h in an ion thruster simulator at a 5.0 kW-equivalent power level using different cathode activation and propellant feed-system procedures. The second pair of cathodes was the main discharge cathode and neutralizer cathode from an ion thruster which have completed an 89-hour life-test at a 5.5 kW power level. The greatest change to the cathode condition was found to be removal of refractory metals, primarily tungsten, and their subsequent deposition on other cathode surfaces. Barium tungstate and barium molybdate were also found in all four cathodes. Criteria for improved cathode longevity and discharge operation are proposed for use in hollow cathode and full thruster testing facilities.

O.G.

A91-45794*# National Aeronautics and Space Administration. Lewis Research Center, Cleveland, OH.

PLUG NOZZLES - THE ULTIMATE CUSTOMER DRIVEN PROPULSION SYSTEM

CARL A. AUKERMAN (NASA, Lewis Research Center, Cleveland; Sverdrup Technology, Inc., Brook Park, OH) AIAA, SAE, ASME, and ASEE, Joint Propulsion Conference, 27th, Sacramento, CA, June 24-26, 1991. 29 p. refs (AIAA PAPER 91-2208) Copyright

This paper presents the results of a study applying the plug cluster nozzle concept to the propulsion system for a typical lunar excursion vehicle. Primary attention for the design criteria is given to user defined factors such as reliability, low volume, and ease of propulsion system development. Total thrust and specific impulse are held constant in the study while other parameters are explored to minimize the design chamber pressure. A brief history of the plug nozzle concept is included to point out the advanced level of technology of the concept and the feasibility of exploiting the variables considered in the study. The plug cluster concept looks very promising as a candidate for consideration for the ultimate customer driven propulsion system.

Author

A91-45795*# National Aeronautics and Space Administration. Lewis Research Center, Cleveland, OH.

HIGH-POWER HYDROGEN ARCJET PERFORMANCE

THOMAS W. HAAG and FRANCIS M. CURRAN (NASA, Lewis Research Center, Cleveland, OH) AIAA, SAE, ASME, and ASEE, Joint Propulsion Conference, 27th, Sacramento, CA, June 24-26, 1991. 23 p. refs (AIAA PAPER 91-2226) Copyright

A hydrogen arcjet was operated at power levels ranging from 5 to 30 kW with three different nozzle geometries. Test results using all three nozzle geometries are reported and include variations of specific impulse with flow rate, and thrust with power. Geometric variables investigated included constrictor diameter, length, and diverging exit angle. The nozzle with a constrictor diameter of 1.78 mm and divergence angle of 20 deg was found to give the highest performance. A specific impulse of 1460 s was attained

20 SPACECRAFT PROPULSION AND POWER

with this nozzle at a thrust efficiency of 29.8 percent. The best efficiency measured was 34.4 percent at a specific impulse of 1045 s. Post test examination of the cathode showed erosion after 28 hours of operation to be small, and limited to the conical tip where steady state arc attachment occurred. Each nozzle was tested to destruction.

Author

A91-45796* # National Aeronautics and Space Administration. Lewis Research Center, Cleveland, OH.

PRELIMINARY PERFORMANCE AND LIFE EVALUATION OF A 2-KW ARCJET

W. E. MORREN and FRANCIS M. CURRAN (NASA Lewis Research Center, Cleveland, OH) AIAA, SAE, ASME, and ASEE, Joint Propulsion Conference, 27th, Sacramento, CA, June 24-26, 1991. 30 p. refs

(AIAA PAPER 91-2228) Copyright

The first results of a program to expand the operational envelope of low-power arcjets to higher specific impulse and power levels are presented. The performance of a kW-class laboratory model arcjet thruster was characterized at three mass flow rates of a 2:1 mixture of hydrogen and nitrogen at power levels ranging from 1.0 to 2.0 kW. This same thruster was then operated for a total of 300 h at a specific impulse and power level of 550 s and 2.0 kW, respectively, in three continuous 100-h sessions. Thruster operation during the three test segments was stable, and no measurable performance degradation was observed during the test series. Substantial cathode erosion was observed during an inspection following the second 100-h test segment. Most notable was the migration of material from the center of the cathode tip to a ring around a large crater. The anode sustained no significant damage during the endurance test segments. Some difficulty was encountered during start-up after disassembly and inspection following the second 100-h test segment, which caused constrictor erosion. This resulted in a reduced flow restriction and arc chamber pressure, which in turn caused a reduction in the arc impedance.

Author

A91-45798* # National Aeronautics and Space Administration. Lewis Research Center, Cleveland, OH.

A PRELIMINARY CHARACTERIZATION OF APPLIED-FIELD MPD THRUSTER PLUMES

ROGER M. MYERS (NASA, Lewis Research Center, Cleveland; Sverdrup Technology, Inc., Brook Park, OH), DAVID WEHRLER, MARK VERNYI, JAMES BIAGLOW, and SHAWN REESE AIAA, SAE, ASME, and ASEE, Joint Propulsion Conference, 27th, Sacramento, CA, June 24-26, 1991. 36 p. refs

(AIAA PAPER 91-2339) Copyright

Electric probes, quantitative imaging, and emission spectroscopy were used to study the plume characteristics of applied-field MPD thrusters. The measurements showed that the applied magnetic field plays the dominant role in establishing the plume structure, followed in importance by the cathode geometry and propellant. The anode radius had no measurable impact on the plume characteristics. For all cases studied the plume was highly ionized, though spectral lines of neutral species were always present. Centerline electron densities and temperatures ranged from 2×10 to the 18th to 8×10 to the 18th cu m and from 7500 to 20,000 K, respectively. The plume was strongly confined by the magnetic field, with radial density gradients increasing monotonically with applied field strength. Plasma potential measurements show a strong effect of the magnetic field on the electrical conductivity and indicate the presence of radial current conduction in the plume.

Author

A91-45802* # National Aeronautics and Space Administration. Lewis Research Center, Cleveland, OH.

EXPERIMENTAL AND ANALYTICAL COMPARISON OF FLOWFIELDS IN A 110 N (25 LBF) H₂/O₂ ROCKET

BRIAN D. REED, PAUL F. PENKO, STEVEN J. SCHNEIDER (NASA, Lewis Research Center, Cleveland, OH), and SUK C. KIM (NASA, Lewis Research Center, Cleveland; Sverdrup Technology, Inc., Brook Park, OH) AIAA, SAE, ASME, and ASEE, Joint

Propulsion Conference, 27th, Sacramento, CA, June 24-26, 1991. 18 p. refs

(AIAA PAPER 91-2283) Copyright

A gaseous hydrogen/gaseous oxygen 110 N (25 lbf) rocket has been examined through the RPLUS code using the full Navier-Stokes equations with finite-rate chemistry. Performance tests were conducted on the rocket in an altitude test facility. Preliminary parametric analyses have been performed for a range of mixture ratios and fuel film cooling percentages. It is shown that the computed values of specific impulse and characteristic exhaust velocity follow the trend of the experimental data. Specific impulse computed by the code is lower than the comparable test values by about two to three percent. The computed characteristic exhaust velocity values are lower than the comparable test values by three to four percent. Thrust coefficients computed by the code are found to be within two percent of the measured values. It is concluded that the discrepancy between computed and experimental performance values could not be attributed to experimental uncertainty.

O.G.

A91-45805* # National Aeronautics and Space Administration. Lewis Research Center, Cleveland, OH.

NUMERICAL SIMULATION OF SELF-FIELD MPD THRUSTERS

MICHAEL R. LA POINTE (NASA, Lewis Research Center, Cleveland; Sverdrup Technology, Inc., Brook Park, OH) AIAA, SAE, ASME, and ASEE, Joint Propulsion Conference, 27th, Sacramento, CA, June 24-26, 1991. 36 p. refs

(AIAA PAPER 91-2341) Copyright

A fully two-dimensional magnetohydrodynamics code has been developed to predict self-field, steady-state MPD thruster performance. The governing equations are outlined, and methods of solution are presented. Model predictions are compared with experimental data for two thruster geometries over a range of discharge currents and mass flow rates. Model limitations are evaluated, and issues concerning quasi-steady versus steady-state thruster comparisons are discussed.

Author

A91-45806* # National Aeronautics and Space Administration. Lewis Research Center, Cleveland, OH.

APPLIED-FIELD MPD THRUSTER GEOMETRY EFFECTS

ROGER M. MYERS (NASA, Lewis Research Center, Cleveland; Sverdrup Technology, Inc., Brook Park, OH) AIAA, SAE, ASME, and ASEE, Joint Propulsion Conference, 27th, Sacramento, CA, June 24-26, 1991. 35 p. refs

(AIAA PAPER 91-2342) Copyright

Eight MPD thruster configurations were used to study the effects of applied-field strength, propellant, and facility pressure on thruster performance. Vacuum facility background pressures higher than about 0.12 Pa were found to significantly influence thruster performance and electrode power deposition. Thrust efficiency and specific impulse increased monotonically with increasing applied field strength. Both cathode and anode radii fundamentally influenced the efficiency-specific impulse relationship, while their lengths influenced only the magnitude of the applied magnetic field required to reach a given performance level. At a given specific impulse, large electrode radii result in lower efficiencies for the operating conditions studied. For all test conditions, anode power deposition was the largest efficiency loss, and represented between 50 percent and 80 percent of the input power. The fraction of the input power deposited into the anode decreased with increasing applied field and anode radius. The highest performance measured, 20 percent efficiency at 3700 seconds specific impulse, was obtained using hydrogen propellant.

Author

A91-45809* # National Aeronautics and Space Administration. Lewis Research Center, Cleveland, OH.

PERFORMANCE AND OPTIMIZATION OF A 'DERATED' ION THRUSTER FOR AUXILIARY PROPULSION

MICHAEL J. PATTERSON (NASA, Lewis Research Center, Cleveland, OH) and JOHN E. FOSTER (Jackson State University, MS) AIAA, SAE, ASME, and ASEE, Joint Propulsion Conference,

27th, Sacramento, CA, June 24-26, 1991. 19 p. refs
(AIAA PAPER 91-2350) Copyright

This paper discusses the characteristics and implications of use of a derated ion thruster for north-south-stationkeeping (NSSK) propulsion. A derated thruster is a 30-cm diameter primary propulsion ion thruster operated at highly throttled conditions appropriate to NSSK functions. The performance characteristics of a 30-cm ion thruster are presented, emphasizing throttled operation at low specific impulse and high thrust-to-power ratio. Performance data and component erosion are compared to other NSSK ion thrusters. Operations benefits derived from the performance advantages of the derated approach are examined assuming an Intelsat VII-type spacecraft. Minimum ground test facility pumping capabilities required to maintain facility enhanced accelerator grid erosion at acceptable levels in a lifetime are quantified as a function of thruster operating condition. Novel approaches to reducing the derated thruster mass and volume are also discussed. Author

A91-45814*# National Aeronautics and Space Administration. Lewis Research Center, Cleveland, OH.

ARCJET THERMAL CHARACTERISTICS

JOHN M. SANKOVIC and FRANCIS M. CURRAN (NASA, Lewis Research Center, Cleveland, OH) AIAA, SAE, ASME, and ASEE, Joint Propulsion Conference, 27th, Sacramento, CA, June 24-26, 1991. 30 p. refs
(AIAA PAPER 91-2456) Copyright

The performance of water-cooled and radiation-cooled arcjet thrusters operating on both 1:2 nitrogen/hydrogen mixtures at 1-2 kW and on pure hydrogen at 1-4 kW are compared. To investigate the effects of test facility background pressure on performance, data were taken for both thrusters operating on hydrogen/nitrogen mixtures at facility background pressures nominally at 0.20 Pa and 20 Pa. It is shown that increasing the background pressure decreased the thruster performance, and simple pressure area corrections alone could not account for the observed degradation in performance. R.E.P.

A91-45817*# Systems Control Technology, Inc., Palo Alto, CA. **DEVELOPMENT OF AN INTELLIGENT DIAGNOSTIC SYSTEM FOR REUSABLE ROCKET ENGINE CONTROL**

R. P. ANEX, J. R. RUSSELL (Systems Control Technology, Inc., Palo Alto, CA), and T.-H. GUO (NASA, Lewis Research Center, Cleveland, OH) AIAA, SAE, ASME, and ASEE, Joint Propulsion Conference, 27th, Sacramento, CA, June 24-26, 1991. 10 p. refs

(Contract NAS3-25823)

(AIAA PAPER 91-2533) Copyright

A description of an intelligent diagnostic system for the Space Shuttle Main Engines (SSME) is presented. This system is suitable for incorporation in an intelligent controller which implements accommodating closed-loop control to extend engine life and maximize available performance. The diagnostic system architecture is a modular, hierarchical, blackboard system which is particularly well suited for real-time implementation of a system which must be repeatedly updated and extended. The diagnostic problem is formulated as a hierarchical classification problem in which the failure hypotheses are represented in terms of predefined data patterns. The diagnostic expert system incorporates techniques for priority-based diagnostics, the combination of analytical and heuristic knowledge for diagnosis, integration of different AI systems, and the implementation of hierarchical distributed systems. A prototype reusable rocket engine diagnostic system (ReREDS) has been implemented. The prototype user interface and diagnostic performance using SSME test data are described. Author

A91-48843* Sverdrup Technology, Inc., Brook Park, OH.

PERFORMANCE AND FLOW CALCULATIONS FOR A GASEOUS H₂/O₂ THRUSTER

S. C. KIM (Sverdrup Technology, Inc., Brook Park, OH) and T. J. VANOVERBEKE (NASA, Lewis Research Center, Cleveland, OH) Journal of Spacecraft and Rockets (ISSN 0022-4650), vol. 28,

July-Aug. 1991, p. 433-438. Previously cited in issue 21, p. 3335. Accession no. A90-47224. refs
(Contract NAS3-25266) Copyright

A91-52309* National Aeronautics and Space Administration. Lewis Research Center, Cleveland, OH.

LIQUID OXYGEN COOLING OF HYDROCARBON FUELED ROCKET THRUST CHAMBERS

ELIZABETH A. RONCACE (NASA, Lewis Research Center, Cleveland, OH) Journal of Propulsion and Power (ISSN 0748-4658), vol. 7, Sept.-Oct. 1991, p. 717-723. Previously cited in issue 21, p. 3298, Accession no. A89-49686. refs
Copyright

A91-52311 National Aeronautics and Space Administration. Lewis Research Center, Cleveland, OH.

ENERGY DEPOSITION IN LOW-POWER COAXIAL PLASMA THRUSTERS

R. M. MYERS (NASA, Lewis Research Center; Sverdrup Technology, Inc., Cleveland, OH), A. J. KELLY, and R. G. JAHN (Princeton University, NJ) Journal of Propulsion and Power (ISSN 0748-4658), vol. 7, Sept.-Oct. 1991, p. 732-739. Research supported by Rocket Research, Inc., Hercules Aerospace Co., and DOE. refs
(Contract JPL-954997) Copyright

An experimental examination of energy deposition in self-field, coaxial plasma thrusters revealed that the thrust efficiency ranged from 2-9 percent and that the dominant losses resulted from electrode heating and propellant ionization. Sensible enthalpy and radiative losses were negligible. Thruster specific impulse increased with current, ranging from 550-1750 seconds. Spectroscopic studies of the plume plasma showed that the electron temperature ranged from 0.5-2.5 eV and that the dominant species were singly and doubly ionized argon. Attempts to raise thruster efficiency by increasing the chamber pressure resulted in reduced electrode losses and lowered I(sp), but the thrust efficiency decreased because of a current redistribution that lowered the thrust beyond expectations. Author

A91-52312* National Aeronautics and Space Administration. Lewis Research Center, Cleveland, OH.

FIVE-KILOWATT ARCJET POWER ELECTRONICS

R. P. GRUBER, R. W. GOTT, and T. W. HAAG (NASA, Lewis Research Center, Cleveland, OH) Journal of Propulsion and Power (ISSN 0748-4658), vol. 7, Sept.-Oct. 1991, p. 740-748. Previously cited in issue 21, p. 3208, Accession no. A89-49685. refs
Copyright

A91-52313* National Aeronautics and Space Administration. Lewis Research Center, Cleveland, OH.

ANTIPROTON POWERED PROPULSION WITH MAGNETICALLY CONFINED PLASMA ENGINES

MICHAEL R. LAPOINTE (NASA, Lewis Research Center, Cleveland; Sverdrup Technology, Inc., Brook Park, OH) Journal of Propulsion and Power (ISSN 0748-4658), vol. 7, Sept.-Oct. 1991, p. 749-759. Previously cited in issue 20, p. 3114, Accession no. A89-46758. refs
Copyright

A91-52314 National Aeronautics and Space Administration. Lewis Research Center, Cleveland, OH.

CATHODE PHENOMENA IN A LOW-POWER MAGNETOPLASMA DYNAMIC THRUSTER

R. M. MYERS (NASA, Lewis Research Center; Sverdrup Technology, Inc., Cleveland, OH), N. SUZUKI (NASA, Johnson Space Center; Rockwell International Corp., Houston, TX), A. J. KELLY, and R. G. JAHN (Princeton University, NJ) Journal of Propulsion and Power (ISSN 0748-4658), vol. 7, Sept.-Oct. 1991, p. 760-766. Research supported by Rocket Research, Inc., Hercules Aerospace Co., and DOE. Previously cited in issue 04,

20 SPACECRAFT PROPULSION AND POWER

p. 491, Accession no. A89-16481. refs
(Contract JPL-954997)
Copyright

A91-52326*# National Aeronautics and Space Administration.
Lewis Research Center, Cleveland, OH.

PERFORMANCE IMPACT ON NUCLEAR THERMAL PROPULSION OF PILOTED MARS MISSIONS WITH SHORT TRANSIT TIMES

T. J. WICKENHEISER, K. S. GESSNER, and S. W. ALEXANDER
(NASA, Lewis Research Center, Cleveland, OH) AIAA, NASA, and OAI, Conference on Advanced SEI Technologies, Cleveland, OH, Sept. 4-6, 1991. 22 p. refs
(AIAA PAPER 91-3401) Copyright

The requirements of nuclear thermal propulsion (NTP) are examined with respect to a specific mission scenario derived from Stafford Committee recommendations. The recommended mission scenario is a split/sprint opposition mission which includes a piloted vehicle and a cargo vehicle, and the baseline mission is developed from a reference trajectory. Key mission parameters are developed from the baseline mission, including engine-thrust levels, mission opportunity, and engine burn-time requirements. The impact of engine failure is also considered in terms of burn-time requirements, and other mission-performance issues considered include propulsion-technology assumptions, triple-perigee earth-departure burns, and Mars parking-orbit selection. The engine requirements call for a 50-75-kib engine-thrust level, maximum single burn time of 0.6 hours, and a maximum total-mission burn time of 1.7 hours. For a crew of 6, a 475-day total-mission trip with a 90-day stay at Mars is possible.
C.C.S.

A91-52335*# National Aeronautics and Space Administration.
Lewis Research Center, Cleveland, OH.

THE NASA/DOE/DOD NUCLEAR ROCKET PROPULSION PROJECT - FY 1991 STATUS

JOHN S. CLARK and THOMAS J. MILLER (NASA, Lewis Research Center, Cleveland, OH) AIAA, NASA, and OAI, Conference on Advanced SEI Technologies, Cleveland, OH, Sept. 4-6, 1991. 5 p. refs
(AIAA PAPER 91-3413) Copyright

NASA has initiated planning and critical technology development for nuclear rocket propulsion systems for Space Exploration Initiative missions to the moon and to Mars. Interagency agreements are being negotiated between NASA, the Department of Energy, and the Department of Defense for joint technology development activities. This paper summarizes the activities of the NASA project planning team in FY 1990 that led to the draft Nuclear Propulsion Project Plan, outlines the FY 1991 Interagency activities, and describes the current status of the project plan.

Author

A91-52351*# National Aeronautics and Space Administration.
Lewis Research Center, Cleveland, OH.

PLANS FOR THE DEVELOPMENT OF CRYOGENIC ENGINES FOR SPACE EXPLORATION

JAMES R. STONE, LORETTA M. SHAW (NASA, Lewis Research Center, Cleveland, OH), and CARL A. AUKERMAN (NASA, Lewis Research Center; Sverdrup Technology, Inc., Cleveland, OH) AIAA, NASA, and OAI, Conference on Advanced SEI Technologies, Cleveland, OH, Sept. 4-6, 1991. 20 p. refs
(AIAA PAPER 91-3438) Copyright

The NASA Lewis Research Center (LeRC) is conducting a broad range of basic research and focused technology development activities in both aeronautical and space propulsion. By virtue of the successful conduct of these programs, LeRC is strongly qualified to lead Advanced Development and subsequent development programs on cryogenic space propulsion systems in support of the Space Exploration Initiative. This paper provides a review of technology status, including recent progress in the ongoing activities, and a top level description of the proposed program.
Author

A91-52352*# National Aeronautics and Space Administration.
Lewis Research Center, Cleveland, OH.

HYDROGEN/OXYGEN AUXILIARY PROPULSION TECHNOLOGY

BRIAN D. REED and STEVEN J. SCHNEIDER (NASA, Lewis Research Center, Cleveland, OH) AIAA, NASA, and OAI, Conference on Advanced SEI Technologies, Cleveland, OH, Sept. 4-6, 1991. 37 p. refs
(AIAA PAPER 91-3440) Copyright

This paper provides a survey of hydrogen/oxygen (H/O) auxiliary propulsion system (APS) concepts and low thrust H/O rocket technology. A review of H/O APS studies performed for the Space Shuttle, Space Tug, Space Station Freedom, and Advanced Manned Launch System programs is given. The survey also includes a review of low thrust H/O rocket technology programs, covering liquid H/O and gaseous H/O rocket technology, ranging from 6600 N to 440 mN thrust. Ignition concepts for H/O thrusters and high-temperature, oxidation-resistant chamber materials are also reviewed.
Author

A91-52353*# National Aeronautics and Space Administration.
Lewis Research Center, Cleveland, OH.

BLAZING THE TRAILWAY - NUCLEAR ELECTRIC PROPULSION AND ITS TECHNOLOGY PROGRAM PLANS

MICHAEL P. DOHERTY (NASA, Lewis Research Center, Cleveland, OH) AIAA, NASA, and OAI, Conference on Advanced SEI Technologies, Cleveland, OH, Sept. 4-6, 1991. 21 p. refs
(AIAA PAPER 91-3441) Copyright

An overview is given of the plans for a program in nuclear electric propulsion (NEP) technology for outer space applications being considered by NASA, DOE, and DOD. Possible missions using NEP are examined, and NEP technology plans are addressed regarding concept development, systems engineering, nuclear fuels, power conversion, thermal management, power management and distribution, electric thrusters, facilities, and issues related to safety and environment. The programmatic characteristics are considered.
C.D.

A91-52355*# National Aeronautics and Space Administration.
Lewis Research Center, Cleveland, OH.

THE NASA LEWIS RESEARCH CENTER ELECTRIC PROPULSION PROGRAM

DAVID C. BYERS (NASA, Lewis Research Center, Cleveland, OH) AIAA, NASA, and OAI, Conference on Advanced SEI Technologies, Cleveland, OH, Sept. 4-6, 1991. 12 p. refs
(AIAA PAPER 91-3443) Copyright

The Lewis Research Center conducts an electric propulsion program aimed at a broad class of space missions. The program is structured in an evolutionary fashion in order to both maximize expectations for the acceptance of developed concepts and accommodate anticipated developments of critical system technologies. Recent efforts have assisted in the acceptance of low power electric rockets. Primary electric propulsion concepts are also being developed for both Solar Electric Propulsion Systems and Nuclear Electric Propulsion Systems class space missions, and the paper briefly describes the concepts under evaluation for potential Space Exploration Initiative missions.
Author

A91-52369*# National Aeronautics and Space Administration.
Lewis Research Center, Cleveland, OH.

SEI NEEDS FOR SPACE NUCLEAR POWER

H. W. BRANDHORST and R. L. CATALDO (NASA, Lewis Research Center, Cleveland, OH) AIAA, NASA, and OAI, Conference on Advanced SEI Technologies, Cleveland, OH, Sept. 4-6, 1991. 10 p. refs
(AIAA PAPER 91-3459)

The use of nuclear electric propulsion (NEP) and nuclear thermal propulsion (NTP) for transportation to the moon and Mars is examined, and the use on Mars and moon bases of thermal conversion subsystems based on either a Brayton or a Stirling cycle is examined. It is shown that both cycles are attractive alternatives for those applications where continuous field operation

is desired. Nuclear power systems have a clear advantage with regard to the moon and a lesser one with regard to Mars. C.D.

A91-52382*# McDonnell-Douglas Space Systems Co., Houston, TX.

CRYOGENIC PROPELLANT MANAGEMENT SYSTEM REQUIREMENTS FOR SPACE STATION FREEDOM

R. J. SAUCILLO (McDonnell Douglas Space Systems Co., Houston, TX), S. M. STEVENSON, and R. R. CORBAN (NASA, Lewis Research Center, Cleveland, OH) AIAA, NASA, and OAI, Conference on Advanced SEI Technologies, Cleveland, OH, Sept. 4-6, 1991. 9 p. refs
(AIAA PAPER 91-3476) Copyright

Specific propellant management system requirements have been identified for each facility category of SSF. Distributed systems have been analyzed to identify momentum management, guidance, and traffic management requirements associated with the guidance, navigation, and control system; space-to-space communications and enhanced tracking requirements associated with the communications and tracking system; and propellant management system utility requirements associated with the electrical power system. Flight element analyses determined attach structure, utility distribution, and structural integrity requirements for the pre-integrated truss and high mass manipulation and translation requirements for the mobile base system. O.G.

A91-52384*# McDonnell-Douglas Space Systems Co., Huntington Beach, CA.

FUEL SYSTEMS ARCHITECTURE (FSA) EVALUATION CRITERIA AND CONCEPT EVALUATION METHODOLOGY

J. E. HENDERSHOT (McDonnell Douglas Space Systems Co., Huntington Beach, CA), R. R. CORBAN, and S. M. STEVENSON (NASA, Lewis Research Center, Cleveland, OH) AIAA, NASA, and OAI, Conference on Advanced SEI Technologies, Cleveland, OH, Sept. 4-6, 1991. 9 p. refs
(AIAA PAPER 91-3479) Copyright

Consideration is given to two methods developed for the evaluation, screening, and ranking of concepts for Space Exploration Initiative vehicle propellant management systems. The methods selected for handling this multicriteria decision problem are based on the utility theory which transforms both qualitative and quantitative criteria into a nondimensional utility scale for comparison of dissimilar figures of merit. The development of the resultant FSA evaluation criteria and concept evaluation methodology is summarized. O.G.

A91-52388*# National Aeronautics and Space Administration, Lewis Research Center, Cleveland, OH.

NUCLEAR ELECTRIC PROPULSION MISSION PERFORMANCE FOR FAST PILOTED MARS MISSIONS

K. J. HACK, J. A. GEORGE, and L. A. DUDZINSKI (NASA, Lewis Research Center, Cleveland, OH) AIAA, NASA, and OAI, Conference on Advanced SEI Technologies, Cleveland, OH, Sept. 4-6, 1991. 14 p. refs
(AIAA PAPER 91-3488) Copyright

A mission study aimed at minimizing the time humans would spend in the space environment is presented. The use of nuclear electric propulsion (NEP), when combined with a suitable mission profile, can reduce the trip time to durations competitive with other propulsion systems. Specifically, a split mission profile utilizing an earth crew capture vehicle accounts for a significant portion of the trip time reduction compared to previous studies. NEP is shown to be capable of performing fast piloted missions to Mars at low power levels using near-term technology and is considered to be a viable candidate for these missions. O.G.

A91-52400*# National Aeronautics and Space Administration, Lewis Research Center, Cleveland, OH.

AN OVERVIEW OF TESTED AND ANALYZED NTP CONCEPTS

JAMES T. WALTON (NASA, Lewis Research Center, Cleveland, OH) AIAA, NASA, and OAI, Conference on Advanced SEI Technologies, Cleveland, OH, Sept. 4-6, 1991. 24 p. refs
(AIAA PAPER 91-3503) Copyright

The goals of the Space Exploration Initiative are discussed, and the technologies which enable their attainment are evaluated. The main driving technology is the propulsion system; for interplanetary missions, the safest and most affordable is a Nuclear Thermal Propulsion (NTP) system. This paper presents an overview of the NTP systems which have received detailed conceptual design and, for several, testing. Author

A91-52413*# National Aeronautics and Space Administration, Lewis Research Center, Cleveland, OH.

TRADE STUDIES FOR NUCLEAR SPACE POWER SYSTEMS

JOHN M. SMITH, DAVID J. BENTS, and HARVEY S. BLOOMFIELD (NASA, Lewis Research Center, Cleveland, OH) AIAA, NASA, and OAI, Conference on Advanced SEI Technologies, Cleveland, OH, Sept. 4-6, 1991. 13 p. refs
(AIAA PAPER 91-3518)

As visions of space applications expand and as probes extend further and further out into the universe, the need for power also expands, and missions evolve which are enabled by nuclear power. A broad spectrum of missions which are enhanced or enabled by nuclear power sources are defined. These include earth orbital platforms, deep space platforms, planetary exploration and extraterrestrial resource exploration. The recently proposed Space Exploration Initiative (SEI) to the moon and Mars has more clearly defined these missions and their power requirements. This paper presents results of recent studies of radioisotope and nuclear-reactor energy sources combined with various energy-conversion devices for earth orbital applications, SEI lunar/Mars rover and surface power, and planetary exploration. Author

A91-52443*# National Aeronautics and Space Administration, Lewis Research Center, Cleveland, OH.

ADVANCED ION PROPULSION FOR SPACE EXPLORATION

VINCENT K. RAWLIN (NASA, Lewis Research Center, Cleveland, OH) AIAA, NASA, and OAI, Conference on Advanced SEI Technologies, Cleveland, OH, Sept. 4-6, 1991. 16 p. refs
(AIAA PAPER 91-3567) Copyright

Ion propulsion is one of the numerous technologies proposed for the Space Exploration Initiative. To operate at the megawatt power levels required for Martian cargo and/or piloted missions, ion propulsion must evolve from present technologies. The principles of operation and a brief historical review of this form of propulsion are described. Also presented are the performance of present 50-cm diameter inert gas ion thrusters at power levels and specific impulse values up to 19 kW and 9300 seconds, respectively. These thrusters are applicable to orbit transfer vehicles, planetary probes, and other precursor missions. Author

A91-52444*# National Aeronautics and Space Administration, Lewis Research Center, Cleveland, OH.

MPD THRUSTER TECHNOLOGY

ROGER M. MYERS, MICHAEL R. LAPOINTE (NASA, Lewis Research Center, Cleveland; Sverdrup Technology, Inc., Brook Park, OH), and MARIS A. MANTENIEKS (NASA, Lewis Research Center, Cleveland, OH) AIAA, NASA, and OAI, Conference on Advanced SEI Technologies, Cleveland, OH, Sept. 4-6, 1991. 34 p. refs
(AIAA PAPER 91-3568) Copyright

MPD thrusters have demonstrated between 2000 and 7000 sec specific impulse at efficiencies approaching 40 percent, and have been operated continuously at power levels over 500 kW. These demonstrated capabilities, combined with the simplicity and robustness of the thruster, make them attractive candidates for application to both unmanned and manned orbit raising, lunar, and planetary missions. This work reviews the present status of MPD thruster research, including developments in the measured performance levels and electrode erosion rates, and theoretical studies of the thruster dynamics. Significant progress has been made in establishing empirical scaling laws, performance and lifetime limitations, and in the development of numerical codes to simulate the flowfield and the electrode processes. Author

20 SPACECRAFT PROPULSION AND POWER

A91-52448* Science Applications International Corp., Schaumburg, IL.

NTR VEHICLE COMMONALITY ASSESSMENT FOR PILOTED LUNAR AND MARS MISSIONS

JOHN T. COLLINS, HARVEY FEINGOLD (Science Applications International Corp., Schaumburg, IL), and STANLEY K. BOROWSKI (NASA, Lewis Research Center, Cleveland, OH) AIAA, NASA, and OAI, Conference on Advanced SEI Technologies, Cleveland, OH, Sept. 4-6, 1991. 20 p. refs
(AIAA PAPER 91-3575) Copyright

A study is presented that assesses the feasibility of (1) using common nuclear thermal rocket (NTR) vehicle components to perform a wide range of lunar and Mars missions, and (2) potential performance gains achieved via 'dual-mode' NTR operation, where the nuclear reactor is utilized not only for propulsion but also for electrical power generation. Four vehicle configurations are considered, modular designs with multiple single engine modules and single engine designs with multiple propellant tanks. The standard tank sizes arrived at in the Mars mission mass performance calculations are then applied to cargo and piloted lunar craft to evaluate lunar NTR mass performance against that for chemical propulsion. R.E.P.

A91-52450* National Aeronautics and Space Administration, Lewis Research Center, Cleveland, OH.

COMPUTATIONAL FLUID DYNAMICS STUDIES OF NUCLEAR ROCKET PERFORMANCE

ROBERT M. STUBBS, THOMAS J. BENSON (NASA, Lewis Research Center, Cleveland, OH), and SUK C. KIM (NASA, Lewis Research Center; Sverdrup Technology, Inc., Cleveland, OH) AIAA, NASA, and OAI, Conference on Advanced SEI Technologies, Cleveland, OH, Sept. 4-6, 1991. 12 p. refs
(Contract NAS3-25266)
(AIAA PAPER 91-3577) Copyright

A CFD analysis of a low pressure nuclear rocket concept is presented with the use of an advanced chemical kinetics, Navier-Stokes code. The computations describe the flow field in detail, including gas dynamic, thermodynamic and chemical properties, as well as global performance quantities such as specific impulse. Computational studies of several rocket nozzle shapes are conducted in an attempt to maximize hydrogen recombination. These Navier-Stokes calculations, which include real gas and viscous effects, predict lower performance values than have been reported heretofore. Author

A91-52451* National Aeronautics and Space Administration, Lewis Research Center, Cleveland, OH.

ANALYTICAL STUDY OF NOZZLE PERFORMANCE FOR NUCLEAR THERMAL ROCKETS

KENNETH O. DAVIDIAN and KENNETH J. KACYNSKI (NASA, Lewis Research Center, Cleveland, OH) AIAA, NASA, and OAI, Conference on Advanced SEI Technologies, Cleveland, OH, Sept. 4-6, 1991. 28 p. refs
(AIAA PAPER 91-3578) Copyright

A parametric study has been conducted by the NASA-Lewis Rocket Engine Design Expert System for the convergent-divergent nozzle of the Nuclear Thermal Rocket system, which uses a nuclear reactor to heat hydrogen to high temperature and then expands it through the nozzle. It is established by the study that finite-rate chemical reactions lower performance levels from theoretical levels. Major parametric roles are played by chamber temperature and chamber pressure. A maximum performance of 930 sec is projected at 2700 K, and of 1030 at 3100 K. O.C.

A91-52472* National Aeronautics and Space Administration, Lewis Research Center, Cleveland, OH.

MULTIMEGAWATT NUCLEAR POWER SYSTEMS FOR NUCLEAR ELECTRIC PROPULSION

JEFFREY A. GEORGE (NASA, Lewis Research Center, Cleveland, OH) AIAA, NASA, and OAI, Conference on Advanced SEI Technologies, Cleveland, OH, Sept. 4-6, 1991. 11 p. refs
(AIAA PAPER 91-3607) Copyright

Results from systems analysis studies of multimegawatt nuclear

power systems are presented for application to nuclear electric propulsion. Specific mass estimates are presented for nearer term SP-100 reactor-based potassium Rankine and Brayton power systems for piloted and cargo missions. Growth SP-100/Rankine systems were found to range from roughly 7 to 10 kg/kWe specific mass depending on full power life requirements. The SP-100/Rankine systems were also found to result in a 4-kg/kWe savings in specific mass over SP-100/Brayton systems. The potential of advanced, higher temperature reactor and power conversion technologies for achieving reduced mass Rankine and Brayton systems was also investigated. A target goal of 5 kg/kWe specific mass was deemed reasonable given either 1400 K potassium Rankine with 1500 K lithium-cooled reactors or 2000 K gas cooled reactors with Brayton conversion. Author

A91-52495* National Aeronautics and Space Administration, Lewis Research Center, Cleveland, OH.

NUCLEAR THERMAL PROPULSION TECHNOLOGY - SUMMARY OF FY 1991 INTERAGENCY PANEL PLANNING

JOHN S. CLARK (NASA, Lewis Research Center, Cleveland, OH), PATRICK MCDANIEL (USAF, Phillips Laboratory, Kirtland AFB, NM), STEVEN HOWE (Los Alamos National Laboratory, NM), and MARLAND STANLEY (Idaho National Engineering Laboratory, Idaho Falls) AIAA, NASA, and OAI, Conference on Advanced SEI Technologies, Cleveland, OH, Sept. 4-6, 1991. 11 p. refs
(AIAA PAPER 91-3631) Copyright

An Interagency (NASA/DOE/DOD) technical panel has been working in 1991 to evaluate nuclear thermal propulsion (NTP) concepts on a consistent basis, and to continue technology development project planning for a joint project in nuclear propulsion for Space Exploration Initiative (SEI). This paper summarizes the efforts of the panel to date and summarizes the technology plans defined for NTP. Concepts were categorized based on probable technology readiness data, and innovative 'proof-of-concept' tests and analyses were defined. While further studies will be required to provide a consistent comparison of all of the NTP concepts, the current status of the studies is presented. Author

A91-53706* National Aeronautics and Space Administration, Lewis Research Center, Cleveland, OH.

NUMERICAL PROPULSION SYSTEM SIMULATION - AN INTERDISCIPLINARY APPROACH

LESTER D. NICHOLS and CHRISTOS C. CHAMIS (NASA, Lewis Research Center, Cleveland, OH) AIAA, NASA, and OAI, Conference on Advanced SEI Technologies, Cleveland, OH, Sept. 4-6, 1991. 15 p. Previously announced in STAR as N91-29221. refs
(AIAA PAPER 91-3554) Copyright

The tremendous progress being made in computational engineering and the rapid growth in computing power that is resulting from parallel processing now make it feasible to consider the use of computer simulations to gain insights into the complex interactions in aerospace propulsion systems and to evaluate new concepts early in the design process before a commitment to hardware is made. Described here is a NASA initiative to develop a Numerical Propulsion System Simulation (NPSS) capability. Author

A91-53709* National Aeronautics and Space Administration, Lewis Research Center, Cleveland, OH.

DESIGN ISSUES FOR PROPULSION SYSTEMS USING METALLIZED PROPELLANTS

BRYAN PALASZEWSKI (NASA, Lewis Research Center, Cleveland, OH) and DOUGLAS RAPP (NASA, Lewis Research Center, Cleveland; Sverdrup Technology, Inc., Brook Park, OH) AIAA, NASA, and OAI, Conference on Advanced SEI Technologies, Cleveland, OH, Sept. 4-6, 1991. 26 p. Previously announced in STAR as N91-29220. refs
(AIAA PAPER 91-3484) Copyright

Metallized propellants are liquid propellants that contain metal particles. These particles are suspended in a gelled fuel or oxidizer. Aluminum is used as the metal additive. The addition of metal to

conventional propellants can increase their specific impulse and their density over conventional propellants, and consequently, the payload delivered on Mars and lunar transportation vehicles, Earth-to-Orbit vehicles and upper stages for robotic planetary missions. Gelled fuels also provide increased safety during accidental propellant leakage or spills. To take full advantage of these potential performance increases, there are changes that must be made to the vehicle design. The differences are discussed between metallized propellant and traditional liquid propellants and their effect on the propulsion system design. These differences include the propellant density, mixture ratio, engine performance, and propellant rheology. Missions related to the Space Exploration Initiative are considered as design examples to illustrate these issues. Author

A91-53712* National Aeronautics and Space Administration. Lewis Research Center, Cleveland, OH.

EVOLVING THE SP-100 REACTOR IN ORDER TO BOOST LARGE PAYLOADS TO GEO AND TO LOW LUNAR ORBIT VIA NUCLEAR-ELECTRIC PROPULSION

ROBERT E. ENGLISH (NASA, Lewis Research Center, Cleveland, OH) AIAA, NASA, and OAI, Conference on Advanced SEI Technologies, Cleveland, OH, Sept. 4-6, 1991. 13 p. Previously announced in STAR as N91-27212. refs (AIAA PAPER 91-3562) Copyright

In striving to reduce exploration cost and exploration risks, a crucial aspect of the plans is program continuity, i.e., the continuing application of a given technology over a long period so that experience will accumulate from extended testing here on earth and from a diversity of applications in space. An integrated view needs to be formed of the missions SEI will carry out, near term as well as far, and of the ways in which these missions can mutually support one another. Near term programs should be so constituted as to provide for the long term missions both the enabling technologies and the accumulation of experience they need. In achieving this, missions in earth orbit should both evolve and show the technologies crucial to long term missions on the lunar surfaces, and the program for the lunar labs should evolve and show the enabling technologies for exploration of the surface of Mars and for flights of human beings to Mars and return. In the near term, the program for the Space Station should be directed and funded to develop and demonstrate the solar Brayton power plant that will be most useful as the power generator for the SP-100 nuclear reactor. Author

N91-10117* National Aeronautics and Space Administration. Lewis Research Center, Cleveland, OH.

ANALYSIS OF 5 KHZ COMBUSTION INSTABILITIES IN 40K METHANE/LOX COMBUSTION CHAMBERS

KEVIN J. BREISACHER and RICHARD J. PRIEM (Sverdrup Technology, Inc., Cleveland, OH.) 1988 12 p Presented at the 25th JANNAF Combustion Meeting, Huntsville, AL, 24-28 Oct. 1988

(Contract SVERDRUP-5324-85; RTOP 582-01-21) (NASA-TM-101368; E-4407; NAS 1.15:101368) Avail: NTIS HC/MF A03 CSCL 21H

In 40K methane/LOX 5 KHz engine tests, (first transverse mode) combustion instabilities observed by Rocketdyne are analyzed using Heidmann and Wieber's vaporization model to include LOX flow oscillations. The LOX flow oscillations are determined by including acoustic waves in the feed system analysis. The major parameter controlling stability is the distance (or time delay) associated with atomizing the LOX stream in the coaxial injection system. Results of the analysis that show the influence of mixture ratio, oxidizer and fuel injection velocities, burning time and combustion chamber/injector dimensions on stability are used to explain the existing data. Calculated results to predict the influence of design changes being made for the next set of experiments are also presented. Author

N91-10118* National Aeronautics and Space Administration. Lewis Research Center, Cleveland, OH.

PERFORMANCE CHARACTERIZATION OF A SEGMENTED ANODE ARCJET THRUSTER

FRANCIS M. CURRAN, DAVID H. MANZELLA (Sverdrup Technology, Inc., Brook Park, OH.), and ERIC J. PENCIL Jul. 1990 18 p Presented at the 21st International Electric Propulsion Conference, Orlando, FL, 18-20 Jul. 1990; sponsored in part by AIAA, DGLR, and JSASS

(Contract RTOP 506-42-31) (NASA-TM-103227; E-5643; NAS 1.15:103227; AIAA PAPER 90-2582) Avail: NTIS HC/MF A03 CSCL 21H

A modular, 1 to 2 kW class arcjet thruster incorporating a segmented anode/nozzle was operated on a thrust stand to obtain performance characteristics of the device and further study its operating characteristics under a number of experimental conditions. The nozzle was composed of five axial conducting segments isolated from one another by boron nitride spacers. The electrical configuration allowed the current delivered to the arcjet to be collected at any combination of segments. Both the current collected by each segment, and the potential difference between the cathode and each segment were monitored throughout the test period. As in previous tests a similar device, current appeared to attach diffusely in the anode when all of the segments were allowed to conduct. Improvements to the device allowed long term (4 to 8 hour) operation at steady-state and operating characteristics were repeatable over extended periods. Performance characteristics indicated that the segmented anode reasonably simulates the behavior of solid anodes of similar geometry. Current distribution depended on flow rate as the arc attachment moved downstream in the nozzle with increases in the mass flow rate. The current level had little effect on current distribution on the anode segments. Thrust measurements indicated that the current distribution in the nozzle did not significantly affect performance of the device. Author

N91-10119* National Aeronautics and Space Administration. Lewis Research Center, Cleveland, OH.

DEVELOPMENTS IN REDES: THE ROCKET ENGINE DESIGN EXPERT SYSTEM

KENNETH O. DAVIDIAN 1990 11 p Presented at the 27th JANNAF Combustion Meeting, Cheyenne, WY, 5-9 Nov. 1990 (Contract RTOP 506-42-11)

(NASA-TM-103657; E-5848; NAS 1.15:103657) Avail: NTIS HC/MF A03 CSCL 21H

The Rocket Engine Design Expert System (REDES) is being developed at the NASA-Lewis to collect, automate, and perpetuate the existing expertise of performing a comprehensive rocket engine analysis and design. Currently, REDES uses the rigorous JANNAF methodology to analyze the performance of the thrust chamber and perform computational studies of liquid rocket engine problems. The following computer codes were included in REDES: a gas properties program named GASP, a nozzle design program named RAO, a regenerative cooling channel performance evaluation code named RTE, and the JANNAF standard liquid rocket engine performance prediction code TDK (including performance evaluation modules ODE, ODK, TDE, TDK, and BLM). Computational analyses are being conducted by REDES to provide solutions to liquid rocket engine thrust chamber problems. REDES is built in the Knowledge Engineering Environment (KEE) expert system shell and runs on a Sun 4/110 computer. Author

N91-11058* National Aeronautics and Space Administration. Lewis Research Center, Cleveland, OH.

PRELIMINARY RESULTS FROM THE ADVANCED PHOTOVOLTAIC EXPERIMENT FLIGHT TEST

DAVID J. BRINKER, RUSSELL E. HART, JR., and JOHN R. HICKEY (Eppey Lab., Inc., Newport, RI.) May 1990 12 p Presented at the 21st Photovoltaic Specialists Conference, Kissimmee, FL, 21-25 May 1990; sponsored in part by IEEE

(Contract RTOP 506-41-11) (NASA-TM-103269; E-5709; NAS 1.15:103269) Avail: NTIS HC/MF A03 CSCL 21H

20 SPACECRAFT PROPULSION AND POWER

The Advanced Photovoltaic Experiment is a space flight test designed to provide reference cell standards for photovoltaic measurement as well as to investigate the solar spectrum and the effect of the space environment on solar cells. After a flight of 69 months in low earth orbit as part of the Long Duration Exposure Facility set of experiments, it was retrieved in January, 1990. The electronic data acquisition system functioned as designed, measuring and recording cell performance data over the first 358 days of flight; limited by battery lifetime. Significant physical changes are also readily apparent, including erosion of front surface paint, micrometeoroid and debris catering and contamination.

Author

N91-11059* National Aeronautics and Space Administration, Lewis Research Center, Cleveland, OH.

A LIFE COMPARISON OF TUBE AND CHANNEL COOLING PASSAGES FOR THRUST CHAMBERS

R. S. JANKOVSKY and J. M. KAZAROFF 1990 9 p Presented at the 1990 JANNAF Propulsion Meeting, Anaheim, CA, 3-5 Oct. 1990

(Contract RTOP 591-41-21)

(NASA-TM-103613; E-5724; NAS 1.15:103613) Avail: NTIS

HC/MF A02 CSCL 21H

The life analysis used to compare copper tubes and milled copper channels for rocket engine cooling passages is described. Copper tubes were chosen as a possible replacement for the existing milled copper channel configuration because (1) they offer increased surface area for additional enthalpy extraction; (2) they have ideal pressure vessel characteristics; and (3) the shape of the tube is believed to allow free expansion, thus accommodating the strain resulting from thermal expansion. The analysis was a two-dimensional elastic-plastic comparison, using a finite element method, to illustrate that, under the same thermal and pressure loading, the compliant shape of the tube increases the life of the chamber. The analysis indicates that for a hot-gas-side-wall temperature of 100 F the critical strain decreases from 1.25 percent in the channel to 0.94 percent in the tube. Since the life of rocket thrust chambers is most often limited by cyclic strain or strain range, this decrease corresponds to an expected tube life which is nearly twice the channel life.

Author

N91-11060* National Aeronautics and Space Administration, Lewis Research Center, Cleveland, OH.

INVESTIGATION OF THE ARCJET PLUME NEAR FIELD USING ELECTROSTATIC PROBES

JOHN M. SANKOVIC Nov. 1990 19 p Presented at the 1990 JANNAF Propulsion Meeting, Anaheim, CA, 2-4 Oct. 1990

(Contract RTOP 506-42-31)

(NASA-TM-103638; E-5817; NAS 1.15:103638) Avail: NTIS

HC/MF A03 CSCL 21H

The near field plume of a 1 kW class arcjet thruster was investigated using electrostatic probes of various geometries. The electron number densities and temperatures were determined in a simulated hydrazine plume at axial distances between 3 cm (1.2 in) and 15 cm (5.9 in) and radial distances extending to 10 cm (3.9 in) off centerline. Values of electron number densities obtained using cylindrical and spherical probes of different geometries agreed very well. The electron density on centerline followed a source flow approximation for axial distances as near as 3 cm (1.2 in) from the nozzle exit plane. The model agreed well with previously obtained data in the far field. The effects of propellant mass flow rate and input power level were also studied. Cylindrical probes were used to obtain ion streamlines by changing the probe orientation with respect to the flow. The effects of electrical configuration on the plasma characteristics of the plume were also investigated by using a segmented anode/nozzle thruster. The results showed that the electrical configuration in the nozzle affected the distribution of electrons in the plume.

Author

N91-11061* National Aeronautics and Space Administration, Lewis Research Center, Cleveland, OH.

PHOTOVOLTAIC OPTIONS FOR SOLAR ELECTRIC PROPULSION

PAUL M. STELLA (Jet Propulsion Lab., California Inst. of Tech., Pasadena.) and DENNIS J. FLOOD Jul. 1990 16 p Presented at the 26th Joint Propulsion Conference, Orlando, FL, 16-18 Jul. 1990; sponsored in part by AIAA, ASME, SAE, and ASEE (Contract RTOP 506-41-11)

(NASA-TM-103284; E-5739; NAS 1.15:103284) Avail: NTIS HC/MF A03 CSCL 21H

During the past decade, a number of advances have occurred in solar cell and array technology. These advances have led to performance improvement for both conventional space arrays and for advanced technology arrays. Performance enhancements have occurred in power density, specific power, and environmental capability. Both state-of-the-art and advanced development cells and array technology are discussed. Present technology will include rigid, rollout, and foldout flexible substrate designs, with silicon and GaAs solar cells. The use of concentrator array systems is also discussed based on both DOD and NASA efforts. The benefits of advanced lightweight array technology, for both near term and far term utilization, and of advanced high efficiency, thin, radiation resistant cells is examined. This includes gallium arsenide on germanium substrates, indium phosphide, and thin film devices such as copper indium diselenide.

Author

N91-11796* National Aeronautics and Space Administration, Lewis Research Center, Cleveland, OH.

STATUS OF STRUCTURAL ANALYSIS OF 30 CM DIAMETER ION OPTICS

GREGORY S. MACRAE and GARY T. HERING 1990 17 p Presented at the 21st International Electric Propulsion Conference, Orlando, FL, 18-20 Jul. 1990; cosponsored by AIAA, DGLR, and JSASS

(Contract RTOP 506-42-31)

(NASA-TM-103618; E-5775; NAS 1.15:103618; AIAA PAPER 90-2649) Avail: NTIS HC/MF A03 CSCL 21/8

Three structural finite element programs are compared with theory, experimental data, and each other to evaluate their usefulness for modeling the thermomechanical deflection of ion engine electrodes. Two programs, NASTRAN and MARC, used a Cray XMP and the third, Algor, used an IBM compatible personal computer. The shape of the applied temperature gradient greatly affects off-axis displacement, implying that an accurate temperature distribution is required to analyze new designs. The use of bulk material constants to model the perforated electrodes was investigated. The stress and displacement predictions are shown to be sensitive to the temperature gradient and the Young's modulus, and insensitive to number of nodes, above some minimum value, and the Poisson ratio used. The models are shown to be useful tools for evaluating designs. Experimental measurements of temperatures and displacements was identified as the most critical area.

Author

N91-11797* National Aeronautics and Space Administration, Lewis Research Center, Cleveland, OH.

ADVANCED LAUNCH VEHICLE UPPER STAGES USING LIQUID PROPULSION AND METALLIZED PROPELLANTS

B. A. PALASZEWSKI 1990 24 p Presented at the 1990 JANNAF Propulsion Meeting, Anaheim, CA, 3-5 Oct. 1990

(Contract RTOP 506-42-00)

(NASA-TM-103622; E-5779; NAS 1.15:103622) Avail: NTIS HC/MF A03 CSCL 21/8

Metallized propellants are liquid propellants with a metal additive suspended in a gelled fuel or oxidizer. Typically, aluminum particles are the metal additives. These propellants provide increase in the density and/or the specific impulse of the propulsion system. Using metallized propellants for volume- and mass-constrained upper stages can deliver modest increases in performance for Low Earth Orbit to Geosynchronous Earth Orbit and other Earth orbital transfer missions. Metallized propellants, however, can enable very fast planetary missions with a single-stage upper stage system. Trade studies comparing metallized propellant stage performance with non-metallized upper stages and the Inertial Upper Stage are presented. These upper stages are both one- and two-stage vehicles that provide the added energy to send

payloads to altitudes and onto trajectories that are unattainable with only the launch vehicle. The stage designs are controlled by the volume and the mass constraints of the Space Transportation System and Space Transportation System-Cargo launch vehicles. The influences of the density and specific impulse increases enabled by metallized propellants are examined for a variety of different stage and propellant combinations. Author

N91-11798*# National Aeronautics and Space Administration. Lewis Research Center, Cleveland, OH.
XENON ION PROPULSION FOR ORBIT TRANSFER
 V. K. RAWLIN, M. J. PATTERSON, and R. P. GRUBER Jul. 1990 30 p Presented at the 21st International Electric Propulsion Conference, Orlando, FL, 18-20 Jul. 1990; sponsored in part by AIAA, DGLR, and JSASS
 (Contract RTOP 506-42-31)
 (NASA-TM-103193; E-5586; NAS 1.15:103193; AIAA PAPER 90-2527) Avail: NTIS HC/MF A03 CSCL 21/8

For more than 30 years, NASA has conducted an ion propulsion program which has resulted in several experimental space flight demonstrations and the development of many supporting technologies. Technologies appropriate for geosynchronous stationkeeping, earth-orbit transfer missions, and interplanetary missions are defined and evaluated. The status of critical ion propulsion system elements is reviewed. Electron bombardment ion thrusters for primary propulsion have evolved to operate on xenon in the 5 to 10 kW power range. Thruster efficiencies of 0.7 and specific impulse values of 4000 s were documented. The baseline thruster currently under development by NASA LeRC includes ring-cusp magnetic field plasma containment and dished two-grid ion optics. Based on past experience and demonstrated simplifications, power processors for these thrusters should have approximately 500 parts, a mass of 40 kg, and an efficiency near 0.94. Thrust vector control, via individual thruster gimbals, is a mature technology. High pressure, gaseous xenon propellant storage and control schemes, using flight qualified hardware, result in propellant tankage fractions between 0.1 and 0.2. In-space and ground integration testing has demonstrated that ion propulsion systems can be successfully integrated with their host spacecraft. Ion propulsion system technologies are mature and can significantly enhance and/or enable a variety of missions in the nation's space propulsion program. Author

N91-11799*# National Aeronautics and Space Administration. Lewis Research Center, Cleveland, OH.
UNSTEADY BLADE-SURFACE PRESSURES ON A LARGE-SCALE ADVANCED PROPELLER: PREDICTION AND DATA
 M. NALLASAMY (Sverdrup Technology, Inc., Brook Park, OH.) and J. F. GROENEWEG Jul. 1990 15 p Presented at the 26th Joint Propulsion Conference, Orlando, FL, 16-18 Jul. 1990; sponsored in part by AIAA, SAE, ASME, and ASEE Previously announced in IAA as A90-47220 Original contains color illustrations
 (Contract NAS3-24105; RTOP 505-62-4D)
 (NASA-TM-103218; E-5630; NAS 1.15:103218) Avail: NTIS HC/MF A03; 1 functional color page CSCL 21/8

An unsteady 3-D Euler analysis technique is employed to compute the flow field of an advanced propeller operating at an angle of attack. The predicted blade pressure waveforms are compared with wind tunnel data at two Mach numbers, 0.5 and 0.2. The inflow angle is three degrees. For an inflow Mach number of 0.5, the predicted pressure response is in fair agreement with data: the predicted phases of the waveforms are in close agreement with data while the magnitudes are underpredicted. At the low Mach number of 0.2 (takeoff), the numerical solution shows the formation of a leading edge vortex which is in qualitative agreement with measurements. However, the highly nonlinear pressure response measured on the blade suction surface is not captured in the present inviscid analysis. Author

N91-11800*# National Aeronautics and Space Administration. Lewis Research Center, Cleveland, OH.
METALLIZED PROPELLANTS FOR THE HUMAN EXPLORATION OF MARS
 BRYAN A. PALASZEWSKI Nov. 1990 14 p
 (Contract RTOP 506-42-00)
 (NASA-TP-3062; E-5544; NAS 1.60:3062) Avail: NTIS HC/MF A03 CSCL 21/8

Advanced chemical propulsion using Metallized Propellants (MP) can lead to significant reductions in launch mass for piloted Mars missions. MP allow the propellant density or the specific impulse I_{sp} of the propulsion system, or both, to increase. It can reduce the propellant mass and the propulsion system dry mass. Detailed mass-scaling equations and estimates of the I_{sp} for several MP combinations are presented. The most significant savings with MP are derived from increasing the payload delivered to Mars. For the mass in low Earth orbit (LEO), a metallized Mars transfer vehicle can deliver 20 to 22 percent additional payload. This 20-percent payload increase reduces the total number of Mars flights and therefore significantly reduces the number of Space Transportation System-Cargo launches for the entire Mars architecture. Using MP to reduce the mass in LEO per flight is not as effective as increasing the payload delivery capacity. The mass saving per flight, while delivering the same payload with a higher I_{sp} system, is much smaller. Using MP in all of the Mars propulsion systems would produce a modest 3.3 percent LEO mass saving. This translates into a saving of 38,000 kg over the mass required with O₂/H₂ propulsion. A Mars excursion vehicle using Earth- or space-storable propellants for the ascent can be an alternative to storing cryogenic H₂ on Mars. A space-storable system using oxygen/monomethyl hydrazine/aluminum (O₂/MMH/Al) would deliver the lowest mass penalty over O₂/H₂. For lower-energy expedition missions the LEO mass penalty for using metallized O₂/MMH/Al would be only 3 to 5 percent. Author

N91-11801*# National Aeronautics and Space Administration. Lewis Research Center, Cleveland, OH.
REAPPRAISAL OF SOLID SELECTIVE EMITTERS
 DONALD L. CHUBB May 1990 16 p Presented at the 21st Photovoltaic Specialists Conference, Kissimmee, FL, 21-25 May 1990; sponsored in part by IEEE
 (Contract RTOP 506-41-11)
 (NASA-TM-103290; E-5750; NAS 1.15:103290) Avail: NTIS HC/MF A03 CSCL 21/8

New rare earth oxide emitters show greater efficiency than previous emitters. As a result, based on a simple model the efficiency of these emitters was calculated. Results indicate that the emission band of the selective emitter must be at relatively low energy (less than or equal to .52 eV) to obtain maximum efficiency at moderate emitter temperatures (less than or equal to 1500 K). Thus low bandgap energy PV materials are required to obtain an efficient thermophotovoltaic (TPV) system. Of the 4 specific rare earths (Nd, Ho, Er, Yb) studied Ho has the largest efficiency at moderate temperatures (72 percent at 1500 K). A comparison was made between a selective emitter TPV system and a TPV system that uses a thermal emitter plus a band pass filter to make the thermal emitter behave like a selective emitter. Results of the comparison indicate that only for very optimistic filter and thermal emitter properties will the filter TPV system have a greater efficiency than the selective emitter system. Author

N91-11802*# National Aeronautics and Space Administration. Lewis Research Center, Cleveland, OH.
A 10,000-HR LIFE TEST OF AN ENGINEERING MODEL RESISTOJET
 RODGER J. SLUTZ Oct. 1990 17 p
 (Contract RTOP 474-52-01)
 (NASA-TM-103216; E-5627; NAS 1.15:103216) Avail: NTIS HC/MF A03 CSCL 21/8

One of the major issues associated with using resistojet thrusters on Space Station Freedom is the long life required. An engineering model resistojet was life-tested to determine if it was

20 SPACECRAFT PROPULSION AND POWER

capable of meeting that requirement. This thruster, which was designed for 10,000 hr of operation at 2552.4 F (1400 C) or less under cyclical thermal conditions, successfully operated for 10,036 hr at 1836 F (1002 C) while undergoing 141 thermal cycles.

Author

N91-13491* National Aeronautics and Space Administration. Lewis Research Center, Cleveland, OH.

JANNAF LIQUID ROCKET COMBUSTION INSTABILITY PANEL RESEARCH RECOMMENDATIONS

MARK D. KLEM 1990 12 p Presented at the 27th JANNAF Combustion Meeting, Cheyenne, WY, 5-9 Nov. 1990

(Contract RTOP 506-42-00)

(NASA-TM-103653; E-5826; NAS 1.15:103653) Avail: NTIS

HC/MF A03 CSCL 21/8

The Joint Army, Navy, NASA, Air Force (JANNAF) Liquid Rocket Combustion Instability Panel was formed in 1988, drawing its members from industry, academia, and government experts. The panel was chartered to address the needs of near-term engine development programs and to make recommendations whose implementation would provide not only sufficient data but also the analysis capabilities to design stable and efficient engines. The panel was also chartered to make long-term recommendations toward developing mechanistic analysis models that would not be limited by design geometry or operating regime. These models would accurately predict stability and thereby minimize the amount of subscale testing for anchoring. The panel has held workshops on acoustic absorbing devices, combustion instability mechanisms, instability test hardware, and combustion instability computational methods. At these workshops, research projects that would meet the panel's charter were suggested. The JANNAF Liquid Rocket Combustion Instability Panel's conclusions about the work that needs to be done and recommendations on how to approach it, based on evaluation of the suggested research projects, are presented.

Author

N91-15301* National Aeronautics and Space Administration. Lewis Research Center, Cleveland, OH.

NEW METHOD OF MAKING ADVANCED TUBE-BUNDLE ROCKET THRUST CHAMBERS

JOHN M. KAZAROFF, ALBERT J. PAVLI, and GLENN A. MALONE (Electroformed Nickel, Inc., Corona, CA.) 1990 15 p Presented at the 1990 JANNAF Propulsion Meeting, Anaheim, CA, 3-5 Oct. 1990

(Contract RTOP 591-41-21)

(NASA-TM-103617; E-5723; NAS 1.15:103617) Avail: NTIS

HC/MF A03 CSCL 21/8

An improved method of fabrication rocket chambers for future space applications is described. Included are fabrication demonstrator and test chambers produced by this method. This concept offers the promise of improved cyclic life, reusability, and performance. The performance is improved because of the enhanced enthalpy extraction. The improved cyclic life, reusability, and reliability is improved because of the structural compliance inherent in the construction. The method of construction involves the forming of the combustion chamber by a tube-bundle of high conductivity copper or copper alloy tubes and the bonding of these tubes by a unique electroforming operation. Furthermore, the method of fabrication reduces chamber complexity by incorporating manifolds, and structural stiffeners while having the potential for thrust chamber cost and weight reduction.

Author

N91-15303* National Aeronautics and Space Administration. Lewis Research Center, Cleveland, OH.

THE AERODYNAMIC CHARACTERISTICS OF VORTEX INGESTION FOR THE F/A-18 INLET DUCT

BERNHARD H. ANDERSON Jan. 1991 40 p Presented at the 29th Aerospace Sciences Meeting, Reno, NV, 7-10 Jan. 1991; sponsored in part by AIAA

(Contract RTOP 505-62-52)

(NASA-TM-103703; E-5925; NAS 1.15:103703; AIAA PAPER

91-0130) Avail: NTIS HC/MF A03 CSCL 01/3

A Reduced Navier-Stokes (RNS) solution technique was

successfully combined with the concept of partitioned geometry and mesh generation to form a very efficient 3D RNS code aimed at the analysis-design engineering environment. Partitioned geometry and mesh generation is a pre-processor to augment existing geometry and grid generation programs which allows the solver to (1) recluster an existing gridfile mesh lattice, and (2) perturb an existing gridfile definition to alter the cross-sectional shape and inlet duct centerline distribution without returning to the external geometry and grid generator. The present results provide a quantitative validation of the initial value space marching 3D RNS procedure and demonstrates accurate predictions of the engine face flow field, with a separation present in the inlet duct as well as when vortex generators are installed to suppress flow separation. The present results also demonstrate the ability of the 3D RNS procedure to analyze the flow physics associated with vortex ingestion in general geometry ducts such as the F/A-18 inlet. At the conditions investigated, these interactions are basically inviscid like, i.e., the dominant aerodynamic characteristics have their origin in inviscid flow theory.

Author

N91-15306* National Aeronautics and Space Administration. Lewis Research Center, Cleveland, OH.

EFFECT OF EMITTER PARAMETER VARIATION ON THE PERFORMANCE OF HETEROEPIITAXIAL INDIUM PHOSPHIDE SOLAR CELLS

RAJ K. JAIN and DENNIS J. FLOOD Dec. 1990 15 p Presented at the 21st Photovoltaics Specialists Conference, Kissimmee, FL, 21-25 May 1990; sponsored by IEEE

(Contract RTOP 506-41-11)

(NASA-TM-103619; E-5776; NAS 1.15:103619) Avail: NTIS

HC/MF A03 CSCL 10/1

Metallorganic chemical-vapor-deposited heteroepitaxial indium phosphide (InP) solar cell experimental results were simulated by using a PC-1D computer model. The effect of emitter parameter variation on the performance of $n(+)/p/p(+)$ heteroepitaxial InP/GaAs solar cell was presented. The thinner and lighter doped emitters were observed to offer higher cell efficiencies. The influence of emitter thickness and minority carrier diffusion length on the cell efficiency with respect to dislocation density was studied. Heteroepitaxial cells with efficiencies similar to present day homojunction InP efficiencies (greater than 16 percent AMO) were shown to be attainable if a dislocation density lower than $10(\exp 6)/\text{sq cm}$ could be achieved. A realistic optimized design study yielded InP solar cells of over 22 percent AMO efficiency at 25 C.

Author

N91-15308* National Aeronautics and Space Administration. Lewis Research Center, Cleveland, OH.

LUNAR MISSIONS USING CHEMICAL PROPULSION: SYSTEM DESIGN ISSUES

BRYAN PALASZEWSKI Jan. 1991 13 p Presented at the 26th Joint Propulsion Conference, Orlando, FL, 16-18 Jul. 1990; sponsored in part by AIAA, ASME, SAE, and ASEE Previously announced as A90-47221

(Contract RTOP 506-42-51)

(NASA-TP-3065; E-5542; NAS 1.60:3065) Avail: NTIS HC/MF A03 CSCL 21/8

To transport lunar base elements to the Moon, large high-energy propulsion systems will be required. Advanced propulsion systems for lunar missions can significantly reduce launch mass and increase the delivered payload, resulting in significant launch cost savings. In this report, the masses in low Earth orbit (LEO) are compared for several propulsion systems: nitrogen tetroxide/monomethyl hydrazine (NTO/MMH), oxygen/methane (O_2/CH_4), oxygen/hydrogen (O_2/H_2), and metallized $\text{O}_2/\text{H}_2/\text{Al}$ propellants. Also addressed are payload mass increases enabled with these systems; system design issues involving the engine thrust levels, engine commonality between the transfer vehicle and the excursion vehicle; the number of launches to place the lunar mission vehicles into LEO; and analyses of small lunar missions launched from a single Space Transportation System-Cargo (STS-C) flight.

Author

N91-17129* National Aeronautics and Space Administration. Lewis Research Center, Cleveland, OH.

A ROCKET ENGINE DESIGN EXPERT SYSTEM

KENNETH J. DAVIDIAN In Johns Hopkins Univ., The 26th JANNAF Combustion Meeting, Volume 2 p 293-300 Oct. 1989
 Avail: NTIS HC/MF A18 CSCL 20/4

The overall structure and capabilities of an expert system designed to evaluate rocket engine performance are described. The expert system incorporates a JANNAF standard reference computer code to determine rocket engine performance and a state of the art finite element computer code to calculate the interactions between propellant injection, energy release in the combustion chamber, and regenerative cooling heat transfer. Rule-of-thumb heuristics were incorporated for the H₂-O₂ coaxial injector design, including a minimum gap size constraint on the total number of injector elements. One dimensional equilibrium chemistry was used in the energy release analysis of the combustion chamber. A 3-D conduction and/or 1-D advection analysis is used to predict heat transfer and coolant channel wall temperature distributions, in addition to coolant temperature and pressure drop. Inputting values to describe the geometry and state properties of the entire system is done directly from the computer keyboard. Graphical display of all output results from the computer code analyses is facilitated by menu selection of up to five dependent variables per plot. Author

N91-19175* National Aeronautics and Space Administration. Lewis Research Center, Cleveland, OH.

ADVANCED CHEMICAL PROPULSION AT NASA LEWIS: METALLIZED AND HIGH ENERGY DENSITY PROPELLANTS

BRYAN A. PALASZEWSKI Feb. 1991 7 p Presented at the High Energy Density Materials Contractor's Meeting, Albuquerque, NM, 24-27 Feb. 1991; sponsored in part by AF
 (Contract RTOP 506-42-00)
 (NASA-TM-103771; E-6034; NAS 1.15:103771) Avail: NTIS HC/MF A02 CSCL 21/9

Two of the programs at the NASA Lewis Research Center investigating advanced systems for future space missions are the Metallized Propellant Program and the Advanced Concepts Program. Each program includes both experimental and theoretical studies of future propellants and the associated vehicle impacts and significant payload benefits for many types of space transportation. These programs are described. Author

N91-19176* National Aeronautics and Space Administration. Lewis Research Center, Cleveland, OH.

RADIATION RESISTANCE OF THIN-FILM SOLAR CELLS FOR SPACE PHOTOVOLTAIC POWER

JAMES R. WOODYARD (Wayne State Univ., Detroit, MI.) and GEOFFREY A. LANDIS Jan. 1991 35 p Sponsored in part by Wayne State Univ., Detroit, MI
 (Contract NAS3-25266; NAG3-833; RTOP 506-41-11)
 (NASA-TM-103715; E-5948; NAS 1.15:103715) Avail: NTIS HC/MF A03 CSCL 10/2

Copper indium diselenide, cadmium telluride, and amorphous silicon alloy solar cells have achieved noteworthy performance and are currently being studied for space power applications. Cadmium sulfide cells had been the subject of much effort but are no longer considered for space applications. A review is presented of what is known about the radiation degradation of thin film solar cells in space. Experimental cadmium telluride and amorphous silicon alloy cells are reviewed. Damage mechanisms and radiation induced defect generation and passivation in the amorphous silicon alloy cell are discussed in detail due to the greater amount of experimental data available. Author

N91-19177* National Aeronautics and Space Administration. Lewis Research Center, Cleveland, OH.

MULTI-DIMENSIONAL MODELING OF A THERMAL ENERGY STORAGE CANISTER M.S. Thesis - Cleveland State Univ., Dec. 1990

THOMAS W. KERSLAKE Jan. 1991 192 p

(Contract RTOP 474-52-10)

(NASA-TM-103731; E-5966; NAS 1.15:103731) Avail: NTIS HC/MF A09 CSCL 10/3

The Solar Dynamic Power Module being developed for Space Station Freedom uses a eutectic mixture of LiF-CaF₂ phase change material (PCM) contained in toroidal canisters for thermal energy storage. Presented are the results from heat transfer analyses of a PCM containment canister. One and two dimensional finite difference computer models are developed to analyze heat transfer in the canister walls, PCM, void, and heat engine working fluid coolant. The modes of heat transfer considered include conduction in canister walls and solid PCM, conduction and pseudo-free convection in liquid PCM, conduction and radiation across PCM vapor filled void regions, and forced convection in the heat engine working fluid. Void shape, location, growth or shrinkage (due to density difference between the solid and liquid PCM phases) are prescribed based on engineering judgment. The PCM phase change process is analyzed using the enthalpy method. The discussion of the results focuses on how canister thermal performance is affected by free convection in the liquid PCM and void heat transfer. Characterizing these effects is important for interpreting the relationship between ground-based canister performance (in 1-g) and expected on-orbit performance (in micro-g). Void regions accentuate canister hot spots and temperature gradients due to their large thermal resistance. Free convection reduces the extent of PCM superheating and lowers canister temperatures during a portion of the PCM thermal charge period. Surprisingly small differences in canister thermal performance result from operation on the ground and operation on-orbit. This lack of a strong gravity dependency is attributed to the large contribution of container walls in overall canister energy redistribution by conduction. Author

N91-19178* National Aeronautics and Space Administration. Lewis Research Center, Cleveland, OH.

SOLAR ELECTRIC PROPULSION FOR MARS TRANSPORT VEHICLES

J. M. HICKMAN, H. B. CURTIS, S. W. ALEXANDER, J. H. GILLAND (Sverdrup Technology, Inc., Brook Park, OH.), K. J. HACK, C. LAWRENCE, and C. K. SWARTZ Sep. 1990 17 p
 (Contract RTOP 326-31-15)
 (NASA-TM-103234; E-5654; NAS 1.15:103234) Avail: NTIS HC/MF A03 CSCL 13/6

Solar electric propulsion (SEP) is an alternative to chemical and nuclear powered propulsion systems for both piloted and unpiloted Mars transport vehicles. Photovoltaic solar cell and array technologies were evaluated as components of SEP power systems. Of the systems considered, the SEP power system composed of multijunction solar cells in an ENTECH domed fresnel concentrator array had the least array mass and area. Trip times to Mars optimized for minimum propellant mass were calculated. Additionally, a preliminary vehicle concept was designed. Author

N91-19179* National Aeronautics and Space Administration. Lewis Research Center, Cleveland, OH.

KEY ISSUES IN SPACE NUCLEAR POWER

HENRY W. BRANDHORST Jan. 1991 8 p Presented at the 8th Symposium on Space Nuclear Power Systems, Albuquerque, NM, 6-10 Jan. 1991; sponsored in part by New Mexico Univ., Strategic Defense Initiative Organization, DOE, AF
 (Contract RTOP 590-13-11)
 (NASA-TM-103656; E-5847; NAS 1.15:103656) Avail: NTIS HC/MF A02 CSCL 10/2

The future appears rich in missions that will extend the frontiers of knowledge, human presence in space, and opportunities for profitable commerce. Key to the success of these ventures is the availability of plentiful, cost effective electric power and assured, low cost access to space. While forecasts of space power needs are problematic, an assessment of future needs based on terrestrial experience has been made. These needs fall into three broad categories: survival, self sufficiency, and industrialization. The cost of delivering payloads to orbital locations from LEO to Mars has been determined and future launch cost reductions projected. From

20 SPACECRAFT PROPULSION AND POWER

these factors, then, projections of the performance necessary for future solar and nuclear space power options has been made. These goals are largely dependent upon orbital location and energy storage needs. Finally the cost of present space power systems has been determined and projections made for future systems.

Author

N91-19180* National Aeronautics and Space Administration. Lewis Research Center, Cleveland, OH.

A 5-KW XENON ION THRUSTER LIFETEST

MICHAEL J. PATTERSON and TIMOTHY R. VERHEY (Sverdrup Technology, Inc., Brook Park, OH.) 1990 53 p Presented at the 21st International Electric Propulsion Conference, Orlando, FL, 18-20 Jul. 1990; sponsored by AIAA, DGLR, and JSASS Previously announced in IAA as A90-52564

(Contract RTOP 506-42-31)

(NASA-TM-103191; E-5579; NAS 1.15:103191; AIAA PAPER 90-2543) Avail: NTIS HC/MF A04 CSCL 21/8

The results of the first life test of a high power ring-cusp ion thruster are presented. A 30-cm laboratory model thruster was operated steady-state at a nominal beam power of 5 kW on xenon propellant for approximately 900 hours. This test was conducted to identify life-timing erosion modifications, and to demonstrate operation using simplified power processing. The results from this test are described including the conclusions derived from extensive post-test analyses of the thruster. Modifications to the thruster and ground support equipment, which were incorporated to solve problems identified by the lifetest, are also described.

Author

N91-19182* National Aeronautics and Space Administration. Lewis Research Center, Cleveland, OH.

SPACE PHOTOVOLTAIC RESEARCH AND TECHNOLOGY, 1989

Washington Jan. 1991 515 p Tenth conference held in Cleveland, OH, 7-9 Nov. 1989

(Contract RTOP 506-41-11)

(NASA-CP-3107; E-5728; NAS 1.55:3107) Avail: NTIS HC/MF A22 CSCL 10/2

Remarkable progress on a wide variety of approaches in space photovoltaics, for both near and far term applications is reported. Papers were presented in a variety of technical areas, including multi-junction cell technology, GaAs and InP cells, system studies, cell and array development, and non-solar direct conversion. Five workshops were held to discuss the following topics: mechanical versus monolithic multi-junction cells; strategy in space flight experiments; non-solar direct conversion; indium phosphide cells; and space cell theory and modeling.

N91-20204* National Aeronautics and Space Administration. Lewis Research Center, Cleveland, OH.

EFFECTS OF DUST ACCUMULATION AND REMOVAL ON RADIATOR SURFACES ON MARS

JAMES R. GAIER, MARLA E. PEREZ-DAVIS, SHARON K. RUTLEDGE, DEBORAH HOTES, and RAYMOND M. OLLE (Cleveland State Univ., OH.) Jan. 1991 10 p Presented at the 8th Symposium on Space Nuclear Power Systems, Albuquerque, NM, 6-10 Jan. 1991; sponsored by NASA, New Mexico Univ., Strategic Defense Initiative Organization, DOE, and the AF

(Contract NCC3-19; RTOP 591-14-41)

(NASA-TM-103704; E-5841; NAS 1.15:103704) Avail: NTIS HC/MF A02 CSCL 10/2

Tests were carried out to assess the impact of wind blown dust accumulation and abrasion on radiator surfaces on Mars. High emittance arc-textured copper and niobium-1 percent-zirconium samples were subjected to basaltic dust laden wind at Martian pressure (1000 Pa) at speeds varying from 19 to 97 m/s in the Martian Surface Wind Tunnel. The effect of accumulated dust was also observed by pre-dusting some of the samples before the test. Radiator degradation was determined by measuring the change in the emittance after dust was deposited and/or removed. The principle mode of degradation was abrasion.

Arc textured Nb-1 percent-Zr proved to be more susceptible to degradation than Cu, and pre-dusting appeared to have lessened the abrasion.

Author

N91-20206* National Aeronautics and Space Administration. Lewis Research Center, Cleveland, OH.

COMPUTER CODE FOR SINGLE-POINT THERMODYNAMIC ANALYSIS OF HYDROGEN/OXYGEN EXPANDER-CYCLE ROCKET ENGINES

ARTHUR J. GLASSMAN (Toledo Univ., OH.) and SCOTT M. JONES Washington Apr. 1991 19 p

(Contract RTOP 505-69-01)

(NASA-TM-4275; E-5652; NAS 1.15:4275) Avail: NTIS HC/MF A03 CSCL 21/8

This analysis and this computer code apply to full, split, and dual expander cycles. Heat regeneration from the turbine exhaust to the pump exhaust is allowed. The combustion process is modeled as one of chemical equilibrium in an infinite-area or a finite-area combustor. Gas composition in the nozzle may be either equilibrium or frozen during expansion. This report, which serves as a users guide for the computer code, describes the system, the analysis methodology, and the program input and output. Sample calculations are included to show effects of key variables such as nozzle area ratio and oxidizer-to-fuel mass ratio.

Author

N91-20689* National Aeronautics and Space Administration. Lewis Research Center, Cleveland, OH.

AUTONOMOUS POWER EXPERT SYSTEM ADVANCED DEVELOPMENT

TODD M. QUINN (Sverdrup Technology, Inc., Brook Park, OH.) and JERRY L. WALTERS In NASA, Lyndon B. Johnson Space Center, Fourth Annual Workshop on Space Operations Applications and Research (SOAR 90) p 383-390 Jan. 1991

Avail: NTIS HC/MF A21 CSCL 10/2

The autonomous power expert (APEX) system is being developed at Lewis Research Center to function as a fault diagnosis advisor for a space power distribution test bed. APEX is a rule-based system capable of detecting faults and isolating the probable causes. APEX also has a justification facility to provide natural language explanations about conclusions reached during fault isolation. To help maintain the health of the power distribution system, additional capabilities were added to APEX. These capabilities allow detection and isolation of incipient faults and enable the expert system to recommend actions/procedure to correct the suspected fault conditions. New capabilities for incipient fault detection consist of storage and analysis of historical data and new user interface displays. After the cause of a fault is determined, appropriate recommended actions are selected by rule-based inferencing which provides corrective/extended test procedures. Color graphics displays and improved mouse-selectable menus were also added to provide a friendlier user interface. A discussion of APEX in general and a more detailed description of the incipient detection, recommended actions, and user interface developments during the last year are presented.

Author

N91-21233* National Aeronautics and Space Administration. Lewis Research Center, Cleveland, OH.

COOLING OF IN-SITU PROPELLANT ROCKET ENGINES FOR MARS MISSION M.S. Thesis - Cleveland State Univ.

ELIZABETH S. ARMSTRONG Jan. 1991 98 p

(Contract RTOP 590-21-21)

(NASA-TM-103729; E-5963; NAS 1.15:103729) Avail: NTIS HC/MF A05 CSCL 21/8

One propulsion option of a Mars ascent/descent vehicle is multiple high-pressure, pump-fed rocket engines using in-situ propellants, which have been derived from substances available on the Martian surface. The chosen in-situ propellant combination for this analysis is carbon monoxide as the fuel and oxygen as the oxidizer. Both could be extracted from carbon dioxide, which makes up 96 percent of the Martian atmosphere. A pump-fed rocket engine allows for higher chamber pressure than a pressure-fed engine, which in turn results in higher thrust and in

higher heat flux in the combustion chamber. The heat flowing through the wall cannot be sufficiently dissipated by radiation cooling and, therefore, a regenerative coolant may be necessary to avoid melting the rocket engine. The two possible fluids for this coolant scheme, carbon monoxide and oxygen, are compared analytically. To determine their heat transfer capability, they are evaluated based upon their heat transfer and fluid flow characteristics. Author

N91-21240*# National Aeronautics and Space Administration. Lewis Research Center, Cleveland, OH.

POWER TECHNOLOGIES AND THE SPACE FUTURE

KARL A. FAYMON, J. STUART FORDYCE, and HENRY W. BRANDHORST, JR. Apr. 1991 24 p Submitted for publication

(Contract RTOP 506-49-21)

(NASA-TM-103649; E-5835; NAS 1.15:103649) Avail: NTIS

HC/MF A03 CSCL 21/8

Advancements in space power and energy technologies are critical to serve space development needs and help solve problems on Earth. The availability of low cost power and energy in space will be the hallmark of this advance. Space power will undergo a dramatic change for future space missions. The power systems which have served the U.S. space program so well in the past will not suffice for the missions of the future. This is especially true if the space commercialization is to become a reality. New technologies, and new and different space power architectures and topologies will replace the lower power, low-voltage systems of the past. Efficiencies will be markedly improved, specific powers will be greatly increased, and system lifetimes will be markedly extended. Space power technology is discussed - its past, its current status, and predictions about where it will go in the future. A key problem for power and energy is its cost of affordability. Power must be affordable or it will not serve future needs adequately. This aspect is also specifically addressed. Author

N91-22161*# National Aeronautics and Space Administration. Lewis Research Center, Cleveland, OH.

EXPLORING THE NOTION OF SPACE COUPLING PROPULSION

MARC G. MILLIS *In its Vision-21: Space Travel for the Next Millennium* p 307-316 Apr. 1990

Avail: NTIS HC/MF A25 CSCL 21/8

All existing methods of space propulsion are based on expelling a reaction mass (propellant) to induce motion. Alternatively, 'space coupling propulsion' refers to speculations about reacting with space-time itself to generate propulsive forces. Conceivably, the resulting increases in payload, range, and velocity would constitute a breakthrough in space propulsion. Such speculations are still considered science fiction for a number of reasons: (1) it appears to violate conservation of momentum; (2) no reactive media appear to exist in space; (3) no 'Grand Uniform Theories' exist to link gravity, an acceleration field, to other phenomena of nature such as electrodynamics. The rationale behind these objectives is the focus of interest. Various methods to either satisfy or explore these issues are presented along with secondary considerations. It is found that it may be useful to consider alternative conventions of science to further explore speculations of space coupling propulsion. Author

N91-22163*# National Aeronautics and Space Administration. Lewis Research Center, Cleveland, OH.

REACTIONLESS PROPULSION USING TETHERS

GEOFFREY A. LANDIS *In its Vision-21: Space Travel for the Next Millennium* p 330-340 Apr. 1990

Avail: NTIS HC/MF A25 CSCL 21/8

An orbiting tethered satellite can propel itself by reaction against the gravitational gradient, with expenditure of energy but with no use of on-board reaction mass. Energy can be added to the orbit by pumping the tether length in the same way as pumping a swing. Examples of tether propulsion in orbit without use of reaction mass are discussed, including: (1) using tether extension to reposition a satellite in orbit without fuel expenditure by extending

a mass on the end of a tether; (2) using a tether for eccentricity pumping to add energy to the orbit for boosting an orbital transfer; and (3) length modulation of a spinning tether to transfer angular momentum between the orbit and tether spin, thus allowing changes in orbital angular momentum. Author

N91-22176*# National Aeronautics and Space Administration. Lewis Research Center, Cleveland, OH.

THE THEORY OF AN AUTO-RESONANT FIELD EMISSION CATHODE RELATIVISTIC ELECTRON ACCELERATOR FOR HIGH EFFICIENCY MICROWAVE TO DIRECT CURRENT POWER CONVERSION

ROBERT M. MANNING *In its Vision-21: Space Travel for the Next Millennium* p 468-476 Apr. 1990

Avail: NTIS HC/MF A25 CSCL 21/8

A novel method of microwave power conversion to direct current is discussed that relies on a modification of well known resonant linear relativistic electron accelerator techniques. An analysis is presented that shows how, by establishing a 'slow' electromagnetic field in a waveguide, electrons liberated from an array of field emission cathodes, are resonantly accelerated to several times their rest energy, thus establishing an electric current over a large potential difference. Such an approach is not limited to the relatively low frequencies that characterize the operation of rectennas, and can, with appropriate waveguide and slow wave structure design, be employed in the 300 to 600 GHz range where much smaller transmitting and receiving antennas are needed. Author

N91-22367*# National Aeronautics and Space Administration. Lewis Research Center, Cleveland, OH.

EVALUATION OF THERMAL CONTROL COATINGS FOR USE ON SOLAR DYNAMIC RADIATORS IN LOW EARTH ORBIT

JOYCE A. DEVER, ELVIN RODRIGUEZ, WAYNE S. SLEMP, and JOSEPH E. STOYACK (LTV Missiles and Electronics Group, Grand Prairie, TX.) 1991 13 p Proposed for presentation at the 26th Thermophysics Conference, Honolulu, HI, 24-26 Jun. 1991; sponsored by AIAA

(Contract RTOP 474-52-10)

(NASA-TM-104335; E-6103; NAS 1.15:104335; AIAA PAPER 91-1327) Avail: NTIS HC/MF A03 CSCL 10/2

Thermal control coatings with high thermal emittance and low solar absorptance are needed for Space Station Freedom (SSF) solar dynamic power module radiator (SDR) surfaces for efficient heat rejection. Additionally, these coatings must be durable to low earth orbital (LEO) environmental effects of atomic oxygen, ultraviolet radiation and deep thermal cycles which occur as a result of start-up and shut-down of the solar dynamic power system. Eleven candidate coatings were characterized for their solar absorptance and emittance before and after exposure to ultraviolet (UV) radiation (200 to 400 nm), vacuum UV (VUV) radiation (100 to 200 nm) and atomic oxygen. Results indicated that the most durable and best performing coatings were white paint thermal control coatings Z-93, zinc oxide pigment in potassium silicate binder, and YB-71, zinc orthotitanate pigment in potassium silicate binder. Optical micrographs of these materials exposed to the individual environmental effects of atomic oxygen and vacuum thermal cycling showed that no surface cracking occurred. Author

N91-22370*# National Aeronautics and Space Administration. Lewis Research Center, Cleveland, OH.

FINDINGS OF THE JOINT WORKSHOP ON EVALUATION OF IMPACTS OF SPACE STATION FREEDOM GROUND CONFIGURATIONS

DALE C. FERGUSON, DAVID B. SNYDER, and RALPH CARRUTH (National Aeronautics and Space Administration. Marshall Space Flight Center, Huntsville, AL.) 1990 9 p Presented at the Space Environment Analysis Workshop, Noordwijk, Netherlands, 9-12 Oct. 1990; sponsored by ESA

(Contract RTOP 506-41-41)

(NASA-TM-103717; E-5950; NAS 1.15:103717) Avail: NTIS HC/MF A02 CSCL 22/2

A workshop to consider the effects of various proposed Space

20 SPACECRAFT PROPULSION AND POWER

Station Freedom (SSF) grounding schemes was held. Expert from the plasma interactions community evaluated the impacts of environmental interactions on SSF under each of three proposed grounding schemes. The choice of the grounding scheme for the SSF power system was found to have important implications for SSF design. Interactions of the SSF power system and structure with the low earth orbit (LEO) plasma differ significantly between different grounding schemes. Environmental constraints will require modification of current SSF designs under any grounding scheme. Maintaining the present negative ground scheme may compromise SSF safety, structural integrity, and electromagnetic compatibility, and will increase contamination rates over alternate schemes. Positive grounding of the array requires redesign of the primary power system. Floating the array reduces the number of circuit changes in the primary power system but adds new hardware. Maintaining the present design will affect all parts of SSF. However, no impacts were identified on SSF systems outside of the electrical power system by positively grounding or floating the array.

Author

N91-22371*# National Aeronautics and Space Administration. Lewis Research Center, Cleveland, OH.

FUTURE MISSION OPPORTUNITIES AND REQUIREMENTS FOR ADVANCED SPACE PHOTOVOLTAIC ENERGY CONVERSION TECHNOLOGY

DENNIS J. FLOOD 1990 12 p Presented at the 5th International Photovoltaic Science and Engineering Conference, Kyoto, Japan, 26-30 Nov. 1990; sponsored in part by The Japan Society of Applied Physics, The Inst. of Electrical Engineers of Japan, and Foundation for the Advancement of International Science, Kyoto, Japan, 26-30 November 1990

(Contract RTOP 506-41-11)

(NASA-TM-103661; E-5857; NAS 1.15:103661) Avail: NTIS HC/MF A03 CSCL 10/1

The variety of potential future missions under consideration by NASA will impose a broad range of requirements on space solar arrays, and mandates the development of new solar cells which can offer a wide range of capabilities to mission planners. Major advances in performance have recently been achieved at several laboratories in a variety of solar cell types. Many of those recent advances are reviewed, the areas are examined where possible improvements are yet to be made, and the requirements are discussed that must be met by advanced solar cell if they are to be used in space. The solar cells of interest include single and multiple junction cells which are fabricated from single crystal, polycrystalline and amorphous materials. Single crystal cells on foreign substrates, thin film single crystal cells on superstrates, and multiple junction cells which are either mechanically stacked, monolithically grown, or hybrid structures incorporating both techniques are discussed. Advanced concentrator array technology for space applications is described, and the status of thin film, flexible solar array blanket technology is reported.

Author

N91-22375*# National Aeronautics and Space Administration. Lewis Research Center, Cleveland, OH.

EFFECT OF LEO CYCLING ON 125 AH ADVANCED DESIGN IPV NICKEL-HYDROGEN FLIGHT CELLS. AN UPDATE

JOHN J. SMITHRICK and STEPHEN W. HALL (Naval Weapons Support Center, Crane, IN.) 1991 9 p Presented at the 26th Intersociety Energy Conversion Engineering Conference, Boston, MA, 4-9 Aug. 1991; sponsored by ANS, SAE, American Chemical Society, AIAA, ASME, IEEE, and American Inst. of Chemical Engineers

(Contract RTOP 506-41-21)

(NASA-TM-104384; E-6193; NAS 1.15:104384) Avail: NTIS HC/MF A02 CSCL 21/8

Validation testing of the NASA Lewis 125 Ah advanced design individual pressure vessel (IPV) nickel-hydrogen flight cells was conducted. Work consisted of characterization, storage, and cycle life testing. There was no capacity degradation after 52 days of storage with the cells in the discharged state, an open circuit, 0 C, and a hydrogen pressure of 14.5 psia. The catalyzed wall wick

cells were cycled for over 11,000 cycles with no cell failures in the continuing test. One of the noncatalyzed wall wick cells failed.

Author

N91-22376*# National Aeronautics and Space Administration. Lewis Research Center, Cleveland, OH.

EFFECT OF KOH CONCENTRATION ON LEO CYCLE LIFE OF IPV NICKEL-HYDROGEN FLIGHT CELLS. AN UPDATE

JOHN J. SMITHRICK and STEPHEN W. HALL (Naval Weapons Support Center, Crane, IN.) 1991 8 p Presented at the 26th Intersociety Energy Conversion Engineering Conference, Boston, MA, 4-9 Aug. 1991; sponsored by ANS, SAE, American Chemical Society, AIAA, ASME, IEEE, and American Inst. of Chemical Engineers

(Contract RTOP 506-41-21)

(NASA-TM-104383; E-6192; NAS 1.15:104383) Avail: NTIS HC/MF A02 CSCL 10/2

An update of validation test results confirming the breakthrough in LEO cycle life of nickel-hydrogen cells containing 26 percent potassium hydroxide (KOH) electrolyte is presented. A breakthrough in the LEO cycle life of individual pressure vessel nickel-hydrogen cells is reported. The cycle life of boiler plate cells containing 26 percent KOH electrolyte was about 40,000 LEO cycles compared to 3500 cycles for cells containing 31 percent KOH.

Author

N91-22333*# National Aeronautics and Space Administration. Lewis Research Center, Cleveland, OH.

DESTRUCTIVE PHYSICAL ANALYSIS RESULTS OF NI/H₂ CELLS CYCLED IN LEO REGIME

HONG S. LIM, GABRIELA R. ZELTER, JOHN J. SMITHRICK, and STEPHEN W. HALL (Naval Weapons Support Center, Crane, IN.) 1991 9 p Proposed for presentation at the 26th Intersociety Energy Conversion Engineering Conference, Boston, MA, 4-9 Aug. 1991; cosponsored by ANS, SAE, ACS, AIAA, ASME, IEEE, and AIChE

(Contract NAS3-22238; RTOP 506-41-21)

(NASA-TM-104382; E-6191; NAS 1.15:104382) Avail: NTIS HC/MF A02 CSCL 21/8

Six 48-Ah individual pressure vessel (IPV) Ni/H₂ cells containing 26 and 31 percent KOH electrolyte were life cycle tested in low Earth orbit. All three cells containing 31 percent KOH failed (3729, 4165, and 11,355 cycles), while those with 26 percent KOH were cycled over 14,000 times in the continuing test. Destructive physical analysis (DPA) of the failed cells included visual inspections, measurements of electrode thickness, scanning electron microscopy, chemical analysis, and measurements of nickel electrode capacity in an electrolyte flooded cell. The cycling failure was due to a decrease of nickel electrode capacity. As possible causes of the capacity decrease, researchers observed electrode expansion, rupture, and corrosion of the nickel electrode substrate, active material redistribution, and accumulation of electrochemically undischARGEABLE active material with cycling.

Author

N91-22334*# National Aeronautics and Space Administration. Lewis Research Center, Cleveland, OH.

COMPONENT TECHNOLOGY FOR STIRLING POWER CONVERTERS

LANNY G. THIEME 1991 10 p Presented at the 26th Intersociety Energy Conversion Engineering Conference, Boston, MA, 4-9 Aug. 1991; sponsored by American Nuclear Society, SAE, American Chemical Society, AIAA, ASME, IEEE, and American Inst. of Chemical Engineers

(Contract RTOP 590-13-11)

(NASA-TM-104387; E-6175; NAS 1.15:104387) Avail: NTIS HC/MF A02 CSCL 10/2

NASA Lewis Research Center has organized a component technology program as part of the efforts to develop Stirling converter technology for space power applications. The Stirling Space Power Program is part of the NASA High Capacity Power Project of the Civil Space Technology Initiative (CSTI). NASA Lewis is also providing technical management for the DOE/Sandia program to develop Stirling converters for solar terrestrial power producing electricity for the utility grid. The primary contractors for

the space power and solar terrestrial programs develop component technologies directly related to their goals. This Lewis component technology effort, while coordinated with the main programs, aims at longer term issues, advanced technologies, and independent assessments. An overview of work on linear alternators, engine/alternator/load interactions and controls, heat exchangers, materials, life and reliability, and bearings is presented. Author

N91-24232*# National Aeronautics and Space Administration. Lewis Research Center, Cleveland, OH.

DESIGN OF MULTIHUNDREDWATT DIPS FOR ROBOTIC SPACE MISSIONS

D. J. BENTS, S. M. GENG, J. G. SCHREIBER, C. A. WITHROW, P. C. SCHMITZ, and THOMAS J. MCCOMAS (Florida Univ., Gainesville.) 1991 8 p Proposed for presentation at the 26th Intersociety Energy Conversion Conference, Boston, MA, 4-9 Aug. 1991; cosponsored by ANS, SAE, ACS, AIAA, ASME, IEEE, and AICHE (Contract NAS3-25266; RTOP 590-13-11) (NASA-TM-104401; E-6216; NAS 1.15:104401) Avail: NTIS HC/MF A02 CSCL 21/8

Design of a dynamic isotope power system (DIPS) general purpose heat source (GPHS) and small free piston Stirling engine (FPSE) is being pursued as a potential lower cost alternative to radioisotope thermoelectric generators (RTG's). The design is targeted at the power needs of future unmanned deep space and planetary surface exploration missions ranging from scientific probes to SEI precursor missions. These are multihundredwatt missions. The incentive for any dynamic system is that it can save fuel which reduces cost and radiological hazard. However, unlike a conventional DIPS based on turbomachinery conversions, the small Stirling DIPS can be advantageously scaled to multihundred watt unit size while preserving size and weight competitiveness with RTG's. Stirling conversion extends the range where dynamic systems are competitive to hundreds of watts (a power range not previously considered for dynamic systems). The challenge of course is to demonstrate reliability similar to RTG experience. Since the competitive potential of FPSE as an isotope converter was first identified, work has focused on the feasibility of directly integrating GPHS with the Stirling heater head. Extensive thermal modeling of various radiatively coupled heat source/heater head geometries were performed using data furnished by the developers of FPSE and GPHS. The analysis indicates that, for the 1050 K heater head configurations considered, GPHS fuel clad temperatures remain within safe operating limits under all conditions including shutdown of one engine. Based on these results, preliminary characterizations of multihundred watt units were established. Author

N91-24257*# National Aeronautics and Space Administration. Lewis Research Center, Cleveland, OH.

ADVANCED LAUNCH VEHICLE UPPER STAGES USING LIQUID PROPULSION AND METALLIZED PROPELLANTS

BRYAN A. PALASZEWSKI In Johns Hopkins Univ., The 1990 JANNAF Propulsion Meeting, Volume 2 p 251-271 Oct. 1990 Avail: NTIS HC/MF A20 CSCL 21/8

Metallized propellants are liquid propellants with a metal additive suspended in a gelled fuel or oxidizer. Typically, aluminum (Al) particles are the metal additive. These propellants provide increase in the density and/or the specific impulse of the propulsion system. Using metallized propellant for volume- and mass-constrained upper stages can deliver modest increases in performance for low earth orbit to geosynchronous earth orbit (LEO-GEO) and other earth orbital transfer missions. Metallized propellants, however, can enable very fast planetary missions with a single-stage upper stage system. Trade studies comparing metallized propellant stage performance with non-metallized upper stages and the Inertial Upper Stage (IUS) are presented. These upper stages are both one- and two-stage vehicles that provide the added energy to send payloads to altitudes and onto trajectories that are unattainable with only the launch vehicle. The stage designs are controlled by the volume and the mass constraints of the Space Transportation System (STS) and Space Transportation

System-Cargo (STS-C) launch vehicles. The influences of the density and specific impulse increases enabled by metallized propellants are examined for a variety of different stage and propellant combinations. Author

N91-24258*# National Aeronautics and Space Administration. Lewis Research Center, Cleveland, OH.

A THREE-DIMENSIONAL TURBULENT HEAT TRANSFER ANALYSIS FOR ADVANCED TUBULAR ROCKET THRUST CHAMBERS

KENNETH J. KACYNSKI In Johns Hopkins Univ., The 1990 JANNAF Propulsion Meeting, Volume 2 p 273-279 Oct. 1990 Avail: NTIS HC/MF A20 CSCL 21/8

Heat transfer was analyzed in the throat region of a plug and spool rocket engine for both smooth and corrugated walls. A three-dimensional, Navier-Stokes code was used for the analysis. The turbulence model in the code was modified to handle turbulence suppression in the crevice region of the corrugated wall. Circumferential variations in the wall heat transfer was predicted for the corrugated wall. The overall heat transfer at the throat of the corrugated wall was 34 percent higher than it was for the smooth wall for comparable rocket flow conditions. Author

N91-24270*# National Aeronautics and Space Administration. Lewis Research Center, Cleveland, OH.

INVESTIGATION OF THE ARCJET NEAR FIELD PLUME USING ELECTROSTATIC PROBES

JOHN M. SANKOVIC In Johns Hopkins Univ., The 1990 JANNAF Propulsion Meeting, Volume 2 p 391-406 Oct. 1990 Avail: NTIS HC/MF A20 CSCL 21/8

The near field plume of a 1 kW class arcjet thruster was investigated using electrostatic probes of various geometries. The electron number densities and temperatures were determined in a simulated hydrazine plume at axial distances between 3 cm (1.2 in.) and 15 cm (5.9 in.) and radial distances extending to 10 cm (3.9 in.) off centerline. Values of electron number densities obtained using cylindrical and spherical probes of different geometries agreed very well. The electron density on centerline followed a source flow approximation for axial distances as near as 3 cm (1.2 in.) from the nozzle exit plane. The model agreed well with previously obtained data in the far field. The effects of propellant mass flow rate and input power level were also studied. Cylindrical probes were used to obtain ion streamlines by changing the probe orientation with respect to the flow. The effects of electrical configuration on the plasma characteristics of the plume were also investigated by using a segmented anode/nozzle thruster. The results showed that the electrical configuration in the nozzle affected the distribution of electrons in the plume. Author

N91-24271*# National Aeronautics and Space Administration. Lewis Research Center, Cleveland, OH.

ARCJET NOZZLE AREA RATIO EFFECTS

FRANCIS M. CURRAN, CHARLES J. SARMIENTO, BJORN W. BIRKNER, and JAMES KWASNY (Air Force Academy, CO.) In Johns Hopkins Univ., The 1990 JANNAF Propulsion Meeting, Volume 2 p 407-416 Oct. 1990 Avail: NTIS HC/MF A20 CSCL 21/8

An experimental investigation was conducted to determine the effect of nozzle area ratio on the operating characteristics and performance of a low power dc arcjet thruster. Conical thoriated tungsten nozzle inserts were tested in a modular laboratory arcjet thruster run on hydrogen/nitrogen mixtures simulating the decomposition products of hydrazine. The converging and diverging sides of the inserts had half angles of 30 and 20 degrees, respectively, similar to a flight type unit currently under development. The length of the diverging side was varied to change the area ratio. The nozzle inserts were run over a wide range of specific power. Current, voltage, mass flow rate, and thrust were monitored to provide accurate comparisons between tests. While small differences in performance were observed between the two nozzle inserts, it was determined that for each nozzle insert, arcjet performance improved with increasing nozzle area ratio to the

20 SPACECRAFT PROPULSION AND POWER

highest area ratio tested and that the losses become very pronounced for area ratios below 50. These trends are somewhat different than those obtained in previous experimental and analytical studies of low Re number nozzles. It appears that arcjet performance can be enhanced via area ratio optimization.

Author

N91-24302*# National Aeronautics and Space Administration. Lewis Research Center, Cleveland, OH.

A DUAL-COOLED HYDROGEN-OXYGEN ROCKET ENGINE HEAT TRANSFER ANALYSIS

KENNETH J. KACYNSKI, JOHN M. KAZAROFF, and ROBERT S. JANKOVSKY 1991 17 p Presented at the 27th Joint Propulsion Conference, Sacramento, CA, 24-26 Jun. 1991; sponsored by AIAA, SAE, ASME and the American Society for Electrical Engineers (Contract RTOP 593-12-21)

(NASA-TM-104430; E-6186; NAS 1.15:104430; AIAA PAPER 91-2211) Avail: NTIS HC/MF A03 CSCL 21/8

The potential benefits of simultaneously using hydrogen and oxygen as rocket engine coolants are described. A plug-and-spool rocket engine was examined at heat fluxes ranging from 9290 to 163,500 kW/sq m, using a combined 3-D conduction/advection analysis. Both counter flow and parallel flow cooling arrangements were analyzed. The results indicate that a significant amount of heat transfer to the oxygen occurs, reducing both the hot side wall temperature of the rocket engine and also reducing the exit temperature of the hydrogen coolant. In all heat flux and coolant flow rates examined, the total amount of heat transferred to the oxygen was found to be largely independent of the oxygen coolant flow direction. At low heat flux/low coolant flow (throttled) conditions, the oxygen coolant absorbed more than 30 percent of the overall heat transfer from the rocket engine exhaust gases. Also, hot side wall temperatures were judged to decrease by approximately 120 K in the throat area and up to a 170 K combustion chamber wall temperature reduction is expected if dual cooling is applied. The reduction in combustion chamber wall temperatures at throttled conditions is especially desirable since the analysis indicates that a double temperature maxima, one at the throat and another in the combustion chamber, occurs with a traditional hydrogen cooled only engine. Conversely, a dual cooled engine essentially eliminates any concern for overheating in the combustion chamber.

Author

N91-24303*# National Aeronautics and Space Administration. Lewis Research Center, Cleveland, OH.

CARBON MONOXIDE AND OXYGEN COMBUSTION EXPERIMENTS: A DEMONSTRATION OF MARS IN SITU PROPELLANTS

DIANE L. LINNE 1991 19 p Presented at the 27th Joint Propulsion Conference, Sacramento, CA, 24-27 Jun. 1991; sponsored by AIAA, SAE, ASME, and the American Society for Electrical Engineers

(Contract RTOP 506-42-72)
(NASA-TM-104473; E-6320; NAS 1.15:104473; AIAA PAPER 91-2443) Avail: NTIS HC/MF A03 CSCL 21/8

The feasibility of using carbon monoxide and oxygen as rocket propellants was examined both experimentally and theoretically. The steady-state combustion of carbon monoxide and oxygen was demonstrated for the first time in a subscale rocket engine. Measurements of experimental characteristic velocity, vacuum specific impulse, and thrust coefficient efficiency were obtained over a mixture ratio range of 0.30 to 2.0 and a chamber pressures of 1070 and 530 kPa. The theoretical performance of the propellant combination was studied parametrically over the same mixture ratio range. In addition to one dimensional ideal performance predictions, various performance reduction mechanisms were also modeled, including finite-rate kinetic reactions, two-dimensional divergence effects and viscous boundary layer effects.

Author

N91-24304*# National Aeronautics and Space Administration. Lewis Research Center, Cleveland, OH.

LAUNCH VEHICLE PERFORMANCE USING METALLIZED PROPELLANTS

BRYAN A. PALASZEWSKI and RICHARD POWELL (National Aeronautics and Space Administration. Langley Research Center, Hampton, VA.) 1991 16 p Presented at the 27th Joint Propulsion Conference, Sacramento, CA, 24-27 Jun. 1991; sponsored by AIAA, SAE, ASME, and the American Society for Electrical Engineers

(Contract RTOP 506-42-00)

(NASA-TM-104456; E-6297; NAS 1.15:104456; AIAA PAPER 91-2050) Avail: NTIS HC/MF A03 CSCL 21/8

Metallized propellant propulsion systems are considered as replacements for the solid rocket boosters and liquid sustainer stages on the current launch vehicles: both the Space Transportation System (STS) and the Titan 4. Liquid rocket boosters for the STS were analyzed as replacements for current solid rocket boosters. These boosters can provide a liquid propulsion system within the volume constraints of a solid rocket booster. A replacement for the Space Shuttle Main Engines using metallized O₂/H₂/Al was studied. The liquid stages of the Titan 4 were also investigated; the Aerozine-50 (A-50) fuel was replaced with metallized storable A-50/Al. A metallized propellant is similar to a traditional liquid propellant. However, it has metal particles, such as aluminum, that are suspended in a gelled fuel, such as hydrogen, RP-1, A-50 or monomethyl hydrazine (MMH). The fuels then undergo combustion with liquid oxygen or nitrogen tetroxide (NTO). These propellants provide options for increasing the performance of existing launch vehicle chemical propulsion systems by increasing fuel density or specific impulse or both. These increases in density and specific impulse can significantly reduce the propulsion system liftoff weight and allow a liquid rocket booster to fit into the same volume as an existing solid rocket booster. Also, because gelled fuels are akin to liquid propellants, metallized systems can provide enhanced controllability over solid propulsion systems. Gelling of the propellant also reduces the sensitivity to impacts and consequently reduces the propellant explosion hazard.

Author

N91-24305*# National Aeronautics and Space Administration. Lewis Research Center, Cleveland, OH.

IN-SITU PROPELLANT ROCKET ENGINES FOR MARS MISSION ASCENT VEHICLE

ELIZABETH A. RONCACE 1991 9 p Presented at the 27th Joint Propulsion Conference, Sacramento, CA, 24-27 Jun. 1991; sponsored by AIAA, SAE, ASME, and the American Society for Electrical Engineers

(Contract RTOP 590-21-21)

(NASA-TM-104429; E-6262; NAS 1.15:104429; AIAA PAPER 91-2445) Avail: NTIS HC/MF A02 CSCL 21/8

When contemplating the human exploration of Mars, many scenarios using various propulsion systems have been considered. One propulsion option among them is a vehicle stage with multiple, pump fed rocket engines capable of operating on propellants available on Mars. This reduces the Earth launch mass requirements, resulting in economic and payload benefits. No plentiful sources of hydrogen on Mars have been identified on the surface of Mars, so most commonly used high performance liquid fuels, such as hydrogen and hydrocarbons, can be eliminated as possible in-situ propellants. But 95 pct. of the Martian atmosphere consists of carbon dioxide, which can be converted into carbon monoxide and oxygen. The carbon monoxide oxygen propellant combination is a candidate for a Martian in-situ propellant rocket engine. The feasibility is analyzed of a pump fed engine cycle using the propellant combination of carbon monoxide and oxygen.

Author

N91-24307*# National Aeronautics and Space Administration. Lewis Research Center, Cleveland, OH.

STRUCTURAL INTEGRITY AND DURABILITY OF REUSABLE SPACE PROPULSION SYSTEMS

Apr. 1989 259 p Conference held in Cleveland, OH, 18-19 Apr. 1989

(Contract RTOP 553-13-00)

(NASA-CP-10030; E-4628; NAS 1.55:10030) Avail: NTIS HC/MF A12 CSCL 21/8

Presentations were made by industry, university, and government researchers organized into four sessions: aerothermodynamic loads; instrumentation; fatigue, fracture, and constitutive modeling; and structural dynamics.

N91-24324*# National Aeronautics and Space Administration. Lewis Research Center, Cleveland, OH.

THIN-FILM SENSORS FOR SPACE PROPULSION TECHNOLOGY: FABRICATION AND PREPARATION FOR TESTING

WALTER S. KIM and ALOYSIUS F. HEPP *In its Structural Integrity and Durability of Reusable Space Propulsion Systems* p 123-126 Apr. 1989

Avail: NTIS HC/MF A12 CSCL 21/8

The goal of this work is to develop and test thin-film thermocouples for Space Shuttle Main Engine (SSME) components. Thin-film thermocouples have been developed for aircraft gas turbine engines and are in use for temperature measurement on turbine blades up to 1800 F. Established aircraft engine gas turbine technology is currently being adapted to turbine engine blade materials and the environment encountered in the SSME, especially severe thermal shock from cryogenic fuel to combustion temperatures. Initial results using coupons of MAR M-246 (+Hf) and PWA 1480 have been followed by fabrication of thin-film thermocouples on SSME turbine blades. Current efforts are focused on preparing for testing in the Turbine Blade Tester at the NASA Marshall Space Flight Center (MSFC). Future work will include testing of thin-film thermocouples on SSME blades of single crystal PWA 1480 at MSFC.

Author

N91-25172*# National Aeronautics and Space Administration. Lewis Research Center, Cleveland, OH.

POWER ELECTRONICS FOR LOW POWER ARCJETS

JOHN A. HAMLEY and GERALD M. HILL 1991 17 p Presented at the 27th Joint Propulsion Conference, Sacramento, CA, 24-27 Jun. 1991; sponsored by AIAA, SAE, ASME, and the American Society for Electrical Engineers

(Contract RTOP 506-42-31)
(NASA-TM-104459; E-6300; NAS 1.15:104459; AIAA PAPER 91-1991) Avail: NTIS HC/MF A03 CSCL 21/8

In anticipation of the needs of future light-weight, low-power spacecraft, arcjet power electronics in the 100 to 400 W operating range were developed. Limited spacecraft power and thermal control capacity of these small spacecraft emphasized the need for high efficiency. Power topologies similar to those in the higher 2 kW and 5 to 30 kW power range were implemented, including a four transistor bridge switching circuit, current mode pulse-width modulated control, and an output current averaging inductor with an integral pulse generation winding. Reduction of switching transients was accomplished using a low inductance power distribution network, and no passive snubber circuits were necessary for power switch protection. Phase shift control of the power bridge was accomplished using an improved pulse width modulation to phase shift converter circuit. These features, along with conservative magnetics designs allowed power conversion efficiencies of greater than 92.5 percent to be achieved into resistive loads over the entire operating range of the converter. Electromagnetic compatibility requirements were not considered in this work, and control power for the converter was derived from AC mains. Addition of input filters and control power converters would result in an efficiency of on the order of 90 percent for a flight unit. Due to the developmental nature of arcjet systems at this power level, the exact nature of the thruster/power processor interface was not quantified. Output regulation and current ripple requirements of 1 and 20 percent respectively, as well as starting techniques, were derived from the characteristics of the 2 kW system but an open circuit voltage in excess of 175 V was specified. Arcjet integration tests were performed, resulting in successful starts and stable arcjet operation at power levels as low as 240 W with simulated hydrazine propellants.

Author

N91-25173*# National Aeronautics and Space Administration. Lewis Research Center, Cleveland, OH.

SENSIBLE HEAT RECEIVER FOR SOLAR DYNAMIC SPACE POWER SYSTEM

MARLA E. PEREZ-DAVIS, JAMES R. GAIER, and CHRIS PETREFSKI (Cleveland State Univ., OH.) 1991 6 p Presented at the 26th Intersociety Energy Conversion Engineering Conference, Boston, MA, 4-9 Aug. 1991; sponsored by the American Nuclear Society, SAE, the American Chemical Society, AIAA, ASME, IEEE, and the American Inst. of Chemical Engineers
(Contract RTOP 506-41-41)
(NASA-TM-104393; E-6208; NAS 1.15:104393) Avail: NTIS HC/MF A02 CSCL 10/2

A sensible heat receiver considered in this study uses a vapor grown carbon fiber-carbon (VGCF/C) composite as the thermal storage media and was designed for a 7 kW Brayton engine. The proposed heat receiver stores the required energy to power the system during eclipse in the VGCF/C composite. The heat receiver thermal analysis was conducted through the Systems Improved Numerical Differencing Analyzer and Fluid Integrator (SINDA) software package. The sensible heat receiver compares well with other latent and advanced sensible heat receivers analyzed in other studies while avoiding the problems associated with latent heat storage salts and liquid metal heat pipes. The concept also satisfies the design requirements for a 7 kW Brayton engine system. The weight and size of the system can be optimized by changes in geometry and technology advances for this new material.

Author

N91-25175*# National Aeronautics and Space Administration. Lewis Research Center, Cleveland, OH.

EXPERIMENTAL AND ANALYTICAL STUDIES OF FLOW THROUGH A VENTRAL AND AXIAL EXHAUST NOZZLE SYSTEM FOR STOVL AIRCRAFT

BARBARA S. ESKER and JAMES R. DEBONIS (Sverdrup Technology, Inc., Brook Park, OH.) 1991 20 p Presented at the 27th Joint Propulsion Conference, Sacramento, CA, 24-27 Jun. 1991; sponsored by AIAA, SAE, ASME, and the American Society for Electrical Engineers
(Contract RTOP 505-62-30)

(NASA-TM-104364; E-6160; NAS 1.15:104364; AIAA PAPER 91-2135) Avail: NTIS HC/MF A03 CSCL 21/8

Flow through a combined ventral and axial exhaust nozzle system was studied experimentally and analytically. The work is part of an ongoing propulsion technology effort at NASA Lewis Research Center for short takeoff, vertical landing (STOVL) aircraft. The experimental investigation was done on the NASA Lewis Powered Lift Facility. The experiment consisted of performance testing over a range of tailpipe pressure ratios from 1 to 3.2 and flow visualization. The analytical investigation consisted of modeling the same configuration and solving for the flow using the PARC3D computational fluid dynamics program. The comparison of experimental and analytical results was very good. The ventral nozzle performance coefficients obtained from both the experimental and analytical studies agreed within 1.2 percent. The net horizontal thrust of the nozzle system contained a significant reverse thrust component created by the flow overturning in the ventral duct. This component resulted in a low net horizontal thrust coefficient. The experimental and analytical studies showed very good agreement in the internal flow patterns.

Author

N91-25179*# National Aeronautics and Space Administration. Lewis Research Center, Cleveland, OH.

NUCLEAR ROCKET PROPULSION. NASA PLANS AND PROGRESS, FY 1991

JOHN S. CLARK and THOMAS J. MILLER 1991 8 p Presented at the 26th Intersociety Energy Conversion Engineering Conference, Boston, MA, 4-9 Aug. 1991; cosponsored by the ANS, SAE, ACS, AIAA, ASME, IEEE, and AIChE
(Contract RTOP 593-71-00)

(NASA-TM-104455; E-6296; NAS 1.15:104455) Avail: NTIS HC/MF A02 CSCL 21/8

NASA has initiated planning for a technology development

20 SPACECRAFT PROPULSION AND POWER

project for nuclear rocket propulsion systems for space explorer initiative (SEI) human and robotic missions to the moon and Mars. An interagency project is underway that includes the Department of Energy National Laboratories for nuclear technology development. The activities of the project planning team in FY 1990 and 1991 are summarized. The progress to date is discussed, and the project plan is reviewed. Critical technology issues were identified and include: (1) nuclear fuel temperature, life, and reliability; (2) nuclear system ground test; (3) safety; (4) autonomous system operation and health monitoring; and (5) minimum mass and high specific impulse. Author

N91-25182*# National Aeronautics and Space Administration. Lewis Research Center, Cleveland, OH.

SMALL STIRLING DYNAMIC ISOTOPE POWER SYSTEM FOR MULTIHUNDRED-WATT ROBOTIC MISSIONS

DAVID J. BENTS 1991 16 p Presented at the International Pacific Air and Space Technology Conference, Gifu City, Japan, 7-11 Oct. 1991; sponsored by the Society of Automotive Engineers, Inc.

(Contract RTOP 590-13-11)

(NASA-TM-104460; E-6301; NAS 1.15:104460) Avail: NTIS HC/MF A03 CSCL 10/2

Free piston Stirling Engine (FPSE) and linear alternator (LA) technology is combined with radioisotope heat sources to produce a compact dynamic isotope power system (DIPS) suitable for multihundred watt space application which appears competitive with advanced radioisotope thermoelectric generators (RTGs). The small Stirling DIPS is scalable to multihundred watt power levels or lower. The FPSE/LA is a high efficiency converter in sizes ranging from tens of kilowatts down to only a few watts. At multihundred watt unit size, the FPSE can be directly integrated with the General Purpose Heat Source (GPHS) via radiative coupling; the resulting dynamic isotope power system has a size and weight that compares favorably with the advanced modular (Mod) RTG, but requires less than a third the amount of isotope fuel. Thus the FPSE extends the high efficiency advantage of dynamic systems into a power range never previously considered competitive for DIPS. This results in lower fuel cost and reduced radiological hazard per delivered electrical watt. Author

N91-25183*# National Aeronautics and Space Administration. Lewis Research Center, Cleveland, OH.

EFFECTS OF WINDBLOWN DUST ON PHOTOVOLTAIC SURFACE S ON MARS

JAMES R. GAIER, MARLA E. PEREZ-DAVIS, and ALIA M. MOINUDDIN (Case Western Reserve Univ., Cleveland, OH.) 1991 8 p Presented at the 26th Intersociety Energy Conversion Engineering Conference, Boston, MA, 4-9 Aug. 1991; sponsored by the American Nuclear Society, SAE, the American Chemical Society, AIAA, ASME, IEEE, and the American Inst. of Chemical Engineers

(Contract RTOP 591-14-11)

(NASA-TM-104448; E-6289; NAS 1.15:104448) Avail: NTIS HC/MF A02 CSCL 10/1

Photovoltaic (PV) coverslip material was subjected to Martian dust storm conditions using basaltic dust flowing through the Martian Surface Wind Tunnel at NASA-Ames. Initially dusted and clear coverslips were held at angles from 0 to 90 deg., and the dust laden wind velocity was varied from 20 to 97 m/s. Blowing dust was found to adhere more to the coverslips as the angle was increased. However, dust was partially cleared from surfaces that were initially dusted at substantially lower velocities in dust laden wind than in clear wind. Thus, an equilibrium amount of dust accumulated which was dependent only upon angle and wind velocity and not upon initial concentration of dust. Abrasion was also evident in the coverslips. It increased with wind velocity and angle of attack. It appears that an initial dust layer may help to protect PV surfaces from abrasion. Author

N91-25184*# National Aeronautics and Space Administration. Lewis Research Center, Cleveland, OH.

FULL-SIZE SOLAR DYNAMIC HEAT RECEIVER THERMAL-VACUUM TESTS

L. M. SEDGWICK, K. J. KAUFMANN (Boeing Aerospace and Electronics Co., Seattle, WA.), K. L. MCLALLIN, and THOMAS W. KERSLAKE 1991 8 p Presented at the 26th Intersociety Energy Conversion Engineering Conference, Boston, MA, 4-9 Aug. 1991; sponsored by the American Nuclear Society, SAE, the American Chemical Society, AIAA, ASME, IEEE, and the American Inst. of Chemical Engineers

(Contract RTOP 474-52-10)

(NASA-TM-104486; E-6332; NAS 1.15:104486) Avail: NTIS HC/MF A02 CSCL 10/2

The testing of a full-size, 120 kW, solar dynamic heat receiver utilizing high-temperature thermal energy storage is described. The purpose of the test program was to quantify receiver thermodynamic performance, operating temperatures, and thermal response to changes in environmental and power module interface boundary conditions. The heat receiver was tested in a vacuum chamber with liquid nitrogen cold shrouds and an aperture cold plate to partly simulate a low-Earth-orbit environment. The cavity of the receiver was heated by an infrared quartz lamp heater with 30 independently controllable zones to allow axially and circumferentially varied flux distributions. A closed-Brayton cycle engine simulator conditioned a helium-xenon gas mixture to specific interface conditions to simulate the various operational modes of the solar dynamic power module on the Space Station Freedom. Inlet gas temperature, pressure, and flow rate were independently varied. A total of 58 simulated orbital cycles, each 94 minutes in duration, was completed during the test conduct period. Author

N91-26200*# National Aeronautics and Space Administration. Lewis Research Center, Cleveland, OH.

METHOD OF INJECTING FLUID PROPELLANTS INTO A ROCKET COMBUSTION CHAMBER Patent Application

STEVEN J. SCHNEIDER, inventor (to NASA) 31 May 1991 9 p

(NASA-CASE-LEW-14846-2; NAS 1.71:14846-2;

US-PATENT-APPL-SN-709907) Avail: NTIS HC/MF A02 CSCL 21/8

A rocket injector is provided with multiple sets of manifolds for supplying propellants to injector elements. Sensors transmit the temperatures of the propellants to a suitable controller which is operably connected to valves between these manifolds and propellant storage tanks. Additional valves are opened to furnish propellants to more of the manifolds when cryogenic propellant temperatures are sensed. Only a portion of the valves are opened to furnish propellants to some of the manifolds when lower temperatures are sensed. NASA

N91-26202*# National Aeronautics and Space Administration. Lewis Research Center, Cleveland, OH.

DEVELOPMENT AND TESTING OF A SOURCE SUBSYSTEM FOR THE SUPPORTING DEVELOPMENT PMAD DC TEST BED

ROBERT M. BUTTON 1991 8 p Presented at the 26th Intersociety Energy Conversion Engineering Conference, Boston, MA, 4-9 Aug. 1991; sponsored by ANS, SAE, ACS, AIAA, ASME, IEE, and AIChE

(Contract RTOP 474-42-10)

(NASA-TM-104510; E-6378; NAS 1.15:104510) Avail: NTIS HC/MF A02 CSCL 10/2

The supporting Development Power Management and Distribution (PMAD) DC Test Bed is described. Its benefits to the Space Station Freedom Electrical Power System design are discussed along with a short description of how the PMAD DC Test Bed was systematically integrated. The Source Subsystem of the PMAD DC Test Bed consisting of a Sequential Shunt Unit (SSU) and a Battery Charge/Discharge Unit (BCDU) is introduced. The SSU is described in detail and component level test data is presented. Next, the BCDU's operation and design is given along with component level test data. The Source Subsystem is then

presented and early data given to demonstrate an effective subsystem design. Author

N91-27204*# National Aeronautics and Space Administration. Lewis Research Center, Cleveland, OH.

CONCENTRATOR TESTING USING PROJECTED IMAGES

KENT S. JEFFERIES 1991 16 p Presented at the 26th Intersociety Energy Conversion Engineering Conference, Boston, MA, 4-9 Aug. 1991; sponsored by ANS, AICHE, SAE, ACS, AIAA, ASME, and IEEE

(Contract RTOP 474-12-10)

(NASA-TM-104349; E-6129; NAS 1.15:104349) Avail: NTIS HC/MF A03 CSCL 10/2

The projected image system can be used to evaluate concentrator optical properties by comparing images reflected onto the ceiling of the test facility to theoretical facet outlines. This system was tested by comparing ceiling images to facet outlines computed using facet characteristics measured by the digital image radiometer (DIR) optical measuring system. The agreement was good, confirming the accuracy of both optical systems. Six facets were mounted in the centers of the pie sectors of one hexagonal panel. Differences between the facets and facet nonsymmetries were observed in photographs of the ceiling images of these facets. Author

N91-27206*# National Aeronautics and Space Administration. Lewis Research Center, Cleveland, OH.

AN EMTF SYSTEM LEVEL MODEL OF THE PMAD DC TEST BED

NARAYAN V. DRAVID, THOMAS J. KACPURA, and KWA-SUR TAM (Virginia Polytechnic Inst. and State Univ., Blacksburg.) 1991 9 p Presented at the 26th Intersociety Energy Conversion Engineering Conference, Boston, MA, 4-9 Aug. 1991; sponsored by ANS, SAE, ACS, AIAA, ASME, IEEE, and AICHE

(Contract RTOP 474-42-10)

(NASA-TM-104515; E-6384; NAS 1.15:104515) Avail: NTIS HC/MF A02 CSCL 10/2

A power management and distribution direct current (PMAD DC) test bed was set up at the NASA Lewis Research Center to investigate Space Station Freedom Electric Power Systems issues. Efficiency of test bed operation significantly improves with a computer simulation model of the test bed as an adjunct tool of investigation. Such a model is developed using the Electromagnetic Transients Program (EMTP) and is available to the test bed developers and experimenters. The computer model is assembled on a modular basis. Device models of different types can be incorporated into the system model with only a few lines of code. A library of the various model types is created for this purpose. Simulation results and corresponding test bed results are presented to demonstrate model validity. Author

N91-27207*# National Aeronautics and Space Administration. Lewis Research Center, Cleveland, OH.

THE DEVELOPMENT OF TEST BEDS TO SUPPORT THE DEFINITION AND EVOLUTION OF THE SPACE STATION FREEDOM POWER SYSTEM

JAMES F. SOEDER, ROBERT J. FRYE, and RUDY L. PHILLIPS (Rockwell International Corp., Canoga Park, CA.) 1991 9 p Presented at the 26th Intersociety Energy Conversion Engineering Conference, Boston, MA, 4-9 Aug. 1991; sponsored by ANS, SAE, ACS, AIAA, ASME, IEEE, and AICHE

(Contract RTOP 474-42-10)

(NASA-TM-104504; E-6365; NAS 1.15:104504) Avail: NTIS HC/MF A02 CSCL 10/2

Since the beginning of the Space Station Freedom Program (SSFP), the Lewis Research Center (LeRC) and the Rocketdyne Division of Rockwell International have had extensive efforts underway to develop test beds to support the definition of the detailed electrical power system design. Because of the extensive redirections that have taken place in the Space Station Freedom Program in the past several years, the test bed effort was forced to accommodate a large number of changes. A short history of these program changes and their impact on the LeRC test beds

is presented to understand how the current test bed configuration has evolved. The current test objectives and the development approach for the current DC Test Bed are discussed. A description of the test bed configuration, along with its power and controller hardware and its software components, is presented. Next, the uses of the test bed during the mature design and verification phase of SSFP are examined. Finally, the uses of the test bed in operation and evolution of the SSF are addressed. Author

N91-27208*# National Aeronautics and Space Administration. Lewis Research Center, Cleveland, OH.

UPDATE ON RESULTS OF SPRE TESTING AT NASA LEWIS

JAMES E. CAIRELLI, DIANE M. SWEC, WAYNE A. WONG, THOMAS J. DOEBERLING, and FRANK J. MADI (Sverdrup Technology, Inc., Brook Park, OH.) 1991 8 p Presented at the 26th Intersociety Energy Conversion Engineering Conference, Boston, MA, 4-9 Aug. 1991; sponsored by ANS, SAE, ACS, AIAA, ASME, IEEE, and AICHE

(Contract RTOP 590-13-11)

(NASA-TM-104425; E-6258; NAS 1.15:104425) Avail: NTIS HC/MF A02 CSCL 10/2

The Space Power Research Engine (SPRE), a free-piston Stirling engine with a linear alternator, is being tested at NASA Lewis Research Center as part of the Civilian Space Technology Initiative (CSTI) as a candidate for high capacity space power. Results are presented from recent SPRE tests designed to investigate the effects of variation in the displacer seal clearance and piston centering port area on engine performance and dynamics. The impact of these variations on PV power and efficiency are presented. Comparisons of the displacer seal clearance tests results with HFAST code predictions show good agreement for PV power, but show poor agreement for PV efficiency. Correlations are presented relating the piston midstroke position to the dynamic Delta P across the piston and the centering port area. Test results indicate that a modest improvement in PV power and efficiency may be realized with a reduction in piston centering port area. Author

N91-27209*# National Aeronautics and Space Administration. Lewis Research Center, Cleveland, OH.

GROUND TEST PROGRAM FOR A FULL-SIZE SOLAR DYNAMIC HEAT RECEIVER

L. M. SEDGWICK, K. J. KAUFMANN (Boeing Aerospace and Electronics Co., Seattle, WA.), K. L. MCLALLIN, and T. W. KERSLAKE 1991 8 p Presented at the 26th Intersociety Energy Conversion Engineering Conference, Boston, MA, 4-9 Aug. 1991; sponsored by ANS, SAE, ACS, AIAA, ASME, IEEE, and AICHE

(Contract RTOP 474-52-10)

(NASA-TM-104485; E-6331; NAS 1.15:104485) Avail: NTIS HC/MF A02 CSCL 10/1

Test hardware, facilities, and procedures were developed to conduct ground testing of a full size, solar dynamic heat receiver in a partially simulated, low Earth orbit environment. The heat receiver was designed to supply 102 kW of thermal energy to a helium and xenon gas mixture continuously over a 94 minute orbit, including up to 36 minutes of eclipse. The purpose of the test program was to quantify the receiver thermodynamic performance, its operating temperatures, and thermal response to changes in environmental and power module interface boundary conditions. The heat receiver was tested in a vacuum chamber using liquid nitrogen cold shrouds and an aperture cold plate. Special test equipment were designed to provide the required ranges in interface boundary conditions that typify those expected or required for operation as part of the solar dynamic power module on the Space Station Freedom. The support hardware includes an infrared quartz lamp heater with 30 independently controllable zones and a closed Brayton cycle engine simulator to circulate and condition the helium xenon gas mixture. The test article, test support hardware, facilities, and instrumentation developed to conduct the ground test program are all described. Author

20 SPACECRAFT PROPULSION AND POWER

N91-27212*# National Aeronautics and Space Administration. Lewis Research Center, Cleveland, OH.

EVOLVING THE SP-100 REACTOR IN ORDER TO BOOST LARGE PAYLOADS TO GEO AND TO LOW LUNAR ORBIT VIA NUCLEAR-ELECTRIC PROPULSION

ROBERT E. ENGLISH 1991 14 p Proposed for presentation at the Conference on Advanced Space Exploration Initiative Technologies, Cleveland, OH, 4-6 Sep. 1991; cosponsored by AIAA and OAI

(NASA-TM-104527; E-6401; NAS 1.15:104527; AIAA PAPER 91-3562) Avail: NTIS HC/MF A03 CSCL 18/14

In striving to reduce exploration cost and exploration risks, a crucial aspect of the plans is program continuity, i.e., the continuing application of a given technology over a long period so that experience will accumulate from extended testing here on Earth and from a diversity of applications in space. An integrated view needs to be formed of the missions SEI will carry out, near term as well as far, and of the ways in which these missions can mutually support one another. Near term programs should be so constituted as to provide for the long term missions both the enabling technologies and the accumulation of experience they need. In achieving this, missions in Earth orbit should both evolve and show the technologies crucial to long term missions on the lunar surface, and the program for the lunar labs should evolve and show the enabling technologies for exploration of the surface of Mars and for flights of human beings to Mars and return. In the near term, the program for the Space Station should be directed and funded to develop and demonstrate the solar Brayton power plant that will be most useful as the power generator for the SP-100 nuclear reactor.

Author

N91-27213*# National Aeronautics and Space Administration. Lewis Research Center, Cleveland, OH.

DESIGN CONSIDERATIONS FOR SPACE RADIATORS BASED ON THE LIQUID SHEET (LSR) CONCEPT

ALBERT J. JUHASZ and DONALD L. CHUBB 1991 8 p Presented at the 26th Intersociety Energy Conversion Engineering Conference, Boston, MA, 4-9 Aug. 1991; sponsored by ANS, SAE, ACS, AIAA, ASME, IEEE, and AICHE (Contract RTOP 506-41-51)

(NASA-TM-105158; E-6446; NAS 1.15:105158) Avail: NTIS HC/MF A02 CSCL 10/2

Concept development work on space heat rejection subsystems tailored to the requirements of various space power conversion systems is proceeding over a broad front of technologies at NASA LeRC. Included are orbital and planetary surface based radiator concepts utilizing pumped loops, a variety of heat pipe radiator concepts, and the innovative liquid sheet radiator (LSR). The basic feasibility of the LSR concept was investigated in prior work which generated preliminary information indicating the suitability of the LSR concept for space power systems requiring cycle reject heat to be radiated to the space sink at low-to-mid temperatures (300 to 400 K), with silicon oils used for the radiator working fluid. This study is directed at performing a comparative examination of LSR characteristics as they affect the basic design of low earth orbit solar dynamic power conversion systems. The power systems considered were based on the closed Brayton (CBC) and the Free Piston Stirling (FPS) cycles, each with a power output of 2 kWe and using previously tested silicone oil (Dow-Corning Me2) as the radiator working fluid. Conclusions indicate that, due to its ability for direct cold end cooling, an LSR based heat rejection subsystem is far more compatible with a Stirling space power system than with a CBC, which requires LSR coupling by means of an intermediate gas/liquid heat exchanger and adjustment of cycle operating conditions.

Author

N91-27214*# National Aeronautics and Space Administration. Lewis Research Center, Cleveland, OH.

SOLAR DYNAMIC POWER FOR EARTH ORBITAL AND LUNAR APPLICATIONS

JAMES E. CALOGERAS, MILES O. DUSTIN, and RICHARD R. SECUNDE 1991 12 p Presented at the 26th Intersociety Energy Conversion Engineering Conference, Boston, MA, 4-9 Aug.

1991; sponsored by ANS, SAE, ACS, AIAA, ASME, IEEE, and AICHE

(Contract RTOP 506-41-31)

(NASA-TM-104511; E-6379; NAS 1.15:104511) Avail: NTIS HC/MF A03 CSCL 10/2

Development of solar dynamic (SD) technologies for space over the past 25 years by NASA Lewis Research Center brought SD power to the point where it was selected in the design phase of Space Station Freedom Program as the power source for evolutionary growth. More recent studies showed that large cost savings are possible in establishing manufacturing processes at a Lunar Base if SD is considered as a power source. Technology efforts over the past 5 years have made possible lighter, more durable, SD components for these applications. A review of these efforts and respective benefits is presented.

Author

N91-28212*# National Aeronautics and Space Administration. Lewis Research Center, Cleveland, OH.

ADVANCED CRYO PROPULSION SYSTEMS

WILLIAM K. TABATA /in NASA, Washington, Space Transportation Propulsion Technology Symposium. Volume 2: Symposium Proceedings p 353-364 May 1991

Avail: NTIS HC/MF A99 CSCL 21/8

The following topics are presented in viewgraph form: (1) advanced space engine (ASE) chronology; (2) an ASE description; (3) a single expander; (4) a dual expander; (5) split expander; (6) launch vehicle start; (7) space start; (8) chemical transfer propulsion; and (9) an advanced expander test bed.

K.S.

N91-28215*# National Aeronautics and Space Administration. Lewis Research Center, Cleveland, OH.

FUTURISTIC SYSTEMS: SOLAR AND NUCLEAR ELECTRIC PROPULSION

DAVE BYERS /in NASA, Washington, Space Transportation Propulsion Technology Symposium. Volume 2: Symposium Proceedings p 409-429 May 1991

Avail: NTIS HC/MF A99 CSCL 21/8

The following topics are addressed: (1) in-space propulsion impacts; (2) electric propulsion; (3) mission impacts of electric propulsion; and (4) summaries of electric propulsion status and solar and nuclear propulsion.

K.S.

N91-28246*# National Aeronautics and Space Administration. Lewis Research Center, Cleveland, OH.

OVERALL GOALS

GEORGE BAAKLINI, JOSEPH S. HEYMAN, ERIC MADARAS, CHARLES SALKOWSKI, BERT WESTON, and KEN WOODIS (National Aeronautics and Space Administration. Marshall Space Flight Center, Huntsville, AL.) /in NASA, Washington, Space Transportation Propulsion Technology Symposium. Volume 3: Panel Session Summaries and Presentations p 965-971 May 1991

Avail: NTIS HC/MF A99 CSCL 21/8

Space transportation propulsion systems symposium is discussed. The following subject areas are covered: overall goals; main issues; materials characterization; reduction of manufacturing defects; standards and certification; advanced NDE techniques; designing for inspectability; candidate programs/milestones; and NDE technology potentials.

Author

N91-28247*# National Aeronautics and Space Administration. Lewis Research Center, Cleveland, OH.

CONCURRENT ENGINEERING

C. C. CHAMIS, L. LEGER, D. HUNTER, C. JONES, R. SPRAGUE, L. BERKE, J. NEWELL, and S. SINGHAL (Sverdrup Technology, Inc., Brook Park, OH.) /in NASA, Washington, Space Transportation Propulsion Technology Symposium. Volume 3: Panel Session Summaries and Presentations p 973-988 May 1991

Avail: NTIS HC/MF A99 CSCL 21/8

The following subject areas are covered: issues (liquid rocket propulsion - current development approach, current certification process, and costs of engineering changes); state of the art (DICE information management system, key government participants,

project development strategy, quality management, and numerical propulsion system simulation); needs identified; and proposed program. Author

N91-28277*# National Aeronautics and Space Administration. Lewis Research Center, Cleveland, OH.

SEI POWER SOURCE ALTERNATIVES FOR ROVERS AND OTHER MULTI-KWE DISTRIBUTED SURFACE APPLICATIONS

DAVID J. BENTS, L. L. KOHOUT, BARBARA I. MCKISSOCK, C. D. RODRIGUEZ, C. A. WITHROW, A. COLOZZA, JAMES C. HANLON, and PAUL C. SCHMITZ (Sverdrup Technology, Inc., Brook Park, OH.) 1991 13 p Presented at the European Space Power Conference, Florence, Italy, 2-5 Sep. 1991; sponsored by ESA

(Contract NAS3-25266; RTOP 591-14-11)
(NASA-TM-104360; E-6155; NAS 1.15:104360) Avail: NTIS HC/MF A03 CSCL 10/2

To support the Space Exploration Initiative (SEI), a study was performed to investigate power system alternatives for the rover vehicles and servicers that were subsequently generated for each of these rovers and servicers, candidate power sources incorporating various power generation and energy storage technologies were identified. The technologies were those believed most appropriate to the SEI missions, and included solar, electrochemical, and isotope systems. The candidates were characterized with respect to system mass, deployed area, and volume. For each of the missions a preliminary selection was made. Results of this study depict the available power sources in light of mission requirements as they are currently defined.

Author

N91-28278*# National Aeronautics and Space Administration. Lewis Research Center, Cleveland, OH.

COMPARISON OF DYNAMIC ISOTOPE POWER SYSTEMS FOR DISTRIBUTED PLANET SURFACE APPLICATIONS

DAVID J. BENTS, BARBARA I. MCKISSOCK, JAMES C. HANLON, PAUL C. SCHMITZ (Sverdrup Technology, Inc., Brook Park, OH.), CARLOS D. RODRIGUEZ, and COLLEEN A. WITHROW Washington Aug. 1991 14 p
(Contract RTOP 326-81-10)

(NASA-TM-4303; E-5905; NAS 1.15:4303) Avail: NTIS HC/MF A03 CSCL 10/2

Dynamic isotope power system (DIPS) alternatives were investigated and characterized for the surface mission elements associated with a lunar base and subsequent manned Mars expedition. System designs based on two converter types were studied. These systems were characterized parametrically and compared over the steady-state electrical output power range 0.2 to 20 kWe. Three methods of thermally integrating the heat source and the Stirling heater head were considered, depending on unit size. Figures of merit were derived from the characterizations and compared over the parametric range. Design impacts of mission environmental factors are discussed and quantitatively assessed.

Author

N91-29220*# National Aeronautics and Space Administration. Lewis Research Center, Cleveland, OH.

DESIGN ISSUES FOR PROPULSION SYSTEMS USING METALLIZED PROPELLANTS

BRYAN PALASZEWSKI and DOUGLAS RAPP (Sverdrup Technology, Inc., Brook Park, OH.) 1991 27 p Presented at the Advanced Space Exploration Initiative Technologies, Cleveland, OH, 4-6 Sep. 1991; cosponsored by AIAA and OAI
(Contract RTOP 506-42-00)

(NASA-TM-105190; E-6492; NAS 1.15:105190; AIAA PAPER 91-3484) Avail: NTIS HC/MF A03 CSCL 21/8

Metallized propellants are liquid propellants that contain metal particles. These particles are suspended in a gelled fuel or oxidizer. Aluminum is used as the metal additive. The addition of metal to conventional propellants can increase their specific impulse and their density over conventional propellants, and consequently, the payload delivered on Mars and lunar transportation vehicles, Earth-to-Orbit vehicles and upper stages for robotic planetary

missions. Gelled fuels also provide increased safety during accidental propellant leakage or spills. To take full advantage of these potential performance increases, there are changes that must be made to the vehicle design. The differences are discussed between metallized propellant and traditional liquid propellants and their effect on the propulsion system design. These differences include the propellant density, mixture ratio, engine performance, and propellant rheology. Missions related to the Space Exploration Initiative are considered as design examples to illustrate these issues. Author

N91-29221*# National Aeronautics and Space Administration. Lewis Research Center, Cleveland, OH.

NUMERICAL PROPULSION SYSTEM SIMULATION: AN INTERDISCIPLINARY APPROACH

LESTER D. NICHOLS and CHRISTOS C. CHAMIS 1991 16 p Presented at the Conference on Advanced Space Exploration Initiative Technologies, Cleveland, OH, 4-6 Sep. 1991; cosponsored by AIAA and OAI

(Contract RTOP 509-10-03)
(NASA-TM-105181; E-6359; NAS 1.15:105181; AIAA PAPER 91-3554) Avail: NTIS HC/MF A03 CSCL 21/8

The tremendous progress being made in computational engineering and the rapid growth in computing power that is resulting from parallel processing now make it feasible to consider the use of computer simulations to gain insights into the complex interactions in aerospace propulsion systems and to evaluate new concepts early in the design process before a commitment to hardware is made. Described here is a NASA initiative to develop a Numerical Propulsion System Simulation (NPSS) capability.

Author

N91-29222*# National Aeronautics and Space Administration. Lewis Research Center, Cleveland, OH.

PRODUCTION AND USE OF METALS AND OXYGEN FOR LUNAR PROPULSION

ALOYSIUS F. HEPP, DIANE L. LINNE, GEOFFREY A. LANDIS, MARY F. GROTH, and JAMES E. COLVIN (Arizona Univ., Tucson.) 1991 13 p Presented at the Conference on Advanced Space Exploration Initiative Technologies, Cleveland, OH, 4-6 Sep. 1991; cosponsored by AIAA and OAI

(Contract RTOP 506-41-11)
(NASA-TM-105195; E-6496; NAS 1.15:105195; AIAA PAPER 91-3481) Avail: NTIS HC/MF A03 CSCL 21/8

Production, power, and propulsion technologies for using oxygen and metals derived from lunar resources are discussed. The production process is described, and several of the more developed processes are discussed. Power requirements for chemical, thermal, and electrical production methods are compared. The discussion includes potential impact of ongoing power technology programs on lunar production requirements. The performance potential of several possible metal fuels including aluminum, silicon, iron, and titanium are compared. Space propulsion technology in the area of metal/oxygen rocket engines is discussed. Author

N91-29228*# National Aeronautics and Space Administration. Lewis Research Center, Cleveland, OH.

PRESSURE MEASUREMENTS IN A LOW-DENSITY NOZZLE PLUME FOR CODE VERIFICATION

PAUL F. PENKO, IAIN D. BOYD, DANA L. MEISSNER, and KENNETH J. DEWITT (Toledo Univ., OH.) 1991 18 p Presented at the 27th Joint Propulsion Conference, Sacramento, CA, 24-27 Jun. 1991; sponsored by AIAA, SAE, ASME, and ASEE Previously announced as A91-45783

(Contract RTOP 506-42-31)
(NASA-TM-105170; E-6463; NAS 1.15:105170; AIAA PAPER 91-2110) Avail: NTIS HC/MF A03 CSCL 21/8

Measurements of Pitot pressure were made in the exit plane and plume of a low-density, nitrogen nozzle flow. Two numerical computer codes were used to analyze the flow, including one based on continuum theory using the explicit MacCormack method, and the other on kinetic theory using the method of direct-simulation Monte Carlo (DSMC). The continuum analysis was carried to the

20 SPACECRAFT PROPULSION AND POWER

nozzle exit plane and the results were compared to the measurements. The DSMC analysis was extended into the plume of the nozzle flow and the results were compared with measurements at the exit plane and axial stations 12, 24 and 36 mm into the near-field plume. Two experimental apparatus were used that differed in design and gave slightly different profiles of pressure measurements. The DSMC method compared well with the measurements from each apparatus at all axial stations and provided a more accurate prediction of the flow than the continuum method, verifying the validity of DSMC for such calculations.

Author

N91-29229*# National Aeronautics and Space Administration. Lewis Research Center, Cleveland, OH.

PERFORMANCE AND OPTIMIZATION OF A DERATED ION THRUSTER FOR AUXILIARY PROPULSION

MICHAEL J. PATTERSON and JOHN E. FOSTER (Jackson State Univ., MS.) 1991 18 p Presented at the 27th Joint Propulsion Conference, Sacramento, CA, 24-27 Jun. 1991; sponsored by AIAA, SAE, ASME and ASEE Previously announced as A91-45809 (Contract RTOP 506-42-31) (NASA-TM-105144; E-6419; NAS 1.15:105144; AIAA PAPER 91-2350) Avail: NTIS HC/MF A03 CSCL 21/8

The characteristics and implications of use of a derated ion thruster for north-south stationkeeping (NSSK) propulsion are discussed. A derated thruster is a 30 cm diameter primary propulsion ion thruster operated at highly throttled conditions appropriate to NSSK functions. The performance characteristics of a 30 cm ion thruster are presented, emphasizing throttled operation at low specific impulse and high thrust-to-power ratio. Performance data and component erosion are compared to other NSSK ion thrusters. Operations benefits derived from the performance advantages of the derated approach are examined assuming an INTELSAT 7-type spacecraft. Minimum ground test facility pumping capabilities required to maintain facility enhanced accelerator grid erosion at acceptable levels in a lifetest are quantified as a function of thruster operating condition. Approaches to reducing the derated thruster mass and volume are also discussed.

Author

N91-29230*# National Aeronautics and Space Administration. Lewis Research Center, Cleveland, OH.

EXPERIMENTAL AND ANALYTICAL COMPARISON OF FLOWFIELDS IN A 110 N (25 LBF) H₂/O₂ ROCKET

BRIAN D. REED, PAUL F. PENKO, STEVEN J. SCHNEIDER, and SUK C. KIM (Sverdrup Technology, Inc., Brook Park, OH.) 1991 17 p Presented at the 27th Joint Propulsion Conference, Sacramento, CA, 24-27 Jun. 1991; sponsored by AIAA, SAE, ASME, and ASEE Previously announced as A91-45802 (Contract NAS3-25266; RTOP 506-42-31) (NASA-TM-105175; E-6471; NAS 1.15:105175) Avail: NTIS HC/MF A03 CSCL 21/8

A gaseous hydrogen/gaseous oxygen 110 N (25 lbf) rocket was examined through the RPLUS code using the full Navier-Stokes equations with finite rate chemistry. Performance tests were conducted on the rocket in an altitude test facility. Preliminary parametric analyses were performed for a range of mixture ratios and fuel film cooling pcts. It is shown that the computed values of specific impulse and characteristic exhaust velocity follow the trend of the experimental data. Specific impulse computed by the code is lower than the comparable test values by about two to three percent. The computed characteristic exhaust velocity values are lower than the comparable test values by three to four pct. Thrust coefficients computed by the code are found to be within two pct. of the measured values. It is concluded that the discrepancy between computed and experimental performance values could not be attributed to experimental uncertainty.

Author

N91-29231*# National Aeronautics and Space Administration. Lewis Research Center, Cleveland, OH.

ARCJET THERMAL CHARACTERISTICS

JOHN M. SANKOVIC and FRANCIS M. CURRAN 1991 31 p

Presented at the 27th Joint Propulsion Conference, Sacramento, CA, 24-27 Jun. 1991; sponsored by AIAA, SAE, ASME, and ASEE Previously announced as A91-45814 (Contract RTOP 506-42-31)

(NASA-TM-105156; E-6442; NAS 1.15:105156; AIAA PAPER 91-2456) Copyright Avail: NTIS HC/MF A03 CSCL 21/8

The performance of water-cooled and radiation cooled arcjet thrusters operating on both 1:2 nitrogen/hydrogen mixtures at 1 to 2 kW and on pure hydrogen at 1 to 4 kW are compared. To investigate the effects of test facility background pressure on performance, data were taken for both thruster operating on nitrogen/hydrogen mixtures at facility background pressures nominally at 0.20 Pa and 20 Pa. It is shown that increasing the background pressure decreased the thruster performance, and simple pressure area corrections alone could not account for observed degradation in performance.

Author

N91-30202*# National Aeronautics and Space Administration. Lewis Research Center, Cleveland, OH.

MICROANALYSIS OF EXTENDED-TEST XENON HOLLOW CATHODES

TIMOTHY R. VERHEY (Sverdrup Technology, Inc., Brook Park, OH.) and MICHAEL J. PATTERSON 1991 49 p Presented at the 27th Joint Propulsion Conference, Sacramento, CA, 24-27 Jun. 1991; cosponsored by AIAA, SAE, ASME, and ASEE (Contract RTOP 506-42-31) (NASA-TM-104532; E-6408; NAS 1.15:104532; AIAA PAPER 91-2123) Avail: NTIS HC/MF A03 CSCL 21/8

Four hollow cathode electron sources were analyzed via boroscopy, scanning electron microscopy, energy dispersive x ray analysis, and x ray diffraction analysis. These techniques were used to develop a preliminary understanding of the chemistry of the devices that arise from contamination due to inadequate feed-system integrity and improper insert activation. Two hollow cathodes were operated in an ion thruster simulator at an emission current of 23.0 A for approximately 500 hrs. The two tests differed in propellant-feed systems, discharge power supplies, and activation procedures. Tungsten deposition and barium tungstate formation on the internal cathode surfaces occurred during the first test, which were believed to result from oxygen contamination of the propellant feed-system. Consequently, the test facility was upgraded to reduce contamination, and the test was repeated. The second hollow cathode was found to have experienced significantly less tungsten deposition. A second pair of cathodes examined were the discharge and the neutralizer hollow cathodes used in a life-test of a 30-cm ring-cusp ion thruster at a 5.5 kW power level. The cathodes' test history was documented and the post-test microanalyses are described. The most significant change resulting from the life-test was substantial tungsten deposition on the internal cathode surfaces, as well as removal of material from the insert surface. In addition, barium tungstate and molybdate were found on insert surfaces. As a result of the cathode examinations, procedures and approaches were proposed for improved discharge ignition and cathode longevity.

Author

N91-30203*# National Aeronautics and Space Administration. Lewis Research Center, Cleveland, OH.

SPACE PHOTOVOLTAIC RESEARCH AND TECHNOLOGY CONFERENCE

Aug. 1991 471 p The 11th Conference was held in Cleveland, OH, 7-9 May 1991 (Contract RTOP 506-41-11) (NASA-CP-3121; E-6161; NAS 1.55:3121) Avail: NTIS HC/MF A20 CSCL 10/2

The Eleventh Space Photovoltaic Research and Technology conference was held at NASA Lewis Research Center from May 7 to 9, 1991. The papers and workshop summaries presented here report remarkable progress on a wide variety of approaches in space photovoltaics, both near and far term applications. Papers were presented in a variety of technical areas, including multijunction cell technology, GaAs and InP cells, system studies, cell and array development, and photovoltaics for conversion of

laser radiation. Three workshops were held to discuss thin film cell development, III-V cell development, and space environmental effects.

N91-30223* # National Aeronautics and Space Administration. Lewis Research Center, Cleveland, OH.

KEY RESULTS OF THE MINI-DOME FRESNEL LENS CONCENTRATOR ARRAY DEVELOPMENT PROGRAM UNDER RECENTLY COMPLETED NASA AND SDIO SBIR PROJECTS
MARK J. ONEILL, MICHAEL F. PISZCZOR, and LEWIS M. FRAAS (Boeing Co., Seattle, WA.) *In its Space Photovoltaic Research and Technology Conference* 12 p Aug. 1991
Avail: NTIS HC/MF A20 CSCL 10/2

Since 1986, ENTECH and the NASA Lewis Research Center have been developing a new photovoltaic concentrator system for space power applications. The unique refractive system uses small, dome shaped Fresnel lenses to focus sunlight onto high efficiency photovoltaic concentrator cells which use prismatic cell covers to further increase their performance. Highlights of the five-year development include near Air Mass Zero (AM0) Lear Jet flight testing of mini-dome lenses (90 pct. net optical efficiency achieved); tests verifying sun-pointing error tolerance with negligible power loss; simulator testing of prism-covered GaAs concentrator cells (24 pct. AM0 efficiency); testing of prism-covered Boeing GaAs/GaSb tandem cells (31 pct. AM0 efficiency); and fabrication and outdoor testing of a 36-lens/cell element panel. These test results have confirmed previous analytical predictions which indicate substantial performance improvements for this technology over current array systems. Based on program results to date, it appears that an array power density of 300 watts/sq m and a specific power of 100 watts/kg can be achieved in the near term. All components of the array appear to be readily manufacturable from space-durable materials at reasonable cost. A concise review is presented of the key results leading to the current array, and further development plans for the future are briefly discussed.

Author

N91-30232* # National Aeronautics and Space Administration. Lewis Research Center, Cleveland, OH.

COMPARATIVE MODELING OF INP SOLAR CELL STRUCTURES
R. K. JAIN, I. WEINBERG, and D. J. FLOOD *In its Space Photovoltaic Research and Technology Conference* 9 p Aug. 1991 Prepared in cooperation with National Academy of Sciences/National Research Council, Washington
Avail: NTIS HC/MF A20 CSCL 10/2

The comparative modeling of $p(+)$ n and $n(+)$ p indium phosphide solar cell structures is studied using a numerical program PC-1D. The optimal design study has predicted that the $p(+)$ n structure offers improved cell efficiencies as compared to $n(+)$ p structure, due to higher open-circuit voltage. The various cell material and process parameters to achieve the maximum cell efficiencies are reported. The effect of some of the cell parameters on InP cell I-V characteristics was studied. The available radiation resistance data on $n(+)$ p and $p(+)$ p InP solar cells are also critically discussed.

Author

N91-30233* # National Aeronautics and Space Administration. Lewis Research Center, Cleveland, OH.

A THEORETICAL COMPARISON OF THE NEAR-OPTIMUM DESIGN AND PREDICTED PERFORMANCE OF N/P AND P/N INDIUM PHOSPHIDE HOMOJUNCTION SOLAR CELLS
CHANDRA GORADIA, WILLIAM THESLING, and IRVING WEINBERG *In its Space Photovoltaic Research and Technology Conference* 10 p Aug. 1991 Prepared in cooperation with Cleveland State Univ., OH
Avail: NTIS HC/MF A20 CSCL 10/2

Using a detailed simulation model of $p(+)$ $nn(+)$ and $n(+)$ $pp(+)$ indium phosphide (InP) homojunction solar cells, extensive parametric variation computer simulation runs were performed to aid in making near-optimum designs for these two solar cell configurations. The values of all the geometrical and material parameters corresponding to the near-optimal designs of both these

configurations are presented. The results of parametric variation runs are presented for each configuration showing how the performance parameters $J(\text{sub sc})$, $V(\text{sub oc})$, and η vary with each of the cell design parameters for the near-optimally designed cell. Finally, the theoretically obtained results are discussed, and the relative merits and drawbacks of the two configurations are compared.

Author

N91-30235* # National Aeronautics and Space Administration. Lewis Research Center, Cleveland, OH.

SIGNIFICANT REDUCTION IN ARC FREQUENCY BIASED SOLAR CELLS: OBSERVATIONS, DIAGNOSTICS, AND MITIGATION TECHNIQUE(S)

B. L. UPSCHULTE, G. M. WEYL, W. J. MARINELLI, E. AIFER, D. HASTINGS (Massachusetts Inst. of Tech., Cambridge.), and D. SNYDER *In its Space Photovoltaic Research and Technology Conference* 10 p Aug. 1991
Avail: NTIS HC/MF A20 CSCL 10/2

A variety of experiments were performed which identify key factors contributing to the arcing of negatively biased high voltage solar cells. These efforts have led to reduction of greater than a factor of 100 in the arc frequency of a single cell following proper remediation procedures. Experiments naturally lead to and focussed on the adhesive/encapsulant that is used to bond the protective cover slip to the solar cell. An image-intensified charge coupled device (CCD) camera system recorded UV emission from arc events which occurred exclusively along the interfacial edge between the cover slip and the solar cell. Microscopic inspection of this interfacial region showed a bead of encapsulant along this entire edge. Elimination of this encapsulant bead reduced the arc frequency by two orders of magnitude. Water contamination was also identified as a key contributor which enhances arcing of the encapsulant bead along the solar cell edge. Spectrally resolved measurements of the observable UV light shows a feature assignable to OH(A-X) electronic emission, which is common for water contaminated discharges. Experiments in which the solar cell temperature was raised to 85 C showed a reduced arcing frequency, suggesting desorption of H₂O. Exposing the solar cell to water vapor was shown to increase the arcing frequency. Clean dry gases such as O₂, N₂, and Ar show no enhancement of the arcing rate. Elimination of the exposed encapsulant eliminates any measurable sensitivity to H₂O vapor.

Author

N91-30238* # National Aeronautics and Space Administration. Lewis Research Center, Cleveland, OH.

THE EFFECTS OF LUNAR DUST ACCUMULATION ON THE PERFORMANCE OF PHOTOVOLTAIC ARRAYS
CYNTHIA M. KATZAN, DAVID J. BRINKER, and ROBERT KRESS (Akron Univ., OH.) *In its Space Photovoltaic Research and Technology Conference* 8 p Aug. 1991
(Contract NAS3-25266)
Avail: NTIS HC/MF A20 CSCL 10/2

Lunar base activity, particularly rocket launch and landing, will suspend and transport lunar dust. From preliminary models, the resulting dust accumulation can be significant, even as far as 2 km from the source. For example, at 2 km approximately 0.28 mg/sq cm of dust is anticipated to accumulate after only 10 surface missions with a 26,800 N excursion vehicle. The possible associated penalties in photovoltaic array performance were therefore the subject of experimental as well as theoretical investigation. To evaluate effects of dust accumulation on relative power output, current-voltage characteristics of dust-covered silicon cells were determined under the illumination of a Spectrolab X-25L solar simulator. The dust material used in these experiments was a terrestrial basalt which approximated lunar soil in particle size and composition. Cell short circuit current, an indicator of the penetrating light intensity, was found to decrease exponentially with dust accumulation. This was predicted independently by modeling the light occlusion caused by a growing layer of dust particles. Moreover, the maximum power output of dust-covered cells, derived from the I-V curves, was also found to degrade exponentially. Experimental results are presented and potential implications discussed.

Author

20 SPACECRAFT PROPULSION AND POWER

N91-30239*# National Aeronautics and Space Administration. Lewis Research Center, Cleveland, OH.

RAPID THERMAL CYCLING OF SOLAR ARRAY BLANKET COUPONS FOR SPACE STATION FREEDOM

DAVID A. SCHEIMAN (Sverdrup Technology, Inc., Brook Park, OH.) and BRYAN K. SMITH *In its* Space Photovoltaic Research and Technology Conference 9 p Aug. 1991 (Contract NAS3-25266)

Avail: NTIS HC/MF A20 CSCL 10/2

The NASA Lewis Research Center has been conducting rapid thermal cycling on blanket coupons for Space Station Freedom. This testing includes two designs (8 coupons total) of the solar array. Four coupons were fabricated as part of the Photovoltaic Array Environmental Protection Program (PAEP), NAS3-25079, at Lockheed Missiles and Space Company. These coupons began cycling in early 1989 and have completed 172,000 thermal cycles. Four other coupons were fabricated a year later and included several design changes; cycling of these began in early 1990 and has reached 90,000 cycles. The objective of this testing is to demonstrate the durability or operational lifetime (15 yrs.) of the welded interconnects within a low earth orbit (LEO) thermal cycling environment. The blanket coupons, design changes, test description, status to date including performance and observed anomalies, and any insights related to the testing of these coupons are described. The description of a third design is included.

Author

N91-30248*# National Aeronautics and Space Administration. Lewis Research Center, Cleveland, OH.

LOW EARTH ORBITAL ATOMIC OXYGEN MICROMETEOROID, AND DEBRIS INTERACTIONS WITH PHOTOVOLTAIC ARRAYS

BRUCE A. BANKS, SHARON K. RUTLEDGE, and KIM K. DEGROH *In its* Space Photovoltaic Research and Technology Conference 10 p Aug. 1991

Avail: NTIS HC/MF A20 CSCL 10/2

Polyimide Kapton solar array blankets can be protected from atomic oxygen in low earth orbit if SiO₂ thin film coatings are applied to their surfaces. The useful lifetime of a blanket protected in this manner strongly depends on the number and size of defects in the protective coatings. Atomic oxygen degradation is dominated by undercutting at defects in protective coatings caused by substrate roughness and processing rather than micrometeoroid or debris impacts. Recent findings from the Long Duration Exposure Facility (LDEF) and ground based studies show that interactions between atomic oxygen and silicones may cause grazing and contamination problems which may lead to solar array degradation.

Author

N91-30249*# National Aeronautics and Space Administration. Lewis Research Center, Cleveland, OH.

LEO SPACE PLASMA INTERACTIONS

DALE C. FERGUSON *In its* Space Photovoltaic Research and Technology Conference 11 p Aug. 1991

Avail: NTIS HC/MF A20 CSCL 10/2

Photovoltaic arrays interact with the low earth orbit (LEO) space plasma in two fundamentally different ways. One way is the steady collection of current from the plasma onto exposed conductors and semiconductors. The relative currents collected by different parts of the array will then determine the floating potential of the spacecraft. In addition, these steady state collected currents may lead to sputtering or heating of the array by the ions or electrons collected, respectively. The second kind of interaction is the short time scale arc into the space plasma, which may deplete the array and/or spacecraft of stored charge, damage solar cells, and produce EMI. Such arcs only occur at high negative potentials relative to the space plasma potential, and depend on the steady state ion currents being collected. New high voltage solar arrays being incorporated into advanced spacecraft and space platforms may be endangered by these plasma interactions. Recent advances in laboratory testing and current collection modeling promise the capability of controlling, and perhaps even using, these space plasma interactions to enable design of reliable high voltage space power systems. Some of

the new results may have an impact on solar cell spacing and/or coverslide design. Planned space flight experiments are necessary to confirm the models of high voltage solar array plasma interactions. Finally, computerized, integrated plasma interactions design tools are being constructed to place plasma interactions models into the hands of the spacecraft designer.

Author

N91-30252*# National Aeronautics and Space Administration. Lewis Research Center, Cleveland, OH.

PRELIMINARY PERFORMANCE AND LIFE EVALUATIONS OF A 2-KW ARCJET

W. EARL MORREN and FRANCIS M. CURRAN 1991 31 p Presented at the 27th Joint Propulsion Conference, Sacramento, CA, 24-27 Jun. 1991; sponsored by AIAA, SAE, ASME, and ASEE Previously announced as A91-45796

(Contract RTOP 506-42-31)

(NASA-TM-105149; E-6430; NAS 1.15:105149; AIAA PAPER 91-2228) Copyright Avail: NTIS HC/MF A03 CSCL 21/8

The first results of a program to expand the operational envelope of low-power arcjets to higher specific impulse and power levels are presented. The performance of a kW-class laboratory model arcjet thruster was characterized at three mass flow rates of a 2:1 mixture of hydrogen and nitrogen at power levels ranging from 1.0 to 2.0 kW. This same thruster was then operated for a total of 300 h at a specific impulse and power level of 550 s and 2.0 kW, respectively, in three continuous 100-h sessions. Thruster operation during the three test segments was stable, and no measurable performance degradation was observed during the test series. Substantial cathode erosion was observed during an inspection following the second 100-h test segment. Most notable was the migration of material from the center of the cathode tip to a ring around a large crater. The anode sustained no significant damage during the endurance test segments. Some difficulty was encountered during start-up after disassembly and inspection following the second 100-h test segment, which caused constrictor erosion. This resulted in a reduced flow restriction and arc chamber pressure, which in turn caused a reduction in the arc impedance.

Author

N91-30265*# National Aeronautics and Space Administration. Lewis Research Center, Cleveland, OH.

ON PROTECTION OF FREEDOM'S SOLAR DYNAMIC RADIATOR FROM THE ORBITAL DEBRIS ENVIRONMENT.

PART 2: FURTHER TESTING AND ANALYSES

JENNIFER L. RHATIGAN, ERIC L. CHRISTIANSEN, and MICHAEL L. FLEMING (LTV Missiles and Electronics Group, Dallas, TX.) 1991 11 p Proposed for presentation at the International Solar Energy Conference, Lahaina, Maui, HI, 4-8 Apr. 1992; sponsored by ASME

(Contract RTOP 474-52-10)

(NASA-TM-104514; E-6335; NAS 1.15:104514) Avail: NTIS HC/MF A03 CSCL 21/8

Presented here are results of a test program undertaken to further define the response of the solar dynamic radiator to hypervelocity impact (HVI). Tests were conducted on representative radiator panels (under ambient, nonoperating conditions) over a range of velocity. Target parameters are also varied. Data indicate that analytical penetration predictions are conservative (i.e., pessimistic) for the specific configuration of the solar dynamic radiator. Test results are used to define the solar dynamic radiator reliability with respect to HVI more rigorously than previous studies. Test data, reliability, and survivability results are presented.

Author

N91-30266*# National Aeronautics and Space Administration. Lewis Research Center, Cleveland, OH.

DESCRIPTION OF THE CONTROL SYSTEM DESIGN FOR THE SSF PMAD DC TESTBED

ANASTACIO N. BAEZ and GREG L. KIMNACH 1991 10 p Presented at the 26th Intersociety Energy Conversion Engineering Conference, Boston, MA, 4-9 Aug. 1991; sponsored by ANS, SAE, ACS, AIAA, ASME, IEEE, and AICHE

(Contract RTOP 474-42-10)
(NASA-TM-105202; E-6505; NAS 1.15:105202) Avail: NTIS
HC/MF A02 CSCL 21/8

The Power Management and Distribution (PMAD) DC Testbed Control System for Space Station Freedom was developed using a top down approach based on classical control system and conventional terrestrial power utilities design techniques. The design methodology includes the development of a testbed operating concept. This operating concept describes the operation of the testbed under all possible scenarios. A unique set of operating states was identified and a description of each state, along with state transitions, was generated. Each state is represented by a unique set of attributes and constraints, and its description reflects the degree of system security within which the power system is operating. Using the testbed operating states description, a functional design for the control system was developed. This functional design consists of a functional outline, a text description, and a logical flowchart for all the major control system functions. Described here are the control system design techniques, various control system functions, and the status of the design and implementation. Author

N91-30267* National Aeronautics and Space Administration.
Lewis Research Center, Cleveland, OH.

**TEST AND EVALUATION OF LOAD CONVERTER
TOPOLOGIES USED IN THE SPACE STATION FREEDOM
POWER MANAGEMENT AND DISTRIBUTION DC TEST BED**
RAMON C. LEBRON, ANGELA C. OLIVER, and ROBERT F. BODI
(Analytical Engineering Corp., North Olmsted, OH.) 1991 9 p
Presented at the 26th Intersociety Energy Conversion Engineering
Conference, Boston, MA, 4-9 Aug. 1991; cosponsored by the ANS,
SAE, ACS, AIAA, ASME, IEEE, and AIChE
(Contract RTOP 474-42-10)
(NASA-TM-105217; E-6532; NAS 1.15:105217) Avail: NTIS
HC/MF A02 CSCL 21/8

Power components hardware in support of the Space Station Freedom dc Electrical Power System were tested. One type of breadboard hardware tested is the dc Load Converter Unit, which constitutes the power interface between the electric power system and the actual load. These units are dc to dc converters that provide the final system regulation before power is delivered to the load. Three load converters were tested: a series resonant converter, a series inductor switchmode converter, and a switching full-bridge forward converter. The topology, operation principles, and tests results are described, in general. A comparative analysis of the three units is given with respect to efficiency, regulation, short circuit behavior (protection), and transient characteristics. Author

N91-31208* National Aeronautics and Space Administration.
Lewis Research Center, Cleveland, OH.

**NONLINEAR COMBUSTION INSTABILITY MODEL IN TWO- TO
THREE-DIMENSIONS**
RICHARD J. PRIEM (Priem Consultants, Inc., Cleveland, OH.) and
KEVIN J. BREISACHER 1989 11 p Presented at the 26th
JANNAF Combustion Meeting, Pasadena, CA, 23-27 Oct. 1989
(Contract RTOP 582-01-21)
(NASA-TM-102381; E-5097; NAS 1.15:102381) Avail: NTIS
HC/MF A03 CSCL 21/8

A model is developed on using quasi-steady state equations for the injection, atomization, and vaporization processes that consider the instantaneous local pressures, temperatures, density, and gas velocity vector associated with a 3-L wave. The coupled sets of equations are solved to determine frequency and growth rate of the oscillations as a function of wave amplitude. Calculated results are used to explain the observed instabilities in a 40 Klb LOX/Methane combustor. Author

N91-31212* National Aeronautics and Space Administration.
Lewis Research Center, Cleveland, OH.
**MASS COMPARISONS OF ELECTRIC PROPULSION SYSTEMS
FOR NSSK OF GEOSYNCHRONOUS SPACECRAFT**
VINCENT K. RAWLIN and GREGORY A. MAJCHER (Cleveland

State Univ., OH.) 1991 48 p Presented at the 27th Joint
Propulsion Conference, Sacramento, Ca, 24-27 Jun. 1991;
sponsored by AIAA, SAE, ASME, and ASEE Previously Announced
in IAA as A91-45808

(Contract RTOP 506-42-31)
(NASA-TM-105153; E-6438; NAS 1.15:105153; AIAA PAPER
91-2347) Avail: NTIS HC/MF A03 CSCL 21/8

A model was developed and exercised to allow wet mass comparisons of three axis stabilized communication satellites delivered to geosynchronous transfer orbit. The mass benefits of using advanced chemical propulsion for apogee injection and north-south stationkeeping (NSSK) functions or electric propulsion (hydrazine arcjets and xenon ion thrusters) for NSSK functions are documented. A large derated ion thrusters is proposed which minimizes thruster lifetime concerns and qualification test times when compared to those of smaller ion thrusters planned for NSSK applications. The mass benefits, which depend on the spacecraft mass and mission duration, increase dramatically with arcjet specific impulse in the 500 to 600 s range, but are nearly constant for the derated ion thruster operated in the 2300 to 3000 s range. For a given mission, the mass benefits with an ion system are typically double those of the arcjet system; however, the total thrusting time with arcjets is less than 1/3 that with ion thrusters for the same thruster power. The mass benefits may permit increases in revenue producing payload or reduce launch costs by allowing a move to a smaller launch vehicle. Author

N91-31216* National Aeronautics and Space Administration.
Lewis Research Center, Cleveland, OH.

MEDIUM POWER HYDROGEN ARCJET PERFORMANCE
FRANCIS M. CURRAN, S. RAY BULLOCK, THOMAS W. HAAG,
CHARLES J. SARMIENTO, and JOHN M. SANKOVIC 1991
22 p Presented at the 27th Joint Propulsion Conference,
Sacramento, CA, 24-27 Jun. 1991; sponsored by AIAA, SAE, ASME,
and ASEE
(Contract RTOP 506-42-31)
(NASA-TM-104533; E-6409; NAS 1.15:104533; AIAA PAPER
91-2227) Avail: NTIS HC/MF A03 CSCL 21/8

An experimental investigation was performed to evaluate hydrogen arcjet operating characteristics in the range of 1 to 4 kW. A series of nozzles were operated in modular laboratory thrusters to examine the effects of geometric parameters such as constrictor diameter and nozzle divergence angle. Each nozzle was tested over a range of current and mass flow rates to explore stability and performance. In the range of mass flow rates and power levels tested, specific impulse values between 650 and 1250 sec were obtained at efficiencies between 30 and 40 percent. The performance of the two larger half angle (20, 15 deg) nozzles was similar for each of the two constrictor diameters tested. The nozzles with the smallest half angle (10 deg) were difficult to operate. A restrike mode of operation was identified and described. Damage in the form of melting was observed in the constrictor region of all the nozzle inserts tested. Arcjet ignition was also difficult in many tests and a glow discharge mode that prevents starting was identified. Author

N91-31217* National Aeronautics and Space Administration.
Lewis Research Center, Cleveland, OH.

ADVANCED POWER SYSTEMS FOR EOS
SHEILA G. BAILEY, IRVING WEINBERG, and DENNIS J. FLOOD
1991 8 p Presented at the 26th Intersociety Energy Conversion
Engineering Conference, Boston, MA, 4-9 Aug. 1991; cosponsored
by ANS, SAE, ACS, AIAA, ASME, IEEE, and AIChE
(Contract RTOP 506-41-11)
(NASA-TM-105222; E-6536; NAS 1.15:105222) Avail: NTIS
HC/MF A02 CSCL 21/8

The Earth Observing System, which is part of the International Mission to Planet Earth, is NASA's main contribution to the Global Change Research Program. Five large platforms are to be launched into polar orbit: two by NASA, two by the European Space Agency, and one by the Japanese. In such an orbit the radiation resistance of indium phosphide solar cells combined with the potential of utilizing 5 micron cell structures yields an increase of 10 percent

20 SPACECRAFT PROPULSION AND POWER

in the payload capability. If further combined with the Advanced Photovoltaic Solar Array, the total additional payload capability approaches 12 percent. Author

N91-31218*# National Aeronautics and Space Administration. Lewis Research Center, Cleveland, OH.

THIN FILM, CONCENTRATOR AND MULTI-JUNCTION SPACE SOLAR CELLS: STATUS AND POTENTIAL

DENNIS J. FLOOD 1991 12 p Presented at the European Space Power Conference, Florence, Italy, 3-6 Sep. 1991; sponsored by ESA, the Italian Space Agency, and the European Power Electronics

(Contract RTOP 506-41-11)

(NASA-TM-104505; E-6366; NAS 1.15:104505) Avail: NTIS HC/MF A03 CSCL 21/8

Recent, rapid advances in a variety of solar cell technologies offer the potential for significantly enhancing, or enabling entirely new, mission capabilities. Thin film solar cells are of particular interest in that regard. A review is provided of the status of those thin film cell technologies of interest for space applications, and the issues to be resolved before mission planners can consider them. A short summary is also given of recent developments in concentrator and multi-junction space solar cell and array technology. Author

N91-31220*# National Aeronautics and Space Administration. Lewis Research Center, Cleveland, OH.

ECCENTRICITY EFFECTS ON LEAKAGE OF A BRUSH SEAL AT LOW SPEEDS

JULIE A. SCHLUMBERGER, MARGARET P. PROCTOR, and ROBERT C. HENDRICKS 1991 9 p Proposed for presentation at the 1991 Winter Annual Meeting of the ASME, Atlanta, GA, 1-6 Dec. 1991

(Contract RTOP 506-42-72)

(NASA-TM-105141; E-6414; NAS 1.15:105141) Avail: NTIS HC/MF A02 CSCL 13/11

The effects of eccentricity on brush seal leakage at low rotational speeds were investigated. Included are the leakage results for ambient temperature air and nearly saturated streams at three different rotor eccentricities at both 0 and 400 rpm. A brush seal with a nominal bore diameter of 13.647 cm (5.3730 in.) was used. It had a radial concentric interference of 0.071 cm (0.0028 in.) and a fence height of 0.0927 cm (0.0365 in.). There were 1060 bristles per centimeter of circumference (2690 bristles per inch of circumference). Rotor eccentricities of 0.003, 0.010, 0.038, and 0.043 cm (0.001, 0.004, 0.015, and 0.017 in.) were achieved by using bushings with different offsets. The results were compared with an annular seal model (FLOWCAL) for air and to a standard labyrinth seal model for steam. The annular seal model was also compared with a bulk flow model of a concentric brush seal in air. Large eccentricities did not damage the brush seals or their Haynes 25 bristles. However, the 304 stainless steel rotor did not show wear, indicating a harder surface is needed. Only the stream data showed hysteresis and were affected by shaft rotation. The brush seal had lower leakage rates than those predicted for comparable annular and labyrinth seals (conventional) because of the large clearances those seals require to accommodate large shaft excursions. Author

N91-32158*# National Aeronautics and Space Administration. Lewis Research Center, Cleveland, OH.

ION BEAM SPUTTERING IN ELECTRIC PROPULSION FACILITIES

JAMES S. SOVEY and MICHAEL J. PATTERSON 1991 15 p Presented at the 27th Joint Propulsion Conference, Sacramento, CA, 24-27 Jun. 1991; sponsored by AIAA, SAE, ASME, and ASEE Previously announced in IAA as A91-45785

(Contract RTOP 506-42-31)

(NASA-TM-105145; E-6420; NAS 1.15:105145; AIAA PAPER 91-2117) Avail: NTIS HC/MF A03 CSCL 21/8

Experiments were undertaken to determine sputter yields of potential ion beam target materials, to assess the impact of charge exchange on beam diagnostics in large facilities, and to examine

material erosion and deposition after a 957 hr test of a 5 kW-class ion thruster. The xenon ion sputter yield of flexible graphite was lower than other graphite forms especially at high angles of incidence. Ion beam charge exchange effects were found to hamper beam probe current collection diagnostics even at pressures from 0.7 to 1.7 mPa. Estimates of the xenon ion beam envelope were made and predictions of the thickness of sputter deposited coatings in the facility were compared with measurements. Author

N91-32161*# National Aeronautics and Space Administration. Lewis Research Center, Cleveland, OH.

THE NASA CRYOGENIC FLUID MANAGEMENT TECHNOLOGY PROGRAM PLAN

JAMES R. FADDOUL and STANLEY D. MCINTYRE (National Aeronautics and Space Administration. Marshall Space Flight Center, Huntsville, AL.) Sep. 1991 24 p Presented at the Conference on Advanced Space Exploration Initiative Technologies, Cleveland, OH, 4-6 Sep. 1991; sponsored by AIAA, NASA, and OAI Previously announced in IAA as A91-52436

(Contract RTOP 506-42-73)

(NASA-TM-105256; E-6586; NAS 1.15:105256; AIAA PAPER 91-3553) Avail: NTIS HC/MF A03 CSCL 21/8

During the past three decades, NASA has been designing and using large quantities of cryogenic fluids for propulsion system propellants, coolants for experiments, and for environmental control systems. As a consequence, an erroneous conclusion has been drawn that the technology exists for using large quantities of cryogens in space for long periods of time. The attempt here is to dispel that myth and to present the technology needs that require development in order to support the NASA programs of the future. A NASA program, developed through the impetus of the Marshall Space Flight Center and the Lewis Research Center and supported by all NASA centers is outlined. The current state of the art is discussed along with specific needs for near future missions. Then, using the Space Exploration Initiative mission set, cost/benefit projections are made for the development of advanced cryogenic fluid management techniques. Earth based and space based test programs are discussed relative to the technology requirements for liquid storage, supply, and transfer for fluid transfer and advanced instrumentation. Author

N91-32162*# National Aeronautics and Space Administration. Lewis Research Center, Cleveland, OH.

MPD THRUSTER TECHNOLOGY

ROGER M. MYERS, MARIS A. MANTENIEKS, and MICHAEL R. LAPOINTE (Sverdrup Technology, Inc., Brook Park, OH.) Sep. 1991 36 p Presented at the Conference on Advanced Space Exploration Initiative Technologies, Cleveland OH, 4-6 Sep. 1991; sponsored in part by NASA, AIAA, and OAI

(Contract RTOP 506-42-31)

(NASA-TM-105242; E-6569; NAS 1.15:105242; AIAA PAPER 91-3568) Avail: NTIS HC/MF A03 CSCL 21/8

MPD (MagnetoplasmaDynamic) thrusters demonstrated between 2000 and 7000 seconds specific impulse at efficiencies approaching 40 percent, and were operated continuously at power levels over 500 kW. These demonstrated capabilities, combined with the simplicity and robustness of the thruster, make them attractive candidates for application to both unmanned and manned orbit raising, lunar, and planetary missions. To date, however, only a limited number of thruster configurations, propellants, and operating conditions were studied. The present status of MPD research is reviewed, including developments in the measured performance levels and electrode erosion rates. Theoretical studies of the thruster dynamics are also described. Significant progress was made in establishing empirical scaling laws, performance and lifetime limitations and in the development of numerical codes to simulate the flow field and electrode processes. Author

N91-32163*# National Aeronautics and Space Administration. Lewis Research Center, Cleveland, OH.

FIBER-OPTIC APPLICATIONS FOR SPACE-BASED ENGINES

AMY L. SOVIE, DOUGLAS P. BEWLEY, and MARC G. MILLIS Sep. 1991 9 p Presented at the Conference on Advanced

Space Exploration Initiative Technologies, Cleveland, OH, 4-6 Sep. 1991; cosponsored by AIAA, NASA, and OAI. Previously announced in IAA as A91-52468 (Contract RTOP 590-21-41) (NASA-TM-105235; E-6560; NAS 1.15:105235; AIAA PAPER 91-3602) Copyright Avail: NTIS HC/MF A02 CSCL 21/8

The use of fiber optic technology is discussed with respect to the instrumentation systems for space based rocket engines. Optical fiber technologies are reviewed with specific attention given to the reliability, light weight, small fiber diameter, and operating life of the components in the space environment. An optical system can facilitate the incorporation of an optical health monitoring system, increase the space available for necessary redundancy, and safe high bandwidth communications that are immune to the effects of electromagnetic radiation. Author

N91-32164*# National Aeronautics and Space Administration. Lewis Research Center, Cleveland, OH.

MULTIMEGAWATT ELECTRIC PROPULSION SYSTEM DESIGN CONSIDERATIONS

J. H. GILLAND, ROGER M. MYERS (Sverdrup Technology, Inc., Brook Park, OH.), and MICHAEL J. PATTERSON Aug. 1991 16 p. Presented at the 21st International Electric Propulsion Conference, Orlando, FL, 18-20 Jul. 1990; sponsored in part by AIAA. Previously announced in IAA as A90-52566 (NASA-TM-105152; E-6437; NAS 1.15:105152; AIAA PAPER 90-2552) Avail: NTIS HC/MF A03 CSCL 21/8

Piloted Mars Mission Requirements of relatively short trip times and low initial mass in Earth orbit as identified by the NASA Space Exploration Initiative, indicate the need for multimegawatt electric propulsion systems. The design considerations and results for two thruster types, the argon ion, and hydrogen magnetoplasmadynamic thrusters, are addressed in terms of configuration, performance, and mass projections. Preliminary estimates of power management and distribution for these systems are given. Some assessment of these systems' performance in a reference Space Exploration Initiative piloted mission are discussed. Research and development requirements of these systems are also described. Author

N91-32165*# National Aeronautics and Space Administration. Lewis Research Center, Cleveland, OH.

ORR-SHERBY-DORN CREEP STRENGTHS OF THE REFRACTORY-METAL ALLOYS C-103, ASTAR-811C, W-5RE, AND W-25RE

ROBERT E. ENGLISH 1991 8 p. Prepared for presentation at the 9th Symposium on Space Nuclear Power Systems, Albuquerque, NM, 12-16 Jan. 1992; sponsored in part by New Mexico Univ. (NASA-TM-105228; E-6551; NAS 1.15:105228) Avail: NTIS HC/MF A02 CSCL 21/8

Available creep data for the refractory-metal alloys C-103 (Nb/10 percent Hf/1 percent Ti/0.7 percent Zr), ASTAR-811C (Ta/8 percent W/1 percent Re/0.7 percent Hf/0.025 percent C), W-5Re (W/5 percent Re), and W-25Re (W/25 percent Re) were correlated by the Orr-Sherby-Dorn method and extrapolated to 1 percent creep over 10 years. Useful life was specified to be 2 standard estimates of error below the mean surface through the data. Over the temperature range of 1200 to 1800 K, ASTAR-811C was found to be the strongest of these alloys. In particular, ASTAR-811C was found to have at 1800 K the same creep strength as W-25Re at 1420 K. The difference between these results and those of Horak and Booker likely devolves from the comparative lack of long-time data on tungsten alloys. Author

N91-32167*# National Aeronautics and Space Administration. Lewis Research Center, Cleveland, OH.

SPECTROSCOPIC WEAR DETECTOR Patent Application

GEORGE C. MADZSAR, inventor (to NASA) 27 Jun. 1991 12 p. (NASA-CASE-LEW-15200-1; NAS 1.71:LEW-15200-1; US-PATENT-APPL-SN-722446) Avail: NTIS HC/MF A03 CSCL 21/8

The elemental composition of a material exposed to hot gases and subjected to wear is determined. Atoms of an elemental species not appearing in this material are implanted in a surface at a depth based on the maximum allowable wear. The exhaust gases are spectroscopically monitored to determine the exposure of these atoms when the maximum allowable wear is reached. NASA

23

CHEMISTRY AND MATERIALS (GENERAL)

A91-19720* National Aeronautics and Space Administration. Lewis Research Center, Cleveland, OH.

TRIBOLOGICAL PROPERTIES OF PM212 - A HIGH TEMPERATURE, SELF-LUBRICATING, POWDER METALLURGY COMPOSITE

CHRISTOPHER DELLACORTE and HAROLD E. SLINNEY (NASA, Lewis Research Center, Cleveland, OH) IN: STLE, Annual Meeting, 45th, Denver, CO, May 7-10, 1990, Preprints. Park Ridge, IL, Society of Tribologists and Lubrication Engineers, 1990, 11 p. Previously announced in STAR as N90-12659. refs (STLE PREPRINT 90-AM-4E-1) Copyright

This paper describes a research program to develop and evaluate a new high temperature, self-lubricating powder metallurgy composite, PM212. PM212 has the same composition as the plasma-sprayed coating, PS212, which contains 70 wt percent metal-bonded chromium carbide, 15 wt percent silver and 15 wt percent barium fluoride/calcium fluoride eutectic. The carbide acts as a wear resistant matrix and the silver and fluorides act as low and high temperature lubricants, respectively. The material is prepared by sequential cold press, cold isostatic pressing and sintering techniques. In this study, hemispherically tipped wear pins of PM212 were prepared and slid against superalloy disks at temperatures from 25 to 850 C in air in a pin-on-disk tribometer. Friction coefficients range from 0.29 to 0.38 and the wear of both the composite pins and superalloy disks was moderate to low in the 10(exp -5) to 10(exp -6) cubic mm/N-m range. Preliminary tests indicate that the material has a compressive strength of at least 130 MPa over the entire temperature range of 25 to 900 C. This material has promise for use as seal inserts, bushings, small inside diameter parts and other applications where plasma-sprayed coatings are impractical or too costly. Author

A91-33793* Texas A&M Univ., College Station.

TEMPERATURE DEPENDENCE OF THE ELASTIC MODULI AND DAMPING FOR POLYCRYSTALLINE LiF-22 PCT CAF2 EUTECTIC SALT

A. WOLFENDEN, G. LASTRAPES, M. B. DUGGAN (Texas A & M University, College Station), and S. V. RAJ (NASA, Lewis Research Center, Cleveland, OH) Journal of Materials Science (ISSN 0022-2461), vol. 26, April 1, 1991, p. 1793-1798. refs (Contract NCC3-72) Copyright

Young's and shear moduli and damping were measured for as-cast polycrystalline LiF-(22 mol pct)CaF2 eutectic specimens as a function of temperature using the piezoelectric ultrasonic composite oscillator technique. The shear modulus decreased with increasing temperature from about 40 GPa at 295 K to about 30 GPa at 1000 K, while the Young modulus decreased from about 115 GPa at 295 K to about 35 GPa at 900 K. These values are compared with those derived from the rule of mixtures using elastic moduli data for LiF and CaF2 single crystals. It is shown that, while the shear modulus data agree reasonably well with the predicted trend, there is a large discrepancy between the theoretical calculations and the Young modulus values, where this disagreement increases with increasing temperature. Author

23 CHEMISTRY AND MATERIALS (GENERAL)

A91-38581* National Aeronautics and Space Administration. Lewis Research Center, Cleveland, OH.

ADHESION AT METAL INTERFACES

AMITAVA BANERJEA (NASA, Lewis Research Center, Cleveland; Kent State University, OH), JOHN FERRANTE (NASA, Lewis Research Center, Cleveland, OH), and JOHN R. SMITH (GM Research Laboratories, Warren, MI) IN: Fundamentals of adhesion. New York, Plenum Publishing Corp., 1991, p. 325-348. refs

Copyright

A basic adhesion process is defined, the theory of the properties influencing metallic adhesion is outlined, and theoretical approaches to the interface problem are presented, with emphasis on first-principle calculations as well as jellium-model calculations. The computation of the energies of adhesion as a function of the interfacial separation is performed; fully three-dimensional calculations are presented, and universality in the shapes of the binding energy curves is considered. An embedded-atom method and equivalent-crystal theory are covered in the framework of issues involved in practical adhesion. V.T.

A91-39246* National Aeronautics and Space Administration. Lewis Research Center, Cleveland, OH.

INTRINSIC BOND STRENGTH OF METAL FILMS ON POLYMER SUBSTRATES

DONALD R. WHEELER and HIROYUKI OSAKI (NASA, Lewis Research Center, Cleveland, OH) IN: Metallization of polymers; Proceedings of the Symposium, Montreal, Canada, Sept. 24-28, 1989. Washington, DC, American Chemical Society, 1990, p. 500-512. refs

Copyright

A semiquantitative method for the measurement of the intrinsic bond strength between elastic substrates and elastic films that fail by brittle fracture is described. Measurements on a polyethylene terephthalate (PET)-Ni couple were used to verify the essential features of the analysis. It was found that the interfacial shear strength of Ni on PET doubled after ion etching. K.K.

A91-44284*# National Aeronautics and Space Administration. Lewis Research Center, Cleveland, OH.

DETERMINATION OF ALLOY CONTENT FROM PLUME SPECTRAL MEASUREMENTS

GEORGE C. MADZSAR (NASA, Lewis Research Center, Cleveland, OH) AIAA, SAE, ASME, and ASEE, Joint Propulsion Conference, 27th, Sacramento, CA, June 24-26, 1991. 14 p. Previously announced in STAR as N91-24341. refs

(AIAA PAPER 91-2531) Copyright

The mathematical derivation for a method to determine the identities and amounts of alloys present in a flame where numerous alloys may be present is described. This method is applicable if the total number of elemental species from all alloys that may be in the flame is greater than or equal to the total number of alloys. Arranging the atomic spectral line emission equations for the elemental species as a series of simultaneous equations enables solution for identity and amount of the alloy present in the flame. This technique is intended for identification and quantification of alloy content in the plume of a rocket engine. Spectroscopic measurements reveal the atomic species entrained in the plume. Identification of eroding alloys may lead to the identification of the eroding component. Author

A91-49809* National Aeronautics and Space Administration. Lewis Research Center, Cleveland, OH.

ATOMIC OXYGEN EFFECTS ON REFRACTORY MATERIALS

DALE C. FERGUSON (NASA, Lewis Research Center, Cleveland, OH) IN: Materials degradation in low earth orbit (LEO); Proceedings of the Symposium, 119th Annual Meeting of the Minerals, Metals, and Materials Society, Anaheim, CA, Feb. 17-22, 1990. Warrendale, PA, Minerals, Metals, and Materials Society, 1990, p. 97-105. refs

Copyright

Atomic oxygen in LEO may have undesirable effects on exposed refractory materials, such as are proposed for nuclear reactors in

orbit, high temperature radiators, solar dynamic collectors, etc. Time-resolved measurement of the volatile efflux from such materials at high temperatures is being done in an ultrahigh vacuum atomic oxygen ion beam facility. Results of measurements of the efflux of volatile oxides of molybdenum and niobium-1 percent zirconium at temperatures as high as 1550 K are presented, along with a discussion of the roles of adsorption, desorption, and diffusion in atomic oxygen reactions on surfaces at high temperatures. The dependence of reaction rates for certain materials on the energy of the incident atomic oxygen beam will be emphasized. Author

A91-53704*# National Aeronautics and Space Administration. Lewis Research Center, Cleveland, OH.

ADVANCED MATERIALS FOR SPACE NUCLEAR POWER SYSTEMS

ROBERT H. TITRAN, TONI L. GROBSTEIN (NASA, Lewis Research Center, Cleveland, OH), and DAVID L. ELLIS (Case Western Reserve University, Cleveland, OH) AIAA, NASA, and OAI, Conference on Advanced SEI Technologies, Cleveland, OH, Sept. 4-6, 1991. 18 p. Previously announced in STAR as N91-29298. refs

(AIAA PAPER 91-3530) Copyright

The overall philosophy of the research was to develop and characterize new high temperature power conversion and radiator materials and to provide spacecraft designers with material selection options and design information. Research on three candidate materials (carbide strengthened niobium alloy PWC-11 for fuel cladding, graphite fiber reinforced copper matrix composites for heat rejection fins, and tungsten fiber reinforced niobium matrix composites for fuel containment and structural supports) considered for space power system applications is discussed. Each of these types of materials offers unique advantages for space power applications. Author

A91-56415* National Aeronautics and Space Administration. Lewis Research Center, Cleveland, OH.

HIGH EMITTANCE SURFACES FOR HIGH TEMPERATURE SPACE RADIATOR APPLICATIONS

BRUCE A. BANKS, SHARON K. RUTLEDGE (NASA, Lewis Research Center, Cleveland, OH), and DEBORAH HOTES (Cleveland State University, OH) IN: Optical surfaces resistant to severe environments; Proceedings of the Meeting, San Diego, CA, July 11, 12, 1990. Bellingham, WA, Society of Photo-Optical Instrumentation Engineers, 1990, p. 66-77. refs

Copyright

Surface modification techniques are evaluated for emittance enhancement of radiator surfaces. These techniques include acid etching, heat treating, abrasion, sputter texturing, electrochemical texturing, arc texturing, and atomic oxygen beam texturing. Candidate radiator surface materials under consideration include Nb-1 pct Zr, Cu, Ti, Ti-6 pct Al-4 pct V, 304 stainless steel, Al6061-T6, Mo, W, and Ta. O.G.

N91-11062*# National Aeronautics and Space Administration. Lewis Research Center, Cleveland, OH.

GRAPHITE FLUORIDE FIBERS AND THEIR APPLICATIONS IN THE SPACE INDUSTRY

CHING-CHEN HUNG, MARTIN LONG, and THERESE DEVER (Cleveland State Univ., OH.) Aug. 1990 14 p Presented at the AICHE Summer National Meeting, San Diego, CA, 19-22 Aug. 1990

(Contract RTOP 505-41-41)

(NASA-TM-103265; E-5679; NAS 1.15:103265) Avail: NTIS HC/MF A03 CSCL 07A

Characterization and potential space applications of graphite fluoride fibers from commercially available graphitized carbon fibers are presented. Graphite fluoride fibers with fluorine to carbon ratios of 0.65 and 0.68 were found to have electrical resistivity values of 10(exp 4) and 10(exp 11) Ohms-cm, respectively, and thermal conductivity values of 24 and 5 W/m-K, respectively. At this fluorine content range, the fibers have tensile strength of 0.25 + or - 0.10 GPa (36 + or - 14 ksi), Young's modulus of 170 + or - 30

GPa (25 + or - 5 Msi). The coefficient of thermal expansion value of a sample with fluorine to carbon ratio of 0.61 was found to be 7 ppm/C. These properties change and approach the graphite value as the fluorine content approach 0. Electrically insulative graphite fluoride fiber is at least five times more thermally conductive than fiberglass. Therefore, it can be used as a heat sinking printed circuit board material for low temperature, long life power electronics in spacecraft. Also, partially fluorinated fiber with tailor-made physical properties to meet the requirements of certain engineering design can be produced. For example, a partially fluorinated fiber could have a predetermined CTE value in -1.5 to 7 ppm/C range and would be suitable for use in solar concentrators in solar dynamic power systems. It could also have a predetermined electrical resistivity value suitable for use as a low observable material. Experimental data indicate that slightly fluorinated graphite fibers are more durable in the atomic oxygen environment than pristine graphite. Therefore, fluorination of graphite used in the construction of spacecraft that would be exposed to the low Earth orbit atomic oxygen may protect defect sites in atomic oxygen protective coatings and therefore decrease the rate of degradation of graphite. Author

N91-17141* National Aeronautics and Space Administration. Lewis Research Center, Cleveland, OH.

SUBSTITUTED 1,1,1-TRIARYL-2,2,2-TRIFLUOROETHANES AND PROCESSES FOR THEIR SYNTHESIS Patent

WILLIAM B. ALSTON, inventor (to NASA) and ROY F. GRATZ, inventor (to NASA) 27 Mar. 1990 10 p Filed 30 Dec. 1988 Division of US-Patent-Appl-SN-159071, filed 23 Feb. 1988 which is a division of US-Patent-Appl-SN-924474, filed 29 Oct. 1986 (NASA-CASE-LEW-14345-3; US-PATENT-4,912,238; US-PATENT-APPL-SN-292049; US-PATENT-APPL-SN-159071; US-PATENT-APPL-SN-924474; US-PATENT-CLASS-552-101; INT-PATENT-CLASS-C07C-15/16) Avail: US Patent and Trademark Office CSCL 07/1

Synthetic procedures to tetraalkyls, tetraacids and dianhydrides substituted 1,1,1 triaryl 2,2,2 trifluoroethanes which comprises: (1) 1,1 bis (dialkylaryl) 1 aryl 2,2,2 trifluoroethane, (2) 1,1 bis (dicarboxyaryl) 1 aryl 2,2,2 trifluoro ethane or (3) cyclic dianhydride of diamine of 1,1 bis (dialkylaryl) 1 aryl 2,2,2 trifluoro ethanes. The synthesis of (1) is accomplished by the condensation reaction of an aryltrifluoromethyl ketone with a dialkylaryl compound. The synthesis of (2) is accomplished by oxidation of (1). The synthesis of dianhydride of (3) is accomplished by the conversion of (2) to its corresponding cyclic dianhydride. The synthesis of the diamine is accomplished by the similar reaction of an aryltrifluoromethyl ketone with aniline or alkyl substituted or disubstituted anilines. Also, other derivatives of the above are formed by nucleophilic displacement reactions.

Official Gazette of the U.S. Patent and Trademark Office

N91-19224* National Aeronautics and Space Administration. Lewis Research Center, Cleveland, OH.

TRIBOLOGICAL PROPERTIES OF AG/TI FILMS ON AL₂O₃ CERAMIC SUBSTRATES

CHRISTOPHER DELLACORTE, STEPHEN V. PEPPER, and FRANK S. HONEY 1991 25 p Presented at the International Conference on Metallurgical Coatings and Thin Films, San Diego, CA, 22-26 Apr. 1991; sponsored by American Vacuum Society (Contract RTOP 505-63-1A) (NASA-TM-103784; E-6060; NAS 1.15:103784) Avail: NTIS HC/MF A03 CSCL 07/1

Ag solid lubricant films, with a thin Ti interlayer for enhanced adhesion, were sputter deposited on Al₂O₃ substrate disks to reduce friction and wear. The dual Ag/Ti films were tested at room temperature in a pin-on-disk tribometer sliding against bare, uncoated Al₂O₃ pins under a 4.9 N load at a sliding velocity of 1 m/s. The Ag/Ti films reduced the friction coefficient by 50 percent to about 0.41 compared to unlubricated baseline specimens. Pin wear was reduced by a factor of 140 and disk wear was reduced by a factor of 2.5 compared to the baseline. These films retain their good tribological properties including adhesion after heat treatments at 850 C and thus may be able to lubricate over a

wide temperature range. This lubrication technique is applicable to space lubrication, advanced heat engines, and advanced transportation systems. Author

N91-22377* National Aeronautics and Space Administration. Lewis Research Center, Cleveland, OH.

VISCOELASTIC PROPERTIES OF ADDITION-CURED POLYIMIDES USED IN HIGH TEMPERATURE POLYMER MATRIX COMPOSITES

GARY D. ROBERTS, DIANE C. MALARIK, and JERROLD O. ROBAIDEK (Case Western Reserve Univ., Cleveland, OH.) 1991 11 p Proposed for presentation at the 8th International Conference on Composite Materials, Honolulu, HI, 15-19 Jul. 1991; cosponsored by Society for the Advancement of Material and Process Engineering, American Society of Composites, American Inst. of Metallurgical Engineering, British Composite Society, European Association of Composite Materials, and Japan Society of Composite Materials (Contract RTOP 505-63-1A) (NASA-TM-103768; E-6001; NAS 1.15:103768) Avail: NTIS HC/MF A03 CSCL 11/4

Viscoelastic properties of the addition cured polyimide, PMR-15, were studied using dynamic mechanical and stress relaxation tests. For temperatures below the glass transition temperature, T_{sub g}, the dynamic mechanical properties measured using a temperature scan rate of 10 C/min were strongly affected by the presence of absorbed moisture in the resin. Dynamic mechanical properties measured as a function of time during an isothermal hold provided an indication of chemical changes occurring in the resin. For temperatures above (T_{sub g} + 20 C), the storage modulus increased continuously as a function of time indicating that additional crosslinking is occurring in the resin. Because of these changes in chemical structures, the stress relaxation modulus could not be measured over any useful time interval for temperatures above T_{sub g}. For temperatures below T_{sub g}, dynamic mechanical properties appeared to be unaffected by chemical changes for times exceeding 1 hr. Since the duration of the stress relaxation tests was less than 1 hr, the stress relaxation modulus could be measured. As long as the moisture content of the resin was less than 2 pct, stress relaxation curves measured at different temperatures could be superimposed using horizontal shifts along the log(time) axis with only small shifts along the vertical axis. Author

N91-22379* National Aeronautics and Space Administration. Lewis Research Center, Cleveland, OH.

TRIBOLOGICAL CHARACTERISTICS OF SILICON CARBIDE WHISKER-REINFORCED ALUMINA AT ELEVATED TEMPERATURES

CHRISTOPHER DELLACORTE Apr. 1991 45 p Submitted for publication (Contract RTOP 505-63-1A) (NASA-TM-103799; E-5990; NAS 1.15:103799) Avail: NTIS HC/MF A03 CSCL 07/1

The enhanced fracture toughness of whisker reinforced ceramics makes them attractive candidates for sliding components of advanced heat engines. Examples include piston rings and valve stems for Stirling engines and other low heat rejection devices. However, the tribological behavior of whisker reinforced ceramics is largely unknown. This is especially true for the applications described where use temperatures can vary from below ambient to well over 1000 C. An experimental research program to identify the dominant wear mechanism(s) for a silicon carbide whisker reinforced alumina composite, SiCw-Al₂O₃ is described. In addition, a wear mechanism model is developed to explain and corroborate the experimental results and to provide insight for material improvement. Author

N91-24341* National Aeronautics and Space Administration. Lewis Research Center, Cleveland, OH.

DETERMINATION OF ALLOY CONTENT FROM PLUME SPECTRAL MEASUREMENTS

GEORGE C. MADZSAR 1991 15 p Presented at the 27th

23 CHEMISTRY AND MATERIALS (GENERAL)

Joint Propulsion Conference, Sacramento, CA, 24-27 Jun. 1991; sponsored by AIAA, SAE, ASME, and the American Society for Electrical Engineers
(Contract RTOP 590-21-41)

(NASA-TM-104442; E-6280; NAS 1.15:104442; AIAA PAPER 91-2531) Avail: NTIS HC/MF A03 CSCL 07/1

The mathematical derivation for a method to determine the identities and amounts of alloys present in a flame where numerous alloys may be present is described. This method is applicable if the total number of elemental species from all alloys that may be in the flame is greater than or equal to the total number of alloys. Arranging the atomic spectral line emission equations for the elemental species as a series of simultaneous equations enables solution for identity and amount of the alloy present in the flame. This technique is intended for identification and quantification of alloy content in the plume of a rocket engine. Spectroscopic measurements reveal the atomic species entrained in the plume. Identification of eroding alloys may lead to the identification of the eroding component. Author

N91-25185* National Aeronautics and Space Administration. Lewis Research Center, Cleveland, OH.

SUBSTITUTED 1,1,1-TRIARYL-2,2,2-TRIFLUOROETHANES AND PROCESSES FOR THEIR SYNTHESIS Patent

WILLIAM B. ALSTON, inventor (to NASA) and ROY F. GRATZ, inventor (to NASA) 30 Apr. 1991 10 p Filed 10 Oct. 1989 Division of US-Patent-Appl-SN-292049, filed 30 Dec. 1988 (NASA-CASE-LEW-14345-4; US-PATENT-5,011,955; US-PATENT-APPL-SN-419554; US-PATENT-APPL-SN-292049; US-PATENT-CLASS-552-101; US-PATENT-CLASS-552-108; US-PATENT-CLASS-552-110; US-PATENT-CLASS-552-113; US-PATENT-CLASS-552-115; INT-PATENT-CLASS-C07C-15/16) Avail: US Patent and Trademark Office CSCL 07/1

Synthetic procedures are described for tetraalkyls, tetraacids, and dianhydrides substituted 1,1,1-triaryl-2,2,2-trifluoroethanes which comprises: (1) 1-bis (dialkylaryl)-1-aryl-2,2,2, trifluoroethane, (2) 1,1-bis(dicarboxyaryl) 1 aryl-2,2,2 trifluoroethane, or (3) cyclic dianhydride or diamine of 1,1-bis (dialkylaryl) 1-aryl-2,2,2 trifluoroethanes. The synthesis of (1) is accomplished by the condensation reaction of an aryltrifluoromethyl ketone with a dialkylaryl compound. The synthesis of (2) is accomplished by oxidation of (1). The synthesis dianhydride of (3) is accomplished by the conversion of (2) to its corresponding cyclic dianhydride. The synthesis of the diamine is accomplished by the similar reaction of an aryltrifluoromethyl ketone with aniline or alkyl substituted or disubstituted anilines. Also, other derivatives of the above are formed by nucleophilic displacement reactions.

Official Gazette of the U.S. Patent and Trademark Office

N91-27221*# National Aeronautics and Space Administration. Lewis Research Center, Cleveland, OH.

SLIDING WEAR OF SELF-MATED AL2O3-SiC WHISKER REINFORCED COMPOSITES AT 23-1200 C

SERENE C. FARMER, PATRICIA O. BOOK (Cleveland State Univ., OH.), and CHRISTOPHER DELLACORTE Jul. 1991 29 p (Contract RTOP 505-63-10) (NASA-TM-104490; E-6344; NAS 1.15:104490) Avail: NTIS HC/MF A03 CSCL 07/1

Microstructural changes occurring during sliding wear of self-mated Al₂O₃-SiC whisker reinforced composites were studied using optical, scanning electron microscopy, and transmission electron microscopy. Pin-on-disk specimens were slid in air at 2.7 m/sec sliding velocity under a 26.5 N load for 1 hr. Wear tests were conducted at 23, 600, 800, and 1200 C. Mild wear with a wear factor of 2.4 times 10⁻⁷ to 1.5 times 10⁻⁶ cu mm/Nm was experienced at all test temperatures. The composite shows evidence of wear by fatigue mechanisms at 800 C and below. Tribochemical reaction (SiC oxidation and reaction of SiO₂ and Al₂O₃) leads to intergranular failure at 1200 C. Distinct microstructural differences existing at each test temperature are reported. Author

N91-29235*# National Aeronautics and Space Administration. Lewis Research Center, Cleveland, OH.

AN ANALYSIS OF THE WEAR BEHAVIOR OF SiC WHISKER REINFORCED ALUMINA FROM 25 TO 1200 C

CHRISTOPHER DELLACORTE Aug. 1991 19 p (Contract RTOP 505-63-1A)

(NASA-TM-104489; E-6337; NAS 1.15:104489) Avail: NTIS HC/MF A03 CSCL 11/4

A model is described for predicting the wear behavior of whisker reinforced ceramics. The model was successfully applied to a silicon carbide whisker reinforced alumina ceramic composite subjected to sliding contact. The model compares the friction forces on the whiskers due to sliding, which act to pull or push them out of the matrix, to the clamping or compressive forces on the whiskers due to the matrix, which act to hold the whiskers in the composite. At low temperatures, the whiskers are held strongly in the matrix and are fractured into pieces during the wear process along with the matrix. At elevated temperatures differential thermal expansion between the whiskers and matrix can cause loosening of the whiskers and lead to pullout during the wear process and to higher wear. The model, which represents the combination of elastic stress analysis and a friction heating analysis, predicts a transition temperature at which the strength of the whiskers equals the clamping force holding them in the matrix. Above the transition the whiskers are pulled out of the matrix during sliding, and below the transition the whiskers are simply fractured. The existence of the transition gives rise to a dual wear mode or mechanism behavior for this material which was observed in laboratory experiments. The results from this model correlate well with experimentally observed behavior indicating that the model may be useful in obtaining a better understanding of material behavior and in making material improvements. Author

24

COMPOSITE MATERIALS

Includes physical, chemical, and mechanical properties of laminates and other composite materials.

A91-11815* National Aeronautics and Space Administration. Lewis Research Center, Cleveland, OH.

METAL MATRIX COMPOSITES MICROFRACTURE - COMPUTATIONAL SIMULATION

S. K. MITAL, J. J. CARUSO, and C. C. CHAMIS (NASA, Lewis Research Center, Cleveland, OH) (George Washington University, University of Virginia, and NASA, Symposium on Computational Technology for Flight Vehicles, Washington, DC, Nov. 5-7, 1990) Computers and Structures (ISSN 0045-7949), vol. 37, no. 2, 1990, p. 141-150. Previously announced in STAR as N90-24383. Copyright

Fiber/matrix fracture and fiber-matrix interface debonding in a metal matrix composite (MMC) are computationally simulated. These simulations are part of a research activity to develop computational methods for microfracture, microfracture propagation and fracture toughness of the metal matrix composites. The three-dimensional finite element model used in the simulation consists of a group of nine unidirectional fibers in three by three unit cell array of SiC/Ti₁₅ metal matrix composite with a fiber volume ratio of 0.35. This computational procedure is used to predict the fracture process and establish the hierarchy of fracture modes based on strain energy release rate. It is also used to predict stress redistribution to surrounding matrix-fibers due to initial and progressive fracture of fiber/matrix and due to debonding of fiber-matrix interface. Microfracture results for various loading cases such as longitudinal, transverse, shear and bending are presented and discussed. Step-by-step procedures are outlined to evaluate composite microfracture for a given composite system. Author

A91-16805* National Aeronautics and Space Administration. Lewis Research Center, Cleveland, OH.

IMPACT BEHAVIOR OF A SiC FIBER-REINFORCED REACTION BONDED Si₃N₄ COMPOSITE

J. GRADY, R. BHATT, and S. KLIMA (NASA, Lewis Research Center, Cleveland, OH) IN: 1989 SEM Spring Conference on Experimental Mechanics, Cambridge, MA, May 29-June 1, 1989, Proceedings. Bethel, CT, Society for Experimental Mechanics, Inc., 1989, p. 871-876. refs

Copyright

Impact tests were performed on a series of ceramic plate specimens. Monolithic (unreinforced) and composite specimens with various fiber layups were tested to determine the effect that the fiber reinforcement has on impact damage initiation and dynamic response of the ceramic materials. Results show that a porous surface layer of Si₃N₄ on the composite specimens can enhance the energy absorbing capability of the composite specimens. The addition of SiC fiber reinforcement to the RBSN matrix material is also shown to significantly change the mode of failure and reduce the extent of damage due to impact. Author

A91-16889* Engineering Science Software, Inc., Smithfield, RI. **EQUIVALENCE OF GREEN'S FUNCTION AND THE FOURIER SERIES REPRESENTATION OF COMPOSITES WITH PERIODIC MICROSTRUCTURE**

KEVIN P. WALKER (Engineering Science Software, Inc., Smithfield, RI), ERIC H. JORDAN (Connecticut, University, Storrs), and ALAN D. FREED (NASA, Lewis Research Center, Cleveland, OH) IN: Micromechanics and inhomogeneity - The Toshio Mura 65th anniversary volume; Selected Papers from the Symposium, ASME Winter Annual Meeting, San Francisco, CA, Dec. 10-15, 1989. New York, Springer-Verlag, 1990, p. 535-558. refs

(Contract NAG3-882; DE-AC02-88ER-13895)

Copyright

A computer program which is being developed to analyze the heterogeneous stress and strain history variation at the 'damage critical' locations of a composite structure operating at elevated temperatures is described. The theoretical foundations behind this program are described. The relationship between Fourier series and Green's function approaches is elucidated. K.K.

A91-16880* National Aeronautics and Space Administration. Lewis Research Center, Cleveland, OH.

COMPUTATIONAL SIMULATION OF HIGH-TEMPERATURE METAL MATRIX COMPOSITES CYCLIC BEHAVIOR

CHRISTOS C. CHAMIS, PAPPU L. N. MURTHY, and DALE A. HOPKINS (NASA, Lewis Research Center, Cleveland, OH) IN: Thermal and mechanical behavior of metal matrix and ceramic matrix composites. Philadelphia, PA, American Society for Testing and Materials, 1990, p. 56-69.

Copyright

A procedure was developed and is described that can be used to computationally simulate the cyclic behavior of high-temperature metal matrix composites (HTMMC) and its degradation effects on the structural response. This procedure consists of HTMMC mechanics coupled with a multifactor-interaction constituent material relationship and with an incremental iterative nonlinear analysis. The procedure is implemented in a computer code that can be used to computationally simulate the thermomechanical behavior of HTMMC starting from the fabrication process and proceeding through thermomechanical cycling, accounting for the interface/interphase region. Results show that combined thermal/mechanical cycling, the interphase, and in situ matrix properties have significant effects on the structural integrity of HTMMC. Author

A91-25798* National Aeronautics and Space Administration. Lewis Research Center, Cleveland, OH.

FATIGUE CRACK GROWTH STUDY OF SCS6/Ti-15-3 COMPOSITE

P. KANTZOS and J. TELESMA (NASA, Lewis Research Center, Cleveland, OH) International Journal of Fatigue (ISSN 0142-1123),

vol. 12, Sept. 1990, p. 409-415. refs

Copyright

A study was performed to determine the fatigue crack growth (FCG) behavior and the associated fatigue damage processes in a (0)8- and (90)8-oriented SCS6/Ti-15-3 composite. Companion testing was also done on identically processed Ti-15-3 unreinforced material. The active fatigue crack growth failure processes were very similar for both composite orientations tested. For both orientations, fatigue crack growth was along the fiber direction. It was found that the composite constituent most susceptible to fatigue damage was the interface region and, in particular, the carbon coating surrounding the fiber. The failure of the interface region led to crack initiation and also strongly influenced the FCG behavior in this composite. The failure of the interface region was apparently driven by normal stresses perpendicular to the fiber direction. The FCG rates were considerably higher for the (90)8-oriented CT specimens in comparison to the unreinforced material. Author

A91-27937* National Aeronautics and Space Administration. Lewis Research Center, Cleveland, OH.

REACTION OF Ti AND Ti-AL ALLOYS WITH ALUMINA

AJAY K. MISRA (NASA, Lewis Research Center; Sverdrup Technology, Inc., Cleveland, OH) Metallurgical Transactions A - Physical Metallurgy and Materials Science (ISSN 0360-2133), vol. 22A, March 1991, p. 715-721. refs

Copyright

The reaction of single-crystal Al₂O₃ with pure Ti and Ti-Al alloys with different Al concentrations was examined in the temperature range of 1173 to 1573 K. Significant reaction occurred between Al₂O₃ and the Ti-Al alloys with Al concentrations lower than that corresponding to the gamma-TiAl phase. The reaction mechanism was determined to be simultaneous diffusion of Al and atomic oxygen from Al₂O₃ into Ti and the Ti-Al alloys. Author

A91-28014* Martin Marietta Labs., Baltimore, MD.

COMPRESSION BEHAVIOR OF TiB₂-PARTICULATE-REINFORCED COMPOSITES OF AL₂₂Fe₃Ti₈

M. S. DIPIETRO, K. S. KUMAR (Martin Marietta Laboratories, Baltimore, MD), and J. D. WHITTENBERGER (NASA, Lewis Research Center, Cleveland, OH) Journal of Materials Research (ISSN 0884-2914), vol. 6, March 1991, p. 530-538. refs

(Contract NAS3-25787)

Copyright

The compression behavior of both the monolithic L1(2) compound Al₂₂Fe₃Ti₈ and discontinuous composites obtained by incorporating about 1 micron TiB₂ particles was studied for various volume percent reinforcements as a function of temperature and at high temperatures as a function of strain rate. In this study, by varying the Fe and Ti contents, the nature and volume fraction of the minor phases coexisting with the dominant L1(2) phase were changed and were examined with and without TiB₂ reinforcement. At high strain rates, the TiB₂ reinforcements significantly enhance ambient and warm-temperature strength, although a crossover is observed at about 1000 K, above which the monolithic material is stronger than the composite. At slow strain rates representative of creep conditions, however, the TiB₂-containing composites retain their superiority at least up to 1200 K. Author

A91-31919*# Clarkson Univ., Potsdam, NY.

PROGRESSIVE FRACTURE IN COMPOSITES SUBJECTED TO HYGROTHERMAL ENVIRONMENT

LEVON MINNETYAN (Clarkson University, Potsdam, NY), PAPPU L. N. MURTHY, and CHRISTOS C. CHAMIS (NASA, Lewis Research Center, Cleveland, OH) IN: AIAA/ASME/ASCE/AHS/ASC Structures, Structural Dynamics, and Materials Conference, 32nd, Baltimore, MD, Apr. 8-10, 1991, Technical Papers. Pt. 1. Washington, DC, American Institute of Aeronautics and Astronautics, 1991, p. 867-877. refs

(Contract NAG3-1101)

(AIAA PAPER 91-1140) Copyright

24 COMPOSITE MATERIALS

The effects of temperature and moisture on the load carrying capability and structural response properties of composites are investigated via computational simulation. An integrated computer code is utilized for the simulation of composite structures under loading. Damage initiation, damage growth, fracture progression, and global structural fracture are included in the simulation. Results demonstrate the significance of hygro-thermal effects on composite structural response, toughness, and durability. Author

A91-39553* National Aeronautics and Space Administration. Lewis Research Center, Cleveland, OH.

CONTINUOUS FIBER-REINFORCED TITANIUM ALUMINIDE COMPOSITES

R. A. MACKAY, P. K. BRINDLEY (NASA, Lewis Research Center, Cleveland, OH), and F. H. FROES (Idaho, University, Moscow) JOM (ISSN 1047-4838), vol. 43, May 1991, p. 23-29. refs Copyright

An account is given of the fabrication techniques, microstructural characteristics, and mechanical behavior of a lightweight, high service temperature SiC-reinforced alpha-2 Ti-14Al-21Nb intermetallic-matrix composite. Fabrication techniques under investigation to improve the low-temperature ductility and environmental resistance of this material system, while reducing manufacturing costs to competitive levels, encompass powder-cloth processing, foil-fiber-foil processing, and thermal-spray processing. Attention is given to composite microstructure problems associated with fiber distribution and fiber-matrix interfaces, as well as with mismatches of thermal-expansion coefficient; major improvements are noted to be required in tensile properties, thermal cycling effects, mechanical damage, creep, and environmental effects. O.C.

A91-42297*# National Aeronautics and Space Administration. Lewis Research Center, Cleveland, OH.

EVALUATION OF THERMOMECHANICAL DAMAGE IN SILICON CARBIDE/TITANIUM COMPOSITES

J. E. GRADY and B. A. LERCH (NASA, Lewis Research Center, Cleveland, OH) AIAA Journal (ISSN 0001-1452), vol. 29, June 1991, p. 992-997. Previously cited in issue 11, p. 1639, Accession no. A90-29228. refs Copyright

A91-43232* National Aeronautics and Space Administration. Lewis Research Center, Cleveland, OH.

CONCURRENT TAILORING OF FABRICATION PROCESS AND INTERPHASE LAYER TO REDUCE RESIDUAL STRESSES IN METAL MATRIX COMPOSITES

D. A. SARAVANOS, C. C. CHAMIS (NASA, Lewis Research Center, Cleveland, OH), and M. MOREL (NASA, Lewis Research Center; Sverdrup Technology, Inc., Cleveland, OH) SAMPE Quarterly (ISSN 0036-0821), vol. 22, July 1991, p. 36-44. refs Copyright

A methodology is presented to reduce the residual matrix stresses in continuous fiber metal matrix composites (MMC) by optimizing the fabrication process and interphase layer characteristics. The response of the fabricated MMC was simulated based on nonlinear micromechanics. Application cases include fabrication tailoring, interphase tailoring, and concurrent fabrication-interphase optimization. Two composite systems, silicon carbide/titanium and graphite/copper, are considered. Results illustrate the merits of each approach, indicate that concurrent fabrication/interphase optimization produces significant reductions in the matrix residual stresses and demonstrate the strong coupling between fabrication and interphase tailoring. Author

A91-49943* National Aeronautics and Space Administration. Lewis Research Center, Cleveland, OH.

REACTION OF BETA-PHASE Ni-AL ALLOYS WITH CRB2

AJAY K. MISRA (NASA, Lewis Research Center; Sverdrup Technology, Inc., Cleveland, OH) Journal of Materials Research (ISSN 0884-2914), vol. 6, Aug. 1991, p. 1664-1672. refs Copyright

Reaction of Ni-Al alloys within the beta-NiAl phase with CrB2

was studied at 1473 K as a function of Al concentration in the alloy. Reaction of 49-50 at. pct Al alloys with CrB2 occurred by interdiffusion of Ni into CrB2 and Cr into the alloy without forming a new product phase. On the other hand, a new product phase, rich in Ni and B, formed by the reaction of alloys having Al concentrations 48 at. pct or lower with CrB2. The reaction product was observed both at the CrB2/alloy interface and along the alloy grain boundaries. Author

A91-53552* National Aeronautics and Space Administration. Lewis Research Center, Cleveland, OH.

CERAMIC COMPOSITES FOR ROCKET ENGINE TURBINES

THOMAS P. HERBELL and ANDREW J. ECKEL (NASA, Lewis Research Center, Cleveland, OH) SAE, Aerospace Atlantic Conference, Dayton, OH, Apr. 22-26, 1991. 9 p. Previously announced in STAR as N91-19235. refs (SAE PAPER 911108) Copyright

The use of ceramic materials in the hot section of the fuel turbopump of advanced reusable rocket engines promises increased performance and payload capability, improved component life and economics, and greater design flexibility. Severe thermal transients present during operation of the Space Shuttle Main Engine (SSME), push metallic components to the limit of their capabilities. Future engine requirements might be even more severe. In phase one of this two-phase program, performance benefits were quantified and continuous fiber reinforced ceramic matrix composite components demonstrated a potential to survive the hostile environment of an advanced rocket engine turbopump. Author

A91-55050* National Aeronautics and Space Administration. Lewis Research Center, Cleveland, OH.

PRELIMINARY STUDIES ON NiAl/Nb2Be17 REACTION AND EFFECTIVENESS OF BEO AS AN INTERFACIAL REACTION BARRIER

AJAY K. MISRA (NASA, Lewis Research Center; Sverdrup Technology, Inc., Cleveland, OH) Metallurgical Transactions A - Physical Metallurgy and Materials Science (ISSN 0360-2133), vol. 22A, Oct. 1991, p. 2535-2538. refs Copyright

The interfacial reaction between NiAl and Nb2Be17 (used as a reinforcement for the alloy) was studied by measuring diffusion bonding of NiAl and Nb2Be17 plates in a hot press under a vacuum of 10 exp -5 atm. It was found that, after 2 hrs of hot pressing at 1373 K, the reaction between NiAl and Nb2Be17 was extensive. A 40 to 50-micron-thick reaction zone consisted of three distinct layers at the NiAl/Nb2Be17 interface: layer A next to Nb2Be17, layer B in the middle, and layer C next to NiAl. Results of analysis of the reaction layers using energy dispersive spectroscopy (EDS) were inconclusive because of the inability of EDS to detect Be. I.S.

A91-55900* National Aeronautics and Space Administration. Lewis Research Center, Cleveland, OH.

FACTORS WHICH INFLUENCE TENSILE STRENGTH OF A SiC/Ti-24Al-11Nb (AT. PCT) COMPOSITE

P. K. BRINDLEY, S. L. DRAPER, M. V. NATHAL (NASA, Lewis Research Center, Cleveland, OH), and J. I. ELDRIDGE (Sverdrup Technology, Inc., Middleburg Heights, OH) IN: Fundamental relationships between microstructures and mechanical properties of metal matrix composites; Proceedings of the Symposium, TMS Fall Meeting, Indianapolis, IN, Oct. 1-5, 1989. Warrendale, PA, Minerals, Metals, and Materials Society, 1990, p. 387-401. refs Copyright

Tensile and fiber pullout tests were used in conjunction with SEM to investigate structural and processing effects on SiC fiber, a neat Ti-24Al-11Nb matrix alloy, and a composite fabricated from the two. The effects of oxygen content, fiber spacing, fiber volume fraction, fiber-matrix reaction thickness, Teflon content, and matrix powder size, appear to be smaller than the effects of variability in fiber strength. Fiber spacing did not influence radial crack formation, interfacial bond shear strength, or stress-strain behavior in the

composite. The temperature dependence of composite properties was investigated over the 23-815 C range. O.C.

A91-55906* National Aeronautics and Space Administration. Lewis Research Center, Cleveland, OH.

HIGH TEMPERATURE FATIGUE BEHAVIOR OF TUNGSTEN COPPER COMPOSITES

M. J. VERRILLI, Y.-S. KIM, and T. P. GABB (NASA, Lewis Research Center, Cleveland, OH) IN: Fundamental relationships between microstructures and mechanical properties of metal matrix composites; Proceedings of the Symposium, TMS Fall Meeting, Indianapolis, IN, Oct. 1-5, 1989. Warrendale, PA, Minerals, Metals, and Materials Society, 1990, p. 479-495. refs
Copyright

The present study investigates the high-temperature fatigue behavior of a 9-v/o tungsten fiber-reinforced copper matrix composite. Load-controlled isothermal fatigue at 260 and 560 C and thermomechanical fatigue (TMF) experiments, both in-phase and out-of-phase between 260 and 560 C, were performed. The stress-strain response under all conditions displayed considerable inelasticity. Strain ratchetting was observed during all the fatigue experiments. For the isothermal fatigue and in-phase TMF tests, the ratchetting was always in a tensile direction, continuing until failure. The ratchetting during the out-of-phase TMF test shifted from a tensile to a compressive direction. For all cases, the fatigue lives were found to be controlled by the damage of the copper matrix. On a stress basis, TMF loading substantially reduced lives relative to isothermal cycling. C.A.B.

A91-55907* National Aeronautics and Space Administration. Lewis Research Center, Cleveland, OH.

THE ISOTHERMAL FATIGUE BEHAVIOR OF A UNIDIRECTIONAL SiC/Ti COMPOSITE AND THE Ti ALLOY MATRIX

JOHN GAYDA, T. P. GABB, and A. D. FREED (NASA, Lewis Research Center, Cleveland, OH) IN: Fundamental relationships between microstructures and mechanical properties of metal matrix composites; Proceedings of the Symposium, TMS Fall Meeting, Indianapolis, IN, Oct. 1-5, 1989. Warrendale, PA, Minerals, Metals, and Materials Society, 1990, p. 497-514. refs
Copyright

The high temperature fatigue behavior of a metal matrix composite (MMC) consisting of Ti-15V-3Cr-3Al-3Sn(Ti-15-3) matrix reinforced by 33 volume percent of continuous unidirectional SiC fibers was experimentally and analytically evaluated. Isothermal MMC fatigue tests with constant amplitude loading parallel to the fiber direction were performed at 300 and 550 C. Comparative fatigue tests of the Ti-15-3 matrix alloy were also performed. Composite fatigue behavior and the in situ stress state of the fiber and matrix were analyzed with a micromechanical model, the Concentric Cylinder Model (CCM). The cyclic stress-strain response of the composite was stable at 300 C. However, an increase in cyclic mean strain foreshortened MMC fatigue life at high strain ranges at 550 C. Fatigue tests of the matrix alloy and CCM analyses indicated this response was associated with stress relaxation of the matrix in the composite and subsequent load shedding to the fibers. Author

A91-55918* Rockwell International Corp., Canoga Park, CA. EFFECT OF THERMAL SHOCK ON FIBER-REINFORCED SUPERALLOY COMPOSITES

J. L. YUEN, G. D. SCHNITTGRUND (Rockwell International Corp., Rocketdyne Div., Canoga Park, CA), and D. W. PETRASEK (NASA, Lewis Research Center, Cleveland, OH) IN: Fundamental relationships between microstructures and mechanical properties of metal matrix composites; Proceedings of the Symposium, TMS Fall Meeting, Indianapolis, IN, Oct. 1-5, 1989. Warrendale, PA, Minerals, Metals, and Materials Society, 1990, p. 727-744. refs (Contract NAS3-24380)
Copyright

An evaluation is presented of the thermal shock behavior of tungsten fiber-reinforced superalloy (FRS) composites with respect to the turbine blade requirements of rocket engine turbopumps.

Each composite was reinforced unidirectionally with 40-volume-pct continuous tungsten fibers. The start-up conditions of the first-stage turbine blades of the high-pressure fuel turbopump in the Space Shuttle Main Engine (SSME) were used to investigate the thermal shock behavior of these materials. The FRS composites showed excellent thermal shock resistance, two to nine times better than the turbine blade material used in the SSME. Thermal shock cycling produced microcracks on the surfaces of the irradiated area that were less than 0.13 mm long and 0.005 mm deep. Neither fiber/matrix debonding nor microvoiding was observed. C.A.B.

A91-56254* General Motors Research Labs., Warren, MI. UNIVERSAL ENERGY RELATIONS AND METAL/CERAMIC INTERFACES

JOHN R. SMITH (GM Research Laboratories, Warren, MI), HERBERT SCHLOSSER (Cleveland State University, OH), and JOHN FERRANTE (NASA, Lewis Research Center, Cleveland, OH) IN: Metal-ceramic interfaces; Proceedings of an International Workshop, Santa Barbara, CA, Jan. 16-18, 1989. Oxford, England and Elmsford, NY, Pergamon Press, 1990, p. 15-24. refs
Copyright

Known general relationships between pertinent variables are applied to investigate metal-ceramic interfaces. The adhesive energy is determined. The electronic exchange-correlation energy is found to be the dominant attractive term in the total energy. Results for the adhesive energy are obtained for junctions of all combinations of the low index surfaces of Al, Na, Mg, and Zn. This leads to a variety of curves, all with a single minimum of separation and equilibrium binding energy. Scaling results for 10 contacts fall closely onto a single curve, a universal energy relation for adhesion. The scaled chemisorption curves fall accurately on the same universal form that was found for adhesion. For the case of cohesion, all-first principle results are scaled and again all scaled curves for a variety of metals fall accurately on the universal form for adhesion and chemisorption. An intimate relationship between the energetics of solids and molecules is inferred. C.A.B.

A91-56913* National Aeronautics and Space Administration. Lewis Research Center, Cleveland, OH.

INVESTIGATION OF INTERFACIAL SHEAR STRENGTH IN SiC/Si3N4 COMPOSITES

J. I. ELDRIDGE, R. T. BHATT, and J. D. KISER (NASA, Lewis Research Center, Cleveland, OH) Ceramic Engineering and Science Proceedings (ISSN 0196-6219), vol. 12, July-Aug. 1991, p. 1152-1171. Previously announced in STAR as N91-26233. refs

Copyright

A fiber push-out technique was used to determine fiber/matrix interfacial shear strength (ISS) for silicon carbide fiber reinforced reaction-bonded silicon nitride (SiC/RBSN) composites in the as-fabricated condition and after consolidation by hot isostatic pressing (HIPing). In situ video microscopy and acoustic emission detection greatly aided the interpretation of push-out load/displacement curves. Author

A91-56935* National Aeronautics and Space Administration. Lewis Research Center, Cleveland, OH.

THERMAL SHOCK FIBER-REINFORCED CERAMIC MATRIX COMPOSITES

ANDREW J. ECKEL, THOMAS P. HERBELL, EDWARD R. GENERAZIO (NASA, Lewis Research Center, Cleveland, OH), and JOHN Z. GYKENYESI (Cleveland State University, OH) Ceramic Engineering and Science Proceedings (ISSN 0196-6219), vol. 12, July-Aug. 1991, p. 1500-1508. Previously announced in STAR as N91-19295. refs
Copyright

Monolithic silicon carbide and silicon nitride and a Nicalon fiber reinforced silicon carbide composite were subjected to severe thermal shock conditions via impingement of a hydrogen-oxygen flame. Surface heating rates of 1000 C/sec to 2500 C/sec were generated. The performance of the monolithic reference materials are compared and contrasted to the significantly greater thermal

24 COMPOSITE MATERIALS

shock resistance of the composite. Ultrasonic and radiographic NDE techniques were used to evaluate the integrity of the composite subsequent to thermal shock. Tensile tests were performed to determine the residual tensile strength and modulus. Physical property changes are discussed as a function of number and severity of thermal shock cycles. Author

A91-56937* National Aeronautics and Space Administration. Lewis Research Center, Cleveland, OH.

DYNAMIC FATIGUE PROPERTY OF SILICON CARBIDE WHISKER-REINFORCED SILICON NITRIDE

SUNG R. CHOI (NASA, Lewis Research Center; Cleveland State University, OH), JONATHAN A. SALEM, and JOHN P. GYEKENYESI (NASA, Lewis Research Center, Cleveland, OH) Ceramic Engineering and Science Proceedings (ISSN 0196-6219), vol. 12, July-Aug. 1991, p. 1524-1536. refs Copyright

The dynamic fatigue behavior of 30 vol pct SiC whisker-reinforced silicon nitride was determined in flexure as a function of temperature from 1100 to 1300 C in an air environment. The fatigue susceptibility parameter n decreased from 88.1 to 20.1 with increasing temperature from 1100 to 1300 C. A transition in the dynamic fatigue curve occurred at a lowest stressing rate of 2 MPa/min at a temperature of 1300 C, resulting in a considerably lower value of $n = 5.8$. This transition was primarily due to creep that was enhanced by a combination of high temperature and very slow deformation rate. The fatigue resistance of natural flaws at 1100 C was found to be greater than that of artificial flaws produced by indentation. Author

A91-56942* National Aeronautics and Space Administration. Lewis Research Center, Cleveland, OH.

IN SITU X-RAY MONITORING OF DAMAGE ACCUMULATION IN SiC/RBSN TENSILE SPECIMENS

GEORGE Y. BAAKLINI (NASA, Lewis Research Center, Cleveland, OH) and RAMKRISHNA T. BHATT (NASA, Lewis Research Center; U.S. Army, Propulsion Directorate, Cleveland, OH) Ceramic Engineering and Science Proceedings (ISSN 0196-6219), vol. 12, July-Aug. 1991, p. 1599-1615. Previously announced in STAR as N91-22402. refs Copyright

The room-temperature tensile testing of silicon carbide fiber reinforced reaction-bonded silicon nitride (SiC/RBSN) composite specimens was monitored by using in-situ X-ray film radiography. Radiographic evaluation before, during, and after loading provided data on the effect of preexisting volume flaws (high density impurities, and local density variations) on the fracture behavior of composites. Results from (O)1, (O)3, (O)5, and (O)8 composite specimens showed that X-ray film radiography can monitor damage accumulations during tensile loading. Matrix cracking, fiber-matrix debonding, and fiber pullout were imaged throughout the tensile loading history of the specimens. Further, in-situ film radiography was found to be a helpful and practical technique for estimating interfacial shear strength between the SiC fiber and the RBSN matrix by the matrix crack spacing method. It is concluded that pretest, in-situ, and post-test radiography can provide for a greater understanding of ceramic matrix composite mechanical behavior, a verification of related experimental procedures, and a validation and development of related analytical models. Author

A91-56961* National Aeronautics and Space Administration. Lewis Research Center, Cleveland, OH.

THERMOCHEMICAL ANALYSIS OF CHEMICAL PROCESSES RELEVANT TO THE STABILITY AND PROCESSING OF SiC-REINFORCED Si₃N₄ COMPOSITE

AJAY K. MISRA (NASA, Lewis Research Center; Sverdrup Technology, Inc., Cleveland, OH) Ceramic Engineering and Science Proceedings (ISSN 0196-6219), vol. 12, Sept.-Oct. 1991, p. 1873-1885. refs Copyright

Chemical processes relevant to the stability and processing of SiC-reinforced Si₃N₄ composites have been examined from thermochemical considerations. The thermodynamic stabilities of

various interfaces, such as SiC-Si₃N₄, SiC-Si₃N₄-Si₂ON₂, and SiC-Si₃N₄-SiO₂, have been examined as a function of temperature, and the temperatures above which these interfaces become unstable have been calculated. The degradation of SiC during the processing of the composite has been examined. The processing routes considered in this study include the reaction bonded silicon nitride (RBSN) process and the pressure-assisted sintering processes with suitable sintering additives. Author

N91-10127*# National Aeronautics and Space Administration. Lewis Research Center, Cleveland, OH.

STRUCTURAL PROPERTIES OF LAMINATED DOUGLAS FIR/EPOXY COMPOSITE MATERIAL

DAVID A. SPERA, JACK B. ESGAR, MEADE GOUGEON, and MICHAEL D. ZUTECK (Gougeon Bros., Inc., Bay City, MI.) May 1990 140 p

(Contract NAS3-25266; DE-AI01-76ET-20320; RTOP 776-33-41) (NASA-RP-1236; E-4720; NAS 1.61:1236; DOE/NASA/20320-76) Avail: NTIS HC/MF A07 CSCL 11D

This publication contains a compilation of static and fatigue strength data for laminated-wood material made from Douglas fir and epoxy. Results of tests conducted by several organizations are correlated to provide insight into the effects of variables such as moisture, size, lamina-to-lamina joint design, wood veneer grade, and the ratio of cyclic stress to steady stress during fatigue testing. These test data were originally obtained during development of wood rotor blades for large-scale wind turbines of the horizontal-axis (propeller) configuration. Most of the strength property data in this compilation are not found in the published literature. Test sections ranged from round cylinders 2.25 in. in diameter to rectangular slabs 6 by 24 in. in cross section and approximately 30 ft. long. All specimens were made from Douglas fir veneers 0.10 in. thick, bonded together with the WEST epoxy system developed for fabrication and repair of wood boats. Loading was usually parallel to the grain. Size effects (reduction in strength with increase in test volume) are observed in some of the test data, and a simple mathematical model is presented that includes the probability of failure. General characteristics of the wood/epoxy laminate are discussed, including features that make it useful for a wide variety of applications. Author

N91-10134*# National Aeronautics and Space Administration. Lewis Research Center, Cleveland, OH.

INTERCALATED GRAPHITE FIBER COMPOSITES AS EMI SHIELDS IN AEROSPACE STRUCTURES

JAMES R. GAIER Nov. 1990 31 p Presented at the International Symposium on Carbon, Tsukuba, Japan, 4-8 Nov. 1990; sponsored in part by the Carbon Society of Japan (Contract RTOP 506-41-41)

(NASA-TM-103632; E-5781; NAS 1.15:103632) Avail: NTIS HC/MF A03 CSCL 11D

The requirements for electromagnetic interference (EMI) shielding in aerospace structures are complicated over that of ground structures by their weight limitations. As a result, the best EMI shielding materials must blend low density, high strength, and high elastic modulus with high shielding ability. In addition, fabrication considerations including penetrations and joints play a major role. The EMI shielding properties are calculated for shields formed from pristine and intercalated graphite fiber/epoxy composites and compared to preliminary experimental results and to shields made from aluminum. Calculations indicate that EMI shields could be fabricated from intercalated graphite composites which would have less than 12 percent of the mass of conventional aluminum shields, based on mechanical properties and shielding properties alone. Author

N91-11074*# National Aeronautics and Space Administration. Lewis Research Center, Cleveland, OH.

ELASTIC/PLASTIC ANALYSES OF ADVANCED COMPOSITES INVESTIGATING THE USE OF THE COMPLIANT LAYER CONCEPT IN REDUCING RESIDUAL STRESSES RESULTING FROM PROCESSING

STEVEN M. ARNOLD, VINOD K. ARYA (Toledo Univ., OH.), and

MATTHEW E. MELIS Sep. 1990 51 p
(Contract RTOP 510-01-01)
(NASA-TM-103204; E-5661; NAS 1.15:103204) Avail: NTIS
HC/MF A04 CSCL 11D

High residual stresses within intermetallic and metal matrix composite systems can develop upon cooling from the processing temperature to room temperature due to the coefficient of thermal expansion (CTE) mismatch between the fiber and matrix. As a result, within certain composite systems, radial, circumferential, and/or longitudinal cracks have been observed to form at the fiber-matrix interface. The compliant layer concept (insertion of a compensating interface material between the fiber and matrix) was proposed to reduce or eliminate the residual stress buildup during cooling and thus minimize cracking. The viability of the proposed compliant layer concept is investigated both elastically and elastoplastically. A detailed parametric study was conducted using a unit cell model consisting of three concentric cylinders to determine the required character (i.e., thickness and material properties) of the compliant layer as well as its applicability. The unknown compliant layer mechanical properties were expressed as ratios of the corresponding temperature dependent Ti-24Al-11Nb (a/o) matrix properties. The fiber properties taken were those corresponding to SCS-6 (SiC). Results indicate that the compliant layer can be used to reduce, if not eliminate, radial and circumferential residual stresses within the fiber and matrix and therefore also reduce or eliminate the radial cracking. However, with this decrease in in-plane stresses, one obtains an increase in longitudinal stress, thus potentially initiating longitudinal cracking. Guidelines are given for the selection of a specific compliant material, given a perfectly bonded system. Author

N91-13495* National Aeronautics and Space Administration.
Lewis Research Center, Cleveland, OH.

**RELATIONSHIP BETWEEN VOIDS AND INTERLAMINAR
SHEAR STRENGTH OF POLYMER MATRIX COMPOSITES**

KENNETH J. BOWLES and STEPHEN FRIMPONG 1991 20 p
Proposed for presentation at the 36th International SAMPE
Symposium and Exhibition, San Diego, CA, 15-18 Apr. 1991;
sponsored by Society for the Advancement of Materials and
Process Engineering
(Contract RTOP 510-01-50)
(NASA-TM-103643; E-5825; NAS 1.15:103643) Avail: NTIS
HC/MF A03 CSCL 11/4

The effect of voids on the interlaminar shear strength of a polyimide matrix composite system is described. The AS4 graphite/PMR-15 composite was chosen for study because this system can be readily processed by using the standard specified cure cycle to produce void-free composites and because preliminary work in this study had shown that the processing parameters of this resin matrix system can be altered to produce cured composites of varying void contents. Thirty-eight 12-ply unidirectional composite panels were fabricated for this study. A significant range of void contents (0 to 10 percent) was produced. The panels were mapped, ultrasonically inspected, and sectioned into interlaminar shear, flexure, and fiber content specimens. The density of each specimen was measured and interlaminar shear and flexure strength measurements were then made. The fiber content was measured last. The results of these tests were evaluated by using ultrasonic results, photomicrographs, statistical methods, theoretical relationships derived by other investigators, and comparison of the test data with the Integrated Composite Analyzer (ICAN) computer program developed at the Lewis Research Center for predicting composite ply properties. The testing is described in as much detail as possible in order to help others make realistic comparisons. Author

N91-13502* National Aeronautics and Space Administration.
Lewis Research Center, Cleveland, OH.

**METHOD OF MAKING SINGLE CRYSTAL FIBERS Patent
Application**

LEONARD J. WESTFALL, inventor (to NASA) 23 Aug. 1990
12 p

(NASA-CASE-LEW-14921-1; NAS 1.71:LEW-14921-1;
US-PATENT-APPL-SN-571059) Avail: NTIS HC/MF A03 CSCL
11/4

Single crystal fibers are made from miniature extruded ceramic feed rods. A decomposable binder is mixed with powders to inform a slurry which is extruded into a small rod which may be sintered, either in air or in vacuum, or it may be used in the extruded and dried condition. A pair of laser beams focuses onto the tip of the rod to melt it thereby forming a liquid portion. A single crystal seed fiber of the same material as the feed rod contacts this liquid portion to establish a zone of liquid material between the feed rod and the single crystal seed fiber. The feed rod and the single crystal feed fiber are moved at a predetermined speed to solidify the molten zone onto the seed fiber while simultaneously melting additional feed rod. In this manner a single crystal fiber is formed from the liquid portion. NASA

N91-14426* National Aeronautics and Space Administration.
Lewis Research Center, Cleveland, OH.

LOW VELOCITY IMPACT ANALYSIS WITH NASTRAN

DANIEL A. TROWBRIDGE (Analex Corp., Fairview Park, OH.),
JOSEPH E. GRADY, and ROBERT A. AIELLO Apr. 1990 17 p
Presented at the NASTRAN User's Colloquium, Portland OR, 23-27
Apr. 1990; sponsored in part by COSMIC, and Georgia Univ.
Previously announced as N90-24647
(Contract RTOP 505-63-11)

(NASA-TM-103169; E-5541; NAS 1.15:103169) Avail: NTIS
HC/MF A03 CSCL 11/4

A nonlinear elastic force-displacement relationship is used to calculate the transient impact force and local deformation at the point of contact between impactor and target. The nonlinear analysis and transfer function capabilities of NASTRAN are used to define a finite element model that behaves globally linearly elastic, and locally nonlinear elastic to model the local contact behavior. Results are presented for two different structures: a uniform cylindrical rod impacted longitudinally; and an orthotropic plate impacted transversely. Calculated impact force and transient structural response of the targets are shown to compare well with results measured in experimental tests. Author

N91-15318* National Aeronautics and Space Administration.
Lewis Research Center, Cleveland, OH.

**COMPOSITE BEARING AND SEAL MATERIALS FOR
ADVANCED HEAT ENGINE APPLICATIONS TO 900 C**

HAROLD E. SLINEY Aug. 1990 12 p Presented at the
Workshop on Coatings for Advanced Heat Engines, Castine, ME,
6-9 Aug. 1990

(Contract DE-AI01-85CE-50162; RTOP 778-34-22)

(NASA-TM-103612; E-5769; NAS 1.15:103612;
DOE/NASA/50162-4) Avail: NTIS HC/MF A03 CSCL 11/4

Plasma sprayed composite coatings of metal-bonded chromium carbide with additions of silver and thermochemically stable fluorides were previously reported to be lubricative in pin on disk bench tests from room temperature to 900 C. An early coating formulation of this type, designated as PS200, was successfully tested as a cylinder coating in a Stirling engine at a TRRT of 760 C (1450 F) in a hydrogen atmosphere, and as a backup lubricant for gas bearings to 650 C (1250 F). A subsequent optimization program has shown that tribological properties are further improved by increasing the solid lubricant content. The improved coating is designated as PS212. The same powder formulation has been used to make free-standing powder metallurgy (PM212) parts by sintering or hot isostatic pressing. The process is very attractive for making parts that cannot be readily plasma sprayed such as bushings and cylinders that have small bore diameters and/or high length to diameter ratios. The properties of coatings and free-standing parts fabricated from these powders are reviewed. Author

N91-15320* National Aeronautics and Space Administration.
Lewis Research Center, Cleveland, OH.

**GRAPHITE FLUORIDE FIBER POLYMER COMPOSITE
MATERIAL Patent**

24 COMPOSITE MATERIALS

CHING-CHEH HUNG, inventor (to NASA) 18 Sep. 1990 5 p
Filed 30 Sep. 1988

(NASA-CASE-LEW-14472-1; US-PATENT-4,957,661;
US-PATENT-APPL-SN-251499; US-PATENT-CLASS-252-510;
US-PATENT-CLASS-423-439; US-PATENT-CLASS-423-448;
US-PATENT-CLASS-423-460; US-PATENT-CLASS-423-489;
INT-PATENT-CLASS-H01B-1/06) Avail: US Patent and
Trademark Office CSCL 11/4

Improved graphite fluoride fibers are produced by contact reaction between highly graphitized fibers and fluorine gas. It is preferable to intercalate the fibers with bromine or fluorine and metal fluoride prior to fluorination. These graphite fluoride fibers are bound by an epoxy. The resulting composites have high thermal conductivity, high electric resistivity, and high emissivity.

Official Gazette of the U.S. Patent and Trademark Office

N91-15328* National Aeronautics and Space Administration.
Lewis Research Center, Cleveland, OH.

ICAN SENSITIVITY ANALYSIS

STEPHEN FRIMPONG, GARY D. ROBERTS, and KENNETH J. BOWLES Dec. 1990 24 p

(Contract RTOP 505-63-40)
(NASA-TM-103667; E-5874; NAS 1.15:103667) Avail: NTIS
HC/MF A03 CSCL 11/4

A computer program called Integrated Composite Analyzer (ICAN) was used to predict the properties of high-temperature polymer matrix composites. ICAN is a collection of NASA Lewis Research Center-developed computer codes designed to carry out analysis of multilayered fiber composites. The material properties used as input to the program were those of the thermoset polyimide resin PMR-15 and the carbon fiber Celion 6000. The sensitivity of the predicted composite properties to variations in the resin and fiber properties was examined. In addition, the predicted results were compared with experimental data. In most cases, the effect of changes in resin and fiber properties on composite properties was reasonable. However, the variations in the composite strengths with the moisture content of the PMR-15 resin were inconsistent. The ICAN-predicted composite moduli agreed fairly well with experimental values, but the predicted composite strengths were generally lower than experimental values.

Author

N91-15329* National Aeronautics and Space Administration.
Lewis Research Center, Cleveland, OH.

REINFORCEMENTS: THE KEY TO HIGH PERFORMANCE COMPOSITE MATERIALS

SALVATORE J. GRISAFFE 1990 31 p Presented at the Complex Composites Workshop, Washington, DC, 27 Mar. 1990; sponsored by Japanese Technology Evaluation Center Submitted for publication

(Contract RTOP 505-63-1A)
(NASA-TM-103230; E-5646; NAS 1.15:103230) Avail: NTIS
HC/MF A03 CSCL 11/4

Better high temperature fibers are the key to high performance, light weight composite materials. However, current U.S. and Japanese fibers still have inadequate high temperature strength, creep resistance, oxidation resistance, modulus, stability, and thermal expansion match with some of the high temperature matrices being considered for future aerospace applications. In response to this clear deficiency, both countries have research and development activities underway. Once successful fibers are identified, their production will need to be taken from laboratory scale to pilot plant scale. In such efforts it can be anticipated that the Japanese decisions will be based on longer term criteria than those applied in the U.S. Since the initial markets will be small, short term financial criteria may adversely minimize the number and strength of U.S. aerospace materials suppliers to well into the 21st century. This situation can only be compounded by the Japanese interests in learning to make commercial products with existing materials so that when the required advanced fibers eventually do arrive, their manufacturing skills will be developed.

Author

N91-16075* National Aeronautics and Space Administration.
Lewis Research Center, Cleveland, OH.

EFFECTS OF HIGH PRESSURE NITROGEN ON THE THERMAL STABILITY OF SiC FIBERS

MARTHA H. JASKOWIAK Jan. 1991 18 p Submitted for publication

(Contract RTOP 510-01-01)
(NASA-TM-103245; E-5671; NAS 1.15:103245) Avail: NTIS
HC/MF A03 CSCL 11/4

Polymer-derived SiC fibers were exposed to nitrogen gas pressures of 7 and 50 atm at temperatures up to 1800 C. The fiber weight loss, chemical composition, and tensile strength were then measured at room temperature in order to understand the effects of nitrogen exposure on fiber stability. High pressure nitrogen treatments limited weight loss to 3 percent or less for temperatures up to 1800 C. The bulk Si-C-O chemical composition of the fiber remained relatively constant up to 1800 C with only a slight increase in nitrogen content after treatment at 50 atm; however, fiber strength retention was significantly improved. To further understand the effects of the nitrogen atmosphere on the fiber stability, the results of previous high pressure argon treatments were compared to those of the high pressure nitrogen treatments. High pressure inert gas can temporarily maintain fiber strength by physically inhibiting the evolution of gaseous species which result from internal reactions. In addition to this physical effect, it would appear that high pressure nitrogen further improved fiber temperature capability by chemically reacting with the fiber surface, thereby reducing the rate of gas evolution. Subsequent low pressure argon treatments following the initial nitrogen treatments resulted in stronger fibers than after argon treatment alone, further supporting the chemical reaction mechanism and its beneficial effects on fiber strength.

Author

N91-17143* National Aeronautics and Space Administration.
Lewis Research Center, Cleveland, OH.

METCAN SIMULATION OF CANDIDATE METAL MATRIX COMPOSITES FOR HIGH TEMPERATURE APPLICATIONS

HO-JUN LEE Nov. 1990 21 p

(Contract RTOP 510-01-0A)
(NASA-TM-103636; E-5813; NAS 1.15:103636) Avail: NTIS
HC/MF A03 CSCL 11/4

The METCAN (Metal Matrix Composite Analyzer) computer code is used to simulate the nonlinear behavior of select metal matrix composites in order to assess their potential for high temperature structural applications. Material properties for seven composites are generated at a fiber volume ratio of 0.33 for two bonding conditions (a perfect bond and a weak interphase case) at various temperatures. A comparison of the two bonding conditions studied shows a general reduction in value of all properties (except CTE) for the weak interphase case from the perfect bond case. However, in the weak interphase case, the residual stresses that develop are considerably less than those that form in the perfect bond case. Results of the computational simulation indicate that among the metal matrix composites examined, SiC/NiAl is the best candidate for high temperature applications at the given fiber volume ratio.

Author

N91-17145* National Aeronautics and Space Administration.
Lewis Research Center, Cleveland, OH.

PROCESS FOR HIP CANNING OF COMPOSITES Patent

JOHN J. JUHAS, inventor (to NASA) 25 Dec. 1990 7 p Filed 9 Nov. 1989 Continuation-in-part of abandoned US-Patent-AppI-SN-326757, filed 21 Mar. 1989

(NASA-CASE-LEW-14990-1-CU; US-PATENT-4,980,126;
US-PATENT-APPL-SN-433863; US-PATENT-APPL-SN-326757;
US-PATENT-CLASS-419-49; US-PATENT-CLASS-419-8;
US-PATENT-CLASS-419-24; US-PATENT-CLASS-419-36;
US-PATENT-CLASS-419-37; US-PATENT-CLASS-419-48) Avail:
US Patent and Trademark Office CSCL 11/4

A single step is relied on in the canning process for hot isostatic pressing (HIP) metallurgy composites. The composites are made from arc sprayed and plasma sprayed monolayer. The HIP can is of compatible refractory metal and is sealed at high vacuum and

temperature. This eliminates outgassing during hot isostatic pressing.

Official Gazette of the U.S. Patent and Trademark Office

N91-18192*# National Aeronautics and Space Administration. Lewis Research Center, Cleveland, OH.

REVIEW OF ACOUSTO-ULTRASONIC NDE FOR COMPOSITES
ALEX VARY and HAROLD KAUTZ *In* NASA, Marshall Space Flight Center, Second Conference on NDE for Aerospace Requirements p 33-49 Dec. 1990
Avail: NTIS HC/MF A13 CSCL 11/4

Acousto-ultrasonics utilizes simulated stress waves to detect and quantify defect states, damage conditions, and variations of mechanical properties in fiber reinforced composites. The term acousto-ultrasonics denotes a combination of aspects of acoustic emission methodology with ultrasonic materials characterization. The acousto-ultrasonic approach was developed to deal primarily with evaluation of the integrated effect of minor flaws and diffuse flaw populations of subcritical flaws in composite and bonded structures. These factors singly and collectively also influence acousto-ultrasonic measurements that, in turn, correlate with dynamic response and mechanical property variations. Since it was first introduced, the acousto-ultrasonic approach was successfully applied to a variety of materials, including polymeric, metallic, and ceramic matrix composites; adhesively bonded materials; paper and wood products; cable and rope; and also human bone. Examples of applications and limitations of the approach are reviewed. Basic methods and guidelines are discussed. The underlying hypothesis and theory development needs are indicated. Author

N91-19229*# National Aeronautics and Space Administration. Lewis Research Center, Cleveland, OH.

METCAN UPDATES FOR HIGH TEMPERATURE COMPOSITE BEHAVIOR: SIMULATION/VERIFICATION

H.-J. LEE, P. L. N. MURTHY, and CHRISTOS C. CHAMIS 1991 15 p Presented at the 36th International SAMPE Symposium and Exhibition, San Diego, CA, 15-18 Apr. 1991
(Contract RTOP 510-10-50)
(NASA-TM-103682; E-5899; NAS 1.15:103682) Avail: NTIS HC/MF A03 CSCL 11/4

The continued verification (comparisons with experimental data) of the METCAN (Metal Matrix Composite Analyzer) computer code is updated. Verification includes comparisons at room and high temperatures for two composites, SiC/Ti-15-3 and SiC/Ti-6-4. Specifically, verification of the SiC/Ti-15-3 composite includes comparisons of strength, modulus, and Poisson's ratio as well as stress-strain curves for four laminates at room temperature. High temperature verification includes comparisons of strength and stress-strain curves for two laminates. Verification of SiC/Ti-6-4 is for a transverse room temperature stress-strain curve and comparisons for transverse strength at three temperatures. Results of the verification indicates that METCAN can be used with confidence to simulate the high temperature nonlinear behavior of metal matrix composites. Author

N91-19230*# National Aeronautics and Space Administration. Lewis Research Center, Cleveland, OH.

COMPUTATIONAL SIMULATION OF HOT COMPOSITES STRUCTURES

CHRISTOS C. CHAMIS, P. L. N. MURTHY, and S. N. SINGHAL (Sverdrup Technology, Inc., Brook Park, OH.) 1991 18 p Presented at the Energy-Sources Technology Conference and Exhibition, Houston, TX, 20-24 Jan. 1991; sponsored by ASME
(Contract RTOP 510-01-0A)
(NASA-TM-103681; E-5898; NAS 1.15:103681) Avail: NTIS HC/MF A03 CSCL 11/4

Three different computer codes developed in-house are described for application to hot composite structures. These codes include capabilities for: (1) laminate behavior (METCAN); (2) thermal/structural analysis of hot structures made from high temperature metal matrix composites (HITCAN); and (3) laminate tailoring (MMLT). Results for select sample cases are described

to demonstrate the versatility as well as the application of these codes to specific situations. The sample case results show that METCAN can be used to simulate cyclic life in high temperature metal matrix composites; HITCAN can be used to evaluate the structural performance of curved panels as well as respective sensitivities of various nonlinearities, and MMLT can be used to tailor the fabrication process in order to reduce residual stresses in the matrix upon cool-down. Author

N91-19231*# National Aeronautics and Space Administration. Lewis Research Center, Cleveland, OH.

PROSPECTS FOR USING CARBON-CARBON COMPOSITES FOR EMI SHIELDING

JAMES R. GAIER 1990 6 p Presented at the International Conference on Carbon, Post Symposium on Carbon-Carbon Composites, Tsukuba, Japan, 9 Nov. 1990; sponsored by Carbon Society of Japan
(Contract RTOP 506-41-41)
(NASA-TM-103677; E-5893; NAS 1.15:103677) Avail: NTIS HC/MF A02 CSCL 11/4

Since pyrolyzed carbon has a higher electrical conductivity than most polymers, carbon-carbon composites would be expected to have higher electromagnetic interference (EMI) shielding ability than polymeric resin composites. A rule of mixtures model of composite conductivity was used to calculate the effect on EMI shielding of substituting a pyrolyzed carbon matrix for a polymeric matrix. It was found that the improvements were small, no more than about 2 percent for the lowest conductivity fibers (ex-rayon) and less than 0.2 percent for the highest conductivity fibers (vapor grown carbon fibers). The structure of the rule of mixtures is such that the matrix conductivity would only be important in those cases where it is much higher than the fiber conductivity, as in metal matrix composites. Author

N91-19232*# National Aeronautics and Space Administration. Lewis Research Center, Cleveland, OH.

AN OVERVIEW OF SELF-CONSISTENT METHODS FOR FIBER-REINFORCED COMPOSITES

KURT C. GRAMOLL, ALAN D. FREED, and KEVIN P. WALKER (Engineering Science Software, Inc., Smithfield, RI.) Jan. 1991 29 p
(Contract RTOP 510-01-01)
(NASA-TM-103713; E-5946; NAS 1.15:103713) Avail: NTIS HC/MF A03 CSCL 11/4

The Walker et al. (1989) self-consistent method to predict both the elastic and the inelastic effective material properties of composites is examined and compared with the results of other self-consistent and elastically based solutions. The elastic part of their method is shown to be identical to other self-consistent methods for non-dilute reinforced composite materials; they are the Hill (1965), Budiansky (1965), and Nemat-Nasser et al. (1982) derivations. A simplified form of the non-dilute self-consistent method is also derived. The predicted, elastic, effective material properties for fiber reinforced material using the Walker method was found to deviate from the elasticity solution for the v_{31} , K_{12} , and μ_{31} material properties (fiber is in the 3 direction) especially at the larger volume fractions. Also, the prediction for the transverse shear modulus, μ_{12} , exceeds one of the accepted Hashin bounds. Only the longitudinal elastic modulus E_{33} agrees with the elasticity solution. The differences between the Walker and the elasticity solutions are primarily due to the assumption used in the derivation of the self-consistent method, i.e., the strain fields in the inclusions and the matrix are assumed to remain constant, which is not a correct assumption for a high concentration of inclusions. Author

N91-19233*# National Aeronautics and Space Administration. Lewis Research Center, Cleveland, OH.

LOW-DENSITY, HIGH-STRENGTH INTERMETALLIC MATRIX COMPOSITES BY XD (TRADEMARK) SYNTHESIS

K. S. KUMAR, M. S. DIPIETRO, S. A. BROWN (Martin Marietta Corp., Baltimore, MD.), and J. D. WHITTENBERGER Jan. 1991 100 p

24 COMPOSITE MATERIALS

(Contract NAS3-25787; RTOP 510-01-01)
(NASA-TM-103724; E-5955; NAS 1.15:103724) Avail: NTIS
HC/MF A05 CSCL 11/4

A feasibility study was conducted to evaluate the potential of particulate composites based on low-density, L1(sub 2) trialuminide matrices for high-temperature applications. The compounds evaluated included Al₂₂Fe₃Ti₈ (as a multiphase matrix), Al₆₇Ti₂₅Cr₈, and Al₆₆Ti₂₅Mn₉. The reinforcement consisted of TiB₂ particulates. The TiB₂ composites were processed by ingot and powder metallurgy techniques. Microstructural characterization and mechanical testing were performed in the hot-pressed and hot-isostatic-pressed condition. The casting were sectioned and isothermally forged into pancakes. All the materials were tested in compression as a function of temperature, and at high temperatures as a function of strain rate. The test results are discussed.

Author

N91-19234*# National Aeronautics and Space Administration. Lewis Research Center, Cleveland, OH.

EFFECT OF FIBER REINFORCEMENTS ON THERMO-OXIDATIVE STABILITY AND MECHANICAL PROPERTIES OF POLYMER MATRIX COMPOSITES

KENNETH J. BOWLES Jan. 1991 32 p

(Contract RTOP 505-01-01)

(NASA-TM-103648; E-5834; NAS 1.15:103648) Avail: NTIS
HC/MF A03 CSCL 11/4

A number of studies have investigated the thermo-oxidative behavior of polymer matrix composites. Two significant observations have been made from these research efforts: (1) fiber reinforcement has a significant effect on composite thermal stability; and (2) geometric effects must be considered when evaluating thermal aging data. A compilation of some results from these studies is presented, and this information shows the influence of the reinforcement fibers on the oxidative degradation of various polymer matrix composites. The polyimide PMR-15 was the matrix material that was used in these studies. The control composite material was reinforced with Celion 6000 graphite fiber. T-40R graphite fibers, along with some very stable ceramic fibers were selected as reinforcing fibers because of their high thermal stability. The ceramic fibers were Nicalon (silicon carbide) and Nextel 312 (alumina-silica-boron oxide). The mechanical properties of the two graphite fiber composites were significantly different, probably owing to variations in interfacial bonding between the fibers and the polyimide matrix. The Celion 6000/PMR-15 bond is very tight but the T-40/PMR-15 bond is less tight. Three oxidation mechanisms were observed: (1) the preferential oxidation of the Celion 6000 fiber ends at cut surfaces, leaving a surface of matrix material with holes where the fiber ends were originally situated; (2) preferential oxidation of the composite matrix; and (3) interfacial degradation by oxidation. The latter two mechanisms were also observed on fiber end cut surfaces. The fiber and interface attacks appeared to initiate interfiber cracking along these surfaces.

Author

N91-19235*# National Aeronautics and Space Administration. Lewis Research Center, Cleveland, OH.

CERAMIC COMPOSITES FOR ROCKET ENGINE TURBINES

THOMAS P. HERBELL and ANDREW J. ECKEL 1991 9 p
Presented at the 1991 Aerospace Atlantic Meeting, Dayton, OH, 23-26 Apr. 1991; sponsored by SAE

(Contract RTOP 582-01-11)

(NASA-TM-103743; E-5986; NAS 1.15:103743) Avail: NTIS
HC/MF A02 CSCL 11/4

The use of ceramic materials in the hot section of the fuel turbopump of advanced reusable rocket engines promises increased performance and payload capability, improved component life and economics, and greater design flexibility. Severe thermal transients present during operation of the Space Shuttle Main Engine (SSME), push metallic components to the limit of their capabilities. Future engine requirements might be even more severe. In phase one of this two-phase program, performance benefits were quantified and continuous fiber reinforced ceramic

matrix composite components demonstrated a potential to survive the hostile environment of an advanced rocket engine turbopump.

Author

N91-19236*# National Aeronautics and Space Administration. Lewis Research Center, Cleveland, OH.

PROBABILISTIC MICROMECHANICS AND MACROMECHANICS OF POLYMER MATRIX COMPOSITES

G. T. MASE (General Motors Inst., Flint, MI.), P. L. N. MURTHY, and CHRISTOS C. CHAMIS 1991 20 p
Presented at the 14th Annual Energy-Sources Technology Conference and Exhibition, Houston, TX, 20-24 Jan. 1991; sponsored by ASME
(Contract RTOP 510-01-0A)

(NASA-TM-103669; E-5876; NAS 1.15:103669) Avail: NTIS
HC/MF A03 CSCL 11/4

A probabilistic evaluation of an eight ply graphite-epoxy quasi-isotropic laminate was completed using the Integrated Composite Analyzer (ICAN) in conjunction with Monte Carlo simulation and Fast Probability Integration (FPI) techniques. Probabilistic input included fiber and matrix properties, fiber misalignment, fiber volume ratio, void volume ratio, ply thickness and ply layup angle. Cumulative distribution functions (CDFs) for select laminate properties are given. To reduce the number of simulations, a Fast Probability Integration (FPI) technique was used to generate CDFs for the select properties in the absence of fiber misalignment. These CDFs were compared to a second Monte Carlo simulation done without fiber misalignment effects. It was found that FPI requires fewer simulations to obtain the cumulative distribution functions as opposed to Monte Carlo simulation techniques. Furthermore, FPI provides valuable information regarding the sensitivities of composite properties to the constituent properties, fiber volume ratio and void volume ratio.

Author

N91-19237*# National Aeronautics and Space Administration. Lewis Research Center, Cleveland, OH.

CONCURRENT MICROMECHANICAL TAILORING AND FABRICATION PROCESS OPTIMIZATION FOR METAL-MATRIX COMPOSITES

M. MOREL, D. A. SARAVANOS (Case Western Reserve Univ., Cleveland, OH.), and CHRISTOS C. CHAMIS 1990 17 p
Presented at FEMCAD and Optimization, Los Angeles, CA, 5-6 Nov. 1990; sponsored by Institute for Industrial Technology Transfer

(Contract RTOP 510-01-0A)

(NASA-TM-103670; E-5877; NAS 1.15:103670) Avail: NTIS
HC/MF A03 CSCL 11/4

A method is presented to minimize the residual matrix stresses in metal matrix composites. Fabrication parameters such as temperature and consolidation pressure are optimized concurrently with the characteristics (i.e., modulus, coefficient of thermal expansion, strength, and interphase thickness) of a fiber-matrix interphase. By including the interphase properties in the fabrication process, lower residual stresses are achievable. Results for an ultra-high modulus graphite (P100)/copper composite show a reduction of 21 percent for the maximum matrix microstress when optimizing the fabrication process alone. Concurrent optimization of the fabrication process and interphase properties show a 41 percent decrease in the maximum microstress. Therefore, this optimization method demonstrates the capability of reducing residual microstresses by altering the temperature and consolidation pressure histories and tailoring the interphase properties for an improved composite material. In addition, the results indicate that the consolidation pressures are the most important fabrication parameters, and the coefficient of thermal expansion is the most critical interphase property.

Author

N91-20110*# National Aeronautics and Space Administration. Lewis Research Center, Cleveland, OH.

ADVANCED HIGH TEMPERATURE ENGINE MATERIALS TECHNOLOGY PROGRAM

HUGH R. GRAY *In its* Aeropropulsion 1991 28 p Mar. 1991
Avail: NTIS HC/MF A24 CSCL 11/4

NASA's Advanced High Temperature Engine Materials

Technology Program (HITEMP) is directed towards generating the technology for revolutionary advances in structural materials and analysis to enable the development of 21st century civil aeronautics propulsion systems. Major consideration is being given to propulsion systems that will be economical via reducing fuel consumption per passenger mile, reducing direct operating costs, extending life, and improving reliability. To achieve revolutionary advances in propulsion systems for 21st century transports, high temperatures materials have been identified as the key technology to be addressed. The HITEMP Program is focusing on lightweight composite materials to gain revolutionary advances in the operating temperatures of advanced engines compared to the current state of the art. Emphasis is placed on polymer matrix composites for potential use in fans, casings, and engine control systems. Intermetallic/metal matrix composites are under investigation for application in such areas as compressor and turbine disks, blades, and vanes and in the exhaust nozzle. For extremely high temperature applications, ceramic matrix composites are being explored. Initial applications may include liners for the combustor and exhaust nozzle, and turbine vanes and ultimately turbine blades and disks, or blisks. Author

N91-20111*# National Aeronautics and Space Administration. Lewis Research Center, Cleveland, OH.

**COMPUTATIONAL MATERIALS SCIENCE. AN EXAMPLE:
NUMERICAL MODELING OF CHEMICAL VAPOR DEPOSITION
PROCESSING OF ADVANCED FIBERS**

ARNON CHAIT, SULEYMAN GOKOGLU, MARIA KUCZMARSKI, PANG TSUI, LISA VEITCH, DAVID THOMPSON, and RONALD GAUG (Akron Univ., OH.) *In its Aeropropulsion* 1991 16 p Mar. 1991

Avail: NTIS HC/MF A24 CSCL 11/4

Computational materials science is a rapidly emerging discipline combining aspects from chemistry, fluid dynamics, and materials and computational sciences. The details of initial efforts undertaken in the Materials Division at Lewis Research Center are presented to establish a dedicated facility for numerical and analytical simulations of materials processing. Computation Materials Laboratory activities are currently aimed at understanding and optimizing processes involving transport of heat, fluid, and mass. An ongoing combined experimental and numerical study is presented. It illustrates the growth of advanced fibers for high-temperature composite applications by using dimensional heat and fluid flow inside the reactor along with simultaneous computations of the chemically reacting gas, and fiber surface species are shown to provide an enhanced level of understanding of the process. The difficulties in simulating the entire process, as well as the present accomplishments, are discussed, and future directions are suggested. Author

N91-20228*# National Aeronautics and Space Administration. Lewis Research Center, Cleveland, OH.

**ISOTHERMAL FATIGUE BEHAVIOR OF A (90)(SUB 8)
SiC/Ti-15-3 COMPOSITE AT 426 C**

JOHN GAYDA and TIMOTHY P. GABB Jan. 1991 21 p
(Contract RTOP 505-63-5A)
(NASA-TM-103686; E-5904; NAS 1.15:103686) Avail: NTIS HC/MF A03 CSCL 11/4

The transverse fatigue behavior of a unidirectional, SiC/Ti-15-3 composite (35 v/o SiC, (90)(sub 8)) was evaluated at 426 C. The fatigue behavior of the composite along the fiber direction (0)(sub 8) and of unreinforced Ti-15-3 alloy were also studied for comparison purposes. The (90)(sub 8) composite fatigue life was much shorter than (0)(sub 8) life. Further, (90)(sub 8) fatigue life was also found to be far lower than that of the unreinforced Ti-15-3 alloys. A simple one-dimensional model for (90)(sub 8) fatigue behavior indicated that the short life of the composite in this orientation resulted, in large part, from weak fiber-matrix bond strength. This conclusion was supported by fractographic evidence showing numerous initiation sites along the fiber-matrix interfaces. Author

N91-21243*# National Aeronautics and Space Administration. Lewis Research Center, Cleveland, OH.

**MECHANICAL BEHAVIOR OF FIBER REINFORCED SiC/RBSN
CERAMIC MATRIX COMPOSITES: THEORY AND EXPERIMENT**

ABHISAK CHULYA (Cleveland State Univ., OH.), JOHN P. GYEKENYESI, and RAMAKRISHNA T. BHATT 1991 30 p
Presented at the 36th International Gas Turbine and Aeroengine Congress and Exposition, Orlando, FL, 3-6 Jun. 1991; sponsored by ASME Prepared in cooperation with Army Aviation Systems Command, Cleveland, OH

(Contract NCC3-81; DA PROJ. 1L1-61102-AH-45; RTOP 510-01-50)

(NASA-TM-103688; E-5907; NAS 1.15:103688;
AVSCOM-TR-91-C-004; AD-A235926) Avail: NTIS HC/MF A03 CSCL 11/4

The mechanical behavior of continuous fiber reinforced SiC/RBSN (Reaction Bonded Silicon Nitride) composites with various fiber contents is evaluated. Both catastrophic and noncatastrophic failures are observed in tensile specimens. Damage and failure mechanisms are identified via in-situ monitoring using NDE (nondestructive evaluation) techniques through the loading history. Effects of fiber/matrix interface debonding (splitting) parallel to fibers are discussed. Statistical failure behavior of fibers is also observed, especially when the interface is weak. Micromechanical models incorporating residual stresses to calculate the critical matrix cracking strength, ultimate strength, and work of pull-out are reviewed and used to predict composite response. For selected test problems, experimental measurements are compared to analytical predictions. Author

N91-22396*# National Aeronautics and Space Administration. Lewis Research Center, Cleveland, OH.

SOLID LUBRICANTS

HAROLD E. SLINEY Apr. 1991 37 p Submitted for publication

(Contract RTOP 505-63-5A)

(NASA-TM-102803; E-6094; NAS 1.15:102803) Avail: NTIS HC/MF A03 CSCL 11/4

The state of knowledge of solid lubricants is reviewed. The results of research on solid lubricants from the 1940's to the present are presented from a historical perspective. Emphasis is placed largely, but not exclusively, on work performed at NASA Lewis Research Center with a natural focus on aerospace applications. However, because of the generic nature of the research, the information presented in this review is applicable to most areas where solid lubricant technology is useful. Author

N91-22402*# National Aeronautics and Space Administration. Lewis Research Center, Cleveland, OH.

**IN-SITU X-RAY MONITORING OF DAMAGE ACCUMULATION
IN SiC/RBSN TENSILE SPECIMENS**

GEORGE Y. BAAKLINI and RAMAKRISHNA T. BHATT (Army Aviation Systems Command, Cleveland, OH.) 1991 19 p
Presented at the 15th Annual Conference on Composites and Advanced Ceramics, Cocoa Beach, FL, 13-16 Jan. 1991; sponsored by the American Ceramic Society

(Contract DA PROJ. 1L1-62211-A-47-A; RTOP 510-01-50)

(NASA-TM-103733; E-5971; NAS 1.15:103733;
AVSCOM-TR-91-C-019; AD-A239503) Avail: NTIS HC/MF A03 CSCL 11/4

The room-temperature tensile testing of silicon carbide fiber reinforced reaction-bonded silicon nitride (SiC/RBSN) composite specimens was monitored by using in-situ x ray film radiography. Radiographic evaluation before, during, and after loading provided data on the effect of preexisting volume flaws (high density impurities, and local density variations) on the fracture behavior of composites. Results from (0)1, (0)3, (0)5, and (0)8 composite specimens, showed that x ray film radiography can monitor damage accumulations during tensile loading. Matrix cracking, fiber-matrix debonding, and fiber pullout were imaged throughout the tensile loading history of the specimens. Further, in-situ film radiography was found to be a helpful and practical technique for estimating interfacial shear strength between the SiC fiber and the RBSN

24 COMPOSITE MATERIALS

matrix by the matrix crack spacing method. It is concluded that pretest, in-situ, and post-test radiography can provide for a greater understanding of ceramic matrix composite mechanical behavior, a verification of related experimental procedures, and a validation and development of related analytical models. Author

N91-23040*# National Aeronautics and Space Administration. Lewis Research Center, Cleveland, OH.

INDUSTRIAL APPLICATIONS OF GRAPHITE FLUORIDE FIBERS

CHING-CHEH HUNG and DONALD KUCERA (Cleveland State Univ., OH.) *In* National Aeronautics and Space Administration, Technology 2000, Volume 1 p 156-164 Mar. 1991
Avail: NTIS HC/MF A18 CSCL 11/4

Based on fluorination technology developed during 1934 to 1959, and the fiber technology developed during the 1970s, a new process was developed to produce graphite fluoride fibers. In the process, pitch based graphitized carbon fibers are at first intercalated and deintercalated several times by bromine and iodine, followed by several cycles of nitrogen heating and fluorination at 350 to 370 C. Electrical, mechanical, and thermal properties of this fiber depend on the fluorination process and the fluorine content of the graphite fluoride product. However, these properties are between those of graphite and those of PTFE (Teflon). Therefore, it is considered to be a semiplastic. The physical properties suggest that this new material may have many new and unexplored applications. For example, it can be a thermally conductive electrical insulator. Its coefficient of thermal expansion (CTE) can be adjusted to match that of silicon, and therefore, it can be a heat sinking printed circuit board which is CTE compatible with silicon. Using these fibers in printed circuit boards may provide improved electrical performance and reliability of the electronics on the board over existing designs. Also, since it releases fluorine at 300 C or higher, it can be used as a material to store fluorine and to conduct fluorination. This application may simplify the fluorination process and reduce the risk of handling fluorine. Author

N91-23247*# National Aeronautics and Space Administration. Lewis Research Center, Cleveland, OH.

COMBINED THERMAL AND BENDING FATIGUE OF HIGH-TEMPERATURE METAL-MATRIX COMPOSITES: COMPUTATIONAL SIMULATION

PASCAL K. GOTSIS Jun. 1991 24 p
(Contract RTOP 510-10-01)
(NASA-TM-104354; E-6140; NAS 1.15:104354) Avail: NTIS HC/MF A03 CSCL 11/4

The nonlinear behavior of a high-temperature metal-matrix composite (HT-MMC) was simulated by using the metal matrix composite analyzer (METCAN) computer code. The simulation started with the fabrication process, proceeded to thermomechanical cyclic loading, and ended with the application of a monotonic load. Classical laminate theory and composite micromechanics and macromechanics are used in METCAN, along with a multifactor interaction model for the constituents behavior. The simulation of the stress-strain behavior from the macromechanical and the micromechanical points of view, as well as the initiation and final failure of the constituents and the plies in the composite, were examined in detail. It was shown that, when the fibers and the matrix were perfectly bonded, the fracture started in the matrix and then propagated with increasing load to the fibers. After the fibers fractured, the composite lost its capacity to carry additional load and fractured. Author

N91-24311*# National Aeronautics and Space Administration. Lewis Research Center, Cleveland, OH.

TENSILE AND FATIGUE BEHAVIOR OF TUNGSTEN/COPPER COMPOSITES

MICHAEL J. VERRILLI, TIMOTHY P. GABB, and Y. S. KIM *In* *Its Structural Integrity and Durability of Reusable Space Propulsion Systems* p 25-31 Apr. 1989

Avail: NTIS HC/MF A12 CSCL 11/4

Work on W/Cu unidirectional composites was initiated to study

the behavior of this ductile-ductile composite system under thermomechanical fatigue and to examine the applicability of fatigue-life prediction methods for thermomechanical fatigue of this metal matrix composite. The first step was to characterize the tensile behavior of four ply, 10 vol. percent W/Cu plates at room and elevated temperatures. Fatigue tests were conducted in load control on 0 degree specimens at 260 C. The maximum cyclic stress was varied but the minimum cyclic stress was kept constant. All tests were performed in vacuum. The strain at failure increased with increasing maximum cyclic stress. Author

N91-24345*# National Aeronautics and Space Administration. Lewis Research Center, Cleveland, OH.

APPLICATION OF ARTIFICIAL NEURAL NETWORKS TO COMPOSITE PLY MICROMECHANICS

D. A. BROWN (Wooster Coll., OH.), P. L. N. MURTHY, and L. BERKE 1991 24 p Presented at the Engineering Mechanics Conference, Columbus, OH, 19-22 May 1991; sponsored by the American Society of Civil Engineers
(Contract RTOP 307-50-00)

(NASA-TM-104365; E-6162; NAS 1.15:104365) Avail: NTIS HC/MF A03 CSCL 11/4

Artificial neural networks can provide improved computational efficiency relative to existing methods when an algorithmic description of functional relationships is either totally unavailable or is complex in nature. For complex calculations, significant reductions in elapsed computation time are possible. The primary goal is to demonstrate the applicability of artificial neural networks to composite material characterization. As a test case, a neural network was trained to accurately predict composite hygral, thermal, and mechanical properties when provided with basic information concerning the environment, constituent materials, and component ratios used in the creation of the composite. A brief introduction on neural networks is provided along with a description of the project itself. Author

N91-24359*# National Aeronautics and Space Administration. Lewis Research Center, Cleveland, OH.

INCREASED HEAT TRANSFER TO A CYLINDRICAL LEADING EDGE DUE TO SPANWISE VARIATIONS IN THE FREESTREAM VELOCITY

D. L. RIGBY (Sverdrup Technology, Inc., Brook Park, OH.) and G. J. VANFOSSEN 1991 13 p Presented at the 22nd Fluid Dynamics, Plasma Dynamics and Lasers Conference, Honolulu, HI, 24-26 Jun. 1991; sponsored by AIAA
(Contract NAS3-25266; RTOP 505-62-52)

(NASA-TM-104464; E-6306; NAS 1.15:104464; AIAA PAPER 91-1739) Avail: NTIS HC/MF A03 CSCL 11/4

The present study numerically demonstrates how small spanwise variations in velocity upstream of a body can cause relatively large increases in the spanwise-averaged heat transfer to the leading edge. Vorticity introduced by spanwise variations, first decays as it drifts downstream, then amplifies in the stagnation region as a result of vortex stretching. This amplification can cause a periodic array of 3 D structures, similar to horseshoe vortices, to form. The numerical results indicate that, for the given wavelength, there is an amplitude threshold below which a structure does not form. A one-dimensional analysis, to predict the decay of vorticity in the absence of the body, in conjunction with the full numerical results indicated that the threshold is more accurately stated as minimum level of vorticity required in the leading edge region for a structure to form. It is possible, using the one-dimensional analysis, to compute an optimum wavelength in terms of the maximum vorticity reaching the leading edge region for given amplitude. A discussion is presented which relates experimentally observed trends to the trends of the present phenomena. Author

N91-24360*# National Aeronautics and Space Administration. Lewis Research Center, Cleveland, OH.

HIGH TEMPERATURE TENSION-COMPRESSION FATIGUE BEHAVIOR OF A TUNGSTEN COPPER COMPOSITE

MICHAEL J. VERRILLI and TIMOTHY P. GABB 1990 11 p

Presented at the Fourth Symposium on Composite Materials, Indianapolis, IN, 6-7 May 1991; sponsored by the American Society for Testing and Materials

(Contract RTOP 553-13-00)

(NASA-TM-104370; E-6174; NAS 1.15:104370) Avail: NTIS

HC/MF A03 CSCL 11/4

The high temperature fatigue of a (O)12 tungsten fiber reinforced copper matrix composite was investigated. Specimens having fiber volume percentages of 10 and 36 were fatigued under fully-reversed, strain-controlled conditions at both 260 and 560 C. The fatigue life was found to be independent of fiber volume fraction because fatigue damage preferentially occurred in the matrix. Also, the composite fatigue lives were shorter at 560 C as compared to 260 C due to changes in mode of matrix failure. On a total strain basis, the fatigue life of the composite at 560 C was the same as the life of unreinforced copper, indicating that the presence of the fibers did not degrade the fatigue resistance of the copper matrix in this composite system. Comparison of strain-controlled fatigue data to previously-generated load-controlled data revealed that the strain-controlled fatigue lives were longer because of mean strain and mean stress effects.

Author

N91-24361*# National Aeronautics and Space Administration. Lewis Research Center, Cleveland, OH.

A COMPARISON OF FIBER EFFECTS ON POLYMER MATRIX COMPOSITE OXIDATION

KENNETH J. BOWLES 1991 18 p Presented at the Second Japan International Symposium and Exhibition, Chiba, Japan, 11-14 Dec. 1991; sponsored by the Society for the Advancement of Materials and Process Engineering

(Contract RTOP 510-01-50)

(NASA-TM-104416; E-6248; NAS 1.15:104416) Avail: NTIS

HC/MF A03 CSCL 11/4

A number of thermo-oxidative stability studies addressing the effects of fiber reinforcement on composite thermal stability and influence of geometry on the results of aging studies were performed at NASA-Lewis. The information presented herein, a compilation of some results from these studies, shows the influence of the reinforcement fibers on the oxidative degradation of various PMR-15 composites. Reinforcement of graphite and ceramics were studied and three composite oxidation mechanisms were observed. One was a dominant attack of the reinforcement fiber, the second was the aggressive oxidation of the matrix material, and the third was interfacial degradation.

Author

N91-25186*# National Aeronautics and Space Administration. Lewis Research Center, Cleveland, OH.

QUALITY CONTROL OF THE TRIBOLOGICAL COATING PS212

HAROLD E. SLINEY, CHRISTOPHER DELLACORTE, and DANIEL L. DEADMORE Jun. 1989 20 p

(Contract RTOP 505-63-1A)

(NASA-TM-102067; E-4824; NAS 1.15:102067) Avail: NTIS

HC/MF A03 CSCL 11/4

PS212 is a self-lubricating, composite coating that is applied by the plasma spray process. It is a functional lubricating coating from 25 C (or lower) to 900 C. The coating is prepared from a blend of three different powders with very dissimilar properties. Therefore, the final chemical composition and lubricating effectiveness of the coatings are very sensitive to the process variables used in their preparation. Defined here are the relevant variables. The process and analytical procedures that will result in satisfactory tribological coatings are discussed.

Author

N91-25195*# National Aeronautics and Space Administration. Lewis Research Center, Cleveland, OH.

TENSILE DEFORMATION DAMAGE IN SiC REINFORCED Ti-15V-3Cr-3Al-3Sn

BRADLEY A. LERCH and JAMES F. SALTSMAN Apr. 1991 44 p

(Contract RTOP 510-01-50)

(NASA-TM-103620; E-5778; NAS 1.15:103620) Avail: NTIS HC/MF A03 CSCL 11/4

The damage mechanisms of a laminated, continuous SiC fiber reinforced Ti-15V-3Cr-3Al-3Sn (Ti-15-3) composite were investigated. Specimens consisting of unidirectional as well as cross-ply laminates were pulled in tension to failure at room temperature and 427 C and subsequently examined metallographically. Selected specimens were interrupted at various strain increments and examined to document the development of damage. When possible, a micromechanical stress analysis was performed to aid in the explanation of the observed damage. The analyses provide average constituent microstresses and laminate stresses and strains. It was found that the damage states were dependent upon the fiber architecture.

Author

N91-25198*# National Aeronautics and Space Administration. Lewis Research Center, Cleveland, OH.

MICROFRACTURE IN HIGH TEMPERATURE METAL MATRIX CROSSPLY LAMINATES

SUBODH K. MITAL and CHRISTOS C. CHAMIS 1991 11 p Presented at the Winter Annual Meeting and Symposium on Failure Mechanisms in High Temperature Composites, Atlanta, GA, 1-6 Dec. 1991; sponsored by AME

(Contract NASA ORDER C-99066-G; RTOP 510-10-50)

(NASA-TM-104381; ICOMP-91-8; E-6201; NAS 1.15:104381)

Avail: NTIS HC/MF A03 CSCL 11/4

Microfracture (fiber/matrix fracture, interphase debonding, and inter-ply delamination) in high temperature metal matrix composites (HTMMC), subjected to both mechanical and thermal loading, is computationally simulated. A crossply 0.3 fiber volume ratio SiC/Ti15 composite with 0/90/0 lay-up is evaluated for microfracture using a multicell finite element model. A computational simulation procedure based on strain energy release rates is used to predict the fracture process and establish the hierarchy of fracture modes. Microfracture results for various loading cases are presented and discussed.

Author

N91-25201*# National Aeronautics and Space Administration. Lewis Research Center, Cleveland, OH.

HEAT TRANSFER DEVICE Patent Application

BRUCE A. BANKS, inventor (to NASA) and JAMES R. GAIER, inventor (to NASA) 19 Feb. 1991 10 p

(NASA-CASE-LEW-14162-2; NAS 1.71:LEW-14162-2;

US-PATENT-APPL-SN-657238) Avail: NTIS HC/MF A02 CSCL 11/4

Gas derived graphite fibers are generated by the decomposition of an organic gas. These fibers when joined with a suitable binder are used to make a high thermal conductivity composite material. The fibers may be intercalated. The intercalate can be halogen or halide salt, alkaline metal, or any other species which contributes to the electrical conductivity improvement of the graphite fiber. The heat transfer device may also be made of intercalated highly oriented pyrolytic graphite and machined, rather than made of fibers.

NASA

N91-25202*# National Aeronautics and Space Administration. Lewis Research Center, Cleveland, OH.

METHOD OF APPLYING A THERMAL BARRIER COATING SYSTEM TO A SUBSTRATE Patent Application

ROBERT A. MILLER, inventor (to NASA) 23 May 1991 10 p

(NASA-CASE-LEW-15020-2; NAS 1.71:LEW-15020-2;

US-PATENT-APPL-SN-708255) Avail: NTIS HC/MF A02 CSCL 11/4

A metallic close-out layer is applied to the surface of a thermal barrier coating system to seal the ceramic material in the coating. The close-out layer is glass-bead preened to densify the surface.

NASA

N91-26233*# National Aeronautics and Space Administration. Lewis Research Center, Cleveland, OH.

INVESTIGATION OF INTERFACIAL SHEAR STRENGTH IN SiC/Si3N4 COMPOSITES

J. I. ELDRIDGE, R. T. BHATT (Army Aviation Systems Command,

24 COMPOSITE MATERIALS

Cleveland, OH.), and J. D. KISER 1991 20 p Presented at the 15th Annual Conference on Composites and Advanced Ceramics, Cocoa Beach, FL, 13-16 Jan. 1991; sponsored by the American Ceramic Society
(Contract DA PROJ. 1L1-61102-AH-45; RTOP 510-01-0A)
(NASA-TM-103739; E-5979; NAS 1.15:103739;
AVSCOM-TR-91-C-006; AD-A239502) Avail: NTIS HC/MF A03 CSCL 11/4

A fiber push-out technique was used to determine fiber/matrix interfacial shear strength (ISS) for silicon carbide fiber reinforced reaction-bonded silicon nitride (SiC/RBSN) composites in the as-fabricated condition and after consolidation by hot isostatic pressing (HIPing). In situ video microscopy and acoustic emission detection greatly aided the interpretation of push-out load/displacement curves. Author

N91-26234* National Aeronautics and Space Administration. Lewis Research Center, Cleveland, OH.

POLYMERIC ROUTES TO SILICON CARBIDE AND SILICON OXYCARBIDE CMC

FRANCES I. HURWITZ, PAUL J. HEIMANN, JOHN Z. GYKENYESI, JOHN MASNOVI, and XIN YA BU (Cleveland State Univ., OH.) 1991 13 p Presented at the 15th Annual Conference on Composites and Advanced Ceramics, Cocoa Beach, FL, 13-16 Jan. 1991; sponsored by the American Ceramic Society
(Contract NCC3-63; NAG3-749; RTOP 505-63-31)
(NASA-TM-104372; E-6054; NAS 1.15:104372) Avail: NTIS HC/MF A03 CSCL 11/4

An overview of two approaches to the formation of ceramic composite matrices from polymeric precursors is presented. Copolymerization of alkyl- and alkenylsilanes (RSiH₃) represents a new precursor system for the production of Beta-SiC on pyrolysis, with copolymer composition controlling polymer structure, char yield, and ceramic stoichiometry and morphology. Polysilsesquioxanes which are synthesized readily and can be handled in air serve as precursors to Si-C-O ceramics. Copolymers of phenyl and methyl silsesquioxanes display rheological properties favorable for composite fabrication; these can be tailored by control of pH, water/methoxy ratio and copolymer composition. Composites obtained from these utilize a carbon coated, eight harness satin weave Nicalon cloth reinforcement. The material exhibits nonlinear stress-strain behavior in tension. Author

N91-27244* National Aeronautics and Space Administration. Lewis Research Center, Cleveland, OH.

METHOD OF MAKING CARBIDE/FLUORIDE/SILVER COMPOSITES Patent

HAROLD E. SLINEY, inventor (to NASA) and CHRISTOPHER DELLACORTE, inventor (to NASA) 23 Jul. 1991 10 p Filed 23 Aug. 1990
(NASA-CASE-LEW-14902-1; US-PATENT-5,034,187;
US-PATENT-APPL-SN-571058; US-PATENT-CLASS-419-14;
US-PATENT-CLASS-419-30; US-PATENT-CLASS-419-32;
US-PATENT-CLASS-419-36; US-PATENT-CLASS-419-38;
US-PATENT-CLASS-419-39; US-PATENT-CLASS-419-49) Avail: US Patent and Trademark Office CSCL 11/4

A composition containing 30 to 70 percent chromium carbide, 5 to 20 percent soft noble metal, 5 to 20 percent metal fluorides, and 20 to 60 percent metal binder is used in a powdered metallurgy process for the production of self-lubricating components, such as bearings. The use of the material allows the self-lubricating bearing to maintain its low friction properties over an extended range of operating temperatures.

Official Gazette of the U.S. Patent and Trademark Office

N91-27247* National Aeronautics and Space Administration. Lewis Research Center, Cleveland, OH.

MATRIX PLASTICITY IN SiC/Ti-15-3 COMPOSITE

BRADLEY A. LERCH Jul. 1991 11 p
(Contract RTOP 510-01-50)
(NASA-TM-103760; E-6017; NAS 1.15:103760) Avail: NTIS HC/MF A03 CSCL 11/4

An experimental method is described which allows for the

observation of slip bands due to matrix plasticity in the SiC/Ti-15-3 composite system. A post-test heat treatment and subsequent chemical etch is employed to reveal slip bands in the titanium matrix. Composite specimens of various laminates were examined after tensile testing at room temperature. This method definitively shows that matrix plasticity has occurred in all the laminates investigated and at load/strain levels which were insufficient to cause fiber breakage. Author

N91-28289* National Aeronautics and Space Administration. Lewis Research Center, Cleveland, OH.

APPARATUS FOR INTERCALATING LARGE QUANTITIES OF FIBROUS STRUCTURES Patent Application

JAMES R. GAIER, inventor (to NASA) 24 Jul. 1991 13 p
(NASA-CASE-LEW-15077-2; NAS 1.71:LEW-15077-2;
US-PATENT-APPL-SN-735548) Avail: NTIS HC/MF A03 CSCL 11/4

Apparatus for intercalating large quantities of fibrous structures uses a rotatable reaction chamber containing a liquid phase intercalate. The intercalate liquid phase is controlled by appropriately heating, cooling or pressurizing the reaction. Rotation of the chamber containing the fiber sample ensures total submergence if the fiber during intercalation. Intercalated graphite fibers having metal-like resistivities are produced and are conceivably useful as electrical conductors. NASA

N91-29250* National Aeronautics and Space Administration. Lewis Research Center, Cleveland, OH.

MICROSTRUCTURAL AND STRENGTH STABILITY OF CVD SiC FIBERS IN ARGON ENVIRONMENT

RAMAKRISHNA T. BHATT and DAVID R. HULL 1991 19 p Presented at the 15th Annual Conference on Composites and Advanced Ceramics, Cocoa Beach, FL, 13-16 Jan. 1991; sponsored by the American Ceramic Society
(Contract DA PROJ. 1L1-61102-AH-45; RTOP 510-01-01)
(NASA-TM-103772; E-5957; NAS 1.15:103772;
AVSCOM-TR-91-C-014) Avail: NTIS HC/MF A03 CSCL 11/4

The room temperature tensile strength and microstructure of three types of commercially available chemically vapor deposited silicon carbide fibers were measured after 1, 10, and 100 hour heat treatments under argon pressures of 0.1 to 310 MPa at temperatures to 2100 C. Two types of fiber had carbon-rich surface coatings and the other contained no coating. All three fiber types showed strength degradation beyond 1400 C. Time and temperature of exposure had greater influence on strength degradation than argon pressure. Recrystallization and growth of near stoichiometric SiC grains appears to be the dominant mechanism for the strength degradation. Author

N91-30281* National Aeronautics and Space Administration. Lewis Research Center, Cleveland, OH.

INTERPHASE LAYER OPTIMIZATION FOR METAL MATRIX COMPOSITES WITH FABRICATION CONSIDERATIONS

M. MOREL, D. A. SARAVANOS (Case Western Reserve Univ., Cleveland, OH.), and C. C. CHAMIS 1991 23 p Presented at the 36th International SAMPE Symposium and Exhibition, San Diego, CA, 15-18 Apr. 1991
(Contract RTOP 510-10-50)

(NASA-TM-105166; E-6457; NAS 1.15:105166) Avail: NTIS HC/MF A03 CSCL 11/4

A methodology is presented to reduce the final matrix microstresses for metal matrix composites by concurrently optimizing the interphase characteristics and fabrication process. Application cases include interphase tailoring with and without fabrication considerations for two material systems, graphite/copper and silicon carbide/titanium. Results indicate that concurrent interphase/fabrication optimization produces significant reductions in the matrix residual stresses and strong coupling between interphase and fabrication tailoring. The interphase coefficient of thermal expansion and the fabrication consolidation pressure are the most important design parameters and must be concurrently optimized to further reduce the microstresses to more desirable magnitudes. Author

N91-30282*# National Aeronautics and Space Administration. Lewis Research Center, Cleveland, OH.

THE EFFECTS OF INTERPLY DAMPING LAYERS ON THE DYNAMIC RESPONSE OF COMPOSITE STRUCTURES

D. A. SARAVANOS (Case Western Reserve Univ., Cleveland, OH.) and C. C. CHAMIS 1991 28 p Presented at the 32nd Structures, Structural Dynamics and Materials Conference, Baltimore, MD, 8-10 Apr. 1991; cosponsored by the AIAA, ASME, ASCE, AHS, and ASC Previously announced in IAA as A91-32064

(Contract RTOP 505-63-1B)
(NASA-TM-104497; E-6355; NAS 1.15:104497) Avail: NTIS HC/MF A03 CSCL 11/4

Integrated damping mechanics for composite laminates with constrained interlaminar layers of polymer damping materials are developed. Discrete layer damping mechanics are presented for composite materials with damping layers, in connection with a semi-analytical method for predicting the modal damping in simply-supported specialty composite plates. Several application cases are used to demonstrate the advantages of the method. Damping predictions for graphite-epoxy composite plates of various laminations demonstrate the potential for higher damping than geometrically equivalent aluminum plates. The effects of aspect ratio, damping layer thickness, and fiber volume ratio on static and dynamic characteristics of the composite plate are also investigated. Author

N91-31235*# National Aeronautics and Space Administration. Lewis Research Center, Cleveland, OH.

EXPERIMENTAL AND ANALYTICAL ANALYSIS OF STRESS-STRAIN BEHAVIOR IN A (90/0 DEG)2S, SIC/TI-15-3 LAMINATE

BRADLEY A. LERCH, MATTHEW E. MELIS, and MIKE TONG (Sverdrup Technology, Inc., Brook Park, OH.) Aug. 1991 11 p (Contract RTOP 510-01-50)

(NASA-TM-104470; E-6319; NAS 1.15:104470) Avail: NTIS HC/MF A03 CSCL 11/4

The nonlinear stress strain behavior of 90 degree/0 degree sub 2s, SIC/Ti-15-3 composite laminate was numerically investigated with a finite element, unit cell approach. Tensile stress-strain curves from room temperature experiments depicted three distinct regions of deformation, and these regions were predicted by finite element analysis. The first region of behavior, which was linear elastic, occurred at low applied stresses. As applied stresses increased, fiber/matrix debonding in the 90 degree plies caused a break in the stress-strain curve and initiated a second linear region. In this second region, matrix plasticity in the 90 degree plies developed. The third region, which was typified by nonlinear, stress-strain behavior occurred at high stresses. In this region, the onset of matrix plasticity in the 0 degree plies stiffened the laminate in the direction transverse to the applied load. Metallographic sections confirmed the existence of matrix plasticity in specific areas of the structure. Finite element analysis also predicted these locations of matrix slip. Author

N91-32177*# National Aeronautics and Space Administration. Lewis Research Center, Cleveland, OH.

EFFECT OF LIGHTNING STRIKE ON BROMINE INTERCALATED GRAPHITE FIBER/EPOXY COMPOSITES

JAMES R. GAIER, MELISSA E. SLABE, and NORMAN O. BRINK (Rohr Industries, Inc., Chula Vista, CA.) Aug. 1991 19 p (Contract RTOP 506-41-41)

(NASA-TM-104507; E-6370; NAS 1.15:104507) Avail: NTIS HC/MF A03 CSCL 11/4

Laminar composites were fabricated from pristine and bromine intercalated pitch based graphite fibers. It was found that laminar composites could be fabricated using either pristine or intercalated graphite fibers using standard fabrication techniques. The intercalated graphite fiber composites had electrical properties which were markedly improved over both the corresponding pitch based and polyacrylonitrile (PAN) based composites. Despite composites resistivities more than an order of magnitude lower for pitch based fiber composites, the lightning strike resistance

was poorer than that of the Pan based fiber composites. This leads to the conclusion that the mechanical properties of the pitch fibers are more important than electrical or thermal properties in determining the lightning strike resistance. Based on indicated lightning strike tolerance for high elongation to failure materials, the use of vapor grown, rather than pitch based graphite fibers appears promising. Author

N91-32181*# National Aeronautics and Space Administration. Lewis Research Center, Cleveland, OH.

INTEGRATED MECHANICS FOR THE PASSIVE DAMPING OF POLYMER-MATRIX COMPOSITES AND COMPOSITE STRUCTURES

D. A. SARAVANOS (Case Western Reserve Univ., Cleveland, OH.) and CHRISTOS C. CHAMIS 1991 27 p Presented at the Mechanics and Mechanisms of Materials Damping Conference, Baltimore, MD, 13-15 Mar. 1991; sponsored by the American Society for Testing and Materials

(Contract RTOP 505-63-5B)
(NASA-TM-104346; E-6120; NAS 1.15:104346) Avail: NTIS HC/MF A01 CSCL 11/4

Some recent developments on integrated damping mechanics for unidirectional composites, laminates, and composite structures are reviewed. Simplified damping micromechanics relate the damping of on-axis and off-axis composites to constituent properties, fiber volume ratio, fiber orientation, temperature, and moisture. Laminate and structural damping mechanics for thin composites are summarized. Discrete layer damping mechanics for thick laminates, including the effects of interlaminar shear damping, are developed and semianalytical predictions of modal damping in thick simply supported specialty composite plates are presented. Applications show the advantages of the unified mechanics, and illustrate the effect of fiber volume ratio, fiber orientation, structural geometry, and temperature on the damping. Additional damping properties for composite plates of various laminations, aspect ratios, fiber content, and temperature illustrate the merits and ranges of applicability of each theory (thin or thick laminates). Author

N91-32182*# National Aeronautics and Space Administration. Lewis Research Center, Cleveland, OH.

PROGRESSIVE FRACTURE IN COMPOSITES SUBJECTED TO HYGROTHERMAL ENVIRONMENT

LEVON MINNETYAN (Clarkson Univ., Potsdam, NY.), PAPPU L. N. MURTHY, and CHRISTOS C. CHAMIS 1991 35 p Presented at the 32nd Structures, Structural Dynamics, and Materials Conference, Baltimore, MD, 8-10 Apr. 1991; sponsored in part by AIAA, ASME, ASCE, AHS, and ASC Previously announced in IAA as 91-31919

(Contract RTOP 505-63-5B)
(NASA-TM-105230; E-6553; NAS 1.15:105230) Avail: NTIS HC/MF A03 CSCL 11/4

The influence of hygrothermal environmental conditions on the load carrying ability and response of composite structures are investigated via computational simulation. An integral computer code is utilized for the simulation of composite structural degradation under loading. Damage initiation, damage growth, fracture progression, and global structural fracture are included in the simulation. Results demonstrate the significant hygrothermal effects on composite structural response, toughness, and durability. Author

INORGANIC AND PHYSICAL CHEMISTRY

Includes chemical analysis, e.g., chromatography; combustion theory; electrochemistry; and photochemistry.

A91-12925* Case Western Reserve Univ., Cleveland, OH.
SULFUR AT NICKEL-ALUMINA INTERFACES - MOLECULAR ORBITAL THEORY

S. Y. HONG, ALFRED B. ANDERSON (Case Western Reserve University, Cleveland, OH), and JAMES L. SMIALEK (NASA, Lewis Research Center, Cleveland, OH) Surface Science (ISSN 0039-6028), vol. 230, 1990, p. 175-183. refs (Contract NAG3-688) Copyright

Previous studies on Al-Ni alloys containing sulfur as an impurity suggest that, when S is in the interface between a metal and an oxide scale, it weakens the chemical bonding between them. This paper investigates factors responsible for this effect, using a molecular orbital theory to predict sulfur structures and electronic properties on the Ni-Al₂O₃ interface. It is shown that, in absence of S, the basal plane of Al₂O₃ will bind strongly through the Al(3+) cation surface to Ni (111). When segregated S impurity is present on the Ni surface, there are too few interfacial Al-S bonds to effect good adhesion, leading to an inhibition of the oxide scale adhesion in NiCrAl alloys. I.S.

A91-12927* National Aeronautics and Space Administration, Lewis Research Center, Cleveland, OH.

EVALUATION OF A HYBRID KINETICS/MIXING-CONTROLLED COMBUSTION MODEL FOR TURBULENT PREMIXED AND DIFFUSION COMBUSTION USING KIVA-II

H. LEE NGUYEN (NASA, Lewis Research Center, Cleveland, OH) and MING-JYH WEY (MBR Combustion Research Inc., Princeton, NJ) AIAA, SAE, ASME, and ASCE, Joint Propulsion Conference, 26th, Orlando, FL, July 16-18, 1990. 21 p. Previously announced in STAR as N90-28792. refs (AIAA PAPER 90-2450) Copyright

Two-dimensional calculations were made of spark ignited premixed-charge combustion and direct injection stratified-charge combustion in gasoline fueled piston engines. Results are obtained using kinetic-controlled combustion submodel governed by a four-step global chemical reaction or a hybrid laminar kinetics/mixing-controlled combustion submodel that accounts for laminar kinetics and turbulent mixing effects. The numerical solutions are obtained by using KIVA-2 computer code which uses a kinetic-controlled combustion submodel governed by a four-step global chemical reaction (i.e., it assumes that the mixing time is smaller than the chemistry). A hybrid laminar/mixing-controlled combustion submodel was implemented into KIVA-2. In this model, chemical species approach their thermodynamics equilibrium with a rate that is a combination of the turbulent-mixing time and the chemical-kinetics time. The combination is formed in such a way that the longer of the two times has more influence on the conversion rate and the energy release. An additional element of the model is that the laminar-flame kinetics strongly influence the early flame development following ignition. Author

A91-13439* National Aeronautics and Space Administration, Lewis Research Center, Cleveland, OH.

ACIDIC ATTACK OF PERFLUORINATED ALKYL ETHER LUBRICANT MOLECULES BY METAL OXIDE SURFACES

MICHAEL J. ZEHE and OWEN D. FAUT (NASA, Lewis Research Center, Cleveland, OH) (STLE and ASME, Tribology Conference, 35th, Fort Lauderdale, FL, Oct. 16-19, 1989) STLE Tribology Transactions (ISSN 0569-8197), vol. 33, Oct. 1990, p. 634-640. Previously announced in STAR as N89-19402. refs Copyright

The reactions of linear perfluoropolyalkylether (PFAE) lubricants with alpha-Fe₂O₃ and Fe₂O₃-based solid superacids were studied.

The reaction with alpha-Fe₂O₃ proceeds in two stages. The first stage is an initial slow catalytic decomposition of the fluid. This reaction releases reactive gaseous products which attach the metal oxide and convert it to FeF₃. The second stage is a more rapid decomposition of the fluid, effected by the surface FeF₃. A study of the initial breakdown step was performed using alpha-Fe₂O₃, alpha-Fe₂O₃ preconverted to FeF₃, and sulfate-promoted alpha-Fe₂O₃ superacids. The results indicate that the breakdown reaction involves acidic attack at fluorine atoms on acetal carbons in the linear PFAE. Possible approaches to combat the problem are outlined. Author

A91-19431*# California Univ., La Jolla.
PARTICLE NONUNIFORMITY EFFECTS ON PARTICLE CLOUD FLAMES IN LOW GRAVITY

A. L. BERLAD, V. TANGIRALA, K. SESHADRI (California, University, La Jolla), L. T. FACCA, J. OGRIN, and H. ROSS (NASA, Lewis Research Center, Cleveland, OH) AIAA, Aerospace Sciences Meeting, 29th, Reno, NV, Jan. 7-10, 1991. 8 p. refs (Contract NAG3-925) (AIAA PAPER 91-0718) Copyright

Experimental and analytical studies of particle cloud combustion at reduced gravity reveal the substantial roles that particle cloud nonuniformities may play in particle cloud combustion. Macroscopically uniform, quiescent particle cloud systems (at very low gravitational levels and above) sustain processes which can render them nonuniform on both macroscopic and microscopic scales. It is found that a given macroscopically uniform, quiescent particle cloud flame system can display a range of microscopically nonuniform features which lead to a range of combustion features. Microscopically nonuniform particle cloud distributions are difficult experimentally to detect and characterize. A uniformly distributed lycopodium cloud of particle-enriched microscopic nonuniformities in reduced gravity displays a range of burning velocities for any given overall stoichiometry. The range of observed and calculated burning velocities corresponds to the range of particle enriched concentrations within a characteristic microscopic nonuniformity. Sedimentation effects (even in reduced gravity) are also examined. Author

A91-19432*# National Aeronautics and Space Administration, Lewis Research Center, Cleveland, OH.

RADIATION FROM GAS-JET DIFFUSION FLAMES IN MICROGRAVITY ENVIRONMENTS

M. YOUSEF BAHADORI (NASA, Lewis Research Center, Cleveland, OH; Science Applications International Corp., Torrance, CA), RAYMOND B. EDELMAN (Rockwell International Corp., Rocketdyne Div., Canoga Park, CA), RAYMOND G. SOTOS, and DENNIS P. STOCKER (NASA, Lewis Research Center, Cleveland, OH) AIAA, Aerospace Sciences Meeting, 29th, Reno, NV, Jan. 7-10, 1991. 5 p. refs (Contract NAS3-22822) (AIAA PAPER 91-0719)

This paper presents the first demonstration of quantitative flame-radiation measurement in microgravity environments, with the objective of studying the influences and characteristics of radiative transfer on the behavior of gas-jet diffusion flames with possible application to spacecraft fire detection. Laminar diffusion flames of propane, burning in quiescent air at atmospheric pressure, are studied in the 5.18-Second Zero-Gravity Facility of NASA Lewis Research Center. Radiation from these flames is measured using a wide-view angle, thermopile-detector radiometer, and comparisons are made with normal-gravity flames. The results show that the radiation level is significantly higher in microgravity compared to normal-gravity environments due to larger flame size, enhanced soot formation, and entrapment of combustion products in the vicinity of the flame. These effects are the consequences of the removal of buoyancy which makes diffusion the dominant mechanism of transport. The results show that longer test times may be needed to reach steady state in microgravity environments. Author

A91-19433* National Aeronautics and Space Administration. Lewis Research Center, Cleveland, OH.

N-DECANE DROPLET COMBUSTION IN THE NASA-LEWIS 5 SECOND ZERO-GRAVITY FACILITY - RESULTS IN TEST GAS ENVIRONMENTS OTHER THAN AIR

JOHN B. HAGGARD, BRIAN A. BOROWSKI (NASA, Lewis Research Center, Cleveland, OH), FREDERICK L. DRYER, MUN Y. CHOI (Princeton University, NJ), FORMAN A. WILLIAMS (California, University, La Jolla) et al. AIAA, Aerospace Sciences Meeting, 29th, Reno, NV, Jan. 7-10, 1991. 9 p. refs (AIAA PAPER 91-0720) Copyright

The burning rate of single droplets of n-decane in a microgravity environment of the NASA-Lewis 5 Second Zero-Gravity Facility was investigated as a function of time, together with the flame diameter/droplet diameter ratio, for a wide range of test environments other than normal air conditions, using an engineering model of the flight experiment. Oxygen mole fractions were varied from 18 to 50 percent, the total test chamber pressure was varied from 0.5 to 2 atmospheres, and the initial droplet diameter was varied from 0.98 to 2.41 mm. Measurements showed that the average burning rates for n-decane droplets exhibited the same qualitative trends as are found in two current models. Temporal analysis of the local burning rates showed variable rates of change in local burning as the droplet combustion progressed. The causes and implications of these findings are discussed. I.S.

A91-20219* National Aeronautics and Space Administration. Lewis Research Center, Cleveland, OH.

HIGH TEMPERATURE REACTIONS OF CERAMICS AND METALS WITH CHLORINE AND OXYGEN

N. S. JACOBSON (NASA, Lewis Research Center, Cleveland, OH), M. J. MCNALLAN (Illinois, University, Chicago), and E. R. KREIDLER (Ohio State University, Columbus) High Temperature Science (ISSN 0018-1536), vol. 27, 1990, p. 381-392. refs Copyright

The reactions of chlorine and oxygen with solids are complex and quite dependent on material and reaction conditions. However, there are four reaction schemes that describe many of these reactions. These are direct reaction of chlorine with the oxide layer, penetration of the oxide layer by chlorine, parabolic behavior where oxidation and chlorination are of comparable rates, and finally, gas phase reactions where the volatile chlorides react with oxygen. Examples of chlorine and oxygen reactions with cobalt, nickel, chromium, molybdenum, and silicon carbide illustrate each of these four reaction schemes. Author

A91-20589* California Univ., La Jolla.

PARTICLE CLOUD FLAMES IN ACOUSTIC FIELDS

A. L. BERLAD, V. TANGIRALA (California, University, La Jolla), H. ROSS, and L. FACCA (NASA, Lewis Research Center, Cleveland, OH) Combustion and Flame (ISSN 0010-2180), vol. 82, Dec. 1990, p. 448-450. refs Copyright

Results are presented on a study of flames supported by clouds of particles suspended in air, at pressures about 100 times lower than normal. In the experiment, an acoustic driver (4-in speaker) placed at one end of a closed tube, 0.75-m long and 0.05 m in diameter, disperses a cloud of lycopodium particles during a 0.5-sec powerful acoustic burst. Properties of the particle cloud and the flame were recorded by high-speed motion pictures and optical transmission detectors. Novel flame structures were observed, which owe their features to partial confinement, which encourages flame-acoustic interactions, segregation of particle clouds into laminae, and penetration of the flame's radiative flux density into the unburned particle-cloud regimes. Results of these experiments imply that, for particles in confined spaces, uncontrolled fire and explosion may be a threat even if the $\Phi(0)$ values are below some apparent lean limit. I.S.

A91-21362# National Aeronautics and Space Administration. Lewis Research Center, Cleveland, OH.

COMBUSTION OF LIQUID FUEL DROPLETS IN SUPERCRITICAL CONDITIONS

J. S. SHUEN (NASA, Lewis Research Center; Sverdrup Technology, Inc., Cleveland, OH) and VIGOR YANG (Pennsylvania State University, University Park) AIAA, Aerospace Sciences Meeting, 29th, Reno, NV, Jan. 7-10, 1991. 19 p. Research supported by NASA and Pennsylvania State University. refs (AIAA PAPER 91-0078) Copyright

A comprehensive analysis of liquid-fuel droplet combustion in both sub- and super-critical environments has been conducted. The formulation is based on the complete conservation equations for both gas and liquid phases, and accommodates finite-rate chemical kinetics and a full treatment of liquid-vapor phase equilibrium at the droplet surface. The governing equations and the associated interface boundary conditions are solved numerically using a fully coupled, implicit scheme with the dual time-stepping integration technique. The model is capable of treating the entire droplet history, including the transition from the subcritical to the supercritical state. As a specific example, the combustion of n-pentane fuel droplets in air is studied for pressures of 5-140 atm. Results indicate that the ambient gas pressure exerts significant control of droplet gasification and burning processes through its influences on the fluid transport, gas/liquid interface thermodynamics, and chemical reactions. The droplet gasification rate increases progressively with pressure. However, the data for the overall burnout time exhibits a significant variation near the critical burning pressure, mainly as a result of reduced mass-diffusion rate and latent heat of vaporization with increased pressure. The influence of droplet size on the burning characteristics is also noted. Author

A91-21481*# Carnegie-Mellon Univ., Pittsburgh, PA.

SIMULATION OF MIXING IN THE QUICK QUENCH REGION OF A RICH BURN-QUICK QUENCH MIX-LEAN BURN COMBUSTOR

TOM I.-P. SHIH (Carnegie-Mellon University, Pittsburgh, PA), H. LEE NGUYEN (NASA, Lewis Research Center, Cleveland, OH), GREGORY W. HOWE, and Z. LI AIAA, Aerospace Sciences Meeting, 29th, Reno, NV, Jan. 7-10, 1991. 10 p. refs (Contract NAG3-1009) (AIAA PAPER 91-0410)

A computer program was developed to study the mixing process in the quick quench region of a rich burn-quick quench mix-lean burn combustor. The computer program developed was based on the density-weighted, ensemble-averaged conservation equations of mass, momentum (full compressible Navier-Stokes), total energy, and species, closed by a k-epsilon turbulence model with wall functions. The combustion process was modeled by a two-step global reaction mechanism, and NO(x) formation was modeled by the Zeldovich mechanism. The formulation employed in the computer program and the essence of the numerical method of solution are described. Some results obtained for nonreacting and reacting flows with different main-flow to dilution-jet momentum flux ratios are also presented. Author

A91-30003*# California Univ., La Jolla.

RADIATIVE STRUCTURES OF LYCOPodium-AIR FLAMES IN LOW GRAVITY

A. L. BERLAD, V. TANGIRALA (California, University, La Jolla), H. ROSS, and L. FACCA (NASA, Lewis Research Center, Cleveland, OH) Journal of Propulsion and Power (ISSN 0748-4658), vol. 7, Jan.-Feb. 1991, p. 5-8. Previously cited in issue 09, p. 1315. Accession no. A89-25406. refs Copyright

A91-41749*# National Aeronautics and Space Administration. Lewis Research Center, Cleveland, OH.

A DETAILED NUMERICAL INVESTIGATION OF BURKE-SCHUMANN GASEOUS AND SPRAY FLAMES

M. A. MAWID (NASA, Lewis Research Center, Cleveland, OH) and S. K. AGGARWAL (Illinois, University, Chicago) AIAA, SAE, ASME, and ASSE, Joint Propulsion Conference, 27th, Sacramento, CA, June 24-26, 1991. 11 p. refs (Contract NAG3-796) (AIAA PAPER 91-2311) Copyright

The classical Burke-Schumann gaseous diffusion flame, and the effect of introducing fuel in the form of liquid sprays are investigated numerically. The time-dependent two-dimensional, axisymmetric conservation equations are solved for the gas phase. A Lagrangian approach is used for the dispersed phase. The chemical reactions are modeled through the one-step global reaction scheme. The numerical results show that the computed flame structure is significantly different from that given by the analytical solution. The computed flame is about 15 percent longer and 5 percent narrower than the classical Burke-Schumann flame. The predicted flame shape is, however, in better agreement with experimental observations than the Burke-Schumann flame. The effects of introducing liquid sprays is found to produce thinner and longer flames than its counterpart gaseous flame. A detailed comparison of the structures of gaseous and spray flames is made, and the differences are discussed.

Author

A91-44192*# Pennsylvania State Univ., University Park.
**PRESSURE-COUPLED VAPORIZATION AND COMBUSTION
 RESPONSES OF LIQUID-FUEL DROPLETS IN
 HIGH-PRESSURE ENVIRONMENTS**

VIGOR YANG (Pennsylvania State University, University Park), J. S. SHUEN (NASA, Lewis Research Center; Sverdrup Technology, Inc., Cleveland, OH), and C. C. HSIAO AIAA, SAE, ASME, and ASEE, Joint Propulsion Conference, 27th, Sacramento, CA, June 24-26, 1991. 8 p. refs

(AIAA PAPER 91-2310) Copyright

The dynamic responses of liquid-fuel droplet vaporization and combustion to ambient pressure oscillations are examined. The analysis is based on the complete sets of conservation equations for both gas and liquid phases, and accommodates detailed treatments of finite-rate chemical kinetics and variable properties. With a full account of thermodynamic phase equilibrium at the droplet surface, the model enables a systematic examination of the effects of ambient flow conditions on the droplet behavior. The responses of hydrocarbon fuel droplets in both sub- and super-critical environments are investigated. Results indicate that the droplet gasification and burning mechanisms depend greatly on the ambient pressure. In particular, a rapid enlargement of the vaporization and combustion responses occurs when the droplet surface reaches its critical point, mainly due to the strong variations of latent heat of vaporization and thermophysical properties at the critical state.

Author

A91-45549*# National Aeronautics and Space Administration.
 Lewis Research Center, Cleveland, OH.

**A STUDY OF HYDROGEN DIFFUSION FLAMES USING PDF
 TURBULENCE MODEL**

ANDREW T. HSU (NASA, Lewis Research Center; Sverdrup Technology, Inc., Cleveland, OH) AIAA, Fluid Dynamics, Plasma Dynamics and Lasers Conference, 22nd, Honolulu, HI, June 24-26, 1991. 11 p. refs

(Contract NAS3-25266)

(AIAA PAPER 91-1780) Copyright

The application of probability density function (pdf) turbulence models is addressed in this work. For the purpose of accurate prediction of turbulent combustion, an algorithm that combines a conventional CFD flow solver with the Monte Carlo simulation of the pdf evolution equation has been developed. The algorithm has been validated using experimental data for a heated turbulent plane jet. The study of H₂-F₂ diffusion flames has been carried out using this algorithm. Numerical results compared favorably with experimental data. The computations show that the flame center shifts as the equivalence ratio changes, and that for the same equivalence ratio, similarity solutions for flames exist.

Author

A91-45777*# University of South Florida, Tampa.
**NUMERICAL SIMULATION OF JET-A COMBUSTION
 APPROXIMATED BY IMPROVED PROPANE CHEMICAL
 KINETICS**

SHUH-JING YING (South Florida, University, Tampa, FL) and HUNG LEE NGUYEN (NASA, Lewis Research Center, Cleveland,

OH) AIAA, SAE, ASME, and ASEE, Joint Propulsion Conference, 27th, Sacramento, CA, June 24-26, 1991. 6 p. refs

(Contract NAG3-1112)

(AIAA PAPER 91-1859) Copyright

Through the effort devoted to the chemical kinetics for propane air combustion, three mechanisms are developed. The full mechanism consists of 131 reactions. This mechanism is used as a guide for the evaluation of other mechanisms, but because of the long expected cpu time, it is not to be incorporated into the computer code KIVA-II for actual simulation. Through the sensitivity analysis, a reduced mechanism of 45 reactions is produced. But the calculated results from the 45 reaction mechanism are always low in temperature. Some efforts are devoted to correct this situation and details are included in this report. A simplified mechanism of reactions is successfully improved and computed results are compared with experimental data. Contour plots of physical parameters and species concentrations and results for emission indices of CO and NO_x are presented.

Author

A91-45810*# National Aeronautics and Space Administration.
 Lewis Research Center, Cleveland, OH.

**JET-A REACTION MECHANISM STUDY FOR COMBUSTION
 APPLICATION**

CHI-MING LEE, KRISHNA KUNDU (NASA, Lewis Research Center, Cleveland, OH), and WALDO ACOSTA (NASA, Lewis Research Center; U.S. Army, Propulsion Directorate, Cleveland, OH) AIAA, SAE, ASME, and ASEE, Joint Propulsion Conference, 27th, Sacramento, CA, June 24-26, 1991. 12 p. refs

(AIAA PAPER 91-2355) Copyright

Simplified chemical kinetic reaction mechanisms for the combustion of Jet A fuel are studied. Initially 40 reacting species and 118 elementary chemical reactions were chosen based on the literature review of previous works. Through a sensitivity analysis with the use of LSENS General Kinetics and Sensitivity Analysis Code, 16 species and 21 elementary chemical reactions were determined from this study. This mechanism is first justified by comparison of calculated ignition delay time with available shock tube data, then it is validated by comparison of calculated emissions from plug flow reactor code with in-house flame tube data.

Author

A91-51449*# San Diego State Univ., CA.
**HEAT TRANSFER TO A THIN SOLID COMBUSTIBLE IN
 FLAME SPREADING AT MICROGRAVITY**

S. BHATTACHARJEE (San Diego State University, CA), R. A. ALTENKIRCH (Mississippi State University, Mississippi State), S. L. OLSON, and R. G. SOTOS (NASA, Lewis Research Center, Cleveland, OH) ASME, Transactions, Journal of Heat Transfer (ISSN 0022-1481), vol. 113, Aug. 1991, p. 670-676. refs

(Contract NAS3-23901)

Copyright

The heat transfer rate to a thin solid combustible from an attached diffusion flame, spreading across the surface of the combustible in a quiescent, microgravity environment, was determined from measurements made in the drop tower facility at NASA-Lewis Research Center. With first-order Arrhenius pyrolysis kinetics, the solid-phase mass and energy equations along with the measured spread rate and surface temperature profiles were used to calculate the net heat flux to the surface. Results of the measurements are compared to the numerical solution of the complete set of coupled differential equations that describes the temperature, species, and velocity fields in the gas and solid phases. The theory and experiment agree on the major qualitative features of the heat transfer. Some fundamental differences are attributed to the neglect of radiation in the theoretical model.

Author

N91-19256*# National Aeronautics and Space Administration.
 Lewis Research Center, Cleveland, OH.

**REACTIVITY OF PI-COMPLEXES OF TI, V, AND Nb
 TOWARDS DITHIOACETIC ACID: SYNTHESIS AND
 STRUCTURE OF NOVEL METAL SULFUR-CONTAINING
 COMPLEXES**

STAN A. DURAJ, MARIA T. ANDRAS (Cleveland State Univ., OH.), and ALOYSIUS F. HEPP 1990 6 p Presented at the Fall Meeting of the Materials Research Society, Boston, MA, 26 Nov. - 1 Dec. 1990

(Contract RTOP 307-51-00)

(NASA-TM-103666; E-5873; NAS 1.15:103666) Avail: NTIS HC/MF A02 CSCL 07/4

In order to use sulfur-containing resources economically and with minimal environmental damage, it is important to understand the desulfurization processes. Hydrodesulfurization, for example, is carried out on the surface of a heterogeneous metal sulfide catalyst. Studies of simple, soluble inorganic systems provide information regarding the structure and reactivity of sulfur-containing compounds with metal complexes. Further, consistent with recent trends in materials chemistry, many model compounds warrant further study as catalyst precursors. The reactivity of low-valent organometallic sandwich pi-complexes toward dithiocarboxylic acids is described. For example, treatment of bisbenzene vanadium with CH_3CSSH affords a divanadium tetrakis(dithioacetate) complex. The crystallographically determined V-V bond distance, 2.800(2), is nearly the same as the V-V bond distance in a $\text{V}(\mu\text{-nu squared-S}_2\text{)}_2\text{V}'$ unit in the mineral patonite (VS_4)_n. The stability of the V_2S_4 core in the dimer is demonstrated by evidence of $\text{V}_2\text{S}_4(+)$ in the mass spectrum (70 eV, solid probe) of the vanadium dimer. Several other systems relevant to HDS catalysis are also discussed. Author

N91-22410*# National Aeronautics and Space Administration. Lewis Research Center, Cleveland, OH.

SYNTHESIS AND THERMAL PROPERTIES OF STRONTIUM AND CALCIUM PEROXIDES

WARREN H. PHILIPP and PATRICIA A. KRAFT (Cleveland State Univ., OH.) 1989 14 p Presented at the Annual Meeting of the American Inst. of Chemical Engineers, San Francisco, CA, 6-8 Nov. 1989

(Contract NCC3-111; RTOP 510-01-50)

(NASA-TM-103725; E-5959; NAS 1.15:103725) Avail: NTIS HC/MF A03 CSCL 07/4

A practical synthesis and a discussion of some chemical properties of pure strontium peroxide and calcium peroxide are presented. The general synthesis of these peroxides involves precipitation of their octahydrates by addition of H_2O_2 to aqueous ammoniacal $\text{Sr}(\text{NO}_3)_2$ or CaCl_2 . The octahydrates are converted to the anhydrous peroxides by various dehydration techniques. A new x-ray diffraction powder pattern for $\text{CaO}_2 \cdot 8\text{H}_2\text{O}$ is given from which lattice parameters $a=6.212830$ and $c=11.0090$ were calculated on the basis of the tetragonal crystal system. Author

N91-30210*# National Aeronautics and Space Administration. Lewis Research Center, Cleveland, OH.

HIGH RESOLUTION ELECTROLYTE FOR THINNING INP BY ANODIC DISSOLUTION AND ITS APPLICATIONS TO EC-V PROFILING, DEFECT REVEALING AND SURFACE PASSIVATION

MARIA FAUR, MIRCEA FAUR, IRVING WEINBERG, MANJU GORADIA, and CARLOS VARGAS (Kent State Univ., OH.) In its Space Photovoltaic Research and Technology Conference 12 p Aug. 1991 Prepared in cooperation with Cleveland State Univ., OH

Avail: NTIS HC/MF A20 CSCL 07/4

An extensive experimental study was conducted using various electrolytes in an effort to find an appropriate electrolyte for anodic dissolution of InP. From the analysis of electrochemical characteristics in the dark and under different illumination levels, x ray photoelectron spectroscopy and SEM/Nomarski inspection of the surfaces, it was determined that the anodic dissolution of InP front surface layers by FAP electrolyte is a very good choice for rendering smooth surfaces, free of oxides and contaminants and with good electrical characteristics. The FAP electrolyte, based on HF, CH_3COOH , and H_2O_2 appears to be inherently superior to previously reported electrolytes for performing accurate EC-V profiling of InP at current densities of up to 0.3 mA/sq cm. It can also be used for accurate electrochemical revealing of either

precipitates or dislocation density with application to EPD mapping as a function of depth, and for defect revealing of multilayer InP structures at any depth and/or at the interfaces. Author

26

METALLIC MATERIALS

Includes physical, chemical, and mechanical properties of metals, e.g., corrosion; and metallurgy.

A91-11624* National Aeronautics and Space Administration. Lewis Research Center, Cleveland, OH.

TENSILE PROPERTIES OF HA 230 AND HA 188 AFTER 400 AND 2500 HOUR EXPOSURES TO LiF-22CaF_2 AND VACUUM AT 1093 K

J. DANIEL WHITTENBERGER (NASA, Lewis Research Center, Cleveland, OH) Journal of Materials Engineering (ISSN 0931-7058), vol. 12, Sept. 1990, p. 211-226. refs Copyright

The solid-to-liquid phase transformation of the nominal LiF-20CaF_2 eutectic at 1043 K is considered to be an ideal candidate thermal energy storage mechanism for a space based low temperature Brayton cycle solar dynamic system. Although Co, Fe, and Ni superalloys are thought to be suitable containment materials for LiF based salts, long term containment is of concern because molten fluorides are usually corrosive and Cr can be lost into space through evaporation. Two examples of commercially available superalloys in sheet form, the Ni-base material HA 230 and the Co-base material Ha 88, have been exposed to molten LiF-22CaF_2 , its vapor, and vacuum, at 1093 K, for 400 and 2500 hr. Triplicate tensile testing of specimens subjected to all three environments have been undertaken between 77 to 1200 K. Comparison of the weight gain data, microstructure, and tensile properties indicate that little, if any, difference in behavior can be ascribed to the exposure environment. Author

A91-16869* National Aeronautics and Space Administration. White Sands Test Facility, NM.

SURFACE MODIFICATION OF MONEL K-500 AS A MEANS OF REDUCING FRICTION AND WEAR IN HIGH-PRESSURE OXYGEN

MOHAN GUNAJI (NASA, White Sands Test Facility; Lockheed Engineering and Sciences Co., Las Cruces, NM), JOEL M. STOLTZFUS (NASA, White Sands Test Facility, Las Cruces, NM), LEONARD SCHOENMAN (Aerojet TechSystems Co., Sacramento, CA), and JOHN KAZAROFF (NASA, Lewis Research Center, Cleveland, OH) IN: Flammability and sensitivity of materials in oxygen-enriched atmospheres; Proceedings of the Fourth International Symposium, Las Cruces, NM, Apr. 11-13, 1989. Volume 4. Philadelphia, PA, American Society for Testing and Materials, 1989, p. 332-346. refs Copyright

A study is conducted of the tribological characteristics of Monel K-500 during rubbing in a high pressure oxygen atmosphere, upon surface treatment by ion-implanted oxygen, chromium, lead, and silver, as well as electrolyzed chromium and an electrodeless nickel/SiC composite. The electrolyzed chromium dramatically increased total sample wear, while other surface treatments affected sample wear only moderately. Although the ion-implant treatments reduced the average coefficient of friction at low contact pressure, higher contact pressures eliminated this improvement. O.C.

A91-18674* National Aeronautics and Space Administration. Lewis Research Center, Cleveland, OH.

1300 K COMPRESSIVE PROPERTIES OF A REACTION MILLED NIAL-ALN COMPOSITES

J. DANIEL WHITTENBERGER (NASA, Lewis Research Center, Cleveland, OH), EDUARD ARZT (Max-Planck-Institut fuer

26 METALLIC MATERIALS

Metallforschung, Stuttgart, Federal Republic of Germany), and MICHAEL J. LUTON (Exxon Research and Engineering Co., Annandale, NJ) *Journal of Materials Research* (ISSN 0884-2914), vol. 5, Dec. 1990, p. 2819-2827. refs
Copyright

When B2 crystal-structure nickel aluminide is subjected to high-intensity mechanical ball milling in a liquid nitrogen bath, or 'cryomilling', an NiAl composite is obtained which contains about 10 vol pct AlN particles. This composition arises from the incorporation of N during cryomilling; during subsequent thermomechanical processing, the N reacts with Al. While compressive testing of extruded or isostatically pressed specimens at 1300 K indicated that strength at relatively fast strain rates is slightly dependent on consolidation method, slower strain rates indicate no clear dependency on densification technique: four different consolidation methods were found to yield similar creep strengths. The creep properties of NiAl-AlN are similar to those of the single-crystal Ni-base superalloy NASAIR 100. O.C.

A91-22287* National Aeronautics and Space Administration. Lewis Research Center, Cleveland, OH.

INHOMOGENEOUS DEFORMATION IN INCONEL 718 DURING MONOTONIC AND CYCLIC LOADINGS

D. W. WORTHEM (NASA, Lewis Research Center; Sverdrup Technology, Inc., Cleveland, OH), I. M. ROBERTSON, D. F. SOCIE, C. J. ALTSTETTER (Illinois, University, Urbana), and F. A. LECKIE (California, University, Santa Barbara) *Metallurgical Transactions A - Physical Metallurgy and Materials Science* (ISSN 0360-2133), vol. 21A, Dec. 1990, p. 3215-3220. refs
(Contract DE-AC02-76ER-01198)

Copyright

The paper concentrates on the relation between microstructural observations of the dislocation structures and the macroscopic deformation responses of both aged and homogenized precipitate-hardened alloys at room temperature. The deformation responses are compared to the cyclic deformation response of an aged precipitate-hardened alloy. Early in the deformation, one deformation band per grain and little evidence of work hardening are observed; with increased deformation, work hardening begins, more bands nucleate, and their spacing becomes similar to that in the aged material. It is pointed out that the degree of coarseness of inhomogeneous deformation is not a result of a softening process within the bands due to precipitate shearing, but it is a function of the amount of work hardening within the bands. V.T.

A91-27158* National Aeronautics and Space Administration. Lewis Research Center, Cleveland, OH.

GRAIN BOUNDARY SLIDING BEHAVIOUR OF COPPER AND ALPHA BRASS AT INTERMEDIATE TEMPERATURES

S. V. RAJ (NASA, Lewis Research Center, Cleveland, OH) *Journal of Materials Science* (ISSN 0022-2461), vol. 26, Feb. 15, 1991, p. 1000-1008. DOE-supported research. refs

Copyright

The role of grain boundary sliding in copper and Cu-30 pct Zn in the temperature range 0.50-0.72 T_m, where T_m is the absolute melting point of the material, is examined. First, sliding data obtained on these materials are presented. The results indicate that the stress exponent for sliding is similar to that for lattice deformation, while the activation energy for sliding varies between 0.5 and 1.6 of the activation energy for creep. Several models proposed for grain boundary sliding are discussed, and it is shown that they do not account for the observed results on copper and alpha brass. A phenomenological model is proposed, where it is assumed that grain boundary sliding results from the glide of dislocations on secondary slip planes. Author

A91-27849* Michigan Technological Univ., Houghton. **OXIDATION BEHAVIOR OF CUBIC PHASES FORMED BY ALLOYING AL₃Ti WITH CR AND MN**

L. J. PARFITT, J. P. NIC, D. E. MIKKOLA (Michigan Technological University, Houghton), and J. L. SMIALEK (NASA, Lewis Research Center, Cleveland, OH) *Scripta Metallurgica et Materialia* (ISSN

0956-716X), vol. 25, March 1991, p. 727-731. refs
Copyright

Gravimetric, SEM, and XRD data are presented which document the significant improvement obtainable in the oxidation resistance of Al₃Ti-containing alloys through additions of Cr. The L1(2) Al(67)Cr(8)Ti₂₅ alloy exhibited excellent cyclic oxidation resistance at 1473 K, with the primary oxide formed being the ideally protective alpha-Al₂O₃. The Al(67)Mn(8)Ti(25) alloy also tested for comparison exhibited poor cyclic oxidation resistance, with substantial occurrence of TiO₂ in the protective scales. Catastrophic oxidation was also encountered in the quaternary alloy Al(67)Mn(8)Ti(22)V(3). O.C.

A91-27940* National Aeronautics and Space Administration. Lewis Research Center, Cleveland, OH.

EFFECT OF SULFUR REMOVAL ON AL₂O₃ SCALE ADHESION

JAMES L. SMIALEK (NASA, Lewis Research Center, Cleveland, OH) *Metallurgical Transactions A - Physical Metallurgy and Materials Science* (ISSN 0360-2133), vol. 22A, March 1991, p. 739-752. refs

The effect of removing sulfur impurity on the adhesion of Al₂O₃ scale to NiCrAl was investigated in four experiments. It was found that removing sulfur to concentration less than 1 ppm per weight is sufficient to produce a very significant degree of alpha-Al₂O₃ scale adhesion to undoped NiCrAl alloys. Results of experiments show that repeated oxidation, and polishing after each oxidation cycle, of pure NiCrAl alloy lowered sulfur content from 10 to 2 ppm by weight (presumably by removing the segregated interfacial layer after each cycle); thinner samples became adherent after fewer oxidation-polishing cycles because of more limited supply of sulfur. It was found that spalling in subsequent cyclic oxidation tests was a direct function of the initial sulfur content. The transition between the adherent and nonadherent behavior was modeled in terms of sulfur flux, sulfur content, and sulfur segregation. I.S.

A91-28794* National Aeronautics and Space Administration. Lewis Research Center, Cleveland, OH.

THE EFFECT OF HYDROGEN ON THE LOW CYCLE FATIGUE BEHAVIOR OF A SINGLE CRYSTAL SUPERALLOY

J. GAYDA, T. P. GABB, and R. L. DRESHFIELD (NASA, Lewis Research Center, Cleveland, OH) *IN: Hydrogen effects on material behavior; Proceedings of the 4th International Conference on the Effect of Hydrogen on the Behavior of Materials*, Moran, WY, Sept. 12-15, 1989. Warrendale, PA, Minerals, Metals, and Materials Society, 1990, p. 591-601. refs

Copyright

The present study compares the room temperature fatigue properties of PWA 1480 single crystals containing either normal or elevated hydrogen levels, giving attention to the effects of various levels of HIPing process-controlled porosity on hydrogen-trapping and fatigue life. Hydrogen charging is found to degrade the fatigue lives of alloy samples by an order of magnitude; the magnitude of this degradation is comparable at both high and low porosity. HIPing accomplished a small beneficial effect on the fatigue life of both the hydrogen-charged and uncharged PWA 1480 samples. Fatigue cracks are noted to have consistently initiated at large, near-surface pores. By reducing the size and frequency of the larger pores, HIPing apparently retarded fatigue-crack initiation. O.C.

A91-36214* National Aeronautics and Space Administration. Lewis Research Center, Cleveland, OH.

1000 TO 1300 K SLOW PLASTIC COMPRESSION PROPERTIES OF AL-DEFICIENT NIAL

J. D. WHITTENBERGER (NASA, Lewis Research Center, Cleveland, OH), K. S. KUMAR, and S. K. MANNAN (Martin Marietta Laboratories, Baltimore, MD) *Journal of Materials Science* (ISSN 0022-2461), vol. 26, April 15, 1991, p. 2015-2022. refs
Copyright

Nickel aluminides containing 37, 38.5 and 40 at. pct Al have been fabricated by XD synthesis and hot pressing. Such materials were compression tested in air under constant velocity conditions between 1000 and 1300 K. Examination of the microstructures of hot pressed and compression tested aluminides indicated that the

structure consisted of two phases, gamma-prime and NiAl, for essentially all conditions, where gamma-prime was usually found on the NiAl grain boundaries. The stress-strain behavior of all three intermetallics was similar where flow at a nominally constant stress occurred after about two-percent plastic deformation. Furthermore, the 1000 to 1300 K flow stress-strain rate properties are nearly identical for these materials, and they are much lower than those for XD processed Ni-50Al. The overall deformation of the two phase nickel aluminides appears to be controlled by dislocation climb in NiAl rather than processes in gamma-prime.

Author

A91-39292* National Aeronautics and Space Administration. Lewis Research Center, Cleveland, OH.

THE POTENTIAL FOR DUCTILITY ENHANCEMENT FROM SURFACE AND INTERFACE DISLOCATION SOURCES IN NIAL

R. D. NOEBE, R. R. BOWMAN (NASA, Lewis Research Center, Cleveland, OH), J. T. KIM, M. LARSEN, and R. GIBALA (Michigan, University, Ann Arbor) IN: High temperature aluminides and intermetallics; Proceedings of the 1st Symposium, Indianapolis, IN, Oct. 1-5, 1989. Warrendale, PA, Minerals, Metals and Materials Society, 1990, p. 271-300. University of Michigan-supported research. refs

(Contract NSF DMR-88-10058; NCC3-76)

Copyright

Limited ductility and toughness of NiAl and related aluminides near room temperature pose major problems in their potential application as structural materials. An analysis of these problems is presented as part of a review of the flow and fracture behavior of binary NiAl. Following this discussion is a demonstration that conditions of elastic and plastic constraint associated with phase boundaries afforded by surface films, internal lamellae, or precipitates may introduce sufficient densities of mobile dislocations to enhance the ductility of NiAl-based materials by significant amounts. Examples of this behavior are presented for several model materials, including 001- and 123-oriented single crystals of oxide-coated NiAl, directionally solidified beta-gamma-prime (Ni₇₀Al₃₀) and beta-gamma (Ni₅₀Fe₃₀Al₂₀) in situ composites, and several NiAl/precipitate systems. The nature of the resulting dislocation substructures and the effects of several materials variables are described.

Author

A91-43670*# National Aeronautics and Space Administration. Lewis Research Center, Cleveland, OH.

1000 TO 1200 K TIME-DEPENDENT COMPRESSIVE DEFORMATION OF SINGLE-CRYSTALLINE AND POLYCRYSTALLINE B2 Ni-40Al

J. D. WHITTENBERGER, R. D. NOEBE (NASA, Lewis Research Center, Cleveland, OH), K. S. KUMAR (Martin Marietta Laboratories, Baltimore, MD), S. K. MANNAN (Inco Alloys International, Inc., Huntington, WV), and C. L. CULLERS Metallurgical Transactions A - Physical Metallurgy and Materials Science (ISSN 0360-2133), vol. 22A, July 1991, p. 1595-1607. refs

The 1000-K and 1200-K time-dependent deformation of 100-line-oriented and non-100-line-oriented single crystals of Ni-40Al (made by a modified Bridgman technique) was examined over a large range of strain rates (from 0.1 to 10 to the -7th per sec). The results were compared with those for polycrystalline Ni-40Al made by hot pressing XD synthesized powder. The results from measurements of slow-plastic-strain-rate properties of the two materials show that single crystals offer no strength advantage over polycrystalline material. Both forms were found to deform via a dislocation climb mechanism.

I.S.

A91-46520* National Aeronautics and Space Administration. Lewis Research Center, Cleveland, OH.

RAPID SOLIDIFICATION OF POLYMORPHIC TRANSITION METALS INDUCED BY NANOSECOND LASER PULSES

SATISH VITTA (NASA, Lewis Research Center, Cleveland, OH) Applied Physics Letters (ISSN 0003-6951), vol. 59, July 22, 1991, p. 411-413. refs

Copyright

An Nd-YAG laser giving 5 ns, 266 nm pulses was used to

melt and subsequently quench thin, pure metallic films on a liquid Al/Al₂O₃ substrate at 10 to the 10th - 10 to the 12th K/s. Transmission electron microscopy together with electron diffraction was used to study the competitive nucleation and growth behavior of the crystals from the undercooled melt. In the case of Fe and Co, the high-temperature bcc and fcc structures were retained after laser quenching. Ti and Zr in spite of the structural similarities exhibit different preferences for nucleation from the undercooled melt. In all the metals the solid-state transformations were completely suppressed and the crystal growth was found to be limited by the collisional frequency of the atoms onto the growing interface.

Author

A91-47747* National Aeronautics and Space Administration. Lewis Research Center, Cleveland, OH.

CREEP BEHAVIOUR OF CU-30 PERCENT ZN AT INTERMEDIATE TEMPERATURES

S. V. RAJ (NASA, Lewis Research Center, Cleveland, OH) Journal of Materials Science (ISSN 0022-2461), vol. 26, July 1, 1991, p. 3533-3543. Research supported by DOE. refs

(Contract NCC3-151)

Copyright

The present, intermediate-temperature (573-823 K) range investigation of creep properties for single-phase Cu-30 percent Zn alpha-brass observed inverse, linear, and sigmoidal primary-creep transients above 573 K under stresses that yield minimum creep rates in the 10 to the -7th to 2 x 10 to the -4th range; normal primary creep occurred in all other conditions. In conjunction with a review of the pertinent literature, a detailed analysis of these data suggests that no clearly defined, classes M-to-A-to-M transition exists in this alloy notwithstanding the presence of both classes' characteristics under nominally similar stresses and temperatures.

O.C.

A91-47931* National Aeronautics and Space Administration. Lewis Research Center, Cleveland, OH.

CREEP BEHAVIOR OF COPPER AT INTERMEDIATE TEMPERATURES. II - SURFACE MICROSTRUCTURAL OBSERVATIONS. III - A COMPARISON WITH THEORY

S. V. RAJ (NASA, Lewis Research Center, Cleveland, OH) and T. G. LANGDON (Southern California, University, Los Angeles, CA) Acta Metallurgica et Materialia (ISSN 0956-7151), vol. 39, Aug. 1991, p. 1817-1832. refs

(Contract DE-AM03-76SF-00113; DE-AT03-76ER-10403; NCC3-72)

Copyright

Three different types of microstructural slip features are noted to occur during the creep of Cu at 0.46-0.72 of absolute melting point. While single slip is associated with higher temperatures and lower stresses, complex wavy slip features are observed at higher temperatures and higher stresses as well as with increasing strains: suggesting the importance of cross-slip mechanisms. At lower temperatures and higher stresses the multiple-slip morphologies observed indicate that cross-slip mechanisms may control the creep of polycrystalline Cu only over a limited stress and temperature range. A phenomenological model is proposed which assumes that (1) cell boundaries within subgrains act as both sources of, and obstacles to, gliding dislocations, and (2) dislocation annihilation occurs at the cell boundaries by climb and cross-slip.

O.C.

A91-48509* Florida Univ., Gainesville.

CONSTITUTION OF PSEUDOBINARY HYPOEUTECTIC BETA-NIAL + ALPHA-V ALLOYS

J. D. COTTON, M. J. KAUFMAN (Florida, University, Gainesville), and R. D. NOEBE (NASA, Lewis Research Center, Cleveland, OH) Scripta Metallurgica et Materialia (ISSN 0956-716X), vol. 25, Aug. 1991, p. 1827-1832. refs

(Contract NAG3-1079)

Copyright

The formation of pseudobinary eutectics between NiAl (beta) and V (alpha) at high temperatures was investigated as a possible way of improving the ductility and toughness of the alloy. It is

26 METALLIC MATERIALS

found that a pseudobinary eutectic, characterized by a large beta+alpha field, is formed in the Ni-Al-V ternary system below about 1370 C. The high-temperature solubility of V in beta is about 14 percent, decreasing markedly with decreasing temperature and increasing Al content above 50 at. pct Al. The pseudobinary hypoeutectic exhibits crack resistance under indentation loading.
V.L.

A91-48517* National Aeronautics and Space Administration. Lewis Research Center, Cleveland, OH.

UNIVERSAL BEHAVIOR IN IDEAL SLIP

GUILLERMO BOZZOLO (NASA, Lewis Research Center, Cleveland; Analox Corp., Fairview Park, OH), JOHN FERRANTE (NASA, Lewis Research Center, Cleveland, OH), and JOHN R. SMITH (GM Research Laboratories, Warren, MI) Scripta Metallurgica et Materialia (ISSN 0956-716X), vol. 25, Aug. 1991, p. 1927-1931. refs

Copyright

The slip energies and stresses are computed for defect-free crystals of Ni, Cu, Ag, and Al using the many-atom approach. A simple analytical expression for the slip energies is obtained, leading to a universal form for slip, with the energy scaled by the surface energy and displacement scaled by the lattice constant. Maximum stresses are found to be somewhat larger than but comparable with experimentally determined maximum whisker strengths.
V.L.

A91-48725* National Aeronautics and Space Administration. Lewis Research Center, Cleveland, OH.

A NEW UNIFORMLY VALID ASYMPTOTIC INTEGRATION ALGORITHM FOR ELASTO-PLASTIC CREEP AND UNIFIED VISCOPLASTIC THEORIES INCLUDING CONTINUUM DAMAGE ABHISAK CHULYA (NASA, Lewis Research Center, Cleveland, OH) and KEVIN P. WALKER (Engineering Science Software, Inc., Smithfield, RI) International Journal for Numerical Methods in Engineering (ISSN 0029-5981), vol. 32, Aug. 5, 1991, p. 385-418. Previously announced in STAR as N90-14655. refs

Copyright

A new scheme to integrate a system of stiff differential equations for both the elasto-plastic creep and the unified viscoplastic theories is presented. The method has high stability, allows large time increments, and is implicit and iterative. It is suitable for use with continuum damage theories. The scheme was incorporated into MARC, a commercial finite element code through a user subroutine called HYPELA. Results from numerical problems under complex loading histories are presented for both small and large scale analysis. To demonstrate the scheme's accuracy and efficiency, comparisons to a self-adaptive forward Euler method are made.

Author

A91-53555* National Aeronautics and Space Administration. Lewis Research Center, Cleveland, OH.

ELASTIC RESPONSE OF (001)-ORIENTED PWA 1480 SINGLE CRYSTAL - THE INFLUENCE OF SECONDARY ORIENTATION SREERAMESH KALLURI, ALI ABDUL-AZIS (NASA, Lewis Research Center; Sverdrup Technology, Inc., Cleveland, OH), and MICHAEL MCGAW (NASA, Lewis Research Center, Cleveland, OH) SAE, Aerospace Atlantic Conference, Dayton, OH, Apr. 22-26, 1991. 13 p. Previously announced in STAR as N91-21558. refs

(SAE PAPER 911111) Copyright

The influence of secondary orientation on the elastic response of a zone axis (001)-oriented nickel-base single-crystal superalloy, PWA 1480, was investigated under mechanical loading conditions by applying finite element techniques. Elastic stress analyses were performed with a commercially available finite element code. Secondary orientation of the single-crystal superalloy was offset with respect to the global coordinate system in increments from 0 to 90 deg and stresses developed within the single crystal were determined for each loading condition. The results indicated that the stresses were strongly influenced by the angular offset between the secondary crystal orientation and the global coordinate system.

The degree of influence was found to vary with the type of loading condition (mechanical, thermal, or combined) imposed on the single-crystal superalloy.

Author

A91-55472* Florida Univ., Gainesville.

A SIMPLIFIED METHOD FOR DETERMINING THE NUMBER OF INDEPENDENT SLIP SYSTEMS IN CRYSTALS

J. D. COTTON, M. J. KAUFMAN (Florida, University, Gainesville), and R. D. NOEBE (NASA, Lewis Research Center, Cleveland, OH) Scripta Metallurgica et Materialia (ISSN 0956-716X), vol. 25, Oct. 1991, p. 2395-2398. refs

(Contract NAG3-1079)

Copyright

A novel method for determining the number of independent slip systems for any family or a combination of families of slip systems is proposed, which is more direct than previous approaches. This technique makes it possible to easily determine, from the known operative slip systems, if the material is slip-system-deficient. The method also makes it possible to determine if twinning may contribute additional deformation modes.
I.S.

N91-10149*# National Aeronautics and Space Administration. Lewis Research Center, Cleveland, OH.

HIGH TEMPERATURE CYCLIC OXIDATION DATA. PART 1: TURBINE ALLOYS

CHARLES A. BARRETT, RALPH G. GARLICK, and CARL E. LOWELL Oct. 1989 192 p Revised
(Contract RTOP 505-33-1A)
(NASA-TM-83665; E-1499-PT-1; NAS 1.15:83665) Avail: NTIS HC/MF A09 CSCL 11F

Specific-weight-change-versus-time data and x ray diffraction results are presented derived from high temperature cyclic tests on high temperature, high strength nickel-base gamma/gamma prime and cobalt-base turbine alloys. Each page of data summarizes a complete test on a given alloy sample.
Author

N91-10150*# National Aeronautics and Space Administration. Lewis Research Center, Cleveland, OH.

HIGH-TEMPERATURE CYCLIC OXIDATION DATA. PART 2: TURBINE ALLOYS

CHARLES A. BARRETT and RALPH G. GARLICK Oct. 1989 462 p
(Contract RTOP 505-63-01)
(NASA-TM-101468; E-4263-PT-2; NAS 1.15:101468) Avail: NTIS HC/MF A20 CSCL 11F

Specific-weight-change-versus-time data and x ray diffraction results are presented derived from high temperature cyclic tests on high temperature, high strength nickel-base gamma/gamma prime and cobalt-base turbine alloys. Each page of data summarizes a complete test on a given alloy sample.
Author

N91-14454*# National Aeronautics and Space Administration. Lewis Research Center, Cleveland, OH.

THERMAL STABILITY OF THE MICROSTRUCTURE OF AN AGED NB-ZR-C ALLOY Final Report

MEHMET UZ (Lafayette Coll., Easton, PA.) and ROBERT H. TITRAN Oct. 1990 18 p Presented at the 8th Symposium on Space Nuclear Power Systems, Albuquerque, NM, 7-10 Jan. 1991; sponsored by New Mexico Univ.
(Contract DE-A103-86SF-16310; RTOP 590-13-11)
(NASA-TM-103647; DOE/NASA/16310-14; E-5829; NAS 1.15:103647) Avail: NTIS HC/MF A03 CSCL 11/6

The effects of thermal aging with and without an applied stress on the microstructure of a Nb-Zr-C alloy containing 0.9 wt percent Zr and 0.06 wt percent C were studied. Chemical analysis, metallographic examination, energy dispersive x-ray spectra of the bulk material, and chemical and x-ray analyses of the phase-extracted residue were used to characterize the microstructure. The samples examined were from a creep strength study involving hot and cold working, and various combinations of exposure to temperatures ranging from 1350 to 1755 K with and without applied load for times as long as 34,000 plus hours. The

results showed that the initial microstructure consisted primarily of orthorhombic precipitates of Nb sub 2 C which were partially or completely transformed to face-centered cubic carbides of Nb and Zr, (Zr, Nb)C, upon prolonged exposure to elevated temperatures. Furthermore, it was found that the microstructure of the alloy is extremely stable owing to the very finely distributed precipitates throughout its matrix and along the grain boundaries. The lattice parameters of the cubic carbides were determined to vary from 0.458 to 0.465 nm as the Zr/Nb ratio varied from 38/62 to 75/25. Author

N91-15390*# National Aeronautics and Space Administration. Lewis Research Center, Cleveland, OH.

THERMAL BARRIER COATING EVALUATION NEEDS

WILLIAM J. BRINDLEY and ROBERT A. MILLER 1990 9 p Presented at the Conference on Nondestructive Evaluation of Modern Ceramics, Columbus, OH, 9-12 Jul. 1990; cosponsored by American Ceramic Society and American Society of Nondestructive Testing (Contract RTOP 505-63-1A) (NASA-TM-103708; E-5596; NAS 1.15:103708) Avail: NTIS HC/MF A02 CSCL 11/6

A 0.025 cm (0.010 in) thick thermal barrier coating (TBC) applied to turbine airfoils in a research gas turbine engine provided component temperature reductions of up to 190 C. These impressive temperature reductions can allow increased engine operating temperatures and reduced component cooling to achieve greater engine performance without sacrificing component durability. The significant benefits of TBCs are well established in aircraft gas turbine engine applications and their use is increasing. TBCs are also under intense development for use in the Low Heat Rejection (LHR) diesel engine currently being developed and are under consideration for use in utility and marine gas turbines. However, to fully utilize the benefits of TBCs it is necessary to accurately characterize coating attributes that affect the insulation and coating durability. The purpose there is to discuss areas in which nondestructive evaluation can make significant contributions to the further development and full utilization of TBCs for aircraft gas turbine engines and low heat rejection diesel engines. Author

N91-16128*# National Aeronautics and Space Administration. Lewis Research Center, Cleveland, OH.

TENSILE BEHAVIOR OF TUNGSTEN/NIObIUM COMPOSITES AT 1300 TO 1600 K Final Report

HEE MANN YUN (Cleveland State Univ., OH.) and ROBERT H. TITRAN 1989 25 p Presented at the Fall Meeting of the Metallurgical Society, Indianapolis, IN, 30 Sep. - 6 Oct. 1989 (Contract DE-AI03-86SF-16310; RTOP 590-13-11) (NASA-TM-103727; E-5961; NAS 1.15:103727; DOE/NASA/16310-15) Avail: NTIS HC/MF A03 CSCL 11/6

The tensile behavior of continuous tungsten fiber reinforced niobium composites (W/Nb), fabricated by an arc-spray process, was studied in the 1300 to 1600 K temperature range. The tensile properties of the fiber and matrix components as well as of the composites were measured and were compared to rule of mixtures (ROM) predictions. The deviation from the ROM was found to depend upon the chemistry of the tungsten alloy fibers, with positive deviations for ST300/Nb (i.e., stronger composite strength than the ROM) and negative or zero deviations for 218/Nb. Author

N91-20109*# National Aeronautics and Space Administration. Lewis Research Center, Cleveland, OH.

OVERVIEW OF LEWIS MATERIALS RESEARCH: CONTRIBUTIONS, CURRENT EFFORTS, AND FUTURE DIRECTIONS

SALVATORE J. GRISAFFE and CARL E. LOWELL In its Aeropropulsion 1991 20 p Mar. 1991 Avail: NTIS HC/MF A24 CSCL 11/6

In the 1940's, materials research efforts on high-temperature valve alloys at NASA Lewis Research Center led to the improved lives and performance of piston-engined fighter and bomber aircraft. The metallurgical skills acquired from that work were then applied

to the formulation of high-temperature turbine blade alloys for aircraft gas turbine engines developed in the 1950's. Today, the benefits of superior U.S. engine technology have never been clearer for both commercial and military aircraft. Yet, these superior engines of the 1980's and 1990's now use some of the materials that we helped conceive and evolve in the 1960's and 1970's. NASA Lewis is currently charged with helping industry create, advance, and develop the materials for 21st century engines: 2005 to 2015 plus. Highlights of past work, staff, and facilities are presented. The challenges and new material and process concepts that are currently being worked on as well as plans for the future are summarized. Author

N91-20268*# National Aeronautics and Space Administration. Lewis Research Center, Cleveland, OH.

THERMOMECHANICAL AND BITHERMAL FATIGUE BEHAVIOR OF CAST B1900 + HF AND WROUGHT HAYNES 188

GARY R. HALFORD, MICHAEL J. VERRILLI, SREERAMESH KALLURI, FRANK J. RITZERT, ROB E. DUCKERT (Wisconsin Univ., Madison.), and FREDERIC A. HOLLAND Apr. 1991 22 p (Contract RTOP 553-13-00) (NASA-TM-4225; E-5601; NAS 1.15:4225) Avail: NTIS HC/MF A03 CSCL 11/6

High temperature thermomechanical and bithermal fatigue behavior was investigated for two superalloys: cast nickel-base B1900+Hf and wrought cobalt-base Haynes 188. Experimental results were generated to support development of an advanced thermal fatigue life prediction method. Strain controlled thermomechanical and load-controlled, strain-limited, bithermal fatigue tests were used to determine the fatigue crack initiation and cyclic stress-strain response characteristics of superalloys. Bithermal temperatures of 483 and 871 C were used for B1900+Hf, and 316 and 760 C for Haynes 188. Thermomechanical fatigue tests were conducted by using maximum and minimum temperatures corresponding to those for the bithermal experiments. Lives cover the range from about 10 to 3000 cycles to failure. Isothermal fatigue results obtained previously are also discussed. Author

N91-24312*# National Aeronautics and Space Administration. Lewis Research Center, Cleveland, OH.

CUMULATIVE CREEP FATIGUE DAMAGE IN 316 STAINLESS STEEL

MICHAEL A. MCGAW In its Structural Integrity and Durability of Reusable Space Propulsion Systems p 33-37 Apr. 1989 Avail: NTIS HC/MF A12 CSCL 11/6

The cumulative creep-fatigue damage behavior of 316 stainless steel at 1500 F was experimentally established for the two-level loading cases of fatigue followed by fatigue, creep fatigue followed by fatigue, and fatigue followed by creep fatigue. The two-level loadings were conducted such that the lower life (high strain) cycling was applied first for a controlled number of cycles and the higher life (low strain) cycling was conducted as the second level to failure. The target life levels in this study were 100 cycles to failure for both the fatigue and creep-fatigue lowlife loading, 5000 cycles to failure for the higher life fatigue loading and 10,000 cycles to failure for the higher life creep-fatigue loading. The failed specimens are being examined both fractographically and metallographically to ascertain the nature of the damaging mechanisms that produced failure. Models of creep-fatigue damage accumulation are being evaluated and knowledge of the various damaging mechanisms is necessary to ensure that predictive capability is instilled in the final failure model. Author

N91-24313*# National Aeronautics and Space Administration. Lewis Research Center, Cleveland, OH.

FATIGUE BEHAVIOR OF A SINGLE-CRYSTAL SUPERALLOY SREERAMESH KALLURI (Sverdrup Technology, Inc., Cleveland, OH.) and MICHAEL A. MCGAW In its Structural Integrity and Durability of Reusable Space Propulsion Systems p 39-44 Apr.

26 METALLIC MATERIALS

1989

Avail: NTIS HC/MF A12 CSCL 11/6

A single-crystal superalloy, PWA 1480 is under consideration as a replacement material for the turbine blades of the high pressure fuel turbopump (HPFTP) of the space shuttle main engine (SSME). Three separate experimental programs were conducted to characterize the fatigue behavior of this alloy. Fatigue tests were conducted at room temperature (in air) and at 1000 F (in vacuum) on smooth specimens machined from both cast bars and slabs. The data from all of these programs are consolidated to provide a broader characterization of the fatigue behavior of the single crystal PWA 1480. The zero-mean-stress fatigue relationships are expressed in terms of stress range versus cyclic life lines on log-log plots. Characterization of the fatigue behavior of (001) oriented PWA 1480 single crystal under conditions of tensile mean stress was performed by using the unified approach proposed by Heidmann. In this approach the fatigue life is modified by a mean stress parameter so that a single life relationship can be used to represent both zero and tensile mean stress data.

Author

N91-27324*# National Aeronautics and Space Administration. Lewis Research Center, Cleveland, OH.

PROSPECTS FOR DUCTILITY AND TOUGHNESS ENHANCEMENT OF NIAL BY DUCTILE PHASE REINFORCEMENT

R. D. NOEBE, F. J. RITZERT, A. MISRA, and R. GIBALA (Michigan Univ., Ann Arbor.) Jul. 1991 31 p

(Contract NSF DMR-88-10058; RTOP 510-01-50)

(NASA-TM-103796; E-6022; NAS 1.15:103796) Avail: NTIS HC/MF A03 CSCL 11/6

The use of NiAl as a structural material has been hindered by the fact that this ordered intermetallic does not exhibit significant tensile ductility or toughness at room temperature. A critical review of the operative flow and fracture mechanisms in monolithic NiAl has thus established the need for ductile phase toughening in this order system. Progress in ductile phase reinforced intermetallic systems in general and specifically NiAl-based materials has been reviewed. In addition, further clarification of the primary mechanisms involved in the flow and fracture of ductile phase reinforced alloys has evolved from ongoing investigations of several model NiAl-based materials. The mechanical behavior of these model directionally-solidified alloys (Ni-30Al and Ni-30Fe-20Al) are discussed. Finally, the prospects for developing a ductile phase toughened NiAl-based alloy and the shortcomings presently inherent in these systems are analyzed.

Author

N91-29298*# National Aeronautics and Space Administration. Lewis Research Center, Cleveland, OH.

ADVANCED MATERIALS FOR SPACE NUCLEAR POWER SYSTEMS Final Report

ROBERT H. TITRAN, TONI L. GROBSTEIN, and DAVID L. ELLIS (Case Western Reserve Univ., Cleveland, OH.) 1991 21 p Presented at the Conference on Advanced Space Exploration Initiative Technologies, Cleveland, OH, 4-6 Sep. 1991; sponsored by AIAA, NASA, and OAI

(Contract DE-AL03-86SF-16310)

(NASA-TM-105171; DOE/NASA/16310-16; E-6464; NAS 1.15:105171; AIAA PAPER 91-3530) Avail: NTIS HC/MF A03 CSCL 11/6

The overall philosophy of the research was to develop and characterize new high temperature power conversion and radiator materials and to provide spacecraft designers with material selection options and design information. Research on three candidate materials (carbide strengthened niobium alloy PWC-11 for fuel cladding, graphite fiber reinforced copper matrix composites for heat rejection fins, and tungsten fiber reinforced niobium matrix composites for fuel containment and structural supports considered for space power system applications is discussed. Each of these types of materials offers unique advantages for space power applications.

Author

N91-30318*# National Aeronautics and Space Administration. Lewis Research Center, Cleveland, OH.

EQUIVALENT CRYSTAL THEORY OF ALLOYS

GUILLERMO BOZZOLO (Analex Corp., Fairview Park, OH.) and JOHN FERRANTE Sep. 1991 26 p

(Contract RTOP 505-90-51)

(NASA-TP-3155; E-5996; NAS 1.60:3155) Avail: NTIS HC/MF A03 CSCL 11/6

Equivalent Crystal Theory (ECT) is a new, semi-empirical approach to calculating the energetics of a solid with defects. The theory has successfully reproduced surface energies in metals and semiconductors. The theory of binary alloys to date, both with first-principles and semi-empirical models, has not been very successful in predicting the energetics of alloys. This procedure is used to predict the heats of formation, cohesive energy, and lattice parameter of binary alloys of Cu, Ni, Al, Ag, Au, Pd, and Pt as functions of composition. The procedure accurately reproduces the heats of formation versus composition curves for a variety of binary alloys. The results are then compared with other approaches such as the embedded atom and lattice parameters of alloys from pure metal properties more accurately than Vegard's law is presented.

Author

N91-32204*# National Aeronautics and Space Administration. Lewis Research Center, Cleveland, OH.

A NEW APPROXIMATE SUM RULE FOR BULK ALLOY PROPERTIES

GUILLERMO BOZZOLO (Analex Corp., Brook Park, OH.) and JOHN FERRANTE Oct. 1991 10 p

(Contract RTOP 505-90-51)

(NASA-TM-105282; E-6606; NAS 1.15:105282) Avail: NTIS HC/MF A02 CSCL 11/6

A new, approximate sum rule is introduced for determining bulk properties of multicomponent systems, in terms of the pure components properties. This expression is applied for the study of lattice parameters, cohesive energies, and bulk moduli of binary alloys. The correct experimental trends (i.e., departure from average values) are predicted in all cases.

Author

N91-32215*# National Aeronautics and Space Administration. Lewis Research Center, Cleveland, OH.

THEORETICAL MODELLING OF AFM FOR BIMETALLIC TIP-SUBSTRATE INTERACTIONS

GUILLERMO BOZZOLO (Analex Corp., Brook Park, OH.) and JOHN FERRANTE Oct. 1991 17 p

(Contract RTOP 505-90-52)

(NASA-TM-105280; E-6585; NAS 1.15:105280) Avail: NTIS HC/MF A03 CSCL 11/6

Recently, a new technique for calculating the defect energetics of alloys based on Equivalent Crystal Theory was developed. This new technique successfully predicts the bulk properties for binary alloys as well as segregation energies in the dilute limit. The authors apply this limit for the calculation of energy and force as a function of separation of an atomic force microscope (AFM) tip and substrate. The study was done for different combinations of tip and sample materials. The validity of the universality discovered for the same metal interfaces is examined for the case of different metal interactions.

Author

N91-32216*# National Aeronautics and Space Administration. Lewis Research Center, Cleveland, OH.

LUBRICATION WITH SPUTTERED MOS₂ FILMS: PRINCIPLES, OPERATION, LIMITATIONS

T. SPALVINS 1991 15 p Proposed for presentation at the Advanced Surface Engineering and Technology Conference, Cincinnati, OH, 21-24 Oct. 1991; sponsored by the Surface Engineering Division of ASM International

(Contract RTOP 506-43-11)

(NASA-TM-105292; E-6573; NAS 1.15:105292) Avail: NTIS HC/MF A03 CSCL 11/6

The present practices, limitations, and understanding of thin sputtered MoS₂ films are reviewed. Sputtered MoS₂ films can exhibit remarkable tribological properties such as ultralow friction

coefficients (0.01) and enhanced wear lives (millions of cycles) when used in vacuum or dry air. To achieve these favorable tribological characteristics, the sputtering conditions during deposition must be optimized for adequate film adherence and appropriate structure (morphology) and composition. Author

27

NONMETALLIC MATERIALS

Includes physical, chemical, and mechanical properties of plastics, elastomers, lubricants, polymers, textiles, adhesives, and ceramic materials.

A91-13435* Cedarville Coll., OH.

DETERMINATION OF THE THERMAL STABILITY OF FLUIDS BY TENSIMETRY - INSTRUMENTATION AND PROCEDURE

LARRY S. HELMICK (Cedarville College, OH) and WILLIAM R. JONES, JR. (NASA, Lewis Research Center, Cleveland, OH) (STLE and ASME, Tribology Conference, 35th, Fort Lauderdale, FL, Oct. 16-19, 1989) STLE Tribology Transactions (ISSN 0569-8197), vol. 33, Oct. 1990, p. 519-527; Discussion, p. 527; Authors' Closure, p. 527, 528. Previously announced in STAR as N89-26095. refs

Copyright

A computerized tensimeter and experimental procedure for determination of the thermal decomposition temperature ($T_{sub d}$) of perfluoro alkylethers were developed and tested. Both the apparatus and the procedure are described in detail. Results of testing with bis(2-ethylhexyl) phthalate and trimethylolpropane triheptanoate demonstrate that the reciprocal of the decomposition temperature is a linear function of the logarithm of the gas volume/heated liquid volume ratio. The $T_{sub d}$ obtained for each compound at a gas volume/heated liquid volume ratio of one was similar to the value previously reported using an isoteniscope technique. Results of testing with a polymer of hexafluoropropylene oxide demonstrate that this instrument and procedure can be used to determine the $T_{sub d}$ of perfluoro alkylethers. Author

A91-14409* National Aeronautics and Space Administration. Lewis Research Center, Cleveland, OH.

A REVIEW OF PROPERTIES AND POTENTIAL AEROSPACE APPLICATIONS OF ELECTRICALLY CONDUCTING POLYMERS

MARY ANN B. MEADOR, JAMES R. GAIER, BRIAN S. GOOD, G. RICHARD SHARP, and MICHAEL A. MEADOR (NASA, Lewis Research Center, Cleveland, OH) SAMPE Quarterly (ISSN 0036-0821), vol. 22, Oct. 1990, p. 23-31. refs

Copyright

An overview of current research in conducting polymers is presented. Emphasis is placed on development of materials useful for aeronautic and space applications. Research on organic conducting polymers began in the early 1970s with the discovery of polyacetylene. Since then, many polymers which share structural characteristics with polyacetylene have been prepared which conduct electricity, especially when they are doped with suitable agents. Problems with environmental instability, difficult processing, poor mechanical properties and high cost have slowed the development of conducting polymers. However, practical use of these materials is imminent, based on recent refinements in understanding how polymers conduct, more systematic approaches to the development of new materials, and significant improvements in both the processing and properties. Author

A91-16138* National Aeronautics and Space Administration. Lewis Research Center, Cleveland, OH.

X-RAY PHOTOELECTRON AND MASS SPECTROSCOPIC STUDY OF ELECTRON IRRADIATION AND THERMAL STABILITY OF POLYTETRAFLUOROETHYLENE

DONALD R. WHEELER and STEPHEN V. PEPPER (NASA, Lewis

Research Center, Cleveland, OH) Journal of Vacuum Science and Technology A (ISSN 0734-2101), vol. 8, Nov.-Dec. 1990, p. 4046-4056. refs

Copyright

Polytetrafluoroethylene (PTFE) was subjected to 3 keV electron bombardment and then heated in vacuum to 300 C. The behavior of the material as a function of radiation dose and temperature was studied by X-ray photoelectron spectroscopy (XPS) of the surface and mass spectroscopy of the species evolved. A quantitative comparison of the radiation dose rate with that in other reported studies showed that, for a given total dose, the damage observed by XPS is greater for higher dose rates. Lightly damaged material heated to 300 C evolved saturated fluorocarbon species, whereas unsaturated fluorocarbon species evolved from heavily damaged material. After heating the heavily damaged material, those features in the XPS that were associated with damage diminished, giving the appearance that the radiation damage annealed. The apparent annealing of the radiation damage was found to be due to the covering of the network by saturated fragments that easily diffused through the decomposed material to the surface region upon heating. Author

A91-18675* Case Western Reserve Univ., Cleveland, OH. **THE STRUCTURE OF CARBON IN CHEMICALLY VAPOR DEPOSITED SIC MONOFILAMENTS**

X. J. NING, P. PIROUZ, K. P. D. LAGERLOF (Case Western Reserve University, Cleveland, OH), and J. DICARLO (NASA, Lewis Research Center, Cleveland, OH) Journal of Materials Research (ISSN 0884-2914), vol. 5, Dec. 1990, p. 2865-2876. refs (Contract NCC3-73)

Copyright

Electron diffraction and high resolution TEM have been used to study the microstructures of C-rich regions in CVD SCS-6 SiC fibers. The reciprocal lattice of such structures, and their diffraction patterns, have been ascertained on the basis of geometrical considerations. While the C microstructures in the substrate filament and the outer coating layers of the fabric are consistent with different distributions of Oberlin's (1989) 'basic structural units', the microstructure of the inner substrate coating is consistent with turbostratic C. O.C.

A91-19599* National Aeronautics and Space Administration. Lewis Research Center, Cleveland, OH.

INFLUENCE OF SEVERAL METAL IONS ON THE GELATION ACTIVATION ENERGY OF SILICON TETRAETHOXIDE

NAROTTAM P. BANSAL (NASA, Lewis Research Center, Cleveland, OH) American Ceramic Society, Journal (ISSN 0002-7820), vol. 73, Sept. 1990, p. 2647-2652. Previously announced in STAR as N89-21894. refs

Copyright

The effects of nine metal cations $Li(+)$, $Na(+)$, $Mg(2+)$, $Ca(2+)$, $Sr(2+)$, $Cu(2+)$, $Al(3+)$, $La(3+)$, and $Y(3+)$ on silica gel formation has been investigated by studying the hydrolysis and polycondensation of silicon tetraethoxide (TEOS) in the presence of metal nitrates. The influence of water:TEOS mole ratio, metal ion concentration, and the reaction temperature has been investigated. The overall activation energy for gel formation has been determined from the temperature dependence of the time of gelation for each system. The activation energy for -Si-O-Si-network formation is found to be 54.5 kJ/mol. The gel formation time as well as the activation energy sharply increase in the presence of $Cu(2+)$, $Al(3+)$, $La(3+)$ and $Y(3+)$. In contrast, the presence of $Li(+)$, $Na(+)$, $Mg(2+)$, $Ca(2+)$, or $Sr(2+)$ lowers the gelation time, but has no appreciable effect on the activation energy. This difference may be attributed to the participation or nonparticipation of the metal ions in the formation of the three-dimensional polymeric network during the polycondensation step. The concentration of metal ion $Mg(2+)$, $Ca(2+)$, $Y(3+)$ or the water:TEOS mole ratio had no appreciable effect on the gelation activation energy. A simple test has been proposed to determine whether a metal ion would act as a network intermediate or modifier in silica and other glassy networks. Author

27 NONMETALLIC MATERIALS

A91-19780* National Aeronautics and Space Administration. Lewis Research Center, Cleveland, OH.

EFFECT OF HIGH TEMPERATURE HYDROGEN EXPOSURE ON THE STRENGTH AND MICROSTRUCTURE OF MULLITE

THOMAS P. HERBELL, DAVID HULL (NASA, Lewis Research Center, Cleveland, OH), and GARRY M. HALLUM (Ohio State University, Columbus) IN: Hydrogen effects on material behavior. Warrendale, PA, Minerals, Metals and Materials Society, 1990, p. 351-359. refs

Copyright

The corrosion of near stoichiometric mullite ($3\text{Al}_2\text{O}_3\cdot 2\text{SiO}_2$) by pure dry hydrogen gas was studied at 1050 and 1250 C for times up to 500 hr. The hydrogen preferentially attacked the grain boundaries of the mullite where an aluminosilicate glass was present. Corrosion of the mullite grains was observed after 125 hr at 1250 C. The hydrogen reaction removed SiO_2 from the glassy grain boundaries and the mullite grains resulting in a porous alumina rich surface. At 1250 C the strength increased after short exposure times (at least up to 125 hr) and decreased by 53 percent after 500 hr. At 1050 C, all exposure times (25 to 500 hr) decreased the strength. At 500 hr room temperature strength of mullite exposed to 1050 C was reduced by 22 percent. The strength reduction after short exposure times at 1050 C is attributed to crystallization of the grain boundary glass phase. Author

A91-26506* National Aeronautics and Space Administration. Lewis Research Center, Cleveland, OH.

THERMOCHEMICAL ANALYSIS OF THE SILICON CARBIDE-ALUMINA REACTION WITH REFERENCE TO LIQUID-PHASE SINTERING OF SILICON CARBIDE

AJAY K. MISRA (NASA, Lewis Research Center; Sverdrup Technology, Inc., Cleveland, OH) American Ceramic Society, Journal (ISSN 0002-7820), vol. 74, Feb. 1991, p. 345-351. refs

Copyright

The stabilities of different phases in the Si-Al-C-O system are calculated from thermodynamic considerations with the objective of identifying the liquid phases formed during sintering of SiC in the presence of Al_2O_3 . It is shown that a liquid phase can form at the sintering temperatures by the reaction of SiC with Al_2O_3 . Depending on the carbon activity, the liquid can be either of the following: $\text{Al}_2\text{O}_3 + \text{Al}_4\text{C}_3$, $\text{SiC} + \text{Al}_4\text{C}_3$, or molten aluminum. The stability of the aluminosilicate melts that can form by the reaction of Al_2O_3 with the surface silica layer on SiC powders is also evaluated. Several factors that influence liquid-phase sintering, such as the solubility of SiC in the melts and the generation of gases during sintering, are discussed. The results of the thermodynamic analysis are compared with the observed sintering behavior for SiC. Author

A91-28763* National Aeronautics and Space Administration. Lewis Research Center, Cleveland, OH.

TEMPERATURE DEPENDENCE OF HARDNESS IN YTTRIA-STABILIZED ZIRCONIA SINGLE CRYSTALS

GREGORY N. MORSCHER (NASA, Lewis Research Center; Case Western Reserve University, Cleveland, OH), PIROUZ PIROUZ, and ARTHUR H. HEUER (Case Western Reserve University, Cleveland, OH) American Ceramic Society, Journal (ISSN 0002-7820), vol. 74, March 1991, p. 491-500. refs

(Contract NSF DMR-87-15622)

Copyright

The temperature dependence of hardness and microcracking in single-crystal 9.5-mol pct- Y_2O_3 -fully-stabilized cubic- ZrO_2 was studied as a function of orientation. Crack lengths increased with increased temperature up to 500 C; above 800 C, no cracks were found, indicating an indentation brittle-to-ductile transition of about 800 C. The temperature dependence of hardness was reduced around 500 C. Etching studies to delineate the plastic zone around and below indents identified the operative slip systems. The role of dislocations and their interactions within the plastic zone on the hardness and indentation fracture behavior of cubic- ZrO_2 are discussed. Author

A91-28767* National Aeronautics and Space Administration. Lewis Research Center, Cleveland, OH.

TEMPERATURE-DEPENDENT INDENTATION BEHAVIOR OF TRANSFORMATION-TOUGHENED ZIRCONIA-BASED CERAMICS

VEENA TIKARE (NASA, Lewis Research Center; Case Western Reserve University, Cleveland, OH) and ARTHUR H. HEUER (Case Western Reserve University, Cleveland, OH) American Ceramic Society, Journal (ISSN 0002-7820), vol. 74, March 1991, p. 593-597. refs

(Contract NSF DMR-87-15622)

Copyright

Indentation behavior of Ce-TZP, Y-TZP, and Mg-PSZ between room temperature and 1300 C was investigated. Hardness decreased with increasing temperature for all three materials, but indentation cracking increased with increasing temperature. The opposing temperature dependences are discussed in terms of dislocation and transformation plasticity. Author

A91-28772* National Aeronautics and Space Administration. Lewis Research Center, Cleveland, OH.

WETTABILITY OF PYROLYTIC BORON NITRIDE BY ALUMINUM

FRANCIS P. CHIARAMONTE and BRUCE N. ROSENTHAL (NASA, Lewis Research Center, Cleveland, OH) American Ceramic Society, Communications (ISSN 0002-7820), vol. 74, March 1991, p. 658-661. refs

Copyright

The wetting of pyrolytic boron nitride by molten 99.9999 percent pure aluminum was investigated by using the sessile drop method in a vacuum operating at approximately 660 micro-Pa at temperatures ranging from 700 to 1000 C. The equilibrium contact angle decreased with an increase in temperature. For temperatures at 900 C or less, the equilibrium contact angle was greater than 90 deg. At 1000 C a nonwetting-to-wetting transition occurred and the contact angle stabilized at 49 deg. Author

A91-28783* National Aeronautics and Space Administration. Lewis Research Center, Cleveland, OH.

HYDROGEN-SILICON CARBIDE INTERACTIONS

ANDREW J. ECKEL, AJAY K. MISRA, DONALD L. HUMPHREY (NASA, Lewis Research Center; Sverdrup Technology, Inc., Middleburg Heights, OH), and NATHAN S. JACOBSON (NASA, Lewis Research Center, Cleveland, OH) IN: Hydrogen effects on material behavior; Proceedings of the 4th International Conference on the Effect of Hydrogen on the Behavior of Materials, Moran, WY, Sept. 12-15, 1989. Warrendale, PA, Minerals, Metals, and Materials Society, 1990, p. 341-350. Previously announced in STAR as N90-11144. refs

Copyright

A study of the thermochemistry and kinetics of hydrogen environmental attack of silicon carbide was conducted for temperatures in the range from 1100 C to 1400 C. Thermodynamics maps based on the parameters of pressure and oxygen/moisture content were constructed. With increasing moisture levels, four distinct regions of attack were identified. Each region is defined by the thermodynamically stable solid phases. The theoretically stable solid phases of region 1 are silicon carbide and silicon. Experimental evidence is provided to support this thermodynamic prediction. Silicon carbide is the single stable solid phase in region 2. Active attack of the silicon carbide in this region occurs by the formation of gases of SiO , CO , CH_4 , SiH_4 and SiH . Analyses of the kinetics of reaction for region 2 at 1300 C show the attack of the silicon carbide to be controlled by gas phase diffusion of H_2O to the sample. Silicon carbide and silica are the stable phases common to regions 3 and 4. These two regions are characterized by the passive oxidation of silicon carbide and formation of a protective silica layer. Author

A91-30283* National Aeronautics and Space Administration. Lewis Research Center, Cleveland, OH.

SILSESQUOXANE-DERIVED CERAMIC FIBRES

F. I. HURWITZ, S. C. FARMER, F. M. TEREPA (NASA, Lewis

Research Center, Cleveland, OH), and T. A. LEONHARDT (Sverdrup Technology, Inc., Cleveland, OH) *Journal of Materials Science* (ISSN 0022-2461), vol. 26, March 1, 1991, p. 1247-1252. refs

Copyright

Fibers formed from blends of silsesquioxane polymers were characterized to study the pyrolytic conversion of these precursors to ceramics. The morphology of fibers pyrolyzed to 1400 C revealed primarily amorphous glasses whose conversion to beta-SiC is a function of both blend composition and pyrolysis conditions. Formation of beta-SiC crystallites within the glassy phase is favored by higher than stoichiometric C/Si ratios, while carbothermal reduction of Si-O bonds to form SiC with loss of SiO and CO occurs at higher methyl/phenylpropyl silsesquioxane (lower C/Si) ratios. As the carbothermal reduction is assumed to be diffusion controlled, the fibers can serve as model systems to gain understanding of the silsesquioxane pyrolysis behavior, and therefore are useful in the development of polysilsesquioxane-derived ceramic matrices and coatings as well. Author

A91-35949* National Aeronautics and Space Administration. Lewis Research Center, Cleveland, OH.

RESISTIVITY OF PRISTINE AND INTERCALATED GRAPHITE FIBER EPOXY COMPOSITES

JAMES R. GAIER (NASA, Lewis Research Center, Cleveland, OH), PAUL D. HAMBOURGER, and MELISSA E. SLABE (Cleveland State University, OH) *Carbon* (ISSN 0008-6223), vol. 29, no. 3, 1991, p. 313-320. Previously announced in STAR as N90-21192. refs

(Contract NCC3-19)

Copyright

Laminar composites were fabricated from pristine and bromine intercalated Amoco P-55, P-75, and P-100 graphite fibers and Hysol-Grafil EAG101-1 film epoxy. The thickness and r.f. eddy current resistivity of several samples were measured at grid points and averaged point by point to obtain final values. Although the values obtained this way have high precision (less than 3 percent deviation), the resistivity values appear to be 20 to 90 percent higher than resistivities measured on high aspect ratio samples using multi-point techniques, and by those predicted by theory. The temperature dependence of the resistivity indicates that the fibers are neither damaged nor deintercalated by the composite fabrication process. The resistivity of the composites is a function of sample thickness (i.e., resin content). Composite resistivity is dominated by fiber resistivity, so lowering the resistivity of the fibers, either through increased graphitization or intercalation, results in a lower composite resistivity. A modification of the simple rule of mixtures model appears to predict the conductivity of high aspect ratio samples measured along a fiber direction, but a directional dependence appears which is not predicted by the theory. The resistivity of these materials is clearly more complex than that of homogeneous materials. Author

A91-35952* National Aeronautics and Space Administration. Lewis Research Center, Cleveland, OH.

FUNDAMENTAL CONSIDERATIONS IN ADHESION, FRICTION AND WEAR FOR CERAMIC-METAL CONTACTS

KAZUHISA MIYOSHI (NASA, Lewis Research Center, Cleveland, OH) *Wear* (ISSN 0043-1648), vol. 141, 1990, p. 35-44. refs

Copyright

Fundamental studies of friction, wear and adhesion of ceramics in contact with metals are evaluated. It is shown that friction and adhesion are strongly dependent on the ductility of the metals. The surface energy, friction, adhesion and hardness of a metal are related to its Young's modulus and shear modulus, which have a marked dependence on the electron configuration of the metal. Generally, the greater the shear modulus, the less metal transfer there is to the ceramic. R.E.P.

A91-39242* National Aeronautics and Space Administration. Lewis Research Center, Cleveland, OH.

THERMAL STABILITY OF ELECTRON-IRRADIATED POLY(TETRAFLUOROETHYLENE) - X-RAY PHOTOELECTRON AND MASS SPECTROSCOPIC STUDY

DONALD R. WHEELER and STEPHEN V. PEPPER (NASA, Lewis Research Center, Cleveland, OH) IN: *Metallization of polymers; Proceedings of the Symposium, Montreal, Canada, Sept. 24-28, 1989. Washington, DC, American Chemical Society, 1990, p. 223-234. refs*

Polytetrafluoroethylene (PTFE) was subjected to 3 keV electron bombardment and then heated in vacuum to 300 C. The behavior of the material as a function of radiation dose and temperature was studied by X-ray photoelectron spectroscopy (XPS) of the surface and mass spectroscopy of the species evolved. Lightly damaged material heated to 300 C evolved saturated fluorocarbon species, whereas unsaturated fluorocarbon species were evolved from heavily damaged material. After heating the heavily damaged material, those features in the XPS spectrum that were associated with damage diminished, giving the appearance that the radiation damage had annealed. The observations were interpreted by incorporating mass transport of severed chain fragments and thermal decomposition of severely damaged material into the branched and cross-linked network model of irradiated PTFE. The apparent annealing of the radiation damage was due to covering of the network by saturated fragments that easily diffused through the decomposed material to the surface region upon heating. Author

A91-41516* National Aeronautics and Space Administration. Lewis Research Center, Cleveland, OH.

UNDERCUTTING OF DEFECTS IN THIN FILM PROTECTIVE COATINGS ON POLYMER SURFACES EXPOSED TO ATOMIC OXYGEN

SHARON K. RUTLEDGE (NASA, Lewis Research Center, Cleveland, OH) and JUDITH A. MIHELIC (Cleveland State University, OH) IN: *Metallurgical coatings 1989; Proceedings of the 16th International Conference, San Diego, CA, Apr. 17-21, 1989. Vol. 1. London and New York, Elsevier Applied Science, 1989, p. 607-615. refs*

Copyright

Protection for polymeric surfaces is needed to make them durable in the low earth orbital environment. Thin film coatings of oxides such as SiO₂ are viable candidates to provide this protection, but concern has been voiced over the ability of these coatings to protect when defects are present in the coating due to surface anomalies. When a defected coating protecting a polymer substrate is exposed to atomic oxygen, the defect provides a pathway to the underlying polymer allowing oxidation and subsequent undercutting to occur. Defect undercutting was studied for sputter deposited coatings of SiO₂ on polyimide Kapton. Preliminary results indicate that undercutting may be limited as long as the coating remains intact with the substrate. Therefore, coatings may not need to be defect free to give protection to the underlying surface. Author

A91-49112* National Aeronautics and Space Administration. Lewis Research Center, Cleveland, OH.

AUTOCLAVABLE ADDITION POLYIMIDES FOR 371 C COMPOSITE APPLICATIONS

R. D. VANNUCCI, D. MALARIK, D. PAPADOPOULOS, and J. WATERS (NASA, Lewis Research Center, Cleveland, OH) IN: *International SAMPE Technical Conference, 22nd, Boston, MA, Nov. 6-8, 1990, Proceedings. Covina, CA, Society for the Advancement of Material and Process Engineering, 1990, p. 175-185. Previously announced in STAR as N90-27874. refs*

Copyright

Studies were conducted to improve the thermo-oxidative stability (TOS) of PMR type polyimides by the substitution of para-aminostyrene (PAS) for the nadic ester endcap in second generation PMR polyimides (PMR-2). The nadic endcap which provides the PMR polyimides with their relative ease of fabrication, both by limiting the molecular weight of the prepolymer and by

27 NONMETALLIC MATERIALS

undergoing the final addition cure without volatiles, is also the weak link with regard to TOS. A polyimide formulated with PAS endcaps, called V-CAP, utilizes a two step reaction sequence similar to that of the PMR polyimides and can be easily autoclave molded into low void composite materials. Resin studies included two formulations of both PMR-2 and V-CAP, corresponding to $n = 9$ and $n = 14$ prepolymer stoichiometry. Unidirectional reinforced T40R graphite fiber laminates were fabricated from each of the resins was post-cured in either air at 385 C or nitrogen at 400 C. Composite specimens were aged in air at 371 C and mechanical properties were measured at 371 C before and after exposure.

Author

A91-49801* Universal Energy Systems, Inc., Dayton, OH.
MATERIALS DEGRADATION IN LOW EARTH ORBIT (LEO); PROCEEDINGS OF THE SYMPOSIUM, 119TH ANNUAL MEETING OF THE MINERALS, METALS, AND MATERIALS SOCIETY, ANAHEIM, CA, FEB. 17-22, 1990

V. SRINIVASAN, ED. (Universal Energy Systems, Inc., Dayton, OH) and BRUCE A. BANKS, ED. (NASA, Lewis Research Center, Cleveland, OH) Symposium sponsored by Minerals, Metals, and Materials Society and ASM International. Warrendale, PA, Minerals, Metals, and Materials Society, 1990, 229 p. For individual items see A91-49802 to A91-49816.

Copyright

The current understanding of the effect of space environment on materials and the development of protective coatings is examined in reviews and reports. Consideration is given to hyperthermal atomic oxygen reactions, the effect of atomic oxygen on altered and coated Kapton surfaces for spacecraft applications in LEO, silicon dioxide space coatings studied ellipsometrically, atomic oxygen effects on spacecraft materials, atomic oxygen beam source for erosion simulation, and atomic oxygen effects on refractory materials. Particular attention is given to ellipsometric analysis of materials degradation in space, studies of the interaction of 8 km/s oxygen atoms with selected materials, characterization and calibration of the EOIM-III flight mass spectrometer in a high velocity oxygen atom beam, the reaction efficiency of thermal energy oxygen atoms with polymeric materials, and effects of simulated space environments on the properties of selected materials.

O.G.

A91-49803* National Aeronautics and Space Administration. Lewis Research Center, Cleveland, OH.

ATOMIC OXYGEN UNDERCUTTING OF DEFECTS ON SiO₂ PROTECTED POLYIMIDE SOLAR ARRAY BLANKETS

BRUCE A. BANKS, SHARON K. RUTLEDGE, BRUCE M. AUER (NASA, Lewis Research Center, Cleveland, OH), and FRANK DIFILIPPO (Case Western Reserve University, Cleveland, OH) IN: Materials degradation in low earth orbit (LEO); Proceedings of the Symposium, 119th Annual Meeting of the Minerals, Metals, and Materials Society, Anaheim, CA, Feb. 17-22, 1990. Warrendale, PA, Minerals, Metals, and Materials Society, 1990, p. 15-33. refs

Copyright

Low Earth Orbital (LEO) atomic oxygen can oxidize SiO₂-protected polyimide kapton solar array blanket material which is not totally protected as a result of pinholes or scratches in the SiO₂ coatings. The probability of atomic oxygen reaction upon initial impact is low, thus inviting oxidation by secondary impacts. The secondary impacts can produce atomic oxygen undercutting which may lead to coating mechanical failure and ever increasing mass loss rates of kapton. Comparison of undercutting effects in isotropic plasma asher and directed beam tests are reported. These experimental results are compared with computational undercutting profiles based on Monte Carlo methods and their implication on LEO performance of protected polymers.

Author

A91-49804* National Aeronautics and Space Administration. Lewis Research Center, Cleveland, OH.

THE EFFECT OF ATOMIC OXYGEN ON ALTERED AND COATED KAPTON SURFACES FOR SPACECRAFT APPLICATIONS IN LOW EARTH ORBIT

SHARON K. RUTLEDGE (NASA, Lewis Research Center,

Cleveland, OH) and JUDITH A. MIHELICIC (Cleveland State University, OH) IN: Materials degradation in low earth orbit (LEO); Proceedings of the Symposium, 119th Annual Meeting of the Minerals, Metals, and Materials Society, Anaheim, CA, Feb. 17-22, 1990. Warrendale, PA, Minerals, Metals, and Materials Society, 1990, p. 35-48. refs

Copyright

A commercially applied silicon oxide coating on Kapton and an alternative material with Si groups on the surface were evaluated for durability with respect to atomic oxygen in both a random plasma and a directed atomic oxygen beam system. It is found that the alternative to Kapton, DuPont 93-1, is not adequately protecting to last 15 years in LEO, the desired operation time of the Space Station Freedom. The coated Kapton is considered to be promising due to the adherence of the coating and lack of extensive tearing at undercut defect sites. Fewer defects in the coating and elimination of long scratches and uncoated areas would substantially improve the durability of this material. O.G.

A91-49812* National Aeronautics and Space Administration. Lewis Research Center, Cleveland, OH.

VACUUM ULTRAVIOLET RADIATION AND THERMAL CYCLING EFFECTS ON ATOMIC OXYGEN PROTECTIVE PHOTOVOLTAIC ARRAY BLANKET MATERIALS

J. BRADY and B. BANKS (NASA, Lewis Research Center, Cleveland, OH) IN: Materials degradation in low earth orbit (LEO); Proceedings of the Symposium, 119th Annual Meeting of the Minerals, Metals, and Materials Society, Anaheim, CA, Feb. 17-22, 1990. Warrendale, PA, Minerals, Metals, and Materials Society, 1990, p. 133-143. refs

Copyright

The importance of synergistic environmental exposure is demonstrated through the evaluation of DuPont 93-1 in simulated LEO environment. Changes in optical properties, surface condition, and mass loss data are described. The qualitative results indicate the necessity for exposure of materials to a series of simulated LEO environments in order to properly determine synergistic effects and demonstrate the overall LEO durability of candidate materials. It is shown that synergistic effects may occur with vacuum thermal cycling combined with VUV radiation followed by atomic oxygen exposure. Testing the durability of candidate solar array blanket materials in a test sequence with necessary synergistic effects makes it possible to determine the appropriate material for providing structural support and maintaining the proper operating temperature for solar cells in the SSF Photovoltaic Power System. O.G.

A91-53705*# National Aeronautics and Space Administration. Lewis Research Center, Cleveland, OH.

THERMAL EMITTANCE ENHANCEMENT OF GRAPHITE-COPPER COMPOSITES FOR HIGH TEMPERATURE SPACE BASED RADIATORS

SHARON K. RUTLEDGE (NASA, Lewis Research Center, Cleveland, OH), MARK J. FORKAPA, and JILL M. COOPER (Cleveland State University, OH) AIAA, NASA, and OAI, Conference on Advanced SEI Technologies, Cleveland, OH, Sept. 4-6, 1991. 8 p. Previously announced in STAR as N91-29332. refs

(AIAA PAPER 91-3527) Copyright

Graphite-copper composites are candidate materials for space based radiators. The thermal emittance of this material, however, is a factor of two lower than the desired emittance for these systems of greater than or equal to 0.85. Arc texturing was investigated as a surface modification technique for enhancing the emittance of the composite. Since the outer surface of the composite is copper, and samples of the composite could not be readily obtained for testing, copper was used for optimization testing. Samples were exposed to various frequencies and currents of arcs during texturing. Emittances near the desired goal were achieved at frequencies less than 500 Hz. Arc current did not appear to play a major role under 15 amps. Particulate carbon was observed on the surface, and was easily removed by vibration and handling. In order to determine morphology adherence, ultrasonic cleaning was used to remove the loosely adherent

material. This reduced the emittance significantly. Emittance was found to increase with increasing frequency for the cleaned samples up to 500 Hz. The highest emittance achieved on these samples over the temperature range of interest was 0.5 to 0.6, which is approximately a factor of 25 increase over the untextured copper emittance. Author

A91-55698* National Aeronautics and Space Administration. Lewis Research Center, Cleveland, OH.

HOT CORROSION OF SILICON CARBIDE AND SILICON NITRIDE AT 1000 C

DENNIS S. FOX, NATHAN S. JACOBSON, and JAMES L. SMIALEK (NASA, Lewis Research Center, Cleveland, OH) IN: Corrosion and corrosive degradation of ceramics; Proceedings of the International Symposium, Anaheim, CA, Nov. 1, 2, 1989. Westerville, OH, American Ceramic Society, Inc., 1990, p. 227-249. refs

Copyright

The sodium sulfate hot corrosion of silicon-based ceramics at 1000 C has been extensively studied. Deposition of the sodium sulfate corrodant from combustion products is discussed in relation to sodium air impurity and sulfur fuel impurity content. Corrosion occurs by the combined processes of oxidation to form protective silica scales and dissolution of these scales to form nonprotective sodium silicates. The chemical corrosion mechanisms are presented in terms of acidic/basic dissolution of oxides in molten salts. The reactions are strongly influenced by the presence of free carbon in the ceramic. Strength reductions have been measured and are attributed to pitting in SiC and grain boundary attack in Si₃N₄. Initial results of burner corrosion of two ceramic matrix composites are consistent with the models developed for monolithic ceramics. Author

A91-56905* National Aeronautics and Space Administration. Lewis Research Center, Cleveland, OH.

FIBER CREEP EVALUATION BY STRESS RELAXATION MEASUREMENTS

GREGORY N. MORSCHER, JAMES A. DICARLO, and TIMOTHY WAGNER (NASA, Lewis Research Center, Cleveland, OH) Ceramic Engineering and Science Proceedings (ISSN 0196-6219), vol. 12, July-Aug. 1991, p. 1032-1038. refs

Copyright

A simple bend stress relaxation (BSR) test has been used to measure the creep related properties of a chemically vapor-deposited SiC fiber. Time, temperature, and strain dependent BSR data were analyzed to ascertain the ability of the stress relaxation results to predict tensile creep as a function of the same parameters. The predictions compared very well to actual creep data obtained by axial measurements, indicating that the BSR test could be used for determining both creep and stress relaxation of polycrystalline ceramic fibers under tensile loading. Author

A91-56917* National Aeronautics and Space Administration. Lewis Research Center, Cleveland, OH.

CRYSTALLIZATION AND PROPERTIES OF SR-BA ALUMINOSILICATE GLASS-CERAMIC MATRICES

NAROTTAM P. BANSAL, MARK J. HYATT (NASA, Lewis Research Center, Cleveland, OH), and CHARLES H. DRUMMOND, III (Ohio State University, Columbus) Ceramic Engineering and Science Proceedings (ISSN 0196-6219), vol. 12, July-Aug. 1991, p. 1222-1234. Previously announced in STAR as N91-19308. refs

Copyright

Powders of roller quenched (Sr,Ba)O-Al₂O₃-2SiO₂ glasses of various compositions were uniaxially pressed into bars and hot isostatically pressed at 1350 C for 4 hours or cold isostatically pressed and sintered at different temperatures between 800 to 1500 C for 10 or 20 hours. Densities, flexural strengths, and linear thermal expansion were measured for three compositions. The glass transition and crystallization temperatures were determined by Differential Scanning Calorimetry (DSC). The liquidus and crystallization temperature from the melt were measured using high temperature Differential Thermal Analysis (DTA). Crystalline

phases formed on heat treatment of the glasses were identified by powder X ray diffraction. In Sr containing glasses, the monoclinic celsian phase always crystallized at temperatures above 1000 C. At lower temperatures, the hexagonal analog formed. The temperature for orthorhombic to hexagonal structural transformation increased monotonically with SrO content, from 327 C for BaO-Al₂O₃-2SiO₂ to 758 C for SrO-Al₂O₃-2SiO₂. These glass powders can be sintered to almost full densities and monoclinic celsian phase at a relatively low temperature of 1100 C. Author

A91-56922* National Aeronautics and Space Administration. Lewis Research Center, Cleveland, OH.

POLYMERIC ROUTES TO SILICON CARBIDE AND SILICON OXYCARBIDE CMC

FRANCES I. HURWITZ (NASA, Lewis Research Center, Cleveland, OH), PAULA J. HEIMANN, JOHN Z. GYEKENYESI, JOHN MASNOVI, and XIN Y. BU (Cleveland State University, OH) Ceramic Engineering and Science Proceedings (ISSN 0196-6219), vol. 12, July-Aug. 1991, p. 1292-1303. Previously announced in STAR as N91-26234. refs

Copyright

An overview of two approaches to the formation of ceramic composite matrices from polymeric precursors is presented. Copolymerization of alkyl- and alkenylsilanes (RSiH₃) represents a new precursor system for the production of Beta-SiC on pyrolysis, with copolymer composition controlling polymer structure, char yield, and ceramic stoichiometry and morphology. Polysilsesquioxanes which are synthesized readily and can be handled in air serve as precursors to Si-C-O ceramics. Copolymers of phenyl and methyl silsesquioxanes display rheological properties favorable for composite fabrication; these can be tailored by control of pH, water/methoxy ratio and copolymer composition. Composites obtained from these utilize a carbon coated, eight harness satin weave Nicalon cloth reinforcement. The material exhibits nonlinear stress-strain behavior in tension. Author

A91-56931* National Aeronautics and Space Administration. Lewis Research Center, Cleveland, OH.

INFLUENCE OF THE Si₃N₄ MICROSTRUCTURE ON ITS R-CURVE AND FATIGUE BEHAVIOR

VEENA TIKARE and SUNG R. CHOI (NASA, Lewis Research Center, Cleveland, OH) Ceramic Engineering and Science Proceedings (ISSN 0196-6219), vol. 12, July-Aug. 1991, p. 1437-1447. refs

Copyright

The R-curve and fatigue behavior of a silicon nitride with large, highly elongated grains were compared to those of a silicon nitride with smaller, more equiaxed grains. The former was found to have higher toughness and a slightly rising R-curve which enhanced fatigue resistance, while the latter had constant toughness with crack length. The R-curve was attributed to crack deflection and grain pull-out. The microstructure did not influence the dynamic fatigue properties of the two ceramics, as both had good resistance to dynamic fatigue. The cyclic fatigue resistance of the large-grained Si₃N₄, however, was surprisingly low. Author

A91-56958* National Aeronautics and Space Administration. Lewis Research Center, Cleveland, OH.

MICROSTRUCTURAL AND STRENGTH STABILITY OF CVD SIC FIBERS IN ARGON ENVIRONMENTS

RAMAKRISHNA T. BHATT (NASA, Lewis Research Center; U.S. Army, Propulsion Directorate, Cleveland, OH) and DAVID R. HULL (NASA, Lewis Research Center, Cleveland, OH) Ceramic Engineering and Science Proceedings (ISSN 0196-6219), vol. 12, Sept.-Oct. 1991, p. 1832-1844. Previously announced in STAR as N91-29250. refs

Copyright

The room temperature tensile strength and microstructure of three types of commercially available chemically vapor deposited silicon carbide fibers were measured after 1, 10, and 100 hour heat treatments under argon pressures of 0.1 to 310 MPa at temperatures to 2100 C. Two types of fiber had carbon-rich surface coatings and the other contained no coating. All three fiber types

27 NONMETALLIC MATERIALS

showed strength degradation beyond 1400 C. Time and temperature of exposure had greater influence on strength degradation than argon pressure. Recrystallization and growth of near stoichiometric SiC grains appears to be the dominant mechanism for the strength degradation. Author

A91-56982* Cleveland State Univ., OH.

CRACK HEALING IN SILICON NITRIDE DUE TO OXIDATION

SUNG R. CHOI (Cleveland State University, OH), VEENA TIKARE, and RALPH PAWLIK (NASA, Lewis Research Center, Cleveland, OH) Ceramic Engineering and Science Proceedings (ISSN 0196-6219), vol. 12, Sept.-Oct. 1991, p. 2190-2202. refs Copyright

The crack healing behavior of a commercial, MgO-containing, hot pressed Si₃N₄ was studied as a function of temperature in oxidizing and inert annealing environments. Crack healing occurred at a temperature 800 C or higher due to oxidation regardless of crack size, which ranged from 100 microns (indentation crack) to 1.7 mm (SEPB precrack). The resulting strength and apparent fracture toughness increased at crack healing temperature by 100 percent and 300 percent, respectively. The oxide layer present in the crack plane was found to be highly fatigue resistant, indicating that the oxide is not solely silicate glass, but a mixture of glass, enstatite, and/or cristobalite that was insensitive to fatigue in a room temperature water environment. Author

A91-57058* National Aeronautics and Space Administration. Lewis Research Center, Cleveland, OH.

EVIDENCE FROM TRANSMISSION ELECTRON MICROSCOPY FOR AN OXYNITRIDE LAYER IN OXIDIZED Si₃N₄

LINUS U. J. T. OGBUJI and J. L. SMIALEK (NASA, Lewis Research Center, Cleveland, OH) Electrochemical Society, Journal (ISSN 0013-4651), vol. 138, Oct. 1991, p. L51-L53. refs Copyright

Microstructural and energy dispersive spectrometry evidence is produced, from transmission electron microscopy, to show that a silicon oxynitride inner layer is produced by the oxidation of silicon nitride in dry oxygen at 1350 C as proposed by Tressler et al. (1989). However, details of the microstructures at the oxide/nitride interface do not agree entirely with the rest of the Tressler model for the oxidation of Si₃N₄. Author

A91-57059* National Aeronautics and Space Administration. Lewis Research Center, Cleveland, OH.

OXIDATION INSTABILITY OF SiC AND Si₃N₄ FOLLOWING THERMAL EXCURSIONS

LINUS U. J. T. OGBUJI (NASA, Lewis Research Center, Cleveland, OH) Electrochemical Society, Journal (ISSN 0013-4651), vol. 138, Oct. 1991, p. L53-L56. refs Copyright

The effect of thermal excursion and thermal cycling on the oxidation stability of chemical vapor-deposited (CVD) SiC and Si₃N₄ was studied at 1350 C. Thermal cycling alone produced no noticeable change in oxidation kinetics. However, TEM showed that oxide scales grown in cycles consist of alternating layers of SiO₂ and Si₂N₂O. When the oxidation of CVD SiC or Si₃N₄ at 1350 C was interrupted with a 1.5-h annealing in Ar at 1500 C, the kinetics of reoxidation at 1350 C were found to be drastically increased. The SiC and Si₃N₄ then oxidized essentially at the same rate, which is over 50 times the preannealing rate, and comparable to the expected oxidation rate of these materials at 1500 C. Author

N91-11922*# National Aeronautics and Space Administration. Lewis Research Center, Cleveland, OH.

USES OF AUGER AND X RAY PHOTOELECTRON SPECTROSCOPY IN THE STUDY OF ADHESION AND FRICTION

KAZUHISA MIYOSHI Aug. 1990 13 p Presented at the 1st International Symposium on Industrial Tribology, Chicago, IL, 29-31 Aug. 1990; sponsored in part by NSF (Contract RTOP 506-43-11)

(NASA-TM-103266; E-5631; NAS 1.15:103266) Avail: NTIS HC/MF A03 CSCL 11/3

Three studies are described characterizing the possible contributions of surface science to tribology. These include surface contamination formed by the interaction of a surface with the environment, contaminants obtained with diffusion of compounds, and surface chemical changes resulting from selective thermal evaporation. Surface analytical tools such as Auger electron spectroscopy (AES) and x ray photoelectron spectroscopy (XPS) incorporated directly into adhesion and friction systems are primarily used to define the nature of tribological surfaces before and after tribological experimentation and to characterize the mechanism of solid-to-solid interaction. Emphasis is on fundamental studies involving the role of surfaces in controlling the adhesion and friction properties of materials emerging as a result of the surface analyses. The materials which were studied include metals and ceramics such as elemental metals, amorphous alloys (metallic glasses), and silicon-based ceramics. Author

N91-13566*# National Aeronautics and Space Administration. Lewis Research Center, Cleveland, OH.

VINYL CAPPED ADDITION POLYIMIDES Patent Application

RAYMOND D. VANNUCCI, inventor (to NASA), DIANE C. MALARIK, inventor (to NASA), and PETER DELVIGS, inventor (to NASA) 25 Oct. 1990 14 p (NASA-CASE-LEW-15027-1; NAS 1.71:LEW-15027-1; US-PATENT-APPL-SN-603055) Avail: NTIS HC/MF A03 CSCL 11/7

Polyimide resins having improved thermo-oxidative stability are provided having aromatic vinyl end-caps. The polyimides are prepared by the reaction of a mixture of monomers comprising (1) a diamine, (2) an ester of tetracarboxylic acid and (3) an aromatic vinyl compound in a molar ratio of 1:2:3 of n: (n + 1):2 when the aromatic vinyl compound contains nitrogen and in a ratio of (n + 1):n:2 when the aromatic vinyl compound does not contain nitrogen, wherein n ranges from about 5 to about 20. NASA

N91-14482*# National Aeronautics and Space Administration. Lewis Research Center, Cleveland, OH.

EFFECT OF HYDROGEN ON THE STRENGTH AND MICROSTRUCTURE OF SELECTED CERAMICS

THOMAS P. HERBELL, ANDREW J. ECKEL, DAVID R. HULL, and AJAY K. MISRA (Sverdrup Technology, Inc., Brook Park, OH.) 1990 16 p Presented at the Fall Meeting of the Metallurgical Society, Detroit, MI, 7-11 Oct. 1990 (Contract RTOP 582-01-11) (NASA-TM-103674; E-5702; NAS 1.15:103674) Avail: NTIS HC/MF A03 CSCL 11/3

Ceramics in monolithic form and as composite constituents in the form of fibers, matrices, and coatings are currently being considered for a variety of high-temperature applications in aeronautics and space. Many of these applications involve exposure to a hydrogen-containing environment. The compatibility of selected ceramics in gaseous high-temperature hydrogen is assessed. Environmental stability regimes for the long term use of ceramic materials are defined by the parameters of temperature, pressure, and moisture content. Thermodynamically predicted reactions between hydrogen and several monolithic ceramics are compared with actual performance in a controlled environment. Morphology of hydrogen attack and the corresponding strength degradation is reported for silicon carbide, silicon nitride, alumina, magnesia, and mullite. Author

N91-15402* National Aeronautics and Space Administration. Lewis Research Center, Cleveland, OH.

LADDER POLYMERS FOR USE AS HIGH TEMPERATURE STABLE RESINS OR COATINGS Patent

MARY ANN MEADOR, inventor (to NASA) 7 Aug. 1990 10 p Filed 11 Aug. 1988 (NASA-CASE-LEW-14203-1; US-PATENT-4,946,890; US-PATENT-APPL-SN-231026; US-PATENT-CLASS-524-600;

US-PATENT-CLASS-525-436; US-PATENT-CLASS-528-353;
INT-PATENT-CLASS-C08G-73/10) Avail: US Patent and
Trademark Office CSCL 11/3

An object of the invention is to synthesize a new class of ladder and partial ladder polymers. In accordance with the invention, the new class of ladder and partial ladder polymers are synthesized by polymerizing a bis-dienophile with a bis-diene. Another object of the invention is to provide a fabricated, electrically conducting, void free composite comprising the new class of the ladder and partial ladder polymers described above. The novelty of the invention relates to a new class of ladder and partial ladder polymers and a process for synthesizing these polymers. These polymers are soluble in common organic solvents and are characterized with a unique dehydration property at temperatures of 300 to 400 C to provide thermo-oxidatively stable pentiptycene units along the polymeric backbone. These polymers are further characterized with high softening points and good thermo-oxidative stability properties. Thus these polymers have potential as processable, matrix resins for high temperature composite applications.

Official Gazette of the U.S. Patent and Trademark Office

N91-15412*# National Aeronautics and Space Administration.
Lewis Research Center, Cleveland, OH.

**METALLIC SEAL FOR THERMAL BARRIER COATING
SYSTEMS Patent Application**

ROBERT A. MILLER, inventor (to NASA) 23 Oct. 1990 9 p
(NASA-CASE-LEW-15020-1; NAS 1.71:LEW-15020-1;
US-PATENT-APPL-SN-601957) Avail: NTIS HC/MF A02 CSCL
11/3

The invention is particularly concerned with sealing thermal barrier coating systems of the type in use and being contemplated for use in diesel and other internal combustion engines. The invention also would find application in moderately high temperature regions of gas turbine engines and any other application employing a thermal barrier coating at moderate temperatures. Ni-35Cr-6Al-1Y, Ni-35Cr-6Al-1Yb, or other metallic alloy denoted as MCrAlx is applied over a zirconia-based thermal barrier overlayer. The close-out layer is glass-bead preened to densify its surface. This seals and protects the thermal barrier coating system. NASA

N91-18302*# National Aeronautics and Space Administration.
Lewis Research Center, Cleveland, OH.

**DIAMONDLIKE CARBON AS A MOISTURE BARRIER AND
ANTIREFLECTING COATING ON OPTICAL MATERIALS**

JOHN A. WOOLLAM, BHOLA N. DE, L. Y. CHEN (Nebraska Univ.,
Lincoln.), JOHN J. POUCH, and SAMUEL A. ALTEROVITZ *In its*
Solid State Technology Branch of NASA Lewis Research Center
Second Annual Digest, June 1989 - June 1990 p 232-237 Jun.
1990 Sponsored in part by Control Data Corp.
(Contract NAG3-154; DAAL04-86-C-0030)
Avail: NTIS HC/MF A13 CSCL 11/3

Diamonddike carbon (DLC) is amorphous, hard, semitransparent, and is under consideration for use as a coating material for infrared optics. DLC is also designated as a-C:H to indicate its amorphous nature as well as to indicate the presence of large (20 to 55 percent) amounts of hydrogen in the film. Two important questions arise with respect to use of DLC in infrared optics. Will the lack of grain boundaries help to keep moisture from penetrating the film. Secondly, application as an antireflection coating places restrictions on the allowed values of the index of refraction of the film relative to the particular substrate material being used. Will DLC have the correct index range. These two questions are addressed in this paper. Author

N91-18303*# National Aeronautics and Space Administration.
Lewis Research Center, Cleveland, OH.

**THIN FILM CHARACTERIZATION USING SPECTROSCOPIC
ELLIPSOMETRY**

SAMUEL A. ALTEROVITZ *In its* Solid State Technology Branch
of NASA Lewis Research Center Second Annual Digest, June
1989 - June 1990 p 238 Jun. 1990
Avail: NTIS HC/MF A13 CSCL 11/3

The application of the multiple angle and wavelength (MAW) technique to measure the dielectric function of semiconducting films is discussed. This technique evaluates unambiguously the complex dielectric function, epsilon (E), of the film without any pre-assumptions. In some cases the effective medium approximation (EMA) was used to determine the volume fraction of the film components. Application of the MAW technique to several semiconducting films was published previously. Different applications and examples are given, including metal and insulator films. Author

N91-19292*# National Aeronautics and Space Administration.
Lewis Research Center, Cleveland, OH.

**STRUCTURAL RELIABILITY ANALYSIS OF LAMINATED CMC
COMPONENTS**

STEPHEN F. DUFFY, JOSEPH L. PALKO (Cleveland State Univ.,
OH.), and JOHN P. GYEKENYESI 1991 10 p Proposed for
presentation at the 36th International Gas Turbine and Aeroengine
Congress and Exposition, Orlando, FL, 3-6 Jun. 1991; sponsored
by ASME
(Contract RTOP 505-63-1B)
(NASA-TM-103685; E-5903; NAS 1.15:103685) Avail: NTIS
HC/MF A02 CSCL 11/3

For laminated ceramic matrix composite (CMC) materials to realize their full potential in aerospace applications, design methods and protocols are a necessity. The time independent failure response of these materials is focussed on and a reliability analysis is presented associated with the initiation of matrix cracking. A public domain computer algorithm is highlighted that was coupled with the laminate analysis of a finite element code and which serves as a design aid to analyze structural components made from laminated CMC materials. Issues relevant to the effect of the size of the component are discussed, and a parameter estimation procedure is presented. The estimation procedure allows three parameters to be calculated from a failure population that has an underlying Weibull distribution. Author

N91-19293*# National Aeronautics and Space Administration.
Lewis Research Center, Cleveland, OH.

**COMPARISON OF DYNAMIC FATIGUE BEHAVIOR BETWEEN
SiC WHISKER-REINFORCED COMPOSITE AND MONOLITHIC
SILICON NITRIDES**

SUNG R. CHOI (Cleveland State Univ., OH.) and JONATHAN A.
SALEM Feb. 1991 22 p
(Contract RTOP 505-63-1M)
(NASA-TM-103707; E-5932; NAS 1.15:103707) Avail: NTIS
HC/MF A03 CSCL 11/3

The dynamic fatigue behavior of 30 vol percent silicon nitride whisker-reinforced composite and monolithic silicon nitrides were determined as a function of temperature from 1100 to 1300 C in ambient air. The fatigue susceptibility parameter, n, decreased from 88.1 to 20.1 for the composite material, and from 50.8 to 40.4 for the monolithic, with increasing temperature from 1100 to 1300 C. A transition in the dynamic fatigue curve occurred for the composite material at a low stressing rate of 2 MPa/min at 1300 C, resulting in a very low value of n equals 5.8. Fractographic analysis showed that glassy phases in the slow crack growth region were more pronounced in the composite compared to the monolithic material, implying that SiC whisker addition promotes the formation of glass rich phases at the grain boundaries, thereby enhancing fatigue. These results indicate that SiC whisker addition to Si3 N4 matrix substantially deteriorates fatigue resistance inherent to the matrix base material for this selected material system. Author

N91-19294*# National Aeronautics and Space Administration.
Lewis Research Center, Cleveland, OH.

**LOW EARTH ORBITAL ATOMIC OXYGEN AND ULTRAVIOLET
RADIATION EFFECTS ON POLYMERS**

JOYCE A. DEVER Feb. 1991 15 p
(Contract RTOP 506-43-11)
(NASA-TM-103711; E-5943; NAS 1.15:103711) Avail: NTIS
HC/MF A03 CSCL 11/3

Because atomic oxygen and solar ultraviolet radiation present

27 NONMETALLIC MATERIALS

in the low earth orbital (LEO) environment can alter the chemistry of polymers resulting in degradation, their effects and mechanisms of degradation must be determined in order to determine the long term durability of polymeric surfaces to be exposed on missions such as Space Station Freedom. The effects of atomic oxygen on polymers which contain protective coatings must also be explored, since unique damage mechanisms can occur in areas where the protective coatings has failed. Mechanisms can be determined by utilizing results from previous LEO missions, by performing ground based LEO simulation tests and analysis, and by carrying out focussed space experiments. A survey is presented of the interactions and possible damage mechanisms for environmental atomic oxygen and UV radiation exposure of polymers commonly used in LEO. Author

N91-19295*# National Aeronautics and Space Administration. Lewis Research Center, Cleveland, OH.

THERMAL SHOCK OF FIBER REINFORCED CERAMIC MATRIX COMPOSITES

ANDREW J. ECKEL, JOHN P. GYKENYESI (Cleveland State Univ., OH.), THOMAS P. HERBELL, and EDWARD R. GENERAZIO 1991 13 p Presented at the 15th Annual Conference on Composites and Advanced Ceramics, Cocoa Beach, FL, 13-16 Jan. 1991; sponsored by American Ceramic Society (Contract RTOP 590-21-11) (NASA-TM-103777; E-6006; NAS 1.15:103777) Avail: NTIS HC/MF A03 CSCL 11/3

Monolithic silicon carbide and silicon nitride and a Nicalon fiber reinforced silicon carbide composite were subjected to severe thermal shock conditions via impingement of a hydrogen-oxygen flame. Surface heating rates of 1000 C/sec to 2500 C/sec were generated. The performance of the monolithic reference materials are compared and contrasted to the significantly greater thermal shock resistance of the composite. Ultrasonic and radiographic NDE techniques were used to evaluate the integrity of the composite subsequent to thermal shock. Tensile tests were performed to determine the residual tensile strength and modulus. Physical property changes are discussed as a function of number and severity of thermal shock cycles. Author

N91-19296*# National Aeronautics and Space Administration. Lewis Research Center, Cleveland, OH.

SYNTHESIS AND STRUCTURES OF METAL CHALCOGENIDE PRECURSORS

ALOYSIUS F. HEPP, STAN A. DURAJ, WILLIAM E. ECKLES, and MARIA T. ANDRAS (Cleveland State Univ., OH.) 1990 6 p Presented at the Fall Meeting of the Materials Research Society, Boston, MA, 26 Nov. - 1 Dec. 1990 Sponsored in part by Petroleum Research Fund (Contract NCC3-162; RTOP 307-51-00) (NASA-TM-103665; E-5872; NAS 1.15:103665) Avail: NTIS HC/MF A02 CSCL 11/3

The reactivity of early transition metal sandwich complexes with sulfur-rich molecules such as dithiocarboxylic acids was studied. Researchers recently initiated work on precursors to CuInSe_2 and related chalcopyrite semiconductors. The very high radiation tolerance and the high absorption coefficient of CuInSe_2 makes this material extremely attractive for lightweight space solar cells. Their general approach in early transition metal chemistry, the reaction of low-valent metal complexes or metal powders with sulfur and selenium rich compounds, was extended to the synthesis of chalcopyrite precursors. Here, the researchers describe synthesis, structures, and routes to single molecule precursors to metal chalcogenides. Author

N91-19308*# National Aeronautics and Space Administration. Lewis Research Center, Cleveland, OH.

CRYSTALLIZATION AND PROPERTIES OF SR-BA ALUMINOSILICATE GLASS-CERAMIC MATRICES

NAROTTAM P. BANSAL, MARK J. HYATT, and CHARLES H. DRUMMOND, III (Ohio State Univ., Columbus.) 1991 24 p Presented at the 15th Annual Conference on Composites and Advanced Ceramics, Cocoa Beach, FL, 13-16 Jan. 1991; sponsored

by American Ceramic Society

(Contract RTOP 510-01-01)

(NASA-TM-103764; E-6027; NAS 1.15:103764) Avail: NTIS HC/MF A03 CSCL 11/3

Powders of roller quenched (Sr,Ba)O-Al₂O₃-2SiO₂ glasses of various compositions were uniaxially pressed into bars and hot isostatically pressed at 1350 C for 4 hours or cold isostatically pressed and sintered at different temperatures between 800 to 1500 C for 10 or 20 hours. Densities, flexural strengths, and linear thermal expansion were measured for three compositions. The glass transition and crystallization temperatures were determined by Differential Scanning Calorimetry (DSC). The liquidus and crystallization temperature from the melt were measured using high temperature Differential Thermal Analysis (DTA). Crystalline phases formed on heat treatment of the glasses were identified by powder x ray diffraction. In Sr containing glasses, the monoclinic phase always crystallized at temperatures above 1000 C. At lower temperatures, the hexagonal analog formed. The temperature for orthorhombic to hexagonal structure transformation increased monotonically with SrO content, from 327 C for BaO-Al₂O₃-2SiO₂ to 758 C for SrO-Al₂O₃-2SiO₂. These glass powders can be sintered to almost full densities and monoclinic phase at a relatively low temperature of 1100 C. Author

N91-20107*# National Aeronautics and Space Administration. Lewis Research Center, Cleveland, OH.

TRANSITION-TO-PRACTICE TECHNOLOGIES FOR BRITTLE MATERIALS

EDWARD R. GENERAZIO *In its* Aeropropulsion 1991 18 p Mar. 1991

Avail: NTIS HC/MF A24 CSCL 11/3

Four major technologies are needed to bring brittle ceramic composites up to the level necessary for practical application as aerospace materials. These are mechanical testing, nondestructive evaluation (NDE), mechanical design, and life prediction. An advanced design tool, C-CARES, was developed to assist designers in the mechanical design of structural ceramic components by determining the reliabilities of these components. In situ and in process NDE are being used to enhance/accelerate development of ceramic matrix composites (CMC's). As a very minimum both x-ray and ultrasonic imaging needs to be performed for an accurate NDE. In situ and in process NDE also provides validation of analytical models. Author

N91-21302*# National Aeronautics and Space Administration. Lewis Research Center, Cleveland, OH.

MECHANICAL STRENGTH AND THERMOPHYSICAL PROPERTIES OF PM212: A HIGH TEMPERATURE SELF-LUBRICATING POWDER METALLURGY COMPOSITE Final Report

PHILLIP M. EDWARDS (Case Western Reserve Univ., Cleveland, OH.), HAROLD E. SLINNEY, CHRISTOPHER DELLACORTE, J. DANIEL WHITTENBERGER, and ROBERT R. MARTINEAU Dec. 1990 30 p

(Contract DE-AI01-85CE-50162; RTOP 778-34-22)

(NASA-TM-103694; E-5913; NAS 1.15:103694;

DOE/NASA/50162-5) Avail: NTIS HC/MF A03 CSCL 11/3

A powder metallurgy composite, PM212, composed of metal bonded chromium carbide and solid lubricants is shown to be self-lubricating to a maximum application temperature of 900 C. The high temperature compressive strength, tensile strength, thermal expansion and thermal conductivity data needed to design PM212 sliding contact bearings and seals are reported for sintered and isostatically pressed (HIPed) versions of PM212. Other properties presented are room temperature density, hardness, and elastic modulus. In general, both versions appear to have adequate strength to be considered as sliding contact bearing materials, but the HIPed version, which is fully dense, is much stronger than the sintered version which contains about 20 percent pore volume. The sintered material is less costly to make, but the HIPed version is better where high compressive strength is important. Author

N91-21307*# National Aeronautics and Space Administration. Lewis Research Center, Cleveland, OH. Propulsion Div.
HYDROCARBON-FUEL/COMBUSTION-CHAMBER-LINER MATERIALS COMPATIBILITY Final Report, 31 Oct. 1989 - 31 Mar. 1991

G. DAVID HOMER Apr. 1991 116 p
 (Contract NAS3-25070)
 (NASA-CR-187104; NAS 1.26:187104; KBQ-FR-2; AD-A235644)
 Avail: NTIS HC/MF A06 CSCL 11/3

The results of dynamic tests using methane and NASA-Z copper test specimen under conditions that simulate those expected in the cooling channels of a regeneratively cooled LOX/hydrocarbon booster engine operating at chamber pressures up to 3000 psi are presented. Methane with less than 0.5 ppm sulfur contamination has little or no effect on cooling channel performance. At higher sulfur concentrations, severe corrosion of the NASA-Z copper alloy occurs and the cuprous sulfide Cu₂S, thus formed impedes mass flow rate and heat transfer efficiency. Therefore, it is recommended that the methane specification for this end use set the allowable sulfur content at 0.5 ppm (max). Bulk high purity liquid methane that meets this low sulfur requirement is currently available from only one producer. Pricing, availability, and quality assurance are discussed in detail. Additionally, it was found that dilute sodium cyanide solutions effectively refurbish sulfur corroded cooling channels in only 2 to 5 minutes by completely dissolving all the Cu₂S. Sulfur corroded/sodium cyanide refurbished channels are highly roughened and the increased surface roughness leads to significant improvements in heat transfer efficiency with an attendant loss in mass flow rate. Both the sulfur corrosion and refurbishment effects are discussed in detail. Author

N91-21309*# National Aeronautics and Space Administration. Lewis Research Center, Cleveland, OH.

A SIMPLE TEST FOR THERMOMECHANICAL EVALUATION OF CERAMIC FIBERS

GREGORY N. MORSCHER (Case Western Reserve Univ., Cleveland, OH.) and JAMES A. DICARLO Apr. 1991 10 p
 (Contract RTOP 510-01-50)
 (NASA-TM-103767; E-6029; NAS 1.15:103767) Avail: NTIS HC/MF A02 CSCL 11/3

A simple bend stress relaxation (BSR) test was developed to measure the creep related properties of ceramic fibers and whiskers. The test was applied to a variety of commercial and developmental Si based fibers to demonstrate capabilities and to evaluate the relative creep resistance of the fibers at 1200 to 1400 C. The implications of these results and the advantages of the BSR test over typical tensile creep tests are discussed. Author

N91-22460*# National Aeronautics and Space Administration. Lewis Research Center, Cleveland, OH.

STRUCTURAL DESIGN METHODOLOGIES FOR CERAMIC-BASED MATERIAL SYSTEMS

STEPHEN F. DUFFY, ABHISAK CHULYA (Cleveland State Univ., OH.), and JOHN P. GYKENYESI Mar. 1991 14 p Submitted for publication Original contains color illustrations
 (Contract NCC3-89; RTOP 505-63-1B)
 (NASA-TM-103097; E-5418; NAS 1.15:103097) Avail: NTIS HC/MF A03; 1 functional color page CSCL 11/3

One of the primary pacing items for realizing the full potential of ceramic-based structural components is the development of new design methods and protocols. The focus here is on low temperature, fast-fracture analysis of monolithic, whisker-toughened, laminated, and woven ceramic composites. A number of design models and criteria are highlighted. Public domain computer algorithms, which aid engineers in predicting the fast-fracture reliability of structural components, are mentioned. Emphasis is not placed on evaluating the models, but instead is focused on the issues relevant to the current state of the art. Author

N91-23042*# National Aeronautics and Space Administration. Lewis Research Center, Cleveland, OH.

DUAL ION BEAM PROCESSED DIAMONDLIKE FILMS FOR INDUSTRIAL APPLICATIONS

M. J. MIRTICH, M. T. KUSSMAUL (Sverdrup Technology, Inc., Brook Park, OH.), B. A. BANKS, and J. S. SOVEY In National Aeronautics and Space Administration, Technology 2000, Volume 1 p 173-183 Mar. 1991
 Avail: NTIS HC/MF A18 CSCL 11/3

Single and dual beam ion source systems are used to generate amorphous diamondlike carbon (DLC) films, which were evaluated for a variety of applications including protective coatings on transmitting materials, power electronics as insulated gates and corrosion resistant barriers. A list of the desirable properties of DLC films along with potential applications are presented. Author

N91-23044*# National Aeronautics and Space Administration. Lewis Research Center, Cleveland, OH.

THE PM-200 LUBRICATION SYSTEM

HAROLD E. SLINEY In National Aeronautics and Space Administration, Technology 2000, Volume 1 p 189-196 Mar. 1991
 Avail: NTIS HC/MF A18 CSCL 11/3

Plasma sprayed composite coating of metal-bonded chromium carbide with additions of silver and thermochemically stable fluorides were previously reported to be lubricative in pin on disk bench tests from room temperature to 900 C. An early coating formulation of this type, designated as PS-200, was successfully tested as a cylinder coating in a Stirling engine at a TRRT of 760 C in a hydrogen atmosphere, and as a backup lubricant for gas bearings to 650 C. A subsequent optimization program has shown that tribological properties are further improved by increasing the solid lubricant content. The improved coating is designated as PS-212. The same powder formulation was used to make free-standing powder metallurgy (PM-212) parts by sintering or hot isostatic pressing. The process is very attractive for making parts that cannot be readily plasma sprayed such as bushings and cylinders that have small bore diameters and/or high length to diameter ratios. The properties of coatings and free-standing parts fabricated from these powders are reviewed. Author

N91-23311*# National Aeronautics and Space Administration. Lewis Research Center, Cleveland, OH.

MECHANICAL BEHAVIOR AND FAILURE PHENOMENON OF AN IN SITU-TOUGHENED SILICON NITRIDE

JONATHAN A. SALEM, SUNG R. CHOI, MARC R. FREEDMAN, and MICHAEL G. JENKINS (Oak Ridge National Lab., TN.) 1990 22 p Presented at the 43rd Annual Pacific Coast Meeting, Seattle, WA, 25-27 Oct. 1990; sponsored by the American Ceramic Society
 (Contract DE-AL05-870R-21749; RTOP 505-63-1M)
 (NASA-TM-103741; E-5983; NAS 1.15:103741) Avail: NTIS HC/MF A03 CSCL 11/3

The Weibull modulus, fracture toughness and crack growth resistance of an in-situ toughened, silicon nitride material used to manufacture a turbine combustor were determined from room temperature to 1371 C. The material exhibited an elongated grain structure that resulted in improved fracture toughness, nonlinear crack growth resistance, and good elevated temperature strength. However, low temperature strength was limited by grains of excessive length (30 to 100 microns). These excessively long grains were surrounded by regions rich in sintering additives. Author

N91-24062*# National Aeronautics and Space Administration. Lewis Research Center, Cleveland, OH.

FLEXIBLE FLUOROPOLYMER FILLED PROTECTIVE COATINGS

BRUCE A. BANKS, MICHAEL J. MIRTICH, JAMES S. SOVEY, HENRY NAHRA, and SHARON K. RUTLEDGE In NASA, Washington, Technology 2000, Volume 2 p 179-184 1991
 Avail: NTIS HC/MF A16 CSCL 11/3

Metal oxide films such as SiO₂ are known to provide an effective

27 NONMETALLIC MATERIALS

barrier to the transport of moisture as well as gaseous species through polymeric films. Such thin film coatings have a tendency to crack upon flexure of the polymeric substrate. Sputter co-deposition of SiO₂ with 4 to 15 percent fluoropolymers was demonstrated to produce thin films with glass-like barrier properties that have significant increases in strain to failure over pure glass films which improves their tolerance to flexure on polymeric substrates. Deposition techniques capable of producing these films on polymeric substrates are suitable for durable food packaging and oxidation/corrosion protection applications. Author

N91-25029*# National Aeronautics and Space Administration. Lewis Research Center, Cleveland, OH.

ATOMIC OXYGEN INTERACTIONS WITH FEP TEFLON AND SILICONES ON LDEF Abstract Only

BRUCE A. BANKS and LINDA GEBAUER (Cleveland State Univ., OH.) /in NASA, Langley Research Center, First LDEF Post-Retrieval Symposium Abstracts p 62 Jun. 1991
Avail: NTIS HC/MF A07 CSCL 11/3

The Long Duration Exposure Facility (LDEF) spacecraft represents the first controlled unidirectional exposure of high-fluence atomic oxygen on fluorinated ethylene propylene (FEP Teflon) and silicones. The atomic oxygen erosion yield for FEP Teflon was found to be significantly in excess of previous low fluence orbital data and is an order of magnitude below that of polyimide Kapton. LDEF FEP Teflon erosion yield data as a function of angle of attack is presented. Atomic oxygen interaction with silicon polymers results in crazing of the silicones as well as deposition of dark contaminant oxidation products on adjoining surfaces. Documentation of results and possible mechanistic explanations are presented. Author

N91-25040*# National Aeronautics and Space Administration. Lewis Research Center, Cleveland, OH.

ION BEAM TEXTURED AND COATED SURFACES

EXPERIMENT (IBEX) Abstract Only

MICHAEL J. MIRTICH, NICHOLAS STEVENS, and JAMES MERROW (Cleveland State Univ., OH.) /in NASA, Langley Research Center, First LDEF Post-Retrieval Symposium Abstracts p 73 Jun. 1991

Avail: NTIS HC/MF A07 CSCL 11/3

The IBEX, with 36 samples of various materials, was placed aboard the LDEF. Twenty-seven of the samples had surfaces modified using ion beam technology, and nine were made up of commercially available materials. The materials are in some way useful in space power systems. The various types of materials tested included six categories: (1) ion beam structured surfaces suitable for solar thermal (concentrator) or space radiators; (2) ion beam sputtered conductive coatings for thermal and space charge control; (3) solar reflector surfaces; (4) flexible thin film coatings and solar array blanket material for protection of spacecraft polymers; (5) painted and/or state-of-the-art solar thermal materials; and (6) micrometeoroid sensitive detector. Data analysis presented include the optical properties of each surface before and after exposure to the space environment and the respective backup surfaces. Author

N91-25286*# National Aeronautics and Space Administration. Lewis Research Center, Cleveland, OH.

LONG TERM ISOTHERMAL AGING AND THERMAL ANALYSIS OF N-CYCAP POLYIMIDES

JAMES K. SUTTER, JOHN F. WATERS, and MARLA A. SCHVERMAN (Xavier Univ., Cincinnati, OH.) 1991 8 p
Presented at the High Performance Materials Symposium at the Polymer Technology Conference, Philadelphia, PA, 3-5 Jun. 1991; sponsored by the American Chemical Society
(Contract RTOP 505-10-50)

(NASA-TM-104341; E-6115; NAS 1.15:104341) Avail: NTIS HC/MF A02 CSCL 11/3

The N-CYCAP polyimides utilize a (2,2) paracyclophane endcap that polymerizes and does not generate volatile gases during the cure process. These polyimides have both high glass temperatures (390 C) and an onset of decomposition in air of 560 C. Thermal

oxidative stability (TOS) weight loss studies show that replacing 25 percent by weight of the paraphenylene diamine in the polymer backbone with metaphenylene diamine improves the weight loss characteristics. N-CYCAP neat resin samples performed better than PMR-II-50 when exposed at 343 and 371 C in air for up to 1000 hours. Preliminary composite studies show that both PMR-II-50 and N-CYCAP have better thermal stability when fabricated on T-40R. Higher isothermal aging temperatures of longer aging times are needed to determine the differences in TOS between composite samples of PMR-II-50 and N-CYCAP polyimides. Author

N91-25296* National Aeronautics and Space Administration. Lewis Research Center, Cleveland, OH.

ARC-TEXTURED HIGH EMITTANCE RADIATOR SURFACES

Patent

BRUCE A. BANKS, inventor (to NASA) 30 Apr. 1991 6 p
Filed 18 Jul. 1989 Supersedes N89-28651 (27 - 23, p 3271)
(NASA-CASE-LEW-14679-1; US-PATENT-5,012,062;
US-PATENT-APPL-SN-381240; US-PATENT-CLASS-219-69.11;
INT-PATENT-CLASS-B23H-9/00) Avail: US Patent and
Trademark Office CSCL 11/3

High emittance radiator surfaces are produced by arc-texturing. This process produces such a surface on a metal by scanning it with a low voltage electric arc from a carbon electrode in an inert environment.

Official Gazette of the U.S. Patent and Trademark Office

N91-25298*# National Aeronautics and Space Administration. Lewis Research Center, Cleveland, OH.

CERAMIC COATINGS ON SMOOTH SURFACES Patent

Application

R. A. MILLER, inventor (to NASA), W. J. BRINDLEY, inventor (to NASA), and C. J. ROUGE, inventor (to NASA) 13 May 1991 12 p
(NASA-CASE-LEW-15164-1; NAS 1.71:LEW-15164-1;
US-PATENT-APPL-SN-699130) Avail: NTIS HC/MF A03 CSCL 11/3

A metallic coating is plasma sprayed onto a smooth surface of a metal alloy substitute or on a bond coating. An initial thin ceramic layer is low pressure sprayed onto the smooth surface of the substrate or bond coating. Another ceramic layer is atmospheric plasma sprayed onto the initial ceramic layer. NASA

N91-26375*# National Aeronautics and Space Administration. Lewis Research Center, Cleveland, OH.

OXIDATION RESISTANT COATINGS FOR TITANIUM ALLOYS AND TITANIUM ALLOY MATRIX COMPOSITES Patent

Application

WILLIAM J. BRINDLEY, inventor (to NASA), JAMES L. SMIALEK, inventor (to NASA), and CARL J. ROUGE, inventor (to NASA) 1 Apr. 1991 9 p
(NASA-CASE-LEW-15155-1; NAS 1.71:LEW-15155-1;
US-PATENT-APPL-SN-682160) Avail: NTIS HC/MF A02 CSCL 11/3

An oxidation resistant coating for titanium alloys and titanium alloy matrix composites comprises an MCrAlX material. M is a metal selected from nickel, cobalt, and iron. X is an active element selected from Y, Yb, Zr, and Hf. NASA

N91-26376*# National Aeronautics and Space Administration. Lewis Research Center, Cleveland, OH.

METHOD OF PREPARING A THERMAL BARRIER COATING Patent Application

I. ZAPLATYNSKY, inventor (to NASA) 1 Mar. 1991 10 p
(NASA-CASE-LEW-14999-2; NAS 1.71:LEW-14999-2;
US-PATENT-APPL-SN-662684) Avail: NTIS HC/MF A02 CSCL 11/3

A composite thermal barrier coating is plasma sprayed onto a substrate. This coating has a first layer including a first ceramic material and a second layer including a second ceramic material impregnated with a glass, the glass being a ternary eutectic. The glass may consist of about 14.6 weight percent Al₂O₃, about

23.3 weight percent CaO, and about 62.1 weight percent SiO₂. The first and second ceramic materials may include yttria-stabilized zirconia. NASA

N91-28418*# National Aeronautics and Space Administration. Lewis Research Center, Cleveland, OH.

ELEVATED-TEMPERATURE FRACTURE RESISTANCES (K(SUB IC), R-CURVES, GAMMA SUB (OMEGA OF)) OF MONOLITHIC AND COMPOSITE CERAMICS USING CHEVRON-NOTCHED, BEND TESTS

ASISH GHOSH, M. G. JENKINS, M. K. FERBER, J. PEUSSA (Federation of Finnish Metal, Engineering, and Electronic Technology Industries, Helsinki.), and JONATHAN A. SALEM 1991 2 p Presented at the International Conference Fracture Mechanics of Ceramics, Nagoya (Japan), 15-17 Jul. 1991 (Contract DE-AC05-84OR-21400) (NASA-TM-105090; NAS 1.15:105090; DE91-012961; CONF-9107113-1) Avail: NTIS HC/MF A01 CSCL 11/3

The quasi-static fracture behaviors of monolithic ceramics (SiC, Si₃N₄, MgAl₂O₄), self-reinforced monoliths (acicular grained Si₃N₄, acicular grained mullite), and ceramic matrix composites (SiC whisker/Al₂O₃ matrix, TiB₂ particulate/SiC matrix, SiC fiber/CVI SiC matrix, Al₂O₃ fiber/CVI SiC matrix) were measured over the temperature range of 20 to 1400 C. The chevron notched, bend bar test geometry was essential for characterizing the elevated temperature fracture resistances of this wide range of quasi-brittle materials during stable crack growth. Fractography revealed the differences in the fracture behavior of the different materials at the various temperatures. The fracture resistances of the self-reinforced monoliths were comparable to those of the composites and the fracture mechanisms were found to be similar at room temperature. However at elevated temperatures the differences of the fracture behavior became apparent where the superior fracture resistance of the self-reinforced monoliths were attributed to the minor amounts of glassy, intergranular phases which were often more abundant in the composites and affected the fracture behavior when softened by elevated temperatures. DOE

N91-28423*# National Aeronautics and Space Administration. Lewis Research Center, Cleveland, OH.

PRETREATMENT OF LUBRICATED SURFACES WITH SPUTTERED CADMIUM OXIDE Patent Application

ROBERT L. FUSARO, inventor (to NASA) 24 Jun. 1991 12 p (NASA-CASE-LEW-14474-1; NAS 1.71:LEW-14474-1; US-PATENT-APPL-SN-720133) Avail: NTIS HC/MF A03 CSCL 11/3

Cadmium oxide is used with a dry solid lubricant on a surface to improve wear resistance. The surface topography is first altered by photochemical etching to a predetermined pattern. The cadmium oxide is then sputtered onto the altered surface to form an intermediate layer to more tightly hold the dry lubricant, such as graphite. NASA

N91-29332*# National Aeronautics and Space Administration. Lewis Research Center, Cleveland, OH.

THERMAL EMITTANCE ENHANCEMENT OF GRAPHITE-COPPER COMPOSITES FOR HIGH TEMPERATURE SPACE BASED RADIATORS

SHARON K. RUTLEDGE, MARK J. FORKAPA, and JILL M. COOPER (Cleveland State Univ., OH.) 1991 9 p Presented at the Conference on Advanced Space Exploration Initiative Technologies, Cleveland, OH, 4-6 Sep. 1991; cosponsored by AIAA and OAI (Contract RTOP 590-13-11) (NASA-TM-105178; E-6475; NAS 1.15:105178; AIAA PAPER 91-3527) Avail: NTIS HC/MF A02 CSCL 11/3

Graphite-copper composites are candidate materials for space based radiators. The thermal emittance of this material, however, is a factor of two lower than the desired emittance for these systems of greater than or equal to 0.85. Arc texturing was investigated as a surface modification technique for enhancing the emittance of the composite. Since the outer surface of the

composite is copper, and samples of the composite could not be readily obtained for testing, copper was used for optimization testing. Samples were exposed to various frequencies and currents of arcs during texturing. Emittances near the desired goal were achieved at frequencies less than 500 Hz. Arc current did not appear to play a major role under 15 amps. Particulate carbon was observed on the surface, and was easily removed by vibration and handling. In order to determine morphology adherence, ultrasonic cleaning was used to remove the loosely adherent material. This reduced the emittance significantly. Emittance was found to increase with increasing frequency for the cleaned samples up to 500 Hz. The highest emittance achieved on these samples over the temperature range of interest was 0.5 to 0.6, which is approximately a factor of 25 increase over the untextured copper emittance. Author

N91-32229*# National Aeronautics and Space Administration. Lewis Research Center, Cleveland, OH.

CERAMIC COATINGS ON SMOOTH SURFACES Patent Application

R. A. MILLER, inventor (to NASA), W. J. BRINDLEY, inventor (to NASA), and C. J. ROUGE, inventor (to NASA) 26 Sep. 1991 11 p (NASA-CASE-LEW-15164-2; NAS 1.71:LEW-15164-2; US-PATENT-APPL-SN-766591) Avail: NTIS HC/MF A03 CSCL 11/3

A metal substrate or a bond coating having a smooth surface is covered by a thin ceramic layer of ZrO₂ - 8 pct. Y₂O₃ having a thickness between 0.6 and 1.9 mils. A second ceramic layer of ZrO₂ - 8 pct. Y₂O₃ having a thickness between about four and 15 mils covers the thin ceramic layer. NASA

N91-32230*# National Aeronautics and Space Administration. Lewis Research Center, Cleveland, OH.

ADDITION POLYIMIDES WITH ENHANCED PROCESSABILITY Patent Application

CHUN-HUA CHUANG, inventor (to NASA) and RAYMOND D. VANNUCCI, inventor (to NASA) 7 Oct. 1991 18 p (NASA-CASE-LEW-15043-1; NAS 1.71:LEW-15043-1; US-PATENT-APPL-SN-772181) Avail: NTIS HC/MF A03 CSCL 11/3

The present invention is directed to nonplanar polyimides having improved thermo-oxidative stability and enhanced processability. In a preferred embodiment, high molecular weight polyimides (HMW PMRs (polymerization of monomer reactants)) are obtained by reacting a nonplanar polyphenyl diamine, a diester or dianhydride of a tetracarboxylic acid, and an end capping compound. A second embodiment involves reacting a diamine with a nonplanar diester, or nonplanar dianhydride, of a tetracarboxylic acid, and an end capping compound. The polyimides of this invention overcome processing difficulties involved with using HMW PMRs through their noncoplanar conformation. For example, the noncoplanar conformation helps reduce the melting temperature and melt viscosity normally required and thereby permits substantially increased resin flow in processing of HMW PMRs. The polyimides of the invention possess excellent thermo-oxidative stability at 343 to 371 C for composite applications. In addition, the polyimides of the invention display a low thermal expansion coefficient and a narrow molecular weight distribution at high molecular weights. NASA

PROPELLANTS AND FUELS

Includes rocket propellants, igniters, and oxidizers; their storage and handling procedures; and aircraft fuels.

A91-10112* # McDonnell-Douglas Space Systems Co., Huntington Beach, CA.

CRYOGENIC PROPELLANT MANAGEMENT ARCHITECTURES TO SUPPORT THE SPACE EXPLORATION INITIATIVE

E. C. CADY (McDonnell Douglas Space Systems Co., Huntington Beach, CA), R. R. CORBAN, and S. M. STEVENSON (NASA, Lewis Research Center, Cleveland, OH) AIAA, Space Programs and Technologies Conference, Huntsville, AL, Sept. 25-27, 1990. 11 p.

(Contract NAS3-25810)

(AIAA PAPER 90-3713) Copyright

The initial results of a current study to develop fuel system architectures to support the lunar requirements of the Space Exploration Initiative (SEI) are reported. The study includes the development and assessment of propellant management facility concepts, supporting infrastructure, operations analysis, and identification of impact on current programs, including Space Station Freedom, Earth-to-Orbit vehicles, and the Space Transfer Vehicle. The cryogenic propellant management architectures are evaluated using criteria that have been defined to provide for minimum subjective assessment and effective data reliability.

V.L.

A91-19324* # Michigan Univ., Ann Arbor.

TRANSIENT CRYOGENIC LIQUID DISCHARGE IN NORMAL AND MICRO-GRAVITY

T. P. PURWIN, M. KAVIANY (Michigan, University, Ann Arbor), and J. C. AYDELOTT (NASA, Lewis Research Center, Cleveland, OH) AIAA, Aerospace Sciences Meeting, 29th, Reno, NV, Jan. 7-10, 1991. 12 p. refs

(AIAA PAPER 91-0486) Copyright

Transient discharge of liquid cryogens from partially filled tanks under microgravity is considered. The discharge is made to a low-pressure site through a straight tube. The ultimate objective of the study is to predict the transient mass flow rate. In addition, the pressure history in the tank is of interest, since the pressure falls below the triple point toward the end of the dump, causing solidification in the tank and/or the discharge line. As first steps, experiments have been performed in normal gravity and attempts are made to predict the transient rate and pressure history under this condition. Experiments are performed with liquid nitrogen dumped to sites with pressures below the triple point. Homogeneous equilibrium and nonequilibrium two-phase critical flow models are compared to the experimental results. Equilibrium and nonequilibrium tank pressure history models are also compared to experimental data.

Author

A91-34369* Princeton Univ., NJ.

TWO-DIMENSIONAL IMAGING OF MOLECULAR HYDROGEN IN H₂-AIR DIFFUSION FLAMES USING TWO-PHOTON LASER-INDUCED FLUORESCENCE

W. LEMPERT, V. KUMAR, I. GLESK, R. MILES (Princeton University, NJ), and G. DISKIN (NASA, Langley Research Center, Hampton, VA; Princeton University, NJ) Optics Letters (ISSN 0146-9592), vol. 16, May 1, 1991, p. 660-662. USAF-supported research. refs

Copyright

The use of a tunable ArF laser at 193.26 nm to record simultaneous single-laser-shot, planar images of molecular hydrogen and hot oxygen in a turbulent H₂-air diffusion flame. Excitation spectra of fuel and oxidant-rich flame zones confirm a partial overlap of the two-photon H₂ and single-photon O₂ Schumann-Runge absorption bands. UV Rayleigh scattering images

of flame structure and estimated detection limits for the H₂ two-photon imaging are also presented.

Author

A91-40560* # National Aeronautics and Space Administration. Lewis Research Center, Cleveland, OH.

MECHANISMS AND MODELING OF THE EFFECTS OF ADDITIVES ON THE NITROGEN OXIDES EMISSION

KRISHNA P. KUNDU, H. LEE NGUYEN, and M. PAUL KANG (NASA, Lewis Research Center, Cleveland, OH) AIAA, Aerospace Sciences Meeting, 29th, Reno, NV, Jan. 7-10, 1991. 24 p. Previously announced in STAR as N91-22464. refs

(AIAA PAPER 91-0479) Copyright

A theoretical study on the emission of the oxides of nitrogen in the combustion of hydrocarbons is presented. The current understanding of the mechanisms and the rate parameters for gas phase reactions were used to calculate the NO(x) emission. The possible effects of different chemical species on thermal NO(x), on a long time scale were discussed. The mixing of these additives at various stages of combustion were considered and NO(x) concentrations were calculated; effects of temperatures were also considered. The chemicals such as hydrocarbons, H₂, CH₃OH, NH₃, and other nitrogen species were chosen as additives in this discussion. Results of these calculations can be used to evaluate the effects of these additives on the NO(x) emission in the industrial combustion system.

Author

A91-41631* # National Aeronautics and Space Administration. Lewis Research Center, Cleveland, OH.

CONCEPTUAL STUDY OF ON ORBIT PRODUCTION OF CRYOGENIC PROPELLANTS BY WATER ELECTROLYSIS

MATTHEW E. MORAN (NASA, Lewis Research Center, Cleveland, OH) AIAA, SAE, ASME, and ASEE, Joint Propulsion Conference, 27th, Sacramento, CA, June 24-26, 1991. 11 p. Previously announced in STAR as N91-19317. refs

(AIAA PAPER 91-1844) Copyright

The feasibility is assessed of producing cryogenic propellants on orbit by water electrolysis in support of NASA's proposed Space Exploration Initiative (SEI) missions. Using this method, water launched into low earth orbit (LEO) would be split into gaseous hydrogen and oxygen by electrolysis in an orbiting propellant processor spacecraft. The resulting gases would then be liquefied and stored in cryogenic tanks. Supplying liquid hydrogen and oxygen fuel to space vehicles by this technique has some possible advantages over conventional methods. The potential benefits are derived from the characteristics of water as a payload, and include reduced ground handling and launch risk, denser packaging, and reduced tankage and piping requirements. A conceptual design of a water processor was generated based on related previous studies, and contemporary or near term technologies required. Extensive development efforts would be required to adapt the various subsystems needed for the propellant processor for use in space. Based on the cumulative results, propellant production by on orbit water electrolysis for support of SEI missions is not recommended.

Author

A91-41771* # Washington Univ., Saint Louis, MO.

COMPUTATIONAL MODELING OF THE PRESSURIZATION PROCESS IN A NASP VEHICLE PROPELLANT TANK EXPERIMENTAL SIMULATION

G. P. SASMAL, J. I. HOCHSTEIN, M. C. WENDL (Washington University, Saint Louis, MO), and T. L. HARDY (NASA, Lewis Research Center, Cleveland, OH) AIAA, SAE, ASME, and ASEE, Joint Propulsion Conference, 27th, Sacramento, CA, June 24-26, 1991. 18 p. refs

(Contract NAG3-1156)

(AIAA PAPER 91-2407) Copyright

A multidimensional computational model of the pressurization process in a slush hydrogen propellant storage tank was developed and its accuracy evaluated by comparison to experimental data measured for a 5 ft diameter spherical tank. The fluid mechanic, thermodynamic, and heat transfer processes within the ullage are represented by a finite-volume model. The model was shown to be in reasonable agreement with the experiment data. A parameter

study was undertaken to examine the dependence of the pressurization process on initial ullage temperature distribution and pressurant mass flow rate. It is shown that for a given heat flux rate at the ullage boundary, the pressurization process is nearly independent of initial temperature distribution. Significant differences were identified between the ullage temperature and velocity fields predicted for pressurization of slush and those predicted for pressurization of liquid hydrogen. A simplified model of the pressurization process was constructed in search of a dimensionless characterization of the pressurization process. It is shown that the relationship derived from this simplified model collapses all of the pressure history data generated during this study into a single curve. Author

A91-44197* National Aeronautics and Space Administration. Lewis Research Center, Cleveland, OH.

PARAMAGNETIC PROPELLANT ORIENTATION

R. C. HENDRICKS (NASA, Lewis Research Center, Cleveland, OH) AIAA, SAE, ASME, and ASSE, Joint Propulsion Conference, 27th, Sacramento, CA, June 24-26, 1991. 8 p. Previously announced in STAR as N91-24527. refs (AIAA PAPER 91-2325) Copyright

Deep space or low earth orbital propellant tanks require a fluid orientation system prior to engine firing or transfer. Some propellants such as cryogenic hydrogen, oxygen, and air are paramagnetic and respond to electromagnetic fields. A simple magnetic scheme is described for propellant orientation and a video tape presentation is provided that demonstrates some effects of magnetic fields on liquid air and oxygen in a low gravity simulator using the Leidenfrost phenomenon. When these Leidenfrost drops intersect the field lines, their flight paths are altered, some directly into the poles, some to the edges, and others move out of the field. Author

A91-51914* Battelle Memorial Inst., Columbus, OH.

THE MEASUREMENT, MODELLING AND PREDICTION OF TRACTION FORCES IN A ROCKET PROPELLANT

J. L. TEVAARWERK (Battelle Memorial Institute, Columbus, OH) and C. WOODS (NASA, Lewis Research Center, Cleveland, OH) IN: 1990 SEM Spring Conference on Experimental Mechanics, Albuquerque, NM, June 4-6, 1990, Proceedings. Bethel, CT, Society for Experimental Mechanics, Inc., 1990, p. 155-162. refs Copyright

Traction tests were performed on RPI, a common kerosene-based rocket propellant. Traction data on this fluid are required for purposes of turbopump bearing design, using such codes as SHABERTH. To obtain the traction data, an existing twin disk machine was used, operating under the side slip mode and using elliptical contacts. The resulting traction curves were reduced to fundamental fluid property parameters using the Johnson and Tevaarwerk traction model. Theoretical traction predictions were performed by back substitution of the fundamental properties into the traction model. Comparison of the predicted with the measured curves gives a high degree of confidence in the correctness of the traction model. Author

A91-52362* Argonne National Lab., IL.

DEVELOPMENT OF NUCLEAR FUELS AND MATERIALS FOR PROPULSION SYSTEMS FOR SEI

S. K. BHATTACHARYYA (Argonne National Laboratory, IL), C. S. OLSEN (Idaho National Engineering Laboratory, Idaho Falls), and R. H. TITRAN (NASA, Lewis Research Center, Cleveland, OH) AIAA, NASA, and OAI, Conference on Advanced SEI Technologies, Cleveland, OH, Sept. 4-6, 1991. 11 p. refs (AIAA PAPER 91-3452)

A panel was organized by NASA/DOE/DOD to study nuclear fuels, materials, and related nuclear propulsion technologies for SEI, and the panel findings are discussed. The fuels/materials requirements for nuclear thermal propulsion and nuclear electric propulsions are reviewed, and the development items such as 'element' development and characterization, fabrication process development, nuclear capsule tests, nuclear loop tests, and nuclear furnace tests are examined for selected classes of fuels. C.D.

A91-53710* National Aeronautics and Space Administration. Lewis Research Center, Cleveland, OH.

SLUSH HYDROGEN PROPELLANT PRODUCTION, TRANSFER, AND EXPULSION STUDIES AT THE NASA K-SITE FACILITY

TERRY L. HARDY and MARGARET V. WHALEN (NASA, Lewis Research Center, Cleveland, OH) AIAA, NASA, and OAI, Conference on Advanced SEI Technologies, Cleveland, OH, Sept. 4-6, 1991. 10 p. Previously announced in STAR as N91-28449. refs

(AIAA PAPER 91-3550) Copyright

Slush hydrogen is currently being considered as a fuel for the National Aero-Space Plane (NASP) because it offers the potential for decreased vehicle size and weight. However, no large-scale data was available on the production, transfer, and tank pressure control characteristics required to use the fuel for the NASP. Therefore, experiments were conducted at the NASA Lewis Research Center K-Site Facility to improve the slush hydrogen database. Slush hydrogen was produced using the evaporative cooling, or freeze-thaw, technique in batches of about 800 gallons. This slush hydrogen was pressure transferred to a 5 ft diameter spherical test tank following production, and flow characteristics were measured during this transfer process. The slush hydrogen in the test tank was pressurized and expelled using a pressurized expulsion technique to obtain information on tank pressure control for the NASP. Results from the production, transfer, pressurization, and pressurized expulsion tests are described. Author

A91-53711* National Aeronautics and Space Administration. Lewis Research Center, Cleveland, OH.

PRODUCTION AND USE OF METALS AND OXYGEN FOR LUNAR PROPULSION

ALOYSIUS F. HEPP, DIANE L. LINNE, MARY F. GROTH (NASA, Lewis Research Center, Cleveland, OH), GEOFFREY A. LANDIS (NASA, Lewis Research Center, Cleveland; Sverdrup Technology, Inc., Brook Park, OH), and JAMES E. COLVIN (Arizona, University, Tucson) AIAA, NASA, and OAI, Conference on Advanced SEI Technologies, Cleveland, OH, Sept. 4-6, 1991. 12 p. Previously announced in STAR as N91-29222. refs (AIAA PAPER 91-3481) Copyright

Production, power, and propulsion technologies for using oxygen and metals derived from lunar resources are discussed. The production process is described, and several of the more developed processes are discussed. Power requirements for chemical, thermal, and electrical production methods are compared. The discussion includes potential impact of ongoing power technology programs on lunar production requirements. The performance potential of several possible metal fuels including aluminum, silicon, iron, and titanium are compared. Space propulsion technology in the area of metal/oxygen rocket engines is discussed. Author

N91-15418* National Aeronautics and Space Administration. Lewis Research Center, Cleveland, OH.

IN-FLIGHT AND SIMULATED AIRCRAFT FUEL TEMPERATURE MEASUREMENTS

ROGER A. SVEHLA Dec. 1990 81 p (NASA-TM-103611; E-5765; NAS 1.15:103611) Avail: NTIS HC/MF A05 CSDL 07/4

Fuel tank measurements from ten flights of an L1011 commercial aircraft are reported for the first time. The flights were conducted from 1981 to 1983. A thermocouple rake was installed in an inboard wing tank and another in an outboard tank. During the test periods of either 2 or 5 hr, at altitudes of 10,700 m (35,000 ft) or higher, either the inboard or the outboard tank remained full. Fuel temperature profiles generally developed in the expected manner. The bulk fuel was mixed by natural convection to a nearly uniform temperature, especially in the outboard tank, and a gradient existed at the bottom conduction zone. The data indicated that when full, the upper surface of the inboard tank was wetted and the outboard tank was unwetted. Companion NASA Lewis Research Center tests were conducted in a 0.20 cubic meter (52 gal) tank simulator of the outboard tank, chilled on the top and bottom, and insulated on the sides. Even though the simulator tank had no internal components

28 PROPELLANTS AND FUELS

corresponding to the wing tank, temperatures agreed with the flight measurements for wetted upper surface conditions, but not for unwetted conditions. It was concluded that if boundary conditions are carefully controlled, simulators are a useful way of evaluating actual flight temperatures. Author

N91-19317*# National Aeronautics and Space Administration. Lewis Research Center, Cleveland, OH.

CONCEPTUAL STUDY OF ON ORBIT PRODUCTION OF CRYOGENIC PROPELLANTS BY WATER ELECTROLYSIS

MATTHEW E. MORAN 1991 24 p Proposed for presentation at the 27th Joint Propulsion Conference, Sacramento, CA, 24-27 Jul. 1991; cosponsored by AIAA, SAE, ASME, and ASEE (Contract RTOP 506-48-00) (NASA-TM-103730; E-5964; NAS 1.15:103730) Avail: NTIS HC/MF A03 CSCL 21/9

The feasibility is assessed of producing cryogenic propellants on orbit by water electrolysis in support of NASA's proposed Space Exploration Initiative (SEI) missions. Using this method, water launched into low earth orbit (LEO) would be split into gaseous hydrogen and oxygen by electrolysis in an orbiting propellant processor spacecraft. The resulting gases would then be liquified and stored in cryogenic tanks. Supplying liquid hydrogen and oxygen fuel to space vehicles by this technique has some possible advantages over conventional methods. The potential benefits are derived from the characteristics of water as a payload, and include reduced ground handling and launch risk, denser packaging, and reduced tankage and piping requirements. A conceptual design of a water processor was generated based on related previous studies, and contemporary or near term technologies required. Extensive development efforts would be required to adapt the various subsystems needed for the propellant processor for use in space. Based on the cumulative results, propellant production by on orbit water electrolysis for support of SEI missions is not recommended. Author

N91-20324*# National Aeronautics and Space Administration. Lewis Research Center, Cleveland, OH.

SELF-PRESSURIZATION OF A FLIGHTWEIGHT LIQUID HYDROGEN STORAGE TANK SUBJECTED TO LOW HEAT FLUX

M. M. HASAN, C. S. LIN (Analex Corp., Fairview Park, OH.), and N. T. VANDRESAR 1991 8 p Proposed for presentation at the 1991 ASME/AICHE National Heat Transfer Conference, Minneapolis, MN, 28-31 Jul. 1991 (Contract NAS3-25776)

(NASA-TM-103804; E-6095; NAS 1.15:103804) Avail: NTIS HC/MF A02 CSCL 21/9

Results are presented for an experimental investigation of self-pressurization and thermal stratification of a 4.89 cu m liquid hydrogen (LH2) storage tank subjected to low heat flux (0.35, 2.0, and 3.5 W/sq m) under normal gravity conditions. Tests were performed at fill levels of 83 to 84 percent (by volume). The LH2 tank was representative of future spacecraft tankage, having a low mass-to-volume ratio and high performance multilayer thermal insulation. Results show that the pressure rise rate and thermal stratification increase with increasing heat flux. At the lowest heat flux, the pressure rise rate is comparable to the homogeneous rate, while at the highest heat flux, the rate is more than three times the homogeneous rate. It was found that initial conditions have a significant impact on the initial pressure rise rate. The quasi-steady pressure rise rates are nearly independent of the initial condition after an initial transient period has passed. Author

N91-22464*# National Aeronautics and Space Administration. Lewis Research Center, Cleveland, OH.

MECHANISMS AND MODELING OF THE EFFECTS OF ADDITIVES ON THE NITROGEN OXIDES EMISSION

KRISHNA P. KUNDU, HUNG LEE NGUYEN, and M. PAUL KANG Jan. 1991 24 p Presented at the 29th Aerospace Sciences Meeting, Reno, NV, 7-10 Jan. 1991; sponsored in part by AIAA

(Contract RTOP 537-02-20)

(NASA-TM-103765; E-5969; NAS 1.15:103765; AIAA PAPER 91-0479) Avail: NTIS HC/MF A03 CSCL 20/9

A theoretical study on the emission of the oxides of nitrogen in the combustion of hydrocarbons is presented. The current understanding of the mechanisms and the rate parameters for gas phase reactions were used to calculate the NO(x) emission. The possible effects of different chemical species on thermal NO(x), on a long time scale were discussed. The mixing of these additives at various stages of combustion were considered and NO(x) concentrations were calculated; effects of temperatures were also considered. The chemicals such as hydrocarbons, H2, CH3OH, NH3, and other nitrogen species were chosen as additives in this discussion. Results of these calculations can be used to evaluate the effects of these additives on the NO(x) emission in the industrial combustion system. Author

N91-24263*# National Aeronautics and Space Administration. Lewis Research Center, Cleveland, OH.

THE COLD-SAT EXPERIMENT FOR CRYOGENIC FLUID MANAGEMENT TECHNOLOGY

J. R. SCHUSTER, J. P. WACHTER (Ford Aerospace and Communications Corp., Palo Alto, CA.), and D. M. VENTO /in Johns Hopkins Univ., The 1990 JANNAF Propulsion Meeting, Volume 2 p 317-331 Oct. 1990

(Contract NAS3-25062)

Avail: NTIS HC/MF A20 CSCL 21/9

Future national space transportation missions will depend on the use of cryogenic fluid management technology development needs for these missions. In-space testing will be conducted in order to show low gravity cryogenic fluid management concepts and to acquire a technical data base. Liquid H2 is the preferred test fluid due to its propellant use. The design of COLD-SAT (Cryogenic On-orbit Liquid Depot Storage, Acquisition, and Transfer Satellite), an Expendable Launch Vehicle (ELV) launched orbital spacecraft that will perform subcritical liquid H2 storage and transfer experiments under low gravity conditions is studied. An Atlas launch vehicle will place COLD-SAT into a circular orbit, and the 3-axis controlled spacecraft bus will provide electric power, experiment control, and data management, attitude control, and propulsive accelerations for the experiments. Low levels of acceleration will provide data on the effects that low gravity might have on the heat and mass transfer processes used. The experiment module will contain 3 liquid H2 tanks; fluid transfer, pressurization and venting equipment; and instrumentation. Author

N91-24460*# National Aeronautics and Space Administration. Lewis Research Center, Cleveland, OH.

A PRESSURE CONTROL ANALYSIS OF CRYOGENIC STORAGE SYSTEMS

C.-S. LIN (Analex Corp., Fairview Park, OH.), N. T. VANDRESAR, and M. M. HASAN 1991 10 p Presented at the 27th Joint Propulsion Conference, Sacramento, CA, 24-27 Jun. 1991; cosponsored by AIAA, SAE, ASME, and the American Society for Electrical Engineers (Contract RTOP 506-48-00)

(NASA-TM-104409; E-6235; NAS 1.15:104409; AIAA PAPER 91-2405) Avail: NTIS HC/MF A02 CSCL 21/9

Self-pressurization of cryogenic storage tanks due to heat leak through the thermal protection system is examined along with the performance of various pressure control technologies for application in microgravity environments. Methods of pressure control such as fluid mixing, passive thermodynamic venting, and active thermodynamic venting are analyzed using the homogeneous thermodynamic model. Simplified equations suggested may be used to characterize the performance of various pressure control systems and to design space experiments. Author

N91-25300*# National Aeronautics and Space Administration. Lewis Research Center, Cleveland, OH.

PRESSURIZATION AND EXPULSION OF CRYOGENIC LIQUIDS: GENERIC REQUIREMENTS FOR A LOW GRAVITY EXPERIMENT

NEIL T. VANDRESAR and ROBERT J. STOCHL Jun. 1991
10 p
(Contract RTOP 506-42-73)
(NASA-TM-104417; E-6249; NAS 1.15:104417) Avail: NTIS
HC/MF A02 CSCL 21/9

Requirements are presented for an experiment designed to obtain data for the pressurization and expulsion of a cryogenic supply tank in a low gravity environment. These requirements are of a generic nature and applicable to any cryogenic fluid of interest, condensible or non-condensable pressurants, and various low gravity test platforms such as the Space Shuttle or a free-flyer. Background information, the thermophysical process, preliminary analytical modeling, and experimental requirements are discussed. Key parameters, measurements, hardware requirements, procedures, a test matrix, and data analysis are outlined. Author

N91-27375*# National Aeronautics and Space Administration. Lewis Research Center, Cleveland, OH.
AUTOGENOUS PRESSURIZATION OF CRYOGENIC VESSELS USING SUBMERGED VAPOR INJECTION

ROBERT J. STOCHL, NEIL T. VANDRESAR, and RAYMOND F. LACOVIC 1991 10 p Presented at the Cryogenic Engineering and International Cryogenic Materials Conference, Huntsville, AL, 11-14 Jun. 1991; cosponsored by NASA. Marshall Space Flight Center and Alabama Univ.
(Contract RTOP 591-23-00)
(NASA-TM-104516; E-6386; NAS 1.15:104516) Avail: NTIS
HC/MF A02 CSCL 20/4

Experimental results are reported for submerged injection pressurization and expulsion tests of a 4.89 cu m liquid hydrogen tank. The pressurant injector was positioned near the bottom of the test vessel to simulate liquid engulfment of the pressurant gas inlet; a condition that may occur in low-gravity conditions. Results indicate a substantial reduction in pressurization efficiency, with pressurant gas requirements approximately five times greater than ideal amounts. Consequently, submerged vapor injection should be avoided as a low-gravity autogenous pressurization method whenever possible. The work presented herein validates that pressure requirements are accurately predicted by a homogeneous thermodynamic model when the submerged injection technique is employed. Author

N91-28449*# National Aeronautics and Space Administration. Lewis Research Center, Cleveland, OH.

SLUSH HYDROGEN PROPELLANT PRODUCTION, TRANSFER, AND EXPULSION STUDIES AT THE NASA K-SITE FACILITY
TERRY L. HARDY and MARGARET V. WHALEN 1991 11 p
Presented at the Conference on Advanced Space Exploration Initiative Technologies, Cleveland, OH, 4-6 Sep. 1991; cosponsored by AIAA and OAI
(Contract RTOP 763-22-21)
(NASA-TM-105191; E-6493; NAS 1.15:105191; AIAA PAPER 91-3550) Avail: NTIS HC/MF A03 CSCL 21/9

Slush hydrogen is currently being considered as a fuel for the National AeroSpace Plane (NASP) because it offers the potential for decreased vehicle size and weight. However, no large scale data was available on the production, transfer, and tank pressure control characteristics required to use the fuel for the NASP. Therefore, experiments were conducted at NASA-Lewis K-Site Facility to improve the slush hydrogen data base. Slush hydrogen was produced using the evaporative cooling, or freeze-thaw, technique in batches for approx. 800 gallons. This slush hydrogen was pressure transferred to a 5 ft diameter spherical test tank following production, and flow characteristics were measured during this transfer process. The slush hydrogen in the test tank was pressurized and expelled using a pressurized expulsion technique to obtain information on tank pressure control for the NASP. Results from the production, transfer, pressurization, and pressurized expulsion tests are described. Author

N91-31318*# National Aeronautics and Space Administration. Lewis Research Center, Cleveland, OH.

TECHNICAL PROSPECTS FOR UTILIZING EXTRATERRESTRIAL PROPELLANTS FOR SPACE EXPLORATION

DIANE L. LINNE and MICHAEL L. MEYER 1991 20 p Presented at the 42nd International Astronautical Congress, Montreal, Quebec, 5-11 Oct. 1991; sponsored by International Astronautical Federation
(Contract RTOP 506-42-72)
(NASA-TM-105263; E-6594; NAS 1.15:105263) Avail: NTIS
HC/MF A03 CSCL 21/9

NASA's LeRC has supported several efforts to understand how lunar and Martian produced propellants can be used to their best advantage for space exploration propulsion. A discussion of these efforts and their results is presented. A Manned Mars Mission Analysis Study identified that a more thorough technology base for propellant production is required before the net economic benefits of in situ propellants can be determined. Evaluation of the materials available on the moon indicated metal/oxygen combinations are the most promising lunar propellants. A hazard analysis determined that several lunar metal/LOX monopropellants could be safely worked with in small quantities, and a characterization study was initiated to determine the physical and chemical properties of potential lunar monopropellant formulations. A bipropellant metal/oxygen subscale test engine which utilizes pneumatic injection of powdered metal is being pursued as an alternative to the monopropellant systems. The technology for utilizing carbon monoxide/oxygen, a potential Martian propellant, was studied in subscale ignition and rocket performance experiments. Author

29

MATERIALS PROCESSING

Includes space-based development of products and processes for commercial applications.

A91-19463*# National Aeronautics and Space Administration. Lewis Research Center, Cleveland, OH.

PROGRAMMABLE MULTI-ZONE FURNACE FOR MICROGRAVITY RESEARCH

BRUCE N. ROSENTHAL (NASA, Lewis Research Center, Cleveland, OH) and CATHRYN R. KROLIKOWSKI (Cleveland State University, OH) AIAA, Aerospace Sciences Meeting, 29th, Reno, NV, Jan. 7-10, 1991. 8 p. refs
(AIAA PAPER 91-0781) Copyright

In order to provide new furnace technology to accommodate microgravity research studies and commercial applications in material processes, research has been initiated on the development of the Programmable-Multi-zone Furnace (PMZF). The PMZF is described as a multi-user materials processing furnace facility that is composed of thirty or more heater elements in series on a muffle tube or in a stacked ring-type configuration and independently controlled by a computer. One of the aims of the PMZF project is to allow furnace thermal gradient profiles to be reconfigured without physical modification of the hardware by creating the capability of reconfiguring thermal profiles in response to investigators' requests. The future location of the PMZF facility is discussed; the preliminary science survey results and preliminary conceptual designs for the PMZF are presented; and a review of multi-zone furnace technology is given. L.K.S.

A91-24563*# National Aeronautics and Space Administration. Lewis Research Center, Cleveland, OH.

INTERACTION OF SURFACE RADIATION WITH CONVECTION IN CRYSTAL GROWTH BY PHYSICAL VAPOR TRANSPORT

MOHAMMAD KASSEMI and WALTER M. B. DUVAL (NASA, Lewis Research Center, Cleveland, OH) Journal of Thermophysics

29 MATERIALS PROCESSING

and Heat Transfer (ISSN 0887-8722), vol. 4, Oct. 1990, p. 454-461. Previously cited in issue 11, p. 1624, Accession no. A89-30450. refs
Copyright

A91-26329* National Aeronautics and Space Administration. Lewis Research Center, Cleveland, OH.

A SUMMARY OF EXISTING AND PLANNED EXPERIMENT HARDWARE FOR LOW-GRAVITY FLUIDS RESEARCH

MYRON E. HILL and TERENCE F. O'MALLEY (NASA, Lewis Research Center, Cleveland, OH) AIAA, Aerospace Sciences Meeting, 29th, Reno, NV, Jan. 7-10, 1991. 43 p. refs (AIAA PAPER 91-0777) Copyright

NASA's ground-based and space-based low-gravity facilities are summarized, and an overview of selected experiments that have been developed for use in these facilities is presented. A variety of ground-based facilities (drop towers and aircraft) used to conduct low-gravity experiments for in-space experimentation are described. Capabilities that are available to the researcher and future on-orbit fluids facilities are addressed. The payload bay facilities range from the completely self-contained, relatively small get-away-special canisters to the Materials Science Laboratory and to the larger Spacelab facilities that require crew interaction. Y.P.Q.

A91-42642* National Aeronautics and Space Administration. Lewis Research Center, Cleveland, OH.

THREE-DIMENSIONAL FLOW TRANSPORT MODES IN DIRECTIONAL SOLIDIFICATION DURING SPACE PROCESSING

W. A. ARNOLD, D. A. JACQMIN, R. L. GAUG, and A. CHAIT (NASA, Lewis Research Center, Cleveland, OH) Journal of Spacecraft and Rockets (ISSN 0022-4650), vol. 28, Mar.-Apr. 1991, p. 238-243. Previously cited in issue 09, p. 1295, Accession no. A90-25032. refs
Copyright

A91-53408* Rensselaer Polytechnic Inst., Troy, NY. **ISOTHERMAL DENDRITIC GROWTH EXPERIMENT - SCIENCE, ENGINEERING, AND HARDWARE DEVELOPMENT FOR USMP SPACE FLIGHTS**

M. E. GLICKSMAN, R. C. HAHN, M. B. KOSS, S. H. TIRMIZI, M. E. SELLECK, A. VELOSA (Rensselaer Polytechnic Institute, Troy, NY), and E. WINSA (NASA, Lewis Research Center, Cleveland, OH) (Microgravity research: Material and fluid sciences; Proceedings of Symposium 11 of the COSPAR 28th Plenary Meeting, The Hague, Netherlands, June 25-July 6, 1990. A91-53401 23-29) Advances in Space Research (ISSN 0273-1177), vol. 11, no. 7, 1991, p. 53-57. refs
(Contract NAS3-25368)
Copyright

The Isothermal Dendritic Growth Experiment (IDGE) has been designed to provide microgravity data on dendritic growth for a critical test of theory. This paper updates progress on constructing a crystal growth chamber suitable for space flight. The IDGE chamber is constructed from glass and stainless steel and is hermetically sealed by electron beam welds and glass-metal seals. Initial tests of the chambers sample's melting point plateau show that the new chamber design is capable of preserving the 99.9995 percent purity of succinonitrile. Dendrite growth can be initiated in the center of the IDGE chamber by means of thermo-electric coolers and a capillary injector tube (stinger). The new IDGE chamber is ready for fully integrated tests with the prototype IDGE engineering hardware at NASA's Lewis Research Center. Author

N91-14498* National Aeronautics and Space Administration. Lewis Research Center, Cleveland, OH.

MANIPULATION HARDWARE FOR MICROGRAVITY RESEARCH

J. N. HERNDON, R. L. GLASSELL, P. L. BUTLER, D. M. WILLIAMS, D. A. ROHN, and J. H. MILLER (Sverdrup Technology, Inc., Brook Park, OH.) 1990 14 p Presented at the American Nuclear Society Winter Meeting, Washington, DC, 11-15 Nov. 1990

(Contract DE-AC05-84OR-21400)

(NASA-TM-103423; NAS 1.15:103423; DE91-002871; CONF-901101-46) Avail: NTIS HC/MF A03 CSCL 22/1

The establishment of permanent low earth orbit occupation on the Space Station Freedom will present new opportunities for the introduction of productive flexible automation systems into the microgravity environment of space. The need for robust and reliable robotic systems to support experimental activities normally intended by astronauts will assume great importance. Many experimental modules on the space station are expected to require robotic systems for ongoing experimental operations. When implementing these systems, care must be taken not to introduce deleterious effects on the experiments or on the space station itself. It is important to minimize the acceleration effects on the experimental items being handled while also minimizing manipulator base reaction effects on adjacent experiments and on the space station structure. NASA Lewis Research Center has been performing research on these manipulator applications, focusing on improving the basic manipulator hardware, as well as developing improved manipulator control algorithms. By utilizing the modular manipulator concepts developed during the Laboratory Telerobotic Manipulator program, Oak Ridge National Laboratory has developed an experimental testbed system called the Microgravity Manipulator, incorporating two pitch-yaw modular positioners to provide a 4 dof experimental manipulator arm. A key feature in the design for microgravity manipulation research was the use of traction drives for torque transmission in the modular pitch-yaw differentials.

DOE

N91-19320* National Aeronautics and Space Administration. Lewis Research Center, Cleveland, OH.

GROWTH KINETICS OF PHYSICAL VAPOR TRANSPORT PROCESSES: CRYSTAL GROWTH OF THE OPTOELECTRONIC MATERIAL MERCUROS CHLORIDE

N. B. SINGH (Westinghouse Research and Development Center, Pittsburgh, PA.) and W. M. DUVAL Mar. 1991 31 p
(Contract NAS3-25274; RTOP 674-21-05)
(NASA-TM-103788; E-6065; NAS 1.15:103788) Avail: NTIS HC/MF A03 CSCL 12/1

Physical vapor transport processes were studied for the purpose of identifying the magnitude of convective effects on the crystal growth process. The effects of convection on crystal quality were studied by varying the aspect ratio and those thermal conditions which ultimately affect thermal convection during physical vapor transport. An important outcome of the present study was the observation that the convection growth rate increased up to a certain value and then dropped to a constant value for high aspect ratios. This indicated that a very complex transport had occurred which could not be explained by linear stability theory. Better quality crystals grown at a low Rayleigh number confirmed that improved properties are possible in convectionless environments. Author

N91-21378* National Aeronautics and Space Administration. Lewis Research Center, Cleveland, OH.

AN EXAMINATION OF ANTICIPATED G-JITTER ON SPACE STATION AND ITS EFFECTS ON MATERIALS PROCESSES

EMILY S. NELSON May 1991 118 p
(NASA-TM-103775; E-6042; NAS 1.15:103775) Avail: NTIS HC/MF A06 CSCL 22/1

Discussed here are the effects of g-jitter, the residual acceleration aboard spacecraft, on selected cases of materials processes. In particular, the anticipated acceleration environment aboard Space Station Freedom and its potential effects are analyzed. The topic is covered with a sufficient level of generosity as to apply to other processes and vehicles as well. Key findings of the study are discussed. Author

N91-24464* National Aeronautics and Space Administration. Lewis Research Center, Cleveland, OH.

MICROGRAVITY RESEARCH AT LERC

FRED J. KOHL 1990 7 p Presented at the CSME Mechanical Engineering Forum 1990, Toronto, Ontario, 3-9 Jun. 1990;

sponsored by the Canadian Society for Mechanical Engineering (Contract RTOP 674-29-05)
(NASA-TM-102521; E-5325; NAS 1.15:102521) Avail: NTIS HC/MF A02 CSCL 22/1

The NASA Lewis Research Center is conducting a wide variety of ground-based science and microgravity flight experiments in the disciplines of fluid physics and transport phenomena, combustion science, and materials science. Extensive use is made of low-gravity ground-based facilities such as drop towers and a Learjet aircraft, as well as extensive normal-gravity laboratories. The ground-based facilities are utilized to execute science programs, perform precursor tests to define space experiment science requirements and conceptual designs, and also to perform tests for space experiment technology development and verification. Finally, flight hardware is designed, developed and flown on the Space Shuttle. Author

31

ENGINEERING (GENERAL)

Includes vacuum technology; control engineering; display engineering; cryogenics; and fire prevention.

A91-23108* Pennsylvania State Univ., University Park.

A NEW APPROACH TO CONTROLLER DESIGN FOR MICROGRAVITY ISOLATION SYSTEMS

A. SINHA, C. K. KAO (Pennsylvania State University, University Park), and C. GRODSINSKY (NASA, Lewis Research Center, Cleveland, OH) Acta Astronautica (ISSN 0094-5765), vol. 21, Nov.-Dec. 1990, p. 771-775. refs
(Contract NAG3-949) Copyright

A new method has been developed to design an active vibration isolation system for microgravity space experiments. This method yields the required controller transfer functions for a specified transmissibility. Hence, it is a straightforward task to guarantee that the desired vibration isolation performance is achieved at each frequency. The theory for such a controller design has been presented by considering a single degree of freedom system. The magnitude of the control force required by the new method has been found to be less than that used by a standard phase lead/lag compensator. Author

A91-31842* National Aeronautics and Space Administration. Lewis Research Center, Cleveland, OH.

CONCURRENT MATERIAL-FABRICATION OPTIMIZATION OF METAL-MATRIX LAMINATES UNDER THERMO-MECHANICAL LOADING

D. A. SARAVANOS, M. R. MOREL, and C. C. CHAMIS (NASA, Lewis Research Center, Cleveland, OH) IN: AIAA/ASME/ASCE/AHS/ASC Structures, Structural Dynamics, and Materials Conference, 32nd, Baltimore, MD, Apr. 8-10, 1991, Technical Papers. Pt. 1. Washington, DC, American Institute of Aeronautics and Astronautics, 1991, p. 116-123. refs
(AIAA PAPER 91-1044) Copyright

A methodology is developed to tailor fabrication and material parameters of metal-matrix laminates for maximum loading capacity under thermomechanical loads. The stresses during the thermomechanical response are minimized subject to failure constraints and bounds on the laminate properties. The thermomechanical response of the laminate is simulated using nonlinear composite mechanics. Evaluations of the method on a graphite/copper symmetric cross-ply laminate were performed. The cross-ply laminate required different optimum fabrication procedures than a unidirectional composite. Also, the consideration of the thermomechanical cycle had a significant effect on the predicted optimal process. Author

A91-43444* National Aeronautics and Space Administration. Lewis Research Center, Cleveland, OH.

IMPROVED THERMODYNAMIC MODELLING OF THE NO-VENT FILL PROCESS AND CORRELATION WITH EXPERIMENTAL DATA

W. J. TAYLOR and D. J. CHATO (NASA, Lewis Research Center, Cleveland, OH) AIAA, Thermophysics Conference, 26th, Honolulu, HI, June 24-26, 1991. 19 p. refs
(AIAA PAPER 91-1379) Copyright

The United States plans to establish a permanent manned presence in space and to explore the Solar System have created the need to efficiently handle large quantities of subcritical cryogenic fluids, particularly propellants such as liquid hydrogen and liquid oxygen, in low- to zero-gravity environments. One of the key technologies to be developed for fluid handling is the ability to transfer the cryogenics between storage and spacecraft tanks. The no-vent fill method has been identified as one way to perform this transfer. In order to understand how to apply this method, a model of the no-vent fill process is being developed and correlated with experimental data. The verified models then can be used to design and analyze configurations for tankage and subcritical fluid depots. This paper discusses the development of an improved macroscopic thermodynamic model of the no-vent fill process and correlates the analytical results from the computer program implementation of the model with experimental results for two different test tanks at NASA Lewis Research Center. Author

A91-44336* National Aeronautics and Space Administration. Lewis Research Center, Cleveland, OH.

LN2 SPRAY DROPLET SIZE MEASUREMENT VIA ENSEMBLE DIFFRACTION TECHNIQUE

N. H. SAIYED, D. J. CHATO (NASA, Lewis Research Center, Cleveland, OH), and J. JURNS (NASA, Lewis Research Center, Cleveland; Sverdrup Technology, Inc., Brook Park, OH) AIAA, Thermophysics Conference, 26th, Honolulu, HI, June 24-26, 1991. 13 p. Previously announced in STAR as N91-24470. refs
(AIAA PAPER 91-1381) Copyright

The size of subcooled liquified nitrogen droplets are measured with a 5 mW He-Ne laser as a function of pressure difference (ΔP) across flat spray and full cone pressure atomizing nozzles. For ΔP 's of 3 to 30 psid, the spray sauter mean diameter (SMD) ranged between 250 to 50 microns. The pressure range tested is representative of those expected during cryogenic fluid transfer operations in space. The droplet sizes from the flat spray nozzles were greater than those from the full cone nozzle. A power function of the form, SMD varies as $\Delta P^{(exp a)}$, describes the spray SMD as a function of the ΔP very well. The values of a were -0.36 for the flat spray and -0.87 for the full cone. The reduced dependence of the flat spray SMD on the ΔP was probably because of: (1) the absence of a swirler that generates a turbulence within the nozzle to enhance atomization, and (2) a possible increase in shearing stress resulting from the delayed atomization due to the absence of turbulence. The nitrogen quality, up to 1.5 percent is based on isenthalpic expansion, did not have a distinct and measurable effect on the spray SMD. Both bimodal and monomodal droplet size population distributions were measured. In the bimodal distribution, the frequency of the first mode was much greater than the frequency of the second mode. Also, the frequency of the second mode was low enough such that a monomodal approximation probably would give reasonable results. Author

A91-52430* Michigan Univ., Ann Arbor.

DISCHARGE RATE OF CRYOGENS IN MICROGRAVITY - WHAT GROUND BASED EXPERIMENTATION CANNOT RESOLVE

T. P. PURWIN, M. KAVIANY (Michigan, University, Ann Arbor), and J. C. AYDELOTT (NASA, Lewis Research Center, Cleveland, OH) AIAA, NASA, and OAI, Conference on Advanced SEI Technologies, Cleveland, OH, Sept. 4-6, 1991. 6 p. refs
(AIAA PAPER 91-3545) Copyright

The discharge of cryogenic vapor and liquid from tanks to a

31 ENGINEERING (GENERAL)

vacuum is examined and the effects of the mass quality, length/diameter ratio, supply tank transient and gravitational environment are discussed. Existing model results and normal gravity experiments are presented which indicate that the homogeneous equilibrium model provides an accurate description of two-phase critical flow for a number of conditions likely to be encountered in practical microgravity systems. Nonequilibrium effects are shown to produce flow rates greater than homogeneous equilibrium model predictions for long tubes with low inlet pressure and short tubes with high inlet pressure. R.E.P.

A91-52436# National Aeronautics and Space Administration. Lewis Research Center, Cleveland, OH.

THE NASA CRYOGENIC FLUID MANAGEMENT TECHNOLOGY PROGRAM PLAN

JAMES R. FADDOUL (NASA, Lewis Research Center, Cleveland, OH) and STANLEY D. MCINTYRE (NASA, Marshall Space Flight Center, Huntsville, AL) AIAA, NASA, and OAI, Conference on Advanced SEI Technologies, Cleveland, OH, Sept. 4-6, 1991. 23 p.

(AIAA PAPER 91-3553) Copyright

The status of the NASA Cryogenic Fluid Management Technology Program Plan is discussed along with specific needs for near future missions. Using the Space Exploration Initiative mission set, cost/benefit projections are then made for development of advanced cryogenic fluid management techniques. Space based and earth based test programs are discussed relative to the technology requirements for liquid storage, supply and transfer and for fluid transfer and advanced instrumentation.

R.E.P.

A91-53701*# National Aeronautics and Space Administration. Lewis Research Center, Cleveland, OH.

NASA CRYOGENIC FLUID MANAGEMENT SPACE EXPERIMENT EFFORTS

DANIEL GLOVER (NASA, Lewis Research Center, Cleveland, OH) AIAA, NASA, and OAI, Conference on Advanced SEI Technologies, Cleveland, OH, Sept. 4-6, 1991. 25 p. Previously announced in STAR as N91-30073. refs

(AIAA PAPER 91-3538) Copyright

A history of technological development for subcritical cryogenic fluid management (CFM) through space experiments is given for the period 1960 to 1990. Space experiments with liquid hydrogen were conducted in the early 1960s. Efforts since then have consisted of studies and designs of potential space experiments. A chronology of CFM space experiments and design efforts is included.

Author

N91-11945*# National Aeronautics and Space Administration. Lewis Research Center, Cleveland, OH.

PLASMA-ASSISTED PHYSICAL VAPOR DEPOSITION SURFACE TREATMENTS FOR TRIBOLOGICAL CONTROL

TALIVALDIS SPALVINS 1990 18 p Presented at the TMS Annual Meeting, New Orleans, LA, 17-21 Feb. 1991; sponsored in part by the Minerals, Metals and Materials Society (Contract RTOP 505-63-5A)

(NASA-TM-103652; E-5799; NAS 1.15:103652) Avail: NTIS HC/MF A03 CSCL 13/2

In any mechanical or engineering system where contacting surfaces are in relative motion, adhesion, wear, and friction affect reliability and performance. With the advancement of space age transportation systems, the tribological requirements have dramatically increased. This is due to the optimized design, precision tolerance requirements, and high reliability expected for solid lubricating films in order to withstand hostile operating conditions (vacuum, high-low temperatures, high loads, and space radiation). For these problem areas the ion-assisted deposition/modification processes (plasma-based and ion beam techniques) offer the greatest potential for the synthesis of thin films and the tailoring of adherence and chemical and structural properties for optimized tribological performance. The present practices and new approaches of applying soft solid lubricant and hard wear resistant films to engineering substrates are reviewed.

The ion bombardment treatments have increased film adherence, lowered friction coefficients, and enhanced wear life of the solid lubricating films such as the dichalcogenides (MoS₂) and the soft metals (Au, Ag, Pb). Currently, sputtering is the preferred method of applying MoS₂ films; and ion plating, the soft metallic films. Ultralow friction coefficients (less than 0.01) were achieved with sputtered MoS₂. Further, new diamond-like carbon and BN lubricating films are being developed by using the ion assisted deposition techniques.

Author

N91-14500*# National Aeronautics and Space Administration. Lewis Research Center, Cleveland, OH.

A NUMERICAL AND EXPERIMENTAL ANALYSIS OF REACTOR PERFORMANCE AND DEPOSITION RATES FOR CVD ON MONOFILAMENTS

S. A. GOKOGLU, M. KUCZMARSKI, L. VEITCH, P. TSUI (Sverdrup Technology, Inc., Brook Park, OH.), and A. CHAIT 1990 9 p Presented at the 11th International Conference on Chemical Vapor Deposition, Seattle, WA, 14-19 Oct. 1990; sponsored by Electrochemical Society

(Contract NAS3-25266; RTOP 510-01-01)

(NASA-TM-103631; E-5801; NAS 1.15:103631) Avail: NTIS HC/MF A02 CSCL 13/2

The computational fluid dynamics (CFD) code FLUENT is adopted to simulate a cylindrical upflow reactor designed for chemical vapor deposition (CVD) on monofilaments. Equilibrium temperature profiles along the fiber and quartz reactor wall are experimentally measured and used as boundary conditions in numerical simulations. Two-dimensional axisymmetric flow and temperature fields are calculated for hydrogen and argon; the effect of free convection is assessed. The gas and surface chemistry is included for predicting silicon deposition from silane. The model predictions are compared with experimentally measured silicon CVD rates. Inferences are made for optimum conditions to obtain uniformity.

Author

N91-15424*# National Aeronautics and Space Administration. Lewis Research Center, Cleveland, OH.

LIQUID SHEET RADIATOR APPARATUS Patent

DONALD L. CHUBB, inventor (to NASA) 3 Apr. 1990 9 p Filed 15 Sep. 1988

(NASA-CASE-LEW-14295-1; US-PATENT-4,913,225; US-PATENT-APPL-SN-244377; US-PATENT-CLASS-165-104.31; US-PATENT-CLASS-165-41; US-PATENT-CLASS-165-904; US-PATENT-CLASS-239-597; US-PATENT-CLASS-239-601; US-PATENT-CLASS-244-163; INT-PATENT-CLASS-F8-15/00)

Avail: US Patent and Trademark Office CSCL 13/2

An external flow, liquid sheet radiator apparatus adapted for space applications has as its radiating surface a thin stable liquid sheet formed by fluid flow through a very narrow slit affixed to the sheet generator. As a result of surface tension forces, the sheet has a triangular shape and is collected into a simply designed collector positioned at the apex of the triangle. The specific power for the liquid sheet is virtually the same as the droplet sheet specific power.

Official Gazette of the U.S. Patent and Trademark Office

N91-19324*# National Aeronautics and Space Administration. Lewis Research Center, Cleveland, OH.

DEVELOPMENT OF A VIBRATION ISOLATION PROTOTYPE SYSTEM FOR MICROGRAVITY SPACE EXPERIMENTS

KIRK A. LOGSDON, CARLOS M. GRODSINSKY, and GERALD V. BROWN 1990 8 p Presented at the 28th Plenary Meeting of the Committee on Space Research, The Hague, Netherlands, 25 Jun. - 6 Jul. 1990; cosponsored by COSPAR, ESA, and NASDA

(Contract RTOP 694-03-03)

(NASA-TM-103664; E-5871; NAS 1.15:103664) Avail: NTIS HC/MF A02 CSCL 13/2

The presence of small levels of low-frequency accelerations on the space shuttle orbiters has degraded the microgravity environment for the science community. Growing concern about this microgravity environment has generated interest in systems

that can isolate microgravity science experiments from vibrations. This interest has resulted primarily in studies of isolation systems with active methods of compensation. The development of a magnetically suspended, six-degree-of-freedom active vibration isolation prototype system capable of providing the needed compensation to the orbital environment is presented. A design for the magnetic actuators is described, and the control law for the prototype system that gives a nonintrusive inertial isolation response to the system is also described. Relative and inertial sensors are used to provide an inertial reference for isolating the payload. Author

N91-23340* National Aeronautics and Space Administration. Lewis Research Center, Cleveland, OH.

A SIMPLIFIED DYNAMIC MODEL OF THE SPACE SHUTTLE MAIN ENGINE

AHMET DUYAR, VASFI ELDEM (Florida Atlantic Univ., Boca Raton.), WALTER MERRILL, and TEN-HUEI GUO 1991 12 p Presented at the American Control Conference, Boston, MA, 26-28 Jun. 1991; sponsored by the American Automatic Control Council (Contract RTOP 582-01-11) (NASA-TM-104421; E-6133; NAS 1.15:104421) Avail: NTIS HC/MF A03 CSCL 21/8

A simplified model is presented of the space shuttle main engine (SSME) dynamics valid within the range of operation of the engine. This model is obtained by linking the linearized point models obtained at 25 different operating points of SSME. The simplified model was developed for use with a model-based diagnostic scheme for failure detection and diagnostics studies, as well as control design purposes. Author

N91-24469* National Aeronautics and Space Administration. Lewis Research Center, Cleveland, OH.

ALPHA-CANONICAL FORM REPRESENTATION OF THE OPEN LOOP DYNAMICS OF THE SPACE SHUTTLE MAIN ENGINE

ALMET DUYAR, VASFI ELDEM (Florida Atlantic Univ., Boca Raton.), WALTER C. MERRILL, and TEN-HUEI GUO 1991 22 p Presented at the American Control Conference, Boston, MA, 26-28 Jun. 1991; sponsored by the American Automatic Control Council (Contract RTOP 582-01-11) (NASA-TM-104422; E-6255; NAS 1.15:104422) Avail: NTIS HC/MF A03 CSCL 13/2

A parameter and structure estimation technique for multivariable systems is used to obtain a state space representation of open loop dynamics of the space shuttle main engine in alpha-canonical form. The parameterization being used is both minimal and unique. The simplified linear model may be used for fault detection studies and control system design and development. Author

N91-24470* National Aeronautics and Space Administration. Lewis Research Center, Cleveland, OH.

LN2 SPRAY DROPLET SIZE MEASUREMENT VIA ENSEMBLE DIFFRACTION TECHNIQUE

N. H. SAIYED, J. JURNS (Sverdrup Technology, Inc., Brook Park, OH.), and DAVID J. CHATO 1991 14 p Presented at the 26th Thermophysics Conference, Honolulu, HI, 24-26 Jun. 1991; sponsored by AIAA (Contract RTOP 506-48-00) (NASA-TM-104443; E-6283; NAS 1.15:104443; AIAA PAPER 91-1381) Avail: NTIS HC/MF A03 CSCL 13/2

The size of subcooled liquified nitrogen droplets are measured with a 5 mW He-Ne laser as a function of pressure difference (delta P) across flat spray and full cone pressure atomizing nozzles. For delta P's of 3 to 30 psid, the spray sauter mean diameter (SMD) ranged between 250 to 50 microns. The pressure range tested is representative of those expected during cryogenic fluid transfer operations in space. The droplet sizes from the flat spray nozzles were greater than those from the full cone nozzle. A power function of the form, SMD varies as delta P (exp a), describes the spray SMD as a function of the delta P very well. The values of a were -0.36 for the flat spray and -0.87 for the full cone. The reduced dependence of the flat spray SMD on the delta P was

probably because of: (1) the absence of a swirler that generates turbulence within the nozzle to enhance atomization, and (2) a possible increase in shearing stress resulting from the delayed atomization due to the absence of turbulence. The nitrogen quality, up to 1.5 percent is based on isenthalpic expansion, did not have a distinct and measurable effect on the spray SMD. Both bimodal and monomodal droplet size population distributions were measured. In the bimodal distribution, the frequency of the first mode was much greater than the frequency of the second mode. Also, the frequency of the second mode was low enough such that a monomodal approximation probably would give reasonable results. Author

32

COMMUNICATIONS AND RADAR

Includes radar; land and global communications; communications theory; and optical communications.

A91-17719* National Aeronautics and Space Administration. Lewis Research Center, Cleveland, OH.

COPLANAR-WAVEGUIDE/MICROSTRIP PROBE COUPLER AND APPLICATIONS TO ANTENNAS

R. N. SIMONS and R. Q. LEE (NASA, Lewis Research Center, Cleveland, OH) Electronics Letters (ISSN 0013-5194), vol. 26, Nov. 22, 1990, p. 1998-2000. Copyright

A method to couple microwave power from a coplanar waveguide to a microstrip line on opposite sides of a ground plane is demonstrated. The coupler uses a metallic post which passes through an aperture on the ground plane connecting the strip conductor of the coplanar waveguide to the microstrip line. The measured insertion loss and return loss are about 1 dB and 10 dB, respectively, across the frequency range of 0.045-6.5 GHz. To demonstrate potential applications of the coupler as a feeding network for a microstrip patch array, measured radiation patterns of two rectangular patch antennas with a direct coplanar-waveguide/microstrip feed and with a proximity coupled coplanar-waveguide/microstrip feed are presented. Author

A91-20370* National Aeronautics and Space Administration. Lewis Research Center, Cleveland, OH.

CIRCULAR POLARISATION CHARACTERISTICS OF STACKED MICROSTRIP ANTENNAS

R. Q. LEE (NASA, Lewis Research Center, Cleveland, OH), T. TALTY, and K. F. LEE (Toledo, University, OH) Electronics Letters (ISSN 0013-5194), vol. 26, Dec. 6, 1990, p. 2109, 2110. refs Copyright

Experimental results on the circular polarization (CP) characteristics of a two-layer electromagnetically coupled (EMCP) antenna are presented. Compared to the single CP patch antenna, the two-layer EMCP antenna with proper spacings can provide better axial ratio and directivity. C.D.

A91-24950* National Aeronautics and Space Administration. Lewis Research Center, Cleveland, OH.

BIT ERROR RATE TESTING OF FIBER OPTIC DATA LINKS FOR MMIC-BASED PHASED ARRAY ANTENNAS

K. A. SHALKHAUSER, R. R. KUNATH (NASA, Lewis Research Center, Cleveland, OH), and A. S. DARYOUSH (Drexel University, Philadelphia, PA) IN: Optoelectronic signal processing for phased-array antennas II; Proceedings of the Meeting, Los Angeles, CA, Jan. 16, 17, 1990. Bellingham, WA, Society of Photo-Optical Instrumentation Engineers, 1990, p. 247-254. Previously announced in STAR as N90-21261. Copyright

The measured bit-error-rate (BER) performance of a fiber optic data link to be used in satellite communications systems is presented and discussed. In the testing, the link was measured

32 COMMUNICATIONS AND RADAR

for its ability to carry high burst rate, serial-minimum shift keyed (SMSK) digital data similar to those used in actual space communications systems. The fiber optic data link, as part of a dual-segment injection-locked RF fiber optic link system, offers a means to distribute these signals to the many radiating elements of a phased array antenna. Test procedures, experimental arrangements, and test results are presented. Author

A91-24951* National Aeronautics and Space Administration. Lewis Research Center, Cleveland, OH.

DESIGN OF AN OPTICALLY CONTROLLED KA-BAND GAAS MMIC PHASED-ARRAY ANTENNA

RICHARD R. KUNATH, KUL B. BHASIN (NASA, Lewis Research Center, Cleveland, OH), PAUL C. CLASPY, and MARK A. RICHARD (Case Western Reserve University, Cleveland, OH) IN: Optoelectronic signal processing for phased-array antennas II; Proceedings of the Meeting, Los Angeles, CA, Jan. 16, 17, 1990. Bellingham, WA, Society of Photo-Optical Instrumentation Engineers, 1990, p. 255-259. Previously announced in STAR as N90-26250. refs

Copyright

Phased array antennas long were investigated to support the agile, multibeam radiating apertures with rapid reconfigurability needs of radar and communications. With the development of the Monolithic Microwave Integrated Circuit (MMIC), phased array antennas having the stated characteristics are becoming realizable. However, at K-band frequencies (20 to 40 GHz) and higher, the problem of controlling the MMICs using conventional techniques either severely limits the array size or becomes insurmountable due to the close spacing of the radiating elements necessary to achieve the desired antenna performance. Investigations were made that indicate using fiber optics as a transmission line for control information for the MMICs provides a potential solution. By adding an optical interface circuit to pre-existing MMIC designs, it is possible to take advantage of the small size, lightweight, mechanical flexibility and RFI/EMI resistant characteristics of fiber optics to distribute MMIC control signals. The architecture, circuit development, testing and integration of optically controlled K-band MMIC phased array antennas are described. Author

A91-52341*# National Aeronautics and Space Administration. Lewis Research Center, Cleveland, OH.

KA-BAND MMIC MICROSTRIP ARRAY FOR HIGH RATE COMMUNICATIONS

R. Q. LEE, C. A. RAQUET (NASA, Lewis Research Center, Cleveland, OH), J. B. TOLLESON, and S. M. SANZGIRI (Texas Instruments, Inc., McKinney) AIAA, NASA, and OAI, Conference on Advanced SEI Technologies, Cleveland, OH, Sept. 4-6, 1991. 7 p. Previously announced in STAR as N91-27437. (AIAA PAPER 91-3421) Copyright

In a recent technology assessment of alternative communication systems for the space exploration initiative (SEI), Ka-band (18 to 40 GHz) communication technology was identified to meet the mission requirements of telecommunication, navigation, and information management. Compared to the lower frequency bands, Ka-band antennas offer higher gain and broader bandwidths; thus, they are more suitable for high data rate communications. Over the years, NASA has played an important role in monolithic microwave integrated circuit (MMIC) phased array technology development, and currently, has an ongoing contract with Texas Instrument (TI) to develop a modular Ka-band MMIC microstrip subarray (NAS3-25718). The TI contract emphasizes MMIC integration technology development and stipulates using existing MMIC devices to minimize the array development cost. The objective of this paper is to present array component technologies and integration techniques used to construct the subarray modules. Author

A91-52378*# National Aeronautics and Space Administration. Lewis Research Center, Cleveland, OH.

DESIGN OF AN INFLATABLE, OPTICALLY CONTROLLED AND FED, PHASED ARRAY ANTENNA

RICHARD R. KUNATH and G. R. SHARP (NASA, Lewis Research

Center, Cleveland, OH) AIAA, NASA, and OAI, Conference on Advanced SEI Technologies, Cleveland, OH, Sept. 4-6, 1991. 8 p. refs

(AIAA PAPER 91-3470) Copyright

Initial studies on the antenna requirements of the Space Exploration Initiative (SEI) system architecture have indicated the need for large, lightweight antennas. This paper discusses the design of a modular, inflatable, optically controlled and fed phased array antenna suitable for SEI applications. When high gain antennas are required for space applications, large aperture mesh or collapsible solid antenna reflectors are considered. However, these designs are generally not lightweight, and have complicated deployment mechanisms. Alternatively, the modular, inflatable antenna design discussed here is a lightweight, modular design that incorporates a simple deployment scheme, and after deployment, can be rigidized to enhance its structural integrity. Further, the design features the fiberoptic distribution of both RF and control signals to individual microwave integrated circuit/reflector modules in each of the inflatable, phased array antenna cells. The result of combining these two technologies is a modular, phased array antenna design that is both mechanically and electrically agile and robust. Author

A91-53084* Toledo Univ., OH.

PERFORMANCE EVALUATION OF LAND MOBILE SATELLITE SYSTEM UNDER VEGETATIVE SHADOWING USING DIFFERENTIAL MULTIPLE TCM AND QPSK

JUNGHWAN KIM, D. HASCHART, S. C. KWATRA (Toledo, University, OH), MARK J. VANDERAAR, and G. H. STEVENS (NASA, Lewis Research Center, Cleveland, OH) IN: MILCOM '90 - IEEE Military Communications Conference, Monterey, CA, Sept. 30-Oct. 3, 1990, Conference Record. Vol. 1. New York, Institute of Electrical and Electronics Engineers, Inc., 1990, p. 263-267. refs

(Contract NAG3-157)

Copyright

A comparative analysis by computer simulation of the land mobile satellite system (LMSS) is presented for the uncoded quadrature phase shift keying (QPSK), rate 2/3 8-PSK trellis coded modulation (TCM), and rate 4/6 multiplicity 2 8-PSK TCM schemes. An analytical model is used for simulating the fading channel. The simulation results show that under Rayleigh fades, the TCM designed for the fading channel is superior to uncoded QPSK and to the conventional TCM optimized for the additive white Gaussian noise (AWGN) channel. The performance of differentially detected TCM under AWGN and fading is examined based on the preliminary results. Results of the uncoded QPSK with fading channel modeled with the empirical fade data are given. I.E.

A91-53176* Toledo Univ., OH.

STUDY ON THE SPECTRAL EFFICIENCY OF SFH-GMSK IN LAND MOBILE TELEPHONE COMMUNICATION BY DIRECT SIMULATION

H. BAO, S. C. KWATRA, JUNGHWAN KIM (Toledo, University, OH), and G. H. STEVENS (NASA, Lewis Research Center, Cleveland, OH) IN: GLOBECOM '90 - IEEE Global Telecommunications Conference and Exhibition, San Diego, CA, Dec. 2-5, 1990, Conference Record. Vol. 1. New York, Institute of Electrical and Electronics Engineers, Inc., 1990, p. 507-510. refs

(Contract NAG3-157)

Copyright

A spread spectrum system, slow frequency hopping with GMSK (Gaussian minimum shift keying) modulation (SFH-GMSK), is proposed for mobile telephone communications. The system performance is evaluated using computer simulation and is compared with an unspread system. Results show that under multipath fading conditions, when the signal-to-noise ratio (SNR) is greater than 15 dB, slow frequency hopping gives some bit error rate improvement over the unspread system. Theoretical predictions indicate that a system efficiency of 20-65 users per cell can be achieved in the cellular configuration. Joint use of SFH-GMSK and FM is also investigated. It is shown that FM

interference can cause serious degradation to the SFH-GMSK performance. I.E.

A91-53702*# National Aeronautics and Space Administration. Lewis Research Center, Cleveland, OH.

QUATERNARY PULSE POSITION MODULATION

ELECTRONICS FOR FREE-SPACE LASER COMMUNICATIONS

J. M. BUDINGER, S. D. KERSLAKE, L. A. NAGY, M. J. SHALKHAUSER, N. J. SONI, M. A. CAULEY, J. H. MOHAMED, J. B. STOVER, R. R. ROMANOFISKY (NASA, Lewis Research Center, Cleveland, OH), P. J. LIZANICH (Analex Corp., Brook Park, OH) et al. AIAA, NASA, and OAI, Conference on Advanced SEI Technologies, Cleveland, OH, Sept. 4-6, 1991. 20 p. Previously announced in STAR as N91-29405. refs

(AIAA PAPER 91-3471) Copyright

The development of a high data-rate communications electronic subsystem for future application in free-space, direct-detection laser communications is described. The dual channel subsystem uses quaternary pulse position modulation (GPPM) and operates at a throughput of 650 megabits per second. Transmitting functions described include source data multiplexing, channel data multiplexing, and QPPM symbol encoding. Implementation of a prototype version in discrete gallium arsenide logic, radiofrequency components, and microstrip circuitry is presented. Author

A91-53708*# National Aeronautics and Space Administration. Lewis Research Center, Cleveland, OH.

COMBINATORIAL FSK MODULATION FOR POWER-EFFICIENT HIGH-RATE COMMUNICATIONS

PAUL K. WAGNER, MARK J. VANDERAAR (NASA, Lewis Research Center, Cleveland; Sverdrup Technology, Inc., Brook Park, OH), and JAMES M. BUDINGER (NASA, Lewis Research Center, Cleveland, OH) AIAA, NASA, and OAI, Conference on Advanced SEI Technologies, Cleveland, OH, Sept. 4-6, 1991. 9 p. Previously announced in STAR as N91-29404. refs

(Contract NAS3-25266)

(AIAA PAPER 91-3532) Copyright

Deep-space and satellite communications systems must be capable of conveying high-rate data accurately with low transmitter power, often through dispersive channels. A class of noncoherent Combinatorial Frequency Shift Keying (CFSK) modulation schemes is investigated which address these needs. The bit error rate performance of this class of modulation formats is analyzed and compared to the more traditional modulation types. Candidate modulator, demodulator, and digital signal processing (DSP) hardware structures are examined in detail. System-level issues are also discussed. Author

N91-10208*# National Aeronautics and Space Administration. Lewis Research Center, Cleveland, OH.

EFFECT OF SURFACE DEPOSITS ON ELECTROMAGNETIC WAVES PROPAGATING IN UNIFORM DUCTS

KENNETH J. BAUMEISTER Oct. 1990 13 p Presented at the 4th Biennial IEEE Conference on Electromagnetic Field Computation, Toronto, Ontario, 22-24 Oct. 1990

(NASA-TM-103282; E-5737; NAS 1.15:103282) Avail: NTIS HC/MF A03 CSCL 20N

A finite-element Galerkin formulation was used to study the effect of material surface deposits on the reflective characteristics of straight uniform ducts with PEC (perfectly electric conducting) walls. Over a wide frequency range, the effect of both single and multiple surface deposits on the duct reflection coefficient were examined. The power reflection coefficient was found to be significantly increased by the addition of deposits on the wall. Author

N91-11971*# National Aeronautics and Space Administration. Lewis Research Center, Cleveland, OH.

LBR-2 EARTH STATIONS FOR THE ACTS PROGRAM

MICHAEL OREILLY (Harris Corp., Melbourne, FL.), RUSSELL JIRBERG, and ERNIE SPISZ In JPL, California Inst. of Tech., Proceedings of the Fourteenth NASA Propagation Experimenters Meeting (NAPEX 14) and the Advanced Communications

Technology Satellite (ACTS) Propagation Studies Miniworkshop p 232-239 1 Jul. 1990

Avail: NTIS HC/MF A12 CSCL 20/14

The Low Burst Rate-2 (LBR-2) earth station being developed for NASA's Advanced Communications Technology Satellite (ACTS) is described. The LBR-2 is one of two earth station types that operate through the satellite's baseband processor. The LBR-2 is a small earth terminal (VSAT)-like earth station that is easily sited on a user's premises, and provides up to 1.792 megabits per second (Mbps) of voice, video, and data communications. Addressed here is the design of the antenna, the rf subsystems, the digital processing equipment, and the user interface equipment. Author

N91-11988*# National Aeronautics and Space Administration. Lewis Research Center, Cleveland, OH.

AN EXPERIMENTAL STUDY OF HIGH TC SUPERCONDUCTING MICROSTRIP TRANSMISSION LINES AT 35 GHZ AND THE EFFECT OF FILM MORPHOLOGY

C. M. CHOREY, K. B. BHASIN, J. D. WARNER, J. Y. JOSEFOWICZ, D. B. RENSCH, and C. W. NIEH (Hughes Research Labs., Malibu, CA.) Sep. 1990 7 p Presented at the Applied Superconductivity Conference, Aspen, CO, 24-28 Sep. 1990; sponsored in part by IEEE

(Contract RTOP 506-44-20)

(NASA-TM-103633; E-5758; NAS 1.15:103633) Avail: NTIS HC/MF A02 CSCL 20/14

Microstrip transmission lines in the form of ring resonators were fabricated from a number of in-situ grown laser ablated films and post-annealed co-sputtered YBa₂Cu₃O(7-x) films. The properties of these resonators were measured at 35 GHz and the observed performance is examined in light of the critical temperature (T_c) and film thickness and also the film morphology which is different for the two deposition techniques. It is found that T_c is a major indicator of the film performance for each growth type with film thickness becoming important as it decreases towards 100 Å. It is also found that the films with a mixed grain orientation (both a axis and c axis oriented grains) have poorer microwave properties as compared with the primarily c axis oriented material. This is probably due to the significant number of grain boundaries between the different crystallites, which may act as superconducting weak links and contribute to the surface resistance. Author

N91-13598*# National Aeronautics and Space Administration. Lewis Research Center, Cleveland, OH.

REAL-TIME DATA COMPRESSION OF BROADCAST VIDEO SIGNALS Patent Application

MARY J. SHALKHAUSER, inventor (to NASA), WAYNE A. WHYTE, JR., inventor (to NASA), and SCOTT P. BARNES, inventor (to NASA) (Hughes Aircraft Co., Canoga Park, CA.) 20 Jun. 1990 56 p

(NASA-CASE-LEW-14945-1; NAS 1.71:LEW-14945-1;

US-PATENT-APPL-SN-540976) Avail: NTIS HC/MF A04

A non-adaptive predictor, a nonuniform quantizer, and a multi-level Huffman coder are incorporated into a differential pulse code modulation system for coding and decoding broadcast video signals in real time. NASA

N91-18297*# National Aeronautics and Space Administration. Lewis Research Center, Cleveland, OH.

SOLID STATE TECHNOLOGY BRANCH OF NASA LEWIS RESEARCH CENTER SECOND ANNUAL DIGEST, JUNE 1989 - JUNE 1990

Jun. 1990 289 p

(Contract RTOP 506-59-4C)

(NASA-TM-103226; E-5642; NAS 1.15:103226) Avail: NTIS HC/MF A13 CSCL 20/12

A collection of papers and presentations authored by the branch between June 1989 and June 1990 is presented. The papers are organized into four sections. Section 1 deals with research in microwave circuits and includes full integrated circuits, the demonstration of optical/RF interfaces, and the evaluation of some hybrid circuitry. Section 2 indicates developments in coplanar

32 COMMUNICATIONS AND RADAR

waveguides and their use in breadboard circuits. Section 3 addresses high temperature superconductivity and includes: thin film deposition, transport measurement of film characteristics, RF surface resistant measurements, substrate permittivity measurements, measurements of microstrip line characteristics at cryogenic temperatures, patterning of superconducting films, and evaluation of simple passive microstrip circuitry based on YBaCuO films. Section 4 deals with carbon films, silicon carbide, GaAs/AlGaAs, HgCdTe, and other materials.

N91-19332*# National Aeronautics and Space Administration. Lewis Research Center, Cleveland, OH.

COPLANAR WAVEGUIDE EESOF MICAD MACROS MAKE CIRCUIT LAYOUT EASY

GEORGE E. PONCHAK and NIKOLA VISIC (Cleveland State Univ., OH.) Sep. 1990 39 p

(Contract RTOP 506-44-2B)

(NASA-TM-103272; E-5714; NAS 1.15:103272) Avail: NTIS HC/MF A03 CSCL 09/3

A collection of macro files is presented which permit the layout of coplanar waveguide integrated circuits using EEsoF MICAD CAD software. The files must be added to the user's MICAD.ELE file.

Author

N91-22494*# National Aeronautics and Space Administration. Lewis Research Center, Cleveland, OH.

A STATISTICAL RAIN ATTENUATION PREDICTION MODEL WITH APPLICATION TO THE ADVANCED COMMUNICATION TECHNOLOGY SATELLITE PROJECT. 3: A STOCHASTIC RAIN FADE CONTROL ALGORITHM FOR SATELLITE LINK POWER VIA NON LINEAR MARKOV FILTERING THEORY

ROBERT M. MANNING May 1991 23 p

(Contract RTOP 679-40-00)

(NASA-TM-100243; E-6171; NAS 1.15:100243) Avail: NTIS HC/MF A03 CSCL 20/14

The dynamic and composite nature of propagation impairments that are incurred on Earth-space communications links at frequencies in and above 30/20 GHz Ka band, i.e., rain attenuation, cloud and/or clear air scintillation, etc., combined with the need to counter such degradations after the small link margins have been exceeded, necessitate the use of dynamic statistical identification and prediction processing of the fading signal in order to optimally estimate and predict the levels of each of the deleterious attenuation components. Such requirements are being met in NASA's Advanced Communications Technology Satellite (ACTS) Project by the implementation of optimal processing schemes derived through the use of the Rain Attenuation Prediction Model and nonlinear Markov filtering theory.

Author

N91-23347*# National Aeronautics and Space Administration. Lewis Research Center, Cleveland, OH.

AN ASSESSMENT OF TECHNOLOGY ALTERNATIVES FOR TELECOMMUNICATIONS AND INFORMATION MANAGEMENT FOR THE SPACE EXPLORATION INITIATIVE

DENISE S. PONCHAK and JOHN E. ZUZEK Apr. 1991 25 p

(Contract RTOP 316-30-19)

(NASA-TM-103783; E-6058; NAS 1.15:103783) Avail: NTIS HC/MF A03 CSCL 17/2

On the 20th anniversary of the Apollo 11 lunar landing, President Bush set forth ambitious goals for expanding human presence in the solar system. The Space Exploration Initiative (SEI) addresses these goals beginning with Space Station Freedom, followed by a permanent return to the Moon, and a manned mission to Mars. A well designed, adaptive Telecommunications, Navigation, and Information Management (TNIM) infrastructure is vital to the success of these missions. Utilizing initial projections of user requirements, a team under the direction of NASA's Office of Space Operations developed overall architectures and point designs to implement the TNIM functions for the Lunar and Mars mission scenarios. Based on these designs, an assessment of technology alternatives for the telecommunications and information management functions was performed. This technology assessment identifies technology developments necessary to meet

the telecommunications and information management system requirements for SEI. Technology requirements, technology needs and alternatives, the present level of technology readiness in each area, and a schedule for development are presented. Author

N91-23354*# National Aeronautics and Space Administration. Lewis Research Center, Cleveland, OH.

SYSTEM-LEVEL INTEGRATED CIRCUIT (SLIC) DEVELOPMENT FOR PHASED ARRAY ANTENNA APPLICATIONS

K. A. SHALKHAUSER and C. A. RAQUET 1991 8 p Presented at the International Symposium on Optical Engineering and Photonics, Orlando, FL, 4-5 Apr. 1991; sponsored by Society of Photo-Optical Instrumentation Engineers

(Contract RTOP 650-60-20)

(NASA-TM-104392; E-6207; NAS 1.15:104392) Avail: NTIS HC/MF A02 CSCL 20/14

A microwave/millimeter wave system-level integrated circuit (SLIC) being developed for use in phased array antenna applications is described. The program goal is to design, fabricate, test, and deliver an advanced integrated circuit that merges radio frequency (RF) monolithic microwave integrated circuit (MMIC) technologies with digital, photonic, and analog circuitry that provide control, support, and interface functions. As a whole, the SLIC will offer improvements in RF device performance, uniformity, and stability while enabling accurate, rapid, repeatable control of the RF signal. Furthermore, the SLIC program addresses issues relating to insertion of solid state devices into antenna systems, such as the reduction in number of bias, control, and signal lines. Program goals, approach, and status are discussed.

Author

N91-24067*# National Aeronautics and Space Administration. Lewis Research Center, Cleveland, OH.

DIGITAL CODEC FOR REAL-TIME PROCESSING OF BROADCAST QUALITY VIDEO SIGNALS AT 1.8 BITS/PIXEL

MARY JO SHALKHAUSER and WAYNE A. WHYTE in NASA, Washington, Technology 2000, Volume 2 p 221-228 1991

Previously announced in IAA as A90-51306

Avail: NTIS HC/MF A16 CSCL 17/2

Advances in very large scale integration and recent work in the field of bandwidth efficient digital modulation techniques have combined to make digital video processing technically feasible an potentially cost competitive for broadcast quality television transmission. A hardware implementation was developed for DPCM (differential pulse code modulation)-based digital television bandwidth compression algorithm which processes standard NTSC composite color television signals and produces broadcast quality video in real time at an average of 1.8 bits/pixel. The data compression algorithm and the hardware implementation of the codec are described, and performance results are provided.

Author

N91-27436*# National Aeronautics and Space Administration. Lewis Research Center, Cleveland, OH.

A THREE-DIMENSIONAL FINITE-ELEMENT THERMAL/MECHANICAL ANALYTICAL TECHNIQUE FOR HIGH-PERFORMANCE TRAVELING WAVE TUBES

KAREN F. BARTOS, E. BRIAN FITE, KURT A. SHALKHAUSER, and G. RICHARD SHARP Washington Jun. 1991 17 p

Original contains color illustrations

(Contract RTOP 650-60-20)

(NASA-TP-3081; E-5917; NAS 1.60:3081) Avail: NTIS HC/MF A03; 5 functional color pages CSCL 09/3

Current research in high-efficiency, high-performance traveling wave tubes (TWT's) has led to the development of novel thermal/mechanical computer models for use with helical slow-wave structures. A three-dimensional, finite element computer model and analytical technique used to study the structural integrity and thermal operation of a high-efficiency, diamond-rod, K-band TWT designed for use in advanced space communications systems. This analysis focused on the slow-wave circuit in the radiofrequency section of the TWT, where an inherent localized heating problem existed and where failures were observed during earlier cold

compression, or 'coining' fabrication technique that shows great potential for future TWT development efforts. For this analysis, a three-dimensional, finite element model was used along with MARC, a commercially available finite element code, to simulate the fabrication of a diamond-rod TWT. This analysis was conducted by using component and material specifications consistent with actual TWT fabrication and was verified against empirical data. The analysis is nonlinear owing to material plasticity introduced by the forming process and also to geometric nonlinearities presented by the component assembly configuration. The computer model was developed by using the high efficiency, K-band TWT design but is general enough to permit similar analyses to be performed on a wide variety of TWT designs and styles. The results of the TWT operating condition and structural failure mode analysis, as well as a comparison of analytical results to test data are presented. Author

N91-27437* National Aeronautics and Space Administration. Lewis Research Center, Cleveland, OH.

KA-BAND MMIC MICROSTRIP ARRAY FOR HIGH RATE COMMUNICATIONS

R. Q. LEE, C. A. RAQUET, J. B. TOLLESON, and S. M. SANZGIRI (Texas Instruments, Inc., McKinney.) 1991 8 p Proposed for presentation at the Conference on Advanced Space Exploration Initiative Technologies, Cleveland, OH, 4-6 Sep. 1991; cosponsored by AIAA and OAI (Contract RTOP 650-60-20) (NASA-TM-104500; E-6358; NAS 1.15:104500; AIAA PAPER 91-3421) Avail: NTIS HC/MF A02 CSCL 17/2

In a recent technology assessment of alternative communication systems for the space exploration initiative (SEI), Ka-band (18 to 40 GHz) communication technology was identified to meet the mission requirements of telecommunication, navigation, and information management. Compared to the lower frequency bands, Ka-band antennas offer higher gain and broader bandwidths; thus, they are more suitable for high data rate communications. Over the years, NASA has played an important role in monolithic microwave integrated circuit (MMIC) phased array technology development, and currently, has an ongoing contract with Texas Instrument (TI) to develop a modular Ka-band MMIC microstrip subarray (NAS3-25718). The TI contract emphasizes MMIC integration technology development and stipulates using existing MMIC devices to minimize the array development cost. The objective of this paper is to present array component technologies and integration techniques used to construct the subarray modules. Author

N91-29404* National Aeronautics and Space Administration. Lewis Research Center, Cleveland, OH.

COMBINATORIAL FSK MODULATION FOR POWER-EFFICIENT HIGH-RATE COMMUNICATIONS

PAUL K. WAGNER, JAMES M. BUDINGER, and MARK J. VANDERAAR (Sverdrup Technology, Inc., Brook Park, OH.) 1991 10 p Presented at the Conference on Advanced Space Exploration Initiative Technologies, Cleveland, OH, 4-6 Sep. 1991; cosponsored by AIAA and OAI (Contract NAS3-25266; RTOP 650-60-21) (NASA-TM-105188; E-6490; NAS 1.15:105188; AIAA PAPER 91-3532) Avail: NTIS HC/MF A02 CSCL 17/2

Deep-space and satellite communications systems must be capable of conveying high-rate data accurately with low transmitter power, often through dispersive channels. A class of noncoherent Combinatorial Frequency Shift Keying (CFSK) modulation schemes is investigated which address these needs. The bit error rate performance of this class of modulation formats is analyzed and compared to the more traditional modulation types. Candidate modulator, demodulator, and digital signal processing (DSP) hardware structures are examined in detail. System-level issues are also discussed. Author

N91-29405* National Aeronautics and Space Administration. Lewis Research Center, Cleveland, OH.

QUATERNARY PULSE POSITION MODULATION ELECTRONICS FOR FREE-SPACE LASER COMMUNICATIONS

J. M. BUDINGER, S. D. KERSLAKE, L. A. NAGY, M. J. SHALKHAUSER, N. J. SONI, M. A. CAULEY, J. H. MOHAMED, J. B. STOVER, R. R. ROMANOFKY, P. J. LIZANICH (Analex Corp., Brook Park, OH.) et al. 1991 21 p Presented at the Conference on Advanced Space Exploration Initiative Technologies, Cleveland, OH, 4-6 Sep. 1991; cosponsored by AIAA and OAI (Contract RTOP 650-60-21) (NASA-TM-104502; E-6362; NAS 1.15:104502; AIAA PAPER 91-3471) Avail: NTIS HC/MF A03 CSCL 17/2

The development of a high data-rate communications electronic subsystem for future application in free-space, direct-detection laser communications is described. The dual channel subsystem uses quaternary pulse position modulation (QPPM) and operates at a throughput of 650 megabits per second. Transmitting functions described include source data multiplexing, channel data multiplexing, and QPPM symbol encoding. Implementation of a prototype version in discrete gallium arsenide logic, radiofrequency components, and microstrip circuitry is presented. Author

N91-29431* National Aeronautics and Space Administration. Lewis Research Center, Cleveland, OH.

OPTICAL MULTIPLE ACCESS NETWORK (OMAN) FOR ADVANCED PROCESSING SATELLITE APPLICATIONS

ANTONIO J. MENDEZ, ROBERT M. GAGLIARDI, EUGENE PARK, WILLIAM D. IVANCIC, and BRADLEY D. SHERMAN (McDonnell-Douglas Corp., Long Beach, CA.) 1991 4 p Presented at the Summer Topical Meetings on Spaceborne Photonics: Aerospace Applications of Lasers and Electro-Optics, Newport Beach, CA, 22-24 Jul. 1991; sponsored by IEEE (Contract RTOP 321-01-00) (NASA-TM-105167; E-6458; NAS 1.15:105167) Avail: NTIS HC/MF A01 CSCL 17/2

An OMAN breadboard for exploring advanced processing satellite circuit switch applications is introduced. Network architecture, hardware trade offs, and multiple user interference issues are presented. The breadboard test set up and experimental results are discussed. Author

N91-32247* National Aeronautics and Space Administration. Lewis Research Center, Cleveland, OH.

DATA COMPRESSION FOR FULL MOTION VIDEO TRANSMISSION

WAYNE A. WHYTE, JR. and KHALID SAYOOD (Nebraska Univ., Lincoln.) Sep. 1991 11 p Presented at the Conference on Advanced Space Exploration Initiative Technologies, Cleveland, OH, 4-6 Sep. 1991, cosponsored by the AIAA, NASA, and OAI (Contract RTOP 643-10-01) (NASA-TM-105239; E-6564; NAS 1.15:105239; AIAA PAPER 91-3533) Avail: NTIS HC/MF A03 CSCL 17/2

Clearly transmission of visual information will be a major, if not dominant, factor in determining the requirements for, and assessing the performance of the Space Exploration Initiative (SEI) communications systems. Projected image/video requirements which are currently anticipated for SEI mission scenarios are presented. Based on this information and projected link performance figures, the image/video data compression requirements which would allow link closure are identified. Finally several approaches which could satisfy some of the compression requirements are presented and possible future approaches which show promise for more substantial compression performance improvement are discussed. Author

N91-32287* National Aeronautics and Space Administration. Lewis Research Center, Cleveland, OH.

MILLIMETER WAVELENGTH COMMUNICATIONS APPLICATIONS FOR THE SEI

DENISE S. PONCHAK, JOHN E. ZUZEK, RODNEY L. SPENCE, and WAYNE A. WHYTE, JR. 1991 26 p Presented at the Conference on Advanced Space Exploration Initiative Technologies,

33 ELECTRONICS AND ELECTRICAL ENGINEERING

Cleveland, OH, 4-6 Sep. 1991; sponsored by AIAA, NASA, and OAI. Previously announced in IAA as A91-52458 (Contract RTOP 316-30-19)

(NASA-TM-105275; E-6598; NAS 1.15:105275; AIAA PAPER 91-3589) Copyright Avail: NTIS HC/MF A03 CSCL 17/2

The potentially complex missions of the Space Exploration Initiative (SEI) require advanced lunar communications, navigation, and information systems to provide voice, data, and image transmissions. The objectives here are to determine which SEI telecommunications applications will benefit from millimeter wave technology, assess the state of the art in millimeter wave technology, and describe the technology development shortfalls with respect to potential mission time frames. The assumptions for the analysis as well as other non-performance related issues are also presented. Author

33

ELECTRONICS AND ELECTRICAL ENGINEERING

Includes test equipment and maintainability; components, e.g., tunnel diodes and transistors; microminiaturization; and integrated circuitry.

A91-22987* Michigan Univ., Ann Arbor.

LOW-TEMPERATURE MICROWAVE CHARACTERISTICS OF PSEUDOMORPHIC $\text{In}(x)\text{Ga}(1-x)\text{As}/\text{In}(0.52)\text{Al}(0.48)\text{As}$ MODULATION-DOPED FIELD-EFFECT TRANSISTORS

R. LAI, PALLAB K. BHATTACHARYA (Michigan, University, Ann Arbor), S. A. ALTEROVITZ, A. N. DOWNEY, and C. CHOREY (NASA, Lewis Research Center, Cleveland, OH) IEEE Electron Device Letters (ISSN 0741-3106), vol. 11, Dec. 1990, p. 564-566. refs

(Contract NAG3-988; DAAL03-87-K-0007) Copyright

Low-temperature microwave measurements of both lattice-matched and pseudomorphic $\text{In}(x)\text{Ga}(1-x)\text{As}/\text{In}(0.48)\text{As}$ ($x = 0.53, 0.60$, and 0.70) channel MODFETs on InP substrates were carried out in a cryogenic measurement system. The measurements were done in the temperature range of 77 to 300 K and in the frequency range of 0.5 to 11.0 GHz at different bias conditions. The cutoff frequency (f_T) for the $\text{In}(x)\text{Ga}(1-x)\text{As}/\text{In}(0.52)\text{Al}(0.48)\text{As}$ MODFETs improved from 22 to 29 GHz, 29 to 38 GHz, and 39 to 51 GHz, for $x = 0.53, 0.60$, and 0.70 , respectively, as the temperature was lowered from 300 to 77 K, which is approximately a 31 percent increase at each composition. No degradations were observed in device performance. These results indicate an excellent potential of the pseudomorphic devices at low temperatures. I.E.

A91-25071* National Aeronautics and Space Administration. Lewis Research Center, Cleveland, OH.

SURFACE STUDIES ON SCANDATE CATHODES AND SYNTHESIZED SCANDATES

GARY LESNY (NASA, Lewis Research Center, Cleveland, OH) and RALPH FORMAN (Analex Corp., Fairview Park, OH) (NASA, Tri-Service Cathode Workshop, 7th, Cleveland, OH, Apr. 3-5, 1990) IEEE Transactions on Electron Devices (ISSN 0018-9383), vol. 37, pt. 2, Dec. 1990, p. 2595-2604. refs Copyright

Auger, ESCA, electron emission, evaporation, and desorption measurements were made on three different types of scandate surfaces. They are: (1) an impregnated top layer scandate cathode, (2) an unimpregnated top layer scandate cathode with a deposited barium or barium oxide adsorbate surface layer, and (3) a synthesized scandate surface, which replicates a scandate cathode surface. The purpose of these experiments was to determine the role that Sc_2O_3 plays in making the scandate cathode a more copious electron emitter than the conventional impregnated-type cathode. The synthesized scandate surface experiments consisted

of depositing multilayer scandium on a tungsten surface, oxidizing the scandium, and then depositing either Ba or BaO on the scandium oxide surface. The results of these measurements showed that the low work function portions of the thin-film scandate cathode are where the Sc_2O_3 is the substrate and BaO is the adsorbate. I.E.

A91-25078* National Aeronautics and Space Administration. Lewis Research Center, Cleveland, OH.

A HIGH-EFFICIENCY FERRULELESS COUPLED-CAVITY TRAVELING-WAVE TUBE WITH PHASE-ADJUSTED TAPER

JEFFREY D. WILSON (NASA, Lewis Research Center, Cleveland, OH), HELEN C. LIMBURG, JON A. DAVIS, IVO TAMMARU, and JOHN P. VASZARI (Hughes Aircraft Co., Electron Dynamics Div., Torrance, CA) IEEE Transactions on Electron Devices (ISSN 0018-9383), vol. 37, pt. 2, Dec. 1990, p. 2638-2643. refs Copyright

The design and performance of the first traveling-wave tube (TWT) to be built with a phase-adjusted taper (PAT) is discussed. By adjusting the phase of the electron bunch with respect to the RF wave for strong electron bunch formation at the beginning of the taper and strong power conversion at the end, the PAT achieves a high efficiency of power conversion from the electron beam to the RF wave. A PAT incorporated into the output section of a baseline 29-30 GHz ferruleless coupled-cavity TWT experimentally increased the peak RF power from 420 to 1000 W and the peak RF interaction efficiency from 9.6 to 22.6 percent. I.E.

A91-27331* National Aeronautics and Space Administration. Lewis Research Center, Cleveland, OH.

OPTICAL CONTROL OF MICROWAVE DEVICES

RAINEE SIMONS (NASA, Lewis Research Center, Cleveland, OH) Norwood, MA, Artech House, 1990, 254 p. refs Copyright

Theoretical and applications aspects of optoelectronic control for microwave devices are examined in an introduction for graduate engineering students and practicing engineers. The basic features of optical MMICs are reviewed, and chapters are devoted to laser diodes, electrooptic modulators, photodetectors, microwave fiber-optic links, optoelectronic switching and gating, optoelectronic microwave signal generation, an optoelectronic switch matrix, optoelectronic switching and modulation of oscillators, and optoelectronic injection-locking and tuning of oscillators. Extensive diagrams, drawings, and graphs are provided. D.G.

A91-27529* National Aeronautics and Space Administration. Lewis Research Center, Cleveland, OH.

PULSED RESPONSE OF A TWT

BRIAN D. MAY (NASA, Lewis Research Center, Cleveland, OH) Microwave Journal (ISSN 0192-6225), vol. 34, Feb. 1991, p. 113, 114, 116-118. Copyright

The consequence of frequency domain multiple access channelization in a satellite communications system is that the ground- and space-based components often are required to operate in a linear region to prevent the generation of distortion signals. Components of a time division multiple access (TDMA) satellite system, such as a traveling-wave tube (TWT), can operate in the highest output power state because the channelization technique is relatively insensitive to the distortions resulting from saturated operation. A 30 GHz TWT was tested to determine the suitability of such a device in a TDMA system. Testing was focused on the ability of the TWT's output signal to rise up to full power at the leading edge of TDMA bursts, simulated by a pulse train. A peak power meter was used to display and measure the pulsed signal waveform. Measurements on the TWT output pulse rise time indicate that the TWT lengthened the rise time by 10 to 20 ns. Imposing modulator turn on timing that precedes the data burst by the TWT rise time is a logical approach to coordination of the two subsystem specification. Author

A91-29257* National Aeronautics and Space Administration. Lewis Research Center, Cleveland, OH.

THE PRELIMINARY FEASIBILITY OF INTERCALATED GRAPHITE RAILGUN ARMATURES

JAMES R. GAIER (NASA, Lewis Research Center, Cleveland, OH), CLARENCE E. GOODEN (USAF, Armament Laboratory, Eglin AFB, FL), DOREEN YASHAN (Cleveland State University, OH), and STEVE NAUD (U.S. Navy, Naval Coastal Systems Laboratory, Panama City, FL) (Symposium on Electromagnetic Launcher Technology, 5th, Sandestin, FL, Apr. 3-5, 1990, Proceedings. A91-29205 11-33) IEEE Transactions on Magnetics (ISSN 0018-9464), vol. 27, Jan. 1991, p. 289-293. refs

Graphite intercalation compounds may provide an excellent material for the fabrication of electromagnetic railgun armatures. As a pulse of power is fed into the armature the intercalate could be excited into the plasma state around the edges of the armature, while the bulk of the current would be carried through the graphite block. Such an armature would have both diffuse plasma armatures and bulk conduction armatures. In addition, the highly anisotropic nature of these materials could enable the electrical and thermal conductivity to be tailored to meet the specific requirements of electromagnetic railgun armatures. Preliminary investigations have been performed in an attempt to determine the feasibility of using graphite intercalation compounds as railgun armatures. Issues of fabrication, resistivity, stability, and electrical current spreading have been addressed for the case of highly oriented pyrolytic graphite. I.E.

A91-30893* National Aeronautics and Space Administration. Lewis Research Center, Cleveland, OH.

INDUCTION MOTOR CONTROL

IRVING G. HANSEN (NASA, Lewis Research Center, Cleveland, OH) IN: NAECON 90; Proceedings of the IEEE National Aerospace and Electronics Conference, Dayton, OH, May 21-25, 1990. Vol. 1. New York, Institute of Electrical and Electronics Engineers, Inc., 1990, p. 348-350. Previously announced in STAR as N90-19234.

Electromechanical actuators developed to date have commonly utilized permanent magnet (PM) synchronous motors. More recently switched reluctance (SR) motors have been advocated due to their robust characteristics. Implications of work which utilized induction motors and advanced control techniques are discussed. When induction motors are operated from an energy source capable of controlling voltages and frequencies independently, drive characteristics are obtained which are superior to either PM or SR motors. By synthesizing the machine frequency from a high-frequency carrier (nominally 20 kHz), high efficiencies, low distortion, and rapid torque response are available. At this time multiple horsepower machine drives were demonstrated, and work is on-going to develop a 20 hp average, 40 hp peak class of aerospace actuators. This effort is based upon high-frequency power distribution and management techniques developed by NASA for Space Station Freedom. Author

A91-30901* General Dynamics Corp., San Diego, CA.

CONTROL OF MULTIPLE RESONANT POWER PROCESSORS IN A MULTI-SOURCE SYSTEM

JAMES MILDICE, ALBERT SILVERMAN (General Dynamics Corp., Space Systems Div., San Diego, CA), and BARBARA KENNY (NASA, Lewis Research Center, Cleveland, OH) IN: NAECON 90; Proceedings of the IEEE National Aerospace and Electronics Conference, Dayton, OH, May 21-25, 1990. Vol. 1. New York, Institute of Electrical and Electronics Engineers, Inc., 1990, p. 417-423.

Copyright

Analysis and test results show that phasor-regulated, Mapham-derived resonant inverters can be paralleled to provide standardizing interfaces for multiple sources on a utility-type, aerospace power distribution bus. The basic sources do not require matching in any way, and may have grossly different characteristics. Fully stable system architectures with multiple sources, parallel/redundant distribution buses, and a wide variety of loads can be easily constructed and controlled. The commands and parameters available for system control allow for tight tolerance

bus voltage control, and absolute power-sharing control from the various sources over the full range of possible source and load variations. That level of control enables simplified load power processing hardware and the distribution of losses to optimally load the source thermal control system. Positive control of all system performance and allocation of losses are not required by all missions or vehicles, and overall vehicle considerations do not always require the loads on vehicle energy sources and thermal control systems to be balanced. In those cases, power system control can be simplified, and a hierarchical set of defaults can be substituted for computer-generated or supervisory input commands to allow for stable, fully autonomous system operation. I.E.

A91-31391* National Aeronautics and Space Administration. Lewis Research Center, Cleveland, OH.

HIGH TEMPERATURE SUPERCONDUCTIVE MICROWAVE TECHNOLOGY FOR SPACE APPLICATIONS

R. F. LEONARD, D. J. CONNOLLY, K. B. BHASIN, J. D. WARNER, and S. A. ALTEROVITZ (NASA, Lewis Research Center, Cleveland, OH) IN: Progress in high-temperature superconducting transistors and other devices; Proceedings of the Meeting, Santa Clara, CA, Oct. 4, 5, 1990. Bellingham, WA, Society of Photo-Optical Instrumentation Engineers, 1991, p. 114-125. refs

Copyright

Progress being made on space application technology research on film fabrication, passive microwave circuits, and semiconductor devices for cryogenic circuits is reviewed. Achievements in YBCO and TCBCO films are addressed along with circuit evaluations of microstrip resonators, phase shifters, microstrip filters, dielectric resonator filters, and superconducting antennas. C.D.

A91-32822* National Aeronautics and Space Administration. Lewis Research Center, Cleveland, OH.

MUTUAL COUPLING BETWEEN ELECTROMAGNETICALLY COUPLED RECTANGULAR PATCH ANTENNAS

R. Q. LEE (NASA, Lewis Research Center, Cleveland, OH), T. TALTY, and K. F. LEE (Toledo, University, OH) Electronics Letters (ISSN 0013-5194), vol. 27, March 14, 1991, p. 532, 533.

Copyright

Measured mutual coupling between two X-band electromagnetically coupled rectangular patch antennas is reported. Results are given for both the wideband and high gain regions as well as for E-plane and H-plane couplings. C.D.

A91-32823* National Aeronautics and Space Administration. Lewis Research Center, Cleveland, OH.

NEW COPLANAR WAVEGUIDE/STRIPLINE FEED NETWORK FOR SEVEN PATCH HEXAGONAL CP SUBARRAY

R. N. SIMONS, R. Q. LEE, and G. R. LINDAMOOD (NASA, Lewis Research Center, Cleveland, OH) Electronics Letters (ISSN 0013-5194), vol. 27, March 14, 1991, p. 533-535.

Copyright

A novel CPW-to-stripline post coupler is demonstrated. This device couples the output power from a coax-to-CPW inphase seven-way radial power divider to a balanced stripline line stretcher and together forms a multilayer probe-type feed network. The feed network excites a seven-patch hexagonal circularly polarized (CP) subarray. The measured return loss and insertion loss of the coupler are better than 17 dB and 0.25 dB at the design frequency of 2.875 GHz. The measured on-axis axial ratio for the left hand circular polarization (LHCP) is 1.5 dB and the 3 dB beam widths are 36 deg in the principal planes of the subarray. The gain of the subarray is 13 dB. The input return loss of the subarray is better than 10 dB. Author

A91-35911* Michigan Univ., Ann Arbor.

THEORETICAL AND EXPERIMENTAL CHARACTERIZATION OF COPLANAR WAVEGUIDE DISCONTINUITIES FOR FILTER APPLICATIONS

NIHAD I. DIB, LINDA P. B. KATEHI (Michigan, University, Ann Arbor), GEORGE E. PONCHAK, and RAINEE N. SIMONS (NASA, Lewis Research Center, Cleveland, OH) IEEE Transactions on

33 ELECTRONICS AND ELECTRICAL ENGINEERING

Microwave Theory and Techniques (ISSN 0018-9480), vol. 39, May 1991, p. 873-882. refs

(Contract NSF ECS-86-57951)

Copyright

A full-wave analysis of shielded coplanar waveguide two-port discontinuities based on the solution of an appropriate surface integral equation in the space domain is presented. Frequency-dependent scattering parameters for open-end and short-end coplanar waveguide (CPW) stubs are computed using this method. The numerically derived results are compared with measurements performed in the frequency range 5-25 GHz and show very good agreement. From the scattering parameters, lumped-element equivalent circuits have been derived to model the discontinuities. The inductors and capacitors of these models have been represented by closed-form equations, as functions of the stub length, to compute the circuit element values for these discontinuities.

I.E.

A91-36060* National Aeronautics and Space Administration. Lewis Research Center, Cleveland, OH.

DETERMINATION OF SURFACE RESISTANCE AND MAGNETIC PENETRATION DEPTH OF SUPERCONDUCTING YBA₂Cu₃O(7-DELTA) THIN FILMS BY MICROWAVE POWER TRANSMISSION MEASUREMENTS

K. B. BHASIN, J. D. WARNER (NASA, Lewis Research Center, Cleveland, OH), F. A. MIRANDA, W. L. GORDON (Case Western Reserve University, Cleveland, OH), and H. S. NEWMAN (U.S. Navy, Naval Research Laboratory, Washington, DC) (1990 Applied Superconductivity Conference, Snowmass, CO, Sept. 24-28, 1990, Proceedings. A91-36027 15-33) IEEE Transactions on Magnetics (ISSN 0018-9464), vol. 27, pt. 2, March 1991, p. 1284-1287. Previously announced in STAR as N91-10780. refs

Copyright

A novel waveguide power transmission measurement technique was developed to extract the complex conductivity of superconducting thin films at microwave frequencies. The microwave conductivity was taken of two laser ablated YBa₂Cu₃O(7-delta) thin films on LaAlO₃ with transition temperatures of approximately 86.3 and 82 K, respectively, in the temperature range 25 to 300 K. From the conductivity values, the penetration depth was found to be approximately 0.54 and 0.43 micron, and the surface resistance ($R_{\text{sub s}}$) to be approximately 24 and 36 micro-Ohms at 36 GHz and 76 K for the two films under consideration. The $R_{\text{sub s}}$ values were compared with those obtained from the change in the Q-factor of a 36 GHz Te sub 011-mode (OFHC) copper cavity by replacing one of its end walls with the superconducting sample. This technique allows noninvasive characterization of high transition superconducting thin films at microwave frequencies.

Author

A91-36172*# National Aeronautics and Space Administration. Lewis Research Center, Cleveland, OH.

AN EXPERIMENTAL STUDY OF HIGH TC SUPERCONDUCTING MICROSTRIP TRANSMISSION LINES AT 35 GHZ AND THE EFFECT OF FILM MORPHOLOGY

C. M. CHOREY (NASA, Lewis Research Center, Cleveland; Sverdrup Technology, Inc., Brook Park, OH), K. B. BHASIN, J. D. WARNER (NASA, Lewis Research Center, Cleveland, OH), J. Y. JOSEFOWICZ, D. B. RENSCH (Hughes Research Laboratories, Malibu, CA) et al. (1990 Applied Superconductivity Conference, Snowmass, CO, Sept. 24-28, 1990, Proceedings. A91-36027 15-33) IEEE Transactions on Magnetics (ISSN 0018-9464), vol. 27, pt. 4, March 1991, p. 2940-2943. Previously announced in STAR as N91-11988. refs

Microstrip transmission lines in the form of ring resonators were fabricated from a number of in-situ grown laser ablated films and post-annealed co-sputtered YBa₂Cu₃O(7-x) films. The properties of these resonators were measured at 35 GHz and the observed performance is examined in light of the critical temperature (T_c) and film thickness, and also the film morphology, which is different for the two deposition techniques. It is found that T_c is a major indicator of the film performance for each growth type, with film thickness becoming important as it decreases towards 1000 Å. It

is also found that the films with a mixed grain orientation (both a-axis and c-axis oriented grains) have poorer microwave properties as compared with the primarily c-axis oriented material. This is probably due to the significant number of grain boundaries between the different crystallites, which may act as superconducting weak links and contribute to the surface resistance.

Author

A91-37985* Schafer (W. J.) Associates, Inc., Arlington, VA. LIGHT WEIGHT, HIGH POWER, HIGH VOLTAGE DC/DC CONVERTER TECHNOLOGIES

ROBERT KRAUS (W.J. Schafer Associates, Inc., Arlington, VA), IRA MYERS, and ERIC BAUMANN (NASA, Lewis Research Center, Cleveland, OH) IN: IECEC-90; Proceedings of the 25th Intersociety Energy Conversion Engineering Conference, Reno, NV, Aug. 12-17, 1990. Vol. 1. New York, American Institute of Chemical Engineers, 1990, p. 380-385.

Copyright

Power-conditioning weight reductions by orders of magnitude will be required to enable the megawatt-power-level space systems envisioned by the Strategic Defense Initiative, the Air Force, and NASA. An interagency program has been initiated to develop an 0.1-kg/kW dc/dc converter technology base for these future space applications. Three contractors are in the first phase of a competitive program to develop a megawatt dc/dc converter. Researchers at NASA Lewis Research Center are investigating innovative converter topology control. Three different converter subsystems based on square wave, resonant, and super-resonant topologies are being designed. The components required for the converter designs cover a wide array of technologies. Two different switches, one semiconductor and the other gas, are under development. Issues related to thermal management and material reliability for inductors, transformers, and capacitors are being investigated in order to maximize power density. A brief description of each of the concepts proposed to meet the goals of this program is presented.

I.E.

A91-37987* National Aeronautics and Space Administration. Lewis Research Center, Cleveland, OH.

FIELD ORIENTED CONTROL OF INDUCTION MOTORS

LINDA M. BURROWS, MARY ELLEN ROTH (NASA, Lewis Research Center, Cleveland, OH), and DON S. ZINGER (Akron, University, OH) IN: IECEC-90; Proceedings of the 25th Intersociety Energy Conversion Engineering Conference, Reno, NV, Aug. 12-17, 1990. Vol. 1. New York, American Institute of Chemical Engineers, 1990, p. 391-396. Previously announced in STAR as N90-22731. refs

Copyright

Induction motors have always been known for their simple rugged construction, but until lately were not suitable for variable speed or servo drives due to the inherent complexity of the controls. With the advent of field oriented control (FOC), however, the induction motor has become an attractive option for these types of drive systems. An FOC system which utilizes the pulse population modulation method to synthesize the motor drive frequencies is examined. This system allows for a variable voltage to frequency ratio and enables the user to have independent control of both the speed and torque of an induction motor. A second generation of the control boards were developed and tested with the next point of focus being the minimization of the size and complexity of these controls. Many options were considered with the best approach being the use of a digital signal processor (DSP) due to its inherent ability to quickly evaluate control algorithms. The present test results of the system and the status of the optimization process using a DSP are discussed.

Author

A91-37988* Pittsburgh Univ., Johnstown, PA. HIGH FREQUENCY, HIGH TEMPERATURE SPECIFIC CORE LOSS AND DYNAMIC B-H HYSTERESIS LOOP CHARACTERISTICS OF SOFT MAGNETIC ALLOYS

W. R. WIESERMAN (Pittsburgh, University, Johnstown, PA), G. E. SCHWARZE (NASA, Lewis Research Center, Cleveland, OH), and J. M. NIEDRA (Sverdrup Technology, Inc., Cleveland, OH) IN: IECEC-90; Proceedings of the 25th Intersociety Energy Conversion

Engineering Conference, Reno, NV, Aug. 12-17, 1990. Vol. 1. New York, American Institute of Chemical Engineers, 1990, p. 397-402. Previously announced in STAR as N90-23663. refs
Copyright

Limited experimental data exists for the specific core loss and dynamic B-H loop for soft magnetic materials for the combined conditions of high frequency and high temperature. This experimental study investigates the specific core loss and dynamic B-H loop characteristics of Supermalloy and Metglas 2605SC over the frequency range of 1 to 50 kHz and temperature range of 23 to 300 C under sinusoidal voltage excitation. The experimental setup used to conduct the investigation is described. The effects of the maximum magnetic flux density, frequency, and temperature on the specific core loss and on the size and shape of the B-H loops are examined. Author

A91-37992* National Aeronautics and Space Administration. Lewis Research Center, Cleveland, OH.

ELECTRICAL CHARACTERIZATION OF A MAPHAM INVERTER USING PULSE TESTING TECHNIQUES

E. D. BAUMANN, I. T. MYERS (NASA, Lewis Research Center, Cleveland, OH), and A. N. HAMMOUD (NASA, Lewis Research Center; Sverdrup Technology, Inc., Cleveland, OH) IN: IECEC-90; Proceedings of the 25th Intersociety Energy Conversion Engineering Conference, Reno, NV, Aug. 12-17, 1990. Vol. 1. New York, American Institute of Chemical Engineers, 1990, p. 423-427. SDIO-supported research. (Contract FY1455-89-N-0655)
Copyright

The use of a multiple pulse testing technique to determine the electrical characteristics of large megawatt-level power systems for aerospace missions is proposed. An innovative test method based on the multiple pulse technique is demonstrated on a 2-kW Mapham inverter. The concept of this technique shows that characterization of large power systems under electrical equilibrium at rated power can be accomplished without large costly power supplies. The heat generation that occurs in systems when tested in a continuous mode is eliminated. The results indicate that there is a good agreement between this testing technique and that of steady state testing. I.E.

A91-38162* National Aeronautics and Space Administration. Lewis Research Center, Cleveland, OH.

NEUTRON AND GAMMA IRRADIATION EFFECTS ON POWER SEMICONDUCTOR SWITCHES

G. E. SCHWARZE (NASA, Lewis Research Center, Cleveland, OH) and A. J. FRASCA (Wittenberg University, Springfield, OH) IN: IECEC-90; Proceedings of the 25th Intersociety Energy Conversion Engineering Conference, Reno, NV, Aug. 12-17, 1990. Vol. 6. New York, American Institute of Chemical Engineers, 1990, p. 30-35. Previously announced in STAR as N90-25278. refs
Copyright

The performance characteristics of high-power semiconductor switches subjected to high levels of neutron fluence and gamma dose must be known by the designer of the power conditioning, control and transmission subsystem of space nuclear power systems. Location and the allowable shielding mass budget will determine the level of radiation tolerance required by the switches to meet performance and reliability requirements. Neutron and gamma ray interactions with semiconductor materials and how these interactions affect the electrical and switching characteristics of solid state power switches is discussed. The experimental measurement system and radiation facilities are described. Experimental data showing the effects of neutron and gamma irradiation on the performance characteristics are given for power-type NPN Bipolar Junction Transistors (BJTs), and Metal-Oxide-Semiconductor Field Effect Transistors (MOSFETs). BJTs show a rapid decrease in gain, blocking voltage, and storage time for neutron irradiation, and MOSFETs show a rapid decrease in the gate threshold voltage for gamma irradiation. Author

A91-40272* National Aeronautics and Space Administration. Lewis Research Center, Cleveland, OH.

NEW CHANNELISED COPLANAR WAVEGUIDE TO RECTANGULAR WAVEGUIDE POST AND SLOT COUPLERS

R. N. SIMONS (NASA, Lewis Research Center, Cleveland, OH) Electronics Letters (ISSN 0013-5194), vol. 27, May 9, 1991, p. 856-858.

Copyright

Two new coplanar waveguide to rectangular waveguide couplers with coupling through a post and a slot are experimentally demonstrated. The couplers operate over the Ku-band transmission and X-band reception frequencies that are designated for satellite communications. The measured insertion loss and return loss are about 1 dB, respectively, for both couplers. Author

A91-41889* National Aeronautics and Space Administration. Lewis Research Center, Cleveland, OH.

PEELED FILM GAAS SOLAR CELL DEVELOPMENT

D. M. WILT, R. D. THOMAS, S. G. BAILEY, D. J. BRINKER, F. L. DEANGELO (NASA, Lewis Research Center, Cleveland, OH) et al. IN: IEEE Photovoltaic Specialists Conference, 21st, Kissimmee, FL, May 21-25, 1990, Conference Record. Vol. 1. New York, Institute of Electrical and Electronics Engineers, Inc., 1990, p. 111-114.

Copyright

Thin-film, single-crystal gallium arsenide (GaAs) solar cells could exhibit a specific power approaching 700 W/kg including coverglass. A simple process has been described whereby epitaxial GaAs layers are peeled from a reusable substrate. This process takes advantage of the extreme selectivity of the etching rate of aluminum arsenide (AlAs) over GaAs in dilute hydrofluoric acid. The feasibility of using the peeled film technique to fabricate high-efficiency, low-mass GaAs solar cells is presently demonstrated. A peeled film GaAs solar cell was successfully produced. The device, although fractured and missing the aluminum gallium arsenide window and antireflective coating, had a Voc of 874 mV and a fill factor of 68 percent under AM0 illumination. I.E.

A91-41891* National Aeronautics and Space Administration. Lewis Research Center, Cleveland, OH.

AN ANALYSIS OF THE CONTACT SINTERING PROCESS IN III-V SOLAR CELLS

VICTOR G. WEIZER (NASA, Lewis Research Center, Cleveland, OH) and NAVID S. FATEMI (Sverdrup Technology, Inc., Cleveland, OH) IN: IEEE Photovoltaic Specialists Conference, 21st, Kissimmee, FL, May 21-25, 1990, Conference Record. Vol. 1. New York, Institute of Electrical and Electronics Engineers, Inc., 1990, p. 119-124. Previously announced in STAR as N90-25420. refs (Contract NAS3-25266)
Copyright

The possibility of eliminating the gross mechanical changes that take place during sintering while retaining the processes that reduce contact resistivity is investigated. Before considering the electrical aspects, however, it is necessary to understand the relevant metallurgy. As the sintering process proceeds in the InP-Au system, dramatic color changes that enable a precise measurement of the kinetics of each step occur. A detailed insight into the processes that control each stage in the InP-Au interaction has resulted. It is shown that contact sintering in the InP-Au system consists of three consecutive stages, each of which is controlled by a separate mechanism. Author

A91-41929* Cleveland State Univ., OH.

KEY FACTORS LIMITING THE OPEN CIRCUIT VOLTAGE OF N(+)PP(+) INDIUM PHOSPHIDE SOLAR CELLS

CHANDRA GORADIA, WILLIAM THESLING (Cleveland State University, OH), and IRVING WEINBERG (NASA, Lewis Research Center, Cleveland, OH) IN: IEEE Photovoltaic Specialists Conference, 21st, Kissimmee, FL, May 21-25, 1990, Conference Record. Vol. 1. New York, Institute of Electrical and Electronics Engineers, Inc., 1990, p. 386-393. Previously announced in STAR

33 ELECTRONICS AND ELECTRICAL ENGINEERING

as N91-19206. refs
Copyright

Solar cells made from gallium arsenide (GaAs), with a room temperature bandgap of $E_{\text{sub g}} = 1.43$ eV have exhibited the best measured open circuit voltage ($V_{\text{sub oc}}$) of 1.05 V at 1 AMO, 25 C. The material InP is in many ways similar to GaAs. A simple calculation comparing InP to GaAs then shows that solar cells made from InP, with $E_{\text{sub g}} = 1.35$ at 300 K, should exhibit the best measured $V_{\text{sub oc}}$ of approximately 950 mV at 1 AMO, 300 K. However, to date, the best measured $V_{\text{sub oc}}$ for InP solar cells made by any fabrication method is 899 mV at AM1.5, 25 C which would translate to 912 mV at 1 AMO, 25 C. The $V_{\text{sub oc}}$ of an $n(+)\text{pp}(+)$ InP solar cell is governed by several factors. Of these, some factors, such as the thickness and doping of the emitter and base regions, are easily controlled and can be adjusted to desired values dictated by a good performance optimizing model. Such factors were not considered. There are other factors which also govern $V_{\text{sub oc}}$, and their values are not so easily controlled. The primary ones among these are (1) the indirect or Hall-Shockley-Read lifetimes in the various regions of the cell, (2) the low-doping intrinsic carrier concentration $n_{\text{sub i}}$ of the InP material, (3) the heavy doping factors in the emitter and BSF regions, and (4) the front surface recombination velocity $S_{\text{sub F}}$. The influence of these latter factors on the $V_{\text{sub oc}}$ of the $n(+)\text{pp}(+)$ InP solar cell and the results were used to produce a near-optimum design of the $n(+)\text{pp}(+)$ InP solar cell.

Author

A91-41971*# National Aeronautics and Space Administration. Lewis Research Center, Cleveland, OH.

RECENT RESULTS FROM THE INP HOMOJUNCTION CELL MODULE ON THE LIPS III SPACECRAFT

DAVID J. BRINKER and IRVING WEINBERG (NASA, Lewis Research Center, Cleveland, OH) IN: IEEE Photovoltaic Specialists Conference, 21st, Kissimmee, FL, May 21-25, 1990, Conference Record. Vol. 2. New York, Institute of Electrical and Electronics Engineers, Inc., 1990, p. 1167-1171. refs

The flight performance of the NASA Lewis Research Center's indium phosphide homojunction cell module on the LIPS III spacecraft is presented. Four $n+p$ diffused junction cells, an early product of an InP development program, were flown. The voltage range of the data prohibits determination of the open-circuit voltage or the maximum power point. However, analysis of the 32 months of short-circuit current data reveals a slight increase, not the 4 percent decrease expected from radiation tolerance studies. This increase may be due to continual cleaning of possible prelaunch dust contamination or changes in data acquisition system calibration. For all cells, the average short-circuit current remains below prelaunch values.

I.E.

A91-41984*# National Aeronautics and Space Administration. Lewis Research Center, Cleveland, OH.

EFFECTS OF RADIATION OF INP CELLS EPITAXIALLY GROWN ON SI AND GAAS SUBSTRATES

I. WEINBERG, C. K. SWARTZ, D. J. BRINKER, and D. M. WILT (NASA, Lewis Research Center, Cleveland, OH) IN: IEEE Photovoltaic Specialists Conference, 21st, Kissimmee, FL, May 21-25, 1990, Conference Record. Vol. 2. New York, Institute of Electrical and Electronics Engineers, Inc., 1990, p. 1235-1240. refs

The properties of heteroepitaxial InP cells were determined both before and after 10-MeV proton irradiations. Numerical values, obtained for the diffusion and recombination components of the reverse saturation currents, were found to be consistent with the distribution of dislocations. The radiation resistance of the heteroepitaxial cells was significantly greater than that observed for n/p homoepitaxial InP cells. The carrier removal rate, obtained by C-V measurements, was 1800/cm for 10-MeV protons compared with 2.2/cm for 1-MeV electrons. The high carrier removal rate was found to have no significant effect on the cell's series resistance. It was concluded that the heteroepitaxial cell performance is dominated by the high dislocation density attributable to lattice constant mismatch. Although the efficiencies

of the present cells are low, the recent achievement of 13.7 percent AMO efficiencies using a GaAs substrate demonstrates the marked improvement that can be attained using more appropriate transition layers.

I.E.

A91-42003*# National Aeronautics and Space Administration. Lewis Research Center, Cleveland, OH.

EFFECT OF EMITTER PARAMETER VARIATION ON THE PERFORMANCE OF HETEROEPIITAXIAL INDIUM PHOSPHIDE SOLAR CELLS

R. K. JAIN and D. J. FLOOD (NASA, Lewis Research Center, Cleveland, OH) IN: IEEE Photovoltaic Specialists Conference, 21st, Kissimmee, FL, May 21-25, 1990, Conference Record. Vol. 2. New York, Institute of Electrical and Electronics Engineers, Inc., 1990, p. 1350-1355. Previously announced in STAR as N91-15306. refs

Metalorganic chemical-vapor-deposited heteroepitaxial indium phosphide (InP) solar cell experimental results were simulated by using a PC-1D computer model. The effect of emitter parameter variation on the performance of $n(+)/p/p(+)$ heteroepitaxial InP/GaAs solar cell was presented. The thinner and lighter doped emitters were observed to offer higher cell efficiencies. The influence of emitter thickness and minority carrier diffusion length on the cell efficiency with respect to dislocation density was studied. Heteroepitaxial cells with efficiencies similar to present day homojunction InP efficiencies (greater than 16 percent AMO) were shown to be attainable if a dislocation density lower than $10(\exp 6)/\text{sq cm}$ could be achieved. A realistic optimized design study yielded InP solar cells of over 22 percent AMO efficiency at 25 C.

Author

A91-42694* National Aeronautics and Space Administration. Lewis Research Center, Cleveland, OH.

THE INFLUENCE OF INTERSTITIAL GA AND INTERFACIAL AU2P3 ON THE ELECTRICAL AND METALLURGICAL BEHAVIOR OF AU-CONTACTED III-V SEMICONDUCTORS

VICTOR G. WEIZER (NASA, Lewis Research Center, Cleveland, OH) and NAVID S. FATEMI (NASA, Lewis Research Center; Sverdrup Technology, Inc., Cleveland, OH) Journal of Applied Physics (ISSN 0021-8979), vol. 69, June 15, 1991, p. 8253-8260. refs

(Contract NAS3-25266)

Copyright

The effect of introducing a very small amount of Ga into Au-contacted InP on the behavior of that contact system was investigated. It was found that Ga affected both the metallurgical and the electrical behavior of the system. It is shown that Ga atoms in the interstices of the Au lattice prevent the solid-state reactions that normally take place between Au and InP during contact sintering and cause an order of magnitude reduction in the specific contact resistivity. It is also shown that the presence of Ga affects the reactions of GaP and GaAs with Au contacts.

I.S.

A91-47057* Texas A&M Univ., College Station.

A 29.3-GHZ CAVITY-ENCLOSED APERTURE-COUPLED CIRCULAR-PATCH ANTENNA FOR MICROWAVE CIRCUIT INTEGRATION

JULIO A. NAVARRO, KAI CHANG (Texas A & M University, College Station), JOSEPH TOLLESON, SHASHI SANZGIRI (Texas Instruments, Inc., McKinney), and R. Q. LEE (NASA, Lewis Research Center, Cleveland, OH) IEEE Microwave and Guided Wave Letters (ISSN 1051-8207), vol. 1, July 1991, p. 170, 171. Research supported by Texas Instruments, Inc. and Texas Higher Education Coordinating Board. refs

Copyright

A circular patch antenna fed by an aperture-coupled microstrip line has been demonstrated at 29.3 GHz. The patch was enclosed by a cavity to reduce surface-wave interactions in an array environment and to improve heat dissipation when using active devices. The antenna exhibited a 2:1 input VSWR (voltage standing wave ratio) over a bandwidth of 12 percent from 27.52 to 30.95

GHz. The antenna should have applications in conformal phased arrays at millimeter-wave frequencies. I.E.

A91-50426* National Aeronautics and Space Administration. Lewis Research Center, Cleveland, OH.

SUPERCONDUCTIVITY APPLICATIONS FOR INFRARED AND MICROWAVE DEVICES; PROCEEDINGS OF THE MEETING, ORLANDO, FL, APR. 19, 20, 1990

KUL B. BHASIN, ED. and VERNON O. HEINEN, ED. (NASA, Lewis Research Center, Cleveland, OH) Meeting sponsored by SPIE. Bellingham, WA, Society of Photo-Optical Instrumentation Engineers (SPIE Proceedings. Vol. 1292), 1990, 217 p. For individual items see A91-50427 to A91-50445. (SPIE-1292) Copyright

Various papers on superconductivity applications for IR and microwave devices are presented. The individual topics addressed include: pulsed laser deposition of Ti-Ca-Ba-Cu-O films, patterning of high-Tc superconducting thin films on Si substrates, IR spectra and the energy gap in thin film YBa₂Cu₃O(7- δ), high-temperature superconducting thin film microwave circuits, novel filter implementation utilizing HTS materials, high-temperature superconductor antenna investigations, high-Tc superconducting IR detectors, high-Tc superconducting IR detectors from Y-Ba-Cu-O thin films, Y-Ba-Cu-O thin films as high-speed IR detectors, fabrication of a high-Tc superconducting bolometer, transition-edge microbolometer, photoresponse of YBa₂Cu₃O(7- δ) granular and epitaxial superconducting thin films, fast IR response of YBCO thin films, kinetic inductance effects in high-Tc microstrip circuits at microwave frequencies. C.D.

A91-50433* National Aeronautics and Space Administration. Lewis Research Center, Cleveland, OH.

HIGH TEMPERATURE SUPERCONDUCTING THIN FILM MICROWAVE CIRCUITS - FABRICATION, CHARACTERIZATION, AND APPLICATIONS

K. B. BHASIN, J. D. WARNER, R. R. ROMANOFKY, V. O. HEINEN (NASA, Lewis Research Center, Cleveland, OH), and C. M. CHOREY (NASA, Lewis Research Center; Sverdrup Technology, Inc., Cleveland, OH) IN: Superconductivity applications for infrared and microwave devices; Proceedings of the Meeting, Orlando, FL, Apr. 19, 20, 1990. Bellingham, WA, Society of Photo-Optical Instrumentation Engineers, 1990, p. 71-82. Previously announced in STAR as N90-28786. refs Copyright

Epitaxial YBa₂Cu₃O₇ films were grown on several microwave substrates. Surface resistance and penetration depth measurements were performed to determine the quality of these films. Here, the properties of these films on key microwave substrates are described. The fabrication and characterization of a microwave ring resonator circuit to determine transmission line losses are presented. Lower losses than those observed in gold resonator circuits were observed at temperatures lower than critical transition temperature. Based on these results, potential applications of microwave superconducting circuits such as filters, resonators, oscillators, phase shifters, and antenna elements in space communication systems are identified. Author

A91-50443* Ohio State Univ., Columbus.

PHOTORESPONSE OF YBA₂CU₃O(7- δ) GRANULAR AND EPITAXIAL SUPERCONDUCTING THIN FILMS

G. J. VALCO (Ohio State University, Columbus), P. CLASPY, J. D. WARNER, N. VARALJAY, and K. B. BHASIN (NASA, Lewis Research Center, Cleveland, OH) IN: Superconductivity applications for infrared and microwave devices; Proceedings of the Meeting, Orlando, FL, Apr. 19, 20, 1990. Bellingham, WA, Society of Photo-Optical Instrumentation Engineers, 1990, p. 166-175. Previously announced in STAR as N90-22732. refs (Contract NCC3-105) Copyright

The response is reported of thin films of YBa₂Cu₃O(7- δ) with either a very grainy or a smooth epitaxial morphology to visible radiation. SrTiO₃ substrates were employed for both types of films. The grainy films were formed by sequential multi-layer

electron beam evaporation while the epitaxial films were formed by laser ablation. Both films were patterned into H shaped detectors via a negative photolithographic process employing a Br/ethanol etchant. The bridge region of the H was 50 microns wide. The patterned films formed by laser ablation and sequential evaporation had critical temperatures of 74 K and 72 K respectively. The bridge was current biased and illuminated with chopped He-Ne laser radiation and the voltage developed in response to the illumination was measured. A signal was detected only above the critical temperature and the peak of the response coincided with the resistive transition for both types of films although the correspondence was less exact for the grainy film. The details of the responses and their analysis are presented. Author

A91-51146* Case Western Reserve Univ., Cleveland, OH. **PERFORMANCE OF A 300 MBPS 1:16 SERIAL/PARALLEL OPTOELECTRONIC RECEIVER MODULE**

M. A. RICHARD, P. C. CLASPY (Case Western Reserve University, Cleveland, OH), K. B. BHASIN (NASA, Lewis Research Center, Cleveland, OH), and M. P. BENDETT (Honeywell, Inc., Minneapolis, MN) IN: Optical and digital GaAs technologies for signal-processing applications; Proceedings of the Meeting, Orlando, FL, Apr. 16-18, 1990. Bellingham, WA, Society of Photo-Optical Instrumentation Engineers, 1990, p. 196-202. refs Copyright

Optical interconnects are being considered for the high speed distribution of multiplexed control signals in GaAs MMIC-based phased array antennas. This paper describes the performance of a hybrid GaAs optoelectronic integrated circuit (OEIC), along with a description of its design and fabrication. The OEIC converts a 16-bit serial optical input to a 16 parallel line electrical output using an on-board 1:16 demultiplexer and operates at data rates as high as 305 Mbps. The performance characteristics as well as potential applications of the device are presented. Author

A91-52342*# National Aeronautics and Space Administration. Lewis Research Center, Cleveland, OH.

COPLANAR WAVEGUIDE FEEDS FOR PHASED ARRAY ANTENNAS

RAINEE N. SIMONS (NASA, Lewis Research Center, Cleveland, Sverdrup Technology, Inc., Brook Park, OH) and RICHARD Q. LEE (NASA, Lewis Research Center, Cleveland, OH) AIAA, NASA, and OAI, Conference on Advanced SEI Technologies, Cleveland, OH, Sept. 4-6, 1991. 8 p. Previously announced in STAR as N91-27477. refs (AIAA PAPER 91-3422) Copyright

The design and performance is presented of the following coplanar waveguides (CPW) microwave distribution networks for linear as well as circularly polarized microstrip patches and dipole arrays: (1) CPW/microstrip line feed; (2) CPW/balanced stripline feed; (3) CPW/slotline feed; (4) grounded CPW/balanced coplanar stripline feed; and (5) CPW/slot coupled feed. Typical measured radiation patterns are presented, and their relative advantages and disadvantages are compared. Author

A91-52345*# National Aeronautics and Space Administration. Lewis Research Center, Cleveland, OH.

HIGH EFFICIENCY KA-BAND MMIC AMPLIFIERS

EDWARD J. HAUGLAND (NASA, Lewis Research Center, Cleveland, OH) AIAA, NASA, and OAI, Conference on Advanced SEI Technologies, Cleveland, OH, Sept. 4-6, 1991. 6 p. refs (AIAA PAPER 91-3425) Copyright

This paper describes recent progress in the Ka-band MMIC power amplifier program. New materials, material growth techniques, device designs and circuit design techniques have made it possible to design and fabricate MMIC amplifiers with both high efficiency and high power at Ka-band and higher frequencies. MMIC amplifiers using pseudomorphic AlGaAs/InGaAs/GaAs HEMT devices presently achieve 400 mW with 25 percent efficiency at Ka-band and 1 W, 35 percent efficient amplifiers are being developed. Author

A91-52420* National Aeronautics and Space Administration. Lewis Research Center, Cleveland, OH.

NEUTRON, GAMMA RAY AND POST-IRRADIATION THERMAL ANNEALING EFFECTS ON POWER SEMICONDUCTOR SWITCHES

G. E. SCHWARZE (NASA, Lewis Research Center, Cleveland, OH) and A. J. FRASCA (Wittenberg University, Springfield, OH) AIAA, NASA, and OAI, Conference on Advanced SEI Technologies, Cleveland, OH, Sept. 4-6, 1991. 14 p. (AIAA PAPER 91-3525)

Experimental data showing the effects of neutrons and gamma rays on the performance characteristics of power-type NPN bipolar junction transistors (BJTs), metal-oxide-semiconductor field effect transistors (MOSFETs), and static induction transistors (SITs) are given. These three types of devices were tested at radiation levels which met or exceeded the SP-100 requirements. For the SP-100 radiation requirements, the BJTs were found to be most sensitive to neutrons, the MOSFETs were most sensitive to gamma rays, and the SITs were only slightly sensitive to neutrons. Postirradiation thermal anneals at 300 K and up to 425 K were done on these devices and the effectiveness of these anneals are also discussed. Author

A91-52459* National Aeronautics and Space Administration. Lewis Research Center, Cleveland, OH.

NEW MATERIALS AND TECHNIQUES FOR IMPROVED MM WAVE DEVICES

SAMUEL A. ALTEROVITZ (NASA, Lewis Research Center, Cleveland, OH) AIAA, NASA, and OAI, Conference on Advanced SEI Technologies, Cleveland, OH, Sept. 4-6, 1991. 10 p. refs (AIAA PAPER 91-3590) Copyright

Current research on microwave and mm wave three terminal semiconductor devices is summarized with particular attention given to the development of the pseudomorphic InGaAs modulation-doped field effect transistor (MODFET). Application of the high-indium-concentration MODFET grown on InP in the temperature range of 120-150 K is also described. O.G.

A91-52461* National Aeronautics and Space Administration. Lewis Research Center, Cleveland, OH.

HIGH POWER, HIGH EFFICIENCY MILLIMETER WAVELENGTH TRAVELING WAVE TUBES FOR HIGH RATE COMMUNICATIONS FROM DEEP SPACE

JAMES A. DAYTON, JR. (NASA, Lewis Research Center, Cleveland, OH) AIAA, NASA, and OAI, Conference on Advanced SEI Technologies, Cleveland, OH, Sept. 4-6, 1991. 6 p. refs (AIAA PAPER 91-3593) Copyright

The high-power transmitters needed for high data rate communications from deep space will require a new class of compact, high efficiency traveling wave tubes (TWT's). Many of the recent TWT developments in the microwave frequency range are generically applicable to mm wave devices, in particular much of the technology of computer aided design, cathodes, and multistage depressed collectors. However, because TWT dimensions scale approximately with wavelength, mm wave devices will be physically much smaller with inherently more stringent fabrication tolerances and sensitivity to thermal dissipation. Author

A91-52462* National Aeronautics and Space Administration. Lewis Research Center, Cleveland, OH.

LOW NOISE INP-BASED MMIC RECEIVERS FOR W-BAND

REGIS F. LEONARD (NASA, Lewis Research Center, Cleveland, OH) AIAA, NASA, and OAI, Conference on Advanced SEI Technologies, Cleveland, OH, Sept. 4-6, 1991. 6 p. refs (AIAA PAPER 91-3594) Copyright

A program to develop a monolithic W-band low noise amplifier (a critical element in any W-band communications, sensors, or radar application) is described. Goals of the program include a completely monolithic low noise amplifier, less than a 3.5 dB noise figure, and a monolithic mixer suitable for integration with the LNA. R.E.P.

A91-52485* National Aeronautics and Space Administration. Lewis Research Center, Cleveland, OH.

STATUS OF KA-BAND TWT TRANSMITTER TECHNOLOGY

JAMES A. DAYTON, JR. (NASA, Lewis Research Center, Cleveland, OH) AIAA, NASA, and OAI, Conference on Advanced SEI Technologies, Cleveland, OH, Sept. 4-6, 1991. 5 p. refs (AIAA PAPER 91-3621) Copyright

The TWT types that are available for application to SEI are reviewed and evaluated in terms of their level of development and their suitability for use in space. The NASA OAET program for enhancement of efficiency and lifetime of TWT's is reviewed and the application of this technology to Ka-band devices is illustrated. Author

A91-54526* Cincinnati Univ., OH.

SUBMICRON GATE INP POWER MISFET'S WITH IMPROVED OUTPUT POWER DENSITY AT 18 AND 20 GHZ

MICHAEL D. BIEDENBENDER, VIK J. KAPOOR (Cincinnati, University, OH), KURT A. SHALKHAUSER (NASA, Lewis Research Center, Cleveland, OH), LOUIS J. MESSICK, RICHARD NGUYEN (U.S. Navy, Naval Ocean Systems Center, San Diego, CA), DIETMAR SCHMITZ, and HOLGER JURGENSEN (Aixtron Corp., Aachen, Federal Republic of Germany) IEEE Transactions on Microwave Theory and Techniques (ISSN 0018-9480), vol. 39, Aug. 1991, p. 1368-1375. Research supported by U.S. Navy. Previously announced in STAR as N91-26436. refs Copyright

The microwave characteristics are presented at 18 and 20 GHz of submicron gate indium phosphide (InP) metal-insulator-semiconductor field-effect transistors (MISFETs) for high output power density applications. InP power MISFET's were fabricated and the output power density was investigated as a function of drain-source spacing. The best output power density and gain were obtained for drain-source spacing of 3 micron. The output power density is 2.7 times greater than was previously measured for InP MISFET's at 18 and 20 GHz, and the power-added efficiency also increased. Author

A91-54532* National Aeronautics and Space Administration. Lewis Research Center, Cleveland, OH.

YBCO SUPERCONDUCTING RING RESONATORS AT MILLIMETER-WAVE FREQUENCIES

CHRISTOPHER M. CHOREY (NASA, Lewis Research Center, Cleveland; Sverdrup Technology, Inc., Brook Park, OH), KEON-SHIK KONG (Texas, University, Austin), KUL B. BHASIN, J. D. WARNER (NASA, Lewis Research Center, Cleveland, OH), and TATSUO ITOH (California, University, Los Angeles) IEEE Transactions on Microwave Theory and Techniques (ISSN 0018-9480), vol. 39, Sept. 1991, p. 1480-1487. Previously announced in STAR as N90-18634. refs Copyright

Microstrip ring resonators operating at 35 GHz were fabricated from laser ablated YBCO films deposited on lanthanum aluminate substrates. They were measured over a range of temperatures and their performances compared to identical resonators made of evaporated gold. Below 60 Kelvin the superconducting strip performed better than the gold, reaching an unloaded Q approximately 1.5 times that of gold at 25 K. A shift in the resonant frequency follows the form predicted by the London equations. The Phenomenological Loss Equivalence Method is applied to the ring resonator and the theoretically calculated Q values are compared to the experimental results. Author

A91-54746* National Aeronautics and Space Administration. Lewis Research Center, Cleveland, OH.

HIGH-VOLTAGE 6H-SIC P-N JUNCTION DIODES

L. G. MATUS, J. A. POWELL (NASA, Lewis Research Center, Cleveland, OH), and C. S. SALUPO (Calspan Corp., Middleburg Heights, OH) Applied Physics Letters (ISSN 0003-6951), vol. 59, Sept. 30, 1991, p. 1770-1772. refs Copyright

A chemical vapor deposition (CVD) process has been used to produce device structures of n- and p-type 6H-SiC epitaxial layers

on commercially produced single-crystal 6H-SiC wafers. Mesa-style p-n junction diodes were successfully fabricated from these device structures using reactive ion etching, oxide passivation, and electrical contact metallization techniques. When tested in air, the 6H-SiC diodes displayed excellent rectification characteristics up to the highest temperature tested, 600 C. To observe avalanche breakdown of the p-n junction diodes, testing under a high-electrical-strength liquid was necessary. The avalanche breakdown voltage was 1000 V representing the highest reverse breakdown voltage to be reported for any CVD-grown SiC diode.

Author

N91-14552* National Aeronautics and Space Administration. Lewis Research Center, Cleveland, OH.

UNIVERSAL NONDESTRUCTIVE MM-WAVE INTEGRATED CIRCUIT TEST FIXTURE Patent

ROBERT R. ROMANOFKY, inventor (to NASA) and KURT A. SHALKHAUSER, inventor (to NASA) 25 Dec. 1990 9 p Filed 10 Aug. 1989

(NASA-CASE-LEW-14746-1; US-PATENT-4,980,636; US-PATENT-APPL-SN-392239; US-PATENT-CLASS-324-158F; US-PATENT-CLASS-324-158P; US-PATENT-CLASS-324-601; US-PATENT-CLASS-333-247; INT-PATENT-CLASS-G01R-1/04) Avail: US Patent and Trademark Office CSCL 09/3

Monolithic microwave integrated circuit (MMIC) test includes a bias module having spring-loaded contacts which electrically engage pads on a chip carrier disposed in a recess of a base member. RF energy is applied to and passed from the chip carrier by chamfered edges of ridges in the waveguide passages of housings which are removably attached to the base member. Thru, Delay, and Short calibration standards having dimensions identical to those of the chip carrier assure accuracy and reliability of the test. The MMIC chip fits in an opening in the chip carrier with the boundaries of the MMIC lying on movable reference planes thereby establishing accuracy and flexibility.

Official Gazette of the U.S. Patent and Trademark Office

N91-17043* National Aeronautics and Space Administration. Lewis Research Center, Cleveland, OH.

ADVANCED ELECTRICAL POWER, DISTRIBUTION AND CONTROL FOR THE SPACE TRANSPORTATION SYSTEM

IRVING G. HANSEN and HENRY W. BRANDHORST, JR. In NASA, Washington, Space Transportation Avionics Technology Symposium. Volume 2: Conference Proceedings p 569-579 Aug. 1990

Avail: NTIS HC/MF A99 CSCL 09/3

High frequency power distribution and management is a technology ready state of development. As such, a system employs the fewest power conversion steps, and employs zero current switching for those steps. It results in the most efficiency, and lowest total parts system count when equivalent systems are compared. The operating voltage and frequency are application specific trade off parameters. However, a 20 kHz Hertz system is suitable for wide range systems.

Author

N91-18298* National Aeronautics and Space Administration. Lewis Research Center, Cleveland, OH.

NASA DEVELOPMENTS IN SOLID STATE POWER AMPLIFIERS

REGIS F. LEONARD In its Solid State Technology Branch of NASA Lewis Research Center Second Annual Digest, June 1989 - June 1990 p 3-10 Jun. 1990

Avail: NTIS HC/MF A13 CSCL 09/1

Over the last ten years, NASA has undertaken an extensive program aimed at development of solid state power amplifiers for space applications. Historically, the program may be divided into three phases. The first efforts were carried out in support of the advanced communications technology satellite (ACTS) program, which is developing an experimental version of a Ka-band commercial communications system. These first amplifiers attempted to use hybrid technology. The second phase was still targeted at ACTS frequencies, but concentrated on monolithic implementations, while the current, third phase, is a monolithic

effort that focusses on frequencies appropriate for other NASA programs and stresses amplifier efficiency. The topics covered include: (1) 20 GHz hybrid amplifiers; (2) 20 GHz monolithic MESFET power amplifiers; (3) Texas Instruments' (TI) 20 GHz variable power amplifier; (4) TI 20 GHz high power amplifier; (5) high efficiency monolithic power amplifiers; (6) GHz high efficiency variable power amplifier; (7) TI 32 GHz monolithic power amplifier performance; (8) design goals for Hughes' 32 GHz variable power amplifier; and (9) performance goals for Hughes' pseudomorphic 60 GHz power amplifier.

K.S.

N91-19348* National Aeronautics and Space Administration. Lewis Research Center, Cleveland, OH.

PULSED RESPONSE OF A TRAVELING-WAVE TUBE

BRIAN D. MAY Jan. 1991 15 p

(Contract RTOP 679-40-00)

(NASA-TM-103672; E-5884; NAS 1.15:103672) Avail: NTIS

HC/MF A03 CSCL 09/1

The consequence of frequency-domain multiple access (FDMA) channelization in a satellite communications system is that the ground- and space-based components are often required to operate at reduced output power to prevent the generation of distortions. However, the components of a time-division multiple access (TDMA) satellite system, such as a traveling-wave tube (TWT), can operate at the highest output power because the channelization technique is relatively insensitive to the distortions resulting from saturated operation. A Hughes 30-GHz TWT was tested to determine the suitability of such a device in a TDMA system. Testing was focused on the ability of the TWT to rise up to full power at the leading edge of TDMA bursts, which were simulated by a pulse train. A Wavetek model 8502A peak power meter was used to display and measure the pulsed signal waveform. Measurements of the TWT output signal rise time indicate that the TWT lengthened the rise time by 10 to 20 nsec. Imposing a modulator turn-on time that precedes the data burst by the TWT rise time is a logical approach to coordinating the traveling-wave tube amplifier and modulator specifications.

Author

N91-19349* National Aeronautics and Space Administration. Lewis Research Center, Cleveland, OH.

USING A MODIFIED HEWLETT PACKARD 8410 NETWORK ANALYZER AS AN AUTOMATED FARFIELD ANTENNA RANGE RECEIVER

JOHN D. TERRY and RICHARD R. KUNATH 1990 10 p Presented at the Antenna Measurement Techniques Association Meeting, Philadelphia, PA, 8-11 Oct. 1990

(Contract RTOP 650-60-20)

(NASA-TM-103700; E-5922; NAS 1.15:103700) Avail: NTIS

HC/MF A02 CSCL 09/3

A Hewlett Packard 8410 Network Analyzer was modified to be used as an automated far-field antenna range receiver. By using external mixers, analog to digital signal conversion, and an external computer/controller, the HP8410 is capable of measuring signals as low as -110 dBm. The modified receiver is an integral part of an automated far-field range which features computer controlled test antenna positioning, system measurement parameters, and data acquisition, as well as customized measurement file management. The system described was assembled and made operational, taking advantage of off-the-shelf hardware available at minimal cost.

Author

N91-19351* National Aeronautics and Space Administration. Lewis Research Center, Cleveland, OH.

ELLIPSOMETRIC STUDY OF INGAAS MODFET MATERIAL

S. A. ALTEROVITZ, R. E. SIEG, H. D. YAO, P. G. SNYDER, J. A. WOOLLAM, J. PAMULAPATI, and P. K. BHATTACHARYA (Michigan Univ., Ann Arbor.) 1990 6 p Presented at the 1990 Fall Meeting of the Materials Research Society, Boston, MA, 26 Nov. - 1 Dec. 1990

(Contract RTOP 506-44-21)

(NASA-TM-103286; E-5705; NAS 1.15:103286) Avail: NTIS

HC/MF A02 CSCL 09/3

In(x)Ga(1-x)As based MODFET (modulation doped field effect

33 ELECTRONICS AND ELECTRICAL ENGINEERING

transistor) material was grown by molecular beam epitaxy on semi-insulating InP substrates. Several structures were made, including lattice matched and strained layer InGaAs. All structures also included several layers of In(0.52)Al(0.48)As. Variable angle spectroscopic ellipsometry was used to characterize the structures. The experimental data, together with the calibration function for the constituent materials, were analyzed to yield the thickness of all the layers of the MODFET structure. Results of the ellipsometrically determined thicknesses compare very well with the reflection high energy electron diffraction in situ thickness measurements. Author

N91-19354*# National Aeronautics and Space Administration. Lewis Research Center, Cleveland, OH.

EFFECT OF DISLOCATIONS ON THE OPEN-CIRCUIT VOLTAGE, SHORT-CIRCUIT CURRENT AND EFFICIENCY OF HETEROEPITAXIAL INDIUM PHOSPHIDE SOLAR CELLS

RAJ K. JAIN and DENNIS J. FLOOD 1990 7 p Presented at the 5th International Photovoltaic Science and Engineering Conference, Kyoto, Japan, 26-30 Nov. 1990; sponsored by the Japan Society of Applied Physics, Inst. of Electrical Engineers of Japan, and the Foundation for the Advancement of International Science

(Contract RTOP 506-41-11)

(NASA-TM-103762; E-6024; NAS 1.15:103762) Avail: NTIS HC/MF A02 CSCL 09/3

Excellent radiation resistance of indium phosphide solar cells makes them a promising candidate for space power applications, but the present high cost of starting substrates may inhibit their large scale use. Thin film indium phosphide cells grown on Si or GaAs substrates have exhibited low efficiencies, because of the generation and propagation of large number of dislocations. Dislocation densities were calculated and its influence on the open circuit voltage, short circuit current, and efficiency of heteroepitaxial indium phosphide cells was studied using the PC-1D. Dislocations act as predominant recombination centers and are required to be controlled by proper transition layers and improved growth techniques. It is shown that heteroepitaxial grown cells could achieve efficiencies in excess of 18 percent AMO by controlling the number of dislocations. The effect of emitter thickness and surface recombination velocity on the cell performance parameters vs. dislocation density is also studied. Author

N91-20101*# National Aeronautics and Space Administration. Lewis Research Center, Cleveland, OH.

HIGH TEMPERATURE ELECTRONICS

GARY T. SENG *In its* Aeropropulsion 1991 13 p Mar. 1991
Avail: NTIS HC/MF A24 CSCL 09/3

In recent years, the aerospace propulsion and space power communities have acknowledged a growing need for electronic devices that are capable of sustained high-temperature operation. Aeropropulsion applications for high-temperature electronic devices include engine ground test instrumentation such as multiplexers, analog-to-digital converters, and telemetry systems capable of withstanding hot section engine temperatures in excess of 600 C. Uncooled operation of control and condition monitoring systems in advanced supersonic aircraft would subject the electronics to temperatures in excess of 300 C. Similarly, engine-mounted integrated electronic sensors could reach temperatures which exceed 500 C. In addition to aeronautics, there are many other areas that could benefit from the existence of high-temperature electronic devices. Space applications include power electronic devices for space platforms and satellites. Since power electronics require radiators to shed waste heat, electronic devices that operate at higher temperatures would allow a reduction in radiator size. Terrestrial applications include deep-well drilling instrumentation, high power electronics, and nuclear reactor instrumentation and control. To meet the needs of the applications mentioned previously, the high-temperature electronics (HTE) program at the Lewis Research Center is developing silicon carbide (SiC) as a high-temperature semiconductor material. Research is focused on developing the crystal growth, growth modeling, characterization, and device fabrication technologies necessary to produce a family

of SiC devices. Interest in SiC has grown dramatically in recent years due to solid advances in the technology. Much research remains to be performed, but SiC appears ready to emerge as a useful semiconductor material. Author

N91-20392*# National Aeronautics and Space Administration. Lewis Research Center, Cleveland, OH.

HETEROEPITAXIAL INP SOLAR CELLS ON SI AND GAAS SUBSTRATES

IRVING WEINBERG, CLIFFORD K. SWARTZ, and DAVID J. BRINKER 1990 7 p Presented at the 5th International Photovoltaic Science and Engineering Conference, Kyoto, Japan, 26-30 Nov. 1990; sponsored by the Japan Society of Applied Physics, Inst. of Electrical Engineers of Japan, and the Foundation for the Advancement of International Science

(Contract RTOP 506-41-11)

(NASA-TM-103696; E-5918; NAS 1.15:103696) Avail: NTIS HC/MF A02 CSCL 10/1

The characteristics of InP cells processed from thin layers of InP heteroepitaxially grown on GaAs, on silicon with an intervening GaAs layer, and on GaAs with intervening Ga(x)In(1-x)As layers are described, and the factors affecting cell efficiency are discussed. Under 10 MeV proton irradiations, the radiation resistances of the heteroepitaxial cells were superior to that of homoepitaxial InP cells. The superior radiation resistance is attributed to the high dislocation densities present in the heteroepitaxial cells. Author

N91-20393*# National Aeronautics and Space Administration. Lewis Research Center, Cleveland, OH.

NEAR-FIELD ANTENNA TESTING USING THE HEWLETT PACKARD 8510 AUTOMATED NETWORK ANALYZER

RICHARD R. KUNATH and MICHAEL J. GARRETT (Ohio State Univ., Columbus.) 1990 10 p Presented at the Antenna Measurement Techniques Association Meeting, Philadelphia, PA, 8-11 Oct. 1990

(Contract RTOP 650-60-20)

(NASA-TM-103699; E-5921; NAS 1.15:103699) Avail: NTIS HC/MF A02 CSCL 20/14

Near-field antenna measurements were made using a Hewlett-Packard 8510 automated network analyzer. This system features measurement sensitivity better than -90 dBm, at measurement speeds of one data point per millisecond in the fast data acquisition mode. The system was configured using external, even harmonic mixers and a fiber optic distributed local oscillator signal. Additionally, the time domain capability of the HP8510, made it possible to generate far-field diagnostic results immediately after data acquisition without the use of an external computer. Author

N91-20406*# National Aeronautics and Space Administration. Lewis Research Center, Cleveland, OH.

A SEVEN PATCH HEXAGONAL CP SUBARRAY WITH A CPW/STRIPLINE FEED NETWORK

R. N. SIMONS, R. Q. LEE, and G. R. LINDAMOOD (Akron Univ., OH.) 1991 11 p Prepared for presentation at the North American Radio Science Meeting and International IEEE/AP-S Symposium, London, Ontario, 24-28 Jun. 1991

(Contract NAS3-25266; RTOP 505-44-2C)

(NASA-TM-103802; E-5927; NAS 1.15:103802) Avail: NTIS HC/MF A03 CSCL 09/1

A seven element microstrip subarray of hexagonal geometry were designed and tested at S-band frequencies. The microstrip patch antenna is excited at a single feed position using a direct probe type connection to generate a circularly polarized wave. The RF power is coupled to these feed positions by a novel coplanar waveguide/stripline feeding network. The subarray architecture and the feed network are described in detail. The measured results include the feed network characterization as well as the radiation patterns of the subarray. Author

N91-21433*# National Aeronautics and Space Administration. Lewis Research Center, Cleveland, OH.

OPTIMAL DESIGN STUDY OF HIGH EFFICIENCY INDIUM PHOSPHIDE SPACE SOLAR CELLS

RAJ K. JAIN and DENNIS J. FLOOD Nov. 1990 7 p Presented at the 5th International Photovoltaic Science and Engineering Conference, Kyoto, Japan, 26-30 Nov. 1990; sponsored in part by Japan Society of Applied Physics; the Inst. of Electrical Engineers of Japan; and Foundation for the Advancement of International Science

(Contract RTOP 506-41-11)

(NASA-TM-103763; E-6025; NAS 1.15:103763) Avail: NTIS HC/MF A02 CSCL 10/1

Recently indium phosphide solar cells have achieved beginning of life AMO efficiencies in excess of 19 pct. at 25 C. The high efficiency prospects along with superb radiation tolerance make indium phosphide a leading material for space power requirements. To achieve cost effectiveness, practical cell efficiencies have to be raised to near theoretical limits and thin film indium phosphide cells need to be developed. The optimal design study is described of high efficiency indium phosphide solar cells for space power applications using the PC-1D computer program. It is shown that cells with efficiencies over 22 pct. AMO at 25 C could be fabricated by achieving proper material and process parameters. It is observed that further improvements in cell material and process parameters could lead to experimental cell efficiencies near theoretical limits. The effect of various emitter and base parameters on cell performance was studied. Author

N91-22508*# National Aeronautics and Space Administration. Lewis Research Center, Cleveland, OH.

HIGH TEMPERATURE POWER ELECTRONICS FOR SPACE

AHMAD N. HAMMOUD (Sverdrup Technology, Inc., Brook Park, OH.), ERIC D. BAUMANN, IRA T. MYERS, and ERIC OVERTON 1991 8 p Presented at the First International High Temperature Electronics Conference, Albuquerque, NM, 16-20 Jun. 1991; sponsored by Sandia National Labs., AF Wright Research Development Center and New Mexico Univ.

(Contract NAS3-25266; RTOP 506-41-41)

(NASA-TM-104375; E-6181; NAS 1.15:104375) Avail: NTIS HC/MF A02 CSCL 09/3

A high temperature electronics program at NASA Lewis Research Center focuses on dielectric and insulating materials research, development and testing of high temperature power components, and integration of the developed components and devices into a demonstrable 200 C power system, such as inverter. An overview of the program and a description of the in-house high temperature facilities along with experimental data obtained on high temperature materials are presented. Author

N91-23055*# National Aeronautics and Space Administration. Lewis Research Center, Cleveland, OH.

FOUR QUADRANT CONTROL OF INDUCTION MOTORS

IRVING G. HANSEN In National Aeronautics and Space Administration, Technology 2000, Volume 1 p 279-286 Mar. 1991

Avail: NTIS HC/MF A18 CSCL 09/1

Induction motors are the nation's workhorse, being the motor of choice in most applications due to their simple rugged construction. It has been estimated that 14 to 27 percent of the country's total electricity use could be saved with adjustable speed drives. Until now, induction motors have not been suited well for variable speed or servo-drives, due to the inherent complexity, size, and inefficiency of their variable speed controls. Work at NASA Lewis Research Center on field oriented control of induction motors using pulse population modulation method holds the promise for the desired drive electronics. The system allows for a variable voltage to frequency ratio which enables the user to operate the motor at maximum efficiency, while having independent control of both the speed and torque of an induction motor in all four quadrants of the speed torque map. Multiple horsepower machine drives were demonstrated, and work is on-going to develop

a 20 hp average, 40 hp peak class of machine. The pulse population technique, results to date, and projections for implementation of this existing new motor control technology are discussed. Author

N91-24069*# National Aeronautics and Space Administration. Lewis Research Center, Cleveland, OH.

MICROWAVE INTEGRATED CIRCUITS FOR SPACE APPLICATIONS

REGIS F. LEONARD and ROBERT R. ROMANOFKY In NASA, Washington, Technology 2000, Volume 2 p 242-248 1991

Avail: NTIS HC/MF A16 CSCL 09/3

Monolithic microwave integrated circuits (MMIC), which incorporate all the elements of a microwave circuit on a single semiconductor substrate, offer the potential for drastic reductions in circuit weight and volume and increased reliability, all of which make many new concepts in electronic circuitry for space applications feasible, including phased array antennas. NASA has undertaken an extensive program aimed at development of MMICs for space applications. The first such circuits targeted for development were an extension of work in hybrid (discrete component) technology in support of the Advanced Communication Technology Satellite (ACTS). It focused on power amplifiers, receivers, and switches at ACTS frequencies. More recent work, however, focused on frequencies appropriate for other NASA programs and emphasizes advanced materials in an effort to enhance efficiency, power handling capability, and frequency of operation or noise figure to meet the requirements of space systems. Author

N91-25320*# National Aeronautics and Space Administration. Lewis Research Center, Cleveland, OH.

COMPARATIVE STUDY OF BOLOMETRIC AND NON-BOLOMETRIC SWITCHING ELEMENTS FOR MICROWAVE PHASE SHIFTERS

MASSOOD TABIB-AZAR (Case Western Reserve Univ., Cleveland, OH.), KUL B. BHASIN, and ROBERT R. ROMANOFKY 1991 12 p Presented at the Optical Engineering and Photonics in Aerospace Sensing Symposium, Orlando, FL, 1-5 Apr. 1991; sponsored by the International Society for Optical Engineers (Contract NCC3-203; RC-471035; RTOP 506-44-21)

(NASA-TM-104435; E-6273; NAS 1.15:104435) Avail: NTIS HC/MF A03 CSCL 09/1

The performance of semiconductor and high critical temperature superconductor switches is compared as they are used in delay-line-type microwave and millimeter-wave phase shifters. Such factors as their ratios of the off-to-on resistances, parasitic reactances, power consumption, speed, input-to-output isolation, ease of fabrication, and physical dimensions are compared. Owing to their almost infinite off-to-on resistance ratio and excellent input-to-output isolation, bolometric superconducting switches appear to be quite suitable for use in microwave phase shifters; their only drawbacks are their speed and size. The SUPERFET, a novel device whose operation is based on the electric field effect in high critical temperature ceramic superconductors is also discussed. Preliminary results indicate that the SUPERFET is fast and that it can be scaled; therefore, it can be fabricated with dimensions comparable to semiconductor field-effect transistors. Author

N91-26436*# National Aeronautics and Space Administration. Lewis Research Center, Cleveland, OH.

SUBMICRON GATE INP POWER MISFET'S WITH IMPROVED OUTPUT POWER DENSITY AT 18 AND 20 GHZ

M. D. BIEDENBENDER, VIK J. KAPOOR, K. A. SHALKHAUSER, L. J. MESSICK, R. NGUYEN, D. SCHMITZ, and H. JUERGENSEN (Aixtron Corp., Aachen, Germany, F.R.) In Cincinnati Univ., OH, MMIC Integration Technology Investigation p 44-69 15 Jun. 1991

Avail: NTIS HC/MF A04 CSCL 09/1

The microwave characteristics are presented at 18 and 20 GHz of submicron gate indium phosphide (InP) metal-insulator-semiconductor field-effect transistors (MISFET's) for high output power density applications. InP power MISFET's were

33 ELECTRONICS AND ELECTRICAL ENGINEERING

fabricated and the output power density was investigated as a function of drain-source spacing. The best output power density and gain were obtained for drain-source spacing of 3 microns. The output power density is 2.7 times greater than was previously measured for InP MISFET's at 18 and 20 GHz, and the power-added efficiency also increased. Author

N91-27444*# National Aeronautics and Space Administration. Lewis Research Center, Cleveland, OH.

ELECTRICAL CHARACTERIZATION OF GLASS, TEFLON, AND TANTALUM CAPACITORS AT HIGH TEMPERATURES

A. N. HAMMOUD (Sverdrup Technology, Inc., Brook Park, OH.), E. D. BAUMANN, I. T. MYERS, and E. OVERTON 1991 8 p Presented at the 1991 Conference on Electrical Insulation and Dielectric Phenomena, Knoxville, TN, 20-24 Oct. 1991; sponsored by IEEE

(Contract RTOP 506-41-41)

(NASA-TM-104517; E-6387; NAS 1.15:104517) Avail: NTIS HC/MF A02 CSCL 09/3

Dielectric materials and electrical components and devices employed in radiation fields and the space environment are often exposed to elevated temperatures among other things. Therefore, these systems must withstand the high temperature exposure while still providing good electrical and other functional properties. Experiments were carried out to evaluate glass, teflon, and tantalum capacitors for potential use in high temperature applications. The capacitors were characterized in terms of their capacitance and dielectric loss as a function of temperature up to 200 C. At a given temperature, these properties were obtained in a frequency range of 50 Hz to 100 kHz. The DC leakage current measurements were also performed in a temperature range from 20 to 200 C. The obtained results are discussed and conclusions are made concerning the suitability of the capacitors investigated for high temperature applications. Author

N91-27445*# National Aeronautics and Space Administration. Lewis Research Center, Cleveland, OH.

DESIGN ASPECTS AND COMPARISON BETWEEN HIGH T(SUB C) SUPERCONDUCTING COPLANAR WAVEGUIDE AND MICROSTRIP LINE

K. S. KONG, K. B. BHASIN, and T. ITOH (California Univ., Los Angeles.) 1991 11 p Presented at the Optical Engineering and Photonics in Aerospace Sensing Symposium, Orlando, FL, 1-5 Apr. 1991; sponsored by International Society for Optical Engineers

(Contract NCC3-192; N00014-89-J-1006; RTOP 506-59-4C)

(NASA-TM-105142; E-6416; NAS 1.15:105142) Avail: NTIS HC/MF A03 CSCL 09/3

The high T sub c superconducting microstrip line and coplanar waveguide are compared in terms of the loss characteristics and the design aspects. The quality factor Q values for each structure are compared in respect to the same characteristic impedance with the comparable dimensions of the center conductor of the coplanar waveguide and the strip of the microstrip line. Also, the advantages and disadvantages for each structure are discussed in respect to passive microwave circuit applications. Author

N91-27447*# National Aeronautics and Space Administration. Lewis Research Center, Cleveland, OH.

RECENT PROGRESS IN INP SOLAR CELL RESEARCH

IRVING WEINBERG, D. J. BRINKER, R. K. JAIN, and C. K. SWARTZ 1991 9 p Presented at the 26th Intersociety Energy Conversion Engineering Conference, Boston, MA, 4-9 Aug. 1991; sponsored by ANS, SAE, ACS, AIAA, ASME, IEEE, and AIChE

(Contract RTOP 506-41-11)

(NASA-TM-104509; E-6375; NAS 1.15:104509) Avail: NTIS HC/MF A02 CSCL 10/1

Significant new developments in InP solar cell research are reviewed. Recent accomplishments include monolithic multibandgap two junction cells (three and two terminal) using InP as the top cell and lattice matched GaInAs and GaInAsP as the bottom, low bandgap component. Concentrator cells include the

three terminal multibandgap cell and n + p cell using an InP substrate. The review also includes small scale production of ITO/InP cells and results for n + p InP and ITO/InP cells in space on board the LIPS 3 satellite. Author

N91-27477*# National Aeronautics and Space Administration. Lewis Research Center, Cleveland, OH.

COPLANAR WAVEGUIDE FEEDS FOR PHASED ARRAY ANTENNAS

RAINEE N. SIMONS (Sverdrup Technology, Inc., Brook Park, OH.) and RICHARD Q. LEE 1991 9 p Presented at the Conference on Advanced Space Exploration Initiative Technologies, Cleveland, OH, 4-6 Sep. 1991; sponsored by AIAA, NASA, and OAI (Contract RTOP 506-44-2C)

(NASA-TM-104467; E-6315; NAS 1.15:104467; AIAA PAPER 91-3422) Avail: NTIS HC/MF A02 CSCL 09/3

The design and performance is presented of the following Coplanar Waveguides (CPW) microwave distribution networks for linear as well as circularly polarized microstrip patches and dipole arrays: (1) CPW/Microstrip Line feed; (2) CPW/Balanced Stripline feed; (3) CPW/Slotline feed; (4) Grounded CPW/Balanced coplanar stripline feed; and (5) CPW/Slot coupled feed. Typical measured radiation patterns are presented, and their relative advantages and disadvantages are compared. Author

N91-30426*# National Aeronautics and Space Administration. Lewis Research Center, Cleveland, OH.

MEASUREMENT TECHNIQUES FOR CRYOGENIC KA-BAND MICROSTRIP ANTENNAS

M. A. RICHARD, K. B. BHASIN, C. GILBERT, S. METZLER, and P. C. CLASPY (Case Western Reserve Univ., Cleveland, OH.) 1991 10 p Presented at the 13th Annual Meeting and Symposium of the Antenna Measurement Techniques Association, Boulder, CO, 7-11 Oct. 1991; sponsored by the National Inst. of Standards and Technology Sponsored in part by Ohio Aerospace Inst.

(Contract NGT-40016; RTOP 506-59-4C)

(NASA-TM-105183; E-6479; NAS 1.15:105183) Avail: NTIS HC/MF A02 CSCL 09/3

The measurement of cryogenic antennas poses unique logistical problems since the antenna under test must be embedded in a cooling chamber. A method of measuring the performance of cryogenic microstrip antennas using a closed cycle gas cooled refrigerator in a far field range is described. Antenna patterns showing the performance of gold and superconducting Ka-band microstrip antennas at various temperatures are presented. Author

N91-30427*# National Aeronautics and Space Administration. Lewis Research Center, Cleveland, OH.

MAKEUP AND USES OF A BASIC MAGNET LABORATORY FOR CHARACTERIZING HIGH-TEMPERATURE PERMANENT MAGNETS

JANIS M. NIEDRA (Sverdrup Technology, Inc., Brook Park, OH.) and GENE E. SCHWARZE 1991 8 p Presented at the First International High Temperature Electronics Conference, Albuquerque, NM, 16-20 Jun. 1991; sponsored by Sandia National Laboratories, Wright Research and Development Center, and the Univ. of New Mexico

(Contract RTOP 590-13-11)

(NASA-TM-104508; E-6373; NAS 1.15:104508) Avail: NTIS HC/MF A02 CSCL 09/1

A set of instrumentation for making basic magnetic measurements was assembled in order to characterize high intrinsic coercivity, rare earth permanent magnets with respect to short term demagnetization resistance and long term aging at temperatures up to 300 C. The major specialized components of this set consist of a 13 T peak field, capacitor discharge pulse magnetizer; a 10 in. pole size, variable gap electromagnet; a temperature controlled oven equipped with iron cobalt pole piece extensions and a removable paddle that carries the magnetization and field sensing coils; associated electronic integrators; and sensor standards for field intensity H and magnetic moment M calibration. A 1 cm cubic magnet sample, carried by the paddle,

fits snugly between the pole piece extensions within the electrically heated aluminum oven, where fields up to 3.2 T can be applied by the electromagnet at temperatures up to 300 C. A sample set of demagnetization data for the high energy Sm₂Co₁₇ type of magnet is given for temperatures up to 300 C. These data are reduced to the temperature dependence of the M-H knee field and of the field for a given magnetic induction swing, and they are interpreted to show the limits of safe operation. Author

N91-31529* National Aeronautics and Space Administration. Lewis Research Center, Cleveland, OH.

LOW COST, FORMABLE, HIGH T(SUB C) SUPERCONDUCTING WIRE Patent

JAMES L. SMIALEK, inventor (to NASA) 17 Sep. 1991 5 p Filed 31 Jan. 1989

(NASA-CASE-LEW-14676-1; US-PATENT-5,049,539; US-PATENT-APPL-SN-305675; US-PATENT-CLASS-505-1; US-PATENT-CLASS-505-701; US-PATENT-CLASS-505-702; US-PATENT-CLASS-505-703; US-PATENT-CLASS-505-704; US-PATENT-CLASS-421-209; US-PATENT-CLASS-421-457) Avail: US Patent and Trademark Office CSCL 09/1

A ceramic superconductivity part such as a wire is produced through the partial oxidation of a specially formulated copper alloy in the core. The alloys contain low level quantities of rare earth and alkaline earth dopant elements. Upon oxidation at high temperature, superconducting oxide phases are formed as a thin film. Official Gazette of the U.S. Patent and Trademark Office

N91-32410*# National Aeronautics and Space Administration. Lewis Research Center, Cleveland, OH.

NEUTRON, GAMMA RAY AND POST-IRRADIATION THERMAL ANNEALING EFFECTS ON POWER SEMICONDUCTOR SWITCHES

G. E. SCHWARZE and A. J. FRASCA 1991 15 p Presented at the Conference on Advanced Space Exploration Initiative Technologies, Cleveland, OH, 4-6 Sep. 1991; cosponsored in part by AIAA, NASA, and OAI Previously announced in IAA as A91-52420

(Contract RTOP 590-13-31) (NASA-TM-105248; E-6577; NAS 1.15:105248; AIAA PAPER 91-3525) Avail: NTIS HC/MF A03 CSCL 09/1

The effects of neutron and gamma rays on the electrical and switching characteristics of power semiconductor switches must be known and understood by the designer of the power conditioning, control, and transmission subsystem of space nuclear power systems. The SP-100 radiation requirements at 25 m from the nuclear source are a neutron fluence of 10(exp 13) n/sq cm and a gamma dose of 0.5 Mrads. Experimental data showing the effects of neutrons and gamma rays on the performance characteristics of power-type NPN Bipolar Junction Transistors (BJTs), Metal-Oxide-Semiconductor Field Effect Transistors (MOSFETs), and Static Induction Transistors (SITs) are presented. These three types of devices were tested at radiation levels which met or exceeded the SP-100 requirements. For the SP-100 radiation requirements, the BJTs were found to be most sensitive to neutrons, the MOSFETs were most sensitive to gamma rays, and the SITs were only slightly sensitive to neutrons. Post-irradiation thermal anneals at 300 K and up to 425 K were done on these devices and the effectiveness of these anneals are also discussed. Author

N91-32412*# National Aeronautics and Space Administration. Lewis Research Center, Cleveland, OH.

COMPARISON OF HIGH TEMPERATURE, HIGH FREQUENCY CORE LOSS AND DYNAMIC B-H LOOPS OF TWO 50 NI-FE CRYSTALLINE ALLOYS AND AN IRON-BASED AMORPHOUS ALLOY

W. R. WIESERMAN, G. E. SCHWARZE, and J. M. NIEDRA (Sverdrup Technology, Inc., Brook Park, OH.) Sep. 1991 9 p Presented at the 26th Intersociety Energy Conversion Engineering Conference, Boston, MA, 4-9 Aug. 1991; sponsored by ANS, SAE, ACS, AIAA, ASME, IEEE, and AICHE

(Contract RTOP 590-13-31) (NASA-TM-105205; E-6515; NAS 1.15:105205) Avail: NTIS HC/MF A02 CSCL 09/1

The availability of experimental data that characterizes the performance of soft magnetic materials for the combined conditions of high temperature and high frequency is almost nonexistent. An experimental investigation was conducted over the temperature range of 23 to 300 C and frequency range of 1 to 50 kHz to determine the effects of temperature and frequency on the core loss and dynamic B-H loops of three different soft magnetic materials; and oriented grain 50Ni-50Fe alloy, a nonoriented grain 50Ni-Fe alloy, and an iron based amorphous material (Metglas 2605SC). A comparison of these materials shows that the nonoriented grain 50Ni-50Fe alloy tends to have either the lowest or next lowest core loss for all temperatures and frequencies investigated. Author

34

FLUID MECHANICS AND HEAT TRANSFER

Includes boundary layers; hydrodynamics; fluidics; mass transfer; and ablation cooling.

A91-12971* National Aeronautics and Space Administration. Lewis Research Center, Cleveland, OH.

STABILITY OF AN OSCILLATED FLUID WITH A UNIFORM DENSITY GRADIENT

DAVID JACOMIN (NASA, Lewis Research Center, Cleveland, OH) Journal of Fluid Mechanics (ISSN 0022-1120), vol. 219, Oct. 1990, p. 449-468. refs Copyright

Instabilities in a fluid with a constant density gradient that is subject to arbitrarily oriented oscillatory accelerations are considered. With the Boussinesq approximation and for the case of an unbounded fluid, transformation to Lagrangian coordinates allows the reduction of the problem to an ordinary differential equation for each three-dimensional wavenumber. The problem has three parameters: the nondimensional amplitude R of the base-state oscillation, the nondimensional level of background steady acceleration, which for some cases can be represented in terms of a local (in time) Richardson number Ri, and the Prandtl number Pr. Some general bounds on stability are derived. For Pr = 1 closed-form solutions are found for impulse (delta function) accelerations and a general asymptotic solution is constructed for large R and general imposed accelerations. The asymptotic solution takes advantage of the fact that at large R wave growth is concentrated at 'zero points'. These are times when the effective vertical wavenumber passes through zero. Kelvin-Helmholtz instabilities are found to dominate at low R, while Rayleigh-Taylor instabilities dominate at high R. At high R, the uniform shear of the Kelvin-Helmholtz case tends to distort and weaken instability waves. With unsteady flows, Ri = 1/4 is no longer an instability limit. Significant instabilities have been found for sinusoidal forcing for Ri up to 0.6. Author

A91-13030*# Purdue Univ., West Lafayette, IN.

INFLUENCE OF GEOMETRIC FEATURES ON THE PERFORMANCE OF PRESSURE-SWIRL ATOMIZERS

S. K. CHEN, A. H. LEFEBVRE (Purdue University, West Lafayette, IN), and J. ROLLBUHLER (NASA, Lewis Research Center, Cleveland, OH) ASME, Transactions, Journal of Engineering for Gas Turbines and Power (ISSN 0022-0825), vol. 112, Oct. 1990, p. 579-584. refs Copyright

The spray characteristics of several different simplex pressure-swirl nozzles are examined using water as the working fluid. Measurements of mean drop size, drop-size distribution, effective spray cone angle, and circumferential liquid distribution are carried out over wide ranges of injection pressure. Eight

different nozzles are employed in order to achieve a wide variation in the length/diameter ratio of the final discharge orifice. Generally, it is found that an increase in discharge orifice length/diameter ratio, $l(o)/d(o)$, increases the mean drop size in the spray and reduces the spray cone angle. The circumferential liquid distribution is most uniform when $l(o)/d(o) = 2$. If $l(o)/d(o)$ is raised above or lowered below this optimum value, the circumferential uniformity of the liquid distribution is impaired. The observed effects of $l(o)/d(o)$ on spray characteristics are generally the same regardless of whether the change in $l(o)/d(o)$ is accomplished by varying $l(o)$ or $d(o)$.
Author

A91-13456* Colorado Univ., Boulder.

APPLICATION OF IMPLICIT NUMERICAL TECHNIQUES TO THE SOLUTION OF THE THREE-DIMENSIONAL DIFFUSION EQUATION

LEONARD JOEL PELTIER, SEDAT BIRINGEN (Colorado, University, Boulder), and ARNON CHAIT (NASA, Lewis Research Center, Cleveland, OH) Numerical Heat Transfer, Part B: Fundamentals (ISSN 1040-7790), vol. 18, Oct.-Dec. 1990, p. 205-219. refs

(Contract NAGW-951; NAG1-798)

Copyright

Implicit techniques for calculating three-dimensional, time-dependent heat diffusion in a cube are tested with emphasis on storage efficiency, accuracy, and speed of calculation. For this purpose, a tensor product technique with both Chebyshev collocation and finite differences and a generalized conjugate gradient technique with finite differences are used in conjunction with Crank-Nicolson discretization. An Euler explicit finite difference calculation is performed for use as a benchmark. The implicit techniques are found to be competitive with the Euler explicit method in terms of storage efficiency and speed of calculation and offer advantages both in accuracy and stability. Mesh stretching in the finite difference calculations is shown to markedly improve the accuracy of the solution.
Author

A91-16062* National Aeronautics and Space Administration, Lewis Research Center, Cleveland, OH.

INTERFACIAL DYNAMICS OF TWO LIQUIDS UNDER AN OSCILLATING GRAVITATIONAL FIELD

WALTER M. B. DUVAL and DAVID A. JACQMIN (NASA, Lewis Research Center, Cleveland, OH) AIAA Journal (ISSN 0001-1452), vol. 28, Nov. 1990, p. 1933-1941. refs

Copyright

The evolution of two miscible liquids meeting at an initially sharp interface inside a cavity under microgravity g-jitter conditions is studied numerically. The response of the interface and kinematics of the flowfield to various g-jitter accelerations and aspect ratio variations is shown. The interface region acts like a vortex source sheet, and it can be unstable to Kelvin-Helmholtz and Rayleigh-Taylor instabilities. The vortices produced along the interface can serve as a stirring mechanism to promote local mixing. Below the critical Stokes-Reynolds number, the destabilization of the interface results in deformation into wavy structures. In some parameter regions, these structures oscillate in time; in others, they are quasi-steady. Above the critical Stokes-Reynolds number, 'chaotic' instability results, and the interface breaks into concentration pockets. The morphology of the initial breakup is similar to observed Rayleigh-Taylor instability. Subsequent mixing of the two fluids after the breakup of the interface is then very rapid.
Author

A91-16073* National Aeronautics and Space Administration, Lewis Research Center, Cleveland, OH.

NEW MIXING-LENGTH MODEL FOR SUPERSONIC SHEAR LAYERS

S. C. KIM (NASA, Lewis Research Center, Cleveland, OH) AIAA Journal (ISSN 0001-1452), vol. 28, Nov. 1990, p. 1999, 2000. Previously cited in issue 09, p. 1321, Accession no. A90-25026. refs

(Contract NAS3-25266)

Copyright

A91-18428* Clarkson Univ., Potsdam, NY.

THE MIGRATION OF A COMPOUND DROP DUE TO THERMOCAPILLARITY

DAVID S. MORTON, R. SHANKAR SUBRAMANIAN (Clarkson University, Potsdam, NY), and R. BALASUBRAMANIAM (NASA, Lewis Research Center, Cleveland, OH) Physics of Fluids A (ISSN 0899-8213), vol. 2, Dec. 1990, p. 2119-2133. refs

Copyright

The quasistatic thermocapillary motion of a compound drop in an unbounded fluid possessing a uniform temperature gradient is analyzed. For completeness, gravitational effects are included in the treatment. The general model is formulated, and the equations for the concentric case are solved using spherical polar coordinates, while the eccentric case is handled using bispherical coordinates. Results are given for the velocity of the drop as well as that of the droplet with respect to the drop, along with useful approximations. Illustrative results are presented graphically for the thermocapillary migration of a compound drop in the special case when the droplet is a gas bubble. In addition to the velocities of the drop and the bubble, representative isotherms and streamlines also are presented which display interesting qualitative features.
Author

A91-19138* California Univ., Berkeley.

DROP-TOWER EXPERIMENTS FOR CAPILLARY SURFACES IN AN EXOTIC CONTAINER

PAUL CONCUS (California, University, Berkeley), ROBERT FINN (Stanford University, CA), and MARK WEISLOGEL (NASA, Lewis Research Center, Cleveland, OH) AIAA, Aerospace Sciences Meeting, 29th, Reno, NV, Jan. 7-10, 1991. 6 p. refs

(Contract NAG3-1143; NSF DMS-89-02831;

DE-AC03-76SF-00098)

(AIAA PAPER 91-0107) Copyright

Low-gravity drop-tower experiments are carried out for an 'exotic' rotationally-symmetric container, which admits an entire continuum of distinct equilibrium symmetric capillary free surfaces. It is found that an initial equilibrium planar interface, a member of the continuum, will reorient toward a non-symmetric interface, as predicted by recent mathematical theory.
Author

A91-21452* National Aeronautics and Space Administration, Lewis Research Center, Cleveland, OH.

A COMPARATIVE FLOW VISUALIZATION STUDY OF THERMOCAPILLARY FLOW IN DROPS IN LIQUID-LIQUID SYSTEMS

R. BALASUBRAMANIAM and N. RASHIDNIA (NASA, Lewis Research Center, Cleveland, OH) AIAA, Aerospace Sciences Meeting, 29th, Reno, NV, Jan. 7-10, 1991. 4 p. refs

(AIAA PAPER 91-0311) Copyright

Experiments are performed to visualize thermocapillary flow in drops in an immiscible host liquid. The host liquid used is silicone oil. Drops of three different liquids are used, viz, vegetable oil, water-methanol mixture and pure methanol. Clear evidence of thermocapillary flow is seen in vegetable oil drops. For a mixture of water and methanol (approximately 50-50 by weight), natural convection is seen to dominate the flow outside the drop. Pure methanol drops exhibit thermocapillary flow, but dissolve in silicone oil. A small amount of water added to pure methanol significantly reduces the dissolution. Flow oscillations occur in this system for both isothermal and non-isothermal conditions.
Author

A91-21466* National Aeronautics and Space Administration, Lewis Research Center, Cleveland, OH.

AN EXPERIMENTAL COMPARISON OF NONSWIRLING AND SWIRLING FLOW IN A CIRCULAR-TO-RECTANGULAR TRANSITION DUCT

B. A. REICHERT, W. R. HINGST (NASA, Lewis Research Center, Cleveland, OH), and T. H. OKIISHI (Iowa State University of Science and Technology, Ames) AIAA, Aerospace Sciences Meeting, 29th, Reno, NV, Jan. 7-10, 1991. 14 p. refs

(AIAA PAPER 91-0342) Copyright

Circular-to-rectangular transition duct flows with and without inlet swirl were investigated experimentally in order to determine

the effect of inlet swirl on the transition duct flow field and to provide detailed duct flow data for comparison with numerical code predictions. Coefficients based on detailed measurements of velocity, total pressure and static pressure, acquired in four cross stream planes within a circular-to-rectangular transition duct, with and without inlet swirl, are presented, as are surface static pressure and surface oil film visualization results. V.L.

A91-21467* Wayne State Univ., Detroit, MI.

JET-A FUEL EVAPORATION ANALYSIS IN CONICAL TUBE INJECTORS

M.-C. LAI, T.-H. CHUE, G. ZHU, H. SUN (Wayne State University, Detroit, MI), R. TACINA, K. CHUN, and Y. HICKS (NASA, Lewis Research Center, Cleveland, OH) AIAA, Aerospace Sciences Meeting, 29th, Reno, NV, Jan. 7-10, 1991. 12 p. refs (Contract NAG3-1140) (AIAA PAPER 91-0345) Copyright

A simple one-dimensional drop-life-history analysis and a multidimensional spray calculation using KIVA-II code are applied to the vaporization of Jet-A fuel in multiple tube injectors. Within the assumptions of the analysis, the one-dimensional results are useful for design purposes. The pressure-atomizer breakup models do not accurately predict the dropsize measured experimentally or deduced from the one-dimensional analysis. Cold flow visualization and dropsize measurements show that capillary wave breakup mechanism plays an important role in the spray angle and droplet impingement on the tube wall. Author

A91-21540* National Aeronautics and Space Administration. Lewis Research Center, Cleveland, OH.

MODERN CFD APPLICATIONS FOR THE DESIGN OF A REACTING SHEAR LAYER FACILITY

S. T. YU (NASA, Lewis Research Center; Sverdrup Technology, Inc., Cleveland, OH), C. T. CHANG, and C. J. MAREK (NASA, Lewis Research Center, Cleveland, OH) AIAA, Aerospace Sciences Meeting, 29th, Reno, NV, Jan. 7-10, 1991. 13 p. refs (AIAA PAPER 91-0577) Copyright

The RPLUS2D code, capable of calculating high speed reacting flows, has been adopted to design a compressible shear layer facility. In order to create reacting shear layers at high convective Mach numbers, hot air streams at supersonic speeds, render by converging-diverging nozzles, must be provided. A finite rate chemistry model is used to simulate the nozzle flows. Results are compared with one-dimensional, chemically equilibrium solutions. Additionally, a two equation turbulence model with compressibility effects has been successfully incorporated with the RPLUS code. The model has been applied to simulate a supersonic shear layer. Preliminary results show favorable comparisons with the experimental data. Author

A91-21542* Pennsylvania State Univ., University Park.

A TIME-ACCURATE IMPLICIT METHOD FOR CHEMICALLY REACTING FLOWS AT ALL MACH NUMBERS

J. P. WITHINGTON, V. YANG (Pennsylvania State University, University Park), and J. S. SHUEN (NASA, Lewis Research Center; Sverdrup Technology, Inc., Cleveland, OH) AIAA, Aerospace Sciences Meeting, 29th, Reno, NV, Jan. 7-10, 1991. 13 p. refs (Contract NGT-50532) (AIAA PAPER 91-0581) Copyright

The objective of this work is to develop a unified solution algorithm capable of treating time-accurate chemically reacting flows at all Mach numbers, ranging from molecular diffusion velocities to supersonic speeds. A rescaled pressure term is used in the momentum equation to circumvent the singular behavior of pressure at low Mach numbers. A dual time-stepping integration procedure is established. The system eigenvalues become well behaved and have the same order of magnitude, even in the very low Mach number regime. The computational efficiency for moderate and high speed flow is competitive with the conventional density-based scheme. The capabilities of the algorithm are demonstrated by applying it to selected model problems including nozzle flows and flame dynamics. Y.P.Q.

A91-21556* National Aeronautics and Space Administration. Lewis Research Center, Cleveland, OH.

NONLINEAR REYNOLDS STRESS MODEL FOR TURBULENT SHEAR FLOWS

J. MICHAEL BARTON, R. RUBINSTEIN, and K. R. KIRTLEY (NASA, Lewis Research Center; Sverdrup Technology, Inc., Cleveland, OH) AIAA, Aerospace Sciences Meeting, 29th, Reno, NV, Jan. 7-10, 1991. 14 p. refs (AIAA PAPER 91-0609) Copyright

A nonlinear algebraic Reynolds stress model, derived using the renormalization group, is applied to equilibrium homogeneous shear flow and fully developed flow in a square duct. The model, which is quadratically nonlinear in the velocity gradients, successfully captures the large-scale inhomogeneity and anisotropy of the flows studied. The ratios of normal stresses, as well as the actual magnitudes of the stresses are correctly predicted for equilibrium homogeneous shear flow. Reynolds normal stress anisotropy and attendant turbulence driven secondary flow are predicted for a square duct. Profiles of mean velocity and normal stresses are in good agreement with measurements. Very close to walls, agreement with measurements diminishes. The model has the benefit of containing no arbitrary constants; all values are determined directly from the theory. It seems that near wall behavior is influenced by more than the large scale anisotropy accommodated in the current model. More accurate near wall calculations may well require a model for anisotropic dissipation. Author

A91-22498* National Aeronautics and Space Administration. Lewis Research Center, Cleveland, OH.

MEASUREMENTS AND PREDICTIONS OF A LIQUID SPRAY FROM AN AIR-ASSIST NOZZLE

DANIEL L. BULZAN, YESHAYAHOU LAVY (NASA, Lewis Research Center, Cleveland, OH), SURESH K. AGGARWAL (Illinois, University, Chicago), and SUSHEEL CHITRE AIAA, Aerospace Sciences Meeting, 29th, Reno, NV, Jan. 7-10, 1991. 11 p. Previously announced in STAR as N91-13455. refs (AIAA PAPER 91-0692) Copyright

Droplet size and gas velocity were measured in a water spray using a two-component Phase/Doppler Particle Analyzer. A complete set of measurements was obtained at axial locations from 5 to 50 cm downstream of the nozzle. The nozzle used was a simple axisymmetric air-assist nozzle. The sprays produced, using the atomizer, were extremely fine. Sauter mean diameters were less than 20 microns at all locations. Measurements were obtained for droplets ranging from 1 to 50 microns. The gas phase was seeded with micron sized droplets, and droplets having diameters of 1.4 microns and less were used to represent gas-phase properties. Measurements were compared with predictions from a multi-phase computer model. Initial conditions for the model were taken from measurements at 5 cm downstream. Predictions for both the gas phase and the droplets showed relatively good agreement with the measurements. Author

A91-26191* National Aeronautics and Space Administration. Lewis Research Center, Cleveland, OH.

NUMERICAL STUDY OF SHOCK-WAVE/BOUNDARY LAYER INTERACTIONS IN PREMIXED HYDROGEN-AIR HYPERSONIC FLOWS

SHAYE YUNGSTER (NASA, Lewis Research Center, Cleveland, OH) AIAA, Aerospace Sciences Meeting, 29th, Reno, NV, Jan. 7-10, 1991. 20 p. Previously announced in STAR as N91-14559. refs (AIAA PAPER 91-0413) Copyright

A computational study of shock wave/boundary layer interactions involving premixed combustible gases, and the resulting combustion processes is presented. The analysis is carried out using a new fully implicit, total variation diminishing (TVD) code developed for solving the fully coupled Reynolds-averaged Navier-Stokes equations and species continuity equations in an efficient manner. To accelerate the convergence of the basic iterative procedure, this code is combined with vector extrapolation methods. The chemical nonequilibrium processes are simulated

34 FLUID MECHANICS AND HEAT TRANSFER

by means of a finite-rate chemistry model for hydrogen-air combustion. Several validation test cases are presented and the results compared with experimental data or with other computational results. The code is then applied to study shock wave/boundary layer interactions in a ram accelerator configuration. Results indicate a new combustion mechanism in which a shock wave induces combustion in the boundary layer, which then propagates outwards and downstream. At higher Mach numbers, spontaneous ignition in part of the boundary layer is observed, which eventually extends along the entire boundary layer at still higher values of the Mach number. Author

A91-26328*# National Aeronautics and Space Administration. Lewis Research Center, Cleveland, OH.

TURBULENT BOUNDARY LAYER SEPARATION OVER A REARWARD FACING RAMP AND ITS CONTROL THROUGH MECHANICAL EXCITATION

DANIEL J. MCKINZIE, JR. (NASA, Lewis Research Center, Cleveland, OH) AIAA, Aerospace Sciences Meeting, 29th, Reno, NV, Jan. 7-10, 1991. 27 p. refs (AIAA PAPER 91-0253) Copyright

A vane which oscillates about a fixed point at the inlet to a two-dimensional, 20-deg rearward-facing ramp has been noted to effectively delay the separation of a turbulent boundary layer. A parametric study has been conducted to determine the variation of the maximum values of the static pressure recovery, measured close to the ramp exit as a function of the oscillation frequency of the vane. The resulting curves show a peak value in the maximum static pressure recovery as a function of the vane's oscillation frequency. For the excited cases, corona anemometer measurements in the inner wall regions of the boundary layer along the surface of the ramp show a large range of unsteadiness in the local velocities. Finally, a qualitative explanation of the phenomena of delay of separation is discussed which appears to be supported by the surface static pressure and flow field measurements obtained. O.C.

A91-27166*# Wright State Univ., Dayton, OH.

A PCM/FORCED CONVECTION CONJUGATE TRANSIENT ANALYSIS OF ENERGY STORAGE SYSTEMS WITH ANNULAR AND COUNTERCURRENT FLOWS

Y. CAO, A. FAGHRI (Wright State University, Dayton, OH), and A. JUHASZ (NASA, Lewis Research Center, Cleveland, OH) ASME, Transactions, Journal of Heat Transfer (ISSN 0022-1481), vol. 113, Feb. 1991, p. 37-42. refs (Contract F33615-88-C-2820) Copyright

Latent heat energy storage systems with both annular and countercurrent flows are modeled numerically. The change of phase of the phase-change material (PCM) and the transient forced convective heat transfer for the transfer fluid are solved simultaneously as a conjugate problem. A parametric study and a system optimization are conducted. It is found that the energy storage system with the countercurrent flow is an efficient way to absorb heat energy in a short period for pulsed power load space applications. Author

A91-27175*# National Aeronautics and Space Administration. Lewis Research Center, Cleveland, OH.

ANALYTICAL SOLUTION FOR BOUNDARY HEAT FLUXES FROM A RADIATING RECTANGULAR MEDIUM

R. SIEGEL (NASA, Lewis Research Center, Cleveland, OH) ASME, Transactions, Journal of Heat Transfer (ISSN 0022-1481), vol. 113, Feb. 1991, p. 258-261. refs Copyright

Reference is made to the work of Shah (1979) which demonstrated the possibility of partially integrating the radiative equations analytically to obtain an 'exact' solution. Shah's solution was given as a double integration of the modified Bessel function of order zero. Here, it is shown that the 'exact' solution for a rectangular region radiating to cold black walls can be conveniently derived, and expressed in simple form, by using an integral function,

Sn, analogous to the exponential integral function appearing in plane-layer solutions. V.L.

A91-27946* National Aeronautics and Space Administration. Lewis Research Center, Cleveland, OH.

RENORMALIZATION GROUP ANALYSIS OF ANISOTROPIC DIFFUSION IN TURBULENT SHEAR FLOWS

ROBERT RUBINSTEIN and J. MICHAEL BARTON (NASA, Lewis Research Center; Sverdrup Technology, Inc., Cleveland, OH) Physics of Fluids A (ISSN 0899-8213), vol. 3, March 1991, p. 415-421. refs (Contract NAS3-25266) Copyright

The renormalization group is applied to compute anisotropic corrections to the scalar eddy diffusivity representation of turbulent diffusion of a passive scalar. The corrections are linear in the mean velocity gradients. All model constants are computed theoretically. A form of the theory valid at arbitrary Reynolds number is derived. The theory applies only when convection of the velocity-scalar correlation can be neglected. A ratio of diffusivity components, found experimentally to have a nearly constant value in a variety of shear flows, is computed theoretically for flows in a certain state of equilibrium. The theoretical value is well within the fairly narrow range of experimentally observed values. Theoretical predictions of this diffusivity ratio are also compared with data from experiments and direct numerical simulations of homogeneous shear flows with constant velocity and scalar gradients. Author

A91-29474*# National Aeronautics and Space Administration. Lewis Research Center, Cleveland, OH.

EXTENSION OF TRANSONIC FLOW COMPUTATIONAL CONCEPTS IN THE ANALYSIS OF CAVITATED BEARINGS

D. VIJAYARAGHAVAN (NASA, Lewis Research Center, Cleveland, OH), T. G. KEITH, JR. (Toledo, University, OH), and D. E. BREWE (NASA, Lewis Research Center; U.S. Army, Aviation Research and Technology Activity, Cleveland, OH) ASME and STLE, Joint Tribology Conference, Toronto, Canada, Oct. 7-10, 1990. 8 p. Previously announced in STAR as N91-16304. refs (ASME PAPER 90-TRIB-40)

An analogy between the mathematical modeling of transonic potential flow and the flow in a cavitating bearing is described. Based on the similarities, characteristics of the cavitated region and jump conditions across the film reformation and rupture fronts are developed using the method of weak solutions. The mathematical analogy is extended by utilizing a few computational concepts of transonic flow to numerically model the cavitating bearing. Methods of shock fitting and shock capturing are discussed. Various procedures used in transonic flow computations are adapted to bearing cavitation applications, for example, type differencing, grid transformation, an approximate factorization technique, and Newton's iteration method. These concepts have proved to be successful and have vastly improved the efficiency of numerical modeling of cavitated bearings. Author

A91-31342 National Aeronautics and Space Administration. Lewis Research Center, Cleveland, OH.

ON THE CONTINUOUS SPECTRA OF THE COMPRESSIBLE BOUNDARY LAYER STABILITY EQUATIONS

DAVID E. ASHPIS (NASA, Lewis Research Center, Cleveland, OH) and GORDON ERLEBACHER (NASA, Langley Research Center, Hampton, VA) IN: Instability and transition; Proceedings of the Workshop, Hampton, VA, May 15-June 9, 1989. Vol. 2. New York, Springer-Verlag, 1990, p. 145-159. refs Copyright

The branch cuts in the complex frequency plane (ω) that correspond to the continuous spectrum of the two-dimensional compressible boundary layer stability equations are computed by looking for solutions that are pure oscillatory in the free-stream. In the complex ω -plane there are three compressible and one incompressible branch cuts. The compressible branch cuts are given as solutions of third order polynomials. Computations

are made for a range of Reynolds and Mach numbers, and also for several streamwise wavenumbers. Author

A91-31482* National Aeronautics and Space Administration. Lewis Research Center, Cleveland, OH.

MULTIFREQUENCY EXCITED JETS

REDA R. MANKBADI (NASA, Lewis Research Center, Cleveland, OH) *Physics of Fluids A* (ISSN 0899-8213), vol. 3, April 1991, p. 595-605. refs

Copyright

An analysis of nonlinear wave-wave interactions in turbulent jets based on the integrated energy of each scale of motion in a cross section of the jet shows that two frequency components in the axisymmetric mode can interact with other background frequencies in that mode, thereby amplifying many other frequencies. The present computations produce several features consistent with experimental observations on two-frequency excitation, such as the dependence of the interaction on the initial phase differences between the waves, the enhancement of the momentum thickness under multifrequency forcing, and the increase in background turbulence under forcing. Mixing enhancement is found to be due to turbulence enhancement, rather than the simple amplification of forced-wave components. O.C.

A91-32691* National Aeronautics and Space Administration. Lewis Research Center, Cleveland, OH.

INERTIA EFFECTS IN THIN FILM FLOW WITH A CORRUGATED BOUNDARY

ILTER SERBETCI (NASA, Lewis Research Center, Cleveland, OH) and JOHN A. TICHY (Rensselaer Polytechnic Institute, Troy, NY) *ASME, Transactions, Journal of Applied Mechanics* (ISSN 0021-8936), vol. 58, March 1991, p. 272-277. refs

Copyright

An analytical solution is presented for two-dimensional, incompressible film flow between a sinusoidally grooved (or rough) surface and a flat-surface. The upper grooved surface is stationary whereas the lower, smooth surface moves with a constant speed. The Navier-Stokes equations were solved employing both mapping techniques and perturbation expansions. Due to the inclusion of the inertia effects, a different pressure distribution is obtained than predicted by the classical lubrication theory. In particular, the amplitude of the pressure distribution of the classical lubrication theory is found to be in error by over 100 percent (for modified Reynolds number of 3-4). Author

A91-34132* National Aeronautics and Space Administration. Lewis Research Center, Cleveland, OH.

CALCULATION OF TURBULENCE-DRIVEN SECONDARY MOTION IN DUCTS WITH ARBITRARY CROSS SECTION

A. O. DEMUREN (NASA, Lewis Research Center, Cleveland, OH) *AIAA Journal* (ISSN 0001-1452), vol. 29, April 1991, p. 531-537. Previously cited in issue 06, p. 812, Accession no. A90-19752. refs

(Contract NASA ORDER C-99066-G)

Copyright

A91-34134* National Aeronautics and Space Administration. Lewis Research Center, Cleveland, OH.

CALCULATION OF DIVERGENT CHANNEL FLOWS WITH A MULTIPLE-TIME-SCALE TURBULENCE MODEL

S.-W. KIM (NASA, Lewis Research Center, Cleveland, OH) *AIAA Journal* (ISSN 0001-1452), vol. 29, April 1991, p. 547-554. Previously cited in issue 06, p. 809, Accession no. A90-19649. refs

Copyright

A91-35109* National Aeronautics and Space Administration. Lewis Research Center, Cleveland, OH.

VAPOR CONDENSATION AT THE FREE SURFACE OF AN AXISYMMETRIC LIQUID MIXED BY A LAMINAR JET

CHIN-SHUN LIN (NASA, Lewis Research Center; Analox Corp., Cleveland, OH) *Journal of Thermophysics and Heat Transfer*

(ISSN 0887-8722), vol. 5, Jan. 1991, p. 69-75. refs

Copyright

This paper presents numerical solutions of jet-induced mixing in a partially full cryogenic tank. An axisymmetric laminar jet is discharged from the central part of the tank bottom toward the liquid-vapor interface. Liquid is withdrawn at the same volume flow rate from the outer part of the tank. The jet is at a temperature lower than the interface, which is maintained at a certain saturation temperature. The interface is assumed to be flat and shear free and the condensation-induced velocity is assumed to be negligibly small compared with radial interface velocity. Finite-difference method is used to solve the nondimensional form of steady-state continuity, momentum, and energy equations. Calculations are conducted for jet Reynolds numbers ranging from 150 to 600 and Prandtl numbers ranging from 0.85 to 2.65. The effects of previously stated parameters on the condensation Nusselt and Stanton numbers that characterize the steady-state interface condensation process are investigated. Detailed analysis is performed to gain a better understanding of the fundamentals of fluid mixing and interface condensation. Author

A91-38048* National Aeronautics and Space Administration. Lewis Research Center, Cleveland, OH.

TWO-DIMENSIONAL MODEL OF A SPACE STATION FREEDOM THERMAL ENERGY STORAGE CANISTER

THOMAS W. KERSLAKE (NASA, Lewis Research Center, Cleveland, OH) and MOUNIR B. IBRAHIM (Cleveland State University, OH) IN: *IECEC-90; Proceedings of the 25th Intersociety Energy Conversion Engineering Conference*, Reno, NV, Aug. 12-17, 1990. Vol. 2. New York, American Institute of Chemical Engineers, 1990, p. 151-159. Previously announced in STAR as N90-26279.

Copyright

The Solar Dynamic Power Module being developed for Space Station Freedom uses a eutectic mixture of LiF-CaF₂ phase change salt contained in toroidal canisters for thermal energy storage. Results are presented from heat transfer analyses of the phase-change salt containment canister. A 2-D, axisymmetric finite-difference computer program which models the canister walls, salt, void, and heat engine working fluid coolant was developed. Analyses included effects of conduction in canister walls and solid salt, conduction and free convection in liquid salt, conduction and radiation across salt vapor filled void regions, and forced convection in the heat engine working fluid. Void shape, location, and growth or shrinkage (due to density difference between the solid and liquid salt phases) were prescribed based on engineering judgement. The salt phase change process was modeled using the enthalpy method. Discussion of results focuses on the role of free-convection in the liquid salt on canister heat transfer performance. This role is shown to be important for interpreting the relationship between groundbased canister performance (in 1-g) and expected on-orbit performance (in micro-g). Attention is also focused on the influence of void heat transfer on canister wall temperature distributions. The large thermal resistance of void regions is shown to accentuate canister hot spots and temperature gradients. Author

A91-38126* Space Power, Inc., San Jose, CA.

TWO-DIMENSIONAL SIMULATION OF A TWO-PHASE, REGENERATIVE PUMPED RADIATOR LOOP UTILIZING DIRECT CONTACT HEAT TRANSFER WITH PHASE CHANGE

HYOP S. RHEE, LESTER L. BEGG, JOSEPH R. WETCH (Space Power, Inc., San Jose, CA), JONG H. JANG, and ALBERT J. JUHASZ (NASA, Lewis Research Center, Cleveland, OH) IN: *IECEC-90; Proceedings of the 25th Intersociety Energy Conversion Engineering Conference*, Reno, NV, Aug. 12-17, 1990. Vol. 4. New York, American Institute of Chemical Engineers, 1990, p. 8-13. (Contract NAS3-25208)

Copyright

An innovative pumped loop concept for 600 K space power system radiators utilizing direct contact heat transfer, which facilitates repeated startup/shutdown of the power system without complex and time-consuming coolant thawing during power startup, is under development. The heat transfer process with

34 FLUID MECHANICS AND HEAT TRANSFER

melting/freezing of Li in an NaK flow was studied through two-dimensional time-dependent numerical simulations to characterize and predict the Li/NaK radiator performance during startup (thawing) and shutdown (cold-trapping). Effects of system parameters and the criteria for the plugging domain are presented together with temperature distribution patterns in solid Li and subsequent melting surface profile variations in time. I.E.

A91-38698* Cairo Univ. (Egypt).

HEAT TRANSFER IN OSCILLATING FLOWS

F. EL-MEHLAWY (Cairo University, Egypt) and R. R. MANKBADI (NASA, Lewis Research Center, Cleveland, OH; Cairo University, Egypt) IN: International Symposium on Nonsteady Fluid Dynamics, Toronto, Canada, June 4-7, 1990, Proceedings. New York, American Society of Mechanical Engineers, 1990, p. 329-337. refs

Copyright

The heat transfer in a sudden-expansion flow subjected to upstream periodic disturbances is investigated. In order to study the unsteady turbulent flow for the present symmetrical sudden-expansion flow, the phase-averaging technique of Hussain and Reynolds (1970) is used to derive the governing equations. The imposed periodic disturbances are found to increase the turbulent kinetic energy and the heat transfer rates at the wall. The phenomenon is discovered to be sensitive to the frequency of the imposed disturbances. At the optimum frequency and at a 3 percent disturbance level, the time-averaged heat transfer rate near the reattachment point can be increased by as much as 14 percent. P.D.

A91-38705* National Aeronautics and Space Administration. Lewis Research Center, Cleveland, OH.

NONLINEAR SPATIAL EVOLUTION OF EXTERNALLY EXCITED INSTABILITY WAVES IN FREE SHEAR LAYERS

L. S. HULTGREN and M. E. GOLDSTEIN (NASA, Lewis Research Center, Cleveland, OH) IN: International Symposium on Nonsteady Fluid Dynamics, Toronto, Canada, June 4-7, 1990, Proceedings. New York, American Society of Mechanical Engineers, 1990, p. 417-426. refs

Copyright

The effects of critical-layer nonlinearity on spatially growing instability waves on shear layers between parallel streams are considered. In the two-dimensional incompressible case, the flow in the critical layer is governed by a nonequilibrium, nonlinear vorticity equation. The initial exponential growth of the instability wave is converted into algebraic growth during the streamwise 'aging' of the critical layer into a quasi-equilibrium state. This leads to a next stage of evolution where the instability-wave growth is affected by both mean-flow-divergence and nonlinear effects and is eventually converted to decay. A uniformly valid composite formula for the instability wave amplitude, accounting for both nonparallel and nonlinear effects, is given and compared to experimental results. The inviscid solutions to these equations always end in a singularity at finite downstream distance. Author

A91-38737* National Aeronautics and Space Administration. Lewis Research Center, Cleveland, OH.

TURBULENCE ENHANCEMENT IN FREE SHEAR FLOWS UNDER MULTIFREQUENCY EXCITATION

R. R. MANKBADI (NASA, Lewis Research Center, Cleveland, OH) IN: Forum on Turbulent Flows - 1990; Joint CSME/ASME Spring Meeting, Toronto, Canada, June 4-7, 1990, Proceedings. New York, American Society of Mechanical Engineers, 1990, p. 105-113. refs

Copyright

The interactions of multifrequency wave-packet with the background turbulence in a round jet are studied. The process explains the mechanisms governing the later stages of the laminar-turbulent transitions as well as the effect of multifrequency excitation on turbulent jets. In a multifrequency-excited jet, mixing enhancement was found to be a result of the turbulence enhancement rather than simply the amplification of forced wave components. The excitation waves pump energy from the mean

flow to the turbulence, thus enhancing the latter. The high-frequency wave enhance the turbulence close to the jet exit, but the low-frequency waves are most effective further downstream. Author

A91-38741* National Aeronautics and Space Administration. Lewis Research Center, Cleveland, OH.

CALCULATION OF TURBULENT FLOW IN COMPLEX GEOMETRIES WITH A SECOND-MOMENT CLOSURE MODEL

A. O. DEMUREN (NASA, Lewis Research Center, Cleveland, OH) IN: Forum on Turbulent Flows - 1990; Joint CSME/ASME Spring Meeting, Toronto, Canada, June 4-7, 1990, Proceedings. New York, American Society of Mechanical Engineers, 1990, p. 163-167. refs

Copyright

A full Reynolds stress turbulence model is applied to calculate the flow in various channels with complex cross-section. The model is shown to be more robust and to produce more consistent results than algebraic stress models. The relationship between various versions of the latter is provided. It is shown that differential or algebraic stress models derived from a direct application of a popular linear approximation for the pressure-strain terms in the Reynolds stress equations will always underpredict the secondary motion, and hence the accompanying distortion of other flow properties. A simple approximation which leads to better predictions is presented and related to previous practice. Author

A91-38780* Wisconsin Univ., Milwaukee.

HEAT TRANSFER IN SPACE SYSTEMS; PROCEEDINGS OF THE SYMPOSIUM, AIAA/ASME THERMOPHYSICS AND HEAT TRANSFER CONFERENCE, SEATTLE, WA, JUNE 18-20, 1990

S. H. CHAN, ED. (Wisconsin University, Milwaukee), E. E. ANDERSON, ED. (Texas Tech University, Lubbock), R. J. SIMONEAU, ED. (NASA, Lewis Research Center, Cleveland, OH), C. K. CHAN, ED. (TRW, Inc., Cleveland, OH), D. W. PEPPER, ED. (Marquardt Co., Van Nuys, CA) et al. Symposium sponsored by ASME. New York, American Society of Mechanical Engineers, 1990, 154 p. For individual items see A91-38781 to A91-38798.

Copyright

Theoretical and experimental studies of heat-transfer in a space environment are discussed in reviews and reports. Topics addressed include a small-scale two-phase thermosiphon to cool high-power electronics, a low-pressure-drop heat exchanger with integral heat pipe, an analysis of the thermal performance of heat-pipe radiators, measurements of temperature and concentration fields in a rectangular heat pipe, and a simplified aerothermal heating method for axisymmetric blunt bodies. Consideration is given to entropy production in a shock wave, bubble-slug transition in a two-phase liquid-gas flow under microgravity, plasma arc welding under normal and zero gravity, the Microgravity Thaw Experiment, the flow of a thin film on stationary and rotating disks, an advanced ceramic fabric body-mounted radiator for Space Station Freedom phase 0 design, and lunar radiators with specular reflectors. T.K.

A91-39716* National Aeronautics and Space Administration. Lewis Research Center, Cleveland, OH.

NONLINEAR EVOLUTION OF SUBSONIC AND SUPERSONIC DISTURBANCES ON A COMPRESSIBLE FREE SHEAR LAYER

S. J. LEIB (NASA, Lewis Research Center; Sverdrup Technology, Inc., Cleveland, OH) Journal of Fluid Mechanics (ISSN 0022-1120), vol. 224, March 1991, p. 551-578. refs

Copyright

The effects of a nonlinear-nonequilibrium-viscous critical layer on the spatial evolution of subsonic and supersonic instability modes on a compressible free shear layer is considered. It is shown that the instability wave amplitude is governed by an integrodifferential equation with cubic-type nonlinearity. Numerical and asymptotic solutions to this equation show that the amplitude either ends in a singularity at a finite downstream distance or reaches an equilibrium value, depending on the Prandtl number, viscosity law, viscous parameter and a real parameter which is determined by the linear inviscid stability theory. A necessary

condition for the existence of the equilibrium solution is derived, and whether or not this condition is met is determined numerically for a wide range of physical parameters including both subsonic and supersonic disturbances. It is found that no equilibrium solution exists for the subsonic modes unless the temperature ratio of the low-to-high-speed streams exceeds a critical value, while equilibrium solutions for the most rapidly growing supersonic mode exist over most of the parameter range examined. Author

A91-40793* National Aeronautics and Space Administration. Lewis Research Center, Cleveland, OH.

DEVELOPMENT OF A NEW FLUX SPLITTING SCHEME

MENG-SING LIOU and CHRISTOPHER J. STEFFEN, JR. (NASA, Lewis Research Center, Cleveland, OH) IN: AIAA Computational Fluid Dynamics Conference, 10th, Honolulu, HI, June 24-27, 1991, Technical Papers. Washington, DC, American Institute of Aeronautics and Astronautics, 1991, p. 967, 968.

Copyright

The successful use of a novel splitting scheme, the advection upstream splitting method, for model aerodynamic problems where Van Leer and Roe schemes had failed previously is discussed. The present scheme is based on splitting in which the convective and pressure terms are separated and treated differently depending on the underlying physical conditions. The present method is found to be both simple and accurate. K.K.

A91-41132* National Aeronautics and Space Administration. Lewis Research Center, Cleveland, OH.

THERMOCAPILLARY MIGRATION OF LIQUID DROPLETS IN A TEMPERATURE GRADIENT IN A DENSITY MATCHED SYSTEM

N. RASHIDNIA and R. BALASUBRAMANIAM (NASA, Lewis Research Center, Cleveland, OH) Experiments in Fluids (ISSN 0723-4864), vol. 11, no. 2-3, May 1991, p. 167-174. Previously announced in STAR as N90-14512. refs

Copyright

An experimental investigation of thermocapillary flow in droplets of a vegetable oil (partially hydrogenated soybean oil) immersed in silicone oil was conducted in a test cell with a heated top wall and a cooled bottom wall. The liquids are nearly immiscible and have equal densities at a temperature below the room temperature, thus providing a simulation of low-gravity conditions by reducing the buoyancy forces. The interfacial tension between the two oils was measured in the temperature range 20 to 50 C using a capillary tube and $(d\sigma)/(dT)$ was determined to be negative. Droplets ranging in sizes from 3 mm to 1 cm diameter were injected into the silicone oil. The vertical temperature profile in the bulk liquid (silicone oil) produces temperature variations along the interface which induce variations in the interfacial tension. The flow inside the droplet driven by the resulting interfacial shear stresses was observed using a laser light-sheet flow visualization technique. The flow direction is consistent with the sign of $(d\sigma)/(dT)$. The observed maximum surface velocities are compared to the theoretical predictions of Young et al. (1959). Author

A91-41677* National Aeronautics and Space Administration. Lewis Research Center, Cleveland, OH.

THE DESIGN/ANALYSIS OF FLOWS THROUGH TURBOMACHINERY - A VISCOUS/INVISCID APPROACH

D. P. MILLER and D. R. REDDY (NASA, Lewis Research Center, Cleveland, OH) AIAA, SAE, ASME, and ASEE, Joint Propulsion Conference, 27th, Sacramento, CA, June 24-26, 1991. 11 p. refs

(AIAA PAPER 91-2010) Copyright

A new design/analysis system for the flows through turbomachinery is currently being developed for studying turbomachinery problems with an axisymmetric viscous/invicid 'average-passage' throughflow code. The advantage of this approach, compared to streamline curvature codes, is that the solutions obtained simulate some of the unsteadiness, compressibility and viscous effects of a multistage turbomachine. The design/analysis system consists of three elemental parts, the axisymmetric block grid generator, the blade surface element code,

and the axisymmetric flow code. Each element of the system will be discussed and the flow solutions for three axisymmetric geometries will be shown compared to experimental data where available. The computations are shown to be in very good agreement with test data for SR7 spinner body and transonic boattail geometry obtained in the wind tunnels at NASA Lewis Research Center. The VIADAC Rotor 67 Fan results were compared to PARC2D calculated results and shown to be in very good agreement. Author

A91-41678* National Aeronautics and Space Administration. Lewis Research Center, Cleveland, OH.

VERIFICATION OF THE PROTEUS TWO-DIMENSIONAL NAVIER-STOKES CODE FOR FLAT PLATE AND PIPE FLOWS

JULIANNE M. CONLEY (NASA, Lewis Research Center, Cleveland, OH) and PATRICK L. ZEMAN (USAF, Arnold Engineering and Development Center, Arnold AFB, TN) AIAA, SAE, ASME, and ASEE, Joint Propulsion Conference, 27th, Sacramento, CA, June 24-26, 1991. 8 p. refs

(AIAA PAPER 91-2013) Copyright

The Proteus Navier-Stokes Code is evaluated for two-dimensional/axisymmetric, viscous, incompressible, internal and external flows. The particular cases to be discussed are laminar and turbulent flows over a flat plate, laminar and turbulent developing pipe flows and turbulent pipe flow with swirl. Results are compared with exact solutions, empirical correlations and experimental data. A detailed description of the code set-up, including boundary conditions, initial conditions, grid size and grid packing is given for each case. Author

A91-42286* National Aeronautics and Space Administration. Lewis Research Center, Cleveland, OH.

OSHER'S SCHEME FOR REAL GASES

AMBADY SURESH (NASA, Lewis Research Center; Sverdrup Technology, Inc., Cleveland, OH) and MENG-SING LIOU (NASA, Lewis Research Center, Cleveland, OH) AIAA Journal (ISSN 0001-1452), vol. 29, June 1991, p. 920-926. Previously cited in issue 09, p. 1321, Accession no. A90-25030. refs

(Contract NAS3-25266)

Copyright

A91-42541* National Aeronautics and Space Administration. Lewis Research Center, Cleveland, OH.

STABILITY OF COMPRESSIBLE TAYLOR-COUETTE FLOW

KAI-HSIUNG KAO (NASA, Lewis Research Center, Cleveland, OH) and CHUEN-YEN CHOW (Colorado, University, Boulder) AIAA, Fluid Dynamics, Plasma Dynamics and Lasers Conference, 22nd, Honolulu, HI, June 24-26, 1991. 14 p. refs

(Contract NCC3-168)

(AIAA PAPER 91-1642) Copyright

Compressible stability equations are solved using the spectral collocation method in an attempt to study the effects of temperature difference and compressibility on the stability of Taylor-Couette flow. It is found that the Chebyshev collocation spectral method yields highly accurate results using fewer grid points for solving stability problems. Comparisons are made between the result obtained by assuming small Mach number with a uniform temperature distribution and that based on fully incompressible analysis. K.K.

A91-42549* National Aeronautics and Space Administration. Lewis Research Center, Cleveland, OH.

SIMULATION OF THREE-DIMENSIONAL LIQUID SLOSHING FLOWS USING A STRONGLY IMPLICIT CALCULATION PROCEDURE

K.-H. CHEN (NASA, Lewis Research Center, Cleveland, OH) and R. H. PLETCHER (Iowa State University of Science and Technology, Ames) AIAA, Fluid Dynamics, Plasma Dynamics and Lasers Conference, 22nd, Honolulu, HI, June 24-26, 1991. 14 p. refs

(Contract AF-AFOSR-89-0403)

(AIAA PAPER 91-1661) Copyright

A coupled strongly implicit solution strategy for unsteady

three-dimensional free surface flows has been developed based on an artificial compressibility formulation for the incompressible Navier-Stokes equations. A pseudotime term has been used in the continuity equation to permit time accurate calculations to be achieved. The scheme appears capable of tracking the free surface reasonably accurately inside a partially-filled spherical container undergoing a general rotating motion characteristic of that experienced by a spin-stabilized satellite. Five different free surface calculations have been presented. Some of the results exhibit an interesting Reynolds number dependent oscillatory behavior which is believed to be physical although no experimental results appears to be available for verification to date.

Author

A91-42588* National Aeronautics and Space Administration. Lewis Research Center, Cleveland, OH.

SECOND ORDER MODELING OF BOUNDARY-FREE TURBULENT SHEAR FLOWS

T.-H. SHIH (NASA, Lewis Research Center, Cleveland, OH), J.-Y. CHEN (Sandia National Laboratories, Livermore, CA), and J. L. LUMLEY (Cornell University, Ithaca, NY) AIAA, Fluid Dynamics, Plasma Dynamics and Lasers Conference, 22nd, Honolulu, HI, June 24-26, 1991. 11 p. DOE-supported research. Previously announced in STAR as N91-22524. refs
(Contract AF-AFOSR-89-0226; NAG1-954; NSF DMS-88-14553; NSF MSM-86-11164)

(AIAA PAPER 91-1779) Copyright

A set of realizable second order models for boundary-free turbulent flows is presented. The constraints on second order models based on the realizability principle are re-examined. The rapid terms in the pressure correlations for both the Reynolds stress and the passive scalar flux equations are constructed to exactly satisfy the joint realizability. All other model terms (return-to-isotropy, third moments, and terms in the dissipation equations) already satisfy realizability. To correct the spreading rate of the axisymmetric jet, an extra term is added to the dissipation equation which accounts for the effect of mean vortex stretching on dissipation. The test flows used in this study are the mixing shear layer, plane jet, axisymmetric jet, and plane wake. The numerical solutions show that the unified model equations predict all these flows reasonably. It is expected that these models would be suitable for more complex and critical flows.

Author

A91-42599* National Aeronautics and Space Administration. Lewis Research Center, Cleveland, OH.

UNSTABLE VISCOUS WALL MODES IN ROTATING PIPE FLOW

Z. YANG (NASA, Lewis Research Center, Cleveland, OH) and S. LEIBOVICH (Cornell University, Ithaca, NY) AIAA, Fluid Dynamics, Plasma Dynamics and Lasers Conference, 22nd, Honolulu, HI, June 24-26, 1991. 10 p. refs
(Contract AF-AFOSR-89-0346)

(AIAA PAPER 91-1801) Copyright

Linear stability of flow in a rotating pipe is studied. These flows depend on two parameters, which can be taken as the axial Reynolds number Re and the rotating rate, q . In the region of Re much greater than 1 and $q = O(1)$, the most unstable modes are concentrated near the pipe wall. These wall modes are found to satisfy a simpler set of equations containing two parameters rather than four as in the full linear stability problem. The set of equations is solved numerically and asymptotically over a wide range of the parameters. In the limit of Re approaching infinity, the eigenvalue goes to the inviscid limit. The eigenfunction shows a two-layer structure. It reaches the inviscid limit over the main part of the domain, while near the wall of the pipe, the eigenfunction is represented by a viscous solution of the boundary layer type.

Author

A91-43412* National Aeronautics and Space Administration. Lewis Research Center, Cleveland, OH.

NEW APPROACH IN DIRECT-SIMULATION OF GAS MIXTURES

CHAN-HONG CHUNG (NASA, Lewis Research Center, Cleveland, OH), KENNETH J. DE WITT, and DUEN-REN JENG (Toledo,

University, OH) AIAA, Thermophysics Conference, 26th, Honolulu, HI, June 24-26, 1991. 8 p. refs
(Contract NCC3-171)

(AIAA PAPER 91-1343) Copyright

Results are reported for an investigation of a new direct-simulation Monte Carlo method by which energy transfer and chemical reactions are calculated. The new method, which reduces to the variable cross-section hard sphere model as a special case, allows different viscosity-temperature exponents for each species in a gas mixture when combined with a modified Larsen-Borgnakke phenomenological model. This removes the most serious limitation of the usefulness of the model for engineering simulations. The necessary kinetic theory for the application of the new method to mixtures of monatomic or polyatomic gases is presented, including gas mixtures involving chemical reactions. Calculations are made for the relaxation of a diatomic gas mixture, a plane shock wave in a gas mixture, and a chemically reacting gas flow along the stagnation streamline in front of a hypersonic vehicle. Calculated results show that the introduction of different molecular interactions for each species in a gas mixture produces significant differences in comparison with a common molecular interaction for all species in the mixture. This effect should not be neglected for accurate DSMC simulations in an engineering context.

Author

A91-43429* Elort Corp., Palo Alto, CA.

NUMERICAL AND EXPERIMENTAL INVESTIGATIONS OF RAREFIED NOZZLE AND PLUME FLOWS OF NITROGEN

IAIN D. BOYD (Elort Institute, Palo Alto, CA), PAUL F. PENKO (NASA, Lewis Research Center, Cleveland, OH), and DANA L. MEISSNER (Toledo, University, OH) AIAA, Thermophysics Conference, 26th, Honolulu, HI, June 24-26, 1991. 12 p. refs
(Contract NCC2-582)

(AIAA PAPER 91-1363)

Numerical and experimental investigations are performed for the rarefied flow of nitrogen through a small nozzle which is expanded into near-vacuum conditions. Two different numerical studies are undertaken: the first employs a continuum approach in solving the Navier-Stokes equations, and the second employs a particle approach through use of the direct simulation Monte Carlo method (DSMC). The experimental investigation concerns the measurement of pressure, using a Pitot tube, in the nozzle exit plane and near-field of the plume. Comparison of the experimental and numerical data at the nozzle exit reveals that the DSMC technique provides the more accurate description of the expanding flow. It is discovered that the DSMC solutions are quite sensitive to the model employed to simulate the interaction between the gas and the nozzle wall surface. It is concluded that the simplistic fully diffuse model is quite satisfactory for the present application.

Author

A91-43576* National Aeronautics and Space Administration. Lewis Research Center, Cleveland, OH.

TIME-DERIVATIVE PRECONDITIONING FOR VISCOUS FLOWS

YUNHO CHOI (NASA, Lewis Research Center, Cleveland; Sverdrup Technology, Inc., Brook Park, OH) and CHARLES L. MERKLE (Pennsylvania State University, University Park) AIAA, Fluid Dynamics, Plasma Dynamics and Lasers Conference, 22nd, Honolulu, HI, June 24-26, 1991. 12 p. Previously announced in STAR as N91-24528. refs
(Contract NAS3-25266; NAGW-1356)

(AIAA PAPER 91-1652) Copyright

A time-derivative preconditioning algorithm that is effective over a wide range of flow conditions from inviscid to very diffusive flows and from low speed to supersonic flows was developed. This algorithm uses a viscous set of primary dependent variables to introduce well-conditioned eigenvalues and to avoid having a nonphysical time reversal for viscous flow. The resulting algorithm also provides a mechanism for controlling the inviscid and viscous time step parameters to be of order one for very diffusive flows, thereby ensuring rapid convergence at very viscous flows as well as for inviscid flows. Convergence capabilities are demonstrated through computation of a wide variety of problems.

Author

A91-43623*# National Aeronautics and Space Administration. Lewis Research Center, Cleveland, OH.

INCREASED HEAT TRANSFER TO A CYLINDRICAL LEADING EDGE DUE TO SPANWISE VARIATIONS IN THE FREESTREAM VELOCITY

D. L. RIGBY (NASA, Lewis Research Center, Cleveland; Sverdrup Technology, Inc., Brook Park, OH) and G. J. VAN FOSSEN (NASA, Lewis Research Center, Cleveland, OH) AIAA, Fluid Dynamics, Plasma Dynamics and Lasers Conference, 22nd, Honolulu, HI, June 24-26, 1991. 12 p. Previously announced in STAR as N91-24359. refs (AIAA PAPER 91-1739) Copyright

The present study numerically demonstrates how small spanwise variations in velocity upstream of a body can cause relatively large increases in the spanwise-averaged heat transfer to the leading edge. Vorticity introduced by spanwise variations, first decays as it drifts downstream, then amplifies in the stagnation region as a result of vortex stretching. This amplification can cause a periodic array of 3D structures, similar to horseshoe vortices, to form. The numerical results indicate that, for the given wavelength, there is an amplitude threshold below which a structure does not form. A one-dimensional analysis, to predict the decay of vorticity in the absence of the body, in conjunction with the full numerical results indicated that the threshold is more accurately stated as minimum level of vorticity required in the leading edge region for a structure to form. It is possible, using the one-dimensional analysis, to compute an optimum wavelength in terms of the maximum vorticity reaching the leading edge region for given amplitude. A discussion is presented which relates experimentally observed trends to the trends of the present phenomena.

Author

A91-44057*# National Aeronautics and Space Administration. Lewis Research Center, Cleveland, OH.

NAVIER-STOKES SIMULATION OF THE SUPERSONIC COMBUSTION FLOWFIELD IN A RAM ACCELERATOR

SHAYE YUNGSTER (NASA, Lewis Research Center, Cleveland, OH) AIAA, SAE, ASME, and ASEE, Joint Propulsion Conference, 27th, Sacramento, CA, June 24-26, 1991. 17 p. Previously announced in STAR as N91-24541. refs (AIAA PAPER 91-1916) Copyright

A computational study of the ram accelerator, a ramjet-in-tube device for accelerating projectiles to ultrahigh velocities, is presented. The analysis is performed using a fully implicit TVD scheme that efficiently solves the Reynolds-averaged Navier-Stokes equations and the species continuity equations associated with a finite rate combustion model. The present results indicate that viscous effects are of primary importance in all the cases studied, shock-induced combustion always started in the boundary layer. The effects of Mach number, mixture composition, pressure and turbulence are investigated for various configurations. Two types of combustion processes, one stable and the other unstable, were observed depending on the inflow conditions. The possibility of stabilizing the detonation wave by means of a backward facing step is also investigated. Two numerical techniques were tested: vector extrapolation, to accelerate convergence, and a diagonal formulation that eliminates the expense of inverting large block matrices which arise in chemically reacting flows.

Author

A91-44335*# National Aeronautics and Space Administration. Lewis Research Center, Cleveland, OH.

A NUMERICAL STUDY OF THE DIRECT CONTACT CONDENSATION ON A HORIZONTAL SURFACE

M. M. HASAN (NASA, Lewis Research Center, Cleveland, OH) and C. S. LIN (Analex Corp., Fairview Park, OH) AIAA, Thermophysics Conference, 26th, Honolulu, HI, June 24-26, 1991. 10 p. Previously announced in STAR as N91-24548. refs (AIAA PAPER 91-1307) Copyright

The results of a numerical study of the direct contact condensation on a slowly moving horizontal liquid surface are presented. The geometrical configuration and the input conditions used to obtain numerical solutions are representative to those of

experiments of Celata et al. The effects of Prandtl number (Pr), inflow Reynolds number, and Richardson number on the condensation rate are investigated. Numerical predictions of condensation rate for laminar flow are in good agreement with experimental data. The effect of buoyancy on the condensation rate is characterized by Richardson number. A correlation based on the numerical solutions is developed to predict the average condensation Nusselt number in terms of Richardson number, Peclet number, and inflow Reynolds number.

Author

A91-44337*# National Aeronautics and Space Administration. Lewis Research Center, Cleveland, OH.

SCALING ANALYSIS APPLIED TO THE NORVEX CODE DEVELOPMENT AND THERMAL ENERGY FLIGHT EXPERIMENT

J. R. L. SKARDA, DAVID NAMKOONG, and DOUGLAS DARLING (NASA, Lewis Research Center, Cleveland, OH) AIAA, Thermophysics Conference, 26th, Honolulu, HI, June 24-26, 1991. 12 p. Previously announced in STAR as N91-24549. refs (AIAA PAPER 91-1420) Copyright

A scaling analysis is used to study the dominant flow processes that occur in molten phase change material (PCM) under 1 g and microgravity conditions. Results of the scaling analysis are applied to the development of the NORVEX (NASA Oak Ridge Void Experiment) computer program and the preparation of the Thermal Energy Storage (TES) flight experiment. The NORVEX computer program which is being developed to predict melting and freezing with void formation in a 1 g or microgravity environment of the PCM is described. NORVEX predictions are compared with the scaling and similarity results. The approach to be used to validate NORVEX with TES flight data is also discussed. Similarity and scaling show that the inertial terms must be included as part of the momentum equation in either the 1 g or microgravity environment (a creeping flow assumption is invalid). A 10(exp -4) environment was found to be a suitable microgravity environment for the proposed PCM.

Author

A91-44529*# National Aeronautics and Space Administration. Lewis Research Center, Cleveland, OH.

NAVIER-STOKES ANALYSIS OF TURBINE BLADE HEAT TRANSFER

R. J. BOYLE (NASA, Lewis Research Center, Cleveland, OH) ASME, International Gas Turbine and Aeroengine Congress and Exposition, 35th, Brussels, Belgium, June 11-14, 1990. 16 p. Previously announced in STAR as N90-21300. refs (ASME PAPER 90-GT-42)

Comparisons with experimental heat transfer and surface pressures were made for seven turbine vane and blade geometries using a quasi-three-dimensional thin-layer Navier-Stokes analysis. Comparisons are made for cases with both separated and unseparated flow over a range of Reynolds numbers and freestream turbulence intensities. The analysis used a modified Baldwin-Lomax turbulent eddy viscosity mode. Modifications were made to account for the effects of: (1) freestream turbulence on both transition and leading edge heat transfer; (2) strong favorable pressure gradients on relaminarization; and (3) variable turbulent Prandtl number heat transfer. In addition, the effect of heat transfer on the near wall model of Deissler is compared with the Van Driest model.

Author

A91-44662*# National Aeronautics and Space Administration. Lewis Research Center, Cleveland, OH.

AN EXPERIMENTAL INVESTIGATION OF NOZZLE-EXIT BOUNDARY LAYERS OF HIGHLY HEATED FREE JETS

J. LEPICOVSKY (NASA, Lewis Research Center, Cleveland; Sverdrup Technology Inc., Brook Park, OH) ASME, International Gas Turbine and Aeroengine Congress and Exposition, 35th, Brussels, Belgium, June 11-14, 1990. 10 p. refs (Contract NAS3-23708) (ASME PAPER 90-GT-255)

An experimental investigation of the effects of nozzle operating conditions on the development of nozzle-exit boundary layers of highly heated air free jets is reported in this paper. The total

pressure measurements in the nozzle-exit boundary layer were obtained at a range of jet Mach numbers from 0.1 to 0.97 and jet total temperatures up to 900 K. The analysis of results shows that the nozzle-exit laminar boundary-layer development depends only on the nozzle-exit Reynolds number. For the nozzle-exit turbulent boundary layer, however, it appears that the effects of the jet total temperature on the boundary-layer integral characteristics are independent from the effects of the nozzle-exit Reynolds number. This surprising finding has not yet been reported. Further, laminar boundary-layer profiles were compared with the Pohlhausen solution for a flat-wall converging channel and an acceptable agreement was found only for low Reynolds numbers. For turbulent boundary layers, the dependence of the shape factor on relative Mach numbers at a distance of one momentum thickness from the nozzle wall resembles Spence's prediction. Finally, the calculated total pressure loss coefficient was found to depend on the nozzle-exit Reynolds number for the laminar nozzle-exit boundary layer, while for the turbulent exit boundary layer this coefficient appears to be constant. Author

A91-45327* # National Aeronautics and Space Administration. Lewis Research Center, Cleveland, OH.

GAS PROPERTY EFFECTS ON DROPSIZE OF SIMULATED FUEL SPRAYS

ROBERT D. INGEBO (NASA, Lewis Research Center, Cleveland, OH) Journal of Propulsion and Power (ISSN 0748-4658), vol. 7, July-Aug. 1991, p. 467-472. Previously cited in issue 20, p. 3150. Accession no. A89-46749. refs Copyright

A91-45547* # Sverdrup Technology, Inc., Brook Park, OH. **COMPUTATION OF A CIRCULAR-TO-RECTANGULAR TRANSITION DUCT FLOW FIELD**

J. R. SIRBAUGH (Sverdrup Technology, Inc, Brook Park, OH) and B. A. REICHERT (NASA, Lewis Research Center, Cleveland, OH) AIAA, Fluid Dynamics, Plasma Dynamics and Lasers Conference, 22nd, Honolulu, HI, June 24-26, 1991. 13 p. refs (AIAA PAPER 91-1741) Copyright

This paper presents the results of a Computational Fluid Dynamics (CFD) calibration study of flow through a circular-to-rectangular transition duct. The design of these ducts is critical to the optimum performance of aircraft with rectangular exhaust nozzles, since these ducts transfer the flow from the gas turbine engine to the exhaust nozzle. Two duct inflow conditions are considered, the first with straight inflow and the second with swirling inflow. Both flows contain realistic wall boundary layers. The first case permits examination of the effects of the geometric transition on the flowfield, while the second case adds in the rotational flow effect that can be present from the gas turbine engine. The flowfields associated with the two cases have been shown, both with CFD and experiment, to have significant differences. The Navier-Stokes CFD code PARC with the Baldwin and Lomax turbulence model was used in this study. The turbulence model had to be modified for both cases in order to achieve accurate determination of the edge of the wall bounded vorticity layers and thus turbulent viscosity. The results of this calibration study will be valuable to aircraft designers who rely on CFD to assist in the design and evaluation of propulsion systems. Author

A91-45778* # National Aeronautics and Space Administration. Lewis Research Center, Cleveland, OH.

SIMULATIONS OF FREE SHEAR LAYERS USING A COMPRESSIBLE K-EPSILON MODEL

S. T. YU (NASA, Lewis Research Center, Cleveland; Sverdrup Technology, Inc., Brook Park, OH), C. T. CHANG, and C. J. MAREK (NASA, Lewis Research Center, Cleveland, OH) AIAA, SAE, ASME, and ASEE, Joint Propulsion Conference, 27th, Sacramento, CA, June 24-26, 1991. 10 p. refs (AIAA PAPER 91-1863) Copyright

A two-dimensional, compressible Navier-Stokes equations with a k-epsilon turbulence model are solved numerically to simulate the flows of compressible free shear layers. The appropriate form

of k and epsilon equations for compressible flows are discussed. Sarkar's modeling is adopted to simulate the compressibility effects in the k and epsilon equations. The numerical results show that the spreading rate of the shear layers decreases with increasing convective Mach number. In addition, favorable comparison was found between the calculated results and Goebel and Dutton's experimental data. Author

A91-45790* # National Aeronautics and Space Administration. Lewis Research Center, Cleveland, OH.

TWO-DIMENSIONAL NAVIER-STOKES HEAT TRANSFER ANALYSIS FOR ROUGH TURBINE BLADES

R. J. BOYLE (NASA, Lewis Research Center, Cleveland, OH) and K. C. CIVINSKAS (NASA, Lewis Research Center; U.S. Army, Propulsion Directorate, Cleveland, OH) AIAA, SAE, ASME, and ASEE, Joint Propulsion Conference, 27th, Sacramento, CA, June 24-26, 1991. 12 p. refs (AIAA PAPER 91-2129)

A quasi-three-dimensional thin-layer Navier-Stokes analysis was used to predict heat transfer to rough surfaces. Comparisons are made between predicted and experimental heat transfer for turbine blades and flat plates of known roughness. The effect of surface roughness on heat transfer was modeled using a mixing length approach. The effect of near-wall grid spacing and convergence criteria on the accuracy of the heat transfer predictions are examined. An eddy viscosity mixing length model having an inner and outer layer was used. A discussion of the appropriate model for the crossover between the inner and outer layers is included. The analytic results are compared with experimental data for both flat plates and turbine blade geometries. Comparisons between predicted and experimental heat transfer showed that a modeling roughness effects using a modified mixing length approach results in good predictions of the trends in heat transfer due to roughness. Author

A91-45797* # Carnegie-Mellon Univ., Pittsburgh, PA. **COMPUTATIONS OF THE THREE-DIMENSIONAL FLOW AND HEAT TRANSFER WITHIN A COOLANT PASSAGE OF A RADIAL TURBINE BLADE**

T. I.-P. SHIH (Carnegie Mellon University, Pittsburgh, PA), R. J. ROELKE (NASA, Lewis Research Center, Cleveland, OH), and E. STEINTHORSSON AIAA, SAE, ASME, and ASEE, Joint Propulsion Conference, 27th, Sacramento, CA, June 24-26, 1991. 10 p. refs (Contract NAG3-929) (AIAA PAPER 91-2238)

A numerical code is developed for computing three-dimensional, turbulent, compressible flow within coolant passages of turbine blades. The code is based on a formulation of the compressible Navier-Stokes equations in a rotating frame of reference in which the velocity dependent variable is specified with respect to the rotating frame instead of the inertial frame. The algorithm employed to obtain solutions to the governing equation is a finite-volume LU algorithm that allows convection, source, as well as diffusion terms to be treated implicitly. In this study, all convection terms are upwind differenced by using flux-vector splitting, and all diffusion terms are centrally differenced. This paper describes the formulation and algorithm employed in the code. Some computed solutions for the flow within a coolant passage of a radial turbine are also presented. Author

A91-45811* # Carnegie-Mellon Univ., Pittsburgh, PA. **ALGEBRAIC GRID GENERATION FOR COOLANT PASSAGES OF TURBINE BLADES WITH SERPENTINE CHANNELS AND PIN FINS**

T. I.-P. SHIH (Carnegie Mellon University, Pittsburgh, PA), R. J. ROELKE (NASA, Lewis Research Center, Cleveland, OH), and E. STEINTHORSSON AIAA, SAE, ASME, and ASEE, Joint Propulsion Conference, 27th, Sacramento, CA, June 24-26, 1991. 9 p. refs (Contract NAG3-929) (AIAA PAPER 91-2366)

In order to study numerically details of the flow and heat transfer within coolant passages of turbine blades, a method must first be

developed to generate grid systems within the very complicated geometries involved. In this study, a grid generation package was developed that is capable of generating the required grid systems. The package developed is based on an algebraic grid generation technique that permits the user considerable control over how grid points are to be distributed in a very explicit way. These controls include orthogonality of grid lines next to boundary surfaces and ability to cluster about arbitrary points, lines, and surfaces. This paper describes that grid generation package and shows how it can be used to generate grid systems within complicated-shaped coolant passages via an example. Author

A91-45815* United Technologies Research Center, East Hartford, CT.

EXPERIMENTAL STUDY OF CROSS-STREAM MIXING IN A CYLINDRICAL DUCT

A. VRANOS, D. S. LISCINSKY, B. TRUE (United Technologies Research Center, East Hartford, CT), and J. D. HOLDEMAN (NASA, Lewis Research Center, Cleveland, OH) AIAA, SAE, ASME, and ASEE, Joint Propulsion Conference, 27th, Sacramento, CA, June 24-26, 1991. 14 p. refs
(Contract NAS3-25967)

(AIAA PAPER 91-2459) Copyright

An experimental investigation of cross stream injection and mixing has been conducted with application to a low NO(x) combustor for the HSCT. Mixing in a cylindrical chamber has been studied for transverse injection from slanted slot and round orifice injectors. Momentum ratio, density ratio, and injector geometry were the primary variables. Slanted slots of various size, aspect ratio, and number were studied. Quantitative measurement of injectant concentration distributions were obtained by planar digital imaging of the Mie-scattered light from an aerosol seed uniformly mixed with the injectant. The unmixedness, defined as the ratio of the rms concentration fluctuation to mean concentration in a plane perpendicular to the main flow direction, was found to be primarily a function of momentum ratio and injector spacing. An optimum spacing is indicated. Unmixedness is also a function of orifice size, or mass flow ratio, but the mass flow dependence can be accounted for by normalizing the unmixedness with its maximum theoretical value. The data indicate that density ratio greater than unity retards mixing. It was found that above a certain momentum flux ratio, mixing with slanted slot injectors was better than with round hole injectors. Author

A91-46179* National Aeronautics and Space Administration. Lewis Research Center, Cleveland, OH.

EFFICIENT REAL GAS UPWIND NAVIER-STOKES COMPUTATIONS OF HIGH SPEED FLOWS

WILLIAM J. COIRIER (NASA, Lewis Research Center, Cleveland, OH) AIAA Journal (ISSN 0001-1452), vol. 29, Aug. 1991, p. 1223-1231. refs

Copyright

An efficient method to account for the chemically frozen thermodynamic and transport properties of air in three-dimensional Navier-Stokes calculations has been demonstrated. This approach uses an explicitly specified equation of state (EOS) so that the fluid pressure, temperature, and transport properties are directly related to the flow variables. The method is efficient since no subiterations are required to deduce the pressure and temperature from the flux variables and is modular by allowing different equations of state to be easily supplied to the code. The flexibility of the EOS approach is shown by its implementation into a high-order total variation diminishing upwinding scheme as well as a standard central-differencing scheme. The EOS approach is then demonstrated by computing the hypersonic flow through the corner region of two mutually perpendicular flat plates using both the upwind and central-differencing schemes. Author

A91-47735* National Aeronautics and Space Administration. Lewis Research Center, Cleveland, OH.

ANALYSIS OF THE ONE-DIMENSIONAL TRANSIENT COMPRESSIBLE VAPOR FLOW IN HEAT PIPES

JONG H. JANG (NASA, Lewis Research Center; Sverdrup

Technology, Inc., Cleveland, OH), AMIR FAGHRI (Wright State University, Dayton, OH), and WON S. CHANG (USAF, Wright Research and Development Center, Wright-Patterson AFB, OH) International Journal of Heat and Mass Transfer (ISSN 0017-9310), vol. 34, Aug. 1991, p. 2029-2037. refs

(Contract F33615-88-C-2820)

Copyright

The transient compressible one-dimensional vapor flow dynamics in a heat pipe is modeled. The numerical results are obtained by using the implicit non-iterative Beam-Warming finite difference method. The model is tested for simulated heat pipe vapor flow and actual vapor flow in cylindrical heat pipes. A good comparison of the present transient results for the simulated heat pipe vapor flow with the previous results of a two-dimensional numerical model is achieved and the steady state results are in agreement with the existing experimental data. The transient behavior of the vapor flow under subsonic, sonic, and supersonic speeds as well as high mass flow rates are successfully predicted. Author

A91-48276* National Aeronautics and Space Administration. Lewis Research Center, Cleveland, OH.

FRONTGENESIS DRIVEN BY HORIZONTALLY QUADRATIC DISTRIBUTIONS OF DENSITY

DAVID JACQMIN (NASA, Lewis Research Center, Cleveland, OH) Journal of Fluid Mechanics (ISSN 0022-1120), vol. 228, July 1991, p. 1-24. refs

Copyright

Attention is given to the quadratic density distribution in a channel, which has been established by Simpson and Linden to be the simplest case of the horizontally nonlinear distribution of fluid density required for the production of frontogenesis. The porous-media and Boussinesq flow models are examined, and their evolution equations are reduced to one-dimensional systems. While both the porous-media and the inviscid/nondiffusive Boussinesq systems exhibit classic frontogenesis behavior, the viscous Boussinesq system exhibits a more complex behavior: boundary-layer effects force frontogenesis away from the lower boundary, and at late times the steepest density gradients are close to mid-channel. O.C.

A91-48758* Carnegie-Mellon Univ., Pittsburgh, PA.

ALGEBRAIC GRID GENERATION FOR COMPLEX GEOMETRIES

T. I.-P. SHIH (Carnegie Mellon University, Pittsburgh, PA), R. T. BAILEY (Florida, University, Gainesville), H. L. NGUYEN, and R. J. ROELKE (NASA, Lewis Research Center, Cleveland, OH) International Journal for Numerical Methods in Fluids (ISSN 0271-2091), vol. 13, June 20, 1991, p. 1-31. refs
(Contract NAG3-929; NAG3-997)

Copyright

An efficient computer program called GRID2D/3D has been developed to generate single and composite grid systems within geometrically complex two- and three-dimensional (2D and 3D) spatial domains that can deform with time. GRID2D/3D generates single grid systems by using algebraic grid generation methods based on transfinite interpolation. The distribution of grid points within the spatial domain is controlled by stretching functions and grid lines can intersect boundaries of the spatial domain orthogonally. GRID2D/3D generates composite grid systems by patching together two or more single grid systems. The patching can be discontinuous or continuous. For 2D spatial domains the boundary curves are constructed by using either cubic or tension spline interpolation. For 3D spatial domains the boundary surfaces are constructed by using a new technique, developed in this study, referred to as 3D bidirectional Hermite interpolation. Author

A91-48966* Cleveland State Univ., OH.

FLOW VISUALIZATION AND COMPUTATIONAL STUDIES OF A REVERSE FLOW CIRCULAR COMBUSTOR

B. GHORASHI, F. REARDON, G. MCBEATH (Cleveland State University, OH), and K. CHUN (NASA, Lewis Research Center; Cleveland State University, OH) IN: Heat Transfer and Fluid

34 FLUID MECHANICS AND HEAT TRANSFER

Mechanics Institute, 32nd, Sacramento, CA, June 6, 7, 1991, Proceedings. Sacramento, CA, California State University, 1991, p. 305-324. refs
Copyright

The development of a reverse-flow circular combustor is described in terms of the visualization techniques that are employed to optimize the flow and mixing of fuel and air. The Fluent computer program is used in conjunction with flow visualization studies to investigate the performance of the combustor. The combustor has multiple mini-combustion zones (MCZs) and fuel injection nozzles along its circular geometry, and the fuel injection design is modeled to determine temperature distribution, including the performance at the combustor exit. The yellow dye smoke used in the visualization demonstrated desirable flow patterns with rapid circulation patterns within the MCZs and extensive interaction between the channel flow and the MCZs. The results are similar to those of CFD models, and the main conclusions are that fuel atomization can be further optimized and that the fuel injector nozzle can control swirls, fuel spray angle, and jet penetration.

C.C.S.

A91-50204* National Aeronautics and Space Administration. Lewis Research Center, Cleveland, OH.

NUMERICAL SOLUTION FOR THE VELOCITY-DERIVATIVE SKEWNESS OF A LOW REYNOLDS-NUMBER

TURBULENCE-LIKE DECAYING NAVIER-STOKES FLOW

ROBERT G. DEISSLER (NASA, Lewis Research Center, Cleveland, OH) Computers and Fluids (ISSN 0045-7930), vol. 20, no. 1, 1991, p. 89-91. Previously announced in STAR as N90-27985. refs

Copyright

The variation of the velocity-derivative skewness of a Navier-Stokes flow as the Reynolds number goes toward zero is calculated numerically. The value of the skewness, which has been somewhat controversial, is shown to become small at low Reynolds numbers.

Author

A91-52395*# Space Power, Inc., San Jose, CA.
THE TELESCOPING BOOM RADIATOR CONCEPT FOR MULTIMEGAWATT SPACE POWER SYSTEMS

J. K. KOESTER (Space Power, Inc., San Jose, CA) and A. J. JUHASZ (NASA, Lewis Research Center, Cleveland, OH) AIAA, NASA, and OAI, Conference on Advanced SEI Technologies, Cleveland, OH, Sept. 4-6, 1991. 7 p. refs
(Contract NAS3-25208)

(AIAA PAPER 91-3497) Copyright

Development of the telescoping boom radiator from concept studies through a detailed design is reviewed. Particular attention is given to the scaling law for specific mass of cylindrical radiator geometries and radiator mass projections for large scale heat rejection systems. The concept of the telescoping, cylindrical radiator is identified as a leading candidate for rejecting tens of megawatts of thermal energy while maintaining a reasonable launch.

O.G.

A91-52422*# National Aeronautics and Space Administration. Lewis Research Center, Cleveland, OH.

AN OVERVIEW OF THE LERC CSTI THERMAL MANAGEMENT PROGRAM

ALBERT J. JUHASZ (NASA, Lewis Research Center, Cleveland, OH) AIAA, NASA, and OAI, Conference on Advanced SEI Technologies, Cleveland, OH, Sept. 4-6, 1991. 12 p. refs
(AIAA PAPER 91-3528)

This report presents an integrated multielement project effort, currently being carried out at NASA LeRC, for the development of space heat rejection subsystems, with special emphasis on lightweight radiators, in support of SEI power system technology, and in particular the SP-100 program. Principal project elements include both contracted and in-house efforts. Included in the first category are two contracts aimed at the development of advanced radiator concepts, and demonstration of a flexible fabric heat pipe radiator concept. In-house work is designed to guide and support the overall program by system integration studies, heat pipe testing

and analytical code development, radiator surface morphology alteration for emissivity enhancement, and composite materials research focused on the development of lightweight high conductivity fins.

Author

A91-53714*# National Aeronautics and Space Administration. Lewis Research Center, Cleveland, OH.

CRYOGENIC TRANSFER OPTIONS FOR EXPLORATION MISSIONS

DAVID J. CHATO (NASA, Lewis Research Center, Cleveland, OH) AIAA, NASA, and OAI, Conference on Advanced SEI Technologies, Cleveland, OH, Sept. 4-6, 1991. 11 p. Previously announced in STAR as N91-28538. refs
(AIAA PAPER 91-3541) Copyright

The literature of in-space cryogenic transfer is reviewed in order to propose transportation concepts to support the Space Exploration Initiative (SEI). Forty-nine references are listed and key findings are synopsized. An assessment of the current maturity of cryogenic transfer system technology is made. Although the settled transfer techniques is the most mature technology, the No-Vent Fill technology is maturing rapidly. Future options for development of cryogenic transfer technology are also discussed.

Author

A91-54268* National Aeronautics and Space Administration. Lewis Research Center, Cleveland, OH.

CHARACTERISTICS OF 3D TURBULENT JETS IN CROSSFLOW

A. O. DEMUREN (NASA, Lewis Research Center, Cleveland, OH) IN: Symposium on Turbulence, 12th, Rolla, MO, Sept. 24-26, 1990, Preprints. Rolla, MO, University of Missouri-Rolla, 1990, p. B1-1 to B1-11. Previously announced in STAR as N91-22536. refs
(Contract NASA ORDER C-99066-G)

Copyright

Three dimensional turbulent jets in crossflow at low to medium jet-to-crossflow velocity ratios are computed with a finite volume numerical procedure which utilizes a second-moment closure model to approximate the Reynolds stresses. A multigrid method is used to accelerate the convergence rate of the procedure. Comparison of the computations to measured data show good qualitative agreement. All trends are correctly predicted, though there is some uncertainty on the height of penetration of the jet. The evolution of the vorticity field is used to explore the jet-crossflow interaction.

Author

A91-54958 National Aeronautics and Space Administration. Ames Research Center, Moffett Field, CA.

THE EFFECTS OF ROTATION ON INITIALLY ANISOTROPIC HOMOGENEOUS FLOWS

NAGI N. MANSOUR (NASA, Ames Research Center, Moffett Field, CA), TSAN-HSING SHIH (NASA, Lewis Research Center, Cleveland, OH; Stanford University, CA), and WILLIAM C. REYNOLDS (NASA, Ames Research Center, Moffett Field; Stanford University, CA) Physics of Fluids A (ISSN 0899-8213), vol. 3, Oct. 1991, p. 2421-2425. refs

Copyright

Rotation of initially anisotropic homogeneous flows is studied using a model spectral tensor. It is shown that the anisotropy changes because of the influence of rotation through phase scrambling. Phase scrambling causes the Reynolds stresses to develop with damped oscillations. The final Reynolds stress anisotropy is found to be proportional to the initial structural tensor anisotropy. Closure models for the rapid pressure strain terms should reflect this change in anisotropy, and should drive the anisotropy to reach its final predicted state. Finally, it is shown that long-time integration using direct numerical simulations should be treated with care because phase scrambling effects on a discrete wave space can cause loss of resolution when time becomes large.

Author

N91-10249* National Aeronautics and Space Administration. Lewis Research Center, Cleveland, OH.

A THREE-DIMENSIONAL TURBULENT HEAT TRANSFER ANALYSIS FOR ADVANCED TUBULAR ROCKET THRUST CHAMBERS

KENNETH J. KACYNSKI Oct. 1990 10 p Presented at the JANNAF Propulsion Conference, Anaheim, CA, 3-5 Oct. 1990 (Contract RTOP 591-41-21) (NASA-TM-103293; E-5753; NAS 1.15:103293) Avail: NTIS HC/MF A02 CSCL 20D

Heat transfer was analyzed in the throat region of a plug and spool rocket engine for both smooth and corrugated walls. A three-dimensional, Navier-Stokes code was used for the analysis. The turbulence model in the code was modified to handle turbulence suppression in the crevice region of the corrugated wall. The overall heat transfer at the throat for the corrugated wall was 34 percent higher than it was for the smooth wall for comparable rocket flow conditions. Author

N91-11192* National Aeronautics and Space Administration. Lewis Research Center, Cleveland, OH.

NAVIER-STOKES ANALYSIS OF TRANSONIC CASCADE FLOW

A. ARNONE (Florence Univ., Italy), M.-S. LIOU, and L. POVINELLI Oct. 1990 12 p (Contract NASA ORDER C-99066-G) (NASA-TM-103624; E-5791; NAS 1.15:103624; ICOMP-90-23) Avail: NTIS HC/MF A03 CSCL 20D

A new kind of C-type grid is proposed, this grid is non-periodic on the wake and allows minimum skewness for cascades with high turning and large camber. Reynolds-averaged Navier-Stokes equations are solved on this type of grid using a finite volume discretization and a full multigrid method which uses Runge-Kutta stepping as the driving scheme. The Baldwin-Lomax eddy-viscosity model is used for turbulence closure. A detailed numerical study is proposed for a highly loaded transonic blade. A grid independence analysis is presented in terms of pressure distribution, exit flow angles, and loss coefficient. Comparison with experiments clearly demonstrates the capability of the proposed procedure. Author

N91-12034* National Aeronautics and Space Administration. Lewis Research Center, Cleveland, OH.

A STUDY OF VOID EFFECTS ON THE INTERLAMINAR SHEAR STRENGTH OF UNIDIRECTIONAL GRAPHITE FIBER REINFORCED COMPOSITES

KENNETH J. BOWLES and STEPHEN FRIMPONG Oct. 1990 32 p (Contract RTOP 510-01-01) (NASA-TM-103267; E-5704; NAS 1.15:103267) Avail: NTIS HC/MF A03 CSCL 20/4

A study was conducted to evaluate the effect of voids on the interlaminar shear strength (ILSS) of a polyimide matrix composite system. The graphite/PRM-15 composite was chosen for study because of the extensive amount of experience that has been amassed in the processing of this material. Composite densities and fiber contents of more than thirty different laminates were measured along with ILSS. Void contents were calculated and the void geometry and distribution were noted using microscopic techniques such as those used in metallography. It was found that there was a good empirical correlation between ILSS and composite density. The most acceptable relationship between the ILSS and density was found to be a power equation which closely resembles theoretically derived expressions. An increase in scatter in the strength data was observed as the void content increased. In laminates with low void content, the void appears to be more segregated in one area of the laminate. It was found that void free composites could be processed in matched metal die molds at pressures greater than 1.4 and less than 6.9 MPa. Author

N91-12913* National Aeronautics and Space Administration. Lewis Research Center, Cleveland, OH.

THE EFFECT OF COATINGS AND LINERS ON HEAT TRANSFER IN A DRY SHAFT-BUSH TRIBOSYSTEM

MIHIR K. GHOSH and DAVID E. BREWE (Army Aviation Systems Command, Cleveland, OH.) Aug. 1990 22 p Original contains color illustrations (Contract DA PROJ. 1L1-61102-AH-45; RTOP 505-63-1A) (NASA-TM-102513; E-5316; NAS 1.15:102513; AVSCOM-TR-90-C-006; AD-A229669) Avail: NTIS HC/MF A03; 12 functional color pages CSCL 20/4

The temperatures due to frictional heating within a solid lubricated or coated journal bearing were analyzed by using a finite element method. A solid model of the shaft-bush tribocontact was generated with an eight-node, three-dimensional, first-order isoparametric heat-transfer element and the Patran solid modeler software. The Patran (Patran-Marc) translator was used to help develop the Marc-based finite element program for the system; this software was used on the Cray X-MP supercomputer to perform a finite element analysis of the contact. The analysis was performed for various liner materials, for thin, hard, wear-resistant coated bearings, and for different geometries and thermal cooling boundary conditions. The analyses indicated that thermal conductivity of the liner or coating material is the most vital thermal parameter that controls the interface temperature. In addition to design variations, the proximity of the cooling source to the heat-flux-generating interface is critically important to the temperature control in the system. Author

N91-13638* National Aeronautics and Space Administration. Lewis Research Center, Cleveland, OH.

COMMENT ON LOCAL ENERGY TRANSFER AND NONLOCAL INTERACTIONS IN HOMOGENEOUS, ISOTROPIC TURBULENCE (PHYS. FLUIDS A2, 413 (1990))

ROBERT G. DEISSLER Aug. 1990 7 p (Contract RTOP 505-90-01) (NASA-TM-103263; E-5696; NAS 1.15:103263) Avail: NTIS HC/MF A02 CSCL 20/4

It is argued that the low-Reynolds number results in the subject paper are not congruous with the data of Ling and Huang, and that the spectral transfer should be less local. Author

N91-13668* National Aeronautics and Space Administration. Lewis Research Center, Cleveland, OH.

HEAT TRANSFER DEVICE AND METHOD OF MAKING THE SAME Patent Application

BRUCE A. BANKS, inventor (to NASA) and JAMES R. GAIER, inventor (to NASA) 30 Mar. 1990 11 p (NASA-CASE-LEW-14162-1; NAS 1.71:LEW-14162-1; US-PATENT-APPL-SN-501893) Avail: NTIS HC/MF A03 CSCL 20/4

Gas derived graphite fibers are generated by the decomposition of an organic gas. These fibers when joined with a suitable binder are used to make a high thermal conductivity composite material. The fibers may be intercalated. The intercalate can be halogen or halide salt, alkaline metal, or any other species which contributes to the electrical conductivity improvement of the graphite fiber. The heat transfer device may also be made of intercalated highly oriented pyrolytic graphite and machined, rather than made of fibers. NASA

N91-14556* National Aeronautics and Space Administration. Lewis Research Center, Cleveland, OH.

SURFACE SETTLING IN PARTIALLY FILLED CONTAINERS UPON STEP REDUCTION IN GRAVITY

MARL M. WEISLOGEL and HOWARD D. ROSS Nov. 1990 19 p Submitted for publication (Contract RTOP 674-24-05) (NASA-TM-103641; E-4998; NAS 1.15:103641) Avail: NTIS HC/MF A03 CSCL 20/4

A large literature exists concerning the equilibrium configurations of free liquid/gas surfaces in reduced gravity environments. Such conditions generally yield surfaces of constant curvature meeting

34 FLUID MECHANICS AND HEAT TRANSFER

the container wall at a particular (contact) angle. The time required to reach and stabilize about this configuration is less studied for the case of sudden changes in gravity level, e.g. from normal- to low-gravity, as can occur in many drop tower experiments. The particular interest here was to determine the total reorientation time for such surfaces in cylinders (mainly), as a function primarily of contact angle and kinematic viscosity, in order to aid in the development of drop tower experiment design. A large parametric range of tests were performed and, based on an accompanying scale analysis, the complete data set was correlated. The results of other investigations are included for comparison. Author

N91-14559* National Aeronautics and Space Administration. Lewis Research Center, Cleveland, OH.

NUMERICAL STUDY OF SHOCK-WAVE/BOUNDARY LAYER INTERACTIONS IN PREMIXED HYDROGEN-AIR HYPERSONIC FLOWS

SHAYE YUNGSTER Nov. 1990 21 p Presented at the 29th Aerospace Sciences Meeting, Reno, NV, 7-10 Jan. 1991; sponsored by AIAA Original contains color illustrations (Contract NASA ORDER C-99066-G) (NASA-TM-103273; E-5715; ICOMP-90-22; NAS 1.15:103273; AIAA PAPER 91-0413) Avail: NTIS HC/MF A03; 3 functional color pages CSCL 20/4

A computational study of shock wave/boundary layer interactions involving premixed combustible gases, and the resulting combustion processes is presented. The analysis is carried out using a new fully implicit, total variation diminishing (TVD) code developed for solving the fully coupled Reynolds-averaged Navier-Stokes equations and species continuity equations in an efficient manner. To accelerate the convergence of the basic iterative procedure, this code is combined with vector extrapolation methods. The chemical nonequilibrium processes are simulated by means of a finite-rate chemistry model for hydrogen-air combustion. Several validation test cases are presented and the results compared with experimental data or with other computational results. The code is then applied to study shock wave/boundary layer interactions in a ram accelerator configuration. Results indicate a new combustion mechanism in which a shock wave induces combustion in the boundary layer, which then propagates outwards and downstream. At higher Mach numbers, spontaneous ignition in part of the boundary layer is observed, which eventually extends along the entire boundary layer at still higher values of the Mach number. Author

N91-16304* National Aeronautics and Space Administration. Lewis Research Center, Cleveland, OH.

EXTENSION OF TRANSONIC FLOW COMPUTATIONAL CONCEPTS IN THE ANALYSIS OF CAVITATED BEARINGS

D. VIJAYARAGHAVAN, T. G. KEITH, JR., and D. E. BREWE (Army Aviation Systems Command, Cleveland, OH.) Oct. 1990 14 p Presented at the Joint Tribology Conference, Toronto, Ontario, 7-10 Oct. 1990; cosponsored by the STLE and ASME (Contract DA PROJ. 1L1-61102-AH-45; RTOP 505-63-1A) (NASA-TM-103214; E-5625; NAS 1.15:103214; AVSCOM-TR-91-C-002; AD-A231726) Avail: NTIS HC/MF A03 CSCL 20/4

An analogy between the mathematical modeling of transonic potential flow and the flow in a cavitating bearing is described. Based on the similarities, characteristics of the cavitated region and jump conditions across the film reformation and rupture fronts are developed using the method of weak solutions. The mathematical analogy is extended by utilizing a few computational concepts of transonic flow to numerically model the cavitating bearing. Methods of shock fitting and shock capturing are discussed. Various procedures used in transonic flow computations are adapted to bearing cavitation applications, for example, type differencing, grid transformation, an approximate factorization technique, and Newton's iteration method. These concepts have proved to be successful and have vastly improved the efficiency of numerical modeling of cavitated bearings. Author

N91-19369* National Aeronautics and Space Administration. Lewis Research Center, Cleveland, OH.

TWO REFERENCE TIME SCALES FOR STUDYING THE DYNAMIC CAVITATION OF LIQUID FILMS

D. C. SUN and DAVID E. BREWE (Army Aviation Research and Development Command, Cleveland, OH.) 1991 7 p Presented at the 1991 Cavitation Symposium at the Joint ASME/JSME Fluids Engineering Conference, Portland, OR, 23-26 Jun. 1991 (Contract DA PROJ. 1L1-61102-AH-45; RTOP 505-63-5A) (NASA-TM-103673; E-5885; NAS 1.15:103673; AVSCOM-TR-90-C-030; AD-A231727) Avail: NTIS HC/MF A02 CSCL 20/4

Two formulas, one for characteristic time of filling a void with a vapor of the surrounding liquid, and one of filling the void by diffusion of the dissolved gas in the liquid, are derived. Based on this analysis, it is seen that in an oil film bearing operating under dynamic loads, the content of cavitation region should be oil vapor rather than the air liberated from solution, if the oil is free of entrained air. Author

N91-19370* National Aeronautics and Space Administration. Lewis Research Center, Cleveland, OH.

TURBULENT BOUNDARY LAYER SEPARATION OVER A REARWARD FACING RAMP AND ITS CONTROL THROUGH MECHANICAL EXCITATION

DANIEL J. MCKINZIE, JR. 1991 28 p Presented at the 29th Aerospace Sciences Meeting, Reno, NV, 7-10 Jan. 1991; sponsored by AIAA (NASA-TM-103702; E-5860; NAS 1.15:103702; AIAA PAPER 91-0253) Avail: NTIS HC/MF A03 CSCL 20/4

A vane oscillating about a fixed point at the inlet to a two-dimensional 20 degree rearward facing ramp has proven effective in delaying the separation of a turbulent boundary layer. Measurements of the ramp surface static pressure coefficient obtained under the condition of vane oscillation and constant inlet velocity revealed that two different effects occurred with surface distance along the ramp. In the vicinity of the oscillating vane, the pressure coefficients varied as a negative function of the vane's trailing edge rms velocity; the independent variable on which the rms velocity depends are the vane's oscillation frequency and its displacement amplitude. From a point downstream of the vane to the exit of the ramp; however, the pressure coefficient varied as a more complex function of the two independent variables. That is, it was found to vary as a function of the vane's oscillation frequency throughout the entire range of frequencies covered during the test, but over only a limited range of the trailing edge displacement amplitudes covered. More specifically, the value of the pressure coefficient was independent of increases in the vane's displacement amplitude above approximately 35 inner wall units of the boundary layer. Below this specific amplitude it varied as a function of the vane's trailing edge rms velocity. This height is close to the upper limit of the buffer layer. A parametric study was made to determine the variation of the maximum static pressure recovery as a function of the vane's oscillation frequency, for several ramp inlet velocities and a constant displacement amplitude of the vane's trailing edge. The results indicate that the phenomenon producing the optimum delay of separation may be Strouhal number dependent. Corona anemometer measurements obtained in the inner wall regions of the boundary layer for the excited case reveal a large range of unsteadiness in the local velocities. These measurements imply the existence of inflections in the profiles, which provide a mechanism for resulting inviscid flow instabilities to produce turbulence in the near wall region, thereby delaying separation of the boundary layer. Author

N91-19371* National Aeronautics and Space Administration. Lewis Research Center, Cleveland, OH.

A SUMMARY OF EXISTING AND PLANNED EXPERIMENT HARDWARE FOR LOW-GRAVITY FLUIDS RESEARCH

MYRON E. HILL and TERENCE F. O'MALLEY 1991 44 p Presented at the 29th Aerospace Sciences Meeting, Reno, NV, 7-10 Jan. 1991; sponsored by AIAA

(Contract RTOP 694-03-0A)

(NASA-TM-103706; E-5931; NAS 1.15:103706; AIAA PAPER 91-0777) Avail: NTIS HC/MF A03 CSCL 20/4

An overview is presented of (1) existing ground-based, low gravity research facilities, with examples of hardware capabilities, and (2) existing and planned space-based research facilities, with examples of current and past flight hardware. Low-gravity, ground-based facilities, such as drop towers and aircraft, provide the experimenter with quick turnaround time, easy access to equipment, gravity levels ranging from 10(exp -2) to 10(exp -6) G, and low-gravity durations ranging from 2 to 30 sec. Currently, the only operational space-based facility is the Space Shuttle. The Shuttle's payload bay and middeck facilities are described. Existing and planned low-gravity fluids research facilities are also described with examples of experiments and hardware capabilities. Author

N91-19372*# National Aeronautics and Space Administration. Lewis Research Center, Cleveland, OH.

THE EFFECT OF SMALL STREAMWISE VELOCITY DISTORTION ON THE BOUNDARY LAYER FLOW OVER A THIN FLAT PLATE WITH APPLICATION TO BOUNDARY LAYER STABILITY THEORY

M. E. GOLDSTEIN, S. J. LEIB, and S. J. COWLEY (Cambridge Univ., England) Dec. 1990 37 p

(Contract RTOP 505-62-31)

(NASA-TM-103668; E-5759-1; ICOMP-90-25; NAS 1.15:103668)

Avail: NTIS HC/MF A03 CSCL 20/4

Researchers show how an initially linear spanwise disturbance in the free stream velocity field is amplified by leading edge bluntness effects and ultimately leads to a small amplitude but linear spanwise motion far downstream from the edge. This spanwise motion is imposed on the boundary layer flow and ultimately causes an order-one change in its profile shape. The modified profiles are highly unstable and can support Tollmein-Schlichting wave growth well upstream of the theoretical lower branch of the neutral stability curve for a Blasius boundary layer. Author

N91-19373*# National Aeronautics and Space Administration. Lewis Research Center, Cleveland, OH.

CRITICAL-LAYER NONLINEARITY IN THE RESONANCE GROWTH OF THREE-DIMENSIONAL WAVES IN BOUNDARY LAYERS

REDA R. MANKBADI Nov. 1990 58 p

(Contract RTOP 505-02-22)

(NASA-TM-103639; E-5000; NAS 1.15:103639) Avail: NTIS

HC/MF A04 CSCL 20/4

The nonlinear interactions of a triad of initially linear stability waves are addressed. The triad consisted of a single two-dimensional mode at a given frequency and two oblique modes with equal and opposite spanwise wave numbers. The oblique waves were at half the frequency and streamwise wave number of the two-dimensional mode. Attention was focused on the boundary-layer transition at low frequencies and high Reynolds numbers. A five-zoned structure and low-frequency scaling were used to derive the nonlinear-interaction equations. The initial nonlinear development of the waves was analyzed; the results indicated that the two-dimensional wave behaves according to linear theory. Nonlinear interactions caused exponential-of-an-exponential growth of the oblique modes. This resonant amplification of the subharmonic depended on the initial amplitude of the two-dimensional wave and on the initial phase angle between the two-dimensional wave and the oblique waves. The resonant growth of the oblique modes was more pronounced at lower frequencies than at higher frequencies. The results are in good agreement with experimental results and offer explanations of the observed process. Author

N91-19374*# National Aeronautics and Space Administration. Lewis Research Center, Cleveland, OH.

EXPERIMENTAL INVESTIGATION OF A SINGLE FLUSH-MOUNTED HYPERMIXING NOZZLE

DAVID O. DAVIS, WARREN R. HINGST, and A. ROBERT

PORRO 1990 13 p Presented at the Second International Aerospace Planes Conference, Orlando, FL, 29-31 Oct. 1990; sponsored by AIAA Previously announced in IAA as A91-14466 (Contract RTOP 505-62-31)

(NASA-TM-103726; E-5960; NAS 1.15:103726; AIAA PAPER 90-5240) Avail: NTIS HC/MF A03 CSCL 20/4

The results of an experimental wind tunnel investigation of a circular supersonic jet ($m_{sub j} = 3.47$) injected at a 10 degree angle into a supersonic freestream. The jet penetrates a boundary layer, which has a thickness approximately the same as the jet nozzle exit diameter. Measurements were made for nominal freestream Mach numbers of 1.6, 2.0, 2.5, and 3.0. Three jet total pressures were run at each freestream Mach number, resulting in twelve separate operating conditions. Mean data accumulated by means of static and total pressure probe instrumentation are presented at two axial stations: seven jet nozzle diameters upstream and 15 jet nozzle diameters downstream from where the centerline of the nozzle intersects the wind tunnel wall. For one condition at each freestream Mach number, the jet air was seeded with a hydrocarbon trace gas and the flow was sampled at the downstream measurement plane to quantify the mean mixing of the two streams. Surface oil flow visualization was also used to investigate the flow interaction. All results are for air-to-air mixing. The measurements indicate the presence of two pairs contra-rotating vortices. One pair follows the jet trajectory and tends to split the jet into two streams. A smaller pair, rotating in an opposite sense, develops in the near wall region. Reported results include Mach number and volume fraction distributions in the cross plane, as well as jet penetration and mixing efficiency. Author

N91-19375*# National Aeronautics and Space Administration. Lewis Research Center, Cleveland, OH.

A 2-D OSCILLATING FLOW ANALYSIS IN STIRLING ENGINE HEAT EXCHANGERS

KYUNG H. AHN and MOUNIR B. IBRAHIM (Cleveland State Univ., OH.) 1991 9 p Presented at the 1991 Joint ASME-JSME Fluids Engineering Conference, Portland, OR, 24-26 Jun. 1991

(Contract NASA ORDER C-99066-G)

(NASA-TM-103781; E-6055; ICOMP-91-04; NAS 1.15:103781)

Avail: NTIS HC/MF A02 CSCL 20/4

A two dimensional oscillating flow analysis was conducted, simulating the gas flow inside Stirling heat exchangers. Both laminar and turbulent oscillating pipe flow were investigated numerically for $Re(max) = 1920$ ($Va = 80$), 10800 ($Va = 272$), 19300 ($Va = 272$), and 60800 ($Va = 126$). The results are compared with experimental results of previous investigators. Also, predictions of the flow regime on present oscillating flow conditions were checked by comparing velocity amplitudes and phase differences with those from laminar theory and quasi-steady profile. A high Reynolds number k-epsilon turbulence model was used for turbulent oscillating pipe flow. Finally, performance evaluation of the K-epsilon model was made to explore the applicability of quasi-steady turbulent models to unsteady oscillating flow analysis. Author

N91-20095*# National Aeronautics and Space Administration. Lewis Research Center, Cleveland, OH.

INTERNAL FLUID MECHANICS RESEARCH

LONNIE REID and LOUIS A. POVINELLI *In its* Aeropropulsion 1991 3 p Mar. 1991

Avail: NTIS HC/MF A24 CSCL 20/4

The Internal Fluid Mechanics Division is responsible for computational and experimental research on the internal aerothermodynamics of aeronautical and space propulsion systems. The research focuses on advancing the understanding of the relevant physics associated with improving the state of technology for propulsion system components. Research consists of the development of fast and accurate computational tools and models, the verification of these CFD tools and models through benchmark experiments, and their application to realistic propulsion system components. Advanced computational technologies are used to enhance, accelerate, and integrate computational and

34 FLUID MECHANICS AND HEAT TRANSFER

experimental research. The presentations summarize ongoing work and indicate emphasis in three major research thrusts, namely, inlets, ducts, and nozzles; turbomachinery; and chemical reacting flows.

Author

N91-20096*# National Aeronautics and Space Administration. Lewis Research Center, Cleveland, OH.

INLETS, DUCTS, AND NOZZLES

JAMES R. SCOTT and JOHN M. ABBOTT *In its* Aeropropulsion 1991 27 p Mar. 1991

Avail: NTIS HC/MF A24 CSCL 20/4

The internal fluid mechanics research program in inlets, ducts, and nozzles is a balanced effort between the development and application of computational tools and the conduct of experimental research. The computational effort involves the development and validation of advanced computational fluid dynamics (CFD) codes through comparison with data, the modification of existing codes to extend their range and accuracy, and the application of codes to practical problems to demonstrate their value in design. The experimental research involves both simplified and realistic complex geometries and is used for developing flow physics understanding, for validating advanced numerical analysis codes, and for developing physical models of flow phenomena. The inlet, duct, and nozzle research program is described according to three major classifications of flow phenomena: highly three-dimensional flow fields; shock and high-speed-mixing flow fields; and shear flow control. Specific examples of current and future elements of the research program are described for each of these phenomena. In particular, the highly three-dimensional flow field phenomenon is highlighted by describing the experimental and computational research program in transition ducts having a round-to-rectangular area variation. In the case of shock and high-speed-mixing flow fields, both experimental and computational results are presented for the mixing of a high-speed stream injected into a second high-speed stream. For shear flow control, research in the use of aerodynamic excitation to enhance the jet mixing process is described. In addition, results that stem from using small tabs protruding into a nozzle exit flow stream to enhance mixing are also presented. A three-dimensional, unsteady viscous code development effort that will provide a well-documented, user-friendly flow solver for computing inlet, duct, and nozzle flow fields in the future is described.

Author

N91-20097*# National Aeronautics and Space Administration. Lewis Research Center, Cleveland, OH.

TURBOMACHINERY

ANTHONY J. STRAZISAR, RAYMOND E. GAUGLER, JOHN J. ADAMCZYK, DALE J. ARPASI, and ISAAC LOPEZ (Army Aviation Systems Command, Cleveland, OH.) *In its* Aeropropulsion 1991 8 p Mar. 1991

Avail: NTIS HC/MF A24 CSCL 20/4

Over the last few years a dramatic rise was seen in the capability to computer the 3D flow in turbomachinery, and a program was developed where experimental and computational efforts were applied synergistically to maximize the understanding of the complex flows existing in turbomachinery passages. This improved capability and understanding will lead to significantly better turbomachine designs in the future.

Author

N91-20098*# National Aeronautics and Space Administration. Lewis Research Center, Cleveland, OH.

CHEMICAL REACTING FLOWS

ERWIN A. LEZBERG, EDWARD J. MULARZ (Army Aviation Systems Command, Cleveland, OH.), and MENG-SING LIOU *In its* Aeropropulsion 1991 26 p Mar. 1991

Avail: NTIS HC/MF A24 CSCL 20/4

The objectives and accomplishments of research in chemical reacting flows, including both experimental and computational problems are described. The experimental research emphasizes the acquisition of reliable reacting-flow data for code validation, the development of chemical kinetics mechanisms, and the understanding of two-phase flow dynamics. Typical results from two nonreacting spray studies are presented. The computational

fluid dynamics (CFD) research emphasizes the development of efficient and accurate algorithms and codes, as well as validation of methods and modeling (turbulence and kinetics) for reacting flows. Major developments of the RPLUS code and its application to mixing concepts, the General Electric combustor, and the Government baseline engine for the National Aerospace Plane are detailed. Finally, the turbulence research in the newly established Center for Modeling of Turbulence and Transition (CMOTT) is described.

Author

N91-20417*# National Aeronautics and Space Administration. Lewis Research Center, Cleveland, OH.

A FINITE ELEMENT MODEL OF CONDUCTION, CONVECTION, AND PHASE CHANGE NEAR A SOLID/MELT INTERFACE

Ph.D. Thesis - Michigan Univ.

LARRY A. VITERNA Jan. 1991 185 p

(Contract RTOP 474-12-10)

(NASA-TM-103721; E-5952; NAS 1.15:103721) Avail: NTIS HC/MF A09 CSCL 20/4

Detailed understanding of heat transfer and fluid flow is required for many aerospace thermal systems. These systems often include phase change and operate over a range of accelerations or effective gravitational fields. An approach to analyzing such systems is presented which requires the simultaneous solution of the conservation laws of energy, momentum, and mass, as well as an equation of state. The variable property form of the governing equations are developed in two-dimensional Cartesian coordinates for a Newtonian fluid. A numerical procedure for solving the governing equations is presented and implemented in a computer program. The Galerkin form of the finite element method is used to solve the spatial variation of the field variables, along with the implicit Crank-Nicolson time marching algorithm. Quadratic Lagrangian elements are used for the internal energy and the two components of velocity. Linear Lagrangian elements are used for the pressure. The location of the solid/liquid interface as well as the temperatures are determined from the calculated internal energy and pressure. This approach is quite general in that it can describe heat transfer without phase change, phase change with a sharp interface, and phase change without an interface. Analytical results from this model are compared to those of other researchers studying transient conduction, convection, and phase change and are found to be in good agreement. The numerical procedure presented requires significant computer resources, but this is not unusual when compared to similar studies by other researchers. Several methods are suggested to reduce the computational times.

Author

N91-20445*# National Aeronautics and Space Administration. Lewis Research Center, Cleveland, OH.

TURBULENT FLUID MOTION. PART 1: THE PHENOMENON OF FLUID TURBULENCE

ROBERT G. DEISSLER Feb. 1991 19 p

(Contract RTOP 505-90-01)

(NASA-TM-103723; E-5956; NAS 1.15:103723) Avail: NTIS HC/MF A03 CSCL 20/4

Some introductory material on fluid turbulence is presented. This includes discussions and illustrations of what turbulence is, and how, why, and where turbulence occurs.

Author

N91-21067*# National Aeronautics and Space Administration. Lewis Research Center, Cleveland, OH.

A FINITE-DIFFERENCE, FREQUENCY-DOMAIN NUMERICAL SCHEME FOR THE SOLUTION OF THE LINEARIZED UNSTEADY EULER EQUATIONS

JAMES R. SCOTT and HAFIZ M. ATASSI (Notre Dame Univ., IN.) *In its* Computational Fluid Dynamics Symposium on Aeropropulsion p 55-104 Jan. 1991

Avail: NTIS HC/MF A99; 10 functional color pages CSCL 20/4

A numerical method is developed for solving periodic, three-dimensional, vortical flows around lifting airfoils in subsonic flow. The first-order method, that is presented, fully accounts for the distortion effects of the nonuniform mean flow on the convected upstream vortical disturbances. The unsteady velocity is split into

a vortical component which is a known function of the upstream flow conditions and the Lagrangian coordinates of the mean flow, and an irrotational field whose potential satisfies a nonconstant-coefficient, inhomogeneous, convective wave equation. Using an elliptic coordinate transformation, the unsteady boundary value problem is solved in the frequency domain on grids which are determined as a function of the Mach number and reduced frequency. Extensive comparisons are made with known solutions to unsteady vortical flow problems, and it is seen that the agreement is generally very good for reduced frequencies ranging from 0 up to 4. Author

N91-21069*# National Aeronautics and Space Administration. Lewis Research Center, Cleveland, OH.

SIMULATION OF TURBOMACHINERY FLOWS

JOHN J. ADAMCZYK *In its* Computational Fluid Dynamics Symposium on Aeropropulsion p 119-126 Jan. 1991
 Avail: NTIS HC/MF A99; 10 functional color pages CSCL 20/4

With the interest in jet propulsion at the end of World War II, aerodynamicists were challenged to develop mathematical models which could be used to design turbomachinery components for jets. NASA Lewis engineers and scientists played a major role in meeting this challenge. Some of their accomplishments are highlighted as well as those of others. Several problems are addressed which must be solved if jet propulsion technology is to advance. Author

N91-21071*# National Aeronautics and Space Administration. Lewis Research Center, Cleveland, OH.

TRANSONIC CASCADE FLOW CALCULATIONS USING NON-PERIODIC C-TYPE GRIDS

ANDREA ARNONE, MENG-SING LIOU, and LOUIS A. POVINELLI *In its* Computational Fluid Dynamics Symposium on Aeropropulsion p 143-162 Jan. 1991
 (Contract NASA ORDER C-99066-G)

Avail: NTIS HC/MF A99; 10 functional color pages CSCL 20/4

A new kind of C-type grid is proposed for turbomachinery flow calculations. This grid is nonperiodic on the wake and results in minimum skewness for cascades with high turning and large camber. Euler and Reynolds averaged Navier-Stokes equations are discretized on this type of grid using a finite volume approach. The Baldwin-Lomax eddy-viscosity model is used for turbulence closure. Jameson's explicit Runge-Kutta scheme is adopted for the integration in time, and computational efficiency is achieved through accelerating strategies such as multigriding and residual smoothing. A detailed numerical study was performed for a turbine rotor and for a vane. A grid dependence analysis is presented and the effect of artificial dissipation is also investigated. Comparison of calculations with experiments clearly demonstrates the advantage of the proposed grid. Author

N91-21082*# National Aeronautics and Space Administration. Lewis Research Center, Cleveland, OH.

IMPLICIT SOLUTION OF THREE-DIMENSIONAL INTERNAL TURBULENT FLOWS

V. MICHELASSI, M.-S. LIOU, LOUIS A. POVINELLI, and F. MARTELLI (Florence Univ., Italy) *In its* Computational Fluid Dynamics Symposium on Aeropropulsion p 363-391 Jan. 1991
 (Contract NASA ORDER C-99066-G)

Avail: NTIS HC/MF A99; 10 functional color pages CSCL 20/4

The scalar form of the approximate factorization method was used to develop a new code for the solution of three dimensional internal laminar and turbulent compressible flows. The Navier-Stokes equations in their Reynolds-averaged form were iterated in time until a steady solution was reached. Evidence was given to the implicit and explicit artificial damping schemes that proved to be particularly efficient in speeding up convergence and enhancing the algorithm robustness. A conservative treatment of these terms at the domain boundaries was proposed in order to avoid undesired mass and/or momentum artificial fluxes. Turbulence effects were accounted for by the zero-equation Baldwin-Lomax turbulence model and the q-omega two-equation model. The flow in a developing S-duct was then solved in the

laminar regime in a Reynolds number (Re) of 790 and in the turbulent regime at Re equals 40,000 by using the Baldwin-Lomax model. The Stanitz elbow was then solved by using an inviscid version of the same code at M sub inlet equals 0.4. Grid dependence and convergence rate were investigated, showing that for this solver the implicit damping scheme may play a critical role for convergence characteristics. The same flow at Re equals 2.5 times 10(exp 6) was solved with the Baldwin-Lomax and the q-omega models. Both approaches show satisfactory agreement with experiments, although the q-omega model was slightly more accurate. Author

N91-21083*# National Aeronautics and Space Administration. Lewis Research Center, Cleveland, OH.

NUMERICAL INVESTIGATION OF AN INTERNAL LAYER IN TURBULENT FLOW OVER A CURVED HILL

S.-W. KIM *In its* Computational Fluid Dynamics Symposium on Aeropropulsion p 393-407 Jan. 1991
 (Contract NASA ORDER C-99066-G)

Avail: NTIS HC/MF A99; 10 functional color pages CSCL 20/4

A numerical investigation of incompressible and compressible turbulent flows over strongly curved surfaces is presented. The turbulent flow equations are solved by a pressure based Navier-Stokes equations solver. In the method, the conservation of mass equation is replaced by a pressure correction equation applicable for both compressible and incompressible flows. The turbulence is described by a multiple time scale turbulence model supplemented with a near-wall turbulence model. The numerical results show that the internal layer is a strong turbulence field which is developed beneath the external boundary layer and is located very close to the wall. The development of the internal layer is attributed to the enormous mean flow strain rate caused by the streamline curvature. The external boundary layer flow responds rather slowly to the streamline curvature. Thus, the turbulence field of the forward corner of the curved hill is characterized by two turbulence fields interacting with each other. The turbulence intensity of the internal layer is much stronger than that of the external boundary layer, so that the development of a new boundary layer in the downstream region of the curved hill depends mostly on the internal layer. These numerical results are in good agreement with the measured data, and show that the turbulence model can resolve the turbulence field subjected to the strong streamline curvature. Author

N91-21085*# National Aeronautics and Space Administration. Lewis Research Center, Cleveland, OH.

HEAT TRANSFER, VELOCITY-TEMPERATURE CORRELATION, AND TURBULENT SHEAR STRESS FROM NAVIER-STOKES COMPUTATIONS OF SHOCK WAVE/TURBULENT BOUNDARY LAYER INTERACTION FLOWS

C. R. WANG, W. R. HINGST, and A. R. PORRO *In its* Computational Fluid Dynamics Symposium on Aeropropulsion p 429-456 Jan. 1991

Avail: NTIS HC/MF A99; 10 functional color pages CSCL 20/4

The properties of 2-D shock wave/turbulent boundary layer interaction flows were calculated by using a compressible turbulent Navier-Stokes numerical computational code. Interaction flows caused by oblique shock wave impingement on the turbulent boundary layer flow were considered. The oblique shock waves were induced with shock generators at angles of attack less than 10 degs in supersonic flows. The surface temperatures were kept at near-adiabatic (ratio of wall static temperature to free stream total temperature) and cold wall (ratio of wall static temperature to free stream total temperature) conditions. The computational results were studied for the surface heat transfer, velocity temperature correlation, and turbulent shear stress in the interaction flow fields. Comparisons of the computational results with existing measurements indicated that (1) the surface heat transfer rates and surface pressures could be correlated with Holden's relationship, (2) the mean flow streamwise velocity components and static temperatures could be correlated with Crocco's relationship if flow separation did not occur, and (3) the

34 FLUID MECHANICS AND HEAT TRANSFER

Baldwin-Lomax turbulence model should be modified for turbulent shear stress computations in the interaction flows. Author

N91-21090* National Aeronautics and Space Administration. Lewis Research Center, Cleveland, OH.

DYNAMICS OF LOCAL GRID MANIPULATIONS FOR INTERNAL FLOW PROBLEMS

PETER R. EISEMAN (Program Development Corp., White Plains, NY.), AARON SNYDER, and YUNG K. CHOO *In its* Computational Fluid Dynamics Symposium on Aeropropulsion p 521-546 Jan. 1991

(Contract NAG3-877; F49620-89-C-0096)

Avail: NTIS HC/MF A99; 10 functional color pages CSCL 20/4

The control point method of algebraic grid generation is briefly reviewed. The review proceeds from the general statement of the method in 2-D unencumbered by detailed mathematical formulation. The method is supported by an introspective discussion which provides the basis for confidence in the approach. The more complex 3-D formulation is then presented as a natural generalization. Application of the method is carried out through 2-D examples which demonstrate the technique. Author

N91-21092* National Aeronautics and Space Administration. Lewis Research Center, Cleveland, OH.

THE 3D COMPUTATION OF SINGLE-EXPANSION-RAMP AND SCRAMJET NOZZLES

H. T. LAI *In its* Computational Fluid Dynamics Symposium on Aeropropulsion p 559-582 Jan. 1991

Avail: NTIS HC/MF A99; 10 functional color pages CSCL 20/4

A description of the computations for three-dimensional nonaxisymmetric nozzles and an analysis of the flowfields are presented. Two different types of nozzles are investigated for compressible flows at high Reynolds numbers. These are the single-expansion-ramp and scramjet nozzles. The computation for the single-expansion-ramp nozzle focuses on the condition of low pressure ratio, which requires the simulation for turbulent flow that is not needed at high pressure ratios. The flowfield contains the external quiescent air, and the internal regions of subsonic and low supersonic flows. The second type is the scramjet nozzle, which typically has a very large area ratio and is designed to operate at high speeds and pressure ratios. The freestream external flow has a Mach number of 6, and the internal flow leaving the combustion chamber is at a Mach number of 1.62. The flowfield is mostly supersonic except in the viscous region near walls. The computed results from both cases are compared with experimental data for the surface pressure distributions. Author

N91-21447* National Aeronautics and Space Administration. Lewis Research Center, Cleveland, OH.

CFD FOR HYPERSONIC PROPULSION

LOUIS A. POVINELLI 1990 17 p Presented at the Workshop on Hypersonic Flow, Antibes, France, 22-25 Jan. 1990; cosponsored by National Research Inst. for Information and Automation and Group for Advancement of Numerical Engineering Methods

(Contract RTOP 506-62-21)

(NASA-TM-103791; E-5689; NAS 1.15:103791) Avail: NTIS HC/MF A03 CSCL 20/4

An overview is given of research activity on the application of computational fluid dynamics (CDF) for hypersonic propulsion systems. After the initial consideration of the highly integrated nature of air-breathing hypersonic engines and airframe, attention is directed toward computations carried out for the components of the engine. A generic inlet configuration is considered in order to demonstrate the highly three dimensional viscous flow behavior occurring within rectangular inlets. Reacting flow computations for simple jet injection as well as for more complex combustion chambers are then discussed in order to show the capability of viscous finite rate chemical reaction computer simulations. Finally, the nozzle flow fields are demonstrated, showing the existence of complex shear layers and shock structure in the exhaust plume. The general issues associated with code validation as well as the

specific issue associated with the use of CFD for design are discussed. A prognosis for the success of CFD in the design of future propulsion systems is offered. Author

N91-21448* National Aeronautics and Space Administration. Lewis Research Center, Cleveland, OH.

ON THE ANOMALY OF VELOCITY-PRESSURE DECOUPLING IN COLLOCATED MESH SOLUTIONS

SANG-WOOK KIM (Texas Univ., Arlington.) and THOMAS VANOVERBEKE Mar. 1991 20 p

(Contract RTOP 505-62-52)

(NASA-TM-103769; E-6031; NAS 1.15:103769) Avail: NTIS HC/MF A03 CSCL 20/4

The use of various pressure correction algorithms originally developed for fully staggered meshes can yield a velocity-pressure decoupled solution for collocated meshes. The mechanism that causes velocity-pressure decoupling is identified. It is shown that the use of a partial differential equation for the incremental pressure eliminates such a mechanism and yields a velocity-pressure coupled solution. Example flows considered are a three dimensional lid-driven cavity flow and a laminar flow through a 90 deg bend square duct. Numerical results obtained using the collocated mesh are in good agreement with the measured data and other numerical results. Author

N91-21458* National Aeronautics and Space Administration. Lewis Research Center, Cleveland, OH.

APPLICATION OF COMPUTATIONAL FLUID DYNAMICS IN HIGH SPEED AEROPROPULSION

LOUIS A. POVINELLI 1991 5 p Proposed for presentation at the 13th IMACS World Congress on Computation and Applied Mathematics, Dublin, Ireland, 22-26 Jul. 1991; cosponsored by International Federation for Automatic Control, International Federation for Information Processing International Federation for Operational Research Societies, and International Measurement Confederation

(Contract RTOP 505-62-52)

(NASA-TM-103780; E-6053; NAS 1.15:103780) Avail: NTIS HC/MF A01 CSCL 20/4

The application is described of computational fluid dynamics (CFD) to a hypersonic propulsion system. An overview of the problems associated with a propulsion system of this type is presented, highlighting the special role that CFD plays in the design of said systems. Author

N91-22524* National Aeronautics and Space Administration. Lewis Research Center, Cleveland, OH.

SECOND ORDER MODELING OF BOUNDARY-FREE TURBULENT SHEAR FLOWS

T.-H. SHIH, Y.-Y. CHEN, and J. L. LUMLEY (Cornell Univ., Ithaca, NY.) May 1991 17 p

(Contract NASA ORDER C-99066-G)

(NASA-TM-104369; ICOMP-91-07; E-6170; NAS 1.15:104369; CMOTT-91-02) Avail: NTIS HC/MF A03 CSCL 20/4

A set of realizable second order models for boundary-free turbulent flows is presented. The constraints on second order models based on the realizability principle are re-examined. The rapid terms in the pressure correlations for both the Reynolds stress and the passive scalar flux equations are constructed to exactly satisfy the joint realizability. All other model terms (return-to-isotropy, third moments, and terms in the dissipation equations) already satisfy realizability. To correct the spreading rate of the axisymmetric jet, an extra term is added to the dissipation equation which accounts for the effect of mean vortex stretching on dissipation. The test flows used in this study are the mixing shear layer, plane jet, axisymmetric jet, and plane wake. The numerical solutions show that the unified model equations predict all these flows reasonably. It is expected that these models would be suitable for more complex and critical flows. Author

N91-22536*# National Aeronautics and Space Administration. Lewis Research Center, Cleveland, OH.

CHARACTERISTICS OF 3D TURBULENT JETS IN CROSSFLOW

A. O. DEMUREN Apr. 1991 22 p
(Contract NASA ORDER C-99066-G)
(NASA-TM-104337; ICOMP-91-05; E-6106; NAS 1.15:104337)
Avail: NTIS HC/MF A03 CSCL 20/4

Three dimensional turbulent jets in crossflow at low to medium jet-to-crossflow velocity ratios are computed with a finite volume numerical procedure which utilizes a second-moment closure model to approximate the Reynolds stresses. A multigrid method is used to accelerate the convergence rate of the procedure. Comparison of the computations to measured data show good qualitative agreement. All trends are correctly predicted, though there is some uncertainty on the height of penetration of the jet. The evolution of the vorticity field is used to explore the jet-crossflow interaction. Author

N91-23409*# National Aeronautics and Space Administration. Lewis Research Center, Cleveland, OH.

SIMULATION OF BRUSH INSERT FOR LEADING-EDGE-PASSAGE CONVECTIVE HEAT TRANSFER

R. C. HENDRICKS, M. J. BRAUN, V. CANACCI, and R. L. MULLEN (Case Western Reserve Univ., Cleveland, OH.) 1991 12 p
Presented at the 4th International Symposium on Transport Phenomena in Heat and Mass Transfer, Sydney, Australia, 14-18 Jul. 1991; sponsored by New South Wales Univ.
(Contract RTOP 505-62-52)
(NASA-TM-103801; E-6093; NAS 1.15:103801) Avail: NTIS HC/MF A03 CSCL 20/4

Current and proposed high speed aircraft have high leading edge heat transfer (to 160 MW/sq m, 100 Btu/sq in/sec) and surface temperatures to 1370 K (2000 F). Without cooling, these surfaces could not survive. In one proposal the coolant hydrogen is circulated to the leading edge through a passage and returned to be consumed by the propulsion system. Simulated flow studies and visualizations have shown flow separation within the passage with a stagnation locus that isolates a zone of recirculation at the most critical portion of the passage, namely the leading edge itself. A novel method is described for mitigating the flow separation and the isolated recirculation zones by using a brush insert in the flow passage near the leading edge zone, thus providing a significant increase in heat transfer. Author

N91-23416*# National Aeronautics and Space Administration. Lewis Research Center, Cleveland, OH.

LOW REYNOLDS NUMBER TWO-EQUATION MODELING OF TURBULENT FLOWS

V. MICHELASSI and T.-H. SHIH May 1991 24 p
Presented at the 43d Annual Pacific Coast Meeting, Seattle, WA, 25-27 Oct. 1990; sponsored by the American Ceramic Society
(Contract NASA ORDER C-99066-G)
(NASA-TM-104368; ICOMP-91-06; E-6169; NAS 1.15:104368; CMOTT-91-01) Avail: NTIS HC/MF A03 CSCL 20/4

A k-epsilon model that accounts for viscous and wall effects is presented. The proposed formulation does not contain the local wall distance thereby making very simple the application to complex geometries. The formulation is based on an existing k-epsilon model that proved to fit very well with the results of direct numerical simulation. The new form is compared with nine different two-equation models and with direct numerical simulation for a fully developed channel flow at $Re = 3300$. The simple flow configuration allows a comparison free from numerical inaccuracies. The computed results prove that few of the considered forms exhibit a satisfactory agreement with the channel flow data. The model shows an improvement with respect to the existing formulations. Author

N91-23439*# National Aeronautics and Space Administration. Lewis Research Center, Cleveland, OH.

A SYSTEM-APPROACH TO THE ELASTOHYDRODYNAMIC LUBRICATION POINT-CONTACT PROBLEM

SANG GYU LIM and DAVID E. BREWE (Case Western Reserve Univ., Cleveland, OH.) 1991 17 p
Presented at the Annual Meeting of the Society of Tribologists and Lubrication Engineers, Montreal, Quebec, 29 Apr. - 2 May 1991

(Contract DA PROJ. 1L1-61101-AH-45; RTOP 505-63-5A)
(NASA-TM-104342; E-6116; NAS 1.15:104342; AVSCOM-TR-90-C-031; AD-A237671) Avail: NTIS HC/MF A03 CSCL 20/4

The classical EHL (elastohydrodynamic lubrication) point contact problem is solved using a new system-approach, similar to that introduced by Houpert and Hamrock for the line-contact problem. Introducing a body-fitted coordinate system, the troublesome free-boundary is transformed to a fixed domain. The Newton-Raphson method can then be used to determine the pressure distribution and the cavitation boundary subject to the Reynolds boundary condition. This method provides an efficient and rigorous way of solving the EHL point contact problem with the aid of a supercomputer and a promising method to deal with the transient EHL point contact problem. A typical pressure distribution and film thickness profile are presented and the minimum film thicknesses are compared with the solution of Hamrock and Dowson. The details of the cavitation boundaries for various operating parameters are discussed. Author

N91-24337*# National Aeronautics and Space Administration. Lewis Research Center, Cleveland, OH.

AN UNCONDITIONALLY STABLE RUNGE-KUTTA METHOD FOR UNSTEADY ROTOR-STATOR INTERACTION

RODRICK V. CHIMA and PHILIP C. E. JORGENSON In its Structural Integrity and Durability of Reusable Space Propulsion Systems p 237-246 Apr. 1989 Previously announced in IAA as A89-25180

Avail: NTIS HC/MF A12 CSCL 20/4

A quasi-three-dimensional analysis has been developed for unsteady rotor-stator interaction in turbomachinery. The analysis solves the unsteady Euler or thin-layer Navier-Stokes equations in a body-fitted coordinate system. It accounts for the effects of rotation, radius change, and stress-surface thickness. The Baldwin-Lomax eddy-viscosity model is used for turbulent flows. The equations are integrated in time using an explicit four-stage Runge-Kutta scheme with a constant time step. Implicit residual smoothing is used to increase the stability limit of the time-accurate computations. The scheme is described, and stability and accuracy analyses are given. Author

N91-24338*# National Aeronautics and Space Administration. Lewis Research Center, Cleveland, OH.

AVERAGE-PASSAGE FLOW MODEL DEVELOPMENT

JOHN J. ADAMCZYK, MARK L. CELESTINA, TIM A. BEACH, KEVIN KIRTLEY, and MARK BARNETT (United Technologies Research Center, East Hartford, CT.) In its Structural Integrity and Durability of Reusable Space Propulsion Systems p 247-251 Apr. 1989

Avail: NTIS HC/MF A12 CSCL 20/4

A 3-D model was developed for simulating multistage turbomachinery flows using supercomputers. This average passage flow model described the time averaged flow field within a typical passage of a bladed wheel within a multistage configuration. To date, a number of inviscid simulations were executed to assess the resolution capabilities of the model. Recently, the viscous terms associated with the average passage model were incorporated into the inviscid computer code along with an algebraic turbulence model. A simulation of a stage-and-one-half, low speed turbine was executed. The results of this simulation, including a comparison with experimental data, is discussed. Author

N91-24525*# National Aeronautics and Space Administration. Lewis Research Center, Cleveland, OH.

ADVANCES IN MODELING THE PRESSURE CORRELATION TERMS IN THE SECOND MOMENT EQUATIONS

TSAN-HSING SHIH, AAMIR SHABBIR, and JOHN L. LUMLEY (Cornell Univ., Ithaca, NY.) Jun. 1991 37 p
(Contract NAG1-954; NASA ORDER C-99066-6;

AF-AFOSR-0226-89; NSF DMS-88-14553; NSF MSM-86-11164)
(NASA-TM-104413; ICOMP-91-09; E-6241; NAS 1.15:104413;
CMOTT-91-03) Avail: NTIS HC/MF A03 CSCL 20/4

In developing turbulence models, various model constraints were proposed in an attempt to make the model equations more general (or universal). The most recent of these are the realizability principle, the linearity principle, the rapid distortion theory, and the material indifference principle. Several issues are discussed concerning these principles and special attention is paid to the realizability principle. Realizability (defined as the requirement of non-negative energy and Schwarz' inequality between any fluctuating quantities) is the basic physical and mathematical principle that any modeled equation should obey. Hence, it is the most universal, important and also the minimal requirement for a model equation to prevent it from producing unphysical results. The principle of realizability is described in detail, the realizability conditions are derived for various turbulence models, and the model forms are proposed for the pressure correlation terms in the second moment equations. Detailed comparisons of various turbulence models with experiments and direct numerical simulations are presented. As a special case of turbulence, the two dimensional two-component turbulence modeling is also discussed. Author

N91-24527* # National Aeronautics and Space Administration. Lewis Research Center, Cleveland, OH.

PARAMAGNETIC PROPELLANT ORIENTATION

R. C. HENDRICKS 1991 9 p Presented at the 27th Joint Propulsion Conference, Sacramento, CA, 24-26 Jun. 1991; sponsored by AIAA, SAE, and ASME
(Contract RTOP 505-62-52)

(NASA-TM-104390; E-6165; NAS 1.15:104390; AIAA PAPER 91-2325) Avail: NTIS HC/MF A02 CSCL 20/4

Deep space or low earth orbital propellant tanks require a fluid orientation system prior to engine firing or transfer. Some propellants such as cryogenic hydrogen, oxygen, and air are paramagnetic and respond to electromagnetic fields. A simple magnetic scheme is described for propellant orientation and a video tape presentation is provided that demonstrates some effects of magnetic fields on liquid air and oxygen in a low gravity simulator using the Leidenfrost phenomenon. When these Leidenfrost drops intersect the field lines, their flight paths are altered, some directly into the poles, some to the edges, and others move out of the field. Author

N91-24541* # National Aeronautics and Space Administration. Lewis Research Center, Cleveland, OH.

NAVIER-STOKES SIMULATION OF THE SUPERSONIC COMBUSTION FLOWFIELD IN A RAM ACCELERATOR

SHAYE YUNGSTER 1991 18 p Presented at the 27th Joint Propulsion Conference, Sacramento, CA, 24-27 Jun. 1991; sponsored by AIAA, SAE, ASME, and the American Society for Electrical Engineers Original contains color illustrations
(Contract NASA ORDER C-99066-G)

(NASA-TM-104439; ICOMP-91-10; E-6278; NAS 1.15:104439; AIAA PAPER 91-1916) Avail: NTIS HC/MF A03; 6 functional color pages CSCL 20/4

A computational study of the ram accelerator, a ramjet-in-tube device for accelerating projectiles to ultrahigh velocities, is presented. The analysis is performed using a fully implicit TVD scheme that efficiently solves the Reynolds-averaged Navier-Stokes equations and the species continuity equations associated with a finite rate combustion model. Previous analyses of this concept were based on inviscid assumptions. The present results indicate that viscous effects are of primary importance; in all the cases studied, shock-induced combustion always started in the boundary layer. The effects of Mach number, mixture composition, pressure, and turbulence are investigated for various configurations. Two types of combustion processes, one stable and the other unstable, were observed depending on the inflow conditions. In the unstable case, a detonation wave is formed, which propagates upstream and restarts the ram accelerator. In the stable case, a solution that converges to steady-state is obtained, in which the combustion wave remains stationary with

respect to the ram accelerator projectile. The possibility of stabilizing the detonation wave by means of a backward facing step is also investigated. In addition to these studies, two numerical techniques were tested. These two techniques are vector extrapolation to accelerate convergence, and a diagonal formulation that eliminates the expense of inverting large block matrices that arise in chemically reacting flows. Author

N91-24547* # National Aeronautics and Space Administration. Lewis Research Center, Cleveland, OH.

GROUND TESTING ON THE NONVENTED FILL METHOD OF ORBITAL PROPELLANT TRANSFER: RESULTS OF INITIAL TEST SERIES

DAVID J. CHATO 1991 32 p Presented at the 27th Joint Propulsion Conference, Sacramento, CA, 24-27 Jun. 1991; sponsored by AIAA, SAE, ASME, and the American Society for Electrical Engineers

(Contract RTOP 506-48-00)

(NASA-TM-104444; E-6284; NAS 1.15:104444; AIAA PAPER 91-2326) Avail: NTIS HC/MF A03 CSCL 20/4

The results are presented of a series of no-vent fill experiments conducted on a 175 cu ft flightweight hydrogen tank. The experiments consisted of the nonvented fill of the tankage with liquid hydrogen using two different inlet systems (top spray, and bottom spray) at different tank initial conditions and inflow rates. Nine tests were completed of which six filled in excess of 94 percent. The experiments demonstrated a consistent and repeatable ability to fill the tank in excess of 94 percent using the nonvented fill technique. Ninety-four percent was established as the high level cutoff due to requirements for some tank ullage to prevent rapid tank pressure rise which occurs in a tank filled entirely with liquid. The best fill was terminated at 94 percent full with a tank internal pressure less than 26 psia. Although the baseline initial tank wall temperature criteria was that all portions of the tank wall be less than 40 R, fills were achieved with initial wall temperatures as high as 227 R. Author

N91-24548* # National Aeronautics and Space Administration. Lewis Research Center, Cleveland, OH.

A NUMERICAL STUDY OF THE DIRECT CONTACT CONDENSATION ON A HORIZONTAL SURFACE

M. M. HASAN and C. S. LIN (Analex Corp., Fairview Park, OH.) 1991 11 p Presented at the 26th Thermophysics Conference, Honolulu, HI, 24-26 Jun. 1991; sponsored by AIAA

(Contract NAS3-25776; RTOP 506-48-00)

(NASA-TM-104432; E-6270; NAS 1.15:104432; AIAA PAPER 91-1307) Avail: NTIS HC/MF A03 CSCL 20/4

The results of a numerical study of the direct contact condensation on a slowly moving horizontal liquid surface are presented. The geometrical configuration and the input conditions used to obtain numerical solutions are representative to those of experiments of Celata et al. The effects of Prandtl number (Pr), inflow Reynolds number, and Richardson number on the condensation rate are investigated. Numerical predictions of condensation rate for laminar flow are in good agreement with experimental data. The effect of buoyancy on the condensation rate is characterized by Richardson number. A correlation based on the numerical solutions is developed to predict the average condensation Nusselt number in terms of Richardson number, Peclet number, and inflow Reynolds number. Author

N91-24549* # National Aeronautics and Space Administration. Lewis Research Center, Cleveland, OH.

SCALING ANALYSIS APPLIED TO THE NORVEX CODE DEVELOPMENT AND THERMAL ENERGY FLIGHT EXPERIMENT

J. RAYMOND LEE SKARDA, DAVID NAMKOONG, and DOUGLAS DARLING 1991 13 p Presented at the 26th Thermophysics Conference, Honolulu, HI, 24-26 Jun. 1991; sponsored by AIAA

(Contract RTOP 506-41-31)

(NASA-TM-104462; E-6303; NAS 1.15:104462; AIAA PAPER 91-1420) Avail: NTIS HC/MF A03 CSCL 20/4

A scaling analysis is used to study the dominant flow processes

that occur in molten phase change material (PCM) under 1 g and microgravity conditions. Results of the scaling analysis are applied to the development of the NORVEX (NASA Oak Ridge Ridge Void Experiment) computer program and the preparation of the Thermal Energy Storage (TES) flight experiment. The NORVEX computer program which is being developed to predict melting and freezing with void formation in a 1 g or microgravity environment of the PCM is described. NORVEX predictions are compared with the scaling and similarity results. The approach to be used to validate NORVEX with TES flight data is also discussed. Similarity and scaling show that the inertial terms must be included as part of the momentum equation in either the 1 g or microgravity environment (a creeping flow assumption is invalid). A $10(\text{exp } -4)$ environment was found to be a suitable microgravity environment for the proposed PCM. Author

N91-24550* National Aeronautics and Space Administration. Lewis Research Center, Cleveland, OH.
COMPARISON OF SMAC, PISO, AND ITERATIVE TIME-ADVANCING SCHEMES FOR UNSTEADY FLOWS
 SANG-WOOK KIM (Texas Univ., Arlington.) and THOMAS J. BENSON Jun. 1991 43 p
 (Contract RTOP 505-62-52)
 (NASA-TM-104406; E-6232; NAS 1.15:104406) Avail: NTIS HC/MF A03 CSCL 20/4

Calculations of unsteady flows using a simplified marker and cell (SMAC), a pressure implicit splitting of operators (PSIO), and an iterative time advancing scheme (ITA) are presented. A partial differential equation for incremental pressure is used in each time advancing scheme. Example flows considered are a polar cavity flow starting from rest and self-sustained oscillating flows over a circular and a square cylinder. For a large time step size, the SMAC and ITA are more strongly convergent and yield more accurate results than PSIO. The SMAC is the most efficient computationally. For a small time step size, the three time advancing schemes yield equally accurate Strouhal numbers. The capability of each time advancing scheme to accurately resolve unsteady flows is attributed to the use of new pressure correction algorithm that can strongly enforce the conservation of mass. The numerical results show that the low frequency of the vortex shedding is caused by the growth time of each vortex shed into the wake region. Author

N91-25351* National Aeronautics and Space Administration. Lewis Research Center, Cleveland, OH.
REVIEW AND TEST OF CHILLDOWN METHODS FOR SPACE-BASED CRYOGENIC TANKS
 DAVID J. CHATO and RAFAEL SANABRIA 1991 26 p
 Presented at the 27th Joint Propulsion Conference, Sacramento, CA, 24-27 Jun. 1991; sponsored by AIAA, SAE, ASME, and the American Society for Electrical Engineers
 (Contract RTOP 506-48-00)
 (NASA-TM-104458; E-6299; NAS 1.15:104458; AIAA PAPER 91-1843) Avail: NTIS HC/MF A03 CSCL 20/4

The literature for tank chilldown methods applicable to cryogenic tankage in the zero gravity environment of earth orbit is reviewed. One method is selected for demonstration in a ground based test. The method selected for investigation was the charge-hold-vent method which uses repeated injection of liquid slugs, followed by a hold to allow complete vaporization of the liquid and a vent of the tank to space vacuum to cool tankage to the desired temperature. The test was conducted on a 175 cubic foot, 2219 aluminum walled tank weighing 329 pounds, which was previously outfitted with spray systems to test nonvented fill technologies. To minimize hardware changes, a simple control-by-pressure scheme was implemented to control injected liquid quantities. The tank cooled from 440 R sufficiently in six charge-hold-vent cycles to allow a complete nonvented fill of the test tank. Liquid hydrogen consumed in the process is estimated at 32 pounds. Author

N91-25367* National Aeronautics and Space Administration. Lewis Research Center, Cleveland, OH.

CHARACTERIZATION OF FLOW IN A SCROLL DUCT Final Report, Nov. 1983 - Jan. 1985

E. K. BEGG and J. C. BENNETT Jan. 1985 45 p
 (Contract NAG3-484)

(NASA-CR-188612; NAS 1.26:188612) Avail: NTIS HC/MF A03 CSCL 20/4

A quantitative, flow visualization study was made of a partially elliptic cross section, inward curving duct (scroll duct), with an axial outflow through a vaneless annular cutlet. The working fluid was water, with a $Re(d)$ of 40,000 at the inlet to the scroll duct, this Reynolds number being representative of the conditions in an actual gas turbine scroll. Both still and high speed moving pictures of fluorescein dye injected into the flow and illuminated by an argon ion laser were used to document the flow. Strong secondary flow, similar to the secondary flow in a pipe bend, was found in the bottom half of the scroll within the first 180 degs of turning. The pressure field set up by the turning duct was strong enough to affect the inlet flow condition. At 90 degs downstream, the large scale secondary flow was found to be oscillatory in nature. The exit flow was nonuniform in the annular exit. By 270 degs downstream, the flow appeared unorganized with no distinctive secondary flow pattern. Large scale structures from the upstream core region appeared by 90 degs and continued through the duct to reenter at the inlet section. Author

N91-27487* National Aeronautics and Space Administration. Lewis Research Center, Cleveland, OH.

TURBULENT FLUID MOTION 2: SCALARS, VECTORS, AND TENSORS

ROBERT G. DEISSLER Jul. 1991 14 p
 (Contract RTOP 505-90-01)

(NASA-TM-103756; E-6012; NAS 1.15:103756) Avail: NTIS HC/MF A03 CSCL 20/4

The author shows that the sum or difference of two vectors is a vector. Similarly the sum of any two tensors of the same order is a tensor of that order. No meaning is attached to the sum of tensors of different orders, say $u(\text{sub } i) + u(\text{sub } ij)$; that is not a tensor. In general, an equation containing tensors has meaning only if all the terms in the equation are tensors of the same order, and if the same unreported subscripts appear in all the terms. These facts will be used in obtaining appropriate equations for fluid turbulence. With the foregoing background, the derivation of appropriate continuum equations for turbulence should be straightforward. Author

N91-27489* National Aeronautics and Space Administration. Lewis Research Center, Cleveland, OH.

VISUALIZATION TECHNIQUES TO EXPERIMENTALLY MODEL FLOW AND HEAT TRANSFER IN TURBINE AND AIRCRAFT FLOW PASSAGES

LOUIS M. RUSSELL and STEVEN A. HIPPENSTEELE
 Washington Jun. 1991 19 p Original contains color illustrations

(Contract RTOP 505-62-52)

(NASA-TM-4272; E-5811; NAS 1.15:4272) Avail: NTIS HC/MF A03; 7 functional color pages CSCL 20/4

Increased attention to fuel economy and increased thrust requirements have increased the demand for higher aircraft gas turbine engine efficiency through the use of higher turbine inlet temperatures. These higher temperatures increase the importance of understanding the heat transfer patterns which occur throughout the turbine passages. It is often necessary to use a special coating or some form of cooling to maintain metal temperatures at a level which the metal can withstand for long periods of time. Effective cooling schemes can result in significant fuel savings through higher allowable turbine inlet temperatures and can increase engine life. Before proceeding with the development of any new turbine it is economically desirable to create both mathematical and experimental models to study and predict flow characteristics and temperature distributions. Some of the methods are described used

34 FLUID MECHANICS AND HEAT TRANSFER

to physically model heat transfer patterns, cooling schemes, and other complex flow patterns associated with turbine and aircraft passages.
Author

N91-28538*# National Aeronautics and Space Administration. Lewis Research Center, Cleveland, OH.

CRYOGENIC TRANSFER OPTIONS FOR EXPLORATION MISSIONS

DAVID J. CHATO 1991 12 p Presented at the Conference on Advanced Space Exploration Initiative Technologies, Cleveland, OH, 4-6 Sep. 1991; cosponsored by AIAA and OAI (Contract RTOP 506-48-21) (NASA-TM-105197; E-6499; NAS 1.15:105197; AIAA PAPER 91-3541) Avail: NTIS HC/MF A03 CSCL 20/4

The literature of in-space cryogenic transfer is reviewed in order to propose transportation concepts to support the Space Exploration Initiative (SEI). Forty-nine references are listed and key findings are synopsized. An assessment of the current maturity of cryogenic transfer system technology is made. Although the settled transfer technique is the most mature technology, the No-Vent Fill technology is maturing rapidly. Future options for development of cryogenic transfer technology are also discussed.
Author

N91-29525*# National Aeronautics and Space Administration. Lewis Research Center, Cleveland, OH.

QUALITATIVE INVESTIGATION OF CRYOGENIC INJECTED SHOCK DISSIPATION

R. C. HENDRICKS 1991 8 p Presented at the Cryogenic Engineering Conference, Huntsville, AL, 11-14 Jun. 1991; sponsored by Univ. of Alabama at Huntsville, and NASA, Huntsville (Contract RTOP 505-62-52) (NASA-TM-105140; E-6244; NAS 1.15:105140) Avail: NTIS HC/MF A02 CSCL 20/4

The injection of fluid nitrogen into the flow discharged from a two-dimensional, ambient, static-temperature and static pressure Mach = 2.7 nitrogen flow tunnel was observed. A bow shock stands approximately one diameter off the end of the 3.2 mm o.d. x 1.6 mm i.d. injection tube placed directly into the tunnel exhaust. Cryogenic injection creates a high density region in the injected region and within the bow shock wake but the standoff distance remains unchanged. However as the temperature reaches a critical value the sharp shock interface begins to fade resembling the density gradient seen at the interface of a supercritical fluid and the shock interface begins to move into the supersonic stream. As the injection temperature decreases, the interface continues to move into the supersonic stream and becomes more diffuse; the shock interface can not be distinguished. The phenomena is completely reversible.
Author

N91-30461*# National Aeronautics and Space Administration. Lewis Research Center, Cleveland, OH.

RELATIONSHIP OF OPTICAL COATING ON THERMAL RADIATION CHARACTERISTICS OF NONISOTHERMAL CYLINDRICAL ENCLOSURES

JOSEPH F. BAUMEISTER Aug. 1991 20 p (Contract RTOP 505-62-00) (NASA-TM-104408; E-6234; NAS 1.15:104408) Avail: NTIS HC/MF A03 CSCL 20/4

A numerical ray tracing technique was applied to simulate radiation propagating from various non-isothermal cylindrical cavities to determine the effect of optical coating (surface emissivity). In general, the analysis showed that the optical coating and temperature within a cavity have a significant effect on emitted radiation based on cavity dimension. Temperature thresholds were found to exist where the same optical coating may either reduce or increase cavity performance (apparent emissivity). Parametric values of apparent emissivity results are presented over a wide range of variables to correlate cylindrical cavity radiation for non-uniform cavity emissivity values. A universal curve was developed to aid in selecting wall emissivity values for design considerations.
Author

N91-30462*# National Aeronautics and Space Administration. Lewis Research Center, Cleveland, OH.

VERIFICATION OF THE PROTEUS TWO-DIMENSIONAL NAVIER-STOKES CODE FOR FLAT PLATE AND PIPE FLOWS

JULIANNE M. CONLEY and PATRICK L. ZEMAN (Arnold Engineering Development Center, Arnold Air Force Station, TN.) 1991 9 p Presented at the 27th Joint Propulsion Conference, Sacramento, CA, 24-27 Jun. 1991; sponsored by AIAA, SAE, ASME, and ASEE Previously announced as A91-41678 (NASA-TM-105160; E-6449; NAS 1.15:105160; AIAA PAPER 91-2013) Avail: NTIS HC/MF A02 CSCL 20/4

The Proteus Navier-Stokes Code is evaluated for 2-D/axisymmetric, viscous, incompressible, internal, and external flows. The particular cases to be discussed are laminar and turbulent flows over a flat plate, laminar and turbulent developing pipe flows, and turbulent pipe flow with swirl. Results are compared with exact solutions, empirical correlations, and experimental data. A detailed description of the code set-up, including boundary conditions, initial conditions, grid size, and grid packing is given for each case.
Author

N91-30469*# National Aeronautics and Space Administration. Lewis Research Center, Cleveland, OH.

PARCHED ELASTOHYDRODYNAMIC LUBRICATION: INSTRUMENTATION AND PROCEDURE

BRYAN SCHRITZ, WILLIAM R. JONES, JR., JOSEPH PRAHL, and RALPH JANSEN (Case Western Reserve Univ., Cleveland, OH.) 1991 27 p Presented at the Annual Meeting of the Society of Tribologists and Lubrication Engineers, Philadelphia, PA, 4-7 May 1992

(Contract RTOP 505-63-1A) (NASA-TM-104426; E-6259; NAS 1.15:104426) Avail: NTIS HC/MF A03 CSCL 20/4

A counter rotating bearing rig was designed and constructed to study transient elastohydrodynamic lubrication phenomena. New instrumentation is described and test procedures are documented. Ball and race speed measurement systems and the capacitance (film thickness) measurement system were upgraded. Methods for measuring bearing torque and race temperatures were implemented.
Author

N91-30472*# National Aeronautics and Space Administration. Lewis Research Center, Cleveland, OH.

A LASER-INDUCED HEAT FLUX TECHNIQUE FOR CONVECTIVE HEAT TRANSFER MEASUREMENTS IN HIGH SPEED FLOWS

A. R. PORRO, T. G. KEITH, JR. (Ohio Aerospace Inst., Brook Park.), and W. R. HINGST 1991 12 p Presented at the 14th International Congress on Instrumentation in Aerospace Simulation Facilities, Rockville, MD, 27-31 Oct. 1991; sponsored by IEEE Aerospace and Electronics Systems Society (Contract RTOP 505-62-52)

(NASA-TM-105177; E-6473; NAS 1.15:105177) Avail: NTIS HC/MF A03 CSCL 20/4

A technique is developed to measure the local convective heat transfer coefficient on a model surface in a supersonic flow field. The technique uses a laser to apply a discrete local heat flux at the model test surface, and an infrared camera system determines the local temperature distribution due to the heating. From this temperature distribution and an analysis of the heating process, a local convective heat transfer coefficient is determined. The technique was used to measure the local surface convective heat transfer coefficient distribution on a flat plate at nominal Mach numbers of 2.5, 3.0, 3.5, and 4.0. The flat plate boundary layer initially was laminar and became transitional in the measurement region. The experimentally determined convective heat transfer coefficients were generally higher than the theoretical predictions for flat plate laminar boundary layers. However, the results indicate that this nonintrusive optical measurement technique has the potential to measure surface convective heat transfer coefficients in high speed flow fields.
Author

N91-30473*# National Aeronautics and Space Administration. Lewis Research Center, Cleveland, OH.

A QUALITATIVE VIEW OF CRYOGENIC FLUID INJECTION INTO HIGH SPEED FLOWS

R. C. HENDRICKS, J. SCHLUMBERGER, and M. PROCTOR
1991 8 p Presented at the 18th International Congress of Refrigeration, Montreal, 10-17 Aug. 1991

(Contract RTOP 505-62-52)

(NASA-TM-105139; E-6410; NAS 1.15:105139) Avail: NTIS

HC/MF A02 CSCL 20/4

The injection of supercritical pressure, subcritical temperature fluids, into a 2-D, ambient, static temperature and static pressure supersonic tunnel and free jet supersonic nitrogen flow field was observed. Observed patterns with fluid air were the same as those observed for fluid nitrogen injected into the tunnel at 90 deg to the supersonic flow. The nominal injection pressure was of 6.9 MPa and tunnel Mach number was 2.7. When injected directly into and opposing the tunnel exhaust flow, the observed patterns with fluid air were similar to those observed for fluid nitrogen but appeared more diffusive. Cryogenic injection creates a high density region within the bow shock wake but the standoff distance remains unchanged from the gaseous value. However, as the temperature reaches a critical value, the shock faded and advanced into the supersonic stream. For both fluids, nitrogen and air, the phenomena was completely reversible. Author

N91-30476*# National Aeronautics and Space Administration. Lewis Research Center, Cleveland, OH.

CALCULATION OF A CIRCULAR JET IN CROSSFLOW WITH A MULTIPLE-TIME-SCALE TURBULENCE MODEL

S.-W. KIM (Texas Univ., Arlington.) and T. J. BENSON Jul. 1991 32 p

(Contract NCC3-180; RTOP 505-62-52)

(NASA-TM-104343; E-6117; NAS 1.15:104343) Avail: NTIS

HC/MF A03 CSCL 20/4

Numerical calculation of a three dimensional turbulent flow of a jet in a crossflow using a multiple time scale turbulence model is presented. The turbulence in the forward region of the jet is in a stronger inequilibrium state than that in the wake region of the jet, while the turbulence level in the wake region is higher than that in the front region. The calculated flow and the concentration fields are in very good agreement with the measured data, and it indicated that the turbulent transport of mass, concentration, and momentum is strongly governed by the inequilibrium turbulence. The capability of the multiple time scale turbulence model to resolve the inequilibrium turbulence field is also discussed. Author

N91-31597*# National Aeronautics and Space Administration. Lewis Research Center, Cleveland, OH.

A CRITICAL COMPARISON OF TWO-EQUATION TURBULENCE MODELS

N. J. LANG and T. H. SHIH Sep. 1991 35 p

(Contract NASA ORDER C-99066-G)

(NASA-TM-105237; ICOMP-91-15; E-6562; NAS 1.15:105237;

CMOTT-91-05) Avail: NTIS HC/MF A03 CSCL 20/4

Several two-equation models were proposed and tested against benchmark flows by various researchers. For each study, different numerical methods or codes were used to obtain the results which were reported to be an improvement over other models. However, these comparisons may be overshadowed by the different numerical schemes used to obtain the results. With this in mind, several existing two-equation turbulence models, including k-epsilon, k-tau, k-omega, and q-omega models, are implemented into a common flow solver code for near wall turbulent flows. The quality of each model is based on several criteria, including robustness and accuracy of predicting the turbulent quantities. Author

N91-32440*# National Aeronautics and Space Administration. Lewis Research Center, Cleveland, OH.

A LASER VELOCIMETER INVESTIGATION OF THE NORMAL SHOCK-WAVE BOUNDARY LAYER INTERACTION Ph.D. Thesis, Toledo Univ.

RANDALL M. CHRISS Sep. 1991 123 p

(Contract RTOP 505-62-52)

(NASA-TM-105201; E-6504; NAS 1.15:105201) Avail: NTIS

HC/MF A06 CSCL 20/4

Nonintrusive 3-D measurements were made of a normal shock wave/turbulent boundary layer interaction. The measurements were made through a quadrant of a square test section of a continuous flow supersonic wind tunnel in which a normal shock wave had been stabilized. Two dimensional measurements were made throughout the interaction region while 3-D measurements were made near the corner in the vicinity of the shock where 3-D flow effects were expected to be significant. Laser Doppler velocimetry, surface static pressure measurements, and flow visualization techniques were used for two freestream nominal Mach number test cases: 1.6 and 1.3. No turbulence information was obtained. The mean velocity measurements were converted to Mach number by recording the wind tunnel total temperature. Some shock oscillation was present during both of the test cases. After startup of the wind tunnel, the shock oscillated with an amplitude of approx. + or - 1 cm, however, after reaching steady condition, the shock oscillation amplitude was greatly reduced, as evidenced by the laser velocimeter results. The Mach 1.3 test case resulted in a nearly uniform flow without secondary shock waves and with no or very isolated corner separation. Author

N91-32458*# National Aeronautics and Space Administration. Lewis Research Center, Cleveland, OH.

RESONANT TRIAD IN BOUNDARY-LAYER STABILITY. PART 1: FULLY NONLINEAR INTERACTION

REDA R. MANKBADI Sep. 1991 57 p

(NASA-TM-105208; E-5233-1-PT-1; NAS 1.15:105208) Avail:

NTIS HC/MF A04 CSCL 20/4

A first principles theory is developed to study the nonlinear spatial evolution of a near-resonance triad of instability waves in boundary layer transition. This triad consists of a plane wave at fundamental frequency and a pair of symmetrical, oblique waves at the subharmonic frequency. A low frequency, high Reynolds number asymptotic scaling leads to a distinct critical layer where nonlinearity first becomes important; the development of the triad's waves is determined by the critical layer's nonlinear, viscous dynamics. The resulting theory is fully nonlinear in that all nonlinearly generated oscillatory and nonoscillatory components are accounted for. The presence of the plane wave initially causes exponential of exponential growth of the oblique waves. However, the plane wave continues to follow the linear theory, even when the oblique waves' amplitude attains the same order of magnitude as that of the plane wave. A fully interactive stage then comes into effect when the oblique waves exceed a certain level compared to that of the plane wave. The oblique waves react back on the fundamental, slowing its growth rate. The oblique waves' saturation results from their self-interaction - a mechanism that does not require the presence of the plane wave. The oblique waves' saturation level is independent of their initial level, but decreases as the obliqueness angle increases. Author

N91-32459*# National Aeronautics and Space Administration. Lewis Research Center, Cleveland, OH.

RESONANT TRIAD IN BOUNDARY-LAYER STABILITY. PART 2: COMPOSITE SOLUTION AND COMPARISON WITH OBSERVATIONS

REDA R. MANKBADI Sep. 1991 57 p

(NASA-TM-105209; E-6045-1-PT-2; NAS 1.15:105209) Avail:

NTIS HC/MF A04 CSCL 20/4

Here, numerical results are computed from an asymptotic near-resonance triad analysis. The analysis considers a resonant triad of instability waves consisting of a plane fundamental wave and a pair of symmetrical oblique subharmonic waves. The relevant scaling ensures that nonlinearity is confined to a distinct critical layer. The analysis is first used to form a composite solution that accounts for both the flow divergence and nonlinear effects. It is shown that the backreaction on the plane Tollmien Schlichting (TS) fundamental wave, although fully accounted for, is of little significance. The observed enhancement at the fundamental

frequency disturbance is not in the plane TS wave, but is caused by nonlinearly generated waves at the fundamental frequency that result from nonlinear interactions in the critical layer. The saturation of the oblique waves is caused by their self-interaction. The nonlinear phase-locking phenomenon, the location of resonance with respect to the neutral stability curve, low frequency effects, detuning in the streamwise wave numbers, and nonlinear distortion of the mode shapes are discussed. Nonlinearity modifies the initially two dimensional Blasius profile into a fuller one with spanwise periodicity. The interactions at a wide range of unstable spanwise wave numbers are considered, and the existence of a preferred spanwise wave number is explained by means of the vorticity distribution in the critical layer. Besides presenting novel features of the phenomena and explaining the delicate mechanisms of the interactions, the results of the theory are in excellent agreement with experimental and numerical observations for all stages of the development and for various input parameters. Author

N91-32460* National Aeronautics and Space Administration. Lewis Research Center, Cleveland, OH.

A K-EPSILON MODELING OF NEAR WALL TURBULENCE

Z. YANG and T. H. SHIH Sep. 1991 14 p Presented at the Fourth International Symposium on Computational Fluid Dynamics, Davis, CA, 9-12 Sep. 1991

(Contract NASA ORDER C-99066-G)

(NASA-TM-105238; E-6563; ICOMP-91-16; CMOTT-91-06; NAS 1.15:105238) Avail: NTIS HC/MF A03 CSCL 20/4

A k-epsilon model is proposed for turbulent bounded flows. In this model, the turbulent velocity scale and turbulent time scale are used to define the eddy viscosity. The time scale is shown to be bounded from below by the Kolmogorov time scale. The dissipation equation is reformulated using the time scale, removing the need to introduce the pseudo-dissipation. A damping function is chosen such that the shear stress satisfies the near wall asymptotic behavior. The model constants used are the same as the model constants in the commonly used high turbulent Reynolds number k-epsilon model. Fully developed turbulent channel flows and turbulent boundary layer flows over a flat plate at various Reynolds numbers are used to validate the model. The model predictions were found to be in good agreement with the direct numerical simulation data. Author

35

INSTRUMENTATION AND PHOTOGRAPHY

Includes remote sensors; measuring instruments and gages; detectors; cameras and photographic supplies; and holography.

A91-13046* National Aeronautics and Space Administration. Lewis Research Center, Cleveland, OH.

OPTICAL MEASUREMENT OF UNDUCTED FAN BLADE DEFLECTIONS

A. P. KURKOV (NASA, Lewis Research Center, Cleveland, OH) ASME, Transactions, Journal of Turbomachinery (ISSN 0889-504X), vol. 112, Oct. 1990, p. 751-758. Previously announced in STAR as N88-29142. refs

(ASME PAPER 89-GT-298) Copyright

A nonintrusive optical method for measuring unducted fan (or propeller) blade deflections is described and evaluated. The measurement does not depend on blade surface reflectivity. Deflection of a point at the leading edge and a point at the trailing edge in a plane nearly perpendicular to the pitch axis is obtained with a single light beam generated by a low-power, helium-neon laser. Quantitative analyses are performed from taped signals on a digital computer. Averaging techniques are employed to reduce random errors. Measured static deflections from a series of high-speed wind tunnel tests of a counterrotating unducted fan model are compared with available, predicted deflections, which are also used to evaluate systematic errors. Author

A91-14462* National Aeronautics and Space Administration. Lewis Research Center, Cleveland, OH.

PDCR BASED HIGH TEMPERATURE STATIC STRAIN GAGE

JIH-FEN LEI (NASA, Lewis Research Center; Sverdrup Technology, Inc., Cleveland, OH) and W. D. WILLIAMS (NASA, Lewis Research Center, Cleveland, OH) AIAA, International Aerospace Planes Conference, 2nd, Orlando, FL, Oct. 29-31, 1990. 8 p. refs (AIAA PAPER 90-5236) Copyright

The program at NASA Lewis Research Center to develop a high temperature static strain gage system for the hypersonic vehicle and turbine engine research has emphasized a palladium-13 wt pct chromium (PdCr) alloy. Gages made from this alloy are being developed in both fine wire and thin film form. The wire gage system had platinum wire as a temperature compensator and was coated with a special alumina and zirconia mixture overcoat. This PdCr compensated wire gage responded linearly to the imposed strain to at least 1000 microstrain. The apparent strain varied within 300 microstrain from room temperature to 800 C with a reproducibility within 50 microstrain between thermal cycles to 800 C. The sputtered thin film PdCr strain gage, whose size was 8 x 8 mm and 10 microns thick, has demonstrated the possibility of extending the use of the PdCr strain gage to a temperature of approximately 1000 C. Author

A91-19577* Aurora Optics, Inc., Blue Bell, PA.

FIBER OPTIC PHOTOELASTIC PRESSURE SENSOR FOR HIGH TEMPERATURE GASES

LAURENCE N. WESSON (Aurora Optics, Inc., Blue Bell, PA), ALEX S. REDNER (Strainoptic Technologies, Inc., North Wales, PA), and ROBERT J. BAUMBICK (NASA, Lewis Research Center, Cleveland, OH) IN: Fiber optic and laser sensors VII; Proceedings of the Meeting, Boston, MA, Sept. 5-7, 1989. Bellingham, WA, Society of Photo-Optical Instrumentation Engineers, 1990, p. 270-279. refs

Copyright

A novel fiber optic pressure sensor based on the photoelastic effects has been developed for extremely high temperature gases. At temperatures varying from 25 to 650 C, the sensor experiences no change in the peak pressure of the transfer function and only a 10 percent drop in dynamic range. Refinement of the sensor has resulted in an optoelectronic interface and processor software which can calculate pressure values within 1 percent of full scale at any temperature within the full calibrated temperature range. C.D.

A91-19581* National Aeronautics and Space Administration. Lewis Research Center, Cleveland, OH.

SILICON-ETALON FIBER-OPTIC TEMPERATURE SENSOR

GLENN BEHEIM (NASA, Lewis Research Center, Cleveland, OH), KLAUS FRITSCH (John Carroll University, Cleveland, OH), JOSEPH M. FLATICO, and MASSOOD TABIB AZAR (Case Western Reserve University, Cleveland, OH) IN: Fiber optic and laser sensors VII; Proceedings of the Meeting, Boston, MA, Sept. 5-7, 1989. Bellingham, WA, Society of Photo-Optical Instrumentation Engineers, 1990, p. 504-511. Previously announced in STAR as N90-13381. refs

Copyright

A temperature sensor is described which consists of a silicon etalon that is sputtered directly onto the end of an optical fiber. A two-layer protective cap structure is used to improve the sensor's long-term stability. The sensor's output is wavelength encoded to provide a high degree of immunity from cable and connector effects. This sensor is extremely compact and potentially inexpensive. Author

A91-19582* National Aeronautics and Space Administration. Lewis Research Center, Cleveland, OH.

COMPENSATION FOR EFFECTS OF AMBIENT TEMPERATURE ON RARE-EARTH DOPED FIBER OPTIC THERMOMETER

G. ADAMOVSKY, J. L. SOTOMAYOR, M. J. KRASOWSKI (NASA, Lewis Research Center, Cleveland, OH), and J. G. EUSTACE (John Carroll University, Cleveland, OH) IN: Fiber optic and laser sensors VII; Proceedings of the Meeting, Boston, MA, Sept. 5-7, 1989.

Bellingham, WA, Society of Photo-Optical Instrumentation Engineers, 1990, p. 521-530. Previously announced in STAR as N89-27998. refs
(Contract NAG3-984)
Copyright

Variations in ambient temperature have a negative effect on the performance of any fiber optic sensing system. A change in ambient temperature may alter the design parameters of fiber optic cables, connectors, sources, detectors, and other fiber optic components and eventually the performance of the entire system. The thermal stability of components is especially important in a system which employs intensity modulated sensors. Several referencing schemes have been developed to account for the variable losses that occur within the system. However, none of these conventional compensating techniques can be used to stabilize the thermal drift of the light source in a system based on the spectral properties of the sensor material. The compensation for changes in ambient temperature becomes especially important in fiber optic thermometers doped with rare earths. Different approaches to solving this problem are searched and analyzed.

Author

A91-19604* National Aeronautics and Space Administration. Lewis Research Center, Cleveland, OH.

PARTICLE IMAGE FIELDS AND PARTIAL COHERENCE

ROBERT RUBINSTEIN (NASA, Lewis Research Center; Sverdrup Technology, Inc., Middleburg Heights, OH) and PAUL S. GREENBERG (NASA, Lewis Research Center, Cleveland, OH) Applied Optics (ISSN 0003-6935), vol. 29, Dec. 10, 1990, p. 5282-5291. refs

Copyright

The accuracy of Young's fringe method for reducing velocity field data is compromised by a spatially incoherent background field which originates in the random locations of the seeding particles. The probability density function for the spatial frequency cutoff of this background is derived as a function of the particle count, the distribution governing the power in each frequency interval is derived, and conditions are found under which the Van Cittert-Zernike theorem applies. The background field resembles the far field of a partially coherent source in the high particle count limit, but departs significantly at low and moderate counts.

Author

A91-23005* National Aeronautics and Space Administration. Lewis Research Center, Cleveland, OH.

A FIBER-OPTIC CURRENT SENSOR FOR AEROSPACE APPLICATIONS

RICHARD L. PATTERSON (NASA, Lewis Research Center, Cleveland, OH), A. H. ROSE, D. TANG, and G. W. DAY (NIST, Boulder, CO) IEEE Aerospace and Electronic Systems Magazine (ISSN 0885-8985), vol. 5, Dec. 1990, p. 10-14. Research supported by NASA, Los Alamos National Laboratory, and DNA. Previously announced in STAR as N90-22773. refs

A robust, accurate, broadband, alternating current sensor using fiber optics is being developed for space applications at power frequencies as high as 20 kHz. It can also be used in low and high voltage 60-Hz terrestrial power systems and in 400-Hz aircraft systems. It is intrinsically electromagnetic interference (EMI) immune and has the added benefit of excellent isolation. The sensor uses the Faraday effect in optical fiber and standard polarimetric measurements to sense electrical current. The primary component of the sensor is a specially treated coil of single-mode optical fiber, through which the current carrying conductor passes. Improved precision is accomplished by temperature compensation by means of signals from a novel fiber-optic temperature sensor embedded in the sensing head. The technology used in the sensor is examined and the results of precision tests conducted at various temperatures within the wide operating range are given. The results of early EMI tests are also given.

Author

A91-28968* National Aeronautics and Space Administration. Lewis Research Center, Cleveland, OH.

FIBER OPTIC PHASE STEPPING SYSTEM FOR INTERFEROMETRY

CAROLYN R. MERCER and GLENN BEHEIM (NASA, Lewis Research Center, Cleveland, OH) Applied Optics (ISSN 0003-6935), vol. 30, March 1, 1991, p. 729-734. refs
Copyright

A closed loop phase control system using an all-fiber optical configuration has been developed for use in phase-stepping interferometry. This system drives the relative phase of two interfering beams through a sequence of $\pi/2$ rad increments so that the initial relative phase of these beams can be determined. This phase-stepping system uses optical fibers to provide spatially uniform phase steps from a flexible, easily aligned optical configuration. In addition, this system uses phase feedback to eliminate phase modulator errors and to compensate for phase drifts caused by environmental disturbances.

Author

A91-30371* National Aeronautics and Space Administration. Lewis Research Center, Cleveland, OH.

USE OF ROTATING PINHOLES AND RETICLES FOR CALIBRATION OF CLOUD DROPLET INSTRUMENTATION

EDWARD A. HOVENAC (NASA, Lewis Research Center; Sverdrup Technology, Inc., Cleveland, OH) and E. DAN HIRLEMAN (Arizona State University, Tempe) Journal of Atmospheric and Oceanic Technology (ISSN 0739-0572), vol. 8, Feb. 1991, p. 166-171. refs

Copyright

Calibration devices for the Forward Scattering Spectrometer Probe (FSSP) and the Optical Array Probe (OAP) were developed. The device used with the FSSP is a rotating pinhole calibrator. It utilizes light diffracted by a pinhole of a known diameter to simulate scattered light from a water droplet. This device can be used to calibrate the FSSP, measure the FSSP's optical collection angles and for instrument alignment and troubleshooting. The device used with the OAP is a rotating reticle calibrator. Chrome disks of a known diameter on the reticle are used for calibration of the OAP and for determining the OAP's response to out-of-focus particles in the probe volume.

Author

A91-30634* Aerojet-General Corp., Sacramento, CA.

DEVELOPMENT OF A FABRY-PEROT INTERFEROMETER FOR ROCKET ENGINE PLUME MONITORING

R. L. BICKFORD (Aerojet, Propulsion Div., Sacramento, CA), D. B. DUNCAN (Duncan Technologies, Auburn, CA), and G. MADZSAR (NASA, Lewis Research Center, Cleveland, OH) IN: Annual Health Monitoring Conference for Space Propulsion Systems, 2nd, Cincinnati, OH, Nov. 14, 15, 1990, Proceedings. Cincinnati, OH, University of Cincinnati, 1990, p. 160-168. (Contract NAS3-25624)

Copyright

The development of a lightweight, compact, high-resolution Fabry-Perot interferometer (FPI) based spectrometer capable of detecting the spectral signatures of eroding engine components during test and/or flight operations is discussed. FPI based spectrometers will be designed to be smaller and lighter than grating or prism type devices and to provide greater wavelength resolving capability. The FPI system seeks to combine the features of high line resolution, active background discrimination, smart digital signal processing, and rocket engine flight capability. The design, fabrication, and test of a breadboard FPI spectrometer have been completed and the breadboard instrument has clearly demonstrated the viability of the approach. The breadboard instrument design and test results are also presented.

L.K.S.

A91-30649* National Aeronautics and Space Administration. Lewis Research Center, Cleveland, OH.

HEAT FLUX MEASUREMENT IN SSME TURBINE BLADE TESTER

CURT H. LIEBERT (NASA, Lewis Research Center, Cleveland, OH) IN: Annual Health Monitoring Conference for Space

35 INSTRUMENTATION AND PHOTOGRAPHY

Propulsion Systems, 2nd, Cincinnati, OH, Nov. 14, 15, 1990, Proceedings. Cincinnati, OH, University of Cincinnati, 1990, p. 439-455. Previously announced in STAR as N91-11205. refs

Surface heat flux values were measured in the turbine blade thermal cycling tester located at NASA-Marshall. This is the first time heat flux has been measured in a space shuttle main engine turbopump environment. Plots of transient and quasi-steady state heat flux data over a range of about 0 to 15 MW/sq m are presented. Data were obtained with a miniature heat flux gage device developed at NASA-Lewis. The results from these tests are being incorporated into turbine design models. Also, these gages are being considered for airfoil surface heat flux measurement on turbine vanes mounted in SSME turbopump test bed engine nozzles at Marshall. Heat flux effects that might be observed on degraded vanes are discussed. Author

A91-30652* National Aeronautics and Space Administration. Lewis Research Center, Cleveland, OH.

VIBRATIONAL TESTING OF OPTICAL FIBER CONNECTOR JOINTS

AMY L. SOVIE and GEORGE C. MADZSAR (NASA, Lewis Research Center, Cleveland, OH) IN: Annual Health Monitoring Conference for Space Propulsion Systems, 2nd, Cincinnati, OH, Nov. 14, 15, 1990, Proceedings. Cincinnati, OH, University of Cincinnati, 1990, p. 508-520. Previously announced in STAR as N91-14829.

An experimental study was performed to determine the effects of vibration on the propagation of light through SMA- and ST-type fiber-optic connectors. A multimode, fiber-optic link was vibrated from 0 to 10,000 Hz at a constant peak acceleration along the connector transverse and longitudinal axes. All other environmental parameters were ambient. Transfer characteristics through the connection were examined as a function of vibrational frequency using both laser and light-emitting diode (LED) light to illuminate the system. Slight differences in operation between the SMA and ST connectors were observed with no appreciative attenuation as a result of vibration. Vibration did cause constant-amplitude input light to be modulated in the connector; however, the amplitude of vibration-induced noise was less than 3 standard deviations from the mean. Author

A91-38006* National Aeronautics and Space Administration. Lewis Research Center, Cleveland, OH.

A FIBER-OPTIC CURRENT SENSOR FOR AEROSPACE APPLICATIONS

RICHARD L. PATTERSON (NASA, Lewis Research Center, Cleveland, OH), A. H. ROSE, D. TANG, and G. W. DAY (NIST, Boulder, CO) IN: IECEC-90; Proceedings of the 25th Intersociety Energy Conversion Engineering Conference, Reno, NV, Aug. 12-17, 1990. Vol. 1. New York, American Institute of Chemical Engineers, 1990, p. 500-504. Research supported by NASA, Los Alamos National Laboratory, and DNA. refs

A robust, accurate, broadband, alternating current sensor using fiber optics is being developed for space applications at power frequencies as high as 20 kHz. It can also be used in low- and high-voltage 60-Hz terrestrial power systems and in 400-Hz aircraft systems. It is intrinsically EMI (electromagnetic interference) immune and has the added benefit of excellent isolation. The sensor uses the Faraday effect in optical fiber and standard polarimetric measurements to sense electrical current. The primary component of the sensor is a specially treated coil of single-mode optical fiber, through which the current carrying conductor passes. Improved precision is accomplished by temperature compensation by means of signals from a fiber-optic temperature sensor embedded in the sensing head. The authors report on the technology contained in the sensor and also relate the results of precision tests conducted at various temperatures within the wide operating range. The results of early EMI tests are shown. I.E.

A91-38498* National Aeronautics and Space Administration. Lewis Research Center, Cleveland, OH.

TWO-DIMENSIONAL PARTICLE DISPLACEMENT TRACKING IN PARTICLE IMAGING VELOCIMETRY

MARK P. WERNET (NASA, Lewis Research Center, Cleveland, OH) Applied Optics (ISSN 0003-6935), vol. 30, May 10, 1991, p. 1839-1846. refs

Copyright

A new particle imaging velocimetry data acquisition and analysis system, which is an order of magnitude faster than any previously proposed system, has been constructed and tested. The new particle displacement tracking (PDT) system is an all electronic technique employing a video camera and a large memory buffer frame-grabber board. Using a simple encoding scheme, a time sequence of single exposure images is time-coded into a single image and then processed to track particle displacements and determine two-dimensional velocity vectors. Use of the PDT technique in a counterrotating vortex flow produced over 1100 velocity vectors in 110 s when processed on an 80386 PC.

Author

A91-41921* Varian Associates, Palo Alto, CA.

TEMPERATURE COEFFICIENTS OF MULTIJUNCTION SOLAR CELLS

G. F. VIRSHUP, B.-C. CHUNG, M. LADLE RISTOW, M. S. KURYLA (Varian Research Center, Palo Alto, CA), and D. BRINKER (NASA, Lewis Research Center, Cleveland, OH) IN: IEEE Photovoltaic Specialists Conference, 21st, Kissimmee, FL, May 21-25, 1990, Conference Record. Vol. 1. New York, Institute of Electrical and Electronics Engineers, Inc., 1990, p. 336-338.

Copyright

Temperature coefficients measured in solar simulators with those measured under AM0 solar illumination are compared to illustrate the challenges in making these measurements. It is shown that simulator measurements of the short-circuit current ($\Delta J_{sc}/\Delta T$) are inaccurate due to the mismatch between the solar spectrum and the simulators at the bandgaps of the solar cells. Especially susceptible to error is the $\Delta J_{sc}/\Delta T$ of cells which are components in monolithic multijunction solar cells, such as GaAs filtered by 1.93-eV AlGaAs, which has an AM0 coefficient of 6.82 micro-A/sq cm/deg C, compared to a Xenon simulator coefficient of 22.2 micro-A/sq cm/deg C. I.E.

A91-42849* National Aeronautics and Space Administration. Lewis Research Center, Cleveland, OH.

INVERSE PHOTOELECTRON SPECTROMETER WITH MAGNETICALLY FOCUSED ELECTRON GUN

ISAY L. KRAINSKY (NASA, Lewis Research Center, Cleveland, OH) Review of Scientific Instruments (ISSN 0034-6748), vol. 62, July 1991, p. 1746-1748. refs

Copyright

An inverse photoelectron spectrometer is described which is based on the design of a magnetically focused low energy electron gun. The magnetic lens extends its field over a relatively large segment of the electron trajectory, which could provide a better focusing effect on a high-current-density low-velocity electron beam, providing the magnetic field in the vicinity of the target is reduced sufficiently to preserve the collinearity of the beam. In order to prove the concept, ray tracing is conducted using the Herrmannsfeldt program for solving electron trajectories in electrostatic and magnetostatic focusing systems. The program allows the calculation of the angles of the electron trajectories with the z axis, at the target location. The results of the ray-tracing procedure conducted for this gun are discussed. Some of the advantages of the magnetic focusing are also discussed. S.A.V.

A91-44214* National Aeronautics and Space Administration. Lewis Research Center, Cleveland, OH.

AN EXPERIMENTAL TRACE GAS INVESTIGATION OF FLUID TRANSPORT AND MIXING IN A CIRCULAR-TO-RECTANGULAR TRANSITION DUCT

B. A. REICHERT, W. R. HINGST (NASA, Lewis Research Center, Cleveland, OH), and T. H. OKIISHI (Iowa State University of Science and Technology, Ames) AIAA, SAE, ASME, and ASEE, Joint Propulsion Conference, 27th, Sacramento, CA, June 24-26, 1991. 13 p. refs

(AIAA PAPER 91-2370) Copyright

An ethylene trace gas technique was used to map out fluid transport and mixing within a circular-to-rectangular transition duct. Ethylene gas was injected at several points in a cross stream plane upstream of the transition duct. Ethylene concentration contours were determined at several cross stream measurement planes spaced axially within the duct. The flow involved a uniform inlet flow at a Mach number level of 0.5. Statistical analyses were used to quantitatively interpret the trace gas results. Also, trace gas data were considered along with aerodynamic and surface flow visualization results to ascertain transition duct flow phenomena. Convection of wall boundary layer fluid by vortices produced regions of high total pressure loss in the duct. The physical extent of these high loss regions is governed by turbulent diffusion. Author

A91-44633* Akron Univ., OH.

FLOW VISUALIZATION IN A SIMULATED BRUSH SEAL

M. J. BRAUN, V. CANACCI (Akron, University, OH), and R. C. HENDRICKS (NASA, Lewis Research Center, Cleveland, OH) ASME, International Gas Turbine and Aeroengine Congress and Exposition, 35th, Brussels, Belgium, June 11-14, 1990. 8 p. refs (ASME PAPER 90-GT-217)

A method to visualize and characterize the complex flow fields in simulated brush seals is presented. The brush seal configuration was tested in a water and then in an oil tunnel. The visualization procedure revealed typical regions that are rivering, jetting, vortical or lateral flows and exist upstream, downstream or within the seal. Such flows are engendered by variations in fiber void that are spatial and temporal and affect changes in seal leakage and stability. While the effects of interface motion for linear or cylindrical configurations have not been considered herein, it is believed that the observed flow fields characterize flow phenomenology in both circular and linear brush seals. The axial pressure profiles upstream, across and downstream of the brush in the oil tunnel have been measured under a variety of inlet pressure conditions and the ensuing pressure maps are presented and discussed. Author

A91-45786* National Aeronautics and Space Administration. Lewis Research Center, Cleveland, OH.

LASER INTERFEROMETRIC MEASUREMENT OF ION ELECTRODE SHAPE AND CHARGE EXCHANGE EROSION

GREGORY S. MACRAE and CAROLYN R. MERCER (NASA, Lewis Research Center, Cleveland, OH) AIAA, SAE, ASME, and ASEE, Joint Propulsion Conference, 27th, Sacramento, CA, June 24-26, 1991. 17 p. refs (AIAA PAPER 91-2121) Copyright

A novel projected fringe profilometry system was applied to surface contour measurements of an accelerator electrode from an ion thruster. The system permitted noncontact, nondestructive evaluation of the fine and gross structure of the electrode. A 3D surface map of a dished electrode was generated without altering the electrode surface. The same system was used to examine charge exchange erosion pits near the periphery of the electrode to determine the depth, location, and volume of material lost. This electro-optical measurement system allowed rapid nondestructive digital data acquisition coupled with automated computer data-processing. In addition, variable sensitivity allowed both coarse and fine measurements of objects having various surface finishes. Author

A91-45804* National Aeronautics and Space Administration. Lewis Research Center, Cleveland, OH.

THE DEVELOPMENT OF A FIBER OPTIC RAMAN TEMPERATURE MEASUREMENT SYSTEM FOR ROCKET FLOWS

WIM A. DE GROOT (NASA, Lewis Research Center, Cleveland; Sverdrup Technology, Inc., Brook Park, OH) AIAA, SAE, ASME, and ASEE, Joint Propulsion Conference, 27th, Sacramento, CA, June 24-26, 1991. 24 p. refs (AIAA PAPER 91-2316) Copyright

A fiber-optic Raman diagnostic system for H₂/O₂ rocket flows is currently under development. This system is designed for measurements of temperature and major species concentration in

the combustion chamber and part of the nozzle of a 100 Newton thrust rocket currently undergoing tests. This paper describes a measurement system based on the spontaneous Raman scattering phenomenon. An analysis of the principles behind the technique is given. Software is developed to measure temperature and major species concentration by comparing theoretical Raman scattering spectra with experimentally obtained spectra. Equipment selection and experimental approach are summarized. This experimental effort is part of a program, which is in progress, to evaluate Navier-Stokes based analyses for this class of rockets. Author

A91-51585* National Aeronautics and Space Administration. Lewis Research Center, Cleveland, OH.

SPACELAB QUALIFIED INFRARED IMAGER FOR MICROGRAVITY SCIENCE APPLICATIONS

ALEXANDER D. PLINE and ROBERT L. BUTCHER (NASA, Lewis Research Center, Cleveland, OH) IN: Thermosense XII; Proceedings of the International Conference on Thermal Sensing and Imaging Diagnostic Applications, Orlando, FL, Apr. 18-20, 1990. Bellingham, WA, Society of Photo-Optical Instrumentation Engineers, 1990, p. 250-258. Previously announced in STAR as N90-20352. refs

Copyright

The Lewis Research Center is developing, under contract, a Spacelab (manned module in the Space Shuttle payload bay) qualified infrared imager for noncontact surface temperature measurement in the Surface Tension Driven Convection Experiment, a microgravity fluid physics experiment. A versatile design philosophy was used in order to provide other experiments with essentially an off the shelf Shuttle qualified instrument, eliminating the duplication of the rigorous development and flight qualification processes. An Inframetrics Model 600 Scanning Infrared Radiometer is being modified to satisfy both experimental and flight requirements, while maintaining the basic performance parameters of the commercial instrument. The modifications include an efficient, low power closed cycle cryogenic cooler to cool the detector, a ruggedized scanner mechanism, 8 bit A/D conversion, Mil-STD components (where possible), size and weight optimization, and the addition of a microprocessor to perform automatic gain control. Features such as detector spectral response, the addition of spectral filters, and target temperature ranges could easily be changed to make this instrument useful as both a qualitative and quantitative diagnostic tool for Spacelab microgravity experiments, in combustion and fluid physics. Author

A91-51870* National Aeronautics and Space Administration. Lewis Research Center, Cleveland, OH.

A FIBER OPTIC SENSOR FOR NONCONTACT MEASUREMENT OF SHAFT SPEED, TORQUE AND POWER

GEORGE C. MADZSAR (NASA, Lewis Research Center, Cleveland, OH) IN: International Instrumentation Symposium, 36th, Denver, CO, May 6-10, 1990, Proceedings. Research Triangle Park, NC, Instrument Society of America, 1990, p. 435-444. Previously announced in STAR as N90-21360. refs

Copyright

A fiber optic sensor which enables noncontact measurement of the speed, torque and power of a rotating shaft was fabricated and tested. The sensor provides a direct measurement of shaft rotational speed and shaft angular twist, from which torque and power can be determined. Angles of twist between 0.005 and 10 degrees were measured. Sensor resolution is limited by the sampling rate of the analog to digital converter, while accuracy is dependent on the spot size of the focused beam on the shaft. Increasing the sampling rate improves measurement resolution, and decreasing the focused spot size increases accuracy. Digital processing allows for enhancement of an electronically or optically degraded signal. Author

A91-51930* National Aeronautics and Space Administration. Lewis Research Center, Cleveland, OH.

A RESISTANCE STRAIN GAGE WITH REPEATABLE AND CANCELLABLE APPARENT STRAIN FOR USE TO 1500 F

JIH-FEN LEI (NASA, Lewis Research Center; Sverdrup Technology,

35 INSTRUMENTATION AND PHOTOGRAPHY

Inc., Cleveland, OH) IN: 1990 SEM Spring Conference on Experimental Mechanics, Albuquerque, NM, June 4-6, 1990, Proceedings. Bethel, CT, Society for Experimental Mechanics, Inc., 1990, p. 339-344. refs

Copyright

A temperature compensated static strain gauge, which is fabricated from Pd13Cr alloy and a Pt compensator, is being developed and has been tested over a temperature range to 1500 F at NASA-Lewis. The PdCr compensated strain gage has significantly lower apparent strain to 500 F than other high temperature strain gages. The PdCr compensated gage is protected from oxidation by a flame-sprayed alumina-4 wt pct zirconia overcoating. Test Results to 1500 F indicate apparent strain variations of less than 250 micro-epsilon and reproducibility between thermal cycles within 50 micro-epsilon. The apparent strain of the coated PdCr compensated gage can be predicted and cancelled due to its reproducibility and low value. Author

A91-54388* National Aeronautics and Space Administration. Lewis Research Center, Cleveland, OH.

LAG COMPENSATION OF OPTICAL FIBERS OR THERMOCOUPLES TO ACHIEVE WAVEFORM FIDELITY IN DYNAMIC GAS PYROMETRY

I. WARSHAWSKY (NASA, Lewis Research Center, Cleveland, OH) Review of Scientific Instruments (ISSN 0034-6748), vol. 62, Oct. 1991, p. 2443-2450. refs

Copyright

Fidelity of waveform reproduction requires constant amplitude ratio and constant time lag of a temperature sensor's indication, at all frequencies of interest. However, heat-transfer type sensors usually cannot satisfy these requirements. Equations for the actual indication of a thermocouple and an optical-fiber pyrometer are given explicitly, in terms of sensor and flowing-gas properties. A practical, realistic design of each type of sensor behaves like a first-order system with amplitude-ratio attenuation inversely proportional to frequency when the frequency exceeds the corner frequency. Only at much higher frequencies does the amplitude-ratio attenuation for the optical fiber sensor become inversely proportional to the square root of the frequency. Design options for improving the frequency response are discussed. On-line electrical lag compensation, using a linear amplifier and a passive compensation network, can extend the corner frequency of the thermocouple 100-fold or more; a similar passive network can be used for the optical-fiber sensor. Design details for these networks are presented. Author

A91-54390* University of Eastern Kentucky, Richmond.
AN EXPERIMENTAL APPARATUS FOR MEASURING SURFACE RESISTANCE IN THE SUBMILLIMETER-WAVELENGTH REGION

JERRY D. COOK (Eastern Kentucky University, Richmond, KY), JOHN W. ZWART (Dordt College, Sioux Center, IA), KENWYN J. LONG, VERNON O. HEINEN, and NORBERT STANKIEWICZ (NASA, Lewis Research Center, Cleveland, OH) Review of Scientific Instruments (ISSN 0034-6748), vol. 62, Oct. 1991, p. 2480-2485. Research supported by American Society for Engineering Education. refs

Copyright

A method for measuring the surface electrical resistance of small metallic samples at submillimeter wavelengths is presented which employs a quasi-optical hemispherical resonator fed by an optically pumped far-infrared laser. The small beam size at the sample, which serves as a plane mirror, allows measurements on samples with widths as small as 5 mm. The quality factor is high, and surface resistance losses are readily measurable. V.L.

A91-55530* National Aeronautics and Space Administration. Lewis Research Center, Cleveland, OH.

OPTICAL TECHNIQUES FOR DETERMINATION OF NORMAL SHOCK POSITION IN SUPERSONIC FLOWS FOR AEROSPACE APPLICATIONS

GRIGORY ADAMOVSKY (NASA, Lewis Research Center, Cleveland, OH) and JOHN G. EUSTACE (John Carroll University,

Cleveland, OH) IN: Optical testing and metrology III: Recent advances in industrial optical inspection; Proceedings of the Meeting, San Diego, CA, July 8-13, 1990. Bellingham, WA, Society of Photo-Optical Instrumentation Engineers, 1990, p. 750-756. Previously announced in STAR as N90-25323. refs

(Contract NAG3-984)

Copyright

Techniques for the quantitative determination of shock position in supersonic flows using direct and indirect methods is presented. A description of an experimental setup is also presented, different configurations of shock position sensing systems are explained, and some experimental results are given. All of the methods discussed are analyzed to determine the ease of technology transfer from the laboratory to in-flight operation. Author

A91-55531* National Aeronautics and Space Administration. Lewis Research Center, Cleveland, OH.

TWO-DIMENSIONAL SURFACE STRAIN MEASUREMENT BASED ON A VARIATION OF YAMAGUCHI'S LASER-SPECKLE STRAIN GAUGE

JOHN P. BARRANGER (NASA, Lewis Research Center, Cleveland, OH) IN: Optical testing and metrology III: Recent advances in industrial optical inspection; Proceedings of the Meeting, San Diego, CA, July 8-13, 1990. Bellingham, WA, Society of Photo-Optical Instrumentation Engineers, 1990, p. 757-766. Previously announced in STAR as N90-22784. refs

Copyright

A novel optical method of measuring 2-D surface strain is proposed. Two linear strains along orthogonal axes and the shear strain between those axes is determined by a variation of Yamaguchi's laser-speckle strain gage technique. It offers the advantages of shorter data acquisition times, less stringent alignment requirements, and reduced decorrelation effects when compared to a previously implemented optical strain rosette technique. The method automatically cancels the translational and rotational components of rigid body motion while simplifying the optical system and improving the speed of response. Author

A91-55533* Strainoptic Technologies, Inc., North Wales, PA.
PHOTOELASTIC TRANSDUCER FOR HIGH-TEMPERATURE APPLICATIONS

A. S. REDNER (Strainoptic Technologies, Inc., North Wales, PA), GRIGORY ADAMOVSKY (NASA, Lewis Research Center, Cleveland, OH), and L. N. WESSON (Aurora Optics, Inc., Blue Bell, PA) IN: Optical testing and metrology III: Recent advances in industrial optical inspection; Proceedings of the Meeting, San Diego, CA, July 8-13, 1990. Bellingham, WA, Society of Photo-Optical Instrumentation Engineers, 1990, p. 775-782. refs

(Contract NAS3-25134)

Copyright

A design for a birefringence transducer for high-temperature applications is described. The spring element and the readout instrumentation are addressed. A pressure transducer based on the concept has been built and successfully tested at temperatures up to 600 C. C.D.

A91-56912* National Aeronautics and Space Administration. Lewis Research Center, Cleveland, OH.

ULTRASONIC VELOCITY TECHNIQUE FOR MONITORING PROPERTY CHANGES IN FIBER-REINFORCED CERAMIC MATRIX COMPOSITES

H. E. KAUTZ (NASA, Lewis Research Center, Cleveland, OH) and R. T. BHATT (NASA, Lewis Research Center; U.S. Army, Aviation Research and Technology Activity, Cleveland, OH) Ceramic Engineering and Science Proceedings (ISSN 0196-6219), vol. 12, July-Aug. 1991, p. 1139-1151. Previously announced in STAR as N91-30546. refs

Copyright

A technique for measuring ultrasonic velocity was used to monitor changes that occur during processing and heat treatment of a SiC/RBSM composite. Results indicated that correlations exist between the ultrasonic velocity data and elastic modulus and interfacial shear strength data determined from mechanical tests.

The ultrasonic velocity data can differentiate strength. The advantages and potential of this nondestructive evaluation method for fiber reinforced ceramic matrix composite applications are discussed. Author

N91-10271*# National Aeronautics and Space Administration. Lewis Research Center, Cleveland, OH.

PARTICLE DISPLACEMENT TRACKING FOR PIV

MARK P. WERNET Sep. 1990 25 p

(Contract RTOP 505-62-01)

(NASA-TM-103288; E-5507-1; NAS 1.15:103288) Avail: NTIS

HC/MF A03 CSCL 14B

A new Particle Imaging Velocimetry (PIV) data acquisition and analysis system, which is an order of magnitude faster than any previously proposed system has been constructed and tested. The new Particle Displacement Tracing (PDT) system is an all electronic technique employing a video camera and a large memory buffer frame-grabber board. Using a simple encoding scheme, a time sequence of single exposure images are time coded into a single image and then processed to track particle displacements and determine velocity vectors. Application of the PDT technique to a counter-rotating vortex flow produced over 1100 velocity vectors in 110 seconds when processed on an 80386 PC. Author

N91-11205*# National Aeronautics and Space Administration. Lewis Research Center, Cleveland, OH.

HEAT FLUX MEASUREMENT IN SSME TURBINE BLADE TESTER

CURT H. LIEBERT Nov. 1990 20 p Presented at the 2nd Annual Conference on Health Monitoring for Space Propulsion Systems, Cincinnati, OH, 14-15 Nov. 1990; sponsored in part by Cincinnati Univ.

(Contract RTOP 590-21-11)

(NASA-TM-103274; E-5719; NAS 1.15:103274) Avail: NTIS

HC/MF A03 CSCL 14B

Surface heat flux values were measured in the turbine blade thermal cycling tester located at NASA-Marshall. This is the first time heat flux has been measured in a space shuttle main engine turbopump environment. Plots of transient and quasi-steady state heat flux data over a range of about 0 to 15 MW/sq m are presented. Data were obtained with a miniature heat flux gage device developed at NASA-Lewis. The results from these tests are being incorporated into turbine design models. Also, these gages are being considered for airfoil surface heat flux measurement on turbine vanes mounted in SSME turbopump test bed engine nozzles at Marshall. Heat flux effects that might be observed on degraded vanes are discussed. Author

N91-12064*# National Aeronautics and Space Administration. Lewis Research Center, Cleveland, OH.

DROPSIZE CORRELATION FOR CRYOGENIC LIQUID-JET ATOMIZATION

ROBERT D. INGEBO Jul. 1990 8 p Presented at the 29th Aerospace Sciences Meeting, Reno, NV, 7-10 Jul. 1991; sponsored in part by AIAA

(NASA-TM-103646; E-5828; NAS 1.15:103646; AIAA PAPER 91-0284) Avail: NTIS HC/MF A02 CSCL 14/2

Momentum transfer from high velocity nitrogen gas flow to liquid-nitrogen jets was investigated. A correlation of aerodynamic and liquid-surface forces with characteristic drop diameter was obtained for cryogenic liquid-jet breakup in Mach 1 gas flow. Nitrogen gas mass-flux was varied by using three differently sized two-fluid fuel atomizers with different nozzle diameters. Author

N91-14574*# National Aeronautics and Space Administration. Lewis Research Center, Cleveland, OH.

HIGH RESOLUTION, HIGH FRAME RATE VIDEO TECHNOLOGY

Washington May 1990 102 p Workshop held in Cleveland, OH, 11-12 May 1988 List of attendees included as supplement (Contract RTOP 694-03-03)

(NASA-CP-3080; E-5044; NAS 1.55:3080) Avail: NTIS HC/MF A06 CSCL 14/2

Papers and working group summaries presented at the High Resolution, High Frame Rate Video (HHV) Workshop are compiled. HHV system is intended for future use on the Space Shuttle and Space Station Freedom. The Workshop was held for the dual purpose of: (1) allowing potential scientific users to assess the utility of the proposed system for monitoring microgravity science experiments; and (2) letting technical experts from industry recommend improvements to the proposed near-term HHV system. The following topics are covered: (1) State of the art in the video system performance; (2) Development plan for the HHV system; (3) Advanced technology for image gathering, coding, and processing; (4) Data compression applied to HHV; (5) Data transmission networks; and (6) Results of the users' requirements survey conducted by NASA.

N91-14575*# National Aeronautics and Space Administration. Lewis Research Center, Cleveland, OH.

RESULTS OF THE USERS' REQUIREMENTS SURVEY

ROBERT L. BUTCHER *In its* High Resolution, High Frame Rate Video Technology p 3-17 May 1990

Avail: NTIS HC/MF A06 CSCL 14/2

The objectives of the High Resolution, High Frame Rate Video Technology (HHVT) Users' Requirements Survey were the following: (1) Document the requirements of potential users of the HHVT system; (2) Establish a data base relating key video parameters to HHVT users; (3) Guide the development of a high resolution, high frame rate video system offering high data storage capacity and high data transmission rates; (4) Allow users to compare their requirements to those of other users and to the state-of-the-art technology; and (5) Allow users to reassess, if necessary, their requirements in the light of existing and near-term technology. The results of the Users' Requirements Survey are presented. The diversity of these requirements indicates a need for developing a video system with great flexibility. Y.S.

N91-14578*# National Aeronautics and Space Administration. Lewis Research Center, Cleveland, OH.

STATE OF THE ART IN VIDEO SYSTEM PERFORMANCE

MICHAEL J. LEWIS *In its* High Resolution, High Frame Rate Video Technology p 37-48 May 1990

Avail: NTIS HC/MF A06 CSCL 14/2

The closed circuit television (CCTV) system that is onboard the Space Shuttle has the following capabilities: camera, video signal switching and routing unit (VSU); and Space Shuttle video tape recorder. However, this system is inadequate for use with many experiments that require video imaging. In order to assess the state-of-the-art in video technology and data storage systems, a survey was conducted of the High Resolution, High Frame Rate Video Technology (HHVT) products. The performance of the state-of-the-art solid state cameras and image sensors, video recording systems, data transmission devices, and data storage systems versus users' requirements are shown graphically. Y.S.

N91-14580*# National Aeronautics and Space Administration. Lewis Research Center, Cleveland, OH.

HIGH RESOLUTION, HIGH FRAME RATE VIDEO TECHNOLOGY DEVELOPMENT PLAN AND THE NEAR-TERM SYSTEM CONCEPTUAL DESIGN

ROBERT A. ZIEMKE *In its* High Resolution, High Frame Rate Video Technology p 59-88 May 1990

Avail: NTIS HC/MF A06 CSCL 14/2

The objective of the High Resolution, High Frame Rate Video Technology (HHVT) development effort is to provide technology advancements to remove constraints on the amount of high speed, detailed optical data recorded and transmitted for microgravity science and application experiments. These advancements will enable the development of video systems capable of high resolution, high frame rate video data recording, processing, and transmission. Techniques such as multichannel image scan, video parameter tradeoff, and the use of dual recording media were identified as methods of making the most efficient use of the near-term technology. Author

35 INSTRUMENTATION AND PHOTOGRAPHY

N91-19401*# National Aeronautics and Space Administration. Lewis Research Center, Cleveland, OH.

ROTATING PRESSURE MEASUREMENT SYSTEM USING AN ON BOARD CALIBRATION STANDARD

RICHARD G. SENYITKO, PHILIP Z. BLUMENTHAL (Sverdrup Technology, Inc., Brook Park, OH.), and ROBERT J. FREEDMAN 1991 15 p Proposed for presentation at the 37th International Instrumentation Symposium, San Diego, CA, 5-9 May 1991; sponsored by Instrument Society of America (Contract RTOP 505-62-84) (NASA-TM-103676; E-5892; NAS 1.15:103676) Avail: NTIS HC/MF A03 CSCL 14/2

A computer-controlled multichannel pressure measurement system was developed to acquire detailed flow field measurements on board the Large Low Speed Centrifugal Compressor Research Facility at the NASA Lewis Research Center. A pneumatic slip ring seal assembly is used to transfer calibration pressures to a reference standard transducer on board the compressor rotor in order to measure very low differential pressures with the high accuracy required. A unique data acquisition system was designed and built to convert the analog signal from the reference transducer to the variable frequency required by the multichannel pressure measurement system and also to provide an output for temperature control of the reference transducer. The system also monitors changes in test cell barometric pressure and rotating seal leakage and provides an on screen warning to the operator if limits are exceeded. The methods used for the selection and testing of the reference transducer are discussed, and the data acquisition system hardware and software design are described. The calculated and experimental data for the system measurement accuracy are also presented.

Author

N91-19402*# National Aeronautics and Space Administration. Lewis Research Center, Cleveland, OH.

CRYOGENIC LIQUID-JET BREAKUP IN TWO-FLUID ATOMIZERS

ROBERT D. INGEBO 1991 6 p Proposed for presentation at the 5th International Conference on Liquid Atomization and Spray Systems, Gaithersburg, MD, 15-18 Jul. 1991; sponsored by National Inst. of Standards and Technology (Contract RTOP 505-62-52) (NASA-TM-103734; E-5854; NAS 1.15:103734) Avail: NTIS HC/MF A02 CSCL 20/4

A two-fluid atomizer was used to study the breakup of liquid-nitrogen jets in nitrogen, argon, and helium atomizing gas flows. A scattered-light scanner particle sizing instrument previously developed at NASA Lewis Research Center was further developed and used to determine characteristic drop diameters for the cryogenic sprays. In the breakup regime of aerodynamic-stripping, i.e., sonic-velocity conditions, the following correlation of the reciprocal Sauter mean diameter, $D(\text{sub } 32)\text{exp } -1$, with the atomizing-gas flowrate, $W(\text{g})$, was obtained: $D(\text{sub } 32)\text{exp } -1 = k(\text{sub } c)(W(\text{g})\text{exp } 1.33)$, where $k(\text{sub } c)$ is a proportionality constant evaluated for each atomizing gas. Values of $k(\text{sub } c) = 120, 220$, and 1100 were obtained for argon, nitrogen, and helium gasflows, respectively. The reciprocal Sauter mean diameter and gas flowrate have the units of $1/\text{cm}$ and g/sec , respectively. In the regime of capillary-wave breakup, or subsonic conditions, it was found that $D(\text{sub } 32)\text{exp } -1 = k(\text{g})(W(\text{g})\text{exp } 0.75)$, where $k = 270, 390$, and 880 for argon, nitrogen, and helium gasflows, respectively.

Author

N91-19404*# National Aeronautics and Space Administration. Lewis Research Center, Cleveland, OH.

THREE-DIMENSIONAL COMPUTED TOMOGRAPHY FROM INTERFEROMETRIC MEASUREMENTS WITHIN A NARROW CONE OF VIEWS

ARTHUR J. DECKER and STEVEN H. IZEN (Case Western Reserve Univ., Cleveland, OH.) Mar. 1991 14 p Submitted for publication Original contains color illustrations (Contract NAG3-832; RTOP 505-62-01) (NASA-TM-103257; E-5688; NAS 1.15:103257) Avail: NTIS HC/MF A03; 7 functional color pages CSCL 14/2

A theory to determine the properties of a fluid from measurements of its projections was developed and tested. Viewing cones as small as 10 degrees were evaluated, with the only assumption being that the property was space limited. The results of applying the theory to numerical and actual interferograms of a spherical discontinuity of refractive index are presented. The theory was developed to test the practicality and limits of using three-dimensional computer tomography in internal fluid dynamics.

Author

N91-20100*# National Aeronautics and Space Administration. Lewis Research Center, Cleveland, OH.

PROPULSION INSTRUMENTATION RESEARCH

WILLIAM C. NIEBERDING, DANIEL J. LESCO, and W. DAN WILLIAMS *In its* Aeropropulsion 1991 21 p Mar. 1991 Avail: NTIS HC/MF A24 CSCL 14/2

As was stated in the overview, the goal of the Propulsion Instrumentation Research Program is to provide the instrumentation technology advances needed to support future aeropropulsion research and development. A hallmark of this work is that the sensors and measurement systems being developed are not intended to be used on operational propulsion systems. The systems are aimed at experiments for engine development, component development, and analytical code validation. Although sensors and/or systems for operational engines sometimes grow out of this work, they are not the goal. A further characteristic of this work is that it is frequently blind about whether the application is for aero or space propulsion. Some of the following examples are currently being developed for space propulsion systems, but they are also applicable to aeropropulsion.

Author

N91-20453*# National Aeronautics and Space Administration. Lewis Research Center, Cleveland, OH.

SOFTWARE MANUAL FOR OPERATING PARTICLE DISPLACEMENT TRACKING DATA ACQUISITION AND REDUCTION SYSTEM

MARK P. WERNET Jan. 1991 44 p (Contract RTOP 505-62-50) (NASA-TM-103720; E-5951; NAS 1.15:103720) Avail: NTIS HC/MF A03 CSCL 09/2

The software manual is presented. The necessary steps required to record, analyze, and reduce Particle Image Velocimetry (PIV) data using the Particle Displacement Tracking (PDT) technique are described. The new PDT system is an all electronic technique employing a CCD video camera and a large memory buffer frame-grabber board to record low velocity (less than or equal to 20 cm/s) flows. Using a simple encoding scheme, a time sequence of single exposure images are time coded into a single image and then processed to track particle displacements and determine 2-D velocity vectors. All the PDT data acquisition, analysis, and data reduction software is written to run on an 80386 PC.

Author

N91-24318*# National Aeronautics and Space Administration. Lewis Research Center, Cleveland, OH.

OVERVIEW OF THE INSTRUMENTATION PROGRAM Abstract Only

WILLIAM C. NIEBERDING *In its* Structural Integrity and Durability of Reusable Space Propulsion Systems p 81-82 Apr. 1989 Avail: NTIS HC/MF A12 CSCL 14/2

This program is aimed at developing sensors and measurement systems capable of obtaining the data necessary for the verification of computational models of the structural behavior, the fatigue life, and the environmental conditions pertinent to advanced reusable space propulsion systems. One of the characteristics of measurement systems needed to verify codes is that the sensors must be nonintrusive or at least minimally intrusive so as not to significantly perturb the conditions being measured. This leads to a heavy emphasis on laser optical techniques and on thin-film sensors. Another characteristic of such instruments is that they must be highly accurate and produce very high spatial and temporal resolution of the parameter being measured. The measurement systems needed generally fall into a number of broad categories.

First there are the measurements needed on the surfaces of components such as turbine blades and vanes. Some of the desired parameters are temperature, strain, and heat flux. Another broad category encompasses those measurements needed in the flow environment around these components. Here, the desired results are high resolution maps of such parameters as flow velocity, temperature, density, pressure, and species concentration. The remaining category deals with measurements necessary for monitoring the health of the engine. This category has loomed ever more important since the Challenger disaster. An optical method for determining the characteristics of the plume is presented. Holographic measurement of structural damage is also presented. K.C.D.

N91-24321*# National Aeronautics and Space Administration. Lewis Research Center, Cleveland, OH.

CALIBRATOR TESTS OF HEAT FLUX GAUGES MOUNTED IN SSME BLADES

CURT H. LIEBERT *In its Structural Integrity and Durability of Reusable Space Propulsion Systems* p 99-104 Apr. 1989
 Avail: NTIS HC/MF A12 CSCL 14/2

Measurements of heat flux to space shuttle main engine (SSME) turbine blade surfaces are being made in the Lewis heat flux calibration facility. Surface heat flux information is obtained from transient temperature measurements taken at points within the gauge. A 100-kW Vortek arc lamp is used as a source of thermal radiant energy. Thermoplugs, with diameters of about 0.190 cm and lengths varying from about 0.190 to 0.320 cm, are being investigated. The thermoplug is surrounded on all surfaces except the active surface by a pocket of air located in the circular annulus and under the back cover. Since the thermoplug is insulated, it is assumed that heat is conducted in a one-dimensional manner from the hot active surface to the cooler back side of the thermoplug. It is concluded that the miniature plug-type gauge concept is feasible for measurement of blade surface heat flux. It is suggested that it is important to measure heat flux near the hub on the suction surface and at the throat on SSME blades rotating in engines because stress and heat transfer coefficients are high in this region. Author

N91-25381*# National Aeronautics and Space Administration. Lewis Research Center, Cleveland, OH.

FIBER-OPTIC SENSORS FOR AEROSPACE ELECTRICAL MEASUREMENTS: AN UPDATE

RICHARD L. PATTERSON, A. H. ROSE, D. TANG, and G. W. DAY (National Inst. of Standards and Technology, Boulder, CO.) 1991 6 p Presented at the 26th Intersociety Energy Conversion Engineering Conference, Boston, MA, 4-9 Aug. 1991; sponsored by American Nuclear Society, SAE, American Chemical Society, AIAA, ASME, IEEE, and the American Inst. of Chemical Engineers
 (Contract RTOP 590-13-41)
 (NASA-TM-104454; E-6295; NAS 1.15:104454) Avail: NTIS HC/MF A02 CSCL 14/2

Fiber-optic sensors are being developed for electrical current, voltage, and power measurements in aerospace applications. These sensors are presently designed to cover ac frequencies from 60 Hz to 20 kHz. The current sensor, based on the Faraday effect in optical fiber, is in advanced development after some initial testing. Concentration is on packaging methods and ways to maintain consistent sensitivity with changes in temperature. The voltage sensor, utilizing the Pockels effect in a crystal, has excelled in temperature tests. This paper reports on the development of these sensors, the results of evaluation, improvements now in progress, and the future direction of the work. Author

N91-25382*# National Aeronautics and Space Administration. Lewis Research Center, Cleveland, OH.

PARTICLE IMAGE VELOCIMETRY FOR THE SURFACE TENSION DRIVEN CONVECTION EXPERIMENT USING A PARTICLE DISPLACEMENT TRACKING TECHNIQUE

MARK P. WERNET and ALEXANDER D. PLINE 1991 13 p Presented at the Fourth International Conference on Laser

Anemometry, Cleveland, OH, 5-9 Aug. 1991; sponsored by ASME, European Association for Laser Anemometry, Case Western Reserve Univ., Cleveland State Univ., and the Ohio Aerospace Inst.

(Contract RTOP 505-62-50)
 (NASA-TM-104482; E-6327; NAS 1.15:104482) Avail: NTIS HC/MF A03 CSCL 14/2

The Surface Tension Driven Convection Experiment (STDCE) is a Space Transportation System flight experiment to study both transient and steady thermocapillary fluid flows aboard the USML-1 Spacelab mission planned for 1992. One of the components of data collected during the experiment is a video record of the flow field. This qualitative data is then quantified using an all electronic, two-dimensional particle image velocimetry technique called particle displacement tracking (PDT) which uses a simple space domain particle tracking algorithm. The PDT system is successful in producing velocity vector fields from the raw video data. Application of the PDT technique to a sample data set yielded 1606 vectors in 30 seconds of processing time. A bottom viewing optical arrangement is used to image the illuminated plane, which causes keystone distortion in the final recorded image. A coordinate transformation was incorporated into the system software to correct this viewing angle distortion. PDT processing produced 1.8 percent false identifications, due to random particle locations. A highly successful routine for removing the false identifications was also incorporated, reducing the number of false identifications to 0.2 percent. Author

N91-25387*# National Aeronautics and Space Administration. Lewis Research Center, Cleveland, OH.

PARTICLE DISPLACEMENT TRACKING APPLIED TO AIR FLOWS

MARK P. WERNET 1991 11 p Presented at the Fourth International Conference on Laser Anemometry, Cleveland, OH, 5-9 Aug. 1991; sponsored by NASA Lewis Research Center, ASME, European Association for Laser Anemometry, Case Western Reserve Univ., Cleveland State Univ. and the Oh
 (Contract RTOP 505-62-50)
 (NASA-TM-104481; E-6329; NAS 1.15:104481) Avail: NTIS HC/MF A03 CSCL 14/2

Electronic Particle Image Velocimeter (PIV) techniques offer many advantages over conventional photographic PIV methods such as fast turn around times and simplified data reduction. A new all electronic PIV technique was developed which can measure high speed gas velocities. The Particle Displacement Tracking (PDT) technique employs a single cw laser, small seed particles (1 micron), and a single intensified, gated CCD array frame camera to provide a simple and fast method of obtaining two-dimensional velocity vector maps with unambiguous direction determination. Use of a single CCD camera eliminates registration difficulties encountered when multiple cameras are used to obtain velocity magnitude and direction information. An 80386 PC equipped with a large memory buffer frame-grabber board provides all of the data acquisition and data reduction operations. No array processors of other numerical processing hardware are required. Full video resolution (640x480 pixel) is maintained in the acquired images, providing high resolution video frames of the recorded particle images. The time between data acquisition to display of the velocity vector map is less than 40 sec. The new electronic PDT technique is demonstrated on an air nozzle flow with velocities less than 150 m/s. Author

N91-26490*# National Aeronautics and Space Administration. Lewis Research Center, Cleveland, OH.

APPLIED HIGH-SPEED IMAGING FOR THE ICING RESEARCH PROGRAM AT NASA LEWIS RESEARCH CENTER

HOWARD SLATER, JAY OWENS (Cortez 3 Services Corp., Brook Park, OH.), and JAIWON SHIN 1991 18 p Presented at the 1991 International Symposium on Optical Applied Science and Engineering, San Diego, CA, 21-26 Jul. 1991; sponsored by the Society of Photo-Optical Instrumentation Engineers
 (Contract NAS3-24816)

35 INSTRUMENTATION AND PHOTOGRAPHY

(NASA-TM-104415; E-6246; NAS 1.15:104415) Avail: NTIS HC/MF A03 CSCL 14/2

The Icing Research Tunnel at NASA Lewis Research Center provides scientists a scaled, controlled environment to simulate natural icing events. The closed-loop, low speed, refrigerated wind tunnel offers the experimental capability to test for icing certification requirements, analytical model validation and calibration techniques, cloud physics instrumentation refinement, advanced ice protection systems, and rotorcraft icing methodology development. The test procedures for these objectives all require a high degree of visual documentation, both in real-time data acquisition and post-test image processing. Information is provided to scientific, technical, and industrial imaging specialists as well as to research personnel about the high-speed and conventional imaging systems will be on the recent ice protection technology program. Various imaging examples for some of the tests are presented. Additional imaging examples are available from the NASA Lewis Research Center's Photographic and Printing Branch. Author

N91-27510*# National Aeronautics and Space Administration. Lewis Research Center, Cleveland, OH.

SPRAY MEASUREMENTS OF AEROTHERMODYNAMIC EFFECT ON DISINTEGRATING LIQUID JETS

ROBERT D. INGEBO 1991 9 p Presented at the 1991 Winter Annual Meeting of ASME, Atlanta, GA, 1-6 Dec. 1991 (Contract RTOP 505-62-52) (NASA-TM-104501; E-6361; NAS 1.15:104501) Avail: NTIS HC/MF A02 CSCL 20/4

An experimental investigation was made to determine the effect of atomizing gas mass flux and temperature on liquid jet breakup in sonic velocity gas flow. Characteristic drop size data were obtained by using the following atomizing gases: nitrogen, argon, and helium to breakup water jets in high velocity gas flow. A scattered light scanning instrument developed at Lewis Research Center was used to measure Sauter mean diameter (SMD). The three gases gave a molecular weight range of 4 to 40 and atomizing gas mass flux and temperature were varied from 6 to 50 g/sq cm and 275-400 K, respectively. The ratio of liquid jet diameter to SMD, $D(\text{sub } 0)/D(\text{sub } 32)$, was correlated with aerodynamic and liquid-surface force ratios, i.e., the product of the Weber and Reynolds number, $We Re$, the gas to liquid density ratio, $\rho(\text{sub } g)/\rho(\text{sub } l)$ and also the molecular scale dimensionless group, $\rho(\text{sub } l)(V_m \exp 3)/\mu(\text{sub } l)g$, to give the following expression: $D(\text{sub } 0)/D(\text{sub } 32) = 0.90 \times 10(\exp -8) \times (We Re \rho(\text{sub } g)/\rho(\text{sub } l) \exp 0.44 \times (\rho(\text{sub } l) V_m \exp 3/\mu(\text{sub } l)g) \exp 0.67$ where $We Re = ((\rho(\text{sub } g) \exp 2(D(\text{sub } 0) \exp 2(V(\text{sub } C) \exp 3)/\mu(\text{sub } l) \sigma, \mu(\text{sub } l) \text{ is liquid viscosity, } \sigma \text{ is surface tension, } V(\text{sub } C) \text{ is the acoustic gas velocity, } V(\text{sub } m) \text{ is the RMS velocity of gas molecules, and } g \text{ is the acceleration of gas molecules due to gravity. Good agreement was obtained with atomization theory for liquid-jet breakup in the regime of aerodynamic stripping. Also, due to its low molecular weight and high acoustic velocity, helium was considerably more effective than nitrogen or argon in producing small-droplet sprays with values of } D(\text{sub } 32) \text{ on the order of 5 microns. Author$

N91-27511*# National Aeronautics and Space Administration. Lewis Research Center, Cleveland, OH.

RESEARCH AND DEVELOPMENT OF OPTICAL MEASUREMENT TECHNIQUES FOR AEROSPACE PROPULSION RESEARCH: A NASA LEWIS RESEARCH CENTER PERSPECTIVE

DANIEL J. LESCO 1991 12 p Presented at the Second International Conference on Photomechanics and Speckle Metrology, San Diego, CA, 22-26 Jul. 1991; sponsored by the Society of Photo-Optical Instrumentation Engineers (Contract RTOP 505-62-50) (NASA-TM-104418; E-6251; NAS 1.15:104418) Avail: NTIS HC/MF A03 CSCL 14/2

The applied research effort required to develop new nonintrusive measurement techniques capable of obtaining the data required by aerospace propulsion researchers and of operating in the harsh

environments encountered in research and test facilities is discussed and illustrated through several ongoing projects at NASA's Lewis Research Center. Factors including length of development time, funding levels, and collaborative support from fluid-thermal researchers are cited. Progress in developing new instrumentation via a multi-path approach, including NASA research, grant, and government-sponsored research through mechanisms like the Small Business Innovative Research program, is also described. Author

N91-27521*# National Aeronautics and Space Administration. Lewis Research Center, Cleveland, OH.

HIGH-SPEED LASER ANEMOMETRY BASED ON SPECTRALLY RESOLVED RAYLEIGH SCATTERING

RICHARD G. SEASHOLTZ 1991 9 p Presented at the Fourth International Conference on Laser Anemometry, Cleveland, OH, 5-9 Aug. 1991; sponsored by ASME, the European Association for Laser Anemometry, Case Western Reserve Univ., Cleveland State Univ. and Ohio Aerospace Institute (Contract RTOP 505-62-50) (NASA-TM-104522; E-6395; NAS 1.15:104522) Avail: NTIS HC/MF A02 CSCL 14/2

Laser anemometry in unseeded flows based on the measurement of the spectrum of Rayleigh scattered laser light is reviewed. The use of molecular scattering avoids the well known problems (particle lag, biasing effects, seed generation, seed injection) of seeded flows. The fundamental limits on velocity measurement accuracy are determined using maximum likelihood methods. Measurement of the Rayleigh spectrum with scanning Fabry-Perot interferometers is analyzed and accuracy limits are established for both single pass and multipass configurations. Multipass configurations have much higher selectivity and are needed for measurements where there is a large amount of excess noise caused by stray laser light. It is shown that Rayleigh scattering is particularly useful for supersonic and hypersonic flows. The results of the analysis are compared with measurements obtained with a Rayleigh scattering diagnostic developed for study of the exhaust plume of a small hydrogen-oxygen rocket, where the velocities are in the range of 1000 to 5000 m/sec. Author

N91-30491*# National Aeronautics and Space Administration. Lewis Research Center, Cleveland, OH.

GROUND-BASED PIV AND NUMERICAL FLOW VISUALIZATION RESULTS FROM THE SURFACE TENSION DRIVEN CONVECTION EXPERIMENT

ALEXANDER D. PLINE, MARK P. WERNET, and KWANG-CHUNG HSIEH (Sverdrup Technology, Inc., Brook Park, OH.) 1991 15 p Presented at the 36th Annual International Symposium on Optical and Optoelectronic Applied Science and Engineering, San Diego, CA, 21-26 Jul. 1991; sponsored by the Society of Photo-Optical Instrumentation Engineers (Contract NAS3-25266; RTOP 694-03-00) (NASA-TM-105172; E-6468; NAS 1.15:105172) Avail: NTIS HC/MF A03 CSCL 14/2

The Surface Tension Driven Convection Experiment (STDCE) is a Space Transportation System flight experiment to study both transient and steady thermocapillary fluid flows aboard the United States Microgravity Laboratory-1 (USML-1) Spacelab mission planned for June, 1992. One of the components of data collected during the experiment is a video record of the flow field. This qualitative data is then quantified using an all electric, two dimensional Particle Image Velocimetry (PIV) technique called Particle Displacement Tracking (PDT), which uses a simple space domain particle tracking algorithm. Results using the ground based STDCE hardware, with a radiant flux heating mode, and the PDT system are compared to numerical solutions obtained by solving the axisymmetric Navier Stokes equations with a deformable free surface. The PDT technique is successful in producing a velocity vector field and corresponding stream function from the raw video data which satisfactorily represents the physical flow. A numerical program is used to compute the velocity field and corresponding stream function under identical conditions. Both the PDT system

and numerical results were compared to a streak photograph, used as a benchmark, with good correlation. Author

N91-31605* National Aeronautics and Space Administration. Lewis Research Center, Cleveland, OH.

LASER INTERFEROMETRIC MEASUREMENT OF ION ELECTRODE SHAPE AND CHARGE EXCHANGE EROSION

GREGORY S. MACRAE and CAROLYN R. MERCER 1991 17 p Presented at the 27th Joint Propulsion Conference, Sacramento, CA, 24-27 Jun. 1991; cosponsored by AIAA, SAE, ASME, and ASEE Previously announced in IAA as A91-45786 (Contract RTOP 506-42-31) (NASA-TM-105165; E-6454; NAS 1.15:105165; AIAA PAPER 91-2121) Avail: NTIS HC/MF A03 CSCL 14/2

A projected fringe profilometry system was applied to surface contour measurements of an accelerator electrode from an ion thruster. The system permitted noncontact, nondestructive evaluation of the fine and gross structure of the electrode. A 3-D surface map of a dished electrode was generated without altering the electrode surface. The same system was used to examine charge exchange erosion pits near the periphery of the electrode to determine the depth, location, and volume of material lost. This electro-optical measurement system allowed rapid, nondestructive, digital data acquisition coupled with automated computer data processing. In addition, variable sensitivity allowed both coarse and fine measurements of objects having various surface finishes. Author

N91-31608* National Aeronautics and Space Administration. Lewis Research Center, Cleveland, OH.

PLUG-TYPE HEAT FLUX GAUGE Patent

CURT H. LIEBERT, inventor (to NASA) and JOHN KOCH, JR., inventor (to NASA) 17 Sep. 1991 7 p Filed 31 May 1990 Supersedes N91-13685 (29 -5, p 663) (NASA-CASE-LEW-14967-1; US-PATENT-5,048,973; US-PATENT-APPL-SN-531433; US-PATENT-CLASS-374-29; US-PATENT-CLASS-374-180; US-PATENT-CLASS-374-208; US-PATENT-CLASS-250-356.1; US-PATENT-CLASS-136-200; INT-PATENT-CLASS-G01K-17/16; INT-PATENT-CLASS-G01K-17/06) Avail: US Patent and Trademark Office CSCL 14/2

A plug-type heat flux gauge formed in a material specimen and having a thermoplug integrally formed in the material specimen, and a method for making the same are disclosed. The thermoplug is surrounded by a concentric annulus, through which thermocouple wires are routed. The end of each thermocouple wire is welded to the thermoplug, with each thermocouple wire welded at a different location along the length of the thermoplug. The thermoplug and concentric annulus may be formed in the material specimen by electrical discharge machining and trepanning procedures.

Official Gazette of the U.S. Patent and Trademark Office

36

LASERS AND MASERS

Includes parametric amplifiers.

A91-21614* National Aeronautics and Space Administration. Lewis Research Center, Cleveland, OH.

A PREVIEW OF A MICROGRAVITY LASER LIGHT SCATTERING INSTRUMENT

W. V. MEYER (NASA, Lewis Research Center, Cleveland, OH) and R. R. ANSARI (Case Western Reserve University, Cleveland, OH) AIAA, Aerospace Sciences Meeting, 29th, Reno, NV, Jan. 7-10, 1991. 8 p. refs (AIAA PAPER 91-0779) Copyright

The development of a versatile, miniature, modular light scattering instrument to be used in microgravity is described. The

instrument will measure microscopic particles in the size range of thirty angstroms to above three microns. This modular instrument permits several configurations, each optimized for a particular experiment. In particular, a multiangle instrument will probably be mounted in a rack in the Space Shuttle and on the Space Station. It is possible that a Space Shuttle glove-box and a lap-top computer containing a correlator card can be used to perform a number of experiments and to demonstrate the technology needed for more elaborate investigations. Y.P.Q.

N91-24320* National Aeronautics and Space Administration. Lewis Research Center, Cleveland, OH.

OPTICAL INSPECTION OF SPACE-PROPULSION COMPONENTS USING AN INJECTION SEEDED ND:YAG LASER SYSTEM

ARTHUR J. DECKER *In its Structural Integrity and Durability of Reusable Space Propulsion Systems* p 87-98 Apr. 1989 Avail: NTIS HC/MF A12 CSCL 20/5

A dual-beam, injection-seeded, Nd:YAG laser has been demonstrated for detecting structural defects. This demonstration was part of an on-going project to use dual-reference-beam holographic interferometry to inspect space propulsion components for cracks, structural failures, structural changes, and gas leaks. Potential subjects for inspection include welds, duct work, casings, turbopumps, blades, composites, and ceramics. The maximum dimension of an inspected area ranges from a few centimeters to a meter. The entire optical inspection system is now ready for a demonstration application. Author

37

MECHANICAL ENGINEERING

Includes auxiliary systems (nonpower); machine elements and processes; and mechanical equipment.

A91-14400* Texas A&M Univ., College Station.

USE OF PIEZOELECTRIC ACTUATORS IN ACTIVE VIBRATION CONTROL OF ROTATING MACHINERY

RENG RONG LIN, ALAN B. PALAZZOLO (Texas A & M University, College Station), ALBERT F. KASCAK (NASA, Lewis Research Center; U.S. Army, Cleveland, OH), and GERALD MONTAGUE (Sverdrup Technology, Inc., Middleburg Heights, OH) IN: *Electro-optical materials for switches, coatings, sensor optics, and detectors; Proceedings of the Meeting, Orlando, FL, Apr. 16-20, 1990. Bellingham, WA, Society of Photo-Optical Instrumentation Engineers (SPIE Proceedings. Volume 1307), 1990, p. 199-210. Research supported by the Texas A & M Turbomachinery Research Consortium. refs (Contract NAG3-763) Copyright*

Theoretical and test results for the development of piezoelectric-actuator-based active vibration control (AVC) are presented. The evolution of this technology starts with an ideal model of the actuator and progresses to a more sophisticated model where the pushers force the squirrel cage ball bearing supports of a rotating shaft. The piezoelectric pushers consist of a stack of piezoelectric ceramic disks that are arranged on top of one another and connected in parallel electrically. This model consists of a prescribed displacement that is proportional to the input voltage and a spring that represents the stiffness of the stack of piezoelectric disks. System tests were carried out to stabilize the AVC system, verify its effectiveness in controlling vibration, and confirm the theory presented. R.E.P.

A91-17214* National Aeronautics and Space Administration. Lewis Research Center, Cleveland, OH.

ADVANCED ROTORCRAFT TRANSMISSION PROGRAM

ROBERT C. BILL (NASA, Lewis Research Center; U.S. Army, Propulsion Directorate, Cleveland, OH) IN: *AHS, Annual Forum,*

37 MECHANICAL ENGINEERING

46th, Washington, DC, May 21-23, 1990, Proceedings. Volume 1. Alexandria, VA, American Helicopter Society, 1990, p. 227-238. refs

Copyright

The U.S. Army/NASA Advanced Rotorcraft Transmission (ART) program is charged with developing and demonstrating a light, quiet, and durable drivetrain for next-generation rotorcraft in two classes: a 10,000-20,000 Future Attack Air Vehicle capable of both tactical ground support and air-to-air missions, and a 60,000-80,000 lb Advanced Cargo Aircraft, for heavy-lift field-support operations. Specific ART objectives encompass a 25-percent reduction in drivetrain weight, a 10-dB noise level reduction at the transmission source, and the achievement of a 5000-hr MTBF. Four candidate drivetrain systems have been carried to a conceptual design stage, together with projections of their mission performance and life-cycle costs. O.C.

A91-20938* National Aeronautics and Space Administration. Lewis Research Center, Cleveland, OH.

SIMPLIFIED PROCEDURES FOR DESIGNING ADHESIVELY BONDED COMPOSITE JOINTS

C. C. CHAMIS and P. L. N. MURTHY (NASA, Lewis Research Center, Cleveland, OH) Journal of Reinforced Plastics and Composites (ISSN 0731-6844), vol. 10, Jan. 1991, p. 29-41. Previously announced in STAR as N89-26048. refs

Copyright

Procedures for the preliminary design for composite adhesive joints are described. Typical joints, their respective free body diagrams, and approximate equations for estimating the stresses in each of these typical joints are summarized. Equations are also presented to check the critical conditions of the joint such as minimum length, maximum adhesive shear stress, and peel-off stress. To illustrate the procedure, sample designs are described in step-by-step fashion for a butt joint with single doubler subjected to static loads, cyclic loads, and environmental effects. The results show that unsymmetric adhesive joints are inefficient and should be avoided, and hygrothermal environments and cyclic loads dramatically reduce the structural integrity of the joint and require several joint lengths compared with those for static load with no environmental effects. Author

A91-21071* Akron Univ., OH.

FLOW VISUALIZATION AND QUANTITATIVE VELOCITY AND PRESSURE MEASUREMENTS IN SIMULATED SINGLE AND DOUBLE BRUSH SEALS

M. J. BRAUN, V. A. CANACCI (Akron, University, OH), and R. C. HENDRICKS (NASA, Lewis Research Center, Cleveland, OH) (STLE, Annual Meeting, 45th, Denver, CO, May 7-10, 1990) STLE Tribology Transactions (ISSN 0569-8197), vol. 34, Jan. 1991, p. 70-80. refs

(Contract NAG3-969)

Copyright

A method to visualize and characterize the complex flow fields in simulated single and double brush seals is presented. The brush seal configuration was tested in a gravity fed water tunnel and a pump driven pressurized oil tunnel. Visualization of the flow field revealed regions that are characteristically river jetting, vortical, crossflow and exist upstream, downstream or within the seal. Such flows are especially engendered by variations in fiber void that are spatial and temporal and affect changes in seal leakage and stability. While the effects of interface motion and cylindrical configuration have not been considered herein, it is believed that the observed flow fields and pressure drop patterns characterize flow phenomenology in brush seals. The axial pressure profiles upstream, across and downstream of the brush have been measured under a variety of inlet pressure conditions and the ensuing pressure maps are presented and discussed. Through the application of the Full Flow Field Tracking method developed by the authors, the flow patterns and the accompanying fluid velocities inside the brush were non-intrusively determined and graphically reconstructed. Author

A91-30640*# National Aeronautics and Space Administration. Lewis Research Center, Cleveland, OH.

A MODEL FOR THE SPACE SHUTTLE MAIN ENGINE HIGH PRESSURE OXIDIZER TURBOPUMP SHAFT SEAL SYSTEM

DANIEL E. PAXSON (NASA, Lewis Research Center, Cleveland, OH) IN: Annual Health Monitoring Conference for Space Propulsion Systems, 2nd, Cincinnati, OH, Nov. 14, 15, 1990, Proceedings. Cincinnati, OH, University of Cincinnati, 1990, p. 295-315. refs

A model of the High Pressure Oxidizer Turbopump (HPOTP) shaft seal system on the Space Shuttle Main Engine (SSME) is described. The model predicts the fluid properties and flow rates throughout this system for a number of conditions simulating failed seals. The results agree well with qualitative expectations and redline values but cannot be verified with actual data due to the lack thereof. The results indicate that each failure mode results in a unique distribution of properties throughout the seal system and can therefore be individually identified given the proper instrumentation. Furthermore, the detection process can be built on the principle of qualitative reasoning without the use of exact fluid property values. A simplified implementation of the model which does not include the slinger/labyrinth seal combination has been developed and will be useful for inclusion in a real-time diagnostic system. L.K.S.

A91-33461* National Aeronautics and Space Administration. Lewis Research Center, Cleveland, OH.

ON THE NUMERICAL SOLUTION OF THE DYNAMICALLY LOADED HYDRODYNAMIC LUBRICATION OF THE POINT CONTACT

SANG G. LIM (NASA, Lewis Research Center; Case Western Reserve University, Cleveland, OH), JOSEPH M. PRAHL (Case Western Reserve University, Cleveland, OH), and DAVID E. BREWE (NASA, Lewis Research Center; U.S. Army, Propulsion Directorate, Cleveland, OH) (STLE, Annual Meeting, 45th, Denver, CO, May 7-10, 1990) STLE Tribology Transactions (ISSN 0569-8197), vol. 34, April 1991, p. 195-204. refs

Copyright

A numerical transient solution of the hydrodynamically lubricated point contact problem is obtained using the ball-on-plane model. Results, which include the variation of the minimum film thickness and phase-lag with time as functions of excitation frequency, are compared with the analytic solution of the transient step bearing problem with the same dynamic loading function. I.S.

A91-33600* National Aeronautics and Space Administration. Lewis Research Center, Cleveland, OH.

A NEW TEST MACHINE FOR MEASURING FRICTION AND WEAR IN CONTROLLED ATMOSPHERES TO 1200 C

HAROLD E. SLINNEY and CHRISTOPHER DELLACORTE (NASA, Lewis Research Center, Cleveland, OH) Lubrication Engineering (ISSN 0024-7154), vol. 47, April 1991, p. 314-319. refs

Copyright

This paper describes a new high-temperature friction and wear test apparatus (tribometer). The tribometer can be used as a pin-on-disk or pin-on-ring configuration and is specially designed to measure the tribological properties of ceramics and high temperature metallic alloys from room temperature to 1200 C. Sliding mode can be selected to be either unidirectional at velocities up to 22 m/sec or oscillating at frequencies up to 4.6 Hz and amplitudes up to + or - 60 deg. The test atmosphere is established by a controlled flow rate of a purge gas. All components within the test chamber are compatible with oxidizing, inert or reducing gases. Author

A91-34806*# State Univ. of New York, Binghamton.

A HIGH SPEED PHOTOGRAPHY STUDY OF CAVITATION IN A DYNAMICALLY LOADED JOURNAL BEARING

D. C. SUN (New York, State University, Binghamton) and D. E. BREWE (NASA, Lewis Research Center; U.S. Army, Propulsion Directorate, Cleveland, OH) ASME, Transactions, Journal of Tribology (ISSN 0742-4787), vol. 113, April 1991, p. 287-292;

Discussion, p. 292 - 294. Previously announced in STAR as N90-26338. refs

(ASME PAPER 90-TRIB-19) Copyright

The earlier study made by Jacobson and Hamrock on the cavitation of liquid lubricant films in a dynamically loaded journal bearing was repeated with a quartz sleeve, which was more rigid than the Polymethylmethacrylate (PMMA) sleeve used previously. Various improvements of the test rig were made concomitantly so that the experimental errors could be better controlled and assessed. The updated speed photography experiment and its results are described. Author

A91-38151* National Aeronautics and Space Administration. Lewis Research Center, Cleveland, OH.

RECENT STIRLING ENGINE LOSS-UNDERSTANDING RESULTS

ROY C. TEW, LANNY G. THIEME, and JAMES E. DUDENHOEFER (NASA, Lewis Research Center, Cleveland, OH) IN: IECEC-90; Proceedings of the 25th Intersociety Energy Conversion Engineering Conference, Reno, NV, Aug. 12-17, 1990. Vol. 5. New York, American Institute of Chemical Engineers, 1990, p. 377-385. Previously announced in STAR as N90-21114. refs Copyright

For several years, NASA and other U.S. government agencies have been funding experimental and analytical efforts to improve the understanding of Stirling thermodynamic losses. NASA's objective is to improve Stirling engine design capability to support the development of new engines for space power. An overview of these efforts was last given at the 1988 IECEC. Recent results of this research are reviewed. Author

A91-38154* Pittsburgh Univ., PA.

MULTIDIMENSIONAL COMPUTER SIMULATION OF STIRLING CYCLE ENGINES

C. A. HALL, T. A. PORSCHING, J. MEDLEY (Pittsburgh, University, PA), and R. C. TEW (NASA, Lewis Research Center, Cleveland, OH) IN: IECEC-90; Proceedings of the 25th Intersociety Energy Conversion Engineering Conference, Reno, NV, Aug. 12-17, 1990. Vol. 5. New York, American Institute of Chemical Engineers, 1990, p. 407-411. refs (Contract NAG3-1097) Copyright

The computer code ALGAE (algorithms for the gas equations) treats incompressible, thermally expandable, or locally compressible flows in complicated two-dimensional flow regions. The solution method, finite differencing schemes, and basic modeling of the field equations in ALGAE are applicable to engineering design settings of the type found in Stirling cycle engines. The use of ALGAE to model multiple components of the space power research engine (SPRE) is reported. Videotape computer simulations of the transient behavior of the working gas (helium) in the heater-regenerator-cooler complex of the SPRE demonstrate the usefulness of such a program in providing information on thermal and hydraulic phenomena in multiple component sections of the SPRE. I.E.

A91-41649* National Aeronautics and Space Administration. Lewis Research Center, Cleveland, OH.

EVALUATION OF ADVANCED LUBRICANTS FOR AIRCRAFT APPLICATIONS USING GEAR SURFACE FATIGUE TESTS

DENNIS P. TOWNSEND (NASA, Lewis Research Center, Cleveland, OH) and JOHN SHIMSKI (U.S. Navy, Naval Air Propulsion Center, Trenton, NJ) AIAA, SAE, ASME, and ASEE, Joint Propulsion Conference, 27th, Sacramento, CA, June 24-26, 1991. 12 p. Previously announced in STAR as N91-22568. refs (AIAA PAPER 91-1907) Copyright

Surface pitting fatigue life tests were conducted with five lubricants, using spur gears made from a single lot of consumable-electrode vacuum melted (CVM) AISI 9310 steel. The gears were case carbonized and hardened to a Rockwell c-60 and finish ground. The gear pitch diameter was 8.89 cm. The lot of gears was divided into five groups, each of which was tested with a different lubricant. The test lubricants can be classified as

synthetic polyol-esters with various viscosities and additive packages. Test conditions included bulk gear temperature of 350 K, a maximum Hertz stress of 1.71 GPa (248 ksi) at the pitch line, and a speed of 10,000 RPM. The lubricant with a viscosity that provided a specific film thickness greater than one and with an additive package produced far greater gear surface fatigue lives than lubricants with a viscosity that provided specific film thickness less than one. A low viscosity lubricant with an additive package produced gear surface fatigue lives equivalent to a similar base stock lubricant with 30 percent higher viscosity, but without an additive package. Lubricants with the same viscosity and similar additive packages gave equivalent gear surface fatigue lives. Author

A91-41680* Akron Univ., OH.

ANALYTICAL AND EXPERIMENTAL STUDY OF VIBRATIONS IN A GEAR TRANSMISSION

F. K. CHOY, Y. F. RUAN (Akron, University, OH), J. J. ZAKRAJSEK, F. B. OSWALD, and J. J. COY (NASA, Lewis Research Center, Cleveland, OH) AIAA, SAE, ASME, and ASEE, Joint Propulsion Conference, 27th, Sacramento, CA, June 24-26, 1991. 21 p. Previously announced in STAR as N91-25395. refs (Contract NAS3-25967) (AIAA PAPER 91-2019) Copyright

An analytical simulation of the dynamics of a gear transmission system is presented and compared to experimental results from a gear noise test rig at NASA Lewis. The analytical procedure developed couples the dynamic behaviors of the rotor-bearing-gear system with the response of the gearbox structure. Transient and steady-state vibrations of the gearbox system are presented in the time and frequency domains. The vibration characteristics of a simple single-mesh-gear noise test rig are modeled. The numerical simulations are compared to experimental data measured under typical operating conditions. The system natural frequencies, peak vibration amplitudes, and gear mesh frequencies are generally in good agreement. Author

A91-41681* Akron Univ., OH.

EFFECTS OF RIM THICKNESS ON SPUR GEAR BENDING STRESS

G. D. BIBEL, S. K. REDDY, M. SAVAGE (Akron, University, OH), and R. F. HANDSCHUH (NASA, Lewis Research Center; U.S. Army, Propulsion Directorate, Cleveland, OH) AIAA, SAE, ASME, and ASEE, Joint Propulsion Conference, 27th, Sacramento, CA, June 24-26, 1991. 13 p. Previously announced in STAR as N91-23500. refs (AIAA PAPER 91-2020)

Thin rim gears find application in high-power, light-weight aircraft transmissions. Bending stresses in thin rim spur gear tooth fillets and root areas differ from the stresses in solid gears due to rim deformations. Rim thickness is a significant design parameter for these gears. To study this parameter, a finite element analysis was conducted on a segment of a thin rim gear. The rim thickness was varied and the location and magnitude of the maximum bending stresses reported. Design limits are discussed and compared with the results of other researchers. Author

A91-41682* Akron Univ., OH.

MAXIMUM LIFE SPUR GEAR DESIGN

M. SAVAGE, B. J. MACKULIN (Akron, University, OH), H. H. COE, and J. J. COY (NASA, Lewis Research Center, Cleveland, OH) AIAA, SAE, ASME, and ASEE, Joint Propulsion Conference, 27th, Sacramento, CA, June 24-26, 1991. 13 p. Previously announced in STAR as N91-23514. refs (Contract NAG3-1047) (AIAA PAPER 91-2021) Copyright

Optimization procedures allow one to design a spur gear reduction for maximum life and other end use criteria. A modified feasible directions search algorithm permits a wide variety of inequality constraints and exact design requirements to be met with low sensitivity to initial guess values. The optimization algorithm is described, and the models for gear life and performance are

37 MECHANICAL ENGINEERING

presented. The algorithm is compact and has been programmed for execution on a desk top computer. Two examples are presented to illustrate the method and its application. Author

A91-41683*# Cincinnati Univ., OH.

CONTACT STRESSES IN GEAR TEETH - A NEW METHOD OF ANALYSIS

PAISAN SOMPRAKIT, RONALD L. HUSTON (Cincinnati, University, OH), and FRED B. OSWALD (NASA, Lewis Research Center, Cleveland, OH) AIAA, SAE, ASME, and ASEE, Joint Propulsion Conference, 27th, Sacramento, CA, June 24-26, 1991. 15 p. Previously announced in STAR as N91-22570. refs (Contract NSG-3188)

(AIAA PAPER 91-2022) Copyright

A new, innovative procedure called point load superposition for determining the contact stresses in mating gear teeth is presented. It is believed that this procedure will greatly extend both the range of applicability and the accuracy of gear contact stress analysis. Point load superposition is based upon fundamental solutions from the theory of elasticity. It is an iterative numerical procedure which has distinct advantages over the classical Hertz method, the finite element method, and over existing applications with the boundary element method. Specifically, friction and sliding effects, which are either excluded from or difficult to study with the classical methods, are routinely handled with the new procedure. Presented here are the basic theory and the algorithms. Several examples are given. Results are consistent with those of the classical theories. Applications to spur gears are discussed. Author

A91-41700*# Akron Univ., OH.

EFFECTS OF BRUSH SEAL MORPHOLOGY ON LEAKAGE AND PRESSURE DROPS

M. J. BRAUN, Y. YANG (Akron, University, OH), and R. C. HENDRICKS (NASA, Lewis Research Center, Cleveland, OH) AIAA, SAE, ASME, and ASEE, Joint Propulsion Conference, 27th, Sacramento, CA, June 24-26, 1991. 7 p. refs (Contract NAG3-969)

(AIAA PAPER 91-2106) Copyright

Research on brush seals which was undertaken earlier by Braun et al. (1990) is continued. Particular attention is given to the effects of brush positioning, design, and morphology on sealing surfaces, fluid leakage, and associated pressure drops. It is found that both the structure and the design of the brush are important to its performance. High resistance to the flow of the brush/fence combination can result in catastrophic failure of the brush, while at lower flow resistances, the failure is more gradual. K.K.

A91-41701*# Allied-Signal Aerospace Co., Torrance, CA.

LIQUID HYDROGEN TURBOPUMP FOIL BEARING

M. SAVILLE, A. GU (Allied-Signal Aerospace Co., Aircsearch Los Angeles Div., Torrance, CA), and R. CAPALDI (NASA, Lewis Research Center, Cleveland, OH) AIAA, SAE, ASME, and ASEE, Joint Propulsion Conference, 27th, Sacramento, CA, June 24-26, 1991. 8 p. refs

(AIAA PAPER 91-2108) Copyright

Space transfer vehicles and other power and propulsion systems require long-life turbopumps. Rolling element bearings used in current turbopumps do not have sufficient life for these applications. Process fluid foil bearings have established long life, with exceptional reliability, over a wide range of temperatures and fluids in many high-speed turbomachinery applications. However, liquid hydrogen turbopumps require high-load capacity bearings. An experimental study was conducted to measure foil journal bearing load capacity in liquid hydrogen, using a bearing designed specifically for cryogenic hydrogen turbopump applications. Additional performance parameters such as power loss, stability, cooling flow requirements, and bearing life were measured. These tests showed a load capacity safety factor of approximately 10 for liquid hydrogen turbopump applications. These tests also demonstrated good rotor stability, low power loss and cooling flow, and long life. Author

A91-41800*# Drexel Univ., Philadelphia, PA.

DEVELOPMENT OF BRAIDED ROPE SEALS FOR HYPERSONIC ENGINE APPLICATIONS. II - FLOW MODELING RAJAKKANNU MUTHARASAN, XIAOMING TAO, FRANK KO (Drexel University, Philadelphia, PA), and BRUCE M. STEINETZ (NASA, Lewis Research Center, Cleveland, OH) AIAA, SAE, ASME, and ASEE, Joint Propulsion Conference, 27th, Sacramento, CA, June 24-26, 1991. 12 p. NASA-sponsored research. Previously announced in STAR as N91-22571. refs (AIAA PAPER 91-2495) Copyright

Two models based on the Kozeny-Carmen equation were developed to analyze the fluid flow through a new class of braided rope seals under development for advanced hypersonic engines. A hybrid seal geometry consisting of a braided sleeve and a substantial amount of longitudinal fibers with high packing density was selected for development based on its low leakage rates. The models developed allow prediction of the gas leakage rate as a function of fiber diameter, fiber packing density, gas properties, and pressure drop across the seal. Author

A91-45350*# National Aeronautics and Space Administration. Lewis Research Center, Cleveland, OH.

SURFACE FATIGUE LIFE OF M50N1L AND AISI 9310 GEARS AND ROLLING-CONTACT BARS

DENNIS P. TOWNSEND (NASA, Lewis Research Center, Cleveland, OH) and ERIC N. BAMBERGER (General Electric Co., Cincinnati, OH) Journal of Propulsion and Power (ISSN 0748-4658), vol. 7, July-Aug. 1991, p. 642-649. Previously cited in issue 20, p. 3161, Accession no. A89-47105. refs

Copyright

A91-45820*# National Aeronautics and Space Administration. Lewis Research Center, Cleveland, OH.

SOME PRELIMINARY RESULTS OF BRUSH SEAL/ROTOR INTERFERENCE EFFECTS ON LEAKAGE AT ZERO AND LOW RPM USING A TAPERED-PLUG ROTOR

R. C. HENDRICKS, M. P. PROCTOR, J. A. SCHLUMBERGER (NASA, Lewis Research Center, Cleveland, OH), M. J. BRAUN (Akron, University, OH), and R. L. MULLEN (Case Western Reserve University, Cleveland, OH) AIAA, SAE, ASME, and ASEE, Joint Propulsion Conference, 27th, Sacramento, CA, June 24-26, 1991. 15 p. refs

(AIAA PAPER 91-3390) Copyright

Some preliminary brush seal leakage results for ambient-temperature air are presented. Data for four nominal brush-rotor radial clearances of -0.09, -0.048, -0.008, and 0.035 mm were taken by using a tapered plug rotor at 0 and 400 rpm with rotor runout of 0.127 mm peak to peak. The brush seal nominal bore diameter was 38 mm with 0.05-mm bristles at 200 bristles/mm of circumference and a 0.61-mm fence height. Leakages were greater than predicted, but agreement was reasonable. Leakage rates were not significantly altered by hysteresis or inlet flow variations. Visualization studies showed that the bristles followed the 400-rpm excitation, and loading studies indicated that bristles slid relative to one another. Author

A91-47213*# Akron Univ., OH.

EFFECTS OF GEAR BOX VIBRATION AND MASS IMBALANCE ON THE DYNAMICS OF MULTISTAGE GEAR TRANSMISSION

F. K. CHOY, Y. K. TU (Akron, University, OH), J. J. ZAKRAJSEK, and D. P. TOWNSEND (NASA, Lewis Research Center, Cleveland, OH) ASME, Transactions, Journal of Vibration and Acoustics (ISSN 0739-3717), vol. 113, July 1991, p. 333-344. Previously announced in STAR as N91-21534. refs

Copyright

The dynamic behavior of multistage gear transmission system, with the effects of gear-box-induced vibrations and rotor mass-imbalances is analyzed. The model method, using undamped frequencies and planar mode shapes, is used to reduce the degree-of-freedom of the system. The various rotor-bearing stages as well as lateral and torsional vibrations of each individual stage are coupled through localized gear-mesh-tooth interactions. Gear-box vibrations are coupled to the gear stage dynamics through

bearing support forces. Transient and steady state dynamics of lateral and torsional vibrations of the geared system are examined in both time and frequency domain. A typical three-staged geared system is used as an example. Effects of mass-imbalance and gear box vibrations on the system dynamic behavior are presented in terms of modal excitation functions for both lateral and torsional vibrations. Operational characteristics and conclusions are drawn from the results presented. Author

A91-52811* National Aeronautics and Space Administration. Lewis Research Center, Cleveland, OH.

GEAR NOISE, VIBRATION, AND DIAGNOSTIC STUDIES AT NASA LEWIS RESEARCH CENTER

J. J. ZAKRAJSEK, F. B. OSWALD, D. P. TOWNSEND, and J. J. COY (NASA, Lewis Research Center, Cleveland, OH) IN: Gearbox noise and vibration; Proceedings of the 1st IME International Conference, Cambridge, England, Apr. 9-11, 1990. Bury Saint Edmunds, England, Mechanical Engineering Publications, Ltd., 1990, p. 27-34. Previously announced in STAR as N90-18041. refs

Copyright

The NASA Lewis Research Center and the U.S. Army Aviation Systems Command are involved in a joint research program to advance the technology of rotorcraft transmissions. This program consists of analytical as well as experimental efforts to achieve the overall goals of reducing weight, noise, and vibration, while increasing life and reliability. Recent analytical activities are highlighted in the areas of gear noise, vibration, and diagnostics performed in-house and through NASA and U.S. Army sponsored grants and contracts. These activities include studies of gear tooth profiles to reduce transmission error and vibration as well as gear housing and rotordynamic modeling to reduce structural vibration and transmission and noise radiation, and basic research into current gear failure diagnostic methodologies. Results of these activities are presented along with an overview of near-term research plans in the gear noise, vibration, and diagnostics area. Author

A91-57025*# National Aeronautics and Space Administration. Lewis Research Center, Cleveland, OH.

SPACE MECHANISMS NEEDS FOR FUTURE NASA LONG DURATION SPACE MISSIONS

ROBERT L. FUSARO (NASA, Lewis Research Center, Cleveland, OH) AIAA, NASA, and OAI, Conference on Advanced SEI Technologies, Cleveland, OH, Sept. 4-6, 1991. 10 p. Previously announced in STAR as N91-30532. (AIAA PAPER 91-3428) Copyright

Future NASA long duration missions will require high performance, reliable, long lived mechanical moving systems. In order to develop these systems, high technology components such as bearings, gears, seals, lubricants, etc., will need to be utilized. There has been concern in the NASA community that the current technology level in these mechanical component/tribology areas may not be adequate to meet the goals of long duration NASA mission such as Space Exploration Initiative (SEI). To resolve this concern, NASA-Lewis sent a questionnaire to government and industry workers (who have been involved in space mechanism research, design, and implementation) to ask their opinion if the current space mechanisms technology (mechanical components/tribology) is adequate to meet future NASA Mission needs and goals. In addition, a working group consisting of members from each NASA Center, DoD, and DOE was established to study the technology status. The results of the survey and conclusions of the working group are summarized. Author

N91-12954*# National Aeronautics and Space Administration. Lewis Research Center, Cleveland, OH.

FINITE ELEMENT ANALYSIS OF THERMAL DISTORTION EFFECTS ON OPTICAL PERFORMANCE OF SOLAR DYNAMIC CONCENTRATOR FOR SPACE STATION FREEDOM

MICHAEL P. DOHERTY and VITHAL DALSANIA Jul. 1990 18 p Original contains color illustrations

(Contract RTOP 474-12-10)

(NASA-TM-102504; E-5305; NAS 1.15:102504) Avail: NTIS HC/MF A03; 3 functional color pages CSCL 20/11

An analysis was performed to predict the thermal distortion of the solar dynamic concentrator for Space Station Freedom in low earth orbit and to evaluate the effects of that thermal distortion on concentrator on-orbit performance. The analysis required substructural finite element modeling of critical concentrator structural subsystems, structural finite element modeling of the concentrator, mapping of thermal loading onto the structural finite element model, and the creation of specialized postprocessors to assist in interpreting results. Concentrator temperature distributions and thermally induced displacements and slope errors and the resulting receiver flux distribution profiles are discussed. Results determined for a typical orbit indicate that concentrator facet rotations are less than 0.2 mrad and that the change in facet radius due to thermal flattening is less than 5 percent. The predicted power loss due to thermal distortion effects is less than 0.3 percent. As a consequence the thermal distortions of the solar dynamic concentrator in low earth orbit will have a negligible effect on the flux distribution profiles within the receiver. Author

N91-12956*# National Aeronautics and Space Administration. Lewis Research Center, Cleveland, OH.

EXPERIMENTAL AND ANALYTICAL EVALUATION OF EFFICIENCY OF HELICOPTER PLANETARY STAGE

TIMOTHY L. KRANTZ Nov. 1990 20 p Prepared in cooperation with Army Aviation Systems Command, Cleveland, OH (Contract DA PROJ. 1L1-6221147-A; RTOP 505-63-51) (NASA-TP-3063; E-5268; NAS 1.60:3063; AVSCOM-TR-90-C-001) Avail: NTIS HC/MF A03 CSCL 13/9

The efficiency of a helicopter transmission planetary stage was studied both experimentally and analytically. Experiments were done by using a back-to-back, test-and-slave arrangement. The experiments were a parametric study of the effects of operating conditions on efficiency. In order to enhance the analysis, a model was developed that calculates the power required for the meshing gears to displace oil trapped between the gear teeth. In general, the analysis predicted higher efficiencies than were measured. The results of this study were compared with those of other studies. Author

N91-13732*# National Aeronautics and Space Administration. Lewis Research Center, Cleveland, OH.

PROBE INSERTION APPARATUS WITH INFLATABLE SEAL Patent Application

PAUL A. TRIMARCHI, inventor (to NASA) 23 Aug. 1990 17 p (NASA-CASE-LEW-14965-1; NAS 1.71:LEW-14965-1; US-PATENT-APPL-SN-571062) Avail: NTIS HC/MF A03 CSCL 13/9

A sealing apparatus is disclosed for inserting a probe into a pressure vessel having an elongated opening includes a pair of resiliently deformable seals oppositely disposed in sealing engagement with each other. A retainer is connected to the pressure vessel around the elongated opening and holds the pair of seals rigidly to the pressure vessel. A wedge is engageable with the pair of seals and carries the probe, for longitudinally translating the probe in pressure vessel. NASA

N91-14617* National Aeronautics and Space Administration. Lewis Research Center, Cleveland, OH.

POST CLAMP Patent

JOHN K. RAMSEY, inventor (to NASA) and ERWIN H. MEYN, inventor (to NASA) 7 Aug. 1990 9 p Filed 29 Sep. 1989 (NASA-CASE-LEW-14862-1; US-PATENT-4,946,122; US-PATENT-APPL-SN-414816; US-PATENT-CLASS-248-229; US-PATENT-CLASS-248-230; US-PATENT-CLASS-403-385; US-PATENT-CLASS-403-391; INT-PATENT-CLASS-F16M-13/00) Avail: US and Trademark Office CSCL 13/9

A pair of spaced collars are mounted at right angles on a clamp body by retaining rings which enable the collars to rotate with respect to the clamp body. Mounting posts extend through aligned holes in the collars and clamp body. Each collar can be

37 MECHANICAL ENGINEERING

clamped onto the inserted post while the clamp body remains free to rotate about the post and collar. The clamp body is selectively clamped onto each post.

Official Gazette of the U.S. Patent and Trademark Office

N91-19441*# National Aeronautics and Space Administration. Lewis Research Center, Cleveland, OH.

HIGH TEMPERATURE NASP ENGINE SEAL DEVELOPMENT
BRUCE M. STEINETZ, MATTHEW E. MELIS, DIRK ORLETSKI, and MARK G. TEST (Pratt and Whitney Aircraft, West Palm Beach, FL.) Feb. 1991 21 p Presented at the 9th National Aerospace Plane Technology Symposium, Orlando, FL, 1-2 Nov. 1990 (Contract RTOP 505-63-1B)
(NASA-TM-103716; E-5949; NAS 1.15:103716) Avail: NTIS HC/MF A03 CSCL 13/9

Key to the development of advanced hypersonic engines such as those being considered for the National Aerospace Plane (NASP) is the development and evaluation of high temperature, flexible seals that must seal the many feet of gaps between the articulating and stationary engine panels. Recent seal progress made at NASA-Lewis is reviewed in the areas of seal concept maturation, test rig development, and performance tests. A test fixture was built at NASA capable of subjecting candidate 3 ft long seals to engine simulated temperatures (up to 1500 F), pressures (up to 100 psi), and engine wall distortions (up to 0.15 in only 18 in span). Leakage performance test results at high temperatures are presented for an innovative high temperature, flexible ceramic wafer seal. Also described is a joint Pratt and Whitney/NASA planned test program to evaluate thermal performance of a braided rope seal under engine simulated heat flux rates (up to 400 Btu/sq ft s), and supersonic flow conditions. These conditions are produced by subjecting the seal specimen to hydrogen oxygen rocket exhaust that flows tangent to the specimen.

Author

N91-19442*# National Aeronautics and Space Administration. Lewis Research Center, Cleveland, OH.

A TEST FIXTURE FOR MEASURING HIGH-TEMPERATURE HYPERSONIC-ENGINE SEAL PERFORMANCE

BRUCE M. STEINETZ Dec. 1990 20 p
(Contract RTOP 505-63-1B)
(NASA-TM-103658; E-5780; NAS 1.15:103658) Avail: NTIS HC/MF A03 CSCL 11/1

A test fixture for measuring the performance of several high temperature engine seal concepts was installed at the NASA Lewis Research Center. The test fixture was developed to evaluate seal concepts under development for advanced hypersonic engines such as those being considered for the National Aerospace Plane. The fixture can measure static seal leakage performance from room temperature up to 1500 F and air pressure differentials up to 100 psi. Performance of the seals can be measured while sealing against flat or engine simulated distorted walls, where distortions can be as large as 0.150 in. in only an 18 in. span. The fixture is designed to evaluate seals 3 feet long, a typical engine panel length. The seal channel can be configured to test square, circular, or rectangular seals that are nominally 0.5 in. high. The sensitivity of leakage performance to lateral or axial loading can also be measured using specially designed high temperature lateral and axial bellows preload systems. Leakage data for a candidate ceramic wafer engine seal is provided by way of example to demonstrate the test fixture's capabilities.

Author

N91-19443*# National Aeronautics and Space Administration. Lewis Research Center, Cleveland, OH.

HEAT TRANSFER IN ROTATING SERPENTINE PASSAGES WITH TRIPS NORMAL TO THE FLOW

J. H. WAGNER, B. V. JOHNSON, R. A. GRAZIANI (Pratt and Whitney Aircraft, East Hartford, CT.), and F. C. YEH 1991 15 p Proposed for presentation at the 36th International Gas Turbine and Aeroengine Congress and Exhibition, Orlando, FL, 3-6 Jun. 1991; sponsored by ASME

(Contract NAS3-23691; RTOP 505-62-52)

(NASA-TM-103758; E-6015; NAS 1.15:103758) Avail: NTIS HC/MF A03 CSCL 13/2

Experiments were conducted to determine the effects of buoyancy and Coriolis forces on heat transfer in turbine blade internal coolant passages. The experiments were conducted with a large scale, multipass, heat transfer model with both radially inward and outward flow. Trip strips on the leading and trailing surfaces of the radial coolant passages were used to produce the rough walls. An analysis of the governing flow equations showed that four parameters influence the heat transfer in rotating passages: coolant-to-wall temperature ratio, Rossby number, Reynolds number, and radius-to-passage hydraulic diameter ratio. The first three of these four parameters were varied over ranges which are typical of advanced gas turbine engine operating conditions. Results were correlated and compared to previous results from stationary and rotating similar models with trip strips. The heat transfer coefficients on surfaces, where the heat increased with rotation and buoyancy, varied by as much as a factor of four. Maximum values of the heat transfer coefficients with high rotation were only slightly above the highest levels obtained with the smooth wall model. The heat transfer coefficients on surfaces, where the heat transfer decreased with rotation, varied by as much as a factor of three due to rotation and buoyancy. It was concluded that both Coriolis and buoyancy effects must be considered in turbine blade cooling designs with trip strips and that the effects of rotation were markedly different depending upon the flow direction.

Author

N91-20489*# National Aeronautics and Space Administration. Lewis Research Center, Cleveland, OH.

A MODEL FOR THE SPACE SHUTTLE MAIN ENGINE HIGH PRESSURE OXIDIZER TURBOPUMP SHAFT SEAL SYSTEM

DANIEL E. PAXSON 1990 31 p Presented at the 2nd Annual Conference on Health Monitoring for Space Propulsion Systems, Cincinnati, OH, 14-15 Nov. 1990; sponsored by Cincinnati Univ.

(Contract RTOP 590-21-41)

(NASA-TM-103697; E-5919; NAS 1.15:103697) Avail: NTIS HC/MF A03 CSCL 13/9

A simple static model is presented which solves for the flow properties of pressure, temperature, and mass flow in the Space Shuttle Main Engine pressure Oxidizer Turbopump Shaft Seal Systems. This system includes the primary and secondary turbine seals, the primary and secondary turbine drains, the helium purge seals and feed line, the primary oxygen drain, and the slinger/labyrinth oxygen seal pair. The model predicts the changes in flow variables that occur during and after failures of the various seals. Such information would be particularly useful in a post flight situation where processing of sensor information using this model could identify a particular seal that had experienced excessive wear. Most of the seals in the system are modeled using simple one dimensional equations which can be applied to almost any seal provided that the fluid is gaseous. A failure is modeled as an increase in the clearance between the shaft and the seal. Thus, the model does not attempt to predict how the failure process actually occurs (e.g., wear, seal crack initiation). The results presented were obtained using a FORTRAN implementation of the model running on a VAX computer. Solution for the seal system properties is obtained iteratively; however, a further simplified implementation (which does not include the slinger/labyrinth combination) was also developed which provides fast and reasonable results for most engine operating conditions. Results from the model compare favorably with the limited redline data available.

Author

N91-21531*# National Aeronautics and Space Administration. Lewis Research Center, Cleveland, OH.

ADVANCED ROTORCRAFT TRANSMISSION PROGRAM

ROBERT C. BILL 1990 18 p Presented at the 46th Annual American Helicopter Society Forum, Washington, DC, 21 May 1990 Previously announced in IAA as A91-17214 Prepared in cooperation with Army Aviation Systems Command, Cleveland,

OH

(Contract DA PROJ. 1L1-62211-A-47-A; RTOP 505-62-0K)
(NASA-TM-103276; E-5722; NAS 1.15:103276;
AVSCOM-TR-90-C-015; AD-A235915) Avail: NTIS HC/MF A03
CSCL 13/9

The Advanced Rotorcraft Transmission (ART) program is an Army-funded, joint Army/NASA program to develop and demonstrate lightweight, quiet, durable drivetrain systems for next generation rotorcraft. ART addresses the drivetrain requirements of two distinct next generation aircraft classes: Future Air Attack Vehicle, a 10,000 to 20,000 lb. aircraft capable of undertaking tactical support and air-to-air missions; and Advanced Cargo Aircraft, a 60,000 to 80,000 lb. aircraft capable of heavy life field support operations. Both tiltrotor and more conventional helicopter configurations are included in the ART program. Specific objectives of ART include reduction of drivetrain weight by 25 percent compared to baseline state-of-the-art drive systems configured and sized for the next generation aircraft, reduction of noise level at the transmission source by 10 dB relative to a suitably sized and configured baseline, and attainment of at least a 5000 hr mean-time-between-removal. The technical approach for achieving the ART goals includes application of the latest available component, material, and lubrication technology to advanced concept drivetrains that utilize new ideas in gear configuration, transmission layout, and airframe/drivetrain integration. To date, candidate drivetrain systems were carried to a conceptual design stage, and tradeoff studies were conducted resulting in selection of an ART transmission configuration for each of the four contractors. The final selection was based on comparative weight, noise, and reliability studies. A description of each of the selected ART designs is included. Preliminary design of each of the four selected ART transmission was completed, as have mission impact studies wherein comparisons of aircraft mission performance and life cycle costs are undertaken for the next generation aircraft with ART and with the baseline transmission. Author

N91-21534* National Aeronautics and Space Administration. Lewis Research Center, Cleveland, OH.

EFFECTS OF GEAR BOX VIBRATION AND MASS IMBALANCE ON THE DYNAMICS OF MULTI-STAGE GEAR TRANSMISSIONS

FRED K. CHOY, YU K. TU (Akron Univ., OH.), JAMES J. ZAKRAJSEK, and DENNIS P. TOWNSEND Mar. 1991 33 p
Prepared in cooperation with Army Aviation Systems Command, Cleveland, OH

(Contract DA PROJ. 1L1-62211-A-47-A; RTOP 505-63-51)

(NASA-TM-103695; E-5916; NAS 1.15:103695;

AVSCOM-TR-90-C-022) Avail: NTIS HC/MF A03 CSCL 13/9

The dynamic behavior of multistage gear transmission system, with the effects of gear-box-induced vibrations and rotor mass-imbalances is analyzed. The model method, using undamped frequencies and planar mode shapes, is used to reduce the degree-of-freedom of the system. The various rotor-bearing stages as well as lateral and torsional vibrations of each individual stage are coupled through localized gear-mesh-tooth interactions. Gear-box vibrations are coupled to the gear stage dynamics through bearing support forces. Transient and steady state dynamics of lateral and torsional vibrations of the geared system are examined in both time and frequency domain. A typical three-staged geared system is used as an example. Effects of mass-imbalance and gear box vibrations on the system dynamic behavior are presented in terms of modal excitation functions for both lateral and torsional vibrations. Operational characteristics and conclusions are drawn from the results presented. Author

N91-21540* National Aeronautics and Space Administration. Lewis Research Center, Cleveland, OH.

FULLY ARTICULATED FOUR-POINT-BEND LOADING FIXTURE Patent

ANTHONY M. CALOMINO, inventor (to NASA) 22 Jan. 1991 7 p Filed 28 Dec. 1989 Supersedes N90-15445 (28 - 7, p 940)
(NASA-CASE-LEW-14776-1; US-PATENT-4,986,132;

US-PATENT-APPL-SN-458274; US-PATENT-CLASS-73-852;
INT-PATENT-CLASS-G01N-3/20) Avail: US Patent and
Trademark Office CSCL 13/9

A fully articulated four-point bend loading fixture for Modulus of Rupture (MOR) and fracture toughness specimens utilizes an upper loading plate in combination with a lower loading plate. The lower plate has a pair of spring loaded ball bearings which seat in V-shaped grooves located in the upper plate. The ball bearings are carried in the arms of the lower plate. A load is applied to the specimen through steel rollers, one large roller and one smaller roller each located on both the upper and lower plates. The large rollers have needle roller bearings which enable a single loading roller to rotate relative to the plate to which it is attached.

Official Gazette of the U.S. Patent and Trademark Office

N91-22566* National Aeronautics and Space Administration. Lewis Research Center, Cleveland, OH.

COMPARISON OF ANALYSIS AND EXPERIMENT FOR DYNAMICS OF LOW-CONTACT-RATIO SPUR GEARS

FRED B. OSWALD, BRIAN REBBECCHI, JAMES J. ZAKRAJSEK, DENNIS P. TOWNSEND, and HSIANG HSI LIN (Memphis State Univ., TN.) 1991 9 p Proposed for presentation at the 13th Biennial Conference on Mechanical Vibration and Noise, Miami, FL, 22-25 Sep. 1991; sponsored by ASME

(Contract DA PROJ. 1L1-61102-AH-45; RTOP 505-63-51)

(NASA-TM-103232; E-5648; NAS 1.15:103232;

AVSCOM-TR-90-C-017; AD-A239499) Avail: NTIS HC/MF A02

CSCL 13/9

Low-contact-ratio spur gears were tested in NASA gear-noise-rig to study gear dynamics including dynamic load, tooth bending stress, vibration, and noise. The experimental results were compared with a NASA gear dynamics code to validate the code as a design tool for predicting transmission vibration and noise. Analytical predictions and experimental data for gear-tooth dynamic loads and tooth-root bending stress were compared at 28 operating conditions. Strain gage data were used to compute the normal load between meshing teeth and the bending stress at the tooth root for direct comparison with the analysis. The computed and measured waveforms for dynamic load and stress were compared for several test conditions. These are very similar in shape, which means the analysis successfully simulates the physical behavior of the test gears. The predicted peak value of the dynamic load agrees with the measurement results within an average error of 4.9 percent except at low-torque, high-speed conditions. Predictions of peak dynamic root stress are generally within 10 to 15 percent of the measured values. Author

N91-22567* National Aeronautics and Space Administration. Lewis Research Center, Cleveland, OH.

HIGH TEMPERATURE PERFORMANCE EVALUATION OF A HYPERSONIC ENGINE CERAMIC WAFER SEAL

BRUCE M. STEINETZ Apr. 1991 23 p

(Contract RTOP 505-63-5B)

(NASA-TM-103737; E-5942; NAS 1.15:103737) Avail: NTIS
HC/MF A03 CSCL 13/1

Leakage rates of an innovative hypersonic engine seal were measured using a specially developed static high temperature seal test fixture at NASA Lewis Research Center. The three foot long structural panel-edge seal is designed to minimize leakage of high temperature, high pressure gases past the movable panels of advanced ramjet/scramjet engines. The seal is made of a stack of precision machined ceramic wafer pieces that are inserted into a closely conforming seal channel in the movable engine panel. The wafer seal accommodates the significant distortions in the adjacent engine walls through relative sliding between adjacent wafers. Seal leakage rates are presented for engine simulated air temperatures up to 1350 F and for engine pressures up to 100 psi. Leakage rates are also presented for the seal, sealing both a flat wall condition, and an engine simulated distorted wall condition in which the distortion was 0.15 in. in only an 18 in. span. Seal leakage rates were low, meeting an industry-established tentative leakage limit for all combinations of temperature, pressure, and wall conditions considered. Comparisons are made between the

37 MECHANICAL ENGINEERING

measured leakage rates and leakage rates predicted using a seal leakage model developed from externally-pressurized gas film bearing theory.

Author

N91-22568* National Aeronautics and Space Administration. Lewis Research Center, Cleveland, OH.

EVALUATION OF ADVANCED LUBRICANTS FOR AIRCRAFT APPLICATIONS USING GEAR SURFACE FATIGUE TESTS

DENNIS P. TOWNSEND and JOHN SHIMSKI (Naval Air Propulsion Test Center, Trenton, NJ.) 1991 13 p Proposed for presentation at the 27th Joint Propulsion Conference, Sacramento, CA, 24-26 Jun. 1991; cosponsored by AIAA, SAE, ASEE, and ASME (Contract DA PROJ. 1L1-66211-A-47-A; RTOP 505-63-36) (NASA-TM-104336; E-6044; NAS 1.15:104336; AVSCOM-TR-91-C-007; AD-A239501; AIAA PAPER 91-1907) Avail: NTIS HC/MF A03 CSCL 11/8

Surface pitting fatigue life tests were conducted with five lubricants, using spur gears made from a single lot of consumable-electrode vacuum melted (CVM) AISI 9310 steel. The gears were case carbonized and hardened to a Rockwell c-60 and finish ground. The gear pitch diameter was 8.89 cm. The lot of gears was divided into five groups, each of which was tested with a different lubricant. The test lubricants can be classified as synthetic polyol-esters with various viscosities and additive packages. Test conditions included bulk gear temperature of 350 K, a maximum Hertz stress of 1.71 GPa (248 ksi) at the pitch line, and a speed of 10,000 RPM. The lubricant with a viscosity that provided a specific film thickness greater than one and with an additive package produced far greater gear surface fatigue lives than lubricants with a viscosity that provided specific film thickness less than one. A low viscosity lubricant with an additive package produced gear surface fatigue lives equivalent to a similar base stock lubricant with 30 percent higher viscosity, but without an additive package. Lubricants with the same viscosity and similar additive packages gave equivalent gear surface fatigue lives.

Author

N91-22570* National Aeronautics and Space Administration. Lewis Research Center, Cleveland, OH.

CONTACT STRESSES IN GEAR TEETH: A NEW METHOD OF ANALYSIS

PAISAN SOMPRAKIT, RONALD L. HUSTON (Cincinnati Univ., OH.), and FRED B. OSWALD 1991 16 p Proposed for presentation at the 27th Joint Propulsion Conference, Sacramento, CA, 24-27 Jun. 1991; cosponsored by AIAA, SAE, ASME, and ASEE (Contract NSG-3188; DA PROJ. 1L1-62211-A-47-A; RTOP 505-63-36) (NASA-TM-104397; E-6214; NAS 1.15:104397; AVSCOM-TR-91-C-001; AD-A239497; AIAA PAPER 91-2022) Avail: NTIS HC/MF A03 CSCL 13/9

A new, innovative procedure called point load superposition for determining the contact stresses in mating gear teeth. It is believed that this procedure will greatly extend both the range of applicability and the accuracy of gear contact stress analysis. Point load superposition is based upon fundamental solutions from the theory of elasticity. It is an iterative numerical procedure which has distinct advantages over the classical Hertz method, the finite element method, and over existing applications with the boundary element method. Specifically, friction and sliding effects, which are either excluded from or difficult to study with the classical methods, are routinely handled with the new procedure. Presented here are the basic theory and the algorithms. Several examples are given. Results are consistent with those of the classical theories. Applications to spur gears are discussed.

Author

N91-22571* National Aeronautics and Space Administration. Lewis Research Center, Cleveland, OH.

DEVELOPMENT OF BRAIDED ROPE SEALS FOR HYPERSONIC ENGINE APPLICATIONS. PART 2: FLOW MODELING

RAJAKKANNU MUTHARASAN, BRUCE M. STEINETZ, XIAOMING TAO, and FRANK KO (Drexel Univ., Philadelphia, PA.) 1991

13 p Presented at the 27th Joint Propulsion Conference, Sacramento, CA, 24-26 Jun. 1991; sponsored by AIAA, SAE and ASME

(Contract RTOP 505-63-5B)

(NASA-TM-104371; E-6166-PT-2; NAS 1.15:104371; AIAA PAPER 91-2495-PT-2) Avail: NTIS HC/MF A03 CSCL 11/1

Two models based on the Kozeny-Carmen equation were developed to analyze the fluid flow through a new class of braided rope seals under development for advanced hypersonic engines. A hybrid seal geometry consisting of a braided sleeve and a substantial amount of longitudinal fibers with high packing density was selected for development based on its low leakage rates. The models developed allow prediction of the gas leakage rate as a function of fiber diameter, fiber packing density, gas properties, and pressure drop across the seal.

Author

N91-23500* National Aeronautics and Space Administration. Lewis Research Center, Cleveland, OH.

EFFECTS OF RIM THICKNESS ON SPUR GEAR BENDING STRESS

G. D. BIBEL, S. K. REDDY, M. SAVAGE, and R. F. HANDSCHUH (Army Aviation Systems Command, Cleveland, OH.) 1991 14 p Presented at the 27th Joint Propulsion Conference, Sacramento, CA, 24-26 Jun. 1991; sponsored by AIAA, SAE, and ASME

(Contract DA PROJ. 1L1-62211-A-47-A; RTOP 505-63-36)

(NASA-TM-104388; E-6197; NAS 1.15:104388; AVSCOM-TR-91-C-015; AD-A239500) Avail: NTIS HC/MF A03 CSCL 13/9

Thin rim gears find application in high-power, light-weight aircraft transmissions. Bending stresses in thin rim spur gear tooth fillets and root areas differ from the stresses in solid gears due to rim deformations. Rim thickness is a significant design parameter for these gears. To study this parameter, a finite element analysis was conducted on a segment of a thin rim gear. The rim thickness was varied and the location and magnitude of the maximum bending stresses reported. Design limits are discussed and compared with the results of other researchers.

Author

N91-23501* National Aeronautics and Space Administration. Lewis Research Center, Cleveland, OH.

GOVERNMENT/INDUSTRY RESPONSE TO QUESTIONNAIRE ON SPACE MECHANISMS/TRIBOLOGY TECHNOLOGY NEEDS

ROBERT L. FUSARO May 1991 76 p

(Contract RTOP 307-51-00)

(NASA-TM-104358; E-6148; NAS 1.15:104358) Avail: NTIS HC/MF A05 CSCL 13/9

President Bush has proposed that the U.S. undertake an ambitious mission of manned and robotic exploration of the solar system. This mission will require advanced mechanical moving components, such as bearings, gears, seals, lubricants, etc. There has been concern in the NASA community that the current technology level in these mechanical component/tribology areas may not be adequate to meet the goals of such a mission. To attempt to answer this, NASA-Lewis has sent out a questionnaire to government and industry workers (who have been involved in space mechanism research, design, and implementation) to ask their opinion if the current space mechanisms technology (mechanical components/tribology) is adequate to meet future NASA Missions needs and goals. If they deemed that the technology base inadequate, they were asked to specify the areas of greatest need. The unedited remarks of those who responded to the survey are presented.

Author

N91-23512* National Aeronautics and Space Administration. Lewis Research Center, Cleveland, OH.

QUANTIFYING OIL FILTRATION EFFECTS ON BEARING LIFE

WILLIAM M. NEEDELMAN (Pall Corp., Glen Cove, NY.) and ERWIN V. ZARETSKY Jun. 1991 14 p

(Contract RTOP 505-63-1B)

(NASA-TM-104350; E-5862; NAS 1.15:104350) Avail: NTIS HC/MF A03 CSCL 13/9

Rolling-element bearing life is influenced by the number, size,

and material properties of particles entering the Hertzian contact of the rolling element and raceway. In general, rolling-element bearing life increases with increasing level of oil filtration. Based upon test results, two equations are presented which allow for the adjustment of bearing L_{10} or catalog life based upon oil filter rating. It is recommended that where no oil filtration is used catalog life be reduced by 50 percent. Author

N91-23513*# National Aeronautics and Space Administration. Lewis Research Center, Cleveland, OH.

MODAL ANALYSIS OF MULTISTAGE GEAR SYSTEMS COUPLED WITH GEARBOX VIBRATIONS

F. K. CHOY, Y. F. RUAN, Y. K. TU (Akron Univ., OH.), J. J. ZAKRAJSEK, and D. P. TOWNSEND 1991 34 p Prepared for presentation at the International Conference on Motion and Power Transmissions, Hiroshima, Japan, 24-26 Nov. 1991; sponsored in part by Japan Society of Mechanical Engineers, ASME, I.Mech.E., VDI, I.E.T., CSME (Contract DA PROJ. 1L1-62211-A-47-A; RTOP 505-63-36) (NASA-TM-103797; E-6085; NAS 1.15:103797; AVSCOM-TR-90-C-033) Avail: NTIS HC/MF A03 CSCL 13/9

An analytical procedure to simulate vibrations in gear transmission systems is presented. This procedure couples the dynamics of the rotor-bearing gear system with the vibration in the gear box structure. The model synthesis method is used in solving the overall dynamics of the system, and a variable time-stepping integration scheme is used in evaluating the global transient vibration of the system. Locally each gear stage is modeled as a multimass rotor-bearing system using a discrete model. The modal characteristics are calculated using the matrix-transfer technique. The gearbox structure is represented by a finite element models, and modal parameters are solved by using NASTRAN. The rotor-gear stages are coupled through nonlinear compliance in the gear mesh while the gearbox structure is coupled through the bearing supports of the rotor system. Transient and steady state vibrations of the coupled system are examined in both time and frequency domains. A typical three-gear system is used as an example for demonstration of the developed procedure. Author

N91-23514*# National Aeronautics and Space Administration. Lewis Research Center, Cleveland, OH.

MAXIMUM LIFE SPUR GEAR DESIGN

M. SAVAGE, M. J. MACKULIN (Akron Univ., OH.), H. H. COE, and J. J. COY 1991 14 p Presented at the 27th Joint Propulsion Conference, Sacramento, CA, 24-27 Jun. 1991; cosponsored by AIAA, SAE, ASME, and ASEE Prepared in cooperation with Army Aviation Systems Command, Cleveland, OH

(Contract NAG3-1047; DA PROJ. 1L1-62211-37-A; RTOP 505-63-51) (NASA-TM-104361; E-6157; NAS 1.15:104361; AVSCOM-TR-90-C-024; AD-A237143) Avail: NTIS HC/MF A03 CSCL 13/9

Optimization procedures allow one to design a spur gear reduction for maximum life and other end use criteria. A modified feasible directions search algorithm permits a wide variety of inequality constraints and exact design requirements to be met with low sensitivity to initial guess values. The optimization algorithm is described, and the models for gear life and performance are presented. The algorithm is compact and has been programmed for execution on a desk top computer. Two examples are presented to illustrate the method and its application. Author

N91-23515*# National Aeronautics and Space Administration. Lewis Research Center, Cleveland, OH.

EVALUATION AND RANKING OF CANDIDATE CERAMIC WAFER ENGINE SEAL MATERIALS

BRUCE M. STEINETZ May 1991 26 p (Contract RTOP 505-63-5B) (NASA-TM-103795; E-6082; NAS 1.15:103795) Avail: NTIS HC/MF A03 CSCL 11/1

Modern engineered ceramics offer high temperature capabilities

not found in even the best superalloy metals. The high temperature properties of several selected ceramics including aluminum oxide, silicon carbide, and silicon nitride are reviewed as they apply to hypersonic engine seal design. A ranking procedure is employed to objectively differentiate among four different monolithic ceramic materials considered, including: a cold-pressed and sintered aluminum oxide; a sintered alpha-phase silicon carbide; a hot-isostatically pressed silicon nitride; and a cold-pressed and sintered silicon nitride. This procedure is used to narrow the wide range of potential ceramics considered to an acceptable number for future detailed and costly analyses and tests. The materials are numerically scored according to their high temperature flexural strength; high temperature thermal conductivity; resistance to crack growth; resistance to high heating rates; fracture toughness; Weibull modulus; and finally according to their resistance to leakage flow, where materials having coefficients of thermal expansion closely matching the engine panel material resist leakage flow best. The cold-pressed and sintered material (Kyocera SN-251) ranked the highest in the overall ranking especially when implemented in engine panels made of low expansion rate materials being considered for the engine, including Incoloy and titanium alloys. Author

N91-24593*# National Aeronautics and Space Administration. Lewis Research Center, Cleveland, OH.

COMPARISON OF WEIBULL STRENGTH PARAMETERS FROM FLEXURE AND SPIN TESTS OF BRITTLE MATERIALS

FREDERIC A. HOLLAND, JR. and ERWIN V. ZARETSKY 1991 11 p Presented at the Ninth Biennial Conference on Reliability, Stress Analysis, and Failure Prevention, Miami, FL, 22-25 Sep. 1991; sponsored by ASME (Contract RTOP 505-63-1B)

(NASA-TM-104414; E-6245; NAS 1.15:104414) Avail: NTIS HC/MF A03 CSCL 13/8

Fracture data from five series of four point bend tests of beam and spin tests of flat annular disks were reanalyzed. Silicon nitride and graphite were the test materials. The experimental fracture strengths of the disks were compared with the predicted strengths based on both volume flaw and surface flaw analyses of four point bend data. Volume flaw analysis resulted in a better correlation between disks and beams in three of the five test series than did surface flaw analysis. The Weibull (moduli) and characteristic gage strengths for the disks and beams were also compared. Differences in the experimental Weibull slopes were not statistically significant. It was shown that results from the beam tests can predict the fracture strength of rotating disks. Author

N91-25395*# National Aeronautics and Space Administration. Lewis Research Center, Cleveland, OH.

ANALYTICAL AND EXPERIMENTAL STUDY OF VIBRATIONS IN A GEAR TRANSMISSION

F. K. CHOY, Y. F. RUAN, J. J. ZAKRAJSEK, FRED B. OSWALD, and J. J. COY 1991 21 p Presented at the 27th Joint Propulsion Conference, Sacramento, CA, 24-27 Jun. 1991; sponsored by AIAA, SAE, ASME, and the American Society for Electrical Engineers

(Contract DA PROJ. 1L1-62211-A-47A; RTOP 505-63-56) (NASA-TM-104434; E-6144; NAS 1.15:104434; AVSCOM-TR-90-C-032; AD-A239498; AIAA PAPER 91-219) Avail: NTIS HC/MF A03 CSCL 13/9

An analytical simulation of the dynamics of a gear transmission system is presented and compared to experimental results from a gear noise test rig at the NASA Lewis Research Center. The analytical procedure developed couples the dynamic behaviors of the rotor-bearing-gear system with the response of the gearbox structure. The modal synthesis method is used in solving the overall dynamics of the system. Locally each rotor-gear stage is modeled as an individual rotor-bearing system using the matrix transfer technique. The dynamics of each individual rotor are coupled with other rotor stages through the nonlinear gear mesh forces and with the gearbox structure through bearing support systems. The modal characteristics of the gearbox structure are evaluated using the finite element procedure. A variable time stepping integration

routine is used to calculate the overall time transient behavior of the system in modal coordinates. The global dynamic behavior of the system is expressed in a generalized coordinate system. Transient and steady state vibrations of the gearbox system are presented in the time and frequency domains. The vibration characteristics of a simple single mesh gear noise test rig is modeled. The numerical simulations are compared to experimental data measured under typical operating conditions. The comparison of system natural frequencies, peak vibration amplitudes, and gear mesh frequencies are generally in good agreement. Author

N91-25411* # National Aeronautics and Space Administration. Lewis Research Center, Cleveland, OH.

ACOUSTICAL ANALYSIS OF GEAR HOUSING VIBRATION

A. F. SEYBERT, T. W. WU, X. F. WU (Kentucky Univ., Lexington.), and FRED B. OSWALD Apr. 1991 10 p Presented at the American Helicopter Society Technical Specialists Meeting, Philadelphia, PA, 15-16 Oct. 1991 Original contains color illustrations

(Contract DA PROJ. 1L1-62209-A-47A; RTOP 505-63-51)

(NASA-TM-103691; E-5910; NAS 1.15:103691;

AVSCOM-TR-90-C-002) Avail: NTIS HC/MF A02; 1 functional color page CSCL 13/9

The modal and acoustical analysis of the NASA gear-noise rig is described. Experimental modal analysis techniques were used to determine the modes of vibration of the transmission housing. The resulting modal data were then used in a boundary element method (BEM) analysis to calculate the sound pressure and sound intensity on the surface of the housing as well as the radiation efficiency of each mode. The radiation efficiencies of the transmission housing modes are compared with theoretical results for finite, baffled plates. A method that uses the measured mode shapes and the BEM to predict the effect of simple structural changes on the sound radiation efficiency of the modes of vibration is also described. Author

N91-25412* # National Aeronautics and Space Administration. Lewis Research Center, Cleveland, OH.

ADVANCED ROTORCRAFT TRANSMISSION (ART)

PROGRAM-BOEING HELICOPTERS STATUS REPORT

JOSEPH W. LENSKE, JR. (Boeing Helicopter Co., Philadelphia, PA.) and MARK J. VALCO 1991 26 p Presented at the 27th Joint Propulsion Conference, Sacramento, CA, 24-27 Jun. 1991; sponsored by AIAA, SAE, ASME, and the American Society for Electrical Engineers

(Contract DA PROJ. 1L1-62099-AH-76; RTOP 505-62-OK)

(NASA-TM-104474; E-6321; NAS 1.15:104474;

AVSCOM-TR-91-C-032; AD-A240289) Avail: NTIS HC/MF A03 CSCL 13/9

The Advanced Rotorcraft Transmission (ART) program is structured to incorporate key emerging material and component technologies into an advanced rotorcraft transmission with the intention of making significant improvements in the state of the art (SOA). Specific objectives of ART are: (1) Reduce transmission weight by 25 pct.; (2) Reduce transmission noise by 10 dB; and (3) Improve transmission life and reliability, while extending Mean Time Between Removal to 5000 hr. Boeing selected a transmission sized for the Tactical Tilt Rotor (TTR) aircraft which meets the Future Air Attack Vehicle (FAVV) requirements. Component development testing will be conducted to evaluate the high risk concepts prior to finalizing the advanced transmission configuration. The results of tradeoff studies and development test which were completed are summarized. Author

N91-25413* # National Aeronautics and Space Administration. Lewis Research Center, Cleveland, OH.

MAGNETIC BEARINGS-STATE OF THE ART

DAVID P. FLEMING Jul. 1991 27 p Submitted for publication (Contract RTOP 505-63-5B)

(NASA-TM-104465; E-6309; NAS 1.15:104465) Avail: NTIS HC/MF A03 CSCL 13/11

Magnetic bearings have existed for many years, at least in theory. Earnshaw's theorem, formulated in 1842, concerns stability

of magnetic suspensions, and states that not all axes of a bearing can be stable without some means of active control. In Beam's widely referenced experiments, a tiny (1/64 in diameter) rotor was rotated to the astonishing speed of 800,000 rps while it was suspended in a magnetic field. Despite a long history, magnetic bearings have only begun to see practical application since about 1980. The development that finally made magnetic bearings practical was solid state electronics, enabling power supplies and controls to be reduced in size to where they are now comparable in volume to the bearings themselves. An attempt is made to document the current (1991) state of the art of magnetic bearings. The referenced papers are large drawn from two conferences publications published in 1988 and 1990 respectively. Author

N91-26543* # National Aeronautics and Space Administration. Lewis Research Center, Cleveland, OH.

REMOVABLE HAND HOLD Patent Application

ROBERT D. CORRIGAN, inventor (to NASA) and ROBERT L. HAUER, inventor (to NASA) 15 Apr. 1991 13 p (NASA-CASE-LEW-15196-1; NAS 1.71:LEW-15196-1; US-PATENT-APPL-SN-687606) Avail: NTIS HC/MF A03 CSCL 13/11

A hand hold utilizes joining means which comprises two different mounting brackets that are permanently fastened to a supporting structure. An alignment/capture bracket is disposed at one end of the hand rail or hand hold which mates with one of the mounting brackets. A securing bracket is disposed at the opposite end of the hand rail/hand hold which connects with the other mounting bracket by means of a locking device. The alignment/capture bracket has a central tapered tongue with two matching slots disposed on each side. NASA

N91-27558* # National Aeronautics and Space Administration. Lewis Research Center, Cleveland, OH.

COMPUTERIZED INSPECTION OF REAL SURFACES AND MINIMIZATION OF THEIR DEVIATIONS

FAYDOR L. LITVIN, Y. ZHANG, CHIH-PING KUAN (Illinois Univ., Chicago.), and R. F. HANDSCHUH 1991 12 p Presented at the 5th International Conference on Metrology and Properties of Engineering Surfaces, Leicester, England, 10-12 Apr. 1991 Sponsored in part by Gleason Memorial Fund and Dana Corp. Prepared in cooperation with Air Force Systems Command, Cleveland, OH

(Contract NAG3-964; DA PROJ. 1L1-6221-A-47A; RTOP 505-63-36)

(NASA-TM-103798; E-6086; NAS 1.15:103798;

AVSCOM-TR-91-C-008; AD-A240066) Avail: NTIS HC/MF A03 CSCL 14/4

A method is developed for the minimization of gear tooth surface deviations between theoretical and real surfaces for the improvement of precision of surface manufacture. Coordinate measurement machinery is used to determine a grid of surface coordinates. Theoretical calculations are made for the grid points. A least-square method is used to minimize the deviations between real and theoretical surfaces by altering the manufacturing machine-tool settings. An example is given for a hypoid gear. Author

N91-27559* # National Aeronautics and Space Administration. Lewis Research Center, Cleveland, OH.

SOME PRELIMINARY RESULTS OF BRUSH SEAL/ROTOR INTERFERENCE EFFECTS ON LEAKAGE AT ZERO AND LOW RPM USING A TAPERED-PLUG ROTOR

R. C. HENDRICKS, M. P. PROCTOR, J. A. SCHLUMBERGER, M. J. BRAUN, and R. L. MULLEN (Case Western Reserve Univ., Cleveland, OH.) 1991 16 p Presented at the 27th Joint Propulsion Conference, Sacramento, CA, 24-27 Jun. 1991; sponsored by AIAA, SAE, ASME and ASEE

(Contract RTOP 505-62-52)

(NASA-TM-104396; E-6212; NAS 1.15:104396; AIAA PAPER 91-3390) Avail: NTIS HC/MF A03 CSCL 11/1

Some preliminary brush seal leakage results for ambient temperature air are presented. Data for four nominal brush rotor

radial clearances of -0.09, -0.048, -0.008, and 0.035 mm were taken by using a tapered plug rotor at 0 and 400 rpm with rotor runout of 0.127 mm peak to peak. The brush seal nominal bore diameter was 38 mm with 0.05 mm bristles at 200 bristles/mm of circumference and a 0.61 mm fence height. Leakages were greater than predicted, but agreement was reasonable. Leakage rates were not significantly altered by hysteresis or inlet flow variations. Visualization studies showed that the bristles followed the 400 rpm excitation, and loading studies indicated that bristles slid relative to one another. Author

N91-27560* National Aeronautics and Space Administration. Lewis Research Center, Cleveland, OH.

HIGH-TEMPERATURE, FLEXIBLE, THERMAL BARRIER SEAL Patent

PAUL J. SIROCKY, inventor (to NASA) and BRUCE M. STEINETZ, inventor (to NASA) 14 May 1991 13 p. Filed 27 Nov. 1989 (NASA-CASE-LEW-14672-1; US-PATENT-5,014,917; US-PATENT-APPL-SN-441672; US-PATENT-CLASS-239-265.11; US-PATENT-CLASS-277-34; US-PATENT-CLASS-277-157; US-PATENT-CLASS-277-226; US-PATENT-CLASS-277-229; INT-PATENT-CLASS-B64D-33/04; INT-PATENT-CLASS-F16J-15/46) Avail: US Patent and Trademark Office CSCL 13/9

This device seals the sliding interfaces between structural panels that are roughly perpendicular to each other or whose edges are butted against one another. The nonuniformity of the gap between the panels requires significant flexibility along the seal length. The seal is mounted in a rectangular groove in a movable structural panel. A plurality of particles or balls is densely packed in an outer sheathing. The balls are laterally preloaded to maintain sealing contact with the adjacent wall using a pressurized linear bellows. Distortions in the adjacent panel are accommodated by rearrangement of the particles within the outer sheathing. Leakage through the seal is minimized by densely compacting the internal particles and by maintaining positive preload along the back side of the seal. The braid architecture of the outer sheathing is selected to minimize leakage through the seal and to resist mechanical abrasion.

Official Gazette of the U.S. Patent and Trademark Office

N91-27561* National Aeronautics and Space Administration. Lewis Research Center, Cleveland, OH.

QUICK ACTION CLAMP Patent

FRANK S. CALCO, inventor (to NASA) 16 Jul. 1991 8 p. Filed 30 Mar. 1990 (NASA-CASE-LEW-14887-1; US-PATENT-5,032,045; US-PATENT-APPL-SN-503418; US-PATENT-CLASS-410-80; US-PATENT-CLASS-410-84; US-PATENT-CLASS-292-60; US-PATENT-CLASS-292-61; INT-PATENT-CLASS-B60P-7/15; INT-PATENT-CLASS-E05C-5/04) Avail: US Patent and Trademark Office CSCL 13/11

A quick release toggle clamp that utilizes a spring that requires a deliberate positive action for disengagement is presented. The clamp has a sliding bolt that provides a latching mechanism. The bolt is moved by a handle that tends to remain in an engaged position while under tension.

Official Gazette of the U.S. Patent and Trademark Office

N91-27569*# National Aeronautics and Space Administration. Lewis Research Center, Cleveland, OH.

SURFACE FATIGUE LIFE OF M50NiL AND AISI 9310 SPUR GEARS AND R C BARS

DENNIS P. TOWNSEND and ERIC N. BAMBERGER (General Electric Co., Cincinnati, OH.) 1991 7 p. Presented at the International Conference on Motion and Power Transmissions, Hiroshima, Japan, 24-26 Nov. 1991; sponsored by the Japan Society of Mechanical Engineers with participation of ASME, I. Mech. E., VDI, I.E.T., CSME and other societies (Contract DA PROJ. 1L1-62211-A-47A; RTOP 505-63-36) (NASA-TM-104496; E-6353; NAS 1.15:104496; AVSCOM-TR-91-C-034; AD-A241470) Avail: NTIS HC/MF A02 CSCL 13/11

Spur gear endurance tests and rolling element surface fatigue tests were conducted to study vacuum induction melted, vacuum arc remelted (VIM-VAR) M50NiL steel for use as a gear steel in advanced aircraft applications, to determine its endurance characteristics, and to compare the results with those for standard VAR and VIM-VAR AISI 9310 gear material. Tests were conducted with spur gears and rolling contact bars manufactured from VIM-VAR M50NiL and VAR and VIM-VAR AISI 9310. The gear pitch diameter was 8.9 cm. Gear test conditions were an inlet oil temperature of 320 K, and outlet oil temperature of 350 K, a maximum Hertz stress of 1.71 GPa, and a speed of 10000 rpm. Bench rolling element fatigue tests were conducted at ambient temperatures with a bar speed of 12,500 rpm and a maximum Hertz stress of 4.83 GPa. The VIM-VAR M50NiL gears had a surface fatigue life that was 4.5 and 11.5 times that for VIM-VAR and VAR AISI 9310 gears, respectively. The surface fatigue life of the VIM-VAR M50NiL rolling contact bars was 13.2 and 21.6 times that for the VIM-VAR and VAR AISI 9310, respectively. The VIM-VAR M50NiL material was shown to have good resistance to fracture through a fatigue spall and superior fatigue life to both other gears. Author

N91-27570*# National Aeronautics and Space Administration. Lewis Research Center, Cleveland, OH.

DYNAMIC MEASUREMENTS OF GEAR TOOTH FRICTION AND LOAD

BRIAN REBBECCHI (Australian Aeronautical Research Committee, Melbourne.), FRED B. OSWALD, and DENNIS P. TOWNSEND 1991 14 p. Presented at the Fall Technical Meeting of the American Gear Manufacturers Association, Detroit, MI, 21-23 Oct. 1991

(Contract DA PROJ. 1L1-62211-A-47A; RTOP 505-63-36)

(NASA-TM-103281; E-6020; NAS 1.15:103281;

AVSCOM-TR-90-C-023; AD-A240126) Avail: NTIS HC/MF A03 CSCL 13/11

As part of a program to study fundamental mechanisms of gear noise, static and dynamic gear tooth strain measurements were made on the NASA gear-noise rig. Tooth-fillet strains from low-contact ratio-spur gears were recorded for 28 operating conditions. A method is introduced whereby strain gage measurements taken from both the tension and compression sides of a gear tooth can be transformed into the normal and frictional loads on the tooth. This technique was applied to both the static and dynamic strain data. The static case results showed close agreement with expected results. For the dynamic case, the normal-force computation produced very good results, but the friction results, although promising, were not as accurate. Tooth sliding friction strongly affected the signal from the strain gage on the tensionside of the tooth. The compression gage was affected by friction to a much lesser degree. The potential of the method to measure friction force was demonstrated, but further refinement will be required before this technique can be used to measure friction forces dynamically with an acceptable degree of accuracy. Author

N91-29599*# National Aeronautics and Space Administration. Lewis Research Center, Cleveland, OH.

EFFECT OF TWO SYNTHETIC LUBRICANTS ON LIFE OF AISI 9310 SPUR GEARS

DENNIS P. TOWNSEND and JOHN SHIMSKI (Naval Air Propulsion Test Center, Trenton, NJ.) Jun. 1991 16 p.

(Contract DA PROJ. 1L1-62211-A-47A; RTOP 505-63-36)

(NASA-TM-104352; E-6004; NAS 1.15:104352;

AVSCOM-TR-91-C-011) Avail: NTIS HC/MF A03 CSCL 13/9

Spur-gear fatigue tests were conducted with two lubricants using a single lot of consumable-electrode vacuum-melted (CVM) AISI 9310 spur gears. The gears were case carburized and hardened to Rockwell C60. The gear pitch diameter was 8.89 cm. The lot of gears was divided into two groups, each of which was tested with a different lubricant. The test lubricants can be classified as synthetic polyol-ester-based lubricants. One lubricant was 30 percent more viscous than the other. Both lubricants have similar pressure viscosity coefficients. Test conditions included a bulk gear

37 MECHANICAL ENGINEERING

temperature of 350 K, a maximum Hertz stress of 1.71 GPa at the pitch line, and a speed of 10,000 rpm. The surface fatigue life of gears tested with one lubricant was approximately 2.4 times that for gears tested with the other lubricant. The lubricant with the 30 percent higher viscosity gave a calculated elastohydrodynamic (EHD) film thickness that was 20 percent higher than the other lubricant. This increased EHD film thickness is the most probable reason for the improvement in surface fatigue life of gears tested with this lubricant over gears tested with the less viscous lubricant. Author

N91-29600*# National Aeronautics and Space Administration. Lewis Research Center, Cleveland, OH.

LOCAL SYNTHESIS AND TOOTH CONTACT ANALYSIS OF FACE-MILLED SPIRAL BEVEL GEARS

F. L. LITVIN, Y. ZHANG (Illinois Univ., Chicago.), and R. F. HANDSCHUH 1991 6 p Presented at the 1991 International Conference on Motion and Power Transmissions, Hiroshima, Japan, 24-26 Nov. 1991; sponsored by the Japan Society of Mechanical Engineers

(Contract NAG3-1263; DA PROJ. 1L1-62211-A-47A; RTOP 505-63-36)

(NASA-TM-105182; E-6349; NAS 1.15:105182; AVSCOM-TR-91-C-039; AD-A241588) Avail: NTIS HC/MF A02 CSCL 13/9

A new approach is proposed for the local synthesis of spiral bevel gears. The approach provides contact at the mean contact point with the desired deviation of the transmission error function by a predesigned parabolic function. The orientation of the contact path on the gear tooth surface and the length of the major axis of the instantaneous contact ellipse are also included in the analysis. A tooth contact analysis (TCA) computer program was developed to simulate meshing and contact of the gear tooth surfaces. A numerical example of the process is given. Author

N91-30532*# National Aeronautics and Space Administration. Lewis Research Center, Cleveland, OH.

SPACE MECHANISMS NEEDS FOR FUTURE NASA LONG DURATION SPACE MISSIONS

ROBERT L. FUSARO 1991 12 p Presented at the Conference on Advanced Space Exploration Initiative Technologies, Cleveland, OH, 4-6 Sep. 1991; sponsored by AIAA, NASA, and OAI (Contract RTOP 505-63-5B)

(NASA-TM-105204; E-6507; NAS 1.15:105204) Avail: NTIS HC/MF A03 CSCL 13/9

Future NASA long duration missions will require high performance, reliable, long lived mechanical moving systems. In order to develop these systems, high technology components, such as bearings, gears, seals, lubricants, etc., will need to be utilized. There has been concern in the NASA community that the current technology level in these mechanical component/tribology areas may not be adequate to meet the goals of long duration NASA mission such as Space Exploration Initiative (SEI). To resolve this concern, NASA-Lewis sent a questionnaire to government and industry workers (who have been involved in space mechanism research, design, and implementation) to ask their opinion if the current space mechanisms technology (mechanical components/tribology) is adequate to meet future NASA Mission needs and goals. In addition, a working group consisting of members from each NASA Center, DoD, and DOE was established to study the technology status. The results of the survey and conclusions of the working group are summarized. Author

N91-30533*# National Aeronautics and Space Administration. Lewis Research Center, Cleveland, OH.

TRANSMISSION OVERHAUL ESTIMATES FOR PARTIAL AND FULL REPLACEMENT AT REPAIR

M. SAVAGE (Akron Univ., OH.) and D. G. LEWICKI 1991 8 p Presented at the International Conference on Motion and Power Transmissions, Hiroshima, Japan, 24-26 Nov. 1991; sponsored by the Japan Society of Mechanical Engineers with the participation of ASME, I. Mech. E., VDI, I.E.T., CSME and other societies (Contract DA PROJ. 1L1-62211-A-47A; RTOP 505-63-36)

(NASA-TM-104395; E-6211; NAS 1.15:104395; AVSCOM-TR-91-C-010; AD-A241587) Avail: NTIS HC/MF A02 CSCL 13/9

Timely transmission overhauls increase in-flight service reliability greater than the calculated design reliabilities of the individual aircraft transmission components. Although necessary for aircraft safety, transmission overhauls contribute significantly to aircraft expense. Predictions of a transmission's maintenance needs at the design stage should enable the development of more cost effective and reliable transmissions in the future. The frequency is estimated of overhaul along with the number of transmissions or components needed to support the overhaul schedule. Two methods based on the two parameter Weibull statistical distribution for component life are used to estimate the time between transmission overhauls. These methods predict transmission lives for maintenance schedules which repair the transmission with a complete system replacement or repair only failed components of the transmission. An example illustrates the methods. Author

N91-30537*# National Aeronautics and Space Administration. Lewis Research Center, Cleveland, OH.

HOW TO DETERMINE SPIRAL BEVEL GEAR TOOTH GEOMETRY FOR FINITE ELEMENT ANALYSIS

ROBERT F. HANDSCHUH and FAYDOR L. LITVIN (Illinois Univ., Chicago.) 1991 9 p Proposed for presentation at the International Conference on Motion and Power Transmissions, Hiroshima, Japan, 24-26 Nov. 1991; sponsored by the Japan Society of Mechanical Engineers

(Contract DA PROJ. 1L1-62211-A-47A; RTOP 505-63-36)

(NASA-TM-105150; E-6433; NAS 1.15:105150; AVSCOM-TR-91-C-018) Avail: NTIS HC/MF A02 CSCL 13/9

An analytical method was developed to determine gear tooth surface coordinates of face milled spiral bevel gears. The method combines the basic gear design parameters with the kinematical aspects for spiral bevel gear manufacturing. A computer program was developed to calculate the surface coordinates. From this data a 3-D model for finite element analysis can be determined. Development of the modeling method and an example case are presented. Author

N91-30538*# National Aeronautics and Space Administration. Lewis Research Center, Cleveland, OH.

HIGH TEMPERATURE NASP ENGINE SEALS: A TECHNOLOGY REVIEW

BRUCE M. STEINETZ, CHRISTOPHER DELLACORTE, and MIKE TONG (Sverdrup Technology, Inc., Brook Park, OH.) Aug. 1991 24 p Presented at the 10th National Aerospace Plane Technology Symposium, Monterey, CA, 23-26 Apr. 1991

(Contract RTOP 763-21-41)

(NASA-TM-104468; E-6317; NAS 1.15:104468) Avail: NTIS HC/MF A03 CSCL 11/1

Progress in developing advanced high temperature engine seal concepts and related sealing technologies for advanced hypersonic engines are reviewed. Design attributes and issues requiring further development for both the ceramic wafer seal and the braided ceramic rope seal are examined. Leakage data are presented for these seals for engine simulated pressure and temperature conditions and compared to a target leakage limit. Basic elements of leakage flow models to predict leakage rates for each of these seals over the wide range of pressure and temperature conditions anticipated in the engine are also presented. Author

N91-30539*# National Aeronautics and Space Administration. Lewis Research Center, Cleveland, OH.

PM200/PS200: SELF-LUBRICATING BEARING AND SEAL MATERIALS FOR APPLICATIONS TO 900 C

HAROLD E. SLINNEY Jul. 1991 17 p Sponsored in part by DOE Original contains color illustrations

(Contract RTOP 505-63-5A)

(NASA-TM-103776; E-6043; NAS 1.15:103776) Avail: NTIS HC/MF A03; 13 functional color pages CSCL 13/9

The development of the PS/PM200 class of self-lubricating material is described. The composition of the materials and their

performance under temperature conditions from minus 160 degrees to 900 C (minus 250 to 1650 F) are examined. Applications in areas such as cylinder liner coatings, shaft seals, gas bearings, and airframe thermal expansion joints are proposed. Graphs and tables are provided to show service temperature limits, mechanical strength, linear thermal expansion, and thermal conductivity parameters. M.G.

N91-31648* National Aeronautics and Space Administration. Lewis Research Center, Cleveland, OH.

SPUR-GEAR OPTIMIZATION USING SPUROPT COMPUTER PROGRAM

HAROLD H. COE Sep. 1991 19 p
(Contract DA PROJ. 1L1-62211-A-47A; RTOP 505-63-51)
(NASA-TM-104394; E-6210; NAS 1.15:104394;
AVSCOM-TR-90-C-014) Avail: NTIS HC/MF A03 CSCL 13/9

A computer program developed for optimizing spur gear designs, SPUROPT, was updated by installing a new subroutine that uses AGMA 908-B89 standards to calculate the J-factor for determining tooth-bending stress. The updated SPUROPT program was then used to optimize a spur gear set for maximum fatigue life, minimum dynamic load, or minimum weight. All calculations were made with constraints on as many as 13 parameters by using three design variables: the number of teeth, diametral pitch, and tooth-face width. Results depended largely on constraints values. When the limiting bending stress was set at a high value, the optimal solution was the highest allowable number of teeth. When the allowable bending stress was lowered, the optimal solution moved toward the fewest number of teeth permitted. Final results were also affected by the amount of transmission error. A lower error permitted a higher number of teeth. Author

N91-31654* National Aeronautics and Space Administration. Lewis Research Center, Cleveland, OH.

RECENT MANUFACTURING ADVANCES FOR SPIRAL BEVEL GEARS

ROBERT F. HANDSCHUH and ROBERT C. BILL (Army Aviation Systems Command, Cleveland, OH.) 1991 14 p Presented at the Aerotech 1991, Long Beach, CA, 23-26 Sep. 1991; sponsored by SAE
(Contract DA PROJ. 1L1-62211-A-47A; RTOP 505-63-36)
(NASA-TM-104479; E-6326; NAS 1.15:104479;
AVSCOM-TR-91-C-022; AD-A241256) Avail: NTIS HC/MF A03 CSCL 13/9

The U.S. Army Aviation Systems Command (AVSCOM), through the Propulsion Directorate at NASA LRC, has recently sponsored projects to advance the manufacturing process for spiral bevel gears. This type of gear is a critical component in rotary-wing propulsion systems. Two successfully completed contracted projects are described. The first project addresses the automated inspection of spiral bevel gears through the use of coordinate measuring machines. The second project entails the computer-numerical-control (CNC) conversion of a spiral bevel gear grinding machine that is used for all aerospace spiral bevel gears. The results of these projects are described with regard to the savings effected in manufacturing time. Author

QUALITY ASSURANCE AND RELIABILITY

Includes product sampling procedures and techniques; and quality control.

A91-18596* National Aeronautics and Space Administration. Lewis Research Center, Cleveland, OH.

ULTRASONIC IMAGING OF TEXTURED ALUMINA

D. B. STANG (Sverdrup Technology, Inc., Cleveland, OH), J. A. SALEM, and E. R. GENERAZIO (NASA, Lewis Research Center, Cleveland, OH) Materials Evaluation (ISSN 0025-5327), vol. 48,

Dec. 1990, p. 1478-1482. Previously announced in STAR as N89-28853. refs

Copyright

Ultrasonic images representing the bulk attenuation and velocity of a set of alumina samples were obtained by a pulse-echo contact scanning technique. The samples were taken from larger bodies that were chemically similar but were processed by extrusion or isostatic processing. The crack growth resistance and fracture toughness of the larger bodies were found to vary with processing method and test orientation. The results presented here demonstrate that differences in texture that contribute to variations in structural performance can be revealed by analytic ultrasonic techniques. Author

A91-31064* National Aeronautics and Space Administration. Lewis Research Center, Cleveland, OH.

MODEL-OA WIND TURBINE GENERATOR - FAILURE MODES AND EFFECTS ANALYSIS

WILLIAM E. KLEIN and VINCENT R. LALI (NASA, Lewis Research Center, Cleveland, OH) IN: 1990 Annual Reliability and Maintainability Symposium, Los Angeles, CA, Jan. 23-25, 1990, Proceedings. New York, Institute of Electrical and Electronics Engineers, Inc., 1990, p. 337-340. Previously announced in STAR as N90-12034.
(Contract DE-AB29-79ET-20370)

The results failure modes and effects analysis (FMEA) conducted for wind-turbine generators are presented. The FMEA was performed for the functional modes of each system, subsystem, or component. The single-point failures were eliminated for most of the systems. The blade system was the only exception. The qualitative probability of a blade separating was estimated at level D-remote. Many changes were made to the hardware as a result of this analysis. The most significant change was the addition of the safety system. Operational experience and need to improve machine availability have resulted in subsequent changes to the various systems, which are also reflected in this FMEA. Author

A91-37011* National Aeronautics and Space Administration. Lewis Research Center, Cleveland, OH.

ACOUSTO-ULTRASONICS - RETROSPECTIVE EXHORTATION WITH BIBLIOGRAPHY

ALEX VARY (NASA, Lewis Research Center, Cleveland, OH) Materials Evaluation (ISSN 0025-5327), vol. 49, May 1991, p. 581, 582, 584 (5 ff.). refs
Copyright

Major research on the acousto-ultrasonic (AU) technique (also known as the stress-wave-factor technique) encompassing aspects of acoustic emission and ultrasonic materials characterization methodology is reviewed. AU deals primarily with such factors as the assessment of the integrated effects of diffuse defect states, thermomechanical degradation, and population of subcritical flaws that influence AU measurements correlating with mechanical property variations. AU is used to evaluate fiber-reinforced composites, adhesive bonds, lumber, paper and wood products, cable and rope, and human bone. The AU technique has been demonstrated to be sensitive to interlaminar and adhesive bond strength variations and has been shown to be useful in assessing microporosity and microcracking produced by fatigue cycling. An extensive bibliography ranging from 1985 to 1991 is presented. O.G.

A91-37014* National Aeronautics and Space Administration. Lewis Research Center, Cleveland, OH.

PRELIMINARY INVESTIGATION OF ACOUSTO-ULTRASONIC EVALUATION OF METAL-MATRIX COMPOSITE SPECIMENS

HAROLD E. KAUTZ and BRAD A. LERCH (NASA, Lewis Research Center, Cleveland, OH) Materials Evaluation (ISSN 0025-5327), vol. 49, May 1991, p. 607-612. refs
Copyright

Acoustoultrasonic (AU) measurements were performed on a series of (0)8, (90)8, (+/-30)2s, (+/-60)2s, (0/90)2s, and (90/0)2s tensile specimens composed of eight laminated layers of continuous, SiC-fiber-reinforced Ti-15-3 matrix. The frequency

38 QUALITY ASSURANCE AND RELIABILITY

spectrum was dominated by frequencies of longitudinal wave resonance through the thickness of the specimen at the sending transducer; signal propagation from the sender to the receiver was by shear waves. The magnitude of the frequency spectrum of the AU signal was used for calculating a stress-wave factor (SWF) based upon integrating the spectral distribution function. The SWF was sensitive to fiber-matrix debonding caused by mechanical strain and also to unconstrained thermal cycling. Damage in this metal-matrix composite structure due to tensile loading or thermal cycling was detected by this change in the magnitude of the frequency spectrum. Author

A91-51926* Technology Integration and Development Group, Inc., Billerica, MA.

IN-SERVICE HEALTH MONITORING OF COMPOSITE STRUCTURES

GINO A. PINTO, C. S. VENTRES (Technology Integration and Development Group, Inc., Billerica, MA), CAROL A. GINTY, and CHRISTOS C. CHAMIS (NASA, Lewis Research Center, Cleveland, OH) IN: 1990 SEM Spring Conference on Experimental Mechanics, Albuquerque, NM, June 4-6, 1990, Proceedings. Bethel, CT, Society for Experimental Mechanics, Inc., 1990, p. 304-309. refs Copyright

The aerospace industry is witnessing a vast utilization of composites in critical structural applications and anticipates even more use of them in future aircraft. Therefore, a definite need exists for a composite health monitoring expert system to meet today's current needs and tomorrow's future demands. The primary goal for this conceptual health monitoring system is functional reliability for in-service operation in the environments of various composite structures. The underlying philosophy of this system is to utilize proven vibration techniques to assess the structural integrity of a fibrous composite. Statistical methods are used to determine if the variances in the measured data are acceptable for making a reliable decision on the health status of the composite. The flexible system allows for algorithms describing any composite fatigue or damage behavior characteristic to be provided as an input to the system. Alert thresholds and variances can also be provided as an input to this system and may be updated to allow for future changes/refinements in the composite's structural integrity behavior. Author

A91-53703*# National Aeronautics and Space Administration. Lewis Research Center, Cleveland, OH.

NONDESTRUCTIVE EVALUATION TOOLS AND EXPERIMENTAL STUDIES FOR MONITORING THE HEALTH OF SPACE PROPULSION SYSTEMS

EDWARD R. GENERAZIO (NASA, Lewis Research Center, Cleveland, OH) AIAA, NASA, and OAI, Conference on Advanced SEI Technologies, Cleveland, OH, Sept. 4-6, 1991. 43 p. Previously announced in STAR as N91-28605. refs (AIAA PAPER 91-3433) Copyright

An overview is given of background and information on space propulsion systems on both the programmatic and technical levels. Feasibility experimental studies indicate that nondestructive evaluation tools such as ultrasonic, eddy current and X-ray may be successfully used to monitor the life limiting failure mechanisms of space propulsion systems. Encouraging results were obtained for monitoring the life limiting failure mechanisms for three space propulsion systems: the degradation of tungsten arcjet and magnetoplasmadynamic electrodes; presence and thickness of spallable electrically conducting molybdenum films in ion thrusters; and the degradation of the catalyst in hydrazine thrusters. Author

A91-54553* California State Univ., Fullerton.

K-OUT-OF-N:G SYSTEMS - SOME COST CONSIDERATIONS

RONALD C. SUICH (California State University, Fullerton) and RICHARD L. PATTERSON (NASA, Lewis Research Center, Cleveland, OH) IEEE Transactions on Reliability (ISSN 0018-9529), vol. 40, Aug. 1991, p. 259-264. refs Copyright

The authors provide a tool that an engineer designing a

subsystem can use to decide between one subsystem and a more reliable but more costly one. The authors provide methods for selecting redundancy levels in k-out-of-n:G systems in order to minimize particular cost considerations where the k-out-of-n:G system is a subsystem of a major system. The n and k are chosen to minimize the total cost of the subsystem plus the average loss due to subsystem failure. A BASIC program is available to determine the n and k which find this minimum. Five loss functions are considered, and illustrations are given. I.E.

A91-56972* National Aeronautics and Space Administration. Lewis Research Center, Cleveland, OH.

HIGH RESOLUTION COMPUTED TOMOGRAPHY OF ADVANCED COMPOSITE AND CERAMIC MATERIALS

R. N. YANCEY (Advanced Research and Applications Corp., Fairborn, OH) and S. J. KLIMA (NASA, Lewis Research Center, Cleveland, OH) Ceramic Engineering and Science Proceedings (ISSN 0196-6219), vol. 12, Sept.-Oct. 1991, p. 2029-2041. refs (Contract DNA001-84-C-0046; DNA001-86-C-0010; F33615-85-C-5116) Copyright

Advanced composite and ceramic materials are being developed for use in many new defense and commercial applications. In order to achieve the desired mechanical properties of these materials, the structural elements must be carefully analyzed and engineered. A study was conducted to evaluate the use of high resolution computed tomography (CT) as a macrostructural analysis tool for advanced composite and ceramic materials. Several samples were scanned using a laboratory high resolution CT scanner. Samples were also destructively analyzed at the locations of the scans and the nondestructive and destructive results were compared. The study provides useful information outlining the strengths and limitations of this technique and the prospects for further research in this area. Author

N91-15565*# National Aeronautics and Space Administration. Lewis Research Center, Cleveland, OH.

OVERVIEW OF SPACE PROPULSION SYSTEMS FOR IDENTIFYING NONDESTRUCTIVE EVALUATION AND HEALTH MONITORING OPPORTUNITIES

EDWARD R. GENERAZIO 1991 43 p Prepared for presentation at the JANNAF Nondestructive Evaluation Subcommittee Meeting, Space Issues Panel, Kennedy Space Center, FL, 14-16 May 1991 (Contract RTOP 510-01-0A) (NASA-TM-103614; E-5614; NAS 1.15:103614) Avail: NTIS HC/MF A03 CSCL 14/4

The next generation of space propulsion systems will be designed to incorporate advanced health monitoring and nondestructive inspection capabilities. As a guide to help the nondestructive evaluation (NDE) community impact the development of these space propulsion systems, several questions should be addressed. An overview of background and current information on space propulsion systems at both the programmatic and technical levels is provided. A framework is given that will assist the NDE community in addressing key questions raised during the 2 to 5 April 1990 meeting of the Joint Army-Navy-NASA-Air Force (JANNAF) Nondestructive Evaluation Subcommittee (NDES). Author

N91-17407*# National Aeronautics and Space Administration. Lewis Research Center, Cleveland, OH.

HOW MUCH REDUNDANCY: SOME COST CONSIDERATIONS, INCLUDING EXAMPLES FOR SPACECRAFT SYSTEMS

RONALD C. SUICH (California State Univ., Fullerton) and RICHARD L. PATTERSON 1990 24 p Proposed for presentation at the AIChE Summer National Meeting Session on Space Power Systems Technology, San Diego, CA, 19-22 Aug. 1990; sponsored by American Inst. of Chemical Engineers (Contract NAG3-1100; RTOP 506-41-41) (NASA-TM-103197; E-5592; NAS 1.15:103197) Avail: NTIS HC/MF A03 CSCL 14/4

How much redundancy should be built into a subsystem such as a space power subsystem. How does a reliability or design

engineer choose between a power subsystem with 0.990 reliability and a more costly subsystem with 0.995 reliability. How does the engineer designing a power subsystem for a satellite decide between one power subsystem and a more reliable but heavier power subsystem. High reliability is not necessarily an end in itself. High reliability may be desirable in order to reduce the statistically expected loss due to a subsystem failure. However, this may not be the wisest use of funds since the expected loss due to subsystem failure is not the only cost involved. The subsystem itself may be very costly. The cost of the subsystem or the expected loss due to subsystem failure may not be considered separately. Therefore, the total of the two costs is minimized, i.e., the total of the cost of the subsystem plus the expected loss due to subsystem failure. A specific type of redundant system is considered, called a k-out-of-n: G subsystem. Such a subsystem has n modules, of which k are required to be good for the subsystem to be good. Five models are discussed which can be applied in the design of a power subsystem to select the unique redundancy method which will minimize the total of the cost of the power subsystem plus the expected loss due to the power subsystem failure. A BASIC computer program is available. Author

N91-18193*# National Aeronautics and Space Administration. Lewis Research Center, Cleveland, OH.

ACOUSTO-ULTRASONIC NONDESTRUCTIVE EVALUATION OF MATERIALS USING LASER BEAM GENERATION AND DETECTION

ROBERT D. HUBER, ROBERT E. GREEN, JR. (Johns Hopkins Univ., Baltimore, MD.), ALEX VARY, and HAROLD KAUTZ /in NASA, Marshall Space Flight Center, Second Conference on NDE for Aerospace Requirements p 51-82 Dec. 1990 (Contract NAG3-728)

Avail: NTIS HC/MF A13 CSCL 14/4

Presented in viewgraph format, the possibility of using laser generation and detection of ultrasound to replace piezoelectric transducers for the acousto-ultrasonic technique is advanced. The advantages and disadvantages of laser acousto-ultrasonics are outlined. Laser acousto-ultrasonics complements standard piezoelectric acousto-ultrasonics and offers non-contact nondestructive evaluation. B.G.

N91-19462*# National Aeronautics and Space Administration. Lewis Research Center, Cleveland, OH.

ETARA PC VERSION 3.3 USER'S GUIDE: RELIABILITY, AVAILABILITY, MAINTAINABILITY SIMULATION MODEL

DAVID J. HOFFMAN and LARRY A. VITERNA Feb. 1991 65 p

(Contract RTOP 474-12-10)

(NASA-TM-103751; E-6003; NAS 1.15:103751) Avail: NTIS

HC/MF A04 CSCL 14/4

A user's manual describing an interactive, menu-driven, personal computer based Monte Carlo reliability, availability, and maintainability simulation program called event time availability reliability (ETARA) is discussed. Given a reliability block diagram representation of a system, ETARA simulates the behavior of the system over a specified period of time using Monte Carlo methods to generate block failure and repair intervals as a function of exponential and/or Weibull distributions. Availability parameters such as equivalent availability, state availability (percentage of time as a particular output state capability), continuous state duration and number of state occurrences can be calculated. Initial spares allotment and spares replenishment on a resupply cycle can be simulated. The number of block failures are tabulated both individually and by block type, as well as total downtime, repair time, and time waiting for spares. Also, maintenance man-hours per year and system reliability, with or without repair, at or above a particular output capability can be calculated over a cumulative period of time or at specific points in time. Author

N91-19463*# National Aeronautics and Space Administration. Lewis Research Center, Cleveland, OH.

PROPERTY AND MICROSTRUCTURAL NONUNIFORMITY IN THE YTTRIUM-BARIUM-COPPER-OXIDE SUPERCONDUCTOR DETERMINED FROM ELECTRICAL, MAGNETIC, AND ULTRASONIC MEASUREMENTS Ph.D. Thesis - Case Western Reserve Univ.

DON J. ROTH Jan. 1991 260 p

(Contract RTOP 506-43-11)

(NASA-TM-103732; E-5842; NAS 1.15:103732) Avail: NTIS

HC/MF A12 CSCL 14/4

The purpose of this dissertation was the following: (1) to characterize the effect of pore fraction on a comprehensive set of electrical and magnetic properties for the yttrium-barium-copper-oxide (YBCO) high temperature ceramic superconductor; and (2) to determine the viability of using a room-temperature, nondestructive characterization method to aid in the prediction of superconducting (cryogenic) properties. The latter involved correlating ultrasonic velocity measurements at room temperature with property-affecting pore fraction and oxygen content variations. The use of ultrasonic velocity for estimating pore fraction in YBCO is presented, and other polycrystalline materials are reviewed, modeled, and statistically analyzed. This provides the basis for using ultrasonic velocity to interrogate microstructure. The effect of pore fraction (0.10-0.25) on superconductor properties of YBCO samples was characterized. Spatial (within-sample) variations in microstructure and superconductor properties were investigated, and the effect of oxygen content on elastic behavior was examined. Experimental methods used included a.c. susceptibility, electrical, and ultrasonic velocity measurements. Superconductor properties measured included transition temperature, magnetic transition width, transport and magnetic critical current density, magnetic shielding, a.c. loss, and sharpness of the voltage-current characteristics. An ultrasonic velocity image constructed from measurements at 1mm increments across a YBCO sample revealed microstructural variations that correlated with variations in magnetic shielding and a.c. loss behavior. Destructive examination using quantitative image analysis revealed pore fraction to be the varying microstructural feature. Author

N91-19464*# National Aeronautics and Space Administration. Lewis Research Center, Cleveland, OH.

NDE STANDARDS FOR HIGH TEMPERATURE MATERIALS

ALEX VARY 1991 20 p Presented at the Symposium on Nondestructive Testing Standards 2: New Opportunities for Increased World Trade Through Accepted Standards for NDT and Quality, Gaithersburg, MD, 9-11 Apr. 1991; sponsored by ASTM, NIST, the American Society of Nondestructive Testing, and The American Welding Society

(Contract RTOP 510-01-50)

(NASA-TM-103761; E-6023; NAS 1.15:103761) Avail: NTIS

HC/MF A03 CSCL 14/4

High temperature materials include monolithic ceramics for automotive gas turbine engines and also metallic/intermetallic and ceramic matrix composites for a range of aerospace applications. These are materials that can withstand extreme operating temperatures that will prevail in advanced high-efficiency gas turbine engines. High temperature engine components are very likely to consist of complex composite structures with three-dimensionality interwoven and various intermixed ceramic fibers. The thermomechanical properties of components made of these materials are actually created in-place during processing and fabrication stages. The complex nature of these new materials creates strong incentives for exact standards for unambiguous evaluations of defects and microstructural characteristics. NDE techniques and standards that will ultimately be applicable to production and quality control of high temperature materials and structures are still emerging. The needs range from flaw detection to below 100 micron levels in monolithic ceramics to global imaging of fiber architecture and matrix densification anomalies in composites. The needs are different depending on the processing stage, fabrication method, and nature of the finished product. The

38 QUALITY ASSURANCE AND RELIABILITY

standards are discussed that must be developed in concert with advances in NDE technology, materials processing research, and fabrication development. High temperature materials and structures that fail to meet stringent specifications and standards are unlikely to compete successfully either technologically or in international markets.

Author

N91-21553*# National Aeronautics and Space Administration. Lewis Research Center, Cleveland, OH.

SPATIAL VARIATIONS IN AC SUSCEPTIBILITY AND MICROSTRUCTURE FOR THE YBa₂Cu₃O_{7-x} SUPERCONDUCTOR AND THEIR CORRELATION WITH ROOM-TEMPERATURE ULTRASONIC MEASUREMENTS

DON J. ROTH, MARK R. DEGUIRE, LEONARD E. DOLHERT (Grace, W. R. and Co., Columbia, MD.), and ALOYSIUS F. HEPP May 1991 22 p Presented at the 93rd Annual Meeting of the American Ceramic Society, Cincinnati, OH, 28 Apr. - 2 May 1991 (Contract RTOP 506-43-11)

(NASA-TM-103787; E-6064; NAS 1.15:103787) Avail: NTIS HC/MF A03 CSCL 14/4

The spatial (within-sample) uniformity of superconducting behavior and microstructure in YBa₂Cu₃O_{7-x} specimens over the pore fraction range of 0.10 to 0.25 was examined. The viability of using a room-temperature, nondestructive characterization method (ultrasonic velocity imaging) to predict spatial variability was determined. Spatial variations in superconductor properties were observed for specimens containing 0.10 pore fraction. An ultrasonic velocity image constructed from measurements at 1 mm increments across one such specimen revealed microstructural variation between edge and center locations that correlated with variations in alternating-current shielding and loss behavior. Optical quantitative image analysis on sample cross-sections revealed pore fraction to be the varying microstructural feature.

Author

N91-23050*# National Aeronautics and Space Administration. Lewis Research Center, Cleveland, OH.

RELIABILITY AND RISK ASSESSMENT OF STRUCTURES

C. C. CHAMIS In National Aeronautics and Space Administration, Technology 2000, Volume 1 p 241-248 Mar. 1991

Avail: NTIS HC/MF A18 CSCL 14/4

Development of reliability and risk assessment of structural components and structures is a major activity at Lewis Research Center. It consists of five program elements: (1) probabilistic loads; (2) probabilistic finite element analysis; (3) probabilistic material behavior; (4) assessment of reliability and risk; and (5) probabilistic structural performance evaluation. Recent progress includes: (1) the evaluation of the various uncertainties in terms of cumulative distribution functions for various structural response variables based on known or assumed uncertainties in primitive structural variables; (2) evaluation of the failure probability; (3) reliability and risk-cost assessment; and (4) an outline of an emerging approach for eventual certification of man-rated structures by computational methods. Collectively, the results demonstrate that the structural durability/reliability of man-rated structural components and structures can be effectively evaluated by using formal probabilistic methods.

Author

N91-23521*# National Aeronautics and Space Administration. Lewis Research Center, Cleveland, OH.

A PRELIMINARY INVESTIGATION OF ACOUSTO-ULTRASONIC NDE OF METAL MATRIX COMPOSITE TEST SPECIMENS

HAROLD E. KAUTZ and BRAD A. LERCH May 1991 13 p (Contract RTOP 510-01-01)

(NASA-TM-104339; E-5651-1; NAS 1.15:104339) Avail: NTIS HC/MF A03 CSCL 09/4

Acousto-ultrasonic (AU) measurements were performed on a series of tensile specimens composed of 8 laminated layers of continuous, SiC fiber reinforced Ti-15-3 matrix. The following subject areas are covered: AU signal analysis; tensile behavior; AU and interrupted tensile tests; AU and thermally cycled specimens; AU and stiffness; and AU and specimen geometry.

Author

N91-27575*# National Aeronautics and Space Administration. Lewis Research Center, Cleveland, OH.

ULTRASONIC EVALUATION OF OXIDATION AND REDUCTION EFFECTS ON THE ELASTIC BEHAVIOR AND GLOBAL MICROSTRUCTURE OF YBa₂Cu₃O_{7-x}

DON J. ROTH, MARK R. DEGUIRE, and LEONARD E. DOLHERT (Grace, W. R. and Co., Columbia, MD.) Jul. 1991 29 p (Contract RTOP 506-43-11)

(NASA-TM-104529; E-6282; NAS 1.15:104529) Avail: NTIS HC/MF A03 CSCL 14/4

Ultrasonic velocity measurement techniques were used to evaluate the effects of oxidation and reduction on the elastic properties, global microstructure and oxygen content of the YBa₂Cu₃O_{7-x} ceramic superconductor for samples ranging from 70 to 90 pct. of theoretical density. Bulk density, velocity, and elastic modulus generally increased with increasing oxygen content upon oxidation, and this behavior was reversible. Velocity image patterns were similar after oxidation and reduction treatments for a 90 pct. dense sample, although the velocity value at any given point on the sample was changed following the treatments. The unchanging pattern correlated with destructive measurements showing that the spatial pore distribution (fraction and size) was not measurably altered after the treatments. Changes in superconducting behavior, crystal structure, and grain structure were observed consistent with changes in oxygen content.

Author

N91-28605*# National Aeronautics and Space Administration. Lewis Research Center, Cleveland, OH.

NONDESTRUCTIVE EVALUATION TOOLS AND EXPERIMENTAL STUDIES FOR MONITORING THE HEALTH OF SPACE PROPULSION SYSTEMS

EDWARD R. GENERAZIO 1991 44 p Presented at the Conference on Advanced Space Exploration Initiative Technologies, Cleveland, OH, 4-6 Sep. 1991; cosponsored by AIAA and OAI (Contract RTOP 510-01-1A)

(NASA-TM-105164; E-6453; NAS 1.15:105164; AIAA PAPER 91-3433) Avail: NTIS HC/MF A03 CSCL 14/4

An overview is given of background and information on space propulsion systems on both the programmatic and technical levels. Feasibility experimental studies indicate that nondestructive evaluation tools such as ultrasonic, eddy current and x-ray may be successfully used to monitor the life limiting failure mechanisms of space propulsion systems. Encouraging results were obtained for monitoring the life limiting failure mechanisms for three space propulsion systems; the degradation of tungsten arcjet and magnetoplasmadynamic electrodes; presence and thickness of spallable electrically conducting molybdenum films in ion thrusters; and the degradation of the catalyst in hydrazine thrusters.

Author

N91-29610*# National Aeronautics and Space Administration. Lewis Research Center, Cleveland, OH.

NDE OF CERAMICS AND CERAMIC COMPOSITES

ALEX VARY and STANLEY J. KLIMA (Sverdrup Technology, Inc., Brook Park, OH.) Jul. 1991 15 p (Contract RTOP 510-01-50)

(NASA-TM-104520; E-6390; NAS 1.15:104520) Avail: NTIS HC/MF A03 CSCL 14/4

Although nondestructive evaluation (NDE) techniques for ceramics are fairly well developed, they are difficult to apply in many cases for high probability detection of the minute flaws that can cause failure in monolithic ceramics. Conventional NDE techniques are available for monolithic and fiber reinforced ceramic matrix composites, but more exact quantitative techniques needed are still being investigated and developed. Needs range from flaw detection to below 100 micron levels in monolithic ceramics to global imaging of fiber architecture and matrix densification anomalies in ceramic composites. NDE techniques that will ultimately be applicable to production and quality control of ceramic structures are still emerging from the lab. Needs are different depending on the processing stage, fabrication method, and nature of the finished product. NDE techniques are being developed in

concert with materials processing research where they can provide feedback information to processing development and quality improvement. NDE techniques also serve as research tools for materials characterization and for understanding failure processes, e.g., during thermomechanical testing. Author

N91-30546* National Aeronautics and Space Administration. Lewis Research Center, Cleveland, OH.

ULTRASONIC VELOCITY TECHNIQUE FOR MONITORING PROPERTY CHANGES IN FIBER-REINFORCED CERAMIC MATRIX COMPOSITES

HAROLD E. KAUTZ and RAMAKRISHNA T. BHATT 1991 12 p Presented at the 15th Annual Conference on Composites and Advanced Ceramics, Cocoa Beach, FL, 13-16 Jan. 1991; sponsored by the American Ceramic Society (Contract DA PROJ. 1L1-61102-AH-45; RTOP 510-01-01) (NASA-TM-103806; E-5926; NAS 1.15:103806; AVSCOM-TR-91-C-017) Avail: NTIS HC/MF A03 CSCL 14/4

A technique for measuring ultrasonic velocity was used to monitor changes that occur during processing and heat treatment of a SiC/RBSM composite. Results indicated that correlations exist between the ultrasonic velocity data and elastic modulus and interfacial shear strength data determined from mechanical tests. The ultrasonic velocity data can differentiate strength. The advantages and potential of this nondestructive evaluation method for fiber reinforced ceramic matrix composite applications are discussed. Author

39

STRUCTURAL MECHANICS

Includes structural element design and weight analysis; fatigue; and thermal stress.

A91-12895* National Aeronautics and Space Administration. Lewis Research Center, Cleveland, OH.

MECHANICS OF DAMPING FOR FIBER COMPOSITE LAMINATES INCLUDING HYGROTHERMAL EFFECTS

D. A. SARAVANOS and C. C. CHAMIS (NASA, Lewis Research Center, Cleveland, OH) AIAA Journal (ISSN 0001-1452), vol. 28, Oct. 1990, p. 1813-1819. Previously cited in issue 12, p. 1850, Accession no. A89-30681. refs Copyright

A91-12905* Indian Inst. of Science, Bangalore.
GENERAL PURPOSE PROGRAM TO GENERATE COMPATIBILITY MATRIX FOR THE INTEGRATED FORCE METHOD

J. NAGABHUSANAM (Indian Institute of Science, Bangalore, India) and S. N. PATNAIK (NASA, Lewis Research Center, Cleveland, OH) AIAA Journal (ISSN 0001-1452), vol. 28, Oct. 1990, p. 1838-1842. refs Copyright

An efficient procedure for obtaining the compatibility conditions of finite-element models involves the generation of both field and compatibility conditions from deformation-displacement relations, using (1) the compatibility bandwidth, and (2) the node-determinacy concept. A computer program thus structured will generate sparse and banded compatibility conditions for a structure that is idealized by the finite elements. O.C.

A91-16042* National Aeronautics and Space Administration. Lewis Research Center, Cleveland, OH.

PROBABILISTIC SIMULATION OF UNCERTAINTIES IN THERMAL STRUCTURES

C. C. CHAMIS (NASA, Lewis Research Center, Cleveland, OH) and MICHAEL SHIAO (Sverdrup Technology, Inc., Brook Park, OH) IN: Thermal Structures Conference, 1st, Charlottesville, VA,

Nov. 13-15, 1990, Proceedings. Charlottesville, VA, University of Virginia Light Thermal Structures Center, 1990, p. 313-326. refs Copyright

Development of probabilistic structural analysis methods for hot structures is a major activity at NASA-Lewis, and consists of five program elements: (1) probabilistic loads, (2) probabilistic finite element analysis, (3) probabilistic material behavior, (4) assessment of reliability and risk, and (5) probabilistic structural performance evaluation. Attention is given to quantification of the effects of uncertainties for several variables on High Pressure Fuel Turbopump blade temperature, pressure, and torque of the Space Shuttle Main Engine; the evaluation of the cumulative distribution function for various structural response variables based on assumed uncertainties in primitive structural variables; evaluation of the failure probability; reliability and risk-cost assessment; and an outline of an emerging approach for eventual hot structures certification. Collectively, the results demonstrate that the structural durability/reliability of hot structural components can be effectively evaluated in a formal probabilistic framework. In addition, the approach can be readily extended to computationally simulate certification of hot structures for aerospace environments. Author

A91-16290* National Aeronautics and Space Administration. Lewis Research Center, Cleveland, OH.

SIMPLIFIED PROCEDURES FOR DESIGNING COMPOSITE BOLTED JOINTS

CHRISTOS C. CHAMIS (NASA, Lewis Research Center, Cleveland, OH) Journal of Reinforced Plastics and Composites (ISSN 0731-6844), vol. 9, Nov. 1990, p. 614-626. Previously announced in STAR as N88-15020. refs Copyright

Simplified procedures are described to design and analyze single and multi-bolt composite joints. Numerical examples illustrate the use of these methods. Factors affecting composite bolted joints are summarized. References are cited where more detailed discussion is presented on specific aspects of composite bolted joints. Design variables associated with these joints are summarized in the appendix. Author

A91-19048* Case Western Reserve Univ., Cleveland, OH.
AN INTEGRATED METHODOLOGY FOR OPTIMIZING THE PASSIVE DAMPING OF COMPOSITE STRUCTURES

D. A. SARAVANOS (Case Western Reserve University, Cleveland, OH) and C. C. CHAMIS (NASA, Lewis Research Center, Cleveland, OH) Polymer Composites (ISSN 0272-8397), vol. 11, Dec. 1990, p. 328-336. Previously announced in STAR as N90-11808. refs Copyright

A method is presented for tailoring plate and shell composite structures for optimal forced damped dynamic response. The damping of specific vibration modes is optimized with respect to dynamic performance criteria including placement of natural frequencies and minimization of resonance amplitudes. The structural composite damping is synthesized from the properties of the constituent materials, laminate parameters, and structural geometry based on a specialty finite element. Application studies include the optimization of laminated composite beams and composite shells with fiber volume ratios and ply angles as design variables. The results illustrate the significance of damping tailoring to the dynamic performance of composite structures, and the effectiveness of the method in optimizing the structural dynamic response. Author

A91-23685* National Aeronautics and Space Administration. Lewis Research Center, Cleveland, OH.

SOLUTION AND SENSITIVITY ANALYSIS OF A COMPLEX TRANSCENDENTAL EIGENPROBLEM WITH PAIRS OF REAL EIGENVALUES

D. V. MURTHY (NASA, Lewis Research Center, Cleveland; Toledo, University, OH) IN: Vibration analysis - Techniques and applications; Proceedings of the Twelfth Biennial ASME Conference on Mechanical Vibration and Noise, Montreal, Canada, Sept. 17-21,

39 STRUCTURAL MECHANICS

1989. New York, American Society of Mechanical Engineers, 1989, p. 229-234. Previously announced in STAR as N89-13819. refs
Copyright

This paper considers complex transcendental eigenvalue problems where one is interested in pairs of eigenvalues that are restricted to take real values only. Such eigenvalue problems arise in dynamic stability analysis of nonconservative physical systems, i.e., flutter analysis of aeroelastic systems. Some available solution methods are discussed and a new method is presented. Two computational approaches are described for analytical evaluation of the sensitivities of these eigenvalues when they are dependent on other parameters. The algorithms presented are illustrated through examples. Author

A91-28372* National Aeronautics and Space Administration. Lewis Research Center, Cleveland, OH.

INTEGRATED FORCE METHOD VERSUS DISPLACEMENT METHOD FOR FINITE ELEMENT ANALYSIS

S. N. PATNAIK, L. BERKE (NASA, Lewis Research Center, Cleveland, OH), and R. H. GALLAGHER (Clarkson University, Potsdam, NY) Computers and Structures (ISSN 0045-7949), vol. 38, no. 4, 1991, p. 377-407. Previously announced in STAR as N90-18081. refs
Copyright

A novel formulation termed the integrated force method (IFM) has been developed in recent years for analyzing structures. In this method all the internal forces are taken as independent variables, and the system equilibrium equations (EEs) are integrated with the global compatibility conditions (CCs) to form the governing set of equations. In IFM the CCs are obtained from the strain formulation of St. Venant, and no choices of redundant load systems have to be made, in contrast to the standard force method (SFM). This property of IFM allows the generation of the governing equation to be automated straightforwardly, as it is in the popular stiffness method (SM). In this report IFM and SM are compared relative to the structure of their respective equations, their conditioning, required solution methods, overall computational requirements, and convergence properties as these factors influence the accuracy of the results. Overall, this new version of the force method produces more accurate results than the stiffness method for comparable computational cost. Author

A91-28612* Cleveland State Univ., OH.

DYNAMIC ANALYSIS OF SPACE-RELATED LINEAR AND NON-LINEAR STRUCTURES

PAUL A. BOSELA (Cleveland State University, OH), FRANCIS J. SHAKER (NASA, Lewis Research Center, Cleveland, OH), and DEMETER G. FERTIS (Akron, University, OH) IN: Developments in theoretical and applied mechanics. Vol. 15 - Proceedings of the 15th Southeastern Conference on Theoretical and Applied Mechanics, Atlanta, GA, Mar. 22, 23, 1990. Atlanta, GA, Georgia Institute of Technology, 1990, p. 590-597. Previously announced in STAR as N90-25174. refs
(Contract NAG3-1008)
Copyright

In order to be cost effective, space structures must be extremely light weight, and subsequently, very flexible structures. The power system for Space Station Freedom is such a structure. Each array consists of a deployable truss mast and a split blanket of photo-voltaic solar collectors. The solar arrays are deployed in orbit, and the blanket is stretched into position as the mast is extended. Geometric stiffness due to the preload make this an interesting non-linear problem. The space station will be subjected to various dynamic loads, during shuttle docking, solar tracking, attitude adjustment, etc. Accurate prediction of the natural frequencies and mode shapes of the space station components, including the solar arrays, is critical for determining the structural adequacy of the components, and for designing a dynamic control system. The process used in developing and verifying the finite element dynamic model of the photo-voltaic arrays is documented. Various problems were identified, such as grounding effects due to geometric stiffness, large displacement effects, and pseudo-stiffness (grounding) due to lack of required rigid body

modes. Analysis techniques, such as development of rigorous solutions using continuum mechanics, finite element solution sequence altering, equivalent systems using a curvature basis, Craig-Bampton superelement approach, and modal ordering schemes were utilized. The grounding problems associated with the geometric stiffness are emphasized. Author

A91-31835* Texas Univ., San Antonio.

QUANTIFICATION OF UNCERTAINTIES IN COUPLED MATERIAL DEGRADATION PROCESSES - HIGH TEMPERATURE, FATIGUE AND CREEP

L. BOYCE (Texas, University, San Antonio) and C. C. CHAMIS (NASA, Lewis Research Center, Cleveland, OH) IN: AIAA/ASME/ASCE/AHS/ASC Structures, Structural Dynamics, and Materials Conference, 32nd, Baltimore, MD, Apr. 8-10, 1991, Technical Papers. Pt. 1. Washington, DC, American Institute of Aeronautics and Astronautics, 1991, p. 66-72. refs
(AIAA PAPER 91-0977) Copyright

This paper describes the development of methodology that provides for quantification of uncertainties in lifetime strength of aerospace materials subjected to a number of diverse effects. A probabilistic material degradation model, in the form of a randomized multifactor interaction equation, has been postulated for lifetime strength degradation of structural components of aerospace propulsion systems. The model includes effects that typically reduce lifetime strength and may include temperature, mechanical fatigue, creep and others. The paper also includes the analysis of experimental data from the open literature for Inconel 718. These data are used to provide an initial check for model validity, as well as for calibration of the model's empirical material constants. The model validity check and calibration is carried out for three effects, namely, high temperature, mechanical fatigue and creep. Author

A91-31957* Applied Research Associates, Inc., Raleigh, NC.

PROGRAMMING PROBABILISTIC STRUCTURAL ANALYSIS FOR PARALLEL PROCESSING COMPUTER

ROBERT H. SUES, HEH-CHYUN CHEN, LAWRENCE A. TWISDALE (Applied Research Associates, Inc., Raleigh, NC), CHRISTOS C. CHAMIS, and PAPU L. N. MURTHY (NASA, Lewis Research Center, Cleveland, OH) IN: AIAA/ASME/ASCE/AHS/ASC Structures, Structural Dynamics, and Materials Conference, 32nd, Baltimore, MD, Apr. 8-10, 1991, Technical Papers. Pt. 2. Washington, DC, American Institute of Aeronautics and Astronautics, 1991, p. 1243-1253. refs
(Contract NAS3-28524)
(AIAA PAPER 91-0920) Copyright

The ultimate goal of this research program is to make Probabilistic Structural Analysis (PSA) computationally efficient and hence practical for the design environment by achieving large scale parallelism. The paper identifies the multiple levels of parallelism in PSA, identifies methodologies for exploiting this parallelism, describes the development of a parallel stochastic finite element code, and presents results of two example applications. It is demonstrated that speeds within five percent of those theoretically possible can be achieved. A special-purpose numerical technique, the stochastic preconditioned conjugate gradient method, is also presented and demonstrated to be extremely efficient for certain classes of PSA problems. Author

A91-32032* Michigan Univ., Ann Arbor.

AEROELASTIC MODAL CHARACTERISTICS OF MISTUNED BLADE ASSEMBLIES - MODE LOCALIZATION AND LOSS OF EIGENSTRUCTURE

CHRISTOPHE PIERRE (Michigan, University, Ann Arbor) and DURBHA V. MURTHY (NASA, Lewis Research Center, Cleveland; Toledo, University, OH) IN: AIAA/ASME/ASCE/AHS/ASC Structures, Structural Dynamics, and Materials Conference, 32nd, Baltimore, MD, Apr. 8-10, 1991, Technical Papers. Pt. 3. Washington, DC, American Institute of Aeronautics and Astronautics, 1991, p. 2036-2050. refs
(Contract NAG3-1163)
(AIAA PAPER 91-1218) Copyright

An investigation of the effects of small mistuning on the aeroelastic modes of bladed-disk assemblies with aerodynamic coupling between blades is presented. The cornerstone of the approach is the use and development of perturbation methods that exhibit the crucial role of the interblade coupling and yield general findings regarding mistuning effects. It is shown that blade assemblies with weak aerodynamic interblade coupling are highly sensitive to small blade mistuning, and that their dynamics is qualitatively altered in the following ways: the regular pattern that characterizes the root locus of the tuned aeroelastic eigenvalues in the complex plane is totally lost; the aeroelastic mode shapes become severely localized to only a few blades of the assembly and lose their constant interblade phase angle feature; curve veering phenomena take place when the eigenvalues are plotted versus a mistuning parameter. Author

A91-32064* # National Aeronautics and Space Administration. Lewis Research Center, Cleveland, OH.

THE EFFECTS OF INTERPLY DAMPING LAYERS ON THE DYNAMIC RESPONSE OF COMPOSITE STRUCTURES

D. A. SARAVANOS (NASA, Lewis Research Center, Cleveland, OH) IN: AIAA/ASME/ASCE/AHS/ASC Structures, Structural Dynamics, and Materials Conference, 32nd, Baltimore, MD, Apr. 8-10, 1991, Technical Papers. Pt. 3. Washington, DC, American Institute of Aeronautics and Astronautics, 1991, p. 2363-2370. refs

(AIAA PAPER 91-1124) Copyright

Integrated damping mechanics for composite laminates with interlaminar constrained layers of damping polymer materials are developed. Discrete layer damping mechanics for composite laminates with damping layers, in connection with a semi-analytical method for predicting the modal damping in simply-supported specialty composite plates are presented. Application cases demonstrate the advantages of the method. Damping predictions for graphite/epoxy composite plates of various laminations demonstrate the potential for higher damping than geometrically equivalent aluminum plates. The effects of aspect ratio, damping layer thickness, and fiber volume ratio on static and dynamic characteristics of the composite plate are also investigated.

Author

A91-32087* # SDRC, Inc., San Diego, CA.

SIMULATION OF THE SPACE STATION STRUT-OUT CONDITION

PAUL A. BLELLOCH, NADINE M. MACK (SDRC, Inc., Engineering Services Div., San Diego, CA), and KELLY S. CARNEY (NASA, Lewis Research Center, Cleveland, OH) IN: AIAA/ASME/ASCE/AHS/ASC Structures, Structural Dynamics, and Materials Conference, 32nd, Baltimore, MD, Apr. 8-10, 1991, Technical Papers. Pt. 4. Washington, DC, American Institute of Aeronautics and Astronautics, 1991, p. 2570-2575.

(AIAA PAPER 91-1248) Copyright

A method is presented for reanalyzing a truss structure when one of the truss elements (struts) has failed. The method uses a modal model of the nominal structure coupled with a residual flexibility term to predict the effect of the failed strut without resolving the finite element model. By implementing the method as part of the transient simulation, it is feasible to consider a large number of potential strut failures with a minimum amount of extra effort. Preliminary application of the method to the Space Station indicates excellent agreement with results based on modifying and resolving the finite element model. Author

A91-32099* # Sverdrup Technology, Inc., Brook Park, OH.

COMPUTATIONAL SIMULATION OF ACOUSTIC FATIGUE FOR HOT COMPOSITE STRUCTURES

S. N. SINGHAL, V. K. NAGPAL (Sverdrup Technology, Inc., Brook Park, OH), P. L. N. MURTHY, and C. C. CHAMIS (NASA, Lewis Research Center, Cleveland, OH) IN: AIAA/ASME/ASCE/AHS/ASC Structures, Structural Dynamics, and Materials Conference, 32nd, Baltimore, MD, Apr. 8-10, 1991, Technical Papers. Pt. 4. Washington, DC, American Institute of

Aeronautics and Astronautics, 1991, p. 2709-2719. refs (AIAA PAPER 91-1178) Copyright

This paper presents predictive methods/codes for computational simulation of acoustic fatigue resistance of hot composite structures subjected to acoustic excitation emanating from an adjacent vibrating component. Select codes developed over the past two decades at the NASA Lewis Research Center are used. The codes include computation of (1) acoustic noise generated from a vibrating component, (2) degradation in material properties of the composite laminate at use temperature, (3) dynamic response of acoustically excited hot multilayered composite structure, (4) degradation in the first-ply strength of the excited structure due to acoustic loading, and (5) acoustic fatigue resistance of the excited structure, including propulsion environment. Effects of the laminate lay-up and environment on the acoustic fatigue life are evaluated. The results show that, by keeping the angled plies on the outer surface of the laminate, a substantial increase in the acoustic fatigue life is obtained. The effect of environment (temperature and moisture) is to relieve the residual stresses leading to an increase in the acoustic fatigue life of the excited panel. Author

A91-32129* # Ohio State Univ., Columbus.

FREE VIBRATIONS OF DELAMINATED BEAMS

M.-H. H. SHEN (Ohio State University, Columbus) and J. E. GRADY (NASA, Lewis Research Center, Cleveland, OH) IN: AIAA/ASME/ASCE/AHS/ASC Structures, Structural Dynamics, and Materials Conference, 32nd, Baltimore, MD, Apr. 8-10, 1991, Technical Papers. Pt. 4. Washington, DC, American Institute of Aeronautics and Astronautics, 1991, p. 3017-3025. refs (AIAA PAPER 91-1241) Copyright

Free vibration of laminated composite beams is studied. The effect of interply delaminations on natural frequencies and mode shapes is evaluated both analytically and experimentally. The equation of motion and associated boundary conditions are derived for the free vibration of a composite beam with a delamination of arbitrary size and location. A generalized variational principle is used to formulate the equation of motion, taking into account the interlaminar stress concentration at the crack-tips. This is accomplished by introducing a 'crack function' into the beam's compatibility relations. This function has its maximum value at the crack tip and decays exponentially in the longitudinal direction. The rate of exponential decay is determined by a least-square fit with the experimental results. The effect of coupling between longitudinal vibration and bending vibration is considered in the present study. This coupling effect is found to significantly affect the natural frequencies and mode shapes of the delaminated beam. Author

A91-33096* National Aeronautics and Space Administration. Lewis Research Center, Cleveland, OH.

FIBER PUSHOUT TEST - A THREE-DIMENSIONAL FINITE ELEMENT COMPUTATIONAL SIMULATION

SUBODH K. MITAL and CHRISTOS C. CHAMIS (NASA, Lewis Research Center, Cleveland, OH) Journal of Composites Technology and Research (ISSN 0885-6804), vol. 13, Spring 1991, p. 14-21. Previously announced in STAR as N90-21131. refs Copyright

A fiber pushthrough process was computationally simulated using three-dimensional finite element method. The interface material is replaced by an anisotropic material with greatly reduced shear modulus in order to simulate the fiber pushthrough process using a linear analysis. Such a procedure is easily implemented and is computationally very effective. It can be used to predict fiber pushthrough load for a composite system at any temperature. The average interface shear strength obtained from pushthrough load can easily be separated into its two components: one that comes from frictional stresses and the other that comes from chemical adhesion between fiber and the matrix and mechanical interlocking that develops due to shrinkage of the composite because of phase change during the processing. Step-by-step procedures are described to perform the computational simulation.

39 STRUCTURAL MECHANICS

to establish bounds on interfacial bond strength and to interpret interfacial bond quality. Author

A91-36283* National Aeronautics and Space Administration. Lewis Research Center, Cleveland, OH.

COMPUTATIONAL SIMULATION OF DAMPING IN COMPOSITE STRUCTURES

D. A. SARAVANOS and C. C. CHAMIS (NASA, Lewis Research Center, Cleveland, OH) (National Congress in Mechanics, 2nd, Athens, Greece, June 29-July 1, 1989) Journal of Reinforced Plastics and Composites (ISSN 0731-6844), vol. 10, May 1991, p. 256-278. Previously announced in STAR as N90-20432. refs Copyright

A computational methodology is developed for the prediction of passive damping in composite structures. The method involves multiple levels of damping modeling by integrating micromechanics, laminate, and structural damping theories. The effects of temperature and moisture on structural damping are included. The simulation of damping in the structural level is accomplished with finite-element discretization. Applications are performed on graphite/epoxy composite beams, plates, and shells to illustrate the methodology. Additional parametric studies demonstrate the variation of structural modal damping with respect to ply angles, fiber volume ratio, and temperature. Author

A91-37853*# National Aeronautics and Space Administration. Lewis Research Center, Cleveland, OH.

COMPATIBILITY CONDITIONS OF STRUCTURAL MECHANICS FOR FINITE ELEMENT ANALYSIS

S. N. PATNAIK, L. BERKE (NASA, Lewis Research Center, Cleveland, OH), and R. H. GALLAGHER (Clarkson University, Potsdam, NY) AIAA Journal (ISSN 0001-1452), vol. 29, May 1991, p. 820-829. Previously announced in STAR as N90-17180. refs Copyright

The equilibrium equations and the compatibility conditions are fundamental to the analyses of structures. However, anyone who undertakes even a cursory generic study of the compatibility conditions can discover, with little effort, that historically this facet of structural mechanics had not been adequately researched by the profession. Now the compatibility conditions (CC's) have been researched and are understood to a great extent. For finite element discretizations, the CC's are banded and can be divided into three distinct categories: (1) the interface CC's; (2) the cluster or field CC's; and (3) the external CC's. The generation of CC's requires the separating of a local region, then writing the deformation displacement relation (ddr) for the region, and finally, the eliminating of the displacements from the ddr. The procedure to generate all three types of CC's is presented and illustrated through examples of finite element models. The uniqueness of the CC's thus generated is shown. Author

A91-38754* National Aeronautics and Space Administration. Lewis Research Center, Cleveland, OH.

COMPOSITE LAMINATE TAILORING WITH PROBABILISTIC CONSTRAINTS AND LOADS

P. B. THANEDAR and C. C. CHAMIS (NASA, Lewis Research Center, Cleveland, OH) IN: Composite material technology 1990; Proceedings of the Symposium, 13th ASME Annual Energy-Sources Technology Conference and Exhibition, New Orleans, LA, Jan. 14-18, 1990. New York, American Society of Mechanical Engineers, 1990, p. 11-21. Previously announced in STAR as N90-20138. refs Copyright

A reliability-based structural synthesis procedure was developed to tailor laminates to meet reliability-based (ply) strength requirements and achieve desirable laminate responses. The main thrust is to demonstrate how to integrate the optimization technique in the composite laminate tailoring process to meet reliability design requirements. The question of reliability arises in fiber composite analysis and design because of the inherent scatter that is observed in the constituent (fiber and matrix) material properties during experimentation. Symmetric and asymmetric composite laminates

subject to mechanical loadings are considered as application examples. These application examples illustrate the effectiveness and ease with which reliability considerations can be integrated in the design optimization model for composite laminate tailoring. Author

A91-44319*# National Aeronautics and Space Administration. Lewis Research Center, Cleveland, OH.

LOCALIZATION OF AEROELASTIC MODES IN MISTUNED HIGH-ENERGY TURBINES

CHRISTOPHE PIERRE (NASA, Lewis Research Center, Cleveland, OH; Michigan, University, Ann Arbor), TODD E. SMITH (NASA, Lewis Research Center, Cleveland; Sverdrup Technology, Inc., Brook Park, OH), and DURBHA V. MURTHY (Toledo, University, OH) AIAA, SAE, ASME, and ASEE, Joint Propulsion Conference, 27th, Sacramento, CA, June 24-26, 1991. 36 p. Previously announced in STAR as N91-24659. refs (Contract NAG3-1163; NAG3-742; NAS3-25266) (AIAA PAPER 91-3379) Copyright

The effects of blades mistuning on the aeroelastic vibration characteristics of high energy turbines are investigated, using the first stage of the oxidizer turbopump in the Space Shuttle Main Engine as an example. A model aeroelastic analysis procedure is used in concert with a linearized unsteady aerodynamic theory that accounts for the effects of blade thickness, camber, and steady loading. Extreme sensitivity of the dynamic characteristics of mistuned rotors is demonstrated. In particular, the aeroelastic modes become localized to a few blades, possibly leading to rogue blade failure, and the locus of the aeroelastic eigenvalues loses its structure when small mistunings (of the order present in actual rotors) are introduced. Perturbation analyses that yield physical insights into these phenomena are presented. A powerful but easily calculated stochastic sensitivity measure that allows the global prediction of mistuning effects is developed. Author

A91-48865* Analox Corp., Fairview Park, OH.

LOW VELOCITY IMPACT ANALYSIS WITH NASTRAN

D. A. TROWBRIDGE (Analox Corp., Fairview Park, OH), J. E. GRADY, and R. A. AIELLO (NASA, Lewis Research Center, Cleveland, OH) Computers and Structures (ISSN 0045-7949), vol. 40, no. 4, 1991, p. 977-984. Research supported by U.S. Navy. Previously announced in STAR as N90-24647. refs Copyright

A nonlinear elastic force-displacement relationship is used to calculate the transient impact force and local deformation at the point of contact between impactor and target. The nonlinear analysis and transfer function capabilities of NASTRAN are used to define a finite element model that behaves globally linearly elastic, and locally nonlinear elastic to model the local contact behavior. Results are presented for two different structures: a uniform cylindrical rod impacted longitudinally; and an orthotropic plate impacted transversely. Calculated impact force and transient structural response of the targets are shown to compare well with results measured in experimental tests. Author

A91-48899* National Aeronautics and Space Administration. Lewis Research Center, Cleveland, OH.

A RESISTANCE STRAIN GAGE WITH REPEATABLE APPARENT STRAIN TO 800 C

J.-F. LEI (NASA, Lewis Research Center; Sverdrup Technology, Inc., Cleveland, OH) Experimental Techniques (ISSN 0732-8818), vol. 15, July-Aug. 1991, p. 23-27. refs Copyright

Experimental PdCr temperature-compensated resistance static-strain gages are described. The gages are developed in both fine-wire and thin-film forms. It is found that a PdCr wire strain gage coated with a flame-sprayed mixture of alumina and 4 wt pct zirconia demonstrates the smallest variation in and the best repeatability of apparent strain among the existing gages used at temperatures up to 800 C. Results of preliminary tests indicate uncompensated uncoated thin-film gages have potential usefulness at temperatures up to 1000 C. O.G.

A91-51916* Oak Ridge National Lab., TN.

NUMERICAL, MICRO-MECHANICAL PREDICTION OF CRACK GROWTH RESISTANCE IN A FIBRE-REINFORCED/BRITTLE MATRIX COMPOSITE

MICHAEL G. JENKINS (Oak Ridge National Laboratory, TN), ASISH GHOSH (Philips Display Components Co., Ann Arbor, MI), and JONATHAN A. SALEM (NASA, Lewis Research Center, Cleveland, OH) IN: 1990 SEM Spring Conference on Experimental Mechanics, Albuquerque, NM, June 4-6, 1990, Proceedings. Bethel, CT, Society for Experimental Mechanics, Inc., 1990, p. 179-186. refs
Copyright

Micromechanics fracture models are incorporated into three distinct fracture process zones which contribute to the crack growth resistance of fibrous composites. The frontal process zone includes microcracking, fiber debonding, and some fiber failure. The elastic process zone is related only to the linear elastic creation of new matrix and fiber fracture surfaces. The wake process zone includes fiber bridging, fiber pullout, and fiber breakage. The R-curve predictions of the model compare well with empirical results for a unidirectional, continuous fiber C/C composite. Separating the contributions of each process zone reveals the wake region to contain the dominant crack growth resistance mechanisms. Fractography showed the effects of the micromechanisms on the macroscopic fracture behavior. Author

A91-55137* National Aeronautics and Space Administration. Lewis Research Center, Cleveland, OH.

APPLICATION OF FINITE-ELEMENT-BASED SOLUTION TECHNOLOGIES FOR VISCOPLASTIC STRUCTURAL ANALYSES

VINOD K. ARYA (NASA, Lewis Research Center, Cleveland; Toledo, University, OH) Communications in Applied Numerical Methods (ISSN 0748-8025), vol. 7, Sept. 1991, p. 435-444. refs
Copyright

Finite-element solution technology developed for use in conjunction with advanced viscoplastic models is described. The development of such solution technology is necessary for performing stress/life analyses of engineering structural problems where the complex geometries and loadings make the conventional analytical solutions difficult. The versatility of the solution technology is demonstrated by applying it to viscoplastic models possessing different mathematical structures and encompassing isotropic and anisotropic materials. The computational results qualitatively replicate deformation behavior observed in experiments on prototypical structural components. Author

A91-56365* Toledo Univ., OH.

FINITE ELEMENT ELASTIC-PLASTIC-CREEP AND CYCLIC LIFE ANALYSIS OF A COWL LIP

V. K. ARYA (Toledo, University, OH), M. E. MELIS, and G. R. HALFORD (NASA, Lewis Research Center, Cleveland, OH) Fatigue and Fracture of Engineering Materials and Structures (ISSN 8756-758X), vol. 14, no. 10, 1991, p. 967-977. Previously announced in STAR as N90-22808. refs
Copyright

Results are presented of elastic, elastic-plastic and elastic-plastic-creep analyses of a test-rig component of an actively cooled cowl lip. A cowl lip is part of the leading edge of an engine inlet of proposed hypersonic aircraft and is subject to severe thermal loadings and gradients during flight. Values of stresses calculated by elastic analysis are well above the yield strength of the cowl lip material. Such values are highly unrealistic, and thus elastic stress analyses are inappropriate. The inelastic (elastic-plastic and elastic-plastic-creep) analyses produce more reasonable and acceptable stress and strain distributions in the component. Finally, using the results from these analyses, predictions are made for the cyclic crack initiation life of a cowl lip. A comparison of predicted cyclic lives shows the cyclic life prediction from the elastic-plastic-creep analysis to be the lowest and, hence, most realistic. Author

A91-56540* National Aeronautics and Space Administration. Lewis Research Center, Cleveland, OH.

A DATA ACQUISITION AND CONTROL PROGRAM FOR AXIAL-TORSIONAL FATIGUE TESTING

SREERAMESH KALLURI (NASA, Lewis Research Center; Sverdrup Technology, Inc., Cleveland, OH) and PETER J. BONACUSE (NASA, Lewis Research Center; U.S. Army, Propulsion Directorate, Cleveland, OH) IN: Applications of automation technology to fatigue and fracture testing; Proceedings of the Symposium, Kansas City, MO, May 22, 23, 1989. Philadelphia, PA, American Society for Testing and Materials, 1990, p. 269-287. Previously announced in STAR as N89-28029. refs
Copyright

A computer program was developed for data acquisition and control of axial-torsional fatigue experiments. The multitasked, interrupt-driven program was written in Pascal and Assembly. This program is capable of dual-channel control and six-channel data acquisition. It can be utilized to perform inphase and out-of-phase axial-torsional isothermal fatigue or deformation experiments. The program was successfully used to conduct inphase axial-torsional fatigue experiments on 304 stainless steel at room temperature and on Hastelloy X at 800 C. The details of the software and some of the results generated to date are presented. Author

N91-10332*# National Aeronautics and Space Administration. Lewis Research Center, Cleveland, OH.

CALCULATION OF WEIBULL STRENGTH PARAMETERS, BATDORF FLAW DENSITY CONSTANTS AND RELATED STATISTICAL QUANTITIES USING PC-CARES

STEVEN A. SZATMARY, JOHN P. GYEKENYESI, and NOEL N. NEMETH (Aerospace Design and Fabrication, Inc., Brook Park, OH.) Oct. 1990 111 p
(Contract RTOP 505-63-1B)
(NASA-TM-103247; E-5674; NAS 1.15:103247) Avail: NTIS HC/MF A06 CSCL 20K

This manual describes the operation and theory of the PC-CARES (Personal Computer-Ceramic Analysis and Reliability Evaluation of Structures) computer program for the IBM PC and compatibles running PC-DOS/MS-DOS OR IBM/MS-OS/2 (version 1.1 or higher) operating systems. The primary purpose of this code is to estimate Weibull material strength parameters, the Batdorf crack density coefficient, and other related statistical quantities. Included in the manual is the description of the calculation of shape and scale parameters of the two-parameter Weibull distribution using the least-squares analysis and maximum likelihood methods for volume- and surface-flaw-induced fracture in ceramics with complete and censored samples. The methods for detecting outliers and for calculating the Kolmogorov-Smirnov and the Anderson-Darling goodness-of-fit statistics and 90 percent confidence bands about the Weibull line, as well as the techniques for calculating the Batdorf flaw-density constants are also described. Author

N91-12114*# National Aeronautics and Space Administration. Lewis Research Center, Cleveland, OH.

PROBABILISTIC STRUCTURAL ANALYSIS OF A TRUSS TYPICAL FOR SPACE STATION

SHANTARAM S. PAI Sep. 1990 11 p Presented at the 3rd Air Force/NASA Symposium on Recent Advances in Multidisciplinary Analysis and Optimization, San Francisco, CA, 24-26 Sep. 1990
(Contract RTOP 553-13-00)
(NASA-TM-103277; E-5725; NAS 1.15:103277) Avail: NTIS HC/MF A03 CSCL 20/11

A three-bay, space, cantilever truss is probabilistically evaluated using the computer code NESSUS (Numerical Evaluation of Stochastic Structures Under Stress) to identify and quantify the uncertainties and respective sensitivities associated with corresponding uncertainties in the primitive variables (structural, material, and loads parameters) that defines the truss. The distribution of each of these primitive variables is described in terms of one of several available distributions such as the Weibull, exponential, normal, log-normal, etc. The cumulative distribution

39 STRUCTURAL MECHANICS

function (CDF's) for the response functions considered and sensitivities associated with the primitive variables for given response are investigated. These sensitivities help in determining the dominating primitive variables for that response. Author

N91-12980*# National Aeronautics and Space Administration. Lewis Research Center, Cleveland, OH.

STIRLING ENGINE: AVAILABLE TOOLS FOR LONG-LIFE ASSESSMENT

GARY R. HALFORD and PAUL A. BARTOLOTTA 1991 7 p Presented at the 8th Symposium on Space Nuclear Power Systems, Albuquerque, NM, 6-10 Jan. 1991; sponsored by NASA, New Mexico Univ., Strategic Defense Initiative Organization, DOE, and AF

(Contract RTOP 590-13-11)

(NASA-TM-103660; E-5856; NAS 1.15:103660) Avail: NTIS

HC/MF A02 CSCL 20/11

A review is presented for the durability approaches applicable to long-time life assessment of Stirling engine hot-section components. The crucial elements are experimental techniques for generating long-time materials property data (both monotonic and cyclic flow and failure properties); analytic representations of slow strain rate material stress-strain response characteristics (monotonic and cyclic constitutive relations) at high temperatures and low stresses and strains; analytic creep-fatigue-environmental interaction life prediction methods applicable to long lifetimes at high temperatures and small stresses and strains; and experimental verification of life predictions. Long-lifetime design criteria for materials of interest are woefully lacking. Designing against failures due to creep, creep-rupture, fatigue, environmental attack, and creep-fatigue-environmental interaction will require considerable extrapolation. Viscoplastic constitutive models and time-temperature parameters will have to be calibrated for the hot-section materials of interest. Analysis combined with limited verification testing in a short-time regime will be required to build confidence in long-lifetime durability models. Author

N91-14632*# National Aeronautics and Space Administration. Lewis Research Center, Cleveland, OH.

AXIAL-TORSIONAL FATIGUE: A STUDY OF TUBULAR SPECIMEN THICKNESS EFFECTS

PETER J. BONACUSE and SREERAMESH KALLURI (Sverdrup Technology, Inc., Brook Park, OH.) Dec. 1990 19 p (Contract RTOP 505-63-1B)

(NASA-TM-103637; E-5814; NAS 1.15:103637;

AVSCOM-TM-90-C-014; AD-A231725) Avail: NTIS HC/MF A03 CSCL 20/11

A room-temperature experimental program was conducted on AISI type 316 stainless steel to determine the effect of wall thickness on the cyclic deformation behavior and fatigue life of thin-wall, tubular, axial-torsional fatigue specimens. The following experimental variables were examined in this study: the depth of the surface work-hardened layer produced in specimen machining, and the effects of strain range and axial-torsional strain phasing. Tubular fatigue specimens were fabricated with wall thicknesses of 1.5, 2.0, and 2.5 mm. One as-fabricated specimen from each wall thickness was sectioned for microstructural examination and microhardness measurement. A specimen of each wall thickness was tested at each of three conditions - high strain range in-phase, low strain range in-phase, and low strain range out-of-phase - for a total of nine axial-torsional fatigue experiments. The machining-induced work-hardened zone, as a percentage of the gage section material, was found to have a minimal effect on both deformation behavior and fatigue life. Also, little or no variation in fatigue life or deformation behavior as a function of wall thickness was observed. Out-of-phase fatigue tests displayed shorter fatigue lives and more cyclic hardening than in-phase tests. Author

N91-17415*# National Aeronautics and Space Administration. Lewis Research Center, Cleveland, OH.

A METHODOLOGY FOR EVALUATING THE RELIABILITY AND RISK OF STRUCTURES UNDER COMPLEX SERVICE ENVIRONMENTS

MICHAEL C. SHIAO (Sverdrup Technology, Inc., Brook Park, OH.) and CHRISTOS C. CHAMIS Apr. 1990 17 p Presented at the 31st Structures, Structural Dynamics and Materials Conference, Long Beach, CA, 2-4 Apr. 1990; sponsored in part by AIAA, ASME, ASCE, AHS, and ACS Previously announced in IAA as A90-29332

(Contract RTOP 553-13-00)

(NASA-TM-103244; E-5669; NAS 1.15:103244) Avail: NTIS HC/MF A03 CSCL 20/11

The theoretical basis and numerical implementation of NESSUS (Numerical Evaluation of Stochastic Structures Under Stress), a computer code for probabilistic structural analysis of aerospace components, are described, with an emphasis on the use of NESSUS for reliability and risk assessment. Topics addressed include the structure of probabilistic models of fatigue-crack initiation, risk/cost evaluation, fatigue-fracture analysis, and fatigue-crack initiation. Numerical results from typical applications are presented in graphs and briefly characterized. The usefulness of NESSUS predictions for establishing inspection and retirement schedules and for component certification is indicated. Author

N91-17427*# National Aeronautics and Space Administration. Lewis Research Center, Cleveland, OH.

CURRENT ACTIVITIES IN STANDARDIZATION OF HIGH-TEMPERATURE, LOW-CYCLE-FATIGUE TESTING TECHNIQUES IN THE UNITED STATES

MICHAEL J. VERRILLI, J. RODNEY ELLIS, and ROBERT W. SWINDEMAN (Oak Ridge National Lab., TN.) 1990 21 p Presented at the Harmonisation of Testing Practice for High Temperature Materials, Ispra, Italy, 18-19 Oct. 1990

(Contract RTOP 505-63-52)

(NASA-TM-103675; E-5891; NAS 1.15:103675) Avail: NTIS HC/MF A03 CSCL 20/11

The American Society for Testing and Materials (ASTM) standard E606-80 is the most often used recommended testing practice for low-cycle-fatigue (LCF) testing in the United States. The standard was first adopted in 1977 for LCF testing at room temperature and was modified in 1980 to include high-temperature testing practices. Current activity within ASTM is aimed at extending the E606-80 recommended practices to LCF under thermomechanical conditions, LCF in high-pressure hydrogen, and LCF in metal-matrix composite materials. Interlaboratory testing programs conducted to generate a technical base for modifying E606-80 for the aforementioned LCF test types are discussed. Author

N91-18452*# National Aeronautics and Space Administration. Lewis Research Center, Cleveland, OH.

EFFECT OF TENSILE MEAN STRESS ON FATIGUE BEHAVIOR OF SINGLE-CRYSTAL AND DIRECTIONALLY SOLIDIFIED SUPERALLOYS

SREERAMESH KALLURI (Sverdrup Technology, Inc., Brook Park, OH.) and MICHAEL A. MCGAW 1990 17 p Presented at the Symposium on Cyclic Deformation, Fracture, and Nondestructive Evaluation of Advanced Materials, San Antonio, TX, 12-13 Nov. 1990; sponsored by American Society for Testing and Materials (Contract RTOP 553-13-00)

(NASA-TM-103644; E-5827; NAS 1.15:103644) Avail: NTIS HC/MF A03 CSCL 20/11

Two nickel base superalloys, single crystal PWA 1480 and directionally solidified MAR-M 246 + Hf, were studied in view of the potential usage of the former and usage of the latter as blade materials for the turbomachinery of the space shuttle main engine. The baseline zero mean stress (ZMS) fatigue life (FL) behavior of these superalloys was established, and then the effect of tensile mean stress (TMS) on their FL behavior was characterized. At room temperature these superalloys have lower ductilities and higher strengths than most polycrystalline engineering alloys. The cycle stress-strain response was thus nominally elastic in most of the fatigue tests. Therefore, a stress range based FL prediction approach was used to characterize both the ZMS and TMS fatigue data. In the past, several researchers have developed methods to account for the detrimental effect of tensile mean stress on the

FL for polycrystalline engineering alloys. However, the applicability of these methods to single crystal and directionally solidified superalloys has not been established. In this study, these methods were applied to characterize the TMS fatigue data of single crystal PWA 1480 and directionally solidified MAR-M 246 + Hf and were found to be unsatisfactory. Therefore, a method of accounting for the TMS effect on FL, that is based on a technique proposed by Heidmann and Manson was developed to characterize the TMS fatigue data of these superalloys. Details of this method and its relationship to the conventionally used mean stress methods in FL prediction are discussed. Author

N91-19472*# National Aeronautics and Space Administration. Lewis Research Center, Cleveland, OH.

PROBABILISTIC SIMULATION OF UNCERTAINTIES IN THERMAL STRUCTURES

CHRISTOS C. CHAMIS and MICHAEL SHIAO (Sverdrup Technology, Inc., Brook Park, OH.) 1990 15 p Presented at the First Thermal Structures Conference, Charlottesville, VA, 13-15 Nov. 1990; sponsored by Virginia Univ. (Contract RTOP 553-13-00) (NASA-TM-103680; E-5897; NAS 1.15:103680) Avail: NTIS HC/MF A03 CSCL 20/11

Development of probabilistic structural analysis methods for hot structures is a major activity at Lewis Research Center. It consists of five program elements: (1) probabilistic loads; (2) probabilistic finite element analysis; (3) probabilistic material behavior; (4) assessment of reliability and risk; and (5) probabilistic structural performance evaluation. Recent progress includes: (1) quantification of the effects of uncertainties for several variables on high pressure fuel turbopump (HPFT) blade temperature, pressure, and torque of the Space Shuttle Main Engine (SSME); (2) the evaluation of the cumulative distribution function for various structural response variables based on assumed uncertainties in primitive structural variables; (3) evaluation of the failure probability; (4) reliability and risk-cost assessment, and (5) an outline of an emerging approach for eventual hot structures certification. Collectively, the results demonstrate that the structural durability/reliability of hot structural components can be effectively evaluated in a formal probabilistic framework. In addition, the approach can be readily extended to computationally simulate certification of hot structures for aerospace environments. Author

N91-19473*# National Aeronautics and Space Administration. Lewis Research Center, Cleveland, OH.

APPLICATION OF THERMAL LIFE PREDICTION MODEL TO HIGH-TEMPERATURE AEROSPACE ALLOYS B1900+HF AND HAYNES 188

GARY R. HALFORD, JAMES F. SALTSMAN, MICHAEL J. VERRILLI, and VINOD K. ARYA (Toledo Univ., OH.) Dec. 1990 12 p (Contract RTOP 505-63-1B) (NASA-TM-4226; E-5511; NAS 1.15:4226) Avail: NTIS HC/MF A03 CSCL 20/11

The results of the application of a newly proposed thermomechanical fatigue (TMF) life prediction method to a series of laboratory TMF results on two high-temperature aerospace engine alloys are presented. The method, referred to as TMF/TS-SRP, is based on three relatively recent developments: the total strain version of the method of Strainrange Partitioning (TS-SRP), the bithermal testing technique for characterizing TMF behavior, and advanced viscoplastic constitutive models. The high-temperature data reported in a companion publication are used to evaluate the constants in the model and to provide the TMF verification data to check its accuracy. Predicted lives are in agreement with the experimental lives to within a factor of approximately 2. Author

N91-19475*# National Aeronautics and Space Administration. Lewis Research Center, Cleveland, OH.

CASCADE FLUTTER ANALYSIS WITH TRANSIENT RESPONSE AERODYNAMICS

MILIND A. BAKHLE, APARAJIT J. MAHAJAN, THEO G. KEITH, JR. (Ohio Aerospace Inst., Brook Park.), and GEORGE L. STEFKO Feb. 1991 40 p Previously announced in IAA as A91-19448

(Contract NAG3-1137; RTOP 505-63-5B; RTOP 535-03-10) (NASA-TM-103746; E-5991; NAS 1.15:103746) Avail: NTIS HC/MF A03 CSCL 20/11

Two methods for calculating linear frequency domain aerodynamic coefficients from a time marching Full Potential cascade solver are developed and verified. In the first method, the Influence Coefficient, solutions to elemental problems are superposed to obtain the solutions for a cascade in which all blades are vibrating with a constant interblade phase angle. The elemental problem consists of a single blade in the cascade oscillating while the other blades remain stationary. In the second method, the Pulse Response, the response to the transient motion of a blade is used to calculate influence coefficients. This is done by calculating the Fourier Transforms of the blade motion and the response. Both methods are validated by comparison with the Harmonic Oscillation method and give accurate results. The aerodynamic coefficients obtained from these methods are used for frequency domain flutter calculations involving a typical section blade structural model. An eigenvalue problem is solved for each interblade phase angle mode and the eigenvalues are used to determine aeroelastic stability. Flutter calculations are performed for two examples over a range of subsonic Mach numbers. Author

N91-19476*# National Aeronautics and Space Administration. Lewis Research Center, Cleveland, OH.

ON THE THERMODYNAMICS OF STRESS RATE IN THE EVOLUTION OF BACK STRESS IN VISCOPLASTICITY

ALAN D. FREED, J.-L. CHABOCHE, and K. P. WALKER (Engineering Science Software, Inc., Smithfield, RI.) 1991 8 p Prepared for the 3rd International Symposium on Plasticity, Grenoble, France, 12-16 Aug. 1991; sponsored by the Inst. de Mecanique de Grenoble (Contract RTOP 505-63-52) (NASA-TM-103794; E-6071; NAS 1.15:103794) Avail: NTIS HC/MF A02 CSCL 20/11

A thermodynamic foundation using the concept of internal state variables is presented for the kinematic description of a viscoplastic material. Three different evolution equations for the back stress are considered. The first is that of classical, nonlinear, kinematic hardening. The other two include a contribution that is linear in stress rate. Choosing an appropriate change in variables can remove this stress rate dependence. As a result, one of these two models is shown to be equivalent to the classical, kinematic hardening model; while the other is a new model, one which seems to have favorable characteristics for representing ratchetting behavior. All three models are thermodynamically admissible. Author

N91-19477*# National Aeronautics and Space Administration. Lewis Research Center, Cleveland, OH.

THE METHOD OF LINES IN ANALYZING SOLIDS CONTAINING CRACKS

JOHN P. GYEKENYESI Nov. 1990 22 p Presented at the 1st International Symposium on Methods of Lines, Surfaces, and Dimensional Reduction in Computational Mathematics and Mechanics, Athens, Greece, 25-30 Apr. 1991; sponsored by Polytechnic of Central London (Contract RTOP 505-63-5B) (NASA-TM-103626; E-5794; NAS 1.15:103626) Avail: NTIS HC/MF A03 CSCL 20/11

A semi-numerical method is reviewed for solving a set of coupled partial differential equations subject to mixed and possibly coupled boundary conditions. The line method of analysis is applied to the Navier-Cauchy equations of elastic and elastoplastic equilibrium to calculate the displacement distributions in various, simple geometry bodies containing cracks. The application of this method to the appropriate field equations leads to coupled sets of simultaneous ordinary differential equations whose solutions are

39 STRUCTURAL MECHANICS

obtained along sets of lines in a discretized region. When decoupling of the equations and their boundary conditions is not possible, the use of a successive approximation procedure permits the analytical solution of the resulting ordinary differential equations. The use of this method is illustrated by reviewing and presenting selected solutions of mixed boundary value problems in three dimensional fracture mechanics. These solutions are of great importance in fracture toughness testing, where accurate stress and displacement distributions are required for the calculation of certain fracture parameters. Computations obtained for typical flawed specimens include that for elastic as well as elastoplastic response. Problems in both Cartesian and cylindrical coordinate systems are included. Results are summarized for a finite geometry rectangular bar with a central through-the-thickness or rectangular surface crack under remote uniaxial tension. In addition, stress and displacement distributions are reviewed for finite circular bars with embedded penny-shaped cracks, and rods with external annular or ring cracks under opening mode tension. The results obtained show that the method of lines presents a systematic approach to the solution of some three-dimensional mechanics problems with arbitrary boundary conditions. The advantage of this method over other numerical solutions is that good results are obtained even from the use of a relatively coarse grid.

Author

N91-20104*# National Aeronautics and Space Administration. Lewis Research Center, Cleveland, OH.

OVERVIEW OF STRUCTURES RESEARCH

LARRY D. PINSON *In its* Aeropropulsion 1991 9 p Mar. 1991
Avail: NTIS HC/MF A24 CSCL 20/11

The development of aeronautical and space propulsion systems structures technology is the mission of the Structures Division. The technology required to achieve reliable, high-performance, lightweight structures needed for aerospace propulsion is among the most complex and challenging facing the design engineer. The division staff performs both fundamental and applied research in structural mechanics, fatigue and fracture, structural dynamics, and structural integrity. Research programs include probabilistic analysis and design, nonlinear material properties, symbolic logic, composite micromechanics, aeroelasticity, fatigue and fracture of composite structures, life prediction, and aspects of nondestructive evaluation. These programs, which for the most part are analytically based, are experimentally verified and are used to develop computer codes necessary for the design of complex engine structures. An overview of some of these programs is presented.

Author

N91-20108*# National Aeronautics and Space Administration. Lewis Research Center, Cleveland, OH.

PROGRESS IN MODELING DEFORMATION AND DAMAGE

ALAN D. FREED and STEVEN M. ARNOLD *In its* Aeropropulsion 1991 9 p Mar. 1991

Avail: NTIS HC/MF A24 CSCL 20/11

In hypersonic aircraft, for example, high temperature structures (such as leading edges, inlet cowl, combustor liners, and nozzles) are subjected to thermomechanical deformations. It is believed that such deformations will be a primary cause of structural failure in these components. They arise from large thermal gradients across structural skins that are constrained from free thermal expansion. In order to assess structural life and performance, the material's thermomechanical behavior must be incorporated into the structural design. The laboratories of the Fatigue and Fracture Branch of Lewis Research Center are dedicated to observing the evolution of deformation and damage in laboratory specimens under thermomechanical loading conditions. These observations are used within the branch to guide the development of deformation and life-assessing models.

Author

N91-21558*# National Aeronautics and Space Administration. Lewis Research Center, Cleveland, OH.

ELASTIC RESPONSE OF ZONE AXIS (001)-ORIENTED PWA 1480 SINGLE CRYSTAL: THE INFLUENCE OF SECONDARY ORIENTATION

SREERAMESH KALLURI, ALI ABDUL-AZIZ (Sverdrup Technology, Inc., Brook Park, OH.), and MICHAEL A. MCGAW 1991 13 p
Presented at the 1991 Aerospace Atlantic Meeting, Dayton, OH, 23-26 Apr. 1991; sponsored by SAE
(Contract NAS3-25266; RTOP 553-13-00)
(NASA-TM-103782; E-6057; NAS 1.15:103782) Avail: NTIS
HC/MF A03 CSCL 20/11

The influence of secondary orientation on the elastic response of a zone axis (001)-oriented nickel-base single-crystal superalloy, PWA 1480, was investigated under mechanical loading conditions by applying finite element techniques. Elastic stress analyses were performed with a commercially available finite element code. Secondary orientation of the single-crystal superalloy was offset with respect to the global coordinate system in increments from 0 to 90 deg and stresses developed within the single crystal were determined for each loading condition. The results indicated that the stresses were strongly influenced by the angular offset between the secondary crystal orientation and the global coordinate system. The degree of influence was found to vary with the type of loading condition (mechanical, thermal, or combined) imposed on the single-crystal superalloy.

Author

N91-21559*# National Aeronautics and Space Administration. Lewis Research Center, Cleveland, OH.

APPLICATIONS OF ARTIFICIAL NEURAL NETS IN STRUCTURAL MECHANICS

LASZLO BERKE and PRABHAT HAJELA (Rensselaer Polytechnic Inst., Troy, NY.) 1990 22 p Presented at the Lecture Series on Shape and Layout Optimization of Structural Systems, Udine, Italy, 16-20 Jul. 1990

(Contract RTOP 505-63-1B)

(NASA-TM-102420; E-5941; NAS 1.15:102420) Avail: NTIS
HC/MF A03 CSCL 20/11

A brief introduction to the fundamental of Neural Nets is given, followed by two applications in structural optimization. In the first case, the feasibility of simulating with neural nets the many structural analyses performed during optimization iterations was studied. In the second case, the concept of using neural nets to capture design expertise was studied.

Author

N91-21562*# National Aeronautics and Space Administration. Lewis Research Center, Cleveland, OH.

HITCAN FOR ACTIVELY COOLED HOT-COMPOSITE THERMOSTRUCTURAL ANALYSIS

C. C. CHAMIS, P. L. N. MURTHY, S. N. SINGHAL, and J. J. LACKNEY (Sverdrup Technology, Inc., Brook Park, OH.) 1991 20 p Presented at the 36th International Gas Turbine and Aeroengine Congress and Exposition, Orlando, FL, 3-6 Jun. 1991; sponsored by ASME

(Contract RTOP 763-01-41)

(NASA-TM-103750; E-6002; NAS 1.15:103750) Avail: NTIS
HC/MF A03 CSCL 20/11

A computer code, high temperature composite analyzer (HITCAN), was developed to analyze/design hot metal matrix composite structures. HITCAN is a general purpose code for predicting the global structural and local stress-strain response of multilayered (arbitrarily oriented) metal matrix structures both at the constituent (fiber, matrix, and interphase) and the structural level, including the fabrication process effects. The thermomechanical properties of the constituents are considered to be nonlinearly dependent on several parameters, including temperature, stress, and stress rate. The computational procedure employs an incremental iterative nonlinear approach utilizing a multifactor-interaction material behavior model, i.e., the material properties are expressed in terms of a product of several factors that affect the properties. HITCAN structural analysis capabilities (static, load stepping - a multistep static analysis with material properties updated at each step, modal, and buckling) for cooled hot structures are demonstrated through a specific example problem.

Author

N91-22594*# National Aeronautics and Space Administration. Lewis Research Center, Cleveland, OH.

ANALYSIS OF SOME COMPLIANCE CALIBRATION DATA FOR CHEVRON-NOTCH BAR AND ROD SPECIMENS

THOMAS W. ORANGE, RAYMOND T. BUBSEY, WILLIAM S. PIERCE, and JOHN L. SHANNON, JR. 1991 14 p Presented at the Symposium on Chevron-Notch Fracture Test Experience, Indianapolis, IN, 6 May 1991; sponsored by the American Society for Testing and Materials

(Contract RTOP 505-63-52)

(NASA-TM-104367; E-6167; NAS 1.15:104367) Avail: NTIS

HC/MF A03 CSCL 20/11

A set of equations describing certain fracture mechanics parameters for chevron-notch bar and rod specimens are presented. They are developed by fitting earlier compliance calibration data. The difficulty in determining the minimum stress intensity coefficient and the critical crack length is discussed.

Author

N91-22604*# National Aeronautics and Space Administration. Lewis Research Center, Cleveland, OH.

THE DYNAMIC EFFECTS OF INTERNAL ROBOTS ON SPACE STATION FREEDOM

JEFFREY H. MILLER (Sverdrup Technology, Inc., Brook Park, OH.), CHARLES LAWRENCE, and DOUGLAS A. ROHN 1991 16 p Presented at the Guidance Navigation and Control Conference, New Orleans, LA, 12-14 Aug. 1991; sponsored by AIAA

(Contract RTOP 694-03-03)

(NASA-TM-104345; E-6119; NAS 1.15:104345; AIAA PAPER

91-2822) Avail: NTIS HC/MF A03 CSCL 20/11

Many of the planned experiments of the Space Station Freedom (SSF) will require acceleration levels to be no greater than microgravity (10 exp -6 g) levels for long periods of time. Studies have demonstrated that without adequate control, routine operations may cause disturbances which are large enough to affect on-board experiments. One way to both minimize disturbances and make the SSF more autonomous is to utilize robots instead of astronauts for some operations. The present study addresses the feasibility of using robots for microgravity manipulation. Two methods for minimizing the dynamic disturbances resulting from the robot motions are evaluated. The first method is to use a robot with kinematic redundancy (redundant links). The second method involves the use of a vibration isolation device between the robot and the SSF laboratory module. The results from these methods are presented along with simulations of robots without disturbance control.

Author

N91-23548*# National Aeronautics and Space Administration. Lewis Research Center, Cleveland, OH.

COMPUTATIONAL SIMULATION OF ACOUSTIC FATIGUE FOR HOT COMPOSITE STRUCTURES

SURENDRA N. SINGHAL, PAPPU L. N. MURTHY, CHRISTOS C. CHAMIS, VINOD K. NAGPAL, and EDHI SUTJAHJO (Sverdrup Technology, Inc., Brook Park, OH.) 1991 18 p Presented at the 32nd Structures, Structural Dynamics, and Materials Conference, Baltimore, MD, 8-10 Apr. 1991; cosponsored by AIAA, ASME, ASCE, AHS, and ASC Previously announced in IAA as A91-32099

(Contract NAS3-25266; RTOP 510-01-0A)

(NASA-TM-104379; E-6184; NAS 1.15:104379) Avail: NTIS

HC/MF A03 CSCL 20/11

Predictive methods/computer codes for the computational simulation of acoustic fatigue resistance of hot composite structures subjected to acoustic excitation emanating from an adjacent vibrating component are discussed. Select codes developed over the past two decades at the NASA Lewis Research Center are used. The codes include computation of acoustic noise generated from a vibrating component, degradation in material properties of a composite laminate at use temperature, dynamic response of acoustically excited hot multilayered composite structure, degradation in the first ply strength of the excited structure due to acoustic loading, and acoustic fatigue resistance of the excited structure, including the propulsion environment. Effects of the

laminate lay-up and environment on the acoustic fatigue life are evaluated. The results show that, by keeping the angled plies on the outer surface of the laminate, a substantial increase in the acoustic fatigue life is obtained. The effect of environment (temperature and moisture) is to relieve the residual stresses leading to an increase in the acoustic fatigue life of the excited panel.

Author

N91-23549*# National Aeronautics and Space Administration. Lewis Research Center, Cleveland, OH.

SIMULATION OF PROBABILISTIC WIND LOADS AND BUILDING ANALYSIS

ASHWIN R. SHAH (Sverdrup Technology, Inc., Brook Park, OH.) and CHRISTOS C. CHAMIS 1991 16 p Proposed for presentation at the 9th Biennial Conference on Reliability, Stress Analysis, and Failure Prevention, Miami, FL, 22-25 Sep. 1991; sponsored by ASME

(Contract RTOP 763-01-41)

(NASA-TM-103744; E-5987; NAS 1.15:103744) Avail: NTIS

HC/MF A03 CSCL 20/11

Probabilistic wind loads likely to occur on a structure during its design life are predicted. Described here is a suitable multifactor interactive equation (MFIE) model and its use in the Composite Load Spectra (CLS) computer program to simulate the wind pressure cumulative distribution functions on four sides of a building. The simulated probabilistic wind pressure load was applied to a building frame, and cumulative distribution functions of sway displacements and reliability against overturning were obtained using NESSUS (Numerical Evaluation of Stochastic Structure Under Stress), a stochastic finite element computer code. The geometry of the building and the properties of building members were also considered as random in the NESSUS analysis. The uncertainties of wind pressure, building geometry, and member section property were qualified in terms of their respective sensitivities on the structural response.

Author

N91-23550*# National Aeronautics and Space Administration. Lewis Research Center, Cleveland, OH.

INCORPORATING FINITE ELEMENT ANALYSIS INTO COMPONENT LIFE AND RELIABILITY

RICHARD AUGUST (Sverdrup Technology, Inc., Brook Park, OH.) and ERWIN V. ZARETSKY 1991 9 p Presented at the Ninth Biennial Conference on Reliability, Stress Analysis, and Failure Prevention, Miami, FL, 22-25 Sep. 1991; sponsored by ASME

(Contract NAS3-25266; RTOP 505-63-5B)

(NASA-TM-104400; E-6220; NAS 1.15:104400) Avail: NTIS

HC/MF A02 CSCL 20/11

A method for calculating a component's design survivability by incorporating finite element analysis and probabilistic material properties was developed. The method evaluates design parameters through direct comparisons of component survivability expressed in terms of Weibull parameters. The analysis was applied to a rotating disk with mounting bolt holes. The highest probability of failure occurred at, or near, the maximum shear stress region of the bolt holes. Distribution of failure as a function of Weibull slope affects the probability of survival. Where Weibull parameters are unknown for a rotating disk, it may be permissible to assume Weibull parameters, as well as the stress-life exponent, in order to determine the disk speed where the probability of survival is highest.

Author

N91-24308*# National Aeronautics and Space Administration. Lewis Research Center, Cleveland, OH.

OVERVIEW OF THE FATIGUE/FRACTURE/LIFE WORKING GROUP PROGRAM AT THE LEWIS RESEARCH CENTER

MICHAEL A. MCGAW In its Structural Integrity and Durability of Reusable Space Propulsion Systems p 1-3 Apr. 1989

Avail: NTIS HC/MF A12 CSCL 20/11

Constitutive and life prediction models are developed and verified for materials typically used in hot gas path components of reusable space propulsion systems over the range of relevant operating environments. The efforts were centered on the development of crack initiation life prediction methods, while the

39 STRUCTURAL MECHANICS

efforts of a counterpart group were centered on the development of cyclic crack propagation life prediction methods. The complexion of the active tasks are presented. A significant new task started this year will incorporate the various material constitutive and life prediction models developed in this program into a comprehensive creep-fatigue damage analysis and life assessment computer code. The program will function as a postprocessor to general structural analysis programs (such as finite element or boundary element codes) using the output of such analyses (stress, strain, and temperature fields as functions of time) as the input to the damage analysis and life assessment code. The code will be designed to execute on engineering/scientific workstations and will feature a windowing, mouse-driven user interface. Current plans call for the code to be finished and made available for use in mid 1991.

Author

N91-24319*# National Aeronautics and Space Administration. Lewis Research Center, Cleveland, OH.

TWO-DIMENSIONAL HIGH TEMPERATURE STRAIN MEASUREMENT SYSTEM

CHRISTIAN T. LANT (Sverdrup Technology, Inc., Cleveland, OH.) and JOHN P. BARRANGER *In its* Structural Integrity and Durability of Reusable Space Propulsion Systems p 83-86 Apr. 1989
Avail: NTIS HC/MF A12 CSCL 20/11

Two-dimensional optical strain measurements on high temperature test specimens are presented. This two-dimensional capability is implemented through a rotatable sensitive strain axis. Three components of surface strain can be measured automatically, from which the first and second principal strains are calculated. One- and two-dimensional strain measurements at temperatures beyond 750 C with a resolution of 15 microstrain are demonstrated. The system is based on a one-dimensional speckle shift technique. The speckle shift technique makes use of the linear relationship between surface strain and the differential shift of laser speckle patterns in the diffraction plane. Laser speckle is a phase effect that occurs when spatially coherent light interacts with an optically rough surface. Since speckle is generated by any diffusely reflecting surface, no specimen preparation is needed to obtain a good signal. Testing was done at room temperature on a flat specimen of Inconel 600 mounted in a fatigue testing machine. A load cell measured the stress on the specimen before and after acquiring the speckle data. Strain components were measured at 0 C (parallel to the load axis) and at plus or minus 45 C, and plots indicate the calculated values of the first and second principal strains. The measured values of Young's modulus and Poisson's ratio are in good agreement with handbook values. Good linearity of the principal strain moduli at high temperatures indicate precision and stability of the system. However, a systematic error in the high-temperature test setup introduced a scale factor in the slopes of the two-dimensional stress-strain curves. No high temperature effects, however, have been observed to degrade speckle correlation.

K.C.D.

N91-24326*# National Aeronautics and Space Administration. Lewis Research Center, Cleveland, OH.

PROBABILISTIC STRUCTURAL ANALYSIS: INTRODUCTORY REMARKS Abstract Only

CHRISTOS C. CHAMIS *In its* Structural Integrity and Durability of Reusable Space Propulsion Systems p 137-138 Apr. 1989
Avail: NTIS HC/MF A12 CSCL 20/11

The development of probabilistic structural analysis methodology consists of the following program elements: (1) composite load spectra models, (2) computational probabilistic structural analysis methods, and (3) probabilistic constitutive relationships. The development of the probabilistic structural analysis methodology is a joint program of NASA Lewis in-house and sponsored research. The objective of this session is to illustrate recent progress on the application of this methodology to determine the reliability of structural components for rocket propulsion systems. The session contains descriptions of and progress reports on the following specific activities: (1) The NESSUS computer code, (2) approximate methods, (3) advanced methods, (4) composite load spectra applications, (5) probabilistic fracture

mechanisms, and (6) probability of failure and risk analysis. Collectively, the progress to date demonstrates that the structural durability of hot engine structural components can be effectively evaluated in a formal probabilistic/reliability framework. Author

N91-24334*# National Aeronautics and Space Administration. Lewis Research Center, Cleveland, OH.

OVERVIEW OF AEROTHERMODYNAMIC LOADS DEFINITION STUDY

RAYMOND E. GAUGLER *In its* Structural Integrity and Durability of Reusable Space Propulsion Systems p 209-214 Apr. 1989
Avail: NTIS HC/MF A12 CSCL 20/11

Over the years, NASA has been conducting the Advanced Earth-to-Orbit (AETO) Propulsion Technology Program to provide the knowledge, understanding, and design methodology that will allow the development of advanced Earth-to-orbit propulsion systems with high performance, extended service life, automated operations, and diagnostics for in-flight health monitoring. The objective of the Aerothermodynamic Loads Definition Study is to develop methods to more accurately predict the operating environment in AETO propulsion systems, such as the Space Shuttle Main Engine (SSME) powerhead. The approach taken consists of 2 parts: to modify, apply, and disseminate existing computational fluid dynamics tools in response to current needs and to develop new technology that will enable more accurate computation of the time averaged and unsteady aerothermodynamic loads in the SSME powerhead. The software tools are detailed. Significant progress was made in the area of turbomachinery, where there is an overlap between the AETO efforts and research in the aeronautical gas turbine field. Author

N91-24652*# National Aeronautics and Space Administration. Lewis Research Center, Cleveland, OH.

PROBABILITY APPROACH FOR STRENGTH CALCULATIONS

CHRISTOS C. CHAMIS and T. A. CRUSE (Southwest Research Inst., San Antonio, TX.) *In* AGARD, Analytical Qualification of Aircraft Structures 13 p Apr. 1991

Copyright Avail: NTIS HC/MF A08; Non-NATO Nationals requests available only from AGARD/Scientific Publications Executive CSCL 20/11

The use of probabilistic structural analysis methods (PSAM) to predict structural reliability is the subject of an on-going NASA research program. The elements of the new technology developed to date is reported. Applications of the developed software to structural problems are demonstrated for simple validation problems and for large scale application problems. On-going research to support component and system reliability predictions suitable for analytical certification of aerospace structures is briefly reviewed.

Author

N91-24659*# National Aeronautics and Space Administration. Lewis Research Center, Cleveland, OH.

LOCALIZATION OF AEROELASTIC MODES IN MISTUNED HIGH-ENERGY TURBINES

CHRISTOPHE PIERRE, TODD E. SMITH, and DURBHA V. MURTHY (Toledo Univ., OH.) 1991 37 p Presented at the 27th Joint Propulsion Conference, Sacramento, CA, 24-27 Jun. 1991; sponsored by AIAA, SAE, ASME, and the American Society for Electrical Engineers

(Contract NAS3-25266; NAG3-1163; NAG3-742; NASA ORDER C-99066-G)

(NASA-TM-104445; ICOMP-91-11; E-6285; NAS 1.15:104445; AIAA PAPER 91-3379) Avail: NTIS HC/MF A03 CSCL 20/11

The effects of blade mistuning on the aeroelastic vibration characteristics of high energy turbines are investigated, using the first stage of the oxidizer turbopump in the Space Shuttle Main Engine as an example. A model aeroelastic analysis procedure is used in concert with a linearized unsteady aerodynamic theory that accounts for the effects of blade thickness, camber, and steady loading. Extreme sensitivity of the dynamic characteristics of mistuned rotors is demonstrated. In particular, the aeroelastic modes become localized to a few blades, possibly leading to rogue blade failure, and the locus of the aeroelastic eigenvalues loses

its structure when small mistunings (of the order present in actual rotors) are introduced. Perturbation analyses that yield physical insights into these phenomena are presented. A powerful but easily calculated stochastic sensitivity measure that allows the global prediction of mistuning effects is developed. Author

N91-24660* # National Aeronautics and Space Administration. Lewis Research Center, Cleveland, OH.

MODELING OF CRACK BRIDGING IN A UNIDIRECTIONAL METAL MATRIX COMPOSITE

LOUIS J. GHOSN (Sverdrup Technology, Inc., Brook Park, OH.), PETE KANTZOS, and JACK TELESMA May 1991 22 p (Contract RTOP 510-01-50) (NASA-TM-104355; E-6142; NAS 1.15:104355) Avail: NTIS HC/MF A03 CSCL 20/11

The effective fatigue crack driving force and crack opening profiles were determined analytically for fatigue tested unidirectional composite specimens exhibiting fiber bridging. The crack closure pressure due to bridging was modeled using two approaches; the fiber pressure model and the shear lag model. For both closure models, the Bueckner weight function method and the finite element method were used to calculate crack opening displacements and the crack driving force. The predicted near crack tip opening profile agreed well with the experimentally measured profiles for single edge notch SCS-6/Ti-15-3 metal matrix composite specimens. The numerically determined effective crack driving force, $\Delta K(\text{sup eff})$, was calculated using both models to correlate the measure crack growth rate in the composite. The calculated $\Delta K(\text{sup eff})$ from both models accounted for the crack bridging by showing a good agreement between the measured fatigue crack growth rates of the bridged composite and that of unreinforced, unbridged titanium matrix alloy specimens. Author

N91-25436* # National Aeronautics and Space Administration. Lewis Research Center, Cleveland, OH.

PROBABILITY OF FAILURE AND RISK ASSESSMENT OF PROPULSION STRUCTURAL COMPONENTS

MICHAEL C. SHIAO (Sverdrup Technology, Inc., Cleveland, OH.) and CHRISTOS C. CHAMIS 1989 10 p Presented at the 1989 Joint Army, Navy, NASA, Air Force Propulsion Meeting, Cleveland, OH, 23-25 May 1989 Previously announced as N90-18470

(Contract RTOP 553-13-00) (NASA-TM-102323; E-5019; NAS 1.15:102323) Avail: NTIS HC/MF A02 CSCL 20/11

Because of the increasing need to account for the uncertainties in material properties, loading conditions, geometry, etc., a methodology was developed to determine structural reliability and to assess the associated risk. The methodology consists of a probabilistic structural analysis by a probabilistic finite element computer code, numerical evaluation of stochastic structures under stress (NESSUS), and a generic probabilistic material property model. The methodology is versatile and is equally applicable to structures operating at high and cryogenic temperature environments. Results obtained demonstrate that the issues of structural reliability and risk can be formally evaluated by using the methodology developed which is inclusive of the uncertainties in material properties, structural parameters, and loading conditions. The methodology is described in some detail with illustrative examples. Author

N91-25442* # National Aeronautics and Space Administration. Lewis Research Center, Cleveland, OH.

FATIGUE LIFE PREDICTION OF AN INTERMETALLIC MATRIX COMPOSITE AT ELEVATED TEMPERATURES

PAUL A. BARTOLOTTA 1991 12 p Presented at the 1991 Winter Annual Meeting of ASME, Atlanta, GA, 1-6 Dec. 1991 (Contract RTOP 510-01-50) (NASA-TM-104494; E-6352; NAS 1.15:104494) Avail: NTIS HC/MF A03 CSCL 20/11

A strain-based fatigue life prediction method is proposed for an intermetallic matrix composite (IMC) under tensile cyclic loadings at elevated temperatures. Styled after the Universal Slopes method,

the model utilizes the composite's tensile properties to estimate fatigue life. Factors such as fiber volume ratio, number of plies and temperature dependence are implicitly incorporated into the model through these properties. The model constants are determined by using unidirectional fatigue data at temperatures of 425 and 815 C. Fatigue lives from two independent sources are used to verify the model at temperatures of 650 and 760 C. Cross-ply lives at 760 C are also predicted. It is demonstrated that the correlation between experimental and predicted lives is within a factor of two. Author

N91-27591* # National Aeronautics and Space Administration. Lewis Research Center, Cleveland, OH.

AEROELASTIC MODAL CHARACTERISTICS OF MISTUNED BLADE ASSEMBLIES: MODE LOCALIZATION AND LOSS OF EIGENSTRUCTURE

CHRISTOPHE PIERRE and DURBHA V. MURTHY (Toledo Univ., OH.) Jul. 1991 38 p Previously announced as A91-32032 (Contract NAG3-1163; NAG3-742; NASA ORDER C-99066-G) (NASA-TM-104519; E-6389; NAS 1.15:104519; ICOMP-91-12) Avail: NTIS HC/MF A03 CSCL 20/11

An investigation of the effects of small mistuning on the aeroelastic modes of bladed disk assemblies with aerodynamic coupling between blades is presented. The cornerstone of the approach is the use and development of perturbation methods that exhibit the crucial role of the interblade coupling and yield general findings regarding mistuning effects. It is shown that blade assemblies with weak aerodynamic interblade coupling are highly sensitive to small blade mistuning, and that their dynamics is quantitatively altered in the following ways: the regular pattern that characterizes the root locus of the tuned aeroelastic eigenvalues in the complex plane is totally lost; the aeroelastic mode shapes becomes severely localized to only a few blades of the assembly and lose their constant interblade phase angle feature; and curve veering phenomena take place when the eigenvalues are plotted versus a mistuning parameter. Author

N91-28238* # National Aeronautics and Space Administration. Lewis Research Center, Cleveland, OH.

PROBABILISTIC STRUCTURAL ANALYSIS METHODS FOR SPACE TRANSPORTATION PROPULSION SYSTEMS

C. C. CHAMIS, N. MOORE, C. ANIS, J. NEWELL, V. NAGPAL, and S. SINGHAL (Sverdrup Technology, Inc., Brook Park, OH.) In NASA, Washington, Space Transportation Propulsion Technology Symposium. Volume 3: Panel Session Summaries and Presentations p 895-914 May 1991 Avail: NTIS HC/MF A99 CSCL 20/11

Information on probabilistic structural analysis methods for space propulsion systems is given in viewgraph form. Information is given on deterministic certification methods, probability of failure, component response analysis, stress responses for 2nd stage turbine blades, Space Shuttle Main Engine (SSME) structural durability, and program plans. Author

N91-28622* # National Aeronautics and Space Administration. Lewis Research Center, Cleveland, OH.

VISCOPLASTIC ANALYSIS OF AN EXPERIMENTAL CYLINDRICAL THRUST CHAMBER LINER

VINOD K. ARYA and STEVEN M. ARNOLD Jun. 1991 22 p Submitted for publication LIMITED REPRODUCIBILITY: More than 20% of this document may be affected by color photographs Original contains color illustrations (Contract RTOP 553-13-00) (NASA-TM-103287; E-5746; NAS 1.15:103287) Avail: NTIS HC/MF A03; 10 functional color pages CSCL 20/11

A viscoplastic stress-strain analysis of an experimental cylindrical thrust chamber is presented. A viscoelastic constitutive model incorporating a single internal state variable that represents kinematic hardening was employed to investigate whether such a viscoplastic model could predict the experimentally observed behavior of the thrust chamber. Two types of loading cycles were considered: a short cycle of 3.5 sec. duration that corresponded to the experiments, and an extended loading cycle of 485.1 sec.

39 STRUCTURAL MECHANICS

duration that is typical of the Space Shuttle Main Engine (SSME) operating cycle. The analysis qualitatively replicated the deformation behavior of the component as observed in experiments designed to simulate SSME operating conditions. The analysis also showed that the mode and location in the component may depend on the loading cycle. The results indicate that using viscoplastic models for structural analysis can lead to a more realistic life assessment of thrust chambers. Author

N91-28627* National Aeronautics and Space Administration. Lewis Research Center, Cleveland, OH.

ASTROP2 USERS MANUAL: A PROGRAM FOR AEROELASTIC STABILITY ANALYSIS OF PROPPANS

G. V. NARAYANAN (Sverdrup Technology, Inc., Brook Park, OH.) and K. R. V. KAZA Washington Aug. 1991 75 p
(Contract NAS3-25266; RTOP 505-63-1B; RTOP 535-03-01)
(NASA-TM-4304; E-5768; NAS 1.15:4304) Avail: NTIS HC/MF A04 CSCL 20/11

A user's manual is presented for the aeroelastic stability and response of propulsion systems computer program called ASTROP2. The ASTROP2 code performs aeroelastic stability analysis of rotating propfan blades. This analysis uses a two-dimensional, unsteady cascade aerodynamics model and a three-dimensional, normal-mode structural model. Analytical stability results from this code are compared with published experimental results of a rotating composite advanced turboprop model and of nonrotating metallic wing model. Author

N91-30565* National Aeronautics and Space Administration. Lewis Research Center, Cleveland, OH.

STRUCTURAL DESIGN CONCEPTS FOR A MULTI-MEGAWATT SOLAR ELECTRIC PROPULSION (SEP) SPACECRAFT

CHARLES LAWRENCE and J. MARK HICKMAN Aug. 1991 19 p
(NASA-TM-105148; NAS 1.15:105148) Avail: NTIS HC/MF A03 CSCL 20/11

As a part of the Space Exploratory Initiative (SEI), NASA-Lewis is studying Solar Electric Propulsion (SEP) spacecraft to be used as a cargo transport vehicle to Mars. Two preliminary structural design concepts are offered for SEP spacecraft: a split blanket array configuration, and a ring structure. The split blanket configuration is an expansion of the photovoltaic solar array design proposed for Space Station Freedom and consists of eight independent solar blankets stretched and supported from a central mast. The ring structural concept is a circular design with the solar blanket stretched inside a ring. This concept uses a central mast with guy wires to provide additional support to the ring. The two design concepts are presented, then compared by performing stability, normal modes, and forced response analyses for varying levels of blanket and guy wire preloads. The ring structure configuration is shown to be advantageous because it is much stiffer, more stable, and deflects less under loading than the split blanket concept. Author

N91-30566* National Aeronautics and Space Administration. Lewis Research Center, Cleveland, OH.

FATIGUE BEHAVIOR AND LIFE PREDICTION OF A SiC/Ti-24Al-11Nb COMPOSITE UNDER ISOTHERMAL CONDITIONS Ph.D. Thesis

PAUL A. BAROLOTTA Aug. 1991 141 p
(Contract RTOP 510-01-50)
(NASA-TM-105168; E-6459; NAS 1.15:105168) Avail: NTIS HC/MF A07 CSCL 20/11

Metal Matrix Composites (MMC) and Intermetallic Matrix Composites (IMC) were identified as potential material candidates for advanced aerospace applications. They are especially attractive for high temperature applications which require a low density material that maintains its structural integrity at elevated temperatures. High temperature fatigue resistance plays an important role in determining the structural integrity of the material. This study attempts to examine the relevance of test techniques, failure criterion, and life prediction as they pertain to an IMC material, specifically, unidirectional SiC fiber reinforced titanium

aluminide. A series of strain and load controlled fatigue tests were conducted on unidirectional SiC/Ti-24Al-11Nb composite at 425 and 815 C. Several damage mechanism regimes were identified by using a strain-based representation of the data. Talreja's fatigue life diagram concept. Results of these tests were then used to address issues of test control modes, definition of failure, and testing techniques. Finally, a strain-based life prediction method was proposed for an IMC under tensile cyclic loadings at elevated temperatures. Author

N91-32520* National Aeronautics and Space Administration. Lewis Research Center, Cleveland, OH.

COMPUTATIONAL SIMULATION OF HIGH TEMPERATURE METAL MATRIX COMPOSITE BEHAVIOR

PAPPU L. N. MURTHY and CHRISTOS C. CHAMIS 1991 17 p
Presented at the Eighth International Conference on Composite Materials, Honolulu, HI, 15-19 Jul. 1991; sponsored by the Society for the Advancement of Materials and Process Engineering
(Contract RTOP 510-01-0A)
(NASA-TM-104378; E-6183; NAS 1.15:104378) Avail: NTIS HC/MF A01 CSCL 20/11

Computational procedures are described to simulate the thermal and mechanical behavior of high temperature metal matrix composite (HT MMC) in the following four broad areas: (1) behavior of HT MMC from micromechanics to laminate; (2) HT MMC structural response for simple and complex structural components; (3) HT MMC microfracture; and (4) tailoring of HT MMC behavior for optimum specific performance. Representative results from each area are presented to illustrate the effectiveness of the computational simulation procedures. Relevant reports are referenced for extended discussion regarding the specific area. Author

44

ENERGY PRODUCTION AND CONVERSION

Includes specific energy conversion systems, e.g., fuel cells; global sources of energy; geophysical conversion; and windpower.

A91-38022* National Aeronautics and Space Administration. Lewis Research Center, Cleveland, OH.

NEW DIRECTIONS IN INP SOLAR CELL RESEARCH

I. WEINBERG, C. K. SWARTZ, and D. J. BRINKER (NASA, Lewis Research Center, Cleveland, OH) IN: IECEC-90; Proceedings of the 25th Intersociety Energy Conversion Engineering Conference, Reno, NV, Aug. 12-17, 1990. Vol. 1. New York, American Institute of Chemical Engineers, 1990, p. 593-597. Previously announced in STAR as N90-23662. refs
Copyright

Recent research efforts representing new directions in InP solar cell research are reviewed. These include heteroepitaxial growth on silicon and gallium arsenide substrates, V-grooved cells, large-area high efficiency cells, and surface passivation. Improvements in heteroepitaxial cell efficiency are described together with processing of 19.1 percent, 4 sq cm cells. Recommendations are made for improvements in processing leading to increased efficiencies. Author

A91-38177* National Aeronautics and Space Administration. Lewis Research Center, Cleveland, OH.

MODELING AND OPTIMIZATION OF A REGENERATIVE FUEL CELL SYSTEM USING THE ASPEN PROCESS SIMULATOR

THOMAS M. MALONEY (NASA, Lewis Research Center; Sverdrup Technology, Inc., Brook Park, OH) and HAROLD F. LEIBECKI (NASA, Lewis Research Center, Cleveland, OH) IN: IECEC-90; Proceedings of the 25th Intersociety Energy Conversion Engineering Conference, Reno, NV, Aug. 12-17, 1990. Vol. 6. New

York, American Institute of Chemical Engineers, 1990, p. 114-118. Previously announced in STAR as N90-26396. refs
Copyright

The Hydrogen-Oxygen Regenerative Fuel Cell System was identified as a key component for energy storage in support of future lunar missions. Since the H₂-O₂ regenerative electrochemical conversion technology has not yet been tested in space applications, it is necessary to implement predictive techniques to develop initial feasible system designs. The ASPEN simulation software furnishes a constructive medium for analyzing and optimizing such systems. A rudimentary regenerative fuel cell system design was examined using the ASPEN simulator and this modular approach allows for easy addition of supplementary ancillary components and easy integration with life support systems. The modules included in the preliminary analyses may serve as the fundamental structure for more complicated energy storage systems. Author

A91-38182* National Aeronautics and Space Administration. Lewis Research Center, Cleveland, OH.
PRELIMINARY DESIGNS FOR 25 KWE ADVANCED STIRLING CONVERSION SYSTEMS FOR DISH ELECTRIC APPLICATIONS

RICHARD K. SHALTENS and JEFFREY G. SCHREIBER (NASA, Lewis Research Center, Cleveland, OH) IN: IECEC-90; Proceedings of the 25th Intersociety Energy Conversion Engineering Conference, Reno, NV, Aug. 12-17, 1990. Vol. 6. New York, American Institute of Chemical Engineers, 1990, p. 310-316. Previously announced in STAR as N90-26729. refs
Copyright

Under the Department of Energy's (DOE) Solar Thermal Technology Program, Sandia National Laboratories is evaluating heat engines for terrestrial Solar Distributed Heat Receivers. The Stirling engine has been identified by Sandia as one of the most promising engines for terrestrial applications. The Stirling engine also has the potential to meet DOE's performance and cost goals. The NASA Lewis Research Center is conducting Stirling engine technology development activities directed toward a dynamic power source for space applications. Space power systems requirements include high reliability, very long life, low vibration and high efficiency. The free-piston Stirling engine has the potential for future high power space conversion systems, either nuclear or solar powered. Although both applications appear to be quite different, their requirements complement each other. Preliminary designs feature a free-piston Stirling engine, a liquid metal heat transport system, and a means to provide nominally 25 kW electric power to a utility grid while meeting DOE's performance and long term cost goals. The Cummins design incorporates a linear alternator to provide the electrical output, while the STC design generates electrical power indirectly through a hydraulic pump/motor coupled to an induction generator. Both designs for the ASCS's will use technology which can reasonably be expected to be available in the early 1990's. Author

A91-41966* Midwest Research Inst., Golden, CO.
PRIMARY REFERENCE CELL CALIBRATIONS AT SERI - HISTORY AND METHODS

C. R. OSTERWALD, K. A. EMERY, D. R. MYERS (SERI, Golden, CO), and R. E. HART (NASA, Lewis Research Center, Cleveland, OH) IN: IEEE Photovoltaic Specialists Conference, 21st, Kissimmee, FL, May 21-25, 1990, Conference Record. Vol. 2. New York, Institute of Electrical and Electronics Engineers, Inc., 1990, p. 1062-1067. refs
(Contract DE-AC02-83CH-10093)
Copyright

The tabular calibration method used at the Solar Energy Research Institute (SERI) for primary reference cells is derived and described in detail. An uncertainty analysis shows that the tabular method should have a total uncertainty of + or - 1.0 percent; data from five years of calibrations are then shown to support this analysis. Results from SERI's tabular method are compared with terrestrial calibrations performed by the NASA Lewis Research Center in the late 1970s. I.E.

A91-41978* National Aeronautics and Space Administration. Lewis Research Center, Cleveland, OH.

HIGH ALTITUDE AMO TESTING OF PV CONCENTRATOR LENS ELEMENTS

M. F. PISZCZOR, D. J. BRINKER, E. O. BOYER, R. C. MCKNIGHT, R. J. RANAUDO (NASA, Lewis Research Center, Cleveland, OH) et al. IN: IEEE Photovoltaic Specialists Conference, 21st, Kissimmee, FL, May 21-25, 1990, Conference Record. Vol. 2. New York, Institute of Electrical and Electronics Engineers, Inc., 1990, p. 1203-1207. refs
Copyright

Recently, the NASA Lewis Research Center modified its Lear High Altitude Test Facility to fly two prototype ENTECH minidome Fresnel lens photovoltaic concentrator elements. The tests were highly successful, and the results verified the ability of the Lear High Altitude Facility to measure the optical performance of individual concentrator lens elements and concentrator/cell combinations at near AMO insolation conditions. The two concentrator lenses flown achieved optical efficiencies, based on a gallium arsenide concentrator cell response, of 89.8 percent and 90.0 percent. The flights demonstrated the ability of the aircraft to maintain the pointing accuracy required to obtain useful data. With proper alignment of the collimating tube and the pilot's sunlight, this facility could easily maintain a pointing accuracy of + or - 0.5 deg for a sufficiently long time to obtain accurate, reproducible results. I.E.

A91-41999*# National Aeronautics and Space Administration. Lewis Research Center, Cleveland, OH.
REAPPRAISAL OF SOLID SELECTIVE EMITTERS

DONALD L. CHUBB (NASA, Lewis Research Center, Cleveland, OH) IN: IEEE Photovoltaic Specialists Conference, 21st, Kissimmee, FL, May 21-25, 1990, Conference Record. Vol. 2. New York, Institute of Electrical and Electronics Engineers, Inc., 1990, p. 1326-1333. Previously announced in STAR as N91-11801. refs

New rare earth oxide emitters show greater efficiency than previous emitters. As a result, based on a simple model the efficiency of these emitters was calculated. Results indicate that the emission band of the selective emitter must be at relatively low energy (less than or equal to .52 eV) to obtain maximum efficiency at moderate emitter temperatures (less than or equal to 1500 K). Thus, low bandgap energy PV materials are required to obtain an efficient thermophotovoltaic (TPV) system. Of the 4 specific rare earths (Nd, Ho, Er, Yb) studied, Ho has the largest efficiency at moderate temperatures (72 percent at 1500 K). A comparison was made between a selective emitter TPV system and a TPV system that uses a thermal emitter plus a band pass filter to make the thermal emitter behave like a selective emitter. Results of the comparison indicate that only for very optimistic filter and thermal emitter properties will the filter TPV system have a greater efficiency than the selective emitter system. Author

A91-52339*# Sverdrup Technology, Inc., Cleveland, OH.
LASER PHOTOVOLTAIC POWER SYSTEM SYNERGY FOR SEI APPLICATIONS

GEOFFREY A. LANDIS (Sverdrup Technology, Inc., Cleveland, OH) and J. M. HICKMAN (NASA, Lewis Research Center, Cleveland, OH) AIAA, NASA, and OAI, Conference on Advanced SEI Technologies, Cleveland, OH, Sept. 4-6, 1991. 5 p. refs
(AIAA PAPER 91-3419) Copyright

Solar arrays can provide reliable space power, but do not operate when there is no solar energy. Photovoltaic arrays can also convert laser energy with high efficiency. One proposal to reduce the required mass of energy storage required is to illuminate the photovoltaic arrays by a ground laser system. It is proposed to locate large lasers on cloud-free sites at one or more ground locations, and use large lenses or mirrors with adaptive optical correction to reduce the beam spread due to diffraction or atmospheric turbulence. During the eclipse periods or lunar night, the lasers illuminate the solar arrays to a level sufficient to provide operating power. Author

44 ENERGY PRODUCTION AND CONVERSION

A91-52415*# Rockwell International Corp., Canoga Park, CA.
LUNAR ELECTRIC POWER SYSTEMS UTILIZING THE SP-100 REACTOR COUPLED TO DYNAMIC CONVERSION SYSTEMS
RICHARD B. HARTY, RICHARD E. DURAND (Rockwell International Corp., Rocketdyne Div., Canoga Park, CA), and LEE S. MASON (NASA, Lewis Research Center, Cleveland, OH) AIAA, NASA, and OAI, Conference on Advanced SEI Technologies, Cleveland, OH, Sept. 4-6, 1991. 10 p.
(AIAA PAPER 91-3520) Copyright

An integration study was performed by coupling an SP-100 reactor to either a Brayton or Stirling power conversion subsystem. The application was for a surface power system to supply power requirements to a lunar base. A power level of 550 kWe was selected based on the NASA Space Exploration Initiative 90-day study. Reliability studies were initially performed to determine optimum power-conversion redundancy. This study resulted in selecting three operating engines and one standby unit. Integration-design studies indicated that either the Brayton or Stirling power conversion subsystem could be integrated with the SP-100 reactor. The Stirling system had an integration advantage because of smaller piping size and fewer components. The Stirling engine, however, is more complex and heavier than the Brayton rotating unit, which tends to offset the Stirling integration advantage. From a performance consideration, the Brayton had a 9-percent mass advantage and the Stirling a 50-percent radiator-area advantage.

Author

A91-52487*# Rockwell International Corp., Canoga Park, CA.
DYNAMIC ISOTOPE SURFACE POWER SYSTEMS
MARIBETH E. HUNT, RICHARD D. ROVANG (Rockwell International Corp., Rocketdyne Div., Canoga Park, CA), and ROBERT CATALDO (NASA, Lewis Research Center, Cleveland, OH) AIAA, NASA, and OAI, Conference on Advanced SEI Technologies, Cleveland, OH, Sept. 4-6, 1991. 9 p. refs
(AIAA PAPER 91-3623) Copyright

The Dynamic Isotope Power Systems (DIPS) demonstration program, sponsored by the U.S. Department of Energy (DOE) with support funding from the National Aeronautics and Space Administration (NASA), is currently focused on the development of a standardized 2.5 kWe portable generator for multiple applications on the lunar or Martian surface. A variety of potential remote and mobile applications has been identified by NASA including surface rovers for both short and extended duration missions, remote power to science packages, and backup to central base power. Recent work focused on refining the 2.5 kWe design including assessing compatibility with the Martian environment to assure the design is suitable while imposing only a minor mass penalty on lunar operations. Additional work included a study performed to compare the DIPS with regenerative fuel cell systems for lunar mobile and remote power systems. Power requirements were reviewed and a modular system chosen for the comparison. Finally, a plan and cycle schematic were generated for an early demonstration of a prototypic isotope power Brayton system using the Antarctic as the test bed.

Author

A91-52493*# National Aeronautics and Space Administration.
Lewis Research Center, Cleveland, OH.

THE NASA CSTI HIGH CAPACITY POWER PROGRAM

JERRY M. WINTER (NASA, Lewis Research Center, Cleveland, OH) AIAA, NASA, and OAI, Conference on Advanced SEI Technologies, Cleveland, OH, Sept. 4-6, 1991. 12 p. refs
(AIAA PAPER 91-3629)

NASA's Civil Space Technology Initiative (CSTI) has as its primary goal the improvement of space nuclear power-related technologies and their interactions with the given mission environment. The CSTI High Capacity Power Program supports and advances all nonnuclear aspects of the national SP-100 Space Nuclear Reactor Program, including the demonstration of a 1050 K Stirling Space Power System capable of employing the full output capability of the SP-100 reactor. Thermoelectric technology capable of reaching Z values of 0.001/K with SiGe/GaP will be demonstrated in the course of the program.

O.C.

N91-15628*# National Aeronautics and Space Administration.
Lewis Research Center, Cleveland, OH.

IMPEDANCES OF ELECTROCHEMICALLY IMPREGNATED NICKEL ELECTRODES AS FUNCTIONS OF POTENTIAL, KOH CONCENTRATION, AND IMPREGNATION METHOD

MARGARET A. REID May 1989 12 p Presented at the 1st International Symposium on Electrochemical Impedance Spectroscopy, Bombannes, France, 22-26 May 1989; sponsored in part by the Centre Nationale Research Society, and the University of Paris

(Contract RTOP 506-41-21)

(NASA-TM-103283; E-5738; NAS 1.15:103283) Avail: NTIS HC/MF A03 CSCL 10/1

Impedances of fifteen electrodes from each of the four U.S. manufacturers were measured at 0.200 V vs. the Hg/HgO reference electrode. This corresponds to a voltage of 1.145 for a Ni/H₂ cell. Measurements were also made of a representative sample of these at 0.44 V. At the higher voltage, the impedances were small and very similar, but at the lower voltage there were major differences between manufacturers. Electrodes from the same manufacturers showed only small differences. The impedances of electrodes from two manufacturers were considerably different in 26 percent KOH from those in 31 percent KOH. These preliminary results seen to correlate with the limited data from earlier life testing of cells from these manufacturers. The impedances of cells being tested for Space Station Freedom are being followed, and more impedance measurements of electrodes are being performed as functions of manufacturer, voltage, electrolyte concentration, and cycle history in hopes of finding better correlations of impedance with life.

Author

N91-19189*# National Aeronautics and Space Administration.
Lewis Research Center, Cleveland, OH.

TANDEM CONCENTRATOR SOLAR CELLS WITH 30 PERCENT (AMO) POWER CONVERSION EFFICIENCY

J. E. AVERY, L. M. FRAAS, V. S. SUNDARAM, DAVID J. BRINKER, J. M. GEE, and MARK J. ONEILL (ENTECH Corp., Dallas-Fort Worth Airport, TX.) In its Space Photovoltaic Research and Technology, 1989 p 77-87 Jan. 1991

Avail: NTIS HC/MF A22 CSCL 10/2

Very high efficiency concentrator solar panels are envisioned as economical and reliable electrical power subsystems for space based platforms of the future. GaAs concentrator cells with very high efficiencies and good sub-bandgap transmissions can be fabricated on standard wafers. GaSb booster cell development is progressing very well; performance characteristics are still improving dramatically. Consistent GaAs/GaSb stacked cell AMO efficiencies greater than 30 percent are expected.

Author

N91-19195*# National Aeronautics and Space Administration.
Lewis Research Center, Cleveland, OH.

THERMAL ANNEALING OF GAAS CONCENTRATOR SOLAR CELLS

H. B. CURTIS and DAVID J. BRINKER In its Space Photovoltaic Research and Technology, 1989 p 140-153 Jan. 1991

Avail: NTIS HC/MF A22 CSCL 10/2

Isochronal and isothermal annealing tests were performed on GaAs concentrator cells which were irradiated with electrons of various energies to fluences up to 1×10^{16} e/sq cm. The results include: (1) For cells irradiated with electrons from 0.7 to 2.3 MeV, recovery decreases with increasing electron energy. (2) As determined by the un-annealed fractions, isothermal and isochronal annealing produce the same recovery. Also, cells irradiated to 3×10^{15} or 1×10^{16} e/sq cm recover to similar un-annealed fractions. (3) Some significant annealing is being seen at 150 C although very long times are required.

Author

N91-19198*# National Aeronautics and Space Administration.
Lewis Research Center, Cleveland, OH.

REVIEW OF THIN FILM SOLAR CELL TECHNOLOGY AND APPLICATIONS FOR ULTRA-LIGHT SPACECRAFT SOLAR ARRAYS

GEOFFREY A. LANDIS *In its Space Photovoltaic Research and Technology*, 1989 p 180-203 Jan. 1991
 Avail: NTIS HC/MF A22 CSCL 10/2

Developments in thin-film amorphous and polycrystalline photovoltaic cells are reviewed and discussed with a view to potential applications in space. Two important figures of merit are discussed: efficiency (i.e., what fraction of the incident solar energy is converted to electricity), and specific power (power to weight ratio).
 Author

N91-19200*# National Aeronautics and Space Administration. Lewis Research Center, Cleveland, OH.

DUAL-PURPOSE SELF-DELIVERABLE LUNAR SURFACE PV ELECTRICAL POWER SYSTEM

JACK H. ARNOLD, DAVID W. HARRIS, ELDON R. CROSS (Research Triangle Inst., Research Triangle Park, NC.), and DENNIS J. FLOOD *In its Space Photovoltaic Research and Technology*, 1989 p 212-222 Jan. 1991

Avail: NTIS HC/MF A22 CSCL 10/2

A safe haven and work supported PV power systems on the lunar surface will likely be required by NASA in support of the manned outpost scheduled for the post-2000 lunar/Mars exploration and colonization initiative. Initial system modeling and computer analysis shows that the concept is workable and contains no major high risk technology issues which cannot be resolved in the circa 2000 to 2025 timeframe. A specific selection of the best suited type of electric thruster has not been done; the initial modeling was done using an ion thruster, but Rocketdyne must also evaluate arc and resisto-jets before a final design can be formulated. As a general observation, it appears that such a system can deliver itself to the Moon using many system elements that must be transported as dead payload mass in more conventional delivery modes. It further appears that a larger power system providing a much higher safe haven power level is feasible if this delivery system is implemented, perhaps even sufficient to permit resource prospecting and/or lab experimentation. The concept permits growth and can be expanded to include cargo transport such as habitat and working modules. In short, the combined payload could be manned soon after landing and checkout. NASA has expended substantial resources in the development of electric propulsion concepts and hardware that can be applied to a lunar transport system such as described herein. In short, the paper may represent a viable mission on which previous investments play an invaluable role. A more comprehensive technical paper which embodies second generation analysis and system size will be prepared for near-term presentation.
 Author

N91-19201*# National Aeronautics and Space Administration. Lewis Research Center, Cleveland, OH.

FEASIBILITY OF SOLAR POWER FOR MARS

JOSEPH APPELBAUM and GEOFFREY A. LANDIS *In its Space Photovoltaic Research and Technology*, 1989 p 223-254 Jan. 1991

Avail: NTIS HC/MF A22 CSCL 10/2

NASA, through Project Pathfinder, has put in place an advanced technology program to address future needs of manned space exploration. Included in the missions under study is the establishment of outposts on the surface of Mars. The Surface Power program in Pathfinder is aimed at providing photovoltaic array technology for such an application (as well as for the lunar surface). Another important application is for unmanned precursor missions, such as the photovoltaic-power aircraft, which will scout landing sites and investigate Mars geology for a 1 to 2 year mission without landing on the surface. Effective design and utilization of solar energy depend to a large extent on adequate knowledge of solar radiation characteristics in the region of solar energy system operation. The two major climatic components needed for photovoltaic system designs are the distributions of solar insolation and ambient temperature. These distributions for the Martian climate are given at the two Viking lander locations but can also be used, to the first approximation, for other latitudes. One of the most important results is that there is a large diffuse component of the insolation, even at high optical depth, so that solar energy

system operation is still possible. If the power system is to continue to generate power even on high optical opacity days, it is thus important that the photovoltaic system be designed to collect diffuse irradiance as well as direct. In absence of long term insolation and temperature data for Mars, the data presented can be used until updated data are available. The ambient temperature data are given as measured directly by the temperature sensor; the insolation data are calculated from optical depth measurements of the atmosphere.
 Author

N91-19203*# National Aeronautics and Space Administration. Lewis Research Center, Cleveland, OH.

SEMICONDUCTOR STRUCTURAL DAMAGE ATTENDANT TO CONTACT FORMATION IN III-V SOLAR CELLS

NAVID S. FATEMI (Sverdrup Technology, Inc., Cleveland, OH.) and VICTOR G. WEIZER *In its Space Photovoltaic Research and Technology*, 1989 p 270-279 Jan. 1991

Avail: NTIS HC/MF A22 CSCL 10/2

In order to keep the resistive losses in solar cells to a minimum, it is often necessary for the ohmic contacts to be heat treated to lower the metal-semiconductor contact resistivity to acceptable values. Sintering of the contacts, however can result in extensive mechanical damage of the semiconductor surface under the metallization. An investigation of the detailed mechanisms involved in the process of contact formation during heat treatment may control the structural damage incurred by the semiconductor surface to acceptable levels, while achieving the desired values of contact resistivity for the ohmic contacts. The reaction kinetics of sintered gold contacts to InP were determined. It was found that the Au-InP interaction involves three consecutive stages marked by distinct color changes observed on the surface of the Au, and that each stage is governed by a different mechanism. A detailed description of these mechanisms and options to control them are presented.
 Author

N91-19205*# National Aeronautics and Space Administration. Lewis Research Center, Cleveland, OH.

EFFECTS OF PROTON IRRADIATION ON THE PERFORMANCE OF INP/GAAS SOLAR CELLS

IRVING WEINBERG, C. K. SWARTZ, DAVID J. BRINKER, and D. M. WILT *In its Space Photovoltaic Research and Technology*, 1989 p 289-297 Jan. 1991

Avail: NTIS HC/MF A22 CSCL 10/2

InP solar cells are known to be more radiation resistant than either GaAs or Si. In addition, AMO total area efficiencies approaching 19 percent were attained for InP. However, the present high substrate cost presents a barrier to the eventual widespread use of InP cells in space. In addition, if cell thinning becomes desirable, their relative fragility presents a problem. For these reasons, the NASA Lewis Research Center has initiated a program, aimed at producing thin InP cells, by heteroepitaxial deposition of InP on cheaper, more durable substrates. To date, a short term feasibility study as Spire has resulted in cells processed from InP heteroepitaxially deposited on Si substrates with an intervening thin GaAs layer (InP/GaAs/Si) and cells produced from InP deposited on GaAs (InP/GaAs). As a result of this short study efficiencies of over 7 and 9 percent were achieved for InP/GaAs/Si and InP/GaAs respectively. Although these efficiencies are low, they represent a modest and encouraging starting point for a more intensive program. Obviously, when considering economy and mechanical strength, cells processed on silicon substrates are preferred. However, although the InP/GaAs cells are not the final desirable products of this program, their properties serve to highlight several roadblocks to be overcome in producing cells with the more desirable cost and strength properties. Hence, in the present case, the properties of the InP/GaAs cells before and after irradiation by 10 MeV protons are examined. A similar study of InP/GaAs/Si cells will be reported on at a later date.
 Author

N91-19206*# National Aeronautics and Space Administration. Lewis Research Center, Cleveland, OH.

KEY FACTORS LIMITING THE OPEN CIRCUIT VOLTAGE OF N(+)PP(+) INDIUM PHOSPHIDE SOLAR CELLS

44 ENERGY PRODUCTION AND CONVERSION

CHANDRA GORADIA, WILLIAM THESLING (Cleveland State Univ., OH.), and IRVING WEINBERG *In its Space Photovoltaic Research and Technology*, 1989 p 298-310 Jan. 1991
Avail: NTIS HC/MF A22 CSCL 10/2

Solar cells made from gallium arsenide (GaAs), with a room temperature bandgap of $E(\text{sub } g) = 1.43 \text{ eV}$ have exhibited the best measured open circuit voltage ($V(\text{sub } OC)$) of 1.05 V at 1 AMO, 25 C. The material InP is in many ways similar to GaAs. A simple calculation comparing InP to GaAs then shows that solar cells made from InP, with $E(\text{sub } g) = 1.35$ at 300 K, should exhibit the best measured ($V(\text{sub } OC)$) of approximately 950 mV at 1 AMO, 300 K. However, to date, the best measured $V(\text{sub } OC)$ for InP solar cells made by any fabrication method is 899 mV at AM1.5, 25 C which would translate to 912 mV at 1 AMO, 25 C. The $V(\text{sub } OC)$ of an $n(+)\text{pp}(+)$ InP solar cell is governed by several factors. Of these, some factors, such as the thickness and doping of the emitter and base regions, are easily controlled and can be adjusted to desired values dictated by a good performance optimizing model. Such factors were not considered. There are other factors which also govern $V(\text{sub } OC)$, and their values are not so easily controlled. The primary ones among these are (1) the indirect or Hall-Shockley-Read lifetimes in the various regions of the cell, (2) the low-doping intrinsic carrier concentration $n(\text{sub } i)$ of the InP material, (3) the heavy doping factors in the emitter and BSF regions, and (4) the front surface recombination velocity $S(\text{sub } F)$. The influence of these latter factors on the $V(\text{sub } OC)$ of the $n(+)\text{pp}(+)$ InP solar cell and the results were used to produce a near-optimum design of the $n(+)\text{pp}(+)$ InP solar cell.

Author

N91-19207* # National Aeronautics and Space Administration. Lewis Research Center, Cleveland, OH.

DETERMINATION OF SERIES RESISTANCE OF INDIUM PHOSPHIDE SOLAR CELLS

RAJ K. JAIN and IRVING WEINBERG *In its Space Photovoltaic Research and Technology*, 1989 p 311-315 Jan. 1991
Avail: NTIS HC/MF A22 CSCL 10/2

The series resistance of a solar cell is an important parameter, which must be minimized to achieve high cell efficiencies. The cell series resistance is affected by the starting material, its design, and processing. The theoretical approach proposed by Jia, et. al., is used to calculate the series resistance of indium phosphide solar cells. It is observed that the theoretical approach does not predict the series resistance correctly in all cases. The analysis was modified to include the use of effective junction ideality factor. The calculated results were compared with the available experimental results on indium phosphide solar cells processed by different techniques. It is found that the use of process dependent junction ideality factor leads to better estimation of series resistance. An accurate comprehensive series resistance model is warranted to give proper feedback for modifying the cell processing from the design state.

Author

N91-19208* # National Aeronautics and Space Administration. Lewis Research Center, Cleveland, OH.

INVESTIGATION OF ANODIC AND CHEMICAL OXIDES GROWN ON P-TYPE INP WITH APPLICATIONS TO SURFACE PASSIVATION FOR N(+)-P SOLAR CELL FABRICATION

MARIA FAUR, MIRCEA FAUR, MANJU GORADIA, CHANDRA GORADIA (Cleveland State Univ., OH.), PHILLIP JENKINS, DOUGLAS JAYNE, and IRVING WEINBERG *In its Space Photovoltaic Research and Technology*, 1989 p 316-331 Jan. 1991

Avail: NTIS HC/MF A22 CSCL 10/2

Most of the previously reported InP anodic oxides were grown on a n-type InP with applications to fabrication of MISFET structures and were described as a mixture of In_2O_3 and P_2O_5 stoichiometric compounds or nonstoichiometric phases which have properties similar to crystalline compounds $\text{In}(\text{OH})_3$, InPO_4 , and $\text{In}(\text{PO}_3)_3$. Details of the compositional change of the anodic oxides grown under different anodization conditions were previously reported. The use of P-rich oxides grown either by anodic or chemical oxidation are investigated for surface passivation of p-type InP

and as a protective cap during junction formation by closed-ampoule sulfur diffusion. The investigation is based on but not limited to correlations between PL intensity and X-ray photoelectron spectroscopy (XPS) chemical composition data.

Author

N91-19209* # National Aeronautics and Space Administration. Lewis Research Center, Cleveland, OH.

A COMPARATIVE STUDY OF PERFORMANCE PARAMETERS OF N(+)-P INP SOLAR CELLS MADE BY CLOSED-AMPOULE SULFUR DIFFUSION INTO CD- AND ZN-DOPED P-TYPE INP SUBSTRATES

MIRCEA FAUR, MARIA FAUR, CHANDRA GORADIA, MANJU GORADIA, RALPH D. THOMAS, DAVID J. BRINKER, NAVID S. FATEMI (Sverdrup Technology, Inc., Cleveland, OH.), and FRANK S. HONECY *In its Space Photovoltaic Research and Technology*, 1989 p 332-346 Jan. 1991

Avail: NTIS HC/MF A22 CSCL 10/2

Preliminary results indicate that Cd-doped substrates are better candidates for achieving high efficiency solar cells fabricated by closed-ampoule sulfur (S) diffusion than Zn-doped substrates. The differences in performance parameters (i.e., 14.3 percent efficiency for Cd-doped vs. 11.83 percent in the case of Zn-doped substrates of comparable doping and etch pit densities) were explained in terms of a large increase in dislocation density as a result of S diffusion in the case of Zn-doped as compared to Cd-doped substrates. The $\text{In}(\text{x})\text{S}(\text{y})$ and probably $\text{Zn}(\text{S})$ precipitates in the case of Zn-doped substrates, produce a dead layer which extends deep below the surface and strongly affects the performance parameters. It should be noted that the cells had an unoptimized single layer antireflective coating of SiO_2 , a grid shadowing of 6.25 percent, and somewhat poor contacts, all contributing to a reduction in efficiency. It is believed that by reducing the external losses and further improvement in cell design, efficiencies approaching 17 percent at 1 AMO, 25 degrees should be possible for cells fabricated on these relatively high defect density Cd-doped substrates. Even higher efficiencies, 18 to 19 percent should be possible by using long-lifetime substrates and further improving front surface passivation. If solar cells fabricated on Cd-doped substrates turn out to have comparable radiation tolerance as those reported in the case of cells fabricated on Zn-doped substrates, then for certain space missions 18 to 19 percent efficient cells made by this method of fabrication would be viable.

Author

N91-19219* # National Aeronautics and Space Administration. Lewis Research Center, Cleveland, OH.

MINI-DOME FRESNEL LENS PHOTOVOLTAIC CONCENTRATOR DEVELOPMENT

MARK J. ONEILL (ENTECH Corp., Dallas-Fort Worth Airport, TX.) and MICHAEL F. PISZCZOR, JR. *In its Space Photovoltaic Research and Technology*, 1989 p 443-459 Jan. 1991

Avail: NTIS HC/MF A22 CSCL 10/2

Since 1986 work on a new high-performance, light-weight space photovoltaic concentration array has been conducted. An update on the mini-dome lens concentrator array development program is provided. Recent prototype cell and lens test results indicate that near-term array performance goals of 300 w/sq m and 100 w/kg are feasible, and that a longer-term goal of 200 w/kg is reasonable.

B.G.

N91-19221* # National Aeronautics and Space Administration. Lewis Research Center, Cleveland, OH.

INDIUM PHOSPHIDE SOLAR CELLS

IRVING WEINBERG *In its Space Photovoltaic Research and Technology*, 1989 p 484-486 Jan. 1991

Avail: NTIS HC/MF A22 CSCL 10/2

The direction for InP solar cell research; reduction of cell cost; increase of cell efficiency; measurements needed to better understand cell performance; n/p versus p/n; radiation effects; major problems in cell contacting; and whether the present level of InP solar cell research in the USA should be maintained, decreased, or increased were considered.

B.G.

N91-20732*# National Aeronautics and Space Administration. Lewis Research Center, Cleveland, OH.

ATOMIC OXYGEN INTERACTION WITH SOLAR ARRAY BLANKETS AT PROTECTIVE COATING DEFECT SITES

BRUCE A. BANKS, BRUCE M. AUER, SHARON K. RUTLEDGE, and CAROL M. HILL (Case Western Reserve Univ., Cleveland, OH.) / In NASA, Lyndon B. Johnson Space Center, Fourth Annual Workshop on Space Operations Applications and Research (SOAR 90) p 726-732 Jan. 1991

Avail: NTIS HC/MF A14 CSCL 10/1

Atomic oxygen in the low-Earth-orbital environment oxidizes SiOx protected polyimide Kapton solar array blankets at sites which are not protected such as pin windows or scratches in the protective coatings. The magnitude and shape of the atomic oxygen undercutting which occurs at these sites is dependent upon the exposure environment details such as arrival direction and reaction probability. The geometry of atomic oxygen undercutting at defect sites exposed to atomic oxygen in plasma asher was used to develop a Monte Carlo model to simulate atomic oxygen erosion processes at defect sites in protected Kapton. Comparisons of Monte Carlo predictions and experimental results are presented for plasma asher atomic oxygen exposures for large and small defects as well as for protective coatings on one or both sides of Kapton. The model is used to predict in-space exposure results at defect sites for both directed and sweeping atomic oxygen exposure. A comparison of surface textures predicted by the Monte Carlo model and those experimentally observed from both directed space ram and laboratory plasma asher atomic oxygen exposure indicate substantial agreement. Author

N91-23054*# National Aeronautics and Space Administration. Lewis Research Center, Cleveland, OH.

SOLAR POWERED STIRLING CYCLE ELECTRICAL GENERATOR

RICHARD K. SHALTENS / In National Aeronautics and Space Administration, Technology 2000, Volume 1 p 269-278 Mar. 1991

Avail: NTIS HC/MF A18 CSCL 10/2

Under NASA's Civil Space Technology Initiative (CSTI), the NASA Lewis Research Center is developing the technology needed for free-piston Stirling engines as a candidate power source for space systems in the late 1990's and into the next century. Space power requirements include high efficiency, very long life, high reliability, and low vibration. Furthermore, system weight and operating temperature are important. The free-piston Stirling engine has the potential for a highly reliable engine with long life because it has only a few moving parts, non-contacting gas bearings, and can be hermetically sealed. These attributes of the free-piston Stirling engine also make it a viable candidate for terrestrial applications. In cooperation with the Department of Energy, system designs are currently being completed that feature the free-piston Stirling engine for terrestrial applications. Industry teams were assembled and are currently completing designs for two Advanced Stirling Conversion Systems utilizing technology being developed under the NASA CSTI Program. These systems, when coupled with a parabolic mirror to collect the solar energy, are capable of producing about 25 kW of electricity to a utility grid. Industry has identified a niche market for dish Stirling systems for worldwide remote power application. They believe that these niche markets may play a major role in the introduction of Stirling products into the commercial market. Author

N91-23616*# National Aeronautics and Space Administration. Lewis Research Center, Cleveland, OH.

MATERIAL PROCESSING WITH HYDROGEN AND CARBON MONOXIDE ON MARS

ALOYSIUS F. HEPP, GEOFFREY A. LANDIS (Sverdrup Technology, Inc., Cleveland, OH.), and DIANE L. LINNE 1991 11 p Presented at the 10th Biennial Conference on Space Manufacturing, Princeton, NJ, 15-19 May 1991; sponsored by the Space Studies Inst.

(Contract RTOP 506-41-11)

(NASA-TM-104405; E-6230; NAS 1.15:104405) Avail: NTIS HC/MF A03 CSCL 10/2

Several novel proposals are examined for propellant production from carbon dioxide and monoxide and hydrogen. Potential uses were also examined of CO as a fuel or as a reducing agent in metal oxide processing as obtained or further reduced to carbon. Hydrogen can be reacted with CO to produce a wide variety of hydrocarbons, alcohols, and other organic compounds. Methanol, produced by Fischer-Tropsch chemistry may be useful as a fuel; it is easy to store and handle because it is a liquid at Mars temperatures. The reduction of CO₂ to hydrocarbons such as methane or acetylene can be accomplished with hydrogen. Carbon monoxide and hydrogen require cryogenic temperatures for storage as liquids. Noncryogenic storage of hydrogen may be accomplished using hydrocarbons, inorganic hydrides, or metal hydrides. Noncryogenic storage of CO may be accomplished in the form of iron carbonyl (Fe(CO)₅) or other metal carbonyls. Low hydrogen content fuels such as acetylene (C₂H₂) may be effective propellants with low requirements for earth derived resources. The impact on manned Mars missions of alternative propellant production and utilization is discussed. Author

N91-23617*# National Aeronautics and Space Administration. Lewis Research Center, Cleveland, OH.

SOLAR THERMAL ENERGY RECEIVER Patent Application

KARL W. BAKER, inventor (to NASA) and MILES O. DUSTIN, inventor (to NASA) 27 Mar. 1991 14 p

(NASA-CASE-LEW-14949-1; NAS 1.71:LEW-14949-1;

US-PATENT-APPL-SN-676910) Avail: NTIS HC/MF A03 CSCL 10/1

A plurality of heat pipes in a shell receive concentrated solar energy and transfer the energy to a heat activated system. To provide for even distribution of the energy despite uneven impingement of solar energy on the heat pipes, absence of solar energy at times, or failure of one or more of the heat pipes, energy storage means are disposed on the heat pipes which extend through a heat pipe thermal coupling means into the heat activated device. To enhance energy transfer to the heat activated device, the heat pipe coupling cavity means may be provided with extensions into the device. For use with a Stirling engine having passages for working gas, heat transfer members may be positioned to contact the gas and the heat pipes. The shell may be divided into sections by transverse walls. To prevent cavity working fluid from collecting in the extensions, a porous body is positioned in the cavity. NASA

N91-23620*# National Aeronautics and Space Administration. Lewis Research Center, Cleveland, OH.

SEI ROVER SOLAR-ELECTROCHEMICAL POWER SYSTEM OPTIONS

COLLEEN A. WITHROW, LISA L. KOHOUT, DAVID J. BENTS, and ANTHONY J. COLOZZA (Sverdrup Technology, Inc., Brook Park, OH.) May 1991 19 p Presented at the 26th Intersociety Energy Conversion Engineering Conference, Boston, MA, 4-9 Aug. 1991; sponsored by American Nuclear Society, SAE, American Chemical Society, AIAA, ASME, IEEE, and American Inst. of Chemical Engineers

(Contract NAS3-25266; RTOP 326-81-10)

(NASA-TM-104402; E-6224; NAS 1.15:104402) Avail: NTIS HC/MF A03 CSCL 10/1

A trade study of power system technology for proposed lunar vehicles and servicers is presented. A variety of solar-based power systems were selected and analyzed for each. The analysis determined the power system mass, volume, and deployed area. A comparison was made between periodic refueling/recharging systems and onboard power systems to determine the most practical system. The trade study concluded that the power system significantly impacts the physical characteristics of the vehicle. The refueling/recharging systems were lighter and more compact, but dependent on availability of established lunar base infrastructure. Onboard power systems pay a mass penalty for being fully developed systems. Author

44 ENERGY PRODUCTION AND CONVERSION

N91-25061*# National Aeronautics and Space Administration. Lewis Research Center, Cleveland, OH.

ADVANCED PHOTOVOLTAIC EXPERIMENT, S0014: PRELIMINARY FLIGHT RESULTS AND POST-FLIGHT FINDINGS Abstract Only

DAVID J. BRINKER, JOHN R. HICKEY (Eppley Lab., Inc., Newport, RI.), and DONALD K. BRASTED /in NASA, Langley Research Center, First LDEF Post-Retrieval Symposium Abstracts p 95 Jun. 1991

Avail: NTIS HC/MF A07 CSCL 10/1

The Advanced Photovoltaic Experiment (APEX) is an LDEF experiment designed to provide reference solar cell standards for laboratory measurements as well as to investigate the solar spectrum and the effects of long term exposure of solar cells to the LEO environment. Silicon and gallium arsenide solar cells were flown with the appropriate instrumentation to periodically measure cell performance and temperature. The experimental objectives, the design employed to realize these objectives and the solar cells and instrumentation selected for the flight are presented. A discussion of the flight data returned are included. Preliminary results from the post flight analysis of the absolute cavity radiometer, the digital solar angle sensor, and the Barr Associates narrow bandpass optical filters are also presented. The initial findings of work to determine the chemical nature of contamination layers on APEX are also presented. Author

N91-25062*# National Aeronautics and Space Administration. Lewis Research Center, Cleveland, OH.

DURABILITY EVALUATION OF PHOTOVOLTAIC BLANKET MATERIALS EXPOSED ON LDEF TRAY S1003 Abstract Only

SHARON K. RUTLEDGE and RAYMOND M. OLLE (Cleveland State Univ., OH.) /in NASA, Langley Research Center, First LDEF Post-Retrieval Symposium Abstracts p 96 Jun. 1991

Avail: NTIS HC/MF A07 CSCL 10/1

Several candidate protective coatings on Kapton and uncoated Kapton were exposed to the LEO environment on the LDEF in order to determine whether the coatings could be used to protect polymeric substrates from degradation in the LEO environment. These materials are used for flexible solar array panels in which the polymer is the structural member that supports the solar cell and current carriers. Arrays such as these are used on the Hubble Space Telescope and will be used on Space Station Freedom. The results of the experiments are presented. Author

N91-25510*# National Aeronautics and Space Administration. Lewis Research Center, Cleveland, OH.

STIRLING MACHINE OPERATING EXPERIENCE

BRAD ROSS (Stirling Technology Co., Richland, WA.) and JAMES E. DUDENHOEFER 1991 8 p Presented at the 26th Intersociety Energy Conversion Engineering Conference, Boston, MA, 4-9 Aug. 1991; sponsored by the American Nuclear Society, SAE, the American Chemical Society, AIAA, ASME, IEE, and the American Inst. of Chemical Engineers (Contract RTOP 590-13-11)

(NASA-TM-104487; E-6334; NAS 1.15:104487) Avail: NTIS HC/MF A02 CSCL 10/2

Numerous Stirling machines have been built and operated, but the operating experience of these machines is not well known. It is important to examine this operating experience in detail, because it largely substantiates the claim that Stirling machines are capable of reliable and lengthy lives. The amount of data that exists is impressive, considering that many of the machines that have been built are developmental machines intended to show proof of concept, and were not expected to operate for any lengthy period of time. Some Stirling machines (typically free-piston machines) achieve long life through non-contact bearings, while other Stirling machines (typically kinematic) have achieved long operating lives through regular seal and bearing replacements. In addition to engine and system testing, life testing of critical components is also considered. Author

N91-26592*# National Aeronautics and Space Administration. Lewis Research Center, Cleveland, OH.

A RELIABILITY AND MASS PERSPECTIVE OF SP-100 STIRLING CYCLE LUNAR-BASE POWERPLANT DESIGNS

HARVEY S. BLOOMFIELD Jun. 1991 31 p (Contract RTOP 590-13-11)

(NASA-TM-103736; E-5974; NAS 1.15:103736) Avail: NTIS HC/MF A03 CSCL 10/2

The purpose was to obtain reliability and mass perspectives on selection of space power system conceptual designs based on SP-100 reactor and Stirling cycle power-generation subsystems. The approach taken was to: (1) develop a criterion for an acceptable overall reliability risk as a function of the expected range of emerging technology subsystem unit reliabilities; (2) conduct reliability and mass analyses for a diverse matrix of 800-kWe lunar-base design configurations employing single and multiple powerplants with both full and partial subsystem redundancy combinations; and (3) derive reliability and mass perspectives on selection of conceptual design configurations that meet an acceptable reliability criterion with the minimum system mass increase relative to reference powerplant design. The developed perspectives provided valuable insight into the considerations required to identify and characterize high-reliability and low-mass lunar-base powerplant conceptual design. Author

N91-27611*# National Aeronautics and Space Administration. Lewis Research Center, Cleveland, OH.

PRELIMINARY DESIGN OF A MOBILE LUNAR POWER SUPPLY

PAUL C. SCHMITZ, BARBARA H. KENNY, and CHRISTOPHER R. FULMER (General Dynamics Corp., San Diego, CA.) 1991 13 p Presented at the 26th Intersociety Energy Conversion Engineering Conference, Boston, MA, 4-9 Aug. 1991; sponsored by ANS, SAE, ACS, AIAA, ASME, IEEE, and AIChE (Contract RTOP 590-13-11)

(NASA-TM-104471; E-6376; NAS 1.15:104471) Avail: NTIS HC/MF A03 CSCL 10/2

A preliminary design for a Stirling isotope power system for use as a mobile lunar power supply is presented. Performance and mass of the components required for the system are estimated. These estimates are based on power requirements and the operating environment. Optimizations routines are used to determine minimum mass operational points. Shielding for the isotope system are given as a function of the allowed dose, distance from the source, and the time spent near the source. The technologies used in the power conversion and radiator systems are taken from ongoing research in the Civil Space Technology Initiative (CSTI) program. Author

N91-27614*# National Aeronautics and Space Administration. Lewis Research Center, Cleveland, OH.

THIN SOLAR CELL AND LIGHTWEIGHT ARRAY Patent

HENRY W. BRANDHORST, JR., inventor (to NASA) and IRVING WEINBERG, inventor (to NASA) 28 May 1991 14 p Filed 20 Mar. 1990

(NASA-CASE-LEW-14959-1; US-PATENT-5,019,176; US-PATENT-APPL-SN-495969; US-PATENT-CLASS-136-244; US-PATENT-CLASS-136-249; US-PATENT-CLASS-136-256; US-PATENT-CLASS-357-30; US-PATENT-CLASS-437-2; INT-PATENT-CLASS-H01L-31/42; INT-PATENT-CLASS-H01L-31/18) Avail: US Patent and Trademark Office CSCL 10/1

A thin, lightweight solar cell that utilizes front contact metallization is presented. Both the front light receiving surface of the solar cell and the facing surface of the cover glass are recessed to accommodate this metallization. This enables the two surfaces to meet flush for an optimum seal.

Official Gazette of the U.S. Patent and Trademark Office

N91-30206*# National Aeronautics and Space Administration. Lewis Research Center, Cleveland, OH.

A COMPARATIVE STUDY OF P(+)-JN AND N(+)-JP INP SOLAR CELLS MADE BY A CLOSED AMPOULE DIFFUSION

M. FAUR, M. FAUR, D. J. FLOOD, I. WEINBERG, D. J. BRINKER, C. GORADIA, N. FATEMI (Sverdrup Technology, Inc., Cleveland, OH.), M. GORADIA, and W. THESLING *In its* Space Photovoltaic Research and Technology Conference 12 p Aug. 1991
 Avail: NTIS HC/MF A20 CSCL 10/2

The purpose was to demonstrate the possibility of fabricating thermally diffused p(+)n InP solar cells having high open-circuit voltage without sacrificing the short circuit current. The p(+)n junctions were formed by closed-ampoule diffusion of Cd through a 3 to 5 nm thick anodic or chemical phosphorus-rich oxide cap layer grown on n-InP:S Czochralski LEC grown substrates. For solar cells made by thermal diffusion the p(+)n configuration is expected to have a higher efficiency than the n(+)p configuration. It is predicted that the AM0, BOL efficiencies approaching 19 percent should be readily achieved providing that good ohmic front contacts could be realized on the p(+) emitters of thickness lower than 1 micron. Author

N91-30207*# National Aeronautics and Space Administration. Lewis Research Center, Cleveland, OH.
IMPROVEMENTS IN CONTACT RESISTIVITY AND THERMAL STABILITY OF AU-CONTACTED INP SOLAR CELLS
 NAVID S. FATEMI (Sverdrup Technology, Inc., Brook Park, OH.) and VICTOR G. WEIZER *In its* Space Photovoltaic Research and Technology Conference 7 p Aug. 1991
 Avail: NTIS HC/MF A20 CSCL 10/2

Specific contact resistivities for as-fabricated Au contacts on n-p InP solar cells are typically in the 10(exp -3) ohm/sq cm range, but contact resistivities in the 10(exp -6) ohm/sq cm range can be obtained if the cells are heat treated at 400 C for a few minutes. This heat treatment, however, results in a dramatic drop in the open circuit voltage of the cell due to excessive dissolution of the emitter into the metallization. It was found that low values of contact resistivity can be secured without the accompanying drop in the open circuit voltage by adding Ga and In in the Au metallization. It is shown that Au contacts containing as little as 1 percent atomic Ga can suppress the reaction that takes place at the metal-InP interface during heat treatment, while exhibiting contact resistivity values in the low 10(exp -5) ohm/sq cm. Detailed explanations for the observed superior thermal stability of these contacts are presented. Author

N91-30208*# National Aeronautics and Space Administration. Lewis Research Center, Cleveland, OH.
GROOVED SURFACES ON INP
 SHEILA G. BAILEY, NAVID S. FATEMI, GEOFFREY A. LANDIS, and PHILLIP P. JENKINS (Cleveland State Univ., OH.) *In its* Space Photovoltaic Research and Technology Conference 6 p Aug. 1991
 Avail: NTIS HC/MF A20 CSCL 10/2

Formation of a textured or grooved front surface on a solar cell can increase the efficiency in several ways, including enhanced absorption and light trapping. In III-IV materials the (111) plane is chemically different from the (1'1'1') plane, and both etching and epitaxial deposition behave differently on these surfaces. The current state of profile etching in InP is summarized. Data are presented on novel geometries attainable as a function of etchant temperature and composition, substrate orientation and carrier concentration, and the oxide thickness between the substrate and the photoresist. Depending on dopant concentration, the same etchant can produce either anisotropic or isotropic grooves. V-grooved solar cells were manufactured on InP, and the improved optical absorption was demonstrated. Preferred parameters for various applications are listed and discussed. Author

N91-30209*# National Aeronautics and Space Administration. Lewis Research Center, Cleveland, OH.
EFFECT OF DISLOCATIONS ON PROPERTIES OF HETEROEPITAXIAL INP SOLAR CELLS
 I. WEINBERG, C. K. SWARTZ, H. B. CURTIS, D. J. BRINKER, P. JENKINS, and M. FAUR (Cleveland State Univ., OH.) *In its* Space Photovoltaic Research and Technology Conference 9 p

Aug. 1991

Avail: NTIS HC/MF A20 CSCL 10/2

The apparently unrelated phenomena of temperature dependency, carrier removal and photoluminescence are shown to be affected by the high dislocation densities present in heteroepitaxial InP solar cells. Using homoepitaxial InP cells as a baseline, it is found that the relatively high dislocation densities present in heteroepitaxial InP/GaAs cells lead to increased volumes of dVoc/dt and carrier removal rate and substantial decreases in photoluminescence spectral intensities. With respect to dVoc/dt, the observed effect is attributed to the tendency of dislocations to reduce Voc. Although the basic cause for the observed increase in carrier removal rate is unclear, it is speculated that the decreased photoluminescence intensity is attributable to defect levels introduced by dislocations in the heteroepitaxial cells. Author

N91-31708*# National Aeronautics and Space Administration. Lewis Research Center, Cleveland, OH.
NICKEL-HYDROGEN CELL LOW-EARTH LIFE TEST UPDATE
 DAVID T. FRATE 1991 8 p Presented at the 26th Intersociety Energy Conversion Engineering Conference, Boston, MA, 4-9 Aug. 1991; cosponsored by ANS, SAE, ACS, AIAA, ASME, IEEE, and AICHE
 (Contract RTOP 474-46-10)
 (NASA-TM-105229; E-6552; NAS 1.15:105229) Avail: NTIS HC/MF A02 CSCL 10/1

When individual pressure vessel (IPV) nickel-hydrogen (Ni/H2) cells were selected as the energy storage system for the Space Station Freedom in March of 1986, a limited database existed on life and performance characteristics of these cells in a low earth orbit (LEO) regime. Therefore, NASA LeRC initiated a Ni/H2 cell test program with the primary objectives of building a test facility, procuring cells from existing NASA contracts, and screening several cell designs by life testing in a LEO 35 percent depth of discharge (DOD) scenario. A total of 40 cells incorporating 13 designs were purchased from Yardney, Hughes, and Eagle-Picher. Thirty-two of the cells purchased were 65 A-hr nameplate capacity and eight cells were 50 A-hr. Yardney and Eagle-Picher cells were built with both the Air Force recirculating and the advanced back-to-back electrode stack configurations and incorporated 31 and 26 percent KOH. Acceptance testing of the first delivered cells began in March of 1988, with life testing following in September of that year. Performance comparisons of these cells are made here while specifically addressing life test data relative to the design differences. Author

N91-32549*# National Aeronautics and Space Administration. Lewis Research Center, Cleveland, OH.
SPACE ELECTROCHEMICAL RESEARCH AND TECHNOLOGY
 Sep. 1991 244 p Third Conference held in Cleveland, OH, 9-10 Apr. 1991
 (Contract RTOP 506-41-21)
 (NASA-CP-3125; E-6089; NAS 1.55:3125) Avail: NTIS HC/MF A11 CSCL 10/1

The proceedings of NASA's third Space Electrochemical Research and Technology (SERT) conference are presented. The objective of the conference was to assess the present status and general thrust of research and development in those areas of electrochemical technology required to enable NASA missions in the next century. The conference provided a forum for the exchange of ideas and opinions of those actively involved in the field, in order to define new opportunities for the application of electrochemical processes in future NASA missions. Papers were presented in three technical areas: the electrochemical interface, the next generation in aerospace batteries and fuel cells, and electrochemistry for nonenergy storage applications.

N91-32551*# National Aeronautics and Space Administration. Lewis Research Center, Cleveland, OH.
THE AU CATHODE IN THE SYSTEM LI2CO3-CO2-CO AT 800 TO 900 C
 NORMAN H. HAGEDORN *In its* Space Electrochemical Research

44 ENERGY PRODUCTION AND CONVERSION

and Technology p 7-22 Sep. 1991
Avail: NTIS HC/MF A11 CSCL 10/3

Current results of experimental work to evaluate gold as a possible catalyst for the cathodic reduction of carbon dioxide in molten lithium carbonate are presented. An attempt is then made to rationalize the experimental results by proposing a phenomenological model for the sequence of reactions at and around the electrode. Finally, inferences are made as to the viability of gold as a cathode catalyst for the proposed battery. Author

N91-32556*# National Aeronautics and Space Administration. Lewis Research Center, Cleveland, OH.

RAMAN SPECTRAL OBSERVATION OF A NEW PHASE

OBSERVED IN NICKEL ELECTRODES CYCLED TO FAILURE

PATRICIA L. LOYSELLE, X. SHAN, B. C. CORNILSEN (Michigan Technological Univ., Houghton.), and MARGARET A. REID *In its* Space Electrochemical Research and Technology p 81-87 Sep. 1991

(Contract NAG3-519)

Avail: NTIS HC/MF A11 CSCL 10/2

A new phase is reported in nickel electrodes from Ni/H₂ boilerplate cells which were cycled to failure in electrolyte of variable KOH concentration (21 to 36 percent). Raman spectra clearly show the presence of this phase, and these spectra have been used to estimate the amounts present on these electrodes. Ten of 12 electrodes examined contain this new phase. The cycle life at higher KOH concentrations (31 and 36 percent) was greatly reduced, and nickel electrodes from these cells exhibited extensive amounts of this new phase. The presence of this new phase correlates with cell failure defined by low end of discharge voltages. It is proposed that the lowered capacity and failure of these electrodes was caused by loss of active mass and formation of a phase with reduced electrochemical activity. These results indicate that formation of the new phase is accelerated at higher KOH concentrations. Author

N91-32557*# National Aeronautics and Space Administration. Lewis Research Center, Cleveland, OH.

IMPEDANCES OF NICKEL ELECTRODES CYCLED IN VARIOUS KOH CONCENTRATIONS

MARGARET A. REID and PATRICIA L. LOYSELLE *In its* Space Electrochemical Research and Technology p 89-100 Sep. 1991
Avail: NTIS HC/MF A11 CSCL 10/2

Recent tests at Hughes have shown that Ni/H₂ cells cycled in 26 percent KOH have much longer lives than those cycled in other concentrations. As part of an ongoing program to try to correlate the impedances of nickel electrodes with their life and performance, impedances were measured of a number of electrodes from these tests that had been cycled in concentrations from 21 to 36 percent KOH. These had ranged from about 1000 to 40,000 cycles. After cycling ten times to reduce possible changes due to storage, impedances were measured at five voltages corresponding to low states of charge. The results were analyzed using a standard circuit model including Warburg impedance term. Lower kinetic resistances and Warburg slopes were found for several electrodes which had been cycled in 26 percent KOH even though they had been cycled for a much longer time than the others. Interpretation of the data is complicated by the fact that the cycle lives, storage times, and failure mechanisms varied. Several other circuit models have also been examined, but the best correlations with life were found with parameters obtained from the simple model. Author

N91-32562*# National Aeronautics and Space Administration. Lewis Research Center, Cleveland, OH.

SOME RECENT STUDIES WITH THE SOLID-IONOMER ELECTROCHEMICAL CAPACITOR

S. SARANGAPANI, J. FORCHIONE, A. GRIFFITH, A. B. LACONTI (Giner, Inc., Waltham, MA.), and R. BALDWIN *In its* Space Electrochemical Research and Technology p 175-193 Sep. 1991

(Contract N00014-88-C-0391; NSF ISI-90-60142)

Avail: NTIS HC/MF A11 CSCL 10/2

A high energy density, all solid ionomer electrochemical capacitor was developed, which is completely free of liquid electrolyte. The novel features of this device include a three dimensional metal oxide particulate ionomer composite electrode structure, and a unitized repeating cell element. The composite electrode structures are bonded to opposite sides of a thin sheet of a solid proton conducting ionomer membrane and form an integrally bonded membrane and electrode assembly (MEA). Individual MEAs can be stacked in series as bipolar elements to form a multiple cell device. The discharge characteristics and energy storage properties of these devices are described. Typical capacitance measured for a unit cell is 1 F/sq cm. Life testing of a multicell capacitor on an intermittent basis has shown, that over a 10,000 hour period, the capacitance and resistance of the cell has remained invariant. There has been no maintenance required on the device since it was fabricated. Other multicell units of shorter life duration have exhibited similar reliable performance characteristics. Author

N91-32563*# National Aeronautics and Space Administration. Lewis Research Center, Cleveland, OH.

PERFORMANCE OF A DUAL ANODE NICKEL-HYDROGEN CELL

RANDALL F. GAHN *In its* Space Electrochemical Research and Technology p 195-207 Sep. 1991

Avail: NTIS HC/MF A11 CSCL 10/2

An experimental study was conducted to characterize the voltage performance of a nickel hydrogen cell containing a hydrogen electrode on both sides of the nickel electrode. The dual anode cell was compared with a convenient single anode cell using the same nickel electrode. Higher discharge voltages and lower charge voltages were obtained with the dual anode cell during constant current discharges to 10C, pulse discharges to 8C, and polarization measurements at 50 percent of charge. Author

N91-32569*# National Aeronautics and Space Administration. Lewis Research Center, Cleveland, OH.

STATUS OF NASA'S STIRLING SPACE POWER CONVERTER PROGRAM

JAMES E. DUDENHOEFER and JERRY M. WINTER 1991 8 p Presented at the 26th Intersociety Energy Conversion Engineering Conference, Boston, MA, 4-9 Aug. 1991; sponsored by ANS, SAE, ACS, AIAA, ASME, IEEE, and AIChE (Contract RTOP 590-13-11)

(NASA-TM-104512; E-6381; NAS 1.15:104512) Avail: NTIS HC/MF A02 CSCL 10/2

An overview is presented of the NASA-Lewis Free-Piston Stirling Space Power Converter Technology Program. The goal is to develop the technology base needed to meet the long duration, high capacity power requirements for future NASA space initiatives. Efforts are focused upon increasing system power output and system thermal and electric energy conversion efficiency at least fivefold over current SP-100 technology, and on achieving systems that are compatible with space nuclear reactors. Stirling experience in space and progress toward 1050 and 1300 K Stirling Space Power Converters is discussed. Fabrication is nearly completed for the 1050 K Component Test Power Converters (CTPC); results of motoring tests of cold end (525 K), are presented. The success of these and future designs is dependent upon supporting research and technology efforts including heat pipes, bearings, superalloy joining technologies, high efficiency alternators, life and reliability testing and predictive methodologies. An update is provided of progress in some of these technologies leading off with a discussion of free-piston Stirling experience in space. Author

AEROSPACE MEDICINE

Includes physiological factors; biological effects of radiation; and effects of weightlessness on man and animals.

A91-52331*# Idaho National Engineering Lab., Idaho Falls.
RADIATION DOSE ESTIMATES FOR TYPICAL PILOTED NTR LUNAR AND MARS MISSION ENGINE OPERATIONS
 BRUCE G. SCHNITZLER (Idaho National Engineering Laboratory, Idaho Falls) and STANLEY K. BOROWSKI (NASA, Lewis Research Center, Cleveland, OH) AIAA, NASA, and OAI, Conference on Advanced SEI Technologies, Cleveland, OH, Sept. 4-6, 1991. 14 p. Research supported by NASA. refs
 (Contract DE-AC07-76ID-01570)
 (AIAA PAPER 91-3407) Copyright

The natural and manmade radiation environments to be encountered during lunar and Mars missions are qualitatively summarized. The computational methods available to characterize the radiation environment produced by an operating nuclear propulsion system are discussed. Mission profiles and vehicle configurations are presented for a typical all-propulsive, fully reusable lunar mission and for a typical all-propulsive Mars mission. Estimates of crew location biological doses are developed for all propulsive maneuvers. Post-shutdown dose rates near the nuclear engine are estimated at selected mission times. Author

N91-23032*# National Aeronautics and Space Administration. Lewis Research Center, Cleveland, OH.

ADAPTATION OF NASA TECHNOLOGY FOR THE OPTIMIZATION OF ORTHOPEDIC KNEE IMPLANTS

D. A. SARAVANOS, P. J. MRAZ (Case Western Reserve Univ., Cleveland, OH.), and D. A. HOPKINS /in National Aeronautics and Space Administration, Technology 2000, Volume 1 p 89-98 Mar. 1991
 (Contract NAG3-1027)

Avail: NTIS HC/MF A18 CSCL 05/8

The NASA technology originally developed for the optimization of composite structures (engine blades) is adapted and applied to the optimization of orthopedic knee implants. A method is developed enabling the tailoring of the implant for optimal interaction with the environment of the tibia. The shape of the implant components are optimized, such that the stresses in the bone are favorably controlled to minimize bone degradation and prevent failures. A pilot tailoring system is developed and the feasibility of the concept is elevated. The optimization system is expected to provide the means for improving knee prosthesis and individual implant tailoring for each patient. Author

MAN/SYSTEM TECHNOLOGY AND LIFE SUPPORT

Includes human engineering; biotechnology; and space suits and protective clothing.

N91-20630*# Space Station Engineering and Integration Contractor, North Olmsted, OH.

AN ASSESSMENT OF THE SPACE STATION FREEDOM PROGRAM'S LEAKAGE CURRENT REQUIREMENT Final Report

MICHAEL NAGY Mar. 1991 16 p Prepared for NASA, Lewis Research Center, Cleveland, OH
 (Contract NASW-4300; RTOP 474-17-10)
 (NASA-CR-187077; NAS 1.26:187077; PSL-450-RP91-003A)
 Avail: NTIS HC/MF A03 CSCL 06/11

60 COMPUTER OPERATIONS AND HARDWARE

The Space Station Freedom Program requires leakage currents to be limited to less than human perception level, which NASA presently defines as 5 mA for dc. The origin of this value is traced, and the literature for other dc perception threshold standards is surveyed. It is shown that while many varying standards exist, very little experimental data is available to support them. Author

MATHEMATICAL AND COMPUTER SCIENCES (GENERAL)

N91-24745*# National Aeronautics and Space Administration. Lewis Research Center, Cleveland, OH.

PARALLEL COMPUTING USING A LAGRANGIAN FORMULATION

MAY-FUN LIOU and CHING YUEN LOH 1991 20 p Presented at the Parallel CFD Conference, Stuttgart, Fed. Republic of Germany, 10-12 Jun. 1991; sponsored by NASA, CONVEX, CRAY, debis, GAMNI-SMAI, IBM, INTEL, nCUBE, SIEMENS-NIXDORF, and Thinking Machines
 (Contract RTOP 505-62-52)
 (NASA-TM-104446; E-6286; NAS 1.15:104446) Avail: NTIS HC/MF A03 CSCL 12/1

A new Lagrangian formulation of the Euler equation is adopted for the calculation of 2-D supersonic steady flow. The Lagrangian formulation represents the inherent parallelism of the flow field better than the common Eulerian formulation and offers a competitive alternative on parallel computers. The implementation of the Lagrangian formulation on the Thinking Machines Corporation CM-2 Computer is described. The program uses a finite volume, first-order Godunov scheme and exhibits high accuracy in dealing with multidimensional discontinuities (slip-line and shock). By using this formulation, a better than six times speed-up was achieved on a 8192-processor CM-2 over a single processor of a CRAY-2. Author

COMPUTER OPERATIONS AND HARDWARE

Includes hardware for computer graphics, firmware, and data processing.

A91-35928*# National Aeronautics and Space Administration. Lewis Research Center, Cleveland, OH.

GENERAL-PURPOSE INTERFACE BUS FOR MULTIUSER, MULTITASKING COMPUTER SYSTEM

EDWARD R. GENERAZIO, DON J. ROTH (NASA, Lewis Research Center, Cleveland, OH), and DAVID B. STANG (NASA, Lewis Research Center; Sverdrup Technology, Inc., Cleveland, OH) Materials Evaluation (ISSN 0025-5327), vol. 48, Nov. 1990, p. 1406-1409. refs

The architecture of a multiuser, multitasking, virtual-memory computer system intended for the use by a medium-size research group is described. There are three central processing units (CPU) in the configuration, each with 16 MB memory, and two 474 MB hard disks attached. CPU 1 is designed for data analysis and contains an array processor for fast-Fourier transformations. In addition, CPU 1 shares display images viewed with the image processor. CPU 2 is designed for image analysis and display. CPU 3 is designed for data acquisition and contains 8 GPIB channels and an analog-to-digital conversion input/output interface with 16 channels. Up to 9 users can access the third CPU

61 COMPUTER PROGRAMMING AND SOFTWARE

simultaneously for data acquisition. Focus is placed on the optimization of hardware interfaces and software, facilitating instrument control, data acquisition, and processing. V.T.

61

COMPUTER PROGRAMMING AND SOFTWARE

Includes computer programs, routines, and algorithms, and specific applications, e.g., CAD/CAM.

A91-11819* Clarkson Univ., Potsdam, NY.

COMPOSITE STRUCTURE GLOBAL FRACTURE TOUGHNESS VIA COMPUTATIONAL SIMULATION

L. MINNETYAN (Clarkson University, Potsdam, NY), P. L. N. MURTHY, and C. C. CHAMIS (NASA, Lewis Research Center, Cleveland, OH) (George Washington University, University of Virginia, and NASA, Symposium on Computational Technology for Flight Vehicles, Washington, DC, Nov. 5-7, 1990) Computers and Structures (ISSN 0045-7949), vol. 37, no. 2, 1990, p. 175-180. refs

Copyright

A computational method for the simulation of damage and fracture propagation in laminated composites is presented. A quantitative evaluation of the global fracture toughness of composites is shown as a tool for monitoring the fracture stability of composites under sustained loading. Changes in overall structural properties such as natural frequencies and the fundamental buckling load are also computed with increasing load-induced damage. Structural degradation, delamination, fracture, and damage propagation are included in the simulation. An angle-ply composite plate structure subjected to inplane tensile loading is used as an example to demonstrate some of the feature of the computational method. Author

A91-56538* National Aeronautics and Space Administration. Lewis Research Center, Cleveland, OH.

AUTOMATION SOFTWARE FOR A MATERIALS TESTING LABORATORY

MICHAEL A. MCGAW (NASA, Lewis Research Center, Cleveland, OH) and PETER J. BONACUSE (NASA, Lewis Research Center; U.S. Army, Propulsion Directorate, Cleveland, OH) IN: Applications of automation technology to fatigue and fracture testing; Proceedings of the Symposium, Kansas City, MO, May 22, 23, 1989. Philadelphia, PA, American Society for Testing and Materials, 1990, p. 211-231. refs

Copyright

The software environment in use at the NASA-Lewis Research Center's High Temperature Fatigue and Structures Laboratory is reviewed. This software environment is aimed at supporting the tasks involved in performing materials behavior research. The features and capabilities of the approach to specifying a materials test include static and dynamic control mode switching, enabling multimode test control; dynamic alteration of the control waveform based upon events occurring in the response variables; precise control over the nature of both command waveform generation and data acquisition; and the nesting of waveform/data acquisition strategies so that material history dependencies may be explored. To eliminate repetitive tasks in the conventional research process, a communications network software system is established which provides file interchange and remote console capabilities. O.G.

N91-12215*# National Aeronautics and Space Administration. Lewis Research Center, Cleveland, OH.

SHARED DIRECT MEMORY ACCESS ON THE EXPLORER 2-LX

JEFFREY L. MUSGRAVE Sep. 1990 46 p

(Contract RTOP 582-01-11)

(NASA-TM-103289; E-5747; NAS 1.15:103289) Avail: NTIS HC/MF A03 CSCL 09/2

Advances in Expert System technology and Artificial Intelligence have provided a framework for applying automated Intelligence to the solution of problems which were generally perceived as intractable using more classical approaches. As a result, hybrid architectures and parallel processing capability have become more common in computing environments. The Texas Instruments Explorer II-LX is an example of a machine which combines a symbolic processing environment, and a computationally oriented environment in a single chassis for integrated problem solutions. This user's manual is an attempt to make these capabilities more accessible to a wider range of engineers and programmers with problems well suited to solution in such an environment. Author

N91-20748*# National Aeronautics and Space Administration. Lewis Research Center, Cleveland, OH.

EFFICIENT COMPUTATION OF AERODYNAMIC INFLUENCE COEFFICIENTS FOR AEROELASTIC ANALYSIS ON A TRANSPUTER NETWORK

DAVID C. JANETZKE and DURBHA V. MURTHY (Toledo Univ., OH.) 1991 32 p Presented at the Symposium on Parallel Methods on Large-Scale Structural Analysis and Physics Applications, Hampton, VA, 5-6 Feb. 1991; sponsored by NASA. Langley and AFWL

(Contract RTOP 505-63-5B)

(NASA-TM-103671; E-5883; NAS 1.15:103671) Avail: NTIS

HC/MF A03 CSCL 09/2

Aeroelastic analysis is multi-disciplinary and computationally expensive. Hence, it can greatly benefit from parallel processing. As part of an effort to develop an aeroelastic capability on a distributed memory transputer network, a parallel algorithm for the computation of aerodynamic influence coefficients is implemented on a network of 32 transputers. The aerodynamic influence coefficients are calculated using a 3-D unsteady aerodynamic model and a parallel discretization. Efficiencies up to 85 percent were demonstrated using 32 processors. The effect of subtask ordering, problem size, and network topology are presented. A comparison to results on a shared memory computer indicates that higher speedup is achieved on the distributed memory system. Author

N91-20765*# National Aeronautics and Space Administration. Lewis Research Center, Cleveland, OH.

ALPS: A LINEAR PROGRAM SOLVER

DONALD C. FERENCZ (Case Western Reserve Univ., Cleveland, OH.) and LARRY A. VITERNA Apr. 1991 92 p

(Contract RTOP 474-12-10)

(NASA-TM-104347; E-6122; NAS 1.15:104347) Avail: NTIS

HC/MF A05 CSCL 09/2

ALPS is a computer program which can be used to solve general linear program (optimization) problems. ALPS was designed for those who have minimal linear programming (LP) knowledge and features a menu-driven scheme to guide the user through the process of creating and solving LP formulations. Once created, the problems can be edited and stored in standard DOS ASCII files to provide portability to various word processors or even other linear programming packages. Unlike many math-oriented LP solvers, ALPS contains an LP parser that reads through the LP formulation and reports several types of errors to the user. ALPS provides a large amount of solution data which is often useful in problem solving. In addition to pure linear programs, ALPS can solve for integer, mixed integer, and binary type problems. Pure linear programs are solved with the revised simplex method. Integer or mixed integer programs are solved initially with the revised simplex, and the completed using the branch-and-bound technique. Binary programs are solved with the method of implicit enumeration. This manual describes how to use ALPS to create, edit, and solve linear programming problems. Instructions for installing ALPS on a PC compatible computer are included in the appendices along with a general introduction to linear programming. A programmers guide is also included for assistance in modifying and maintaining the program. Author

N91-22766* # National Aeronautics and Space Administration. Lewis Research Center, Cleveland, OH.

RSM 1.0 USER'S GUIDE: A RESUPPLY SCHEDULER USING INTEGER OPTIMIZATION

LARRY A. VITERNA, ROBERT D. GREEN, and DAVID M. REED (Wittenberg Univ., Springfield, OH.) May 1991 43 p (Contract RTOP 474-12-10) (NASA-TM-104380; E-6185; NAS 1.15:104380) Avail: NTIS HC/MF A03 CSCL 09/2

The Resupply Scheduling Model (RSM) is a PC based, fully menu-driven computer program. It uses integer programming techniques to determine an optimum schedule to replace components on or before a fixed replacement period, subject to user defined constraints such as transportation mass and volume limits or available repair crew time. Principal input for RSJ includes properties such as mass and volume and an assembly sequence. Resource constraints are entered for each period corresponding to the component properties. Though written to analyze the electrical power system on the Space Station Freedom, RSM is quite general and can be used to model the resupply of almost any system subject to user defined resource constraints. Presented here is a step by step procedure for preparing the input, performing the analysis, and interpreting the results. Instructions for installing the program and information on the algorithms are given. Author

N91-24787* # National Aeronautics and Space Administration. Lewis Research Center, Cleveland, OH.

THE DEVELOPMENT OF A POST-TEST DIAGNOSTIC SYSTEM FOR ROCKET ENGINES

JUNE F. ZAKRAJSEK 1991 13 p Presented at the 27th Joint Propulsion Conference, Sacramento, CA, 24-27 Jun. 1991; cosponsored by AIAA, SAE, ASME, and the American Society for Electrical Engineers (Contract RTOP 590-21-41) (NASA-TM-104463; E-6304; NAS 1.15:104463; AIAA PAPER 91-2528) Avail: NTIS HC/MF A03 CSCL 09/2

An effort was undertaken by NASA to develop an automated post-test, post-flight diagnostic system for rocket engines. The automated system is designed to be generic and to automate the rocket engine data review process. A modular, distributed architecture with a generic software core was chosen to meet the design requirements. The diagnostic system is initially being applied to the Space Shuttle Main Engine data review process. The system modules currently under development are the session/message manager, and portions of the applications section, the component analysis section, and the intelligent knowledge server. An overview is presented of a rocket engine data review process, the design requirements and guidelines, the architecture and modules, and the projected benefits of the automated diagnostic system. Author

N91-25630* # National Aeronautics and Space Administration. Lewis Research Center, Cleveland, OH.

GRID3D-V2: AN UPDATED VERSION OF THE GRID2D/3D COMPUTER PROGRAM FOR GENERATING GRID SYSTEMS IN COMPLEX-SHAPED THREE-DIMENSIONAL SPATIAL DOMAINS

E. STEINTHORSSON, T. I.P. SHIH (Carnegie-Mellon Univ., Pittsburgh, PA.), and R. J. ROELKE Jun. 1991 111 p (Contract RTOP 535-05-10) (NASA-TM-103766; E-6028; NAS 1.15:103766) Avail: NTIS HC/MF A06 CSCL 09/2

In order to generate good quality systems for complicated three-dimensional spatial domains, the grid-generation method used must be able to exert rather precise controls over grid-point distributions. Several techniques are presented that enhance control of grid-point distribution for a class of algebraic grid-generation methods known as the two-, four-, and six-boundary methods. These techniques include variable stretching functions from bilinear interpolation, interpolating functions based on tension splines, and normalized K-factors. The techniques developed in this study were incorporated into a new version of GRID3D called GRID3D-v2. The usefulness of GRID3D-v2 was demonstrated by

using it to generate a three-dimensional grid system in the coolant passage of a radial turbine blade with serpentine channels and pin fins. Author

N91-25680* # National Aeronautics and Space Administration. Lewis Research Center, Cleveland, OH.

AN AUTONOMOUS FAULT DETECTION, ISOLATION, AND RECOVERY SYSTEM FOR A 20-KHZ ELECTRIC POWER DISTRIBUTION TEST BED

TODD M. QUINN (Sverdrup Technology, Inc., Brook Park, OH.) and JERRY L. WALTERS Jun. 1991 18 p (Contract NAS3-25266; RTOP 505-12-33) (NASA-TM-104344; E-6118; NAS 1.15:104344) Avail: NTIS HC/MF A03 CSCL 09/2

Future space explorations will require long term human presence in space. Space environments that provide working and living quarters for manned missions are becoming increasingly larger and more sophisticated. Monitor and control of the space environment subsystems by expert system software, which emulate human reasoning processes, could maintain the health of the subsystems and help reduce the human workload. The autonomous power expert (APEX) system was developed to emulate a human expert's reasoning processes used to diagnose fault conditions in the domain of space power distribution. APEX is a fault detection, isolation, and recovery (FDIR) system, capable of autonomous monitoring and control of the power distribution system. APEX consists of a knowledge base, a data base, an inference engine, and various support and interface software. APEX provides the user with an easy-to-use interactive interface. When a fault is detected, APEX will inform the user of the detection. The user can direct APEX to isolate the probable cause of the fault. Once a fault has been isolated, the user can ask APEX to justify its fault isolation and to recommend actions to correct the fault. APEX implementation and capabilities are discussed. Author

N91-32806* # National Aeronautics and Space Administration. Lewis Research Center, Cleveland, OH.

CRAY PERFORMANCE DATA FROM FIVE BENCHMARKS

JAMES A. PENNLINE Sep. 1991 23 p (NASA-TM-105200; E-6503; NAS 1.15:105200) Avail: NTIS HC/MF A03 CSCL 09/2

The five benchmark programs discussed in TM-88956, February 1987, were run on the CRAY X-MP/24 under different operating systems and compilers. Performance data is reported for runs under early versions of UNICOS and CFT77. The most recent data includes a system of configuration for a X-MP hardware upgrade. Performance figures for the Y-MP are shown for comparison. Differences in the figures are analyzed and discussed. Author

COMPUTER SYSTEMS

Includes computer networks and special application computer systems.

A91-56129* National Aeronautics and Space Administration. Lewis Research Center, Cleveland, OH.

ENHANCING AEROPROPULSION RESEARCH WITH HIGH-SPEED INTERACTIVE COMPUTING

JOHN R. SZUCH, DALE J. ARPASI, and ANTHONY J. STRAZISAR (NASA, Lewis Research Center, Cleveland, OH) IN: International Symposium on Air Breathing Engines, 10th, Nottingham, England, Sept. 1-6, 1991, Proceedings. Vol. 1. Washington, DC, American Institute of Aeronautics and Astronautics, 1991, p. 286-298. Previously announced in STAR as N91-24796. refs Copyright

NASA-Lewis has committed to a long range goal of creating a numerical test cell for aeropropulsion research and development.

62 COMPUTER SYSTEMS

Efforts are underway to develop a first generation Numerical Propulsion System Simulation (NPSS). The NPSS will provide a unique capability to numerically simulate advanced propulsion systems from nose to tail. Two essential ingredients to the NPSS are: (1) experimentally validated Computational Fluid Dynamics (CFD) codes; and (2) high performing computing systems (hardware and software) that will permit those codes to be used efficiently. To this end, NASA-Lewis is using high speed, interactive computing as a means for achieving Integrated CFD and Experiments (ICE). The development is described of a prototype ICE system for multistage compressor flow physics research. Author

N91-24796* National Aeronautics and Space Administration. Lewis Research Center, Cleveland, OH.

ENHANCING AEROPROPULSION RESEARCH WITH HIGH-SPEED INTERACTIVE COMPUTING

JOHN R. SZUCH, DALE J. ARPASI, and ANTHONY J. STRAZISAR 1991 18 p Presented at the 10th International Symposium on Air Breathing Engines, Nottingham, England, 1-6 Sep. 1991; sponsored by AIAA (Contract RTOP 505-10-03) (NASA-TM-104374; E-6179; NAS 1.15:104374) Avail: NTIS HC/MF A03 CSCL 09/2

NASA-Lewis has committed to a long range goal of creating a numerical test cell for aeropropulsion research and development. Efforts are underway to develop a first generation Numerical Propulsion System Simulation (NPSS). The NPSS will provide a unique capability to numerically simulate advanced propulsion systems from nose to tail. Two essential ingredients to the NPSS are: (1) experimentally validated Computational Fluid Dynamics (CFD) codes; and (2) high performing computing systems (hardware and software) that will permit those codes to be used efficiently. To this end, NASA-Lewis is using high speed, interactive computing as a means for achieving Integrated CFD and Experiments (ICE). The development is described of a prototype ICE system for multistage compressor flow physics research. Author

N91-28776* National Aeronautics and Space Administration. Lewis Research Center, Cleveland, OH.

DESCRIPTION OF REAL-TIME ADA SOFTWARE IMPLEMENTATION OF A POWER SYSTEM MONITOR FOR THE SPACE STATION FREEDOM PMAD DC TESTBED

KIMBERLY LUDWIG (Sverdrup Technology, Inc., Brook Park, OH.), MICHAEL MACKIN, and THEODORE WRIGHT 1991 8 p Presented at the 26th Intersociety Energy Conversion Engineering Conference, Boston, MA, 4-9 Aug. 1991; cosponsored by ANS, SAE, ACS, AIAA, ASME, IEEE, and AICHE (Contract RTOP 474-42-10) (NASA-TM-105157; E-6444; NAS 1.15:105157) Avail: NTIS HC/MF A02 CSCL 09/2

The Ada language software development to perform the electrical system monitoring functions for the NASA Lewis Research Center's Power Management and Distribution (PMAD) DC testbed is described. The results of the effort to implement this monitor are presented. The PMAD DC testbed is a reduced-scale prototype of the electrical power system to be used in the Space Station Freedom. The power is controlled by smart switches known as power control components (or switchgear). The power control components are currently coordinated by five Compaq 382/20e computers connected through an 802.4 local area network. One of these computers is designated as the control node with the other four acting as subsidiary controllers. The subsidiary controllers are connected to the power control components with a Mil-Std-1553 network. An operator interface is supplied by adding a sixth computer. The power system monitor algorithm is comprised of several functions including: periodic data acquisition, data smoothing, system performance analysis, and status reporting. Data is collected from the switchgear sensors every 100 milliseconds, then passed through a 2 Hz digital filter. System performance analysis includes power interruption and overcurrent detection. The reporting mechanism notifies an operator of any abnormalities in the system. Once per second, the system monitor provides data to the control node for further processing, such as state estimation.

The system monitor required a hardware time interrupt to activate the data acquisition function. The execution time of the code was optimized using an assembly language routine. The routine allows direct vectoring of the processor to Ada language procedures that perform periodic control activities. A summary of the advantages and side effects of this technique are discussed. Author

63

CYBERNETICS

Includes feedback and control theory, artificial intelligence, robotics and expert systems.

A91-26925* National Aeronautics and Space Administration. Lewis Research Center, Cleveland, OH.

AN INTELLIGENT CONTROL SYSTEM FOR ROCKET ENGINES - NEED, VISION, AND ISSUES

CARL F. LORENZO and WALTER C. MERRILL (NASA, Lewis Research Center, Cleveland, OH) IEEE Control Systems Magazine (ISSN 0272-1708), vol. 11, Jan. 1991, p. 42-46. refs Copyright

Several components of intelligence are defined. Within the context of these definitions an intelligent control system for rocket engines is described. The description includes a framework for development of an intelligent control system, including diagnostics, coordination, and direct control. Some current results and issues are presented. I.E.

A91-29181* National Aeronautics and Space Administration. Lewis Research Center, Cleveland, OH.

NEURAL NETWORK ARCHITECTURE FOR CROSSBAR SWITCH CONTROL

TERRY P. TROUDET (NASA, Lewis Research Center; Sverdrup Technology, Inc., Cleveland, OH) and STEPHEN M. WALTERS (Bell Communications Research, Inc., Red Bank, NJ) IEEE Transactions on Circuits and Systems (ISSN 0098-4094), vol. 38, Jan. 1991, p. 42-56. refs Copyright

A Hopfield neural network architecture for the real-time control of a crossbar switch for switching packets at maximum throughput is proposed. The network performance and processing time are derived from a numerical simulation of the transitions of the neural network. A method is proposed to optimize electronic component parameters and synaptic connections, and it is fully illustrated by the computer simulation of a VLSI implementation of 4 x 4 neural net controller. The extension to larger size crossbars is demonstrated through the simulation of an 8 x 8 crossbar switch controller, where the performance of the neural computation is discussed in relation to electronic noise and inhomogeneities of network components. I.E.

A91-29183* Bell Communications Research, Inc., Red Bank, NJ.

A NEURAL NET BASED ARCHITECTURE FOR THE SEGMENTATION OF MIXED GRAY-LEVEL AND BINARY PICTURES

ALI TABATABAI (Bell Communications Research, Inc., Red Bank, NJ) and TERRY P. TROUDET (NASA, Lewis Research Center; Sverdrup Technology, Inc., Cleveland, OH) IEEE Transactions on Circuits and Systems (ISSN 0098-4094), vol. 38, Jan. 1991, p. 66-77. refs Copyright

A neural-net-based architecture is proposed to perform segmentation in real time for mixed gray-level and binary pictures. In this approach, the composite picture is divided into 16 x 16 pixel blocks, which are identified as character blocks or image blocks on the basis of a dichotomy measure computed by an adaptive 16 x 16 neural net. For compression purposes, each image block is further divided into 4 x 4 subblocks; a one-bit

nonparametric quantizer is used to encode 16 x 16 character and 4 x 4 image blocks; and the binary map and quantizer levels are obtained through a neural net segmentor over each block. The efficiency of the neural segmentation in terms of computational speed, data compression, and quality of the compressed picture is demonstrated. The effect of weight quantization is also discussed. VLSI implementations of such adaptive neural nets in CMOS technology are described and simulated in real time for a maximum block size of 256 pixels. I.E.

A91-29784* National Aeronautics and Space Administration. Lewis Research Center, Cleveland, OH.

ROBUST EIGENSPACE ASSIGNMENT USING SINGULAR VALUE SENSITIVITIES

SANJAY GARG (NASA, Lewis Research Center; Sverdrup Technology, Inc., Cleveland, OH) (1989 American Control Conference, 8th, Pittsburgh, PA, June 21-23, 1989, Proceedings. Volume 1, p. 148-158) Journal of Guidance, Control, and Dynamics (ISSN 0731-5090), vol. 14, Mar.-Apr. 1991, p. 416-424. Previously cited in issue 24, p. 3869, Accession no. A89-53958. refs Copyright

A91-30043* Akron Univ., OH.

PARTITIONING METHODS FOR GLOBAL CONTROLLERS

PHILLIP SCHMIDT (Akron, University, OH), SANJAY GARG (Sverdrup Technology, Inc., Cleveland, OH), and CARL LORENZO (NASA, Lewis Research Center, Cleveland, OH) IN: 1990 American Control Conference, 9th, San Diego, CA, May 23-25, 1990, Proceedings. Vol. 1. Piscataway, NJ, Institute of Electrical and Electronics Engineers, 1990, p. 167, 168. refs Copyright

A procedure for partitioning a global (centralized) controller into interconnected decentralized subcontrollers is presented. It is shown that the controller partitioning problem is different than controller order reduction. An example is presented to demonstrate a procedure wherein an integrated flight/propulsion controller is partitioned into separate airframe and engine subcontrollers. Results show that the assembled partitioned subcontrollers closely match the response of the centralized controller in the frequency domain. I.E.

A91-30171* National Aeronautics and Space Administration. Lewis Research Center, Cleveland, OH.

AN EXPERT SYSTEM TO PERFORM ON-LINE CONTROLLER TUNING

JONATHAN LITT (NASA, Lewis Research Center; U.S. Army, Propulsion Directorate, Cleveland, OH) IN: 1990 American Control Conference, 9th, San Diego, CA, May 23-25, 1990, Proceedings. Vol. 2. Piscataway, NJ, Institute of Electrical and Electronics Engineers, 1990, p. 1968-1973. Previously announced in STAR as N90-23991. refs Copyright

An expert system which tunes a proportional-integral-derivative (PID) controller online for a single-input-single-output multiple-lag process with dead time is described. The expert system examines features of the previous transient responses and their corresponding sets of controller parameters. It determines a new set of controller gains to obtain a more desirable time response. This technique can be used to determine and implement a different set of PID gains for each operating regime and, once in steady state, the system can be used to find optimal parameters for load disturbance rejection. The expert system can be applied to any system of the specified form (aerospace, industrial, etc.) and can be expanded to include additional process models. Author

A91-37975* National Aeronautics and Space Administration. Lewis Research Center, Cleveland, OH.

AUTOMATING SECURITY MONITORING AND ANALYSIS FOR SPACE STATION FREEDOM'S ELECTRIC POWER SYSTEM

JAMES L. DOLCE (NASA, Lewis Research Center, Cleveland, OH), DEJAN J. SOBAJIC, and YOH-HAN PAO (Case Western Reserve University, Cleveland, OH) IN: IECEC-90; Proceedings of the 25th Intersociety Energy Conversion Engineering Conference,

Reno, NV, Aug. 12-17, 1990. Vol. 1. New York, American Institute of Chemical Engineers, 1990, p. 296-303. Previously announced in STAR as N90-22324. refs Copyright

Operating a large, space power system requires classifying the system's status and analyzing its security. Conventional algorithms are used by terrestrial electric utilities to provide such information to their dispatchers, but their application aboard Space Station Freedom will consume too much processing time. A novel approach for monitoring and analysis using adaptive pattern techniques is presented. This approach yields an on-line security monitoring and analysis algorithm that is accurate and fast; and thus, it can free the Space Station Freedom's power control computers for other tasks. Author

A91-37976* National Aeronautics and Space Administration. Lewis Research Center, Cleveland, OH.

ELECTRIC POWER SCHEDULING - A DISTRIBUTED PROBLEM-SOLVING APPROACH

PAMELA A. MELLOR, JAMES L. DOLCE (NASA, Lewis Research Center, Cleveland, OH), and JOSEPH C. KRUPP (Decision Science Applications, Inc., Arlington, VA) IN: IECEC-90; Proceedings of the 25th Intersociety Energy Conversion Engineering Conference, Reno, NV, Aug. 12-17, 1990. Vol. 1. New York, American Institute of Chemical Engineers, 1990, p. 304-309. Previously announced in STAR as N90-22323. refs Copyright

Space Station Freedom's power system, along with the spacecraft's other subsystems, needs to carefully conserve its resources and yet strive to maximize overall Station productivity. Due to Freedom's distributed design, each subsystem must work cooperatively within the Station community. There is a need for a scheduling tool which will preserve this distributed structure, allow each subsystem the latitude to satisfy its own constraints, and preserve individual value systems while maintaining Station-wide integrity. Author

A91-53201* Sverdrup Technology, Inc., Brook Park, OH. **NEUROMORPHIC LEARNING OF CONTINUOUS-VALUED MAPPINGS FROM NOISE-CORRUPTED DATA**

T. TROUDET (Sverdrup Technology, Inc., Brook Park, OH) and W. MERRILL (NASA, Lewis Research Center, Cleveland, OH) IEEE Transactions on Neural Networks (ISSN 1045-9227), vol. 2, March 1991, p. 294-301. refs Copyright

The effect of noise on the learning performance of the backpropagation algorithm is analyzed. A selective sampling of the training set is proposed to maximize the learning of control laws by backpropagation, when the data have been corrupted by noise. The training scheme is applied to the nonlinear control of a cart-pole system in the presence of noise. The neural computation provides the neurocontroller with good noise-filtering properties. In the presence of plant noise, the neurocontroller is found to be more stable than the teacher. A novel perspective on the application of neural network technology to control engineering is presented. I.E.

N91-19766* National Aeronautics and Space Administration. Lewis Research Center, Cleveland, OH.

TOWARDS PRACTICAL CONTROL DESIGN USING NEURAL COMPUTATION

TERRY TROUDET, SANJAY GARG, DUANE MATTERN (Sverdrup Technology, Inc., Brook Park, OH.), and WALTER MERRILL 1991 9 p Proposed for presentation at the International Joint Conference on Neural Networks, Seattle, WA, 8-12 Jul. 1991; cosponsored by IEEE and International Neural Network Society (Contract RTOP 582-01-11) (NASA-TM-103785; E-6061; NAS 1.15:103785) Avail: NTIS HC/MF A02 CSCL 09/2

The objective is to develop neural network based control design techniques which address the issue of performance/control effort tradeoff. Additionally, the control design needs to address the important issue of achieving adequate performance in the presence

63 CYBERNETICS

of actuator nonlinearities such as position and rate limits. These issues are discussed using the example of aircraft flight control. Given a set of pilot input commands, a feedforward net is trained to control the vehicle within the constraints imposed by the actuators. This is achieved by minimizing an objective function which is the sum of the tracking errors, control input rates and control input deflections. A tradeoff between tracking performance and control smoothness is obtained by varying, adaptively, the weights of the objective function. The neurocontroller performance is evaluated in the presence of actuator dynamics using a simulation of the vehicle. Appropriate selection of the different weights in the objective function resulted in the good tracking of the pilot commands and smooth neurocontrol. An extension of the neurocontroller design approach is proposed to enhance its practicality. Author

N91-22788*# National Aeronautics and Space Administration. Lewis Research Center, Cleveland, OH.

TECHNIQUES AND IMPLEMENTATION OF THE EMBEDDED RULE-BASED EXPERT SYSTEM USING ADA

EUGENE M. LIBERMAN (Sverdrup Technology, Inc., Brook Park, OH.) and ROBERT E. JONES / In NASA. Goddard Space Flight Center, The 1991 Goddard Conference on Space Applications of Artificial Intelligence p 249-255 May 1991
Avail: NTIS HC/MF A16 CSCL 09/2

Ada is becoming an increasingly popular programming language for large Government-funded software projects. Ada with its portability, transportability, and maintainability lends itself well to today's complex programming environment. In addition, expert systems have also assured a growing role in providing human-like reasoning capability and expertise for computer systems. The integration of expert system technology with Ada programming language, specifically a rule-based expert system using an ART-Ada (Automated Reasoning Tool for Ada) system shell is discussed. The NASA Lewis Research Center was chosen as a beta test site for ART-Ada. The test was conducted by implementing the existing Autonomous Power EXpert System (APEX), a Lisp-base power expert system, in ART-Ada. Three components, the rule-based expert system, a graphics user interface, and communications software make up SMART-Ada (Systems fault Management with ART-Ada). The main objective, to conduct a beta test on the ART-Ada rule-based expert system shell, was achieved. The system is operational. New Ada tools will assist in future successful projects. ART-Ada is one such tool and is a viable alternative to the straight Ada code when an application requires a rule-based or knowledge-based approach. B.G.

N91-24815*# National Aeronautics and Space Administration. Lewis Research Center, Cleveland, OH.

SENSOR FAILURE DETECTION AND RECOVERY BY NEURAL NETWORKS

TEN-HUEI GUO and J. NURRE (Ohio Univ., Athens.) 1991 8 p Presented at the International Joint Conference on Neural Networks, Seattle, WA, 8-12 Jul. 1991; sponsored by the International Neural Network Society and IEEE
(Contract RTOP 505-62-50)
(NASA-TM-104484; E-6330; NAS 1.15:104484) Avail: NTIS HC/MF A02 CSCL 09/2

A new method of sensor failure detection, isolation, and accommodation is described using a neural network approach. In a propulsion system such as the Space Shuttle Main Engine, the dynamics are usually much higher than the order of the system. This built-in redundancy of the sensors can be utilized to detect and correct sensor failure problems. The goal of the proposed scheme is to train a neural network to identify the sensor whose measurement is not consistent with other sensor outputs. Another neural network is trained to recover the value of critical variables when their measurements fail. Techniques for training the network with a limited amount of data are developed. The proposed scheme is tested using the simulated data of the Space Shuttle Main Engine (SSME) inflight sensor group. Author

N91-25696*# National Aeronautics and Space Administration. Lewis Research Center, Cleveland, OH.

A DISTRIBUTED FAULT-DETECTION AND DIAGNOSIS SYSTEM USING ON-LINE PARAMETER ESTIMATION

T.-H. GUO, W. MERRILL, and A. DUYAR (Florida Atlantic Univ., Boca Raton.) 1991 8 p Presented at the International Symposium on Distributed Intelligence Systems, Arlington, VA, 13-15 Aug. 1991; sponsored by the International Federation of Automatic Control Technical Committee on Systems Engineering
(Contract RTOP 582-01-41)
(NASA-TM-104433; E-6271; NAS 1.15:104433) Avail: NTIS HC/MF A02 CSCL 09/2

The development of a model-based fault-detection and diagnosis system (FDD) is reviewed. The system can be used as an integral part of an intelligent control system. It determines the faults of a system from comparison of the measurements of the system with a priori information represented by the model of the system. The method of modeling a complex system is described and a description of diagnosis models which include process faults is presented. There are three distinct classes of fault modes covered by the system performance model equation: actuator faults, sensor faults, and performance degradation. A system equation for a complete model that describes all three classes of faults is given. The strategy for detecting the fault and estimating the fault parameters using a distributed on-line parameter identification scheme is presented. A two-step approach is proposed. The first step is composed of a group of hypothesis testing modules, (HTM) in parallel processing to test each class of faults. The second step is the fault diagnosis module which checks all the information obtained from the HTM level, isolates the fault, and determines its magnitude. The proposed FDD system was demonstrated by applying it to detect actuator and sensor faults added to a simulation of the Space Shuttle Main Engine. The simulation results show that the proposed FDD system can adequately detect the faults and estimate their magnitudes. L.K.S.

N91-31876*# National Aeronautics and Space Administration. Lewis Research Center, Cleveland, OH.

TUNING MAPS FOR SETPOINT CHANGES AND LOAD DISTURBANCE UPSETS IN A THREE CAPACITY PROCESS UNDER MULTIVARIABLE CONTROL

JONATHAN S. LITT and IRA C. SMITH (Westlake High School, OH.) Aug. 1991 19 p
(Contract DA PROJ. 1L1-61102-AH-45; RTOP 505-62-0U)
(NASA-TM-104419; E-6253; NAS 1.15:104419; AVSCOM-TM-90-C-011; AD-A241469) Avail: NTIS HC/MF A03 CSCL 09/2

Tuning maps are an aid in the controller tuning process because they provide a convenient way for the plant operator to determine the consequences of adjusting different controller parameters. In this application the maps provide a graphical representation of the effect of varying the gains in the state feedback matrix on startup and load disturbance transients for a three capacity process. Nominally, the three tank system, represented in diagonal form, has a Proportional-Integral control on each loop. Cross coupling is then introduced between the loops by using non-zero off-diagonal proportional parameters. Changes in transient behavior due to setpoint and load changes are examined by varying the gains of the cross coupling terms. Author

NUMERICAL ANALYSIS

Includes iteration, difference equations, and numerical approximation.

A91-13204* National Aeronautics and Space Administration. Lewis Research Center, Cleveland, OH.

SECOND-ORDER ACCURATE NONOSCILLATORY SCHEMES FOR SCALAR CONSERVATION LAWS

HUNG T. HUYNH (NASA, Lewis Research Center, Cleveland, OH) IN: Numerical methods in laminar and turbulent flow; Proceedings of the Sixth International Conference, Swansea, Wales, July 11-15, 1989. Volume 6, Part 1. Swansea, Wales, Pineridge Press, 1989, p. 25-38. Previously announced in STAR as N89-22573. refs

Copyright

Explicit finite difference schemes for the computation of weak solutions of nonlinear scalar conservation laws is presented and analyzed. These schemes are uniformly second-order accurate and nonoscillatory in the sense that the number of extrema of the discrete solution is not increasing in time. Author

A91-31175* National Aeronautics and Space Administration. Lewis Research Center, Cleveland, OH.

PARALLEL ALGORITHMS FOR BOUNDARY VALUE PROBLEMS

AVI LIN (NASA, Lewis Research Center, Cleveland, OH; Pennsylvania, University, Philadelphia) Journal of Parallel and Distributed Computing (ISSN 0743-7315), vol. 11, April 1991, p. 284-290. Previously announced in STAR as N90-19783. refs (Contract NASA ORDER C-99066-G)

Copyright

A general approach to solve boundary value problems numerically in a parallel environment is discussed. The basic algorithm consists of two steps: the local step where all the P available processors work in parallel, and the global step where one processor solves a tridiagonal linear system of the order P. The main advantages of this approach are twofold. First, this suggested approach is very flexible, especially in the local step and thus the algorithm can be used with any number of processors and with any of the SIMD or MIMD machines. Secondly, the communication complexity is very small and thus can be used as easily with shared memory machines. Several examples for using this strategy are discussed. Author

A91-35956* National Aeronautics and Space Administration. Lewis Research Center, Cleveland, OH.

SOLUTION OF STEADY-STATE, TWO-DIMENSIONAL CONSERVATION LAWS BY MATHEMATICAL PROGRAMMING

JOHN E. LAVERY (NASA, Lewis Research Center, Cleveland, OH; U.S. Navy, Office of Naval Research, Arlington, VA) SIAM Journal on Numerical Analysis (ISSN 0036-1429), vol. 28, Feb. 1991, p. 141-155. refs

Copyright

A truly two-dimensional algorithm is created for solving the steady-state two-dimensional conservation-law problem. An overdetermined system of algebraic equations is obtained through discretization by finite-volume formulas. These equations are perturbed nonsingularly and are solved by an efficient geometrically oriented $l(1)$ procedure. The basic algorithm and the theory for the linear case $f(u) = u$ are presented, and computational results for the nonlinear case $f(u) = \text{sq } u$ are also analyzed. It is noted that the $l(1)$ procedure captures boundary shocks as well as oblique and zigzag interior shocks in bands that are one cell wide, and the solution values are accurate up to the edge of the shock. V.T.

A91-45109*# Carnegie-Mellon Univ., Pittsburgh, PA.
FLUX-VECTOR SPLITTING ALGORITHM FOR CHAIN-RULE CONSERVATION-LAW FORM

T. I.-P. SHIH (Carnegie Mellon University, Pittsburgh, PA), H. L. NGUYEN, E. A. WILLIS (NASA, Lewis Research Center, Cleveland, OH), E. STEINTHORSSON, and Z. LI AIAA Journal (ISSN 0001-1452), vol. 29, July 1991, p. 1101-1107. refs (Contract NAG3-997)

Copyright

A flux-vector splitting algorithm with Newton-Raphson iteration was developed for the 'full compressible' Navier-Stokes equations cast in chain-rule conservation-law form. The algorithm is intended for problems with deforming spatial domains and for problems whose governing equations cannot be cast in strong conservation-law form. The usefulness of the algorithm for such problems was demonstrated by applying it to analyze the unsteady, two- and three-dimensional flows inside one combustion chamber of a Wankel engine under nonfiring conditions. Solutions were obtained to examine the algorithm in terms of conservation error, robustness, and ability to handle complex flows on time-dependent grid systems. Author

N91-14781*# National Aeronautics and Space Administration. Lewis Research Center, Cleveland, OH.

MAPPINGS AND ACCURACY FOR CHEBYSHEV PSEUDO-SPECTRAL APPROXIMATIONS

ALVIN BAYLISS and ELI TURKEL (Tel-Aviv Univ., Israel) Dec. 1990 21 p

(Contract NASA ORDER C-99066-G; NSF ASC-87-19573; NSF DMS-87-01543)

(NASA-TM-103630; ICOMP-90-24; E-5798; NAS 1.15:103630)

Avail: NTIS HC/MF A03 CSCL 12/1

The effect of mappings on the approximation, by Chebyshev collocation, of functions which exhibit localized regions of rapid variation is studied. A general strategy is introduced whereby mappings are adaptively constructed which map specified classes of rapidly varying functions into low order polynomials which can be accurately approximated by Chebyshev polynomial expansions. A particular family of mappings constructed in this way is tested on a variety of rapidly varying functions similar to those occurring in approximations. It is shown that the mapped function can be approximated much more accurately by Chebyshev polynomial approximations than in physical space or where mappings constructed from other strategies are employed. Author

N91-19786*# National Aeronautics and Space Administration. Lewis Research Center, Cleveland, OH.

SPECTRUM TRANSFORMATION FOR DIVERGENT ITERATIONS

MURLI M. GUPTA (George Washington Univ., Washington, DC.) Mar. 1991 18 p

(Contract NASA ORDER C-99066-G)

(NASA-TM-103745; E-5989; ICOMP-91-02; NAS 1.15:103745)

Avail: NTIS HC/MF A03 CSCL 12/1

Certain spectrum transformation techniques are described that can be used to transform a diverging iteration into a converging one. Two techniques are considered called spectrum scaling and spectrum enveloping and how to obtain the optimum values of the transformation parameters is discussed. Numerical examples are given to show how this technique can be used to transform diverging iterations into converging ones; this technique can also be used to accelerate the convergence of otherwise convergent iterations. Author

N91-20830*# National Aeronautics and Space Administration. Lewis Research Center, Cleveland, OH.

ACCURATE MONOTONE CUBIC INTERPOLATION

HUNG T. HUYNH Mar. 1991 63 p

(Contract RTOP 505-62-52)

(NASA-TM-103789; E-6066; NAS 1.15:103789) Avail: NTIS

HC/MF A04 CSCL 12/1

Monotone piecewise cubic interpolants are simple and effective. They are generally third-order accurate, except near strict local extrema where accuracy degenerates to second-order due to the monotonicity constraint. Algorithms for piecewise cubic interpolants, which preserve monotonicity as well as uniform third and

fourth-order accuracy are presented. The gain of accuracy is obtained by relaxing the monotonicity constraint in a geometric framework in which the median function plays a crucial role.

Author

N91-21797*# National Aeronautics and Space Administration. Lewis Research Center, Cleveland, OH.

ASYMPTOTIC INTEGRATION ALGORITHMS FOR NONHOMOGENEOUS, NONLINEAR, FIRST ORDER, ORDINARY DIFFERENTIAL EQUATIONS

K. P. WALKER (Engineering Science Software, Inc., Smithfield, RI.) and A. D. FREED Mar. 1991 45 p
(Contract RTOP 553-13-00)

(NASA-TM-103793; E-6070; NAS 1.15:103793) Avail: NTIS HC/MF A03 CSCL 12/1

New methods for integrating systems of stiff, nonlinear, first order, ordinary differential equations are developed by casting the differential equations into integral form. Nonlinear recursive relations are obtained that allow the solution to a system of equations at time t plus Δt to be obtained in terms of the solution at time t in explicit and implicit forms. Examples of accuracy obtained with the new technique are given by considering systems of nonlinear, first order equations which arise in the study of unified models of viscoplastic behaviors, the spread of the AIDS virus, and predator-prey populations. In general, the new implicit algorithm is unconditionally stable, and has a Jacobian of smaller dimension than that which is acquired by current implicit methods, such as the Euler backward difference algorithm; yet, it gives superior accuracy. The asymptotic explicit and implicit algorithms are suitable for solutions that are of the growing and decaying exponential kinds, respectively, whilst the implicit Euler-Maclaurin algorithm is superior when the solution oscillates, i.e., when there are regions in which both growing and decaying exponential solutions exist.

Author

N91-22814*# National Aeronautics and Space Administration. Lewis Research Center, Cleveland, OH.

A NEW FLUX SPLITTING SCHEME

MENG-SING LIOU and CHRISTOPHER J. STEFFEN, JR. May 1991 33 p

(Contract RTOP 505-61-52)

(NASA-TM-104404; E-6227; NAS 1.15:104404) Avail: NTIS HC/MF A03 CSCL 12/1

A new flux splitting scheme is proposed. The scheme is remarkably simple and yet its accuracy rivals and in some cases surpasses that of Roe's solver in the Euler and Navier-Stokes solutions performed in this study. The scheme is robust and converges as fast as the Roe splitting. An approximately defined cell-face advection Mach number is proposed using values from the two straddling cells via associated characteristic speeds. This interface Mach number is then used to determine the upwind extrapolation for the convective quantities. Accordingly, the name of the scheme is coined as Advection Upstream Splitting Method (AUSM). A new pressure splitting is introduced which is shown to behave successfully, yielding much smoother results than other existing pressure splittings. Of particular interest is the supersonic blunt body problem in which the Roe scheme gives anomalous solutions. The AUSM produces correct solutions without difficulty for a wide range of flow conditions as well as grids.

Author

N91-24817*# National Aeronautics and Space Administration. Lewis Research Center, Cleveland, OH.

THE L SUB 1 FINITE ELEMENT METHOD FOR PURE CONVECTION PROBLEMS

BO-NAN JIANG Apr. 1991 28 p Prepared in cooperation with Computational Physics System, Ann Arbor, MI

(Contract NASA ORDER C-99066-G)

(NASA-TM-103773; E-6039; ICOMP-91-03; NAS 1.15:103773)

Avail: NTIS HC/MF A03 CSCL 12/1

The least squares (L sub 2) finite element method is introduced for 2-D steady state pure convection problems with smooth solutions. It is proven that the L sub 2 method has the same stability estimate as the original equation, i.e., the L sub 2 method

has better control of the streamline derivative. Numerical convergence rates are given to show that the L sub 2 method is almost optimal. This L sub 2 method was then used as a framework to develop an iteratively reweighted L sub 2 finite element method to obtain a least absolute residual (L sub 1) solution for problems with discontinuous solutions. This L sub 1 finite element method produces a nonoscillatory, nondiffusive and highly accurate numerical solution that has a sharp discontinuity in one element on both coarse and fine meshes. A robust reweighting strategy was also devised to obtain the L sub 1 solution in a few iterations. A number of examples solved by using triangle and bilinear elements are presented.

Author

N91-24818*# National Aeronautics and Space Administration. Lewis Research Center, Cleveland, OH.

INSTITUTE FOR COMPUTATIONAL MECHANICS IN PROPULSION (ICOMP) Annual Report No. 5, 1990

CHARLES E. FEILER, ed. May 1991 51 p

(NASA-TM-103790; ICOMP-91-01; E-6067; NAS 1.15:103790)

Avail: NTIS HC/MF A04 CSCL 12/1

The Institute for Computational Mechanics in Propulsion (ICOMP) is operated jointly by Case Western Reserve University and the NASA Lewis Research Center in Cleveland, Ohio. The purpose of ICOMP is to develop techniques to improve problem-solving capabilities in all aspects of computational mechanics related to propulsion. The activities at ICOMP during 1990 are described.

Author

N91-25739*# National Aeronautics and Space Administration. Lewis Research Center, Cleveland, OH.

HIGH-ORDER POLYNOMIAL EXPANSIONS (HOPE) FOR FLUX-VECTOR SPLITTING

MENG-SING LIOU and CHRIS J. STEFFEN, JR. 1991 7 p

Presented at the International Conference on Computational Engineering Science, Melbourne, Australia, 11-16 Aug. 1991

(NASA-TM-104452; E-6293; NAS 1.15:104452) Avail: NTIS

HC/MF A02 CSCL 12/1

The Van Leer flux splitting is known to produce excessive numerical dissipation for Navier-Stokes calculations. Researchers attempt to remedy this deficiency by introducing a higher order polynomial expansion (HOPE) for the mass flux. In addition to Van Leer's splitting, a term is introduced so that the mass diffusion error vanishes at M equals 0. Several splittings for pressure are proposed and examined. The effectiveness of the HOPE scheme is illustrated for 1-D hypersonic conical viscous flow and 2-D supersonic shock-wave boundary layer interactions. Also, the authors give the weakness of the scheme and suggest areas for further investigation.

Author

N91-27886*# National Aeronautics and Space Administration. Lewis Research Center, Cleveland, OH.

FROM DIFFERENTIAL TO DIFFERENCE EQUATIONS FOR FIRST ORDER ODES

ALAN D. FREED and KEVIN P. WALKER (Engineering Science Software, Inc., Smithfield, RI.) Jul. 1991 6 p

(Contract RTOP 553-13-00)

(NASA-TM-104530; E-6406; NAS 1.15:104530) Avail: NTIS

HC/MF A02 CSCL 12/1

When constructing an algorithm for the numerical integration of a differential equation, one should first convert the known ordinary differential equation (ODE) into an ordinary difference equation. Given this difference equation, one can develop an appropriate numerical algorithm. This technical note describes the derivation of two such ordinary difference equations applicable to a first order ODE. The implicit ordinary difference equation has the same asymptotic expansion as the ODE itself, whereas the explicit ordinary difference equation has an asymptotic that is similar in structure but different in value when compared with that of the ODE.

Author

N91-27901*# National Aeronautics and Space Administration. Lewis Research Center, Cleveland, OH.

EXPONENTIAL INTEGRATION ALGORITHMS APPLIED TO VISCOPLASTICITY

ALAN D. FREED and KEVIN P. WALKER (Engineering Science Software, Inc., Smithfield, RI.) 1991 17 p Proposed for presentation at the Third International Conference on Computational Plasticity Fundamentals and Applications (COMPLAS 3), Barcelona, Spain, 6-10 Apr. 1992; sponsored by the Centro Internacional de Metodos Numericos en Ingenieria (Contract RTOP 553-13-00) (NASA-TM-104461; E-6302; NAS 1.15:104461) Avail: NTIS HC/MF A03 CSCL 12/1

Four, linear, exponential, integration algorithms (two implicit, one explicit, and one predictor/corrector) are applied to a viscoplastic model to assess their capabilities. Viscoplasticity comprises a system of coupled, nonlinear, stiff, first order, ordinary differential equations which are a challenge to integrate by any means. Two of the algorithms (the predictor/corrector and one of the implicit) give outstanding results, even for very large time steps. Author

N91-30865*# National Aeronautics and Space Administration. Lewis Research Center, Cleveland, OH.

A COMPARISON OF NUMERICAL METHODS FOR THE RAYLEIGH EQUATION IN UNBOUNDED DOMAINS

W. W. LIU and P. J. MORRIS (Pennsylvania State Univ., University Park.) Aug. 1991 34 p (Contract NASA ORDER C-99066-G) (NASA-TM-105179; ICOMP-91-13; E-6476; NAS 1.15:105179; CMOTT-91-04) Avail: NTIS HC/MF A03 CSCL 12/1

A second-order finite difference and two spectral methods, including a Chebyshev tau and a Chebyshev collocation method were implemented to determine the linear hydrodynamic stability of an unbounded shear flow. The velocity profile of the basic flow in the stability analysis mimicks that of a one-stream free mixing layer. Local and global eigenvalue solution methods are used to determine individual eigenvalues and the eigenvalue spectrum, respectively. The calculated eigenvalue spectrum includes a discrete mode, a continuous spectrum associated with the equation singularity and a continuous spectrum associated with the domain unboundedness. The efficiency and the accuracy of these discretization methods in the prediction of the eigensolutions of the discrete mode were evaluated by comparison with a conventional shooting procedure. Their capabilities in mapping out the continuous eigenvalue spectra are also discussed. Author

N91-30867*# National Aeronautics and Space Administration. Lewis Research Center, Cleveland, OH.

A NEW NUMERICAL FRAMEWORK FOR SOLVING CONSERVATION LAWS: THE METHOD OF SPACE-TIME CONSERVATION ELEMENT AND SOLUTION ELEMENT

SIN-CHUNG CHANG and WAI-MING TO (Sverdrup Technology, Inc., Brook Park, OH.) Aug. 1991 115 p (Contract RTOP 505-62-52) (NASA-TM-104495; E-6403; NAS 1.15:104495) Avail: NTIS HC/MF A06 CSCL 12/1

A new numerical framework for solving conservation laws is being developed. It employs: (1) a nontraditional formulation of the conservation laws in which space and time are treated on the same footing, and (2) a nontraditional use of discrete variables such as numerical marching can be carried out by using a set of relations that represents both local and global flux conservation. Author

N91-31911*# National Aeronautics and Space Administration. Lewis Research Center, Cleveland, OH.

LEAST-SQUARES SOLUTION OF INCOMPRESSIBLE NAVIER-STOKES EQUATIONS WITH THE P-VERSION OF FINITE ELEMENTS

BO-NAN JIANG and VIJAY SONNAD (International Business Machines Corp., Austin, TX.) Sep. 1991 15 p

(Contract NASA ORDER C-99066-G) (NASA-TM-105203; ICOMP-91-14; E-6506; NAS 1.15:105203) Avail: NTIS HC/MF A03 CSCL 12/1

A p-version of the least squares finite element method, based on the velocity-pressure-vorticity formulation, is developed for solving steady state incompressible viscous flow problems. The resulting system of symmetric and positive definite linear equations can be solved satisfactorily with the conjugate gradient method. In conjunction with the use of rapid operator application which avoids the formation of either element or global matrices, it is possible to achieve a highly compact and efficient solution scheme for the incompressible Navier-Stokes equations. Numerical results are presented for two-dimensional flow over a backward facing step. The effectiveness of simple outflow boundary conditions is also demonstrated. Author

66

SYSTEMS ANALYSIS

Includes mathematical modeling; network analysis; and operations research.

A91-30630*# National Aeronautics and Space Administration. Lewis Research Center, Cleveland, OH.

REAL-TIME DIAGNOSTICS OF THE REUSABLE ROCKET ENGINE USING ON-LINE SYSTEM IDENTIFICATION

T.-H. GUO, W. MERRILL (NASA, Lewis Research Center, Cleveland, OH), and A. DUYAR (Florida Atlantic University, Boca Raton) IN: Annual Health Monitoring Conference for Space Propulsion Systems, 2nd, Cincinnati, OH, Nov. 14, 15, 1990, Proceedings. Cincinnati, OH, University of Cincinnati, 1990, p. 75-93. refs

A model-based failure diagnosis system has been proposed for real-time diagnosis of SSME failures. Actuation, sensor, and system degradation failure modes are all considered by the proposed system. In the case of SSME actuation failures, it was shown that real-time identification can effectively be used for failure diagnosis purposes. It is a direct approach since it reduces the detection, isolation, and the estimation of the extent of the failures to the comparison of parameter values before and after the failure. As with any model-based failure detection system, the proposed approach requires a fault model that embodies the essential characteristics of the failure process. The proposed diagnosis approach has the added advantage that it can be used as part of an intelligent control system for failure accommodation purposes. L.K.S.

N91-25749*# National Aeronautics and Space Administration. Lewis Research Center, Cleveland, OH.

DEVELOPMENT OF AN ANALYTICAL TOOL TO STUDY POWER QUALITY OF AC POWER SYSTEMS FOR LARGE SPACECRAFT

L. ALAN KRAFT (Valparaiso Univ., IN.) and M. DAVID KANKAM 1991 7 p Presented at the 26th Intersociety Energy Conversion Engineering Conference, Boston, MA, 4-9 Aug. 1991; sponsored by the American Nuclear Society, SAE, the American Chemical Society, AIAA, ASME, IEEE, and American Inst. of Chemical Engineers (Contract RTOP 506-41-41) (NASA-TM-104451; E-6292; NAS 1.15:104451) Avail: NTIS HC/MF A02 CSCL 12/2

A harmonic power flow program applicable to space power systems with sources of harmonic distortion is described. The algorithm is a modification of the Electric Power Research Institute's HARMFLO program which assumes a three phase, balanced, AC system with loads of harmonic distortion. The modified power flow program can be used with single phase, AC systems. Early results indicate that the required modifications and the models developed are quite adequate for the analysis of a 20 kHz testbed built by

66 SYSTEMS ANALYSIS

General Dynamics Corporation. This is demonstrated by the acceptable correlation of present results with published data. Although the results are not exact, the discrepancies are relatively small.
Author

N91-26870*# National Aeronautics and Space Administration. Lewis Research Center, Cleveland, OH.

COMPARATIVE SURVEY OF DYNAMIC ANALYSES OF FREE-PISTON STIRLING ENGINES

M. DAVID KANKAM and JEFFREY S. RAUCH (Sverdrup Technology, Inc., Brook Park, OH.) 1991 8 p Presented at the 26th Intersociety Energy Conversion Engineering Conference, Boston, MA, 4-9 Aug. 1991; sponsored by ANS, SAE, ACS, AIAA, ASME, IEEE, and AIChE
(Contract RTOP 590-13-11)
(NASA-TM-104491; E-6348; NAS 1.15:104491) Avail: NTIS HC/MF A02 CSCL 12/2

Reported dynamics analyses for evaluating the steady-state response and stability of free-piston Stirling engine (FPSE) systems are compared. Various analytical approaches are discussed to provide guidance on their salient features. Recommendations are made in the recommendations remarks for an approach which captures most of the inherent properties of the engine. Such an approach has the potential for yielding results which will closely match practical FPSE-load systems.
Author

70

PHYSICS (GENERAL)

A91-22894 London Univ. (England).

STRUCTURE OF RANDOM DISCRETE SPACETIME

GRAHAM BRIGHTWELL (London School of Economics and Political Science, England) and RUTH GREGORY (NASA/Fermilab Astrophysics Center, Batavia, IL) Physical Review Letters (ISSN 0031-9007), vol. 66, Jan. 21, 1991, p. 260-263. Research supported by DOE. Previously announced in STAR as N90-28429. refs
(Contract NAGW-1340)
Copyright

The usual picture of spacetime consists of a continuous manifold, together with a metric of Lorentzian signature which imposes a causal structure on the spacetime. A model, first suggested by Bombelli et al., is considered in which spacetime consists of a discrete set of points taken at random from a manifold, with only the causal structure on this set remaining. This structure constitutes a partially ordered set (or poset). Working from the poset alone, it is shown how to construct a metric on the space which closely approximates the metric on the original spacetime manifold, how to define the effective dimension of the spacetime, and how such quantities may depend on the scale of measurement. Possible desirable features of the model are discussed.
Author

N91-26872*# National Aeronautics and Space Administration. Lewis Research Center, Cleveland, OH.

A MODEL FOR THE SCATTERING OF HIGH-FREQUENCY ELECTROMAGNETIC FIELDS FROM DIELECTRICS EXHIBITING THERMALLY-ACTIVATED ELECTRICAL LOSSES

RAIFORD E. HANN May 1991 13 p
(Contract RTOP 505-62-00)
(NASA-TM-104376; E-6040-1; NAS 1.15:104376) Avail: NTIS HC/MF A03 CSCL 20/3

An equivalent circuit model (ECM) approach is used to predict the scattering behavior of temperature-activated, electrically lossy dielectric layers. The total electrical response of the dielectric (relaxation + conductive) is given by the ECM and used in combination with transmission line theory to compute reflectance spectra for a Dallenbach layer configuration. The effects of thermally-activated relaxation processes on the scattering

properties is discussed. Also, the effect of relaxation and conduction activation energy on the electrical properties of the dielectric is described.
Author

71

ACOUSTICS

Includes sound generation, transmission, and attenuation.

A91-12427*# Notre Dame Univ., IN.

ACOUSTIC RADIATION FROM LIFTING AIRFOILS IN COMPRESSIBLE SUBSONIC FLOW

HAFIZ M. ATASSI, SHANKAR SUBRAMANIAM (Notre Dame, University, IN), and JAMES R. SCOTT (NASA, Lewis Research Center, Cleveland, OH) AIAA, Aeroacoustics Conference, 13th, Tallahassee, FL, Oct. 22-24, 1990. 21 p. refs
(Contract NAG3-732)
(AIAA PAPER 90-3911) Copyright

The far field acoustic radiation from a lifting airfoil in a three-dimensional gust is studied. The acoustic pressure is calculated using the Kirchhoff method, instead of using the classical acoustic analogy approach due to Lighthill. The pressure on the Kirchhoff surface is calculated using an existing numerical solution of the unsteady flow field. The far field acoustic pressure is calculated in terms of these values using Kirchhoff's formula. The method is validated against existing semi-analytical results for a flat plate. The method is then used to study the problem of an airfoil in a harmonic three-dimensional gust, for a wide range of Mach numbers. The effect of variation of the airfoil thickness and angle of attack on the acoustic far field is studied. The changes in the mechanism of sound generation and propagation due to the presence of steady loading and non-uniform mean flow are also studied.
Author

A91-12448*# National Aeronautics and Space Administration. Lewis Research Center, Cleveland, OH.

THE EFFECT OF SWIRL RECOVERY VANES ON THE CRUISE NOISE OF AN ADVANCED PROPELLER

JAMES H. DITTMAR (NASA, Lewis Research Center, Cleveland, OH) and DAVID G. HALL (NASA, Lewis Research Center; Sverdrup Technology, Inc., Brook Park, OH) AIAA, Aeroacoustics Conference, 13th, Tallahassee, FL, Oct. 22-24, 1990. 16 p. refs
(AIAA PAPER 90-3932) Copyright

The SR-7A propeller was acoustically tested with and without downstream swirl recovery vanes to determine if any extra noise was caused by the interaction of the propeller wakes and vortices with these vanes. No additional noise was observed at the cruise condition over the angular range tested. The presence of the swirl recovery vanes did unload the propeller and some small peak noise reductions were observed from lower propeller loading noise. The propeller was also tested alone to investigate the behavior of the peak propeller noise with helical tip Mach number. As observed before on other propellers, the peak noise first rose with helical tip Mach number and then leveled off or decreased at higher helical tip Mach numbers. Detailed pressure-time histories indicate that a portion of the primary pressure pulse is progressively cancelled by a secondary pulse as the helical tip Mach number is increased. This cancellation appears to be responsible for the peak noise behavior at high helical tip Mach numbers.
Author

A91-12449*# National Aeronautics and Space Administration. Lewis Research Center, Cleveland, OH.

AEROACOUSTIC EFFECTS OF REDUCED AFT TIP SPEED AT CONSTANT THRUST FOR A MODEL COUNTERROTATION TURBOPROP AT TAKEOFF CONDITIONS

RICHARD P. WOODWARD and CHRISTOPHER E. HUGHES (NASA, Lewis Research Center, Cleveland, OH) AIAA, Aeroacoustics Conference, 13th, Tallahassee, FL, Oct. 22-24, 1990.

19 p. refs

(AIAA PAPER 90-3933) Copyright

A model high-speed, advanced counterrotation propeller, F7/A7, was tested in the NASA Lewis Research Center's 9- by 15-foot anechoic wind tunnel at simulated takeoff and approach conditions of Mach 0.2. The propeller was operated in a baseline configuration with the forward and aft rotor blade setting angles (36.2deg and 35.4 deg) and forward and aft rotational speeds essentially equal. Two additional configurations were tested with the aft rotor at increased blade setting angles and the rotational speed reduced to achieve overall performance similar to that of the baseline configuration. The aft rotor blade angles were adjusted such that the thrust and power absorption for each rotor remained the same as for the baseline configuration. Acoustic data were taken with an axially translating microphone probe that was attached to the tunnel floor. Concurrent aerodynamic data were taken to define propeller operating conditions. The aft rotor fundamental tone was about 6 dB lower with the 36.2 deg and 38.4 deg blade setting angles, and about 9 dB lower with the 36.2 and 41.4 deg blade setting angles. Predicted noise reductions based on tip speed considerations were 5 and 9.5 dB, respectively, for the two altered blade setting angles. Author

A91-12469*# Sverdrup Technology, Inc., Brook Park, OH.
NEAR-FIELD NOISE OF A SINGLE ROTATION PROPPAN AT AN ANGLE OF ATTACK

M. NALLASAMY, E. ENVIA (Sverdrup Technology, Inc., Brook Park, OH), B. J. CLARK, and J. F. GROENEWEG (NASA, Lewis Research Center, Cleveland, OH) AIAA, Aeroacoustics Conference, 13th, Tallahassee, FL, Oct. 22-24, 1990. 18 p. refs
 (AIAA PAPER 90-3953)

The near-field noise characteristics of a propfan operating at an angle of attack are examined utilizing the unsteady pressure field obtained from a three-dimensional Euler simulation of the propfan flowfield. The near-field noise is calculated employing three different procedures: a direct computation method in which the noise field is extracted directly from the Euler solution, and two acoustic-analogy-based frequency domain methods which utilize the computed unsteady pressure distribution on the propfan blades as the source term. The inflow angles considered are -0.4, 1.6, and 4.6 degrees. The results of the direct computation method and one of the frequency domain methods show qualitative agreement with measurements. They show that an increase in the inflow angle is accompanied by an increase in the sound pressure level at the outboard wing boom locations and a decrease in the sound pressure level at the (inboard) fuselage locations. The trends in the computed azimuthal directivities of the noise field also conform to the measured and expected results. Author

A91-12470*# National Aeronautics and Space Administration.
 Lewis Research Center, Cleveland, OH.

PREDICTION OF THE NOISE FROM A PROPELLER AT ANGLE OF ATTACK

EUGENE A. KREJSA (NASA, Lewis Research Center, Cleveland, OH) AIAA, Aeroacoustics Conference, 13th, Tallahassee, FL, Oct. 22-24, 1990. 20 p. refs
 (AIAA PAPER 90-3954) Copyright

An analysis is presented to predict the noise of a propeller at angle of attack. The analysis is an extension of that reported by Mani (1990) which predicted the change in noise due to angle of attack due to both unsteady loading and to azimuthal variation of the radiation efficiency of steady noise sources. Mani's analysis, however, was limited to small angles of attack. The analysis reported herein removes this small angle limitation. Results from the analysis are compared with the data of Woodward (1987, 1988), for a single rotation propeller and for a counter rotating propeller. The comparison shows that including the effect of angle of attack on the steady noise sources significantly improves the agreement with data. Including higher order effects of angle of attack, while changing the predicted noise at far forward and aft angles, has little effect near the propeller plane. Author

A91-12496*# National Aeronautics and Space Administration.
 Lewis Research Center, Cleveland, OH.

NOISE MEASUREMENTS FROM AN EJECTOR SUPPRESSOR NOZZLE IN THE NASA LEWIS 9- BY 15-FOOT LOW SPEED WIND TUNNEL

EUGENE A. KREJSA, BETH A. COOPER (NASA, Lewis Research Center, Cleveland, OH), DAVID G. HALL, and ABBAS KHAVARAN (NASA, Lewis Research Center; Sverdrup Technology, Inc., Brook Park, OH) AIAA, Aeroacoustics Conference, 13th, Tallahassee, FL, Oct. 22-24, 1990. 61 p. refs
 (AIAA PAPER 90-3983) Copyright

Acoustic results are presented on nozzle test experiments conducted in the NASA Lewis 9 x 15-ft anechoic wind tunnel on a 'hypermix' nozzle concept, a two-dimensional lobed mixer nozzle followed by a short ejector section designed to promote rapid mixing of the nozzle flow with the flow induced by the ejector. Acoustic and aerodynamic measurements were carried out to determine the amount of ejector pumping, the degree of mixing, and the noise reduction achieved. Spectra from various nozzle configurations were compared to show the effect of the nozzle geometry on nozzle-alone noise, the benefit of adding an ejector to the mixer nozzles, and the effect of the ejector geometry on ejector/suppressor noise level. I.S.

A91-12533*# National Aeronautics and Space Administration.
 Lewis Research Center, Cleveland, OH.

UNSTEADY BLADE PRESSURE MEASUREMENTS FOR THE SR-7A PROPELLER AT CRUISE CONDITIONS

L. J. HEIDELBERG (NASA, Lewis Research Center, Cleveland, OH) and M. NALLASAMY (NASA, Lewis Research Center; Sverdrup Technology, Inc., Brook Park, OH) AIAA, Aeroacoustics Conference, 13th, Tallahassee, FL, Oct. 22-24, 1990. 16 p. refs
 (AIAA PAPER 90-4022) Copyright

The unsteady blade surface pressures were measured on the SR-7A propeller. The freestream Mach number, inflow angle, and advance ratio were varied while measurements were made at nine blade stations. At a freestream Mach number of 0.8, the data in terms of unsteady pressure coefficient versus azimuth angle are compared to an unsteady three-dimensional Euler solution, yielding very encouraging results. The code predicts the shape (phase) of the waveform very well, while the magnitude is over-predicted in many cases. At tunnel Mach numbers below 0.6, an unusually large response on the suction surface at 0.15 chord and 0.88 radius was observed. The behavior of this response suggests the presence of a leading-edge vortex. Author

A91-12973* National Aeronautics and Space Administration.
 Lewis Research Center, Cleveland, OH.

SPATIAL EVOLUTION OF NONLINEAR ACOUSTIC MODE INSTABILITIES ON HYPERSONIC BOUNDARY LAYERS

M. E. GOLDSTEIN (NASA, Lewis Research Center, Cleveland, OH) and D. W. WUNDROW (NASA, Lewis Research Center; Sverdrup Technology, Inc., Cleveland, OH) Journal of Fluid Mechanics (ISSN 0022-1120), vol. 219, Oct. 1990, p. 585-607. Previously announced in STAR as N90-14517. refs
 Copyright

The effects are considered of strong critical layer nonlinearity on the spatial evolution of an initially linear acoustic mode instability wave on a hypersonic flat plate boundary layer. The analysis shows that nonlinearity, which is initially confined to a thin critical layer, first becomes important when the amplitude of the pressure fluctuations become $O(1/M \exp 4 \ln M \exp 2)$, where M is the free stream Mach number. The flow outside the critical layer is still determined by linear dynamics and therefore takes the form of a linear instability wave, but with its amplitude completely determined by the flow within the critical layer. The latter flow is determined by a coupled set of nonlinear equations, which were solved numerically. Author

A91-14650* National Aeronautics and Space Administration.
 Lewis Research Center, Cleveland, OH.

FLOW INDUCED VIBRATION AND NOISE BY A PAIR OF TANDEM CYLINDERS DUE TO BUFFETING

71 ACOUSTICS

C. M. KIM (NASA, Lewis Research Center, Cleveland; Ohio State University, Columbus) and A. T. CONLISK (Ohio State University, Columbus) *Journal of Fluids and Structures* (ISSN 0889-9746), vol. 4, Sept. 1990, p. 471-493. Research supported by the U.S. Navy. refs

Copyright

The generation of noise by vortex buffeting on a pair of cylinders in tandem in unsteady high-Reynolds-number flow is investigated analytically. The derivation of the governing equations is outlined, and numerical results for several initial vortex configurations are presented in extensive graphs and characterized in detail. Particular attention is given to the possibility of chaotic vortex motion, and it is shown that chaotic motion does not occur when there are three vortices but does appear when there are four. T.K.

A91-18257* Sverdrup Technology, Inc., Brook Park, OH.
PREDICTION OF UNSTEADY BLADE SURFACE PRESSURES ON AN ADVANCED PROPELLER AT AN ANGLE OF ATTACK
M. NALLASAMY (Sverdrup Technology, Inc., Brook Park, OH) and J. F. GROENEWEG (NASA, Lewis Research Center, Cleveland, OH) *Journal of Aircraft* (ISSN 0021-8669), vol. 27, Sept. 1990, p. 785-803. Previously cited in issue 17, p. 2684, Accession no. A89-40473. refs
(Contract NAS3-25266)
Copyright

A91-21547* National Aeronautics and Space Administration. Lewis Research Center, Cleveland, OH.
IN-FLIGHT SOURCE NOISE OF AN ADVANCED FULL-SCALE SINGLE-ROTATION PROPELLER
RICHARD P. WOODWARD and IRVIN J. LOFFLER (NASA, Lewis Research Center, Cleveland, OH) *AIAA, Aerospace Sciences Meeting*, 29th, Reno, NV, Jan. 7-10, 1991. 19 p. refs
(AIAA PAPER 91-0594) Copyright

Flight tests to define the far-field tone source at cruise conditions have been completed on the full-scale SR-7L advanced turboprop, which was installed on the left wing of a Gulfstream II aircraft. These measurements defined source levels for input into long-distance propagation models to predict en route noise. Inflight data were taken for seven test cases. The sideline directivities measured showed expected maximum levels near 105 deg from the propeller upstream axis. However, azimuthal directivities based on the maximum observed sideline tone levels showed highest levels below the aircraft. The tone level reduction associated with reductions in propeller tip speed is shown to be more significant in the horizontal plane than below the aircraft. Author

A91-24317* National Aeronautics and Space Administration. Lewis Research Center, Cleveland, OH.
AEROACOUSTICS OF ADVANCED PROPELLERS
JOHN F. GROENEWEG (NASA, Lewis Research Center, Cleveland, OH) IN: *ICAS, Congress*, 17th, Stockholm, Sweden, Sept. 9-14, 1990, Proceedings. Vol. 1. Washington, DC, American Institute of Aeronautics and Astronautics, Inc., 1990, p. 108-126. Previously announced in STAR as N90-26635. refs
Copyright

The aeroacoustics of advanced, high speed propellers (propfans) are reviewed from the perspective of NASA research conducted in support of the Advanced Turboprop Program. Aerodynamic and acoustic components of prediction methods for near and far field noise are summarized for both single and counterrotation propellers in uninstalled and configurations. Experimental results from tests at both takeoff/approach and cruise conditions are reviewed with emphasis on: (1) single and counterrotation model tests in the NASA Lewis 9 by 15 (low speed) and 8 by 6 (high speed) wind tunnels, and (2) full scale flight tests of a 9 ft (2.74 m) diameter single rotation wing mounted tractor and a 11.7 ft (3.57 m) diameter counterrotation aft mounted pusher propeller. Comparisons of model data projected to flight with full scale flight data show good agreement validating the scale model wind tunnel approach. Likewise, comparisons of measured and predicted noise level show excellent agreement for both single and counterrotation propellers. Progress in describing

angle of attack and installation effects is also summarized. Finally, the aeroacoustic issues associated with ducted propellers (very high bypass fans) are discussed. Author

A91-45106* National Aeronautics and Space Administration. Lewis Research Center, Cleveland, OH.
CONTROL OF LAMINAR SEPARATION OVER AIRFOILS BY ACOUSTIC EXCITATION
K. B. M. Q. ZAMAN and D. J. MCKINZIE (NASA, Lewis Research Center, Cleveland, OH) *AIAA Journal* (ISSN 0001-1452), vol. 29, July 1991, p. 1075-1083. Previously cited in issue 09, p. 1284, Accession no. A89-25454. refs
Copyright

A91-45111* National Aeronautics and Space Administration. Lewis Research Center, Cleveland, OH.
AXISYMMETRIC JET FORCED BY FUNDAMENTAL AND SUBHARMONIC TONES
GANESH RAMAN (NASA, Lewis Research Center; Sverdrup Technology, Inc., Cleveland, OH) and EDWARD J. RICE (NASA, Lewis Research Center, Cleveland, OH) *AIAA Journal* (ISSN 0001-1452), vol. 29, July 1991, p. 1114-1122. Previously cited in issue 15, p. 2311, Accession no. A89-37825. refs
Copyright

A91-48227* National Aeronautics and Space Administration. Lewis Research Center, Cleveland, OH.
ACOUSTO-ULTRASONICS
ALEX VARY (NASA, Lewis Research Center, Cleveland, OH) IN: *Non-destructive testing of fibre-reinforced plastics composites*. Vol. 2. London and New York, Elsevier Applied Science, 1990, p. 1-54. refs
Copyright

The theoretical development, methodology, and potential applications of acousto-ultrasonic nondestructive testing are set forth in an overview to assess the effectiveness of the technique. Stochastic wave propagation is utilized to isolate and describe defects in fiber-reinforced composites, particularly emphasizing the integrated effects of diffuse populations of subcritical flaws. The generation and nature of acousto-ultrasonic signals are described in detail, and stress-wave factor analysis of the signals is discussed. Applications of acousto-ultrasonics are listed including the prediction of failure sites, assessing fatigue and impact damage, calculating ultimate tensile strength, and determining interlaminar bond strength. The method can identify subtle but important variations in fiber-reinforced composites, and development of the related instrumentation technology is emphasized. C.C.S.

N91-10703* National Aeronautics and Space Administration. Lewis Research Center, Cleveland, OH.
AEROACOUSTIC EFFECTS OF REDUCED AFT TIP SPEED AT CONSTANT THRUST FOR A MODEL COUNTERROTATION TURBOPROP AT TAKEOFF CONDITIONS
RICHARD P. WOODWARD and CHRISTOPHER E. HUGHES Oct. 1990 21 p. Presented at the 13th Aeroacoustics Conference, Tallahassee, FL, 22-24 Oct. 1990; sponsored in part by AIAA (Contract RTOP 505-62-4D)
(NASA-TM-103608; E-5732; NAS 1.15:103608; AIAA PAPER 90-3933) Avail: NTIS HC/MF A03 CSCL 20A

A model high-speed, advanced counterrotation propeller, F7/A7, was tested in the anechoic wind tunnel at simulated takeoff and approach conditions of Mach 0.2. The propeller was operated in a baseline configuration with the forward and aft rotor blade setting angles and forward and aft rotational speeds essentially equal. Two additional configurations were tested with the aft rotor at increased blade setting angles and the rotational speed reduced to achieve overall performance similar to that of the baseline configuration. Acoustic data were taken with an axially translating microphone probe that was attached to the tunnel floor. Concurrent aerodynamic data were taken to define propeller operating conditions. Author

N91-11493*# National Aeronautics and Space Administration. Lewis Research Center, Cleveland, OH.

NOISE MEASUREMENTS FROM AN EJECTOR SUPPRESSOR NOZZLE IN THE NASA LEWIS 9- BY 15-FOOT LOW SPEED WIND TUNNEL

EUGENE A. KREJSA, BETH A. COOPER, DAVID G. HALL, and ABBAS KHAVARAN (Sverdrup Technology, Inc., Brook Park, OH.) Oct. 1990 62 p Presented at the 13th Aeroacoustics Conference, Tallahassee, FL, 22-24 Oct. 1990; sponsored in part by AIAA

(Contract RTOP 505-62-40)

(NASA-TM-103628; E-5717; NAS 1.15:103628; AIAA PAPER 90-3983) Avail: NTIS HC/MF A04 CSCL 20A

Acoustic results are presented of a cooperative nozzle test program between NASA and Pratt and Whitney, conducted in the NASA-Lewis 9 x 15 ft Anechoic Wind Tunnel. The nozzle tested was the P and W Hypermix Nozzle concept, a 2-D lobed mixer nozzle followed by a short ejector section made to promote rapid mixing of the induced ejector nozzle flow. Acoustic and aerodynamic measurements were made to determine the amount of ejector pumping, degree of mixing, and noise reduction achieved. A series of tests were run to verify the acoustic quality of this tunnel. The results indicated that the tunnel test section is reasonably anechoic but that background noise can limit the amount of suppression observed from suppressor nozzles. Also, a possible internal noise was observed in the air supply system. The P and W ejector suppressor nozzle demonstrated the potential of this concept to significantly reduce jet noise. Significant reduction in low frequency noise was achieved by increasing the peak jet noise frequency. This was accomplished by breaking the jet into segments with smaller dimensions than those of the baseline nozzle. Variations in ejector parameters had little effect on the noise for the geometries and the range of temperatures and pressure ratios tested. Author

N91-11494*# National Aeronautics and Space Administration. Lewis Research Center, Cleveland, OH.

THE EFFECT OF SWIRL RECOVERY VANES ON THE CRUISE NOISE OF AN ADVANCED PROPELLER

JAMES H. DITTMAR and DAVID G. HALL (Sverdrup Technology, Inc., Brook Park, OH.) 1990 18 p Presented at the 13th Aeroacoustics Conference, Tallahassee, FL, 22-24 Oct. 1990; sponsored by AIAA

(Contract RTOP 535-03-10)

(NASA-TM-103625; E-5731; NAS 1.15:103625; AIAA PAPER 90-3932) Avail: NTIS HC/MF A03 CSCL 20A

The SR-7A propeller was acoustically tested with and without downstream swirl recovery vanes to determine if any extra noise was caused by the interaction of the propeller wakes and vortices with these vanes. No additional noise was observed at the cruise condition over the angular range tested. The presence of the swirl recovery vanes did unload the propeller and some small peak noise reductions were observed from lower propeller loading noise. The propeller was also tested alone to investigate the behavior of the peak propeller noise with helical tip Mach number. As observed before on other propellers, the peak noise first rose with helical tip Mach number and then leveled off or decreased at higher helical tip Mach numbers. Detailed pressure-time histories indicate that a portion of the primary pressure pulse is progressively cancelled by a secondary pulse as the helical tip Mach number is increased. This cancellation appears to be responsible for the peak noise behavior at high helical tip Mach numbers. Author

N91-11495*# National Aeronautics and Space Administration. Lewis Research Center, Cleveland, OH.

PREDICTION OF THE NOISE FROM A PROPELLER AT ANGLE OF ATTACK

EUGENE A. KREJSA Oct. 1990 22 p Presented at the 13th Aeroacoustics Conference, Tallahassee, FL, 22-24 Oct. 1990; sponsored in part by AIAA

(Contract RTOP 505-62-4D)

(NASA-TM-103627; E-5795; NAS 1.15:103627; AIAA PAPER 90-3954) Avail: NTIS HC/MF A03 CSCL 20A

An analysis is presented to predict the noise of a propeller at angle of attack. The analysis is an extension of that reported by Mani which predicted the change in noise due to angle of attack to both unsteady loading and to azimuthal variation of the radiation efficiency of steady noise sources. Mani's analysis, however, was limited to small angles of attack. The analysis reported herein removes this small angle limitation. Results from the analysis are compared with the data of Woodward for a single rotation propeller and a counter rotating propeller. The comparison shows that including the effect of angle of attack on the steady noise sources significantly improves the agreement with data. Including higher order effects of angle of attack, while changing the predicted noise at far forward and aft angles, has little effect near the propeller plane. Author

N91-12316*# National Aeronautics and Space Administration. Lewis Research Center, Cleveland, OH.

NEAR-FIELD NOISE OF A SINGLE-ROTATION PROPFAN AT AN ANGLE OF ATTACK

M. NALLASAMY, E. ENVIA (Sverdrup Technology, Inc., Brook Park, OH.), B. J. CLARK, and J. F. GROENEWEG Oct. 1990 20 p Presented at the 13th Aeroacoustics Conference, Tallahassee, FL, 22-24 Oct. 1990; sponsored in part by AIAA

(Contract RTOP 505-62-4D)

(NASA-TM-103645; E-5805; NAS 1.15:103645; AIAA PAPER 90-3953) Avail: NTIS HC/MF A03 CSCL 20/1

The near field noise characteristics of a propfan operating at an angle of attack are examined utilizing the unsteady pressure field obtained from a 3-D Euler simulation of the propfan flowfield. The near field noise is calculated employing three different procedures: a direct computation method in which the noise field is extracted directly from the Euler solution, and two acoustic-analogy-based frequency domain methods which utilize the computed unsteady pressure distribution on the propfan blades as the source term. The inflow angles considered are -0.4, 1.6, and 4.6 degrees. The results of the direct computation method and one of the frequency domain methods show qualitative agreement with measurements. They show that an increase in the inflow angle is accompanied by an increase in the sound pressure level at the outboard wing boom locations and a decrease in the sound pressure level at the (inboard) fuselage locations. The trends in the computed azimuthal directivities of the noise field also conform to the measured and expected results. Author

N91-12317*# National Aeronautics and Space Administration. Lewis Research Center, Cleveland, OH.

EMERGING APPLICATIONS OF HIGH TEMPERATURE SUPERCONDUCTORS FOR SPACE COMMUNICATIONS

VERNON O. HEINEN, KUL B. BHASIN, and KENWYN J. LONG Sep. 1990 12 p Presented at the World Congress on Superconductivity, Houston, TX, 10-13 Sep. 1990

(Contract RTOP 506-44-00)

(NASA-TM-103629; E-5797; NAS 1.15:103629) Avail: NTIS HC/MF A03 CSCL 20/1

Proposed space missions require longevity of communications system components, high input power levels, and high speed digital logic devices. The complexity of these missions calls for a high data bandwidth capacity. Incorporation of high temperature superconducting (HTS) thin films into some of these communications system components may provide a means of meeting these requirements. Space applications of superconducting technology has previously been limited by the requirement of cooling to near liquid helium temperatures. Development of HTS materials with transition temperatures above 77 K along with the natural cooling ability of space suggest that space applications may lead the way in the applications of high temperature superconductivity. In order for HTS materials to be incorporated into microwave and millimeter wave devices, the material properties such as electrical conductivity, current density, surface resistivity and others as a function of temperature and frequency must be well characterized and understood. The millimeter wave conductivity and surface resistivity were well characterized, and at 77 K are better than copper. Basic microwave circuits such as ring

71 ACOUSTICS

resonators were used to determine transmission line losses. Higher Q values than those of gold resonator circuits were observed below the transition temperature. Several key HTS circuits including filters, oscillators, phase shifters and phased array antenna feeds are feasible in the near future. For technology to improve further, good quality, large area films must be reproducibly grown on low dielectric constant, low loss microwave substrates. Author

N91-15842*# National Aeronautics and Space Administration. Lewis Research Center, Cleveland, OH.

POTENTIAL REDUCTION OF EN ROUTE NOISE FROM AN ADVANCED TURBOPROP AIRCRAFT

JAMES H. DITTMAR Dec. 1990 19 p
(Contract RTOP 535-03-10)

(NASA-TM-103635; E-5809; NAS 1.15:103635) Avail: NTIS HC/MF A03 CSCL 20/1

When the en route noise of a representative aircraft powered by an eight-blade SR-7 propeller was previously calculated, the noise level was cited as a possible concern associated with the acceptance of advanced turboprop aircraft. Some potential methods for reducing the en route noise were then investigated and are reported. Source noise reductions from increasing the blade number and from operating at higher rotative speed to reach a local minimum noise point were investigated. Greater atmospheric attenuations for higher blade passing frequencies were also indicated. Potential en route noise reductions from these methods were calculated as 9.5 dB (6.5 dB(A)) for a 10-blade redesigned propeller and 15.5 dB (11 dB(A)) for a 12-blade redesigned propeller. Author

N91-15848*# National Aeronautics and Space Administration. Lewis Research Center, Cleveland, OH.

MONOGRAPH ON PROPAGATION OF SOUND WAVES IN CURVED DUCTS

WOJCIECH ROSTAFINSKI Jan. 1991 97 p

(Contract RTOP 505-69-61)

(NASA-RP-1248; E-5480; NAS 1.61:1248) Avail: NTIS HC/MF A05 CSCL 20/1

After reviewing and evaluating the existing material on sound propagation in curved ducts without flow, it seems strange that, except for Lord Rayleigh in 1878, no book on acoustics has treated the case of wave motion in bends. This monograph reviews the available analytical and experimental material, nearly 30 papers published on this subject so far, and concisely summarizes what has been learned about the motion of sound in hard-wall and acoustically lined cylindrical bends. Author

N91-16679*# National Aeronautics and Space Administration. Langley Research Center, Hampton, VA.

WIND TURBINE ACOUSTICS

HARVEY H. HUBBARD and KEVIN P. SHEPHERD Dec. 1990 49 p Submitted for publication Prepared in cooperation with NASA, Lewis Research Center and American Society of Mechanical Engineers

(Contract DE-AI01-76ET-20320; RTOP 776-33-41)

(NASA-TP-3057; E-5663; DOE/NASA/20320-77; NAS 1.60:3057) Avail: NTIS HC/MF A03 CSCL 20/1

Available information on the physical characteristics of the noise generated by wind turbines is summarized, with example sound pressure time histories, narrow- and broadband frequency spectra, and noise radiation patterns. Reviewed are noise measurement standards, analysis technology, and a method of characterizing wind turbine noise. Prediction methods are given for both low-frequency rotational harmonics and broadband noise components. Also included are atmospheric propagation data showing the effects of distance and refraction by wind shear. Human perception thresholds, based on laboratory and field tests, are given. Building vibration analysis methods are summarized. The bibliography of this report lists technical publications on all aspects of wind turbine acoustics. Author

N91-19825*# National Aeronautics and Space Administration. Lewis Research Center, Cleveland, OH.

UNSTEADY BLADE PRESSURE MEASUREMENTS FOR THE SR-7A PROPELLER AT CRUISE CONDITIONS

L. J. HEIDELBERG and M. NALLASAMY (Sverdrup Technology, Inc., Brook Park, OH.) 1990 17 p Presented at the 13th Aeroacoustics Conference, Tallahassee, FL, 22-24 Oct. 1990; sponsored by AIAA Previously announced in IAA as A91-12533 (Contract NAS3-24105; RTOP 505-62-4D)

(NASA-TM-103606; E-5754; NAS 1.15:103606; AIAA PAPER 90-4022) Avail: NTIS HC/MF A03 CSCL 20/1

The unsteady blade surface pressures were measured on the SR-7A propeller. The freestream Mach no., inflow angle, and advance ratio were varied while measurements were made at nine blade stations. At a freestream Mach no. of 0.8, the data in terms of unsteady pressure coefficient vs. azimuth angle are compared to an unsteady 3-D Euler solution, yielding very encouraging results. The code predicts the shape (phase) of the waveform very well, while the magnitude is over-predicted in many cases. At tunnel Mach nos. below 0.6, an unusually large response on the suction surface at 0.15 chord and 0.88 radius was observed. The behavior of this response suggests the presence of a leading edge vortex. The midchord measuring stations on the suction surface exhibit a response that leads the forcing function while most other locations show a phase lag. Author

N91-25817*# National Aeronautics and Space Administration. Lewis Research Center, Cleveland, OH.

TUNED OPTIMIZATION OF EXTENDED REACTING ACOUSTIC LINERS

KENNETH J. BAUMEISTER 1991 9 p Presented at the 1991 Winter Annual Meeting of ASME, Atlanta, GA, 1-6 Dec. 1991

(Contract RTOP 505-62-52)

(NASA-TM-104431; E-6265; NAS 1.15:104431) Avail: NTIS HC/MF A02 CSCL 20/1

A finite element Galerkin formulation was employed to study the optimum attenuation and reflection characteristics of acoustic waves propagating in two dimensional straight ducts with extended reacting absorbing walls without a mean flow. The reflection and transmission of acoustic energy at the entrance and the exit of the duct were determined by coupling the finite element solutions in the absorbing portion of the duct to the eigenfunctions of an infinite, uniform, hard wall duct. In the frequency range where the duct height and acoustic wave length are nearly equal, power attenuation contours were examined to determine conditions for minimizing acoustic transmission through the duct. The extended reacting liners were found to significantly minimize the reflective characteristics of the duct rather than to increase absorption in the liner. Thus, extended reacting wall liner properties can be theoretically chosen to yield large impedance mismatches in an open straight duct. Author

72

ATOMIC AND MOLECULAR PHYSICS

Includes atomic structure, electron properties, and molecular spectra.

A91-33236* National Aeronautics and Space Administration. Lewis Research Center, Cleveland, OH.

GLOBAL EXPRESSION FOR REPRESENTING DIATOMIC POTENTIAL-ENERGY CURVES

JOHN FERRANTE (NASA, Lewis Research Center, Cleveland, OH), HERBERT SCHLOSSER (Cleveland State University, OH), and JOHN R. SMITH (GM Research Laboratories, Warren, MI) Physical Review A (ISSN 1050-2947), vol. 43, April 1, 1991, p. 3487-3494. refs

Copyright

NUCLEAR AND HIGH-ENERGY PHYSICS

Includes elementary and nuclear particles; and reactor theory.

N91-18799* National Aeronautics and Space Administration. Lewis Research Center, Cleveland, OH.

CONSTRUCTION AND TESTING OF CERAMIC FABRIC HEAT PIPE WITH WATER WORKING FLUID

ZENEN I. ANTONIAK, BRENT J. WEBB, JAMES M. BATES, and MATTHEW F. COOPER Jan. 1991 7 p Presented at the 8th Symposium on Space Nuclear Power Systems, Albuquerque, NM, 6-10 Jan. 1991 Prepared in cooperation with NASA, Lyndon B. Johnson Space Center, and Pacific Northwest Lab., Richland, WA Sponsored in part by Air Force (Contract DE-AC06-76RL-01830) (NASA-TM-103332; NAS 1.15:103332; DE91-006716; PNL-SA-18805; CONF-910116-16) Avail: NTIS HC/MF A02 CSDL 20/8

A prototype ceramic fabric/titanium water heat pipe has been constructed and tested; it transported 25 to 80 W of power at 423 K. Component development and testing is continuing with the aim of providing an improved prototype, with a 38 micron stainless steel liner covered by a biaxially-braided Nextel (trademark) sleeve that is approximately 300 microns thick. This fabric has been tested to 800 K, and its emittance is about 0.5 at that temperature. Advanced versions of the water heat pipe will probably require a coating over the ceramic fabric in order to increase this emittance to the 0.8 to 0.9 range. DOE

OPTICS

Includes light phenomena; and optical devices.

A91-41995* National Aeronautics and Space Administration. Lewis Research Center, Cleveland, OH.

A LIGHT-TRAPPING SOLAR CELL COVERGLASS

GEOFFREY A. LANDIS (NASA, Lewis Research Center, Cleveland, OH) IN: IEEE Photovoltaic Specialists Conference, 21st, Kissimmee, FL, May 21-25, 1990, Conference Record. Vol. 2. New York, Institute of Electrical and Electronics Engineers, Inc., 1990, p. 1304-1307. refs Copyright

A novel method of reducing surface reflectivity which eliminates the need to texturize the surface of the cell is presented. A double light pass is achieved by using a light-trapping coverglass which redirects reflected light back to the cell surface by total internal reflection. This technique allows low-reflectance surfaces to be used on planar solar cells, including GaAs and InP, with the benefit of increasing the possible short-circuit current (and hence the efficiency) by 6 to 10 percent with no additional steps added to the cell manufacturing process. The coverglass design also has applications to reduction of grid shadowing and to light trapping within the cell. I.E.

N91-13996* National Aeronautics and Space Administration. Lewis Research Center, Cleveland, OH.

MONOLITHIC MM-WAVE PHASE SHIFTER USING OPTICALLY ACTIVATED SUPERCONDUCTING SWITCHES Patent

Application

ROBERT R. ROMANOFKY, inventor (to NASA) and KUL B. BHASIN, inventor (to NASA) 25 Sep. 1990 16 p (NASA-CASE-LEW-14878-1; NAS 1.71:LEW-14878-1; US-PATENT-APPL-SN-587921) Avail: NTIS HC/MF A03 CSDL 20/6

A three-parameter expression that gives an accurate fit to diatomic potential curves over the entire range of separation for charge transfers between 0 and 1. It is based on a generalization of the universal binding-energy relation of Smith et al. (1989) with a modification that describes the crossover from a partially ionic state to the neutral state at large separations. The expression is tested by comparison with first-principles calculations of the potential curves ranging from covalently bonded to ionically bonded. The expression is also used to calculate spectroscopic constants from a curve fit to the first-principles curves. A comparison is made with experimental values of the spectroscopic constants.

Author

N91-20735* National Aeronautics and Space Administration. Lewis Research Center, Cleveland, OH.

THE EFFECT OF ATOMIC OXYGEN ON POLYSILOXANE-POLYIMIDE FOR SPACECRAFT APPLICATIONS IN LOW EARTH ORBIT

SHARON K. RUTLEDGE, JILL M. COOPER, and RAYMOND M. OLLE (Cleveland State Univ., OH.) IN NASA, Lyndon B. Johnson Space Center, Fourth Annual Workshop on Space Operations Applications and Research (SOAR 90) p 755-762 Jan. 1991 Avail: NTIS HC/MF A14 CSDL 20/8

Polysiloxane-polyimide films are of interest as a replacement for polyimide Kapton in the Space Station Freedom solar array blanket. The blanket provides the structural support for the solar cells as well as providing transport of heat away from the back of the cells. Polyimide Kapton would be an ideal material to use; however, its high rate of degradation due to attack by atomic oxygen in low Earth orbit, at the altitudes Space Station Freedom will fly, is of such magnitude that if left unprotected, the blanket will undergo structural failure in much less than the desired 15 year operating life. Polysiloxane-polyimide is of interest as a replacement material because it should form its own protective silicon dioxide coating upon exposure to atomic oxygen. Mass, optical, and photomicrographic data obtained in the evaluation of the durability of polysiloxane-polyimide to an atomic oxygen environment are presented. Author

N91-25027* National Aeronautics and Space Administration. Lewis Research Center, Cleveland, OH.

ATOMIC OXYGEN UNDERCUTTING OF LDEF ALUMINIZED KAPTON MULTILAYER INSULATION Abstract Only

KIM K. DEGROH IN NASA, Langley Research Center, First LDEF Post-Retrieval Symposium Abstracts p 60 Jun. 1991 Avail: NTIS HC/MF A07 CSDL 20/8

Atomic oxygen undercutting is a potential threat to vulnerable spacecraft materials which have been shielded with an atomic oxygen protective coating. This is due to atomic oxygen attack of oxidizable materials at the point of microscopic defects in the protective coatings which occur during fabrication and handling, or from micrometeoroid and debris bombardment in space. An aluminized Kapton multilayer insulation sample which was flown on the leading edge of the Long Duration Exposure Facility (LDEF) was used to study low Earth orbit (LEO) directed ram oxygen undercutting. Cracks in the aluminized coatings around the vent holes provided excellent locations for evaluation of atomic oxygen undercutting. The undercutting profiles were compared to Monte Carlo models which predict LEO ram atomic oxygen attack. The shape of the undercutting profile was found to vary with crack width, which is proportional to the number of atomic oxygen atoms entering the crack. The resulting atomic oxygen undercut profiles which occurred on LDEF indicated wide undercut cavities in spite of the fixed ram orientation. Potential causes of the observed undercutting profiles will be presented. Implications of the undercutting profiles relevant to Space Station Freedom will also be discussed. Author

A phase shifter is disclosed having a reference path and a delay path, light sources, and superconductive switches. Each of the superconductive switches is terminated in a virtual short circuit, which may be a radial stub. Switching between the reference path and delayed path is accomplished by illuminating the superconductive switches connected to the desired path, while not illuminating the superconductive switches connected to the other path.

NASA

N91-14829* # National Aeronautics and Space Administration. Lewis Research Center, Cleveland, OH.

VIBRATIONAL TESTING OF OPTICAL FIBER CONNECTOR JOINTS

AMY L. SOVIE and GEORGE C. MADZSAR 1990 10 p
Presented at the 2nd Annual Conference on Health Monitoring for Space Propulsion Systems, Cincinnati, OH, 14-15 Nov. 1990; sponsored by Cincinnati Univ.

(Contract RTOP 553-13-00)

(NASA-TM-103654; E-5845; NAS 1.15:103654) Avail: NTIS HC/MF A02 CSCL 20/6

An experimental study was performed to determine the effects of vibration on the propagation of light through SMA- and ST-type fiber-optic connectors. A multimode, fiber-optic link was vibrated from 0 to 10,000 Hz at a constant peak acceleration along the connector transverse and longitudinal axes. All other environmental parameters were ambient. Transfer characteristics through the connection were examined as a function of vibrational frequency using both laser and light-emitting diode (LED) light to illuminate the system. Slight differences in operation between the SMA and ST connectors were observed with no appreciative attenuation as a result of vibration. Vibration did cause the constant-amplitude input light to be modulated in the connector; however, the amplitude of vibration-induced noise was less than 3 standard deviations from the mean.

Author

N91-18305* # National Aeronautics and Space Administration. Lewis Research Center, Cleveland, OH.

OPTICAL DISPERSION RELATIONS FOR DIAMONDLIKE CARBON FILMS

SAMUEL A. ALTEROVITZ, ROBERT M. SIEG, NEIL S. SHOEMAKER (Case Western Reserve Univ., Cleveland, OH.), and JOHN J. POUCH *In its* Solid State Technology Branch of NASA Lewis Research Center Second Annual Digest, June 1989 - June 1990 p 240-245 Jun. 1990 Previously announced as N90-10738

Avail: NTIS HC/MF A13 CSCL 20/6

Ellipsometric measurements on plasma deposited diamondlike amorphous carbon (a-C:H) films were taken in the visible, (E = 1.75 to 3.5 eV). The films were deposited on Si and their properties were varied using high temperature (up to 750 C) anneals. The real (n) and imaginary (k) parts of the complex index of refraction, N, were obtained simultaneously. Following the theory of Forouhi and Bloomer, a least squares fit was used to find the dispersion relations n(E) and k(E). Reasonably good fits were obtained, showing that the theory can be used for a-C:H films. Moreover, the value of the energy gap, E_g, obtained in this way was compared the the E_g value using conventional Tauc plots and reasonably good agreement was obtained.

Author

N91-18306* # National Aeronautics and Space Administration. Lewis Research Center, Cleveland, OH.

DIAMONDLIKE CARBON APPLICATIONS IN INFRARED OPTICS AND MICROELECTRONICS

JOHN A. WOOLLAM, BHOLA N. DE, S. ORZESZKO, N. J. IANNO, PAUL G. SNYDER, SAMUEL A. ALTEROVITZ, JOHN J. POUCH, R. L. C. WU, and D. C. INGRAM (Universal Energy Systems, Inc., Dayton, OH.) *In its* Solid State Technology Branch of NASA Lewis Research Center Second Annual Digest, June 1989 - June 1990 p 246-276 Jun. 1990

Avail: NTIS HC/MF A13 CSCL 20/6

The use of diamondlike carbon (DLC) as a protective coating in harsh environments is addressed. There are three topics presented. The first is a description of the preparation of DLC on

seven different infrared transmitting materials, and the possibility of using DLC as an antireflecting coating at commonly used wavelengths. DLC doesn't bond easily to all materials, and special techniques for bonding are presented. The second topic deals with how well DLC will protect a substrate from moisture penetration. This is an important aspect in numerous uses of DLC, including both infrared optics and integrated circuits. The third topic is the effect of particulate impact on film performance and integrity.

Author

N91-20102* # National Aeronautics and Space Administration. Lewis Research Center, Cleveland, OH.

FIBER-OPTIC-BASED CONTROLS

GARY T. SENG *In its* Aeropropulsion 1991 11 p Mar. 1991
Avail: NTIS HC/MF A24 CSCL 20/6

The challenge of those involved in control-system hardware development is to accommodate an ever-increasing complexity in aircraft control, while limiting the size and weight of the components and improving system reliability. A technology that displays promise towards this end is the area of fiber optics. The primary advantages of employing optical fibers, passive optical sensors, and optically controlled actuators over conventional control systems are greater immunity from electromagnetic effects, weight and volume reduction, non-radiating characteristics, superior bandwidth capabilities, and freedom from short circuits and sparking contacts. Since 1975, NASA Lewis has been performing in-house, contract, and grant research in fiber-optic sensors, high-temperature electro-optic switches, and fly-by-light control system architecture. Passive optical sensor development is an essential yet challenging area of work and has therefore received much attention during this period. A major effort to develop and demonstrate fly-by-light control system technology, known as the fiber optic control system integration (FOCSI) program, was initiated in 1985. Phase 1 of FOCSI, A NASA-DOD effort completed in 1986, was aimed at the design of a fiber optic propulsion/flight control system. Phase 2, a NASA Navy effort currently in progress, will provide the system design, subcomponent and system development, and system ground tests. Phase 3, flight demonstration, was also initiated and will culminate in full FOCSI system flight tests. In addition to a summary of the benefits of fiber optics, the FOCSI program, sensor advances, and future directions in the NASA Lewis program are discussed.

Author

N91-21871* National Aeronautics and Space Administration. Lewis Research Center, Cleveland, OH.

FIBER OPTIC SENSING SYSTEM Patent

GRIGORY ADAMOVSKY, inventor (to NASA) 26 Feb. 1991
8 p Filed 7 Sep. 1989 Supersedes N90-15733 (28 - 7, p 992)
(NASA-CASE-LEW-14795-1; US-PATENT-4,995,697;
US-PATENT-APPL-SN-404291; US-PATENT-CLASS-350-96.29;
US-PATENT-CLASS-356-345; US-PATENT-CLASS-250-227;
INT-PATENT-CLASS-G02B-6/02;
INT-PATENT-CLASS-G02B-6/16;
INT-PATENT-CLASS-G01B-9/02) Avail: US Patent and
Trademark Office CSCL 20/6

A fiber optic interferometer utilizes a low coherence light emitting diode (LED) laser as a light source which is filtered and driven at two RF frequencies, high and low, that are specific to the initial length of the resonator chamber. A displacement of a reflecting mirror changes the length traveled by the nonreferencing signal. The low frequency light undergoes destructive interference which reduces the average intensity of the wave while the high frequency light undergoes constructive interference which increases the average intensity of the wave. The ratio of these two intensity measurements is proportional to the displacement incurred.

Official Gazette of the U.S. Patent and Trademark Office

PLASMA PHYSICS

Includes magnetohydrodynamics and plasma fusion.

N91-17734* National Aeronautics and Space Administration. Lewis Research Center, Cleveland, OH.

THE ENVIRONMENT POWER SYSTEM ANALYSIS TOOL DEVELOPMENT PROGRAM

GARY A. JONGEWARD, ROBERT A. KUHARSKI, ERIC M. KENNEDY, N. JOHN STEVENS, RAND M. PUTNAM, JAMES C. ROCHE, and KATHERINE G. WILCOX (Systems Science and Software, La Jolla, CA.) In NASA, Marshall Space Flight Center, Current Collection from Space Plasmas p 352-357 Dec. 1990
 Avail: NTIS HC/MF A16 CSCL 20/9

The Environment Power System Analysis Tool (EPSAT) is being developed to provide space power system design engineers with an analysis tool for determining system performance of power systems in both naturally occurring and self-induced environments. The program is producing an easy to use computer aided engineering (CAE) tool general enough to provide a vehicle for technology transfer from space scientists and engineers to power system design engineers. The results of the project after two years of a three year development program are given. The EPSAT approach separates the CAE tool into three distinct functional units: a modern user interface to present information, a data dictionary interpreter to coordinate analysis, and a data base for storing system designs and results of analysis. Author

N91-25875* National Aeronautics and Space Administration. Lewis Research Center, Cleveland, OH.

PLASMA GUN WITH COAXIAL POWDER FEED AND ADJUSTABLE CATHODE Patent

ISIDOR ZAPLATYNSKY, inventor (to NASA) 5 Feb. 1991 6 p
 Filed 7 Jul. 1989 Supersedes N90-10718 (28 - 1, p 126)
 (NASA-CASE-LEW-14901-1; US-PATENT-4,990,739;
 US-PATENT-APPL-SN-376488; US-PATENT-CLASS-219-121.47;
 US-PATENT-CLASS-219-121.52; US-PATENT-CLASS-219-121.48;
 US-PATENT-CLASS-219-75; US-PATENT-CLASS-219-76.16;
 US-PATENT-CLASS-427-34; INT-PATENT-CLASS-B23K-9/00)
 Avail: US Patent and Trademark Office CSCL 20/9

An improved plasma gun coaxially injects particles of ceramic materials having high melting temperatures into the central portion of a plasma jet. This results in a more uniform and higher temperature and velocity distribution of the sprayed particles. The position of the cathode is adjustable to facilitate optimization of the performance of the gun wherein grains of the ceramic material are melted at lower power input levels.

Official Gazette of the U.S. Patent and Trademark Office

SOLID-STATE PHYSICS

Includes superconductivity.

A91-13767* National Aeronautics and Space Administration. Lewis Research Center, Cleveland, OH.

AEROSPACE APPLICATIONS OF HIGH TEMPERATURE SUPERCONDUCTIVITY

D. J. CONNOLLY, V. O. HEINEN, P. R. ARON (NASA, Lewis Research Center, Cleveland, OH), J. LAZAR (Argonne National Laboratory, IL), and ROBERT R. ROMANOFKY (NASA, Washington, DC) IAF, International Astronautical Congress, 41st, Dresden, Federal Republic of Germany, Oct. 6-12, 1990. 6 p. refs
 (IAF PAPER 90-054) Copyright

A review is presented of all the applications that are part of the NASA program to develop space technology capitalizing on the potential benefit of high temperature superconducting materials. The applications in three major areas are being pursued: sensors and cryogenic systems, space communications, and propulsion and power systems. This review places emphasis on space communications applications and the propulsion and power applications. It is concluded that the power and propulsion applications will eventually be limited by structural considerations rather than by the availability of suitable superconductors. A cursory examination of structural limitations implied by the virial theorem suggested that there is an upper limit to the size of high field magnetic systems that are feasible in space. R.E.P.

A91-16105* National Aeronautics and Space Administration. Lewis Research Center, Cleveland, OH.

TIME DEVELOPMENT OF A PERTURBED-SPHERICAL NUCLEUS IN A PURE SUPERCOOLED LIQUID. I - POWER-LAW GROWTH OF MORPHOLOGICAL INSTABILITIES. II - NONLINEAR DEVELOPMENT

V. PINES, M. ZLATKOWSKI, and A. CHAIT (NASA, Lewis Research Center, Cleveland, OH) Physical Review A (ISSN 1050-2947), vol. 42, Nov. 15, 1990, p. 6129-6150. refs
 Copyright

The linear growth stage of the morphological instabilities developing at the liquid-solid interface during crystal growth from an axisymmetric spherical nucleus is analyzed. The corresponding growth rate parameters are calculated numerically, and it is shown that morphological instabilities for free growth evolve according to a power law in agreement with WKB results and contrary to an exponential law found in a quasi-stationary approximation. The time evolution of an arbitrary perturbed liquid-solid interface from a linear into the nonlinear stage is studied. The initial perturbations include the eigenfunctions for the linear problem, localized perturbations of the grain-boundary type, and a stochastic noise. It is shown that the perturbations grow and spread in a wavelike manner. The formation of a predendritic growth stage is characterized by establishment of constant values of tip radius and velocity. C.D.

A91-19820* National Aeronautics and Space Administration. Lewis Research Center, Cleveland, OH.

ELECTRICAL TRANSPORT MEASUREMENTS ON POLYCRYSTALLINE SUPERCONDUCTING Y-Ba-Cu-O FILMS

M. A. STAN, S. A. ALTEROVITZ, and D. IGNJATOVIC (NASA, Lewis Research Center, Cleveland, OH) IN: Superconductivity and applications. New York, Plenum Press, 1990, p. 139-152. refs
 Copyright

The current-voltage, I-V, characteristics of polycrystalline Y-Ba-Cu-O films have been measured as a function of temperature. The I-V characteristics are interpreted using a model based upon an array of weak links with a statistical distribution of critical currents. In addition, evidence is found that the supercurrents flow in nearly independent filaments near T_c . Various criteria are discussed with respect to the definition of the transport critical current, I_c , in these films. A temperature dependence for I_c has also been deduced from the I-V data by appealing to an empirical scaling law. It is proposed that this temperature dependence is representative of the weaker links within the critical current distribution. Author

A91-26989* National Aeronautics and Space Administration. Lewis Research Center, Cleveland, OH.

ELECTROMIGRATION FAILURE IN YBa2Cu3O(7-X) THIN FILMS

SATISH VITTA, M. A. STAN, J. D. WARNER, and S. A. ALTEROVITZ (NASA, Lewis Research Center, Cleveland, OH) Applied Physics Letters (ISSN 0003-6951), vol. 58, Feb. 18, 1991, p. 759-761. refs
 Copyright

Electromigration failure in highly oriented YBa2Cu3O(7-x) thin films below the superconducting transition temperature is reported

here for the first time. The film on SrTiO₃ failed at 86 K, 230,000 A/sq cm, while that on LaAlO₃ failed at 84 K, 930,000 A/sq cm. Scanning electron microscopy and energy dispersive X-ray analysis of the films after failure shows that Cu migrates preferentially away from the failure region toward the electrode. Author

A91-35449* National Aeronautics and Space Administration. Lewis Research Center, Cleveland, OH.

PREPARATION OF 110K (Bi, Pb)-SR-CA-CU-O SUPERCONDUCTOR FROM GLASS PRECURSOR

NAROTTAM P. BANSAL (NASA, Lewis Research Center, Cleveland, OH) IN: Superconductivity and ceramic superconductors. Westerville, OH, American Ceramic Society, Inc. (Ceramic Transactions. Vol. 13), 1990, p. 339-347. Previously announced in STAR as N90-14108. refs Copyright

The Bi_{1.5}Pb_{0.5}Sr₂Ca₂Cu₃O(x) glass, prepared by rapid quenching of the melt, showed T_{sub g} of 383 C, crystallization temperature of approx. 446 C, melting temperature of approx. 855 C, and bulk density of 5.69 g/cu. cm. in air. The as-quenched glass was oxygen deficient. On heating in O₂, it showed a slow, irreversible, and continuous weight gain starting at approx. 530 C. The influence of annealing conditions on the formation of various phases was investigated by XRD and electrical resistivity measurements. The 110K-T_{sub c} phase did not form below 840 C. The amount of this phase increased with the sintering time at 840 C. A sample annealed at 840 C for 243 h in air and furnace cooled showed the highest T_{sub c} (R=0) of 107.2 K and transition width delta T_{sub c} (10 to 90 percent) of approx. 2 K. Author

A91-36047* National Aeronautics and Space Administration. Lewis Research Center, Cleveland, OH.

TEMPERATURE DEPENDENCE OF THE ANISOTROPY IN MAGNETIC RELAXATION IN YBa₂Cu₃O(7-x) THIN FILMS

SATISH VITTA, M. A. STAN, and S. A. ALTEROVITZ (NASA, Lewis Research Center, Cleveland, OH) (1990 Applied Superconductivity Conference, Snowmass, CO, Sept. 24-28, 1990, Proceedings. A91-36027 15-33) IEEE Transactions on Magnetics (ISSN 0018-9464), vol. 27, pt. 2, March 1991, p. 1083-1085. refs Copyright

The relaxation of diamagnetic magnetization in the c-axis-aligned YBa₂Cu₃O(7-x) thin film is studied as a function of orientation and temperature in the range of 5-50 K at H = 0.2 T. The magnetization M(T,H) in the orientations H parallel to c and H perpendicular to c and at all the temperatures is found to decrease logarithmically with time t. The activation energy for the movement of flux lines U is found to be 30-110 meV in the range 5-50 K. For H parallel c, U increases continuously with T, whereas for H perpendicular c, U has two apparent maxima: at T = 10 K and T greater than 50 K. These results are discussed in terms of the thermally activated flux motion model. I.E.

A91-41893* Cleveland State Univ., OH.
STUDY OF SURFACE PASSIVATION AS A FUNCTION OF INP CLOSED-AMPOULE SOLAR CELL FABRICATION PROCESSING VARIABLES

MIRCEA FAUR, MARIA FAUR, PHILLIP JENKINS, MANJU GORADIA, CHANDRA GORADIA (Cleveland State University, OH), SHEILA BAILEY, IRVING WEINBERG (NASA, Lewis Research Center, Cleveland, OH), and DOUGLAS JAYNE (Case Western Reserve University, Cleveland, OH) IN: IEEE Photovoltaic Specialists Conference, 21st, Kissimmee, FL, May 21-25, 1990, Conference Record. Vol. 1. New York, Institute of Electrical and Electronics Engineers, Inc., 1990, p. 130-137. refs (Contract NAG3-2696) Copyright

The effects of various surface preparation procedures, including chemical treatment and anodic or chemical oxidation, closed-ampoule diffusion conditions, and post-diffusion surface preparation and annealing conditions, on the passivating properties of InP have been investigated in order to optimize the fabrication procedures of n(+)-p InP solar cells made by closed-ampoule

diffusion of sulfur into p-type InP. The InP substrates used were p-type Cd-doped to a level of 1.7 x 10 to the 16th/cu cm, Zn-doped to levels of 2.2 x 10 to the 16th and 1.2 x 10 to the 18th/cu cm, and n-type S-doped to 4.4 x 10 to the 18th/cu cm. The passivating properties have been evaluated from photoluminescence (PL) and conductance-voltage (G-V) data. Good agreement was found between the level of surface passivation and the composition of different surface layers as revealed by X-ray photoelectron spectroscopy (XPS) analysis. I.E.

A91-41931* Cleveland State Univ., OH.

MEASUREMENT OF SURFACE RECOMBINATION VELOCITY ON HEAVILY DOPED INDIUM PHOSPHIDE

PHILLIP JENKINS, MANJU GHALLA-GORADIA, MIRCEA FAUR, MARIA FAUR (Cleveland State University, OH), and SHEILA BAILEY (NASA, Lewis Research Center, Cleveland, OH) IN: IEEE Photovoltaic Specialists Conference, 21st, Kissimmee, FL, May 21-25, 1990, Conference Record. Vol. 1. New York, Institute of Electrical and Electronics Engineers, Inc., 1990, p. 399-403. refs Copyright

Surface recombination velocity (SRV) on heavily doped n-type and p-type InP was measured as a function of surface treatment. For the limited range of substrates and surface treatments studied, SRV and surface stability depend strongly on the surface treatment. SRVs of 100,000 cm/sec in both p-type and n-type InP are obtainable, but in n-type the low-SRV surfaces were unstable, and the only stable surfaces on n-type had SRVs of more than 10 to the 6th cm/sec. I.E.

A91-42170* Auburn Univ., AL.

SELECTIVE AND LOW TEMPERATURE SYNTHESIS OF POLYCRYSTALLINE DIAMOND

R. RAMESHAM, T. ROPPEL, C. ELLIS, W. BAUGH (Auburn University, AL), and D. A. JAWORSKE (NASA, Lewis Research Center, Cleveland, OH) Journal of Materials Research (ISSN 0884-2914), vol. 6, June 1991, p. 1278-1286. Research supported by SDIO and Auburn University. refs (Contract N60921-86-C-A226) Copyright

Polycrystalline diamond thin films have been deposited on single-crystal silicon substrates at low temperatures (not above 600 C) using a mixture of hydrogen and methane gases by high-pressure microwave plasma-assisted chemical vapor deposition. Low-temperature deposition has been achieved by cooling the substrate holder with nitrogen gas. For deposition at reduced substrate temperature, it has been found that nucleation of diamond will not occur unless the methane/hydrogen ratio is increased significantly from its value at higher substrate temperature. Selective deposition of polycrystalline diamond thin films has been achieved at 600 C. Decrease in the diamond particle size and growth rate and an increase in surface smoothness have been observed with decreasing substrate temperature during the growth of thin films. As-deposited films are identified by Raman spectroscopy, and the morphology is analyzed by scanning electron microscopy. Author

A91-45713* National Aeronautics and Space Administration. Lewis Research Center, Cleveland, OH.

CONTROLLED GROWTH OF 3C-SIC AND 6H-SIC FILMS ON LOW-TILT-ANGLE VICINAL (0001) 6H-SIC WAFERS

J. A. POWELL, J. B. PETIT, J. H. EDGAR, I. G. JENKINS, L. G. MATUS (NASA, Lewis Research Center, Cleveland, OH) et al. Applied Physics Letters (ISSN 0003-6951), vol. 59, July 15, 1991, p. 333-335. refs Copyright

It has been found that, with proper pregrowth surface treatment, 6H-SiC single-crystal films can be grown by chemical vapor deposition (CVD) at 1450 C on vicinal (0001) 6H-SiC with tilt angles as small as 0.1 deg. Previously, tilt angles of greater than 1.5 deg were required to achieve 6H on 6H at this growth temperature. In addition, 3C-SiC could be induced to grow within selected regions on the 6H substrate. the 3C regions contained few (or zero)

double-positioning boundaries and a low density of stacking faults. A new growth model is proposed to explain the control of SiC polytype in this epitaxial film growth process. Author

A91-45881* National Aeronautics and Space Administration. Lewis Research Center, Cleveland, OH.

APPLICATION OF OXIDATION TO THE STRUCTURAL CHARACTERIZATION OF SiC EPITAXIAL FILMS

J. A. POWELL, J. B. PETIT, J. H. EDGAR, I. G. JENKINS, L. G. MATUS (NASA, Lewis Research Center, Cleveland, OH) et al. Applied Physics Letters (ISSN 0003-6951), vol. 59, July 8, 1991, p. 183-185. refs
Copyright

Both 3C-SiC and 6H-SiC single-crystal films can be grown on vicinal (0001) 6H-SiC wafers. It is found that oxidation can be a powerful diagnostic process for (1) 'color mapping' the 3C and 6H regions of these films, (2) decorating stacking faults in the films, (3) enhancing the decoration of double positioning boundaries, and (4) decorating polishing damage. Contrary to previously published oxidation results, proper oxidation conditions can yield interference colors that provide a definitive map of the polytype distribution for both the Si face and C face of SiC films. Author

A91-52349*# National Aeronautics and Space Administration. Lewis Research Center, Cleveland, OH.

ELECTRICALLY CONDUCTING POLYMERS FOR AEROSPACE APPLICATIONS

MARY ANN B. MEADOR, JAMES R. GAIER, BRIAN S. GOOD, G. R. SHARP, and MICHAEL A. MEADOR (NASA, Lewis Research Center, Cleveland, OH) AIAA, NASA, and OAI, Conference on Advanced SEI Technologies, Cleveland, OH, Sept. 4-6, 1991. 12 p. refs
(AIAA PAPER 91-3432) Copyright

Current research on electrically conducting polymers from 1974 to the present is reviewed focusing on the development of materials for aeronautic and space applications. Problems discussed include extended pi-systems, pyrolytic polymers, charge-transfer systems, conductive matrix resins for composite materials, and prospects for the use of conducting polymers in space photovoltaics. O.G.

A91-53235* National Aeronautics and Space Administration. Lewis Research Center, Cleveland, OH.

ELLIPSOMETRIC STUDY OF YBa₂Cu₃O_{7-x} LASER ABLATED AND CO-EVAPORATED FILMS

S. A. ALTEROVITZ, J. D. WARNER, S. VITTA (NASA, Lewis Research Center, Cleveland, OH), M. A. STAN (Kent State University, Cleveland, OH), and R. M. SIEG International Conference on Electronic Materials, 2nd, Newark, NJ, Sept. 17-19, 1990, Paper. p. a. Previously announced in STAR as N90-26682. refs
Copyright

High temperature superconducting films of YBa₂Cu₃O_{7-x} (YBCO) were grown on SrTiO₃, LaAlO₃, and YSZ substrates using two techniques: excimer laser ablation with in situ annealing and co-evaporation of Y, Cu, and BaF₂ with ex-situ annealing. Film thicknesses were typically 5000 Å, with predominant c-axis alignment perpendicular to the substrate. Critical temperatures up to T_c(R = 0) = 90 K were achieved by both techniques. Ellipsometric measurements were taken in the range 1.6 to 4.3 eV using a variable angle spectroscopic ellipsometer. The complex dielectric function of the laser ablated films was reproducible from run to run, and was found to be within 10 percent of that previously reported for (001) oriented single crystals. A dielectric overlayer was observed in these films, with an index of refraction of approximately 1.55 and nearly zero absorption. For the laser ablated films the optical properties were essentially independent of substrate material. The magnitude of the dielectric function obtained for the co-evaporated films was much lower than the value reported for single crystals, and was sample dependent. Author

A91-53236* National Aeronautics and Space Administration. Lewis Research Center, Cleveland, OH.

DIELECTRIC FUNCTION OF INGAAS IN THE VISIBLE

S. A. ALTEROVITZ (NASA, Lewis Research Center, Cleveland, OH), H. D. YAO (NASA, Lewis Research Center, Cleveland, OH), P. G. SNYDER, J. A. WOOLAM (Nebraska, University, Lincoln), J. PAMULAPATI, P. K. BHATTACHARYA (Michigan, University, Ann Arbor), P. A. SEKULA-MOISE (Spire Corp., Bedford, MA), and R. E. SIEG International Conference on Electronic Materials, 2nd, Newark, NJ, Sept. 17-19, 1990, Paper. p. a. Previously announced in STAR as N90-26683. refs
(Contract NAG3-988; NAS3-25867)
Copyright

Measurements are reported of the dielectric function of thermodynamically stable In_xGa_(1-x)As in the composition range 0.3 equal to or less than X = to or less than 0.7. The optically thick samples of InGaAs were made by molecular beam epitaxy (MBE) in the range 0.4 = to or less than X = to or less than 0.7 and by metal-organic chemical vapor deposition (MOCVD) for X = 0.3. The MBE made samples, usually 1 micron thick, were grown on semi-insulating InP and included a strain release structure. The MOCVD sample was grown on GaAs and was 2 microns thick. The dielectric functions were measured by variable angle spectroscopic ellipsometry in the range 1.55 to 4.4 eV. The data was analyzed assuming an optically thick InGaAs material with an oxide layer on top. The thickness of this layer was estimated by comparing the results for the InP lattice matched material, i.e., X = 0.53, with results published in the literature. The top oxide layer mathematically for X = 0.3 and X = 0.53 was removed to get the dielectric function of the bare InGaAs. In addition, the dielectric function of GaAs in vacuum, after a protective arsenic layer was removed. The dielectric functions for X = 0, 0.3, and 0.53 together with the X = 1 result from the literature to evaluate an algorithm for calculating the dielectric function of InGaAs for an arbitrary value of X (0 = to or less than X = to or less than 1) were used. Results of the dielectric function calculated using the algorithm were compared with experimental data. Author

A91-53707*# National Aeronautics and Space Administration. Lewis Research Center, Cleveland, OH.

HIGH TEMPERATURE SUPERCONDUCTOR ANALOG ELECTRONICS FOR MILLIMETER-WAVELENGTH COMMUNICATIONS

R. R. ROMANOFKY and K. B. BHASIN (NASA, Lewis Research Center, Cleveland, OH) AIAA, NASA, and OAI, Conference on Advanced SEI Technologies, Cleveland, OH, Sept. 4-6, 1991. 7 p. Previously announced in STAR as N91-29982. refs
(AIAA PAPER 91-3592) Copyright

The performance of high temperature superconductor (HTS) passive microwave circuits up to X-band was encouraging when compared to their metallic counterparts. The extremely low surface resistance of HTS films up to about 10 GHz enables a reduction in loss by as much as 100 times compared to copper when both materials are kept at about 77 K. However, a superconductor's surface resistance varies in proportion to the frequency squared. Consequently, the potential benefit of HTS materials to millimeter-wave communications requires careful analysis. A simple ring resonator was used to evaluate microstrip losses at Ka-band. Additional promising components were investigated such as antennas and phase shifters. Prospects for HTS to favorable impact millimeter-wave communications systems are discussed. Author

A91-54969* National Aeronautics and Space Administration. Lewis Research Center, Cleveland, OH.

SPATIAL VARIATIONS IN A.C. SUSCEPTIBILITY AND MICROSTRUCTURE FOR THE YBa₂Cu₃O_{7-x} SUPERCONDUCTOR AND THEIR CORRELATION WITH ROOM-TEMPERATURE ULTRASONIC MEASUREMENTS

DON J. ROTH, ALOYSIUS F. HEPP (NASA, Lewis Research Center, Cleveland, OH), MARK R. DEGUIRE (Case Western Reserve University, Cleveland, OH), and LEONARD E. DOLHERT (W.R. Grace and Co., Columbia, MD) Journal of Materials

Research (ISSN 0884-2914), vol. 6, Oct. 1991, p. 2041-2053. Previously announced in STAR as N91-21553. refs Copyright

The spatial (within-sample) uniformity of superconducting behavior and microstructure in $\text{YBa}_2\text{Cu}_3\text{O}_{7-x}$ specimens over the pore fraction range of 0.10 to 0.25 was examined. The viability of using a room-temperature, nondestructive characterization method (ultrasonic velocity imaging) to predict spatial variability was determined. Spatial variations in superconductor properties were observed for specimens containing 0.10 pore fraction. An ultrasonic velocity image constructed from measurements at 1 mm increments across one such specimen revealed microstructural variation between edge and center locations that correlated with variations in alternating-current shielding and loss behavior. Optical quantitative image analysis on sample cross-sections revealed pore fraction to be the varying microstructural feature. Author

N91-10780* National Aeronautics and Space Administration. Lewis Research Center, Cleveland, OH.

DETERMINATION OF SURFACE RESISTANCE AND MAGNETIC PENETRATION DEPTH OF SUPERCONDUCTING $\text{YBa}_2\text{Cu}_3\text{O}_{7-\Delta}$ THIN FILMS BY MICROWAVE POWER TRANSMISSION MEASUREMENTS

K. B. BHASIN, J. D. WARNER, F. A. MIRANDA, W. L. GORDON, and H. S. NEWMAN (Naval Research Lab., Washington, DC.) Sep. 1990 7 p Presented at the Applied Superconductivity Conference, Aspen, CO, 24-28 Sep. 1990; sponsored in part by IEEE

(Contract RTOP 506-44-20)

(NASA-TM-103616; E-5743; NAS 1.15:103616) Avail: NTIS HC/MF A02 CSCL 20L

A novel waveguide power transmission measurement technique was developed to extract the complex conductivity of superconducting thin films at microwave frequencies. The microwave conductivity was taken of two laser ablated $\text{YBa}_2\text{Cu}_3\text{O}_{7-\Delta}$ thin films on LaAlO_3 with transition temperatures of approx. 86.3 and 82 K, respectively, in the temperature range 25 to 300 K. From the conductivity values, the penetration depth was found to be approx. 0.54 and 0.43 micron, and the surface resistance ($R_{\text{sub s}}$) to be approx. 24 and 36 micro-Ohms at 36 GHz and 76 K for the two films under consideration. The $R_{\text{sub s}}$ values were compared with those obtained from the change in the Q-factor of a 36 GHz Te sub 011-mode (OFHC) copper cavity by replacing one of its end walls with the superconducting sample. This technique allows noninvasive characterization of high transition temperature superconducting thin films at microwave frequencies. Author

N91-11555* National Aeronautics and Space Administration. Lewis Research Center, Cleveland, OH.

MIS CAPACITOR STUDIES ON SILICON CARBIDE SINGLE CRYSTALS Final Report, 8 May - 8 Nov. 1989

J. J. KOPANSKI (National Inst. of Standards and Technology, Gaithersburg, MD.) Sep. 1990 43 p (Contract NASA ORDER C-30018-M; NASA ORDER C-30007-K) (NASA-CR-187350; NAS 1.26:187350; PB90-257718; NISTIR-4352) Avail: NTIS HC/MF A03 CSCL 20L

Cubic SiC metal-insulator-semiconductor (MIS) capacitors with thermally grown or chemical-vapor-deposited (CVD) insulators were characterized by capacitance-voltage (C-V), conductance-voltage (G-V), and current-voltage (I-V) measurements. The purpose of these measurements was to determine the four charge densities commonly present in an MIS capacitor (oxide fixed charge, $N(\text{f})$; interface trap level density, $D(\text{it})$; oxide trapped charge, $N(\text{ot})$; and mobile ionic charge, $N(\text{m})$) and to determine the stability of the device properties with electric-field stress and temperature. The section headings in the report include the following: Capacitance-voltage and conductance-voltage measurements; Current-voltage measurements; Deep-level transient spectroscopy; and Conclusions (Electrical characteristics of SiC MIS capacitors).

GRA

N91-14050* National Aeronautics and Space Administration. Lewis Research Center, Cleveland, OH.

AN X RAY PHOTOELECTRON SPECTROSCOPY STUDY OF $\text{Au}(\text{X})\text{IN}(\text{Y})$ ALLOYS

DOUGLAS T. JAYNE, NAVID S. FATEMI (Sverdrup Technology, Inc., Brook Park, OH.), and VICTOR G. WEIZER Nov. 1990 18 p Presented at the 37th Annual National Symposium, Toronto, Ontario, 8-12 Oct. 1990; sponsored by the American Vacuum Society

(Contract NAS3-25266; NAG3-696; RTOP 505-43-11)

(NASA-TM-103659; E-5745; NAS 1.15:103659) Avail: NTIS HC/MF A03 CSCL 20/12

Four gold-indium alloys were studied by x ray photoelectron spectroscopy. The binding energies and intensity ratios of the $\text{Au } 4f_{7/2}$ and $\text{In } 3d_{5/2}$ core levels were determined for the bulk alloy compositions of $\text{Au}(10 \text{ percent In})$, Au_3In , AuIn , and AuIn_2 . These values were determined for the native oxides on the materials, for the surfaces prepared by ion bombardment to remove the oxide and for surfaces scraped in-situ with a ceramic tool to expose the bulk composition. These results furnish calibration values that allow determination of the composition of thin films of this alloy system. In addition the binding energies add to the data base for understanding the effect of alloying on core level binding energies. As an illustration, these results are used to determine the composition of a series of alloy films formed by incongruent evaporation of an alloy charge. Author

N91-14850* National Aeronautics and Space Administration. Lewis Research Center, Cleveland, OH.

SILICON CARBIDE, A SEMICONDUCTOR FOR SPACE POWER ELECTRONICS

J. ANTHONY POWELL and LAWRENCE G. MATUS 1991 8 p Presented at the 8th Symposium on Space Nuclear Power Systems, Albuquerque, NM, 6-10 Jan. 1991; cosponsored by New Mexico Univ., Strategic Defense Initiative Organization, DOE, and AF (Contract RTOP 505-62-50)

(NASA-TM-103655; NAS 1.15:103655) Avail: NTIS HC/MF A02 CSCL 20/12

After many years of promise as a high temperature semiconductor, silicon carbide (SiC) is finally emerging as a useful electronic material. Recent significant progress that has led to this emergence has been in the areas of crystal growth and device fabrication technology. High quality single-crystal SiC wafers, up to 25 mm in diameter, can now be produced routinely from boules grown by a high temperature (2700 K) sublimation process. Device fabrication processes, including chemical vapor deposition (CVD), in situ doping during CVD, reactive ion etching, oxidation, metallization, etc. have been used to fabricate p-n junction diodes and MOSFETs. The diode was operated to 870 K and the MOSFET to 770 K. Author

N91-18299* National Aeronautics and Space Administration. Lewis Research Center, Cleveland, OH.

SURFACE AND IMPLANTATION EFFECTS ON P-N JUNCTIONS

SAMUEL E. SCHACHAM and ELIEZER FINKMAN (Technion - Israel Inst. of Tech., Haifa.) In its Solid State Technology Branch of NASA Lewis Research Center Second Annual Digest, June 1989 - June 1990 p 201-204 Jun. 1990 Avail: NTIS HC/MF A13 CSCL 20/12

The contribution of the graded region of implanted p-n junctions is analyzed using an exponential profile. Though previously neglected, it was recently shown that this contribution to the saturation current of HgCdTe diodes is significant. Assuming a dominant Auger recombination, an analytical solution to the continuity equation is obtained. An expression for the current generation by the graded region is presented for both ohmic and reflecting boundary conditions. A revised condition for a wide region is derived. When the region is narrow, the current differs drastically from that of the zero-gradient case. The effects of the junction depth and the substrate and surface concentrations on the current are investigated. It is shown that the reverse current does not saturate. Author

N91-18300*# National Aeronautics and Space Administration. Lewis Research Center, Cleveland, OH.

PROPERTIES OF INSULATOR INTERFACES WITH P-HGCDTE
SAMUEL E. SCHACHAM and ELIEZER FINKMAN (Technion - Israel Inst. of Tech., Haifa.) *In its* Solid State Technology Branch of NASA Lewis Research Center Second Annual Digest, June 1989 - June 1990 p 205-207 Jun. 1990 Repr. from Journal of Vacuum Science Technology, v. 8, no. 2, Mar./Apr. 1990
Avail: NTIS HC/MF A13 CSCL 20/12

Heat treatment at 70 C of low carrier concentration p-type HgCdTe samples ($p_{sub} = 8 \times 10^{14}/cm^3$) generates an inverted surface layer. A two day anneal process below 95 C did not affect the Hall coefficient, whereas an almost complete recovery was obtained by annealing at 120 C. While bulk electron mobility, obtained from PEM data, remained high (about 9×10^4 cm²/V s at 77 K), surface mobility is lower by more than an order of magnitude. Surface recombination velocity indicates a continuous improvement with increased temperature, and the activation energy remains equal to the vacancies energy level. The proposed mechanism is that of positive changes in the sulfide migrating towards the interface and generating an image inversion layer.

Author

N91-18301*# National Aeronautics and Space Administration. Lewis Research Center, Cleveland, OH.

SURFACE ELECTRONS IN INVERTED LAYERS OF P-HGCDTE
SAMUEL E. SCHACHAM and ELIEZER FINKMAN (Technion - Israel Inst. of Tech., Haifa.) *In its* Solid State Technology Branch of NASA Lewis Research Center Second Annual Digest, June 1989 - June 1990 p 208-214 Jun. 1990
Avail: NTIS HC/MF A13 CSCL 20/12

Anodic oxide passivation of p-type HgCdTe generates an inversion layer. Extremely high Hall mobility data for electrons in this layer indicated the presence of a two-dimensional electron gas. This is verified by use of the Shubnikov-de Haas effect from 1.45 to 4.15 K. Data are extracted utilizing a numerical second derivative of dc measurement. Three sub-bands are detected. Their relative occupancies are in excellent agreement with theory and with experimental results obtained on anodic oxide as accumulation layers of n-type HgCdTe. The effective mass derived is comparable to what was expected.

Author

N91-18304*# National Aeronautics and Space Administration. Lewis Research Center, Cleveland, OH.

ELLIPSOMETRIC STUDY OF CUBIC SiC Abstract Only
SAMUEL A. ALTEROVITZ, NEIL S. SHOEMAKER, and J. A. POWELL *In its* Solid State Technology Branch of NASA Lewis Research Center Second Annual Digest, June 1989 - June 1990 p 239 Jun. 1990
Avail: NTIS HC/MF A13 CSCL 20/12

Variable angle spectroscopic ellipsometry (VASE) was applied to cubic SiC. This technique gives absolute values of the refractive index (n) and the extinction coefficient (k) of a substrate and/or a thin film of unknown material. The samples were grown by chemical vapor deposition (CVD) on p-type silicon. The substrate was aligned either on the (001) axis or 1 degree of (001). Several growth temperatures and growth durations were used. The samples were divided into two groups: (1) thick films of order 10 microns grown near optimal conditions of temperature, flow, and gas ratio; and (2) thin films of order 100 Å grown at various temperatures. The ellipsometric results for samples in group 1 were analyzed using a two-phase model (substrate and ambient). Results show that for wavelengths in the visible, the refractive index of these CVD samples is equal to that reported for single crystal cubic SiC, within the experimental error, which is on the order of 1 percent. However, the extinction coefficient has a relatively large value, even above the band gap. The absorption is sample dependent and has a broad peak in the visible. The results for samples in group 2 were analyzed using a three-phase model (substrate, film, and ambient). The dielectric functions of the film, deducted from the measured n and k , were further analyzed using the effective medium approximation. The results show that the films contain 30

to 40 vol. percent amorphous silicon, i.e., silicon with only short-range order.
Author

N91-19935*# National Aeronautics and Space Administration. Lewis Research Center, Cleveland, OH.

STUDY OF INGAAS BASED MODFET STRUCTURES USING VARIABLE ANGLE SPECTROSCOPIC ELLIPSOMETRY

S. A. ALTEROVITZ, R. M. SIEG, H. D. YAO, P. G. SNYDER, J. A. WOOLLAM, J. PAMULAPATI, P. K. BHATTACHARYA, and P. A. SEKULA-MOISE (Spire Corp., Bedford, MA.) Apr. 1991 14 p Presented at the International Conference on Metallurgical Coatings and Thin Films, San Diego, CA, 22-26 Apr. 1991; sponsored by American Vacuum Society (Contract RTOP 506-44-21) (NASA-TM-103792; E-6069; NAS 1.15:103792) Avail: NTIS HC/MF A03 CSCL 20/12

Variable angle spectroscopic ellipsometry was used to estimate the thicknesses of all layers within the optical penetration depth of InGaAs based MODFET structures. Strained and unstrained InGaAs channels were made by MBE on InP substrates and by MOCVD on GaAs substrates. In most cases, ellipsometrically determined thicknesses were within 10 percent of the growth calibration results. The MBE made InGaAs strained layers showed large strain effects, indicating a probable shift in the critical points of their dielectric function toward the InP lattice matched concentration.
Author

N91-21910*# National Aeronautics and Space Administration. Lewis Research Center, Cleveland, OH.

THE SERIES $Bi_2Sr_2Ca(n-1)Cu(n)O(2n+4)$ (1 LESS THAN OR EQUAL TO n LESS THAN OR EQUAL TO 5): PHASE STABILITY AND SUPERCONDUCTING PROPERTIES
MARK R. DEGUIRE, NAROTTAM P. BANSAL, DAVID E. FARRELL, VALERIE FINAN, CHEOL J. KIM, BETHANIE J. HILLS, and CHRISTOPHER J. ALLEN (Case Western Reserve Univ., Cleveland, OH.) 1989 20 p Presented at the 91st Annual Meeting of the American Ceramic Society, Indianapolis, IN, 23-27 Apr. 1989 (Contract RTOP 307-51-00) (NASA-TM-103749; E-6000; NAS 1.15:103749) Avail: NTIS HC/MF A03 CSCL 20/12

Phase relations at 850 and 870 C, melting transitions in air, oxygen, and helium were studied for $Bi(2.1)Sr(1.9)CuO_6$ and for the $Bi_2Sr_2Ca(n-1)Cu(n)O(2n+4)$ for $n = 1, 2, 3, 4, 5$, and infinity ($CaCuO_2$). Up to 870 C, the $n = 2$ composition resides in the compatibility tetrahedron bounded by $Bi(2+x)(Sr,Ca)(3-y)Cu_2O_8$, $(Sr,Ca)_{14}Cu_{24}O_{41}$, Ca_2CuO_3 , and a Bi-Sr-Ca-O phase. The n is greater than or equal to 3 compositions reside in the compatibility tetrahedron $Bi(2+x)(Sr,Ca)(3-y)Cu_2O_8 - (Sr,Ca)_{14}Cu_{24}O_{41} - Ca_2CuO_3 - CuO$ up to 850 C. However, $Bi(2+x)Sr(4-y)Cu_3O_{10}$ forms for n is greater than or equal to 3 after extended heating at 870 C. $Bi(2+x)Sr(2-y)CuO_6$ and $Bi(2+x)(Sr,Ca)(3-y)Cu_2O_8$ melt in air at 914 C and 895 C respectively. During melting, all of the compositions studied lose 1 to 2 percent by weight of oxygen from the reduction of copper. $Bi(2+x)Sr(2-y)CuO_6$, $Bi(2+n)(Sr,Ca)(3-y)Cu_2O_8$, and $Bi(2+x)(Sr,Ca)(4-y)Cu_3O_{10}$ exhibit crystallographic alignment in a magnetic field, with the c-axes orienting parallel to the field.
Author

N91-22179*# National Aeronautics and Space Administration. Lewis Research Center, Cleveland, OH.

APPLICATIONS OF THIN FILM TECHNOLOGY TOWARD A LOW-MASS SOLAR POWER SATELLITE

GEOFFREY A. LANDIS (Sverdrup Technology, Inc., Brook Park, OH.) and RONALD C. CULL *In its* Vision-21: Space Travel for the Next Millennium p 494-500 Apr. 1990
Avail: NTIS HC/MF A25 CSCL 20/12

Previous concepts for solar power satellites have used conventional-technology photovoltaics and microwave tubes. The authors propose using thin film photovoltaics and an integrated solid state phased array to design an ultra-lightweight solar power satellite, resulting in a potential reduction in weight by a factor of ten to a hundred over conventional concepts for solar power satellites.
Author

N91-22921*# National Aeronautics and Space Administration. Lewis Research Center, Cleveland, OH.

DEVELOPMENT OF SILICON CARBIDE SEMICONDUCTOR DEVICES FOR HIGH TEMPERATURE APPLICATIONS

LAWRENCE G. MATUS, J. ANTHONY POWELL, and JEREMY B. PETIT (Sverdrup Technology, Inc., Brook Park, OH.) 1991 9 p
Presented at the First International High Temperature Electronics Conference, Albuquerque, NM, 16-20 Jun. 1991; sponsored by Sandia National Labs., AF Wright Research and Development Center, and New Mexico Univ.
(Contract RTOP 505-62-50)

(NASA-TM-104398; E-6217; NAS 1.15:104398) Avail: NTIS HC/MF A02 CSCL 20/12

The semiconducting properties of electronic grade silicon carbide crystals, such as wide energy bandgap, make it particularly attractive for high temperature applications. Applications for high temperature electronic devices include instrumentation for engines under development, engine control and condition monitoring systems, and power conditioning and control systems for space platforms and satellites. Discrete prototype SiC devices were fabricated and tested at elevated temperatures. Grown p-n junction diodes demonstrated very good rectification characteristics at 870 K. A depletion-mode metal-oxide-semiconductor field-effect transistor was also successfully fabricated and tested at 770 K. While optimization of SiC fabrication processes remain, it is believed that SiC is an enabling high temperature electronic technology.

Author

N91-23946*# National Aeronautics and Space Administration. Lewis Research Center, Cleveland, OH.

ADVANCES IN SILICON CARBIDE CHEMICAL VAPOR DEPOSITION (CVD) FOR SEMICONDUCTOR DEVICE FABRICATION

J. ANTHONY POWELL, JEREMY B. PETIT (Sverdrup Technology, Inc., Brook Park, OH.), and LAWRENCE G. MATUS 1991 8 p
Presented at the First International High Temperature Electronics Conference, Albuquerque, NM, 16-20 Jun. 1991; sponsored by Sandia National Labs., AF Wright Research and Development Center, and New Mexico Univ.
(Contract RTOP 505-62-50)

(NASA-TM-104410; E-6237; NAS 1.15:104410) Avail: NTIS HC/MF A02 CSCL 20/12

Improved SiC chemical vapor deposition films of both 3C and 6H polytypes were grown on vicinal (0001) 6H-SiC wafers cut from single-crystal boules. These films were produced from silane and propane in hydrogen at one atmosphere at a temperature of 1725 K. Among the more important factors which affected the structure and morphology of the grown films were the tilt angle of the substrate, the polarity of the growth surface, and the pregrowth surface treatment of the substrate. With proper pregrowth surface treatment, 6H films were grown on 6H substrates with tilt angles as small as 0.1 degrees. In addition, 3C could be induced to grow within selected regions on a 6H substrate. The polarity of the substrate was a large factor in the incorporation of dopants during epitaxial growth. A new growth model is discussed which explains the control of SiC polytype in epitaxial growth on vicinal (0001) SiC substrates.

Author

N91-24061*# National Aeronautics and Space Administration. Lewis Research Center, Cleveland, OH.

SILICON CARBIDE, AN EMERGING HIGH TEMPERATURE SEMICONDUCTOR

LAWRENCE G. MATUS and J. ANTHONY POWELL *In* NASA, Washington, Technology 2000, Volume 2 p 171-178 1991
Avail: NTIS HC/MF A16 CSCL 20/12

In recent years, the aerospace propulsion and space power communities have expressed a growing need for electronic devices that are capable of sustained high temperature operation. Applications for high temperature electronic devices include development instrumentation within engines, engine control, and condition monitoring systems, and power conditioning and control systems for space platforms and satellites. Other earth-based applications include deep-well drilling instrumentation, nuclear

reactor instrumentation and control, and automotive sensors. To meet the needs of these applications, the High Temperature Electronics Program at the Lewis Research Center is developing silicon carbide (SiC) as a high temperature semiconductor material. Research is focussed on developing the crystal growth, characterization, and device fabrication technologies necessary to produce a family of silicon carbide electronic devices and integrated sensors. The progress made in developing silicon carbide is presented, and the challenges that lie ahead are discussed.

Author

N91-24080*# National Aeronautics and Space Administration. Lewis Research Center, Cleveland, OH.

AEROSPACE APPLICATIONS OF HIGH TEMPERATURE SUPERCONDUCTIVITY

V. O. HEINEN and D. J. CONNOLLY *In* NASA, Washington, Technology 2000, Volume 2 p 343-345 1991

Avail: NTIS HC/MF A16 CSCL 20/12

Space application of high temperature superconducting (HTS) materials may occur before most terrestrial applications because of the passive cooling possibilities in space and because of the economic feasibility of introducing an expensive new technology which has a significant system benefit in space. NASA Lewis Research Center has an ongoing program to develop space technology capitalizing on the potential benefit of HTS materials. The applications being pursued include space communications, power and propulsion systems, and magnetic bearings. In addition, NASA Lewis is pursuing materials research to improve the performance of HTS materials for space applications.

Author

N91-24081*# National Aeronautics and Space Administration. Lewis Research Center, Cleveland, OH.

SUPERCONDUCTING MICROWAVE ELECTRONICS AT LEWIS RESEARCH CENTER

JOSEPH D. WARNER, KUL B. BHASIN, and REGIS F. LEONARD *In* NASA, Washington, Technology 2000, Volume 2 p 346-354 1991

Avail: NTIS HC/MF A16 CSCL 20/12

Over the last three years, NASA Lewis Research Center has investigated the application of newly discovered high temperature superconductors to microwave electronics. Using thin films of YBa₂Cu₃O_{7-delta} and Tl₂Ca₂Ba₂Cu₃O_x deposited on a variety of substrates, including strontium titanate, lanthanum gallate, lanthanum aluminate and magnesium oxide, a number of microwave circuits have been fabricated and evaluated. These include a cavity resonator at 60 GHz, microstrip resonators at 35 GHz, a superconducting antenna array at 35 GHz, a dielectric resonator at 9 GHz, and a microstrip filter at 5 GHz. Performance of some of these circuits as well as suggestions for other applications are reported.

Author

N91-26966*# National Aeronautics and Space Administration. Lewis Research Center, Cleveland, OH.

PROCESS FOR THE CONTROLLED GROWTH OF SINGLE-CRYSTAL FILMS OF SILICON CARBIDE POLYTYPES ON SILICON CARBIDE WAFERS Patent Application

J. ANTHONY POWELL, inventor (to NASA) 12 Jun. 1991 20 p
(NASA-CASE-LEW-15222-1; NAS 1.71:LEW-15222-1; US-PATENT-APPL-SN-718315) Avail: NTIS HC/MF A03 CSCL 20/11

This invention is a method for the controlled growth of single-crystal semiconductor device quality films of SiC polytypes on vicinal (0001) SiC wafers with low tilt angles. Both homoepitaxial and heteroepitaxial SiC films can be produced on the same wafer. In particular, 3C-SiC and 6H-SiC films can be produced within selected areas of the same 6H-SiC wafer.

NASA

N91-26967*# National Aeronautics and Space Administration. Lewis Research Center, Cleveland, OH.

PROCESS FOR THE HOMOEPITAXIAL GROWTH OF SINGLE-CRYSTAL SILICON CARBIDE FILMS ON SILICON CARBIDE WAFERS Patent Application

J. ANTHONY POWELL, inventor (to NASA) 12 Jun. 1991 15 p

(NASA-CASE-LEW-15223-1; NAS 1.71:LEW-15223-1; US-PATENT-APPL-SN-718314) Avail: NTIS HC/MF A03 CSCL 20/12

The invention is a method for growing homoepitaxial films of SiC on low tilt angle vicinal (0001) SiC wafers. The invention proposes and teaches a new theoretical model for the homoepitaxial growth of SiC films on (0001) SiC substrates. The inventive method consists of (1) preparing the growth surface of SiC wafers slightly off-axis (from less the 0.1 to 6 deg) from the (0001) plane, (2) subjecting the growth surface to a suitable etch, and then (3) growing the homoepitaxial film using conventional SiC growth techniques. NASA

N91-29982* National Aeronautics and Space Administration. Lewis Research Center, Cleveland, OH.

HIGH TEMPERATURE SUPERCONDUCTOR ANALOG ELECTRONICS FOR MILLIMETER-WAVELENGTH COMMUNICATIONS

R. R. ROMANOFFSKY and K. B. BHASIN 1991 8 p Presented at the Conference on Advanced Space Exploration Initiative Technologies, Cleveland, OH, 4-6 Sep. 1991; cosponsored by AIAA and OAI

(Contract RTOP 506-44-21)

(NASA-TM-105184; E-6481; NAS 1.15:105184; AIAA PAPER 91-3592) Avail: NTIS HC/MF A02 CSCL 20/12

The performance of high temperature superconductor (HTS) passive microwave circuits up to X-band was encouraging when compared to their metallic counterparts. The extremely low surface resistance of HTS films up to about 10 GHz enables a reduction in loss by as much as 100 times compared to copper when both materials are kept at about 77 K. However, a superconductor's surface resistance varies in proportion to the frequency squared. Consequently, the potential benefit of HTS materials to millimeter-wave communications requires careful analysis. A simple ring resonator was used to evaluate microstrip losses at Ka-band. Additional promising components were investigated such as antennas and phase shifters. Prospects for HTS to favorable impact millimeter-wave communications systems are discussed. Author

N91-31962* National Aeronautics and Space Administration. Lewis Research Center, Cleveland, OH.

CRYSTALLIZATION AND CHARACTERIZATION OF Y2O3-SiO2 GLASSES

CHARLES H. DRUMMOND, III, WILLIAM E. LEE (Ohio State Univ., Columbus.), W. A. SANDERS, and J. D. KISER In Ohio State Univ., Crystallization of the Glassy Grain Boundary Phase in Silicon Nitride Ceramics 18 p Aug. 1991 Repr. from Ceram. Eng. Sci. Proc., 9(9-10) 1988 p 1343-1354 Previously announced in IAA as A89-19486

Avail: NTIS HC/MF A05 CSCL 20/2

Glasses in the yttria-silica system with 20 to 40 mol pct Y2O3 were subjected to recrystallization studies after melting at 1900 to 2100 C in W crucibles in 1 and 50 atm N2. The TEM and XRD results obtained indicate the presence of the delta, gamma, gamma prime, and beta-Y2Si2O7 crystalline phases, depending on melting and quenching conditions. Heat treatment in air at 1100 to 1600 C increased the amount of crystallization, and led to the formation of Y2SiO5, cristaballite, and polymorphs of Y2Si2O7. Also investigated were the effects of 5 and 10 wt pct zirconia additions. Author

N91-31977* National Aeronautics and Space Administration. Lewis Research Center, Cleveland, OH.

NEAR-EDGE STUDY OF GOLD-SUBSTITUTED YBa2Cu3O(7-DELTA)

MARK W. RUCKMAN (Brookhaven National Lab., Upton, NY.) and ALOYSIUS F. HEPP Sep. 1991 11 p (Contract DE-AC02-76CH-00016; DE-AC05-80ER-10742; RTOP 506-41-11)

(NASA-TM-105220; E-6509; NAS 1.15:105220) Avail: NTIS HC/MF A03 CSCL 20/12

The valence of Cu and Au in YBa2Au0.3Cu2.7O7-delta was investigated using x-ray absorption near edge structure (XANES).

X-ray and neutron diffraction studies indicate that Au goes on the Cu(1) site and Cu K-edge XANES shows that this has little effect on the oxidation state of the remaining copper. The Au L3 edge develops a white line feature whose position lies between that of trivalent gold oxide and monovalent potassium gold cyanide, and whose height relative to the edge step is smaller than in the two reference compounds. The appearance of the Au L3 edge suggests that fewer Au 3d states are involved in forming the Au-O bond in YBa2Au0.3Cu2.7O7-delta than in trivalent gold oxide. Author

77

THERMODYNAMICS AND STATISTICAL PHYSICS

Includes quantum mechanics; theoretical physics; and Bose and Fermi statistics.

A91-16103* National Aeronautics and Space Administration. Lewis Research Center, Cleveland, OH.

CRITICAL-POINT ANALYSIS OF THE LIQUID-VAPOR INTERFACIAL SURFACE TENSION

R. E. SALVINO (NASA, Lewis Research Center; Sverdrup Technology, Inc., Cleveland, OH) Physical Review A (ISSN 1050-2947), vol. 42, Nov. 15, 1990, p. 6079-6086. refs (Contract NAS3-25266)

Copyright

The interfacial surface tension of the liquid-vapor system is analyzed near the critical point in a manner similar to bulk thermodynamic critical-point analyses. This is accomplished by a critical-point analysis of the single-phase hard-wall surface tension. Both a Landau expansion and a scaling theory equation of state are investigated. Some general exponent relations are derived and, in addition, some thermodynamically defined correlation lengths are discussed. Author

A91-19495* National Aeronautics and Space Administration. Lewis Research Center, Cleveland, OH.

NEWTONIAN MECHANICS OF A MANY-PARTICLE ASSEMBLY COUPLED TO AN EXTERNAL BODY POTENTIAL

R. E. SALVINO (NASA, Lewis Research Center; Sverdrup Technology, Inc., Cleveland, OH) Physical Review A (ISSN 1050-2947), vol. 42, Dec. 15, 1990, p. 7236-7243. refs (Contract NAS3-25266)

The Newtonian mechanics of a many-particle system evolving in time under the influence of an external body potential, that is, an external potential that couples to the center of mass only, is examined. The lack of any other external fields allows the complete separation of the center-of-mass (or external-field-dependent) equations from the internal (or external-field-independent) dynamics. The complete solution of the center-of-mass motion then allows an analytical evaluation of the external body potential contributions to the thermophysical properties of the system. The phenomena of field-induced heating, Taylor-Aris hydrodynamic form for the diffusion tensor, and an analogous hydrodynamic form for the viscosity tensor are derived from microscopic principles. A brief and model-dependent description of equilibrium phenomena is also presented. Author

81

ADMINISTRATION AND MANAGEMENT

Includes management planning and research.

A91-16900* National Aeronautics and Space Administration. Lewis Research Center, Cleveland, OH.
SPECULATING ON SPACE FUTURES

82 DOCUMENTATION AND INFORMATION SCIENCE

MARC G. MILLIS (NASA, Lewis Research Center, Cleveland, OH)
Space Policy (ISSN 0265-9646), vol. 6, Nov. 1990, p. 353-356.
Copyright

A volunteer group of engineers and scientists at NASA's Lewis Research Center is trying to push the frontiers of aerospace science and technology beyond the realm of conventional methods and concepts. The first step is to provide a supportive environment for ideas that are too speculative or high risk to warrant formal organizational responsibility. This report describes the motivation, birth and experiences of this group. Author

82

DOCUMENTATION AND INFORMATION SCIENCE

Includes information management; information storage and retrieval technology; technical writing; graphic arts; and micrography.

N91-10798*# National Aeronautics and Space Administration. Lewis Research Center, Cleveland, OH.

BIBLIOGRAPHY OF LEWIS RESEARCH CENTER TECHNICAL PUBLICATIONS ANNOUNCED IN 1989

May 1990 399 p
(NASA-TM-102542; E-5352; NAS 1.15:102542) Avail: NTIS HC/MF A17 CSCL 05B

This compilation of abstracts describes and indexes the technical reporting that resulted from the scientific and engineering work performed and managed by the Lewis Research Center in 1989. All the publications were announced in the 1989 issues of STAR (Scientific and Technical Aerospace Reports) and/or IAA (International Aerospace Abstracts). Included are research reports, journal articles, conference presentations, patents and patent applications, and theses. Author

83

ECONOMICS AND COST ANALYSIS

Includes cost effectiveness studies.

N91-24952*# National Aeronautics and Space Administration. Lewis Research Center, Cleveland, OH.

BALANCING RELIABILITY AND COST TO CHOOSE THE BEST POWER SUBSYSTEM

RONALD C. SUICH (California State Univ., Fullerton.) and RICHARD L. PATTERSON 1991 7 p Presented at the 26th Intersociety Energy Conversion Engineering Conference, Boston, MA, 4-9 Aug. 1991; sponsored by the American Nuclear Society, SAE, the American Chemical Society, AIAA, ASME, IEE, and the American Inst. of Chemical Engineers
(Contract NAG3-1100; RTOP 506-41-41)
(NASA-TM-104453; E-6294; NAS 1.15:104453) Avail: NTIS HC/MF A02 CSCL 05/3

A mathematical model is presented for computing total (spacecraft) subsystem cost including both the basic subsystem cost and the expected cost due to the failure of the subsystem. This model is then used to determine power subsystem cost as a function of reliability and redundancy. Minimum cost and maximum reliability and/or redundancy are not generally equivalent. Two example cases are presented. One is a small satellite, and the other is an interplanetary spacecraft. Author

N91-33014*# National Aeronautics and Space Administration. Lewis Research Center, Cleveland, OH.

RELIABILITY AND COST: A SENSITIVITY ANALYSIS

RONALD C. SUICH (California State Univ., Fullerton.) and RICHARD L. PATTERSON Oct. 1991 14 p

(Contract NAG3-1100; RTOP 506-41-41)

(NASA-TM-105293; E-6631; NAS 1.15:105293) Avail: NTIS HC/MF A03 CSCL 05/3

In the design phase of a system, how a design engineer or manager choose between a subsystem with .990 reliability and a more costly subsystem with .995 reliability is examined, along with the justification of the increased cost. High reliability is not necessarily an end in itself but may be desirable in order to reduce the expected cost due to subsystem failure. However, this may not be the wisest use of funds since the expected cost due to subsystem failure is not the only cost involved. The subsystem itself may be very costly. The cost of the subsystem nor the expected cost due to subsystem failure should not be considered separately but the total of the two costs should be maximized, i.e., the total of the cost of the subsystem plus the expected cost due to subsystem failure. Author

85

URBAN TECHNOLOGY AND TRANSPORTATION

Includes applications of space technology to urban problems; technology transfer; technology assessment; and surface and mass transportation.

N91-31023*# National Aeronautics and Space Administration. Lewis Research Center, Cleveland, OH.

STATUS OF THE ADVANCED STIRLING CONVERSION SYSTEM PROJECT FOR 25 KW DISH STIRLING APPLICATIONS Final Report

RICHARD K. SHALTENS and JEFFREY G. SCHREIBER 1991 11 p Presented at the 26th Intersociety Energy Conversion Engineering Conference, Boston, MA, 4-9 Aug. 1991; cosponsored by ANS, SAE, ACS, AIAA, ASME, IEEE, and AIChE
(Contract DE-AL04-85AL-33408; RTOP 776-81-63)
(NASA-TM-104528; E-6404; DOE/NASA/33408-5; NAS 1.15:104528) Avail: NTIS HC/MF A03 CSCL 10/2

Heat engines were evaluated for terrestrial Solar Distributed Heat Receivers. The Stirling engine was identified as one of the most promising heat engines for terrestrial applications. Technology development is also conducted for Stirling convertors directed toward a dynamic power source for space applications. Space power requirements include high reliability with very long life, low vibration, and high system efficiency. The free-piston Stirling engine has the potential for future high power space conversion systems, either nuclear or solar powered. Although both applications appear to be quite different, their requirements complement each other. Author

90

ASTROPHYSICS

Includes cosmology; celestial mechanics; space plasmas; and interstellar and interplanetary gases and dust.

A91-12343* Chicago Univ., IL.

CHARACTERISTIC MICROWAVE-BACKGROUND DISTORTIONS FROM COLLAPSING SPHERICAL DOMAIN WALLS

GUENTER GOETZ and DIRK NOTZOLD (Chicago, University; NASA/Fermilab Astrophysics Center, Batavia, IL) Physical Review Letters (ISSN 0031-9007), vol. 65, Oct. 29, 1990, p. 2229-2232. refs

(Contract NSF AST-88-22595; NAGW-1321; NAGW-1340)
Copyright

The redshift distortion induced by collapsing spherical domain

walls is calculated. The most frequent microwave background distortions are found to occur at large angles in the form of blue disks. This is the angular region currently measured by the COBE satellite. COBE could therefore detect signals predicted here for domain walls with surface energy density of the order of MeV. Such values for σ are proposed in the late-time phase-transition scenario of Hill et al. (1989). C.D.

A91-19545* Massachusetts Inst. of Tech., Cambridge.

NATURAL INFLATION WITH PSEUDO NAMBU-GOLDSTONE BOSONS

KATHERINE FREESE (MIT, Cambridge, MA), JOSHUA A. FRIEMAN, and ANGELA V. OLINTO (NASA/Fermilab Astrophysics Center, Batavia, IL) Physical Review Letters (ISSN 0031-9007), vol. 65, Dec. 24, 1990, p. 3233-3236. Research supported by NSF, Alfred P. Sloan Foundation, and DOE. refs (Contract NAGW-1320; NAGW-1340)

Copyright

It is shown that a pseudo-Nambu-Goldstone boson of given potential can naturally give rise to an epoch of inflation in the early universe. Mass scales which arise in particle physics models with a gauge group that becomes strongly interacting at a certain scales are shown to be conditions for successful inflation. The density fluctuation spectrum is nonscale-invariant, with extra power on large length scales. C.D.

A91-20430* Fermi National Accelerator Lab., Batavia, IL.

COHERENT PECULIAR VELOCITIES AND PERIODIC REDSHIFTS

CHRISTOPHER T. HILL (Fermi National Accelerator Laboratory, Batavia, IL), PAUL J. STEINHARDT (Pennsylvania, University, Philadelphia), and MICHAEL S. TURNER (NASA/Fermilab Astrophysics Center, Batavia; Chicago, University, IL) Astrophysical Journal, Part 2 - Letters (ISSN 0004-637X), vol. 366, Jan. 10, 1991, p. L57-L60. Research supported by DOE. refs (Contract NAGW-1340)

Copyright

A coherent, sinusoidal peculiar velocity field of 0.003 amplitude and wavelength of 128/h Mpc could explain the apparent redshift periodicity seen in the recent pencil-beam survey of Broadhurst et al. (1990). Such a peculiar velocity field could arise if the power spectrum of density perturbations has a strong feature at about this wavelength. This explanation has additional predictions: the phase, period, and strength of the periodicity should vary in different directions; the strength of the periodicity should decrease at higher redshifts; and there should be more 'thin' structures perpendicular to the line of sight than parallel to it. Author

A91-20491 National Aeronautics and Space Administration. Lewis Research Center, Cleveland, OH.

INFLATIONARY AXION COSMOLOGY

MICHAEL S. TURNER (NASA/Fermilab Astrophysics Center, Batavia; Chicago, University, IL) and FRANK WILCZEK (Institute for Advanced Study, Princeton, NJ) Physical Review Letters (ISSN 0031-9007), vol. 66, Jan. 7, 1991, p. 5-8. Research supported by DOE and NSF. refs (Contract NAGW-1340)

Copyright

If Peccei-Quinn (PQ) symmetry is broken after inflation, the initial axion angle is a random variable on cosmological scales; based on this fact, estimates of the relic-axion mass density give too large a value if the axion mass is less than about 10 to the -6th eV. This bound can be evaded if the universe underwent inflation after PQ-symmetry breaking and if the observable universe happens to be a region where the initial axion angle was atypically small. Consideration of fluctuations induced during inflation severely constrains the latter alternative is shown. Author

A91-26361 National Aeronautics and Space Administration. Lewis Research Center, Cleveland, OH.

THE DYNAMIC INSTABILITY OF ADIABATIC BLAST WAVES

DONGSU RYU (NASA/Fermilab Astrophysics Center, Batavia, IL) and ETHAN T. VISHNIAC (Texas, University, Austin) Astrophysical

Journal, Part 1 (ISSN 0004-637X), vol. 368, Feb. 20, 1991, p. 411-425. Research supported by DOE. Previously announced in STAR as N90-23679. refs

(Contract NAGW-1340)

Copyright

Adiabatic blastwaves, which have a total energy injected from the center E varies as $t^{(\sup q)}$ and propagate through a preshock medium with a density $\rho(\sub E)$ varies as $r(\sup -\omega)$ are described by a family of similarity solutions. Previous work has shown that adiabatic blastwaves with increasing or constant postshock entropy behind the shock front are susceptible to an oscillatory instability, caused by the difference between the nature of the forces on the two sides of the dense shell behind the shock front. This instability sets in if the dense postshock layer is sufficiently thin. The stability of adiabatic blastwaves with a decreasing postshock entropy is considered. Such blastwaves, if they are decelerating, always have a region behind the shock front which is subject to convection. Some accelerating blastwaves also have such region, depending on the values of q , ω , and γ where γ is the adiabatic index. However, since the shock interface stabilizes dynamically induced perturbations, blastwaves become convectively unstable only if the convective zone is localized around the origin or a contact discontinuity far from the shock front. On the other hand, the contact discontinuity of accelerating blastwaves is subject to a strong Rayleigh-Taylor instability. The frequency spectra of the nonradial, normal modes of adiabatic blastwaves have been calculated. The results have been applied to the shocks propagating through supernovae envelopes. It is shown that the metal/He and He/H interfaces are strongly unstable against the Rayleigh-Taylor instability. This instability will induce mixing in supernovae envelopes. In addition the implications of this work for the evolution of planetary nebulae is discussed. Author

A91-28714 Chicago Univ., IL.

TELESCOPE SEARCH FOR A 3-EV TO 8-EV AXION

MATTHEW A. BERSHADY (Chicago, University, IL), M. TED RESSELL, and MICHAEL S. TURNER (NASA/Fermilab Astrophysics Center, Batavia; Chicago, University, IL) Physical Review Letters (ISSN 0031-9007), vol. 66, March 18, 1991, p. 1398-1401. Research supported by DOE and NSF. refs (Contract NAGW-1340)

Copyright

Axions of mass 3-8 eV should have a cosmological abundance of about 50/cu cm and reside in rich clusters of galaxies. Their decays to two photons will produce a line at a wavelength of about 3100-8300 A. This effort has searched unsuccessfully for such a feature in the tergalactic light of three rich clusters, closing this 'window', and leaving open only the window from 10 to the -6th to 0.001 eV. This implies that if the axion exists, it likely comprises the dark matter. The present flux limits are of relevance to other relics whose decays produce monoenergetic photons. Author

A91-33573 Clemson Univ., SC.

THE SHOCK PROCESS AND LIGHT-ELEMENT PRODUCTION IN SUPERNOVA ENVELOPES

LAWRENCE E. BROWN (Clemson University, SC), DAVID S. DEARBORN (Lawrence Livermore National Laboratory, Livermore, CA), DAVID N. SCHRAMM (NASA/Fermilab Astrophysics Center, Batavia; Chicago, University, IL), JON T. LARSEN (Cascade Applied Sciences, Boulder, CO), and SHIN KUOKAWA (Chicago, University, IL) Astrophysical Journal, Part 1 (ISSN 0004-637X), vol. 371, April 20, 1991, p. 648-664. DOE-supported research. Previously announced in STAR as N90-28471. refs (Contract NAGW-1340)

Copyright

Detailed hydrodynamic modeling of the passage of supernova shocks through the hydrogen envelopes of blue and red progenitor stars was carried out to explore the sensitivity to model conditions of light element production (specifically Li7 and B-11) which was noted by Dearborn, Schramm, Steigman and Truran (1989) (DSST). It is found that, for stellar models with M is less than or

approximately 100 M solar mass, current state of the art supernova shocks do not produce significant light element yields by hydrodynamic processes alone. The dependence of this conclusion on stellar models and on shock strengths is explored. Preliminary implications for Galactic evolution of lithium are discussed, and it is suspected that intermediate mass red giant stars may be the most consistent production site for lithium. Author

A91-37428* National Aeronautics and Space Administration. Lewis Research Center, Cleveland, OH.

BIG BANG NUCLEOSYNTHESIS - THE STANDARD MODEL AND ALTERNATIVES

DAVID N. SCHRAMM (NASA/Fermilab Astrophysics Center, Batavia; Chicago, University, IL) (The birth and early evolution of our universe; Proceedings of Nobel Symposium 79, Graftavallen, Sweden, June 11-16, 1990. A91-37426 15-90) Physica Scripta (ISSN 0281-1847), vol. T36, 1991, p. 22-29. refs

(Contract NSF AST-88-22595; NAGW-1321; NAGW-1340)

Copyright

The standard homogeneous-isotropic calculation of the big bang cosmological model is reviewed, and alternate models are discussed. The standard model is shown to agree with the light element abundances for He-4, H-2, He-3, and Li-7 that are available. Improved observational data from recent LEP collider and SLC results are discussed. The data agree with the standard model in terms of the number of neutrinos, and provide improved information regarding neutron lifetimes. Alternate models are reviewed which describe different scenarios for decaying matter or quark-hadron induced inhomogeneities. The baryonic density relative to the critical density in the alternate models is similar to that of the standard model when they are made to fit the abundances. This reinforces the conclusion that the baryonic density relative to critical density is about 0.06, and also reinforces the need for both nonbaryonic dark matter and dark baryonic matter. C.C.S.

A91-37444* National Aeronautics and Space Administration. Lewis Research Center, Cleveland, OH.

FIRST-ORDER INFLATION

EDWARD W. KOLB (NASA/Fermilab Astrophysics Center, Batavia; Chicago, University, IL) (The birth and early evolution of our universe; Proceedings of Nobel Symposium 79, Graftavallen, Sweden, June 11-16, 1990. A91-37426 15-90) Physica Scripta (ISSN 0281-1847), vol. T36, 1991, p. 199-217. refs

(Contract NAGW-1340)

Copyright

In the original proposal, inflation occurred in the process of a strongly first-order phase transition. This model was soon demonstrated to be fatally flawed. Subsequent models for inflation involved phase transitions that were second-order, or perhaps weakly first-order; some even involved no phase transition at all. Recently the possibility of inflation during a strongly first-order phase transition has been revived. In this paper, some models for first-order inflation are discussed, and unique signatures that result if inflation is realized in a first-order transition are emphasized. Some of the history of inflation is reviewed to demonstrate how first-order inflation differs from other models. Author

A91-43291 National Aeronautics and Space Administration. Lewis Research Center, Cleveland, OH.

ASTROPHYSICS AND COSMOLOGY CONFRONT THE 17-KEV NEUTRINO

EDWARD W. KOLB and MICHAEL S. TURNER (NASA/Fermilab Astrophysics Center, Batavia; Chicago, University, IL) Physical Review Letters (ISSN 0031-9007), vol. 67, July 1, 1991, p. 5-8. DOE-supported research. Previously announced in STAR as N91-22981. refs

(Contract NAGW-1340)

Copyright

A host of astrophysical and cosmological arguments severely constrain the properties of a 17 keV Dirac neutrino. Such a neutrino must have interactions beyond those of the standard electroweak theory to reduce its cosmic abundance (through decay or

annihilation) by a factor of two hundred. A predicament arises because the additional helicity states of the neutrino necessary to construct a Dirac mass must have interactions strong enough to evade the astrophysical bound from SN 1987A, but weak enough to avoid violating the bound from primordial nucleosynthesis.

Author

A91-45907 Harvard-Smithsonian Center for Astrophysics, Cambridge, MA.

PRIMORDIAL NUCLEOSYNTHESIS REDUX

TERRY P. WALKER (Harvard-Smithsonian Center for Astrophysics, Cambridge, MA; Ohio State University, Columbus), GARY STEIGMAN, HO-SHIK KANG (Ohio State University, Columbus), DAVID M. SCHRAMM (NASA/Fermilab Astrophysics Center, Batavia; Chicago, University, IL), and KEITH A. OLIVE (Minnesota, University, Minneapolis; CNRS, Laboratoire d'Annecy-le-Vieux de Physique des Particules, France) Astrophysical Journal, Part 1 (ISSN 0004-637X), vol. 376, July 20, 1991, p. 51-69. refs

(Contract NSG-931; NAGW-1321; NSF AST-88-20595;

DE-AC02-76ER-01545; DE-AC02-83ER-40105)

Copyright

The abundances of D, He-3, He-4, and Li-7, are presently recalculated within the framework of primordial nucleosynthesis in the standard hot big bang model, in order to estimate the primordial abundances of the light elements. A comparison between theory and experiment demonstrates the consistency of standard model predictions; the baryon density parameter is constrained on the basis of a nucleon-to-photon ratio of 2.8-4.0. These bounds imply that the bulk of the baryons in the universe are dark, requiring that the universe be dominated by nonbaryonic matter. O.C.

A91-46543 National Aeronautics and Space Administration. Lewis Research Center, Cleveland, OH.

CONSTRAINTS FROM PRIMORDIAL NUCLEOSYNTHESIS ON THE MASS OF THE TAU NEUTRINO

EDWARD W. KOLB, MICHAEL S. TURNER, A. CHAKRAVORTY, and DAVID N. SCHRAMM (NASA/Fermilab Astrophysics Center, Batavia; Chicago, University, IL) Physical Review Letters (ISSN 0031-9007), vol. 67, July 29, 1991, p. 533-536. Research supported by DOE and NSF. refs

(Contract NAGW-1340; NAGW-1321)

Copyright

It is shown that primordial nucleosynthesis excludes a tau-neutrino mass from 0.3 to 25 MeV (Dirac) and 0.5 to 25 MeV (Majorana) provided that its lifetime is not less than about 1 sec, and from 0.3 to 30 MeV (Dirac) and 0.5 to 32 MeV (Majorana) for a lifetime of not less than about 1000 sec. A modest improvement in the laboratory mass limit - from 35 to 25 MeV - would imply that the tau-neutrino mass must be less than 0.5 MeV (provided the lifetime is not less than about 1 sec). Author

A91-54201 National Aeronautics and Space Administration. Lewis Research Center, Cleveland, OH.

BARYON ISOCURVATURE SCENARIO IN INFLATIONARY COSMOLOGY - A PARTICLE PHYSICS MODEL AND ITS ASTROPHYSICAL IMPLICATIONS

JUN'ICHI YOKOYAMA (NASA/Fermilab Astrophysics Center, Batavia, IL; Tokyo, University, Japan) and YASUSHI SUTO (Kyoto University, Uji, Japan) Astrophysical Journal, Part 1 (ISSN 0004-637X), vol. 379, Oct. 1, 1991, p. 427-439. Research supported by DOE. refs

(Contract MOESC-02740189; NAGW-1340)

Copyright

A phenomenological model to produce isocurvature baryon-number fluctuations is proposed in the framework of inflationary cosmology. The resulting spectrum of density fluctuation is very different from the conventional Harrison-Zel'dovich shape. The model, with the parameters satisfying several requirements from particle physics and cosmology, provides an appropriate initial condition for the minimal baryon isocurvature scenario of galaxy formation discussed by Peebles. Author

N91-25975*# National Aeronautics and Space Administration. Lewis Research Center, Cleveland, OH.

OUTLINE OF THE SOLAR SYSTEM: ACTIVITIES FOR ELEMENTARY STUDENTS

J. HARTSFIELD and M. SELLERS 1990 43 p
(NASA-TM-104965; NAS 1.15:104965; PB91-140814) Avail:
NTIS HC/MF A03 CSCL 03/2

An introduction to the solar system for the elementary school student is given. The introduction contains historical background, facts, and pertinent symbols concerning the sun, the nine major planets and their moons, and information about comets and asteroids. Aids to teaching are given, including a solar system crossword puzzle with answers. Author

N91-26058*# National Aeronautics and Space Administration. Lewis Research Center, Cleveland, OH.

NEAR-EARTH ASTEROIDS: METALS OCCURRENCE, EXTRACTION, AND FABRICATION Abstract Only

RICHARD WESTFALL In Arizona Univ., Resources of Near-Earth Space: Abstracts p 22 1991
Avail: NTIS HC/MF A04 CSCL 03/2

Near-earth asteroids occur in three principle types of orbits: Amor, Apollo, and Aten. Amor asteroids make relatively close (within 0.3 AU) approaches to the earth's orbit, but do not actually overlap it. Apollo asteroids spend most of their time outside the earth's orbital path, but at some point of close approach to the sun, they cross the orbit of the earth. Aten asteroids are those whose orbits remain inside the earth's path for the majority of their time, with semi-major axes less than 0.1 AU. Near-earth orbit asteroids include: stones, stony-irons, irons, carbonaceous, and super-carbonaceous. Metals within these asteroids include: iron, nickel, cobalt, the platinum group, aluminum, titanium, and others. Focus is on the extraction of ferrous and platinum group metals from the stony-iron asteroids, and the iron asteroids. Extraction of the metal fraction can be accomplished through the use of tunnel-boring-machines (TBM) in the case of the stony-irons. The metals within the stony-iron asteroids occur as dispersed granules, which can be separated from the stony fraction through magnetic and gaseous digestion separation techniques. The metal asteroids are processed by drilling and gaseous digestion or by gaseous digestion alone. Manufacturing of structures, housings, framing networks, pressure vessels, mirrors, and other products is accomplished through the chemical vapor deposition (CVD) of metal coating on advanced composites and on the inside of contour-defining inflatables (CDI). Metal coatings on advanced composites provide: resistance to degradation in the hostile environments of space; superior optical properties; superior heat dissipation; service as wear coatings; and service as evidential coatings. Metal coatings on the inside of CDI produce metal load-bearing products. Fibers such as graphite, kevlar, glass, ceramic, metal, etc., can be incorporated in the metal coatings on the inside of CDI producing metal matrix products which exhibit high strength and resist crack propagation. Author

91

LUNAR AND PLANETARY EXPLORATION

Includes planetology; and manned and unmanned flights.

N91-14259*# National Aeronautics and Space Administration. Lewis Research Center, Cleveland, OH.

DESIGN CONSIDERATIONS FOR LUNAR BASE PHOTOVOLTAIC POWER SYSTEMS

J. MARK HICKMAN, HENRY B. CURTIS, and GEOFFREY A. LANDIS 1990 10 p Presented at the 21st Photovoltaic Specialists Conference, Kissimmee, FL, 21-25 May 1990; sponsored by IEEE
(Contract RTOP 326-81-10)

(NASA-TM-103642; E-5823; NAS 1.15:103642) Avail: NTIS HC/MF A02 CSCL 03/2

A survey was made of factors that may affect the design of photovoltaic arrays for a lunar base. These factors, which include the lunar environment and system design criteria, are examined. A photovoltaic power system design with a triangular array geometry is discussed and compared to a nuclear reactor power systems and a power system utilizing both nuclear and solar power sources. Author

N91-20015*# National Aeronautics and Space Administration. Lewis Research Center, Cleveland, OH.

CHEMICAL APPROACHES TO CARBON DIOXIDE UTILIZATION FOR MANNED MARS MISSIONS

ALOYSIUS F. HEPP, GEOFFREY A. LANDIS, and CLIFFORD P. KUBIAK (Purdue Univ., West Lafayette, IN.) 1991 22 p Presented at the 2nd Annual Symposium of the UA/NASA Space Engineering Research Center, Tucson, AZ, 7-10 Jan. 1991 (Contract NAS3-25266; RTOP 506-41-11)
(NASA-TM-103728; E-5962; NAS 1.15:103728) Avail: NTIS HC/MF A03 CSCL 03/2

Use of resources available in situ is a critical enabling technology for a permanent human presence in space. A permanent presence on Mars, e.g., requires a large infrastructure to sustain life under hostile conditions. As a resource on Mars, atmospheric CO₂ is as follows: abundant; available at all points on the surface; of known presence; chemically simple; and can be obtained by simple compression. Many studies focus on obtaining O₂ and the various uses for O₂ including life support and fuel; discussion of CO, the coproduct from CO₂ fixation revolves around its uses as a fuel, being oxidized back to CO₂. Several new proposals are studied for CO₂ fixation through chemical, photochemical, and photoelectrochemical means. For example, the reduction of CO₂ to hydrocarbons such as acetylene (C₂H₂) can be accomplished with H₂. C₂H₂ has a theoretical vacuum specific impulse of approx. 375 secs. Potential uses were also studied of CO₂, as obtained or further reduced to carbon, as a reducing agent in metal oxide processing to form metals or metal carbides for use as structural or power materials; the CO₂ can be recycled to generate O₂ and CO. Author

N91-26073*# National Aeronautics and Space Administration. Lewis Research Center, Cleveland, OH.

CHEMICAL APPROACHES TO CARBON DIOXIDE

UTILIZATION FOR MANNED MARS MISSIONS Abstract Only

ALOYSIUS F. HEPP, GEOFFREY A. LANDIS, and CLIFFORD P. KUBIAK (Purdue Univ., West Lafayette, IN.) In Arizona Univ., Resources of Near-Earth Space: Abstracts p 30 1991
Avail: NTIS HC/MF A04 CSCL 03/2

Utilization of resources available in situ is a critical enabling technology for permanent human presence in space. A permanent presence on Mars, for example, requires a tremendous infrastructure to sustain life under hostile conditions (low oxygen, partial pressure, ultraviolet radiation, low temperature, etc.). There are numerous studies on the most accessible of Martian resources: atmospheric carbon dioxide. As a resource on Mars, atmospheric CO₂ is: (1) abundant; (2) available at all points on the surface; (3) of known presence, requiring no precursor mission to verify; (4) chemically simple; and (5) can be obtained by simple compression, with no requirements of mining or beneficiation equipment operation. Several novel proposals are presented for CO₂ fixation through chemical, photochemical, and photoelectrochemical means. Author

N91-27061*# National Aeronautics and Space Administration. Lewis Research Center, Cleveland, OH.

EFFECTS OF MARTIAN DUST ON POWER SYSTEM COMPONENTS

J. R. GAIER and M. E. PEREZ-DAVIS In NASA. Ames Research Center, Sand and Dust on Mars p 18-19 May 1991
Avail: NTIS HC/MF A04 CSCL 03/2

Before large power systems for manned exploration of the Martian surface can be put into place, it must be determined how

91 LUNAR AND PLANETARY EXPLORATION

their performance will be affected by the Martian environment. A program was started to assess the impact of these environmental factors on power system performance, and to find ways to mitigate the degradative effects. The effects of blowing dust on photovoltaic (PV) and radiator surfaces is studied. Extensive use was made of the Martian Surface Wind Tunnel (MARSWIT) located at NASA-Ames to simulate Martian winds. Two basic types of experiment sets were run. In the first, the threshold clearing velocity of dust deposited on PV coverslip material and high emissivity radiator materials in clear Martian-like winds was examined. In the second, dust was dropped near the inlet of the wind tunnel and the winds were allowed to carry the dust past the samples, simulating a dust storm. A summary of results is given. Author

N91-27068* # National Aeronautics and Space Administration. Lewis Research Center, Cleveland, OH.

ELECTRICAL SYSTEM/ENVIRONMENT INTERACTIONS ON THE PLANET MARS

J. C. KOLECKI, G. B. HILLARD, and D. C. FERGUSON *In* NASA. Ames Research Center, Sand and Dust on Mars p 34-35 May 1991

Avail: NTIS HC/MF A04 CSCL 03/2

The Martian environment is a diverse environment with which systems will interact in numerous ways. Preliminary thoughts on electrical system/environment interactions which might be of interest to system designers at all stages of system design are presented. These interactions are primarily related to electrical charging, contamination, and Martian surface sand and dust.

Author

92

SOLAR PHYSICS

Includes solar activity, solar flares, solar radiation and sunspots.

A91-28153* National Aeronautics and Space Administration. Lewis Research Center, Cleveland, OH.

SOLAR RADIATION ON MARS

JOSEPH APPELBAUM and DENNIS J. FLOOD (NASA, Lewis Research Center, Cleveland, OH) Solar Energy (ISSN 0038-092X), vol. 45, no. 6, 1990, p. 353-363. Previously announced in STAR as N89-27623. refs

Copyright

Detailed information on solar radiation characteristics on Mars are necessary for effective design of future planned solar energy systems operating on the surface of Mars. Presented here is a procedure and solar radiation related data from which the diurnally, hourly and daily variation of the global, direct beam and diffuse insolation on Mars are calculated. The radiation data are based on measured optical depth of the Martian atmosphere derived from images taken of the sun with a special diode on the Viking cameras; and computation based on multiple wavelength and multiple scattering of the solar radiation. Author

N91-15117* # National Aeronautics and Space Administration. Lewis Research Center, Cleveland, OH.

SOLAR RADIATION ON MARS: UPDATE 1990

JOSEPH APPELBAUM (Tel-Aviv Univ., Israel) and DENNIS J. FLOOD Oct. 1990 36 p

(Contract NAGW-2022; RTOP 506-41-11)

(NASA-TM-103623; E-5783; NAS 1.15:103623) Avail: NTIS HC/MF A03 CSCL 03/2

Detailed information on solar radiation characteristics on Mars are necessary for effective design of future planned solar energy systems operating on the surface of Mars. The authors present a procedure and solar radiation related data from which the diurnally and daily variation of the global, direct beam and diffuse insolation on Mars are calculated. The radiation data are based on measured optical depth of the Martian atmosphere derived from images taken

of the Sun with a special diode on the Viking Lander cameras and computation based on multiple wavelength and multiple scattering of the solar radiation. This work is an update to NASA-TM-102299 and includes a refinement of the solar radiation model. Author

N91-33046* # National Aeronautics and Space Administration. Lewis Research Center, Cleveland, OH.

SOLAR RADIATION ON MARS: UPDATE 1991

JOSEPH APPELBAUM and GEOFFREY A. LANDIS (Sverdrup Technology, Inc., Brook Park, OH.) Sep. 1991 48 p Presented at the European Space Power Conference, Florence, Italy, 2-6 Sep. 1991; sponsored by ESA

(Contract NAS3-25266; NAGW-2022; RTOP 506-41-11)

(NASA-TM-105216; E-6465; NAS 1.15:105216) Avail: NTIS

HC/MF A03 CSCL 03/2

Detailed information on solar radiation characteristics on Mars are necessary for effective design of future planned solar energy systems operating on the surface of Mars. A procedure and solar radiation related data are presented from which the daily variation of the global, direct beam and diffuse insolation on Mars are calculated. Given the optical depth of the Mars atmosphere, the global radiation is calculated from the normalized net flux function based on multiple wavelength and multiple scattering of the solar radiation. The direct beam was derived from the optical depth using Beer's law, and the diffuse component was obtained from the difference of the global and the direct beam radiation. The optical depths of the Mars atmosphere were derived from images taken of the Sun with a special diode on the cameras used on the two Viking Landers. Author

99

GENERAL

A91-53713* # National Aeronautics and Space Administration. Lewis Research Center, Cleveland, OH.

HISTORICAL PERSPECTIVES - THE ROLE OF THE NASA LEWIS RESEARCH CENTER IN THE NATIONAL SPACE NUCLEAR POWER PROGRAMS

H. S. BLOOMFIELD and R. J. SOVIE (NASA, Lewis Research Center, Cleveland, OH) AIAA, NASA, and OAI, Conference on Advanced SEI Technologies, Cleveland, OH, Sept. 4-6, 1991. 7 p. Previously announced in STAR as N91-29138. refs

(AIAA PAPER 91-3462) Copyright

The history of the NASA Lewis Research Center's role in space nuclear power programs is reviewed. Lewis has provided leadership in research, development, and the advancement of space power and propulsion systems. Lewis' pioneering efforts in nuclear reactor technology, shielding, high temperature materials, fluid dynamics, heat transfer, mechanical and direct energy conversion, high-energy propellants, electric propulsion and high performance rocket fuels and nozzles have led to significant technical and management roles in many natural space nuclear power and propulsion programs. Author

N91-20087* # National Aeronautics and Space Administration. Lewis Research Center, Cleveland, OH.

LEWIS AEROPROPULSION TECHNOLOGY: REMEMBERING THE PAST AND CHALLENGING THE FUTURE

NEAL T. SAUNDERS and ARTHUR J. GLASSMAN *In its* Aeropropulsion 1991 21 p Mar. 1991

Avail: NTIS HC/MF A24 CSCL 05/4

It was on January 23, 1941, less than two years after the first flight of a jet-propelled aircraft, that ground was broken in Cleveland for the NACA Aircraft Engine Research Laboratory (AERL). Originally envisioned as a laboratory for fundamental research on piston engines, the new NACA laboratory never actually fulfilled

this role. From the first test in 1942 until the end of the war in 1945, primary emphasis was on trouble-shooting to solve the problems of engines in production for the war effort. By the end of the war, the transition from piston to jet propulsion was well underway, and with it went the direction of the laboratory's program. Some of the major accomplishments over the past fifty years are reviewed and the challenges of the future examined. From piston engines through environmentally acceptable high-speed propulsion systems, efforts have included and will continue to include discipline, component, and engine activities along with provision of facilities to carry out the programs. Author

N91-23072*# National Aeronautics and Space Administration. Lewis Research Center, Cleveland, OH.

RESEARCH AND TECHNOLOGY

1990 149 p

(NASA-TM-103759; NAS 1.15:103759) Avail: NTIS HC/MF A07 CSCL 05/2

A brief but comprehensive review is given of the technical accomplishments of the NASA Lewis Research Center during the past year. Topics covered include instrumentation and controls technology; internal fluid dynamics; aerospace materials, structures, propulsion, and electronics; space flight systems; cryogenic fluids; Space Station Freedom systems engineering, photovoltaic power module, electrical systems, and operations; and engineering and computational support. Author

N91-29138*# National Aeronautics and Space Administration. Lewis Research Center, Cleveland, OH.

HISTORICAL PERSPECTIVES: THE ROLE OF THE NASA LEWIS RESEARCH CENTER IN THE NATIONAL SPACE NUCLEAR POWER PROGRAMS

H. S. BLOOMFIELD and R. J. SOVIE 1991 8 p Presented at the Conference on Advanced Space Exploration Initiative Technologies, Cleveland, OH, 4-6 Sep. 1991; cosponsored by AIAA and OAI

(Contract RTOP 593-31-1A)

(NASA-TM-105196; E-6498; NAS 1.15:105196; AIAA PAPER 91-3462) Avail: NTIS HC/MF A02 CSCL 05/4

The history of the NASA Lewis Research Center's role in space nuclear power programs is reviewed. Lewis has provided leadership in research, development, and the advancement of space power and propulsion systems. Lewis' pioneering efforts in nuclear reactor technology, shielding, high temperature materials, fluid dynamics, heat transfer, mechanical and direct energy conversion, high-energy propellants, electric propulsion and high performance rocket fuels and nozzles have led to significant technical and management roles in many national space nuclear power and propulsion programs. Author

N91-30073*# National Aeronautics and Space Administration. Lewis Research Center, Cleveland, OH.

NASA CRYOGENIC FLUID MANAGEMENT SPACE EXPERIMENT EFFORTS, 1960-1990

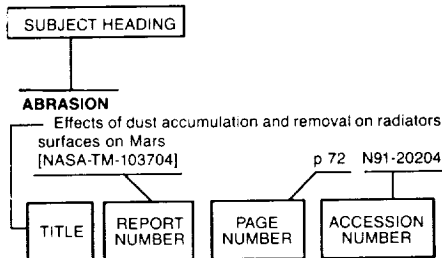
DANIEL GLOVER 1991 29 p Presented at the Conference on Advanced Space Exploration Initiative Technologies, Cleveland, OH, 4-6 Sep. 1991; cosponsored by AIAA and OAI

(Contract RTOP 506-48-00)

(NASA-TM-103752; E-6005; NAS 1.15:103752; AIAA PAPER 91-3538) Avail: NTIS HC/MF A03 CSCL 05/4

A history of technological development for subcritical cryogenic fluid management (CFM) through space experiments is given for the period 1960 to 1990. Space experiments with liquid hydrogen were conducted in the early 1960's. Efforts since then have consisted of studies and designs of potential space experiments. A chronology of CFM space experiments and design efforts is included. Author

Typical Subject Index Listing



The subject heading is a key to the subject content of the document. Titles, report numbers, and accession numbers of pertinent documents are provided under each subject heading. When the title is insufficiently descriptive of document content, a title extension is added, separated from the title by three hyphens. The report number helps to indicate the type of document cited (e.g., NASA report, NASA translation, NASA contractor report). The accession number is the number by which the document abstracts are arranged in this journal and by which the document is sold or requested. The titles, with title extensions if present, are arranged under each subject heading in ascending accession number order. The subject headings have been selected from the latest revision of the *NASA Thesaurus*.

A

- ABLATION**
Ellipsometric study of YBa₂Cu₃O_{7-x} laser ablated and co-evaporated films p 233 A91-53235
- ABRASION**
Effects of dust accumulation and removal on radiators surfaces on Mars [NASA-TM-103704] p 72 N91-20204
- ABUNDANCE**
Primordial nucleosynthesis redux p 240 A91-45907
- AC GENERATORS**
Update on results of SPRE testing at NASA p 56 A91-38140
Component technology for stirling power converters [NASA-TM-104387] p 74 N91-23234
Development of an analytical tool to study power quality of AC power systems for large spacecraft [NASA-TM-104451] p 223 N91-25749
Update on results of SPRE testing at NASA Lewis [NASA-TM-104425] p 79 N91-27208
- ACCELERATION (PHYSICS)**
Presentation on a Space Acceleration Measurement System (SAMS) p 50 N91-12417
An examination of anticipated g-jitter on space station and its effects on materials processes [NASA-TM-103775] p 128 N91-21378
- ACCELEROMETERS**
Vibration environment - Acceleration mapping strategy and microgravity requirements for Spacelab and Space Station p 39 A91-13991
[IAF PAPER 90-350] p 39 A91-13991
Presentation on a Space Acceleration Measurement System (SAMS) p 50 N91-12417
- ACETIC ACID**
High resolution electrolyte for thinning InP by anodic dissolution and its applications to EC-V profiling, defect revealing and surface passivation p 107 N91-30210

ACOUSTIC ATTENUATION

- Tuned optimization of extended reacting acoustic liners [NASA-TM-104431] p 228 N91-25817

ACOUSTIC DUCTS

- Monograph on propagation of sound waves in curved ducts [NASA-RP-1248] p 228 N91-15848
Tuned optimization of extended reacting acoustic liners [NASA-TM-104431] p 228 N91-25817

ACOUSTIC EMISSION

- Acousto-ultrasonics - Retrospective exhortation with bibliography p 191 A91-37011
Preliminary investigation of acousto-ultrasonic evaluation of metal-matrix composite specimens p 191 A91-37014
Acousto-ultrasonics p 226 A91-48227
Review of acousto-ultrasonic NDE for composites p 97 N91-18192
Acousto-ultrasonic nondestructive evaluation of materials using laser beam generation and detection p 193 N91-18193

ACOUSTIC EXCITATION

- Effect of acoustic excitation on stalled flows over an airfoil [AIAA PAPER 90-4009] p 1 A91-12521
Particle cloud flames in acoustic fields p 105 A91-20589
A steady effect of acoustic excitation on transitory stall [AIAA PAPER 91-0043] p 2 A91-22499
Control of laminar separation over airfoils by acoustic excitation p 226 A91-45106
Axisymmetric jet forced by fundamental and subharmonic tones p 226 A91-45111
Effect of acoustic excitation on stalled flows over an airfoil [NASA-TM-103183] p 10 N91-11675
A steady effect of acoustic excitation on transitory stall [NASA-TM-103689] p 11 N91-13420
Naturally occurring and forced azimuthal modes in a turbulent jet [NASA-TM-103692] p 11 N91-17000
Computational simulation of acoustic fatigue for hot composite structures [NASA-TM-104379] p 203 N91-23548

ACOUSTIC FATIGUE

- Computational simulation of acoustic fatigue for hot composite structures [AIAA PAPER 91-1178] p 197 A91-32099
Computational simulation of acoustic fatigue for hot composite structures [NASA-TM-104379] p 203 N91-23548

ACOUSTIC INSTABILITY

- Spatial evolution of nonlinear acoustic mode instabilities on hypersonic boundary layers p 225 A91-12973

ACOUSTIC MEASUREMENT

- A preliminary investigation of acousto-ultrasonic NDE of metal matrix composite test specimens [NASA-TM-104339] p 194 N91-23521

ACOUSTIC PROPAGATION

- Monograph on propagation of sound waves in curved ducts [NASA-RP-1248] p 228 N91-15848
Tuned optimization of extended reacting acoustic liners [NASA-TM-104431] p 228 N91-25817

ACOUSTIC PROPERTIES

- Tuned optimization of extended reacting acoustic liners [NASA-TM-104431] p 228 N91-25817

ACOUSTIC VELOCITY

- Prediction of the noise from a propeller at angle of attack [NASA-TM-103627] p 227 N91-11495

ACOUSTICS

- Wind turbine acoustics [NASA-TP-3057] p 228 N91-16679

- Control of an axisymmetric turbulent jet by multi-modal excitation [NASA-TM-104483] p 17 N91-26121

ACTIVATION ENERGY

- Influence of several metal ions on the gelation activation energy of silicon tetraethoxide p 113 A91-19599
A model for the scattering of high-frequency electromagnetic fields from dielectrics exhibiting thermally-activated electrical losses [NASA-TM-104376] p 224 N91-26872

ACTIVE CONTROL

- Modern developments in shear flow control with swirl p 3 A91-24519
Autonomous power expert system p 54 A91-37972
Microgravity vibration isolation: An optimal control law for the one-dimensional case p 49 N91-21206

ACTS

- Advanced Communications Technology Satellite (ACTS) p 44 A91-14056
[IAF PAPER 90-481] p 44 A91-14056
Evaluation of components, subsystems, and networks for high rate, high frequency space communications [AIAA PAPER 91-3423] p 41 A91-52343
LBR-2 Earth stations for the ACTS program p 133 N91-11971

ACTUATION

- Electromechanical actuation for thrust vector control applications p 52 A91-31026

ACTUATORS

- Use of piezoelectric actuators in active vibration control of rotating machinery p 179 A91-14400
Advanced launch system (ALS) - Electrical actuation and power systems improve operability and cost picture p 51 A91-31025
Civil air transport - A fresh look at power-by-wire and fly-by-light p 36 A91-31030
Field oriented control of induction motors p 138 A91-37987
Towards practical control design using neural computation [NASA-TM-103785] p 219 N91-19766

ADA (PROGRAMMING LANGUAGE)

- Techniques and implementation of the embedded rule-based expert system using Ada p 220 N91-22788
Description of real-time Ada software implementation of a power system monitor for the Space Station Freedom PMAD DC testbed [NASA-TM-105157] p 218 N91-28776

ADAPTIVE CONTROL

- An expert system to perform on-line controller restructuring for abrupt model changes p 36 A91-29466

ADDITION RESINS

- Autoclavable addition polyimides for 371 C composite applications p 115 A91-49112
Vinyl capped addition polyimides [NASA-CASE-LEW-15027-1] p 118 N91-13566

ADDITIVES

- Mechanisms and modeling of the effects of additives on the nitrogen oxides emission [AIAA PAPER 91-0479] p 124 A91-40560
Evaluation of advanced lubricants for aircraft applications using gear surface fatigue tests [AIAA PAPER 91-1907] p 181 A91-41649
Mechanisms and modeling of the effects of additives on the nitrogen oxides emission [NASA-TM-103765] p 126 N91-22464
Evaluation of advanced lubricants for aircraft applications using gear surface fatigue tests [NASA-TM-104336] p 186 N91-22568

ADHESION

- Fundamental considerations in adhesion, friction and wear for ceramic-metal contacts p 115 A91-35952
Adhesion at metal interfaces p 88 A91-38581
Uses of Auger and x ray photoelectron spectroscopy in the study of adhesion and friction [NASA-TM-103266] p 118 N91-11922
Lubrication with sputtered MoS₂ films: Principles, operation, limitations [NASA-TM-105292] p 112 N91-32216

ADHESION TESTS

ADHESION TESTS

Simplified procedures for designing adhesively bonded composite joints p 180 A91-20938

ADHESIVE BONDING

Simplified procedures for designing adhesively bonded composite joints p 180 A91-20938
Effect of sulfur removal on Al₂O₃ scale adhesion p 108 A91-27940
Intrinsic bond strength of metal films on polymer substrates p 88 A91-39246
Universal energy relations and metal/ceramic interfaces p 93 A91-56254

ADHESIVES

Significant reduction in arc frequency biased solar cells. Observations, diagnostics, and mitigation technique(s) p 83 N91-30235

ADVANCED LAUNCH SYSTEM (STS)

Advanced launch system (ALS) - Electrical actuation and power systems improve operability and cost picture p 51 A91-31025
Advanced launch vehicle upper stages using liquid propulsion and metallized propellants p 75 N91-24257

AEOLIAN TONES

Aeolian removal of dust types from photovoltaic surfaces on Mars p 47 N91-19156

AEROACOUSTICS

Aeroacoustic effects of reduced aft tip speed at constant thrust for a model counterrotation turboprop at takeoff conditions [AIAA PAPER 90-3933] p 224 A91-12449
Flow induced vibration and noise by a pair of tandem cylinders due to buffeting p 225 A91-14650
In-flight source noise of an advanced full-scale single-rotation propeller [AIAA PAPER 91-0594] p 226 A91-21547
Aeroacoustics of advanced propellers p 226 A91-24317
Control of laminar separation over airfoils by acoustic excitation p 226 A91-45106
Inflight source noise of an advanced full-scale single-rotation propeller [NASA-TM-103687] p 12 N91-19045
Ultra-high bypass research p 30 N91-20117

AERODYNAMIC BALANCE

A review of ice accretion data from a model rotor icing test and comparison with theory [AIAA PAPER 91-0661] p 19 A91-22500
A review of ice accretion data from a model rotor icing test and comparison with theory [NASA-TM-103712] p 11 N91-13421
Model rotor icing tests in the NASA Lewis icing research tunnel [NASA-TM-104351] p 32 N91-23184

AERODYNAMIC CHARACTERISTICS

The aerodynamic characteristics of vortex ingestion for the F/A-18 inlet duct [AIAA PAPER 91-0130] p 3 A91-26192
Comparison of a quasi-3D analysis and experimental performance for three compact radial turbines [AIAA PAPER 91-2128] p 25 A91-45789
Aeroacoustic effects of reduced aft tip speed at constant thrust for a model counterrotation turboprop at takeoff conditions [NASA-TM-103608] p 226 N91-10703
The aerodynamic characteristics of vortex ingestion for the F/A-18 inlet duct [NASA-TM-103703] p 70 N91-15303
Prediction of ice shapes and their effect on airfoil performance [NASA-TM-103701] p 12 N91-19047
Overview of high performance aircraft propulsion p 28 N91-20089

AERODYNAMIC COEFFICIENTS

Cascade flutter analysis with transient response aerodynamics [AIAA PAPER 91-0747] p 21 A91-19448
Cascade flutter analysis with transient response aerodynamics [NASA-TM-103746] p 201 N91-19475
Efficient computation of aerodynamic influence coefficients for aeroelastic analysis on a transputer network [NASA-TM-103671] p 216 N91-20748

AERODYNAMIC CONFIGURATIONS

Advanced rotorcraft transmission program [NASA-TM-103276] p 184 N91-21531

AERODYNAMIC DRAG

Prediction of ice shapes and their effect on airfoil performance [AIAA PAPER 91-0264] p 3 A91-26330
Prediction of ice shapes and their effect on airfoil performance [NASA-TM-103701] p 12 N91-19047

AERODYNAMIC HEAT TRANSFER

Heat transfer in oscillating flows p 152 A91-38698

Simulation of brush insert for leading-edge-passage convective heat transfer [NASA-TM-103801] p 165 N91-23409

AERODYNAMIC INTERFERENCE

Transonic wind-tunnel wall interference prediction code p 38 A91-26112

AERODYNAMIC LOADS

Semianalytical technique for sensitivity analysis of unsteady aerodynamic computations p 7 A91-48816
Simulation of iced wing aerodynamics [NASA-TM-104362] p 15 N91-23086
Overview of aerothermodynamic loads definition study p 204 N91-24334

AERODYNAMIC NOISE

Unsteady blade pressure measurements for the SR-7A propeller at cruise conditions [AIAA PAPER 90-4022] p 225 A91-12533
Unsteady blade pressure measurements for the SR-7A propeller at cruise conditions [NASA-TM-103606] p 228 N91-19825

AERODYNAMIC STABILITY

ASTROP2 users manual: A program for aeroelastic stability analysis of propfans [NASA-TM-4304] p 206 N91-28627

AERODYNAMIC STALLING

Effect of acoustic excitation on stalled flows over an airfoil [AIAA PAPER 90-4009] p 1 A91-12521
A steady effect of acoustic excitation on transitory stall [AIAA PAPER 91-0043] p 2 A91-22499
Effect of acoustic excitation on stalled flows over an airfoil [NASA-TM-103183] p 10 N91-11675
A steady effect of acoustic excitation on transitory stall [NASA-TM-103689] p 11 N91-13420

AERODYNAMICS

Development of a new flux splitting scheme p 153 A91-40793
Aerodynamics and heat transfer investigations on a high Reynolds number turbine cascade [NASA-TM-103260] p 11 N91-15134
Transonic aerodynamics of dense gases [NASA-TM-103722] p 13 N91-20045
Simulation of iced wing aerodynamics [NASA-TM-104362] p 15 N91-23086
Icing simulation: A survey of computer models and experimental facilities [NASA-TM-104366] p 15 N91-23087

AEROELASTICITY

Cascade flutter analysis with transient response aerodynamics [AIAA PAPER 91-0747] p 21 A91-19448
Experimental investigation of propfan aeroelastic response in off-axis flow with mistuning p 22 A91-30015
Aeroelastic modal characteristics of mistuned blade assemblies - Mode localization and loss of eigenstructure [AIAA PAPER 91-1218] p 196 A91-32032
Influence of thickness and camber on the aeroelastic stability of supersonic throughflow fans p 5 A91-42814
Localization of aeroelastic modes in mistuned high-energy turbines [AIAA PAPER 91-3379] p 198 A91-44319
Application of an efficient hybrid scheme for aeroelastic analysis of advanced propellers p 7 A91-52315
Optical measurement of unducted fan flutter [NASA-TM-103285] p 27 N91-15174
Propulsion aeroelasticity, vibration control, and dynamic system modeling p 29 N91-20105
Efficient computation of aerodynamic influence coefficients for aeroelastic analysis on a transputer network [NASA-TM-103671] p 216 N91-20748
Localization of aeroelastic modes in mistuned high-energy turbines [NASA-TM-104445] p 204 N91-24659
Aeroelastic modal characteristics of mistuned blade assemblies: Mode localization and loss of eigenstructure [NASA-TM-104519] p 205 N91-27591
ASTROP2 users manual: A program for aeroelastic stability analysis of propfans [NASA-TM-4304] p 206 N91-28627

AERONAUTICAL ENGINEERING

Bibliography of Lewis Research Center technical publications announced in 1989 [NASA-TM-102542] p 238 N91-10798

AERONAUTICAL SATELLITES

Characteristics of a future aeronautical satellite communications system [NASA-TM-104389] p 20 N91-23102

AEROSPACE ENGINEERING

A review of properties and potential aerospace applications of electrically conducting polymers p 113 A91-14409
High temperature superconductive microwave technology for space applications p 137 A91-31391
Optical techniques for determination of normal shock position in supersonic flows for aerospace applications p 174 A91-55530
Space mechanisms needs for future NASA long duration space missions [AIAA PAPER 91-3428] p 183 A91-57025
Bibliography of Lewis Research Center technical publications announced in 1989 [NASA-TM-102542] p 238 N91-10798
NDE standards for high temperature materials [NASA-TM-103761] p 193 N91-19464
Government/industry response to questionnaire on space mechanisms/tribology technology needs [NASA-TM-104358] p 186 N91-23501
Aerospace applications of high temperature superconductivity p 236 N91-24080
Update on results of SPRE testing at NASA Lewis [NASA-TM-104425] p 79 N91-27208
Space mechanisms needs for future NASA long duration space missions [NASA-TM-105204] p 190 N91-30532

AEROSPACE ENVIRONMENTS

Preliminary flight test results from the advanced photovoltaic experiment p 56 A91-38163
Heat transfer in space systems, Proceedings of the Symposium, AIAA/ASME Thermophysics and Heat Transfer Conference, Seattle, WA, June 18-20, 1990 p 152 A91-38780
Preliminary results from the advanced photovoltaic experiment flight test [NASA-TM-103269] p 67 N91-11058
The effect of the low Earth orbit environment on space solar cells [NASA-TM-103735] p 48 N91-19165
Findings of the Joint Workshop on Evaluation of Impacts of Space Station Freedom Ground Configurations [NASA-TM-103717] p 73 N91-22370
Ion beam textured and coated surfaces experiment (IBEX) p 122 N91-25040
Advanced photovoltaic experiment, S0014: Preliminary flight results and post-flight findings p 212 N91-25061
An autonomous fault detection, isolation, and recovery system for a 20-kHz electric power distribution test bed [NASA-TM-104344] p 217 N91-25680
Space Photovoltaic Research and Technology Conference [NASA-CP-3121] p 82 N91-30203

AEROSPACE INDUSTRY

Aerospace applications of high temperature superconductivity [IAF PAPER 90-054] p 231 A91-13767

AEROSPACE PLANES

3D computation of hypersonic nozzle [AIAA PAPER 90-5203] p 1 A91-14429
Overview of the Beta II two-stage-to-orbit vehicle design [AIAA PAPER 91-3175] p 43 A91-54088
Overview of hypersonic/transatmospheric vehicle propulsion technology p 28 N91-20092
Overview of NASP nozzle research p 28 N91-20093
Chemical reacting flows p 162 N91-20098
High temperature NASP engine seals: A technology review [NASA-TM-104468] p 190 N91-30538

AEROSPACE SAFETY

Space engine safety system [AIAA PAPER 91-3604] p 44 A91-52470
Findings of the Joint Workshop on Evaluation of Impacts of Space Station Freedom Ground Configurations p 48 N91-20728

AEROSPACE SCIENCES

Speculating on space futures p 237 A91-16900
Bibliography of Lewis Research Center technical publications announced in 1989 [NASA-TM-102542] p 238 N91-10798

AEROSPACE SYSTEMS

A fiber-optic current sensor for aerospace applications p 172 A91-38006
NASA Aerospace Flight Battery Systems Program p 56 A91-38088
Preliminary designs for 25 kWe advanced Stirling conversion systems for dish electric applications p 207 A91-38182
Nondestructive evaluation tools and experimental studies for monitoring the health of space propulsion systems [AIAA PAPER 91-3433] p 192 A91-53703

Overview of space propulsion systems for identifying nondestructive evaluation and health monitoring opportunities

[NASA-TM-103614] p 192 N91-15565

How much redundancy: Some cost considerations, including examples for spacecraft systems

[NASA-TM-103197] p 192 N91-17407

Space reactor/Stirling cycle systems for high power lunar application

[NASA-TM-103698] p 40 N91-19112

Internal fluid mechanics research p 161 N91-20095

Propulsion instrumentation research

p 176 N91-20100

Nondestructive evaluation tools and experimental studies for monitoring the health of space propulsion systems

[NASA-TM-105164] p 194 N91-28605

AEROSPACE VEHICLES

Computational simulation of propulsion structures

performance and reliability p 29 N91-20106

AEROTHERMODYNAMICS

Turbine blading designed for high heat load space propulsion applications

p 50 A91-10338

Heat transfer in oscillating flows p 152 A91-38698

Probabilistic modeling for simulation of aerodynamic uncertainties in propulsion systems p 58 A91-42725

Navier-Stokes analysis of turbine blade heat transfer

[ASME PAPER 90-GT-42] p 155 A91-44529

Flux splitting algorithms for two-dimensional viscous flows with finite-rate chemistry p 10 N91-10894

Internal fluid mechanics research p 161 N91-20095

Overview of aerothermodynamic loads definition study

p 204 N91-24334

Spray measurements of aerothermodynamic effect on disintegrating liquid jets

[NASA-TM-104501] p 178 N91-27510

AGING (MATERIALS)

Effect of fiber reinforcements on thermo-oxidative stability and mechanical properties of polymer matrix composites

[NASA-TM-103648] p 98 N91-19234

A comparison of fiber effects on polymer matrix composite oxidation

[NASA-TM-104416] p 101 N91-24361

Long term isothermal aging and thermal analysis of N-CYCAP polyimides

[NASA-TM-104341] p 122 N91-25286

AGING (METALLURGY)

Makeup and uses of a basic magnet laboratory for characterizing high-temperature permanent magnets

[NASA-TM-104508] p 146 N91-30427

AIR

Numerical study of shock-wave/boundary layer interactions in premixed hydrogen-air hypersonic flows

[AIAA PAPER 91-0413] p 149 A91-26191

Numerical study of shock-wave/boundary layer interactions in premixed hydrogen-air hypersonic flows

[NASA-TM-103273] p 160 N91-14559

AIR BREATHING BOOSTERS

Mach 6.5 air induction system design for the Beta II Two-Stage-to-Orbit booster vehicle

[AIAA PAPER 91-3196] p 43 A91-54099

AIR BREATHING ENGINES

Feedback linearization for control of air breathing engines

[AIAA PAPER 91-2000] p 23 A91-41671

Enhancing aeropropulsion research with high-speed interactive computing p 217 A91-56129

Aeropropulsion 1991

[NASA-CP-10063] p 27 N91-20086

CFD for hypersonic propulsion

[NASA-TM-103791] p 164 N91-21447

NASA aeropropulsion research in support of propulsion systems of the 21st century

[NASA-TM-104403] p 15 N91-23083

Enhancing aeropropulsion research with high-speed interactive computing

[NASA-TM-104374] p 218 N91-24796

AIR FLOW

Radiative structures of lycopodium-air flames in low gravity

p 105 A91-30003

Progress toward synergistic hypermixing nozzles

[AIAA PAPER 91-2264] p 25 A91-45800

Particle displacement tracking applied to air flows

[NASA-TM-104481] p 177 N91-25387

Progress toward synergistic hypermixing nozzles

[NASA-TM-105169] p 18 N91-29150

A qualitative view of cryogenic fluid injection into high speed flows

[NASA-TM-105139] p 169 N91-30473

AIR INTAKES

Mach 6.5 air induction system design for the Beta II Two-Stage-to-Orbit booster vehicle

[AIAA PAPER 91-3196] p 43 A91-54099

AIR POLLUTION

Mechanisms and modeling of the effects of additives on the nitrogen oxides emission

[AIAA PAPER 91-0479] p 124 A91-40560

Mechanisms and modeling of the effects of additives on the nitrogen oxides emission

[NASA-TM-103765] p 126 N91-22464

AIR TRANSPORTATION

Propulsion challenges for a 21st century economically viable, environmentally compatible High-Speed Civil Transport

p 25 A91-56109

Overview of supersonic cruise propulsion research

p 27 N91-20088

Engine technology challenges for a 21st century high speed civil transport

[NASA-TM-104363] p 19 N91-23098

AIRBORNE/SPACEBORNE COMPUTERS

Description of real-time Ada software implementation of a power system monitor for the Space Station Freedom

PMAD DC testbed

[NASA-TM-105157] p 218 N91-28776

AIRCRAFT CONFIGURATIONS

A comparison of arrow, trapezoidal and M wing concepts using a Mach 2 supersonic cruise transport mission

[AIAA PAPER 91-3102] p 7 A91-54027

Advanced rotorcraft transmission program

[NASA-TM-103276] p 184 N91-21531

AIRCRAFT CONSTRUCTION MATERIALS

Reinforcements: The key to high performance composite materials

[NASA-TM-103230] p 96 N91-15329

Transition-to-practice technologies for brittle materials

p 120 N91-20107

Progress in modeling deformation and damage

p 202 N91-20108

Overview of Lewis materials research: Contributions, current efforts, and future directions

p 111 N91-20109

Advanced high temperature engine materials technology program

p 98 N91-20110

Research and technology

[NASA-TM-103759] p 243 N91-23072

Fatigue behavior and life prediction of a SiC/Ti-24Al-11Nb composite under isothermal conditions

[NASA-TM-105168] p 206 N91-30566

AIRCRAFT CONTROL

Digital angular position sensor using wavelength division multiplexing

p 21 A91-19580

Effects of horizontal tail ice on longitudinal aerodynamic derivatives

p 36 A91-38547

A linear control design structure to maintain loop properties during limit operation in a multi-nozzle turbofan engine

[AIAA PAPER 91-1997] p 24 A91-45780

Neural network application to aircraft control system design

[AIAA PAPER 91-2715] p 36 A91-49676

Neural network application to aircraft control system design

[NASA-TM-105151] p 37 N91-27167

A linear control design structure to maintain loop properties during limit operation in a multi-nozzle turbofan engine

[NASA-TM-105163] p 35 N91-29188

AIRCRAFT DESIGN

NASA's High Speed Research Program - An introduction and status report

[SAE PAPER 901923] p 1 A91-48605

Application of an integrated flight/propulsion control design methodology to a STOVL aircraft

[AIAA PAPER 91-2792] p 36 A91-49793

V/STOL gets a lift

p 20 A91-52835

A comparison of arrow, trapezoidal and M wing concepts using a Mach 2 supersonic cruise transport mission

[AIAA PAPER 91-3102] p 7 A91-54027

Aeropropulsion 1991

[NASA-CP-10063] p 27 N91-20086

Overview of high performance aircraft propulsion

p 28 N91-20089

Application of an integrated flight/propulsion control design methodology to a STOVL aircraft

[NASA-TM-105254] p 37 N91-32143

AIRCRAFT ENGINES

Partitioning methods for global controllers

p 219 A91-30043

Fuel-rich, catalytic reaction experimental results --- fuel development for high-speed civil transport aircraft

[AIAA PAPER 91-2463] p 24 A91-44250

Computation of a circular-to-rectangular transition duct flow field

[AIAA PAPER 91-1741] p 156 A91-45547

Design and experimental evaluation of compact radial-inflow turbines

[AIAA PAPER 91-2127] p 24 A91-45788

Comparison of turbine bypass and mixed flow turbofan engines for a high-speed civil transport

[AIAA PAPER 91-3132] p 25 A91-54051

Three-dimensional flows in a transonic compressor rotor

p 8 A91-56152

An AD100 implementation of a real-time STOVL aircraft propulsion system

[NASA-TM-103683] p 26 N91-13457

Combustor technology for future aircraft

[NASA-TM-103268] p 26 N91-14349

Thermal barrier coating evaluation needs

[NASA-TM-103708] p 111 N91-15390

Aeropropulsion 1991

[NASA-CP-10063] p 27 N91-20086

Lewis aeropropulsion technology: Remembering the past and challenging the future

p 242 N91-20087

Overview of high performance aircraft propulsion

p 28 N91-20089

High temperature electronics

p 144 N91-20101

Advanced aeropropulsion controls technology

p 29 N91-20103

Propulsion aeroelasticity, vibration control, and dynamic system modeling

p 29 N91-20105

Computational simulation of propulsion structures performance and reliability

p 29 N91-20106

Advanced high temperature engine materials technology program

p 98 N91-20110

Rotary engine technology

p 30 N91-20114

Overview of subsonic transport propulsion technology

p 30 N91-20116

High-efficiency core technology

p 30 N91-20118

Performance of a high-work, low-aspect-ratio turbine stator tested with a realistic inlet radial temperature gradient

[NASA-TM-103738] p 31 N91-20126

Application of computational fluid dynamics in high speed aeropropulsion

[NASA-TM-103780] p 164 N91-21458

NASA aeropropulsion research in support of propulsion systems of the 21st century

[NASA-TM-104403] p 15 N91-23083

Engine technology challenges for a 21st century high speed civil transport

[NASA-TM-104363] p 19 N91-23098

Fuel-rich, catalytic reaction experimental results

[NASA-TM-104423] p 33 N91-24203

Visualization techniques to experimentally model flow and heat transfer in turbine and aircraft flow passages

[NASA-TM-4272] p 167 N91-27489

AIRCRAFT FUELS

In-flight and simulated aircraft fuel temperature measurements

[NASA-TM-103611] p 125 N91-15418

AIRCRAFT HAZARDS

NASA's aircraft icing technology program

p 19 N91-20120

Icing simulation: A survey of computer models and experimental facilities

[NASA-TM-104366] p 15 N91-23087

Calculated performance of the NASA Lewis icing research tunnel

[NASA-TM-105173] p 39 N91-29199

AIRCRAFT INSTRUMENTS

A resistance strain gage with repeatable apparent strain to 800 C

p 198 A91-48899

AIRCRAFT LANDING

Integrated flight/propulsion control system design based on a centralized approach

p 36 A91-22950

Integrated flight/propulsion control system design based on a decentralized, hierarchical approach

[NASA-TM-103678] p 31 N91-21137

AIRCRAFT MODELS

Results of a sub-scale model rotor icing test

[AIAA PAPER 91-0660] p 19 A91-26190

Results of a sub-scale model rotor icing test

[NASA-TM-103709] p 11 N91-14309

Model rotor icing tests in the NASA Lewis icing research tunnel

[NASA-TM-104351] p 32 N91-23184

AIRCRAFT NOISE

Aeroacoustic effects of reduced aft tip speed at constant thrust for a model counterrotation turboprop at takeoff conditions

[AIAA PAPER 90-3933] p 224 A91-12449

Near-field noise of a single rotation propfan at an angle of attack

[AIAA PAPER 90-3953] p 225 A91-12469

Near-field noise of a single-rotation propfan at an angle of attack

[NASA-TM-103645] p 227 N91-12316

Inflight source noise of an advanced full-scale single-rotation propeller

[NASA-TM-103687] p 12 N91-19045

AIRCRAFT PERFORMANCE

Experimental water droplet impingement data on modern aircraft surfaces
[AIAA PAPER 91-0445] p 2 A91-21493

AIRCRAFT POWER SUPPLIES

Civil air transport - A fresh look at power-by-wire and fly-by-light p 36 A91-31030
Civil air transport: A fresh look at power-by-wire and fly-by-light p 37 A91-23053

AIRCRAFT STABILITY

Effects of horizontal tail ice on longitudinal aerodynamic derivatives p 36 A91-38547

AIRCRAFT STRUCTURES

Progress in modeling deformation and damage p 202 A91-20108
Probability approach for strength calculations p 204 A91-24652
PM200/PS200: Self-lubricating bearing and seal materials for applications to 900 C [NASA-TM-103776] p 190 A91-30539

AIRFOIL OSCILLATIONS

The aerodynamics of an oscillating cascade in a compressible flow field [ASME PAPER 89-GT-271] p 1 A91-13047
Experimental investigation of oscillating cascade aerodynamics p 3 A91-27801

AIRFOIL PROFILES

Control of laminar separation over airfoils by acoustic excitation p 226 A91-45106
Effect of acoustic excitation on stalled flows over an airfoil [NASA-TM-103183] p 10 A91-11675
Compressible flows with periodic vortical disturbances around lifting airfoils [NASA-TM-103742] p 14 A91-21060

AIRFOILS

Acoustic radiation from lifting airfoils in compressible subsonic flow [AIAA PAPER 90-3911] p 224 A91-12427
Effect of acoustic excitation on stalled flows over an airfoil [AIAA PAPER 90-4009] p 1 A91-12521
A steady effect of acoustic excitation on transitory stall [AIAA PAPER 91-0043] p 2 A91-22499
Prediction of ice shapes and their effect on airfoil performance [AIAA PAPER 91-0264] p 3 A91-26330
Elevator deflections on the icing process p 20 A91-35427
Influence of thickness and camber on the aeroelastic stability of supersonic throughflow fans p 5 A91-42814

Progress toward the development of an airfoil icing analysis capability p 9 A91-10866
A steady effect of acoustic excitation on transitory stall [NASA-TM-103689] p 11 A91-13420
Thermal barrier coating evaluation needs [NASA-TM-103708] p 111 A91-15390
Icing characteristics of a natural-laminar-flow, a medium-speed, and a swept, medium-speed airfoil [NASA-TM-103693] p 12 A91-19046
Prediction of ice shapes and their effect on airfoil performance [NASA-TM-103701] p 12 A91-19047

Acoustic radiation from lifting airfoils in compressible subsonic flow [NASA-TM-103650] p 13 A91-19053
Wind tunnel wall effects in a linear oscillating cascade [NASA-TM-103690] p 27 A91-19098
Transonic aerodynamics of dense gases [NASA-TM-103722] p 13 A91-20045
Compressible flows with periodic vortical disturbances around lifting airfoils [NASA-TM-103742] p 14 A91-21060
A finite-difference, frequency-domain numerical scheme for the solution of the linearized unsteady Euler equations p 162 A91-21067
Icing simulation: A survey of computer models and experimental facilities [NASA-TM-104366] p 15 A91-23087
Advanced ice protection systems test in the NASA Lewis icing research tunnel [NASA-TM-103757] p 32 A91-23183

AIRFRAMES
IMPAC: An Integrated Methodology for Propulsion and Airframe Control [NASA-TM-103805] p 30 A91-20122
CFD for hypersonic propulsion [NASA-TM-103791] p 164 A91-21447

AIRSPEED
High alpha inlets p 28 A91-20091

ALGEBRA
Dynamics of local grid manipulations for internal flow problems p 164 A91-21090

ALGORITHMS

Use of piezoelectric actuators in active vibration control of rotating machinery p 179 A91-14400
Parallel algorithms for boundary value problems p 221 A91-31175

Automating security monitoring and analysis for Space Station Freedom's electric power system p 219 A91-37975

Time-derivative preconditioning for viscous flows [AIAA PAPER 91-1652] p 154 A91-43576
The application of neural networks to the SSME startup transient [AIAA PAPER 91-2530] p 60 A91-44283

A new uniformly valid asymptotic integration algorithm for elasto-plastic creep and unified viscoplastic theories including continuum damage p 110 A91-48725
Flux splitting algorithms for two-dimensional viscous flows with finite-rate chemistry p 10 A91-10894

Efficient computation of aerodynamic influence coefficients for aeroelastic analysis on a transputer network [NASA-TM-103671] p 216 A91-20748
Microgravity vibration isolation: An optimal control law for the one-dimensional case p 49 A91-21206

On the anomaly of velocity-pressure decoupling in collocated mesh solutions [NASA-TM-103769] p 164 A91-21448
Asymptotic integration algorithms for nonhomogeneous, nonlinear, first order, ordinary differential equations [NASA-TM-103793] p 222 A91-21797

The NASA Lewis integrated propulsion and flight control simulator [NASA-TM-105147] p 21 A91-27157
From differential to difference equations for first order ODEs [NASA-TM-104530] p 222 A91-27886

Exponential integration algorithms applied to viscoplasticity [NASA-TM-104461] p 223 A91-27901

ALIGNMENT
The series Bi₂Sr₂Ca_(n-1)Cu_(n)O_(2n+4) (1 less than or equal to n less than or equal to 5): Phase stability and superconducting properties [NASA-TM-103749] p 235 A91-21910

ALKYL COMPOUNDS
Substituted 1,1,1-triaryl-2,2,2-trifluoroethanes and processes for their synthesis [NASA-CASE-LEW-14345-4] p 90 A91-25185

ALKYLATES
Determination of the thermal stability of fluids by tensimetry - Instrumentation and procedure p 113 A91-13435

ALLOYING
Oxidation behavior of cubic phases formed by alloying Al₃Ti with Cr and Mn p 108 A91-27849

ALTERNATING CURRENT
Spatial variations in a.c. susceptibility and microstructure for the YBa₂Cu₃O_(7-x) superconductor and their correlation with room-temperature ultrasonic measurements p 233 A91-54969
Spatial variations in ac susceptibility and microstructure for the YBa₂Cu₃O_(7-x) superconductor and their correlation with room-temperature ultrasonic measurements [NASA-TM-103787] p 194 A91-21553

ALUMINIDES
1300 K compressive properties of a reaction milled NiAl-AIN composites p 107 A91-18674
1000 to 1300 K slow plastic compression properties of Al-deficient NiAl p 108 A91-36214
The potential for ductility enhancement from surface and interface dislocation sources in NiAl p 109 A91-39292

Continuous fiber-reinforced titanium aluminide composites p 92 A91-39553
1000 to 1200 K time-dependent compressive deformation of single-crystalline and polycrystalline B2 Ni-40Al p 109 A91-43670

Low-density, high-strength intermetallic matrix composites by XD (trademark) synthesis [NASA-TM-103724] p 97 A91-19233
Fatigue behavior and life prediction of a SiC/Ti-24Al-11Nb composite under isothermal conditions [NASA-TM-105168] p 206 A91-30566

ALUMINUM
Wettability of pyrolytic boron nitride by aluminum p 114 A91-28772
Launch vehicle performance using metallized propellants [AIAA PAPER 91-2050] p 58 A91-44106
Launch vehicle performance using metallized propellants [NASA-TM-104456] p 76 A91-24304

Atomic oxygen undercutting of LDEF aluminized Kapton multilayer insulation p 229 A91-25027

ALUMINUM ALLOYS

Sulfur at nickel-alumina interfaces - Molecular orbital theory p 104 A91-12925
Oxidation behavior of cubic phases formed by alloying Al₃Ti with Cr and Mn p 108 A91-27849
Reaction of Ti and Ti-Al alloys with alumina p 91 A91-27937

Effect of sulfur removal on Al₂O₃ scale adhesion p 108 A91-27940
Compression behavior of TiB₂-particulate-reinforced composites of Al₂Fe₃Ti₈ p 91 A91-28014
Reaction of beta-phase Ni-Al alloys with CrB₂ p 92 A91-49943

Preliminary studies on NiAl/Nb₂Be₁₇ reaction and effectiveness of BeO as an interfacial reaction barrier p 92 A91-55050
A simplified method for determining the number of independent slip systems in crystals p 110 A91-55472

Factors which influence tensile strength of a SiC/Ti-24Al-11Nb (at pct) composite p 92 A91-55900
Prospects for ductility and toughness enhancement of NiAl by ductile phase reinforcement [NASA-TM-103796] p 112 A91-27324

ALUMINUM GALLIUM ARSENIDES
Monolithic and mechanical multijunction space solar cells p 54 A91-38020
23.5 percent thin-film space concentrator cells p 58 A91-42002

ALUMINUM NITRIDES
1300 K compressive properties of a reaction milled NiAl-AIN composites p 107 A91-18674

ALUMINUM OXIDES
Sulfur at nickel-alumina interfaces - Molecular orbital theory p 104 A91-12925
Ultrasonic imaging of textured alumina p 191 A91-18596

Thermochemical analysis of the silicon carbide-alumina reaction with reference to liquid-phase sintering of silicon carbide p 114 A91-26506
Reaction of Ti and Ti-Al alloys with alumina p 91 A91-27937

Effect of sulfur removal on Al₂O₃ scale adhesion p 108 A91-27940
Tribological properties of Ag/Ti films on Al₂O₃ ceramic substrates [NASA-TM-103784] p 89 A91-19224

Tribological characteristics of silicon carbide whisker-reinforced alumina at elevated temperatures [NASA-TM-103799] p 89 A91-22379
Sliding wear of self-mated Al₂O₃-SiC whisker reinforced composites at 23-1200 C [NASA-TM-104490] p 90 A91-27221

An analysis of the wear behavior of SiC whisker reinforced alumina from 25 to 1200 C [NASA-TM-104489] p 90 A91-29235

AMBIENT TEMPERATURE
Compensation for effects of ambient temperature on rare-earth doped fiber optic thermometer p 170 A91-19582

AMMETERS
A fiber-optic current sensor for aerospace applications p 171 A91-23005

AMORPHOUS MATERIALS
Diamondlike carbon as a moisture barrier and antireflecting coating on optical materials p 119 A91-18302
Optical dispersion relations for diamondlike carbon films p 230 A91-18305

Dual ion beam processed diamondlike films for industrial applications p 121 A91-23042

AMPOULES
A comparative study of p(i) n and n(i) p InP solar cells made by a closed ampoule diffusion p 212 A91-30206

ANALOG CIRCUITS
High temperature superconductor analog electronics for millimeter-wavelength communications [AIAA PAPER 91-3592] p 233 A91-53707
High temperature superconductor analog electronics for millimeter-wavelength communications [NASA-TM-105184] p 237 A91-29982

ANALOGIES
Extension of transonic flow computational concepts in the analysis of cavitated bearings [ASME PAPER 90-TRIB-40] p 150 A91-29474
Extension of transonic flow computational concepts in the analysis of cavitated bearings [NASA-TM-103214] p 160 A91-16304

ANGLE OF ATTACK
Near-field noise of a single rotation propfan at an angle of attack [AIAA PAPER 90-3953] p 225 A91-12469
Prediction of the noise from a propeller at angle of attack [AIAA PAPER 90-3954] p 225 A91-12470

- Prediction of unsteady blade surface pressures on an advanced propeller at an angle of attack p 226 A91-18257
- Prediction of the noise from a propeller at angle of attack [NASA-TM-103627] p 227 N91-11495
- Prediction of ice shapes and their effect on airfoil performance [NASA-TM-103701] p 12 N91-19047
- ANHYDRIDES**
- Substituted 1,1,1-triaryl-2,2,2-trifluoroethanes and processes for their synthesis [NASA-CASE-LEW-14345-3] p 89 N91-17141
- Substituted 1,1,1-triaryl-2,2,2-trifluoroethanes and processes for their synthesis [NASA-CASE-LEW-14345-4] p 90 N91-25185
- Addition polyimides with enhanced processability [NASA-CASE-LEW-15043-1] p 123 N91-32230
- ANILINE**
- Substituted 1,1,1-triaryl-2,2,2-trifluoroethanes and processes for their synthesis [NASA-CASE-LEW-14345-4] p 90 N91-25185
- ANISOTROPIC FLUIDS**
- Renormalization group analysis of anisotropic diffusion in turbulent shear flows p 150 A91-27946
- ANISOTROPIC MEDIA**
- The effects of rotation on initially anisotropic homogeneous flows p 158 A91-54958
- ANISOTROPY**
- Temperature dependence of the anisotropy in magnetic relaxation in YBa₂Cu₃O(7-x) thin films p 232 A91-36047
- ANNEALING**
- Neutron, gamma ray and post-irradiation thermal annealing effects on power semiconductor switches [AIAA PAPER 91-3525] p 142 A91-52420
- Ellipsometric study of YBa₂Cu₃O(7-x) laser ablated and co-evaporated films p 233 A91-53235
- Thermal annealing of GaAs concentrator solar cells p 208 N91-19195
- Neutron, gamma ray and post-irradiation thermal annealing effects on power semiconductor switches [NASA-TM-105248] p 147 N91-32410
- ANNIHILATION REACTIONS**
- Antiproton powered propulsion with magnetically confined plasma engines p 63 A91-52313
- ANNUAL FLOW**
- A PCM/forced convection conjugate transient analysis of energy storage systems with annular and countercurrent flows p 150 A91-27166
- Three-component laser anemometer measurement systems [NASA-TP-3080] p 13 N91-19057
- ANODES**
- Performance characterization of a segmented anode arcjet thruster [NASA-TM-103227] p 67 N91-10118
- Investigation of anodic and chemical oxides grown on p-type InP with applications to surface passivation for n(+)p solar cell fabrication p 210 N91-19208
- High resolution electrolyte for thinning InP by anodic dissolution and its applications to EC-V profiling, defect revealing and surface passivation p 107 N91-30210
- ANOMALIES**
- On the anomaly of velocity-pressure decoupling in collocated mesh solutions [NASA-TM-103769] p 164 N91-21448
- ANTENNA ARRAYS**
- Design of an optically controlled Ka-band GaAs MMIC phased-array antenna p 132 A91-24951
- New coplanar waveguide/stripline feed network for seven patch hexagonal CP subarray p 137 A91-32823
- Ka-band MMIC microstrip array for high rate communications [AIAA PAPER 91-3421] p 132 A91-52341
- Coplanar waveguide feeds for phased array antennas [AIAA PAPER 91-3422] p 141 A91-52342
- Design of an inflatable, optically controlled and fed, phased array antenna [AIAA PAPER 91-3470] p 132 A91-52378
- High temperature superconductor analog electronics for millimeter-wavelength communications [AIAA PAPER 91-3592] p 233 A91-53707
- A seven patch hexagonal CP subarray with a CPW/stripline feed network [NASA-TM-103802] p 144 N91-20406
- System-Level Integrated Circuit (SLIC) development for phased array antenna applications [NASA-TM-104392] p 134 N91-23354
- Ka-band MMIC microstrip array for high rate communications [NASA-TM-104500] p 135 N91-27437
- Coplanar waveguide feeds for phased array antennas [NASA-TM-104467] p 146 N91-27477
- High temperature superconductor analog electronics for millimeter-wavelength communications [NASA-TM-105184] p 237 N91-29982
- ANTENNA COUPLERS**
- Mutual coupling between electromagnetically coupled rectangular patch antennas p 137 A91-32822
- ANTENNA DESIGN**
- Design of an inflatable, optically controlled and fed, phased array antenna [AIAA PAPER 91-3470] p 132 A91-52378
- ATDRS payload technology R & D p 45 A91-53188
- Designs for the ATDRSS tri-band reflector antenna [NASA-TM-103754] p 48 N91-20184
- A seven patch hexagonal CP subarray with a CPW/stripline feed network [NASA-TM-103802] p 144 N91-20406
- A new fabrication method for precision antenna reflectors for space flight and ground test [NASA-TP-3078] p 48 N91-21185
- Characteristics of a future aeronautical satellite communications system [NASA-TM-104389] p 20 N91-23102
- ANTENNA FEEDS**
- Coplanar waveguide/microstrip probe coupler and applications to antennas p 131 A91-17719
- Mutual coupling between electromagnetically coupled rectangular patch antennas p 137 A91-32822
- New coplanar waveguide/stripline feed network for seven patch hexagonal CP subarray p 137 A91-32823
- A 29.3-GHz cavity-enclosed aperture-coupled circular-patch antenna for microwave circuit integration p 140 A91-47057
- Coplanar waveguide feeds for phased array antennas [AIAA PAPER 91-3422] p 141 A91-52342
- ATDRS payload technology R & D p 45 A91-53188
- Designs for the ATDRSS tri-band reflector antenna [NASA-TM-103754] p 48 N91-20184
- Coplanar waveguide feeds for phased array antennas [NASA-TM-104467] p 146 N91-27477
- ANTENNA RADIATION PATTERNS**
- Circular polarisation characteristics of stacked microstrip antennas p 131 A91-20370
- Mutual coupling between electromagnetically coupled rectangular patch antennas p 137 A91-32822
- A 29.3-GHz cavity-enclosed aperture-coupled circular-patch antenna for microwave circuit integration p 140 A91-47057
- Measurement techniques for cryogenic Ka-band microstrip antennas [NASA-TM-105183] p 146 N91-30426
- ANTIFRICTION BEARINGS**
- PM200/PS200: Self-lubricating bearing and seal materials for applications to 900 C [NASA-TM-103776] p 190 N91-30539
- ANTIMATTER**
- Antiproton powered propulsion with magnetically confined plasma engines p 63 A91-52313
- ANTI-PROTONS**
- Antiproton powered propulsion with magnetically confined plasma engines p 63 A91-52313
- ANTIREFLECTION COATINGS**
- A light-trapping solar cell coverglass p 229 A91-41995
- Diamondlike carbon as a moisture barrier and antireflecting coating on optical materials p 119 N91-18302
- Diamondlike carbon applications in infrared optics and microelectronics p 230 N91-18306
- Relationship of optical coating on thermal radiation characteristics of nonisothermal cylindrical enclosures [NASA-TM-104408] p 168 N91-30461
- APPLICATIONS PROGRAMS (COMPUTERS)**
- 3-D Navier-Stokes analysis of crossing, glancing shocks/turbulent boundary layer interactions [AIAA PAPER 91-1758] p 6 A91-43631
- Algebraic grid generation for complex geometries p 157 A91-48758
- A data acquisition and control program for axial-torsional fatigue testing p 199 A91-56540
- Computational simulation of hot composites structures [NASA-TM-103681] p 97 N91-19230
- ALPS: A Linear Program Solver [NASA-TM-104347] p 216 N91-20765
- The 3-D Navier-Stokes analysis of crossing, glancing shocks/turbulent boundary layer interactions [NASA-TM-104469] p 16 N91-24130
- The design/analysis of flows through turbomachinery: A viscous/inviscid approach [NASA-TM-104447] p 33 N91-25148
- Probability of failure and risk assessment of propulsion structural components [NASA-TM-102323] p 205 N91-25436
- GRID3D-v2: An updated version of the GRID2D/3D computer program for generating grid systems in complex-shaped three-dimensional spatial domains [NASA-TM-103766] p 217 N91-25630
- Development of an analytical tool to study power quality of AC power systems for large spacecraft [NASA-TM-104451] p 223 N91-25749
- Comparison of a quasi-3D analysis and experimental performance for three compact radial turbines [NASA-TM-105155] p 35 N91-30142
- Comparative modeling of InP solar cell structures p 83 N91-30232
- Verification of the proteus two-dimensional Navier-Stokes code for flat plate and pipe flows [NASA-TM-105160] p 168 N91-30462
- ARC DISCHARGES**
- Significant reduction in arc frequency biased solar cells: Observations, diagnostics, and mitigation techniques p 83 N91-30235
- ARC JET ENGINES**
- Performance and lifetime assessment of magnetoplasmadynamic arc thruster technology p 51 A91-30013
- Power electronics for low power arcjets [AIAA PAPER 91-1991] p 60 A91-45779
- Nonequilibrium in a low power arcjet nozzle [AIAA PAPER 91-2113] p 61 A91-45784
- High-power hydrogen arcjet performance [AIAA PAPER 91-2226] p 61 A91-45795
- Preliminary performance and life evaluation of a 2-kW arcjet [AIAA PAPER 91-2228] p 62 A91-45796
- Arcjet thermal characteristics [AIAA PAPER 91-2456] p 63 A91-45814
- Five-kilowatt arcjet power electronics p 63 A91-52312
- Performance characterization of a segmented anode arcjet thruster [NASA-TM-103227] p 67 N91-10118
- Investigation of the arcjet plume near field using electrostatic probes [NASA-TM-103638] p 68 N91-11060
- Investigation of the arcjet near field plume using electrostatic probes p 75 N91-24270
- Arcjet nozzle area ratio effects p 75 N91-24271
- Power electronics for low power arcjets [NASA-TM-104459] p 77 N91-25172
- Arcjet thermal characteristics [NASA-TM-105156] p 82 N91-29231
- Preliminary performance and life evaluations of a 2-kW arcjet [NASA-TM-105149] p 84 N91-30252
- Medium power hydrogen arcjet performance [NASA-TM-104533] p 85 N91-31216
- ARC SPRAYING**
- Tensile behavior of tungsten/nibium composites at 1300 to 1600 K [NASA-TM-103727] p 111 N91-16128
- Process for HIP canning of composites [NASA-CASE-LEW-14990-1-CU] p 96 N91-17145
- ARCHITECTURE (COMPUTERS)**
- Neural network architecture for crossbar switch control p 218 A91-29181
- A neural net based architecture for the segmentation of mixed gray-level and binary pictures p 218 A91-29183
- ARGON**
- Microstructural and strength stability of CVD SiC fibers in argon environments p 117 A91-56958
- Microstructural and strength stability of CVD SiC fibers in argon environment [NASA-TM-103772] p 102 N91-29250
- ARMATURES**
- The preliminary feasibility of intercalated graphite railgun armatures p 137 A91-29257
- ARROW WINGS**
- A comparison of arrow, trapezoidal and M wing concepts using a Mach 2 supersonic cruise transport mission [AIAA PAPER 91-3102] p 7 A91-54027
- ARTIFICIAL GRAVITY**
- Design strategies for the International Space University's variable gravity research facility p 42 N91-22171
- ARTIFICIAL INTELLIGENCE**
- An intelligent control system for rocket engines - Need, vision, and issues p 218 A91-26925
- Technologies for unattended network operations [AIAA PAPER 91-3534] p 45 A91-52425
- Applications of artificial neural nets in structural mechanics [NASA-TM-102420] p 202 N91-21559
- Techniques and implementation of the embedded rule-based expert system using Ada p 220 N91-22788
- Application of artificial neural networks to composite ply micromechanics [NASA-TM-104365] p 100 N91-24345

ASCENT PROPULSION SYSTEMS

- In-situ propellant rocket engines for Mars missions ascent vehicle
[AIAA PAPER 91-2445] p 60 A91-44247
In-situ propellant rocket engines for Mars mission ascent vehicle
[NASA-TM-104429] p 76 N91-24305

ASTEROIDS

- Outline of the Solar System: Activities for elementary students
[NASA-TM-104965] p 241 N91-25975
Near-Earth asteroids: Metals occurrence, extraction, and fabrication p 241 N91-26058

ASTRONOMICAL MODELS

- Baryon isocurvature scenario in inflationary cosmology
- A particle physics model and its astrophysical implications p 240 A91-54201

ASTRONOMICAL SPECTROSCOPY

- Telescope search for a 3-eV to 8-eV axion p 239 A91-28714

ASTROPHYSICS

- Astrophysics and cosmology confront the 17-keV neutrino p 240 A91-43291
Constraints from primordial nucleosynthesis on the mass of the tau neutrino p 240 A91-46543
Baryon isocurvature scenario in inflationary cosmology
- A particle physics model and its astrophysical implications p 240 A91-54201

ASYMPTOTIC METHODS

- A new uniformly valid asymptotic integration algorithm for elasto-plastic creep and unified viscoplastic theories including continuum damage p 110 A91-48725
Asymptotic integration algorithms for nonhomogeneous, nonlinear, first order, ordinary differential equations
[NASA-TM-103793] p 222 N91-21797
A k-epsilon modeling of near wall turbulence
[NASA-TM-105238] p 170 N91-32460

ASYMPTOTIC SERIES

- Resonant triad in boundary-layer stability. Part 2: Composite solution and comparison with observations
[NASA-TM-105209] p 169 N91-32459

ATMOSPHERIC ATTENUATION

- A statistical rain attenuation prediction model with application to the advanced communication technology satellite project. 3: A stochastic rain fade control algorithm for satellite link power via non linear Markov filtering theory
[NASA-TM-100243] p 134 N91-22494

ATMOSPHERIC COMPOSITION

- Chemical approaches to carbon dioxide utilization for manned Mars missions
[NASA-TM-103728] p 241 N91-20015
Chemical approaches to carbon dioxide utilization for manned Mars missions p 241 N91-26073

ATMOSPHERIC DENSITY

- Frontogenesis driven by horizontally quadratic distributions of density p 157 A91-48276

ATOMIZERS

- Jet-A fuel evaporation analysis in conical tube injectors
[AIAA PAPER 91-0345] p 149 A91-21467
Measurements and predictions of a liquid spray from an air-assist nozzle
[AIAA PAPER 91-0692] p 149 A91-22498
Measurements and predictions of a liquid spray from an air-assist nozzle
[NASA-TM-103640] p 26 N91-13455
Cryogenic liquid-jet breakup in two-fluid atomizers
[NASA-TM-103734] p 176 N91-19402

ATOMIZING

- Effects of nozzle lip geometry on spray atomization and emissions advanced gas turbine combustors
[AIAA PAPER 91-2201] p 24 A91-44153
Fuel-rich, catalytic reaction experimental results --- fuel development for high-speed civil transport aircraft
[AIAA PAPER 91-2463] p 24 A91-44250
Gas property effects on droplet size of simulated fuel sprays p 156 A91-45327
Fuel-rich, catalytic reaction experimental results
[NASA-TM-104423] p 33 N91-24203

ATTENUATION COEFFICIENTS

- Ellipsometric study of cubic SiC p 235 N91-18304

AUGER SPECTROSCOPY

- Uses of Auger and x ray photoelectron spectroscopy in the study of adhesion and friction
[NASA-TM-103266] p 118 N91-11922

AUGMENTATION

- Control of an axisymmetric turbulent jet by multi-modal excitation
[NASA-TM-104483] p 17 N91-26121

AUTOCCLAVING

- Autoclavable addition polyimides for 371 C composite applications p 115 A91-49112

AUTOMATIC CONTROL

- Partitioning methods for global controllers p 219 A91-30043

- Automated electric power management and control for Space Station Freedom p 53 A91-37970

- Automated design of controlled diffusion blades p 9 N91-10883

- Automatic control study of the icing research tunnel refrigeration system
[NASA-TM-4257] p 40 N91-19115

- Autonomous power expert system advanced development p 72 N91-20689

AUTOMATIC TEST EQUIPMENT

- Recent manufacturing advances for spiral bevel gears
[NASA-TM-104479] p 191 N91-31654

AUTOMATION

- Automation software for a materials testing laboratory p 216 A91-56538

AUTONOMY

- Autonomous power expert system p 54 A91-37972

AUXILIARY POWER SOURCES

- SEI power source alternatives for rovers and other multi-kWe distributed surface applications
[NASA-TM-104360] p 81 N91-28277

AUXILIARY PROPULSION

- Performance and optimization of a 'derated' ion thruster for auxiliary propulsion
[AIAA PAPER 91-2350] p 62 A91-45809
Hydrogen/oxygen auxiliary propulsion technology
[AIAA PAPER 91-3440] p 64 A91-52352
Performance and optimization of a derated ion thruster for auxiliary propulsion
[NASA-TM-105144] p 82 N91-29229
Preliminary performance and life evaluations of a 2-kW arcjet
[NASA-TM-105149] p 84 N91-30252

AVIONICS

- Digital angular position sensor using wavelength division multiplexing p 21 A91-19580
Advanced launch system (ALS) - Electrical actuation and power systems improve operability and cost picture p 51 A91-31025

AXIAL FLOW

- Improved visualization of flow field measurements
[AIAA PAPER 91-0273] p 3 A91-26331
Experimental investigation of propan aeroelastic response in off-axis flow with mistuning p 22 A91-30015

AXIAL STRAIN

- A data acquisition and control program for axial-torsional fatigue testing p 199 A91-56540
Axial-torsional fatigue: A study of tubular specimen thickness effects
[NASA-TM-103637] p 200 N91-14632

AXISYMMETRIC FLOW

- Vapor condensation at the free surface of an axisymmetric liquid mixed by a laminar jet p 151 A91-35109
Computational analysis of underexpanded jets in the hypersonic regime p 4 A91-37421
Axisymmetric jet forced by fundamental and subharmonic tones p 226 A91-45111
A numerical and experimental analysis of reactor performance and deposition rates for CVD on monofilaments
[NASA-TM-103631] p 130 N91-14500
The design/analysis of flows through turbomachinery: A viscous/inviscid approach
[NASA-TM-104447] p 33 N91-25148
Effect of tabs on the evolution of an axisymmetric jet
[NASA-TM-104472] p 34 N91-27159
An experimental study of natural and forced modes in an axisymmetric jet
[NASA-TM-105225] p 18 N91-32074

AZIMUTH

- Naturally occurring and forced azimuthal modes in a turbulent jet
[NASA-TM-103692] p 11 N91-17000

B**BACKWARD FACING STEPS**

- A steady effect of acoustic excitation on transitory stall
[AIAA PAPER 91-0043] p 2 A91-22499
Turbulent boundary layer separation over a rearward facing ramp and its control through mechanical excitation
[AIAA PAPER 91-0253] p 150 A91-26328
A steady effect of acoustic excitation on transitory stall
[NASA-TM-103689] p 11 N91-13420
Least-squares solution of incompressible Navier-Stokes equations with the p-version of finite elements
[NASA-TM-105203] p 223 N91-31911

BALANCING

- Balancing reliability and cost to choose the best power subsystem
[NASA-TM-104453] p 238 N91-24952

BALL BEARINGS

- Fully articulated four-point-bend loading fixture
[NASA-CASE-LEW-14776-1] p 185 N91-21540
Quantifying oil filtration effects on bearing life
[NASA-TM-104350] p 186 N91-23512
Parched elastohydrodynamic lubrication: Instrumentation and procedure
[NASA-TM-104426] p 168 N91-30469

BANDWIDTH

- Digital CODEC for real-time processing of broadcast quality video signals at 1.8 bits/pixel p 134 N91-24067

BARIIUM OXIDES

- Photoresponse of YBa₂Cu₃O₇(δ) granular and epitaxial superconducting thin films p 141 A91-50443
Ellipsometric study of YBa₂Cu₃O_{7-x} laser ablated and co-evaporated films p 233 A91-53235
Near-edge study of gold-substituted YBa₂Cu₃O₇(δ)
[NASA-TM-105220] p 237 N91-31977

BARRIERS

- High-temperature, flexible, thermal barrier seal
[NASA-CASE-LEW-14672-1] p 189 N91-27560

BARS

- Surface fatigue life of M50NiL and AISI 9310 spur gears and R C bars
[NASA-TM-104496] p 189 N91-27569

BARYONS

- Baryon isocurvature scenario in inflationary cosmology
- A particle physics model and its astrophysical implications p 240 A91-54201

BEACONS

- GaAs monolithic RF modules for SRSAT distress beacons
[NASA-TM-104338] p 46 N91-21184

BEAM INTERACTIONS

- Ion beam sputtering in electric propulsion facilities
[AIAA PAPER 91-2117] p 61 A91-45785

BEAMS (SUPPORTS)

- Dynamic analysis of space-related linear and non-linear structures p 196 A91-28612

BEARINGS

- Extension of transonic flow computational concepts in the analysis of cavitated bearings
[ASME PAPER 90-TRIB-40] p 150 A91-29474
Extension of transonic flow computational concepts in the analysis of cavitated bearings
[NASA-TM-103214] p 160 N91-16304
Advanced Rotorcraft Transmission (ART) program-Boeing helicopters status report
[NASA-TM-104474] p 188 N91-25412

BEND TESTS

- Fiber creep evaluation by stress relaxation measurements p 117 A91-56905
A simple test for thermomechanical evaluation of ceramic fibers
[NASA-TM-103767] p 121 N91-21309
Fully articulated four-point-bend loading fixture
[NASA-CASE-LEW-14776-1] p 185 N91-21540
Comparison of Weibull strength parameters from flexure and spin tests of brittle materials
[NASA-TM-104414] p 187 N91-24593
Elevated-temperature fracture resistances (K(sub IC), R-curves, gamma sub (omega OF)) of monolithic and composite ceramics using chevron-notched, bend tests
[NASA-TM-105090] p 123 N91-28418

BENDING

- Monograph on propagation of sound waves in curved ducts
[NASA-RP-1248] p 228 N91-15848

BENDING FATIGUE

- Effects of rim thickness on spur gear bending stress
[AIAA PAPER 91-2020] p 181 A91-41681
Comparison of analysis and experiment for dynamics of low-contact-ratio spur gears
[NASA-TM-103232] p 185 N91-22566
Combined thermal and bending fatigue of high-temperature metal-matrix composites: Computational simulation
[NASA-TM-104354] p 100 N91-23247
Effects of rim thickness on spur gear bending stress
[NASA-TM-104388] p 186 N91-23500

BERYLLIUM ALLOYS

- Preliminary studies on NiAl/Nb₂B₆ reaction and effectiveness of BeO as an interfacial reaction barrier p 92 A91-55050

BIS

- Magnetic bearings with zero bias p 48 N91-21194

BIBLIOGRAPHIES

- Acousto-ulasonics - Retrospective exhortation with bibliography p 191 A91-37011

- Bibliography of Lewis Research Center technical publications announced in 1989
[NASA-TM-102542] p 238 N91-10798
- Magnetic bearings-state of the art
[NASA-TM-104465] p 188 N91-25413
- BIG BANG COSMOLOGY**
- Big bang nucleosynthesis - The standard model and alternatives p 240 A91-37428
- Primordial nucleosynthesis redux p 240 A91-45907
- BIMETALS**
- Theoretical modelling of AFM for bimetallic tip-substrate interactions
[NASA-TM-105280] p 112 N91-32215
- BINARY ALLOYS**
- Equivalent crystal theory of alloys
[NASA-TP-3155] p 112 N91-30318
- A new approximate sum rule for bulk alloy properties
[NASA-TM-105282] p 112 N91-32204
- Theoretical modelling of AFM for bimetallic tip-substrate interactions
[NASA-TM-105280] p 112 N91-32215
- BINDERS (MATERIALS)**
- Method of making single crystal fibers
[NASA-CASE-LEW-14921-1] p 95 N91-13502
- Heat transfer device and method of making the same
[NASA-CASE-LEW-14162-1] p 159 N91-13668
- Method of making carbide/fluoride/silver composites
[NASA-CASE-LEW-14902-1] p 102 N91-27244
- BIPOLAR TRANSISTORS**
- Neutron and gamma irradiation effects on power semiconductor switches p 139 A91-38162
- BIREFRINGENCE**
- Photoelastic transducer for high-temperature applications p 174 A91-55533
- Fiber-optic sensors for aerospace electrical measurements: An update
[NASA-TM-104454] p 177 N91-25381
- BIT ERROR RATE**
- Bit error rate testing of fiber optic data links for MMIC-based phased array antennas p 131 A91-24950
- Combinatorial FSK modulation for power-efficient high-rate communications
[AIAA PAPER 91-3532] p 133 A91-53708
- Combinatorial FSK modulation for power-efficient high-rate communications
[NASA-TM-105188] p 135 N91-29404
- BLADE TIPS**
- Optical measurement of unducted fan flutter
[NASA-TM-103285] p 27 N91-15174
- BLADE-VORTEX INTERACTION**
- Navier-Stokes simulation of transonic blade-vortex interactions p 2 A91-21065
- BLUE STARS**
- The shock process and light-element production in supernova envelopes p 239 A91-33573
- BOLTED JOINTS**
- Simplified procedures for designing composite bolted joints p 195 A91-16290
- BONDING**
- Ceramic coatings on smooth surfaces
[NASA-CASE-LEW-15164-1] p 122 N91-25298
- BOOSTER ROCKETS**
- The design and performance estimates for the propulsion module for the booster of a TSTO vehicle
[AIAA PAPER 91-3136] p 43 A91-54054
- BORON ISOTOPIES**
- The shock process and light-element production in supernova envelopes p 239 A91-33573
- BORON NITRIDES**
- Wettability of pyrolytic boron nitride by aluminum p 114 A91-28772
- BORON REINFORCED MATERIALS**
- Compression behavior of TiB₂-particulate-reinforced composites of Al₂O₃/Fe₃TiB p 91 A91-28014
- BOSONS**
- Natural inflation with pseudo Nambu-Goldstone bosons p 239 A91-19545
- BOUNDARY CONDITIONS**
- General purpose program to generate compatibility matrix for the integrated force method p 195 A91-12905
- Numerical analysis of flow through oscillating cascade sections p 9 N91-10884
- The method of lines in analyzing solids containing cracks
[NASA-TM-103626] p 201 N91-19477
- A system-approach to the elastohydrodynamic lubrication point-contact problem
[NASA-TM-104342] p 165 N91-23439
- Full-size solar dynamic heat receiver thermal-vacuum tests
[NASA-TM-104486] p 78 N91-25184
- BOUNDARY ELEMENT METHOD**
- Acoustical analysis of gear housing vibration
[NASA-TM-103691] p 188 N91-25411
- BOUNDARY LAYER CONTROL**
- Turbulent boundary layer separation over a rearward facing ramp and its control through mechanical excitation
[NASA-TM-103702] p 160 N91-19370
- A study of three dimensional turbulent boundary layer separation and vortex flow control using the reduced Navier Stokes equations
[NASA-TM-104407] p 16 N91-23089
- BOUNDARY LAYER EQUATIONS**
- Analytical solution for boundary heat fluxes from a radiating rectangular medium p 150 A91-27175
- On the continuous spectra of the compressible boundary layer stability equations p 150 A91-31342
- BOUNDARY LAYER FLOW**
- Spatial evolution of nonlinear acoustic mode instabilities on hypersonic boundary layers p 225 A91-12973
- An experimental investigation of nozzle-exit boundary layers of highly heated free jets
[ASME PAPER 90-GT-255] p 155 A91-44662
- Comparison of a quasi-3D analysis and experimental performance for three compact radial turbines
[AIAA PAPER 91-2128] p 25 A91-45789
- The effect of varying Mach number on crossing, glancing shocks/turbulent boundary-layer interactions
[AIAA PAPER 91-2157] p 6 A91-45792
- The effect of small streamwise velocity distortion on the boundary layer flow over a thin flat plate with application to boundary layer stability theory
[NASA-TM-103668] p 161 N91-19372
- Numerical investigation of an internal layer in turbulent flow over a curved hill p 163 N91-21083
- Heat transfer, velocity-temperature correlation, and turbulent shear stress from Navier-Stokes computations of shock wave/turbulent boundary layer interaction flows p 163 N91-21085
- A laser-induced heat flux technique for convective heat transfer measurements in high speed flows
[NASA-TM-105177] p 168 N91-30472
- A laser velocimeter investigation of the normal shock-wave boundary layer interaction
[NASA-TM-105201] p 169 N91-32440
- BOUNDARY LAYER SEPARATION**
- Turbulent boundary layer separation over a rearward facing ramp and its control through mechanical excitation
[AIAA PAPER 91-0253] p 150 A91-26328
- Effect of acoustic excitation on stalled flows over an airfoil
[NASA-TM-103183] p 10 N91-11675
- Turbulent boundary layer separation over a rearward facing ramp and its control through mechanical excitation
[NASA-TM-103702] p 160 N91-19370
- A study of three dimensional turbulent boundary layer separation and vortex flow control using the reduced Navier Stokes equations
[NASA-TM-104407] p 16 N91-23089
- BOUNDARY LAYER STABILITY**
- Spatial evolution of nonlinear acoustic mode instabilities on hypersonic boundary layers p 225 A91-12973
- On the continuous spectra of the compressible boundary layer stability equations p 150 A91-31342
- The effect of small streamwise velocity distortion on the boundary layer flow over a thin flat plate with application to boundary layer stability theory
[NASA-TM-103668] p 161 N91-19372
- Resonant triad in boundary-layer stability. Part 1: Fully nonlinear interaction
[NASA-TM-105208] p 169 N91-32458
- Resonant triad in boundary-layer stability. Part 2: Composite solution and comparison with observations
[NASA-TM-105209] p 169 N91-32459
- BOUNDARY LAYER TRANSITION**
- Critical-layer nonlinearity in the resonance growth of three-dimensional waves in boundary layers
[NASA-TM-103639] p 161 N91-19373
- Experimental study of boundary layer transition on a heated flat plate
[NASA-TM-103779] p 14 N91-21061
- Resonant triad in boundary-layer stability. Part 1: Fully nonlinear interaction p 169 N91-32458
- Resonant triad in boundary-layer stability. Part 2: Composite solution and comparison with observations
[NASA-TM-105209] p 169 N91-32459
- BOUNDARY LAYERS**
- Numerical study of shock-wave/boundary layer interactions in premixed hydrogen-air hypersonic flows
[AIAA PAPER 91-0413] p 149 A91-26191
- Numerical flux formulas for the Euler and Navier-Stokes equations. II - Progress in flux-vector splitting
[AIAA PAPER 91-1566] p 5 A91-40740
- A Navier-Stokes study of shock-boundary layer interaction and flow separation inside a transonic compressor p 8 A91-56115
- Numerical study of shock-wave/boundary layer interactions in premixed hydrogen-air hypersonic flows
[NASA-TM-103273] p 160 N91-14559
- Aerodynamics and heat transfer investigations on a high Reynolds number turbine cascade
[NASA-TM-103260] p 11 N91-15134
- Prediction of ice shapes and their effect on airfoil performance p 12 N91-19047
- [NASA-TM-103701] p 12 N91-19047
- Numerical flux formulas for the Euler and Navier-Stokes equations. 2: Progress in flux-vector splitting
[NASA-TM-104353] p 15 N91-22084
- Evaluation of a technique to generate artificially thickened boundary layers in supersonic and hypersonic flows
[NASA-TP-3142] p 17 N91-28136
- An experimental study of natural and forced modes in an axisymmetric jet
[NASA-TM-105225] p 18 N91-32074
- BOUNDARY LUBRICATION**
- Inertia effects in thin film flow with a corrugated boundary p 151 A91-32691
- On the numerical solution of the dynamically loaded hydrodynamic lubrication of the point contact p 180 A91-33461
- A system-approach to the elastohydrodynamic lubrication point-contact problem
[NASA-TM-104342] p 165 N91-23439
- BOUNDARY VALUE PROBLEMS**
- Parallel algorithms for boundary value problems p 221 A91-31175
- The method of lines in analyzing solids containing cracks
[NASA-TM-103626] p 201 N91-19477
- Compressible flows with periodic turbulent disturbances around lifting airfoils
[NASA-TM-103742] p 14 N91-21060
- BOUSSINESQ APPROXIMATION**
- Stability of an oscillated fluid with a uniform density gradient p 147 A91-12971
- BOW WAVES**
- Qualitative investigation of cryogenic injected shock dissipation
[NASA-TM-105140] p 168 N91-29525
- BRACKETS**
- Removable hand hold
[NASA-CASE-LEW-15196-1] p 188 N91-26543
- BRASSES**
- Grain boundary sliding behaviour of copper and alpha brass at intermediate temperatures p 108 A91-27158
- BRAYTON CYCLE**
- Lunar electric power systems utilizing the SP-100 reactor coupled to dynamic conversion systems
[AIAA PAPER 91-3520] p 208 A91-52415
- Dynamic Isotope Surface Power Systems
[AIAA PAPER 91-3623] p 208 A91-52487
- Evolving the SP-100 reactor in order to boost large payloads to GEO and to low lunar orbit via nuclear-electric propulsion p 67 A91-53712
- [AIAA PAPER 91-3562] p 67 A91-53712
- Full-size solar dynamic heat receiver thermal-vacuum tests
[NASA-TM-104486] p 78 N91-25184
- Evolving the SP-100 reactor in order to boost large payloads to GEO and to low lunar orbit via nuclear-electric propulsion
[NASA-TM-104527] p 80 N91-27212
- Design considerations for space radiators based on the liquid sheet (LSR) concept p 80 N91-27213
- [NASA-TM-105158] p 80 N91-27213
- Comparison of dynamic isotope power systems for distributed planet surface applications
[NASA-TM-4303] p 81 N91-28278
- BREADBOARD MODELS**
- Five-kilowatt arcjet power electronics p 63 A91-52312
- Optical Multiple Access Network (OMAN) for advanced processing satellite applications
[NASA-TM-105167] p 135 N91-29431
- Test and evaluation of load converter topologies used in the Space Station Freedom Power Management and distribution DC test bed
[NASA-TM-105217] p 85 N91-30267
- BRITTLE MATERIALS**
- Transition-to-practice technologies for brittle materials p 120 N91-20107
- Comparison of Weibull strength parameters from flexure and spin tests of brittle materials
[NASA-TM-104414] p 187 N91-24593
- BROADCASTING**
- Real-time data compression of broadcast video signals
[NASA-CASE-LEW-14945-1] p 133 N91-13598
- BROKEN SYMMETRY**
- Inflationary axion cosmology p 239 A91-20491

BROMINE

BROMINE

- Effect of lightning strike on bromine intercalated graphite fiber/epoxy composites
[NASA-TM-104507] p 103 N91-32177

BRUSH SEALS

- Flow visualization in a simulated brush seal
[ASME PAPER 90-GT-217] p 173 A91-44633
Some preliminary results of brush seal/rotor interference effects on leakage at zero and low rpm using a tapered-plug rotor
[AIAA PAPER 91-3390] p 182 A91-45820
Eccentricity effects on leakage of a brush seal at low speeds
[NASA-TM-105141] p 86 N91-31220

BRUSHES

- Simulation of brush insert for leading-edge-passage convective heat transfer
[NASA-TM-103801] p 165 N91-23409
Some preliminary results of brush seal/rotor interference effects on leakage at zero and low RPM using a tapered-plug rotor
[NASA-TM-104396] p 188 N91-27559

BUBBLES

- The migration of a compound drop due to thermocapillarity p 148 A91-18428

BUFFETING

- Flow induced vibration and noise by a pair of tandem cylinders due to buffeting p 225 A91-14650

BUILDINGS

- Simulation of probabilistic wind loads and building analysis
[NASA-TM-103744] p 203 N91-23549

BUOYANCY

- A numerical study of the direct contact condensation on a horizontal surface
[AIAA PAPER 91-1307] p 155 A91-44335
Heat transfer in rotating serpentine passages with trips normal to the flow
[NASA-TM-103758] p 184 N91-19443
A numerical study of the direct contact condensation on a horizontal surface
[NASA-TM-104432] p 166 N91-24548

BURNING RATE

- Particle nonuniformity effects on particle cloud flames in low gravity
[AIAA PAPER 91-0718] p 104 A91-19431
N-decane droplet combustion in the NASA-Lewis 5 Second Zero-Gravity Facility - Results in test gas environments other than air
[AIAA PAPER 91-0720] p 105 A91-19433

BUSHINGS

- Eccentricity effects on leakage of a brush seal at low speeds
[NASA-TM-105141] p 86 N91-31220

BUTT JOINTS

- Simplified procedures for designing adhesively bonded composite joints p 180 A91-20938

BYPASS RATIO

- Ultra-high bypass research p 30 N91-20117

C

CADMIUM

- A comparative study of $p(+)$ and $n(+)$ InP solar cells made by a closed ampoule diffusion p 212 N91-30206

CADMIUM COMPOUNDS

- Pretreatment of lubricated surfaces with sputtered cadmium oxide
[NASA-CASE-LEW-14474-1] p 123 N91-28423

CALCIUM COMPOUNDS

- Synthesis and thermal properties of strontium and calcium peroxides
[NASA-TM-103725] p 107 N91-22410

CALCIUM FLUORIDES

- Tensile properties of HA 230 and HA 188 after 400 and 2500 hour exposures to LiF-22CaF₂ and vacuum at 1093 K p 207 A91-11624
Temperature dependence of the elastic moduli and damping for polycrystalline LiF-22 pct CaF₂ eutectic salt p 87 A91-33797

CALIBRATING

- Use of rotating pinholes and reticles for calibration of cloud droplet instrumentation p 171 A91-30371
Primary reference cell calibrations at SERI - History and methods ... solar cells p 207 A91-41966
High altitude AM0 testing of PV concentrator lens elements ... Air Mass Zero p 207 A91-41978
An x ray photoelectron spectroscopy study of Au(x)In(y) alloys
[NASA-TM-103659] p 234 N91-14050
Rotating pressure measurement system using an on board calibration standard
[NASA-TM-103676] p 176 N91-19401

Overview of high performance aircraft propulsion p 28 N91-20089

- Calibrator tests of heat flux gauges mounted in SSME blades p 177 N91-24321
Applied high-speed imaging for the icing research program at the NASA Lewis Research Center
[NASA-TM-104415] p 177 N91-26490
Makeup and uses of a basic magnet laboratory for characterizing high-temperature permanent magnets
[NASA-TM-104508] p 146 N91-30427

CAMBER

- Influence of thickness and camber on the aeroelastic stability of supersonic throughflow fans p 5 A91-42814

CANONICAL FORMS

- Alpha-canonical form representation of the open loop dynamics of the Space Shuttle main engine
[NASA-TM-104422] p 131 N91-24469

CANS

- Two-dimensional model of a Space Station Freedom thermal energy storage canister p 151 A91-38048
Process for HIP canning of composites
[NASA-CASE-LEW-14990-1-CU] p 96 N91-17145
Multi-dimensional modeling of a thermal energy storage canister
[NASA-TM-103731] p 71 N91-19177

CANTILEVER BEAMS

- Free vibrations of delaminated beams
[AIAA PAPER 91-1241] p 197 A91-32129

CAPACITANCE

- Electrical characterization of glass, teflon, and tantalum capacitors at high temperatures
[NASA-TM-104517] p 146 N91-27444
Parched elastohydrodynamic lubrication: Instrumentation and procedure
[NASA-TM-104426] p 168 N91-30469
Some recent studies with the solid-ionomer electrochemical capacitor p 214 N91-32562

CAPACITORS

- MIS capacitor studies on silicon carbide single crystals
[NASA-CR-187350] p 234 N91-11555
Electrical characterization of glass, teflon, and tantalum capacitors at high temperatures
[NASA-TM-104517] p 146 N91-27444
Some recent studies with the solid-ionomer electrochemical capacitor p 214 N91-32562

CAPILLARY FLOW

- The migration of a compound drop due to thermocapillarity p 148 A91-18428
Drop-tower experiments for capillary surfaces in an exotic container
[AIAA PAPER 91-0107] p 148 A91-19138
A comparative flow visualization study of thermocapillary flow in drops in liquid-liquid systems
[AIAA PAPER 91-0311] p 148 A91-21452
Particle image velocimetry for the surface tension driven convection experiment using a particle displacement tracking technique
[NASA-TM-104482] p 177 N91-25382
Ground-based PIV and numerical flow visualization results from the surface tension driven convection experiment
[NASA-TM-105172] p 178 N91-30491

CARBIDES

- Thermal stability of the microstructure of an aged Nb-Zr-C alloy
[NASA-TM-103647] p 110 N91-14454

CARBON

- Diamondlike carbon as a moisture barrier and antireflecting coating on optical materials p 119 N91-18302
Optical dispersion relations for diamondlike carbon films p 230 N91-18305
Diamondlike carbon applications in infrared optics and microelectronics p 230 N91-18306
Dual ion beam processed diamondlike films for industrial applications p 121 N91-23042

CARBON DIOXIDE

- Fire suppression in human-crew spacecraft
[NASA-TM-104334] p 44 N91-21182
Cooling of in-situ propellant rocket engines for Mars mission
[NASA-TM-103729] p 72 N91-21233
Material processing with hydrogen and carbon monoxide on Mars
[NASA-TM-104405] p 211 N91-23616
Chemical approaches to carbon dioxide utilization for manned Mars missions p 241 N91-26073
The Au cathode in the system Li₂CO₃-CO₂-CO at 800 to 900 C p 213 N91-32551

CARBON DIOXIDE CONCENTRATION

- Chemical approaches to carbon dioxide utilization for manned Mars missions
[NASA-TM-103728] p 241 N91-20015
Chemical approaches to carbon dioxide utilization for manned Mars missions p 241 N91-26073

CARBON FIBER REINFORCED PLASTICS

- Effect of fiber reinforcements on thermo-oxidative stability and mechanical properties of polymer matrix composites
[NASA-TM-103648] p 98 N91-19234

CARBON FIBERS

- Graphite fluoride fibers and their applications in the space industry
[NASA-TM-103265] p 88 N91-11062
ICAN sensitivity analysis
[NASA-TM-103667] p 96 N91-15328
Prospects for using carbon-carbon composites for EMI shielding
[NASA-TM-103677] p 97 N91-19231
Industrial applications of graphite fluoride fibers p 100 N91-23040
Sensible heat receiver for solar dynamic space power system
[NASA-TM-104393] p 77 N91-25173
Apparatus for intercalating large quantities of fibrous structures
[NASA-CASE-LEW-15077-2] p 102 N91-28289

CARBON MONOXIDE

- Carbon monoxide and oxygen combustion experiments - A demonstration of Mars in situ propellants
[AIAA PAPER 91-2443] p 60 A91-44246
Cooling of in-situ propellant rocket engines for Mars mission
[NASA-TM-103729] p 72 N91-21233
Material processing with hydrogen and carbon monoxide on Mars
[NASA-TM-104405] p 211 N91-23616
Carbon monoxide and oxygen combustion experiments. A demonstration of Mars in situ propellants
[NASA-TM-104473] p 76 N91-24303
The Au cathode in the system Li₂CO₃-CO₂-CO at 800 to 900 C p 213 N91-32551

CARBON-CARBON COMPOSITES

- Numerical, micro-mechanical prediction of crack growth resistance in a fibre-reinforced/brittle matrix composite p 199 A91-51916
Prospects for using carbon-carbon composites for EMI shielding
[NASA-TM-103677] p 97 N91-19231
Sensible heat receiver for solar dynamic space power system
[NASA-TM-104393] p 77 N91-25173

CARRIER DENSITY (SOLID STATE)

- Study of surface passivation as a function of InP closed-ampoule solar cell fabrication processing variables p 232 A91-41893
Key factors limiting the open circuit voltage of $n(+)$ and $p(-)$ indium phosphide solar cells p 139 A91-41929
Key factors limiting the open circuit voltage of $n(+)$ and $p(-)$ indium phosphide solar cells p 209 N91-19206

CASCADE FLOW

- Oscillating cascade aerodynamics by an experimental influence coefficient technique p 1 A91-10339
The aerodynamics of an oscillating cascade in a compressible flow field
[ASME PAPER 89-GT-271] p 1 A91-13047
Cascade flutter analysis with transient response aerodynamics
[AIAA PAPER 91-0747] p 21 A91-19448
Experimental investigation of oscillating cascade aerodynamics p 3 A91-27801
Numerical simulations of supersonic flow through oscillating cascade sections p 4 A91-28590
Influence of thickness and camber on the aeroelastic stability of supersonic throughflow fans p 5 A91-42814
Flutter analysis of cascades using a two dimensional Euler solver
[AIAA PAPER 91-1681] p 6 A91-45548
Multigrid calculation of three-dimensional viscous cascade flows
[AIAA PAPER 91-3238] p 7 A91-53754
Numerical analysis of flow through oscillating cascade sections p 9 N91-10884
Navier-Stokes analysis of transonic cascade flow
[NASA-TM-103624] p 159 N91-11192
Aerodynamics and heat transfer investigations on a high Reynolds number turbine cascade
[NASA-TM-103260] p 11 N91-15134
Cascade flutter analysis with transient response aerodynamics
[NASA-TM-103746] p 201 N91-19475
Transonic cascade flow calculations using non-periodic C-type grids p 163 N91-21071

CAST ALLOYS

- Thermomechanical and bithermal fatigue behavior of cast B1900 + Hf and wrought Haynes 188
[NASA-TM-4225] p 111 N91-20268

SUBJECT INDEX

CATALYSIS

Reactivity of pi-complexes of Ti, V, and Nb towards dithioacetic acid: Synthesis and structure of novel metal sulfur-containing complexes
[NASA-TM-103666] p 106 N91-19256

CATALYSTS

Fuel-rich, catalytic reaction experimental results --- fuel development for high-speed civil transport aircraft
[AIAA PAPER 91-2463] p 24 A91-44250

Reactivity of pi-complexes of Ti, V, and Nb towards dithioacetic acid: Synthesis and structure of novel metal sulfur-containing complexes
[NASA-TM-103666] p 106 N91-19256

Fuel-rich, catalytic reaction experimental results
[NASA-TM-104423] p 33 N91-24203

The Au cathode in the system $\text{Li}_2\text{CO}_3\text{-CO}_2\text{-CO}$ at 800 to 900 C
p 213 N91-32551

CATHODES

Surface studies on scandate cathodes and synthesized scandates
p 136 A91-25071

The theory of an auto-resonant field emission cathode relativistic electron accelerator for high efficiency microwave to direct current power conversion
p 73 N91-22176

Plasma gun with coaxial powder feed and adjustable cathode
[NASA-CASE-LEW-14901-1] p 231 N91-25875

CAVITATION FLOW

Extension of transonic flow computational concepts in the analysis of cavitated bearings
[ASME PAPER 90-TRIB-40] p 150 A91-29474

A high speed photography study of cavitation in a dynamically loaded journal bearing
[ASME PAPER 90-TRIB-19] p 180 A91-34806

Extension of transonic flow computational concepts in the analysis of cavitated bearings
[NASA-TM-103214] p 160 N91-16304

Two reference time scales for studying the dynamic cavitation of liquid films
[NASA-TM-103673] p 160 N91-19369

CAVITIES

Relationship of optical coating on thermal radiation characteristics of nonisothermal cylindrical enclosures
[NASA-TM-104408] p 168 N91-30461

CAVITY RESONATORS

Superconducting microwave electronics at Lewis Research Center
p 236 N91-24081

CELL ANODES

Performance of a dual anode nickel-hydrogen cell
p 214 N91-32563

CELL CATHODES

The Au cathode in the system $\text{Li}_2\text{CO}_3\text{-CO}_2\text{-CO}$ at 800 to 900 C
p 213 N91-32551

CENTER OF MASS

Newtonian mechanics of a many-particle assembly coupled to an external body potential
p 237 A91-19495

CENTRAL PROCESSING UNITS

Parallel algorithms for boundary value problems
p 221 A91-31175

CENTRIFUGAL COMPRESSORS

Rotating pressure measurement system using an on board calibration standard
[NASA-TM-103676] p 176 N91-19401

NASA low-speed centrifugal compressor for 3-D viscous code assessment and fundamental flow physics research
[NASA-TM-103710] p 13 N91-20044

CENTRIFUGAL FORCE

Optical measurement of unducted fan flutter
[NASA-TM-103285] p 27 N91-15174

CERAMIC BONDING

Universal energy relations and metal/ceramic interfaces
p 93 A91-56254

CERAMIC COATINGS

Ceramic coatings on smooth surfaces
[NASA-CASE-LEW-15164-1] p 122 N91-25298

Ceramic coatings on smooth surfaces
[NASA-CASE-LEW-15164-2] p 123 N91-32229

CERAMIC FIBERS

The structure of carbon in chemically vapor deposited SiC monofilaments
p 113 A91-18675

Silsesquioxane-derived ceramic fibres
p 114 A91-30283

Fiber creep evaluation by stress relaxation measurements
p 117 A91-56905

Investigation of interfacial shear strength in SiC/Si₃N₄ composites
p 93 A91-56913

Microstructural and strength stability of CVD SiC fibers in argon environments
p 117 A91-56958

High resolution computed tomography of advanced composite and ceramic materials
p 192 A91-56972

A simple test for thermomechanical evaluation of ceramic fibers
[NASA-TM-103767] p 121 N91-21309

A preliminary investigation of acousto-ultrasonic NDE of metal matrix composite test specimens
[NASA-TM-104339] p 194 N91-23521

Investigation of interfacial shear strength in SiC/Si₃N₄ composites
[NASA-TM-103739] p 101 N91-26233

Microstructural and strength stability of CVD SiC fibers in argon environment
[NASA-TM-103772] p 102 N91-29250

CERAMIC MATRIX COMPOSITES

Impact behavior of a SiC fiber-reinforced reaction bonded Si₃N₄ composite
p 91 A91-16805

Silsesquioxane-derived ceramic fibres
p 114 A91-30283

Continuous fiber-reinforced titanium aluminide composites
p 92 A91-39553

Ceramic composites for rocket engine turbines
[SAE PAPER 911108] p 92 A91-53552

Ultrasonic velocity technique for monitoring property changes in fiber-reinforced ceramic matrix composites
p 174 A91-56912

Investigation of interfacial shear strength in SiC/Si₃N₄ composites
p 93 A91-56913

Polymeric routes to silicon carbide and silicon oxycarbide CMC
p 117 A91-56922

Thermal shock fiber-reinforced ceramic matrix composites
p 93 A91-56935

Thermochemical analysis of chemical processes relevant to the stability and processing of SiC-reinforced Si₃N₄ composite
p 94 A91-56961

Ceramic composites for rocket engine turbines
[NASA-TM-103743] p 98 N91-19235

Structural reliability analysis of laminated CMC components
[NASA-TM-103685] p 119 N91-19292

Thermal shock of fiber reinforced ceramic matrix composites
[NASA-TM-103777] p 120 N91-19295

NDE standards for high temperature materials
[NASA-TM-103761] p 193 N91-19464

Transition-to-practice technologies for brittle materials
p 120 N91-20107

Mechanical behavior of fiber reinforced SiC/RBSN ceramic matrix composites: Theory and experiment
[NASA-TM-103688] p 99 N91-21243

Investigation of interfacial shear strength in SiC/Si₃N₄ composites
[NASA-TM-103739] p 101 N91-26233

Polymeric routes to silicon carbide and silicon oxycarbide CMC
[NASA-TM-104372] p 102 N91-26234

An analysis of the wear behavior of SiC whisker reinforced alumina from 25 to 1200 C
[NASA-TM-104489] p 90 N91-29235

NDE of ceramics and ceramic composites
[NASA-TM-104520] p 194 N91-29610

Ultrasonic velocity technique for monitoring property changes in fiber-reinforced ceramic matrix composites
[NASA-TM-103806] p 195 N91-30546

CERAMICS

High temperature reactions of ceramics and metals with chlorine and oxygen
p 105 A91-20219

Temperature-dependent indentation behavior of transformation-toughened zirconia-based ceramics
p 114 A91-28767

Preparation of 110K (Bi, Pb)-Sr-Ca-Cu-O superconductor from glass precursor
p 232 A91-35449

Fundamental considerations in adhesion, friction and wear for ceramic-metal contacts
p 115 A91-35952

Thermal and structural assessments of a ceramic wafer seal in hypersonic engine
[AIAA PAPER 91-2494] p 23 A91-41799

Spatial variations in a.c. susceptibility and microstructure for the YBa₂Cu₃O_{7-x} superconductor and their correlation with room-temperature ultrasonic measurements
p 233 A91-54969

Crystallization and properties of Sr-Ba aluminosilicate glass-ceramic matrices
p 117 A91-56917

Influence of the Si₃N₄ microstructure on its R-curve and fatigue behavior
p 117 A91-56931

Crack healing in silicon nitride due to oxidation
p 118 A91-56982

Calculation of Weibull strength parameters, Batdorf flaw density constants and related statistical quantities using PC-CARES
[NASA-TM-103247] p 199 N91-10332

Thermal and structural assessments of a ceramic wafer seal in hypersonic engines
[NASA-TM-103651] p 26 N91-13456

Method of making single crystal fibers
[NASA-CASE-LEW-14921-1] p 95 N91-13502

An x ray photoelectron spectroscopy study of Au(x)In(y) alloys
[NASA-TM-103659] p 234 N91-14050

Effect of hydrogen on the strength and microstructure of selected ceramics
[NASA-TM-103674] p 118 N91-14482

Metallic seal for thermal barrier coating systems
[NASA-CASE-LEW-15020-1] p 119 N91-15412

Construction and testing of ceramic fabric heat pipe with water working fluid
[NASA-TM-103332] p 229 N91-18799

Tribological properties of Ag/Ti films on Al₂O₃ ceramic substrates
[NASA-TM-103784] p 89 N91-19224

Crystallization and properties of Sr-Ba aluminosilicate glass-ceramic matrices
[NASA-TM-103764] p 120 N91-19308

Property and microstructural nonuniformity in the yttrium-barium-copper-oxide superconductor determined from electrical, magnetic, and ultrasonic measurements
[NASA-TM-103732] p 193 N91-19463

NDE standards for high temperature materials
[NASA-TM-103761] p 193 N91-19464

Turbomachinery and combustor technology for small engines
p 29 N91-20113

Spatial variations in ac susceptibility and microstructure for the YBa₂Cu₃O_{7-x} superconductor and their correlation with room-temperature ultrasonic measurements
[NASA-TM-103787] p 194 N91-21553

Structural design methodologies for ceramic-based material systems
[NASA-TM-103097] p 121 N91-22460

High temperature performance evaluation of a hypersonic engine ceramic wafer seal
[NASA-TM-103737] p 185 N91-22567

Evaluation and ranking of candidate ceramic wafer engine seal materials
[NASA-TM-103795] p 187 N91-23515

Comparison of Weibull strength parameters from flexure and spin tests of brittle materials
[NASA-TM-104414] p 187 N91-24593

Method of applying a thermal barrier coating system to a substrate
[NASA-CASE-LEW-15020-2] p 101 N91-25202

Ceramic coatings on smooth surfaces
[NASA-CASE-LEW-15164-1] p 122 N91-25298

Plasma gun with coaxial powder feed and adjustable cathode
[NASA-CASE-LEW-14901-1] p 231 N91-25875

Method of preparing a thermal barrier coating
[NASA-CASE-LEW-14999-2] p 122 N91-26376

Elevated-temperature fracture resistances (K(sub IC), R-curves, gamma sub (omega OF)) of monolithic and composite ceramics using chevron-notched, bend tests
[NASA-TM-105090] p 123 N91-28418

NDE of ceramics and ceramic composites
[NASA-TM-104520] p 194 N91-29610

Low cost, formable, high T(sub c) superconducting wire
[NASA-CASE-LEW-14676-1] p 147 N91-31529

CERTIFICATION

Probability approach for strength calculations
p 204 N91-24652

CHALCOGENIDES

Synthesis and structures of metal chalcogenide precursors
[NASA-TM-103665] p 120 N91-19296

CHANNEL FLOW

Calculation of divergent channel flows with a multiple-time-scale turbulence model
p 151 A91-34134

Mixing of multiple jets with a confined subsonic crossflow - Summary of NASA-supported experiments and modeling
[AIAA PAPER 91-2458] p 7 A91-45813

Frontogenesis driven by horizontally quadratic distributions of density
p 157 A91-48276

Low Reynolds number two-equation modeling of turbulent flows
[NASA-TM-104368] p 165 N91-23416

Mixing of multiple jets with a confined subsonic crossflow. Summary of NASA-supported experiments and modeling
[NASA-TM-104412] p 33 N91-24202

A k-epsilon modeling of near wall turbulence
[NASA-TM-105238] p 170 N91-32460

CHANNELS (DATA TRANSMISSION)

General-purpose interface bus for multiuser, multitasking computer system
p 215 A91-35928

Quaternary pulse position modulation electronics for free-space laser communications
[AIAA PAPER 91-3471] p 133 A91-53702

Quaternary pulse position modulation electronics for free-space laser communications
[NASA-TM-104502] p 135 N91-29405

CHARACTERIZATION

CHARACTERIZATION

High temperature superconducting thin film microwave circuits - Fabrication, characterization, and applications
[NASA-TM-103236] p 141 N91-50433

Application of artificial neural networks to composite ply micromechanics
[NASA-TM-104365] p 100 N91-24345

CHARGE COUPLED DEVICES

Optical techniques for determination of normal shock position in supersonic flows for aerospace applications
p 174 N91-55530

CHARGE DISTRIBUTION

MIS capacitor studies on silicon carbide single crystals
[NASA-CR-187350] p 234 N91-11555

CHARGE EFFICIENCY

Performance of a dual anode nickel-hydrogen cell
p 214 N91-32563

CHARGE EXCHANGE

Global expression for representing diatomic potential-energy curves
p 228 N91-33236

Laser interferometric measurement of ion electrode shape and charge exchange erosion
[AIAA PAPER 91-2121] p 173 N91-45786

Laser interferometric measurement of ion electrode shape and charge exchange erosion
[NASA-TM-105165] p 179 N91-31605

Ion beam sputtering in electric propulsion facilities
[NASA-TM-105145] p 86 N91-32158

CHARGE TRANSFER

Electrically conducting polymers for aerospace applications
[AIAA PAPER 91-3432] p 233 N91-52349

CHEBYSHEV APPROXIMATION

Mappings and accuracy for Chebyshev pseudo-spectral approximations
[NASA-TM-103630] p 221 N91-14781

A comparison of numerical methods for the Rayleigh equation in unbounded domains
[NASA-TM-105179] p 223 N91-30865

CHEMICAL ANALYSIS

Thermal stability of the microstructure of an aged Nb-Zr-C alloy
[NASA-TM-103647] p 110 N91-14454

CHEMICAL COMPOSITION

Investigation of anodic and chemical oxides grown on p-type InP with applications to surface passivation for n(+)-p solar cell fabrication
p 210 N91-19208

Spectroscopic wear detector
[NASA-CASE-LEW-15200-1] p 87 N91-32167

CHEMICAL EQUILIBRIUM

Computer code for single-point thermodynamic analysis of hydrogen/oxygen expander-cycle rocket engines
[NASA-TM-4275] p 72 N91-20206

A new approximate sum rule for bulk alloy properties
[NASA-TM-105282] p 112 N91-32204

CHEMICAL PROPERTIES

Synthesis and thermal properties of strontium and calcium peroxides
[NASA-TM-103725] p 107 N91-22410

CHEMICAL PROPULSION

Mass comparisons of electric propulsion systems for NSSK of geosynchronous spacecraft --- North-South Station Keeping
[AIAA PAPER 91-2347] p 47 N91-45808

Production and use of metals and oxygen for lunar propulsion
[AIAA PAPER 91-3481] p 125 N91-53711

Lunar missions using chemical propulsion: System design issues
[NASA-TP-3065] p 70 N91-15308

Advanced chemical propulsion at NASA Lewis: Metallized and high energy density propellants
[NASA-TM-103771] p 71 N91-19175

Production and use of metals and oxygen for lunar propulsion
[NASA-TM-105195] p 81 N91-29222

Mass comparisons of electric propulsion systems for NSSK of geosynchronous spacecraft
[NASA-TM-105153] p 85 N91-31212

CHEMICAL REACTION CONTROL

Acidic attack of perfluorinated alkyl ether lubricant molecules by metal oxide surfaces
p 104 N91-13439

CHEMICAL REACTIONS

Influence of several metal ions on the gelation activation energy of silicon tetraethoxide
p 113 N91-19599

High temperature reactions of ceramics and metals with chlorine and oxygen
p 105 N91-20219

A time-accurate implicit method for chemically reacting flows at all Mach numbers
[AIAA PAPER 91-0581] p 149 N91-21542

Reaction of Ti and Ti-Al alloys with alumina
p 91 N91-27937

Flux splitting algorithms for two-dimensional viscous flows with finite-rate chemistry
p 10 N91-10894

Application of mixing-controlled combustion models to gas turbine combustors
[NASA-TM-103236] p 31 N91-22126

Substituted 1,1,1-triaryl-2,2,2-trifluoroethanes and processes for their synthesis
[NASA-CASE-LEW-14345-4] p 90 N91-25185

Improvements in contact resistivity and thermal stability of Au-contacted InP solar cells
p 213 N91-30207

Jet-A reaction mechanism study for combustion application
[NASA-TM-104441] p 35 N91-31181

A numerical and experimental analysis of reactor performance and deposition rates for CVD on monofilaments
[NASA-TM-103631] p 130 N91-14500

CHEMICAL REACTORS

High temperature reactions of ceramics and metals with chlorine and oxygen
p 105 N91-20219

CHLORINE

Thermal stability of the microstructure of an aged Nb-Zr-C alloy
[NASA-TM-103647] p 110 N91-14454

CHROMIUM

Effect of sulfur removal on Al₂O₃ scale adhesion
p 108 N91-27940

CHROMIUM ALLOYS

Reaction of beta-phase Ni-Al alloys with CrB₂
p 92 N91-49943

CHROMIUM BORIDES

Composite bearing and seal materials for advanced heat engine applications to 900 C
[NASA-TM-103612] p 95 N91-15318

Mechanical strength and thermophysical properties of PM212: A high temperature self-lubricating powder metallurgy composite
[NASA-TM-103694] p 120 N91-21302

The PM-200 lubrication system
p 121 N91-23044

Method of making carbide/fluoride/silver composites
[NASA-CASE-LEW-14902-1] p 102 N91-27244

CHROMIUM COMPOUNDS

PdCr based high temperature static strain gage
[AIAA PAPER 90-5236] p 170 N91-14462

CIRCUIT DIAGRAMS

Design aspects and comparison between high T(sub c) superconducting coplanar waveguide and microstrip line
[NASA-TM-105142] p 146 N91-27445

CIRCULAR CYLINDERS

Numerical study of unsteady shockwave reflections using an upwind TVD scheme
[NASA-TM-103251] p 10 N91-11676

Surface settling in partially filled containers upon step reduction in gravity
[NASA-TM-103641] p 159 N91-14556

Relationship of optical coating on thermal radiation characteristics of nonisothermal cylindrical enclosures
[NASA-TM-104408] p 168 N91-30461

CIRCULAR POLARIZATION

Circular polarisation characteristics of stacked microstrip antennas
p 131 N91-20370

New coplanar waveguide/stripline feed network for seven patch hexagonal CP subarray
p 137 N91-32823

A seven patch hexagonal CP subarray with a CPW/stripline feed network
[NASA-TM-103802] p 144 N91-20406

CIRCULATION CONTROL AIRFOILS

Control of flow separation and mixing by aerodynamic excitation
p 2 N91-24360

CIVIL AVIATION

Civil air transport - A fresh look at power-by-wire and fly-by-light
p 36 N91-31030

NASA's High Speed Research Program - An introduction and status report
[SAE PAPER 901923] p 1 N91-48605

Overview of the NASA-sponsored HSCT propulsion system studies --- High Speed Civil Transport
[AIAA PAPER 91-3329] p 20 N91-53871

Propulsion challenges for a 21st century economically viable, environmentally compatible High-Speed Civil Transport
p 25 N91-56109

Advanced high temperature engine materials technology program
p 98 N91-20110

Overview of rotorcraft and general aviation propulsion technology
p 29 N91-20112

Civil air transport: A fresh look at power-by-wire and fly-by-light
p 37 N91-23053

Engine technology challenges for a 21st century high speed civil transport
[NASA-TM-104363] p 19 N91-23098

CLADDING

Advanced materials for space nuclear power systems
[AIAA PAPER 91-3530] p 88 N91-53704

Advanced materials for space nuclear power systems
[NASA-TM-105171] p 112 N91-29298

CLAMPS

Post clamp
[NASA-CASE-LEW-14862-1] p 183 N91-14617

Quick action clamp
[NASA-CASE-LEW-14887-1] p 189 N91-27561

CLASSIFICATIONS

Inlets, ducts, and nozzles
p 162 N91-20096

CLIMBING FLIGHT

icing characteristics of a natural-laminar-flow, a medium-speed, and a swept, medium-speed airfoil
[NASA-TM-103693] p 12 N91-19046

CLOSED CIRCUIT TELEVISION

State of the art in video system performance
p 175 N91-14578

COATING

Ceramic coatings on smooth surfaces
[NASA-CASE-LEW-15164-1] p 122 N91-25298

COATINGS

Quality control of the tribological coating PS212
[NASA-TM-102067] p 101 N91-25186

Lubrication with sputtered MoS₂ films: Principles, operation, limitations
[NASA-TM-105292] p 112 N91-32216

COBALT

Thermomechanical and bithermal fatigue behavior of cast B1900 + Hf and wrought Haynes 188
[NASA-TM-4225] p 111 N91-20268

COBALT ALLOYS

High temperature cyclic oxidation data. Part 1: Turbine alloys
[NASA-TM-83665] p 110 N91-10149

High-temperature cyclic oxidation data. Part 2: Turbine alloys
[NASA-TM-101468] p 110 N91-10150

CODE DIVISION MULTIPLE ACCESS

Optical Multiple Access Network (OMAN) for advanced processing satellite applications
[NASA-TM-105167] p 135 N91-29431

CODES

Numerical simulations of supersonic flow through oscillating cascade sections
p 4 N91-28590

CODING

Quaternary pulse position modulation electronics for free-space laser communications
[AIAA PAPER 91-3471] p 133 N91-53702

Software manual for operating particle displacement tracking data acquisition and reduction system
[NASA-TM-103720] p 176 N91-20453

Quaternary pulse position modulation electronics for free-space laser communications
[NASA-TM-104502] p 135 N91-29405

COERCIVITY

Makeup and uses of a basic magnet laboratory for characterizing high-temperature permanent magnets
[NASA-TM-104508] p 146 N91-30427

COHESION

Equivalent crystal theory of alloys
[NASA-TP-3155] p 112 N91-30318

COLLOCATION

Mappings and accuracy for Chebyshev pseudo-spectral approximations
[NASA-TM-103630] p 221 N91-14781

A comparison of numerical methods for the Rayleigh equation in unbounded domains
[NASA-TM-105179] p 223 N91-30865

COLOR

An analysis of the contact sintering process in III-V solar cells
p 139 N91-41891

COLOR TELEVISION

Digital CODEC for real-time processing of broadcast quality video signals at 1.8 bits/pixel
p 134 N91-24067

COMBUSTIBLE FLOW

A time-accurate implicit method for chemically reacting flows at all Mach numbers
[AIAA PAPER 91-0581] p 149 N91-21542

A detailed numerical investigation of Burke-Schumann gaseous and spray flames
[AIAA PAPER 91-2311] p 105 N91-41749

A study of hydrogen diffusion flames using PDF turbulence model
[AIAA PAPER 91-1780] p 106 N91-45549

The development of a fiber optic Raman temperature measurement system for rocket flows
[AIAA PAPER 91-2316] p 173 N91-45804

An imaging system for PLIF/Mie measurements for a combustor flow
[NASA-TM-103714] p 27 N91-20084

Computational Fluid Dynamics Symposium on Aeropropulsion
[NASA-CP-3078] p 14 N91-21062

Modern CFD applications for the design of a reacting shear layer facility
[NASA-TM-104523] p 34 N91-27164

COMBUSTION

- Fuel-rich, catalytic reaction experimental results --- fuel development for high-speed civil transport aircraft [AIAA PAPER 91-2463] p 24 A91-44250
- Fire suppression in human-crew spacecraft [NASA-TM-104334] p 44 N91-21182
- Fuel-rich, catalytic reaction experimental results [NASA-TM-104423] p 33 N91-24203

COMBUSTION CHAMBERS

- Numerical study of supersonic combustors by multi-block grids with mismatched interfaces [AIAA PAPER 90-5204] p 21 A91-14430
- Simulation of mixing in the quick quench region of a rich burn-quick quench mix-lean burn combustor [AIAA PAPER 91-0410] p 105 A91-21481
- A CFD study of jet mixing in reduced flow areas for lower combustor emissions [AIAA PAPER 91-2460] p 23 A91-41788
- Effects of nozzle lip geometry on spray atomization and emissions advanced gas turbine combustors [AIAA PAPER 91-2201] p 24 A91-44153
- A dual-cooled hydrogen-oxygen rocket engine heat transfer analysis [AIAA PAPER 91-2211] p 59 A91-44156
- Flux-vector splitting algorithm for chain-rule conservation-law form p 221 A91-45109
- Analytical combustion/emissions research related to the NASA High-Speed Research Program [AIAA PAPER 91-2252] p 25 A91-45799
- Mixing of multiple jets with a confined subsonic crossflow - Summary of NASA-supported experiments and modeling [AIAA PAPER 91-2458] p 7 A91-45813
- Experimental study of cross-stream mixing in a cylindrical duct [AIAA PAPER 91-2459] p 157 A91-45815
- Flow visualization and computational studies of a reverse flow circular combustor p 157 A91-48966
- Liquid oxygen cooling of hydrocarbon fueled rocket thrust chambers p 63 A91-52309
- Design of an Advanced Expander Test Bed --- for future space engines [AIAA PAPER 91-3437] p 42 A91-52350
- Hydrogen/oxygen auxiliary propulsion technology [AIAA PAPER 91-3440] p 64 A91-52352
- Analysis of 5 KHz combustion instabilities in 40K methane/LOX combustion chambers [NASA-TM-101368] p 67 N91-10117
- Combustor technology for future aircraft [NASA-TM-103268] p 26 N91-14349
- A rocket engine design expert system p 71 N91-17129
- Turbomachinery and combustor technology for small engines p 29 N91-20113
- Computational Fluid Dynamics Symposium on Aeropropulsion [NASA-CP-3078] p 14 N91-21062
- Application of mixing-controlled combustion models to gas turbine combustors [NASA-TM-103236] p 31 N91-22126
- A CFD study of jet mixing in reduced flow areas for lower combustor emissions [NASA-TM-104411] p 32 N91-23185
- Mechanical behavior and failure phenomenon of an in situ-toughened silicon nitride p 121 N91-23311
- [NASA-TM-103741] p 121 N91-23311
- A simplified dynamic model of the Space Shuttle main engine [NASA-TM-104421] p 131 N91-23340
- Mixing of multiple jets with a confined subsonic crossflow. Summary of NASA-supported experiments and modeling p 33 N91-24202
- [NASA-TM-104412] p 33 N91-24202
- A dual-cooled hydrogen-oxygen rocket engine heat transfer analysis p 76 N91-24302
- [NASA-TM-104430] p 76 N91-24302
- CFD analysis of jet mixing in low NOx flammability combustors [NASA-TM-104466] p 33 N91-26146
- Method of injecting fluid propellants into a rocket combustion chamber [NASA-CASE-LEW-14846-2] p 78 N91-26200
- Analytical combustion/emissions research related to the NASA high-speed research program p 34 N91-27165
- [NASA-TM-104521] p 34 N91-27165
- Experimental study of cross-stream mixing in a cylindrical duct [NASA-TM-105180] p 34 N91-29187
- COMBUSTION CHEMISTRY**
- Mechanisms and modeling of the effects of additives on the nitrogen oxides emission [AIAA PAPER 91-0479] p 124 A91-40560
- Numerical simulation of Jet-A combustion approximated by improved propane chemical kinetics [AIAA PAPER 91-1859] p 106 A91-45777

- Jet-A reaction mechanism study for combustion application [AIAA PAPER 91-2355] p 106 A91-45810
- Mechanisms and modeling of the effects of additives on the nitrogen oxides emission [NASA-TM-103765] p 126 N91-22464
- Jet-A reaction mechanism study for combustion application [NASA-TM-104441] p 35 N91-31181

COMBUSTION EFFICIENCY

- N-decane droplet combustion in the NASA-Lewis 5 Second Zero-Gravity Facility - Results in test gas environments other than air [AIAA PAPER 91-0720] p 105 A91-19433
- A CFD study of jet mixing in reduced flow areas for lower combustor emissions [AIAA PAPER 91-2460] p 23 A91-41788
- Fuel-rich, catalytic reaction experimental results --- fuel development for high-speed civil transport aircraft [AIAA PAPER 91-2463] p 24 A91-44250
- A CFD study of jet mixing in reduced flow areas for lower combustor emissions [NASA-TM-104411] p 32 N91-23185
- Fuel-rich, catalytic reaction experimental results [NASA-TM-104423] p 33 N91-24203

COMBUSTION PHYSICS

- Combustion of liquid fuel droplets in supercritical conditions [AIAA PAPER 91-0078] p 105 A91-21362
- Numerical study of shock-wave/boundary layer interactions in premixed hydrogen-air hypersonic flows [AIAA PAPER 91-0413] p 149 A91-26191
- Navier-Stokes simulation of the supersonic combustion flowfield in a ram accelerator [AIAA PAPER 91-1916] p 155 A91-44057
- Analytical combustion/emissions research related to the NASA High-Speed Research Program [AIAA PAPER 91-2252] p 25 A91-45799
- Spacelab qualified infrared imager for microgravity science applications p 173 A91-51585
- Numerical study of shock-wave/boundary layer interactions in premixed hydrogen-air hypersonic flows [NASA-TM-103273] p 160 N91-14559
- Application of mixing-controlled combustion models to gas turbine combustors [NASA-TM-103236] p 31 N91-22126
- Microgravity research at LeRC [NASA-TM-102521] p 128 N91-24464
- Navier-Stokes simulation of the supersonic combustion flowfield in a ram accelerator [NASA-TM-104439] p 166 N91-24541
- Analytical combustion/emissions research related to the NASA high-speed research program [NASA-TM-104521] p 34 N91-27165

COMBUSTION PRODUCTS

- Mechanisms and modeling of the effects of additives on the nitrogen oxides emission [AIAA PAPER 91-0479] p 124 A91-40560
- Application of mixing-controlled combustion models to gas turbine combustors [NASA-TM-103236] p 31 N91-22126
- Mechanisms and modeling of the effects of additives on the nitrogen oxides emission [NASA-TM-103765] p 126 N91-22464

COMBUSTION STABILITY

- A study of hydrogen diffusion flames using PDF turbulence model [AIAA PAPER 91-1780] p 106 A91-45549
- Analysis of 5 KHz combustion instabilities in 40K methane/LOX combustion chambers [NASA-TM-101368] p 67 N91-10117
- JANNAF liquid rocket combustion instability panel research recommendations [NASA-TM-103653] p 70 N91-13491
- Nonlinear combustion instability model in two- to three-dimensions [NASA-TM-102381] p 85 N91-31208

COMMERCIAL AIRCRAFT

- Engine technology challenges for a 21st century high speed civil transport [NASA-TM-104363] p 19 N91-23098
- Analytical combustion/emissions research related to the NASA high-speed research program [NASA-TM-104521] p 34 N91-27165

COMMUNICATION EQUIPMENT

- Overview of Ka-band communications technology requirements for the Space Exploration Initiative [AIAA PAPER 91-3424] p 45 A91-52344

COMMUNICATION NETWORKS

- Evaluation of components, subsystems, and networks for high rate, high frequency space communications [AIAA PAPER 91-3423] p 41 A91-52343
- Technologies for unattended network operations [AIAA PAPER 91-3534] p 45 A91-52425

- Development of technology needs for the SEI TNM network [AIAA PAPER 91-3536] p 45 A91-52427

- Optical Multiple Access Network (OMAN) for advanced processing satellite applications [NASA-TM-105167] p 135 N91-29431

COMMUNICATION SATELLITES

- A charging study of the ACTS satellite using NASCAP [AIAA PAPER 91-1471] p 46 A91-42522
- Mass comparisons of electric propulsion systems for NSSK of geosynchronous spacecraft --- North-South Station Keeping [AIAA PAPER 91-2347] p 47 A91-45808
- Overview of Ka-band communications technology requirements for the Space Exploration Initiative [AIAA PAPER 91-3424] p 45 A91-52344
- Millimeter wavelength communications applications for the SEI [AIAA PAPER 91-3589] p 45 A91-52458
- A new fabrication method for precision antenna reflectors for space flight and ground test [NASA-TP-3078] p 48 N91-21185
- Microwave integrated circuits for space applications p 145 N91-24069

COMPATIBILITY

- General purpose program to generate compatibility matrix for the integrated force method p 195 A91-12905
- Compatibility conditions of structural mechanics for finite element analysis p 198 A91-37853

COMPILERS

- Cray performance data from five benchmarks [NASA-TM-105200] p 217 N91-32806

COMPLEX VARIABLES

- Solution and sensitivity analysis of a complex transcendental eigenproblem with pairs of real eigenvalues p 195 A91-23685

COMPONENT RELIABILITY

- Review of the transmissions of the Soviet helicopters [NASA-TM-103634] p 20 N91-15146
- Incorporating finite element analysis into component life and reliability [NASA-TM-104400] p 203 N91-23550
- Probability approach for strength calculations p 204 N91-24652

COMPOSITE MATERIALS

- Simplified procedures for designing composite bolted joints p 195 A91-16290
- Equivalence of Green's function and the Fourier series representation of composites with periodic microstructure p 91 A91-16889
- Thermal emittance enhancement of graphite-copper composites for high temperature space based radiators [AIAA PAPER 91-3527] p 116 A91-53705
- Heat transfer device and method of making the same [NASA-CASE-LEW-14162-1] p 159 N91-13668
- Composite bearing and seal materials for advanced heat engine applications to 900 C p 95 N91-15318
- [NASA-TM-103612] p 95 N91-15318
- Graphite fluoride fiber polymer composite material [NASA-CASE-LEW-14472-1] p 95 N91-15320
- Reinforcements: The key to high performance composite materials p 96 N91-15329
- [NASA-TM-103230] p 96 N91-15329
- An overview of self-consistent methods for fiber-reinforced composites [NASA-TM-103713] p 97 N91-19232
- Isothermal fatigue behavior of a (90)(sub 8) SiC/Ti-15-3 composite at 426 C p 99 N91-20228
- [NASA-TM-103686] p 99 N91-20228
- Mechanical strength and thermophysical properties of PM212: A high temperature self-lubricating powder metallurgy composite p 120 N91-21302
- [NASA-TM-103694] p 120 N91-21302
- Application of artificial neural networks to composite ply micromechanics [NASA-TM-104365] p 100 N91-24345
- Heat transfer device [NASA-CASE-LEW-14162-2] p 101 N91-25201
- Elevated-temperature fracture resistances (K(sub IC), R-curves, gamma sub (omega OF)) of monolithic and composite ceramics using chevron-notched, bend tests [NASA-TM-105090] p 123 N91-28418
- Thermal emittance enhancement of graphite-copper composites for high temperature space based radiators [NASA-TM-105178] p 123 N91-29332
- Progressive fracture in composites subjected to hygrothermal environment [NASA-TM-105230] p 103 N91-32182

COMPOSITE STRUCTURES

- Composite structure global fracture toughness via computational simulation p 216 A91-11819
- An integrated methodology for optimizing the passive damping of composite structures p 195 A91-19048

- Progressive fracture in composites subjected to hydrothermal environment p 91 A91-31919
[AIAA PAPER 91-1140]
- Computational simulation of acoustic fatigue for hot composite structures p 197 A91-32099
[AIAA PAPER 91-1178]
- Free vibrations of delaminated beams p 197 A91-32129
[AIAA PAPER 91-1241]
- Computational simulation of damping in composite structures p 198 A91-36283
- In-service health monitoring of composite structures p 192 A91-51926
- Structural properties of laminated Douglas fir/epoxy composite material p 94 A91-10127
[NASA-RP-1236]
- Relationship between voids and interlaminar shear strength of polymer matrix composites p 95 A91-13495
[NASA-TM-103643]
- Process for HIP canning of composites p 96 A91-17145
[NASA-CASE-LEW-14990-1-CU]
- Review of acousto-ultrasonic NDE for composites p 97 A91-18192
- Computational simulation of hot composites structures p 97 A91-19230
[NASA-TM-103681]
- HITCAN for actively cooled hot-composite thermostructural analysis p 202 A91-21562
[NASA-TM-103750]
- Computational simulation of acoustic fatigue for hot composite structures p 203 A91-23548
[NASA-TM-104379]
- Integrated mechanics for the passive damping of polymer-matrix composites and composite structures p 103 A91-32181
[NASA-TM-104346]
- Progressive fracture in composites subjected to hydrothermal environment p 103 A91-32182
[NASA-TM-105230]
- COMPRESSED GAS**
- Effects of high pressure nitrogen on the thermal stability of SiC fibers p 96 A91-16075
[NASA-TM-103245]
- COMPRESSIBILITY**
- High temperature tension-compression fatigue behavior of a tungsten copper composite p 100 A91-24360
[NASA-TM-104370]
- COMPRESSIBILITY EFFECTS**
- Modern CFD applications for the design of a reacting shear layer facility p 34 A91-27164
[NASA-TM-104523]
- COMPRESSIBLE BOUNDARY LAYER**
- On the continuous spectra of the compressible boundary layer stability equations p 150 A91-31342
- Nonlinear evolution of subsonic and supersonic disturbances on a compressible free shear layer p 152 A91-39716
- COMPRESSIBLE FLOW**
- Acoustic radiation from lifting airfoils in compressible subsonic flow p 224 A91-12427
[AIAA PAPER 90-3911]
- The aerodynamics of an oscillating cascade in a compressible flow field p 1 A91-13047
[ASME PAPER 89-GT-271]
- Multidimensional computer simulation of Stirling cycle engines p 181 A91-38154
- Stability of compressible Taylor-Couette flow p 153 A91-42541
[AIAA PAPER 91-1642]
- Simulations of free shear layers using a compressible k-epsilon model p 156 A91-45778
[AIAA PAPER 91-1863]
- Computations of the three-dimensional flow and heat transfer within a coolant passage of a radial turbine blade p 156 A91-45797
[AIAA PAPER 91-2238]
- Primitive variable, strongly implicit calculation procedure for viscous flows at all speeds p 7 A91-46181
- Analysis of the one-dimensional transient compressible vapor flow in heat pipes p 157 A91-47735
- Acoustic radiation from lifting airfoils in compressible subsonic flow p 13 A91-19053
[NASA-TM-103650]
- Implicit solution of three-dimensional internal turbulent flows p 163 A91-21087
- The 3D computation of single-expansion-ramp and scramjet nozzles p 164 A91-21092
- Euler flow predictions for an oscillating cascade using a high resolution wave-split scheme p 16 A91-24107
[NASA-TM-104377]
- Evaluation of a technique to generate artificially thickened boundary layers in supersonic and hypersonic flows p 17 A91-28136
[NASA-TP-3142]
- COMPRESSION LOADS**
- 1000 to 1200 K time-dependent compressive deformation of single-crystalline and polycrystalline B2 Ni-40Al p 109 A91-43670

COMPRESSION TESTS

- 1300 K compressive properties of a reaction milled NiAl-AlN composites p 107 A91-18674
- 1000 to 1300 K slow plastic compression properties of Al-deficient NiAl p 108 A91-36214

COMPRESSIVE STRENGTH

- Compression behavior of TiB₂-particulate-reinforced composites of Al₂Fe₃Ti₈ p 91 A91-28014
- 1000 to 1300 K slow plastic compression properties of Al-deficient NiAl p 108 A91-36214
- Mechanical strength and thermophysical properties of PM212: A high temperature self-lubricating powder metallurgy composite p 120 A91-21302
[NASA-TM-103694]

COMPRESSOR BLADES

- Automated design of controlled diffusion blades p 9 A91-10883

COMPRESSOR ROTORS

- Effects of inlet distortion on the development of secondary flows in a subsonic axial inlet compressor rotor p 31 A91-23179
[NASA-TM-104356]
- An unconditionally stable Runge-Kutta method for unsteady rotor-stator interaction p 165 A91-24337

COMPRESSORS

- Turbomachinery and combustor technology for small engines p 29 A91-20113

COMPUTATION

- Institute for Computational Mechanics in Propulsion (ICOMP) p 222 A91-24818
[NASA-TM-103790]

COMPUTATIONAL FLUID DYNAMICS

- Numerical study of supersonic combustors by multi-block grids with mismatched interfaces p 21 A91-14430
[AIAA PAPER 90-5204]
- Navier-Stokes simulation of transonic blade-vortex interactions p 2 A91-21065
- Flow studies in close-coupled ventral nozzles for STOVL aircraft p 2 A91-21242
[SAE PAPER 901033]
- Modern CFD applications for the design of a reacting shear layer facility p 149 A91-21540
[AIAA PAPER 91-0577]
- Transonic wind-tunnel wall interference prediction code p 38 A91-26112
- The aerodynamic characteristics of vortex ingestion for the F/A-18 inlet duct p 3 A91-26192
[AIAA PAPER 91-0130]
- Extension of transonic flow computational concepts in the analysis of cavitating bearings p 150 A91-29474
[ASME PAPER 90-TRIB-40]
- Three-dimensional viscous flow computations of high area ratio nozzles for hypersonic propulsion p 4 A91-30014
- On the continuous spectra of the compressible boundary layer stability equations p 150 A91-31342
- Calculation of turbulence-driven secondary motion in ducts with arbitrary cross section p 151 A91-34132
- Role of artificial viscosity in Euler and Navier-Stokes solvers p 4 A91-34135
- Development of a new flux splitting scheme p 153 A91-40793
- CFD analysis of a hydrogen fueled ramjet engine at Mach 3.44 p 23 A91-41653
[AIAA PAPER 91-1919]
- The design/analysis of flows through turbomachinery - A viscous/inviscid approach p 153 A91-41677
[AIAA PAPER 91-2010]
- Verification of the Proteus two-dimensional Navier-Stokes code for flat plate and pipe flows p 153 A91-41678
[AIAA PAPER 91-2013]
- A three-dimensional Navier-Stokes stage analysis of the flow through a compact radial turbine p 23 A91-41815
[AIAA PAPER 91-2564]
- Osher's scheme for real gases p 153 A91-42286
- Stability of compressible Taylor-Couette flow p 153 A91-42541
[AIAA PAPER 91-1642]
- Large-scale advanced propeller blade pressure distributions - Prediction and data p 5 A91-42820
- New approach in direct-simulation of gas mixtures p 154 A91-43412
[AIAA PAPER 91-1343]
- An analysis of the viscous flow through a compact radial turbine by the average passage approach p 6 A91-44545
[ASME PAPER 90-GT-64]
- Flux-vector splitting algorithm for chain-rule conservation-law form p 221 A91-45109
- Computation of a circular-to-rectangular transition duct flow field p 156 A91-45547
[AIAA PAPER 91-1741]
- A study of hydrogen diffusion flames using PDF turbulence model p 106 A91-45549
[AIAA PAPER 91-1780]
- Simulations of free shear layers using a compressible k-epsilon model p 156 A91-45778
[AIAA PAPER 91-1863]

- Three-dimensional calculation of the mixing of radial jets from slanted slots with a reactive cylindrical crossflow p 24 A91-45782
[AIAA PAPER 91-2081]
- Algebraic grid generation for coolant passages of turbine blades with serpentine channels and pin fins p 156 A91-45811
[AIAA PAPER 91-2366]
- Efficient real gas upwind Navier-Stokes computations of high speed flows p 157 A91-46179
- Algebraic grid generation for complex geometries p 157 A91-48758
- Semanalytical technique for sensitivity analysis of unsteady aerodynamic computations p 7 A91-48816
- Performance and flow calculations for a gaseous H₂/O₂ thruster p 63 A91-48843
- Flow visualization and computational studies of a reverse flow circular combustor p 157 A91-48966
- Computational fluid dynamics studies of nuclear rocket performance p 66 A91-52450
[AIAA PAPER 91-3577]
- Multigrid calculation of three-dimensional viscous cascade flows p 7 A91-53754
[AIAA PAPER 91-3238]
- Characteristics of 3D turbulent jets in crossflow p 158 A91-54268
- A Navier-Stokes study of shock-boundary layer interaction and flow separation inside a transonic compressor p 8 A91-56115
- Enhancing aeropropulsion research with high-speed interactive computing p 217 A91-56129
- Three-dimensional flows in a transonic compressor rotor p 8 A91-56152
- Computational fluid dynamics at the Lewis Research Center: An overview p 8 A91-10842
- Progress toward the development of an airfoil icing analysis capability p 9 A91-10866
- The breakup of trailing-line vortices p 9 A91-10867
- Simulation of turbomachinery flows p 9 A91-10880
- Numerical analysis of flow through oscillating cascade sections p 9 A91-10884
- CFD analysis for high speed inlets p 10 A91-10888
- Navier-Stokes analysis of transonic cascade flow p 159 A91-11192
[NASA-TM-103624]
- A numerical and experimental analysis of reactor performance and deposition rates for CVD on monofilaments p 130 A91-14500
[NASA-TM-103631]
- The aerodynamic characteristics of vortex ingestion for the F/A-18 inlet duct p 70 A91-15303
[NASA-TM-103703]
- Extension of transonic flow computational concepts in the analysis of cavitating bearings p 160 A91-16304
[NASA-TM-103214]
- Implementation of control point form of algebraic grid-generation technique p 13 A91-19054
[NASA-TM-103748]
- NASA low-speed centrifugal compressor for 3-D viscous code assessment and fundamental flow physics research p 13 A91-20044
[NASA-TM-103710]
- A comparison of CFD predictions and experimental results for a Mach 5 inlet p 28 A91-20094
- Internal fluid mechanics research p 161 A91-20095
- Inlets, ducts, and nozzles p 162 A91-20096
- Turbomachinery p 162 A91-20097
- Chemical reacting flows p 162 A91-20098
- A finite element model of conduction, convection, and phase change near a solid/melt interface p 162 A91-20417
[NASA-TM-103721]
- Compressible flows with periodic vortical disturbances around lifting airfoils p 14 A91-21060
[NASA-TM-103742]
- Computational Fluid Dynamics Symposium on Aeropropulsion p 14 A91-21062
[NASA-CP-3078]
- Transonic cascade flow calculations using non-periodic C-type grids p 163 A91-21071
- Implicit solution of three-dimensional internal turbulent flows p 163 A91-21082
- Numerical investigation of an internal layer in turbulent flow over a curved hill p 163 A91-21083
- CFD for hypersonic propulsion p 164 A91-21447
[NASA-TM-103791]
- Application of computational fluid dynamics in high speed aeropropulsion p 164 A91-21458
[NASA-TM-103780]
- Characteristics of 3D turbulent jets in crossflow p 165 A91-22536
[NASA-TM-104337]
- Computational modeling and validation for hypersonic inlets p 16 A91-23162
- A three-dimensional Navier-Stokes stage analysis of the flow through a compact radial turbine p 32 A91-23186
[NASA-TM-104420]
- Advances in modeling the pressure correlation terms in the second moment equations p 165 A91-24525
[NASA-TM-104413]

- Parallel computing using a Lagrangian formulation
[NASA-TM-104446] p 215 N91-24745
- Enhancing aeropropulsion research with high-speed interactive computing
[NASA-TM-104374] p 218 N91-24796
- The design/analysis of flows through turbomachinery: A viscous/inviscid approach
[NASA-TM-104447] p 33 N91-25148
- CFD analysis of jet mixing in low NOx flametube combustors
[NASA-TM-104466] p 33 N91-26146
- COMPUTATIONAL GRIDS**
- Numerical study of supersonic combustors by multi-block grids with mismatched interfaces
[AIAA PAPER 90-5204] p 21 A91-14430
- Resistivity of pristine and intercalated graphite fiber epoxy composites
p 115 A91-35949
- Navier-Stokes analysis of transonic cascade flow
[NASA-TM-103624] p 159 N91-11192
- Implementation of control point form of algebraic grid-generation technique
[NASA-TM-103748] p 13 N91-19054
- Transonic cascade flow calculations using non-periodic C-type grids
p 163 N91-21071
- Implicit solution of three-dimensional internal turbulent flows
p 163 N91-21082
- Dynamics of local grid manipulations for internal flow problems
p 164 N91-21090
- On the anomaly of velocity-pressure decoupling in collocated mesh solutions
[NASA-TM-103769] p 164 N91-21448
- A new flux splitting scheme
[NASA-TM-104044] p 222 N91-22814
- GRID3D-v2: An updated version of the GRID2D/3D computer program for generating grid systems in complex-shaped three-dimensional spatial domains
[NASA-TM-103766] p 217 N91-25630
- A new numerical framework for solving conservation laws: The method of space-time conservation element and solution element
[NASA-TM-104495] p 223 N91-30867
- COMPUTER AIDED DESIGN**
- Modeling and optimization of a regenerative fuel cell system using the ASPEN process simulator
p 206 A91-38177
- Maximum life spur gear design
[AIAA PAPER 91-2021] p 181 A91-41682
- Numerical study of high-area-ratio H₂/O₂ rocket nozzles
[AIAA PAPER 91-2434] p 57 A91-41780
- Developments in REDES: The rocket engine design expert system
[NASA-TM-103657] p 67 N91-10119
- The environment power system analysis tool development program
p 231 N91-17734
- Structural reliability analysis of laminated CMC components
[NASA-TM-103685] p 119 N91-19292
- Coplanar waveguide EEsF MICAD macros make circuit layout easy
[NASA-TM-103272] p 134 N91-19332
- Overview of structures research
p 202 N91-20104
- Computational simulation of propulsion structures performance and reliability
p 29 N91-20106
- Transition-to-practice technologies for brittle materials
p 120 N91-20107
- The environment workbench: A design tool for Space Station Freedom
p 48 N91-20727
- Optimal design study of high efficiency indium phosphide space solar cells
[NASA-TM-103763] p 145 N91-21433
- HITCAN for actively cooled hot-composite thermostructural analysis
[NASA-TM-103750] p 202 N91-21562
- Maximum life spur gear design
[NASA-TM-104361] p 187 N91-23514
- Spur-gear optimization using SPUROPT computer program
[NASA-TM-104394] p 191 N91-31648
- COMPUTER AIDED MANUFACTURING**
- Recent manufacturing advances for spiral bevel gears
[NASA-TM-104479] p 191 N91-31654
- COMPUTER AIDED TOMOGRAPHY**
- High resolution computed tomography of advanced composite and ceramic materials
p 192 A91-56972
- Three-dimensional computed tomography from interferometric measurements within a narrow cone of views
[NASA-TM-103257] p 176 N91-19404
- COMPUTER GRAPHICS**
- Implementation of control point form of algebraic grid-generation technique
[NASA-TM-103748] p 13 N91-19054
- COMPUTER NETWORKS**
- Shared direct memory access on the Explorer 2-LX
[NASA-TM-103289] p 216 N91-12215

COMPUTER PROGRAMMING

- Programming probabilistic structural analysis for parallel processing computer
[AIAA PAPER 91-0920] p 196 A91-31957
- Techniques and implementation of the embedded rule-based expert system using Ada
p 220 N91-22788

COMPUTER PROGRAMS

- Simulation of mixing in the quick quench region of a rich burn-quick quench mix-lean burn combustor
[AIAA PAPER 91-0410] p 105 A91-21481
- Numerical simulation of ice growth on a MS-317 swept wing geometry
[AIAA PAPER 91-0263] p 19 A91-26193
- Composite laminate tailoring with probabilistic constraints and loads
p 198 A91-38754
- Scaling analysis applied to the NORVEX code development and thermal energy flight experiment
[AIAA PAPER 91-1420] p 155 A91-44337
- An analysis of the viscous flow through a compact radial turbine by the average passage approach
[ASME PAPER 90-GT-64] p 6 A91-44545
- Analytical combustion/emissions research related to the NASA High-Speed Research Program
[AIAA PAPER 91-2252] p 25 A91-45799
- Developments in REDES: The rocket engine design expert system
[NASA-TM-103657] p 67 N91-10119
- Calculation of Weibull strength parameters, Batdorf flow density constants and related statistical quantities using PC-CARES
[NASA-TM-103247] p 199 N91-10332
- Progress toward the development of an airfoil icing analysis capability
p 9 N91-10866
- Analysis of three-dimensional viscous flow in a supersonic throughflow fan
p 10 N91-10885
- Numerical study of unsteady shockwave reflections using an upwind TVD scheme
[NASA-TM-103251] p 10 N91-11676
- Probabilistic structural analysis of a truss typical for space station
[NASA-TM-103277] p 199 N91-12114
- An AD100 implementation of a real-time STOVLA aircraft propulsion system
[NASA-TM-103683] p 26 N91-13457
- Relationship between voids and interlaminar shear strength of polymer matrix composites
[NASA-TM-103643] p 95 N91-13495
- Numerical simulation of ice growth on a MS-317 swept wing geometry
[NASA-TM-103705] p 11 N91-14310
- ICAN sensitivity analysis
[NASA-TM-103667] p 96 N91-15328
- A rocket engine design expert system
p 71 N91-17129
- METCAN simulation of candidate metal matrix composites for high temperature applications
[NASA-TM-103636] p 96 N91-17143
- The environment power system analysis tool development program
p 231 N91-17734
- Implementation of control point form of algebraic grid-generation technique
[NASA-TM-103748] p 13 N91-19054
- METCAN updates for high temperature composite behavior: Simulation/verification
[NASA-TM-103682] p 97 N91-19229
- Transonic aerodynamics of dense gases
[NASA-TM-103722] p 13 N91-20045
- Aeropropulsion 1991
[NASA-CP-10063] p 27 N91-20086
- Turbomachinery
p 162 N91-20097
- Computer code for single-point thermodynamic analysis of hydrogen/oxygen expander-cycle rocket engines
[NASA-TM-4275] p 72 N91-20206
- Software manual for operating particle displacement tracking data acquisition and reduction system
[NASA-TM-103720] p 176 N91-20453
- Optimal design study of high efficiency indium phosphide space solar cells
[NASA-TM-103763] p 145 N91-21433
- Euler flow predictions for an oscillating cascade using a high resolution wave-split scheme
[NASA-TM-104377] p 16 N91-24107
- Overview of the fatigue/fracture/life working group program at the Lewis Research Center
p 203 N91-24308
- Overview of aerothermodynamic loads definition study
p 204 N91-24334
- Scaling analysis applied to the NORVEX code development and thermal energy flight experiment
[NASA-TM-104462] p 166 N91-24549
- Analytical combustion/emissions research related to the NASA high-speed research program
[NASA-TM-104521] p 34 N91-27165

- The development of test beds to support the definition and evolution of the Space Station Freedom power system
[NASA-TM-104504] p 79 N91-27207
- A three-dimensional finite-element thermal/mechanical analytical technique for high-performance traveling wave tubes
[NASA-TP-3081] p 134 N91-27436
- ASTROP2 users manual: A program for aeroelastic stability analysis of propfans
[NASA-TM-4304] p 206 N91-28627
- Divergence thrust loss calculations for convergent-divergent nozzles: Extensions to the classical case
[NASA-TM-105176] p 34 N91-29181
- Calculated performance of the NASA Lewis icing research tunnel
[NASA-TM-105173] p 39 N91-29199
- Pressure measurements in a low-density nozzle plume for code verification
[NASA-TM-105170] p 81 N91-29228
- Local synthesis and tooth contact analysis of face-milled spiral bevel gears
[NASA-TM-105182] p 190 N91-29600
- The Navy/NASA Engine Program (NNEP89): A user's manual
[NASA-TM-105186] p 35 N91-30141
- Spur-gear optimization using SPUROPT computer program
[NASA-TM-104394] p 191 N91-31648
- Progressive fracture in composites subjected to hygrothermal environment
[NASA-TM-105230] p 103 N91-32182
- COMPUTER SYSTEMS DESIGN**
- The environment workbench: A design tool for Space Station Freedom
p 48 N91-20727
- COMPUTER SYSTEMS PERFORMANCE**
- Enhancing aeropropulsion research with high-speed interactive computing
p 217 A91-56129
- Enhancing aeropropulsion research with high-speed interactive computing
p 218 N91-24796
- [NASA-TM-104374] p 218 N91-24796
- Cray performance data from five benchmarks
[NASA-TM-105200] p 217 N91-32806
- COMPUTER SYSTEMS PROGRAMS**
- Enhancing aeropropulsion research with high-speed interactive computing
p 217 A91-56129
- Techniques and implementation of the embedded rule-based expert system using Ada
p 220 N91-22788
- Enhancing aeropropulsion research with high-speed interactive computing
[NASA-TM-104374] p 218 N91-24796
- An autonomous fault detection, isolation, and recovery system for a 20-kHz electric power distribution test bed
[NASA-TM-104344] p 217 N91-25680
- COMPUTER TECHNIQUES**
- Particle displacement tracking applied to air flows
[NASA-TM-104481] p 177 N91-25387
- Computerized inspection of real surfaces and minimization of their deviations
[NASA-TM-103798] p 188 N91-27558
- COMPUTERIZED SIMULATION**
- Metal matrix composites microfracture - Computational simulation
p 90 A91-11815
- Composite structure global fracture toughness via computational simulation
p 216 A91-11819
- Probabilistic simulation of uncertainties in thermal structures
p 195 A91-16042
- Computational simulation of high-temperature metal matrix composites cyclic behavior
p 91 A91-18680
- Measurements and predictions of a liquid spray from an air-assist nozzle
[AIAA PAPER 91-0692] p 149 A91-22498
- Numerical simulation of ice growth on a MS-317 swept wing geometry
[AIAA PAPER 91-0263] p 19 A91-26193
- A model for the Space Shuttle Main Engine High Pressure Oxidizer Turbopump shaft seal system
p 180 A91-30640
- Progressive fracture in composites subjected to hygrothermal environment
[AIAA PAPER 91-1140] p 91 A91-31919
- Simulation of the Space Station strut-out condition
[AIAA PAPER 91-1248] p 197 A91-32087
- Fiber pushout test - A three-dimensional finite element computational simulation
p 197 A91-33096
- Modeling of Space Station electric power system with EMT
p 55 A91-38040
- An expert system for simulating electric loads aboard Space Station Freedom
p 55 A91-38041
- Multidimensional computer simulation of Stirling cycle engines
p 181 A91-38154
- Modeling and optimization of a regenerative fuel cell system using the ASPEN process simulator
p 206 A91-38177

- Computational modeling of the pressurization process in a NASP vehicle propellant tank experimental simulation
[AIAA PAPER 91-2407] p 124 A91-41771
- A CFD study of jet mixing in reduced flow areas for lower combustor emissions
[AIAA PAPER 91-2460] p 23 A91-41788
- A three-dimensional Navier-Stokes stage analysis of the flow through a compact radial turbine
[AIAA PAPER 91-2564] p 23 A91-41815
- Effect of emitter parameter variation on the performance of heteroepitaxial indium phosphide solar cells
p 140 A91-42003
- Flow visualization studies of the internal flow characteristics in a simulated mixed flow vectored thrust ASTOVL engine configuration
[AIAA PAPER 91-1689] p 23 A91-42556
- New approach in direct-simulation of gas mixtures
[AIAA PAPER 91-1343] p 154 A91-43412
- Numerical and experimental investigations of rarefied nozzle and plume flows of nitrogen
[AIAA PAPER 91-1363] p 154 A91-43429
- Navier-Stokes simulation of the supersonic combustion flowfield in a ram accelerator
[AIAA PAPER 91-1916] p 155 A91-44057
- Numerical simulation of self-field MPD thrusters
[AIAA PAPER 91-2341] p 62 A91-45805
- Results from computational analysis of a mixed compression supersonic inlet
p 7 A91-45818
- Study on the spectral efficiency of SFH-GMSK in land mobile telephone communication by direct simulation
p 132 A91-53176
- Numerical propulsion system simulation - An interdisciplinary approach
[AIAA PAPER 91-3554] p 66 A91-53706
- Enhancing aeropropulsion research with high-speed interactive computing
p 217 A91-56129
- The breakup of trailing-line vortices
p 9 A91-10867
- Simulation of turbomachinery flows
p 9 A91-10880
- Numerical study of unsteady shockwave reflections using an upwind TVD scheme
[NASA-TM-103251] p 10 A91-11676
- Measurements and predictions of a liquid spray from an air-assist nozzle
[NASA-TM-103640] p 26 A91-13455
- Numerical simulation of ice growth on a MS-317 swept wing geometry
[NASA-TM-103705] p 11 A91-14310
- Effect of emitter parameter variation on the performance of heteroepitaxial indium phosphide solar cells
[NASA-TM-103619] p 70 A91-15306
- METCAN simulation of candidate metal matrix composites for high temperature applications
[NASA-TM-103636] p 96 A91-17143
- Multi-dimensional modeling of a thermal energy storage canister
[NASA-TM-103731] p 71 A91-19177
- On the anomaly of velocity-pressure decoupling in collocated mesh solutions
[NASA-TM-103769] p 164 A91-21448
- Icing simulation: A survey of computer models and experimental facilities
[NASA-TM-104366] p 15 A91-23087
- A CFD study of jet mixing in reduced flow areas for lower combustor emissions
[NASA-TM-104411] p 32 A91-23185
- A three-dimensional Navier-Stokes stage analysis of the flow through a compact radial turbine
[NASA-TM-104420] p 32 A91-23186
- A simplified dynamic model of the Space Shuttle main engine
[NASA-TM-104421] p 131 A91-23340
- Computational simulation of acoustic fatigue for hot composite structures
[NASA-TM-104379] p 203 A91-23548
- Simulation of probabilistic wind loads and building analysis
[NASA-TM-103744] p 203 A91-23549
- Average-passage flow model development
p 165 A91-24338
- Navier-Stokes simulation of the supersonic combustion flowfield in a ram accelerator
[NASA-TM-104439] p 166 A91-24541
- Enhancing aeropropulsion research with high-speed interactive computing
[NASA-TM-104374] p 218 A91-24796
- A distributed fault-detection and diagnosis system using on-line parameter estimation
[NASA-TM-104433] p 220 A91-25696
- An EMTF system level model of the PMAD DC test bed
[NASA-TM-104515] p 79 A91-27206
- Numerical propulsion system simulation: An interdisciplinary approach
[NASA-TM-105181] p 81 A91-29221
- Pressure measurements in a low-density nozzle plume for code verification
[NASA-TM-105170] p 81 A91-29228
- Progressive fracture in composites subjected to hygrothermal environment
[NASA-TM-105230] p 103 A91-32182
- ### CONCENTRATORS
- The mini-dome Fresnel lens photovoltaic concentrator array - Current status of component and prototype panel testing
p 57 A91-41989
- Finite element analysis of thermal distortion effects on optical performance of solar dynamic concentrator for Space Station Freedom
[NASA-TM-102504] p 183 A91-12954
- Mini-dome Fresnel lens photovoltaic concentrator development
p 210 A91-19219
- Future mission opportunities and requirements for advanced space photovoltaic energy conversion technology
[NASA-TM-103661] p 74 A91-22371
- Concentrator testing using projected images
[NASA-TM-104349] p 79 A91-27204
- Key results of the mini-dome Fresnel lens concentrator array development program under recently completed NASA and SDO SBIR projects
p 83 A91-30223
- Thin film, concentrator and multijunction space solar cells: Status and potential
[NASA-TM-104505] p 86 A91-31218
- ### CONDENSATION
- A numerical study of the direct contact condensation on a horizontal surface
[AIAA PAPER 91-1307] p 155 A91-44335
- A numerical study of the direct contact condensation on a horizontal surface
[NASA-TM-104432] p 166 A91-24548
- ### CONDUCTING POLYMERS
- A review of properties and potential aerospace applications of electrically conducting polymers
p 113 A91-14409
- Electrically conducting polymers for aerospace applications
[AIAA PAPER 91-3432] p 233 A91-52349
- ### CONDUCTIVITY
- A finite element model of conduction, convection, and phase change near a solid/melt interface
[NASA-TM-103721] p 162 A91-20417
- ### CONFERENCES
- Heat transfer in space systems; Proceedings of the Symposium, AIAA/ASME Thermophysics and Heat Transfer Conference, Seattle, WA, June 18-20, 1990
p 152 A91-38780
- Materials degradation in low earth orbit (LEO); Proceedings of the Symposium, 119th Annual Meeting of the Minerals, Metals, and Materials Society, Anaheim, CA, Feb. 17-22, 1990
p 116 A91-49801
- Superconductivity applications for infrared and microwave devices; Proceedings of the Meeting, Orlando, FL, Apr. 19, 20, 1990
[SPIE-1292] p 141 A91-50426
- Space Photovoltaic Research and Technology, 1989
[NASA-CP-3107] p 72 A91-19182
- Computational Fluid Dynamics Symposium on Aeropropulsion
[NASA-CP-3078] p 14 A91-21062
- Vision-21: Space Travel for the Next Millennium
[NASA-CP-10059] p 40 A91-22139
- Findings of the Joint Workshop on Evaluation of Impacts of Space Station Freedom Ground Configurations
[NASA-TM-103717] p 73 A91-22370
- Structural Integrity and Durability of Reusable Space Propulsion Systems
[NASA-CP-10030] p 76 A91-24307
- Space Photovoltaic Research and Technology Conference
[NASA-CP-3121] p 82 A91-30203
- ### CONICAL FLOW
- High-Order Polynomial Expansions (HOPE) for flux-vector splitting
[NASA-TM-104452] p 222 A91-25739
- ### CONICAL NOZZLES
- Arjet nozzle area ratio effects
p 75 A91-24271
- ### CONJUGATE GRADIENT METHOD
- Generalized conjugate-gradient methods for the Navier-Stokes equations
[AIAA PAPER 91-1556] p 5 A91-40730
- Least-squares solution of incompressible Navier-Stokes equations with the p-version of finite elements
[NASA-TM-105203] p 223 A91-31911
- ### CONNECTORS
- Vibrational testing of optical fiber connector joints
[NASA-TM-103654] p 172 A91-30652
- Vibrational testing of optical fiber connector joints
p 230 A91-14829
- ### CONSERVATION
- Exploring the notion of space coupling propulsion
p 73 A91-22161
- ### CONSERVATION EQUATIONS
- A detailed numerical investigation of Burke-Schumann gaseous and spray flames
[AIAA PAPER 91-2311] p 105 A91-41749
- ### CONSERVATION LAWS
- Second-order accurate nonoscillatory schemes for scalar conservation laws
p 221 A91-13204
- Solution of steady-state, two-dimensional conservation laws by mathematical programming
p 221 A91-35956
- Flux-vector splitting algorithm for chain-rule conservation-law form
p 221 A91-45109
- A new numerical framework for solving conservation laws: The method of space-time conservation element and solution element
[NASA-TM-104495] p 223 A91-30867
- ### CONSTRUCTION
- Recent advances in Lewis aeropropulsion facilities
p 38 A91-20121
- ### CONSTRUCTION MATERIALS
- METCAN simulation of candidate metal matrix composites for high temperature applications
[NASA-TM-103636] p 96 A91-17143
- ### CONTACT LOADS
- On the numerical solution of the dynamically loaded hydrodynamic lubrication of the point contact
p 180 A91-33461
- A system-approach to the elastohydrodynamic lubrication point-contact problem
[NASA-TM-104342] p 165 A91-23439
- ### CONTACT RESISTANCE
- Determination of surface resistance and magnetic penetration depth of superconducting YBa₂Cu₃O₇(δ) thin films by microwave power transmission measurements
p 138 A91-36060
- An analysis of the contact sintering process in III-V solar cells
p 139 A91-41891
- Determination of surface resistance and magnetic penetration depth of superconducting YBa₂Cu₃O₇(δ) thin films by microwave power transmission measurements
[NASA-TM-103616] p 234 A91-10780
- ### CONTAINERS
- Drop-tower experiments for capillary surfaces in an exotic container
[AIAA PAPER 91-0107] p 148 A91-19138
- ### CONTAINMENT
- Advanced materials for space nuclear power systems
[AIAA PAPER 91-3530] p 82 A91-53704
- Advanced materials for space nuclear power systems
[NASA-TM-105171] p 112 A91-29298
- ### CONTAMINATION
- Microanalysis of extended-test xenon hollow cathodes
[NASA-TM-104532] p 82 A91-30202
- Significant reduction in arc frequency biased solar cells. Observations, diagnostics, and mitigation technique(s)
p 83 A91-30235
- ### CONTINUOUS WAVE LASERS
- Particle displacement tracking applied to air flows
[NASA-TM-104481] p 177 A91-25387
- ### CONTINUUM MECHANICS
- Mechanics of damping for fiber composite laminates including hygrothermal effects
p 195 A91-12895
- A new uniformly valid asymptotic integration algorithm for elasto-plastic creep and unified viscoplastic theories including continuum damage
p 110 A91-48725
- ### CONTRACT MANAGEMENT
- Status of the advanced Stirling conversion system project for 25 kW dish Stirling applications
[NASA-TM-104528] p 238 A91-31023
- ### CONTROL SIMULATION
- The NASA Lewis integrated propulsion and flight control simulator
[AIAA PAPER 91-2969] p 38 A91-47847
- ### CONTROL STABILITY
- Robust eigenspace assignment using singular value sensitivities
p 219 A91-29784
- Integrated flight/propulsion control system design for a STOVL aircraft using H-infinity control design techniques
[NASA-TM-104340] p 31 A91-21140
- ### CONTROL SYSTEMS DESIGN
- Use of piezoelectric actuators in active vibration control of rotating machinery
p 179 A91-14400
- Integrated flight/propulsion control system design based on a centralized approach
p 36 A91-22950
- An intelligent control system for rocket engines - Need, vision, and issues
p 218 A91-26925
- Optical control of microwave devices - Book
p 136 A91-27331
- Dynamic analysis of space-related linear and non-linear structures
p 196 A91-28612
- An expert system to perform on-line controller restructuring for abrupt model changes
p 36 A91-29466
- Robust eigenspace assignment using singular value sensitivities
p 219 A91-29784
- Induction motor control
p 137 A91-30893

Hot gas ingestion test results of a two-poster vectored thrust concept with flow visualization in the NASA Lewis 9- by 15-foot low speed wind tunnel
[AIAA PAPER 90-2268] p 4 A91-40561

Feedback linearization for control of air breathing engines
[AIAA PAPER 91-2000] p 23 A91-41671

Preliminary thermal design of the COLD-SAT spacecraft
[AIAA PAPER 91-1305] p 46 A91-45550

A linear control design structure to maintain loop properties during limit operation in a multi-nozzle turbofan engine
[AIAA PAPER 91-1997] p 24 A91-45780

The NASA Lewis integrated propulsion and flight control simulator
[AIAA PAPER 91-2969] p 38 A91-47847

Neural network application to aircraft control system design
[AIAA PAPER 91-2715] p 36 A91-49676

Application of an integrated flight/propulsion control design methodology to a STOVL aircraft
[AIAA PAPER 91-2792] p 36 A91-49793

Automation software for a materials testing laboratory
p 216 A91-56538

Towards practical control design using neural computation
[NASA-TM-103785] p 219 N91-19766

Aeropropulsion 1991
[NASA-CP-10063] p 27 N91-20086

Instrumentation and controls overview
p 38 N91-20099

Fiber-optic-based controls
p 230 N91-20102

Advanced aeropropulsion controls technology
p 29 N91-20103

A method for partitioning centralized controllers
[NASA-TM-4276] p 36 N91-20133

Hot gas ingestion test results of a two-poster vectored thrust concept with flow visualization in the NASA Lewis 9- x 15-foot low speed wind tunnel
[NASA-TM-103258] p 15 N91-21116

Integrated flight/propulsion control system design based on a decentralized, hierarchical approach
[NASA-TM-103678] p 31 N91-21137

Integrated flight/propulsion control design for a STOVL aircraft using H-infinity control design techniques
[NASA-TM-104340] p 31 N91-21140

Microgravity vibration isolation: An optimal control law for the one-dimensional case
p 49 N91-21206

Life extending control: A concept paper
[NASA-TM-104391] p 37 N91-22135

Alpha-canonical form representation of the open loop dynamics of the Space Shuttle main engine
[NASA-TM-104422] p 131 N91-24469

Preliminary thermal design of the COLD-SAT spacecraft
[NASA-TM-104440] p 49 N91-25161

A distributed fault-detection and diagnosis system using on-line parameter estimation
[NASA-TM-104433] p 220 N91-25696

Control of an axisymmetric turbulent jet by multi-modal excitation
[NASA-TM-104483] p 17 N91-26121

Development and testing of a source subsystem for the supporting development PMAD DC test bed
[NASA-TM-104510] p 78 N91-26202

Neural network application to aircraft control system design
[NASA-TM-105151] p 37 N91-27167

The development of test beds to support the definition and evolution of the Space Station Freedom power system
[NASA-TM-104504] p 79 N91-27207

Apparatus for intercalating large quantities of fibrous structures
[NASA-CASE-LEW-10577-2] p 102 N91-28289

A linear control design structure to maintain loop properties during limit operation in a multi-nozzle turbofan engine
[NASA-TM-105163] p 35 N91-29188

Description of the control system design for the SSF PMAD DC testbed
[NASA-TM-105202] p 84 N91-30266

Application of an integrated flight/propulsion control design methodology to a STOVL aircraft
[NASA-TM-105254] p 37 N91-32143

CONTROL THEORY

Development of a vibration isolation prototype system for microgravity space experiments
p 47 A91-53403

Implementation of control point form of algebraic grid-generation technique
[NASA-TM-103748] p 13 N91-19054

Development of a vibration isolation prototype system for microgravity space experiments
[NASA-TM-103664] p 130 N91-19324

IMPAC: An Integrated Methodology for Propulsion and Airframe Control
[NASA-TM-103805] p 30 N91-20122

CONTROL VALVES

Automatic control study of the icing research tunnel refrigeration system
[NASA-TM-4257] p 40 N91-19115

A high-frequency servosystem for fuel control in hypersonic engines
[NASA-TM-104333] p 35 N91-31178

CONTROLLERS

Neural network architecture for crossbar switch control
p 218 A91-29181

An expert system to perform on-line controller restructuring for abrupt model changes
p 36 A91-29466

Partitioning methods for global controllers
p 219 A91-30043

An expert system to perform on-line controller tuning
p 219 A91-30171

Field oriented control of induction motors
p 138 A91-37987

Automatic control study of the icing research tunnel refrigeration system
[NASA-TM-4257] p 40 N91-19115

A method for partitioning centralized controllers
[NASA-TM-4276] p 36 N91-20133

Magnetic bearings with zero bias
p 48 N91-21194

Method of injecting fluid propellants into a rocket combustion chamber
[NASA-CASE-LEW-14846-2] p 78 N91-26200

Description of the control system design for the SSF PMAD DC testbed
[NASA-TM-105202] p 84 N91-30266

Tuning maps for setpoint changes and load disturbance upsets in a three capacity process under multivariable control
[NASA-TM-104419] p 220 N91-31876

CONVECTION

Interaction of surface radiation with convection in crystal growth by physical vapor transport
p 127 A91-24563

The dynamic instability of adiabatic blast waves
p 239 A91-26361

Spacelab qualified infrared imager for microgravity science applications
p 173 A91-51585

A finite element model of conduction, convection, and phase change near a solid/melt interface
[NASA-TM-103721] p 162 N91-20417

A new flux splitting scheme
[NASA-TM-104404] p 222 N91-22814

The L sub 1 finite element method for pure convection problems
[NASA-TM-103773] p 222 N91-24817

Particle image velocimetry for the surface tension driven convection experiment using a particle displacement tracking technique
[NASA-TM-104482] p 177 N91-25382

Ground-based PIV and numerical flow visualization results from the surface tension driven convection experiment
[NASA-TM-105172] p 178 N91-30491

CONVECTIVE HEAT TRANSFER

Turbine blading designed for high heat load space propulsion applications
p 50 A91-10338

Development of a laser-induced heat flux technique for measurement of convective heat transfer coefficients in a supersonic flowfield
[NASA-TM-103778] p 13 N91-19063

Heat transfer in rotating serpentine passages with trips normal to the flow
[NASA-TM-103758] p 184 N91-19443

Simulation of brush insert for leading-edge-passage convective heat transfer
[NASA-TM-103801] p 165 N91-23409

A laser-induced heat flux technique for convective heat transfer measurements in high speed flows
[NASA-TM-105177] p 168 N91-30472

CONVERGENCE

Time-derivative preconditioning for viscous flows
[AIAA PAPER 91-1652] p 154 A91-43576

Spectrum transformation for divergent iterations
[NASA-TM-103745] p 221 N91-19786

Comparison of SMAC, PISO, and iterative time-advancing schemes for unsteady flows
[NASA-TM-104406] p 167 N91-24550

CONVERGENT-DIVERGENT NOZZLES

Supersonic jet mixing enhancement by vortex generators
[AIAA PAPER 91-2263] p 5 A91-41738

Modern CFD applications for the design of a reacting shear layer facility
[NASA-TM-104523] p 34 N91-27164

Divergence thrust loss calculations for convergent-divergent nozzles: Extensions to the classical case
[NASA-TM-105176] p 34 N91-29181

CONVEXITY

Wind tunnel wall effects in a linear oscillating cascade
[NASA-TM-103690] p 27 N91-19098

COOLANTS

Computations of the three-dimensional flow and heat transfer within a coolant passage of a radial turbine blade
[AIAA PAPER 91-2238] p 156 A91-45797

Algebraic grid generation for coolant passages of turbine blades with serpentine channels and pin fins
[AIAA PAPER 91-2366] p 156 A91-45811

Cooling of in-situ propellant rocket engines for Mars mission
[NASA-TM-103729] p 72 N91-21233

The NASA cryogenic fluid management technology program plan
[NASA-TM-105256] p 86 N91-32161

COOLING

Review and test of chilldown methods for space-based cryogenic tanks
[AIAA PAPER 91-1843] p 60 A91-45776

A life comparison of tube and channel cooling passages for thrust chambers
[NASA-TM-103613] p 68 N91-11059

A unique high heat flux facility for testing hypersonic engine components
[NASA-TM-103238] p 38 N91-11770

Cooling of in-situ propellant rocket engines for Mars mission
[NASA-TM-103729] p 72 N91-21233

Hydrocarbon-fuel/combustion-chamber-liner materials compatibility
[NASA-CR-187104] p 121 N91-21307

Review and test of chilldown methods for space-based cryogenic tanks
[NASA-TM-104458] p 167 N91-25351

COOLING SYSTEMS

A dual-cooled hydrogen-oxygen rocket engine heat transfer analysis
[AIAA PAPER 91-2211] p 59 A91-44156

Heat transfer in rotating serpentine passages with trips normal to the flow
[NASA-TM-103758] p 184 N91-19443

A dual-cooled hydrogen-oxygen rocket engine heat transfer analysis
[NASA-TM-104430] p 76 N91-24302

Advanced cryo propulsion systems
p 80 N91-28212

COORDINATE TRANSFORMATIONS

Algebraic grid generation for complex geometries
p 157 A91-48758

Compressible flows with periodic vortical disturbances around lifting airfoils
[NASA-TM-103742] p 14 N91-21060

Turbulent fluid motion 2: Scalars, vectors, and tensors
[NASA-TM-103756] p 167 N91-27487

Computerized inspection of real surfaces and minimization of their deviations
[NASA-TM-103798] p 188 N91-27558

COPOLYMERIZATION

Polymeric routes to silicon carbide and silicon oxycarbide
CMC p 117 A91-56922

Polymeric routes to silicon carbide and silicon oxycarbide
CMC [NASA-TM-104372] p 102 N91-26234

COPOLYMERS

Polymeric routes to silicon carbide and silicon oxycarbide
CMC p 117 A91-56922

Polymeric routes to silicon carbide and silicon oxycarbide
CMC [NASA-TM-104372] p 102 N91-26234

COPPER

Thermal emittance enhancement of graphite-copper composites for high temperature space based radiators
[AIAA PAPER 91-3527] p 116 A91-53705

High temperature tension-compression fatigue behavior of a tungsten copper composite
[NASA-TM-104370] p 100 N91-24360

Thermal emittance enhancement of graphite-copper composites for high temperature space based radiators
[NASA-TM-105178] p 123 N91-29332

Near-edge study of gold-substituted YBa₂Cu₃O(7-delta)
[NASA-TM-105220] p 237 N91-31977

COPPER ALLOYS

Grain boundary sliding behaviour of copper and alpha brass at intermediate temperatures
p 108 A91-27158

Creep behaviour of Cu-30 percent Zn at intermediate temperatures
p 109 A91-47747

Creep behavior of copper at intermediate temperatures. II - Surface microstructural observations. III - A comparison with theory
p 109 A91-47931

High temperature fatigue behavior of tungsten copper composites
p 93 A91-55906

Hydrocarbon-fuel/combustion-chamber-liner materials compatibility
[NASA-CR-187104] p 121 N91-21307

- Tensile and fatigue behavior of tungsten/copper composites p 100 N91-24311
Low cost, formable, high T(sub c) superconducting wire [NASA-CASE-LEW-14676-1] p 147 N91-31529
- COPPER OXIDES**
Electromigration failure in YBa₂Cu₃O(7-x) thin films p 231 A91-26989
Determination of surface resistance and magnetic penetration depth of superconducting YBa₂Cu₃O(7-delta) thin films by microwave power transmission measurements p 138 A91-36060
Photoresponse of YBa₂Cu₃O(7-delta) granular and epitaxial superconducting thin films p 141 A91-50443
Ellipsometric study of YBa₂Cu₃O(7-x) laser ablated and co-evaporated films p 233 A91-53235
Determination of surface resistance and magnetic penetration depth of superconducting YBa₂Cu₃O(7-delta) thin films by microwave power transmission measurements [NASA-TM-103616] p 234 N91-10780
Near-edge study of gold-substituted YBa₂Cu₃O(7-delta) [NASA-TM-105220] p 237 N91-31977
- COPPER SULFIDES**
Hydrocarbon-fuel/combustion-chamber-liner materials compatibility [NASA-CR-187104] p 121 N91-21307
- COROLIS EFFECT**
Heat transfer in rotating serpentine passages with trips normal to the flow [NASA-TM-103758] p 184 N91-19443
- CORNER FLOW**
Efficient real gas upwind Navier-Stokes computations of high speed flows p 157 A91-46179
- CORRELATION**
Dropsize correlation for cryogenic liquid-jet atomization [NASA-TM-103646] p 175 N91-12064
Advances in modeling the pressure correlation terms in the second moment equations [NASA-TM-104413] p 165 N91-24525
Orr-Sherby-Dorn creep strengths of the refractory-metal alloys C-103, ASTAR-811C, W-5Re, and W-25Re [NASA-TM-105228] p 87 N91-32165
- CORROSION**
Hydrocarbon-fuel/combustion-chamber-liner materials compatibility [NASA-CR-187104] p 121 N91-21307
- CORROSION RESISTANCE**
Effect of high temperature hydrogen exposure on the strength and microstructure of mullite p 114 A91-19780
- CORROSION TESTS**
The effect of atomic oxygen on polysiloxane-polyimide for spacecraft applications in low Earth orbit p 229 N91-20735
- COSMOCHEMISTRY**
Big bang nucleosynthesis - The standard model and alternatives p 240 A91-37428
- COSMOLOGY**
Natural inflation with pseudo Nambu-Goldstone bosons p 239 A91-19545
Inflationary axion cosmology p 239 A91-20491
First-order inflation --- in cosmology p 240 A91-37444
Astrophysics and cosmology confront the 17-keV neutrino p 240 A91-43291
Baryon isocurvature scenario in inflationary cosmology - A particle physics model and its astrophysical implications p 240 A91-54201
- COST ANALYSIS**
k-out-of-n:G systems - Some cost considerations p 192 A91-54553
How much redundancy: Some cost considerations, including examples for spacecraft systems [NASA-TM-103197] p 192 N91-17407
Balancing reliability and cost to choose the best power subsystem [NASA-TM-104453] p 238 N91-24952
Reliability and cost: A sensitivity analysis [NASA-TM-105293] p 238 N91-33014
- COST EFFECTIVENESS**
Propulsion challenges for a 21st century economically viable, environmentally compatible High-Speed Civil Transport p 25 A91-56109
Key issues in space nuclear power [NASA-TM-103656] p 71 N91-19179
Power technologies and the space future [NASA-TM-103649] p 73 N91-21240
Balancing reliability and cost to choose the best power subsystem [NASA-TM-104453] p 238 N91-24952
- COST REDUCTION**
Evolving the SP-100 reactor in order to boost large payloads to GEO and to low lunar orbit via nuclear-electric propulsion [AIAA PAPER 91-3562] p 67 A91-53712
Key issues in space nuclear power [NASA-TM-103656] p 71 N91-19179
Indium phosphide solar cells p 210 N91-19221
Evolving the SP-100 reactor in order to boost large payloads to GEO and to low lunar orbit via nuclear-electric propulsion [NASA-TM-104527] p 80 N91-27212
- COSTS**
Preliminary designs for 25 kWe advanced Stirling conversion systems for dish electric applications p 207 N91-38182
- COUETTE FLOW**
Stability of compressible Taylor-Couette flow [AIAA PAPER 91-1642] p 153 A91-42541
- COUNTER ROTATION**
Aeroacoustic effects of reduced alt tip speed at constant thrust for a model counterrotation turboprop at takeoff conditions [NASA-TM-103608] p 226 N91-10703
Optical measurement of unducted fan flutter [NASA-TM-103285] p 27 N91-15174
- COUNTERFLOW**
A PCM/forced convection conjugate transient analysis of energy storage systems with annular and countercurrent flows p 150 A91-27166
- COUPLED MODES**
A high-efficiency ferruleless coupled-cavity traveling-wave tube with phase-adjusted taper p 136 A91-25078
- COUPLES**
Modal analysis of multistage gear systems coupled with gearbox vibrations [NASA-TM-103797] p 187 N91-23513
- CRACK CLOSURE**
Crack healing in silicon nitride due to oxidation p 118 A91-56982
- CRACK OPENING DISPLACEMENT**
Analysis of some compliance calibration data for chevron-notch bar and rod specimens [NASA-TM-104367] p 203 N91-22594
- CRACK PROPAGATION**
Ultrasonic imaging of textured alumina p 191 A91-18596
Fatigue crack growth study of SC56/Ti-15-3 composite p 91 A91-25798
Numerical, micro-mechanical prediction of crack growth resistance in a fibre-reinforced/brittle matrix composite p 199 A91-51916
Influence of the Si₃N₄ microstructure on its R-curve and fatigue behavior p 117 A91-56931
Comparison of dynamic fatigue behavior between SiC whisker-reinforced composite and monolithic silicon nitrides [NASA-TM-103707] p 119 N91-19293
Analysis of some compliance calibration data for chevron-notch bar and rod specimens [NASA-TM-104367] p 203 N91-22594
Mechanical behavior and failure phenomenon of an in situ-toughened silicon nitride [NASA-TM-103741] p 121 N91-23311
Modeling of crack bridging in a unidirectional metal matrix composite [NASA-TM-104355] p 205 N91-24660
Elevated-temperature fracture resistances (K(sub IC), R-curves, gamma sub (omega OF)) of monolithic and composite ceramics using chevron-notched, bend tests [NASA-TM-105090] p 123 N91-28418
- CRACKING (FRACTURING)**
Elastic/plastic analyses of advanced composites investigating the use of the compliant layer concept in reducing residual stresses resulting from processing [NASA-TM-103204] p 94 N91-11074
- CRACKS**
Calculation of Weibull strength parameters, Batdorf flaw density constants and related statistical quantities using PC-CARES [NASA-TM-103247] p 199 N91-10332
Modeling of crack bridging in a unidirectional metal matrix composite [NASA-TM-104355] p 205 N91-24660
Atomic oxygen undercutting of LDEF aluminized Kapton multilayer insulation p 229 N91-25027
- CRAY COMPUTERS**
Cray performance data from five benchmarks [NASA-TM-105200] p 217 N91-32806
- CREEP ANALYSIS**
Orr-Sherby-Dorn creep strengths of the refractory-metal alloys C-103, ASTAR-811C, W-5Re, and W-25Re [NASA-TM-105228] p 87 N91-32165
- CREEP PROPERTIES**
Quantification of uncertainties in coupled material degradation processes - High temperature, fatigue and creep [AIAA PAPER 91-0977] p 196 A91-31835
Creep behaviour of Cu-30 percent Zn at intermediate temperatures p 109 A91-47747
Creep behavior of copper at intermediate temperatures. II - Surface microstructural observations. III - A comparison with theory p 109 A91-47931
Fiber creep evaluation by stress relaxation measurements p 117 A91-56905
Cumulative creep fatigue damage in 316 stainless steel p 111 N91-24312
Orr-Sherby-Dorn creep strengths of the refractory-metal alloys C-103, ASTAR-811C, W-5Re, and W-25Re [NASA-TM-105228] p 87 N91-32165
- CREEP STRENGTH**
Thermal stability of the microstructure of an aged Nb-Zr-C alloy [NASA-TM-103647] p 110 N91-14454
Reinforcements: The key to high performance composite materials [NASA-TM-103230] p 96 N91-15329
A simple test for thermomechanical evaluation of ceramic fibers [NASA-TM-103767] p 121 N91-21309
Orr-Sherby-Dorn creep strengths of the refractory-metal alloys C-103, ASTAR-811C, W-5Re, and W-25Re [NASA-TM-105228] p 87 N91-32165
- CREEP TESTS**
1300 K compressive properties of a reaction milled NiAl-AlN composites p 107 A91-18674
Automation software for a materials testing laboratory p 216 A91-56538
- CRITICAL FLOW**
Critical-layer nonlinearity in the resonance growth of three-dimensional waves in boundary layers [NASA-TM-103639] p 161 N91-19373
- CRITICAL TEMPERATURE**
An experimental study of high Tc superconducting microstrip transmission lines at 35 GHz and the effect of film morphology p 138 A91-36172
An experimental study of high Tc superconducting microstrip transmission lines at 35 GHz and the effect of film morphology [NASA-TM-103633] p 133 N91-11988
- CROSS COUPLING**
Tuning maps for setpoint changes and load disturbance upsets in a three capacity process under multivariable control [NASA-TM-104419] p 220 N91-31876
- CROSS FLOW**
Three-dimensional calculation of the mixing of radial jets from slanted slots with a reactive cylindrical crossflow [AIAA PAPER 91-2081] p 24 A91-45782
Mixing of multiple jets with a confined subsonic crossflow - Summary of NASA-supported experiments and modeling [AIAA PAPER 91-2458] p 7 A91-45813
Experimental study of cross-stream mixing in a cylindrical duct [AIAA PAPER 91-2459] p 157 A91-45815
Characteristics of 3D turbulent jets in crossflow p 158 A91-54268
Characteristics of 3D turbulent jets in crossflow [NASA-TM-104337] p 165 N91-22536
Mixing of multiple jets with a confined subsonic crossflow. Summary of NASA-supported experiments and modeling [NASA-TM-104412] p 33 N91-24202
Experimental study of cross-stream mixing in a cylindrical duct [NASA-TM-105180] p 34 N91-29187
Calculation of a circular jet in crossflow with a multiple-time-scale turbulence model [NASA-TM-104343] p 169 N91-30476
- CRUISING FLIGHT**
The effect of swirl recovery vanes on the cruise noise of an advanced propeller [AIAA PAPER 90-3932] p 224 A91-12448
Cruise noise of an advanced single-rotation propeller measured from an adjacent aircraft p 22 A91-28265
- CRYOGENIC COOLING**
Hydrogen/oxygen auxiliary propulsion technology [AIAA PAPER 91-3440] p 64 A91-52352
Advanced cryo propulsion systems p 80 N91-28212
- CRYOGENIC EQUIPMENT**
High temperature superconductive microwave technology for space applications p 137 A91-31391
Measurement techniques for cryogenic Ka-band microstrip antennas [NASA-TM-105183] p 146 N91-30426
The NASA cryogenic fluid management technology program plan [NASA-TM-105256] p 86 N91-32161

CRYOGENIC FLUID STORAGE

- The COLD-SAT experiment for cryogenic fluid management technology p 46 A91-29799
- Improved thermodynamic modelling of the non-vent fill process and correlation with experimental data [AIAA PAPER 91-1379] p 129 A91-43444
- A pressure control analysis of cryogenic storage systems [AIAA PAPER 91-2405] p 59 A91-44228
- A numerical study of the direct contact condensation on a horizontal surface [AIAA PAPER 91-1307] p 155 A91-44335
- Review and test of chilldown methods for space-based cryogenic tanks [AIAA PAPER 91-1843] p 60 A91-45776
- Thermal performance of a liquid hydrogen tank multilayer insulation system at warm boundary temperatures of 630, 530, and 152 R [AIAA PAPER 91-2400] p 43 A91-45812
- Discharge rate of cryogenics in microgravity - What ground based experimentation cannot resolve [AIAA PAPER 91-3545] p 129 A91-52430
- The NASA Cryogenic Fluid Management Technology Program Plan [AIAA PAPER 91-3553] p 130 A91-52436
- Slush hydrogen propellant production, transfer, and expulsion studies at the NASA K-Site Facility [AIAA PAPER 91-3550] p 125 A91-53710
- A pressure control analysis of cryogenic storage systems [NASA-TM-104409] p 126 N91-24460
- A numerical study of the direct contact condensation on a horizontal surface [NASA-TM-104432] p 166 N91-24548
- Pressurization and expulsion of cryogenic liquids: Generic requirements for a low gravity experiment [NASA-TM-104417] p 126 N91-25300
- Review and test of chilldown methods for space-based cryogenic tanks [NASA-TM-104458] p 167 N91-25351
- Slush hydrogen propellant production, transfer, and expulsion studies at the NASA K-Site Facility [NASA-TM-105191] p 127 N91-28449
- The NASA cryogenic fluid management technology program plan [NASA-TM-105256] p 86 N91-32161
- CRYOGENIC FLUIDS**
- Drops size correlation for cryogenic liquid-jet atomization [AIAA PAPER 91-0284] p 51 A91-19218
- Transient cryogenic liquid discharge in normal and micro-gravity [AIAA PAPER 91-0486] p 124 A91-19324
- Vapor condensation at the free surface of an axisymmetric liquid mixed by a laminar jet p 151 A91-35109
- LN₂ spray droplet size measurement via ensemble diffraction technique [AIAA PAPER 91-1381] p 129 A91-44336
- Preliminary thermal design of the COLD-SAT spacecraft [AIAA PAPER 91-1305] p 46 A91-45550
- Discharge rate of cryogenics in microgravity - What ground based experimentation cannot resolve [AIAA PAPER 91-3545] p 129 A91-52430
- The NASA Cryogenic Fluid Management Technology Program Plan [AIAA PAPER 91-3553] p 130 A91-52436
- NASA cryogenic fluid management space experiment efforts [AIAA PAPER 91-3538] p 130 A91-53701
- Cryogenic liquid-jet breakup in two-fluid atomizers [NASA-TM-103734] p 176 N91-19402
- The COLD-SAT experiment for cryogenic fluid management technology p 126 N91-24263
- LN₂ spray droplet size measurement via ensemble diffraction technique [NASA-TM-104443] p 131 N91-24470
- Preliminary thermal design of the COLD-SAT spacecraft [NASA-TM-104440] p 49 N91-25161
- Pressurization and expulsion of cryogenic liquids: Generic requirements for a low gravity experiment [NASA-TM-104417] p 126 N91-25300
- NASA cryogenic fluid management space experiment efforts, 1960-1990 [NASA-TM-103752] p 243 N91-30073
- The NASA cryogenic fluid management technology program plan [NASA-TM-105256] p 86 N91-32161
- CRYOGENIC ROCKET PROPELLANTS**
- Cryogenic propellant management architectures to support the Space Exploration Initiative [AIAA PAPER 90-3713] p 124 A91-10112
- The COLD-SAT experiment for cryogenic fluid management technology p 46 A91-29799

- Conceptual study of on orbit production of cryogenic propellants by water electrolysis [AIAA PAPER 91-1844] p 124 A91-41631
- Plans for the development of cryogenic engines for space exploration [AIAA PAPER 91-3438] p 64 A91-52351
- Cryogenic propellant management system requirements for Space Station Freedom [AIAA PAPER 91-3476] p 65 A91-52382
- Fuel Systems Architecture (FSA) evaluation criteria and concept evaluation methodology [AIAA PAPER 91-3479] p 65 A91-52384
- Cryogenic transfer options for exploration missions [AIAA PAPER 91-3541] p 158 A91-53714
- Conceptual study of on orbit production of cryogenic propellants by water electrolysis [NASA-TM-103730] p 126 N91-19317
- Advanced cryo propulsion systems p 80 N91-28212
- Cryogenic transfer options for exploration missions [NASA-TM-105197] p 168 N91-28538
- CRYOGENIC STORAGE**
- Cryogenic transfer options for exploration missions [AIAA PAPER 91-3541] p 158 A91-53714
- Cryogenic transfer options for exploration missions [NASA-TM-105197] p 168 N91-28538
- CRYOGENIC TEMPERATURE**
- Low-temperature microwave characteristics of pseudomorphic In(x)Ga(1-x)As/In(0.52)Al(0.48)As modulation-doped field-effect transistors p 136 A91-22987
- CRYOGENICS**
- Advanced launch system (ALS) - Electrical actuation and power systems improve operability and cost picture p 51 A91-31025
- Paramagnetic propellant orientation [AIAA PAPER 91-2325] p 125 A91-44197
- Ground testing of the nonvented fill method of orbital propellant transfer - Results of initial test series [AIAA PAPER 91-2326] p 59 A91-44198
- Cryogenic transfer options for exploration missions [AIAA PAPER 91-3541] p 158 A91-53714
- Drops size correlation for cryogenic liquid-jet atomization [NASA-TM-103646] p 175 N91-12064
- Research and technology [NASA-TM-103759] p 243 N91-23072
- Paramagnetic propellant orientation [NASA-TM-104390] p 166 N91-24527
- Ground testing on the nonvented fill method of orbital propellant transfer: Results of initial test series [NASA-TM-104444] p 166 N91-24547
- Pressurization and expulsion of cryogenic liquids: Generic requirements for a low gravity experiment [NASA-TM-104417] p 126 N91-25300
- Autogenous pressurization of cryogenic vessels using submerged vapor injection [NASA-TM-104516] p 127 N91-27375
- Cryogenic transfer options for exploration missions [NASA-TM-105197] p 168 N91-28538
- Qualitative investigation of cryogenic injected shock dissipation [NASA-TM-105140] p 168 N91-29525
- The NASA cryogenic fluid management technology program plan [NASA-TM-105256] p 86 N91-32161
- CRYSTAL DEFECTS**
- Equivalent crystal theory of alloys [NASA-TP-3155] p 112 N91-30318
- CRYSTAL DISLOCATIONS**
- Temperature dependence of hardness in yttria-stabilized zirconia single crystals p 114 A91-28763
- The potential for ductility enhancement from surface and interface dislocation sources in NiAl p 109 A91-39292
- A simplified method for determining the number of independent slip systems in crystals p 110 A91-55472
- Effect of dislocations on the open-circuit voltage, short-circuit current and efficiency of heteroepitaxial indium phosphide solar cells [NASA-TM-103762] p 144 N91-19354
- Heteroepitaxial InP solar cells on Si and GaAs substrates [NASA-TM-103696] p 144 N91-20392
- Effect of dislocations on properties of heteroepitaxial InP solar cells p 213 N91-30209
- CRYSTAL GROWTH**
- Time development of a perturbed-spherical nucleus in a pure supercooled liquid. I - Power-law growth of morphological instabilities. II - Nonlinear development p 231 A91-16105
- Interaction of surface radiation with convection in crystal growth by physical vapor transport p 127 A91-24563
- Controlled growth of 3C-SiC and 6H-SiC films on low-tilt-angle vicinal (0001) 6H-SiC wafers p 232 A91-45713

- Isothermal Dendritic Growth Experiment - Science, engineering, and hardware development for USMP space flights p 128 A91-53408
- Silicon carbide, a semiconductor for space power electronics [NASA-TM-103655] p 234 N91-14850
- Ellipsometric study of cubic SiC p 235 N91-18304
- Growth kinetics of physical vapor transport processes: Crystal growth of the optoelectronic material mercurous chloride [NASA-TM-103788] p 128 N91-19320
- High temperature electronics p 144 N91-20101
- An examination of anticipated g-jitter on space station and its effects on materials processes [NASA-TM-103775] p 128 N91-21378
- Process for the controlled growth of single-crystal films of silicon carbide polytypes on silicon carbide wafers [NASA-CASE-LEW-15222-1] p 236 N91-26966
- CRYSTAL LATTICES**
- The structure of carbon in chemically vapor deposited SiC monofilaments p 113 A91-18675
- Universal behavior in ideal slip p 110 A91-48517
- Equivalent crystal theory of alloys [NASA-TP-3155] p 112 N91-30318
- CRYSTAL STRUCTURE**
- Grain boundary sliding behaviour of copper and alpha brass at intermediate temperatures p 108 A91-27158
- A simplified method for determining the number of independent slip systems in crystals p 110 A91-55472
- Ellipsometric study of InGaAs MODFET material [NASA-TM-103286] p 143 N91-19351
- Solid lubricants [NASA-TM-102803] p 99 N91-22396
- Synthesis and thermal properties of strontium and calcium peroxides [NASA-TM-103725] p 107 N91-22410
- Equivalent crystal theory of alloys [NASA-TP-3155] p 112 N91-30318
- CRYSTALLINITY**
- Selective and low temperature synthesis of polycrystalline diamond p 232 A91-42170
- Investigation of anodic and chemical oxides grown on p-type InP with applications to surface passivation for n(+)-p solar cell fabrication p 210 N91-19208
- CRYSTALLIZATION**
- Crystallization and properties of Sr-Ba aluminosilicate glass-ceramic matrices p 117 A91-56917
- Crystallization and properties of Sr-Ba aluminosilicate glass-ceramic matrices [NASA-TM-103764] p 120 N91-19308
- CRYSTALS**
- Growth kinetics of physical vapor transport processes: Crystal growth of the optoelectronic material mercurous chloride [NASA-TM-103788] p 128 N91-19320
- Development of silicon carbide semiconductor devices for high temperature applications [NASA-TM-104398] p 236 N91-22921
- Theoretical modelling of AFM for bimetallic tip-substrate interactions [NASA-TM-105280] p 112 N91-32215
- CUBIC EQUATIONS**
- Accurate monotone cubic interpolation [NASA-TM-103789] p 221 N91-20830
- CUBIC LATTICES**
- Oxidation behavior of cubic phases formed by alloying Al₃Ti with Cr and Mn p 108 A91-27849
- Ellipsometric study of cubic SiC p 235 N91-18304
- CUMULATIVE DAMAGE**
- In-service health monitoring of composite structures p 192 A91-51926
- CURRENT DENSITY**
- Aerospace applications of high temperature superconductivity [IAF PAPER 90-054] p 231 A91-13767
- Surface studies on scandate cathodes and synthesized scandates p 136 A91-25071
- CURVATURE**
- Surface settling in partially filled containers upon step reduction in gravity [NASA-TM-103641] p 159 N91-14556
- Numerical investigation of an internal layer in turbulent flow over a curved hill p 163 N91-21083
- CURVE FITTING**
- Analysis of some compliance calibration data for chevron-notch bar and rod specimens [NASA-TM-104367] p 203 N91-22594
- CURVES**
- Monograph on propagation of sound waves in curved ducts [NASA-RP-1248] p 228 N91-15848
- CYCLIC LOADS**
- Simplified procedures for designing adhesively bonded composite joints p 180 A91-20938

- Inhomogeneous deformation in INCONEL 718 during monotonic and cyclic loadings p 108 A91-22287
The effect of hydrogen on the low cycle fatigue behavior of a single crystal superalloy p 108 A91-28794
Cumulative creep fatigue damage in 316 stainless steel p 111 N91-24312
Probabilistic structural analysis: Introductory remarks p 204 N91-24326

CYLINDRICAL BODIES

- Flow induced vibration and noise by a pair of tandem cylinders due to buffeting p 225 A91-14650
Increased heat transfer to a cylindrical leading edge due to spanwise variations in the freestream velocity [AIAA PAPER 91-1739] p 155 A91-43623
Low velocity impact analysis with NASTRAN p 198 A91-48865
Low velocity impact analysis with NASTRAN [NASA-TM-103169] p 95 N91-14426
Increased heat transfer to a cylindrical leading edge due to spanwise variations in the freestream velocity [NASA-TM-104464] p 100 N91-24359
Experimental study of cross-stream mixing in a cylindrical duct [NASA-TM-105180] p 34 N91-29187

CYLINDRICAL CHAMBERS

- Viscoplastic analysis of an experimental cylindrical thrust chamber liner [NASA-TM-103287] p 205 N91-28622

CZCCHRALSKI METHOD

- A comparative study of $p(+)$ and $n(+)$ in p solar cells made by a closed ampoule diffusion p 212 N91-30206

D**DAMAGE**

- A new uniformly valid asymptotic integration algorithm for elastoplastic creep and unified viscoplastic theories including continuum damage p 110 A91-48725
Review of acousto-ultrasonic NDE for composites p 97 N91-18192
Semiconductor structural damage attendant to contact formation in III-V solar cells p 209 N91-19203
Atomic oxygen undercutting of LDEF aluminized Kapton multilayer insulation p 229 N91-25027

DAMAGE ASSESSMENT

- Fatigue crack growth study of SCS6/Ti-15-3 composite p 91 A91-25798
In situ X-ray monitoring of damage accumulation in SiC/RBSN tensile specimens p 94 A91-56942
In-situ x-ray monitoring of damage accumulation in SiC/RBSN tensile specimens [NASA-TM-103733] p 99 N91-22402

DAMPING

- An integrated methodology for optimizing the passive damping of composite structures p 195 A91-19048

DARK MATTER

- Telescope search for a 3-eV to 8-eV axion p 239 A91-28714

DATA ACQUISITION

- Two-dimensional particle displacement tracking in particle imaging velocimetry p 172 A91-38498
A data acquisition and control program for axial-torsional fatigue testing p 199 A91-56540
Rotating pressure measurement system using an on board calibration standard [NASA-TM-103676] p 176 N91-19401
Chemical reacting flows p 162 N91-20098
Software manual for operating particle displacement tracking data acquisition and reduction system [NASA-TM-103720] p 176 N91-20453

DATA BASES

- Overview of high performance aircraft propulsion p 28 N91-20089
High alpha inlets p 28 N91-20091

DATA COMPRESSION

- Data compression for full motion video transmission [AIAA PAPER 91-3533] p 45 A91-52424
Real-time data compression of broadcast video signals [NASA-CASE-LEW-14945-1] p 133 N91-13598
High Resolution, High Frame Rate Video Technology [NASA-CP-3080] p 175 N91-14574
Digital CODEC for real-time processing of broadcast quality video signals at 1.8 bits/pixel p 134 N91-24067
Data compression for full motion video transmission [NASA-TM-105239] p 135 N91-32247

DATA LINKS

- Bit error rate testing of fiber optic data links for MMIC-based phased array antennas p 131 A91-24950
A comparison of optical technologies for a high data rate Mars link [AIAA PAPER 91-3469] p 45 A91-52377

- Millimeter wavelength communications applications for the SEI [NASA-TM-105275] p 135 N91-32287

DATA PROCESSING

- Neuromorphic learning of continuous-valued mappings from noise-corrupted data p 219 A91-53201
A model for the space shuttle main engine high pressure oxidizer turbopump shaft seal system [NASA-TM-103697] p 184 N91-20489

DATA SYSTEMS

- Rotating pressure measurement system using an on board calibration standard [NASA-TM-103676] p 176 N91-19401

DATA TRANSMISSION

- LBR-2 Earth stations for the ACTS program p 133 N91-11971
High Resolution, High Frame Rate Video Technology [NASA-CP-3080] p 175 N91-14574
Results of the users' requirements survey p 175 N91-14575
State of the art in video system performance p 175 N91-14578
High resolution, high frame rate video technology development plan and the near-term system conceptual design p 175 N91-14580
Data compression for full motion video transmission [NASA-TM-105239] p 135 N91-32247
Millimeter wavelength communications applications for the SEI [NASA-TM-105275] p 135 N91-32287

DECOMPOSITION

- Arjet nozzle area ratio effects p 75 N91-24271

DECOUPLING

- On the anomaly of velocity-pressure decoupling in collocated mesh solutions [NASA-TM-103769] p 164 N91-21448

DEFECTS

- Calculation of Weibull strength parameters, Batdorf flaw density constants and related statistical quantities using PC-CARES [NASA-TM-103247] p 199 N91-10332
Review of acousto-ultrasonic NDE for composites p 97 N91-18192
A comparative study of performance parameters of $n(+)$ and p InP solar cells made by closed-ampoule sulfur diffusion into Cd- and Zn-doped p-type InP substrates p 210 N91-19209
Low Earth orbital atomic oxygen micrometeoroid, and debris interactions with photovoltaic arrays p 84 N91-30248
Theoretical modelling of AFM for bimetallic tip-substrate interactions [NASA-TM-105280] p 112 N91-32215

DEFENSE PROGRAM

- Multidisciplinary research overview (IHPTET/NPSS) p 30 N91-20119

DEFLECTION

- Status of structural analysis of 30 cm diameter ion optics [NASA-TM-103618] p 68 N91-11796
Optical measurement of propeller blade deflections in a spin facility [NASA-TM-103115] p 12 N91-17002

DEFORMATION

- Effects of rim thickness on spur gear bending stress [AIAA PAPER 91-2020] p 181 A91-41681
Low velocity impact analysis with NASTRAN p 198 A91-48865
A simplified method for determining the number of independent slip systems in crystals p 110 A91-55472
Probe insertion apparatus with inflatable seal [NASA-CASE-LEW-14965-1] p 183 N91-13732
Low velocity impact analysis with NASTRAN [NASA-TM-103169] p 95 N91-14426
Axial-torsional fatigue: A study of tubular specimen thickness effects [NASA-TM-103637] p 200 N91-14632
Progress in modeling deformation and damage p 202 N91-20108
Effects of rim thickness on spur gear bending stress [NASA-TM-104388] p 186 N91-23500
Experimental and analytical analysis of stress-strain behavior in a (90/0 deg)₂s, SiC/Ti-15-3 laminate [NASA-TM-104470] p 103 N91-31235

DEGRADATION

- Materials degradation in low earth orbit (LEO): Proceedings of the Symposium, 119th Annual Meeting of the Minerals, Metals, and Materials Society, Anaheim, CA, Feb. 17-22, 1990 p 116 A91-49801
Tensile behavior of tungsten/nitrogen composites at 1300 to 1600 K [NASA-TM-103727] p 111 N91-16128
Effect of LEO cycling on 125 Ah advanced design IPV nickel-hydrogen flight cells: An update [NASA-TM-104384] p 74 N91-22375

- Environmental interactions of the Space Station Freedom electric power system [NASA-TM-104373] p 49 N91-24225

DEICERS

- Advanced ice protection systems test in the NASA Lewis icing research tunnel [NASA-TM-103757] p 32 N91-23183

DEICING

- Progress toward the development of an airfoil icing analysis capability p 9 N91-10866
NASA's aircraft icing technology program p 19 N91-20120
Icing simulation: A survey of computer models and experimental facilities [NASA-TM-104366] p 15 N91-23087
Advanced ice protection systems test in the NASA Lewis icing research tunnel [NASA-TM-103757] p 32 N91-23183

DELAMINATING

- Composite structure global fracture toughness via computational simulation p 216 A91-11819
Free vibrations of delaminated beams [AIAA PAPER 91-1241] p 197 A91-32129

DEMAGNETIZATION

- Makeup and uses of a basic magnet laboratory for characterizing high-temperature permanent magnets [NASA-TM-104508] p 146 N91-30427

DENDRITIC CRYSTALS

- Isothermal Dendritic Growth Experiment - Science, engineering, and hardware development for USMP space flights p 128 A91-53408

DENSITY DISTRIBUTION

- Frontogenesis driven by horizontally quadratic distributions of density p 157 A91-48276
High resolution computed tomography of advanced composite and ceramic materials p 192 A91-56972

DEPLOYMENT

- Satellite relocation by tether deployment p 40 A91-22966

DEPOSITION

- Simulation of Martian dust accumulation on surfaces p 47 N91-19160
Lubrication with sputtered MoS₂ films: Principles, operation, limitations [NASA-TM-105292] p 112 N91-32216

DEPOSITS

- Effect of surface deposits on electromagnetic waves propagating in uniform ducts [NASA-TM-103282] p 133 N91-10208

DEPTH

- Determination of surface resistance and magnetic penetration depth of superconducting YBa₂Cu₃O_{7-δ} thin films by microwave power transmission measurements p 138 A91-36060
Determination of surface resistance and magnetic penetration depth of superconducting YBa₂Cu₃O_{7-δ} thin films by microwave power transmission measurements [NASA-TM-103616] p 234 N91-10780

DESIGN ANALYSIS

- Simplified procedures for designing composite bolted joints p 195 A91-16290
An integrated methodology for optimizing the passive damping of composite structures p 195 A91-19048
Composite laminate tailoring with probabilistic constraints and loads p 198 A91-38754
Effects of rim thickness on spur gear bending stress [AIAA PAPER 91-2020] p 181 A91-41681
Maximum life spur gear design [AIAA PAPER 91-2021] p 181 A91-41682
Design considerations for lunar base photovoltaic power systems p 41 A91-41987
Effect of emitter parameter variation on the performance of heteroepitaxial indium phosphide solar cells p 140 A91-42003
Stirling engine: Available tools for long-life assessment [NASA-TM-103660] p 200 N91-12980
Design considerations for lunar base photovoltaic power systems [NASA-TM-103642] p 241 N91-14259
Effect of emitter parameter variation on the performance of heteroepitaxial indium phosphide solar cells [NASA-TM-103619] p 70 N91-15306
ETARA PC version 3.3 user's guide: Reliability, availability, maintainability simulation model [NASA-TM-103751] p 193 N91-19462
A new fabrication method for precision antenna reflectors for space flight and ground test [NASA-TP-3078] p 48 N91-21185
HITCAN for actively cooled hot-composite thermostructural analysis [NASA-TM-103750] p 202 N91-21562
Structural design methodologies for ceramic-based material systems [NASA-TM-103097] p 121 N91-22460

- Effects of rim thickness on spur gear bending stress
[NASA-TM-104388] p 186 N91-23500
- Maximum life spur gear design
[NASA-TM-104361] p 187 N91-23514
- Incorporating finite element analysis into component life and reliability
[NASA-TM-104400] p 203 N91-23550
- A reliability and mass perspective of SP-100 Stirling cycle lunar-base powerplant designs
[NASA-TM-103736] p 212 N91-26592
- Comparison of dynamic isotope power systems for distributed planet surface applications
[NASA-TM-4303] p 81 N91-28278
- The NASA Lewis Research Center Internal Fluid Mechanics Facility
[NASA-TM-105187] p 39 N91-30163
- Reliability and cost: A sensitivity analysis
[NASA-TM-105293] p 238 N91-33014
- DESTRUCTION**
Destructive physical analysis results of Ni/H₂ cells cycled in LEO regime
[NASA-TM-104382] p 74 N91-23233
- DESULFURIZING**
Reactivity of pi-complexes of Ti, V, and Nb towards dithioacetic acid: Synthesis and structure of novel metal sulfur-containing complexes
[NASA-TM-103666] p 106 N91-19256
- DETECTION**
Sensor failure detection and recovery by neural networks
[NASA-TM-104484] p 220 N91-24815
- DETONABLE GAS MIXTURES**
Particle cloud flames in acoustic fields
p 105 A91-20589
- DIAGNOSIS**
Gear noise, vibration, and diagnostic studies at NASA Lewis Research Center
p 183 A91-52811
- DIAMINES**
Vinyl capped addition polyimides
[NASA-CASE-LEW-15027-1] p 118 N91-13566
- Substituted 1,1,1-triaryl-2,2,2-trifluoroethanes and processes for their synthesis
[NASA-CASE-LEW-14345-4] p 90 N91-25185
- Addition polyimides with enhanced processability
[NASA-CASE-LEW-15043-1] p 123 N91-32230
- DIAMONDS**
Selective and low temperature synthesis of polycrystalline diamond
p 232 A91-42170
- Diamondlike carbon as a moisture barrier and antireflecting coating on optical materials
p 119 N91-18302
- Optical dispersion relations for diamondlike carbon films
p 230 N91-18305
- Diamondlike carbon applications in infrared optics and microelectronics
p 230 N91-18306
- Dual ion beam processed diamondlike films for industrial applications
p 121 N91-23042
- DIATOMIC MOLECULES**
Global expression for representing diatomic potential-energy curves
p 228 A91-33236
- DIELECTRIC PROPERTIES**
Ellipsometric study of YBa₂Cu₃O_{7-x} laser ablated and co-evaporated films
p 233 A91-53235
- Dielectric function of InGaAs in the visible
p 233 A91-53236
- Thin film characterization using spectroscopic ellipsometry
p 119 N91-18303
- Ellipsometric study of cubic SiC
p 235 N91-18304
- Study of InGaAs based MODFET structures using variable angle spectroscopic ellipsometry
[NASA-TM-103792] p 235 N91-19935
- Electrical characterization of glass, teflon, and tantalum capacitors at high temperatures
[NASA-TM-104517] p 146 N91-27444
- DIELECTRICS**
A model for the scattering of high-frequency electromagnetic fields from dielectrics exhibiting thermally-activated electrical losses
[NASA-TM-104376] p 224 N91-26872
- DIESEL ENGINES**
Thermal barrier coating evaluation needs
[NASA-TM-103708] p 111 N91-15390
- DIFFERENCE EQUATIONS**
From differential to difference equations for first order ODEs
[NASA-TM-104530] p 222 N91-27886
- DIFFERENTIAL EQUATIONS**
Numerical flux formulas for the Euler and Navier-Stokes equations. II - Progress in flux-vector splitting
[AIAA PAPER 91-1566] p 5 A91-40740
- Asymptotic integration algorithms for nonhomogeneous, nonlinear, first order, ordinary differential equations
[NASA-TM-103793] p 222 N91-21797
- Numerical flux formulas for the Euler and Navier-Stokes equations. 2: Progress in flux-vector splitting
[NASA-TM-104353] p 15 N91-22084
- From differential to difference equations for first order ODEs
[NASA-TM-104530] p 222 N91-27886
- Exponential integration algorithms applied to viscoplasticity
[NASA-TM-104461] p 223 N91-27901
- Tuning maps for setpoint changes and load disturbance upsets in a three capacity process under multivariable control
[NASA-TM-104419] p 220 N91-31876
- DIFFERENTIAL PULSE CODE MODULATION**
Real-time data compression of broadcast video signals
[NASA-CASE-LEW-14945-1] p 133 N91-13598
- DIFFUSERS**
A steady effect of acoustic excitation on transitory stall
[AIAA PAPER 91-0043] p 2 A91-22499
- A steady effect of acoustic excitation on transitory stall
[NASA-TM-103689] p 11 N91-13420
- DIFFUSION**
Automated design of controlled diffusion blades
p 9 N91-10883
- A comparative study of performance parameters of n(+)-p InP solar cells made by closed-ampoule sulfur diffusion into Cd- and Zn-doped p-type InP substrates
p 210 N91-19209
- DIFFUSION FLAMES**
Radiation from gas-jet diffusion flames in microgravity environments
[AIAA PAPER 91-0719] p 104 A91-19432
- Two-dimensional imaging of molecular hydrogen in H₂-air diffusion flames using two-photon laser-induced fluorescence
p 124 A91-34369
- A detailed numerical investigation of Burke-Schumann gaseous and spray flames
[AIAA PAPER 91-2311] p 105 A91-41749
- A study of hydrogen diffusion flames using PDF turbulence model
[AIAA PAPER 91-1780] p 106 A91-45549
- Heat transfer to a thin solid combustible in flame spreading at microgravity
p 106 A91-51449
- DIGITAL DATA**
Bit error rate testing of fiber optic data links for MMIC-based phased array antennas
p 131 A91-24950
- DIGITAL SIMULATION**
Numerical simulation of Jet-A combustion approximated by improved propane chemical kinetics
[AIAA PAPER 91-1859] p 106 A91-45777
- The effects of rotation on initially anisotropic homogeneous flows
p 158 A91-54958
- Automatic control study of the icing research tunnel refrigeration system
[NASA-TM-4257] p 40 N91-19115
- DIGITAL SYSTEMS**
ATDRS payload technology R & D
p 45 A91-53188
- DIGITAL TECHNIQUES**
Software manual for operating particle displacement tracking data acquisition and reduction system
[NASA-TM-103720] p 176 N91-20453
- Digital CODEC for real-time processing of broadcast quality video signals at 1.8 bits/pixel
p 134 N91-24067
- DIMENSIONAL ANALYSIS**
Fiber pushout test - A three-dimensional finite element computational simulation
p 197 A91-33096
- DIRECT CURRENT**
An assessment of the Space Station Freedom program's leakage current requirement
[NASA-CR-187077] p 215 N91-20630
- The theory of an auto-resonant field emission cathode relativistic electron accelerator for high efficiency microwave to direct current power conversion
p 73 N91-22176
- An EMTP system level model of the PMAD DC test bed
[NASA-TM-104515] p 79 N91-27206
- The development of test beds to support the definition and evolution of the Space Station Freedom power system
[NASA-TM-104504] p 79 N91-27207
- DIRECTIONAL SOLIDIFICATION (CRYSTALS)**
Three-dimensional flow transport modes in directional solidification during space processing
p 128 A91-42642
- Effect of tensile mean stress on fatigue behavior of single-crystal and directionally solidified superalloys
[NASA-TM-103644] p 200 N91-18452
- DISCHARGE COEFFICIENT**
Experimental and analytical studies of flow through a ventral and axial exhaust nozzle system for STOV_L aircraft
[AIAA PAPER 91-2135] p 25 A91-45791
- Experimental and analytical studies of flow through a ventral and axial exhaust nozzle system for STOV_L aircraft
[NASA-TM-104364] p 77 N91-25175
- DISCONNECT DEVICES**
Quick action clamp
[NASA-CASE-LEW-14887-1] p 189 N91-27561
- DISCONTINUITY**
The dynamic instability of adiabatic blast waves
p 239 A91-26361
- Theoretical and experimental characterization of coplanar waveguide discontinuities for filter applications
p 137 A91-35911
- The L sub 1 finite element method for pure convection problems
[NASA-TM-103773] p 222 N91-24817
- DISCRETE FUNCTIONS**
Structure of random discrete spacetime
p 224 A91-22894
- DISPLACEMENT**
Integrated force method versus displacement method for finite element analysis
p 196 A91-28372
- Particle displacement tracking for PIV
[NASA-TM-103288] p 175 N91-10271
- DISPLACEMENT MEASUREMENT**
Optical measurement of unducted fan blade deflections
[ASME PAPER 89-GT-298] p 170 A91-13046
- DISPLAY DEVICES**
An Electronic Pressure Profile Display system for aeronautic test facilities
p 38 A91-51858
- DISSOLVING**
High resolution electrolyte for thinning InP by anodic dissolution and its applications to EC-V profiling, defect revealing and surface passivation
p 107 N91-30210
- DISTORTION**
Finite element analysis of thermal distortion effects on optical performance of solar dynamic concentrator for Space Station Freedom
[NASA-TM-102504] p 183 N91-12954
- Naturally occurring and forced azimuthal modes in a turbulent jet
[NASA-TM-103692] p 11 N91-17000
- A test fixture for measuring high-temperature hypersonic-engine seal performance
[NASA-TM-103658] p 184 N91-19442
- Compressible flows with periodic vortical disturbances around lifting airfoils
[NASA-TM-103742] p 14 N91-21060
- DISTRIBUTED PARAMETER SYSTEMS**
Autonomous power expert system
p 54 A91-37972
- A distributed fault-detection and diagnosis system using on-line parameter estimation
[NASA-TM-104433] p 220 N91-25696
- DISTRIBUTED PROCESSING**
The development of a post-test diagnostic system for rocket engines
[AIAA PAPER 91-2528] p 60 A91-44281
- The development of a post-test diagnostic system for rocket engines
[NASA-TM-104463] p 217 N91-24787
- DISTRIBUTION FUNCTIONS**
Probabilistic structural analysis of a truss typical for space station
[NASA-TM-103277] p 199 N91-12114
- Simulation of probabilistic wind loads and building analysis
[NASA-TM-103744] p 203 N91-23549
- DIVERGENCE**
Spectrum transformation for divergent iterations
[NASA-TM-103745] p 221 N91-19786
- DOPED CRYSTALS**
Measurement of surface recombination velocity on heavily doped indium phosphide
p 232 A91-41931
- Advances in silicon carbide Chemical Vapor Deposition (CVD) for semiconductor device fabrication
[NASA-TM-104410] p 236 N91-23946
- DRAW**
Icing characteristics of a natural-laminar-flow, a medium-speed, and a swept, medium-speed airfoil
[NASA-TM-103693] p 12 N91-19046
- DRAW COEFFICIENTS**
Icing characteristics of a natural-laminar-flow, a medium-speed, and a swept, medium-speed airfoil
[AIAA PAPER 91-0447] p 3 A91-26327
- DRAW REDUCTION**
Solar array orientations for a space station in low earth orbit
p 46 A91-30019
- Overview of NASP nozzle research
p 28 N91-20093
- DROP SIZE**
Influence of geometric features on the performance of pressure-swirl atomizers
p 147 A91-13030
- Measurements and predictions of a liquid spray from an air-assist nozzle
[AIAA PAPER 91-0692] p 149 A91-22498

- LN2 spray droplet size measurement via ensemble diffraction technique
[AIAA PAPER 91-1381] p 129 A91-44336
- Gas property effects on droplet size of simulated fuel sprays
[NASA-TM-103640] p 156 A91-45327
- Measurements and predictions of a liquid spray from an air-assist nozzle
[NASA-TM-103640] p 26 N91-13455
- Cryogenic liquid-jet breakup in two-fluid atomizers
[NASA-TM-103734] p 176 N91-19402
- LN2 spray droplet size measurement via ensemble diffraction technique
[NASA-TM-104443] p 131 N91-24470
- DROP TOWERS**
- Drop-tower experiments for capillary surfaces in an exotic container
[AIAA PAPER 91-0107] p 148 A91-19138
- A summary of existing and planned experiment hardware for low-gravity fluids research
[AIAA PAPER 91-0777] p 128 A91-26329
- Surface settling in partially filled containers upon step reduction in gravity
[NASA-TM-103641] p 159 N91-14556
- DROPS (LIQUIDS)**
- The migration of a compound drop due to thermocapillarity
[AIAA PAPER 91-0078] p 105 A91-21362
- Combustion of liquid fuel droplets in supercritical conditions
[AIAA PAPER 91-0078] p 105 A91-21362
- A comparative flow visualization study of thermocapillary flow in drops in liquid-liquid systems
[AIAA PAPER 91-0311] p 148 A91-21452
- Experimental water droplet impingement data on modern aircraft surfaces
[AIAA PAPER 91-0445] p 2 A91-21493
- Measurements and predictions of a liquid spray from an air-assist nozzle
[AIAA PAPER 91-0692] p 149 A91-22498
- Thermocapillary migration of liquid droplets in a temperature gradient in a density matched system
[AIAA PAPER 91-0692] p 153 A91-41132
- Pressure-coupled vaporization and combustion responses of liquid-fuel droplets in high-pressure environments
[AIAA PAPER 91-2310] p 106 A91-44192
- Measurements and predictions of a liquid spray from an air-assist nozzle
[NASA-TM-103640] p 26 N91-13455
- DUCT GEOMETRY**
- Computation of a circular-to-rectangular transition duct flow field
[AIAA PAPER 91-1741] p 156 A91-45547
- Experimental investigation of turbulent flow through a circular-to-rectangular transition duct
[NASA-TM-105210] p 18 N91-31106
- DUCTED FAN ENGINES**
- Ultra-high bypass research
[NASA-TM-105210] p 30 N91-20117
- DUCTED FLOW**
- An experimental comparison of nonswirling and swirling flow in a circular-to-rectangular transition duct
[AIAA PAPER 91-0342] p 148 A91-21466
- Calculation of turbulence-driven secondary motion in ducts with arbitrary cross section
[AIAA PAPER 91-0342] p 151 A91-34132
- An experimental trace gas investigation of fluid transport and mixing in a circular-to-rectangular transition duct
[AIAA PAPER 91-2370] p 172 A91-44214
- Computation of a circular-to-rectangular transition duct flow field
[AIAA PAPER 91-1741] p 156 A91-45547
- Mixing of multiple jets with a confined subsonic crossflow - Summary of NASA-supported experiments and modeling
[AIAA PAPER 91-2458] p 7 A91-45813
- Experimental study of cross-stream mixing in a cylindrical duct
[AIAA PAPER 91-2459] p 157 A91-45815
- An experimental comparison of nonswirling and swirling flow in a circular-to-rectangular transition duct
[NASA-TM-104359] p 14 N91-21115
- Mixing of multiple jets with a confined subsonic crossflow. Summary of NASA-supported experiments and modeling
[NASA-TM-104412] p 33 N91-24202
- Characterization of flow in a scroll duct
[NASA-CR-188612] p 167 N91-25367
- A study of high speed flows in an aircraft transition duct
[NASA-TM-104449] p 17 N91-26122
- An experimental trace gas investigation of fluid transport and mixing in a circular-to-rectangular transition duct
[NASA-TM-104499] p 17 N91-27129
- Experimental study of cross-stream mixing in a cylindrical duct
[NASA-TM-105180] p 34 N91-29187

- The NASA Lewis Research Center Internal Fluid Mechanics Facility
[NASA-TM-105187] p 39 N91-30163
- Experimental investigation of turbulent flow through a circular-to-rectangular transition duct
[NASA-TM-105210] p 18 N91-31106
- DUCTILITY**
- The potential for ductility enhancement from surface and interface dislocation sources in NiAl
[AIAA PAPER 91-0130] p 109 A91-39292
- Continuous fiber-reinforced titanium aluminide composites
[AIAA PAPER 91-0130] p 92 A91-39553
- Constitution of pseudobinary hypoeutectic beta-NiAl + alpha-V alloys
[AIAA PAPER 91-0130] p 109 A91-48509
- Prospects for ductility and toughness enhancement of NiAl by ductile phase reinforcement
[NASA-TM-103796] p 112 N91-27324
- DUCTS**
- The aerodynamic characteristics of vortex ingestion for the F/A-18 inlet duct
[AIAA PAPER 91-0130] p 3 A91-26192
- Evaluation of panel code predictions with experimental results of inlet performance for a 17-inch ducted prop/fan simulator operating at Mach 0.2
[AIAA PAPER 91-3354] p 7 A91-45819
- Effect of surface deposits on electromagnetic waves propagating in uniform ducts
[NASA-TM-103282] p 133 N91-10208
- The aerodynamic characteristics of vortex ingestion for the F/A-18 inlet duct
[NASA-TM-103703] p 70 N91-15303
- Inlets, ducts, and nozzles
[AIAA PAPER 91-0130] p 162 N91-20096
- An experimental comparison of nonswirling and swirling flow in a circular-to-rectangular transition duct
[NASA-TM-104359] p 14 N91-21115
- Evaluation of panel code predictions with experimental results of inlet performance for a 17-inch ducted prop/fan simulator operating at Mach 0.2
[NASA-TM-104428] p 17 N91-25106
- A study of high speed flows in an aircraft transition duct
[NASA-TM-104449] p 17 N91-26122
- DURABILITY**
- Probabilistic structural analysis: Introductory remarks
[AIAA PAPER 91-24326] p 204 N91-24326
- Durability evaluation of photovoltaic blanket materials exposed on LDEF tray S1003
[NASA-TM-105062] p 212 N91-25062
- DUST**
- Aeolian removal of dust types from photovoltaic surfaces on Mars
[AIAA PAPER 91-19156] p 47 N91-19156
- Simulation of Martian dust accumulation on surfaces
[AIAA PAPER 91-19160] p 47 N91-19160
- Effects of dust accumulation and removal on radiators surfaces on Mars
[NASA-TM-103704] p 72 N91-20204
- Effects of windblown dust on photovoltaic surfaces on Mars
[NASA-TM-104448] p 78 N91-25183
- Effects of Martian dust on power system components
[AIAA PAPER 91-27061] p 241 N91-27061
- Electrical system/environment interactions on the planet Mars
[AIAA PAPER 91-27068] p 242 N91-27068
- DUST STORMS**
- Design considerations for Mars photovoltaic power systems
[AIAA PAPER 91-19156] p 41 A91-41988
- Aeolian removal of dust types from photovoltaic surfaces on Mars
[AIAA PAPER 91-19156] p 47 N91-19156
- Effects of Martian dust on power system components
[AIAA PAPER 91-27061] p 241 N91-27061
- DYNAMIC CHARACTERISTICS**
- High frequency, high temperature specific core loss and dynamic B-H hysteresis loop characteristics of soft magnetic alloys
[AIAA PAPER 91-37988] p 138 A91-37988
- Effects of gear box vibration and mass imbalance on the dynamics of multistage gear transmission
[AIAA PAPER 91-47213] p 182 A91-47213
- Comparison of dynamic fatigue behavior between SiC whisker-reinforced composite and monolithic silicon nitrides
[NASA-TM-103707] p 119 N91-19293
- Effects of gear box vibration and mass imbalance on the dynamics of multi-stage gear transmissions
[NASA-TM-103695] p 185 N91-21534
- DYNAMIC CONTROL**
- Dynamic analysis of space-related linear and non-linear structures
[AIAA PAPER 91-28612] p 196 A91-28612
- DYNAMIC LOADS**
- Two reference time scales for studying the dynamic cavitation of liquid films
[NASA-TM-103673] p 160 N91-19369
- Comparison of analysis and experiment for dynamics of low-contact-ratio spur gears
[NASA-TM-103232] p 185 N91-22566
- Dynamic measurements of gear tooth friction and load
[NASA-TM-103281] p 189 N91-27570

DYNAMIC MODELS

- An AD100 implementation of a real-time STOV aircraft propulsion system
[NASA-TM-103683] p 26 N91-13457
- Propulsion aeroelasticity, vibration control, and dynamic system modeling
[NASA-TM-103683] p 29 N91-20105

DYNAMIC RESPONSE

- Experimental investigation of propfan aeroelastic response in off-axis flow with mistuning
[AIAA PAPER 91-30015] p 22 A91-30015
- The effects of interply damping layers on the dynamic response of composite structures
[AIAA PAPER 91-1124] p 197 A91-32064
- Pressure-coupled vaporization and combustion responses of liquid-fuel droplets in high-pressure environments
[AIAA PAPER 91-2310] p 106 A91-44192
- Computational simulation of acoustic fatigue for hot composite structures
[NASA-TM-104379] p 203 N91-23548
- The effects of interply damping layers on the dynamic response of composite structures
[NASA-TM-104497] p 103 N91-30282

DYNAMIC STRUCTURAL ANALYSIS

- Simulation of the Space Station strut-out condition
[AIAA PAPER 91-1248] p 197 A91-32087
- Computational simulation of acoustic fatigue for hot composite structures
[AIAA PAPER 91-1178] p 197 A91-32099
- Computational simulation of damping in composite structures
[AIAA PAPER 91-36283] p 198 A91-36283
- Low velocity impact analysis with NASTRAN
[NASA-TM-103169] p 95 N91-14426
- Wind turbine acoustics
[NASA-TP-3057] p 228 N91-16679
- Overview of structures research
[AIAA PAPER 91-20104] p 202 N91-20104
- Propulsion aeroelasticity, vibration control, and dynamic system modeling
[AIAA PAPER 91-20105] p 29 N91-20105
- Computational simulation of propulsion structures performance and reliability
[AIAA PAPER 91-20106] p 29 N91-20106
- Structural Integrity and Durability of Reusable Space Propulsion Systems
[NASA-CP-10030] p 76 N91-24307

DYNAMIC TESTS

- Hydrocarbon-fuel/combustion-chamber-liner materials compatibility
[NASA-CR-187104] p 121 N91-21307

E

EARTH MAGNETOSPHERE

- A charging study of the ACTS satellite using NASCAP
[AIAA PAPER 91-1471] p 46 A91-42522

EARTH OBSERVING SYSTEM (EOS)

- Advanced power systems for EOS
[NASA-TM-105222] p 85 N91-31217

EARTH ORBITAL ENVIRONMENTS

- Evolutionary use of nuclear electric propulsion
[AIAA PAPER 90-3821] p 50 A91-10174
- Solar array orientations for a space station in low earth orbit
[AIAA PAPER 91-30019] p 46 A91-30019
- Undercutting of defects in thin film protective coatings on polymer surfaces exposed to atomic oxygen
[AIAA PAPER 91-41516] p 115 A91-41516
- Materials degradation in low earth orbit (LEO); Proceedings of the Symposium, 119th Annual Meeting of the Minerals, Metals, and Materials Society, Anaheim, CA, Feb. 17-22, 1990
[AIAA PAPER 91-49801] p 116 A91-49801
- The effect of atomic oxygen on altered and coated Kapton surfaces for spacecraft applications in low earth orbit
[AIAA PAPER 91-49804] p 116 A91-49804
- Atomic oxygen effects on refractory materials
[AIAA PAPER 91-49809] p 88 A91-49809
- The effect of the near earth micrometeoroid environment on a mirror surface after 20 years in space
[AIAA PAPER 91-49810] p 47 A91-49810
- Vacuum ultraviolet radiation and thermal cycling effects on atomic oxygen protective photovoltaic array blanket materials
[AIAA PAPER 91-49812] p 116 A91-49812
- Low Earth orbital atomic oxygen and ultraviolet radiation effects on polymers
[NASA-TM-103711] p 119 N91-19294
- Environmental interactions of the Space Station Freedom electric power system
[NASA-TM-104373] p 49 N91-24225
- Durability evaluation of photovoltaic blanket materials exposed on LDEF tray S1003
[NASA-TM-105062] p 212 N91-25062
- Full-size solar dynamic heat receiver thermal-vacuum tests
[NASA-TM-104486] p 78 N91-25184
- Rapid thermal cycling of solar array blanket coupons for Space Station Freedom
[NASA-TM-103239] p 84 N91-30239
- Nickel-hydrogen cell low-Earth life test update
[NASA-TM-105229] p 213 N91-31708

EARTH ORBITS

Conceptual study of on orbit production of cryogenic propellants by water electrolysis
[AIAA PAPER 91-1844] p 124 A91-41631

Evaluation of thermal control coatings for use on solar dynamic radiators in low earth orbit
[AIAA PAPER 91-1327] p 58 A91-43397

Review and test of chilldown methods for space-based cryogenic tanks
[AIAA PAPER 91-1843] p 60 A91-45776

Advanced launch vehicle upper stages using liquid propulsion and metallized propellants
[NASA-TM-103622] p 68 N91-11797

Metallized propellants for the human exploration of Mars
[NASA-TP-3062] p 69 N91-11800

Conceptual study of on orbit production of cryogenic propellants by water electrolysis
[NASA-TM-103730] p 126 N91-19317

Evaluation of thermal control coatings for use on solar dynamic radiators in low Earth orbit
[NASA-TM-104335] p 73 N91-22367

Effect of LEO cycling on 125 Ah advanced design IPV nickel-hydrogen flight cells. An update
[NASA-TM-104384] p 74 N91-22375

Destructive physical analysis results of Ni/H₂ cells cycled in LEO regime
[NASA-TM-104382] p 74 N91-23233

Atomic oxygen undercutting of LDEF aluminized Kapton multilayer insulation
p 229 N91-25027

Review and test of chilldown methods for space-based cryogenic tanks
[NASA-TM-104458] p 167 N91-25351

Low Earth orbital atomic oxygen micrometeoroid, and debris interactions with photovoltaic arrays
p 84 N91-30248

Leo space plasma interactions p 84 N91-30249

EARTH TERMINALS

LBR-2 Earth stations for the ACTS program
p 133 N91-11971

ECCENTRICITY

Eccentricity effects on leakage of a brush seal at low speeds
[NASA-TM-105141] p 86 N91-31220

ECLIPSE PROJECT

Satellite eclipse power by laser illumination
[IAF PAPER 90-053] p 50 A91-13766

EDDY CURRENTS

Nondestructive evaluation tools and experimental studies for monitoring the health of space propulsion systems
[AIAA PAPER 91-3433] p 192 A91-53703

Magnetic bearings with zero bias p 48 N91-21194

Nondestructive evaluation tools and experimental studies for monitoring the health of space propulsion systems
[NASA-TM-105164] p 194 N91-28605

EDDY VISCOSITY

An algebraic RNG-based turbulence model for three-dimensional turbomachinery flows
[AIAA PAPER 91-0172] p 2 A91-21393

Navier-Stokes analysis of transonic cascade flow
[NASA-TM-103624] p 159 N91-11192

Transonic cascade flow calculations using non-periodic C-type grids p 163 N91-21071

EDGE DISLOCATIONS

Universal behavior in ideal slip p 110 A91-48517

EDUCATION

Outline of the Solar System: Activities for elementary students
[NASA-TM-104965] p 241 N91-25975

EIGENVALUES

Solution and sensitivity analysis of a complex transcendental eigenproblem with pairs of real eigenvalues p 195 A91-23685

Robust eigenspace assignment using singular value sensitivities p 219 A91-29784

Aeroelastic modal characteristics of mistuned blade assemblies - Mode localization and loss of eigenstructure
[AIAA PAPER 91-1218] p 196 A91-32032

Aeroelastic modal characteristics of mistuned blade assemblies: Mode localization and loss of eigenstructure
[NASA-TM-104519] p 205 N91-27591

A comparison of numerical methods for the Rayleigh equation in unbounded domains p 223 N91-30865

EIGENVECTORS

Robust eigenspace assignment using singular value sensitivities p 219 A91-29784

EJECTORS

Noise measurements from an ejector suppressor nozzle in the NASA Lewis 9- by 15-foot low speed wind tunnel [AIAA PAPER 90-3983] p 225 A91-12496

Static performance tests of a flight-type STOVL ejector

[AIAA PAPER 91-1902] p 24 A91-44050

Transient flow thrust prediction for an ejector propulsion concept p 24 A91-45326

Noise measurements from an ejector suppressor nozzle in the NASA Lewis 9- by 15-foot low speed wind tunnel [NASA-TM-103628] p 227 N91-11493

Static performance tests of a flight-type STOVL ejector [NASA-TM-104437] p 33 N91-24201

ELASTIC DEFORMATION

Inhomogeneous deformation in INCONEL 718 during monotonic and cyclic loadings p 108 A91-22287

ELASTIC PROPERTIES

Elastic response of (001)-oriented PWA 1480 single crystal - The influence of secondary orientation [SAE PAPER 911111] p 110 A91-53555

A life comparison of tube and channel cooling passages for thrust chambers p 68 N91-11059

An overview of self-consistent methods for fiber-reinforced composites p 97 N91-19232

Elastic response of zone axis (001)-oriented PWA 1480 single crystal: The influence of secondary orientation [NASA-TM-103782] p 202 N91-21558

ELASTIC WAVES

Unsteady blade-surface pressures on a large-scale advanced propeller: Prediction and data [NASA-TM-103218] p 69 N91-11799

ELASTOHYDRODYNAMICS

A system-approach to the elasto-hydrodynamic lubrication point-contact problem [NASA-TM-104342] p 165 N91-23439

Parched elasto-hydrodynamic lubrication: Instrumentation and procedure [NASA-TM-104426] p 168 N91-30469

ELASTOPLASTICITY

The potential for ductility enhancement from surface and interface dislocation sources in NiAl p 109 A91-39292

A new uniformly valid asymptotic integration algorithm for elasto-plastic creep and unified viscoplastic theories including continuum damage p 110 A91-48725

Elastic/plastic analyses of advanced composites investigating the use of the compliant layer concept in reducing residual stresses resulting from processing [NASA-TM-103204] p 94 N91-11074

The method of lines in analyzing solids containing cracks [NASA-TM-103626] p 201 N91-19477

ELECTRIC BATTERIES

Power electronic applications for Space Station Freedom p 52 A91-36832

Development and testing of a source subsystem for the supporting development PMAD DC test bed [NASA-TM-104510] p 78 N91-26202

Space Electrochemical Research and Technology [NASA-CP-3125] p 213 N91-32549

ELECTRIC BRIDGES

Five-kilowatt arcjet power electronics p 63 A91-52312

ELECTRIC CONTACTS

A system-approach to the elasto-hydrodynamic lubrication point-contact problem [NASA-TM-104342] p 165 N91-23439

Improvements in contact resistivity and thermal stability of Au-contacted InP solar cells p 213 N91-30207

ELECTRIC CONTROL

A high-frequency servosystem for fuel control in hypersonic engines [NASA-TM-104333] p 35 N91-31178

ELECTRIC CURRENT

A fiber-optic current sensor for aerospace applications p 171 A91-23005

An assessment of the Space Station Freedom program's leakage current requirement [NASA-CR-187077] p 215 N91-20630

The theory of an auto-resonant field emission cathode relativistic electron accelerator for high efficiency microwave to direct current power conversion p 73 N91-22176

Fiber-optic sensors for aerospace electrical measurements: An update [NASA-TM-104454] p 177 N91-25381

ELECTRIC DISCHARGES

Performance of a dual anode nickel-hydrogen cell p 214 N91-32563

ELECTRIC FIELD STRENGTH

MIS capacitor studies on silicon carbide single crystals [NASA-CR-187350] p 234 N91-11555

ELECTRIC GENERATORS

Control of multiple resonant power processors in a multi-source system p 137 A91-30901

Solar powered Stirling cycle electrical generator p 211 N91-23054

ELECTRIC POTENTIAL

Impedances of electrochemically impregnated nickel electrodes as functions of potential, KOH concentration, and impregnation method p 208 N91-15628

ELECTRIC POWER SUPPLIES

Advanced launch system (ALS) - Electrical actuation and power systems improve operability and cost picture p 51 A91-31025

Nuclear technology and the space exploration missions p 53 A91-37939

Electrical characterization of a Mapham inverter using pulse testing techniques p 139 A91-37992

SEI needs for space nuclear power [AIAA PAPER 91-3459] p 64 A91-52369

Trade studies for nuclear space power systems [AIAA PAPER 91-3518] p 65 A91-52413

Lunar electric power systems utilizing the SP-100 reactor coupled to dynamic conversion systems [AIAA PAPER 91-3520] p 208 A91-52415

Advanced electrical power, distribution and control for the Space Transportation System p 143 N91-17043

How much redundancy: Some cost considerations, including examples for spacecraft systems [NASA-TM-103197] p 192 N91-17407

ETARA PC version 3.3 user's guide: Reliability, availability, maintainability simulation model [NASA-TM-103751] p 193 N91-19462

ELECTRIC POWER TRANSMISSION

An expert system for simulating electric loads aboard Space Station Freedom p 55 A91-38041

Advanced electrical power, distribution and control for the Space Transportation System p 143 N91-17043

ELECTRIC PROPULSION

Performance and lifetime assessment of magnetoplasmadynamic arc thruster technology p 51 A91-30013

Ion beam sputtering in electric propulsion facilities [AIAA PAPER 91-2117] p 61 A91-45785

Mass comparisons of electric propulsion systems for NNSK of geosynchronous spacecraft --- North-South Station Keeping [AIAA PAPER 91-2347] p 47 A91-45808

Historical perspectives - The role of the NASA Lewis Research Center in the national space nuclear power programs [AIAA PAPER 91-3462] p 242 A91-53713

A 10,000-hr life test of an engineering model resistorjet [NASA-TM-103216] p 69 N91-11802

Dual-purpose self-deliverable lunar surface PV electrical power system p 209 N91-19200

Historical perspectives: The role of the NASA Lewis Research Center in the national space nuclear power programs [NASA-TM-105196] p 243 N91-29138

Mass comparisons of electric propulsion systems for NNSK of geosynchronous spacecraft [NASA-TM-105153] p 85 N91-31212

Multimegawatt electric propulsion system design considerations [NASA-TM-105152] p 87 N91-32164

ELECTRIC ROCKET ENGINES

Performance characterization of a segmented anode arcjet thruster [NASA-TM-103227] p 67 N91-10118

Investigation of the arcjet near field plume using electrostatic probes p 75 N91-24270

Arcjet nozzle area ratio effects p 75 N91-24271

Preliminary performance and life evaluations of a 2-kW arcjet [NASA-TM-105149] p 84 N91-30252

MPD thruster technology [NASA-TM-105242] p 86 N91-32162

ELECTRIC SWITCHES

Neutron, gamma ray and post-irradiation thermal annealing effects on power semiconductor switches [AIAA PAPER 91-3525] p 142 A91-52420

ELECTRICAL FAULTS

Electrical system/environment interactions on the planet Mars p 242 N91-27068

ELECTRICAL GROUNDING

Findings of the Joint Workshop on Evaluation of Impacts of Space Station Freedom Ground Configurations p 48 N91-20728

Findings of the Joint Workshop on Evaluation of Impacts of Space Station Freedom Ground Configurations [NASA-TM-103717] p 73 N91-22370

ELECTRICAL IMPEDANCE

Impedances of Ni electrodes and Ni/H₂ cells from different manufacturers p 55 A91-38082

Impedances of nickel electrodes cycled in various KOH concentrations p 214 N91-32557

ELECTRICAL INSULATION

Thin film characterization using spectroscopic ellipsometry p 119 N91-18303

ELECTRICAL MEASUREMENT

- A fiber-optic current sensor for aerospace applications p 171 A91-23005
- Impedances of Ni electrodes and Ni/H₂ cells from different manufacturers p 55 A91-38082
- Fiber-optic sensors for aerospace electrical measurements: An update [NASA-TM-104454] p 177 N91-25381
- ELECTRICAL PROPERTIES**
- Electrical transport measurements on polycrystalline superconducting Y-Ba-Cu-O films p 231 A91-19820
- High temperature superconductive microwave technology for space applications p 137 A91-31391
- The influence of interstitial Ga and interfacial Au₂P₃ on the electrical and metallurgical behavior of Au-contacted III-V semiconductors p 140 A91-42694
- Properly and microstructural nonuniformity in the yttrium-barium-copper-oxide superconductor determined from electrical, magnetic, and ultrasonic measurements [NASA-TM-103732] p 193 N91-19463
- Industrial applications of graphite fluoride fibers p 100 N91-23040
- A model for the scattering of high-frequency electromagnetic fields from dielectrics exhibiting thermally-activated electrical losses [NASA-TM-104376] p 224 N91-26872
- Electrical system/environment interactions on the planet Mars p 242 N91-27068
- ELECTRICAL RESISTANCE**
- An experimental apparatus for measuring surface resistance in the submillimeter-wavelength region p 174 A91-54390
- Comparative study of bolometric and non-bolometric switching elements for microwave phase shifters [NASA-TM-104435] p 145 N91-25320
- ELECTRICAL RESISTIVITY**
- Resistivity of pristine and intercalated graphite fiber epoxy composites p 115 A91-35949
- An analysis of the contact sintering process in III-V solar cells p 139 A91-41891
- Heat transfer device and method of making the same [NASA-CASE-LEW-14162-1] p 159 N91-13668
- Semiconductor structural damage attendant to contact formation in III-V solar cells p 209 N91-19203
- Determination of series resistance of indium phosphide solar cells p 210 N91-19207
- Improvements in contact resistivity and thermal stability of Au-contacted InP solar cells p 213 N91-30207
- ELECTRO-OPTICS**
- Fiber-optic-based controls p 230 N91-20102
- Laser interferometric measurement of ion electrode shape and charge exchange erosion [NASA-TM-105165] p 179 N91-31605
- ELECTROCHEMISTRY**
- Impedances of electrochemically impregnated nickel electrodes as functions of potential, KOH concentration, and impregnation method [NASA-TM-103283] p 208 N91-15628
- High resolution electrolyte for thinning InP by anodic dissolution and its applications to EC-V profiling, defect revealing and surface passivation p 107 N91-30210
- Space Electrochemical Research and Technology [NASA-CP-3125] p 213 N91-32549
- ELECTRODE MATERIALS**
- Surface studies on scandate cathodes and synthesized scandates p 136 A91-25071
- Impedances of Ni electrodes and Ni/H₂ cells from different manufacturers p 55 A91-38082
- Microanalyses of extended-test xenon hollow cathodes --- in ion thruster simulators [AIAA PAPER 91-2123] p 61 A91-45787
- ELECTRODEPOSITION**
- Raman spectral observation of a new phase observed in nickel electrodes cycled to failure p 214 N91-32556
- ELECTRODES**
- Effect of LEO cycling on 125 Ah advanced design IPV nickel-hydrogen battery cells p 55 A91-38077
- Laser interferometric measurement of ion electrode shape and charge exchange erosion [AIAA PAPER 91-2121] p 173 A91-45786
- Status of structural analysis of 30 cm diameter ion optics [NASA-TM-103618] p 68 N91-11796
- Impedances of electrochemically impregnated nickel electrodes as functions of potential, KOH concentration, and impregnation method [NASA-TM-103283] p 208 N91-15628
- Destructive physical analysis results of Ni/H₂ cells cycled in LEO regime [NASA-TM-104382] p 74 N91-23233
- Laser interferometric measurement of ion electrode shape and charge exchange erosion [NASA-TM-105165] p 179 N91-31605
- Raman spectral observation of a new phase observed in nickel electrodes cycled to failure p 214 N91-32556
- Impedances of nickel electrodes cycled in various KOH concentrations p 214 N91-32557
- Some recent studies with the solid-ionomer electrochemical capacitor p 214 N91-32562
- ELECTRODYNAMICS**
- Exploring the notion of space coupling propulsion p 73 N91-22161
- ELECTROFORMING**
- New method of making advanced tube-bundle rocket thrust chambers [NASA-TM-103617] p 70 N91-15301
- ELECTROLYSIS**
- Conceptual study of on orbit production of cryogenic propellants by water electrolysis [AIAA PAPER 91-1844] p 124 A91-41631
- Conceptual study of on orbit production of cryogenic propellants by water electrolysis [NASA-TM-103730] p 126 N91-19317
- ELECTROLYTES**
- Effect of KOH concentration on LEO cycle life of IPV nickel-hydrogen flight battery cells p 55 A91-38076
- Effect of LEO cycling on 125 Ah advanced design IPV nickel-hydrogen battery cells p 55 A91-38077
- Effect of KOH concentration on LEO cycle life of IPV nickel-hydrogen flight cells. An update [NASA-TM-104383] p 74 N91-22376
- Destructive physical analysis results of Ni/H₂ cells cycled in LEO regime [NASA-TM-104382] p 74 N91-23233
- High resolution electrolyte for thinning InP by anodic dissolution and its applications to EC-V profiling, defect revealing and surface passivation p 107 N91-30210
- Raman spectral observation of a new phase observed in nickel electrodes cycled to failure p 214 N91-32556
- ELECTROMAGNETIC ABSORPTION**
- Grooved surfaces on InP p 213 N91-30208
- ELECTROMAGNETIC ACCELERATION**
- The preliminary feasibility of intercalated graphite railgun armatures p 137 A91-29257
- ELECTROMAGNETIC COMPATIBILITY**
- Power electronics for low power arcjets [AIAA PAPER 91-1991] p 60 A91-45779
- Power electronics for low power arcjets [NASA-TM-104459] p 77 N91-25172
- ELECTROMAGNETIC COUPLING**
- Circular polarisation characteristics of stacked microstrip antennas p 131 A91-20370
- Mutual coupling between electromagnetically coupled rectangular patch antennas p 137 A91-32822
- ELECTROMAGNETIC FIELDS**
- Paramagnetic propellant orientation [AIAA PAPER 91-2325] p 125 A91-44197
- Paramagnetic propellant orientation [NASA-TM-104390] p 166 N91-24527
- A model for the scattering of high-frequency electromagnetic fields from dielectrics exhibiting thermally-activated electrical losses [NASA-TM-104376] p 224 N91-26872
- ELECTROMAGNETIC INTERFERENCE**
- Coplanar-waveguide/microstrip probe coupler and applications to antennas p 131 A91-17719
- Intercalated graphite fiber composites as EMI shields in aerospace structures [NASA-TM-103632] p 94 N91-10134
- Prospects for using carbon-carbon composites for EMI shielding [NASA-TM-103677] p 97 N91-19231
- ELECTROMAGNETIC RADIATION**
- Effect of surface deposits on electromagnetic waves propagating in uniform ducts [NASA-TM-103282] p 133 N91-10208
- ELECTROMAGNETIC SHIELDING**
- Intercalated graphite fiber composites as EMI shields in aerospace structures [NASA-TM-103632] p 94 N91-10134
- Prospects for using carbon-carbon composites for EMI shielding [NASA-TM-103677] p 97 N91-19231
- ELECTROMECHANICAL DEVICES**
- Induction motor control p 137 A91-30893
- Electromechanical actuation for thrust vector control applications p 52 A91-31026
- ELECTROMIGRATION**
- Electromigration failure in YBa₂Cu₃O_{7-x} thin films p 231 A91-26989
- ELECTRON ACCELERATORS**
- The theory of an auto-resonant field emission cathode relativistic electron accelerator for high efficiency microwave to direct current power conversion p 73 N91-22176

ELECTRON BEAMS

- A high-efficiency ferruleless coupled-cavity traveling-wave tube with phase-adjusted taper p 136 A91-25078
- Inverse photoelectron spectrometer with magnetically focused electron gun p 172 A91-42849
- ELECTRON BUNCHING**
- A high-efficiency ferruleless coupled-cavity traveling-wave tube with phase-adjusted taper p 136 A91-25078
- ELECTRON DENSITY (CONCENTRATION)**
- Investigation of the arcjet plume near field using electrostatic probes [NASA-TM-103638] p 68 N91-11060
- Investigation of the arcjet near field plume using electrostatic probes p 75 N91-24270
- ELECTRON DIFFRACTION**
- The structure of carbon in chemically vapor deposited SiC monofilaments p 113 A91-18675
- ELECTRON EMISSION**
- Surface studies on scandate cathodes and synthesized scandates p 136 A91-25071
- ELECTRON GUNS**
- Inverse photoelectron spectrometer with magnetically focused electron gun p 172 A91-42849
- ELECTRON IRRADIATION**
- X-ray photoelectron and mass spectroscopic study of electron irradiation and thermal stability of polytetrafluoroethylene p 113 A91-16138
- Thermal stability of electron-irradiated poly(tetrafluoroethylene) - X-ray photoelectron and mass spectroscopic study p 115 A91-39242
- Space Photovoltaic Research and Technology Conference [NASA-CP-3121] p 82 N91-30203
- ELECTRON MICROSCOPY**
- Evidence from transmission electron microscopy for an oxynitride layer in oxidized Si₃N₄ p 118 A91-57058
- ELECTRON MOBILITY**
- Properties of insulator interfaces with p-HgCdTe p 235 N91-18300
- Surface electrons in inverted layers of p-HgCdTe p 235 N91-18301
- ELECTRONIC CONTROL**
- Turbofan engine demonstration of sensor failure detection p 22 A91-29775
- ELECTRONIC EQUIPMENT**
- An Electronic Pressure Profile Display system for aeronautic test facilities p 38 A91-51858
- High temperature power electronics for space [NASA-TM-104375] p 145 N91-22508
- Electrical system/environment interactions on the planet Mars p 242 N91-27068
- ELECTRONIC EQUIPMENT TESTS**
- Power systems testing [NASA-TM-104513] p 42 N91-30186
- ELECTRONS**
- The theory of an auto-resonant field emission cathode relativistic electron accelerator for high efficiency microwave to direct current power conversion p 73 N91-22176
- ELECTROSTATIC BONDING**
- Thin solar cell and lightweight array [NASA-CASE-LEW-14959-1] p 212 N91-27614
- ELECTROSTATIC PROBES**
- Investigation of the arcjet plume near field using electrostatic probes [NASA-TM-103638] p 68 N91-11060
- Investigation of the arcjet near field plume using electrostatic probes p 75 N91-24270
- ELEMENTARY PARTICLES**
- Comment on 'Negative matter propulsion' p 52 A91-37424
- Primordial nucleosynthesis redux p 240 A91-45907
- ELEVATORS (CONTROL SURFACES)**
- Elevator deflections on the icing process p 20 A91-35427
- ELLIPSOMETERS**
- Ellipsometric study of YBa₂Cu₃O_{7-x} laser ablated and co-evaporated films p 233 A91-53235
- ELLIPSOMETRY**
- Thin film characterization using spectroscopic ellipsometry p 119 N91-18303
- Ellipsometric study of InGaAs MODFET material [NASA-TM-103286] p 143 N91-19351
- Study of InGaAs based MODFET structures using variable angle spectroscopic ellipsometry [NASA-TM-103792] p 235 N91-19935
- EMBEDDED COMPUTER SYSTEMS**
- Techniques and implementation of the embedded rule-based expert system using Ada p 220 N91-22788
- EMITTANCE**
- Thermal emittance enhancement of graphite-copper composites for high temperature space based radiators [AIAA PAPER 91-3527] p 116 A91-53705

SUBJECT INDEX

- Thermal emittance enhancement of graphite-copper composites for high temperature space based radiators [NASA-TM-105178] p 123 N91-29332
- EMITTERS**
- Reappraisal of solid selective emitters --- for thermovoltaic energy conversion p 207 A91-41999
- Effect of emitter parameter variation on the performance of heteroepitaxial indium phosphide solar cells p 140 A91-42003
- Reappraisal of solid selective emitters [NASA-TM-103290] p 69 N91-11801
- Effect of emitter parameter variation on the performance of heteroepitaxial indium phosphide solar cells [NASA-TM-103619] p 70 N91-15306
- ENERGY CONVERSION**
- A comparison of energy conversion systems for meeting the power requirements of manned rover for Mars missions p 53 A91-37932
- ENERGY CONVERSION EFFICIENCY**
- A high-efficiency ferruleless coupled-cavity traveling-wave tube with phase-adjusted taper p 136 A91-25078
- Component and prototype panel testing of the mini-dome Fresnel lens photovoltaic concentrator array p 54 A91-38023
- Effects of radiation of InP cells epitaxially grown on Si and GaAs substrates p 140 A91-41984
- The mini-dome Fresnel lens photovoltaic concentrator array - Current status of component and prototype panel testing p 57 A91-41989
- Lightweight concentrator module with 30 percent AM0 efficient GaAs/GaSb tandem cells p 57 A91-41990
- Effect of emitter parameter variation on the performance of heteroepitaxial indium phosphide solar cells p 140 A91-42003
- Applied-field MPD thruster geometry effects [AIAA PAPER 91-2342] p 62 A91-45806
- Effect of emitter parameter variation on the performance of heteroepitaxial indium phosphide solar cells [NASA-TM-103619] p 70 N91-15306
- Tandem concentrator solar cells with 30 percent (AM0) power conversion efficiency p 208 N91-19189
- Review of thin film solar cell technology and applications for ultra-light spacecraft solar arrays p 208 N91-19198
- Determination of series resistance of indium phosphide solar cells p 210 N91-19207
- A comparative study of performance parameters of n(+) - p InP solar cells made by closed-ampoule sulfur diffusion into Cd- and Zn-doped p-type InP substrates p 210 N91-19209
- Effect of dislocations on the open-circuit voltage, short-circuit current and efficiency of heteroepitaxial indium phosphide solar cells [NASA-TM-103762] p 144 N91-19354
- Optimal design study of high efficiency indium phosphide space solar cells [NASA-TM-103763] p 145 N91-21433
- Status of NASA's Stirling Space Power Converter Program [NASA-TM-104512] p 214 N91-32569
- ENERGY DISSIPATION**
- Magnetic bearings with zero bias p 48 N91-21194
- Qualitative investigation of cryogenic injected shock dissipation [NASA-TM-105140] p 168 N91-29525
- ENERGY DISTRIBUTION**
- Description of real-time Ada software implementation of a power system monitor for the Space Station Freedom PMAD DC testbed [NASA-TM-105157] p 218 N91-28776
- ENERGY GAPS (SOLID STATE)**
- Monolithic and mechanical multijunction space solar cells p 54 A91-38020
- Key factors limiting the open circuit voltage of n(+) - pp(+) indium phosphide solar cells p 139 A91-41929
- Key factors limiting the open circuit voltage of n(+) - pp(+) indium phosphide solar cells p 209 N91-19206
- ENERGY OF FORMATION**
- Equivalent crystal theory of alloys [NASA-TP-3155] p 112 N91-30318
- ENERGY STORAGE**
- Satellite eclipse power by laser illumination [IAF PAPER 90-053] p 50 A91-13766
- A PCM/forced convection conjugate transient analysis of energy storage systems with annular and countercurrent flows p 150 A91-27166
- Lunar orbiting microwave beam power system p 56 A91-38158
- Design considerations for Mars photovoltaic power systems p 41 A91-41988
- Scaling analysis applied to the NORVEX code development and thermal energy flight experiment [AIAA PAPER 91-1420] p 155 A91-44337
- Trade studies for nuclear space power systems [AIAA PAPER 91-3518] p 65 A91-52413

- Solar thermal energy receiver [NASA-CASE-LEW-14949-1] p 211 N91-23617
- SEI rover solar-electrochemical power system options [NASA-TM-104402] p 211 N91-23620
- Scaling analysis applied to the NORVEX code development and thermal energy flight experiment [NASA-TM-104462] p 166 N91-24549
- ENERGY TECHNOLOGY**
- Nuclear power technology requirements for NASA exploration missions p 53 A91-37940
- Light weight, high power, high voltage dc/dc converter technologies p 138 A91-37985
- Feasibility of solar power for Mars p 209 N91-19201
- Power technologies and the space future [NASA-TM-103649] p 73 N91-21240
- ENERGY TRANSFER**
- Multifrequency excited jets p 151 A91-31482
- New approach in direct-simulation of gas mixtures [AIAA PAPER 91-1343] p 154 A91-43412
- Comment on local energy transfer and nonlocal interactions in homogeneous, isotropic turbulence (Phys. Fluids A2, 413 (1990)) p 159 N91-13638
- [NASA-TM-103263] p 159 N91-13638
- Multi-heat addition turbine engine [NASA-CASE-LEW-15094-1] p 32 N91-23180
- Solar thermal energy receiver [NASA-CASE-LEW-14949-1] p 211 N91-23617
- ENGINE CONTROL**
- Sensor failure detection for jet engines p 22 A91-37593
- Feedback linearization for control of air breathing engines [AIAA PAPER 91-2000] p 23 A91-41671
- Fiber-optic applications for space-based rocket engines [AIAA PAPER 91-3602] p 49 A91-52468
- A method for partitioning centralized controllers [NASA-TM-4276] p 36 N91-20133
- Integrated flight/propulsion control system design based on a decentralized, hierarchical approach [NASA-TM-103678] p 31 N91-21137
- A simplified dynamic model of the Space Shuttle main engine [NASA-TM-104421] p 131 N91-23340
- Fiber-optic applications for space-based engines [NASA-TM-105235] p 86 N91-32163
- ENGINE COOLANTS**
- A dual-cooled hydrogen-oxygen rocket engine heat transfer analysis [AIAA PAPER 91-2211] p 59 A91-44156
- Liquid oxygen cooling of hydrocarbon fueled rocket thrust chambers p 63 A91-52309
- A dual-cooled hydrogen-oxygen rocket engine heat transfer analysis [NASA-TM-104430] p 76 N91-24302
- ENGINE DESIGN**
- Turbine blading designed for high heat load space propulsion applications p 50 A91-10338
- STOVL Hot Gas Ingestion control technology [ASME PAPER 89-GT-323] p 22 A91-23642
- An update of engine system research at the Army Propulsion Directorate p 22 A91-29452
- Recent Stirling engine loss-understanding results p 181 A91-38151
- Preliminary designs for 25 kWe advanced Stirling conversion systems for dish electric applications p 207 A91-38182
- CFD analysis of a hydrogen fueled ramjet engine at Mach 3.44 [AIAA PAPER 91-1919] p 23 A91-41653
- Design and experimental evaluation of compact radial-inflow turbines p 24 A91-45788
- Applied-field MPD thruster geometry effects [AIAA PAPER 91-2342] p 62 A91-45806
- Energy deposition in low-power coaxial plasma thrusters p 63 A91-52311
- Comparison of turbine bypass and mixed flow turbofan engines for a high-speed civil transport [AIAA PAPER 91-3132] p 25 A91-54051
- Mach 6.5 air induction system design for the Beta II Two-Stage-to-Orbit booster vehicle [AIAA PAPER 91-3196] p 43 A91-54099
- A three-dimensional turbulent heat transfer analysis for advanced tubular rocket thrust chambers [NASA-TM-103293] p 159 N91-10249
- Automated design of controlled diffusion blades p 9 N91-10883
- An update of engine system research at the Army Propulsion Directorate [NASA-TM-103278] p 26 N91-11752
- JANNAF liquid rocket combustion instability panel research recommendations [NASA-TM-103653] p 70 N91-13491

ENGINE MONITORING INSTRUMENTS

- The selection of convertible engines with current gas generator technology for high speed rotorcraft [NASA-TM-103774] p 27 N91-19097
- High temperature NASP engine seal development [NASA-TM-103716] p 184 N91-19441
- A test fixture for measuring high-temperature hypersonic-engine seal performance [NASA-TM-103658] p 184 N91-19442
- Overview of supersonic cruise propulsion research p 27 N91-20088
- Overview of high performance aircraft propulsion p 28 N91-20089
- Overview of hypersonic/transatmospheric vehicle propulsion technology p 28 N91-20092
- Propulsion instrumentation research p 176 N91-20100
- Computational simulation of propulsion structures performance and reliability p 29 N91-20106
- Overview of rotorcraft and general aviation propulsion technology p 29 N91-20112
- Turbomachinery and combustor technology for small engines p 29 N91-20113
- High-efficiency core technology p 30 N91-20118
- Multidisciplinary research overview (IHPTET/NPSS) p 30 N91-20119
- NASA aeropropulsion research in support of propulsion systems of the 21st century [NASA-TM-104403] p 15 N91-23083
- Evaluation and ranking of candidate ceramic wafer engine seal materials [NASA-TM-103795] p 187 N91-23515
- Design of multihundredwatt DIPS for robotic space missions [NASA-TM-104401] p 75 N91-24232
- The Navy/NASA Engine Program (NNEP89): A user's manual [NASA-TM-105186] p 35 N91-30141
- High temperature NASP engine seals: A technology review [NASA-TM-104468] p 190 N91-30538
- Status of the advanced Stirling conversion system project for 25 kW dish Stirling applications [NASA-TM-104528] p 238 N91-31023
- Medium power hydrogen arcjet performance [NASA-TM-104533] p 85 N91-31216
- Status of NASA's Stirling Space Power Converter Program [NASA-TM-104512] p 214 N91-32569
- ENGINE FAILURE**
- Turbofan engine demonstration of sensor failure detection p 22 A91-29775
- Sensor failure detection for jet engines p 22 A91-37593
- ENGINE INLETS**
- A design strategy for the use of vortex generators to manage inlet-engine distortion using computational fluid dynamics [AIAA PAPER 91-2474] p 6 A91-44259
- Evaluation of panel code predictions with experimental results of inlet performance for a 17-inch ducted prop/fan simulator operating at Mach 0.2 [AIAA PAPER 91-3354] p 7 A91-45819
- Finite element elastic-plastic-creep and cyclic life analysis of a cowl lip p 199 A91-56365
- A numerical study of the hot gas environment around a STOVL aircraft in ground proximity p 10 N91-10887
- CFD analysis for high speed inlets p 10 N91-10888
- High alpha inlets p 28 N91-20091
- Performance of a high-work, low-aspect-ratio turbine stator tested with a realistic inlet radial temperature gradient [NASA-TM-103738] p 31 N91-20126
- A study of three dimensional turbulent boundary layer separation and vortex flow control using the reduced Navier Stokes equations [NASA-TM-104407] p 16 N91-23089
- A design strategy for the use of vortex generators to manage inlet-engine distortion using computational fluid dynamics [NASA-TM-104436] p 16 N91-24131
- Evaluation of panel code predictions with experimental results of inlet performance for a 17-inch ducted prop/fan simulator operating at Mach 0.2 [NASA-TM-104428] p 17 N91-25106
- ENGINE MONITORING INSTRUMENTS**
- Turbofan engine demonstration of sensor failure detection p 22 A91-29775
- Development of a Fabry-Perot interferometer for rocket engine plume monitoring p 171 A91-30634
- The development of a post-test diagnostic system for rocket engines [AIAA PAPER 91-2528] p 60 A91-44281
- Space Shuttle Main Engine nozzle mounted optic for throat plane spectroscopy [AIAA PAPER 91-2524] p 49 A91-45816

- Technology readiness assessment of advanced space engine integrated controls and health monitoring
[AIAA PAPER 91-3601] p 49 A91-52467
- Fiber-optic applications for space-based rocket engines
[AIAA PAPER 91-3602] p 49 A91-52468
- The development of a post-test diagnostic system for rocket engines
[NASA-TM-104463] p 217 N91-24787
- Fiber-optic applications for space-based engines
[NASA-TM-105235] p 86 N91-32163
- ENGINE NOISE**
- Near-field noise of a single rotation propfan at an angle of attack
[AIAA PAPER 90-3953] p 225 A91-12469
- ENGINE PARTS**
- A unique high heat flux facility for testing hypersonic engine components
[AIAA PAPER 90-5228] p 37 A91-14454
- Further two-dimensional code development for Stirling space engine components p 56 A91-38184
- A unique high heat flux facility for testing hypersonic engine components
[NASA-TM-103238] p 38 N91-11770
- Stirling engine: Available tools for long-life assessment
[NASA-TM-103660] p 200 N91-12980
- Advanced high temperature engine materials technology program p 98 N91-20110
- High temperature performance evaluation of a hypersonic engine ceramic water seal
[NASA-TM-103737] p 185 N91-22567
- Evaluation and ranking of candidate ceramic water engine seal materials
[NASA-TM-103795] p 187 N91-23515
- Probability of failure and risk assessment of propulsion structural components
[NASA-TM-102323] p 205 N91-25436
- High-temperature, flexible, thermal barrier seal
[NASA-CASE-LEW-14672-1] p 189 N91-27560
- Status of the advanced Stirling conversion system project for 25 kW dish Stirling applications
[NASA-TM-104528] p 238 N91-31023
- A high-frequency servosystem for fuel control in hypersonic engines
[NASA-TM-104333] p 35 N91-31178
- ENGINE TESTS**
- STOVL Hot Gas Ingestion control technology
[ASME PAPER 89-GT-323] p 22 A91-23642
- An update of engine system research at the Army Propulsion Directorate p 22 A91-29452
- Real-time diagnostics of the reusable rocket engine using on-line system identification p 223 A91-30630
- Test-cell pressure effects on the performance of resistojets p 38 A91-37417
- The development of a post-test diagnostic system for rocket engines
[AIAA PAPER 91-2528] p 60 A91-44281
- Experimental and analytical comparison of flowfields in a 110 N (25 lbf) H₂/O₂ rocket
[AIAA PAPER 91-2283] p 62 A91-45802
- Design of an Advanced Expander Test Bed --- for future space engines
[AIAA PAPER 91-3437] p 42 A91-52350
- Test facilities for high power electric propulsion
[AIAA PAPER 91-3499] p 42 A91-52396
- Analysis of 5 KHz combustion instabilities in 40K methane/LOX combustion chambers
[NASA-TM-101368] p 67 N91-10117
- An update of engine system research at the Army Propulsion Directorate
[NASA-TM-103278] p 26 N91-11752
- NASA low-speed centrifugal compressor for 3-D viscous code assessment and fundamental flow physics research
[NASA-TM-103710] p 13 N91-20044
- High temperature performance evaluation of a hypersonic engine ceramic water seal
[NASA-TM-103737] p 185 N91-22567
- The development of a post-test diagnostic system for rocket engines
[NASA-TM-104463] p 217 N91-24787
- Stirling machine operating experience
[NASA-TM-104487] p 212 N91-25510
- Experimental and analytical comparison of flowfields in a 110 N (25 lbf) H₂/O₂ rocket
[NASA-TM-105175] p 82 N91-29230
- Medium power hydrogen arcjet performance
[NASA-TM-104533] p 85 N91-31216
- ENTHALPY**
- A life comparison of tube and channel cooling passages for thrust chambers
[NASA-TM-103613] p 68 N91-11059
- ENTROPY**
- The dynamic instability of adiabatic blast waves p 239 A91-26361
- ENVIRONMENT EFFECTS**
- Flow visualization and hot gas ingestion characteristics of a vectored thrust STOVL concept p 28 N91-20090
- ENVIRONMENTAL SIMULATION**
- Hydrocarbon-fuel/combustion-chamber-liner materials compatibility
[NASA-CR-187104] p 121 N91-21307
- ENVIRONMENTAL TESTS**
- The effect of hydrogen on the low cycle fatigue behavior of a single crystal superalloy p 108 A91-28794
- Preliminary flight test results from the advanced photovoltaic experiment p 56 A91-38163
- Preliminary results from the advanced photovoltaic experiment flight test
[NASA-TM-103269] p 67 N91-11058
- Rapid thermal cycling of solar array blanket coupons for Space Station Freedom p 84 N91-30239
- Nickel-hydrogen cell low-Earth life test update
[NASA-TM-105229] p 213 N91-31708
- EPITAXY**
- New directions in InP solar cell research p 206 A91-38022
- Peeled film GaAs solar cell development p 139 A91-41889
- Application of oxidation to the structural characterization of SiC epitaxial films p 233 A91-45881
- High-voltage 6H-SiC p-n junction diodes p 142 A91-54746
- Effect of dislocations on the open-circuit voltage, short-circuit current and efficiency of heteroepitaxial indium phosphide solar cells
[NASA-TM-103762] p 144 N91-19354
- Heteroepitaxial InP solar cells on Si and GaAs substrates
[NASA-TM-103696] p 144 N91-20392
- Advances in silicon carbide Chemical Vapor Deposition (CVD) for semiconductor device fabrication
[NASA-TM-104410] p 236 N91-23946
- Silicon carbide, an emerging high temperature semiconductor p 236 N91-24061
- Process for the homoepitaxial growth of single-crystal silicon carbide films on silicon carbide wafers
[NASA-CASE-LEW-15223-1] p 236 N91-26967
- Effect of dislocations on properties of heteroepitaxial InP solar cells p 213 N91-30209
- EPOXY MATRIX COMPOSITES**
- Resistivity of pristine and intercalated graphite fiber epoxy composites p 115 A91-35949
- EPOXY RESINS**
- Structural properties of laminated Douglas fir/epoxy composite material
[NASA-RP-1236] p 94 N91-10127
- EQUILIBRIUM EQUATIONS**
- Integrated force method versus displacement method for finite element analysis p 196 A91-28372
- Compatibility conditions of structural mechanics for finite element analysis p 198 A91-37853
- EQUILIBRIUM FLOW**
- Least-squares solution of incompressible Navier-Stokes equations with the p-version of finite elements
[NASA-TM-105203] p 223 N91-31911
- EQUIPMENT SPECIFICATIONS**
- Use of rotating pinholes and reticles for calibration of cloud droplet instrumentation p 171 A91-30371
- EQUIVALENT CIRCUITS**
- Impedances of nickel electrodes cycled in various KOH concentrations p 214 N91-32557
- EROSION**
- Preliminary flight test results from the advanced photovoltaic experiment p 56 A91-38163
- Laser interferometric measurement of ion electrode shape and charge exchange erosion
[AIAA PAPER 91-2121] p 173 A91-45786
- Preliminary results from the advanced photovoltaic experiment flight test
[NASA-TM-103269] p 67 N91-11058
- Atomic oxygen interactions with FEP Teflon and silicones on LDEF p 122 N91-25029
- Laser interferometric measurement of ion electrode shape and charge exchange erosion
[NASA-TM-105165] p 179 N91-31605
- ERROR ANALYSIS**
- Orr-Sherby-Dorn creep strengths of the refractory-metal alloys C-103, ASTAR-811C, W-5Re, and W-25Re
[NASA-TM-105228] p 87 N91-32165
- ERROR CORRECTING CODES**
- An autonomous fault detection, isolation, and recovery system for a 20-kHz electric power distribution test bed
[NASA-TM-104344] p 217 N91-25680
- ERROR DETECTION CODES**
- An autonomous fault detection, isolation, and recovery system for a 20-kHz electric power distribution test bed
[NASA-TM-104344] p 217 N91-25680
- ERROR FUNCTIONS**
- Local synthesis and tooth contact analysis of face-milled spiral bevel gears
[NASA-TM-105182] p 190 N91-29600
- ESTERS**
- Addition polyimides with enhanced processability
[NASA-CASE-LEW-15043-1] p 123 N91-32230
- ETCHING**
- Flexible fluoropolymer filled protective coatings p 121 N91-24062
- Process for the homoepitaxial growth of single-crystal silicon carbide films on silicon carbide wafers
[NASA-CASE-LEW-15223-1] p 236 N91-26967
- Grooved surfaces on InP p 213 N91-30208
- ETHANE**
- Substituted 1,1,1-triaryl-2,2,2-trifluoroethanes and processes for their synthesis
[NASA-CASE-LEW-14345-3] p 89 N91-17141
- Substituted 1,1,1-triaryl-2,2,2-trifluoroethanes and processes for their synthesis
[NASA-CASE-LEW-14345-4] p 90 N91-25185
- ETHYLENE**
- An experimental trace gas investigation of fluid transport and mixing in a circular-to-rectangular transition duct
[AIAA PAPER 91-2370] p 172 A91-44214
- Atomic oxygen interactions with FEP Teflon and silicones on LDEF p 122 N91-25029
- EULER EQUATIONS OF MOTION**
- Numerical simulations of supersonic flow through oscillating cascade sections p 4 A91-28590
- Role of artificial viscosity in Euler and Navier-Stokes solvers p 4 A91-34135
- Flutter analysis of cascades using a two dimensional Euler solver
[AIAA PAPER 91-1681] p 6 A91-45548
- Application of an efficient hybrid scheme for aeroelastic analysis of advanced propellers p 7 A91-52315
- Numerical analysis of flow through oscillating cascade sections p 9 N91-10884
- A finite-difference, frequency-domain numerical scheme for the solution of the linearized unsteady Euler equations p 162 N91-21067
- A new flux splitting scheme
[NASA-TM-104404] p 222 N91-22814
- Euler flow predictions for an oscillating cascade using a high resolution wave-split scheme
[NASA-TM-104377] p 16 N91-24107
- Three-dimensional Euler time accurate simulations of fan rotor-stator interactions
[NASA-TM-102528] p 16 N91-24124
- Parallel computing using a Lagrangian formulation
[NASA-TM-104446] p 215 N91-24745
- EUTECTIC ALLOYS**
- Constitution of pseudobinary hypoeutectic beta-NiAl - alpha-V alloys p 109 A91-48509
- EUTECTIC COMPOSITES**
- Tribological properties of Pt*212 - A high temperature, self-lubricating, powder metallurgy composite
[STLE PREPRINT 90-AM-4E-1] p 87 A91-19720
- Temperature dependence of the elastic moduli and damping for polycrystalline LiF-22 pct CaF₂ eutectic salt p 87 A91-33793
- EUTECTICS**
- Two-dimensional model of a Space Station Freedom thermal energy storage canister p 151 A91-38048
- Method of preparing a thermal barrier coating
[NASA-CASE-LEW-14999-2] p 122 N91-26376
- EVAPORATION**
- Ellipsometric study of YBa₂Cu₃O_{7-x} laser ablated and co-evaporated films p 233 A91-53235
- EXCITATION**
- Control of an axisymmetric turbulent jet by multi-modal excitation
[NASA-TM-104483] p 17 N91-26121
- EXHAUST EMISSION**
- A CFD study of jet mixing in reduced flow areas for lower combustor emissions
[AIAA PAPER 91-2460] p 23 A91-41788
- NASA's High Speed Research Program - An introduction and status report
[SAE PAPER 901923] p 1 A91-48605
- Application of mixing-controlled combustion models to gas turbine combustors
[NASA-TM-103236] p 31 N91-22126
- A CFD study of jet mixing in reduced flow areas for lower combustor emissions
[NASA-TM-104411] p 32 N91-23185
- EXHAUST GASES**
- Application of mixing-controlled combustion models to gas turbine combustors
[NASA-TM-103236] p 31 N91-22126
- EXHAUST NOZZLES**
- An experimental comparison of nonswirling and swirling flow in a circular-to-rectangular transition duct
[AIAA PAPER 91-0342] p 148 A91-21466

- Hot gas ingestion test results of a two-poster vectored thrust concept with flow visualization in the NASA Lewis 9- by 15-foot low speed wind tunnel
[AIAA PAPER 90-2268] p 4 A91-40561
- Computation of a circular-to-rectangular transition duct flow field
[AIAA PAPER 91-1741] p 156 A91-45547
- Pressure measurements in a low-density nozzle plume for code verification
[AIAA PAPER 91-2110] p 61 A91-45783
- Experimental and analytical studies of flow through a ventral and axial exhaust nozzle system for STOVL aircraft
[AIAA PAPER 91-2135] p 25 A91-45791
- Space Shuttle Main Engine nozzle mounted optic for throat plane spectroscopy
[AIAA PAPER 91-2524] p 49 A91-45816
- Overview of the NASA-sponsored HSCST propulsion system studies --- High Speed Civil Transport
[AIAA PAPER 91-3329] p 20 A91-53871
- Noise measurements from an ejector suppressor nozzle in the NASA Lewis 9- by 15-foot low speed wind tunnel
[NASA-TM-103628] p 227 N91-11493
- An experimental comparison of nonswirling and swirling flow in a circular-to-rectangular transition duct
[NASA-TM-104359] p 14 N91-21115
- Hot gas ingestion test results of a two-poster vectored thrust concept with flow visualization in the NASA Lewis 9- x 15-foot low speed wind tunnel
[NASA-TM-103258] p 15 N91-21116
- Experimental and analytical studies of flow through a ventral and axial exhaust nozzle system for STOVL aircraft
[NASA-TM-104364] p 77 N91-25175
- Pressure measurements in a low-density nozzle plume for code verification
[NASA-TM-105170] p 81 N91-29228
- EXHAUST SYSTEMS**
Experimental and analytical studies of flow through a ventral and axial exhaust nozzle system for STOVL aircraft
[AIAA PAPER 91-2135] p 25 A91-45791
- Experimental and analytical studies of flow through a ventral and axial exhaust nozzle system for STOVL aircraft
[NASA-TM-104364] p 77 N91-25175
- EXHAUST VELOCITY**
Experimental and analytical comparison of flowfields in a 110 N (25 lbf) H₂/O₂ rocket
[NASA-TM-105175] p 82 N91-29230
- EXOBIOLOGY**
The International Space University's variable gravity research facility design
[NASA-TM-105224] p 44 N91-31196
- EXPERT SYSTEMS**
An expert system to perform on-line controller restructuring for abrupt model changes
p 36 A91-29466
- An expert system to perform on-line controller tuning
p 219 A91-30171
- Automated electric power management and control for Space Station Freedom
p 53 A91-37970
- Autonomous power expert system
p 54 A91-37972
- An expert system for simulating electric loads aboard Space Station Freedom
p 55 A91-38041
- Development of an intelligent diagnostic system for reusable rocket engine control
[AIAA PAPER 91-2533] p 63 A91-45817
- Developments in REDES: The rocket engine design expert system
[NASA-TM-103657] p 67 N91-10119
- A rocket engine design expert system
p 71 N91-17129
- Autonomous power expert system advanced development
p 72 N91-20689
- Techniques and implementation of the embedded rule-based expert system using Ada
p 220 N91-22788
- An autonomous fault detection, isolation, and recovery system for a 20-kHz electric power distribution test bed
[NASA-TM-104344] p 217 N91-25680
- EXPOSURE**
Space Photovoltaic Research and Technology Conference
[NASA-CP-3121] p 82 N91-30203
- EXPULSION**
Pressurization and expulsion of cryogenic liquids: Generic requirements for a low gravity experiment
[NASA-TM-104417] p 126 N91-25300
- EXTINGUISHING**
Fire suppression in human-crew spacecraft
[NASA-TM-104334] p 44 N91-21182
- EXTRACTION**
Near-Earth asteroids: Metals occurrence, extraction, and fabrication
p 241 N91-26058

EXTRATERRESTRIAL RESOURCES

- Material processing with hydrogen and carbon monoxide on Mars
[NASA-TM-104405] p 211 N91-23616
- Near-Earth asteroids: Metals occurrence, extraction, and fabrication
p 241 N91-26058
- Chemical approaches to carbon dioxide utilization for manned Mars missions
p 241 N91-26073
- Technical prospects for utilizing extraterrestrial propellants for space exploration
[NASA-TM-105263] p 127 N91-31318
- EXTREMELY HIGH FREQUENCIES**
Ka-band MMIC microstrip array for high rate communications
[AIAA PAPER 91-3421] p 132 A91-52341
- Evaluation of components, subsystems, and networks for high rate, high frequency space communications
[AIAA PAPER 91-3423] p 41 A91-52343
- Overview of Ka-band communications technology requirements for the Space Exploration Initiative
[AIAA PAPER 91-3424] p 45 A91-52344
- High efficiency Ka-band MMIC amplifiers
[AIAA PAPER 91-3425] p 141 A91-52345
- Status of Ka-band TWT transmitter technology
[AIAA PAPER 91-3621] p 142 A91-52485
- A statistical rain attenuation prediction model with application to the advanced communication technology satellite project. 3: A stochastic rain fade control algorithm for satellite link power via non linear Markov filtering theory
[NASA-TM-100243] p 134 N91-22494
- Characteristics of a future aeronautical satellite communications system
[NASA-TM-104389] p 20 N91-23102
- Ka-band MMIC microstrip array for high rate communications
[NASA-TM-104500] p 135 N91-27437
- EXTRUDING**
Method of making single crystal fibers
[NASA-CASE-LEW-14921-1] p 95 N91-13502

F**F-18 AIRCRAFT**

- The aerodynamic characteristics of vortex ingestion for the F/A-18 inlet duct
[AIAA PAPER 91-0130] p 3 A91-26192
- The aerodynamic characteristics of vortex ingestion for the F/A-18 inlet duct
[NASA-TM-103703] p 70 N91-15303

FABRICATION

- Concurrent material-fabrication optimization of metal-matrix laminates under thermo-mechanical loading
[AIAA PAPER 91-1044] p 129 A91-31842
- Key factors limiting the open circuit voltage of n(+)-pp(+)-indium phosphide solar cells
p 139 A91-41929
- Concurrent tailoring of fabrication process and interphase layer to reduce residual stresses in metal matrix composites
p 92 A91-43232
- High temperature superconducting thin film microwave circuits - Fabrication, characterization, and applications
p 141 A91-50433
- YBCO superconducting ring resonators at millimeter-wave frequencies
p 142 A91-54532
- Structural properties of laminated Douglas fir/epoxy composite material
[NASA-RP-1236] p 94 N91-10127
- Relationship between voids and interlaminar shear strength of polymer matrix composites
[NASA-TM-103643] p 95 N91-13495
- New method of making advanced tube-bundle rocket thrust chambers
[NASA-TM-103617] p 70 N91-15301
- Tandem concentrator solar cells with 30 percent (AMO) power conversion efficiency
p 208 N91-19189
- Key factors limiting the open circuit voltage of n(+)-pp(+)-indium phosphide solar cells
p 209 N91-19206
- Investigation of anodic and chemical oxides grown on p-type InP with applications to surface passivation for n(+)-p solar cell fabrication
p 210 N91-19208
- A comparative study of performance parameters of n(+)-p InP solar cells made by closed-ampoule sulfur diffusion into Cd- and Zn-doped p-type InP substrates
p 210 N91-19209
- Concurrent micromechanical tailoring and fabrication process optimization for metal-matrix composites
[NASA-TM-103670] p 98 N91-19237
- A new fabrication method for precision antenna reflectors for space flight and ground test
[NASA-TP-3078] p 48 N91-21185
- Development of silicon carbide semiconductor devices for high temperature applications
[NASA-TM-104398] p 236 N91-22921

- System-Level Integrated Circuit (SLIC) development for phased array antenna applications
[NASA-TM-104392] p 134 N91-23354
- Method of preparing a thermal barrier coating
[NASA-CASE-LEW-14999-2] p 122 N91-26376
- A comparative study of p(+)-n and n(+)-p InP solar cells made by a closed ampoule diffusion
p 212 N91-30206

- Interphase layer optimization for metal matrix composites with fabrication considerations
[NASA-TM-105166] p 102 N91-30281

FABRICS

- Construction and testing of ceramic fabric heat pipe with water working fluid
[NASA-TM-103332] p 229 N91-18799

FABRY-PEROT INTERFEROMETERS

- Development of a Fabry-Perot interferometer for rocket engine plume monitoring
p 171 A91-30634
- Optical techniques for determination of normal shock position in supersonic flows for aerospace applications
p 174 A91-55530

- High-speed laser anemometry based on spectrally resolved Rayleigh scattering
[NASA-TM-104522] p 178 N91-27521

FACSIMILE COMMUNICATION

- A neural net based architecture for the segmentation of mixed gray-level and binary pictures
p 218 A91-29183

FACTORIZATION

- Implicit solution of three-dimensional internal turbulent flows
p 163 N91-21082

FAILURE

- Localization of aeroelastic modes in mistuned high-energy turbines
[AIAA PAPER 91-3379] p 198 A91-44319
- Nondestructive evaluation tools and experimental studies for monitoring the health of space propulsion systems
[AIAA PAPER 91-3433] p 192 A91-53703
- Effect of LEO cycling on 125 Ah advanced design IPV nickel-hydrogen flight cells. An update
[NASA-TM-104384] p 74 N91-22375
- Destructive physical analysis results of Ni/H₂ cells cycled in LEO regime
[NASA-TM-104382] p 74 N91-23233
- Mechanical behavior and failure phenomenon of an in situ-toughened silicon nitride
[NASA-TM-103741] p 121 N91-23311
- Localization of aeroelastic modes in mistuned high-energy turbines
[NASA-TM-104445] p 204 N91-24659
- Nondestructive evaluation tools and experimental studies for monitoring the health of space propulsion systems
[NASA-TM-105164] p 194 N91-28605
- FAILURE ANALYSIS**
Metal matrix composites microfracture - Computational simulation
p 90 A91-11815
- Electromigration failure in YBa₂Cu₃O_{7-x} thin films
p 231 A91-26989
- Real-time diagnostics of the reusable rocket engine using on-line system identification
p 223 A91-30630
- Model-OA wind turbine generator - Failure modes and effects analysis
p 191 A91-31064
- Sensor failure detection for jet engines
p 22 A91-37593

- Effect of KOH concentration on LEO cycle life of IPV nickel-hydrogen flight battery cells
p 55 A91-38076
- Thermal and structural assessments of a ceramic wafer seal in hypersonic engine
[AIAA PAPER 91-2494] p 23 A91-41799
- In situ X-ray monitoring of damage accumulation in SiC/RBSN tensile specimens
p 94 A91-56942
- Thermal and structural assessments of a ceramic wafer seal in hypersonic engines
[NASA-TM-103651] p 26 N91-13456
- Probabilistic simulation of uncertainties in thermal structures
[NASA-TM-103680] p 201 N91-19472
- Progress in modeling deformation and damage
p 202 N91-20108
- In situ x-ray monitoring of damage accumulation in SiC/RBSN tensile specimens
[NASA-TM-103733] p 99 N91-22402
- Combined thermal and bending fatigue of high-temperature metal-matrix composites: Computational simulation
[NASA-TM-104354] p 100 N91-23247
- A simplified dynamic model of the Space Shuttle main engine
[NASA-TM-104421] p 131 N91-23340
- Incorporating finite element analysis into component life and reliability
p 203 N91-23550
- Cumulative creep fatigue damage in 316 stainless steel
p 111 N91-24312

- Probabilistic structural analysis: Introductory remarks p 204 N91-24326
- High temperature tension-compression fatigue behavior of a tungsten copper composite [NASA-TM-104370] p 100 N91-24360
- Sensor failure detection and recovery by neural networks [NASA-TM-104484] p 220 N91-24815
- Tensile deformation damage in SiC reinforced Ti-15V-3Cr-3Al-3Sn [NASA-TM-103620] p 101 N91-25195
- Microfracture in high temperature metal matrix crossply laminates [NASA-TM-104381] p 101 N91-25198
- Probability of failure and risk assessment of propulsion structural components [NASA-TM-102323] p 205 N91-25436
- An autonomous fault detection, isolation, and recovery system for a 20-kHz electric power distribution test bed [NASA-TM-104344] p 217 N91-25680
- A distributed fault-detection and diagnosis system using on-line parameter estimation [NASA-TM-104433] p 220 N91-25696
- A three-dimensional finite-element thermal/mechanical analytical technique for high-performance traveling wave tubes [NASA-TP-3081] p 134 N91-27436
- Probabilistic structural analysis methods for space transportation propulsion systems p 205 N91-28238
- Fatigue behavior and life prediction of a SiC/Ti-24Al-11Nb composite under isothermal conditions [NASA-TM-105168] p 206 N91-30566
- FAILURE MODES**
- A model for the Space Shuttle Main Engine High Pressure Oxidizer Turbopump shaft seal system p 180 A91-30640
- Model-OA wind turbine generator - Failure modes and effects analysis p 191 A91-31064
- Impedances of Ni electrodes and Ni/H₂ cells from different manufacturers p 55 A91-38082
- Linear quadratic servo control of a reusable rocket engine [AIAA PAPER 91-1999] p 57 A91-41670
- Adaptation of NASA technology for the optimization of orthopedic knee implants p 215 N91-23032
- FAN BLADES**
- Optical measurement of unducted fan blade deflections [ASME PAPER 89-GT-298] p 170 A91-13046
- Analysis of three-dimensional viscous flow in a supersonic throughflow fan p 10 N91-10885
- FANS**
- Influence of thickness and camber on the aeroelastic stability of supersonic throughflow fans p 5 A91-42814
- FAR FIELDS**
- Investigation of the arcjet plume near field using electrostatic probes [NASA-TM-103638] p 68 N91-11060
- Using a modified Hewlett Packard 8410 network analyzer as an automated farfield antenna range receiver [NASA-TM-103700] p 143 N91-19349
- Investigation of the arcjet near field plume using electrostatic probes p 75 N91-24270
- FAR ULTRAVIOLET RADIATION**
- Vacuum ultraviolet radiation and thermal cycling effects on atomic oxygen protective photovoltaic array blanket materials p 116 A91-49812
- FARADAY EFFECT**
- A fiber-optic current sensor for aerospace applications p 172 A91-38006
- Fiber-optic sensors for aerospace electrical measurements: An update [NASA-TM-104454] p 177 N91-25381
- FATIGUE (MATERIALS)**
- The isothermal fatigue behavior of a unidirectional SiC/Ti composite and the Ti alloy matrix p 93 A91-55907
- Influence of the Si₃N₄ microstructure on its R-curve and fatigue behavior p 117 A91-56931
- Dynamic fatigue property of silicon carbide whisker-reinforced silicon nitride p 94 A91-56937
- A methodology for evaluating the reliability and risk of structures under complex service environments [NASA-TM-103244] p 200 N91-17415
- Current activities in standardization of high-temperature, low-cycle-fatigue testing techniques in the United States [NASA-TM-103675] p 200 N91-17427
- Comparison of dynamic fatigue behavior between SiC whisker-reinforced composite and monolithic silicon nitrides [NASA-TM-103707] p 119 N91-19293
- Overview of the fatigue/fracture/life working group program at the Lewis Research Center p 203 N91-24308
- Modeling of crack bridging in a unidirectional metal matrix composite [NASA-TM-104355] p 205 N91-24660
- FATIGUE LIFE**
- Quantification of uncertainties in coupled material degradation processes - High temperature, fatigue and creep [AIAA PAPER 91-0977] p 196 A91-31835
- Computational simulation of acoustic fatigue for hot composite structures [AIAA PAPER 91-1178] p 197 A91-32099
- Evaluation of advanced lubricants for aircraft applications using gear surface fatigue tests [AIAA PAPER 91-1907] p 181 A91-41649
- Surface fatigue life of M50NiL and AISI 9310 gears and rolling-contact bars p 182 A91-45350
- In-service health monitoring of composite structures p 192 A91-51926
- Axial-torsional fatigue: A study of tubular specimen thickness effects [NASA-TM-103637] p 200 N91-14632
- Application of thermal life prediction model to high-temperature aerospace alloys B1900 + Hf and Haynes 188 [NASA-TM-4226] p 201 N91-19473
- Isothermal fatigue behavior of a (90)(sub 8) SiC/Ti-15-3 composite at 426 C [NASA-TM-103686] p 99 N91-20228
- Thermomechanical and bithermal fatigue behavior of cast B1900 + Hf and wrought Haynes 188 [NASA-TM-4225] p 111 N91-20268
- Life extending control: A concept paper [NASA-TM-104391] p 37 N91-22135
- Evaluation of advanced lubricants for aircraft applications using gear surface fatigue tests [NASA-TM-104336] p 186 N91-22568
- Computational simulation of acoustic fatigue for hot composite structures [NASA-TM-104379] p 203 N91-23548
- Fatigue life prediction of an intermetallic matrix composite at elevated temperatures [NASA-TM-104494] p 205 N91-25442
- Surface fatigue life of M50NiL and AISI 9310 spur gears and R C bars [NASA-TM-104496] p 189 N91-27569
- Effect of two synthetic lubricants on life of AISI 9310 spur gears [NASA-TM-104352] p 189 N91-29599
- Fatigue behavior and life prediction of a SiC/Ti-24Al-11Nb composite under isothermal conditions [NASA-TM-105168] p 206 N91-30566
- FATIGUE TESTS**
- Fatigue crack growth study of SCS6/Ti-15-3 composite p 91 A91-25798
- The effect of hydrogen on the low cycle fatigue behavior of a single crystal superalloy p 108 A91-28794
- Evaluation of advanced lubricants for aircraft applications using gear surface fatigue tests [AIAA PAPER 91-1907] p 181 A91-41649
- Surface fatigue life of M50NiL and AISI 9310 gears and rolling-contact bars p 182 A91-45350
- Automation software for a materials testing laboratory p 216 A91-56538
- A data acquisition and control program for axial-torsional fatigue testing p 199 A91-56540
- Axial-torsional fatigue: A study of tubular specimen thickness effects [NASA-TM-103637] p 200 N91-14632
- Current activities in standardization of high-temperature, low-cycle-fatigue testing techniques in the United States [NASA-TM-103675] p 200 N91-17427
- Effect of tensile mean stress on fatigue behavior of single-crystal and directionally solidified superalloys [NASA-TM-103644] p 200 N91-18452
- Thermomechanical and bithermal fatigue behavior of cast B1900 + Hf and wrought Haynes 188 [NASA-TM-4225] p 111 N91-20268
- Evaluation of advanced lubricants for aircraft applications using gear surface fatigue tests [NASA-TM-104336] p 186 N91-22568
- Cumulative creep fatigue damage in 316 stainless steel p 111 N91-24312
- Fatigue behavior of a single-crystal superalloy p 111 N91-24313
- Two-dimensional high temperature strain measurement system p 204 N91-24319
- Modeling of crack bridging in a unidirectional metal matrix composite [NASA-TM-104355] p 205 N91-24660
- Furnace for tensile/fatigue testing [NASA-CASE-LEW-14848-1] p 42 N91-27175
- Surface fatigue life of M50NiL and AISI 9310 spur gears and R C bars [NASA-TM-104496] p 189 N91-27569
- Effect of two synthetic lubricants on life of AISI 9310 spur gears [NASA-TM-104352] p 189 N91-29599
- Fatigue behavior and life prediction of a SiC/Ti-24Al-11Nb composite under isothermal conditions [NASA-TM-105168] p 206 N91-30566
- FAULT TOLERANCE**
- Autonomous power expert system advanced development p 72 N91-20689
- FEASIBILITY ANALYSIS**
- Programming probabilistic structural analysis for parallel processing computer [AIAA PAPER 91-0920] p 196 A91-31957
- Neural network application to aircraft control system design [AIAA PAPER 91-2715] p 36 A91-49676
- The dynamic effects of internal robots on Space Station Freedom [AIAA PAPER 91-2822] p 40 A91-49764
- Low-density, high-strength intermetallic matrix composites by XD (trademark) synthesis [NASA-TM-103724] p 97 N91-19233
- The dynamic effects of internal robots on Space Station Freedom [NASA-TM-104345] p 203 N91-22604
- Neural network application to aircraft control system design [NASA-TM-105151] p 37 N91-27167
- FEED SYSTEMS**
- Microanalysis of extended-test xenon hollow cathodes [NASA-TM-104532] p 82 N91-30202
- FEEDBACK CONTROL**
- Use of piezoelectric actuators in active vibration control of rotating machinery p 179 A91-14400
- Fiber optic phase stepping system for interferometry p 171 A91-28968
- Robust eigenspace assignment using singular value sensitivities p 219 A91-29784
- Partitioning methods for global controllers p 219 A91-30043
- Feedback linearization for control of air breathing engines [AIAA PAPER 91-2000] p 23 A91-41671
- A linear control design structure to maintain loop properties during limit operation in a multi-nozzle turbofan engine [AIAA PAPER 91-1997] p 24 A91-45780
- Integrated flight/propulsion control system design based on a decentralized, hierarchical approach [NASA-TM-103678] p 31 N91-21137
- Alpha-canonical form representation of the open loop dynamics of the Space Shuttle main engine [NASA-TM-104422] p 131 N91-24469
- Applied high-speed imaging for the icing research program at NASA Lewis Research Center [NASA-TM-104415] p 177 N91-26490
- A linear control design structure to maintain loop properties during limit operation in a multi-nozzle turbofan engine [NASA-TM-105163] p 35 N91-29188
- FEEDERS**
- Plasma gun with coaxial powder feed and adjustable cathode [NASA-CASE-LEW-14901-1] p 231 N91-25875
- FEEDFORWARD CONTROL**
- The application of neural networks to the SSME startup transient [AIAA PAPER 91-2530] p 60 A91-44283
- Neural network application to aircraft control system design [AIAA PAPER 91-2715] p 36 A91-49676
- Towards practical control design using neural computation [NASA-TM-103785] p 219 N91-19766
- Neural network application to aircraft control system design [NASA-TM-105151] p 37 N91-27167
- FIBER COMPOSITES**
- Mechanics of damping for fiber composite laminates including hygrothermal effects p 195 A91-12895
- Impact behavior of a SiC fiber-reinforced reaction bonded Si₃N₄ composite p 91 A91-16805
- Computational simulation of high-temperature metal matrix composites cyclic behavior p 91 A91-18680
- An integrated methodology for optimizing the passive damping of composite structures p 195 A91-19048
- Simplified procedures for designing adhesively bonded composite joints p 180 A91-20938
- Composite laminate tailoring with probabilistic constraints and loads p 198 A91-38754
- Continuous fiber-reinforced titanium aluminide composites p 92 A91-39553
- Evaluation of thermomechanical damage in silicon carbide/titanium composites p 92 A91-42297

- Concurrent tailoring of fabrication process and interphase layer to reduce residual stresses in metal matrix composites p 92 A91-43232
- Acousto-ultrasonics p 226 A91-48227
- Reaction of beta-phase Ni-Al alloys with CrB₂ p 92 A91-49943
- Numerical, micro-mechanical prediction of crack growth resistance in a fibre-reinforced/brittle matrix composite p 199 A91-51916
- In-service health monitoring of composite structures p 192 A91-51926
- Advanced materials for space nuclear power systems [AIAA PAPER 91-3530] p 88 A91-53704
- The isothermal fatigue behavior of a unidirectional SiC/Ti composite and the Ti alloy matrix p 93 A91-55907
- Effect of thermal shock on fiber-reinforced superalloy composites p 93 A91-55918
- Ultrasonic velocity technique for monitoring property changes in fiber-reinforced ceramic matrix composites p 174 A91-56912
- Investigation of interfacial shear strength in SiC/Si₃N₄ composites p 93 A91-56913
- In situ X-ray monitoring of damage accumulation in SiC/RBSN tensile specimens p 94 A91-56942
- High resolution computed tomography of advanced composite and ceramic materials p 192 A91-56972
- Intercalated graphite fiber composites as EMI shields in aerospace structures [NASA-TM-103632] p 94 A91-10134
- ICAN sensitivity analysis [NASA-TM-103667] p 96 A91-15328
- Tensile behavior of tungsten/nitrogen composites at 1300 to 1600 K [NASA-TM-103727] p 111 A91-16128
- Review of acousto-ultrasonic NDE for composites p 97 A91-18192
- An overview of self-consistent methods for fiber-reinforced composites [NASA-TM-103713] p 97 A91-19232
- Effect of fiber reinforcements on thermo-oxidative stability and mechanical properties of polymer matrix composites [NASA-TM-103648] p 98 A91-19234
- Computational materials science. An example: Numerical modeling of chemical vapor deposition processing of advanced fibers p 99 A91-20111
- Mechanical behavior of fiber reinforced SiC/RBSN ceramic matrix composites: Theory and experiment [NASA-TM-103688] p 99 A91-21243
- In-situ x-ray monitoring of damage accumulation in SiC/RBSN tensile specimens [NASA-TM-103733] p 99 A91-22402
- A preliminary investigation of acousto-ultrasonic NDE of metal matrix composite test specimens [NASA-TM-104339] p 194 A91-23521
- High temperature tension-compression fatigue behavior of a tungsten copper composite p 100 A91-24360
- A comparison of fiber effects on polymer matrix composite oxidation [NASA-TM-104416] p 101 A91-24361
- Sensible heat receiver for solar dynamic space power system [NASA-TM-104393] p 77 A91-25173
- Tensile deformation damage in SiC reinforced Ti-15V-3Cr-3Al-3Sn p 101 A91-25195
- Investigation of interfacial shear strength in SiC/Si₃N₄ composites [NASA-TM-103739] p 101 A91-26233
- Advanced materials for space nuclear power systems [NASA-TM-105171] p 112 A91-29298
- NDE of ceramics and ceramic composites [NASA-TM-104520] p 194 A91-29610
- Ultrasonic velocity technique for monitoring property changes in fiber-reinforced ceramic matrix composites [NASA-TM-103806] p 195 A91-30546
- Fatigue behavior and life prediction of a SiC/Ti-24Al-11Nb composite under isothermal conditions [NASA-TM-105168] p 206 A91-30566
- Effect of lightning strike on bromine intercalated graphite fiber/epoxy composites [NASA-TM-104507] p 103 A91-32177
- FIBER OPTICS**
- Fiber optic photoelastic pressure sensor for high temperature gases p 170 A91-19577
- Silicon-etalon fiber-optic temperature sensor p 170 A91-19581
- Compensation for effects of ambient temperature on rare-earth doped fiber optic thermometer p 170 A91-19582
- A fiber-optic current sensor for aerospace applications p 171 A91-23005
- Bit error rate testing of fiber optic data links for MMIC-based phased array antennas p 131 A91-24950
- Design of an optically controlled Ka-band GaAs MMIC phased-array antenna p 132 A91-24951
- Optical control of microwave devices --- Book p 136 A91-27331
- Fiber optic phase stepping system for interferometry p 171 A91-28968
- Vibrational testing of optical fiber connector joints p 172 A91-30652
- Civil air transport - A fresh look at power-by-wire and fly-by-light p 36 A91-31030
- A fiber-optic current sensor for aerospace applications p 172 A91-38006
- The development of a fiber optic Raman temperature measurement system for rocket flows [AIAA PAPER 91-2316] p 173 A91-45804
- Space Shuttle Main Engine nozzle mounted optic for throat plane spectroscopy p 49 A91-45816
- [AIAA PAPER 91-2524] p 173 A91-45816
- A fiber optic sensor for noncontact measurement of shaft speed, torque and power p 173 A91-51870
- Design of an inflatable, optically controlled and fed, phased array antenna [AIAA PAPER 91-3470] p 132 A91-52378
- Fiber-optic applications for space-based rocket engines [AIAA PAPER 91-3602] p 49 A91-52468
- Vibrational testing of optical fiber connector joints [NASA-TM-103654] p 230 A91-14829
- Fiber-optic-based controls p 230 A91-20102
- Fiber optic sensing system [NASA-CASE-LEW-14795-1] p 230 A91-21871
- Civil air transport: A fresh look at power-by-wire and fly-by-light p 37 A91-23053
- Fiber-optic sensors for aerospace electrical measurements: An update [NASA-TM-104454] p 177 A91-25381
- Fiber-optic applications for space-based engines [NASA-TM-105235] p 86 A91-32163
- FIBER ORIENTATION**
- Resistivity of pristine and intercalated graphite fiber epoxy composites p 115 A91-35949
- An overview of self-consistent methods for fiber-reinforced composites [NASA-TM-103713] p 97 A91-19232
- Isothermal fatigue behavior of a (90)(sub 8) SiC/Ti-15-3 composite at 426 C [NASA-TM-103686] p 99 A91-20228
- FIBER STRENGTH**
- Effects of high pressure nitrogen on the thermal stability of SiC fibers [NASA-TM-103245] p 96 A91-16075
- FIBERS**
- Fiber pushout test - A three-dimensional finite element computational simulation p 197 A91-33096
- Development of braided rope seals for hypersonic engine applications. II - Flow modeling [AIAA PAPER 91-2495] p 182 A91-41800
- A numerical and experimental analysis of reactor performance and deposition rates for CVD on monofilaments p 130 A91-14500
- [NASA-TM-103631] p 130 A91-14500
- Graphite fluoride fiber polymer composite material [NASA-CASE-LEW-14472-1] p 95 A91-15320
- Reinforcements: The key to high performance composite materials [NASA-TM-103230] p 96 A91-15329
- Development of braided rope seals for hypersonic engine applications. Part 2: Flow modeling [NASA-TM-104371] p 186 A91-22571
- FIELD EFFECT TRANSISTORS**
- Neutron and gamma irradiation effects on power semiconductor switches p 139 A91-38162
- Submicron gate InP power MISFET's with improved output power density at 18 and 20 GHz p 142 A91-54526
- Silicon carbide, a semiconductor for space power electronics [NASA-TM-103655] p 234 A91-14850
- Development of silicon carbide semiconductor devices for high temperature applications [NASA-TM-104398] p 236 A91-22921
- Microwave integrated circuits for space applications p 145 A91-24069
- Submicron gate InP power MISFET's with improved output power density at 18 and 20 GHz p 145 A91-26436
- FIELD EMISSION**
- The theory of an auto-resonant field emission cathode relativistic electron accelerator for high efficiency microwave to direct current power conversion p 73 A91-22176
- FIGHTER AIRCRAFT**
- Integrated flight/propulsion control system design based on a decentralized, hierarchical approach [NASA-TM-103678] p 31 A91-21137
- FILM THICKNESS**
- Ellipsometric study of YBa₂Cu₃O(7-x) laser ablated and co-evaporated films p 233 A91-53235
- FILTRATION**
- Quantifying oil filtration effects on bearing life [NASA-TM-104350] p 186 A91-23512
- FINITE DIFFERENCE THEORY**
- Numerical simulations of supersonic flow through oscillating cascade sections p 4 A91-28590
- Two-dimensional model of a Space Station Freedom thermal energy storage canister p 151 A91-38048
- A finite-difference, frequency-domain numerical scheme for the solution of the linearized unsteady Euler equations p 162 A91-21067
- A comparison of numerical methods for the Rayleigh equation in unbounded domains [NASA-TM-105179] p 223 A91-30865
- FINITE ELEMENT METHOD**
- Metal matrix composites microfracture - Computational simulation p 90 A91-11815
- General purpose program to generate compatibility matrix for the integrated force method p 195 A91-12905
- Integrated force method versus displacement method for finite element analysis p 196 A91-28372
- Fiber pushout test - A three-dimensional finite element computational simulation p 197 A91-33096
- Compatibility conditions of structural mechanics for finite element analysis p 198 A91-37853
- Analytical and experimental study of vibrations in a gear transmission [AIAA PAPER 91-2019] p 181 A91-41680
- Effects of rim thickness on spur gear bending stress [AIAA PAPER 91-2020] p 181 A91-41681
- Thermal and structural assessments of a ceramic wafer seal in hypersonic engine [AIAA PAPER 91-2494] p 23 A91-41799
- Low velocity impact analysis with NASTRAN p 198 A91-48865
- Elastic response of (001)-oriented PWA 1480 single crystal - The influence of secondary orientation [SAE PAPER 911111] p 110 A91-53555
- Application of finite-element-based solution technologies for viscoplastic structural analyses p 199 A91-55137
- Finite element elastic-plastic-creep and cyclic life analysis of a coil lip p 199 A91-56365
- Effect of surface deposits on electromagnetic waves propagating in uniform ducts [NASA-TM-103282] p 133 A91-10208
- A life comparison of tube and channel cooling passages for thrust chambers [NASA-TM-103613] p 68 A91-11059
- Status of structural analysis of 30 cm diameter ion optics [NASA-TM-103618] p 68 A91-11796
- The effect of coatings and liners on heat transfer in a dry shaft-bush tribosystem [NASA-TM-102513] p 159 A91-12913
- Finite element analysis of thermal distortion effects on optical performance of solar dynamic concentrator for Space Station Freedom [NASA-TM-102504] p 183 A91-12954
- Thermal and structural assessments of a ceramic wafer seal in hypersonic engines [NASA-TM-103651] p 26 A91-13456
- Low velocity impact analysis with NASTRAN [NASA-TM-103169] p 95 A91-14426
- Probabilistic simulation of uncertainties in thermal structures [NASA-TM-103680] p 201 A91-19472
- A finite element model of conduction, convection, and phase change near a solid/melt interface [NASA-TM-103721] p 162 A91-20417
- Elastic response of zone axis (001)-oriented PWA 1480 single crystal: The influence of secondary orientation [NASA-TM-103782] p 202 A91-21558
- Reliability and risk assessment of structures p 194 A91-23050
- Effects of rim thickness on spur gear bending stress [NASA-TM-104388] p 186 A91-23500
- Modal analysis of multistage gear systems coupled with gearbox vibrations [NASA-TM-103797] p 187 A91-23513
- Incorporating finite element analysis into component life and reliability [NASA-TM-104400] p 203 A91-23550
- Probabilistic structural analysis: Introductory remarks p 204 A91-24326
- The L sub 1 finite element method for pure convection problems [NASA-TM-103773] p 222 A91-24817
- Microfracture in high temperature metal matrix crossply laminates [NASA-TM-104381] p 101 A91-25198

- Analytical and experimental study of vibrations in a gear transmission
[NASA-TM-104434] p 187 N91-25395
- Probability of failure and risk assessment of propulsion structural components
[NASA-TM-102323] p 205 N91-25436
- Tuned optimization of extended reacting acoustic liners
[NASA-TM-104431] p 228 N91-25817
- A three-dimensional finite-element thermal/mechanical analytical technique for high-performance traveling wave tubes
[NASA-TP-3081] p 134 N91-27436
- How to determine spiral bevel gear tooth geometry for finite element analysis
[NASA-TM-105150] p 190 N91-30537
- Least-squares solution of incompressible Navier-Stokes equations with the p-version of finite elements
[NASA-TM-105203] p 223 N91-31911
- FINITE VOLUME METHOD**
- Calculation of turbulence-driven secondary motion in ducts with arbitrary cross section p 151 A91-34132
- Solution of steady-state, two-dimensional conservation laws by mathematical programming p 221 A91-35956
- Computational modeling of the pressurization process in a NASP vehicle propellant tank experimental simulation
[AIAA PAPER 91-2407] p 124 A91-41771
- Performance and flow calculations for a gaseous H₂/O₂ thruster p 63 A91-48843
- FINIS**
- Advanced materials for space nuclear power systems
[AIAA PAPER 91-3530] p 88 A91-53704
- Advanced materials for space nuclear power systems
[NASA-TM-105171] p 112 N91-29298
- FIRE PREVENTION**
- Radiation from gas-jet diffusion flames in microgravity environments
[AIAA PAPER 91-0719] p 104 A91-19432
- FIRES**
- Fire suppression in human-crew spacecraft
[NASA-TM-104334] p 44 N91-21182
- FLAME PROPAGATION**
- Particle cloud flames in acoustic fields p 105 A91-20589
- Radiative structures of lycopodium-air flames in low gravity p 105 A91-30003
- A study of hydrogen diffusion flames using PDF turbulence model
[AIAA PAPER 91-1780] p 106 A91-45549
- Heat transfer to a thin solid combustible in flame spreading at microgravity p 106 A91-51449
- FLAME SPECTROSCOPY**
- Radiation from gas-jet diffusion flames in microgravity environments
[AIAA PAPER 91-0719] p 104 A91-19432
- FLAME TEMPERATURE**
- A CFD study of jet mixing in reduced flow areas for lower combustor emissions
[AIAA PAPER 91-2460] p 23 A91-41788
- A CFD study of jet mixing in reduced flow areas for lower combustor emissions
[NASA-TM-104411] p 32 N91-23185
- FLAMES**
- Determination of alloy content from plume spectral measurements
[AIAA PAPER 91-2531] p 88 A91-44284
- Determination of alloy content from plume spectral measurements
[NASA-TM-104442] p 89 N91-24341
- FLAT PLATES**
- Verification of the Proteus two-dimensional Navier-Stokes code for flat plate and pipe flows
[AIAA PAPER 91-2013] p 153 A91-41678
- Development of a laser-induced heat flux technique for measurement of convective heat transfer coefficients in a supersonic flowfield
[NASA-TM-103778] p 13 N91-19063
- Wind tunnel wall effects in a linear oscillating cascade
[NASA-TM-103690] p 27 N91-19098
- Experimental study of boundary layer transition on a heated flat plate
[NASA-TM-103779] p 14 N91-21061
- Verification of the proteus two-dimensional Navier-Stokes code for flat plate and pipe flows
[NASA-TM-105160] p 168 N91-30462
- A k-epsilon modeling of near wall turbulence
[NASA-TM-105238] p 170 N91-32460
- FLEXIBILITY**
- Flexible fluoropolymer filled protective coatings p 121 N91-24062
- FLEXIBLE BODIES**
- High-temperature, flexible, thermal barrier seal
[NASA-CASE-LEW-14672-1] p 189 N91-27560

FLIGHT CONTROL

- Integrated flight/propulsion control system design based on a centralized approach p 36 A91-22950
- Civil air transport - A fresh look at power-by-wire and fly-by-light p 36 A91-31030
- The NASA Lewis integrated propulsion and flight control simulator
[AIAA PAPER 91-2969] p 38 A91-47847
- Application of an integrated flight/propulsion control design methodology to a STOVL aircraft
[AIAA PAPER 91-2792] p 36 A91-49793
- Fiber-optic-based controls p 230 N91-20102
- Advanced aeropropulsion controls technology p 29 N91-20103
- IMPAC: An Integrated Methodology for Propulsion and Airframe Control
[NASA-TM-103805] p 30 N91-20122
- A method for partitioning centralized controllers
[NASA-TM-4276] p 36 N91-20133
- Integrated flight/propulsion control system design based on a decentralized, hierarchical approach
[NASA-TM-103678] p 31 N91-21137
- Integrated flight/propulsion control design for a STOVL aircraft using H-infinity control design techniques
[NASA-TM-104340] p 31 N91-21140
- Civil air transport: A fresh look at power-by-wire and fly-by-light p 37 N91-23053
- The NASA Lewis integrated propulsion and flight control simulator
[NASA-TM-105147] p 21 N91-27157
- Application of an integrated flight/propulsion control design methodology to a STOVL aircraft
[NASA-TM-105254] p 37 N91-32143
- FLIGHT PATHS**
- Paramagnetic propellant orientation
[AIAA PAPER 91-2325] p 125 A91-44197
- Paramagnetic propellant orientation
[NASA-TM-104390] p 166 N91-24527
- FLIGHT SAFETY**
- NASA's aircraft icing technology program p 19 N91-20120
- FLIGHT SIMULATION**
- An AD100 implementation of a real-time STOVL aircraft propulsion system
[NASA-TM-103683] p 26 N91-13457
- NASA's aircraft icing technology program p 19 N91-20120
- The NASA Lewis integrated propulsion and flight control simulator
[NASA-TM-105147] p 21 N91-27157
- FLIGHT SIMULATORS**
- The NASA Lewis integrated propulsion and flight control simulator
[AIAA PAPER 91-2969] p 38 A91-47847
- FLIGHT TESTS**
- In-flight source noise of an advanced full-scale single-rotation propeller
[AIAA PAPER 91-0594] p 226 A91-21547
- Aeroacoustics of advanced propellers p 226 A91-24317
- Effects of horizontal tail ice on longitudinal aerodynamic derivatives p 36 A91-38547
- Recent results from the InP homojunction cell module on the LIPS III spacecraft p 140 A91-41971
- High altitude AMO testing of PV concentrator lens elements - Air Mass Zero p 207 A91-41978
- Preliminary results from the Advanced Photovoltaic Experiment flight test p 39 A91-41980
- Static performance tests of a flight-type STOVL ejector
[AIAA PAPER 91-1902] p 24 A91-44050
- Inflight source noise of an advanced full-scale single-rotation propeller
[NASA-TM-103687] p 12 N91-19045
- Static performance tests of a flight-type STOVL ejector
[NASA-TM-104437] p 33 N91-24201
- FLOW CHARACTERISTICS**
- A time-accurate implicit method for chemically reacting flows at all Mach numbers
[AIAA PAPER 91-0581] p 149 A91-21542
- Flow visualization studies of the internal flow characteristics in a simulated mixed flow vectored thrust ASTOVL engine configuration
[AIAA PAPER 91-1689] p 23 A91-42556
- Unstable viscous wall modes in rotating pipe flow
[AIAA PAPER 91-1801] p 154 A91-42599
- Slush hydrogen propellant production, transfer, and expulsion studies at the NASA K-Site Facility
[AIAA PAPER 91-3550] p 125 A91-53710
- Stirling engine: Available tools for long-life assessment
[NASA-TM-103660] p 200 N91-12980
- A comparison of CFD predictions and experimental results for a Mach 5 inlet p 28 N91-20094

- A model for the space shuttle main engine high pressure oxidizer turbopump shaft seal system
[NASA-TM-103697] p 184 N91-20489
- An unconditionally stable Runge-Kutta method for unsteady rotor-stator interaction p 165 N91-24337
- Slush hydrogen propellant production, transfer, and expulsion studies at the NASA K-Site Facility
[NASA-TM-105191] p 127 N91-28449
- FLOW DISTORTION**
- A design strategy for the use of vortex generators to manage inlet-engine distortion using computational fluid dynamics
[AIAA PAPER 91-2474] p 6 A91-44259
- Effects of inlet distortion on the development of secondary flows in a subsonic axial inlet compressor rotor
[NASA-TM-104356] p 31 N91-23179
- A design strategy for the use of vortex generators to manage inlet-engine distortion using computational fluid dynamics
[NASA-TM-104436] p 16 N91-24131
- FLOW DISTRIBUTION**
- Effect of acoustic excitation on stalled flows over an airfoil
[AIAA PAPER 90-4009] p 1 A91-12521
- Spatial evolution of nonlinear acoustic mode instabilities on hypersonic boundary layers p 225 A91-12973
- Experimental investigation of a single flush-mounted hypermixing nozzle
[AIAA PAPER 90-5240] p 21 A91-14466
- Modern CFD applications for the design of a reacting shear layer facility
[AIAA PAPER 91-0577] p 149 A91-21540
- A steady effect of acoustic excitation on transitory stall
[AIAA PAPER 91-0043] p 2 A91-22499
- The aerodynamic characteristics of vortex ingestion for the F/A-18 inlet duct
[AIAA PAPER 91-0130] p 3 A91-26192
- Numerical simulation of ice growth on a MS-317 swept wing geometry
[AIAA PAPER 91-0263] p 19 A91-26193
- Calculation of turbulent flow in complex geometries with a second-moment closure model p 152 A91-38741
- Hot gas ingestion test results of a two-poster vectored thrust concept with flow visualization in the NASA Lewis 9- by 15-foot low speed wind tunnel
[AIAA PAPER 90-2268] p 4 A91-40561
- CFD analysis of a hydrogen fueled ramjet engine at Mach 3.44
[AIAA PAPER 91-1919] p 23 A91-41653
- A three-dimensional Navier-Stokes stage analysis of the flow through a compact radial turbine
[AIAA PAPER 91-2564] p 23 A91-41815
- Navier-Stokes simulation of the supersonic combustion flowfield in a ram accelerator
[AIAA PAPER 91-1916] p 155 A91-44057
- A design strategy for the use of vortex generators to manage inlet-engine distortion using computational fluid dynamics
[AIAA PAPER 91-2474] p 6 A91-44259
- An analysis of the viscous flow through a compact radial turbine by the average passage approach
[ASME PAPER 90-GT-64] p 6 A91-44545
- Flow visualization in a simulated brush seal
[ASME PAPER 90-GT-217] p 173 A91-44633
- Experimental and analytical comparison of flowfields in a 110 N (25 Lbf) H₂/O₂ rocket
[AIAA PAPER 91-2283] p 62 A91-45802
- Mixing of multiple jets with a confined subsonic crossflow - Summary of NASA-supported experiments and modeling
[AIAA PAPER 91-2458] p 7 A91-45813
- Space Shuttle Main Engine nozzle mounted optic for throat plane spectroscopy
[AIAA PAPER 91-2524] p 49 A91-45816
- Results from computational analysis of a mixed compression supersonic inlet
[AIAA PAPER 91-2581] p 7 A91-45818
- Application of an efficient hybrid scheme for aeroelastic analysis of advanced propellers p 7 A91-52315
- VSTOL ground effects testing with flow visualization and image enhancement
[AIAA PAPER 91-3145] p 8 A91-54061
- Computational fluid dynamics at the Lewis Research Center: An overview p 8 N91-10842
- A numerical study of the hot gas environment around a STOVL aircraft in ground proximity p 10 N91-10887
- CFD analysis for high speed inlets p 10 N91-10888
- Effect of acoustic excitation on stalled flows over an airfoil
[NASA-TM-103183] p 10 N91-11675
- Unsteady blade-surface pressures on a large-scale advanced propeller: Prediction and data
[NASA-TM-103218] p 69 N91-11799

- Near-field noise of a single-rotation propfan at an angle of attack
[NASA-TM-103645] p 227 N91-12316
- A steady effect of acoustic excitation on transitory stall
[NASA-TM-103689] p 11 N91-13420
- Numerical simulation of ice growth on a MS-317 swept wing geometry
[NASA-TM-103705] p 11 N91-14310
- A numerical and experimental analysis of reactor performance and deposition rates for CVD on monofilaments
[NASA-TM-103631] p 130 N91-14500
- The aerodynamic characteristics of vortex ingestion for the F/A-18 inlet duct
[NASA-TM-103703] p 70 N91-15303
- Improved visualization of flow field measurements
[NASA-TM-103679] p 12 N91-19044
- Development of a laser-induced heat flux technique for measurement of convective heat transfer coefficients in a supersonic flowfield
[NASA-TM-103778] p 13 N91-19063
- Wind tunnel wall effects in a linear oscillating cascade
[NASA-TM-103690] p 27 N91-19098
- Experimental investigation of a single flush-mounted hypermixing nozzle
[NASA-TM-103726] p 161 N91-19374
- A 2-D oscillating flow analysis in Stirling engine heat exchangers
[NASA-TM-103781] p 161 N91-19375
- Rotating pressure measurement system using an on board calibration standard
[NASA-TM-103676] p 176 N91-19401
- Unsteady blade pressure measurements for the SR-7A propeller at cruise conditions
[NASA-TM-103606] p 228 N91-19825
- NASA low-speed centrifugal compressor for 3-D viscous code assessment and fundamental flow physics research
[NASA-TM-103710] p 13 N91-20044
- An imaging system for PLIF/Mie measurements for a combustor flow
[NASA-TM-103714] p 27 N91-20084
- A comparison of CFD predictions and experimental results for a Mach 5 inlet
[NASA-TM-103791] p 164 N91-21447
- Inlets, ducts, and nozzles
[NASA-TM-103780] p 164 N91-21458
- Turbomachinery
[NASA-TM-103738] p 31 N91-20126
- Performance of a high-work, low-aspect-ratio turbine stator tested with a realistic inlet radial temperature gradient
[NASA-TM-103738] p 31 N91-20126
- Simulation of turbomachinery flows
[NASA-TM-103258] p 15 N91-21116
- The 3D computation of single-expansion-ramp and scramjet nozzles
[NASA-TM-103791] p 164 N91-21447
- Hot gas ingestion test results of a two-poster vectored thrust concept with flow visualization in the NASA Lewis 9- x 15-foot low speed wind tunnel
[NASA-TM-103258] p 15 N91-21116
- CFD for hypersonic propulsion
[NASA-TM-103791] p 164 N91-21447
- Application of computational fluid dynamics in high speed aeropropulsion
[NASA-TM-103780] p 164 N91-21458
- Effects of inlet distortion on the development of secondary flows in a subsonic axial inlet compressor rotor
[NASA-TM-104356] p 31 N91-23179
- A three-dimensional Navier-Stokes stage analysis of the flow through a compact radial turbine
[NASA-TM-104420] p 32 N91-23186
- Three-dimensional Euler time accurate simulations of fan rotor-stator interactions
[NASA-TM-102528] p 16 N91-24124
- A design strategy for the use of vortex generators to manage inlet-engine distortion using computational fluid dynamics
[NASA-TM-104436] p 16 N91-24131
- Mixing of multiple jets with a confined subsonic crossflow. Summary of NASA-supported experiments and modeling
[NASA-TM-104412] p 33 N91-24202
- Average-passage flow model development
[NASA-TM-104436] p 16 N91-24131
- Navier-Stokes simulation of the supersonic combustion flowfield in a ram accelerator
[NASA-TM-104439] p 166 N91-24541
- Comparison of SMAC, PISO, and iterative time-advancing schemes for unsteady flows
[NASA-TM-104406] p 167 N91-24550
- Parallel computing using a Lagrangian formulation
[NASA-TM-104446] p 215 N91-24745
- The design/analysis of flows through turbomachinery: A viscous/inviscid approach
[NASA-TM-104447] p 33 N91-25148
- Characterization of flow in a scroll duct
[NASA-CR-188612] p 167 N91-25367
- An experimental trace gas investigation of fluid transport and mixing in a circular-to-rectangular transition duct
[NASA-TM-104499] p 17 N91-27129
- Effect of tabs on the evolution of an axisymmetric jet
[NASA-TM-104472] p 34 N91-27159
- High-speed laser anemometry based on spectrally resolved Rayleigh scattering
[NASA-TM-104522] p 178 N91-27521
- Experimental and analytical comparison of flowfields in a 110 N (25 lbf) H2/O2 rocket
[NASA-TM-105175] p 82 N91-29230
- A laser-induced heat flux technique for convective heat transfer measurements in high speed flows
[NASA-TM-105177] p 168 N91-30472
- A qualitative view of cryogenic fluid injection into high speed flows
[NASA-TM-105139] p 169 N91-30473
- Calculation of a circular jet in crossflow with a multiple-time-scale turbulence model
[NASA-TM-104343] p 169 N91-30476
- Ground-based PIV and numerical flow visualization results from the surface tension driven convection experiment
[NASA-TM-105172] p 178 N91-30491
- Unsteady flowfield of a propfan at takeoff conditions
[NASA-TM-105223] p 18 N91-32075
- FLOW EQUATIONS**
- Second-order accurate nonoscillatory schemes for scalar conservation laws
[NASA-TM-105177] p 168 N91-30472
- Heat transfer in rotating serpentine passages with trips normal to the flow
[NASA-TM-103758] p 184 N91-19443
- Numerical investigation of an internal layer in turbulent flow over a curved hill
[NASA-TM-105223] p 18 N91-32075
- FLOW GEOMETRY**
- An experimental comparison of nonswirling and swirling flow in a circular-to-rectangular transition duct
[AIAA PAPER 91-0342] p 148 N91-21466
- Calculation of turbulence-driven secondary motion in ducts with arbitrary cross section
[NASA-TM-104359] p 14 N91-21115
- The design/analysis of flows through turbomachinery - A viscous/inviscid approach
[AIAA PAPER 91-2010] p 153 N91-41677
- Mixing of multiple jets with a confined subsonic crossflow - Summary of NASA-supported experiments and modeling
[AIAA PAPER 91-2458] p 7 N91-45813
- An experimental comparison of nonswirling and swirling flow in a circular-to-rectangular transition duct
[NASA-TM-104359] p 14 N91-21115
- Mixing of multiple jets with a confined subsonic crossflow. Summary of NASA-supported experiments and modeling
[NASA-TM-104412] p 33 N91-24202
- FLOW MEASUREMENT**
- Improved visualization of flow field measurements
[AIAA PAPER 91-0273] p 3 A91-26331
- Progress toward synergistic hypermixing nozzles
[AIAA PAPER 91-2264] p 25 A91-45800
- NASA low-speed centrifugal compressor for 3-D viscous code assessment and fundamental flow physics research
[NASA-TM-103710] p 13 N91-20044
- An imaging system for PLIF/Mie measurements for a combustor flow
[NASA-TM-103714] p 27 N91-20084
- Effects of inlet distortion on the development of secondary flows in a subsonic axial inlet compressor rotor
[NASA-TM-104356] p 31 N91-23179
- Progress toward synergistic hypermixing nozzles
[NASA-TM-105169] p 18 N91-26310
- Experimental investigation of turbulent flow through a circular-to-rectangular transition duct
[NASA-TM-105210] p 18 N91-31106
- FLOW STABILITY**
- Modern developments in shear flow control with swirl
[NASA-TM-104412] p 33 N91-24202
- Nonlinear spatial evolution of externally excited instability waves in free shear layers
[NASA-TM-104356] p 31 N91-23179
- Nonlinear evolution of subsonic and supersonic disturbances on a compressible free shear layer
[NASA-TM-105169] p 18 N91-26310
- Stability of compressible Taylor-Couette flow
[AIAA PAPER 91-1642] p 153 A91-42541
- Influence of thickness and camber on the aeroelastic stability of supersonic throughflow fans
[NASA-TM-104412] p 33 N91-24202
- The effects of rotation on initially anisotropic homogeneous flows
[NASA-TM-104412] p 33 N91-24202
- Turbulent boundary layer separation over a rearward facing ramp and its control through mechanical excitation
[NASA-TM-103702] p 160 N91-19370
- A comparison of numerical methods for the Rayleigh equation in unbounded domains
[NASA-TM-105179] p 223 N91-30865
- FLOW THEORY**
- The aerodynamic characteristics of vortex ingestion for the F/A-18 inlet duct
[AIAA PAPER 91-0130] p 3 A91-26192
- The aerodynamic characteristics of vortex ingestion for the F/A-18 inlet duct
[NASA-TM-103703] p 70 N91-15303
- FLOW VELOCITY**
- Particle image fields and partial coherence
[NASA-TM-103703] p 70 N91-15303
- Performance characterization of a segmented anode arcjet thruster
[NASA-TM-103227] p 67 N91-10118
- Improved visualization of flow field measurements
[NASA-TM-103679] p 12 N91-19044
- Effects of inlet distortion on the development of secondary flows in a subsonic axial inlet compressor rotor
[NASA-TM-104356] p 31 N91-23179
- High-speed laser anemometry based on spectrally resolved Rayleigh scattering
[NASA-TM-104522] p 178 N91-27521
- FLOW VISUALIZATION**
- Flow visualization and quantitative velocity and pressure measurements in simulated single and double brush seals
[AIAA PAPER 91-0311] p 148 N91-21452
- A comparative flow visualization study of thermocapillary flow in drops in liquid-liquid systems
[AIAA PAPER 91-0273] p 3 A91-26331
- Hot gas ingestion test results of a two-poster vectored thrust concept with flow visualization in the NASA Lewis 9- by 15-foot low speed wind tunnel
[AIAA PAPER 90-2268] p 4 A91-40561
- Effects of brush seal morphology on leakage and pressure drops
[AIAA PAPER 91-2106] p 182 A91-41700
- Flow visualization studies of the internal flow characteristics in a simulated mixed flow vectored thrust ASTOVL engine configuration
[AIAA PAPER 91-1689] p 23 A91-42556
- Flow visualization of a rocket injector spray using gelled propellant simulants
[AIAA PAPER 91-2198] p 59 A91-44151
- Flow visualization in a simulated brush seal
[ASME PAPER 90-GT-217] p 173 A91-44633
- Some preliminary results of brush seal/rotor interference effects on leakage at zero and low rpm using a tapered-plug rotor
[AIAA PAPER 91-3390] p 182 A91-45820
- VSTOL ground effects testing with flow visualization and image enhancement
[AIAA PAPER 91-3145] p 8 A91-54061
- Improved visualization of flow field measurements
[NASA-TM-103679] p 12 N91-19044
- An imaging system for PLIF/Mie measurements for a combustor flow
[NASA-TM-103714] p 27 N91-20084
- Flow visualization and hot gas ingestion characteristics of a vectored thrust STOV concept
[NASA-TM-103258] p 15 N91-21116
- Hot gas ingestion test results of a two-poster vectored thrust concept with flow visualization in the NASA Lewis 9- x 15-foot low speed wind tunnel
[NASA-TM-103258] p 15 N91-21116
- Visualization techniques to experimentally model flow and heat transfer in turbine and aircraft flow passages
[NASA-TM-4272] p 167 N91-27489
- FLUE GASES**
- Mechanisms and modeling of the effects of additives on the nitrogen oxides emission
[AIAA PAPER 91-0479] p 124 A91-40560
- Mechanisms and modeling of the effects of additives on the nitrogen oxides emission
[NASA-TM-103765] p 126 N91-22464
- FLUID DYNAMICS**
- Interfacial dynamics of two liquids under an oscillating gravitational field
[AIAA PAPER 91-1566] p 5 A91-40740
- Numerical flux formulas for the Euler and Navier-Stokes equations. II - Progress in flux-vector splitting
[AIAA PAPER 91-1566] p 5 A91-40740
- Numerical solution for the velocity-derivative skewness of a low Reynolds-number turbulent-like decaying Navier-Stokes flow
[NASA-TM-103765] p 126 N91-22464
- Spacelab qualified infrared imager for microgravity science applications
[NASA-TM-103765] p 126 N91-22464
- Numerical simulation of nonlinear development of instability waves
[E-4658] p 8 N91-10849

- Three-dimensional computed tomography from interferometric measurements within a narrow cone of views
[NASA-TM-103257] p 176 N91-19404
- Numerical flux formulas for the Euler and Navier-Stokes equations. 2: Progress in flux-vector splitting
[NASA-TM-104353] p 15 N91-22084
- Research and technology
[NASA-TM-103759] p 243 N91-23072
- Microgravity research at LeRC
[NASA-TM-102521] p 128 N91-24464
- Turbulent fluid motion 2: Scalars, vectors, and tensors
[NASA-TM-103756] p 167 N91-27487
- Calculation of a circular jet in crossflow with a multiple-time-scale turbulence model
[NASA-TM-104343] p 169 N91-30476
- A comparison of numerical methods for the Rayleigh equation in unbounded domains
[NASA-TM-105179] p 223 N91-30865
- A critical comparison of two-equation turbulence models
[NASA-TM-105237] p 169 N91-31597
- A k-epsilon modeling of near wall turbulence
[NASA-TM-105238] p 170 N91-32460
- FLUID FILMS**
- Extension of transonic flow computational concepts in the analysis of cavitated bearings
[ASME PAPER 90-TRIB-40] p 150 A91-29474
- Inertia effects in thin film flow with a corrugated boundary
p 151 A91-32691
- On the numerical solution of the dynamically loaded hydrodynamic lubrication of the point contact
p 180 A91-33461
- A high speed photography study of cavitation in a dynamically loaded journal bearing
[ASME PAPER 90-TRIB-19] p 180 A91-34806
- Extension of transonic flow computational concepts in the analysis of cavitated bearings
[NASA-TM-103214] p 160 N91-16304
- Two reference time scales for studying the dynamic cavitation of liquid films
[NASA-TM-103673] p 160 N91-19369
- A system-approach to the elastohydrodynamic lubrication point-contact problem
[NASA-TM-104342] p 165 N91-23439
- FLUID FLOW**
- Generalized conjugate-gradient methods for the Navier-Stokes equations
[AIAA PAPER 91-1556] p 5 A91-40730
- Development of braided rope seals for hypersonic engine applications. II - Flow modeling
[AIAA PAPER 91-2495] p 182 A91-41800
- Liquid sheet radiator apparatus
[NASA-CASE-LEW-14295-1] p 130 N91-15424
- A finite element model of conduction, convection, and phase change near a solid/melt interface
[NASA-TM-103721] p 162 N91-20417
- Development of braided rope seals for hypersonic engine applications. Part 2: Flow modeling
[NASA-TM-104371] p 186 N91-22571
- A study of high speed flows in an aircraft transition duct
[NASA-TM-104449] p 17 N91-26122
- The NASA Lewis Research Center Internal Fluid Mechanics Facility
[NASA-TM-105187] p 39 N91-30163
- Ground-based PIV and numerical flow visualization results from the surface tension driven convection experiment
[NASA-TM-105172] p 178 N91-30491
- FLUID INJECTION**
- A qualitative view of cryogenic fluid injection into high speed flows
[NASA-TM-105139] p 169 N91-30473
- FLUID JETS**
- Cryogenic liquid-jet breakup in two-fluid atomizers
[NASA-TM-103734] p 176 N91-19402
- CFD analysis of jet mixing in low NO_x flametube combustors
[NASA-TM-104466] p 33 N91-26146
- Spray measurements of aerothermodynamic effect on disintegrating liquid jets
[NASA-TM-104501] p 178 N91-27510
- FLUID MANAGEMENT**
- Transient cryogenic liquid discharge in normal and micro-gravity
[AIAA PAPER 91-0486] p 124 A91-19324
- The COLD-SAT experiment for cryogenic fluid management technology
p 46 A91-29799
- Improved thermodynamic modelling of the no-vent fill process and correlation with experimental data
[AIAA PAPER 91-1379] p 129 A91-43444
- Fuel Systems Architecture (FSA) evaluation criteria and concept evaluation methodology
[AIAA PAPER 91-3479] p 65 A91-52384
- The NASA Cryogenic Fluid Management Technology Program Plan
[AIAA PAPER 91-3553] p 130 A91-52436
- NASA cryogenic fluid management space experiment efforts
[AIAA PAPER 91-3538] p 130 A91-53701
- The COLD-SAT experiment for cryogenic fluid management technology
p 126 N91-24263
- NASA cryogenic fluid management space experiment efforts, 1960-1990
[NASA-TM-103752] p 243 N91-30073
- The NASA cryogenic fluid management technology program plan
[NASA-TM-105256] p 86 N91-32161
- FLUID MECHANICS**
- Optical techniques for determination of normal shock position in supersonic flows for aerospace applications
p 174 A91-55530
- Simulation of turbomachinery flows
p 9 N91-10880
- A summary of existing and planned experiment hardware for low-gravity fluids research
[NASA-TM-103706] p 160 N91-19371
- Aeropropulsion 1991
[NASA-CP-10063] p 27 N91-20086
- Internal fluid mechanics research
p 161 N91-20095
- Inlets, ducts, and nozzles
p 162 N91-20096
- The NASA Lewis Research Center Internal Fluid Mechanics Facility
[NASA-TM-105187] p 39 N91-30163
- FLUORIDES**
- Graphite fluoride fibers and their applications in the space industry
[NASA-TM-103265] p 88 N91-11062
- Composite bearing and seal materials for advanced heat engine applications to 900 C
[NASA-TM-103612] p 95 N91-15318
- Graphite fluoride fiber polymer composite material
[NASA-CASE-LEW-14472-1] p 95 N91-15320
- Industrial applications of graphite fluoride fibers
p 100 N91-23040
- The PM-200 lubrication system
p 121 N91-23044
- FLUORINATION**
- Graphite fluoride fibers and their applications in the space industry
[NASA-TM-103265] p 88 N91-11062
- Industrial applications of graphite fluoride fibers
p 100 N91-23040
- FLUORINE COMPOUNDS**
- Substituted 1,1,1-triaryl-2,2,2-trifluoroethanes and processes for their synthesis
[NASA-CASE-LEW-14345-4] p 90 N91-25185
- FLUOROHYDROCARBONS**
- Substituted 1,1,1-triaryl-2,2,2-trifluoroethanes and processes for their synthesis
[NASA-CASE-LEW-14345-3] p 89 N91-17141
- FLUOROPOLYMERS**
- Flexible fluoropolymer filled protective coatings
p 121 N91-24062
- FLUTTER**
- Localization of aeroelastic modes in mistuned high-energy turbines
[AIAA PAPER 91-3379] p 198 A91-44319
- Optical measurement of unducted fan flutter
[NASA-TM-103285] p 27 N91-15174
- Localization of aeroelastic modes in mistuned high-energy turbines
[NASA-TM-104445] p 204 N91-24659
- FLUTTER ANALYSIS**
- Cascade flutter analysis with transient response aerodynamics
[AIAA PAPER 91-0747] p 21 A91-19448
- Flutter analysis of cascades using a two dimensional Euler solver
[AIAA PAPER 91-1681] p 6 A91-45548
- Cascade flutter analysis with transient response aerodynamics
[NASA-TM-103746] p 201 N91-19475
- FLUX (RATE)**
- Self-pressurization of a lightweight liquid hydrogen storage tank subjected to low heat flux
[NASA-TM-103804] p 126 N91-20324
- FLUX DENSITY**
- High frequency, high temperature specific core loss and dynamic B-H hysteresis loop characteristics of soft magnetic alloys
p 138 A91-37988
- FLUX VECTOR SPLITTING**
- Numerical flux formulas for the Euler and Navier-Stokes equations. II - Progress in flux-vector splitting
[AIAA PAPER 91-1566] p 5 A91-40740
- Development of a new flux splitting scheme
p 153 A91-40793
- Flux-vector splitting algorithm for chain-rule conservation-law form
p 221 A91-45109
- Flux splitting algorithms for two-dimensional viscous flows with finite-rate chemistry
p 10 N91-10894
- Numerical flux formulas for the Euler and Navier-Stokes equations. 2: Progress in flux-vector splitting
[NASA-TM-104353] p 15 N91-22084
- A new flux splitting scheme
[NASA-TM-104404] p 222 N91-22814
- High-Order Polynomial Expansions (HOPE) for flux-vector splitting
[NASA-TM-104452] p 222 N91-25739
- FLY BY WIRE CONTROL**
- Civil air transport: A fresh look at power-by-wire and fly-by-light
p 37 N91-23053
- FOIL BEARINGS**
- Liquid hydrogen turbopump foil bearing
[AIAA PAPER 91-2108] p 182 A91-41701
- FOLDING STRUCTURES**
- The telescoping boom radiator concept for multimegawatt space power systems
[AIAA PAPER 91-3497] p 158 A91-52395
- FORCED CONVECTION**
- Turbine blading designed for high heat load space propulsion applications
p 50 A91-10338
- A PCM/forced convection conjugate transient analysis of energy storage systems with annular and countercurrent flows
p 150 A91-27166
- FORCED VIBRATION**
- Euler flow predictions for an oscillating cascade using a high resolution wave-split scheme
[NASA-TM-104377] p 16 N91-24107
- FORECASTING**
- Key issues in space nuclear power
[NASA-TM-103656] p 71 N91-19179
- FORMULATIONS**
- Numerical simulation of nonlinear development of instability waves
[E-4658] p 8 N91-10849
- FORWARD SCATTERING**
- Use of rotating pinholes and reticles for calibration of cloud droplet instrumentation
p 171 A91-30371
- FOURIER SERIES**
- Equivalence of Green's function and the Fourier series representation of composites with periodic microstructure
p 91 A91-16889
- FRACTOGRAPHY**
- Comparison of dynamic fatigue behavior between SiC whisker-reinforced composite and monolithic silicon nitrides
[NASA-TM-103707] p 119 N91-19293
- FRACTURE MECHANICS**
- Progressive fracture in composites subjected to hygrothermal environment
[AIAA PAPER 91-1140] p 91 A91-31919
- The potential for ductility enhancement from surface and interface dislocation sources in NiAl
p 109 A91-39292
- Hot corrosion of silicon carbide and silicon nitride at 1000 C
p 117 A91-55698
- In situ X-ray monitoring of damage accumulation in SiC/RBSN tensile specimens
p 94 A91-56942
- Effects of high pressure nitrogen on the thermal stability of SiC fibers
[NASA-TM-103245] p 96 N91-16075
- The method of lines in analyzing solids containing cracks
[NASA-TM-103626] p 201 N91-19477
- In-situ x-ray monitoring of damage accumulation in SiC/RBSN tensile specimens
[NASA-TM-103733] p 99 N91-22402
- Structural design methodologies for ceramic-based material systems
[NASA-TM-103097] p 121 N91-22460
- Analysis of some compliance calibration data for chevron-notch bar and rod specimens
[NASA-TM-104367] p 203 N91-22594
- Overview of the fatigue/fracture/life working group program at the Lewis Research Center
p 203 N91-24308
- Prospects for ductility and toughness enhancement of NiAl by ductile phase reinforcement
[NASA-TM-103796] p 112 N91-27324
- FRACTURE STRENGTH**
- Composite structure global fracture toughness via computational simulation
p 216 A91-11819
- Ultrasonic imaging of textured alumina
p 191 A91-18596
- Effect of high temperature hydrogen exposure on the strength and microstructure of mullite
p 114 A91-19780
- Intrinsic bond strength of metal films on polymer substrates
p 88 A91-39246
- 1000 to 1200 K time-dependent compressive deformation of single-crystalline and polycrystalline B2 Ni-40Al
p 109 A91-43670
- Numerical, micro-mechanical prediction of crack growth resistance in a fibre-reinforced/brittle matrix composite
p 199 A91-51916
- Influence of the Si3N4 microstructure on its R-curve and fatigue behavior
p 117 A91-56931

- Comparison of dynamic fatigue behavior between SiC whisker-reinforced composite and monolithic silicon nitrides
[NASA-TM-103707] p 119 N91-19293
- The method of lines in analyzing solids containing cracks
[NASA-TM-103626] p 201 N91-19477
- Fully articulated four-point-bend loading fixture
[NASA-CASE-LEW-14776-1] p 185 N91-21540
- Analysis of some compliance calibration data for chevron-notch bar and rod specimens
[NASA-TM-104367] p 203 N91-22594
- Mechanical behavior and failure phenomenon of an in situ-toughened silicon nitride
[NASA-TM-103741] p 121 N91-23311
- Evaluation and ranking of candidate ceramic wafer engine seal materials
[NASA-TM-103795] p 187 N91-23515
- Computational simulation of acoustic fatigue for hot composite structures
[NASA-TM-104379] p 203 N91-23548
- Comparison of Weibull strength parameters from flexure and spin tests of brittle materials
[NASA-TM-104414] p 187 N91-24593
- Surface fatigue life of M50NiL and AISI 9310 spur gears and R C bars
[NASA-TM-104496] p 189 N91-27569
- Elevated-temperature fracture resistances (K(sub IC), R-curves, gamma sub (omega OF)) of monolithic and composite ceramics using chevron-notched, bend tests
[NASA-TM-105090] p 123 N91-28418
- FRACTURES (MATERIALS)**
- Metal matrix composites microfracture - Computational simulation p 90 A91-11815
- Microfracture in high temperature metal matrix crossply laminates
[NASA-TM-104381] p 101 N91-25198
- FRACTURING**
- Calculation of Weibull strength parameters, Batdorf flaw density constants and related statistical quantities using PC-CARES
[NASA-TM-103247] p 199 N91-10332
- Prospects for ductility and toughness enhancement of NiAl by ductile phase reinforcement
[NASA-TM-103796] p 112 N91-27324
- Progressive fracture in composites subjected to hygrothermal environment
[NASA-TM-105230] p 103 N91-32182
- FRAMES (DATA PROCESSING)**
- High Resolution, High Frame Rate Video Technology
[NASA-CP-3080] p 175 N91-14574
- Results of the users' requirements survey p 175 N91-14575
- FREE BOUNDARIES**
- A system-approach to the elastohydrodynamic lubrication point-contact problem
[NASA-TM-104342] p 165 N91-23439
- FREE FLOW**
- Experimental investigation of a single flush-mounted hypermixing nozzle
[AIAA PAPER 90-5240] p 21 A91-14466
- Turbulence enhancement in free shear flows under multifrequency excitation p 152 A91-38737
- Increased heat transfer to a cylindrical leading edge due to spanwise variations in the freestream velocity
[AIAA PAPER 91-1739] p 155 A91-43623
- The effect of small streamwise velocity distortion on the boundary layer flow over a thin flat plate with application to boundary layer stability theory p 161 N91-19372
- [NASA-TM-103668] p 161 N91-19372
- Experimental study of boundary layer transition on a heated flat plate p 14 N91-21061
- [NASA-TM-103779] p 14 N91-21061
- Increased heat transfer to a cylindrical leading edge due to spanwise variations in the freestream velocity
[NASA-TM-104464] p 100 N91-24359
- FREE JETS**
- An experimental investigation of nozzle-exit boundary layers of highly heated free jets
[ASME PAPER 90-GT-255] p 155 A91-44662
- A qualitative view of cryogenic fluid injection into high speed flows
[NASA-TM-105139] p 169 N91-30473
- FREE VIBRATION**
- Free vibrations of delaminated beams
[AIAA PAPER 91-1241] p 197 A91-32129
- FREE-PISTON ENGINES**
- Solar powered Stirling cycle electrical generator p 211 N91-23054
- Design of multihundredwatt DIPS for robotic space missions
[NASA-TM-104401] p 75 N91-24232
- Small Stirling dynamic isotope power system for multihundred-watt robotic missions
[NASA-TM-104460] p 78 N91-25182
- Comparative survey of dynamic analyses of free-piston Stirling engines
[NASA-TM-104491] p 224 N91-26870
- Update on results of SPRE testing at NASA Lewis
[NASA-TM-104425] p 79 N91-27208
- Status of NASA's Stirling Space Power Converter Program
[NASA-TM-104512] p 214 N91-32569
- FREEZING**
- Icing tests of a model main rotor p 18 A91-17218
- FREQUENCY ASSIGNMENT**
- NASA developments in solid state power amplifiers p 143 N91-18298
- FREQUENCY DISTRIBUTION**
- Induction motor control p 137 A91-30893
- FREQUENCY HOPPING**
- Study on the spectral efficiency of SFH-GMSK in land mobile telephone communication by direct simulation p 132 A91-53176
- FREQUENCY MODULATION**
- Combinatorial FSK modulation for power-efficient high-rate communications
[AIAA PAPER 91-3532] p 133 A91-53708
- Combinatorial FSK modulation for power-efficient high-rate communications
[NASA-TM-105188] p 135 N91-29404
- FREQUENCY RANGES**
- Comparison of high temperature, high frequency core loss and dynamic B-H loops of two 50 Ni-Fe crystalline alloys and an iron-based amorphous alloy
[NASA-TM-105205] p 147 N91-32412
- FREQUENCY RESPONSE**
- Significant reduction in arc frequency biased solar cells: Observations, diagnostics, and mitigation technique(s) p 83 N91-30235
- FREQUENCY SHIFT KEYING**
- Combinatorial FSK modulation for power-efficient high-rate communications
[AIAA PAPER 91-3532] p 133 A91-53708
- Combinatorial FSK modulation for power-efficient high-rate communications
[NASA-TM-105188] p 135 N91-29404
- FRESNEL LENSES**
- Component and prototype panel testing of the mini-dome Fresnel lens photovoltaic concentrator array p 54 A91-38023
- High altitude AM0 testing of PV concentrator lens elements --- Air Mass Zero p 207 A91-41978
- The mini-dome Fresnel lens photovoltaic concentrator array - Current status of component and prototype panel testing p 57 A91-41989
- Mini-dome Fresnel lens photovoltaic concentrator development p 210 N91-19219
- Key results of the mini-dome Fresnel lens concentrator array development program under recently completed NASA and SDIO SBIR projects p 83 N91-30223
- FRICTION**
- Contact stresses in gear teeth - A new method of analysis p 182 A91-41683
- [AIAA PAPER 91-2022] p 182 A91-41683
- Uses of Auger and x ray photoelectron spectroscopy in the study of adhesion and friction p 118 N91-11922
- [NASA-TM-103266] p 118 N91-11922
- Tribological characteristics of silicon carbide whisker-reinforced alumina at elevated temperatures
[NASA-TM-103799] p 89 N91-22379
- Contact stresses in gear teeth: A new method of analysis p 186 N91-22570
- [NASA-TM-104397] p 186 N91-22570
- Dynamic measurements of gear tooth friction and load
[NASA-TM-103281] p 189 N91-27570
- An analysis of the wear behavior of SiC whisker reinforced alumina from 25 to 1200 C
[NASA-TM-104489] p 90 N91-29235
- FRICTION FACTOR**
- Fiber pushout test - A three-dimensional finite element computational simulation p 197 A91-33096
- The effect of coatings and liners on heat transfer in a dry shaft-bush tribosystem
[NASA-TM-102513] p 159 N91-12913
- FRICTION MEASUREMENT**
- A new test machine for measuring friction and wear in controlled atmospheres to 1200 C p 180 A91-33600
- FRICTION REDUCTION**
- Surface modification of Monel K-500 as a means of reducing friction and wear in high-pressure oxygen p 107 A91-16869
- Tribological properties of Ag/Ti films on Al₂O₃ ceramic substrates
[NASA-TM-103784] p 89 N91-19224
- FRONTS (METEOROLOGY)**
- Frontogenesis driven by horizontally quadratic distributions of density p 157 A91-48276
- FUEL CELLS**
- Space Electrochemical Research and Technology
[NASA-CP-3125] p 213 N91-32549
- The Au cathode in the system Li₂CO₃-CO₂-CO at 800 to 900 C p 213 N91-32551
- FUEL COMBUSTION**
- Evaluation of a hybrid kinetics/mixing-controlled combustion model for turbulent premixed and diffusion combustion using KIVA-II p 104 A91-12927
- [AIAA PAPER 90-2450] p 104 A91-12927
- Particle nonuniformity effects on particle cloud flames in low gravity p 104 A91-19431
- [AIAA PAPER 91-0718] p 104 A91-19431
- Radiative structures of lycopodium-air flames in low gravity p 105 A91-30003
- Pressure-coupled vaporization and combustion responses of liquid-fuel droplets in high-pressure environments p 106 A91-44192
- [AIAA PAPER 91-2310] p 106 A91-44192
- Fuel-rich, catalytic reaction experimental results --- fuel development for high-speed civil transport aircraft
[AIAA PAPER 91-2463] p 24 A91-44250
- Fuel-rich, catalytic reaction experimental results
[NASA-TM-104423] p 33 N91-24203
- Analytical combustion/emissions research related to the NASA high-speed research program
[NASA-TM-104521] p 34 N91-27165
- Nonlinear combustion instability model in two- to three-dimensions p 85 N91-31208
- [NASA-TM-102381] p 85 N91-31208
- FUEL CONSUMPTION**
- Prediction of the noise from a propeller at angle of attack p 225 A91-12470
- [AIAA PAPER 90-3954] p 225 A91-12470
- Civil air transport - A fresh look at power-by-wire and fly-by-light p 36 A91-31030
- FUEL CONTROL**
- A high-frequency servosystem for fuel control in hypersonic engines
[NASA-TM-104333] p 35 N91-31178
- FUEL CORROSION**
- Hot corrosion of silicon carbide and silicon nitride at 1000 C p 117 A91-55698
- FUEL INJECTION**
- Evaluation of a hybrid kinetics/mixing-controlled combustion model for turbulent premixed and diffusion combustion using KIVA-II p 104 A91-12927
- [AIAA PAPER 90-2450] p 104 A91-12927
- Jet-A fuel evaporation analysis in conical tube injectors p 149 A91-21467
- [AIAA PAPER 91-0345] p 149 A91-21467
- Effects of nozzle lip geometry on spray atomization and emissions advanced gas turbine combustors
[AIAA PAPER 91-2201] p 24 A91-44153
- Experimental study of cross-stream mixing in a cylindrical duct p 157 A91-45815
- [AIAA PAPER 91-2459] p 157 A91-45815
- Flow visualization and computational studies of a reverse flow circular combustor p 157 A91-48966
- Method of injecting fluid propellants into a rocket combustion chamber
[NASA-CASE-LEW-14846-2] p 78 N91-26200
- Experimental study of cross-stream mixing in a cylindrical duct p 34 N91-29187
- [NASA-TM-105180] p 34 N91-29187
- FUEL PRODUCTION**
- Production and use of metals and oxygen for lunar propulsion p 125 A91-53711
- [AIAA PAPER 91-3481] p 125 A91-53711
- Production and use of metals and oxygen for lunar propulsion p 81 N91-29222
- [NASA-TM-105195] p 81 N91-29222
- Technical prospects for utilizing extraterrestrial propellants for space exploration
[NASA-TM-105263] p 127 N91-31318
- FUEL SPRAYS**
- Jet-A fuel evaporation analysis in conical tube injectors p 149 A91-21467
- [AIAA PAPER 91-0345] p 149 A91-21467
- Radiative structures of lycopodium-air flames in low gravity p 105 A91-30003
- A detailed numerical investigation of Burke-Schumann gaseous and spray flames p 105 A91-41749
- [AIAA PAPER 91-2311] p 105 A91-41749
- Gas property effects on droplet size of simulated fuel sprays p 156 A91-45327
- Cryogenic transfer options for exploration missions
[AIAA PAPER 91-3541] p 158 A91-53714
- Cryogenic liquid-jet breakup in two-fluid atomizers
[NASA-TM-103734] p 176 N91-19402
- Spray measurements of aerothermodynamic effect on disintegrating liquid jets p 178 N91-27510
- [NASA-TM-104501] p 178 N91-27510
- Cryogenic transfer options for exploration missions
[NASA-TM-105197] p 168 N91-28538
- FUEL SYSTEMS**
- Fuel Systems Architecture (FSA) evaluation criteria and concept evaluation methodology
[AIAA PAPER 91-3479] p 65 A91-52384

FUEL TANK PRESSURIZATION

SUBJECT INDEX

FUEL TANK PRESSURIZATION

Computational modeling of the pressurization process in a NASP vehicle propellant tank experimental simulation

[AIAA PAPER 91-2407] p 124 A91-41771

A pressure control analysis of cryogenic storage systems

[AIAA PAPER 91-2405] p 59 A91-44228

A pressure control analysis of cryogenic storage systems

[NASA-TM-104409] p 126 N91-24460

FUEL TANKS

A review of candidate multilayer insulation systems for potential use on wet-launched LH2 tankage for the Space Exploration Initiative lunar missions

[AIAA PAPER 91-2176] p 43 A91-45793

Thermal performance of a liquid hydrogen tank multilayer insulation system at warm boundary temperatures of 630, 530, and 152 R

[AIAA PAPER 91-2400] p 43 A91-45812

Cryogenic transfer options for exploration missions

[AIAA PAPER 91-3541] p 158 A91-53714

In-flight and simulated aircraft fuel temperature measurements

[NASA-TM-103611] p 125 N91-15418

Thermal performance of a liquid hydrogen tank multilayer insulation system at warm boundary temperatures of 630, 530, and 152 R

[NASA-TM-104476] p 43 N91-25159

Cryogenic transfer options for exploration missions

[NASA-TM-105197] p 168 N91-28538

FUEL TESTS

Jet-A reaction mechanism study for combustion application

[AIAA PAPER 91-2355] p 106 A91-45810

FULL SCALE TESTS

Turbofan engine demonstration of sensor failure detection

[AIAA PAPER 91-2375] p 22 A91-29775

FUNCTIONAL DESIGN SPECIFICATIONS

Integrated flight/propulsion control system design based on a decentralized, hierarchical approach

[NASA-TM-103678] p 31 N91-21137

Characteristics of a future aeronautical satellite communications system

[NASA-TM-104389] p 20 N91-23102

FUNCTIONS (MATHEMATICS)

Mappings and accuracy for Chebyshev pseudo-spectral approximations

[NASA-TM-103630] p 221 N91-14781

FURNACES

Programmable multi-zone furnace for microgravity research

[AIAA PAPER 91-0781] p 127 A91-19463

Furnace for tensile/fatigue testing

[NASA-CASE-LEW-14848-1] p 42 N91-27175

FUSELAGES

A review of ice accretion data from a model rotor icing test and comparison with theory

[AIAA PAPER 91-0661] p 19 A91-22500

A review of ice accretion data from a model rotor icing test and comparison with theory

[NASA-TM-103712] p 11 N91-13421

G

GALACTIC CLUSTERS

Telescope search for a 3-eV to 8-eV axion

[AIAA PAPER 91-2874] p 239 A91-28714

GALACTIC EVOLUTION

The shock process and light-element production in supernova envelopes

[AIAA PAPER 91-33573] p 239 A91-33573

GALERKIN METHOD

Effect of surface deposits on electromagnetic waves propagating in uniform ducts

[NASA-TM-103282] p 133 N91-10208

A finite element model of conduction, convection, and phase change near a solid/melt interface

[NASA-TM-103721] p 162 N91-20417

Tuned optimization of extended reacting acoustic liners

[NASA-TM-104431] p 228 N91-25817

GALLIUM

The influence of interstitial Ga and interfacial Au₂P₃ on the electrical and metallurgical behavior of Au-contacted III-V semiconductors

[AIAA PAPER 91-42694] p 140 A91-42694

GALLIUM ANTIMONIDES

Lightweight concentrator module with 30 percent AMO efficient GaAs/GaSb tandem cells

[AIAA PAPER 91-41990] p 57 A91-41990

GALLIUM ARSENIDES

Low-temperature microwave characteristics of pseudomorphic In(x)Ga(1-x)As/In(0.52)Al(0.48)As modulation-doped field-effect transistors

[AIAA PAPER 91-22987] p 136 A91-22987

Peeled film GaAs solar cell development

[AIAA PAPER 91-41889] p 139 A91-41889

Temperature coefficients of multijunction solar cells

[AIAA PAPER 91-41921] p 172 A91-41921

Lightweight concentrator module with 30 percent AMO efficient GaAs/GaSb tandem cells

[AIAA PAPER 91-41990] p 57 A91-41990

Photovoltaic superiority for Space Station Freedom power in the 21st century

[AIAA PAPER 91-42004] p 58 A91-42004

Three-dimensional flow transport modes in directional solidification during space processing

[AIAA PAPER 91-42642] p 128 A91-42642

Performance of a 300 Mbps 1:16 serial/parallel optoelectronic receiver module

[AIAA PAPER 91-51146] p 141 A91-51146

New materials and techniques for improved mm wave devices

[AIAA PAPER 91-3590] p 142 A91-52459

Dielectric function of InGaAs in the visible

[AIAA PAPER 91-53236] p 233 A91-53236

Thermal annealing of GaAs concentrator solar cells

[AIAA PAPER 91-19195] p 208 N91-19195

Effects of proton irradiation on the performance of InP/GaAs solar cells

[AIAA PAPER 91-19205] p 209 N91-19205

Ellipsometric study of InGaAs MODFET material

[AIAA PAPER 91-19351] p 143 N91-19351

Study of InGaAs based MODFET structures using variable angle spectroscopic ellipsometry

[AIAA PAPER 91-19935] p 235 N91-19935

Heteroepitaxial InP solar cells on Si and GaAs substrates

[AIAA PAPER 91-20392] p 144 N91-20392

GaAs monolithic RF modules for SARSAT distress beacons

[AIAA PAPER 91-21184] p 46 N91-21184

Future mission opportunities and requirements for advanced space photovoltaic energy conversion technology

[AIAA PAPER 91-22371] p 74 N91-22371

Microwave integrated circuits for space applications

[AIAA PAPER 91-24069] p 145 N91-24069

Advanced photovoltaic experiment, S0014: Preliminary flight results and post-flight findings

[AIAA PAPER 91-25061] p 212 N91-25061

Recent progress in InP solar cell research

[AIAA PAPER 91-27447] p 146 N91-27447

Key results of the mini-dome Fresnel lens concentrator array development program under recently completed NASA and SDIO SBIR projects

[AIAA PAPER 91-30223] p 83 N91-30223

GAMMA RAYS

Neutron and gamma irradiation effects on power semiconductor switches

[AIAA PAPER 91-38162] p 139 A91-38162

Neutron, gamma ray and post-irradiation thermal annealing effects on power semiconductor switches

[AIAA PAPER 91-35251] p 142 A91-52420

Neutron, gamma ray and post-irradiation thermal annealing effects on power semiconductor switches

[NASA-TM-105248] p 147 N91-32410

GAS BEARINGS

Composite bearing and seal materials for advanced heat engine applications to 900 C

[NASA-TM-103612] p 95 N91-15318

GAS DENSITY

Gas property effects on droplet size of simulated fuel sprays

[AIAA PAPER 91-45327] p 156 A91-45327

Transonic aerodynamics of dense gases

[NASA-TM-103722] p 13 N91-20045

GAS FLOW

An experimental trace gas investigation of fluid transport and mixing in a circular-to-rectangular transition duct

[AIAA PAPER 91-2370] p 172 A91-44214

Cryogenic liquid-jet breakup in two-fluid atomizers

[NASA-TM-103734] p 176 N91-19402

Transonic aerodynamics of dense gases

[NASA-TM-103722] p 13 N91-20045

GAS GENERATORS

The selection of convertible engines with current gas generator technology for high speed rotorcraft

[NASA-TM-103774] p 27 N91-19097

GAS INJECTION

An experimental trace gas investigation of fluid transport and mixing in a circular-to-rectangular transition duct

[AIAA PAPER 91-2370] p 172 A91-44214

Qualitative investigation of cryogenic injected shock dissipation

[NASA-TM-105140] p 168 N91-29525

GAS IONIZATION

High voltage interactions of a sounding rocket with the ambient and system-generated environments

[AIAA PAPER 91-23077] p 46 A91-23077

GAS JETS

Radiation from gas-jet diffusion flames in microgravity environments

[AIAA PAPER 91-0719] p 104 A91-19432

GAS MIXTURES

Numerical study of shock-wave/boundary layer interactions in premixed hydrogen-air hypersonic flows

[AIAA PAPER 91-0413] p 149 A91-26191

New approach in direct-simulation of gas mixtures

[AIAA PAPER 91-1343] p 154 A91-43412

Preliminary performance and life evaluation of a 2-kW arcjet

[AIAA PAPER 91-2228] p 62 A91-45796

Numerical study of shock-wave/boundary layer interactions in premixed hydrogen-air hypersonic flows

[NASA-TM-103273] p 160 N91-14559

Ground test program for a full-size solar dynamic heat receiver

[NASA-TM-104485] p 79 N91-27209

GAS PRESSURE

Effects of high pressure nitrogen on the thermal stability of SiC fibers

[NASA-TM-103245] p 96 N91-16075

A test fixture for measuring high-temperature hypersonic-engine seal performance

[NASA-TM-103658] p 184 N91-19442

GAS TRANSPORT

An experimental trace gas investigation of fluid transport and mixing in a circular-to-rectangular transition duct

[NASA-TM-104499] p 17 N91-27129

GAS TURBINE ENGINES

Effects of nozzle lip geometry on spray atomization and emissions advanced gas turbine combustors

[AIAA PAPER 91-2201] p 24 A91-44153

Fuel-rich, catalytic reaction experimental results ... fuel development for high-speed civil transport aircraft

[AIAA PAPER 91-2463] p 24 A91-44250

Computation of a circular-to-rectangular transition duct flow field

[AIAA PAPER 91-1741] p 156 A91-45547

Analytical combustion/emissions research related to the NASA High-Speed Research Program

[AIAA PAPER 91-2252] p 25 A91-45799

Mixing of multiple jets with a confined subsonic crossflow

Summary of NASA-supported experiments and modeling

[AIAA PAPER 91-2458] p 7 A91-45813

Some preliminary results of brush seal/rotor interference effects on leakage at zero and low rpm using a tapered-plug rotor

[AIAA PAPER 91-3390] p 182 A91-45820

Hot corrosion of silicon carbide and silicon nitride at 1000 C

[AIAA PAPER 91-55698] p 117 A91-55698

Stirling engine: Available tools for long-life assessment

[NASA-TM-103660] p 200 N91-12980

Combustor technology for future aircraft

[NASA-TM-103268] p 26 N91-14349

Thermal barrier coating evaluation needs

[NASA-TM-103708] p 111 N91-15390

NASA low-speed centrifugal compressor for 3-D viscous code assessment and fundamental flow physics research

[NASA-TM-103710] p 13 N91-20044

Turbomachinery and combustor technology for small engines

[NASA-TM-103708] p 29 N91-20113

Rotary engine technology

[NASA-TM-103710] p 30 N91-20114

Mixing of multiple jets with a confined subsonic crossflow. Summary of NASA-supported experiments and modeling

[NASA-TM-104412] p 33 N91-24202

Fuel-rich, catalytic reaction experimental results

[NASA-TM-104423] p 33 N91-24203

Analytical combustion/emissions research related to the NASA high-speed research program

[NASA-TM-104521] p 34 N91-27165

Visualization techniques to experimentally model flow and heat transfer in turbine and aircraft flow passages

[NASA-TM-4272] p 167 N91-27489

GAS TURBINES

Application of mixing-controlled combustion models to gas turbine combustors

[NASA-TM-103236] p 31 N91-22126

Multi-heat addition turbine engine

[NASA-CASE-LEW-15094-1] p 32 N91-23180

CFD analysis of jet mixing in low NOx flame tube combustors

[NASA-TM-104466] p 33 N91-26146

GASEOUS DIFFUSION

A detailed numerical investigation of Burke-Schumann gaseous and spray flames

[AIAA PAPER 91-2311] p 105 A91-41749

GASEOUS ROCKET PROPELLANTS

Performance and flow calculations for a gaseous H₂/O₂ thruster

[AIAA PAPER 91-48843] p 63 A91-48843

GEAR TEETH

Contact stresses in gear teeth - A new method of analysis

[AIAA PAPER 91-2022] p 182 A91-41683

Gear noise, vibration, and diagnostic studies at NASA Lewis Research Center

[AIAA PAPER 91-52811] p 183 A91-52811

Comparison of analysis and experiment for dynamics of low-contact-ratio spur gears

[NASA-TM-103232] p 185 N91-22566

Contact stresses in gear teeth: A new method of analysis

[NASA-TM-104397] p 186 N91-22570

- Computerized inspection of real surfaces and minimization of their deviations
[NASA-TM-103798] p 188 N91-27558
- Dynamic measurements of gear tooth friction and load
[NASA-TM-103281] p 189 N91-27570
- Local synthesis and tooth contact analysis of face-milled spiral bevel gears
[NASA-TM-105182] p 190 N91-29600
- How to determine spiral bevel gear tooth geometry for finite element analysis
[NASA-TM-105150] p 190 N91-30537
- Spur-gear optimization using SPUROPT computer program
[NASA-TM-104394] p 191 N91-31648
- GEARS**
- Evaluation of advanced lubricants for aircraft applications using gear surface fatigue tests
[AIAA PAPER 91-1907] p 181 A91-41649
- Analytical and experimental study of vibrations in a gear transmission
[AIAA PAPER 91-2019] p 181 A91-41680
- Effects of rim thickness on spur gear bending stress
[AIAA PAPER 91-2020] p 181 A91-41681
- Maximum life spur gear design
[AIAA PAPER 91-2021] p 181 A91-41682
- Contact stresses in gear teeth - A new method of analysis
[AIAA PAPER 91-2022] p 182 A91-41683
- Surface fatigue life of M50NiL and AISI 9310 gears and rolling-contact bars
p 182 A91-45350
- Gear noise, vibration, and diagnostic studies at NASA Lewis Research Center
p 183 A91-52811
- Comparison of analysis and experiment for dynamics of low-contact-ratio spur gears
[NASA-TM-103232] p 185 N91-22566
- Evaluation of advanced lubricants for aircraft applications using gear surface fatigue tests
[NASA-TM-104336] p 186 N91-22568
- Contact stresses in gear teeth: A new method of analysis
[NASA-TM-104397] p 186 N91-22570
- Effects of rim thickness on spur gear bending stress
[NASA-TM-104388] p 186 N91-23500
- Modal analysis of multistage gear systems coupled with gearbox vibrations
[NASA-TM-103797] p 187 N91-23513
- Maximum life spur gear design
[NASA-TM-104361] p 187 N91-23514
- Analytical and experimental study of vibrations in a gear transmission
[NASA-TM-104434] p 187 N91-25395
- Acoustical analysis of gear housing vibration
[NASA-TM-103691] p 188 N91-25411
- Advanced Rotorcraft Transmission (ART) program-Boeing helicopters status report
[NASA-TM-104474] p 188 N91-25412
- Surface fatigue life of M50NiL and AISI 9310 spur gears and R C bars
[NASA-TM-104496] p 189 N91-27569
- Effect of two synthetic lubricants on life of AISI 9310 spur gears
[NASA-TM-104352] p 189 N91-29599
- Local synthesis and tooth contact analysis of face-milled spiral bevel gears
[NASA-TM-105182] p 190 N91-29600
- How to determine spiral bevel gear tooth geometry for finite element analysis
[NASA-TM-105150] p 190 N91-30537
- Spur-gear optimization using SPUROPT computer program
[NASA-TM-104394] p 191 N91-31648
- Recent manufacturing advances for spiral bevel gears
[NASA-TM-104479] p 191 N91-31654
- GELATION**
- Influence of several metal ions on the gelation activation energy of silicon tetraethoxide
p 113 A91-19599
- GELLED PROPELLANTS**
- Advanced launch vehicle upper stages using liquid propulsion and metallized propellants
p 75 N91-24257
- GELLED ROCKET PROPELLANTS**
- Launch vehicle performance using metallized propellants
[AIAA PAPER 91-2050] p 58 A91-44106
- Flow visualization of a rocket injector spray using gelled propellant simulants
[AIAA PAPER 91-2198] p 59 A91-44151
- Advanced chemical propulsion at NASA Lewis: Metallized and high energy density propellants
[NASA-TM-103771] p 71 N91-19175
- Launch vehicle performance using metallized propellants
[NASA-TM-104456] p 76 N91-24304
- GENERAL AVIATION AIRCRAFT**
- Overview of rotorcraft and general aviation propulsion technology
p 29 N91-20112
- GEOMETRICAL OPTICS**
- Concentrator testing using projected images
[NASA-TM-104349] p 79 N91-27204
- GEOSYNCHRONOUS ORBITS**
- Satellite eclipse power by laser illumination
[IAF PAPER 90-053] p 50 A91-13766
- GERMANIUM**
- Photovoltaic superiority for Space Station Freedom power in the 21st century
p 58 A91-42004
- GET AWAY SPECIALS (STS)**
- A summary of existing and planned experiment hardware for low-gravity fluids research
[AIAA PAPER 91-0777] p 128 A91-26329
- GLASS**
- Preparation of 110K (Bi, Pb)-Sr-Ca-Cu-O superconductor from glass precursor
p 232 A91-35449
- Crystallization and properties of Sr-Ba aluminosilicate glass-ceramic matrices
p 117 A91-56917
- Crystallization and properties of Sr-Ba aluminosilicate glass-ceramic matrices
[NASA-TM-103764] p 120 N91-19308
- Method of preparing a thermal barrier coating
[NASA-CASE-LEW-14999-2] p 122 N91-26376
- Electrical characterization of glass, teflon, and tantalum capacitors at high temperatures
[NASA-TM-104517] p 146 N91-27444
- Thin solar cell and lightweight array
[NASA-CASE-LEW-14959-1] p 212 N91-27614
- GLASS COATINGS**
- A light-trapping solar cell coverglass
p 229 A91-41995
- 23.5 percent thin-film space concentrator cells
p 58 A91-42002
- GLASS TRANSITION TEMPERATURE**
- Viscoelastic properties of addition-cured polyimides used in high temperature polymer matrix composites
[NASA-TM-103768] p 89 N91-22377
- GLAZES**
- Modeling of surface roughness effects on glaze ice accretion
p 19 A91-35107
- GOLD**
- An analysis of the contact sintering process in III-V solar cells
p 139 A91-41891
- The influence of interstitial Ga and interfacial Au₂P₃ on the electrical and metallurgical behavior of Au-contacted III-V semiconductors
p 140 A91-42694
- Improvements in contact resistivity and thermal stability of Au-contacted InP solar cells
p 213 N91-30207
- The Au cathode in the system Li₂CO₃-CO₂-CO at 800 to 900 C
p 213 N91-32551
- GOLD ALLOYS**
- An x ray photoelectron spectroscopy study of Au(x)In(y) alloys
[NASA-TM-103659] p 234 N91-14050
- GOVERNMENT/INDUSTRY RELATIONS**
- Government/industry response to questionnaire on space mechanisms/tribology technology needs
[NASA-TM-104358] p 186 N91-23501
- GRAIN BOUNDARIES**
- Grain boundary sliding behaviour of copper and alpha brass at intermediate temperatures
p 108 A91-27158
- Thermal stability of the microstructure of an aged Nb-Zr-C alloy
[NASA-TM-103647] p 110 N91-14454
- GRAPHITE**
- Resistivity of pristine and intercalated graphite fiber epoxy composites
p 115 A91-35949
- Thermal emittance enhancement of graphite-copper composites for high temperature space based radiators
[AIAA PAPER 91-3527] p 116 A91-53705
- Graphite fluoride fibers and their applications in the space industry
[NASA-TM-103265] p 88 N91-11062
- Solid lubricants
[NASA-TM-102803] p 99 N91-22396
- Industrial applications of graphite fluoride fibers
p 100 N91-23040
- Apparatus for intercalating large quantities of fibrous structures
[NASA-CASE-LEW-15077-2] p 102 N91-28289
- Thermal emittance enhancement of graphite-copper composites for high temperature space based radiators
[NASA-TM-105178] p 123 N91-29332
- Ion beam sputtering in electric propulsion facilities
[NASA-TM-105145] p 86 N91-32158
- GRAPHITE-EPOXY COMPOSITES**
- The effects of interply damping layers on the dynamic response of composite structures
[AIAA PAPER 91-1124] p 197 A91-32064
- Intercalated graphite fiber composites as EMI shields in aerospace structures
[NASA-TM-103632] p 94 N91-10134
- Probabilistic micromechanics and macromechanics of polymer matrix composites
[NASA-TM-103669] p 98 N91-19236
- The effects of interply damping layers on the dynamic response of composite structures
[NASA-TM-104497] p 103 N91-30282
- Effect of lightning strike on bromine intercalated graphite fiber/epoxy composites
[NASA-TM-104507] p 103 N91-32177
- GRAPHITE-POLYIMIDE COMPOSITES**
- A study of void effects on the interlaminar shear strength of unidirectional graphite fiber reinforced composites
[NASA-TM-103267] p 159 N91-12034
- GRAPHITIZATION**
- Graphite fluoride fiber polymer composite material
[NASA-CASE-LEW-14472-1] p 95 N91-15320
- Industrial applications of graphite fluoride fibers
p 100 N91-23040
- GRAVITATION**
- Exploring the notion of space coupling propulsion
p 73 N91-22161
- GRAVITATIONAL COLLAPSE**
- Characteristic microwave-background distortions from collapsing spherical domain walls
p 238 A91-12343
- GRAVITATIONAL EFFECTS**
- Reactionless orbital propulsion using tether deployment
[IAF PAPER 90-254] p 51 A91-13908
- Interfacial dynamics of two liquids under an oscillating gravitational field
p 148 A91-16062
- The migration of a compound drop due to thermocapillarity
p 148 A91-18428
- Scaling analysis applied to the NORVEX code development and thermal energy flight experiment
[AIAA PAPER 91-1420] p 155 A91-44337
- Spacelab qualified infrared imager for microgravity science applications
p 173 A91-51585
- Development of a vibration isolation prototype system for microgravity space experiments
p 47 A91-53403
- Multi-dimensional modeling of a thermal energy storage canister
[NASA-TM-103731] p 71 N91-19177
- Development of a vibration isolation prototype system for microgravity space experiments
[NASA-TM-103664] p 130 N91-19324
- The COLD-SAT experiment for cryogenic fluid management technology
p 126 N91-24263
- Microgravity research at LeRC
[NASA-TM-102521] p 128 N91-24464
- Scaling analysis applied to the NORVEX code development and thermal energy flight experiment
[NASA-TM-104462] p 166 N91-24549
- GRAVITATIONAL PHYSIOLOGY**
- The International Space University's variable gravity research facility design
[NASA-TM-105224] p 44 N91-31196
- GRAY SCALE**
- A neural net based architecture for the segmentation of mixed gray-level and binary pictures
p 218 A91-29183
- GREEN'S FUNCTIONS**
- Equivalence of Green's function and the Fourier series representation of composites with periodic microstructure
p 91 A91-16889
- GRID GENERATION (MATHEMATICS)**
- The aerodynamic characteristics of vortex ingestion for the F/A-18 inlet duct
[AIAA PAPER 91-0130] p 3 A91-26192
- Algebraic grid generation for coolant passages of turbine blades with serpentine channels and pin fins
[AIAA PAPER 91-2366] p 156 A91-45811
- Algebraic grid generation for complex geometries
p 157 A91-48758
- The aerodynamic characteristics of vortex ingestion for the F/A-18 inlet duct
[NASA-TM-103703] p 70 N91-15303
- Implementation of control point form of algebraic grid-generation technique
[NASA-TM-103748] p 13 N91-19054
- Computational Fluid Dynamics Symposium on Aeropropulsion
[NASA-CP-3078] p 14 N91-21062
- Dynamics of local grid manipulations for internal flow problems
p 164 N91-21090
- The design/analysis of flows through turbomachinery: A viscous/inviscid approach
[NASA-TM-104447] p 33 N91-25148
- GRID3D-v2: An updated version of the GRID2D/3D computer program for generating grid systems in complex-shaped three-dimensional spatial domains
[NASA-TM-103766] p 217 N91-25630
- GRINDING MACHINES**
- Recent manufacturing advances for spiral bevel gears
[NASA-TM-104479] p 191 N91-31654
- GROOVES**
- Grooved surfaces on InP
p 213 N91-30208

GROUND EFFECT (AERODYNAMICS)

- VSTOL ground effects testing with flow visualization and image enhancement
[AIAA PAPER 91-3145] p 8 A91-54061
A numerical study of the hot gas environment around a STOL aircraft in ground proximity p 10 N91-10887
- GROUND TESTS**
Ground testing of the nonvented fill method of orbital propellant transfer - Results of initial test series
[AIAA PAPER 91-2326] p 59 A91-44198
Ground testing on the nonvented fill method of orbital propellant transfer: Results of initial test series
[NASA-TM-104444] p 166 N91-24547
Ground test program for a full-size solar dynamic heat receiver
[NASA-TM-104485] p 79 N91-27209
- GROUND WIND**
Effects of dust accumulation and removal on radiators surfaces on Mars
[NASA-TM-103704] p 72 N91-20204
- GUIDE VANES**
Turbulent boundary layer separation over a rearward facing ramp and its control through mechanical excitation
[NASA-TM-103702] p 160 N91-19370
- GUST LOADS**
Acoustic radiation from lifting airfoils in compressible subsonic flow
[NASA-TM-103650] p 13 N91-19053

H**HALL EFFECT**

- Properties of insulator interfaces with p-HgCdTe
p 235 N91-18300
Surface electrons in inverted layers of p-HgCdTe
p 235 N91-18301

HARDNESS

- Temperature dependence of hardness in yttria-stabilized zirconia single crystals p 114 A91-28763

HARDWARE

- A summary of existing and planned experiment hardware for low-gravity fluids research
[NASA-TM-103706] p 160 N91-19371
Fiber-optic-based controls p 230 N91-20102

HARMONIC MOTION

- Euler flow predictions for an oscillating cascade using a high resolution wave-split scheme
[NASA-TM-104377] p 16 N91-24107

HARMONIC OSCILLATION

- Wind tunnel wall effects in a linear oscillating cascade
[NASA-TM-103690] p 27 N91-19098

HARMONICS

- Wind turbine acoustics
[NASA-TP-3057] p 228 N91-16679

HEAT EXCHANGERS

- Two-dimensional model of a Space Station Freedom thermal energy storage canister p 151 A91-38048
A dual-cooled hydrogen-oxygen rocket engine heat transfer analysis
[AIAA PAPER 91-2211] p 59 A91-44156
An overview of the LeRC CSTI thermal management program
[AIAA PAPER 91-3528] p 158 A91-52422
A 2-D oscillating flow analysis in Stirling engine heat exchangers
[NASA-TM-103781] p 161 N91-19375
A dual-cooled hydrogen-oxygen rocket engine heat transfer analysis
[NASA-TM-104430] p 76 N91-24302

HEAT FLUX

- A comparative flow visualization study of thermocapillary flow in drops in liquid-liquid systems
[AIAA PAPER 91-0311] p 148 A91-21452
Analytical solution for boundary heat fluxes from a radiating rectangular medium p 150 A91-27175
Heat flux measurement in SSME turbine blade tester p 171 A91-30649
Heat flux measurement in SSME turbine blade tester
[NASA-TM-103274] p 175 N91-11205
A unique high heat flux facility for testing hypersonic engine components
[NASA-TM-103238] p 38 N91-11770
Development of a laser-induced heat flux technique for measurement of convective heat transfer coefficients in a supersonic flowfield
[NASA-TM-103778] p 13 N91-19063
Self-pressurization of a lightweight liquid hydrogen storage tank subjected to low heat flux
[NASA-TM-103804] p 126 N91-20324
Calibrator tests of heat flux gauges mounted in SSME blades p 177 N91-24321
A laser-induced heat flux technique for convective heat transfer measurements in high speed flows
[NASA-TM-105177] p 168 N91-30472

- Plug-type heat flux gauge
[NASA-CASE-LEW-14967-1] p 179 N91-31608

HEAT MEASUREMENT

- Development of a laser-induced heat flux technique for measurement of convective heat transfer coefficients in a supersonic flowfield
[NASA-TM-103778] p 13 N91-19063

HEAT PIPES

- Analysis of the one-dimensional transient compressible vapor flow in heat pipes p 157 A91-47735
An overview of the LeRC CSTI thermal management program
[AIAA PAPER 91-3528] p 158 A91-52422
Construction and testing of ceramic fabric heat pipe with water working fluid
[NASA-TM-103332] p 229 N91-18799
Solar thermal energy receiver
[NASA-CASE-LEW-14949-1] p 211 N91-23617

HEAT RADIATORS

- Two-dimensional simulation of a two-phase, regenerative pumped radiator loop utilizing direct contact heat transfer with phase change p 151 A91-38126
Thermal emittance enhancement of graphite-copper composites for high temperature space based radiators
[AIAA PAPER 91-3527] p 116 A91-53705
Effects of dust accumulation and removal on radiators surfaces on Mars
[NASA-TM-103704] p 72 N91-20204
Arc-textured high emittance radiator surfaces
[NASA-CASE-LEW-14679-1] p 122 N91-25296
Thermal emittance enhancement of graphite-copper composites for high temperature space based radiators
[NASA-TM-105178] p 123 N91-29332
On protection of Freedom's solar dynamic radiator from the orbital debris environment. Part 2: Further testing and analyses
[NASA-TM-104514] p 84 N91-30265

HEAT RESISTANT ALLOYS

- Tensile properties of HA 230 and HA 188 after 400 and 2500 hour exposures to LiF-22CaF₂ and vacuum at 1093 K p 107 A91-11624
Computational simulation of high-temperature metal matrix composites cyclic behavior p 91 A91-18680
Elastic response of (001)-oriented PWA 1480 single crystal: The influence of secondary orientation
[SAE PAPER 911111] p 110 A91-53555
Effect of thermal shock on fiber-reinforced superalloy composites p 93 A91-55918
High temperature cyclic oxidation data. Part 1: Turbine alloys
[NASA-TM-83665] p 110 N91-10149
High-temperature cyclic oxidation data. Part 2: Turbine alloys
[NASA-TM-101468] p 110 N91-10150
Effect of tensile mean stress on fatigue behavior of single-crystal and directionally solidified superalloys
[NASA-TM-103644] p 200 N91-18452
Application of thermal life prediction model to high-temperature aerospace alloys B1900 + Hf and Haynes 188
[NASA-TM-4226] p 201 N91-19473
Thermomechanical and bithermal fatigue behavior of cast B1900 + Hf and wrought Haynes 188
[NASA-TM-4225] p 111 N91-20268
Elastic response of zone axis (001)-oriented PWA 1480 single crystal: The influence of secondary orientation
[NASA-TM-103782] p 202 N91-21558
Evaluation and ranking of candidate ceramic wafer engine seal materials
[NASA-TM-103795] p 187 N91-23515
Fatigue behavior of a single-crystal superalloy p 111 N91-24313

HEAT SOURCES

- Dynamic Isotope Surface Power Systems
[AIAA PAPER 91-3623] p 208 A91-52487
Comparison of dynamic isotope power systems for distributed planet surface applications
[NASA-TM-4303] p 81 N91-28278

HEAT STORAGE

- Two-dimensional model of a Space Station Freedom thermal energy storage canister p 151 A91-38048
Multi-dimensional modeling of a thermal energy storage canister
[NASA-TM-103731] p 71 N91-19177
Sensible heat receiver for solar dynamic space power system
[NASA-TM-104393] p 77 N91-25173
Full-size solar dynamic heat receiver thermal-vacuum tests
[NASA-TM-104486] p 78 N91-25184
Ground test program for a full-size solar dynamic heat receiver
[NASA-TM-104485] p 79 N91-27209

HEAT TRANSFER

- Two-dimensional model of a Space Station Freedom thermal energy storage canister p 151 A91-38048

- Two-dimensional simulation of a two-phase, regenerative pumped radiator loop utilizing direct contact heat transfer with phase change p 151 A91-38126
Preliminary designs for 25 kW advanced Stirling conversion systems for dish electric applications p 207 A91-38182
Further two-dimensional code development for Stirling space engine components p 56 A91-38184
Heat transfer in space systems: Proceedings of the Symposium, AIAA/ASME Thermophysics and Heat Transfer Conference, Seattle, WA, June 18-20, 1990 p 152 A91-38780
Increased heat transfer to a cylindrical leading edge due to spanwise variations in the freestream velocity
[AIAA PAPER 91-1739] p 155 A91-43623
A dual-cooled hydrogen-oxygen rocket engine heat transfer analysis
[AIAA PAPER 91-2211] p 59 A91-44156
A pressure control analysis of cryogenic storage systems
[AIAA PAPER 91-2405] p 59 A91-44228
Navier-Stokes analysis of turbine blade heat transfer
[ASME PAPER 90-GT-42] p 155 A91-44529
Two-dimensional Navier-Stokes heat transfer analysis for rough turbine blades
[AIAA PAPER 91-2129] p 156 A91-45790
Computations of the three-dimensional flow and heat transfer within a coolant passage of a radial turbine blade
[AIAA PAPER 91-2238] p 156 A91-45797
Algebraic grid generation for coolant passages of turbine blades with serpentine channels and pin fins
[AIAA PAPER 91-2366] p 156 A91-45811
Thermal performance of a liquid hydrogen tank multilayer insulation system at warm boundary temperatures of 630, 530, and 152 R
[AIAA PAPER 91-2400] p 43 A91-45812
Heat transfer to a thin solid combustible in flame spreading at microgravity p 106 A91-51449
The effect of coatings and liners on heat transfer in a dry shaft-bush tribosystem
[NASA-TM-102513] p 159 N91-12913
Heat transfer device and method of making the same
[NASA-CASE-LEW-14162-1] p 159 N91-13668
Aerodynamics and heat transfer investigations on a high Reynolds number turbine cascade
[NASA-TM-103260] p 11 N91-15134
Multi-dimensional modeling of a thermal energy storage canister
[NASA-TM-103731] p 71 N91-19177
Heat transfer, velocity-temperature correlation, and turbulent shear stress from Navier-Stokes computations of shock wave/turbulent boundary layer interaction flows p 163 N91-21085
Cooling of in-situ propellant rocket engines for Mars mission
[NASA-TM-103729] p 72 N91-21233
Multi-heat addition turbine engine
[NASA-CASE-LEW-15094-1] p 32 N91-23180
Solar thermal energy receiver
[NASA-CASE-LEW-14949-1] p 211 N91-23617
A three-dimensional turbulent heat transfer analysis for advanced tubular rocket thrust chambers p 75 N91-24258
A dual-cooled hydrogen-oxygen rocket engine heat transfer analysis
[NASA-TM-104430] p 76 N91-24302
Calibrator tests of heat flux gauges mounted in SSME blades p 177 N91-24321
Increased heat transfer to a cylindrical leading edge due to spanwise variations in the freestream velocity
[NASA-TM-104464] p 100 N91-24359
A pressure control analysis of cryogenic storage systems
[NASA-TM-104409] p 126 N91-24460
Thermal performance of a liquid hydrogen tank multilayer insulation system at warm boundary temperatures of 630, 530, and 152 R
[NASA-TM-104476] p 43 N91-25159
Heat transfer device
[NASA-CASE-LEW-14162-2] p 101 N91-25201
Visualization techniques to experimentally model flow and heat transfer in turbine and aircraft flow passages
[NASA-TM-4272] p 167 N91-27489
Arcjet thermal characteristics
[NASA-TM-105156] p 82 N91-29231
- HEAT TRANSFER COEFFICIENTS**
Development of a laser-induced heat flux technique for measurement of convective heat transfer coefficients in a supersonic flowfield
[NASA-TM-103778] p 13 N91-19063
A laser-induced heat flux technique for convective heat transfer measurements in high speed flows
[NASA-TM-105177] p 168 N91-30472

HEAT TRANSMISSION

Analytical solution for boundary heat fluxes from a radiating rectangular medium p 150 A91-27175

HEAT TREATMENT

Tensile properties of HA 230 and HA 188 after 400 and 2500 hour exposures to LiF-22CaF₂ and vacuum at 1093 K p 107 A91-11624

Crystallization and properties of Sr-Ba aluminosilicate glass-ceramic matrices p 117 A91-56917

Properties of insulator interfaces with p-HgCdTe p 235 N91-18300

Semiconductor structural damage attendant to contact formation in III-V solar cells p 209 N91-19203

Crystallization and properties of Sr-Ba aluminosilicate glass-ceramic matrices p 120 N91-19308

Matrix plasticity in SiC/Ti-15-3 composite p 102 N91-27247

Improvements in contact resistivity and thermal stability of Au-contacted InP solar cells p 213 N91-30207

HEATING

The effect of coatings and liners on heat transfer in a dry shaft-bush tribosystem p 159 N91-12913

The series Bi₂Sr₂Ca(n-1)Cu(n)O(2n+4) (1 less than or equal to n less than or equal to 5): Phase stability and superconducting properties p 235 N91-21910

Furnace for tensile/fatigue testing p 42 N91-27175

HELICAL FLOW

An experimental study of natural and forced modes in an axisymmetric jet p 18 N91-32074

HELICOPTER CONTROL

An expert system to perform on-line controller restructuring for abrupt model changes p 36 A91-29466

HELICOPTER DESIGN

Advanced rotorcraft transmission program p 184 N91-21531

HELICOPTER PROPELLER DRIVE

Experimental and analytical evaluation of efficiency of helicopter planetary stage p 183 N91-12956

Review of the transmissions of the Soviet helicopters p 20 N91-15146

Advanced rotorcraft transmission program p 184 N91-21531

Advanced Rotorcraft Transmission (ART) program-Boeing helicopters status report p 188 N91-25412

HELICOPTERS

Experimental and analytical evaluation of efficiency of helicopter planetary stage p 183 N91-12956

HERMITIAN POLYNOMIAL

Accurate monotone cubic interpolation p 221 N91-20830

HETEROJUNCTIONS

Temperature coefficients of multijunction solar cells p 172 A91-41921

HIERARCHIES

Development and testing of a source subsystem for the supporting development PMAD DC test bed p 78 N91-26202

HIGH ENERGY PROPELLANTS

Advanced chemical propulsion at NASA Lewis: Metalized and high energy density propellants p 71 N91-19175

HIGH FREQUENCIES

Control of multiple resonant power processors in a multi-source system p 137 A91-30901

High frequency, high temperature specific core loss and dynamic B-H hysteresis loop characteristics of soft magnetic alloys p 138 A91-37988

A model for the scattering of high-frequency electromagnetic fields from dielectrics exhibiting thermally-activated electrical losses p 224 N91-26872

HIGH POWER LASERS

Satellite eclipse power by laser illumination p 50 A91-13766

HIGH PRESSURE

Pressure-coupled vaporization and combustion responses of liquid-fuel droplets in high-pressure environments p 106 A91-44192

Effects of high pressure nitrogen on the thermal stability of SiC fibers p 96 N91-16075

Current activities in standardization of high-temperature, low-cycle-fatigue testing techniques in the United States p 200 N91-17427

A model for the space shuttle main engine high pressure oxidizer turbopump shaft seal system p 184 N91-20489

HIGH PRESSURE OXYGEN

Surface modification of Monel K-500 as a means of reducing friction and wear in high-pressure oxygen p 107 A91-16869

HIGH RESOLUTION

High Resolution, High Frame Rate Video Technology p 175 N91-14574

Results of the users' requirements survey p 175 N91-14575

High resolution, high frame rate video technology development plan and the near-term system conceptual design p 175 N91-14580

Euler flow predictions for an oscillating cascade using a high resolution wave-split scheme p 16 N91-24107

High resolution electrolyte for thinning InP by anodic dissolution and its applications to EC-V profiling, defect revealing and surface passivation p 107 N91-30210

HIGH REYNOLDS NUMBER

Aerodynamics and heat transfer investigations on a high Reynolds number turbine cascade p 11 N91-15134

Critical-layer nonlinearity in the resonance growth of three-dimensional waves in boundary layers p 161 N91-19373

The 3D computation of single-expansion-ramp and scramjet nozzles p 164 N91-21092

Calculated performance of the NASA Lewis icing research tunnel p 39 N91-29199

An experimental study of natural and forced modes in an axisymmetric jet p 18 N91-32074

HIGH SPEED

The selection of convertible engines with current gas generator technology for high speed rotorcraft p 27 N91-19097

A study of high speed flows in an aircraft transition duct p 17 N91-26122

Applied high-speed imaging for the icing research program at NASA Lewis Research Center p 177 N91-26490

HIGH SPEED PHOTOGRAPHY

A high speed photography study of cavitation in a dynamically loaded journal bearing p 180 A91-34806

HIGH STRENGTH ALLOYS

High temperature cyclic oxidation data. Part 1: Turbine alloys p 110 N91-10149

High-temperature cyclic oxidation data. Part 2: Turbine alloys p 110 N91-10150

HIGH TEMPERATURE

Quantification of uncertainties in coupled material degradation processes - High temperature, fatigue and creep p 196 A91-31835

Determination of surface resistance and magnetic penetration depth of superconducting YBa₂Cu₃O(7- δ) thin films by microwave power transmission measurements p 138 A91-36060

High frequency, high temperature specific core loss and dynamic B-H hysteresis loop characteristics of soft magnetic alloys p 138 A91-37988

High temperature superconducting thin film microwave circuits - Fabrication, characterization, and applications p 141 A91-50433

Advanced materials for space nuclear power systems p 88 A91-53704

Thermal emittance enhancement of graphite-copper composites for high temperature space based radiators p 116 A91-53705

Photoelastic transducer for high-temperature applications p 174 A91-55533

Reinforcements: The key to high performance composite materials p 96 N91-15329

Current activities in standardization of high-temperature, low-cycle-fatigue testing techniques in the United States p 200 N91-17427

A test fixture for measuring high-temperature hypersonic-engine seal performance p 184 N91-19442

NDE standards for high temperature materials p 193 N91-19464

High temperature electronics p 144 N91-20101

Tribological characteristics of silicon carbide whisker-reinforced alumina at elevated temperatures p 89 N91-22379

Aerospace applications of high temperature superconductivity p 236 N91-24080

HIGH TEMPERATURE SUPERCONDUCTORS

High temperature tension-compression fatigue behavior of a tungsten copper composite p 100 N91-24360

Microfracture in high temperature metal matrix crossply laminates p 101 N91-25198

Electrical characterization of glass, teflon, and tantalum capacitors at high temperatures p 146 N91-27444

Advanced materials for space nuclear power systems p 112 N91-29298

Thermal emittance enhancement of graphite-copper composites for high temperature space based radiators p 123 N91-29332

High temperature NASP engine seals: A technology review p 190 N91-30538

HIGH TEMPERATURE AIR

An experimental investigation of nozzle-exit boundary layers of highly heated free jets p 155 A91-44662

HIGH TEMPERATURE ENVIRONMENTS

Probabilistic simulation of uncertainties in thermal structures p 195 A91-16042

Heat flux measurement in SSME turbine blade tester p 171 A91-30649

High emittance surfaces for high temperature space radiator applications p 88 A91-56415

Heat flux measurement in SSME turbine blade tester p 175 N91-11205

High temperature electronics p 144 N91-20101

High temperature power electronics for space p 145 N91-22508

Development of silicon carbide semiconductor devices for high temperature applications p 236 N91-22921

Silicon carbide, an emerging high temperature semiconductor p 236 N91-24061

HIGH TEMPERATURE GASES

Fiber optic photoelastic pressure sensor for high temperature gases p 170 A91-19577

Effect of high temperature hydrogen exposure on the strength and microstructure of mullite p 114 A91-19780

High temperature reactions of ceramics and metals with chlorine and oxygen p 105 A91-20219

STOVL Hot Gas Ingestion control technology p 22 A91-23642

Hot gas ingestion test results of a two-poster vectored thrust concept with flow visualization in the NASA Lewis 9- by 15-foot low speed wind tunnel p 4 A91-40561

Flow visualization and hot gas ingestion characteristics of a vectored thrust STOVL concept p 28 N91-20090

Hot gas ingestion test results of a two-poster vectored thrust concept with flow visualization in the NASA Lewis 9- x 15-foot low speed wind tunnel p 15 N91-21116

Spectroscopic wear detector p 87 N91-32167

HIGH TEMPERATURE RESEARCH

Progress in modeling deformation and damage p 202 N91-20108

Overview of Lewis materials research: Contributions, current efforts, and future directions p 111 N91-20109

Silicon carbide, an emerging high temperature semiconductor p 236 N91-24061

HIGH TEMPERATURE SUPERCONDUCTORS

High temperature superconductivity technology for advanced space power systems p 50 A91-13447

Aerospace applications of high temperature superconductivity p 231 A91-13767

Electrical transport measurements on polycrystalline superconducting Y-Ba-Cu-O films p 231 A91-19820

Electromigration failure in YBa₂Cu₃O(7-x) thin films p 231 A91-26989

High temperature superconductive microwave technology for space applications p 137 A91-31391

Preparation of 110K (Bi, Pb)-Sr-Ca-Cu-O superconductor from glass precursor p 232 A91-35449

Temperature dependence of the anisotropy in magnetic relaxation in YBa₂Cu₃O(7-x) thin films p 232 A91-36047

An experimental study of high T_c superconducting microstrip transmission lines at 35 GHz and the effect of film morphology p 138 A91-36172

Superconductivity applications for infrared and microwave devices; Proceedings of the Meeting, Orlando, FL, Apr. 19, 20, 1990 p 141 A91-50426

High temperature superconductor analog electronics for millimeter-wavelength communications p 233 A91-53707

- Determination of surface resistance and magnetic penetration depth of superconducting $\text{YBa}_2\text{Cu}_3\text{O}_{7-\delta}$ thin films by microwave power transmission measurements
[NASA-TM-103616] p 234 N91-10780
- An experimental study of high T_c superconducting microstrip transmission lines at 35 GHz and the effect of film morphology
[NASA-TM-103633] p 133 N91-11988
- Emerging applications of high temperature superconductors for space communications
[NASA-TM-103629] p 227 N91-12317
- Solid State Technology Branch of NASA Lewis Research Center Second Annual Digest, June 1989 - June 1990
[NASA-TM-103226] p 133 N91-18297
- Property and microstructural nonuniformity in the yttrium-barium-copper-oxide superconductor determined from electrical, magnetic, and ultrasonic measurements
[NASA-TM-103732] p 193 N91-19463
- Instrumentation and controls overview p 38 N91-20099
- The series $\text{Bi}_2\text{Sr}_2\text{Ca}(n-1)\text{Cu}(n)\text{O}(2n+4)$ (1 less than or equal to n less than or equal to 5): Phase stability and superconducting properties
[NASA-TM-103749] p 235 N91-21910
- Aerospace applications of high temperature superconductivity p 236 N91-24080
- Superconducting microwave electronics at Lewis Research Center p 236 N91-24081
- Design aspects and comparison between high T (sub c) superconducting coplanar waveguide and microstrip line
[NASA-TM-105142] p 146 N91-27445
- Ultrasonic evaluation of oxidation and reduction effects on the elastic behavior and global microstructure of $\text{YBa}_2\text{Cu}_3\text{O}_{7-x}$
[NASA-TM-104529] p 194 N91-27575
- High temperature superconductor analog electronics for millimeter-wavelength communications
[NASA-TM-105184] p 237 N91-29982
- ### HIGH TEMPERATURE TESTS
- A unique high heat flux facility for testing hypersonic engine components
[AIAA PAPER 90-5228] p 37 A91-14454
- Equivalence of Green's function and the Fourier series representation of composites with periodic microstructure p 91 A91-16889
- A new test machine for measuring friction and wear in controlled atmospheres to 1200 C p 180 A91-33600
- A resistance strain gage with repeatable and cancellable apparent strain for use to 1500 F p 173 A91-51930
- High temperature fatigue behavior of tungsten copper composites p 93 A91-55906
- Dynamic fatigue property of silicon carbide whisker-reinforced silicon nitride p 94 A91-56937
- High temperature power electronics for space
[NASA-TM-104375] p 145 N91-22508
- Development of silicon carbide semiconductor devices for high temperature applications
[NASA-TM-104398] p 236 N91-22921
- Two-dimensional high temperature strain measurement system p 204 N91-24319
- Makeup and uses of a basic magnet laboratory for characterizing high-temperature permanent magnets
[NASA-TM-104508] p 146 N91-30427
- ### HIGH VOLTAGES
- High voltage interactions of a sounding rocket with the ambient and system-generated environments p 46 A91-23077
- Significant reduction in arc frequency biased solar cells: Observations, diagnostics, and mitigation technique(s)
[NASA-TM-104508] p 83 N91-30235
- ### HIGHLY MANEUVERABLE AIRCRAFT
- High alpha inlets p 28 N91-20091
- ### HISTORIES
- Historical perspectives - The role of the NASA Lewis Research Center in the national space nuclear power programs
[AIAA PAPER 91-3462] p 242 A91-53713
- Historical perspectives: The role of the NASA Lewis Research Center in the national space nuclear power programs
[NASA-TM-105196] p 243 N91-29138
- ### HOLDERS
- Post clamp
[NASA-CASE-LEW-14862-1] p 183 N91-14617
- Removable hand hold
[NASA-CASE-LEW-15196-1] p 188 N91-26543
- ### HOLES (MECHANICS)
- Incorporating finite element analysis into component life and reliability
[NASA-TM-104400] p 203 N91-23550
- ### HOLLOW CATHODES
- Microanalyses of extended-test xenon hollow cathodes --- in ion thruster simulators
[AIAA PAPER 91-2123] p 61 A91-45787
- Microanalysis of extended-test xenon hollow cathodes
[NASA-TM-104532] p 82 N91-30202
- ### HOLOGRAPHIC INTERFEROMETRY
- Optical inspection of space-propulsion components using an injection seeded Nd:YAG laser system p 179 N91-24320
- ### HOLOGRAPHY
- Three-dimensional computed tomography from interferometric measurements within a narrow cone of views
[NASA-TM-103257] p 176 N91-19404
- ### HOMOGENEOUS TURBULENCE
- Comment on local energy transfer and nonlocal interactions in homogeneous, isotropic turbulence (Phys. Fluids A2, 413 (1990))
[NASA-TM-103263] p 159 N91-13638
- ### HOMOJUNCTIONS
- Recent results from the InP homojunction cell module on the LIPS III spacecraft p 140 A91-41971
- Effect of emitter parameter variation on the performance of heteroepitaxial indium phosphide solar cells p 140 A91-42003
- Effect of emitter parameter variation on the performance of heteroepitaxial indium phosphide solar cells
[NASA-TM-103619] p 70 N91-15306
- A theoretical comparison of the near-optimum design and predicted performance of n/p and p/n indium phosphide homojunction solar cells p 83 N91-30233
- ### HONEYCOMB STRUCTURES
- Evaluation of a technique to generate artificially thickened boundary layers in supersonic and hypersonic flows
[NASA-TP-3142] p 17 N91-28136
- ### HORSESHOE VORTICES
- Increased heat transfer to a cylindrical leading edge due to spanwise variations in the freestream velocity
[AIAA PAPER 91-1739] p 155 A91-43623
- Increased heat transfer to a cylindrical leading edge due to spanwise variations in the freestream velocity
[NASA-TM-104464] p 100 N91-24359
- ### HOT CORROSION
- High temperature reactions of ceramics and metals with chlorine and oxygen p 105 A91-20219
- Hot corrosion of silicon carbide and silicon nitride at 1000 C p 117 A91-55698
- ### HOT ISOSTATIC PRESSING
- Crystallization and properties of Sr-Ba aluminosilicate glass-ceramic matrices p 117 A91-56917
- Composite bearing and seal materials for advanced heat engine applications to 900 C
[NASA-TM-103612] p 95 N91-15318
- Process for HIP canning of composites
[NASA-CASE-LEW-14990-1-CU] p 96 N91-17145
- Crystallization and properties of Sr-Ba aluminosilicate glass-ceramic matrices
[NASA-TM-103764] p 120 N91-19308
- Mechanical strength and thermophysical properties of PM212: A high temperature self-lubricating powder metallurgy composite
[NASA-TM-103694] p 120 N91-21302
- ### HOT-WIRE ANEMOMETERS
- Experimental investigation of turbulent flow through a circular-to-rectangular transition duct
[NASA-TM-105210] p 18 N91-31106
- ### HOUSINGS
- Gear noise, vibration, and diagnostic studies at NASA Lewis Research Center p 183 A91-52811
- Acoustical analysis of gear housing vibration
[NASA-TM-103691] p 188 N91-25411
- ### HUMAN BODY
- Design strategies for the International Space University's variable gravity research facility p 42 N91-22171
- ### HYDRAULIC CONTROL
- A high-frequency servosystem for fuel control in hypersonic engines
[NASA-TM-104333] p 35 N91-31178
- ### HYDRAULIC TEST TUNNELS
- A review of ice accretion data from a model rotor icing test and comparison with theory
[AIAA PAPER 91-0661] p 19 A91-22500
- A review of ice accretion data from a model rotor icing test and comparison with theory
[NASA-TM-103712] p 11 N91-13421
- ### HYDRAZINES
- Lunar missions using chemical propulsion: System design issues
[NASA-TP-3065] p 70 N91-15308
- Arcjet nozzle area ratio effects p 75 N91-24271
- ### HYDROCARBON COMBUSTION
- Combustion of liquid fuel droplets in supercritical conditions
[AIAA PAPER 91-0078] p 105 A91-21362
- Mechanisms and modeling of the effects of additives on the nitrogen oxides emission
[AIAA PAPER 91-0479] p 124 A91-40560
- Numerical simulation of Jet-A combustion approximated by improved propane chemical kinetics
[AIAA PAPER 91-1859] p 106 A91-45777
- Analytical combustion/emissions research related to the NASA High-Speed Research Program
[AIAA PAPER 91-2252] p 25 A91-45799
- Mechanisms and modeling of the effects of additives on the nitrogen oxides emission
[NASA-TM-103765] p 126 N91-22464
- ### HYDROCARBON FUELS
- Fuel-rich, catalytic reaction experimental results --- fuel development for high-speed civil transport aircraft
[AIAA PAPER 91-2463] p 24 A91-44250
- Liquid oxygen cooling of hydrocarbon fueled rocket thrust chambers p 63 A91-52309
- Fuel-rich, catalytic reaction experimental results
[NASA-TM-104423] p 33 N91-24203
- ### HYDRODYNAMICS
- Naturally occurring and forced azimuthal modes in a turbulent jet
[NASA-TM-103692] p 11 N91-17000
- ### HYDROFLUORIC ACID
- High resolution electrolyte for thinning InP by anodic dissolution and its applications to EC-V profiling, defect revealing and surface passivation p 107 N91-30210
- ### HYDROGEN
- Effect of high temperature hydrogen exposure on the strength and microstructure of mullite p 114 A91-19780
- Numerical study of shock-wave/boundary layer interactions in premixed hydrogen-air hypersonic flows
[AIAA PAPER 91-0413] p 149 A91-26191
- Hydrogen-silicon carbide interactions p 114 A91-28783
- Two-dimensional imaging of molecular hydrogen in H_2 -air diffusion flames using two-photon laser-induced fluorescence p 124 A91-34369
- Effect of hydrogen on the strength and microstructure of selected ceramics p 118 N91-14482
- Numerical study of shock-wave/boundary layer interactions in premixed hydrogen-air hypersonic flows
[NASA-TM-103273] p 160 N91-14559
- Material processing with hydrogen and carbon monoxide on Mars
[NASA-TM-104405] p 211 N91-23616
- Arcjet thermal characteristics p 82 N91-29231
- Performance of a dual anode nickel-hydrogen cell p 214 N91-32563
- ### HYDROGEN EMBRITTLEMENT
- The effect of hydrogen on the low cycle fatigue behavior of a single crystal superalloy p 108 A91-28794
- ### HYDROGEN ENGINES
- CFD analysis of a hydrogen fueled ramjet engine at Mach 3.44
[AIAA PAPER 91-1919] p 23 A91-41653
- High-power hydrogen arcjet performance
[AIAA PAPER 91-2226] p 61 A91-45795
- Medium power hydrogen arcjet performance
[NASA-TM-104533] p 85 N91-31216
- ### HYDROGEN FUELS
- Material processing with hydrogen and carbon monoxide on Mars
[NASA-TM-104405] p 211 N91-23616
- ### HYDROGEN OXYGEN ENGINES
- The Advanced Expander Test Bed
[AIAA PAPER 90-3708] p 50 A91-10107
- A unique high heat flux facility for testing hypersonic engine components
[AIAA PAPER 90-5228] p 37 A91-14454
- Spectrally resolved Rayleigh scattering diagnostic for hydrogen-oxygen rocket plume studies
[AIAA PAPER 91-0462] p 51 A91-21498
- Numerical study of high-area-ratio H_2/O_2 rocket nozzles
[AIAA PAPER 91-2434] p 57 A91-41780
- A dual-cooled hydrogen-oxygen rocket engine heat transfer analysis
[AIAA PAPER 91-2211] p 59 A91-44156
- Experimental and analytical comparison of flowfields in a 110 N (25 Lbf) H_2/O_2 rocket
[AIAA PAPER 91-2283] p 62 A91-45802
- The development of a fiber optic Raman temperature measurement system for rocket flows
[AIAA PAPER 91-2316] p 173 A91-45804
- Performance and flow calculations for a gaseous H_2/O_2 thruster p 63 A91-48843
- Design of an Advanced Expander Test Bed --- for future space engines
[AIAA PAPER 91-3437] p 42 A91-52350
- Plans for the development of cryogenic engines for space exploration
[AIAA PAPER 91-3438] p 64 A91-52351
- Hydrogen/oxygen auxiliary propulsion technology
[AIAA PAPER 91-3440] p 64 A91-52352

- Technology readiness assessment of advanced space engine integrated controls and health monitoring [AIAA PAPER 91-3601] p 49 A91-52467
- A unique high heat flux facility for testing hypersonic engine components [NASA-TM-103238] p 38 N91-11770
- A rocket engine design expert system p 71 N91-17129
- Computer code for single-point thermodynamic analysis of hydrogen/oxygen expander-cycle rocket engines [NASA-TM-4275] p 72 N91-20206
- A dual-cooled hydrogen-oxygen rocket engine heat transfer analysis [NASA-TM-104430] p 76 N91-24302
- Advanced cryo propulsion systems p 80 N91-28212
- Experimental and analytical comparison of flowfields in a 110 N (25 lbf) H₂/O₂ rocket [NASA-TM-105175] p 82 N91-29230
- HYDROGEN OXYGEN FUEL CELLS**
- SEI rover solar-electrochemical power system options [NASA-TM-104402] p 211 N91-23620
- HYDROGEN PEROXIDE**
- High resolution electrolyte for thinning InP by anodic dissolution and its applications to EC-V profiling, defect revealing and surface passivation p 107 N91-30210
- HYDROGEN PRODUCTION**
- Slush hydrogen propellant production, transfer, and expulsion studies at the NASA K-Site Facility [AIAA PAPER 91-3550] p 125 A91-53710
- Slush hydrogen propellant production, transfer, and expulsion studies at the NASA K-Site Facility [NASA-TM-105191] p 127 N91-28449
- HYDROGENATION**
- Chemical approaches to carbon dioxide utilization for manned Mars missions [NASA-TM-103728] p 241 N91-20015
- HYDROTHERMAL STRESS ANALYSIS**
- Progressive fracture in composites subjected to hydrothermal environment [NASA-TM-105230] p 103 N91-32182
- HYGRAL PROPERTIES**
- Mechanics of damping for fiber composite laminates including hygrothermal effects p 195 A91-12895
- Progressive fracture in composites subjected to hydrothermal environment [AIAA PAPER 91-1140] p 91 A91-31919
- HYPERCUBE MULTIPROCESSORS**
- Shared direct memory access on the Explorer 2-LX [NASA-TM-103289] p 216 N91-12215
- HYPERSONIC FLIGHT**
- CFD for hypersonic propulsion [NASA-TM-103791] p 164 N91-21447
- Application of computational fluid dynamics in high speed aeropropulsion [NASA-TM-103780] p 164 N91-21458
- HYPERSONIC FLOW**
- Spatial evolution of nonlinear acoustic mode instabilities on hypersonic boundary layers p 225 A91-12973
- Numerical study of shock-wave/boundary layer interactions in premixed hydrogen-air hypersonic flows [AIAA PAPER 91-0413] p 149 A91-26191
- Three-dimensional viscous flow computations of high area ratio nozzles for hypersonic propulsion p 4 A91-30014
- Computational analysis of underexpanded jets in the hypersonic regime p 4 A91-37421
- A new Lagrangian random choice method for steady two-dimensional supersonic/hypersonic flow [AIAA PAPER 91-1546] p 5 A91-40721
- Numerical flux formulas for the Euler and Navier-Stokes equations. II - Progress in flux-vector splitting [AIAA PAPER 91-1566] p 5 A91-40740
- Efficient real gas upwind Navier-Stokes computations of high speed flows p 157 A91-46179
- Numerical study of shock-wave/boundary layer interactions in premixed hydrogen-air hypersonic flows [NASA-TM-103273] p 160 N91-14559
- Numerical flux formulas for the Euler and Navier-Stokes equations. 2: Progress in flux-vector splitting [NASA-TM-104353] p 15 N91-22084
- High-Order Polynomial Expansions (HOPE) for flux-vector splitting [NASA-TM-104452] p 222 N91-25739
- Evaluation of a technique to generate artificially thickened boundary layers in supersonic and hypersonic flows [NASA-TP-3142] p 17 N91-28136
- HYPERSONIC INLETS**
- 3-D Navier-Stokes analysis of crossing, glancing shocks/turbulent boundary layer interactions [AIAA PAPER 91-1758] p 6 A91-43631
- CFD analysis for high speed inlets p 10 N91-10888
- Computational modeling and validation for hypersonic inlets p 16 N91-23162
- The 3-D Navier-Stokes analysis of crossing, glancing shocks/turbulent boundary layer interactions [NASA-TM-104469] p 16 N91-24130
- HYPERSONIC NOZZLES**
- 3D computation of hypersonic nozzle [AIAA PAPER 90-5203] p 1 A91-14429
- HYPERSONIC SPEED**
- A comparison of CFD predictions and experimental results for a Mach 5 inlet p 28 N91-20094
- HYPERSONIC VEHICLES**
- A unique high heat flux facility for testing hypersonic engine components [AIAA PAPER 90-5228] p 37 A91-14454
- Development of braided rope seals for hypersonic engine applications. II - Flow modeling [AIAA PAPER 91-2495] p 182 A91-41800
- A unique high heat flux facility for testing hypersonic engine components [NASA-TM-103238] p 38 N91-11770
- High temperature NASP engine seal development [NASA-TM-103716] p 184 N91-19441
- Overview of hypersonic/transatmospheric vehicle propulsion technology p 28 N91-20092
- Development of braided rope seals for hypersonic engine applications. Part 2: Flow modeling [NASA-TM-104371] p 186 N91-22571
- A high-frequency servosystem for fuel control in hypersonic engines [NASA-TM-104333] p 35 N91-31178
- HYPERSONICS**
- Thermal and structural assessments of a ceramic wafer seal in hypersonic engine [AIAA PAPER 91-2494] p 23 A91-41799
- Thermal and structural assessments of a ceramic wafer seal in hypersonic engines [NASA-TM-103651] p 26 N91-13456
- A test fixture for measuring high-temperature hypersonic-engine seal performance [NASA-TM-103658] p 184 N91-19442
- CFD for hypersonic propulsion [NASA-TM-103791] p 164 N91-21447
- Evaluation and ranking of candidate ceramic wafer engine seal materials [NASA-TM-103795] p 187 N91-23515
- HYPERVELOCITY IMPACT**
- On protection of Freedom's solar dynamic radiator from the orbital debris environment. Part 2: Further testing and analyses [NASA-TM-104514] p 84 N91-30265
- HYSTERESIS**
- High frequency, high temperature specific core loss and dynamic B-H hysteresis loop characteristics of soft magnetic alloys p 138 A91-37988
- A data acquisition and control program for axial-torsional fatigue testing p 199 A91-56540
- Eccentricity effects on leakage of a brush seal at low speeds [NASA-TM-105141] p 86 N91-31220
- ICE**
- A review of ice accretion data from a model rotor icing test and comparison with theory [NASA-TM-103712] p 11 N91-13421
- Simulation of iced wing aerodynamics [NASA-TM-104362] p 15 N91-23086
- Icing simulation: A survey of computer models and experimental facilities [NASA-TM-104366] p 15 N91-23087
- Advanced ice protection systems test in the NASA Lewis icing research tunnel [NASA-TM-103757] p 32 N91-23183
- Model rotor icing tests in the NASA Lewis icing research tunnel [NASA-TM-104351] p 32 N91-23184
- ICE CLOUDS**
- Use of rotating pinholes and reticles for calibration of cloud droplet instrumentation p 171 A91-30371
- ICE FORMATION**
- Icing tests of a model main rotor p 18 A91-17218
- A review of ice accretion data from a model rotor icing test and comparison with theory [AIAA PAPER 91-0661] p 19 A91-22500
- Results of a sub-scale model rotor icing test [AIAA PAPER 91-0660] p 19 A91-26190
- Numerical simulation of ice growth on a MS-317 swept wing geometry [AIAA PAPER 91-0263] p 19 A91-26193
- Icing characteristics of a natural-laminar-flow, a medium-speed, and a swept, medium-speed airfoil [AIAA PAPER 91-0447] p 3 A91-26327
- Prediction of ice shapes and their effect on airfoil performance [AIAA PAPER 91-0264] p 3 A91-26330
- Modeling of surface roughness effects on glaze ice accretion p 19 A91-35107
- Elevator deflections on the icing process p 20 A91-35427
- Effects of horizontal tail ice on longitudinal aerodynamic derivatives p 36 A91-38547
- Progress toward the development of an airfoil icing analysis capability p 9 N91-10866
- A review of ice accretion data from a model rotor icing test and comparison with theory [NASA-TM-103712] p 11 N91-13421
- Results of a sub-scale model rotor icing test [NASA-TM-103709] p 11 N91-14309
- Numerical simulation of ice growth on a MS-317 swept wing geometry [NASA-TM-103705] p 11 N91-14310
- Icing characteristics of a natural-laminar-flow, a medium-speed, and a swept, medium-speed airfoil [NASA-TM-103693] p 12 N91-19046
- Prediction of ice shapes and their effect on airfoil performance [NASA-TM-103701] p 12 N91-19047
- Automatic control study of the icing research tunnel refrigeration system [NASA-TM-4257] p 40 N91-19115
- Simulation of iced wing aerodynamics [NASA-TM-104362] p 15 N91-23086
- Icing simulation: A survey of computer models and experimental facilities [NASA-TM-104366] p 15 N91-23087
- Advanced ice protection systems test in the NASA Lewis icing research tunnel [NASA-TM-103757] p 32 N91-23183
- Model rotor icing tests in the NASA Lewis icing research tunnel [NASA-TM-104351] p 32 N91-23184
- Applied high-speed imaging for the icing research program at NASA Lewis Research Center [NASA-TM-104415] p 177 N91-26490
- Calculated performance of the NASA Lewis icing research tunnel [NASA-TM-105173] p 39 N91-29199
- ICE PREVENTION**
- Experimental water droplet impingement data on modern aircraft surfaces [AIAA PAPER 91-0445] p 2 A91-21493
- Progress toward the development of an airfoil icing analysis capability p 9 N91-10866
- NASA's aircraft icing technology program p 19 N91-20120
- Icing simulation: A survey of computer models and experimental facilities [NASA-TM-104366] p 15 N91-23087
- Advanced ice protection systems test in the NASA Lewis icing research tunnel [NASA-TM-103757] p 32 N91-23183
- ILLUMINATION**
- Satellite eclipse power by laser illumination [IAF PAPER 90-053] p 50 A91-13766
- IMAGE ANALYSIS**
- Spatial variations in a.c. susceptibility and microstructure for the YBa₂Cu₃O_{7-x} superconductor and their correlation with room-temperature ultrasonic measurements p 233 A91-54969
- Spatial variations in ac susceptibility and microstructure for the YBa₂Cu₃O_{7-x} superconductor and their correlation with room-temperature ultrasonic measurements [NASA-TM-103787] p 194 N91-21553
- Concentrator testing using projected images [NASA-TM-104349] p 79 N91-27204
- IMAGE ENHANCEMENT**
- VSTOL ground effects testing with flow visualization and image enhancement [AIAA PAPER 91-3145] p 8 A91-54061
- IMAGE PROCESSING**
- A neural net based architecture for the segmentation of mixed gray-level and binary pictures p 218 A91-29183
- Two-dimensional imaging of molecular hydrogen in H₂-air diffusion flames using two-photon laser-induced fluorescence p 124 A91-34369
- Particle displacement tracking for PIV [NASA-TM-103286] p 175 N91-10271
- High Resolution, High Frame Rate Video Technology [NASA-CP-3080] p 175 N91-14574
- High resolution, high frame rate video technology development plan and the near-term system conceptual design p 175 N91-14580
- Improved visualization of flow field measurements [NASA-TM-103679] p 12 N91-19044
- Software manual for operating particle displacement tracking data acquisition and reduction system [NASA-TM-103720] p 176 N91-20453

IMAGING TECHNIQUES

Applied high-speed imaging for the icing research program at NASA Lewis Research Center
[NASA-TM-104415] p 177 N91-26490

IMAGING TECHNIQUES

Particle image fields and partial coherence
p 171 A91-19604
Two-dimensional particle displacement tracking in particle imaging velocimetry
p 172 A91-38498
Particle displacement tracking for PIV
[NASA-TM-103288] p 175 N91-10271
High Resolution, High Frame Rate Video Technology
[NASA-CP-3080] p 175 N91-14574
An imaging system for PLIF/Mie measurements for a combustor flow
[NASA-TM-103714] p 27 N91-20084
Particle image velocimetry for the surface tension driven convection experiment using a particle displacement tracking technique
[NASA-TM-104482] p 177 N91-25382
Particle displacement tracking applied to air flows
[NASA-TM-104481] p 177 N91-25387
Applied high-speed imaging for the icing research program at NASA Lewis Research Center
[NASA-TM-104415] p 177 N91-26490

IMPACT TESTS

Impact behavior of a SiC fiber-reinforced reaction bonded Si₃N₄ composite
p 91 A91-16805
Low velocity impact analysis with NASTRAN
[NASA-TM-103169] p 95 N91-14426

IMPACTORS

Low velocity impact analysis with NASTRAN
p 198 A91-48865
Low velocity impact analysis with NASTRAN
[NASA-TM-103169] p 95 N91-14426

IMPEDANCE

Impedances of electrochemically impregnated nickel electrodes as functions of potential, KOH concentration, and impregnation method
[NASA-TM-103283] p 208 N91-15628

IMPEDANCE MATCHING

Design aspects and comparison between high T(sub c) superconducting coplanar waveguide and microstrip line
[NASA-TM-105142] p 146 N91-27445

IMPEDANCE MEASUREMENT

Impedances of nickel electrodes cycled in various KOH concentrations
p 214 N91-32557

IMPINGEMENT

Experimental water droplet impingement data on modern aircraft surfaces
[AIAA PAPER 91-0445] p 2 A91-21493
Icing characteristics of a natural-laminar-flow, a medium-speed, and a swept, medium-speed airfoil
[NASA-TM-103693] p 12 N91-19046

IMPLANTATION

Surface and implantation effects on p-n junctions
p 234 N91-18299
Adaptation of NASA technology for the optimization of orthopedic knee implants
p 215 N91-23032

IMPREGNATING

Impedances of electrochemically impregnated nickel electrodes as functions of potential, KOH concentration, and impregnation method
[NASA-TM-103283] p 208 N91-15628

IN-FLIGHT MONITORING

In-flight source noise of an advanced full-scale single-rotation propeller
[AIAA PAPER 91-0594] p 226 A91-21547
In-flight and simulated aircraft fuel temperature measurements
[NASA-TM-103611] p 125 N91-15418

INCOMPRESSIBLE FLOW

Multidimensional computer simulation of Stirling cycle engines
p 181 A91-38154
Further two-dimensional code development for Stirling space engine components
p 56 A91-38184
Numerical solution for the velocity-derivative skewness of a low Reynolds-number turbulent-like decaying Navier-Stokes flow
p 158 A91-50204
Time dependent viscous incompressible Navier-Stokes equations
p 9 N91-10854
On the anomaly of velocity-pressure decoupling in collocated mesh solutions
[NASA-TM-103769] p 164 N91-21448
Experimental investigation of turbulent flow through a circular-to-rectangular transition duct
[NASA-TM-105210] p 18 N91-31106
Least-squares solution of incompressible Navier-Stokes equations with the p-version of finite elements
[NASA-TM-105203] p 223 N91-31911

INCONEL (TRADEMARK)

Inhomogeneous deformation in INCONEL 718 during monotonic and cyclic loadings
p 108 A91-22287
Two-dimensional high temperature strain measurement system
p 204 N91-24319

INDENTATION

Temperature-dependent indentation behavior of transformation-toughened zirconia-based ceramics
p 114 A91-28767

INDEXES (DOCUMENTATION)

Bibliography of Lewis Research Center technical publications announced in 1989
[NASA-TM-102542] p 238 N91-10798

INDIUM ALLOYS

An x ray photoelectron spectroscopy study of Au(x)In(y) alloys
[NASA-TM-103659] p 234 N91-14050

INDIUM ARSENIDES

New materials and techniques for improved mm wave devices
[AIAA PAPER 91-3590] p 142 A91-52459
Ellipsometric study of InGaAs MODFET material
[NASA-TM-103286] p 143 N91-19351
Study of InGaAs based MODFET structures using variable angle spectroscopic ellipsometry
[NASA-TM-103792] p 235 N91-19935
Recent progress in InP solar cell research
[NASA-TM-104509] p 146 N91-27447

INDIUM COMPOUNDS

Dielectric function of InGaAs in the visible
p 233 A91-53236

INDIUM PHOSPHIDES

New directions in InP solar cell research
p 206 A91-38022
An analysis of the contact sintering process in III-V solar cells
p 139 A91-41891
Study of surface passivation as a function of InP closed-ampoule solar cell fabrication processing variables
p 232 A91-41891
Key factors limiting the open circuit voltage of n(+)/pp(+/-) indium phosphide solar cells
p 139 A91-41929
Measurement of surface recombination velocity on heavily doped indium phosphide
p 232 A91-41931
Recent results from the InP homojunction cell module on the LIPS III spacecraft
p 140 A91-41971
Effects of radiation of InP cells epitaxially grown on Si and GaAs substrates
p 140 A91-41984
Effect of emitter parameter variation on the performance of heteroepitaxial indium phosphide solar cells
p 140 A91-42003
The influence of interstitial Ga and interfacial Au₂P₃ on the electrical and metallurgical behavior of Au-contacted III-V semiconductors
p 140 A91-42694
Low noise InP-based MMIC receivers for W-band
[AIAA PAPER 91-3594] p 142 A91-52462
Submicron gate InP power MISFET's with improved output power density at 18 and 20 GHz
p 142 A91-54526

Effect of emitter parameter variation on the performance of heteroepitaxial indium phosphide solar cells
[NASA-TM-103619] p 70 N91-15306
Effects of proton irradiation on the performance of InP/GaAs solar cells
p 209 N91-19205
Key factors limiting the open circuit voltage of n(+)/pp(+/-) indium phosphide solar cells
p 209 N91-19206
Determination of series resistance of indium phosphide solar cells
p 210 N91-19207
Indium phosphide solar cells
p 210 N91-19221
Effect of dislocations on the open-circuit voltage, short-circuit current and efficiency of heteroepitaxial indium phosphide solar cells
[NASA-TM-103762] p 144 N91-19354
Heteroepitaxial InP solar cells on Si and GaAs substrates
[NASA-TM-103696] p 144 N91-20392
Optimal design study of high efficiency indium phosphide space solar cells
[NASA-TM-103763] p 145 N91-21433
Future mission opportunities and requirements for advanced space photovoltaic energy conversion technology
[NASA-TM-103661] p 74 N91-22371
Submicron gate InP power MISFET's with improved output power density at 18 and 20 GHz
p 145 N91-26436

Recent progress in InP solar cell research
[NASA-TM-104509] p 146 N91-27447
A comparative study of p(+)/n and n(+)/p InP solar cells made by a closed ampoule diffusion
p 212 N91-30206

Improvements in contact resistivity and thermal stability of Au-contacted InP solar cells
p 213 N91-30207
Grooved surfaces on InP
p 213 N91-30208
Effect of dislocations on properties of heteroepitaxial InP solar cells
p 213 N91-30209
Comparative modeling of InP solar cell structures
p 83 N91-30232
A theoretical comparison of the near-optimum design and predicted performance of n/p and p/n indium phosphide homojunction solar cells
p 83 N91-30233

Advanced power systems for EOS
[NASA-TM-105222] p 85 N91-31217

INDUCTION MOTORS

Induction motor control
p 137 A91-30893
Electromechanical actuation for thrust vector control applications
p 52 A91-31026
Field oriented control of induction motors
p 138 A91-37987
Four quadrant control of induction motors
p 145 N91-23055

INERTIA

Inertia effects in thin film flow with a corrugated boundary
p 151 A91-32691

INERTIAL UPPER STAGE

Advanced launch vehicle upper stages using liquid propulsion and metallized propellants
[NASA-TM-103622] p 68 N91-11797
Advanced launch vehicle upper stages using liquid propulsion and metallized propellants
p 75 N91-24257

INFERENCE

An autonomous fault detection, isolation, and recovery system for a 20-kHz electric power distribution test bed
[NASA-TM-104344] p 217 N91-25680

INFLATABLE SPACECRAFT

Design of an inflatable, optically controlled and fed, phased array antenna
[AIAA PAPER 91-3470] p 132 A91-52378

INFLUENCE COEFFICIENT

Oscillating cascade aerodynamics by an experimental influence coefficient technique
p 1 A91-10339
Cascade flutter analysis with transient response aerodynamics
[AIAA PAPER 91-0747] p 21 A91-19448
Cascade flutter analysis with transient response aerodynamics
[NASA-TM-103746] p 201 N91-19475
Efficient computation of aerodynamic influence coefficients for aeroelastic analysis on a transputer network
[NASA-TM-103671] p 216 N91-20748

INFORMATION MANAGEMENT

A technology assessment of alternative communications systems for the space exploration initiative
[AIAA PAPER 90-3681] p 44 A91-11472
Development of technology needs for the SEI TNIM network
[AIAA PAPER 91-3536] p 45 A91-52427
An assessment of technology alternatives for telecommunications and information management for the space exploration initiative
[NASA-TM-103783] p 134 N91-23347

INFORMATION SYSTEMS

Millimeter wavelength communications applications for the SEI
[NASA-TM-105275] p 135 N91-32287

INFORMATION TRANSFER

A comparison of optical technologies for a high data rate Mars link
[AIAA PAPER 91-3469] p 45 A91-52377

INFRARED DETECTORS

Superconductivity applications for infrared and microwave devices, Proceedings of the Meeting, Orlando, FL, Apr. 19, 20, 1990
[SPIE-1292] p 141 A91-50426

INFRARED INSTRUMENTS

Diamondlike carbon applications in infrared optics and microelectronics
p 230 N91-18306

INFRARED LASERS

An experimental apparatus for measuring surface resistance in the submillimeter-wavelength region
p 174 A91-54390

INGESTION (ENGINES)

STOVL Hot Gas Ingestion control technology
[ASME PAPER 89-GT-323] p 22 A91-23642
VSTOL ground effects testing with flow visualization and image enhancement
[AIAA PAPER 91-3145] p 8 A91-54061
A numerical study of the hot gas environment around a STOVL aircraft in ground proximity
p 10 N91-10887

INJECTION

Review and test of chilldown methods for space-based cryogenic tanks
[AIAA PAPER 91-1843] p 60 A91-45776
Cryogenic transfer options for exploration missions
[AIAA PAPER 91-3541] p 158 A91-53714
Review and test of chilldown methods for space-based cryogenic tanks
[NASA-TM-104458] p 167 N91-25351
Autogenous pressurization of cryogenic vessels using submerged vapor injection
[NASA-TM-104516] p 127 N91-27375
Cryogenic transfer options for exploration missions
[NASA-TM-105197] p 168 N91-28538

SUBJECT INDEX

INJECTORS

- Flow visualization of a rocket injector spray using gelled propellant simulants
[AIAA PAPER 91-2198] p 59 A91-44151
- Progress toward synergistic hypermixing nozzles
[AIAA PAPER 91-2264] p 25 A91-45800
- Method of injecting fluid propellants into a rocket combustion chamber
[NASA-CASE-LEW-14846-2] p 78 N91-26200
- Progress toward synergistic hypermixing nozzles
[NASA-TM-105169] p 18 N91-29150

INLET FLOW

- Hot gas ingestion test results of a two-poster vectored thrust concept with flow visualization in the NASA Lewis 9- by 15-foot low speed wind tunnel
[AIAA PAPER 90-2268] p 4 A91-40561
- An experimental trace gas investigation of fluid transport and mixing in a circular-to-rectangular transition duct
[AIAA PAPER 91-2370] p 172 A91-44214
- Design and experimental evaluation of compact radial-inflow turbines
[AIAA PAPER 91-2127] p 24 A91-45788
- Some preliminary results of brush seal/rotor interference effects on leakage at zero and low rpm using a tapered-plug rotor
[AIAA PAPER 91-3390] p 182 A91-45820
- Turbulent boundary layer separation over a rearward facing ramp and its control through mechanical excitation
[NASA-TM-103702] p 160 N91-19370
- A comparison of CFD predictions and experimental results for a Mach 5 inlet
p 28 N91-20094
- Hot gas ingestion test results of a two-poster vectored thrust concept with flow visualization in the NASA Lewis 9- x 15-foot low speed wind tunnel
[NASA-TM-103258] p 15 N91-21116
- A study of three dimensional turbulent boundary layer separation and vortex flow control using the reduced Navier Stokes equations
[NASA-TM-104407] p 16 N91-23089
- Computational modeling and validation for hypersonic inlets
p 16 N91-23162
- Effects of inlet distortion on the development of secondary flows in a subsonic axial inlet compressor rotor
[NASA-TM-104356] p 31 N91-23179
- Characterization of flow in a scroll duct
[NASA-CR-188612] p 167 N91-25367
- An experimental trace gas investigation of fluid transport and mixing in a circular-to-rectangular transition duct
[NASA-TM-104499] p 17 N91-27129
- Some preliminary results of brush seal/rotor interference effects on leakage at zero and low RPM using a tapered-plug rotor
[NASA-TM-104396] p 188 N91-27559
- Unsteady flowfield of a propfan at takeoff conditions
[NASA-TM-105223] p 18 N91-32075

INLET NOZZLES

- Overview of hypersonic/transatmospheric vehicle propulsion technology
p 28 N91-20092
- Overview of NASP nozzle research
p 28 N91-20093
- Inlets, ducts, and nozzles
p 162 N91-20096

INLET PRESSURE

- Flow visualization in a simulated brush seal
[ASME PAPER 90-GT-217] p 173 A91-44633

INLET TEMPERATURE

- Visualization techniques to experimentally model flow and heat transfer in turbine and aircraft flow passages
[NASA-TM-4272] p 167 N91-27489

INORGANIC PEROXIDES

- Synthesis and thermal properties of strontium and calcium peroxides
[NASA-TM-103725] p 107 N91-22410

INSOLATION

- Solar radiation on Mars
p 242 A91-28153
- Solar radiation on Mars: Update 1990
[NASA-TM-103623] p 242 N91-15117

INSPECTION

- Overview of space propulsion systems for identifying nondestructive evaluation and health monitoring opportunities
[NASA-TM-103614] p 192 N91-15565
- A methodology for evaluating the reliability and risk of structures under complex service environments
[NASA-TM-103244] p 200 N91-17415
- Computerized inspection of real surfaces and minimization of their deviations
[NASA-TM-103798] p 188 N91-27558

INSTRUMENT COMPENSATION

- Advanced Communications Technology Satellite (ACTS)
[IAF PAPER 90-481] p 44 A91-14056

INSULATORS

- Properties of insulator interfaces with p-HgCdTe
p 235 N91-18300

- Thin film characterization using spectroscopic ellipsometry
p 119 N91-18303

INTAKE SYSTEMS

- A numerical study of the hot gas environment around a STOVL aircraft in ground proximity
p 10 N91-10887

INTEGERS

- RSM 1.0 user's guide: A resupply scheduler using integer optimization
[NASA-TM-104380] p 217 N91-22766

INTEGRATED CIRCUITS

- Design of an optically controlled Ka-band GaAs MMIC phased-array antenna
p 132 A91-24951
- Optical control of microwave devices --- Book
p 136 A91-27331

- Performance of a 300 Mbps 1:16 serial/parallel optoelectronic receiver module
p 141 A91-51146

- Ka-band MMIC microstrip array for high rate communications
[AIAA PAPER 91-3421] p 132 A91-52341

- High efficiency Ka-band MMIC amplifiers
[AIAA PAPER 91-3425] p 141 A91-52345

- Low noise InP-based MMIC receivers for W-band
[AIAA PAPER 91-3594] p 142 A91-52462

- Universal nondestructive mm-wave integrated circuit test fixture
[NASA-CASE-LEW-14746-1] p 143 N91-14552

- Solid State Technology Branch of NASA Lewis Research Center Second Annual Digest, June 1989 - June 1990
[NASA-TM-103226] p 133 N91-18297

- Coplanar waveguide EEsof MICAD macros make circuit layout easy
[NASA-TM-103272] p 134 N91-19332

- System-Level Integrated Circuit (SLIC) development for phased array antenna applications
[NASA-TM-104392] p 134 N91-23354

- Microwave integrated circuits for space applications
p 145 N91-24069

- Ka-band MMIC microstrip array for high rate communications
[NASA-TM-104500] p 135 N91-27437

INTEGRATED OPTICS

- Optical control of microwave devices --- Book
p 136 A91-27331

INTERACTIONAL AERODYNAMICS

- The design/analysis of flows through turbomachinery - A viscous/inviscid approach
[AIAA PAPER 91-2010] p 153 A91-41677

- The effect of varying Mach number on crossing, glancing shocks/turbulent boundary-layer interactions
[AIAA PAPER 91-2157] p 6 A91-45792

- Primitive variable, strongly implicit calculation procedure for viscous flows at all speeds
p 7 A91-46181

- Three-dimensional Euler time accurate simulations of fan rotor-stator interactions
[NASA-TM-102528] p 16 N91-24124

INTERACTIVE CONTROL

- Presentation on a Space Acceleration Measurement System (SAMS)
p 50 N91-12417

INTERCALATION

- The preliminary feasibility of intercalated graphite railgun armatures
p 137 A91-29257

- Resistivity of pristine and intercalated graphite fiber epoxy composites
p 115 A91-35949

- Intercalated graphite fiber composites as EMI shields in aerospace structures
[NASA-TM-103632] p 94 N91-10134

- Apparatus for intercalating large quantities of fibrous structures
[NASA-CASE-LEW-15077-2] p 102 N91-28289

INTERFACE STABILITY

- Adhesion at metal interfaces
p 88 A91-38581

- Preliminary studies on NiAl/Nb2Be17 reaction and effectiveness of BeO as an interfacial reaction barrier
p 92 A91-55050

- Interphase layer optimization for metal matrix composites with fabrication considerations
[NASA-TM-105166] p 102 N91-30281

INTERFACES

- Drop-tower experiments for capillary surfaces in an exotic container
[AIAA PAPER 91-0107] p 148 A91-19138

- Theoretical modelling of AFM for bimetallic tip-substrate interactions
[NASA-TM-105280] p 112 N91-32215

INTERFACIAL TENSION

- Critical-point analysis of the liquid-vapor interfacial surface tension
p 237 A91-16103

- Thermocapillary migration of liquid droplets in a temperature gradient in a density matched system
p 153 A91-41132

- Spacelab qualified infrared imager for microgravity science applications
p 173 A91-51585

- Particle image velocimetry for the surface tension driven convection experiment using a particle displacement tracking technique
[NASA-TM-104482] p 177 N91-25382

- Ground-based PIV and numerical flow visualization results from the surface tension driven convection experiment
[NASA-TM-105172] p 178 N91-30491

INTERFERENCE IMMUNITY

- Prospects for using carbon-carbon composites for EMI shielding
[NASA-TM-103677] p 97 N91-19231

INTERFEROMETERS

- Fiber optic sensing system
[NASA-CASE-LEW-14795-1] p 230 N91-21871

INTERFEROMETRY

- Three-dimensional computed tomography from interferometric measurements within a narrow cone of views
[NASA-TM-103257] p 176 N91-19404

INTERLAYERS

- The effects of interply damping layers on the dynamic response of composite structures
[AIAA PAPER 91-1124] p 197 A91-32064

- The effects of interply damping layers on the dynamic response of composite structures
[NASA-TM-104497] p 103 N91-30282

INTERMETALLICS

- Oxidation behavior of cubic phases formed by alloying Al3Ti with Cr and Mn
p 108 A91-27849

- 1000 to 1300 K slow plastic compression properties of Al-deficient NiAl
p 108 A91-36214

- The potential for ductility enhancement from surface and interface dislocation sources in NiAl
p 109 A91-39292

- Continuous fiber-reinforced titanium aluminum composites
p 92 A91-39553

- A simplified method for determining the number of independent slip systems in crystals
p 110 A91-55472

- Low-density, high-strength intermetallic matrix composites by XD (trademark) synthesis
[NASA-TM-103724] p 97 N91-19233

- NDE standards for high temperature materials
[NASA-TM-103761] p 193 N91-19464

- Prospects for ductility and toughness enhancement of NiAl by ductile phase reinforcement
[NASA-TM-103796] p 112 N91-27324

- Fatigue behavior and life prediction of a SiC/Ti-24Al-11Nb composite under isothermal conditions
[NASA-TM-105168] p 206 N91-30566

INTERPLANETARY COMMUNICATION

- A comparison of optical technologies for a high data rate Mars link
[AIAA PAPER 91-3469] p 45 A91-52377

- Technologies for unattended network operations
[AIAA PAPER 91-3534] p 45 A91-52425

INTERPLANETARY FLIGHT

- Electrical characterization of a Mapham inverter using pulse testing techniques
p 139 A91-37992

INTERPLANETARY SPACECRAFT

- Synergistic use of high and low thrust propulsion systems for piloted missions to Mars
[AIAA PAPER 91-2346] p 39 A91-45807

INTERPOLATION

- Accurate monotone cubic interpolation
[NASA-TM-103789] p 221 N91-20830

INTERPROCESSOR COMMUNICATION

- General-purpose interface bus for multiuser, multitasking computer system
p 215 A91-35928

- Performance of a 300 Mbps 1:16 serial/parallel optoelectronic receiver module
p 141 A91-51146

INTERSTITIALS

- The influence of interstitial Ga and interfacial Au2P3 on the electrical and metallurgical behavior of Au-contacted III-V semiconductors
p 140 A91-42694

INVERSIONS

- Surface electrons in inverted layers of p-HgCdTe
p 235 N91-18301

INVISCID FLOW

- Numerical flux formulas for the Euler and Navier-Stokes equations. II - Progress in flux-vector splitting
[AIAA PAPER 91-1566] p 5 A91-40740

- The design/analysis of flows through turbomachinery - A viscous/inviscid approach
[AIAA PAPER 91-2010] p 153 A91-41677

- Time-derivative preconditioning for viscous flows
[AIAA PAPER 91-1652] p 154 A91-43576

- Numerical flux formulas for the Euler and Navier-Stokes equations. 2: Progress in flux-vector splitting
[NASA-TM-104353] p 15 N91-22084

- The design/analysis of flows through turbomachinery: A viscous/inviscid approach
[NASA-TM-104447] p 33 N91-25148

ION BEAMS

- Ion beam sputtering in electric propulsion facilities
[AIAA PAPER 91-2117] p 61 A91-45785

- Dual ion beam processed diamondlike films for industrial applications
p 121 N91-23042

- Ion beam textured and coated surfaces experiment (IBEX)
p 122 N91-25040

- Ion beam sputtering in electric propulsion facilities
[NASA-TM-105145] p 86 N91-32158
- ION ENGINES**
- Ion beam sputtering in electric propulsion facilities
[AIAA PAPER 91-2117] p 61 A91-45785
- Laser interferometric measurement of ion electrode shape and charge exchange erosion
[AIAA PAPER 91-2121] p 173 A91-45786
- Microanalyses of extended-test xenon hollow cathodes --- in ion thruster simulators
[AIAA PAPER 91-2123] p 61 A91-45787
- Performance and optimization of a 'derated' ion thruster for auxiliary propulsion
[AIAA PAPER 91-2350] p 62 A91-45809
- Energy deposition in low-power coaxial plasma thrusters
p 63 A91-52311
- Status of structural analysis of 30 cm diameter ion optics
[NASA-TM-103618] p 68 N91-11796
- Solar electric propulsion for Mars transport vehicles
[NASA-TM-103234] p 71 N91-19178
- Performance and optimization of a derated ion thruster for auxiliary propulsion
[NASA-TM-105144] p 82 N91-29229
- Microanalysis of extended-test xenon hollow cathodes
[NASA-TM-104532] p 82 N91-30202
- Laser interferometric measurement of ion electrode shape and charge exchange erosion
[NASA-TM-105165] p 179 N91-31605
- Multimegawatt electric propulsion system design considerations
[NASA-TM-105152] p 87 N91-32164
- ION EXCHANGE MEMBRANE ELECTROLYTES**
- Some recent studies with the solid-ionomer electrochemical capacitor
p 214 N91-32562
- ION PLATING**
- Plasma-assisted physical vapor deposition surface treatments for tribological control
[NASA-TM-103652] p 130 N91-11945
- ION PROPULSION**
- Evolutionary use of nuclear electric propulsion
[AIAA PAPER 90-3821] p 50 A91-10174
- Advanced ion propulsion for space exploration
[AIAA PAPER 91-3567] p 65 A91-52443
- Xenon ion propulsion for orbit transfer
[NASA-TM-103193] p 69 N91-11798
- A 5-kW xenon ion thruster lifetest
[NASA-TM-103191] p 72 N91-19180
- Dual-purpose self-deliverable lunar surface PV electrical power system
p 209 N91-19200
- Performance and optimization of a derated ion thruster for auxiliary propulsion
[NASA-TM-105144] p 82 N91-29229
- Microanalysis of extended-test xenon hollow cathodes
[NASA-TM-104532] p 82 N91-30202
- Ion beam sputtering in electric propulsion facilities
[NASA-TM-105145] p 86 N91-32158
- ION SOURCES**
- Dual ion beam processed diamondlike films for industrial applications
p 121 N91-23042
- IRON ALLOYS**
- Compression behavior of TiB₂-particulate-reinforced composites of Al₂Fe₃TiB
p 91 A91-28014
- Comparison of high temperature, high frequency core loss and dynamic B-H loops of two 50 Ni-Fe crystalline alloys and an iron-based amorphous alloy
[NASA-TM-105205] p 147 N91-32412
- IRON COMPOUNDS**
- Near-Earth asteroids: Metals occurrence, extraction, and fabrication
p 241 N91-26058
- IRRADIATION**
- Neutron and gamma irradiation effects on power semiconductor switches
p 139 A91-38162
- Thermal annealing of GaAs concentrator solar cells
p 208 N91-19195
- ISOLATION**
- Sensor failure detection and recovery by neural networks
[NASA-TM-104484] p 220 N91-24815
- ISOTHERMAL PROCESSES**
- Long term isothermal aging and thermal analysis of N-CYCAP polyimides
[NASA-TM-104341] p 122 N91-25286
- ISOTOPES**
- Design of multihundredwatt DIPS for robotic space missions
[NASA-TM-104401] p 75 N91-24232
- Preliminary design of a mobile lunar power supply
[NASA-TM-104471] p 212 N91-27611
- ISOTROPIC TURBULENCE**
- Comment on local energy transfer and nonlocal interactions in homogeneous, isotropic turbulence (Phys. Fluids A2, 413 (1990))
[NASA-TM-103263] p 159 N91-13638

ITERATION

- Spectrum transformation for divergent iterations
[NASA-TM-103745] p 221 N91-19786

ITO (SEMICONDUCTORS)

- Recent progress in InP solar cell research
[NASA-TM-104509] p 146 N91-27447

J

JET BOUNDARIES

- Naturally occurring and forced azimuthal modes in a turbulent jet
[NASA-TM-103692] p 11 N91-17000

JET ENGINE FUELS

- Fuel-rich, catalytic reaction experimental results --- fuel development for high-speed civil transport aircraft
[AIAA PAPER 91-2463] p 24 A91-44250
- Jet-A reaction mechanism study for combustion application
[AIAA PAPER 91-2355] p 106 A91-45810
- Fuel-rich, catalytic reaction experimental results
[NASA-TM-104423] p 33 N91-24203
- Jet-A reaction mechanism study for combustion application
[NASA-TM-104441] p 35 N91-31181

JET ENGINES

- Sensor failure detection for jet engines
p 22 A91-37593
- Numerical simulation of Jet-A combustion approximated by improved propane chemical kinetics
[AIAA PAPER 91-1859] p 106 A91-45777

JET FLOW

- Dropsize correlation for cryogenic liquid-jet atomization
[AIAA PAPER 91-0284] p 51 A91-19218
- Computational analysis of underexpanded jets in the hypersonic regime
p 4 A91-37421
- Second order modeling of boundary-free turbulent shear flows
[AIAA PAPER 91-1779] p 154 A91-42588
- Axisymmetric jet forced by fundamental and subharmonic tones
p 226 A91-45111
- Dropsize correlation for cryogenic liquid-jet atomization
[NASA-TM-103646] p 175 N91-12064
- Second order modeling of boundary-free turbulent shear flows
[NASA-TM-104369] p 164 N91-22524
- Effect of tabs on the evolution of an axisymmetric jet
[NASA-TM-104472] p 34 N91-27159
- Spray measurements of aerothermodynamic effect on disintegrating liquid jets
[NASA-TM-104501] p 178 N91-27510
- A qualitative view of cryogenic fluid injection into high speed flows
[NASA-TM-105139] p 169 N91-30473

JET IMPINGEMENT

- Icing characteristics of a natural-laminar-flow, a medium-speed, and a swept, medium-speed airfoil
[AIAA PAPER 91-0447] p 3 A91-26327

JET MIXING FLOW

- Experimental investigation of a single flush-mounted hypermixing nozzle
[AIAA PAPER 90-5240] p 21 A91-14466
- Jet-A fuel evaporation analysis in conical tube injectors
[AIAA PAPER 91-0345] p 149 A91-21467
- Control of flow separation and mixing by aerodynamic excitation
p 2 A91-24360
- Vapor condensation at the free surface of an axisymmetric liquid mixed by a laminar jet
p 151 A91-35109
- Supersonic jet mixing enhancement by vortex generators
[AIAA PAPER 91-2263] p 5 A91-41738
- A CFD study of jet mixing in reduced flow areas for lower combustor emissions
[AIAA PAPER 91-2460] p 23 A91-41788
- Progress toward synergistic hypermixing nozzles
[AIAA PAPER 91-2264] p 25 A91-45800
- Mixing of multiple jets with a confined subsonic crossflow - Summary of NASA-supported experiments and modeling
[AIAA PAPER 91-2458] p 7 A91-45813
- Experimental investigation of a single flush-mounted hypermixing nozzle
[NASA-TM-103726] p 161 N91-19374
- A CFD study of jet mixing in reduced flow areas for lower combustor emissions
[NASA-TM-104411] p 32 N91-23185
- Mixing of multiple jets with a confined subsonic crossflow. Summary of NASA-supported experiments and modeling
[NASA-TM-104412] p 33 N91-24202
- CFD analysis of jet mixing in low NO_x flametube combustors
[NASA-TM-104466] p 33 N91-26146

- Effect of tabs on the evolution of an axisymmetric jet
[NASA-TM-104472] p 34 N91-27159
- Progress toward synergistic hypermixing nozzles
[NASA-TM-105169] p 18 N91-29150

JET NOZZLES

- An experimental investigation of nozzle-exit boundary layers of highly heated free jets
[ASME PAPER 90-GT-255] p 155 A91-44662

JET PROPULSION

- Lewis aeropropulsion technology Remembering the past and challenging the future
p 242 N91-20087
- Simulation of turbomachinery flows
p 163 N91-21069

JOINTS (JUNCTIONS)

- Fiber pushout test - A three-dimensional finite element computational simulation
p 197 A91-33096

JOURNAL BEARINGS

- A high speed photography study of cavitation in a dynamically loaded journal bearing
[ASME PAPER 90-TRIB-19] p 180 A91-34806
- The effect of coatings and liners on heat transfer in a dry shaft-bush tribosystem
[NASA-TM-102513] p 159 N91-12913
- Two reference time scales for studying the dynamic cavitation of liquid films
[NASA-TM-103673] p 160 N91-19369

JUNCTION DIODES

- High-voltage 6H-SiC p-n junction diodes
p 142 A91-54746
- Development of silicon carbide semiconductor devices for high temperature applications
[NASA-TM-104398] p 236 N91-22921

JUNCTION TRANSISTORS

- Neutron and gamma irradiation effects on power semiconductor switches
p 139 A91-38162

K

K-EPSILON TURBULENCE MODEL

- Simulation of mixing in the quick quench region of a rich burn-quick quench mix-lean burn combustor
[AIAA PAPER 91-0410] p 105 A91-21481
- Simulations of free shear layers using a compressible k-epsilon model
[AIAA PAPER 91-1863] p 156 A91-45778
- A 2-D oscillating flow analysis in Stirling engine heat exchangers
[NASA-TM-103781] p 161 N91-19375
- Low Reynolds number two-equation modeling of turbulent flows
[NASA-TM-104368] p 165 N91-23416
- A critical comparison of two-equation turbulence models
[NASA-TM-105237] p 169 N91-31597
- A k-epsilon modeling of near wall turbulence
[NASA-TM-105238] p 170 N91-32460

KAPTON (TRADEMARK)

- The effect of atomic oxygen on altered and coated Kapton surfaces for spacecraft applications in low earth orbit
p 116 A91-49804
- Atomic oxygen interaction with solar array blankets at protective coating defect sites
p 211 N91-20732
- Atomic oxygen undercutting of LDEF aluminized Kapton multilayer insulation
p 229 N91-25027
- Low Earth orbital atomic oxygen micrometeoroid, and debris interactions with photovoltaic arrays
p 84 N91-30248

KELVIN-HELMHOLTZ INSTABILITY

- Stability of an oscillated fluid with a uniform density gradient
p 147 A91-12971

KETONES

- Substituted 1,1,1-triaryl-2,2,2-trifluoroethanes and processes for their synthesis
[NASA-CASE-LEW-14345-4] p 90 N91-25185

KINEMATICS

- Surface settling in partially filled containers upon step reduction in gravity
[NASA-TM-103641] p 159 N91-14556
- Viscoplastic analysis of an experimental cylindrical thrust chamber liner
[NASA-TM-103287] p 205 N91-28622

KINETICS

- Growth kinetics of physical vapor transport processes. Crystal growth of the optoelectronic material mercurous chloride
[NASA-TM-103788] p 128 N91-19320

KNEE (ANATOMY)

- Adaptation of NASA technology for the optimization of orthopedic knee implants
p 215 N91-23032

L

LABORATORIES

Computational materials science. An example:
Numerical modeling of chemical vapor deposition
processing of advanced fibers p 99 N91-20111

LABYRINTH SEALS

Eccentricity effects on leakage of a brush seal at low
speeds
[NASA-TM-105141] p 86 N91-31220

LAMINAR BOUNDARY LAYER

Naturally occurring and forced azimuthal modes in a
turbulent jet
[NASA-TM-103692] p 11 N91-17000

LAMINAR FLOW

Vapor condensation at the free surface of an
axisymmetric liquid mixed by a laminar jet
p 151 A91-35109

Further two-dimensional code development for Stirling
space engine components p 56 A91-38184

A detailed numerical investigation of Burke-Schumann
gaseous and spray flames
[AIAA PAPER 91-2311] p 105 A91-41749

A numerical study of the direct contact condensation
on a horizontal surface
[AIAA PAPER 91-1307] p 155 A91-44335

Control of laminar separation over airfoils by acoustic
excitation p 226 A91-45106

Icing characteristics of a natural-laminar-flow, a
medium-speed, and a swept, medium-speed airfoil
[NASA-TM-103693] p 12 N91-19046

Implicit solution of three-dimensional internal turbulent
flows p 163 N91-21082

A numerical study of the direct contact condensation
on a horizontal surface
[NASA-TM-104432] p 166 N91-24548

LAMINAR FLOW AIRFOILS

Icing characteristics of a natural-laminar-flow, a
medium-speed, and a swept, medium-speed airfoil
[AIAA PAPER 91-0447] p 3 A91-26327

LAMINATES

Mechanics of damping for fiber composite laminates
including hygrothermal effects p 195 A91-12895

Concurrent material-fabrication optimization of
metal-matrix laminates under thermo-mechanical loading
[AIAA PAPER 91-1044] p 129 A91-31842

The effects of interply damping layers on the dynamic
response of composite structures
[AIAA PAPER 91-1124] p 197 A91-32064

Free vibrations of delaminated beams
[AIAA PAPER 91-1241] p 197 A91-32129

Structural properties of laminated Douglas fir/epoxy
composite material
[NASA-RP-1236] p 94 N91-10127

A study of void effects on the interlaminar shear strength
of unidirectional graphite fiber reinforced composites
[NASA-TM-103267] p 159 N91-12034

METCAN updates for high temperature composite
behavior: Simulation/verification
[NASA-TM-103682] p 97 N91-19229

Probabilistic micromechanics and macromechanics of
polymer matrix composites
[NASA-TM-103669] p 98 N91-19236

Structural reliability analysis of laminated CMC
components
[NASA-TM-103685] p 119 N91-19292

Structural design methodologies for ceramic-based
material systems
[NASA-TM-103097] p 121 N91-22460

Tensile deformation damage in SiC reinforced
Ti-15V-3Cr-3Al-3Sn
[NASA-TM-103620] p 101 N91-25195

Microfracture in high temperature metal matrix crossply
laminates
[NASA-TM-104381] p 101 N91-25198

Matrix plasticity in SiC/Ti-15-3 composite
[NASA-TM-103760] p 102 N91-27247

The effects of interply damping layers on the dynamic
response of composite structures
[NASA-TM-104497] p 103 N91-30282

Experimental and analytical analysis of stress-strain
behavior in a (90/0 deg)_{2s} SiC/Ti-15-3 laminate
[NASA-TM-104470] p 103 N91-31235

Effect of lightning strike on bromine intercalated graphite
fiber/epoxy composites
[NASA-TM-104507] p 103 N91-32177

Integrated mechanics for the passive damping of
polymer-matrix composites and composite structures
[NASA-TM-104346] p 103 N91-32181

Computational simulation of high temperature metal
matrix composite behavior
[NASA-TM-104378] p 206 N91-32520

LAND MOBILE SATELLITE SERVICE

Performance evaluation of land mobile satellite system
under vegetative shadowing using differential multiple TCM
and QPSK p 132 A91-53084

LANDING SITES

Feasibility of solar power for Mars
p 209 N91-19201

LARGE SPACE STRUCTURES

Dynamic analysis of space-related linear and non-linear
structures p 196 A91-28612

Advanced power systems for EOS
[NASA-TM-105222] p 85 N91-31217

LASER ANEMOMETERS

Improved visualization of flow field measurements
[AIAA PAPER 91-0273] p 3 A91-26331

Improved visualization of flow field measurements
[NASA-TM-103679] p 12 N91-19044

Three-component laser anemometer measurement
systems
[NASA-TP-3080] p 13 N91-19057

High-speed laser anemometry based on spectrally
resolved Rayleigh scattering
[NASA-TM-104522] p 178 N91-27521

LASER APPLICATIONS

Hot gas ingestion test results of a two-poster vectored
thrust concept with flow visualization in the NASA Lewis
9- by 15-foot low speed wind tunnel
[AIAA PAPER 90-2268] p 4 A91-40561

LN2 spray droplet size measurement via ensemble
diffraction technique
[AIAA PAPER 91-1381] p 129 A91-44336

Ellipsometric study of YBa₂Cu₃O_{7-x} laser ablated and
co-evaporated films p 233 A91-53235

Quaternary pulse position modulation electronics for
free-space laser communications
[AIAA PAPER 91-3471] p 133 A91-53702

Optical measurement of propeller blade deflections in
a spin facility
[NASA-TM-103115] p 12 N91-17002

An imaging system for PLIF/Mie measurements for a
combusting flow
[NASA-TM-103714] p 27 N91-20084

Hot gas ingestion test results of a two-poster vectored
thrust concept with flow visualization in the NASA Lewis
9- by 15-foot low speed wind tunnel
[NASA-TM-103258] p 15 N91-21116

LN2 spray droplet size measurement via ensemble
diffraction technique
[NASA-TM-104443] p 131 N91-24470

Particle displacement tracking applied to air flows
[NASA-TM-104481] p 177 N91-25387

Quaternary pulse position modulation electronics for
free-space laser communications
[NASA-TM-104502] p 135 N91-29405

Laser interferometric measurement of ion electrode
shape and charge exchange erosion
[NASA-TM-105165] p 179 N91-31605

LASER BEAMS

Optical measurement of unducted fan blade
deflections
[ASME PAPER 89-GT-298] p 170 A91-13046

A preview of a microgravity laser light scattering
instrument
[AIAA PAPER 91-0779] p 179 A91-21614

Acousto-ultrasonic nondestructive evaluation of
materials using laser beam generation and detection
p 193 N91-18193

LASER DOPPLER VELOCIMETERS

Three-component laser anemometer measurement
systems
[NASA-TP-3080] p 13 N91-19057

LASER HEATING

A laser-induced heat flux technique for convective heat
transfer measurements in high speed flows
[NASA-TM-105177] p 168 N91-30472

LASER INDUCED FLUORESCENCE

Two-dimensional imaging of molecular hydrogen in
H₂-air diffusion flames using two-photon laser-induced
fluorescence p 124 A91-34369

An imaging system for PLIF/Mie measurements for a
combusting flow
[NASA-TM-103714] p 27 N91-20084

LASER INTERFEROMETRY

Laser interferometric measurement of ion electrode
shape and charge exchange erosion
[AIAA PAPER 91-2121] p 173 A91-45786

Three-component laser anemometer measurement
systems
[NASA-TP-3080] p 13 N91-19057

Laser interferometric measurement of ion electrode
shape and charge exchange erosion
[NASA-TM-105165] p 179 N91-31605

LASER OUTPUTS

Fiber optic sensing system
[NASA-CASE-LEW-14795-1] p 230 N91-21871

LASER PROPULSION

Laser photovoltaic power system synergy for SEI
applications
[AIAA PAPER 91-3419] p 207 A91-52339

LASERS

An experimental study of high T_c superconducting
microstrip transmission lines at 35 GHz and the effect of
film morphology p 138 A91-36172

YBCO superconducting ring resonators at
millimeter-wave frequencies p 142 A91-54532

An experimental study of high T_c superconducting
microstrip transmission lines at 35 GHz and the effect of
film morphology
[NASA-TM-103633] p 133 N91-11988

LATCHES

Quick action clamp
[NASA-CASE-LEW-14887-1] p 189 N91-27561

LATTICE PARAMETERS

Universal behavior in ideal slip p 110 A91-48517

Thermal stability of the microstructure of an aged
Nb-Zr-C alloy
[NASA-TM-103647] p 110 N91-14454

Equivalent crystal theory of alloys
[NASA-TP-3155] p 112 N91-30318

A new approximate sum rule for bulk alloy properties
[NASA-TM-105282] p 112 N91-32204

LAUNCH VEHICLES

Advanced launch system (ALS) - Electrical actuation
and power systems improve operability and cost picture
p 51 A91-31025

Electromechanical actuation for thrust vector control
applications p 52 A91-31026

The design and performance estimates for the
propulsion module for the booster of a TSTO vehicle
[AIAA PAPER 91-3136] p 43 A91-54054

Advanced launch vehicle upper stages using liquid
propulsion and metallized propellants
[NASA-TM-103622] p 68 N91-11797

Advanced launch vehicle upper stages using liquid
propulsion and metallized propellants
p 75 N91-24257

LAUNCHING

Metallized propellants for the human exploration of
Mars
[NASA-TP-3062] p 69 N91-11800

LAY-UP

Probabilistic micromechanics and macromechanics of
polymer matrix composites
[NASA-TM-103669] p 98 N91-19236

LEADING EDGES

Finite element elastic-plastic-creep and cyclic life
analysis of a cowl lip p 199 A91-56365

The effect of small streamwise velocity distortion on
the boundary layer flow over a thin flat plate with application
to boundary layer stability theory
[NASA-TM-103668] p 161 N91-19372

Simulation of iced wing aerodynamics
[NASA-TM-104362] p 15 N91-23086

Simulation of brush insert for leading-edge-passage
convective heat transfer
[NASA-TM-103801] p 165 N91-23409

Atomic oxygen undercutting of LDEF aluminized Kapton
multilayer insulation p 229 N91-25027

LEAKAGE

Effects of brush seal morphology on leakage and
pressure drops
[AIAA PAPER 91-2106] p 182 A91-41700

Development of braided rope seals for hypersonic
engine applications. II - Flow modeling
[AIAA PAPER 91-2495] p 182 A91-41800

Some preliminary results of brush seal/rotor interference
effects on leakage at zero and low rpm using a tapered-plug
rotor
[AIAA PAPER 91-3390] p 182 A91-45820

A test fixture for measuring high-temperature
hypersonic-engine seal performance
[NASA-TM-103658] p 184 N91-19442

An assessment of the Space Station Freedom program's
leakage current requirement
[NASA-CR-187077] p 215 N91-20630

High temperature performance evaluation of a
hypersonic engine ceramic wafer seal
[NASA-TM-103737] p 185 N91-22567

Development of braided rope seals for hypersonic
engine applications. Part 2: Flow modeling
[NASA-TM-104371] p 186 N91-22571

Thermal performance of a liquid hydrogen tank multilayer
insulation system at warm boundary temperatures of 630,
530, and 152 R
[NASA-TM-104476] p 43 N91-25159

Some preliminary results of brush seal/rotor interference
effects on leakage at zero and low RPM using a
tapered-plug rotor
[NASA-TM-104396] p 188 N91-27559

High temperature NASP engine seals: A technology
review
[NASA-TM-104468] p 190 N91-30538

Eccentricity effects on leakage of a brush seal at low
speeds
[NASA-TM-105141] p 86 N91-31220

LEAST SQUARES METHOD

- The L sub 1 finite element method for pure convection problems
[NASA-TM-103773] p 222 N91-24817
- Least-squares solution of incompressible Navier-Stokes equations with the p-version of finite elements
[NASA-TM-105203] p 223 N91-31911
- LEIDENFROST PHENOMENON**
- Paramagnetic propellant orientation
[AIAA PAPER 91-2325] p 125 A91-44197
- Paramagnetic propellant orientation
[NASA-TM-104390] p 166 N91-24527
- LIFE (DURABILITY)**
- Effect of KOH concentration on LEO cycle life of IPV nickel-hydrogen flight battery cells p 55 A91-38076
- Maximum life spur gear design
[AIAA PAPER 91-2021] p 181 A91-41682
- Finite element elastic-plastic-creep and cyclic life analysis of a cow lip p 199 A91-56365
- Stirling engine: Available tools for long-life assessment
[NASA-TM-103660] p 200 N91-12980
- New method of making advanced tube-bundle rocket thrust chambers
[NASA-TM-103617] p 70 N91-15301
- Computational simulation of hot composites structures
[NASA-TM-103681] p 97 N91-19230
- Application of thermal life prediction model to high-temperature aerospace alloys B1900+Hf and Haynes 188
[NASA-TM-4226] p 201 N91-19473
- Transition-to-practice technologies for brittle materials p 120 N91-20107
- Progress in modeling deformation and damage p 202 N91-20108
- Life extending control: A concept paper
[NASA-TM-104391] p 37 N91-22135
- Effect of KOH concentration on LEO cycle life of IPV nickel-hydrogen flight cells. An update
[NASA-TM-104383] p 74 N91-22376
- Destructive physical analysis results of Ni/H₂ cells cycled in LEO regime
[NASA-TM-104382] p 74 N91-23233
- Quantifying oil filtration effects on bearing life
[NASA-TM-104350] p 186 N91-23512
- Maximum life spur gear design
[NASA-TM-104361] p 187 N91-23514
- Incorporating finite element analysis into component life and reliability
[NASA-TM-104400] p 203 N91-23550
- Structural Integrity and Durability of Reusable Space Propulsion Systems
[NASA-CP-10030] p 76 N91-24307
- Overview of the fatigue/fracture/life working group program at the Lewis Research Center p 203 N91-24308
- Tensile and fatigue behavior of tungsten/copper composites p 100 N91-24311
- Arc-textured high emittance radiator surfaces
[NASA-CASE-LEW-14679-1] p 122 N91-25296
- Stirling machine operating experience
[NASA-TM-104487] p 212 N91-25510
- Rapid thermal cycling of solar array blanket coupons for Space Station Freedom p 84 N91-30239
- Fatigue behavior and life prediction of a SiC/Ti-24Al-11Nb composite under isothermal conditions
[NASA-TM-105168] p 206 N91-30566
- Nickel-hydrogen cell low-Earth life test update
[NASA-TM-105229] p 213 N91-31708
- LIFT**
- Acoustic radiation from lifting airfoils in compressible subsonic flow
[AIAA PAPER 90-3911] p 224 A91-12427
- Acoustic radiation from lifting airfoils in compressible subsonic flow
[NASA-TM-103650] p 13 N91-19053
- LIFTING BODIES**
- A finite-difference, frequency-domain numerical scheme for the solution of the linearized unsteady Euler equations p 162 N91-21067
- LIGHT AIRCRAFT**
- Rotary engine technology p 30 N91-20114
- LIGHT BEAMS**
- High-speed laser anemometry based on spectrally resolved Rayleigh scattering
[NASA-TM-104522] p 178 N91-27521
- LIGHT ELEMENTS**
- The shock process and light-element production in supernova envelopes p 239 A91-33573
- LIGHT EMITTING DIODES**
- Compensation for effects of ambient temperature on rare-earth doped fiber optic thermometer p 170 A91-19582
- High-voltage 6H-SiC p-n junction diodes p 142 A91-54746
- Fiber optic sensing system
[NASA-CASE-LEW-14795-1] p 230 N91-21871

LIGHT SCATTERING

- A preview of a microgravity laser light scattering instrument
[AIAA PAPER 91-0779] p 179 A91-21614

LIGHT TRANSMISSION

- Vibrational testing of optical fiber connector joints p 172 A91-30652
- Vibrational testing of optical fiber connector joints
[NASA-TM-103654] p 230 N91-14829

LIGHTNING SUPPRESSION

- Effect of lightning strike on bromine intercalated graphite fiber/epoxy composites
[NASA-TM-104507] p 103 N91-32177

LINE SPECTRA

- Determination of alloy content from plume spectral measurements
[AIAA PAPER 91-2531] p 88 A91-44284
- Determination of alloy content from plume spectral measurements
[NASA-TM-104442] p 89 N91-24341

LINEAR ACCELERATORS

- The theory of an auto-resonant field emission cathode relativistic electron accelerator for high efficiency microwave to direct current power conversion p 73 N91-22176

LINEAR PROGRAMMING

- ALPS: A Linear Program Solver
[NASA-TM-104347] p 216 N91-20765

LINEAR QUADRATIC GAUSSIAN CONTROL

- Integrated flight/propulsion control system design based on a centralized approach p 36 A91-22950
- Linear quadratic servo control of a reusable rocket engine
[AIAA PAPER 91-1999] p 57 A91-41670

LINEAR QUADRATIC REGULATOR

- Microgravity vibration isolation: An optimal control law for the one-dimensional case p 49 N91-21206

LINEAR SYSTEMS

- Parallel algorithms for boundary value problems p 221 A91-31175

LINEARIZATION

- Feedback linearization for control of air breathing engines
[AIAA PAPER 91-2000] p 23 A91-41671

LININGS

- The effect of coatings and liners on heat transfer in a dry shaft-bush tribosystem
[NASA-TM-102513] p 159 N91-12913
- Tuned optimization of extended reacting acoustic liners
[NASA-TM-104431] p 228 N91-25817

LIQUID ATOMIZATION

- Influence of geometric features on the performance of pressure-swirl atomizers p 147 A91-13030
- Dropsize correlation for cryogenic liquid-jet atomization
[AIAA PAPER 91-0284] p 51 A91-19218
- Flow visualization of a rocket injector spray using gelled propellant simulants
[AIAA PAPER 91-2198] p 59 A91-44151
- Cryogenic liquid-jet breakup in two-fluid atomizers
[NASA-TM-103734] p 176 N91-19402
- Spray measurements of aerothermodynamic effect on disintegrating liquid jets
[NASA-TM-104501] p 178 N91-27510

LIQUID COOLING

- Arcjet thermal characteristics
[AIAA PAPER 91-2456] p 63 A91-45814

LIQUID FLOW

- Spray measurements of aerothermodynamic effect on disintegrating liquid jets
[NASA-TM-104501] p 178 N91-27510

LIQUID FUELS

- Combustion of liquid fuel droplets in supercritical conditions
[AIAA PAPER 91-0078] p 105 A91-21362
- Pressure-coupled vaporization and combustion responses of liquid-fuel droplets in high-pressure environments
[AIAA PAPER 91-2310] p 106 A91-44192
- Spray measurements of aerothermodynamic effect on disintegrating liquid jets
[NASA-TM-104501] p 178 N91-27510

LIQUID HYDROGEN

- Liquid hydrogen turbopump foil bearing
[AIAA PAPER 91-2108] p 182 A91-41701
- Improved thermodynamic modelling of the no-vent fill process and correlation with experimental data
[AIAA PAPER 91-1379] p 129 A91-43444
- Ground testing of the nonvented fill method of orbital propellant transfer - Results of initial test series
[AIAA PAPER 91-2326] p 59 A91-44198
- A review of candidate multilayer insulation systems for potential use on wet-launched LH₂ tankage for the Space Exploration Initiative lunar missions
[AIAA PAPER 91-2176] p 43 A91-45793

Thermal performance of a liquid hydrogen tank multilayer insulation system at warm boundary temperatures of 630, 530, and 152 R

- [AIAA PAPER 91-2400] p 43 A91-45812
- NASA cryogenic fluid management space experiment efforts
[AIAA PAPER 91-3538] p 130 A91-53701
- Self-pressurization of a lightweight liquid hydrogen storage tank subjected to low heat flux
[NASA-TM-103804] p 126 N91-20324
- Simulation of brush insert for leading-edge-passage convective heat transfer
[NASA-TM-103801] p 165 N91-23409
- The COLD-SAT experiment for cryogenic fluid management technology p 126 N91-24263
- Ground testing on the nonvented fill method of orbital propellant transfer: Results of initial test series
[NASA-TM-104444] p 166 N91-24547
- Thermal performance of a liquid hydrogen tank multilayer insulation system at warm boundary temperatures of 630, 530, and 152 R
[NASA-TM-104476] p 43 N91-25159
- Autogenous pressurization of cryogenic vessels using submerged vapor injection
[NASA-TM-104516] p 127 N91-27375
- NASA cryogenic fluid management space experiment efforts, 1960-1990
[NASA-TM-103752] p 243 N91-30073

LIQUID METAL COOLED REACTORS

- Multimegawatt nuclear power systems for nuclear electric propulsion
[AIAA PAPER 91-3607] p 66 A91-52472

LIQUID NITROGEN

- Dropsize correlation for cryogenic liquid-jet atomization
[AIAA PAPER 91-0284] p 51 A91-19218
- LN₂ spray droplet size measurement via ensemble diffraction technique
[AIAA PAPER 91-1381] p 129 A91-44336
- Dropsize correlation for cryogenic liquid-jet atomization
[NASA-TM-103646] p 175 N91-12064
- Cryogenic liquid-jet breakup in two-fluid atomizers
[NASA-TM-103734] p 176 N91-19402
- LN₂ spray droplet size measurement via ensemble diffraction technique
[NASA-TM-104443] p 131 N91-24470
- A qualitative view of cryogenic fluid injection into high speed flows
[NASA-TM-105139] p 169 N91-30473

LIQUID OXYGEN

- Improved thermodynamic modelling of the no-vent fill process and correlation with experimental data
[AIAA PAPER 91-1379] p 129 A91-43444
- Carbon monoxide and oxygen combustion experiments - A demonstration of Mars in situ propellants
[AIAA PAPER 91-2443] p 60 A91-44246
- Liquid oxygen cooling of hydrocarbon fueled rocket thrust chambers p 63 A91-52309
- Analysis of 5 KHz combustion instabilities in 40K methane/LOX combustion chambers
[NASA-TM-101368] p 67 N91-10117
- Carbon monoxide and oxygen combustion experiments. A demonstration of Mars in situ propellants
[NASA-TM-104473] p 76 N91-24303

LIQUID PHASES

- Thermochemical analysis of the silicon carbide-alumina reaction with reference to liquid-phase sintering of silicon carbide p 114 A91-26506
- Two-dimensional model of a Space Station Freedom thermal energy storage canister p 151 A91-38048
- Apparatus for intercalating large quantities of fibrous structures
[NASA-CASE-LEW-15077-2] p 102 N91-28289

LIQUID PROPELLANT ROCKET ENGINES

- Launch vehicle performance using metallized propellants
[AIAA PAPER 91-2050] p 58 A91-44106
- Carbon monoxide and oxygen combustion experiments - A demonstration of Mars in situ propellants
[AIAA PAPER 91-2443] p 60 A91-44246
- Liquid oxygen cooling of hydrocarbon fueled rocket thrust chambers p 63 A91-52309
- Developments in REDES: The rocket engine design expert system
[NASA-TM-103657] p 67 N91-10119
- JANNAF liquid rocket combustion instability panel research recommendations
[NASA-TM-103653] p 70 N91-13491
- Carbon monoxide and oxygen combustion experiments. A demonstration of Mars in situ propellants
[NASA-TM-104473] p 76 N91-24303
- Launch vehicle performance using metallized propellants
[NASA-TM-104456] p 76 N91-24304

LIQUID ROCKET PROPELLANTS

- Launch vehicle performance using metallized propellants
[AIAA PAPER 91-2050] p 58 A91-44106
- Ground testing of the nonvented fill method of orbital propellant transfer - Results of initial test series
[AIAA PAPER 91-2326] p 59 A91-44198
- Carbon monoxide and oxygen combustion experiments - A demonstration of Mars in situ propellants
[AIAA PAPER 91-2443] p 60 A91-44246
- The measurement, modelling and prediction of traction forces in a rocket propellant
p 125 A91-51914
- Design issues for propulsion systems using metallized propellants
[AIAA PAPER 91-3484] p 66 A91-53709
- Carbon monoxide and oxygen combustion experiments: A demonstration of Mars in situ propellants
[NASA-TM-104473] p 76 N91-24303
- Launch vehicle performance using metallized propellants
[NASA-TM-104456] p 76 N91-24304
- Ground testing on the nonvented fill method of orbital propellant transfer: Results of initial test series
[NASA-TM-104444] p 166 N91-24547
- Design issues for propulsion systems using metallized propellants
[NASA-TM-105190] p 81 N91-29220
- LIQUID SLOSHING**
- Simulation of three-dimensional liquid sloshing flows using a strongly implicit calculation procedure
[AIAA PAPER 91-1661] p 153 A91-42549
- LIQUID SURFACES**
- A numerical study of the direct contact condensation on a horizontal surface
[AIAA PAPER 91-1307] p 155 A91-44335
- Surface settling in partially filled containers upon step reduction in gravity
[NASA-TM-103641] p 159 N91-14556
- A numerical study of the direct contact condensation on a horizontal surface
[NASA-TM-104432] p 166 N91-24548
- LIQUID-LIQUID INTERFACES**
- Interfacial dynamics of two liquids under an oscillating gravitational field
p 148 A91-16062
- LIQUID-VAPOR INTERFACES**
- Critical-point analysis of the liquid-vapor interfacial surface tension
p 237 A91-16103
- Vapor condensation at the free surface of an axisymmetric liquid mixed by a laminar jet
p 151 A91-35109
- A numerical study of the direct contact condensation on a horizontal surface
[AIAA PAPER 91-1307] p 155 A91-44335
- A numerical study of the direct contact condensation on a horizontal surface
[NASA-TM-104432] p 166 N91-24548
- LITHIUM**
- The Au cathode in the system $\text{Li}_2\text{CO}_3\text{-CO}_2\text{-CO}$ at 800 to 900 C
p 213 N91-32551
- LITHIUM FLUORIDES**
- Tensile properties of HA 230 and HA 188 after 400 and 2500 hour exposures to LiF-22CaF_2 and vacuum at 1093 K
p 107 A91-11624
- Temperature dependence of the elastic moduli and damping for polycrystalline LiF-22 pct CaF_2 eutectic salt
p 87 A91-33793
- LITHIUM ISOTOPES**
- The shock process and light-element production in supernova envelopes
p 239 A91-33573
- LOAD DISTRIBUTION (FORCES)**
- Overview of aerothermodynamic loads definition study
p 204 N91-24334
- LOAD TESTING MACHINES**
- Fully articulated four-point-bend loading fixture
[NASA-CASE-LEW-14776-1] p 185 N91-21540
- LOAD TESTS**
- A data acquisition and control program for axial-torsional fatigue testing
p 199 A91-56540
- LOADS (FORCES)**
- Integrated force method versus displacement method for finite element analysis
p 196 A91-28372
- Concurrent material-fabrication optimization of metal-matrix laminates under thermo-mechanical loading
[AIAA PAPER 91-1044] p 129 A91-31842
- An analysis of space power system masses
p 54 A91-38003
- An expert system for simulating electric loads aboard Space Station Freedom
p 55 A91-38041
- Composite laminate tailoring with probabilistic constraints and loads
p 198 A91-38754
- Contact stresses in gear teeth - A new method of analysis
[AIAA PAPER 91-2022] p 162 A91-41683
- Contact stresses in gear teeth: A new method of analysis
[NASA-TM-104397] p 186 N91-22570

- Simulation of probabilistic wind loads and building analysis
[NASA-TM-103744] p 203 N91-23549
- Tuning maps for setpoint changes and load disturbance upsets in a three capacity process under multivariable control
[NASA-TM-104419] p 220 N91-31876
- LOCAL AREA NETWORKS**
- Description of real-time Ada software implementation of a power system monitor for the Space Station Freedom PMAD DC testbed
[NASA-TM-105157] p 218 N91-28776
- LOCKING**
- Removable hand hold
[NASA-CASE-LEW-15196-1] p 188 N91-26543
- Quick action clamp
[NASA-CASE-LEW-14887-1] p 189 N91-27561
- LONG DURATION EXPOSURE FACILITY**
- Preliminary flight test results from the advanced photovoltaic experiment
p 56 A91-38163
- Preliminary results from the advanced photovoltaic experiment flight test
[NASA-TM-103269] p 67 N91-11058
- The effect of the low Earth orbit environment on space solar cells
[NASA-TM-103735] p 48 N91-19165
- Atomic oxygen undercutting of LDEF aluminized Kapton multilayer insulation
p 229 N91-25027
- Atomic oxygen interactions with FEP Teflon and silicones on LDEF
p 122 N91-25029
- Ion beam textured and coated surfaces experiment (IBEX)
p 122 N91-25040
- Advanced photovoltaic experiment, S0014: Preliminary flight results and post-flight findings
p 212 N91-25061
- Durability evaluation of photovoltaic blanket materials exposed on LDEF tray S1003
p 212 N91-25062
- Low Earth orbital atomic oxygen micrometeoroid, and debris interactions with photovoltaic arrays
p 84 N91-30248
- LONG DURATION SPACE FLIGHT**
- Space mechanisms needs for future NASA long duration space missions
[AIAA PAPER 91-3428] p 183 A91-57025
- Space mechanisms needs for future NASA long duration space missions
[NASA-TM-105204] p 190 N91-30532
- LONG TERM EFFECTS**
- Space mechanisms needs for future NASA long duration space missions
[AIAA PAPER 91-3428] p 183 A91-57025
- Space mechanisms needs for future NASA long duration space missions
[NASA-TM-105204] p 190 N91-30532
- LOOPS**
- Tuning maps for setpoint changes and load disturbance upsets in a three capacity process under multivariable control
[NASA-TM-104419] p 220 N91-31876
- LOSSES**
- High frequency, high temperature specific core loss and dynamic B-H hysteresis loop characteristics of soft magnetic alloys
p 138 A91-37988
- Comparison of high temperature, high frequency core loss and dynamic B-H loops of two 50 Ni-Fe crystalline alloys and an iron-based amorphous alloy
[NASA-TM-105205] p 147 N91-32412
- LOW FREQUENCIES**
- Critical-layer nonlinearity in the resonance growth of three-dimensional waves in boundary layers
[NASA-TM-103639] p 161 N91-19373
- LOW NOISE**
- Low noise InP-based MMIC receivers for W-band
[AIAA PAPER 91-3594] p 142 A91-52462
- LOW REYNOLDS NUMBER**
- Numerical solution for the velocity-derivative skewness of a low Reynolds-number turbulent-like decaying Navier-Stokes flow
p 158 A91-50204
- Comment on local energy transfer and nonlocal interactions in homogeneous, isotropic turbulence (Phys. Fluids A2, 413 (1990))
[NASA-TM-103263] p 159 N91-13638
- Experimental study of boundary layer transition on a heated flat plate
[NASA-TM-103779] p 14 N91-21061
- Low Reynolds number two-equation modeling of turbulent flows
[NASA-TM-104368] p 165 N91-23416
- LOW SPEED**
- Low velocity impact analysis with NASTRAN
p 198 A91-48865
- NASA low-speed centrifugal compressor for 3-D viscous code assessment and fundamental flow physics research
[NASA-TM-103710] p 13 N91-20044

LOW SPEED WIND TUNNELS

- Noise measurements from an ejector suppressor nozzle in the NASA Lewis 9- by 15-foot low speed wind tunnel
[AIAA PAPER 90-3983] p 225 A91-12496
- Evaluation of panel code predictions with experimental results of inlet performance for a 17-inch ducted prop/fan simulator operating at Mach 0.2
[AIAA PAPER 91-3354] p 7 A91-45819
- Evaluation of panel code predictions with experimental results of inlet performance for a 17-inch ducted prop/fan simulator operating at Mach 0.2
[NASA-TM-104428] p 17 N91-25106
- Applied high-speed imaging for the icing research program at NASA Lewis Research Center
[NASA-TM-104415] p 177 N91-26490
- LOW TEMPERATURE**
- Selective and low temperature synthesis of polycrystalline diamond
p 232 A91-42170
- LOW TEMPERATURE TESTS**
- Measurement techniques for cryogenic Ka-band microstrip antennas
[NASA-TM-105183] p 146 N91-30426
- LOW THRUST PROPULSION**
- Plans for the development of cryogenic engines for space exploration
[AIAA PAPER 91-3438] p 64 A91-52351
- The NASA Lewis Research Center electric propulsion program
[AIAA PAPER 91-3443] p 64 A91-52355
- LOW WEIGHT**
- Light weight, high power, high voltage dc/dc converter technologies
p 138 A91-37985
- LUBRICANT TESTS**
- Effect of two synthetic lubricants on life of AISI 9310 spur gears
[NASA-TM-104352] p 189 N91-29599
- PM200/PS200: Self-lubricating bearing and seal materials for applications to 900 C
[NASA-TM-103776] p 190 N91-30539
- LUBRICANTS**
- A high speed photography study of cavitation in a dynamically loaded journal bearing
[ASME PAPER 90-TRIB-19] p 180 A91-34806
- Evaluation of advanced lubricants for aircraft applications using gear surface fatigue tests
[AIAA PAPER 91-1907] p 181 A91-41649
- Composite bearing and seal materials for advanced heat engine applications to 900 C
[NASA-TM-103612] p 95 N91-15318
- Evaluation of advanced lubricants for aircraft applications using gear surface fatigue tests
[NASA-TM-104336] p 186 N91-22568
- Quality control of the tribological coating PS212
[NASA-TM-102067] p 101 N91-25186
- Effect of two synthetic lubricants on life of AISI 9310 spur gears
[NASA-TM-104352] p 189 N91-29599
- LUBRICATION**
- Evaluation of advanced lubricants for aircraft applications using gear surface fatigue tests
[AIAA PAPER 91-1907] p 181 A91-41649
- Evaluation of advanced lubricants for aircraft applications using gear surface fatigue tests
[NASA-TM-104336] p 186 N91-22568
- Pretreatment of lubricated surfaces with sputtered cadmium oxide
[NASA-CASE-LEW-14474-1] p 123 N91-28423
- Parched elastohydrodynamic lubrication: Instrumentation and procedure
[NASA-TM-104426] p 168 N91-30469
- High temperature NASP engine seals: A technology review
[NASA-TM-104468] p 190 N91-30538
- Lubrication with sputtered MoS₂ films: Principles, operation, limitations
[NASA-TM-105292] p 112 N91-32216
- LUBRICATION SYSTEMS**
- Acidic attack of perfluorinated alkyl ether lubricant molecules by metal oxide surfaces
p 104 A91-13439
- The PM-200 lubrication system
p 121 N91-23044
- LUMINOUS INTENSITY**
- The effects of lunar dust accumulation on the performance of photovoltaic arrays
p 83 N91-30238
- LUNAR BASED EQUIPMENT**
- The effects of lunar dust accumulation on the performance of photovoltaic arrays
p 83 N91-30238
- LUNAR BASES**
- Proposal for a sun-following moonbase
p 41 A91-27356
- Power system requirements and definition for lunar and Mars outposts
p 52 A91-37930
- Electrical characterization of a Mapham inverter using pulse testing techniques
p 139 A91-37992
- Design considerations for lunar base photovoltaic power systems
p 41 A91-41987

LUNAR DUST

- Lunar electric power systems utilizing the SP-100 reactor coupled to dynamic conversion systems
[AIAA PAPER 91-3520] p 208 A91-52415
- Design considerations for lunar base photovoltaic power systems
[NASA-TM-103642] p 241 N91-14259
- Lunar missions using chemical propulsion: System design issues
[NASA-TP-3065] p 70 N91-15308
- Space reactor/Stirling cycle systems for high power lunar application
[NASA-TM-103698] p 40 N91-19112
- Component technology for stirling power converters
[NASA-TM-104387] p 74 N91-23234
- Solar dynamic power for Earth orbital and lunar applications
[NASA-TM-104511] p 80 N91-27214
- SEI power source alternatives for rovers and other multi-kWe distributed surface applications
[NASA-TM-104360] p 81 N91-28277
- LUNAR DUST**
- The effects of lunar dust accumulation on the performance of photovoltaic arrays p 83 N91-30238
- LUNAR EXPLORATION**
- Technical prospects for utilizing extraterrestrial propellants for space exploration
[NASA-TM-105263] p 127 N91-31318
- LUNAR FLIGHT**
- A review of candidate multilayer insulation systems for potential use on wet-launched LH2 tankage for the Space Exploration Initiative lunar missions
[AIAA PAPER 91-2176] p 43 A91-45793
- Radiation dose estimates for typical piloted NTR lunar and Mars mission engine operations
[AIAA PAPER 91-3407] p 215 A91-52331
- LUNAR ORBITS**
- Lunar orbiting microwave beam power system p 56 A91-38158
- LUNAR RESOURCES**
- Production and use of metals and oxygen for lunar propulsion
[AIAA PAPER 91-3481] p 125 A91-53711
- Production and use of metals and oxygen for lunar propulsion
[NASA-TM-105195] p 81 N91-29222
- Technical prospects for utilizing extraterrestrial propellants for space exploration
[NASA-TM-105263] p 127 N91-31318
- LUNAR ROVING VEHICLES**
- SEI rover solar-electrochemical power system options
[NASA-TM-104402] p 211 N91-23620
- SEI power source alternatives for rovers and other multi-kWe distributed surface applications
[NASA-TM-104360] p 81 N91-28277
- LUNAR SPACECRAFT**
- The rationale/benefits of nuclear thermal rocket propulsion for NASA's lunar space transportation system
[AIAA PAPER 91-2052] p 39 A91-45781
- Plug nozzles - The ultimate customer driven propulsion system --- applied to manned lunar and Martian landers
[AIAA PAPER 91-2208] p 61 A91-45794
- LUNAR SURFACE**
- Dual-purpose self-deliverable lunar surface PV electrical power system p 209 N91-19200
- Preliminary design of a mobile lunar power supply
[NASA-TM-104471] p 212 N91-27611
- LUNAR SURFACE VEHICLES**
- Dual-purpose self-deliverable lunar surface PV electrical power system p 209 N91-19200

M

MACH NUMBER

- A time-accurate implicit method for chemically reacting flows at all Mach numbers
[AIAA PAPER 91-0581] p 149 A91-21542
- The effect of varying Mach number on crossing, glancing shocks/turbulent boundary-layer interactions
[AIAA PAPER 91-2157] p 6 A91-45792
- Experimental investigation of a single flush-mounted hypermixing nozzle
[NASA-TM-103726] p 161 N91-19374
- Effect of tabs on the evolution of an axisymmetric jet
[NASA-TM-104472] p 34 N91-27159

MACHINE LEARNING

- Neuromorphic learning of continuous-valued mappings from noise-corrupted data p 219 A91-53201

MACHINE TOOLS

- Computerized inspection of real surfaces and minimization of their deviations
[NASA-TM-103798] p 188 N91-27558

MACHINING

- Plug-type heat flux gauge
[NASA-CASE-LEW-14967-1] p 179 N91-31608

MAGNETIC BEARINGS

- Magnetic bearings with zero bias p 48 N91-21194
- Magnetic bearings-state of the art
[NASA-TM-104465] p 188 N91-25413

MAGNETIC COMPRESSION

- Antiproton powered propulsion with magnetically confined plasma engines p 63 A91-52313

MAGNETIC EFFECTS

- Paramagnetic propellant orientation
[AIAA PAPER 91-2325] p 125 A91-44197
- Paramagnetic propellant orientation
[NASA-TM-104390] p 166 N91-24527

MAGNETIC ENERGY STORAGE

- High temperature superconductivity technology for advanced space power systems p 50 A91-13447

MAGNETIC FIELD CONFIGURATIONS

- Anode power deposition in an applied-field segmented anode MPD thruster
[AIAA PAPER 91-2343] p 59 A91-44204

MAGNETIC FIELDS

- The series $\text{BiSr}_2\text{Ca}_{(n-1)}\text{Cu}_{(n)}\text{O}_{(2n+4)}$ (1 less than or equal to n less than or equal to 5): Phase stability and superconducting properties
[NASA-TM-103749] p 235 N91-21910
- Magnetic bearings-state of the art
[NASA-TM-104465] p 188 N91-25413

MAGNETIC FLUX

- High frequency, high temperature specific core loss and dynamic B-H hysteresis loop characteristics of soft magnetic alloys p 138 A91-37988

MAGNETIC MATERIALS

- Comparison of high temperature, high frequency core loss and dynamic B-H loops of two 50 Ni-Fe crystalline alloys and an iron-based amorphous alloy
[NASA-TM-105205] p 147 N91-32412

MAGNETIC MEASUREMENT

- High frequency, high temperature specific core loss and dynamic B-H hysteresis loop characteristics of soft magnetic alloys p 138 A91-37988

MAGNETIC PERMEABILITY

- Spatial variations in a.c. susceptibility and microstructure for the $\text{YBa}_2\text{Cu}_3\text{O}_{(7-x)}$ superconductor and their correlation with room-temperature ultrasonic measurements p 233 A91-54969
- Spatial variations in ac susceptibility and microstructure for the $\text{YBa}_2\text{Cu}_3\text{O}_{(7-x)}$ superconductor and their correlation with room-temperature ultrasonic measurements
[NASA-TM-103787] p 194 N91-21553

MAGNETIC PROPERTIES

- Property and microstructural nonuniformity in the yttrium-barium-copper-oxide superconductor determined from electrical, magnetic, and ultrasonic measurements
[NASA-TM-103732] p 193 N91-19463

MAGNETIC RELAXATION

- Temperature dependence of the anisotropy in magnetic relaxation in $\text{YBa}_2\text{Cu}_3\text{O}_{(7-x)}$ thin films p 232 A91-36047

MAGNETIC STORMS

- A charging study of the ACTS satellite using NASCAP
[AIAA PAPER 91-1471] p 46 A91-42522

MAGNETIC SUSPENSION

- Development of a vibration isolation prototype system for microgravity space experiments p 47 A91-53403
- Development of a vibration isolation prototype system for microgravity space experiments
[NASA-TM-103664] p 130 N91-19324
- Magnetic bearings-state of the art
[NASA-TM-104465] p 188 N91-25413

MAGNETOHYDRODYNAMIC FLOW

- Nonequilibrium in a low power arcjet nozzle
[AIAA PAPER 91-2113] p 61 A91-45784

MAGNETOPLASMADYNAMICS

- Evolutionary use of nuclear electric propulsion
[AIAA PAPER 90-3821] p 50 A91-10174
- Performance and lifetime assessment of magnetoplasmadynamic arc thruster technology p 51 A91-30013
- Thrust stand for high-power electric propulsion devices p 41 A91-36239
- Anode power deposition in an applied-field segmented anode MPD thruster
[AIAA PAPER 91-2343] p 59 A91-44204
- A preliminary characterization of applied-field MPD thruster plumes
[AIAA PAPER 91-2339] p 62 A91-45798
- Numerical simulation of self-field MPD thrusters
[AIAA PAPER 91-2341] p 62 A91-45805
- Applied-field MPD thruster geometry effects
[AIAA PAPER 91-2342] p 62 A91-45806
- Cathode phenomena in a low-power magnetoplasmadynamic thruster p 63 A91-52314
- Nondestructive evaluation tools and experimental studies for monitoring the health of space propulsion systems
[AIAA PAPER 91-3433] p 192 A91-53703

SUBJECT INDEX

- Nondestructive evaluation tools and experimental studies for monitoring the health of space propulsion systems
[NASA-TM-105164] p 194 N91-28605
- MPD thruster technology
[NASA-TM-105242] p 86 N91-32162
- MAINTENANCE**
- Structural properties of laminated Douglas fir/epoxy composite material
[NASA-RP-1236] p 94 N91-10127
- Transmission overhaul estimates for partial and full replacement at repair
[NASA-TM-104395] p 190 N91-30533
- MAN MACHINE SYSTEMS**
- Tuning maps for setpoint changes and load disturbance upsets in a three capacity process under multivariable control
[NASA-TM-104419] p 220 N91-31876
- MAN-COMPUTER INTERFACE**
- General-purpose interface bus for multiuser, multitasking computer system p 215 A91-35928
- MANAGEMENT SYSTEMS**
- Automated electric power management and control for Space Station Freedom p 53 A91-37970
- Autonomous power expert system advanced development p 72 N91-20689
- An assessment of technology alternatives for telecommunications and information management for the space exploration initiative
[NASA-TM-103783] p 134 N91-23347
- MANEUVERABILITY**
- Overview of high performance aircraft propulsion p 28 N91-20089
- MANIFOLDS (MATHEMATICS)**
- Structure of random discrete spacetime p 224 A91-22894
- MANIPULATORS**
- Manipulation hardware for microgravity research
[NASA-TM-103423] p 128 N91-14498
- MANNED MARS MISSIONS**
- Preliminary assessments in the power requirements of a manned rover for Mars missions p 41 A91-27702
- Power system requirements and definition for lunar and Mars outposts p 52 A91-37930
- A comparison of energy conversion systems for meeting the power requirements of manned rover for Mars missions p 53 A91-37932
- Synergistic use of high and low thrust propulsion systems for piloted missions to Mars
[AIAA PAPER 91-2346] p 39 A91-45807
- Performance impact on nuclear thermal propulsion of piloted Mars missions with short transit times
[AIAA PAPER 91-3401] p 64 A91-52326
- Radiation dose estimates for typical piloted NTR lunar and Mars mission engine operations
[AIAA PAPER 91-3407] p 215 A91-52331
- A comparison of optical technologies for a high data rate Mars link
[AIAA PAPER 91-3469] p 45 A91-52377
- Nuclear electric propulsion mission performance for fast piloted Mars missions
[AIAA PAPER 91-3488] p 65 A91-52388
- NTR vehicle commonality assessment for piloted lunar and Mars missions
[AIAA PAPER 91-3575] p 66 A91-52448
- Metallized propellants for the human exploration of Mars
[NASA-TP-3062] p 69 N91-11800
- Design strategies for the International Space University's variable gravity research facility p 42 N91-22171
- An assessment of technology alternatives for telecommunications and information management for the space exploration initiative
[NASA-TM-103783] p 134 N91-23347
- Chemical approaches to carbon dioxide utilization for manned Mars missions p 241 N91-26073
- Technical prospects for utilizing extraterrestrial propellants for space exploration
[NASA-TM-105263] p 127 N91-31318
- Multimegawatt electric propulsion system design considerations
[NASA-TM-105152] p 87 N91-32164
- MANNED SPACECRAFT**
- Power electronic applications for Space Station Freedom p 52 A91-36832
- MANUFACTURING**
- Review of the transmissions of the Soviet helicopters
[NASA-TM-103634] p 20 N91-15146
- Reinforcements: The key to high performance composite materials
[NASA-TM-103230] p 96 N91-15329
- MAPPING**
- Mappings and accuracy for Chebyshev pseudo-spectral approximations
[NASA-TM-103630] p 221 N91-14781

MARKET RESEARCH

- Reinforcements: The key to high performance composite materials
[NASA-TM-103230] p 96 N91-15329

MARKOV PROCESSES

- A statistical rain attenuation prediction model with application to the advanced communication technology satellite project. 3: A stochastic rain fade control algorithm for satellite link power via non linear Markov filtering theory
[NASA-TM-100243] p 134 N91-22494

MARS (PLANET)

- Solar radiation on Mars p 242 A91-28153
Effects of dust accumulation and removal on radiators surfaces on Mars
[NASA-TM-103704] p 72 N91-20204
Material processing with hydrogen and carbon monoxide on Mars
[NASA-TM-104405] p 211 N91-23616
Chemical approaches to carbon dioxide utilization for manned Mars missions p 241 N91-26073

MARS ATMOSPHERE

- Solar radiation on Mars p 242 A91-28153
Microwave beam powered Mars airplane
p 52 A91-37931
In-situ propellant rocket engines for Mars missions ascent vehicle
[AIAA PAPER 91-2445] p 60 A91-44247
Solar radiation on Mars: Update 1990
[NASA-TM-103623] p 242 N91-15117
Chemical approaches to carbon dioxide utilization for manned Mars missions
[NASA-TM-103728] p 241 N91-20015
Cooling of in-situ propellant rocket engines for Mars mission
[NASA-TM-103729] p 72 N91-21233
In-situ propellant rocket engines for Mars mission ascent vehicle
[NASA-TM-104429] p 76 N91-24305
Effects of Martian dust on power system components
p 241 N91-27061
Solar radiation on Mars: Update 1991
[NASA-TM-105216] p 242 N91-33046

MARS ENVIRONMENT

- Simulation of Martian dust accumulation on surfaces
p 47 N91-19160
Electrical system/environment interactions on the planet Mars
p 242 N91-27068

MARS LANDING

- Cooling of in-situ propellant rocket engines for Mars mission
[NASA-TM-103729] p 72 N91-21233

MARS PROBES

- Solar electric propulsion for Mars transport vehicles
[NASA-TM-103234] p 71 N91-19178

MARS SURFACE

- Systems analysis of Mars solar electric propulsion vehicles
[AIAA PAPER 90-3824] p 40 A91-10176
Solar radiation on Mars p 242 A91-28153
Microwave beam powered Mars airplane
p 52 A91-37931
Electrical characterization of a Mapham inverter using pulse testing techniques
p 139 A91-37992
Design considerations for Mars photovoltaic power systems
p 41 A91-41988
Solar radiation on Mars: Update 1990
[NASA-TM-103623] p 242 N91-15117
Aeolian removal of dust types from photovoltaic surfaces on Mars
p 47 N91-19156
Simulation of Martian dust accumulation on surfaces
p 47 N91-19160
Feasibility of solar power for Mars
p 209 N91-19201
Effects of dust accumulation and removal on radiators surfaces on Mars
[NASA-TM-103704] p 72 N91-20204
Effects of windblown dust on photovoltaic surfaces on Mars
[NASA-TM-104448] p 78 N91-25183
Effects of Martian dust on power system components
p 241 N91-27061
Electrical system/environment interactions on the planet Mars
p 242 N91-27068
Solar radiation on Mars: Update 1991
[NASA-TM-105216] p 242 N91-33046
- MASS BALANCE**
Effects of gear box vibration and mass imbalance on the dynamics of multistage gear transmission
p 182 A91-47213
Effects of gear box vibration and mass imbalance on the dynamics of multi-stage gear transmissions
[NASA-TM-103695] p 185 N91-21534

MASS FLOW

- Experimental study of cross-stream mixing in a cylindrical duct
[AIAA PAPER 91-2459] p 157 A91-45815
Experimental study of cross-stream mixing in a cylindrical duct
[NASA-TM-105180] p 34 N91-29187

MASS FLOW RATE

- Transient cryogenic liquid discharge in normal and micro-gravity
[AIAA PAPER 91-0486] p 124 A91-19324
Performance characterization of a segmented anode arcjet thruster
[NASA-TM-103227] p 67 N91-10118

MASS SPECTROSCOPY

- X-ray photoelectron and mass spectroscopic study of electron irradiation and thermal stability of polytetrafluoroethylene
p 113 A91-16138

MATERIALS RECOVERY

- Near-Earth asteroids: Metals occurrence, extraction, and fabrication
p 241 N91-26058

MATERIALS SCIENCE

- Materials degradation in low earth orbit (LEO); Proceedings of the Symposium, 119th Annual Meeting of the Minerals, Metals, and Materials Society, Anaheim, CA, Feb. 17-22, 1990
p 116 A91-49801
Computational materials science. An example: Numerical modeling of chemical vapor deposition processing of advanced fibers
p 99 N91-20111
- MATERIALS TESTS**
Automation software for a materials testing laboratory
p 216 A91-56538

MATHEMATICAL MODELS

- Metal matrix composites microfracture - Computational simulation
p 90 A91-11815
Evaluation of a hybrid kinetics/mixing-controlled combustion model for turbulent premixed and diffusion combustion using KIVA-II
[AIAA PAPER 90-2450] p 104 A91-12927
An integrated methodology for optimizing the passive damping of composite structures
p 195 A91-19048
Numerical simulation of ice growth on a MS-317 swept wing geometry
[AIAA PAPER 91-0263] p 19 A91-26193
Computational simulation of damping in composite structures
p 198 A91-36283
Mechanisms and modeling of the effects of additives on the nitrogen oxides emission
[AIAA PAPER 91-0479] p 124 A91-40560
Computational modeling of the pressurization process in a NASP vehicle propellant tank experimental simulation
[AIAA PAPER 91-2407] p 124 A91-41771
Effect of emitter parameter variation on the performance of heteroepitaxial indium phosphide solar cells
p 140 A91-42003
Effects of gear box vibration and mass imbalance on the dynamics of multistage gear transmission
p 182 A91-47213
MPD thruster technology
[AIAA PAPER 91-3568] p 65 A91-52444
Dielectric function of InGaAs in the visible
p 233 A91-53236
In situ X-ray monitoring of damage accumulation in SiC/RBSN tensile specimens
p 94 A91-56942
Structural properties of laminated Douglas fir/epoxy composite material
[NASA-RP-1236] p 94 N91-10127
Simulation of turbomachinery flows
p 9 N91-10880
The effect of coatings and liners on heat transfer in a dry shaft-bush tribosystem
[NASA-TM-102513] p 159 N91-12913
Finite element analysis of thermal distortion effects on optical performance of solar dynamic concentrator for Space Station Freedom
[NASA-TM-102504] p 183 N91-12954
Stirling engine: Available tools for long-life assessment
[NASA-TM-103660] p 200 N91-12980
Numerical simulation of ice growth on a MS-317 swept wing geometry
[NASA-TM-103705] p 11 N91-14310
Effect of emitter parameter variation on the performance of heteroepitaxial indium phosphide solar cells
[NASA-TM-103619] p 70 N91-15306
Multi-dimensional modeling of a thermal energy storage canister
[NASA-TM-103731] p 71 N91-19177
Determination of series resistance of indium phosphide solar cells
p 210 N91-19207
Application of thermal life prediction model to high-temperature aerospace alloys B1900 + Hf and Haynes 188
[NASA-TM-4226] p 201 N91-19473
Turbomachinery
p 162 N91-20097
Progress in modeling deformation and damage
p 202 N91-20108

- Computational materials science. An example: Numerical modeling of chemical vapor deposition processing of advanced fibers
p 99 N91-20111

- Isothermal fatigue behavior of a (90)(sub 8) SiC/Ti-15-3 composite at 426 C
[NASA-TM-103686] p 99 N91-20228

- A finite element model of conduction, convection, and phase change near a solid/melt interface
[NASA-TM-103721] p 162 N91-20417

- Simulation of turbomachinery flows
p 163 N91-21069

- Dynamics of local grid manipulations for internal flow problems
p 164 N91-21090

- Effects of gear box vibration and mass imbalance on the dynamics of multi-stage gear transmissions
[NASA-TM-103695] p 185 N91-21534

- Application of mixing-controlled combustion models to gas turbine combustors
[NASA-TM-103236] p 31 N91-22126

- Reactionless propulsion using tethers
p 73 N91-22163

- In-situ x-ray monitoring of damage accumulation in SiC/RBSN tensile specimens
[NASA-TM-103733] p 99 N91-22402

- Mechanisms and modeling of the effects of additives on the nitrogen oxides emission
p 126 N91-22464

- A statistical rain attenuation prediction model with application to the advanced communication technology satellite project. 3: A stochastic rain fade control algorithm for satellite link power via non linear Markov filtering theory
[NASA-TM-100243] p 134 N91-22494

- A new flux splitting scheme
[NASA-TM-104404] p 222 N91-22814

- A simplified dynamic model of the Space Shuttle main engine
[NASA-TM-104421] p 131 N91-23340

- Modal analysis of multistage gear systems coupled with gearbox vibrations
[NASA-TM-103797] p 187 N91-23513

- Overview of the fatigue/fracture/life working group program at the Lewis Research Center
p 203 N91-24308

- Modeling of crack bridging in a unidirectional metal matrix composite
[NASA-TM-104355] p 205 N91-24660

- Institute for Computational Mechanics in Propulsion (ICOMP)
[NASA-TM-103790] p 222 N91-24818

- Balancing reliability and cost to choose the best power subsystem
[NASA-TM-104453] p 238 N91-24952

- Microfracture in high temperature metal matrix crossply laminates
[NASA-TM-104381] p 101 N91-25198

- GRID3D-v2: An updated version of the GRID2D/3D computer program for generating grid systems in complex-shaped three-dimensional spatial domains
[NASA-TM-103766] p 217 N91-25630

- A distributed fault-detection and diagnosis system using on-line parameter estimation
[NASA-TM-104433] p 220 N91-25696

- Development of an analytical tool to study power quality of AC power systems for large spacecraft
[NASA-TM-104451] p 223 N91-25749

- Applied high-speed imaging for the icing research program at NASA Lewis Research Center
[NASA-TM-104415] p 177 N91-26490

- Comparative survey of dynamic analyses of free-piston Stirling engines
[NASA-TM-104491] p 224 N91-26870

- Process for the homoepitaxial growth of single-crystal silicon carbide films on silicon carbide wafers
[NASA-CASE-LEW-15223-1] p 236 N91-26967

- Visualization techniques to experimentally model flow and heat transfer in turbine and aircraft flow passages
[NASA-TM-4272] p 167 N91-27489

- Viscoplastic analysis of an experimental cylindrical thrust chamber liner
[NASA-TM-103287] p 205 N91-28622

- Comparative modeling of InP solar cell structures
p 83 N91-30232

- The effects of interply damping layers on the dynamic response of composite structures
[NASA-TM-104497] p 103 N91-30282

- Nonlinear combustion instability model in two- to three-dimensions
[NASA-TM-102381] p 85 N91-31208

- Theoretical modelling of AFM for bimetallic tip-substrate interactions
[NASA-TM-105280] p 112 N91-32215

- MATHEMATICAL PROGRAMMING**
Solution of steady-state, two-dimensional conservation laws by mathematical programming
p 221 A91-35956

MATRIX MATERIALS

- Composite laminate tailoring with probabilistic constraints and loads p 198 A91-38754
- Polymeric routes to silicon carbide and silicon oxycarbide CMC p 117 A91-56922
- Reinforcements. The key to high performance composite materials
- [NASA-TM-103230] p 96 N91-15329
- Probabilistic micromechanics and macromechanics of polymer matrix composites
- [NASA-TM-103669] p 98 N91-19236
- Comparison of dynamic fatigue behavior between SiC whisker-reinforced composite and monolithic silicon nitrides
- [NASA-TM-103707] p 119 N91-19293
- Mechanical behavior of fiber reinforced SiC/RBSN ceramic matrix composites. Theory and experiment
- [NASA-TM-103688] p 99 N91-21243
- Polymeric routes to silicon carbide and silicon oxycarbide CMC
- [NASA-TM-104372] p 102 N91-26234
- Computational simulation of high temperature metal matrix composite behavior
- [NASA-TM-104378] p 206 N91-32520

MATRIX METHODS

- General purpose program to generate compatibility matrix for the integrated force method

- p 195 A91-12905
- In situ X-ray monitoring of damage accumulation in SiC/RBSN tensile specimens p 94 A91-56942
- In-situ x-ray monitoring of damage accumulation in SiC/RBSN tensile specimens
- [NASA-TM-103733] p 99 N91-22402

MATTER-ANTIMATTER PROPULSION

- Antiproton powered propulsion with magnetically confined plasma engines p 63 A91-52313

MAXIMUM LIKELIHOOD ESTIMATES

- Calculation of Weibull strength parameters, Batdorf flaw density constants and related statistical quantities using PC-CARES
- [NASA-TM-103247] p 199 N91-10332

MEASURE AND INTEGRATION

- Asymptotic integration algorithms for nonhomogeneous, nonlinear, first order, ordinary differential equations
- [NASA-TM-103793] p 222 N91-21797

MEASURING INSTRUMENTS

- Using a modified Hewlett Packard 8410 network analyzer as an automated farfield antenna range receiver
- [NASA-TM-103700] p 143 N91-19349
- Rotating pressure measurement system using an on board calibration standard
- [NASA-TM-103676] p 176 N91-19401

- Instrumentation and controls overview
- p 38 N91-20099
- Overview of the instrumentation program
- p 176 N91-24318

- Fiber-optic sensors for aerospace electrical measurements: An update
- [NASA-TM-104454] p 177 N91-25381
- Research and development of optical measurement techniques for aerospace propulsion research: A NASA Lewis Research Center perspective
- [NASA-TM-104418] p 178 N91-27511
- Plug-type heat flux gauge
- [NASA-CASE-LEW-14967-1] p 179 N91-31608

MECHANICAL DEVICES

- Space mechanisms needs for future NASA long duration space missions
- [AIAA PAPER 91-3428] p 183 A91-57025
- Space mechanisms needs for future NASA long duration space missions
- [NASA-TM-105204] p 190 N91-30532

MECHANICAL DRIVES

- Advanced Rotorcraft Transmission Program
- p 179 A91-17214
- Advanced rotorcraft transmission program
- [NASA-TM-103276] p 184 N91-21531

- Four quadrant control of induction motors
- p 145 N91-23055
- Computerized inspection of real surfaces and minimization of their deviations
- [NASA-TM-103798] p 188 N91-27558

- How to determine spiral bevel gear tooth geometry for finite element analysis
- [NASA-TM-105150] p 190 N91-30537

MECHANICAL PROPERTIES

- A review of properties and potential aerospace applications of electrically conducting polymers
- p 113 A91-14409
- Computational simulation of high-temperature metal matrix composites cyclic behavior
- p 91 A91-18680
- Fundamental considerations in adhesion, friction and wear for ceramic-metal contacts
- p 115 A91-35952
- Effect of thermal shock on fiber-reinforced superalloy composites
- p 93 A91-55918

- Crystallization and properties of Sr-Ba aluminosilicate glass-ceramic matrices
- p 117 A91-56917

- In situ X-ray monitoring of damage accumulation in SiC/RBSN tensile specimens
- p 94 A91-56942
- Calculation of Weibull strength parameters, Batdorf flaw density constants and related statistical quantities using PC-CARES

- [NASA-TM-103247] p 199 N91-10332
- Stirling engine: Available tools for long-life assessment
- [NASA-TM-103660] p 200 N91-12980

- ICAN sensitivity analysis
- [NASA-TM-103667] p 96 N91-15328
- Effect of fiber reinforcements on thermo-oxidative stability and mechanical properties of polymer matrix composites

- [NASA-TM-103648] p 98 N91-19234
- Crystallization and properties of Sr-Ba aluminosilicate glass-ceramic matrices

- [NASA-TM-103764] p 120 N91-19308
- In-situ x-ray monitoring of damage accumulation in SiC/RBSN tensile specimens

- [NASA-TM-103733] p 99 N91-22402
- Industrial applications of graphite fluoride fibers
- p 100 N91-23040

MELTING

- The series $\text{Bi}_2\text{Sr}_2\text{Ca}_{(n-1)}\text{Cu}(n)\text{O}_{(2n+4)}$ (1 less than or equal to n less than or equal to 5): Phase stability and superconducting properties
- [NASA-TM-103749] p 235 N91-21910

MELTING POINTS

- Creep behavior of copper at intermediate temperatures. II - Surface microstructural observations. III - A comparison with theory
- p 109 A91-47931

MEMBRANES

- Some recent studies with the solid-ionomer electrochemical capacitor
- p 214 N91-32562

MERCURY CADMIUM TELLURIDES

- Surface and implantation effects on p-n junctions
- p 234 N91-18299
- Properties of insulator interfaces with p-HgCdTe
- p 235 N91-18300
- Surface electrons in inverted layers of p-HgCdTe
- p 235 N91-18301

METAL BONDING

- Universal energy relations and metal/ceramic interfaces
- p 93 A91-56254

METAL COATINGS

- Metallic seal for thermal barrier coating systems
- [NASA-CASE-LEW-15020-1] p 119 N91-15412
- Ceramic coatings on smooth surfaces
- [NASA-CASE-LEW-15164-1] p 122 N91-25298

METAL FATIGUE

- Inhomogeneous deformation in INCONEL 718 during monotonic and cyclic loadings
- p 108 A91-22287
- Surface fatigue life of M50NiL and AISI 9310 gears and rolling-contact bars
- p 182 A91-45350
- Effect of tensile mean stress on fatigue behavior of single-crystal and directionally solidified superalloys
- [NASA-TM-103644] p 200 N91-18452
- Tensile and fatigue behavior of tungsten/copper composites
- p 100 N91-24311
- Cumulative creep fatigue damage in 316 stainless steel
- p 111 N91-24312
- Fatigue behavior of a single-crystal superalloy
- p 111 N91-24313
- Fatigue life prediction of an intermetallic matrix composite at elevated temperatures
- [NASA-TM-104494] p 205 N91-25442

METAL FILMS

- Advanced materials for space nuclear power systems
- [AIAA PAPER 91-3530] p 86 A91-53704
- High temperature fatigue behavior of tungsten copper composites
- p 93 A91-55906
- Effect of thermal shock on fiber-reinforced superalloy composites
- p 93 A91-55918
- Advanced materials for space nuclear power systems
- [NASA-TM-105171] p 112 N91-29298

METAL FILMS

- Intrinsic bond strength of metal films on polymer substrates
- p 88 A91-39246
- Rapid solidification of polymorphic transition metals induced by nanosecond laser pulses
- p 109 A91-46520

METAL FLUORIDES

- Method of making carbide/fluoride/silver composites
- [NASA-CASE-LEW-14902-1] p 102 N91-27244

METAL FUELS

- Production and use of metals and oxygen for lunar propulsion
- [AIAA PAPER 91-3481] p 125 A91-53711
- Production and use of metals and oxygen for lunar propulsion
- [NASA-TM-105195] p 81 N91-29222

METAL IONS

- Influence of several metal ions on the gelation activation energy of silicon tetraethoxide
- p 113 A91-19599

METAL MATRIX COMPOSITES

- Metal matrix composites microfracture - Computational simulation
- p 90 A91-11815
- 1300 K compressive properties of a reaction milled NiAl-AIN composites
- p 107 A91-18674
- Computational simulation of high-temperature metal matrix composites cyclic behavior
- p 91 A91-18680
- Fatigue crack growth study of SCS6/Ti-15-3 composite
- p 91 A91-25798
- Compression behavior of TiB2-particulate-reinforced composites of Al22Fe3Ti8
- p 91 A91-28014
- Concurrent material-fabrication optimization of metal-matrix laminates under thermo-mechanical loading
- [AIAA PAPER 91-1044] p 129 A91-31842
- Preliminary investigation of acousto-ultrasonic evaluation of metal-matrix composite specimens
- p 191 A91-37014
- Evaluation of thermomechanical damage in silicon carbide/titanium composites
- p 92 A91-42297
- Concurrent tailoring of fabrication process and interphase layer to reduce residual stresses in metal matrix composites
- p 92 A91-43232
- Preliminary studies on NiAl/Nb2Be17 reaction and effectiveness of BeO as an interfacial reaction barrier
- p 92 A91-55050
- Factors which influence tensile strength of a SiC/Ti-24Al-11Nb (at. pct) composite
- p 92 A91-55900
- High temperature fatigue behavior of tungsten copper composites
- p 93 A91-55906
- The isothermal fatigue behavior of a unidirectional SiC/Ti composite and the Ti alloy matrix
- p 93 A91-55907
- Elastic/plastic analyses of advanced composites investigating the use of the compliant layer concept in reducing residual stresses resulting from processing
- [NASA-TM-103204] p 94 N91-11074
- METCAN simulation of candidate metal matrix composites for high temperature applications
- [NASA-TM-103636] p 96 N91-17143
- Current activities in standardization of high-temperature, low-cycle-fatigue testing techniques in the United States
- [NASA-TM-103675] p 200 N91-17427
- METCAN updates for high temperature composite behavior: Simulation/verification
- [NASA-TM-103682] p 97 N91-19229
- Computational simulation of hot composites structures
- [NASA-TM-103681] p 97 N91-19230
- Low-density, high-strength intermetallic matrix composites by XD (trademark) synthesis
- [NASA-TM-103724] p 97 N91-19233
- Concurrent micromechanical tailoring and fabrication process optimization for metal-matrix composites
- [NASA-TM-103670] p 98 N91-19237
- HITCAN for actively cooled hot-composite thermostructural analysis
- [NASA-TM-103750] p 202 N91-21562
- Combined thermal and bending fatigue of high-temperature metal-matrix composites. Computational simulation
- [NASA-TM-104354] p 100 N91-23247
- A preliminary investigation of acousto-ultrasonic NDE of metal matrix composite test specimens
- [NASA-TM-104339] p 194 N91-23521
- Tensile and fatigue behavior of tungsten/copper composites
- p 100 N91-24311
- High temperature tension-compression fatigue behavior of a tungsten copper composite
- [NASA-TM-104370] p 100 N91-24360
- Modeling of crack bridging in a unidirectional metal matrix composite
- [NASA-TM-104355] p 205 N91-24660
- Microfracture in high temperature metal matrix crossply laminates
- [NASA-TM-104381] p 101 N91-25198
- Fatigue life prediction of an intermetallic matrix composite at elevated temperatures
- [NASA-TM-104494] p 205 N91-25442
- Oxidation resistant coatings for titanium alloys and titanium alloy matrix composites
- [NASA-CASE-LEW-15155-1] p 122 N91-26375
- Matrix plasticity in SiC/Ti-15-3 composite
- [NASA-TM-103760] p 102 N91-27247
- Interphase layer optimization for metal matrix composites with fabrication considerations
- [NASA-TM-105166] p 102 N91-30281
- Fatigue behavior and life prediction of a SiC/Ti-24Al-11Nb composite under isothermal conditions
- [NASA-TM-105168] p 206 N91-30566
- Experimental and analytical analysis of stress-strain behavior in a (90/0 deg)2s, SiC/Ti-15-3 laminate
- [NASA-TM-104470] p 103 N91-31235
- Computational simulation of high temperature metal matrix composite behavior
- [NASA-TM-104378] p 206 N91-32520

METAL OXIDE SEMICONDUCTORS

- Neutron and gamma irradiation effects on power semiconductor switches
- p 139 A91-38162

- Development of silicon carbide semiconductor devices for high temperature applications
[NASA-TM-104398] p 236 N91-22921
- METAL OXIDES**
Acidic attack of perfluorinated alkyl ether lubricant molecules by metal oxide surfaces p 104 A91-13439
Production and use of metals and oxygen for lunar propulsion
[AIAA PAPER 91-3481] p 125 A91-53711
Production and use of metals and oxygen for lunar propulsion
[NASA-TM-105195] p 81 N91-29222
- METAL PARTICLES**
Launch vehicle performance using metallized propellants
[AIAA PAPER 91-2050] p 58 A91-44106
Design issues for propulsion systems using metallized propellants
[AIAA PAPER 91-3484] p 66 A91-53709
Advanced launch vehicle upper stages using liquid propulsion and metallized propellants
p 75 N91-24257
Launch vehicle performance using metallized propellants
[NASA-TM-104456] p 76 N91-24304
Design issues for propulsion systems using metallized propellants
[NASA-TM-105190] p 81 N91-29220
- METAL PLATES**
The effects of interply damping layers on the dynamic response of composite structures
[AIAA PAPER 91-1124] p 197 A91-32064
- METAL POWDER**
Tribological properties of PM212 - A high temperature, self-lubricating, powder metallurgy composite
[STLE PREPRINT 90-AM-4E-1] p 87 A91-19720
Synthesis and structures of metal chalcogenide precursors
[NASA-TM-103665] p 120 N91-19296
- METAL PROPELLANTS**
Launch vehicle performance using metallized propellants
[AIAA PAPER 91-2050] p 58 A91-44106
Design issues for propulsion systems using metallized propellants
[AIAA PAPER 91-3484] p 66 A91-53709
Production and use of metals and oxygen for lunar propulsion
[AIAA PAPER 91-3481] p 125 A91-53711
Advanced launch vehicle upper stages using liquid propulsion and metallized propellants
[NASA-TM-103622] p 68 N91-11797
Metallized propellants for the human exploration of Mars
[NASA-TP-3062] p 69 N91-11800
Lunar missions using chemical propulsion: System design issues
[NASA-TP-3065] p 70 N91-15308
Advanced chemical propulsion at NASA Lewis: Metallized and high energy density propellants
[NASA-TM-103771] p 71 N91-19175
Advanced launch vehicle upper stages using liquid propulsion and metallized propellants
p 75 N91-24257
Launch vehicle performance using metallized propellants
[NASA-TM-104456] p 76 N91-24304
Design issues for propulsion systems using metallized propellants
[NASA-TM-105190] p 81 N91-29220
Production and use of metals and oxygen for lunar propulsion
[NASA-TM-105195] p 81 N91-29222
- METAL SURFACES**
Surface modification of Monel K-500 as a means of reducing friction and wear in high-pressure oxygen
p 107 A91-16869
Fundamental considerations in adhesion, friction and wear for ceramic-metal contacts p 115 A91-35952
The effect of the near earth micrometeoroid environment on a mirror surface after 20 years in space
p 47 A91-49810
Reactivity of pi-complexes of Ti, V, and Nb towards dithioacetic acid: Synthesis and structure of novel metal sulfur-containing complexes
[NASA-TM-103666] p 106 N91-19256
Arc-textured high emittance radiator surfaces
[NASA-CASE-LEW-14679-1] p 122 N91-25296
Ceramic coatings on smooth surfaces
[NASA-CASE-LEW-15164-1] p 122 N91-25298
- METAL-METAL BONDING**
Adhesion at metal interfaces p 88 A91-38581
- METALLIZING**
Semiconductor structural damage attendant to contact formation in III-V solar cells p 209 N91-19203
- Thin solar cell and lightweight array
[NASA-CASE-LEW-14959-1] p 212 N91-27614
- METALLOGRAPHY**
Thermal stability of the microstructure of an aged Nb-Zr-C alloy
[NASA-TM-103647] p 110 N91-14454
Experimental and analytical analysis of stress-strain behavior in a (90/0 deg)2s, SiC/Ti-15-3 laminate
[NASA-TM-104470] p 103 N91-31235
- METALS**
High temperature reactions of ceramics and metals with chlorine and oxygen p 105 A91-20219
Near-Earth asteroids: Metals occurrence, extraction, and fabrication p 241 N91-26058
- METEORITIC DAMAGE**
Preliminary flight test results from the advanced photovoltaic experiment p 56 A91-38163
Preliminary results from the advanced photovoltaic experiment flight test
[NASA-TM-103269] p 67 N91-11058
- METEOROID HAZARDS**
The effect of the near earth micrometeoroid environment on a mirror surface after 20 years in space
p 47 A91-49810
- METHANE**
Analysis of 5 KHz combustion instabilities in 40K methane/LOX combustion chambers
[NASA-TM-101368] p 67 N91-10117
Hydrocarbon-fuel/combustion-chamber-liner materials compatibility
[NASA-CR-187104] p 121 N91-21307
- METRIC SPACE**
Structure of random discrete spacetime
p 224 A91-22894
- MICROANALYSIS**
Microanalyses of extended-test xenon hollow cathodes --- in ion thruster simulators
[AIAA PAPER 91-2123] p 61 A91-45787
Microanalysis of extended-test xenon hollow cathodes
[NASA-TM-104532] p 82 N91-30202
- MICROCRACKS**
Metal matrix composites microfracture - Computational simulation p 90 A91-11815
Microfracture in high temperature metal matrix crossply laminates
[NASA-TM-104381] p 101 N91-25198
- MICROELECTRONICS**
Diamondlike carbon applications in infrared optics and microelectronics p 230 N91-18306
- MICROGRAVITY APPLICATIONS**
Transient cryogenic liquid discharge in normal and micro-gravity
[AIAA PAPER 91-0486] p 124 A91-19324
Programmable multi-zone furnace for microgravity research
[AIAA PAPER 91-0781] p 127 A91-19463
Microgravity research at LeRC
[NASA-TM-102521] p 128 N91-24464
- MICROMECHANICS**
Computational simulation of damping in composite structures p 198 A91-36283
Composite laminate tailoring with probabilistic constraints and loads p 198 A91-38754
Probabilistic micromechanics and macromechanics of polymer matrix composites
[NASA-TM-103669] p 98 N91-19236
Concurrent micromechanical tailoring and fabrication process optimization for metal-matrix composites
[NASA-TM-103670] p 98 N91-19237
Combined thermal and bending fatigue of high-temperature metal-matrix composites: Computational simulation
[NASA-TM-104354] p 100 N91-23247
Application of artificial neural networks to composite ply micromechanics
[NASA-TM-104365] p 100 N91-24345
Integrated mechanics for the passive damping of polymer-matrix composites and composite structures
[NASA-TM-104346] p 103 N91-32181
Computational simulation of high temperature metal matrix composite behavior
[NASA-TM-104378] p 206 N91-32520
- MICROMETEORIODS**
The effect of the near earth micrometeoroid environment on a mirror surface after 20 years in space
p 47 A91-49810
Atomic oxygen undercutting of LDEF aluminized Kapton multilayer insulation p 229 N91-25027
Low Earth orbital atomic oxygen micrometeoroid, and debris interactions with photovoltaic arrays
p 84 N91-30248
- MICROSCOPES**
Theoretical modelling of AFM for bimetallic tip-substrate interactions
[NASA-TM-105280] p 112 N91-32215
- MICROSTRIP ANTENNAS**
Circular polarisation characteristics of stacked microstrip antennas p 131 A91-20370
A 29.3-GHz cavity-enclosed aperture-coupled circular-patch antenna for microwave circuit integration
p 140 A91-47057
Ka-band MMIC microstrip array for high rate communications
[AIAA PAPER 91-3421] p 132 A91-52341
Coplanar waveguide feeds for phased array antennas
[AIAA PAPER 91-3422] p 141 A91-52342
A seven patch hexagonal CP subarray with a CPW/stripline feed network
[NASA-TM-103802] p 144 N91-20406
Ka-band MMIC microstrip array for high rate communications
[NASA-TM-104500] p 135 N91-27437
Coplanar waveguide feeds for phased array antennas
[NASA-TM-104467] p 146 N91-27477
Measurement techniques for cryogenic Ka-band microstrip antennas
[NASA-TM-105183] p 146 N91-30426
- MICROSTRIP TRANSMISSION LINES**
Coplanar-waveguide/microstrip probe coupler and applications to antennas p 131 A91-17719
An experimental study of high Tc superconducting microstrip transmission lines at 35 GHz and the effect of film morphology p 138 A91-36172
A 29.3-GHz cavity-enclosed aperture-coupled circular-patch antenna for microwave circuit integration
p 140 A91-47057
An experimental study of high Tc superconducting microstrip transmission lines at 35 GHz and the effect of film morphology
[NASA-TM-103633] p 133 N91-11988
Comparative study of bolometric and non-bolometric switching elements for microwave phase shifters
[NASA-TM-104435] p 145 N91-25320
Design aspects and comparison between high T(sub c) superconducting coplanar waveguide and microstrip line
[NASA-TM-105142] p 146 N91-27445
- MICROSTRUCTURE**
Equivalence of Green's function and the Fourier series representation of composites with periodic microstructure p 91 A91-16889
The structure of carbon in chemically vapor deposited SiC monofilaments p 113 A91-18675
Effect of high temperature hydrogen exposure on the strength and microstructure of mullite
p 114 A91-19780
Continuous fiber-reinforced titanium aluminide composites p 92 A91-39553
Creep behavior of copper at intermediate temperatures. II - Surface microstructural observations. III - A comparison with theory p 109 A91-47931
Spatial variations in a.c. susceptibility and microstructure for the YBa2Cu3O(7-x) superconductor and their correlation with room-temperature ultrasonic measurements p 233 A91-54969
Influence of the Si3N4 microstructure on its R-curve and fatigue behavior p 117 A91-56931
Microstructural and strength stability of CVD SiC fibers in argon environments p 117 A91-56958
Evidence from transmission electron microscopy for an oxyntide layer in oxidized Si3N4 p 118 A91-57058
Thermal stability of the microstructure of an aged Nb-Zr-C alloy
[NASA-TM-103647] p 110 N91-14454
Effect of hydrogen on the strength and microstructure of selected ceramics
[NASA-TM-103674] p 118 N91-14482
Property and microstructural nonuniformity in the yttrium-barium-copper-oxide superconductor determined from electrical, magnetic, and ultrasonic measurements
[NASA-TM-103732] p 193 N91-19463
Spatial variations in ac susceptibility and microstructure for the YBa2Cu3O(7-x) superconductor and their correlation with room-temperature ultrasonic measurements
[NASA-TM-103787] p 194 N91-21553
Ultrasonic evaluation of oxidation and reduction effects on the elastic behavior and global microstructure of YBa2Cu3O7-x
[NASA-TM-104529] p 194 N91-27575
Microstructural and strength stability of CVD SiC fibers in argon environment
[NASA-TM-103772] p 102 N91-29250
Experimental and analytical analysis of stress-strain behavior in a (90/0 deg)2s, SiC/Ti-15-3 laminate
[NASA-TM-104470] p 103 N91-31235
- MICROWAVE AMPLIFIERS**
High efficiency Ka-band MMIC amplifiers
[AIAA PAPER 91-3425] p 141 A91-52345
Low noise InP-based MMIC receivers for W-band
[AIAA PAPER 91-3594] p 142 A91-52462

MICROWAVE ANTENNAS

- Design of an optically controlled Ka-band GaAs MMIC phased-array antenna p 132 A91-24951
 Ka-band MMIC microstrip array for high rate communications p 132 A91-52341
 [AIAA PAPER 91-3421] p 132 A91-52341
 Overview of Ka-band communications technology requirements for the Space Exploration Initiative p 45 A91-52344
 [AIAA PAPER 91-3424] p 45 A91-52344
 Using a modified Hewlett Packard 8410 network analyzer as an automated farfield antenna range receiver [NASA-TM-103700] p 143 N91-19349
 Superconducting microwave electronics at Lewis Research Center p 236 N91-24081
 Ka-band MMIC microstrip array for high rate communications [NASA-TM-104500] p 135 N91-27437
- MICROWAVE CIRCUITS**
 Coplanar-waveguide/microstrip probe coupler and applications to antennas p 131 A91-17719
 Low-temperature microwave characteristics of pseudomorphic $\text{In(x)Ga(1-x)As/In(0.52)Al(0.48)As}$ modulation-doped field-effect transistors p 136 A91-22987
 Optical control of microwave devices --- Book p 136 A91-27331
 High temperature superconductive microwave technology for space applications p 137 A91-31391
 A 29.3-GHz cavity-enclosed aperture-coupled circular-patch antenna for microwave circuit integration p 140 A91-47057
 High temperature superconducting thin film microwave circuits - Fabrication, characterization, and applications p 141 A91-50433
 Ka-band MMIC microstrip array for high rate communications [AIAA PAPER 91-3421] p 132 A91-52341
 High temperature superconductor analog electronics for millimeter-wavelength communications [AIAA PAPER 91-3592] p 233 A91-53707
 Universal nondestructive mm-wave integrated circuit test fixture [NASA-CASE-LEW-14746-1] p 143 N91-14552
 Solid State Technology Branch of NASA Lewis Research Center Second Annual Digest, June 1989 - June 1990 [NASA-TM-103226] p 133 N91-18297
 System-Level Integrated Circuit (SLIC) development for phased array antenna applications [NASA-TM-104392] p 134 N91-23354
 Microwave integrated circuits for space applications p 145 N91-24069
 Superconducting microwave electronics at Lewis Research Center p 236 N91-24081
 Comparative study of bolometric and non-bolometric switching elements for microwave phase shifters [NASA-TM-104435] p 145 N91-25320
 Ka-band MMIC microstrip array for high rate communications [NASA-TM-104500] p 135 N91-27437
 Design aspects and comparison between high T(sub c) superconducting coplanar waveguide and microstrip line [NASA-TM-105142] p 146 N91-27445
 High temperature superconductor analog electronics for millimeter-wavelength communications [NASA-TM-105184] p 237 N91-29982
- MICROWAVE COUPLING**
 New channelised coplanar waveguide to rectangular waveguide post and slot couplers p 139 A91-40272
 A 29.3-GHz cavity-enclosed aperture-coupled circular-patch antenna for microwave circuit integration p 140 A91-47057
- MICROWAVE EQUIPMENT**
 Superconductivity applications for infrared and microwave devices; Proceedings of the Meeting, Orlando, FL, Apr. 19, 20, 1990 [SPIE-1292] p 141 A91-50426
 Using a modified Hewlett Packard 8410 network analyzer as an automated farfield antenna range receiver [NASA-TM-103700] p 143 N91-19349
- MICROWAVE FILTERS**
 Theoretical and experimental characterization of coplanar waveguide discontinuities for filter applications p 137 A91-35911
- MICROWAVE OSCILLATORS**
 High temperature superconducting thin film microwave circuits - Fabrication, characterization, and applications p 141 A91-50433
- MICROWAVE POWER BEAMING**
 High temperature superconductivity technology for advanced space power systems p 50 A91-13447
 Determination of surface resistance and magnetic penetration depth of superconducting $\text{YBa}_2\text{Cu}_3\text{O}(7\text{-delta})$ thin films by microwave power transmission measurements p 138 A91-36060

- Microwave beam powered Mars airplane p 52 A91-37931
 Lunar orbiting microwave beam power system p 56 A91-38158
 Determination of surface resistance and magnetic penetration depth of superconducting $\text{YBa}_2\text{Cu}_3\text{O}(7\text{-delta})$ thin films by microwave power transmission measurements [NASA-TM-103616] p 234 N91-10780
- MICROWAVE SCATTERING**
 Theoretical and experimental characterization of coplanar waveguide discontinuities for filter applications p 137 A91-35911
- MICROWAVE SWITCHING**
 Comparative study of bolometric and non-bolometric switching elements for microwave phase shifters [NASA-TM-104435] p 145 N91-25320
- MICROWAVE TRANSMISSION**
 Emerging applications of high temperature superconductors for space communications [NASA-TM-103629] p 227 N91-12317
- MICROWAVES**
 Coplanar waveguide EEsof MICAD macros make circuit layout easy [NASA-TM-103272] p 134 N91-19332
 Near-field antenna testing using the Hewlett Packard 8510 automated network analyzer [NASA-TM-103699] p 144 N91-20393
 GaAs monolithic RF modules for SRSAT distress beacons [NASA-TM-104338] p 46 N91-21184
 The theory of an auto-resonant field emission cathode relativistic electron accelerator for high efficiency microwave to direct current power conversion p 73 N91-22176
- MIE SCATTERING**
 An imaging system for PLIF/Mie measurements for a combustor flow [NASA-TM-103714] p 27 N91-20084
- MILITARY AIRCRAFT**
 V/STOL gets a lift p 20 A91-52835
 Overview of rotorcraft and general aviation propulsion technology p 29 N91-20112
 Multidisciplinary research overview (IHPTET/NPSS) p 30 N91-20119
- MILLIMETER WAVES**
 Millimeter wavelength communications applications for the SEI [AIAA PAPER 91-3589] p 45 A91-52458
 New materials and techniques for improved mm wave devices [AIAA PAPER 91-3590] p 142 A91-52459
 High power, high efficiency millimeter wavelength traveling wave tubes for high rate communications from deep space [AIAA PAPER 91-3593] p 142 A91-52461
 High temperature superconductor analog electronics for millimeter-wavelength communications [AIAA PAPER 91-3592] p 233 A91-53707
 YBCO superconducting ring resonators at millimeter-wave frequencies p 142 A91-54532
 Emerging applications of high temperature superconductors for space communications [NASA-TM-103629] p 227 N91-12317
 Monolithic mm-wave phase shifter using optically activated superconducting switches [NASA-CASE-LEW-14878-1] p 229 N91-13996
 Universal nondestructive mm-wave integrated circuit test fixture [NASA-CASE-LEW-14746-1] p 143 N91-14552
 High temperature superconductor analog electronics for millimeter-wavelength communications [NASA-TM-105184] p 237 N91-29982
 Millimeter wavelength communications applications for the SEI [NASA-TM-105275] p 135 N91-32287
- MILLING (MACHINING)**
 How to determine spiral bevel gear tooth geometry for finite element analysis [NASA-TM-105150] p 190 N91-30537
- MINIATURIZATION**
 Method of making single crystal fibers [NASA-CASE-LEW-14921-1] p 95 N91-13502
- MIRRORS**
 The effect of the near earth micrometeoroid environment on a mirror surface after 20 years in space p 47 A91-49810
- MIS (SEMICONDUCTORS)**
 Submicron gate InP power MISFET's with improved output power density at 18 and 20 GHz p 142 A91-54526
 MIS capacitor studies on silicon carbide single crystals [NASA-CR-187350] p 234 N91-11555
 Submicron gate InP power MISFET's with improved output power density at 18 and 20 GHz p 145 N91-26436

MISSION PLANNING

- Cryogenic propellant management architectures to support the Space Exploration Initiative [AIAA PAPER 90-3713] p 124 A91-10112
 NASA's future space power needs and requirements p 52 A91-37929
 Nuclear power technology requirements for NASA exploration missions p 53 A91-37940
 Performance impact on nuclear thermal propulsion of piloted Mars missions with short transit times [AIAA PAPER 91-3401] p 64 A91-52326
 The NASA/DOE/DOD nuclear rocket propulsion project - FY 1991 status p 64 A91-52335
 [AIAA PAPER 91-3413] p 64 A91-52335
 Nuclear electric propulsion mission performance for fast piloted Mars missions [AIAA PAPER 91-3488] p 65 A91-52388
 Evolving the SP-100 reactor in order to boost large payloads to GEO and to low lunar orbit via nuclear-electric propulsion [AIAA PAPER 91-3562] p 67 A91-53712
 Metallized propellants for the human exploration of Mars [NASA-TP-3062] p 69 N91-11800
 Vision-21: Space Travel for the Next Millennium [NASA-CP-10059] p 40 N91-22139
 Evolving the SP-100 reactor in order to boost large payloads to GEO and to low lunar orbit via nuclear-electric propulsion [NASA-TM-104527] p 80 N91-27212
 Thin film, concentrator and multijunction space solar cells: Status and potential [NASA-TM-104505] p 86 N91-31218
 Multimegawatt electric propulsion system design considerations [NASA-TM-105152] p 87 N91-32164
- MIXED OXIDES**
 Electrical transport measurements on polycrystalline superconducting Y-Ba-Cu-O films p 231 A91-19820
 Electromigration failure in $\text{YBa}_2\text{Cu}_3\text{O}(7\text{-x})$ thin films p 231 A91-26989
 Superconductivity applications for infrared and microwave devices; Proceedings of the Meeting, Orlando, FL, Apr. 19, 20, 1990 [SPIE-1292] p 141 A91-50426
 Property and microstructural nonuniformity in the yttrium-barium-copper-oxide superconductor determined from electrical, magnetic, and ultrasonic measurements [NASA-TM-103732] p 193 N91-19463
- MIXING**
 Simulation of mixing in the quick quench region of a rich burn-quick quench mix-lean burn combustor [AIAA PAPER 91-0410] p 105 A91-21481
 Experimental study of cross-stream mixing in a cylindrical duct [NASA-TM-105180] p 34 N91-29187
- MIXING LAYERS (FLUIDS)**
 Second order modeling of boundary-free turbulent shear flows [AIAA PAPER 91-1779] p 154 A91-42588
 A pressure control analysis of cryogenic storage systems [AIAA PAPER 91-2405] p 59 A91-44228
 Second order modeling of boundary-free turbulent shear flows [NASA-TM-104369] p 164 N91-22524
 A pressure control analysis of cryogenic storage systems [NASA-TM-104409] p 126 N91-24460
 A comparison of numerical methods for the Rayleigh equation in unbounded domains [NASA-TM-105179] p 223 N91-30865
- MIXING LENGTH FLOW THEORY**
 New mixing-length model for supersonic shear layers p 148 A91-16073
- MOBILE COMMUNICATION SYSTEMS**
 Study on the spectral efficiency of SFH-GMSK in land mobile telephone communication by direct simulation p 132 A91-53176
- MODAL RESPONSE**
 Aeroelastic modal characteristics of mistuned blade assemblies - Mode localization and loss of eigenstructure [AIAA PAPER 91-1218] p 196 A91-32032
 Aeroelastic modal characteristics of mistuned blade assemblies: Mode localization and loss of eigenstructure [NASA-TM-104519] p 205 N91-27591
- MODELS**
 A 10,000-hr life test of an engineering model resistor [NASA-TM-103216] p 69 N91-11802
- MODFETS**
 Low-temperature microwave characteristics of pseudomorphic $\text{In(x)Ga(1-x)As/In(0.52)Al(0.48)As}$ modulation-doped field-effect transistors p 136 A91-22987

- New materials and techniques for improved mm wave devices
[AIAA PAPER 91-3590] p 142 A91-52459
- Ellipsometric study of InGaAs MODFET material
[NASA-TM-103286] p 143 N91-19351
- Study of InGaAs based MODFET structures using variable angle spectroscopic ellipsometry
[NASA-TM-103792] p 235 N91-19935
- MODULATORS**
GaAs monolithic RF modules for SRSAT distress beacons
[NASA-TM-104338] p 46 N91-21184
- MODULUS OF ELASTICITY**
Temperature dependence of the elastic moduli and damping for polycrystalline LiF-22 pct CaF₂ eutectic salt
p 87 A91-33793
- Analysis of some compliance calibration data for chevron-notch bar and rod specimens
[NASA-TM-104367] p 203 N91-22594
- Ultrasonic evaluation of oxidation and reduction effects on the elastic behavior and global microstructure of YBa₂Cu₃O_{7-x}
[NASA-TM-104529] p 194 N91-27575
- MOISTURE CONTENT**
Viscoelastic properties of addition-cured polyimides used in high temperature polymer matrix composites
[NASA-TM-103768] p 89 N91-22377
- MOLECULAR BEAM EPITAXY**
Low-temperature microwave characteristics of pseudomorphic In(x)Ga(1-x)As/In(0.52)Al(0.48)As modulation-doped field-effect transistors
p 136 A91-22987
- Dielectric function of InGaAs in the visible
p 233 A91-53236
- MOLECULAR CHAINS**
Ladder polymers for use as high temperature stable resins or coatings
[NASA-CASE-LEW-14203-1] p 118 N91-15402
- MOLECULAR FLOW**
High-speed laser anemometry based on spectrally resolved Rayleigh scattering
[NASA-TM-104522] p 178 N91-27521
- MOLECULAR IONS**
Global expression for representing diatomic potential-energy curves
p 228 A91-33236
- MOLECULAR ORBITALS**
Sulfur at nickel-alumina interfaces - Molecular orbital theory
p 104 A91-12925
- MOLECULAR WEIGHT**
Addition polyimides with enhanced processability
[NASA-CASE-LEW-15043-1] p 123 N91-32230
- MOLTEN SALTS**
Two-dimensional simulation of a two-phase, regenerative pumped radiator loop utilizing direct contact heat transfer with phase change
p 151 A91-38126
- MOLYBDENUM DISULFIDES**
Solid lubricants
[NASA-TM-102803] p 99 N91-22396
- Lubrication with sputtered MoS₂ films: Principles, operation, limitations
[NASA-TM-105292] p 112 N91-32216
- MOMENT DISTRIBUTION**
Advances in modeling the pressure correlation terms in the second moment equations
[NASA-TM-104413] p 165 N91-24525
- MOMENTUM**
Experimental study of boundary layer transition on a heated flat plate
[NASA-TM-103779] p 14 N91-21061
- Exploring the notion of space coupling propulsion
p 73 N91-22161
- MONITORS**
Automating security monitoring and analysis for Space Station Freedom's electric power system
p 219 A91-37975
- Nondestructive evaluation tools and experimental studies for monitoring the health of space propulsion systems
[AIAA PAPER 91-3433] p 192 A91-53703
- Overview of space propulsion systems for identifying nondestructive evaluation and health monitoring opportunities
[NASA-TM-103614] p 192 N91-15565
- Overview of the instrumentation program
p 176 N91-24318
- Nondestructive evaluation tools and experimental studies for monitoring the health of space propulsion systems
[NASA-TM-105164] p 194 N91-28605
- Description of real-time Ada software implementation of a power system monitor for the Space Station Freedom PMAD DC testbed
[NASA-TM-105157] p 218 N91-28776
- MONOMERS**
Addition polyimides with enhanced processability
[NASA-CASE-LEW-15043-1] p 123 N91-32230
- MONOTONE FUNCTIONS**
Second-order accurate nonoscillatory schemes for scalar conservation laws
p 221 A91-13204
- Accurate monotone cubic interpolation
[NASA-TM-103789] p 221 N91-20830
- MONTE CARLO METHOD**
Numerical and experimental investigations of rarefied nozzle and plume flows of nitrogen
[AIAA PAPER 91-1363] p 154 A91-43429
- ETARA PC version 3.3 user's guide: Reliability, availability, maintainability simulation model
[NASA-TM-103751] p 193 N91-19462
- Pressure measurements in a low-density nozzle plume for code verification
[NASA-TM-105170] p 81 N91-29228
- MORPHOLOGY**
Photoresponse of YBa₂Cu₃O₇(δ) granular and epitaxial superconducting thin films
p 141 A91-50443
- Polymeric routes to silicon carbide and silicon oxycarbide
CMC
p 117 A91-56922
- Polymeric routes to silicon carbide and silicon oxycarbide
CMC
[NASA-TM-104372] p 102 N91-26234
- MOUNTING**
Post clamp
[NASA-CASE-LEW-14862-1] p 183 N91-14617
- Removable hand hold
[NASA-CASE-LEW-15196-1] p 188 N91-26543
- MULLITES**
Effect of high temperature hydrogen exposure on the strength and microstructure of mullite
p 114 A91-19780
- MULTIBEAM ANTENNAS**
Advanced Communications Technology Satellite (ACTS)
[IAF PAPER 90-481] p 44 A91-14056
- MULTIGRID METHODS**
Multigrid calculation of three-dimensional viscous cascade flows
[AIAA PAPER 91-3238] p 7 A91-53754
- Characteristics of 3D turbulent jets in crossflow
p 158 A91-54268
- Characteristics of 3D turbulent jets in crossflow
[NASA-TM-104337] p 165 N91-22536
- MULTILAYER INSULATION**
A review of candidate multilayer insulation systems for potential use on wet-launched LH₂ tankage for the Space Exploration Initiative lunar missions
[AIAA PAPER 91-2176] p 43 A91-45793
- Thermal performance of a liquid hydrogen tank multilayer insulation system at warm boundary temperatures of 630, 530, and 152 R
[AIAA PAPER 91-2400] p 43 A91-45812
- Atomic oxygen undercutting of LDEF aluminized Kapton multilayer insulation
p 229 N91-25027
- Thermal performance of a liquid hydrogen tank multilayer insulation system at warm boundary temperatures of 630, 530, and 152 R
[NASA-TM-104476] p 43 N91-25159
- MULTIPHASE FLOW**
Dropsize correlation for cryogenic liquid-jet atomization
[NASA-TM-103646] p 175 N91-12064
- MULTIPLE ACCESS**
ATDRS payload technology R & D
p 45 A91-53188
- MULTIPLEXING**
Quaternary pulse position modulation electronics for free-space laser communications
[AIAA PAPER 91-3471] p 133 A91-53702
- Quaternary pulse position modulation electronics for free-space laser communications
[NASA-TM-104502] p 135 N91-29405
- MULTIPROGRAMMING**
General-purpose interface bus for multiuser, multitasking computer system
p 215 A91-35928
- MULTISTAGE ROCKET VEHICLES**
Overview of the Beta II two-stage-to-orbit vehicle design
[AIAA PAPER 91-3175] p 43 A91-54088
- MULTIVARIABLE CONTROL**
A linear control design structure to maintain loop properties during limit operation in a multi-nozzle turbofan engine
[AIAA PAPER 91-1997] p 24 A91-45780
- A linear control design structure to maintain loop properties during limit operation in a multi-nozzle turbofan engine
[NASA-TM-105163] p 35 N91-29188
- Tuning maps for setpoint changes and load disturbance upsets in a three capacity process under multivariable control
[NASA-TM-104419] p 220 N91-31876
- N-TYPE SEMICONDUCTORS**
Improvements in contact resistivity and thermal stability of Au-contacted InP solar cells
p 213 N91-30207
- NASA PROGRAMS**
NASA's High Speed Research Program - An introduction and status report
[SAE PAPER 901923] p 1 A91-48605
- An overview of the LeRC CSTI thermal management program
[AIAA PAPER 91-3528] p 158 A91-52422
- The NASA CSTI High Capacity Power Program
[AIAA PAPER 91-3629] p 208 A91-52493
- Historical perspectives - The role of the NASA Lewis Research Center in the national space nuclear power programs
[AIAA PAPER 91-3462] p 242 A91-53713
- Simulation of turbomachinery flows
p 9 N91-10880
- NASA developments in solid state power amplifiers
p 143 N91-18298
- Advanced chemical propulsion at NASA Lewis: Metallized and high energy density propellants
[NASA-TM-103771] p 71 N91-19175
- Overview of structures research
p 202 N91-20104
- Propulsion aeroelasticity, vibration control, and dynamic system modeling
p 29 N91-20105
- Overview of Lewis materials research: Contributions, current efforts, and future directions
p 111 N91-20109
- Computational materials science. An example: Numerical modeling of chemical vapor deposition processing of advanced fibers
p 99 N91-20111
- Overview of rotorcraft and general aviation propulsion technology
p 29 N91-20112
- Rotary engine technology
p 30 N91-20114
- Overview of subsonic transport propulsion technology
p 30 N91-20116
- Ultra-high bypass research
p 30 N91-20117
- High-efficiency core technology
p 30 N91-20118
- Multidisciplinary research overview (IHPTET/NPSS)
p 30 N91-20119
- NASA's aircraft icing technology program
p 19 N91-20120
- Recent advances in Lewis aeropropulsion facilities
p 38 N91-20121
- IMPAC: An Integrated Methodology for Propulsion and Airframe Control
[NASA-TM-103805] p 30 N91-20122
- Microwave integrated circuits for space applications
p 145 N91-24069
- Historical perspectives: The role of the NASA Lewis Research Center in the national space nuclear power programs
[NASA-TM-105196] p 243 N91-29138
- NASA SPACE PROGRAMS**
Cryogenic propellant management architectures to support the Space Exploration Initiative
[AIAA PAPER 90-3713] p 124 A91-10112
- Evolutionary use of nuclear electric propulsion
[AIAA PAPER 90-3821] p 50 A91-10174
- Advanced Communications Technology Satellite (ACTS)
[IAF PAPER 90-481] p 44 A91-14056
- Speculating on space futures
p 237 A91-16900
- NASA's future space power needs and requirements
p 52 A91-37929
- Nuclear power technology requirements for NASA exploration missions
p 53 A91-37940
- The NASA/DOE/DOD nuclear rocket propulsion project - FY 1991 status
[AIAA PAPER 91-3413] p 64 A91-52335
- A comparison of optical technologies for a high data rate Mars link
[AIAA PAPER 91-3469] p 45 A91-52377
- Nuclear rocket propulsion. NASA plans and progress, FY 1991
[NASA-TM-104455] p 77 N91-25179
- NASTRAN**
Low velocity impact analysis with NASTRAN
p 198 A91-48865
- Application of an efficient hybrid scheme for aeroelastic analysis of advanced propellers
p 7 A91-52315
- Low velocity impact analysis with NASTRAN
[NASA-TM-103169] p 95 N91-14426
- Modal analysis of multistage gear systems coupled with gearbox vibrations
[NASA-TM-103797] p 187 N91-23513
- NATIONAL AEROSPACE PLANE PROGRAM**
High temperature NASP engine seal development
[NASA-TM-103716] p 184 N91-19441
- A test fixture for measuring high-temperature hypersonic-engine seal performance
[NASA-TM-103658] p 184 N91-19442
- Overview of NASP nozzle research
p 28 N91-20093

Chemical reacting flows p 162 N91-20098

NAVIER-STOKES EQUATION

Navier-Stokes simulation of transonic blade-vortex interactions p 2 A91-21065

Flow studies in close-coupled ventral nozzles for STOL aircraft

[SAE PAPER 901033] p 2 A91-21242

Simulation of mixing in the quick quench region of a rich burn-quick quench mix-lean burn combustor

[AIAA PAPER 91-0410] p 105 A91-21481

The aerodynamic characteristics of vortex ingestion for the F/A-18 inlet duct

[AIAA PAPER 91-0130] p 3 A91-26192

Role of artificial viscosity in Euler and Navier-Stokes solvers p 4 A91-34135

Generalized conjugate-gradient methods for the Navier-Stokes equations

[AIAA PAPER 91-1556] p 5 A91-40730

Numerical flux formulas for the Euler and Navier-Stokes equations. II - Progress in flux-vector splitting

[AIAA PAPER 91-1566] p 5 A91-40740

Verification of the Proteus two-dimensional Navier-Stokes code for flat plate and pipe flows

[AIAA PAPER 91-2013] p 153 A91-41678

A three-dimensional Navier-Stokes stage analysis of the flow through a compact radial turbine

[AIAA PAPER 91-2564] p 23 A91-41815

Numerical and experimental investigations of rarefied nozzle and plume flows of nitrogen

[AIAA PAPER 91-1363] p 154 A91-43429

3-D Navier-Stokes analysis of crossing, glancing shocks/turbulent boundary layer interactions

[AIAA PAPER 91-1758] p 6 A91-43631

Navier-Stokes simulation of the supersonic combustion flowfield in a ram accelerator

[AIAA PAPER 91-1916] p 155 A91-44057

A design strategy for the use of vortex generators to manage inlet-engine distortion using computational fluid dynamics

[AIAA PAPER 91-2474] p 6 A91-44259

Navier-Stokes analysis of turbine blade heat transfer

[ASME PAPER 90-GT-42] p 155 A91-44529

Two-dimensional Navier-Stokes heat transfer analysis for rough turbine blades

[AIAA PAPER 91-2129] p 156 A91-45790

Primitive variable, strongly implicit calculation procedure for viscous flows at all speeds p 7 A91-46181

Performance and flow calculations for a gaseous H₂/O₂ thruster p 63 A91-48843

Numerical solution for the velocity-derivative skewness of a low Reynolds-number turbulent-like decaying Navier-Stokes flow p 158 A91-50204

A Navier-Stokes study of shock-boundary layer interaction and flow separation inside a transonic compressor p 8 A91-56115

A three-dimensional turbulent heat transfer analysis for advanced tubular rocket thrust chambers

[NASA-TM-103293] p 159 N91-10249

Time dependent viscous incompressible Navier-Stokes equations p 9 N91-10854

Numerical analysis of flow through oscillating cascade sections p 9 N91-10884

Navier-Stokes analysis of transonic cascade flow

[NASA-TM-103624] p 159 N91-11192

The aerodynamic characteristics of vortex ingestion for the F/A-18 inlet duct

[NASA-TM-103703] p 70 N91-15303

Performance of a high-work, low-aspect-ratio turbine stator tested with a realistic inlet radial temperature gradient

[NASA-TM-103738] p 31 N91-20126

Turbulent fluid motion. Part 1: The phenomenon of fluid turbulence

[NASA-TM-103723] p 162 N91-20445

Transonic cascade flow calculations using non-periodic C-type grids p 163 N91-21071

Implicit solution of three-dimensional internal turbulent flows p 163 N91-21082

Numerical investigation of an internal layer in turbulent flow over a curved hill p 163 N91-21083

Numerical flux formulas for the Euler and Navier-Stokes equations. 2: Progress in flux-vector splitting

[NASA-TM-104353] p 15 N91-22084

A new flux splitting scheme

[NASA-TM-104404] p 222 N91-22814

A study of three dimensional turbulent boundary layer separation and vortex flow control using the reduced Navier Stokes equations

[NASA-TM-104407] p 16 N91-23089

Computational modeling and validation for hypersonic inlets p 16 N91-23162

A three-dimensional Navier-Stokes stage analysis of the flow through a compact radial turbine

[NASA-TM-104420] p 32 N91-23186

The 3-D Navier-Stokes analysis of crossing, glancing shocks/turbulent boundary layer interactions

[NASA-TM-104469] p 16 N91-24130

A design strategy for the use of vortex generators to manage inlet-engine distortion using computational fluid dynamics

[NASA-TM-104436] p 16 N91-24131

Navier-Stokes simulation of the supersonic combustion flowfield in a ram accelerator

[NASA-TM-104439] p 166 N91-24541

Comparison of SMAC, PISO, and iterative time-advancing schemes for unsteady flows

[NASA-TM-104406] p 167 N91-24550

High-Order Polynomial Expansions (HOPE) for flux-vector splitting

[NASA-TM-104452] p 222 N91-25739

Verification of the proteus two-dimensional Navier-Stokes code for flat plate and pipe flows

[NASA-TM-105160] p 168 N91-30462

Least-squares solution of incompressible Navier-Stokes equations with the p-version of finite elements

[NASA-TM-105203] p 223 N91-31911

NAVIGATION

A technology assessment of alternative communications systems for the space exploration initiative

[AIAA PAPER 90-3681] p 44 A91-11472

NEAR FIELDS

Near-field noise of a single rotation propfan at an angle of attack

[AIAA PAPER 90-3953] p 225 A91-12469

Investigation of the arcjet plume near field using electrostatic probes

[NASA-TM-103638] p 68 N91-11060

Near-field noise of a single-rotation propfan at an angle of attack

[NASA-TM-103645] p 227 N91-12316

Near-field antenna testing using the Hewlett Packard 8510 automated network analyzer

[NASA-TM-103699] p 144 N91-20393

Investigation of the arcjet near field plume using electrostatic probes p 75 N91-24270

NEGATIVE MATTER PROPULSION

Comment on 'Negative matter propulsion'

p 52 A91-37424

NEODYMIUM LASERS

Optical inspection of space-propulsion components using an injection seeded Nd:YAG laser system

p 179 N91-24320

NETWORK ANALYSIS

Using a modified Hewlett Packard 8410 network analyzer as an automated farfield antenna range receiver

[NASA-TM-103700] p 143 N91-19349

NETWORK CONTROL

Neural network architecture for crossbar switch control p 218 A91-29181

Neural network application to aircraft control system design

[AIAA PAPER 91-2715] p 36 A91-49676

Towards practical control design using neural computation

[NASA-TM-103785] p 219 N91-19766

Neural network application to aircraft control system design

[NASA-TM-105151] p 37 N91-27167

NEURAL NETS

Neural network architecture for crossbar switch control p 218 A91-29181

A neural net based architecture for the segmentation of mixed gray-level and binary pictures

p 218 A91-29183

The application of neural networks to the SSME startup transient

[AIAA PAPER 91-2530] p 60 A91-44283

Neural network application to aircraft control system design

[AIAA PAPER 91-2715] p 36 A91-49676

Neuromorphic learning of continuous-valued mappings from noise-corrupted data p 219 A91-53201

Towards practical control design using neural computation

[NASA-TM-103785] p 219 N91-19766

Applications of artificial neural nets in structural mechanics

[NASA-TM-102420] p 202 N91-21559

Application of artificial neural networks to composite ply micromechanics

[NASA-TM-104365] p 100 N91-24345

Sensor failure detection and recovery by neural networks

[NASA-TM-104484] p 220 N91-24815

Neural network application to aircraft control system design

[NASA-TM-105151] p 37 N91-27167

NEUTRINOS

Astrophysics and cosmology confront the 17-keV neutrino p 240 A91-43291

Constraints from primordial nucleosynthesis on the mass of the tau neutrino p 240 A91-46543

NEUTRON DIFFRACTION

Near-edge study of gold-substituted YBa₂Cu₃O₇(δ)

[NASA-TM-105220] p 237 N91-31977

NEUTRON IRRADIATION

Neutron and gamma irradiation effects on power semiconductor switches p 139 A91-38162

Neutron, gamma ray and post-irradiation thermal annealing effects on power semiconductor switches

[AIAA PAPER 91-3525] p 142 A91-52420

NEUTRONS

Neutron, gamma ray and post-irradiation thermal annealing effects on power semiconductor switches

[NASA-TM-105248] p 147 N91-32410

NEWTONIAN FLUIDS

Newtonian mechanics of a many-particle assembly coupled to an external body potential

p 237 A91-19495

A finite element model of conduction, convection, and phase change near a solid/melt interface

[NASA-TM-103721] p 162 N91-20417

NICKEL

Raman spectral observation of a new phase observed in nickel electrodes cycled to failure

p 214 N91-32556

Impedances of nickel electrodes cycled in various KOH concentrations p 214 N91-32557

NICKEL ALLOYS

Sulfur at nickel-alumina interfaces - Molecular orbital theory p 104 A91-12925

1300 K compressive properties of a reaction milled NiAl-AIN composites p 107 A91-18674

Effect of sulfur removal on Al₂O₃ scale adhesion

p 108 A91-27940

The effect of hydrogen on the low cycle fatigue behavior of a single crystal superalloy p 108 A91-28794

1000 to 1300 K slow plastic compression properties of Al-deficient NiAl p 108 A91-36214

1000 to 1200 K time-dependent compressive deformation of single-crystalline and polycrystalline B2 Ni-40Al p 109 A91-43670

Reaction of beta-phase Ni-Al alloys with CrB₂

p 92 A91-49943

Preliminary studies on NiAl/Nb₂Be₁₇ reaction and effectiveness of BeO as an interfacial reaction barrier

p 92 A91-55050

A simplified method for determining the number of independent slip systems in crystals

p 110 A91-55472

High temperature cyclic oxidation data. Part 1: Turbine alloys

[NASA-TM-83665] p 110 N91-10149

High-temperature cyclic oxidation data. Part 2: Turbine alloys

[NASA-TM-101468] p 110 N91-10150

Effect of tensile mean stress on fatigue behavior of single-crystal and directionally solidified superalloys

[NASA-TM-103644] p 200 N91-18452

Thermomechanical and bithermal fatigue behavior of cast B1900 + Hf and wrought Haynes 188

[NASA-TM-4225] p 111 N91-20268

Prospects for ductility and toughness enhancement of NiAl by ductile phase reinforcement

[NASA-TM-103796] p 112 N91-27324

Comparison of high temperature, high frequency core loss and dynamic B-H loops of two 50 Ni-Fe crystalline alloys and an iron-based amorphous alloy

[NASA-TM-105205] p 147 N91-32412

NICKEL CADMIUM BATTERIES

NASA Aerospace Flight Battery Systems Program

p 56 A91-38088

NICKEL COMPOUNDS

The potential for ductility enhancement from surface and interface dislocation sources in NiAl p 109 A91-39292

NICKEL HYDROGEN BATTERIES

Effect of KOH concentration on LEO cycle life of IPV nickel-hydrogen flight battery cells p 55 A91-38076

Effect of LEO cycling on 125 Ah advanced design IPV nickel-hydrogen battery cells p 55 A91-38077

Impedances of Ni electrodes and Ni/H₂ cells from different manufacturers

p 55 A91-38082

NASA Aerospace Flight Battery Systems Program

p 56 A91-38088

Photovoltaic power for Space Station Freedom

p 57 A91-41878

Impedances of electrochemically impregnated nickel electrodes as functions of potential, KOH concentration, and impregnation method

[NASA-TM-103283] p 208 N91-15628

Effect of LEO cycling on 125 Ah advanced design IPV nickel-hydrogen flight cells. An update

[NASA-TM-104384] p 74 N91-22375

- Effect of KOH concentration on LEO cycle life of IPV nickel-hydrogen flight cells. An update
[NASA-TM-104383] p 74 N91-22376
- Destructive physical analysis results of Ni/H₂ cells cycled in LEO regime
[NASA-TM-104382] p 74 N91-23233
- Nickel-hydrogen cell low-Earth life test update
[NASA-TM-105229] p 213 N91-31708
- Raman spectral observation of a new phase observed in nickel electrodes cycled to failure
p 214 N91-32556
- Performance of a dual anode nickel-hydrogen cell
p 214 N91-32563
- NIOBIUM**
- Thermal stability of the microstructure of an aged Nb-Zr-C alloy
[NASA-TM-103647] p 110 N91-14454
- Tensile behavior of tungsten/niobium composites at 1300 to 1600 K
[NASA-TM-103727] p 111 N91-16128
- NIOBIUM ALLOYS**
- Preliminary studies on NiAl/Nb2Be17 reaction and effectiveness of BeO as an interfacial reaction barrier
p 92 A91-55050
- Factors which influence tensile strength of a SiC/Ti-24Al-11Nb (at. pct) composite p 92 A91-55900
- Reactivity of pi-complexes of Ti, V, and Nb towards dithioacetic acid: Synthesis and structure of novel metal sulfur-containing complexes
[NASA-TM-103666] p 106 N91-19256
- NITRIC OXIDE**
- Simulation of mixing in the quick quench region of a rich burn-quick quench mix-lean burn combustor
[AIAA PAPER 91-0410] p 105 A91-21481
- NITROGEN**
- Dropsizes correlation for cryogenic liquid-jet atomization
[AIAA PAPER 91-0284] p 51 A91-19218
- Dropsizes correlation for cryogenic liquid-jet atomization
[NASA-TM-103646] p 175 N91-12064
- Effects of high pressure nitrogen on the thermal stability of SiC fibers
[NASA-TM-103245] p 96 N91-16075
- Arjet thermal characteristics
[NASA-TM-105156] p 82 N91-29231
- Qualitative investigation of cryogenic injected shock dissipation
[NASA-TM-105140] p 168 N91-29525
- Crystallization and characterization of Y2O3-SiO2 glasses
p 237 N91-31962
- NITROGEN OXIDES**
- Mechanisms and modeling of the effects of additives on the nitrogen oxides emission
[AIAA PAPER 91-0479] p 124 A91-40560
- Experimental study of cross-stream mixing in a cylindrical duct
[AIAA PAPER 91-2459] p 157 A91-45815
- Mechanisms and modeling of the effects of additives on the nitrogen oxides emission
[NASA-TM-103765] p 126 N91-22464
- CFD analysis of jet mixing in low NOx flametube combustors
[NASA-TM-104466] p 33 N91-26146
- Experimental study of cross-stream mixing in a cylindrical duct
[NASA-TM-105180] p 34 N91-29187
- NITROUS OXIDES**
- A CFD study of jet mixing in reduced flow areas for lower combustor emissions
[AIAA PAPER 91-2460] p 23 A91-41788
- A CFD study of jet mixing in reduced flow areas for lower combustor emissions
[NASA-TM-104411] p 32 N91-23185
- NOISE (SOUND)**
- Computational simulation of acoustic fatigue for hot composite structures
[NASA-TM-104379] p 203 N91-23548
- NOISE GENERATORS**
- In-flight source noise of an advanced full-scale single-rotation propeller
[AIAA PAPER 91-0594] p 226 A91-21547
- Cruise noise of an advanced single-rotation propeller measured from an adjacent aircraft p 22 A91-28265
- NOISE INTENSITY**
- Aeroacoustics of advanced propellers
p 226 A91-24317
- NOISE MEASUREMENT**
- Noise measurements from an ejector suppressor nozzle in the NASA Lewis 9- by 15-foot low speed wind tunnel
[AIAA PAPER 90-3983] p 225 A91-12496
- Cruise noise of an advanced single-rotation propeller measured from an adjacent aircraft p 22 A91-28265
- Aeroacoustic effects of reduced aft tip speed at constant thrust for a model counterrotation turboprop at takeoff conditions
[NASA-TM-103608] p 226 N91-10703
- Noise measurements from an ejector suppressor nozzle in the NASA Lewis 9- by 15-foot low speed wind tunnel
[NASA-TM-103628] p 227 N91-11493
- Wind turbine acoustics
[NASA-TP-3057] p 228 N91-16679
- NOISE PREDICTION (AIRCRAFT)**
- Prediction of the noise from a propeller at angle of attack
[AIAA PAPER 90-3954] p 225 A91-12470
- Aeroacoustics of advanced propellers
p 226 A91-24317
- Prediction of the noise from a propeller at angle of attack
[NASA-TM-103627] p 227 N91-11495
- Acoustical analysis of gear housing vibration
[NASA-TM-103691] p 188 N91-25411
- NOISE REDUCTION**
- Noise measurements from an ejector suppressor nozzle in the NASA Lewis 9- by 15-foot low speed wind tunnel
[AIAA PAPER 90-3983] p 225 A91-12496
- Advanced Rotorcraft Transmission Program
p 179 A91-17214
- NASA's High Speed Research Program - An introduction and status report
[SAE PAPER 901923] p 1 A91-48605
- Overview of the NASA-sponsored HSCST propulsion system studies --- High Speed Civil Transport
[AIAA PAPER 91-3329] p 20 A91-53871
- Noise measurements from an ejector suppressor nozzle in the NASA Lewis 9- by 15-foot low speed wind tunnel
[NASA-TM-103628] p 227 N91-11493
- The effect of swirl recovery vanes on the cruise noise of an advanced propeller
[NASA-TM-103625] p 227 N91-11494
- Prediction of the noise from a propeller at angle of attack
[NASA-TM-103627] p 227 N91-11495
- Potential reduction of en route noise from an advanced turboprop aircraft
[NASA-TM-103635] p 228 N91-15842
- Advanced rotorcraft transmission program
[NASA-TM-103276] p 184 N91-21531
- NONDESTRUCTIVE TESTS**
- Ultrasonic imaging of textured alumina
p 191 A91-18596
- Fiber optic phase stepping system for interferometry
p 171 A91-28968
- Acousto-ultrasonics - Retrospective exhortation with bibliography
p 191 A91-37011
- Preliminary investigation of acousto-ultrasonic evaluation of metal-matrix composite specimens
p 191 A91-37014
- Acousto-ultrasonics
p 226 A91-48227
- Nondestructive evaluation tools and experimental studies for monitoring the health of space propulsion systems
[AIAA PAPER 91-3433] p 192 A91-53703
- Spatial variations in a.c. susceptibility and microstructure for the YBa2Cu3O(7-x) superconductor and their correlation with room-temperature ultrasonic measurements
p 233 A91-54969
- Two-dimensional surface strain measurement based on a variation of Yamaguchi's laser-speckle strain gauge
p 174 A91-55531
- Ultrasonic velocity technique for monitoring property changes in fiber-reinforced ceramic matrix composites
p 174 A91-56912
- High resolution computed tomography of advanced composite and ceramic materials
p 192 A91-56972
- Universal nondestructive mm-wave integrated circuit test fixture
[NASA-CASE-LEW-14746-1] p 143 N91-14552
- Overview of space propulsion systems for identifying nondestructive evaluation and health monitoring opportunities
[NASA-TM-103614] p 192 N91-15565
- Review of acousto-ultrasonic NDE for composites
p 97 N91-18192
- Acousto-ultrasonic nondestructive evaluation of materials using laser beam generation and detection
p 193 N91-18193
- NDE standards for high temperature materials
[NASA-TM-103761] p 193 N91-19464
- Transition-to-practice technologies for brittle materials
p 120 N91-20107
- Mechanical behavior of fiber reinforced SiC/RBSN ceramic matrix composites: Theory and experiment
[NASA-TM-103688] p 99 N91-21243
- Spatial variations in ac susceptibility and microstructure for the YBa2Cu3O(7-x) superconductor and their correlation with room-temperature ultrasonic measurements
[NASA-TM-103787] p 194 N91-21553
- Optical inspection of space-propulsion components using an injection seeded Nd:YAG laser system
p 179 N91-24320
- Overall goals
p 80 N91-28246
- Nondestructive evaluation tools and experimental studies for monitoring the health of space propulsion systems
[NASA-TM-105164] p 194 N91-28605
- NDE of ceramics and ceramic composites
[NASA-TM-104520] p 194 N91-29610
- Ultrasonic velocity technique for monitoring property changes in fiber-reinforced ceramic matrix composites
[NASA-TM-103806] p 195 N91-30546
- Spectroscopic wear detector
[NASA-CASE-LEW-15200-1] p 87 N91-32167
- NONEQUILIBRIUM FLOW**
- Nonequilibrium in a low power arcjet nozzle
[AIAA PAPER 91-2113] p 61 A91-45784
- NONLINEAR EQUATIONS**
- Time development of a perturbed-spherical nucleus in a pure supercooled liquid. I - Power-law growth of morphological instabilities. II - Nonlinear development
p 231 A91-16105
- Neuromorphic learning of continuous-valued mappings from noise-corrupted data
p 219 A91-53201
- Asymptotic integration algorithms for nonhomogeneous, nonlinear, first order, ordinary differential equations
[NASA-TM-103793] p 222 N91-21797
- Nonlinear combustion instability model in two- to three-dimensions
[NASA-TM-102381] p 85 N91-31208
- NONLINEAR EVOLUTION EQUATIONS**
- Nonlinear spatial evolution of externally excited instability waves in free shear layers
p 152 A91-38705
- Nonlinear evolution of subsonic and supersonic disturbances on a compressible free shear layer
p 152 A91-39716
- NONLINEARITY**
- Dynamic analysis of space-related linear and non-linear structures
p 196 A91-28612
- Numerical simulation of nonlinear development of instability waves
[E-4658] p 8 N91-10849
- Optical measurement of unducted fan flutter
[NASA-TM-103285] p 27 N91-15174
- Critical-layer nonlinearity in the resonance growth of three-dimensional waves in boundary layers
[NASA-TM-103639] p 161 N91-19373
- Asymptotic integration algorithms for nonhomogeneous, nonlinear, first order, ordinary differential equations
[NASA-TM-103793] p 222 N91-21797
- Exponential integration algorithms applied to viscoplasticity
[NASA-TM-104461] p 223 N91-27901
- Resonant triad in boundary-layer stability. Part 1: Fully nonlinear interaction
[NASA-TM-105208] p 169 N91-32458
- Resonant triad in boundary-layer stability. Part 2: Composite solution and comparison with observations
[NASA-TM-105209] p 169 N91-32459
- NONOSCILLATORY ACTION**
- Second-order accurate nonoscillatory schemes for scalar conservation laws
p 221 A91-13204
- NONUNIFORMITY**
- Property and microstructural nonuniformity in the yttrium-barium-copper-oxide superconductor determined from electrical, magnetic, and ultrasonic measurements
[NASA-TM-103732] p 193 N91-19463
- NORMAL SHOCK WAVES**
- A laser velocimeter investigation of the normal shock-wave boundary layer interaction
[NASA-TM-105201] p 169 N91-32440
- NOTCH STRENGTH**
- Analysis of some compliance calibration data for chevron-notch bar and rod specimens
[NASA-TM-104367] p 203 N91-22594
- NOZZLE DESIGN**
- Numerical study of high-area-ratio H₂/O₂ rocket nozzles
[AIAA PAPER 91-2434] p 57 A91-41780
- Comparison of a quasi-3D analysis and experimental performance for three compact radial turbines
[AIAA PAPER 91-2128] p 25 A91-45789
- Analytical study of nozzle performance for nuclear thermal rockets
[AIAA PAPER 91-3578] p 66 A91-52451
- Overview of the NASA-sponsored HSCST propulsion system studies --- High Speed Civil Transport
[AIAA PAPER 91-3329] p 20 A91-53871
- Overview of NASP nozzle research
p 28 N91-20093
- Inlets, ducts, and nozzles
p 162 N91-20096
- Comparison of a quasi-3D analysis and experimental performance for three compact radial turbines
[NASA-TM-105155] p 35 N91-30142

NOZZLE FLOW

- Hot gas ingestion test results of a two-poster vectored thrust concept with flow visualization in the NASA Lewis 9- by 15-foot low speed wind tunnel
[AIAA PAPER 90-2268] p 4 A91-40561
- Numerical and experimental investigations of rarefied nozzle and plume flows of nitrogen
[AIAA PAPER 91-1363] p 154 A91-43429
- Pressure measurements in a low-density nozzle plume for code verification
[AIAA PAPER 91-2110] p 61 A91-45783
- Nonequilibrium in a low power arcjet nozzle
[AIAA PAPER 91-2113] p 61 A91-45784
- Experimental and analytical studies of flow through a ventral and axial exhaust nozzle system for STOVL aircraft
[AIAA PAPER 91-2135] p 25 A91-45791
- Noise measurements from an ejector suppressor nozzle in the NASA Lewis 9- by 15-foot low speed wind tunnel
[NASA-TM-103628] p 227 N91-11493
- Nozzles, ducts, and nozzles p 162 N91-20096
- Hot gas ingestion test results of a two-poster vectored thrust concept with flow visualization in the NASA Lewis 9- x 15-foot low speed wind tunnel
[NASA-TM-103258] p 15 N91-21116
- CFD for hypersonic propulsion
[NASA-TM-103791] p 164 N91-21447
- Experimental and analytical studies of flow through a ventral and axial exhaust nozzle system for STOVL aircraft
[NASA-TM-104364] p 77 N91-25175
- Effect of tabs on the evolution of an axisymmetric jet
[NASA-TM-104472] p 34 N91-27159
- Modern CFD applications for the design of a reacting shear layer facility
[NASA-TM-104523] p 34 N91-27164
- Pressure measurements in a low-density nozzle plume for code verification
[NASA-TM-105170] p 81 N91-29228
- An experimental study of natural and forced modes in an axisymmetric jet
[NASA-TM-105225] p 18 N91-32074
- NOZZLE GEOMETRY**
- Noise measurements from an ejector suppressor nozzle in the NASA Lewis 9- by 15-foot low speed wind tunnel
[AIAA PAPER 90-3983] p 225 A91-12496
- Influence of geometric features on the performance of pressure-swirl atomizers p 147 A91-13030
- 3D computation of hypersonic nozzle
[AIAA PAPER 90-5203] p 1 A91-14429
- Experimental investigation of a single flush-mounted hypermixing nozzle
[AIAA PAPER 90-5240] p 21 A91-14466
- Flow studies in close-coupled ventral nozzles for STOVL aircraft
[SAE PAPER 901033] p 2 A91-21242
- An experimental comparison of nonswirling and swirling flow in a circular-to-rectangular transition duct
[AIAA PAPER 91-0342] p 148 A91-21466
- Three-dimensional viscous flow computations of high area ratio nozzles for hypersonic propulsion p 4 A91-30014
- Effects of nozzle lip geometry on spray atomization and emissions advanced gas turbine combustors
[AIAA PAPER 91-2201] p 24 A91-44153
- A linear control design structure to maintain loop properties during limit operation in a multi-nozzle turbofan engine
[AIAA PAPER 91-1997] p 24 A91-45780
- High-power hydrogen arcjet performance
[AIAA PAPER 91-2226] p 61 A91-45795
- Progress toward synergistic hypermixing nozzles
[AIAA PAPER 91-2264] p 25 A91-45800
- Experimental investigation of a single flush-mounted hypermixing nozzle
[NASA-TM-103726] p 161 N91-19374
- An experimental comparison of nonswirling and swirling flow in a circular-to-rectangular transition duct
[NASA-TM-104359] p 14 N91-21115
- Progress toward synergistic hypermixing nozzles
[NASA-TM-105169] p 18 N91-29150
- Divergence thrust loss calculations for convergent-divergent nozzles: Extensions to the classical case
[NASA-TM-105176] p 34 N91-29181
- Medium power hydrogen arcjet performance
[NASA-TM-104533] p 85 N91-31216
- NOZZLE INSERTS**
- Arcjet nozzle area ratio effects p 75 N91-24271
- NOZZLE THRUST COEFFICIENTS**
- Experimental and analytical studies of flow through a ventral and axial exhaust nozzle system for STOVL aircraft
[AIAA PAPER 91-2135] p 25 A91-45791

- Experimental and analytical studies of flow through a ventral and axial exhaust nozzle system for STOVL aircraft
[NASA-TM-104364] p 77 N91-25175
- NUCLEAR AUXILIARY POWER UNITS**
- Design of multihundredwatt DIPS for robotic space missions
[NASA-TM-104401] p 75 N91-24232
- NUCLEAR BINDING ENERGY**
- An x-ray photoelectron spectroscopy study of Au(x)In(y) alloys
[NASA-TM-103659] p 234 N91-14050
- NUCLEAR ELECTRIC POWER GENERATION**
- Nuclear technology and the space exploration missions p 53 A91-37939
- Photovoltaic superiority for Space Station Freedom power in the 21st century p 58 A91-42004
- Lunar electric power systems utilizing the SP-100 reactor coupled to dynamic conversion systems
[AIAA PAPER 91-3520] p 208 A91-52415
- The NASA CSTI High Capacity Power Program
[AIAA PAPER 91-3629] p 208 A91-52493
- Design of multihundredwatt DIPS for robotic space missions
[NASA-TM-104401] p 75 N91-24232
- Small Stirling dynamic isotope power system for multihundred-watt robotic missions
[NASA-TM-104460] p 78 N91-25182
- NUCLEAR ELECTRIC PROPULSION**
- Evolutionary use of nuclear electric propulsion
[AIAA PAPER 90-3821] p 50 A91-10174
- Blazing the trailway - Nuclear electric propulsion and its technology program plans
[AIAA PAPER 91-3441] p 64 A91-52353
- The NASA Lewis Research Center electric propulsion program
[AIAA PAPER 91-3443] p 64 A91-52355
- SEI needs for space nuclear power
[AIAA PAPER 91-3459] p 64 A91-52369
- Nuclear electric propulsion mission performance for fast piloted Mars missions
[AIAA PAPER 91-3488] p 65 A91-52388
- Test facilities for high power electric propulsion
[AIAA PAPER 91-3499] p 42 A91-52396
- Multimegawatt nuclear power systems for nuclear electric propulsion
[AIAA PAPER 91-3607] p 66 A91-52472
- Evolving the SP-100 reactor in order to boost large payloads to GEO and to low lunar orbit via nuclear-electric propulsion
[AIAA PAPER 91-3562] p 67 A91-53712
- Nuclear rocket propulsion. NASA plans and progress, FY 1991
[NASA-TM-104455] p 77 N91-25179
- Evolving the SP-100 reactor in order to boost large payloads to GEO and to low lunar orbit via nuclear-electric propulsion
[NASA-TM-104527] p 80 N91-27212
- Futuristic systems: Solar and nuclear electric propulsion p 80 N91-28215
- MPD thruster technology
[NASA-TM-105242] p 86 N91-32162
- NUCLEAR ENERGY**
- Nuclear power technology requirements for NASA exploration missions p 53 A91-37940
- NUCLEAR FUELS**
- Development of nuclear fuels and materials for propulsion systems for SEI
[AIAA PAPER 91-3452] p 125 A91-52362
- NUCLEAR FUSION**
- Big bang nucleosynthesis - The standard model and alternatives p 240 A91-37428
- Astrophysics and cosmology confront the 17-keV neutrino p 240 A91-43291
- Primordial nucleosynthesis redux p 240 A91-45907
- Constraints from primordial nucleosynthesis on the mass of the tau neutrino p 240 A91-46543
- NUCLEAR POWER REACTORS**
- Key issues in space nuclear power
[NASA-TM-103656] p 71 N91-19179
- Effects of dust accumulation and removal on radiators surfaces on Mars
[NASA-TM-103704] p 72 N91-20204
- NUCLEAR PROPULSION**
- Nuclear power systems for lunar and Mars exploration
[IAF PAPER 90-200] p 51 A91-13868
- Nuclear technology and the space exploration missions p 53 A91-37939
- The rationale/benefits of nuclear thermal rocket propulsion for NASA's lunar space transportation system
[AIAA PAPER 91-2052] p 39 A91-45781
- Performance impact on nuclear thermal propulsion of piloted Mars missions with short transit times
[AIAA PAPER 91-3401] p 64 A91-52326

- Radiation dose estimates for typical piloted NTR lunar and Mars mission engine operations
[AIAA PAPER 91-3407] p 215 A91-52331
- The NASA/DOE/DOD nuclear rocket propulsion project - FY 1991 status
[AIAA PAPER 91-3413] p 64 A91-52335
- Development of nuclear fuels and materials for propulsion systems for SEI
[AIAA PAPER 91-3452] p 125 A91-52362
- An overview of tested and analyzed NTP concepts
[AIAA PAPER 91-3503] p 65 A91-52400
- Nuclear Thermal Propulsion technology - Summary of FY 1991 Interagency panel planning
[AIAA PAPER 91-3631] p 66 A91-52495
- Vision-21: Space Travel for the Next Millennium
[NASA-CP-10059] p 40 N91-22139
- Nuclear rocket propulsion. NASA plans and progress, FY 1991
[NASA-TM-104455] p 77 N91-25179
- NUCLEAR REACTOR CONTROL**
- High temperature electronics p 144 N91-20101
- NUCLEAR REACTORS**
- Preliminary assessment of the power requirements of a manned rover for Mars missions p 41 A91-27702
- Trade studies for nuclear space power systems
[AIAA PAPER 91-3518] p 65 A91-52413
- Lunar electric power systems utilizing the SP-100 reactor coupled to dynamic conversion systems
[AIAA PAPER 91-3520] p 208 A91-52415
- Historical perspectives - The role of the NASA Lewis Research Center in the national space nuclear power programs
[AIAA PAPER 91-3462] p 242 A91-53713
- Space reactor/Stirling cycle systems for high power lunar application
[NASA-TM-103698] p 40 N91-19112
- Vision-21: Space Travel for the Next Millennium
[NASA-CP-10059] p 40 N91-22139
- A reliability and mass perspective of SP-100 Stirling cycle lunar-base powerplant designs
[NASA-TM-103736] p 212 N91-26592
- Historical perspectives: The role of the NASA Lewis Research Center in the national space nuclear power programs
[NASA-TM-105196] p 243 N91-29138
- NUCLEAR ROCKET ENGINES**
- The rationale/benefits of nuclear thermal rocket propulsion for NASA's lunar space transportation system
[AIAA PAPER 91-2052] p 39 A91-45781
- The NASA/DOE/DOD nuclear rocket propulsion project - FY 1991 status
[AIAA PAPER 91-3413] p 64 A91-52335
- NTR vehicle commonality assessment for piloted lunar and Mars missions
[AIAA PAPER 91-3575] p 66 A91-52448
- Computational fluid dynamics studies of nuclear rocket performance
[AIAA PAPER 91-3577] p 66 A91-52450
- Analytical study of nozzle performance for nuclear thermal rockets
[AIAA PAPER 91-3578] p 66 A91-52451
- Nuclear Thermal Propulsion technology - Summary of FY 1991 Interagency panel planning
[AIAA PAPER 91-3631] p 66 A91-52495
- Nuclear rocket propulsion. NASA plans and progress, FY 1991
[NASA-TM-104455] p 77 N91-25179
- NUMERICAL ANALYSIS**
- Increased heat transfer to a cylindrical leading edge due to spanwise variations in the freestream velocity
[AIAA PAPER 91-1739] p 155 A91-43623
- A numerical and experimental analysis of reactor performance and deposition rates for CVD on monofilaments
[NASA-TM-103631] p 130 N91-14500
- Increased heat transfer to a cylindrical leading edge due to spanwise variations in the freestream velocity
[NASA-TM-104464] p 100 N91-24359
- Institute for Computational Mechanics in Propulsion (ICOMP)
[NASA-TM-103790] p 222 N91-24818
- A critical comparison of two-equation turbulence models
[NASA-TM-105237] p 169 N91-31597
- NUMERICAL FLOW VISUALIZATION**
- Simulation of three-dimensional liquid sloshing flows using a strongly implicit calculation procedure
[AIAA PAPER 91-1661] p 153 A91-42549
- Flow visualization and computational studies of a reverse flow circular combustor p 157 A91-48966
- Ground-based PIV and numerical flow visualization results from the surface tension driven convection experiment
[NASA-TM-105172] p 178 N91-30491

NUMERICAL INTEGRATION

- From differential to difference equations for first order ODEs
[NASA-TM-104530] p 222 N91-27886
- Exponential integration algorithms applied to viscoplasticity
[NASA-TM-104461] p 223 N91-27901

NUMERICAL STABILITY

- The L sub 1 finite element method for pure convection problems
[NASA-TM-103773] p 222 N91-24817

O

OBLIQUE SHOCK WAVES

- Heat transfer, velocity-temperature correlation, and turbulent shear stress from Navier-Stokes computations of shock wave/turbulent boundary layer interaction flows
p 163 N91-21085

OILS

- Thermocapillary migration of liquid droplets in a temperature gradient in a density matched system
p 153 A91-41132
- Quantifying oil filtration effects on bearing life
[NASA-TM-104350] p 186 N91-23512

ON-LINE SYSTEMS

- An expert system to perform on-line controller restructuring for abrupt model changes
p 36 A91-29466
- An expert system to perform on-line controller tuning
p 219 A91-30171
- Automating security monitoring and analysis for Space Station Freedom's electric power system
p 219 A91-37975

OPEN CIRCUIT VOLTAGE

- Key factors limiting the open circuit voltage of $n(+)$ pp(+) indium phosphide solar cells
p 139 A91-41929
- Key factors limiting the open circuit voltage of $n(+)$ pp(+) indium phosphide solar cells
p 209 N91-19206
- Effect of dislocations on the open-circuit voltage, short-circuit current and efficiency of heteroepitaxial indium phosphide solar cells
[NASA-TM-103762] p 144 N91-19354
- Comparative modeling of InP solar cell structures
p 83 N91-30232

OPERATING TEMPERATURE

- NDE standards for high temperature materials
[NASA-TM-103761] p 193 N91-19464

OPERATORS (PERSONNEL)

- Tuning maps for setpoint changes and load disturbance upsets in a three capacity process under multivariable control
[NASA-TM-104419] p 220 N91-31876

OPTICAL COMMUNICATION

- A comparison of optical technologies for a high data rate Mars link
[AIAA PAPER 91-3469] p 45 A91-52377
- Quaternary pulse position modulation electronics for free-space laser communications
[AIAA PAPER 91-3471] p 133 A91-53702
- Quaternary pulse position modulation electronics for free-space laser communications
[NASA-TM-104502] p 135 N91-29405
- Optical Multiple Access Network (OMAN) for advanced processing satellite applications
[NASA-TM-105167] p 135 N91-29431

OPTICAL EQUIPMENT

- Diamondlike carbon applications in infrared optics and microelectronics
p 230 N91-18306
- Research and development of optical measurement techniques for aerospace propulsion research: A NASA Lewis Research Center perspective
[NASA-TM-104418] p 178 N91-27511

OPTICAL FIBERS

- Compensation for effects of ambient temperature on rare-earth doped fiber optic thermometer
p 170 A91-19582
- Lag compensation of optical fibers or thermocouples to achieve waveform fidelity in dynamic gas pyrometry
p 174 A91-54388
- Fiber-optic-based controls
p 230 N91-20102

OPTICAL MATERIALS

- Diamondlike carbon as a moisture barrier and antireflecting coating on optical materials
p 119 N91-18302

OPTICAL MEASUREMENT

- LN2 spray droplet size measurement via ensemble diffraction technique
[AIAA PAPER 91-1381] p 129 A91-44336
- Optical measurement of unducted fan flutter
[NASA-TM-103285] p 27 N91-15174
- Optical measurement of propeller blade deflections in a spin facility
[NASA-TM-103115] p 12 N91-17002

- LN2 spray droplet size measurement via ensemble diffraction technique
[NASA-TM-104443] p 131 N91-24470

- Research and development of optical measurement techniques for aerospace propulsion research: A NASA Lewis Research Center perspective
[NASA-TM-104418] p 178 N91-27511

OPTICAL MEASURING INSTRUMENTS

- Optical measurement of unducted fan blade deflections
[ASME PAPER 89-GT-298] p 170 A91-13046
- Compensation for effects of ambient temperature on rare-earth doped fiber optic thermometer
p 170 A91-19582
- Use of rotating pinholes and reticles for calibration of cloud droplet instrumentation
p 171 A91-30371
- Fiber-optic-based controls
p 230 N91-20102
- Optical inspection of space-propulsion components using an injection seeded Nd:YAG laser system
p 179 N91-24320

OPTICAL PROPERTIES

- Ellipsometric study of YBaCuO(7-x) laser ablated and co-evaporated films
p 233 A91-53235
- Ion beam textured and coated surfaces experiment (IBEX)
p 122 N91-25040
- Relationship of optical coating on thermal radiation characteristics of nonisothermal cylindrical enclosures
[NASA-TM-104408] p 168 N91-30461

OPTICAL PUMPING

- An experimental apparatus for measuring surface resistance in the submillimeter-wavelength region
p 174 A91-54390

OPTICAL THICKNESS

- Solar radiation on Mars: Update 1990
[NASA-TM-103623] p 242 N91-15117

OPTIMAL CONTROL

- Neural network application to aircraft control system design
[AIAA PAPER 91-2715] p 36 A91-49676
- A statistical rain attenuation prediction model with application to the advanced communication technology satellite project. 3: A stochastic rain fade control algorithm for satellite link power via non linear Markov filtering theory
[NASA-TM-100243] p 134 N91-22494
- Neural network application to aircraft control system design
[NASA-TM-105151] p 37 N91-27167

OPTIMIZATION

- An integrated methodology for optimizing the passive damping of composite structures
p 195 A91-19048
- Concurrent material-fabrication optimization of metal-matrix laminates under thermo-mechanical loading
[AIAA PAPER 91-1044] p 129 A91-31842
- Modeling and optimization of a regenerative fuel cell system using the ASPEN process simulator
p 206 A91-38177
- Composite laminate tailoring with probabilistic constraints and loads
p 198 A91-38754
- Maximum life spur gear design
[AIAA PAPER 91-2021] p 181 A91-41682
- Performance and optimization of a 'derated' ion thruster for auxiliary propulsion
[AIAA PAPER 91-2350] p 62 A91-45809
- Concurrent micromechanical tailoring and fabrication process optimization for metal-matrix composites
[NASA-TM-103670] p 98 N91-19237
- ALPS: A Linear Program Solver
[NASA-TM-104347] p 216 N91-20765
- Applications of artificial neural nets in structural mechanics
[NASA-TM-102420] p 202 N91-21559
- RSM 1.0 user's guide: A resupply scheduler using integer optimization
[NASA-TM-104380] p 217 N91-22766
- Adaptation of NASA technology for the optimization of orthopedic knee implants
p 215 N91-23032
- Maximum life spur gear design
[NASA-TM-104361] p 187 N91-23514
- Arjet nozzle area ratio effects
p 75 N91-24271

OPTOELECTRONIC DEVICES

- A fiber-optic current sensor for aerospace applications
p 171 A91-23005
- Optical control of microwave devices --- Book
p 136 A91-27331
- Performance of a 300 Mbps 1:16 serial/parallel optoelectronic receiver module
p 141 A91-51146
- Growth kinetics of physical vapor transport processes: Crystal growth of the optoelectronic material mercurous chloride
[NASA-TM-103788] p 128 N91-19320
- Fiber-optic sensors for aerospace electrical measurements: An update
[NASA-TM-104454] p 177 N91-25381

ORBIT TRANSFER VEHICLES

- Mach 6.5 air induction system design for the Beta II Two-Stage-to-Orbit booster vehicle
[AIAA PAPER 91-3196] p 43 A91-54099

ORGANIC CHEMISTRY

- Substituted 1,1,1-triaryl-2,2,2-trifluoroethanes and processes for their synthesis
[NASA-CASE-LEW-14345-3] p 89 N91-17141

ORGANIC SEMICONDUCTORS

- A review of properties and potential aerospace applications of electrically conducting polymers
p 113 A91-14409

ORIENTATION

- Elastic response of (001)-oriented PWA 1480 single crystal - The influence of secondary orientation
[SAE PAPER 911111] p 110 A91-53555
- Elastic response of zone axis (001)-oriented PWA 1480 single crystal: The influence of secondary orientation
[NASA-TM-103782] p 202 N91-21558

ORIFICE FLOW

- Three-dimensional calculation of the mixing of radial jets from slanted slots with a reactive cylindrical crossflow
[AIAA PAPER 91-2081] p 24 A91-45782
- Experimental study of cross-stream mixing in a cylindrical duct
[NASA-TM-105180] p 34 N91-29187

ORTHOPEDICS

- Adaptation of NASA technology for the optimization of orthopedic knee implants
p 215 N91-23032

ORTHOTROPIC PLATES

- Low velocity impact analysis with NASTRAN
p 198 A91-48865
- Low velocity impact analysis with NASTRAN
[NASA-TM-103169] p 95 N91-14426

OSCILLATING FLOW

- Stability of an oscillated fluid with a uniform density gradient
p 147 A91-12971
- The aerodynamics of an oscillating cascade in a compressible flow field
[ASME PAPER 89-GT-271] p 1 A91-13047
- Interfacial dynamics of two liquids under an oscillating gravitational field
p 148 A91-16062
- On the continuous spectra of the compressible boundary layer stability equations
p 150 A91-31342
- Further two-dimensional code development for Stirling space engine components
p 56 A91-38184
- Heat transfer in oscillating flows
p 152 A91-38698
- A 2-D oscillating flow analysis in Stirling engine heat exchangers
[NASA-TM-103781] p 161 N91-19375

OSCILLATIONS

- Oscillating cascade aerodynamics by an experimental influence coefficient technique
p 1 A91-10339
- Numerical analysis of flow through oscillating cascade sections
p 9 N91-10884
- A laser velocimeter investigation of the normal shock-wave boundary layer interaction
[NASA-TM-105201] p 169 N91-32440

OSCILLATORS

- Near-field antenna testing using the Hewlett Packard 8510 automated network analyzer
[NASA-TM-103699] p 144 N91-20393

OUTGASSING

- Process for HIP canning of composites
[NASA-CASE-LEW-14990-1-CU] p 96 N91-17145

OXIDATION

- Hydrogen-silicon carbide interactions
p 114 A91-28783
- Application of oxidation to the structural characterization of SiC epitaxial films
p 233 A91-45881
- Crack healing in silicon nitride due to oxidation
p 118 A91-56982
- High temperature cyclic oxidation data. Part 1: Turbine alloys
[NASA-TM-83665] p 110 N91-10149
- High-temperature cyclic oxidation data. Part 2: Turbine alloys
[NASA-TM-101468] p 110 N91-10150
- Vinyl capped addition polyimides
[NASA-CASE-LEW-15027-1] p 118 N91-13566
- Investigation of anodic and chemical oxides grown on p-type InP with applications to surface passivation for $n(+)$ -p solar cell fabrication
p 210 N91-19208
- Atomic oxygen interaction with solar array blankets at protective coating defect sites
p 211 N91-20732
- A comparison of fiber effects on polymer matrix composite oxidation
[NASA-TM-104416] p 101 N91-24361
- Atomic oxygen interactions with FEP Teflon and silicones on LDEF
p 122 N91-25029
- Oxidation resistant coatings for titanium alloys and titanium alloy matrix composites
[NASA-CASE-LEW-15155-1] p 122 N91-26375
- Sliding wear of self-mated Al₂O₃-SiC whisker reinforced composites at 23-1200 C
[NASA-TM-104490] p 90 N91-27221

- Low cost, formable, high T(sub c) superconducting wire
[NASA-CASE-LEW-14676-1] p 147 N91-31529
Near-edge study of gold-substituted YBa₂Cu₃O₇(δ)
[NASA-TM-105220] p 237 N91-31977
- OXIDATION RESISTANCE**
Oxidation behavior of cubic phases formed by alloying Al₃Ti with Cr and Mn p 108 A91-27849
A resistance strain gage with repeatable apparent strain to 800 C p 198 A91-48899
Oxidation instability of SiC and Si₃N₄ following thermal excursions p 118 A91-57059
Reinforcements: The key to high performance composite materials
[NASA-TM-103230] p 96 N91-15329
Effect of fiber reinforcements on thermo-oxidative stability and mechanical properties of polymer matrix composites
[NASA-TM-103648] p 98 N91-19234
The effect of atomic oxygen on polysiloxane-polyimide for spacecraft applications in low Earth orbit p 229 N91-20735
Long term isothermal aging and thermal analysis of N-CYCOP polyimides
[NASA-TM-104341] p 122 N91-25286
Oxidation resistant coatings for titanium alloys and titanium alloy matrix composites
[NASA-CASE-LEW-15155-1] p 122 N91-26375
- OXIDATION-REDUCTION REACTIONS**
Ultrasonic evaluation of oxidation and reduction effects on the elastic behavior and global microstructure of YBa₂Cu₃O_{7-x}
[NASA-TM-104529] p 194 N91-27575
The Au cathode in the system Li₂CO₃-CO₂-CO at 800 to 900 C p 213 N91-32551
- OXIDE FILMS**
Application of oxidation to the structural characterization of SiC epitaxial films p 233 A91-45881
- OXIDES**
Preparation of 110K (Bi, Pb)-Sr-Ca-Cu-O superconductor from glass precursor p 232 A91-35449
Investigation of anodic and chemical oxides grown on p-type InP with applications to surface passivation for n(+)-p solar cell fabrication p 210 N91-19208
Pretreatment of lubricated surfaces with sputtered cadmium oxide
[NASA-CASE-LEW-14474-1] p 123 N91-28423
- OXIDIZERS**
A model for the Space Shuttle Main Engine High Pressure Oxidizer Turbopump shaft seal system p 180 A91-30640
A model for the space shuttle main engine high pressure oxidizer turbopump shaft seal system
[NASA-TM-103697] p 184 N91-20489
- OXYGEN**
High temperature reactions of ceramics and metals with chlorine and oxygen p 105 A91-20219
Two-dimensional imaging of molecular hydrogen in H₂-air diffusion flames using two-photon laser-induced fluorescence p 124 A91-34369
Cooling of in-situ propellant rocket engines for Mars mission
[NASA-TM-103729] p 72 N91-21233
Atomic oxygen undercutting of LDEF aluminized Kapton multilayer insulation p 229 N91-25027
- OXYGEN ATOMS**
Undercutting of defects in thin film protective coatings on polymer surfaces exposed to atomic oxygen p 115 A91-41516
Evaluation of thermal control coatings for use on solar dynamic radiators in low earth orbit
[AIAA PAPER 91-1327] p 58 A91-43397
Atomic oxygen undercutting of defects on SiO₂ protected polyimide solar array blankets p 116 A91-49803
The effect of atomic oxygen on altered and coated Kapton surfaces for spacecraft applications in low earth orbit p 116 A91-49804
Atomic oxygen effects on refractory materials p 88 A91-49809
Vacuum ultraviolet radiation and thermal cycling effects on atomic oxygen protective photovoltaic array blanket materials p 116 A91-49812
Graphite fluoride fibers and their applications in the space industry
[NASA-TM-103265] p 88 N91-11062
Low Earth orbital atomic oxygen and ultraviolet radiation effects on polymers
[NASA-TM-103711] p 119 N91-19294
Atomic oxygen interaction with solar array blankets at protective coating defect sites p 211 N91-20732
The effect of atomic oxygen on polysiloxane-polyimide for spacecraft applications in low Earth orbit p 229 N91-20735

- Evaluation of thermal control coatings for use on solar dynamic radiators in low Earth orbit
[NASA-TM-104335] p 73 N91-22367
Atomic oxygen undercutting of LDEF aluminized Kapton multilayer insulation p 229 N91-25027
Atomic oxygen interactions with FEP Teflon and silicones on LDEF p 122 N91-25029
Low Earth orbital atomic oxygen micrometeoroid, and debris interactions with photovoltaic arrays p 84 N91-30248

OXYGEN PRODUCTION

- Production and use of metals and oxygen for lunar propulsion
[AIAA PAPER 91-3481] p 125 A91-53711
Chemical approaches to carbon dioxide utilization for manned Mars missions p 241 N91-26073
Production and use of metals and oxygen for lunar propulsion
[NASA-TM-105195] p 81 N91-29222

OXYGEN-HYDROCARBON ROCKET ENGINES

- In-situ propellant rocket engines for Mars missions ascent vehicle
[AIAA PAPER 91-2445] p 60 A91-44247
Liquid oxygen cooling of hydrocarbon fueled rocket thrust chambers p 63 A91-52309
Hydrocarbon-fuel/combustion-chamber-liner materials compatibility
[NASA-CR-187104] p 121 N91-21307
In-situ propellant rocket engines for Mars mission ascent vehicle
[NASA-TM-104429] p 76 N91-24305

OXYNITRIDES

- Evidence from transmission electron microscopy for an oxynitride layer in oxidized Si₃N₄ p 118 A91-57058

P**P-N JUNCTIONS**

- High-voltage 6H-SiC p-n junction diodes p 142 A91-54746
Silicon carbide, a semiconductor for space power electronics
[NASA-TM-103655] p 234 N91-14850
Surface and implantation effects on p-n junctions p 234 N91-18299
A comparative study of p(+)-n and n(+)-p InP solar cells made by a closed ampoule diffusion p 121 N91-30206
Comparative modeling of InP solar cell structures p 83 N91-30232

P-TYPE SEMICONDUCTORS

- Properties of insulator interfaces with p-HgCdTe p 235 N91-18300
Surface electrons in inverted layers of p-HgCdTe p 235 N91-18301

PACKINGS (SEALS)

- PM200/PS200: Self-lubricating bearing and seal materials for applications to 900 C
[NASA-TM-103776] p 190 N91-30539

PAIN SENSITIVITY

- An assessment of the Space Station Freedom program's leakage current requirement
[NASA-CR-187077] p 215 N91-20630

PAINTS

- Evaluation of thermal control coatings for use on solar dynamic radiators in low earth orbit
[AIAA PAPER 91-1327] p 58 A91-43397
Evaluation of thermal control coatings for use on solar dynamic radiators in low Earth orbit
[NASA-TM-104335] p 73 N91-22367

PALLADIUM COMPOUNDS

- PdCr based high temperature static strain gage
[AIAA PAPER 90-5236] p 170 A91-14462

PANEL METHOD (FLUID DYNAMICS)

- Evaluation of panel code predictions with experimental results of inlet performance for a 17-inch ducted prop/fan simulator operating at Mach 0.2
[AIAA PAPER 91-3354] p 7 A91-45819
Evaluation of panel code predictions with experimental results of inlet performance for a 17-inch ducted prop/fan simulator operating at Mach 0.2
[NASA-TM-104428] p 17 N91-25106

PANELS

- Relationship between voids and interlaminar shear strength of polymer matrix composites
[NASA-TM-103643] p 95 N91-13495

PARABOLIC REFLECTORS

- Status of the advanced Stirling conversion system project for 25 kW dish Stirling applications
[NASA-TM-104528] p 238 N91-31023

PARABOLOID MIRRORS

- Solar powered Stirling cycle electrical generator p 211 N91-23054

PARALLEL COMPUTERS

- Parallel computing using a Lagrangian formulation
[NASA-TM-104446] p 215 N91-24745

PARALLEL FLOW

- Nonlinear spatial evolution of externally excited instability waves in free shear layers p 152 A91-38705

PARALLEL PROCESSING (COMPUTERS)

- Parallel algorithms for boundary value problems p 221 A91-31175
Programming probabilistic structural analysis for parallel processing computer
[AIAA PAPER 91-0920] p 196 A91-31957
Numerical propulsion system simulation - An interdisciplinary approach
[AIAA PAPER 91-3554] p 66 A91-53706
Enhancing aeropropulsion research with high-speed interactive computing p 217 A91-56129
Shared direct memory access on the Explorer 2-LX
[NASA-TM-103289] p 216 N91-12215
Efficient computation of aerodynamic influence coefficients for aeroelastic analysis on a transputer network
[NASA-TM-103671] p 216 N91-20748
Application of artificial neural networks to composite ply micromechanics
[NASA-TM-104365] p 100 N91-24345
Parallel computing using a Lagrangian formulation
[NASA-TM-104446] p 215 N91-24745
Enhancing aeropropulsion research with high-speed interactive computing p 218 N91-24796
Numerical propulsion system simulation: An interdisciplinary approach
[NASA-TM-105181] p 81 N91-29221

PARALLEL PROGRAMMING

- Programming probabilistic structural analysis for parallel processing computer
[AIAA PAPER 91-0920] p 196 A91-31957

PARAMETER IDENTIFICATION

- A distributed fault-detection and diagnosis system using on-line parameter estimation
[NASA-TM-104433] p 220 N91-25696

PARAMETERIZATION

- Effect of emitter parameter variation on the performance of heteroepitaxial indium phosphide solar cells p 140 A91-42003
Effect of emitter parameter variation on the performance of heteroepitaxial indium phosphide solar cells
[NASA-TM-103619] p 70 N91-15306
Alpha-canonical form representation of the open loop dynamics of the Space Shuttle main engine
[NASA-TM-104422] p 131 N91-24469

PARTIAL DIFFERENTIAL EQUATIONS

- Mappings and accuracy for Chebyshev pseudo-spectral approximations
[NASA-TM-103630] p 221 N91-14781
The method of lines in analyzing solids containing cracks
[NASA-TM-103626] p 201 N91-19477
On the anomaly of velocity-pressure decoupling in collocated mesh solutions
[NASA-TM-103769] p 164 N91-21448

PARTICLE INTERACTIONS

- Natural inflation with pseudo Nambu-Goldstone bosons p 239 A91-19545

PARTICLE LADEN JETS

- Particle image fields and partial coherence p 171 A91-19604

PARTICLE MASS

- Comment on 'Negative matter propulsion' p 52 A91-37424
Constraints from primordial nucleosynthesis on the mass of the tau neutrino p 240 A91-46543

PARTICLE MOTION

- Newtonian mechanics of a many-particle assembly coupled to an external body potential p 237 A91-19495

- Two-dimensional particle displacement tracking in particle imaging velocimetry p 172 A91-38498

- Software manual for operating particle displacement tracking data acquisition and reduction system
[NASA-TM-103720] p 176 N91-20453

- Particle displacement tracking applied to air flows
[NASA-TM-104481] p 177 N91-25387

PARTICLE THEORY

- Inflationary axion cosmology p 239 A91-20491

PARTICLE TRACKS

- Particle displacement tracking for PIV
[NASA-TM-103288] p 175 N91-10271

PARTICLE TRAJECTORIES

- Experimental water droplet impingement data on modern aircraft surfaces
[AIAA PAPER 91-0445] p 2 A91-21493

- Particle image velocimetry for the surface tension driven convection experiment using a particle displacement tracking technique
[NASA-TM-104482] p 177 N91-25382
- Particle displacement tracking applied to air flows
[NASA-TM-104481] p 177 N91-25387
- PARTICULATE REINFORCED COMPOSITES**
Compression behavior of TiB₂-particulate-reinforced composites of Al₂₂Fe₃Ti₈ p 91 A91-28014
- PARTICULATES**
Particle nonuniformity effects on particle cloud flames in low gravity
[AIAA PAPER 91-0718] p 104 A91-19431
- Particle cloud flames in acoustic fields
p 105 A91-20589
- Low-density, high-strength intermetallic matrix composites by XD (trademark) synthesis
[NASA-TM-103724] p 97 N91-19233
- PARTITIONS (MATHEMATICS)**
Partitioning methods for global controllers
p 219 A91-30043
- A method for partitioning centralized controllers
[NASA-TM-4276] p 36 N91-20133
- PASSIVITY**
New directions in InP solar cell research
p 206 A91-38022
- Surface electrons in inverted layers of p-HgCdTe
p 235 N91-18301
- Radiation resistance of thin-film solar cells for space photovoltaic power
[NASA-TM-103715] p 71 N91-19176
- A comparative study of performance parameters of n(+)-p InP solar cells made by closed-ampoule sulfur diffusion into Cd- and Zn-doped p-type InP substrates
p 210 N91-19209
- PAYLOADS**
ATDRS payload technology R & D p 45 A91-53188
- Metalized propellants for the human exploration of Mars
[NASA-TP-3062] p 69 N91-11800
- Lunar missions using chemical propulsion: System design issues
[NASA-TP-3065] p 70 N91-15308
- PECULIAR STARS**
Coherent peculiar velocities and periodic redshifts
p 239 A91-20430
- PEELING**
Peeled film GaAs solar cell development
p 139 A91-41889
- PENETRATION**
Determination of surface resistance and magnetic penetration depth of superconducting YBa₂Cu₃O₇(δ) thin films by microwave power transmission measurements
p 138 A91-36060
- Determination of surface resistance and magnetic penetration depth of superconducting YBa₂Cu₃O₇(δ) thin films by microwave power transmission measurements
[NASA-TM-103616] p 234 N91-10780
- On protection of Freedom's solar dynamic radiator from the orbital debris environment. Part 2: Further testing and analyses
[NASA-TM-104514] p 84 N91-30265
- PERFLUORO COMPOUNDS**
Determination of the thermal stability of fluids by tensimetry - Instrumentation and procedure
p 113 A91-13435
- PERFORMANCE PREDICTION**
Modeling and optimization of a regenerative fuel cell system using the ASPEN process simulator
p 206 A91-38177
- Key factors limiting the open circuit voltage of n(+)-pp(+)-indium phosphide solar cells
p 139 A91-41929
- Transient flow thrust prediction for an ejector propulsion concept
p 24 A91-45326
- MPD thruster technology
[AIAA PAPER 91-3568] p 65 A91-52444
- Key factors limiting the open circuit voltage of n(+)-pp(+)-indium phosphide solar cells
p 209 N91-19206
- Comparison of a quasi-3D analysis and experimental performance for three compact radial turbines
[NASA-TM-105155] p 35 N91-30142
- The effects of lunar dust accumulation on the performance of photovoltaic arrays
p 83 N91-30238
- PERFORMANCE TESTS**
Flow studies in close-coupled ventral nozzles for STOVL aircraft
[SAE PAPER 901033] p 2 A91-21242
- An experimental study of high T_c superconducting microstrip transmission lines at 35 GHz and the effect of film morphology
[NASA-TM-103633] p 133 N91-11988
- A 5-kW xenon ion thruster lifetest
[NASA-TM-103191] p 72 N91-19180
- Thermal annealing of GaAs concentrator solar cells
p 208 N91-19195
- Effects of proton irradiation on the performance of InP/GaAs solar cells
p 209 N91-19205
- Near-field antenna testing using the Hewlett Packard 8510 automated network analyzer
[NASA-TM-103699] p 144 N91-20393
- Industrial applications of graphite fluoride fibers
p 100 N91-23040
- Concentrator testing using projected images
[NASA-TM-104349] p 79 N91-27204
- Test and evaluation of load converter topologies used in the Space Station Freedom Power Management and distribution DC test bed
[NASA-TM-105217] p 85 N91-30267
- PERMANENT MAGNETS**
Induction motor control
p 137 A91-30893
- Makeup and uses of a basic magnet laboratory for characterizing high-temperature permanent magnets
[NASA-TM-104508] p 146 N91-30427
- PERTURBATION THEORY**
Aeroelastic modal characteristics of mistuned blade assemblies - Mode localization and loss of eigenstructure
[AIAA PAPER 91-1218] p 196 A91-32032
- Aeroelastic modal characteristics of mistuned blade assemblies: Mode localization and loss of eigenstructure
[NASA-TM-104519] p 205 N91-27591
- PHASE CHANGE MATERIALS**
A PCM/forced convection conjugate transient analysis of energy storage systems with annular and countercurrent flows
p 150 A91-27166
- Scaling analysis applied to the NORVEX code development and thermal energy flight experiment
[AIAA PAPER 91-1420] p 155 A91-44337
- Scaling analysis applied to the NORVEX code development and thermal energy flight experiment
[NASA-TM-104462] p 166 N91-24549
- Full-size solar dynamic heat receiver thermal-vacuum tests
[NASA-TM-104486] p 78 N91-25184
- Ground test program for a full-size solar dynamic heat receiver
[NASA-TM-104485] p 79 N91-27209
- PHASE CONTROL**
A high-efficiency ferruleless coupled-cavity traveling-wave tube with phase-adjusted taper
p 136 A91-25078
- Fiber optic phase stepping system for interferometry
p 171 A91-28968
- PHASE DIAGRAMS**
Thermochemical analysis of the silicon carbide-alumina reaction with reference to liquid-phase sintering of silicon carbide
p 114 A91-26506
- PHASE SHIFT CIRCUITS**
Power electronics for low power arcjets
[AIAA PAPER 91-1991] p 60 A91-45779
- Power electronics for low power arcjets
[NASA-TM-104459] p 77 N91-25172
- Comparative study of bolometric and non-bolometric switching elements for microwave phase shifters
[NASA-TM-104435] p 145 N91-25320
- PHASE STABILITY (MATERIALS)**
Reaction of beta-phase Ni-Al alloys with CrB₂
p 92 A91-49943
- PHASE TRANSFORMATIONS**
Tensile properties of HA 230 and HA 188 after 400 and 2500 hour exposures to LiF-22CaF₂ and vacuum at 1093 K
p 107 A91-11624
- Temperature-dependent indentation behavior of transformation-toughened zirconia-based ceramics
p 114 A91-28767
- First-order inflation --- in cosmology
p 240 A91-37444
- Rapid solidification of polymorphic transition metals induced by nanosecond laser pulses
p 109 A91-46520
- Constitution of pseudobinary hypoeutectic beta-NiAl + alpha-V alloys
p 109 A91-48509
- A finite element model of conduction, convection, and phase change near a solid/melt interface
[NASA-TM-103721] p 162 N91-20417
- Crystallization and characterization of Y₂O₃-SiO₂ glasses
p 237 N91-31962
- Raman spectral observation of a new phase observed in nickel electrodes cycled to failure
p 214 N91-32556
- PHASED ARRAYS**
Bit error rate testing of fiber optic data links for MMIC-based phased array antennas
p 131 A91-24950
- Design of an optically controlled Ka-band GaAs MMIC phased-array antenna
p 132 A91-24951
- Performance of a 300 Mbps 1:16 serial/parallel optoelectronic receiver module
p 141 A91-51146
- Ka-band MMIC microstrip array for high rate communications
[AIAA PAPER 91-3421] p 132 A91-52341
- Coplanar waveguide feeds for phased array antennas
[AIAA PAPER 91-3422] p 141 A91-52342
- Design of an inflatable, optically controlled and fed, phased array antenna
[AIAA PAPER 91-3470] p 132 A91-52378
- ATDRS payload technology R & D p 45 A91-53188
- High temperature superconductor analog electronics for millimeter-wavelength communications
[AIAA PAPER 91-3592] p 233 A91-53707
- Applications of thin film technology toward a low-mass solar power satellite
p 235 N91-22179
- System-Level Integrated Circuit (SLIC) development for phased array antenna applications
[NASA-TM-104392] p 134 N91-23354
- Ka-band MMIC microstrip array for high rate communications
[NASA-TM-104500] p 135 N91-27437
- Coplanar waveguide feeds for phased array antennas
[NASA-TM-104467] p 146 N91-27477
- High temperature superconductor analog electronics for millimeter-wavelength communications
[NASA-TM-105184] p 237 N91-29982
- PHENOMENOLOGY**
YBCO superconducting ring resonators at millimeter-wave frequencies
p 142 A91-54532
- PHOTOCONDUCTIVITY**
Grooved surfaces on InP
p 213 N91-30208
- PHOTODIODES**
Optical techniques for determination of normal shock position in supersonic flows for aerospace applications
p 174 A91-55530
- Surface and implantation effects on p-n junctions
p 234 N91-18299
- PHOTOELASTICITY**
Fiber optic photoelastic pressure sensor for high temperature gases
p 170 A91-19577
- Photoelastic transducer for high-temperature applications
p 174 A91-55533
- PHOTOELECTROCHEMISTRY**
Material processing with hydrogen and carbon monoxide on Mars
[NASA-TM-104405] p 211 N91-23616
- PHOTOELECTRON SPECTROSCOPY**
X-ray photoelectron and mass spectroscopic study of electron irradiation and thermal stability of polytetrafluoroethylene
p 113 A91-16138
- Inverse photoelectron spectrometer with magnetically focused electron gun
p 172 A91-42849
- Uses of Auger and x ray photoelectron spectroscopy in the study of adhesion and friction
[NASA-TM-103266] p 118 N91-11922
- An x ray photoelectron spectroscopy study of Au(x)In(y) alloys
[NASA-TM-103659] p 234 N91-14050
- PHOTOLITHOGRAPHY**
Photoresponse of YBa₂Cu₃O₇(δ) granular and epitaxial superconducting thin films
p 141 A91-50443
- PHOTOLUMINESCENCE**
Effect of dislocations on properties of heteroepitaxial InP solar cells
p 213 N91-30209
- PHOTOMETERS**
Optical control of microwave devices --- Book
p 136 A91-27331
- Optical measurement of propeller blade deflections in a spin facility
[NASA-TM-103115] p 12 N91-17002
- PHOTONS**
Telescope search for a 3-eV to 8-eV axion
p 239 A91-28714
- PHOTOTHERMAL CONVERSION**
Sensible heat receiver for solar dynamic space power system
[NASA-TM-104393] p 77 N91-25173
- PHOTOVOLTAIC CELLS**
Component and prototype panel testing of the mini-dome Fresnel lens photovoltaic concentrator array
p 54 A91-38023
- Design considerations for lunar base photovoltaic power systems
p 41 A91-41987
- Photovoltaic superiority for Space Station Freedom power in the 21st century
p 58 A91-42004
- Laser photovoltaic power system synergy for SEI applications
[AIAA PAPER 91-3419] p 207 A91-52339

- Design considerations for lunar base photovoltaic power systems
[NASA-TM-103642] p 241 N91-14259
- Aeolian removal of dust types from photovoltaic surfaces on Mars p 47 N91-19156
- Space Photovoltaic Research and Technology, 1989 [NASA-CP-3107] p 72 N91-19182
- Dual-purpose self-deliverable lunar surface PV electrical power system p 209 N91-19200
- Feasibility of solar power for Mars p 209 N91-19201
- Mini-dome Fresnel lens photovoltaic concentrator development p 210 N91-19219
- Effects of windblown dust on photovoltaic surface s on Mars
[NASA-TM-104448] p 78 N91-25183
- Key results of the mini-dome Fresnel lens concentrator array development program under recently completed NASA and SDIO SBIR projects p 83 N91-30223
- PHOTOVOLTAIC CONVERSION**
- An evolutionary path to satellite solar power systems p 51 A91-26063
- Power electronic applications for Space Station Freedom p 52 A91-36832
- Rapid thermal cycling of new technology solar array blanket coupons p 54 A91-38019
- Preliminary results from the Advanced Photovoltaic Experiment flight test p 39 A91-41980
- Design considerations for Mars photovoltaic power systems p 41 A91-41988
- The mini-dome Fresnel lens photovoltaic concentrator array - Current status of component and prototype panel testing p 57 A91-41989
- Space Photovoltaic Research and Technology, 1989 [NASA-CP-3107] p 72 N91-19182
- Feasibility of solar power for Mars p 209 N91-19201
- Applications of thin film technology toward a low-mass solar power satellite p 235 N91-22179
- Space Photovoltaic Research and Technology Conference [NASA-CP-3121] p 82 N91-30203
- PHOTOVOLTAIC EFFECT**
- Reappraisal of solid selective emitters --- for thermovoltaic energy conversion p 207 A91-41999
- Reappraisal of solid selective emitters [NASA-TM-103290] p 69 N91-11801
- Radiation resistance of thin-film solar cells for space photovoltaic power [NASA-TM-103715] p 71 N91-19176
- PHYSICAL PROPERTIES**
- A review of properties and potential aerospace applications of electrically conducting polymers p 113 A91-14409
- PIEZOELECTRIC CERAMICS**
- Use of piezoelectric actuators in active vibration control of rotating machinery p 179 A91-14400
- PILOTLESS AIRCRAFT**
- Microwave beam powered Mars airplane p 52 A91-37931
- PIPE FLOW**
- Verification of the Proteus two-dimensional Navier-Stokes code for flat plate and pipe flows [AIAA PAPER 91-2013] p 153 A91-41678
- Unstable viscous wall modes in rotating pipe flow [AIAA PAPER 91-1801] p 154 A91-42599
- Analysis of the one-dimensional transient compressible vapor flow in heat pipes p 157 A91-47735
- Turbulent fluid motion. Part 1: The phenomenon of fluid turbulence [NASA-TM-103723] p 162 N91-20445
- Verification of the proteus two-dimensional Navier-Stokes code for flat plate and pipe flows [NASA-TM-105160] p 168 N91-30462
- PIPES (TUBES)**
- Axial-torsional fatigue: A study of tubular specimen thickness effects [NASA-TM-103637] p 200 N91-14632
- New method of making advanced tube-bundle rocket thrust chambers [NASA-TM-103617] p 70 N91-15301
- PISTON ENGINES**
- Lewis aeropropulsion technology: Remembering the past and challenging the future p 242 N91-20087
- Rotary engine technology p 30 N91-20114
- Stirling machine operating experience [NASA-TM-104487] p 212 N91-25510
- Status of the advanced Stirling conversion system project for 25 kW dish Stirling applications [NASA-TM-104528] p 238 N91-31023
- PLASTICS**
- Undercutting of defects in thin film protective coatings on polymer surfaces exposed to atomic oxygen p 115 A91-41516
- PLATES**
- Fully articulated four-point-bend loading fixture [NASA-CASE-LEW-14776-1] p 185 N91-21540
- PLATES (STRUCTURAL MEMBERS)**
- The effects of interply damping layers on the dynamic response of composite structures [NASA-TM-104497] p 103 N91-30282
- PLATINUM COMPOUNDS**
- Near-Earth asteroids: Metals occurrence, extraction, and fabrication p 241 N91-26058
- PLUG NOZZLES**
- Plug nozzles - The ultimate customer driven propulsion system --- applied to manned lunar and Martian landers [AIAA PAPER 91-2208] p 61 A91-45794
- Divergence thrust loss calculations for convergent-divergent nozzles: Extensions to the classical case [NASA-TM-105176] p 34 N91-29181
- PLUGS**
- Some preliminary results of brush seal/rotor interference effects on leakage at zero and low RPM using a tapered-plug rotor [NASA-TM-104396] p 188 N91-27559
- PLUMES**
- Experimental evaluation of resistojel thruster plume shields p 51 A91-30010
- Development of a Fabry-Perot interferometer for rocket engine plume monitoring p 171 A91-30634
- Computational analysis of underexpanded jets in the hypersonic regime p 4 A91-37421
- Numerical and experimental investigations of rarefied nozzle and plume flows of nitrogen [AIAA PAPER 91-1363] p 154 A91-43429
- Determination of alloy content from plume spectral measurements [AIAA PAPER 91-2531] p 88 A91-44284
- Pressure measurements in a low-density nozzle plume for code verification [AIAA PAPER 91-2110] p 61 A91-45783
- A preliminary characterization of applied-field MPD thruster plumes [AIAA PAPER 91-2339] p 62 A91-45798
- Investigation of the arcjet plume near field using electrostatic probes [NASA-TM-103638] p 68 N91-11060
- Investigation of the arcjet near field plume using electrostatic probes p 75 N91-24270
- Determination of alloy content from plume spectral measurements [NASA-TM-104442] p 89 N91-24341
- Pressure measurements in a low-density nozzle plume for code verification [NASA-TM-105170] p 81 N91-29228
- PNEUMATICS**
- Advanced ice protection systems test in the NASA Lewis icing research tunnel [NASA-TM-103757] p 32 N91-23183
- POLYACRYLONITRILE**
- Effect of lightning strike on bromine intercalated graphite fiber/epoxy composites [NASA-TM-104507] p 103 N91-32177
- POLYCRYSTALS**
- Electrical transport measurements on polycrystalline superconducting Y-Ba-Cu-O films p 231 A91-19820
- Temperature dependence of the elastic moduli and damping for polycrystalline LiF-22 pct CaF2 eutectic salt p 87 A91-33793
- Selective and low temperature synthesis of polycrystalline diamond p 232 A91-42170
- 1000 to 1200 K time-dependent compressive deformation of single-crystalline and polycrystalline B2 Ni-40Al p 109 A91-43670
- POLYETHYLENE TEREPHTHALATE**
- Intrinsic bond strength of metal films on polymer substrates p 88 A91-39246
- PITTING**
- Evaluation of advanced lubricants for aircraft applications using gear surface fatigue tests [AIAA PAPER 91-1907] p 181 A91-41649
- Evaluation of advanced lubricants for aircraft applications using gear surface fatigue tests [NASA-TM-104336] p 186 N91-22568
- PLANE WAVES**
- Resonant triad in boundary-layer stability. Part 1: Fully nonlinear interaction [NASA-TM-105208] p 169 N91-32458
- Resonant triad in boundary-layer stability. Part 2: Composite solution and comparison with observations [NASA-TM-105209] p 169 N91-32459
- PLANETARY BASES**
- Power system requirements and definition for lunar and Mars outposts p 52 A91-37930
- PLANETARY NEBULAE**
- The dynamic instability of adiabatic blast waves p 239 A91-26361
- PLANETARY SURFACES**
- Comparison of dynamic isotope power systems for distributed planet surface applications [NASA-TM-4303] p 81 N91-28278
- PLANETS**
- Outline of the Solar System: Activities for elementary students [NASA-TM-104965] p 241 N91-25975
- PLASMA CONDUCTIVITY**
- Leo space plasma interactions p 84 N91-30249
- PLASMA CURRENTS**
- High voltage interactions of a sounding rocket with the ambient and system-generated environments p 46 A91-23077
- PLASMA ENGINES**
- Antiproton powered propulsion with magnetically confined plasma engines p 63 A91-52313
- MPD thruster technology [AIAA PAPER 91-3568] p 65 A91-52444
- Multimegawatt electric propulsion system design considerations [NASA-TM-105152] p 87 N91-32164
- PLASMA GUNS**
- Plasma gun with coaxial powder feed and adjustable cathode [NASA-CASE-LEW-14901-1] p 231 N91-25875
- PLASMA INTERACTION EXPERIMENT**
- Leo space plasma interactions p 84 N91-30249
- PLASMA INTERACTIONS**
- Findings of the Joint Workshop on Evaluation of Impacts of Space Station Freedom Ground Configurations p 48 N91-20728
- Findings of the Joint Workshop on Evaluation of Impacts of Space Station Freedom Ground Configurations [NASA-TM-103717] p 73 N91-22370
- Leo space plasma interactions p 84 N91-30249
- PLASMA JETS**
- Energy deposition in low-power coaxial plasma thrusters p 63 A91-52311
- PLASMA POTENTIALS**
- Leo space plasma interactions p 84 N91-30249
- PLASMA PROPULSION**
- Performance and lifetime assessment of magnetoplasma dynamic arc thruster technology p 51 A91-30013
- Thrust stand for high-power electric propulsion devices p 41 A91-36239
- Anode power deposition in an applied-field segmented anode MPD thruster [AIAA PAPER 91-2343] p 59 A91-44204
- Nonequilibrium in a low power arcjet nozzle [AIAA PAPER 91-2113] p 61 A91-45784
- Numerical simulation of self-field MPD thrusters [AIAA PAPER 91-2341] p 62 A91-45805
- Energy deposition in low-power coaxial plasma thrusters p 63 A91-52311
- Cathode phenomena in a low-power magnetoplasma dynamic thruster p 63 A91-52314
- MPD thruster technology [AIAA PAPER 91-3568] p 65 A91-52444
- MPD thruster technology [NASA-TM-105242] p 86 N91-32162
- PLASMA SPRAYING**
- Composite bearing and seal materials for advanced heat engine applications to 900 C [NASA-TM-103612] p 95 N91-15318
- Process for HIP canning of composites [NASA-CASE-LEW-14990-1-CU] p 96 N91-17145
- The PM-200 lubrication system p 121 N91-23044
- Quality control of the tribological coating PS212 [NASA-TM-102067] p 101 N91-25186
- Plasma gun with coaxial powder feed and adjustable cathode [NASA-CASE-LEW-14901-1] p 231 N91-25875
- Method of preparing a thermal barrier coating [NASA-CASE-LEW-14999-2] p 122 N91-26376
- PLASMA-ELECTROMAGNETIC INTERACTION**
- A preliminary characterization of applied-field MPD thruster plumes [AIAA PAPER 91-2339] p 62 A91-45798
- PLASMAS (PHYSICS)**
- Ceramic coatings on smooth surfaces [NASA-CASE-LEW-15164-1] p 122 N91-25298
- PLASTIC DEFORMATION**
- 1000 to 1300 K slow plastic compression properties of Al-deficient NiAl p 108 A91-36214
- PLASTIC PROPERTIES**
- Matrix plasticity in SiC/Ti-15-3 composite [NASA-TM-103760] p 102 N91-27247
- Experimental and analytical analysis of stress-strain behavior in a (90/0 deg)2s, SiC/Ti-15-3 laminate [NASA-TM-104470] p 103 N91-31235

POLYIMIDE RESINS

- Autoclavable addition polyimides for 371 C composite applications p 115 A91-49112
- Atomic oxygen undercutting of defects on SiO₂ protected polyimide solar array blankets p 116 A91-49803
- Vinyl capped addition polyimides [NASA-CASE-LEW-15027-1] p 118 N91-13566
- Addition polyimides with enhanced processability [NASA-CASE-LEW-15043-1] p 123 N91-32230

POLYIMIDES

- Viscoelastic properties of addition-cured polyimides used in high temperature polymer matrix composites [NASA-TM-103768] p 89 N91-22377
- A comparison of fiber effects on polymer matrix composite oxidation [NASA-TM-104416] p 101 N91-24361
- Long term isothermal aging and thermal analysis of N-CYCAP polyimides p 122 N91-25286
- [NASA-TM-104341] p 122 N91-25286
- Low Earth orbital atomic oxygen micrometeoroid, and debris interactions with photovoltaic arrays p 84 N91-30248

POLYMER CHEMISTRY

- Ladder polymers for use as high temperature stable resins or coatings [NASA-CASE-LEW-14203-1] p 118 N91-15402
- Low Earth orbital atomic oxygen and ultraviolet radiation effects on polymers [NASA-TM-103711] p 119 N91-19294

POLYMER MATRIX COMPOSITES

- Intrinsic bond strength of metal films on polymer substrates p 88 A91-39246
- Relationship between voids and interlaminar shear strength of polymer matrix composites [NASA-TM-103643] p 95 N91-13495
- ICAN sensitivity analysis p 96 N91-15328
- Effect of fiber reinforcements on thermo-oxidative stability and mechanical properties of polymer matrix composites [NASA-TM-103648] p 98 N91-19234
- Probabilistic micromechanics and macromechanics of polymer matrix composites [NASA-TM-103669] p 98 N91-19236
- Viscoelastic properties of addition-cured polyimides used in high temperature polymer matrix composites [NASA-TM-103768] p 89 N91-22377
- A comparison of fiber effects on polymer matrix composite oxidation [NASA-TM-104416] p 101 N91-24361
- Integrated mechanics for the passive damping of polymer-matrix composites and composite structures [NASA-TM-104346] p 103 N91-32181

POLYMERIC FILMS

- Low Earth orbital atomic oxygen and ultraviolet radiation effects on polymers [NASA-TM-103711] p 119 N91-19294

POLYMERIZATION

- Graphite fluoride fiber polymer composite material [NASA-CASE-LEW-14472-1] p 95 N91-15320
- Ladder polymers for use as high temperature stable resins or coatings [NASA-CASE-LEW-14203-1] p 118 N91-15402
- Addition polyimides with enhanced processability [NASA-CASE-LEW-15043-1] p 123 N91-32230

POLYMERS

- Solid lubricants [NASA-TM-102803] p 99 N91-22396
- Long term isothermal aging and thermal analysis of N-CYCAP polyimides [NASA-TM-104341] p 122 N91-25286
- Some recent studies with the solid-ionomer electrochemical capacitor p 214 N91-32562

POLYMORPHISM

- Rapid solidification of polymorphic transition metals induced by nanosecond laser pulses p 109 A91-46520

POLYNOMIALS

- Mappings and accuracy for Chebyshev pseudo-spectral approximations [NASA-TM-103630] p 221 N91-14781
- High-Order Polynomial Expansions (HOPE) for flux-vector splitting [NASA-TM-104452] p 222 N91-25739

POLYPHENYLS

- Addition polyimides with enhanced processability [NASA-CASE-LEW-15043-1] p 123 N91-32230

POLYTETRAFLUOROETHYLENE

- X-ray photoelectron and mass spectroscopic study of electron irradiation and thermal stability of polytetrafluoroethylene p 113 A91-16138
- Thermal stability of electron-irradiated poly(tetrafluoroethylene) - X-ray photoelectron and mass spectroscopic study p 115 A91-39242

POROSITY

- Frontogenesis driven by horizontally quadratic distributions of density p 157 A91-48276

POROUS MATERIALS

- Development of braided rope seals for hypersonic engine applications. II - Flow modeling [AIAA PAPER 91-2495] p 182 A91-41800
- Development of braided rope seals for hypersonic engine applications. Part 2: Flow modeling [NASA-TM-104371] p 186 N91-22571

POSITION (LOCATION)

- Optical techniques for determination of normal shock position in supersonic flows for aerospace applications p 174 A91-55530

POSITION SENSING

- Digital angular position sensor using wavelength division multiplexing p 21 A91-19580
- Optical techniques for determination of normal shock position in supersonic flows for aerospace applications p 174 A91-55530

POSTFLIGHT ANALYSIS

- The development of a post-test diagnostic system for rocket engines [AIAA PAPER 91-2528] p 60 A91-44281
- The development of a post-test diagnostic system for rocket engines [NASA-TM-104463] p 217 N91-24787

POTASSIUM HYDROXIDES

- Effect of KOH concentration on LEO cycle life of IPV nickel-hydrogen flight battery cells p 55 A91-38076
- Effect of LEO cycling on 125 Ah advanced design IPV nickel-hydrogen battery cells p 55 A91-38077
- Impedances of electrochemically impregnated nickel electrodes as functions of potential, KOH concentration, and impregnation method [NASA-TM-103283] p 208 N91-15628
- Effect of KOH concentration on LEO cycle life of IPV nickel-hydrogen flight cells. An update [NASA-TM-104383] p 74 N91-22376
- Destructive physical analysis results of Ni/H₂ cells cycled in LEO regime [NASA-TM-104382] p 74 N91-23233
- Impedances of nickel electrodes cycled in various KOH concentrations p 214 N91-32557

POTENTIAL ENERGY

- Global expression for representing diatomic potential-energy curves p 228 A91-33236

POTENTIAL FLOW

- Extension of transonic flow computational concepts in the analysis of cavitated bearings [ASME PAPER 90-TRIB-40] p 150 A91-29474
- Aerodynamics and heat transfer investigations on a high Reynolds number turbine cascade [NASA-TM-103260] p 11 N91-15134
- Extension of transonic flow computational concepts in the analysis of cavitated bearings [NASA-TM-103214] p 160 N91-16304

POTENTIAL THEORY

- Cascade flutter analysis with transient response aerodynamics [NASA-TM-103746] p 201 N91-19475

POWDER (PARTICLES)

- Crystallization and properties of Sr-Ba aluminosilicate glass-ceramic matrices p 117 A91-56917
- Method of making single crystal fibers [NASA-CASE-LEW-14921-1] p 95 N91-13502
- Composite bearing and seal materials for advanced heat engine applications to 900 C [NASA-TM-103612] p 95 N91-15318
- Crystallization and properties of Sr-Ba aluminosilicate glass-ceramic matrices [NASA-TM-103764] p 120 N91-19308

POWDER METALLURGY

- Tribological properties of PM212 - A high temperature, self-lubricating, powder metallurgy composite [STLE PREPRINT 90-AM-4E-1] p 87 A91-19720
- Low-density, high-strength intermetallic matrix composites by XD (trademark) synthesis [NASA-TM-103724] p 97 N91-19233
- Mechanical strength and thermophysical properties of PM212: A high temperature self-lubricating powder metallurgy composite [NASA-TM-103694] p 120 N91-21302
- The PM-200 lubrication system p 121 N91-23044
- Method of making carbide/fluoride/silver composites [NASA-CASE-LEW-14902-1] p 102 N91-27244
- PM200/PS200: Self-lubricating bearing and seal materials for applications to 900 C [NASA-TM-103776] p 190 N91-30539

POWDERED ALUMINUM

- Design issues for propulsion systems using metallized propellants [AIAA PAPER 91-3484] p 66 A91-53709
- Design issues for propulsion systems using metallized propellants [NASA-TM-105190] p 81 N91-29220

POWER AMPLIFIERS

- NASA developments in solid state power amplifiers p 143 N91-18298
- GaAs monolithic RF modules for SARSAT distress beacons [NASA-TM-104338] p 46 N91-21184

POWER CONDITIONING

- Control of multiple resonant power processors in a multi-source system p 137 A91-30901
- Power electronic applications for Space Station Freedom p 52 A91-36832
- A comparison of energy conversion systems for meeting the power requirements of manned rover for Mars missions p 53 A91-37932
- Electric power scheduling - A distributed problem-solving approach p 219 A91-37976
- An analysis of space power system masses p 54 A91-38003

- Power electronics for low power arcjets [AIAA PAPER 91-1991] p 60 A91-45779
- Five-kilowatt arcjet power electronics p 63 A91-52312

- Xenon ion propulsion for orbit transfer [NASA-TM-103193] p 69 N91-11798
- High temperature power electronics for space [NASA-TM-104375] p 145 N91-22508

- Power electronics for low power arcjets [NASA-TM-104459] p 77 N91-25172
- Development of an analytical tool to study power quality of AC power systems for large spacecraft [NASA-TM-104451] p 223 N91-25749

- Neutron, gamma ray and post-irradiation thermal annealing effects on power semiconductor switches [NASA-TM-105248] p 147 N91-32410
- Comparison of high temperature, high frequency core loss and dynamic B-H loops of two 50 Ni-Fe crystalline alloys and an iron-based amorphous alloy [NASA-TM-105205] p 147 N91-32412

POWER CONVERTERS

- Control of multiple resonant power processors in a multi-source system p 137 A91-30901
- Programmatic status of NASA's CSTI High Capacity Power Stirling Space Power Converter Program p 53 A91-37933
- Power electronics for low power arcjets [AIAA PAPER 91-1991] p 60 A91-45779
- Five-kilowatt arcjet power electronics p 63 A91-52312
- Component technology for Stirling power converters [NASA-TM-104387] p 74 N91-23234
- Power electronics for low power arcjets [NASA-TM-104459] p 77 N91-25172
- Status of NASA's Stirling Space Power Converter Program [NASA-TM-104512] p 214 N91-32569

POWER EFFICIENCY

- Power electronics for low power arcjets [AIAA PAPER 91-1991] p 60 A91-45779
- Tandem concentrator solar cells with 30 percent (AMO) power conversion efficiency p 208 N91-19189
- Balancing reliability and cost to choose the best power subsystem [NASA-TM-104453] p 238 N91-24952
- Power electronics for low power arcjets [NASA-TM-104459] p 77 N91-25172

POWER FACTOR CONTROLLERS

- Development of an analytical tool to study power quality of AC power systems for large spacecraft [NASA-TM-104451] p 223 N91-25749

POWER LOSS

- Experimental and analytical evaluation of efficiency of helicopter planetary stage [NASA-TP-3063] p 183 N91-12956

POWER REACTORS

- Preliminary assessment of the power requirements of a manned rover for Mars missions p 41 A91-27702

POWER SERIES

- Time development of a perturbed-spherical nucleus in a pure supercooled liquid. I - Power-law growth of morphological instabilities. II - Nonlinear development p 231 A91-16105

POWER SUPPLIES

- SEI power source alternatives for rovers and other multi-kWe distributed surface applications [NASA-TM-104360] p 81 N91-28277

POWERED LIFT AIRCRAFT

- Static performance tests of a flight-type STOVL ejector [AIAA PAPER 91-1902] p 24 A91-44050
- Static performance tests of a flight-type STOVL ejector [NASA-TM-104437] p 33 N91-24201

POWERED MODELS

- Results of a sub-scale model rotor icing test [AIAA PAPER 91-0660] p 19 A91-26190

Results of a sub-scale model rotor icing test
[NASA-TM-103709] p 11 N91-14309

PRANDTL NUMBER

Stability of an oscillated fluid with a uniform density gradient p 147 A91-12971

PRECIPITATION HARDENING

Inhomogeneous deformation in INCONEL 718 during monotonic and cyclic loadings p 108 A91-22287

PRECONDITIONING

Time-derivative preconditioning for viscous flows
[AIAA PAPER 91-1652] p 154 A91-43576

PREDICTION ANALYSIS TECHNIQUES

Aeroacoustics of advanced propellers p 226 A91-24317

Results of a sub-scale model rotor icing test
[AIAA PAPER 91-0660] p 19 A91-26190

Modeling and optimization of a regenerative fuel cell system using the ASPEN process simulator p 206 A91-38177

The application of neural networks to the SSME startup transient
[AIAA PAPER 91-2530] p 60 A91-44283

Computational fluid dynamics at the Lewis Research Center: An overview p 8 N91-10842

Unsteady blade-surface pressures on a large-scale advanced propeller: Prediction and data
[NASA-TM-103218] p 69 N91-11799

Stirling engine: Available tools for long-life assessment
[NASA-TM-103660] p 200 N91-12980

Results of a sub-scale model rotor icing test
[NASA-TM-103709] p 11 N91-14309

Wind turbine acoustics p 228 N91-16679

Prediction of ice shapes and their effect on airfoil performance
[NASA-TM-103701] p 12 N91-19047

ETARA PC version 3.3 user's guide: Reliability, availability, maintainability simulation model
[NASA-TM-103751] p 193 N91-19462

Application of thermal life prediction model to high-temperature aerospace alloys B1900 + Hf and Haynes 188 p 201 N91-19473

A comparison of CFD predictions and experimental results for a Mach 5 inlet p 28 N91-20094

Overview of structures research p 202 N91-20104

Transition-to-practice technologies for brittle materials p 120 N91-20107

Progress in modeling deformation and damage p 202 N91-20108

Thermomechanical and bithermal fatigue behavior of cast B1900 + Hf and wrought Haynes 188
[NASA-TM-4225] p 111 N91-20268

The environment workbench: A design tool for Space Station Freedom p 48 N91-20727

Mechanical behavior of fiber reinforced SiC/RBSN ceramic matrix composites: Theory and experiment
[NASA-TM-103688] p 99 N91-21243

Comparison of analysis and experiment for dynamics of low-contact-ratio spur gears
[NASA-TM-103232] p 185 N91-22566

Structural Integrity and Durability of Reusable Space Propulsion Systems p 76 N91-24307

Overview of the fatigue/fracture/life working group program at the Lewis Research Center p 203 N91-24308

Tensile and fatigue behavior of tungsten/copper composites p 100 N91-24311

Comparison of a quasi-3D analysis and experimental performance for three compact radial turbines
[NASA-TM-105155] p 35 N91-30142

Fatigue behavior and life prediction of a SiC/Ti-24Al-11Nb composite under isothermal conditions
[NASA-TM-105168] p 206 N91-30566

PREDICTIONS

Measurements and predictions of a liquid spray from an air-assist nozzle
[AIAA PAPER 91-0692] p 149 A91-22498

A review of ice accretion data from a model rotor icing test and comparison with theory
[AIAA PAPER 91-0661] p 19 A91-22500

A review of ice accretion data from a model rotor icing test and comparison with theory
[NASA-TM-103712] p 11 N91-13421

Measurements and predictions of a liquid spray from an air-assist nozzle
[NASA-TM-103640] p 26 N91-13455

Relationship between voids and interlaminar shear strength of polymer matrix composites
[NASA-TM-103643] p 95 N91-13495

Application of thermal life prediction model to high-temperature aerospace alloys B1900 + Hf and Haynes 188
[NASA-TM-4226] p 201 N91-19473

Life extending control: A concept paper
[NASA-TM-104391] p 37 N91-22135

A statistical rain attenuation prediction model with application to the advanced communication technology satellite project 3: A stochastic rain fade control algorithm for satellite link power via non linear Markov filtering theory
[NASA-TM-100243] p 134 N91-22494

Fatigue behavior and life prediction of a SiC/Ti-24Al-11Nb composite under isothermal conditions
[NASA-TM-105168] p 206 N91-30566

PREMIXED FLAMES

Particle nonuniformity effects on particle cloud flames in low gravity
[AIAA PAPER 91-0718] p 104 A91-19431

PREMIXING

Numerical study of shock-wave/boundary layer interactions in premixed hydrogen-air hypersonic flows
[AIAA PAPER 91-0413] p 149 A91-26191

Numerical study of shock-wave/boundary layer interactions in premixed hydrogen-air hypersonic flows
[NASA-TM-103273] p 160 N91-14559

POLYMERS

Autoclavable addition polyimides for 371 C composite applications p 115 A91-49112

PRESSURE DISTRIBUTION

Prediction of unsteady blade surface pressures on an advanced propeller at an angle of attack p 226 A91-18257

Numerical flux formulas for the Euler and Navier-Stokes equations. II - Progress in flux-vector splitting
[AIAA PAPER 91-1566] p 5 A91-40740

Large-scale advanced propeller blade pressure distributions - Prediction and data p 5 A91-42820

An Electronic Pressure Profile Display system for aeronautic test facilities p 38 A91-51858

Near-field noise of a single-rotation propfan at an angle of attack
[NASA-TM-103645] p 227 N91-12316

Aerodynamics and heat transfer investigations on a high Reynolds number turbine cascade
[NASA-TM-103260] p 11 N91-15134

Numerical flux formulas for the Euler and Navier-Stokes equations. 2: Progress in flux-vector splitting
[NASA-TM-104353] p 15 N91-22084

Simulation of probabilistic wind loads and building analysis
[NASA-TM-103744] p 203 N91-23549

Advances in modeling the pressure correlation terms in the second moment equations
[NASA-TM-104413] p 165 N91-24525

Characterization of flow in a scroll duct
[NASA-CR-188612] p 167 N91-25367

PRESSURE EFFECTS

Test-cell pressure effects on the performance of resistojets p 38 A91-37417

Effects of high pressure nitrogen on the thermal stability of SiC fibers
[NASA-TM-103245] p 96 N91-16075

Unsteady blade pressure measurements for the SR-7A propeller at cruise conditions
[NASA-TM-103606] p 228 N91-19825

PRESSURE GRADIENTS

Determination of the thermal stability of fluids by tensimetry - Instrumentation and procedure p 113 A91-13435

PRESSURE MEASUREMENT

Unsteady blade pressure measurements for the SR-7A propeller at cruise conditions
[AIAA PAPER 90-4022] p 225 A91-12533

Flow visualization and quantitative velocity and pressure measurements in simulated single and double brush seals p 180 A91-21071

Pressure measurements in a low-density nozzle plume for code verification
[AIAA PAPER 91-2110] p 61 A91-45783

Probe insertion apparatus with inflatable seal
[NASA-CASE-LEW-14965-1] p 183 N91-13732

Rotating pressure measurement system using an on board calibration standard
[NASA-TM-103676] p 176 N91-19401

Unsteady blade pressure measurements for the SR-7A propeller at cruise conditions
[NASA-TM-103606] p 228 N91-19825

Pressure measurements in a low-density nozzle plume for code verification
[NASA-TM-105170] p 81 N91-29228

PRESSURE OSCILLATIONS

Pressure-coupled vaporization and combustion responses of liquid-fuel droplets in high-pressure environments
[AIAA PAPER 91-2310] p 106 A91-44192

Unsteady blade-surface pressures on a large-scale advanced propeller: Prediction and data
[NASA-TM-103218] p 69 N91-11799

PRESSURE RATIO

The 3D computation of single-expansion-ramp and scramjet nozzles p 164 N91-21092

PRESSURE REDUCTION

Effects of brush seal morphology on leakage and pressure drops
[AIAA PAPER 91-2106] p 182 A91-41700

PRESSURE SENSORS

Unsteady blade pressure measurements for the SR-7A propeller at cruise conditions
[AIAA PAPER 90-4022] p 225 A91-12533

Fiber optic photoelastic pressure sensor for high temperature gases p 170 A91-19577

Photoelastic transducer for high-temperature applications p 174 A91-55533

PRESSURE VESSELS

Effect of LEO cycling on 125 Ah advanced design IPV nickel-hydrogen battery cells p 55 A91-38077

Probe insertion apparatus with inflatable seal
[NASA-CASE-LEW-14965-1] p 183 N91-13732

Effect of LEO cycling on 125 Ah advanced design IPV nickel-hydrogen flight cells. An update
[NASA-TM-104384] p 74 N91-22375

Destructive physical analysis results of Ni/H₂ cells cycled in LEO regime
[NASA-TM-104382] p 74 N91-23233

Autogenous pressurization of cryogenic vessels using submerged vapor injection
[NASA-TM-104516] p 127 N91-27375

Nickel-hydrogen cell low-Earth life test update
[NASA-TM-105229] p 213 N91-31708

PRESSURIZING

Self-pressurization of a lightweight liquid hydrogen storage tank subjected to low heat flux
[NASA-TM-103804] p 126 N91-20324

Pressurization and expulsion of cryogenic liquids: Generic requirements for a low gravity experiment
[NASA-TM-104417] p 126 N91-25300

Autogenous pressurization of cryogenic vessels using submerged vapor injection
[NASA-TM-104516] p 127 N91-27375

PRIMARY BATTERIES

NASA Aerospace Flight Battery Systems Program p 56 A91-38088

PRIMITIVE EQUATIONS

Probabilistic structural analysis of a truss typical for space station
[NASA-TM-103277] p 199 N91-12114

PROBABILITY DENSITY FUNCTIONS

A study of hydrogen diffusion flames using PDF turbulence model
[AIAA PAPER 91-1780] p 106 A91-45549

PROBABILITY DISTRIBUTION FUNCTIONS

Structure of random discrete spacetime p 224 A91-22894

PROBABILITY THEORY

Probabilistic simulation of uncertainties in thermal structures p 195 A91-16042

Programming probabilistic structural analysis for parallel processing computer
[AIAA PAPER 91-0920] p 196 A91-31957

Probabilistic modeling for simulation of aerodynamic uncertainties in propulsion systems p 58 A91-42725

Probabilistic structural analysis of a truss typical for space station
[NASA-TM-103277] p 199 N91-12114

Probabilistic micromechanics and macromechanics of polymer matrix composites
[NASA-TM-103669] p 98 N91-19236

Probabilistic simulation of uncertainties in thermal structures
[NASA-TM-103680] p 201 N91-19472

Reliability and risk assessment of structures p 194 N91-23050

Probabilistic structural analysis: Introductory remarks p 204 N91-24326

Probability approach for strength calculations p 204 N91-24652

Probability of failure and risk assessment of propulsion structural components
[NASA-TM-102323] p 205 N91-25436

Probabilistic structural analysis methods for space transportation propulsion systems p 205 N91-28238

PROBLEM SOLVING

Automated electric power management and control for Space Station Freedom p 53 A91-37970

Autonomous power expert system p 54 A91-37972

PROCEDURES

Current activities in standardization of high-temperature, low-cycle-fatigue testing techniques in the United States
[NASA-TM-103675] p 200 N91-17427

PROCESS CONTROL (INDUSTRY)

A numerical and experimental analysis of reactor performance and deposition rates for CVD on monofilaments
[NASA-TM-103631] p 130 N91-14500

SUBJECT INDEX

Quality control of the tribological coating PS212
[NASA-TM-102067] p 101 N91-25186

PRODUCTION ENGINEERING

Production and use of metals and oxygen for lunar propulsion
[AIAA PAPER 91-3481] p 125 A91-53711

Production and use of metals and oxygen for lunar propulsion
[NASA-TM-105195] p 81 N91-29222

PROFILOMETERS

Laser interferometric measurement of ion electrode shape and charge exchange erosion
[NASA-TM-105165] p 179 N91-31605

PROGRAM VERIFICATION (COMPUTERS)

Pressure measurements in a low-density nozzle plume for code verification
[AIAA PAPER 91-2110] p 61 A91-45783

Enhancing aeropropulsion research with high-speed interactive computing p 217 A91-56129

Turbomachinery p 162 N91-20097

Overview of the instrumentation program p 176 N91-24318

Enhancing aeropropulsion research with high-speed interactive computing p 218 N91-24796

Verification of the proteus two-dimensional Navier-Stokes code for flat plate and pipe flows
[NASA-TM-105160] p 168 N91-30462

PROJECT MANAGEMENT

Concurrent engineering p 80 N91-28247

PROJECT PLANNING

Power system requirements and definition for lunar and Mars outposts p 52 A91-37930

Plans for the development of cryogenic engines for space exploration p 64 A91-52351

JANNAF liquid rocket combustion instability panel research recommendations p 70 N91-13491

Vision-21: Space Travel for the Next Millennium
[NASA-CP-10059] p 40 N91-22139

Civil air transport: A fresh look at power-by-wire and fly-by-light p 37 N91-23053

Nuclear rocket propulsion. NASA plans and progress, FY 1991 p 77 N91-25179

PROJECTILES

Navier-Stokes simulation of the supersonic combustion flowfield in a ram accelerator p 155 A91-44057

Navier-Stokes simulation of the supersonic combustion flowfield in a ram accelerator p 166 N91-24541

PROP-FAN TECHNOLOGY

Near-field noise of a single rotation propfan at an angle of attack p 225 A91-12469

Optical measurement of unducted fan blade deflections
[ASME PAPER 89-GT-298] p 170 A91-13046

Aeroacoustics of advanced propellers p 226 A91-24317

Experimental investigation of propfan aeroelastic response in off-axis flow with mistuning p 22 A91-30015

Large-scale advanced propeller blade pressure distributions - Prediction and data p 5 A91-42820

Optical measurement of propeller blade deflections in a spin facility p 12 N91-17002

Inflight source noise of an advanced full-scale single-rotation propeller p 12 N91-19045

The selection of convertible engines with current gas generator technology for high speed rotorcraft
[NASA-TM-103774] p 27 N91-19097

Ultra-high bypass research p 30 N91-20117

ASTROP2 users manual: A program for aeroelastic stability analysis of propanes p 206 N91-28627

Unsteady flowfield of a propfan at takeoff conditions
[NASA-TM-105223] p 18 N91-32075

PROPANE

Radiation from gas-jet diffusion flames in microgravity environments p 104 A91-19432

Numerical simulation of Jet-A combustion approximated by improved propane chemical kinetics
[AIAA PAPER 91-1859] p 106 A91-45777

PROPELLANT ADDITIVES

Launch vehicle performance using metallized propellants p 58 A91-44106

Advanced launch vehicle upper stages using liquid propulsion and metallized propellants
[NASA-TM-103622] p 68 N91-11797

Lunar missions using chemical propulsion: System design issues p 70 N91-15308

Advanced launch vehicle upper stages using liquid propulsion and metallized propellants p 75 N91-24257

Launch vehicle performance using metallized propellants p 76 N91-24304

PROPELLANT CHEMISTRY

Material processing with hydrogen and carbon monoxide on Mars
[NASA-TM-104405] p 211 N91-23616

PROPELLANT COMBUSTION

Carbon monoxide and oxygen combustion experiments - A demonstration of Mars in situ propellants
[AIAA PAPER 91-2443] p 60 A91-44246

Computer code for single-point thermodynamic analysis of hydrogen/oxygen expander-cycle rocket engines
[NASA-TM-4275] p 72 N91-20206

Carbon monoxide and oxygen combustion experiments: A demonstration of Mars in situ propellants
[NASA-TM-104473] p 76 N91-24303

PROPELLANT STORABILITY

The COLD-SAT experiment for cryogenic fluid management technology p 126 N91-24263

PROPELLANT TANKS

Computational modeling of the pressurization process in a NASP vehicle propellant tank experimental simulation p 124 A91-41771

Paramagnetic propellant orientation
[AIAA PAPER 91-2325] p 125 A91-44197

Paramagnetic propellant orientation
[NASA-TM-104390] p 166 N91-24527

PROPELLANT TESTS

The measurement, modelling and prediction of traction forces in a rocket propellant p 125 A91-51914

PROPELLANT TRANSFER

Ground testing of the nonvented fill method of orbital propellant transfer - Results of initial test series
[AIAA PAPER 91-2326] p 59 A91-44198

Slush hydrogen propellant production, transfer, and expulsion studies at the NASA K-Site Facility
[AIAA PAPER 91-3550] p 125 A91-53710

Ground testing on the nonvented fill method of orbital propellant transfer: Results of initial test series
[NASA-TM-104444] p 166 N91-24547

Slush hydrogen propellant production, transfer, and expulsion studies at the NASA K-Site Facility
[NASA-TM-105191] p 127 N91-28449

PROPELLANTS

Paramagnetic propellant orientation
[AIAA PAPER 91-2325] p 125 A91-44197

Investigation of the arcjet near field plume using electrostatic probes p 75 N91-24270

Paramagnetic propellant orientation
[NASA-TM-104390] p 166 N91-24527

Method of injecting fluid propellants into a rocket combustion chamber p 78 N91-26200

The NASA cryogenic fluid management technology program plan
[NASA-TM-105256] p 86 N91-32161

PROPELLER BLADES

The effect of swirl recovery vanes on the cruise noise of an advanced propeller p 224 A91-12448

Unsteady blade pressure measurements for the SR-7A propeller at cruise conditions p 225 A91-12533

Prediction of unsteady blade surface pressures on an advanced propeller at an angle of attack p 226 A91-18257

Large-scale advanced propeller blade pressure distributions - Prediction and data p 5 A91-42820

Application of an efficient hybrid scheme for aeroelastic analysis of advanced propellers p 7 A91-52315

Unsteady blade-surface pressures on a large-scale advanced propeller: Prediction and data
[NASA-TM-103218] p 69 N91-11799

Potential reduction of en route noise from an advanced turboprop aircraft p 228 N91-15842

Optical measurement of propeller blade deflections in a spin facility p 12 N91-17002

Unsteady blade pressure measurements for the SR-7A propeller at cruise conditions
[NASA-TM-103606] p 228 N91-19825

PROPELLER EFFICIENCY

Application of an efficient hybrid scheme for aeroelastic analysis of advanced propellers p 7 A91-52315

PROPELLER FANS

Aeroacoustics of advanced propellers p 226 A91-24317

PROPULSION SYSTEM CONFIGURATIONS

Aeroacoustic effects of reduced aft tip speed at constant thrust for a model counterrotation turboprop at takeoff conditions p 226 N91-10703

Near-field noise of a single-rotation propfan at an angle of attack p 227 N91-12316

Inflight source noise of an advanced full-scale single-rotation propeller p 12 N91-19045

The selection of convertible engines with current gas generator technology for high speed rotorcraft
[NASA-TM-103774] p 27 N91-19097

Ultra-high bypass research p 30 N91-20117

ASTROP2 users manual: A program for aeroelastic stability analysis of propanes p 206 N91-28627

Unsteady flowfield of a propfan at takeoff conditions
[NASA-TM-105223] p 18 N91-32075

PROPELLER NOISE

The effect of swirl recovery vanes on the cruise noise of an advanced propeller
[AIAA PAPER 90-3932] p 224 A91-12448

Prediction of the noise from a propeller at angle of attack p 225 A91-12470

In-flight source noise of an advanced full-scale single-rotation propeller p 226 A91-21547

Cruise noise of an advanced single-rotation propeller measured from an adjacent aircraft p 22 A91-28265

The effect of swirl recovery vanes on the cruise noise of an advanced propeller p 227 N91-11494

Prediction of the noise from a propeller at angle of attack p 227 N91-11495

Potential reduction of en route noise from an advanced turboprop aircraft p 228 N91-15842

PROPELLERS

Aeroacoustic effects of reduced aft tip speed at constant thrust for a model counterrotation turboprop at takeoff conditions p 224 A91-12449

Aeroacoustics of advanced propellers p 226 A91-24317

Structural properties of laminated Douglas fir/epoxy composite material
[NASA-RP-1236] p 94 N91-10127

The effect of swirl recovery vanes on the cruise noise of an advanced propeller p 227 N91-11494

Inflight source noise of an advanced full-scale single-rotation propeller p 12 N91-19045

PROPULSION

Computational fluid dynamics at the Lewis Research Center: An overview p 8 N91-10842

An AD100 implementation of a real-time STOVL aircraft propulsion system p 26 N91-13457

Propulsion aeroelasticity, vibration control, and dynamic system modeling p 29 N91-20105

Research and technology p 243 N91-23072

Institute for Computational Mechanics in Propulsion (ICOMP) p 222 N91-24818

PROPULSION SYSTEM CONFIGURATIONS

Cryogenic propellant management architectures to support the Space Exploration Initiative p 124 A91-10112

Nuclear power systems for lunar and Mars exploration
[IAF PAPER 90-200] p 51 A91-13668

An update of engine system research at the Army Propulsion Directorate p 22 A91-29452

In-situ propellant rocket engines for Mars missions ascent vehicle p 60 A91-44247

The rationale/benefits of nuclear thermal rocket propulsion for NASA's lunar space transportation system
[AIAA PAPER 91-2052] p 39 A91-45781

Plug nozzles - The ultimate customer driven propulsion system --- applied to manned lunar and Martian landers
[AIAA PAPER 91-2208] p 61 A91-45794

Synergistic use of high and low thrust propulsion systems for piloted missions to Mars p 39 A91-45807

Application of an integrated flight/propulsion control design methodology to a STOVL aircraft
[AIAA PAPER 91-2792] p 36 A91-49793

Plans for the development of cryogenic engines for space exploration p 64 A91-52351

The NASA Lewis Research Center electric propulsion program
[AIAA PAPER 91-3443] p 64 A91-52355
Cryogenic propellant management system requirements for Space Station Freedom
[AIAA PAPER 91-3476] p 65 A91-52382
Nondestructive evaluation tools and experimental studies for monitoring the health of space propulsion systems
[AIAA PAPER 91-3433] p 192 A91-53703
Numerical propulsion system simulation - An interdisciplinary approach
[AIAA PAPER 91-3554] p 66 A91-53706
Design issues for propulsion systems using metallized propellants
[AIAA PAPER 91-3484] p 66 A91-53709
Historical perspectives - The role of the NASA Lewis Research Center in the national space nuclear power programs
[AIAA PAPER 91-3462] p 242 A91-53713
Comparison of turbine bypass and mixed flow turbofan engines for a high-speed civil transport
[AIAA PAPER 91-3132] p 25 A91-54051
Computational fluid dynamics at the Lewis Research Center: An overview p 8 A91-10842
An update of engine system research at the Army Propulsion Directorate
[NASA-TM-103278] p 26 A91-11752
Xenon ion propulsion for orbit transfer
[NASA-TM-103193] p 69 A91-11798
Lunar missions using chemical propulsion: System design issues
[NASA-TP-3065] p 70 A91-15308
Overview of space propulsion systems for identifying nondestructive evaluation and health monitoring opportunities
[NASA-TM-103614] p 192 A91-15565
The selection of convertible engines with current gas generator technology for high speed rotorcraft
[NASA-TM-103774] p 27 A91-19097
Solar electric propulsion for Mars transport vehicles
[NASA-TM-103234] p 71 A91-19178
Aeropropulsion 1991
[NASA-CP-10063] p 27 A91-20086
Lewis aeropropulsion technology: Remembering the past and challenging the future p 242 A91-20087
High alpha inlets p 28 A91-20091
Overview of hypersonic/transatmospheric vehicle propulsion technology p 28 A91-20092
A comparison of CFD predictions and experimental results for a Mach 5 inlet p 28 A91-20094
Internal fluid mechanics research p 161 A91-20095
Instrumentation and controls overview p 38 A91-20099
Propulsion instrumentation research p 176 A91-20100
Advanced aeropropulsion controls technology p 29 A91-20103
Overview of structures research p 202 A91-20104
Propulsion aeroelasticity, vibration control, and dynamic system modeling p 29 A91-20105
Computational simulation of propulsion structures performance and reliability p 29 A91-20106
Ultra-high bypass research p 30 A91-20117
IMPAC: An Integrated Methodology for Propulsion and Airframe Control
[NASA-TM-103805] p 30 A91-20122
CFD for hypersonic propulsion
[NASA-TM-103791] p 164 A91-21447
NASA aeropropulsion research in support of propulsion systems of the 21st century
[NASA-TM-104403] p 15 A91-23083
Engine technology challenges for a 21st century high speed civil transport
[NASA-TM-104363] p 19 A91-23098
In-situ propellant rocket engines for Mars mission ascent vehicle
[NASA-TM-104429] p 76 A91-24305
Structural Integrity and Durability of Reusable Space Propulsion Systems
[NASA-CP-10030] p 76 A91-24307
Probabilistic structural analysis: Introductory remarks p 204 A91-24326
The NASA Lewis integrated propulsion and flight control simulator
[NASA-TM-105147] p 21 A91-27157
Advanced cryo propulsion systems p 80 A91-28212
Probabilistic structural analysis methods for space transportation propulsion systems p 205 A91-28238
Overall goals p 80 A91-28246
Concurrent engineering p 80 A91-28247
Nondestructive evaluation tools and experimental studies for monitoring the health of space propulsion systems
[NASA-TM-105164] p 194 A91-28605

Historical perspectives: The role of the NASA Lewis Research Center in the national space nuclear power programs
[NASA-TM-105196] p 243 A91-29138
Design issues for propulsion systems using metallized propellants
[NASA-TM-105190] p 81 A91-29220
Numerical propulsion system simulation: An interdisciplinary approach
[NASA-TM-105181] p 81 A91-29221
Mass comparisons of electric propulsion systems for NSSK of geosynchronous spacecraft
[NASA-TM-105153] p 85 A91-31212
Medium power hydrogen arcjet performance
[NASA-TM-104533] p 85 A91-31216
Application of an integrated flight/propulsion control design methodology to a STOVL aircraft
[NASA-TM-105254] p 37 A91-32143
MPD thruster technology
[NASA-TM-105242] p 86 A91-32162
PROPULSION SYSTEM PERFORMANCE
The Advanced Expander Test Bed
[AIAA PAPER 90-3708] p 50 A91-10107
Integrated flight/propulsion control system design based on a centralized approach p 36 A91-22950
An update of engine system research at the Army Propulsion Directorate p 22 A91-29452
Three-dimensional viscous flow computations of high area ratio nozzles for hypersonic propulsion p 4 A91-30014
Computational simulation of acoustic fatigue for hot composite structures
[AIAA PAPER 91-1178] p 197 A91-32099
Probabilistic modeling for simulation of aerodynamic uncertainties in propulsion systems p 58 A91-42725
Launch vehicle performance using metallized propellants
[AIAA PAPER 91-2050] p 58 A91-44106
Carbon monoxide and oxygen combustion experiments - A demonstration of Mars in situ propellants
[AIAA PAPER 91-2443] p 60 A91-44246
In-situ propellant rocket engines for Mars missions ascent vehicle
[AIAA PAPER 91-2445] p 60 A91-44247
Experimental and analytical studies of flow through a ventral and axial exhaust nozzle system for STOVL aircraft
[AIAA PAPER 91-2135] p 25 A91-45791
Applied-field MPD thruster geometry effects
[AIAA PAPER 91-2342] p 62 A91-45806
Synergistic use of high and low thrust propulsion systems for piloted missions to Mars
[AIAA PAPER 91-2346] p 39 A91-45807
Performance and optimization of a 'derated' ion thruster for auxiliary propulsion
[AIAA PAPER 91-2350] p 62 A91-45809
MPD thruster technology
[AIAA PAPER 91-3568] p 65 A91-52444
Computational fluid dynamics studies of nuclear rocket performance
[AIAA PAPER 91-3577] p 66 A91-52450
Nondestructive evaluation tools and experimental studies for monitoring the health of space propulsion systems
[AIAA PAPER 91-3433] p 192 A91-53703
Numerical propulsion system simulation - An interdisciplinary approach
[AIAA PAPER 91-3554] p 66 A91-53706
Historical perspectives - The role of the NASA Lewis Research Center in the national space nuclear power programs
[AIAA PAPER 91-3462] p 242 A91-53713
Overview of the NASA-sponsored HSCT propulsion system studies --- High Speed Civil Transport
[AIAA PAPER 91-3329] p 20 A91-53871
The design and performance estimates for the propulsion module for the booster of a TSTO vehicle
[AIAA PAPER 91-3136] p 43 A91-54054
Computational fluid dynamics at the Lewis Research Center: An overview p 8 A91-10842
An update of engine system research at the Army Propulsion Directorate
[NASA-TM-103278] p 26 A91-11752
Xenon ion propulsion for orbit transfer
[NASA-TM-103193] p 69 A91-11798
Lunar missions using chemical propulsion: System design issues
[NASA-TP-3065] p 70 A91-15308
Overview of space propulsion systems for identifying nondestructive evaluation and health monitoring opportunities
[NASA-TM-103614] p 192 A91-15565
The selection of convertible engines with current gas generator technology for high speed rotorcraft
[NASA-TM-103774] p 27 A91-19097

Lewis aeropropulsion technology: Remembering the past and challenging the future p 242 A91-20087
Overview of supersonic cruise propulsion research p 27 A91-20088
Internal fluid mechanics research p 161 A91-20095
Propulsion instrumentation research p 176 A91-20100
Overview of structures research p 202 A91-20104
Computational simulation of propulsion structures performance and reliability p 29 A91-20106
Advanced high temperature engine materials technology program p 98 A91-20110
Overview of rotorcraft and general aviation propulsion technology p 29 A91-20112
Overview of subsonic transport propulsion technology p 30 A91-20116
High-efficiency core technology p 30 A91-20118
Multidisciplinary research overview (IHPTET/NPSS) p 30 A91-20119
IMPAC: An Integrated Methodology for Propulsion and Airframe Control
[NASA-TM-103805] p 30 A91-20122
Computational Fluid Dynamics Symposium on Aeropropulsion
[NASA-CP-3078] p 14 A91-21062
CFD for hypersonic propulsion
[NASA-TM-103791] p 164 A91-21447
Application of computational fluid dynamics in high speed aeropropulsion
[NASA-TM-103780] p 164 A91-21458
NASA aeropropulsion research in support of propulsion systems of the 21st century
[NASA-TM-104403] p 15 A91-23083
Carbon monoxide and oxygen combustion experiments: A demonstration of Mars in situ propellants
[NASA-TM-104473] p 76 A91-24303
Launch vehicle performance using metallized propellants
[NASA-TM-104456] p 76 A91-24304
In-situ propellant rocket engines for Mars mission ascent vehicle
[NASA-TM-104429] p 76 A91-24305
Experimental and analytical studies of flow through a ventral and axial exhaust nozzle system for STOVL aircraft
[NASA-TM-104364] p 77 A91-25175
Probability of failure and risk assessment of propulsion structural components
[NASA-TM-102323] p 205 A91-25436
The NASA Lewis integrated propulsion and flight control simulator
[NASA-TM-105147] p 21 A91-27157
Probabilistic structural analysis methods for space transportation propulsion systems p 205 A91-28238
Overall goals p 80 A91-28246
Concurrent engineering p 80 A91-28247
Nondestructive evaluation tools and experimental studies for monitoring the health of space propulsion systems
[NASA-TM-105164] p 194 A91-28605
Historical perspectives: The role of the NASA Lewis Research Center in the national space nuclear power programs
[NASA-TM-105196] p 243 A91-29138
Numerical propulsion system simulation: An interdisciplinary approach
[NASA-TM-105181] p 81 A91-29221
Performance and optimization of a derated ion thruster for auxiliary propulsion
[NASA-TM-105144] p 82 A91-29229
Mass comparisons of electric propulsion systems for NSSK of geosynchronous spacecraft
[NASA-TM-105153] p 85 A91-31212
Medium power hydrogen arcjet performance
[NASA-TM-104533] p 85 A91-31216
PROPULSIVE EFFICIENCY
Overview of subsonic transport propulsion technology p 30 A91-20116
High-efficiency core technology p 30 A91-20118
Application of computational fluid dynamics in high speed aeropropulsion p 164 A91-21458
[NASA-TM-103780] p 164 A91-21458
Advanced Rotorcraft Transmission (ART) program-Boeing helicopters status report
[NASA-TM-104474] p 188 A91-25412
PROPYLENE
Atomic oxygen interactions with FEP Teflon and silicones on LDEF p 122 A91-25029
PROTECTION
On protection of Freedom's solar dynamic radiator from the orbital debris environment. Part 2: Further testing and analyses
[NASA-TM-104514] p 84 A91-30265

PROTECTIVE COATINGS

- Undercutting of defects in thin film protective coatings on polymer surfaces exposed to atomic oxygen p 115 A91-41516
- Atomic oxygen undercutting of defects on SiO₂ protected polyimide solar array blankets p 116 A91-49803
- The effect of atomic oxygen on altered and coated Kapton surfaces for spacecraft applications in low earth orbit p 116 A91-49804
- The effect of coatings and liners on heat transfer in a dry shaft-bush tribosystem p 159 N91-12913
- [NASA-TM-102513] p 159 N91-12913
- Metallic seal for thermal barrier coating systems p 119 N91-15412
- [NASA-CASE-LEW-15020-1] p 119 N91-15412
- Diamondlike carbon as a moisture barrier and antireflecting coating on optical materials p 119 N91-18302
- Diamondlike carbon applications in infrared optics and microelectronics p 230 N91-18306
- Atomic oxygen interaction with solar array blankets at protective coating defect sites p 211 N91-20732
- The effect of atomic oxygen on polysiloxane-polyimide for spacecraft applications in low Earth orbit p 229 N91-20735
- Solid lubricants p 99 N91-22396
- [NASA-TM-102803] p 99 N91-22396
- Flexible fluoropolymer filled protective coatings p 121 N91-24062
- Atomic oxygen undercutting of LDEF aluminized Kapton multilayer insulation p 229 N91-25027
- Durability evaluation of photovoltaic blanket materials exposed on LDEF tray S1003 p 212 N91-25062
- Oxidation resistant coatings for titanium alloys and titanium alloy matrix composites p 122 N91-26375
- [NASA-CASE-LEW-15155-1] p 122 N91-26375
- Low Earth orbital atomic oxygen micrometeoroid, and debris interactions with photovoltaic arrays p 84 N91-30248
- Ceramic coatings on smooth surfaces p 123 N91-32229
- [NASA-CASE-LEW-15164-2] p 123 N91-32229
- PROTON IRRADIATION**
- Effects of radiation of InP cells epitaxially grown on Si and GaAs substrates p 140 A91-41984
- Effects of proton irradiation on the performance of InP/GaAs solar cells p 209 N91-19205
- Heteroepitaxial InP solar cells on Si and GaAs substrates p 144 N91-20392
- [NASA-TM-103696] p 144 N91-20392
- Space Photovoltaic Research and Technology Conference p 82 N91-30203
- [NASA-CP-3121] p 82 N91-30203
- PROTOTYPES**
- Development of a vibration isolation prototype system for microgravity space experiments p 47 A91-53403
- Development of a vibration isolation prototype system for microgravity space experiments p 130 N91-19324
- [NASA-TM-103664] p 130 N91-19324
- PULSE COMMUNICATION**
- Pulsed response of a TWT p 136 A91-27529
- PULSE DURATION**
- Pulsed response of a traveling-wave tube p 143 N91-19348
- [NASA-TM-103672] p 143 N91-19348
- PULSE DURATION MODULATION**
- Power electronics for low power arcjets p 60 A91-45779
- [AIAA PAPER 91-1991] p 60 A91-45779
- Power electronics for low power arcjets p 77 N91-25172
- [NASA-TM-104459] p 77 N91-25172
- PULSE POSITION MODULATION**
- Quaternary pulse position modulation electronics for free-space laser communications p 133 A91-53702
- [AIAA PAPER 91-3471] p 133 A91-53702
- Quaternary pulse position modulation electronics for free-space laser communications p 135 N91-29405
- [NASA-TM-104502] p 135 N91-29405
- PULSED LASERS**
- Rapid solidification of polymorphic transition metals induced by nanosecond laser pulses p 109 A91-46520
- PYROLYSIS**
- Wettability of pyrolytic boron nitride by aluminum p 114 A91-28772
- Polymeric routes to silicon carbide and silicon oxycarbide p 117 A91-56922
- CMC p 102 N91-26234
- [NASA-TM-104372] p 102 N91-26234
- PYROLYTIC GRAPHITE**
- The preliminary feasibility of intercalated graphite railgun armatures p 137 A91-29257
- Heat transfer device and method of making the same p 159 N91-13668
- [NASA-CASE-LEW-14162-1] p 159 N91-13668
- Heat transfer device p 101 N91-25201
- [NASA-CASE-LEW-14162-2] p 101 N91-25201

PYROMETERS

- Lag compensation of optical fibers or thermocouples to achieve waveform fidelity in dynamic gas pyrometry p 174 A91-54388

Q**QUADRATURE PHASE SHIFT KEYING**

- Performance evaluation of land mobile satellite system under vegetative shadowing using differential multiple TCM and QPSK p 132 A91-53084

QUALIFICATIONS

- Spacelab qualified infrared imager for microgravity science applications p 173 A91-51585

QUALITY CONTROL

- Optical inspection of space-propulsion components using an injection seeded Nd:YAG laser system p 179 N91-24320

- Quality control of the tribological coating PS212 p 101 N91-25186

QUANTUM CHROMODYNAMICS

- Inflationary axion cosmology p 239 A91-20491

QUANTUM EFFICIENCY

- Study of surface passivation as a function of InP closed-ampoule solar cell fabrication processing variables p 232 A91-41893

QUANTUM MECHANICS

- Adhesion at metal interfaces p 88 A91-38581

QUARTZ

- A numerical and experimental analysis of reactor performance and deposition rates for CVD on monofilaments p 130 N91-14500

- [NASA-TM-103631] p 130 N91-14500

R**RADIAL FLOW**

- A three-dimensional Navier-Stokes stage analysis of the flow through a compact radial turbine p 23 A91-41815

- [AIAA PAPER 91-2564] p 23 A91-41815

- Design and experimental evaluation of compact radial-inflow turbines p 24 A91-45788

- [AIAA PAPER 91-2127] p 24 A91-45788

- Comparison of a quasi-3D analysis and experimental performance for three compact radial turbines p 25 A91-45789

- [AIAA PAPER 91-2128] p 25 A91-45789

- A three-dimensional Navier-Stokes stage analysis of the flow through a compact radial turbine p 32 N91-23186

- [NASA-TM-104420] p 32 N91-23186

- Comparison of a quasi-3D analysis and experimental performance for three compact radial turbines p 35 N91-30142

- [NASA-TM-105155] p 35 N91-30142

- Unsteady flowfield of a propfan at takeoff conditions p 18 N91-32075

- [NASA-TM-105223] p 18 N91-32075

RADIANT COOLING

- Arcjet thermal characteristics p 63 A91-45814

- [AIAA PAPER 91-2456] p 63 A91-45814

- Liquid sheet radiator apparatus p 130 N91-15424

- [NASA-CASE-LEW-14295-1] p 130 N91-15424

- Cooling of in-situ propellant rocket engines for Mars mission p 72 N91-21233

- [NASA-TM-103729] p 72 N91-21233

RADIATION DAMAGE

- Radiation resistance of thin-film solar cells for space photovoltaic power p 71 N91-19176

- [NASA-TM-103715] p 71 N91-19176

- Space Photovoltaic Research and Technology Conference p 82 N91-30203

- [NASA-CP-3121] p 82 N91-30203

- Leo space plasma interactions p 84 N91-30249

RADIATION DOSAGE

- Neutron and gamma irradiation effects on power semiconductor switches p 139 A91-38162

- [NASA-TM-103733] p 139 A91-38162

- Radiation dose estimates for typical piloted NTR lunar and Mars mission engine operations p 215 A91-52331

- [AIAA PAPER 91-3407] p 215 A91-52331

RADIATION EFFECTS

- Effects of radiation of InP cells epitaxially grown on Si and GaAs substrates p 140 A91-41984

- [NASA-TM-103715] p 140 A91-41984

- Neutron, gamma ray and post-irradiation thermal annealing effects on power semiconductor switches p 142 A91-52420

- [AIAA PAPER 91-3525] p 142 A91-52420

- Effects of proton irradiation on the performance of InP/GaAs solar cells p 209 N91-19205

- [NASA-TM-104502] p 209 N91-19205

- Indium phosphide solar cells p 210 N91-19221

- [NASA-TM-104460] p 210 N91-19221

- Low Earth orbital atomic oxygen and ultraviolet radiation effects on polymers p 119 N91-19294

- [NASA-TM-103711] p 119 N91-19294

- Heteroepitaxial InP solar cells on Si and GaAs substrates p 144 N91-20392

- [NASA-TM-103696] p 144 N91-20392

- Environmental interactions of the Space Station Freedom electric power system p 49 N91-24225

- [NASA-TM-104373] p 49 N91-24225

- Advanced photovoltaic experiment, S0014: Preliminary flight results and post-flight findings p 212 N91-25061
- Neutron, gamma ray and post-irradiation thermal annealing effects on power semiconductor switches p 147 N91-32410
- [NASA-TM-105248] p 147 N91-32410

RADIATION MEASUREMENT

- Solar radiation on Mars p 242 A91-28153

RADIATION PROTECTION

- Radiation dose estimates for typical piloted NTR lunar and Mars mission engine operations p 215 A91-52331

- [AIAA PAPER 91-3407] p 215 A91-52331

RADIATION SHIELDING

- Neutron and gamma irradiation effects on power semiconductor switches p 139 A91-38162

RADIATION TOLERANCE

- Neutron and gamma irradiation effects on power semiconductor switches p 139 A91-38162

- Effects of radiation of InP cells epitaxially grown on Si and GaAs substrates p 140 A91-41984

- [NASA-TM-103715] p 140 A91-41984

- Radiation resistance of thin-film solar cells for space photovoltaic power p 71 N91-19176

- [NASA-TM-103715] p 71 N91-19176

- Effects of proton irradiation on the performance of InP/GaAs solar cells p 209 N91-19205

- [NASA-TM-104502] p 209 N91-19205

- A comparative study of performance parameters of n(+)-p InP solar cells made by closed-ampoule sulfur diffusion into Cd- and Zn-doped p-type InP substrates p 210 N91-19209

- [NASA-TM-103762] p 210 N91-19209

- Effect of dislocations on the open-circuit voltage, short-circuit current and efficiency of heteroepitaxial indium phosphide solar cells p 144 N91-19354

- [NASA-TM-103762] p 144 N91-19354

- Advanced power systems for EOS p 85 N91-31217

- [NASA-TM-105222] p 85 N91-31217

RADIATIVE HEAT TRANSFER

- Interaction of surface radiation with convection in crystal growth by physical vapor transport p 127 A91-24563

- [NASA-TM-103762] p 127 A91-24563

- Analytical solution for boundary heat fluxes from a radiating rectangular medium p 150 A91-27175

- [NASA-TM-103762] p 150 A91-27175

RADIO COMMUNICATION

- High temperature superconductor analog electronics for millimeter-wavelength communications p 233 A91-53707

- [AIAA PAPER 91-3592] p 233 A91-53707

- High temperature superconductor analog electronics for millimeter-wavelength communications p 237 N91-29982

- [NASA-TM-105184] p 237 N91-29982

RADIO FREQUENCIES

- LBR-2 Earth stations for the ACTS program p 133 N91-11971

- [NASA-TM-103802] p 133 N91-11971

- A seven patch hexagonal CP subarray with a CPW/stripline feed network p 144 N91-20406

- [NASA-TM-103802] p 144 N91-20406

- GaAs monolithic RF modules for SRSAT distress beacons p 46 N91-21184

- [NASA-TM-104338] p 46 N91-21184

- Fiber optic sensing system p 230 N91-21871

- [NASA-CASE-LEW-14795-1] p 230 N91-21871

- System-Level Integrated Circuit (SLIC) development for phased array antenna applications p 134 N91-23354

- [NASA-TM-104392] p 134 N91-23354

RADIO RECEIVERS

- Using a modified Hewlett Packard 8410 network analyzer as an automated farfield antenna range receiver p 143 N91-19349

- [NASA-TM-103700] p 143 N91-19349

RADIOGRAPHY

- In situ X-ray monitoring of damage accumulation in SiC/RBSN tensile specimens p 94 A91-56942

- [NASA-TM-103733] p 94 A91-56942

- In-situ x-ray monitoring of damage accumulation in SiC/RBSN tensile specimens p 99 N91-22402

- [NASA-TM-103733] p 99 N91-22402

- NDE of ceramics and ceramic composites p 194 N91-29610

- [NASA-TM-104520] p 194 N91-29610

RADIOISOTOPE BATTERIES

- SEI needs for space nuclear power p 64 A91-52369

- [AIAA PAPER 91-3459] p 64 A91-52369

- Trade studies for nuclear space power systems p 65 A91-52413

- [AIAA PAPER 91-3518] p 65 A91-52413

- Dynamic Isotope Surface Power Systems p 208 A91-52487

- [AIAA PAPER 91-3623] p 208 A91-52487

- Small Stirling dynamic isotope power system for multihundred-watt robotic missions p 78 N91-25182

- [NASA-TM-104460] p 78 N91-25182

RADIOMETERS

- Concentrator testing using projected images p 79 N91-27204

- [NASA-TM-104349] p 79 N91-27204

RAILGUN ACCELERATORS

- The preliminary feasibility of intercalated graphite railgun armatures p 137 A91-29257

- [NASA-TM-104349] p 137 A91-29257

RAILS

- Removable hand hold p 188 N91-26543

- [NASA-CASE-LEW-15196-1] p 188 N91-26543

RAIN

A statistical rain attenuation prediction model with application to the advanced communication technology satellite project. 3: A stochastic rain fade control algorithm for satellite link power via non linear Markov filtering theory

[NASA-TM-100243] p 134 N91-22494

RAMAN SPECTRA

The development of a fiber optic Raman temperature measurement system for rocket flows

[AIAA PAPER 91-2316] p 173 A91-45804

RAMJET ENGINES

Overview of hypersonic/transatmospheric vehicle propulsion technology

p 28 N91-20092

High temperature performance evaluation of a hypersonic engine ceramic wafer seal

[NASA-TM-103737] p 185 N91-22567

RAMPS (STRUCTURES)

Turbulent boundary layer separation over a rearward facing ramp and its control through mechanical excitation

[NASA-TM-103702] p 160 N91-19370

RANKING

Evaluation and ranking of candidate ceramic wafer engine seal materials

[NASA-TM-103795] p 187 N91-23515

RAPID QUENCHING (METALLURGY)

Rapid solidification of polymorphic transition metals induced by nanosecond laser pulses

p 109 A91-46520

RARE EARTH COMPOUNDS

Reappraisal of solid selective emitters ... for thermovoltaic energy conversion

p 207 A91-41999

Reappraisal of solid selective emitters

[NASA-TM-103290] p 69 N91-11801

RARE EARTH ELEMENTS

Reappraisal of solid selective emitters ... for thermovoltaic energy conversion

p 207 A91-41999

Reappraisal of solid selective emitters

[NASA-TM-103290] p 69 N91-11801

RAREFIED GAS DYNAMICS

Numerical and experimental investigations of rarefied nozzle and plume flows of nitrogen

[AIAA PAPER 91-1363] p 154 A91-43429

RATES (PER TIME)

Quaternary pulse position modulation electronics for free-space laser communications

[AIAA PAPER 91-3471] p 133 A91-53702

Quaternary pulse position modulation electronics for free-space laser communications

[NASA-TM-104502] p 135 N91-29405

RATINGS

Quantifying oil filtration effects on bearing life

[NASA-TM-104350] p 186 N91-23512

RAY TRACING

Inverse photoelectron spectrometer with magnetically focused electron gun

p 172 A91-42849

Relationship of optical coating on thermal radiation characteristics of nonisothermal cylindrical enclosures

[NASA-TM-104408] p 168 N91-30461

RAYLEIGH EQUATIONS

A comparison of numerical methods for the Rayleigh equation in unbounded domains

[NASA-TM-105179] p 223 N91-30865

RAYLEIGH SCATTERING

Spectrally resolved Rayleigh scattering diagnostic for hydrogen-oxygen rocket plume studies

[AIAA PAPER 91-0462] p 51 A91-21498

High-speed laser anemometry based on spectrally resolved Rayleigh scattering

[NASA-TM-104522] p 178 N91-27521

REACTING FLOW

Three-dimensional calculation of the mixing of radial jets from slanted slots with a reactive cylindrical crossflow

[AIAA PAPER 91-2081] p 24 A91-45782

Experimental and analytical comparison of flowfields in a 110 N (25 Lbf) H₂/O₂ rocket

[AIAA PAPER 91-2283] p 62 A91-45802

Experimental and analytical comparison of flowfields in a 110 N (25 lbf) H₂/O₂ rocket

[NASA-TM-105175] p 82 N91-29230

REACTION BONDING

Impact behavior of a SiC fiber-reinforced reaction bonded Si₃N₄ composite

p 91 A91-16805

REACTION KINETICS

Evaluation of a hybrid kinetics/mixing-controlled combustion model for turbulent premixed and diffusion combustion using KIVA-II

[AIAA PAPER 90-2450] p 104 A91-12927

Combustion of liquid fuel droplets in supercritical conditions

[AIAA PAPER 91-0078] p 105 A91-21362

Hydrogen-silicon carbide interactions

p 114 A91-28783

An analysis of the contact sintering process in III-V solar cells

p 139 A91-41891

Fuel-rich, catalytic reaction experimental results ... fuel development for high-speed civil transport aircraft

[AIAA PAPER 91-2463] p 24 A91-44250

Numerical simulation of Jet-A combustion approximated by improved propane chemical kinetics

[AIAA PAPER 91-1859] p 106 A91-45777

Jet-A reaction mechanism study for combustion application

[AIAA PAPER 91-2355] p 106 A91-45810

Effects of high pressure nitrogen on the thermal stability of SiC fibers

[NASA-TM-103245] p 96 N91-16075

Chemical reacting flows

p 162 N91-20098

Computer code for single-point thermodynamic analysis of hydrogen/oxygen expander-cycle rocket engines

[NASA-TM-104275] p 72 N91-20206

Fuel-rich, catalytic reaction experimental results

[NASA-TM-104423] p 33 N91-24203

Analytical combustion/emissions research related to the NASA high-speed research program

[NASA-TM-104521] p 34 N91-27165

Jet-A reaction mechanism study for combustion application

[NASA-TM-104441] p 35 N91-31181

REACTIVITY

Reactivity of pi-complexes of Ti, V, and Nb towards dithioacetic acid: Synthesis and structure of novel metal sulfur-containing complexes

[NASA-TM-103666] p 106 N91-19256

Synthesis and structures of metal chalcogenide precursors

[NASA-TM-103665] p 120 N91-19296

REACTOR DESIGN

An overview of tested and analyzed NTP concepts

[AIAA PAPER 91-3503] p 65 A91-52400

Multimegawatt nuclear power systems for nuclear electric propulsion

[AIAA PAPER 91-3607] p 66 A91-52472

Nuclear Thermal Propulsion technology - Summary of FY 1991 Interagency panel planning

[AIAA PAPER 91-3631] p 66 A91-52495

Vision-21: Space Travel for the Next Millennium

[NASA-CP-10059] p 40 N91-22139

A reliability and mass perspective of SP-100 Stirling cycle lunar-base powerplant designs

[NASA-TM-103736] p 212 N91-26592

REACTOR MATERIALS

Development of nuclear fuels and materials for propulsion systems for SEI

[AIAA PAPER 91-3452] p 125 A91-52362

Orr-Sherby-Dorn creep strengths of the refractory-metal alloys C-103, ASTAR-811C, W-5Re, and W-25Re

[NASA-TM-105228] p 87 N91-32165

REACTOR TECHNOLOGY

Vision-21: Space Travel for the Next Millennium

[NASA-CP-10059] p 40 N91-22139

REAL GASES

Osher's scheme for real gases

p 153 A91-42286

Efficient real gas upwinded Navier-Stokes computations of high speed flows

p 157 A91-46179

REAL TIME OPERATION

Real-time diagnostics of the reusable rocket engine using on-line system identification

p 223 A91-30630

Autonomous power expert system

p 54 A91-37972

Effect of KOH concentration on LEO cycle life of IPV nickel-hydrogen flight battery cells

p 55 A91-38076

An Electronic Pressure Profile Display system for aeronautics test facilities

p 38 A91-51858

An AD100 implementation of a real-time STOV_L aircraft propulsion system

[NASA-TM-103683] p 26 N91-13457

Real-time data compression of broadcast video signals

[NASA-CASE-LEW-14945-1] p 133 N91-13598

The NASA Lewis integrated propulsion and flight control simulator

[NASA-TM-105147] p 21 N91-27157

Description of real-time Ada software implementation of a power system monitor for the Space Station Freedom

PMAD DC testbed

[NASA-TM-105157] p 218 N91-28776

REATTACHED FLOW

Calculation of divergent channel flows with a multiple-time-scale turbulence model

p 151 A91-34134

RECEIVERS

Solar thermal energy receiver

[NASA-CASE-LEW-14949-1] p 211 N91-23617

Sensible heat receiver for solar dynamic space power system

[NASA-TM-104393] p 77 N91-25173

RECOMBINATION COEFFICIENT

Measurement of surface recombination velocity on heavily doped indium phosphide

p 232 A91-41931

RECRYSTALLIZATION

Crystallization and characterization of Y₂O₃-SiO₂ glasses

p 237 N91-31962

RECTANGULAR WAVEGUIDES

Mutual coupling between electromagnetically coupled rectangular patch antennas

p 137 A91-32822

New channelised coplanar waveguide to rectangular waveguide post and slot couplers

p 139 A91-40272

RECTENNAS

Lunar orbiting microwave beam power system

p 56 A91-38158

The theory of an auto-resonant field emission cathode relativistic electron accelerator for high efficiency microwave to direct current power conversion

p 73 N91-22176

RED GIANT STARS

The shock process and light-element production in supernova envelopes

p 239 A91-33573

RED SHIFT

Characteristic microwave-background distortions from collapsing spherical domain walls

p 238 A91-12343

Coherent peculiar velocities and periodic redshifts

p 239 A91-20430

REDUCED GRAVITY

Interfacial dynamics of two liquids under an oscillating gravitational field

p 148 A91-16062

Drop-tower experiments for capillary surfaces in an exotic container

[AIAA PAPER 91-0107] p 148 A91-19138

Transient cryogenic liquid discharge in normal and micro-gravity

[AIAA PAPER 91-0486] p 124 A91-19324

Particle nonuniformity effects on particle cloud flames in low gravity

[AIAA PAPER 91-0718] p 104 A91-19431

Radiation from gas-jet diffusion flames in microgravity environments

[AIAA PAPER 91-0719] p 104 A91-19432

Particle cloud flames in acoustic fields

p 105 A91-20589

A preview of a microgravity laser light scattering instrument

[AIAA PAPER 91-0779] p 179 A91-21614

A new approach to controller design for microgravity isolation systems

p 129 A91-23108

The COLD-SAT experiment for cryogenic fluid management technology

p 46 A91-29799

Radiative structures of lycopodium-air flames in low gravity

p 105 A91-30003

Thermocapillary migration of liquid droplets in a temperature gradient in a density matched system

p 153 A91-41132

Three-dimensional flow transport modes in directional solidification during space processing

p 128 A91-42642

Paramagnetic propellant orientation

[AIAA PAPER 91-2325] p 125 A91-44197

The dynamic effects of internal robots on Space Station Freedom

[AIAA PAPER 91-2822] p 40 A91-49764

Heat transfer to a thin solid combustible in flame spreading at microgravity

p 106 A91-51449

Discharge rate of cryogens in microgravity - What ground based experimentation cannot resolve

[AIAA PAPER 91-3545] p 129 A91-52430

The NASA Cryogenic Fluid Management Technology Program Plan

[AIAA PAPER 91-3553] p 130 A91-52436

Development of a vibration isolation prototype system for microgravity space experiments

p 47 A91-53403

Isothermal Dendritic Growth Experiment - Science, engineering, and hardware development for USMP space flights

p 128 A91-53408

Cryogenic transfer options for exploration missions

[AIAA PAPER 91-3541] p 158 A91-53714

Manipulation hardware for microgravity research

[NASA-TM-103423] p 128 N91-14498

Surface settling in partially filled containers upon step reduction in gravity

[NASA-TM-103641] p 159 N91-14556

Development of a vibration isolation prototype system for microgravity space experiments

[NASA-TM-103664] p 130 N91-19324

A summary of existing and planned experiment hardware for low-gravity fluids research

[NASA-TM-103706] p 160 N91-19371

Fire suppression in human-crew spacecraft

[NASA-TM-104334] p 44 N91-21182

Microgravity vibration isolation: An optimal control law for the one-dimensional case

p 49 N91-21206

An examination of anticipated g-jitter on space station and its effects on materials processes

[NASA-TM-103775] p 128 N91-21378

The dynamic effects of internal robots on Space Station Freedom

[NASA-TM-104345] p 203 N91-22604

Microgravity research at LeRC
[NASA-TM-102521] p 128 N91-24464

Paramagnetic propellant orientation
[NASA-TM-104390] p 166 N91-24527

Pressurization and expulsion of cryogenic liquids:
Generic requirements for a low gravity experiment
[NASA-TM-104417] p 126 N91-25300

Autogenous pressurization of cryogenic vessels using
submerged vapor injection
[NASA-TM-104516] p 127 N91-27375

Cryogenic transfer options for exploration missions
[NASA-TM-105197] p 168 N91-28538

Ground-based PIV and numerical flow visualization
results from the surface tension driven convection
experiment
[NASA-TM-105172] p 178 N91-30491

The International Space University's variable gravity
research facility design
[NASA-TM-105224] p 44 N91-31196

REDUNDANCY

Sensor failure detection for jet engines
p 22 A91-37593

k-out-of-n:G systems - Some cost considerations
p 192 A91-54553

How much redundancy: Some cost considerations,
including examples for spacecraft systems
[NASA-TM-103197] p 192 N91-17407

Reliability and cost: A sensitivity analysis
[NASA-TM-105293] p 238 N91-33014

REFLECTANCE

A model for the scattering of high-frequency
electromagnetic fields from dielectrics exhibiting
thermally-activated electrical losses
[NASA-TM-104376] p 224 N91-26872

REFLECTOR ANTENNAS

New coplanar waveguide/stripline feed network for
seven patch hexagonal CP subarray
p 137 A91-32823

Designs for the ATDRSS tri-band reflector antenna
[NASA-TM-103754] p 48 N91-20184

A new fabrication method for precision antenna
reflectors for space flight and ground test
[NASA-TP-3078] p 48 N91-21185

REFLECTORS

A new fabrication method for precision antenna
reflectors for space flight and ground test
[NASA-TP-3078] p 48 N91-21185

REFRACTIVITY

Optical techniques for determination of normal shock
position in supersonic flows for aerospace applications
p 174 A91-55530

Ellipsometric study of cubic SiC
p 235 N91-18304

Optical dispersion relations for diamondlike carbon
films
p 230 N91-18305

Three-dimensional computed tomography from
interferometric measurements within a narrow cone of
views
[NASA-TM-103257] p 176 N91-19404

REFRACTORY MATERIALS

Tribological properties of PM212 - A high temperature,
self-lubricating, powder metallurgy composite
[STLE PREPRINT 90-AM-4E-1] p 87 A91-19720

Atomic oxygen effects on refractory materials
p 88 A91-49809

METCAN simulation of candidate metal matrix
composites for high temperature applications
[NASA-TM-103636] p 96 N91-17143

NDE standards for high temperature materials
[NASA-TM-103761] p 193 N91-19464

Advanced high temperature engine materials technology
program
p 98 N91-20110

High temperature power electronics for space
[NASA-TM-104375] p 145 N91-22508

Combined thermal and bending fatigue of
high-temperature metal-matrix composites: Computational
simulation
[NASA-TM-104354] p 100 N91-23247

REFRACTORY METAL ALLOYS

Orr-Sherby-Dorn creep strengths of the refractory-metal
alloys C-103, ASTAR-811C, W-5Re, and W-25Re
[NASA-TM-105228] p 87 N91-32165

REFRIGERANTS

Automatic control study of the icing research tunnel
refrigeration system
[NASA-TM-4257] p 40 N91-19115

REFRIGERATING

Automatic control study of the icing research tunnel
refrigeration system
[NASA-TM-4257] p 40 N91-19115

REGENERATIVE FUEL CELLS

Modeling and optimization of a regenerative fuel cell
system using the ASPEN process simulator
p 206 A91-38177

SEI rover solar-electrochemical power system options
[NASA-TM-104402] p 211 N91-23620

REGENERATORS

Turbomachinery and combustor technology for small
engines p 29 N91-20113

REINFORCING FIBERS

An overview of self-consistent methods for
fiber-reinforced composites
[NASA-TM-103713] p 97 N91-19232

Effect of fiber reinforcements on thermo-oxidative
stability and mechanical properties of polymer matrix
composites
[NASA-TM-103648] p 98 N91-19234

Computational materials science. An example:
Numerical modeling of chemical vapor deposition
processing of advanced fibers
p 99 N91-20111

Mechanical behavior of fiber reinforced SiC/RBSN
ceramic matrix composites: Theory and experiment
[NASA-TM-103688] p 99 N91-21243

Tribological characteristics of silicon carbide
whisker-reinforced alumina at elevated temperatures
[NASA-TM-103799] p 89 N91-22379

Modeling of crack bridging in a unidirectional metal matrix
composite
[NASA-TM-104355] p 205 N91-24660

Tensile deformation damage in SiC reinforced
Ti-15V-3Cr-3Al-3Sn
[NASA-TM-103620] p 101 N91-25195

RELATIVITY

Exploring the notion of space coupling propulsion
p 73 N91-22161

RELAY SATELLITES

Technologies for unattended network operations
[AIAA PAPER 91-3534] p 45 A91-52425

Millimeter wavelength communications applications for
the SEI
[AIAA PAPER 91-3589] p 45 A91-52458

Millimeter wavelength communications applications for
the SEI
[NASA-TM-105275] p 135 N91-32287

RELEASING

Quick action clamp
[NASA-CASE-LEW-14887-1] p 189 N91-27561

RELIABILITY

Preliminary designs for 25 kWe advanced Stirling
conversion systems for dish electric applications
p 207 A91-38182

A methodology for evaluating the reliability and risk of
structures under complex service environments
[NASA-TM-103244] p 200 N91-17415

Balancing reliability and cost to choose the best power
subsystem
[NASA-TM-104453] p 238 N91-24952

On protection of Freedom's solar dynamic radiator from
the orbital debris environment. Part 2: Further testing and
analyses
[NASA-TM-104514] p 84 N91-30265

RELIABILITY ANALYSIS

k-out-of-n:G systems - Some cost considerations
p 192 A91-54553

ETARA PC version 3.3 user's guide: Reliability,
availability, maintainability simulation model
[NASA-TM-103751] p 193 N91-19462

The environment workbench: A design tool for Space
Station Freedom
p 48 N91-20727

Reliability and risk assessment of structures
p 194 N91-23050

Probability approach for strength calculations
p 204 N91-24652

A reliability and mass perspective of SP-100 Stirling cycle
lunar-base powerplant designs
[NASA-TM-103736] p 212 N91-26592

RELIABILITY ENGINEERING

How much redundancy: Some cost considerations,
including examples for spacecraft systems
[NASA-TM-103197] p 192 N91-17407

Reliability and cost: A sensitivity analysis
[NASA-TM-105293] p 238 N91-33014

RELIC RADIATION

Characteristic microwave-background distortions from
collapsing spherical domain walls
p 238 A91-12343

Coherent peculiar velocities and periodic redshifts
p 239 A91-20430

Big bang nucleosynthesis - The standard model and
alternatives
p 240 A91-37428

RELOCATION

Satellite relocation by tether deployment
p 40 A91-22966

RENORMALIZATION GROUP METHODS

An algebraic RNG-based turbulence model for
three-dimensional turbomachinery flows
[AIAA PAPER 91-0172] p 2 A91-21393

Nonlinear Reynolds stress model for turbulent shear
flows
[AIAA PAPER 91-0609] p 149 A91-21556

Renormalization group analysis of anisotropic diffusion
in turbulent shear flows
p 150 A91-27946

RESEARCH AIRCRAFT

Effects of horizontal tail ice on longitudinal aerodynamic
derivatives p 36 A91-38547

RESEARCH AND DEVELOPMENT

Programmable multi-zone furnace for microgravity
research
[AIAA PAPER 91-0781] p 127 A91-19463

Bibliography of Lewis Research Center technical
publications announced in 1989
[NASA-TM-102542] p 238 N91-10798

JANNAF liquid rocket combustion instability panel
research recommendations
[NASA-TM-103653] p 70 N91-13491

Instrumentation and controls overview
p 38 N91-20099

Overview of Lewis materials research: Contributions,
current efforts, and future directions
p 111 N91-20109

Computational materials science. An example:
Numerical modeling of chemical vapor deposition
processing of advanced fibers
p 99 N91-20111

Turbomachinery and combustor technology for small
engines p 29 N91-20113

Rotary engine technology p 30 N91-20114

Overview of subsonic transport propulsion technology
p 30 N91-20116

Multidisciplinary research overview (IHPTET/NPSS)
p 30 N91-20119

NASA's aircraft icing technology program
p 19 N91-20120

Recent advances in Lewis aer propulsion facilities
p 38 N91-20121

High temperature power electronics for space
[NASA-TM-104375] p 145 N91-22508

Institute for Computational Mechanics in Propulsion
(ICOMP)
[NASA-TM-103790] p 222 N91-24818

Research and development of optical measurement
techniques for aerospace propulsion research: A NASA
Lewis Research Center perspective
[NASA-TM-104418] p 178 N91-27511

Concurrent engineering
p 80 N91-28247

MPD thruster technology
[NASA-TM-105242] p 86 N91-32162

RESEARCH FACILITIES

A summary of existing and planned experiment hardware
for low-gravity fluids research
[NASA-TM-103706] p 160 N91-19371

Overview of Lewis materials research: Contributions,
current efforts, and future directions
p 111 N91-20109

Recent advances in Lewis aer propulsion facilities
p 38 N91-20121

Design strategies for the International Space University's
variable gravity research facility
p 42 N91-22171

Research and technology
[NASA-TM-103759] p 243 N91-23072

The International Space University's variable gravity
research facility design
[NASA-TM-105224] p 44 N91-31196

RESEARCH MANAGEMENT

Research and development of optical measurement
techniques for aerospace propulsion research: A NASA
Lewis Research Center perspective
[NASA-TM-104418] p 178 N91-27511

RESEARCH PROJECTS

JANNAF liquid rocket combustion instability panel
research recommendations
[NASA-TM-103653] p 70 N91-13491

Overview of structures research
p 202 N91-20104

Overview of Lewis materials research: Contributions,
current efforts, and future directions
p 111 N91-20109

Multidisciplinary research overview (IHPTET/NPSS)
p 30 N91-20119

Status of the advanced Stirling conversion system
project for 25 kW dish Stirling applications
[NASA-TM-104528] p 238 N91-31023

RESIDUAL STRENGTH

Thermal shock fiber-reinforced ceramic matrix
composites
p 93 A91-56935

Thermal shock of fiber reinforced ceramic matrix
composites
[NASA-TM-103777] p 120 N91-19295

RESIDUAL STRESS

Fiber pushout test - A three-dimensional finite element
computational simulation
p 197 A91-33096

Concurrent tailoring of fabrication process and
interphase layer to reduce residual stresses in metal matrix
composites
p 92 A91-43232

Elastic/plastic analyses of advanced composites
investigating the use of the compliant layer concept in
reducing residual stresses resulting from processing
[NASA-TM-103204] p 94 N91-11074

- Tensile behavior of tungsten/niobium composites at 1300 to 1600 K
[NASA-TM-103727] p 111 N91-16128
- METCAN simulation of candidate metal matrix composites for high temperature applications
[NASA-TM-103636] p 96 N91-17143
- Computational simulation of hot composites structures
[NASA-TM-103681] p 97 N91-19230
- Concurrent micromechanical tailoring and fabrication process optimization for metal-matrix composites
[NASA-TM-103670] p 98 N91-19237
- Elevated-temperature fracture resistances (K_{IC}), R-curves, gamma sub (omega OF) of monolithic and composite ceramics using chevron-notched, bend tests
[NASA-TM-105090] p 123 N91-28418
- Interphase layer optimization for metal matrix composites with fabrication considerations
[NASA-TM-105166] p 102 N91-30281
- RESIN MATRIX COMPOSITES**
- Electrically conducting polymers for aerospace applications
[AIAA PAPER 91-3432] p 233 A91-52349
- Ladder polymers for use as high temperature stable resins or coatings
[NASA-CASE-LEW-14203-1] p 118 N91-15402
- RESISTOJET ENGINES**
- Experimental evaluation of resistojet thruster plume shields p 51 A91-30010
- Test-cell pressure effects on the performance of resistojets p 38 A91-37417
- A 10,000-hr life test of an engineering model resistojet
[NASA-TM-103216] p 69 N91-11802
- RESONANCE**
- Resonant triad in boundary-layer stability. Part 2: Composite solution and comparison with observations
[NASA-TM-105209] p 169 N91-32459
- RESONANT FREQUENCIES**
- Dynamic analysis of space-related linear and non-linear structures p 196 A91-28612
- YBCO superconducting ring resonators at millimeter-wave frequencies p 142 A91-54532
- RESONATORS**
- An experimental study of high T_c superconducting microstrip transmission lines at 35 GHz and the effect of film morphology p 138 A91-36172
- YBCO superconducting ring resonators at millimeter-wave frequencies p 142 A91-54532
- An experimental study of high T_c superconducting microstrip transmission lines at 35 GHz and the effect of film morphology
[NASA-TM-103633] p 133 N91-11988
- RESOURCE ALLOCATION**
- Automated electric power management and control for Space Station Freedom p 53 A91-37970
- REUSABLE ROCKET ENGINES**
- An intelligent control system for rocket engines - Need, vision, and issues p 218 A91-26925
- Linear quadratic servo control of a reusable rocket engine
[AIAA PAPER 91-1999] p 57 A91-41670
- Development of an intelligent diagnostic system for reusable rocket engine control
[AIAA PAPER 91-2533] p 63 A91-45817
- Structural Integrity and Durability of Reusable Space Propulsion Systems
[NASA-CP-10030] p 76 N91-24307
- REUSABLE SPACECRAFT**
- Real-time diagnostics of the reusable rocket engine using on-line system identification p 223 A91-30630
- Cryogenic propellant management system requirements for Space Station Freedom
[AIAA PAPER 91-3476] p 65 A91-52382
- REVERSED FLOW**
- Flow visualization and computational studies of a reverse flow circular combustor p 157 A91-48966
- REYNOLDS EQUATION**
- Navier-Stokes simulation of the supersonic combustion flowfield in a ram accelerator
[AIAA PAPER 91-1916] p 155 A91-44057
- A system-approach to the elastohydrodynamic lubrication point-contact problem
[NASA-TM-104342] p 165 N91-23439
- Navier-Stokes simulation of the supersonic combustion flowfield in a ram accelerator
[NASA-TM-104439] p 166 N91-24541
- REYNOLDS NUMBER**
- Navier-Stokes analysis of turbine blade heat transfer
[ASME PAPER 90-GT-42] p 155 A91-44529
- Characterization of flow in a scroll duct
[NASA-CR-188612] p 167 N91-25367
- REYNOLDS STRESS**
- Nonlinear Reynolds stress model for turbulent shear flows
[AIAA PAPER 91-0609] p 149 A91-21556
- Calculation of turbulent flow in complex geometries with a second-moment closure model p 152 A91-38741
- Second order modeling of boundary-free turbulent shear flows
[AIAA PAPER 91-1779] p 154 A91-42588
- The effects of rotation on initially anisotropic homogeneous flows p 158 A91-54958
- Second order modeling of boundary-free turbulent shear flows
[NASA-TM-104369] p 164 N91-22524
- Experimental investigation of turbulent flow through a circular-to-rectangular transition duct
[NASA-TM-105210] p 18 N91-31106
- RHEOLOGY**
- Polymeric routes to silicon carbide and silicon oxycarbide CMC p 117 A91-56922
- Polymeric routes to silicon carbide and silicon oxycarbide CMC
[NASA-TM-104372] p 102 N91-26234
- RICHARDSON NUMBER**
- Stability of an oscillated fluid with a uniform density gradient p 147 A91-12971
- RING STRUCTURES**
- Structural design concepts for a multi-megawatt Solar Electric Propulsion (SEP) spacecraft
[NASA-TM-105148] p 206 N91-30565
- RISK**
- A methodology for evaluating the reliability and risk of structures under complex service environments
[NASA-TM-103244] p 200 N91-17415
- Dual-purpose self-deliverable lunar surface PV electrical power system p 209 N91-19200
- Reliability and risk assessment of structures p 194 N91-23050
- ROBOT CONTROL**
- The dynamic effects of internal robots on Space Station Freedom
[AIAA PAPER 91-2822] p 40 A91-49764
- The dynamic effects of internal robots on Space Station Freedom
[NASA-TM-104345] p 203 N91-22604
- ROBOTICS**
- Manipulation hardware for microgravity research
[NASA-TM-103423] p 128 N91-14498
- ROBOTS**
- The dynamic effects of internal robots on Space Station Freedom
[AIAA PAPER 91-2822] p 40 A91-49764
- Manipulation hardware for microgravity research
[NASA-TM-103423] p 128 N91-14498
- The dynamic effects of internal robots on Space Station Freedom
[NASA-TM-104345] p 203 N91-22604
- ROBUSTNESS (MATHEMATICS)**
- Partitioning methods for global controllers p 219 A91-30043
- Integrated flight/propulsion control design for a STOVL aircraft using H-infinity control design techniques
[NASA-TM-104340] p 31 N91-21140
- ROCKET ENGINE CONTROL**
- Linear quadratic servo control of a reusable rocket engine
[AIAA PAPER 91-1999] p 57 A91-41670
- Development of an intelligent diagnostic system for reusable rocket engine control
[AIAA PAPER 91-2533] p 63 A91-45817
- ROCKET ENGINE DESIGN**
- Real-time diagnostics of the reusable rocket engine using on-line system identification p 223 A91-30630
- Numerical simulation of self-field MPD thrusters
[AIAA PAPER 91-2341] p 62 A91-45805
- Design of an Advanced Expander Test Bed --- for future space engines
[AIAA PAPER 91-3437] p 42 A91-52350
- Blazing the trailway - Nuclear electric propulsion and its technology program plans
[AIAA PAPER 91-3441] p 64 A91-52353
- An overview of tested and analyzed NTP concepts
[AIAA PAPER 91-3503] p 65 A91-52400
- Advanced ion propulsion for space exploration
[AIAA PAPER 91-3567] p 65 A91-52443
- NTR vehicle commonality assessment for piloted lunar and Mars missions
[AIAA PAPER 91-3575] p 66 A91-52448
- Computational fluid dynamics studies of nuclear rocket performance
[AIAA PAPER 91-3577] p 66 A91-52450
- Fiber-optic applications for space-based rocket engines
[AIAA PAPER 91-3602] p 49 A91-52468
- Space engine safety system
[AIAA PAPER 91-3604] p 44 A91-52470
- Developments in REDES: The rocket engine design expert system
[NASA-TM-103657] p 67 N91-10119
- A rocket engine design expert system p 71 N91-17129
- Fiber-optic applications for space-based engines
[NASA-TM-105235] p 86 N91-32163
- Multimegawatt electric propulsion system design considerations
[NASA-TM-105152] p 87 N91-32164
- ROCKET ENGINES**
- Development of a Fabry-Perot interferometer for rocket engine plume monitoring p 171 A91-30634
- Flow visualization of a rocket injector spray using gelled propellant simulants
[AIAA PAPER 91-2198] p 59 A91-44151
- A dual-cooled hydrogen-oxygen rocket engine heat transfer analysis
[AIAA PAPER 91-2211] p 59 A91-44156
- Determination of alloy content from plume spectral measurements
[AIAA PAPER 91-2531] p 88 A91-44284
- Cathode phenomena in a low-power magnetoplasmadynamic thruster p 63 A91-52314
- A three-dimensional turbulent heat transfer analysis for advanced tubular rocket thrust chambers
[NASA-TM-103293] p 159 N91-10249
- Cooling of in-situ propellant rocket engines for Mars mission
[NASA-TM-103729] p 72 N91-21233
- A three-dimensional turbulent heat transfer analysis for advanced tubular rocket thrust chambers p 75 N91-24258
- A dual-cooled hydrogen-oxygen rocket engine heat transfer analysis
[NASA-TM-104430] p 76 N91-24302
- Probabilistic structural analysis: Introductory remarks p 204 N91-24326
- Determination of alloy content from plume spectral measurements
[NASA-TM-104442] p 89 N91-24341
- ROCKET EXHAUST**
- Spectrally resolved Rayleigh scattering diagnostic for hydrogen-oxygen rocket plume studies
[AIAA PAPER 91-0462] p 51 A91-21498
- ROCKET NOZZLES**
- Numerical study of high-area-ratio H_2/O_2 rocket nozzles
[AIAA PAPER 91-2434] p 57 A91-41780
- Analytical study of nozzle performance for nuclear thermal rockets
[AIAA PAPER 91-3578] p 66 A91-52451
- ROCKET PROPELLANTS**
- Historical perspectives - The role of the NASA Lewis Research Center in the national space nuclear power programs
[AIAA PAPER 91-3462] p 242 A91-53713
- Cooling of in-situ propellant rocket engines for Mars mission
[NASA-TM-103729] p 72 N91-21233
- Historical perspectives: The role of the NASA Lewis Research Center in the national space nuclear power programs
[NASA-TM-105196] p 243 N91-29138
- Technical prospects for utilizing extraterrestrial propellants for space exploration
[NASA-TM-105263] p 127 N91-31318
- MPD thruster technology
[NASA-TM-105242] p 86 N91-32162
- ROCKET TEST FACILITIES**
- The Advanced Expander Test Bed
[AIAA PAPER 90-3708] p 50 A91-10107
- Design of an Advanced Expander Test Bed --- for future space engines
[AIAA PAPER 91-3437] p 42 A91-52350
- Test facilities for high power electric propulsion
[AIAA PAPER 91-3499] p 42 A91-52396
- ROCKET THRUST**
- A three-dimensional turbulent heat transfer analysis for advanced tubular rocket thrust chambers
[NASA-TM-103293] p 159 N91-10249
- A life comparison of tube and channel cooling passages for thrust chambers
[NASA-TM-103613] p 68 N91-11059
- New method of making advanced tube-bundle rocket thrust chambers
[NASA-TM-103617] p 70 N91-15301
- A three-dimensional turbulent heat transfer analysis for advanced tubular rocket thrust chambers p 75 N91-24258
- RODS**
- Low velocity impact analysis with NASTRAN p 198 A91-48865
- Low velocity impact analysis with NASTRAN
[NASA-TM-103169] p 95 N91-14426
- ROLLER BEARINGS**
- Quantifying oil filtration effects on bearing life
[NASA-TM-104350] p 186 N91-23512
- ROLLERS**
- Fully articulated four-point-bend loading fixture
[NASA-CASE-LEW-14776-1] p 185 N91-21540

ROLLING CONTACT LOADS

- Surface fatigue life of M50NiL and AISI 9310 gears and rolling-contact bars p 182 A91-45350
- Surface fatigue life of M50NiL and AISI 9310 spur gears and R C bars p 189 N91-27569

ROOM TEMPERATURE

- Matrix plasticity in SiC/Ti-15-3 composite p 102 N91-27247

ROTARY WING AIRCRAFT

- The breakup of trailing-line vortices p 9 N91-10867
- The selection of convertible engines with current gas generator technology for high speed rotorcraft p 27 N91-19097
- Overview of rotorcraft and general aviation propulsion technology p 29 N91-20112
- Advanced rotorcraft transmission program p 184 N91-21531

ROTARY WINGS

- Results of a sub-scale model rotor icing test p 19 A91-26190
- Results of a sub-scale model rotor icing test p 11 N91-14309
- Recent manufacturing advances for spiral bevel gears p 191 N91-31654

ROTATING BODIES

- In-flight source noise of an advanced full-scale single-rotation propeller p 226 A91-21547

ROTATING DISKS

- Incorporating finite element analysis into component life and reliability p 203 N91-23550

ROTATING FLUIDS

- Unstable viscous wall modes in rotating pipe flow p 154 A91-42599
- The effects of rotation on initially anisotropic homogeneous flows p 158 A91-54958
- A study of high speed flows in an aircraft transition duct p 17 N91-26122

ROTATING SHAFTS

- A fiber optic sensor for noncontact measurement of shaft speed, torque and power p 173 A91-51870
- Eccentricity effects on leakage of a brush seal at low speeds p 86 N91-31220

ROTATION

- Apparatus for intercalating large quantities of fibrous structures p 102 N91-28289

ROTOR AERODYNAMICS

- Prediction of unsteady blade surface pressures on an advanced propeller at an angle of attack p 226 A91-18257

- A review of ice accretion data from a model rotor icing test and comparison with theory p 19 A91-22500

- Results of a sub-scale model rotor icing test p 19 A91-26190

- A review of ice accretion data from a model rotor icing test and comparison with theory p 11 N91-13421

- Results of a sub-scale model rotor icing test p 11 N91-14309

- Model rotor icing tests in the NASA Lewis icing research tunnel p 32 N91-23184

- Calculated performance of the NASA Lewis icing research tunnel p 39 N91-29199

- Model rotor icing tests in the NASA Lewis icing research tunnel p 32 N91-23184

- Calculated performance of the NASA Lewis icing research tunnel p 39 N91-29199

- Model rotor icing tests in the NASA Lewis icing research tunnel p 32 N91-23184

- Calculated performance of the NASA Lewis icing research tunnel p 39 N91-29199

- Model rotor icing tests in the NASA Lewis icing research tunnel p 32 N91-23184

- Calculated performance of the NASA Lewis icing research tunnel p 39 N91-29199

- Model rotor icing tests in the NASA Lewis icing research tunnel p 32 N91-23184

- Calculated performance of the NASA Lewis icing research tunnel p 39 N91-29199

- Model rotor icing tests in the NASA Lewis icing research tunnel p 32 N91-23184

- Calculated performance of the NASA Lewis icing research tunnel p 39 N91-29199

- Model rotor icing tests in the NASA Lewis icing research tunnel p 32 N91-23184

- Calculated performance of the NASA Lewis icing research tunnel p 39 N91-29199

- Model rotor icing tests in the NASA Lewis icing research tunnel p 32 N91-23184

- Calculated performance of the NASA Lewis icing research tunnel p 39 N91-29199

- Model rotor icing tests in the NASA Lewis icing research tunnel p 32 N91-23184

- Calculated performance of the NASA Lewis icing research tunnel p 39 N91-29199

- Model rotor icing tests in the NASA Lewis icing research tunnel p 32 N91-23184

- Calculated performance of the NASA Lewis icing research tunnel p 39 N91-29199

- Model rotor icing tests in the NASA Lewis icing research tunnel p 32 N91-23184

- Calculated performance of the NASA Lewis icing research tunnel p 39 N91-29199

- Model rotor icing tests in the NASA Lewis icing research tunnel p 32 N91-23184

- Calculated performance of the NASA Lewis icing research tunnel p 39 N91-29199

- Model rotor icing tests in the NASA Lewis icing research tunnel p 32 N91-23184

- Calculated performance of the NASA Lewis icing research tunnel p 39 N91-29199

- Model rotor icing tests in the NASA Lewis icing research tunnel p 32 N91-23184

- Calculated performance of the NASA Lewis icing research tunnel p 39 N91-29199

- Model rotor icing tests in the NASA Lewis icing research tunnel p 32 N91-23184

- Calculated performance of the NASA Lewis icing research tunnel p 39 N91-29199

- Model rotor icing tests in the NASA Lewis icing research tunnel p 32 N91-23184

- Calculated performance of the NASA Lewis icing research tunnel p 39 N91-29199

- Model rotor icing tests in the NASA Lewis icing research tunnel p 32 N91-23184

- Calculated performance of the NASA Lewis icing research tunnel p 39 N91-29199

- Model rotor icing tests in the NASA Lewis icing research tunnel p 32 N91-23184

- Calculated performance of the NASA Lewis icing research tunnel p 39 N91-29199

- Model rotor icing tests in the NASA Lewis icing research tunnel p 32 N91-23184

- Calculated performance of the NASA Lewis icing research tunnel p 39 N91-29199

- Model rotor icing tests in the NASA Lewis icing research tunnel p 32 N91-23184

- Calculated performance of the NASA Lewis icing research tunnel p 39 N91-29199

- Model rotor icing tests in the NASA Lewis icing research tunnel p 32 N91-23184

- Calculated performance of the NASA Lewis icing research tunnel p 39 N91-29199

- Model rotor icing tests in the NASA Lewis icing research tunnel p 32 N91-23184

- Calculated performance of the NASA Lewis icing research tunnel p 39 N91-29199

- Model rotor icing tests in the NASA Lewis icing research tunnel p 32 N91-23184

ROTORS

- A review of ice accretion data from a model rotor icing test and comparison with theory p 19 A91-22500

- Localization of aeroelastic modes in mistuned high-energy turbines p 198 A91-44319

- A review of ice accretion data from a model rotor icing test and comparison with theory p 11 N91-13421

- Optical measurement of unducted fan flutter p 27 N91-15174

- Modal analysis of multistage gear systems coupled with gearbox vibrations p 187 N91-23513

- Localization of aeroelastic modes in mistuned high-energy turbines p 204 N91-24659

- Some preliminary results of brush seal/rotor interference effects on leakage at zero and low RPM using a tapered-plug rotor p 188 N91-27559

- Calculated performance of the NASA Lewis icing research tunnel p 39 N91-29199

- Eccentricity effects on leakage of a brush seal at low speeds p 86 N91-31220

- [NASA-TM-105141] p 86 N91-31220

- [NASA-TM-105141] p 86 N91-31220

- [NASA-TM-105141] p 86 N91-31220

- [NASA-TM-105141] p 86 N91-31220

- [NASA-TM-105141] p 86 N91-31220

- [NASA-TM-105141] p 86 N91-31220

- [NASA-TM-105141] p 86 N91-31220

- [NASA-TM-105141] p 86 N91-31220

- [NASA-TM-105141] p 86 N91-31220

- [NASA-TM-105141] p 86 N91-31220

- [NASA-TM-105141] p 86 N91-31220

- [NASA-TM-105141] p 86 N91-31220

- [NASA-TM-105141] p 86 N91-31220

- [NASA-TM-105141] p 86 N91-31220

- [NASA-TM-105141] p 86 N91-31220

- [NASA-TM-105141] p 86 N91-31220

- [NASA-TM-105141] p 86 N91-31220

- [NASA-TM-105141] p 86 N91-31220

- [NASA-TM-105141] p 86 N91-31220

- [NASA-TM-105141] p 86 N91-31220

- [NASA-TM-105141] p 86 N91-31220

- [NASA-TM-105141] p 86 N91-31220

- [NASA-TM-105141] p 86 N91-31220

- [NASA-TM-105141] p 86 N91-31220

- [NASA-TM-105141] p 86 N91-31220

- [NASA-TM-105141] p 86 N91-31220

- [NASA-TM-105141] p 86 N91-31220

- [NASA-TM-105141] p 86 N91-31220

- [NASA-TM-105141] p 86 N91-31220

- [NASA-TM-105141] p 86 N91-31220

- [NASA-TM-105141] p 86 N91-31220

- [NASA-TM-105141] p 86 N91-31220

- [NASA-TM-105141] p 86 N91-31220

- [NASA-TM-105141] p 86 N91-31220

- [NASA-TM-105141] p 86 N91-31220

- [NASA-TM-105141] p 86 N91-31220

- [NASA-TM-105141] p 86 N91-31220

- [NASA-TM-105141] p 86 N91-31220

- [NASA-TM-105141] p 86 N91-31220

- [NASA-TM-105141] p 86 N91-31220

- [NASA-TM-105141] p 86 N91-31220

- [NASA-TM-105141] p 86 N91-31220

- [NASA-TM-105141] p 86 N91-31220

- [NASA-TM-105141] p 86 N91-31220

- [NASA-TM-105141] p 86 N91-31220

- [NASA-TM-105141] p 86 N91-31220

- [NASA-TM-105141] p 86 N91-31220

- [NASA-TM-105141] p 86 N91-31220

- [NASA-TM-105141] p 86 N91-31220

- [NASA-TM-105141] p 86 N91-31220

- [NASA-TM-105141] p 86 N91-31220

- [NASA-TM-105141] p 86 N91-31220

- [NASA-TM-105141] p 86 N91-31220

- [NASA-TM-105141] p 86 N91-31220

- [NASA-TM-105141] p 86 N91-31220

- [NASA-TM-105141] p 86 N91-31220

- [NASA-TM-105141] p 86 N91-31220

- [NASA-TM-105141] p 86 N91-31220

- [NASA-TM-105141] p 86 N91-31220

- [NASA-TM-105141] p 86 N91-31220

- [NASA-TM-105141] p 86 N91-31220

- [NASA-TM-105141] p 86 N91-31220

- [NASA-TM-105141] p 86 N91-31220

- [NASA-TM-105141] p 86 N91-31220

- [NASA-TM-105141] p 86 N91-31220

- [NASA-TM-105141] p 86 N91-31220

- [NASA-TM-105141] p 86 N91-31220

- [NASA-TM-105141] p 86 N91-31220

- [NASA-TM-105141] p 86 N91-31220

- [NASA-TM-105141] p 86 N91-31220

- [NASA-TM-105141] p 86 N91-31220

- [NASA-TM-105141] p 86 N91-31220

- [NASA-TM-105141] p 86 N91-31220

- [NASA-TM-105141] p 86 N91-31220

- [NASA-TM-105141] p 86 N91-31220

- [NASA-TM-105141] p 86 N91-31220

- [NASA-TM-105141] p 86 N91-31220

- [NASA-TM-105141] p 86 N91-31220

- [NASA-TM-105141] p 86 N91-31220

- [NASA-TM-105141] p 86 N91-31220

- [NASA-TM-105141] p 86 N91-31220

- [NASA-TM-105141] p 86 N91-31220

- [NASA-TM-105141] p 86 N91-31220

- [NASA-TM-105141] p 86 N91-31220

- [NASA-TM-105141] p 86 N91-31220

- [NASA-TM-105141] p 86 N91-31220

- [NASA-TM-105141] p 86 N91-31220

- [NASA-TM-105141] p 86 N91-31220

- [NASA-TM-105141] p 86 N91-31220

- [NASA-TM-105141] p 86 N91-31220

S**SAFETY MANAGEMENT**

- Space engine safety system p 44 A91-52470

- [AIAA PAPER 91-3604] p 44 A91-52470

- [AIAA PAPER 91-3604] p 44 A91-52470

- [AIAA PAPER 91-3604] p 44 A91-52470

- [AIAA PAPER 91-3604] p 44 A91-52470

- [AIAA PAPER 91-3604] p 44 A91-52470

- [AIAA PAPER 91-3604] p 44 A91-52470

- [AIAA PAPER 91-3604] p 44 A91-52470

- [AIAA PAPER 91-3604] p 44 A91-52470

- [AIAA PAPER 91-3604] p 44 A91-52470

- [AIAA PAPER 91-3604] p 44 A91-52470

- [AIAA PAPER 91-3604] p 44 A91-52470

- [AIAA PAPER 91-3604] p 44 A91-52470

- [AIAA PAPER 91-3604] p 44 A91-52470

- [AIAA PAPER 91-3604] p 44 A91-52470

- [AIAA PAPER 91-3604] p 44 A91-52470

- [AIAA PAPER 91-3604] p 44 A91-52470

- [AIAA PAPER 91-3604] p 44 A91-52470

- [AIAA PAPER 91-3604] p 44 A91-52470

- [AIAA PAPER 91-3604] p 44 A91-52470

- [AIAA PAPER 91-3604] p 44 A91-52470

- [AIAA PAPER 91-3604] p 44 A91-52470

- [AIAA PAPER 91-3604] p 44 A91-52470

- [AIAA PAPER 91-3604] p 44 A91-52470

SECONDARY FLOW

- Development of braided rope seals for hypersonic engine applications: Part 2: Flow modeling
[NASA-TM-104371] p 186 N91-22571
- High-temperature, flexible, thermal barrier seal
[NASA-CASE-LEW-14672-1] p 189 N91-27560
- High temperature NASP engine seals: A technology review
[NASA-TM-104468] p 190 N91-30538
- ### SECONDARY FLOW
- Characterization of flow in a scroll duct
[NASA-CR-188612] p 167 N91-25367
- ### SECURITY
- Automating security monitoring and analysis for Space Station Freedom's electric power system
p 219 A91-37975
- ### SEGMENTS
- Performance characterization of a segmented anode arcjet thruster
[NASA-TM-103227] p 67 N91-10118
- ### SELENIUM COMPOUNDS
- Synthesis and structures of metal chalcogenide precursors
[NASA-TM-103665] p 120 N91-19296
- ### SELF LUBRICATING MATERIALS
- Tribological properties of PM212 - A high temperature, self-lubricating, powder metallurgy composite
[STLE PREPRINT 90-AM-4E-1] p 87 A91-19720
- PM200/PS200: Self-lubricating bearing and seal materials for applications to 900 C
[NASA-TM-103776] p 190 N91-30539
- ### SELF TESTS
- Electromechanical actuation for thrust vector control applications
p 52 A91-31026
- ### SEMICONDUCTING FILMS
- Controlled growth of 3C-SiC and 6H-SiC films on low-tilt-angle vicinal (0001) 6H-SiC wafers
p 232 A91-45713
- Thin film characterization using spectroscopic ellipsometry
p 119 N91-18303
- Ellipsometric study of cubic SiC
p 235 N91-18304
- ### SEMICONDUCTOR DEVICES
- Neutron, gamma ray and post-irradiation thermal annealing effects on power semiconductor switches
[AIAA PAPER 91-3525] p 142 A91-52420
- New materials and techniques for improved mm wave devices
[AIAA PAPER 91-3590] p 142 A91-52459
- Development of silicon carbide semiconductor devices for high temperature applications
[NASA-TM-104398] p 236 N91-22921
- Advances in silicon carbide Chemical Vapor Deposition (CVD) for semiconductor device fabrication
[NASA-TM-104410] p 236 N91-23946
- Silicon carbide, an emerging high temperature semiconductor
p 236 N91-24061
- Process for the controlled growth of single-crystal films of silicon carbide polytypes on silicon carbide wafers
[NASA-CASE-LEW-15222-1] p 236 N91-26966
- ### SEMICONDUCTOR JUNCTIONS
- Monolithic and mechanical multijunction space solar cells
p 54 A91-38020
- Thin solar cell and lightweight array
[NASA-CASE-LEW-14959-1] p 212 N91-27614
- ### SEMICONDUCTOR LASERS
- Fiber optic sensing system
[NASA-CASE-LEW-14795-1] p 230 N91-21871
- ### SEMICONDUCTORS (MATERIALS)
- Programmable multi-zone furnace for microgravity research
[AIAA PAPER 91-0781] p 127 A91-19463
- Neutron and gamma irradiation effects on power semiconductor switches
p 139 A91-38162
- An analysis of the contact sintering process in III-V solar cells
p 139 A91-41891
- The influence of interstitial Ga and interfacial Au₂P₃ on the electrical and metallurgical behavior of Au-contacted III-V semiconductors
p 140 A91-42694
- Silicon carbide, a semiconductor for space power electronics
[NASA-TM-103655] p 234 N91-14850
- Solid State Technology Branch of NASA Lewis Research Center Second Annual Digest, June 1989 - June 1990
[NASA-TM-103226] p 133 N91-18297
- Semiconductor structural damage attendant to contact formation in III-V solar cells
p 209 N91-19203
- Synthesis and structures of metal chalcogenide precursors
[NASA-TM-103665] p 120 N91-19296
- High temperature electronics
p 144 N91-20101
- Silicon carbide, an emerging high temperature semiconductor
p 236 N91-24061
- Leo space plasma interactions
p 84 N91-30249
- ### SENSITIVITY
- Solution and sensitivity analysis of a complex transcendental eigenproblem with pairs of real eigenvalues
p 195 A91-23685

SENSORY PERCEPTION

- An assessment of the Space Station Freedom program's leakage current requirement
[NASA-CR-187077] p 215 N91-20630

SEPARATED FLOW

- Effect of acoustic excitation on stalled flows over an airfoil
[AIAA PAPER 90-4009] p 1 A91-12521
- A steadying effect of acoustic excitation on transitory stall
[AIAA PAPER 91-0043] p 2 A91-22499
- Control of flow separation and mixing by aerodynamic excitation
p 2 A91-24360
- Navier-Stokes analysis of turbine blade heat transfer
[ASME PAPER 90-GT-42] p 155 A91-44529
- Control of laminar separation over airfoils by acoustic excitation
p 226 A91-45106
- A Navier-Stokes study of shock-boundary layer interaction and flow separation inside a transonic compressor
p 8 A91-56115
- A steadying effect of acoustic excitation on transitory stall
[NASA-TM-103689] p 11 N91-13420
- Simulation of brush insert for leading-edge-passage convective heat transfer
[NASA-TM-103801] p 165 N91-23409

SERVICE LIFE

- In-service health monitoring of composite structures
p 192 A91-51926
- A 5-kW xenon ion thruster lifetest
[NASA-TM-103191] p 72 N91-19180
- The effect of atomic oxygen on polysiloxane-polyimide for spacecraft applications in low Earth orbit
p 229 N91-20735
- Effect of LEO cycling on 125 Ah advanced design IPV nickel-hydrogen flight cells: An update
[NASA-TM-104384] p 74 N91-22375
- Advanced Rotorcraft Transmission (ART) program-Boeing helicopters status report
[NASA-TM-104474] p 188 N91-25412
- Microanalysis of extended-test xenon hollow cathodes
[NASA-TM-104532] p 82 N91-30202
- Transmission overhaul estimates for partial and full replacement at repair
[NASA-TM-104395] p 190 N91-30533
- Mass comparisons of electric propulsion systems for NSSK of geosynchronous spacecraft
[NASA-TM-105153] p 85 N91-31212

SERVOCONTROL

- Linear quadratic servo control of a reusable rocket engine
[AIAA PAPER 91-1999] p 57 A91-41670
- A high-frequency servosystem for fuel control in hypersonic engines
[NASA-TM-104333] p 35 N91-31178

SERVOMECHANISMS

- Four quadrant control of induction motors
p 145 N91-23055
- A high-frequency servosystem for fuel control in hypersonic engines
[NASA-TM-104333] p 35 N91-31178

SETTLING

- Surface settling in partially filled containers upon step reduction in gravity
[NASA-TM-103641] p 159 N91-14556

SHADOWGRAPH PHOTOGRAPHY

- Optical techniques for determination of normal shock position in supersonic flows for aerospace applications
p 174 A91-55530

SHAFTS (MACHINE ELEMENTS)

- Review of the transmissions of the Soviet helicopters
[NASA-TM-103634] p 20 N91-15146
- A model for the space shuttle main engine high pressure oxidizer turbopump shaft seal system
[NASA-TM-103697] p 184 N91-20489

SHEAR FLOW

- Nonlinear Reynolds stress model for turbulent shear flows
[AIAA PAPER 91-0609] p 149 A91-21556
- Control of flow separation and mixing by aerodynamic excitation
p 2 A91-24360
- Modern developments in shear flow control with swirl
p 3 A91-24519
- Renormalization group analysis of anisotropic diffusion in turbulent shear flows
p 150 A91-27946
- Multifrequency excited jets
p 151 A91-31482
- Turbulence enhancement in free shear flows under multifrequency excitation
p 152 A91-38737
- Second order modeling of boundary-free turbulent shear flows
[AIAA PAPER 91-1779] p 154 A91-42588
- Second order modeling of boundary-free turbulent shear flows
[NASA-TM-104369] p 164 N91-22524

- A comparison of numerical methods for the Rayleigh equation in unbounded domains
[NASA-TM-105179] p 223 N91-30865

SHEAR LAYERS

- Stability of an oscillated fluid with a uniform density gradient
p 147 A91-12971
- New mixing-length model for supersonic shear layers
p 148 A91-16073
- Modern CFD applications for the design of a reacting shear layer facility
[AIAA PAPER 91-0577] p 149 A91-21540
- Calculation of divergent channel flows with a multiple-time-scale turbulence model
p 151 A91-34134
- Nonlinear spatial evolution of externally excited instability waves in free shear layers
p 152 A91-38705
- Nonlinear evolution of subsonic and supersonic disturbances on a compressible free shear layer
p 152 A91-39716
- Second order modeling of boundary-free turbulent shear flows
[AIAA PAPER 91-1779] p 154 A91-42588
- Axisymmetric jet forced by fundamental and subharmonic tones
p 226 A91-45111
- Simulations of free shear layers using a compressible k-epsilon model
[AIAA PAPER 91-1863] p 156 A91-45778
- Numerical simulation of nonlinear development of instability waves
[E-4658] p 8 N91-10849
- Second order modeling of boundary-free turbulent shear flows
[NASA-TM-104369] p 164 N91-22524
- Control of an axisymmetric turbulent jet by multi-modal excitation
[NASA-TM-104483] p 17 N91-26121
- Modern CFD applications for the design of a reacting shear layer facility
[NASA-TM-104523] p 34 N91-27164
- An experimental study of natural and forced modes in an axisymmetric jet
[NASA-TM-105225] p 18 N91-32074

SHEAR STRAIN

- Two-dimensional surface strain measurement based on a variation of Yamaguchi's laser-speckle strain gauge
p 174 A91-55531

SHEAR STRENGTH

- Fiber pushout test - A three-dimensional finite element computational simulation
p 197 A91-33096
- Investigation of interfacial shear strength in SiC/Si₃N₄ composites
p 93 A91-56913
- A study of void effects on the interlaminar shear strength of unidirectional graphite fiber reinforced composites
[NASA-TM-103267] p 159 N91-12034
- Relationship between voids and interlaminar shear strength of polymer matrix composites
[NASA-TM-103643] p 95 N91-13495
- Investigation of interfacial shear strength in SiC/Si₃N₄ composites
[NASA-TM-103739] p 101 N91-26233

SHEAR STRESS

- Heat transfer, velocity-temperature correlation, and turbulent shear stress from Navier-Stokes computations of shock wave/turbulent boundary layer interaction flows
p 163 N91-21085

SHOCK FRONTS

- The dynamic instability of adiabatic blast waves
p 239 A91-26361
- Optical techniques for determination of normal shock position in supersonic flows for aerospace applications
p 174 A91-55530

SHOCK LAYERS

- Numerical study of shock-wave/boundary layer interactions in premixed hydrogen-air hypersonic flows
[AIAA PAPER 91-0413] p 149 A91-26191
- Numerical study of shock-wave/boundary layer interactions in premixed hydrogen-air hypersonic flows
[NASA-TM-103273] p 160 N91-14559
- A laser velocimeter investigation of the normal shock-wave boundary layer interaction
[NASA-TM-105201] p 169 N91-32440

SHOCK RESISTANCE

- Thermal shock fiber-reinforced ceramic matrix composites
p 93 A91-56935
- Thermal shock of fiber reinforced ceramic matrix composites
[NASA-TM-103777] p 120 N91-19295

SHOCK WAVE INTERACTION

- Numerical study of shock-wave/boundary layer interactions in premixed hydrogen-air hypersonic flows
[AIAA PAPER 91-0413] p 149 A91-26191
- 3-D Navier-Stokes analysis of crossing, glancing shocks/turbulent boundary layer interactions
[AIAA PAPER 91-1758] p 6 A91-43631

- The effect of varying Mach number on crossing, glancing shocks/turbulent boundary-layer interactions
[AIAA PAPER 91-2157] p 6 A91-45792
- Primitive variable, strongly implicit calculation procedure for viscous flows at all speeds p 7 A91-46181
- A Navier-Stokes study of shock-boundary layer interaction and flow separation inside a transonic compressor p 8 A91-56115
- Numerical study of shock-wave/boundary layer interactions in premixed hydrogen-air hypersonic flows [NASA-TM-103273] p 160 N91-14559
- Computational modeling and validation for hypersonic inlets p 16 N91-23162
- The 3-D Navier-Stokes analysis of crossing, glancing shocks/turbulent boundary layer interactions [NASA-TM-104469] p 16 N91-24130
- SHOCK WAVE PROPAGATION**
- Qualitative investigation of cryogenic injected shock dissipation [NASA-TM-105140] p 168 N91-29525
- SHOCK WAVES**
- Navier-Stokes simulation of transonic blade-vortex interactions p 2 A91-21065
- Numerical study of shock-wave/boundary layer interactions in premixed hydrogen-air hypersonic flows [AIAA PAPER 91-0413] p 149 A91-26191
- The shock process and light-element production in supernova envelopes p 239 A91-33573
- Solution of steady-state, two-dimensional conservation laws by mathematical programming p 221 A91-35956
- Results from computational analysis of a mixed compression supersonic inlet [AIAA PAPER 91-2581] p 7 A91-45818
- Optical techniques for determination of normal shock position in supersonic flows for aerospace applications p 174 A91-55530
- Numerical study of unsteady shockwave reflections using an upwind TVD scheme [NASA-TM-103251] p 10 N91-11676
- Numerical study of shock-wave/boundary layer interactions in premixed hydrogen-air hypersonic flows [NASA-TM-103273] p 160 N91-14559
- High-Order Polynomial Expansions (HOPE) for flux-vector splitting [NASA-TM-104452] p 222 N91-25739
- Qualitative investigation of cryogenic injected shock dissipation [NASA-TM-105140] p 168 N91-29525
- A qualitative view of cryogenic fluid injection into high speed flows [NASA-TM-105139] p 169 N91-30473
- SHORT CIRCUIT CURRENTS**
- High altitude AM0 testing of PV concentrator lens elements --- Air Mass Zero p 207 A91-41978
- Effect of dislocations on the open-circuit voltage, short-circuit current and efficiency of heteroepitaxial indium phosphide solar cells [NASA-TM-103762] p 144 N91-19354
- SHROUDED PROPELLERS**
- Evaluation of panel code predictions with experimental results of inlet performance for a 17-inch ducted prop/fan simulator operating at Mach 0.2 [AIAA PAPER 91-3354] p 7 A91-45819
- Ultra-high bypass research p 30 N91-20117
- Evaluation of panel code predictions with experimental results of inlet performance for a 17-inch ducted prop/fan simulator operating at Mach 0.2 [NASA-TM-104428] p 17 N91-25106
- SHUTTLE DERIVED VEHICLES**
- Overview of the Beta II two-stage-to-orbit vehicle design [AIAA PAPER 91-3175] p 43 A91-54088
- SIGNAL ENCODING**
- Data compression for full motion video transmission [AIAA PAPER 91-3533] p 45 A91-52424
- Digital CODEC for real-time processing of broadcast quality video signals at 1.8 bits/pixel p 134 N91-24067
- SIGNAL FADING**
- A statistical rain attenuation prediction model with application to the advanced communication technology satellite project 3: A stochastic rain fade control algorithm for satellite link power via non linear Markov filtering theory [NASA-TM-100243] p 134 N91-22494
- SIGNAL MEASUREMENT**
- Using a modified Hewlett Packard 8410 network analyzer as an automated farfield antenna range receiver [NASA-TM-103700] p 143 N91-19349
- SIGNAL PROCESSING**
- Field oriented control of induction motors p 138 A91-37987
- Combinatorial FSK modulation for power-efficient high-rate communications [AIAA PAPER 91-3532] p 133 A91-53708
- Real-time data compression of broadcast video signals [NASA-CASE-LEW-14945-1] p 133 N91-13598
- Near-field antenna testing using the Hewlett Packard 8510 automated network analyzer [NASA-TM-103699] p 144 N91-20393
- Combinatorial FSK modulation for power-efficient high-rate communications [NASA-TM-105188] p 135 N91-29404
- SIGNAL TO NOISE RATIOS**
- Neuromorphic learning of continuous-valued mappings from noise-corrupted data p 219 A91-53201
- SIKORSKY AIRCRAFT**
- Results of a sub-scale model rotor icing test [AIAA PAPER 91-0660] p 19 A91-26190
- Results of a sub-scale model rotor icing test [NASA-TM-103709] p 11 N91-14309
- Model rotor icing tests in the NASA Lewis icing research tunnel [NASA-TM-104351] p 32 N91-23184
- SILANES**
- A numerical and experimental analysis of reactor performance and deposition rates for CVD on monofilaments [NASA-TM-103631] p 130 N91-14500
- SILICA GEL**
- Influence of several metal ions on the gelation activation energy of silicon tetraethoxide p 113 A91-19599
- SILICA GLASS**
- Crystallization and characterization of Y2O3-SiO2 glasses p 237 N91-31962
- SILICON**
- Silicon-etaion fiber-optic temperature sensor p 170 A91-19581
- Advanced photovoltaic experiment, S0014: Preliminary flight results and post-flight findings p 212 N91-25061
- SILICON CARBIDES**
- Impact behavior of a SiC fiber-reinforced reaction bonded Si3N4 composite p 91 A91-16805
- The structure of carbon in chemically vapor deposited SiC monofilaments p 113 A91-18675
- Thermochemical analysis of the silicon carbide-alumina reaction with reference to liquid-phase sintering of silicon carbide p 114 A91-26506
- Hydrogen-silicon carbide interactions p 114 A91-28783
- Silsesquioxane-derived ceramic fibres p 114 A91-30283
- Evaluation of thermomechanical damage in silicon carbide/titanium composites p 92 A91-42297
- Controlled growth of 3C-SiC and 6H-SiC films on low-tilt-angle vicinal (0001) 6H-SiC wafers p 232 A91-45713
- Application of oxidation to the structural characterization of SiC epitaxial films p 233 A91-45881
- High-voltage 6H-SiC p-n junction diodes p 142 A91-54746
- Hot corrosion of silicon carbide and silicon nitride at 1000 C p 117 A91-55698
- Factors which influence tensile strength of a SiC/Ti-24Al-11Nb (at. pct) composite p 92 A91-55900
- The isothermal fatigue behavior of a unidirectional SiC/Ti composite and the Ti alloy matrix p 93 A91-55907
- Fiber creep evaluation by stress relaxation measurements p 117 A91-56905
- Investigation of interfacial shear strength in SiC/Si3N4 composites p 93 A91-56913
- Polymeric routes to silicon carbide and silicon oxycarbide CMC p 117 A91-56922
- Thermal shock fiber-reinforced ceramic matrix composites p 93 A91-56935
- Dynamic fatigue property of silicon carbide whisker-reinforced silicon nitride p 94 A91-56937
- In situ X-ray monitoring of damage accumulation in SiC/RBSN tensile specimens p 94 A91-56942
- Microstructural and strength stability of CVD SiC fibers in argon environments p 117 A91-56958
- Thermochemical analysis of chemical processes relevant to the stability and processing of SiC-reinforced Si3N4 composite p 94 A91-56961
- Oxidation instability of SiC and Si3N4 following thermal excursions p 118 A91-57059
- MIS capacitor studies on silicon carbide single crystals [NASA-CR-187350] p 234 N91-11555
- Silicon carbide, a semiconductor for space power electronics [NASA-TM-103655] p 234 N91-14850
- Effects of high pressure nitrogen on the thermal stability of SiC fibers [NASA-TM-103245] p 96 N91-16075
- Ellipsometric study of cubic SiC p 235 N91-18304
- METCAN updates for high temperature composite behavior: Simulation/verification [NASA-TM-103682] p 97 N91-19229
- Thermal shock of fiber reinforced ceramic matrix composites [NASA-TM-103777] p 120 N91-19295
- High temperature electronics p 144 N91-20101
- Isothermal fatigue behavior of a (90)(sub 8) SiC/Ti-15-3 composite at 426 C [NASA-TM-103686] p 99 N91-20228
- Mechanical behavior of fiber reinforced SiC/RBSN ceramic matrix composites: Theory and experiment [NASA-TM-103688] p 99 N91-21243
- Tribological characteristics of silicon carbide whisker-reinforced alumina at elevated temperatures [NASA-TM-103799] p 89 N91-22379
- In-situ x-ray monitoring of damage accumulation in SiC/RBSN tensile specimens p 99 N91-22402
- Development of silicon carbide semiconductor devices for high temperature applications [NASA-TM-104398] p 236 N91-22921
- A preliminary investigation of acousto-ultrasonic NDE of metal matrix composite test specimens [NASA-TM-104339] p 194 N91-23521
- Advances in silicon carbide Chemical Vapor Deposition (CVD) for semiconductor device fabrication [NASA-TM-104410] p 236 N91-23946
- Silicon carbide, an emerging high temperature semiconductor p 236 N91-24061
- Tensile deformation damage in SiC reinforced Ti-15V-3Cr-3Al-3Sn [NASA-TM-103620] p 101 N91-25195
- Investigation of interfacial shear strength in SiC/Si3N4 composites [NASA-TM-103739] p 101 N91-26233
- Polymeric routes to silicon carbide and silicon oxycarbide CMC [NASA-TM-104372] p 102 N91-26234
- Process for the controlled growth of single-crystal films of silicon carbide polytypes on silicon carbide wafers [NASA-CASE-LEW-15222-1] p 236 N91-26966
- Process for the homoepitaxial growth of single-crystal silicon carbide films on silicon carbide wafers [NASA-CASE-LEW-15223-1] p 236 N91-26967
- Matrix plasticity in SiC/Ti-15-3 composite [NASA-TM-103760] p 102 N91-27247
- An analysis of the wear behavior of SiC whisker reinforced alumina from 25 to 1200 C [NASA-TM-104489] p 90 N91-29235
- Microstructural and strength stability of CVD SiC fibers in argon environment [NASA-TM-103772] p 102 N91-29250
- SILICON DIOXIDE**
- Atomic oxygen undercutting of defects on SiO2 protected polyimide solar array blankets p 116 A91-49803
- Flexible fluoropolymer filled protective coatings p 121 N91-24062
- Sliding wear of self-mated Al2O3-SiC whisker reinforced composites at 23-1200 C [NASA-TM-104490] p 90 N91-27221
- SILICON NITRIDES**
- Impact behavior of a SiC fiber-reinforced reaction bonded Si3N4 composite p 91 A91-16805
- Hot corrosion of silicon carbide and silicon nitride at 1000 C p 117 A91-55698
- Investigation of interfacial shear strength in SiC/Si3N4 composites p 93 A91-56913
- Influence of the Si3N4 microstructure on its R-curve and fatigue behavior p 117 A91-56931
- Thermal shock fiber-reinforced ceramic matrix composites p 93 A91-56935
- Dynamic fatigue property of silicon carbide whisker-reinforced silicon nitride p 94 A91-56937
- In situ X-ray monitoring of damage accumulation in SiC/RBSN tensile specimens p 94 A91-56942
- Thermochemical analysis of chemical processes relevant to the stability and processing of SiC-reinforced Si3N4 composite p 94 A91-56961
- Crack healing in silicon nitride due to oxidation p 118 A91-56982
- Evidence from transmission electron microscopy for an oxyntide layer in oxidized Si3N4 p 118 A91-57058
- Oxidation instability of SiC and Si3N4 following thermal excursions p 118 A91-57059
- Comparison of dynamic fatigue behavior between SiC whisker-reinforced composite and monolithic silicon nitrides [NASA-TM-103707] p 119 N91-19293
- Thermal shock of fiber reinforced ceramic matrix composites [NASA-TM-103777] p 120 N91-19295
- In-situ x-ray monitoring of damage accumulation in SiC/RBSN tensile specimens p 99 N91-22402
- [NASA-TM-103733] p 99 N91-22402
- Mechanical behavior and failure phenomenon of an in situ-toughened silicon nitride [NASA-TM-103741] p 121 N91-23311

- Investigation of interfacial shear strength in SiC/Si₃N₄ composites [NASA-TM-103739] p 101 N91-26233
- SILICON POLYMERS**
- Atomic oxygen interactions with FEP Teflon and silicones on LDEF p 122 N91-25029
- SILICONES**
- A comparative flow visualization study of thermocapillary flow in drops in liquid-liquid systems [AIAA PAPER 91-0311] p 148 A91-21452
- Atomic oxygen interactions with FEP Teflon and silicones on LDEF p 122 N91-25029
- Design considerations for space radiators based on the liquid sheet (LSR) concept [NASA-TM-105158] p 80 N91-27213
- SILVER**
- Composite bearing and seal materials for advanced heat engine applications to 900 C [NASA-TM-103612] p 95 N91-15318
- The PM-200 lubrication system p 121 N91-23044
- SILVER COMPOUNDS**
- Method of making carbide/fluoride/silver composites [NASA-CASE-LEW-14902-1] p 102 N91-27244
- SIMPLIFICATION**
- Two-dimensional surface strain measurement based on a variation of Yamaguchi's laser-speckle strain gauge p 174 A91-55531
- SIMULATION**
- Computational simulation of damping in composite structures p 198 A91-36283
- Thermocapillary migration of liquid droplets in a temperature gradient in a density matched system p 153 A91-41132
- Numerical simulation of nonlinear development of instability waves [E-4658] p 8 N91-10849
- Simulation of iced wing aerodynamics [NASA-TM-104362] p 15 N91-23086
- SIMULATORS**
- Evaluation of panel code predictions with experimental results of inlet performance for a 17-inch ducted prop/fan simulator operating at Mach 0.2 [AIAA PAPER 91-3354] p 7 A91-45819
- In-flight and simulated aircraft fuel temperature measurements [NASA-TM-103611] p 125 N91-15418
- Evaluation of panel code predictions with experimental results of inlet performance for a 17-inch ducted prop/fan simulator operating at Mach 0.2 [NASA-TM-104428] p 17 N91-25106
- SIMULTANEOUS EQUATIONS**
- Determination of alloy content from plume spectral measurements [AIAA PAPER 91-2531] p 88 A91-44284
- Determination of alloy content from plume spectral measurements [NASA-TM-104442] p 89 N91-24341
- SINGLE CRYSTALS**
- Reaction of Ti and Ti-Al alloys with alumina p 91 A91-27937
- Temperature dependence of hardness in yttria-stabilized zirconia single crystals p 114 A91-28763
- The effect of hydrogen on the low cycle fatigue behavior of a single crystal superalloy p 108 A91-28794
- 1000 to 1200 K time-dependent compressive deformation of single-crystalline and polycrystalline B2 Ni-40Al p 109 A91-43670
- Application of oxidation to the structural characterization of SiC epitaxial films p 233 A91-45881
- Elastic response of (001)-oriented PWA 1480 single crystal - The influence of secondary orientation [SAE PAPER 91-1111] p 110 A91-53555
- MIS capacitor studies on silicon carbide single crystals [NASA-CR-187350] p 234 N91-11555
- Method of making single crystal fibers [NASA-CASE-LEW-14921-1] p 95 N91-13502
- Effect of tensile mean stress on fatigue behavior of single-crystal and directionally solidified superalloys [NASA-TM-103644] p 200 N91-18452
- Elastic response of zone axis (001)-oriented PWA 1480 single crystal: The influence of secondary orientation [NASA-TM-103782] p 202 N91-21558
- Fatigue behavior of a single-crystal superalloy p 111 N91-24313
- Process for the controlled growth of single-crystal films of silicon carbide polytypes on silicon carbide wafers [NASA-CASE-LEW-15222-1] p 236 N91-26966
- Process for the homoepitaxial growth of single-crystal silicon carbide films on silicon carbide wafers [NASA-CASE-LEW-15223-1] p 236 N91-26967
- SINTERING**
- Thermochemical analysis of the silicon carbide-alumina reaction with reference to liquid-phase sintering of silicon carbide p 114 A91-26506
- An analysis of the contact sintering process in III-V solar cells p 139 A91-41891
- Crystallization and properties of Sr-Ba aluminosilicate glass-ceramic matrices p 117 A91-56917
- Method of making single crystal fibers [NASA-CASE-LEW-14921-1] p 95 N91-13502
- Composite bearing and seal materials for advanced heat engine applications to 900 C [NASA-TM-103612] p 95 N91-15318
- Semiconductor structural damage attendant to contact formation in III-V solar cells p 209 N91-19203
- Crystallization and properties of Sr-Ba aluminosilicate glass-ceramic matrices [NASA-TM-103764] p 120 N91-19308
- Mechanical behavior and failure phenomenon of an in situ-toughened silicon nitride [NASA-TM-103741] p 121 N91-23311
- SISO (CONTROL SYSTEMS)**
- An expert system to perform on-line controller tuning p 219 A91-30171
- SIZE DETERMINATION**
- LN2 spray droplet size measurement via ensemble diffraction technique [AIAA PAPER 91-1381] p 129 A91-44336
- LN2 spray droplet size measurement via ensemble diffraction technique [NASA-TM-104443] p 131 N91-24470
- SKEWNESS**
- Numerical solution for the velocity-derivative skewness of a low Reynolds-number turbulent-like decaying Navier-Stokes flow p 158 A91-50204
- SLEWING**
- Magnetic bearings with zero bias p 48 N91-21194
- SLIDING**
- Contact stresses in gear teeth - A new method of analysis [AIAA PAPER 91-2022] p 182 A91-41683
- Contact stresses in gear teeth: A new method of analysis [NASA-TM-104397] p 186 N91-22570
- Sliding wear of self-mated Al₂O₃-SiC whisker reinforced composites at 23-1200 C [NASA-TM-104490] p 90 N91-27221
- An analysis of the wear behavior of SiC whisker reinforced alumina from 25 to 1200 C [NASA-TM-104489] p 90 N91-29235
- SLUSH HYDROGEN**
- Slush hydrogen propellant production, transfer, and expulsion studies at the NASA K-Site Facility [AIAA PAPER 91-3550] p 125 A91-53710
- Overview of hypersonic/transatmospheric vehicle propulsion technology p 28 N91-20092
- Slush hydrogen propellant production, transfer, and expulsion studies at the NASA K-Site Facility [NASA-TM-105191] p 127 N91-28449
- SMART STRUCTURES**
- In-service health monitoring of composite structures p 192 A91-51926
- SODIUM SULFUR BATTERIES**
- SEI rover solar-electrochemical power system options [NASA-TM-104402] p 211 N91-23620
- SOFTWARE ENGINEERING**
- Automation software for a materials testing laboratory p 216 A91-56538
- SOFTWARE TOOLS**
- Internal fluid mechanics research p 161 N91-20095
- Inlets, ducts, and nozzles p 162 N91-20096
- SOL-GEL PROCESSES**
- Influence of several metal ions on the gelation activation energy of silicon tetraethoxide p 113 A91-19599
- SOLAR ARRAYS**
- Dynamic analysis of space-related linear and non-linear structures p 196 A91-28612
- Solar array orientations for a space station in low earth orbit p 46 A91-30019
- Rapid thermal cycling of new technology solar array blanket coupons p 54 A91-38019
- Component and prototype panel testing of the mini-dome Fresnel lens photovoltaic concentrator array p 54 A91-38023
- Photovoltaic power for Space Station Freedom p 57 A91-41878
- Design considerations for lunar base photovoltaic power systems p 41 A91-41987
- Design considerations for Mars photovoltaic power systems p 41 A91-41988
- Vacuum ultraviolet radiation and thermal cycling effects on atomic oxygen protective photovoltaic array blanket materials p 116 A91-49812
- Laser photovoltaic power system synergy for SEI applications [AIAA PAPER 91-3419] p 207 A91-52339
- Photovoltaic options for solar electric propulsion [NASA-TM-103284] p 68 N91-11061
- Design considerations for lunar base photovoltaic power systems [NASA-TM-103642] p 241 N91-14259
- Space Photovoltaic Research and Technology, 1989 [NASA-CP-3107] p 72 N91-19182
- Review of thin film solar cell technology and applications for ultra-light spacecraft solar arrays p 208 N91-19198
- Feasibility of solar power for Mars p 209 N91-19201
- Mini-dome Fresnel lens photovoltaic concentrator development p 210 N91-19219
- Future mission opportunities and requirements for advanced space photovoltaic energy conversion technology [NASA-TM-103661] p 74 N91-22371
- Durability evaluation of photovoltaic blanket materials exposed on LDEF tray S1003 p 212 N91-25062
- Thin solar cell and lightweight array [NASA-CASE-LEW-14959-1] p 212 N91-27614
- The effects of lunar dust accumulation on the performance of photovoltaic arrays p 83 N91-30238
- Rapid thermal cycling of solar array blanket coupons for Space Station Freedom p 84 N91-30239
- Low Earth orbital atomic oxygen micrometeoroid, and debris interactions with photovoltaic arrays p 84 N91-30248
- Leo space plasma interactions p 84 N91-30249
- Structural design concepts for a multi-megawatt Solar Electric Propulsion (SEP) spacecraft [NASA-TM-105148] p 206 N91-30565
- Advanced power systems for EOS [NASA-TM-105222] p 85 N91-31217
- Thin film, concentrator and multijunction space solar cells: Status and potential [NASA-TM-104505] p 86 N91-31218
- SOLAR BLANKETS**
- Rapid thermal cycling of new technology solar array blanket coupons p 54 A91-38019
- Atomic oxygen undercutting of defects on SiO₂ protected polyimide solar array blankets p 116 A91-49803
- Vacuum ultraviolet radiation and thermal cycling effects on atomic oxygen protective photovoltaic array blanket materials p 116 A91-49812
- Atomic oxygen interaction with solar array blankets at protective coating defect sites p 211 N91-20732
- The effect of atomic oxygen on polysiloxane-polyimide for spacecraft applications in low Earth orbit p 229 N91-20735
- Durability evaluation of photovoltaic blanket materials exposed on LDEF tray S1003 p 212 N91-25062
- Structural design concepts for a multi-megawatt Solar Electric Propulsion (SEP) spacecraft [NASA-TM-105148] p 206 N91-30565
- SOLAR CELLS**
- Systems analysis of Mars solar electric propulsion vehicles [AIAA PAPER 90-3824] p 40 A91-10176
- Power electronic applications for Space Station Freedom p 52 A91-36832
- Automating security monitoring and analysis for Space Station Freedom's electric power system p 219 A91-37975
- Monolithic and mechanical multijunction space solar cells p 54 A91-38020
- New directions in InP solar cell research p 206 A91-38022
- Preliminary flight test results from the advanced photovoltaic experiment p 56 A91-38163
- Peeled film GaAs solar cell development p 139 A91-41889
- Study of surface passivation as a function of InP closed-ampoule solar cell fabrication processing variables p 232 A91-41893
- Temperature coefficients of multijunction solar cells p 172 A91-41921
- Key factors limiting the open circuit voltage of n(+)-p(p+)-indium phosphide solar cells p 139 A91-41929
- Measurement of surface recombination velocity on heavily doped indium phosphide p 232 A91-41931
- Primary reference cell calibrations at SERI - History and methods --- solar cells p 207 A91-41966
- Recent results from the InP homojunction cell module on the LIPS III spacecraft p 140 A91-41971
- High altitude AM0 testing of PV concentrator lens elements --- Air Mass Zero p 207 A91-41978
- Preliminary results from the Advanced Photovoltaic Experiment flight test p 39 A91-41980
- Effects of radiation of InP cells epitaxially grown on Si and GaAs substrates p 140 A91-41984
- Lightweight concentrator module with 30 percent AM0 efficient GaAs/GaSb tandem cells p 57 A91-41990
- A light-trapping solar cell coverglass p 229 A91-41995
- 23.5 percent thin-film space concentrator cells p 58 A91-42002

Effect of emitter parameter variation on the performance of heteroepitaxial indium phosphide solar cells p 140 A91-42003

Electrically conducting polymers for aerospace applications [AIAA PAPER 91-3432] p 233 A91-52349

Preliminary results from the advanced photovoltaic experiment flight test [NASA-TM-103269] p 67 N91-11058

Photovoltaic options for solar electric propulsion [NASA-TM-103284] p 68 N91-11061

Effect of emitter parameter variation on the performance of heteroepitaxial indium phosphide solar cells [NASA-TM-103619] p 70 N91-15306

The environment power system analysis tool development program p 231 N91-17734

The effect of the low Earth orbit environment on space solar cells [NASA-TM-103735] p 48 N91-19165

Radiation resistance of thin-film solar cells for space photovoltaic power [NASA-TM-103715] p 71 N91-19176

Solar electric propulsion for Mars transport vehicles [NASA-TM-103234] p 71 N91-19178

Space Photovoltaic Research and Technology, 1989 [NASA-CP-3107] p 72 N91-19182

Tandem concentrator solar cells with 30 percent (AMO) power conversion efficiency p 208 N91-19189

Thermal annealing of GaAs concentrator solar cells p 208 N91-19195

Review of thin film solar cell technology and applications for ultra-light spacecraft solar arrays p 208 N91-19198

Semiconductor structural damage attendant to contact formation in III-V solar cells p 209 N91-19203

Effects of proton irradiation on the performance of InP/GaAs solar cells p 209 N91-19205

Key factors limiting the open circuit voltage of n(+)-pp(+)-indium phosphide solar cells p 209 N91-19206

Determination of series resistance of indium phosphide solar cells p 210 N91-19207

Investigation of anodic and chemical oxides grown on p-type InP with applications to surface passivation for n(+)-p solar cell fabrication p 210 N91-19208

A comparative study of performance parameters of n(+)-p InP solar cells made by closed-ampoule sulfur diffusion into Cd- and Zn-doped p-type InP substrates p 210 N91-19209

Indium phosphide solar cells p 210 N91-19221

Effect of dislocations on the open-circuit voltage, short-circuit current and efficiency of heteroepitaxial indium phosphide solar cells [NASA-TM-103762] p 144 N91-19354

Heteroepitaxial InP solar cells on Si and GaAs substrates [NASA-TM-103696] p 144 N91-20392

Optimal design study of high efficiency indium phosphide space solar cells [NASA-TM-103763] p 145 N91-21433

Future mission opportunities and requirements for advanced space photovoltaic energy conversion technology [NASA-TM-103661] p 74 N91-22371

SEI rover solar-electrochemical power system options [NASA-TM-104402] p 211 N91-23620

Advanced photovoltaic experiment, S0014: Preliminary flight results and post-flight findings p 212 N91-25061

Durability evaluation of photovoltaic blanket materials exposed on LDEF tray S1003 p 212 N91-25062

Design considerations for space radiators based on the liquid sheet (LSR) concept [NASA-TM-105158] p 80 N91-27213

Recent progress in InP solar cell research [NASA-TM-104509] p 146 N91-27447

Thin solar cell and lightweight array [NASA-CASE-LEW-14959-1] p 212 N91-27614

Space Photovoltaic Research and Technology Conference [NASA-CP-3121] p 82 N91-30203

A comparative study of p(+)-n and n(+)-p InP solar cells made by a closed ampoule diffusion p 212 N91-30206

Improvements in contact resistivity and thermal stability of Au-contacted InP solar cells p 213 N91-30207

Grooved surfaces on InP p 213 N91-30208

Effect of dislocations on properties of heteroepitaxial InP solar cells p 213 N91-30209

Key results of the mini-dome Fresnel lens concentrator array development program under recently completed NASA and SDIO SBIR projects p 83 N91-30223

Comparative modeling of InP solar cell structures p 83 N91-30232

A theoretical comparison of the near-optimum design and predicted performance of n/p and p/n indium phosphide homojunction solar cells p 83 N91-30233

Significant reduction in arc frequency biased solar cells: Observations, diagnostics, and mitigation technique(s) p 83 N91-30235

The effects of lunar dust accumulation on the performance of photovoltaic arrays p 83 N91-30238

Description of the control system design for the SSF PMAD DC testbed [NASA-TM-105202] p 84 N91-30266

Thin film, concentrator and multijunction space solar cells: Status and potential [NASA-TM-104505] p 86 N91-31218

Solar radiation on Mars: Update 1991 [NASA-TM-105216] p 242 N91-33046

SOLAR COLLECTORS

Dynamic analysis of space-related linear and non-linear structures p 196 A91-28612

Preliminary designs for 25 kWe advanced Stirling conversion systems for dish electric applications p 207 A91-38182

Solar powered Stirling cycle electrical generator p 211 N91-23054

Full-size solar dynamic heat receiver thermal-vacuum tests [NASA-TM-104486] p 78 N91-25184

Concentrator testing using projected images [NASA-TM-104349] p 79 N91-27204

Ground test program for a full-size solar dynamic heat receiver [NASA-TM-104485] p 79 N91-27209

Status of the advanced Stirling conversion system project for 25 kW dish Stirling applications [NASA-TM-104528] p 238 N91-31023

Thin film, concentrator and multijunction space solar cells: Status and potential [NASA-TM-104505] p 86 N91-31218

SOLAR DYNAMIC POWER SYSTEMS

An evolutionary path to satellite solar power systems p 51 A91-26063

Photovoltaic power for Space Station Freedom p 57 A91-41878

Sensible heat receiver for solar dynamic space power system [NASA-TM-104393] p 77 N91-25173

Full-size solar dynamic heat receiver thermal-vacuum tests [NASA-TM-104486] p 78 N91-25184

Concentrator testing using projected images [NASA-TM-104349] p 79 N91-27204

Ground test program for a full-size solar dynamic heat receiver [NASA-TM-104485] p 79 N91-27209

Design considerations for space radiators based on the liquid sheet (LSR) concept [NASA-TM-105158] p 80 N91-27213

Solar dynamic power for Earth orbital and lunar applications [NASA-TM-104511] p 80 N91-27214

SOLAR ELECTRIC PROPULSION

Systems analysis of Mars solar electric propulsion vehicles [AIAA PAPER 90-3824] p 40 A91-10176

The NASA Lewis Research Center electric propulsion program [AIAA PAPER 91-3443] p 64 A91-52355

Test facilities for high power electric propulsion [AIAA PAPER 91-3499] p 42 A91-52396

Photovoltaic options for solar electric propulsion [NASA-TM-103284] p 68 N91-11061

Solar electric propulsion for Mars transport vehicles [NASA-TM-103234] p 71 N91-19178

Futuristic systems: Solar and nuclear electric propulsion p 80 N91-28215

Structural design concepts for a multi-megawatt Solar Electric Propulsion (SEP) spacecraft [NASA-TM-105148] p 206 N91-30565

SOLAR ENERGY

Solar radiation on Mars p 242 A91-28153

Lunar orbiting microwave beam power system p 56 A91-38158

Review of thin film solar cell technology and applications for ultra-light spacecraft solar arrays p 208 N91-19198

Solar thermal energy receiver [NASA-CASE-LEW-14949-1] p 211 N91-23617

SOLAR ENERGY ABSORBERS

Evaluation of thermal control coatings for use on solar dynamic radiators in low earth orbit [AIAA PAPER 91-1327] p 58 A91-43397

Evaluation of thermal control coatings for use on solar dynamic radiators in low Earth orbit [NASA-TM-104335] p 73 N91-22367

SOLAR ENERGY CONVERSION

Electric power scheduling - A distributed problem-solving approach p 219 A91-37976

Monolithic and mechanical multijunction space solar cells p 54 A91-38020

Photovoltaic superiority for Space Station Freedom power in the 21st century p 58 A91-42004

Feasibility of solar power for Mars p 209 N91-19201

Future mission opportunities and requirements for advanced space photovoltaic energy conversion technology [NASA-TM-103661] p 74 N91-22371

Component technology for Stirling power converters [NASA-TM-104387] p 74 N91-23234

The effects of lunar dust accumulation on the performance of photovoltaic arrays p 83 N91-30238

Solar radiation on Mars: Update 1991 [NASA-TM-105216] p 242 N91-33046

SOLAR GENERATORS

Automating security monitoring and analysis for Space Station Freedom's electric power system p 219 A91-37975

An analysis of space power system masses p 54 A91-38003

The environment power system analysis tool development program p 231 N91-17734

Solar powered Stirling cycle electrical generator p 211 N91-23054

Solar radiation on Mars: Update 1991 [NASA-TM-105216] p 242 N91-33046

SOLAR POWER SATELLITES

Applications of thin film technology toward a low-mass solar power satellite p 235 N91-22179

SOLAR RADIATION

Solar radiation on Mars p 242 A91-28153

Solar radiation on Mars: Update 1990 [NASA-TM-103623] p 242 N91-15117

Solar radiation on Mars: Update 1991 [NASA-TM-105216] p 242 N91-33046

SOLAR REFLECTORS

Ion beam textured and coated surfaces experiment (IBEX) p 122 N91-25040

SOLAR SIMULATORS

Temperature coefficients of multijunction solar cells p 172 A91-41921

SOLAR SPECTRA

Preliminary flight test results from the advanced photovoltaic experiment p 56 A91-38163

Preliminary results from the Advanced Photovoltaic Experiment flight test p 39 A91-41980

Preliminary results from the advanced photovoltaic experiment flight test [NASA-TM-103269] p 67 N91-11058

Advanced photovoltaic experiment, S0014: Preliminary flight results and post-flight findings p 212 N91-25061

SOLAR SYSTEM

Outline of the Solar System: Activities for elementary students [NASA-TM-104965] p 241 N91-25975

SOLID ELECTROLYTES

Some recent studies with the solid-ionomer electrochemical capacitor p 214 N91-32562

SOLID LUBRICANTS

Plasma-assisted physical vapor deposition surface treatments for tribological control [NASA-TM-103652] p 130 N91-11945

Composite bearing and seal materials for advanced heat engine applications to 900 C [NASA-TM-103612] p 95 N91-15318

Tribological properties of Ag/Ti films on Al₂O₃ ceramic substrates [NASA-TM-103784] p 89 N91-19224

Mechanical strength and thermophysical properties of PM212: A high temperature self-lubricating powder metallurgy composite [NASA-TM-103694] p 120 N91-21302

Solid lubricants [NASA-TM-102803] p 99 N91-22396

The PM-200 lubrication system p 121 N91-23044

Pretreatment of lubricated surfaces with sputtered cadmium oxide [NASA-CASE-LEW-14474-1] p 123 N91-28423

SOLID PROPELLANT COMBUSTION

Heat transfer to a thin solid combustible in flame spreading at microgravity p 106 A91-51449

SOLID STATE DEVICES

Solid State Technology Branch of NASA Lewis Research Center Second Annual Digest, June 1989 - June 1990 [NASA-TM-103226] p 133 N91-18297

NASA developments in solid state power amplifiers p 143 N91-18298

SOLID-SOLID INTERFACES

Fundamental considerations in adhesion, friction and wear for ceramic-metal contacts p 115 A91-35952

Adhesion at metal interfaces p 88 A91-38581

Universal energy relations and metal/ceramic interfaces p 93 A91-56254

Investigation of interfacial shear strength in SiC/Si₃N₄ composites p 93 A91-56913

- Evidence from transmission electron microscopy for an oxynitride layer in oxidized Si₃N₄ p 118 A91-57058
- Elastic/plastic analyses of advanced composites investigating the use of the compliant layer concept in reducing residual stresses resulting from processing [NASA-TM-103204] p 94 A91-11074
- Investigation of interfacial shear strength in SiC/Si₃N₄ composites [NASA-TM-103739] p 101 A91-26233
- Interphase layer optimization for metal matrix composites with fabrication considerations [NASA-TM-105166] p 102 A91-30281
- SOLIDIFICATION**
- Time development of a perturbed-spherical nucleus in a pure supercooled liquid. I - Power-law growth of morphological instabilities. II - Nonlinear development p 231 A91-16105
- SOLIDS**
- The method of lines in analyzing solids containing cracks [NASA-TM-103626] p 201 A91-19477
- SOLUBILITY**
- Interfacial dynamics of two liquids under an oscillating gravitational field p 148 A91-16062
- Constitution of pseudobinary hypoeutectic beta-NiAl + alpha-V alloys p 109 A91-48509
- SOLUTIONS**
- Solution and sensitivity analysis of a complex transcendental eigenproblem with pairs of real eigenvalues p 195 A91-23685
- SOUND PROPAGATION**
- Monograph on propagation of sound waves in curved ducts [NASA-RP-1248] p 228 A91-15848
- SOUND WAVES**
- Acoustic radiation from lifting airfoils in compressible subsonic flow [AIAA PAPER 90-3911] p 224 A91-12427
- Gear noise, vibration, and diagnostic studies at NASA Lewis Research Center p 183 A91-52811
- Monograph on propagation of sound waves in curved ducts [NASA-RP-1248] p 228 A91-15848
- Wind turbine acoustics [NASA-TP-3057] p 228 A91-16679
- Acoustic radiation from lifting airfoils in compressible subsonic flow [NASA-TM-103650] p 13 A91-19053
- SOUNDING ROCKETS**
- High voltage interactions of a sounding rocket with the ambient and system-generated environments p 46 A91-23077
- SPACE**
- Exploring the notion of space coupling propulsion p 73 A91-22161
- SPACE COLONIES**
- Proposal for a sun-following moonbase p 41 A91-27356
- SPACE COMMERCIALIZATION**
- SP-100 nuclear space power systems with application to space commercialization p 57 A91-38933
- Key issues in space nuclear power [NASA-TM-103656] p 71 A91-19179
- SPACE COMMUNICATION**
- Evaluation of components, subsystems, and networks for high rate, high frequency space communications [AIAA PAPER 91-3423] p 41 A91-52343
- Overview of Ka-band communications technology requirements for the Space Exploration Initiative [AIAA PAPER 91-3424] p 45 A91-52344
- High efficiency Ka-band MMIC amplifiers [AIAA PAPER 91-3425] p 141 A91-52345
- Data compression for full motion video transmission [AIAA PAPER 91-3533] p 45 A91-52424
- Millimeter wavelength communications applications for the SEI [AIAA PAPER 91-3589] p 45 A91-52458
- High power, high efficiency millimeter wavelength traveling wave tubes for high rate communications from deep space [AIAA PAPER 91-3593] p 142 A91-52461
- Status of Ka-band TWT transmitter technology [AIAA PAPER 91-3621] p 142 A91-52485
- Emerging applications of high temperature superconductors for space communications [NASA-TM-103629] p 227 A91-12317
- NASA developments in solid state power amplifiers p 143 A91-18298
- Microwave integrated circuits for space applications p 145 A91-24069
- Data compression for full motion video transmission [NASA-TM-105239] p 135 A91-32247
- SPACE DEBRIS**
- Preliminary results from the Advanced Photovoltaic Experiment flight test p 39 A91-41980

- Atomic oxygen undercutting of LDEF aluminized Kapton multilayer insulation p 229 A91-25027
- Low Earth orbital atomic oxygen micrometeoroid, and debris interactions with photovoltaic arrays p 84 A91-30248
- On protection of Freedom's solar dynamic radiator from the orbital debris environment. Part 2: Further testing and analyses [NASA-TM-104514] p 84 A91-30265
- SPACE ENVIRONMENT SIMULATION**
- Test-cell pressure effects on the performance of resistojets p 38 A91-37417
- Aeolian removal of dust types from photovoltaic surfaces on Mars p 47 A91-19156
- Simulation of Martian dust accumulation on surfaces p 47 A91-19160
- Low Earth orbital atomic oxygen and ultraviolet radiation effects on polymers [NASA-TM-103711] p 119 A91-19294
- Full-size solar dynamic heat receiver thermal-vacuum tests [NASA-TM-104486] p 78 A91-25184
- SPACE EXPLORATION**
- A technology assessment of alternative communications systems for the space exploration initiative [AIAA PAPER 90-3681] p 44 A91-11472
- Nuclear power systems for lunar and Mars exploration [IAF PAPER 90-200] p 51 A91-13868
- Nuclear power technology requirements for NASA exploration missions p 53 A91-37940
- A review of candidate multilayer insulation systems for potential use on wet-launched LH₂ tankage for the Space Exploration Initiative lunar missions [AIAA PAPER 91-2176] p 43 A91-45793
- The NASA/DOE/DOD nuclear rocket propulsion project - FY 1991 status [AIAA PAPER 91-3413] p 64 A91-52335
- Laser photovoltaic power system synergy for SEI applications [AIAA PAPER 91-3419] p 207 A91-52339
- Plans for the development of cryogenic engines for space exploration [AIAA PAPER 91-3438] p 64 A91-52351
- The NASA Lewis Research Center electric propulsion program [AIAA PAPER 91-3443] p 64 A91-52355
- Development of nuclear fuels and materials for propulsion systems for SEI [AIAA PAPER 91-3452] p 125 A91-52362
- SEI needs for space nuclear power [AIAA PAPER 91-3459] p 64 A91-52369
- Technologies for unattended network operations [AIAA PAPER 91-3534] p 45 A91-52425
- Development of technology needs for the SEI TNIM network [AIAA PAPER 91-3536] p 45 A91-52427
- Advanced ion propulsion for space exploration [AIAA PAPER 91-3567] p 85 A91-52443
- Millimeter wavelength communications applications for the SEI [AIAA PAPER 91-3589] p 45 A91-52458
- Evolving the SP-100 reactor in order to boost large payloads to GEO and to low lunar orbit via nuclear-electric propulsion [AIAA PAPER 91-3562] p 67 A91-53712
- Space mechanisms needs for future NASA long duration space missions [AIAA PAPER 91-3428] p 183 A91-57025
- Feasibility of solar power for Mars p 209 A91-19201
- Vision-21: Space Travel for the Next Millennium [NASA-CP-10059] p 40 A91-22139
- An assessment of technology alternatives for telecommunications and information management for the space exploration initiative [NASA-TM-103783] p 134 A91-23347
- Government/industry response to questionnaire on space mechanisms/tribology technology needs [NASA-TM-104358] p 186 A91-23501
- Evolving the SP-100 reactor in order to boost large payloads to GEO and to low lunar orbit via nuclear-electric propulsion [NASA-TM-104527] p 80 A91-27212
- Space mechanisms needs for future NASA long duration space missions [NASA-TM-105204] p 190 A91-30532
- The NASA cryogenic fluid management technology program plan [NASA-TM-105256] p 86 A91-32161
- Millimeter wavelength communications applications for the SEI [NASA-TM-105275] p 135 A91-32287

SPACE LABORATORIES

- Vibration environment - Acceleration mapping strategy and microgravity requirements for Spacelab and Space Station [IAF PAPER 90-350] p 39 A91-13991
- SPACE MISSIONS**
- Nuclear technology and the space exploration missions p 53 A91-37939
- The NASA CSTI High Capacity Power Program [AIAA PAPER 91-3629] p 208 A91-52493
- Advanced launch vehicle upper stages using liquid propulsion and metallized propellants [NASA-TM-103622] p 68 A91-11797
- A comparative study of performance parameters of n(+) - p InP solar cells made by closed-ampoule sulfur diffusion into Cd- and Zn-doped p-type InP substrates p 210 A91-19209
- Power technologies and the space future [NASA-TM-103649] p 73 A91-21240
- Government/industry response to questionnaire on space mechanisms/tribology technology needs [NASA-TM-104358] p 186 A91-23501
- Advanced launch vehicle upper stages using liquid propulsion and metallized propellants p 75 A91-24257
- SPACE NAVIGATION**
- Development of technology needs for the SEI TNIM network [AIAA PAPER 91-3536] p 45 A91-52427
- Millimeter wavelength communications applications for the SEI [AIAA PAPER 91-3589] p 45 A91-52458
- Millimeter wavelength communications applications for the SEI [NASA-TM-105275] p 135 A91-32287
- SPACE PLASMAS**
- Leo space plasma interactions p 84 A91-30249
- SPACE PLATFORMS**
- Leo space plasma interactions p 84 A91-30249
- Advanced power systems for EOS [NASA-TM-105222] p 85 A91-31217
- SPACE POWER REACTORS**
- Nuclear technology and the space exploration missions p 53 A91-37939
- Nuclear power technology requirements for NASA exploration missions p 53 A91-37940
- SP-100 nuclear space power systems with application to space commercialization p 57 A91-38933
- SEI needs for space nuclear power [AIAA PAPER 91-3459] p 64 A91-52369
- Trade studies for nuclear space power systems [AIAA PAPER 91-3518] p 65 A91-52413
- Analytical study of nozzle performance for nuclear thermal rockets [AIAA PAPER 91-3578] p 66 A91-52451
- Multimegawatt nuclear power systems for nuclear electric propulsion [AIAA PAPER 91-3607] p 66 A91-52472
- Advanced materials for space nuclear power systems [AIAA PAPER 91-3530] p 88 A91-53704
- Evolving the SP-100 reactor in order to boost large payloads to GEO and to low lunar orbit via nuclear-electric propulsion [AIAA PAPER 91-3562] p 67 A91-53712
- Space reactor/Stirling cycle systems for high power lunar application [NASA-TM-103698] p 40 A91-19112
- A reliability and mass perspective of SP-100 Stirling cycle lunar-base powerplant designs [NASA-TM-103736] p 212 A91-26592
- Evolving the SP-100 reactor in order to boost large payloads to GEO and to low lunar orbit via nuclear-electric propulsion [NASA-TM-104527] p 80 A91-27212
- Advanced materials for space nuclear power systems [NASA-TM-105171] p 112 A91-29298
- Neutron, gamma ray and post-irradiation thermal annealing effects on power semiconductor switches [NASA-TM-105248] p 147 A91-32410
- Status of NASA's Stirling Space Power Converter Program [NASA-TM-104512] p 214 A91-32569
- SPACE PROCESSING**
- Programmable multi-zone furnace for microgravity research [AIAA PAPER 91-0781] p 127 A91-19463
- A summary of existing and planned experiment hardware for low-gravity fluids research [AIAA PAPER 91-0777] p 128 A91-26329
- Three-dimensional flow transport modes in directional solidification during space processing p 128 A91-42642
- Isothermal Dendritic Growth Experiment - Science, engineering, and hardware development for USMP space flights p 128 A91-53408

- An examination of anticipated g-jitter on space station and its effects on materials processes
[NASA-TM-103775] p 128 N91-21378
- SPACE PROGRAMS**
- Speculating on space futures p 237 A91-16900
Power technologies and the space future
[NASA-TM-103649] p 73 N91-21240
- SPACE RENDEZVOUS**
- Evolutionary use of nuclear electric propulsion
[AIAA PAPER 90-3821] p 50 A91-10174
- SPACE SHUTTLE MAIN ENGINE**
- An intelligent control system for rocket engines - Need, vision, and issues p 218 A91-26925
A model for the Space Shuttle Main Engine High Pressure Oxidizer Turbopump shaft seal system p 180 A91-30640
Heat flux measurement in SSME turbine blade tester p 171 A91-30649
The development of a post-test diagnostic system for rocket engines
[AIAA PAPER 91-2528] p 60 A91-44281
The application of neural networks to the SSME startup transient
[AIAA PAPER 91-2530] p 60 A91-44283
Localization of aeroelastic modes in mistuned high-energy turbines
[AIAA PAPER 91-3379] p 198 A91-44319
Space Shuttle Main Engine nozzle mounted optic for throat plane spectroscopy
[AIAA PAPER 91-2524] p 49 A91-45816
Development of an intelligent diagnostic system for reusable rocket engine control
[AIAA PAPER 91-2533] p 63 A91-45817
Ceramic composites for rocket engine turbines
[SAE PAPER 911108] p 92 A91-53552
Heat flux measurement in SSME turbine blade tester
[NASA-TM-103274] p 175 N91-11205
Aerodynamics and heat transfer investigations on a high Reynolds number turbine cascade
[NASA-TM-103260] p 11 N91-15134
Ceramic composites for rocket engine turbines
[NASA-TM-103743] p 98 N91-19235
Probabilistic simulation of uncertainties in thermal structures
[NASA-TM-103680] p 201 N91-19472
A model for the space shuttle main engine high pressure oxidizer turbopump shaft seal system
[NASA-TM-103697] p 184 N91-20489
A simplified dynamic model of the Space Shuttle main engine
[NASA-TM-104421] p 131 N91-23340
Overview of the instrumentation program p 176 N91-24318
Calibrator tests of heat flux gauges mounted in SSME blades p 177 N91-24321
Thin-film sensors for space propulsion technology: Fabrication and preparation for testing p 77 N91-24324
Alpha-canonical form representation of the open loop dynamics of the Space Shuttle main engine
[NASA-TM-104422] p 131 N91-24469
Localization of aeroelastic modes in mistuned high-energy turbines
[NASA-TM-104445] p 204 N91-24659
The development of a post-test diagnostic system for rocket engines
[NASA-TM-104463] p 217 N91-24787
Probabilistic structural analysis methods for space transportation propulsion systems p 205 N91-28238
Viscoplastic analysis of an experimental cylindrical thrust chamber liner
[NASA-TM-103287] p 205 N91-28622
- SPACE SHUTTLE PAYLOADS**
- Spacelab qualified infrared imager for microgravity science applications p 173 A91-51585
- SPACE SHUTTLES**
- State of the art in video system performance p 175 N91-14578
Pressurization and expulsion of cryogenic liquids: Generic requirements for a low gravity experiment
[NASA-TM-104417] p 126 N91-25300
- SPACE STATION FREEDOM**
- National space test centers - Lewis Research Center Facilities
[AIAA PAPER 90-3593] p 41 A91-11471
Vibration environment - Acceleration mapping strategy and microgravity requirements for Spacelab and Space Station
[IAF PAPER 90-350] p 39 A91-13991
Dynamic analysis of space-related linear and non-linear structures p 196 A91-28612
Power electronic applications for Space Station Freedom p 52 A91-36832
Automated electric power management and control for Space Station Freedom p 53 A91-37970
Autonomous power expert system p 54 A91-37972
- Automating security monitoring and analysis for Space Station Freedom's electric power system p 219 A91-37975
Electric power scheduling - A distributed problem-solving approach p 219 A91-37976
An analysis of space power system masses p 54 A91-38003
Rapid thermal cycling of new technology solar array blanket coupons p 54 A91-38019
An expert system for simulating electric loads aboard Space Station Freedom p 55 A91-38041
Two-dimensional model of a Space Station Freedom thermal energy storage canister p 151 A91-38048
Photovoltaic power for Space Station Freedom p 57 A91-41878
Photovoltaic superiority for Space Station Freedom power in the 21st century p 58 A91-42004
The dynamic effects of internal robots on Space Station Freedom
[AIAA PAPER 91-2822] p 40 A91-49764
Cryogenic propellant management system requirements for Space Station Freedom
[AIAA PAPER 91-3476] p 65 A91-52382
Fuel Systems Architecture (FSA) evaluation criteria and concept evaluation methodology p 65 A91-52384
[AIAA PAPER 91-3479] p 65 A91-52384
Finite element analysis of thermal distortion effects on optical performance of solar dynamic concentrator for Space Station Freedom
[NASA-TM-102504] p 183 N91-12954
Multi-dimensional modeling of a thermal energy storage canister
[NASA-TM-103731] p 71 N91-19177
An assessment of the Space Station Freedom program's leakage current requirement
[NASA-CR-187077] p 215 N91-20630
The environment workbench: A design tool for Space Station Freedom p 48 N91-20727
Findings of the Joint Workshop on Evaluation of Impacts of Space Station Freedom Ground Configurations p 48 N91-20728
The effect of atomic oxygen on polysiloxane-polyimide for spacecraft applications in low Earth orbit p 229 N91-20735
Fire suppression in human-crew spacecraft
[NASA-TM-104334] p 44 N91-21182
An examination of anticipated g-jitter on space station and its effects on materials processes
[NASA-TM-103775] p 128 N91-21378
Findings of the Joint Workshop on Evaluation of Impacts of Space Station Freedom Ground Configurations
[NASA-TM-103717] p 73 N91-22370
The dynamic effects of internal robots on Space Station Freedom
[NASA-TM-104345] p 203 N91-22604
RSM 1.0 user's guide: A resupply scheduler using integer optimization p 217 N91-22766
[NASA-TM-104380] p 217 N91-22766
Research and technology p 243 N91-23072
[NASA-TM-103759] p 243 N91-23072
Environmental interactions of the Space Station Freedom electric power system p 49 N91-24225
[NASA-TM-104373] p 49 N91-24225
Development and testing of a source subsystem for the supporting development PMAD DC test bed
[NASA-TM-104510] p 78 N91-26202
An EMTP system level model of the PMAD DC test bed
[NASA-TM-104515] p 79 N91-27206
The development of test beds to support the definition and evolution of the Space Station Freedom power system
[NASA-TM-104504] p 79 N91-27207
Solar dynamic power for Earth orbital and lunar applications p 80 N91-27214
Description of real-time Ada software implementation of a power system monitor for the Space Station Freedom PMAD DC testbed
[NASA-TM-105157] p 218 N91-28776
Power systems testing p 42 N91-30186
[NASA-TM-104513] p 42 N91-30186
Test and evaluation of load converter topologies used in the Space Station Freedom Power Management and distribution DC test bed p 85 N91-30267
[NASA-TM-105217] p 85 N91-30267
Nickel-hydrogen cell low-Earth life test update
[NASA-TM-105229] p 213 N91-31708
- SPACE STATION POWER SUPPLIES**
- High temperature superconductivity technology for advanced space power systems p 50 A91-13447
Automated electric power management and control for Space Station Freedom p 53 A91-37970
Electric power scheduling - A distributed problem-solving approach p 219 A91-37976
- Light weight, high power, high voltage dc/dc converter technologies p 138 A91-37985
Rapid thermal cycling of new technology solar array blanket coupons p 54 A91-38019
Monolithic and mechanical multijunction space solar cells p 54 A91-38020
Modeling of Space Station electric power system with EMTP p 55 A91-38040
Photovoltaic power for Space Station Freedom p 57 A91-41878
Photovoltaic superiority for Space Station Freedom power in the 21st century p 58 A91-42004
Development and testing of a source subsystem for the supporting development PMAD DC test bed
[NASA-TM-104510] p 78 N91-26202
Concentrator testing using projected images
[NASA-TM-104349] p 79 N91-27204
An EMTP system level model of the PMAD DC test bed
[NASA-TM-104515] p 79 N91-27206
The development of test beds to support the definition and evolution of the Space Station Freedom power system
[NASA-TM-104504] p 79 N91-27207
Solar dynamic power for Earth orbital and lunar applications p 80 N91-27214
Description of real-time Ada software implementation of a power system monitor for the Space Station Freedom PMAD DC testbed
[NASA-TM-105157] p 218 N91-28776
Power systems testing p 42 N91-30186
[NASA-TM-104513] p 42 N91-30186
Test and evaluation of load converter topologies used in the Space Station Freedom Power Management and distribution DC test bed p 85 N91-30267
[NASA-TM-105217] p 85 N91-30267
Nickel-hydrogen cell low-Earth life test update
[NASA-TM-105229] p 213 N91-31708
- SPACE STATION PROPULSION**
- Performance and flow calculations for a gaseous H₂/O₂ thruster p 63 A91-48843
- SPACE STATION STRUCTURES**
- Simulation of the Space Station strut-out condition
[AIAA PAPER 91-1248] p 197 A91-32087
Environmental interactions of the Space Station Freedom electric power system
[NASA-TM-104373] p 49 N91-24225
- SPACE STATIONS**
- National space test centers - Lewis Research Center Facilities
[AIAA PAPER 90-3593] p 41 A91-11471
Vibration environment - Acceleration mapping strategy and microgravity requirements for Spacelab and Space Station
[IAF PAPER 90-350] p 39 A91-13991
Dynamic analysis of space-related linear and non-linear structures p 196 A91-28612
Solar array orientations for a space station in low earth orbit p 46 A91-30019
Induction motor control p 137 A91-30893
Autonomous power expert system p 54 A91-37972
Automating security monitoring and analysis for Space Station Freedom's electric power system p 219 A91-37975
An analysis of space power system masses p 54 A91-38003
An expert system for simulating electric loads aboard Space Station Freedom p 55 A91-38041
Two-dimensional model of a Space Station Freedom thermal energy storage canister p 151 A91-38048
Photovoltaic power for Space Station Freedom p 57 A91-41878
Evaluation of thermal control coatings for use on solar dynamic radiators in low earth orbit
[AIAA PAPER 91-1327] p 58 A91-43397
A 10,000-hr life test of an engineering model resistojel
[NASA-TM-103216] p 69 N91-11802
Impedances of electrochemically impregnated nickel electrodes as functions of potential, KOH concentration, and impregnation method p 208 N91-15628
[NASA-TM-103283] p 208 N91-15628
Multi-dimensional modeling of a thermal energy storage canister p 71 N91-19177
[NASA-TM-103731] p 71 N91-19177
Low Earth orbital atomic oxygen and ultraviolet radiation effects on polymers p 119 N91-19294
[NASA-TM-103711] p 119 N91-19294
ETARA PC version 3.3 user's guide: Reliability, availability, maintainability simulation model
[NASA-TM-103751] p 193 N91-19462
An assessment of the Space Station Freedom program's leakage current requirement
[NASA-CR-187077] p 215 N91-20630
Autonomous power expert system advanced development p 72 N91-20689

- The environment workbench: A design tool for Space Station Freedom p 48 N91-20727
- Findings of the Joint Workshop on Evaluation of Impacts of Space Station Freedom Ground Configurations p 48 N91-20728
- Atomic oxygen interaction with solar array blankets at protective coating defect sites p 211 N91-20732
- The effect of atomic oxygen on polysiloxane-polyimide for spacecraft applications in low Earth orbit p 229 N91-20735
- Fire suppression in human-crew spacecraft [NASA-TM-104334] p 44 N91-21182
- An examination of anticipated g-jitter on space station and its effects on materials processes [NASA-TM-103775] p 128 N91-21378
- Evaluation of thermal control coatings for use on solar dynamic radiators in low Earth orbit [NASA-TM-104335] p 73 N91-22367
- Findings of the Joint Workshop on Evaluation of Impacts of Space Station Freedom Ground Configurations [NASA-TM-103717] p 73 N91-22370
- The dynamic effects of internal robots on Space Station Freedom [NASA-TM-104345] p 203 N91-22604
- RSM 1.0 user's guide: A resupply scheduler using integer optimization [NASA-TM-104380] p 217 N91-22766
- Research and technology [NASA-TM-103759] p 243 N91-23072
- An assessment of technology alternatives for telecommunications and information management for the space exploration initiative [NASA-TM-103783] p 134 N91-23347
- Atomic oxygen undercutting of LDEF aluminized Kapton multilayer insulation p 229 N91-25027
- Durability evaluation of photovoltaic blanket materials exposed on LDEF tray S1003 p 212 N91-25062
- Full-size solar dynamic heat receiver thermal-vacuum tests [NASA-TM-104486] p 78 N91-25184
- Development and testing of a source subsystem for the supporting development PMAD DC test bed [NASA-TM-104510] p 78 N91-26202
- An EMTP system level model of the PMAD DC test bed [NASA-TM-104515] p 79 N91-27206
- The development of test beds to support the definition and evolution of the Space Station Freedom power system [NASA-TM-104504] p 79 N91-27207
- Ground test program for a full-size solar dynamic heat receiver [NASA-TM-104485] p 79 N91-27209
- On protection of Freedom's solar dynamic radiator from the orbital debris environment. Part 2: Further testing and analyses [NASA-TM-104514] p 84 N91-30265
- Description of the control system design for the SSF PMAD DC testbed [NASA-TM-105202] p 84 N91-30266
- SPACE TECHNOLOGY EXPERIMENTS**
- NASA cryogenic fluid management space experiment efforts [AIAA PAPER 91-3538] p 130 A91-53701
- NASA cryogenic fluid management space experiment efforts, 1960-1990 [NASA-TM-103752] p 243 N91-30073
- SPACE TRANSPORTATION**
- The COLD-SAT experiment for cryogenic fluid management technology p 46 A91-29799
- Metallized propellants for the human exploration of Mars [NASA-TP-3062] p 69 N91-11800
- Lunar missions using chemical propulsion: System design issues [NASA-TP-3065] p 70 N91-15308
- SPACE TRANSPORTATION SYSTEM**
- The rationale/benefits of nuclear thermal rocket propulsion for NASA's lunar space transportation system [AIAA PAPER 91-2052] p 39 A91-45781
- Advanced electrical power, distribution and control for the Space Transportation System p 143 N91-17043
- Probabilistic structural analysis methods for space transportation propulsion systems p 205 N91-28238
- Overall goals p 80 N91-28246
- SPACE TRANSPORTATION SYSTEM FLIGHTS**
- Ground-based PIV and numerical flow visualization results from the surface tension driven convection experiment [NASA-TM-105172] p 178 N91-30491
- SPACE-TIME FUNCTIONS**
- Structure of random discrete spacetime p 224 A91-22894
- A new numerical framework for solving conservation laws: The method of space-time conservation element and solution element [NASA-TM-104495] p 223 N91-30867
- SPACEBORNE EXPERIMENTS**
- Vibration environment - Acceleration mapping strategy and microgravity requirements for Spacelab and Space Station [IAF PAPER 90-350] p 39 A91-13991
- A summary of existing and planned experiment hardware for low-gravity fluids research [AIAA PAPER 91-0777] p 128 A91-26329
- An expert system for simulating electric loads aboard Space Station Freedom p 55 A91-38041
- Development of a vibration isolation prototype system for microgravity space experiments p 47 A91-53403
- NASA cryogenic fluid management space experiment efforts [AIAA PAPER 91-3538] p 130 A91-53701
- Computational fluid dynamics at the Lewis Research Center: An overview p 8 N91-10842
- Presentation on a Space Acceleration Measurement System (SAMS) p 50 N91-12417
- The effect of the low Earth orbit environment on space solar cells [NASA-TM-103735] p 48 N91-19165
- Development of a vibration isolation prototype system for microgravity space experiments [NASA-TM-103664] p 130 N91-19324
- A summary of existing and planned experiment hardware for low-gravity fluids research [NASA-TM-103706] p 160 N91-19371
- Research and technology [NASA-TM-103759] p 243 N91-23072
- Advanced photovoltaic experiment, S0014: Preliminary flight results and post-flight findings p 212 N91-25061
- Durability evaluation of photovoltaic blanket materials exposed on LDEF tray S1003 p 212 N91-25062
- NASA cryogenic fluid management space experiment efforts, 1960-1990 [NASA-TM-103752] p 243 N91-30073
- Leo space plasma interactions p 84 N91-30249
- SPACEBORNE LASERS**
- A preview of a microgravity laser light scattering instrument [AIAA PAPER 91-0779] p 179 A91-21614
- SPACECRAFT ANTENNAS**
- Design of an inflatable, optically controlled and fed, phased array antenna [AIAA PAPER 91-3470] p 132 A91-52378
- SPACECRAFT CHARGING**
- High voltage interactions of a sounding rocket with the ambient and system-generated environments p 46 A91-23077
- A charging study of the ACTS satellite using NASCAP [AIAA PAPER 91-1471] p 46 A91-42522
- SPACECRAFT COMMUNICATION**
- Quaternary pulse position modulation electronics for free-space laser communications [AIAA PAPER 91-3471] p 133 A91-53702
- Quaternary pulse position modulation electronics for free-space laser communications [NASA-TM-104502] p 135 N91-29405
- SPACECRAFT COMPONENTS**
- Space mechanisms needs for future NASA long duration space missions [AIAA PAPER 91-3428] p 183 A91-57025
- Government/industry response to questionnaire on space mechanisms/tribology technology needs [NASA-TM-104358] p 186 N91-23501
- Optical inspection of space-propulsion components using an injection seeded Nd:YAG laser system p 179 N91-24320
- Space mechanisms needs for future NASA long duration space missions [NASA-TM-105204] p 190 N91-30532
- SPACECRAFT CONFIGURATIONS**
- NTR vehicle commonality assessment for piloted lunar and Mars missions [AIAA PAPER 91-3575] p 66 A91-52448
- Findings of the Joint Workshop on Evaluation of Impacts of Space Station Freedom Ground Configurations p 48 N91-20728
- SPACECRAFT CONSTRUCTION MATERIALS**
- The effect of atomic oxygen on altered and coated Kapton surfaces for spacecraft applications in low earth orbit p 116 A91-49804
- Graphite fluoride fibers and their applications in the space industry [NASA-TM-103265] p 88 N91-11062
- Reinforcements: The key to high performance composite materials [NASA-TM-103230] p 96 N91-15329
- Transition-to-practice technologies for brittle materials p 120 N91-20107
- Overview of Lewis materials research: Contributions, current efforts, and future directions p 111 N91-20109
- The effect of atomic oxygen on polysiloxane-polyimide for spacecraft applications in low Earth orbit p 229 N91-20735
- Research and technology [NASA-TM-103759] p 243 N91-23072
- Ion beam textured and coated surfaces experiment (IBEX) p 122 N91-25040
- Overall goals p 80 N91-28246
- SPACECRAFT CONTAMINATION**
- Experimental evaluation of resistojet thruster plume shields p 51 A91-30010
- SPACECRAFT CONTROL**
- Technology readiness assessment of advanced space engine integrated controls and health monitoring [AIAA PAPER 91-3601] p 49 A91-52467
- Description of real-time Ada software implementation of a power system monitor for the Space Station Freedom PMAD DC testbed [NASA-TM-105157] p 218 N91-28776
- SPACECRAFT DESIGN**
- The Advanced Expander Test Bed [AIAA PAPER 90-3708] p 50 A91-10107
- SP-100 nuclear space power systems with application to space commercialization p 57 A91-38933
- A charging study of the ACTS satellite using NASCAP [AIAA PAPER 91-1471] p 46 A91-42522
- Overview of the Beta II two-stage-to-orbit vehicle design [AIAA PAPER 91-3175] p 43 A91-54088
- The environment workbench: A design tool for Space Station Freedom p 48 N91-20727
- Findings of the Joint Workshop on Evaluation of Impacts of Space Station Freedom Ground Configurations p 48 N91-20728
- The development of test beds to support the definition and evolution of the Space Station Freedom power system [NASA-TM-104504] p 79 N91-27207
- Power systems testing [NASA-TM-104513] p 42 N91-30186
- Structural design concepts for a multi-megawatt Solar Electric Propulsion (SEP) spacecraft [NASA-TM-105148] p 206 N91-30565
- The International Space University's variable gravity research facility design [NASA-TM-105224] p 44 N91-31196
- SPACECRAFT ENVIRONMENTS**
- Radiation from gas-jet diffusion flames in microgravity environments [AIAA PAPER 91-0719] p 104 A91-19432
- High emittance surfaces for high temperature space radiator applications p 88 A91-56415
- The environment workbench: A design tool for Space Station Freedom p 48 N91-20727
- SPACECRAFT INSTRUMENTS**
- Fiber-optic applications for space-based rocket engines [AIAA PAPER 91-3602] p 49 A91-52468
- Overview of the instrumentation program p 176 N91-24318
- Fiber-optic applications for space-based engines [NASA-TM-105235] p 86 N91-32163
- SPACECRAFT LAUNCHING**
- Advanced launch system (ALS) - Electrical actuation and power systems improve operability and cost picture p 51 A91-31025
- Key issues in space nuclear power [NASA-TM-103656] p 71 N91-19179
- Advanced launch vehicle upper stages using liquid propulsion and metallized propellants p 75 N91-24257
- SPACECRAFT MAINTENANCE**
- RSM 1.0 user's guide: A resupply scheduler using integer optimization [NASA-TM-104380] p 217 N91-22766
- SPACECRAFT POWER SUPPLIES**
- Nuclear power systems for lunar and Mars exploration [IAF PAPER 90-200] p 51 A91-13868
- An evolutionary path to satellite solar power systems p 51 A91-26063
- Power electronic applications for Space Station Freedom p 52 A91-36832
- NASA's future space power needs and requirements p 52 A91-37929
- Power system requirements and definition for lunar and Mars outposts p 52 A91-37930
- A comparison of energy conversion systems for meeting the power requirements of manned rover for Mars missions p 53 A91-37932
- Programmatic status of NASA's CSTI High Capacity Power Stirling Space Power Converter Program p 53 A91-37933

- Automating security monitoring and analysis for Space Station Freedom's electric power system p 219 A91-37975
- Electrical characterization of a Mapham inverter using pulse testing techniques p 139 A91-37992
- An analysis of space power system masses p 54 A91-38003
- Component and prototype panel testing of the mini-dome Fresnel lens photovoltaic concentrator array p 54 A91-38023
- Effect of LEO cycling on 125 Ah advanced design IPV nickel-hydrogen battery cells p 55 A91-38077
- Impedances of Ni electrodes and Ni/H₂ cells from different manufacturers p 55 A91-38082
- NASA Aerospace Flight Battery Systems Program p 56 A91-38088
- Two-dimensional simulation of a two-phase, regenerative pumped radiator loop utilizing direct contact heat transfer with phase change p 151 A91-38126
- Update on results of SPRE testing at NASA p 56 A91-38140
- Recent Stirling engine loss-understanding results p 181 A91-38151
- Lunar orbiting microwave beam power system p 56 A91-38158
- SP-100 nuclear space power systems with application to space commercialization p 57 A91-38933
- Conceptual study of on orbit production of cryogenic propellants by water electrolysis [AIAA PAPER 91-1844] p 124 A91-41631
- Lightweight concentrator module with 30 percent AMO efficient GaAs/GaSb tandem cells p 57 A91-41990
- 23.5 percent thin-film space concentrator cells p 58 A91-42002
- Laser photovoltaic power system synergy for SEI applications [AIAA PAPER 91-3419] p 207 A91-52339
- The telescoping boom radiator concept for multimegawatt space power systems [AIAA PAPER 91-3497] p 158 A91-52395
- Advanced materials for space nuclear power systems [AIAA PAPER 91-3530] p 88 A91-53704
- Historical perspectives - The role of the NASA Lewis Research Center in the national space nuclear power programs [AIAA PAPER 91-3462] p 242 A91-53713
- Silicon carbide, a semiconductor for space power electronics [NASA-TM-103655] p 234 A91-14850
- The environment power system analysis tool development program p 231 A91-17734
- Simulation of Martian dust accumulation on surfaces p 47 A91-19160
- Radiation resistance of thin-film solar cells for space photovoltaic power [NASA-TM-103715] p 71 A91-19176
- Key issues in space nuclear power [NASA-TM-103656] p 71 A91-19179
- Space Photovoltaic Research and Technology, 1989 [NASA-CP-3107] p 72 A91-19182
- Review of thin film solar cell technology and applications for ultra-light spacecraft solar arrays p 208 A91-19198
- Dual-purpose self-deliverable lunar surface PV electrical power system p 209 A91-19200
- Conceptual study of on orbit production of cryogenic propellants by water electrolysis [NASA-TM-103730] p 126 A91-19317
- ETARA PC version 3.3 user's guide: Reliability, availability, maintainability simulation model [NASA-TM-103751] p 193 A91-19462
- Autonomous power expert system advanced development p 72 A91-20689
- Findings of the Joint Workshop on Evaluation of Impacts of Space Station Freedom Ground Configurations p 48 A91-20728
- Future mission opportunities and requirements for advanced space photovoltaic energy conversion technology [NASA-TM-103661] p 74 A91-22371
- Research and technology [NASA-TM-103759] p 243 A91-23072
- Design of multihundredwatt DIPS for robotic space missions [NASA-TM-104401] p 75 A91-24232
- Balancing reliability and cost to choose the best power subsystem [NASA-TM-104453] p 238 A91-24952
- Sensible heat receiver for solar dynamic space power system [NASA-TM-104393] p 77 A91-25173
- Small Stirling dynamic isotope power system for multihundred-watt robotic missions [NASA-TM-104460] p 78 A91-25182
- Development of an analytical tool to study power quality of AC power systems for large spacecraft [NASA-TM-104451] p 223 A91-25749
- Effects of Martian dust on power system components p 241 A91-27061
- Design considerations for space radiators based on the liquid sheet (LSR) concept [NASA-TM-105158] p 80 A91-27213
- Solar dynamic power for Earth orbital and lunar applications [NASA-TM-104511] p 80 A91-27214
- Recent progress in InP solar cell research [NASA-TM-104509] p 146 A91-27447
- Comparison of dynamic isotope power systems for distributed planet surface applications [NASA-TM-4303] p 81 A91-28278
- Historical perspectives: The role of the NASA Lewis Research Center in the national space nuclear power programs [NASA-TM-105196] p 243 A91-29138
- Advanced materials for space nuclear power systems [NASA-TM-105171] p 112 A91-29298
- Space Photovoltaic Research and Technology Conference [NASA-CP-3121] p 82 A91-30203
- Leo space plasma interactions p 84 A91-30249
- Description of the control system design for the SSF PMAD DC testbed [NASA-TM-105202] p 84 A91-30266
- Advanced power systems for EOS [NASA-TM-105222] p 85 A91-31217
- SPACECRAFT PROPULSION**
- The Advanced Expander Test Bed [AIAA PAPER 90-3708] p 50 A91-10107
- Cryogenic propellant management architectures to support the Space Exploration Initiative [AIAA PAPER 90-3713] p 124 A91-10112
- National space test centers - Lewis Research Center Facilities [AIAA PAPER 90-3593] p 41 A91-11471
- Reactionless orbital propulsion using tether deployment [IAF PAPER 90-254] p 51 A91-13908
- Performance and lifetime assessment of magnetoplasmadynamic arc thruster technology p 51 A91-30013
- Thrust stand for high-power electric propulsion devices p 41 A91-36239
- Comment on 'Negative matter propulsion' p 52 A91-37424
- Probabilistic modeling for simulation of aerodynamic uncertainties in propulsion systems p 58 A91-42725
- Anode power deposition in an applied-field segmented anode MPD thruster [AIAA PAPER 91-2343] p 59 A91-44204
- Carbon monoxide and oxygen combustion experiments - A demonstration of Mars in situ propellants [AIAA PAPER 91-2443] p 60 A91-44246
- Nonequilibrium in a low power arcjet nozzle [AIAA PAPER 91-2113] p 61 A91-45784
- Ion beam sputtering in electric propulsion facilities [AIAA PAPER 91-2117] p 61 A91-45785
- Plug nozzles - The ultimate customer driven propulsion system --- applied to manned lunar and Martian landers [AIAA PAPER 91-2208] p 61 A91-45794
- High-power hydrogen arcjet performance [AIAA PAPER 91-2226] p 61 A91-45795
- Preliminary performance and life evaluation of a 2-kW arcjet [AIAA PAPER 91-2228] p 62 A91-45796
- Performance impact on nuclear thermal propulsion of piloted Mars missions with short transit times [AIAA PAPER 91-3401] p 64 A91-52326
- Laser photovoltaic power system synergy for SEI applications [AIAA PAPER 91-3419] p 207 A91-52339
- Hydrogen/oxygen auxiliary propulsion technology [AIAA PAPER 91-3440] p 64 A91-52352
- Blazing the trailway - Nuclear electric propulsion and its technology program plans [AIAA PAPER 91-3441] p 64 A91-52353
- Development of nuclear fuels and materials for propulsion systems for SEI [AIAA PAPER 91-3452] p 125 A91-52362
- SEI needs for space nuclear power [AIAA PAPER 91-3459] p 64 A91-52369
- Test facilities for high power electric propulsion [AIAA PAPER 91-3499] p 42 A91-52396
- An overview of tested and analyzed NTP concepts [AIAA PAPER 91-3503] p 65 A91-52400
- Advanced ion propulsion for space exploration [AIAA PAPER 91-3567] p 65 A91-52443
- Nuclear Thermal Propulsion technology - Summary of FY 1991 interagency panel planning [AIAA PAPER 91-3631] p 66 A91-52495
- Nondestructive evaluation tools and experimental studies for monitoring the health of space propulsion systems [AIAA PAPER 91-3433] p 192 A91-53703
- Numerical propulsion system simulation - An interdisciplinary approach [AIAA PAPER 91-3554] p 86 A91-53706
- The design and performance estimates for the propulsion module for the booster of a TSTO vehicle [AIAA PAPER 91-3136] p 43 A91-54054
- Advanced chemical propulsion at NASA Lewis: Metallized and high energy density propellants [NASA-TM-103771] p 71 A91-19175
- High temperature electronics p 144 A91-20101
- Overview of structures research p 202 A91-20104
- Propulsion aeroelasticity, vibration control, and dynamic system modeling p 29 A91-20105
- Computational simulation of propulsion structures performance and reliability p 29 A91-20106
- Cooling of in-situ propellant rocket engines for Mars mission [NASA-TM-103729] p 72 A91-21233
- Vision-21: Space Travel for the Next Millennium [NASA-CP-10059] p 40 A91-22139
- Exploring the notion of space coupling propulsion p 73 A91-22161
- Reactionless propulsion using tethers p 73 A91-22163
- Research and technology [NASA-TM-103759] p 243 A91-23072
- Carbon monoxide and oxygen combustion experiments: A demonstration of Mars in situ propellants [NASA-TM-104473] p 76 A91-24303
- Overview of the instrumentation program p 176 A91-24318
- Overview of aerothermodynamic loads definition study p 204 A91-24334
- Sensor failure detection and recovery by neural networks [NASA-TM-104484] p 220 A91-24815
- Nuclear rocket propulsion: NASA plans and progress, FY 1991 [NASA-TM-104455] p 77 A91-25179
- Research and development of optical measurement techniques for aerospace propulsion research: A NASA Lewis Research Center perspective [NASA-TM-104418] p 178 A91-27511
- Advanced cryo propulsion systems p 80 A91-28212
- Futuristic systems: Solar and nuclear electric propulsion p 80 A91-28215
- Concurrent engineering p 80 A91-28247
- Nondestructive evaluation tools and experimental studies for monitoring the health of space propulsion systems [NASA-TM-105164] p 194 A91-28605
- Numerical propulsion system simulation: An interdisciplinary approach [NASA-TM-105181] p 81 A91-29221
- Performance and optimization of a derated ion thruster for auxiliary propulsion [NASA-TM-105144] p 82 A91-29229
- Preliminary performance and life evaluations of a 2-kW arcjet [NASA-TM-105149] p 84 A91-30252
- Technical prospects for utilizing extraterrestrial propellants for space exploration [NASA-TM-105263] p 127 A91-31318
- MPD thruster technology [NASA-TM-105242] p 86 A91-32162
- Multimegawatt electric propulsion system design considerations [NASA-TM-105152] p 87 A91-32164
- SPACECRAFT RADIATORS**
- The telescoping boom radiator concept for multimegawatt space power systems [AIAA PAPER 91-3497] p 158 A91-52395
- An overview of the LeRC CSTI thermal management program [AIAA PAPER 91-3528] p 158 A91-52422
- High emittance surfaces for high temperature space radiator applications p 88 A91-56415
- Liquid sheet radiator apparatus [NASA-CASE-LEW-14295-1] p 130 A91-15424
- Design considerations for space radiators based on the liquid sheet (LSR) concept [NASA-TM-105158] p 80 A91-27213
- SPACECRAFT RELIABILITY**
- Technology readiness assessment of advanced space engine integrated controls and health monitoring [AIAA PAPER 91-3601] p 49 A91-52467
- Space engine safety system [AIAA PAPER 91-3604] p 44 A91-52470
- The environment workbench: A design tool for Space Station Freedom p 48 A91-20727

SPACECRAFT SHIELDING

- Experimental evaluation of resistojet thruster plume shields p 51 A91-30010
 Interlaced graphite fiber composites as EMI shields in aerospace structures p 94 N91-10134 [NASA-TM-103632]
 Atomic oxygen interaction with solar array blankets at protective coating defect sites p 211 N91-20732
 The effect of atomic oxygen on polysiloxane-polyimide for spacecraft applications in low Earth orbit p 229 N91-20735

SPACECRAFT STRUCTURES

- Probabilistic simulation of uncertainties in thermal structures p 195 A91-16042
 Dynamic analysis of space-related linear and non-linear structures p 196 A91-28612
 Undercutting of defects in thin film protective coatings on polymer surfaces exposed to atomic oxygen p 115 A91-41516
 Probabilistic simulation of uncertainties in thermal structures [NASA-TM-103680] p 201 N91-19472
 PM200/PS200: Self-lubricating bearing and seal materials for applications to 900 C [NASA-TM-103776] p 190 N91-30539

SPACECRAFT TEMPERATURE

- Preliminary thermal design of the COLD-SAT spacecraft [AIAA PAPER 91-1305] p 46 A91-45550
 Preliminary thermal design of the COLD-SAT spacecraft [NASA-TM-104440] p 49 N91-25161

SPACELAB

- Spacelab qualified infrared imager for microgravity science applications p 173 A91-51585
 Ground-based PIV and numerical flow visualization results from the surface tension driven convection experiment [NASA-TM-105172] p 178 N91-30491

SPARK IGNITION

- Evaluation of a hybrid kinetics/mixing-controlled combustion model for turbulent premixed and diffusion combustion using KIVA-II [AIAA PAPER 90-2450] p 104 A91-12927

SPATIAL DISTRIBUTION

- Spatial evolution of nonlinear acoustic mode instabilities on hypersonic boundary layers p 225 A91-12973

SPECIFIC IMPULSE

- High-power hydrogen arcjet performance [AIAA PAPER 91-2226] p 61 A91-45795
 Energy deposition in low-power coaxial plasma thrusters p 63 A91-52311
 Design issues for propulsion systems using metallized propellants [AIAA PAPER 91-3484] p 66 A91-53709
 Design issues for propulsion systems using metallized propellants [NASA-TM-105190] p 81 N91-29220
 Experimental and analytical comparison of flowfields in a 110 N (25 lbf) H₂/O₂ rocket [NASA-TM-105175] p 82 N91-29230
 Preliminary performance and life evaluations of a 2-kW arcjet [NASA-TM-105149] p 84 N91-30252

SPECKLE HOLOGRAPHY

- Two-dimensional high temperature strain measurement system p 204 N91-24319

SPECKLE INTERFEROMETRY

- Fiber optic phase stepping system for interferometry p 171 A91-28968

SPECKLE PATTERNS

- Two-dimensional surface strain measurement based on a variation of Yamaguchi's laser-speckle strain gauge p 174 A91-55531

SPECTRA

- Wind turbine acoustics [NASA-TP-3057] p 228 N91-16679

SPECTRAL LINE WIDTH

- A preliminary characterization of applied-field MPD thruster plumes [AIAA PAPER 91-2339] p 62 A91-45798

SPECTRAL METHODS

- Mappings and accuracy for Chebyshev pseudo-spectral approximations [NASA-TM-103630] p 221 N91-14781
 A comparison of numerical methods for the Rayleigh equation in unbounded domains [NASA-TM-105179] p 223 N91-30865

SPECTROSCOPIC ANALYSIS

- Spectroscopic wear detector [NASA-CASE-LEW-15200-1] p 87 N91-32167

SPECTROSCOPY

- Determination of alloy content from plume spectral measurements [AIAA PAPER 91-2531] p 88 A91-44284

- Thin film characterization using spectroscopic ellipsometry p 119 N91-18303
 Study of InGaAs based MODFET structures using variable angle spectroscopic ellipsometry [NASA-TM-103792] p 235 N91-19935
 Determination of alloy content from plume spectral measurements [NASA-TM-104442] p 89 N91-24341

SPECTRUM ANALYSIS

- Determination of alloy content from plume spectral measurements [AIAA PAPER 91-2531] p 88 A91-44284
 Determination of alloy content from plume spectral measurements [NASA-TM-104442] p 89 N91-24341

SPEED CONTROL

- Four quadrant control of induction motors p 145 N91-23055

SPIN TESTS

- Comparison of Weibull strength parameters from flexure and spin tests of brittle materials [NASA-TM-104414] p 187 N91-24593

SPLITTING

- A new flux splitting scheme [NASA-TM-104404] p 222 N91-22814

SPONTANEOUS COMBUSTION

- Particle cloud flames in acoustic fields p 105 A91-20589

SPRAY CHARACTERISTICS

- Influence of geometric features on the performance of pressure-swirl atomizers p 147 A91-13030
 Flow visualization of a rocket injector spray using gelled propellant simulants [AIAA PAPER 91-2198] p 59 A91-44151
 Spray measurements of aerothermodynamic effect on disintegrating liquid jets [NASA-TM-104501] p 178 N91-27510

SPRAY NOZZLES

- Influence of geometric features on the performance of pressure-swirl atomizers p 147 A91-13030
 LN₂ spray droplet size measurement via ensemble diffraction technique [AIAA PAPER 91-1381] p 129 A91-44336
 LN₂ spray droplet size measurement via ensemble diffraction technique [NASA-TM-104443] p 131 N91-24470

SPRAYED COATINGS

- Composite bearing and seal materials for advanced heat engine applications to 900 C [NASA-TM-103612] p 95 N91-15318
 The PM-200 lubrication system p 121 N91-23044

SPRAYERS

- Measurements and predictions of a liquid spray from an air-assist nozzle [AIAA PAPER 91-0692] p 149 A91-22498
 Cryogenic transfer options for exploration missions [AIAA PAPER 91-3541] p 158 A91-53714
 Measurements and predictions of a liquid spray from an air-assist nozzle [NASA-TM-103640] p 26 N91-13455
 Cryogenic transfer options for exploration missions [NASA-TM-105197] p 168 N91-28538

SPREAD SPECTRUM TRANSMISSION

- Study on the spectral efficiency of SFH-GMSK in land mobile telephone communication by direct simulation p 132 A91-53176

SPREADING

- Naturally occurring and forced azimuthal modes in a turbulent jet [NASA-TM-103692] p 11 N91-17000

SPUTTERING

- Ion beam sputtering in electric propulsion facilities [AIAA PAPER 91-2117] p 61 A91-45785
 Plasma-assisted physical vapor deposition surface treatments for tribological control [NASA-TM-103652] p 130 N91-11945
 Flexible fluoropolymer filled protective coatings p 121 N91-24062
 Leo space plasma interactions p 84 N91-30249
 Ion beam sputtering in electric propulsion facilities [NASA-TM-105145] p 86 N91-32158
 Lubrication with sputtered MoS₂ films: Principles, operation, limitations [NASA-TM-105292] p 112 N91-32216

STABILITY

- Vinyl capped addition polyimides [NASA-CASE-LEW-15027-1] p 118 N91-13566
 High alpha inlets p 28 N91-20091
 The series Bi₂Sr₂Ca(n-1)Cu(n)O(2n+4) (1 less than or equal to n less than or equal to 5): Phase stability and superconducting properties [NASA-TM-103749] p 235 N91-21910

STABILITY TESTS

- MIS capacitor studies on silicon carbide single crystals [NASA-CR-187350] p 234 N91-11555

STAINLESS STEELS

- Axial-torsional fatigue: A study of tubular specimen thickness effects [NASA-TM-103637] p 200 N91-14632
 Cumulative creep fatigue damage in 316 stainless steel p 111 N91-24312

STANDARD DEVIATION

- Vibrational testing of optical fiber connector joints p 172 A91-30652
 Vibrational testing of optical fiber connector joints [NASA-TM-103654] p 230 N91-14829

STANDARDIZATION

- Current activities in standardization of high-temperature, low-cycle-fatigue testing techniques in the United States [NASA-TM-103675] p 200 N91-17427

STANDARDS

- Primary reference cell calibrations at SERI - History and methods --- solar cells p 207 A91-41966
 NDE standards for high temperature materials [NASA-TM-103761] p 193 N91-19464

STATE ESTIMATION

- Alpha-canonical form representation of the open loop dynamics of the Space Shuttle main engine [NASA-TM-104422] p 131 N91-24469

STATIC DEFORMATION

- Optical measurement of unducted fan blade deflections [ASME PAPER 89-GT-298] p 170 A91-13046

STATIC LOADS

- Simplified procedures for designing adhesively bonded composite joints p 180 A91-20938

STATIC MODELS

- A model for the space shuttle main engine high pressure oxidizer turbopump shaft seal system [NASA-TM-103697] p 184 N91-20489

STATIC PRESSURE

- Turbulent boundary layer separation over a rearward facing ramp and its control through mechanical excitation [AIAA PAPER 91-0253] p 150 A91-26326
 Unsteady flowfield of a propfan at takeoff conditions [NASA-TM-105223] p 18 N91-32075

STATIC TESTS

- Static performance tests of a flight-type STOVL ejector [AIAA PAPER 91-1902] p 24 A91-44050
 Static performance tests of a flight-type STOVL ejector [NASA-TM-104437] p 33 N91-24201

STATIONKEEPING

- Mass comparisons of electric propulsion systems for NSSK of geosynchronous spacecraft --- North-South Station Keeping [AIAA PAPER 91-2347] p 47 A91-45808
 Xenon ion propulsion for orbit transfer [NASA-TM-103193] p 69 N91-11798
 Mass comparisons of electric propulsion systems for NSSK of geosynchronous spacecraft [NASA-TM-105153] p 85 N91-31212

STATISTICAL ANALYSIS

- Relationship between voids and interlaminar shear strength of polymer matrix composites [NASA-TM-103643] p 95 N91-13495

STATORS

- Performance of a high-work, low-aspect-ratio turbine stator tested with a realistic inlet radial temperature gradient [NASA-TM-103738] p 31 N91-20126
 Three-dimensional Euler time accurate simulations of fan rotor-stator interactions [NASA-TM-102528] p 16 N91-24124

STEADY FLOW

- A new Lagrangian random choice method for steady two-dimensional supersonic/hypersonic flow [AIAA PAPER 91-1546] p 5 A91-40721
 Parallel computing using a Lagrangian formulation [NASA-TM-104446] p 215 N91-24745
 Experimental investigation of turbulent flow through a circular-to-rectangular transition duct [NASA-TM-105210] p 18 N91-31106

STEELS

- Evaluation of advanced lubricants for aircraft applications using gear surface fatigue tests [AIAA PAPER 91-1907] p 181 A91-41649
 Surface fatigue life of M50NiL and AISI 9310 gears and rolling-contact bars p 182 A91-45350
 Evaluation of advanced lubricants for aircraft applications using gear surface fatigue tests [NASA-TM-104336] p 186 N91-22568
 Surface fatigue life of M50NiL and AISI 9310 spur gears and R C bars [NASA-TM-104496] p 189 N91-27569

STIFFNESS

- Integrated force method versus displacement method for finite element analysis p 196 A91-28372

STIRLING CYCLE

- Recent Stirling engine loss-understanding results
p 181 A91-38151
- Preliminary designs for 25 kW advanced Stirling conversion systems for dish electric applications
p 207 A91-38182
- Lunar electric power systems utilizing the SP-100 reactor coupled to dynamic conversion systems
[AIAA PAPER 91-3520] p 208 A91-52415
- Space reactor/Stirling cycle systems for high power lunar application
[NASA-TM-103698] p 40 N91-19112
- Solar powered Stirling cycle electrical generator
p 211 N91-23054
- Component technology for Stirling power converters
[NASA-TM-104387] p 74 N91-23234
- Small Stirling dynamic isotope power system for multihundred-watt robotic missions
[NASA-TM-104460] p 78 N91-25182
- Stirling machine operating experience
[NASA-TM-104487] p 212 N91-25510
- A reliability and mass perspective of SP-100 Stirling cycle lunar-base powerplant designs
[NASA-TM-103736] p 212 N91-26592
- Design considerations for space radiators based on the liquid sheet (LSR) concept
[NASA-TM-105158] p 80 N91-27213
- Preliminary design of a mobile lunar power supply
[NASA-TM-104471] p 212 N91-27611
- Comparison of dynamic isotope power systems for distributed planet surface applications
[NASA-TM-4303] p 81 N91-28278
- Status of the advanced Stirling conversion system project for 25 kW dish Stirling applications
[NASA-TM-104528] p 238 N91-31023
- Status of NASA's Stirling Space Power Converter Program
[NASA-TM-104512] p 214 N91-32569

STIRLING ENGINES

- Programmatic status of NASA's CSTI High Capacity Power Stirling Space Power Converter Program
p 53 A91-37933
- Update on results of SPRE testing at NASA
p 56 A91-38140
- Recent Stirling engine loss-understanding results
p 181 A91-38151
- Multidimensional computer simulation of Stirling cycle engines
p 181 A91-38154
- Preliminary designs for 25 kW advanced Stirling conversion systems for dish electric applications
p 207 A91-38182
- Further two-dimensional code development for Stirling space engine components
p 56 A91-38184
- Stirling engine: Available tools for long-life assessment
[NASA-TM-103660] p 200 N91-12980
- Composite bearing and seal materials for advanced heat engine applications to 900 C
[NASA-TM-103612] p 95 N91-15318
- A 2-D oscillating flow analysis in Stirling engine heat exchangers
[NASA-TM-103781] p 161 N91-19375
- Solar powered Stirling cycle electrical generator
p 211 N91-23054
- Solar thermal energy receiver
[NASA-CASE-LEW-14949-1] p 211 N91-23617
- Design of multihundredwatt DIPS for robotic space missions
[NASA-TM-104401] p 75 N91-24232
- Small Stirling dynamic isotope power system for multihundred-watt robotic missions
[NASA-TM-104460] p 78 N91-25182
- Comparative survey of dynamic analyses of free-piston Stirling engines
[NASA-TM-104491] p 224 N91-26870
- Update on results of SPRE testing at NASA Lewis
[NASA-TM-104425] p 79 N91-27208
- Status of the advanced Stirling conversion system project for 25 kW dish Stirling applications
[NASA-TM-104528] p 238 N91-31023
- STOCHASTIC PROCESSES**
- Localization of aeroelastic modes in mistuned high-energy turbines
[AIAA PAPER 91-3379] p 198 A91-44319
- A methodology for evaluating the reliability and risk of structures under complex service environments
[NASA-TM-103244] p 200 N91-17415
- Localization of aeroelastic modes in mistuned high-energy turbines
[NASA-TM-104445] p 204 N91-24659
- STORAGE BATTERIES**
- Photovoltaic power for Space Station Freedom
p 57 A91-41878
- STORAGE STABILITY**
- Effect of LEO cycling on 125 Ah advanced design IPV nickel-hydrogen flight cells. An update
[NASA-TM-104384] p 74 N91-22375

STORAGE TANKS

- Improved thermodynamic modelling of the no-vent fill process and correlation with experimental data
[AIAA PAPER 91-1379] p 129 A91-43444
- Preliminary thermal design of the COLD-SAT spacecraft
[AIAA PAPER 91-1305] p 46 A91-45550
- Review and test of chilldown methods for space-based cryogenic tanks
[AIAA PAPER 91-1843] p 60 A91-45776
- Self-pressurization of a lightweight liquid hydrogen storage tank subjected to low heat flux
[NASA-TM-103804] p 126 N91-20324
- Preliminary thermal design of the COLD-SAT spacecraft
[NASA-TM-104440] p 49 N91-25161
- Pressurization and expulsion of cryogenic liquids: Generic requirements for a low gravity experiment
[NASA-TM-104417] p 126 N91-25300
- Review and test of chilldown methods for space-based cryogenic tanks
[NASA-TM-104458] p 167 N91-25351
- Autogenous pressurization of cryogenic vessels using submerged vapor injection
[NASA-TM-104516] p 127 N91-27375
- STOVL AIRCRAFT**
- Experimental and analytical studies of flow through a ventral and axial exhaust nozzle system for STOVL aircraft
[AIAA PAPER 91-2135] p 25 A91-45791
- The NASA Lewis integrated propulsion and flight control simulator
[AIAA PAPER 91-2969] p 38 A91-47847
- Application of an integrated flight/propulsion control design methodology to a STOVL aircraft
[AIAA PAPER 91-2792] p 36 A91-49793
- Experimental and analytical studies of flow through a ventral and axial exhaust nozzle system for STOVL aircraft
[NASA-TM-104364] p 77 N91-25175
- Application of an integrated flight/propulsion control design methodology to a STOVL aircraft
[NASA-TM-105254] p 37 N91-32143
- STRAIN DISTRIBUTION**
- Finite element elastic-plastic-creep and cyclic life analysis of a cowl lip
p 199 A91-56365
- STRAIN GAGES**
- PdCr based high temperature static strain gage
[AIAA PAPER 90-5236] p 170 A91-14462
- A resistance strain gage with repeatable apparent strain to 800 C
p 198 A91-48899
- A resistance strain gage with repeatable and cancellable apparent strain for use to 1500 F
p 173 A91-51930
- Two-dimensional surface strain measurement based on a variation of Yamaguchi's laser-speckle strain gauge
p 174 A91-55531
- STRAIN HARDENING**
- On the thermodynamics of stress rate in the evolution of back stress in viscoplasticity
[NASA-TM-103794] p 201 N91-19476
- STRAIN MEASUREMENT**
- Two-dimensional surface strain measurement based on a variation of Yamaguchi's laser-speckle strain gauge
p 174 A91-55531
- Two-dimensional high temperature strain measurement system
p 204 N91-24319
- Dynamic measurements of gear tooth friction and load
[NASA-TM-103281] p 189 N91-27570
- STREAK PHOTOGRAPHY**
- Ground-based PIV and numerical flow visualization results from the surface tension driven convection experiment
[NASA-TM-105172] p 178 N91-30491
- STREAMS**
- Experimental study of cross-stream mixing in a cylindrical duct
[NASA-TM-105180] p 34 N91-29187
- STRESS ANALYSIS**
- Contact stresses in gear teeth - A new method of analysis
[AIAA PAPER 91-2022] p 182 A91-41683
- Elastic response of (001)-oriented PWA 1480 single crystal - The influence of secondary orientation
[SAE PAPER 911111] p 110 A91-53555
- Application of finite-element-based solution technologies for viscoplastic structural analyses
p 199 A91-55137
- On the thermodynamics of stress rate in the evolution of back stress in viscoplasticity
[NASA-TM-103794] p 201 N91-19476
- Elastic response of zone axis (001)-oriented PWA 1480 single crystal: The influence of secondary orientation
[NASA-TM-103782] p 202 N91-21558
- Comparison of analysis and experiment for dynamics of low-contact-ratio spur gears
[NASA-TM-103232] p 185 N91-22566

- Contact stresses in gear teeth: A new method of analysis
[NASA-TM-104397] p 186 N91-22570
- An unconditionally stable Runge-Kutta method for unsteady rotor-stator interaction
p 165 N91-24337
- Tensile deformation damage in SiC reinforced Ti-15V-3Cr-3Al-3Sn
[NASA-TM-103620] p 101 N91-25195
- An analysis of the wear behavior of SiC whisker reinforced alumina from 25 to 1200 C
[NASA-TM-104489] p 90 N91-29235
- STRESS CYCLES**
- Cumulative creep fatigue damage in 316 stainless steel
p 111 N91-24312
- STRESS DISTRIBUTION**
- Creep behavior of copper at intermediate temperatures. II - Surface microstructural observations. III - A comparison with theory
p 109 A91-47931
- Universal behavior in ideal slip
p 110 A91-48517
- Finite element elastic-plastic-creep and cyclic life analysis of a cowl lip
p 199 A91-56365
- The method of lines in analyzing solids containing cracks
[NASA-TM-103626] p 201 N91-19477
- STRESS INTENSITY FACTORS**
- Analysis of some compliance calibration data for chevron-notch bar and rod specimens
[NASA-TM-104367] p 203 N91-22594
- STRESS MEASUREMENT**
- Two-dimensional high temperature strain measurement system
p 204 N91-24319
- STRESS RELAXATION**
- Concurrent tailoring of fabrication process and interphase layer to reduce residual stresses in metal matrix composites
p 92 A91-43232
- Fiber creep evaluation by stress relaxation measurements
p 117 A91-56905
- A simple test for thermomechanical evaluation of ceramic fibers
[NASA-TM-103767] p 121 N91-21309
- Viscoelastic properties of addition-cured polyimides used in high temperature polymer matrix composites
[NASA-TM-103768] p 89 N91-22377
- STRESS WAVES**
- Acousto-ultrasonics
p 226 A91-48227
- Review of acousto-ultrasonic NDE for composites
p 97 N91-18192
- STRESS-STRAIN DIAGRAMS**
- METCAN updates for high temperature composite behavior: Simulation/verification
[NASA-TM-103682] p 97 N91-19229
- STRESS-STRAIN RELATIONSHIPS**
- Polymeric routes to silicon carbide and silicon oxycarbide CMC
p 117 A91-56922
- Stirling engine: Available tools for long-life assessment
[NASA-TM-103660] p 200 N91-12980
- On the thermodynamics of stress rate in the evolution of back stress in viscoplasticity
[NASA-TM-103794] p 201 N91-19476
- Thermomechanical and bithermal fatigue behavior of cast B1900 + Hf and wrought Haynes 188
[NASA-TM-4225] p 111 N91-20268
- HITCAN for actively cooled hot-composite thermostructural analysis
[NASA-TM-103750] p 202 N91-21562
- Combined thermal and bending fatigue of high-temperature metal-matrix composites: Computational simulation
[NASA-TM-104354] p 100 N91-23247
- Two-dimensional high temperature strain measurement system
p 204 N91-24319
- Polymeric routes to silicon carbide and silicon oxycarbide CMC
[NASA-TM-104372] p 102 N91-26234
- Viscoplastic analysis of an experimental cylindrical thrust chamber liner
[NASA-TM-103287] p 205 N91-28622
- Experimental and analytical analysis of stress-strain behavior in a (90/0 deg)2s, SiC/Ti-15-3 laminate
[NASA-TM-104470] p 103 N91-31235
- STRONTIUM COMPOUNDS**
- Synthesis and thermal properties of strontium and calcium peroxides
[NASA-TM-103725] p 107 N91-22410
- STRUCTURAL ANALYSIS**
- General purpose program to generate compatibility matrix for the integrated force method
p 195 A91-12905
- Probabilistic simulation of uncertainties in thermal structures
p 195 A91-16042
- Integrated force method versus displacement method for finite element analysis
p 196 A91-28372
- Progressive fracture in composites subjected to hygrothermal environment
[AIAA PAPER 91-1140] p 91 A91-31919

- Programming probabilistic structural analysis for parallel processing computer
[AIAA PAPER 91-0920] p 196 A91-31957
- Compatibility conditions of structural mechanics for finite element analysis p 198 A91-37853
- Thermal and structural assessments of a ceramic wafer seal in hypersonic engine
[AIAA PAPER 91-2494] p 23 A91-41799
- Evaluation of thermomechanical damage in silicon carbide/titanium composites p 92 A91-42297
- Application of finite-element-based solution technologies for viscoplastic structural analyses p 199 A91-55137
- Status of structural analysis of 30 cm diameter ion optics
[NASA-TM-103618] p 68 N91-11796
- Probabilistic structural analysis of a truss typical for space station
[NASA-TM-103277] p 199 N91-12114
- Thermal and structural assessments of a ceramic wafer seal in hypersonic engines
[NASA-TM-103651] p 26 N91-13456
- A methodology for evaluating the reliability and risk of structures under complex service environments
[NASA-TM-103244] p 200 N91-17415
- Computational simulation of hot composites structures
[NASA-TM-103681] p 97 N91-19230
- Structural reliability analysis of laminated CMC components
[NASA-TM-103685] p 119 N91-19292
- Probabilistic simulation of uncertainties in thermal structures
[NASA-TM-103680] p 201 N91-19472
- Applications of artificial neural nets in structural mechanics
[NASA-TM-102420] p 202 N91-21559
- HITCAN for actively cooled hot-composite thermostructural analysis
[NASA-TM-103750] p 202 N91-21562
- Overview of the fatigue/fracture/life working group program at the Lewis Research Center p 203 N91-24308
- Probabilistic structural analysis: Introductory remarks p 204 N91-24326
- Probability approach for strength calculations p 204 N91-24652
- Acoustical analysis of gear housing vibration
[NASA-TM-103691] p 188 N91-25411
- Probability of failure and risk assessment of propulsion structural components
[NASA-TM-102323] p 205 N91-25436
- Probabilistic structural analysis methods for space transportation propulsion systems p 205 N91-28238
- Viscoplastic analysis of an experimental cylindrical thrust chamber liner
[NASA-TM-103287] p 205 N91-28622
- STRUCTURAL DESIGN**
- A new approach to controller design for microgravity isolation systems p 129 A91-23108
- Dynamic analysis of space-related linear and non-linear structures p 196 A91-28612
- The COLD-SAT experiment for cryogenic fluid management technology p 46 A91-29799
- Tandem concentrator solar cells with 30 percent (AMC) power conversion efficiency p 208 N91-19189
- Thermal annealing of GaAs concentrator solar cells p 208 N91-19195
- Dual-purpose self-deliverable lunar surface PV electrical power system p 209 N91-19200
- Structural reliability analysis of laminated CMC components
[NASA-TM-103685] p 119 N91-19292
- Aeropropulsion 1991
[NASA-CP-10063] p 27 N91-20086
- Structural design methodologies for ceramic-based material systems
[NASA-TM-103097] p 121 N91-22460
- Reliability and risk assessment of structures p 194 N91-23050
- STRUCTURAL FAILURE**
- A three-dimensional finite-element thermal/mechanical analytical technique for high-performance traveling wave tubes
[NASA-TP-3081] p 134 N91-27436
- Fatigue behavior and life prediction of a SiC/Ti-24Al-11Nb composite under isothermal conditions
[NASA-TM-105168] p 206 N91-30566
- STRUCTURAL RELIABILITY**
- Thermal and structural assessments of a ceramic wafer seal in hypersonic engine
[AIAA PAPER 91-2494] p 23 A91-41799
- Thermal and structural assessments of a ceramic wafer seal in hypersonic engines
[NASA-TM-103651] p 26 N91-13456
- Structural reliability analysis of laminated CMC components
[NASA-TM-103685] p 119 N91-19292
- Reliability and risk assessment of structures p 194 N91-23050
- Probability of failure and risk assessment of propulsion structural components
[NASA-TM-102323] p 205 N91-25436
- STRUCTURAL STABILITY**
- Integrated force method versus displacement method for finite element analysis p 196 A91-28372
- Structural design concepts for a multi-megawatt Solar Electric Propulsion (SEP) spacecraft
[NASA-TM-105148] p 206 N91-30565
- STRUCTURAL VIBRATION**
- A new approach to controller design for microgravity isolation systems p 129 A91-23108
- Computational simulation of damping in composite structures p 198 A91-36283
- Gear noise, vibration, and diagnostic studies at NASA Lewis Research Center p 183 A91-52811
- An examination of anticipated g-jitter on space station and its effects on materials processes
[NASA-TM-103775] p 128 N91-21378
- Integrated mechanics for the passive damping of polymer-matrix composites and composite structures
[NASA-TM-104346] p 103 N91-32181
- STRUTS**
- Simulation of the Space Station strut-out condition
[AIAA PAPER 91-1248] p 197 A91-32087
- STUDENTS**
- Outline of the Solar System: Activities for elementary students
[NASA-TM-104965] p 241 N91-25975
- SUBMERGING**
- Apparatus for intercalating large quantities of fibrous structures
[NASA-CASE-LEW-15077-2] p 102 N91-28289
- SUBMILLIMETER WAVES**
- An experimental apparatus for measuring surface resistance in the submillimeter-wavelength region p 174 A91-54390
- SUBROUTINES**
- Spur-gear optimization using SPUROPT computer program
[NASA-TM-104394] p 191 N91-31648
- SUBSONIC AIRCRAFT**
- Overview of subsonic transport propulsion technology p 30 N91-20116
- High-efficiency core technology p 30 N91-20118
- SUBSONIC FLOW**
- Acoustic radiation from lifting airfoils in compressible subsonic flow
[AIAA PAPER 90-3911] p 224 A91-12427
- Experimental investigation of oscillating cascade aerodynamics p 3 A91-27801
- Nonlinear evolution of subsonic and supersonic disturbances on a compressible free shear layer p 152 A91-39716
- Acoustic radiation from lifting airfoils in compressible subsonic flow
[NASA-TM-103650] p 13 N91-19053
- Wind tunnel wall effects in a linear oscillating cascade
[NASA-TM-103690] p 27 N91-19098
- A finite-difference, frequency-domain numerical scheme for the solution of the linearized unsteady Euler equations p 162 N91-21067
- SUBSONIC SPEED**
- Evaluation of panel code predictions with experimental results of inlet performance for a 17-inch ducted prop/fan simulator operating at Mach 0.2
[AIAA PAPER 91-3354] p 7 A91-45819
- Aeroacoustic effects of reduced aft tip speed at constant thrust for a model counterrotation turboprop at takeoff conditions
[NASA-TM-103608] p 226 N91-10703
- High alpha inlets p 28 N91-20091
- Evaluation of panel code predictions with experimental results of inlet performance for a 17-inch ducted prop/fan simulator operating at Mach 0.2
[NASA-TM-104428] p 17 N91-25106
- SUBSONIC WIND TUNNELS**
- Automatic control study of the icing research tunnel refrigeration system
[NASA-TM-4257] p 40 N91-19115
- SUBSTRATES**
- New directions in InP solar cell research p 206 A91-38022
- A comparative study of performance parameters of n(+)-p InP solar cells made by closed-ampoule sulfur diffusion into Cd- and Zn-doped p-type InP substrates p 210 N91-19209
- Heteroepitaxial InP solar cells on Si and GaAs substrates
[NASA-TM-103696] p 144 N91-20392
- Advances in silicon carbide Chemical Vapor Deposition (CVD) for semiconductor device fabrication
[NASA-TM-104410] p 236 N91-23946
- Method of applying a thermal barrier coating system to a substrate
[NASA-CASE-LEW-15020-2] p 101 N91-25202
- Ceramic coatings on smooth surfaces
[NASA-CASE-LEW-15164-2] p 123 N91-32229
- SULFUR**
- Sulfur at nickel-alumina interfaces - Molecular orbital theory p 104 A91-12925
- Effect of sulfur removal on Al₂O₃ scale adhesion p 108 A91-27940
- A comparative study of performance parameters of n(+)-p InP solar cells made by closed-ampoule sulfur diffusion into Cd- and Zn-doped p-type InP substrates p 210 N91-19209
- Hydrocarbon-fuel/combustion-chamber-liner materials compatibility
[NASA-CR-187104] p 121 N91-21307
- SULFUR COMPOUNDS**
- Synthesis and structures of metal chalcogenide precursors
[NASA-TM-103665] p 120 N91-19296
- SUM RULES**
- A new approximate sum rule for bulk alloy properties
[NASA-TM-105282] p 112 N91-32204
- SUN**
- Outline of the Solar System: Activities for elementary students
[NASA-TM-104965] p 241 N91-25975
- SUNLIGHT**
- Primary reference cell calibrations at SERI - History and methods --- solar cells p 207 A91-41966
- SUPERCONDUCTING FILMS**
- Aerospace applications of high temperature superconductivity
[IAF PAPER 90-054] p 231 A91-13767
- Electrical transport measurements on polycrystalline superconducting Y-Ba-Cu-O films p 231 A91-19820
- Electromigration failure in YBa₂Cu₃O_{7-x} thin films p 231 A91-26989
- Temperature dependence of the anisotropy in magnetic relaxation in YBa₂Cu₃O_{7-x} thin films p 232 A91-36047
- An experimental study of high T_c superconducting microstrip transmission lines at 35 GHz and the effect of film morphology p 138 A91-36172
- Photoresponse of YBa₂Cu₃O_{7-delta} granular and epitaxial superconducting thin films p 141 A91-50443
- Ellipsometric study of YBa₂Cu₃O_{7-x} laser ablated and co-evaporated films p 233 A91-53235
- High temperature superconductor analog electronics for millimeter-wavelength communications
[AIAA PAPER 91-3592] p 233 A91-53707
- An experimental study of high T_c superconducting microstrip transmission lines at 35 GHz and the effect of film morphology
[NASA-TM-103633] p 133 N91-11988
- Emerging applications of high temperature superconductors for space communications
[NASA-TM-103629] p 227 N91-12317
- Solid State Technology Branch of NASA Lewis Research Center Second Annual Digest, June 1989 - June 1990
[NASA-TM-103226] p 133 N91-18297
- High temperature superconductor analog electronics for millimeter-wavelength communications
[NASA-TM-105184] p 237 N91-29982
- SUPERCONDUCTIVITY**
- High temperature superconducting thin film microwave circuits - Fabrication, characterization, and applications p 141 A91-50433
- Photoresponse of YBa₂Cu₃O_{7-delta} granular and epitaxial superconducting thin films p 141 A91-50443
- YBCO superconducting ring resonators at millimeter-wave frequencies p 142 A91-54532
- Monolithic mm-wave phase shifter using optically activated superconducting switches p 229 N91-13996
- [NASA-CASE-LEW-14678-1] p 229 N91-13996
- The series Bi₂Sr₂Ca(n-1)Cu(n)O(2n+4) (1 less than or equal to n less than or equal to 5): Phase stability and superconducting properties
[NASA-TM-103749] p 235 N91-21910
- Aerospace applications of high temperature superconductivity p 236 N91-24080
- Superconducting microwave electronics at Lewis Research Center p 236 N91-24081
- Low cost, formable, high T_{sub c} superconducting wire
[NASA-CASE-LEW-14676-1] p 147 N91-31529
- SUPERCONDUCTORS**
- Determination of surface resistance and magnetic penetration depth of superconducting YBa₂Cu₃O_{7-delta} thin films by microwave power transmission measurements p 138 A91-36060

- High temperature superconducting thin film microwave circuits - Fabrication, characterization, and applications p 141 A91-50433
- Spatial variations in a.c. susceptibility and microstructure for the YBa₂Cu₃O_{7-x} superconductor and their correlation with room-temperature ultrasonic measurements p 233 A91-54969
- Spatial variations in ac susceptibility and microstructure for the YBa₂Cu₃O_{7-x} superconductor and their correlation with room-temperature ultrasonic measurements [NASA-TM-103787] p 194 N91-21553
- Low cost, formable, high T(sub c) superconducting wire [NASA-CASE-LEW-14676-1] p 147 N91-31529
- Near-edge study of gold-substituted YBa₂Cu₃O_{7-delta} [NASA-TM-105220] p 237 N91-31977
- SUPERCOOLING**
- Time development of a perturbed-spherical nucleus in a pure supercooled liquid. I - Power-law growth of morphological instabilities. II - Nonlinear development p 231 A91-16105
- SUPERHIGH FREQUENCIES**
- Submicron gate InP power MISFET's with improved output power density at 18 and 20 GHz p 142 A91-54526
- Submicron gate InP power MISFET's with improved output power density at 18 and 20 GHz p 145 N91-26436
- SUPERNOVAE**
- The dynamic instability of adiabatic blast waves p 239 A91-26361
- The shock process and light-element production in supernova envelopes p 239 A91-33573
- SUPERSONIC BOUNDARY LAYERS**
- High-Order Polynomial Expansions (HOPE) for flux-vector splitting [NASA-TM-104452] p 222 N91-25739
- SUPERSONIC COMBUSTION**
- Navier-Stokes simulation of the supersonic combustion flowfield in a ram accelerator [AIAA PAPER 91-1916] p 155 A91-44057
- Navier-Stokes simulation of the supersonic combustion flowfield in a ram accelerator [NASA-TM-104439] p 166 N91-24541
- SUPERSONIC COMBUSTION RAMJET ENGINES**
- Numerical study of supersonic combustors by multi-block grids with mismatched interfaces [AIAA PAPER 90-5204] p 21 A91-14430
- CFD analysis of a hydrogen fueled ramjet engine at Mach 3.44 [AIAA PAPER 91-1919] p 23 A91-41653
- Progress toward synergistic hypermixing nozzles [AIAA PAPER 91-2264] p 25 A91-45800
- The 3D computation of single-expansion-ramp and scramjet nozzles p 164 N91-21092
- High temperature performance evaluation of a hypersonic engine ceramic water seal [NASA-TM-103737] p 185 N91-22567
- SUPERSONIC COMMERCIAL AIR TRANSPORT**
- Comparison of turbine bypass and mixed flow turbofan engines for a high-speed civil transport [AIAA PAPER 91-3132] p 25 A91-54051
- SUPERSONIC FLOW**
- New mixing-length model for supersonic shear layers p 148 A91-16073
- Numerical simulations of supersonic flow through oscillating cascade sections p 4 A91-28590
- Nonlinear evolution of subsonic and supersonic disturbances on a compressible free shear layer p 152 A91-39716
- A new Lagrangian random choice method for steady two-dimensional supersonic/hypersonic flow [AIAA PAPER 91-1546] p 5 A91-40721
- Supersonic jet mixing enhancement by vortex generators [AIAA PAPER 91-2263] p 5 A91-41738
- Influence of thickness and camber on the aeroelastic stability of supersonic throughflow fans p 5 A91-42814
- Optical techniques for determination of normal shock position in supersonic flows for aerospace applications p 174 A91-55530
- Analysis of three-dimensional viscous flow in a supersonic throughflow fan p 10 N91-10885
- Development of a laser-induced heat flux technique for measurement of convective heat transfer coefficients in a supersonic flowfield [NASA-TM-103778] p 13 N91-19063
- Parallel computing using a Lagrangian formulation [NASA-TM-104446] p 215 N91-24745
- Evaluation of a technique to generate artificially thickened boundary layers in supersonic and hypersonic flows [NASA-TP-3142] p 17 N91-28136
- A laser-induced heat flux technique for convective heat transfer measurements in high speed flows [NASA-TM-105177] p 168 N91-30472
- A qualitative view of cryogenic fluid injection into high speed flows [NASA-TM-105139] p 169 N91-30473
- SUPERSONIC INLETS**
- Results from computational analysis of a mixed compression supersonic inlet [AIAA PAPER 91-2581] p 7 A91-45818
- CFD analysis for high speed inlets p 10 N91-10888
- SUPERSONIC JET FLOW**
- Experimental investigation of a single flush-mounted hypermixing nozzle [AIAA PAPER 90-5240] p 21 A91-14466
- Experimental investigation of a single flush-mounted hypermixing nozzle [NASA-TM-103726] p 161 N91-19374
- Progress toward synergistic hypermixing nozzles [NASA-TM-105169] p 18 N91-29150
- SUPERSONIC NOZZLES**
- Experimental investigation of a single flush-mounted hypermixing nozzle [NASA-TM-103726] p 161 N91-19374
- The 3D computation of single-expansion-ramp and scramjet nozzles p 164 N91-21092
- Modern CFD applications for the design of a reacting shear layer facility [NASA-TM-104523] p 34 N91-27164
- SUPERSONIC TRANSPORTS**
- NASA's High Speed Research Program - An introduction and status report [SAE PAPER 901923] p 1 A91-48605
- Overview of the NASA-sponsored HSCST propulsion system studies --- High Speed Civil Transport [AIAA PAPER 91-3329] p 20 A91-53871
- A comparison of arrow, trapezoidal and M wing concepts using a Mach 2 supersonic cruise transport mission [AIAA PAPER 91-3102] p 7 A91-54027
- Overview of supersonic cruise propulsion research p 27 N91-20088
- Engine technology challenges for a 21st century high speed civil transport [NASA-TM-104363] p 19 N91-23098
- SUPERSYMMETRY**
- Inflationary axion cosmology p 239 A91-20491
- SUPPORT SYSTEMS**
- Hot gas ingestion test results of a two-poster vectored thrust concept with flow visualization in the NASA Lewis 9- by 15-foot low speed wind tunnel [AIAA PAPER 90-2268] p 4 A91-40561
- Hot gas ingestion test results of a two-poster vectored thrust concept with flow visualization in the NASA Lewis 9- x 15-foot low speed wind tunnel [NASA-TM-103258] p 15 N91-21116
- SUPPORTS**
- Post clamp [NASA-CASE-LEW-14862-1] p 183 N91-14617
- SURFACE CRACKS**
- The method of lines in analyzing solids containing cracks [NASA-TM-103626] p 201 N91-19477
- SURFACE DEFECTS**
- Atomic oxygen interaction with solar array blankets at protective coating defect sites p 211 N91-20732
- SURFACE ENERGY**
- Universal behavior in ideal slip p 110 A91-48517
- Universal energy relations and metal/ceramic interfaces p 93 A91-56254
- SURFACE FINISHING**
- Metallic seal for thermal barrier coating systems [NASA-CASE-LEW-15020-1] p 119 N91-15412
- SURFACE LAYERS**
- Properties of insulator interfaces with p-HgCdTe p 235 N91-18300
- Surface electrons in inverted layers of p-HgCdTe p 235 N91-18301
- Pretreatment of lubricated surfaces with sputtered cadmium oxide [NASA-CASE-LEW-14474-1] p 123 N91-28423
- High resolution electrolyte for thinning InP by anodic dissolution and its applications to EC-V profiling, defect revealing and surface passivation p 107 N91-30210
- SURFACE PROPERTIES**
- Interaction of surface radiation with convection in crystal growth by physical vapor transport p 127 A91-24563
- Surface studies on scandate cathodes and synthesized scandates p 136 A91-25071
- Measurement of surface recombination velocity on heavily doped indium phosphide p 232 A91-41931
- Creep behavior of copper at intermediate temperatures. II - Surface microstructural observations. III - A comparison with theory p 109 A91-47931
- An experimental apparatus for measuring surface resistance in the submillimeter-wavelength region p 174 A91-54390
- High emittance surfaces for high temperature space radiator applications p 88 A91-56415
- Uses of Auger and x ray photoelectron spectroscopy in the study of adhesion and friction [NASA-TM-103266] p 118 N91-11922
- Effect of two synthetic lubricants on life of AISI 9310 spur gears [NASA-TM-104352] p 189 N91-29599
- Grooved surfaces on InP p 213 N91-30208
- Relationship of optical coating on thermal radiation characteristics of nonisothermal cylindrical enclosures [NASA-TM-104408] p 168 N91-30461
- SURFACE REACTIONS**
- Surface and implantation effects on p-n junctions p 234 N91-18299
- Arc-textured high emittance radiator surfaces [NASA-CASE-LEW-14679-1] p 122 N91-25296
- SURFACE ROUGHNESS**
- Two-dimensional Navier-Stokes heat transfer analysis for rough turbine blades p 156 A91-45790
- [AIAA PAPER 91-2129] p 156 A91-45790
- Low Earth orbital atomic oxygen micrometeoroid, and debris interactions with photovoltaic arrays p 84 N91-30248
- SURFACE ROUGHNESS EFFECTS**
- Inertia effects in thin film flow with a corrugated boundary p 151 A91-32691
- Modeling of surface roughness effects on glaze ice accretion p 19 A91-35107
- SURFACE TEMPERATURE**
- Cathode phenomena in a low-power magnetoplasmadynamic thruster p 63 A91-52314
- Heat transfer, velocity-temperature correlation, and turbulent shear stress from Navier-Stokes computations of shock wave/turbulent boundary layer interaction flows p 163 N91-21085
- Simulation of brush insert for leading-edge-passage convective heat transfer [NASA-TM-103801] p 165 N91-23409
- SURFACE TREATMENT**
- Surface modification of Monel K-500 as a means of reducing friction and wear in high-pressure oxygen p 107 A91-16869
- Study of surface passivation as a function of InP closed-ampoule solar cell fabrication processing variables p 232 A91-41893
- SURFACE VEHICLES**
- Systems analysis of Mars solar electric propulsion vehicles [AIAA PAPER 90-3824] p 40 A91-10176
- SURFACES**
- Numerical investigation of an internal layer in turbulent flow over a curved hill p 163 N91-21083
- SURVEYS**
- Design considerations for lunar base photovoltaic power systems p 41 A91-41987
- Design considerations for lunar base photovoltaic power systems [NASA-TM-103642] p 241 N91-14259
- Results of the users' requirements survey p 175 N91-14575
- State of the art in video system performance p 175 N91-14578
- Comparative survey of dynamic analyses of free-piston Stirling engines [NASA-TM-104491] p 224 N91-26870
- SWIRLING**
- The effect of swirl recovery vanes on the cruise noise of an advanced propeller [AIAA PAPER 90-3932] p 224 A91-12448
- Influence of geometric features on the performance of pressure-swirl atomizers p 147 A91-13030
- An experimental comparison of nonswirling and swirling flow in a circular-to-rectangular transition duct [AIAA PAPER 91-0342] p 148 A91-21466
- Modern developments in shear flow control with swirl p 3 A91-24519
- An experimental comparison of nonswirling and swirling flow in a circular-to-rectangular transition duct [NASA-TM-104359] p 14 N91-21115
- A study of high speed flows in an aircraft transition duct [NASA-TM-104449] p 17 N91-26122
- SWITCHES**
- Neutron and gamma irradiation effects on power semiconductor switches p 139 A91-38162
- Monolithic mm-wave phase shifter using optically activated superconducting switches [NASA-CASE-LEW-14878-1] p 229 N91-13996
- SWITCHING**
- Induction motor control p 137 A91-30893
- SWITCHING CIRCUITS**
- Neural network architecture for crossbar switch control p 218 A91-29181
- Advanced electrical power, distribution and control for the Space Transportation System p 143 N91-17043

- Comparative study of bolometric and non-bolometric switching elements for microwave phase shifters
[NASA-TM-104435] p 145 N91-25320
- Optical Multiple Access Network (OMAN) for advanced processing satellite applications
[NASA-TM-105167] p 135 N91-29431
- Neutron, gamma ray and post-irradiation thermal annealing effects on power semiconductor switches
[NASA-TM-105248] p 147 N91-32410
- SYMBOLIC PROGRAMMING**
- Shared direct memory access on the Explorer 2-LX
[NASA-TM-103289] p 216 N91-12215
- SYNCHRONOUS MOTORS**
- Induction motor control p 137 A91-30893
- SYNCHRONOUS SATELLITES**
- A charging study of the ACTS satellite using NASCAP
[AIAA PAPER 91-1471] p 46 A91-42522
- SYNTHESIS (CHEMISTRY)**
- Ladder polymers for use as high temperature stable resins or coatings
[NASA-CASE-LEW-14203-1] p 118 N91-15402
- Substituted 1,1,1-triaryl-2,2,2-trifluoroethanes and processes for their synthesis
[NASA-CASE-LEW-14345-3] p 89 N91-17141
- Reactivity of pi-complexes of Ti, V, and Nb towards dithioacetic acid: Synthesis and structure of novel metal sulfur-containing complexes
[NASA-TM-103666] p 106 N91-19256
- Synthesis and structures of metal chalcogenide precursors
[NASA-TM-103665] p 120 N91-19296
- The series $\text{Bi}_2\text{Sr}_2\text{Ca}(n-1)\text{Cu}(n)\text{O}(2n+4)$ (1 less than or equal to n less than or equal to 5): Phase stability and superconducting properties
[NASA-TM-103749] p 235 N91-21910
- Synthesis and thermal properties of strontium and calcium peroxides
[NASA-TM-103725] p 107 N91-22410
- Substituted 1,1,1-triaryl-2,2,2-trifluoroethanes and processes for their synthesis
[NASA-CASE-LEW-14345-4] p 90 N91-25185
- SYSTEM EFFECTIVENESS**
- Experimental and analytical evaluation of efficiency of helicopter planetary stage
[NASA-TP-3063] p 183 N91-12956
- SYSTEM FAILURES**
- k-out-of-n:G systems - Some cost considerations
p 192 A91-54553
- A distributed fault-detection and diagnosis system using on-line parameter estimation
[NASA-TM-104433] p 220 N91-25696
- SYSTEM GENERATED ELECTROMAGNETIC PULSES**
- High voltage interactions of a sounding rocket with the ambient and system-generated environments
p 46 A91-23077
- SYSTEM IDENTIFICATION**
- Real-time diagnostics of the reusable rocket engine using on-line system identification p 223 A91-30630
- SYSTEMS ANALYSIS**
- Systems analysis of Mars solar electric propulsion vehicles
[AIAA PAPER 90-3824] p 40 A91-10176
- An update of engine system research at the Army Propulsion Directorate p 22 A91-29452
- Electric power scheduling - A distributed problem-solving approach p 219 A91-37976
- An update of engine system research at the Army Propulsion Directorate
[NASA-TM-103278] p 26 N91-11752
- The environment power system analysis tool development program p 231 N91-17734
- Computer code for single-point thermodynamic analysis of hydrogen/oxygen expander-cycle rocket engines
[NASA-TM-4275] p 72 N91-20206
- Environmental interactions of the Space Station Freedom electric power system
[NASA-TM-104373] p 49 N91-24225
- Comparative survey of dynamic analyses of free-piston Stirling engines
[NASA-TM-104491] p 224 N91-26870
- Reliability and cost: A sensitivity analysis
[NASA-TM-105293] p 238 N91-33014
- SYSTEMS ENGINEERING**
- National space test centers - Lewis Research Center Facilities
[AIAA PAPER 90-3593] p 41 A91-11471
- Proposal for a sun-following moonbase p 41 A91-27356
- An Electronic Pressure Profile Display system for aeronautic test facilities p 38 A91-51858
- Research and technology
[NASA-TM-103759] p 243 N91-23072
- SYSTEMS INTEGRATION**
- Integrated flight/propulsion control system design based on a centralized approach p 36 A91-22950

- The NASA Lewis integrated propulsion and flight control simulator
[AIAA PAPER 91-2969] p 38 A91-47847
- Application of an integrated flight/propulsion control design methodology to a STOVLC aircraft
[AIAA PAPER 91-2792] p 36 A91-49793
- Technology readiness assessment of advanced space engine integrated controls and health monitoring
[AIAA PAPER 91-3601] p 49 A91-52467
- Fiber-optic-based controls p 230 N91-20102
- Advanced aeropropulsion controls technology p 29 N91-20103
- IMPAC: An Integrated Methodology for Propulsion and Airframe Control
[NASA-TM-103805] p 30 N91-20122
- Integrated flight/propulsion control system design based on a decentralized, hierarchical approach
[NASA-TM-103678] p 31 N91-21137
- The NASA Lewis integrated propulsion and flight control simulator
[NASA-TM-105147] p 21 N91-27157
- Application of an integrated flight/propulsion control design methodology to a STOVLC aircraft
[NASA-TM-105254] p 37 N91-32143
- SYSTEMS MANAGEMENT**
- Techniques and implementation of the embedded rule-based expert system using Ada p 220 N91-22788
- An EMTP system level model of the PMAD DC test bed
[NASA-TM-104515] p 79 N91-27206
- SYSTEMS SIMULATION**
- Probabilistic modeling for simulation of aerodynamic uncertainties in propulsion systems p 58 A91-42725

T

- TABLES (DATA)**
- Cray performance data from five benchmarks
[NASA-TM-105200] p 217 N91-32806
- TABS (CONTROL SURFACES)**
- Effect of tabs on the evolution of an axisymmetric jet
[NASA-TM-104472] p 34 N91-27159
- TAIL ROTORS**
- Model rotor icing tests in the NASA Lewis icing research tunnel
[NASA-TM-104351] p 32 N91-23184
- TAKEOFF**
- Flow visualization and hot gas ingestion characteristics of a vectored thrust STOVLC concept p 28 N91-20090
- TANKS (CONTAINERS)**
- Ground testing of the nonvented fill method of orbital propellant transfer - Results of initial test series
[AIAA PAPER 91-2326] p 59 A91-44198
- Review and test of chilldown methods for space-based cryogenic tanks
[AIAA PAPER 91-1843] p 60 A91-45776
- Ground testing on the nonvented fill method of orbital propellant transfer: Results of initial test series
[NASA-TM-104444] p 166 N91-24547
- Review and test of chilldown methods for space-based cryogenic tanks
[NASA-TM-104458] p 167 N91-25351
- TANTALUM**
- Electrical characterization of glass, teflon, and tantalum capacitors at high temperatures
[NASA-TM-104517] p 146 N91-27444
- TARGETS**
- Low velocity impact analysis with NASTRAN p 198 A91-48865
- Low velocity impact analysis with NASTRAN
[NASA-TM-103169] p 95 N91-14426
- TAYLOR INSTABILITY**
- The dynamic instability of adiabatic blast waves p 239 A91-26361
- TDR SATELLITES**
- ATDRS payload technology R & D p 45 A91-53188
- Designs for the ATDRSS tri-band reflector antenna
[NASA-TM-103754] p 48 N91-20184
- TECHNOLOGICAL FORECASTING**
- Speculating on space futures p 237 A91-16900
- NASA's future space power needs and requirements p 52 A91-37929
- TECHNOLOGY ASSESSMENT**
- A technology assessment of alternative communications systems for the space exploration initiative
[AIAA PAPER 90-3681] p 44 A91-11472
- Blazing the trailway - Nuclear electric propulsion and its technology program plans
[AIAA PAPER 91-3441] p 64 A91-52353
- MPD thruster technology
[AIAA PAPER 91-3568] p 65 A91-52444
- Technology readiness assessment of advanced space engine integrated controls and health monitoring
[AIAA PAPER 91-3601] p 49 A91-52467
- Status of Ka-band TWT transmitter technology
[AIAA PAPER 91-3621] p 142 A91-52485
- An assessment of technology alternatives for telecommunications and information management for the space exploration initiative
[NASA-TM-103783] p 134 N91-23347
- MPD thruster technology
[NASA-TM-105242] p 86 N91-32162
- TECHNOLOGY UTILIZATION**
- Preliminary designs for 25 kWe advanced Stirling conversion systems for dish electric applications p 207 A91-38182
- Photovoltaic options for solar electric propulsion
[NASA-TM-103284] p 68 N91-11061
- Review of thin film solar cell technology and applications for ultra-light spacecraft solar arrays p 208 N91-19198
- High temperature electronics p 144 N91-20101
- Microwave integrated circuits for space applications p 145 N91-24069
- Aerospace applications of high temperature superconductivity p 236 N91-24080
- Solar dynamic power for Earth orbital and lunar applications p 80 N91-27214
- Thin film, concentrator and multijunction space solar cells: Status and potential
[NASA-TM-104505] p 86 N91-31218
- TEETERING**
- Model rotor icing tests in the NASA Lewis icing research tunnel
[NASA-TM-104351] p 32 N91-23184
- TEFLON (TRADEMARK)**
- Atomic oxygen interactions with FEP Teflon and silicones on LDEF p 122 N91-25029
- Electrical characterization of glass, teflon, and tantalum capacitors at high temperatures
[NASA-TM-104517] p 146 N91-27444
- TELECOMMUNICATION**
- A technology assessment of alternative communications systems for the space exploration initiative
[AIAA PAPER 90-3681] p 44 A91-11472
- Development of technology needs for the SEI TNIM network
[AIAA PAPER 91-3536] p 45 A91-52427
- Millimeter wavelength communications applications for the SEI
[AIAA PAPER 91-3589] p 45 A91-52458
- TELEPHONY**
- Study on the spectral efficiency of SFH-GMSK in land mobile telephone communication by direct simulation p 132 A91-53176
- TELESCOPES**
- Telescope search for a 3-eV to 8-eV axion p 239 A91-28714
- TELEVISION SYSTEMS**
- State of the art in video system performance p 175 N91-14578
- TELEVISION TRANSMISSION**
- Data compression for full motion video transmission
[AIAA PAPER 91-3533] p 45 A91-52424
- Digital CODEC for real-time processing of broadcast quality video signals at 1.8 bits/pixel p 134 N91-24067
- TEMPERATURE COMPENSATION**
- Compensation for effects of ambient temperature on rare-earth doped fiber optic thermometer p 170 A91-19582
- A resistance strain gage with repeatable apparent strain to 800 C p 198 A91-48899
- TEMPERATURE CONTROL**
- Preliminary thermal design of the COLD-SAT spacecraft
[AIAA PAPER 91-1305] p 46 A91-45550
- Power electronics for low power arcjets
[AIAA PAPER 91-1991] p 60 A91-45779
- An overview of the LeRC CSTI thermal management program p 158 A91-52422
- The effect of coatings and liners on heat transfer in a dry shaft-bush tribosystem p 159 N91-12913
- Preliminary thermal design of the COLD-SAT spacecraft
[NASA-TM-104440] p 49 N91-25161
- Power electronics for low power arcjets
[NASA-TM-104459] p 77 N91-25172
- TEMPERATURE DEPENDENCE**
- Temperature dependence of hardness in yttria-stabilized zirconia single crystals p 114 A91-28763
- Temperature-dependent indentation behavior of transformation-toughened zirconia-based ceramics p 114 A91-28767
- Temperature dependence of the elastic moduli and damping for polycrystalline LiF-22 pct CaF₂ eutectic salt p 87 A91-33793

Temperature dependence of the anisotropy in magnetic relaxation in YBa₂Cu₃O(7-x) thin films

p 232 A91-36047

Temperature coefficients of multijunction solar cells

p 172 A91-41921

TEMPERATURE DISTRIBUTION

Application of implicit numerical techniques to the solution of the three-dimensional diffusion equation

p 148 A91-13456

Finite element analysis of thermal distortion effects on optical performance of solar dynamic concentrator for Space Station Freedom

[NASA-TM-102504] p 183 N91-12954

A numerical and experimental analysis of reactor performance and deposition rates for CVD on monofilaments

[NASA-TM-103631] p 130 N91-14500

TEMPERATURE EFFECTS

The migration of a compound drop due to thermocapillarity

p 148 A91-18428

Progressive fracture in composites subjected to hygrothermal environment

[AIAA PAPER 91-1140] p 91 A91-31919

Thermal performance of a liquid hydrogen tank multilayer insulation system at warm boundary temperatures of 630, 530, and 152 R

[AIAA PAPER 91-2400] p 43 A91-45812

Elastic/plastic analyses of advanced composites investigating the use of the compliant layer concept in reducing residual stresses resulting from processing

[NASA-TM-103204] p 94 N91-11074

MIS capacitor studies on silicon carbide single crystals

[NASA-CR-187350] p 234 N91-11555

Finite element analysis of thermal distortion effects on optical performance of solar dynamic concentrator for Space Station Freedom

[NASA-TM-102504] p 183 N91-12954

Aerodynamics and heat transfer investigations on a high Reynolds number turbine cascade

[NASA-TM-103260] p 11 N91-15134

METCAN updates for high temperature composite behavior: Simulation/verification

[NASA-TM-103682] p 97 N91-19229

Computational simulation of hot composites structures

[NASA-TM-103681] p 97 N91-19230

High temperature NASP engine seal development

[NASA-TM-103716] p 184 N91-19441

HITCAN for actively cooled hot-composite thermostructural analysis

[NASA-TM-103750] p 202 N91-21562

The COLD-SAT experiment for cryogenic fluid management technology

[NASA-TM-104378] p 126 N91-24263

Thermal performance of a liquid hydrogen tank multilayer insulation system at warm boundary temperatures of 630, 530, and 152 R

[NASA-TM-104476] p 43 N91-25159

Electrical characterization of glass, teflon, and tantalum capacitors at high temperatures

[NASA-TM-104517] p 146 N91-27444

Elevated-temperature fracture resistances (K(sub IC), R-curves, gamma sub (omega OF)) of monolithic and composite ceramics using chevron-notched, bend tests

[NASA-TM-105090] p 123 N91-28418

Measurement techniques for cryogenic Ka-band microstrip antennas

[NASA-TM-105183] p 146 N91-30426

Computational simulation of high temperature metal matrix composite behavior

[NASA-TM-104378] p 206 N91-32520

TEMPERATURE GRADIENTS

Determination of the thermal stability of fluids by tensimetry - Instrumentation and procedure

p 113 A91-13435

Thermocapillary migration of liquid droplets in a temperature gradient in a density matched system

p 153 A91-41132

In-flight and simulated aircraft fuel temperature measurements

[NASA-TM-103611] p 125 N91-15418

TEMPERATURE MEASUREMENT

The development of a fiber optic Raman temperature measurement system for rocket flows

[AIAA PAPER 91-2316] p 173 A91-45804

Spacelab qualified infrared imager for microgravity science applications

p 173 A91-51585

Cathode phenomena in a low-power magnetoplasmadynamic thruster

p 63 A91-52314

In-flight and simulated aircraft fuel temperature measurements

[NASA-TM-103611] p 125 N91-15418

Plug-type heat flux gauge

[NASA-CASE-LEW-14967-1] p 179 N91-31608

TEMPERATURE MEASURING INSTRUMENTS

Silicon-etalon fiber-optic temperature sensor

p 170 A91-19581

Calibrator tests of heat flux gauges mounted in SSME blades

p 177 N91-24321

TEMPERATURE PROFILES

A numerical and experimental analysis of reactor performance and deposition rates for CVD on monofilaments

[NASA-TM-103631] p 130 N91-14500

In-flight and simulated aircraft fuel temperature measurements

[NASA-TM-103611] p 125 N91-15418

TEMPERATURE SENSORS

A fiber-optic current sensor for aerospace applications

p 172 A91-38006

Lag compensation of optical fibers or thermocouples to achieve waveform fidelity in dynamic gas pyrometry

p 174 A91-54388

TENSILE DEFORMATION

Tensile deformation damage in SiC reinforced Ti-15V-3Cr-3Al-3Sn

[NASA-TM-103620] p 101 N91-25195

TENSILE PROPERTIES

Tensile behavior of tungsten/niobium composites at 1300 to 1600 K

[NASA-TM-103727] p 111 N91-16128

Mechanical behavior of fiber reinforced SiC/RBSN ceramic matrix composites: Theory and experiment

[NASA-TM-103688] p 99 N91-21243

Tensile and fatigue behavior of tungsten/copper composites

p 100 N91-24311

Furnace for tensile/fatigue testing

[NASA-CASE-LEW-14848-1] p 42 N91-27175

TENSILE STRENGTH

Factors which influence tensile strength of a SiC/Ti-24Al-11Nb (at. pct) composite

p 92 A91-55900

Thermal shock fiber-reinforced ceramic matrix composites

p 93 A91-56935

Microstructural and strength stability of CVD SiC fibers in argon environments

p 117 A91-56958

Effects of high pressure nitrogen on the thermal stability of SiC fibers

p 96 N91-16075

Thermal shock of fiber reinforced ceramic matrix composites

p 120 N91-19295

Mechanical strength and thermophysical properties of PM212: A high temperature self-lubricating powder metallurgy composite

p 120 N91-21302

Microstructural and strength stability of CVD SiC fibers in argon environment

p 102 N91-29250

TENSILE STRESS

Effect of tensile mean stress on fatigue behavior of single-crystal and directionally solidified superalloys

[NASA-TM-103644] p 200 N91-18452

Fatigue behavior of a single-crystal superalloy

p 111 N91-24313

TENSILE TESTS

Tensile properties of HA 230 and HA 188 after 400 and 2500 hour exposures to LiF-22CaF₂ and vacuum at 1093 K

p 107 A91-11624

Inhomogeneous deformation in INCONEL 718 during monotonic and cyclic loadings

p 108 A91-22287

Thermal shock fiber-reinforced ceramic matrix composites

p 93 A91-56935

Thermal shock of fiber reinforced ceramic matrix composites

p 120 N91-19295

A preliminary investigation of acousto-ultrasonic NDE of metal matrix composite test specimens

[NASA-TM-104339] p 194 N91-23521

Tensile deformation damage in SiC reinforced Ti-15V-3Cr-3Al-3Sn

p 101 N91-25195

Furnace for tensile/fatigue testing

p 42 N91-27175

Experimental and analytical analysis of stress-strain behavior in a (90/0 deg)2s, SiC/Ti-15-3 laminate

[NASA-TM-104470] p 103 N91-31235

TENSORS

Turbulent fluid motion 2: Scalars, vectors, and tensors

[NASA-TM-103756] p 167 N91-27487

TERNARY ALLOYS

Constitution of pseudobinary hypoeutectic beta-NiAl + alpha-V alloys

p 109 A91-48509

TEST CHAMBERS

New method of making advanced tube-bundle rocket thrust chambers

[NASA-TM-103617] p 70 N91-15301

TEST EQUIPMENT

A unique high heat flux facility for testing hypersonic engine components

[AIAA PAPER 90-5228] p 37 A91-14454

The NASA Lewis Research Center Internal Fluid Mechanics Facility

p 39 N91-30163

TEST FACILITIES

National space test centers - Lewis Research Center Facilities

[AIAA PAPER 90-3593] p 41 A91-11471

N-decane droplet combustion in the NASA-Lewis 5 Second Zero-Gravity Facility - Results in test gas environments other than air

[AIAA PAPER 91-0720] p 105 A91-19433

Modern CFD applications for the design of a reacting shear layer facility

[AIAA PAPER 91-0577] p 149 A91-21540

Thrust stand for high-power electric propulsion devices

p 41 A91-36239

Effects of brush seal morphology on leakage and pressure drops

[AIAA PAPER 91-2106] p 182 A91-41700

A unique high heat flux facility for testing hypersonic engine components

[NASA-TM-103238] p 38 N91-11770

NASA low-speed centrifugal compressor for 3-D viscous code assessment and fundamental flow physics research

[NASA-TM-103710] p 13 N91-20044

Overview of Lewis materials research: Contributions, current efforts, and future directions

p 111 N91-20109

Recent advances in Lewis aeropropulsion facilities

p 38 N91-20121

Modern CFD applications for the design of a reacting shear layer facility

[NASA-TM-104523] p 34 N91-27164

The NASA Lewis Research Center Internal Fluid Mechanics Facility

[NASA-TM-105187] p 39 N91-30163

The International Space University's variable gravity research facility design

[NASA-TM-105224] p 44 N91-31196

TEST FIRING

The application of neural networks to the SSME startup transient

[AIAA PAPER 91-2530] p 60 A91-44283

TEST STANDS

Autonomous power expert system advanced development

p 72 N91-20689

The development of test beds to support the definition and evolution of the Space Station Freedom power system

[NASA-TM-104504] p 79 N91-27207

TETHERED SATELLITES

Reactionless orbital propulsion using tether deployment

[IAF PAPER 90-254] p 51 A91-13908

Reactionless propulsion using tethers

p 73 N91-22163

TETHERING

Reactionless propulsion using tethers

p 73 N91-22163

TETHERLINES

Satellite relocation by tether deployment

p 40 A91-22966

THERMAL ANALYSIS

Probabilistic simulation of uncertainties in thermal structures

p 195 A91-16042

Preliminary thermal design of the COLD-SAT spacecraft

[AIAA PAPER 91-1305] p 46 A91-45550

Computational simulation of hot composites structures

[NASA-TM-103681] p 97 N91-19230

Probabilistic simulation of uncertainties in thermal structures

[NASA-TM-103680] p 201 N91-19472

Preliminary thermal design of the COLD-SAT spacecraft

[NASA-TM-104440] p 49 N91-25161

Sensible heat receiver for solar dynamic space power system

[NASA-TM-104393] p 77 N91-25173

Long term isothermal aging and thermal analysis of N-CYCOP polyimides

[NASA-TM-104341] p 122 N91-25286

A three-dimensional finite-element thermal/mechanical analytical technique for high-performance traveling wave tubes

[NASA-TP-3081] p 134 N91-27436

Arjet thermal characteristics

[NASA-TM-105156] p 82 N91-29231

THERMAL BOUNDARY LAYER

Experimental study of boundary layer transition on a heated flat plate

[NASA-TM-103779] p 14 N91-21061

THERMAL CONDUCTIVITY

An overview of the LeRC CSTI thermal management program

[AIAA PAPER 91-3528] p 158 A91-52422

- The effect of coatings and liners on heat transfer in a dry shaft-bush tribosystem
[NASA-TM-102513] p 159 N91-12913
- Heat transfer device and method of making the same
[NASA-CASE-LEW-14162-1] p 159 N91-13668
- Evaluation and ranking of candidate ceramic wafer engine seal materials
[NASA-TM-103795] p 187 N91-23515
- Heat transfer device
[NASA-CASE-LEW-14162-2] p 101 N91-25201
- THERMAL CONTROL COATINGS**
- Evaluation of thermal control coatings for use on solar dynamic radiators in low earth orbit
[AIAA PAPER 91-1327] p 58 A91-43397
- Thermal barrier coating evaluation needs
[NASA-TM-103708] p 111 N91-15390
- Metallic seal for thermal barrier coating systems
[NASA-CASE-LEW-15020-1] p 119 N91-15412
- Evaluation of thermal control coatings for use on solar dynamic radiators in low Earth orbit
[NASA-TM-104335] p 73 N91-22367
- Ion beam textured and coated surfaces experiment (IBEX) p 122 N91-25040
- Method of applying a thermal barrier coating system to a substrate
[NASA-CASE-LEW-15020-2] p 101 N91-25202
- Method of preparing a thermal barrier coating
[NASA-CASE-LEW-14999-2] p 122 N91-26376
- THERMAL CYCLING TESTS**
- Computational simulation of high-temperature metal matrix composites cyclic behavior p 91 A91-18680
- Heat flux measurement in SSME turbine blade tester
p 171 A91-30649
- Rapid thermal cycling of new technology solar array blanket coupons p 54 A91-38019
- Vacuum ultraviolet radiation and thermal cycling effects on atomic oxygen protective photovoltaic array blanket materials p 116 A91-49812
- Oxidation instability of SiC and Si₃N₄ following thermal excursions p 118 A91-57059
- Heat flux measurement in SSME turbine blade tester
[NASA-TM-103274] p 175 N91-11205
- A preliminary investigation of acousto-ultrasonic NDE of metal matrix composite test specimens
[NASA-TM-104339] p 194 N91-23521
- Thin-film sensors for space propulsion technology: Fabrication and preparation for testing p 77 N91-24324
- Rapid thermal cycling of solar array blanket coupons for Space Station Freedom p 84 N91-30239
- THERMAL DECOMPOSITION**
- Determination of the thermal stability of fluids by tensimetry - instrumentation and procedure p 113 A91-13435
- THERMAL DEGRADATION**
- Quantification of uncertainties in coupled material degradation processes - High temperature, fatigue and creep
[AIAA PAPER 91-0977] p 196 A91-31835
- THERMAL DIFFUSION**
- Application of implicit numerical techniques to the solution of the three-dimensional diffusion equation p 148 A91-13456
- A comparative study of p(+)n and n(+)p InP solar cells made by a closed ampoule diffusion p 212 N91-30206
- THERMAL EMISSION**
- Evaluation of thermal control coatings for use on solar dynamic radiators in low earth orbit
[AIAA PAPER 91-1327] p 58 A91-43397
- Thermal emittance enhancement of graphite-copper composites for high temperature space based radiators
[AIAA PAPER 91-3527] p 116 A91-53705
- Evaluation of thermal control coatings for use on solar dynamic radiators in low Earth orbit
[NASA-TM-104335] p 73 N91-22367
- Arc-textured high emittance radiator surfaces
[NASA-CASE-LEW-14679-1] p 122 N91-25296
- Thermal emittance enhancement of graphite-copper composites for high temperature space based radiators
[NASA-TM-105178] p 123 N91-29332
- THERMAL ENERGY**
- Scaling analysis applied to the NORVEX code development and thermal energy flight experiment
[AIAA PAPER 91-1420] p 155 A91-44337
- Multi-dimensional modeling of a thermal energy storage canister
[NASA-TM-103731] p 71 N91-19177
- Thermal annealing of GaAs concentrator solar cells p 208 N91-19195
- Solar thermal energy receiver
[NASA-CASE-LEW-14949-1] p 211 N91-23617
- Scaling analysis applied to the NORVEX code development and thermal energy flight experiment
[NASA-TM-104462] p 166 N91-24549
- Ground test program for a full-size solar dynamic heat receiver
[NASA-TM-104485] p 79 N91-27209
- THERMAL EXPANSION**
- A life comparison of tube and channel cooling passages for thrust chambers
[NASA-TM-103613] p 68 N91-11059
- Elastic/plastic analyses of advanced composites investigating the use of the compliant layer concept in reducing residual stresses resulting from processing
[NASA-TM-103204] p 94 N91-11074
- THERMAL FATIGUE**
- Quantification of uncertainties in coupled material degradation processes - High temperature, fatigue and creep
[AIAA PAPER 91-0977] p 196 A91-31835
- High temperature fatigue behavior of tungsten copper composites p 93 A91-55906
- Dynamic fatigue property of silicon carbide whisker-reinforced silicon nitride p 94 A91-56937
- Thermomechanical and bithermal fatigue behavior of cast B1900 + Hf and wrought Haynes 188
[NASA-TM-4225] p 111 N91-20268
- Combined thermal and bending fatigue of high-temperature metal-matrix composites: Computational simulation
[NASA-TM-104354] p 100 N91-23247
- High temperature tension-compression fatigue behavior of a tungsten copper composite p 100 N91-24360
- Fatigue life prediction of an intermetallic matrix composite at elevated temperatures
[NASA-TM-104494] p 205 N91-25442
- THERMAL INSULATION**
- Thermal barrier coating evaluation needs
[NASA-TM-103708] p 111 N91-15390
- Ceramic coatings on smooth surfaces
[NASA-CASE-LEW-15164-2] p 123 N91-32229
- THERMAL PROTECTION**
- Metallic seal for thermal barrier coating systems
[NASA-CASE-LEW-15020-1] p 119 N91-15412
- High-temperature, flexible, thermal barrier seal
[NASA-CASE-LEW-14672-1] p 189 N91-27560
- THERMAL RADIATION**
- Relationship of optical coating on thermal radiation characteristics of nonisothermal cylindrical enclosures
[NASA-TM-104408] p 168 N91-30461
- THERMAL RESISTANCE**
- A resistance strain gage with repeatable apparent strain to 800 C p 198 A91-48899
- THERMAL SHOCK**
- Effect of thermal shock on fiber-reinforced superalloy composites p 93 A91-55918
- Thermal shock fiber-reinforced ceramic matrix composites p 93 A91-56935
- Thermal shock of fiber reinforced ceramic matrix composites
[NASA-TM-103777] p 120 N91-19295
- THERMAL STABILITY**
- Mechanics of damping for fiber composite laminates including hygrothermal effects p 195 A91-12895
- Determination of the thermal stability of fluids by tensimetry - instrumentation and procedure p 113 A91-13435
- Acidic attack of perfluorinated alkyl ether lubricant molecules by metal oxide surfaces p 104 A91-13439
- X-ray photoelectron and mass spectroscopic study of electron irradiation and thermal stability of polytetrafluoroethylene p 113 A91-16138
- Thermal stability of electron-irradiated poly(tetrafluoroethylene) - X-ray photoelectron and mass spectroscopic study p 115 A91-39242
- Application of finite-element-based solution technologies for viscoplastic structural analyses p 199 A91-55137
- Thermochemical analysis of chemical processes relevant to the stability and processing of SiC-reinforced Si₃N₄ composite p 94 A91-56961
- Thermal stability of the microstructure of an aged Nb-Zr-C alloy
[NASA-TM-103647] p 110 N91-14454
- Effects of high pressure nitrogen on the thermal stability of SiC fibers p 96 N91-16075
- Effect of fiber reinforcements on thermo-oxidative stability and mechanical properties of polymer matrix composites
[NASA-TM-103648] p 98 N91-19234
- A comparison of fiber effects on polymer matrix composite oxidation
[NASA-TM-104416] p 101 N91-24361
- Long term isothermal aging and thermal analysis of N-CYCAP polyimides
[NASA-TM-104341] p 122 N91-25286
- THERMAL STRESSES**
- A unique high heat flux facility for testing hypersonic engine components
[AIAA PAPER 90-5228] p 37 A91-14454
- Concurrent material-fabrication optimization of metal-matrix laminates under thermo-mechanical loading
[AIAA PAPER 91-1044] p 129 A91-31842
- Fiber pushout test - A three-dimensional finite element computational simulation p 197 A91-33096
- A resistance strain gage with repeatable and cancellable apparent strain for use to 1500 F p 173 A91-51930
- Overview of aerothermodynamic loads definition study p 204 N91-24334
- THERMAL VACUUM TESTS**
- Full-size solar dynamic heat receiver thermal-vacuum tests
[NASA-TM-104486] p 78 N91-25184
- THERMIONIC CATHODES**
- Cathode phenomena in a low-power magnetoplasmadynamic thruster p 63 A91-52314
- THERMOCHEMICAL PROPERTIES**
- Thermochemical analysis of chemical processes relevant to the stability and processing of SiC-reinforced Si₃N₄ composite p 94 A91-56961
- THERMOCHEMISTRY**
- Thermochemical analysis of the silicon carbide-alumina reaction with reference to liquid-phase sintering of silicon carbide p 114 A91-26506
- Hydrogen-silicon carbide interactions p 114 A91-28783
- THERMOCOUPLES**
- Lag compensation of optical fibers or thermocouples to achieve waveform fidelity in dynamic gas pyrometry p 174 A91-54388
- Thin-film sensors for space propulsion technology: Fabrication and preparation for testing p 77 N91-24324
- Plug-type heat flux gauge
[NASA-CASE-LEW-14967-1] p 179 N91-31608
- THERMODYNAMIC CYCLES**
- The Navy/NASA Engine Program (NNEP89): A user's manual
[NASA-TM-105186] p 35 N91-30141
- THERMODYNAMIC EFFICIENCY**
- Overview of subsonic transport propulsion technology p 30 N91-20116
- THERMODYNAMIC PROPERTIES**
- Improved thermodynamic modelling of the no-vent fill process and correlation with experimental data
[AIAA PAPER 91-1379] p 129 A91-43444
- Arcjet thermal characteristics
[AIAA PAPER 91-2456] p 63 A91-45814
- Synthesis and thermal properties of strontium and calcium peroxides
[NASA-TM-103725] p 107 N91-22410
- Industrial applications of graphite fluoride fibers p 100 N91-23040
- THERMODYNAMICS**
- Critical-point analysis of the liquid-vapor interfacial surface tension p 237 A91-16103
- Status of structural analysis of 30 cm diameter ion optics
[NASA-TM-103618] p 68 N91-11796
- Current activities in standardization of high-temperature, low-cycle-fatigue testing techniques in the United States
[NASA-TM-103675] p 200 N91-17427
- Application of thermal life prediction model to high-temperature aerospace alloys B1900 + Hf and Haynes 188
[NASA-TM-4226] p 201 N91-19473
- On the thermodynamics of stress rate in the evolution of back stress in viscoplasticity
[NASA-TM-103794] p 201 N91-19476
- Transonic aerodynamics of dense gases
[NASA-TM-103722] p 13 N91-20045
- Computer code for single-point thermodynamic analysis of hydrogen/oxygen expander-cycle rocket engines
[NASA-TM-4275] p 72 N91-20206
- Thermomechanical and bithermal fatigue behavior of cast B1900 + Hf and wrought Haynes 188
[NASA-TM-4225] p 111 N91-20268
- Autogenous pressurization of cryogenic vessels using submerged vapor injection
[NASA-TM-104516] p 127 N91-27375
- THERMOELECTRIC GENERATORS**
- Small Stirling dynamic isotope power system for multihundred-watt robotic missions
[NASA-TM-104460] p 78 N91-25182
- Preliminary design of a mobile lunar power supply
[NASA-TM-104471] p 212 N91-27611
- Comparison of dynamic isotope power systems for distributed planet surface applications
[NASA-TM-4303] p 81 N91-28278
- THERMOELECTRIC MATERIALS**
- The NASA CSTI High Capacity Power Program
[AIAA PAPER 91-3629] p 208 A91-52493

THERMOELECTRIC POWER GENERATION

- Dynamic Isotope Surface Power Systems
[AIAA PAPER 91-3623] p 208 A91-52487
- Sensible heat receiver for solar dynamic space power system
[NASA-TM-104393] p 77 N91-25173

THERMOELECTRICITY

- The NASA CSTI High Capacity Power Program
[AIAA PAPER 91-3629] p 208 A91-52493

THERMOHYDRAULICS

- A comparative flow visualization study of thermocapillary flow in drops in liquid-liquid systems
[AIAA PAPER 91-0311] p 148 A91-21452

THERMOMETERS

- Compensation for effects of ambient temperature on rare-earth doped fiber optic thermometer
p 170 A91-19582

THERMOPHYSICAL PROPERTIES

- Newtonian mechanics of a many-particle assembly coupled to an external body potential
p 237 A91-19495

THERMOSETTING RESINS

- Long term isothermal aging and thermal analysis of N-CYCAP polyimides
[NASA-TM-104341] p 122 N91-25286

THICKNESS

- Effects of rim thickness on spur gear bending stress
[AIAA PAPER 91-2020] p 181 A91-41681
- Influence of thickness and camber on the aeroelastic stability of supersonic throughflow fans
p 5 A91-42814
- Effects of rim thickness on spur gear bending stress
[NASA-TM-104388] p 186 N91-23500

THIN FILMS

- Determination of surface resistance and magnetic penetration depth of superconducting YBa₂Cu₃O₇(δ) thin films by microwave power transmission measurements
p 138 A91-36060
- Undercutting of defects in thin film protective coatings on polymer surfaces exposed to atomic oxygen
p 115 A91-41516
- Peeled film GaAs solar cell development
p 139 A91-41889
- 23.5 percent thin-film space concentrator cells
p 58 A91-42002
- Selective and low temperature synthesis of polycrystalline diamond
p 232 A91-42170
- Application of oxidation to the structural characterization of SiC epitaxial films
p 233 A91-45881
- High temperature superconducting thin film microwave circuits - Fabrication, characterization, and applications
p 141 A91-50433
- Photoresponse of YBa₂Cu₃O₇(δ) granular and epitaxial superconducting thin films
p 141 A91-50443
- Determination of surface resistance and magnetic penetration depth of superconducting YBa₂Cu₃O₇(δ) thin films by microwave power transmission measurements
p 234 N91-10780
- Plasma-assisted physical vapor deposition surface treatments for tribological control
[NASA-TM-103652] p 130 N91-11945
- Emerging applications of high temperature superconductors for space communications
[NASA-TM-103629] p 227 N91-12317
- Liquid sheet radiator apparatus
[NASA-CASE-LEW-14295-1] p 130 N91-15424
- Diamondlike carbon as a moisture barrier and antireflecting coating on optical materials
p 119 N91-18302
- Thin film characterization using spectroscopic ellipsometry
p 119 N91-18303
- Optical dispersion relations for diamondlike carbon films
p 230 N91-18305
- Review of thin film solar cell technology and applications for ultra-light spacecraft solar arrays
p 208 N91-19198
- Tribological properties of Ag/Ti films on Al₂O₃ ceramic substrates
[NASA-TM-103784] p 89 N91-19224
- Applications of thin film technology toward a low-mass solar power satellite
p 235 N91-22179
- Dual ion beam processed diamondlike films for industrial applications
p 121 N91-23042
- Flexible fluoropolymer filled protective coatings
p 121 N91-24062
- Superconducting microwave electronics at Lewis Research Center
p 236 N91-24081
- Thin-film sensors for space propulsion technology: Fabrication and preparation for testing
p 77 N91-24324
- Process for the controlled growth of single-crystal films of silicon carbide polytypes on silicon carbide wafers
[NASA-CASE-LEW-15222-1] p 236 N91-26966

- Low Earth orbital atomic oxygen micrometeoroid, and debris interactions with photovoltaic arrays
p 84 N91-30248

- Thin film, concentrator and multijunction space solar cells: Status and potential
[NASA-TM-104505] p 86 N91-31218
- Low cost, formable, high T(sub c) superconducting wire
[NASA-CASE-LEW-14676-1] p 147 N91-31529
- Lubrication with sputtered MoS₂ films: Principles, operation, limitations
[NASA-TM-105292] p 112 N91-32216

THREE AXIS STABILIZATION

- Mass comparisons of electric propulsion systems for NSSK of geosynchronous spacecraft --- North-South Station Keeping
[AIAA PAPER 91-2347] p 47 A91-45808

THREE DIMENSIONAL BOUNDARY LAYER

- The effect of small streamwise velocity distortion on the boundary layer flow over a thin flat plate with application to boundary layer stability theory
[NASA-TM-103668] p 161 N91-19372
- Critical-layer nonlinearity in the resonance growth of three-dimensional waves in boundary layers
[NASA-TM-103639] p 161 N91-19373
- A study of three dimensional turbulent boundary layer separation and vortex flow control using the reduced Navier Stokes equations
[NASA-TM-104407] p 16 N91-23089

THREE DIMENSIONAL FLOW

- An algebraic RNG-based turbulence model for three-dimensional turbomachinery flows
[AIAA PAPER 91-0172] p 2 A91-21393
- Three-dimensional viscous flow computations of high area ratio nozzles for hypersonic propulsion
p 4 A91-30014
- Simulation of three-dimensional liquid sloshing flows using a strongly implicit calculation procedure
[AIAA PAPER 91-1861] p 153 A91-42549
- Three-dimensional flow transport modes in directional solidification during space processing
p 128 A91-42642
- 3-D Navier-Stokes analysis of crossing, glancing shocks/turbulent boundary layer interactions
[AIAA PAPER 91-1758] p 6 A91-43631
- Three-dimensional calculation of the mixing of radial jets from slanted slots with a reactive cylindrical crossflow
[AIAA PAPER 91-2081] p 24 A91-45782
- Computations of the three-dimensional flow and heat transfer within a coolant passage of a radial turbine blade
[AIAA PAPER 91-2238] p 156 A91-45797
- Efficient real gas upwinded Navier-Stokes computations of high speed flows
p 157 A91-46179
- Multigrad calculation of three-dimensional viscous cascade flows
[AIAA PAPER 91-3238] p 7 A91-53754
- Three-dimensional flows in a transonic compressor rotor
p 8 A91-56152
- Analysis of three-dimensional viscous flow in a supersonic throughflow fan
p 10 N91-10885
- CFD analysis for high speed inlets
p 10 N91-10888
- Three-component laser anemometer measurement systems
[NASA-TP-3080] p 13 N91-19057
- A comparison of CFD predictions and experimental results for a Mach 5 inlet
p 28 N91-20094
- Turbomachinery
p 162 N91-20097
- Compressible flows with periodic vortical disturbances around lifting airfoils
[NASA-TM-103742] p 14 N91-21060
- A finite-difference, frequency-domain numerical scheme for the solution of the linearized unsteady Euler equations
p 162 N91-21067
- Implicit solution of three-dimensional internal turbulent flows
p 163 N91-21082
- CFD for hypersonic propulsion
[NASA-TM-103791] p 164 N91-21447
- Three-dimensional Euler time accurate simulations of fan rotor-stator interactions
[NASA-TM-102528] p 16 N91-24124
- The 3-D Navier-Stokes analysis of crossing, glancing shocks/turbulent boundary layer interactions
[NASA-TM-104469] p 16 N91-24130
- Calculation of a circular jet in crossflow with a multiple-time-scale turbulence model
[NASA-TM-104343] p 169 N91-30476
- Nonlinear combustion instability model in two- to three-dimensions
[NASA-TM-102381] p 85 N91-31208

THREE DIMENSIONAL MODELS

- Metal matrix composites microfracture - Computational simulation
p 90 A91-11815
- Application of implicit numerical techniques to the solution of the three-dimensional diffusion equation
p 148 A91-13456

- 3D computation of hypersonic nozzle
[AIAA PAPER 90-5203] p 1 A91-14429
- Three-dimensional flow transport modes in directional solidification during space processing
p 128 A91-42642
- An analysis of the viscous flow through a compact radial turbine by the average passage approach
[ASME PAPER 90-GT-64] p 6 A91-44545
- Algebraic grid generation for complex geometries
p 157 A91-48758
- A three-dimensional turbulent heat transfer analysis for advanced tubular rocket thrust chambers
p 75 N91-24258
- GRID3D-v2: An updated version of the GRID2D/3D computer program for generating grid systems in complex-shaped three-dimensional spatial domains
[NASA-TM-103766] p 217 N91-25630
- A three-dimensional finite-element thermal/mechanical analytical technique for high-performance traveling wave tubes
[NASA-TP-3081] p 134 N91-27436
- How to determine spiral bevel gear tooth geometry for finite element analysis
[NASA-TM-105150] p 190 N91-30537

THRESHOLDS (PERCEPTION)

- An assessment of the Space Station Freedom program's leakage current requirement
[NASA-CR-187077] p 215 N91-20630

THRUST

- Aeroacoustic effects of reduced aft tip speed at constant thrust for a model counterrotation turboprop at takeoff conditions
[AIAA PAPER 90-3933] p 224 A91-12449
- Divergence thrust loss calculations for convergent-divergent nozzles: Extensions to the classical case
[NASA-TM-105176] p 34 N91-29181

THRUST AUGMENTATION

- Transient flow thrust prediction for an ejector propulsion concept
p 24 A91-45326

THRUST CHAMBERS

- Anode power deposition in an applied-field segmented anode MPD thruster
[AIAA PAPER 91-2343] p 59 A91-44204
- A life comparison of tube and channel cooling passages for thrust chambers
[NASA-TM-103613] p 68 N91-11059
- New method of making advanced tube-bundle rocket thrust chambers
[NASA-TM-103617] p 70 N91-15301
- A three-dimensional turbulent heat transfer analysis for advanced tubular rocket thrust chambers
p 75 N91-24258
- Method of injecting fluid propellants into a rocket combustion chamber
[NASA-CASE-LEW-14846-2] p 78 N91-26200
- Viscoplastic analysis of an experimental cylindrical thrust chamber liner
[NASA-TM-103287] p 205 N91-28622

THRUST MEASUREMENT

- Thrust stand for high-power electric propulsion devices
p 41 A91-36239
- Preliminary performance and life evaluation of a 2-kW arcjet
[AIAA PAPER 91-2228] p 62 A91-45796
- Performance characterization of a segmented anode arcjet thruster
[NASA-TM-103227] p 67 N91-10118
- Preliminary performance and life evaluations of a 2-kW arcjet
[NASA-TM-105149] p 84 N91-30252

THRUST VECTOR CONTROL

- Electromechanical actuation for thrust vector control applications
p 52 A91-31026
- Hot gas ingestion test results of a two-poster vectored thrust concept with flow visualization in the NASA Lewis 9- by 15-foot low speed wind tunnel
[AIAA PAPER 90-2268] p 4 A91-40561
- Flow visualization studies of the internal flow characteristics in a simulated mixed flow vectored thrust ASTOVL engine configuration
[AIAA PAPER 91-1689] p 23 A91-42556
- Xenon ion propulsion for orbit transfer
[NASA-TM-103193] p 69 N91-11798
- Flow visualization and hot gas ingestion characteristics of a vectored thrust STOVL concept
p 28 N91-20090
- Hot gas ingestion test results of a two-poster vectored thrust concept with flow visualization in the NASA Lewis 9- by 15-foot low speed wind tunnel
[NASA-TM-103258] p 15 N91-21116

THRUSTORS

- Thrust stand for high-power electric propulsion devices
p 41 A91-36239
- A preliminary characterization of applied-field MPD thruster plumes
[AIAA PAPER 91-2339] p 62 A91-45798

- Hydrogen/oxygen auxiliary propulsion technology
[AIAA PAPER 91-3440] p 64 A91-52352
- Performance and optimization of a derated ion thruster for auxiliary propulsion
[NASA-TM-105144] p 82 N91-29229
- Multimegawatt electric propulsion system design considerations
[NASA-TM-105152] p 87 N91-32164
- TILT ROTOR AIRCRAFT**
The selection of convertible engines with current gas generator technology for high speed rotorcraft
[NASA-TM-103774] p 27 N91-19097
- TIME**
Exploring the notion of space coupling propulsion
p 73 N91-22161
- TIME DEPENDENCE**
Time dependent viscous incompressible Navier-Stokes equations
p 9 N91-10854
- TIME DIVISION MULTIPLE ACCESS**
Pulsed response of a TWT
p 136 A91-27529
- LBR-2 Earth stations for the ACTS program
p 133 N91-11971
- Pulsed response of a traveling-wave tube
[NASA-TM-103672] p 143 N91-19348
- TIME LAG**
Lag compensation of optical fibers or thermocouples to achieve waveform fidelity in dynamic gas pyrometry
p 174 A91-54388
- TIME MARCHING**
Time-derivative preconditioning for viscous flows
[AIAA PAPER 91-1652] p 154 A91-43576
- Cascade flutter analysis with transient response aerodynamics
[NASA-TM-103746] p 201 N91-19475
- TIME RESPONSE**
Pulsed response of a traveling-wave tube
[NASA-TM-103672] p 143 N91-19348
- TIP SPEED**
Aeroacoustic effects of reduced aft tip speed at constant thrust for a model counterrotation turboprop at takeoff conditions
[NASA-TM-103608] p 226 N91-10703
- TITANIUM**
Construction and testing of ceramic fabric heat pipe with water working fluid
[NASA-TM-103332] p 229 N91-18799
- Matrix plasticity in SiC/Ti-15-3 composite
[NASA-TM-103760] p 102 N91-27247
- Fatigue behavior and life prediction of a SiC/Ti-24Al-11Nb composite under isothermal conditions
[NASA-TM-105168] p 206 N91-30566
- TITANIUM ALLOYS**
Fatigue crack growth study of SCS6/Ti-15-3 composite
p 91 A91-25798
- Oxidation behavior of cubic phases formed by alloying Al₃Ti with Cr and Mn
p 108 A91-27849
- Reaction of Ti and Ti-Al alloys with alumina
p 91 A91-27937
- Compression behavior of TiB₂-particulate-reinforced composites of Al₂Fe₃Ti₈
p 91 A91-28014
- Evaluation of thermomechanical damage in silicon carbide/titanium composites
p 92 A91-42297
- Factors which influence tensile strength of a SiC/Ti-24Al-11Nb (at. pct) composite
p 92 A91-55900
- The isothermal fatigue behavior of a unidirectional SiC/Ti composite and the Ti alloy matrix
p 93 A91-55907
- Isothermal fatigue behavior of a (90)(sub 8) SiC/Ti-15-3 composite at 426 C
[NASA-TM-103686] p 99 N91-20228
- Oxidation resistant coatings for titanium alloys and titanium alloy matrix composites
[NASA-CASE-LEW-15155-1] p 122 N91-26375
- TITANIUM BORIDES**
Low-density, high-strength intermetallic matrix composites by XD (trademark) synthesis
[NASA-TM-103724] p 97 N91-19233
- TITANIUM COMPOUNDS**
Continuous fiber-reinforced titanium aluminide composites
p 92 A91-39553
- METCAN updates for high temperature composite behavior: Simulation/verification
[NASA-TM-103682] p 97 N91-19229
- TOLLMIE-SCHLICHTING WAVES**
The effect of small streamwise velocity distortion on the boundary layer flow over a thin flat plate with application to boundary layer stability theory
[NASA-TM-103668] p 161 N91-19372
- TOMOGRAPHY**
Three-dimensional computed tomography from interferometric measurements within a narrow cone of views
[NASA-TM-103257] p 176 N91-19404
- TOPOLOGY**
Power electronics for low power arcjets
[AIAA PAPER 91-1991] p 60 A91-45779
- Power electronics for low power arcjets
[NASA-TM-104459] p 77 N91-25172
- TORQUE**
A fiber optic sensor for noncontact measurement of shaft speed, torque and power
p 173 A91-51870
- Four quadrant control of induction motors
p 145 N91-23055
- TORQUEMETERS**
A fiber optic sensor for noncontact measurement of shaft speed, torque and power
p 173 A91-51870
- TORSION**
A data acquisition and control program for axial-torsional fatigue testing
p 199 A91-56540
- TOUGHNESS**
Constitution of pseudobinary hypoeutectic beta-NiAl + alpha-V alloys
p 109 A91-48509
- Prospects for ductility and toughness enhancement of NiAl by ductile phase reinforcement
[NASA-TM-103796] p 112 N91-27324
- TRACE CONTAMINANTS**
An experimental trace gas investigation of fluid transport and mixing in a circular-to-rectangular transition duct
[NASA-TM-104499] p 17 N91-27129
- TRACE ELEMENTS**
An experimental trace gas investigation of fluid transport and mixing in a circular-to-rectangular transition duct
[AIAA PAPER 91-2370] p 172 A91-44214
- TRACKING (POSITION)**
Two-dimensional particle displacement tracking in particle imaging velocimetry
p 172 A91-38498
- Particle image velocimetry for the surface tension driven convection experiment using a particle displacement tracking technique
[NASA-TM-104482] p 177 N91-25382
- TRACTION**
The measurement, modeling and prediction of traction forces in a rocket propellant
p 125 A91-51914
- TRADEOFFS**
Towards practical control design using neural computation
[NASA-TM-103785] p 219 N91-19766
- Characteristics of a future aeronautical satellite communications system
[NASA-TM-104389] p 20 N91-23102
- TRAILING EDGES**
Turbulent boundary layer separation over a rearward facing ramp and its control through mechanical excitation
[AIAA PAPER 91-0253] p 150 A91-26328
- TRANSATMOSPHERIC VEHICLES**
The design and performance estimates for the propulsion module for the booster of a TSTO vehicle
[AIAA PAPER 91-3136] p 43 A91-54054
- TRANSCENDENTAL FUNCTIONS**
Solution and sensitivity analysis of a complex transcendental eigenproblem with pairs of real eigenvalues
p 195 A91-23685
- TRANSDUCERS**
Photoelastic transducer for high-temperature applications
p 174 A91-55533
- Rotating pressure measurement system using an on board calibration standard
[NASA-TM-103676] p 176 N91-19401
- TRANSFER ORBITS**
Turbine blading designed for high heat load space propulsion applications
p 50 A91-10338
- Mass comparisons of electric propulsion systems for NSSK of geosynchronous spacecraft --- North-South Station Keeping
[AIAA PAPER 91-2347] p 47 A91-45808
- Advanced launch vehicle upper stages using liquid propulsion and metallized propellants
[NASA-TM-103622] p 68 N91-11797
- Xenon ion propulsion for orbit transfer
[NASA-TM-103193] p 69 N91-11798
- Mass comparisons of electric propulsion systems for NSSK of geosynchronous spacecraft
[NASA-TM-105153] p 85 N91-31212
- TRANSFORMATIONS (MATHEMATICS)**
Spectrum transformation for divergent iterations
[NASA-TM-103745] p 221 N91-19786
- TRANSIENT LOADS**
Modeling of Space Station electric power system with EMTP
p 55 A91-38040
- TRANSIENT RESPONSE**
Cascade flutter analysis with transient response aerodynamics
[AIAA PAPER 91-0747] p 21 A91-19448
- An expert system to perform on-line controller tuning
p 219 A91-30171
- On the numerical solution of the dynamically loaded hydrodynamic lubrication of the point contact
p 180 A91-33461
- The application of neural networks to the SSME startup transient
[AIAA PAPER 91-2530] p 60 A91-44283
- Transient flow thrust prediction for an ejector propulsion concept
p 24 A91-45326
- Low velocity impact analysis with NASTRAN
p 198 A91-48865
- Low velocity impact analysis with NASTRAN
[NASA-TM-103169] p 95 N91-14426
- TRANSISTORS**
Neutron, gamma ray and post-irradiation thermal annealing effects on power semiconductor switches
[AIAA PAPER 91-3525] p 142 A91-52420
- TRANSITION FLIGHT**
Application of an integrated flight/propulsion control design methodology to a STOVL aircraft
[NASA-TM-105254] p 37 N91-32143
- TRANSITION FLOW**
Turbulence enhancement in free shear flows under multifrequency excitation
p 152 A91-38737
- Computation of a circular-to-rectangular transition duct flow field
[AIAA PAPER 91-1741] p 156 A91-45547
- TRANSITION METALS**
Rapid solidification of polymorphic transition metals induced by nanosecond laser pulses
p 109 A91-46520
- Synthesis and structures of metal chalcogenide precursors
[NASA-TM-103665] p 120 N91-19296
- TRANSMISSION LINES**
Coplanar waveguide EESoF MICAD macros make circuit layout easy
[NASA-TM-103272] p 134 N91-19332
- TRANSMISSION LOSS**
Design aspects and comparison between high T(sub c) superconducting coplanar waveguide and microstrip line
[NASA-TM-105142] p 146 N91-27445
- TRANSMISSIONS (MACHINE ELEMENTS)**
Advanced Rotorcraft Transmission Program
p 179 A91-17214
- On the numerical solution of the dynamically loaded hydrodynamic lubrication of the point contact
p 180 A91-33461
- Analytical and experimental study of vibrations in a gear transmission
[AIAA PAPER 91-2019] p 181 A91-41680
- Effects of gear box vibration and mass imbalance on the dynamics of multistage gear transmission
p 182 A91-47213
- Experimental and analytical evaluation of efficiency of helicopter planetary stage
[NASA-TP-3063] p 183 N91-12956
- Review of the transmissions of the Soviet helicopters
[NASA-TM-103634] p 20 N91-15146
- Advanced rotorcraft transmission program
[NASA-TM-103276] p 184 N91-21531
- Effects of gear box vibration and mass imbalance on the dynamics of multi-stage gear transmissions
[NASA-TM-103695] p 185 N91-21534
- Analytical and experimental study of vibrations in a gear transmission
[NASA-TM-104434] p 187 N91-25395
- Acoustical analysis of gear housing vibration
[NASA-TM-103691] p 188 N91-25411
- Advanced Rotorcraft Transmission (ART) program-Boeing helicopters status report
[NASA-TM-104474] p 188 N91-25412
- Transmission overhaul estimates for partial and full replacement at repair
[NASA-TM-104395] p 190 N91-30533
- Recent manufacturing advances for spiral bevel gears
[NASA-TM-104479] p 191 N91-31654
- TRANSMITTANCE**
Simulation of Martian dust accumulation on surfaces
p 47 N91-19160
- TRANSMITTERS**
Status of Ka-band TWT transmitter technology
[AIAA PAPER 91-3621] p 142 A91-52485
- Combinatorial FSK modulation for power-efficient high-rate communications
[AIAA PAPER 91-3532] p 133 A91-53708
- Combinatorial FSK modulation for power-efficient high-rate communications
[NASA-TM-105188] p 135 N91-29404
- TRANSONIC COMPRESSORS**
A Navier-Stokes study of shock-boundary layer interaction and flow separation inside a transonic compressor
p 8 A91-56115
- TRANSONIC FLOW**
Navier-Stokes simulation of transonic blade-vortex interactions
p 2 A91-21065
- Improved visualization of flow field measurements
[AIAA PAPER 91-0273] p 3 A91-26331
- Experimental investigation of oscillating cascade aerodynamics
p 3 A91-27801

- Extension of transonic flow computational concepts in the analysis of cavitated bearings
[ASME PAPER 90-TRIB-40] p 150 A91-29474
- Navier-Stokes analysis of transonic cascade flow
[NASA-TM-103624] p 159 N91-11192
- Extension of transonic flow computational concepts in the analysis of cavitated bearings
[NASA-TM-103214] p 160 N91-16304
- Transonic aerodynamics of dense gases
[NASA-TM-103722] p 13 N91-20045
- Transonic cascade flow calculations using non-periodic C-type grids p 163 N91-21071
- Euler flow predictions for an oscillating cascade using a high resolution wave-split scheme
[NASA-TM-104377] p 16 N91-24107
- TRANSONIC WIND TUNNELS**
- Transonic wind-tunnel wall interference prediction code p 38 A91-26112
- TRANSPORT AIRCRAFT**
- Civil air transport - A fresh look at power-by-wire and fly-by-light p 36 A91-31030
- Effects of nozzle lip geometry on spray atomization and emissions advanced gas turbine combustors
[AIAA PAPER 91-2201] p 24 A91-44153
- Overview of subsonic transport propulsion technology p 30 N91-20116
- High-efficiency core technology p 30 N91-20118
- Civil air transport: A fresh look at power-by-wire and fly-by-light p 37 N91-23053
- TRANSPORT VEHICLES**
- Solar electric propulsion for Mars transport vehicles
[NASA-TM-103234] p 71 N91-19178
- Overview of supersonic cruise propulsion research p 27 N91-20088
- TRANSPUTERS**
- Efficient computation of aerodynamic influence coefficients for aeroelastic analysis on a transputer network
[NASA-TM-103671] p 216 N91-20748
- TRAPEZOIDAL WINGS**
- A comparison of arrow, trapezoidal and M wing concepts using a Mach 2 supersonic cruise transport mission
[AIAA PAPER 91-3102] p 7 A91-54027
- TRAPPING**
- Grooved surfaces on InP p 213 N91-30208
- TRAVELING WAVE AMPLIFIERS**
- Pulsed response of a TWT p 136 A91-27529
- TRAVELING WAVE TUBES**
- A high-efficiency ferruleless coupled-cavity traveling-wave tube with phase-adjusted taper p 136 A91-25078
- Pulsed response of a TWT p 136 A91-27529
- High power, high efficiency millimeter wavelength traveling wave tubes for high rate communications from deep space p 142 A91-52461
- [AIAA PAPER 91-3593] p 142 A91-52461
- Status of Ka-band TWT transmitter technology
[AIAA PAPER 91-3621] p 142 A91-52485
- Pulsed response of a traveling-wave tube p 143 N91-19348
- [NASA-TM-103672] p 143 N91-19348
- A three-dimensional finite-element thermal/mechanical analytical technique for high-performance traveling wave tubes
[NASA-TP-3081] p 134 N91-27436
- TRELLIS CODING**
- Performance evaluation of land mobile satellite system under vegetative shadowing using differential multiple TCM and QPSK p 132 A91-53084
- TRENDS**
- Advanced aeropropulsion controls technology p 29 N91-20103
- TRIBOLOGY**
- Acidic attack of perfluorinated alkyl ether lubricant molecules by metal oxide surfaces p 104 A91-13439
- Tribological properties of PM212 - A high temperature, self-lubricating, powder metallurgy composite
[STLE PREPRINT 90-AM-4E-1] p 87 A91-19720
- A new test machine for measuring friction and wear in controlled atmospheres to 1200 C p 180 A91-33600
- Space mechanisms needs for future NASA long duration space missions p 183 A91-57025
- [AIAA PAPER 91-3428] p 183 A91-57025
- Composite bearing and seal materials for advanced heat engine applications to 900 C
[NASA-TM-103612] p 95 N91-15318
- Tribological properties of Ag/Ti films on Al₂O₃ ceramic substrates p 89 N91-19224
- [NASA-TM-103784] p 89 N91-19224
- Tribological characteristics of silicon carbide whisker-reinforced alumina at elevated temperatures
[NASA-TM-103799] p 89 N91-22379
- Solid lubricants p 99 N91-22396
- [NASA-TM-102803] p 99 N91-22396
- Government/industry response to questionnaire on space mechanisms/tribology technology needs
[NASA-TM-104358] p 186 N91-23501
- Quality control of the tribological coating PS212
[NASA-TM-102067] p 101 N91-25186
- Space mechanisms needs for future NASA long duration space missions p 190 N91-30532
- [NASA-TM-105204] p 190 N91-30532
- Lubrication with sputtered MoS₂ films: Principles, operation, limitations
[NASA-TM-105292] p 112 N91-32216
- TRUSSES**
- Dynamic analysis of space-related linear and non-linear structures p 196 A91-28612
- Simulation of the Space Station strut-out condition
[AIAA PAPER 91-1248] p 197 A91-32087
- Probabilistic structural analysis of a truss typical for space station
[NASA-TM-103277] p 199 N91-12114
- TUNGSTEN**
- High temperature tension-compression fatigue behavior of a tungsten copper composite
[NASA-TM-104370] p 100 N91-24360
- TUNGSTEN ALLOYS**
- High temperature fatigue behavior of tungsten copper composites p 93 A91-55906
- Effect of thermal shock on fiber-reinforced superalloy composites p 93 A91-55918
- Tensile behavior of tungsten/nickel composites at 1300 to 1600 K
[NASA-TM-103727] p 111 N91-16128
- Tensile and fatigue behavior of tungsten/copper composites p 100 N91-24311
- TUNGSTEN COMPOUNDS**
- Solid lubricants
[NASA-TM-102803] p 99 N91-22396
- TUNING**
- Localization of aeroelastic modes in mistuned high-energy turbines
[AIAA PAPER 91-3379] p 198 A91-44319
- Localization of aeroelastic modes in mistuned high-energy turbines
[NASA-TM-104445] p 204 N91-24659
- Tuning maps for setpoint changes and load disturbance upsets in a three capacity process under multivariable control
[NASA-TM-104419] p 220 N91-31876
- TURBINE BLADES**
- Turbine blading designed for high heat load space propulsion applications p 50 A91-10338
- Heat flux measurement in SSME turbine blade tester p 171 A91-30649
- Model-OA wind turbine generator - Failure modes and effects analysis p 191 A91-31064
- Navier-Stokes analysis of turbine blade heat transfer
[ASME PAPER 90-GT-42] p 155 A91-44529
- Design and experimental evaluation of compact radial-inflow turbines p 24 A91-45788
- [AIAA PAPER 91-2127] p 24 A91-45788
- Two-dimensional Navier-Stokes heat transfer analysis for rough turbine blades p 156 A91-45790
- [AIAA PAPER 91-2129] p 156 A91-45790
- Computations of the three-dimensional flow and heat transfer within a coolant passage of a radial turbine blade p 156 A91-45797
- [AIAA PAPER 91-2238] p 156 A91-45797
- Algebraic grid generation for coolant passages of turbine blades with serpentine channels and pin fins p 156 A91-45811
- [AIAA PAPER 91-2366] p 156 A91-45811
- Heat flux measurement in SSME turbine blade tester
[NASA-TM-103274] p 175 N91-11205
- Heat transfer in rotating serpentine passages with trips normal to the flow p 184 N91-19443
- [NASA-TM-103758] p 184 N91-19443
- Calibrator tests of heat flux gauges mounted in SSME blades p 177 N91-24321
- Thin-film sensors for space propulsion technology: Fabrication and preparation for testing p 77 N91-24324
- Comparison of a quasi-3D analysis and experimental performance for three compact radial turbines
[NASA-TM-105155] p 35 N91-30142
- TURBINE ENGINES**
- Comparison of a quasi-3D analysis and experimental performance for three compact radial turbines
[AIAA PAPER 91-2128] p 25 A91-45789
- Three-dimensional flows in a transonic compressor rotor p 8 A91-56152
- High-efficiency core technology p 30 N91-20118
- Multidisciplinary research overview (IHPTET/NPSS) p 30 N91-20119
- Multi-heat addition turbine engine
[NASA-CASE-LEW-15094-1] p 32 N91-23180
- The Navy/NASA Engine Program (NNEP8): A user's manual p 35 N91-30141
- [NASA-TM-105186] p 35 N91-30141
- TURBINE PUMPS**
- Heat flux measurement in SSME turbine blade tester p 171 A91-30649
- Liquid hydrogen turbopump foil bearing
[AIAA PAPER 91-2108] p 182 A91-41701
- Localization of aeroelastic modes in mistuned high-energy turbines
[AIAA PAPER 91-3379] p 198 A91-44319
- Ceramic composites for rocket engine turbines
[SAE PAPER 911108] p 92 A91-53552
- Heat flux measurement in SSME turbine blade tester
[NASA-TM-103274] p 175 N91-11205
- Ceramic composites for rocket engine turbines
[NASA-TM-103743] p 98 N91-19235
- A model for the space shuttle main engine high pressure oxidizer turbopump shaft seal system
[NASA-TM-103697] p 184 N91-20489
- Localization of aeroelastic modes in mistuned high-energy turbines
[NASA-TM-104445] p 204 N91-24659
- TURBINE WHEELS**
- Aeroelastic modal characteristics of mistuned blade assemblies - Mode localization and loss of eigenstructure
[AIAA PAPER 91-1218] p 196 A91-32032
- A three-dimensional Navier-Stokes stage analysis of the flow through a compact radial turbine p 23 A91-41815
- [AIAA PAPER 91-2564] p 23 A91-41815
- A three-dimensional Navier-Stokes stage analysis of the flow through a compact radial turbine p 32 N91-23186
- [NASA-TM-104420] p 32 N91-23186
- An unconditionally stable Runge-Kutta method for unsteady rotor-stator interaction p 165 N91-24337
- Average-passage flow model development p 165 N91-24338
- Aeroelastic modal characteristics of mistuned blade assemblies: Mode localization and loss of eigenstructure
[NASA-TM-104519] p 205 N91-27591
- Comparison of a quasi-3D analysis and experimental performance for three compact radial turbines
[NASA-TM-105155] p 35 N91-30142
- TURBINES**
- A three-dimensional Navier-Stokes stage analysis of the flow through a compact radial turbine
[AIAA PAPER 91-2564] p 23 A91-41815
- Localization of aeroelastic modes in mistuned high-energy turbines
[AIAA PAPER 91-3379] p 198 A91-44319
- An analysis of the viscous flow through a compact radial turbine by the average passage approach
[ASME PAPER 90-GT-64] p 6 A91-44545
- High temperature cyclic oxidation data. Part 1: Turbine alloys p 110 N91-10149
- [NASA-TM-83665] p 110 N91-10149
- High-temperature cyclic oxidation data. Part 2: Turbine alloys p 110 N91-10150
- [NASA-TM-101468] p 110 N91-10150
- Aerodynamics and heat transfer investigations on a high Reynolds number turbine cascade p 11 N91-15134
- [NASA-TM-103260] p 11 N91-15134
- Performance of a high-work, low-aspect-ratio turbine stator tested with a realistic inlet radial temperature gradient p 31 N91-20126
- [NASA-TM-103738] p 31 N91-20126
- A three-dimensional Navier-Stokes stage analysis of the flow through a compact radial turbine
[NASA-TM-104420] p 32 N91-23186
- Mechanical behavior and failure phenomenon of an in situ-toughened silicon nitride p 121 N91-23311
- [NASA-TM-103741] p 121 N91-23311
- Localization of aeroelastic modes in mistuned high-energy turbines
[NASA-TM-104445] p 204 N91-24659
- TURBOCOMPRESSORS**
- Three-dimensional flows in a transonic compressor rotor p 8 A91-56152
- Automated design of controlled diffusion blades p 9 N91-10883
- TURBOFAN ENGINES**
- Turbofan engine demonstration of sensor failure detection p 22 A91-29775
- A linear control design structure to maintain loop properties during limit operation in a multi-nozzle turbofan engine p 24 A91-45780
- [AIAA PAPER 91-1997] p 24 A91-45780
- Comparison of turbine bypass and mixed flow turbofan engines for a high-speed civil transport
[AIAA PAPER 91-3132] p 25 A91-54051
- NASA aeropropulsion research in support of propulsion systems of the 21st century p 15 N91-23083
- [NASA-TM-104403] p 15 N91-23083
- A linear control design structure to maintain loop properties during limit operation in a multi-nozzle turbofan engine p 35 N91-29188
- [NASA-TM-105163] p 35 N91-29188
- TURBOFANS**
- Analysis of three-dimensional viscous flow in a supersonic throughflow fan p 10 N91-10885

- Improved visualization of flow field measurements
[NASA-TM-103679] p 12 N91-19044
Calculated performance of the NASA Lewis icing
research tunnel
[NASA-TM-105173] p 39 N91-29199

TURBOMACHINERY

- An algebraic RNG-based turbulence model for
three-dimensional turbomachinery flows
[AIAA PAPER 91-0172] p 2 A91-21393
Effects of brush seal morphology on leakage and
pressure drops
[AIAA PAPER 91-2106] p 182 A91-41700
Simulation of turbomachinery flows p 9 N91-10880
Three-component laser anemometer measurement
systems
[NASA-TP-3080] p 13 N91-19057
Turbomachinery p 162 N91-20097
Turbomachinery and combustor technology for small
engines p 29 N91-20113
Computational Fluid Dynamics Symposium on
Aeropropulsion
[NASA-CP-3078] p 14 N91-21062
Simulation of turbomachinery flows

- Transonic cascade flow calculations using non-periodic
C-type grids p 163 N91-21071
Overview of aerothermodynamic loads definition study
p 204 N91-24334
An unconditionally stable Runge-Kutta method for
unsteady rotor-stator interaction p 165 N91-24337
The design/analysis of flows through turbomachinery:
A viscous/inviscid approach
[NASA-TM-104447] p 33 N91-25148
Comparison of a quasi-3D analysis and experimental
performance for three compact radial turbines
[NASA-TM-105155] p 35 N91-30142

TURBOPROP AIRCRAFT

- Prediction of the noise from a propeller at angle of
attack
[AIAA PAPER 90-3954] p 225 A91-12470
Cruise noise of an advanced single-rotation propeller
measured from an adjacent aircraft p 22 A91-28265
Potential reduction of en route noise from an advanced
turboprop aircraft
[NASA-TM-103635] p 228 N91-15842

TURBOSHAFTS

- A model for the Space Shuttle Main Engine High
Pressure Oxidizer Turbopump shaft seal system
p 180 A91-30640

TURBULENCE

- Transonic cascade flow calculations using non-periodic
C-type grids p 163 N91-21071
Numerical investigation of an internal layer in turbulent
flow over a curved hill p 163 N91-21083
Application of mixing-controlled combustion models to
gas turbine combustors
[NASA-TM-103236] p 31 N91-22126
A three-dimensional turbulent heat transfer analysis for
advanced tubular rocket thrust chambers

- p 75 N91-24258
Turbulent fluid motion 2: Scalars, vectors, and tensors
[NASA-TM-103756] p 167 N91-27487

TURBULENCE EFFECTS

- Turbulent fluid motion. Part 1: The phenomenon of fluid
turbulence
[NASA-TM-103723] p 162 N91-20445
A laser velocimeter investigation of the normal
shock-wave boundary layer interaction
[NASA-TM-105201] p 169 N91-32440

TURBULENCE MODELS

- An algebraic RNG-based turbulence model for
three-dimensional turbomachinery flows
[AIAA PAPER 91-0172] p 2 A91-21393
Modern CFD applications for the design of a reacting
shear layer facility
[AIAA PAPER 91-0577] p 149 A91-21540
Calculation of turbulence-driven secondary motion in
ducts with arbitrary cross section p 151 A91-34132
Calculation of divergent channel flows with a
multiple-time-scale turbulence model

- p 151 A91-34134
Calculation of turbulent flow in complex geometries with
a second-moment closure model p 152 A91-38741
A study of hydrogen diffusion flames using PDF
turbulence model

- [AIAA PAPER 91-1780] p 106 A91-45549
A three-dimensional turbulent heat transfer analysis for
advanced tubular rocket thrust chambers

- [NASA-TM-103293] p 159 N91-10249
Analysis of three-dimensional viscous flow in a
supersonic throughflow fan p 10 N91-10885
Navier-Stokes analysis of transonic cascade flow

- [NASA-TM-103624] p 159 N91-11192
Computational Fluid Dynamics Symposium on
Aeropropulsion

- [NASA-CP-3078] p 14 N91-21062

- Implicit solution of three-dimensional internal turbulent
flows p 163 N91-21082

- Numerical investigation of an internal layer in turbulent
flow over a curved hill p 163 N91-21083

- Heat transfer, velocity-temperature correlation, and
turbulent shear stress from Navier-Stokes computations
of shock wave/turbulent boundary layer interaction flows
p 163 N91-21085

- Computational modeling and validation for hypersonic
inlets p 16 N91-23162

- A three-dimensional turbulent heat transfer analysis for
advanced tubular rocket thrust chambers

- p 75 N91-24258
Average-passage flow model development

- p 165 N91-24338
Advances in modeling the pressure correlation terms
in the second moment equations

- [NASA-TM-104413] p 165 N91-24525
Modern CFD applications for the design of a reacting
shear layer facility

- [NASA-TM-104523] p 34 N91-27164
Calculation of a circular jet in crossflow with a
multiple-time-scale turbulence model

- [NASA-TM-104343] p 169 N91-30476

TURBULENT BOUNDARY LAYER

- Turbulent boundary layer separation over a rearward
facing ramp and its control through mechanical
excitation

- [AIAA PAPER 91-0253] p 150 A91-26328
3-D Navier-Stokes analysis of crossing, glancing
shocks/turbulent boundary layer interactions

- [AIAA PAPER 91-1758] p 6 A91-43631
The effect of varying Mach number on crossing, glancing
shocks/turbulent boundary-layer interactions

- [AIAA PAPER 91-2157] p 6 A91-45792
Results from computational analysis of a mixed
compression supersonic inlet

- [AIAA PAPER 91-2581] p 7 A91-45818
Naturally occurring and forced azimuthal modes in a
turbulent jet

- [NASA-TM-103692] p 11 N91-17000
Turbulent boundary layer separation over a rearward
facing ramp and its control through mechanical
excitation

- [NASA-TM-103702] p 160 N91-19370
Experimental study of boundary layer transition on a
heated flat plate

- [NASA-TM-103779] p 14 N91-21061
Heat transfer, velocity-temperature correlation, and
turbulent shear stress from Navier-Stokes computations
of shock wave/turbulent boundary layer interaction flows

- p 163 N91-21085
A study of three dimensional turbulent boundary layer
separation and vortex flow control using the reduced Navier
Stokes equations

- [NASA-TM-104407] p 16 N91-23089
The 3-D Navier-Stokes analysis of crossing, glancing
shocks/turbulent boundary layer interactions

- [NASA-TM-104469] p 16 N91-24130
Evaluation of a technique to generate artificially
thickened boundary layers in supersonic and hypersonic
flows

- [NASA-TP-3142] p 17 N91-28136
A k-epsilon modeling of near wall turbulence

- [NASA-TM-105238] p 170 N91-32460

TURBULENT DIFFUSION

- Renormalization group analysis of anisotropic diffusion
in turbulent shear flows p 150 A91-27946

- An experimental trace gas investigation of fluid transport
and mixing in a circular-to-rectangular transition duct

- [NASA-TM-104499] p 17 N91-27129

TURBULENT FLOW

- Nonlinear Reynolds stress model for turbulent shear
flows

- [AIAA PAPER 91-0609] p 149 A91-21556
Renormalization group analysis of anisotropic diffusion
in turbulent shear flows

- p 150 A91-27946
Calculation of turbulence-driven secondary motion in
ducts with arbitrary cross section p 151 A91-34132

- Calculation of divergent channel flows with a
multiple-time-scale turbulence model

- p 151 A91-34134
Calculation of turbulent flow in complex geometries with
a second-moment closure model p 152 A91-38741

- Verification of the Proteus two-dimensional
Navier-Stokes code for flat plate and pipe flows

- [AIAA PAPER 91-2013] p 153 A91-41678
Second order modeling of boundary-free turbulent shear
flows

- [AIAA PAPER 91-1779] p 154 A91-42588
Simulations of free shear layers using a compressible
k-epsilon model

- [AIAA PAPER 91-1863] p 156 A91-45778

- Computations of the three-dimensional flow and heat
transfer within a coolant passage of a radial turbine
blade

- [AIAA PAPER 91-2238] p 156 A91-45797
Numerical solution for the velocity-derivative skewness
of a low Reynolds-number turbulent-like decaying
Navier-Stokes flow

- p 158 A91-50204
The effects of rotation on initially anisotropic
homogeneous flows p 158 A91-54958

- A numerical study of the hot gas environment around
a STOVL aircraft in ground proximity p 10 N91-10887

- A 2-D oscillating flow analysis in Stirling engine heat
exchangers

- [NASA-TM-103781] p 161 N91-19375
Turbulent fluid motion. Part 1: The phenomenon of fluid
turbulence

- [NASA-TM-103723] p 162 N91-20445
Implicit solution of three-dimensional internal turbulent
flows

- p 163 N91-21082
Numerical investigation of an internal layer in turbulent
flow over a curved hill p 163 N91-21083

- Second order modeling of boundary-free turbulent shear
flows

- [NASA-TM-104369] p 164 N91-22524
Low Reynolds number two-equation modeling of
turbulent flows

- [NASA-TM-104368] p 165 N91-23416
Advances in modeling the pressure correlation terms
in the second moment equations

- [NASA-TM-104413] p 165 N91-24525
Calculation of a circular jet in crossflow with a
multiple-time-scale turbulence model

- [NASA-TM-104343] p 169 N91-30476
Experimental investigation of turbulent flow through a
circular-to-rectangular transition duct

- [NASA-TM-105210] p 18 N91-31106
A critical comparison of two-equation turbulence
models

- [NASA-TM-105237] p 169 N91-31597
A k-epsilon modeling of near wall turbulence

- [NASA-TM-105238] p 170 N91-32460

TURBULENT HEAT TRANSFER

- A three-dimensional turbulent heat transfer analysis for
advanced tubular rocket thrust chambers

- [NASA-TM-103293] p 159 N91-10249
A three-dimensional turbulent heat transfer analysis for
advanced tubular rocket thrust chambers

- p 75 N91-24258

TURBULENT JETS

- Modern developments in shear flow control with swirl

- p 3 A91-24519
Multifrequency excited jets p 151 A91-31482

- Turbulence enhancement in free shear flows under
multifrequency excitation p 152 A91-38737

- Transient flow thrust prediction for an ejector propulsion
concept p 24 A91-45326

- Three-dimensional calculation, of the mixing of radial jets
from slanted slots with a reactive cylindrical crossflow

- [AIAA PAPER 91-2081] p 24 A91-45782
Characteristics of 3D turbulent jets in crossflow

- p 158 A91-54268
Numerical simulation of nonlinear development of
instability waves

- [E-4658] p 8 N91-10849
Naturally occurring and forced azimuthal modes in a
turbulent jet

- [NASA-TM-103692] p 11 N91-17000
Characteristics of 3D turbulent jets in crossflow

- [NASA-TM-104337] p 165 N91-22536
Control of an axisymmetric turbulent jet by multi-modal
excitation

- [NASA-TM-104483] p 17 N91-26121
An experimental study of natural and forced modes in
an axisymmetric jet

- [NASA-TM-105225] p 18 N91-32074

TURBULENT MIXING

- An experimental trace gas investigation of fluid transport
and mixing in a circular-to-rectangular transition duct

- [NASA-TM-104499] p 17 N91-27129
An experimental study of natural and forced modes in
an axisymmetric jet

- [NASA-TM-105225] p 18 N91-32074

TURBULENT WAKES

- Second order modeling of boundary-free turbulent shear
flows

- [AIAA PAPER 91-1779] p 154 A91-42588
Second order modeling of boundary-free turbulent shear
flows

- [NASA-TM-104369] p 164 N91-22524

TVD SCHEMES

- Numerical study of shock-wave/boundary layer
interactions in premixed hydrogen-air hypersonic flows

- [AIAA PAPER 91-0413] p 149 A91-26191
Navier-Stokes simulation of the supersonic combustion
flowfield in a ram accelerator

- [AIAA PAPER 91-1916] p 155 A91-44057

- Numerical study of unsteady shockwave reflections using an upwind TVD scheme
[NASA-TM-103251] p 10 N91-11676
- Numerical study of shock-wave/boundary layer interactions in premixed hydrogen-air hypersonic flows [NASA-TM-103273] p 160 N91-14559
- Navier-Stokes simulation of the supersonic combustion flowfield in a ram accelerator
[NASA-TM-104439] p 166 N91-24541

TWO DIMENSIONAL BOUNDARY LAYER

- On the continuous spectra of the compressible boundary layer stability equations p 150 A91-31342

TWO DIMENSIONAL FLOW

- Inertia effects in thin film flow with a corrugated boundary p 151 A91-32691
- Multidimensional computer simulation of Stirling cycle engines p 181 A91-38154
- A new Lagrangian random choice method for steady two-dimensional supersonic/hypersonic flow
[AIAA PAPER 91-1546] p 5 A91-40721
- Verification of the Proteus two-dimensional Navier-Stokes code for flat plate and pipe flows
[AIAA PAPER 91-2013] p 153 A91-41678
- Flutter analysis of cascades using a two dimensional Euler solver
[AIAA PAPER 91-1681] p 6 A91-45548
- Simulations of free shear layers using a compressible k-epsilon model
[AIAA PAPER 91-1863] p 156 A91-45778
- Two-dimensional Navier-Stokes heat transfer analysis for rough turbine blades
[AIAA PAPER 91-2129] p 156 A91-45790
- Primitive variable, strongly implicit calculation procedure for viscous flows at all speeds p 7 A91-46181
- Flux splitting algorithms for two-dimensional viscous flows with finite-rate chemistry p 10 N91-10894
- A numerical and experimental analysis of reactor performance and deposition rates for CVD on monofilaments
[NASA-TM-103631] p 130 N91-14500
- A 2-D oscillating flow analysis in Stirling engine heat exchangers
[NASA-TM-103781] p 161 N91-19375
- Transonic aerodynamics of dense gases
[NASA-TM-103722] p 13 N91-20045
- Verification of the proteus two-dimensional Navier-Stokes code for flat plate and pipe flows
[NASA-TM-105160] p 168 N91-30462
- Least-squares solution of incompressible Navier-Stokes equations with the p-version of finite elements
[NASA-TM-105203] p 223 N91-31911

TWO DIMENSIONAL MODELS

- Solution of steady-state, two-dimensional conservation laws by mathematical programming p 221 A91-35956
- A comparison of CFD predictions and experimental results for a Mach 5 inlet p 28 N91-20094

TWO PHASE FLOW

- Dropsize correlation for cryogenic liquid-jet atomization
[AIAA PAPER 91-0284] p 51 A91-19218
- Particle image fields and partial coherence p 171 A91-19604
- Gas property effects on dropsizes of simulated fuel sprays p 156 A91-45327
- Chemical reacting flows p 162 N91-20098

TWO REFLECTOR ANTENNAS

- Designs for the ATRSS tri-band reflector antenna
[NASA-TM-103754] p 48 N91-20184

U**UH-60A HELICOPTER**

- A review of ice accretion data from a model rotor icing test and comparison with theory
[AIAA PAPER 91-0661] p 19 A91-22500
- A review of ice accretion data from a model rotor icing test and comparison with theory p 11 N91-13421

ULTRAHIGH FREQUENCIES

- GaAs monolithic RF modules for SARSSAT distress beacons
[NASA-TM-104338] p 46 N91-21184

ULTRASONIC FLAW DETECTION

- Acousto-ultrasonics - Retrospective exhortation with bibliography p 191 A91-37011
- Preliminary investigation of acousto-ultrasonic evaluation of metal-matrix composite specimens p 191 A91-37014
- Acousto-ultrasonics p 226 A91-48227
- Ultrasonic velocity technique for monitoring property changes in fiber-reinforced ceramic matrix composites p 174 A91-56912
- Review of acousto-ultrasonic NDE for composites p 97 N91-18192

- Acousto-ultrasonic nondestructive evaluation of materials using laser beam generation and detection p 193 N91-18193

- Ultrasonic velocity technique for monitoring property changes in fiber-reinforced ceramic matrix composites [NASA-TM-103806] p 195 N91-30546

ULTRASONIC TESTS

- Preliminary investigation of acousto-ultrasonic evaluation of metal-matrix composite specimens p 191 A91-37014

- Spatial variations in a.c. susceptibility and microstructure for the YBa₂Cu₃O(7-x) superconductor and their correlation with room-temperature ultrasonic measurements p 233 A91-54969

- Spatial variations in ac susceptibility and microstructure for the YBa₂Cu₃O(7-x) superconductor and their correlation with room-temperature ultrasonic measurements [NASA-TM-103787] p 194 N91-21553

- A preliminary investigation of acousto-ultrasonic NDE of metal matrix composite test specimens [NASA-TM-104339] p 194 N91-23521

- Ultrasonic evaluation of oxidation and reduction effects on the elastic behavior and global microstructure of YBa₂Cu₃O(7-x) [NASA-TM-104529] p 194 N91-27575

- NDE of ceramics and ceramic composites [NASA-TM-104520] p 194 N91-29610

ULTRASONICS

- Ultrasonic imaging of textured alumina p 191 A91-18596
- Advanced electrical power, distribution and control for the Space Transportation System p 143 N91-17043

ULTRAVIOLET RADIATION

- Low Earth orbital atomic oxygen and ultraviolet radiation effects on polymers [NASA-TM-103711] p 119 N91-19294

UNIVERSE

- Primordial nucleosynthesis redux p 240 A91-45907

UNIVERSITY PROGRAM

- The International Space University's variable gravity research facility design [NASA-TM-105224] p 44 N91-31196

UNSTEADY AERODYNAMICS

- Oscillating cascade aerodynamics by an experimental influence coefficient technique p 1 A91-10339
- Acoustic radiation from lifting airfoils in compressible subsonic flow [AIAA PAPER 90-3911] p 224 A91-12427
- The aerodynamics of an oscillating cascade in a compressible flow field [ASME PAPER 89-GT-271] p 1 A91-13047
- Control of flow separation and mixing by aerodynamic excitation p 2 A91-24360
- Experimental investigation of oscillating cascade aerodynamics p 3 A91-27801
- Role of artificial viscosity in Euler and Navier-Stokes solvers p 4 A91-34135
- Influence of thickness and camber on the aeroelastic stability of supersonic throughflow fans p 5 A91-42814

- Localization of aeroelastic modes in mistuned high-energy turbines [AIAA PAPER 91-3379] p 198 A91-44319

- Semianalytical technique for sensitivity analysis of unsteady aerodynamic computations p 7 A91-48816
- Numerical analysis of flow through oscillating cascade sections p 9 N91-10884

- Unsteady blade-surface pressures on a large-scale advanced propeller: Prediction and data [NASA-TM-103218] p 69 N91-11799

- Near-field noise of a single-rotation propfan at an angle of attack [NASA-TM-103645] p 227 N91-12316

- Acoustic radiation from lifting airfoils in compressible subsonic flow [NASA-TM-103650] p 13 N91-19053

- Wind tunnel wall effects in a linear oscillating cascade [NASA-TM-103690] p 27 N91-19098

- Three-dimensional Euler time accurate simulations of fan rotor-stator interactions [NASA-TM-102528] p 16 N91-24124

- Localization of aeroelastic modes in mistuned high-energy turbines [NASA-TM-104445] p 204 N91-24659

UNSTEADY FLOW

- Unsteady blade pressure measurements for the SR-7A propeller at cruise conditions [AIAA PAPER 90-4022] p 225 A91-12533

- Flow induced vibration and noise by a pair of tandem cylinders due to buffeting p 225 A91-14650

- Unstable viscous wall modes in rotating pipe flow [AIAA PAPER 91-1801] p 154 A91-42599

- Flux-vector splitting algorithm for chain-rule conservation-law form p 221 A91-45109

- Transient flow thrust prediction for an ejector propulsion concept p 24 A91-45326

- Time dependent viscous incompressible Navier-Stokes equations p 9 N91-10854

- Compressible flows with periodic vortical disturbances around lifting airfoils [NASA-TM-103742] p 14 N91-21060

- Euler flow predictions for an oscillating cascade using a high resolution wave-split scheme [NASA-TM-104377] p 16 N91-24107

- Comparison of SMAC, PISO, and iterative time-advancing schemes for unsteady flows [NASA-TM-104406] p 167 N91-24550

- Unsteady flowfield of a propfan at takeoff conditions [NASA-TM-105223] p 18 N91-32075

UPPER STAGE ROCKET ENGINES

- Advanced chemical propulsion at NASA Lewis: Metallized and high energy density propellants [NASA-TM-103771] p 71 N91-19175

USER MANUALS (COMPUTER PROGRAMS)

- Shared direct memory access on the Explorer 2-LX [NASA-TM-103289] p 216 N91-12215

- ETARA PC version 3.3 user's guide: Reliability, availability, maintainability simulation model [NASA-TM-103751] p 193 N91-19462

- Computer code for single-point thermodynamic analysis of hydrogen/oxygen expander-cycle rocket engines [NASA-TM-4275] p 72 N91-20206

- Software manual for operating particle displacement tracking data acquisition and reduction system [NASA-TM-103720] p 176 N91-20453

- ALPS: A Linear Program Solver [NASA-TM-104347] p 216 N91-20765

- ASTROP2 users manual: A program for aeroelastic stability analysis of propfans [NASA-TM-4304] p 206 N91-28627

- The Navy/NASA Engine Program (NNEP89): A user's manual [NASA-TM-105186] p 35 N91-30141

USER REQUIREMENTS

- Plug nozzles - The ultimate customer driven propulsion system --- applied to manned lunar and Martian landers [AIAA PAPER 91-2208] p 61 A91-45794
- Results of the users' requirements survey p 175 N91-14575

V**V/STOL AIRCRAFT**

- Flow studies in close-coupled ventral nozzles for STOVL aircraft [SAE PAPER 901033] p 2 A91-21242

- STOVL Hot Gas Ingestion control technology [ASME PAPER 89-GT-323] p 22 A91-23642

- Flow visualization studies of the internal flow characteristics in a simulated mixed flow vectored thrust ASTOVL engine configuration [AIAA PAPER 91-1689] p 23 A91-42556

- Static performance tests of a flight-type STOVL ejector [AIAA PAPER 91-1902] p 24 A91-44050

- V/STOL gets a lift p 20 A91-52835

- VSTOL ground effects testing with flow visualization and image enhancement [AIAA PAPER 91-3145] p 8 A91-54061

- A numerical study of the hot gas environment around a STOVL aircraft in ground proximity p 10 N91-10887

- An AD100 implementation of a real-time STOVL aircraft propulsion system [NASA-TM-103683] p 26 N91-13457

- Flow visualization and hot gas ingestion characteristics of a vectored thrust STOVL concept p 28 N91-20090

- IMPAC: An Integrated Methodology for Propulsion and Airframe Control [NASA-TM-103805] p 30 N91-20122

- Integrated flight/propulsion control design for a STOVL aircraft using H-infinity control design techniques [NASA-TM-104340] p 31 N91-21140

- Static performance tests of a flight-type STOVL ejector [NASA-TM-104437] p 33 N91-24201

VACUUM CHAMBERS

- Full-size solar dynamic heat receiver thermal-vacuum tests [NASA-TM-104486] p 78 N91-25184

VACUUM EFFECTS

- First-order inflation --- in cosmology p 240 A91-37444

- Discharge rate of cryogens in microgravity - What ground based experimentation cannot resolve [AIAA PAPER 91-3545] p 129 A91-52430

VALENCE

- Near-edge study of gold-substituted YBa₂Cu₃O(7-delta) [NASA-TM-105220] p 237 N91-31977

VALVES

- Method of injecting fluid propellants into a rocket combustion chamber
[NASA-CASE-LEW-14846-2] p 78 N91-26200

VANADIUM

- Reactivity of pi-complexes of Ti, V, and Nb towards dithioacetic acid: Synthesis and structure of novel metal sulfur-containing complexes
[NASA-TM-103666] p 106 N91-19256

VANES

- The effect of swirl recovery vanes on the cruise noise of an advanced propeller
[AIAA PAPER 90-3932] p 224 A91-12448
Navier-Stokes analysis of turbine blade heat transfer
[ASME PAPER 90-GT-42] p 155 A91-44529
The effect of swirl recovery vanes on the cruise noise of an advanced propeller
[NASA-TM-103625] p 227 N91-11494

VAPOR DEPOSITION

- The structure of carbon in chemically vapor deposited SiC monofilaments p 113 A91-18675
Interaction of surface radiation with convection in crystal growth by physical vapor transport p 127 A91-24563
Selective and low temperature synthesis of polycrystalline diamond p 232 A91-42170
Controlled growth of 3C-SiC and 6H-SiC films on low-tit-angle vicinal (0001) 6H-SiC wafers p 232 A91-45713
Dielectric function of InGaAs in the visible p 233 A91-53236
High-voltage 6H-SiC p-n junction diodes p 142 A91-54746
Oxidation instability of SiC and Si₃N₄ following thermal excursions p 118 A91-57059
Plasma-assisted physical vapor deposition surface treatments for tribological control
[NASA-TM-103652] p 130 N91-11945
A numerical and experimental analysis of reactor performance and deposition rates for CVD on monofilaments
[NASA-TM-103631] p 130 N91-14500
Silicon carbide, a semiconductor for space power electronics
[NASA-TM-103655] p 234 N91-14850
Ellipsometric study of cubic SiC p 235 N91-18304
Computational materials science. An example: Numerical modeling of chemical vapor deposition processing of advanced fibers p 99 N91-20111
Advances in silicon carbide Chemical Vapor Deposition (CVD) for semiconductor device fabrication
[NASA-TM-104410] p 236 N91-23946

VAPOR PHASES

- Measurements and predictions of a liquid spray from an air-assist nozzle
[AIAA PAPER 91-0692] p 149 A91-22498
Measurements and predictions of a liquid spray from an air-assist nozzle
[NASA-TM-103640] p 26 N91-13455

VAPORIZING

- Jet-A fuel evaporation analysis in conical tube injectors
[AIAA PAPER 91-0345] p 149 A91-21467
Pressure-coupled vaporization and combustion responses of liquid-fuel droplets in high-pressure environments
[AIAA PAPER 91-2310] p 106 A91-44192
Fuel-rich, catalytic reaction experimental results --- fuel development for high-speed civil transport aircraft
[AIAA PAPER 91-2463] p 24 A91-44250
Fuel-rich, catalytic reaction experimental results
[NASA-TM-104423] p 33 N91-24203

VAPORS

- Analysis of the one-dimensional transient compressible vapor flow in heat pipes p 157 A91-47735
Growth kinetics of physical vapor transport processes: Crystal growth of the optoelectronic material mercurous chloride
[NASA-TM-103788] p 128 N91-19320
Autogenous pressurization of cryogenic vessels using submerged vapor injection
[NASA-TM-104516] p 127 N91-27375

VEGETATION

- Performance evaluation of land mobile satellite system under vegetative shadowing using differential multiple TCM and QPSK p 132 A91-53084

VELOCITY DISTRIBUTION

- Effects of inlet distortion on the development of secondary flows in a subsonic axial inlet compressor rotor
[NASA-TM-104356] p 31 N91-23179
Comparison of SMAC, PISO, and iterative time-advancing schemes for unsteady flows
[NASA-TM-104406] p 167 N91-24550

- Ground-based PIV and numerical flow visualization results from the surface tension driven convection experiment
[NASA-TM-105172] p 178 N91-30491
A comparison of numerical methods for the Rayleigh equation in unbounded domains
[NASA-TM-105179] p 223 N91-30865

VELOCITY MEASUREMENT

- Particle image fields and partial coherence p 171 A91-19604
Flow visualization and quantitative velocity and pressure measurements in simulated single and double brush seals p 180 A91-21071
Two-dimensional particle displacement tracking in particle imaging velocimetry p 172 A91-38498
A fiber optic sensor for noncontact measurement of shaft speed, torque and power p 173 A91-51870
Particle displacement tracking for PIV
[NASA-TM-103288] p 175 N91-10271
Software manual for operating particle displacement tracking data acquisition and reduction system
[NASA-TM-103720] p 176 N91-20453
Particle image velocimetry for the surface tension driven convection experiment using a particle displacement tracking technique
[NASA-TM-104482] p 177 N91-25382
Particle displacement tracking applied to air flows
[NASA-TM-104481] p 177 N91-25387

VENTING

- A pressure control analysis of cryogenic storage systems
[AIAA PAPER 91-2405] p 59 A91-44228
A pressure control analysis of cryogenic storage systems
[NASA-TM-104409] p 126 N91-24460

VERTICAL LANDING

- Flow studies in close-coupled ventral nozzles for STOVL aircraft
[SAE PAPER 901033] p 2 A91-21242
Static performance tests of a flight-type STOVL ejector
[AIAA PAPER 91-1902] p 24 A91-44050
Overview of high performance aircraft propulsion p 28 N91-20089
Flow visualization and hot gas ingestion characteristics of a vectored thrust STOVL concept p 28 N91-20090
Static performance tests of a flight-type STOVL ejector
[NASA-TM-104437] p 33 N91-24201

VIBRATION

- Vibrational testing of optical fiber connector joints p 172 A91-30652
Analytical and experimental study of vibrations in a gear transmission
[AIAA PAPER 91-2019] p 181 A91-41680
Development of a vibration isolation prototype system for microgravity space experiments p 47 A91-53403
Vibrational testing of optical fiber connector joints
[NASA-TM-103654] p 230 N91-14829
Development of a vibration isolation prototype system for microgravity space experiments
[NASA-TM-103664] p 130 N91-19324
Modal analysis of multistage gear systems coupled with gearbox vibrations
[NASA-TM-103797] p 187 N91-23513
Computational simulation of acoustic fatigue for hot composite structures
[NASA-TM-104379] p 203 N91-23548
Analytical and experimental study of vibrations in a gear transmission
[NASA-TM-104434] p 187 N91-25395

VIBRATION DAMPING

- The effects of interply damping layers on the dynamic response of composite structures
[AIAA PAPER 91-1124] p 197 A91-32064
Computational simulation of damping in composite structures p 198 A91-36283
Propulsion aeroelasticity, vibration control, and dynamic system modeling p 29 N91-20105
Microgravity vibration isolation: An optimal control law for the one-dimensional case p 49 N91-21206
The effects of interply damping layers on the dynamic response of composite structures
[NASA-TM-104497] p 103 N91-30282
Integrated mechanics for the passive damping of polymer-matrix composites and composite structures
[NASA-TM-104346] p 103 N91-32181

VIBRATION EFFECTS

- Flow induced vibration and noise by a pair of tandem cylinders due to buffeting p 225 A91-14650
Effects of gear box vibration and mass imbalance on the dynamics of multistage gear transmission
[NASA-TM-103695] p 185 N91-21534
Effects of gear box vibration and mass imbalance on the dynamics of multi-stage gear transmissions

VIBRATION ISOLATORS

- A new approach to controller design for microgravity isolation systems p 129 A91-23108
The dynamic effects of internal robots on Space Station Freedom
[AIAA PAPER 91-2822] p 40 A91-49764
Development of a vibration isolation prototype system for microgravity space experiments p 47 A91-53403
Development of a vibration isolation prototype system for microgravity space experiments
[NASA-TM-103664] p 130 N91-19324
The dynamic effects of internal robots on Space Station Freedom
[NASA-TM-104345] p 203 N91-22604

VIBRATION MEASUREMENT

- Use of piezoelectric actuators in active vibration control of rotating machinery p 179 A91-14400

VIBRATION MODE

- The aerodynamics of an oscillating cascade in a compressible flow field
[ASME PAPER 89-GT-271] p 1 A91-13047
Dynamic analysis of space-related linear and non-linear structures p 196 A91-28612
Simulation of the Space Station strut-out condition
[AIAA PAPER 91-1248] p 197 A91-32087
Effects of gear box vibration and mass imbalance on the dynamics of multistage gear transmission
[NASA-TM-104519] p 182 A91-47213
Optical measurement of unducted fan flutter
[NASA-TM-103285] p 27 N91-15174
Effects of gear box vibration and mass imbalance on the dynamics of multi-stage gear transmissions
[NASA-TM-103695] p 185 N91-21534
Acoustical analysis of gear housing vibration
[NASA-TM-103691] p 188 N91-25411
Aeroelastic modal characteristics of mistuned blade assemblies: Mode localization and loss of eigenstructure
[NASA-TM-104519] p 205 N91-27591

VIBRATION TESTS

- Vibrational testing of optical fiber connector joints p 172 A91-30652
Evaluation of thermomechanical damage in silicon carbide/titanium composites p 92 A91-42297
Vibrational testing of optical fiber connector joints
[NASA-TM-103654] p 230 N91-14829

VIBRATIONAL STRESS

- Experimental investigation of propfan aeroelastic response in off-axis flow with mistuning p 22 A91-30015
Computational simulation of acoustic fatigue for hot composite structures
[AIAA PAPER 91-1178] p 197 A91-32099

VIDEO COMMUNICATION

- Data compression for full motion video transmission
[NASA-TM-105239] p 135 N91-32247

VIDEO DATA

- Data compression for full motion video transmission
[AIAA PAPER 91-3533] p 45 A91-52424
LBR-2 Earth stations for the ACTS program p 133 N91-11971
High Resolution, High Frame Rate Video Technology
[NASA-CP-3080] p 175 N91-14574
Results of the users' requirements survey p 175 N91-14575

- High resolution, high frame rate video technology development plan and the near-term system conceptual design p 175 N91-14580
Ground-based PIV and numerical flow visualization results from the surface tension driven convection experiment
[NASA-TM-105172] p 178 N91-30491
Data compression for full motion video transmission
[NASA-TM-105239] p 135 N91-32247

VIDEO EQUIPMENT

- High resolution, high frame rate video technology development plan and the near-term system conceptual design p 175 N91-14580

VIDEO SIGNALS

- Real-time data compression of broadcast video signals
[NASA-CASE-LEW-14945-1] p 133 N91-13598
State of the art in video system performance p 175 N91-14578
Digital CODEC for real-time processing of broadcast quality video signals at 1.8 bits/pixel p 134 N91-24067

- Data compression for full motion video transmission
[NASA-TM-105239] p 135 N91-32247

VIKING LANDER SPACECRAFT

- Design considerations for Mars photovoltaic power systems p 41 A91-41988

VIRTUAL MEMORY SYSTEMS

- General-purpose interface bus for multiuser, multitasking computer system p 215 A91-35928

VISCOELASTICITY

Viscoelastic properties of addition-cured polyimides used in high temperature polymer matrix composites
[NASA-TM-103768] p 89 N91-22377

Viscoplastic analysis of an experimental cylindrical thrust chamber liner
[NASA-TM-103287] p 205 N91-28622

VISCOPLASTICITY

A new uniformly valid asymptotic integration algorithm for elasto-plastic creep and unified viscoplastic theories including continuum damage p 110 A91-48725

Application of finite-element-based solution technologies for viscoplastic structural analyses p 199 A91-55137

Application of thermal life prediction model to high-temperature aerospace alloys B1900+Hf and Haynes 188 p 201 N91-19473

On the thermodynamics of stress rate in the evolution of back stress in viscoplasticity p 201 N91-19476

Exponential integration algorithms applied to viscoplasticity p 223 N91-27901

Viscoplastic analysis of an experimental cylindrical thrust chamber liner p 205 N91-28622

VISCOSITY

Evaluation of advanced lubricants for aircraft applications using gear surface fatigue tests p 181 A91-41649

Flow visualization of a rocket injector spray using gelled propellant simulants p 59 A91-44151

Evaluation of advanced lubricants for aircraft applications using gear surface fatigue tests p 186 N91-22568

VISCIOUS FLOW

Three-dimensional viscous flow computations of high area ratio nozzles for hypersonic propulsion p 4 A91-30014

Role of artificial viscosity in Euler and Navier-Stokes solvers p 4 A91-34135

Numerical flux formulas for the Euler and Navier-Stokes equations. II - Progress in flux-vector splitting p 5 A91-40740

The design/analysis of flows through turbomachinery - A viscous/inviscid approach p 153 A91-41677

Unstable viscous wall modes in rotating pipe flow p 154 A91-42599

Time-derivative preconditioning for viscous flows p 154 A91-43576

3-D Navier-Stokes analysis of crossing, glancing shocks/turbulent boundary layer interactions p 6 A91-43631

An analysis of the viscous flow through a compact radial turbine by the average passage approach p 6 A91-44545

Primitive variable, strongly implicit calculation procedure for viscous flows at all speeds p 7 A91-46181

Frontogenesis driven by horizontally quadratic distributions of density p 157 A91-48276

Multigrid calculation of three-dimensional viscous cascade flows p 7 A91-53754

Time dependent viscous incompressible Navier-Stokes equations p 9 N91-10854

Analysis of three-dimensional viscous flow in a supersonic throughflow fan p 10 N91-10885

Flux splitting algorithms for two-dimensional viscous flows with finite-rate chemistry p 10 N91-10894

CFD for hypersonic propulsion p 164 N91-21447

Numerical flux formulas for the Euler and Navier-Stokes equations. 2: Progress in flux-vector splitting p 15 N91-22084

Low Reynolds number two-equation modeling of turbulent flows p 165 N91-23416

The 3-D Navier-Stokes analysis of crossing, glancing shocks/turbulent boundary layer interactions p 16 N91-24130

Average-passage flow model development p 165 N91-24338

The design/analysis of flows through turbomachinery: A viscous/inviscid approach p 33 N91-25148

High-Order Polynomial Expansions (HOPE) for flux-vector splitting p 222 N91-25739

Least-squares solution of incompressible Navier-Stokes equations with the p-version of finite elements p 223 N91-31911

VITREOUS MATERIALS

Crystallization and characterization of Y2O3-SiO2 glasses p 237 N91-31962

VOIDS

Scaling analysis applied to the NORVEX code development and thermal energy flight experiment p 155 A91-44337

A study of void effects on the interlaminar shear strength of unidirectional graphite fiber reinforced composites p 159 N91-12034

Relationship between voids and interlaminar shear strength of polymer matrix composites p 95 N91-13495

Multi-dimensional modeling of a thermal energy storage canister p 71 N91-19177

Two reference time scales for studying the dynamic cavitation of liquid films p 160 N91-19369

Scaling analysis applied to the NORVEX code development and thermal energy flight experiment p 166 N91-24549

VOLT-AMPERE CHARACTERISTICS

Low-temperature microwave characteristics of pseudomorphic $\text{In}_x\text{Ga}_{1-x}\text{As}/\text{In}(0.52)\text{Al}(0.48)\text{As}$ modulation-doped field-effect transistors p 136 A91-22987

Recent results from the InP homojunction cell module on the LIPS III spacecraft p 140 A91-41971

Preliminary results from the Advanced Photovoltaic Experiment flight test p 39 A91-41980

Lightweight concentrator module with 30 percent AM0 efficient GaAs/GaSb tandem cells p 57 A91-41990

23.5 percent thin-film space concentrator cells p 58 A91-42002

Comparative modeling of InP solar cell structures p 83 N91-30232

The Au cathode in the system $\text{Li}_2\text{CO}_3\text{-CO}_2\text{-CO}$ at 800 to 900 C p 213 N91-32551

Performance of a dual anode nickel-hydrogen cell p 214 N91-32563

VOLTAGE CONVERTERS (DC TO DC)

Light weight, high power, high voltage dc/dc converter technologies p 138 A91-37985

Test and evaluation of load converter topologies used in the Space Station Freedom Power Management and distribution DC test bed p 85 N91-30267

VOLTAGE REGULATORS

Control of multiple resonant power processors in a multi-source system p 137 A91-30901

VORTEX BREAKDOWN

Modern developments in shear flow control with swirl p 3 A91-24519

VORTEX GENERATORS

Supersonic jet mixing enhancement by vortex generators p 5 A91-41738

A design strategy for the use of vortex generators to manage inlet-engine distortion using computational fluid dynamics p 6 A91-44259

A design strategy for the use of vortex generators to manage inlet-engine distortion using computational fluid dynamics p 16 N91-24131

Effect of tabs on the evolution of an axisymmetric jet p 34 N91-27159

VORTEX SHEDDING

Comparison of SMAC, PISO, and iterative time-advancing schemes for unsteady flows p 167 N91-24550

VORTICES

The aerodynamic characteristics of vortex ingestion for the F/A-18 inlet duct p 3 A91-26192

Second order modeling of boundary-free turbulent shear flows p 154 A91-42588

The breakup of trailing-line vortices p 9 N91-10867

The aerodynamic characteristics of vortex ingestion for the F/A-18 inlet duct p 70 N91-15303

Compressible flows with periodic vortical disturbances around lifting airfoils p 14 N91-21060

A finite-difference, frequency-domain numerical scheme for the solution of the linearized unsteady Euler equations p 162 N91-21067

Second order modeling of boundary-free turbulent shear flows p 164 N91-22524

A study of three dimensional turbulent boundary layer separation and vortex flow control using the reduced Navier Stokes equations p 16 N91-23089

A study of high speed flows in an aircraft transition duct p 17 N91-26122

Effect of tabs on the evolution of an axisymmetric jet p 34 N91-27159

VORTICITY

Flow induced vibration and noise by a pair of tandem cylinders due to buffeting p 225 A91-14650

Renormalization group analysis of anisotropic diffusion in turbulent shear flows p 150 A91-27946

Increased heat transfer to a cylindrical leading edge due to spanwise variations in the freestream velocity p 155 A91-43623

Characteristics of 3D turbulent jets in crossflow p 158 A91-54268

The breakup of trailing-line vortices p 9 N91-10867

Characteristics of 3D turbulent jets in crossflow p 165 N91-22536

Increased heat transfer to a cylindrical leading edge due to spanwise variations in the freestream velocity p 100 N91-24359

W

WAFERS

Thermal and structural assessments of a ceramic wafer seal in hypersonic engine p 23 A91-41799

Controlled growth of 3C-SiC and 6H-SiC films on low-tilt-angle vicinal (0001) 6H-SiC wafers p 232 A91-45713

Thermal and structural assessments of a ceramic wafer seal in hypersonic engines p 26 N91-13456

Silicon carbide, a semiconductor for space power electronics p 234 N91-14850

High temperature performance evaluation of a hypersonic engine ceramic wafer seal p 185 N91-22567

Evaluation and ranking of candidate ceramic wafer engine seal materials p 187 N91-23515

Advances in silicon carbide Chemical Vapor Deposition (CVD) for semiconductor device fabrication p 236 N91-23946

Process for the controlled growth of single-crystal films of silicon carbide polytypes on silicon carbide wafers p 236 N91-26966

Process for the homoepitaxial growth of single-crystal silicon carbide films on silicon carbide wafers p 236 N91-26967

WAKES

Navier-Stokes analysis of transonic cascade flow p 159 N91-11192

Calculation of a circular jet in crossflow with a multiple-time-scale turbulence model p 169 N91-30476

WALL FLOW

Unstable viscous wall modes in rotating pipe flow p 154 A91-42599

Low Reynolds number two-equation modeling of turbulent flows p 165 N91-23416

Progress toward synergistic hypermixing nozzles p 18 N91-29150

A critical comparison of two-equation turbulence models p 169 N91-31597

WALLS

Surface settling in partially filled containers upon step reduction in gravity p 159 N91-14556

Axial-torsional fatigue: A study of tubular specimen thickness effects p 200 N91-14632

A k-epsilon modeling of near wall turbulence p 170 N91-32460

WANKEL ENGINES

Flux-vector splitting algorithm for chain-rule conservation-law form p 221 A91-45109

Rotary engine technology p 30 N91-20114

WASTE HEAT

High temperature electronics p 144 N91-20101

WATER

Experimental water droplet impingement data on modern aircraft surfaces p 2 A91-21493

Conceptual study of on orbit production of cryogenic propellants by water electrolysis p 124 A91-41631

Construction and testing of ceramic fabric heat pipe with water working fluid p 229 N91-18799

- Conceptual study of on orbit production of cryogenic propellants by water electrolysis
[NASA-TM-103730] p 126 N91-19317
- Characterization of flow in a scroll duct
[NASA-CR-188612] p 167 N91-25367
- WATER SPLITTING**
- Conceptual study of on orbit production of cryogenic propellants by water electrolysis
[AIAA PAPER 91-1844] p 124 A91-41631
- Conceptual study of on orbit production of cryogenic propellants by water electrolysis
[NASA-TM-103730] p 126 N91-19317
- WATER VAPOR**
- Significant reduction in arc frequency biased solar cells: Observations, diagnostics, and mitigation technique(s)
p 83 N91-30235
- WATERPROOFING**
- Diamondlike carbon as a moisture barrier and antireflecting coating on optical materials
p 119 N91-18302
- Diamondlike carbon applications in infrared optics and microelectronics
p 230 N91-18306
- WAVE DISPERSION**
- Optical dispersion relations for diamondlike carbon films
p 230 N91-18305
- WAVE EQUATIONS**
- Monograph on propagation of sound waves in curved ducts
[NASA-RP-1248] p 228 N91-15848
- Compressible flows with periodic vortical disturbances around lifting airfoils
[NASA-TM-103742] p 14 N91-21060
- Nonlinear combustion instability model in two- to three-dimensions
[NASA-TM-102381] p 85 N91-31208
- WAVE EXCITATION**
- Modern developments in shear flow control with swirl
p 3 A91-24519
- WAVE GENERATION**
- Nonlinear spatial evolution of externally excited instability waves in free shear layers
p 152 A91-38705
- WAVE INTERACTION**
- Multifrequency excited jets
p 151 A91-31482
- Critical-layer nonlinearity in the resonance growth of three-dimensional waves in boundary layers
[NASA-TM-103639] p 161 N91-19373
- WAVE PACKETS**
- Turbulence enhancement in free shear flows under multifrequency excitation
p 152 A91-38737
- WAVE PROPAGATION**
- Effect of surface deposits on electromagnetic waves propagating in uniform ducts
[NASA-TM-103282] p 133 N91-10208
- Numerical simulation of nonlinear development of instability waves
[E-4658] p 8 N91-10849
- Resonant triad in boundary-layer stability. Part 1: Fully nonlinear interaction
[NASA-TM-105208] p 169 N91-32458
- WAVEGUIDE ANTENNAS**
- New coplanar waveguide/stripline feed network for seven patch hexagonal CP subarray
p 137 A91-32823
- WAVEGUIDE FILTERS**
- Theoretical and experimental characterization of coplanar waveguide discontinuities for filter applications
p 137 A91-35911
- WAVEGUIDES**
- Coplanar-waveguide/microstrip probe coupler and applications to antennas
p 131 A91-17719
- Universal nondestructive mm-wave integrated circuit test fixture
[NASA-CASE-LEW-14746-1] p 143 N91-14552
- Solid State Technology Branch of NASA Lewis Research Center Second Annual Digest, June 1989 - June 1990
[NASA-TM-103226] p 133 N91-18297
- Coplanar waveguide EEsoF MICAD macros make circuit layout easy
[NASA-TM-103272] p 134 N91-19332
- WAVELENGTH DIVISION MULTIPLEXING**
- Digital angular position sensor using wavelength division multiplexing
p 21 A91-19580
- WEAK ENERGY INTERACTIONS**
- Constraints from primordial nucleosynthesis on the mass of the tau neutrino
p 240 A91-46543
- WEAR**
- Tribological properties of Ag/Ti films on Al₂O₃ ceramic substrates
[NASA-TM-103784] p 89 N91-19224
- Tribological characteristics of silicon carbide whisker-reinforced alumina at elevated temperatures
[NASA-TM-103799] p 89 N91-22379
- Sliding wear of self-mated Al₂O₃-SiC whisker reinforced composites at 23-1200 C
[NASA-TM-104490] p 90 N91-27221

- An analysis of the wear behavior of SiC whisker reinforced alumina from 25 to 1200 C
[NASA-TM-104489] p 90 N91-29235
- Eccentricity effects on leakage of a brush seal at low speeds
[NASA-TM-105141] p 86 N91-31220
- Spectroscopic wear detector
[NASA-CASE-LEW-15200-1] p 87 N91-32167
- Lubrication with sputtered MoS₂ films: Principles, operation, limitations
[NASA-TM-105292] p 112 N91-32216
- WEAR RESISTANCE**
- Surface modification of Monel K-500 as a means of reducing friction and wear in high-pressure oxygen
p 107 A91-16869
- Fundamental considerations in adhesion, friction and wear for ceramic-metal contacts
p 115 A91-35952
- Pretreatment of lubricated surfaces with sputtered cadmium oxide
[NASA-CASE-LEW-14474-1] p 123 N91-28423
- WEAR TESTS**
- Tribological properties of PM212 - A high temperature, self-lubricating, powder metallurgy composite
[STLE PREPRINT 90-AM-4E-1] p 87 A91-19720
- A new test machine for measuring friction and wear in controlled atmospheres to 1200 C
p 180 A91-33600
- Sliding wear of self-mated Al₂O₃-SiC whisker reinforced composites at 23-1200 C
[NASA-TM-104490] p 90 N91-27221
- WEAVING**
- Structural design methodologies for ceramic-based material systems
[NASA-TM-103097] p 121 N91-22460
- WEIBULL DENSITY FUNCTIONS**
- Thermal and structural assessments of a ceramic wafer seal in hypersonic engine
[AIAA PAPER 91-2494] p 23 A91-41799
- Calculation of Weibull strength parameters, Batdorf flaw density constants and related statistical quantities using PC-CARES
[NASA-TM-103247] p 199 N91-10332
- Thermal and structural assessments of a ceramic wafer seal in hypersonic engines
[NASA-TM-103651] p 26 N91-13456
- Mechanical behavior and failure phenomenon of an in situ-toughened silicon nitride
[NASA-TM-103741] p 121 N91-23311
- Comparison of Weibull strength parameters from flexure and spin tests of brittle materials
[NASA-TM-104414] p 187 N91-24593
- Transmission overhaul estimates for partial and full replacement at repair
[NASA-TM-104395] p 190 N91-30533
- WEIGHT REDUCTION**
- Review of the transmissions of the Soviet helicopters
[NASA-TM-103634] p 20 N91-15146
- WEIGHTLESSNESS**
- Vibration environment - Acceleration mapping strategy and microgravity requirements for Spacelab and Space Station
[IAF PAPER 90-350] p 39 A91-13991
- N-decane droplet combustion in the NASA-Lewis 5 Second Zero-Gravity Facility - Results in test gas environments other than air
[AIAA PAPER 91-0720] p 105 A91-19433
- A summary of existing and planned experiment hardware for low-gravity fluids research
[AIAA PAPER 91-0777] p 128 A91-26329
- Review and test of chilldown methods for space-based cryogenic tanks
[AIAA PAPER 91-1843] p 60 A91-45776
- Design strategies for the International Space University's variable gravity research facility
p 42 N91-22171
- Review and test of chilldown methods for space-based cryogenic tanks
[NASA-TM-104458] p 167 N91-25351
- The International Space University's variable gravity research facility design
[NASA-TM-105224] p 44 N91-31196
- WELDED JOINTS**
- Rapid thermal cycling of solar array blanket coupons for Space Station Freedom
p 84 N91-30239
- WETTABILITY**
- Wettability of pyrolytic boron nitride by aluminum
p 114 A91-28772
- WHISKER COMPOSITES**
- Dynamic fatigue property of silicon carbide whisker-reinforced silicon nitride
p 94 A91-56937
- Comparison of dynamic fatigue behavior between SiC whisker-reinforced composite and monolithic silicon nitrides
[NASA-TM-103707] p 119 N91-19293
- Tribological characteristics of silicon carbide whisker-reinforced alumina at elevated temperatures
[NASA-TM-103799] p 89 N91-22379

- Structural design methodologies for ceramic-based material systems
[NASA-TM-103097] p 121 N91-22460
- Sliding wear of self-mated Al₂O₃-SiC whisker reinforced composites at 23-1200 C
[NASA-TM-104490] p 90 N91-27221
- An analysis of the wear behavior of SiC whisker reinforced alumina from 25 to 1200 C
[NASA-TM-104489] p 90 N91-29235
- WHISKERS (CRYSTALS)**
- A simple test for thermomechanical evaluation of ceramic fibers
[NASA-TM-103767] p 121 N91-21309
- WIND EFFECTS**
- Effects of windblown dust on photovoltaic surface s on Mars
[NASA-TM-104448] p 78 N91-25183
- WIND PRESSURE**
- Simulation of probabilistic wind loads and building analysis
[NASA-TM-103744] p 203 N91-23549
- WIND SHEAR**
- Wind turbine acoustics
[NASA-TP-3057] p 228 N91-16679
- WIND TUNNEL APPARATUS**
- Probe insertion apparatus with inflatable seal
[NASA-CASE-LEW-14965-1] p 183 N91-13732
- WIND TUNNEL MODELS**
- Evaluation of a technique to generate artificially thickened boundary layers in supersonic and hypersonic flows
[NASA-TP-3142] p 17 N91-28136
- WIND TUNNEL TESTS**
- Experimental investigation of a single flush-mounted hypermixing nozzle
[AIAA PAPER 90-5240] p 21 A91-14466
- Icing tests of a model main rotor
p 18 A91-17218
- Transonic wind-tunnel wall interference prediction code
p 38 A91-26112
- Icing characteristics of a natural-laminar-flow, a medium-speed, and a swept, medium-speed airfoil
[AIAA PAPER 91-0447] p 3 A91-26327
- Modeling of surface roughness effects on glaze ice accretion
p 19 A91-35107
- The effect of varying Mach number on crossing, glancing shocks/turbulent boundary-layer interactions
[AIAA PAPER 91-2157] p 6 A91-45792
- Noise measurements from an ejector suppressor nozzle in the NASA Lewis 9- by 15-foot low speed wind tunnel
[NASA-TM-103628] p 227 N91-11493
- The effect of swirl recovery vanes on the cruise noise of an advanced propeller
[NASA-TM-103625] p 227 N91-11494
- Wind tunnel wall effects in a linear oscillating cascade
[NASA-TM-103690] p 27 N91-19098
- Experimental investigation of a single flush-mounted hypermixing nozzle
[NASA-TM-103726] p 161 N91-19374
- A laser velocimeter investigation of the normal shock-wave boundary layer interaction
[NASA-TM-105201] p 169 N91-32440
- WIND TUNNEL WALLS**
- Wind tunnel wall effects in a linear oscillating cascade
[NASA-TM-103690] p 27 N91-19098
- WIND TUNNELS**
- Recent advances in Lewis aeropropulsion facilities
p 38 N91-20121
- WIND TURBINES**
- Model-OA wind turbine generator - Failure modes and effects analysis
p 191 A91-31064
- Wind turbine acoustics
[NASA-TP-3057] p 228 N91-16679
- WIND VELOCITY**
- Aeolian removal of dust types from photovoltaic surfaces on Mars
p 47 N91-19156
- Effects of windblown dust on photovoltaic surface s on Mars
[NASA-TM-104448] p 78 N91-25183
- WIND OSCILLATIONS**
- Euler flow predictions for an oscillating cascade using a high resolution wave-split scheme
[NASA-TM-104377] p 16 N91-24107
- WING TANKS**
- In-flight and simulated aircraft fuel temperature measurements
[NASA-TM-103611] p 125 N91-15418
- WINGS**
- Simulation of iced wing aerodynamics
[NASA-TM-104362] p 15 N91-23086
- WIRE**
- Low cost, formable, high T(sub c) superconducting wire
[NASA-CASE-LEW-14676-1] p 147 N91-31529

SUBJECT INDEX

WOOD

Structural properties of laminated Douglas fir/epoxy composite material p 94 N91-10127
[NASA-RP-1236]

WORKING FLUIDS

Two-dimensional model of a Space Station Freedom thermal energy storage canister p 151 A91-38048
Construction and testing of ceramic fabric heat pipe with water working fluid p 229 N91-18799
[NASA-TM-103332]
Cooling of in-situ propellant rocket engines for Mars mission p 72 N91-21233
[NASA-TM-103729]
Design considerations for space radiators based on the liquid sheet (LSR) concept p 80 N91-27213
[NASA-TM-105158]

X

X RAY ABSORPTION

Near-edge study of gold-substituted YBa₂Cu₃O(7-delta) p 237 N91-31977
[NASA-TM-105220]

X RAY ANALYSIS

Thermal stability of the microstructure of an aged Nb-Zr-C alloy p 110 N91-14454
[NASA-TM-103647]

X RAY SPECTROSCOPY

X-ray photoelectron and mass spectroscopic study of electron irradiation and thermal stability of polytetrafluoroethylene p 113 A91-16138
Uses of Auger and x ray photoelectron spectroscopy in the study of adhesion and friction p 118 N91-11922
[NASA-TM-103266]
An x ray photoelectron spectroscopy study of Au(x)In(y) alloys p 234 N91-14050
[NASA-TM-103659]

X RAYS

Nondestructive evaluation tools and experimental studies for monitoring the health of space propulsion systems p 192 A91-53703
[AIAA PAPER 91-3433]
In situ X-ray monitoring of damage accumulation in SiC/RBSN tensile specimens p 94 A91-56942
In-situ x-ray monitoring of damage accumulation in SiC/RBSN tensile specimens p 99 N91-22402
[NASA-TM-103733]
Nondestructive evaluation tools and experimental studies for monitoring the health of space propulsion systems p 194 N91-28605
[NASA-TM-105164]
Near-edge study of gold-substituted YBa₂Cu₃O(7-delta) p 237 N91-31977
[NASA-TM-105220]

X WING ROTORS

Results of a sub-scale model rotor icing test p 19 A91-26190
[AIAA PAPER 91-0660]
Results of a sub-scale model rotor icing test p 11 N91-14309
[NASA-TM-103709]

X-30 VEHICLE

Overview of hypersonic/transatmospheric vehicle propulsion technology p 28 N91-20092

XENON

Microanalyses of extended-test xenon hollow cathodes --- in ion thruster simulators p 61 A91-45787
[AIAA PAPER 91-2123]
Xenon ion propulsion for orbit transfer p 69 N91-11798
[NASA-TM-103193]
A 5-kW xenon ion thruster lifetest p 72 N91-19180
[NASA-TM-103191]
Microanalysis of extended-test xenon hollow cathodes p 82 N91-30202
[NASA-TM-104532]

Y

YAG LASERS

Optical inspection of space-propulsion components using an injection seeded Nd:YAG laser system p 179 N91-24320

YTTERBIUM COMPOUNDS

Photoresponse of YBa₂Cu₃O(7-delta) granular and epitaxial superconducting thin films p 141 A91-50443
Ellipsometric study of YBa₂Cu₃O(7-x) laser ablated and co-evaporated films p 233 A91-53235

YTTRIUM OXIDES

Electrical transport measurements on polycrystalline superconducting Y-Ba-Cu-O films p 231 A91-19820
Temperature dependence of hardness in yttria-stabilized zirconia single crystals p 114 A91-28763
Temperature dependence of the anisotropy in magnetic relaxation in YBa₂Cu₃O(7-x) thin films p 232 A91-36047
Crystallization and characterization of Y₂O₃-SiO₂ glasses p 237 N91-31962

Near-edge study of gold-substituted YBa₂Cu₃O(7-delta) p 237 N91-31977
[NASA-TM-105220]

Z

ZINC ALLOYS

Grain boundary sliding behaviour of copper and alpha brass at intermediate temperatures p 108 A91-27158
Creep behaviour of Cu-30 percent Zn at intermediate temperatures p 109 A91-47747

ZIRCONIUM

Thermal stability of the microstructure of an aged Nb-Zr-C alloy p 110 N91-14454
[NASA-TM-103647]

ZIRCONIUM OXIDES

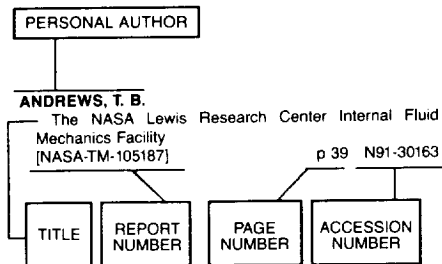
Temperature dependence of hardness in yttria-stabilized zirconia single crystals p 114 A91-28763
Temperature-dependent indentation behavior of transformation-toughened zirconia-based ceramics p 114 A91-28767
Metallic seal for thermal barrier coating systems p 119 N91-15412
[NASA-CASE-LEW-15020-1]
Ceramic coatings on smooth surfaces p 123 N91-32229
[NASA-CASE-LEW-15164-2]

ZONE MELTING

Method of making single crystal fibers p 95 N91-13502
[NASA-CASE-LEW-14921-1]

PERSONAL AUTHOR INDEX

Typical Personal Author Index Listing



Listings in this index are arranged alphabetically by personal author. The accession number denotes the number by which the citation is identified.

A

- ABBOTT, JOHN M.**
Control of flow separation and mixing by aerodynamic excitation p 2 A91-24360
Inlets, ducts, and nozzles p 162 A91-20096
- ABDELWAHAB, MAHMOOD**
Turbofan engine demonstration of sensor failure detection p 22 A91-29775
- ABDUL-AZIS, ALI**
Elastic response of (001)-oriented PWA 1480 single crystal - The influence of secondary orientation [SAE PAPER 911111] p 110 A91-53555
- ABDUL-AZIZ, ALI**
Elastic response of zone axis (001)-oriented PWA 1480 single crystal: The influence of secondary orientation [NASA-TM-103782] p 202 A91-21558
- ACOSTA, WALDO**
Jet-A reaction mechanism study for combustion application [AIAA PAPER 91-2355] p 106 A91-45810
Jet-A reaction mechanism study for combustion application [NASA-TM-104441] p 35 A91-31181
- ADAMCZYK, JOHN J.**
Simulation of turbomachinery flows p 9 A91-10880
Turbomachinery p 162 A91-20097
Simulation of turbomachinery flows p 163 A91-21069
Average-passage flow model development p 165 A91-24338
- ADAMOVSKY, G.**
Compensation for effects of ambient temperature on rare-earth doped fiber optic thermometer p 170 A91-19582
- ADAMOVSKY, GRIGORY**
Optical techniques for determination of normal shock position in supersonic flows for aerospace applications p 174 A91-55530
Photoelastic transducer for high-temperature applications p 174 A91-55533
Fiber optic sensing system [NASA-CASE-LEW-14795-1] p 230 A91-21871

- AGGARWAL, S. K.**
A detailed numerical investigation of Burke-Schumann gaseous and spray flames [AIAA PAPER 91-2311] p 105 A91-41749
- AGGARWAL, SURESH K.**
Measurements and predictions of a liquid spray from an air-assist nozzle [AIAA PAPER 91-0692] p 149 A91-22498
Measurements and predictions of a liquid spray from an air-assist nozzle [NASA-TM-103640] p 26 A91-13455
- AHN, KYUNG H.**
A 2-D oscillating flow analysis in Stirling engine heat exchangers [NASA-TM-103781] p 161 A91-19375
- AIELLO, R. A.**
Low velocity impact analysis with NASTRAN p 198 A91-48865
- AIELLO, ROBERT A.**
Low velocity impact analysis with NASTRAN [NASA-TM-103169] p 95 A91-14426
- AIFER, E.**
Significant reduction in arc frequency biased solar cells: Observations, diagnostics, and mitigation technique(s) p 83 A91-30235
- AJMANI, KUMUD**
Generalized conjugate-gradient methods for the Navier-Stokes equations [AIAA PAPER 91-1556] p 5 A91-40730
- ALEXANDER, S. W.**
Performance impact on nuclear thermal propulsion of piloted Mars missions with short transit times [AIAA PAPER 91-3401] p 64 A91-52326
Solar electric propulsion for Mars transport vehicles [NASA-TM-103234] p 71 A91-19178
- ALLAIRE, PAUL E.**
Microgravity vibration isolation: An optimal control law for the one-dimensional case p 49 A91-21206
- ALLEN, CHRISTOPHER J.**
The series Bi₂SrCa(n-1)Cu(n)O(2n+4) (1 less than or equal to n less than or equal to 5): Phase stability and superconducting properties [NASA-TM-103749] p 235 A91-21910
- ALSTON, WILLIAM B.**
Substituted 1,1,1-triaryl-2,2,2-trifluoroethanes and processes for their synthesis [NASA-CASE-LEW-14345-3] p 89 A91-17141
Substituted 1,1,1-triaryl-2,2,2-trifluoroethanes and processes for their synthesis [NASA-CASE-LEW-14345-4] p 90 A91-25185
- ALTENKIRCH, R. A.**
Heat transfer to a thin solid combustible in flame spreading at microgravity p 106 A91-51449
- ALTEROVITZ, S. A.**
Electrical transport measurements on polycrystalline superconducting Y-Ba-Cu-O films p 231 A91-19820
Low-temperature microwave characteristics of pseudomorphic In(x)Ga(1-x) As/In(0.52)Al(0.48)As modulation-doped field-effect transistors p 136 A91-22987
Electromigration failure in YBa₂Cu₃O(7-x) thin films p 231 A91-26989
High temperature superconductive microwave technology for space applications p 137 A91-31391
Temperature dependence of the anisotropy in magnetic relaxation in YBa₂Cu₃O(7-x) thin films p 232 A91-36047
Ellipsometric study of YBa₂Cu₃O(7-x) laser ablated and co-evaporated films p 233 A91-53235
Dielectric function of InGaAs in the visible p 233 A91-53236
Ellipsometric study of InGaAs MODFET material [NASA-TM-103286] p 143 A91-19351
Study of InGaAs based MODFET structures using variable angle spectroscopic ellipsometry [NASA-TM-103792] p 235 A91-19935
- ALTEROVITZ, SAMUEL A.**
New materials and techniques for improved mm wave devices [AIAA PAPER 91-3590] p 142 A91-52459

- Diamondlike carbon as a moisture barrier and antireflecting coating on optical materials p 119 A91-18302
Thin film characterization using spectroscopic ellipsometry p 119 A91-18303
Ellipsometric study of cubic SiC p 235 A91-18304
Optical dispersion relations for diamondlike carbon films p 230 A91-18305
Diamondlike carbon applications in infrared optics and microelectronics p 230 A91-18306
- ALTSTETTER, C. J.**
Inhomogeneous deformation in INCONEL 718 during monotonic and cyclic loadings p 108 A91-22287
- AMUEDO, K. C.**
STOVL Hot Gas Ingestion control technology [ASME PAPER 89-GT-323] p 22 A91-23642
- AMUEDO, KURT C.**
Hot gas ingestion test results of a two-poster vectored thrust concept with flow visualization in the NASA Lewis 9- by 15-foot low speed wind tunnel [AIAA PAPER 90-2268] p 4 A91-40561
Hot gas ingestion test results of a two-poster vectored thrust concept with flow visualization in the NASA Lewis 9- x 15-foot low speed wind tunnel [NASA-TM-103258] p 15 A91-21116
- ANDERSON, ALFRED B.**
Sulfur at nickel-alumina interfaces - Molecular orbital theory p 104 A91-12925
- ANDERSON, BERNHARD H.**
The aerodynamic characteristics of vortex ingestion for the F/A-18 inlet duct [AIAA PAPER 91-0130] p 3 A91-26192
A design strategy for the use of vortex generators to manage inlet-engine distortion using computational fluid dynamics [AIAA PAPER 91-2474] p 6 A91-44259
The aerodynamic characteristics of vortex ingestion for the F/A-18 inlet duct [NASA-TM-103703] p 70 A91-15303
High alpha inlets p 28 A91-20091
A study of three dimensional turbulent boundary layer separation and vortex flow control using the reduced Navier Stokes equations [NASA-TM-104407] p 16 A91-23089
A design strategy for the use of vortex generators to manage inlet-engine distortion using computational fluid dynamics [NASA-TM-104436] p 16 A91-24131
- ANDERSON, E. E.**
Heat transfer in space systems: Proceedings of the Symposium, AIAA/ASME Thermophysics and Heat Transfer Conference, Seattle, WA, June 18-20, 1990 p 152 A91-38780
- ANDRAS, MARIA T.**
Reactivity of pi-complexes of Ti, V, and Nb towards dithioacetic acid: Synthesis and structure of novel metal sulfur-containing complexes [NASA-TM-103666] p 106 A91-19256
Synthesis and structures of metal chalcogenide precursors [NASA-TM-103665] p 120 A91-19296
- ANDREWS, T. B.**
The NASA Lewis Research Center Internal Fluid Mechanics Facility [NASA-TM-105187] p 39 A91-30163
- ANDRO, M.**
ATDRS payload technology R & D p 45 A91-53188
- ANEX, R. P.**
Development of an intelligent diagnostic system for reusable rocket engine control [AIAA PAPER 91-2533] p 63 A91-45817
- ANIS, C.**
Probabilistic structural analysis methods for space transportation propulsion systems p 205 A91-28238
- ANSARI, R. R.**
A preview of a microgravity laser light scattering instrument [AIAA PAPER 91-0779] p 179 A91-21614
- ANTONIAK, ZENEN I.**
Construction and testing of ceramic fabric heat pipe with water working fluid [NASA-TM-103332] p 229 A91-18799

- ANZIC, G.**
ATDRS payload technology R & D p 45 A91-53188
- APPELBAUM, JOSEPH**
Solar radiation on Mars p 242 A91-28153
Design considerations for Mars photovoltaic power systems p 41 A91-41988
Solar radiation on Mars: Update 1990
[NASA-TM-103623] p 242 N91-15117
Feasibility of solar power for Mars p 209 N91-19201
Solar radiation on Mars: Update 1991
[NASA-TM-105216] p 242 N91-33046
- ARIF, HUGH**
Preliminary thermal design of the COLD-SAT spacecraft
[AIAA PAPER 91-1305] p 46 A91-45550
Preliminary thermal design of the COLD-SAT spacecraft
[NASA-TM-104440] p 49 N91-25161
- ARMSTRONG, ELIZABETH S.**
Cooling of in-situ propellant rocket engines for Mars mission
[NASA-TM-103729] p 72 N91-21233
- ARNOLD, JACK H.**
Dual-purpose self-deliverable lunar surface PV electrical power system p 209 N91-19200
- ARNOLD, STEVEN M.**
Elastic/plastic analyses of advanced composites investigating the use of the compliant layer concept in reducing residual stresses resulting from processing
[NASA-TM-103204] p 94 N91-11074
Progress in modeling deformation and damage p 202 N91-20108
Viscoplastic analysis of an experimental cylindrical thrust chamber liner
[NASA-TM-103287] p 205 N91-28622
- ARNOLD, W. A.**
Three-dimensional flow transport modes in directional solidification during space processing p 128 A91-42642
- ARNONE, A.**
Multigrid calculation of three-dimensional viscous cascade flows
[AIAA PAPER 91-3238] p 7 A91-53754
Navier-Stokes analysis of transonic cascade flow
[NASA-TM-103624] p 159 N91-11192
- ARNONE, ANDREA**
Transonic cascade flow calculations using non-periodic C-type grids p 163 N91-21071
- ARON, P. R.**
Aerospace applications of high temperature superconductivity
[IAF PAPER 90-054] p 231 A91-13767
- ARPASI, DALE J.**
Enhancing aeropropulsion research with high-speed interactive computing p 217 A91-56129
Turbomachinery p 162 N91-20097
Enhancing aeropropulsion research with high-speed interactive computing
[NASA-TM-104374] p 218 N91-24796
- ARYA, V. K.**
Finite element elastic-plastic-creep and cyclic life analysis of a cow lip p 199 A91-56365
- ARYA, VINOD K.**
Application of finite-element-based solution technologies for viscoplastic structural analyses p 199 A91-55137
Elastic/plastic analyses of advanced composites investigating the use of the compliant layer concept in reducing residual stresses resulting from processing
[NASA-TM-103204] p 94 N91-11074
Application of thermal life prediction model to high-temperature aerospace alloys B1900 + Hf and Haynes 188
[NASA-TM-4226] p 201 N91-19473
Viscoplastic analysis of an experimental cylindrical thrust chamber liner
[NASA-TM-103287] p 205 N91-28622
- ARZT, EDUARD**
1300 K compressive properties of a reaction milled NiAl-AIN composites p 107 A91-18674
- ASHPIS, DAVID E.**
On the continuous spectra of the compressible boundary layer stability equations p 150 A91-31342
- ATASSI, HAFIZ M.**
Acoustic radiation from lifting airfoils in compressible subsonic flow
[AIAA PAPER 90-3911] p 224 A91-12427
Acoustic radiation from lifting airfoils in compressible subsonic flow
[NASA-TM-103650] p 13 N91-19053
A finite-difference, frequency-domain numerical scheme for the solution of the linearized unsteady Euler equations p 162 N91-21067

- AUER, BRUCE M.**
Atomic oxygen undercutting of defects on SiO₂ protected polyimide solar array blankets p 116 A91-49803
Atomic oxygen interaction with solar array blankets at protective coating defect sites p 211 N91-20732
- AUGUST, RICHARD**
Incorporating finite element analysis into component life and reliability
[NASA-TM-104400] p 203 N91-23550
- AUKERMAN, CARL A.**
Plug nozzles - The ultimate customer driven propulsion system
[AIAA PAPER 91-2208] p 61 A91-45794
Plans for the development of cryogenic engines for space exploration
[AIAA PAPER 91-3438] p 64 A91-52351
- AVERY, J. E.**
Lightweight concentrator module with 30 percent AMO efficient GaAs/GaSb tandem cells p 57 A91-41990
Tandem concentrator solar cells with 30 percent (AMO) power conversion efficiency p 208 N91-19189
- AYDELOTT, J. C.**
Transient cryogenic liquid discharge in normal and micro-gravity
[AIAA PAPER 91-0486] p 124 A91-19324
Discharge rate of cryogenics in microgravity - What ground based experimentation cannot resolve
[AIAA PAPER 91-3545] p 129 A91-52430

B

- BAAKLINI, GEORGE**
Overall goals p 80 N91-28246
- BAAKLINI, GEORGE Y.**
In situ X-ray monitoring of damage accumulation in SiC/RBSN tensile specimens p 94 A91-56942
In-situ x-ray monitoring of damage accumulation in SiC/RBSN tensile specimens
[NASA-TM-103733] p 99 N91-22402
- BAEZ, ANASTACIO N.**
Description of the control system design for the SSF PMAD DC testbed
[NASA-TM-105202] p 84 N91-30266
- BAHADORI, M. YOUSEF**
Radiation from gas-jet diffusion flames in microgravity environments
[AIAA PAPER 91-0719] p 104 A91-19432
- BAILEY, ALLAN B.**
Experimental evaluation of resistojet thruster plume shields p 51 A91-30010
- BAILEY, R. T.**
Algebraic grid generation for complex geometries p 157 A91-48758
- BAILEY, S. G.**
Peel film GaAs solar cell development p 139 A91-41889
- BAILEY, SHEILA**
Study of surface passivation as a function of InP closed-amoule solar cell fabrication processing variables p 232 A91-41893
Measurement of surface recombination velocity on heavily doped indium phosphide p 232 A91-41931
- BAILEY, SHEILA G.**
Photovoltaic superiority for Space Station Freedom power in the 21st century p 58 A91-42004
Design strategies for the International Space University's variable gravity research facility p 42 N91-22171
Grooved surfaces on InP p 213 N91-30208
The International Space University's variable gravity research facility design
[NASA-TM-105224] p 44 N91-31196
Advanced power systems for EOS
[NASA-TM-105222] p 85 N91-31217
- BAKER, KARL W.**
Solar thermal energy receiver
[NASA-CASE-LEW-14949-1] p 211 N91-23617
- BAKHLE, MILIND A.**
Cascade flutter analysis with transient response aerodynamics
[AIAA PAPER 91-0747] p 21 A91-19448
Flutter analysis of cascades using a two dimensional Euler solver
[AIAA PAPER 91-1681] p 6 A91-45548
Cascade flutter analysis with transient response aerodynamics
[NASA-TM-103746] p 201 N91-19475
- BALASUBRAMANIAM, R.**
The migration of a compound drop due to thermocapillarity p 148 A91-18428
A comparative flow visualization study of thermocapillary flow in drops in liquid-liquid systems
[AIAA PAPER 91-0311] p 148 A91-21452
- Thermocapillary migration of liquid droplets in a temperature gradient in a density matched system p 153 A91-41132
- BALDWIN, R.**
Some recent studies with the solid-ionomer electrochemical capacitor p 214 N91-32562
- BALOMBIN, JOSEPH R.**
Advanced Communications Technology Satellite (ACTS)
[IAF PAPER 90-481] p 44 A91-14055
- BAMBERGER, ERIC N.**
Surface fatigue life of M50NiL and AISI 9310 gears and rolling-contact bars p 182 A91-45350
Surface fatigue life of M50NiL and AISI 9310 spur gears and R C bars
[NASA-TM-104496] p 189 N91-27569
- BANERJEE, AMITAVA**
Adhesion at metal interfaces p 88 A91-38581
- BANKS, B.**
Vacuum ultraviolet radiation and thermal cycling effects on atomic oxygen protective photovoltaic array blanket materials p 116 A91-49812
- BANKS, B. A.**
Dual ion beam processed diamondlike films for industrial applications p 121 N91-23042
- BANKS, BRUCE A.**
Materials degradation in low earth orbit (LEO). Proceedings of the Symposium, 119th Annual Meeting of the Minerals, Metals, and Materials Society, Anaheim, CA, Feb. 17-22, 1990 p 116 A91-49801
Atomic oxygen undercutting of defects on SiO₂ protected polyimide solar array blankets p 116 A91-49803
High emittance surfaces for high temperature space radiator applications p 88 A91-56415
Heat transfer device and method of making the same
[NASA-CASE-LEW-14162-1] p 159 N91-13668
Atomic oxygen interaction with solar array blankets at protective coating defect sites p 211 N91-20732
Flexible fluoropolymer filled protective coatings p 121 N91-24062
Atomic oxygen interactions with FEP Teflon and silicones on LDEF p 122 N91-25029
Heat transfer device
[NASA-CASE-LEW-14162-2] p 101 N91-25201
Arc-textured high emittance radiator surfaces
[NASA-CASE-LEW-14679-1] p 122 N91-25296
Low Earth orbital atomic oxygen micrometeoroid, and debris interactions with photovoltaic arrays p 84 N91-30248
- BANSAL, NAROTTAM P.**
Influence of several metal ions on the gelation activation energy of silicon tetraethoxide p 113 A91-19599
Preparation of 110K (Bi, Pb)-Sr-Ca-Cu-O superconductor from glass precursor p 232 A91-35449
Crystallization and properties of Sr-Ba aluminosilicate glass-ceramic matrices p 117 A91-56917
Crystallization and properties of Sr-Ba aluminosilicate glass-ceramic matrices
[NASA-TM-103764] p 120 N91-19308
The series Bi₂Sr₂Ca(n-1)Cu(n)O(2n+4) (1 less than or equal to n less than or equal to 5): Phase stability and superconducting properties
[NASA-TM-103749] p 235 N91-21910
- BAO, H.**
Study on the spectral efficiency of SFH-GMSK in land mobile telephone communication by direct simulation p 132 A91-53176
- BARANKIEWICZ, WENDY S.**
Static performance tests of a flight-type STOVL ejector
[AIAA PAPER 91-1902] p 24 A91-44050
Static performance tests of a flight-type STOVL ejector
[NASA-TM-104437] p 33 N91-24201
- BARAONA, COSMO R.**
Photovoltaic power for Space Station Freedom p 57 A91-41878
- BARNES, SCOTT P.**
Real-time data compression of broadcast video signals
[NASA-CASE-LEW-14945-1] p 133 N91-13598
- BARNETT, MARK**
Average-passage flow model development p 165 N91-24338
- BARRANGER, JOHN P.**
Two-dimensional surface strain measurement based on a variation of Yamaguchi's laser-speckle strain gauge p 174 A91-55531
Two-dimensional high temperature strain measurement system p 204 N91-24319
- BARRETT, CHARLES A.**
High temperature cyclic oxidation data. Part 1. Turbine alloys
[NASA-TM-83665] p 110 N91-10149

- High-temperature cyclic oxidation data. Part 2: Turbine alloys
[NASA-TM-101468] p 110 N91-10150
- BARTOLOTTA, PAUL A.**
Stirling engine: Available tools for long-life assessment
[NASA-TM-103660] p 200 N91-12980
Fatigue life prediction of an intermetallic matrix composite at elevated temperatures
[NASA-TM-104494] p 205 N91-25442
Fatigue behavior and life prediction of a SiC/Ti-24Al-11Nb composite under isothermal conditions
[NASA-TM-105168] p 206 N91-30566
- BARTON, J. MICHAEL**
Nonlinear Reynolds stress model for turbulent shear flows
[AIAA PAPER 91-0609] p 149 A91-21556
Renormalization group analysis of anisotropic diffusion in turbulent shear flows p 150 A91-27946
- BARTOS, KAREN F.**
A three-dimensional finite-element thermal/mechanical analytical technique for high-performance traveling wave tubes
[NASA-TP-3081] p 134 N91-27436
- BATES, JAMES M.**
Construction and testing of ceramic fabric heat pipe with water working fluid
[NASA-TM-103332] p 229 N91-18799
- BATTERSON, J. G.**
Effects of horizontal tail ice on longitudinal aerodynamic derivatives p 36 A91-38547
- BATTERTON, PETER G.**
Overview of high performance aircraft propulsion p 28 N91-20089
- BAUGH, W.**
Selective and low temperature synthesis of polycrystalline diamond p 232 A91-42170
- BAUGHER, CHARLES R.**
Vibration environment - Acceleration mapping strategy and microgravity requirements for Spacelab and Space Station
[IAF PAPER 90-350] p 39 A91-13991
- BAUMANN, E. D.**
Electrical characterization of a Mapham inverter using pulse testing techniques p 139 A91-37992
Electrical characterization of glass, teflon, and tantalum capacitors at high temperatures
[NASA-TM-104517] p 146 N91-27444
- BAUMANN, ERIC**
Light weight, high power, high voltage dc/dc converter technologies p 138 A91-37985
- BAUMANN, ERIC D.**
High temperature power electronics for space
[NASA-TM-104375] p 145 N91-22508
- BAUMBICK, ROBERT J.**
Fiber optic photoelastic pressure sensor for high temperature gases p 170 A91-19577
- BAUMEISTER, JOSEPH F.**
Relationship of optical coating on thermal radiation characteristics of nonisothermal cylindrical enclosures
[NASA-TM-104408] p 168 N91-30461
- BAUMEISTER, KENNETH J.**
Effect of surface deposits on electromagnetic waves propagating in uniform ducts
[NASA-TM-103282] p 133 N91-10208
Tuned optimization of extended reacting acoustic liners
[NASA-TM-104431] p 228 N91-25817
- BAYLISS, ALVIN**
Mappings and accuracy for Chebyshev pseudo-spectral approximations
[NASA-TM-103630] p 221 N91-14781
- BEACH, TIM A.**
Average-passage flow model development p 165 N91-24338
- BEACH, TIMOTHY A.**
An analysis of the viscous flow through a compact radial turbine by the average passage approach
[ASME PAPER 90-GT-64] p 6 A91-44545
- BEGG, E. K.**
Characterization of flow in a scroll duct
[NASA-CR-188612] p 167 N91-25367
- BEGG, LESTER L.**
Two-dimensional simulation of a two-phase, regenerative pumped radiator loop utilizing direct contact heat transfer with phase change p 151 A91-38126
- BEHEIM, GLENN**
Digital angular position sensor using wavelength division multiplexing p 21 A91-19580
Silicon-etalon fiber-optic temperature sensor p 170 A91-19581
Fiber optic phase stepping system for interferometry p 171 A91-28968
- BENCIC, TIMOTHY J.**
Hot gas ingestion test results of a two-poster vectored thrust concept with flow visualization in the NASA Lewis 9- by 15-foot low speed wind tunnel
[AIAA PAPER 90-2268] p 4 A91-40561
Flow visualization and hot gas ingestion characteristics of a vectored thrust STOVL concept p 28 N91-20090
Hot gas ingestion test results of a two-poster vectored thrust concept with flow visualization in the NASA Lewis 9- by 15-foot low speed wind tunnel
[NASA-TM-103258] p 15 N91-21116
- BENDETT, M. P.**
Performance of a 300 Mbps 1:16 serial/parallel optoelectronic receiver module p 141 A91-51146
- BENNETT, J. C.**
Characterization of flow in a scroll duct
[NASA-CR-188612] p 167 N91-25367
- BENSON, T. J.**
Calculation of a circular jet in crossflow with a multiple-time-scale turbulence model
[NASA-TM-104343] p 169 N91-30476
- BENSON, THOMAS J.**
Computational fluid dynamics studies of nuclear rocket performance
[AIAA PAPER 91-3577] p 66 A91-52450
Comparison of SMAC, PISO, and iterative time-advancing schemes for unsteady flows
[NASA-TM-104406] p 167 N91-24550
- BENSON, TOM**
CFD analysis for high speed inlets p 10 N91-10888
- BENTS, D. J.**
Design of multihundredwatt DIPS for robotic space missions
[NASA-TM-104401] p 75 N91-24232
- BENTS, DAVID J.**
Trade studies for nuclear space power systems
[AIAA PAPER 91-3518] p 65 A91-52413
SEI rover solar-electrochemical power system options
[NASA-TM-104402] p 211 N91-23620
Small Stirling dynamic isotope power system for multihundred-watt robotic missions
[NASA-TM-104460] p 78 N91-25182
SEI power source alternatives for rovers and other multi-kWe distributed surface applications
[NASA-TM-104360] p 81 N91-28277
Comparison of dynamic isotope power systems for distributed planet surface applications
[NASA-TM-4303] p 81 N91-28278
- BERKE, L.**
Integrated force method versus displacement method for finite element analysis p 196 A91-28372
Compatibility conditions of structural mechanics for finite element analysis p 198 A91-37853
Application of artificial neural networks to composite ply micromechanics
[NASA-TM-104365] p 100 N91-24345
Concurrent engineering p 80 N91-28247
- BERKE, LASZLO**
Applications of artificial neural nets in structural mechanics
[NASA-TM-102420] p 202 N91-21559
- BERKOWITZ, BRIAN**
Prediction of ice shapes and their effect on airfoil performance
[AIAA PAPER 91-0264] p 3 A91-26330
Modeling of surface roughness effects on glaze ice accretion p 19 A91-35107
Prediction of ice shapes and their effect on airfoil performance
[NASA-TM-103701] p 12 N91-19047
- BERKOWITZ, BRIAN M.**
Progress toward the development of an airfoil icing analysis capability p 9 N91-10866
- BERLAD, A. L.**
Particle nonuniformity effects on particle cloud flames in low gravity
[AIAA PAPER 91-0718] p 104 A91-19431
Particle cloud flames in acoustic fields p 105 A91-20589
Radiative structures of lycopodium-air flames in low gravity p 105 A91-30003
- BERSHADY, MATTHEW A.**
Telescope search for a 3-eV to 8-eV axion p 239 A91-28714
- BERTON, JEFFREY J.**
Comparison of turbine bypass and mixed flow turbofan engines for a high-speed civil transport
[AIAA PAPER 91-3132] p 25 A91-54051
Divergence thrust loss calculations for convergent-divergent nozzles: Extensions to the classical case
[NASA-TM-105176] p 34 N91-29181
- BEWLEY, DOUGLAS P.**
Fiber-optic applications for space-based rocket engines
[AIAA PAPER 91-3602] p 49 A91-52468
- Fiber-optic applications for space-based engines
[NASA-TM-105235] p 86 N91-32163
- BHASIN, K. B.**
High temperature superconductive microwave technology for space applications p 137 A91-31391
Determination of surface resistance and magnetic penetration depth of superconducting YBa₂Cu₃O₇(δ) thin films by microwave power transmission measurements p 138 A91-36060
An experimental study of high T_c superconducting microstrip transmission lines at 35 GHz and the effect of film morphology p 138 A91-36172
High temperature superconducting thin film microwave circuits - Fabrication, characterization, and applications p 141 A91-50433
Photoresponse of YBa₂Cu₃O₇(δ) granular and epitaxial superconducting thin films p 141 A91-50443
Performance of a 300 Mbps 1:16 serial/parallel optoelectronic receiver module p 141 A91-51146
High temperature superconductor analog electronics for millimeter-wavelength communications
[AIAA PAPER 91-3592] p 233 A91-53707
Determination of surface resistance and magnetic penetration depth of superconducting YBa₂Cu₃O₇(δ) thin films by microwave power transmission measurements p 234 N91-10780
An experimental study of high T_c superconducting microstrip transmission lines at 35 GHz and the effect of film morphology p 133 N91-11988
[NASA-TM-103633] p 133 N91-11988
Design aspects and comparison between high T_c superconducting coplanar waveguide and microstrip line
[NASA-TM-105142] p 146 N91-27445
High temperature superconductor analog electronics for millimeter-wavelength communications p 237 N91-29982
[NASA-TM-105184] p 237 N91-29982
Measurement techniques for cryogenic Ka-band microstrip antennas
[NASA-TM-105183] p 146 N91-30426
- BHASIN, KUL B.**
Design of an optically controlled Ka-band GaAs MMIC phased-array antenna p 132 A91-24951
Superconductivity applications for infrared and microwave devices; Proceedings of the Meeting, Orlando, FL, Apr. 19, 20, 1990 p 141 A91-50426
[SPIE-1292] p 141 A91-50426
YBCO superconducting ring resonators at millimeter-wave frequencies p 142 A91-54532
Emerging applications of high temperature superconductors for space communications
[NASA-TM-103629] p 227 N91-12317
Monolithic mm-wave phase shifter using optically activated superconducting switches
[NASA-CASE-LEW-14878-1] p 229 N91-13996
Superconducting microwave electronics at Lewis Research Center p 236 N91-24081
Comparative study of bolometric and non-bolometric switching elements for microwave phase shifters
[NASA-TM-104435] p 145 N91-25320
- BHATT, R.**
Impact behavior of a SiC fiber-reinforced reaction bonded Si₃N₄ composite p 91 A91-16805
- BHATT, R. T.**
Ultrasonic velocity technique for monitoring property changes in fiber-reinforced ceramic matrix composites p 174 A91-56912
Investigation of interfacial shear strength in SiC/Si₃N₄ composites p 93 A91-56913
Investigation of interfacial shear strength in SiC/Si₃N₄ composites p 101 N91-26233
[NASA-TM-103739] p 101 N91-26233
- BHATT, RAMAKRISHNA T.**
Microstructural and strength stability of CVD SiC fibers in argon environments p 117 A91-56958
Mechanical behavior of fiber reinforced SiC/RBSN ceramic matrix composites: Theory and experiment
[NASA-TM-103688] p 99 N91-21243
In-situ x-ray monitoring of damage accumulation in SiC/RBSN tensile specimens p 99 N91-22402
[NASA-TM-103733] p 99 N91-22402
Microstructural and strength stability of CVD SiC fibers in argon environment p 102 N91-29250
[NASA-TM-103772] p 102 N91-29250
Ultrasonic velocity technique for monitoring property changes in fiber-reinforced ceramic matrix composites
[NASA-TM-103806] p 195 N91-30546
- BHATT, RAMKRISHNA T.**
In situ X-ray monitoring of damage accumulation in SiC/RBSN tensile specimens p 94 A91-56942
- BHATTACHARJEE, S.**
Heat transfer to a thin solid combustible in flame spreading at microgravity p 106 A91-51449

BHATTACHARYA, P. K.

- Dielectric function of InGaAs in the visible
p 233 A91-53236
- Ellipsometric study of InGaAs MODFET material
[NASA-TM-103286] p 143 N91-19351
- Study of InGaAs based MODFET structures using
variable angle spectroscopic ellipsometry
[NASA-TM-103792] p 235 N91-19935

BHATTACHARYA, PALLAB K.

- Low-temperature microwave characteristics of
pseudomorphic $\text{In}_x\text{Ga}_{1-x}\text{As}/\text{In}_{0.52}\text{Al}_{0.48}\text{As}$
modulation-doped field-effect transistors
p 136 A91-22987

BHATTACHARYYA, S. K.

- Development of nuclear fuels and materials for
propulsion systems for SEI
[AIAA PAPER 91-3452] p 125 A91-52362

BIAGLOW, JAMES

- A preliminary characterization of applied-field MPD
thruster plumes
[AIAA PAPER 91-2339] p 62 A91-45798

BIBEL, G. D.

- Effects of rim thickness on spur gear bending stress
[AIAA PAPER 91-2020] p 181 A91-41681
- Effects of rim thickness on spur gear bending stress
[NASA-TM-104388] p 186 N91-23500

BICKFORD, R. L.

- Development of a Fabry-Perot interferometer for rocket
engine plume monitoring p 171 A91-30634
- Space Shuttle Main Engine nozzle mounted optic for
throat plane spectroscopy
[AIAA PAPER 91-2524] p 49 A91-45816

BIDWELL, C. S.

- Numerical simulation of ice growth on a MS-317 swept
wing geometry
[AIAA PAPER 91-0263] p 19 A91-26193
- Numerical simulation of ice growth on a MS-317 swept
wing geometry
[NASA-TM-103705] p 11 N91-14310

BIDWELL, COLIN S.

- Experimental water droplet impingement data on modern
aircraft surfaces
[AIAA PAPER 91-0445] p 2 A91-21493
- Icing characteristics of a natural-laminar-flow, a
medium-speed, and a swept, medium-speed airfoil
[AIAA PAPER 91-0447] p 3 A91-26327
- Progress toward the development of an airfoil icing
analysis capability p 9 N91-10866
- Icing characteristics of a natural-laminar-flow, a
medium-speed, and a swept, medium-speed airfoil
[NASA-TM-103693] p 12 N91-19046

BIEDENBENDER, M. D.

- Submicron gate InP power MISFET's with improved
output power density at 18 and 20 GHz
p 145 N91-26436

BIEDENBENDER, MICHAEL D.

- Submicron gate InP power MISFET's with improved
output power density at 18 and 20 GHz
p 142 A91-54526

BIESIADNY, THOMAS J.

- Overview of high performance aircraft propulsion
p 28 N91-20089

BIESIADNY, TOM

- V-STOL gets a lift p 20 A91-52835

BILL, ROBERT C.

- Advanced Rotorcraft Transmission Program
p 179 A91-17214
- Advanced rotorcraft transmission program
[NASA-TM-103276] p 184 N91-21531
- Recent manufacturing advances for spiral bevel gears
[NASA-TM-104479] p 191 N91-31654

BIRINGEN, SEDAT

- Application of implicit numerical techniques to the
solution of the three-dimensional diffusion equation
p 148 A91-13456

BIRKNER, BJORN W.

- Arjet nozzle area ratio effects p 75 N91-24271

BLAIR, A. B., JR.

- Evaluation of a technique to generate artificially
thickened boundary layers in supersonic and hypersonic
flows
[NASA-TP-3142] p 17 N91-28136

BLELLOCH, PAUL A.

- Simulation of the Space Station strut-out condition
[AIAA PAPER 91-1248] p 197 A91-32087

BLISS, DONALD B.

- Role of artificial viscosity in Euler and Navier-Stokes
solvers p 4 A91-34135

BLOOMFIELD, H. S.

- Historical perspectives - The role of the NASA Lewis
Research Center in the national space nuclear power
programs
[AIAA PAPER 91-3462] p 242 A91-53713

- Historical perspectives. The role of the NASA Lewis
Research Center in the national space nuclear power
programs
[NASA-TM-105196] p 243 N91-29138

BLOOMFIELD, HARVEY

- Preliminary assessment of the power requirements of
a manned rover for Mars missions p 41 A91-27702
- A comparison of energy conversion systems for meeting
the power requirements of manned rover for Mars
missions p 53 A91-37932

BLOOMFIELD, HARVEY S.

- Nuclear power technology requirements for NASA
exploration missions p 53 A91-37940
- Trade studies for nuclear space power systems
[AIAA PAPER 91-3518] p 65 A91-52413
- A reliability and mass perspective of SP-100 Stirling cycle
lunar-base powerplant designs
[NASA-TM-103736] p 212 N91-26592

BLUMENTHAL, PHILIP Z.

- Rotating pressure measurement system using an on
board calibration standard
[NASA-TM-103676] p 176 N91-19401

BOBER, L. J.

- Large-scale advanced propeller blade pressure
distributions - Prediction and data p 5 A91-42820

BOBER, LAWRENCE J.

- Turbomachinery and combustor technology for small
engines p 29 N91-20113

BOBULA, GEORGE A.

- An update of engine system research at the Army
Propulsion Directorate p 22 A91-29452
- An update of engine system research at the Army
Propulsion Directorate
[NASA-TM-103278] p 26 N91-11752

BODI, ROBERT F.

- Test and evaluation of load converter topologies used
in the Space Station Freedom Power Management and
distribution DC test bed
[NASA-TM-105217] p 85 N91-30267

BOLDMAN, D. R.

- Evaluation of panel code predictions with experimental
results of inlet performance for a 17-inch ducted prop/fan
simulator operating at Mach 0.2
[AIAA PAPER 91-3354] p 7 A91-45819
- Evaluation of panel code predictions with experimental
results of inlet performance for a 17-inch ducted prop/fab
simulator operating at Mach 0.2
[NASA-TM-104428] p 17 N91-25106

BONACUSE, PETER J.

- Automation software for a materials testing laboratory
p 216 A91-56538
- A data acquisition and control program for axial-torsional
fatigue testing p 199 A91-56540
- Axial-torsional fatigue: A study of tubular specimen
thickness effects
[NASA-TM-103637] p 200 N91-14632

BOND, T. H.

- Effects of horizontal tail ice on longitudinal aerodynamic
derivatives p 36 A91-38547

BOND, THOMAS H.

- Icing tests of a model main rotor p 18 A91-17218
- A review of ice accretion data from a model rotor icing
test and comparison with theory
[AIAA PAPER 91-0661] p 19 A91-22500

Results of a sub-scale model rotor icing test

- [AIAA PAPER 91-0660] p 19 A91-26190

- A review of ice accretion data from a model rotor icing
test and comparison with theory
[NASA-TM-103712] p 11 N91-13421

Results of a sub-scale model rotor icing test

- [NASA-TM-103709] p 11 N91-14309

- Advanced ice protection systems test in the NASA Lewis
icing research tunnel
[NASA-TM-103757] p 32 N91-23183

- Model rotor icing tests in the NASA Lewis icing research
tunnel
[NASA-TM-104351] p 32 N91-23184

BOOK, PATRICIA O.

- Sliding wear of self-mated $\text{Al}_2\text{O}_3\text{-SiC}$ whisker reinforced
composites at 23-1200 C
[NASA-TM-104490] p 90 N91-27221

BORETTI, A. A.

- Three-dimensional Euler time accurate simulations of
fan rotor-stator interactions
[NASA-TM-102528] p 16 N91-24124

BOROWSKI, BRIAN A.

- N-decane droplet combustion in the NASA-Lewis 5
Second Zero-Gravity Facility - Results in test gas
environments other than air
[AIAA PAPER 91-0720] p 105 A91-19433

BOROWSKI, STANLEY K.

- The rationale/benefits of nuclear thermal rocket
propulsion for NASA's lunar space transportation system
[AIAA PAPER 91-2052] p 39 A91-45781

- Radiation dose estimates for typical piloted NTR lunar
and Mars mission engine operations
[AIAA PAPER 91-3407] p 215 A91-52331

- NTR vehicle commonality assessment for piloted lunar
and Mars missions
[AIAA PAPER 91-3575] p 66 A91-52448

BOSELA, PAUL A.

- Dynamic analysis of space-related linear and non-linear
structures p 196 A91-28612

BOWLES, KENNETH J.

- A study of void effects on the interlaminar shear strength
of unidirectional graphite fiber reinforced composites
[NASA-TM-103267] p 159 N91-12034
- Relationship between voids and interlaminar shear
strength of polymer matrix composites
[NASA-TM-103643] p 95 N91-13495

ICAN sensitivity analysis

- [NASA-TM-103667] p 96 N91-15328

- Effect of fiber reinforcements on thermo-oxidative
stability and mechanical properties of polymer matrix
composites
[NASA-TM-103648] p 98 N91-19234

- A comparison of fiber effects on polymer matrix
composite oxidation
[NASA-TM-104416] p 101 N91-24361

BOWMAN, R. R.

- The potential for ductility enhancement from surface and
interface dislocation sources in NiAl p 109 A91-39292

BOYCE, L.

- Quantification of uncertainties in coupled material
degradation processes - High temperature, fatigue and
creep
[AIAA PAPER 91-0977] p 196 A91-31835

BOYD, IAIN D.

- Numerical and experimental investigations of rarefied
nozzle and plume flows of nitrogen
[AIAA PAPER 91-1363] p 154 A91-43429
- Pressure measurements in a low-density nozzle plume
for code verification
[AIAA PAPER 91-2110] p 61 A91-45783
- Pressure measurements in a low-density nozzle plume
for code verification
[NASA-TM-105170] p 81 N91-29228

BOYER, E. O.

- High altitude AMO testing of PV concentrator lens
elements p 207 A91-41978

BOYLE, R. J.

- Turbine blading designed for high heat load space
propulsion applications p 50 A91-10338
- Navier-Stokes analysis of turbine blade heat transfer
[ASME PAPER 90-GT-42] p 155 A91-44529
- Comparison of a quasi-3D analysis and experimental
performance for three compact radial turbines
[AIAA PAPER 91-2128] p 25 A91-45789
- Two-dimensional Navier-Stokes heat transfer analysis
for rough turbine blades
[AIAA PAPER 91-2129] p 156 A91-45790
- Comparison of a quasi-3D analysis and experimental
performance for three compact radial turbines
[NASA-TM-105155] p 35 N91-30142

BOZEK, J. M.

- Nuclear power systems for lunar and Mars exploration
[IAF PAPER 90-200] p 51 A91-13868
- Power system requirements and definition for lunar and
Mars outposts p 52 A91-37930

BOZZOLO, GUILLERMO

- Universal behavior in ideal slip p 110 A91-48517
- Equivalent crystal theory of alloys
[NASA-TP-3155] p 112 N91-30318
- A new approximate sum rule for bulk alloy properties
[NASA-TM-105282] p 112 N91-32204
- Theoretical modelling of AFM for bimetallic tip-substrate
interactions
[NASA-TM-105280] p 112 N91-32215

BRABBS, THEODORE A.

- Multi-heat addition turbine engine
[NASA-CASE-LEW-15094-1] p 32 N91-23180

BRADY, J.

- Vacuum ultraviolet radiation and thermal cycling effects
on atomic oxygen protective photovoltaic array blanket
materials p 116 A91-49812

BRAGG, M. B.

- Simulation of iced wing aerodynamics
[NASA-TM-104362] p 15 N91-23086

BRANDHORST, H. W.

- SEI needs for space nuclear power
[AIAA PAPER 91-3459] p 64 A91-52369

BRANDHORST, HENRY W.

- Nuclear technology and the space exploration
missions p 53 A91-37939
- Key issues in space nuclear power
[NASA-TM-103656] p 71 N91-19179

BRANDHORST, HENRY W., JR.

- Advanced electrical power, distribution and control for
the Space Transportation System p 143 N91-17043

- Power technologies and the space future
[NASA-TM-103649] p 73 N91-21240
Thin solar cell and lightweight array
[NASA-CASE-LEW-14959-1] p 212 N91-27614
- BRASTED, DONALD K.**
The effect of the low Earth orbit environment on space solar cells
[NASA-TM-103735] p 48 N91-19165
Advanced photovoltaic experiment, S0014: Preliminary flight results and post-flight findings p 212 N91-25061
- BRAUN, M. J.**
Flow visualization and quantitative velocity and pressure measurements in simulated single and double brush seals p 180 A91-21071
Effects of brush seal morphology on leakage and pressure drops p 182 A91-41700
Flow visualization in a simulated brush seal
[ASME PAPER 90-GT-217] p 173 A91-44633
Some preliminary results of brush seal/rotor interference effects on leakage at zero and low rpm using a tapered-plug rotor
[AIAA PAPER 91-3390] p 182 A91-45820
Simulation of brush insert for leading-edge-passage convective heat transfer p 165 N91-23409
[NASA-TM-103801] p 165 N91-23409
Some preliminary results of brush seal/rotor interference effects on leakage at zero and low RPM using a tapered-plug rotor
[NASA-TM-104396] p 188 N91-27559
- BREER, MARLIN D.**
Experimental water droplet impingement data on modern aircraft surfaces
[AIAA PAPER 91-0445] p 2 A91-21493
- BREISACHER, KEVIN J.**
Analysis of 5 KHz combustion instabilities in 40K methane/LOX combustion chambers p 67 N91-10117
Nonlinear combustion instability model in two- to three-dimensions p 85 N91-31208
[NASA-TM-102381] p 85 N91-31208
- BREWE, D. E.**
Extension of transonic flow computational concepts in the analysis of cavitated bearings p 150 A91-29474
[ASME PAPER 90-TRIB-40] p 150 A91-29474
A high speed photography study of cavitation in a dynamically loaded journal bearing p 180 A91-34806
[ASME PAPER 90-TRIB-19] p 180 A91-34806
Extension of transonic flow computational concepts in the analysis of cavitated bearings p 160 N91-16304
[NASA-TM-103214] p 160 N91-16304
- BREWE, DAVID E.**
On the numerical solution of the dynamically loaded hydrodynamic lubrication of the point contact p 180 A91-33461
[NASA-TM-103442] p 165 N91-23439
- The effect of coatings and liners on heat transfer in a dry shaft-bush tribosystem p 159 N91-12913
[NASA-TM-102513] p 159 N91-12913
Two reference time scales for studying the dynamic cavitation of liquid films p 160 N91-19369
[NASA-TM-103673] p 160 N91-19369
A system-approach to the elastohydrodynamic lubrication point-contact problem p 165 N91-23439
[NASA-TM-104342] p 165 N91-23439
- BRIGHT, MICHELLE M.**
The NASA Lewis integrated propulsion and flight control simulator
[AIAA PAPER 91-2969] p 38 A91-47847
The NASA Lewis integrated propulsion and flight control simulator
[NASA-TM-105147] p 21 N91-27157
- BRIGHTWELL, GRAHAM**
Structure of random discrete spacetime p 224 A91-22894
- BRILEY, W. R.**
Navier-Stokes simulation of transonic blade-vortex interactions p 2 A91-21065
- BRINDLEY, P. K.**
Continuous fiber-reinforced titanium aluminide composites p 92 A91-39553
Factors which influence tensile strength of a SiC/Ti-24Al-11Nb (at. pct) composite p 92 A91-55900
- BRINDLEY, PAMELA K.**
Furnace for tensile/fatigue testing
[NASA-CASE-LEW-14848-1] p 42 N91-27175
- BRINDLEY, W. J.**
Ceramic coatings on smooth surfaces
[NASA-CASE-LEW-15164-1] p 122 N91-25298
Ceramic coatings on smooth surfaces
[NASA-CASE-LEW-15164-2] p 123 N91-32229
- BRINDLEY, WILLIAM J.**
Thermal barrier coating evaluation needs
[NASA-TM-103708] p 111 N91-15390
Oxidation resistant coatings for titanium alloys and titanium alloy matrix composites p 122 N91-26375
[NASA-CASE-LEW-15155-1] p 122 N91-26375
- BRINK, NORMAN O.**
Effect of lightning strike on bromine intercalated graphite fiber/epoxy composites p 103 N91-32177
[NASA-TM-104507] p 103 N91-32177
- BRINKER, D.**
Temperature coefficients of multijunction solar cells p 172 A91-41921
- BRINKER, D. J.**
New directions in InP solar cell research p 206 A91-38022
Peeled film GaAs solar cell development p 139 A91-41889
High altitude AM0 testing of PV concentrator lens elements p 207 A91-41978
Effects of radiation of InP cells epitaxially grown on Si and GaAs substrates p 140 A91-41984
Lightweight concentrator module with 30 percent AM0 efficient GaAs/GaSb tandem cells p 57 A91-41990
23.5 percent thin-film space concentrator cells p 58 A91-42002
Recent progress in InP solar cell research
[NASA-TM-104509] p 146 N91-27447
A comparative study of p(+)/n and n(+)/p InP solar cells made by a closed ampoule diffusion p 212 N91-30206
Effect of dislocations on properties of heteroepitaxial InP solar cells p 213 N91-30209
- BRINKER, DAVID J.**
Preliminary flight test results from the advanced photovoltaic experiment p 56 A91-38163
Recent results from the InP homojunction cell module on the LIPS III spacecraft p 140 A91-41971
Preliminary results from the Advanced Photovoltaic Experiment flight test p 39 A91-41980
Preliminary results from the advanced photovoltaic experiment flight test
[NASA-TM-103269] p 67 N91-11058
The effect of the low Earth orbit environment on space solar cells p 48 N91-19165
[NASA-TM-103735] p 48 N91-19165
Tandem concentrator solar cells with 30 percent (AM0) power conversion efficiency p 208 N91-19189
Thermal annealing of GaAs concentrator solar cells p 208 N91-19195
Effects of proton irradiation on the performance of InP/GaAs solar cells p 209 N91-19205
A comparative study of performance parameters of n(+)-p InP solar cells made by closed-ampoule sulfur diffusion into Cd- and Zn-doped p-type InP substrates p 210 N91-19209
Heteroepitaxial InP solar cells on Si and GaAs substrates p 144 N91-20392
[NASA-TM-103696] p 144 N91-20392
Advanced photovoltaic experiment, S0014: Preliminary flight results and post-flight findings p 212 N91-25061
The effects of lunar dust accumulation on the performance of photovoltaic arrays p 83 N91-30238
- BRITTON, RANDALL K.**
Icing tests of a model main rotor p 18 A91-17218
A review of ice accretion data from a model rotor icing test and comparison with theory p 19 A91-22500
[AIAA PAPER 91-0661] p 19 A91-22500
Results of a sub-scale model rotor icing test p 19 A91-26190
[AIAA PAPER 91-0660] p 19 A91-26190
Elevator deflections on the icing process p 20 A91-35427
A review of ice accretion data from a model rotor icing test and comparison with theory p 11 N91-13421
[NASA-TM-103712] p 11 N91-13421
Results of a sub-scale model rotor icing test p 11 N91-14309
[NASA-TM-103709] p 11 N91-14309
Model rotor icing tests in the NASA Lewis icing research tunnel p 32 N91-23184
[NASA-TM-104351] p 32 N91-23184
- BROWN, D. A.**
Application of artificial neural networks to composite ply micromechanics p 100 N91-24345
[NASA-TM-104365] p 100 N91-24345
- BROWN, G. V.**
Development of a vibration isolation prototype system for microgravity space experiments p 47 A91-53403
- BROWN, GERALD V.**
Development of a vibration isolation prototype system for microgravity space experiments p 130 N91-19324
[NASA-TM-103664] p 130 N91-19324
Magnetic bearings with zero bias p 48 N91-21194
- BROWN, LAWRENCE E.**
The shock process and light-element production in supernova envelopes p 239 A91-33573
- BROWN, S. A.**
Low-density, high-strength intermetallic matrix composites by XD (trademark) synthesis
[NASA-TM-103724] p 97 N91-19233
- BU, XIN Y.**
Polymeric routes to silicon carbide and silicon oxycarbide CMC p 117 A91-56922
- BU, XIN YA**
Polymeric routes to silicon carbide and silicon oxycarbide CMC
[NASA-TM-104372] p 102 N91-26234
- BUBSEY, RAYMOND T.**
Analysis of some compliance calibration data for chevron-notch bar and rod specimens
[NASA-TM-104367] p 203 N91-22594
- BUDINGER, J. M.**
Quaternary pulse position modulation electronics for free-space laser communications p 133 A91-53702
[AIAA PAPER 91-3471] p 133 A91-53702
Quaternary pulse position modulation electronics for free-space laser communications
[NASA-TM-104502] p 135 N91-29405
- BUDINGER, JAMES M.**
Combinatorial FSK modulation for power-efficient high-rate communications p 133 A91-53708
[AIAA PAPER 91-3532] p 133 A91-53708
Combinatorial FSK modulation for power-efficient high-rate communications
[NASA-TM-105188] p 135 N91-29404
- BUFFUM, D. H.**
The aerodynamics of an oscillating cascade in a compressible flow field
[ASME PAPER 89-GT-271] p 1 A91-13047
- BUFFUM, DANIEL H.**
Oscillating cascade aerodynamics by an experimental influence coefficient technique p 1 A91-10339
Experimental investigation of oscillating cascade aerodynamics p 3 A91-27801
Wind tunnel wall effects in a linear oscillating cascade
[NASA-TM-103690] p 27 N91-19098
- BULLARD, RANDY**
Integrated flight/propulsion control system design based on a decentralized, hierarchical approach p 31 N91-21137
[NASA-TM-103678] p 31 N91-21137
- BULLARD, RANDY E.**
Integrated flight/propulsion control system design based on a centralized approach p 36 A91-22950
- BULLOCK, S. RAY**
Medium power hydrogen arcjet performance
[NASA-TM-105533] p 85 N91-31216
- BULZAN, DANIEL L.**
Measurements and predictions of a liquid spray from an air-assist nozzle p 149 A91-22498
[AIAA PAPER 91-0692] p 149 A91-22498
Measurements and predictions of a liquid spray from an air-assist nozzle p 26 N91-13455
[NASA-TM-103640] p 26 N91-13455
- BURLEY, RICHARD R.**
High alpha inlets p 28 N91-20091
- BURROWS, LINDA M.**
Field oriented control of induction motors p 138 A91-37987
- BUTCHER, ROBERT L.**
Spacelab qualified infrared imager for microgravity science applications p 173 A91-51585
Results of the users' requirements survey p 175 N91-14575
- BUTLER, P. L.**
Manipulation hardware for microgravity research
[NASA-TM-103423] p 128 N91-14498
- BUTTON, ROBERT M.**
Development and testing of a source subsystem for the supporting development PMAD DC test bed
[NASA-TM-104510] p 78 N91-26202
- BYERS, DAVE**
Futuristic systems: Solar and nuclear electric propulsion p 80 N91-28215
- BYERS, DAVID C.**
The NASA Lewis Research Center electric propulsion program
[AIAA PAPER 91-3443] p 64 A91-52355

C

- CADY, E. C.**
Cryogenic propellant management architectures to support the Space Exploration Initiative
[AIAA PAPER 90-3713] p 124 A91-10112
- CAIRELLI, JAMES E.**
Update on results of SPRE testing at NASA p 56 A91-38140
Update on results of SPRE testing at NASA Lewis
[NASA-TM-104425] p 79 N91-27208
- CALCO, FRANK S.**
Quick action clamp
[NASA-CASE-LEW-14887-1] p 189 N91-27561
- CALOGERAS, JAMES E.**
Solar dynamic power for Earth orbital and lunar applications
[NASA-TM-104511] p 80 N91-27214

CALOMINO, ANTHONY M.
Fully articulated four-point-bend loading fixture
[NASA-CASE-LEW-14776-1] p 185 N91-21540

CANACCI, V.
Flow visualization in a simulated brush seal
[ASME PAPER 90-GT-217] p 173 A91-44633
Simulation of brush insert for leading-edge-passage convective heat transfer
[NASA-TM-103801] p 165 N91-23409

CANACCI, V. A.
Flow visualization and quantitative velocity and pressure measurements in simulated single and double brush seals
p 180 A91-21071

CAO, Y.
A PCM/forced convection conjugate transient analysis of energy storage systems with annular and countercurrent flows
p 150 A91-27166

CAPALDI, R.
Liquid hydrogen turbopump foil bearing
[AIAA PAPER 91-2108] p 182 A91-41701

CARBONI, JEANNE D.
Overview of NASP nozzle research
p 28 N91-20093

CARNEY, KELLY S.
Simulation of the Space Station strut-out condition
[AIAA PAPER 91-1248] p 197 A91-32087

CARNEY, LYNNETTE M.
Experimental evaluation of resistojet thruster plume shields
p 51 A91-30010

CARRUTH, RALPH
Findings of the Joint Workshop on Evaluation of Impacts of Space Station Freedom Ground Configurations
p 48 N91-20728
Findings of the Joint Workshop on Evaluation of Impacts of Space Station Freedom Ground Configurations
[NASA-TM-103717] p 73 N91-22370

CARUSO, J. J.
Metal matrix composites microfracture - Computational simulation
p 90 A91-11815

CASHMAN, WILLIAM F.
Advanced Communications Technology Satellite (ACTS)
[IAF PAPER 90-481] p 44 A91-14056

CATALDO, R. L.
Power system requirements and definition for lunar and Mars outposts
p 52 A91-37930
SEI needs for space nuclear power
[AIAA PAPER 91-3459] p 64 A91-52369

CATALDO, ROBERT
Preliminary assessment of the power requirements of a manned rover for Mars missions
p 41 A91-27702
A comparison of energy conversion systems for meeting the power requirements of manned rover for Mars missions
p 53 A91-37932
Dynamic Isotope Surface Power Systems
[AIAA PAPER 91-3623] p 208 A91-52487

CAULEY, M. A.
Quaternary pulse position modulation electronics for free-space laser communications
[AIAA PAPER 91-3471] p 133 A91-53702
Quaternary pulse position modulation electronics for free-space laser communications
[NASA-TM-104502] p 135 N91-29405

CAULEY, MICHAEL A.
GaAs monolithic RF modules for SARSAT distress beacons
[NASA-TM-104338] p 46 N91-21184

CEBECI, TUNCER
Prediction of ice shapes and their effect on airfoil performance
[AIAA PAPER 91-0264] p 3 A91-26330
Prediction of ice shapes and their effect on airfoil performance
[NASA-TM-103701] p 12 N91-19047

CELESTINA, MARK L.
Three-dimensional flows in a transonic compressor rotor
p 8 A91-56152
Average-passage flow model development
p 165 N91-24338

CHABOCHE, J.-L.
On the thermodynamics of stress rate in the evolution of back stress in viscoplasticity
[NASA-TM-103794] p 201 N91-19476

CHAIKO, LEV I.
Review of the transmissions of the Soviet helicopters
[NASA-TM-103634] p 20 N91-15146

CHAIT, A.
Time development of a perturbed-spherical nucleus in a pure supercooled liquid. I - Power-law growth of morphological instabilities. II - Nonlinear development
p 231 A91-16105
Three-dimensional flow transport modes in directional solidification during space processing
p 128 A91-42642

A numerical and experimental analysis of reactor performance and deposition rates for CVD on monofilaments
[NASA-TM-103631] p 130 N91-14500

CHAIT, ARNON
Application of implicit numerical techniques to the solution of the three-dimensional diffusion equation
p 148 A91-13456
Computational materials science. An example: Numerical modeling of chemical vapor deposition processing of advanced fibers
p 99 N91-20111

CHAKRAVORTY, A.
Constraints on primordial nucleosynthesis on the mass of the tau neutrino
p 240 A91-46543

CHAMIS, C. C.
Metal matrix composites microfracture - Computational simulation
p 90 A91-11815
Composite structure global fracture toughness via computational simulation
p 216 A91-11819
Mechanics of damping for fiber composite laminates including hygrothermal effects
p 195 A91-12895
Probabilistic simulation of uncertainties in thermal structures
p 195 A91-16042
An integrated methodology for optimizing the passive damping of composite structures
p 195 A91-19048
Simplified procedures for designing adhesively bonded composite joints
p 180 A91-20938
Quantification of uncertainties in coupled material degradation processes - High temperature, fatigue and creep
[AIAA PAPER 91-0977] p 196 A91-31835
Concurrent material-fabrication optimization of metal-matrix laminates under thermo-mechanical loading
[AIAA PAPER 91-1044] p 129 A91-31842
Computational simulation of acoustic fatigue for hot composite structures
[AIAA PAPER 91-1178] p 197 A91-32099
Computational simulation of damping in composite structures
p 198 A91-36283
Composite laminate tailoring with probabilistic constraints and loads
p 198 A91-38754
Probabilistic modeling for simulation of aerodynamic uncertainties in propulsion systems
p 58 A91-42725
Concurrent tailoring of fabrication process and interphase layer to reduce residual stresses in metal matrix composites
p 92 A91-43232
HITCAN for actively cooled hot-composite thermosstructural analysis
[NASA-TM-103750] p 202 N91-21562
Reliability and risk assessment of structures
p 194 A91-23050
Probabilistic structural analysis methods for space transportation propulsion systems
p 205 N91-28238
Concurrent engineering
p 80 N91-28247
Interphase layer optimization for metal matrix composites with fabrication considerations
[NASA-TM-105166] p 102 N91-30281
The effects of interply damping layers on the dynamic response of composite structures
[NASA-TM-104497] p 103 N91-30282

CHAMIS, CHRISTOS C.
Simplified procedures for designing composite bolted joints
p 195 A91-16290
Computational simulation of high-temperature metal matrix composites cyclic behavior
p 91 A91-18680
Progressive fracture in composites subjected to hygrothermal environment
[AIAA PAPER 91-1140] p 91 A91-31919
Programming probabilistic structural analysis for parallel processing computer
[AIAA PAPER 91-0920] p 196 A91-31957
Fiber pushout test - A three-dimensional finite element computational simulation
p 197 A91-33096
In-service health monitoring of composite structures
p 192 A91-51926
Numerical propulsion system simulation - An interdisciplinary approach
[AIAA PAPER 91-3554] p 66 A91-53706
A methodology for evaluating the reliability and risk of structures under complex service environments
[NASA-TM-103244] p 200 N91-17415
METCAN updates for high temperature composite behavior: Simulation/verification
[NASA-TM-103682] p 97 N91-19229
Computational simulation of hot composites structures
[NASA-TM-103681] p 97 N91-19230
Probabilistic micromechanics and macromechanics of polymer matrix composites
[NASA-TM-103669] p 98 N91-19236
Concurrent micromechanical tailoring and fabrication process optimization for metal-matrix composites
[NASA-TM-103670] p 98 N91-19237
Probabilistic simulation of uncertainties in thermal structures
[NASA-TM-103680] p 201 N91-19472

Computational simulation of acoustic fatigue for hot composite structures
[NASA-TM-104379] p 203 N91-23548
Simulation of probabilistic wind loads and building analysis
[NASA-TM-103744] p 203 N91-23549
Probabilistic structural analysis: Introductory remarks
p 204 N91-24326
Probability approach for strength calculations
p 204 N91-24652
Microfracture in high temperature metal matrix crossply laminates
[NASA-TM-104381] p 101 N91-25198
Probability of failure and risk assessment of propulsion structural components
[NASA-TM-102323] p 205 N91-25436
Numerical propulsion system simulation: An interdisciplinary approach
[NASA-TM-105181] p 81 N91-29221
Integrated mechanics for the passive damping of polymer-matrix composites and composite structures
[NASA-TM-104346] p 103 N91-32181
Progressive fracture in composites subjected to hygrothermal environment
[NASA-TM-105230] p 103 N91-32182
Computational simulation of high temperature metal matrix composite behavior
[NASA-TM-104378] p 206 N91-32520

CHAN, C. K.
Heat transfer in space systems; Proceedings of the Symposium, AIAA/ASME Thermophysics and Heat Transfer Conference, Seattle, WA, June 18-20, 1990
p 152 A91-38780

CHAN, S. H.
Heat transfer in space systems; Proceedings of the Symposium, AIAA/ASME Thermophysics and Heat Transfer Conference, Seattle, WA, June 18-20, 1990
p 152 A91-38780

CHANG, C. T.
Modern CFD applications for the design of a reacting shear layer facility
[AIAA PAPER 91-0577] p 149 A91-21540
Simulations of free shear layers using a compressible k-epsilon model
[AIAA PAPER 91-1863] p 156 A91-45778
Modern CFD applications for the design of a reacting shear layer facility
[NASA-TM-104523] p 34 N91-27164

CHANG, KAI
A 29.3-GHz cavity-enclosed aperture-coupled circular-patch antenna for microwave circuit integration
p 140 A91-47057

CHANG, SIN-CHUNG
A new numerical framework for solving conservation laws: The method of space-time conservation element and solution element
[NASA-TM-104495] p 223 N91-30867

CHANG, WON S.
Analysis of the one-dimensional transient compressible vapor flow in heat pipes
p 157 A91-47735

CHASE, THEODORE L.
Presentation on a Space Acceleration Measurement System (SAMS)
p 50 N91-12417

CHATO, D. J.
Improved thermodynamic modelling of the no-vent fill process and correlation with experimental data
[AIAA PAPER 91-1379] p 129 A91-43444
LN2 spray droplet size measurement via ensemble diffraction technique
[AIAA PAPER 91-1381] p 129 A91-44336

CHATO, DAVID J.
Ground testing of the nonvented fill method of orbital propellant transfer - Results of initial test series
[AIAA PAPER 91-2326] p 59 A91-44198
Review and test of chilldown methods for space-based cryogenic tanks
[AIAA PAPER 91-1843] p 60 A91-45776
Cryogenic transfer options for exploration missions
[AIAA PAPER 91-3541] p 158 A91-53714
LN2 spray droplet size measurement via ensemble diffraction technique
[NASA-TM-104443] p 131 N91-24470
Ground testing on the nonvented fill method of orbital propellant transfer: Results of initial test series
[NASA-TM-104444] p 166 N91-24547
Review and test of chilldown methods for space-based cryogenic tanks
[NASA-TM-104458] p 167 N91-25351
Cryogenic transfer options for exploration missions
[NASA-TM-105197] p 168 N91-28538

CHEN, HEH-CHYUN
Programming probabilistic structural analysis for parallel processing computer
[AIAA PAPER 91-0920] p 196 A91-31957

- CHEN, HSUN**
Prediction of ice shapes and their effect on airfoil performance
[NASA-TM-103701] p 12 N91-19047
- CHEN, HSUN H.**
Prediction of ice shapes and their effect on airfoil performance
[AIAA PAPER 91-0264] p 3 A91-26330
- CHEN, J.-Y.**
Second order modeling of boundary-free turbulent shear flows
[AIAA PAPER 91-1779] p 154 A91-42588
- CHEN, K.-H.**
Simulation of three-dimensional liquid sloshing flows using a strongly implicit calculation procedure
[AIAA PAPER 91-1661] p 153 A91-42549
Primitive variable, strongly implicit calculation procedure for viscous flows at all speeds p 7 A91-46181
- CHEN, L. Y.**
Diamondlike carbon as a moisture barrier and antireflecting coating on optical materials p 119 N91-18302
- CHEN, S. K.**
Influence of geometric features on the performance of pressure-swirl atomizers p 147 A91-13030
- CHEN, Y.-Y.**
Second order modeling of boundary-free turbulent shear flows
[NASA-TM-104369] p 164 N91-22524
- CHIARAMONTE, FRANCIS P.**
Wettability of pyrolytic boron nitride by aluminum p 114 A91-28772
Design strategies for the International Space University's variable gravity research facility p 42 N91-22171
The International Space University's variable gravity research facility design
[NASA-TM-105224] p 44 N91-31196
- CHIMA, RODRICK V.**
Analysis of three-dimensional viscous flow in a supersonic throughflow fan p 10 N91-10885
An unconditionally stable Runge-Kutta method for unsteady rotor-stator interaction p 165 N91-24337
- CHITRE, SUSHEEL**
Measurements and predictions of a liquid spray from an air-assist nozzle
[AIAA PAPER 91-0692] p 149 A91-22498
Measurements and predictions of a liquid spray from an air-assist nozzle
[NASA-TM-103640] p 26 N91-13455
- CHOI, MUN Y.**
N-decane droplet combustion in the NASA-Lewis 5 Second Zero-Gravity Facility - Results in test gas environments other than air
[AIAA PAPER 91-0720] p 105 A91-19433
- CHOI, SUNG R.**
Influence of the Si₃N₄ microstructure on its R-curve and fatigue behavior p 117 A91-56931
Dynamic fatigue property of silicon carbide whisker-reinforced silicon nitride p 94 A91-56937
Crack healing in silicon nitride due to oxidation p 118 A91-56982
Comparison of dynamic fatigue behavior between SiC whisker-reinforced composite and monolithic silicon nitrides
[NASA-TM-103707] p 119 N91-19293
Mechanical behavior and failure phenomenon of an in situ-toughened silicon nitride
[NASA-TM-103741] p 121 N91-23311
- CHOI, YUNHO**
Time-derivative preconditioning for viscous flows
[AIAA PAPER 91-1652] p 154 A91-43576
- CHOO, YUNG K.**
Implementation of control point form of algebraic grid-generation technique
[NASA-TM-103748] p 13 N91-19054
Dynamics of local grid manipulations for internal flow problems p 164 N91-21090
- CHOREY, C.**
Low-temperature microwave characteristics of pseudomorphic In(x)Ga(1-x) As/In(0.52)Al(0.48)As modulation-doped field-effect transistors p 136 A91-22987
- CHOREY, C. M.**
An experimental study of high T_c superconducting microstrip transmission lines at 35 GHz and the effect of film morphology p 138 A91-36172
High temperature superconducting thin film microwave circuits - Fabrication, characterization, and applications p 141 A91-50433
An experimental study of high T_c superconducting microstrip transmission lines at 35 GHz and the effect of film morphology
[NASA-TM-103633] p 133 N91-11988
- CHOREY, CHRISTOPHER M.**
YBCO superconducting ring resonators at millimeter-wave frequencies p 142 A91-54532
- CHOW, CHUEN-YEN**
Stability of compressible Taylor-Couette flow
[AIAA PAPER 91-1642] p 153 A91-42541
- CHOY, F. K.**
Analytical and experimental study of vibrations in a gear transmission
[AIAA PAPER 91-2019] p 181 A91-41680
Effects of gear box vibration and mass imbalance on the dynamics of multistage gear transmission p 182 A91-47213
Modal analysis of multistage gear systems coupled with gearbox vibrations
[NASA-TM-103797] p 187 N91-23513
Analytical and experimental study of vibrations in a gear transmission
[NASA-TM-104434] p 187 N91-25395
- CHOY, FRED K.**
Effects of gear box vibration and mass imbalance on the dynamics of multi-stage gear transmissions
[NASA-TM-103695] p 185 N91-21534
- CHRISS, RANDALL M.**
Development of a laser-induced heat flux technique for measurement of convective heat transfer coefficients in a supersonic flowfield
[NASA-TM-103778] p 13 N91-19063
A laser velocimeter investigation of the normal shock-wave boundary layer interaction
[NASA-TM-105201] p 169 N91-32440
- CHRISTIANSEN, ERIC L.**
On protection of Freedom's solar dynamic radiator from the orbital debris environment. Part 2: Further testing and analyses
[NASA-TM-104514] p 84 N91-30265
- CHUANG, CHUN-HUA**
Addition polyimides with enhanced processability
[NASA-CASE-LEW-15043-1] p 123 N91-32230
- CHUBB, DONALD L.**
Reappraisal of solid selective emitters p 207 A91-41999
Reappraisal of solid selective emitters
[NASA-TM-103290] p 69 N91-11801
Liquid sheet radiator apparatus
[NASA-CASE-LEW-14295-1] p 130 N91-15424
Design considerations for space radiators based on the liquid sheet (LSR) concept
[NASA-TM-105158] p 80 N91-27213
- CHUE, T.-H.**
Jet-A fuel evaporation analysis in conical tube injectors
[AIAA PAPER 91-0345] p 149 A91-21467
- CHULYA, ABHISAK**
A new uniformly valid asymptotic integration algorithm for elasto-plastic creep and unified viscoplastic theories including continuum damage p 110 A91-48725
Mechanical behavior of fiber reinforced SiC/RBSN ceramic matrix composites: Theory and experiment
[NASA-TM-103688] p 99 N91-21243
Structural design methodologies for ceramic-based material systems
[NASA-TM-103097] p 121 N91-22460
- CHUM, K.**
Jet-A fuel evaporation analysis in conical tube injectors
[AIAA PAPER 91-0345] p 149 A91-21467
Flow visualization and computational studies of a reverse flow circular combustor p 157 A91-48966
- CHUNG, B.-C.**
Temperature coefficients of multijunction solar cells p 172 A91-41921
- CHUNG, CHAN-HONG**
New approach in direct-simulation of gas mixtures
[AIAA PAPER 91-1343] p 154 A91-43412
- CIVINSKAS, K. C.**
Turbine blading designed for high heat load space propulsion applications p 50 A91-10338
Two-dimensional Navier-Stokes heat transfer analysis for rough turbine blades
[AIAA PAPER 91-2129] p 156 A91-45790
- CLARK, B. J.**
Near-field noise of a single rotation propfan at an angle of attack
[AIAA PAPER 90-3953] p 225 A91-12469
Near-field noise of a single-rotation propfan at an angle of attack
[NASA-TM-103645] p 227 N91-12316
- CLARK, JOHN S.**
The NASA/DOE/DOD nuclear rocket propulsion project - FY 1991 status p 64 A91-52335
Nuclear Thermal Propulsion technology - Summary of FY 1991 Interagency panel planning
[AIAA PAPER 91-3631] p 66 A91-52495
Nuclear rocket propulsion. NASA plans and progress, FY 1991 p 77 N91-25179
[NASA-TM-104455]
- CLASPY, P.**
Photoreponse of YBa₂Cu₃O(7-delta) granular and epitaxial superconducting thin films p 141 A91-50443
- CLASPY, P. C.**
Performance of a 300 Mbps 1:16 serial/parallel optoelectronic receiver module p 141 A91-51146
Measurement techniques for cryogenic Ka-band microstrip antennas
[NASA-TM-105183] p 146 N91-30426
- CLASPY, PAUL C.**
Design of an optically controlled Ka-band GaAs MMIC phased-array antenna p 132 A91-24951
- COE, H. H.**
Maximum life spur gear design
[AIAA PAPER 91-2021] p 181 A91-41682
Maximum life spur gear design
[NASA-TM-104361] p 187 N91-23514
- COE, HAROLD H.**
Spur-gear optimization using SPUROPT computer program
[NASA-TM-104394] p 191 N91-31648
- COIRIER, WILLIAM J.**
Numerical flux formulas for the Euler and Navier-Stokes equations. II - Progress in flux-vector splitting
[AIAA PAPER 91-1566] p 5 A91-40740
Efficient real gas upwind Navier-Stokes computations of high speed flows p 157 A91-46179
Numerical flux formulas for the Euler and Navier-Stokes equations. 2: Progress in flux-vector splitting
[NASA-TM-104353] p 15 N91-22084
- COLLINS, JOHN T.**
NTR vehicle commonality assessment for piloted lunar and Mars missions
[AIAA PAPER 91-3575] p 66 A91-52448
- COLOZZA, A.**
SEI power source alternatives for rovers and other multi-kWe distributed surface applications
[NASA-TM-104360] p 81 N91-28277
- COLOZZA, ANTHONY J.**
SEI rover solar-electrochemical power system options
[NASA-TM-104402] p 211 N91-23620
- COLVIN, JAMES E.**
Production and use of metals and oxygen for lunar propulsion
[AIAA PAPER 91-3481] p 125 A91-53711
Production and use of metals and oxygen for lunar propulsion
[NASA-TM-105195] p 81 N91-29222
- CONCUS, PAUL**
Drop-tower experiments for capillary surfaces in an exotic container
[AIAA PAPER 91-0107] p 148 A91-19138
- CONLEY, JULIANNE M.**
Verification of the Proteus two-dimensional Navier-Stokes code for flat plate and pipe flows
[AIAA PAPER 91-2013] p 153 A91-41678
Verification of the proteus two-dimensional Navier-Stokes code for flat plate and pipe flows
[NASA-TM-105160] p 168 N91-30462
- CONLISK, A. T.**
Flow induced vibration and noise by a pair of tandem cylinders due to buffeting p 225 A91-14650
- CONNOLLY, D. J.**
Aerospace applications of high temperature superconductivity
[IAF PAPER 90-054] p 231 A91-13767
High temperature superconductive microwave technology for space applications p 137 A91-31391
ATDRS payload technology R & D p 45 A91-53188
Aerospace applications of high temperature superconductivity p 236 N91-24080
- CONNOLLY, DENIS J.**
High temperature superconductivity technology for advanced space power systems p 50 A91-13447
- COOK, JERRY D.**
An experimental apparatus for measuring surface resistance in the submillimeter-wavelength region p 174 A91-54390
- COOPER, BETH A.**
Noise measurements from an ejector suppressor nozzle in the NASA Lewis 9- by 15-foot low speed wind tunnel
[AIAA PAPER 90-3983] p 225 A91-12496
Noise measurements from an ejector suppressor nozzle in the NASA Lewis 9- by 15-foot low speed wind tunnel
[NASA-TM-103628] p 227 N91-11493
- COOPER, JILL M.**
Thermal emittance enhancement of graphite-copper composites for high temperature space based radiators
[AIAA PAPER 91-3527] p 116 A91-53705
The effect of atomic oxygen on polysiloxane-polyimide for spacecraft applications in low Earth orbit p 229 N91-20735
Thermal emittance enhancement of graphite-copper composites for high temperature space based radiators
[NASA-TM-105178] p 123 N91-29332

- COOPER, MATTHEW F.**
Construction and testing of ceramic fabric heat pipe with water working fluid
[NASA-TM-103332] p 229 N91-18799
- CORBAN, R. R.**
Cryogenic propellant management architectures to support the Space Exploration Initiative
[AIAA PAPER 90-3713] p 124 A91-10112
Cryogenic propellant management system requirements for Space Station Freedom
[AIAA PAPER 91-3476] p 65 A91-52382
Fuel Systems Architecture (FSA) evaluation criteria and concept evaluation methodology
[AIAA PAPER 91-3479] p 65 A91-52384
- CORNILSEN, B. C.**
Raman spectral observation of a new phase observed in nickel electrodes cycled to failure
p 214 N91-32556
- CORRIGAN, ROBERT D.**
Removable hand hold
[NASA-CASE-LEW-15196-1] p 188 N91-26543
- COTTON, J. D.**
Constitution of pseudobinary hypoeutectic beta-NiAl + alpha-V alloys p 109 A91-48509
A simplified method for determining the number of independent slip systems in crystals p 110 A91-55472
- COWLEY, S. J.**
The effect of small streamwise velocity distortion on the boundary layer flow over a thin flat plate with application to boundary layer stability theory
[NASA-TM-103668] p 161 N91-19372
- COY, J. J.**
Analytical and experimental study of vibrations in a gear transmission
[AIAA PAPER 91-2019] p 181 A91-41680
Maximum life spur gear design
[AIAA PAPER 91-2021] p 181 A91-41682
Gear noise, vibration, and diagnostic studies at NASA Lewis Research Center p 183 A91-52811
Maximum life spur gear design
[NASA-TM-104361] p 187 N91-23514
Analytical and experimental study of vibrations in a gear transmission
[NASA-TM-104434] p 187 N91-25395
- COY, JOHN J.**
Overview of rotorcraft and general aviation propulsion technology p 29 N91-20112
- CRAIG, NEIL C.**
Experimental water droplet impingement data on modern aircraft surfaces
[AIAA PAPER 91-0445] p 2 A91-21493
- CROSS, ELDON R.**
Dual-purpose self-deliverable lunar surface PV electrical power system p 209 N91-19200
- CRUSE, T. A.**
Probability approach for strength calculations p 204 N91-24652
- CULL, RONALD C.**
An analysis of space power system masses p 54 A91-38003
Lunar orbiting microwave beam power system p 56 A91-38158
Applications of thin film technology toward a low-mass solar power satellite p 235 N91-22179
- CULLERS, C. L.**
1000 to 1200 K time-dependent compressive deformation of single-crystalline and polycrystalline B2 Ni-40Al p 109 A91-43670
- CURRAN, FRANCIS M.**
High-power hydrogen arcjet performance
[AIAA PAPER 91-2226] p 61 A91-45795
Preliminary performance and life evaluation of a 2-kW arcjet
[AIAA PAPER 91-2228] p 62 A91-45796
Arcjet thermal characteristics
[AIAA PAPER 91-2456] p 63 A91-45814
Performance characterization of a segmented anode arcjet thruster
[NASA-TM-103227] p 67 N91-10118
Arcjet nozzle area ratio effects p 75 N91-24271
Arcjet thermal characteristics
[NASA-TM-105156] p 82 N91-29231
Preliminary performance and life evaluations of a 2-kW arcjet
[NASA-TM-105149] p 84 N91-30252
Medium power hydrogen arcjet performance
[NASA-TM-104533] p 85 N91-31216
- CURTIS, H. B.**
Systems analysis of Mars solar electric propulsion vehicles
[AIAA PAPER 90-3824] p 40 A91-10176
Lightweight concentrator module with 30 percent AMO efficient GaAs/GaSb tandem cells p 57 A91-41990
23.5 percent thin-film space concentrator cells p 58 A91-42002
- Solar electric propulsion for Mars transport vehicles
[NASA-TM-103234] p 71 N91-19178
Thermal annealing of GaAs concentrator solar cells p 208 N91-19195
Effect of dislocations on properties of heteroepitaxial InP solar cells p 213 N91-30209
- CURTIS, HENRY B.**
Design considerations for lunar base photovoltaic power systems p 41 A91-41987
Design considerations for lunar base photovoltaic power systems
[NASA-TM-103642] p 241 N91-14259
- ## D
- DALSANIA, VITHAL**
Finite element analysis of thermal distortion effects on optical performance of solar dynamic concentrator for Space Station Freedom
[NASA-TM-102504] p 183 N91-12954
- DARLING, DOUGLAS**
Scaling analysis applied to the NORVEX code development and thermal energy flight experiment
[AIAA PAPER 91-1420] p 155 A91-44337
Scaling analysis applied to the NORVEX code development and thermal energy flight experiment
[NASA-TM-104462] p 166 N91-24549
- DARYOUSH, A. S.**
Bit error rate testing of fiber optic data links for MMIC-based phased array antennas p 131 A91-24950
- DAVIDIAN, KENNETH J.**
A rocket engine design expert system p 71 N91-17129
Design strategies for the International Space University's variable gravity research facility p 42 N91-22171
The International Space University's variable gravity research facility design
[NASA-TM-105224] p 44 N91-31196
- DAVIDIAN, KENNETH O.**
Analytical study of nozzle performance for nuclear thermal rockets
[AIAA PAPER 91-3578] p 66 A91-52451
Developments in REDES: The rocket engine design expert system
[NASA-TM-103657] p 67 N91-10119
- DAVIS, D. O.**
Experimental investigation of a single flush-mounted hypermixing nozzle
[AIAA PAPER 90-5240] p 21 A91-14466
Progress toward synergistic hypermixing nozzles
[AIAA PAPER 91-2264] p 25 A91-45800
Evaluation of a technique to generate artificially thickened boundary layers in supersonic and hypersonic flows
[NASA-TP-3142] p 17 N91-28136
Progress toward synergistic hypermixing nozzles
[NASA-TM-105169] p 18 N91-29150
- DAVIS, DAVID O.**
Experimental investigation of a single flush-mounted hypermixing nozzle
[NASA-TM-103726] p 161 N91-19374
Experimental investigation of turbulent flow through a circular-to-rectangular transition duct
[NASA-TM-105210] p 18 N91-31106
- DAVIS, JON A.**
A high-efficiency ferruleless coupled-cavity traveling-wave tube with phase-adjusted taper p 136 A91-25078
- DAVOUDZADEH, F.**
Navier-Stokes simulation of transonic blade-vortex interactions p 2 A91-21065
- DAY, G. W.**
A fiber-optic current sensor for aerospace applications p 171 A91-23005
A fiber-optic current sensor for aerospace applications p 172 A91-38006
Fiber-optic sensors for aerospace electrical measurements: An update
[NASA-TM-104454] p 177 N91-25381
- DAYTON, JAMES A., JR.**
High power, high efficiency millimeter wavelength traveling wave tubes for high rate communications from deep space
[AIAA PAPER 91-3593] p 142 A91-52461
Status of Ka-band TWT transmitter technology
[AIAA PAPER 91-3621] p 142 A91-52485
- DE GROOT, WIM A.**
The development of a fiber optic Raman temperature measurement system for rocket flows
[AIAA PAPER 91-2316] p 173 A91-45804
- DE WITT, K. J.**
Test-cell pressure effects on the performance of resistojets p 38 A91-37417
- DE WITT, KENNETH J.**
New approach in direct-simulation of gas mixtures
[AIAA PAPER 91-1343] p 154 A91-43412
- DE, BHOLA N.**
Diamondlike carbon as a moisture barrier and antireflecting coating on optical materials p 119 N91-18302
Diamondlike carbon applications in infrared optics and microelectronics p 230 N91-18306
- DEADMORE, DANIEL L.**
Quality control of the tribological coating PS212
[NASA-TM-102067] p 101 N91-25186
- DEANGELO, F. L.**
Peeled film GaAs solar cell development p 139 A91-41889
- DEARBORN, DAVID S.**
The shock process and light-element production in supernova envelopes p 239 A91-33573
- DEBONIS, JAMES R.**
Experimental and analytical studies of flow through a ventral and axial exhaust nozzle system for STOVL aircraft
[AIAA PAPER 91-2135] p 25 A91-45791
Experimental and analytical studies of flow through a ventral and axial exhaust nozzle system for STOVL aircraft
[NASA-TM-104364] p 77 N91-25175
- DECKER, ARTHUR J.**
Three-dimensional computed tomography from interferometric measurements within a narrow cone of views
[NASA-TM-103257] p 176 N91-19404
Optical inspection of space-propulsion components using an injection seeded Nd:YAG laser system p 179 N91-24320
- DEGROH, KIM K.**
Atomic oxygen undercutting of LDEF aluminized Kapton multilayer insulation p 229 N91-25027
Low Earth orbital atomic oxygen micrometeoroid, and debris interactions with photovoltaic arrays p 84 N91-30248
- DEGUIRE, MARK R.**
Spatial variations in a.c. susceptibility and microstructure for the YBa₂Cu₃O_{7-x} superconductor and their correlation with room-temperature ultrasonic measurements p 233 A91-54969
Spatial variations in a.c. susceptibility and microstructure for the YBa₂Cu₃O_{7-x} superconductor and their correlation with room-temperature ultrasonic measurements
[NASA-TM-103787] p 194 N91-21553
The series Bi₂Si₂Ca(n-1) Cu(n)O(2n+4) (1 less than or equal to n less than or equal to 5): Phase stability and superconducting properties
[NASA-TM-103749] p 235 N91-21910
Ultrasonic evaluation of oxidation and reduction effects on the elastic behavior and global microstructure of YBa₂Cu₃O_{7-x}
[NASA-TM-104529] p 194 N91-27575
- DESSLER, ROBERT G.**
Numerical solution for the velocity-derivative skewness of a low Reynolds-number turbulent-like decaying Navier-Stokes flow p 158 A91-50204
Comment on local energy transfer and nonlocal interactions in homogeneous, isotropic turbulence (Phys. Fluids A2, 413 (1990)) p 159 N91-13638
Turbulent fluid motion: Part 1: The phenomenon of fluid turbulence
[NASA-TM-103723] p 162 N91-20445
Turbulent fluid motion 2: Scalars, vectors, and tensors
[NASA-TM-103756] p 167 N91-27487
- DELAAT, JOHN C.**
Turbolane engine demonstration of sensor failure detection p 22 A91-29775
- DELLACORTE, CHRISTOPHER**
Tribological properties of PM212 - A high temperature, self-lubricating, powder metallurgy composite
[STLE PREPRINT 90-AM-4E-1] p 87 A91-19720
A new test machine for measuring friction and wear in controlled atmospheres to 1200 C p 180 A91-33600
Tribological properties of Ag/Ti films on Al₂O₃ ceramic substrates
[NASA-TM-103784] p 89 N91-19224
Mechanical strength and thermophysical properties of PM212: A high temperature self-lubricating powder metallurgy composite
[NASA-TM-103694] p 120 N91-21302
Tribological characteristics of silicon carbide whisker-reinforced alumina at elevated temperatures
[NASA-TM-103799] p 89 N91-22379
Quality control of the tribological coating PS212
[NASA-TM-102067] p 101 N91-25186
Sliding wear of self-mated Al₂O₃-SiC whisker reinforced composites at 23-1200 C
[NASA-TM-104490] p 90 N91-27221

- Method of making carbide/fluoride/silver composites
[NASA-CASE-LEW-14902-1] p 102 N91-27244
An analysis of the wear behavior of SiC whisker reinforced alumina from 25 to 1200 C
[NASA-TM-104489] p 90 N91-29235
High temperature NASP engine seals: A technology review
[NASA-TM-104468] p 190 N91-30538
- DELOMBARD, RICHARD**
Vibration environment - Acceleration mapping strategy and microgravity requirements for Spacelab and Space Station
[IAF PAPER 90-350] p 39 A91-13991
- DELVIGS, PETER**
Vinyl capped addition polyimides
[NASA-CASE-LEW-15027-1] p 118 N91-13566
- DEMUREN, A. O.**
Calculation of turbulence-driven secondary motion in ducts with arbitrary cross section p 151 A91-34132
Calculation of turbulent flow in complex geometries with a second-moment closure model p 152 A91-38741
Characteristics of 3D turbulent jets in crossflow p 158 A91-54268
Characteristics of 3D turbulent jets in crossflow
[NASA-TM-104337] p 165 N91-22536
- DEVER, JOYCE A.**
Evaluation of thermal control coatings for use on solar dynamic radiators in low earth orbit
[AIAA PAPER 91-1327] p 58 A91-43397
Low Earth orbital atomic oxygen and ultraviolet radiation effects on polymers
[NASA-TM-103711] p 119 N91-19294
Evaluation of thermal control coatings for use on solar dynamic radiators in low Earth orbit
[NASA-TM-104335] p 73 N91-22367
- DEVER, THERESE**
Graphite fluoride fibers and their applications in the space industry
[NASA-TM-103265] p 88 N91-11062
- DEWITT, KENNETH**
Three-dimensional flows in a transonic compressor rotor p 8 A91-56152
- DEWITT, KENNETH J.**
Pressure measurements in a low-density nozzle plume for code verification
[AIAA PAPER 91-2110] p 61 A91-45783
Pressure measurements in a low-density nozzle plume for code verification
[NASA-TM-105170] p 81 N91-29228
- DIB, NIHAD I.**
Theoretical and experimental characterization of coplanar waveguide discontinuities for filter applications p 137 A91-35911
- DICARLO, J.**
The structure of carbon in chemically vapor deposited SiC monofilaments p 113 A91-18675
- DICARLO, JAMES A.**
Fiber creep evaluation by stress relaxation measurements p 117 A91-56905
A simple test for thermomechanical evaluation of ceramic fibers
[NASA-TM-103767] p 121 N91-21309
- DIETRICH, DANIEL L.**
Fire suppression in human-crew spacecraft
[NASA-TM-104334] p 44 N91-21182
- DIFILIPPO, FRANK**
Atomic oxygen undercutting of defects on SiO₂ protected polyimide solar array blankets p 116 A91-49803
- DINGLE, B. D.**
23.5 percent thin-film space concentrator cells p 58 A91-42002
- DIPIETRO, M. S.**
Compression behavior of TiB₂-particulate-reinforced composites of Al₂Fe₃Ti₈ p 91 A91-28014
Low-density, high-strength intermetallic matrix composites by XD (trademark) synthesis
[NASA-TM-103724] p 97 N91-19233
- DISKIN, G.**
Two-dimensional imaging of molecular hydrogen in H₂-air diffusion flames using two-photon laser-induced fluorescence p 124 A91-34369
- DITTMAR, JAMES H.**
The effect of swirl recovery vanes on the cruise noise of an advanced propeller
[AIAA PAPER 90-3932] p 224 A91-12448
The effect of swirl recovery vanes on the cruise noise of an advanced propeller
[NASA-TM-103625] p 227 N91-11494
Potential reduction of en route noise from an advanced turboprop aircraft
[NASA-TM-103635] p 228 N91-15842
Ultra-high bypass research p 30 N91-20117
- DOEBERLING, THOMAS J.**
Update on results of SPRE testing at NASA Lewis
[NASA-TM-104425] p 79 N91-27208
- DOHERTY, MICHAEL P.**
Blazing the railway - Nuclear electric propulsion and its technology program plans p 64 A91-52353
[AIAA PAPER 91-3441]
Finite element analysis of thermal distortion effects on optical performance of solar dynamic concentrator for Space Station Freedom
[NASA-TM-102504] p 183 N91-12954
- DOLCE, JAMES L.**
Automated electric power management and control for Space Station Freedom p 53 A91-37970
Automating security monitoring and analysis for Space Station Freedom's electric power system p 219 A91-37975
Electric power scheduling - A distributed problem-solving approach p 219 A91-37976
An expert system for simulating electric loads aboard Space Station Freedom p 55 A91-38041
- DOLHERT, LEONARD E.**
Spatial variations in a.c. susceptibility and microstructure for the YBa₂Cu₃O_{7-x} superconductor and their correlation with room-temperature ultrasonic measurements p 233 A91-54969
Spatial variations in ac susceptibility and microstructure for the YBa₂Cu₃O_{7-x} superconductor and their correlation with room-temperature ultrasonic measurements p 194 N91-21553
[NASA-TM-103787]
Ultrasonic evaluation of oxidation and reduction effects on the elastic behavior and global microstructure of YBa₂Cu₃O_{7-x}
[NASA-TM-104529] p 194 N91-27575
- DOWELL, EARL H.**
Role of artificial viscosity in Euler and Navier-Stokes solvers p 4 A91-34135
- DOWNEY, A. N.**
Low-temperature microwave characteristics of pseudomorphic In(x)Ga(1-x) As/In(0.52)Al(0.48)As modulation-doped field-effect transistors p 136 A91-22987
- DRAPER, S. L.**
Factors which influence tensile strength of a SiC/Ti-24Al-11Nb (at. pct) composite p 92 A91-55900
- DRAVID, NARAYAN V.**
Modeling of Space Station electric power system with EMTF p 55 A91-38040
An EMTF system level model of the PMAD DC test bed
[NASA-TM-104515] p 79 N91-27206
- DRESHFIELD, R. L.**
The effect of hydrogen on the low cycle fatigue behavior of a single crystal superalloy p 108 A91-28794
- DRUMMOND, CHARLES H., III**
Crystallization and properties of Sr-Ba aluminosilicate glass-ceramic matrices p 117 A91-56917
Crystallization and properties of Sr-Ba aluminosilicate glass-ceramic matrices
[NASA-TM-103764] p 120 N91-19308
Crystallization and characterization of Y₂O₃-SiO₂ glasses p 237 N91-31962
- DRUMMOND, COLIN K.**
Transient flow thrust prediction for an ejector propulsion concept p 24 A91-45326
An AD100 implementation of a real-time STOVLC aircraft propulsion system
[NASA-TM-103683] p 26 N91-13457
- DRYER, FREDERICK L.**
N-decane droplet combustion in the NASA-Lewis 5 Second Zero-Gravity Facility - Results in test gas environments other than air p 105 A91-19433
[AIAA PAPER 91-0720]
- DUCKERT, ROB E.**
Thermomechanical and bithermal fatigue behavior of cast B1900 + Hf and wrought Haynes 188
[NASA-TM-4225] p 111 N91-20268
- DUDENHOEFER, JAMES E.**
Programmatic status of NASA's CSTI High Capacity Power Stirling Space Power Converter Program p 53 A91-37933
Recent Stirling engine loss-understanding results p 181 A91-38151
Further two-dimensional code development for Stirling space engine components p 56 A91-38184
Stirling machine operating experience p 212 N91-25510
[NASA-TM-104487]
Status of NASA's Stirling Space Power Converter Program p 214 N91-32569
[NASA-TM-104512]
- DUDZINSKI, L. A.**
Nuclear electric propulsion mission performance for fast piloted Mars missions
[AIAA PAPER 91-3488] p 65 A91-52388
- DUFFY, STEPHEN F.**
Structural reliability analysis of laminated CMC components p 119 N91-19292
[NASA-TM-103685]
- Structural design methodologies for ceramic-based material systems p 121 N91-22460
[NASA-TM-103097]
- DUGGAN, M. B.**
Temperature dependence of the elastic moduli and damping for polycrystalline LiF-22 pct CaF₂ eutectic salt p 87 A91-33793
- DUNCAN, BEVERLY**
CFD analysis of a hydrogen fueled ramjet engine at Mach 3.44 p 23 A91-41653
[AIAA PAPER 91-1919]
- DUNCAN, D. B.**
Development of a Fabry-Perot interferometer for rocket engine plume monitoring p 171 A91-30634
Space Shuttle Main Engine nozzle mounted optic for throat plane spectroscopy p 49 A91-45816
[AIAA PAPER 91-2524]
- DURAJ, STAN A.**
Reactivity of pi-complexes of Ti, V, and Nb towards dithioacetic acid: Synthesis and structure of novel metal sulfur-containing complexes p 106 N91-19256
[NASA-TM-103666]
Synthesis and structures of metal chalcogenide precursors p 120 N91-19296
[NASA-TM-103665]
- DURAND, RICHARD E.**
Lunar electric power systems utilizing the SP-100 reactor coupled to dynamic conversion systems p 208 A91-52415
[AIAA PAPER 91-3520]
- DUSTIN, MILES O.**
Solar thermal energy receiver p 211 N91-23617
[NASA-CASE-LEW-14949-1]
Solar dynamic power for Earth orbital and lunar applications p 80 N91-27214
[NASA-TM-104511]
- DUVAL, W. M.**
Growth kinetics of physical vapor transport processes: Crystal growth of the optoelectronic material mercurous chloride p 128 N91-19320
[NASA-TM-103788]
- DUVAL, WALTER M. B.**
Interfacial dynamics of two liquids under an oscillating gravitational field p 148 A91-16062
Interaction of surface radiation with convection in crystal growth by physical vapor transport p 127 A91-24563
- DUYAR, A.**
Real-time diagnostics of the reusable rocket engine using on-line system identification p 223 A91-30630
A distributed fault-detection and diagnosis system using on-line parameter estimation p 220 N91-25696
[NASA-TM-104433]
- DUYAR, AHMET**
A simplified dynamic model of the Space Shuttle main engine p 131 N91-23340
[NASA-TM-104421]
- DUYAR, ALMET**
Alpha-canonical form representation of the open loop dynamics of the Space Shuttle main engine p 131 N91-24469
[NASA-TM-104422]

E

- ECKEL, ANDREW J.**
Hydrogen-silicon carbide interactions p 114 A91-28783
Ceramic composites for rocket engine turbines
[SAE PAPER 911108] p 92 A91-53552
Thermal shock fiber-reinforced ceramic matrix composites p 93 A91-56935
Effect of hydrogen on the strength and microstructure of selected ceramics p 118 N91-14482
[NASA-TM-103674]
Ceramic composites for rocket engine turbines p 98 N91-19235
[NASA-TM-103743]
Thermal shock of fiber reinforced ceramic matrix composites p 120 N91-19295
[NASA-TM-103777]
- ECKLES, WILLIAM E.**
Synthesis and structures of metal chalcogenide precursors p 120 N91-19296
[NASA-TM-103665]
- EDELMAN, RAYMOND B.**
Radiation from gas-jet diffusion flames in microgravity environments p 104 A91-19432
[AIAA PAPER 91-0719]
- EDGAR, J. H.**
Controlled growth of 3C-SiC and 6H-SiC films on low-tilt-angle vicinal (0001) 6H-SiC wafers p 232 A91-45713
Application of oxidation to the structural characterization of SiC epitaxial films p 233 A91-45881

F

EDWARDS, PHILLIP M.

Mechanical strength and thermophysical properties of PM212: A high temperature self-lubricating powder metallurgy composite
[NASA-TM-103694] p 120 N91-21302

EISEMAN, PETER R.

Dynamics of local grid manipulations for internal flow problems p 164 N91-21090

EISENBERG, JOSEPH D.

The selection of convertible engines with current gas generator technology for high speed rotorcraft
[NASA-TM-103774] p 27 N91-19097
Overview of rotorcraft and general aviation propulsion technology p 29 N91-20112

EL-GENK, MOHAMED S.

Preliminary assessment of the power requirements of a manned rover for Mars missions p 41 A91-27702
A comparison of energy conversion systems for meeting the power requirements of manned rover for Mars missions p 53 A91-37932

EL-MEHLAWY, F.

Heat transfer in oscillating flows p 152 A91-38698

ELDEM, VASFI

A simplified dynamic model of the Space Shuttle main engine
[NASA-TM-104421] p 131 N91-23340
Alpha-canonical form representation of the open loop dynamics of the Space Shuttle main engine
[NASA-TM-104422] p 131 N91-24469

ELDRIDGE, J. I.

Factors which influence tensile strength of a SiC/Ti-24Al-11Nb (at pct) composite p 92 A91-55900
Investigation of interfacial shear strength in SiC/Si3N4 composites p 93 A91-56913
Investigation of interfacial shear strength in SiC/Si3N4 composites
[NASA-TM-103739] p 101 N91-26233

ELLIS, C.

Selective and low temperature synthesis of polycrystalline diamond p 232 A91-42170

ELLIS, DAVID L.

Advanced materials for space nuclear power systems
[AIAA PAPER 91-3530] p 88 A91-53704
Advanced materials for space nuclear power systems
[NASA-TM-105171] p 112 N91-29298

ELLIS, J. RODNEY

Current activities in standardization of high-temperature, low-cycle-fatigue testing techniques in the United States
[NASA-TM-103675] p 200 N91-17427

EMERY, K. A.

Primary reference cell calibrations at SERI - History and methods p 207 A91-41966

ENGLISH, ROBERT E.

Evolving the SP-100 reactor in order to boost large payloads to GEO and to low lunar orbit via nuclear-electric propulsion
[AIAA PAPER 91-3562] p 67 A91-53712
Evolving the SP-100 reactor in order to boost large payloads to GEO and to low lunar orbit via nuclear-electric propulsion
[NASA-TM-104527] p 80 N91-27212
On-Sherby-Dorn creep strengths of the refractory-metal alloys C-103, ASTAR-811C, W-5Re, and W-25Re
[NASA-TM-105228] p 87 N91-32165

ENVIA, E.

Near-field noise of a single rotation propfan at an angle of attack
[AIAA PAPER 90-3953] p 225 A91-12469
Near-field noise of a single-rotation propfan at an angle of attack
[NASA-TM-103645] p 227 N91-12316

ERLEBACHER, GORDON

On the continuous spectra of the compressible boundary layer stability equations p 150 A91-31342

ESGAR, JACK B.

Structural properties of laminated Douglas fir/epoxy composite material
[NASA-RP-1236] p 94 N91-10127

ESKER, BARBARA S.

Experimental and analytical studies of flow through a ventral and axial exhaust nozzle system for STOVL aircraft
[AIAA PAPER 91-2135] p 25 A91-45791
Experimental and analytical studies of flow through a ventral and axial exhaust nozzle system for STOVL aircraft
[NASA-TM-104364] p 77 N91-25175

EUSTACE, J. G.

Compensation for effects of ambient temperature on rare-earth doped fiber optic thermometer p 170 A91-19582

EUSTACE, JOHN G.

Optical techniques for determination of normal shock position in supersonic flows for aerospace applications p 174 A91-55530

FACCA, L.

Particle cloud flames in acoustic fields p 105 A91-20589

FACCA, L. T.

Radiative structures of lycopodium-air flames in low gravity p 105 A91-30003

Particle nonuniformity effects on particle cloud flames in low gravity
[AIAA PAPER 91-0718] p 104 A91-19431

FADDOUL, JAMES R.

The NASA Cryogenic Fluid Management Technology Program Plan
[AIAA PAPER 91-3553] p 130 A91-52436
The NASA cryogenic fluid management technology program plan
[NASA-TM-105256] p 86 N91-32161

FAGHRI, A.

A PCM/forced convection conjugate transient analysis of energy storage systems with annular and countercurrent flows p 150 A91-27166

FAGHRI, AMIR

Analysis of the one-dimensional transient compressible vapor flow in heat pipes p 157 A91-47735

FARMER, S. C.

Silsesquioxane-derived ceramic fibres p 114 A91-30283

FARMER, SERENE C.

Sliding wear of self-mated Al2O3-SiC whisker reinforced composites at 23-1200 C
[NASA-TM-104490] p 90 N91-27221

FAROKHI, S.

Modern developments in shear flow control with swirl p 3 A91-24519

FAROKHI, SAEED

A study of three dimensional turbulent boundary layer separation and vortex flow control using the reduced Navier Stokes equations
[NASA-TM-104407] p 16 N91-23089

FARRELL, DAVID E.

The series Bi2Sr2Ca(n-1)Cu(n)O(2n+4) (1 less than or equal to n less than or equal to 5): Phase stability and superconducting properties
[NASA-TM-103749] p 235 N91-21910

FATEMI, N.

A comparative study of p(+)n and n(+)p InP solar cells made by a closed ampoule diffusion p 212 N91-30206

FATEMI, NAVID S.

An analysis of the contact sintering process in III-V solar cells p 139 A91-41891
The influence of interstitial Ga and interfacial Au2P3 on the electrical and metallurgical behavior of Au-contacted III-V semiconductors p 140 A91-42694
An x ray photoelectron spectroscopy study of Au(x)In(y) alloys
[NASA-TM-103659] p 234 N91-14050
Semiconductor structural damage attendant to contact formation in III-V solar cells p 209 N91-19203
A comparative study of performance parameters of n(+)p InP solar cells made by closed-ampoule sulfur diffusion into Cd- and Zn-doped p-type InP substrates p 210 N91-19209
Improvements in contact resistivity and thermal stability of Au-contacted InP solar cells p 213 N91-30207
Grooved surfaces on InP p 213 N91-30208

FAUR, M.

A comparative study of p(+)n and n(+)p InP solar cells made by a closed ampoule diffusion p 212 N91-30206
A comparative study of p(+)n and n(+)p InP solar cells made by a closed ampoule diffusion p 212 N91-30206

Effect of dislocations on properties of heteroepitaxial InP solar cells p 213 N91-30209

FAUR, MARIA

Study of surface passivation as a function of InP closed-ampoule solar cell fabrication processing variables p 232 A91-41893
Measurement of surface recombination velocity on heavily doped indium phosphide p 232 A91-41931
Investigation of anodic and chemical oxides grown on p-type InP with applications to surface passivation for n(+)p solar cell fabrication p 210 N91-19208
A comparative study of performance parameters of n(+)p InP solar cells made by closed-ampoule sulfur diffusion into Cd- and Zn-doped p-type InP substrates p 210 N91-19209
High resolution electrolyte for thinning InP by anodic dissolution and its applications to EC-V profiling, defect revealing and surface passivation p 107 N91-30210

FAUR, MIRCEA

Study of surface passivation as a function of InP closed-ampoule solar cell fabrication processing variables p 232 A91-41893

Measurement of surface recombination velocity on heavily doped indium phosphide p 232 A91-41931
Investigation of anodic and chemical oxides grown on p-type InP with applications to surface passivation for n(+)p solar cell fabrication p 210 N91-19208
A comparative study of performance parameters of n(+)p InP solar cells made by closed-ampoule sulfur diffusion into Cd- and Zn-doped p-type InP substrates p 210 N91-19209

High resolution electrolyte for thinning InP by anodic dissolution and its applications to EC-V profiling, defect revealing and surface passivation p 107 N91-30210

FAUT, OWEN D.

Acidic attack of perfluorinated alkyl ether lubricant molecules by metal oxide surfaces p 104 A91-13439

FAY, EDGAR H.

Lunar orbiting microwave beam power system p 56 A91-38158

FAYMON, KARL A.

High temperature superconductivity technology for advanced space power systems p 50 A91-13447
Microwave beam powered Mars airplane p 52 A91-37931

Power technologies and the space future
[NASA-TM-103649] p 73 N91-21240

FEILER, CHARLES E.

Institute for Computational Mechanics in Propulsion (ICOMP)
[NASA-TM-103790] p 222 N91-24818

FEINGOLD, HARVEY

NTR vehicle commonality assessment for piloted lunar and Mars missions
[AIAA PAPER 91-3575] p 66 A91-52448

FERBER, M. K.

Elevated-temperature fracture resistances (K(sub IC), R-curves, gamma sub (omega OF)) of monolithic and composite ceramics using chevron-notched, bend tests
[NASA-TM-105090] p 123 N91-28418

FERENCZ, DONALD C.

ALPS: A Linear Program Solver
[NASA-TM-104347] p 216 N91-20765

FERGUSON, D. C.

Electrical system/environment interactions on the planet Mars p 242 N91-27068

FERGUSON, DALE C.

Atomic oxygen effects on refractory materials p 88 A91-49809
Findings of the Joint Workshop on Evaluation of Impacts of Space Station Freedom Ground Configurations p 48 N91-20728
Findings of the Joint Workshop on Evaluation of Impacts of Space Station Freedom Ground Configurations
[NASA-TM-103717] p 73 N91-22370
Leo space plasma interactions p 84 N91-30249

FERRANTE, JOHN

Global expression for representing diatomic potential-energy curves p 228 A91-33236
Adhesion at metal interfaces p 88 A91-38581
Universal behavior in ideal slip p 110 A91-48517
Universal energy relations and metal/ceramic interfaces p 93 A91-56254
Equivalent crystal theory of alloys
[NASA-TP-3155] p 112 N91-30318
A new approximate sum rule for bulk alloy properties
[NASA-TM-105282] p 112 N91-32204
Theoretical modelling of AFM for bimetallic tip-substrate interactions
[NASA-TM-105280] p 112 N91-32215

FERRARO, P. J.

Flow visualization studies of the internal flow characteristics in a simulated mixed flow vectored thrust ASTOVL engine configuration
[AIAA PAPER 91-1689] p 23 A91-42556

FERTIS, DEMETER G.

Dynamic analysis of space-related linear and non-linear structures p 196 A91-28612

FINAN, VALERIE

The series Bi2Sr2Ca(n-1)Cu(n)O(2n+4) (1 less than or equal to n less than or equal to 5): Phase stability and superconducting properties
[NASA-TM-103749] p 235 N91-21910

FINKMAN, ELIEZER

Surface and implantation effects on p-n junctions p 234 N91-18299
Properties of insulator interfaces with p-HgCdTe p 235 N91-18300
Surface electrons in inverted layers of p-HgCdTe p 235 N91-18301

FINN, ROBERT

Drop-tower experiments for capillary surfaces in an exotic container
[AIAA PAPER 91-0107] p 148 A91-19138

FITE, E. BRIAN

A three-dimensional finite-element thermal/mechanical analytical technique for high-performance traveling wave tubes
[NASA-TP-3081] p 134 N91-27436

FLATICO, JOSEPH M.

Silicon-etalon fiber-optic temperature sensor
p 170 A91-19581

FLEETER, S.

The aerodynamics of an oscillating cascade in a compressible flow field
[ASME PAPER 89-GT-271] p 1 A91-13047

FLEETER, SANFORD

Oscillating cascade aerodynamics by an experimental influence coefficient technique p 1 A91-10339
Experimental investigation of oscillating cascade aerodynamics p 3 A91-27801
Wind tunnel wall effects in a linear oscillating cascade [NASA-TM-103690] p 27 N91-19098

FLEMING, DAVID P.

Magnetic bearings-state of the art
[NASA-TM-104465] p 188 N91-25413

FLEMING, MICHAEL L.

On protection of Freedom's solar dynamic radiator from the orbital debris environment. Part 2: Further testing and analyses
[NASA-TM-104514] p 84 N91-30265

FLEMMING, ROBERT J.

Icing tests of a model main rotor p 18 A91-17218
Results of a sub-scale model rotor icing test p 140 A91-26190
[AIAA PAPER 91-0660] p 19 A91-26190
Results of a sub-scale model rotor icing test [NASA-TM-103709] p 11 N91-14309
Model rotor icing tests in the NASA Lewis icing research tunnel [NASA-TM-104351] p 32 N91-23184

FLOOD, D. J.

Effect of emitter parameter variation on the performance of heteroepitaxial indium phosphide solar cells
p 140 A91-42003
A comparative study of p(+)n and n(+)p InP solar cells made by a closed ampoule diffusion p 212 N91-30206
Comparative modeling of InP solar cell structures p 83 N91-30232

FLOOD, DENNIS J.

Solar radiation on Mars p 242 A91-28153
Monolithic and mechanical multijunction space solar cells p 54 A91-38020
Photovoltaic options for solar electric propulsion [NASA-TM-103284] p 68 N91-11061
Solar radiation on Mars: Update 1990 [NASA-TM-103623] p 242 N91-15117
Effect of emitter parameter variation on the performance of heteroepitaxial indium phosphide solar cells [NASA-TM-103619] p 70 N91-15306
Dual-purpose self-deliverable lunar surface PV electrical power system p 209 N91-19200
Effect of dislocations on the open-circuit voltage, short-circuit current and efficiency of heteroepitaxial indium phosphide solar cells [NASA-TM-103762] p 144 N91-19354
Optimal design study of high efficiency indium phosphide space solar cells [NASA-TM-103763] p 145 N91-21433
Future mission opportunities and requirements for advanced space photovoltaic energy conversion technology [NASA-TM-103661] p 74 N91-22371
Advanced power systems for EOS [NASA-TM-105222] p 85 N91-31217
Thin film, concentrator and multijunction space solar cells: Status and potential [NASA-TM-104505] p 86 N91-31218

FLOOD, J. D.

STOVL Hot Gas Ingestion control technology [ASME PAPER 89-GT-323] p 22 A91-23642
Flow visualization studies of the internal flow characteristics in a simulated mixed flow vectored thrust ASTOVL engine configuration [AIAA PAPER 91-1689] p 23 A91-42556

FLOOD, JOSEPH D.

Hot gas ingestion test results of a two-poster vectored thrust concept with flow visualization in the NASA Lewis 9- by 15-foot low speed wind tunnel [AIAA PAPER 90-2268] p 4 A91-40561
Hot gas ingestion test results of a two-poster vectored thrust concept with flow visualization in the NASA Lewis 9- x 15-foot low speed wind tunnel [NASA-TM-103258] p 15 N91-21116

FORCHIONE, J.

Some recent studies with the solid-ionomer electrochemical capacitor p 214 N91-32562

FORDYCE, J. STUART

Power technologies and the space future [NASA-TM-103649] p 73 N91-21240

FORKAPA, MARK J.

Thermal emittance enhancement of graphite-copper composites for high temperature space based radiators [AIAA PAPER 91-3527] p 116 A91-53705
Thermal emittance enhancement of graphite-copper composites for high temperature space based radiators [NASA-TM-105178] p 123 N91-29332

FORMAN, RALPH

Surface studies on scandate cathodes and synthesized scandates p 136 A91-25071

FOSTER, JOHN E.

Performance and optimization of a 'derated' ion thruster for auxiliary propulsion p 62 A91-45809
[AIAA PAPER 91-2350] p 62 A91-45809
Performance and optimization of a derated ion thruster for auxiliary propulsion [NASA-TM-105144] p 82 N91-29229

FOX, DENNIS S.

Hot corrosion of silicon carbide and silicon nitride at 1000 C p 117 A91-55698

FRAAS, L. M.

The mini-dome Fresnel lens photovoltaic concentrator array - Current status of component and prototype panel testing p 57 A91-41989
Lightweight concentrator module with 30 percent AM0 efficient GaAs/GaSb tandem cells p 57 A91-41990
Tandem concentrator solar cells with 30 percent (AM0) power conversion efficiency p 208 N91-19189

FRAAS, LEWIS M.

Key results of the mini-dome Fresnel lens concentrator array development program under recently completed NASA and SDIO SBIR projects p 83 N91-30223

FRANCISCU, LEO C.

Multi-heat addition turbine engine [NASA-CASE-LEW-15094-1] p 32 N91-23180

FRASCA, A. J.

Neutron and gamma irradiation effects on power semiconductor switches p 139 A91-38162
Neutron, gamma ray and post-irradiation thermal annealing effects on power semiconductor switches [AIAA PAPER 91-3525] p 142 A91-52420
Neutron, gamma ray and post-irradiation thermal annealing effects on power semiconductor switches [NASA-TM-105248] p 147 N91-32410

FRATE, DAVID T.

Nickel-hydrogen cell low-Earth life test update [NASA-TM-105229] p 213 N91-31708

FREDMONSKI, A. J.

Design and experimental evaluation of compact radial-inflow turbines [AIAA PAPER 91-2127] p 24 A91-45788

FREED, A. D.

The isothermal fatigue behavior of a unidirectional SiC/Ti composite and the Ti alloy matrix p 93 A91-55907
Asymptotic integration algorithms for nonhomogeneous, nonlinear, first order, ordinary differential equations [NASA-TM-103793] p 222 N91-21797

FREED, ALAN D.

Equivalence of Green's function and the Fourier series representation of composites with periodic microstructure p 91 A91-16889
An overview of self-consistent methods for fiber-reinforced composites [NASA-TM-103713] p 97 N91-19232
On the thermodynamics of stress rate in the evolution of back stress in viscoplasticity [NASA-TM-103794] p 201 N91-19476
Progress in modeling deformation and damage p 202 N91-20108

From differential to difference equations for first order ODES [NASA-TM-104530] p 222 N91-27886

Exponential integration algorithms applied to viscoplasticity [NASA-TM-104461] p 223 N91-27901

FREEDMAN, MARC R.

Mechanical behavior and failure phenomenon of an in situ-toughened silicon nitride [NASA-TM-103741] p 121 N91-23311

FREEDMAN, ROBERT J.

Rotating pressure measurement system using an on board calibration standard [NASA-TM-103676] p 176 N91-19401

FREESSE, KATHERINE

Natural inflation with pseudo Nambu-Goldstone bosons p 239 A91-19545

FRICKER, DAVID M.

Flow visualization and hot gas ingestion characteristics of a vectored thrust STOVL concept p 28 N91-20090

FRIEDMAN, ROBERT

Fire suppression in human-crew spacecraft [NASA-TM-104334] p 44 N91-21182

FRIEMAN, JOSHUA A.

Natural inflation with pseudo Nambu-Goldstone bosons p 239 A91-19545

FRIMPONG, STEPHEN

A study of void effects on the interlaminar shear strength of unidirectional graphite fiber reinforced composites [NASA-TM-103267] p 159 N91-12034
Relationship between voids and interlaminar shear strength of polymer matrix composites [NASA-TM-103643] p 95 N91-13495
ICAN sensitivity analysis [NASA-TM-103667] p 96 N91-15328
FRITSCH, KLAUS
Digital angular position sensor using wavelength division multiplexing p 21 A91-19580
Silicon-etalon fiber-optic temperature sensor p 170 A91-19581

FROES, F. H.

Continuous fiber-reinforced titanium aluminide composites p 92 A91-39553

FRYE, ROBERT J.

The development of test beds to support the definition and evolution of the Space Station Freedom power system [NASA-TM-104504] p 79 N91-27207

FUJIKAWA, G.

ATDRS payload technology R & D p 45 A91-53188

FUJIKAWA, GENE

Designs for the ATDRSS tri-band reflector antenna [NASA-TM-103754] p 48 N91-20184

FULMER, CHRISTOPHER R.

Preliminary design of a mobile lunar power supply [NASA-TM-104471] p 212 N91-27611

FUSARO, ROBERT L.

Space mechanisms needs for future NASA long duration space missions [AIAA PAPER 91-3428] p 183 A91-57025
Government/industry response to questionnaire on space mechanisms/tribology technology needs [NASA-TM-104358] p 186 N91-23501
Pretreatment of lubricated surfaces with sputtered cadmium oxide [NASA-CASE-LEW-14474-1] p 123 N91-28423
Space mechanisms needs for future NASA long duration space missions [NASA-TM-105204] p 190 N91-30532

G**GABB, T. P.**

The effect of hydrogen on the low cycle fatigue behavior of a single crystal superalloy p 108 A91-28794
High temperature fatigue behavior of tungsten copper composites p 93 A91-55906
The isothermal fatigue behavior of a unidirectional SiC/Ti composite and the Ti alloy matrix p 93 A91-55907

GABB, TIMOTHY P.

Isothermal fatigue behavior of a (90)(sub 8) SiC/Ti-15-3 composite at 426 C p 99 N91-20228
[NASA-TM-103686] p 99 N91-20228
Tensile and fatigue behavior of tungsten/copper composites p 100 N91-24311
High temperature tension-compression fatigue behavior of a tungsten copper composite [NASA-TM-104370] p 100 N91-24360

GAGLIARDI, ROBERT M.

Optical Multiple Access Network (OMAN) for advanced processing satellite applications [NASA-TM-105167] p 135 N91-29431

GAHN, RANDALL F.

Performance of a dual anode nickel-hydrogen cell p 214 N91-32563

GAIER, J. R.

Effects of Martian dust on power system components p 241 N91-27061

GAIER, JAMES R.

A review of properties and potential aerospace applications of electrically conducting polymers p 113 A91-14409
The preliminary feasibility of intercalated graphite railgun armatures p 137 A91-29257
Resistivity of pristine and intercalated graphite fiber epoxy composites p 115 A91-35949
Electrically conducting polymers for aerospace applications [AIAA PAPER 91-3432] p 233 A91-52349
Intercalated graphite fiber composites as EMI shields in aerospace structures [NASA-TM-103632] p 94 N91-10134
Heat transfer device and method of making the same [NASA-CASE-LEW-14162-1] p 159 N91-13668
Aeolian removal of dust types from photovoltaic surfaces on Mars p 47 N91-19156
Simulation of Martian dust accumulation on surfaces p 47 N91-19160
Prospects for using carbon-carbon composites for EMI shielding [NASA-TM-103677] p 97 N91-19231

- Effects of dust accumulation and removal on radiators surfaces on Mars
[NASA-TM-103704] p 72 N91-20204
- Sensible heat receiver for solar dynamic space power system
[NASA-TM-104393] p 77 N91-25173
- Effects of windblown dust on photovoltaic surfaces on Mars
[NASA-TM-104448] p 78 N91-25183
- Heat transfer device
[NASA-CASE-LEW-14162-2] p 101 N91-25201
- Apparatus for intercalating large quantities of fibrous structures
[NASA-CASE-LEW-15077-2] p 102 N91-28289
- Effect of lightning strike on bromine intercalated graphite fiber/epoxy composites
[NASA-TM-104507] p 103 N91-32177
- GALE, R. P.**
23.5 percent thin-film space concentrator cells
p 58 A91-42002
- GALLAGHER, R. H.**
Integrated force method versus displacement method for finite element analysis p 196 A91-28372
- Compatibility conditions of structural mechanics for finite element analysis p 198 A91-37853
- GALLIMORE, A. D.**
Anode power deposition in an applied-field segmented anode MPD thruster
[AIAA PAPER 91-2343] p 59 A91-44204
- GARG, SANJAY**
Integrated flight/propulsion control system design based on a centralized approach p 36 A91-22950
- Robust eigenspace assignment using singular value sensitivities p 219 A91-29784
- Partitioning methods for global controllers p 219 A91-30043
- Neural network application to aircraft control system design
[AIAA PAPER 91-2715] p 36 A91-49676
- Application of an integrated flight/propulsion control design methodology to a STOVL aircraft
[AIAA PAPER 91-2792] p 36 A91-49793
- Towards practical control design using neural computation
[NASA-TM-103785] p 219 N91-19766
- IMPAC: An Integrated Methodology for Propulsion and Airframe Control
[NASA-TM-103805] p 30 N91-20122
- A method for partitioning centralized controllers
[NASA-TM-4276] p 36 N91-20133
- Integrated flight/propulsion control system design based on a decentralized, hierarchical approach
[NASA-TM-103678] p 31 N91-21137
- Integrated flight/propulsion control design for a STOVL aircraft using H-infinity control design techniques
[NASA-TM-104340] p 31 N91-21140
- Neural network application to aircraft control system design
[NASA-TM-105151] p 37 N91-27167
- Application of an integrated flight/propulsion control design methodology to a STOVL aircraft
[NASA-TM-105254] p 37 N91-32143
- GARLICK, RALPH G.**
High temperature cyclic oxidation data. Part 1: Turbine alloys
[NASA-TM-83665] p 110 N91-10149
- High-temperature cyclic oxidation data. Part 2: Turbine alloys
[NASA-TM-101468] p 110 N91-10150
- GARRETT, MICHAEL J.**
Near-field antenna testing using the Hewlett Packard 8510 automated network analyzer
[NASA-TM-103699] p 144 N91-20393
- GAUG, R. L.**
Three-dimensional flow transport modes in directional solidification during space processing p 128 A91-42642
- GAUG, RONALD**
Computational materials science. An example: Numerical modeling of chemical vapor deposition processing of advanced fibers p 99 N91-20111
- GAUGLER, RAYMOND E.**
Turbomachinery p 162 N91-20097
- Overview of aerothermodynamic loads definition study p 204 N91-24334
- GAYDA, J.**
The effect of hydrogen on the low cycle fatigue behavior of a single crystal superalloy p 108 A91-28794
- GAYDA, JOHN**
The isothermal fatigue behavior of a unidirectional SiC/Ti composite and the Ti alloy matrix p 93 A91-55907
- Isothermal fatigue behavior of a (90)(sub 8) SiC/Ti-15-3 composite at 426 C p 99 N91-20228
- GEBAUER, LINDA**
Atomic oxygen interactions with FEP Teflon and silicones on LDEF p 122 N91-25029
- GEDNEY, RICHARD T.**
Advanced Communications Technology Satellite (ACTS)
[IAF PAPER 90-481] p 44 A91-14056
- GEE, J. M.**
Tandem concentrator solar cells with 30 percent (AMO) power conversion efficiency p 208 N91-19189
- GENERAZIO, E. R.**
Ultrasonic imaging of textured alumina p 191 A91-18596
- GENERAZIO, EDWARD R.**
General-purpose interface bus for multiuser, multitasking computer system p 215 A91-35928
- Nondestructive evaluation tools and experimental studies for monitoring the health of space propulsion systems
[AIAA PAPER 91-3433] p 192 A91-53703
- Thermal shock fiber-reinforced ceramic matrix composites p 93 A91-56935
- Overview of space propulsion systems for identifying nondestructive evaluation and health monitoring opportunities
[NASA-TM-103614] p 192 N91-15565
- Thermal shock of fiber reinforced ceramic matrix composites
[NASA-TM-103777] p 120 N91-19295
- Transition-to-practice technologies for brittle materials p 120 N91-20107
- Nondestructive evaluation tools and experimental studies for monitoring the health of space propulsion systems
[NASA-TM-105164] p 194 N91-28605
- GENG, S. M.**
Design of multihundredwatt DIPS for robotic space missions
[NASA-TM-104401] p 75 N91-24232
- GEORGE, J. A.**
Evolutionary use of nuclear electric propulsion
[AIAA PAPER 90-3821] p 50 A91-10174
- Nuclear electric propulsion mission performance for fast piloted Mars missions
[AIAA PAPER 91-3488] p 65 A91-52388
- GEORGE, JEFFREY A.**
Multimegawatt nuclear power systems for nuclear electric propulsion
[AIAA PAPER 91-3607] p 66 A91-52472
- GEISSNER, K. S.**
Performance impact on nuclear thermal propulsion of piloted Mars missions with short transit times
[AIAA PAPER 91-3401] p 64 A91-52326
- GHALLA-GORADIA, MANJU**
Measurement of surface recombination velocity on heavily doped indium phosphide p 232 A91-41931
- GHORASHI, B.**
Flow visualization and computational studies of a reverse flow circular combustor p 157 A91-48966
- An imaging system for PLIF/Mie measurements for a combustor flow
[NASA-TM-103714] p 27 N91-20084
- GHOSH, ASISH**
Numerical, micro-mechanical prediction of crack growth resistance in a fibre-reinforced/brittle matrix composite p 199 A91-51916
- Elevated-temperature fracture resistances (K(sub IC), R-curves, gamma sub (omega OF)) of monolithic and composite ceramics using chevron-notched, bend tests
[NASA-TM-105090] p 123 N91-28418
- GHOSH, MIHIR K.**
The effect of coatings and liners on heat transfer in a dry shaft-bush tribosystem
[NASA-TM-102513] p 159 N91-12913
- GHOSH, LOUIS J.**
Modeling of crack bridging in a unidirectional metal matrix composite
[NASA-TM-104355] p 205 N91-24660
- GIBALA, R.**
The potential for ductility enhancement from surface and interface dislocation sources in NiAl p 109 A91-39292
- Prospects for ductility and toughness enhancement of NiAl by ductile phase reinforcement
[NASA-TM-103796] p 112 N91-27324
- GILBERT, C.**
Measurement techniques for cryogenic Ka-band microstrip antennas
[NASA-TM-105183] p 146 N91-30426
- GILLAND, J. H.**
Evolutionary use of nuclear electric propulsion
[AIAA PAPER 90-3821] p 50 A91-10174
- Solar electric propulsion for Mars transport vehicles
[NASA-TM-103234] p 71 N91-19178
- Multimegawatt electric propulsion system design considerations
[NASA-TM-105152] p 87 N91-32164
- GILLAND, JAMES H.**
Synergistic use of high and low thrust propulsion systems for piloted missions to Mars
[AIAA PAPER 91-2346] p 39 A91-45807
- GINTY, CAROL A.**
In-service health monitoring of composite structures p 192 A91-51926
- GLADDEN, HERBERT J.**
A unique high heat flux facility for testing hypersonic engine components
[AIAA PAPER 90-5228] p 37 A91-14454
- A unique high heat flux facility for testing hypersonic engine components
[NASA-TM-103238] p 38 N91-11770
- GLASSELL, R. L.**
Manipulation hardware for microgravity research
[NASA-TM-103423] p 128 N91-14498
- GLASSMAN, ARTHUR J.**
Lewis aeropropulsion technology: Remembering the past and challenging the future p 242 N91-20087
- Computer code for single-point thermodynamic analysis of hydrogen/oxygen expander-cycle rocket engines
[NASA-TM-4275] p 72 N91-20206
- GLESK, I.**
Two-dimensional imaging of molecular hydrogen in H2-air diffusion flames using two-photon laser-induced fluorescence p 124 A91-34369
- GLICKSMAN, M. E.**
Isothermal Dendritic Growth Experiment - Science, engineering, and hardware development for USMP space flights p 128 A91-53408
- GLOVER, DANIEL**
NASA cryogenic fluid management space experiment efforts
[AIAA PAPER 91-3538] p 130 A91-53701
- NASA cryogenic fluid management space experiment efforts, 1960-1990
[NASA-TM-103752] p 243 N91-30073
- GOETZ, GUENTER**
Characteristic microwave-background distortions from collapsing spherical domain walls p 238 A91-12343
- GOKOGLU, S. A.**
A numerical and experimental analysis of reactor performance and deposition rates for CVD on monofilaments
[NASA-TM-103631] p 130 N91-14500
- GOKOGLU, SULEYMAN**
Computational materials science. An example: Numerical modeling of chemical vapor deposition processing of advanced fibers p 99 N91-20111
- GOLDMAN, LOUIS J.**
Three-component laser anemometer measurement systems
[NASA-TP-3080] p 13 N91-19057
- GOLDSTEIN, M. E.**
Spatial evolution of nonlinear acoustic mode instabilities on hypersonic boundary layers p 225 A91-12973
- Nonlinear spatial evolution of externally excited instability waves in free shear layers p 152 A91-38705
- The effect of small streamwise velocity distortion on the boundary layer flow over a thin flat plate with application to boundary layer stability theory
[NASA-TM-103668] p 161 N91-19372
- GOOD, BRIAN S.**
A review of properties and potential aerospace applications of electrically conducting polymers p 113 A91-14409
- Electrically conducting polymers for aerospace applications
[AIAA PAPER 91-3432] p 233 A91-52349
- GOODEN, CLARENCE E.**
The preliminary feasibility of intercalated graphite railgun armatures p 137 A91-29257
- GOODRICH, JOHN W.**
Time dependent viscous incompressible Navier-Stokes equations p 9 N91-10854
- GORADIA, C.**
A comparative study of p(+)-In and n(+)-p InP solar cells made by a closed ampoule diffusion p 212 N91-30206
- GORADIA, CHANDRA**
Study of surface passivation as a function of InP closed-ampoule solar cell fabrication processing variables p 232 A91-41893
- Key factors limiting the open circuit voltage of n(+)-pp(+)-indium phosphide solar cells p 139 A91-41929
- Key factors limiting the open circuit voltage of n(+)-pp(+)-indium phosphide solar cells p 209 N91-19206
- Investigation of anodic and chemical oxides grown on p-type InP with applications to surface passivation for n(+)-p solar cell fabrication p 210 N91-19208
- A comparative study of performance parameters of n(+)-p InP solar cells made by closed-ampoule sulfur diffusion into Cd- and Zn-doped p-type InP substrates p 210 N91-19209

- A theoretical comparison of the near-optimum design and predicted performance of n/p and p/n indium phosphide homojunction solar cells p 83 N91-30233
- GORADIA, M.**
A comparative study of p(+)-n and n(+)-p InP solar cells made by a closed ampoule diffusion p 212 N91-30206
- GORADIA, MANJU**
Study of surface passivation as a function of InP closed-ampoule solar cell fabrication processing variables p 232 A91-41893
Investigation of anodic and chemical oxides grown on p-type InP with applications to surface passivation for n(+)-p solar cell fabrication p 210 N91-19208
A comparative study of performance parameters of n(+)-p InP solar cells made by closed-ampoule sulfur diffusion into Cd- and Zn-doped p-type InP substrates p 210 N91-19209
High resolution electrolyte for thinning InP by anodic dissolution and its applications to EC-V profiling, defect revealing and surface passivation p 107 N91-30210
- GORDON, W. L.**
Determination of surface resistance and magnetic penetration depth of superconducting YBa₂Cu₃O₇(δ) thin films by microwave power transmission measurements p 138 A91-36060
Determination of surface resistance and magnetic penetration depth of superconducting YBa₂Cu₃O₇(δ) thin films by microwave power transmission measurements [NASA-TM-103616] p 234 N91-10780
- GOTSIS, PASCAL K.**
Combined thermal and bending fatigue of high-temperature metal-matrix composites: Computational simulation [NASA-TM-104354] p 100 N91-23247
- GOTT, R. W.**
Five-kilowatt arcjet power electronics p 63 A91-52312
- GOUGEON, MEADE**
Structural properties of laminated Douglas fir/epoxy composite material [NASA-RP-1236] p 94 N91-10127
- GRADY, J.**
Impact behavior of a SiC fiber-reinforced reaction bonded Si₃N₄ composite p 91 A91-16805
- GRADY, J. E.**
Free vibrations of delaminated beams [AIAA PAPER 91-1241] p 197 A91-32129
Evaluation of thermomechanical damage in silicon carbide/titanium composites p 92 A91-42297
Low velocity impact analysis with NASTRAN p 198 A91-48865
- GRADY, JOSEPH E.**
Low velocity impact analysis with NASTRAN [NASA-TM-103169] p 95 N91-14426
- GRAMOLL, KURT C.**
An overview of self-consistent methods for fiber-reinforced composites [NASA-TM-103713] p 97 N91-19232
- GRATZ, ROY F.**
Substituted 1,1,1-triaryl-2,2,2-trifluoroethanes and processes for their synthesis [NASA-CASE-LEW-14345-3] p 89 N91-17141
Substituted 1,1,1-triaryl-2,2,2-trifluoroethanes and processes for their synthesis [NASA-CASE-LEW-14345-4] p 90 N91-25185
- GRAY, HUGH R.**
Advanced high temperature engine materials technology program p 98 N91-20110
- GRAZIANI, R. A.**
Heat transfer in rotating serpentine passages with trips normal to the flow [NASA-TM-103758] p 184 N91-19443
- GREEN, JAMES M.**
Flow visualization of a rocket injector spray using gelled propellant simulants [AIAA PAPER 91-2198] p 59 A91-44151
- GREEN, ROBERT D.**
RSM 1.0 user's guide: A resupply scheduler using integer optimization [NASA-TM-104380] p 217 N91-22766
- GREEN, ROBERT E., JR.**
Acousto-ultrasonic nondestructive evaluation of materials using laser beam generation and detection p 193 N91-18193
- GREENBERG, PAUL S.**
Particle image fields and partial coherence p 171 A91-19604
- GREGORY, RUTH**
Structure of random discrete spacetime p 224 A91-22894
- GREY, R. E.**
Flow visualization studies of the internal flow characteristics in a simulated mixed flow vectored thrust ASTOVL engine configuration [AIAA PAPER 91-1689] p 23 A91-42556
- GRIFFITH, A.**
Some recent studies with the solid-ionomer electrochemical capacitor p 214 N91-32562
- GRIMALDA, JUSTUS**
Simulation of Martian dust accumulation on surfaces p 47 N91-19160
- GRISAFFE, SALVATORE J.**
Reinforcements: The key to high performance composite materials [NASA-TM-103230] p 96 N91-15329
Overview of Lewis materials research: Contributions, current efforts, and future directions p 111 N91-20109
- GRISNIK, STANLEY P.**
Test facilities for high power electric propulsion [AIAA PAPER 91-3499] p 42 A91-52396
- GROBSTEIN, TONI L.**
Advanced materials for space nuclear power systems [AIAA PAPER 91-3530] p 88 A91-53704
Advanced materials for space nuclear power systems [NASA-TM-105171] p 112 N91-29298
- GRODSINSKY, C.**
A new approach to controller design for microgravity isolation systems p 129 A91-23108
- GRODSINSKY, C. M.**
Development of a vibration isolation prototype system for microgravity space experiments p 47 A91-53403
- GRODSINSKY, CARLOS M.**
Development of a vibration isolation prototype system for microgravity space experiments [NASA-TM-103664] p 130 N91-19324
Magnetic bearings with zero bias p 48 N91-21194
Microgravity vibration isolation: An optimal control law for the one-dimensional case p 49 N91-21206
- GROENEWEG, J. F.**
Near-field noise of a single rotation propfan at an angle of attack [AIAA PAPER 90-3953] p 225 A91-12469
Prediction of unsteady blade surface pressures on an advanced propeller at an angle of attack p 226 A91-18257
Unsteady blade-surface pressures on a large-scale advanced propeller: Prediction and data [NASA-TM-103218] p 69 N91-11799
Near-field noise of a single-rotation propfan at an angle of attack [NASA-TM-103645] p 227 N91-12316
Unsteady flowfield of a propfan at takeoff conditions [NASA-TM-105223] p 18 N91-32075
- GROENEWEG, JOHN F.**
Aeroacoustics of advanced propellers p 226 A91-24317
Overview of subsonic transport propulsion technology p 30 N91-20116
- GROTH, MARY F.**
Production and use of metals and oxygen for lunar propulsion [AIAA PAPER 91-3481] p 125 A91-53711
Production and use of metals and oxygen for lunar propulsion [NASA-TM-105195] p 81 N91-29222
- GRUBER, R. P.**
Five-kilowatt arcjet power electronics p 63 A91-52312
Xenon ion propulsion for orbit transfer [NASA-TM-103193] p 69 N91-11798
- GU, A.**
Liquid hydrogen turbopump foil bearing [AIAA PAPER 91-2108] p 182 A91-41701
- GUNAJI, MOHAN**
Surface modification of Monel K-500 as a means of reducing friction and wear in high-pressure oxygen p 107 A91-16869
- GUO, T.-H.**
Real-time diagnostics of the reusable rocket engine using on-line system identification p 223 A91-30630
Development of an intelligent diagnostic system for reusable rocket engine control [AIAA PAPER 91-2533] p 63 A91-45817
A distributed fault-detection and diagnosis system using on-line parameter estimation [NASA-TM-104433] p 220 N91-25696
- GUO, TEN-HUEI**
A simplified dynamic model of the Space Shuttle main engine [NASA-TM-104421] p 131 N91-23340
Alpha-canonical form representation of the open loop dynamics of the Space Shuttle main engine [NASA-TM-104422] p 131 N91-24469
- Sensor failure detection and recovery by neural networks [NASA-TM-104484] p 220 N91-24815
- GUPTA, MURLI M.**
Spectrum transformation for divergent iterations [NASA-TM-103745] p 221 N91-19786
- GYEKENYESI, JOHN P.**
Dynamic fatigue property of silicon carbide whisker-reinforced silicon nitride p 94 A91-56937
Calculation of Weibull strength parameters, Batdorf flaw density constants and related statistical quantities using PC-CARES [NASA-TM-103247] p 199 N91-10332
Structural reliability analysis of laminated CMC components [NASA-TM-103685] p 119 N91-19292
Thermal shock of fiber reinforced ceramic matrix composites [NASA-TM-103777] p 120 N91-19295
The method of lines in analyzing solids containing cracks [NASA-TM-103626] p 201 N91-19477
Mechanical behavior of fiber reinforced SiC/RBSN ceramic matrix composites: Theory and experiment [NASA-TM-103688] p 99 N91-21243
Structural design methodologies for ceramic-based material systems [NASA-TM-103097] p 121 N91-22460
- GYEKENYESI, JOHN Z.**
Polymeric routes to silicon carbide and silicon oxycarbide CMC p 117 A91-56922
Thermal shock fiber-reinforced ceramic matrix composites p 93 A91-56935
Polymeric routes to silicon carbide and silicon oxycarbide CMC [NASA-TM-104372] p 102 N91-26234

H

- HAAG, T. W.**
Thrust stand for high-power electric propulsion devices p 41 A91-36239
Five-kilowatt arcjet power electronics p 63 A91-52312
- HAAG, THOMAS W.**
High-power hydrogen arcjet performance [AIAA PAPER 91-2226] p 61 A91-45795
Medium power hydrogen arcjet performance [NASA-TM-104533] p 85 N91-31216
- HACK, K. J.**
Evolutionary use of nuclear electric propulsion [AIAA PAPER 90-3821] p 50 A91-10174
Nuclear electric propulsion mission performance for fast piloted Mars missions [AIAA PAPER 91-3488] p 65 A91-52388
Solar electric propulsion for Mars transport vehicles [NASA-TM-103234] p 71 N91-19178
- HAGEDORN, NORMAN H.**
The Au cathode in the system Li₂CO₃-CO₂-CO at 800 to 900 C p 213 N91-32551
- HAGGARD, JOHN B.**
N-decane droplet combustion in the NASA-Lewis 5 Second Zero-Gravity Facility - Results in test gas environments other than air [AIAA PAPER 91-0720] p 105 A91-19433
- HAH, CHUNILL**
A Navier-Stokes study of shock-boundary layer interaction and flow separation inside a transonic compressor p 8 A91-56115
- HAHN, R. C.**
Isothermal Dendritic Growth Experiment - Science, engineering, and hardware development for USMP space flights p 128 A91-53408
- HAJELA, PRABHAT**
Applications of artificial neural nets in structural mechanics [NASA-TM-102420] p 202 N91-21559
- HALFORD, G. R.**
Finite element elastic-plastic-creep and cyclic life analysis of a cowl lip p 199 A91-56365
- HALFORD, GARY R.**
Stirling engine: Available tools for long-life assessment [NASA-TM-103660] p 200 N91-12980
Application of thermal life prediction model to high-temperature aerospace alloys B1900 + Hf and Haynes 188 [NASA-TM-4226] p 201 N91-19473
Thermomechanical and bithermal fatigue behavior of cast B1900 + Hf and wrought Haynes 188 [NASA-TM-4225] p 111 N91-20268
- HALL, C. A.**
Multidimensional computer simulation of Stirling cycle engines p 181 A91-38154

HALL, DAVID G.

- The effect of swirl recovery vanes on the cruise noise of an advanced propeller
[AIAA PAPER 90-3932] p 224 A91-12448
- Noise measurements from an ejector suppressor nozzle in the NASA Lewis 9- by 15-foot low speed wind tunnel
[AIAA PAPER 90-3983] p 225 A91-12496
- Noise measurements from an ejector suppressor nozzle in the NASA Lewis 9- by 15-foot low speed wind tunnel
[NASA-TM-103628] p 227 N91-11493
- The effect of swirl recovery vanes on the cruise noise of an advanced propeller
[NASA-TM-103625] p 227 N91-11494

HALL, STEPHEN W.

- Effect of KOH concentration on LEO cycle life of IPV nickel-hydrogen flight battery cells p 55 A91-38076
- Effect of LEO cycling on 125 Ah advanced design IPV nickel-hydrogen battery cells p 55 A91-38077
- Effect of LEO cycling on 125 Ah advanced design IPV nickel-hydrogen flight cells. An update
[NASA-TM-104384] p 74 N91-22375
- Effect of KOH concentration on LEO cycle life of IPV nickel-hydrogen flight cells. An update
[NASA-TM-104383] p 74 N91-22376
- Destructive physical analysis results of Ni/H₂ cells cycled in LEO regime
[NASA-TM-104382] p 74 N91-22323

HALLER, WILLIAM J.

- Comparison of turbine bypass and mixed flow turbofan engines for a high-speed civil transport
[AIAA PAPER 91-3132] p 25 A91-54051

HALLUM, GARRY M.

- Effect of high temperature hydrogen exposure on the strength and microstructure of mullite
p 114 A91-19780

HAMBOURGER, PAUL D.

- Resistivity of pristine and intercalated graphite fiber epoxy composites p 115 A91-35949

HAMED, A.

- Probabilistic modeling for simulation of aerodynamic uncertainties in propulsion systems p 58 A91-42725

HAMLEY, JOHN A.

- Power electronics for low power arcjets
[AIAA PAPER 91-1991] p 60 A91-45779
- Power electronics for low power arcjets
[NASA-TM-104459] p 77 N91-25172

HAMMOUD, A. N.

- Electrical characterization of a Mapham inverter using pulse testing techniques p 139 A91-37992
- Electrical characterization of glass, teflon, and tantalum capacitors at high temperatures
[NASA-TM-104517] p 146 N91-27444

HAMMOUD, AHMAD N.

- High temperature power electronics for space
[NASA-TM-104375] p 145 N91-22508

HAMPTON, RICHARD D.

- Microgravity vibration isolation: An optimal control law for the one-dimensional case p 49 N91-21206

HANDSCHUH, R. F.

- Effects of rim thickness on spur gear bending stress
[AIAA PAPER 91-2020] p 181 A91-41681
- Effects of rim thickness on spur gear bending stress
[NASA-TM-104388] p 186 N91-23500
- Computerized inspection of real surfaces and minimization of their deviations
[NASA-TM-103798] p 188 N91-27558
- Local synthesis and tooth contact analysis of face-milled spiral bevel gears
[NASA-TM-105182] p 190 N91-29600

HANDSCHUH, ROBERT F.

- How to determine spiral bevel gear tooth geometry for finite element analysis
[NASA-TM-105150] p 190 N91-30537
- Recent manufacturing advances for spiral bevel gears
[NASA-TM-104479] p 191 N91-31654

HANLON, JAMES C.

- SEI power source alternatives for rovers and other multi-kWe distributed surface applications
[NASA-TM-104360] p 81 N91-28277
- Comparison of dynamic isotope power systems for distributed planet surface applications
[NASA-TM-4303] p 81 N91-28278

HANN, RAIFORD E.

- A model for the scattering of high-frequency electromagnetic fields from dielectrics exhibiting thermally-activated electrical losses
[NASA-TM-104376] p 224 N91-26872

HANSEN, IRVING G.

- Induction motor control p 137 A91-30893
- Advanced electrical power, distribution and control for the Space Transportation System p 143 N91-17043
- Four quadrant control of induction motors p 145 N91-23055

HANSMAN, R. JOHN, JR.

- Modeling of surface roughness effects on glaze ice accretion p 19 A91-35107

HARDY, T. L.

- Computational modeling of the pressurization process in a NASP vehicle propellant tank experimental simulation
[AIAA PAPER 91-2407] p 124 A91-41771

HARDY, TERRY L.

- Slush hydrogen propellant production, transfer, and expulsion studies at the NASA K-Site Facility
[AIAA PAPER 91-3550] p 125 A91-53710
- Slush hydrogen propellant production, transfer, and expulsion studies at the NASA K-Site Facility
[NASA-TM-105191] p 127 N91-28449

HARLOFF, G. J.

- Three-dimensional viscous flow computations of high area ratio nozzles for hypersonic propulsion p 4 A91-30014

HARLOFF, GARY J.

- High alpha inlets p 28 N91-20091

HARRIS, DAVID W.

- Dual-purpose self-deliverable lunar surface PV electrical power system p 209 N91-19200

HART, R. E.

- Primary reference cell calibrations at SERI - History and methods p 207 A91-41966

HART, RUSSELL E., JR.

- Preliminary results from the Advanced Photovoltaic Experiment flight test p 39 A91-41980
- Preliminary results from the advanced photovoltaic experiment flight test
[NASA-TM-103269] p 67 N91-11058

HARTSFIELD, J.

- Outline of the Solar System: Activities for elementary students
[NASA-TM-104965] p 241 N91-25975

HARTY, RICHARD B.

- Lunar electric power systems utilizing the SP-100 reactor coupled to dynamic conversion systems
[AIAA PAPER 91-3520] p 208 A91-52415

HASAN, M. M.

- A pressure control analysis of cryogenic storage systems
[AIAA PAPER 91-2405] p 59 A91-44228
- A numerical study of the direct contact condensation on a horizontal surface
[AIAA PAPER 91-1307] p 155 A91-44335
- Self-pressurization of a lightweight liquid hydrogen storage tank subjected to low heat flux
[NASA-TM-103804] p 126 N91-20324
- A pressure control analysis of cryogenic storage systems
[NASA-TM-104409] p 126 N91-24460
- A numerical study of the direct contact condensation on a horizontal surface
[NASA-TM-104432] p 166 N91-24548

HASCHART, D.

- Performance evaluation of land mobile satellite system under vegetative shadowing using differential multiple TCM and QPSK p 132 A91-53084

HASTINGS, D.

- Significant reduction in arc frequency biased solar cells: Observations, diagnostics, and mitigation technique(s) p 83 N91-30235

HATHAWAY, M. D.

- NASA low-speed centrifugal compressor for 3-D viscous code assessment and fundamental flow physics research
[NASA-TM-103710] p 13 N91-20044

HAUER, ROBERT L.

- Removable hand hold
[NASA-CASE-LEW-15196-1] p 188 N91-26543

HAUGLAND, EDWARD J.

- High efficiency Ka-band MMIC amplifiers
[AIAA PAPER 91-3425] p 141 A91-52345

HEIDELBERG, L. J.

- Unsteady blade pressure measurements for the SR-7A propeller at cruise conditions
[AIAA PAPER 90-4022] p 225 A91-12533
- Unsteady blade pressure measurements for the SR-7A propeller at cruise conditions
[NASA-TM-103606] p 228 N91-19825

HEIDMANN, JAMES D.

- A three-dimensional Navier-Stokes stage analysis of the flow through a compact radial turbine
[AIAA PAPER 91-2564] p 23 A91-41815
- An analysis of the viscous flow through a compact radial turbine by the average passage approach
[ASME PAPER 90-GT-64] p 6 A91-44545
- A three-dimensional Navier-Stokes stage analysis of the flow through a compact radial turbine
[NASA-TM-104420] p 32 N91-23186

HEIMANN, PAUL J.

- Polymeric routes to silicon carbide and silicon oxycarbide CMC
[NASA-TM-104372] p 102 N91-26234

HEIMANN, PAULA J.

- Polymeric routes to silicon carbide and silicon oxycarbide CMC p 117 A91-56922

HEINEN, V. O.

- Aerospace applications of high temperature superconductivity
[IAF PAPER 90-054] p 231 A91-13767
- High temperature superconducting thin film microwave circuits - Fabrication, characterization, and applications p 141 A91-50433
- Aerospace applications of high temperature superconductivity p 236 N91-24080

HEINEN, VERNON O.

- Superconductivity applications for infrared and microwave devices; Proceedings of the Meeting, Orlando, FL, Apr. 19, 20, 1990 p 141 A91-50426
- An experimental apparatus for measuring surface resistance in the submillimeter-wavelength region p 174 A91-54390
- Emerging applications of high temperature superconductors for space communications
[NASA-TM-103629] p 227 N91-12317

HELMICK, LARRY S.

- Determination of the thermal stability of fluids by tensimetry - Instrumentation and procedure p 113 A91-13435

HENDERSHOT, J. E.

- Fuel Systems Architecture (FSA) evaluation criteria and concept evaluation methodology
[AIAA PAPER 91-3479] p 65 A91-52384

HENDRICKS, R. C.

- Flow visualization and quantitative velocity and pressure measurements in simulated single and double brush seals p 180 A91-21071
- Effects of brush seal morphology on leakage and pressure drops
[AIAA PAPER 91-2106] p 182 A91-41700
- Paramagnetic propellant orientation
[AIAA PAPER 91-2325] p 125 A91-44197
- Flow visualization in a simulated brush seal
[ASME PAPER 90-GT-217] p 173 A91-44633
- Some preliminary results of brush seal/rotor interference effects on leakage at zero and low rpm using a tapered-plug rotor
[AIAA PAPER 91-3390] p 182 A91-45820
- Simulation of brush insert for leading-edge-passage convective heat transfer
[NASA-TM-103801] p 165 N91-23409
- Paramagnetic propellant orientation
[NASA-TM-104390] p 166 N91-24527
- Some preliminary results of brush seal/rotor interference effects on leakage at zero and low RPM using a tapered-plug rotor
[NASA-TM-104396] p 188 N91-27559
- Qualitative investigation of cryogenic injected shock dissipation
[NASA-TM-105140] p 168 N91-29525
- A qualitative view of cryogenic fluid injection into high speed flows
[NASA-TM-105139] p 169 N91-30473

HENDRICKS, ROBERT C.

- Eccentricity effects on leakage of a brush seal at low speeds
[NASA-TM-105141] p 86 N91-31220

HEPP, ALOYSIUS F.

- Production and use of metals and oxygen for lunar propulsion
[AIAA PAPER 91-3481] p 125 A91-53711
- Spatial variations in a.c. susceptibility and microstructure for the YBa₂Cu₃O_{7-x} superconductor and their correlation with room-temperature ultrasonic measurements p 233 A91-54969
- Reactivity of pi-complexes of Ti, V, and Nb towards dithioacetic acid: Synthesis and structure of novel metal sulfur-containing complexes
[NASA-TM-103666] p 106 N91-19256
- Synthesis and structures of metal chalcogenide precursors
[NASA-TM-103665] p 120 N91-19296
- Chemical approaches to carbon dioxide utilization for manned Mars missions
[NASA-TM-103728] p 241 N91-20015
- Spatial variations in ac susceptibility and microstructure for the YBa₂Cu₃O_{7-x} superconductor and their correlation with room-temperature ultrasonic measurements
[NASA-TM-103787] p 194 N91-21553
- Material processing with hydrogen and carbon monoxide on Mars
[NASA-TM-104405] p 211 N91-23616
- Thin-film sensors for space propulsion technology: Fabrication and preparation for testing p 77 N91-24324
- Chemical approaches to carbon dioxide utilization for manned Mars missions p 241 N91-26073

- Production and use of metals and oxygen for lunar propulsion
[NASA-TM-105195] p 81 N91-29222
- Near-edge study of gold-substituted YBa₂Cu₃O(7- δ)
[NASA-TM-105220] p 237 N91-31977
- HERBELL, THOMAS P.**
Effect of high temperature hydrogen exposure on the strength and microstructure of mullite
p 114 A91-19780
- Ceramic composites for rocket engine turbines
[SAE PAPER 911108] p 92 A91-53552
- Thermal shock fiber-reinforced ceramic matrix composites
p 93 A91-56935
- Effect of hydrogen on the strength and microstructure of selected ceramics
[NASA-TM-103674] p 118 N91-14482
- Ceramic composites for rocket engine turbines
[NASA-TM-103743] p 98 N91-19235
- Thermal shock of fiber reinforced ceramic matrix composites
[NASA-TM-103777] p 120 N91-19295
- HERING, GARY T.**
Status of structural analysis of 30 cm diameter ion optics
[NASA-TM-103618] p 68 N91-11796
- HERNDON, J. N.**
Manipulation hardware for microgravity research
[NASA-TM-103423] p 128 N91-14498
- HERR, JOEL L.**
A charging study of the ACTS satellite using NASCAP
[AIAA PAPER 91-1471] p 46 A91-42522
- HEUER, ARTHUR H.**
Temperature dependence of hardness in yttria-stabilized zirconia single crystals
p 114 A91-28763
- Temperature-dependent indentation behavior of transformation-toughened zirconia-based ceramics
p 114 A91-28767
- HEYMAN, JOSEPH S.**
Overall goals
p 80 N91-28246
- HICKEY, JOHN R.**
Preliminary flight test results from the advanced photovoltaic experiment
p 56 A91-38163
- Preliminary results from the Advanced Photovoltaic Experiment flight test
p 39 A91-41980
- Preliminary results from the advanced photovoltaic experiment flight test
[NASA-TM-103269] p 67 N91-11058
- The effect of the low Earth orbit environment on space solar cells
[NASA-TM-103735] p 48 N91-19165
- Advanced photovoltaic experiment, S0014: Preliminary flight results and post-flight findings
p 212 N91-25061
- HICKMAN, J. M.**
Systems analysis of Mars solar electric propulsion vehicles
[AIAA PAPER 90-3824] p 40 A91-10176
- Design considerations for lunar base photovoltaic power systems
p 41 A91-41987
- Laser photovoltaic power system synergy for SEI applications
[AIAA PAPER 91-3419] p 207 A91-52339
- Solar electric propulsion for Mars transport vehicles
[NASA-TM-103234] p 71 N91-19178
- HICKMAN, J. MARK**
Design considerations for lunar base photovoltaic power systems
[NASA-TM-103642] p 241 N91-14259
- Structural design concepts for a multi-megawatt Solar Electric Propulsion (SEP) spacecraft
[NASA-TM-105148] p 206 N91-30565
- HICKS, Y.**
Jet-A fuel evaporation analysis in conical tube injectors
[AIAA PAPER 91-0345] p 149 A91-21467
- HILL, CAROL M.**
Atomic oxygen interaction with solar array blankets at protective coating defect sites
p 211 N91-20732
- HILL, CHRISTOPHER T.**
Coherent peculiar velocities and periodic redshifts
p 239 A91-20430
- HILL, GERALD M.**
Power electronics for low power arcjets
[AIAA PAPER 91-1991] p 60 A91-45779
- Power electronics for low power arcjets
[NASA-TM-104459] p 77 N91-25172
- HILL, MYRON E.**
A summary of existing and planned experiment hardware for low-gravity fluids research
[AIAA PAPER 91-0777] p 128 A91-26329
- A summary of existing and planned experiment hardware for low-gravity fluids research
[NASA-TM-103706] p 160 N91-19371
- HILLARD, G. B.**
Electrical system/environment interactions on the planet Mars
p 242 N91-27068
- HILLS, BETHANIE J.**
The series Bi₂Sr₂Ca(n-1) Cu(n)O(2n+4) (1 less than or equal to n less than or equal to 5): Phase stability and superconducting properties
[NASA-TM-103749] p 235 N91-21910
- HINGST, W. R.**
Experimental investigation of a single flush-mounted hypermixing nozzle
[AIAA PAPER 90-5240] p 21 A91-14466
- An experimental comparison of nonswirling and swirling flow in a circular-to-rectangular transition duct
[AIAA PAPER 91-0342] p 148 A91-21466
- An experimental trace gas investigation of fluid transport and mixing in a circular-to-rectangular transition duct
[AIAA PAPER 91-2370] p 172 A91-44214
- The effect of varying Mach number on crossing, glancing shocks/turbulent boundary-layer interactions
[AIAA PAPER 91-2157] p 6 A91-45792
- Progress toward synergistic hypermixing nozzles
[AIAA PAPER 91-2264] p 25 A91-45800
- Heat transfer, velocity-temperature correlation, and turbulent shear stress from Navier-Stokes computations of shock wave/turbulent boundary layer interaction flows
p 163 N91-21085
- An experimental comparison of nonswirling and swirling flow in a circular-to-rectangular transition duct
[NASA-TM-104359] p 14 N91-21115
- An experimental trace gas investigation of fluid transport and mixing in a circular-to-rectangular transition duct
[NASA-TM-104499] p 17 N91-27129
- Evaluation of a technique to generate artificially thickened boundary layers in supersonic and hypersonic flows
[NASA-TP-3142] p 17 N91-28136
- Progress toward synergistic hypermixing nozzles
[NASA-TM-105169] p 18 N91-29150
- The NASA Lewis Research Center Internal Fluid Mechanics Facility
[NASA-TM-105187] p 39 N91-30163
- A laser-induced heat flux technique for convective heat transfer measurements in high speed flows
[NASA-TM-105177] p 168 N91-30472
- HINGST, WARREN R.**
Development of a laser-induced heat flux technique for measurement of convective heat transfer coefficients in a supersonic flowfield
[NASA-TM-103778] p 13 N91-19063
- Experimental investigation of a single flush-mounted hypermixing nozzle
[NASA-TM-103726] p 161 N91-19374
- HIPPENSTEELE, STEVEN A.**
Visualization techniques to experimentally model flow and heat transfer in turbine and aircraft flow passages
[NASA-TM-4272] p 167 N91-27489
- HIRLEMAN, E. DAN**
Use of rotating pinholes and reticles for calibration of cloud droplet instrumentation
p 171 A91-30371
- HOCHSTEIN, J. I.**
Computational modeling of the pressurization process in a NASP vehicle propellant tank experimental simulation
[AIAA PAPER 91-2407] p 124 A91-41771
- HOFFMAN, DAVID J.**
ETARA PC version 3.3 user's guide: Reliability, availability, maintainability simulation model
[NASA-TM-103751] p 193 N91-19462
- HOLDEN, J. D.**
A CFD study of jet mixing in reduced flow areas for lower combustor emissions
[AIAA PAPER 91-2460] p 23 A91-41788
- Experimental study of cross-stream mixing in a cylindrical duct
[AIAA PAPER 91-2459] p 157 A91-45815
- A CFD study of jet mixing in reduced flow areas for lower combustor emissions
[NASA-TM-104411] p 32 N91-23185
- CFD analysis of jet mixing in low NO_x flametube combustors
[NASA-TM-104466] p 33 N91-26146
- Experimental study of cross-stream mixing in a cylindrical duct
[NASA-TM-105180] p 34 N91-29187
- HOLDEMAN, JAMES D.**
Mixing of multiple jets with a confined subsonic crossflow - Summary of NASA-supported experiments and modeling
[AIAA PAPER 91-2458] p 7 A91-45813
- A numerical study of the hot gas environment around a STOVL aircraft in ground proximity
p 10 N91-10887
- Mixing of multiple jets with a confined subsonic crossflow. Summary of NASA-supported experiments and modeling
[NASA-TM-104412] p 33 N91-24202
- HOLDRIDGE, MARK**
Technologies for unattended network operations
[AIAA PAPER 91-3534] p 45 A91-52425
- HOLLAND, FREDERIC A.**
Thermomechanical and bithermal fatigue behavior of cast B1900 + Hf and wrought Haynes 188
[NASA-TM-4225] p 111 N91-20268
- HOLLAND, FREDERIC A., JR.**
Comparison of Weibull strength parameters from flexure and spin tests of brittle materials
[NASA-TM-104414] p 187 N91-24593
- HOMER, G. DAVID**
Hydrocarbon-fuel/combustion-chamber-liner materials compatibility
[NASA-CR-187104] p 121 N91-21307
- HONECY, FRANK S.**
A comparative study of performance parameters of n(+)-p InP solar cells made by closed-ampoule sulfur diffusion into Cd- and Zn-doped p-type InP substrates
p 210 N91-19209
- Tribological properties of Ag/Ti films on Al₂O₃ ceramic substrates
[NASA-TM-103784] p 89 N91-19224
- HONG, S. Y.**
Sulfur at nickel-alumina interfaces - Molecular orbital theory
p 104 A91-12925
- HOPKINS, D. A.**
Adaptation of NASA technology for the optimization of orthopedic knee implants
p 215 N91-23032
- HOPKINS, DALE A.**
Computational simulation of high-temperature metal matrix composites cyclic behavior
p 91 A91-18680
- Computational simulation of propulsion structures performance and reliability
p 29 N91-20106
- NOTES, DEBORAH**
High emittance surfaces for high temperature space radiator applications
p 88 A91-56415
- Effects of dust accumulation and removal on radiators surfaces on Mars
[NASA-TM-103704] p 72 N91-20204
- HOVENAC, EDWARD A.**
Use of rotating pinholes and reticles for calibration of cloud droplet instrumentation
p 171 A91-30371
- HOWE, GREGORY W.**
Simulation of mixing in the quick quench region of a rich burn-quick quench mix-lean burn combustor
[AIAA PAPER 91-0410] p 105 A91-21481
- HOWE, STEVEN**
Nuclear Thermal Propulsion technology - Summary of FY 1991 interagency panel planning
[AIAA PAPER 91-3631] p 66 A91-52495
- HRACH, FRANK J.**
Satellite relocation by tether deployment
p 40 A91-22966
- HSIAO, C. C.**
Pressure-coupled vaporization and combustion responses of liquid-fuel droplets in high-pressure environments
[AIAA PAPER 91-2310] p 106 A91-44192
- HSIEH, KWANG-CHUNG**
Ground-based PIV and numerical flow visualization results from the surface tension driven convection experiment
[NASA-TM-105172] p 178 N91-30491
- HSU, ANDREW T.**
Computational analysis of underexpanded jets in the hypersonic regime
p 4 A91-37421
- A study of hydrogen diffusion flames using PDF turbulence model
[AIAA PAPER 91-1780] p 106 A91-45549
- Numerical study of unsteady shockwave reflections using an upwind TVD scheme
[NASA-TM-103251] p 10 N91-11676
- HUBBARD, HARVEY H.**
Wind turbine acoustics
[NASA-TP-3057] p 228 N91-16679
- HUBER, F. W.**
Design and experimental evaluation of compact radial-inflow turbines
[AIAA PAPER 91-2127] p 24 A91-45788
- HUBER, ROBERT D.**
Acousto-ultrasonic nondestructive evaluation of materials using laser beam generation and detection
p 193 N91-18193
- HUFF, D. L.**
Application of an efficient hybrid scheme for aeroelastic analysis of advanced propellers
p 7 A91-52315
- HUFF, DENNIS L.**
Numerical simulations of supersonic flow through oscillating cascade sections
p 4 A91-28590
- Flutter analysis of cascades using a two dimensional Euler solver
[AIAA PAPER 91-1681] p 6 A91-45548
- Numerical analysis of flow through oscillating cascade sections
p 9 N91-10884
- Euler flow predictions for an oscillating cascade using a high resolution wave-split scheme
[NASA-TM-104377] p 16 N91-24107

HUGHES, CHRISTOPHER E.

Aerodynamic effects of reduced aft tip speed at constant thrust for a model counterrotation turboprop at takeoff conditions

[AIAA PAPER 90-3933] p 224 A91-12449

Aerodynamic effects of reduced aft tip speed at constant thrust for a model counterrotation turboprop at takeoff conditions

[NASA-TM-103608] p 226 N91-10703

HUI, W. H.

A new Lagrangian random choice method for steady two-dimensional supersonic/hypersonic flow

[AIAA PAPER 91-1546] p 5 A91-40721

HULL, DAVID

Effect of high temperature hydrogen exposure on the strength and microstructure of mullite

p 114 A91-19780

HULL, DAVID R.

Microstructural and strength stability of CVD SiC fibers in argon environments

p 117 A91-56958

Effect of hydrogen on the strength and microstructure of selected ceramics

[NASA-TM-103674] p 118 N91-14482

Microstructural and strength stability of CVD SiC fibers in argon environment

[NASA-TM-103772] p 102 N91-29250

HULTGREN, L. S.

Nonlinear spatial evolution of externally excited instability waves in free shear layers

p 152 A91-38705

HUMPHREY, DONALD L.

Hydrogen-silicon carbide interactions

p 114 A91-28783

HUNG, CHING-CHEH

Graphite fluoride fiber polymer composite material

[NASA-CASE-LEW-14472-1] p 95 N91-15320

Industrial applications of graphite fluoride fibers

p 100 N91-23040

HUNG, CHING-CHEH

Graphite fluoride fibers and their applications in the space industry

[NASA-TM-103265] p 88 N91-11062

HUNT, MARIBETH E.

Dynamic Isotope Surface Power Systems

[AIAA PAPER 91-3623] p 208 A91-52487

HUNTER, D.

Concurrent engineering

p 80 N91-28247

HURWITZ, F. I.

Silsesquioxane-derived ceramic fibres

p 114 A91-30283

HURWITZ, FRANCES I.

Polymeric routes to silicon carbide and silicon oxycarbide CMC

p 117 A91-56922

Polymeric routes to silicon carbide and silicon oxycarbide CMC

[NASA-TM-104372] p 102 N91-26234

HUSTON, RONALD L.

Contact stresses in gear teeth - A new method of analysis

[AIAA PAPER 91-2022] p 182 A91-41683

Contact stresses in gear teeth: A new method of analysis

[NASA-TM-104397] p 186 N91-22570

HUYNH, HUNG T.

Second-order accurate nonoscillatory schemes for scalar conservation laws

p 221 A91-13204

Accurate monotone cubic interpolation

[NASA-TM-103789] p 221 N91-20830

HWANG, D. P.

Evaluation of panel code predictions with experimental results of inlet performance for a 17-inch ducted prop/fan simulator operating at Mach 0.2

[AIAA PAPER 91-3354] p 7 A91-45819

Evaluation of panel code predictions with experimental results of inlet performance for a 17-inch ducted prop/fan simulator operating at Mach 0.2

[NASA-TM-104428] p 17 N91-25106

HYATT, MARK J.

Crystallization and properties of Sr-Ba aluminosilicate glass-ceramic matrices

p 117 A91-56917

Crystallization and properties of Sr-Ba aluminosilicate glass-ceramic matrices

[NASA-TM-103764] p 120 N91-19308

IANNO, N. J.

Diamondlike carbon applications in infrared optics and microelectronics

p 230 N91-18306

IBRAHIM, MOUNIR

Further two-dimensional code development for Stirling space engine components

p 56 A91-38184

IBRAHIM, MOUNIR B.

Two-dimensional model of a Space Station Freedom thermal energy storage canister

p 151 A91-38048

A 2-D oscillating flow analysis in Stirling engine heat exchangers

[NASA-TM-103781] p 161 N91-19375

IEK, C.

Evaluation of panel code predictions with experimental results of inlet performance for a 17-inch ducted prop/fan simulator operating at Mach 0.2

[AIAA PAPER 91-3354] p 7 A91-45819

Evaluation of panel code predictions with experimental results of inlet performance for a 17-inch ducted prop/fan simulator operating at Mach 0.2

[NASA-TM-104428] p 17 N91-25106

IGNJATOVIC, D.

Electrical transport measurements on polycrystalline superconducting Y-Ba-Cu-O films

p 231 A91-19820

INGEBO, ROBERT D.

Drops size correlation for cryogenic liquid-jet atomization

[AIAA PAPER 91-0284] p 51 A91-19218

Gas property effects on drops size of simulated fuel sprays

p 156 A91-45327

Drops size correlation for cryogenic liquid-jet atomization

[NASA-TM-103646] p 175 N91-12064

Cryogenic liquid-jet breakup in two-fluid atomizers

[NASA-TM-103734] p 176 N91-19402

Spray measurements of aerothermodynamic effect on disintegrating liquid jets

[NASA-TM-104501] p 178 N91-27510

INGRAM, D. C.

Diamondlike carbon applications in infrared optics and microelectronics

p 230 N91-18306

ITO, T.

Design aspects and comparison between high T(sub c) superconducting coplanar waveguide and microstrip line

[NASA-TM-105142] p 146 N91-27445

ITO, TATSUO

YBCO superconducting ring resonators at millimeter-wave frequencies

p 142 A91-54532

IVANCIC, WILLIAM D.

Evaluation of components, subsystems, and networks for high rate, high frequency space communications

[AIAA PAPER 91-3423] p 41 A91-52343

Optical Multiple Access Network (OMAN) for advanced processing satellite applications

[NASA-TM-105167] p 135 N91-29431

IZEN, STEVEN H.

Three-dimensional computed tomography from interferometric measurements within a narrow cone of views

[NASA-TM-103257] p 176 N91-19404

J

JACOBSON, N. S.

High temperature reactions of ceramics and metals with chlorine and oxygen

p 105 A91-20219

JACOBSON, NATHAN S.

Hydrogen-silicon carbide interactions

p 114 A91-28783

Hot corrosion of silicon carbide and silicon nitride at 1000 C

p 117 A91-55698

JACOMIN, D. A.

Three-dimensional flow transport modes in directional solidification during space processing

p 128 A91-42642

JACOMIN, DAVID

Stability of an oscillated fluid with a uniform density gradient

p 147 A91-12971

Frontogenesis driven by horizontally quadratic distributions of density

p 157 A91-48276

The breakup of trailing-line vortices

p 9 N91-10867

JACOMIN, DAVID A.

Interfacial dynamics of two liquids under an oscillating gravitational field

p 148 A91-16062

JAHN, R. G.

Anode power deposition in an applied-field segmented anode MPD thruster

[AIAA PAPER 91-2343] p 59 A91-44204

Energy deposition in low-power coaxial plasma thrusters

p 63 A91-52311

Cathode phenomena in a low-power magnetoplasmadynamic thruster

p 63 A91-52314

JAIN, R. K.

Effect of emitter parameter variation on the performance of heteroepitaxial indium phosphide solar cells

p 140 A91-42003

Recent progress in InP solar cell research

[NASA-TM-104509] p 146 N91-27447

Comparative modeling of InP solar cell structures

p 83 N91-30232

JAIN, RAJ K.

Monolithic and mechanical multijunction space solar cells

p 54 A91-38020

Effect of emitter parameter variation on the performance of heteroepitaxial indium phosphide solar cells

[NASA-TM-103619] p 70 N91-15306

Determination of series resistance of indium phosphide solar cells

p 210 N91-19207

Effect of dislocations on the open-circuit voltage, short-circuit current and efficiency of heteroepitaxial indium phosphide solar cells

[NASA-TM-103762] p 144 N91-19354

Optimal design study of high efficiency indium phosphide space solar cells

[NASA-TM-103763] p 145 N91-21433

JANETZKE, DAVID C.

Efficient computation of aerodynamic influence coefficients for aeroelastic analysis on a transputer network

[NASA-TM-103671] p 216 N91-20748

JANG, JONG H.

Two-dimensional simulation of a two-phase, regenerative pumped radiator loop utilizing direct contact heat transfer with phase change

p 151 A91-38126

Analysis of the one-dimensional transient compressible vapor flow in heat pipes

p 157 A91-47735

JANKOVSKY, R. S.

A life comparison of tube and channel cooling passages for thrust chambers

[NASA-TM-103613] p 68 N91-11059

JANKOVSKY, ROBERT S.

A dual-cooled hydrogen-oxygen rocket engine heat transfer analysis

[AIAA PAPER 91-2211] p 59 A91-44156

A dual-cooled hydrogen-oxygen rocket engine heat transfer analysis

[NASA-TM-104430] p 76 N91-24302

JANSEN, RALPH

Patched elastohydrodynamic lubrication: Instrumentation and procedure

[NASA-TM-104426] p 168 N91-30469

JASKOWIAK, MARTHA H.

Effects of high pressure nitrogen on the thermal stability of SiC fibers

[NASA-TM-103245] p 96 N91-16075

JAWORSKE, D. A.

Selective and low temperature synthesis of polycrystalline diamond

p 232 A91-42170

JAWORSKI, ALLAN

Technologies for unattended network operations

[AIAA PAPER 91-3534] p 45 A91-52425

JAYNE, DOUGLAS

Study of surface passivation as a function of InP closed-ampoule solar cell fabrication processing variables

p 232 A91-41893

Investigation of anodic and chemical oxides grown on p-type InP with applications to surface passivation for n(+)-p solar cell fabrication

p 210 N91-19208

JAYNE, DOUGLAS T.

An x ray photoelectron spectroscopy study of Au(x)In(y) alloys

[NASA-TM-103659] p 234 N91-14050

JEFFERIES, KENT S.

Concentrator testing using projected images

[NASA-TM-104349] p 79 N91-27204

JENG, DUEN-REN

New approach in direct-simulation of gas mixtures

[AIAA PAPER 91-1343] p 154 A91-43412

JENKINS, I. G.

Controlled growth of 3C-SiC and 6H-SiC films on low-tilt-angle vicinal (0001) 6H-SiC wafers

p 232 A91-45713

Application of oxidation to the structural characterization of SiC epitaxial films

p 233 A91-45881

JENKINS, M. G.

Elevated-temperature fracture resistances (K(sub IC), R-curves, gamma sub (omega OF)) of monolithic and composite ceramics using chevron-notched, bend tests

[NASA-TM-105090] p 123 N91-28418

JENKINS, MICHAEL G.

Numerical, micro-mechanical prediction of crack growth resistance in a fibre-reinforced/brittle matrix composite

p 199 A91-51916

Mechanical behavior and failure phenomenon of an in situ-toughened silicon nitride

[NASA-TM-103741] p 121 N91-23311

JENKINS, P.

Effect of dislocations on properties of heteroepitaxial InP solar cells

p 213 N91-30209

JENKINS, PHILLIP

Study of surface passivation as a function of InP closed-ampoule solar cell fabrication processing variables

p 232 A91-41893

Measurement of surface recombination velocity on heavily doped indium phosphide

p 232 A91-41931

Investigation of anodic and chemical oxides grown on p-type InP with applications to surface passivation for n(+)-p solar cell fabrication

p 210 N91-19208

- JENKINS, PHILLIP P.**
Grooved surfaces on InP p 213 N91-30208
- JERACKI, R. J.**
Evaluation of panel code predictions with experimental results of inlet performance for a 17-inch ducted prop/fan simulator operating at Mach 0.2 [AIAA PAPER 91-3354] p 7 A91-45819
Evaluation of panel code predictions with experimental results of inlet performance for a 17-inch ducted prop/fan simulator operating at Mach 0.2 [NASA-TM-104428] p 17 N91-25106
- JERACKI, ROBERT J.**
Ultra-high bypass research p 30 N91-20117
- JIANG, BO-NAN**
The L sub 1 finite element method for pure convection problems [NASA-TM-103773] p 222 N91-24817
Least-squares solution of incompressible Navier-Stokes equations with the p-version of finite elements [NASA-TM-105203] p 223 N91-31911
- JIRBERG, RUSSELL**
LBR-2 Earth stations for the ACTS program p 133 N91-11971
- JOHNS, A. L.**
STOVL Hot Gas Ingestion control technology [ASME PAPER 89-GT-323] p 22 A91-23642
- JOHNS, ALBERT L.**
Hot gas ingestion test results of a two-poster vectored thrust concept with flow visualization in the NASA Lewis 9- x 15-foot low speed wind tunnel [AIAA PAPER 90-2268] p 4 A91-40561
VSTOL ground effects testing with flow visualization and image enhancement [AIAA PAPER 91-3145] p 8 A91-54061
Flow visualization and hot gas ingestion characteristics of a vectored thrust STOVL concept p 28 N91-20090
Hot gas ingestion test results of a two-poster vectored thrust concept with flow visualization in the NASA Lewis 9- x 15-foot low speed wind tunnel [NASA-TM-103258] p 15 N91-21116
- JOHNSON, B. V.**
Heat transfer in rotating serpentine passages with trips normal to the flow [NASA-TM-103758] p 184 N91-19443
- JOHNSON, SUSAN M.**
Multidisciplinary research overview (IHPTET/NPSS) p 30 N91-20119
- JONES, C.**
Concurrent engineering p 80 N91-28247
- JONES, ROBERT E.**
Techniques and implementation of the embedded rule-based expert system using Ada p 220 N91-22788
- JONES, SCOTT M.**
Computer code for single-point thermodynamic analysis of hydrogen/oxygen expander-cycle rocket engines [NASA-TM-4275] p 72 N91-20206
- JONES, WILLIAM R., JR.**
Determination of the thermal stability of fluids by tensimetry - Instrumentation and procedure p 113 A91-13435
Parched elastohydrodynamic lubrication: Instrumentation and procedure [NASA-TM-104426] p 168 N91-30469
- JONGEWARD, GARY A.**
High voltage interactions of a sounding rocket with the ambient and system-generated environments p 46 A91-23077
The environment power system analysis tool development program p 231 N91-17734
The environment workbench: A design tool for Space Station Freedom p 48 N91-20727
- JORDAN, ERIC H.**
Equivalence of Green's function and the Fourier series representation of composites with periodic microstructure p 91 A91-16889
- JORGENSEN, PHILIP C. E.**
An unconditionally stable Runge-Kutta method for unsteady rotor-stator interaction p 165 N91-24337
- JOSEFOWICZ, J. Y.**
An experimental study of high Tc superconducting microstrip transmission lines at 35 GHz and the effect of film morphology p 138 A91-36172
An experimental study of high Tc superconducting microstrip transmission lines at 35 GHz and the effect of film morphology [NASA-TM-103633] p 133 N91-11988
- JUERGENSEN, H.**
Submicron gate InP power MISFET's with improved output power density at 18 and 20 GHz p 145 N91-26436
- JUHAS, JOHN J.**
Process for HIP canning of composites [NASA-CASE-LEW-14990-1-CU] p 96 N91-17145
- JUHASZ, A.**
A PCM/forced convection conjugate transient analysis of energy storage systems with annular and countercurrent flows p 150 A91-27166
- JUHASZ, A. J.**
The telescoping boom radiator concept for multimegawatt space power systems [AIAA PAPER 91-3497] p 158 A91-52395
- JUHASZ, ALBERT J.**
Two-dimensional simulation of a two-phase, regenerative pumped radiator loop utilizing direct contact heat transfer with phase change p 151 A91-38126
An overview of the LeRC CSTI thermal management program [AIAA PAPER 91-3528] p 158 A91-52422
Design considerations for space radiators based on the liquid sheet (LSR) concept [NASA-TM-105158] p 80 N91-27213
- JURGENSEN, HOLGER**
Submicron gate InP power MISFET's with improved output power density at 18 and 20 GHz p 142 A91-54526
- JURNS, J.**
LN2 spray droplet size measurement via ensemble diffraction technique [AIAA PAPER 91-1381] p 129 A91-44336
LN2 spray droplet size measurement via ensemble diffraction technique [NASA-TM-104443] p 131 N91-24470

K

- KACUPURA, THOMAS J.**
An EMTP system level model of the PMAD DC test bed [NASA-TM-104515] p 79 N91-27206
- KACZYNSKI, KENNETH J.**
A dual-cooled hydrogen-oxygen rocket engine heat transfer analysis [AIAA PAPER 91-2211] p 59 A91-44156
Analytical study of nozzle performance for nuclear thermal rockets [AIAA PAPER 91-3578] p 66 A91-52451
A three-dimensional turbulent heat transfer analysis for advanced tubular rocket thrust chambers [NASA-TM-103293] p 159 N91-10249
A three-dimensional turbulent heat transfer analysis for advanced tubular rocket thrust chambers p 75 N91-24258
A dual-cooled hydrogen-oxygen rocket engine heat transfer analysis [NASA-TM-104430] p 76 N91-24302
- KALLURI, SREERAMESH**
Elastic response of (001)-oriented PWA 1480 single crystal - The influence of secondary orientation [SAE PAPER 911111] p 110 A91-53555
A data acquisition and control program for axial-torsional fatigue testing p 199 A91-56540
Axial-torsional fatigue: A study of tubular specimen thickness effects [NASA-TM-103637] p 200 N91-14632
Effect of tensile mean stress on fatigue behavior of single-crystal and directionally solidified superalloys [NASA-TM-103644] p 200 N91-18452
Thermomechanical and bithermal fatigue behavior of cast B1900 + Hf and wrought Haynes 188 [NASA-TM-4225] p 111 N91-20268
Elastic response of zone axis (001)-oriented PWA 1480 single crystal: The influence of secondary orientation [NASA-TM-103782] p 202 N91-21558
Fatigue behavior of a single-crystal superalloy p 111 N91-24313
- KANG, HO-SHIK**
Primordial nucleosynthesis redux p 240 A91-45907
- KANG, M. PAUL**
Mechanisms and modeling of the effects of additives on the nitrogen oxides emission [AIAA PAPER 91-0479] p 124 A91-40560
Mechanisms and modeling of the effects of additives on the nitrogen oxides emission [NASA-TM-103765] p 126 N91-22464
- KANKAM, M. D.**
An analysis of space power system masses p 54 A91-38003
- KANKAM, M. DAVID**
Development of an analytical tool to study power quality of AC power systems for large spacecraft [NASA-TM-104451] p 223 N91-25749
Comparative survey of dynamic analyses of free-piston Stirling engines [NASA-TM-104491] p 224 N91-26870
- KANTZOS, P.**
Fatigue crack growth study of SCS6/Ti-15-3 composite p 91 A91-25798
- KANTZOS, PETE**
Modeling of crack bridging in a unidirectional metal matrix composite [NASA-TM-104355] p 205 N91-24660
- KA0, C. K.**
A new approach to controller design for microgravity isolation systems p 129 A91-23108
- KA0, KAI-HSIUNG**
Stability of compressible Taylor-Couette flow [AIAA PAPER 91-1642] p 153 A91-42541
- KAPOOR, VIK J.**
Submicron gate InP power MISFET's with improved output power density at 18 and 20 GHz p 142 A91-54526
Submicron gate InP power MISFET's with improved output power density at 18 and 20 GHz p 145 N91-26436
- KASCAK, ALBERT F.**
Use of piezoelectric actuators in active vibration control of rotating machinery p 179 A91-14400
- KASSEMI, MOHAMMAD**
Interaction of surface radiation with convection in crystal growth by physical vapor transport p 127 A91-24563
- KATEHI, LINDA P. B.**
Theoretical and experimental characterization of coplanar waveguide discontinuities for filter applications p 137 A91-35911
- KATZAN, CYNTHIA M.**
The effects of lunar dust accumulation on the performance of photovoltaic arrays p 83 N91-30238
- KAUFMAN, M. J.**
Constitution of pseudobinary hypoeutectic beta-NiAl + alpha-V alloys p 109 A91-48509
A simplified method for determining the number of independent slip systems in crystals p 110 A91-55472
- KAUFMANN, K. J.**
Full-size solar dynamic heat receiver thermal-vacuum tests [NASA-TM-104486] p 78 N91-25184
Ground test program for a full-size solar dynamic heat receiver [NASA-TM-104485] p 79 N91-27209
- KAUTZ, H. E.**
Ultrasonic velocity technique for monitoring property changes in fiber-reinforced ceramic matrix composites p 174 A91-56912
- KAUTZ, HAROLD**
Review of acousto-ultrasonic NDE for composites p 97 N91-18192
Acousto-ultrasonic nondestructive evaluation of materials using laser beam generation and detection p 193 N91-18193
- KAUTZ, HAROLD E.**
Preliminary investigation of acousto-ultrasonic evaluation of metal-matrix composite specimens p 191 A91-37014
A preliminary investigation of acousto-ultrasonic NDE of metal matrix composite test specimens [NASA-TM-104339] p 194 N91-23521
Ultrasonic velocity technique for monitoring property changes in fiber-reinforced ceramic matrix composites [NASA-TM-103806] p 195 N91-30546
- KAVIANY, M.**
Transient cryogenic liquid discharge in normal and micro-gravity [AIAA PAPER 91-0486] p 124 A91-19324
Discharge rate of cryogenics in microgravity - What ground based experimentation cannot resolve [AIAA PAPER 91-3545] p 129 A91-52430
- KAYTEN, GERALD G.**
NASA's High Speed Research Program - An introduction and status report [SAE PAPER 901923] p 1 A91-48605
- KAZA, K. R. V.**
ASTROP2 users manual: A program for aeroelastic stability analysis of propanes [NASA-TM-4304] p 206 N91-28627
- KAZA, KRISHNA R. V.**
Semi-analytical technique for sensitivity analysis of unsteady aerodynamic computations p 7 A91-48816
- KAZAROFF, J. M.**
A life comparison of tube and channel cooling passages for thrust chambers [NASA-TM-103613] p 68 N91-11059
- KAZAROFF, JOHN**
Surface modification of Monel K-500 as a means of reducing friction and wear in high-pressure oxygen p 107 A91-16869
- KAZAROFF, JOHN M.**
A dual-cooled hydrogen-oxygen rocket engine heat transfer analysis [AIAA PAPER 91-2211] p 59 A91-44156
New method of making advanced tube-bundle rocket thrust chambers [NASA-TM-103617] p 70 N91-15301

- A dual-cooled hydrogen-oxygen rocket engine heat transfer analysis
[NASA-TM-104430] p 76 N91-24302
- KEGELMAN, JEROME T.**
VSTOL ground effects testing with flow visualization and image enhancement
[AIAA PAPER 91-3145] p 8 A91-54061
Flow visualization and hot gas ingestion characteristics of a vectored thrust STOVL concept p 28 N91-20090
- KEITH, T. G., JR.**
Extension of transonic flow computational concepts in the analysis of cavitating bearings
[ASME PAPER 90-TRIB-40] p 150 A91-29474
Test-cell pressure effects on the performance of resistojets p 38 A91-37417
Results from computational analysis of a mixed compression supersonic inlet
[AIAA PAPER 91-2581] p 7 A91-45818
Extension of transonic flow computational concepts in the analysis of cavitating bearings
[NASA-TM-103214] p 160 N91-16304
A laser-induced heat flux technique for convective heat transfer measurements in high speed flows
[NASA-TM-105177] p 168 N91-30472
- KEITH, THEO**
Three-dimensional flows in a transonic compressor rotor p 8 A91-56152
- KEITH, THEO G., JR.**
Cascade flutter analysis with transient response aerodynamics
[AIAA PAPER 91-0747] p 21 A91-19448
Development of a laser-induced heat flux technique for measurement of convective heat transfer coefficients in a supersonic flowfield
[NASA-TM-103778] p 13 N91-19063
Cascade flutter analysis with transient response aerodynamics
[NASA-TM-103746] p 201 N91-19475
- KELLY, A. J.**
Anode power deposition in an applied-field segmented anode MPD thruster
[AIAA PAPER 91-2343] p 59 A91-44204
Energy deposition in low-power coaxial plasma thrusters p 63 A91-52311
Cathode phenomena in a low-power magnetoplasmadynamic thruster p 63 A91-52314
- KENNEDY, ERIC M.**
The environment power system analysis tool development program p 231 N91-17734
- KENNY, B. H.**
Systems analysis of Mars solar electric propulsion vehicles
[AIAA PAPER 90-3824] p 40 A91-10176
- KENNY, BARBARA**
Control of multiple resonant power processors in a multi-source system p 137 A91-30901
- KENNY, BARBARA H.**
An analysis of space power system masses p 54 A91-38003
Preliminary design of a mobile lunar power supply
[NASA-TM-104471] p 212 N91-27611
- KERCZEWSKI, ROBERT J.**
Evaluation of components, subsystems, and networks for high rate, high frequency space communications
[AIAA PAPER 91-3423] p 41 A91-52343
- KERSLAKE, S. D.**
Quaternary pulse position modulation electronics for free-space laser communications
[AIAA PAPER 91-3471] p 133 A91-53702
Quaternary pulse position modulation electronics for free-space laser communications
[NASA-TM-104502] p 135 N91-29405
- KERSLAKE, T. W.**
Ground test program for a full-size solar dynamic heat receiver
[NASA-TM-104485] p 79 N91-27209
- KERSLAKE, THOMAS W.**
Two-dimensional model of a Space Station Freedom thermal energy storage canister p 151 A91-38048
Multi-dimensional modeling of a thermal energy storage canister
[NASA-TM-103731] p 71 N91-19177
Full-size solar dynamic heat receiver thermal-vacuum tests
[NASA-TM-104486] p 78 N91-25184
- KERSLAKE, WILLIAM R.**
The effect of the near earth micrometeoroid environment on a mirror surface after 20 years in space p 47 A91-49810
- KETELSEN, DEAN A.**
A new fabrication method for precision antenna reflectors for space flight and ground test
[NASA-TP-3078] p 48 N91-21185
- KHAVARAN, ABBAS**
Noise measurements from an ejector suppressor nozzle in the NASA Lewis 9- by 15-foot low speed wind tunnel
[AIAA PAPER 90-3983] p 225 A91-12496
Noise measurements from an ejector suppressor nozzle in the NASA Lewis 9- by 15-foot low speed wind tunnel
[NASA-TM-103628] p 227 N91-11493
- KIEFFER, ARTHUR W.**
Automatic control study of the icing research tunnel refrigeration system
[NASA-TM-4257] p 40 N91-19115
- KIM, C. M.**
Flow induced vibration and noise by a pair of tandem cylinders due to buffeting p 225 A91-14650
- KIM, CHEOL J.**
The series Bi₂Sr₂Ca(n-1) Cu(n)O(2n+4) (1 less than or equal to n less than or equal to 5): Phase stability and superconducting properties
[NASA-TM-103749] p 235 N91-21910
- KIM, J. T.**
The potential for ductility enhancement from surface and interface dislocation sources in NiAl p 109 A91-39292
- KIM, JUNGHWAN**
Performance evaluation of land mobile satellite system under vegetative shadowing using differential multiple TCM and QPSK p 132 A91-53084
Study on the spectral efficiency of SFH-GMSK in land mobile telephone communication by direct simulation p 132 A91-53176
- KIM, S. C.**
New mixing-length model for supersonic shear layers p 148 A91-16073
Numerical study of high-area-ratio H₂/O₂ rocket nozzles
[AIAA PAPER 91-2434] p 57 A91-41780
Performance and flow calculations for a gaseous H₂/O₂ thruster p 63 A91-48843
- KIM, S.-W.**
Calculation of divergent channel flows with a multiple-time-scale turbulence model p 151 A91-34134
Numerical investigation of an internal layer in turbulent flow over a curved hill p 163 N91-21083
Calculation of a circular jet in crossflow with a multiple-time-scale turbulence model p 169 N91-30476
- KIM, SANG-WOOK**
On the anomaly of velocity-pressure decoupling in collocated mesh solutions
[NASA-TM-103769] p 164 N91-21448
Comparison of SMAC, PISO, and iterative time-advancing schemes for unsteady flows
[NASA-TM-104406] p 167 N91-24550
- KIM, SUK C.**
Experimental and analytical comparison of flowfields in a 110 N (25 Lbf) H₂/O₂ rocket
[AIAA PAPER 91-2283] p 62 A91-45802
Computational fluid dynamics studies of nuclear rocket performance
[AIAA PAPER 91-3577] p 66 A91-52450
Experimental and analytical comparison of flowfields in a 110 N (25 lbf) H₂/O₂ rocket
[NASA-TM-105175] p 82 N91-29230
- KIM, WALTER S.**
Thin-film sensors for space propulsion technology: Fabrication and preparation for testing p 77 N91-24324
- KIM, Y. S.**
Tensile and fatigue behavior of tungsten/copper composites p 100 N91-24311
- KIM, Y.-S.**
High temperature fatigue behavior of tungsten copper composites p 93 A91-55906
- KIMNACH, GREG L.**
Description of the control system design for the SSF PMAD DC testbed
[NASA-TM-105202] p 84 N91-30266
- KIRTLEY, K. R.**
An algebraic RNG-based turbulence model for three-dimensional turbomachinery flows
[AIAA PAPER 91-0172] p 2 A91-21393
Nonlinear Reynolds stress model for turbulent shear flows
[AIAA PAPER 91-0609] p 149 A91-21556
- KIRTLEY, KEVIN**
Average-passage flow model development p 165 N91-24338
- KISER, J. D.**
Investigation of interfacial shear strength in SiC/Si₃N₄ composites p 93 A91-56913
Investigation of interfacial shear strength in SiC/Si₃N₄ composites
[NASA-TM-103739] p 101 N91-26233
Crystallization and characterization of Y₂O₃-SiO₂ glasses p 237 N91-31962
- KISH, JAMES A.**
Automated electric power management and control for Space Station Freedom p 53 A91-37970
- KLEIN, WILLIAM E.**
Model-OA wind turbine generator - Failure modes and effects analysis p 191 A91-31064
- KLEM, MARK D.**
JANNAF liquid rocket combustion instability panel research recommendations
[NASA-TM-103653] p 70 N91-13491
- KLIMA, S.**
Impact behavior of a SiC fiber-reinforced reaction bonded Si₃N₄ composite p 91 A91-16805
- KLIMA, S. J.**
High resolution computed tomography of advanced composite and ceramic materials p 192 A91-56972
- KLIMA, STANLEY J.**
NDE of ceramics and ceramic composites
[NASA-TM-104520] p 194 N91-29610
- KNIP, GERALD, JR.**
High-efficiency core technology p 30 N91-20118
- KNOLL, RICHARD H.**
A review of candidate multilayer insulation systems for potential use on wet-launched LH₂ tankage for the Space Exploration Initiative lunar missions
[AIAA PAPER 91-2176] p 43 A91-45793
Thermal performance of a liquid hydrogen tank multilayer insulation system at warm boundary temperatures of 630, 530, and 152 R
[AIAA PAPER 91-2400] p 43 A91-45812
Thermal performance of a liquid hydrogen tank multilayer insulation system at warm boundary temperatures of 630, 530, and 152 R
[NASA-TM-104476] p 43 N91-25159
- KNOSPE, CARL R.**
Microgravity vibration isolation: An optimal control law for the one-dimensional case p 49 N91-21206
- KO, FRANK**
Development of braided rope seals for hypersonic engine applications. II - Flow modeling
[AIAA PAPER 91-2495] p 182 A91-41800
Development of braided rope seals for hypersonic engine applications. Part 2: Flow modeling
[NASA-TM-104371] p 186 N91-22571
- KOCH, JOHN, JR.**
Plug-type heat flux gauge
[NASA-CASE-LEW-14967-1] p 179 N91-31608
- KOESTER, J. K.**
The telescoping boom radiator concept for multimegawatt space power systems
[AIAA PAPER 91-3497] p 158 A91-52395
- KOHL, FRED J.**
Microgravity research at LeRC
[NASA-TM-102521] p 128 N91-24464
- KOHOUT, L. L.**
SEI power source alternatives for rovers and other multi-kWe distributed surface applications
[NASA-TM-104360] p 81 N91-28277
- KOHOUT, LISA L.**
SEI rover solar-electrochemical power system options
[NASA-TM-104402] p 211 N91-23620
- KOLB, EDWARD W.**
First-order inflation p 240 A91-37444
Astrophysics and cosmology confront the 17-keV neutrino p 240 A91-43291
Constraints from primordial nucleosynthesis on the mass of the tau neutrino p 240 A91-46543
- KOLECKI, J. C.**
Electrical system/environment interactions on the planet Mars p 242 N91-27068
- KONG, K. S.**
Design aspects and comparison between high T(sub c) superconducting coplanar waveguide and microstrip line
[NASA-TM-105142] p 146 N91-27445
- KONG, KEON-SHIK**
YBCO superconducting ring resonators at millimeter-wave frequencies p 142 A91-54532
- KOPANSKI, J. J.**
MIS capacitor studies on silicon carbide single crystals
[NASA-CR-187350] p 234 N91-11555
- KOSS, M. B.**
Isothermal Dendritic Growth Experiment - Science, engineering, and hardware development for USMP space flights p 128 A91-53408
- KRAFT, L. ALAN**
Development of an analytical tool to study power quality of AC power systems for large spacecraft
[NASA-TM-104451] p 223 N91-25749
- KRAFT, PATRICIA A.**
Synthesis and thermal properties of strontium and calcium peroxides
[NASA-TM-103725] p 107 N91-22410
- KRAINSKY, ISAY L.**
Inverse photoelectron spectrometer with magnetically focused electron gun p 172 A91-42849

- KRANTZ, TIMOTHY L.**
Experimental and analytical evaluation of efficiency of helicopter planetary stage
[NASA-TP-3063] p 183 N91-12956
- KRASOWSKI, M. J.**
Compensation for effects of ambient temperature on rare-earth doped fiber optic thermometer
p 170 A91-19582
- KRAUS, ROBERT**
Light weight, high power, high voltage dc/dc converter technologies
p 138 A91-37985
- KREIDLER, E. R.**
High temperature reactions of ceramics and metals with chlorine and oxygen
p 105 A91-20219
- KREJSA, EUGENE A.**
Prediction of the noise from a propeller at angle of attack
[AIAA PAPER 90-3954] p 225 A91-12470
Noise measurements from an ejector suppressor nozzle in the NASA Lewis 9- by 15-foot low speed wind tunnel
[AIAA PAPER 90-3983] p 225 A91-12496
Noise measurements from an ejector suppressor nozzle in the NASA Lewis 9- by 15-foot low speed wind tunnel
[NASA-TM-103628] p 227 N91-11493
Prediction of the noise from a propeller at angle of attack
[NASA-TM-103627] p 227 N91-11495
- KRESS, ROBERT**
Simulation of Martian dust accumulation on surfaces
p 47 N91-19180
The effects of lunar dust accumulation on the performance of photovoltaic arrays
p 83 N91-30238
- KROLIKOWSKI, CATHRYN R.**
Programmable multi-zone furnace for microgravity research
[AIAA PAPER 91-0781] p 127 A91-19463
- KRUPP, JOSEPH C.**
Electric power scheduling - A distributed problem-solving approach
p 219 A91-37976
- KUAN, CHIHPIING**
Computerized inspection of real surfaces and minimization of their deviations
[NASA-TM-103798] p 188 N91-27558
- KUBIAK, CLIFFORD P.**
Chemical approaches to carbon dioxide utilization for manned Mars missions
[NASA-TM-103728] p 241 N91-20015
Chemical approaches to carbon dioxide utilization for manned Mars missions
p 241 N91-26073
- KUCERA, DONALD**
Industrial applications of graphite fluoride fibers
p 100 N91-23040
- KUCZMARSKI, M.**
A numerical and experimental analysis of reactor performance and deposition rates for CVD on monofilaments
[NASA-TM-103631] p 130 N91-14500
- KUCZMARSKI, MARIA**
Computational materials science. An example: Numerical modeling of chemical vapor deposition processing of advanced fibers
p 99 N91-20111
- KUHARSKI, ROBERT A.**
High voltage interactions of a sounding rocket with the ambient and system-generated environments
p 46 A91-23077
The environment power system analysis tool development program
p 231 N91-17734
The environment workbench: A design tool for Space Station Freedom
p 48 N91-20727
- KUKICH, GEORGE**
An expert system for simulating electric loads aboard Space Station Freedom
p 55 A91-38041
- KUMAR, K. S.**
Compression behavior of TiB₂-particulate-reinforced composites of Al₂₂Fe₃Ti₈
p 91 A91-28014
1000 to 1300 K slow plastic compression properties of Al-deficient NiAl
p 108 A91-36214
1000 to 1200 K time-dependent compressive deformation of single-crystalline and polycrystalline B2 Ni-40Al
p 109 A91-43670
Low-density, high-strength intermetallic matrix composites by XD (trademark) synthesis
[NASA-TM-103724] p 97 N91-19233
- KUMAR, V.**
Two-dimensional imaging of molecular hydrogen in H₂-air diffusion flames using two-photon laser-induced fluorescence
p 124 A91-34369
- KUNATH, R. R.**
Bit error rate testing of fiber optic data links for MMIC-based phased array antennas
p 131 A91-24950
ATDRS payload technology R & D
p 45 A91-53188
- KUNATH, RICHARD R.**
Design of an optically controlled Ka-band GaAs MMIC phased-array antenna
p 132 A91-24951
- Design of an inflatable, optically controlled and fed, phased array antenna
[AIAA PAPER 91-3470] p 132 A91-52378
Using a modified Hewlett Packard 8410 network analyzer as an automated farfield antenna range receiver
[NASA-TM-103700] p 143 N91-19349
Near-field antenna testing using the Hewlett Packard 8510 automated network analyzer
[NASA-TM-103699] p 144 N91-20393
- KUNDU, KRISHNA**
Jet-A reaction mechanism study for combustion application
[AIAA PAPER 91-2355] p 106 A91-45810
Jet-A reaction mechanism study for combustion application
[NASA-TM-104441] p 35 N91-31181
- KUNDU, KRISHNA P.**
Mechanisms and modeling of the effects of additives on the nitrogen oxides emission
[AIAA PAPER 91-0479] p 124 A91-40580
Mechanisms and modeling of the effects of additives on the nitrogen oxides emission
[NASA-TM-103785] p 126 N91-22464
- KURKOV, A. P.**
Optical measurement of unducted fan blade deflections
[ASME PAPER 89-GT-298] p 170 A91-13046
- KURKOV, ANATOLE P.**
Optical measurement of unducted fan flutter
[NASA-TM-103285] p 27 N91-15174
Optical measurement of propeller blade deflections in a spin facility
[NASA-TM-103115] p 12 N91-17002
- KURLAND, RICHARD M.**
Rapid thermal cycling of new technology solar array blanket coupons
p 54 A91-38019
- KUROKAWA, SHIN**
The shock process and light-element production in supernova envelopes
p 239 A91-33573
- KURYLE, M. S.**
Temperature coefficients of multijunction solar cells
p 172 A91-41921
- KUSSMAUL, M. T.**
Dual ion beam processed diamondlike films for industrial applications
p 121 N91-23042
- KUTINA, FRANK J., JR.**
Recent advances in Lewis aeropropulsion facilities
p 38 N91-20121
- KWASNY, JAMES**
Arcjet nozzle area ratio effects
p 75 N91-24271
- KWATRA, S. C.**
Performance evaluation of land mobile satellite system under vegetative shadowing using differential multiple TCM and QPSK
p 132 A91-53084
Study on the spectral efficiency of SFH-GMSK in land mobile telephone communication by direct simulation
p 132 A91-53176
- KWON, O. J.**
Simulation of iced wing aerodynamics
[NASA-TM-104362] p 15 N91-23086
- L**
- LA POINTE, MICHAEL R.**
Numerical simulation of self-field MPD thrusters
[AIAA PAPER 91-2341] p 62 A91-45805
- LACKNEY, J. J.**
HITCAN for actively cooled hot-composite thermostructural analysis
[NASA-TM-103750] p 202 N91-21562
- LACONTI, A. B.**
Some recent studies with the solid-ionomer electrochemical capacitor
p 214 N91-32562
- LACOVIC, RAYMOND F.**
Autogenous pressurization of cryogenic vessels using submerged vapor injection
[NASA-TM-104516] p 127 N91-27375
- LADLE RISTOW, M.**
Temperature coefficients of multijunction solar cells
p 172 A91-41921
- LAGERLOF, K. P. D.**
The structure of carbon in chemically vapor deposited SiC monofilaments
p 113 A91-18675
- LAI, H. T.**
3D computation of hypersonic nozzle
[AIAA PAPER 90-5203] p 1 A91-14429
The 3D computation of single-expansion-ramp and scramjet nozzles
p 164 N91-21092
- LAI, M. C.**
CFD analysis of jet mixing in low NO_x flame tube combustors
[NASA-TM-104466] p 33 N91-26146
- LAI, M.-C.**
Jet-A fuel evaporation analysis in conical tube injectors
[AIAA PAPER 91-0345] p 149 A91-21467
- LAI, R.**
Low-temperature microwave characteristics of pseudomorphic In(x)Ga(1-x) As/In(0.52)Al(0.48)As modulation-doped field-effect transistors
p 136 A91-22987
- LALI, VINCENT R.**
Model-OA wind turbine generator - Failure modes and effects analysis
p 191 A91-31064
- LANDIS, G. A.**
Proposal for a sun-following moonbase
p 41 A91-27356
- LANDIS, GEOFFREY A.**
Satellite eclipse power by laser illumination
[IAF PAPER 90-053] p 50 A91-13766
Reactionless orbital propulsion using tether deployment
[IAF PAPER 90-254] p 51 A91-13908
Satellite relocation by tether deployment
p 40 A91-22966
An evolutionary path to satellite solar power systems
p 51 A91-26063
Solar array orientations for a space station in low earth orbit
p 46 A91-30019
Comment on 'Negative matter propulsion'
p 52 A91-37424
Design considerations for lunar base photovoltaic power systems
p 41 A91-41987
Design considerations for Mars photovoltaic power systems
p 41 A91-41988
A light-trapping solar cell coverglass
p 229 A91-41995
Photovoltaic superiority for Space Station Freedom power in the 21st century
p 58 A91-42004
Laser photovoltaic power system synergy for SEI applications
[AIAA PAPER 91-3419] p 207 A91-52339
Production and use of metals and oxygen for lunar propulsion
[AIAA PAPER 91-3481] p 125 A91-53711
Design considerations for lunar base photovoltaic power systems
[NASA-TM-103642] p 241 N91-14259
Radiation resistance of thin-film solar cells for space photovoltaic power
[NASA-TM-103715] p 71 N91-19176
Review of thin film solar cell technology and applications for ultra-light spacecraft solar arrays
p 208 N91-19198
Feasibility of solar power for Mars
p 209 N91-19201
Chemical approaches to carbon dioxide utilization for manned Mars missions
[NASA-TM-103728] p 241 N91-20015
Vision-21: Space Travel for the Next Millennium
[NASA-CP-10059] p 40 N91-22139
Reactionless propulsion using tethers
p 73 N91-22163
Applications of thin film technology toward a low-mass solar power satellite
p 235 N91-22179
Material processing with hydrogen and carbon monoxide on Mars
[NASA-TM-104405] p 211 N91-23616
Chemical approaches to carbon dioxide utilization for manned Mars missions
p 241 N91-26073
Production and use of metals and oxygen for lunar propulsion
[NASA-TM-105195] p 81 N91-29222
Grooved surfaces on InP
p 213 N91-30208
Solar radiation on Mars: Update 1991
[NASA-TM-105216] p 242 N91-33046
- LANG, N. J.**
A critical comparison of two-equation turbulence models
[NASA-TM-105237] p 169 N91-31597
- LANGDON, T. G.**
Creep behavior of copper at intermediate temperatures. II - Surface microstructural observations. III - A comparison with theory
p 109 A91-47931
- LANT, CHRISTIAN T.**
Two-dimensional high temperature strain measurement system
p 204 N91-24319
- LAPOINTE, MICHAEL R.**
Antiproton powered propulsion with magnetically confined plasma engines
p 63 A91-52313
MPD thruster technology
[AIAA PAPER 91-3568] p 65 A91-52444
MPD thruster technology
[NASA-TM-105242] p 86 N91-32162

LARKIN, M.

Evaluation of panel code predictions with experimental results of inlet performance for a 17-inch ducted prop/fan simulator operating at Mach 0.2
[AIAA PAPER 91-3354] p 7 A91-45819

Evaluation of panel code predictions with experimental results of inlet performance for a 17-inch ducted prop/fan simulator operating at Mach 0.2
[NASA-TM-104428] p 17 N91-25106

LARSEN, JON T.

The shock process and light-element production in supernova envelopes p 239 A91-33573

LARSEN, M.

The potential for ductility enhancement from surface and interface dislocation sources in NiAl p 109 A91-39292

LASTRAPES, G.

Temperature dependence of the elastic moduli and damping for polycrystalline LiF-22 pct CaF₂ eutectic salt p 87 A91-33793

LAVERY, JOHN E.

Solution of steady-state, two-dimensional conservation laws by mathematical programming p 221 A91-35956

LAVY, YESHAYAHOU

Measurements and predictions of a liquid spray from an air-assist nozzle
[AIAA PAPER 91-0692] p 149 A91-22498

LAWRENCE, C.

Solar electric propulsion for Mars transport vehicles
[NASA-TM-103234] p 71 N91-19178

LAWRENCE, CHARLES

The dynamic effects of internal robots on Space Station Freedom
[AIAA PAPER 91-2822] p 40 A91-49764

The dynamic effects of internal robots on Space Station Freedom
[NASA-TM-104345] p 203 N91-22604

Structural design concepts for a multi-megawatt Solar Electric Propulsion (SEP) spacecraft
[NASA-TM-105148] p 206 N91-30565

LAZAR, J.

Aerospace applications of high temperature superconductivity
[IAF PAPER 90-054] p 231 A91-13767

LAZBIN, IGOR

Power electronic applications for Space Station Freedom p 52 A91-36832

LEBRON, RAMON C.

Test and evaluation of load converter topologies used in the Space Station Freedom Power Management and distribution DC test bed
[NASA-TM-105217] p 85 N91-30267

LECKIE, F. A.

Inhomogeneous deformation in INCONEL 718 during monotonic and cyclic loadings p 108 A91-22287

LEE, CHI-MING

Jet-A reaction mechanism study for combustion application
[AIAA PAPER 91-2355] p 106 A91-45810

Jet-A reaction mechanism study for combustion application
[NASA-TM-104441] p 35 N91-31181

LEE, H.-J.

METCAN updates for high temperature composite behavior: Simulation/verification
[NASA-TM-103682] p 97 N91-19229

LEE, HO-JUN

METCAN simulation of candidate metal matrix composites for high temperature applications
[NASA-TM-103636] p 96 N91-17143

LEE, K. F.

Circular polarisation characteristics of stacked microstrip antennas p 131 A91-20370

Mutual coupling between electromagnetically coupled rectangular patch antennas p 137 A91-32822

LEE, R. Q.

Coplanar-waveguide/microstrip probe coupler and applications to antennas p 131 A91-17719

Circular polarisation characteristics of stacked microstrip antennas p 131 A91-20370

Mutual coupling between electromagnetically coupled rectangular patch antennas p 137 A91-32822

New coplanar waveguide/stripline feed network for seven patch hexagonal CP subarray p 137 A91-32823

A 29.3-GHz cavity-enclosed aperture-coupled circular-patch antenna for microwave circuit integration p 140 A91-47057

Ka-band MMIC microstrip array for high rate communications
[AIAA PAPER 91-3421] p 132 A91-52341

A seven patch hexagonal CP subarray with a CPW/stripline feed network
[NASA-TM-103802] p 144 N91-20406

Ka-band MMIC microstrip array for high rate communications
[NASA-TM-104500] p 135 N91-27437

LEE, RICHARD Q.

Coplanar waveguide feeds for phased array antennas
[AIAA PAPER 91-3422] p 141 A91-52342

Coplanar waveguide feeds for phased array antennas
[NASA-TM-104467] p 146 N91-27477

LEE, SHUNG-WU

Designs for the ATRSS tri-band reflector antenna
[NASA-TM-103754] p 48 N91-20184

LEE, WILLIAM E.

Crystallization and characterization of Y2O3-SiO2 glasses p 237 N91-31962

LEFEBVRE, A. H.

Influence of geometric features on the performance of pressure-swirl atomizers p 147 A91-13030

LEGER, L.

Concurrent engineering p 80 N91-28247

LEI, J.-F.

A resistance strain gage with repeatable apparent strain to 800 C p 198 A91-48899

LEI, JIH-FEN

PdCr based high temperature static strain gage
[AIAA PAPER 90-5236] p 170 A91-14462

A resistance strain gage with repeatable and cancellable apparent strain for use to 1500 F p 173 A91-51930

LEIB, S. J.

Nonlinear evolution of subsonic and supersonic disturbances on a compressible free shear layer p 152 A91-39716

The effect of small streamwise velocity distortion on the boundary layer flow over a thin flat plate with application to boundary layer stability theory
[NASA-TM-103668] p 161 N91-19372

LEIBECKI, HAROLD F.

Modeling and optimization of a regenerative fuel cell system using the ASPEN process simulator p 206 A91-38177

LEIBOVICH, S.

Unstable viscous wall modes in rotating pipe flow
[AIAA PAPER 91-1801] p 154 A91-42599

LEMPERT, W.

Two-dimensional imaging of molecular hydrogen in H₂-air diffusion flames using two-photon laser-induced fluorescence p 124 A91-34369

LENSKI, JOSEPH W., JR.

Advanced Rotorcraft Transmission (ART) program-Boeing helicopters status report
[NASA-TM-104474] p 188 N91-25412

LEONARD, R. F.

High temperature superconductive microwave technology for space applications p 137 A91-31391

LEONARD, REGIS F.

Low noise InP-based MMIC receivers for W-band
[AIAA PAPER 91-3594] p 142 A91-52462

NASA developments in solid state power amplifiers p 143 N91-18298

Microwave integrated circuits for space applications p 145 N91-24069

Superconducting microwave electronics at Lewis Research Center p 236 N91-24081

LEONHARDT, T. A.

Sisessquioxane-derived ceramic fibres p 114 A91-30283

LEPICOVSKY, J.

An experimental investigation of nozzle-exit boundary layers of highly heated free jets
[ASME PAPER 90-GT-255] p 155 A91-44662

LERCH, B. A.

Evaluation of thermomechanical damage in silicon carbide/titanium composites p 92 A91-42297

LERCH, BRAD A.

Preliminary investigation of acousto-ultrasonic evaluation of metal-matrix composite specimens p 191 A91-37014

A preliminary investigation of acousto-ultrasonic NDE of metal matrix composite test specimens
[NASA-TM-104339] p 194 N91-23521

LERCH, BRADLEY A.

Tensile deformation damage in SiC reinforced Ti-15V-3Cr-3Al-3Sn
[NASA-TM-103620] p 101 N91-25195

Matrix plasticity in SiC/Ti-15-3 composite
[NASA-TM-103760] p 102 N91-27247

Experimental and analytical analysis of stress-strain behavior in a (90/0 deg)2s, SiC/Ti-15-3 laminate
[NASA-TM-104470] p 103 N91-31235

LESCO, DANIEL J.

Propulsion instrumentation research p 176 N91-20100

Research and development of optical measurement techniques for aerospace propulsion research: A NASA Lewis Research Center perspective
[NASA-TM-104418] p 178 N91-27511

LESNY, GARY

Surface studies on scandate cathodes and synthesized scandates p 136 A91-25071

LEVY, RALPH

A design strategy for the use of vortex generators to manage inlet-engine distortion using computational fluid dynamics
[AIAA PAPER 91-2474] p 6 A91-44259

A design strategy for the use of vortex generators to manage inlet-engine distortion using computational fluid dynamics
[NASA-TM-104436] p 16 N91-24131

LEVY, YESHAYAHOU

Measurements and predictions of a liquid spray from an air-assist nozzle
[NASA-TM-103640] p 26 N91-13455

LEWICKI, D. G.

Transmission overhaul estimates for partial and full replacement at repair
[NASA-TM-104395] p 190 N91-30533

LEWIS, DAVID W.

Microgravity vibration isolation: An optimal control law for the one-dimensional case p 49 N91-21206

LEWIS, MICHAEL J.

State of the art in video system performance p 175 N91-14578

LEZBERG, ERWIN A.

Chemical reacting flows p 162 N91-20098

LI, Z.

Simulation of mixing in the quick quench region of a rich burn-quick quench mix-lean burn combustor
[AIAA PAPER 91-0410] p 105 A91-21481

Flux-vector splitting algorithm for chain-rule conservation-law form p 221 A91-45109

LIBERMAN, EUGENE M.

Techniques and implementation of the embedded rule-based expert system using Ada p 220 N91-22788

LIEBERT, CURT H.

Heat flux measurement in SSME turbine blade tester p 171 A91-30649

Heat flux measurement in SSME turbine blade tester
[NASA-TM-103274] p 175 N91-11205

Calibrator tests of heat flux gauges mounted in SSME blades p 177 N91-24321

Plug-type heat flux gauge
[NASA-CASE-LEW-14967-1] p 179 N91-31608

LIM, HONG S.

Destructive physical analysis results of Ni/H₂ cells cycled in LEO regime
[NASA-TM-104382] p 74 N91-23233

LIM, SANG G.

On the numerical solution of the dynamically loaded hydrodynamic lubrication of the point contact p 180 A91-33461

LIM, SANG GYU

A system-approach to the elastohydrodynamic lubrication point-contact problem
[NASA-TM-104342] p 165 N91-23439

LIMBURG, HELEN C.

A high-efficiency ferruleless coupled-cavity traveling-wave tube with phase-adjusted taper p 136 A91-25078

LIN, AVI

Parallel algorithms for boundary value problems p 221 A91-31175

LIN, C. S.

A numerical study of the direct contact condensation on a horizontal surface
[AIAA PAPER 91-1307] p 155 A91-44335

Self-pressurization of a lightweight liquid hydrogen storage tank subjected to low heat flux
[NASA-TM-103804] p 126 N91-20324

A numerical study of the direct contact condensation on a horizontal surface
[NASA-TM-104432] p 166 N91-24548

LIN, C.-S.

A pressure control analysis of cryogenic storage systems
[AIAA PAPER 91-2405] p 59 A91-44228

A pressure control analysis of cryogenic storage systems
[NASA-TM-104409] p 126 N91-24460

LIN, CHIN-SHUN

Vapor condensation at the free surface of an axisymmetric liquid mixed by a laminar jet p 151 A91-35109

LIN, HSIANG HSI

Comparison of analysis and experiment for dynamics of low-contact-ratio spur gears
[NASA-TM-103232] p 185 N91-22566

LIN, RENG RONG

Use of piezoelectric actuators in active vibration control of rotating machinery p 179 A91-14400

LINDAMOOD, G. R.

New coplanar waveguide/stripline feed network for seven patch hexagonal CP subarray p 137 A91-32823

M

- A seven patch hexagonal CP subarray with a CPW/stripline feed network
[NASA-TM-103802] p 144 N91-20406
- LINNE, DIANE L.**
Carbon monoxide and oxygen combustion experiments - A demonstration of Mars in situ propellants
[AIAA PAPER 91-2443] p 60 A91-44246
Production and use of metals and oxygen for lunar propulsion
[AIAA PAPER 91-3481] p 125 A91-53711
Material processing with hydrogen and carbon monoxide on Mars
[NASA-TM-104405] p 211 N91-23616
Carbon monoxide and oxygen combustion experiments: A demonstration of Mars in situ propellants
[NASA-TM-104473] p 76 N91-24303
Production and use of metals and oxygen for lunar propulsion
[NASA-TM-105195] p 81 N91-29222
Technical prospects for utilizing extraterrestrial propellants for space exploration
[NASA-TM-105263] p 127 N91-31318
- LIU, M.-S.**
Multigrid calculation of three-dimensional viscous cascade flows
[AIAA PAPER 91-3238] p 7 A91-53754
Navier-Stokes analysis of transonic cascade flow
[NASA-TM-103624] p 159 N91-11192
Implicit solution of three-dimensional internal turbulent flows
p 163 N91-21082
- LIU, MAY-FUN**
Parallel computing using a Lagrangian formulation
[NASA-TM-104446] p 215 N91-24745
- LIU, MENG-SING**
Computational analysis of underexpanded jets in the hypersonic regime p 4 A91-37421
Generalized conjugate-gradient methods for the Navier-Stokes equations
[AIAA PAPER 91-1556] p 5 A91-40730
Development of a new flux splitting scheme
p 153 A91-40793
Osher's scheme for real gases p 153 A91-42286
Flux splitting algorithms for two-dimensional viscous flows with finite-rate chemistry p 10 N91-10894
Numerical study of unsteady shockwave reflections using an upwind TVD scheme
[NASA-TM-103251] p 10 N91-11676
Chemical reacting flows p 162 N91-20098
Transonic cascade flow calculations using non-periodic C-type grids p 163 N91-21071
A new flux splitting scheme
[NASA-TM-104404] p 222 N91-22814
High-Order Polynomial Expansions (HOPE) for flux-vector splitting
[NASA-TM-104452] p 222 N91-25739
- LIU, W. W.**
A comparison of numerical methods for the Rayleigh equation in unbounded domains
[NASA-TM-105179] p 223 N91-30865
- LISCINSKY, D. S.**
Experimental study of cross-stream mixing in a cylindrical duct
[AIAA PAPER 91-2459] p 157 A91-45815
Experimental study of cross-stream mixing in a cylindrical duct
[NASA-TM-105180] p 34 N91-29187
- LITT, JONATHAN**
An expert system to perform on-line controller restructuring for abrupt model changes
p 36 A91-29466
An expert system to perform on-line controller tuning
p 219 A91-30171
- LITT, JONATHAN S.**
Tuning maps for setpoint changes and load disturbance upsets in a three capacity process under multivariable control
[NASA-TM-104419] p 220 N91-31876
- LITVIN, F. L.**
Local synthesis and tooth contact analysis of face-milled spiral bevel gears
[NASA-TM-105182] p 190 N91-29600
- LITVIN, FAYDOR L.**
Computerized inspection of real surfaces and minimization of their deviations
[NASA-TM-103798] p 188 N91-27558
How to determine spiral bevel gear tooth geometry for finite element analysis
[NASA-TM-105150] p 190 N91-30537
- LIU, N.-S.**
Navier-Stokes simulation of transonic blade-vortex interactions
p 2 A91-21065
- LIZANICH, P. J.**
Quaternary pulse position modulation electronics for free-space laser communications
[AIAA PAPER 91-3471] p 133 A91-53702
- Quaternary pulse position modulation electronics for free-space laser communications
[NASA-TM-104502] p 135 N91-29405
- LOEFFLER, IRVIN J.**
Cruise noise of an advanced single-rotation propeller measured from an adjacent aircraft p 22 A91-28265
Inflight source noise of an advanced full-scale single-rotation propeller
[NASA-TM-103687] p 12 N91-19045
- LOFFLER, IRVIN J.**
In-flight source noise of an advanced full-scale single-rotation propeller
[AIAA PAPER 91-0594] p 226 A91-21547
- LOGSDON, K. A.**
Development of a vibration isolation prototype system for microgravity space experiments p 47 A91-53403
- LOGSDON, KIRK A.**
Development of a vibration isolation prototype system for microgravity space experiments
[NASA-TM-103664] p 130 N91-19324
- LOH, C. Y.**
A new Lagrangian random choice method for steady two-dimensional supersonic/hypersonic flow
[AIAA PAPER 91-1546] p 5 A91-40721
- LOH, CHING YUEN**
Parallel computing using a Lagrangian formulation
[NASA-TM-104446] p 215 N91-24745
- LONG, KENWYN J.**
An experimental apparatus for measuring surface resistance in the submillimeter-wavelength region
p 174 A91-54390
Emerging applications of high temperature superconductors for space communications
[NASA-TM-103629] p 227 N91-12317
- LONG, MARTIN**
Graphite fluoride fibers and their applications in the space industry
[NASA-TM-103265] p 88 N91-11062
- LOPEZ, ISAAC**
Turbomachinery p 162 N91-20097
- LORENZO, CARL**
Partitioning methods for global controllers
p 219 A91-30043
- LORENZO, CARL F.**
An intelligent control system for rocket engines - Need, vision, and issues p 218 A91-26925
Advanced aeropropulsion controls technology
p 29 N91-20103
IMPAC: An Integrated Methodology for Propulsion and Airframe Control
[NASA-TM-103805] p 30 N91-20122
A method for partitioning centralized controllers
[NASA-TM-4276] p 36 N91-20133
Life extending control: A concept paper
[NASA-TM-104391] p 37 N91-22135
- LOWELL, CARL E.**
High temperature cyclic oxidation data. Part 1: Turbine alloys
[NASA-TM-83665] p 110 N91-10149
Overview of Lewis materials research: Contributions, current efforts, and future directions
p 111 N91-20109
- LOYSELLE, PATRICIA L.**
Raman spectral observation of a new phase observed in nickel electrodes cycled to failure
p 214 N91-32556
Impedances of nickel electrodes cycled in various KOH concentrations
p 214 N91-32557
- LU, CHENG-YI**
Solar array orientations for a space station in low earth orbit p 46 A91-30019
Environmental interactions of the Space Station Freedom electric power system
[NASA-TM-104373] p 49 N91-24225
- LUDWIG, KIMBERLY**
Description of real-time Ada software implementation of a power system monitor for the Space Station Freedom PMAD DC testbed
[NASA-TM-105157] p 218 N91-28776
- LUMLEY, J. L.**
Second order modeling of boundary-free turbulent shear flows
[AIAA PAPER 91-1779] p 154 A91-42588
Second order modeling of boundary-free turbulent shear flows
[NASA-TM-104369] p 164 N91-22524
- LUMLEY, JOHN L.**
Advances in modeling the pressure correlation terms in the second moment equations
[NASA-TM-104413] p 165 N91-24525
- LUTON, MICHAEL J.**
1300 K compressive properties of a reaction milled NiAl-AIN composites p 107 A91-18674
- MACK, NADINE M.**
Simulation of the Space Station strut-out condition
[AIAA PAPER 91-1248] p 197 A91-32087
- MACKAY, R. A.**
Continuous fiber-reinforced titanium aluminide composites p 92 A91-39553
- MACKIN, MICHAEL**
Description of real-time Ada software implementation of a power system monitor for the Space Station Freedom PMAD DC testbed
[NASA-TM-105157] p 218 N91-28776
- MACKULIN, B. J.**
Maximum life spur gear design
[AIAA PAPER 91-2021] p 181 A91-41682
- MACKULIN, M. J.**
Maximum life spur gear design
[NASA-TM-104361] p 187 N91-23514
- MACRAE, GREGORY S.**
Laser interferometric measurement of ion electrode shape and charge exchange erosion
[AIAA PAPER 91-2121] p 173 A91-45786
Status of structural analysis of 30 cm diameter ion optics
[NASA-TM-103618] p 68 N91-11796
Laser interferometric measurement of ion electrode shape and charge exchange erosion
[NASA-TM-105165] p 179 N91-31605
- MADARAS, ERIC**
Overall goals p 80 N91-28246
- MADI, FRANK J.**
Update on results of SPRE testing at NASA Lewis
[NASA-TM-104425] p 79 N91-27208
- MADZSAR, G.**
Development of a Fabry-Perot interferometer for rocket engine plume monitoring p 171 A91-30634
Space Shuttle Main Engine nozzle mounted optic for throat plane spectroscopy
[AIAA PAPER 91-2524] p 49 A91-45816
- MADZSAR, GEORGE C.**
Vibrational testing of optical fiber connector joints
p 172 A91-30652
Determination of alloy content from plume spectral measurements
[AIAA PAPER 91-2531] p 88 A91-44284
A fiber optic sensor for noncontact measurement of shaft speed, torque and power p 173 A91-51870
Vibrational testing of optical fiber connector joints
[NASA-TM-103654] p 230 N91-14829
Determination of alloy content from plume spectral measurements
[NASA-TM-104442] p 89 N91-24341
Spectroscopic wear detector
[NASA-CASE-LEW-15200-1] p 87 N91-32167
- MAHAJAN, APARAJIT J.**
Cascade flutter analysis with transient response aerodynamics
[AIAA PAPER 91-0747] p 21 A91-19448
Role of artificial viscosity in Euler and Navier-Stokes solvers p 4 A91-34135
Cascade flutter analysis with transient response aerodynamics
[NASA-TM-103746] p 201 N91-19475
- MAJCHER, G. A.**
Mass comparisons of electric propulsion systems for NSSK of geosynchronous spacecraft
[AIAA PAPER 91-2347] p 47 A91-45808
- MAJCHER, GREGORY A.**
Mass comparisons of electric propulsion systems for NSSK of geosynchronous spacecraft
[NASA-TM-105153] p 85 N91-31212
- MALARIK, D.**
Autoclavable addition polyimides for 371 C composite applications p 115 A91-49112
- MALARIK, DIANE C.**
Vinyl capped addition polyimides
[NASA-CASE-LEW-15027-1] p 118 N91-13566
Viscoelastic properties of addition-cured polyimides used in high temperature polymer matrix composites
[NASA-TM-103768] p 89 N91-22377
- MALDONADO, JAIME J.**
The design and performance estimates for the propulsion module for the booster of a TSTO vehicle
[AIAA PAPER 91-3136] p 43 A91-54054
- MALONE, GLENN A.**
New method of making advanced tube-bundle rocket thrust chambers
[NASA-TM-103617] p 70 N91-15301
- MALONEY, THOMAS M.**
Modeling and optimization of a regenerative fuel cell system using the ASPEN process simulator
p 206 A91-38177
- MANKBADI, R. R.**
Heat transfer in oscillating flows p 152 A91-38698

- Turbulence enhancement in free shear flows under multifrequency excitation p 152 A91-38737
- MANKBADI, REDA R.**
Multifrequency excited jets p 151 A91-31482
Numerical simulation of nonlinear development of instability waves p 8 N91-10849
[E-4658]
Critical-layer nonlinearity in the resonance growth of three-dimensional waves in boundary layers [NASA-TM-103639] p 161 N91-19373
Resonant triad in boundary-layer stability. Part 1: Fully nonlinear interaction [NASA-TM-105208] p 169 N91-32458
Resonant triad in boundary-layer stability. Part 2: Composite solution and comparison with observations [NASA-TM-105209] p 169 N91-32459
- MANNAN, S. K.**
1000 to 1300 K slow plastic compression properties of Al-deficient NiAl p 108 A91-36214
1000 to 1200 K time-dependent compressive deformation of single-crystalline and polycrystalline B2 Ni-40Al p 109 A91-43670
- MANNING, ROBERT M.**
The theory of an auto-resonant field emission cathode relativistic electron accelerator for high efficiency microwave to direct current power conversion p 73 N91-22176
A statistical rain attenuation prediction model with application to the advanced communication technology satellite project. 3. A stochastic rain fade control algorithm for satellite link power via non linear Markov filtering theory [NASA-TM-100243] p 134 N91-22494
- MANSOORI, N.**
Lightweight concentrator module with 30 percent AMO efficient GaAs/GaSb tandem cells p 57 A91-41990
- MANSOUR, NAGI N.**
The effects of rotation on initially anisotropic homogeneous flows p 158 A91-54958
- MANTENIEKS, MARIS A.**
Performance and lifetime assessment of magnetoplasmadynamic arc thruster technology p 51 A91-30013
MPD thruster technology [AIAA PAPER 91-3568] p 65 A91-52444
MPD thruster technology [NASA-TM-105242] p 86 N91-32162
- MANZELLA, D. H.**
Test-cell pressure effects on the performance of resistojets p 38 A91-37417
- MANZELLA, DAVID H.**
Performance characterization of a segmented anode arcjet thruster [NASA-TM-103227] p 67 N91-10118
- MANZO, MICHELLE A.**
NASA Aerospace Flight Battery Systems Program p 56 A91-38088
- MARCUM, DON C., JR.**
A comparison of arrow, trapezoidal and M wing concepts using a Mach 2 supersonic cruise transport mission [AIAA PAPER 91-3102] p 7 A91-54027
- MAREK, C. J.**
Modern CFD applications for the design of a reacting shear layer facility [AIAA PAPER 91-0577] p 149 A91-21540
Simulations of free shear layers using a compressible k-epsilon model [AIAA PAPER 91-1863] p 156 A91-45778
An imaging system for PLIF/Mie measurements for a combustor flow [NASA-TM-103714] p 27 N91-20084
Modern CFD applications for the design of a reacting shear layer facility [NASA-TM-104523] p 34 N91-27164
- MARINELLI, W. J.**
Significant reduction in arc frequency biased solar cells: Observations, diagnostics, and mitigation technique(s) p 83 N91-30235
- MARTELLI, F.**
Implicit solution of three-dimensional internal turbulent flows p 163 N91-21082
- MARTIN, GARY L.**
Vibration environment - Acceleration mapping strategy and microgravity requirements for Spacelab and Space Station [IAF PAPER 90-350] p 39 A91-13991
- MARTIN, GLENN L.**
A comparison of arrow, trapezoidal and M wing concepts using a Mach 2 supersonic cruise transport mission [AIAA PAPER 91-3102] p 7 A91-54027
- MARTINEAU, ROBERT R.**
Mechanical strength and thermophysical properties of PM212: A high temperature self-lubricating powder metallurgy composite [NASA-TM-103694] p 120 N91-21302
- MASE, G. T.**
Probabilistic micromechanics and macromechanics of polymer matrix composites [NASA-TM-103669] p 98 N91-19236
- MASNOVI, JOHN**
Polymeric routes to silicon carbide and silicon oxycarbide CMC p 117 A91-56922
Polymeric routes to silicon carbide and silicon oxycarbide CMC [NASA-TM-104372] p 102 N91-26234
- MASON, LEE S.**
Lunar electric power systems utilizing the SP-100 reactor coupled to dynamic conversion systems [AIAA PAPER 91-3520] p 208 A91-52415
Space reactor/Stirling cycle systems for high power lunar application [NASA-TM-103698] p 40 N91-19112
- MASTERS, ARTHUR I.**
The Advanced Expander Test Bed [AIAA PAPER 90-3708] p 50 A91-10107
Design of an Advanced Expander Test Bed [AIAA PAPER 91-3437] p 42 A91-52350
- MATTERN, DUANE**
Feedback linearization for control of air breathing engines [AIAA PAPER 91-2000] p 23 A91-41671
A linear control design structure to maintain loop properties during limit operation in a multi-nozzle turbofan engine [AIAA PAPER 91-1997] p 24 A91-45780
Towards practical control design using neural computation [NASA-TM-103785] p 219 N91-19766
Integrated flight/propulsion control system design based on a decentralized, hierarchical approach [NASA-TM-103678] p 31 N91-21137
A linear control design structure to maintain loop properties during limit operation in a multi-nozzle turbofan engine [NASA-TM-105163] p 35 N91-29188
- MATTERN, DUANE L.**
Integrated flight/propulsion control system design based on a centralized approach p 36 A91-22950
Application of an integrated flight/propulsion control design methodology to a STOVL aircraft [AIAA PAPER 91-2792] p 36 A91-49793
IMPAC: An Integrated Methodology for Propulsion and Airframe Control [NASA-TM-103805] p 30 N91-20122
Application of an integrated flight/propulsion control design methodology to a STOVL aircraft [NASA-TM-105254] p 37 N91-32143
- MATUS, L. G.**
Controlled growth of 3C-SiC and 6H-SiC films on low-tilt-angle vicinal (0001) 6H-SiC wafers p 232 A91-45713
Application of oxidation to the structural characterization of SiC epitaxial films p 233 A91-45881
High-voltage 6H-SiC p-n junction diodes p 142 A91-54746
- MATUS, LAWRENCE G.**
Silicon carbide, a semiconductor for space power electronics [NASA-TM-103655] p 234 N91-14850
Development of silicon carbide semiconductor devices for high temperature applications [NASA-TM-104398] p 236 N91-22921
Advances in silicon carbide Chemical Vapor Deposition (CVD) for semiconductor device fabrication [NASA-TM-104410] p 236 N91-23946
Silicon carbide, an emerging high temperature semiconductor p 236 N91-24061
- MAUL, WILLIAM A.**
The application of neural networks to the SSME startup transient [AIAA PAPER 91-2530] p 60 A91-44283
Space engine safety system [AIAA PAPER 91-3604] p 44 A91-52470
- MAWID, M. A.**
A detailed numerical investigation of Burke-Schumann gaseous and spray flames [AIAA PAPER 91-2311] p 105 A91-41749
- MAY, BRIAN D.**
Pulsed response of a TWT p 136 A91-27529
Pulsed response of a traveling-wave tube [NASA-TM-103672] p 143 N91-19348
- MCARDLE, JACK G.**
Flow studies in close-coupled ventral nozzles for STOVL aircraft [SAE PAPER 901033] p 2 A91-21242
- MCBEATH, G.**
Flow visualization and computational studies of a reverse flow circular combustor p 157 A91-48966
- MCCELLELAND, R. W.**
23.5 percent thin-film space concentrator cells p 58 A91-42002
- MCCOMAS, THOMAS J.**
Design of multihundredwatt DIPS for robotic space missions [NASA-TM-104401] p 75 N91-24232
- MCCONNAUGHEY, H. V.**
Turbine blading designed for high heat load space propulsion applications p 50 A91-10338
- MCDANAL, A. J.**
The mini-dome Fresnel lens photovoltaic concentrator array - Current status of component and prototype panel testing p 57 A91-41989
- MCDANIEL, PATRICK**
Nuclear Thermal Propulsion technology - Summary of FY 1991 Interagency panel planning [AIAA PAPER 91-3631] p 66 A91-52495
- MCFADDEN, JOHN J.**
Rotary engine technology p 30 N91-20114
- MCFARLAND, ERIC**
Aerodynamics and heat transfer investigations on a high Reynolds number turbine cascade [NASA-TM-103260] p 11 N91-15134
- MCGAW, MICHAEL**
Elastic response of (001)-oriented PWA 1480 single crystal - The influence of secondary orientation [SAE PAPER 911111] p 110 A91-53555
- MCGAW, MICHAEL A.**
Automation software for a materials testing laboratory p 216 A91-56538
Effect of tensile mean stress on fatigue behavior of single-crystal and directionally solidified superalloys [NASA-TM-103644] p 200 N91-18452
Elastic response of zone axis (001)-oriented PWA 1480 single crystal: The influence of secondary orientation [NASA-TM-103782] p 202 N91-21558
Overview of the fatigue/fracture/life working group program at the Lewis Research Center p 203 N91-24308
Cumulative creep fatigue damage in 316 stainless steel p 111 N91-24312
Fatigue behavior of a single-crystal superalloy p 111 N91-24313
- MCINTYRE, STANLEY D.**
The NASA Cryogenic Fluid Management Technology Program Plan [AIAA PAPER 91-3553] p 130 A91-52436
The NASA cryogenic fluid management technology program plan [NASA-TM-105256] p 86 N91-32161
- MCKINZIE, D. J.**
Control of laminar separation over airfoils by acoustic excitation p 226 A91-45106
- MCKINZIE, DANIEL J., JR.**
Turbulent boundary layer separation over a rearward facing ramp and its control through mechanical excitation [AIAA PAPER 91-0253] p 150 A91-26328
Turbulent boundary layer separation over a rearward facing ramp and its control through mechanical excitation [NASA-TM-103702] p 160 N91-19370
- MCKISSOCK, BARBARA I.**
SEI power source alternatives for rovers and other multi-kWe distributed surface applications [NASA-TM-104360] p 81 N91-28277
Comparison of dynamic isotope power systems for distributed planet surface applications [NASA-TM-4203] p 81 N91-28278
- MCKNIGHT, R. C.**
High altitude AMO testing of PV concentrator lens elements p 207 A91-41978
- MCLALLIN, K. L.**
Full-size solar dynamic heat receiver thermal-vacuum tests [NASA-TM-104486] p 78 N91-25184
Ground test program for a full-size solar dynamic heat receiver [NASA-TM-104485] p 79 N91-27209
- MCNALLAN, M. J.**
High temperature reactions of ceramics and metals with chlorine and oxygen p 105 A91-20219
- MEADOR, MARY ANN**
Ladder polymers for use as high temperature stable resins or coatings [NASA-CASE-LEW-14203-1] p 118 N91-15402
- MEADOR, MARY ANN B.**
A review of properties and potential aerospace applications of electrically conducting polymers p 113 A91-14409
Electrically conducting polymers for aerospace applications [AIAA PAPER 91-3432] p 233 A91-52349
- MEADOR, MICHAEL A.**
A review of properties and potential aerospace applications of electrically conducting polymers p 113 A91-14409

- Electrically conducting polymers for aerospace applications
[AIAA PAPER 91-3432] p 233 A91-52349
- MEDLEY, J.**
Multidimensional computer simulation of Stirling cycle engines p 181 A91-38154
- MEHMED, ORAL**
Experimental investigation of propfan aeroelastic response in off-axis flow with mistuning p 22 A91-30015
Optical measurement of unducted fan flutter [NASA-TM-103285] p 27 N91-15174
Optical measurement of propeller blade deflections in a spin facility [NASA-TM-103115] p 12 N91-17002
- MEISSNER, DANA L.**
Numerical and experimental investigations of rarefied nozzle and plume flows of nitrogen [AIAA PAPER 91-1363] p 154 A91-43429
Pressure measurements in a low-density nozzle plume for code verification [AIAA PAPER 91-2110] p 61 A91-45783
Pressure measurements in a low-density nozzle plume for code verification [NASA-TM-105170] p 81 N91-29228
- MELIS, M. E.**
Finite element elastic-plastic-creep and cyclic life analysis of a cowl lip p 199 A91-56365
- MELIS, MATTHEW E.**
A unique high heat flux facility for testing hypersonic engine components [AIAA PAPER 90-5228] p 37 A91-14454
Elastic/plastic analyses of advanced composites investigating the use of the compliant layer concept in reducing residual stresses resulting from processing [NASA-TM-103204] p 94 N91-11074
A unique high heat flux facility for testing hypersonic engine components [NASA-TM-103238] p 38 N91-11770
High temperature NASP engine seal development [NASA-TM-103716] p 184 N91-19441
Experimental and analytical analysis of stress-strain behavior in a (90/0 deg)2s, SiC/Ti-15-3 laminate [NASA-TM-104470] p 103 N91-31235
- MELLOR, PAMELA A.**
Automated electric power management and control for Space Station Freedom p 53 A91-37970
Electric power scheduling - A distributed problem-solving approach p 219 A91-37976
- MENDEZ, ANTONIO J.**
Optical Multiple Access Network (OMAN) for advanced processing satellite applications [NASA-TM-105167] p 135 N91-29431
- MERCER, CAROLYN R.**
Fiber optic phase stepping system for interferometry p 171 A91-28968
Laser interferometric measurement of ion electrode shape and charge exchange erosion [AIAA PAPER 91-2121] p 173 A91-45786
Laser interferometric measurement of ion electrode shape and charge exchange erosion [NASA-TM-105165] p 179 N91-31605
- MERKLE, CHARLES L.**
Time-derivative preconditioning for viscous flows [AIAA PAPER 91-1652] p 154 A91-43576
- MERRILL, W.**
Real-time diagnostics of the reusable rocket engine using on-line system identification p 223 A91-30630
Neuromorphic learning of continuous-valued mappings from noise-corrupted data p 219 A91-53201
A distributed fault-detection and diagnosis system using on-line parameter estimation [NASA-TM-104433] p 220 N91-25696
- MERRILL, WALTER**
Towards practical control design using neural computation [NASA-TM-103785] p 219 N91-19766
A simplified dynamic model of the Space Shuttle main engine [NASA-TM-104421] p 131 N91-23340
- MERRILL, WALTER C.**
An intelligent control system for rocket engines - Need, vision, and issues p 218 A91-26925
Turbofan engine demonstration of sensor failure detection p 22 A91-29775
Sensor failure detection for jet engines p 22 A91-37593
Neural network application to aircraft control system design [AIAA PAPER 91-2715] p 36 A91-49676
Life extending control: A concept paper [NASA-TM-104391] p 37 N91-22135
Alpha-canonical form representation of the open loop dynamics of the Space Shuttle main engine [NASA-TM-104422] p 131 N91-24469
- Neural network application to aircraft control system design [NASA-TM-105151] p 37 N91-27167
- MERROW, JAMES**
Ion beam textured and coated surfaces experiment (IBEX) p 122 N91-25040
- MESANDER, GEERT A.**
Advanced ice protection systems test in the NASA Lewis icing research tunnel [NASA-TM-103757] p 32 N91-23183
- MESCH, HANS G.**
Rapid thermal cycling of new technology solar array blanket coupons p 54 A91-38019
- MESSICK, L. J.**
Submicron gate InP power MISFET's with improved output power density at 18 and 20 GHz p 145 N91-26436
- MESSICK, LOUIS J.**
Submicron gate InP power MISFET's with improved output power density at 18 and 20 GHz p 142 A91-54526
- METZLER, S.**
Measurement techniques for cryogenic Ka-band microstrip antennas [NASA-TM-105183] p 146 N91-30426
- MEYER, CLAUDIA M.**
The application of neural networks to the SSME startup transient [AIAA PAPER 91-2530] p 60 A91-44283
Space engine safety system [AIAA PAPER 91-3604] p 44 A91-52470
- MEYER, MICHAEL L.**
Technical prospects for utilizing extraterrestrial propellants for space exploration [NASA-TM-105263] p 127 N91-31318
- MEYER, W. V.**
A preview of a microgravity laser light scattering instrument [AIAA PAPER 91-0779] p 179 A91-21614
- MEYN, ERWIN H.**
Post clamp [NASA-CASE-LEW-14862-1] p 183 N91-14617
Optical measurement of propeller blade deflections in a spin facility [NASA-TM-103115] p 12 N91-17002
- MICHELASSI, V.**
Implicit solution of three-dimensional internal turbulent flows p 163 N91-21082
Low Reynolds number two-equation modeling of turbulent flows [NASA-TM-104368] p 165 N91-23416
- MICKLOW, GERALD J.**
Effects of nozzle lip geometry on spray atomization and emissions advanced gas turbine combustors [AIAA PAPER 91-2201] p 24 A91-44153
- MIDEA, ANTHONY C.**
Mach 6.5 air induction system design for the Beta II Two-Stage-to-Orbit booster vehicle [AIAA PAPER 91-3196] p 43 A91-54099
- MIHLEIC, JUDITH A.**
Undercutting of defects in thin film protective coatings on polymer surfaces exposed to atomic oxygen p 115 A91-41516
The effect of atomic oxygen on altered and coated Kapton surfaces for spacecraft applications in low earth orbit p 116 A91-49804
- MIKKOLA, D. E.**
Oxidation behavior of cubic phases formed by alloying Al3Ti with Cr and Mn p 108 A91-27849
- MILDICE, JAMES**
Control of multiple resonant power processors in a multi-source system p 137 A91-30901
- MILES, JEFFREY HILTON**
Improved visualization of flow field measurements [AIAA PAPER 91-0273] p 3 A91-26331
Improved visualization of flow field measurements [NASA-TM-103679] p 12 N91-19044
- MILES, R.**
Two-dimensional imaging of molecular hydrogen in H2-air diffusion flames using two-photon laser-induced fluorescence p 124 A91-34369
- MILLER, CHRISTOPHER J.**
Ultra-high bypass research p 30 N91-20117
- MILLER, D. P.**
The design/analysis of flows through turbomachinery - A viscous/inviscid approach [AIAA PAPER 91-2010] p 153 A91-41677
The design/analysis of flows through turbomachinery: A viscous/inviscid approach [NASA-TM-104447] p 33 N91-25148
- MILLER, DAVID P.**
Implementation of control point form of algebraic grid-generation technique [NASA-TM-103748] p 13 N91-19054
- MILLER, EDWARD F.**
Overview of Ka-band communications technology requirements for the Space Exploration Initiative [AIAA PAPER 91-3424] p 45 A91-52344
- MILLER, J. H.**
Manipulation hardware for microgravity research [NASA-TM-103423] p 128 N91-14498
- MILLER, JEFFREY H.**
The dynamic effects of internal robots on Space Station Freedom [AIAA PAPER 91-2822] p 40 A91-49764
The dynamic effects of internal robots on Space Station Freedom [NASA-TM-104345] p 203 N91-22604
- MILLER, R. A.**
Ceramic coatings on smooth surfaces [NASA-CASE-LEW-15164-1] p 122 N91-25298
Ceramic coatings on smooth surfaces [NASA-CASE-LEW-15164-2] p 123 N91-32229
- MILLER, ROBERT A.**
Thermal barrier coating evaluation needs [NASA-TM-103708] p 111 N91-15390
Metallic seal for thermal barrier coating systems [NASA-CASE-LEW-15020-1] p 119 N91-15412
Method of applying a thermal barrier coating system to a substrate [NASA-CASE-LEW-15020-2] p 101 N91-25202
- MILLER, THOMAS J.**
The NASA/DOE/DOD nuclear rocket propulsion project - FY 1991 status p 64 A91-52335
Nuclear rocket propulsion. NASA plans and progress, FY 1991 [NASA-TM-104455] p 77 N91-25179
- MILLIS, MARC G.**
Speculating on space futures p 237 A91-16900
Technology readiness assessment of advanced space engine integrated controls and health monitoring [AIAA PAPER 91-3601] p 49 A91-52467
Fiber-optic applications for space-based rocket engines [AIAA PAPER 91-3602] p 49 A91-52468
Exploring the notion of space coupling propulsion p 73 N91-22161
Fiber-optic applications for space-based engines [NASA-TM-105235] p 86 N91-32163
- MINNETYAN, L.**
Composite structure global fracture toughness via computational simulation p 216 A91-11819
- MINNETYAN, LEVON**
Progressive fracture in composites subjected to hygrothermal environment [AIAA PAPER 91-1140] p 91 A91-31919
Progressive fracture in composites subjected to hygrothermal environment [NASA-TM-105230] p 103 N91-32182
- MIRANDA, F. A.**
Determination of surface resistance and magnetic penetration depth of superconducting YBa2Cu3O(7-delta) thin films by microwave power transmission measurements p 138 A91-36060
Determination of surface resistance and magnetic penetration depth of superconducting YBa2Cu3O(7-delta) thin films by microwave power transmission measurements [NASA-TM-103616] p 234 N91-10780
- MIRTICH, M. J.**
Dual ion beam processed diamondlike films for industrial applications p 121 N91-23042
- MIRTICH, MICHAEL J.**
The effect of the near earth micrometeoroid environment on a mirror surface after 20 years in space p 47 A91-49810
Flexible fluoropolymer filled protective coatings p 121 N91-24062
Ion beam textured and coated surfaces experiment (IBEX) p 122 N91-25040
- MISRA, A.**
Prospects for ductility and toughness enhancement of NiAl by ductile phase reinforcement [NASA-TM-103796] p 112 N91-27324
- MISRA, AJAY K.**
Thermochemical analysis of the silicon carbide-alumina reaction with reference to liquid-phase sintering of silicon carbide p 114 A91-26506
Reaction of Ti and Ti-Al alloys with alumina p 91 A91-27937
Hydrogen-silicon carbide interactions p 114 A91-28783
Reaction of beta-phase Ni-Al alloys with CrB2 p 92 A91-49943
Preliminary studies on NiAl/Nb2Be17 reaction and effectiveness of BeO as an interfacial reaction barrier p 92 A91-55050

- Thermochemical analysis of chemical processes relevant to the stability and processing of SiC-reinforced Si3N4 composite p 94 A91-56961
Effect of hydrogen on the strength and microstructure of selected ceramics [NASA-TM-103674] p 118 N91-14482
- MITAL, S. K.**
Metal matrix composites microfracture - Computational simulation p 90 A91-11815
- MITAL, SUBODH K.**
Fiber pushout test - A three-dimensional finite element computational simulation p 197 A91-33096
Microfracture in high temperature metal matrix crossply laminates [NASA-TM-104381] p 101 N91-25198
- MIYOSHI, KAZUHIKA**
Fundamental considerations in adhesion, friction and wear for ceramic-metal contacts p 115 A91-35952
Uses of Auger and x ray photoelectron spectroscopy in the study of adhesion and friction [NASA-TM-103266] p 118 N91-11922
- MOEYKENS, S. A.**
Three-dimensional calculation of the mixing of radial jets from slanted slots with a reactive cylindrical crossflow [AIAA PAPER 91-2081] p 24 A91-45782
- MOHAMED, J. H.**
Quaternary pulse position modulation electronics for free-space laser communications [AIAA PAPER 91-3471] p 133 A91-53702
Quaternary pulse position modulation electronics for free-space laser communications [NASA-TM-104502] p 135 N91-29405
- MOINUDDIN, ALIA M.**
Effects of windblown dust on photovoltaic surface s on Mars [NASA-TM-104448] p 78 N91-25183
- MONTAGUE, GERALD**
Use of piezoelectric actuators in active vibration control of rotating machinery p 179 A91-14400
- MOON, YOUNG J.**
Numerical study of supersonic combustors by multi-block grids with mismatched interfaces [AIAA PAPER 90-5204] p 21 A91-14430
- MOORE, N.**
Probabilistic structural analysis methods for space transportation propulsion systems p 205 N91-28238
- MORAN, MATTHEW E.**
Conceptual study of on orbit production of cryogenic propellants by water electrolysis [AIAA PAPER 91-1844] p 124 A91-41631
Conceptual study of on orbit production of cryogenic propellants by water electrolysis [NASA-TM-103730] p 126 N91-19317
- MOREL, M.**
Concurrent tailoring of fabrication process and interphase layer to reduce residual stresses in metal matrix composites p 92 A91-43232
Concurrent micromechanical tailoring and fabrication process optimization for metal-matrix composites [NASA-TM-103670] p 98 N91-19237
Interphase layer optimization for metal matrix composites with fabrication considerations [NASA-TM-105166] p 102 N91-30281
- MOREL, M. R.**
Concurrent material-fabrication optimization of metal-matrix laminates under thermo-mechanical loading [AIAA PAPER 91-1044] p 129 A91-31842
- MORLEY, NICHOLAS**
A comparison of energy conversion systems for meeting the power requirements of manned rover for Mars missions p 53 A91-37932
- MORLEY, NICHOLAS J.**
Preliminary assessment of the power requirements of a manned rover for Mars missions p 41 A91-27702
- MORREN, SYBIL HUANG**
Transonic aerodynamics of dense gases [NASA-TM-103722] p 13 N91-20045
- MORREN, W. E.**
Preliminary performance and life evaluation of a 2-kW arcjet [AIAA PAPER 91-2228] p 62 A91-45796
- MORREN, W. EARL**
Preliminary performance and life evaluations of a 2-kW arcjet [NASA-TM-105149] p 84 N91-30252
- MORRIS, P. J.**
A comparison of numerical methods for the Rayleigh equation in unbounded domains [NASA-TM-105179] p 223 N91-30865
- MORSCHER, GREGORY N.**
Temperature dependence of hardness in yttria-stabilized zirconia single crystals p 114 A91-28763
Fiber creep evaluation by stress relaxation measurements p 117 A91-56905
- A simple test for thermomechanical evaluation of ceramic fibers [NASA-TM-103767] p 121 N91-21309
- MORTON, DAVID S.**
The migration of a compound drop due to thermocapillarity p 148 A91-18428
- MRAZ, P. J.**
Adaptation of NASA technology for the optimization of orthopedic knee implants p 215 N91-23032
- MULARZ, EDWARD J.**
Chemical reacting flows p 162 N91-20098
- MULLEN, R. L.**
Some preliminary results of brush seal/rotor interference effects on leakage at zero and low rpm using a tapered-plug rotor [AIAA PAPER 91-3390] p 182 A91-45820
Simulation of brush insert for leading-edge-passage convective heat transfer [NASA-TM-103801] p 165 N91-23409
Some preliminary results of brush seal/rotor interference effects on leakage at zero and low RPM using a tapered-plug rotor [NASA-TM-104396] p 188 N91-27559
- MURTHY, D. V.**
Solution and sensitivity analysis of a complex transcendental eigenproblem with pairs of real eigenvalues p 195 A91-23685
- MURTHY, DURBHA V.**
Experimental investigation of propan aeroelastic response in off-axis flow with mistuning p 22 A91-30015
Aeroelastic modal characteristics of mistuned blade assemblies - Mode localization and loss of eigenstructure [AIAA PAPER 91-1218] p 196 A91-32032
Localization of aeroelastic modes in mistuned high-energy turbines [AIAA PAPER 91-3379] p 198 A91-44319
Semi-analytical technique for sensitivity analysis of unsteady aerodynamic computations p 7 A91-48816
Efficient computation of aerodynamic influence coefficients for aeroelastic analysis on a transputer network [NASA-TM-103671] p 216 N91-20748
Localization of aeroelastic modes in mistuned high-energy turbines [NASA-TM-104445] p 204 N91-24659
Aeroelastic modal characteristics of mistuned blade assemblies: Mode localization and loss of eigenstructure [NASA-TM-104519] p 205 N91-27591
- MURTHY, P. L. N.**
Composite structure global fracture toughness via computational simulation p 216 A91-11819
Simplified procedures for designing adhesively bonded composite joints p 180 A91-20938
Computational simulation of acoustic fatigue for hot composite structures [AIAA PAPER 91-1178] p 197 A91-32099
METCAN updates for high temperature composite behavior: Simulation/verification [NASA-TM-103682] p 97 N91-19229
Computational simulation of hot composites structures [NASA-TM-103681] p 97 N91-19230
Probabilistic micromechanics and macromechanics of polymer matrix composites [NASA-TM-103669] p 98 N91-19236
HITCAN for actively cooled hot-composite thermostructural analysis [NASA-TM-103750] p 202 N91-21562
Application of artificial neural networks to composite ply micromechanics [NASA-TM-104365] p 100 N91-24345
- MURTHY, PAPPU L. N.**
Computational simulation of high-temperature metal matrix composites cyclic behavior p 91 A91-18680
Progressive fracture in composites subjected to hygrothermal environment [AIAA PAPER 91-1140] p 91 A91-31919
Computational simulation of acoustic fatigue for hot composite structures [NASA-TM-104379] p 203 N91-23548
Progressive fracture in composites subjected to hygrothermal environment [NASA-TM-105230] p 103 N91-32182
Computational simulation of high temperature metal matrix composite behavior [NASA-TM-104378] p 206 N91-32520
- MURTHY, PAPU L. N.**
Programming probabilistic structural analysis for parallel processing computer [AIAA PAPER 91-0920] p 196 A91-31957
- MUSGRAVE, JEFFREY L.**
Linear quadratic servo control of a reusable rocket engine [AIAA PAPER 91-1999] p 57 A91-41670
- Shared direct memory access on the Explorer 2-LX [NASA-TM-103289] p 216 N91-12215
- MUTHARASAN, RAJAKKANNU**
Development of braided rope seals for hypersonic engine applications. II - Flow modeling [AIAA PAPER 91-2495] p 182 A91-41800
Development of braided rope seals for hypersonic engine applications. Part 2: Flow modeling [NASA-TM-104371] p 186 N91-22571
- MYERS, D. R.**
Primary reference cell calibrations at SERI - History and methods p 207 A91-41966
- MYERS, I. T.**
Electrical characterization of a Mapham inverter using pulse testing techniques p 139 A91-37992
Electrical characterization of glass, teflon, and tantalum capacitors at high temperatures [NASA-TM-104517] p 146 N91-27444
- MYERS, IRA**
Light weight, high power, high voltage dc/dc converter technologies p 138 A91-37985
- MYERS, IRA T.**
High temperature superconductivity technology for advanced space power systems p 50 A91-13447
High temperature power electronics for space [NASA-TM-104375] p 145 N91-22508
- MYERS, R. M.**
Anode power deposition in an applied-field segmented anode MPD thruster [AIAA PAPER 91-2343] p 59 A91-44204
Energy deposition in low-power coaxial plasma thrusters p 63 A91-52311
Cathode phenomena in a low-power magnetoplasmadynamic thruster p 63 A91-52314
- MYERS, ROGER M.**
Nonequilibrium in a low power arcjet nozzle [AIAA PAPER 91-2113] p 61 A91-45784
A preliminary characterization of applied-field MPD thruster plumes [AIAA PAPER 91-2339] p 62 A91-45798
Applied-field MPD thruster geometry effects [AIAA PAPER 91-2342] p 62 A91-45806
Test facilities for high power electric propulsion [AIAA PAPER 91-3499] p 42 A91-52396
MPD thruster technology [AIAA PAPER 91-3568] p 65 A91-52444
MPD thruster technology [NASA-TM-105242] p 86 N91-32162
Multimegawatt electric propulsion system design considerations [NASA-TM-105152] p 87 N91-32164

N

- NAGABHUSANAM, J.**
General purpose program to generate compatibility matrix for the integrated force method p 195 A91-12905
- NAGPAL, V.**
Probabilistic structural analysis methods for space transportation propulsion systems p 205 N91-28238
- NAGPAL, V. K.**
Computational simulation of acoustic fatigue for hot composite structures [AIAA PAPER 91-1178] p 197 A91-32099
- NAGPAL, VINOD K.**
Computational simulation of acoustic fatigue for hot composite structures [NASA-TM-104379] p 203 N91-23548
- NAGY, L. A.**
Quaternary pulse position modulation electronics for free-space laser communications [AIAA PAPER 91-3471] p 133 A91-53702
Quaternary pulse position modulation electronics for free-space laser communications [NASA-TM-104502] p 135 N91-29405
- NAGY, MICHAEL**
An assessment of the Space Station Freedom program's leakage current requirement [NASA-CR-187077] p 215 N91-20630
- NAHRA, HENRY**
Flexible fluoropolymer filled protective coatings p 121 N91-24062
- NAHRA, HENRY K.**
Environmental interactions of the Space Station Freedom electric power system [NASA-TM-104373] p 49 N91-24225
- NALLASAMY, M.**
Near-field noise of a single rotation propfan at an angle of attack [AIAA PAPER 90-3953] p 225 A91-12469
Unsteady blade pressure measurements for the SR-7A propeller at cruise conditions [AIAA PAPER 90-4022] p 225 A91-12533



- Prediction of unsteady blade surface pressures on an advanced propeller at an angle of attack p 226 A91-18257
- Unsteady blade-surface pressures on a large-scale advanced propeller: Prediction and data [NASA-TM-103218] p 69 N91-11799
- Near-field noise of a single-rotation propfan at an angle of attack [NASA-TM-103645] p 227 N91-12316
- Unsteady blade pressure measurements for the SR-7A propeller at cruise conditions [NASA-TM-103606] p 228 N91-19825
- Unsteady flowfield of a propfan at takeoff conditions [NASA-TM-105223] p 18 N91-32075
- NALLASAMY, N.**
Large-scale advanced propeller blade pressure distributions - Prediction and data p 5 A91-42820
- NAMKOONG, DAVID**
Scaling analysis applied to the NORVEX code development and thermal energy flight experiment [AIAA PAPER 91-1420] p 155 A91-44337
- Scaling analysis applied to the NORVEX code development and thermal energy flight experiment [NASA-TM-104462] p 166 N91-24549
- NARAYANAN, G. V.**
ASTROP2 users manual: A program for aeroelastic stability analysis of propfans [NASA-TM-4304] p 206 N91-28627
- NATHAL, M. V.**
Factors which influence tensile strength of a SiC/Ti-24Al-11Nb (at. pct) composite p 92 A91-55900
- NAUD, STEVE**
The preliminary feasibility of intercalated graphite railgun armatures p 137 A91-29257
- NAVARRO, JULIO A.**
A 29.3-GHz cavity-enclosed aperture-coupled circular-patch antenna for microwave circuit integration p 140 A91-47057
- NEEDELMAN, WILLIAM M.**
Quantifying oil filtration effects on bearing life [NASA-TM-104350] p 186 N91-23512
- NEINER, GEORGE**
Hot gas ingestion test results of a two-poster vectored thrust concept with flow visualization in the NASA Lewis 9- by 15-foot low speed wind tunnel [AIAA PAPER 90-2268] p 4 A91-40561
- Hot gas ingestion test results of a two-poster vectored thrust concept with flow visualization in the NASA Lewis 9- x 15-foot low speed wind tunnel [NASA-TM-103258] p 15 N91-21116
- NEINER, GEORGE H.**
Flow visualization and hot gas ingestion characteristics of a vectored thrust STOV concept p 28 N91-20090
- NELSON, EMILY S.**
An examination of anticipated g-jitter on space station and its effects on materials processes [NASA-TM-103775] p 128 N91-21378
- NEMETH, NOEL N.**
Calculation of Weibull strength parameters, Batdorf flow density constants and related statistical quantities using PC-CARES [NASA-TM-103247] p 199 N91-10332
- NEWELL, J.**
Probabilistic structural analysis methods for space transportation propulsion systems p 205 N91-28238
- Concurrent engineering p 80 N91-28247
- NEWMAN, H. S.**
Determination of surface resistance and magnetic penetration depth of superconducting YBa₂Cu₃O₇(δ) thin films by microwave power transmission measurements p 138 A91-36060
- Determination of surface resistance and magnetic penetration depth of superconducting YBa₂Cu₃O₇(δ) thin films by microwave power transmission measurements [NASA-TM-103616] p 234 N91-10780
- NG, WING-FAI**
Generalized conjugate-gradient methods for the Navier-Stokes equations [AIAA PAPER 91-1556] p 5 A91-40730
- NGUYEN, H. L.**
Effects of nozzle lip geometry on spray atomization and emissions advanced gas turbine combustors [AIAA PAPER 91-2201] p 24 A91-44153
- Flux-vector splitting algorithm for chain-rule conservation-law form p 221 A91-45109
- Three-dimensional calculation of the mixing of radial jets from slanted slots with a reactive cylindrical crossflow [AIAA PAPER 91-2081] p 24 A91-45782
- Analytical combustion/emissions research related to the NASA High-Speed Research Program [AIAA PAPER 91-2252] p 25 A91-45799
- Algebraic grid generation for complex geometries p 157 A91-48758
- NGUYEN, H. LEE**
Evaluation of a hybrid kinetics/mixing-controlled combustion model for turbulent premixed and diffusion combustion using KIVA-II [AIAA PAPER 90-2450] p 104 A91-12927
- Simulation of mixing in the quick quench region of a rich burn-quick quench mix-lean burn combustor [AIAA PAPER 91-0410] p 105 A91-21481
- Mechanisms and modeling of the effects of additives on the nitrogen oxides emission [AIAA PAPER 91-0479] p 124 A91-40560
- Analytical combustion/emissions research related to the NASA high-speed research program [NASA-TM-104521] p 34 N91-27165
- NGUYEN, HUNG LEE**
Numerical simulation of Jet-A combustion approximated by improved propane chemical kinetics [AIAA PAPER 91-1859] p 106 A91-45777
- Application of mixing-controlled combustion models to gas turbine combustors [NASA-TM-103236] p 31 N91-22126
- Mechanisms and modeling of the effects of additives on the nitrogen oxides emission [NASA-TM-103765] p 126 N91-22464
- NGUYEN, R.**
Submicron gate InP power MISFET's with improved output power density at 18 and 20 GHz p 145 N91-26436
- NGUYEN, RICHARD**
Submicron gate InP power MISFET's with improved output power density at 18 and 20 GHz p 142 A91-54526
- NIC, J. P.**
Oxidation behavior of cubic phases formed by alloying Al₃Ti with Cr and Mn p 108 A91-27849
- NICHOLS, LESTER D.**
Numerical propulsion system simulation - An interdisciplinary approach [AIAA PAPER 91-3554] p 66 A91-53706
- Multidisciplinary research overview (IHPTET/NPSS) p 30 N91-20119
- Numerical propulsion system simulation: An interdisciplinary approach [NASA-TM-105181] p 81 N91-29221
- NIEBERDING, WILLIAM C.**
Propulsion instrumentation research p 176 N91-20100
- Overview of the instrumentation program p 176 N91-24318
- NIEDRA, J. M.**
High frequency, high temperature specific core loss and dynamic B-H hysteresis loop characteristics of soft magnetic alloys p 138 A91-37988
- Comparison of high temperature, high frequency core loss and dynamic B-H loops of two 50 Ni-Fe crystalline alloys and an iron-based amorphous alloy [NASA-TM-105205] p 147 N91-32412
- NIEDRA, JANIS M.**
Makeup and uses of a basic magnet laboratory for characterizing high-temperature permanent magnets [NASA-TM-104508] p 146 N91-30427
- NIEDZWIECKI, RICHARD W.**
Turbomachinery and combustor technology for small engines p 29 N91-20113
- NIEH, C. W.**
An experimental study of high T_c superconducting microstrip transmission lines at 35 GHz and the effect of film morphology [NASA-TM-103633] p 133 N91-11988
- NING, X. J.**
The structure of carbon in chemically vapor deposited SiC monofilaments p 113 A91-18675
- NOEBE, R. D.**
The potential for ductility enhancement from surface and interface dislocation sources in NiAl p 109 A91-39292
- 1000 to 1200 K time-dependent compressive deformation of single-crystalline and polycrystalline B2 Ni-40Al p 109 A91-43670
- Constitution of pseudobinary hypoeutectic beta-NiAl + α -V alloys p 109 A91-48509
- A simplified method for determining the number of independent slip systems in crystals p 110 A91-55472
- Prospects for ductility and toughness enhancement of NiAl by ductile phase reinforcement [NASA-TM-103796] p 112 N91-27324
- NOTZOLD, DIRK**
Characteristic microwave-background distortions from collapsing spherical domain walls p 238 A91-12343
- NURRE, J.**
Sensor failure detection and recovery by neural networks [NASA-TM-104484] p 220 N91-24815
- O'DONNELL, PATRICIA M.**
NASA Aerospace Flight Battery Systems Program p 56 A91-38088
- O'MALLEY, TERENCE F.**
A summary of existing and planned experiment hardware for low-gravity fluids research [AIAA PAPER 91-0777] p 128 A91-26329
- O'MARA, T. M.**
Effects of horizontal tail ice on longitudinal aerodynamic derivatives p 36 A91-38547
- O'NEILL, M. J.**
The mini-dome Fresnel lens photovoltaic concentrator array - Current status of component and prototype panel testing p 57 A91-41989
- Lightweight concentrator module with 30 percent AMO efficient GaAs/GaSb tandem cells p 57 A91-41990
- O'NEILL, MARK J.**
Component and prototype panel testing of the mini-dome Fresnel lens photovoltaic concentrator array p 54 A91-38023
- ODUBIYI, JIDE**
Technologies for unattended network operations [AIAA PAPER 91-3534] p 45 A91-52425
- OGBUJI, LINUS U. J. T.**
Evidence from transmission electron microscopy for an oxyntide layer in oxidized Si₃N₄ p 118 A91-57058
- Oxidation instability of SiC and Si₃N₄ following thermal excursions p 118 A91-57059
- OGRIN, J.**
Particle nonuniformity effects on particle cloud flames in low gravity [AIAA PAPER 91-0718] p 104 A91-19431
- OKIISHI, T. H.**
An experimental comparison of nonswirling and swirling flow in a circular-to-rectangular transition duct [AIAA PAPER 91-0342] p 148 A91-21466
- An experimental trace gas investigation of fluid transport and mixing in a circular-to-rectangular transition duct [AIAA PAPER 91-2370] p 172 A91-44214
- An experimental comparison of nonswirling and swirling flow in a circular-to-rectangular transition duct [NASA-TM-104359] p 14 N91-21115
- An experimental trace gas investigation of fluid transport and mixing in a circular-to-rectangular transition duct [NASA-TM-104499] p 17 N91-27129
- OLINTO, ANGELA V.**
Natural inflation with pseudo Nambu-Goldstone bosons p 239 A91-19545
- OLIVE, KEITH A.**
Primordial nucleosynthesis redux p 240 A91-45907
- OLIVER, ANGELA C.**
Test and evaluation of load converter topologies used in the Space Station Freedom Power Management and distribution DC test bed [NASA-TM-105217] p 85 N91-30267
- OLLE, RAYMOND M.**
Effects of dust accumulation and removal on radiators surfaces on Mars [NASA-TM-103704] p 72 N91-20204
- The effect of atomic oxygen on polysiloxane-polyimide for spacecraft applications in low Earth orbit p 229 N91-20735
- Durability evaluation of photovoltaic blanket materials exposed on LDEF tray S1003 p 212 N91-25062
- OLSEN, C. S.**
Development of nuclear fuels and materials for propulsion systems for SEI [AIAA PAPER 91-3452] p 125 A91-52362
- OLSON, S. L.**
Heat transfer to a thin solid combustible in flame spreading at microgravity p 106 A91-51449
- OMALLEY, TERENCE F.**
A summary of existing and planned experiment hardware for low-gravity fluids research [NASA-TM-103706] p 160 N91-19371
- ONEILL, MARK J.**
Tandem concentrator solar cells with 30 percent (AMO) power conversion efficiency p 208 N91-19189
- Mini-dome Fresnel lens photovoltaic concentrator development p 210 N91-19219
- Key results of the mini-dome Fresnel lens concentrator array development program under recently completed NASA and SDIO SBIR projects p 83 N91-30223
- ORANGE, THOMAS W.**
Analysis of some compliance calibration data for chevron-notch bar and rod specimens [NASA-TM-104367] p 203 N91-22594
- OREILLY, MICHAEL**
LBR-2 Earth stations for the ACTS program p 133 N91-11971
- ORLETSKI, DIRK**
High temperature NASP engine seal development [NASA-TM-103716] p 184 N91-19441

ORZESZKO, S.

Diamondlike carbon applications in infrared optics and microelectronics p 230 N91-18306

OSAKI, HIROYUKI

Intrinsic bond strength of metal films on polymer substrates p 88 A91-39246

OSTERWALD, C. R.

Primary reference cell calibrations at SERI - History and methods p 207 A91-41966

OSWALD, F. B.

Analytical and experimental study of vibrations in a gear transmission [AIAA PAPER 91-2019] p 181 A91-41680

Gear noise, vibration, and diagnostic studies at NASA Lewis Research Center p 183 A91-52811

OSWALD, FRED B.

Contact stresses in gear teeth - A new method of analysis [AIAA PAPER 91-2022] p 182 A91-41683

Comparison of analysis and experiment for dynamics of low-contact-ratio spur gears [NASA-TM-103232] p 185 N91-22566

Contact stresses in gear teeth: A new method of analysis [NASA-TM-104397] p 186 N91-22570

Analytical and experimental study of vibrations in a gear transmission [NASA-TM-104434] p 187 N91-25395

Acoustical analysis of gear housing vibration [NASA-TM-103691] p 188 N91-25411

Dynamic measurements of gear tooth friction and load [NASA-TM-103281] p 189 N91-27570

OUZTS, PETER

A linear control design structure to maintain loop properties during limit operation in a multi-nozzle turbofan engine [AIAA PAPER 91-1997] p 24 A91-45780

A linear control design structure to maintain loop properties during limit operation in a multi-nozzle turbofan engine [NASA-TM-105163] p 35 N91-29188

OUZTS, PETER J.

An AD100 implementation of a real-time STOVL aircraft propulsion system [NASA-TM-103683] p 26 N91-13457

IMPAC: An Integrated Methodology for Propulsion and Airframe Control [NASA-TM-103805] p 30 N91-20122

Integrated flight/propulsion control design for a STOVL aircraft using H-infinity control design techniques [NASA-TM-104340] p 31 N91-21140

OVERTON, E.

Electrical characterization of glass, teflon, and tantalum capacitors at high temperatures [NASA-TM-104517] p 146 N91-27444

OVERTON, ERIC

High temperature power electronics for space [NASA-TM-104375] p 145 N91-22508

OWEN, ALBERT K.

Effects of inlet distortion on the development of secondary flows in a subsonic axial inlet compressor rotor [NASA-TM-104356] p 31 N91-23179

OWENS, JAY

Applied high-speed imaging for the icing research program at NASA Lewis Research Center [NASA-TM-104415] p 177 N91-26490

P

PAI, SHANTARAM S.

Probabilistic structural analysis of a truss typical for space station [NASA-TM-103277] p 199 N91-12114

PALASZEWSKI, B. A.

Advanced launch vehicle upper stages using liquid propulsion and metallized propellants [NASA-TM-103622] p 68 N91-11797

PALASZEWSKI, BRYAN

Launch vehicle performance using metallized propellants [AIAA PAPER 91-2050] p 58 A91-44106

Design issues for propulsion systems using metallized propellants [AIAA PAPER 91-3484] p 66 A91-53709

Lunar missions using chemical propulsion: System design issues [NASA-TP-3065] p 70 N91-15308

Design issues for propulsion systems using metallized propellants [NASA-TM-105190] p 81 N91-29220

PALASZEWSKI, BRYAN A.

Metallized propellants for the human exploration of Mars [NASA-TP-3062] p 69 N91-11800

Advanced chemical propulsion at NASA Lewis: Metallized and high energy density propellants [NASA-TM-103771] p 71 N91-19175

Advanced launch vehicle upper stages using liquid propulsion and metallized propellants p 75 N91-24257

Launch vehicle performance using metallized propellants [NASA-TM-104456] p 76 N91-24304

PALAZZOLO, ALAN B.

Use of piezoelectric actuators in active vibration control of rotating machinery p 179 A91-14400

PALKO, JOSEPH L.

Structural reliability analysis of laminated CMC components [NASA-TM-103685] p 119 N91-19292

PAMULAPATI, J.

Dielectric function of InGaAs in the visible p 233 A91-53236

Ellipsometric study of InGaAs MODFET material [NASA-TM-103286] p 143 N91-19351

Study of InGaAs based MODFET structures using variable angle spectroscopic ellipsometry [NASA-TM-103792] p 235 N91-19935

PAO, YOH-HAN

Automating security monitoring and analysis for Space Station Freedom's electric power system p 219 A91-37975

PAPADAKIS, MICHAEL

Experimental water droplet impingement data on modern aircraft surfaces [AIAA PAPER 91-0445] p 2 A91-21493

PAPADOPOULOS, D.

Autoclavable addition polyimides for 371 C composite applications p 115 A91-49112

PARFITT, L. J.

Oxidation behavior of cubic phases formed by alloying Al3Ti with Cr and Mn p 108 A91-27849

PARK, EUGENE

Optical Multiple Access Network (OMAN) for advanced processing satellite applications [NASA-TM-105167] p 135 N91-29431

PARKES, JAMES E.

Test facilities for high power electric propulsion [AIAA PAPER 91-3499] p 42 A91-52396

PATNAIK, S. N.

General purpose program to generate compatibility matrix for the integrated force method p 195 A91-12905

Integrated force method versus displacement method for finite element analysis p 196 A91-28372

Compatibility conditions of structural mechanics for finite element analysis p 198 A91-37853

PATTERSON, M. J.

Xenon ion propulsion for orbit transfer [NASA-TM-103193] p 69 N91-11798

PATTERSON, MICHAEL J.

Ion beam sputtering in electric propulsion facilities [AIAA PAPER 91-2117] p 61 A91-45785

Microanalyses of extended-test xenon hollow cathodes [AIAA PAPER 91-2123] p 61 A91-45787

Performance and optimization of a 'derated' ion thruster for auxiliary propulsion [AIAA PAPER 91-2350] p 62 A91-45809

A 5-kW xenon ion thruster lifetest [NASA-TM-103191] p 72 N91-19180

Performance and optimization of a derated ion thruster for auxiliary propulsion [NASA-TM-105144] p 82 N91-29229

Microanalysis of extended-test xenon hollow cathodes [NASA-TM-104532] p 82 N91-30202

Ion beam sputtering in electric propulsion facilities [NASA-TM-105145] p 86 N91-32158

Multimegawatt electric propulsion system design considerations [NASA-TM-105152] p 87 N91-32164

PATTERSON, RICHARD L.

A fiber-optic current sensor for aerospace applications p 171 A91-23005

A fiber-optic current sensor for aerospace applications p 172 A91-38006

k-out-of-n:G systems - Some cost considerations p 192 A91-54553

How much redundancy: Some cost considerations, including examples for spacecraft systems [NASA-TM-103197] p 192 N91-17407

Balancing reliability and cost to choose the best power subsystem [NASA-TM-104453] p 238 N91-24952

Fiber-optic sensors for aerospace electrical measurements: An update [NASA-TM-104454] p 177 N91-25381

Reliability and cost: A sensitivity analysis [NASA-TM-105293] p 238 N91-33014

PAVLI, ALBERT J.

New method of making advanced tube-bundle rocket thrust chambers [NASA-TM-103617] p 70 N91-15301

PAWLIK, RALPH

Crack healing in silicon nitride due to oxidation p 118 A91-56982

PAXSON, DANIEL E.

A model for the Space Shuttle Main Engine High Pressure Oxidizer Turbopump shaft seal system p 180 A91-30640

A model for the space shuttle main engine high pressure oxidizer turbopump shaft seal system [NASA-TM-103697] p 184 N91-20489

PELTIER, LEONARD JOEL

Application of implicit numerical techniques to the solution of the three-dimensional diffusion equation p 148 A91-13456

PENCIL, ERIC J.

Performance characterization of a segmented anode arcjet thruster [NASA-TM-103227] p 67 N91-10118

PENKO, P. F.

Test-cell pressure effects on the performance of resistojets p 38 A91-37417

PENKO, PAUL F.

Numerical and experimental investigations of rarefied nozzle and plume flows of nitrogen [AIAA PAPER 91-1363] p 154 A91-43429

Pressure measurements in a low-density nozzle plume for code verification [AIAA PAPER 91-2110] p 61 A91-45783

Experimental and analytical comparison of flowfields in a 110 N (25 Lbf) H2/O2 rocket [AIAA PAPER 91-2283] p 62 A91-45802

Pressure measurements in a low-density nozzle plume for code verification [NASA-TM-105170] p 81 N91-29228

Experimental and analytical comparison of flowfields in a 110 N (25 lbf) H2/O2 rocket [NASA-TM-105175] p 82 N91-29230

PENNLIN, JAMES A.

Cray performance data from five benchmarks [NASA-TM-105200] p 217 N91-32806

PEPPER, D. W.

Heat transfer in space systems. Proceedings of the Symposium, AIAA/ASME Thermophysics and Heat Transfer Conference, Seattle, WA, June 18-20, 1990 p 152 A91-38780

PEPPER, STEPHEN V.

X-ray photoelectron and mass spectroscopic study of electron irradiation and thermal stability of polytetrafluoroethylene p 113 A91-16138

Thermal stability of electron-irradiated poly(tetrafluoroethylene) - X-ray photoelectron and mass spectroscopic study p 115 A91-39242

Tribological properties of Ag/Ti films on Al2O3 ceramic substrates [NASA-TM-103784] p 89 N91-19224

PEREZ-DAVIS, M. E.

Effects of Martian dust on power system components p 241 N91-27061

PEREZ-DAVIS, MARLA E.

Aeolian removal of dust types from photovoltaic surfaces on Mars p 47 N91-19156

Simulation of Martian dust accumulation on surfaces p 47 N91-19160

Effects of dust accumulation and removal on radiators surfaces on Mars [NASA-TM-103704] p 72 N91-20204

Sensible heat receiver for solar dynamic space power system [NASA-TM-104393] p 77 N91-25173

Effects of windblown dust on photovoltaic surfaces on Mars [NASA-TM-104448] p 78 N91-25183

PERINO, MARIA A.

Photovoltaic superiority for Space Station Freedom power in the 21st century p 58 A91-42004

PETIT, J. B.

Controlled growth of 3C-SiC and 6H-SiC films on low-tilt-angle vicinal (0001) 6H-SiC wafers p 232 A91-45713

Application of oxidation to the structural characterization of SiC epitaxial films p 233 A91-45881

PETIT, JEREMY B.

Development of silicon carbide semiconductor devices for high temperature applications [NASA-TM-104398] p 236 N91-22921

Advances in silicon carbide Chemical Vapor Deposition (CVD) for semiconductor device fabrication [NASA-TM-104410] p 236 N91-23946

PETRASEK, D. W.

Effect of thermal shock on fiber-reinforced superalloy composites p 93 A91-55918

- PETREFSKI, CHRIS**
Sensible heat receiver for solar dynamic space power system
[NASA-TM-104393] p 77 N91-25173
- PETRI, D. A.**
Power system requirements and definition for lunar and Mars outposts p 52 A91-37930
- PEUSSA, J.**
Elevated-temperature fracture resistances (K_{sub} IC), R-curves, gamma sub (ω OF) of monolithic and composite ceramics using chevron-notched, bend tests [NASA-TM-105090] p 123 N91-28418
- PHILIPP, WARREN H.**
Synthesis and thermal properties of strontium and calcium peroxides
[NASA-TM-103725] p 107 N91-22410
- PHILLIPS, PAMELA S.**
Transonic wind-tunnel wall interference prediction code p 38 A91-26112
- PHILLIPS, RUDY L.**
The development of test beds to support the definition and evolution of the Space Station Freedom power system
[NASA-TM-104504] p 79 N91-27207
- PHILLIPS, STEPHEN**
Feedback linearization for control of air breathing engines
[AIAA PAPER 91-2000] p 23 A91-41671
- PICKRELL, ROY L.**
Power electronic applications for Space Station Freedom p 52 A91-36832
- PIERCE, WILLIAM S.**
Analysis of some compliance calibration data for chevron-notch bar and rod specimens
[NASA-TM-104367] p 203 N91-22594
- PIERRE, CHRISTOPHE**
Aeroelastic modal characteristics of mistuned blade assemblies - Mode localization and loss of eigenstructure
[AIAA PAPER 91-1218] p 196 A91-32032
Localization of aeroelastic modes in mistuned high-energy turbines
[AIAA PAPER 91-3379] p 198 A91-44319
Localization of aeroelastic modes in mistuned high-energy turbines
[NASA-TM-104445] p 204 N91-24659
Aeroelastic modal characteristics of mistuned blade assemblies: Mode localization and loss of eigenstructure
[NASA-TM-104519] p 205 N91-27591
- PINES, V.**
Time development of a perturbed-spherical nucleus in a pure supercooled liquid. I - Power-law growth of morphological instabilities. II - Nonlinear development p 231 A91-16105
- PINSON, LARRY D.**
Overview of structures research p 202 N91-20104
- PINTO, GINO A.**
In-service health monitoring of composite structures p 192 A91-51926
- PIROUZ, P.**
The structure of carbon in chemically vapor deposited SiC monofilaments p 113 A91-18675
- PIROUZ, PIROUZ**
Temperature dependence of hardness in yttria-stabilized zirconia single crystals p 114 A91-28763
- PISZCZOR, M. F.**
High altitude AM0 testing of PV concentrator lens elements p 207 A91-41978
The mini-dome Fresnel lens photovoltaic concentrator array - Current status of component and prototype panel testing p 57 A91-41989
- PISZCZOR, MICHAEL F.**
Component and prototype panel testing of the mini-dome Fresnel lens photovoltaic concentrator array p 54 A91-38023
Key results of the mini-dome Fresnel lens concentrator array development program under recently completed NASA and SDIO SBIR projects p 83 N91-30223
- PISZCZOR, MICHAEL F., JR.**
Mini-dome Fresnel lens photovoltaic concentrator development p 210 N91-19219
- PLENCNER, ROBERT M.**
Overview of the Beta II two-stage-to-orbit vehicle design
[AIAA PAPER 91-3175] p 43 A91-54088
High-efficiency core technology p 30 N91-20118
The Navy/NASA Engine Program (NNEP89): A user's manual
[NASA-TM-105186] p 35 N91-30141
- PLETCHER, R. H.**
Simulation of three-dimensional liquid sloshing flows using a strongly implicit calculation procedure
[AIAA PAPER 91-1661] p 153 A91-42549
Primitive variable, strongly implicit calculation procedure for viscous flows at all speeds p 7 A91-46181
- PLINE, ALEXANDER D.**
Spacelab qualified infrared imager for microgravity science applications p 173 A91-51585
Particle image velocimetry for the surface tension driven convection experiment using a particle displacement tracking technique
[NASA-TM-104482] p 177 N91-25382
Ground-based PIV and numerical flow visualization results from the surface tension driven convection experiment
[NASA-TM-105172] p 178 N91-30491
- PONCHAK, DENISE S.**
A technology assessment of alternative communications systems for the space exploration initiative
[AIAA PAPER 90-3681] p 44 A91-11472
Millimeter wavelength communications applications for the SEI
[AIAA PAPER 91-3589] p 45 A91-52458
An assessment of technology alternatives for telecommunications and information management for the space exploration initiative
[NASA-TM-103783] p 134 N91-23347
Millimeter wavelength communications applications for the SEI
[NASA-TM-105275] p 135 N91-32287
- PONCHAK, GEORGE E.**
Theoretical and experimental characterization of coplanar waveguide discontinuities for filter applications p 137 A91-35911
Coplanar waveguide EEsof MICAD macros make circuit layout easy
[NASA-TM-103272] p 134 N91-19332
- PORRO, A. R.**
Experimental investigation of a single flush-mounted hypermixing nozzle
[AIAA PAPER 90-5240] p 21 A91-14466
Heat transfer, velocity-temperature correlation, and turbulent shear stress from Navier-Stokes computations of shock wave/turbulent boundary layer interaction flows p 163 N91-21085
Evaluation of a technique to generate artificially thickened boundary layers in supersonic and hypersonic flows
[NASA-TP-3142] p 17 N91-28136
The NASA Lewis Research Center Internal Fluid Mechanics Facility
[NASA-TM-105187] p 39 N91-30163
A laser-induced heat flux technique for convective heat transfer measurements in high speed flows
[NASA-TM-105177] p 168 N91-30472
- PORRO, A. ROBERT**
Development of a laser-induced heat flux technique for measurement of convective heat transfer coefficients in a supersonic flowfield
[NASA-TM-103778] p 13 N91-19063
Experimental investigation of a single flush-mounted hypermixing nozzle
[NASA-TM-103726] p 161 N91-19374
- PORSCHING, T. A.**
Multidimensional computer simulation of Stirling cycle engines p 181 A91-38154
- POTAPCZUK, M. G.**
Numerical simulation of ice growth on a MS-317 swept wing geometry
[AIAA PAPER 91-0263] p 19 A91-26193
Numerical simulation of ice growth on a MS-317 swept wing geometry
[NASA-TM-103705] p 11 N91-14310
Simulation of iced wing aerodynamics
[NASA-TM-104362] p 15 N91-23086
Icing simulation: A survey of computer models and experimental facilities
[NASA-TM-104366] p 15 N91-23087
- POTAPCZUK, MARK**
Modeling of surface roughness effects on glaze ice accretion p 19 A91-35107
- POTAPCZUK, MARK G.**
Progress toward the development of an airfoil icing analysis capability p 9 N91-10866
- POUCH, JOHN J.**
Diamondlike carbon as a moisture barrier and antireflecting coating on optical materials p 119 N91-18302
Optical dispersion relations for diamondlike carbon films p 230 N91-18305
Diamondlike carbon applications in infrared optics and microelectronics p 230 N91-18306
- POVINELLI, L.**
Navier-Stokes analysis of transonic cascade flow
[NASA-TM-103624] p 159 N91-11192
- POVINELLI, L. A.**
Multigrid calculation of three-dimensional viscous cascade flows
[AIAA PAPER 91-3238] p 7 A91-53754
- POVINELLI, LOUIS A.**
Internal fluid mechanics research p 161 N91-20095
- Transonic cascade flow calculations using non-periodic C-type grids p 163 N91-21071
Implicit solution of three-dimensional internal turbulent flows p 163 N91-21082
CFD for hypersonic propulsion
[NASA-TM-103791] p 164 N91-21447
Application of computational fluid dynamics in high speed aeropropulsion
[NASA-TM-103780] p 164 N91-21458
Computational modeling and validation for hypersonic inlets p 16 N91-23162
- POWELL, J. A.**
Controlled growth of 3C-SiC and 6H-SiC films on low-tilt-angle vicinal (0001) 6H-SiC wafers p 232 A91-45713
Application of oxidation to the structural characterization of SiC epitaxial films p 233 A91-45881
High-voltage 6H-SiC p-n junction diodes p 142 A91-54746
Ellipsometric study of cubic SiC p 235 N91-18304
- POWELL, J. ANTHONY**
Silicon carbide, a semiconductor for space power electronics
[NASA-TM-103655] p 234 N91-14850
Development of silicon carbide semiconductor devices for high temperature applications
[NASA-TM-104398] p 236 N91-22921
Advances in silicon carbide Chemical Vapor Deposition (CVD) for semiconductor device fabrication
[NASA-TM-104410] p 236 N91-23946
Silicon carbide, an emerging high temperature semiconductor p 236 N91-24061
Process for the controlled growth of single-crystal films of silicon carbide polytypes on silicon carbide wafers
[NASA-CASE-LEW-15222-1] p 236 N91-26966
Process for the homoepitaxial growth of single-crystal silicon carbide films on silicon carbide wafers
[NASA-CASE-LEW-15223-1] p 236 N91-26967
- POWELL, RICHARD**
Launch vehicle performance using metallized propellants
[AIAA PAPER 91-2050] p 58 A91-44106
Launch vehicle performance using metallized propellants
[NASA-TM-104456] p 76 N91-24304
- PRAHL, JOSEPH**
Parched elastohydrodynamic lubrication: Instrumentation and procedure p 168 N91-30469
[NASA-TM-104426]
- PRAHL, JOSEPH M.**
On the numerical solution of the dynamically loaded hydrodynamic lubrication of the point contact p 180 A91-33461
- PRATHER, MICHAEL J.**
NASA's High Speed Research Program - An introduction and status report
[SAE PAPER 901923] p 1 A91-48605
- PRIEM, RICHARD J.**
Analysis of 5 KHz combustion instabilities in 40K methane/LOX combustion chambers
[NASA-TM-101368] p 67 N91-10117
Nonlinear combustion instability model in two- to three-dimensions
[NASA-TM-102381] p 85 N91-31208
- PROCTOR, M.**
A qualitative view of cryogenic fluid injection into high speed flows
[NASA-TM-105139] p 169 N91-30473
- PROCTOR, M. P.**
Some preliminary results of brush seal/rotor interference effects on leakage at zero and low rpm using a tapered-plug rotor
[AIAA PAPER 91-3390] p 182 A91-45820
Some preliminary results of brush seal/rotor interference effects on leakage at zero and low RPM using a tapered-plug rotor
[NASA-TM-104396] p 188 N91-27559
- PROCTOR, MARGARET P.**
Eccentricity effects on leakage of a brush seal at low speeds
[NASA-TM-105141] p 86 N91-31220
- PURWIN, T. P.**
Transient cryogenic liquid discharge in normal and micro-gravity
[AIAA PAPER 91-0486] p 124 A91-19324
Discharge rate of cryogenics in microgravity - What ground based experimentation cannot resolve
[AIAA PAPER 91-3545] p 129 A91-52430
- PUTERBAUGH, STEVEN L.**
A Navier-Stokes study of shock-boundary layer interaction and flow separation inside a transonic compressor p 8 A91-56115
- PUTNAM, RAND M.**
The environment power system analysis tool development program p 231 N91-17734

Q

QUINN, TODD M.

- Autonomous power expert system p 54 A91-37972
 Autonomous power expert system advanced development p 72 N91-20689
 An autonomous fault detection, isolation, and recovery system for a 20-kHz electric power distribution test bed [NASA-TM-104344] p 217 N91-25680

R

RAJ, S. V.

- Grain boundary sliding behaviour of copper and alpha brass at intermediate temperatures p 108 A91-27158
 Temperature dependence of the elastic moduli and damping for polycrystalline LiF-22 pct CaF₂ eutectic salt p 87 A91-33793
 Creep behaviour of Cu-30 percent Zn at intermediate temperatures p 109 A91-47747
 Creep behavior of copper at intermediate temperatures. II - Surface microstructural observations. III - A comparison with theory p 109 A91-47931

RAMAN, GANESH

- Axisymmetric jet forced by fundamental and subharmonic tones p 226 A91-45111
 Naturally occurring and forced azimuthal modes in a turbulent jet [NASA-TM-103692] p 11 N91-17000
 Control of an axisymmetric turbulent jet by multi-modal excitation [NASA-TM-104483] p 17 N91-26121
 An experimental study of natural and forced modes in an axisymmetric jet [NASA-TM-105225] p 18 N91-32074

RAMESHAM, R.

- Selective and low temperature synthesis of polycrystalline diamond p 232 A91-42170

RAMSEY, JOHN K.

- Influence of thickness and camber on the aeroelastic stability of supersonic throughflow fans p 5 A91-42814

- Post clamp [NASA-CASE-LEW-14862-1] p 183 N91-14617
 Optical measurement of propeller blade deflections in a spin facility [NASA-TM-103115] p 12 N91-17002

RANAUDO, R. J.

- Effects of horizontal tail ice on longitudinal aerodynamic derivatives p 36 A91-38547
 High altitude AMO testing of PV concentrator lens elements p 207 A91-41978

RANAUDO, RICHARD J.

- Cruise noise of an advanced single-rotation propeller measured from an adjacent aircraft p 22 A91-28265

RANKIN, THOMAS V.

- High voltage interactions of a sounding rocket with the ambient and system-generated environments p 46 A91-23077
 The environment workbench: A design tool for Space Station Freedom p 48 N91-20727

RAPP, DOUGLAS

- Design issues for propulsion systems using metallized propellants [AIAA PAPER 91-3484] p 66 A91-53709
 Design issues for propulsion systems using metallized propellants [NASA-TM-105190] p 81 N91-29220

RAPP, DOUGLAS C.

- Flow visualization of a rocket injector spray using gelled propellant simulants [AIAA PAPER 91-2198] p 59 A91-44151

RAQUET, C. A.

- Ka-band MMIC microstrip array for high rate communications [AIAA PAPER 91-3421] p 132 A91-52341
 System-Level Integrated Circuit (SLIC) development for phased array antenna applications [NASA-TM-104392] p 134 N91-23354
 Ka-band MMIC microstrip array for high rate communications [NASA-TM-104500] p 135 N91-27437

RASHIDNIA, N.

- A comparative flow visualization study of thermocapillary flow in drops in liquid-liquid systems [AIAA PAPER 91-0311] p 148 A91-21452
 Thermocapillary migration of liquid droplets in a temperature gradient in a density matched system p 153 A91-41132

RAUCH, JEFFREY S.

- Update on results of SPRE testing at NASA p 56 A91-38140
 Comparative survey of dynamic analyses of free-piston Stirling engines [NASA-TM-104491] p 224 N91-26870

RAWLIN, V. K.

- Mass comparisons of electric propulsion systems for NSSK of geosynchronous spacecraft [AIAA PAPER 91-2347] p 47 A91-45808
 Xenon ion propulsion for orbit transfer [NASA-TM-103193] p 69 N91-11798

RAWLIN, VINCENT K.

- Advanced ion propulsion for space exploration [AIAA PAPER 91-3567] p 65 A91-52443
 Mass comparisons of electric propulsion systems for NSSK of geosynchronous spacecraft [NASA-TM-105153] p 85 N91-31212

REARDON, F.

- Flow visualization and computational studies of a reverse flow circular combustor p 157 A91-48966

REBBECCHI, BRIAN

- Comparison of analysis and experiment for dynamics of low-contact-ratio spur gears [NASA-TM-103232] p 185 N91-22566
 Dynamic measurements of gear tooth friction and load [NASA-TM-103281] p 189 N91-27570

REDDY, D. R.

- Three-dimensional viscous flow computations of high area ratio nozzles for hypersonic propulsion p 4 A91-30014
 The design/analysis of flows through turbomachinery - A viscous/inviscid approach [AIAA PAPER 91-2010] p 153 A91-41677
 3-D Navier-Stokes analysis of crossing, glancing shocks/turbulent boundary layer interactions [AIAA PAPER 91-1758] p 6 A91-43631
 A comparison of CFD predictions and experimental results for a Mach 5 inlet p 28 N91-20094
 The 3-D Navier-Stokes analysis of crossing, glancing shocks/turbulent boundary layer interactions [NASA-TM-104469] p 16 N91-24130
 The design/analysis of flows through turbomachinery: A viscous/inviscid approach [NASA-TM-104447] p 33 N91-25148

REDDY, S. K.

- Effects of rim thickness on spur gear bending stress [AIAA PAPER 91-2020] p 181 A91-41681
 Effects of rim thickness on spur gear bending stress [NASA-TM-104388] p 186 N91-23500

REDDY, T. S. R.

- Numerical simulations of supersonic flow through oscillating cascade sections p 4 A91-28590
 Flutter analysis of cascades using a two dimensional Euler solver [AIAA PAPER 91-1681] p 6 A91-45548
 Application of an efficient hybrid scheme for aeroelastic analysis of advanced propellers p 7 A91-52315
 Euler flow predictions for an oscillating cascade using a high resolution wave-split scheme [NASA-TM-104377] p 16 N91-24107

REDNER, A. S.

- Photoelastic transducer for high-temperature applications p 174 A91-55533

REDNER, ALEX S.

- Fiber optic photoelastic pressure sensor for high temperature gases p 170 A91-19577

REED, BRIAN D.

- Experimental and analytical comparison of flowfields in a 110 N (25 Lbf) H₂/O₂ rocket [AIAA PAPER 91-2283] p 62 A91-45802
 Hydrogen/oxygen auxiliary propulsion technology [AIAA PAPER 91-3440] p 64 A91-52352
 Experimental and analytical comparison of flowfields in a 110 N (25 Lbf) H₂/O₂ rocket [NASA-TM-105175] p 82 N91-29230

REED, DAVID M.

- RSM 1.0 user's guide: A resupply scheduler using integer optimization [NASA-TM-104380] p 217 N91-22766

REEDER, M. F.

- Supersonic jet mixing enhancement by vortex generators [AIAA PAPER 91-2263] p 5 A91-41738
 Effect of tabs on the evolution of an axisymmetric jet [NASA-TM-104472] p 34 N91-27159

REEHORST, A. L.

- Effects of horizontal tail ice on longitudinal aerodynamic derivatives p 36 A91-38547

REESE, SHAWN

- A preliminary characterization of applied-field MPD thruster plumes [AIAA PAPER 91-2339] p 62 A91-45798

REICHERT, B. A.

- An experimental comparison of nonswirling and swirling flow in a circular-to-rectangular transition duct [AIAA PAPER 91-0342] p 148 A91-21466
 An experimental trace gas investigation of fluid transport and mixing in a circular-to-rectangular transition duct [AIAA PAPER 91-2370] p 172 A91-44214

- Computation of a circular-to-rectangular transition duct flow field [AIAA PAPER 91-1741] p 156 A91-45547

- An experimental comparison of nonswirling and swirling flow in a circular-to-rectangular transition duct [NASA-TM-104359] p 14 N91-21115
 An experimental trace gas investigation of fluid transport and mixing in a circular-to-rectangular transition duct [NASA-TM-104499] p 17 N91-27129

REICHERT, BRUCE A.

- A study of high speed flows in an aircraft transition duct [NASA-TM-104449] p 17 N91-26122

REID, LONNIE

- Three-dimensional flows in a transonic compressor rotor p 8 A91-56152
 Internal fluid mechanics research p 161 N91-20095

REID, MARGARET A.

- Impedances of Ni electrodes and Ni/H₂ cells from different manufacturers p 55 A91-38082
 Impedances of electrochemically impregnated nickel electrodes as functions of potential, KOH concentration, and impregnation method [NASA-TM-103283] p 208 N91-15628
 Raman spectral observation of a new phase observed in nickel electrodes cycled to failure p 214 N91-32556

- Impedances of nickel electrodes cycled in various KOH concentrations p 214 N91-32557

REINMANN, J. J.

- Icing simulation: A survey of computer models and experimental facilities [NASA-TM-104366] p 15 N91-23087

REINMANN, JOHN J.

- NASA's aircraft icing technology program p 19 N91-20120

RENO, CHARLES J.

- Implementation of control point form of algebraic grid-generation technique [NASA-TM-103748] p 13 N91-19054

RENSCH, D. B.

- An experimental study of high T_c superconducting microstrip transmission lines at 35 GHz and the effect of film morphology p 138 A91-36172
 An experimental study of high T_c superconducting microstrip transmission lines at 35 GHz and the effect of film morphology [NASA-TM-103633] p 133 N91-11988

RESHOTKO, E.

- Experimental study of boundary layer transition on a heated flat plate [NASA-TM-103779] p 14 N91-21061

RESHOTKO, ELI

- Naturally occurring and forced azimuthal modes in a turbulent jet [NASA-TM-103692] p 11 N91-17000
 Control of an axisymmetric turbulent jet by multi-modal excitation [NASA-TM-104483] p 17 N91-26121
 An experimental study of natural and forced modes in an axisymmetric jet [NASA-TM-105225] p 18 N91-32074

RESSELL, M. TED

- Telescope search for a 3-eV to 8-eV axion p 239 A91-28714

REYNOLDS, WILLIAM C.

- The effects of rotation on initially anisotropic homogeneous flows p 158 A91-54958

RHATIGAN, JENNIFER L.

- On protection of Freedom's solar dynamic radiator from the orbital debris environment. Part 2: Further testing and analyses [NASA-TM-104514] p 84 N91-30265

RHEE, HYOP S.

- Two-dimensional simulation of a two-phase, regenerative pumped radiator loop utilizing direct contact heat transfer with phase change p 151 A91-38126

RICE, E. J.

- Modern developments in shear flow control with swirl p 3 A91-24519

RICE, EDWARD J.

- Control of flow separation and mixing by aerodynamic excitation p 2 A91-24360
 Axisymmetric jet forced by fundamental and subharmonic tones p 226 A91-45111
 Naturally occurring and forced azimuthal modes in a turbulent jet [NASA-TM-103692] p 11 N91-17000
 Control of an axisymmetric turbulent jet by multi-modal excitation [NASA-TM-104483] p 17 N91-26121
 An experimental study of natural and forced modes in an axisymmetric jet [NASA-TM-105225] p 18 N91-32074

- RICHARD, M. A.**
Performance of a 300 Mbps 1:16 serial/parallel optoelectronic receiver module p 141 A91-51146
Measurement techniques for cryogenic Ka-band microstrip antennas [NASA-TM-105183] p 146 N91-30426
- RICHARD, MARK A.**
Design of an optically controlled Ka-band GaAs MMIC phased-array antenna p 132 A91-24951
- RIEHL, J. P.**
Evolutionary use of nuclear electric propulsion [AIAA PAPER 90-3821] p 50 A91-10174
- RIGBY, D. L.**
Increased heat transfer to a cylindrical leading edge due to spanwise variations in the freestream velocity [AIAA PAPER 91-1739] p 155 A91-43623
Increased heat transfer to a cylindrical leading edge due to spanwise variations in the freestream velocity [NASA-TM-104464] p 100 N91-24359
- RINGER, MARK J.**
Autonomous power expert system p 54 A91-37972
- RITZERT, F. J.**
Prospects for ductility and toughness enhancement of NiAl by ductile phase reinforcement [NASA-TM-103796] p 112 N91-27324
- RITZERT, FRANK J.**
Thermomechanical and bithermal fatigue behavior of cast B1900 + Hf and wrought Haynes 188 [NASA-TM-4225] p 111 N91-20268
- ROBAIDEK, JERROLD O.**
Viscoelastic properties of addition-cured polyimides used in high temperature polymer matrix composites [NASA-TM-103768] p 89 N91-22377
- ROBERTS, GARY D.**
ICAN sensitivity analysis [NASA-TM-103667] p 96 N91-15328
- ROBERTS, GARY D.**
Viscoelastic properties of addition-cured polyimides used in high temperature polymer matrix composites [NASA-TM-103768] p 89 N91-22377
- ROBERTSON, I. M.**
Inhomogeneous deformation in INCONEL 718 during monotonic and cyclic loadings p 108 A91-22287
- ROCHE, JAMES C.**
High voltage interactions of a sounding rocket with the ambient and system-generated environments p 46 A91-23077
The environment power system analysis tool development program p 231 N91-17734
The environment workbench: A design tool for Space Station Freedom p 48 N91-20727
- RODRIGUEZ, C. D.**
SEI power source alternatives for rovers and other multi-kWe distributed surface applications [NASA-TM-104360] p 81 N91-28277
- RODRIGUEZ, CARLOS D.**
Comparison of dynamic isotope power systems for distributed planet surface applications [NASA-TM-4303] p 81 N91-28278
- RODRIGUEZ, ELVIN**
Evaluation of thermal control coatings for use on solar dynamic radiators in low earth orbit [AIAA PAPER 91-1327] p 58 A91-43397
Evaluation of thermal control coatings for use on solar dynamic radiators in low Earth orbit [NASA-TM-104335] p 73 N91-22367
- ROELKE, R. J.**
Design and experimental evaluation of compact radial-inflow turbines [AIAA PAPER 91-2127] p 24 A91-45788
Computations of the three-dimensional flow and heat transfer within a coolant passage of a radial turbine blade [AIAA PAPER 91-2238] p 156 A91-45797
Algebraic grid generation for coolant passages of turbine blades with serpentine channels and pin fins [AIAA PAPER 91-2366] p 156 A91-45811
Algebraic grid generation for complex geometries p 157 A91-48758
GRID3D-v2: An updated version of the GRID2D/3D computer program for generating grid systems in complex-shaped three-dimensional spatial domains [NASA-TM-103766] p 217 N91-25630
- ROHDE, JOHN E.**
Overview of hypersonic/transatmospheric vehicle propulsion technology p 28 N91-20092
- ROHN, D. A.**
Manipulation hardware for microgravity research [NASA-TM-103423] p 128 N91-14498
- ROHN, DOUGLAS A.**
The dynamic effects of internal robots on Space Station Freedom [AIAA PAPER 91-2822] p 40 A91-49764
The dynamic effects of internal robots on Space Station Freedom [NASA-TM-104345] p 203 N91-22604
- ROLLBUHLER, J.**
Influence of geometric features on the performance of pressure-swirl atomizers p 147 A91-13030
- ROLLBUHLER, JIM**
Fuel-rich, catalytic reaction experimental results [AIAA PAPER 91-2463] p 24 A91-44250
- ROLLBUHLER, R. JAMES**
Fuel-rich, catalytic reaction experimental results [NASA-TM-104423] p 33 N91-24203
- ROMANOFSKY, R. R.**
High temperature superconducting thin film microwave circuits - Fabrication, characterization, and applications p 141 A91-50433
Quaternary pulse position modulation electronics for free-space laser communications [AIAA PAPER 91-3471] p 133 A91-53702
High temperature superconductor analog electronics for millimeter-wavelength communications [AIAA PAPER 91-3592] p 233 A91-53707
Quaternary pulse position modulation electronics for free-space laser communications [NASA-TM-104502] p 135 N91-29405
High temperature superconductor analog electronics for millimeter-wavelength communications [NASA-TM-105184] p 237 N91-29982
- ROMANOFSKY, ROBERT R.**
Aerospace applications of high temperature superconductivity [IAF PAPER 90-054] p 231 A91-13767
Monolithic mm-wave phase shifter using optically activated superconducting switches [NASA-CASE-LEW-14878-1] p 229 N91-13996
Universal nondestructive mm-wave integrated circuit test fixture [NASA-CASE-LEW-14746-1] p 143 N91-14552
Microwave integrated circuits for space applications p 145 N91-24069
Comparative study of bolometric and non-bolometric switching elements for microwave phase shifters [NASA-TM-104435] p 145 N91-25320
- RONCACE, ELIZABETH A.**
In-situ propellant rocket engines for Mars missions ascent vehicle [AIAA PAPER 91-2445] p 60 A91-44247
Liquid oxygen cooling of hydrocarbon fueled rocket thrust chambers p 63 A91-52309
In-situ propellant rocket engines for Mars mission ascent vehicle [NASA-TM-104429] p 76 N91-24305
- RONCACE, JAMES**
Flow visualization of a rocket injector spray using gelled propellant simulants [AIAA PAPER 91-2198] p 59 A91-44151
- ROPPEL, T.**
Selective and low temperature synthesis of polycrystalline diamond p 232 A91-42170
- ROSE, A. H.**
A fiber-optic current sensor for aerospace applications p 171 A91-23005
A fiber-optic current sensor for aerospace applications p 172 A91-38006
Fiber-optic sensors for aerospace electrical measurements: An update [NASA-TM-104454] p 177 N91-25381
- ROSENTHAL, BRUCE N.**
Programmable multi-zone furnace for microgravity research [AIAA PAPER 91-0781] p 127 A91-19463
Wettability of pyrolytic boron nitride by aluminum p 114 A91-28772
- ROSKILLY, RONALD R.**
National space test centers - Lewis Research Center Facilities [AIAA PAPER 90-3593] p 41 A91-11471
- ROSS, BRAD**
Stirling machine operating experience [NASA-TM-104487] p 212 N91-25510
- ROSS, H.**
Particle nonuniformity effects on particle cloud flames in low gravity [AIAA PAPER 91-0718] p 104 A91-19431
Particle cloud flames in acoustic fields p 105 A91-20589
Radiative structures of lycopodium-air flames in low gravity p 105 A91-30003
- ROSS, HOWARD D.**
Surface settling in partially filled containers upon step reduction in gravity [NASA-TM-103641] p 159 N91-14556
- ROSTAFINSKI, WOJCIECH**
Monograph on propagation of sound waves in curved ducts [NASA-RP-1248] p 228 N91-15848
- ROTH, DON J.**
General-purpose interface bus for multiuser, multitasking computer system p 215 A91-35928
- Spatial variations in a.c. susceptibility and microstructure for the YBa₂Cu₃O(7-x) superconductor and their correlation with room-temperature ultrasonic measurements p 233 A91-54969
Property and microstructural nonuniformity in the yttrium-barium-copper-oxide superconductor determined from electrical, magnetic, and ultrasonic measurements [NASA-TM-103732] p 193 N91-19463
Spatial variations in ac susceptibility and microstructure for the YBa₂Cu₃O(7-x) superconductor and their correlation with room-temperature ultrasonic measurements [NASA-TM-103787] p 194 N91-21553
Ultrasonic evaluation of oxidation and reduction effects on the elastic behavior and global microstructure of YBa₂Cu₃O_{7-x} [NASA-TM-104529] p 194 N91-27575
- ROTH, MARY ELLEN**
Electromechanical actuation for thrust vector control applications p 52 A91-31026
Field oriented control of induction motors p 138 A91-37987
- ROUGE, C. J.**
Ceramic coatings on smooth surfaces [NASA-CASE-LEW-15164-1] p 122 N91-25298
Ceramic coatings on smooth surfaces [NASA-CASE-LEW-15164-2] p 123 N91-32229
- ROUGE, CARL J.**
Oxidation resistant coatings for titanium alloys and titanium alloy matrix composites [NASA-CASE-LEW-15155-1] p 122 N91-26375
- ROVANG, RICHARD D.**
Dynamic Isotope Surface Power Systems [AIAA PAPER 91-3623] p 208 A91-52487
- ROYCHOUDHURY, SUBIR**
Effects of nozzle lip geometry on spray atomization and emissions advanced gas turbine combustors [AIAA PAPER 91-2201] p 24 A91-44153
- RUAN, Y. F.**
Analytical and experimental study of vibrations in a gear transmission [AIAA PAPER 91-2019] p 181 A91-41680
Modal analysis of multistage gear systems coupled with gearbox vibrations [NASA-TM-103797] p 187 N91-23513
Analytical and experimental study of vibrations in a gear transmission [NASA-TM-104434] p 187 N91-25395
- RUBINSTEIN, R.**
Nonlinear Reynolds stress model for turbulent shear flows [AIAA PAPER 91-0609] p 149 A91-21556
- RUBINSTEIN, ROBERT**
Particle image fields and partial coherence p 171 A91-19604
Renormalization group analysis of anisotropic diffusion in turbulent shear flows p 150 A91-27946
- RUCKMAN, MARK W.**
Near-edge study of gold-substituted YBa₂Cu₃O(7-delta) [NASA-TM-105220] p 237 N91-31977
- RUSSELL, J. R.**
Development of an intelligent diagnostic system for reusable rocket engine control [AIAA PAPER 91-2533] p 63 A91-45817
- RUSSELL, LOUIS M.**
Visualization techniques to experimentally model flow and heat transfer in turbine and aircraft flow passages [NASA-TM-4272] p 167 N91-27489
- RUTLEDGE, SHARON K.**
Undercutting of defects in thin film protective coatings on polymer surfaces exposed to atomic oxygen p 115 A91-41516
Atomic oxygen undercutting of defects on SiO₂ protected polyimide solar array blankets p 116 A91-49803
The effect of atomic oxygen on altered and coated Kapton surfaces for spacecraft applications in low earth orbit p 116 A91-49804
Thermal emittance enhancement of graphite-copper composites for high temperature space based radiators [AIAA PAPER 91-3527] p 116 A91-53705
High emittance surfaces for high temperature space radiator applications p 88 A91-56415
Effects of dust accumulation and removal on radiators surfaces on Mars [NASA-TM-103704] p 72 N91-20204
Atomic oxygen interaction with solar array blankets at protective coating defect sites p 211 N91-20732
The effect of atomic oxygen on polysiloxane-polyimide for spacecraft applications in low Earth orbit p 229 N91-20735
Flexible fluoropolymer filled protective coatings p 121 N91-24062
Durability evaluation of photovoltaic blanket materials exposed on LDEF tray S1003 p 212 N91-25062

Thermal emittance enhancement of graphite-copper composites for high temperature space based radiators [NASA-TM-105178] p 123 N91-29332
Low Earth orbital atomic oxygen micrometeoroid, and debris interactions with photovoltaic arrays p 84 N91-30248

RYU, DONGSU

The dynamic instability of adiabatic blast waves p 239 A91-26361

S

SAIYED, N. H.

LN2 spray droplet size measurement via ensemble diffraction technique [AIAA PAPER 91-1381] p 129 A91-44336
LN2 spray droplet size measurement via ensemble diffraction technique [NASA-TM-104443] p 131 N91-24470

SALEM, J. A.

Ultrasonic imaging of textured alumina p 191 A91-18596

SALEM, JONATHAN A.

Numerical, micro-mechanical prediction of crack growth resistance in a fibre-reinforced/brittle matrix composite p 199 A91-51916

Dynamic fatigue property of silicon carbide whisker-reinforced silicon nitride p 94 A91-56937

Comparison of dynamic fatigue behavior between SiC whisker-reinforced composite and monolithic silicon nitrides [NASA-TM-103707] p 119 N91-19293

Mechanical behavior and failure phenomenon of an in situ-toughened silicon nitride [NASA-TM-103741] p 121 N91-23311

Elevated-temperature fracture resistances (K(sub IC), R-curves, gamma sub (omega OF)) of monolithic and composite ceramics using chevron-notched, bend tests [NASA-TM-105090] p 123 N91-28418

SALKOWSKI, CHARLES

Overall goals p 80 N91-28246

SALTSMAN, JAMES F.

Application of thermal life prediction model to high-temperature aerospace alloys B1900 + Hf and Haynes 188 [NASA-TM-4226] p 201 N91-19473

Tensile deformation damage in SiC reinforced Ti-15V-3Cr-3Al-3Sn [NASA-TM-103620] p 101 N91-25195

SALUPO, C. S.

High-voltage 6H-SiC p-n junction diodes p 142 A91-54746

SALVINO, R. E.

Critical-point analysis of the liquid-vapor interfacial surface tension p 237 A91-16103

Newtonian mechanics of a many-particle assembly coupled to an external body potential p 237 A91-19495

SAMIMY, M.

Supersonic jet mixing enhancement by vortex generators [AIAA PAPER 91-2263] p 5 A91-41738

Effect of tabs on the evolution of an axisymmetric jet [NASA-TM-104472] p 34 N91-27159

SANABRIA, RAFAEL

Review and test of chilldown methods for space-based cryogenic tanks [AIAA PAPER 91-1843] p 60 A91-45776

A review of candidate multilayer insulation systems for potential use on wet-launched LH2 tankage for the Space Exploration Initiative lunar missions [AIAA PAPER 91-2176] p 43 A91-45793

Review and test of chilldown methods for space-based cryogenic tanks [NASA-TM-104458] p 167 N91-25351

SANDERS, W. A.

Crystallization and characterization of Y2O3-SiO2 glasses p 237 N91-31962

SANKAR, L. N.

Simulation of iced wing aerodynamics [NASA-TM-104362] p 15 N91-23086

SANKAR, LAKSHMI N.

Application of an efficient hybrid scheme for aeroelastic analysis of advanced propellers p 7 A91-52315

SANKOVIC, JOHN M.

Arjet thermal characteristics [AIAA PAPER 91-2456] p 63 A91-45814

Investigation of the arcjet plume near field using electrostatic probes [NASA-TM-103638] p 68 N91-11060

Investigation of the arcjet near field plume using electrostatic probes p 75 N91-24270

Arjet thermal characteristics [NASA-TM-105156] p 82 N91-29231

Medium power hydrogen arcjet performance [NASA-TM-104533] p 85 N91-31216

SANZ, JOSE M.

Automated design of controlled diffusion blades p 9 N91-10883

SANZGIRI, S. M.

Ka-band MMIC microstrip array for high rate communications [AIAA PAPER 91-3421] p 132 A91-52341

Ka-band MMIC microstrip array for high rate communications [NASA-TM-104500] p 135 N91-27437

SANZGIRI, SHASHI

A 29.3-GHz cavity-enclosed aperture-coupled circular-patch antenna for microwave circuit integration p 140 A91-47057

SARANGAPANI, S.

Some recent studies with the solid-ionomer electrochemical capacitor p 214 N91-32562

SARAVANOS, D. A.

Mechanics of damping for fiber composite laminates including hygrothermal effects p 195 A91-12895

An integrated methodology for optimizing the passive damping of composite structures p 195 A91-19048

Concurrent material-fabrication optimization of metal-matrix laminates under thermo-mechanical loading [AIAA PAPER 91-1044] p 129 A91-31842

The effects of interply damping layers on the dynamic response of composite structures [AIAA PAPER 91-1124] p 197 A91-32064

Computational simulation of damping in composite structures p 198 A91-36283

Concurrent tailoring of fabrication process and interphase layer to reduce residual stresses in metal matrix composites p 92 A91-43232

Concurrent micromechanical tailoring and fabrication process optimization for metal-matrix composites [NASA-TM-103670] p 98 N91-19237

Adaptation of NASA technology for the optimization of orthopedic knee implants p 215 N91-23032

Interphase layer optimization for metal matrix composites with fabrication considerations [NASA-TM-105166] p 102 N91-30281

The effects of interply damping layers on the dynamic response of composite structures [NASA-TM-104497] p 103 N91-30282

Integrated mechanics for the passive damping of polymer-matrix composites and composite structures [NASA-TM-104346] p 103 N91-32181

SARIPALLI, K. R.

Flow visualization studies of the internal flow characteristics in a simulated mixed flow vectored thrust ASTOVL engine configuration [AIAA PAPER 91-1689] p 23 A91-42556

SARMIENTO, CHARLES J.

Arjet nozzle area ratio effects p 75 N91-24271

Medium power hydrogen arcjet performance [NASA-TM-104533] p 85 N91-31216

SASMAL, G. P.

Computational modeling of the pressurization process in a NASP vehicle propellant tank experimental simulation [AIAA PAPER 91-2407] p 124 A91-41771

SAUCILLO, R. J.

Cryogenic propellant management system requirements for Space Station Freedom [AIAA PAPER 91-3476] p 65 A91-52382

SAUNDERS, J. D.

Results from computational analysis of a mixed compression supersonic inlet [AIAA PAPER 91-2581] p 7 A91-45818

SAUNDERS, NEAL T.

Lewis aeropropulsion technology: Remembering the past and challenging the future p 242 N91-20087

SAVAGE, M.

Effects of rim thickness on spur gear bending stress [AIAA PAPER 91-2020] p 181 A91-41681

Maximum life spur gear design [AIAA PAPER 91-2021] p 181 A91-41682

Effects of rim thickness on spur gear bending stress [NASA-TM-104388] p 186 N91-23500

Maximum life spur gear design [NASA-TM-104361] p 187 N91-23514

Transmission overhaul estimates for partial and full replacement at repair [NASA-TM-104395] p 190 N91-30533

SAVILLE, M.

Liquid hydrogen turbopump foil bearing [AIAA PAPER 91-2108] p 182 A91-41701

SAYOOD, KHALID

Data compression for full motion video transmission [AIAA PAPER 91-3533] p 45 A91-52424

Data compression for full motion video transmission [NASA-TM-105239] p 135 N91-32247

SCHACHAM, SAMUEL E.

Surface and implantation effects on p-n junctions p 234 N91-18299

Properties of insulator interfaces with p-HgCdTe p 235 N91-18300

Surface electrons in inverted layers of p-HgCdTe p 235 N91-18301

SCHEIMAN, DAVID A.

Rapid thermal cycling of new technology solar array blanket coupons p 54 A91-38019

Rapid thermal cycling of solar array blanket coupons for Space Station Freedom p 84 N91-30239

SCHLOSSER, HERBERT

Global expression for representing diatomic potential-energy curves p 228 A91-33236

Universal energy relations and metal/ceramic interfaces p 93 A91-56254

SCHLUMBERGER, J.

A qualitative view of cryogenic fluid injection into high speed flows [NASA-TM-105139] p 169 N91-30473

SCHLUMBERGER, J. A.

Some preliminary results of brush seal/rotor interference effects on leakage at zero and low rpm using a tapered-plug rotor [AIAA PAPER 91-3390] p 182 A91-45820

Some preliminary results of brush seal/rotor interference effects on leakage at zero and low RPM using a tapered-plug rotor [NASA-TM-104396] p 188 N91-27559

SCHLUMBERGER, JULIE A.

Eccentricity effects on leakage of a brush seal at low speeds [NASA-TM-105141] p 86 N91-31220

SCHMIDT, FRED

Characteristics of a future aeronautical satellite communications system [NASA-TM-104389] p 20 N91-23102

SCHMIDT, PHILLIP

Partitioning methods for global controllers p 219 A91-30043

A method for partitioning centralized controllers [NASA-TM-4276] p 36 N91-20133

SCHMITZ, D.

Submicron gate InP power MISFET's with improved output power density at 18 and 20 GHz p 145 N91-26436

SCHMITZ, DIETMAR

Submicron gate InP power MISFET's with improved output power density at 18 and 20 GHz p 142 A91-54526

SCHMITZ, P. C.

Design of multihundredwatt DIPS for robotic space missions [NASA-TM-104401] p 75 N91-24232

SCHMITZ, PAUL C.

Space reactor/Stirling cycle systems for high power lunar application [NASA-TM-103698] p 40 N91-19112

Preliminary design of a mobile lunar power supply [NASA-TM-104471] p 212 N91-27611

SEI power source alternatives for rovers and other multi-kWe distributed surface applications [NASA-TM-104360] p 81 N91-28277

Comparison of dynamic isotope power systems for distributed planet surface applications [NASA-TM-4303] p 81 N91-28278

SCHNEIDER, S. J.

Spectrally resolved Rayleigh scattering diagnostic for hydrogen-oxygen rocket plume studies [AIAA PAPER 91-0462] p 51 A91-21498

SCHNEIDER, STEVEN J.

Experimental and analytical comparison of flowfields in a 110 N (25 Lbf) H2/O2 rocket [AIAA PAPER 91-2283] p 62 A91-45802

Hydrogen/oxygen auxiliary propulsion technology [AIAA PAPER 91-3440] p 64 A91-52352

Method of injecting fluid propellants into a rocket combustion chamber [NASA-CASE-LEW-14846-2] p 78 N91-26200

Experimental and analytical comparison of flowfields in a 110 N (25 lbf) H2/O2 rocket [NASA-TM-105175] p 82 N91-29230

SCHNITTGRUND, G. D.

Effect of thermal shock on fiber-reinforced superalloy composites p 93 A91-55918

SCHNITZER, BRUCE G.

Radiation dose estimates for typical piloted NTR lunar and Mars mission engine operations [AIAA PAPER 91-3407] p 215 A91-52331

SCHNYER, A. D.

NASA's future space power needs and requirements p 52 A91-37929

- SCHOBEIRI, TAHER**
Aerodynamics and heat transfer investigations on a high Reynolds number turbine cascade
[NASA-TM-103260] p 11 N91-15134
- SCHOENMAN, LEONARD**
Surface modification of Monel K-500 as a means of reducing friction and wear in high-pressure oxygen
p 107 A91-16869
- SCHRAMM, DAVID M.**
Primordial nucleosynthesis redux p 240 A91-45907
- SCHRAMM, DAVID N.**
The shock process and light-element production in supernova envelopes p 239 A91-33573
Big bang nucleosynthesis - The standard model and alternatives p 240 A91-37428
Constraints from primordial nucleosynthesis on the mass of the tau neutrino p 240 A91-46543
- SCHREIBER, J. G.**
Design of multihundredwatt DIPS for robotic space missions
[NASA-TM-104401] p 75 N91-24232
- SCHREIBER, JEFFREY G.**
Preliminary designs for 25 kWe advanced Stirling conversion systems for dish electric applications p 207 A91-38182
Status of the advanced Stirling conversion system project for 25 kW dish Stirling applications
[NASA-TM-104528] p 238 N91-31023
- SCHRIITZ, BRYAN**
Patched elasto-hydrodynamic lubrication: Instrumentation and procedure
[NASA-TM-104426] p 168 N91-30469
- SCHUSTER, J. R.**
The COLD-SAT experiment for cryogenic fluid management technology p 46 A91-29799
The COLD-SAT experiment for cryogenic fluid management technology p 126 N91-24263
- SCHVERMAN, MARLA A.**
Long term isothermal aging and thermal analysis of N-CYCAP polyimides
[NASA-TM-104341] p 122 N91-25286
- SCHWAB, JOHN R.**
Performance of a high-work, low-aspect-ratio turbine stator tested with a realistic inlet radial temperature gradient
[NASA-TM-103738] p 31 N91-20126
- SCHWARZE, G. E.**
High frequency, high temperature specific core loss and dynamic B-H hysteresis loop characteristics of soft magnetic alloys p 138 A91-37988
Neutron and gamma irradiation effects on power semiconductor switches p 139 A91-38162
Neutron, gamma ray and post-irradiation thermal annealing effects on power semiconductor switches
[AIAA PAPER 91-3525] p 142 A91-52420
Neutron, gamma ray and post-irradiation thermal annealing effects on power semiconductor switches
[NASA-TM-105248] p 147 N91-32410
Comparison of high temperature, high frequency core loss and dynamic B-H loops of two 50 Ni-Fe crystalline alloys and an iron-based amorphous alloy
[NASA-TM-105205] p 147 N91-32412
- SCHWARZE, GENE E.**
Makeup and uses of a basic magnet laboratory for characterizing high-temperature permanent magnets
[NASA-TM-104508] p 146 N91-30427
- SCOTT, JAMES R.**
Acoustic radiation from lifting airfoils in compressible subsonic flow
[AIAA PAPER 90-3911] p 224 A91-12427
Acoustic radiation from lifting airfoils in compressible subsonic flow
[NASA-TM-103650] p 13 N91-19053
Inlets, ducts, and nozzles p 162 N91-20096
Compressible flows with periodic vortical disturbances around lifting airfoils
[NASA-TM-103742] p 14 N91-21060
A finite-difference, frequency-domain numerical scheme for the solution of the linearized unsteady Euler equations p 162 N91-21067
- SEABLOM, KIRK D.**
Development of a laser-induced heat flux technique for measurement of convective heat transfer coefficients in a supersonic flowfield
[NASA-TM-103778] p 13 N91-19063
- SEASHOLTZ, R. G.**
Spectrally resolved Rayleigh scattering diagnostic for hydrogen-oxygen rocket plume studies
[AIAA PAPER 91-0462] p 51 A91-21498
- SEASHOLTZ, RICHARD G.**
High-speed laser anemometry based on spectrally resolved Rayleigh scattering
[NASA-TM-104522] p 178 N91-27521
- SECUNDE, RICHARD R.**
Solar dynamic power for Earth orbital and lunar applications
[NASA-TM-104511] p 80 N91-27214
- SEDGWICK, L. M.**
Full-size solar dynamic heat receiver thermal-vacuum tests
[NASA-TM-104486] p 78 N91-25184
Ground test program for a full-size solar dynamic heat receiver
[NASA-TM-104485] p 79 N91-27209
- SEFCIK, R. J.**
Systems analysis of Mars solar electric propulsion vehicles
[AIAA PAPER 90-3824] p 40 A91-10176
- SEIDEL, JONATHAN A.**
A comparison of arrow, trapezoidal and M wing concepts using a Mach 2 supersonic cruise transport mission
[AIAA PAPER 91-3102] p 7 A91-54027
Comparison of turbine bypass and mixed flow turbofan engines for a high-speed civil transport
[AIAA PAPER 91-3132] p 25 A91-54051
- SEKULA-MOISE, P. A.**
Dielectric function of InGaAs in the visible
p 233 A91-53236
Study of InGaAs based MODFET structures using variable angle spectroscopic ellipsometry
[NASA-TM-103792] p 235 N91-19935
- SELLECK, M. E.**
Isothermal Dendritic Growth Experiment - Science, engineering, and hardware development for USMP space flights p 128 A91-53408
- SELLERS, M.**
Outline of the Solar System: Activities for elementary students
[NASA-TM-104965] p 241 N91-25875
- SENG, GARY T.**
High temperature electronics p 144 N91-20101
Fiber-optic-based controls p 230 N91-20102
- SENYITKO, RICHARD G.**
Rotating pressure measurement system using an on board calibration standard
[NASA-TM-103676] p 176 N91-19401
- SERBETCI, ILTER**
Inertia effects in thin film flow with a corrugated boundary p 151 A91-32691
- SESHADRI, K.**
Particle nonuniformity effects on particle cloud flames in low gravity
[AIAA PAPER 91-0718] p 104 A91-19431
- SEYBERT, A. F.**
Acoustical analysis of gear housing vibration
[NASA-TM-103691] p 188 N91-25411
- SHABBI, AAMIR**
Advances in modeling the pressure correlation terms in the second moment equations
[NASA-TM-104413] p 165 N91-24525
- SHAH, ASHWIN R.**
Simulation of probabilistic wind loads and building analysis
[NASA-TM-103744] p 203 N91-23549
- SHAKER, FRANCIS J.**
Dynamic analysis of space-related linear and non-linear structures p 196 A91-28612
- SHALKHAUSER, K. A.**
Bit error rate testing of fiber optic data links for MMIC-based phased array antennas
p 131 A91-24950
System-Level Integrated Circuit (SLIC) development for phased array antenna applications
[NASA-TM-104392] p 134 N91-23354
Submicron gate InP power MISFET's with improved output power density at 18 and 20 GHz
p 145 N91-26436
- SHALKHAUSER, KURT A.**
Submicron gate InP power MISFET's with improved output power density at 18 and 20 GHz
p 142 A91-54526
Universal nondestructive mm-wave integrated circuit test fixture
[NASA-CASE-LEW-14746-1] p 143 N91-14552
A three-dimensional finite-element thermal/mechanical analytical technique for high-performance traveling wave tubes
[NASA-TP-3081] p 134 N91-27436
- SHALKHAUSER, M. J.**
Quaternary pulse position modulation electronics for free-space laser communications
[AIAA PAPER 91-3471] p 133 A91-53702
Quaternary pulse position modulation electronics for free-space laser communications
[NASA-TM-104502] p 135 N91-29405
- SHALKHAUSER, MARY J.**
Real-time data compression of broadcast video signals
[NASA-CASE-LEW-14945-1] p 133 N91-13598
- SHALKHAUSER, MARY JO**
Digital CODEC for real-time processing of broadcast quality video signals at 1.8 bits/pixel p 134 N91-24067
- SHALTENS, RICHARD K.**
Preliminary designs for 25 kWe advanced Stirling conversion systems for dish electric applications
p 207 A91-38182
Solar powered Stirling cycle electrical generator
p 211 N91-23054
Status of the advanced Stirling conversion system project for 25 kW dish Stirling applications
[NASA-TM-104528] p 238 N91-31023
- SHAMROTH, S. J.**
Navier-Stokes simulation of transonic blade-vortex interactions p 2 A91-21065
- SHAN, X.**
Raman spectral observation of a new phase observed in nickel electrodes cycled to failure p 214 N91-32556
- SHANNON, JOHN L., JR.**
Analysis of some compliance calibration data for chevron-notch bar and rod specimens
[NASA-TM-104367] p 203 N91-22594
- SHARP, G. R.**
Electrically conducting polymers for aerospace applications
[AIAA PAPER 91-3432] p 233 A91-52349
Design of an inflatable, optically controlled and fed, phased array antenna
[AIAA PAPER 91-3470] p 132 A91-52378
ATDRS payload technology R & D p 45 A91-53188
- SHARP, G. RICHARD**
A review of properties and potential aerospace applications of electrically conducting polymers
p 113 A91-14409
Designs for the ATDRSS tri-band reflector antenna
[NASA-TM-103754] p 48 N91-20184
A new fabrication method for precision antenna reflectors for space flight and ground test
[NASA-TP-3078] p 48 N91-21185
A three-dimensional finite-element thermal/mechanical analytical technique for high-performance traveling wave tubes
[NASA-TP-3081] p 134 N91-27436
- SHAW, LORETTA M.**
Plans for the development of cryogenic engines for space exploration
[AIAA PAPER 91-3438] p 64 A91-52351
- SHAW, R. J.**
Overview of supersonic cruise propulsion research p 27 N91-20088
- SHAW, ROBERT J.**
Propulsion challenges for a 21st century economically viable, environmentally compatible High-Speed Civil Transport p 25 A91-56109
Engine technology challenges for a 21st century high speed civil transport
[NASA-TM-104363] p 19 N91-23098
- SHEN, M.-H. H.**
Free vibrations of delaminated beams
[AIAA PAPER 91-1241] p 197 A91-32129
- SHEPHERD, KEVIN P.**
Wind turbine acoustics
[NASA-TP-3057] p 228 N91-16679
- SHERMAN, BRADLEY D.**
Optical Multiple Access Network (OMAN) for advanced processing satellite applications
[NASA-TM-105167] p 135 N91-29431
- SHIAO, MICHAEL**
Probabilistic simulation of uncertainties in thermal structures p 195 A91-16042
Probabilistic simulation of uncertainties in thermal structures
[NASA-TM-103680] p 201 N91-19472
- SHIAO, MICHAEL C.**
A methodology for evaluating the reliability and risk of structures under complex service environments
[NASA-TM-103244] p 200 N91-17415
Probability of failure and risk assessment of propulsion structural components
[NASA-TM-102323] p 205 N91-25436
- SHIH, T. H.**
A critical comparison of two-equation turbulence models
[NASA-TM-105237] p 169 N91-31597
A k-epsilon modeling of near wall turbulence
[NASA-TM-105238] p 170 N91-32460
- SHIH, T. I.-P.**
Flux-vector splitting algorithm for chain-rule conservation-law form p 221 A91-45109
Computations of the three-dimensional flow and heat transfer within a coolant passage of a radial turbine blade
[AIAA PAPER 91-2238] p 156 A91-45797

- Algebraic grid generation for coolant passages of turbine blades with serpentine channels and pin fins
[AIAA PAPER 91-2366] p 156 A91-45811
- Algebraic grid generation for complex geometries
[NASA-TM-103766] p 157 A91-48758
- SHIH, T. I-P.**
GRID3D-v2: An updated version of the GRID2D/3D computer program for generating grid systems in complex-shaped three-dimensional spatial domains
[NASA-TM-103766] p 217 A91-25630
- SHIH, T.-H.**
Second order modeling of boundary-free turbulent shear flows
[AIAA PAPER 91-1779] p 154 A91-42588
Second order modeling of boundary-free turbulent shear flows
[NASA-TM-104369] p 164 A91-22524
Low Reynolds number two-equation modeling of turbulent flows
[NASA-TM-104368] p 165 A91-23416
- SHIH, TOM I.-P.**
Simulation of mixing in the quick quench region of a rich burn-quick quench mix-lean burn combustor
[AIAA PAPER 91-0410] p 105 A91-21481
- SHIH, TSAN-HSING**
The effects of rotation on initially anisotropic homogeneous flows
p 158 A91-54958
Advances in modeling the pressure correlation terms in the second moment equations
[NASA-TM-104413] p 165 A91-24525
- SHIMSKI, JOHN**
Evaluation of advanced lubricants for aircraft applications using gear surface fatigue tests
[AIAA PAPER 91-1907] p 181 A91-41649
Evaluation of advanced lubricants for aircraft applications using gear surface fatigue tests
[NASA-TM-104336] p 186 A91-22568
Effect of two synthetic lubricants on life of AISI 9310 spur gears
[NASA-TM-104352] p 189 A91-29599
- SHIN, JAIWON**
Prediction of ice shapes and their effect on airfoil performance
[AIAA PAPER 91-0264] p 3 A91-26330
Prediction of ice shapes and their effect on airfoil performance
[NASA-TM-103701] p 12 A91-19047
Advanced ice protection systems test in the NASA Lewis icing research tunnel
[NASA-TM-103757] p 32 A91-23183
Applied high-speed imaging for the icing research program at NASA Lewis Research Center
[NASA-TM-104415] p 177 A91-26490
- SHOEMAKER, NEIL S.**
Ellipsometric study of cubic SiC p 235 A91-18304
Optical dispersion relations for diamondlike carbon films
p 230 A91-18305
- SHUEN, J. S.**
Combustion of liquid fuel droplets in supercritical conditions
[AIAA PAPER 91-0078] p 105 A91-21362
A time-accurate implicit method for chemically reacting flows at all Mach numbers
[AIAA PAPER 91-0581] p 149 A91-21542
Pressure-coupled vaporization and combustion responses of liquid-fuel droplets in high-pressure environments
[AIAA PAPER 91-2310] p 106 A91-44192
- SHUEN, JIAN-SHUN**
Flux splitting algorithms for two-dimensional viscous flows with finite-rate chemistry
p 10 A91-10894
- SHYNE, RICKEY J.**
Overview of NASP nozzle research
p 28 A91-20093
- SIEG, R. E.**
Dielectric function of InGaAs in the visible
p 233 A91-53236
Ellipsometric study of InGaAs MODFET material
[NASA-TM-103286] p 143 A91-19351
- SIEG, R. M.**
Ellipsometric study of YBa₂Cu₃O_{7-x} laser ablated and co-evaporated films
p 233 A91-53235
Study of InGaAs based MODFET structures using variable angle spectroscopic ellipsometry
[NASA-TM-103792] p 235 A91-19935
- SIEG, ROBERT M.**
Optical dispersion relations for diamondlike carbon films
p 230 A91-18305
- SIEGEL, R.**
Analytical solution for boundary heat fluxes from a radiating rectangular medium
p 150 A91-27175
- SILVERMAN, ALBERT**
Control of multiple resonant power processors in a multi-source system
p 137 A91-30901
- SIMON, DONALD L.**
The NASA Lewis integrated propulsion and flight control simulator
[AIAA PAPER 91-2969] p 38 A91-47847
The NASA Lewis integrated propulsion and flight control simulator
[NASA-TM-105147] p 21 A91-27157
A high-frequency servosystem for fuel control in hypersonic engines
[NASA-TM-104333] p 35 A91-31178
- SIMONEAU, R. J.**
Heat transfer in space systems; Proceedings of the Symposium, AIAA/ASME Thermophysics and Heat Transfer Conference, Seattle, WA, June 18-20, 1990
p 152 A91-38780
- SIMONS, R. N.**
Coplanar-waveguide/microstrip probe coupler and applications to antennas
p 131 A91-17719
New coplanar waveguide/stripline feed network for seven patch hexagonal CP subarray
p 137 A91-32823
New channelised coplanar waveguide to rectangular waveguide post and slot couplers
p 139 A91-40272
A seven patch hexagonal CP subarray with a CPW/stripline feed network
[NASA-TM-103802] p 144 A91-20406
- SIMONS, RAINEE**
Optical control of microwave devices
p 136 A91-27331
- SIMONS, RAINEE N.**
Theoretical and experimental characterization of coplanar waveguide discontinuities for filter applications
p 137 A91-35911
Coplanar waveguide feeds for phased array antennas
[AIAA PAPER 91-3422] p 141 A91-52342
Coplanar waveguide feeds for phased array antennas
[NASA-TM-104467] p 146 A91-27477
- SIMONYI, P. S.**
Comparison of a quasi-3D analysis and experimental performance for three compact radial turbines
[AIAA PAPER 91-2128] p 25 A91-45789
Comparison of a quasi-3D analysis and experimental performance for three compact radial turbines
[NASA-TM-105155] p 35 A91-30142
- SIMONYI, S.**
Design and experimental evaluation of compact radial-inflow turbines
[AIAA PAPER 91-2127] p 24 A91-45788
- SINGH, N. B.**
Growth kinetics of physical vapor transport processes: Crystal growth of the optoelectronic material mercurous chloride
[NASA-TM-103788] p 128 A91-19320
- SINGHAL, S.**
Probabilistic structural analysis methods for space transportation propulsion systems
p 205 A91-28238
Concurrent engineering
p 80 A91-28247
- SINGHAL, S. N.**
Computational simulation of acoustic fatigue for hot composite structures
[AIAA PAPER 91-1178] p 197 A91-32099
Computational simulation of hot composites structures
[NASA-TM-103681] p 97 A91-19230
HITCAN for actively cooled hot-composite thermostructural analysis
[NASA-TM-103750] p 202 A91-21562
- SINGHAL, SURENDRA N.**
Computational simulation of acoustic fatigue for hot composite structures
[NASA-TM-104379] p 203 A91-23548
- SINHA, A.**
A new approach to controller design for microgravity isolation systems
p 129 A91-23108
- SIRBAUGH, J. R.**
Computation of a circular-to-rectangular transition duct flow field
[AIAA PAPER 91-1741] p 156 A91-45547
- SIROCKY, PAUL J.**
High-temperature, flexible, thermal barrier seal
[NASA-CASE-LEW-14672-1] p 189 A91-27560
- SKARDA, J. R. L.**
Scaling analysis applied to the NORVEX code development and thermal energy flight experiment
[AIAA PAPER 91-1420] p 155 A91-44337
- SKARDA, J. RAYMOND LEE**
Scaling analysis applied to the NORVEX code development and thermal energy flight experiment
[NASA-TM-104462] p 166 A91-24549
- SKUPINSKI, ROBERT C.**
Update on results of SPRE testing at NASA
p 56 A91-38140
- SLABE, MELISSA E.**
Resistivity of pristine and intercalated graphite fiber epoxy composites
p 115 A91-35949
- Effect of lightning strike on bromine intercalated graphite fiber/epoxy composites
[NASA-TM-104507] p 103 A91-32177
- SLATER, HOWARD**
Applied high-speed imaging for the icing research program at NASA Lewis Research Center
[NASA-TM-104415] p 177 A91-26490
- SLEMP, WAYNE S.**
Evaluation of thermal control coatings for use on solar dynamic radiators in low earth orbit
[AIAA PAPER 91-1327] p 58 A91-43397
Evaluation of thermal control coatings for use on solar dynamic radiators in low Earth orbit
[NASA-TM-104335] p 73 A91-22367
- SLINEY, HAROLD E.**
Tribological properties of PM212 - A high temperature, self-lubricating, powder metallurgy composite
[STLE PREPRINT 90-AM-4E-1] p 87 A91-19720
A new test machine for measuring friction and wear in controlled atmospheres to 1200 C
p 180 A91-33600
Composite bearing and seal materials for advanced heat engine applications to 900 C
[NASA-TM-103612] p 95 A91-15318
Mechanical strength and thermophysical properties of PM212: A high temperature self-lubricating powder metallurgy composite
[NASA-TM-103694] p 120 A91-21302
Solid lubricants
[NASA-TM-102803] p 99 A91-22396
The PM-200 lubrication system
p 121 A91-23044
Quality control of the tribological coating PS212
[NASA-TM-102067] p 101 A91-25186
Method of making carbide/fluoride/silver composites
[NASA-CASE-LEW-14902-1] p 102 A91-27244
PM200/PS200: Self-lubricating bearing and seal materials for applications to 900 C
[NASA-TM-103776] p 190 A91-30539
- SLUTZ, RODGER J.**
A 10,000-hr life test of an engineering model resistojet
[NASA-TM-103216] p 69 A91-11802
- SMIALEK, J. L.**
Oxidation behavior of cubic phases formed by alloying Al₃Ti with Cr and Mn
p 108 A91-27849
Evidence from transmission electron microscopy for an oxynitride layer in oxidized Si₃N₄
p 118 A91-57058
- SMIALEK, JAMES L.**
Sulfur at nickel-alumina interfaces - Molecular orbital theory
p 104 A91-12925
Effect of sulfur removal on Al₂O₃ scale adhesion
p 108 A91-27940
Hot corrosion of silicon carbide and silicon nitride at 1000 C
p 117 A91-55698
Oxidation resistant coatings for titanium alloys and titanium alloy matrix composites
[NASA-CASE-LEW-15155-1] p 122 A91-26375
Low cost, formable, high T(sub c) superconducting wire
[NASA-CASE-LEW-14676-1] p 147 A91-31529
- SMITH, BRYAN K.**
Rapid thermal cycling of new technology solar array blanket coupons
p 54 A91-38019
Rapid thermal cycling of solar array blanket coupons for Space Station Freedom
p 84 A91-30239
- SMITH, C. E.**
A CFD study of jet mixing in reduced flow areas for lower combustor emissions
[AIAA PAPER 91-2460] p 23 A91-41788
A CFD study of jet mixing in reduced flow areas for lower combustor emissions
[NASA-TM-104411] p 32 A91-23185
CFD analysis of jet mixing in low NO_x flame tube combustors
[NASA-TM-104466] p 33 A91-26146
- SMITH, C. FREDERIC**
Flow studies in close-coupled ventral nozzles for STOV aircraft
[SAE PAPER 901033] p 2 A91-21242
High alpha inlets
p 28 A91-20091
- SMITH, IRA C.**
Tuning maps for setpoint changes and load disturbance upsets in a three capacity process under multivariable control
[NASA-TM-104419] p 220 A91-31876
- SMITH, J. M.**
SP-100 nuclear space power systems with application to space commercialization
p 57 A91-38933
- SMITH, JOHN M.**
Trade studies for nuclear space power systems
[AIAA PAPER 91-3518] p 65 A91-52413
- SMITH, JOHN R.**
Global expression for representing diatomic potential-energy curves
p 228 A91-33236
Adhesion at metal interfaces
p 88 A91-38581
Universal behavior in ideal slip
p 110 A91-48517
Universal energy relations and metal/ceramic interfaces
p 93 A91-56254

- SMITH, TODD E.**
Localization of aeroelastic modes in mistuned high-energy turbines [AIAA PAPER 91-3379] p 198 A91-44319
Localization of aeroelastic modes in mistuned high-energy turbines [NASA-TM-104445] p 204 A91-24659
- SMITHRICK, JOHN J.**
Effect of KOH concentration on LEO cycle life of IPV nickel-hydrogen flight battery cells p 55 A91-38076
Effect of LEO cycling on 125 Ah advanced design IPV nickel-hydrogen battery cells p 55 A91-38077
Effect of LEO cycling on 125 Ah advanced design IPV nickel-hydrogen flight cells. An update [NASA-TM-104384] p 74 A91-22375
Effect of KOH concentration on LEO cycle life of IPV nickel-hydrogen flight cells. An update [NASA-TM-104383] p 74 A91-22376
Destructive physical analysis results of Ni/H₂ cells cycled in LEO regime [NASA-TM-104382] p 74 A91-23233
- SNYDER, AARON**
Dynamics of local grid manipulations for internal flow problems p 164 A91-21090
- SNYDER, CHRISTOPHER A.**
The design and performance estimates for the propulsion module for the booster of a TSTO vehicle [AIAA PAPER 91-3136] p 43 A91-54054
The Navy/NASA Engine Program (NNEP89): A user's manual [NASA-TM-105186] p 35 A91-30141
- SNYDER, D.**
Significant reduction in arc frequency biased solar cells: Observations, diagnostics, and mitigation technique(s) p 83 A91-30235
- SNYDER, DAVID B.**
Findings of the Joint Workshop on Evaluation of Impacts of Space Station Freedom Ground Configurations p 48 A91-20728
Findings of the Joint Workshop on Evaluation of Impacts of Space Station Freedom Ground Configurations [NASA-TM-103717] p 73 A91-22370
- SNYDER, P. G.**
Dielectric function of InGaAs in the visible p 233 A91-53236
Ellipsometric study of InGaAs MODFET material [NASA-TM-103286] p 143 A91-19351
Study of InGaAs based MODFET structures using variable angle spectroscopic ellipsometry [NASA-TM-103792] p 235 A91-19935
- SNYDER, PAUL G.**
Diamondlike carbon applications in infrared optics and microelectronics p 230 A91-18306
- SOBAJIC, DEJAN J.**
Automating security monitoring and analysis for Space Station Freedom's electric power system p 219 A91-37975
- SOCIE, D. F.**
Inhomogeneous deformation in INCONEL 718 during monotonic and cyclic loadings p 108 A91-22287
- SOEDER, JAMES F.**
The development of test beds to support the definition and evolution of the Space Station Freedom power system [NASA-TM-104504] p 79 A91-27207
- SOEDER, RONALD H.**
Automatic control study of the icing research tunnel refrigeration system [NASA-TM-4257] p 40 A91-19115
- SOHN, K. H.**
Experimental study of boundary layer transition on a heated flat plate [NASA-TM-103779] p 14 A91-21061
- SOHN, PHILIP Y.**
A technology assessment of alternative communications systems for the space exploration initiative [AIAA PAPER 90-3681] p 44 A91-11472
Advanced Communications Technology Satellite (ACTS) [IAF PAPER 90-481] p 44 A91-14056
Characteristics of a future aeronautical satellite communications system [NASA-TM-104389] p 20 A91-23102
- SOMPRAKIT, PAISAN**
Contact stresses in gear teeth - A new method of analysis [AIAA PAPER 91-2022] p 182 A91-41683
Contact stresses in gear teeth: A new method of analysis [NASA-TM-104397] p 186 A91-22570
- SONI, N. J.**
Quaternary pulse position modulation electronics for free-space laser communications [AIAA PAPER 91-3471] p 133 A91-53702
- Quaternary pulse position modulation electronics for free-space laser communications [NASA-TM-104502] p 135 A91-29405
- SONNAD, VIJAY**
Least-squares solution of incompressible Navier-Stokes equations with the p-version of finite elements [NASA-TM-105203] p 223 A91-31911
- SORIN, G.**
Evaluation of panel code predictions with experimental results of inlet performance for a 17-inch ducted prop/fab simulator operating at Mach 0.2 [NASA-TM-104428] p 17 A91-25106
- SOTOMAYOR, J. L.**
Compensation for effects of ambient temperature on rare-earth doped fiber optic thermometer p 170 A91-19582
- SOTOMAYOR, JORGE**
Digital angular position sensor using wavelength division multiplexing p 21 A91-19580
- SOTOS, R. G.**
Heat transfer to a thin solid combustible in flame spreading at microgravity p 106 A91-51449
- SOTOS, RAYMOND G.**
Radiation from gas-jet diffusion flames in microgravity environments [AIAA PAPER 91-0719] p 104 A91-19432
- SOVEY, J. S.**
Dual ion beam processed diamondlike films for industrial applications p 121 A91-23042
- SOVEY, JAMES S.**
Performance and lifetime assessment of magnetoplasmadynamic arc thruster technology p 51 A91-30013
Ion beam sputtering in electric propulsion facilities [AIAA PAPER 91-2117] p 61 A91-45785
Test facilities for high power electric propulsion [AIAA PAPER 91-3499] p 42 A91-52396
Flexible fluoropolymer filled protective coatings p 121 A91-24062
Ion beam sputtering in electric propulsion facilities [NASA-TM-105145] p 86 A91-32158
- SOVIE, AMY L.**
Vibrational testing of optical fiber connector joints p 172 A91-30652
Fiber-optic applications for space-based rocket engines [AIAA PAPER 91-3602] p 49 A91-52468
Vibrational testing of optical fiber connector joints [NASA-TM-103654] p 230 A91-14829
Fiber-optic applications for space-based engines [NASA-TM-105235] p 86 A91-32163
- SOVIE, R. J.**
Nuclear power systems for lunar and Mars exploration [IAF PAPER 90-200] p 51 A91-13868
Historical perspectives - The role of the NASA Lewis Research Center in the national space nuclear power programs [AIAA PAPER 91-3462] p 242 A91-53713
Historical perspectives: The role of the NASA Lewis Research Center in the national space nuclear power programs [NASA-TM-105196] p 243 A91-29138
- SOVIE, RONALD J.**
NASA's future space power needs and requirements p 52 A91-37929
Nuclear technology and the space exploration missions p 53 A91-37939
- SPALVINS, T.**
Lubrication with sputtered MoS₂ films: Principles, operation, limitations [NASA-TM-105292] p 112 A91-32216
- SPALVINS, TALIVALDIS**
Plasma-assisted physical vapor deposition surface treatments for tribological control [NASA-TM-103652] p 130 A91-11945
- SPENCE, RODNEY L.**
A technology assessment of alternative communications systems for the space exploration initiative [AIAA PAPER 90-3681] p 44 A91-11472
A comparison of optical technologies for a high data rate Mars link [AIAA PAPER 91-3469] p 45 A91-52377
Millimeter wavelength communications applications for the SEI [AIAA PAPER 91-3589] p 45 A91-52458
Millimeter wavelength communications applications for the SEI [NASA-TM-105275] p 135 A91-32287
- SPERA, DAVID A.**
Structural properties of laminated Douglas fir/epoxy composite material [NASA-RP-1236] p 94 A91-10127
- SPISZ, ERNIE**
LBR-2 Earth stations for the ACTS program p 133 A91-11971
- SPITZER, M. B.**
23.5 percent thin-film space concentrator cells p 58 A91-42002
- SPRAGUE, R.**
Concurrent engineering p 80 A91-28247
- SRINIVASAN, V.**
Materials degradation in low earth orbit (LEO); Proceedings of the Symposium, 119th Annual Meeting of the Minerals, Metals, and Materials Society, Anaheim, CA, Feb. 17-22, 1990 p 116 A91-49801
- SRIVASTAVA, R.**
Application of an efficient hybrid scheme for aeroelastic analysis of advanced propellers p 7 A91-52315
- STABE, ROY G.**
Performance of a high-work, low-aspect-ratio turbine stator tested with a realistic inlet radial temperature gradient [NASA-TM-103738] p 31 A91-20126
- STAN, M. A.**
Electrical transport measurements on polycrystalline superconducting Y-Ba-Cu-O films p 231 A91-19820
Electromigration failure in YBa₂Cu₃O_{7-x} thin films p 231 A91-26989
Temperature dependence of the anisotropy in magnetic relaxation in YBa₂Cu₃O_{7-x} thin films p 232 A91-36047
Ellipsometric study of YBa₂Cu₃O_{7-x} laser ablated and co-evaporated films p 233 A91-53235
- STANG, D. B.**
Ultrasonic imaging of textured alumina p 191 A91-18596
- STANG, DAVID B.**
General-purpose interface bus for multiuser, multitasking computer system p 215 A91-35928
- STANKIEWICZ, NORBERT**
An experimental apparatus for measuring surface resistance in the submillimeter-wavelength region p 174 A91-54390
- STANLEY, MARLAND**
Nuclear Thermal Propulsion technology - Summary of FY 1991 Interagency panel planning [AIAA PAPER 91-3631] p 66 A91-52495
- STEFFEN, CHRIS J., JR.**
High-Order Polynomial Expansions (HOPE) for flux-vector splitting [NASA-TM-104452] p 222 A91-25739
- STEFFEN, CHRISTOPHER J., JR.**
Development of a new flux splitting scheme p 153 A91-40793
A new flux splitting scheme [NASA-TM-104404] p 222 A91-22814
- STEFKO, GEORGE L.**
Cascade flutter analysis with transient response aerodynamics [AIAA PAPER 91-0747] p 21 A91-19448
Cascade flutter analysis with transient response aerodynamics [NASA-TM-103746] p 201 A91-19475
- STEIGMAN, GARY**
Primordial nucleosynthesis redux p 240 A91-45907
- STEINETZ, BRUCE**
Thermal and structural assessments of a ceramic wafer seal in hypersonic engine [AIAA PAPER 91-2494] p 23 A91-41799
- STEINETZ, BRUCE M.**
Development of braided rope seals for hypersonic engine applications. II - Flow modeling [AIAA PAPER 91-2495] p 182 A91-41800
Thermal and structural assessments of a ceramic wafer seal in hypersonic engines [NASA-TM-103651] p 26 A91-13456
High temperature NASP engine seal development [NASA-TM-103716] p 184 A91-19441
A test fixture for measuring high-temperature hypersonic-engine seal performance [NASA-TM-103658] p 184 A91-19442
Propulsion aeroelasticity, vibration control, and dynamic system modeling p 29 A91-20105
High temperature performance evaluation of a hypersonic engine ceramic wafer seal [NASA-TM-103737] p 185 A91-22567
Development of braided rope seals for hypersonic engine applications. Part 2: Flow modeling [NASA-TM-104371] p 186 A91-22571
Evaluation and ranking of candidate ceramic wafer engine seal materials [NASA-TM-103795] p 187 A91-23515
High-temperature, flexible, thermal barrier seal [NASA-CASE-LEW-14672.1] p 189 A91-27560
High temperature NASP engine seals: A technology review [NASA-TM-104468] p 190 A91-30538
- STEINHARDT, PAUL J.**
Coherent peculiar velocities and periodic redshifts p 239 A91-20430

STEINTHORSSON, E.

- Flux-vector splitting algorithm for chain-rule conservation-law form p 221 A91-45109
- Computations of the three-dimensional flow and heat transfer within a coolant passage of a radial turbine blade
[AIAA PAPER 91-2238] p 156 A91-45797
- Algebraic grid generation for coolant passages of turbine blades with serpentine channels and pin fins
[AIAA PAPER 91-2366] p 156 A91-45811
- GRID3D-v2: An updated version of the GRID2D/3D computer program for generating grid systems in complex-shaped three-dimensional spatial domains
[NASA-TM-103766] p 217 N91-25630

STELLA, PAUL M.

- Photovoltaic options for solar electric propulsion
[NASA-TM-103284] p 68 N91-11061

STERN, ALAN

- Characteristics of a future aeronautical satellite communications system
[NASA-TM-104389] p 20 N91-23102

STEVENS, G. H.

- Performance evaluation of land mobile satellite system under vegetative shadowing using differential multiple TCM and QPSK p 132 A91-53084
- Study on the spectral efficiency of SFH-GMSK in land mobile telephone communication by direct simulation p 132 A91-53176

STEVENS, N. JOHN

- The environment power system analysis tool development program p 231 N91-17734

STEVENS, NICHOLAS

- Ion beam textured and coated surfaces experiment (IBEX) p 122 N91-25040

STEVENSON, S. M.

- Cryogenic propellant management architectures to support the Space Exploration Initiative
[AIAA PAPER 90-3713] p 124 A91-10112
- Cryogenic propellant management system requirements for Space Station Freedom
[AIAA PAPER 91-3476] p 65 A91-52382
- Fuel Systems Architecture (FSA) evaluation criteria and concept evaluation methodology
[AIAA PAPER 91-3479] p 65 A91-52384

STOCHL, ROBERT J.

- A review of candidate multilayer insulation systems for potential use on wet-launched LH2 tankage for the Space Exploration Initiative lunar missions
[AIAA PAPER 91-2176] p 43 A91-45793
- Thermal performance of a liquid hydrogen tank multilayer insulation system at warm boundary temperatures of 630, 530, and 152 R
[AIAA PAPER 91-2400] p 43 A91-45812
- Thermal performance of a liquid hydrogen tank multilayer insulation system at warm boundary temperatures of 630, 530, and 152 R
[NASA-TM-104476] p 43 N91-25159

- Pressurization and expulsion of cryogenic liquids: Generic requirements for a low gravity experiment
[NASA-TM-104417] p 126 N91-25300
- Autogenous pressurization of cryogenic vessels using submerged vapor injection
[NASA-TM-104516] p 127 N91-27375

STOCKER, DENNIS P.

- Radiation from gas-jet diffusion flames in microgravity environments
[AIAA PAPER 91-0719] p 104 A91-19432

STOLTZFUS, JOEL M.

- Surface modification of Monel K-500 as a means of reducing friction and wear in high-pressure oxygen
p 107 A91-16869

STONE, JAMES R.

- Plans for the development of cryogenic engines for space exploration
[AIAA PAPER 91-3438] p 64 A91-52351

STOVER, J. B.

- Quaternary pulse position modulation electronics for free-space laser communications
[AIAA PAPER 91-3471] p 133 A91-53702
- Quaternary pulse position modulation electronics for free-space laser communications
[NASA-TM-104502] p 135 N91-29405

STOYACK, JOSEPH E.

- Evaluation of thermal control coatings for use on solar dynamic radiators in low earth orbit
[AIAA PAPER 91-1327] p 58 A91-43397
- Evaluation of thermal control coatings for use on solar dynamic radiators in low Earth orbit
[NASA-TM-104335] p 73 N91-22367

STRACK, WILLIAM C.

- Overview of the NASA-sponsored HSCT propulsion system studies
[AIAA PAPER 91-3329] p 20 A91-53871

STRAZISAR, ANTHONY J.

- Enhancing aeropropulsion research with high-speed interactive computing p 217 A91-56129

- Turbomachinery p 162 N91-20097
- Enhancing aeropropulsion research with high-speed interactive computing
[NASA-TM-104374] p 218 N91-24796

STROCK, THOMAS W.

- Hot gas ingestion test results of a two-poster vectored thrust concept with flow visualization in the NASA Lewis 9- x 15-foot low speed wind tunnel
[NASA-TM-103258] p 15 N91-21116

STUBBS, ROBERT M.

- Computational fluid dynamics studies of nuclear rocket performance
[AIAA PAPER 91-3577] p 66 A91-52450
- Computational fluid dynamics at the Lewis Research Center: An overview p 8 N91-10842

SUBRAMANIAM, SHANKAR

- Acoustic radiation from lifting airfoils in compressible subsonic flow
[AIAA PAPER 90-3911] p 224 A91-12427
- Acoustic radiation from lifting airfoils in compressible subsonic flow
[NASA-TM-103650] p 13 N91-19053

SUBRAMANIAN, R. SHANKAR

- The migration of a compound drop due to thermocapillarity p 148 A91-18428

SUES, ROBERT H.

- Programming probabilistic structural analysis for parallel processing computer
[AIAA PAPER 91-0920] p 196 A91-31957

SUICH, RONALD C.

- k-out-of-n-G systems - Some cost considerations p 192 A91-54553

- How much redundancy: Some cost considerations, including examples for spacecraft systems
[NASA-TM-103197] p 192 N91-17407

- Balancing reliability and cost to choose the best power subsystem
[NASA-TM-104453] p 238 N91-24952
- Reliability and cost: A sensitivity analysis
[NASA-TM-105293] p 238 N91-33014

SUN, D. C.

- A high speed photography study of cavitation in a dynamically loaded journal bearing
[ASME PAPER 90-TRIB-19] p 180 A91-34806
- Two reference time scales for studying the dynamic cavitation of liquid films
[NASA-TM-103673] p 160 N91-19369

SUN, H.

- Jet-A fuel evaporation analysis in conical tube injectors
[AIAA PAPER 91-0345] p 149 A91-21467

SUNDARAM, V. S.

- Lightweight concentrator module with 30 percent AMO efficient GaAs/GaSb tandem cells p 57 A91-41990
- Tandem concentrator solar cells with 30 percent (AMO) power conversion efficiency p 208 N91-19189

SUNDBERG, GALE R.

- Advanced launch system (ALS) - Electrical actuation and power systems improve operability and cost picture p 51 A91-31025
- Civil air transport - A fresh look at power-by-wire and fly-by-light p 36 A91-31030
- Civil air transport: A fresh look at power-by-wire and fly-by-light p 37 N91-23053

SURESH, AMBADI

- Osher's scheme for real gases p 153 A91-42286

SUTJAHJO, EDHI

- Computational simulation of acoustic fatigue for hot composite structures
[NASA-TM-104379] p 203 N91-23548

SUTO, YASUSHI

- Baryon isocurvature scenario in inflationary cosmology - A particle physics model and its astrophysical implications p 240 A91-54201

SUTTER, JAMES K.

- Long term isothermal aging and thermal analysis of N-CYCAP polyimides
[NASA-TM-104341] p 122 N91-25286

SUZUKI, N.

- Cathode phenomena in a low-power magnetoplasma dynamic thruster p 63 A91-52314

SVEHLA, ROGER A.

- In-flight and simulated aircraft fuel temperature measurements
[NASA-TM-103611] p 125 N91-15418

SWAFFORD, TIMOTHY W.

- Flutter analysis of cascades using a two dimensional Euler solver
[AIAA PAPER 91-1681] p 6 A91-45548
- Euler flow predictions for an oscillating cascade using a high resolution wave-split scheme
[NASA-TM-104377] p 16 N91-24107

SWARTZ, C. K.

- New directions in InP solar cell research p 206 A91-38022

- Effects of radiation of InP cells epitaxially grown on Si and GaAs substrates p 140 A91-41984

- The mini-dome Fresnel lens photovoltaic concentrator array - Current status of component and prototype panel testing p 57 A91-41989

- Solar electric propulsion for Mars transport vehicles
[NASA-TM-103234] p 71 N91-19178

- Effects of proton irradiation on the performance of InP/GaAs solar cells p 209 N91-19205
- Recent progress in InP solar cell research
[NASA-TM-104509] p 146 N91-27447

- Effect of dislocations on properties of heteroepitaxial InP solar cells p 213 N91-30209

SWARTZ, CLIFFORD K.

- Component and prototype panel testing of the mini-dome Fresnel lens photovoltaic concentrator array p 54 A91-38023

- Heteroepitaxial InP solar cells on Si and GaAs substrates
[NASA-TM-103696] p 144 N91-20392

SWEC, DIANE M.

- Update on results of SPRE testing at NASA p 56 A91-38140

- Update on results of SPRE testing at NASA Lewis
[NASA-TM-104425] p 79 N91-27208

SWINDEMAN, ROBERT W.

- Current activities in standardization of high-temperature, low-cycle-fatigue testing techniques in the United States
[NASA-TM-103675] p 200 N91-17427

SZATMARY, STEVEN A.

- Calculation of Weibull strength parameters, Batdorf flaw density constants and related statistical quantities using PC-CARES
[NASA-TM-103247] p 199 N91-10332

SZUCH, JOHN R.

- Enhancing aeropropulsion research with high-speed interactive computing p 217 A91-56129
- Enhancing aeropropulsion research with high-speed interactive computing
[NASA-TM-104374] p 218 N91-24796

T**TABATA, WILLIAM K.**

- The Advanced Expander Test Bed
[AIAA PAPER 90-3708] p 50 A91-10107
- Design of an Advanced Expander Test Bed
[AIAA PAPER 91-3437] p 42 A91-52350
- Advanced cryo propulsion systems p 80 N91-28212

TABATABAI, ALI

- A neural net based architecture for the segmentation of mixed gray-level and binary pictures p 218 A91-29183

TABIB AZAR, MASSOOD

- Silicon-etalon fiber-optic temperature sensor p 170 A91-19581

TABIB-AZAR, MASSOOD

- Comparative study of bolometric and non-bolometric switching elements for microwave phase shifters
[NASA-TM-104435] p 145 N91-25320

TACINA, R.

- Jet-A fuel evaporation analysis in conical tube injectors
[AIAA PAPER 91-0345] p 149 A91-21467

TACINA, ROBERT R.

- Combustor technology for future aircraft
[NASA-TM-103268] p 26 N91-14349

TAGHAVI, R.

- Modern developments in shear flow control with swirl p 3 A91-24519

TALPALLIKAR, M. V.

- A CFD study of jet mixing in reduced flow areas for lower combustor emissions
[AIAA PAPER 91-2460] p 23 A91-41788

- A CFD study of jet mixing in reduced flow areas for lower combustor emissions
[NASA-TM-104411] p 32 N91-23185

- CFD analysis of jet mixing in low NOx flametube combustors
[NASA-TM-104466] p 33 N91-26146

TALTY, T.

- Circular polarisation characteristics of stacked microstrip antennas p 131 A91-20370
- Mutual coupling between electromagnetically coupled rectangular patch antennas p 137 A91-32822

TAM, KWA-SUR

- Modeling of Space Station electric power system with EMTF p 55 A91-38040
- An EMTF system level model of the PMAD DC test bed
[NASA-TM-104515] p 79 N91-27206

TAMMARU, IVO

- A high-efficiency ferruleless coupled-cavity traveling-wave tube with phase-adjusted taper p 136 A91-25078

- TANG, D.**
A fiber-optic current sensor for aerospace applications p 171 A91-23005
A fiber-optic current sensor for aerospace applications p 172 A91-38006
Fiber-optic sensors for aerospace electrical measurements: An update [NASA-TM-104454] p 177 N91-25381
- TANGIRALA, V.**
Particle nonuniformity effects on particle cloud flames in low gravity [AIAA PAPER 91-0718] p 104 A91-19431
Particle cloud flames in acoustic fields p 105 A91-20589
Radiative structures of lycopodium-air flames in low gravity p 105 A91-30003
- TAO, XIAOMING**
Development of braided rope seals for hypersonic engine applications. II - Flow modeling [AIAA PAPER 91-2495] p 182 A91-41800
Development of braided rope seals for hypersonic engine applications. Part 2: Flow modeling [NASA-TM-104371] p 186 N91-22571
- TAYLOR, W. J.**
Improved thermodynamic modelling of the no-vent fill process and correlation with experimental data [AIAA PAPER 91-1379] p 129 A91-43444
- TELESMA, J.**
Fatigue crack growth study of SCS6/Ti-15-3 composite p 91 A91-25798
- TELESMA, JACK**
Modeling of crack bridging in a unidirectional metal matrix composite [NASA-TM-104355] p 205 N91-24660
- TEREPKA, F. M.**
Silsesquioxane-derived ceramic fibres p 114 A91-30283
- TERRY, JOHN D.**
Using a modified Hewlett Packard 8410 network analyzer as an automated farfield antenna range receiver [NASA-TM-103700] p 143 N91-19349
- TEST, MARK G.**
High temperature NASP engine seal development [NASA-TM-103716] p 184 N91-19441
- TEVAARWERK, J. L.**
The measurement, modelling and prediction of traction forces in a rocket propellant p 125 A91-51914
- TEW, R. C.**
Multidimensional computer simulation of Stirling cycle engines p 181 A91-38154
- TEW, ROY C.**
Recent Stirling engine loss-understanding results p 181 A91-38151
Further two-dimensional code development for Stirling space engine components p 56 A91-38184
- THANEDAR, P. B.**
Composite laminate tailoring with probabilistic constraints and loads p 198 A91-38754
- THESLING, W.**
A comparative study of $p(+)$ and $n(+)$ p/n solar cells made by a closed ampoule diffusion p 212 N91-30206
- THESLING, WILLIAM**
Key factors limiting the open circuit voltage of $n(+)$ ppp(+) indium phosphide solar cells p 139 A91-41929
Key factors limiting the open circuit voltage of $n(+)$ ppp(+) indium phosphide solar cells p 209 N91-19206
A theoretical comparison of the near-optimum design and predicted performance of n/p and p/n indium phosphide homojunction solar cells p 83 N91-30233
- THIEME, LANNY G.**
Recent Stirling engine loss-understanding results p 181 A91-38151
Component technology for Stirling power converters [NASA-TM-104387] p 74 N91-23234
- THOMAS, R. D.**
Peeled film GaAs solar cell development p 139 A91-41889
- THOMAS, RALPH D.**
A comparative study of performance parameters of $n(+)$ -p InP solar cells made by closed-ampoule sulfur diffusion into Cd- and Zn-doped p-type InP substrates p 210 N91-19209
- THOMPSON, DAVID**
Computational materials science. An example: Numerical modeling of chemical vapor deposition processing of advanced fibers p 99 N91-20111
- TICE, DAVID C.**
A comparison of arrow, trapezoidal and M wing concepts using a Mach 2 supersonic cruise transport mission [AIAA PAPER 91-3102] p 7 A91-54027
- TICHEY, JOHN A.**
Inertia effects in thin film flow with a corrugated boundary p 151 A91-32691
- TIKARE, VEENA**
Temperature-dependent indentation behavior of transformation-toughened zirconia-based ceramics p 114 A91-28767
Influence of the Si₃N₄ microstructure on its R-curve and fatigue behavior p 117 A91-56931
Crack healing in silicon nitride due to oxidation p 118 A91-56982
- TIRMIZI, S. H.**
Isothermal Dendritic Growth Experiment - Science, engineering, and hardware development for USMP space flights p 128 A91-53408
- TITRAN, R. H.**
Development of nuclear fuels and materials for propulsion systems for SEI [AIAA PAPER 91-3452] p 125 A91-52362
- TITRAN, ROBERT H.**
Advanced materials for space nuclear power systems [AIAA PAPER 91-3530] p 88 A91-53704
Thermal stability of the microstructure of an aged Nb-Zr-C alloy [NASA-TM-103647] p 110 N91-14454
Tensile behavior of tungsten/niobium composites at 1300 to 1600 K [NASA-TM-103727] p 111 N91-16128
Advanced materials for space nuclear power systems [NASA-TM-105171] p 112 N91-29298
- TO, WAI-MING**
A new numerical framework for solving conservation laws: The method of space-time conservation element and solution element [NASA-TM-104495] p 223 N91-30867
- TOLLESON, J. B.**
Ka-band MMIC microstrip array for high rate communications [AIAA PAPER 91-3421] p 132 A91-52341
Ka-band MMIC microstrip array for high rate communications [NASA-TM-104500] p 135 N91-27437
- TOLLESON, JOSEPH**
A 29.3-GHz cavity-enclosed aperture-coupled circular-patch antenna for microwave circuit integration p 140 A91-47057
- TONG, MIKE**
Thermal and structural assessments of a ceramic wafer seal in hypersonic engine [AIAA PAPER 91-2494] p 23 A91-41799
High temperature NASP engine seals: A technology review [NASA-TM-104468] p 190 N91-30538
Experimental and analytical analysis of stress-strain behavior in a (90/0 deg)2s, SiC/Ti-15-3 laminate [NASA-TM-104470] p 103 N91-31235
- TONG, MIKE T.**
Thermal and structural assessments of a ceramic wafer seal in hypersonic engines [NASA-TM-103651] p 26 N91-13456
- TOWNSEND, D. P.**
Effects of gear box vibration and mass imbalance on the dynamics of multistage gear transmission p 182 A91-47213
Gear noise, vibration, and diagnostic studies at NASA Lewis Research Center p 183 A91-52811
Modal analysis of multistage gear systems coupled with gearbox vibrations [NASA-TM-103797] p 187 N91-23513
- TOWNSEND, DENNIS P.**
Evaluation of advanced lubricants for aircraft applications using gear surface fatigue tests [AIAA PAPER 91-1907] p 181 A91-41649
Surface fatigue life of M50NiL and AISI 9310 spur gears and rolling-contact bars p 182 A91-45350
Effects of gear box vibration and mass imbalance on the dynamics of multi-stage gear transmissions [NASA-TM-103695] p 185 N91-21534
Comparison of analysis and experiment for dynamics of low-contact-ratio spur gears [NASA-TM-103232] p 185 N91-22566
Evaluation of advanced lubricants for aircraft applications using gear surface fatigue tests [NASA-TM-104336] p 186 N91-22568
Surface fatigue life of M50NiL and AISI 9310 spur gears and R C bars [NASA-TM-104496] p 189 N91-27569
Dynamic measurements of gear tooth friction and load [NASA-TM-103281] p 189 N91-27570
Effect of two synthetic lubricants on life of AISI 9310 spur gears [NASA-TM-104352] p 189 N91-29599
- TREFFNY, CHARLES J.**
Overview of NASP nozzle research p 28 N91-20093
- TRIMARCHI, PAUL A.**
Probe insertion apparatus with inflatable seal [NASA-CASE-LEW-14965-1] p 183 N91-13732
- TROUDET, T.**
Neuromorphic learning of continuous-valued mappings from noise-corrupted data p 219 A91-53201
- TROUDET, TERRY**
Neural network application to aircraft control system design [AIAA PAPER 91-2715] p 36 A91-49676
Towards practical control design using neural computation [NASA-TM-103785] p 219 N91-19766
Neural network application to aircraft control system design [NASA-TM-105151] p 37 N91-27167
- TROUDET, TERRY P.**
Neural network architecture for crossbar switch control p 218 A91-29181
A neural net based architecture for the segmentation of mixed gray-level and binary pictures p 218 A91-29183
- TROWBRIDGE, D. A.**
Low velocity impact analysis with NASTRAN p 198 A91-48865
- TROWBRIDGE, DANIEL A.**
Low velocity impact analysis with NASTRAN [NASA-TM-103169] p 95 N91-14426
- TRUE, B.**
Experimental study of cross-stream mixing in a cylindrical duct [AIAA PAPER 91-2459] p 157 A91-45815
Experimental study of cross-stream mixing in a cylindrical duct [NASA-TM-105180] p 34 N91-29187
- TSUI, P.**
A numerical and experimental analysis of reactor performance and deposition rates for CVD on monofilaments [NASA-TM-103631] p 130 N91-14500
- TSUI, PANG**
Computational materials science. An example: Numerical modeling of chemical vapor deposition processing of advanced fibers p 99 N91-20111
- TU, Y. K.**
Effects of gear box vibration and mass imbalance on the dynamics of multistage gear transmission p 182 A91-47213
Modal analysis of multistage gear systems coupled with gearbox vibrations [NASA-TM-103797] p 187 N91-23513
- TU, YU K.**
Effects of gear box vibration and mass imbalance on the dynamics of multi-stage gear transmissions [NASA-TM-103695] p 185 N91-21534
- TURKEL, ELI**
Mappings and accuracy for Chebyshev pseudo-spectral approximations [NASA-TM-103630] p 221 N91-14781
- TURNER, MICHAEL S.**
Coherent peculiar velocities and periodic redshifts p 239 A91-20430
Inflationary axion cosmology p 239 A91-20491
Telescope search for a 3-eV to 8-eV axion p 239 A91-28714
Astrophysics and cosmology confront the 17-keV neutrino p 240 A91-43291
Constraints from primordial nucleosynthesis on the mass of the tau neutrino p 240 A91-46543
- TWISDALE, LAWRENCE A.**
Programming probabilistic structural analysis for parallel processing computer [AIAA PAPER 91-0920] p 196 A91-31957

U

- UPSCHULTE, B. L.**
Significant reduction in arc frequency biased solar cells: Observations, diagnostics, and mitigation technique(s) p 83 N91-30235

- UZ, MEHMET**
Thermal stability of the microstructure of an aged Nb-Zr-C alloy [NASA-TM-103647] p 110 N91-14454

V

- VALCO, G. J.**
Photoresponse of YBa₂Cu₃O₇(δ) granular and epitaxial superconducting thin films p 141 A91-50443
- VALCO, MARK J.**
Advanced Rotorcraft Transmission (ART) program-Boeing helicopters status report [NASA-TM-104474] p 188 N91-25412

VAN DRESAR, N. T.

A pressure control analysis of cryogenic storage systems
[AIAA PAPER 91-2405] p 59 A91-44228

VAN FOSSEN, G. J.

Increased heat transfer to a cylindrical leading edge due to spanwise variations in the freestream velocity
[AIAA PAPER 91-1739] p 155 A91-43623

VAN LEER, BRAM

Numerical flux formulas for the Euler and Navier-Stokes equations. II - Progress in flux-vector splitting
[AIAA PAPER 91-1566] p 5 A91-40740

VANDERAAR, MARK J.

Performance evaluation of land mobile satellite system under vegetative shadowing using differential multiple TCM and QPSK p 132 A91-53084

Combinatorial FSK modulation for power-efficient high-rate communications
[AIAA PAPER 91-3532] p 133 A91-53708

Combinatorial FSK modulation for power-efficient high-rate communications
[NASA-TM-105188] p 135 N91-29404

VANDRESAR, N. T.

Self-pressurization of a lightweight liquid hydrogen storage tank subjected to low heat flux
[NASA-TM-103804] p 126 N91-20324

A pressure control analysis of cryogenic storage systems
[NASA-TM-104409] p 126 N91-24460

VANDRESAR, NEIL T.

Pressurization and expulsion of cryogenic liquids: Generic requirements for a low gravity experiment
[NASA-TM-104417] p 126 N91-25300

Autogenous pressurization of cryogenic vessels using submerged vapor injection
[NASA-TM-104516] p 127 N91-27375

VANFOSSEN, G. J.

Increased heat transfer to a cylindrical leading edge due to spanwise variations in the freestream velocity
[NASA-TM-104464] p 100 N91-24359

VANLEER, BRAM

Numerical flux formulas for the Euler and Navier-Stokes equations. 2: Progress in flux-vector splitting
[NASA-TM-104353] p 15 N91-22084

VANNUCCI, R. D.

Autoclavable addition polyimides for 371 C composite applications p 115 A91-49112

VANNUCCI, RAYMOND D.

Vinyl capped addition polyimides
[NASA-CASE-LEW-15027-1] p 118 N91-13566

Addition polyimides with enhanced processability
[NASA-CASE-LEW-15043-1] p 123 N91-32230

VANOVERBEKE, T. J.

Performance and flow calculations for a gaseous H₂/O₂ thruster p 63 A91-48843

VANOVERBEKE, THOMAS

On the anomaly of velocity-pressure decoupling in collocated mesh solutions
[NASA-TM-103769] p 164 N91-21448

VANOVERBEKE, THOMAS J.

A numerical study of the hot gas environment around a STOVL aircraft in ground proximity p 10 N91-10887

VARALJAY, N.

Photoreponse of YBa₂Cu₃O₇(δ) granular and epitaxial superconducting thin films p 141 A91-50443

VARGAS, CARLOS

High resolution electrolyte for thinning InP by anodic dissolution and its applications to EC-V profiling, defect revealing and surface passivation p 107 N91-30210

VARY, ALEX

Acousto-ultrasonics - Retrospective exhortation with bibliography p 191 A91-37011
Acousto-ultrasonics p 226 A91-48227
Review of acousto-ultrasonic NDE for composites p 97 N91-18192

Acousto-ultrasonic nondestructive evaluation of materials using laser beam generation and detection p 193 N91-18193

NDE standards for high temperature materials
[NASA-TM-103761] p 193 N91-19464

NDE of ceramics and ceramic composites
[NASA-TM-104520] p 194 N91-29610

VASZARI, JOHN P.

A high-efficiency ferruleless coupled-cavity traveling-wave tube with phase-adjusted taper p 136 A91-25078

VEITCH, L.

A numerical and experimental analysis of reactor performance and deposition rates for CVD on monofilaments
[NASA-TM-103631] p 130 N91-14500

VEITCH, LISA

Computational materials science. An example: Numerical modeling of chemical vapor deposition processing of advanced fibers p 99 N91-20111

VELOSA, A.

Isothermal Dendritic Growth Experiment - Science, engineering, and hardware development for USMP space flights p 128 A91-53408

VENTO, D. M.

The COLD-SAT experiment for cryogenic fluid management technology p 46 A91-29799

The COLD-SAT experiment for cryogenic fluid management technology p 126 N91-24263

VENTRES, C. S.

In-service health monitoring of composite structures p 192 A91-51926

VERHEY, TIMOTHY R.

Microanalyses of extended-test xenon hollow cathodes
[AIAA PAPER 91-2123] p 61 A91-45787

A 5-kW xenon ion thruster lifetest
[NASA-TM-103191] p 72 N91-19180

Microanalysis of extended-test xenon hollow cathodes
[NASA-TM-104532] p 82 N91-30202

VERNYI, MARK

A preliminary characterization of applied-field MPD thruster plumes
[AIAA PAPER 91-2339] p 62 A91-45798

VERRILLI, M. J.

High temperature fatigue behavior of tungsten copper composites p 93 A91-55906

VERRILLI, MICHAEL J.

Current activities in standardization of high-temperature, low-cycle-fatigue testing techniques in the United States
[NASA-TM-103675] p 200 N91-17427

Application of thermal life prediction model to high-temperature aerospace alloys B1900 + Hf and Haynes 188
[NASA-TM-4226] p 201 N91-19473

Thermomechanical and bithermal fatigue behavior of cast B1900 + Hf and wrought Haynes 188
[NASA-TM-4225] p 111 N91-20268

Tensile and fatigue behavior of tungsten/copper composites p 100 N91-24311

High temperature tension-compression fatigue behavior of a tungsten copper composite
[NASA-TM-104370] p 100 N91-24360

VETRONE, ROBERT H.

Test facilities for high power electric propulsion
[AIAA PAPER 91-3499] p 42 A91-52396

VJAYARAGHAVAN, D.

Extension of transonic flow computational concepts in the analysis of cavitated bearings
[ASME PAPER 90-TRIB-40] p 150 A91-29474

Extension of transonic flow computational concepts in the analysis of cavitated bearings
[NASA-TM-103214] p 160 N91-16304

VIRSHUP, G. F.

Temperature coefficients of multijunction solar cells p 172 A91-41921

VISHNIAC, ETHAN T.

The dynamic instability of adiabatic blast waves p 239 A91-26361

VISIC, NIKOLA

Coplanar waveguide EEsoF MICAD macros make circuit layout easy
[NASA-TM-103272] p 134 N91-19332

VITERNA, LARRY A.

ETARA PC version 3.3 user's guide: Reliability, availability, maintainability simulation model
[NASA-TM-103751] p 193 N91-19462

A finite element model of conduction, convection, and phase change near a solid/melt interface
[NASA-TM-103721] p 162 N91-20417

ALPS: A Linear Program Solver

[NASA-TM-104347] p 216 N91-20765

RSM 1.0 user's guide: A resupply scheduler using integer optimization
[NASA-TM-104380] p 217 N91-22766

Calculated performance of the NASA Lewis icing research tunnel
[NASA-TM-105173] p 39 N91-29199

VITTA, S.

Ellipsometric study of YBa₂Cu₃O₇(δ) laser ablated and co-evaporated films p 233 A91-53235

VITTA, SATISH

Electromigration failure in YBa₂Cu₃O₇(δ) thin films p 231 A91-26989

Temperature dependence of the anisotropy in magnetic relaxation in YBa₂Cu₃O₇(δ) thin films p 232 A91-36047

Rapid solidification of polymorphic transition metals induced by nanosecond laser pulses p 109 A91-46520

VRANOS, A.

Experimental study of cross-stream mixing in a cylindrical duct
[AIAA PAPER 91-2459] p 157 A91-45815

Experimental study of cross-stream mixing in a cylindrical duct
[NASA-TM-105180] p 34 N91-29187

W**WACHS, M. R.**

Development of technology needs for the SEI TNIM network
[AIAA PAPER 91-3536] p 45 A91-52427

WACHTER, J. P.

The COLD-SAT experiment for cryogenic fluid management technology p 46 A91-29799

The COLD-SAT experiment for cryogenic fluid management technology p 126 N91-24263

WAGGONER, EDGAR G.

Transonic wind-tunnel wall interference prediction code p 38 A91-26112

WAGNER, J. H.

Heat transfer in rotating serpentine passages with trips normal to the flow
[NASA-TM-103758] p 184 N91-19443

WAGNER, PAUL K.

Combinatorial FSK modulation for power-efficient high-rate communications
[AIAA PAPER 91-3532] p 133 A91-53708

Combinatorial FSK modulation for power-efficient high-rate communications
[NASA-TM-105188] p 135 N91-29404

WAGNER, TIMOTHY

Fiber creep evaluation by stress relaxation measurements p 117 A91-56905

WALKER, K. P.

On the thermodynamics of stress rate in the evolution of back stress in viscoplasticity
[NASA-TM-103794] p 201 N91-19476

Asymptotic integration algorithms for nonhomogeneous, nonlinear, first order, ordinary differential equations
[NASA-TM-103793] p 222 N91-21797

WALKER, KEVIN P.

Equivalence of Green's function and the Fourier series representation of composites with periodic microstructure p 91 A91-16869

A new uniformly valid asymptotic integration algorithm for elasto-plastic creep and unified viscoplastic theories including continuum damage p 110 A91-48725

An overview of self-consistent methods for fiber-reinforced composites p 97 N91-19232

From differential to difference equations for first order ODEs
[NASA-TM-104530] p 222 N91-27886

Exponential integration algorithms applied to viscoplasticity
[NASA-TM-104461] p 223 N91-27901

WALKER, TERRY P.

Primordial nucleosynthesis redux p 240 A91-45907

WALTERS, JERRY L.

Autonomous power expert system advanced development p 72 N91-20689

An autonomous fault detection, isolation, and recovery system for a 20-kHz electric power distribution test bed
[NASA-TM-104344] p 217 N91-25680

WALTERS, STEPHEN M.

Neural network architecture for crossbar switch control p 218 A91-29181

WALTON, JAMES T.

An overview of tested and analyzed NTP concepts
[AIAA PAPER 91-3503] p 65 A91-52400

WANG, C. R.

Heat transfer, velocity-temperature correlation, and turbulent shear stress from Navier-Stokes computations of shock wave/turbulent boundary layer interaction flows p 163 N91-21085

WANHAINEN, JOYCE S.

A new fabrication method for precision antenna reflectors for space flight and ground test
[NASA-TP-3078] p 48 N91-21185

WARNER, J. D.

Electromigration failure in YBa₂Cu₃O₇(δ) thin films p 231 A91-26989

High temperature superconductive microwave technology for space applications p 137 A91-31391

Determination of surface resistance and magnetic penetration depth of superconducting YBa₂Cu₃O₇(δ) thin films by microwave power transmission measurements p 138 A91-36060

An experimental study of high T_c superconducting microstrip transmission lines at 35 GHz and the effect of film morphology p 138 A91-36172

High temperature superconducting thin film microwave circuits - Fabrication, characterization, and applications p 141 A91-50433

Photoreponse of YBa₂Cu₃O₇(δ) granular and epitaxial superconducting thin films p 141 A91-50443

- Ellipsometric study of YBa₂Cu₃O(7-x) laser ablated and co-evaporated films p 233 A91-53235
YBCO superconducting ring resonators at millimeter-wave frequencies p 142 A91-54532
Determination of surface resistance and magnetic penetration depth of superconducting YBa₂Cu₃O(7-delta) thin films by microwave power transmission measurements p 234 N91-10780
[NASA-TM-103616]
An experimental study of high T_c superconducting microstrip transmission lines at 35 GHz and the effect of film morphology p 133 N91-11988
[NASA-TM-103633]
WARNER, JOSEPH D.
Superconducting microwave electronics at Lewis Research Center p 236 N91-24081
WARSHAWSKY, I.
Lag compensation of optical fibers or thermocouples to achieve waveform fidelity in dynamic gas pyrometry p 174 A91-54388
WARS, S.
Large-scale advanced propeller blade pressure distributions - Prediction and data p 5 A91-42820
WASSERBAUER, C. A.
NASA low-speed centrifugal compressor for 3-D viscous code assessment and fundamental flow physics research p 13 N91-20044
[NASA-TM-103710]
The NASA Lewis Research Center Internal Fluid Mechanics Facility p 39 N91-30163
[NASA-TM-105187]
WATERS, J.
Autoclavable addition polyimides for 371 C composite applications p 115 A91-49112
WATERS, JOHN F.
Long term isothermal aging and thermal analysis of N-CYCAP polyimides p 122 N91-25286
[NASA-TM-104341]
WAZYNIAK, J. A.
Flow visualization studies of the internal flow characteristics in a simulated mixed flow vectored thrust ASTOVL engine configuration p 23 A91-42556
[AIAA PAPER 91-1689]
WEBB, BRENT J.
Construction and testing of ceramic fabric heat pipe with water working fluid p 229 N91-18799
[NASA-TM-103332]
WEHRLE, DAVID
A preliminary characterization of applied-field MPD thruster plumes p 62 A91-45798
[AIAA PAPER 91-2339]
WEINBERG, I.
New directions in InP solar cell research p 206 A91-38022
Effects of radiation of InP cells epitaxially grown on Si and GaAs substrates p 140 A91-41984
A comparative study of p(+)n and n(+)p InP solar cells made by a closed ampoule diffusion p 212 N91-30206
Effect of dislocations on properties of heteroepitaxial InP solar cells p 213 N91-30209
Comparative modeling of InP solar cell structures p 83 N91-30232
WEINBERG, IRVING
Study of surface passivation as a function of InP closed-ampoule solar cell fabrication processing variables p 232 A91-41893
Key factors limiting the open circuit voltage of n(+)jpp(+) indium phosphide solar cells p 139 A91-41929
Recent results from the InP homojunction cell module on the LIPS III spacecraft p 140 A91-41971
Effects of proton irradiation on the performance of InP/GaAs solar cells p 209 N91-19205
Key factors limiting the open circuit voltage of n(+)jpp(+) indium phosphide solar cells p 209 N91-19206
Determination of series resistance of indium phosphide solar cells p 210 N91-19207
Investigation of anodic and chemical oxides grown on p-type InP with applications to surface passivation for n(+)p solar cell fabrication p 210 N91-19208
Indium phosphide solar cells p 210 N91-19221
Heteroepitaxial InP solar cells on Si and GaAs substrates p 144 N91-20392
[NASA-TM-103696]
Recent progress in InP solar cell research p 146 N91-27447
[NASA-TM-104509]
Thin solar cell and lightweight array p 212 N91-27614
[NASA-CASE-LEW-14959-1]
High resolution electrolyte for thinning InP by anodic dissolution and its applications to EC-V profiling, defect revealing and surface passivation p 107 N91-30210
A theoretical comparison of the near-optimum design and predicted performance of n/p and p/n indium phosphide homojunction solar cells p 83 N91-30233
Advanced power systems for EOS p 85 N91-31217
[NASA-TM-105222]
WEIR, LOIS J.
A comparison of CFD predictions and experimental results for a Mach 5 inlet p 28 N91-20094
WEISLOGEL, MARK
Drop-tower experiments for capillary surfaces in an exotic container p 148 A91-19138
[AIAA PAPER 91-0107]
WEISLOGEL, MARL M.
Surface settling in partially filled containers upon step reduction in gravity p 159 N91-14556
[NASA-TM-103641]
WEIZER, VICTOR G.
An analysis of the contact sintering process in III-V solar cells p 139 A91-41891
The influence of interstitial Ga and interfacial Au₂P₃ on the electrical and metallurgical behavior of Au-contacted III-V semiconductors p 140 A91-42694
An x ray photoelectron spectroscopy study of Au(x)In(y) alloys p 234 N91-14050
[NASA-TM-103659]
Semiconductor structural damage attendant to contact formation in III-V solar cells p 209 N91-19203
Improvements in contact resistivity and thermal stability of Au-contacted InP solar cells p 213 N91-30207
WENDL, M. C.
Computational modeling of the pressurization process in a NASP vehicle propellant tank experimental simulation p 124 A91-41771
[AIAA PAPER 91-2407]
WENGER, NORMAN C.
Instrumentation and controls overview p 38 N91-20099
WERNET, MARK P.
Two-dimensional particle displacement tracking in particle imaging velocimetry p 172 A91-38498
Particle displacement tracking for PIV p 175 N91-10271
[NASA-TM-103288]
Software manual for operating particle displacement tracking data acquisition and reduction system p 176 N91-20453
[NASA-TM-103720]
Particle image velocimetry for the surface tension driven convection experiment using a particle displacement tracking technique p 177 N91-25382
[NASA-TM-104482]
Particle displacement tracking applied to air flows p 177 N91-25387
[NASA-TM-104481]
Ground-based PIV and numerical flow visualization results from the surface tension driven convection experiment p 178 N91-30491
[NASA-TM-105172]
WESOKY, HOWARD L.
NASA's High Speed Research Program - An introduction and status report p 1 A91-48605
[SAE PAPER 901923]
WESSON, L. N.
Photoelastic transducer for high-temperature applications p 174 A91-55533
WESSON, LAURENCE N.
Fiber optic photoelastic pressure sensor for high temperature gases p 170 A91-19577
WESTFALL, LEONARD J.
Method of making single crystal fibers p 95 N91-13502
[NASA-CASE-LEW-14921-1]
WESTFALL, RICHARD
Near-Earth asteroids: Metals occurrence, extraction, and fabrication p 241 N91-26058
WESTON, BERT
Overall goals p 80 N91-28246
WETCH, JOSEPH R.
Two-dimensional simulation of a two-phase, regenerative pumped radiator loop utilizing direct contact heat transfer with phase change p 151 A91-38126
WEY, C.
An imaging system for PLIF/Mie measurements for a combustor flow p 27 N91-20084
[NASA-TM-103714]
WEY, C. C.
An imaging system for PLIF/Mie measurements for a combustor flow p 27 N91-20084
[NASA-TM-103714]
WEY, MING-JYH
Evaluation of a hybrid kinetics/mixing-controlled combustion model for turbulent premixed and diffusion combustion using KIVA-II p 104 A91-12927
[AIAA PAPER 90-2450]
WEYL, G. M.
Significant reduction in arc frequency biased solar cells: Observations, diagnostics, and mitigation technique(s) p 83 N91-30235
WHALEN, MARGARET V.
Slush hydrogen propellant production, transfer, and expulsion studies at the NASA K-Site Facility p 125 A91-53710
[AIAA PAPER 91-3550]
Slush hydrogen propellant production, transfer, and expulsion studies at the NASA K-Site Facility p 127 N91-28449
[NASA-TM-105191]
WHEELER, DONALD R.
X-ray photoelectron and mass spectroscopic study of electron irradiation and thermal stability of polytetrafluoroethylene p 113 A91-16138
Thermal stability of electron-irradiated poly(tetrafluoroethylene) - X-ray photoelectron and mass spectroscopic study p 115 A91-39242
Intrinsic bond strength of metal films on polymer substrates p 88 A91-39246
WHITTENBERGER, J. D.
Compression behavior of TiB₂-particulate-reinforced composites of Al₂Fe₃Ti₈ p 91 A91-28014
1000 to 1300 K slow plastic compression properties of Al-deficient NiAl p 108 A91-36214
1000 to 1200 K time-dependent compressive deformation of single-crystalline and polycrystalline B2 Ni-40Al p 109 A91-43670
Low-density, high-strength intermetallic matrix composites by XD (trademark) synthesis p 97 N91-19233
[NASA-TM-103724]
WHITTENBERGER, J. DANIEL
Tensile properties of HA 230 and HA 188 after 400 and 2500 hour exposures to LiF-22CaF₂ and vacuum at 1093 K p 107 A91-11624
1300 K compressive properties of a reaction milled NiAl-AIN composites p 107 A91-18674
Mechanical strength and thermophysical properties of PM212: A high temperature self-lubricating powder metallurgy composite p 120 N91-21302
[NASA-TM-103694]
WHYTE, WAYNE A.
Digital CODEC for real-time processing of broadcast quality video signals at 1.8 bits/pixel p 134 N91-24067
WHYTE, WAYNE A., JR.
A technology assessment of alternative communications systems for the space exploration initiative p 44 A91-11472
[AIAA PAPER 90-3681]
Data compression for full motion video transmission p 45 A91-52424
[AIAA PAPER 91-3533]
Millimeter wavelength communications applications for the SEI p 45 A91-52458
[AIAA PAPER 91-3589]
Real-time data compression of broadcast video signals p 133 N91-13598
[NASA-CASE-LEW-14945-1]
Data compression for full motion video transmission p 135 N91-32247
[NASA-TM-105239]
Millimeter wavelength communications applications for the SEI p 135 N91-32287
[NASA-TM-105275]
WICKENHEISER, T. J.
Performance impact on nuclear thermal propulsion of piloted Mars missions with short transit times p 64 A91-52326
[AIAA PAPER 91-3401]
WIESERMAN, W. R.
High frequency, high temperature specific core loss and dynamic B-H hysteresis loop characteristics of soft magnetic alloys p 138 A91-37988
Comparison of high temperature, high frequency core loss and dynamic B-H loops of two 50 Ni-Fe crystalline alloys and an iron-based amorphous alloy p 147 N91-32412
[NASA-TM-105205]
WILCOX, KATHERINE G.
High voltage interactions of a sounding rocket with the ambient and system-generated environments p 46 A91-23077
The environment power system analysis tool development program p 231 N91-17734
The environment workbench: A design tool for Space Station Freedom p 48 N91-20727
WILCZEK, FRANK
Inflationary axion cosmology p 239 A91-20491
WILLIAMS, B. R.
STOVL Hot Gas Ingestion control technology p 22 A91-23642
[ASME PAPER 89-GT-323]
WILLIAMS, D. M.
Manipulation hardware for microgravity research p 128 N91-14498
[NASA-TM-103423]
WILLIAMS, FORMAN A.
N-decane droplet combustion in the NASA-Lewis 5 Second Zero-Gravity Facility - Results in test gas environments other than air p 105 A91-19433
[AIAA PAPER 91-0720]
WILLIAMS, K. E.
The effect of varying Mach number on crossing, glancing shocks/turbulent boundary-layer interactions p 6 A91-45792
[AIAA PAPER 91-2157]
WILLIAMS, W. D.
PdCr based high temperature static strain gage p 170 A91-14462
[AIAA PAPER 90-5236]
WILLIAMS, W. DAN
Propulsion instrumentation research p 176 N91-20100

- WILLIS, E. A.**
Flux-vector splitting algorithm for chain-rule conservation-law form p 221 A91-45109
- WILLIS, EDWARD A.**
Rotary engine technology p 30 N91-20114
NASA aeropropulsion research in support of propulsion systems of the 21st century [NASA-TM-104403] p 15 N91-23083
- WILSON, JEFFREY D.**
A high-efficiency ferruleless coupled-cavity traveling-wave tube with phase-adjusted taper p 136 A91-25078
- WILT, D. M.**
Peel film GaAs solar cell development p 139 A91-41889
Effects of radiation of InP cells epitaxially grown on Si and GaAs substrates p 140 A91-41984
Effects of proton irradiation on the performance of InP/GaAs solar cells p 209 N91-19205
- WINOWICH, N. S.**
Three-dimensional calculation of the mixing of radial jets from slanted slots with a reactive cylindrical crossflow [AIAA PAPER 91-2081] p 24 A91-45782
- WINSA, E.**
Isothermal Dendritic Growth Experiment - Science, engineering, and hardware development for USMP space flights p 128 A91-53408
- WINTER, JERRY M.**
The NASA CSTI High Capacity Power Program [AIAA PAPER 91-3629] p 208 A91-52493
Status of NASA's Stirling Space Power Converter Program [NASA-TM-104512] p 214 N91-32569
- WITHINGTON, J. P.**
A time-accurate implicit method for chemically reacting flows at all Mach numbers [AIAA PAPER 91-0581] p 149 A91-21542
- WITHROW, C. A.**
Design of multihundredwatt DIPS for robotic space missions [NASA-TM-104401] p 75 N91-24232
SEI power source alternatives for rovers and other multi-kWe distributed surface applications [NASA-TM-104360] p 81 N91-28277
- WITHROW, COLLEEN A.**
SEI rover solar-electrochemical power system options [NASA-TM-104402] p 211 N91-23620
Comparison of dynamic isotope power systems for distributed planet surface applications [NASA-TM-4303] p 81 N91-28278
- WOIKE, MARK R.**
An Electronic Pressure Profile Display system for aeronautic test facilities p 38 A91-51858
- WOLFENDEN, A.**
Temperature dependence of the elastic moduli and damping for polycrystalline LiF-22 pct CaF₂ eutectic salt p 87 A91-33793
- WONG, WAYNE A.**
Update on results of SPRE testing at NASA Lewis [NASA-TM-104425] p 79 N91-27208
- WOOD, J. R.**
NASA low-speed centrifugal compressor for 3-D viscous code assessment and fundamental flow physics research [NASA-TM-103710] p 13 N91-20044
- WOODIS, KEN**
Overall goals p 80 N91-28246
- WOODS, C.**
The measurement, modelling and prediction of traction forces in a rocket propellant p 125 A91-51914
- WOODWARD, RICHARD P.**
Aeroacoustic effects of reduced aft tip speed at constant thrust for a model counterrotation turboprop at takeoff conditions [AIAA PAPER 90-3933] p 224 A91-12449
In-flight source noise of an advanced full-scale single-rotation propeller [AIAA PAPER 91-0594] p 226 A91-21547
Cruise noise of an advanced single-rotation propeller measured from an adjacent aircraft p 22 A91-28265
Aeroacoustic effects of reduced aft tip speed at constant thrust for a model counterrotation turboprop at takeoff conditions [NASA-TM-103608] p 226 N91-10703
Inflight source noise of an advanced full-scale single-rotation propeller [NASA-TM-103687] p 12 N91-19045
- WOODYARD, JAMES R.**
Radiation resistance of thin-film solar cells for space photovoltaic power [NASA-TM-103715] p 71 N91-19176
- WOOLLAM, J. A.**
Dielectric function of InGaAs in the visible p 233 A91-53236
- WOOLLAM, J. A.**
Ellipsometric study of InGaAs MODFET material [NASA-TM-103286] p 143 N91-19351
Study of InGaAs based MODFET structures using variable angle spectroscopic ellipsometry [NASA-TM-103792] p 235 N91-19935
- WOOLLAM, JOHN A.**
Diamondlike carbon as a moisture barrier and antireflecting coating on optical materials p 119 N91-18302
Diamondlike carbon applications in infrared optics and microelectronics p 230 N91-18306
- WORTHEN, D. W.**
Inhomogeneous deformation in INCONEL 718 during monotonic and cyclic loadings p 108 A91-22287
- WRIGHT, DAVID L.**
Advanced Communications Technology Satellite (ACTS) [IAF PAPER 90-481] p 44 A91-14056
- WRIGHT, THEODORE**
Description of real-time Ada software implementation of a power system monitor for the Space Station Freedom PMAD DC testbed [NASA-TM-105157] p 218 N91-28776
- WU, R. L. C.**
Diamondlike carbon applications in infrared optics and microelectronics p 230 N91-18306
- WU, T. W.**
Acoustical analysis of gear housing vibration [NASA-TM-103691] p 188 N91-25411
- WU, X. F.**
Acoustical analysis of gear housing vibration [NASA-TM-103691] p 188 N91-25411
- WUNDROW, D. W.**
Spatial evolution of nonlinear acoustic mode instabilities on hypersonic boundary layers p 225 A91-12973

Y

- YAMAGUCHI, KEIKO**
Modeling of surface roughness effects on glaze ice accretion p 19 A91-35107
- YAMAMOTO, O.**
Large-scale advanced propeller blade pressure distributions - Prediction and data p 5 A91-42820
- YANCEY, R. N.**
High resolution computed tomography of advanced composite and ceramic materials p 192 A91-56972
- YANG, LIFENG**
Modeling of Space Station electric power system with EMT p 55 A91-38040
- YANG, V.**
A time-accurate implicit method for chemically reacting flows at all Mach numbers [AIAA PAPER 91-0581] p 149 A91-21542
- YANG, VIGOR**
Combustion of liquid fuel droplets in supercritical conditions [AIAA PAPER 91-0078] p 105 A91-21362
Pressure-coupled vaporization and combustion responses of liquid-fuel droplets in high-pressure environments [AIAA PAPER 91-2310] p 106 A91-44192
- YANG, Y.**
Effects of brush seal morphology on leakage and pressure drops [AIAA PAPER 91-2106] p 182 A91-41700
- YANG, Z.**
Unstable viscous wall modes in rotating pipe flow [AIAA PAPER 91-1801] p 154 A91-42599
A k-epsilon modeling of near wall turbulence [NASA-TM-105238] p 170 N91-32460
- YAO, H. D.**
Dielectric function of InGaAs in the visible p 233 A91-53236
Ellipsometric study of InGaAs MODFET material [NASA-TM-103286] p 143 N91-19351
Study of InGaAs based MODFET structures using variable angle spectroscopic ellipsometry [NASA-TM-103792] p 235 N91-19935
- YASHAN, DOREEN**
The preliminary feasibility of intercalated graphite railgun armatures p 137 A91-29257
- YEH, F. C.**
Heat transfer in rotating serpentine passages with trips normal to the flow [NASA-TM-103758] p 184 N91-19443
- YEH, FREDERICK**
Aerodynamics and heat transfer investigations on a high Reynolds number turbine cascade [NASA-TM-103260] p 11 N91-15134
- YERKES, J. W.**
Lightweight concentrator module with 30 percent AM0 efficient GaAs/GaSb tandem cells p 57 A91-41990

YING, SHUH-JING

- Numerical simulation of Jet-A combustion approximated by improved propane chemical kinetics [AIAA PAPER 91-1859] p 106 A91-45777
- YOKOYAMA, JUN'ICHI**
Baryon isocurvature scenario in inflationary cosmology - A particle physics model and its astrophysical implications p 240 A91-54201
- YU, S. T.**
Modern CFD applications for the design of a reacting shear layer facility [AIAA PAPER 91-0577] p 149 A91-21540
Simulations of free shear layers using a compressible k-epsilon model [AIAA PAPER 91-1863] p 156 A91-45778
Modern CFD applications for the design of a reacting shear layer facility [NASA-TM-104523] p 34 N91-27164
- YUEN, J. L.**
Effect of thermal shock on fiber-reinforced superalloy composites p 93 A91-55918
- YUN, HEE MANN**
Tensile behavior of tungsten/niobium composites at 1300 to 1600 K [NASA-TM-103727] p 111 N91-16128
- YUNGSTER, SHAYE**
Numerical study of shock-wave/boundary layer interactions in premixed hydrogen-air hypersonic flows [AIAA PAPER 91-0413] p 149 A91-26191
Navier-Stokes simulation of the supersonic combustion flowfield in a ram accelerator [AIAA PAPER 91-1916] p 155 A91-44057
Numerical study of shock-wave/boundary layer interactions in premixed hydrogen-air hypersonic flows [NASA-TM-103273] p 160 N91-14559
Navier-Stokes simulation of the supersonic combustion flowfield in a ram accelerator [NASA-TM-104439] p 166 N91-24541

Z

- ZAKRAJSEK, J. J.**
Analytical and experimental study of vibrations in a gear transmission [AIAA PAPER 91-2019] p 181 A91-41680
Effects of gear box vibration and mass imbalance on the dynamics of multistage gear transmission p 182 A91-47213
Gear noise, vibration, and diagnostic studies at NASA Lewis Research Center p 183 A91-52811
Modal analysis of multistage gear systems coupled with gearbox vibrations [NASA-TM-103797] p 187 N91-23513
Analytical and experimental study of vibrations in a gear transmission [NASA-TM-104434] p 187 N91-25395
- ZAKRAJSEK, JAMES J.**
Effects of gear box vibration and mass imbalance on the dynamics of multi-stage gear transmissions [NASA-TM-103695] p 185 N91-21534
Comparison of analysis and experiment for dynamics of low-contact-ratio spur gears [NASA-TM-103232] p 185 N91-22566
- ZAKRAJSEK, JUNE F.**
The development of a post-test diagnostic system for rocket engines [AIAA PAPER 91-2528] p 60 A91-44281
The development of a post-test diagnostic system for rocket engines [NASA-TM-104463] p 217 N91-24787
- ZAMAN, K. B. M. Q.**
Effect of acoustic excitation on stalled flows over an airfoil [AIAA PAPER 90-4009] p 1 A91-12521
A steady effect of acoustic excitation on transitory stall [AIAA PAPER 91-0043] p 2 A91-22499
Supersonic jet mixing enhancement by vortex generators [AIAA PAPER 91-2263] p 5 A91-41738
Control of laminar separation over airfoils by acoustic excitation p 226 A91-45106
Effect of acoustic excitation on stalled flows over an airfoil [NASA-TM-103183] p 10 N91-11675
A steady effect of acoustic excitation on transitory stall [NASA-TM-103689] p 11 N91-13420
Experimental study of boundary layer transition on a heated flat plate [NASA-TM-103779] p 14 N91-21061
Effect of tabs on the evolution of an axisymmetric jet [NASA-TM-104472] p 34 N91-27159

ZAPLATYNSKY, I.

Method of preparing a thermal barrier coating
[NASA-CASE-LEW-14999-2] p 122 N91-26376

ZAPLATYNSKY, ISIDOR

Plasma gun with coaxial powder feed and adjustable cathode
[NASA-CASE-LEW-14901-1] p 231 N91-25875

ZARETSKY, ERWIN V.

Quantifying oil filtration effects on bearing life
[NASA-TM-104350] p 186 N91-23512
Incorporating finite element analysis into component life and reliability

[NASA-TM-104400] p 203 N91-23550
Comparison of Weibull strength parameters from flexure and spin tests of brittle materials
[NASA-TM-104414] p 187 N91-24593

ZEHE, MICHAEL J.

Acidic attack of perfluorinated alkyl ether lubricant molecules by metal oxide surfaces p 104 A91-13439

ZELTER, GABRIELA R.

Destructive physical analysis results of Ni/H₂ cells cycled in LEO regime
[NASA-TM-104382] p 74 N91-23233

ZEMAN, PATRICK L.

Verification of the Proteus two-dimensional Navier-Stokes code for flat plate and pipe flows
[AIAA PAPER 91-2013] p 153 A91-41678
Verification of the proteus two-dimensional Navier-Stokes code for flat plate and pipe flows
[NASA-TM-105160] p 168 N91-30462

ZHANG, Y.

Computerized inspection of real surfaces and minimization of their deviations
[NASA-TM-103798] p 188 N91-27558
Local synthesis and tooth contact analysis of face-milled spiral bevel gears
[NASA-TM-105182] p 190 N91-29600

ZHU, G.

Jet-A fuel evaporation analysis in conical tube injectors
[AIAA PAPER 91-0345] p 149 A91-21467

ZIEMIANSKI, JOSEPH A.

NASA aeropropulsion research in support of propulsion systems of the 21st century
[NASA-TM-104403] p 15 N91-23083

ZIEMKE, ROBERT A.

High resolution, high frame rate video technology development plan and the near-term system conceptual design p 175 N91-14580

ZIMMERMAN, MARTIN L.

Designs for the ATDRSS tri-band reflector antenna
[NASA-TM-103754] p 48 N91-20184

ZINGER, DON S.

Field oriented control of induction motors p 138 A91-37987

ZLATKOWSKI, M.

Time development of a perturbed-spherical nucleus in a pure supercooled liquid. I - Power-law growth of morphological instabilities. II - Nonlinear development p 231 A91-16105

ZUBE, DIETER M.

Nonequilibrium in a low power arcjet nozzle
[AIAA PAPER 91-2113] p 61 A91-45784

ZUPANC, F. J.

Spectrally resolved Rayleigh scattering diagnostic for hydrogen-oxygen rocket plume studies
[AIAA PAPER 91-0462] p 51 A91-21498

ZUTECK, MICHAEL D.

Structural properties of laminated Douglas fir/epoxy composite material
[NASA-RP-1236] p 94 N91-10127

ZUZEK, J. E.

Development of technology needs for the SEI TNIM network
[AIAA PAPER 91-3536] p 45 A91-52427

ZUZEK, JOHN

Technologies for unattended network operations
[AIAA PAPER 91-3534] p 45 A91-52425

ZUZEK, JOHN E.

A technology assessment of alternative communications systems for the space exploration initiative
[AIAA PAPER 90-3681] p 44 A91-11472

Evaluation of components, subsystems, and networks for high rate, high frequency space communications
[AIAA PAPER 91-3423] p 41 A91-52343

Millimeter wavelength communications applications for the SEI
[AIAA PAPER 91-3589] p 45 A91-52458

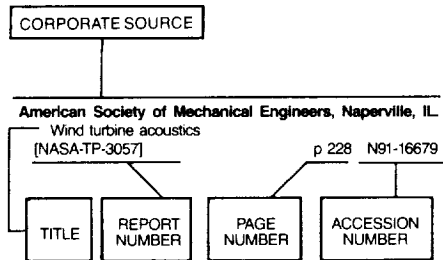
An assessment of technology alternatives for telecommunications and information management for the space exploration initiative
[NASA-TM-103783] p 134 N91-23347

Millimeter wavelength communications applications for the SEI
[NASA-TM-105275] p 135 N91-32287

ZWART, JOHN W.

An experimental apparatus for measuring surface resistance in the submillimeter-wavelength region p 174 A91-54390

Typical Corporate Source Index Listing



Listings in this index are arranged alphabetically by corporate source. The title of the document provides the user with a brief description of the subject matter. The report number helps to indicate the type of document cited (e.g., NASA report, translation, NASA contractor report). The accession number denotes the number by which the citation is identified. The titles are arranged under each corporate source in ascending accession number order.

A

- Aeritalia S.p.A., Turin (Italy).**
Photovoltaic superiority for Space Station Freedom power in the 21st century p 58 A91-42004
- Aerojet-General Corp., Sacramento, CA.**
Development of a Fabry-Perot interferometer for rocket engine plume monitoring p 171 A91-30634
Space Shuttle Main Engine nozzle mounted optic for throat plane spectroscopy p 49 A91-45816
[AIAA PAPER 91-2524]
- Aerojet TechSystems Co., Sacramento, CA.**
Surface modification of Monel K-500 as a means of reducing friction and wear in high-pressure oxygen p 107 A91-16869
- Air Force Aero Propulsion Lab., Wright-Patterson AFB, OH.**
A Navier-Stokes study of shock-boundary layer interaction and flow separation inside a transonic compressor p 8 A91-56115
- Air Force Armament Lab., Eglin AFB, FL.**
The preliminary feasibility of intercalated graphite railgun armatures p 137 A91-29257
- Air Force Systems Command, Cleveland, OH.**
Ultrasonic velocity technique for monitoring property changes in fiber-reinforced ceramic matrix composites p 174 A91-56912
Computerized inspection of real surfaces and minimization of their deviations p 188 A91-27558
[NASA-TM-103798]
- Air Force Systems Command, Kirtland AFB, NM.**
Nuclear Thermal Propulsion technology - Summary of FY 1991 Interagency panel planning p 66 A91-52495
[AIAA PAPER 91-3631]
- Akron Univ., OH.**
Flow visualization and quantitative velocity and pressure measurements in simulated single and double brush seals p 180 A91-21071
Dynamic analysis of space-related linear and non-linear structures p 196 A91-28612

- Partitioning methods for global controllers p 219 A91-30043
- Field oriented control of induction motors p 138 A91-37987
- Analytical and experimental study of vibrations in a gear transmission p 181 A91-41680
[AIAA PAPER 91-2019]
Effects of rim thickness on spur gear bending stress p 181 A91-41681
[AIAA PAPER 91-2020]
Maximum life spur gear design p 181 A91-41682
[AIAA PAPER 91-2021]
Effects of brush seal morphology on leakage and pressure drops p 182 A91-41700
[AIAA PAPER 91-2106]
Flow visualization in a simulated brush seal p 173 A91-44633
[ASME PAPER 90-GT-217]
Some preliminary results of brush seal/rotor interference effects on leakage at zero and low rpm using a tapered-plug rotor p 182 A91-45820
[AIAA PAPER 91-3390]
Effects of gear box vibration and mass imbalance on the dynamics of multistage gear transmission p 182 A91-47213
- Allied-Signal Aerospace Co., Torrance, CA.**
Liquid hydrogen turbopump foil bearing p 182 A91-41701
[AIAA PAPER 91-2108]
- American Society of Mechanical Engineers, Naperville, IL.**
Wind turbine acoustics p 228 A91-16679
[NASA-TP-3057]
- Analex Corp., Cleveland, OH.**
Vapor condensation at the free surface of an axisymmetric liquid mixed by a laminar jet p 151 A91-35109
Quaternary pulse position modulation electronics for free-space laser communications p 133 A91-53702
[AIAA PAPER 91-3471]
- Analex Corp., Fairview Park, OH.**
Surface studies on scandate cathodes and synthesized scandates p 136 A91-25071
Power electronic applications for Space Station Freedom p 52 A91-36832
A pressure control analysis of cryogenic storage systems p 59 A91-44228
[AIAA PAPER 91-2405]
A numerical study of the direct contact condensation on a horizontal surface p 155 A91-44335
[AIAA PAPER 91-1307]
Universal behavior in ideal slip p 110 A91-48517
Low velocity impact analysis with NASTRAN p 198 A91-48865
- Analytical Engineering Corp., North Olmsted, OH.**
An expert system for simulating electric loads aboard Space Station Freedom p 55 A91-38041
- Applied Research Associates, Inc., Raleigh, NC.**
Programming probabilistic structural analysis for parallel processing computer p 196 A91-31957
[AIAA PAPER 91-0920]
- Argonne National Lab., IL.**
Aerospace applications of high temperature superconductivity p 231 A91-13767
[IAF PAPER 90-054]
Development of nuclear fuels and materials for propulsion systems for SEI p 125 A91-52362
[AIAA PAPER 91-3452]
- Arizona State Univ., Tempe.**
Use of rotating pinholes and reticles for calibration of cloud droplet instrumentation p 171 A91-30371
- Arizona Univ., Tucson.**
Production and use of metals and oxygen for lunar propulsion p 125 A91-53711
[AIAA PAPER 91-3481]
- Ary Aviation Systems Command, Cleveland, OH.**
Use of piezoelectric actuators in active vibration control of rotating machinery p 179 A91-14400
Advanced Rotorcraft Transmission Program p 179 A91-17214
An update of engine system research at the Army Propulsion Directorate p 22 A91-29452
An expert system to perform on-line controller restructuring for abrupt model changes p 36 A91-29466

- Extension of transonic flow computational concepts in the analysis of cavitated bearings p 150 A91-29474
[ASME PAPER 90-TRIB-40]
An expert system to perform on-line controller tuning p 219 A91-30171
- Effects of rim thickness on spur gear bending stress p 181 A91-41681
[AIAA PAPER 91-2020]
Two-dimensional Navier-Stokes heat transfer analysis for rough turbine blades p 156 A91-45790
[AIAA PAPER 91-2129]
Jet-A reaction mechanism study for combustion application p 106 A91-45810
[AIAA PAPER 91-2355]
The NASA Lewis integrated propulsion and flight control simulator p 38 A91-47847
[AIAA PAPER 91-2969]
Automation software for a materials testing laboratory p 216 A91-56538
A data acquisition and control program for axial-torsional fatigue testing p 199 A91-56540
In situ X-ray monitoring of damage accumulation in SiC/RBSN tensile specimens p 94 A91-56942
Microstructural and strength stability of CVD SiC fibers in argon environments p 117 A91-56958
An update of engine system research at the Army Propulsion Directorate p 26 A91-11752
[NASA-TM-103278]
Experimental and analytical evaluation of efficiency of helicopter planetary stage p 183 A91-12956
[NASA-TP-3063]
Review of the transmissions of the Soviet helicopters p 20 A91-15146
[NASA-TM-103634]
Mechanical behavior of fiber reinforced SiC/RBSN ceramic matrix composites: Theory and experiment p 99 A91-21243
[NASA-TM-103688]
Advanced rotorcraft transmission program p 184 A91-21531
[NASA-TM-103276]
Effects of gear box vibration and mass imbalance on the dynamics of multi-stage gear transmissions p 185 A91-21534
[NASA-TM-103695]
Effects of inlet distortion on the development of secondary flows in a subsonic axial inlet compressor rotor p 31 A91-23179
[NASA-TM-104356]
Maximum life spur gear design p 187 A91-23514
[NASA-TM-104361]
- Army Propulsion Lab., Cleveland, OH.**
On the numerical solution of the dynamically loaded hydrodynamic lubrication of the point contact p 180 A91-33461
[NASA-TM-104361]
- A high speed photography study of cavitation in a dynamically loaded journal bearing p 180 A91-34806
[ASME PAPER 90-TRIB-19]
- Arnold Engineering Development Center, Arnold Air Force Station, TN.**
Verification of the Proteus two-dimensional Navier-Stokes code for flat plate and pipe flows p 153 A91-41678
[AIAA PAPER 91-2013]
- Auburn Univ., AL.**
Selective and low temperature synthesis of polycrystalline diamond p 232 A91-42170
- Aurora Optics, Inc., Blue Bell, PA.**
Fiber optic photoelastic pressure sensor for high temperature gases p 170 A91-19577
Photoelastic transducer for high-temperature applications p 174 A91-55533

B

- Battelle Memorial Inst., Columbus, OH.**
The measurement, modelling and prediction of traction forces in a rocket propellant p 125 A91-51914
- Bell Communications Research, Inc., Red Bank, NJ.**
Neural network architecture for crossbar switch control p 218 A91-29181
A neural net based architecture for the segmentation of mixed gray-level and binary pictures p 218 A91-29183

Boeing Co., Seattle, WA.

- The mini-dome Fresnel lens photovoltaic concentrator array - Current status of component and prototype panel testing p 57 A91-41989
 Lightweight concentrator module with 30 percent AMO efficient GaAs/GaSb tandem cells p 57 A91-41990

Boeing Co., Wichita, KS.

- Experimental water droplet impingement data on modern aircraft surfaces
 [AIAA PAPER 91-0445] p 2 A91-21493

C**Cairo Univ. (Egypt).**

- Heat transfer in oscillating flows p 152 A91-38698

California State Univ., Fullerton.

- k-out-of-n-G systems - Some cost considerations
 p 192 A91-54553

California State Univ., Long Beach.

- Prediction of ice shapes and their effect on airfoil performance
 [AIAA PAPER 91-0264] p 3 A91-26330

California Univ., Berkeley.

- Drop-tower experiments for capillary surfaces in an exotic container
 [AIAA PAPER 91-0107] p 148 A91-19138

California Univ., La Jolla.

- Particle nonuniformity effects on particle cloud flames in low gravity
 [AIAA PAPER 91-0718] p 104 A91-19431
 N-decane droplet combustion in the NASA-Lewis 5 Second Zero-Gravity Facility - Results in test gas environments other than air
 [AIAA PAPER 91-0720] p 105 A91-19433
 Particle cloud flames in acoustic fields p 105 A91-20589
 Radiative structures of lycopodium-air flames in low gravity p 105 A91-30003

California Univ., Los Angeles.

- YBCO superconducting ring resonators at millimeter-wave frequencies p 142 A91-54532

California Univ., Santa Barbara.

- Inhomogeneous deformation in INCONEL 718 during monotonic and cyclic loadings p 108 A91-22287

Calspan Corp., Arnold AFS, TN.

- Experimental evaluation of resistojet thruster plume shields p 51 A91-30010

Carnegie-Mellon Univ., Pittsburgh, PA.

- Simulation of mixing in the quick quench region of a rich burn-quick quench mix-lean burn combustor
 [AIAA PAPER 91-0410] p 105 A91-21481
 Flux-vector splitting algorithm for chain-rule conservation-law form p 221 A91-45109
 Computations of the three-dimensional flow and heat transfer within a coolant passage of a radial turbine blade
 [AIAA PAPER 91-2238] p 156 A91-45797
 Algebraic grid generation for coolant passages of turbine blades with serpentine channels and pin fins
 [AIAA PAPER 91-2366] p 156 A91-45811
 Algebraic grid generation for complex geometries p 157 A91-48758

Cascade Applied Sciences, Boulder, CO.

- The shock process and light-element production in supernova envelopes p 239 A91-33573

Case Western Reserve Univ., Cleveland, OH.

- Sulfur at nickel-alumina interfaces - Molecular orbital theory p 104 A91-12925
 The structure of carbon in chemically vapor deposited SiC monofilaments p 113 A91-18675
 An integrated methodology for optimizing the passive damping of composite structures p 195 A91-19048
 Silicon-etalon fiber-optic temperature sensor p 170 A91-19581
 A preview of a microgravity laser light scattering instrument
 [AIAA PAPER 91-0779] p 179 A91-21614
 Design of an optically controlled Ka-band GaAs MMIC phased-array antenna p 132 A91-24951
 Temperature dependence of hardness in yttria-stabilized zirconia single crystals p 114 A91-28763
 Temperature-dependent indentation behavior of transformation-toughened zirconia-based ceramics p 114 A91-28767
 On the numerical solution of the dynamically loaded hydrodynamic lubrication of the point contact p 180 A91-33461
 Determination of surface resistance and magnetic penetration depth of superconducting YBa₂Cu₃O_{7-δ} thin films by microwave power transmission measurements p 138 A91-36060
 Automating security monitoring and analysis for Space Station Freedom's electric power system p 219 A91-37975

Feedback linearization for control of air breathing engines

- [AIAA PAPER 91-2000] p 23 A91-41671
 Study of surface passivation as a function of InP closed-ampoule solar cell fabrication processing variables p 232 A91-41893
 Some preliminary results of brush seal/rotor interference effects on leakage at zero and low rpm using a tapered-plug rotor
 [AIAA PAPER 91-3390] p 182 A91-45820
 Atomic oxygen undercutting of defects on SiO₂ protected polyimide solar array blankets p 116 A91-49803
 Performance of a 300 Mbps 1:16 serial/parallel optoelectronic receiver module p 141 A91-51146
 Advanced materials for space nuclear power systems [AIAA PAPER 91-3530] p 88 A91-53704
 Spatial variations in a.c. susceptibility and microstructure for the YBa₂Cu₃O_{7-x} superconductor and their correlation with room-temperature ultrasonic measurements p 233 A91-54969

Cedarville Coll., OH.

- Determination of the thermal stability of fluids by tensimetry - Instrumentation and procedure p 113 A91-13435

Centre National de la Recherche Scientifique, Annecy-le-Vieux (France).

- Primordial nucleosynthesis redux p 240 A91-45907

CFD Research Corp., Huntsville, AL.

- A CFD study of jet mixing in reduced flow areas for lower combustor emissions
 [AIAA PAPER 91-2460] p 23 A91-41788

Chicago Univ., IL.

- Characteristic microwave-background distortions from collapsing spherical domain walls p 238 A91-12343
 Coherent peculiar velocities and periodic redshifts p 239 A91-20430
 Inflationary axion cosmology p 239 A91-20491
 Telescope search for a 3-eV to 8-eV axion p 239 A91-28714
 The shock process and light-element production in supernova envelopes p 239 A91-33573
 Big bang nucleosynthesis - The standard model and alternatives p 240 A91-37428
 First-order inflation p 240 A91-37444
 Astrophysics and cosmology confront the 17-keV neutrino p 240 A91-43291
 Primordial nucleosynthesis redux p 240 A91-45907
 Constraints from primordial nucleosynthesis on the mass of the tau neutrino p 240 A91-46543

Cincinnati Univ., OH.

- Contact stresses in gear teeth - A new method of analysis
 [AIAA PAPER 91-2022] p 182 A91-41683
 Probabilistic modeling for simulation of aerodynamic uncertainties in propulsion systems p 58 A91-42725
 Submicron gate InP power MISFET's with improved output power density at 18 and 20 GHz p 142 A91-54526

Clarkson Univ., Potsdam, NY.

- Composite structure global fracture toughness via computational simulation p 216 A91-11819
 The migration of a compound drop due to thermocapillarity p 148 A91-18428
 Integrated force method versus displacement method for finite element analysis p 196 A91-28372
 Progressive fracture in composites subjected to hygrothermal environment
 [AIAA PAPER 91-1140] p 91 A91-31919
 Compatibility conditions of structural mechanics for finite element analysis p 198 A91-37853

Clemson Univ., SC.

- The shock process and light-element production in supernova envelopes p 239 A91-33573

Cleveland State Univ., OH.

- Programmable multi-zone furnace for microgravity research
 [AIAA PAPER 91-0781] p 127 A91-19463
 Dynamic analysis of space-related linear and non-linear structures p 196 A91-28612
 The preliminary feasibility of intercalated graphite railgun armatures p 137 A91-29257
 Global expression for representing diatomic potential-energy curves p 228 A91-33236
 Resistivity of pristine and intercalated graphite fiber epoxy composites p 115 A91-35949
 Two-dimensional model of a Space Station Freedom thermal energy storage canister p 151 A91-38048
 Further two-dimensional code development for Stirling space engine components p 56 A91-38184
 Undercutting of defects in thin film protective coatings on polymer surfaces exposed to atomic oxygen p 115 A91-41516
 Study of surface passivation as a function of InP closed-ampoule solar cell fabrication processing variables p 232 A91-41893

Key factors limiting the open circuit voltage of n(+)/pp(+)

- indium phosphide solar cells p 139 A91-41929
 Measurement of surface recombination velocity on heavily doped indium phosphide p 232 A91-41931
 Evaluation of thermal control coatings for use on solar dynamic radiators in low earth orbit
 [AIAA PAPER 91-1327] p 58 A91-43397
 Mass comparisons of electric propulsion systems for NSSK of geosynchronous spacecraft
 [AIAA PAPER 91-2347] p 47 A91-45808
 Flow visualization and computational studies of a reverse flow circular combustor p 157 A91-48966
 The effect of atomic oxygen on altered and coated Kapton surfaces for spacecraft applications in low earth orbit p 116 A91-49804
 Thermal emittance enhancement of graphite-copper composites for high temperature space based radiators [AIAA PAPER 91-3527] p 116 A91-53705
 Universal energy relations and metal/ceramic interfaces p 93 A91-56254
 High emittance surfaces for high temperature space radiator applications p 88 A91-56415
 Polymeric routes to silicon carbide and silicon oxycarbide CMC p 117 A91-56922
 Thermal shock fiber-reinforced ceramic matrix composites p 93 A91-56935
 Dynamic fatigue property of silicon carbide whisker-reinforced silicon nitride p 94 A91-56937
 Crack healing in silicon nitride due to oxidation p 118 A91-56982

- High resolution electrolyte for thinning InP by anodic dissolution and its applications to EC-V profiling, defect revealing and surface passivation p 107 A91-30210
 A theoretical comparison of the near-optimum design and predicted performance of n/p and p/n indium phosphide homojunction solar cells p 83 A91-30233

Colorado Univ., Boulder.

- Application of implicit numerical techniques to the solution of the three-dimensional diffusion equation p 148 A91-13456
 Stability of compressible Taylor-Couette flow
 [AIAA PAPER 91-1642] p 153 A91-42541

Computational Physics System, Ann Arbor, MI.

- The L sub 1 finite element method for pure convection problems
 [NASA-TM-103773] p 222 A91-24817

Connecticut Univ., Storrs.

- Equivalence of Green's function and the Fourier series representation of composites with periodic microstructure p 91 A91-16889

Cornell Univ., Ithaca, NY.

- Second order modeling of boundary-free turbulent shear flows
 [AIAA PAPER 91-1779] p 154 A91-42588
 Unstable viscous wall modes in rotating pipe flow
 [AIAA PAPER 91-1801] p 154 A91-42599

D**Decision-Science Applications, Inc., Arlington, VA.**

- Electric power scheduling - A distributed problem-solving approach p 219 A91-37976

Dordt Coll., Sioux Center, IA.

- An experimental apparatus for measuring surface resistance in the submillimeter-wavelength region p 174 A91-54390

Drexel Univ., Philadelphia, PA.

- Bit error rate testing of fiber optic data links for MMIC-based phased array antennas p 131 A91-24950

- Development of braided rope seals for hypersonic engine applications. II - Flow modeling
 [AIAA PAPER 91-2495] p 182 A91-41800

Duke Univ., Durham, NC.

- Role of artificial viscosity in Euler and Navier-Stokes solvers p 4 A91-34135

Duncan Technologies, Auburn, CA.

- Space Shuttle Main Engine nozzle mounted optic for throat plane spectroscopy
 [AIAA PAPER 91-2524] p 49 A91-45816

E**Eloret Corp., Moffett Field, CA.**

- Pressure measurements in a low-density nozzle plume for code verification
 [AIAA PAPER 91-2110] p 61 A91-45783

Eloret Corp., Palo Alto, CA.

- Numerical and experimental investigations of rarefied nozzle and plume flows of nitrogen
 [AIAA PAPER 91-1363] p 154 A91-43429

Engineering Science Software, Inc., Smithfield, RI.

Equivalence of Green's function and the Fourier series representation of composites with periodic microstructure p 91 A91-16889

A new uniformly valid asymptotic integration algorithm for elasto-plastic creep and unified viscoplastic theories including continuum damage p 110 A91-48725

ENTECH Corp., Dallas-Fort Worth Airport, TX.

Component and prototype panel testing of the mini-dome Fresnel lens photovoltaic concentrator array p 54 A91-38023

The mini-dome Fresnel lens photovoltaic concentrator array - Current status of component and prototype panel testing p 57 A91-41989

Lightweight concentrator module with 30 percent AMO efficient GaAs/GaSb tandem cells p 57 A91-41990

Eppley Lab., Inc., Newport, RI.

Preliminary flight test results from the advanced photovoltaic experiment p 56 A91-38163

Preliminary results from the Advanced Photovoltaic Experiment flight test p 39 A91-41980

Exxon Research and Engineering Co., Annandale, NJ.

1300 K compressive properties of a reaction milled NiAl-AlN composites p 107 A91-18674

F**Fermi National Accelerator Lab., Batavia, IL.**

Characteristic microwave-background distortions from collapsing spherical domain walls p 238 A91-12343

Natural inflation with pseudo Nambu-Goldstone bosons p 239 A91-19545

Coherent peculiar velocities and periodic redshifts p 239 A91-20430

Inflationary axion cosmology p 239 A91-20491

Structure of random discrete spacetime p 224 A91-22894

The dynamic instability of adiabatic blast waves p 239 A91-26361

Telescope search for a 3-eV to 8-eV axion p 239 A91-28714

The shock process and light-element production in supernova envelopes p 239 A91-33573

Big bang nucleosynthesis - The standard model and alternatives p 240 A91-37428

First-order inflation p 240 A91-37444

Astrophysics and cosmology confront the 17-keV neutrino p 240 A91-43291

Primordial nucleosynthesis redux p 240 A91-45907

Constraints from primordial nucleosynthesis on the mass of the tau neutrino p 240 A91-46543

Baryon isocurvature scenario in inflationary cosmology - A particle physics model and its astrophysical implications p 240 A91-54201

Florence Univ. (Italy).

Multigrid calculation of three-dimensional viscous cascade flows [AIAA PAPER 91-3238] p 7 A91-53754

Florida Atlantic Univ., Boca Raton.

Real-time diagnostics of the reusable rocket engine using on-line system identification p 223 A91-30630

Florida Univ., Gainesville.

Effects of nozzle lip geometry on spray atomization and emissions advanced gas turbine combustors [AIAA PAPER 91-2201] p 24 A91-44153

Constitution of pseudobinary hypoeutectic beta-NiAl + alpha-V alloys p 109 A91-48509

Algebraic grid generation for complex geometries p 157 A91-48758

A simplified method for determining the number of independent slip systems in crystals p 110 A91-55472

Ford Aerospace Corp., Palo Alto, CA.

The COLD-SAT experiment for cryogenic fluid management technology p 46 A91-29799

G**General Dynamics Corp., San Diego, CA.**

The COLD-SAT experiment for cryogenic fluid management technology p 46 A91-29799

Control of multiple resonant power processors in a multi-source system p 137 A91-30901

General Electric Co., Cincinnati, OH.

Surface fatigue life of M50NiL and AISI 9310 gears and rolling-contact bars p 182 A91-45350

General Electric Co., Princeton, NJ.

Advanced Communications Technology Satellite (ACTS) [IAF PAPER 90-481] p 44 A91-14056

General Motors Research Labs., Warren, MI.

Global expression for representing diatomic potential-energy curves p 228 A91-33236

Adhesion at metal interfaces p 88 A91-38581

Universal behavior in ideal slip p 110 A91-48517

Universal energy relations and metal/ceramic interfaces p 93 A91-56254

George Washington Univ., Washington, DC.

Effects of horizontal tail ice on longitudinal aerodynamic derivatives p 36 A91-38547

Georgia Inst. of Tech., Atlanta.

Application of an efficient hybrid scheme for aeroelastic analysis of advanced propellers p 7 A91-52315

Grace (W. R.) and Co., Columbia, MD.

Spatial variations in a.c. susceptibility and microstructure for the YBaCu3O(7-x) superconductor and their correlation with room-temperature ultrasonic measurements p 233 A91-54969

H**Harvard-Smithsonian Center for Astrophysics, Cambridge, MA.**

Primordial nucleosynthesis redux p 240 A91-45907

Honeywell, Inc., Minneapolis, MN.

Performance of a 300 Mbps 1:16 serial/parallel optoelectronic receiver module p 141 A91-51146

Hughes Aircraft Co., El Segundo, CA.

Development of technology needs for the SEI TNIM network [AIAA PAPER 91-3536] p 45 A91-52427

Hughes Aircraft Co., Torrance, CA.

A high-efficiency ferruleless coupled-cavity traveling-wave tube with phase-adjusted taper p 136 A91-25078

Hughes Research Labs., Malibu, CA.

An experimental study of high Tc superconducting microstrip transmission lines at 35 GHz and the effect of film morphology p 138 A91-36172

I**Idaho National Engineering Lab., Idaho Falls.**

Radiation dose estimates for typical piloted NTR lunar and Mars mission engine operations [AIAA PAPER 91-3407] p 215 A91-52331

Development of nuclear fuels and materials for propulsion systems for SEI [AIAA PAPER 91-3452] p 125 A91-52362

Nuclear Thermal Propulsion technology - Summary of FY 1991 Interagency panel planning [AIAA PAPER 91-3631] p 66 A91-52495

Idaho Univ., Moscow.

Continuous fiber-reinforced titanium aluminide composites p 92 A91-39553

Illinois Univ., Chicago.

High temperature reactions of ceramics and metals with chlorine and oxygen p 105 A91-20219

Measurements and predictions of a liquid spray from an air-assist nozzle [AIAA PAPER 91-0692] p 149 A91-22498

A detailed numerical investigation of Burke-Schumann gaseous and spray flames [AIAA PAPER 91-2311] p 105 A91-41749

Illinois Univ., Urbana.

Inhomogeneous deformation in INCONEL 718 during monotonic and cyclic loadings p 108 A91-22287

Inco Alloys International, Inc., Huntington, WV.

1000 to 1200 K time-dependent compressive deformation of single-crystalline and polycrystalline B2 Ni-40Al p 109 A91-43670

Indian Inst. of Science, Bangalore.

General purpose program to generate compatibility matrix for the integrated force method p 195 A91-12905

Institute for Advanced Study, Princeton, NJ.

Inflationary axion cosmology p 239 A91-20491

Iowa State Univ. of Science and Technology, Ames.

An experimental comparison of nonswirling and swirling flow in a circular-to-rectangular transition duct [AIAA PAPER 91-0342] p 148 A91-21466

Simulation of three-dimensional liquid sloshing flows using a strongly implicit calculation procedure [AIAA PAPER 91-1661] p 153 A91-42549

An experimental trace gas investigation of fluid transport and mixing in a circular-to-rectangular transition duct [AIAA PAPER 91-2370] p 172 A91-44214

Primitive variable, strongly implicit calculation procedure for viscous flows at all speeds p 7 A91-46181

J**Jackson State Univ., MS.**

Performance and optimization of a 'derated' ion thruster for auxiliary propulsion [AIAA PAPER 91-2350] p 62 A91-45809

John Carroll Univ., Cleveland, OH.

Digital angular position sensor using wavelength division multiplexing p 21 A91-19580

Silicon-etalon fiber-optic temperature sensor p 170 A91-19581

Compensation for effects of ambient temperature on rare-earth doped fiber optic thermometer p 170 A91-19582

Optical techniques for determination of normal shock position in supersonic flows for aerospace applications p 174 A91-55530

K**Kansas Univ., Lawrence.**

Modern developments in shear flow control with swirl p 3 A91-24519

Kent State Univ., OH.

Adhesion at metal interfaces p 88 A91-38581

Ellipsometric study of YBaCu3O(7-x) laser ablated and co-evaporated films p 233 A91-53235

Kopin Corp., Taunton, MA.

23.5 percent thin-film space concentrator cells p 58 A91-42002

Kyoto Univ., Uji (Japan).

Baryon isocurvature scenario in inflationary cosmology - A particle physics model and its astrophysical implications p 240 A91-54201

L**Lawrence Livermore National Lab., CA.**

The shock process and light-element production in supernova envelopes p 239 A91-33573

Lockheed Engineering and Sciences Co., Hampton, VA.

A comparison of arrow, trapezoidal and M wing concepts using a Mach 2 supersonic cruise transport mission [AIAA PAPER 91-3102] p 7 A91-54027

Lockheed Engineering and Sciences Co., Las Cruces, NM.

Surface modification of Monel K-500 as a means of reducing friction and wear in high-pressure oxygen p 107 A91-16869

London Univ. (England).

Structure of random discrete spacetime p 224 A91-22894

Loral AeroSys, Seabrook, MD.

Technologies for unattended network operations [AIAA PAPER 91-3534] p 45 A91-52425

Los Alamos National Lab., NM.

Nuclear Thermal Propulsion technology - Summary of FY 1991 Interagency panel planning [AIAA PAPER 91-3631] p 66 A91-52495

LTV Missiles and Electronics Group, Grand Prairie, TX.

Evaluation of thermal control coatings for use on solar dynamic radiators in low earth orbit [AIAA PAPER 91-1327] p 58 A91-43397

M**Maine Univ., Orono.**

Three-dimensional calculation of the mixing of radial jets from slanted slots with a reactive cylindrical crossflow [AIAA PAPER 91-2081] p 24 A91-45782

Marquardt Corp., Van Nuys, CA.

Heat transfer in space systems; Proceedings of the Symposium, AIAA/ASME Thermophysics and Heat Transfer Conference, Seattle, WA, June 18-20, 1990 p 152 A91-38780

Martin Marietta Labs., Baltimore, MD.

Compression behavior of TiB2-particulate-reinforced composites of Al22Fe3Ti8 p 91 A91-28014

1000 to 1300 K slow plastic compression properties of Al-deficient NiAl p 108 A91-36214

1000 to 1200 K time-dependent compressive deformation of single-crystalline and polycrystalline B2 Ni-40Al p 109 A91-43670

Massachusetts Inst. of Tech., Cambridge.

Natural inflation with pseudo Nambu-Goldstone bosons p 239 A91-19545

Modeling of surface roughness effects on glaze ice accretion p 19 A91-35107

Max-Planck-Inst. fuer Metallforschung, Stuttgart (Germany, F.R.).

1300 K compressive properties of a reaction milled NiAl-AlN composites p 107 A91-18674

Maxwell Labs., Inc., San Diego, CA.

High voltage interactions of a sounding rocket with the ambient and system-generated environments p 46 A91-23077

MBR Combustion Research, Inc., Princeton, NJ.

Evaluation of a hybrid kinetics/mixing-controlled combustion model for turbulent premixed and diffusion combustion using KIVA-II

[AIAA PAPER 90-2450] p 104 A91-12927

McDonnell Aircraft Co., Saint Louis, MO.

STOVL Hot Gas Ingestion control technology

[ASME PAPER 89-GT-323] p 22 A91-23642

Hot gas ingestion test results of a two-poster vectored thrust concept with flow visualization in the NASA Lewis 9- by 15-foot low speed wind tunnel

[AIAA PAPER 90-2268] p 4 A91-40561

Flow visualization studies of the internal flow characteristics in a simulated mixed flow vectored thrust ASTOVL engine configuration

[AIAA PAPER 91-1689] p 23 A91-42556

McDonnell-Douglas Research Labs., Saint Louis, MO.

Flow visualization studies of the internal flow characteristics in a simulated mixed flow vectored thrust ASTOVL engine configuration

[AIAA PAPER 91-1689] p 23 A91-42556

VSTOL ground effects testing with flow visualization and image enhancement

[AIAA PAPER 91-3145] p 8 A91-54061

McDonnell-Douglas Space Systems Co., Houston, TX.

Cryogenic propellant management system requirements for Space Station Freedom

[AIAA PAPER 91-3476] p 65 A91-52382

McDonnell-Douglas Space Systems Co., Huntington Beach, CA.

Cryogenic propellant management architectures to support the Space Exploration Initiative

[AIAA PAPER 90-3713] p 124 A91-10112

Fuel Systems Architecture (FSA) evaluation criteria and concept evaluation methodology

[AIAA PAPER 91-3479] p 65 A91-52384

Michigan Technological Univ., Houghton.

Oxidation behavior of cubic phases formed by alloying Al₃Ti with Cr and Mn

p 108 A91-27849

Michigan Univ., Ann Arbor.

Transient cryogenic liquid discharge in normal and micro-gravity

[AIAA PAPER 91-0486] p 124 A91-19324

Low-temperature microwave characteristics of pseudomorphic In(x)Ga(1-x)As/In(0.52)Al(0.48)As modulation-doped field-effect transistors

p 136 A91-22987

Aeroelastic modal characteristics of mistuned blade assemblies - Mode localization and loss of eigenstructure

[AIAA PAPER 91-1218] p 196 A91-32032

Theoretical and experimental characterization of coplanar waveguide discontinuities for filter applications

p 137 A91-35911

The potential for ductility enhancement from surface and interface dislocation sources in NiAl

p 109 A91-39292

Numerical flux formulas for the Euler and Navier-Stokes equations. II - Progress in flux-vector splitting

[AIAA PAPER 91-1566] p 5 A91-40740

Localization of aeroelastic modes in mistuned high-energy turbines

[AIAA PAPER 91-3379] p 198 A91-44319

Discharge rate of cryogenics in microgravity - What ground based experimentation cannot resolve

[AIAA PAPER 91-3545] p 129 A91-52430

Dielectric function of InGaAs in the visible

p 233 A91-53236

Midwest Research Inst., Golden, CO.

Primary reference cell calibrations at SERI - History and methods

p 207 A91-41966

Minnesota Univ., Minneapolis.

Primordial nucleosynthesis redux

p 240 A91-45907

Mississippi State Univ., Mississippi State.

Flutter analysis of cascades using a two dimensional Euler solver

[AIAA PAPER 91-1681] p 6 A91-45548

Heat transfer to a thin solid combustible in flame spreading at microgravity

p 106 A91-51449

N

National Academy of Sciences - National Research Council, Washington, DC.

Comparative modeling of InP solar cell structures

p 83 A91-30232

National Aeronautics and Space Administration, Washington, DC.

Aerospace applications of high temperature superconductivity

[IAF PAPER 90-054] p 231 A91-13767

Vibration environment - Acceleration mapping strategy and microgravity requirements for Spacelab and Space Station

[IAF PAPER 90-350] p 39 A91-13991

NASA's future space power needs and requirements

p 52 A91-37929

NASA's High Speed Research Program - An introduction and status report

[SAE PAPER 901923] p 1 A91-48605

National Aeronautics and Space Administration. Ames Research Center, Moffett Field, CA.

Pressure measurements in a low-density nozzle plume for code verification

[AIAA PAPER 91-2110] p 61 A91-45783

The effects of rotation on initially anisotropic homogeneous flows

p 158 A91-54958

National Aeronautics and Space Administration. Goddard Inst. for Space Studies, New York, NY.

NASA's High Speed Research Program - An introduction and status report

[SAE PAPER 901923] p 1 A91-48605

National Aeronautics and Space Administration. Lyndon B. Johnson Space Center, Houston, TX.

Power system requirements and definition for lunar and Mars outposts

p 52 A91-37930

Cathode phenomena in a low-power magnetoplasmadynamic thruster

p 63 A91-52314

Construction and testing of ceramic fabric heat pipe with water working fluid

[NASA-TM-103332] p 229 A91-18799

National Aeronautics and Space Administration. Langley Research Center, Hampton, VA.

On the continuous spectra of the compressible boundary layer stability equations

p 150 A91-31342

Effects of horizontal tail ice on longitudinal aerodynamic derivatives

p 36 A91-38547

Evaluation of thermal control coatings for use on solar dynamic radiators in low earth orbit

[AIAA PAPER 91-1327] p 58 A91-43397

Launch vehicle performance using metallized propellants

[AIAA PAPER 91-2050] p 58 A91-44106

A comparison of arrow, trapezoidal and M wing concepts using a Mach 2 supersonic cruise transport mission

[AIAA PAPER 91-3102] p 7 A91-54027

Wind turbine acoustics

[NASA-TP-3057] p 228 A91-16679

National Aeronautics and Space Administration. Marshall Space Flight Center, Huntsville, AL.

Turbine blading designed for high heat load space propulsion applications

p 50 A91-10338

Vibration environment - Acceleration mapping strategy and microgravity requirements for Spacelab and Space Station

[IAF PAPER 90-350] p 39 A91-13991

The NASA Cryogenic Fluid Management Technology Program Plan

[AIAA PAPER 91-3553] p 130 A91-52436

National Aeronautics and Space Administration. White Sands Test Facility, NM.

Surface modification of Monel K-500 as a means of reducing friction and wear in high-pressure oxygen

p 107 A91-16869

National Inst. of Standards and Technology, Boulder, CO.

A fiber-optic current sensor for aerospace applications

p 171 A91-23005

A fiber-optic current sensor for aerospace applications

p 172 A91-38006

Naval Air Propulsion Test Center, Trenton, NJ.

Evaluation of advanced lubricants for aircraft applications using gear surface fatigue tests

[AIAA PAPER 91-1907] p 181 A91-41649

Naval Coastal Systems Center, Panama City, FL.

The preliminary feasibility of intercalated graphite railgun armatures

p 137 A91-29257

Naval Ocean Systems Center, San Diego, CA.

Submicron gate InP power MISFET's with improved output power density at 18 and 20 GHz

p 142 A91-54526

Naval Research Lab., Washington, DC.

Determination of surface resistance and magnetic penetration depth of superconducting YBa₂Cu₃O₇(δ) thin films by microwave power transmission measurements

p 138 A91-36060

Naval Weapons Support Center, Crane, IN.

Effect of KOH concentration on LEO cycle life of IPV nickel-hydrogen flight battery cells

p 55 A91-38076

Effect of LEO cycling on 125 Ah advanced design IPV nickel-hydrogen battery cells

p 55 A91-38077

Nebraska Univ., Lincoln.

Data compression for full motion video transmission

[AIAA PAPER 91-3533] p 45 A91-52424

Dielectric function of InGaAs in the visible

p 233 A91-53236

New Mexico Univ., Albuquerque.

Preliminary assessment of the power requirements of a manned rover for Mars missions

p 41 A91-27702

A comparison of energy conversion systems for meeting the power requirements of manned rover for Mars missions

p 53 A91-37932

Notre Dame Univ., IN.

Acoustic radiation from lifting airfoils in compressible subsonic flow

[AIAA PAPER 90-3911] p 224 A91-12427

O

Oak Ridge National Lab., TN.

Numerical, micro-mechanical prediction of crack growth resistance in a fibre-reinforced/brittle matrix composite

p 199 A91-51916

Office of Naval Research, Arlington, VA.

Solution of steady-state, two-dimensional conservation laws by mathematical programming

p 221 A91-35956

Ohio Aerospace Inst., Brook Park.

Results from computational analysis of a mixed compression supersonic inlet

[AIAA PAPER 91-2581] p 7 A91-45818

Ohio State Univ., Columbus.

Flow induced vibration and noise by a pair of tandem cylinders due to buffeting

p 225 A91-14650

Effect of high temperature hydrogen exposure on the strength and microstructure of mullite

p 114 A91-19780

High temperature reactions of ceramics and metals with chlorine and oxygen

p 105 A91-20219

Free vibrations of delaminated beams

[AIAA PAPER 91-1241] p 197 A91-32129

Supersonic jet mixing enhancement by vortex generators

[AIAA PAPER 91-2263] p 5 A91-41738

Primordial nucleosynthesis redux

p 240 A91-45907

Photoresponse of YBa₂Cu₃O₇(δ) granular and epitaxial superconducting thin films

p 141 A91-50443

Crystallization and properties of Sr-Ba aluminosilicate glass-ceramic matrices

p 117 A91-56917

P

Pacific Northwest Lab., Richland, WA.

Construction and testing of ceramic fabric heat pipe with water working fluid

[NASA-TM-103332] p 229 A91-18799

Pennsylvania State Univ., University Park.

Combustion of liquid fuel droplets in supercritical conditions

[AIAA PAPER 91-0078] p 105 A91-21362

A time-accurate implicit method for chemically reacting flows at all Mach numbers

[AIAA PAPER 91-0581] p 149 A91-21542

A new approach to controller design for microgravity isolation systems

p 129 A91-23108

Time-derivative preconditioning for viscous flows

[AIAA PAPER 91-1652] p 154 A91-43576

Pressure-coupled vaporization and combustion responses of liquid-fuel droplets in high-pressure environments

[AIAA PAPER 91-2310] p 106 A91-44192

Pennsylvania Univ., Philadelphia.

Coherent peculiar velocities and periodic redshifts

p 239 A91-20430

Parallel algorithms for boundary value problems

p 221 A91-31175

Philips Display Components Co., Ann Arbor, MI.

Numerical, micro-mechanical prediction of crack growth resistance in a fibre-reinforced/brittle matrix composite

p 199 A91-51916

Pittsburgh Univ., Johnstown, PA.

High frequency, high temperature specific core loss and dynamic B-H hysteresis loop characteristics of soft magnetic alloys

p 138 A91-37988

Pittsburgh Univ., PA.

Multidimensional computer simulation of Stirling cycle engines

p 181 A91-38154

Pratt and Whitney Aircraft, East Hartford, CT.

Evaluation of panel code predictions with experimental results of inlet performance for a 17-inch ducted prop/fan simulator operating at Mach 0.2

[AIAA PAPER 91-3354] p 7 A91-45819

Pratt and Whitney Aircraft Group, East Hartford, CT.

Flow visualization studies of the internal flow characteristics in a simulated mixed flow vectored thrust ASTOVL engine configuration

[AIAA PAPER 91-1689] p 23 A91-42556

Pratt and Whitney Aircraft Group, West Palm Beach, FL.

The Advanced Expander Test Bed

[AIAA PAPER 90-3708] p 50 A91-10107

Design and experimental evaluation of compact radial-inflow turbines

[AIAA PAPER 91-2127] p 24 A91-45788

- Design of an Advanced Expander Test Bed
[AIAA PAPER 91-3437] p 42 A91-52350
- Princeton Univ., NJ.**
N-decane droplet combustion in the NASA-Lewis 5 Second Zero-Gravity Facility - Results in test gas environments other than air
[AIAA PAPER 91-0720] p 105 A91-19433
- Two-dimensional imaging of molecular hydrogen in H₂-air diffusion flames using two-photon laser-induced fluorescence
p 124 A91-34369
- Anode power deposition in an applied-field segmented anode MPD thruster
[AIAA PAPER 91-2343] p 59 A91-44204
- Energy deposition in low-power coaxial plasma thrusters
p 63 A91-52311
- Cathode phenomena in a low-power magnetoplasmadynamic thruster
p 63 A91-52314
- Purdue Univ., West Lafayette, IN.**
Oscillating cascade aerodynamics by an experimental influence coefficient technique
p 1 A91-10339
- Influence of geometric features on the performance of pressure-swirl atomizers
p 147 A91-13030
- The aerodynamics of an oscillating cascade in a compressible flow field
[ASME PAPER 89-GT-271] p 1 A91-13047
- Experimental investigation of oscillating cascade aerodynamics
p 3 A91-27801

R

- Rensselaer Polytechnic Inst., Troy, NY.**
Inertia effects in thin film flow with a corrugated boundary
p 151 A91-32691
- Isothermal Dendritic Growth Experiment - Science, engineering, and hardware development for USMP space flights
p 128 A91-53408
- Rockwell International Corp., Canoga Park, CA.**
Radiation from gas-jet diffusion flames in microgravity environments
[AIAA PAPER 91-0719] p 104 A91-19432
- Lunar electric power systems utilizing the SP-100 reactor coupled to dynamic conversion systems
[AIAA PAPER 91-3520] p 208 A91-52415
- Dynamic Isotope Surface Power Systems
[AIAA PAPER 91-3623] p 208 A91-52487
- Effect of thermal shock on fiber-reinforced superalloy composites
p 93 A91-55918
- Rockwell International Corp., Houston, TX.**
Cathode phenomena in a low-power magnetoplasmadynamic thruster
p 63 A91-52314

S

- San Diego State Univ., CA.**
Heat transfer to a thin solid combustible in flame spreading at microgravity
p 106 A91-51449
- Sandia National Labs., Livermore, CA.**
Second order modeling of boundary-free turbulent shear flows
[AIAA PAPER 91-1779] p 154 A91-42588
- Schafer (W. J.) Associates, Inc., Arlington, VA.**
Light weight, high power, high voltage dc/dc converter technologies
p 138 A91-37985
- Science Applications International Corp., Schaumburg, IL.**
NTR vehicle commonality assessment for piloted lunar and Mars missions
[AIAA PAPER 91-3575] p 66 A91-52448
- Science Applications International Corp., Torrance, CA.**
Radiation from gas-jet diffusion flames in microgravity environments
[AIAA PAPER 91-0719] p 104 A91-19432
- Scientific Research Associates, Inc., Glastonbury, CT.**
Navier-Stokes simulation of transonic blade-vortex interactions
p 2 A91-21065
- A design strategy for the use of vortex generators to manage inlet-engine distortion using computational fluid dynamics
[AIAA PAPER 91-2474] p 6 A91-44259
- SDRC, Inc., San Diego, CA.**
Simulation of the Space Station strut-out condition
[AIAA PAPER 91-1248] p 197 A91-32087
- Sikorsky Aircraft, Stratford, CT.**
Icing tests of a model main rotor
p 18 A91-17218
- Results of a sub-scale model rotor icing test
[AIAA PAPER 91-0660] p 19 A91-26190
- Space Power, Inc., San Jose, CA.**
Two-dimensional simulation of a two-phase, regenerative pumped radiator loop utilizing direct contact heat transfer with phase change
p 151 A91-38126
- The telescoping boom radiator concept for multimewatt space power systems
[AIAA PAPER 91-3497] p 158 A91-52395

- Space Station Engineering and Integration Contractor, North Olmsted, OH.**
An assessment of the Space Station Freedom program's leakage current requirement
[NASA-CR-187077] p 215 N91-20630
- Spire Corp., Bedford, MA.**
Dielectric function of InGaAs in the visible
p 233 A91-53236
- Stanford Univ., CA.**
Drop-tower experiments for capillary surfaces in an exotic container
[AIAA PAPER 91-0107] p 148 A91-19138
- The effects of rotation on initially anisotropic homogeneous flows
p 158 A91-54958
- State Univ. of New York, Binghamton.**
A high speed photography study of cavitation in a dynamically loaded journal bearing
[ASME PAPER 90-TRIB-19] p 180 A91-34806
- Strainoptic Technologies, Inc., North Wales, PA.**
Fiber optic photoelastic pressure sensor for high temperature gases
p 170 A91-19577
- Photoelastic transducer for high-temperature applications
p 174 A91-55533
- Sverdrup Technology, Inc., Brook Park, OH.**
The effect of swirl recovery vanes on the cruise noise of an advanced propeller
[AIAA PAPER 90-3932] p 224 A91-12448
- Near-field noise of a single rotation propfan at an angle of attack
[AIAA PAPER 90-3953] p 225 A91-12469
- Noise measurements from an ejector suppressor nozzle in the NASA Lewis 9- by 15-foot low speed wind tunnel
[AIAA PAPER 90-3983] p 225 A91-12496
- Unsteady blade pressure measurements for the SR-7A propeller at cruise conditions
[AIAA PAPER 90-4022] p 225 A91-12533
- Probabilistic simulation of uncertainties in thermal structures
p 195 A91-16042
- Prediction of unsteady blade surface pressures on an advanced propeller at an angle of attack
p 226 A91-18257
- An algebraic RNG-based turbulence model for three-dimensional turbomachinery flows
[AIAA PAPER 91-0172] p 2 A91-21393
- A review of ice accretion data from a model rotor icing test and comparison with theory
[AIAA PAPER 91-0661] p 19 A91-22500
- Prediction of ice shapes and their effect on airfoil performance
[AIAA PAPER 91-0264] p 3 A91-26330
- Three-dimensional viscous flow computations of high area ratio nozzles for hypersonic propulsion
p 4 A91-30014
- Computational simulation of acoustic fatigue for hot composite structures
[AIAA PAPER 91-1178] p 197 A91-32099
- An experimental study of high T_c superconducting microstrip transmission lines at 35 GHz and the effect of film morphology
p 138 A91-36172
- Rapid thermal cycling of new technology solar array blanket coupons
p 54 A91-38019
- Update on results of SPRE testing at NASA
p 56 A91-38140
- Lunar orbiting microwave beam power system
p 56 A91-38158
- Modeling and optimization of a regenerative fuel cell system using the ASPEN process simulator
p 206 A91-38177
- CFD analysis of a hydrogen fueled ramjet engine at Mach 3.44
[AIAA PAPER 91-1919] p 23 A91-41653
- Feedback linearization for control of air breathing engines
[AIAA PAPER 91-2000] p 23 A91-41671
- Thermal and structural assessments of a ceramic wafer seal in hypersonic engine
[AIAA PAPER 91-2494] p 23 A91-41799
- Photovoltaic superiority for Space Station Freedom power in the 21st century
p 58 A91-42004
- A charging study of the ACTS satellite using NASCAP
[AIAA PAPER 91-1471] p 46 A91-42522
- Large-scale advanced propeller blade pressure distributions - Prediction and data
p 5 A91-42820
- Time-derivative preconditioning for viscous flows
[AIAA PAPER 91-1652] p 154 A91-43576
- Increased heat transfer to a cylindrical leading edge due to spanwise variations in the freestream velocity
[AIAA PAPER 91-1739] p 155 A91-43623
- Flow visualization of a rocket injector spray using gelled propellant simulants
[AIAA PAPER 91-2198] p 59 A91-44151
- Anode power deposition in an applied-field segmented anode MPD thruster
[AIAA PAPER 91-2343] p 59 A91-44204

- The application of neural networks to the SSME startup transient
[AIAA PAPER 91-2530] p 60 A91-44283
- Localization of aeroelastic modes in mistuned high-energy turbines
[AIAA PAPER 91-3379] p 198 A91-44319
- LN₂ spray droplet size measurement via ensemble diffraction technique
[AIAA PAPER 91-1381] p 129 A91-44336
- An experimental investigation of nozzle-exit boundary layers of highly heated free jets
[ASME PAPER 90-GT-255] p 155 A91-44662
- Computation of a circular-to-rectangular transition duct flow field
[AIAA PAPER 91-1741] p 156 A91-45547
- Simulations of free shear layers using a compressible k-epsilon model
[AIAA PAPER 91-1863] p 156 A91-45778
- A linear control design structure to maintain loop properties during limit operation in a multi-nozzle turbofan engine
[AIAA PAPER 91-1997] p 24 A91-45780
- Nonequilibrium in a low power arcjet nozzle
[AIAA PAPER 91-2113] p 61 A91-45784
- Microanalyses of extended-test xenon hollow cathodes
[AIAA PAPER 91-2123] p 61 A91-45787
- Design and experimental evaluation of compact radial-inflow turbines
[AIAA PAPER 91-2127] p 24 A91-45788
- Comparison of a quasi-3D analysis and experimental performance for three compact radial turbines
[AIAA PAPER 91-2128] p 25 A91-45789
- Experimental and analytical studies of flow through a ventral and axial exhaust nozzle system for STOVL aircraft
[AIAA PAPER 91-2135] p 25 A91-45791
- Plug nozzles - The ultimate customer driven propulsion system
[AIAA PAPER 91-2208] p 61 A91-45794
- A preliminary characterization of applied-field MPD thruster plumes
[AIAA PAPER 91-2339] p 62 A91-45798
- Experimental and analytical comparison of flowfields in a 110 N (25 Lbf) H₂/O₂ rocket
[AIAA PAPER 91-2283] p 62 A91-45802
- The development of a fiber optic Raman temperature measurement system for rocket flows
[AIAA PAPER 91-2316] p 173 A91-45804
- Numerical simulation of self-field MPD thrusters
[AIAA PAPER 91-2341] p 62 A91-45805
- Applied-field MPD thruster geometry effects
[AIAA PAPER 91-2342] p 62 A91-45806
- Synergistic use of high and low thrust propulsion systems for piloted missions to Mars
[AIAA PAPER 91-2346] p 39 A91-45807
- Performance and flow calculations for a gaseous H₂/O₂ thruster
p 63 A91-48843
- The dynamic effects of internal robots on Space Station Freedom
[AIAA PAPER 91-2822] p 40 A91-49764
- The effect of the near earth micrometeoroid environment on a mirror surface after 20 years in space
p 47 A91-49810
- Coplanar waveguide feeds for phased array antennas
[AIAA PAPER 91-3422] p 141 A91-52342
- MPD thruster technology
[AIAA PAPER 91-3568] p 65 A91-52444
- Space engine safety system
[AIAA PAPER 91-3604] p 44 A91-52470
- Neuromorphic learning of continuous-valued mappings from noise-corrupted data
p 219 A91-53201
- Combinatorial FSK modulation for power-efficient high-rate communications
[AIAA PAPER 91-3532] p 133 A91-53708
- Design issues for propulsion systems using metallized propellants
[AIAA PAPER 91-3484] p 66 A91-53709
- Production and use of metals and oxygen for lunar propulsion
[AIAA PAPER 91-3481] p 125 A91-53711
- YBCO superconducting ring resonators at millimeter-wave frequencies
p 142 A91-54532
- Sverdrup Technology, Inc., Cleveland, OH.**
Evolutionary use of nuclear electric propulsion
[AIAA PAPER 90-3821] p 50 A91-10174
- Spatial evolution of nonlinear acoustic mode instabilities on hypersonic boundary layers
p 225 A91-12973
- Satellite eclipse power by laser illumination
[IAF PAPER 90-053] p 50 A91-13766
- Reactionless orbital propulsion using tether deployment
[IAF PAPER 90-254] p 51 A91-13908
- 3D computation of hypersonic nozzle
[AIAA PAPER 90-5203] p 1 A91-14429

Numerical study of supersonic combustors by multi-block grids with mismatched interfaces [AIAA PAPER 90-5204] p 21 A91-14430

PoCr based high temperature static strain gage [AIAA PAPER 90-5236] p 170 A91-14462

Critical-point analysis of the liquid-vapor interfacial surface tension p 237 A91-16103

Icing tests of a model main rotor p 18 A91-17218

Ultrasonic imaging of textured alumina p 191 A91-18596

Newtonian mechanics of a many-particle assembly coupled to an external body potential p 237 A91-19495

Flow studies in close-coupled ventral nozzles for STOVL aircraft [SAE PAPER 901033] p 2 A91-21242

Combustion of liquid fuel droplets in supercritical conditions [AIAA PAPER 91-0078] p 105 A91-21362

Modern CFD applications for the design of a reacting shear layer facility [AIAA PAPER 91-0577] p 149 A91-21540

A time-accurate implicit method for chemically reacting flows at all Mach numbers [AIAA PAPER 91-0581] p 149 A91-21542

Nonlinear Reynolds stress model for turbulent shear flows [AIAA PAPER 91-0609] p 149 A91-21556

Inhomogeneous deformation in INCONEL 718 during monotonic and cyclic loadings p 108 A91-22287

Integrated flight/propulsion control system design based on a centralized approach p 36 A91-22950

Modern developments in shear flow control with swirl p 3 A91-24519

An evolutionary path to satellite solar power systems p 51 A91-26063

Results of a sub-scale model rotor icing test [AIAA PAPER 91-0660] p 19 A91-26190

Thermochemical analysis of the silicon carbide-alumina reaction with reference to liquid-phase sintering of silicon carbide p 114 A91-26506

Reaction of Ti and Ti-Al alloys with alumina p 91 A91-27937

Renormalization group analysis of anisotropic diffusion in turbulent shear flows p 150 A91-27946

Neural network architecture for crossbar switch control p 218 A91-29181

A neural net based architecture for the segmentation of mixed gray-level and binary pictures p 218 A91-29183

Robust eigenspace assignment using singular value sensitivities p 219 A91-29784

Partitioning methods for global controllers p 219 A91-30043

Silsesquioxane-derived ceramic fibres p 114 A91-30283

Use of rotating pinholes and reticles for calibration of cloud droplet instrumentation p 171 A91-30371

General-purpose interface bus for multiuser, multitasking computer system p 215 A91-35928

Test-cell pressure effects on the performance of resistojets p 38 A91-37417

Computational analysis of underexpanded jets in the hypersonic regime p 4 A91-37421

Comment on 'Negative matter propulsion' p 52 A91-37424

Autonomous power expert system p 54 A91-37972

High frequency, high temperature specific core loss and dynamic B-H hysteresis loop characteristics of soft magnetic alloys p 138 A91-37988

Electrical characterization of a Mapham inverter using pulse testing techniques p 139 A91-37992

An analysis of space power system masses p 54 A91-38003

Nonlinear evolution of subsonic and supersonic disturbances on a compressible free shear layer p 152 A91-39716

Numerical study of high-area-ratio H₂/O₂ rocket nozzles [AIAA PAPER 91-2434] p 57 A91-41780

An analysis of the contact sintering process in III-V solar cells p 139 A91-41891

Osher's scheme for real gases p 153 A91-42286

The influence of interstitial Ga and interfacial Au₂P₃ on the electrical and metallurgical behavior of Au-contacted III-V semiconductors p 140 A91-42694

Concurrent tailoring of fabrication process and interphase layer to reduce residual stresses in metal matrix composites p 92 A91-43232

Pressure-coupled vaporization and combustion responses of liquid-fuel droplets in high-pressure environments [AIAA PAPER 91-2310] p 106 A91-44192

An analysis of the viscous flow through a compact radial turbine by the average passage approach [ASME PAPER 90-GT-64] p 6 A91-44545

Axisymmetric jet forced by fundamental and subharmonic tones p 226 A91-45111

A study of hydrogen diffusion flames using PDF turbulence model [AIAA PAPER 91-1780] p 106 A91-45549

Analysis of the one-dimensional transient compressible vapor flow in heat pipes p 157 A91-47735

A resistance strain gage with repeatable apparent strain to 800 C p 198 A91-48899

Reaction of beta-phase Ni-Al alloys with CrB₂ p 92 A91-49943

High temperature superconducting thin film microwave circuits - Fabrication, characterization, and applications p 141 A91-50433

A resistance strain gage with repeatable and cancellable apparent strain for use to 1500 F p 173 A91-51930

Energy deposition in low-power coaxial plasma thrusters p 63 A91-52311

Antiproton powered propulsion with magnetically confined plasma engines p 63 A91-52313

Cathode phenomena in a low-power magnetoplasma dynamic thruster p 63 A91-52314

Laser photovoltaic power system synergy for SEI applications [AIAA PAPER 91-3419] p 207 A91-52339

Coplanar waveguide feeds for phased array antennas [AIAA PAPER 91-3422] p 141 A91-52342

Plans for the development of cryogenic engines for space exploration [AIAA PAPER 91-3438] p 64 A91-52351

Test facilities for high power electric propulsion [AIAA PAPER 91-3499] p 42 A91-52396

Computational fluid dynamics studies of nuclear rocket performance [AIAA PAPER 91-3577] p 66 A91-52450

Elastic response of (001)-oriented PWA 1480 single crystal - The influence of secondary orientation [SAE PAPER 911111] p 110 A91-53555

Mach 6.5 air induction system design for the Beta II Two-Stage-to-Orbit booster vehicle [AIAA PAPER 91-3196] p 43 A91-54099

Preliminary studies on NiAl/Nb₂Be₁₇ reaction and effectiveness of BeO as an interfacial reaction barrier p 92 A91-55050

Three-dimensional flows in a transonic compressor rotor p 8 A91-56152

A data acquisition and control program for axial-torsional fatigue testing p 199 A91-56540

Thermochemical analysis of chemical processes relevant to the stability and processing of SiC-reinforced Si₃N₄ composite p 94 A91-56961

Sverdrup Technology, Inc., Middleburg Heights, OH.

Use of piezoelectric actuators in active vibration control of rotating machinery p 179 A91-14400

Particle image fields and partial coherence p 171 A91-19604

Hydrogen-silicon carbide interactions p 114 A91-28783

Modeling of surface roughness effects on glaze ice accretion p 19 A91-35107

Factors which influence tensile strength of a SiC/Ti-24Al-11Nb (at. pct) composite p 92 A91-55900

Systems Control Technology, Inc., Palo Alto, CA.

Development of an intelligent diagnostic system for reusable rocket engine control [AIAA PAPER 91-2533] p 63 A91-45817

T

Technology Integration and Development Group, Inc., Billerica, MA.

In-service health monitoring of composite structures p 192 A91-51926

Texas A&M Univ., College Station.

Use of piezoelectric actuators in active vibration control of rotating machinery p 179 A91-14400

Temperature dependence of the elastic moduli and damping for polycrystalline LiF-22 pct CaF₂ eutectic salt p 87 A91-33793

A 29.3-GHz cavity-enclosed aperture-coupled circular-patch antenna for microwave circuit integration p 140 A91-47057

Texas Instruments, Inc., McKinney.

A 29.3-GHz cavity-enclosed aperture-coupled circular-patch antenna for microwave circuit integration p 140 A91-47057

Ka-band MMIC microstrip array for high rate communications [AIAA PAPER 91-3421] p 132 A91-52341

Texas Technological Univ., Lubbock.

Heat transfer in space systems; Proceedings of the Symposium, AIAA/ASME Thermophysics and Heat Transfer Conference, Seattle, WA, June 18-20, 1990 p 152 A91-38780

Texas Univ., Austin.

The dynamic instability of adiabatic blast waves p 239 A91-26361

YBCO superconducting ring resonators at millimeter-wave frequencies p 142 A91-54532

Texas Univ., San Antonio.

Quantification of uncertainties in coupled material degradation processes - High temperature, fatigue and creep [AIAA PAPER 91-0977] p 196 A91-31835

Tokyo Univ. (Japan).

Baryon isocurvature scenario in inflationary cosmology - A particle physics model and its astrophysical implications p 240 A91-54201

Toledo Univ., OH.

Cascade flutter analysis with transient response aerodynamics [AIAA PAPER 91-0747] p 21 A91-19448

Circular polarsation characteristics of stacked microstrip antennas p 131 A91-20370

Solution and sensitivity analysis of a complex transcendental eigenproblem with pairs of real eigenvalues p 195 A91-23685

Numerical simulations of supersonic flow through oscillating cascade sections p 4 A91-28590

Extension of transonic flow computational concepts in the analysis of cavitated bearings [ASME PAPER 90-TRIB-40] p 150 A91-29474

Experimental investigation of proplan aeroelastic response in off-axis flow with mistuning p 22 A91-30015

Aeroelastic modal characteristics of mistuned blade assemblies - Mode localization and loss of eigenstructure [AIAA PAPER 91-1218] p 196 A91-32032

Mutual coupling between electromagnetically coupled rectangular patch antennas p 137 A91-32822

Test-cell pressure effects on the performance of resistojets p 38 A91-37417

New approach in direct-simulation of gas mixtures [AIAA PAPER 91-1343] p 154 A91-43412

Numerical and experimental investigations of rarefied nozzle and plume flows of nitrogen [AIAA PAPER 91-1363] p 154 A91-43429

Localization of aeroelastic modes in mistuned high-energy turbines [AIAA PAPER 91-3379] p 198 A91-44319

Flutter analysis of cascades using a two dimensional Euler solver [AIAA PAPER 91-1681] p 6 A91-45548

Pressure measurements in a low-density nozzle plume for code verification [AIAA PAPER 91-2110] p 61 A91-45783

Primitive variable, strongly implicit calculation procedure for viscous flows at all speeds p 7 A91-46181

Semianalytical technique for sensitivity analysis of unsteady aerodynamic computations p 7 A91-48816

Application of an efficient hybrid scheme for aeroelastic analysis of advanced propellers p 7 A91-52315

Performance evaluation of land mobile satellite system under vegetative shadowing using differential multiple TCM and QPSK p 132 A91-53084

Study on the spectral efficiency of SFH-GMSK in land mobile telephone communication by direct simulation p 132 A91-53176

Application of finite-element-based solution technologies for viscoplastic structural analyses p 199 A91-55137

Three-dimensional flows in a transonic compressor rotor p 8 A91-56152

Finite element elastic-plastic-creep and cyclic life analysis of a cowl lip p 199 A91-56365

TRW, Inc., Cleveland, OH.

Heat transfer in space systems; Proceedings of the Symposium, AIAA/ASME Thermophysics and Heat Transfer Conference, Seattle, WA, June 18-20, 1990 p 152 A91-38780

TRW, Inc., Redondo Beach, CA.

Rapid thermal cycling of new technology solar array blanket coupons p 54 A91-38019

U

United Technologies Research Center, East Hartford, CT.

Experimental study of cross-stream mixing in a cylindrical duct [AIAA PAPER 91-2459] p 157 A91-45815

Universal Energy Systems, Inc., Dayton, OH.

Materials degradation in low earth orbit (LEO); Proceedings of the Symposium, 119th Annual Meeting of the Minerals, Metals, and Materials Society, Anaheim, CA, Feb. 17-22, 1990 p 116 A91-49801

University of Eastern Kentucky, Richmond.

An experimental apparatus for measuring surface resistance in the submillimeter-wavelength region
p 174 A91-54390

University of South Florida, Tampa.

Numerical simulation of Jet-A combustion approximated by improved propane chemical kinetics
[AIAA PAPER 91-1859] p 106 A91-45777

University of Southern California, Los Angeles.

Creep behavior of copper at intermediate temperatures.
II - Surface microstructural observations. III - A comparison with theory p 109 A91-47931

V**Varian Associates, Palo Alto, CA.**

Temperature coefficients of multijunction solar cells
p 172 A91-41921

Virginia Polytechnic Inst. and State Univ., Blacksburg.

Modeling of Space Station electric power system with EMTP p 55 A91-38040
Generalized conjugate-gradient methods for the Navier-Stokes equations
[AIAA PAPER 91-1556] p 5 A91-40730

W**Washington Univ., Saint Louis, MO.**

Computational modeling of the pressurization process in a NASP vehicle propellant tank experimental simulation
[AIAA PAPER 91-2407] p 124 A91-41771

Waterloo Univ. (Ontario).

A new Lagrangian random choice method for steady two-dimensional supersonic/hypersonic flow
[AIAA PAPER 91-1546] p 5 A91-40721

Wayne State Univ., Detroit, MI.

Jet-A fuel evaporation analysis in conical tube injectors
[AIAA PAPER 91-0345] p 149 A91-21467

Wichita State Univ., KS.

Experimental water droplet impingement data on modern aircraft surfaces
[AIAA PAPER 91-0445] p 2 A91-21493

Wisconsin Univ., Milwaukee.

Heat transfer in space systems; Proceedings of the Symposium, AIAA/ASME Thermophysics and Heat Transfer Conference, Seattle, WA, June 18-20, 1990
p 152 A91-38780

Wittenberg Univ., Springfield, OH.

Neutron and gamma irradiation effects on power semiconductor switches p 139 A91-38162
Neutron, gamma ray and post-irradiation thermal annealing effects on power semiconductor switches
[AIAA PAPER 91-3525] p 142 A91-52420

Wright Research Development Center,**Wright-Patterson AFB, OH.**

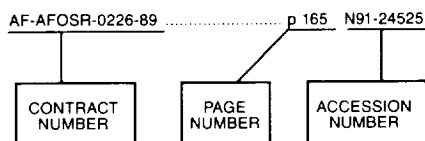
Analysis of the one-dimensional transient compressible vapor flow in heat pipes p 157 A91-47735

Wright State Univ., Dayton, OH.

A PCM/forced convection conjugate transient analysis of energy storage systems with annular and countercurrent flows p 150 A91-27166
Analysis of the one-dimensional transient compressible vapor flow in heat pipes p 157 A91-47735

CONTRACT NUMBER INDEX

Typical Contract Number Index Listing



Listings in this index are arranged alphanumerically by contract number. Under each contract number the accession numbers denoting documents that have been produced as a result of research done under that contract are arranged in ascending order. The accession number denotes the number by which the citation is identified.

AF-AFOSR-0226-89 p 165 N91-24525
 AF-AFOSR-89-0226 p 154 A91-42588
 AF-AFOSR-89-0346 p 154 A91-42599
 AF-AFOSR-89-0403 p 153 A91-42549
 p 7 A91-46181
 DA PROJ. 1L1-61101-AH-45 p 165 N91-23439
 DA PROJ. 1L1-61102-AH-45 p 159 N91-12913
 p 20 N91-15146
 p 160 N91-16304
 p 160 N91-19369
 p 13 N91-20044
 p 99 N91-21243
 p 185 N91-22566
 p 31 N91-23179
 p 101 N91-26233
 p 102 N91-29250
 p 195 N91-30546
 p 35 N91-31178
 p 220 N91-31876
 DA PROJ. 1L1-62099-AH-76 p 188 N91-25412
 DA PROJ. 1L1-62209-A-47A p 188 N91-25411
 DA PROJ. 1L1-6221-A-47A p 188 N91-27558
 DA PROJ. 1L1-62211-A-47-A p 26 N91-11752
 p 184 N91-21531
 p 185 N91-21534
 p 99 N91-22402
 p 186 N91-22570
 p 186 N91-23500
 p 187 N91-23513
 DA PROJ. 1L1-62211-A-47A p 187 N91-25395
 p 189 N91-27569
 p 189 N91-27570
 p 189 N91-29599
 p 190 N91-29600
 p 190 N91-30533
 p 190 N91-30537
 p 35 N91-31181
 p 191 N91-31648
 p 191 N91-31654
 DA PROJ. 1L1-62211-37-A p 187 N91-23514
 DA PROJ. 1L1-6221147-A p 183 N91-12956
 DA PROJ. 1L1-66211-A-47-A p 186 N91-22568
 DAAL03-87-K-0007 p 136 A91-22987
 DAAL04-86-C-0030 p 119 N91-18302
 DE-AB29-79ET-20370 p 191 A91-31064
 DE-AC02-76CH-00016 p 237 N91-31977
 DE-AC02-76ER-01198 p 108 A91-22287
 DE-AC02-76ER-01545 p 240 A91-45907
 DE-AC02-83CH-10093 p 207 A91-41966
 DE-AC02-83ER-40105 p 240 A91-45907
 DE-AC02-88ER-13895 p 91 A91-16889

DE-AC03-76SF-00098 p 148 A91-19138
 DE-AC05-80ER-10742 p 237 N91-31977
 DE-AC05-84OR-21400 p 128 N91-14498
 p 123 N91-28418
 DE-AC06-76RL-01830 p 229 N91-18799
 DE-AC07-76ID-01570 p 215 A91-52331
 DE-AI01-76ET-20320 p 94 N91-10127
 p 228 N91-16679
 DE-AI01-85CE-50162 p 95 N91-15318
 p 120 N91-21302
 DE-AI03-86SF-16310 p 111 N91-16128
 p 112 N91-29298
 DE-AI04-85AL-33408 p 238 N91-31023
 DE-AI05-87OR-21749 p 121 N91-23311
 DE-AM03-76SF-00113 p 109 A91-47931
 DE-AT03-76ER-10403 p 109 A91-47931
 DE-A103-86SF-16310 p 110 N91-14454
 DNA001-84-C-0046 p 192 A91-56972
 DNA001-86-C-0010 p 192 A91-56972
 FY1455-89-N-0655 p 139 A91-37992
 F33615-85-C-5116 p 192 A91-56972
 F33615-88-C-2820 p 150 A91-27166
 p 157 A91-47735
 F49620-89-C-0096 p 164 N91-21090
 JPL-954997 p 63 A91-52311
 p 63 A91-52314
 MOESC-02740189 p 240 A91-54201
 NAGW-1320 p 239 A91-19545
 NAGW-1321 p 238 A91-12343
 p 240 A91-37428
 p 240 A91-45907
 p 240 A91-46543
 NAGW-1340 p 238 A91-12343
 p 239 A91-19545
 p 239 A91-20430
 p 239 A91-20491
 p 224 A91-22894
 p 239 A91-26361
 p 239 A91-28714
 p 239 A91-33573
 p 240 A91-37428
 p 240 A91-37444
 p 240 A91-43291
 p 240 A91-46543
 p 240 A91-54201
 NAGW-1356 p 154 A91-43576
 NAGW-2022 p 242 N91-15117
 p 242 N91-33046
 NAGW-951 p 148 A91-13456
 NAGW-798 p 148 A91-13456
 NAGW-954 p 154 A91-42588
 p 165 N91-24525
 NAG3-1008 p 196 A91-28612
 NAG3-1009 p 105 A91-21481
 NAG3-1027 p 215 N91-23032
 NAG3-1047 p 181 A91-41682
 p 187 N91-23514
 NAG3-1079 p 109 A91-48509
 p 110 A91-55472
 NAG3-1097 p 181 A91-38154
 NAG3-1098 p 3 A91-24519
 NAG3-1100 p 192 N91-17407
 p 238 N91-24952
 p 238 N91-33014
 NAG3-1101 p 91 A91-31919
 NAG3-1112 p 106 A91-45777
 NAG3-1115 p 24 A91-45782
 NAG3-1120 p 55 A91-38040
 NAG3-1137 p 6 A91-45548
 p 201 N91-19475
 NAG3-1140 p 149 A91-21467
 NAG3-1143 p 148 A91-19138
 NAG3-1156 p 124 A91-41771
 NAG3-1163 p 196 A91-32032
 p 198 A91-44319
 p 204 N91-24659
 p 205 N91-27591
 NAG3-1232 p 23 A91-41671
 NAG3-1263 p 190 N91-29600
 NAG3-154 p 119 N91-18302
 NAG3-157 p 132 A91-53084
 p 132 A91-53176
 NAG3-230 p 14 N91-21061

NAG3-2696 p 232 A91-41893
 NAG3-3139 p 6 A91-45548
 NAG3-376 p 18 N91-31106
 NAG3-484 p 167 N91-25367
 NAG3-519 p 214 N91-32556
 NAG3-566 p 2 A91-21493
 NAG3-571 p 21 A91-19580
 NAG3-577 p 38 A91-37417
 NAG3-666 p 19 A91-35107
 NAG3-688 p 104 A91-12925
 NAG3-696 p 234 N91-14050
 NAG3-724 p 4 A91-34135
 NAG3-728 p 193 N91-18193
 NAG3-730 p 7 A91-52315
 NAG3-732 p 224 A91-12427
 NAG3-742 p 198 A91-44319
 p 204 N91-24659
 p 205 N91-27591
 p 102 N91-26234
 NAG3-749 p 179 A91-14400
 NAG3-763 p 105 A91-41749
 NAG3-796 p 176 N91-19404
 NAG3-832 p 71 N91-19176
 NAG3-833 p 164 N91-21090
 NAG3-877 p 91 A91-16889
 NAG3-882 p 104 A91-19431
 NAG3-925 p 156 A91-45797
 NAG3-929 p 156 A91-45811
 p 157 A91-48758
 NAG3-949 p 129 A91-23108
 NAG3-964 p 188 N91-27558
 NAG3-969 p 180 A91-21071
 p 182 A91-41700
 NAG3-983 p 6 A91-45548
 NAG3-984 p 170 A91-19582
 p 174 A91-55530
 NAG3-988 p 136 A91-22987
 p 233 A91-53236
 NAG3-992 p 41 A91-27702
 p 53 A91-37932
 NAG3-997 p 221 A91-45109
 p 157 A91-48758
 NASA ORDER C-30004-J p 51 A91-30010
 NASA ORDER C-30007-K p 234 N91-11555
 NASA ORDER C-30018-M p 234 N91-11555
 NASA ORDER C-99066-G p 221 A91-31175
 p 151 A91-34132
 p 58 A91-42725
 p 158 A91-54268
 p 159 N91-11192
 p 160 N91-14559
 p 221 N91-14781
 p 161 N91-19375
 p 221 N91-19786
 p 163 N91-21071
 p 163 N91-21082
 p 163 N91-21083
 p 164 N91-22524
 p 165 N91-22536
 p 165 N91-23416
 p 16 N91-24124
 p 166 N91-24541
 p 204 N91-24659
 p 222 N91-24817
 p 101 N91-25198
 p 205 N91-27591
 p 223 N91-30865
 p 169 N91-31597
 p 223 N91-31911
 p 170 N91-32460
 p 165 N91-24525
 NASA ORDER C-99066-6 p 215 N91-20630
 NASW-4300 p 2 A91-21065
 NAS2-12635 p 74 N91-23233
 NAS3-22238 p 104 A91-19432
 NAS3-22822 p 184 N91-19443
 NAS3-23691 p 155 A91-44662
 NAS3-23708 p 106 A91-51449
 NAS3-23901 p 1 A91-14429
 NAS3-24105 p 4 A91-30014
 p 69 N91-11799
 p 228 N91-19825
 NAS3-24380 p 93 A91-55918

CONTRACT

C-5

NAS3-24816

CONTRACT NUMBER INDEX

NAS3-24816	p 177	N91-26490	NCC3-192	p 146	N91-27445		p 224	N91-26872
NAS3-25062	p 46	A91-29799	NCC3-19	p 115	A91-35949		p 168	N91-30461
	p 126	N91-24263		p 72	N91-20204	RTOP 505-62-01	p 175	N91-10271
NAS3-25070	p 121	N91-21307	NCC3-203	p 145	N91-25320		p 176	N91-19404
NAS3-25134	p 174	A91-55533	NCC3-56	p 3	A91-24519		p 36	N91-20133
NAS3-25208	p 151	A91-38126	NCC3-63	p 102	N91-26234	RTOP 505-62-10	p 33	N91-25148
	p 158	A91-52395	NCC3-72	p 87	A91-33793	RTOP 505-62-12	p 15	N91-23083
NAS3-25226	p 54	A91-38019		p 109	A91-47931	RTOP 505-62-38	p 40	N91-19115
NAS3-25266	p 1	A91-14429	NCC3-73	p 113	A91-18675		p 31	N91-20126
	p 21	A91-14430	NCC3-76	p 109	A91-39292	RTOP 505-62-30	p 77	N91-25175
	p 148	A91-16073	NCC3-81	p 99	N91-21243	RTOP 505-62-31	p 161	N91-19372
	p 237	A91-16103	NCC3-89	p 121	N91-22460		p 161	N91-19374
	p 226	A91-18257	NGL-22-009-640	p 19	A91-35107	RTOP 505-62-4D	p 226	N91-10703
	p 237	A91-19495	NGT-40016	p 146	N91-30426		p 227	N91-11495
	p 2	A91-21393	NGT-50532	p 149	A91-21542		p 69	N91-11799
	p 150	A91-27946	NSF ASC-87-19573	p 221	N91-14781		p 227	N91-12316
	p 4	A91-30014	NSF AST-88-20595	p 240	A91-45907		p 228	N91-19825
	p 54	A91-37972	NSF AST-88-22595	p 238	A91-12343	RTOP 505-62-40	p 227	N91-11493
	p 54	A91-38003		p 240	A91-37428		p 18	N91-29150
	p 57	A91-41780	NSF DMR-87-15622	p 114	A91-28763	RTOP 505-62-41	p 26	N91-13455
	p 139	A91-41891		p 114	A91-28767	RTOP 505-62-50	p 234	N91-14850
	p 153	A91-42286	NSF DMR-88-10058	p 109	A91-39292		p 30	N91-20122
	p 46	A91-42522		p 112	N91-27324		p 176	N91-20453
	p 140	A91-42694	NSF DMS-87-01543	p 221	N91-14781		p 31	N91-21137
	p 154	A91-43576	NSF DMS-88-14553	p 154	A91-42588		p 31	N91-21140
	p 59	A91-44151		p 165	N91-24525		p 37	N91-22135
	p 60	A91-44283	NSF DMS-89-02831	p 148	A91-19138		p 236	N91-22921
	p 198	A91-44319	NSF ECS-86-57951	p 137	A91-35911		p 236	N91-23946
	p 106	A91-45549	NSF ISI-90-60142	p 214	N91-32562		p 220	N91-24815
	p 25	A91-45789	NSF MSM-86-11164	p 154	A91-42588		p 177	N91-25382
	p 63	A91-48843		p 165	N91-24525		p 177	N91-25387
	p 66	A91-52450	NSG-3139	p 21	A91-19448		p 21	N91-27157
	p 133	A91-53708	NSG-3188	p 182	A91-41683		p 37	N91-27167
	p 43	A91-54099		p 186	N91-22570		p 178	N91-27511
	p 94	N91-10127	NSG-931	p 240	A91-45907		p 178	N91-27521
	p 11	N91-13421	N00014-88-C-0391	p 214	N91-32562		p 35	N91-29188
	p 234	N91-14050	N00014-89-J-1006	p 146	N91-27445		p 37	N91-32143
	p 130	N91-14500	N60921-86-C-A226	p 232	A91-42170	RTOP 505-62-52	p 70	N91-15303
	p 11	N91-17000	RC-471035	p 145	N91-25320		p 11	N91-17000
	p 71	N91-19176	RTOP 307-50-00	p 100	N91-24345		p 13	N91-19053
	p 241	N91-20015	RTOP 307-51-00	p 106	N91-19256		p 13	N91-19063
	p 27	N91-20084		p 120	N91-19296		p 176	N91-19402
	p 144	N91-20406		p 235	N91-21910		p 184	N91-19443
	p 44	N91-21182		p 186	N91-23501		p 221	N91-20830
	p 202	N91-21558	RTOP 316-30-19	p 134	N91-23347		p 14	N91-21060
	p 145	N91-22508		p 135	N91-32287		p 14	N91-21061
	p 203	N91-23548	RTOP 316-60-13	p 48	N91-20184		p 164	N91-21448
	p 203	N91-23550	RTOP 321-01-00	p 135	N91-29431		p 164	N91-21458
	p 211	N91-23620	RTOP 323-53-62	p 44	N91-21182		p 15	N91-22084
	p 75	N91-24232	RTOP 326-31-15	p 71	N91-19178		p 16	N91-23089
	p 100	N91-24359	RTOP 326-81-10	p 241	N91-14259		p 31	N91-23179
	p 204	N91-24659		p 211	N91-23620		p 165	N91-23409
	p 217	N91-25680		p 81	N91-28278		p 16	N91-24130
	p 34	N91-27164	RTOP 342-02-00	p 46	N91-21184		p 16	N91-24131
	p 81	N91-28277	RTOP 474-12-10	p 183	N91-12954		p 100	N91-24359
	p 206	N91-28627		p 193	N91-19462		p 166	N91-24527
	p 35	N91-29188		p 162	N91-20417		p 167	N91-24550
	p 82	N91-29230		p 216	N91-20765		p 215	N91-24745
	p 135	N91-29404		p 217	N91-22766		p 228	N91-25617
	p 35	N91-30142		p 49	N91-24225		p 17	N91-26121
	p 83	N91-30238		p 79	N91-27204		p 34	N91-27159
	p 84	N91-30239		p 39	N91-29199		p 167	N91-27489
	p 178	N91-30491	RTOP 474-17-10	p 215	N91-20630		p 178	N91-27510
	p 18	N91-32075	RTOP 474-42-10	p 78	N91-26202		p 188	N91-27559
	p 242	N91-33046		p 79	N91-27206		p 168	N91-29525
NAS3-25274	p 128	N91-19320		p 79	N91-27207		p 39	N91-30163
NAS3-25347	p 48	N91-20727		p 218	N91-28776		p 168	N91-30472
NAS3-25366	p 6	A91-43631		p 84	N91-30266		p 169	N91-30473
NAS3-25368	p 128	A91-53408		p 85	N91-30267		p 169	N91-30476
NAS3-25624	p 171	A91-30634	RTOP 474-46-10	p 213	N91-31708		p 223	N91-30867
NAS3-25629	p 8	A91-54061	RTOP 474-52-01	p 69	N91-11802		p 18	N91-31106
NAS3-25776	p 126	N91-20324	RTOP 474-52-10	p 71	N91-19177		p 18	N91-32074
	p 166	N91-24548		p 73	N91-22367	RTOP 505-62-71	p 169	N91-32440
NAS3-25787	p 91	A91-28014		p 78	N91-25184		p 26	N91-13457
	p 97	N91-19233		p 79	N91-27209		p 15	N91-21116
NAS3-25799	p 52	A91-31026		p 84	N91-30265		p 33	N91-24201
NAS3-25810	p 124	A91-10112	RTOP 474-74-10	p 42	N91-30186	RTOP 505-62-84	p 176	N91-19401
NAS3-25823	p 63	A91-45817	RTOP 505-01-01	p 98	N91-19234	RTOP 505-62-91	p 14	N91-21115
NAS3-25834	p 33	N91-26146	RTOP 505-02-22	p 161	N91-19373		p 17	N91-26122
NAS3-25867	p 233	A91-53236	RTOP 505-05-10	p 32	N91-23186		p 17	N91-27129
NAS3-25960	p 42	A91-52350	RTOP 505-10-03	p 218	N91-24796	RTOP 505-63-01	p 110	N91-10150
NAS3-25967	p 181	A91-41680	RTOP 505-10-50	p 122	N91-25286	RTOP 505-63-1A	p 159	N91-12913
	p 23	A91-41788	RTOP 505-12-33	p 217	N91-25680		p 96	N91-15329
	p 157	A91-45815	RTOP 505-33-1A	p 110	N91-10149		p 111	N91-15390
	p 32	N91-23185	RTOP 505-41-41	p 88	N91-11062		p 160	N91-16304
	p 34	N91-29187	RTOP 505-43-11	p 234	N91-14050		p 89	N91-19224
NAS3-28524	p 196	A91-31957	RTOP 505-44-2C	p 144	N91-20406		p 89	N91-22377
NCC2-582	p 154	A91-43429	RTOP 505-61-52	p 27	N91-20084		p 89	N91-22379
NCC3-105	p 141	A91-50443		p 222	N91-22814		p 101	N91-25186
NCC3-111	p 107	N91-22410	RTOP 505-62-OK	p 26	N91-11752		p 90	N91-29235
NCC3-151	p 109	A91-47747		p 20	N91-15146		p 168	N91-30469
NCC3-153	p 13	N91-19054		p 188	N91-25412	RTOP 505-63-1B	p 199	N91-10332
NCC3-162	p 120	N91-19296		p 35	N91-31178		p 200	N91-14632
NCC3-168	p 153	A91-42541	RTOP 505-62-OK	p 184	N91-21531		p 27	N91-15174
NCC3-171	p 154	A91-43412	RTOP 505-62-OU	p 220	N91-31876		p 12	N91-17002
NCC3-180	p 169	N91-30476	RTOP 505-62-00	p 27	N91-20086		p 119	N91-19292

CONTRACT NUMBER INDEX

RTOP 591-14-11

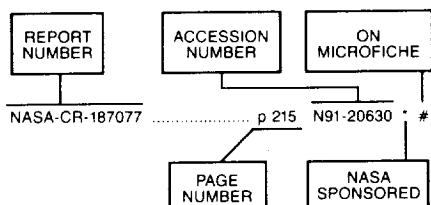
	p 184 N91-19441		p 242 N91-33046		p 102 N91-29250
	p 184 N91-19442	RTOP 506-41-21	p 208 N91-15628		p 195 N91-30546
	p 201 N91-19473		p 74 N91-22375	RTOP 510-01-1A	p 194 N91-28605
	p 202 N91-21559		p 74 N91-22376	RTOP 510-01-50	p 95 N91-13495
	p 121 N91-22460		p 74 N91-23233		p 193 N91-19464
	p 186 N91-23512	RTOP 506-41-31	p 213 N91-32549		p 99 N91-21243
	p 187 N91-24593		p 166 N91-24549		p 121 N91-21309
	p 206 N91-28627	RTOP 506-41-41	p 80 N91-27214		p 99 N91-22402
	p 103 N91-30282		p 94 N91-10134		p 107 N91-22410
RTOP 505-63-1M	p 119 N91-19293		p 192 N91-17407		p 101 N91-24361
	p 121 N91-23311		p 97 N91-19231		p 205 N91-24660
RTOP 505-63-10	p 90 N91-27221		p 73 N91-22370		p 101 N91-25195
RTOP 505-63-113	p 26 N91-13456		p 145 N91-22508		p 205 N91-25442
RTOP 505-63-11	p 95 N91-14426		p 238 N91-24952		p 102 N91-27247
RTOP 505-63-31	p 102 N91-26234		p 77 N91-25173		p 112 N91-27324
RTOP 505-63-36	p 186 N91-22568		p 223 N91-25749		p 194 N91-29610
	p 186 N91-22570		p 146 N91-27444		p 206 N91-30566
	p 186 N91-23500		p 103 N91-32177		p 103 N91-31235
	p 187 N91-23513		p 238 N91-33014	RTOP 510-10-01	p 100 N91-23247
	p 188 N91-27558	RTOP 506-41-51	p 80 N91-27213	RTOP 510-10-50	p 97 N91-19229
	p 189 N91-27569	RTOP 506-42-00	p 68 N91-11797		p 101 N91-25198
	p 189 N91-27570		p 69 N91-11800		p 102 N91-30281
	p 189 N91-29599		p 70 N91-13491	RTOP 535-03-01	p 12 N91-19045
	p 190 N91-29600		p 71 N91-19175		p 16 N91-24107
	p 190 N91-30533		p 76 N91-24304		p 206 N91-28627
	p 190 N91-30537		p 81 N91-29220	RTOP 535-03-10	p 227 N91-11494
	p 191 N91-31654	RTOP 506-42-11	p 67 N91-10119		p 228 N91-15842
RTOP 505-63-40	p 96 N91-15328	RTOP 506-42-31	p 67 N91-10118		p 201 N91-19475
RTOP 505-63-5A	p 130 N91-11945		p 68 N91-11060		p 17 N91-25106
	p 160 N91-19369		p 68 N91-11796		p 18 N91-32075
	p 99 N91-20228		p 69 N91-11798	RTOP 535-05-01	p 26 N91-14349
	p 99 N91-22396		p 72 N91-19180		p 27 N91-19098
	p 165 N91-23439		p 77 N91-25172	RTOP 535-05-10	p 217 N91-25630
	p 190 N91-30539		p 81 N91-29228		p 35 N91-30142
RTOP 505-63-5B	p 201 N91-19475		p 82 N91-29229	RTOP 537-01-11	p 33 N91-24203
	p 201 N91-19477		p 82 N91-29230		p 35 N91-31181
	p 216 N91-20748		p 82 N91-29231	RTOP 537-01-22	p 34 N91-29181
	p 185 N91-22567		p 82 N91-30202	RTOP 537-02-00	p 19 N91-23098
	p 186 N91-22571		p 84 N91-30252	RTOP 537-02-11	p 31 N91-22126
	p 187 N91-23515		p 85 N91-31212	RTOP 537-02-20	p 126 N91-22464
	p 203 N91-23550		p 85 N91-31216		p 34 N91-27165
	p 188 N91-25413		p 179 N91-31605	RTOP 537-02-21	p 32 N91-23185
	p 190 N91-30532		p 86 N91-32158		p 33 N91-24202
	p 103 N91-32181		p 86 N91-32162		p 33 N91-26146
RTOP 505-63-51	p 103 N91-32182	RTOP 506-42-51	p 70 N91-15308		p 34 N91-29187
	p 183 N91-12956	RTOP 506-42-72	p 76 N91-24303	RTOP 553-13-00	p 199 N91-12114
	p 185 N91-21534		p 86 N91-31220		p 230 N91-14829
	p 185 N91-22566		p 127 N91-31318		p 200 N91-17415
	p 187 N91-23514	RTOP 506-42-73	p 126 N91-25300		p 200 N91-18452
	p 188 N91-25411		p 86 N91-32161		p 201 N91-19472
	p 191 N91-31648	RTOP 506-43-11	p 118 N91-11922		p 111 N91-20268
RTOP 505-63-52	p 200 N91-17427		p 119 N91-19294		p 202 N91-21558
	p 201 N91-19476		p 193 N91-19463		p 222 N91-21797
	p 203 N91-22594		p 194 N91-21553		p 76 N91-24307
RTOP 505-63-56	p 187 N91-25395		p 194 N91-27575		p 100 N91-24360
RTOP 505-68-10	p 11 N91-14310		p 112 N91-32216		p 205 N91-25436
	p 12 N91-19046	RTOP 506-44-00	p 227 N91-12317		p 222 N91-27886
	p 12 N91-19047	RTOP 506-44-2B	p 134 N91-19332		p 223 N91-27901
	p 15 N91-23086	RTOP 506-44-2C	p 146 N91-27477		p 205 N91-28622
	p 15 N91-23087	RTOP 506-44-20	p 234 N91-10780	RTOP 582-01-11	p 216 N91-12215
RTOP 505-68-11	p 11 N91-13421		p 133 N91-11988		p 118 N91-14482
	p 11 N91-14309	RTOP 506-44-21	p 143 N91-19351		p 98 N91-19235
	p 32 N91-23183		p 235 N91-19935		p 219 N91-19766
	p 32 N91-23184		p 145 N91-25320		p 131 N91-23340
RTOP 505-69-01	p 72 N91-20206		p 237 N91-29982		p 131 N91-24469
RTOP 505-69-50	p 35 N91-30141	RTOP 506-48-00	p 126 N91-19317	RTOP 582-01-21	p 67 N91-10117
RTOP 505-69-51	p 27 N91-19097		p 126 N91-24460		p 85 N91-31208
RTOP 505-69-61	p 228 N91-15848		p 131 N91-24470	RTOP 582-01-41	p 220 N91-25696
RTOP 505-80-21	p 17 N91-28136		p 166 N91-24547	RTOP 590-13-11	p 200 N91-12980
RTOP 505-90-01	p 159 N91-13638		p 166 N91-24548		p 110 N91-14454
	p 162 N91-20445		p 49 N91-25161		p 111 N91-16128
	p 167 N91-27487		p 167 N91-25351		p 40 N91-19112
RTOP 505-90-51	p 112 N91-30318		p 243 N91-30073		p 71 N91-19179
	p 112 N91-32204	RTOP 506-48-21	p 168 N91-28538		p 74 N91-23234
RTOP 505-90-52	p 112 N91-32215	RTOP 506-49-21	p 73 N91-21240		p 75 N91-24232
RTOP 506-41-11	p 67 N91-11058	RTOP 506-59-4C	p 133 N91-18297		p 78 N91-25182
	p 68 N91-11061		p 146 N91-27445		p 212 N91-25510
	p 69 N91-11801		p 146 N91-30426		p 212 N91-26592
	p 242 N91-15117	RTOP 506-62-21	p 164 N91-21447		p 224 N91-26870
	p 70 N91-15306	RTOP 509-10-03	p 81 N91-29221		p 79 N91-27208
	p 48 N91-19165	RTOP 510-01-0A	p 192 N91-15565		p 212 N91-27611
	p 71 N91-19176		p 96 N91-17143		p 123 N91-29332
	p 72 N91-19182		p 97 N91-19230		p 146 N91-30427
	p 144 N91-19354		p 98 N91-19236		p 214 N91-32569
	p 241 N91-20015		p 98 N91-19237	RTOP 590-13-31	p 147 N91-32410
	p 144 N91-20392		p 203 N91-23548		p 147 N91-32412
	p 145 N91-21433		p 101 N91-26233	RTOP 590-13-41	p 177 N91-25381
	p 74 N91-22371		p 206 N91-32520	RTOP 590-21-11	p 175 N91-11205
	p 211 N91-23616	RTOP 510-01-01	p 94 N91-11074		p 120 N91-19295
	p 146 N91-27447		p 159 N91-12034	RTOP 590-21-21	p 72 N91-21233
	p 81 N91-29222		p 130 N91-14500		p 76 N91-24305
	p 82 N91-30203		p 96 N91-16075	RTOP 590-21-41	p 184 N91-20489
	p 44 N91-31196		p 97 N91-19232		p 89 N91-24341
	p 85 N91-31217		p 97 N91-19233		p 217 N91-24787
	p 86 N91-31218		p 120 N91-19308		p 86 N91-32163
	p 237 N91-31977		p 194 N91-23521	RTOP 591-14-11	p 78 N91-25183

RTOP 591-14-41
CONTRACT NUMBER INDEX

RTOP 591-14-41	p 81	N91-28277
RTOP 591-23-00	p 72	N91-20204
RTOP 591-41-21	p 127	N91-27375
	p 159	N91-10249
	p 68	N91-11059
	p 70	N91-15301
	p 13	N91-20045
RTOP 593-12-21	p 76	N91-24302
RTOP 593-21-00	p 43	N91-25159
RTOP 593-31-1A	p 243	N91-29138
RTOP 593-71-00	p 77	N91-25179
RTOP 643-10-01	p 135	N91-32247
RTOP 650-60-20	p 143	N91-19349
	p 144	N91-20393
	p 48	N91-21185
	p 134	N91-23354
	p 134	N91-27436
	p 135	N91-27437
RTOP 650-60-21	p 135	N91-29404
	p 135	N91-29405
RTOP 674-21-05	p 128	N91-19320
RTOP 674-24-05	p 159	N91-14556
RTOP 674-29-05	p 128	N91-24464
RTOP 679-40-00	p 143	N91-19348
	p 134	N91-22494
	p 20	N91-23102
RTOP 694-03-0A	p 160	N91-19371
RTOP 694-03-00	p 178	N91-30491
RTOP 694-03-03	p 175	N91-14574
	p 130	N91-19324
	p 203	N91-22604
RTOP 763-01-41	p 38	N91-11770
	p 202	N91-21562
	p 203	N91-23549
RTOP 763-21-41	p 190	N91-30538
RTOP 763-22-21	p 127	N91-28449
RTOP 776-33-41	p 94	N91-10127
	p 228	N91-16679
RTOP 776-81-63	p 238	N91-31023
RTOP 778-34-22	p 95	N91-15318
	p 120	N91-21302
SVERDRUP-5324-85	p 67	N91-10117
505-62-21	p 133	N91-10208
	p 159	N91-11192
	p 10	N91-11675
	p 10	N91-11676
	p 175	N91-12064
	p 11	N91-13420
	p 160	N91-14559
	p 221	N91-14781
	p 11	N91-15134
	p 125	N91-15418
	p 12	N91-19044
	p 13	N91-19054
	p 160	N91-19370
	p 161	N91-19375
	p 221	N91-19786
	p 13	N91-20044
	p 14	N91-21062
	p 40	N91-22139
	p 164	N91-22524
	p 165	N91-22536
	p 165	N91-23416
	p 16	N91-24124
	p 165	N91-24525
	p 166	N91-24541
	p 204	N91-24659
	p 222	N91-24817
	p 222	N91-24818
	p 222	N91-25739
	p 34	N91-27164
	p 205	N91-27591
	p 168	N91-30462
	p 223	N91-30865
	p 169	N91-31597
	p 223	N91-31911
	p 169	N91-32458
	p 169	N91-32459
	p 170	N91-32460

REPORT/ACCESSION NUMBER INDEX

Typical Report Number
Index Listing



Listings in this index are arranged alphanumerically by report number. The accession number denotes the number by which the citation is identified. An asterisk (*) indicates that the item is a NASA report. A pound sign (#) indicates that the item is available on microfiche.

AD-A229668 p 26 N91-11752 * #
 AD-A229669 p 159 N91-12913 * #
 AD-A231725 p 200 N91-14632 * #
 AD-A231726 p 160 N91-16304 * #
 AD-A231727 p 160 N91-19369 * #
 AD-A235644 p 121 N91-21307 * #
 AD-A235915 p 184 N91-21531 * #
 AD-A235926 p 99 N91-21243 * #
 AD-A237143 p 187 N91-23514 * #
 AD-A237671 p 165 N91-23439 * #
 AD-A239497 p 186 N91-22570 * #
 AD-A239498 p 187 N91-25395 * #
 AD-A239499 p 185 N91-22566 * #
 AD-A239500 p 186 N91-23500 * #
 AD-A239501 p 186 N91-22568 * #
 AD-A239502 p 101 N91-26233 * #
 AD-A239503 p 99 N91-22402 * #
 AD-A240066 p 188 N91-27558 * #
 AD-A240071 p 21 N91-27157 * #
 AD-A240126 p 189 N91-27570 * #
 AD-A240289 p 188 N91-25412 * #
 AD-A240930 p 31 N91-23179 * #
 AD-A241256 p 191 N91-31654 * #
 AD-A241468 p 35 N91-31178 * #
 AD-A241469 p 220 N91-31876 * #
 AD-A241470 p 189 N91-27569 * #
 AD-A241587 p 190 N91-30533 * #
 AD-A241588 p 190 N91-29600 * #
 AD-A242473 p 13 N91-20044 * #

AIAA PAPER 89-3519 p 31 N91-21137 * #
 AIAA PAPER 90-2268 p 4 A91-40561 * #
 AIAA PAPER 90-2268 p 15 N91-21116 * #
 AIAA PAPER 90-2400 p 26 N91-14349 * #
 AIAA PAPER 90-2450 p 104 A91-12927 * #
 AIAA PAPER 90-2527 p 69 N91-11798 * #
 AIAA PAPER 90-2543 p 72 N91-19180 * #
 AIAA PAPER 90-2552 p 87 N91-32164 * #
 AIAA PAPER 90-2582 p 67 N91-10118 * #
 AIAA PAPER 90-2649 p 68 N91-11796 * #
 AIAA PAPER 90-3593 p 41 A91-11471 * #
 AIAA PAPER 90-3681 p 44 A91-11472 * #
 AIAA PAPER 90-3708 p 50 A91-10107 * #
 AIAA PAPER 90-3713 p 124 A91-10112 * #
 AIAA PAPER 90-3821 p 50 A91-10174 * #
 AIAA PAPER 90-3824 p 40 A91-10176 * #
 AIAA PAPER 90-3911 p 224 A91-12427 * #
 AIAA PAPER 90-3911 p 13 N91-19053 * #
 AIAA PAPER 90-3932 p 224 A91-12448 * #
 AIAA PAPER 90-3932 p 227 N91-11494 * #
 AIAA PAPER 90-3933 p 224 A91-12449 * #
 AIAA PAPER 90-3933 p 226 N91-10703 * #
 AIAA PAPER 90-3953 p 225 A91-12469 * #
 AIAA PAPER 90-3953 p 227 N91-12316 * #
 AIAA PAPER 90-3954 p 225 A91-12470 * #

AIAA PAPER 90-3954 p 227 N91-11495 * #
 AIAA PAPER 90-3983 p 225 A91-12496 * #
 AIAA PAPER 90-3983 p 227 N91-11493 * #
 AIAA PAPER 90-4009 p 1 A91-12521 * #
 AIAA PAPER 90-4010 p 10 N91-11675 * #
 AIAA PAPER 90-4022 p 225 A91-12533 * #
 AIAA PAPER 90-4022 p 228 N91-19825 * #
 AIAA PAPER 90-5203 p 1 A91-14429 * #
 AIAA PAPER 90-5204 p 21 A91-14430 * #
 AIAA PAPER 90-5228 p 37 A91-14454 * #
 AIAA PAPER 90-5236 p 170 A91-14462 * #
 AIAA PAPER 90-5240 p 21 A91-14466 * #
 AIAA PAPER 90-5240 p 161 N91-19374 * #
 AIAA PAPER 91-0043 p 2 A91-22499 * #
 AIAA PAPER 91-0043 p 11 N91-13420 * #
 AIAA PAPER 91-0078 p 105 A91-21362 * #
 AIAA PAPER 91-0107 p 148 A91-19138 * #
 AIAA PAPER 91-0130 p 3 A91-26192 * #
 AIAA PAPER 91-0130 p 70 N91-15303 * #
 AIAA PAPER 91-0172 p 2 A91-21393 * #
 AIAA PAPER 91-0253 p 150 A91-26328 * #
 AIAA PAPER 91-0253 p 160 N91-19370 * #
 AIAA PAPER 91-0263 p 19 A91-26193 * #
 AIAA PAPER 91-0263 p 11 N91-14310 * #
 AIAA PAPER 91-0264 p 3 A91-26330 * #
 AIAA PAPER 91-0264 p 12 N91-19047 * #
 AIAA PAPER 91-0273 p 3 A91-26331 * #
 AIAA PAPER 91-0273 p 12 N91-19044 * #
 AIAA PAPER 91-0284 p 51 A91-19218 * #
 AIAA PAPER 91-0284 p 175 N91-12064 * #
 AIAA PAPER 91-0311 p 148 A91-21452 * #
 AIAA PAPER 91-0342 p 148 A91-21466 * #
 AIAA PAPER 91-0342 p 14 N91-21115 * #
 AIAA PAPER 91-0345 p 149 A91-21467 * #
 AIAA PAPER 91-0410 p 105 A91-21481 * #
 AIAA PAPER 91-0413 p 149 A91-26191 * #
 AIAA PAPER 91-0413 p 160 N91-14559 * #
 AIAA PAPER 91-0445 p 2 A91-21493 * #
 AIAA PAPER 91-0447 p 3 A91-26327 * #
 AIAA PAPER 91-0447 p 12 N91-19046 * #
 AIAA PAPER 91-0462 p 51 A91-21498 * #
 AIAA PAPER 91-0479 p 124 A91-40560 * #
 AIAA PAPER 91-0479 p 126 N91-22464 * #
 AIAA PAPER 91-0486 p 124 A91-19324 * #
 AIAA PAPER 91-0577 p 149 A91-21540 * #
 AIAA PAPER 91-0577 p 34 N91-27164 * #
 AIAA PAPER 91-0581 p 149 A91-21542 * #
 AIAA PAPER 91-0594 p 226 A91-21547 * #
 AIAA PAPER 91-0594 p 12 N91-19045 * #
 AIAA PAPER 91-0609 p 149 A91-21556 * #
 AIAA PAPER 91-0660 p 19 A91-26190 * #
 AIAA PAPER 91-0660 p 11 N91-14309 * #
 AIAA PAPER 91-0661 p 19 A91-22500 * #
 AIAA PAPER 91-0661 p 11 N91-13421 * #
 AIAA PAPER 91-0692 p 149 A91-22498 * #
 AIAA PAPER 91-0692 p 26 N91-13455 * #
 AIAA PAPER 91-0718 p 104 A91-19431 * #
 AIAA PAPER 91-0719 p 104 A91-19432 * #
 AIAA PAPER 91-0720 p 105 A91-19433 * #
 AIAA PAPER 91-0747 p 21 A91-19448 * #
 AIAA PAPER 91-0777 p 128 A91-26329 * #
 AIAA PAPER 91-0777 p 160 N91-19371 * #
 AIAA PAPER 91-0779 p 179 A91-21614 * #
 AIAA PAPER 91-0781 p 127 A91-19463 * #
 AIAA PAPER 91-0920 p 196 A91-31957 * #
 AIAA PAPER 91-0977 p 196 A91-31835 * #
 AIAA PAPER 91-1044 p 129 A91-31842 * #
 AIAA PAPER 91-1124 p 197 A91-32064 * #
 AIAA PAPER 91-1140 p 91 A91-31919 * #
 AIAA PAPER 91-1178 p 197 A91-32099 * #
 AIAA PAPER 91-1218 p 196 A91-32032 * #
 AIAA PAPER 91-1241 p 197 A91-32129 * #
 AIAA PAPER 91-1248 p 197 A91-32087 * #
 AIAA PAPER 91-1305 p 46 A91-45550 * #
 AIAA PAPER 91-1305 p 49 N91-25161 * #
 AIAA PAPER 91-1307 p 155 A91-44335 * #
 AIAA PAPER 91-1307 p 166 N91-24548 * #
 AIAA PAPER 91-1327 p 58 A91-43397 * #
 AIAA PAPER 91-1327 p 73 N91-22367 * #
 AIAA PAPER 91-1343 p 154 A91-43412 * #
 AIAA PAPER 91-1363 p 154 A91-43429 * #
 AIAA PAPER 91-1379 p 129 A91-43444 * #
 AIAA PAPER 91-1381 p 129 A91-44336 * #

AIAA PAPER 91-1381 p 131 N91-24470 * #
 AIAA PAPER 91-1420 p 155 A91-44337 * #
 AIAA PAPER 91-1420 p 166 N91-24549 * #
 AIAA PAPER 91-1471 p 46 A91-42522 * #
 AIAA PAPER 91-1546 p 5 A91-40721 * #
 AIAA PAPER 91-1556 p 5 A91-40730 * #
 AIAA PAPER 91-1566 p 5 A91-40740 * #
 AIAA PAPER 91-1566 p 15 N91-22084 * #
 AIAA PAPER 91-1642 p 153 A91-42541 * #
 AIAA PAPER 91-1652 p 154 A91-43576 * #
 AIAA PAPER 91-1661 p 153 A91-42549 * #
 AIAA PAPER 91-1681 p 6 A91-45548 * #
 AIAA PAPER 91-1689 p 23 A91-42556 * #
 AIAA PAPER 91-1739 p 155 A91-43623 * #
 AIAA PAPER 91-1739 p 100 N91-24359 * #
 AIAA PAPER 91-1741 p 156 A91-45547 * #
 AIAA PAPER 91-1758 p 6 A91-43631 * #
 AIAA PAPER 91-1758 p 16 N91-24130 * #
 AIAA PAPER 91-1779 p 154 A91-42588 * #
 AIAA PAPER 91-1780 p 106 A91-45549 * #
 AIAA PAPER 91-1801 p 154 A91-42599 * #
 AIAA PAPER 91-1843 p 60 A91-45776 * #
 AIAA PAPER 91-1843 p 167 N91-25351 * #
 AIAA PAPER 91-1844 p 124 A91-41631 * #
 AIAA PAPER 91-1859 p 106 A91-45777 * #
 AIAA PAPER 91-1863 p 156 A91-45778 * #
 AIAA PAPER 91-1902 p 24 A91-44050 * #
 AIAA PAPER 91-1902 p 33 N91-24201 * #
 AIAA PAPER 91-1907 p 181 A91-41649 * #
 AIAA PAPER 91-1907 p 186 N91-22568 * #
 AIAA PAPER 91-1916 p 155 A91-44057 * #
 AIAA PAPER 91-1916 p 166 N91-24541 * #
 AIAA PAPER 91-1919 p 23 A91-41653 * #
 AIAA PAPER 91-1991 p 60 A91-45779 * #
 AIAA PAPER 91-1991 p 77 N91-25172 * #
 AIAA PAPER 91-1997 p 24 A91-45780 * #
 AIAA PAPER 91-1997 p 35 N91-29188 * #
 AIAA PAPER 91-1999 p 57 A91-41670 * #
 AIAA PAPER 91-2000 p 23 A91-41671 * #
 AIAA PAPER 91-2010 p 153 A91-41677 * #
 AIAA PAPER 91-2010 p 33 N91-25148 * #
 AIAA PAPER 91-2013 p 153 A91-41678 * #
 AIAA PAPER 91-2013 p 168 N91-30462 * #
 AIAA PAPER 91-2019 p 181 A91-41680 * #
 AIAA PAPER 91-2019 p 187 N91-25395 * #
 AIAA PAPER 91-2020 p 181 A91-41681 * #
 AIAA PAPER 91-2021 p 181 A91-41682 * #
 AIAA PAPER 91-2022 p 182 A91-41683 * #
 AIAA PAPER 91-2022 p 186 N91-22570 * #
 AIAA PAPER 91-2050 p 58 A91-44106 * #
 AIAA PAPER 91-2050 p 76 N91-24304 * #
 AIAA PAPER 91-2052 p 39 A91-45781 * #
 AIAA PAPER 91-2081 p 24 A91-45782 * #
 AIAA PAPER 91-2106 p 182 A91-41700 * #
 AIAA PAPER 91-2108 p 182 A91-41701 * #
 AIAA PAPER 91-2110 p 61 A91-45783 * #
 AIAA PAPER 91-2110 p 81 N91-29228 * #
 AIAA PAPER 91-2113 p 61 A91-45784 * #
 AIAA PAPER 91-2117 p 61 A91-45785 * #
 AIAA PAPER 91-2117 p 86 N91-32158 * #
 AIAA PAPER 91-2121 p 173 A91-45786 * #
 AIAA PAPER 91-2121 p 179 N91-31605 * #
 AIAA PAPER 91-2123 p 61 A91-45787 * #
 AIAA PAPER 91-2123 p 82 N91-30202 * #
 AIAA PAPER 91-2127 p 24 A91-45788 * #
 AIAA PAPER 91-2128 p 25 A91-45789 * #
 AIAA PAPER 91-2128 p 35 N91-30142 * #
 AIAA PAPER 91-2129 p 156 A91-45790 * #
 AIAA PAPER 91-2135 p 25 A91-45791 * #
 AIAA PAPER 91-2135 p 77 N91-25175 * #
 AIAA PAPER 91-2157 p 6 A91-45792 * #
 AIAA PAPER 91-2176 p 43 A91-45793 * #
 AIAA PAPER 91-2198 p 59 A91-44151 * #
 AIAA PAPER 91-2201 p 24 A91-44153 * #
 AIAA PAPER 91-2208 p 61 A91-45794 * #
 AIAA PAPER 91-2211 p 59 A91-44156 * #
 AIAA PAPER 91-2211 p 76 N91-24302 * #
 AIAA PAPER 91-2226 p 61 A91-45795 * #
 AIAA PAPER 91-2227 p 85 N91-31216 * #
 AIAA PAPER 91-2228 p 62 A91-45796 * #
 AIAA PAPER 91-2228 p 84 N91-30252 * #
 AIAA PAPER 91-2238 p 156 A91-45797 * #
 AIAA PAPER 91-2252 p 25 A91-45799 * #

AIAA PAPER 91-2252	p 34	N91-27165 * #	AIAA PAPER 91-3438	p 64	A91-52351 * #	AVSCOM-TR-90-C-021	p 26	N91-11752 * #
AIAA PAPER 91-2263	p 5	A91-41738 * #	AIAA PAPER 91-3440	p 64	A91-52352 * #	AVSCOM-TR-90-C-022	p 185	N91-21534 * #
AIAA PAPER 91-2264	p 25	A91-45800 * #	AIAA PAPER 91-3441	p 64	A91-52353 * #	AVSCOM-TR-90-C-023	p 189	N91-27570 * #
AIAA PAPER 91-2264	p 18	N91-29150 * #	AIAA PAPER 91-3443	p 64	A91-52355 * #	AVSCOM-TR-90-C-024	p 187	N91-23514 * #
AIAA PAPER 91-2283	p 62	A91-45802 * #	AIAA PAPER 91-3452	p 125	A91-52362 * #	AVSCOM-TR-90-C-030	p 160	N91-19369 * #
AIAA PAPER 91-2310	p 106	A91-44192 * #	AIAA PAPER 91-3459	p 64	A91-52369 * #	AVSCOM-TR-90-C-031	p 165	N91-23439 * #
AIAA PAPER 91-2311	p 105	A91-41749 * #	AIAA PAPER 91-3462	p 242	A91-53713 * #	AVSCOM-TR-90-C-032	p 187	N91-25395 * #
AIAA PAPER 91-2316	p 173	A91-45804 * #	AIAA PAPER 91-3462	p 243	N91-29138 * #	AVSCOM-TR-90-C-033	p 187	N91-23513 * #
AIAA PAPER 91-2325	p 125	A91-44197 * #	AIAA PAPER 91-3469	p 45	A91-52377 * #	AVSCOM-TR-91-C-001	p 186	N91-22570 * #
AIAA PAPER 91-2325	p 166	N91-24527 * #	AIAA PAPER 91-3470	p 132	A91-52378 * #	AVSCOM-TR-91-C-002	p 160	N91-16304 * #
AIAA PAPER 91-2326	p 59	A91-44198 * #	AIAA PAPER 91-3471	p 133	A91-53702 * #	AVSCOM-TR-91-C-003	p 13	N91-20044 * #
AIAA PAPER 91-2326	p 166	N91-24547 * #	AIAA PAPER 91-3471	p 135	N91-29405 * #	AVSCOM-TR-91-C-004	p 99	N91-21243 * #
AIAA PAPER 91-2339	p 62	A91-45798 * #	AIAA PAPER 91-3476	p 65	A91-52382 * #	AVSCOM-TR-91-C-006	p 101	N91-26233 * #
AIAA PAPER 91-2341	p 62	A91-45805 * #	AIAA PAPER 91-3479	p 65	A91-52384 * #	AVSCOM-TR-91-C-007	p 186	N91-22568 * #
AIAA PAPER 91-2342	p 62	A91-45806 * #	AIAA PAPER 91-3481	p 125	A91-53711 * #	AVSCOM-TR-91-C-008	p 188	N91-27558 * #
AIAA PAPER 91-2343	p 59	A91-44204 * #	AIAA PAPER 91-3481	p 81	N91-29222 * #	AVSCOM-TR-91-C-010	p 190	N91-30533 * #
AIAA PAPER 91-2346	p 39	A91-45807 * #	AIAA PAPER 91-3484	p 66	A91-53709 * #	AVSCOM-TR-91-C-011	p 189	N91-29599 * #
AIAA PAPER 91-2347	p 47	A91-45808 * #	AIAA PAPER 91-3484	p 81	N91-29220 * #	AVSCOM-TR-91-C-014	p 102	N91-29250 * #
AIAA PAPER 91-2347	p 85	N91-31212 * #	AIAA PAPER 91-3488	p 65	A91-52388 * #	AVSCOM-TR-91-C-015	p 186	N91-23500 * #
AIAA PAPER 91-2350	p 62	A91-45809 * #	AIAA PAPER 91-3497	p 158	A91-52395 * #	AVSCOM-TR-91-C-016	p 35	N91-31178 * #
AIAA PAPER 91-2350	p 82	N91-29229 * #	AIAA PAPER 91-3499	p 42	A91-52396 * #	AVSCOM-TR-91-C-017	p 195	N91-30546 * #
AIAA PAPER 91-2355	p 106	A91-45810 * #	AIAA PAPER 91-3503	p 65	A91-52400 * #	AVSCOM-TR-91-C-018	p 190	N91-30537 * #
AIAA PAPER 91-2355	p 35	N91-31181 * #	AIAA PAPER 91-3518	p 65	A91-52413 * #	AVSCOM-TR-91-C-019	p 99	N91-22402 * #
AIAA PAPER 91-2366	p 156	A91-45811 * #	AIAA PAPER 91-3520	p 208	A91-52415 * #	AVSCOM-TR-91-C-022	p 191	N91-31654 * #
AIAA PAPER 91-2370	p 172	A91-44214 * #	AIAA PAPER 91-3525	p 142	A91-52420 * #	AVSCOM-TR-91-C-029	p 35	N91-31181 * #
AIAA PAPER 91-2370	p 17	N91-27129 * #	AIAA PAPER 91-3525	p 147	N91-32410 * #	AVSCOM-TR-91-C-032	p 188	N91-25412 * #
AIAA PAPER 91-2400	p 43	A91-45812 * #	AIAA PAPER 91-3527	p 116	A91-53705 * #	AVSCOM-TR-91-C-034	p 189	N91-27569 * #
AIAA PAPER 91-2400	p 43	N91-25159 * #	AIAA PAPER 91-3527	p 123	N91-29332 * #	AVSCOM-TR-91-C-037	p 21	N91-27157 * #
AIAA PAPER 91-2405	p 59	A91-44228 * #	AIAA PAPER 91-3528	p 158	A91-52422 * #	AVSCOM-TR-91-C-039	p 190	N91-29600 * #
AIAA PAPER 91-2405	p 126	N91-24460 * #	AIAA PAPER 91-3530	p 88	A91-53704 * #			
AIAA PAPER 91-2407	p 124	A91-41771 * #	AIAA PAPER 91-3530	p 112	N91-29298 * #	CMOTT-91-01	p 165	N91-23416 * #
AIAA PAPER 91-2434	p 57	A91-41780 * #	AIAA PAPER 91-3532	p 133	A91-53708 * #	CMOTT-91-02	p 164	N91-22524 * #
AIAA PAPER 91-2443	p 60	A91-44246 * #	AIAA PAPER 91-3532	p 135	N91-29404 * #	CMOTT-91-03	p 165	N91-24525 * #
AIAA PAPER 91-2443	p 76	N91-24303 * #	AIAA PAPER 91-3533	p 45	A91-52424 * #	CMOTT-91-04	p 223	N91-30865 * #
AIAA PAPER 91-2445	p 60	A91-44247 * #	AIAA PAPER 91-3533	p 135	N91-32247 * #	CMOTT-91-05	p 169	N91-31597 * #
AIAA PAPER 91-2445	p 76	N91-24305 * #	AIAA PAPER 91-3534	p 45	A91-52425 * #	CMOTT-91-06	p 170	N91-32460 * #
AIAA PAPER 91-2456	p 63	A91-45814 * #	AIAA PAPER 91-3536	p 45	A91-52427 * #			
AIAA PAPER 91-2456	p 82	N91-29231 * #	AIAA PAPER 91-3538	p 130	A91-53701 * #	CONF-901101-46	p 128	N91-14498 * #
AIAA PAPER 91-2458	p 7	A91-45813 * #	AIAA PAPER 91-3538	p 243	N91-30073 * #	CONF-910116-16	p 229	N91-18799 * #
AIAA PAPER 91-2458	p 33	N91-24202 * #	AIAA PAPER 91-3541	p 158	A91-53714 * #	CONF-9107113-1	p 123	N91-28418 * #
AIAA PAPER 91-2459	p 157	A91-45815 * #	AIAA PAPER 91-3541	p 168	N91-28538 * #			
AIAA PAPER 91-2459	p 34	N91-29187 * #	AIAA PAPER 91-3545	p 129	A91-52430 * #	DE91-002871	p 128	N91-14498 * #
AIAA PAPER 91-2460	p 23	A91-41788 * #	AIAA PAPER 91-3550	p 125	A91-53710 * #	DE91-006716	p 229	N91-18799 * #
AIAA PAPER 91-2460	p 32	N91-23185 * #	AIAA PAPER 91-3550	p 127	N91-28449 * #	DE91-012961	p 123	N91-28418 * #
AIAA PAPER 91-2463	p 24	A91-44250 * #	AIAA PAPER 91-3553	p 130	A91-52436 * #			
AIAA PAPER 91-2463	p 33	N91-24203 * #	AIAA PAPER 91-3553	p 86	N91-32161 * #	DOE/NASA/16310-14	p 110	N91-14454 * #
AIAA PAPER 91-2474	p 6	A91-44259 * #	AIAA PAPER 91-3554	p 66	A91-53706 * #	DOE/NASA/16310-15	p 111	N91-16128 * #
AIAA PAPER 91-2474	p 16	N91-24131 * #	AIAA PAPER 91-3554	p 81	N91-29221 * #	DOE/NASA/16310-16	p 112	N91-29298 * #
AIAA PAPER 91-2494	p 23	A91-41799 * #	AIAA PAPER 91-3562	p 67	A91-53712 * #	DOE/NASA/20320-76	p 94	N91-10127 * #
AIAA PAPER 91-2495-PT-2	p 186	N91-22571 * #	AIAA PAPER 91-3562	p 80	N91-27212 * #	DOE/NASA/20320-77	p 228	N91-16679 * #
AIAA PAPER 91-2495	p 182	A91-41800 * #	AIAA PAPER 91-3567	p 65	A91-52443 * #	DOE/NASA/33408-5	p 238	N91-31023 * #
AIAA PAPER 91-2524	p 49	A91-45816 * #	AIAA PAPER 91-3568	p 65	A91-52444 * #	DOE/NASA/50162-4	p 95	N91-15318 * #
AIAA PAPER 91-2528	p 60	A91-44281 * #	AIAA PAPER 91-3568	p 86	N91-32162 * #	DOE/NASA/50162-5	p 120	N91-21302 * #
AIAA PAPER 91-2528	p 217	N91-24787 * #	AIAA PAPER 91-3575	p 66	A91-52448 * #			
AIAA PAPER 91-2530	p 60	A91-44283 * #	AIAA PAPER 91-3577	p 66	A91-52450 * #	E-1499-PT-1	p 110	N91-10149 * #
AIAA PAPER 91-2531	p 88	A91-44284 * #	AIAA PAPER 91-3578	p 66	A91-52451 * #	E-4263-PT-2	p 110	N91-10150 * #
AIAA PAPER 91-2531	p 89	N91-24341 * #	AIAA PAPER 91-3589	p 45	A91-52458 * #	E-4407	p 67	N91-10117 * #
AIAA PAPER 91-2533	p 63	A91-45817 * #	AIAA PAPER 91-3589	p 135	N91-32287 * #	E-4628	p 76	N91-24307 * #
AIAA PAPER 91-2564	p 23	A91-41815 * #	AIAA PAPER 91-3590	p 142	A91-52459 * #	E-4658	p 8	N91-10849 * #
AIAA PAPER 91-2581	p 7	A91-45818 * #	AIAA PAPER 91-3592	p 233	A91-53707 * #	E-4720	p 94	N91-10127 * #
AIAA PAPER 91-2715	p 36	A91-49676 * #	AIAA PAPER 91-3592	p 237	N91-29982 * #	E-4824	p 101	N91-25186 * #
AIAA PAPER 91-2792	p 36	A91-49793 * #	AIAA PAPER 91-3593	p 142	A91-52461 * #	E-4998	p 159	N91-14556 * #
AIAA PAPER 91-2792	p 37	N91-32143 * #	AIAA PAPER 91-3594	p 142	A91-52462 * #	E-5000	p 161	N91-19373 * #
AIAA PAPER 91-2822	p 40	A91-49764 * #	AIAA PAPER 91-3601	p 49	A91-52467 * #	E-5019	p 205	N91-25436 * #
AIAA PAPER 91-2822	p 203	N91-22604 * #	AIAA PAPER 91-3602	p 49	A91-52468 * #	E-5044	p 175	N91-14574 * #
AIAA PAPER 91-2969	p 38	A91-47847 * #	AIAA PAPER 91-3602	p 86	N91-32163 * #	E-5097	p 85	N91-31208 * #
AIAA PAPER 91-3102	p 7	A91-54027 * #	AIAA PAPER 91-3604	p 44	A91-52470 * #	E-5176	p 48	N91-21185 * #
AIAA PAPER 91-3132	p 25	A91-54051 * #	AIAA PAPER 91-3607	p 66	A91-52472 * #	E-5233-1-PT-1	p 169	N91-32458 * #
AIAA PAPER 91-3136	p 43	A91-54054 * #	AIAA PAPER 91-3621	p 142	A91-52485 * #	E-5268	p 183	N91-12956 * #
AIAA PAPER 91-3145	p 8	A91-54061 * #	AIAA PAPER 91-3623	p 208	A91-52487 * #	E-5296	p 14	N91-21062 * #
AIAA PAPER 91-3175	p 43	A91-54088 * #	AIAA PAPER 91-3629	p 208	A91-52493 * #	E-5305	p 183	N91-12954 * #
AIAA PAPER 91-3196	p 43	A91-54099 * #	AIAA PAPER 91-3631	p 66	A91-52495 * #	E-5316	p 159	N91-12913 * #
AIAA PAPER 91-3238	p 7	A91-53754 * #				E-5325	p 128	N91-24464 * #
AIAA PAPER 91-3329	p 20	A91-53871 * #	ASME PAPER 89-GT-271	p 1	A91-13047 * #	E-5338	p 16	N91-24124 * #
AIAA PAPER 91-3354	p 7	A91-45819 * #	ASME PAPER 89-GT-298	p 170	A91-13046 * #	E-5352	p 238	N91-10798 * #
AIAA PAPER 91-3354	p 17	N91-25106 * #	ASME PAPER 89-GT-323	p 22	A91-23642 * #	E-5418	p 121	N91-22460 * #
AIAA PAPER 91-3379	p 198	A91-44319 * #	ASME PAPER 90-GT-217	p 173	A91-44633 * #	E-5439	p 12	N91-17002 * #
AIAA PAPER 91-3379	p 204	N91-24659 * #	ASME PAPER 90-GT-255	p 155	A91-44662 * #	E-5480	p 228	N91-15848 * #
AIAA PAPER 91-3390	p 182	A91-45820 * #	ASME PAPER 90-GT-42	p 155	A91-44529 * #	E-5507-1	p 175	N91-10271 * #
AIAA PAPER 91-3390	p 188	N91-27559 * #	ASME PAPER 90-GT-64	p 6	A91-44545 * #	E-5511	p 201	N91-19473 * #
AIAA PAPER 91-3401	p 64	A91-52326 * #	ASME PAPER 90-TRIB-19	p 180	A91-34806 * #	E-5526	p 13	N91-19057 * #
AIAA PAPER 91-3407	p 215	A91-52331 * #	ASME PAPER 90-TRIB-40	p 150	A91-29474 * #	E-5541	p 95	N91-14426 * #
AIAA PAPER 91-3413	p 64	A91-52335 * #				E-5542	p 70	N91-15308 * #
AIAA PAPER 91-3419	p 207	A91-52339 * #	ASME-91-GT-217	p 33	N91-26146 * #	E-5544	p 69	N91-11800 * #
AIAA PAPER 91-3421	p 132	A91-52341 * #				E-5563	p 10	N91-11675 * #
AIAA PAPER 91-3421	p 135	N91-27437 * #	AVSCOM-TM-90-C-011	p 220	N91-31876 * #	E-5579	p 72	N91-19180 * #
AIAA PAPER 91-3422	p 141	A91-52342 * #	AVSCOM-TM-90-C-014	p 200	N91-14632 * #	E-5583	p 31	N91-23179 * #
AIAA PAPER 91-3422	p 146	N91-27477 * #	AVSCOM-TM-90-C-015	p 20	N91-15146 * #	E-5586	p 69	N91-11798 * #
AIAA PAPER 91-3423	p 41	A91-52343 * #				E-5588	p 40	N91-19115 * #
AIAA PAPER 91-3424	p 45	A91-52344 * #	AVSCOM-TR-90-C-001	p 183	N91-12956 * #	E-5592	p 192	N91-17407 * #
AIAA PAPER 91-3425	p 141	A91-52345 * #	AVSCOM-TR-90-C-002	p 188	N91-25411 * #	E-5596	p 111	N91-15390 * #
AIAA PAPER 91-3428	p 183	A91-57025 * #	AVSCOM-TR-90-C-006	p 159	N91-12913 * #	E-5601	p 111	N91-20268 * #
AIAA PAPER 91-3432	p 233	A91-52349 * #	AVSCOM-TR-90-C-012	p 31	N91-23179 * #	E-5614	p 192	N91-15565 * #
AIAA PAPER 91-3433	p 192	A91-53703 * #	AVSCOM-TR-90-C-014	p 191	N91-31648 * #	E-5625	p 160	N91-16304 * #
AIAA PAPER 91-3433	p 194	N91-28605 * #	AVSCOM-TR-90-C-015	p 184	N91-21531 * #	E-5627	p 69	N91-11802 * #
AIAA PAPER 91-3437	p 42	A91-52350 * #	AVSCOM-TR-90-C-017	p 185	N91-22566 * #	E-5630	p 69	N91-11799 * #

E-5631	p 118	N91-11922 * #	E-5857	p 74	N91-22371 * #	E-6012	p 167	N91-27487 * #
E-5642	p 133	N91-18297 * #	E-5860	p 160	N91-19370 * #	E-6013	p 32	N91-23183 * #
E-5643	p 67	N91-10118 * #	E-5862	p 186	N91-23512 * #	E-6015	p 184	N91-19443 * #
E-5646	p 96	N91-15329 * #	E-5871	p 130	N91-19324 * #	E-6017	p 102	N91-27247 * #
E-5648	p 185	N91-22566 * #	E-5872	p 120	N91-19296 * #	E-6020	p 189	N91-27570 * #
E-5649	p 31	N91-22126 * #	E-5873	p 106	N91-19256 * #	E-6022	p 112	N91-27324 * #
E-5651-1	p 194	N91-23521 * #	E-5874	p 96	N91-15328 * #	E-6023	p 193	N91-19464 * #
E-5652	p 72	N91-20206 * #	E-5876	p 98	N91-19236 * #	E-6024	p 144	N91-19354 * #
E-5654	p 71	N91-19178 * #	E-5877	p 98	N91-19237 * #	E-6025	p 145	N91-21433 * #
E-5657	p 38	N91-11770 * #	E-5883	p 216	N91-20748 * #	E-6027	p 120	N91-19308 * #
E-5660	p 17	N91-28136 * #	E-5884	p 143	N91-19348 * #	E-6028	p 217	N91-25630 * #
E-5661	p 94	N91-11074 * #	E-5885	p 160	N91-19369 * #	E-6029	p 121	N91-21309 * #
E-5663	p 228	N91-16679 * #	E-5887	p 27	N91-20084 * #	E-6031	p 164	N91-21448 * #
E-5669	p 200	N91-17415 * #	E-5891	p 200	N91-17427 * #	E-6034	p 71	N91-19175 * #
E-5671	p 96	N91-16075 * #	E-5892	p 176	N91-19401 * #	E-6035	p 30	N91-20122 * #
E-5674	p 199	N91-10332 * #	E-5893	p 97	N91-19231 * #	E-6039	p 222	N91-24817 * #
E-5679	p 88	N91-11062 * #	E-5895	p 31	N91-21137 * #	E-6040-1	p 224	N91-26872 * #
E-5680	p 10	N91-11676 * #	E-5896	p 12	N91-19044 * #	E-6041	p 27	N91-19097 * #
E-5688	p 176	N91-19404 * #	E-5897	p 201	N91-19472 * #	E-6042	p 128	N91-21378 * #
E-5689	p 164	N91-21447 * #	E-5898	p 97	N91-19230 * #	E-6043	p 190	N91-30539 * #
E-5690	p 15	N91-21116 * #	E-5899	p 97	N91-19229 * #	E-6044	p 186	N91-22568 * #
E-5696	p 159	N91-13638 * #	E-5901	p 26	N91-13457 * #	E-6045-1-PT-2	p 169	N91-32459 * #
E-5702	p 118	N91-14482 * #	E-5903	p 119	N91-19292 * #	E-6049	p 13	N91-19063 * #
E-5704	p 159	N91-12034 * #	E-5904	p 99	N91-20228 * #	E-6050	p 14	N91-21061 * #
E-5705	p 143	N91-19351 * #	E-5905	p 81	N91-28278 * #	E-6053	p 164	N91-21458 * #
E-5707	p 26	N91-14349 * #	E-5906	p 12	N91-19045 * #	E-6054	p 102	N91-26234 * #
E-5709	p 67	N91-11058 * #	E-5907	p 99	N91-21243 * #	E-6055	p 161	N91-19375 * #
E-5714	p 134	N91-19332 * #	E-5908	p 11	N91-13420 * #	E-6057	p 202	N91-21558 * #
E-5715	p 160	N91-14559 * #	E-5909	p 27	N91-19098 * #	E-6058	p 134	N91-23347 * #
E-5717	p 227	N91-11493 * #	E-5910	p 188	N91-25411 * #	E-6060	p 89	N91-19224 * #
E-5719	p 175	N91-11205 * #	E-5911	p 11	N91-17000 * #	E-6061	p 219	N91-19766 * #
E-5722	p 184	N91-21531 * #	E-5912	p 12	N91-19046 * #	E-6064	p 194	N91-21553 * #
E-5723	p 70	N91-15301 * #	E-5913	p 120	N91-21302 * #	E-6065	p 128	N91-19320 * #
E-5724	p 68	N91-11059 * #	E-5916	p 185	N91-21534 * #	E-6066	p 221	N91-20830 * #
E-5725	p 199	N91-12114 * #	E-5917	p 134	N91-27436 * #	E-6067	p 222	N91-24818 * #
E-5726	p 26	N91-11752 * #	E-5918	p 144	N91-20392 * #	E-6069	p 235	N91-19935 * #
E-5728	p 72	N91-19182 * #	E-5919	p 184	N91-20489 * #	E-6070	p 222	N91-21797 * #
E-5731	p 227	N91-11494 * #	E-5920	p 40	N91-19112 * #	E-6071	p 201	N91-19476 * #
E-5732	p 226	N91-10703 * #	E-5921	p 144	N91-20393 * #	E-6082	p 187	N91-23513 * #
E-5737	p 133	N91-10208 * #	E-5922	p 143	N91-19349 * #	E-6085	p 187	N91-23513 * #
E-5738	p 208	N91-15628 * #	E-5924	p 12	N91-19047 * #	E-6086	p 188	N91-27558 * #
E-5739	p 68	N91-11061 * #	E-5925	p 70	N91-15303 * #	E-6089	p 213	N91-32549 * #
E-5741	p 27	N91-15174 * #	E-5926	p 195	N91-30546 * #	E-6091	p 18	N91-32074 * #
E-5743	p 234	N91-10780 * #	E-5927	p 144	N91-20406 * #	E-6093	p 165	N91-23409 * #
E-5745	p 234	N91-14050 * #	E-5928	p 11	N91-14310 * #	E-6094	p 99	N91-22396 * #
E-5746	p 205	N91-28622 * #	E-5930	p 11	N91-13421 * #	E-6095	p 126	N91-20324 * #
E-5747	p 216	N91-12215 * #	E-5931	p 160	N91-19371 * #	E-6098	p 35	N91-31178 * #
E-5750	p 69	N91-11801 * #	E-5932	p 119	N91-19293 * #	E-6100	p 44	N91-21182 * #
E-5753	p 159	N91-10249 * #	E-5933	p 16	N91-24107 * #	E-6103	p 73	N91-22367 * #
E-5754	p 228	N91-19825 * #	E-5935	p 11	N91-14309 * #	E-6106	p 165	N91-22536 * #
E-5758	p 133	N91-11988 * #	E-5937	p 11	N91-15134 * #	E-6107	p 46	N91-21184 * #
E-5759-1	p 161	N91-19372 * #	E-5938	p 13	N91-20044 * #	E-6113	p 31	N91-21140 * #
E-5765	p 125	N91-15418 * #	E-5941	p 202	N91-21559 * #	E-6115	p 122	N91-25286 * #
E-5768	p 206	N91-28627 * #	E-5942	p 185	N91-22567 * #	E-6116	p 165	N91-23439 * #
E-5769	p 95	N91-15318 * #	E-5943	p 119	N91-19294 * #	E-6117	p 169	N91-30476 * #
E-5775	p 68	N91-11796 * #	E-5946	p 97	N91-19232 * #	E-6118	p 217	N91-25680 * #
E-5776	p 70	N91-15306 * #	E-5948	p 71	N91-19176 * #	E-6119	p 203	N91-22604 * #
E-5778	p 101	N91-25195 * #	E-5949	p 184	N91-19441 * #	E-6120	p 103	N91-32181 * #
E-5779	p 68	N91-11797 * #	E-5950	p 73	N91-22370 * #	E-6122	p 216	N91-20765 * #
E-5780	p 184	N91-19442 * #	E-5951	p 176	N91-20453 * #	E-6125	p 34	N91-27159 * #
E-5781	p 94	N91-10134 * #	E-5952	p 162	N91-20417 * #	E-6129	p 79	N91-27204 * #
E-5783	p 242	N91-15117 * #	E-5953	p 13	N91-20045 * #	E-6131	p 33	N91-24201 * #
E-5791	p 159	N91-11192 * #	E-5954	p 27	N91-20086 * #	E-6133	p 131	N91-23340 * #
E-5794	p 201	N91-19477 * #	E-5955	p 97	N91-19233 * #	E-6136	p 32	N91-23184 * #
E-5795	p 227	N91-11495 * #	E-5956	p 162	N91-20445 * #	E-6138	p 15	N91-22084 * #
E-5797	p 227	N91-12317 * #	E-5957	p 102	N91-29250 * #	E-6140	p 100	N91-23247 * #
E-5798	p 221	N91-14781 * #	E-5959	p 107	N91-22410 * #	E-6142	p 205	N91-24660 * #
E-5799	p 130	N91-11945 * #	E-5960	p 161	N91-19374 * #	E-6144	p 187	N91-25395 * #
E-5800	p 36	N91-20133 * #	E-5961	p 111	N91-16128 * #	E-6148	p 186	N91-23501 * #
E-5801	p 130	N91-14500 * #	E-5962	p 241	N91-20015 * #	E-6149	p 14	N91-21115 * #
E-5803	p 20	N91-15146 * #	E-5963	p 72	N91-21233 * #	E-6155	p 81	N91-28277 * #
E-5805	p 227	N91-12316 * #	E-5964	p 126	N91-19317 * #	E-6157	p 187	N91-23514 * #
E-5809	p 228	N91-15842 * #	E-5966	p 71	N91-19177 * #	E-6158	p 15	N91-23086 * #
E-5811	p 167	N91-27489 * #	E-5969	p 126	N91-22464 * #	E-6159	p 19	N91-23098 * #
E-5813	p 96	N91-17143 * #	E-5971	p 99	N91-22402 * #	E-6160	p 77	N91-25175 * #
E-5814	p 200	N91-14632 * #	E-5973	p 48	N91-19165 * #	E-6161	p 82	N91-30203 * #
E-5817	p 68	N91-11060 * #	E-5974	p 212	N91-26592 * #	E-6162	p 100	N91-24345 * #
E-5821	p 26	N91-13455 * #	E-5975	p 31	N91-20126 * #	E-6164	p 15	N91-23087 * #
E-5823	p 241	N91-14259 * #	E-5979	p 101	N91-26233 * #	E-6165	p 166	N91-24527 * #
E-5825	p 95	N91-13495 * #	E-5983	p 121	N91-23311 * #	E-6166-PT-2	p 186	N91-22571 * #
E-5826	p 70	N91-13491 * #	E-5984	p 14	N91-21060 * #	E-6167	p 203	N91-22594 * #
E-5827	p 200	N91-18452 * #	E-5986	p 98	N91-19235 * #	E-6169	p 165	N91-23416 * #
E-5828	p 175	N91-12064 * #	E-5987	p 203	N91-23549 * #	E-6170	p 164	N91-22524 * #
E-5829	p 110	N91-14454 * #	E-5989	p 221	N91-19786 * #	E-6171	p 134	N91-22494 * #
E-5830	p 13	N91-19053 * #	E-5990	p 89	N91-22379 * #	E-6174	p 100	N91-24360 * #
E-5834	p 98	N91-19234 * #	E-5991	p 201	N91-19475 * #	E-6175	p 74	N91-23234 * #
E-5835	p 73	N91-21240 * #	E-5996	p 112	N91-30318 * #	E-6177	p 49	N91-24225 * #
E-5838	p 40	N91-22139 * #	E-5997	p 13	N91-19054 * #	E-6179	p 218	N91-24796 * #
E-5840	p 26	N91-13456 * #	E-6000	p 235	N91-21910 * #	E-6181	p 145	N91-22508 * #
E-5841	p 72	N91-20204 * #	E-6001	p 89	N91-22377 * #	E-6183	p 206	N91-32520 * #
E-5842	p 193	N91-19463 * #	E-6002	p 202	N91-21562 * #	E-6184	p 203	N91-23548 * #
E-5845	p 230	N91-14829 * #	E-6003	p 193	N91-19462 * #	E-6185	p 217	N91-22766 * #
E-5847	p 71	N91-19179 * #	E-6004	p 189	N91-29599 * #	E-6186	p 76	N91-24302 * #
E-5848	p 67	N91-10119 * #	E-6005	p 243	N91-30073 * #	E-6191	p 74	N91-23233 * #
E-5854	p 176	N91-19402 * #	E-6006	p 120	N91-19295 * #	E-6192	p 74	N91-22376 * #
E-5856	p 200	N91-12980 * #	E-6008	p 48	N91-20184 * #	E-6193	p 74	N91-22375 * #

E-6197	p 186	N91-23500 * #	E-6359	p 81	N91-29221 * #	E-6594	p 127	N91-31318 * #
E-6200	p 20	N91-23102 * #	E-6361	p 178	N91-27510 * #	E-6598	p 135	N91-32287 * #
E-6201	p 101	N91-25198 * #	E-6362	p 135	N91-29405 * #	E-6606	p 112	N91-32204 * #
E-6206	p 37	N91-22135 * #	E-6365	p 79	N91-27207 * #	E-6631	p 238	N91-33014 * #
E-6207	p 134	N91-23354 * #	E-6366	p 86	N91-31218 * #			
E-6208	p 77	N91-25173 * #	E-6370	p 103	N91-32177 * #	IAF PAPER 90-053	p 50	A91-13766 * #
E-6210	p 191	N91-31648 * #	E-6373	p 146	N91-30427 * #	IAF PAPER 90-054	p 231	A91-13767 * #
E-6211	p 190	N91-30533 * #	E-6375	p 146	N91-27447 * #	IAF PAPER 90-200	p 51	A91-13868 * #
E-6212	p 188	N91-27559 * #	E-6376	p 212	N91-27611 * #	IAF PAPER 90-254	p 51	A91-13908 * #
E-6214	p 186	N91-22570 * #	E-6378	p 78	N91-26202 * #	IAF PAPER 90-350	p 39	A91-13991 * #
E-6216	p 75	N91-24232 * #	E-6379	p 80	N91-27214 * #	IAF PAPER 90-481	p 44	A91-14056 * #
E-6217	p 236	N91-22921 * #	E-6381	p 214	N91-32569 * #			
E-6220	p 203	N91-23550 * #	E-6383	p 42	N91-30186 * #	ICOMP-90-08	p 16	N91-24124 * #
E-6224	p 211	N91-23620 * #	E-6384	p 79	N91-27206 * #	ICOMP-90-22	p 160	N91-14559 * #
E-6226	p 15	N91-23083 * #	E-6386	p 127	N91-27375 * #	ICOMP-90-23	p 159	N91-11192 * #
E-6227	p 222	N91-22814 * #	E-6387	p 146	N91-27444 * #	ICOMP-90-24	p 221	N91-14781 * #
E-6230	p 211	N91-23616 * #	E-6389	p 205	N91-27591 * #	ICOMP-90-25	p 161	N91-19372 * #
E-6232	p 167	N91-24550 * #	E-6390	p 194	N91-29610 * #	ICOMP-91-01	p 221	N91-24818 * #
E-6233	p 16	N91-23089 * #	E-6392	p 34	N91-27165 * #	ICOMP-91-02	p 221	N91-19786 * #
E-6234	p 168	N91-30461 * #	E-6395	p 178	N91-27521 * #	ICOMP-91-03	p 222	N91-24817 * #
E-6235	p 126	N91-24460 * #	E-6396	p 34	N91-27164 * #	ICOMP-91-04	p 161	N91-19375 * #
E-6237	p 236	N91-23946 * #	E-6401	p 80	N91-27212 * #	ICOMP-91-05	p 165	N91-22536 * #
E-6238	p 32	N91-23185 * #	E-6403	p 223	N91-30867 * #	ICOMP-91-06	p 165	N91-23416 * #
E-6239	p 33	N91-24202 * #	E-6404	p 238	N91-31023 * #	ICOMP-91-07	p 164	N91-22524 * #
E-6241	p 165	N91-24525 * #	E-6406	p 222	N91-27886 * #	ICOMP-91-09	p 165	N91-24525 * #
E-6243	p 17	N91-26121 * #	E-6408	p 82	N91-30202 * #	ICOMP-91-10	p 166	N91-24541 * #
E-6244	p 168	N91-29525 * #	E-6409	p 85	N91-31216 * #	ICOMP-91-11	p 204	N91-24659 * #
E-6245	p 187	N91-24593 * #	E-6410	p 169	N91-30473 * #	ICOMP-91-12	p 205	N91-27591 * #
E-6246	p 177	N91-26490 * #	E-6414	p 86	N91-31220 * #	ICOMP-91-13	p 223	N91-30865 * #
E-6247	p 49	N91-25161 * #	E-6416	p 146	N91-27445 * #	ICOMP-91-14	p 223	N91-31911 * #
E-6248	p 101	N91-24361 * #	E-6419	p 82	N91-29229 * #	ICOMP-91-15	p 169	N91-31597 * #
E-6249	p 126	N91-25300 * #	E-6420	p 86	N91-32158 * #	ICOMP-91-16	p 170	N91-32460 * #
E-6251	p 178	N91-27511 * #	E-6423	p 21	N91-27157 * #	ICOMP-91-8	p 101	N91-25198 * #
E-6253	p 220	N91-31876 * #	E-6430	p 84	N91-30252 * #			
E-6254	p 32	N91-23188 * #	E-6433	p 190	N91-30537 * #	INT-PATENT-CLASS-B23H-9/00	p 122	N91-25296 * #
E-6255	p 131	N91-24469 * #	E-6435	p 37	N91-27167 * #	INT-PATENT-CLASS-B23K-9/00	p 231	N91-25875 * #
E-6256	p 33	N91-24203 * #	E-6437	p 87	N91-32164 * #	INT-PATENT-CLASS-B60P-7/15	p 189	N91-27561 * #
E-6258	p 79	N91-27208 * #	E-6438	p 85	N91-31212 * #	INT-PATENT-CLASS-B64D-33/04	p 189	N91-27560 * #
E-6259	p 168	N91-30469 * #	E-6441	p 35	N91-30142 * #			
E-6261	p 17	N91-25106 * #	E-6442	p 82	N91-29231 * #	INT-PATENT-CLASS-C07C-15/16	p 89	N91-17141 * #
E-6262	p 76	N91-24305 * #	E-6444	p 218	N91-28776 * #	INT-PATENT-CLASS-C07C-15/16	p 90	N91-25185 * #
E-6265	p 228	N91-25817 * #	E-6446	p 80	N91-27213 * #	INT-PATENT-CLASS-C08G-73/10	p 118	N91-15402 * #
E-6270	p 166	N91-24548 * #	E-6449	p 168	N91-30462 * #			
E-6271	p 220	N91-25696 * #	E-6452	p 35	N91-29188 * #	INT-PATENT-CLASS-E05C-5/04	p 189	N91-27561 * #
E-6273	p 145	N91-25320 * #	E-6453	p 194	N91-28605 * #			
E-6275	p 16	N91-24131 * #	E-6454	p 179	N91-31605 * #	INT-PATENT-CLASS-F16J-15/46	p 189	N91-27560 * #
E-6278	p 166	N91-24541 * #	E-6457	p 102	N91-30281 * #	INT-PATENT-CLASS-F16M-13/00	p 183	N91-14617 * #
E-6279	p 35	N91-31181 * #	E-6458	p 135	N91-29431 * #	INT-PATENT-CLASS-F27B-5/14	p 42	N91-27175 * #
E-6280	p 89	N91-24341 * #	E-6459	p 206	N91-30566 * #	INT-PATENT-CLASS-F27D-11/10	p 42	N91-27175 * #
E-6282	p 194	N91-27575 * #	E-6461	p 18	N91-29150 * #	INT-PATENT-CLASS-F8-15/00	p 130	N91-15424 * #
E-6283	p 131	N91-24470 * #	E-6463	p 81	N91-29228 * #			
E-6284	p 166	N91-24547 * #	E-6464	p 112	N91-29298 * #	INT-PATENT-CLASS-G01B-9/02	p 230	N91-21871 * #
E-6285	p 204	N91-24659 * #	E-6465	p 242	N91-33046 * #	INT-PATENT-CLASS-G01K-17/06	p 179	N91-31608 * #
E-6286	p 215	N91-24745 * #	E-6468	p 178	N91-30491 * #	INT-PATENT-CLASS-G01K-17/16	p 179	N91-31608 * #
E-6288	p 33	N91-25148 * #	E-6469	p 39	N91-29199 * #	INT-PATENT-CLASS-G01N-3/08	p 42	N91-27175 * #
E-6289	p 78	N91-25183 * #	E-6471	p 82	N91-29230 * #	INT-PATENT-CLASS-G01N-3/20	p 185	N91-21540 * #
E-6290	p 17	N91-26122 * #	E-6472	p 34	N91-29181 * #	INT-PATENT-CLASS-G01R-1/04	p 143	N91-14552 * #
E-6292	p 223	N91-25749 * #	E-6473	p 168	N91-30472 * #	INT-PATENT-CLASS-G02B-6/02	p 230	N91-21871 * #
E-6293	p 222	N91-25739 * #	E-6475	p 123	N91-29332 * #	INT-PATENT-CLASS-G02B-6/16	p 230	N91-21871 * #
E-6294	p 238	N91-24952 * #	E-6476	p 223	N91-30865 * #			
E-6295	p 177	N91-25381 * #	E-6478	p 34	N91-29187 * #	INT-PATENT-CLASS-H01B-1/06	p 95	N91-15320 * #
E-6296	p 77	N91-25179 * #	E-6479	p 146	N91-30426 * #	INT-PATENT-CLASS-H01L-31/18	p 212	N91-27614 * #
E-6297	p 76	N91-24304 * #	E-6481	p 237	N91-29982 * #	INT-PATENT-CLASS-H01L-31/42	p 212	N91-27614 * #
E-6299	p 167	N91-25351 * #	E-6484	p 35	N91-30141 * #			
E-6300	p 77	N91-25172 * #	E-6487	p 39	N91-30163 * #	KBQ-FR-2	p 121	N91-21307 * #
E-6301	p 78	N91-25182 * #	E-6490	p 135	N91-29404 * #			
E-6302	p 223	N91-27901 * #	E-6492	p 81	N91-29220 * #	NAS 1.15:100243	p 134	N91-22494 * #
E-6303	p 166	N91-24549 * #	E-6493	p 127	N91-28449 * #	NAS 1.15:101368	p 67	N91-10117 * #
E-6304	p 217	N91-24787 * #	E-6496	p 81	N91-29222 * #	NAS 1.15:101468	p 110	N91-10150 * #
E-6306	p 100	N91-24359 * #	E-6498	p 243	N91-29138 * #	NAS 1.15:102067	p 101	N91-25186 * #
E-6309	p 188	N91-25413 * #	E-6499	p 168	N91-28538 * #	NAS 1.15:102323	p 205	N91-25436 * #
E-6313	p 33	N91-26146 * #	E-6503	p 217	N91-32806 * #	NAS 1.15:102381	p 85	N91-31208 * #
E-6315	p 146	N91-27477 * #	E-6504	p 169	N91-32440 * #	NAS 1.15:102420	p 202	N91-21559 * #
E-6317	p 190	N91-30538 * #	E-6505	p 84	N91-30266 * #	NAS 1.15:102504	p 183	N91-12954 * #
E-6318	p 16	N91-24130 * #	E-6506	p 223	N91-31911 * #	NAS 1.15:102513	p 159	N91-12913 * #
E-6319	p 103	N91-31235 * #	E-6507	p 190	N91-30532 * #	NAS 1.15:102521	p 128	N91-24464 * #
E-6320	p 76	N91-24303 * #	E-6509	p 237	N91-31977 * #	NAS 1.15:102528	p 16	N91-24124 * #
E-6321	p 188	N91-25412 * #	E-6515	p 147	N91-32412 * #	NAS 1.15:102542	p 238	N91-10798 * #
E-6323	p 43	N91-25159 * #	E-6522	p 18	N91-31106 * #	NAS 1.15:102803	p 99	N91-22396 * #
E-6326	p 191	N91-31654 * #	E-6532	p 85	N91-30267 * #	NAS 1.15:103097	p 121	N91-22460 * #
E-6327	p 177	N91-25382 * #	E-6536	p 85	N91-31217 * #	NAS 1.15:103115	p 12	N91-17002 * #
E-6329	p 177	N91-25387 * #	E-6540	p 18	N91-32075 * #	NAS 1.15:103169	p 95	N91-14426 * #
E-6330	p 220	N91-24815 * #	E-6541	p 44	N91-31196 * #	NAS 1.15:103183	p 10	N91-11675 * #
E-6331	p 79	N91-27209 * #	E-6551	p 87	N91-32165 * #	NAS 1.15:103191	p 72	N91-19180 * #
E-6332	p 78	N91-25184 * #	E-6552	p 213	N91-31708 * #	NAS 1.15:103193	p 69	N91-11798 * #
E-6334	p 212	N91-25510 * #	E-6553	p 103	N91-32182 * #	NAS 1.15:103197	p 192	N91-17407 * #
E-6335	p 84	N91-30265 * #	E-6560	p 86	N91-32163 * #	NAS 1.15:103204	p 94	N91-11074 * #
E-6337	p 90	N91-29235 * #	E-6562	p 169	N91-31597 * #	NAS 1.15:103214	p 160	N91-16304 * #
E-6344	p 90	N91-27221 * #	E-6563	p 170	N91-32460 * #	NAS 1.15:103216	p 69	N91-11802 * #
E-6348	p 224	N91-26870 * #	E-6564	p 135	N91-32247 * #	NAS 1.15:103218	p 69	N91-11799 * #
E-6349	p 190	N91-29600 * #	E-6569	p 86	N91-32162 * #	NAS 1.15:103226	p 133	N91-18297 * #
E-6352	p 205	N91-25442 * #	E-6573	p 112	N91-32216 * #	NAS 1.15:103227	p 67	N91-10118 * #
E-6353	p 189	N91-27569 * #	E-6577	p 147	N91-32410 * #	NAS 1.15:103230	p 96	N91-15329 * #
E-6355	p 103	N91-30282 * #	E-6583	p 37	N91-32143 * #	NAS 1.15:103232	p 185	N91-22566 * #
E-6356	p 17	N91-27129 * #	E-6585	p 112	N91-32215 * #	NAS 1.15:103234	p 71	N91-19178 * #
E-6358	p 135	N91-27437 * #	E-6586	p 86	N91-32161 * #	NAS 1.15:103236	p 31	N91-22126 * #

REPORT NUMBER INDEX

NAS 1.15:104409

NAS 1.15:103238	p 38	N91-11770 *	NAS 1.15:103676	p 176	N91-19401 *	NAS 1.15:103780	p 164	N91-21458 *
NAS 1.15:103244	p 200	N91-17415 *	NAS 1.15:103677	p 97	N91-19231 *	NAS 1.15:103781	p 161	N91-19375 *
NAS 1.15:103245	p 96	N91-16075 *	NAS 1.15:103678	p 31	N91-21137 *	NAS 1.15:103782	p 202	N91-21558 *
NAS 1.15:103247	p 199	N91-10332 *	NAS 1.15:103679	p 12	N91-19044 *	NAS 1.15:103783	p 134	N91-23347 *
NAS 1.15:103251	p 10	N91-11676 *	NAS 1.15:103680	p 201	N91-19472 *	NAS 1.15:103784	p 89	N91-19224 *
NAS 1.15:103257	p 176	N91-19404 *	NAS 1.15:103681	p 97	N91-19230 *	NAS 1.15:103785	p 219	N91-19766 *
NAS 1.15:103258	p 15	N91-21116 *	NAS 1.15:103682	p 97	N91-19229 *	NAS 1.15:103787	p 194	N91-21553 *
NAS 1.15:103260	p 11	N91-15134 *	NAS 1.15:103683	p 26	N91-13457 *	NAS 1.15:103788	p 128	N91-19320 *
NAS 1.15:103263	p 159	N91-13638 *	NAS 1.15:103685	p 119	N91-19292 *	NAS 1.15:103789	p 221	N91-20830 *
NAS 1.15:103265	p 88	N91-11062 *	NAS 1.15:103686	p 99	N91-20228 *	NAS 1.15:103790	p 222	N91-24818 *
NAS 1.15:103266	p 118	N91-11922 *	NAS 1.15:103687	p 12	N91-19045 *	NAS 1.15:103791	p 164	N91-21447 *
NAS 1.15:103267	p 159	N91-12034 *	NAS 1.15:103688	p 99	N91-21243 *	NAS 1.15:103792	p 235	N91-19935 *
NAS 1.15:103268	p 26	N91-14349 *	NAS 1.15:103689	p 11	N91-13420 *	NAS 1.15:103793	p 222	N91-21797 *
NAS 1.15:103269	p 67	N91-11058 *	NAS 1.15:103690	p 27	N91-19098 *	NAS 1.15:103794	p 201	N91-19476 *
NAS 1.15:103272	p 134	N91-19332 *	NAS 1.15:103691	p 188	N91-25411 *	NAS 1.15:103795	p 187	N91-23515 *
NAS 1.15:103273	p 160	N91-14559 *	NAS 1.15:103692	p 11	N91-17000 *	NAS 1.15:103796	p 112	N91-27324 *
NAS 1.15:103274	p 175	N91-11205 *	NAS 1.15:103693	p 12	N91-19046 *	NAS 1.15:103797	p 187	N91-23513 *
NAS 1.15:103276	p 184	N91-21531 *	NAS 1.15:103694	p 120	N91-21302 *	NAS 1.15:103798	p 188	N91-27558 *
NAS 1.15:103277	p 199	N91-12114 *	NAS 1.15:103695	p 185	N91-21534 *	NAS 1.15:103799	p 89	N91-22379 *
NAS 1.15:103278	p 26	N91-11752 *	NAS 1.15:103696	p 144	N91-20392 *	NAS 1.15:103801	p 165	N91-23409 *
NAS 1.15:103281	p 189	N91-27570 *	NAS 1.15:103697	p 184	N91-20489 *	NAS 1.15:103802	p 144	N91-20406 *
NAS 1.15:103282	p 133	N91-10208 *	NAS 1.15:103698	p 40	N91-19112 *	NAS 1.15:103804	p 126	N91-20324 *
NAS 1.15:103283	p 208	N91-15628 *	NAS 1.15:103699	p 144	N91-20393 *	NAS 1.15:103805	p 30	N91-20122 *
NAS 1.15:103284	p 68	N91-11061 *	NAS 1.15:103700	p 143	N91-19349 *	NAS 1.15:103806	p 195	N91-30546 *
NAS 1.15:103285	p 27	N91-15174 *	NAS 1.15:103701	p 12	N91-19047 *	NAS 1.15:104333	p 35	N91-31178 *
NAS 1.15:103286	p 143	N91-19351 *	NAS 1.15:103702	p 160	N91-19370 *	NAS 1.15:104334	p 44	N91-21182 *
NAS 1.15:103287	p 205	N91-28622 *	NAS 1.15:103703	p 70	N91-15303 *	NAS 1.15:104335	p 73	N91-22367 *
NAS 1.15:103288	p 175	N91-10271 *	NAS 1.15:103704	p 72	N91-20204 *	NAS 1.15:104336	p 186	N91-22568 *
NAS 1.15:103289	p 216	N91-12215 *	NAS 1.15:103705	p 11	N91-14310 *	NAS 1.15:104337	p 165	N91-22536 *
NAS 1.15:103290	p 69	N91-11801 *	NAS 1.15:103706	p 160	N91-19371 *	NAS 1.15:104338	p 46	N91-21184 *
NAS 1.15:103293	p 159	N91-10249 *	NAS 1.15:103707	p 119	N91-19293 *	NAS 1.15:104339	p 194	N91-23521 *
NAS 1.15:103332	p 229	N91-18799 *	NAS 1.15:103708	p 111	N91-15390 *	NAS 1.15:104340	p 31	N91-21140 *
NAS 1.15:103423	p 128	N91-14498 *	NAS 1.15:103709	p 11	N91-14309 *	NAS 1.15:104341	p 122	N91-25286 *
NAS 1.15:103606	p 228	N91-19825 *	NAS 1.15:103710	p 13	N91-20044 *	NAS 1.15:104342	p 165	N91-23439 *
NAS 1.15:103608	p 226	N91-10703 *	NAS 1.15:103711	p 119	N91-19294 *	NAS 1.15:104343	p 169	N91-30476 *
NAS 1.15:103611	p 125	N91-15418 *	NAS 1.15:103712	p 11	N91-13421 *	NAS 1.15:104344	p 217	N91-25680 *
NAS 1.15:103612	p 95	N91-15318 *	NAS 1.15:103713	p 97	N91-19232 *	NAS 1.15:104345	p 203	N91-22604 *
NAS 1.15:103613	p 68	N91-11059 *	NAS 1.15:103714	p 27	N91-20084 *	NAS 1.15:104346	p 103	N91-32181 *
NAS 1.15:103614	p 192	N91-15565 *	NAS 1.15:103715	p 71	N91-19176 *	NAS 1.15:104347	p 216	N91-20765 *
NAS 1.15:103616	p 234	N91-10780 *	NAS 1.15:103716	p 184	N91-19441 *	NAS 1.15:104349	p 79	N91-27204 *
NAS 1.15:103617	p 70	N91-15301 *	NAS 1.15:103717	p 73	N91-22370 *	NAS 1.15:104350	p 186	N91-23512 *
NAS 1.15:103618	p 68	N91-11796 *	NAS 1.15:103720	p 176	N91-20453 *	NAS 1.15:104351	p 32	N91-23184 *
NAS 1.15:103619	p 70	N91-15306 *	NAS 1.15:103721	p 162	N91-20417 *	NAS 1.15:104352	p 189	N91-29599 *
NAS 1.15:103620	p 101	N91-25195 *	NAS 1.15:103722	p 13	N91-20045 *	NAS 1.15:104353	p 15	N91-22084 *
NAS 1.15:103622	p 68	N91-11797 *	NAS 1.15:103723	p 162	N91-20445 *	NAS 1.15:104354	p 100	N91-23247 *
NAS 1.15:103623	p 242	N91-15117 *	NAS 1.15:103724	p 97	N91-19233 *	NAS 1.15:104355	p 205	N91-24660 *
NAS 1.15:103624	p 159	N91-11192 *	NAS 1.15:103725	p 107	N91-22410 *	NAS 1.15:104356	p 31	N91-23179 *
NAS 1.15:103625	p 227	N91-11494 *	NAS 1.15:103726	p 161	N91-19374 *	NAS 1.15:104358	p 186	N91-23501 *
NAS 1.15:103626	p 201	N91-19477 *	NAS 1.15:103727	p 111	N91-16128 *	NAS 1.15:104359	p 14	N91-21115 *
NAS 1.15:103627	p 227	N91-11495 *	NAS 1.15:103728	p 241	N91-20015 *	NAS 1.15:104360	p 81	N91-28277 *
NAS 1.15:103628	p 227	N91-11493 *	NAS 1.15:103729	p 72	N91-21233 *	NAS 1.15:104361	p 187	N91-23514 *
NAS 1.15:103629	p 227	N91-12317 *	NAS 1.15:103730	p 126	N91-19317 *	NAS 1.15:104362	p 15	N91-23086 *
NAS 1.15:103630	p 221	N91-14781 *	NAS 1.15:103731	p 71	N91-19177 *	NAS 1.15:104363	p 19	N91-23098 *
NAS 1.15:103631	p 130	N91-14500 *	NAS 1.15:103732	p 193	N91-19463 *	NAS 1.15:104364	p 77	N91-25175 *
NAS 1.15:103632	p 94	N91-10134 *	NAS 1.15:103733	p 99	N91-22402 *	NAS 1.15:104365	p 100	N91-24345 *
NAS 1.15:103633	p 133	N91-11988 *	NAS 1.15:103734	p 176	N91-19402 *	NAS 1.15:104366	p 15	N91-23087 *
NAS 1.15:103634	p 20	N91-15146 *	NAS 1.15:103735	p 48	N91-19165 *	NAS 1.15:104367	p 203	N91-22594 *
NAS 1.15:103635	p 228	N91-15842 *	NAS 1.15:103736	p 212	N91-26592 *	NAS 1.15:104368	p 165	N91-23416 *
NAS 1.15:103636	p 96	N91-17143 *	NAS 1.15:103737	p 185	N91-22567 *	NAS 1.15:104369	p 164	N91-22524 *
NAS 1.15:103637	p 200	N91-14632 *	NAS 1.15:103738	p 31	N91-20126 *	NAS 1.15:104370	p 100	N91-24360 *
NAS 1.15:103638	p 68	N91-11060 *	NAS 1.15:103739	p 101	N91-26233 *	NAS 1.15:104371	p 186	N91-22571 *
NAS 1.15:103639	p 161	N91-19373 *	NAS 1.15:103741	p 121	N91-23311 *	NAS 1.15:104372	p 102	N91-26234 *
NAS 1.15:103640	p 26	N91-13455 *	NAS 1.15:103742	p 14	N91-21060 *	NAS 1.15:104373	p 49	N91-24225 *
NAS 1.15:103641	p 159	N91-14556 *	NAS 1.15:103743	p 98	N91-19235 *	NAS 1.15:104374	p 218	N91-24796 *
NAS 1.15:103642	p 241	N91-14259 *	NAS 1.15:103744	p 203	N91-23549 *	NAS 1.15:104375	p 145	N91-22508 *
NAS 1.15:103643	p 95	N91-13495 *	NAS 1.15:103745	p 221	N91-19786 *	NAS 1.15:104376	p 224	N91-26872 *
NAS 1.15:103644	p 200	N91-18452 *	NAS 1.15:103746	p 201	N91-19475 *	NAS 1.15:104377	p 16	N91-24107 *
NAS 1.15:103645	p 227	N91-12316 *	NAS 1.15:103747	p 13	N91-19054 *	NAS 1.15:104378	p 206	N91-32520 *
NAS 1.15:103646	p 175	N91-12064 *	NAS 1.15:103749	p 235	N91-21910 *	NAS 1.15:104379	p 203	N91-23548 *
NAS 1.15:103647	p 110	N91-14454 *	NAS 1.15:103750	p 202	N91-21562 *	NAS 1.15:104380	p 217	N91-22766 *
NAS 1.15:103648	p 98	N91-19234 *	NAS 1.15:103751	p 193	N91-19462 *	NAS 1.15:104381	p 101	N91-25198 *
NAS 1.15:103649	p 73	N91-21240 *	NAS 1.15:103752	p 243	N91-30073 *	NAS 1.15:104382	p 74	N91-23233 *
NAS 1.15:103650	p 13	N91-19053 *	NAS 1.15:103754	p 48	N91-20184 *	NAS 1.15:104383	p 74	N91-22376 *
NAS 1.15:103651	p 26	N91-13456 *	NAS 1.15:103756	p 167	N91-27487 *	NAS 1.15:104384	p 74	N91-22375 *
NAS 1.15:103652	p 130	N91-11945 *	NAS 1.15:103757	p 32	N91-23183 *	NAS 1.15:104387	p 74	N91-23234 *
NAS 1.15:103653	p 70	N91-13491 *	NAS 1.15:103758	p 184	N91-19443 *	NAS 1.15:104388	p 186	N91-23500 *
NAS 1.15:103654	p 230	N91-14829 *	NAS 1.15:103759	p 243	N91-23072 *	NAS 1.15:104389	p 20	N91-23102 *
NAS 1.15:103655	p 234	N91-14850 *	NAS 1.15:103760	p 102	N91-27247 *	NAS 1.15:104390	p 166	N91-24527 *
NAS 1.15:103656	p 71	N91-19179 *	NAS 1.15:103761	p 193	N91-19464 *	NAS 1.15:104391	p 37	N91-22135 *
NAS 1.15:103657	p 67	N91-10119 *	NAS 1.15:103762	p 144	N91-19354 *	NAS 1.15:104392	p 134	N91-23354 *
NAS 1.15:103658	p 184	N91-19442 *	NAS 1.15:103763	p 145	N91-21433 *	NAS 1.15:104393	p 77	N91-25173 *
NAS 1.15:103659	p 234	N91-14050 *	NAS 1.15:103764	p 120	N91-19308 *	NAS 1.15:104394	p 191	N91-31648 *
NAS 1.15:103660	p 200	N91-12980 *	NAS 1.15:103765	p 126	N91-22464 *	NAS 1.15:104395	p 190	N91-30533 *
NAS 1.15:103661	p 74	N91-22371 *	NAS 1.15:103766	p 217	N91-25630 *	NAS 1.15:104396	p 188	N91-27559 *
NAS 1.15:103664	p 120	N91-19324 *	NAS 1.15:103767	p 121	N91-21309 *	NAS 1.15:104397	p 186	N91-22570 *
NAS 1.15:103665	p 130	N91-19296 *	NAS 1.15:103768	p 89	N91-22377 *	NAS 1.15:104398	p 236	N91-22921 *
NAS 1.15:103666	p 106	N91-19256 *	NAS 1.15:103769	p 164	N91-21448 *	NAS 1.15:104400	p 203	N91-23550 *
NAS 1.15:103667	p 96	N91-15328 *	NAS 1.15:103771	p 71	N91-19175 *	NAS 1.15:104401	p 75	N91-24232 *
NAS 1.15:103668	p 161	N91-19372 *	NAS 1.15:103772	p 102	N91-29250 *	NAS 1.15:104402	p 211	N91-23620 *
NAS 1.15:103669	p 98	N91-19236 *	NAS 1.15:103773	p 222	N91-24817 *	NAS 1.15:104403	p 15	N91-23083 *
NAS 1.15:103670	p 98	N91-19237 *	NAS 1.15:103774	p 27	N91-19097 *	NAS 1.15:104404	p 222	N91-22814 *
NAS 1.15:103671	p 216	N91-20748 *	NAS 1.15:103775	p 128	N91-21378 *	NAS 1.15:104405	p 211	N91-23616 *
NAS 1.15:103672	p 143	N91-19348 *	NAS 1.15:103776	p 190	N91-30539 *	NAS 1.15:104406	p 167	N91-24550 *
NAS 1.15:103673	p 160	N91-19369 *	NAS 1.15:103777	p 120	N91-19295 *	NAS 1.15:104407	p 16	N91-23089 *
NAS 1.15:103674	p 118	N91-14482 *	NAS 1.15:103778	p 13	N91-19063 *	NAS 1.15:104408	p 168	N91-30461 *
NAS 1.15:103675	p 200	N91-17427 *	NAS 1.15:103779	p 14	N91-21061 *	NAS 1.15:104409	p 126	N91-24460 *

NAS 1.15:104410	p 236	N91-23946 * #	NAS 1.15:104522	p 178	N91-27521 * #	NAS 1.15:4303	p 81	N91-28278 * #
NAS 1.15:104411	p 32	N91-23185 * #	NAS 1.15:104523	p 34	N91-27164 * #	NAS 1.15:4304	p 206	N91-28627 * #
NAS 1.15:104412	p 33	N91-24202 * #	NAS 1.15:104527	p 80	N91-27212 * #	NAS 1.15:83665	p 110	N91-10149 * #
NAS 1.15:104413	p 165	N91-24525 * #	NAS 1.15:104528	p 238	N91-31023 * #	NAS 1.26:187077	p 215	N91-20630 * #
NAS 1.15:104414	p 187	N91-24593 * #	NAS 1.15:104529	p 194	N91-27575 * #	NAS 1.26:187104	p 121	N91-21307 * #
NAS 1.15:104415	p 177	N91-26490 * #	NAS 1.15:104530	p 222	N91-27886 * #	NAS 1.26:187350	p 234	N91-11555 * #
NAS 1.15:104416	p 101	N91-24361 * #	NAS 1.15:104532	p 82	N91-30202 * #	NAS 1.26:188612	p 167	N91-25367 * #
NAS 1.15:104417	p 126	N91-25300 * #	NAS 1.15:104533	p 85	N91-31216 * #	NAS 1.55:10030	p 76	N91-24307 * #
NAS 1.15:104418	p 178	N91-27511 * #	NAS 1.15:104965	p 241	N91-25975 * #	NAS 1.55:10059	p 40	N91-22139 * #
NAS 1.15:104419	p 220	N91-31876 * #	NAS 1.15:105090	p 123	N91-28418 * #	NAS 1.55:10063	p 27	N91-20086 * #
NAS 1.15:104420	p 32	N91-23186 * #	NAS 1.15:105139	p 169	N91-30473 * #	NAS 1.55:3078	p 14	N91-21062 * #
NAS 1.15:104421	p 131	N91-23340 * #	NAS 1.15:105140	p 168	N91-29525 * #	NAS 1.55:3080	p 175	N91-14574 * #
NAS 1.15:104422	p 131	N91-24469 * #	NAS 1.15:105141	p 86	N91-31220 * #	NAS 1.55:3107	p 72	N91-19182 * #
NAS 1.15:104423	p 33	N91-24203 * #	NAS 1.15:105142	p 146	N91-27445 * #	NAS 1.55:3121	p 82	N91-30203 * #
NAS 1.15:104425	p 79	N91-27208 * #	NAS 1.15:105144	p 82	N91-29229 * #	NAS 1.55:3125	p 213	N91-32549 * #
NAS 1.15:104426	p 168	N91-30469 * #	NAS 1.15:105145	p 86	N91-32158 * #	NAS 1.60:3057	p 228	N91-16679 * #
NAS 1.15:104428	p 17	N91-25106 * #	NAS 1.15:105147	p 21	N91-27157 * #	NAS 1.60:3062	p 69	N91-11800 * #
NAS 1.15:104429	p 76	N91-24305 * #	NAS 1.15:105148	p 206	N91-30565 * #	NAS 1.60:3063	p 183	N91-12956 * #
NAS 1.15:104430	p 76	N91-24302 * #	NAS 1.15:105149	p 84	N91-30252 * #	NAS 1.60:3065	p 70	N91-15308 * #
NAS 1.15:104431	p 228	N91-25817 * #	NAS 1.15:105150	p 190	N91-30537 * #	NAS 1.60:3078	p 48	N91-21185 * #
NAS 1.15:104432	p 166	N91-24548 * #	NAS 1.15:105151	p 37	N91-27167 * #	NAS 1.60:3080	p 13	N91-19057 * #
NAS 1.15:104433	p 220	N91-25696 * #	NAS 1.15:105152	p 87	N91-32164 * #	NAS 1.60:3081	p 134	N91-27436 * #
NAS 1.15:104434	p 187	N91-25395 * #	NAS 1.15:105153	p 85	N91-31212 * #	NAS 1.60:3142	p 17	N91-28136 * #
NAS 1.15:104435	p 145	N91-25320 * #	NAS 1.15:105155	p 35	N91-30142 * #	NAS 1.60:3155	p 112	N91-30318 * #
NAS 1.15:104436	p 16	N91-24131 * #	NAS 1.15:105156	p 82	N91-29231 * #	NAS 1.61:1236	p 94	N91-10127 * #
NAS 1.15:104437	p 33	N91-24201 * #	NAS 1.15:105157	p 218	N91-28776 * #	NAS 1.61:1248	p 228	N91-15848 * #
NAS 1.15:104439	p 166	N91-24541 * #	NAS 1.15:105158	p 80	N91-27213 * #	NAS 1.71 LEW-14162-1	p 159	N91-13668 * #
NAS 1.15:104440	p 49	N91-25161 * #	NAS 1.15:105160	p 168	N91-30462 * #	NAS 1.71 LEW-14162-2	p 101	N91-25201 * #
NAS 1.15:104441	p 35	N91-31181 * #	NAS 1.15:105163	p 35	N91-29188 * #	NAS 1.71 LEW-14474-1	p 123	N91-28423 * #
NAS 1.15:104442	p 89	N91-24341 * #	NAS 1.15:105164	p 194	N91-28605 * #	NAS 1.71 LEW-14878-1	p 229	N91-13996 * #
NAS 1.15:104443	p 131	N91-24470 * #	NAS 1.15:105165	p 179	N91-31605 * #	NAS 1.71 LEW-14921-1	p 95	N91-13502 * #
NAS 1.15:104444	p 166	N91-24547 * #	NAS 1.15:105166	p 102	N91-30281 * #	NAS 1.71 LEW-14945-1	p 133	N91-13598 * #
NAS 1.15:104445	p 204	N91-24659 * #	NAS 1.15:105167	p 135	N91-29431 * #	NAS 1.71 LEW-14949-1	p 211	N91-23617 * #
NAS 1.15:104446	p 215	N91-24745 * #	NAS 1.15:105168	p 206	N91-30566 * #	NAS 1.71 LEW-14965-1	p 183	N91-13732 * #
NAS 1.15:104447	p 33	N91-25148 * #	NAS 1.15:105169	p 18	N91-29150 * #	NAS 1.71 LEW-14999-2	p 122	N91-26376 * #
NAS 1.15:104448	p 78	N91-25183 * #	NAS 1.15:105170	p 81	N91-29228 * #	NAS 1.71 LEW-15020-1	p 119	N91-15412 * #
NAS 1.15:104449	p 17	N91-26122 * #	NAS 1.15:105171	p 112	N91-29298 * #	NAS 1.71 LEW-15020-2	p 101	N91-25202 * #
NAS 1.15:104451	p 223	N91-25749 * #	NAS 1.15:105172	p 178	N91-30491 * #	NAS 1.71 LEW-15027-1	p 118	N91-13566 * #
NAS 1.15:104452	p 222	N91-25739 * #	NAS 1.15:105173	p 39	N91-29199 * #	NAS 1.71 LEW-15043-1	p 123	N91-32230 * #
NAS 1.15:104453	p 238	N91-24952 * #	NAS 1.15:105175	p 82	N91-29230 * #	NAS 1.71 LEW-15077-2	p 102	N91-28289 * #
NAS 1.15:104454	p 177	N91-25381 * #	NAS 1.15:105176	p 34	N91-29181 * #	NAS 1.71 LEW-15094-1	p 32	N91-23180 * #
NAS 1.15:104455	p 77	N91-25179 * #	NAS 1.15:105177	p 168	N91-30472 * #	NAS 1.71 LEW-15155-1	p 122	N91-26375 * #
NAS 1.15:104456	p 76	N91-24304 * #	NAS 1.15:105178	p 123	N91-29332 * #	NAS 1.71 LEW-15164-1	p 122	N91-25298 * #
NAS 1.15:104458	p 167	N91-25351 * #	NAS 1.15:105179	p 223	N91-30865 * #	NAS 1.71 LEW-15164-2	p 123	N91-32229 * #
NAS 1.15:104459	p 77	N91-25172 * #	NAS 1.15:105180	p 34	N91-29187 * #	NAS 1.71 LEW-15196-1	p 188	N91-26543 * #
NAS 1.15:104460	p 78	N91-25182 * #	NAS 1.15:105181	p 81	N91-29221 * #	NAS 1.71 LEW-15200-1	p 87	N91-32167 * #
NAS 1.15:104461	p 223	N91-27901 * #	NAS 1.15:105182	p 190	N91-29600 * #	NAS 1.71 LEW-15222-1	p 236	N91-26966 * #
NAS 1.15:104462	p 166	N91-24549 * #	NAS 1.15:105183	p 146	N91-30426 * #	NAS 1.71 LEW-15223-1	p 236	N91-26967 * #
NAS 1.15:104463	p 217	N91-24787 * #	NAS 1.15:105184	p 237	N91-29982 * #	NAS 1.71:14846-2	p 78	N91-26200 * #
NAS 1.15:104464	p 100	N91-24359 * #	NAS 1.15:105186	p 35	N91-30141 * #			
NAS 1.15:104465	p 188	N91-25413 * #	NAS 1.15:105187	p 39	N91-30163 * #	NASA-CASE-LEW-14162-1	p 159	N91-13668 * #
NAS 1.15:104466	p 33	N91-26146 * #	NAS 1.15:105188	p 135	N91-29404 * #	NASA-CASE-LEW-14162-2	p 101	N91-25201 * #
NAS 1.15:104467	p 146	N91-27477 * #	NAS 1.15:105190	p 81	N91-29220 * #	NASA-CASE-LEW-14203-1	p 118	N91-15402 * #
NAS 1.15:104468	p 190	N91-30538 * #	NAS 1.15:105191	p 127	N91-28449 * #	NASA-CASE-LEW-14295-1	p 130	N91-15424 * #
NAS 1.15:104469	p 16	N91-24130 * #	NAS 1.15:105195	p 81	N91-29222 * #	NASA-CASE-LEW-14345-3	p 89	N91-17141 * #
NAS 1.15:104470	p 103	N91-31235 * #	NAS 1.15:105196	p 243	N91-29138 * #	NASA-CASE-LEW-14345-4	p 90	N91-25185 * #
NAS 1.15:104471	p 212	N91-27611 * #	NAS 1.15:105197	p 168	N91-28538 * #	NASA-CASE-LEW-14472-1	p 95	N91-15320 * #
NAS 1.15:104472	p 34	N91-27159 * #	NAS 1.15:105200	p 217	N91-32806 * #	NASA-CASE-LEW-14474-1	p 123	N91-28423 * #
NAS 1.15:104473	p 76	N91-24303 * #	NAS 1.15:105201	p 169	N91-32440 * #	NASA-CASE-LEW-14672-1	p 189	N91-27560 * #
NAS 1.15:104474	p 188	N91-25412 * #	NAS 1.15:105202	p 84	N91-30266 * #	NASA-CASE-LEW-14676-1	p 147	N91-31529 * #
NAS 1.15:104475	p 43	N91-25159 * #	NAS 1.15:105203	p 223	N91-31911 * #	NASA-CASE-LEW-14679-1	p 122	N91-25296 * #
NAS 1.15:104476	p 191	N91-31654 * #	NAS 1.15:105204	p 190	N91-30532 * #	NASA-CASE-LEW-14746-1	p 143	N91-14552 * #
NAS 1.15:104481	p 177	N91-25387 * #	NAS 1.15:105205	p 147	N91-32412 * #	NASA-CASE-LEW-14776-1	p 185	N91-21540 * #
NAS 1.15:104482	p 177	N91-25382 * #	NAS 1.15:105208	p 169	N91-32458 * #	NASA-CASE-LEW-14795-1	p 230	N91-21871 * #
NAS 1.15:104483	p 17	N91-26121 * #	NAS 1.15:105209	p 169	N91-32459 * #	NASA-CASE-LEW-14846-2	p 78	N91-26200 * #
NAS 1.15:104484	p 220	N91-24815 * #	NAS 1.15:105210	p 18	N91-31106 * #	NASA-CASE-LEW-14848-1	p 42	N91-27175 * #
NAS 1.15:104485	p 79	N91-27209 * #	NAS 1.15:105216	p 242	N91-33046 * #	NASA-CASE-LEW-14862-1	p 183	N91-14617 * #
NAS 1.15:104486	p 78	N91-25184 * #	NAS 1.15:105217	p 85	N91-30267 * #	NASA-CASE-LEW-14878-1	p 229	N91-13996 * #
NAS 1.15:104487	p 212	N91-25510 * #	NAS 1.15:105220	p 237	N91-31977 * #	NASA-CASE-LEW-14887-1	p 189	N91-27561 * #
NAS 1.15:104489	p 90	N91-29235 * #	NAS 1.15:105222	p 85	N91-31217 * #	NASA-CASE-LEW-14901-1	p 231	N91-25875 * #
NAS 1.15:104490	p 90	N91-27221 * #	NAS 1.15:105223	p 18	N91-32075 * #	NASA-CASE-LEW-14902-1	p 102	N91-27244 * #
NAS 1.15:104491	p 224	N91-26870 * #	NAS 1.15:105224	p 44	N91-31196 * #	NASA-CASE-LEW-14921-1	p 95	N91-13502 * #
NAS 1.15:104494	p 205	N91-25442 * #	NAS 1.15:105225	p 18	N91-32074 * #	NASA-CASE-LEW-14945-1	p 133	N91-13598 * #
NAS 1.15:104495	p 223	N91-30867 * #	NAS 1.15:105228	p 87	N91-32165 * #	NASA-CASE-LEW-14949-1	p 211	N91-23617 * #
NAS 1.15:104496	p 189	N91-27569 * #	NAS 1.15:105229	p 213	N91-31708 * #	NASA-CASE-LEW-14959-1	p 212	N91-27614 * #
NAS 1.15:104497	p 103	N91-30282 * #	NAS 1.15:105230	p 103	N91-32182 * #	NASA-CASE-LEW-14965-1	p 183	N91-13732 * #
NAS 1.15:104499	p 17	N91-27129 * #	NAS 1.15:105235	p 86	N91-32163 * #	NASA-CASE-LEW-14967-1	p 179	N91-31608 * #
NAS 1.15:104500	p 135	N91-27437 * #	NAS 1.15:105237	p 169	N91-31597 * #	NASA-CASE-LEW-14990-1-CU	p 96	N91-17145 * #
NAS 1.15:104501	p 178	N91-27510 * #	NAS 1.15:105238	p 170	N91-32460 * #	NASA-CASE-LEW-14999-2	p 122	N91-26376 * #
NAS 1.15:104502	p 135	N91-29405 * #	NAS 1.15:105239	p 135	N91-32247 * #	NASA-CASE-LEW-15020-1	p 119	N91-15412 * #
NAS 1.15:104504	p 79	N91-27207 * #	NAS 1.15:105242	p 86	N91-32162 * #	NASA-CASE-LEW-15020-2	p 101	N91-25202 * #
NAS 1.15:104505	p 86	N91-31218 * #	NAS 1.15:105248	p 147	N91-32410 * #	NASA-CASE-LEW-15027-1	p 118	N91-13566 * #
NAS 1.15:104507	p 103	N91-32177 * #	NAS 1.15:105254	p 37	N91-32143 * #	NASA-CASE-LEW-15043-1	p 123	N91-32230 * #
NAS 1.15:104508	p 146	N91-30427 * #	NAS 1.15:105256	p 86	N91-32161 * #	NASA-CASE-LEW-15077-2	p 102	N91-28289 * #
NAS 1.15:104509	p 146	N91-27447 * #	NAS 1.15:105263	p 127	N91-31318 * #	NASA-CASE-LEW-15094-1	p 32	N91-23180 * #
NAS 1.15:104510	p 78	N91-26202 * #	NAS 1.15:105275	p 135	N91-32287 * #	NASA-CASE-LEW-15155-1	p 122	N91-26375 * #
NAS 1.15:104511	p 80	N91-27214 * #	NAS 1.15:105280	p 112	N91-32215 * #	NASA-CASE-LEW-15164-1	p 122	N91-25298 * #
NAS 1.15:104512	p 214	N91-32569 * #	NAS 1.15:105282	p 112	N91-32204 * #	NASA-CASE-LEW-15164-2	p 123	N91-32229 * #
NAS 1.15:104513	p 42	N91-30186 * #	NAS 1.15:105292	p 112	N91-32216 * #	NASA-CASE-LEW-15196-1	p 188	N91-26543 * #
NAS 1.15:104514	p 84	N91-30265 * #	NAS 1.15:105293	p 238	N91-33014 * #	NASA-CASE-LEW-15200-1	p 87	N91-32167 * #
NAS 1.15:104515	p 79	N91-27206 * #	NAS 1.15:4225	p 111	N91-20268 * #	NASA-CASE-LEW-15222-1	p 236	N91-26966 * #
NAS 1.15:104516	p 127	N91-27375 * #	NAS 1.15:4226	p 201	N91-19473 * #	NASA-CASE-LEW-15223-1	p 236	N91-26967 * #
NAS 1.15:104517	p 146	N91-27444 * #	NAS 1.15:4257	p 40	N91-19115 * #			
NAS 1.15:104519	p 205	N91-27591 * #	NAS 1.15:4272	p 167	N91-27489 * #	NASA-CP-10030	p 76	

REPORT NUMBER INDEX

NASA-TM-104361

NASA-CP-10063	p 27	N91-20086 *	NASA-TM-103629	p 227	N91-12317 *	NASA-TM-103730	p 126	N91-19317 *
NASA-CP-3078	p 14	N91-21062 *	NASA-TM-103630	p 221	N91-14781 *	NASA-TM-103731	p 71	N91-19177 *
NASA-CP-3080	p 175	N91-14574 *	NASA-TM-103631	p 130	N91-14500 *	NASA-TM-103732	p 193	N91-19463 *
NASA-CP-3107	p 72	N91-19182 *	NASA-TM-103632	p 94	N91-10134 *	NASA-TM-103733	p 99	N91-22402 *
NASA-CP-3121	p 82	N91-30203 *	NASA-TM-103633	p 133	N91-11988 *	NASA-TM-103734	p 176	N91-19402 *
NASA-CP-3125	p 213	N91-32549 *	NASA-TM-103634	p 20	N91-15146 *	NASA-TM-103735	p 48	N91-19165 *
			NASA-TM-103635	p 228	N91-15842 *	NASA-TM-103736	p 212	N91-26592 *
NASA-CR-187077	p 215	N91-20630 *	NASA-TM-103636	p 96	N91-17143 *	NASA-TM-103737	p 185	N91-22567 *
NASA-CR-187104	p 121	N91-21307 *	NASA-TM-103637	p 200	N91-14632 *	NASA-TM-103738	p 31	N91-20126 *
NASA-CR-187350	p 234	N91-11555 *	NASA-TM-103638	p 68	N91-11060 *	NASA-TM-103739	p 101	N91-26233 *
NASA-CR-188612	p 167	N91-25367 *	NASA-TM-103639	p 161	N91-19373 *	NASA-TM-103741	p 121	N91-23311 *
			NASA-TM-103640	p 26	N91-13455 *	NASA-TM-103742	p 14	N91-21060 *
NASA-RP-1236	p 94	N91-10127 *	NASA-TM-103641	p 159	N91-14556 *	NASA-TM-103743	p 98	N91-19235 *
NASA-RP-1248	p 228	N91-15848 *	NASA-TM-103642	p 241	N91-14259 *	NASA-TM-103744	p 203	N91-23549 *
			NASA-TM-103643	p 95	N91-13495 *	NASA-TM-103745	p 221	N91-19786 *
NASA-TM-100243	p 134	N91-22494 *	NASA-TM-103644	p 200	N91-18452 *	NASA-TM-103746	p 201	N91-19475 *
NASA-TM-101368	p 67	N91-10117 *	NASA-TM-103645	p 227	N91-12316 *	NASA-TM-103748	p 13	N91-19054 *
NASA-TM-101468	p 110	N91-10150 *	NASA-TM-103646	p 175	N91-12064 *	NASA-TM-103749	p 235	N91-21910 *
NASA-TM-102067	p 101	N91-25186 *	NASA-TM-103647	p 110	N91-14454 *	NASA-TM-103750	p 202	N91-21562 *
NASA-TM-102323	p 205	N91-25436 *	NASA-TM-103648	p 98	N91-19234 *	NASA-TM-103751	p 193	N91-19462 *
NASA-TM-102381	p 85	N91-31208 *	NASA-TM-103649	p 73	N91-21240 *	NASA-TM-103752	p 243	N91-30073 *
NASA-TM-102420	p 202	N91-21559 *	NASA-TM-103650	p 13	N91-19053 *	NASA-TM-103754	p 48	N91-20184 *
NASA-TM-102504	p 183	N91-12954 *	NASA-TM-103651	p 26	N91-13456 *	NASA-TM-103756	p 167	N91-27487 *
NASA-TM-102513	p 159	N91-12913 *	NASA-TM-103652	p 130	N91-11945 *	NASA-TM-103757	p 32	N91-23183 *
NASA-TM-102521	p 128	N91-24464 *	NASA-TM-103653	p 70	N91-13491 *	NASA-TM-103758	p 184	N91-19443 *
NASA-TM-102528	p 16	N91-24124 *	NASA-TM-103654	p 230	N91-14829 *	NASA-TM-103759	p 243	N91-23072 *
NASA-TM-102542	p 238	N91-10798 *	NASA-TM-103655	p 234	N91-14850 *	NASA-TM-103760	p 102	N91-27247 *
NASA-TM-102803	p 99	N91-22396 *	NASA-TM-103656	p 71	N91-19179 *	NASA-TM-103761	p 193	N91-19464 *
NASA-TM-103097	p 121	N91-22460 *	NASA-TM-103657	p 67	N91-10119 *	NASA-TM-103762	p 144	N91-19354 *
NASA-TM-103115	p 12	N91-17002 *	NASA-TM-103658	p 184	N91-19442 *	NASA-TM-103763	p 145	N91-21433 *
NASA-TM-103169	p 95	N91-14426 *	NASA-TM-103659	p 234	N91-14050 *	NASA-TM-103764	p 120	N91-19308 *
NASA-TM-103183	p 10	N91-11675 *	NASA-TM-103660	p 200	N91-12980 *	NASA-TM-103765	p 126	N91-22464 *
NASA-TM-103191	p 72	N91-19180 *	NASA-TM-103661	p 74	N91-22371 *	NASA-TM-103766	p 217	N91-25630 *
NASA-TM-103193	p 69	N91-11798 *	NASA-TM-103662	p 130	N91-19324 *	NASA-TM-103767	p 121	N91-21309 *
NASA-TM-103197	p 192	N91-17407 *	NASA-TM-103663	p 120	N91-19296 *	NASA-TM-103768	p 89	N91-22377 *
NASA-TM-103204	p 94	N91-11074 *	NASA-TM-103664	p 106	N91-19256 *	NASA-TM-103769	p 164	N91-21448 *
NASA-TM-103214	p 160	N91-16304 *	NASA-TM-103665	p 96	N91-15328 *	NASA-TM-103771	p 71	N91-19175 *
NASA-TM-103216	p 69	N91-11802 *	NASA-TM-103666	p 161	N91-19372 *	NASA-TM-103772	p 102	N91-29250 *
NASA-TM-103218	p 69	N91-11799 *	NASA-TM-103667	p 98	N91-19236 *	NASA-TM-103773	p 222	N91-24817 *
NASA-TM-103226	p 133	N91-18297 *	NASA-TM-103668	p 98	N91-19237 *	NASA-TM-103774	p 27	N91-19097 *
NASA-TM-103227	p 67	N91-10118 *	NASA-TM-103669	p 216	N91-20748 *	NASA-TM-103775	p 128	N91-21378 *
NASA-TM-103230	p 96	N91-15329 *	NASA-TM-103670	p 143	N91-19348 *	NASA-TM-103776	p 190	N91-30539 *
NASA-TM-103232	p 185	N91-22566 *	NASA-TM-103671	p 160	N91-19369 *	NASA-TM-103777	p 120	N91-19295 *
NASA-TM-103234	p 71	N91-19178 *	NASA-TM-103672	p 118	N91-14482 *	NASA-TM-103778	p 13	N91-19063 *
NASA-TM-103236	p 31	N91-22126 *	NASA-TM-103673	p 200	N91-17427 *	NASA-TM-103779	p 14	N91-21061 *
NASA-TM-103238	p 38	N91-11770 *	NASA-TM-103674	p 176	N91-19401 *	NASA-TM-103780	p 164	N91-21458 *
NASA-TM-103244	p 200	N91-17415 *	NASA-TM-103675	p 97	N91-19231 *	NASA-TM-103781	p 161	N91-19375 *
NASA-TM-103245	p 96	N91-16075 *	NASA-TM-103676	p 31	N91-21137 *	NASA-TM-103782	p 202	N91-21558 *
NASA-TM-103247	p 199	N91-10332 *	NASA-TM-103677	p 12	N91-19044 *	NASA-TM-103783	p 134	N91-23347 *
NASA-TM-103251	p 10	N91-11676 *	NASA-TM-103678	p 201	N91-19472 *	NASA-TM-103784	p 89	N91-19224 *
NASA-TM-103257	p 176	N91-19404 *	NASA-TM-103679	p 97	N91-19230 *	NASA-TM-103785	p 219	N91-19766 *
NASA-TM-103258	p 15	N91-21116 *	NASA-TM-103680	p 97	N91-19229 *	NASA-TM-103786	p 194	N91-21553 *
NASA-TM-103260	p 11	N91-15134 *	NASA-TM-103681	p 26	N91-13457 *	NASA-TM-103787	p 128	N91-19320 *
NASA-TM-103263	p 159	N91-13638 *	NASA-TM-103682	p 119	N91-19292 *	NASA-TM-103788	p 221	N91-20830 *
NASA-TM-103265	p 88	N91-11062 *	NASA-TM-103683	p 99	N91-20228 *	NASA-TM-103789	p 222	N91-24818 *
NASA-TM-103266	p 118	N91-11922 *	NASA-TM-103684	p 12	N91-19045 *	NASA-TM-103790	p 164	N91-21447 *
NASA-TM-103267	p 159	N91-12034 *	NASA-TM-103685	p 99	N91-21243 *	NASA-TM-103791	p 235	N91-19935 *
NASA-TM-103268	p 26	N91-14349 *	NASA-TM-103686	p 11	N91-13420 *	NASA-TM-103792	p 222	N91-21797 *
NASA-TM-103269	p 67	N91-11058 *	NASA-TM-103687	p 27	N91-19098 *	NASA-TM-103793	p 201	N91-19476 *
NASA-TM-103272	p 134	N91-19332 *	NASA-TM-103688	p 188	N91-25411 *	NASA-TM-103794	p 187	N91-23515 *
NASA-TM-103273	p 160	N91-14559 *	NASA-TM-103689	p 11	N91-17000 *	NASA-TM-103795	p 112	N91-27324 *
NASA-TM-103274	p 175	N91-11205 *	NASA-TM-103690	p 12	N91-19046 *	NASA-TM-103796	p 187	N91-23513 *
NASA-TM-103276	p 184	N91-21531 *	NASA-TM-103691	p 120	N91-21302 *	NASA-TM-103797	p 188	N91-27558 *
NASA-TM-103277	p 199	N91-12114 *	NASA-TM-103692	p 185	N91-21534 *	NASA-TM-103798	p 89	N91-22379 *
NASA-TM-103278	p 26	N91-11752 *	NASA-TM-103693	p 144	N91-20382 *	NASA-TM-103799	p 165	N91-23409 *
NASA-TM-103281	p 189	N91-27570 *	NASA-TM-103694	p 184	N91-20489 *	NASA-TM-103800	p 144	N91-20406 *
NASA-TM-103282	p 133	N91-10208 *	NASA-TM-103695	p 40	N91-19112 *	NASA-TM-103801	p 126	N91-20324 *
NASA-TM-103283	p 208	N91-15628 *	NASA-TM-103696	p 144	N91-20393 *	NASA-TM-103802	p 30	N91-20122 *
NASA-TM-103284	p 68	N91-11061 *	NASA-TM-103697	p 143	N91-19349 *	NASA-TM-103803	p 195	N91-30546 *
NASA-TM-103285	p 27	N91-15174 *	NASA-TM-103700	p 12	N91-19047 *	NASA-TM-103804	p 35	N91-31178 *
NASA-TM-103286	p 143	N91-19351 *	NASA-TM-103701	p 160	N91-19370 *	NASA-TM-103805	p 44	N91-21182 *
NASA-TM-103287	p 205	N91-28622 *	NASA-TM-103702	p 70	N91-15303 *	NASA-TM-103806	p 73	N91-22367 *
NASA-TM-103288	p 175	N91-10271 *	NASA-TM-103703	p 72	N91-20204 *	NASA-TM-103807	p 186	N91-22568 *
NASA-TM-103289	p 216	N91-12215 *	NASA-TM-103704	p 11	N91-14310 *	NASA-TM-103808	p 165	N91-22536 *
NASA-TM-103290	p 69	N91-11801 *	NASA-TM-103705	p 160	N91-19371 *	NASA-TM-103809	p 46	N91-21184 *
NASA-TM-103293	p 159	N91-10249 *	NASA-TM-103706	p 119	N91-19293 *	NASA-TM-103810	p 194	N91-23521 *
NASA-TM-103332	p 229	N91-18799 *	NASA-TM-103707	p 111	N91-15390 *	NASA-TM-103811	p 31	N91-21140 *
NASA-TM-103423	p 128	N91-14498 *	NASA-TM-103708	p 11	N91-14309 *	NASA-TM-103812	p 122	N91-25286 *
NASA-TM-103606	p 228	N91-19825 *	NASA-TM-103709	p 13	N91-20044 *	NASA-TM-103813	p 165	N91-23439 *
NASA-TM-103608	p 226	N91-10703 *	NASA-TM-103710	p 119	N91-19294 *	NASA-TM-103814	p 169	N91-30476 *
NASA-TM-103611	p 125	N91-15418 *	NASA-TM-103711	p 11	N91-13421 *	NASA-TM-103815	p 217	N91-25680 *
NASA-TM-103612	p 95	N91-15318 *	NASA-TM-103712	p 97	N91-19232 *	NASA-TM-103816	p 203	N91-22604 *
NASA-TM-103613	p 68	N91-11059 *	NASA-TM-103713	p 27	N91-20084 *	NASA-TM-103817	p 103	N91-32181 *
NASA-TM-103614	p 192	N91-15565 *	NASA-TM-103714	p 71	N91-19176 *	NASA-TM-103818	p 216	N91-20765 *
NASA-TM-103616	p 234	N91-10780 *	NASA-TM-103715	p 184	N91-19441 *	NASA-TM-103819	p 79	N91-27204 *
NASA-TM-103617	p 70	N91-15301 *	NASA-TM-103716	p 73	N91-22370 *	NASA-TM-103820	p 186	N91-23512 *
NASA-TM-103618	p 68	N91-11796 *	NASA-TM-103717	p 176	N91-20453 *	NASA-TM-103821	p 32	N91-23184 *
NASA-TM-103619	p 70	N91-15306 *	NASA-TM-103718	p 162	N91-20417 *	NASA-TM-103822	p 189	N91-29599 *
NASA-TM-103620	p 101	N91-25195 *	NASA-TM-103719	p 13	N91-20045 *	NASA-TM-103823	p 15	N91-22084 *
NASA-TM-103622	p 68	N91-11797 *	NASA-TM-103720	p 162	N91-20445 *	NASA-TM-103824	p 100	N91-23247 *
NASA-TM-103623	p 242	N91-15117 *	NASA-TM-103721	p 97	N91-19233 *	NASA-TM-103825	p 205	N91-24660 *
NASA-TM-103624	p 159	N91-11192 *	NASA-TM-103722	p 107	N91-22410 *	NASA-TM-103826	p 31	N91-23179 *
NASA-TM-103625	p 227	N91-11494 *	NASA-TM-103723	p 161	N91-19374 *	NASA-TM-103827	p 186	N91-23501 *
NASA-TM-103626	p 201	N91-19477 *	NASA-TM-103724	p 111	N91-16128 *	NASA-TM-103828	p 14	N91-21115 *
NASA-TM-103627	p 227	N91-11495 *	NASA-TM-103725	p 241	N91-20015 *	NASA-TM-103829	p 81	N91-28277 *
NASA-TM-103628	p 227	N91-11493 *	NASA-TM-103726	p 72	N91-21233 *	NASA-TM-103830	p 187	N91-23514 *

NASA-TM-104362	p 15	N91-23086 * #	NASA-TM-104466	p 33	N91-26146 * #	NASA-TM-105188	p 135	N91-29404 * #
NASA-TM-104363	p 19	N91-23098 * #	NASA-TM-104467	p 146	N91-27477 * #	NASA-TM-105190	p 81	N91-29220 * #
NASA-TM-104364	p 77	N91-25175 * #	NASA-TM-104468	p 190	N91-30538 * #	NASA-TM-105191	p 127	N91-28449 * #
NASA-TM-104365	p 100	N91-24345 * #	NASA-TM-104469	p 16	N91-24130 * #	NASA-TM-105195	p 81	N91-29222 * #
NASA-TM-104366	p 15	N91-23087 * #	NASA-TM-104470	p 103	N91-31235 * #	NASA-TM-105196	p 243	N91-29138 * #
NASA-TM-104367	p 203	N91-22594 * #	NASA-TM-104471	p 212	N91-27611 * #	NASA-TM-105197	p 168	N91-28538 * #
NASA-TM-104368	p 165	N91-23416 * #	NASA-TM-104472	p 34	N91-27159 * #	NASA-TM-105200	p 217	N91-32806 * #
NASA-TM-104369	p 164	N91-22524 * #	NASA-TM-104473	p 76	N91-24303 * #	NASA-TM-105201	p 169	N91-32440 * #
NASA-TM-104370	p 100	N91-24360 * #	NASA-TM-104474	p 188	N91-25412 * #	NASA-TM-105202	p 84	N91-30266 * #
NASA-TM-104371	p 186	N91-22571 * #	NASA-TM-104476	p 43	N91-25159 * #	NASA-TM-105203	p 223	N91-31911 * #
NASA-TM-104372	p 102	N91-26234 * #	NASA-TM-104479	p 191	N91-31654 * #	NASA-TM-105204	p 190	N91-30532 * #
NASA-TM-104373	p 49	N91-24225 * #	NASA-TM-104481	p 177	N91-25387 * #	NASA-TM-105205	p 147	N91-32412 * #
NASA-TM-104374	p 218	N91-24796 * #	NASA-TM-104482	p 177	N91-25382 * #	NASA-TM-105208	p 169	N91-32458 * #
NASA-TM-104375	p 145	N91-22508 * #	NASA-TM-104483	p 17	N91-26121 * #	NASA-TM-105209	p 169	N91-32459 * #
NASA-TM-104376	p 224	N91-26872 * #	NASA-TM-104484	p 220	N91-24815 * #	NASA-TM-105210	p 18	N91-31106 * #
NASA-TM-104377	p 16	N91-24107 * #	NASA-TM-104485	p 79	N91-27209 * #	NASA-TM-105216	p 242	N91-33046 * #
NASA-TM-104378	p 206	N91-32520 * #	NASA-TM-104486	p 78	N91-25184 * #	NASA-TM-105217	p 85	N91-30267 * #
NASA-TM-104379	p 203	N91-23548 * #	NASA-TM-104487	p 212	N91-25510 * #	NASA-TM-105220	p 237	N91-31977 * #
NASA-TM-104380	p 217	N91-22766 * #	NASA-TM-104489	p 90	N91-29235 * #	NASA-TM-105222	p 85	N91-31217 * #
NASA-TM-104381	p 101	N91-25198 * #	NASA-TM-104490	p 90	N91-27221 * #	NASA-TM-105223	p 18	N91-32075 * #
NASA-TM-104382	p 74	N91-23233 * #	NASA-TM-104491	p 224	N91-26870 * #	NASA-TM-105224	p 44	N91-31196 * #
NASA-TM-104383	p 74	N91-22376 * #	NASA-TM-104494	p 205	N91-25442 * #	NASA-TM-105225	p 18	N91-32074 * #
NASA-TM-104384	p 74	N91-22375 * #	NASA-TM-104495	p 223	N91-30867 * #	NASA-TM-105228	p 87	N91-32165 * #
NASA-TM-104387	p 74	N91-23234 * #	NASA-TM-104496	p 189	N91-27569 * #	NASA-TM-105229	p 213	N91-31708 * #
NASA-TM-104388	p 186	N91-23500 * #	NASA-TM-104497	p 103	N91-30282 * #	NASA-TM-105230	p 103	N91-32182 * #
NASA-TM-104389	p 20	N91-23102 * #	NASA-TM-104499	p 17	N91-27129 * #	NASA-TM-105235	p 86	N91-32163 * #
NASA-TM-104390	p 166	N91-24527 * #	NASA-TM-104500	p 135	N91-27437 * #	NASA-TM-105237	p 169	N91-31597 * #
NASA-TM-104391	p 37	N91-22135 * #	NASA-TM-104501	p 178	N91-27510 * #	NASA-TM-105238	p 170	N91-32460 * #
NASA-TM-104392	p 134	N91-23354 * #	NASA-TM-104502	p 135	N91-29405 * #	NASA-TM-105239	p 135	N91-32247 * #
NASA-TM-104393	p 77	N91-25173 * #	NASA-TM-104504	p 79	N91-27207 * #	NASA-TM-105242	p 86	N91-32162 * #
NASA-TM-104394	p 191	N91-31648 * #	NASA-TM-104505	p 86	N91-31218 * #	NASA-TM-105248	p 147	N91-32410 * #
NASA-TM-104395	p 190	N91-30533 * #	NASA-TM-104507	p 103	N91-32177 * #	NASA-TM-105254	p 37	N91-32143 * #
NASA-TM-104396	p 188	N91-27559 * #	NASA-TM-104508	p 146	N91-30427 * #	NASA-TM-105256	p 86	N91-32161 * #
NASA-TM-104397	p 186	N91-22570 * #	NASA-TM-104509	p 146	N91-27447 * #	NASA-TM-105263	p 127	N91-31318 * #
NASA-TM-104398	p 236	N91-22921 * #	NASA-TM-104510	p 78	N91-26202 * #	NASA-TM-105275	p 135	N91-32287 * #
NASA-TM-104400	p 203	N91-23550 * #	NASA-TM-104511	p 80	N91-27214 * #	NASA-TM-105280	p 112	N91-32215 * #
NASA-TM-104401	p 75	N91-24232 * #	NASA-TM-104512	p 214	N91-32569 * #	NASA-TM-105282	p 112	N91-32204 * #
NASA-TM-104402	p 211	N91-23620 * #	NASA-TM-104513	p 42	N91-30186 * #	NASA-TM-105292	p 112	N91-32216 * #
NASA-TM-104403	p 15	N91-23083 * #	NASA-TM-104514	p 84	N91-30265 * #	NASA-TM-105293	p 238	N91-33014 * #
NASA-TM-104404	p 222	N91-22814 * #	NASA-TM-104515	p 79	N91-27206 * #	NASA-TM-4225	p 111	N91-20268 * #
NASA-TM-104405	p 211	N91-23616 * #	NASA-TM-104516	p 127	N91-27375 * #	NASA-TM-4226	p 201	N91-19473 * #
NASA-TM-104406	p 167	N91-24550 * #	NASA-TM-104517	p 146	N91-27444 * #	NASA-TM-4257	p 40	N91-19115 * #
NASA-TM-104407	p 16	N91-23089 * #	NASA-TM-104519	p 205	N91-27591 * #	NASA-TM-4272	p 167	N91-27489 * #
NASA-TM-104408	p 168	N91-30461 * #	NASA-TM-104520	p 194	N91-29610 * #	NASA-TM-4275	p 72	N91-20206 * #
NASA-TM-104409	p 126	N91-24460 * #	NASA-TM-104521	p 34	N91-27165 * #	NASA-TM-4276	p 36	N91-20133 * #
NASA-TM-104410	p 236	N91-23946 * #	NASA-TM-104522	p 178	N91-27521 * #	NASA-TM-4303	p 81	N91-28278 * #
NASA-TM-104411	p 32	N91-23185 * #	NASA-TM-104523	p 34	N91-27164 * #	NASA-TM-4304	p 206	N91-28627 * #
NASA-TM-104412	p 33	N91-24202 * #	NASA-TM-104527	p 80	N91-27212 * #	NASA-TM-83665	p 110	N91-10149 * #
NASA-TM-104413	p 165	N91-24525 * #	NASA-TM-104528	p 238	N91-31023 * #			
NASA-TM-104414	p 187	N91-24593 * #	NASA-TM-104529	p 194	N91-27575 * #	NASA-TP-3057	p 228	N91-16679 * #
NASA-TM-104415	p 177	N91-26490 * #	NASA-TM-104530	p 222	N91-27886 * #	NASA-TP-3062	p 69	N91-11800 * #
NASA-TM-104416	p 101	N91-24361 * #	NASA-TM-104532	p 82	N91-30202 * #	NASA-TP-3063	p 183	N91-12956 * #
NASA-TM-104417	p 126	N91-25300 * #	NASA-TM-104533	p 85	N91-31216 * #	NASA-TP-3065	p 70	N91-15308 * #
NASA-TM-104418	p 178	N91-27511 * #	NASA-TM-104965	p 241	N91-25975 * #	NASA-TP-3078	p 48	N91-21185 * #
NASA-TM-104419	p 220	N91-31876 * #	NASA-TM-105090	p 123	N91-28418 * #	NASA-TP-3080	p 13	N91-19057 * #
NASA-TM-104420	p 32	N91-23186 * #	NASA-TM-105139	p 169	N91-30473 * #	NASA-TP-3081	p 134	N91-27436 * #
NASA-TM-104421	p 131	N91-23340 * #	NASA-TM-105140	p 168	N91-29525 * #	NASA-TP-3142	p 17	N91-28136 * #
NASA-TM-104422	p 131	N91-24469 * #	NASA-TM-105141	p 86	N91-31220 * #	NASA-TP-3155	p 112	N91-30318 * #
NASA-TM-104423	p 33	N91-24203 * #	NASA-TM-105142	p 146	N91-27445 * #			
NASA-TM-104425	p 79	N91-27208 * #	NASA-TM-105144	p 82	N91-29229 * #	NISTIR-4352	p 234	N91-11555 * #
NASA-TM-104426	p 168	N91-30469 * #	NASA-TM-105145	p 86	N91-32158 * #			
NASA-TM-104428	p 17	N91-25106 * #	NASA-TM-105147	p 21	N91-27157 * #	PB90-257718	p 234	N91-11555 * #
NASA-TM-104429	p 76	N91-24305 * #	NASA-TM-105148	p 206	N91-30565 * #	PB91-140814	p 241	N91-25975 * #
NASA-TM-104430	p 76	N91-24302 * #	NASA-TM-105149	p 84	N91-30252 * #			
NASA-TM-104431	p 228	N91-25817 * #	NASA-TM-105150	p 190	N91-30537 * #	PNL-SA-18805	p 229	N91-18799 * #
NASA-TM-104432	p 166	N91-24548 * #	NASA-TM-105151	p 37	N91-27167 * #			
NASA-TM-104433	p 220	N91-25696 * #	NASA-TM-105152	p 87	N91-32164 * #	PSL-450-RP91-003A	p 215	N91-20630 * #
NASA-TM-104434	p 187	N91-25395 * #	NASA-TM-105153	p 85	N91-31212 * #			
NASA-TM-104435	p 145	N91-25320 * #	NASA-TM-105155	p 35	N91-30142 * #	SAE PAPER 901033	p 2	A91-21242 *
NASA-TM-104436	p 16	N91-24131 * #	NASA-TM-105156	p 82	N91-29231 * #	SAE PAPER 901923	p 1	A91-48605
NASA-TM-104437	p 33	N91-24201 * #	NASA-TM-105157	p 218	N91-28776 * #	SAE PAPER 911108	p 92	A91-53552 *
NASA-TM-104439	p 166	N91-24541 * #	NASA-TM-105158	p 80	N91-27213 * #	SAE PAPER 911111	p 110	A91-53555 *
NASA-TM-104440	p 49	N91-25161 * #	NASA-TM-105160	p 168	N91-30462 * #			
NASA-TM-104441	p 35	N91-31181 * #	NASA-TM-105163	p 35	N91-29188 * #	SPIE-1292	p 141	A91-50426 *
NASA-TM-104442	p 89	N91-24341 * #	NASA-TM-105164	p 194	N91-28605 * #			
NASA-TM-104443	p 131	N91-24470 * #	NASA-TM-105165	p 179	N91-31605 * #	STLE PREPRINT 90-AM-4E-1	p 87	A91-19720 *
NASA-TM-104444	p 166	N91-24547 * #	NASA-TM-105166	p 102	N91-30281 * #			
NASA-TM-104445	p 204	N91-24659 * #	NASA-TM-105167	p 135	N91-29431 * #	US-PATENT-APPL-SN-159071	p 89	N91-17141 *
NASA-TM-104446	p 215	N91-24745 * #	NASA-TM-105168	p 206	N91-30566 * #	US-PATENT-APPL-SN-231026	p 118	N91-15402 *
NASA-TM-104447	p 33	N91-25148 * #	NASA-TM-105169	p 18	N91-29150 * #	US-PATENT-APPL-SN-244377	p 130	N91-15424 *
NASA-TM-104448	p 78	N91-25183 * #	NASA-TM-105170	p 81	N91-29228 * #	US-PATENT-APPL-SN-251499	p 95	N91-15320 *
NASA-TM-104449	p 17	N91-26122 * #	NASA-TM-105171	p 112	N91-29298 * #	US-PATENT-APPL-SN-292049	p 89	N91-17141 *
NASA-TM-104451	p 223	N91-25749 * #	NASA-TM-105172	p 178	N91-30491 * #	US-PATENT-APPL-SN-292049	p 90	N91-25185 *
NASA-TM-104452	p 222	N91-25739 * #	NASA-TM-105173	p 39	N91-29199 * #	US-PATENT-APPL-SN-305675	p 147	N91-31529 *
NASA-TM-104453	p 238	N91-24952 * #	NASA-TM-105175	p 82	N91-29230 * #	US-PATENT-APPL-SN-326757	p 96	N91-17145 *
NASA-TM-104454	p 177	N91-25381 * #	NASA-TM-105176	p 34	N91-29181 * #	US-PATENT-APPL-SN-376488	p 231	N91-25875 *
NASA-TM-104455	p 77	N91-25179 * #	NASA-TM-105177	p 168	N91-30472 * #	US-PATENT-APPL-SN-381240	p 122	N91-25296 *
NASA-TM-104456	p 76	N91-24304 * #	NASA-TM-105178	p 123	N91-29332 * #	US-PATENT-APPL-SN-382885	p 42	N91-27175 *
NASA-TM-104458	p 167	N91-25351 * #	NASA-TM-105179	p 223	N91-30865 * #	US-PATENT-APPL-SN-392239	p 143	N91-14552 *
NASA-TM-104459	p 77	N91-25172 * #	NASA-TM-105180	p 34	N91-29187 * #	US-PATENT-APPL-SN-404291	p 230	N91-21871 *
NASA-TM-104460	p 78	N91-25182 * #	NASA-TM-105181	p 81	N91-29221 * #	US-PATENT-APPL-SN-414816	p 183	N91-14617 *
NASA-TM-104461	p 223	N91-27901 * #	NASA-TM-105182	p 190	N91-29600 * #	US-PATENT-APPL-SN-419554	p 90	N91-25185 *
NASA-TM-104462	p 166	N91-24549 * #	NASA-TM-105183	p 146	N91-30426 * #	US-PATENT-APPL-SN-433863	p 96	N91-17145 *
NASA-TM-104463	p 217	N91-24787 * #	NASA-TM-105184	p 237	N91-29982 * #	US-PATENT-APPL-SN-441672	p 189	N91-27560 *
NASA-TM-104464	p 100	N91-24359 * #	NASA-TM-105186	p 35	N91-30141 * #	US-PATENT-APPL-SN-458274	p 185	N91-21540 *
NASA-TM-104465	p 188	N91-25413 * #	NASA-TM-105187	p 39	N91-30163 * #	US-PATENT-APPL-SN-495969	p 212	N91-27614 *

US-PATENT-APPL-SN-501893	p 159	N91-13668 *	US-PATENT-CLASS-505-702	p 147	N91-31529 *
US-PATENT-APPL-SN-503418	p 189	N91-27561 *	US-PATENT-CLASS-505-703	p 147	N91-31529 *
US-PATENT-APPL-SN-531433	p 179	N91-31608 *	US-PATENT-CLASS-505-704	p 147	N91-31529 *
US-PATENT-APPL-SN-540976	p 133	N91-13598 *	US-PATENT-CLASS-524-600	p 118	N91-15402 *
US-PATENT-APPL-SN-571058	p 102	N91-27244 *	US-PATENT-CLASS-525-436	p 118	N91-15402 *
US-PATENT-APPL-SN-571059	p 95	N91-13502 *	US-PATENT-CLASS-528-353	p 118	N91-15402 *
US-PATENT-APPL-SN-571062	p 183	N91-13732 *	US-PATENT-CLASS-552-101	p 89	N91-17141 *
US-PATENT-APPL-SN-587921	p 229	N91-13996 *	US-PATENT-CLASS-552-101	p 90	N91-25185 *
US-PATENT-APPL-SN-601957	p 119	N91-15412 *	US-PATENT-CLASS-552-108	p 90	N91-25185 *
US-PATENT-APPL-SN-603055	p 118	N91-13566 *	US-PATENT-CLASS-552-110	p 90	N91-25185 *
US-PATENT-APPL-SN-647902	p 32	N91-23180 *	US-PATENT-CLASS-552-113	p 90	N91-25185 *
US-PATENT-APPL-SN-657238	p 101	N91-25201 *	US-PATENT-CLASS-552-115	p 90	N91-25185 *
US-PATENT-APPL-SN-662684	p 122	N91-26376 *	US-PATENT-CLASS-73-826	p 42	N91-27175 *
US-PATENT-APPL-SN-676910	p 211	N91-23617 *	US-PATENT-CLASS-73-852	p 185	N91-21540 *
US-PATENT-APPL-SN-682160	p 122	N91-26375 *			
US-PATENT-APPL-SN-687606	p 188	N91-26543 *	US-PATENT-4,912,238	p 89	N91-17141 *
US-PATENT-APPL-SN-699130	p 122	N91-25298 *	US-PATENT-4,913,225	p 130	N91-15424 *
US-PATENT-APPL-SN-708255	p 101	N91-25202 *	US-PATENT-4,946,122	p 183	N91-14617 *
US-PATENT-APPL-SN-709907	p 78	N91-26200 *	US-PATENT-4,946,890	p 118	N91-15402 *
US-PATENT-APPL-SN-718314	p 236	N91-26967 *	US-PATENT-4,957,661	p 95	N91-15320 *
US-PATENT-APPL-SN-718315	p 236	N91-26966 *	US-PATENT-4,980,126	p 96	N91-17145 *
US-PATENT-APPL-SN-720133	p 123	N91-28423 *	US-PATENT-4,980,636	p 143	N91-14552 *
US-PATENT-APPL-SN-722446	p 87	N91-32167 *	US-PATENT-4,986,132	p 185	N91-21540 *
US-PATENT-APPL-SN-735548	p 102	N91-28289 *	US-PATENT-4,990,739	p 231	N91-25875 *
US-PATENT-APPL-SN-766591	p 123	N91-32229 *	US-PATENT-4,995,697	p 230	N91-21871 *
US-PATENT-APPL-SN-772181	p 123	N91-32230 *	US-PATENT-5,011,955	p 90	N91-25185 *
US-PATENT-APPL-SN-924474	p 89	N91-17141 *	US-PATENT-5,012,062	p 122	N91-25296 *
			US-PATENT-5,014,917	p 189	N91-27560 *
US-PATENT-CLASS-136-200	p 179	N91-31608 *	US-PATENT-5,015,825	p 42	N91-27175 *
US-PATENT-CLASS-136-244	p 212	N91-27614 *	US-PATENT-5,019,176	p 212	N91-27614 *
US-PATENT-CLASS-136-249	p 212	N91-27614 *	US-PATENT-5,032,045	p 189	N91-27561 *
US-PATENT-CLASS-136-256	p 212	N91-27614 *	US-PATENT-5,034,187	p 102	N91-27244 *
US-PATENT-CLASS-165-104.31	p 130	N91-15424 *	US-PATENT-5,048,973	p 179	N91-31608 *
US-PATENT-CLASS-165-41	p 130	N91-15424 *	US-PATENT-5,049,539	p 147	N91-31529 *
US-PATENT-CLASS-165-904	p 130	N91-15424 *			
US-PATENT-CLASS-219-121.47	p 231	N91-25875 *			
US-PATENT-CLASS-219-121.48	p 231	N91-25875 *			
US-PATENT-CLASS-219-121.52	p 231	N91-25875 *			
US-PATENT-CLASS-219-390	p 42	N91-27175 *			
US-PATENT-CLASS-219-69.11	p 122	N91-25296 *			
US-PATENT-CLASS-219-75	p 231	N91-25875 *			
US-PATENT-CLASS-219-76.16	p 231	N91-25875 *			
US-PATENT-CLASS-239-265.11	p 189	N91-27560 *			
US-PATENT-CLASS-239-597	p 130	N91-15424 *			
US-PATENT-CLASS-239-601	p 130	N91-15424 *			
US-PATENT-CLASS-244-163	p 130	N91-15424 *			
US-PATENT-CLASS-248-229	p 183	N91-14617 *			
US-PATENT-CLASS-248-230	p 183	N91-14617 *			
US-PATENT-CLASS-250-227	p 230	N91-21871 *			
US-PATENT-CLASS-250-356.1	p 179	N91-31608 *			
US-PATENT-CLASS-252-510	p 95	N91-15320 *			
US-PATENT-CLASS-277-157	p 189	N91-27560 *			
US-PATENT-CLASS-277-226	p 189	N91-27560 *			
US-PATENT-CLASS-277-229	p 189	N91-27560 *			
US-PATENT-CLASS-277-34	p 189	N91-27560 *			
US-PATENT-CLASS-292-60	p 189	N91-27561 *			
US-PATENT-CLASS-292-61	p 189	N91-27561 *			
US-PATENT-CLASS-324-158F	p 143	N91-14552 *			
US-PATENT-CLASS-324-158P	p 143	N91-14552 *			
US-PATENT-CLASS-324-601	p 143	N91-14552 *			
US-PATENT-CLASS-333-247	p 143	N91-14552 *			
US-PATENT-CLASS-350-96.29	p 230	N91-21871 *			
US-PATENT-CLASS-356-345	p 230	N91-21871 *			
US-PATENT-CLASS-357-30	p 212	N91-27614 *			
US-PATENT-CLASS-374-180	p 179	N91-31608 *			
US-PATENT-CLASS-374-208	p 179	N91-31608 *			
US-PATENT-CLASS-374-29	p 179	N91-31608 *			
US-PATENT-CLASS-374-49	p 42	N91-27175 *			
US-PATENT-CLASS-374-50	p 42	N91-27175 *			
US-PATENT-CLASS-403-385	p 183	N91-14617 *			
US-PATENT-CLASS-403-391	p 183	N91-14617 *			
US-PATENT-CLASS-410-80	p 189	N91-27561 *			
US-PATENT-CLASS-410-84	p 189	N91-27561 *			
US-PATENT-CLASS-419-14	p 102	N91-27244 *			
US-PATENT-CLASS-419-24	p 96	N91-17145 *			
US-PATENT-CLASS-419-30	p 102	N91-27244 *			
US-PATENT-CLASS-419-32	p 102	N91-27244 *			
US-PATENT-CLASS-419-36	p 96	N91-17145 *			
US-PATENT-CLASS-419-36	p 102	N91-27244 *			
US-PATENT-CLASS-419-37	p 96	N91-17145 *			
US-PATENT-CLASS-419-38	p 102	N91-27244 *			
US-PATENT-CLASS-419-39	p 102	N91-27244 *			
US-PATENT-CLASS-419-48	p 96	N91-17145 *			
US-PATENT-CLASS-419-49	p 96	N91-17145 *			
US-PATENT-CLASS-419-49	p 102	N91-27244 *			
US-PATENT-CLASS-419-8	p 96	N91-17145 *			
US-PATENT-CLASS-421-209	p 147	N91-31529 *			
US-PATENT-CLASS-421-457	p 147	N91-31529 *			
US-PATENT-CLASS-423-439	p 95	N91-15320 *			
US-PATENT-CLASS-423-448	p 95	N91-15320 *			
US-PATENT-CLASS-423-460	p 95	N91-15320 *			
US-PATENT-CLASS-423-489	p 95	N91-15320 *			
US-PATENT-CLASS-427-34	p 231	N91-25875 *			
US-PATENT-CLASS-437-2	p 212	N91-27614 *			
US-PATENT-CLASS-505-1	p 147	N91-31529 *			
US-PATENT-CLASS-505-701	p 147	N91-31529 *			

REPORT DOCUMENTATION PAGE			Form Approved OMB No. 0704-0188	
Public reporting burden for this collection of information is estimated to average 1 hour per response, including the time for reviewing instructions, searching existing data sources, gathering and maintaining the data needed, and completing and reviewing the collection of information. Send comments regarding this burden estimate or any other aspect of this collection of information, including suggestions for reducing this burden, to Washington Headquarters Services, Directorate for Information Operations and Reports, 1215 Jefferson Davis Highway, Suite 1204, Arlington, VA 22202-4302, and to the Office of Management and Budget, Paperwork Reduction Project (0704-0188), Washington, DC 20503.				
1. AGENCY USE ONLY (Leave blank)		2. REPORT DATE October 1992		3. REPORT TYPE AND DATES COVERED Technical Memorandum
4. TITLE AND SUBTITLE Bibliography of Lewis Research Center Technical Publications Announced in 1991			5. FUNDING NUMBERS None	
6. AUTHOR(S)				
7. PERFORMING ORGANIZATION NAME(S) AND ADDRESS(ES) National Aeronautics and Space Administration Lewis Research Center Cleveland, Ohio 44135-3191			8. PERFORMING ORGANIZATION REPORT NUMBER E-6928	
9. SPONSORING/MONITORING AGENCY NAMES(S) AND ADDRESS(ES) National Aeronautics and Space Administration Washington, D.C. 20546-0001			10. SPONSORING/MONITORING AGENCY REPORT NUMBER NASA TM-105595	
11. SUPPLEMENTARY NOTES Compiled by Technical Information Services Division, Lewis Research Center.				
12a. DISTRIBUTION/AVAILABILITY STATEMENT Unclassified - Unlimited Subject Category 82			12b. DISTRIBUTION CODE	
13. ABSTRACT (Maximum 200 words) This compilation of abstracts describes and indexes the technical reporting that resulted from the scientific and engineering work performed and managed by the Lewis Research Center in 1991. All the publications were announced in the 1991 issues of STAR (Scientific and Technical Aerospace Reports) and/or IAA (International Aerospace Abstracts). Included are research reports, journal articles, conference presentations, patents and patent applications, and theses.				
14. SUBJECT TERMS Bibliographies; Abstracts; Documentation; Indexes (Documentation)			15. NUMBER OF PAGES 402	
			16. PRICE CODE A18	
17. SECURITY CLASSIFICATION OF REPORT Unclassified	18. SECURITY CLASSIFICATION OF THIS PAGE Unclassified	19. SECURITY CLASSIFICATION OF ABSTRACT Unclassified	20. LIMITATION OF ABSTRACT	

National Aeronautics and
Space Administration
Lewis Research Center
Cleveland, Ohio 44135-3191

Official Business
Penalty for Private Use, \$300

FOURTH CLASS MAIL

ADDRESS CORRECTION REQUESTED



Postage and Fees Paid
National Aeronautics and
Space Administration
NASA-451

NASA
